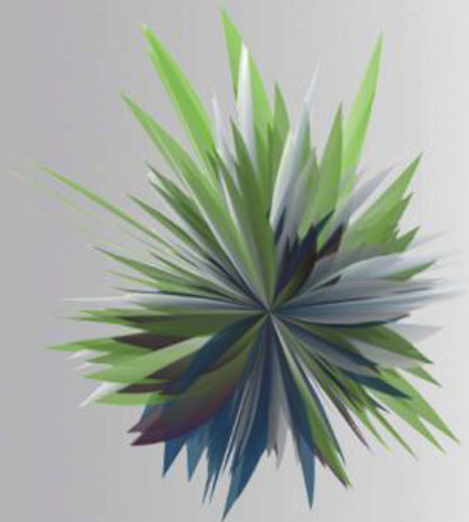# Handbook of Imaging the Alzheimer Brain

Edited by

J. Wesson Ashford
Allyson Rosen
Maheen Adamson
Peter Bayley

Osama Sabri
Ansgar Furst
Sandra E. Black
Michael Weiner

IOS Press

HANDBOOK OF IMAGING THE ALZHEIMER BRAIN

Advances in Alzheimer's Disease

Advances in Alzheimer's Disease brings together the latest insights in Alzheimer's disease research in specific areas in which major advances have been made. This book series assembles and builds on work recently published in the *Journal of Alzheimer's Disease* (JAD) and also includes further contributions to ensure comprehensive coverage of the topic. The emphasis is on the development of novel approaches to understanding and treating Alzheimer's and related diseases.

Series Editors:
George Perry, Ph.D. and Mark A. Smith, Ph.D.†

Volume 2

Previously published in this series

Handbook of Imaging the Alzheimer Brain

Edited by

J. Wesson Ashford, M.D., Ph.D.
Stanford/VA Palo Alto HCS, USA

Allyson Rosen, Ph.D.
Stanford/VA Palo Alto HCS, USA

Maheen Adamson, Ph.D.
Stanford/VA Palo Alto HCS, USA

Peter Bayley
Stanford/VA Palo Alto HCS, USA

Osama Sabri, M.D.Ph.D.
Leipzig University, Germany

Ansgar Furst, Ph.D.
Stanford/VA Palo Alto HCS, USA

Sandra E. Black M.D. FRCP(C)
Sunnybrook, University of Toronto, Canada

and

Michael Weiner, M.D.
UC San Francisco / VA San Francisco, USA

PRINTED IN THE NETHERLANDS

Dedication

This book is dedicated to Veterans who have returned from combat with traumatic brain injuries (TBI), post-traumatic stress disorder (PTSD), and other war-related illnesses and injuries that may cause cognitive dysfunction and increase the risk for developing dementia in the future. TBI and PTSD may contribute to brain degeneration and AD through attacking common neural substrates. Veterans have made great sacrifices for the welfare of others, and we are deeply grateful to the Veterans who've served their countries and who dedicate themselves to helping future generations through participating in dementia research.

Considerable support for the organization of this volume was provided by the U.S. Department of Veterans Affairs, including the War Related Illness and Injury Study Center (WRIISC) at the Veterans Affairs Palo Alto Health Care System (Drs. Maheen Adamson, J. Wesson Ashford, Peter Bayley, Ansgar Furst, Ahmad Salehi), based in the VA Office of Public Health and Environmental Hazards, and the Department of Veterans Affairs Sierra-Pacific Mental Illness Research, Education, and Clinical Center (MIRECC) (Drs. Ruth O'Hara, Allyson Rosen, Michael Weiner, Jerome Yesavage).

It is hoped that the advances in brain imaging for Alzheimer's disease described in this book will not only lead to benefits for people with and predisposed to dementing disorders, but will also help Veterans with TBI and PTSD, as well as patients with other brain disorders.

A special note is made here to honor the memory of Dr. Mark A. Smith, the late Editor in Chief of the *Journal of Alzheimer's Disease*, who contributed a great deal toward the organization of the systems that led to the creation of this book.

Commendation is given to Rasjel van der Holst, a publisher at IOS Press, who conceptualized the idea of this book, participated in the recruitment of the editors, and worked diligently to make this book a reality.

This book was made possible by the efforts and work of Beth Kumar, Managing Editor of the *Journal of Alzheimer's Disease*, and Dr. George Perry, Editor in Chief of the *Journal of Alzheimer's Disease*.

Thanks is due to all of the co-editors and section editors who willingly volunteered their time to create this volume. Further, there are over 400 individual authors from many countries around the world who contributed their hard work to research and manuscript writing to provide the important content presented here, and their efforts are also very much appreciated.

A final thank you goes to all research participants, both normal individuals and patients with various serious conditions, who contributed to the research that made this volume possible. Since there is no true animal model for Alzheimer's disease, it is absolutely essential for people, including younger and older individuals without known problems as well as patients with Alzheimer's disease, to participate in this kind of research for us to make progress against the devastating conditions that impair our mental functions in our later years.

J. Wesson Ashford, M.D., Ph.D.
Director, War Related Illness and Injury Study Center, VA Palo Alto Health Care System
Clinical Professor (affiliated), Department of Psychiatry and Behavioral Sciences, Stanford University

This page intentionally left blank

Preface

Alois Alzheimer first described the syndrome associated with his name in a conference in 1906 and then published a paper that accurately described this condition, both the clinical presentation and the pathology, in 1907. The patient who he described was 51 years of age when she first presented to him with dementia and psychosis, at an age close to the average life-expectancy of that region of Germany at that time. He also described her presentation as a rare, presenile form of dementia, and pathologically she had severe atherosclerosis as well as a form of changes in the brain that he saw for the first time due to the newly available silver stains, senile plaques and neurofibrillary changes, which are now the pathological hallmarks of this disease. Two factors have brought Alzheimer's disease from a rare condition to what is now the leading factor associated with death in the developed world: 1) the presence of the senile plaques and neurofibrillary changes in the most common form of dementia in the elderly, and 2) the progressive increase in life-expectancy (about 25 years since Alzheimer's time) leading to a huge growth in the elderly population in the age range which is most susceptible to this condtion.

The great developments that have led to this handbook are the advances in the technology for imaging the brain of the living person. In the last 50 years, a wide variety of techniques have emerged, including measurement of electromagnetic signals, anatomy, functional activity, chemical composition, and neuropathological changes. These techniques are not yet able to image individually the senile plaques and neurofibrillary changes that are seen by the pathologists at autopsy, but they are reflecting Alzheimer pathological changes more and more closely. Now, these techniques allow imaging of brain regions that estimates the presence of senile plaques that are seen by the pathologists at autopsy, and ligands for neurofibrillary changes are under active development, so new techniques are able to report more and more accurate estimations of pathological changes of Alzheimer's disease. Other techniques reviewed in this handbook are able to convey critical information about the function and connectivity of the brain that is disrupted by Alzheimer pathology.

This handbook was developed to provide an overview of the state of the art of brain-imaging approaches that have recently emerged to reveal the critical characteristics of brains of patients with Alzheimer's disease. The book was initially conceived as an opportunity to present the major findings produced from the Alzheimer's Disease Neuroimaging Initiative (ADNI), which has been led by Michael Weiner, and has led to the publication over 200 hundred papers on imaging the brains of individuals along the transition from elderly normal to mild cognitive impairment to mild dementia. This book provides numerous chapters that examine this critical phase of Alzheimer's disease, but chapters also discuss diagnosis, early biomarkers, late changes, the role of vascular disease, and treatment. The book drew from presentations at the International Conference on Alzheimer's Disease (ICAD), which met in Hawaii in July, 2010, and the associated Alzheimer's Imaging Consortium, chaired by Sandra Black and Giovanni Frisoni.

This book is organized in 10 sections. Each section addresses a particular neuroimaging modality that has been found to be useful in understanding or diagnosing Alzheimer's disease. Each section has an introduction to the particular technique and how it has the potential for informing clinical care or evaluating novel therapies for Alzheimer's patients. The chapters provide clinicians with specific information as to how the particular neuroimaging technique is or can be useful in a clinical setting, including the gamut from Radiology to Primary Care and address specific advances in the various types of neuroimaging. The book includes brief overviews of imaging of Alzheimer's disease and reviews fundamental principles for neuroimaging pathological changes that it causes, with an emphasis on practical and future applications.

The basic concept of this compendium is that each section provides an overview of the use of brain imaging in the specific area of Alzheimer's disease neuroimaging. The chapters in this book provide the field with perspectives on the value of the various imaging techniques for screening for Alzheimer's disease, determining the early markers of the disease, making the diagnosis, following the progression of the disease, determining the variability of the manifestation of Alzheimer's disease, and estimating the utility of these metrics of disease

severity for examining the effects of treatments. However, this work has not addressed all of the numerous complexities of Alzheimer's disease, including co-occurrence, Parkinson's disease, fronto-temporal dementia, etc., and only briefly touches on vascular risk factors and subcortical ischemic vasculopathy.

The target audience for this book is the clinical community, including medical students, residents-in-training with an interest in neuroimaging, as well as clinicians and faculty in fields where neuroimaging of Alzheimer's disease is and will become even more critical as automatic quatnification methods start coming on-line and available for practicing clinicians taking care of the affected patients (Family Practitioners, Geriatric Medicine, Neurologists, Radiologist, Psychiatrists). The overview is relatively brief but highly accessible for students, clinicians, and other researchers studying Alzheimer's disease, since a need to understand the clinical aspects of the disease are critical for guiding basic investigations.

Alzheimer's disease is a common problem which is becoming progressively more prevalent and burdensome to the World. Through better recognition of this disease and more precise diagnosis, led by brain imaging in the appropriate clinical context, it is our sincere hope that mankind can conquer this terrible disease.

J. Wesson Ashford, Sandra E. Black, Giovanni Frisoni and George Perry

Contents

**Section 3: Imaging of Cerebral Blood Flow, Glucose Metabolism, Amyloid Plaques and Neurofibrillary
Tangles in AD**

Section 4: Current Advances in Functional Magnetic Resonance Imaging for Detecting Alzheimer's Disease

Section 5: Electromagnetic Brain Mapping

Section 7: Magenetic Resonance Spectroscopy

Section 8: Longitudinal Neuroimaging Measures: Windows into Progression of Disease and Potential Endpoints for Clinical Trials

This page intentionally left blank

Section 1
Imaging the Alzheimer Brain: The Pathology and Pathophysiolgical Bases of Alzheimer's Disease: Implications for Advancing Diagnostic Imaging

This page intentionally left blank

Introduction

Section 1: Imaging the Alzheimer Brain: The Pathology and Pathophysiological Bases of Alzheimer's Disease: Implications for Advancing Diagnostic Imaging

J. Wesson Ashford*, Ahmad Salehi, Ansgar Furst and Peter Bayley
War Related Illness and Injury Study Center, VA Palo Alto Health Care System, Department of Psychiatry and Behavioral Sciences, Stanford University, Palo Alto, CA, USA

Abstract. Alzheimer's disease (AD), first described by Alois Alzheimer in 1906, is a combination of neuropathological processes, which is devastating the world socially and economically. The distinct neuropathological observations are the senile plaques, composed predominantly of the amyloid-beta protein, and the neurofibrillary changes (threads and tangles), made of hyperphosphorlyated micro-tubule associate protein tau. Autosomal-dominant genetic factors can cause AD under 60 years of age, and Apo-lipo-protein E factors are strongly related to risk after age 60. AD affects basic neuronal plasticity mechanisms leading to relentless loss of memory function that causes insidious and progressive dementia. Recent conceptualizations have emphasized the progression of AD from the earliest abnormal preclinical changes, through appearances of memory and other cognitive impairments, leading to losses of function associated with dementia. This brief summary introduces a compendium of articles on AD which examines the advances in the science, engineering, and technology of imaging the brain to better understand and diagnose AD and develop treatments and cures. This introduction emphasizes the primary importance of understanding pathology, pathophysiology, and causation, genetic and environmental. The approaches described in this compendium are arranged according to widely used practices, including structural and functional imaging techniques as well as electro-magneto-encephalography and magnetic resonance spectroscopy, with additional chapters focusing on vascular factors, techniques for assessing longitudinal change, and multi-modal integration for the future. Advances in brain imaging hold the promise to contribute understanding of AD for development of therapies to prevent the disease at its earliest stages, halt its progression, and reverse its dementia.

Keywords: Alzheimer's disease, amyloid beta-peptides, neurofibrillary tangles, magnetic resonance imaging, positron-emission tomography, electroencephalography, apolipoproteins E, synapses, neuronal plasticity, leptin

On November 3, 1906, in a presentation for the South-West German Society of Alienists (the term used

---

*Correspondence to: J. Wesson Ashford, E-mail: ashford@stanford.edu.

at that time for superintendents of insane asylums) in Tübingen, Germany, Alois Alzheimer, presented a paper entitled "Über eine eigenartige Erkrankung der Hirnrinde" ("regarding a curious disease of the cortex"). In this paper, he described for the first

time a constellation of symptoms in a 51 year-old woman that was associated at autopsy with several new neuropathological changes. This patient initially showed suspiciousness of her husband, and then soon developed a rapidly increasing memory impairment, disorientation, and further paranoia with progressive agitation. Clinically, the most severe disturbance was in her ability to encode information, immediately forgetting things after clearly perceiving them. The condition progressed to utter bewilderment with complete disorientation to time and place, leading to a terminal state after 4.5 years. The original description of her brain included both macro and microscopic pathology. Although postmortem examination showed generalized atrophy of the brain, there was no macroscopic focal degeneration. Upon preparation of tissue samples, neuritic plaques, neurofibrillary tangles, neuropil threads, and reactive gliosis were evident and appeared to be occurring with the deposition of a "pathological metabolic substance in the neuron" [1, 2].

The modern era of interest was ushered in when in 1968 Blessed, Tomlinson, and Roth linked the common, progressive dementia found in the elderly to the same type of pathology described originally by Alzheimer [3]. Today, the disease originally described by Alzheimer in a younger individual is no longer unique or infrequent. The incidence of Alzheimer's disease (AD) has progressively increased with the great extension of longevity in most parts of the world over the last 100 years [4]. Now, AD is the most common cause of dementia, and reported as the sixth leading cause of all deaths in the United States (Centers for Disease Control (CDC) mortality data, 74,632 deaths attributed to AD in 2007). However, by another analysis, AD is now associated with more deaths than heart disease (in 2007, the CDC reported 2,423,712 total deaths and 616,067 deaths related to heart disease, 25.4% of all US deaths, but at the same time, the Alzheimer's Association estimated that 5 million individuals had AD in the US, with an 8 year life expectancy, leading to the calculation that 625,000 deaths would be AD-related, which is 25.8% of all deaths). According to the World Health Organization (WHO), in 2008, there were more than a half million deaths in the world attributed to AD, a number still greatly under-estimating the occurrence of AD.

These already grim figures do not take into account the psychological and social burdens of AD. Overall, AD patients are more likely to have mental health conditions, neurological conditions, cognitive disorders, cerebrovascular disease, diabetes with acute complications, and injuries resulting in annual costs for AD patients being 34% higher than for matched controls [5]. Individuals with AD have higher healthcare costs and utilization than demographically-matched Medicare beneficiaries and even after adjusting for co-morbid illnesses sustain more emergency room visits and inpatient admissions [6]. As the US population ages, AD rates are expected to quadruple over the next 50 years [7]. In order to diminish or even sustain the current level of the devastating worldwide social and economic impact of AD, there is an urgent need to further our understanding and expedite research and development on all aspect of AD.

Thanks to enormous advances in science, engineering and technology in recent decades, new imaging methods have been developed. The purpose of the *Handbook of Imaging the Alzheimer Brain* is to present the developments and advances in numerous imaging modalities that are currently being used to increase our understanding of the pathophysiological basis of AD and drive us toward new therapies for this multi-system disorder. The chapters of this collection clearly show that multiple imaging systems are now available for helping understand, diagnose, and treat AD.

UNDERSTANDING THE PATHOLOGICAL BASIS OF AD

The fundamental pathological changes in AD are senile plaques, both primitive and neuritic (SPs) and neurofibrillary pathology (NP), which include both tangles and neuropil threads (see [8]). The SPs are thought to progress from a primitive to a neuritic form which is composed of several pathological entities including aggregated amyloid-β (Aβ) protein, inflammatory glial cells, and pathological neurites containing hyper-phosphorylated microtubule-associated protein tau [9, 10]. The NP is composed principally of paired-helical filaments (PHFs) which are composed of hyper-phosphorylated tau [10, 11]. The relationship between these two pathological entities, SPs and NP, is not fully understood. The neuropil threads are actually in dendrites and linked from the neuropil to the neuronal cell bodies which contain the neurofibrillary tangles [12]. These fundamental pathological entities are thought to begin their formation long before the first psycho-social symptoms appear [13].

A core concern in understanding AD has been the question of the nature, origin, and development of

Alzheimer pathology. There have been two schools of thought concerning the development of Alzheimer pathology, one that has focused on the amyloid pathology of AD [14] and another that has considered the neurofibrillary pathology to be the fundamental problem [13]. Resolution of the relationship between these components may lead to the understanding of AD that has so far eluded research.

THE NEW PERSPECTIVE ON THE CONTINUUM OF AD

A new perspective has been developing in this field, that there must be consideration for the earliest developments of pathological changes associated with this disease. The pioneering discovery in this direction was from the Nun Study that showed the linguistic ability evident in the writing in women in their early 20's could be associated with their later development of AD-related dementia [15]. This finding is complemented by recent pathological studies which have found that Aβ decreases in the spinal fluid likely occur as early as the fourth decade of life [16] and pathological findings of neurofibrillary pathology in individuals in their third decade [13]. Further AD-related changes can even be found in the entorhinal cortex of children [17]. This new perspective has led to the recent division of AD into preclinical [18], mild cognitive impairment [19], and dementia [20], with a particular focus on biomarkers and brain imaging [21]. Now AD can be seen as a continuum [22] that is influenced by factors early in life, including genetics [23, 24] and education [25].

The purpose of this *Handbook of Imaging the Alzheimer Brain* is to present the numerous modalities that are currently being used to estimate the degree of Alzheimer pathology in the brains of living individuals who are at risk for developing dementia or have already suffered from the impairments caused by this pathological condition. Conceptualizing the continuum of AD is likely to provide greater understanding of this disease and help to advance diagnosis and the quest for prevention and treatment.

DEFINING THE CRITICAL AREAS OF AD STUDY

A central theme of this book is the imaging of the brain along the continuum of AD, from young individuals who have early AD changes or have developed a predisposition, through early signs of cognitive impairment, through mild to profound dementia. Associated issues include genetic factors and environmental events that predispose an individual to develop Aβ or neurofibrillary pathology as well as the associated dementia.

Neurofibrillary pathology

Neurofibrillary pathology relates to the severity of dementia. The selective appearance of neurofibrillary changes in specific regions of the brain [26] and its progression through the brain [13] correspond closely to the distribution of loss of perfusion [27] (Fig. 1) and metabolism (Sections 3 and 4 in this volume). The abnormalities of metabolism are seen prior to the development of dementia in association with the APOE ε4 genetic factor [28, 29] (see below). Even though the neurofibrillary changes are closely related to dementia, they do not have a clear relationship to genetic factors. However, they do seem to be stimulated by at least one environmental factor, trauma. A specific PET ligand, FDDNP is able to show the distribution of neurofibrillary pathology in humans (see Shin et al., in Section 3 of this volume).

Amyloid-β accumulation and neurofibrillary degeneration

Aβ plaques constitute an important aspect of AD pathology. While rare genetic mutations associated with the production of Aβ suggest an important role for Aβ in AD in the affected younger individuals (see Reiman et al., Section 8 of this volume), the relationship of Aβ to AD in older patients has been less clear. AD is characterized by Aβ accumulation in the brain of affected individuals, and Aβ depositions are associated with the predisposition to dementia. However, Aβ depositions relate poorly to the severity of dementia, and neither Aβ accumulation nor the number of plaques has been strongly linked to the severity of cognitive dysfunction in AD (see [30]). The deposition of Aβ in the brain can now be imaged with PET ligands. PET ligands, such as ^{11}C-labelled Pittsburgh compound B (PIB) and ^{18}F-labelled Aβ ligands (florbetapir F18 (^{18}F-AV-45), ^{18}F-flutemetamol (^{18}F-GE067), florbetaben (^{18}F-BAY94-9172), and ^{18}F-FDDNP) (see Section 3 in this volume).

Synaptic loss

Synapses are the dynamic infrastructures of cognitive processes. The anabolic production, maintenance,
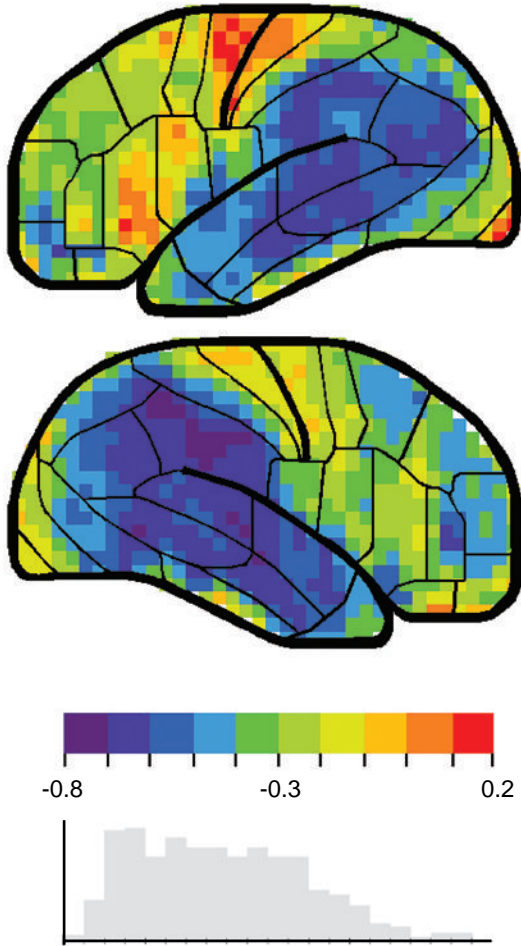
Fig. 1. Lateral view of the cortical surface (left side is on top). Scale indicates range for Peason corrletions with single decimal precision with "time-indexed" estimation of dementia severity in 30 probable AD male patients with a broad range of severity. Bottom graph shows relative frequency of each decimal range [27].

remodeling, and removal of these important entities are crucial for normal cognitive function [31]. Numerous studies have shown that AD is linked to a significant loss of synapses and synaptic markers in a variety of brain regions [32]. The loss of synapses is not only due to neuronal loss but also is linked to reduced number of synapses per neurons, likely related to the accumulation of hyperphosphorylated tau in dendrites [12]. Indeed compared with other pathological hallmarks of AD, the severity of synaptic loss correlates best with the severity of cognitive dysfunction in AD [32]. Excessive synaptic loss in the AD brain is associated with a cascade of pathology, including hypofunction (decreased metabolism and blood flow), atrophy, and alteration in the chemical composition in vari-

ous brain regions. For this reason, imaging modalities that can detect either structural (Section 2), metabolic (Section 3), functional (Section 4), electro-magneto-encephalographic (Section 5), axonal tract (Section 6), or chemical (Section 7) alterations in the brain are critical in detecting and assessing these pathological changes.

Neuronal loss and/or hypofunction of specific systems

In addition to significant loss of neurons in the cortex and hippocampus, AD is also characterized by a significant loss and dysfunction of subcortical neurons projecting extensively to the hippocampus and cortex (Section 1). These losses are some of the most critical early changes in the AD brain and may contribute to the development of pathology in the cerebrum. For example, degeneration of cholinergic neurons in the nucleus basalis of Meynert occurs early in the course of AD [33, 34]. Indeed, cholinergic drugs represent the most successful class of pharmaceuticals yet developed to treat AD. Other neurotransmitter systems are also affected early in AD, including, the serotonin nuclei, particularly in the dorsal raphe nucleus, which may be affected significantly before any cerebral changes occur [35], and the noradrenergic neurons of the locus coeruleus (see Milan et al., in Section 1 of this volume). The loss of markers and atrophy of these neurons in AD may specifically lead to degeneration and dysfunction in both hippocampus and cortex. These structural and functional changes are easily detected by MRI and fMRI (Sections 2 and 4). Furthermore, the significant loss of neurons will also reflect the loss of extensive connections between these regions which can be detected by EEG [36] (see Babiloni et al., in Section 5 of this volume) and DTI (Section 6).

Metabolic disorders

Apolipoprotein E (ApoE) polymorphism constitutes the strongest genetic risk factor linked to the sporadic form of AD [23, 24]. Interestingly, ApoE ε4 alleles increase the risk of AD in a dose dependent manner. Although the exact mechanism by which ApoE4 alleles lead to increased risk of AD remains to be determined, a link to amyloid binding and neuroplastic mechanisms appears likely, particularly the high, constant frequency of synapse creation and removal [24, 37]. Further, decreased neuronal activity related to ApoE ε4 alleles is one of the most significant associations

between any contributing factor and AD pathophysiology [38]. Indeed, abnormalities of metabolism are seen prior to the development of dementia in association with the APOE ε4 [28, 29]. Numerous studies have shown the link between ApoE ε4 alleles and cerebral metabolic rate for glucose (CMRgl) in brain regions including posterior cingulate, precuneus, parietal, temporal, and prefrontal brain regions in ApoE ε4 carriers [39] (Sections 3 and 4).

The relationship of AD to the general status of cerebral metabolism is also of potential importance. Links to glucose metabolism and insulin mechanisms have been of considerable interest (see Section 10). There is also a potential link to fat metabolism and leptin that is still under investigation [40]. Further, there are potential associations between risk and sex hormones. The relationship of AD to vascular factors is also of great importance (see Section 9 of this volume).

Environmental factors, traumatic brain injury, and complex stimulation

While there are clearly genetic factors predisposing to AD, there are numerous environmental factors that have been considered to have a possible relationship to AD causation. Questions of great interest in this handbook are which factors could be better studied through brain imaging and whether brain imaging can help to determine if the manipulation of those factors would lead to measurable alterations of the course of AD pathology development.

The relationship between repetitive brain trauma and progressive neurological abnormalities has long been established. Chronic traumatic encephalopathy seems to be a major contributor in cognitive dysfunction seen in athletes, particularly boxers and probably several other groups. Brain trauma may lead to significant atrophy of multiple brain regions including cortical and hippocampal areas and enlargement of ventricles. Microscopically, this condition is characterized by neuronal loss, gliosis, the occurrence of neurofibrillay degeneration, particularly in superficial cortical layer neurons, and tau-positive astrocytes [41].

Another recent finding is that combat veterans suffering from post-traumatic stress disorder (PTSD) have a two fold increase risk of dementia [42]. Of note, PTSD is also significantly associated with head trauma in this population.

Environmental stimulation such as education [25] may decrease the risk of dementia. Further, as described by Rosen et al. and Forster et al. in Sec-

tion 8 of this volume, cognitive stimulation may have positive effects on dementia that can be measured by brain imaging techniques.

IDENTIFYING BIOMARKERS AND DEVELOPING EARLY DETECTION METHODS

The strongest genetic factor associated with AD in older individuals is the APOE genotype, with the variation in incidence between the ε4/4 to ε3/3 to ε2/2 individuals potentially explaining 95% of the causation of AD [24]. Recent data from the Alzheimer's Disease Neuroimaging Initiative (ADNI) had initially suggested that CSF Aβ and tau levels were associated with the transition from "normal" to "MCI" to "mild dementia". However, re-examination of the data by genotype indicated that only the tau measures were associated with dementia, while the Aβ levels were associated with APOE genotype [43]. Further, the initial association of Aβ to diagnosis turned out to be an artifact related to the small number of individuals with the APOE ε4 allele in the normal group, an intermediate number in the MCI group, and a large number in the mild dementia group) (Tables 1, 2). Age was also a contributing variable (Table 3). This point is critical to understand because many studies that examine Alzheimer patients and compare their results to normal individuals do not address the issue of specific APOE genotype and age, which appears to be critical for the diagnosis of AD and for establishing the links leading to its causation.

There is a further problem with the APOE genotype that should be mentioned here. While the APOE protein is a cholesterol transport protein, it appears to bind to Aβ, with the APOE ε4 protein binding most strongly to it (see [24, 37] for reviews). Such strong binding could explain why the APOE ε4 individuals have lower Aβ in their cerebro-spinal fluid and more Aβ deposition in the brain. However, Aβ deposition in the brain has a high relationship to AD risk but not to

Table 1
ADNI data on CSF biomarkers, mean ± SD

	Tau	Aβ	P-Tau-[181]P
AD ($n = 102$)	122 ± 58	143 ± 41	42 ± 20
MCI ($n = 200$)	103 ± 61	164 ± 55	35 ± 18
Normal ($n = 114$)	70 ± 30	206 ± 55	25 ± 15

$p < 0.0001$, for each of the 3 biomarker tests for AD vs. Normal and for MCI vs. Normal. For AD vs. MCI: $p < 0.005$, Tau; $p < 0.01$, Aβ; $p < 0.01$, P-Tau-181P. Mann-Whitney test (ADNI data, 2008).

Table 2
When the same data is analyzed by APOE genotype, different results are found, mean ± SD

APOE genotype	Normal	MCI	Mild AD
CSF Aβ levels			
33	212.4 ± 48.4	189.1 ± 59.8	168.8 ± 52.3
34	156.0 ± 47.8	148.4 ± 42.4	139.0 ± 27.2
44	126.0 ± 2.8	119.8 ± 23.5	116.2 ± 22.3
CSF P-Tau levels			
33	67.8 ± 26.9	83.6 ± 40.8	123.8 ± 68.6
34	81.8 ± 42.6	122.4 ± 72.7	113.3 ± 42.0
44	71.0 ± 2.8	110.6 ± 45.9	128.9 ± 53.1
	p-value		
Aβ comparison			
33 vs. 34	<0.0001		
33 vs. 44	<0.0001		
34 vs. 44	0.08		
Normal vs. MCI	0.57		
Normal vs. Mild AD	0.15		
MCI vs. Mild AD	0.20		
	p-value		
P-Tau comparison			
33 vs. 34	0.07		
33 vs. 44	0.67		
34 vs. 44	0.99		
Normal vs. MCI	0.05		
Normal vs. Mild AD	<0.01		
MCI vs. Mild AD	0.06		
APOE εgenotype	Normal	MCI	Mild AD
3/3	67 (72%)	82 (44%)	29 (31%)
3/4	24 (26%)	81 (44%)	42 (45%)
4/4	2 (2%)	22 (12%)	22 (24%)

Number of subjects (note more ε4 alleles with higher grade of AD diagnosis

Table 3
Ages of ADNI CSF subjects in each APOE genotype and subject group, mean ± SD

APOE ε4 genotype	Normal	MCI	Mild AD
3/3	75.8 ± 5.0	75.4 ± 8.4	76.3 ± 8.6
3/4	75.8 ± 6.0	73.9 ± 6.7	75.6 ± 6.6
4/4	77.0 ± 1.4	72.2 ± 6.0	69.8 ± 7.0

AD dementia (see Section 3 of this volume). Accordingly, there is a question of what the causal link is between Aβ and dementia. While Aβ is considered toxic, that toxicity may just be a normal aspect of neuroplasticity [37, 44–46]. It is the loss of synapses which is most closely associated with dementia [32], followed by the neurofibrillary pathology [3], with the neurofibrillary pathology likely leading to the synapse loss [12]. The question then is whether the Aβ somehow leads to the neurofibrillary pathology [47] or whether some associated factor, even an adjacent gene like Translocase of outer mitochondrial membrane 40 homolog

(*TOMM-40*) [48], which affects mitochondrial function, leads to the NCs.

EFFECTIVE METHODS OF EVALUATION OF THERAPIES

Having access to methods that allow unbiased evaluation of different therapeutic strategies is an important aspect of developing a successful strategy for treating any disorder. Numerous therapeutic strategies, both invasive and non-invasive, have been used for the treatment of AD. These methods have focused either on reducing accumulation of specific proteins and/or elements, restoring the function of specific systems, increasing the function of neurons using trophic factors, or reducing the reaction of the brain to protein accumulation and toxicity. Although a few intervention strategies have shown promising effects and have reached advanced stages of clinical trials, the only approved methods for countering cognitive dysfunction in AD are drugs that increase cholinergic tone (tacrine, donepezil, galantamine, rivastigmine) and a drug that affects glutamate neurotransmission by modulating *N-methyl-D-aspartate* (NMDA) receptor activation (memantine). Advanced imaging methods have been instrumental in verifying the effects of different treatments in AD. Section 8 discusses important considerations for utilizing the developments in brain imaging to more effectively evaluate the benefit of treatments for AD.

The development of treatments for AD should begin with better understanding of the pathophysiology and more accurate assessments of the state and rate of progression of the disease. The earliest factors in the AD course are genetic (for example, see Reiman et al., in Section 8 of this volume), and the APOE genotype appears to reflect a factor that is highly related to the predisposition to AD, though there have been no treatments yet that appear to block this predisposition yet that appear to block this predisposition. Since APOE-related brain changes may be detected in childhood, interventions addressing this factor should begin very early in life (the best model may be the management of phenyl-ketonuria). The changes related to Aβ have been suggested to occur in middle adulthood [16], so therapeutic strategies that address Aβ would greatly benefit from brain imaging techniques that can detect Aβ deposition at this middle phase of the disease. For therapies that target prevention of dementia progression (a later phase of the newly conceived

AD continuum) early in its course, a greater focus on measuring atrophy, metabolism, and tau would be of most utility [49]. Recent data suggest that blocking tau hyperphosphorylation may be sufficient to prevent the progression to dementia [50]. Consequently, the brain imaging approaches most associated with neurofibrillary pathology would be of most relevance for assessing the benefits of therapies that target the transmission from the state of normal cognitive function to dementia.

FUTURE DIRECTIONS OF AD RESEARCH AND CLINICAL DEVELOPMENT

The concordance of the changes seen with pathological analysis, brain imaging, and neurocognitive testing indicate that the visualization of AD has progressed far, but discovering the cause of AD and developing appropriate interventions for cure and prevention have remained elusive. Future efforts will be needed to continue the incredible advances in neuroimaging (see Section 10). However, there needs to be more focus on the fundamental causative mechanisms leading to AD. In particular, advances in genetics need to determine the specific contributions of genetic factors to all of the pathological changes observed both biologically and psycho-socially. Since all adults with Down syndrome have AD pathology by age 40, there should be more emphasis on understanding the pathophysiological basis of Down syndrome which is considered a genetic model of AD. Understanding of how numerous environmental factors affect AD progression from an apparently normal state toward dementia also needs to be defined. Further refinements are also needed to improve the measurements of cognitive function to the point were cognitive measures accurately and precisely reflect the pathological changes seen in brain imaging and other biomarkers.

REFERENCES

[1]   Alzheimer A (1907) Über eine eigenartige Erkrankung der Hirnrinde. *Allgemeine Zeitschrift für Psychiatrie* **64**, 146-148.
[2]   Azheimler A, Stelzmann RA, Schnitzlein HN, Murtagh FR (1995) An English translation of Alzheimer's 1907 paper, "Uber eine eigenartige Erkankung der Hirnrinde". *Clin Anat* **8**, 429-431.
[3]   Blessed G, Tomlinson BE, Roth M (1968) The association between quantitative measures of dementia and of senile change in the cerebral grey matter of elderly subjects. *Br J Psychiatry* **114**, 797-811.
[4]   Ashford JW (2008) Screening for memory disorder, dementia, and Alzheimer's disease. *Aging Health* **4**, 399-432.
[5]   Kuo TC, Zhao Y, Weir S, Kramer MS, Ash AS (2008) Implications of comorbidity on costs for patients with Alzheimer disease. *Med Care* **46**, 839-846.
[6]   Zhao Y, Kuo TC, Weir S, Kramer MS, Ash AS (2008) Healthcare costs and utilization for Medicare beneficiaries with Alzheimer's. *BMC Health Serv Res* **8**, 108.
[7]   Aupperle PM (2006) Navigating patients and caregivers through the course of Alzheimer's disease. *J Clin Psychiatry* **67 Suppl 3**, 8-14; quiz 23.
[8]   Geddes JW, Tekirian TL, Soultanian NS, Ashford JW, Davis DG, Markesbery WR (1997) Comparison of neuropathologic criteria for the diagnosis of Alzheimer's disease. *Neurobiol Aging* **18**, S99-S105.
[9]   Stromer T, Serpell LC (2005) Structure and morphology of the Alzheimer's amyloid fibril. *Microsc Res Tech* **67**, 210-217.
[10] Perl DP (2000) Neuropathology of Alzheimer's disease and related disorders. *Neurol Clin* **18**, 847-864.
[11] Schochet SS Jr (1998) Neuropathology of aging. *Neurol Clin* **16**, 569-580.
[12] Ashford JW, Soultanian NS, Zhang SX, Geddes JW (1998) Neuropil threads are collinear with MAP2 immunostaining in neuronal dendrites of Alzheimer brain. *J Neuropathol Exp Neurol* **57**, 972-978.
[13] Braak H, Braak E (1997) Frequency of stages of Alzheimer-related lesions in different age categories. *Neurobiol Aging* **18**, 351-357.
[14] Hardy J, Selkoe DJ (2002) The amyloid hypothesis of Alzheimer's disease: progress and problems on the road to therapeutics. *Science* **297**, 353-356.
[15] Snowdon DA, Kemper SJ, Mortimer JA, Greiner LH, Wekstein DR, Markesbery WR (1996) Linguistic ability in early life and cognitive function and Alzheimer's disease in late life it Findings from the Nun Study. *Jama* **275**, 528-532.
[16] Morris JC, Roe CM, Xiong C, Fagan AM, Goate AM, Holtzman DM, Mintun MA (2010) APOE predicts amyloid-beta but not tau Alzheimer pathology in cognitively normal aging. *Ann Neurol* **67**, 122-131.
[17] Shaw P, Lerch JP, Pruessner JC, Taylor KN, Rose AB, Greenstein D, Clasen L, Evans A, Rapoport JL, Giedd JN (2007) Cortical morphology in children and adolescents with different apolipoprotein E gene polymorphisms: an observational study. *Lancet Neurol* **6**, 494-500.
[18] Sperling RA, Aisen PS, Beckett LA, Bennett DA, Craft S, Fagan AM, Iwatsubo T, Jack CR Jr, Kaye J, Montine TJ, Park DC, Reiman EM, Rowe CC, Siemers E, Stern Y, Yaffe K, Carrillo MC, Thies B, Morrison-Bogorad M, Wagster MV, Phelps CH (2011) Toward defining the preclinical stages of Alzheimer's disease: Recommendations from the National Institute on Aging-Alzheimer's Association workgroups on diagnostic guidelines for Alzheimer's disease. *Alzheimers Dement* **7**, 280-292.
[19] Albert MS, Dekosky ST, Dickson D, Dubois B, Feldman HH, Fox NC, Gamst A, Holtzman DM, Jagust WJ, Petersen RC, Snyder PJ, Carrillo MC, Thies B, Phelps CH (2011) The diagnosis of mild cognitive impairment due to Alzheimer's disease: Recommendations from the National Institute on Aging-Alzheimer's Association workgroups on diagnostic guidelines for Alzheimer's disease. *Alzheimers Dement* **7**, 270-279.
[20] McKhann GM, Knopman DS, Chertkow H, Hyman BT, Jack CR Jr, Kawas CH, Klunk WE, Koroshetz WJ, Manly JJ, Mayeux R, Mohs RC, Morris JC, Rossor MN, Scheltens P, Carrillo MC, Thies B, Weintraub S, Phelps CH (2011) The diagnosis of dementia due to Alzheimer's dis-

ease: Recommendations from the National Institute on Aging-Alzheimer's Association workgroups on diagnostic guidelines for Alzheimer's disease. *Alzheimers Dement* **7**, 263-269.

[21] Jack CR Jr, Albert MS, Knopman DS, McKhann GM, Sperling RA, Carrillo MC, Thies B, Phelps CH (2011) Introduction to the recommendations from the National Institute on Aging-Alzheimer's Association workgroups on diagnostic guidelines for Alzheimer's disease. *Alzheimers Dement* **7**, 257-262.

[22] Ashford JW, Schmitt FA (2001) Modeling the time-course of Alzheimer dementia. *Curr Psychiatry Rep* **3**, 20-28.

[23] Ashford JW (2004) APOE genotype effects on Alzheimer's disease onset and epidemiology. *J Mol Neurosci* **23**, 157-165.

[24] Raber J, Huang Y, Ashford JW (2004) ApoE genotype accounts for the vast majority of AD risk and AD pathology. *Neurobiol Aging* **25**, 641-650.

[25] Butler SM, Ashford JW, Snowdon DA (1996) Age, education, and changes in the Mini-Mental State Exam scores of older women: findings from the Nun Study. *J Am Geriatr Soc* **44**, 675-681.

[26] Brun A, Englund E (1981) Regional pattern of degeneration in Alzheimer's disease: neuronal loss and histopathological grading. *Histopathology* **5**, 549-564.

[27] Ashford JW, Shih WJ, Coupal J, Shetty R, Schneider A, Cool C, Aleem A, Kiefer VH, Mendiondo MS, Schmitt FA (2000) Single SPECT measures of cerebral cortical perfusion reflect time-index estimation of dementia severity in Alzheimer's disease. *J Nucl Med* **41**, 57-64.

[28] Small GW, Kepe V, Ercoli LM, Siddarth P, Bookheimer SY, Miller KJ, Lavretsky H, Burggren AC, Cole GM, Vinters HV, Thompson PM, Huang SC, Satyamurthy N, Phelps ME, Barrio (2006) PET of brain amyloid and tau in mild cognitive impairment. *N Engl J Med* **355**, 2652-2663.

[29] Reiman EM, Caselli RJ, Yun LS, Chen K, Bandy D, Minoshima S, Thibodeau SN, Osborne D (1996) Preclinical evidence of Alzheimer's disease in persons homozygous for the epsilon 4 allele for apolipoprotein E. *N Engl J Med* **334**, 752-758.

[30] Furst AJ, Rabinovici GD, Rostomian AH, Steed T, Alkalay A, Racine C, Miller BL, Jagust WJ (2010) Cognition, glucose metabolism and amyloid burden in Alzheimer's disease. *Neurobiol Aging*, doi:10.1016/j.neurobiolaging.2010.03.011, 2010 Apr 22 [Epub ahead of print].

[31] Ashford JW, Coburn, KL, Fuster, JM (1998) Functional cognitive networks in primates. *In fundamentals of Neural Networks: Neuropsychology and Cognitive Neuroscience*, Parks RW, Levine DS, eds. The MIT Press, Cambridge, Mass.

[32] Scheff SW, Price DA, Schmitt FA, Scheff MA, Mufson EJ (2011) Synaptic loss in the inferior temporal gyrus in mild cognitive impairment and Alzheimer's disease. *J Alzheimers Dis* **24**, 547-557.

[33] Whitehouse PJ, Price DL, Struble RG, Clark AW, Coyle JT, Delon MR (1982) Alzheimer's disease and senile dementia: loss of neurons in the basal forebrain. *Science* **215**, 1237-1239.

[34] Struble RG, Cork LC, Whitehouse PJ, Price DL (1982) Cholinergic innervation in neuritic plaques. *Science* **216**, 413-415.

[35] Grinberg LT, Rub U, Ferretti RE, Nitrini R, Farfel JM, Polichiso L, Gierga K, Jacob-Filho W, Heinsen H (2009) The dorsal raphe nucleus shows phospho-tau neurofibrillary changes before the transentorhinal region in Alzheimer's dis-

ease. A precocious onset? *Neuropathol Appl Neurobiol* **35**, 406-416.

[36] Babiloni C, Pievani M, Vecchio F, Geroldi C, Eusebi F, Fracassi C, Fletcher E, De Carli C, Boccardi M, Rossini PM, Frisoni GB (2009) White-matter lesions along the cholinergic tracts are related to cortical sources of EEG rhythms in amnesic mild cognitive impairment. *Hum Brain Mapp* **30**, 1431-1443.

[37] Teter B, Ashford JW (2002) Neuroplasticity in Alzheimer's disease. *J Neurosci Res* **70**, 402-437.

[38] Salehi A, Dubelaar EJ, Mulder M, Swaab DF (1998) Aggravated decrease in the activity of nucleus basalis neurons in Alzheimer's disease is apolipoprotein E-type dependent. *Proc Natl Acad Sci U S A* **95**, 11445-11449.

[39] Silverman DH, Small GW, Chang CY, Lu CS, Kung De Aburto MA, Chen W, Czernin J, Rapoport SI, Pietrini P, Alexander GE, Schapiro MB, Jagust WJ, Hoffman JM, Welsh-Bohmer KA, Alavi A, Clark CM, Salmon E, de Leon MJ, Mielke R, Cummings JL, Kowell AP, Gambhir SS, Hoh CK, Phelps ME (2001) Positron emission tomography in evaluation of dementia: Regional brain metabolism and long-term outcome. *JAMA* **286**, 2120-2127.

[40] Tezapsidis N, Johnston JM, Smith MA, Ashford JW, Casadesus G, Robakis NK, Wolozin B, Perry G, Zhu X, Greco SJ, Sarkar S (2009) Leptin: a novel therapeutic strategy for Alzheimer's disease. *J Alzheimers Dis* **16**, 731-740.

[41] McKee AC, Cantu RC, Nowinski CJ, Hedley-Whyte ET, Gavett BE, Budson AE, Santini VE, Lee HS, Kubilus CA, Stern RA (2009) Chronic traumatic encephalopathy in athletes: progressive tauopathy after repetitive head injury. *J Neuropathol Exp Neurol* **68**, 709-735.

[42] Yaffe K, Vittinghoff E, Lindquist K, Barnes D, Covinsky KE, Neylan T, Kluse M, Marmar C (2010) Posttraumatic stress disorder and risk of dementia among US veterans. *Arch Gen Psychiatry* **67**, 608-613.

[43] Kim S, Swaminathan S, Shen L, Risacher SL, Nho K, Foroud T, Shaw LM, Trojanowski JQ, Potkin SG, Huentelman MJ, Craig DW, DeChairo BM, Aisen PS, Petersen RC, Weiner MW, Saykin AJ (2011) Genome-wide association study of CSF biomarkers Abeta1-42, *t*-tau, and *p*-tau181p in the ADNI cohort. *Neurology* **76**, 69-79.

[44] Struble RG, Ala T, Patrylo PR, Brewer GJ, Yan XX (2010) Is brain amyloid production a cause or a result of dementia of the Alzheimer's type? *J Alzheimers Dis* **22**, 393-399.

[45] Parihar MS, Brewer GJ (2010) Amyloid-beta as a modulator of synaptic plasticity. *J Alzheimers Dis* **22**, 741-763.

[46] Ashford JW (2002) ApoE4: is it the absence of good or the presence of bad? *J Alzheimers Dis* **4**, 141-143.

[47] Oddo S, Billings L, Kesslak JP, Cribbs DH, LaFerla FM (2004) Abeta immunotherapy leads to clearance of early, but not late, hyperphosphorylated tau aggregates via the proteasome. *Neuron* **43**, 321-332.

[48] Roses AD (2010) An inherited variable poly-T repeat genotype in TOMM40 in Alzheimer disease. *Arch Neurol* **67**, 536-541.

[49] Jack CR Jr, Knopman DS, Jagust WJ, Shaw LM, Aisen PS, Weiner MW, Petersen RC, Trojanowski JQ (2010) Hypothetical model of dynamic biomarkers of the Alzheimer's pathological cascade. *Lancet Neurol* **9**, 119-128.

[50] Roberson ED, Halabisky B, Yoo JW, Yao J, Chin J, Yan F, Wu T, Hamto P, Devidze N, Yu GQ, Palop JJ, Noebels JL, Mucke L (2011) Amyloid-beta/Fyn-induced synaptic, network, and cognitive impairments depend on tau levels in multiple mouse models of Alzheimer's disease. *J Neurosci* **31**, 700-711.

Hippocampal Network Alterations in Alzheimer's Disease and Down Syndrome: From Structure to Therapy

Martha Millan Sanchez[a,b,*], Sarah Moghadam[a], Priyanka Naik[a], Kara J. Martin[a] and Ahmad Salehi[a,b]
[a]*VA Palo Alto Health Care System, Palo Alto, CA, USA*
[b]*Department of Psychiatry and Behavioral Sciences, Stanford University School of Medicine, Stanford, CA, USA*

Abstract. Hippocampal structural and functional alterations in Alzheimer's disease (AD), detected by advanced imaging methods, have been linked to significant abnormalities in multiple internal and external networks in this critical brain region. Uncovering the temporal and anatomical pattern of these network alterations would provide important clues into understanding the pathophysiology of AD and suggest new therapeutic strategies for this multi-system and prevalent disorder. Over the last decade, we have focused on studying brain structures that provide major projections to the hippocampus (HC) and the pattern of de-afferentation of this area in mouse models of AD and a related neurodegenerative disorder, i.e. Down syndrome (DS). Our studies have revealed that major inputs into the hippocampal structure undergo significant age-dependent alterations. Studying locus coeruleus (LC), the sole source of noradrenergic terminals for the HC, it has been shown that these neurons show significant age-dependent degeneration in both mouse models of DS and AD. Furthermore, increasing noradrenergic signaling was able to restore cognitive function by improving synaptic plasticity, and possibly promoting microglia recruitment, and amyloid β (Aβ) clearance in transgenic (tg) mouse models of AD. Here, we re-examine the effects of alterations in major inputs to the hippocampal region and their structural and functional consequences in mouse models of neurodegenerative disorders. We will conclude that improving the function of major hippocampal inputs could lead to a significant improvement in cognitive function in both AD and DS.

Keywords: Alzheimer's disease, amyloid precursor protein, contextual learning, Down syndrome, L-DOPS, locus coeruleus, norepinephrine, perforant path, xamoterol

LIST OF ABBREVIATIONS

MHPG	3-methoxy-4-hydroxyphenylglycol
ACh	Acetylcholine
ARs	Adrenergic receptors
AD	Alzheimer's disease
APP	Amyloid precursor protein
Aβ	Amyloid β
BFCNs	Basal forebrain cholinergic neurons
BBB	Blood brain barrier
BDNF	Brain-derived neurotrophic factor
COMT	Catechol O-methyltransferase
CNS	Central nervous system
CSTB	Cystatin B
DGCL	Dentate granule cell layer
DG	Dentate gyrus
DHPG	Dihydroxyphenylglycol
DDC	Dopa-decarboxylase
DA	Dopamine
DBH	Dopamine β-hydroxylase
DR	Dorsal raphe
DS	Down syndrome
DSCAM	Down syndrome cell adhesion molecule
DYRK1A	Dual-specificity tyrosine-(Y)-phosphorylation regulated kinase lA

*Correspondence to: Martha Millan Sanchez, M.D., Department of Psychiatry and Behavioral Sciences, Stanford University School of Medicine, VA Palo Alto Health Care System, 3801 Miranda Ave, 151Y, Palo Alto, CA 94304, USA. Tel.: +650 493 5000 (68918); Fax: +650 852 3297; E-mail: marnemil@stanford.edu.

EC	Entorhinal cortex
EPSP	Excitatory postsynaptic potential
HC	Hippocampus
HSA21	Human chromosome 21
iNOS	Inducible nitric oxide synthase
IDE	Insulin degrading enzyme
ISO	Isoproterenol
IFNAR1 and 2	Interferon (α and β) receptor 1 and 2
AAAD	L-amino acid decarboxylase
L-DOPA	L-dihydroxyphenylalanine
L-DOPS	L-threo-3, 4-dihydroxyphenylserine
LC	Locus coeruleus
LTP	Long-term potentiation
MEC	Medial EC
LEC	Lateral EC
MRN	Median raphe nuclei
MML	Middle molecular layer
MCI	Mild cognitive impairment
MMSE	Mini-mental state examination
ML	Molecular layer
MAO	Monoamine oxidase
DSP4	*N*-(2-chloroethyl)-*N*-ethyl-2 bromobenzylamine
NCAM2	Neural cell adhesion molecule 2
NGF	Nerve growth factor
NT-3	Neurotrophin-3
NE	Norepinephrine
PrH	Nucleus prepositus hypoglossi
OLIG2	Oligodendrocyte transcription factor 2
LPGi	Paragigantocellularis lateralis
PPT	Pedunculopontine tegmental nucleus
KCNE1	Potassium voltage-gated channel, Isk-related family, member 1
PP	Perforant path
PS1	Presenilin1
RN	Raphe nuclei
REM	Rapid eye movement
RRP1	Ribosomal RNA processing 1 homolog
SNP	Single nucleotide polymorphism
SUMA	Supramamillary area
tg	Transgenic
TMPRSS2	Transmembrane protease, serine 2
TMN	Tuberomamillary nucleus
TH	Tyrosine hydroxylase
USP25	Ubiquitin specific peptidase 25
VLPO	Ventrolateral preoptic area
VMAT	Vesicular monoamine transporter

NEUROBIOLOGICAL BASIS OF COGNITIVE DYSFUNCTION IN ALZHEIMER'S DISEASE AND DOWN SYNDROME

All individuals with Down syndrome (DS) show neuropathological changes of Alzheimer's disease (AD) by age 40 [1] and most demonstrate significant cognitive decline by the sixth decade [2, 3]. Furthermore, overexpression of amyloid precursor protein *(APP)*, a gene whose mutations lead to familial form of AD, has been linked to the occurrence of Alzheimer

pathology in aged DS individuals [4]. This suggests that DS consistently shows pathogenic mechanisms very similar to that of AD [5, 6]. Neuropathologically, both AD and DS are characterized by significant degeneration of the hippocampal formation, a region that plays a conspicuous role in a variety of higher cognitive functions particularly, spatial and contextual learning [7]. The proper function of the hippocampus (HC) depends on the integrity of intra-and extrahippocampal circuits and their extensive projections from these regions to the HC. The role of mostly unidirectional intra-hippocampal circuits in the proper function of the HC has been extensively studied [8]. Most extra-hippocampal circuits are formed by subcortical regions that project extensively to the HC. These include basal forebrain cholinergic neurons (BFCNs) [9], noradrenergic neurons of locus coeruleus (LC) [10], serotonergic neurons of raphe nuclei (RN) [11], and neurons of the supramamillary area (SUMA) [12]. These rather large neurons project extensively to specific subregions of the HC. The densest cholinergic inputs to the HC in rodents are found in the immediate vicinity of the dentate granule cell layer (DGCL) [13]. It should be noted that hippocampal inputs from the basal forebrain are not exclusively cholinergic. A large number of interneurons in the hippocampus, particularly in the dentate gyrus (DG), also receive dense GABA-ergic terminals [14]. Using retrograde labeling, it has been shown that a majority of these terminals originate in the lateral septum of the basal forebrain [15]. The majority of these terminals end in the subgranular layer of the DG (e.g., GABA-ergic chandelier and basket cells) in the polymorphic layer of the DG [16]. All noradrenergic terminals to the HC originate from LC neurons [17]. The majority of these terminals end in the DG (polymorphic and the middle molecular layer (MML)) and stratum lucidum of the CA3 area [10]. Most serotonergic innervation of the HC originates from the dorsal raphe (DR) and median raphe nuclei (MRN) [18]. Projections from the RN in the DG are found in the subgranular area in the polymorphic layer of DG and in the hilar border of the stratum granulosum [19]. The mostly calretinin-positive neurons of the SUMA send major projections either directly or indirectly through basal forebrain to the DG [20] of the HC. The majority of these neurons terminate in the supragranular region of the molecular layer (ML) in the immediate vicinity of DG cell layer, making synapses with the primary dendrites of DG cells [12]. Furthermore, the pyramidal layer of the CA2 area also receives heavy innervations from SUMA neurons [20] (Fig. 1).
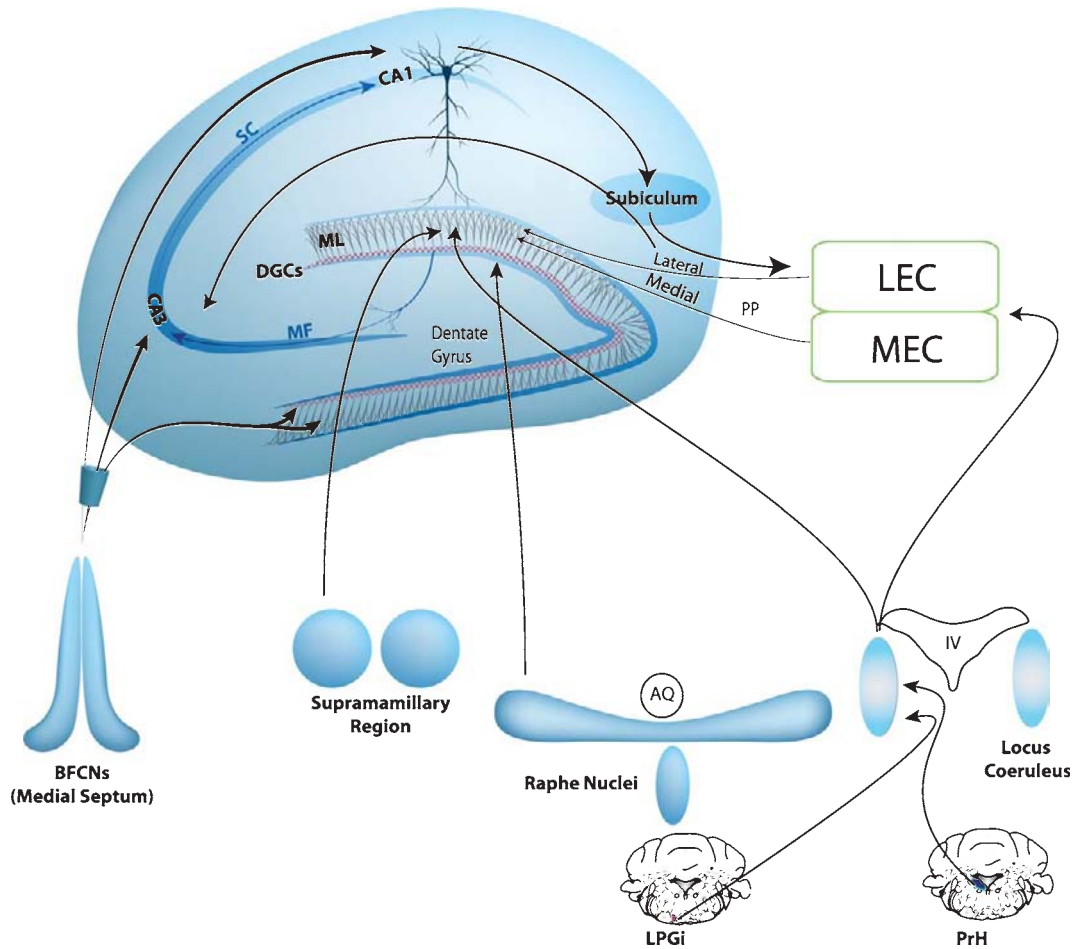
Fig. 1. Multiple subcortical regions innervate the hippocampus. The hippocampal formation receives major afferents from multiple sub-cortical systems. These systems include the cholinergic system originating from medial septum nucleus (MSN), noradrenergic system coming from locus coeruleus (LC), serotonergic neurons coming from the raphe nuclei (RN) and mainly the histaminergic neurons of supramamillary area (SUMA). Except basal ganglia, most brain regions in rodents receive inputs from the LC. Major afferents of LC are located in the rostral aspect of the medulla: paragiganto cellularis lateralis (LPGi) and nucleus prepositus hypoglossi (PrH). LC hippocampal efferents mainly end in the dentate gyrus (DG) reaching via cingulum bundle (ventral DG), and fornix (to the septal pole of DG and via ventral amygdalofugal (midseptotemporal aspects of the DG). CA$_1$; Cornu Ammonis l, CA$_3$; Cornu Ammonis 3, SC; Schaffer collaterals, ML; molecular layer, MF; mossy fibers, DGCs; dentate granule cells, PP; perforant path, LEC; lateral entorhinal cortex, MEC; medial entorhinal cortex, III; the third ventricle, AQ; aqueduct of Sylvius, IV; the fourth ventricle.

The structural and functional integrity of these major inputs to the HC play a crucial role in its normal physiology. Studying these subcortical structures, one could notice the following characteristics:

1) BFCNs, RN, LC, and SUMA neurons all retrogradely transport and are responsive to neurotrophins [21–23]. For instance, it has been shown that BFCNs and SUMA retrogradely transport nerve growth factor (NGF) from HC in rodents. Furthermore, injecting brain-derived neurotrophic factor (BDNF) in either HC or

entorhinal cortex (EC) leads to retrograde labeling of LC, SUMA, BFCNs, and RN, which in some cases acts as a survival factor for these populations [23]. In addition to NGF and BDNF, neurotrophin-3 (NT-3) is also retrogradely transported from HC to SUMA and BFCN cell bodies [21, 24]. These data indicate that all these subcortical regions with extensive projections to the HC are able to retrogradely transport neurotrophins.

2) Although it is not uniform, it has been suggested that there is an inverse relationship between

the levels of myelination and the severity of degeneration [25]. For instance, the entorhinal and hippocampal regions, which are poorly myelinated, are generally heavily affected in AD [26–28], while sensory primary and motor primary fields that are heavily myelinated are scarcely affected by AD-related pathology. It is of note that BFCNs [29], LC [30], RN [31], and SUMA neurons have generally thin and poorly myelinated axons.

3) The axon terminals of subcortical regions projecting to the HC travel relatively large distances to reach the HC.

4) Degeneration of subcortical regions with extensive projections to the HC leads to failed cognitive function. Indeed, it has been shown that lesion or inactivation of SUMA [32], septum [33], MRN [34], and LC [35] will be followed by impaired learning and memory in rodents.

5) All of these regions, including the cholinergic neurons of nucleus basalis of Meynert, LC, RN [36], and neurons of the tuberomamillary nucleus (TMN), which anatomically belong to the mamillary complex [37, 38] show extensive atrophy and degeneration in AD [39] and DS [40, 41].

These observations support the fact that the proper function of the HC depends on a number of vulnerable neuronal populations. In this review, we will focus on noradrenergic system and show that restoring the proper function of this vulnerable neuronal population could be a successful strategy in restoring the physiological role of the HC in mouse models of neurodegenerative disorders.

HUMAN CHROMOSOME 21 IN ALZHEIMER'S DISEASE AND DOWN SYNDROME

Complete sequencing of human chromosome 21 (HSA21) by Hattori and colleagues [42] revealed the presence of 225 genes and 59 pseudogenes on this chromosome (38.3 mb). However, it has been predicted that the number of genes to be significantly higher (552 genes) [43]. Among genes with known functions on HSA21 are a variety of kinases (e.g. *DYRKA1)*, members of ubiquitination pathway (e.g. *USP25)*, cell adhesion molecules (e.g. *NCAM2* and *DSCAM*), transcription factors (e.g. *OLIG2)*, ion chan-

nels (e.g. *KCNE1)*, members of interferon receptor family *(IFNAR1* and *2)*, proteases (e.g. *TMPRSS2)*, protease inhibitors (e.g. *CSTB)*, and genes involved in RNA processing (e.g. *RRP1)*. For this reason, overexpression of all these genes in DS leads to abnormalities in multiple systems and organs [44]. An important gene on HSA21 with multiple functions is *APP* gene. Alternative splicing of *APP* mRNA leads to synthesis of three isoforms of App695, 751 and 770, from which 695 predominantly expresses in neurons. Both AD and DS have been strongly linked to abnormalities in *APP* metabolism or expression. For instance, so far 32 point mutations in 85 families have been linked to the familial forms of AD (see [45]). Furthermore, the triplication of *APP* has been shown to be necessary for the occurrence of AD-related pathology in adults with DS [4]. Our investigation on mouse models of DS has shown that overexpression of *App* is both necessary and sufficient to lead to failed NGF axonal transport in basal forebrain cholinergic neurons [46]. Another important issue that might play a significant role in the clinical picture presented in DS is the presence of single nucleotide polymorphism (SNP) in genes on HSA21. These substitutions, when located on critical sites, can lead to significant alterations in the outcome (Millan et al., submitted). There are a large number SNPs on human *APP* gene from which several could play a significant role in alterations in gene function. For instance, although yet to be replicated, it has been reported that individuals with DS with 3 copies of the tetranucleotide repeat in intron 7 of *APP* (attt6) show a significantly earlier age of onset of dementia [47].

NORADRENERGIC SYSTEM IN HUMANS AND RODENTS

The monoaminergic system in the rodents' brain was mapped approximately 40 years ago by Dahlström and Fuxe using histofluorescence techniques. According to this classification, catecholamine-ergic neurons (cell groups A1-A7) are found in medulla oblongata and pons, cell groups A8 in reticular formation, A9 in substantia nigra, A10 in the mesencephalon, and A11 and A12 in the diencephalon. Serotonergic neurons (cell groups B1-B9) are found in medulla oblongata, pons, and mesencephalon [48]. For the purpose of this review, we will mainly focus on noradrenergic neurons located in LC (cell group A6). LC consists of a population of relatively small neurons located in the brainstem (rostral pons in the two corners of the fourth ventricle)
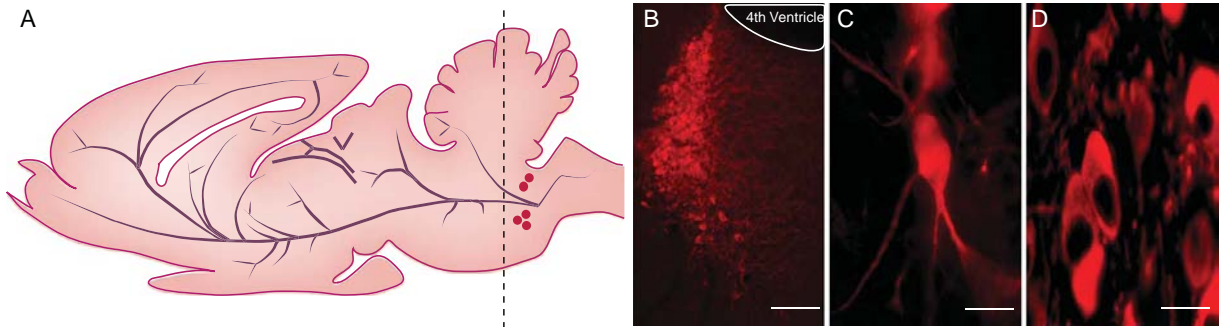
Fig. 2. Locus coeruleus neurons in the mouse brain. (A) Anatomical localization of LC and its inputs and outputs in the rodent brain. Immuno-cytochemical visualization of LC neurons in a 2N mouse using a polyclonal antibody against tyrosine hydroxylase (TH). TH-positive neurons are located in the proximity of the two corners of the 4th ventricle. Scale bar = 200 μm (B), and 20 μm (C and D).

(Fig. 2). It contains around 1,500 neurons in rodents [49] and up to 50,000 pigmented neurons in humans [50]. Due to the presence of melanin neurons [51], LC is easily visible in the human brain. With the exception of basal ganglia, most brain regions receive inputs from LC neurons. This enables these cells to exert an extraordinary modulatory effect on most brain regions [49, 52–54]. LC neurons are considered the sole source of noradrenergic terminals for the HC [17], projecting to this region through the ventral amygdaloid pathway (15%), the fornix (15%), and the cingulum bundle (70%) [55]. Although, LC neurons send extensive projections to the rest of the brain, they receive very few inputs. The two major afferents of LC originate in medulla oblongata from paragigantocellularis lateralis (LPGi) and nucleus prepositus hypoglossi (PrH) [56]. Unlike LPGi that sends excitatory terminals to LC [57], PrH provides major inhibitory inputs for this region [58, 59] (Fig. 1). Functionally, PrH plays a major role in controlling eye movements [60], while LPGi conveys sympathetic excitatory stimuli to LC [61]. Together, LPGi and PrH play a role in attention [61, 62].

Norepinephrine

The synthesis of norepinephrine (NE) involves several enzymatic steps that start with L-phenylalanine converted to tyrosine. Tyrosine is converted to dihydroxyphenylalalanine (L-DOPA) by tyrosine hydroxylase (TH), a rate-limiting enzyme found in catecholaminergic cells. L-DOPA is then decarboxylated to dopamine (DA), the immediate precursor of NE, by dopa-decarboxylase (DDC), also referred as L-aromatic amino acid decarboxylase (AADC) found in catecholamine and serotonergic neurons. DA is con-

verted to NE by dopamine β-hydroxylase (DBH) found in both membrane-bound and soluble forms. Interestingly, it has been shown that DBH null mice show a significant failure in hippocampal-mediated contextual learning [63]. Once formed, NE is transported into synaptic vesicles by the vesicular monoamine transporter (VMAT) and released to bind to adrenergic receptors (ARs), α and β [64]. The control of the NE signaling involves reuptake [65] and enzymatic action [66] via monoamine oxidase (MAO) and aldehyde reductase which leads to the formation of dihydroxyphenylglycol (DHPG). DHPG is converted to 3-methoxy-4-hydroxyphenylglycol (MHPG) by catechol O-methyltransferase (COMT) [64]. The released NE is generally re-uptaken by NE transporter (NET), encoded by *SLC6A2* gene (solute carrier family). There are nine ARs receptors, including α1 (A, B, and D subtypes), which signal through Gq/11 family of G-proteins: α2 (A, B, and C subtypes), signaling through Gi heterodimeric G protein and β (1, 2, and 3), which are members of a G-protein coupled receptor family characterized by seven transmembrane, three intracellular, and three extracellular domains. The transmembrane domains are involved in ligand binding and G protein activation. All three α1 receptors have been found in the brain with only α1D in the HC [67]. Between α2 receptors, α2A is widely expressed in the brain, followed by α2C. α2B receptors have only been found in the spinal cord. Among β-ARs, only β1 and β2 have been found in the central nervous system (CNS), particularly in the CA1 and CA3 areas of the HC [68], while all three express in peripheral organs. β3-ARS are mostly found in adipose tissue [67]. Binding NE to α2-ARs on presynaptic sites reduces adenyl cyclase, thus it is believed that the α2-ARs play a role as

feedback inhibitors [69]. However, it has been shown that α2-ARs, also located on postsynaptic sites, play a significant role in prefrontal cortex-mediated working memory [70]. Post-synaptic β1 activation leads to increased levels of cAMP from ATP [64, 71]. β-AR activation in the HC plays an important role in synaptic plasticity and memory formation [72]. Although it has been shown that activation of β-ARs leads to the induction of a late phase of long-term potentiation (LTP), blockade of β-ARs in the CA1 region impairs consolidation of contextual and spatial learning [73, 74]. Similarly, the activation of β-ARs by either NE or β1/β2 agonists increases BDNF levels in astrocytes [75], whereas β1-2 ARs antagonists (e.g. atenolol) significantly reduce BDNF levels in rat cortical astrocytes [76]. Interestingly, Nagahara and colleagues recently showed that BDNF gene delivery to the EC, which receives extensive inputs from LC and innervates, HC leads to a significant improvement in cognitive functions in mouse models of AD [77]. This suggests that there is reciprocal positive relationship between β-AR signaling and BDNF production and release.

Physiology of noradrenergic system

Direct and indirect connections between LC and other major regions involved in wakefulness including the TMN, DR, the ventral tegmental area, ventral periaqueductal grey, ventrolateral preoptic area (VLPO), lateral hypothalamus, and pedunculopontine tegmental nucleus (PPT) place LC in a position to play a significant role in the sleep-wake cycle [78, 79]. Indeed, LC neurons activity varies during sleep-wake cycles. These neurons display a tonic fire pattern during arousal [80] and no detectable activity during rapid eye movement (REM) sleep. It is believed that by disinhibiting a wakefulness-promoting region like TMN, LC neurons promote wakefulness. For this reason, medications targeting LC neurons significantly affect sleep-wake cycle. For instance, modafinil, a widely used drug for the treatment of excessive daytime sleepiness and narcolepsy, has been shown to activate LC neurons [81]. LC neurons undergo significant degeneration in AD [36], a potential explanation for sleep disturbances among approximately 25% of individuals with AD [82], including sleep fragmentation and reduced REM sleep [83].

For the purpose of this review, we will mainly focus on the role of the LC-noradrenergic system in cognition and particularly contextual learning.

Role of locus coeruleus-norepinephrine in cognition

NE plays a key role in the acquisition [84], retrieval, and encoding [85] of fear [86]; contextual [17]; and emotional memories [87, 88]. Pre-training inactivation of LC neurons by lidocaine in rats led to a significant failure in Morris Water Maze tasks, while post-training had no significant effects [84]. The release of NE in amygdala is essential for the encoding and retention of emotion-related memories [88]. Activation of β-ARs within the brain [63] contributes to the modulation of memory by NE [88] and synaptic plasticity [17, 89–91]. Indeed, the use of β-ARs agonists leads to restoration of cognitive deficits caused by reduced NE levels [63, 92, 93] or LC degeneration [94]. Conversely, the use of β-ARs antagonists [90] has shown to impair the formation of LTP in HC and retrieval of new [95] and emotional memories [96]. Murchison and colleagues found that β-receptor antagonists ((+)-propranolol and (-)-propranolol) delivered specifically into the HC prior to testing could also impair contextual memory retrieval [63]. Interestingly, delivering these antagonists into the lateral ventricles or even cortex had no effects on memory retrieval, which indicates that intra-hippocampal function of β-ARs plays a major role in memory retrieval.

It has been suggested that there is an interaction between NE and acetylcholine (ACh)-ergic systems. BFCNs receive inputs from noradrenergic neurons of LC [49]. The use of α2-ARs agonists has been shown to inhibit ACh release from these cells [97], while systemic administration of α2-ARs antagonists increase ACh release from cortical neurons [98]. Furthermore, partial lesion of LC leads to a significant reduction in the effects of selective α2-ARs antagonist on cortical ACh release [98]. Indeed, it has been shown that clonidine, i.e., a selective α2-ARs agonist, is able to cause delayed cognitive dysfunction in aged primates with lesioned prefrontal cortex [99]. The inter-relationship between the cholinergic and noradrenergic systems was recently supported by a study showing that degeneration of LC terminals accelerates degeneration of cholinergic neurons in the Ts65Dn mouse model of DS [100]. This suggests that NE-based therapies might also improve cholinergic function in AD and DS. Indeed, α2-ARs antagonist yohimbine, which primarily targets α2-ARs, has shown to improve noradrenergic transmission in individuals with AD [101]. However, combining acetylcholinesterase inhibitor treatment with yohim-

bine in a small sample group of AD patients did not result in an overall benefit [102]. These results suggest that more extensive studies using drugs targeting specific ARs are needed.

The role of norepinephrine in contextual learning

There are multiple studies indicating that NE plays a significant role in contextual learning [63, 94, 103–105]. This type of learning is formed when the subject combines sensory and spatial information to build a frame in which the learning occurs (see [106]). Indeed, keeping the animal aware of changes in the environment is crucial to its survival. In doing so, the animal needs to integrate multiple types of cues and information in one place, which is believed to be the HC. The gateway for the HC to channel different types of information is the EC [107]. Based on the cytoar-

chitecture, this area is divided into two major parts, medial EC (MEC) and lateral EC (LEC) [108]. MEC (Brodmann's area 28 b) is in the caudomedial, and LEC (Brodmann's area 28 a) is in the rostrolateral part of the EC [109]. MEC receives its major inputs from dorsal thalamus, claustrum, and olfactory areas while LEC receives its inputs from olfactory bulb, amygdala, and claustrum [110]. For this reason, the MEC channels spatial information while LEC provides mostly sensory information to the HC [111, 112]. Both MEC and LEC give rise to perforant path (PP), which travels mainly parallel to the CA regions to the DG [107]. PP can also be divided into two pathways. Lateral PP carry the information from the LEC and mostly end up in the outer 1/3 of the ML of DG. Medial PP carries spatial information from the MEC and makes synapses with DGCs dendrites in the middle 1/3 of the ML [113] (Fig. 3). It has been shown that the release
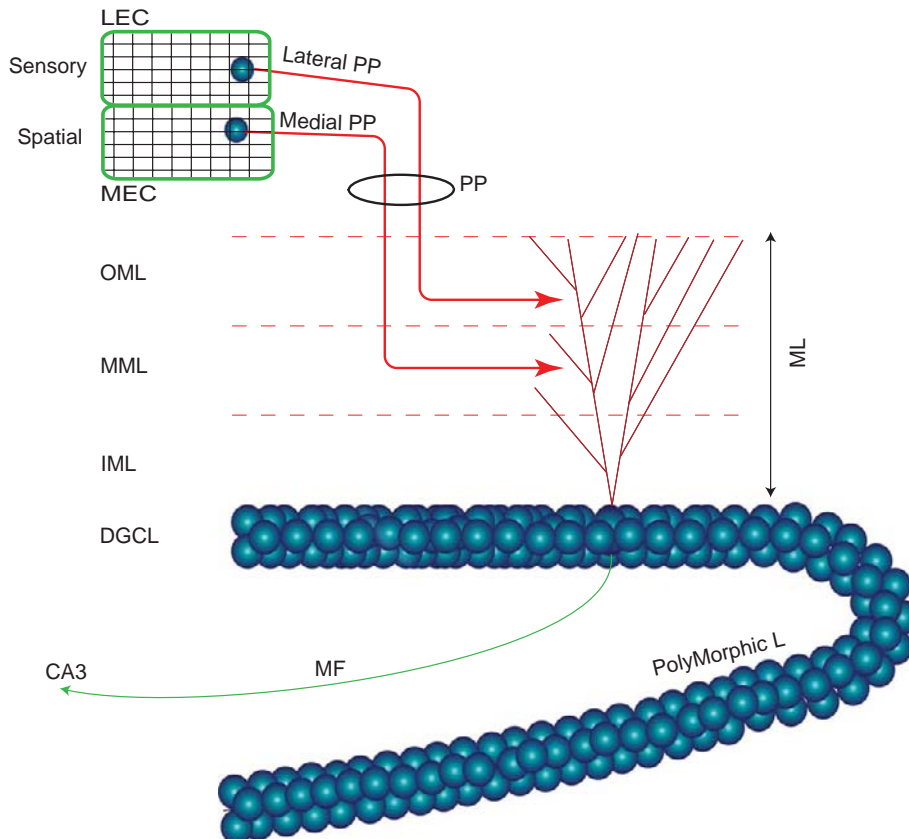
Fig. 3. Mechanism of effects of norepinephrine on contextual learning in the hippocampus. Schematic representation of major inputs to the molecular layer of the dentate gyrus (DG) in the hippocampus (HC). Perforant path (PP) carrying both sensory and spatial information from the entorhinal cortex (EC) end in the inner 1/3 and outer 1/3 of the molecular layer (ML) of the DG. It has been shown that releasing NE in this region lead to differential effects on the dentate granule cells. LEC; lateral entorhinal cortex, MEC; medial entorhinal cortex, PP; perforant path, OML; outer molecular layer, MML; middle molecular layer, IML; inner molecular layer, DGCL; dentate granule cell layer, CA$_3$; Cornu Ammonis 3, MF; mossy fibers, PolyMorphic L; polymorphic layer, ML; molecular layer, *; $p = 0.007$.

of NE can have a differential effect on medial perforant path (MPP) versus lateral perforant path (LPP). Indeed, the use of NE or isoproterenol (ISO), a β-AR agonist, leads to persistent potentiation of the excitatory postsynaptic potential (EPSP) in DGCs caused by the stimulation of the PP [114, 115]; whereas the response evoked by stimulation of the lateral PP causes long-lasting depression in the presence of either NE or ISO [116]. This suggests that by changing the balance between sensory versus spatial inputs in the DG, NE plays a significant role in attention and thus cognitive function.

DEGENERATION OF LOCUS COERULEUS NEURONS IN DOWN SYNDROME AND ALZHEIMER'S DISEASE

Locus coeruleus degeneration in Alzheimer's disease

Individuals with AD present cognitive dysfunction and behavioral disturbances that contribute to caregiver burden and a high demand for institutionalization [117, 118]. In the 1980s, Bondareff and colleagues reported a significant loss of LC neurons in AD [78], which may occur even at early stages of the disease [119]. Indeed,

individuals with mild cognitive impairment (MCI) also exhibit neurofibrillary degeneration in LC neurons that negatively correlates with changes of mini-mental state examination (MMSE) scores [120]. It has been shown that the majority of the cell loss in LC occurs in the caudal part of this area in AD [121], a pattern similar to our observation in the Ts65Dn model of DS. It is important to note that most cortical and hippocampal terminals of LC originate from the caudal part of this area (Fig. 4). It has been shown the significant loss of LC neurons in AD and DS is associated with a moderate number of amyloid plaques and both early and late stages of neurofibrillary degeneration as shown by AT8 and silver staining in this region [120, 122, 123]. The loss of LC neurons in AD results in decreased NE levels [120, 123–126], which positively correlates with the duration of the disease [121] and severity of cognitive deficits as shown by MMSE in the affected individuals [120]. Interestingly, LC degeneration in AD patients was found to be even more extensive (68% loss) than that of BFCNs (40% loss) [127]. It appears that there is a compensatory increase in the activity of remaining LC neurons in AD as shown by quantifying MHPG/NE ratio [128] and increased density of binding site for α2-ARs at the presynaptic level in the DG of the HC [126] in those inflicted with AD.
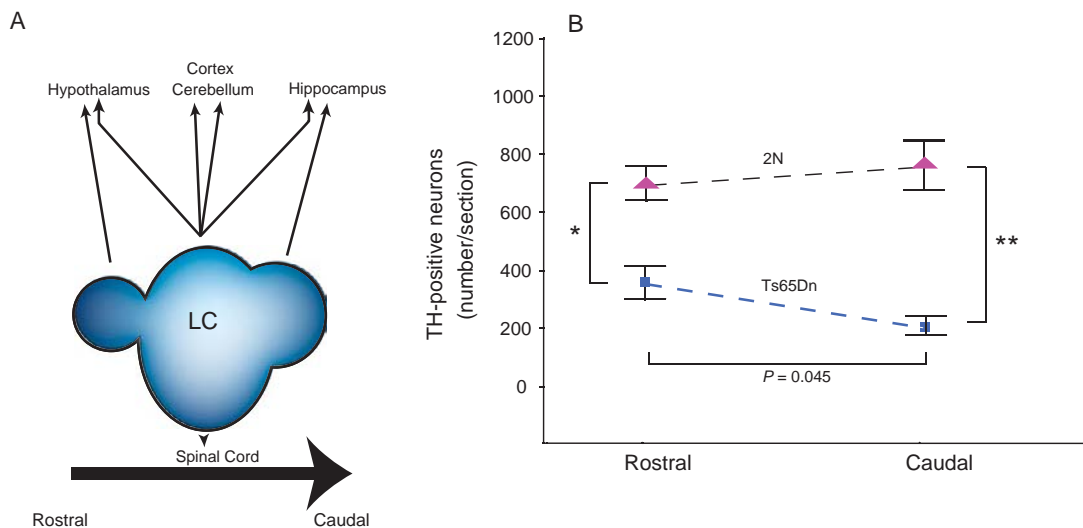
Fig. 4. The pattern of the loss of tyrosine hydroxylase positive neurons in Ts6 sDn mice. (A) Schematic representation of LC projections to cortical and subcortical targets. The rostral part of the LC in rodents projects to the hypothalamus. However, the core of the LC projects to the hypothalamus, cortex, and spinal cord, and the caudal part of the LC projects exclusively to the HC. (C) Density of TH-immunoreactive neurons (IR) across the rostral-caudal axis of the LC in 6-month-old 2N and Ts65Dn mice. Although there was a reduction in neuronal density across the rostral-caudal axis of the LC, degeneration of TH neurons was more severe in the caudal part of the LC. There was a significant reduction in the density of TH-positive neurons in Ts65Dn mice relative to the rostral region of the LC. *; *p = 0.0002,* **; *p = o.ooooi. (Published in Salehi et ah, 2009 Science Translational Medicine 18;1(7):7ra17).*

Multiple studies support the reciprocal relationship between *APP*/Aβ levels and NE in the context of AD. Animal models of AD overexpressing either mutant *APP* (V717F) [129] or a combination of APP and presenilin1 (*PS1*) [130] show significant degeneration of LC neurons and decreased microglial activation [131]. Moreover, inducing noradrenergic neuronal loss of transgenic (tg) mouse models of AD has shown to increase the severity of AD-like pathology (amyloid load) [132]. Conversely, NE levels have shown to reduce inflammation in these mice. Rats receiving two intraperitoneal (IP) injections of *N*-(2-chloroethyl)-*N*-ethyl-2 bromobenzylamine (DSP4), which induces LC cell loss and cortical NE depletion, show a significant increase in the expression of inflammatory genes, including inducible nitric oxide synthase (iNOS) and, cyclooxygenase-2 (COX-2). Interestingly, Aβ injection in these rats leads to significant exacerbation of these inflammatory responses [133]. Increasing β adrenergic signaling has shown to lead to decreased levels of amyloid accumulation by microglia [134]. Although microglia cells have β1-ARs, [135], it has been suggested that the effects of NE or adrenergic agonists (e.g. ISO) are mediated through β2-ARs rather than β1 or 3 receptors. Interestingly, β2 activation following the promotion of adrenergic signaling also leads to a minor increase in the expression of insulin degrading enzyme (IDE) [136]. This suggests that increasing NE signaling might reduce Aβ levels either by increasing Aβ inter nalization or increasing the levels of enzymes involved in Aβ degradation i.e., IDE.

Age-dependent degeneration of locus coeruleus neurons in mouse models of Down syndrome

Several mouse models have been generated to model DS, from which, the Ts65Dn mouse is best characterized [44]. The Ts65Dn mouse has an extra copy of approximately 140 mouse genes in chromosome 16 orthologous to those on HSA21. Changes in hippocampal-mediated cognitive function [137–142] have been reported in these mice, as are changes in the structure and function of hippocampal neurons [143] and in induction of hippocampal LTP [144, 145]. Similar to DS, alterations in specific brain pathways have also been reported in these mice [146–149]. We found significant age-related degeneration of BFCNs in these mice [46, 149], features that also characterize both AD and DS [150]. In order to maintain their function and morphology, mature BFCNs are dependent

on the constant supply of neurotrophins, particularly NGF [151]. Interestingly, we found that BFCN degeneration in Ts65Dn mice was associated with a dramatic decrease in retrograde transport of NGF from their axon terminals in the HC to their cell bodies [46]. Remarkably, when NGF was infused into the lateral ventricles, to directly reach BFCN cell bodies, even advanced degenerative changes in the mouse model of DS were reversed [149]. A significant reduction in NGF axonal transport was also found in *APP* tg mouse models of AD [46]. A compelling case can thus be made that failed NGF transport is responsible for the degeneration of BFCNs. This may well explain the cholinergic de-afferentation of the HC and cognitive decline in patients with AD and in elderly people with DS (see [44, 46]. In a study that focused on the pathogenic mechanism for BFCNs degeneration, we showed that the disruption of NGF transport and degeneration of BFCNs could both be linked to increased gene dose for *App* in these mice [46]. These findings strongly suggest that increased expression of *App* in DS leads to reduced NGF transport with resulting BFCN degeneration and hippocampal cholinergic de-afferentation [44]. Since there is a direct interaction between cholinergic and noradrenergic systems (see above), we questioned whether an increased expression of *App* in Ts65Dn mice is also responsible for the degeneration of noradrenergic neurons. We investigated LC neuronal number and size in Ts65Dn mice and found that both TH-immunoreactive (IR) cell number and cell profile area were significantly lower in young adult Ts65Dn mice (6 months of age). Interestingly, the loss of TH-IR neurons in Ts65Dn mice was found to be age dependent, i.e. no significant loss of LC neurons at 3 months of age, and significantly more severe degeneration at 18 months of age (Fig. 5). To ask whether changes in LC neuron cell bodies could be linked to alterations in HC innervation, we examined monoaminergic terminals in HC by examining and quantifying staining for vesicular monoamine transporter 2 (VMAT2). Comparing Ts65Dn and 2 N mice at age 6 months, VMAT2 staining showed an overall decrease of ∼20% in comparison to 2 N mice in the ML of the DG (Fig. 6). These observations suggest that changes in LC terminals precede those detected in neuronal somas. Degeneration of LC neurons in Ts65Dn mice was recently confirmed [100].

Our previous data have shown that degeneration of BFCNs in Ts65Dn mice can be linked to *App* overexpression [46]. To test whether *App* overexpression can also be linked to LC degeneration in Ts65Dn
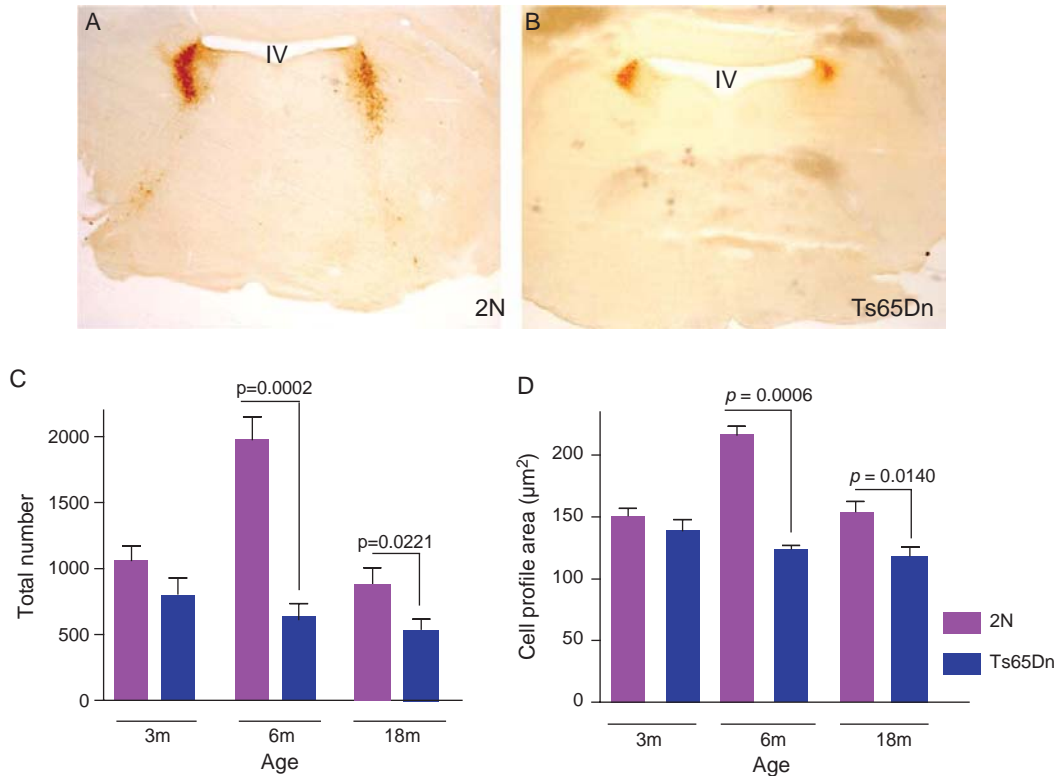
Fig. 5. Degeneration of locus coeruleus neurons in Ts65Dn mouse model of Down syndrome. Immunocytochemical visualization of TH-positive neurons in a 2N (A) and a Ts65Dn (B) mouse. Using unbiased stereological methods, the total number (C) and the size (D) of TH-positive neurons in 3, 6, and 18 month-old Ts65Dn and their controls (2N) were quantified and showed a significant reduction in the size and number of TH-positive neurons in LC in Ts65Dn mice. *(Published in Salehi et al, 2009 Science Translational Medicine 18;1(7):7ra17).*
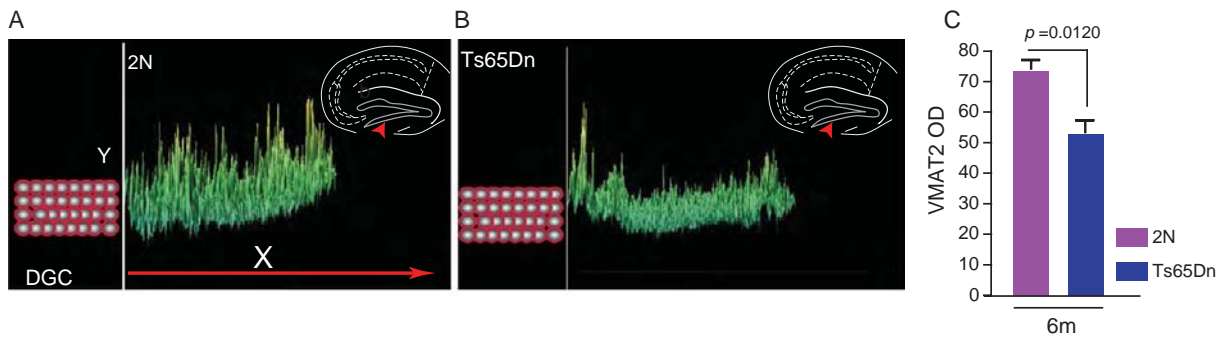
Fig. 6. Alterations in monaminergic terminals in the hippocampus of Ts6sDn mice. (A) Surface imaging of vesicular monoamine transporter 2 (VMAT2) optical density in the inner molecular layer of DG in a 6-month-old 2N (A) and Ts65Dn mice (B). The Y axis indicates VMAT2 optical density and the X axis depicts the anatomical localization starting from dentate granule cell layer toward the pyramidal cell layer of the HC. (C) Quantification of the optical density for VMAT2 in this region indicated a significant reduction in the molecular layer of DG in Ts65Dn mice compared with 2N controls. DGC; dentate granular cell. VMAT2-OD; vesicular monoamine transporter-optical density. The arrow heads indicate where in the molecular layer (ML) the measurements were performed *(Published in Salehi et al., 2009 Science Translational Medicine 18;1(7):7ra17).*

mice, we compared mouse models of DS harboring different triplicated fragments of mouse chromosome 16. Ts1Cje mice, which have triplication of a shorter

fragment of mouse chromosome 16 compared with Ts65Dn mice [44], showed no significant changes in size or number of LC neurons. This suggested the
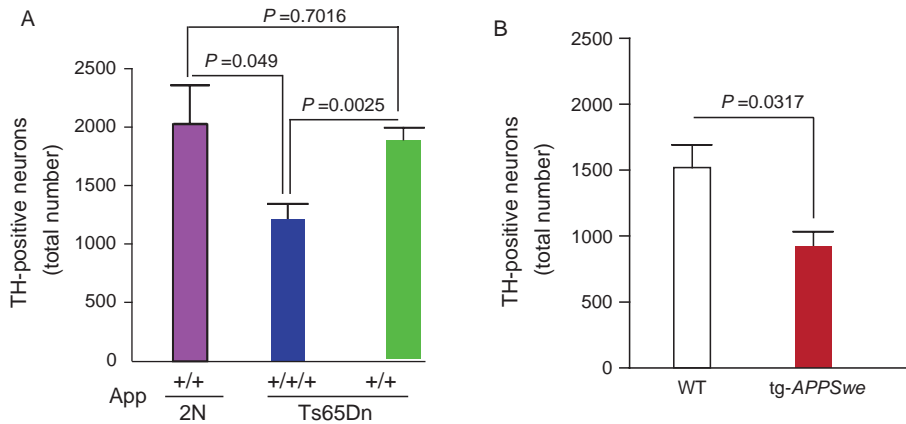
Fig. 7. The relationship between *amyloid precursor protein* overexpression and the loss of tyrosine hydroxylase-positive neurons. (A) The quantification of the total number of TH positive neurons in LC of Ts65Dn mice with either 3 (Ts65Dn *App* +/+/+) or 2 (Ts65Dn *App* +/+/−) copies of *App* and their 2N controls. Deleting an extra copy of *App* in Ts65Dn mice led to a significant improvement in the number of LC neurons. As a result, most significant differences were found between Ts65Dn *App* +/+/− and their 2N control. (B) Quantification of the total number of TH positive neurons in 18-month-old APP_{swe} tg mice showed a significant loss of TH positive neurons indicating that the overexpression of *APP* is both necessary and sufficient to cause LC degeneration. *(Published in Salehi et al., 2009 Science Translational Medicine 18;1(7):7ra17).*

responsible gene(s) is located on the MMU16 fragment between *Gabpa* and *Sodi*. This fragment contains approximately 32 genes including the *App* gene. To test whether an increased dose for *App* contributes to LC degeneration, we examined these neurons in Ts65Dn mice bearing either two or three copies of *App*. Deleting the third copy of *App* in Ts65Dn mice eliminated the decrease in the number of LC neurons, suggesting that *App* overexpression is necessary for LC degeneration. To ask whether or not *App* overexpression is sufficient to cause LC degeneration, we examined mice that overexpress a mutant APP_{Swe} transgene. There was a significant decrease in LC neurons in these mice (Fig. 7). This latter finding is consistent with a recent report showing degeneration of LC neurons in amyloid precursor protein/presenilini *(APP/PS1)* tg mice [132]. Taken together, the findings are evidence that the *APP* gene overexpression plays a conspicuous role in the degeneration of LC neurons. The mechanisms by which *App* overexpression leads to LC degeneration in Ts65Dn mice have yet to be explored. Our investigation on the role of *App* overexpression on BFCNs degeneration suggested that *App* overexpression leads to a significant failure in axonal transport in BFCNs, affecting the size of early endosomes [46]. Possibly a similar mechanism occurs in LC neurons. Based on this, *App* overexpression in Ts65Dn mice and Aβ accumulation in the HC of *APP* tg mice, lead to alterations in early endosomes structure or function, diminishing the retrograde transport of neurotrophins (e.g. BDNF) in

these neurons. Indeed, it has been shown that increased levels of Aβ oligomers lead to failed BDNF retrograde transport in APP tg mouse models of AD [152]. It is important to note that most AD mouse models overexpress mutant APP which eventually leads to increased Aβ levels, whereas the Ts65Dn mouse model of DS bears triplication of wild type mouse *App* (50% increase in dose) (see [44]) with no elevated levels of Aβ [46].

RESTORING NORADRENERGIC SYSTEM AS A TREATMENT FOR DOWN SYNDROME AND ALZHEIMER'S DISEASE

Significant degeneration of LC neurons in adult Ts65Dn mice suggests failure in NE signaling in these mice. However, investigations on the status of β1-ARs in the HC of Ts65Dn mice have demosntrated a significant increase in the number of β1-positive neurons in the polymorphic layer of the DG in young adult Ts65Dn mice [94]. This suggested that in spite of significant LC degeneration in young adult Ts65Dn mice, the machinery of ARs signaling is still intact in these mice. A logical strategy for restoring NE levels would be the use of NE; however, NE does not cross the blood brain barrier (BBB) [153]. Furthermore, due to the presence of ARs on blood vessels, heart, kidneys, stomach, bladder, and several other peripheral organs, increasing NE signaling would lead to significant peripheral side effects in the treated ani-

mals. For this reason, one would need to use an NE prodrug that is able to cross the BBB [154] without causing significant peripheral side effects. L-threo-3, 4-dihydroxyphenylserine (L-DOPS) is an NE-prodrug that has shown to have both requirements [155]. L-DOPS was synthesized in the early 1900s and has been used in Japan since 1989 for the treatment of Parkin-

son's disease and neurogenic orthostatic hypotension. Using aromatic L-amino acid decarboxylase (AAAD), also known as DDC, L-DOPS is converted to NE. In order to limit the effects of L-DOPS to the CNS, L-DOPS is generally given in combination with carbidopa, a peripheral DDC inhibitor that does not cross the BBB [156] (Fig. 8A).
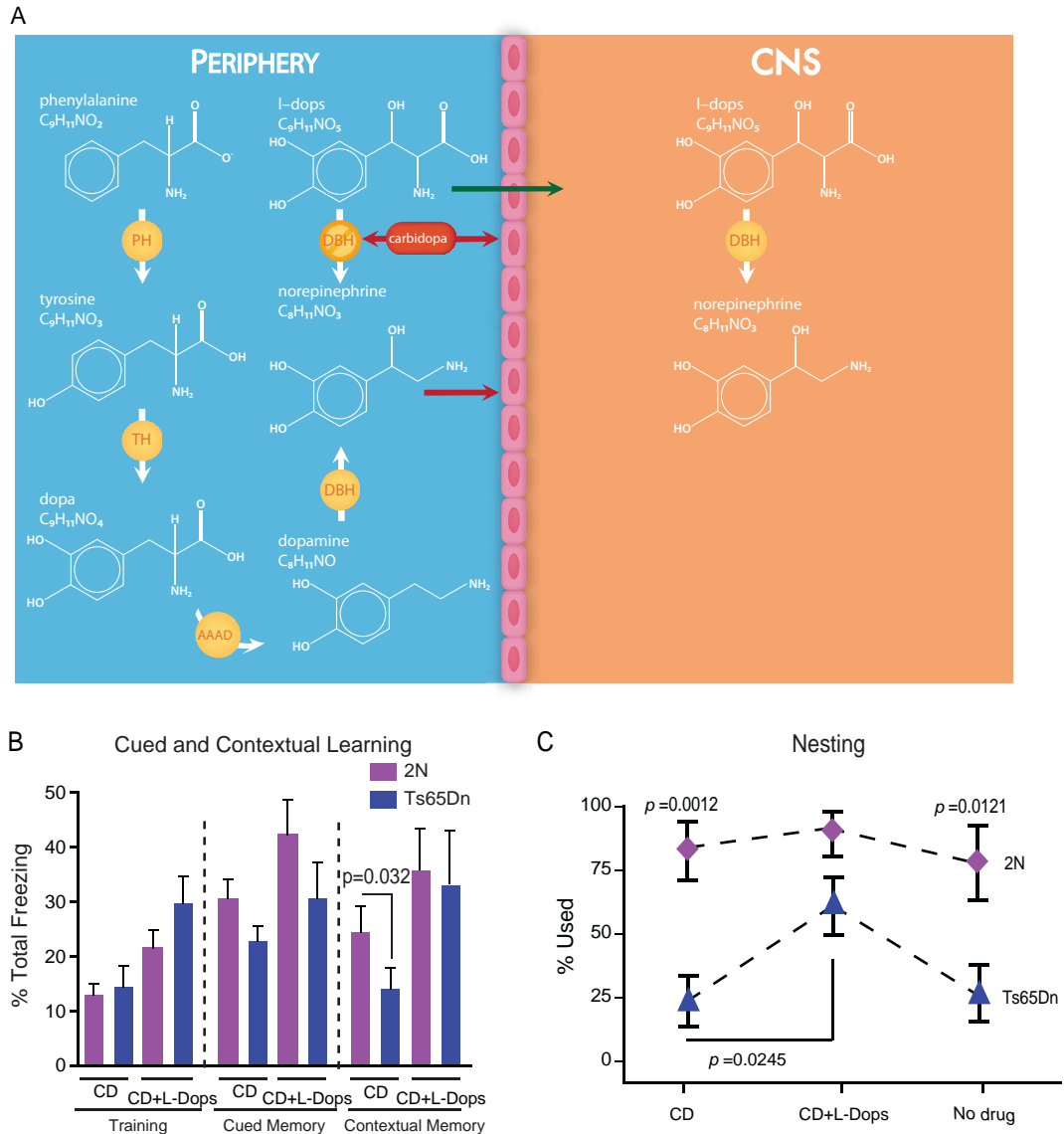
Fig. 8. Effects of L-DOPS on contextual learning. (A) Schematic representation of drug therapy using L-DOPS in combination with carbidopa to block the peripheral effects of this prodrug for NE. (B) Restoration of cognitive function in Ts65Dn mouse model of DS using L-DOPS. 2N mice used a larger percentage of their nesting material compared with Ts65Dn mice which indicates the integrity of their hippocampal function. L-DOPS treatment in Ts65Dn mice improved the nesting behavior and restored failed contextual learning in Ts65Dn mice. (C) Quantification of nesting and fear conditioning behavior after the treatment with L-DOPS in Ts65Dn mouse models of DS. Phenylalanine; $C_9H_{11}NO_2$, Tyrosine; $C_9H_{11}NO_3$, DOPA; $C_9H_{11}NO_4$, Dopamine; $C_8H_{11}NO$, Norepinephrine; $C_8H_{11}NO_3$, L-DOPS; $C_9H_{11}NO_5$, PH; Phenylalanine Hydroxylase, TH; Tyrosine Hydroxylase, AAAD; Aromatic L-Amino Acid Decarboxylase. Also known as DOPA Decarboxylase (DDC), DBH; Dopamine β-hydroxylase. CD (carboxidopa). *(Published in Salehi et al., 2009 Science Translational Medicine 18;1(7):7ra17).*
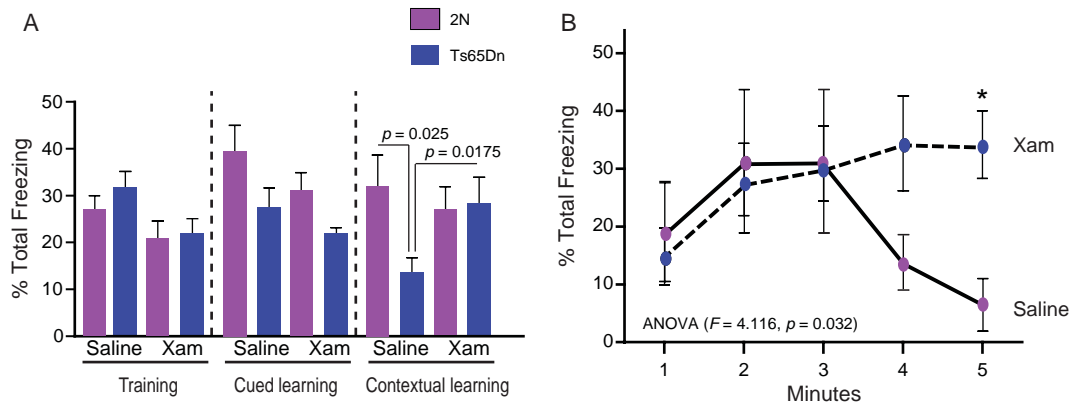
Fig. 9. The use of β1 agonist improves contextual learning in Ts6sDn mice. (A) The comparison of percentage of total freezing in 2N and Ts65Dn mice treated with a β1-AR partial agonist, xamoterol (3 mg/kg) vs. saline. (B) Restoration of failed contextual learning in Ts65Dn mice treated with xamoterol in a similar manner to L-DOPS. This suggests that β1-ARs play a significant role in cognitive effects of NE. *(Published in Salehi et al., 2009 Science Translational Medicine 18;1(7):7ra17).*

Testing fear conditioning in Ts65Dn mice showed a significant failure in contextual learning while cued learning remained relatively intact. Using L-DOPS before training and during cued and contextual learning in young adult Ts65Dn mice showed that failed contextual learning can be successfully restored in these mice (Fig. 8B). Indeed contextual learning was not the sole hippocampal-dependent behavior that can be restored in Ts65Dn mice. We found that treating Ts65Dn mice with L-DOPS also significantly restored the ability to build nests in these mice (Fig. 8C) though the positive effects of L-DOPS on nesting vanished two weeks after discontinuing the treatment. Up-regulation of β 1-ARs in the DG of the Ts65Dn mice and the positive effects of β1-ARs agonists on contextual learning [63] suggests that the positive effects of NE in Ts65Dn mice occur through β1-AR signaling. This idea was supported by the fact that the use of a β1-ARs partial agonist (i.e. xamoterol) had similar positive effects on restoring contextual learning in young adult Ts65Dn mice (Fig. 9).

Increasing β-AR signaling has also been shown to have significant beneficial effects in mouse models of AD. Using DSP4 to deplete brain NE levels in double *(APP/PS1)* tg mice led to a significant increase in brain Aβ accumulation in the HC without affecting Aβ production. Furthermore, it was linked to a significant cognitive dysfunction in *APP/PSi* tg mice [132]. Increasing the hippocampal and cortical levels of NE by using L-DOPS was able to prevent decreased microglial migration and improve Aβ phagocytosis in these mice [134].

CONCLUSIONS

Major therapeutic strategies for AD have either been focused on restoring the levels of ACh (e.g. acetyl-cholinesterase inhibitors) or targeting Aβ levels and reducing AD-related pathology. Unfortunately, none of these two therapeutic strategies have been able to fundamentally change the course of the disease. The data presented here suggests that NE-based therapy may be an attractive alternative to consider.

At the synaptic levels, increasing the levels of NE and/or improving NE signaling within the critical areas of the brain would improve synaptic plasticity and thus cognitive function, whereas extra-synaptically, it would reduce Aβ accumulation via enhanced microglia migration and Aβ clearance. As for negative effects of increasing NE levels, it has been shown that increased density of both α2 and β1-ARs in the cerebellar cortex can be associated with aggression in individuals with AD [157]. In addition, the use of mainly α2 antagonist, e.g. yohimbine, which leads to a significant increase in NE levels in cerebral spinal fluid (CSF), was linked to increased excitement and tension in both healthy individuals and AD patients, with a more pronounced effect in AD [158]. Therefore, there is a need to synthesize or identify β-ARs agonists or small molecules that easily cross the BBB, lack peripheral side effects mediated by ARs, and specifically target β-ARs bearing hippocampal neurons, an area affected by amyloid accumulation and decreased synaptic function in mouse models of AD. Similar molecules might be used to stimulate PP and

EC causing a beneficial effect on DG cells (Fig. 3). Together, these strategies aim to increase NE levels and/or improve β-adrenergic signaling would be able to restore the function of LC neurons and provide additional neuroprotection by reducing Aβ accumulation.

Since all individuals affected by DS will eventually develop AD pathology, an alternative approach to the use of this strategy in advanced cases of AD is to begin treatment before the age of 40 years in individuals affected with DS or those presenting with MCI.

The question on the molecular mechanisms of basic vulnerability of LC neurons in both AD and DS remains unanswered. Data from both the Ts65Dn mice [46] and *App* tg mice [159] suggest that LC degeneration is a retrograde process initiated in the HC. Although the retrograde degeneration of LC neurons in *APP* tg mice could be associated with Aβ accumulation in the HC, the lack of accumulation of Aβ40 and Aβ42 in Ts65Dn mice [46] indicates that the apparent retrograde degeneration of LC neurons in *APP* tg mice and Ts65Dn mice might involve different mechanisms.

The fact that increasing β-adrenergic signaling might both improve synaptic function and reduce amyloid accumulation should encourage further research on the feasibility of the use of this strategy in AD and adults with DS. The availability of multiple widely prescribed drugs on the market able to improve β-adrenergic signaling should further facilitate and expedite these trials. Although extensive studies presented here all suggest positive effects of increased b-adrenergic drugs in mouse models of AD and DS, further inclusive and well-planned studies are needed to support this strategy in the clinical setting. The fact that there is a significant positive interaction between NA-ergic and cholinergic systems supports that adjunct therapy targeting both systems might have a better success rate. Furthermore, the results summarized in this review also suggest that drugs targeting *App* gene expression in DS and/or Aβ levels in AD, in combination with NE drugs, might be able to fundamentally alter the course of both disorders.

ACKNOWLEDGMENTS

REFERENCES

[1] Wisniewski KE, Wisniewski HM, Wen GY (1985) Occurrence of neuropathological changes and dementia of Alzheimer's disease in Down's syndrome. *Ann Neurol* **17**, 278-282.

[2] Lai F, Williams RS (1989) A prospective study of Alzheimer disease in Down syndrome. *Arch Neurol* **46**, 849-853.

[3] Chapman RS, Hesketh LJ (2000) Behavioral phenotype of individuals with Down syndrome. *Ment Retard Dev Disabil Res Rev* **6**, 84-95.

[4] Prasher VP, Farrer MJ, Kessling AM, Fisher EM, West RJ, Barber PC, Butler AC (1998) Molecular mapping of Alzheimer-type dementia in Down's syndrome. *Ann Neurol* **43**, 380-383.

[5] Roizen NJ, Patterson D (2003) Down's syndrome. *Lancet* **361**, 1281-1289.

[6] Salehi A. PB, Mobley WC. (2008) Down syndrome/ Trisomy 21. 2008. In *The New Encyclopedia of Neuroscience* Elsevier.

[7] Chun MM, Jiang Y (2003) Implicit, long-term spatial contextual memory. *J Exp Psychol Learn Mem Cogn* **29**, 224-234.

[8] Lawrence JJ, McBain CJ (2003) Interneuron diversity series: containing the detonation—feedforward inhibition in the CA3 hippocampus. *Trends Neurosci* **26**, 631-640.

[9] Whitehouse PJ, Price DL, Struble RG, Clark AW, Coyle JT, Delon MR (1982) Alzheimer's disease and senile dementia: loss of neurons in the basal forebrain. *Science* **215**, 1237-1239.

[10] Moudy AM, Kunkel DD, Schwartzkroin PA (1993) Development of dopamine-beta-hydroxylase-positive fiber innervation of the rat hippocampus. *Synapse* **15**, 307-318.

[11] Jacobs BL, Azmitia EC (1992) Structure and function of the brain serotonin system. *Physiol Rev* **72**, 165-229.

[12] Haglund L, Swanson LW, Kohler C (1984) The projection of the supramammillary nucleus to the hippocampal formation: an immunohistochemical and anterograde transport study with the lectin PHA-L in the rat. *J Comp Neurol* **229**, 171-185.

[13] Clarke DJ (1985) Cholinergic innervation of the rat dentate gyrus: an immunocytochemical and electron microscopical study. *Brain Res* **360**, 349-354.

[14] Freund TF, Antal M (1988) GABA-containing neurons in the septum control inhibitory interneurons in the hippocampus. *Nature* **336**, 170-173.

[15] Kohler C, Chan-Palay V (1983) Distribution of gamma aminobutyric acid containing neurons and terminals in the septal area. an immunohistochemical study using antibodies to glutamic acid decarboxylase in the rat brain. *Anat Embryol (Berl)* **167**, 53-65.

[16] Amaral DG, Menno P.Witter. (1995) Hippocampal Formation In *The Rat Nervous System*, Paxinos G, ed. Academic Press.

[17] Sara SJ (2009) The locus coeruleus and noradrenergic modulation of cognition. *Nat Rev Neurosci* **10**, 211-223.

[18] Tork I (1990) Anatomy of the serotonergic system. *Ann N Y Acad Sci* **600**, 9-34; discussion 34-35.

[19] Freund TF, Gulyas AI, Acsady L, Gores T, Toth K (1990) Serotonergic control of the hippocampus via local inhibitory interneurons. *Proc Natl Acad Sci USA* **87**, 8501-8505.

[20] Nitsch R, Leranth C (1993) Calretinin immunoreactivity in the monkey hippocampal formation—ii. Intrinsic GABAergic and hypothalamic non-GABAergic systems: an

experimental tracing and co-existence study. *Neuroscience* **55**, 797-812.

[21] Mufson EJ, Kroin JS, Sendera TJ, Sobreviela T (1999) Distribution and retrograde transport of trophic factors in the central nervous system: functional implications for the treatment of neurodegenerative diseases. *Prog Neurobiol* **57**, 451-484.

[22] Celada P, Siuciak JA, Tran TM, Altar CA, Tepper JM (1996) Local infusion of brain-derived neurotrophic factor modifies the firing pattern of dorsal raphe serotonergic neurons. *Brain Res* **712**, 293-298.

[23] Friedman WJ, Ibanez CF, Hallbook F, Persson H, Cain LD, Dreyfus CF, Black IB (1993) Differential actions of neurotrophins in the locus coeruleus and basal forebrain. *Exp Neurol* **119**, 72-78.

[24] Sobreviela T, Pagcatipunan M, Kroin JS, Mufson EJ (1996) Retrograde transport of brain-derived neurotrophic factor (BDNF) following infusion in neo- and limbic cortex in rat: relationship to BDNF mRNA expressing neurons. *J Comp Neurol* **375**, 417-444.

[25] Braak H, Del Tredici K, Schultz C, Braak E (2000) Vulnerability of select neuronal types to Alzheimer's disease. *Ann N Y Acad Sci* **924**, 53-61.

[26] Morys J, Sadowski M, Barcikowska M, Maciejewska B, Narkiewicz O (1994) The second layer neurones of the entorhinal cortex and the perforant path in physiological ageing and Alzheimer's disease. *Acta Neurobiol Exp (Wars)* **54**, 47-53.

[27] Oliveira PP, Jr., Nitrini R, Busatto G, Buchpiguel C, Sato JR, Amaro E, Jr. (2010) Use of SVM methods with surface-based cortical and volumetric subcortical measurements to detect Alzheimer's disease. *JAlzheimers Dis* **19**, 1263-1272.

[28] Abraham H, Vincze A, Jewgenow I, Veszpremi B, Kravjak A, Gomori E, Seress L (2010) Myelination in the human hippocampal formation from midgestation to adulthood. *Int J Dev Neurosci* **28**, 401-410.

[29] Oda Y (1999) Choline acetyltransferase: the structure, distribution and pathologic changes in the central nervous system. *Pathol Int* **49**, 921-937.

[30] Aston-Jones G, Segal M, Bloom FE (1980) Brain aminergic axons exhibit marked variability in conduction velocity. *Brain Res* **195**, 215-222.

[31] Leranth C, Hajszan T (2007) Extrinsic afferent systems to the dentate gyms. *Prog Brain Res* **163**, 63-84.

[32] Shahidi S, Motamedi F, Naghdi N (2004) Effect of reversible inactivation of the supramammillary nucleus on spatial learning and memory in rats. *Brain Res* **1026**, 267-274.

[33] Moreau PH, Cosquer B, Jeltsch H, Cassel JC, Mathis C (2008) Neuroanatomical and behavioral effects of a novel version of the cholinergic immunotoxin mu p75-saporin in mice. *Hippocampus* **18**, 610-622.

[34] Borelli KG, Gargaro AC, dos Santos JM, Brandao ML (2005) Effects of inactivation of serotonergic neurons of the median raphe nucleus on learning and performance of contextual fear conditioning. *Neurosci Lett* **387**, 105-110.

[35] Compton DM, Dietrich KL, Smith JS, Davis BK (1995) Spatial and non-spatial learning in the rat following lesions to the nucleus locus coeruleus. *Neuroreport* **7**, 177-182.

[36] Mann DM (1985) The neuropathology of Alzheimer's disease: a review with pathogenetic, aetiological and therapeutic considerations. *Mech Ageing Dev* **31**, 213-255.

[37] Amaral DG. (2010) Memory: Anatomical Organization of Candidate Brain Regions. In *Comprehensive Physiology*. Wiley, pp. 211-294.

[38] Nakamura S, Takemura M, Ohnishi K, Suenaga T, Nishimura M, Akiguchi I, Kimura J, Kimura T (1993) Loss of large neurons and occurrence of neurofibrillary tangles in the tuberomammillary nucleus of patients with Alzheimer's disease. *Neurosci Lett* **151**, 196-199.

[39] Salehi A, Heyn S, Gonatas NK, Swaab DF (1995) Decreased protein synthetic activity of the hypothalamic tuberomamillary nucleus in Alzheimer's disease as suggested by smaller Golgi apparatus. *Neurosci Lett* **193**, 29-32.

[40] Schliebs R, Arendt T (2010) The cholinergic system in aging and neuronal degeneration. *Behav Brain Res*.

[41] Mann DM, Yates PO, Marcyniuk B, Ravindra CR (1987) Loss of neurones from cortical and subcortical areas in Down's syndrome patients at middle age. Quantitative comparisons with younger Down's patients and patients with Alzheimer's disease. *J Neurol Sci* **80**, 79-89.

[42] Hattori M, Fujiyama A, Taylor TD, Watanabe H, Yada T, Park HS, Toyoda A, Ishii K, Totoki Y, Choi DK, Groner Y, Soeda E, Ohki M, Takagi T, Sakaki Y, Taudien S, Blechschmidt K, Polley A, Menzel U, Delabar J, Kumpf K, Lehmann R, Patterson D, Reichwald K, Rump A, Schillhabel M, Schudy A, Zimmermann W, Rosenthal A, Kudoh J, Schibuya K, Kawasaki K, Asakawa S, Shintani A, Sasaki T, Nagamine K, Mitsuyama S, Antonarakis SE, Minoshima S, Shimizu N, Nordsiek G, Hornischer K, Brant P, Scharfe M, Schon O, Desario A, Reichelt J, Kauer G, Blocker H, Ramser J, Beck A, Klages S, Hennig S, Riesselmann L, Dagand E, Haaf T, Wehrmeyer S, Borzym K, Gardiner K, Nizetic D, Francis F, Lehrach H, Reinhardt R, Yaspo ML (2000) The DNA sequence of human chromosome 21 . *Nature* **405**, 311-319.

[43] Sturgeon X, Gardiner KJ (2011) Transcript catalogs of human chromosome 21 and orthologous chimpanzee and mouse regions. *Mamm Genome*.

[44] Salehi A, Faizi M, Belichenko PV, Mobley WC (2007) Using mouse models to explore genotype-phenotype relationship in Down syndrome. *Merit Retard Dev Disabil Res Rev* **13**, 207-214.

[45] Bekris LM, Yu CE, Bird TD, Tsuang DW (2010) Genetics of Alzheimer disease. *J Geriatr Psychiatry Neurol* **23**, 213-227.

[46] Salehi A, Delcroix JD, Belichenko PV, Zhan K, Wu C, Valletta JS, Takimoto-Kimura R, Kleschevnikov AM, Sambamurti K, Chung PP, Xia W, Villar A, Campbell WA, Kulnane LS, Nixon RA, Lamb BT, Epstein CJ, Stokin GB, Goldstein LS, Mobley WC (2006) Increased App expression in a mouse model of Down's syndrome disrupts NGF transport and causes cholinergic neuron degeneration. *Neuron* **51**, 29-42.

[47] Bullido MJ, Ramos MC, Ruiz-Gomez A, Tutor AS, Sastre I, Frank A, Coria F, Gil P, Mayor F, Valdivieso F (2004) Polymorphism in genes involved in adrenergic signaling associated with Alzheimer's. *Neurobiol Aging* **25**, 853-859.

[48] Dahlstroem A, Fuxe K (1964) EVIDENCE FOR THE EXISTENCE OF MONOAMINE-CONTAINING NEURONS IN THE CENTRAL NERVOUS SYSTEM. i. demonstration of monoamines in the cell bodies of brain stem neurons. *Ada Physiol Scand Suppl* (232), 231-255.

[49] Berridge CW, Waterhouse BD (2003) The locus coeruleus-noradrenergic system: modulation of behavioral state and state-dependent cognitive processes. *Brain Res Brain Res Rev* **42**, 33-84.

[50] Mouton PR, Pakkenberg B, Gundersen HJ, Price DL (1994) Absolute number and size of pigmented locus coeruleus neu-

rons in young and aged individuals. *J Chem Neuroanat* **7**, 185-190.

[51] Palmer AM, DeKosky ST (1993) Monoamine neurons in aging and Alzheimer's disease. *J Neural Transm Gen Sect* **91**, 135-159.

[52] Jones BE, Yang TZ (1985) The efferent projections from the reticular formation and the locus coeruleus studied by anterograde and retrograde axonal transport in the rat. *J Comp Neurol* **242**, 56-92.

[53] Foote SL, Morrison JH (1987) Extrathalamic modulation of cortical function. *Annu Rev Neurosci* **10**, 67-95.

[54] Zaborszky L, Cullinan WE, Luine VN (1993) Catecho-laminergic-cholinergic interaction in the basal forebrain. *Prog Brain Res* **98**, 31-49.

[55] Loy R, Koziell DA, Lindsey JD, Moore RY (1980) Noradrenergic innervation of the adult rat hippocampal formation. *J Comp Neurol* **189**, 699-710.

[56] Aston-Jones G, Ennis M, Pieribone VA, Nickell WT, Shipley MT (1986) The brain nucleus locus coeruleus: restricted afferent control of a broad efferent network. *Science* **234**, 734-737.

[57] Ennis M, Aston-Jones G (1988) Activation of locus coeruleus from nucleus paragigantocellularis: a new excitatory amino acid pathway in brain. *J Neurosci* **8**, 3644-3657.

[58] Ennis M, Aston-Jones G (1989) Potent inhibitory input to locus coeruleus from the nucleus prepositus hypoglossi. *Brain Res Bull* **22**, 793-803.

[59] Ennis M, Aston-Jones G (1989) GABA-mediated inhibition of locus coeruleus from the dorsomedial rostral medulla. *J Neurosci* **9**, 2973-2981.

[60] Gaymard B, Pierrot-Deseilligny C (1999) Neurology of saccades and smooth pursuit. *Curr Opin Neurol* **12**, 13-19.

[61] Van Bockstaele EJ, Aston-Jones G (1995) Integration in the ventral medulla and coordination of sympathetic, pain and arousal functions. *Clin Exp Hypertens* **17**, 153-165.

[62] Aston-Jones G, Shipley MT, Chouvet G, Ennis M, van Bockstaele E, Pieribone V, Shiekhattar R, Akaoka H, Drolet G, Astier B, et al. (1991) Afferent regulation of locus coeruleus neurons: anatomy, physiology and pharmacology. *Prog Brain Res* **88**, 47-75.

[63] Murchison CF, Zhang XY, Zhang WP, Ouyang M, Lee A, Thomas SA (2004) A distinct role for norepinephrine in memory retrieval. *Cell* **117**, 131-143.

[64] Herrmann N, Lanctot KL, Khan LR (2004) The role of norepinephrine in the behavioral and psychological symptoms of dementia. *J Neuropsychiatry Clin Neurosci* **16**, 261-276.

[65] Amara SG, Kuhar MJ (1993) Neurotransmitter transporters: recent progress. *Anna Rev Neurosci* **16**, 73-93.

[66] Benarroch EE (2009) The locus ceruleus norepinephrine system: functional organization and potential clinical significance. *Neurology* **73**, 1699-1704.

[67] Gilsbach R, Hein L (2008) Presynaptic metabotropic receptors for acetylcholine and adrenaline/noradrenaline. *Handb Exp Pharmacol*, 261-288.

[68] Duncan GE, Little KY, Koplas PA, Kirkman JA, Breese GR, Stumpf WE (1991) Beta-adrenergic receptor distribution in human and rat hippocampal formation: marked species differences. *Brain Res* **561**, 84-92.

[69] Starke K (2001) Presynaptic autoreceptors in the third decade: focus on alpha2-adrenoceptors. *J Neurochem* **78**, 685-693.

[70] Arnsten AF, Steere JC, Hunt RD (1996) The contribution of alpha 2-noradrenergic mechanisms of prefrontal cortical cognitive function. Potential significance for attention-deficit hyperactivity disorder. *Arch Gen Psychiatry* **53**, 448-455.

[71] Nestler EJ, Alreja M, Aghajanian GK (1999) Molecular control of locus coeruleus neurotransmission. *Biol Psychiatry* **46**, 1131-1139.

[72] Devauges V, Sara SJ (1991) Memory retrieval enhancement by locus coeruleus stimulation: evidence for mediation by beta-receptors. *Behav Brain Res* **43**, 93-97.

[73] Ji JZ, Wang XM, Li BM (2003) Deficit in long-term contextual fear memory induced by blockade of beta-adrenoceptors in hippocampal CA1 region. *Eur J Neurosci* **17**, 1947-1952.

[74] Ji JZ, Zhang XH, Li BM (2003) Deficient spatial memory induced by blockade of beta-adrenoceptors in the hippocampal CA1 region. *Behav Neurosci* **117**, 1378-1384.

[75] Juric DM, Miklic S, Carman-Krzan M (2006) Monoaminergic neuronal activity up-regulates BDNF synthesis in cultured neonatal rat astrocytes. *Brain Res* **1108**, 54-62.

[76] Juric DM, Loncar D, Carman-Krzan M (2008) Noradrenergic stimulation of BDNF synthesis in astrocytes: mediation via alphai- and betai/beta2-adrenergic receptors. *Neurochem Int* **52**, 297-306.

[77] Nagahara AH, Merrill DA, Coppola G, Tsukada S, Schroeder BE, Shaked GM, Wang L, Blesch A, Kim A, Conner JM, Rockenstein E, Chao MV, Koo EH, Geschwind D, Masliah E, Chiba AA, Tuszynski MH (2009) Neuroprotective effects of brain-derived neurotrophic factor in rodent and primate models of Alzheimer's disease. *Nat Med* **15**, 331-337.

[78] Bondareff W, Mountjoy CQ, Roth M (1982) Loss of neurons of origin of the adrenergic projection to cerebral cortex (nucleus locus ceruleus) in senile dementia. *Neurology* **32**, 164-168.

[79] Mitchell HA, Weinshenker D. Good night and good luck: norepinephrine in sleep pharmacology. *Biochem Pharmacol* **79**, 801-809.

[80] Aston-Jones G, Bloom FE (1981) Norepinephrine-containing locus coeruleus neurons in behaving rats exhibit pronounced responses to non-noxious environmental stimuli. *J Neurosci* **1**, 887-900.

[81] Minzenberg MJ, Watrous AJ, Yoon JH, Ursu S, Carter CS (2008) Modafinil shifts human locus coeruleus to low-tonic, high-phasic activity during functional mri. *Science* **322**, 1700-1702.

[82] Bliwise DL (2004) Sleep disorders in Alzheimer's disease and other dementias. *Clin Cornerstone* **6(Suppl 1A)**, 16-28.

[83] Maurizi CP (1987) Dementia—the failure of hippocampal plasticity and dreams. Is there a preventative role for melatonin? *Med Hypotheses* **24**, 59-68.

[84] Khakpour-Taleghani B, Lashgari R, Motamedi F, Naghdi N (2009) Effect of reversible inactivation of locus ceruleus on spatial reference and working memory. *Neuroscience* **158**, 1284-1291.

[85] van Stegeren AH (2008) The role of the noradrenergic system in emotional memory. *Acta Psychol (Amst)* **127**, 532-541.

[86] Rodrigues SM, LeDoux JE, Sapolsky RM (2009) The influence of stress hormones on fear circuitry. *Annu Rev Neurosci* **32**, 289-313.

[87] Sterpenich V, D'Argembeau A, Desseilles M, Balteau E, Albouy G, Vandewalle G, Degueldre C, Luxen A, Collette F, Maquet P (2006) The locus ceruleus is involved in the successful retrieval of emotional memories in humans. *J Neurosci* **26**, 7416-7423.

[88] Tully K, Bolshakov VY (Brain) Emotional enhancement of memory: how norepinephrine enables synaptic plasticity. *Mol* **3**, 15.

[89] Hu H, Real E, Takamiya K, Kang MG, Ledoux J, Huganir RL, Malinow R (2007) Emotion enhances learning via norepinephrine regulation of AMPA-receptor trafficking. *Cell* **131**, 160-173.

[90] Ikegaya Y, Nakanishi K, Saito H, Abe K (1997) Amygdala beta-noradrenergic influence on hippocampal long-term potentiation *in vivo*. *Neuroreport* **8**, 3143-3146.

[91] Harley CW (2007) Norepinephrine and the dentate gyms. *Prog Brain Res* **163**, 299-318.

[92] Crowe SF, Shaw S (1997) Salbutamol overcomes the effect of the noradrenergic neurotoxin DSP-4 on memory function in the day-old chick. *Behav Pharmacol* **8**, 216-222.

[93] Gibbs ME, Maksel D, Gibbs Z, Hou X, Summers RJ, Small DH. Memory loss caused by beta-amyloid protein is rescued by a beta(3)-adrenoceptor agonist. *Neurobiol Aging* **31**, 614-624.

[94] Salehi A, Faizi M, Colas D, Valletta J, Laguna J, Takimoto-Kimura R, Kleschevnikov A, Wagner SL, Aisen P, Shamloo M, Mobley WC (2009) Restoration of norepinephrine-modulated contextual memory in a mouse model of Down syndrome. *Sci Transl Med* **1**, 7ra17.

[95] Gliebus G, Lippa CF (2007) The influence of beta-blockers on delayed memory function in people with cognitive impairment. *Am J Alzheimers Dis Other Demen* **22**, 57-61.

[96] Cahill L, Prins B, Weber M, McGaugh JL (1994) Beta-adrenergic activation and memory for emotional events. *Nature* **371**, 702-704.

[97] Siniscalchi A, Badini I, Bianchi C, Beani L (1994) Mono-amines modulate the electrically-evoked efflux of 3H-choline from slices of guinea pig nucleus basalis magnocellularis. *Naunyn Schmiedebergs Arch Pharmacol* **350**, 10-14.

[98] Tellez S, Colpaert F, Marien M (1999) Alpha2-adrenoceptor modulation of cortical acetylcholine release *in vivo*. *Neuroscience* **89**, 1041-1050.

[99] Arnsten AF, Goldman-Rakic PS (1985) Alpha 2-adrenergic mechanisms in prefrontal cortex associated with cognitive decline in aged nonhuman primates. *Science* **230**, 1273-1276.

[100] Lockrow J, Boger H, Gerhardt G, Bachman D, Granholm AC. A Noradrenergic Lesion Exacerbates Neurodegeneration in a Down syndrome Mouse Model. *J Alzheimers Dis*.

[101] Peskind ER, Elrod R, Dobie DJ, Pascualy M, Petrie E, Jensen C, Brodkin K, Murray S, Veith RC, Raskind MA (1998) Cerebrospinal fluid epinephrine in Alzheimer's disease and normal aging. *Neuropsychopharmacology* **19**, 465-471.

[102] Bierer LM, Aisen PS, Davidson M, Ryan TM, Stern RG, Schmeidler J, Davis KL (1993) A pilot study of oral physostigmine plus yohimbine in patients with Alzheimer disease. *Alzheimer Dis Assoc Disord* **7**, 98-104.

[103] Davis JA, Gould TJ (2007) Atomoxetine reverses nicotine withdrawal-associated deficits in contextual fear conditioning. *Neuropsychopharmacology* **32**, 2011-2019.

[104] Murchison CF, Schutsky K, Jin SH, Thomas SA (2011) Norepinephrine and betai-adrenergic signaling facilitate activation of hippocampal cai pyramidal neurons during contextual memory retrieval. *Neuroscience*.

[105] Olson VG, Rockett HR, Reh RK, Redila VA, Tran PM, Venkov HA, Defino MC, Hague C, Peskind ER, Szot P, Raskind MA (2011) The role of norepinephrine in differential response to stress in an animal model of posttraumatic stress disorder. *Biol Psychiatry*,.

[106] Hull C (1993) 1. Teaching and learning (ii). how adults learn. *Nurs Times* **89**, i-viii.

[107] Witter MP, Naber PA, van Haeften T, Machielsen WC, Rombouts SA, Barkhof F, Scheltens P, Lopes da Silva FH (2000) Cortico-hippocampal communication by way of parallel parahippocampal-subicular pathways. *Hippocampus* **10**, 398-410.

[108] Beckstead RM (1978) Afferent connections of the entorhinal area in the rat as demonstrated by retrograde cell-labeling with horseradish peroxidase. *Brain Res* **152**, 249-264.

[109] Dolorfo CL, Amaral DG (1998) Entorhinal cortex of the rat: topographic organization of the cells of origin of the perforant path projection to the dentate gyrus. *J Comp Neurol* **398**, 25-48.

[110] Kerr KM, Agster KL, Furtak SC, Burwell RD (2007) Functional neuroanatomy of the parahippocampal region: the lateral and medial entorhinal areas. *Hippocampus* **17**, 697-708.

[111] Hafting T, Fyhn M, Molden S, Moser MB, Moser EI (2005) Microstructure of a spatial map in the entorhinal cortex. *Nature* **436**, 801-806.

[112] Steffenach HA, Witter M, Moser MB, Moser EI (2005) Spatial memory in the rat requires the dorsolateral band of the entorhinal cortex. *Neuron* **45**, 301-313.

[113] Harley CH. (2007) norepinephrine and the dentate gyrus *In Progress in Brain Research*, Scharfman HE, ed. Elsevier.

[114] Lacaille JC, Harley CW (1985) The action of norepinephrine in the dentate gyrus: beta-mediated facilitation of evoked potentials *in vitro*. *Brain Res* **358**, 210-220.

[115] Stanton PK, Sarvey JM (1985) Blockade of norepinephrine-induced long-lasting potentiation in the hippocampal dentate gyrus by an inhibitor of protein synthesis. *Brain Res* **361**, 276-283.

[116] Dahl D, Sarvey JM (1989) Norepinephrine induces pathway-specific long-lasting potentiation and depression in the hippocampal dentate gyrus. *Proc Natl Acad Sci USA* **86**, 4776-4780.

[117] Papastavrou E, Kalokerinou A, Papacostas SS, Tsangari H, Sourtzi P (2007) Caring for a relative with dementia: family caregiver burden. *J Adv Nurs* **58**, 446-457.

[118] Gaugler JE, Yu F, Krichbaum K, Wyman JF (2009) Predictors of nursing home admission for persons with dementia. *Med Care* **47**, 191-198.

[119] Palmer AM, Francis PT, Bowen DM, Benton JS, Neary D, Mann DM, Snowden JS (1987) Catecholaminergic neurones assessed ante-mortem in Alzheimer's disease. *Brain Res* **414**, 365-375.

[120] Grudzien A, Shaw P, Weintraub S, Bigio E, Mash DC, Mesulam MM (2007) Locus coeruleus neurofibrillary degeneration in aging, mild cognitive impairment and early Alzheimer's disease. *Neurobiol Aging* **28**, 327-335.

[121] German DC, Manaye KF, White CL, Woodward DJ, Mclntire DD, Smith WK, Kalaria RN, Mann DM (1992) Disease-specific patterns of locus coeruleus cell loss. *Ann Neurol* **32**, 667-676.

[122] Cole G, Neal JW, Singhrao SK, Jasani B, Newman GR (1993) The distribution of amyloid plaques in the cerebellum and brain stem in Down's syndrome and Alzheimer's disease: a light microscopical analysis. *Ada Neuropathol* **85**, 542-552.

[123] Hoogendijk WJ, Pool CW, Troost D, van Zwieten E, Swaab DF (1995) Image analyser-assisted morphometry of the locus coeruleus in Alzheimer's disease, Parkinson's disease and amyotrophic lateral sclerosis. *Brain* **118**(1), 131-143.

[124] Iversen LL, Rossor MN, Reynolds GP, Hills R, Roth M, Mountjoy CQ, Foote SL, Morrison JH, Bloom FE (1983) Loss of pigmented dopamine-beta-hydroxylase positive cells from locus coeruleus in senile dementia of Alzheimer's type. *Neurosci Lett* **39**, 95-100.

[125] Matthews KL, Chen CP, Esiri MM, Keene J, Minger SL, Francis PT (2002) Noradrenergic changes, aggressive behavior, and cognition in patients with dementia. *Biol Psychiatry* **51**, 407-416.

[126] Szot P, White SS, Greenup JL, Leverenz JB, Peskind ER, Raskind MA (2006) Compensatory changes in the noradrenergic nervous system in the locus ceruleus and hippocampus of postmortem subjects with Alzheimer's disease and dementia with lewy bodies. *J Neurosci* **26**, 467-478.

[127] Zarow C, Lyness SA, Mortimer JA, Chui HC (2003) Neuronal loss is greater in the locus coeruleus than nucleus basalis and substantia nigra in Alzheimer and parkinson diseases. *Arch Neurol* **60**, 337-341.

[128] Hoogendijk WJ, Feenstra MG, Botterblom MH, Gilhuis J, Sommer IE, Kamphorst W, Eikelenboom P, Swaab DF (1999) Increased activity of surviving locus ceruleus neurons in Alzheimer's disease. *Ann Neurol* **45**, 82-91.

[129] Kalinin S, Gavrilyuk V, Polak PE, Vasser R, Zhao J, Heneka MT, Feinstein DL (Aging) (2007) Noradrenaline deficiency in brain increases beta-amyloid plaque burden in an animal model of Alzheimer's disease. *Neurobiol* **28**, 1206-1214.

[130] O'Neil JN, Mouton PR, Tizabi Y, Ottinger MA, Lei DL, Ingram DK, Manaye KF (2007) Catecholaminergic neuronal loss in locus coeruleus of aged female dtg APP/PS1 mice. *J Chem Neuroanat* **34**, 102-107.

[131] Heneka MT, Ramanathan M, Jacobs AH, Dumitrescu-Ozimek L, Bilkei-Gorzo A, Debeir T, Sastre M, Galldiks N, Zimmer A, Hoehn M, Heiss WD, Klockgether T, Staufenbiel M (2006) Locus ceruleus degeneration promotes Alzheimer pathogenesis in amyloid precursor protein 23 transgenic mice. *J Neurosci* **26**, 1343-1354.

[132] Jardanhazi-Kurutz D, Kummer MP, Terwel D, Vogel K, Dyrks T, Thiele A, Heneka MT. Induced LC degeneration in APP/PSi transgenic mice accelerates early cerebral amyloidosis and cognitive deficits. *Neurochem Int* **57**, 375-382.

[133] Heneka MT, Galea E, Gavriluyk V, Dumitrescu-Ozimek L, Daeschner J, O'Banion MK, Weinberg G, Klockgether T, Feinstein DL (2002) Noradrenergic depletion potentiates beta-amyloid-induced cortical inflammation: implications for Alzheimer's disease. *J Neurosci* **22**, 2434-2442.

[134] Heneka MT, Nadrigny F, Regen T, Martinez-Hernandez A, Dumitrescu-Ozimek L, Terwel D, Jardanhazi-Kurutz D, Walter J, Kirchhoff F, Hanisch UK, Kummer MP. Locus ceruleus controls Alzheimer's disease pathology by modulating microglial functions through norepinephrine. *Proc Natl Acad Sci USA* **107**, 6058-6063.

[135] Tanaka KF, Kashima H, Suzuki H, Ono K, Sawada M (2002) Existence of functional beta1- and beta2-adrenergic receptors on microglia. *J Neurosci Res* **70**, 232-237.

[136] Kong Y, Ruan L, Qian L, Liu X, Le Y (2010) Norepinephrine promotes microglia to uptake and degrade amyloid beta peptide through upregulation of mouse formyl peptide receptor 2 and induction of insulin-degrading enzyme. *J Neurosci* **30**, 11848-11857.

[137] Reeves TM, Lyeth BG, Povlishock JT (1995) Long-term potentiation deficits and excitability changes following traumatic brain injury. *Exp Brain Res* **106**, 248-256.

[138] Escorihuela RM, Fernandez-Teruel A, Vallina IF, Baamonde C, Lumbreras MA, Dierssen M, Tobena A, Florez J (1995) A behavioral assessment of Ts65Dn mice: a putative Down syndrome model. *Neurosci Lett* **199**, 143-146.

[139] Escorihuela RM, Vallina IF, Martinez-Cue C, Baamonde C, Dierssen M, Tobena A, Florez J, Fernandez-Teruel A (1998) Impaired short- and long-term memory in Ts65Dn mice, a model for Down syndrome. *Neurosci Lett* **247**, 171-174.

[140] Demas GE, Nelson RJ, Krueger BK, Yarowsky PJ (1998) Impaired spatial working and reference memory in segmental trisomy (Ts65Dn) mice. *Behau Brain Res* **90**, 199-201.

[141] Sago H, Carlson EJ, Smith DJ, Rubin EM, Crnic LS, Huang TT, Epstein CJ (2000) Genetic dissection of region associated with behavioral abnormalities in mouse models for Down syndrome. *Pediatr Res* **48**, 606-613.

[142] Hyde LA, Frisone DF, Crnic LS (2001) Ts65Dn mice, a model for Down syndrome, have deficits in context discrimination learning suggesting impaired hippocampal function. *Behau Brain Res* **118**, 53-60.

[143] Belichenko PV, Masliah E, Kleschevnikov AM, Villar AJ, Epstein CJ, Salehi A, Mobley WC (2004) Synaptic structural abnormalities in the Ts65Dn mouse model of Down Syndrome. *J Comp Neurol* **480**, 281-298.

[144] Siarey RJ, Carlson EJ, Epstein CJ, Balbo A, Rapoport SI, Galdzicki Z (1999) Increased synaptic depression in the Ts65Dn mouse, a model for mental retardation in Down syndrome. *Neuropharmacology* **38**, 1917-1920.

[145] Kleschevnikov AM, Belichenko PV, Villar AJ, Epstein CJ, Malenka RC, Mobley WC (2004) Hippocampal long-term potentiation suppressed by increased inhibition in the Ts65Dn mouse, a genetic model of Down syndrome. *J Neurosci* **24**, 8153-8160.

[146] Holtzman DM, Santucci D, Kilbridge J, Chua-Couzens J, Fontana DJ, Daniels SE, Johnson RM, Chen K, Sun Y, Carlson E, Alleva E, Epstein CJ, Mobley WC (1996) Developmental abnormalities and age-related neurodegeneration in a mouse model of Down syndrome. *Proc Natl Acad Sci USA* **93**, 13333-13338.

[147] Dierssen M, Vallina IF, Baamonde C, Garcia-Calatayud S, Lumbreras MA, Florez J (1997) Alterations of central noradrenergic transmission in Ts65Dn mouse, a model for Down syndrome. *Brain Res* **749**, 238-244.

[148] Granholm AC, Sanders LA, Crnic LS (2000) Loss of cholinergic phenotype in basal forebrain coincides with cognitive decline in a mouse model of Down's syndrome. *Exp Neurol* **161**, 647-663.

[149] Cooper JD, Salehi A, Delcroix JD, Howe CL, Belichenko PV, Chua-Couzens J, Kilbridge JF, Carlson EJ, Epstein CJ, Mobley WC (2001) Failed retrograde transport of ngf in a mouse model of Down's syndrome: reversal of cholinergic neurodegenerative pheno types following NGF infusion. *Proc Natl Acad Sci USA* **98**, 10439-10444.

[150] Salehi A, Lucassen PJ, Pool CW, Gonatas NK, Ravid R, Swaab DF (1994) Decreased neuronal activity in the nucleus basalis of meynert in Alzheimer's disease as suggested by the size of the Golgi apparatus. *Neuroscience* **59**, 871-880.

[151] Sofroniew MV, Howe CL, Mobley WC (2001) Nerve growth factor signaling, neuroprotection, and neural repair. *Annu Rev Neurosci* **24**, 1217-1281.

[152] Poon WW, Blurton-Jones M, Tu CH, Feinberg LM, Chabrier MA, Harris JW, Jeon NL, Cotman CW (2009) Beta-amyloid impairs axonal BDNF retrograde trafficking. *Neurobiol Aging*.

[153] Weil-Malherbe H, Whitby LG, Axelrod J (1961) The uptake of circulating [3H]norepinephrine by the pituitary gland and various areas of the brain. *J Neurochem* **8**, 55-64.

[154] Kato T, Karai N, Katsuyama M, Nakamura M, Katsube J (1987) Studies on the activity of L-threo-3,4-dihydroxyphenylserine (L-DOPS) as a catecholamine precursor in the brain. Comparison with that of L-dopa. *Biochem Pharmacol* **36**, 3051-3057.

[155] Goldstein DS (2006) L-dihydroxyphenylserine (L-DOPS): a norepinephrine prodrug. *Cardiovasc Drug Rev* **24**, 189-203.

[156] Kaufmann H (2006) The discovery of the pressor effect of DOPS and its blunting by decarboxylase inhibitors. *J Neural Transm Suppl*, 477-484.

[157] Russo-Neustadt A, Cotman CW (1997) Adrenergic receptors in Alzheimer's disease brain: selective increases in the cerebella of aggressive patients. *J Neurosci* **17**, 5573-5580.

[158] Peskind ER, Wingerson D, Murray S, Pascualy M, Dobie DJ, Le Corre P, Le Verge R, Veith RC, Raskind MA (1995) Effects of Alzheimer's disease and normal aging on cerebrospinal fluid norepinephrine responses to yohimbine and clonidine. *Arch Gen Psychiatry* **52**, 774-782.

[159] Liu Y, Yoo MJ, Savonenko A, Stirling W, Price DL, Borchelt DR, Mamounas L, Lyons WE, Blue ME, Lee MK (2008) Amyloid pathology is associated with progressive monoaminergic neurodegeneration in a transgenic mouse model of Alzheimer's disease. *J Neurosci* **28**, 13805-13814.

This page intentionally left blank

Cerebrospinal Fluid Biomarkers of Neurodegenerative and Ventricular Changes in the Elderly

Ronald A. Cohen[a,*], Assawin Gongvatana[a], Brian R. Ott[b,*] and Alzheimer's Disease Neuroimaging Initiative[1]

[a]*Department of Psychiatry and Human Behavior, Werren Alpert Medical school of Brown University, Providence, RI, USA*
[b]*Department of Neurology, Warren Alpert Medical School of Brown University, Providence, RI, USA*

Abstract. Ventricular enlargement is a common finding among patients with Alzheimer's disease (AD), and has recently been shown to occur from an early disease stage. A possible pathophysiological link between ventricular enlargement and AD has been suggested, with faulty cerebrospinal fluid (CSF) clearance implicated as one possible mechanism. We examined whether ventricular enlargement is associated with CSF amyloid beta (Aβ) early in the disease, even before cognitive symptoms are present, as one would expect to observe this relationship if CSF clearance is impaired. Baseline CSF biomarker data (Aβ, tau, and phosphorylated tau) and MRI brain volumetric measures were obtained from the Alzheimer's Disease Neuroimaging Initiative (ADNI). Data from 288 participants classified as cognitively asymptomatic ($n = 87$), mild cognitive impairment (MCI; $n = 136$), or mild AD ($n = 65$) were analyzed by multiple linear regression with brain volumes and age as independent variables, and each biomarker as dependent variables. Ventricular volume was negatively associated with CSF Aβ in APOE ε4-positive cognitively asymptomatic participants. In contrast, ventricular volume was not associated with Aβ among ε4-positive MCI or AD patients. Tau concentrations were negatively associated with ventricular volume among ε4-positive AD patients. These findings indicate that increased ventricular volume is associated with decreased CSF Aβ among cognitively asymptomatic people who are at risk for AD based on ε4 genotype. The effects of APOE ε4 genotype on these relationships are currently not well understood, but may involve impaired CSF clearance and possibly CSF-blood-brain barrier dysfunction.

Keywords: Alzheimer's, MRI, cerebrospinal fluid, A-beta

*Correspondence to: Brian R. Ott, MD, The Alzheimer's Disease & Memory Disorders Center, Rhode Island Hospital, APC-6, 593 Eddy Street, Providence, RI 02903, USA. Tel.: +1 401 444 6440; Fax: +1 401 444 6858; E-mail: BOtt@lifespan.org. or Ronald A. Cohen, PhD, ABPP, ABCN, Neuropsychology, Coro Bldg. 100-East, Point St., Providence, RI 02906, USA. Tel.: +1 401 793 8787; E-mail: RCohen@lifespan.org.

INTRODUCTION

The neuropathological mechanisms underlying the development of Alzheimer's disease (AD) remain the subject of intense research inquiry. Considerable emphasis has been placed on the role of amyloid beta (Aβ) and tau proteins in AD [1–5], though the link between these biomarkers and the neurodegenerative process is still not fully understood. Other lines of research have focused on the role of apolipoprotein E (APOE), specifically the association between the ε4 genotype and the development of AD [6–10]. Neuropathological processes related to the cerebral spinal fluid (CSF) disturbances, CSF-blood-brain-

barrier dysfunction, and ventricular enlargement, have also been studied as possible contributors. There is evidence suggesting that these factors are linked in AD, though the nature of their pathophysiological interrelationship and how they influence the expression of cognitive dysfunction remains an open question.

Ventricular enlargement is a hallmark structural brain abnormality apparent on neuroimaging that is often associated with AD. When concurrent with brain atrophy, this enlargement of CSF space can reflect a compensation for the loss of brain parenchyma (i.e., hydrocephalus ex vacuo). Yet, ventricular enlargement may also reflect active neuropathological processes beyond changes secondary to atrophy. Normal pressure hydrocephalus (NPH), a clinical syndrome characterized by the triad of gait disturbance, bladder incontinence, and later dementia, involves ventricular dilation in which expansion of ventricles is out of proportion to the degree of cortical atrophy. However, unlike acute obstructive hydrocephalus in which there is an increased ventricular pressure, and rapid symptom relief with shunting, NPH tends to occur in elderly patients without apparent cause, and many of these patients have evidence of degenerative brain disease postmortem, most commonly AD. Given the frequent co-occurrence of AD pathology, ranging from 31–75% of patients with clinically diagnosed NPH who have been biopsied [11–13], comorbidity between AD and NPH may reflect common pathophysiological mechanisms among certain people. Silverberg et al. coined the term "NPH-AD" to describe a subset of patients with overlapping clinical features of AD and NPH [14].

Clinical and experimental studies have been conducted to examine a possible link between AD and NPH [15–16]. One mechanism that has been explored is a defect in homeostasis involving CSF dynamics in the choroid plexus of AD that affects the clearance of Aβ from interstitial fluid into vascular space [17]. It is well recognized that Aβ levels are decreased, whereas levels of tau and phosphorylated-tau (p-tau) are elevated in the CSF of AD patients compared to normal controls. Furthermore, abnormalities in these biomarkers have been demonstrated in the preclinical stage of mild cognitive impairment (MCI) [1], and are being explored as potentially useful biomarkers of disease progression in AD.

Tau probably arises from degeneration of neurofibrillary tangle-laden neurons and axons. It is elevated not only in AD, but also in other conditions including acute stroke, multiple sclerosis, AIDS dementia, head trauma, amyotrophic lateral sclerosis, frontotemporal dementias, corticobasal degeneration, and prion diseases [2, 3]. Aβ is the major constituent of neuritic plaques in AD and appears to be deposited extracellularly in the brain very early in the pathological process of AD. There is evidence that this occurs in the preclinical stage of disease, many years before the onset of dementia symptoms. The "amyloid hypothesis", a prevailing theory of AD pathogenesis, holds that Aβ deposition is a seminal event leading to a toxic cascade of neurodegenerative processes that culminate eventually in loss of synapses and neuronal death [4, 5].

Why Aβ levels in the CSF decline in AD is not well understood, though this could occur secondary to cerebral Aβ aggregation due to faulty clearance mechanism. Resistance to CSF absorption, a mechanism for reduced CSF turnover in NPH would be expected to result in interstitial Aβ accumulation in susceptible patient [18]. Since amyloid accumulates in the arachnoid membranes of AD patients [19, 20], it is possible that that reduced absorption or production of CSF could contribute to amyloid toxicity or other neuronal metabolic disturbances among people with AD for whom overproduction of Aβ is not the primary problem. If reduced absorption rather than reduced production is the primary mechanism of CSF stagnation in AD, then one would expect to see ventricular dilation out of proportion to cortical atrophy together with reduced Aβ levels in the CSF due to a trapping mechanism.

At this point, relatively little data exists regarding the pathophysiological relationship between ventricular enlargement, CSF Aβ levels, and the clinical course of functional deterioration and neurodegeneration in AD. Furthermore, it is not known whether these neuropathological associations are linked to the genetic risk for AD incurred by the APOE ε4 genotype. We propose that ventricular enlargement in AD serves as a marker of altered CSF dynamics that can be used as a biologic proxy for faulty CSF clearance mechanisms. If so, then a close relationship should exist between degree of ventricular dilation in AD and levels of Aβ in CSF. If such a relationship can be demonstrated, then therapies aimed at restoring normal CSF dynamics may prove to be palliative or even effective in slowing disease progression.

Of note, a recent controlled trial of shunting patients with AD failed to demonstrate efficacy, possibly due to insensitivity of the global end point (Global Deterioration Scale) over the nine months of the double-blind portion of the study [21]. Another reason for this failure may have been related to enrollment of too many

moderate to severe patients. Like a number of current anti-amyloid experimental therapies that have failed in clinical trials, the intervention may also have been tried too late to restore or slow a well-established neurodegenerative cascade. Therefore, we examined the relationship of Aβ and ventricular volumes in persons with MCI and aged controls as well as those with well-established AD.

The goals of this study were to demonstrate that there is a significant relationship between ventricular enlargement and CSF Aβ levels. We predicted that this relationship would be more significant for patients with AD than for cognitively asymptomatic controls, and that the strength of the relationship would be intermediate for those with MCI. We also predicted that these effects would be most evident among people with the APOE ε4 genotype, who may be at increased risk for Aβ disturbances.

MATERIALS AND METHODS

Subjects

Data were obtained from the Alzheimer's Disease Neuroimaging Initiative (ADNI) database (http://adni.loni.ucla.edu). The ADNI was launched in 2003 by the National Institute on Aging, the National Institute of Biomedical Imaging and Bioengineering, the Food and Drug Administration, private pharmaceutical companies and non-profit organizations, as a $60 million, 5-year public-private partnership. The primary goal of ADNI has been to test whether serial MRI, PET, other biological markers, and clinical and neuropsychological assessments can be combined to measure the progression of MCI and early AD. Determination of sensitive and specific markers of very early AD progression is intended to aid researchers and clinicians to develop new treatments and monitor their effectiveness, as well as lessen the time and cost of clinical trials [17, 18]. All participants undergo neuropsychological and behavioral evaluations every six months over three years, as well as periodic neuroimaging with MRI and PET, blood and urine samples. Over 50% are providing periodic lumbar CSF samples as well. The biomarkers being studied include APOE genotype, tau and phosphorylated tau$_{181p}$ (p-tau), Aβ, isoprostanes, and homocysteine.

Demographic, cognitive, CSF, and MRI volumetric measures were obtained from ADNI for 288 participants, consisting of 87 cognitively asymptomatic individuals, 136 with mild cognitive impairment (MCI),

and 65 with mild AD. All participants underwent an extensive clinical evaluation, including basic mental status tests, neuropsychological tests, physical and neurological examinations. Global cognitive function was measured by the Mini Mental State Examination (MMSE) [24]. Dementia severity was graded by the Clinical Dementia Rating (CDR) [25]. All AD patients satisfied NINCDS-ADRDA diagnostic criteria [26] for probable AD and had questionable to very mild (CDR 0.5) or mild (CDR 1) dementia. MCI subjects score 24–30 on the MMSE, had a CDR of 0.5, and had memory complaints as well as objective evidence of memory impairment based on education-adjusted scores on the Wechsler Logical Memory II memory scale. By study entry criteria, "any significant neurologic disease, such as Parkinson's disease, multi-infarct dementia, Huntington's disease, normal pressure hydrocephalus, brain tumor, progressive supranuclear palsy, seizure disorder, subdural hematoma, multiple sclerosis, or history of significant head trauma followed by persistent neurologic defaults or known structural brain abnormalities". In this manner, cases with normal pressure hydrocephalus were excluded by clinical criteria without a specific radiologic exclusion of any person with enlarged ventricles.

Biomarkers

CSF specimens for biomarkers were processed by the Biomarker Core of ADNI at the Department of Pathology & Laboratory Medicine at the University of Pennsylvania Medical School. Methods for measuring CSF biomarkers have been described previously [27]. The Luminex multiplex immunoassay platform was used for measurements of Aβ, tau, and p-tau. Over 50 studies have demonstrated clinical sensitivity and specificity for these biomarkers at greater than 80% each [28]. Routine laboratory measurements of CSF included total protein, glucose, and cell counts.

Magnetic resonance imaging

Image acquisition, quality control, image correction, and phantom based scaling methods are described in detail on the ADNI website. Briefly, after image acquisition, phantom scans were used to correct for gradient nonlinearities, followed by image intensity normalization. Brain segmentation was performed on 3D T1-weighted MRI volumes using an automated whole-brain segmentation procedure for obtaining delineations of different neuroanatomical

structures, including hippocampus, amygdala, thalamus, cerebellum, putamen, globus pallidus, whole brain and all ventricles [29, 30]. Neuroanatomical labels are assigned to each voxel based on probabilistic information estimated from an atlas, thus allowing estimation of volumetric measures of each anatomical structures. The accuracy of this procedure has been shown to be comparable to that of manual labeling and sensitive to subtle changes in AD [29] and normal aging [31]. These methods are publicly available through the FreeSurfer package [32]. The volumetric measures so acquired, were then uploaded to the ADNI website for public access.

Total ventricular volume and total brain volume were the primary variables of interest. Total brain volume represents a summary measure of total brain parenchyma. In addition, total intracranial volume measure was obtained to control for head size variability between subjects. This measure was intended to be insensitive to cerebral atrophy and to reflect the intracranial volume regardless of age or disease progression. This measure was derived by combining the segmented grey matter, white matter, and CSF. To account for spatial discontinuity, the combined mask was repeatedly smoothed with a Gaussian kernel to produce a connected uniform mask extending to but excluding the skull.

Statistical analyses

Pearson correlation coefficients were examined comparing ventricle to whole brain volumes. For the entire sample, there was a significant relationship between the two volume measurements ($r = 0.17$, $p < 0.005$). Significant positive correlations between ventricle and whole brain volumes were seen in all three subject groups, suggesting a common relationship to overall head size (see Table 1).

To adjust for inter-subject differences in brain size, ventricle/whole brain volume ratio was derived as a secondary independent variable. Correction procedures are often necessary in volumetric MRI studies

to account for such difference between individuals; however, there is no clearly preferred method. The ventricle/whole brain volume ratio has been shown to have more robust relationships with neuropsychological performance than either volume alone in a study of dementia and elderly control subjects [33]. In another study, ventricle/whole brain volume ratio performed better than ventricle/total intracranial volume ratio and better than uncorrected ventricular volume in distinguishing dementia subjects from elderly controls [34].

A series of multivariable linear regression models were then analyzed using stepwise subtraction of independent variables with significance levels of $p > 0.05$. The CSF biomarkers were the dependent variables in these models. Independent variables included ventricle and whole brain parenchymal volumes, as well as age. Total intracranial volume was also included as an additional covariate to account for head size variability between subjects. After accomplishing these analyses, the same analyses were repeated with ventricle/brain parenchymal volume ratio substituting for the separate ventricle and brain parenchymal volumes, and the two set of results were compared. To assess whether ventricle volume may be simply a proxy for lateral ventricle expansion secondary to early degeneration and atrophy of medial temporal structures, significant relationships between biomarkers and hippocampal and entorhinal cortex volumes were examined as well. Hippocampal atrophy has been shown to be a stronger predictor of progression from MCI to AD than whole brain volume [35].

Group analyses according to APOE genotype were defined according to presence or absence of at least one APOE ε4 allele. Statistical analyses were performed using Stata SE, version 10, software. Graphs were created using the same software.

RESULTS

Demographic information for the study sample is provided in Table 2. The sample included 87 control subjects, 136 MCI subjects, and 65 AD subjects. Global cognitive impairment for the AD subjects was mild, with a mean MMSE of 23.7 ± 2.0, compared to 27.1 ± 1.8 for MCI subjects and 29.1 ± 1.1 for controls.

Tau, Aβ, and ventricular volume

Mean measurements for the biomarkers and MRI volumes are provided in Table 3. Similar summary

Table 1
Ventricle and whole brain volume correlations: Pearson correlation coefficients and N

	All subjects	APOE ε4 positive subjects	APOE ε4 negative subjects
Controls	0.03 (87)*	0.15 (21)*	0.01 (66)
MCI	0.03 (136)	0.02 (74)	0.04 (62)*
AD	0.07 (65)*	0.11 (44)*	0.03 (21)

* $p < 0.05$.

Table 2
Demographic data subclassified by presence of APOE ε4 genotype

	Normal older controls			Mild cognitive impairment			Alzheimer's disease		
	ε 4-	ε 4+	All	ε 4-	ε 4+	All	ε 4-	ε 4+	All
Sample size: N	66	21	87	62	74	136	21	44	65
Sex: female N (proportion)	30 (0.45)	15 (0.71)	45 (0.52)	47 (0.52)	42 (0.57)	89 (0.65)	11 (0.52)	25 (0.57)	36 (0.55)
Age: years mean (S.D.)	75.9 (5.3)	75.4 (6.3)	75.8 (5.5)	75.8 (8.1)	73.2 (6.7)	74.4 (7.4)	75.0 (9.2)	74.9 (6.8)	74.9 (7.6)
Education: years mean (S.D)	15.7 (2.7)	15.7 (3.6)	15.7 (2.9)	15.9 (2.9)	15.8 (2.9)	15.9 (2.9)	16.9 (2.5)	14.5 (3.6)	15.3 (3.5)
MMSE: score mean (S.D.)	29.1 (1.0)	28.9 (1.2)	29.1 (1.1)	27.0 (1.9)	27.2 (1.8)	27.1 (1.8)	23.6 (1.9)	23.7 (2.0)	23.7 (2.0)

Table 3
CSF biomarkers and MRI volumes subclassified by diagnosis and presence of APOE ε4 genotype

	Normal older controls			Mild cognitive impairment			Alzheimer's disease		
	ε 4-	ε 4+	All	ε 4-	ε 4+	All	ε 4-	ε 4+	All
CSF $A\beta_{1-42}$ (pg/ml.± S.D.)	220.7 (47.9)	156.9 (48.5)	205.6 (55.1)	187.5 (59.3)	143.0 (40.9)	163.7 (54.9)	170.0 (52.3)	131.0 (27.2)	143.0 (40.8)
CSF Tau (pg/ml.± S.D.)	66.3 (25.9)	80.4 (40.2)	69.6 (30.3)	86.2 (47.2)	118.4 (67.3)	103.5 (60.9)	124.9 (68.7)	120.1 (52.3)	121.6 (57.6)
CSF P-Tau$_{181}$ (pg/ml.± S.D.)	22.5 (11.1)	32.3 (21.0)	24.8 (14.6)	29.7 (16.3)	40.5 (18.0)	35.5 (18.0)	41.5 (22.1)	41.7 (18.8)	41.6 (19.8)
CSF Protein (g/dl.± S.D.)	46.0 (18.8)	39.8 (21.1)	44.3 (19.6)	45.0 (20.7)	38.2 (18.5)	41.6 (19.8)	47.3 (21.3)	47.6 (34.3)	47.5 (29.7)
Ventricular volume (mean ml.± S.D.)	37.3 (19.2)	36.0 (22.3)	37.0 (20.0)	46.1 (23.4)	44.0 (19.6)	45.0 (21.3)	48.0 (21.7)	49.1 (22.4)	48.7 (22.0)
Whole brain volume (mean ml.± S.D.)	997.1 (99.1)	999.8 (97.7)	997.9 (98.4)	998.3 (110.0)	993.5 (109.7)	995.6 (109.7)	946.0 (110.1)	955.3 (92.8)	952.3 (98.6)
Ventricles/brain volume (proportion + S.D.)	0.038 (0.019)	0.036 (0.020)	0.037 (0.020)	0.046 (0.022)	0.045 (0.020)	0.045 (0.021)	0.051 (0.023)	0.051 (0.022)	0.051 (0.023)

data from a cross-sectional study of 399 subjects using ADNI data have been previously presented [31]. As expected, CSF Aβ levels declined and tau levels rose progressively among normal, MCI, and AD groups. Ventricular volumes increased and brain volumes declined progressively among normal, MCI, and AD groups.

For the entire sample, ventricles ($t = -2.90$; $p = 0.004$) and age ($t = 2.29$; $p = 0.02$) were significantly related to CSF Aβ. Similar results were found for ventricle/brain ratio ($t = -2.94$; $p = 0.004$) and age ($t = 2.39$; $p = 0.02$). Tau was significantly related to whole brain volume ($t = -2.70$; $p = 0.007$) but not ventricle volume or age. There was a trend toward relationship between p-tau and whole brain ($t = -1.82$; $p = 0.07$). CSF total protein was not significantly associated with any brain or ventricular volume in any of the analyses.

Tau, Aβ, and ventricular volume by diagnostic group

The models containing significant variables ($p < 0.05$) for diagnostic subgroups are shown in

Table 4. The ventricle/brain volume ratio proved to be an equivalent or more significant predictor than ventricular volume alone, so these ratios are shown in the table.

Cognitive asymptomatic

Ventricular volume was significantly associated with Aβ, but not age, in the APOE ε4 positive cognitive healthy controls. Ventricular volume was not significantly associated with Aβ for cognitively healthy controls who were APOE ε4 negative, or for the control group as a whole. Aβ was also not associated with whole brain volume for the group as a whole or as a function of APOE genotype. The relationship between Aβ levels and ventricular volume in the APOE ε4 positive healthy controls is shown in Fig. 1, with a scatter plot of data points relative to the regression line.

In contrast with findings for Aβ, both ventricular volume and age were significantly associated with CSF tau levels in the APOE ε4 negative cognitively healthy controls. Yet, tau levels were not significantly associated with ventricular volume for either APOE ε4

Table 4
Summary of multiple regression models by disease category and APOE ε4 genotype.

	N	F	Probability > F	R^2	CSF Biomarker	Region	t	p
Controls								
ε4+	21	(1,19) = 5.95	0.025	0.24	A-beta	Ventricles/brain	−2.44	0.025
ε4-	66	(2,63) = 4.24	0.02	0.12	Tau	Ventricles/brain	−2.54	0.01
						Age	2.05	0.04
All	87	(2,84) = 4.34	0.02	0.09	Tau	Ventricles/brain	−2.32	0.02
						Age	2.45	0.02
MCI								
All	133	(1,131) = 8.24	0.005	0.06	Tau	Brain	−2.87	0.005
All	133	(1,135) = 4.40	0.04	0.03	*P*-tau	Brain	−2.10	0.04
AD								
ε4+	43	(1,41) = 11.95	0.001	0.23	Tau	Ventricles/brain	−3.46	0.001
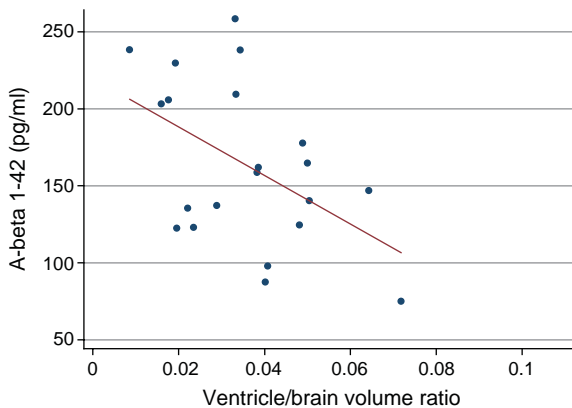
Fig. 1. Aβ levels and ventricle/brain volume in APOE ε4 positive healthy controls.

Fig. 2. Tau levels and ventricle/brain volume in APOE ε4 positive AD patients.

positive healthy controls or the group as a whole. There was no interaction between age and MRI volumetric variables.

There was not a significant relationship between either Aβ or tau and total hippocampal or entorhinal volumes among APOE ε4 positive cognitively healthy controls. A significant relationship was found between tau and right hippocampal volume in APOE ε4 negative controls ($p < 0.05$) but not for left hippocampal volume or entorhinal cortex in either hemisphere. Smaller right hippocampal volume was associated with greater CSF tau among the healthy controls.

Mild cognitive impairment

Significant associations were found between whole brain volume and both CSF tau and CSF p-tau for the MCI group as a whole. However, ventricular volume was not significantly associated with either tau or p-tau for MCI patients. Furthermore, neither whole brain nor ventricular volume were associated with any biomarkers (Aβ, tau, p-tau) as a function of APOE ε4 status among people with MCI.

Alzheimer disease

Ventricular volume was significantly associated with tau levels among APOE ε4 positive patients with AD (see Fig. 2). In contrast, ventricular volume was not associated with Aβ in APOE ε4 positive subjects.

Aβ and tau were not significantly related to whole brain volume among the AD patients. There was no significant relationship between Aβ and tau and volume measurements of either hippocampus or entorhinal cortex, among APOE ε4 positive control and AD subjects. There was no significant effect of total intracranial volume when entered as a covariate in any of the models above.

DISCUSSION

As expected, a significant negative relationship between ventricular volume and CSF Aβ levels existed for this ADNI sample as a whole. AD patients exhibited greatest ventricular volumes and lowest CSF Aβ levels, healthy controls had the smallest ventricles and highest

CSF Aβ levels, whereas MCI patients fell in between on both of these measures. This finding is consistent with widely accepted thinking regarding the relationship between CSF Aβ levels and neuropathological findings in AD [27] and provides additional evidence that this relationship holds for ventricular volume.

We also expected that this relationship would be strongest among patients with AD, but surprisingly found the opposite relationship. Neither the MCI or AD patients exhibited a significant association between Aβ levels and ventricular volumes, where as the cognitively asymptomatic group did. This paradoxical finding may point to important issues regarding the relationships between biomarkers and AD pathogenesis. AD neuropathology occurring at different stages of the disease may produce different relationships between CSF Aβ and ventricular volume.

The current findings suggest that the greatest effects of Aβ sequestration in the brain relative to ventricular enlargement occur very early in the disease process, when people are largely asymptomatic. By the time people develop cognitive and functional impairments that lead to a diagnosis of MCI or AD, Aβ dynamics in the CSF relative to ventricular function are less operative. It is also possible that MCI and AD patients for whom Aβ CSF and ventricular volume were most strongly associated were excluded based on symptoms and radiological signs of NPH, as the presence of NPH was one of the exclusion criteria for ADNI study. This possibility does not seem very likely because presumably only patients with clinical symptoms of NPH in addition to large ventricles would have been excluded and not patients with ventricles which were proportionate to their overall brain atrophy.

As expected, CSF tau concentrations were elevated as a function of disease stage. Furthermore, the fact that increased tau concentrations were associated with ventricular volume when the entire ADNI sample was considered suggests a general relationship between disease stage, ventricular enlargement and levels of this biomarker. Tau sequestration continues to occur and CSF levels increase as the disease progresses. However, tau was more strongly associated with whole brain volume than ventricular volume among MCI patients, suggesting that this aspect of AD neuropathology may be more directly linked to neuronal changes resulting in brain atrophy rather than ventricular pathology.

We were surprised not to see a similar relationship among patients with AD. We suspect that this may reflect a ceiling effect, whereby tau saturation in CSF

is reached once people exhibit AD. To illustrate this point, among APOE ε4 positive subjects, CSF tau increased by 48% between normal and MCI groups, but only by 2% between MCI and AD groups, while ventricular volume increased 25% between normal and MCI groups, and by 13% between MCI and AD groups.

Our findings partially replicate another recent study showing a relationship between elevated levels of CSF tau and p-tau and whole brain volume in a mixed group of 21 subjects with very mild (CDR 0.5) AD and 8 subjects with mild (CDR 1.0) AD. Among 69 cognitively normal subjects CSF Aβ-42 was positively correlated with whole brain volume, though ventricular volume was not examined in that study, limiting comparison with the current findings [37].

One of the most intriguing findings from this analysis was the negative association between CSF Aβ levels and ventricular volume among cognitively asymptomatic controls who were positive for the APOE ε4 allele. CSF Aβ levels decreased as ventricular volume increased. In fact, this relationship was only found among the controls. That a significant relationship was not found for APOE ε4 positive MCI subjects suggests that the transition with respect to the sequestering Aβ in the brain and its relationship to ventricular enlargement occur during the prodromal stage of the disease among people with a genetic risk for AD. Along similar lines, amyloid deposition in brain has been shown by PiB amyloid PET imaging studies to occur frequently in cognitively normal elderly, however, the causes and prognostic significance of such cases of early amyloid deposition are unknown [38].

We propose that altered CSF-blood-brain barrier functions may account for these complex relationships. There is increasing evidence of blood-brain barrier compromise [39] as well as microvascular damage occurring early in AD [27, 40, 41]. Apolipoprotein E is essential for both blood-brain barrier integrity and for deposition of fibrillary Aβ. Both APOE and Aβ are ligands for low-density lipoprotein receptor-related protein 1 (LRP-1), a major transporter of Aβ out of brain, and all three proteins are located in plaques. Most plaques are in close proximity to the cerebral microvessels, leading to potentially complex interactions affecting clearance of Aβ. In AD, LRP-1 is downregulated at the blood-brain barrier, which is likely one of the mechanisms of reduced Aβ clearance from the brain [42]. There is evidence to suggest that APOE ε4 enhances vascular and parenchymal deposition of Aβ in the brain [43] and may influence both

transport and permeability of the blood-brain barrier [39, 44].

CSF protein concentration was consistently higher in AD compared to MCI and controls. This likely reflects enhanced blood-brain barrier permeability to albumin, but there was no correlation between blood-brain barrier function, measured as the CSF total protein level, and any brain or ventricular volume. This finding suggests that blood-brain barrier dysfunction is not directly related to brain atrophy. Aβ-induced disruptions of blood-brain barrier and choroid plexus permeability and transport would be expected to destabilize interstitial and CSF dynamics (and ventricle size) thereby impairing brain metabolism and blood flow [45, 46].

Enhancement of vascular amyloid deposition by APOE ε4 in arachnoid granulations may have a role in reducing Aβ clearance from brain via CSF circulation. This may account for the observation of increased APOE ε4 allele frequency in NPH patients with dementia [47] and a role for hydrocephalus in the pathogenesis of AD in some patients. Alternatively APOE ε4 may serve as just a marker of earlier onset and more severe AD pathology and not be directly involved in the mechanisms of Aβ clearance via CSF. In further support of a hydrocephalic mechanism for AD is a recent report of Aβ$_{42}$ and hyperphosphorylated tau pathology occurrence in a kaolin-induced hydrocephalus model of the aged rat [48, 49].

Little is known about compartmentalization of tau in the course of AD, but this data suggests that as neurodegeneration becomes established by cascading pathogenic events, tau becomes sequestered at a later time in those with well-established disease. Tau sequestration in AD may be related to similar mechanisms described previously for Aβ, which occur much earlier than tau in the pathogenic cascade.

Finally, among APOE ε4 negative controls we found a negative relationship between CSF tau and ventricular volume. In this group, age and hippocampal volume were also associated with tau levels, suggesting that age-related atrophy rather than APOE genetic mechanisms may be driving this relationship. Since this group of subjects likely includes many who would never go on to develop AD, the relevance of this relationship to our understanding of biomarkers for AD is limited.

The results of this study should be interpreted with caution for a number of reasons. The measure of ventricular volume is a global measure of the entire ventricular system. We cannot exclude the possibility that the ventricle volume is merely a proxy for brain atrophy in specific adjacent brain regions such as the medial temporal lobe, which could affect mainly the temporal horn. While the lack of relationship to brain volume in this area in our APOE ε4 positive subjects argues against this possibility, further analyses using segmented ventricle volumes [50] and ventricular shape data [51] could provide more definitive evidence for a primary role of ventricular pathology leading to Aβ deposition.

The analyses here were only cross-sectional, due to the limited availability of longitudinal CSF biomarker data in ADNI. Future studies examining sequential changes in biomarkers compared to brain and ventricular volumes in prodromal AD may shed more light on the mechanisms we propose based on baseline data. Also to be noted, the sample size of 21 in the APOE ε4 positive control group is particularly small. While the relationship between ventricle/brain ratio and CSF Aβ is one of the most interesting observations, these results need verification from studies involving larger samples of older cognitively normal subjects.

Experimental evidence using animal models of hydrocephalus and APOE may shed light on the exact nature of these relationships. If indeed altered CSF clearance mechanisms in the prodromal stage of AD caused by interaction of APOE ε4 and epithelial/vascular function in the choroid plexus and/or arachnoid villi leads to sequestration of Aβ in the brain, setting off a cascade of pathologic events, then efforts to interrupt these mechanisms may prove fruitful in disease prevention.

While this exploration of the ADNI data provides evidence of a potential hydrocephalic mechanism early in AD for some patients as well as a potential explanation of amyloid deposition in NPH, we were unable to examine actual CSF production, which is reduced in aging and AD [18, 52], and how this too may affect Aβ, tau, or other brain-derived proteins. These are rich areas of potential future research.

An alternative explanation to the proposed obstructive hydrocephalic mechanism is that enlarged ventricles relative to the rest of brain tissue reflect central atrophy involving white matter volume changes which are more dramatic in APOE ε4 carriers. This could be explored further by examining volumetric measurements of white matter on MRI in comparison to CSF biomarkers.

Ventricular volume [50, 53] and ventricular volume change [54] in aging, MCI, and AD is emerging as an important biological indicator of disease progression. As previously mentioned, ventricular volume has

been shown to be a more robust correlate of cognitive function in AD and MCI than other whole brain measures. The reason for this significant relationship is not well understood but deserves further investigation, as ventricular volume may be a useful biomarker outcome for early disease intervention and prevention trials, particularly for those at genetic risk due to APOE ε4 genotype.

SUPPORT ACKNOWLEDGMENTS

REFERENCES

[1] Chong MS, Lim WS, Sahadevan S, (2006) Biomarkers in preclinical Alzheimer's disease. *Curr Opin Investig Drugs* **7**, 600-607. e:ag

[2] Clark CM, Xie S, Chittams J, Ewbank D, Peskind E, Galasko D, Morris JC, McKeel DW Jr., Farlow M, Weitlauf SL, Quinn J, Kaye J, Knopman D, Arai H, Doody RS, DeCarli C, Leight S, Lee VM, Trojanowski JQ (2003) Cerebrospinal fluid tau and beta-amyloid: how well do these biomarkers reflect autopsy-confirmed dementia diagnoses? *Arch Neurol* **60**, 1696-1702.

[3] Formichi P, Battisti C, Radi E, Federico A (2006) Cerebrospinal fluid tau, A beta, and phosphorylated tau protein for the diagnosis of Alzheimer's disease. *J Cell Physiol* **208**, 39-46.

[4] Hardy JA, Higgins GA (1992) Alzheimer's disease: the amyloid cascade hypothesis. *Science* **256**, 184-185.

[5] Selkoe DJ (2000) Toward a comprehensive theory for Alzheimer's disease. Hypothesis: Alzheimer's disease is caused by the cerebral accumulation and cytotoxicity of amyloid beta-protein. *Ann N Y Acad Sci* **924**, 17-25.

[6] Roses AD (1994) Apolipoprotein E is a relevant susceptibility gene that affects the rate of expression of Alzheimer's disease. *Neurobiol Aging* **15** Suppl 2, S165-S167.

[7] Saunders AM, Strittmatter WJ, Schmechel D, George-Hyslop PH, Pericak-Vance MA, Joo SH, Rosi BL, Gusella JF, Crapper-MacLachlan DR, Alberts MJ, et al. (1993) Association of apolipoprotein E allele epsilon 4 with late-onset familial and sporadic Alzheimer's disease. *Neurology. Aug* **43**, 1467-1472.

[8] Strittmatter WJ, Saunders AM, Schmechel D, Pericak-Vance M, Enghild J, Salvesen GS, Roses AD (1993) Apolipoprotein E: high-avidity binding to beta-amyloid and increased frequency of type 4 allele in late-onset familial alzheimer disease. *Proc Natl Acad Sci U S A* **90**, 1977-1981.

[9] Tamaoka A, Miyatake F, Matsuno S, Ishii K, Nagase S, Sahara N, Ono S, Mori H, Wakabayashi K, Tsuji S, Takahashi H, Shoji S (2000) Apolipoprotein E allele-dependent antioxidant activity in brains with Alzheimer's disease. *Neurology* **54**(12), 2319-2321.

[10] Lehtovirta M, Laakso MP, Frisoni GB, Soininen H (2000) How does the apolipoprotein E genotype modulate the brain in aging and in Alzheimer's disease? a review of neuroimaging studies. *Neurobiol Aging* **21**(2), 293-300.

[11] Golomb J, Wisoff J, Miller DC, Boksay I, Kluger A, Weiner H, Salton J, Graves W (2000) Alzheimer's disease comorbidity in normal pressure hydrocephalus: prevalence and shunt response. *J Neurol Neurosurg Psychiatry* **68**, 778-781.

[12] Leinonen V, Alafuzoff I, Aalto S, Suotunen T, Savolainen S, Nagren K, Tapiola T, Pirttila T, Rinne J, Jaaskelainen JE, Soininen H, Rinne JO (2008) Assessment of beta-amyloid in a frontal cortical brain biopsy specimen and by positron emission tomography with carbon 11-labeled pittsburgh Compound B. *Arch Neurol* **65**, 1304-1309.

[13] Savolainen S, Paljarvi L, Vapalahti M (1999) Prevalence of Alzheimer's disease in patients investigated for presumed normal pressure hydrocephalus: a clinical and neuropathological study. *Acta Neurochir (Wien)* **141**, 849-853.

[14] Silverberg GD, Mayo M, Saul T, Rubenstein E, McGuire D (2003) Alzheimer's disease, normal-pressure hydrocephalus, and senescent changes in CSF circulatory physiology: a hypothesis. *Lancet Neurol* **2**, 506-511.

[15] Chakravarty A (2004) Unifying concept for Alzheimer's disease, vascular dementia and normal pressure hydrocephalus - a hypothesis. *Med Hypotheses* **63**, 827-833.

[16] Wostyn P, Audenaert K, De Deyn PP (2008) Alzheimer's disease-related changes in diseases characterized by elevation of intracranial or intraocular pressure. *Clin Neurol Neurosurg* **110**, 101-109.

[17] Johanson C, McMillan P, Tavares R, Spangenberger A, Duncan J, Silverberg G, Stopa E (2004) Homeostatic capabilities of the choroid plexus epithelium in Alzheimer's disease. *Cerebrospinal Fluid Res* **1**, 3.

[18] Silverberg GD, Mayo M, Saul T, Rubenstein E, McGuire D (2003) Alzheimer's disease, normal-pressure hydrocephalus, and senescent changes in CSF circulatory physiology: a hypothesis. *Lancet Neurol* **2**, 506-511.

[19] Kalaria RN, Premkumar DR, Pax AB, Cohen DL, Lieberburg I (1996) Production and increased detection of amyloid beta protein and amyloidogenic fragments in brain microvessels,

meningeal vessels and choroid plexus in Alzheimer's disease. *Brain Res Mol Brain Res* **35**, 58-68.

[20] Stopa EG, Berzin TM, Kim S, Song P, Kuo-LeBlanc V, Rodriguez-Wolf M, Baird A, Johanson CE (2001) Human choroid plexus growth factors: what are the implications for CSF dynamics in Alzheimer's disease? *Exp Neurol* **167**, 40-47.

[21] Silverberg GD, Mayo M, Saul T, Fellmann J, Carvalho J, McGuire D (2008) Continuous CSF drainage in AD: results of a double-blind, randomized, placebo-controlled study. *Neurology* **71**, 202-209.

[22] Mueller SG, Weiner MW, Thal LJ, Petersen RC, Jack CR, Jagust W, Trojanowski JQ, Toga AW, Beckett L (2005) Ways toward an early diagnosis in Alzheimer's disease: The Alzheimer's Disease Neuroimaging Initiative (ADNI). *Alzheimers Dement* **1**, 55-66.

[23] Mueller SG, Weiner MW, Thal LJ, Petersen RC, Jack C, Jagust W, Trojanowski JQ, Toga AW, Beckett L (2005) The Alzheimer's disease neuroimaging initiative. *Neuroimaging Clin N Am* **15**, 869-872.

[24] Folstein MF, Folstein SE, McHugh PR (1975) "Mini-mental state". A practical method for grading the cognitive state of patients for the clinician. *J Psychiatr Res* **12**, 189-198.

[25] Morris JC (1997) Clinical dementia rating: a reliable and valid diagnostic and staging measure for dementia of the alzheimer type. *Int Psychogeriatr* **9 Suppl 1**, 173-176.

[26] McKhann G, Drachman D, Folstein M, Katzman R, Price D, Stadlan EM (1984) Clinical diagnosis of Alzheimer's disease: report of the NINCDS-ADRDA Work Group Under the Auspices of Department of Health and Human Services Task Force on Alzheimer's disease. *Neurology* **34**, 939-944.

[27] Shaw LM, Vanderstichele H, Knapik-Czajka M, Clark CM, Aisen PS, Petersen RC, Blennow K, Soares H, Simon A, Lewczuk P, Dean R, Siemers E, Potter W, Lee VM, Trojanowski JQ (2009) Cerebrospinal fluid biomarker signature in Alzheimer's disease neuroimaging initiative subjects. *Ann Neurol* **65**, 403-413.

[28] Shaw LM (2008) PENN biomarker core of the Alzheimer's disease Neuroimaging Initiative. *Neurosignals* **16**, 19-23.

[29] Fischl B, Salat DH, Busa E, Albert M, Dieterich M, Haselgrove C, van der KA, Killiany R, Kennedy D, Klaveness S, Montillo A, Makris N, Rosen B, Dale AM (2002) Whole brain segmentation: automated labeling of neuroanatomical structures in the human brain. *Neuron* **33**, 341-355.

[30] Fischl B, Salat DH, van der Kouwe AJ, Makris N, Segonne F, Quinn BT, Dale AM (2004) Sequence-independent segmentation of magnetic resonance images. *Neuroimage* **23**, S69-S84.

[31] Walhovd KB, Fjell AM, Reinvang I, Lundervold A, Dale AM, Eilertsen DE, Quinn BT, Salat D, Makris N, Fischl B (2005) Effects of age on volumes of cortex, white matter and subcortical structures. *Neurobiol Aging* **26**, 1261-1270.

[32] Dale AM, Fischl B, Sereno MI (1999) Cortical surface-based analysis. I. Segmentation and surface reconstruction. *Neuroimage* **9**, 179-194.

[33] Bigler ED, Neeley ES, Miller MJ, Tate DF, Rice SA, Cleavinger H, Wolfson L, Tschanz J, Welsh-Bohmer K (2004) Cerebral volume loss, cognitive deficit and neuropsychological performance: comparative measures of brain atrophy: I. Dementia. *J Int Neuropsychol Soc* **10**, 442-452.

[34] Bigler ED, Tate DF (2001) Brain volume, intracranial volume, and dementia. *Invest Radiol* **36**, 539-546.

[35] Henneman WJ, Sluimer JD, Barnes J, van der Flier WM, Sluimer IC, Fox NC, Scheltens P, Vrenken H, Barkhof F (2009) Hippocampal atrophy rates in Alzheimer disease: added value over whole brain volume measures. *Neurology* **72**, 999-1007.

[36] Vemuri P, Wiste HJ, Weigand SD, Shaw LM, Trojanowski JQ, Weiner MW, Knopman DS, Petersen RC, Jack CR Jr (2009) MRI and CSF biomarkers in normal, MCI, and AD subjects: diagnostic discrimination and cognitive correlations. *Neurology* **73**, 287-293.

[37] Fagan AM, Head D, Shah AR, Marcus D, Mintun M, Morris JC, Holtzman DM (2009) Decreased cerebrospinal fluid Abeta(42) correlates with brain atrophy in cognitively normal elderly. *Ann Neurol* **65**, 176-183.

[38] Aizenstein HJ, Nebes RD, Saxton JA, Price JC, Mathis CA, Tsopelas ND, Ziolko SK, James JA, Snitz BE, Houck PR, Bi W, Cohen AD, Lopresti BJ, DeKosky ST, Halligan EM, Klunk WE (2008) Frequent amyloid deposition without significant cognitive impairment among the elderly. *Arch Neurol* **65**, 1509-1517.

[39] Donahue JE, Johanson CE (2008) Apolipoprotein E, amyloid-beta, and blood-brain barrier permeability in Alzheimer disease. *J Neuropathol Exp Neurol* **67**, 261-270.

[40] Stopa EG, Butala P, Salloway S, Johanson CE, Gonzalez L, Tavares R, Hovanesian V, Hulette CM, Vitek MP, Cohen RA (2008) Cerebral cortical arteriolar angiopathy, vascular beta-amyloid, smooth muscle actin, braak stage, and APOE genotype. *Stroke* **39**, 814-821.

[41] Kalaria RN, Premkumar DR, Pax AB, Cohen DL, Lieberburg I (1996) Production and increased detection of amyloid beta protein and amyloidogenic fragments in brain microvessels, meningeal vessels and choroid plexus in Alzheimer's disease. *Brain Res Mol Brain Res* **35**, 58-68.

[42] Donahue JE, Flaherty SL, Johanson CE, Duncan JA III, Silverberg GD, Miller MC, Tavares R, Yang W, Wu Q, Sabo E, Hovanesian V, Stopa EG (2006) RAGE, LRP-1, and amyloid-beta protein in Alzheimer's disease. *Acta Neuropathol* **112**, 405-415.

[43] Fryer JD, Simmons K, Parsadanian M, Bales KR, Paul SM, Sullivan PM, Holtzman DM (2005) Human apolipoprotein E4 alters the amyloid-beta 40 : 42 ratio and promotes the formation of cerebral amyloid angiopathy in an amyloid precursor protein transgenic model. *J Neurosci* **25**, 2803-2810.

[44] Deane R, Sagare A, Hamm K, Parisi M, Lane S, Finn MB, Holtzman DM, Zlokovic BV (2008) aPOE isoform-specific disruption of amyloid beta peptide clearance from mouse brain. *J Clin Invest* **118**, 4002-4013.

[45] Deane R, Bell RD, Sagare A, Zlokovic BV (2009) Clearance of amyloid-beta peptide across the blood-brain barrier: implication for therapies in Alzheimer's disease. *CNS Neurol Disord Drug Targets* **8**, 16-30.

[46] Serot JM, Bene MC, Faure GC (2003) Choroid plexus, aging of the brain, and Alzheimer's disease. *Front Biosci* **8**, s515-s521.

[47] Nacmias B, Tedde A, Guarnieri BM, Petruzzi C, Ortenzi L, Serio A, Amaducci L, Sorbi S (1997) Analysis of apolipoprotein E, alpha1-antichymotrypsin and presenilin-1 genes polymorphisms in dementia caused by normal pressure hydrocephalus in man. *Neurosci Lett* **229**, 177-180.

[48] Klinge PM, Heile M, Slone S, Johanson CE, Miller M, Duncan JA, Brinker T, Silverberg GD (2009) Evidence of TAU pathology in kaolin-induced hydrocephalus model of the aged rat. *Cerebrospinal Fluid Res* **6**, S37.

[49] Klinge PM, Samii A, Niescken S, Brinker T, Silverberg GD (2006) Brain amyloid accumulates in aged rats with kaolin-induced hydrocephalus. *Neuroreport* **17**, 657-660.

[50] Chou YY, Lepore N, Avedissian C, Madsen SK, Parikshak N, Hua X, Shaw LM, Trojanowski JQ, Weiner MW, Toga AW, Thompson PM (2009) Mapping correlations between ventricular expansion and CSF amyloid and tau biomarkers in 240 subjects with Alzheimer's disease, mild cognitive impairment and elderly controls. *Neuroimage* **46**, 394-410.

[51] Qiu A, Fennema-Notestine C, Dale AM, Miller MI (2009) Regional shape abnormalities in mild cognitive impairment and Alzheimer's disease. *Neuroimage* **45**, 656-661.

[52] Johanson CE, Duncan JA, Klinge PM, Brinker T, Stopa EG, Silverberg GD (2008) Multiplicity of cerebrospinal fluid functions: new challenges in health and disease. *Cerebrospinal Fluid Res* **5**, 10.

[53] Nestor SM, Rupsingh R, Borrie M, Smith M, Accomazzi V, Wells JL, Fogarty J, Bartha R (2008) Ventricular enlargement as a possible measure of Alzheimer's disease progression validated using the Alzheimer's disease neuroimaging initiative database. *Brain* **131**, 2443-2454.

[54] Carmichael OT, Kuller LH, Lopez OL, Thompson PM, Dutton RA, Lu A, Lee SE, Lee JY, Aizenstein HJ, Meltzer CC, Liu Y, Toga AW, Becker JT (2007) Cerebral ventricular changes associated with transitions between normal cognitive function, mild cognitive impairment, and dementia. *Alzheimer Dis Assoc Disord* **21**, 14-24.

This page intentionally left blank

Section 2
Structural Imaging to Diagnose and Measure
Alzheimer-Related Brain Changes

This page intentionally left blank

Introduction

Section 2: Structural Imaging

Peter J. Bayley[a,*], Giovanni B. Frisoni[b] and Clifford R. Jack Jr[c]

[a]*Stanford/VA Aging Clinical Research Center, VA Palo Alto Health Care System, Palo Alto, CA, USA*
[b]*LENITEM - Laboratory of Epidemiology Neuroimaging and Telemedicine, IRCCS Centro San Giovanni di Dio FBF, The National Centre for Research and Care of Alzheimer's and Mental Diseases, Brescia, Italy*
[c]*Department of Radiology, Mayo Clinic, Rochester, MN, USA*

Structural MRI provides a measure of the cerebral atrophy that is a central feature of Alzheimer's disease (AD). Atrophy in AD is a result of neurodegenerative processes involving dendritic pruning and loss of synapses, as well as neuronal cell body degeneration and death, with related loss of axons [1, 2]. A body of literature suggests that neurodegeneration in AD is a relatively late event, and is preceded by abnormalities in CSF, tau, Aβ, and FDG-PET [3]. While the rate of change of some of these other biomarkers may slow before the appearance of structural atrophy, abnormalities in neurodegeneration on MRI accelerate as clinical symptoms appear, and then parallel cognitive decline. As a result, volumetric or voxel-based measures of brain atrophy retain a close relationship with cognitive performance across a broad range of AD severity, and rates of neuronal and synaptic loss indicated by brain atrophy correlate strongly with rates of concurrent cognitive decline [4]. In addition, the degree of atrophy correlates well with Braak staging at autopsy [5–7] and the topographic distribution of atrophy on MRI maps well onto Braak's staging of NFT pathology in patients who have undergone post-mortem staging [8]. Many of these themes are explored in the chapters of this Section. For example, brain atrophy and its relationship to cognitive performance in patients with AD and MCI is examined in two chapters by Thomann et al. AD is traditionally considered to be the prototypical "cortical" (limbic as well as neocortical) dementia which arises through degeneration of the cerebral cortex and is typically associated with severe memory loss. Thomann et al. demonstrate that this may be an oversimplification, and that although recall and recognition in AD patients are indeed related to cortical atrophy in the bilateral medial temporal lobe and posterior cingulate, they are also related to degeneration in subcortical regions including the thalamus. The same group of researchers also identified reduced grey matter density in the olfactory bulb and tract suggesting that this brain region may be a potentially useful marker of neurodegeneration in AD and MCI.

One of the difficulties of diagnosing AD is that it shares many clinical symptoms with other types of dementia and the value of structural MRI in the diagnosis of AD is explored by several groups. For example, Lehmann et al. show that although widespread cortical thinning occurs in AD, the specific pattern of thinning varies between patients with typical and atypical presentations of AD. However, thinning of the posterior cingulate was a distinctive feature in both typical and atypical cases of AD but not in frontotemporal lobar degeneration. Cortical thickness was also examined by Fennema-Notestine et al. in relation to ApoE genotype in healthy middle-aged men. The ApoE E4 allele was associated with significantly thinner frontal cortex in this group, which may help explain the greater susceptibility to AD in individuals with the E4 allele. Firbank et al. examined the use of high resolution structural imaging of the hippocampus to differentiate between

*Correspondence to: Peter J. Bayley, Stanford/VA Aging Clinical Research Center, VA Palo Alto Health Care System, 3801 Miranda Avenue, Palo Alto, CA 94304-1290, USA. E-mail: peter.bayley@va.gov.

AD and dementia with Lewy bodies (DLB). They identified three structural abnormalities that differentiated AD from DLB and aged healthy subjects that included the subiculum, CA1, and a hypointense line between CA1 and CA3/4. Oliveira et al. used image analysis algorithms in order to automatically discriminate between AD patients and controls using cortical thickness and volumetric data. Results demonstrated that this method could successfully distinguish between AD patients and controls (sensitivity = 93%; specificity = 85%). Although the patient sample size in this study was relatively small, this and other specialized statistical classification methods based on image analysis are promising techniques which have the potential to improve the diagnosis and monitoring of AD.

Although automated procedures are increasingly used in the segmentation of structural images, manual segmentation remains the gold standard. However, as reviewed by Boccardi et al., the results obtained by manual segmentation depends strongly on which protocol is used – and can result in up to 2.5-fold volume differences when evaluating hippocampal atrophy in AD. As a step in addressing this issue, Boccardi et al. highlight some of the differences between 12 published protocols for hippocampal segmentation.

The relationship between biomarkers of AD and rates of cortical thinning are also explored. It is known that patients with AD have reduced amyloid ($A\beta_{1-42}$), elevated phosphorylated tau (p-tau) and elevated total tau in cerebrospinal fluid. Two groups (Tosun-Turgut et al. and Brys et al.) both show that longitudinal rates of brain atrophy increase in the presence of lower $A\beta_{1-42}$ levels and higher p-tau levels. Combining CSF biomarkers and structural imaging biomarkers significantly increases the overall predictive accuracy of conversion of MCI to AD and supports the hypothesis that CSF $A\beta_{1-42}$ and tau are measures of early AD pathology. In this context, it should be noted that a long standing issue in AD is the uncertain relationship between the senile plaque pathology associated with $A\beta$ and the neurofibrillary pathology associated with tau. Recent data have suggested that the $A\beta$ pathology is more closely associated with the ApoE genotype and the predisposition to AD and develops over decades, while the tau pathology is more closely related to cognitive function and develops over the course of dementia [9]. In view of this, the different time courses of these various biomarkers must be taken into account when using combined measures to estimate where an individual lies on the continuum of AD.

Finally, new technologies are on the horizon for structural imaging in AD, including the routine use of ultra-high field MRI. Kerchner reviews two AD-related applications for 7T MRI: direct visualization of cortical plaques, and high resolution hippocampal imaging. Together, these tools promise to provide an ever greater insight for the diagnosis and treatment of AD.

REFERENCES

[1] Bobinski M, de Leon MJ, Wegiel J, Desanti S, Convit A, Saint Louis LA, Rusinek H, Wisniewski HM (2000) The histological validation of post mortem magnetic resonance imaging-determined hippocampal volume in Alzheimer's disease. *Neuroscience* **95**, 721-725.

[2] Ashford JW, Soultanian NS, Zhang SX, Geddes JW (1998) Neuropil threads are collinear with MAP2 immunostaining in neuronal dendrites of Alzheimer brain. *J Neuropathol Exp Neurol* **57**, 972-978.

[3] Jack CR Jr, Knopman DS, Jagust WJ, Shaw LM, Aisen PS, Weiner MW, Petersen RC, Trojanowski JQ (2010) Hypothetical model of dynamic biomarkers of the Alzheimer's pathological cascade. *Lancet Neurol* **9**, 119-128.

[4] Fox NC, Scahill RI, Crum WR, Rossor MN (1999) Correlation between rates of brain atrophy and cognitive decline in AD. *Neurology* **52**, 1687-1689.

[5] Jack CR Jr, Dickson DW, Parisi JE, Xu YC, Cha RH, O'Brien PC, Edland SD, Smith GE, Boeve BF, Tangalos EG, Kokmen E, Petersen RC (2002) Antemortem MRI findings correlate with hippocampal neuropathology in typical aging and dementia. *Neurology* **58**, 750-757.

[6] Silbert LC, Quinn JF, Moore MM, Corbridge E, Ball MJ, Murdoch G, Sexton G, Kaye JA (2003) Changes in premorbid brain volume predict Alzheimer's disease pathology. *Neurology* **61**, 487-492.

[7] Braak H, Braak E (1991) Neuropathological staging of Alzheimer-related changes. *(Berlin) Acta Neuropathol* **82**, 239-259.

[8] Whitwell JL, Josephs KA, Murray ME, Kantarci K, Przybelski SA, Weigand SD, Vemuri P, Senjem ML, Parisi JE, Knopman DS, Boeve BF, Petersen RC, Dickson DW, Jack CR Jr (2008) MRI correlates of neurofibrillary tangle pathology at autopsy: a voxel-based morphometry study. *Neurology* **71**, 743-749.

[9] Morris JC, Roe CM, Xiong C, Fagan AM, Goate AM, Holtzman DM, Mintun MA (2010) APOE predicts amyloid-beta but not tau Alzheimer pathology in cognitively normal aging. *Ann Neurol* **67**, 122-131.

Cognitive Performance and Its Relation to Brain Morphology in MCI and AD

Philipp A. Thomann[a,b,*], Vasco Dos Santos[b], Torsten Wüstenberg[c], Ulrich Seidl[b], Marco Essig[d] and Johannes Schröder[b]

[a]*Structural Neuroimaging Group, Center of Psychosocial Medicine, Department of General Psychiatry, University of Heidelberg, Heidelberg, Germany*
[b]*Section of Geriatric Psychiatry, University of Heidelberg, Heidelberg, Germany*
[c]*Department of Psychiatry and Psychotherapy, Charité Universitätsmedizin Berlin, Campus Mitte, Germany*
[d]*German Cancer Research Center, Heidelberg, Germany*

Abstract. The aim of the present study was to examine the relationship between cerebral morphological changes and cognitive deficits as determined by the CERAD neuropsychological test battery in a large group of patients with MCI and with AD and otherwise healthy elderly controls. Patients were recruited among typical memory clinic referrals and carefully matched for age, gender and educational level. Optimized voxel based morphometry was used to reveal gray matter differences between groups and to investigate the association of neuropsychological deficits with brain structural alterations. When compared to controls, AD patients and, to a lesser extent, patients with MCI showed significant atrophy predominantly in the medial temporal lobe. Deficits in verbal fluency and word finding were significantly correlated with left fronto-temporal and left temporal (including the hippocampus) changes, respectively. Decreased scores in immediate and delayed recall and in delayed recognition were associated with several cortical and subcortical areas including the parahippocampal and posterior cingulate gyrus, the right thalamus, and the right hippocampus, whereas deficits in constructional praxis and constructional praxis recall referred to regions in the left thalamus and cerebellum, and the temporal cortices, respectively. These findings lend further support to medial temporal lobe degeneration in MCI and AD and suggest that cognitive deficits reflect morphological alterations in widespread cortico-subcortical networks.

INTRODUCTION

Alzheimer's disease (AD), the most common cause of dementia, is a neurodegenerative disorder characterized by cerebral deposition of neurofibrillary tangles and senile plaques accompanied by neuron cell loss in specific brain regions. Longitudinal studies confirmed the clinical impression that the majority of individuals affected by AD undergo a longstanding preclinical phase where cognitive deficits are still less obvious before manifest dementia is diagnosed [1]. This transitional phase between health and onset of AD is generally referred to as mild cognitive impairment (MCI). According to large representative studies, around 40–60% of MCI patients develop AD within the first 5 years [2].

The CERAD-NP neuropsychological test battery was developed by the Consortium for the Etablishment of a Registry for Alzheimer´s disease in 1986 [3, 4] to address a broad range of neuropsychological deficits typically found in MCI and AD: verbal fluency (animal category), naming, word list immediate/delayed recall, constructional praxis, constructional praxis recall, and also includes the Mini Mental State Examination

*Correspondence to: PD Dr. med. Philipp A. Thomann, Structural Neuroimaging Group, Center of Psychosocial Medicine, Department of General Psychiatry, University of Heidelberg, Voßstr. 4, 69115 Heidelberg, Germany. Tel.: +49 6221 56 38091; Fax: +49 6221 56 1742; E-mail: philipp.thomann@med.uni-heidelberg.de.

(MMSE) [5]. While the CERAD-NP is generally considered as a easy to use, comprehensive test battery with good psychometric properties [6–8], its potential cerebral correlates have so far only scarcely been addressed. A positron emission tomography (PET) study with 18F-2-deoxyglucose (FDG) as a tracer, found measures of episodic memory, verbal fluency, naming and drawing to be related to a decreased glucose uptake in left-hemispheric temporal, prefrontal and inferior parietal regions in 30 patients with AD [9]. However, patients with MCI and mild AD, in whom neuropsychological assessment is of particular importance for early diagnosis, were not included. Most recently, Schmidt-Wilcke et al. [10] conducted a voxel based morphometry (VBM) study in a small sample of MCI subjects ($n = 18$) and demonstrated impaired CERAD-NP performance to be accompanied by gray matter loss predominantly in the medial temporal lobe.

The aim of our study was to identify the cerebral correlates of neuropsychological deficits as assessed by the CERAD-NP test battery in a large sample including healthy subjects and both, patients with MCI and AD.

MATERIALS AND METHODS

Patients and control subjects

Thirty-four patients with mild AD, 60 with MCI and 32 cognitively unaffected controls were consecutively recruited through the memory clinic of the Section of Geriatric Psychiatry at Heidelberg University, Germany. All subjects were carefully matched for age, gender, ethnicity and education. Patients fulfilled the NINCDS-ADRDA criteria for probable AD [11] or the criteria of aging-associated cognitive decline (AACD) [1, 12]. The latter consider decline in a broad potential range of cognitive domains and have been confirmed as a stable and broad concept for MCI, predictive for the development of dementia [13, 14]. Clinical evaluation included ascertainment of personal and family history and detailed physical and neurological examination. None of the participants had a lifetime history of neurological or severe systemic illness, head injury or substance abuse. The investigations were approved by the local ethics committee. Written informed consent was obtained from all participants after the procedures of the study had been fully explained.

Neuropsychological assessment

Cognitive functions were investigated using the German version of the CERAD-NP test battery. Raw values were z-transformed by referring to the age and gender specific norms obtained in a large sample of healthy Swiss subjects [15]. Further methodological details are described elsewhere [16, 17].

Magnetic resonance imaging

MRI-data were obtained at the German Cancer Research Center with a 1.5-T Magnetom Symphony MR scanner (Siemens Medical Solutions, Erlangen, Germany). To exclude secondary causes of dementia and ischemic changes a 2D T2-weighted Fast-Spin Echo (TR = 4500 ms, TE = 90 ms) sequence was performed in axial orientation. For structural analysis, a T1-weighted 3D magnetization prepared rapid gradient echo (MP-RAGE) sequence was performed with the following parameters: 126 coronar slices, image matrix = 256×256, voxel size = 0.98 mm $\times$ 0.98 mm $\times$ [33]1.8 mm, TR = 10 msec, TE = 4 msec.

Voxel based morphometry

The optimized VBM protocol proposed by Good and colleagues [18] was applied for the preprocessing of imaging data. This method minimizes the probability of misclassifications within the tissue segmentation by the introduction of additional preprocessing steps prior to normalization and subsequent segmentation.

Statistical analysis

SPSS for Windows version 14 was used for statistical analysis; p-values less than 0.05 were considered significant. Analyses of variance with post hoc Duncan's tests were calculated in order to compare the demographic and clinical data between the diagnostic groups. The gender distribution was analyzed by the χ^2-test.

Using the general linear approach as implemented in the statistical parametric mapping program SPM2 (http://www.fil.ion.ucl.ac.uk/spm), diagnostic groups were compared for significant gray matter differences. Subsequently, neuropsychological test performance was correlated with gray matter density values. This was done across all three diagnostic groups, since MCI forms a continuum between healthy aging and mild AD

Regional correlations between local gray matter density and cognitive performance were assessed by a voxel-wise regression analysis containing the results of each individual (z-values of CERAD subtests, respectively) as explanatory variables. T-maps were thresholded for a significance level of $p < 0.001$ uncorrected and a spatial extend of 200 voxels. Finally, these t-maps were masked with the above mentioned mask images to exclude all voxels with a gray matter density distribution significantly correlated with the variables of no interest. In a second – and statistically more stringent – step, we repeated the aforementioned analysis by applying a family-wise error correction for multiple comparisons over the whole brain ($p < 0.05$).

RESULTS

Demographic and clinical data

The clinical characteristics of the diagnostic groups are reported in Table 1. As expected, MMSE scores differed significantly between the three groups while no significant differences arose with respect to age, gender, and education, respectively. Similarly, all CERAD subtests showed significant differences with the MCI patients taking an intermediate position between AD patients and controls (Table 1, Fig. 1). The largest differences were obtained for the CERAD subtests 'delayed recall', 'recognition', and 'constructional praxis recall', respectively.

Morphometric between-group comparisons

When compared with healthy controls, patients with MCI showed significant gray matter changes in the gyri temporalis medius and superior bilaterally, the right insula, left gyrus temporalis superior, left anterior cingulate gyrus, and the left cerebellum. Patients with AD demonstrated significant lower gray matter density values in the right gyrus temporalis inferior and medius, right gyrus precentralis, right cingulate gyrus, left entorhinal cortex, and left gyrus temporalis superior than the MCI patients. When contrasted with the healthy controls, the AD patients were characterized by significantly lower gray matter density values in the right thalamus and cuneus, right gyrus frontalis superior and inferior, left hippocampus and left gyrus fusiformis extending to the left gyrus temporalis inferior (Table 2, Fig. 2).

Neuropsychological performance and gray matter density

Impaired performance in the CERAD subtest 'verbal fluency' was correlated with reduced gray matter density values in the left dorsolateral prefrontal cortex (including Brodmann area 44), gyrus temporalis superior, and right thalamus, while performance deficits in the naming subtest referred to reductions in the left – and to a lesser extent – right temporal cortex including the hippocampus (bilaterally). Deficits in the CERAD subtests 'immediate recall' and 'delayed recall' referred to left – and to a somewhat lesser

Table 1
Subject demographics, clinical and neuropsychological characteristics

Variable	Controls (1) (n = 32)	MCI (2) (n = 60)	AD (3) (n = 34)	F	df	p	Duncan test (5%)
Sex	17 F/15 M	34 F/26 M	23 F/11 M	1.636[a]	2	0.44	n.a.
Age, years	68.69 ± 7.36	70.33 ± 6.32	70.32 ± 5.73	0.775	2,123	0.46	1 = 2 = 3
Education, years	10.15 ± 2.04	9.40 ± 1.59	9.35 ± 1.66	6.049[a]	2	0.42	n.a
GDeteriorationS[b]	1.13 ± 0.33	3.00 ± 0.00	3.06 ± 0.23	981.733	2,123	<0.001	1 > 2 > 3
CDR[c]	0.00 ± 0.00	0.50 ± 0.00	0.82 ± 0.24	359.918	2,123	<0.001	1 > 2 > 3
GDepressionS[d]	2.75 ± 0.95	2.88 ± 0.69	2.62 ± 0.95	1.116	2,123	0.033	1 = 2 = 3
MMSE[e]	29.22 ± 0.792	26.38 ± 1.78	21.41 ± 2.176	177.285	2,123	<0.001	1 > 2 > 3
Verbal fluency[e]	0.57 ± 0.96	−0.58 ± 1.13	−1.44 ± 0.77	30.38	2,123	<0.001	1 > 2 > 3
BNT[e]	0.41 ± 0.76	−0.81 ± 1.55	−1.95 ± 2.53	15.17	2,123	<0.001	1 > 2 > 3
WL immediate recall[e]	0.16 ± 0.90	−1.67 ± 1.36	−3.59 ± 2.40	43.79	2,123	<0.001	1 > 2 > 3
WL delayed recall[e]	0.24 ± 0.88	−1.57 ± 1.37	−3.37 ± 1.58	82.66	2,123	<0.001	1 > 2 > 3
WL recognition[e]	0.33 ± 0.43	−1.85 ± 2.81	−5.80 ± 3.56	44.94	2,123	<0.001	1 > 2 > 3
CP[e]	0.16 ± 1.47	−0.35 ± 1.49	−1.47 ± 2.02	8.78	2,123	<0.001	1 = 2 > 3
CP recall[e]	0.57 ± 1.36	−0.96 ± 1.65	−3.50 ± 1.40	47.58	2,123	<0.001	1 > 2 > 3

MCI = Mild cognitive impairment, AD = Alzheimer's disease; df = degrees of freedom; [a]Pearsons-χ^2-test; n.a.not applicable; [b]Global Deterioration Scale, [c]Clinical Dementia Rating, [d]Geriatric Depression Scale, [e]CERAD test battery (mean z-scores except for MMSE); MMSE = Mini Mental State Examination; BNT = Boston Naming Test; WL = word list; CP = constructional praxis
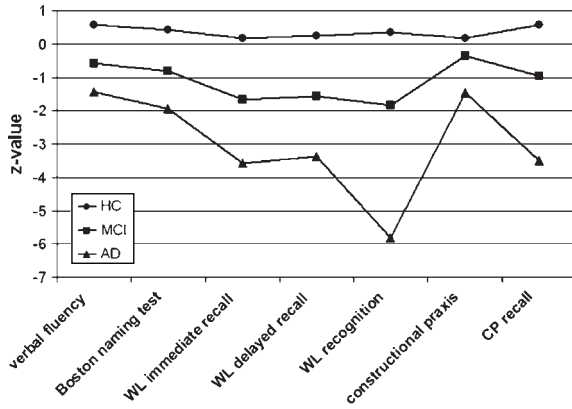
Fig. 1. CERAD-subtest performance in healthy controls, subjects with MCI and patients with AD.

lateral prefrontal cortex (bihemispheric), respectively. A reduced performance in the subtest 'constructional praxis' involved changes in the temporal cortices (predominantly on the left hemisphere), the thalamus and the cerebellum, while deficits in the subtest 'constructional praxis recall' were correlated with changes of temporal lobes and mediofrontal cortices predominantly in the left hemisphere (Table 3, Fig. 3).

Subsequently, the respective analyses were repeated for each diagnostic group separately. Each of these analyses yielded – though at lower significance levels – similar findings as obtained in the whole group (data not shown).

DISCUSSION

The aim of the present study was to examine the relationship between cerebral morphological changes and cognitive deficits as determined by the CERAD

extend – right temporal lobe changes including the hippocampus, those in the subtest 'recognition' to gray matter reductions in the left hippocampus and dorso-

Table 2
Anatomical structures showing significant differences in gray matter density between the three groups

Comparison	Anatomical structure	Cluster size (voxels)	T-value	Peak coordinates (x,y,z)
HC > AD	**Left hippocampus**	327921 (**87511**)	8.46	−29, −13, −18
	Left gyrus fusiformis extending to gyrus temporalis inferior	58041 (**2101**)	7.74	−33, −13, −38
	Right thalamus	2237 (**1360**)	5.81	8, −16, 0
	Right gyrus frontalis inferior	289 (**277**)	5.43	41, 9, 33
HC > MCI	**Right gyrus temporalis medius extending to insula**	128667 (**552**)	5.67	42, −7, −8
	Left gyrus temporalis superior	708 (**124**)	5.50	−26, 12, −44
MCI > AD	Left entorhinal cortex	5912	5.72	−27, −14, −33
	Right gyrus temporalis inferior	444	4.98	29, −13, −34
	Right amygdala	311	4.77	22, −2, −15
	Left gyrus temporalis medius	251	4.75	−50, −9, −15

Height threshold $p < 0.001$ uncorrected; extent threshold = 100 voxels. Regions surviving $p < 0.05$ FWE-correction and corresponding cluster sizes in bold.
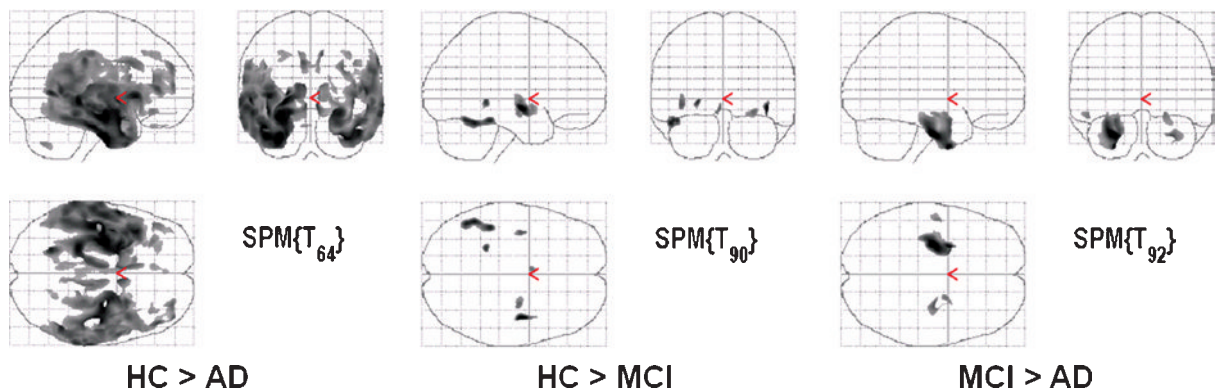
Fig. 2. Brain regions showing significant gray matter differences between the three study groups.

Table 3
Significant associations between gray matter density and cognitive performance

Test	Anatomical structure	Cluster size (voxel)	T-value	Peak coordinates (x,y,z)
Verbal	Left thalamus	1515	5.93	–12, –30, 3
Fluency	Left insula	3146	5.36	–41, –5, 8
	Left gyrus parahippocampalis	469	5.11	–22, 3, –17
	Left gyrus frontalis inferior	217	5.08	–54, 13, 16
	Left gyrus temporalis superior	908	5.07	–53, 13, 16
	Left gyrus parahippocampalis	211	4.92	–27, –13, –36
	Right thalamus	246	4.91	13, –29, 3
	Left hippocampus	477	4.69	–27, –11, –16
Boston naming test	Left gyrus inferior temporal extending to gyrus parahippocampalis	11449	6.42	–29, –10, –40
	Left hippocampus	314	4.74	–27, –35, –6
Word list immediate recall	Right hippocampus	197794	7.59	21, –5, –14
	Right thalamus	1769	6.62	11, –28, 2
	Left gyrus middle frontalis	4194	5.67	–45, 35, 20
	Left precuneus	985	5.50	–10, –70, 26
	Right gyrus middle frontalis	573	5.45	30, 33, 43
	Right gyrus superior frontalis	883	5.04	28, 52, 28
	Right gyrus middle frontalis	242	4.81	39, 12, 51
	Right posterior cingulate gyrus	1468	4.69	5, –48, 29
Word list delayed recall	Left gyrus parahippocampalis	100362	8.62	–21, 1, –15
	Right gyurs parahippocampalis	67074	8.25	22, –4, –14
	Left gyrus middle frontalis	6295	6.24	–45, 35, 20
	Right gyrus superior frontalis	2784	6.17	35, 52, 22
	Left anterior cingulate gyrus	621	5.84	–8, 15, 38
	Right thalamus	1580	5.78	13, –28, –2
	Left posterior cingulate gyrus	685	5.30	–1, –33, 30
	Left cerebellum	4080	5.28	–45, –62, –45
Word list recognition	Left hippocampus	7001	6.03	–30, –34, –6
	Right precentral gyrus	937	5.69	45, 19, 7
	Left gyrus superior temporal	1232	5.47	–56, 0, 2
	Right gyrus parahippocampalis	1887	5.62	25, 3, –23
	Right gyrus middle frontalis	640	5.27	49, –55, 10
	Right gyrus fusiformis	229	5.20	44, –27, –25
	Left gyrus inferior frontalis	308	5.05	–49, 10, 21
	Left gyrus middle temporalis	410	4.95	–48, –55, 11
	Right gyrus inferior temporali	218	4.65	59, –24, –22
	Right gyrus supramarginalis	376	4.57	58, –45, 24
Constructional praxis	Left thalamus	742	5.00	–11, –22, 12
	Left cerebellum	381	4.94	–13, –82, –45
Constructional praxis recall	Left hippocampus	9721	7.30	–24, –38, –2
	Right gyrus inferior temporalis	3320	5.61	45, –15, –31
	Left gyrus middle temporalis	2480	5.86	–54, –27, –13
	Left gyrus middle temporalis	517	5.54	–67, –40, –4
	Right gyrus parahippocampalis	1318	5.38	20, –4, –15
	Left insula	1460	5.28	–40, 11, 0
	Right gyrus parahippocampalis	263	5.15	30, –37, –10

Height threshold $p < 0.05$, FWE-corrected; extent threshold = 100 voxels.

neuropsychological test battery in a large group of patients with MCI and with AD and otherwise healthy elderly controls. Patients were recruited among typical memory clinic referrals and carefully matched for age, gender and educational levels; the pattern of cognitive deficits is similar to that previously observed in an independent sample [16]. We analyzed high-resolution MRI datasets by using optimized VBM which enabled us to account for potential changes in gray matter density throughout the entire brain.

Observed between group structural changes were generally in line with previous findings in that AD patients and – to a lower extent – individuals with MCI were characterized by atrophic processes predominantly in temporal lobe regions when compared with healthy control subjects [19–21].
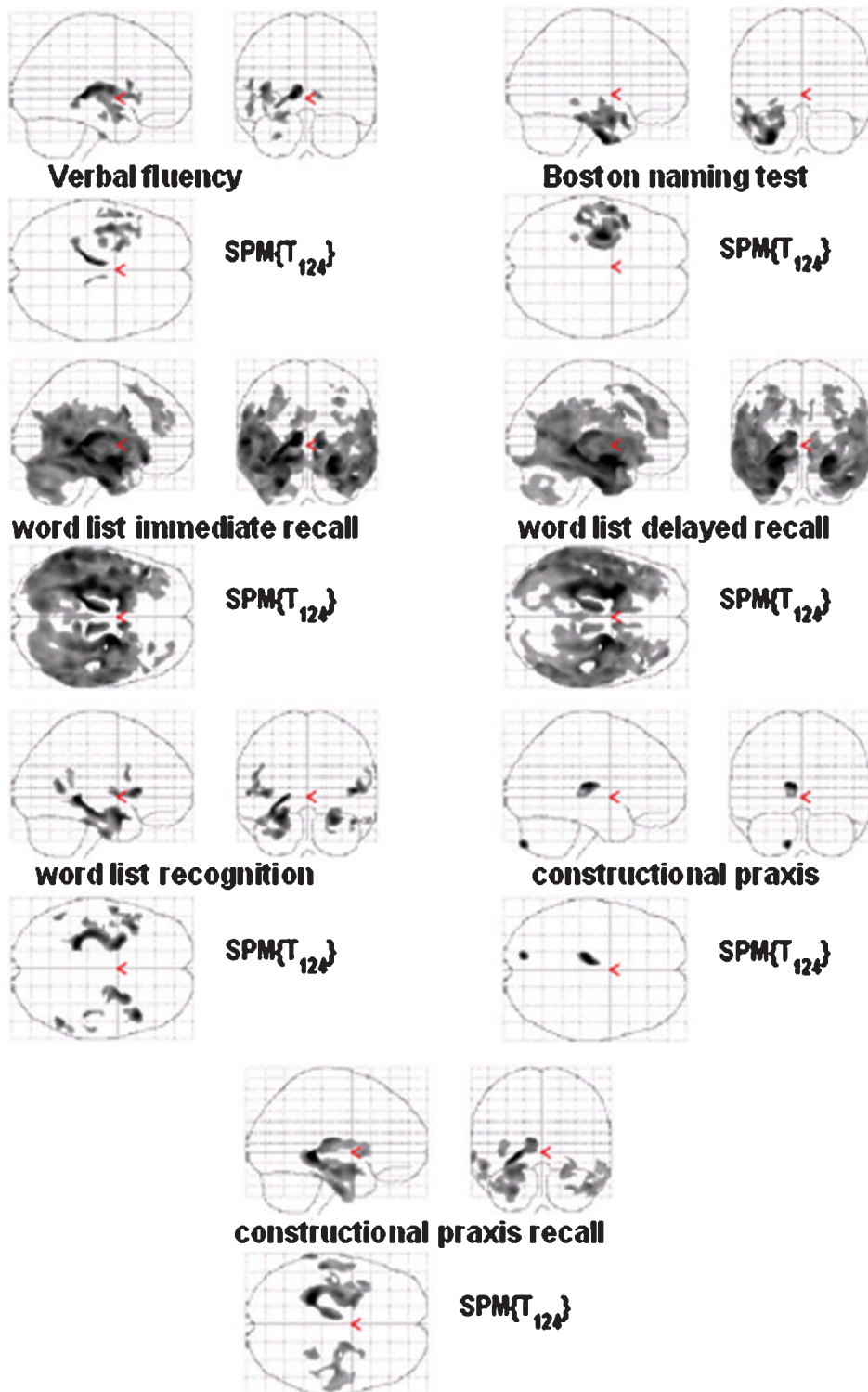
Fig. 3. Brain regions showing significant correlation between gray matter density and CERAD-subtest performance in controls, MCI and AD.

The association found between reduced verbal fluency and reduced gray matter values in the left prefrontal and superior temporal cortices is supported by the results of two previous MRI studies which used manual segmentation [22, 23]. A recent study which applied a surface-based computational anatomy technique in 19 patients with mild AD and 5 MCI patients found deficits in a verbal fluency task to be significantly correlated with predominantly left hemispheric changes which involved the frontal (including Broca's are), parietal and temporal cortices [24]. The semantic verbal fluency task was similar to that used in the present study. Significant associations between deficits in verbal fluency and left frontal cortex changes were also reported in FDG-PET studies [9, 25, 26] and point towards the functional relevance of the respective sites including Broca's region for word generation and speech.

Deficits in the naming subtest referred to changes in the temporal lobes including the hippocampi which predominantly involved the left hemisphere. An association of deficits in naming and left temporal atrophy was also reported in a previous study of our group which evaluated the MRI obtained in 50 patients from all stages of AD by using manual segmentation [23]. The aforementioned MRI study using surface analysis [24] found both temporal cortices to be involved in naming deficits although a marked lateralization of findings to the left hemisphere was also evident. These discrepancies are likely to be accounted for by methodological differences, in particular the restrictions to preselected and often rather large cerebral structures inherent to manual segmentation. In addition, the stage of disease has to be considered as another important factor since AD also involves compensatory mechanisms, such as dedifferentiation of neural functioning with contralateral sites supporting tasks which were primarily served by lateralized sites [27]. Actually, patients investigated here and by Apostolova and colleagues were in the early or even preclinical phases of AD, while the sample of our previous study also comprised patients in more advanced stages. Similarly, a recent FDG-PET study which involved 30 patients in all stages of AD identified the left temporal posterior cortex as an important site for naming deficits [9].

Deficits in immediate recall corresponded to changes in the temporal lobes including their medial substructures. Changes involved both hemispheres although they were predominantly associated with the left side. An association between verbal memory and hippocampal integrity was reported in one of the early

pioneer studies which investigated the hippocampus in 20 patients with mild to moderate AD by using manual segmentation [28]. More recently, immediate recall of a word list was found to be significantly correlated with left entorhinal changes in 18 patients with moderate AD by using optimized VBM [29]. A correlation between deficits to immediately recall a story and a decreased glucose uptake in the temporal cortices was described in a sample of 19 patients with mild-to-moderate AD [25], while Teipel and colleagues [9] found associations rather lateralized in the left prefrontal and temporal cortices.

Failures in delayed recall were related to bihemispheric atrophic changes in both temporal lobes which extended to the medial frontal, occipital and parietal cortices. In contrast, the aforementioned study solely reported significant correlations for left prefrontal and temporal cortices [9]. It is generally accepted that episodic memory should not be conceptualized as reflecting a unitary or highly localized process but, rather, as involving different stages and brain regions [30, 31]. Within declarative memory two critical processes (encoding vs. retrieval) and two major branches (episodic vs. semantic) are differentiated. The cerebral circuitries underlying these aspects of declarative memory functioning are only partly understood. According to the model of "hemispheric encoding/retrieval asymmetry" [32], left and right frontal cortical areas are differentially involved in encoding into episodic memory and retrieval of information from episodic memory, respectively. This hemispheric asymmetry model is generally consistent with PET studies [32–34] in healthy subjects that revealed an activation of right prefrontal and temporal areas in episodic memory retrieval. Actually in AD, reported correlations between regional callosal atrophy and severity of dementia [35, 36] support the assumption that interhemispheric cortico-cortical disconnection may contribute to the dementia syndrome.

Functional neuroimaging studies indicate that the lateralization of prefrontal cortex activations tends to be reduced by aging, a finding which was conceptualized in terms of a model called Hemispheric Asymmetry Reduction in Old Adults, or HAROLD [37]. While the HAROLD model was supported by functional neuroimaging studies in a variety of cognitive domains, including episodic memory retrieval, up to now it was not related to structural changes. However, it is generally accepted that recovery of function after unilateral brain damage frequently involves the recruitment of the unaffected hemisphere. In healthy

aging and in MCI, increased bilaterality could help counteract deficits in a compensatory effort. This supposition is corroborated by the association of deficits in immediate and delayed recall with bihemispheric prefrontal and temporal changes as demonstrated in the present study. According to the compensation hypothesis one may expect hemispheric asymmetry reductions to be greater for difficult than for easier tasks. This hypothesis corresponds to our finding of a more lateralized pattern of structural changes.

An impairment of constructional praxis was related to reduced thalamic and cerebellar gray matter densities. From a neuroanatomical standpoint, this association seems plausible since these regions are known to be crucial for both visuospatial and fine motor skills [38, 39]. In contrast, the recall of geometric figures was significantly associated with structural alterations in regions typically involved in memory functioning, namely the hippocampus, the parahippocampal gyrus, the insula, and the inferior and middle temporal gyrus, respectively.

Age, gender and educational level had to be considered as potential confounding factors. However, the correlations obtained between test performance and density reductions in MRI were corrected for these variables. The term "MCI" was originally introduced by Flicker and colleagues to describe a syndrome in the elderly with impairments in recent and remote memory, language function, concept formation and visuospatial praxis which tended to deteriorate at follow-up [40]. Similarly, AACD criteria consider deficits in five important cognitive domains. AACD criteria were developed by a working party of the International Psychogeriatric Association in 1994 and compare with the revised MCI criteria proposed by Winblad and colleagues in 2004 [41]. Recent epidemiological and clinical studies confirm the reliability and prognostic validity of the AACD criteria [14, 16, 21] and indicate that "broad" definitions of MCI may provide better psychometric properties than narrowly defined criteria.

In conclusion, we found impaired cognitive performance as assessed with the CERAD test battery to be associated with reduced gray matter densities in a variety of cerebral sites, likely reflecting the fact that cognitive impairment in AD and in its presumable precursor MCI is not simple related to degenerative processes in a few distinct brain regions. The respective associations are generally in line with findings of previous functional imaging studies in both healthy individual and patients with cognitive impairment and

can also facilitate the interpretation of neuropsychological and MRI findings in clinical practise. However, for the interpretation of the present results it is important to bear in mind that we related cerebral-structural to individual-cognitive data and hence, drawing brain-functional conclusions is somewhat speculative. To overcome these limitations, future studies might combine neuropsychological, brain structural and brain functional assessments in order to elucidate how they specifically relate to each other.

ACKNOWLEDGMENTS

REFERENCES

[1] Schröder J, Kratz B, Pantel J, Minnemann E, Lehr U, Sauer H (1998) Prevalence of mild cognitive impairment in an elderly community sample. *J Neural Transm Suppl* **54**, 51-59.

[2] De Carli C (2003) Mild cognitive impairment: prevalence, prognosis, aetiology, and treatment. *Lancet Neurol* **2**, 15-21.

[3] Heyman A, Peterson B, Fillenbaum G, Pieper C (1997) Predictors of time to predictors of time to institutionalization of patients with Alzheimer's disease: the CERAD experience, part XVII. *Neurology* **48**, 1304-1309.

[4] Morris JC, Heyman A, Mohs RC, Hughes JP, van Belle G, Fillenbaum G, Mellits ED, Clark C (1989) The consortium to establish a registry for Alzheimer's disease (CERAD). Part I Clinical and neuropsychological assessment of Alzheimer's disease. *Neurology* **39**, 1159-1165.

[5] Folstein MF, Folstein SE, McHugh PR (1975) "Mini-mental state". A practical method for grading the cognitive state of patients for the clinician. *J Psychiatr Res* **12**, 189-198.

[6] Welsh K, Butters N, Hughes J, Mohs R, Heyman A (1991) Detection of abnormal memory decline in mild cases of Alzheimer´s disease using CERAD-NP neuropsychological measures. *Arch Neurol* **48**, 278-281.

[7] Welsh K, Butters N, Hughes J, Mohs R, Heyman A (1992) Detection and staging of dementia in Alzheimer's disease: Use of neuropsychological measures developed for the consortium to establish a registry for Alzheimer's disease. *Arch Neurol* **49**, 448-452.

[8] Satzger W, Hampel H, Padberg F, Bürger K, Nolde T, Ingrassia G, Engel R (2001) Zur praktischen Anwendung der CERAD-NP Testbatterie als neuropsychologisches Demenzscreening. *Nervenarzt* **72**, 196-203.

[9] Teipel SJ, Willoch F, Ishii K, Bürger K, Drzezga A, Engel R, Bartenstein P, Möller HJ, Schwaiger M, Hampel H (2006) Resting state glucose utilization and the CERAD cognitive battery in patients with Alzheimer's disease. *Neurobiol Aging* **27**, 681-690.

[10] Schmidt-Wilcke T, Poljansky S, Hierlmeier S, Hausner J, Ibach B (2009) Memory performance correlates with gray matter density in the ento-/perirhinal cortex and posterior hippocampus in patients with mild cognitive impairment and healthy controls–a voxel based morphometry study. *Neuroimage* **47**, 1914-1920.

[11] McKhann G, Drachman D, Folstein M, Katzman R, Price D, Stadlan EM (1984) Clinical diagnosis of Alzheimer's disease: report of the NINCDS-ADRDA work group under the auspices of department of health and human services task force on Alzheimer's disease. *Neurology* **34**, 939-944.

[12] Levy R (1994) Aging-associated cognitive decline. Working party of the international psychogeriatric association in collaboration with the world health organization int. *Psychogeriatr* **6**, 63-68.

[13] Ritchie K, Ledesert B, Touchon J (2000) Subclinical cognitive impairment: epidemiology and clinical characteristics. *Compr Psychiatry* **41**, 61-65.

[14] Schönknecht P, Pantel J, Kruse A, Schröder J (2005) Prevalence and natural course of aging-associated cognitive decline in a population-based sample of young-old subjects. *Am J Psychiatry* **162**, 2071-2077.

[15] Thalmann B, Monsch A (1997) CERAD-NP-Neuropsychologische Testbatterie: Vorläufige Normen. *Basel: Memory Clini*.

[16] Barth S, Schönknecht P, Pantel J, Schröder J (2005) Neuropsychologische Profile in der Demenzdiagnostik: Eine Untersuchung mit der CERAD-NP-Testbatterie. *Fortschr Neurol Psychiatr* **73**, 568-576.

[17] Aebi C (2002) Validierung der neuropsychologischen Testbatterie CERAD-NP. *Dissertationsschrift, Universität Basel*.

[18] Good CD, Johnsrude IS, Ashburner J, Henson RN, Friston KJ, Frackowiak RS (2001) A voxel-based morphometric study of ageing in 465 normal adult human brains. *Neuroimage* **14**, 21-36.

[19] De Santi S, de Leon MJ, Rusinek H, Convit A, Tarshish CY, Roche A, Tsui WH, Kandil E, Boppana M, Daisley K, Wang GJ, Schlyer D, Fowle RJ (2001) Hippocampal formation glucose metabolism and volume losses in MCI and AD. *Neurobiol Aging* **22**, 529-539.

[20] Killiany RJ, Hyman BT, Gomez-Isla T, Moss MB, Kikinis R, Jolesz F, Tanzi R, Jones K, Albert MS (2002) MRI measures of entorhinal cortex vs hippocampus in preclinical AD. *Neurology* **58**, 1188-1196.

[21] Pantel J, Kratz B, Essig M, Schröder J (2003) Parahippocampal volume deficits in subjects with aging-associated cognitive decline. *Am J Psychiatry* **160**, 379-382.

[22] Fama R, Sullivan E, Shear P, Marsh L, Yesavage J, Tinklenberg J, Lim K, Pfefferbaum A (1997) Selective cortical and hippocampal volume correlates of mattis dementia rating scale in Alzheimer disease. *Arch Neurol* **54**, 719-728.

[23] Pantel J, Schönknecht P, Essig M, Schröder J (2004) Distribution of cerebral atrophy assessed by magnetic resonance imaging reflects patterns of neuropsychological deficits in Alzheimer's dementia. *Neurosci Lett* **361**, 17-20.

[24] Apostolova LG, Lu P, Rogers S, Dutton RA, Hayashi KM, Toga AW, Cummings JL, Thompson PM (2008) 3D mapping of language networks in clinical and pre-clinical Alzheimer's disease. *Brain Lang* **104**, 33-41.

[25] Desgranges B, Baron J, Eustache F (1998) The functional neuroanatomy of episodic memory: the role of the frontal lobes, the hippocampal formation, and other areas. *Neuroimage* **8**, 198-213.

[26] Welsh KA, Hoffman JM, Earl NL, Hanson MW (1994) Neural correlates of dementia: regional brain metabolism (FDG-PET) and the CERAD neuropsychological battery. *Arch Clin Neuropsychol* **9**, 395-409.

[27] Schröder J, Buchsbaum MS, Shihabuddin L, Tang C, Wie T, Spiegel-Cohen J, Hazlett EA, Abel L, Luu-Hsia C, Ciaravolo TM, Marin D, Davis KL (2001) Patterns of cortical activity and memory performance in Alzheimer's disease. *Biol Psychiatry* **49**, 426-436.

[28] Pantel J, Schröder J, Schad L, Friedlinger M, Knopp M, Schmitt R, Geissler M, Blüml S, Klemenz M, Essig M, Sauer H (1997) Quantitative magnetic resonance imaging and neuropsychological functions in dementia of the Alzheimer type. *Psychol Med* **27**, 221-229.

[29] Di Paola M, Macaluso E, Carlesimo GA, Tomaiuolo F, Worsley KJ, Fadda L, Caltagirone C (2007) Episodic memory impairment in patients with Alzheimer's disease is correlated with entorhinal cortex atrophy. A voxel-based morphometry study. *J Neurol* **254**, 774-781.

[30] Markowitsch H (1995) Which brain regions are critically involved in the retrieval of old episodic memory?. *Brain Res Rev* **21**, 117-127.

[31] Squire L (1986) Mechanisms of memory. *Science* **232**, 1612-1619.

[32] Tulving E, Kapur S, Markowitsch H, Craik F, Habib R, Houle S (1994) Neuroanatomical correlates of retrieval in episodic memory: auditory sentence recognition. *Proc Natl Acad Sci* **91**, 2012-2015.

[33] Andreasen N, O'Leary D, Cizadlo T, Arndt S, Rezai K, Watkins G, Ponto L, Hichwa R (1995) II PET studies of memory novel versus practiced free recall of word lists. *Neuroimage* **2**, 296-305.

[34] Squire L (1992) Memory and the hippocampus: a synthesis from findings with rats, monkeys, and humans. *Psychol Rev* **99**, 195-231.

[35] Pantel J, Schröder J, Jauss M, Essig M, Minakaran R, Schönknecht P, Schneider G, Schad L, Knopp M (1999) Topography of callosal atrophy reflects distribution of regional cerebral volume reduction in Alzheimer´s disease. *Psychiatry Res* **90**, 181-192.

[36] Thomann PA, Wüstenberg T, Pantel J, Essig M, Schröder J (2006) Structural changes of the corpus callosum in mild cognitive impairment and Alzheimer´s disease. *Dement Geriatr Cogn Disord* **21**, 215-220.

[37] Cabeza R (2002) Hemispheric asymmetry reduction in older adults: the HAROLD model. *Psychol Aging* **17**, 85-100.

[38] Schmahmann JD, Sherman JC (1998) The cerebellar cognitive affective syndrome. *Brain* **121**, 561-579.

[39] Tavano A, Grasso R, Gagliardi C, Triulzi F, Bresolin N, Fabbro F, Borgatti R (2007) Disorders of cognitive and affective development in cerebellar malformations. *Brain* **130**, 2646-2660.

[40] Flicker C, Ferris SH, Reisberg B (1991) Mild cognitive impairment in the elderly: predictors of dementia. *Neurology* **41**, 1006-1009.

[41] Winblad B, Palmer K, Kivipelto M, Jelic V, Fratiglioni L, Wahlund LO, Nordberg A, Backman L, Albert M, Almkvist O, Arai H, Basun H, Blennow K, de Leon M, DeCarli C, Erkinjuntti T, Giacobini E, Graff C, Hardy J, Jack C, Jorm A, Ritchie K, van Duijn C, Visser P, Petersen RC (2004) Mild cognitive impairment – beyond controversies, towards a consensus: report of the international working group on mild cognitive impairment. *J Intern Med* **256**, 240-246.

This page intentionally left blank

Patterns of Cortical Thickness in Pathologically-Confirmed Typical and Atypical Alzheimer's Disease

Manja Lehmann[a,*], Jonathan D. Rohrer[a], Matthew J. Clarkson[a,b], Gerard R. Ridgway[a], Rachael I. Scahill[a], Marc Modat[b], Jason D. Warren[a], Sebastien Ourselin[a,b], Josephine Barnes[a], Martin N. Rossor[a] and Nick C. Fox[a]

[a]*Dementia Research Centre, UCL Institute of Neurology, Queen Square, London, UK*
[b]*Centre for Medical Image Computing, University College London, Gower Street, London, UK*

Abstract. Alzheimer's disease (AD) can be difficult to differentiate clinically from other forms of dementia, such as frontotemporal lobar degeneration (FTLD), due to overlapping symptoms. Research studies often base their diagnostic inclusion criteria on clinical rather than pathological data which may mean some subjects are misdiagnosed and misclassified. Recently, methods measuring cortical thickness using magnetic resonance imaging (MRI) have been suggested to be effective in differentiating between clinically-defined AD and frontotemporal dementia (FTD) in addition to showing disease-related patterns of atrophy. In this study, cortical thickness was measured in 28 pathologically-confirmed AD patients, of which 11 had a typical amnestic presentation and 17 an atypical presentation during life, 23 pathologically-confirmed FTLD subjects, and 25 healthy controls. Patients with AD pathology, irrespective of clinical diagnosis, showed reduced cortical thickness bilaterally in the medial temporal lobe, posterior cingulate gyrus, precuneus, posterior parietal lobe, and frontal pole compared with controls. Lower cortical thickness in the posterior cingulate gyrus, parietal lobe and frontal pole was shown to be suggestive of AD pathology in patients with behavioural or language deficits. In contrast, lower cortical thickness in the anterior temporal lobe and frontal lobe is indicative of the presence of FTLD pathology in patients with a clinical presentation of FTD. Reduced cortical thickness in the posterior cingulate gyrus is characteristic of AD pathology in patients with typical and atypical clinical presentations of AD, and may assist a clinical distinction of AD pathology from FTLD pathology.

Keywords: Alzheimer's disease, cortical thickness, pathology, magnetic resonance imaging, FreeSurfer, Frontotemporal lobar degeneration

INTRODUCTION

Alzheimer's disease (AD) is characterised by the presence of extracellular amyloid plaques and intra-neuronal neurofibrillary tangles [1]. One of the effects of this pathology is tissue loss or atrophy which is initially localised to temporal lobes and subsequently spreads to the cortex. Such macroscopic atrophy can be visualised using magnetic resonance imaging (MRI). There are now a large number of studies demonstrating reduced volumes of various structures of the temporal lobe including hippocampus, entorhinal cortex, amygdala and parahippocampus [2, 3], as well as cingulate gyrus [4] and whole brain [5]. Furthermore, volume loss is reflected in expansion of the lateral ventricles in

---

*Correspondence to: Manja Lehmann, UCL Institute of Neurology, Box 16 National Hospital for Neurology and Neurosurgery, Queen Square, London WC1N 3BG, UK. Tel.: +44 207 837 3611; Fax: +44 207 676 2066; E-mail: lehmann@drc.ion.ucl.ac.uk.

individuals with AD compared with healthy controls [5].

Typically, patients with AD pathology present with memory deficits which gradually progress to involve multiple cognitive domains [6]. However, an increasing number of studies stress the importance of 'atypical' forms of AD, i.e. dementia in which the underlying pathology is AD, but in which memory is not the primary deficit [7]. Some patients with AD pathology may present with visuospatial and visuoperceptual problems and are diagnosed with posterior cortical atrophy (PCA) [8]; whilst others present with marked behavioural features (so called 'frontal-variant AD') [9]; yet others have a predominantly language presentation which often has features of logopenic progressive aphasia (LPA) [10]. These atypical behavioural and language presentations of AD can be difficult to distinguish from patients with Frontotemporal lobar degeneration (FTLD) pathology.

FTLD, although less prevalent overall, is almost as common as AD in patients under the age of 65 years [11, 12]. It is characterized by the presence of non-AD histopathology, most commonly either tau-positive inclusions or ubiquitin-positive, TDP-43-positive inclusions [13]. Clinically, patients with underlying AD and FTLD pathology may present with overlapping symptoms. Patients with underlying FTLD pathology may also present with a range of different clinical symptoms. The clinical heterogeneity of FTLD is enshrined in diagnostic criteria which explicitly describe different clinical subtypes or variants. Three main clinical syndromes are distinguished: behavioural variant frontotemporal dementia (bvFTD), semantic dementia (SD), and progressive non-fluent aphasia (PNFA); the latter two are often referred to as primary progressive aphasia (PPA) [14].

Recent work has included the assessment of cortical thickness as a marker of degenerative disease. Automated *in vivo* techniques have been developed to estimate cortical thickness on MRI [15–18]. These methods aim to identify differences in the width of the cortical grey matter on the surface of the brain and, unlike the relatively laborious region-of-interest approach, they have the advantage of being more automated, improving reproducibility and greatly reducing operator time. Vertex-wise statistical analysis allows one to derive local patterns of significant atrophy without requiring hypothesized regions of interest [19]. A number of studies have shown a reduction in cortical thickness in individuals with AD compared with controls [16, 18], as well as in mild cognitive impair-

ment (MCI) subjects [20]. A study conducted by Du et al. showed cortical thinning in bilateral frontal, parietal, temporal and occipital regions in AD patients compared with controls, and thinner cortex in bilateral frontal and temporal regions in behavioural variant FTLD patients [21].

These patterns of atrophy may aid diagnosis – *in vivo* an atrophy 'signature' in life may predict the underlying pathology [22]. In many research studies, however, autopsy confirmation is lacking and 'clinically diagnosed' patients are included. Clinical prediction of histopathology is inevitably imperfect; more importantly there is a risk of circularity. Clinically diagnosed subjects reflect 'typical' presentations of these diseases as the purpose of clinical criteria is to describe the most typical presentations to reduce misdiagnosis. Furthermore, future disease-modifying treatments are likely to target specific pathologies. It is therefore important to understand atrophy patterns associated with different pathologies rather than clinical phenotypes.

We investigated atrophy patterns in patients with pathological confirmation including atypical and typical clinical presentations of AD and FTLD. We wished to incorporate non-amnestic presentations of AD including language and behavioural presentations which are more likely to overlap with FTLD in terms of atrophy. The aim of this study was to assess the commonality of cortical thickness patterns between patients with AD pathology who presented with either typical amnestic deficits or atypical non-amnestic deficits during life. We further investigated patients clinically diagnosed as FTD to assess whether there were differences in cortical atrophy patterns between those who were subsequently found to have AD pathology and those with FTLD pathology.

MATERIALS AND METHODS

Subjects

We initially selected 62 patients from a database of pathologically-confirmed cases: 32 individuals with a pathological diagnosis of AD and 30 subjects with pathologically-confirmed FTLD who had undergone volumetric MR imaging as part of their diagnostic work-up. Twenty-five healthy controls that had undergone MRI assessment were also included. After image processing, 11 subjects were excluded (see below). The study therefore included 28 AD patients, 23 with FTLD, and 25 controls: the demographics of the 76

Table 1
Subject demographics

	N	Gender[†NS]	Age in years at scan[± NS]	MMSE at scan[±*¥]	Disease duration at scan [± NS]	Time to death from scan[± NS†]	Scanner			
		% male	mean (SD)	mean (SD)	mean (SD)	mean (SD)	a	b	c	d
Controls	25	68%	64.2 (9.4)	29.3 (0.9)	–	–	6	15	0	4
Typical AD	11	73%	68.0 (10.5)	14.4 (7.0)	3.6 (2.3)	3.8 (2.7)	4	7	0	0
Atypical AD	17	53%	59.2 (6.5)	17.7 (6.9)	3.7 (1.5)	4.7 (1.7)	0	14	3	0
PPA	9	67%	58.6 (6.9)	16.6 (7.1)	3.8 (1.2)	3.5 (1.3)	0	7	2	0
PCA	6	33%	60.2 (7.5)	22.2 (4.3)	3.4 (2.2)	6.0 (0.9)	0	5	1	0
bvFTD	2	50%	59.0 (1.4)	9.5 (0.7)	4.4 (1.0)	6.6	0	2	0	0
FTLD	23	57%	62.5 (10.1)	23.4 (5.6)	4.3 (2.1)	6.0 (3.4)	0	18	2	3
SD	11	55%	65.9 (6.0)	22.2 (5.6)	4.3 (2.4)	8.0 (3.0)	0	7	1	3
bvFTD	8	50%	58.3 (14.2)	22.7 (5.1)	4.3 (2.3)	3.6 (2.3)	0	7	1	0
PNFA	4	75%	62.8 (6.9)	27.7 (1.2)	4.4 (0.7)	4.0 (2.6)	0	4	0	0

[†] Fisher's Exact test;[±] ANOVA; [*]$p < 0.001$; [†]available in 10 typical AD; 13 atypical AD (7PPA, 5 PCA, 1 bvFTD); 21 FTLD (11SD, 7 bvFTD, 3 bvFTD); [¥]available in 12 controls; all typical and atypical AD; 20 FTLD (10 SD, 7 bvFTD, 3 PNFA); a, b, c, d – different 1.5 T GE scanners; NS – not significant.

subjects included are summarized in Table 1. All clinically affected subjects had attended the Specialist Cognitive Disorders Clinic at the National Hospital for Neurology and Neurosurgery, London, UK. Informed consent was obtained from all subjects and the study had local ethics committee approval. Some of these patients have been included in previous imaging studies [23–25]. All patients underwent comprehensive clinical assessment which included the Mini-Mental State Examination (MMSE) [26]. We excluded subjects with mixed AD and dementia with Lewy body pathology.

Pathologically-confirmed AD subjects were divided into 'typical' and 'atypical' AD patients based on their clinical ante-mortem presentation. Typical AD patients were defined as those who presented with amnestic deficits during life, whereas atypical patients presented predominantly with language, behavioural or visuop-
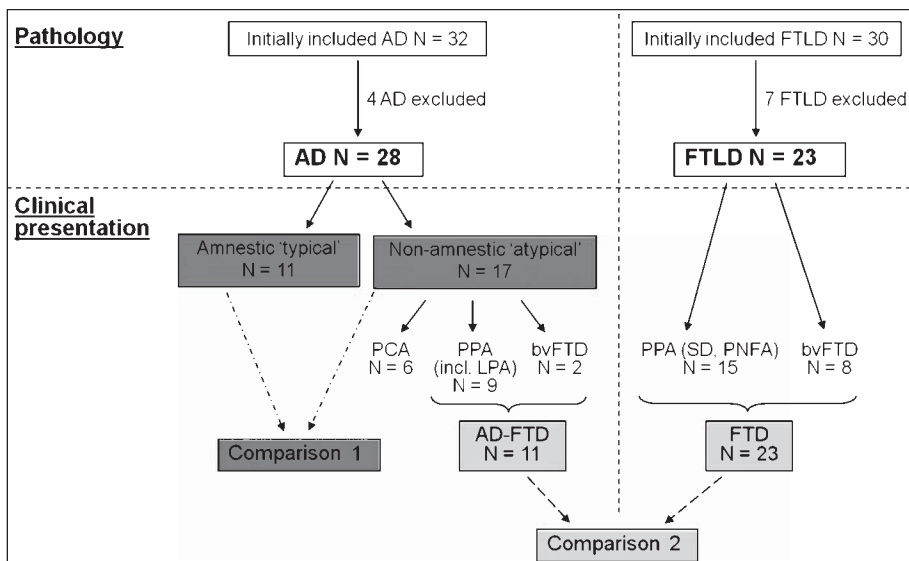
Fig. 1. Overview groups and comparisons. Comparison 1 assessed differences in cortical thickness between patients with underlying AD pathology but different clinical presentations ('typical' amnestic vs. 'atypical' non-amnestic), whereas comparison 2 assessed differences in cortical thickness between patients with a clinic presentation of FTD but different underlying pathologies, i.e. AD pathology (AD-FTD) vs. FTLD pathology (FTD). PPA – primary progressive aphasia; LPA – logopenic progressive aphasia; PCA – posterior cortical atrophy; SD – semantic dementia; PNFA – progressive non-fluent aphasia; bvFTD – behavioural variant frontotemporal dementia.

erceptual and visuospatial deficits (Fig. 1). Of the 11 typical AD subjects, 10 had post-mortem and 1 had brain biopsy confirmation. All of these AD patients had been diagnosed ante-mortem with AD according to NINCDS-ADRDA criteria [6]. Of the 17 atypical AD subjects, 12 had post-mortem confirmation and 5 had biopsy confirmation. This group consisted of 9 patients who had a clinical diagnosis of PPA, 6 patients with PCA, and 2 patients with bvFTD. The 11 patients with PPA and bvFTD are collectively referred to as AD-FTD (see Fig. 1). Of the 23 pathologically-confirmed FTLD subjects, 20 had post-mortem confirmation and 3 had brain biopsy. The FTLD group comprised 10 tau-positive patients (5 bvFTD, 4 PNFA, 1 atypical SD) and 13 tau-negative, ubiquitin-positive patients (10 SD and 3 bvFTD). All FTLD subjects had been clinically-diagnosed with FTD [14].

MRI acquisition

T1-weighted volumetric MR scans were performed on 1.5 Tesla Signa units (General Electric, Milwaukee) using a volumetric spoiled gradient recalled (SPGR) sequence with 1.5 mm thick slices covering the head (except one FTLD subject with 1.7 mm thick slices).

Image processing

Cortical thickness measurements were made using the freely-available software FreeSurfer, version 4.0.3. (http://surfer.nmr.mgh.harvard.edu/). The detailed procedure for the surface construction has been described and validated in previous publications [15, 27]. Cortical thickness was smoothed with a 20 mm full-width at half height Gaussian kernel to reduce local variations in the measurements for further analysis. Two modifications to the standard FreeSurfer processing stream were undertaken: a locally-generated brain mask was used for skull stripping and FreeSurfer ventricular segmentations were added to the white matter mask to improve cortical segmentation [28].

All images were visually inspected and on average edited and re-run three times as suggested (http://surfer.nmr.mgh.harvard.edu/fswiki/FsTutorial/TroubleshootingData). At this stage, as mentioned above, four individuals with AD and seven with FTLD were excluded due to poor image quality causing poor segmentations.

Statistical analysis

Regional cortical thickness variations between the patient groups and the control group were assessed using a vertex-by-vertex general linear model (GLM), performed with the SurfStat software (http://www.stat.uchicago.edu/~worsley/surfstat/). Cortical thickness (C) was modelled as a function of group, controlling for age, gender and scanner by their inclusion as covariates. We used separate models for the two comparisons of interest.

Comparison 1 assessed cortical thickness in typical and atypical AD, and was modelled $C = \beta_1$ (controls) $+ \beta_2$ (typical AD) $+ \beta_3$ (atypical AD) $+ \beta_4$ age $+ \beta_5$ gender $+ \beta_6$ scanner $+ \varepsilon$ (where ε is error), contrasting β_1 vs. β_2 (controls vs. typical AD), β_1 vs. β_3 (controls vs. atypical AD), and β_2 vs. β_3 (typical AD vs. atypical AD; see Fig. 1). Contrasts were calculated using two-tailed t-tests.

Comparison 2 assessed cortical thickness in AD-FTD (including the clinically diagnosed PPA and bvFTD patients with AD pathology) vs. FTLD, and was modelled $C = \beta_1$ (controls) $+ \beta_2$ (AD-FTD) $+ \beta_3$ (FTLD) $+ \beta_4$ age $+ \beta_5$ gender $+ \beta_6$ scanner $+ \varepsilon$, contrasting β_1 vs. β_2 (controls vs. AD-FTD), β_1 vs. β_3 (controls vs. FTLD), and β_2 vs. β_3 (AD-FTD vs. FTLD, see Fig. 1). Maps were produced showing percentage differences in average cortical thickness and statistically significant differences with false discovery rate (FDR) correction at $p < 0.05$ [29]. Intersection maps highlight regions which two patient groups compared with controls had in common.

Support vector machine

A linear support vector machine (SVM) was used to classify subjects [30, 31], implemented with LIBSVM version 2.89 [32] under MATLAB (version 7.2.0). The same scans as in the vertex-wise statistical comparisons described above were used for this analysis. The comparison of interest was the classification of the FTLD and AD-FTD groups (which relates to comparison 2 described above, see Fig. 1), i.e. assessing how well patients with a clinical diagnosis of FTD who were subsequently found to have either AD or FTLD pathology can be classified into their respective group.

Subjects were represented as points in an n-dimensional space, where $n = 299881$ is the total number of vertices in the cortical surface (including left and right hemispheres, but excluding the medial wall). SVMs identify an optimal separating hyperplane

in this space such that subjects from each group lie as far as possible from the hyperplane, on opposite sides. Once the hyperplane has been defined scores can be generated by projecting the points onto the normal of the hyperplane; the direction of the normal can be visualised as an image, showing the relative weights and signs of vertices' contributions to the classifier scores. We use the C-SVM formulation, employing a two-level nested cross-validation to optimize the misclassification penalty parameter C using a leave-one-out procedure within the main leave-one-out loop [33]. This ensures an unbiased estimation of generalisation accuracy by leaving each scan in turn entirely out of the training procedure.

RESULTS

Subjects

No significant differences across groups were found for gender, disease duration and time to death (Table 1). Age difference across all groups was not significant, however, the atypical AD group was significantly younger than controls ($p < 0.05$). MMSE scores across patient groups differed significantly ($p < 0.05$) which was mainly driven by the high MMSE scores in the FTLD group which differed from the typical and atypical AD groups ($p < 0.001$ and $p < 0.01$ respectively).

Comparison 1: typical vs. atypical AD

Compared with controls, typical AD showed lower thickness across the cortex, with the most prominent reduction bilaterally in the medial and posterior temporal regions, posterior cingulate gyrus, and frontal lobe regions (Fig. 2A). The atypical AD group showed reduced cortical thickness bilaterally in the medial temporal lobe, posterior cingulate gyrus, precuneus, posterior parietal lobe, and frontal pole (Fig. 2B). The intersection map shows areas of reduced cortical thickness common to both typical and atypical AD compared with controls (Fig. 2C) bilaterally in the medial temporal lobe, posterior cingulate gyrus, precuneus, posterior parietal lobe, and frontal pole.

The direct comparison of typical and atypical AD showed lower cortical thickness predominantly in the left posterior temporal lobe and left occipital lobe in the typical AD group compared with atypical AD (Fig. 3A). However, this difference was reduced when including disease duration as covariate, and disappeared completely when correcting for MMSE. No regions were found to be significantly thinner in the atypical AD group compared with typical AD. However, the percent difference maps indicate trends towards lower cortical thickness bilaterally in the precuneus and superior parietal lobe in the atypical compared with typical AD group (Fig. 3B).

Comparison 2: AD-FTD vs. FTLD

Compared with controls, AD-FTD patients showed lower cortical thickness in the left superior temporal lobe, as well as bilaterally in the posterior cingulate gyrus, precuneus, left posterior parietal lobe and bilateral frontal pole (Fig. 4A). The FTLD group showed
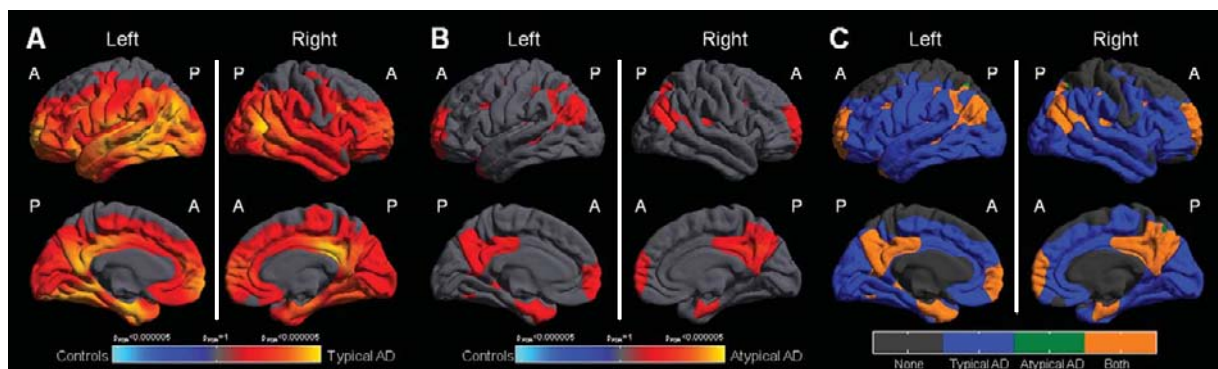
Fig. 2. Reduced cortical thickness in typical and atypical AD compared with controls. The figure shows differences in cortical thickness between **A)** typical AD and controls, and **B)** atypical AD and controls. The colour scale represents FDR-corrected p values thresholded at a 0.05 significance level. Red and yellow represent lower cortical thickness in the patient group, whereas blue represents lower cortical thickness in the control group. **C)** Intersection map showing regional differences in cortical thickness between typical AD and controls, and atypical AD and controls. Blue represents areas which are reduced in the typical AD group only, green represents regions which are reduced in atypical AD only, and orange shows areas which are reduced in both typical and atypical AD compared with controls.
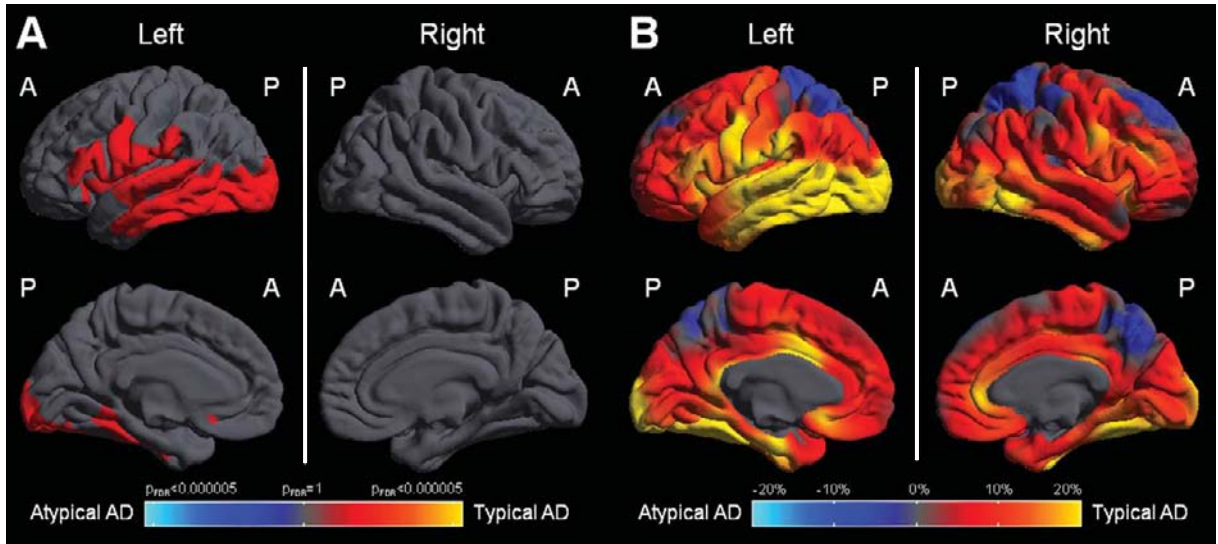
Fig. 3. Differences in cortical thickness between typical and atypical AD. Differences in cortical thickness between typical and atypical AD are shown as **A)** statistical difference map, and **B)** percent difference map. The colour scale of the statistical difference map represents FDR-corrected p values thresholded at a 0.05 significance level whereas the colour bar for percent difference represents magnitude of cortical thickness group difference expressed as a percentage of mean thickness across both groups (adjusted for age, gender and scanner). Red and yellow represent lower cortical thickness in the typical AD group, whereas blue represents lower cortical thickness in the atypical AD group.
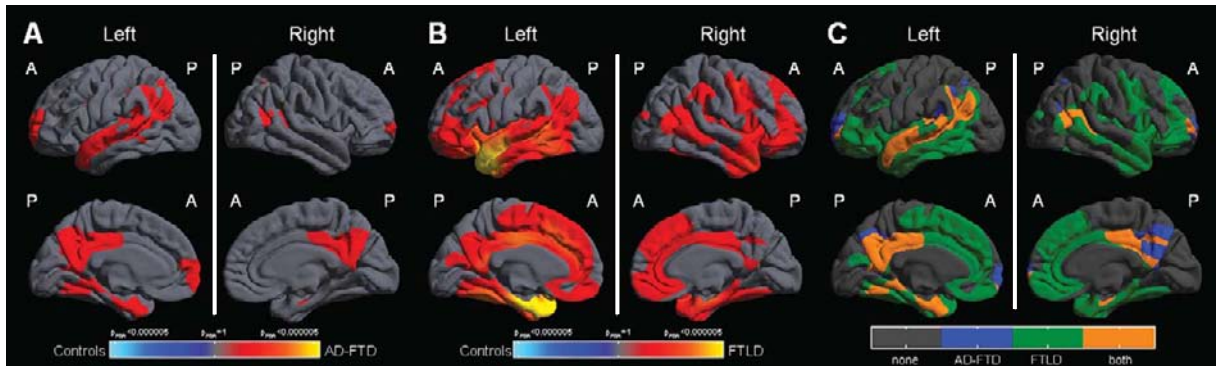
Fig. 4. Reduced cortical thickness in AD-FTD and FTLD compared with controls. Differences in cortical thickness are shown between **A)** AD-FTD and controls, and **B)** FTLD and controls. The colour scale represents FDR-corrected p values thresholded at a 0.05 significance level. Red and yellow represent lower cortical thickness in the patient group, whereas blue represents lower cortical thickness in the controls. **C)** Intersection map showing regional differences in cortical thickness between AD-FTD and controls, and FTLD and controls. Blue represents areas which are reduced in the AD-FTD group only, green represents regions which are reduced in FTLD only, and orange shows areas which are reduced in both AD-FTD and FTLD compared with controls.

widespread thinning with the most prominent reductions found bilaterally in the anterior temporal lobe (Fig. 4B). The intersection map reveals regions in which both AD-FTD and FTLD show reduced cortical thickness compared with controls which include the bilateral posterior cingulate gyrus, left superior temporal lobe and left medial temporal lobe (Fig. 4C).

Differences in cortical thickness between AD-FTD and FTLD in a direct comparison did not reach statistical significance after FDR correction. However, percent difference maps show tendencies of reduced thickness bilaterally in the anterior temporal lobe and frontal lobe regions in the FTLD group compared with AD-FTD, whereas the AD-FTD group showed lower cortical thickness in left posterior pari-
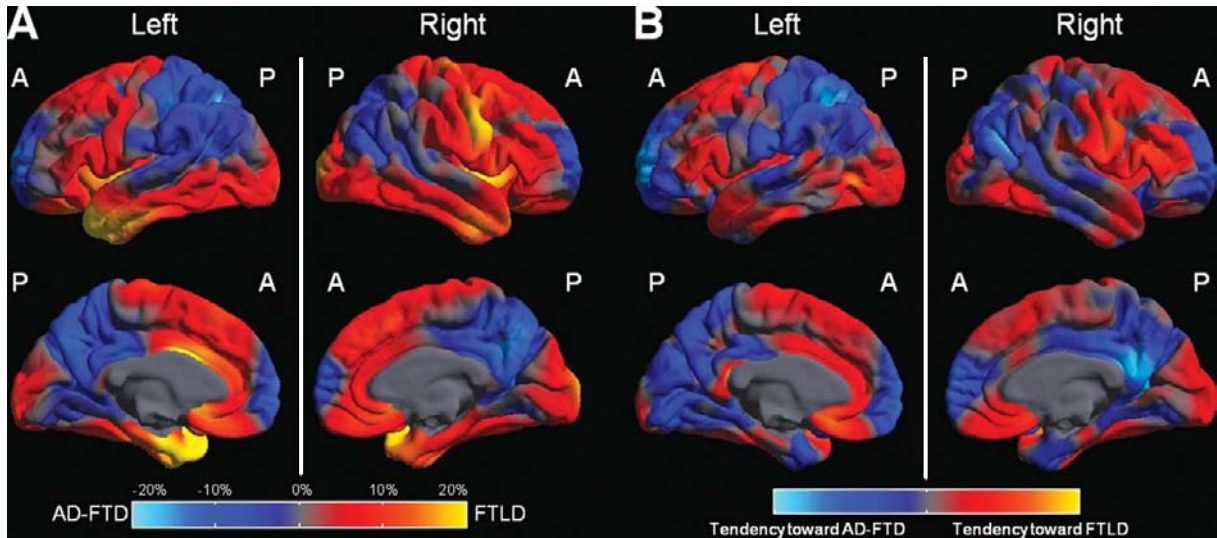
Fig. 5. Differences in cortical thickness between AD-FTD and FTLD. **A)** Regional differences in cortical thickness between AD-FTD and FTLD shown as percent difference map. The colour bar represents magnitude of cortical thickness group difference expressed as a percentage of mean thickness of the two groups. Red and yellow represent lower cortical thickness in the FTLD group, whereas blue represents lower cortical thickness in the AD-FTD group. **B)** Classification map showing regions that were most influential in making a classification between AD-FTD and FTLD. Red represents areas where low cortical thickness indicates FTLD, whereas blue shows areas where lower cortical thickness indicates AD-FTD.

etal regions, bilaterally in the precuneus, posterior cingulate gyrus and frontal pole compared with FTLD (Fig. 5A).

The classification analysis produced a classification accuracy of 79.4% with 95% confidence intervals [62.1%, 91.3%]. Of the AD-FTD patients 54.5% [23.4%, 83.3%] were correctly classified (sensitivity), whereas 91.3% [72.0%, 98.9%] of the FTLD patients were correctly classified (specificity). The area under the receiver operating characteristic (ROC) curve is 0.87 (Fig. 6). Areas in which reduced cortical thickness contributed most to the classification of AD-FTD were shown bilaterally in the posterior cingulate gyrus, posterior parietal lobe, precuneus, medial temporal lobe, and frontal pole (Fig. 5B). In contrast, regions which contributed most towards a classification of FTLD were shown bilaterally in frontal lobe regions and the lateral temporal lobe.

DISCUSSION

This study describes patterns of cortical thinning in pathologically-confirmed AD and FTLD patients. Patients with AD pathology and a typical amnestic presentation during life showed reduced cortical thickness bilaterally in the medial temporal lobe, posterior cin-
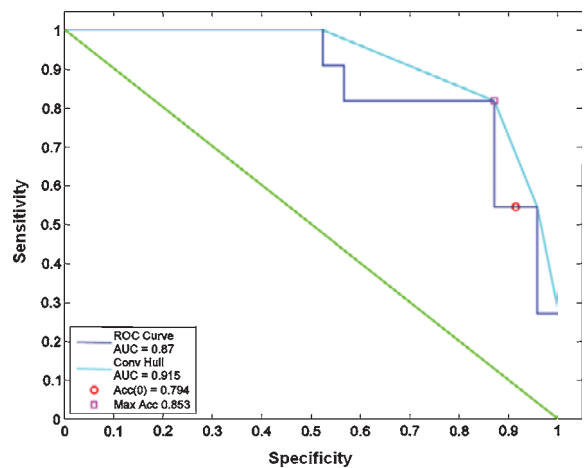
Fig. 6. ROC curve for comparison of AD-FTD vs. FTLD classification. Shown is the tradeoff between sensitivity and specificity. The receiver operating characteristic (ROC) curve is plotted by varying the decision threshold. The low sensitivity reported in the main results arises from unbalanced group numbers, which allow high accuracy from high specificity. The ROC curve shows that relatively high sensitivity and specificity are simultaneously achievable if the threshold is altered. AUC – area under the curve, acc – accuracy.

gulate gyrus, precuneus, posterior parietal regions, and frontal lobe. The association of an amnestic presentation of AD with medial temporal lobe atrophy was

expected [2, 21, 34]. The finding of prominent thinning in the posterior cingulate cortex and precuneus concurs with increasing recognition that atrophy as well as hypometabolism in these regions is characteristic of AD [24, 35]. However, frontal pole involvement was less expected.

A similar pattern of cortical thinning, compared with controls, was found in patients with AD pathology who had a different ante-mortem clinical diagnosis; however, thinning was less widespread, perhaps reflecting the mix of 'focal' presentations of AD in this group. A direct comparison between the two patient groups revealed greater loss in left posterior temporal lobe and left occipital lobe in the typical AD group compared with atypical AD. The fact that this difference is diminished after correcting for disease duration and MMSE may suggest that these differences simply reflect severity differences. However, mean disease duration was almost identical between groups. Disease progression in typical and atypical forms of AD may vary which means that disease duration is not a very accurate marker of disease severity. MMSE is also an imperfect indicator of disease severity in dementias with different cognitive profiles, and the high mean MMSE in atypical AD subjects is largely driven by the PCA subjects included.

The intersection analysis illustrates the commonality of cortical thinning in typical and atypical AD. Cortical thickness was reduced in both the typical and atypical AD groups, compared with controls, bilaterally in the medial temporal lobe, posterior cingulate gyrus, precuneus, posterior parietal lobe and frontal pole. Cortical thinning in these regions appears to indicate the presence of AD pathology irrespective of clinical presentation. Cortical thinning in the medial temporal lobe in typical and atypical AD is consistent with the presence of memory deficits at the time of scan in both groups. Our general AD-specific findings are in accordance with previous imaging studies which investigated differences in cortical thickness [18, 21] and grey matter volume using voxel-based morphometry [36, 37] in typical forms of AD.

A strong involvement of the posterior cingulate gyrus in AD has been shown in a number of structural [4, 24, 36, 38] and functional imaging studies [39]. Most functional imaging studies (PET, SPECT and fMRI) have reported reduced activity in this region in early stages of the disease [40–42]. The regions showing reduced cortical thickness in pathologically-confirmed AD patients in our study are consistent with those associated with the 'default mode' network [43].

Our finding adds to the growing number of studies suggesting that functional imaging findings are not as dissociated from atrophy as was once thought; temporal associations, however, remain unclear [44].

The involvement of the frontal lobe in AD, and more specifically of the prefrontal cortex and frontal pole, remains controversial. A number of studies have shown reduced cortical thickness [18, 21] and grey matter volumes [36, 37, 45] in this region. However, a number of studies have failed to show involvement of any frontal areas [for an overview see 46]. Our study with the advantage of pathology confirmation does support frontal pole atrophy in AD. There is always the theoretical possibility that this could be an artefact of the analysis technique, however, after careful visual inspection of this area in each subject we could not see any signal drop off or any kind of fault in the FreeSurfer surfaces which would explain reduced cortical thickness in this region.

The second subject group comparison revealed that patients with AD pathology and a clinical diagnosis of FTD during life (either behavioural or language variant) had, despite their atypical presentation, a thinner cortex in the medial temporal lobe, posterior parietal regions, posterior cingulate gyrus and frontal pole than patients with FTLD pathology. In contrast, patients with FTLD pathology showed reduced cortical thickness predominantly in anterior temporal and frontal lobe regions. The highly significant reduction in the anterior temporal lobe in the FTLD group is possibly driven by the high proportion of semantic dementia patients in this group who are known to have marked atrophy in this region [38, 47, 48]. The patterns of cortical thinning observed in the FTLD group are consistent with previous histopathological and volumetric MRI studies [46, 48–50].

Although differences in the direct comparison between AD-FTD and FTLD did not reach statistical significance, tendencies of cortical thinning as shown in the percent difference maps are consistent with the patterns observed in the control comparisons. Thinner cortex in the posterior cingulate gyrus, parietal lobe and frontal pole suggests the presence of AD pathology, whereas cortical thinning in the anterior temporal lobe and frontal lobe regions suggests the presence of FTLD pathology. Our classification algorithm showed that subjects could be correctly classified on the basis of the MRI scans alone in 79% of cases despite having had similar (FTD) clinical diagnoses in life. The ROC curve illustrates that although the original sensitivity is relatively low, this is probably driven by the

imbalance in subject numbers between the two groups. The high area under the curve reveals that the classifier performs well, and a more favourable balance of sensitivity and specificity could be obtained by altering the threshold. The pattern of cortical thinning shown to separate the two patient groups best was consistent with that observed in the direct comparison between AD-FTD and FTLD.

One strength of this study is that all AD and FTLD cases had pathological confirmation. This is particularly important considering that accuracies for the clinical diagnosis of AD can vary between 60-90% [51, 52]. Consequently, a number of individuals included in studies of AD and FTLD will inevitably have a different type of pathology. A post-mortem study further revealed 30% of patients diagnosed with a language subtype of FTLD (i.e. PNFA, SD) had AD pathology [53]. It is noteworthy, however, that the inclusion of only pathologically-confirmed cases inevitably limits subject numbers, reducing the power to detect differences between disease groups. Pathology confirmation was not obtained for the whole control group and it may be that some controls had a neurological condition but were asymptomatic. This is, however, unlikely and would only have reduced our ability to detect differences.

Another limitation is the variety in image acquisition which has been shown to affect thickness measures [54]. We therefore adjusted for scanner type in our statistical models. It should also be noted that there was an imbalance in scanner type between groups, with scanner A being present only in the control and typical AD group. However, excluding subjects imaged using scanner A from the analysis gave very similar results. Our groups were matched for disease duration, but not for disease severity as measured by MMSE. As expected, MMSE scores varied significantly between individual groups owing to the weighting of questions towards memory and orientation.

In summary, this study describes patterns of cortical thickness in patients with AD pathology but different clinical presentations. Common areas of lower cortical thickness were found in patients with AD pathology despite different clinical symptoms. These areas included the medial temporal lobe, posterior cingulate gyrus, precuneus, posterior parietal cortex and frontal pole. In contrast, lower cortical thickness in the anterior temporal lobe and frontal lobe regions is indicative of the presence of FTLD pathology in patients with a clinical presentation of FTD. Furthermore, patients with a frontal presentation during life and AD pathology at

post-mortem show lower cortical thickness in posterior regions than patients with FTLD pathology. These findings suggest that atrophy not only in the medial temporal lobe but also in the posterior cingulate gyrus might be indicative of the presence of AD pathology irrespective of clinical diagnosis. Assessing atrophy in this and other posterior regions might therefore aid the differential diagnosis between AD and FTD.

REFERENCES

[1] Braak H, Braak E (1991) Neuropathological staging of Alzheimer related changes. *Acta Neuropathol* **82**(4), 239-259.
[2] Teipel SJ, Pruessner JC, Faltraco F, Born C, Rocha-Unold M, Evans A, Moller HJ, Hampel H (2006) Comprehensive dissection of the medial temporal lobe in AD: measurement of hippocampus, amygdala, entorhinal, perirhinal and parahippocampal cortices using MRI. *J Neurol* **253**(6), 794-800.
[3] Du AT, Schuff N, Kramer JH, Ganzer S, Zhu XP, Jagust WJ, Miller BL, Reed BR, Mungas D, Yaffe K, Chui HC, Weiner MW (2004) Higher atrophy rate of entorhinal cortex than hippocampus in AD. *Neurology* **62**(3), 422-427.
[4] Jones BF, Barnes J, Uylings HBM, Fox NC, Frost C, Witter MP, Scheltens P (2006) Differential regional atrophy of the cingulate gyrus in Alzheimer disease: A volumetric MRI study. *Cereb Cortex* **16**(12), 1701-1708.
[5] Fox NC, Freeborough PA, Rossor MN (1996) Visualisation and quantification of rates of atrophy in Alzheimer's disease. *Lancet* **348**(9020), 94-97.
[6] McKhann G, Drachman D, Folstein M, Katzman R, Price D, Stadlan EM (1984) Clinical diagnosis of Alzheimer's disease: report of the NINCDS-ADRDA work group under the auspices of Department of Health and Human Services Task Force on Alzheimer's disease. *Neurology* **34**(7), 939-944.
[7] Galton CJ, Patterson K, Xuereb JH, Hodges JR (2000) Atypical and typical presentations of Alzheimer's disease: a

clinical, neuropsychological, neuroimaging and pathological study of 13 cases. *Brain* **123**, 484-498.

[8] Benson F, Davis J, Snyder BD (1988) Posterior cortical atrophy. *Arch Neurol* **45**, 789-793.

[9] Johnson JK, Head E, Kim R, Starr A, Cotman CW (1999) Clinical and pathological evidence for a frontal variant of Alzheimer disease. *Arch Neurol* **56**(10), 1233-1239.

[10] Gorno-Tempini ML, Brambati SM, Ginex V, Ogar J, Dronkers NF, Marcone A, Perani D, Garibotto V, Cappa SF, Miller BL (2008) The logopenic/phonological variant of primary progressive aphasia. *Neurology* **71**(16), 1227-1234.

[11] Harvey RJ, Skelton-Robinson M, Rossor MN (2003) The prevalence and causes of dementia in people under the age of 65 years. *J Neurol Neurosurg Psychiatry* **74**(9), 1206-1209.

[12] Ratnavalli E, Brayne C, Dawson K, Hodges JR (2002) The prevalence of frontotemporal dementia. *Neurology* **58**(11), 1615-1621.

[13] Cairns NJ, Bigio EH, Mackenzie IR, Neumann M, Lee VM, Hatanpaa KJ, White CL III, Schneider JA, Grinberg LT, Halliday G, Duyckaerts C, Lowe JS, Holm IE, Tolnay M, Okamoto K, Yokoo H, Murayama S, Woulfe J, Munoz DG, Dickson DW, Ince PG, Trojanowski JQ, Mann DM (2007) Neuropathologic diagnostic and nosologic criteria for frontotemporal lobar degeneration: consensus of the Consortium for Frontotemporal Lobar Degeneration. *Acta Neuropathol* **114**(1), 5-22.

[14] Neary D, Snowden JS, Gustafson L, Passant U, Stuss D, Black S, Freedman M, Kertesz A, Robert PH, Albert M, Boone K, Miller BL, Cummings J, Benson DF (1998) Frontotemporal lobar degeneration – a consensus on clinical diagnostic criteria. *Neurology* **51**(6), 1546-1554.

[15] Fischl B, Sereno MI, Dale AM (1999) Cortical surface-based analysis – II: Inflation, flattening, and a surface-based coordinate system. *Neuroimage* **9**(2), 195-207.

[16] Thompson PM, Mega MS, Woods RP, Zoumalan CI, Lindshield CJ, Blanton RE, Moussai J, Holmes CJ, Cummings JL, Toga AW (2001) Cortical change in Alzheimer's disease detected with a disease-specific population-based brain atlas. *Cereb Cortex* **11**(1), 1-16.

[17] MacDonald D, Kabani N, Avis D, Evans AC (2000) Automated 3-D extraction of inner and outer surfaces of cerebral cortex from MRI. *Neuroimage* **12**(3), 340-356.

[18] Lerch JP, Pruessner JC, Zijdenbos A, Hampel H, Teipel SJ, Evans AC (2005) Focal decline of cortical thickness in Alzheimer's disease identified by computational neuroanatomy. *Cereb Cortex* **15**(7), 995-1001.

[19] Worsley KJ, Taylor JE, Carbonell F, Chung ML, Duerden E, Bernhardt B, Lyttelton O, Boucher M, Evans AC (2009) SurfStat: A Matlab toolbox for the statistical analysis of univariate and multivariate surface and volumetric data using linear mixed effects models and random field theory. *Neuroimage* **47**(Supplementary 1), S102.

[20] Singh V, Chertkow H, Lerch JP, Evans AC, Dorr AE, Kabani NJ (2006) Spatial patterns of cortical thinning in mild cognitive impairment and Alzheimer's disease. *Brain* **129**, 2885-2893.

[21] Du AT, Schuff N, Kramer JH, Rosen HJ, Gorno-Tempini ML, Rankin K, Miller BL, Weiner MW (2007) Different regional patterns of cortical thinning in Alzheimer's disease and frontotemporal dementia. *Brain* **130**, 1159-1166.

[22] Likeman M, Anderson VM, Stevens JM, Waldman AD, Godbolt AK, Frost C, Rossor MN, Fox NC (2005) Visual assessment of atrophy on magnetic resonance imaging in the diagnosis of pathologically confirmed young-onset dementias. *Arch Neurol* **62**(9), 1410-1415.

[23] Kloppel S, Stonnington CM, Chu C, Draganski B, Scahill RI, Rohrer JD, Fox NC, Jack CR, Ashburner J, Frackowiak RS (2008) Automatic classification of MR scans in Alzheimer's disease. *Brain* **131**(Pt 3), 681-689.

[24] Barnes J, Godbolt AK, Frost C, Boyes RG, Jones BF, Scahill RI, Rossor MN, Fox NC (2007) Atrophy rates of the cingulate gyrus and hippocampus in AD and FTLD. *Neurobiol Aging* **28**(1), 20-28.

[25] Rohrer JD, Warren JD, Modat M, Ridgway GR, Douiri A, Rossor MN, Ourselin S, Fox NC (2009) Patterns of cortical thinning in the language variants of frontotemporal lobar degeneration. *Neurology* **72**(18), 1562-1569.

[26] Folstein MF, Folstein SE, Mchugh PR (1975) Mini-mental state – practical method for grading cognitive state of patients for clinician. *J Psychiatr Res* **12**(3), 189-198.

[27] Dale AM, Fischl B, Sereno MI (1999) Cortical surface-based analysis – I. Segmentation and surface reconstruction. *Neuroimage* **9**(2), 179-194.

[28] Lehmann M, Crutch SJ, Ridgway GR, Ridha BH, Barnes J, Warrington EK, Rossor MN, Fox NC (2009) Cortical thickness and voxel-based morphometry in posterior cortical atrophy and typical Alzheimer's disease. *Neurobiol Aging*, in press, doi:10.1016/j.neurobiolaging.2009.08.017.

[29] Genovese CR, Lazar NA, Nichols T (2002) Thresholding of statistical maps in functional neuroimaging using the false discovery rate. *Neuroimage* **15**(4), 870-878.

[30] Vapnik V (1995) *The nature of statistical learning theory*, Springer, New York.

[31] Vapnik V (1998) *Statistical learning theory*, John Wiley and Sons, New York.

[32] Chang CC, Lin CJ (2001) Training nu-support vector classifiers: Theory and algorithms. *Neural Comput* **13**(9), 2119-2147.

[33] Wilson SM, Ogar JM, Laluz V, Growdon M, Jang J, Glenn S, Miller BL, Weiner MW, Gorno-Tempini ML (2009) Automated MRI-based classification of primary progressive aphasia variants. *Neuroimage* **47**(4), 1558-1567.

[34] Ridha BH, Barnes J, Bartlett JW, Godbolt A, Pepple T, Rossor MN, Fox NC (2006) Tracking atrophy progression in familial Alzheimer's disease: a serial MRI study. *Lancet Neurol* **5**(10), 828-834.

[35] Nestor PJ, Caine D, Fryer TD, Clarke J, Hodges JR (2003) The topography of metabolic deficits in posterior cortical atrophy (the visual variant of Alzheimer's disease) with FDG-PET. *J Neurol Neurosurg Psychiatry* **74**(11), 1521-1529.

[36] Baron JC, Chetelat G, Desgranges B, Perchey G, Landeau B, De La Sayette V, Eustache F (2001) *In vivo* mapping of gray matter loss with voxel-based morphometry in mild Alzheimer's disease. *Neuroimage* **14**, 298-309.

[37] Busatto GE, Garrido GEJ, Almeida OP, Castro CC, Camargo CHP, Cid CG, Buchpiguel CA, Furuie S, Bottino CM (2003) A voxel-based morphometry study of temporal lobe gray matter reductions in Alzheimer's disease. *Neurobiol Aging* **24**(2), 221-231.

[38] Boxer AL, Rankin KP, Miller BL, Schuff N, Weiner M, Gorno-Tempini ML, Rosen HJ (2003) Cinguloparietal atrophy distinguishes Alzheimer disease from semantic dementia. *Arch Neurol* **60**(7), 949-956.

[39] Lustig C, Snyder AZ, Bhakta M, O'Brien KC, McAvoy M, Raichle ME, Morris JC, Buckner RL (2003) Functional deactivations: change with age and dementia of the Alzheimer type. *Proc Natl Acad Sci USA* **100**(24), 14504-14509.

[40] Johnson KA, Jones K, Holman BL, Becker JA, Spiers PA, Satlin A, Albert MS (1998) Preclinical prediction of Alzheimer's disease using SPECT. *Neurology* **50**(6), 1563-1571.

[41] Matsuda H (2001) Cerebral blood flow and metabolic abnormalities in Alzheimer's disease. *Ann Nucl Med* **15**(2), 85-92.

[42] Minoshima S, Giordani B, Berent S, Frey KA, Foster NL, Kuhl DE (1997) Metabolic reduction in the posterior cingulate cortex in very early Alzheimer's disease. *Ann Neurol* **42**(1), 85-94.

[43] Greicius MD, Srivastava G, Reiss AL, Menon V (2004) Default-mode network activity distinguishes Alzheimer's disease from healthy aging: evidence from functional MRI. *Proc Natl Acad Sci USA* **101**(13), 4637-4642.

[44] Villain N, Desgranges B, Viader F, De La Sayette V, Mezenge F, Landeau B, Baron JC, Eustache F, Chetelat G (2008) Relationships between hippocampal atrophy, white matter disruption, and gray matter hypometabolism in Alzheimer's disease. *J Neurosci* **28**(24), 6174-6181.

[45] Davatzikos C, Resnick SM, Wu X, Parmpi P, Clark CM (2008) Individual patient diagnosis of AD and FTD via high-dimensional pattern classification of MRI. *Neuroimage* **41**(4), 1220-1227.

[46] Whitwell JL, Jack CR Jr. (2005) Comparisons between Alzheimer disease, frontotemporal lobar degeneration, and normal aging with brain mapping. *Top Magn Reson Imaging* **16**, 409-425.

[47] Chan D, Fox N, Scahill R, Crum W, Whitwell J, Cipolotti L, Rossor MN (2001) Patterns of temporal lobe atrophy in semantic dementia and Alzheimer's disease. *J Neurol Neurosurg Psychiatry* 70(2), 276.

[48] Rosen HJ, Gorno-Tempini ML, Goldman WP, Perry RJ, Schuff N, Weiner M, Feiwell R, Kramer JH, Miller BL (2002) Patterns of brain atrophy in frontotemporal dementia and semantic dementia. *Neurology* **58**(2), 198-208.

[49] Broe M, Hodges JR, Schofield E, Shepherd CE, Kril JJ, Halliday GM (2003) Staging disease severity in pathologically confirmed cases of frontotemporal dementia. *Neurology* **60**(6), 1005-1011.

[50] Grossman M, McMillan C, Moore P, Ding LJ, Glossner G, Work M, Gee J (2004) What's in a name: voxel-based morphometric analyses of MRI and naming difficulty in Alzheimer's disease, frontotemporal dementia and corticobasal degeneration. *Brain* **127**, 628-649.

[51] Brayne C, Richardson K, Matthews FE, Fleming J, Hunter S, Xuereb JH, Paykel E, Mukaetova-Ladinska EB, Huppert FA, O'Sullivan A, Dening T (2009) Neuropathological correlates of dementia in over-80-year-old brain donors from the population-based Cambridge city over-75 s cohort (CC75C) study. *J Alzheimers Dis* **18**(3), 645-658.

[52] Jellinger KA (2006) Clinicopathological analysis of dementia disorders in the elderly–an update. *J Alzheimers Dis 9(3 Suppl)*, 61-70.

[53] Knibb JA, Xuereb JH, Patterson K, Hodges JR (2006) Clinical and pathological characterization of progressive aphasia. *Ann Neurol* **59**(1), 156-165.

[54] Han X, Jovicich J, Salat D, van der Kouwe A, Quinn B, Czanner S, Busa E, Pacheco J, Albert M, Killiany R, Maguire P, Rosas D, Makris N, Dale A, Dickerson B, Fischl B (2006) Reliability of MRI-derived measurements of human cerebral cortical thickness: The effects of field strength, scanner upgrade and manufacturer. *Neuroimage* **32**(1), 180-194.

This page intentionally left blank

Volumetry of the Olfactory Bulb and Tract: Relation to Medial Temporal Lobe Atrophy and to Cognitive Performance in MCI and AD

Philipp A. Thomann[a,b,*], Vasco Dos Santos[b], Torsten Wüstenberg[c], Ulrich Seidl[b], Elmar Kaiser[b], Pablo Toro[b], Marco Essig[d] and Johannes Schröder[b]

[a]*Structural Neuroimaging Group, Center of Psychosocial Medicine, Department of General Psychiatry, University of Heidelberg, Heidelberg, Germany*
[b]*Section of Geriatric Psychiatry, University of Heidelberg, Heidelberg, Germany*
[c]*Department of Psychiatry and Psychotherapy, Charité Universitätsmedizin, Berlin, Campus Mitte, Germany*
[d]*German Cancer Research Center, Heidelberg, Germany*

Abstract. Neuropathological research consistently revealed that the olfactory bulb and tract (OBT) is subjected to degenerative processes in Alzheimer's disease (AD). In the present study, we assessed OBT volumes in individuals with mild cognitive impairment (MCI), in patients with probable AD, and in healthy comparison subjects using high-resolution magnetic resonance imaging. In both MCI and AD patients OBT volumes were significantly lower compared to controls with atrophy being most prominent in the AD group. In the patient group, lower mean OBT volumes were associated with a decreased gray matter density in the MTL bilaterally. Further, OBT volumes in patients were significantly correlated with cognitive performance. Our findings suggest the OBT volume as a potentially useful marker of AD and MCI related neurodegeneration.

INTRODUCTION

The term 'mild cognitive impairment' refers to cognitive deficits in the elderly which exceed age-related cognitive decline but do not fulfill criteria of dementia. Affected subjects are assumed to be at higher risk for development of dementia, particularly of Alzheimer's disease (AD) as the most common cause of dementia beyond the age of 65 years.

Neuropathologically, AD is characterized by neuronal loss and deposition of amyloid plaques and neurofibrillary tangles (NFT) in the cerebral cortex. As demonstrated in post-mortem studies, this destructive process generally follows a specific regional pattern, with the substructures of the medial temporal lobe (MTL) to be the earliest affected, even before the onset of any clinical symptoms [1, 2].

There is increasing evidence that the olfactory bulb and tract (OBT) is – besides the MTL – a primary focus of AD typical histopathological changes [3–7]. The olfactory bulb is the main relay station in the olfactory pathways. It is located on the cribriform plate of the ethmoid and beneath the inferior surface of the frontal lobe. The olfactory tract constitutes the caudal outflow pathway of the olfactory bulb.

Structural magnetic resonance imaging (MRI) enables us to study morphological brain changes

*Correspondence to: PD Dr. med. Philipp A. Thomann, Structural Neuroimaging Group, Center of Psychosocial Medicine, Department of General Psychiatry, University of Heidelberg, Voßstr. 4, 69115 Heidelberg, Germany. Tel.: +49 6221 56 38091; Fax: +49 6221 56 1742; E-mail: philipp.thomann@med.uni-heidelberg.de

in-vivo. While significant atrophy of the MTL in AD and, to a lower extent, in mild cognitive impairment, is a well established finding [8–12], potential alterations of the OBT have so far only scarcely been addressed, although this structure can be reliably ascertained on appropriate MR images [13–17]. In a first MRI study of our own group, manually determined OBT volumes were significantly reduced in AD patients when compared to healthy comparison subjects [18], a finding likely reflecting the neurodegenerative changes described above. Since these alterations appear to be a feature of incipient or even preclinical AD, the purpose of the present study was to examine whether OBT atrophy can already be detected in subjects with mild cognitive impairment and thus might have potential value as a new surrogate marker in AD. In a second step, we tested for the association of OBT atrophy with morphological changes in other cerebral sites by using voxel based morphometry (VBM), an unbiased and almost fully automated imaging technique that is not restricted to predefined specific regions but allows examining the entire brain. Given the anatomical and functional connectivity between the OBT and the MTL, and their involvement early in the course of the disease, we hypothesized that there might be correlations between atrophic changes in the OBT and the MTL in mild cognitive impairment and AD.

MATERIALS AND METHODS

Patients and control subjects

This analysis includes data from 86 individuals consecutively recruited at the Section of Geriatric Psychiatry, University of Heidelberg, Germany, between 2003 and 2004: Twenty-nine patients with mild cognitive impairment defined according to the concept of aging-associated cognitive decline (AACD) [19], 27 patients with probable AD (NINCDS-ADRDA criteria) [20], and 30 healthy controls. The AACD concept considers decline in a broad potential range of cognitive domains, namely memory and learning, attention and concentration, abstract thinking, language, and visuospatial functioning. Subjects with AACD were identified according to the following criteria:

(i) Performance of at least 1 standard deviation below the age-adjusted norm on a standardized test of cognition, involving at least one of the aforementioned domains

(ii) Exclusion of any medical, neurological or psychiatric disorder that could lead to cognitive deterioration as determined by history and/or clinical examination
(iii) Normal activities of daily living
(iv) Exclusion of dementia.

Particular care was taken to exclude any subject with ICD 10 mild cognitive disorder which refers to cognitive changes secondary to cerebral disorders other than AD. This was done by thorough clinical and neuropsychological investigation, MRI, and if clinically necessary, CSF analyses (including tau and phospho-tau concentrations).

All investigations were approved by the local Institutional Review Board. Depending on the level of cognitive impairment, written informed consent was obtained from either participants or caregivers after the planned procedures had been fully explained by a geriatric psychiatrist who was not involved in the study.

Clinical evaluation

The clinical evaluation of all subjects included ascertainment of personal and family history as well as physical, neurological and neuropsychological examination. Global cognitive deficits were assessed using the Mini Mental State Examination (MMSE) [21]. Cognitive performance was investigated with the German version of a standardized extensive neuropsychological test battery (CERAD) [22].

Magnetic resonance imaging

The MRI-data were obtained at the German Cancer Research Center with a 1.5-T Magnetom Symphony MR scanner (Siemens Medical Solutions, Erlangen, Germany). To exclude secondary causes of dementia and ischemic changes a 2D T2-weighted Fast-Spin Echo ($TR = 4500$ ms, $TE = 90$ ms) sequence was performed in axial orientation. For structural analysis, a T1-weighted 3D magnetization prepared rapid gradient echo (MP-RAGE) sequence was performed with the following parameters: 126 coronar slices, image matrix $= 256 \times 256$, voxel size $= 0.98$ mm $\times 0.98$ mm $\times 1.8$ mm, $TR = 10$ msec, $TE = 4$ msec.

Manual segmentation

Measurements of the OBT were obtained using the manual segmentation function of BRAINS2 software [23]. Delineation was performed in coronal view
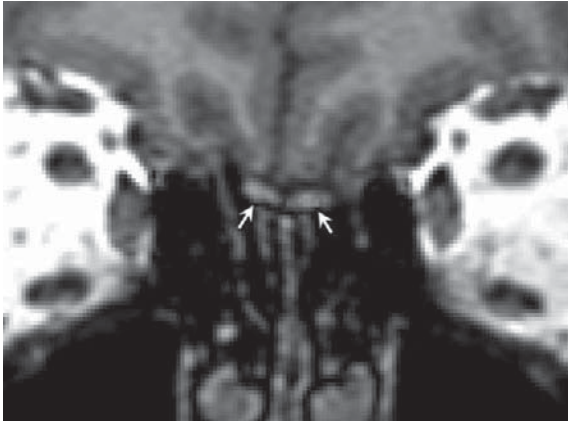
Fig. 1. Coronal T1-weighted MRI scan with arrows pointing to the olfactory bulbs.

(Fig. 1). The olfactory bulb was identified at the anterior cribriform plate and traced on consecutive slices; posteriorly, the olfactory tract extends to enter the brain below the rostral part of the corpus callosum. The rater (V.D.S.) was blind to the diagnoses. A sufficient inter- and intrarater reliability of the applied protocol has been established previously [18].

Voxel based morphometry

SPM2 software (http://www.fil.ion.ucl.ac.uk/spm) was used for voxel based analysis. Before pre-processing, all structural images were checked for artefacts and realigned regarding midsagittal plane and anterior–posterior commissure line.

The VBM protocol proposed by Good et al. [24] was applied for preprocessing of MRI data in order to minimize the probability of misclassifications within the tissue segmentation.

Statistical analysis

SPSS for Windows version 14 was used for statistical analysis; p-values less than 0.05 were considered significant. To address inter-individual differences in head size, the OBT volumes were corrected by dividing them by each subject's intracranial volume. The latter was estimated by the SPM2-derived sum of gray matter, white matter and cerebrospinal fluid volumes. Analyses of variance with post hoc Duncan's tests were calculated in order to compare the demographic, clinical and morphometric data between the diagnostic groups. The gender distribution was analyzed by the χ^2-test.

In the patient group, regional correlations between corrected mean OBT volumes and local GM density values were assessed with a voxel-wise regression analysis including potential confounding factors, i.e. age, gender, and education as nuisance covariates. In order to control for the rate of false-positive results, t-maps were thresholded at $p < 0.05$, corrected for multiple comparisons (family-wise error correction over the whole brain as defined in SPM), with an extent threshold of 100 voxels.

The relationship between mean OBT volume and global cognitive performance (as determined by the MMSE score) was assessed by using Pearson's correlation coefficient. The sensitivity of OBT measurements in distinguishing the three clinical groups (healthy controls, AD, AACD) was calculated at a fixed specificity of 80%.

RESULTS

Demographics, clinical characteristics and OBT measures are summarized in Table 1. According to statistical analysis, there were no significant differences between the three groups (controls, AACD, AD) with respect to age, gender distribution, and level of education. As expected, neuropsychological measures (mean MMSE scores and other CERAD subtests) differed significantly among all three groups with the AACD subjects ranking in between AD patients and healthy controls. Analyses of variance yielded no significant differences for the intracranial volume, but for the right, left and mean OBT volume, the latter differentiating among all three groups with highest values in controls and lowest values in AD patients.

In patients with AACD and AD, VBM revealed lower mean OBT volumes to be significantly correlated with a reduced gray matter density in the left-hemispheric amygdala, hippocampus and parahippocampal gyrus, and in the right-sided amygdala and parahippocampal gyrus, respectively (Figs 2 and 3 A and B, Table 2). In patients, mean OBT volumes were furthermore significantly associated with the MMSE score according to Pearson's moment correlation (whole patient group: $r = 0.59$, $p < 0.01$ (Fig. 4); AACD group: $r = 0.59$, $p < 0.01$; AD group: $r = 0.61$, $p < 0.01$).

OBT related measures of sensitivity at a fixed specificity of 80% and of diagnostic accuracy were as follows: controls vs. AD: 78% and 79%, controls vs. AACD: 50% and 65%, and AACD vs. AD: 46% and 63%, respectively.

Table 1
Subject demographics, clinical characteristics and morphometric measures

Variable	Controls (1) ($n = 30$)	AACD (2) ($n = 29$)	AD (3) ($n = 27$)	F	df	p	Duncan test (5%)
Sex	14 F / 16 M	16 F / 13 M	15 F / 12 M				n.sig.[a]
Age, years	70.50 ± 5.48	71.38 ± 6.14	71.44 ± 3.94	0.29	2, 83	0.75	1 = 2 = 3
Education, years	9.97 ± 1.71	10.21 ± 1.88	9.70 ± 1.68	0.57	2, 83	0.57	1 = 2 = 3
MMSE[b]	29.17 ± 0.75	26.17 ± 1.63	20.85 ± 3.07	123.57	2, 83	<0.001	1 > 2 > 3
Verbal fluency[b]	0.61 ± 0.98	-0.71 ± 1.29	-1.47 ± 0.81	28.62	2, 83	<0.001	1 > 2 > 3
BNT[b]	0.51 ± 0.66	-0.92 ± 1.68	-1.73 ± 1.76	17.79	2, 83	<0.001	1 > 2 > 3
WL immediate recall[b]	0.17 ± 0.92	-1.66 ± 1.36	-3.69 ± 2.66	33.85	2, 83	<0.001	1 > 2 > 3
WL delayed recall[b]	0.26 ± 0.91	-1.77 ± 1.22	-3.32 ± 0.90	88.20	2, 83	<0.001	1 > 2 > 3
WL recognition[b]	0.38 ± 0.35	-2.06 ± 2.63	-5.57 ± 3.84	36.23	2, 83	<0.001	1 > 2 > 3
CP[b]	0.13 ± 1.52	-0.36 ± 1.46	-1.40 ± 1.85	6.55	2, 83	0.002	1, 2 > 3[b]
CP recall[b]	0.51 ± 1.37	-0.84 ± 1.63	-3.02 ± 1.34	42.27	2, 83	<0.001	1 > 2 > 3
ICV (dm³)	1.39 ± 0.09	1.35 ± 0.09	1.34 ± 0.10	2.24	2, 83	0.11	1 = 2 = 3
Right OBT[c]	95.69 ± 10.08	91.16 ± 9.40	85.95 ± 8.35	7.74	2, 83	0.001	1, 2 > 3
Left OBT[c]	95.76 ± 9.68	90.46 ± 9.24	85.89 ± 8.07	8.50	2, 83	<0.001	1 > 2, 3
Mean OBT[c]	95.73 ± 9.77	90.81 ± 9.27	85.92 ± 8.18	8.21	2, 83	0.001	1 > 2 > 3

AACD = aging-associated cognitive decline; *AD* = Alzheimer's disease; *df* = degrees of freedom; n.sig.=not significant; [a] = χ^2-test; [b] = CERAD test battery (mean z-scores except for MMSE); *MMSE* = Mini Mental State Examination; *BNT* = Boston Naming Test; *WL* = word list; *CP* = constructional praxis; *ICV* = intracranial volume; *OBT* = olfactory bulb and tract; [c] = corrected by intracranial volume
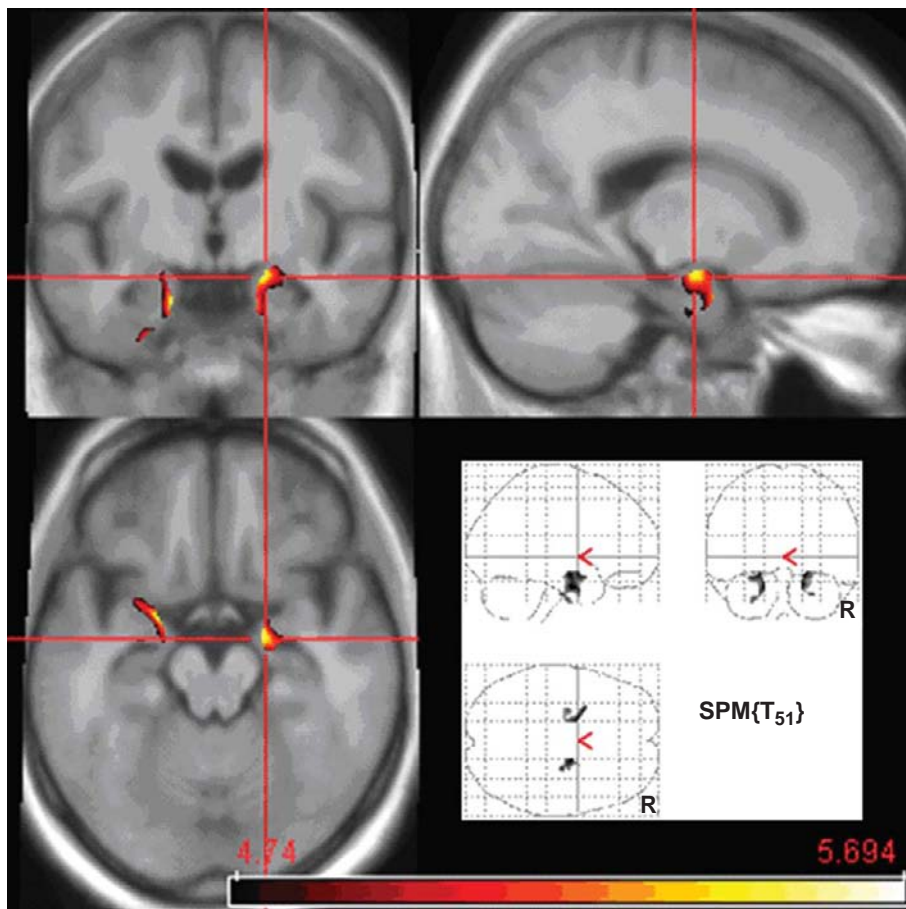
Fig. 2. Brain regions showing significant correlation between gray matter density and olfactory bulb and tract volume in subjects with mild cognitive impairment/AACD and patients with AD (height threshold $p < 0.05$, corrected for multiple comparisons; extent *threshold* = 100 voxels).

Table 2
Anatomical structures showing significant correlation between OBT volume and gray matter density in patients with mild cognitive impairment/AACD and AD

Anatomical structure	Cluster size (voxel)	T	Peak coordinates (x, y, z)
Left amygdala, extending to hippocampus and parahippocampal gyrus	994	5.69	−26, −6, −14
Right amygdala, extending to parahippocampal gyrus	823	5.60	19, −8, −13

Height threshold $p < 0.05$, corrected for multiple comparisons; extent *threshold* = 100 voxels.
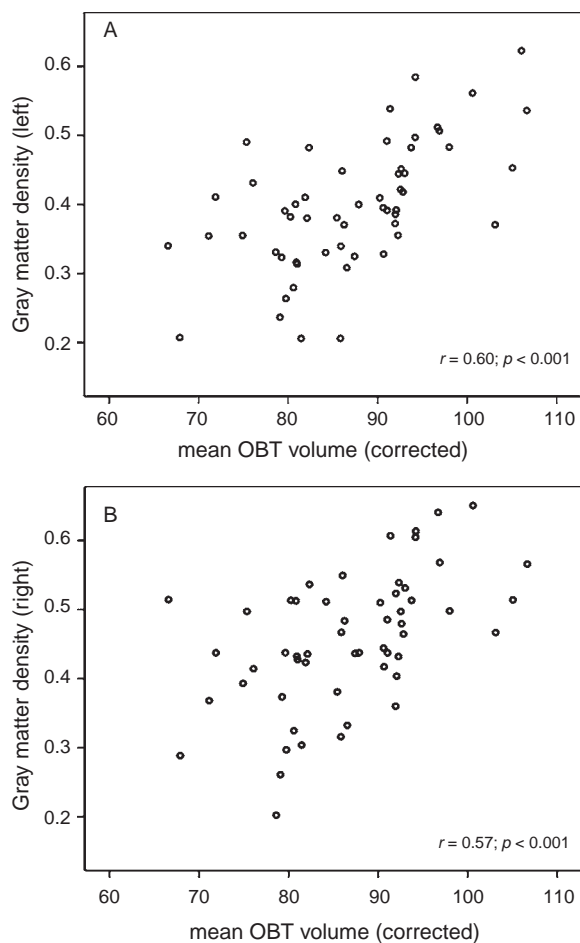
Fig. 3. Scatter plots showing the association of olfactory bulb and tract volume with gray matter density in subjects with mild cognitive impairment/AACD and patients with AD at A) left and B) right peak coordinates.

Fig. 4. Association of olfactory bulb and tract volume with MMSE score in subjects with mild cognitive impairment/AACD and patients with AD.

(i) In both AACD and AD patients OBT volumes were significantly lower compared to controls with atrophy being most prominent in the AD group.
(ii) In the patient group, lower mean OBT volumes were associated with a decreased gray matter density in the MTL bilaterally.
(iii) In patients, the OBT volume was significantly correlated with cognitive performance.

DISCUSSION

Our study assessed OBT volumes in individuals with mild cognitive impairment according to AACD criteria [19], in patients with probable AD, and in healthy comparison subjects using high-resolution MRI. We yielded three major findings:

Neuropathological research consistently revealed that the OBT is subject to degenerative processes in AD [3, 5, 7]. According to these studies, the respective changes (i.e. deposition of amyloid plaques and NFT) are not restricted to the advanced stages, but appear very early in the course of AD. Based on histopathological findings, the traditional 'Braak model' differentiates three main stages during the clinical course of AD [1]: In the earliest and almost symptom-free transentorhinal stage (Braak stages 1 and 2), morphological changes selectively affect the parahippocampal regions. The destructive process then spreads into additional structures of the MTL/limbic system, mainly involving the hippocampal formation

(Braak stages 3 and 4). Eventually, the pathological alterations encroach the isocortex until major parts of the temporal, parietal, and frontal cortical areas are affected (Braak stages 5 and 6). In their post-mortem study on 93 individuals, Tsuboi et al. [7] found olfactory tau pathology in one-third of the cases with Braak stage 2. A similar result (NFT in the OBT of 36.4% of the Braak stages 2) was reported by Attems and Jellinger [3] after examination of 273 autopsy cases. In a post-mortem study by Kovacs et al. [5], AD pathology was present in the OBT even without any affection of the entorhinal area. Taken together, these findings clearly emphasize that the OBT is a primary focus of AD pathology. Hence, our result of significant OBT atrophy in mild cognitive impairment likely reflects the neurodegenerative changes described above.

In both, AD and AACD patients, lower mean OBT volumes were significantly associated with poorer MMSE performance. This result indicates that atrophy of the OBT might be related to disease severity, likely reflecting the histopathological finding of NFT density increasing with higher Braak stages [3, 5, 7]. With a sensitivity and an overall correct classification of approximately 80%, OBT volume appeared to be a good measure for distinguishing controls and patients with AD. On the other hand, its contribution to an accurate diagnosis of mild cognitive impairment was rather poor and inferior to MRI measurements derived from the MTL [25–27]. However, for the interpretation of the latter result it is relevant to have in mind that it might underlie numerous potential confounding factors such as age, education, patients' disease state, sample size, mode of recruitment and classification, or image acquisition and analysis. Thus, future studies should volumetrically assess both MTL subregions and the OBT concomitantly in order to determine comparable measures of sensitivity, specificity, and diagnostic accuracy, respectively.

VBM analysis revealed that reduced OBT volumes in AD and AACD patients are related to reduced gray matter densities in the right- and left-hemispheric MTL, while there are no associations with other brain regions. Within the MTL, correlation with OBT volumes was most significant for the amygdala bilaterally. One might assume that this finding is at least partly related to the given anatomical connectivity between the olfactory bulb and the amygdala, with anterior olfactory nucleus neurons projecting to the amygdala [28]. Histopathological evidence that neurodegeneration in these two anatomical regions is linked comes from a study by Fujishiro et al. [29], who found

significant correlations between tau and α-synuclein pathology in the olfactory bulb and the amygdala in AD.

The olfactory bulb constitutes the first synaptic relay in the olfactory pathway [30]. Olfactory processing is mediated by many of the same MTL areas of the brain that have been implicated in incipient AD. Correspondingly, the hypothesis that AD patients develop an olfactory dysfunction early in the course of the disease gains support by an increasing body of research [31]. Olfactory deficits increase with disease severity [6, 32–34], aid in discriminating AD from major depression [35], and predict future development of manifest dementia in individuals with mild cognitive impairment [36]. It is generally assumed that impaired olfaction in AD refers to the appearance of neurofibrillary tangles and accompanying atrophic changes in olfactory-related brain regions. However, this assumption has still to be confirmed in neuropathological studies. With respect to neuroimaging, a first structural MRI study in 13 patients with AD and 22 age-matched controls revealed that deficits in olfaction correlate with atrophy in MTL regions [37], indicating that the grade of olfactory behavioral impairment indeed reflects the degree of neuronal damage in AD. This hypothesis is indirectly supported by our finding that OBT atrophy is associated with reductions of grey matter densities in the MTL. However, since the present study did not assess olfactory function, this interpretation is highly speculative and the link between impaired olfaction and neurodegenerative alterations in OBT and MTL regions in patients with mild cognitive impairment and AD has yet to be established.

In summary, the results confirm our prior finding of a significant OBT atrophy in manifest AD [18]. Since this atrophy was, to a lower extent, already present in mild cognitive impairment, and correlated with morphological changes in MTL regions, our findings suggest that the OBT volume might be a useful marker of neurodegeneration. Future studies, combining measures of olfactory function with neuroimaging may provide important additional insights on the interaction of these factors and thus facilitate the early and accurate diagnosis of AD.

ACKNOWLEDGMENTS

No actual or potential conflicts of interest to be declared by any of the authors.

REFERENCES

[1] Braak H, Braak E (1991) Neuropathological stageing of Alzheimer-related changes. *Acta Neuropathol (Berl)* **82**, 239-259.

[2] Van Hoesen GW, Augustinack JC, Dierking J, Redman SJ, Thangavel R (2000) The parahippocampal gyrus in Alzheimer's disease. Clinical and preclinical neuroanatomical correlates. *Ann N Y Acad Sci* **911**, 254-274.

[3] Attems J, Jellinger KA (2006) Olfactory tau pathology in Alzheimer disease and mild cognitive impairment. *Clin Neuropathol* **25**, 265-271.

[4] Hyman BT, Arriagada PV, Van Hoesen GW (1991) Pathologic changes in the olfactory system in aging and Alzheimer's disease. *Ann N Y Acad Sci* **640**, 14-19.

[5] Kovacs T, Cairns NJ, Lantos PL (1999) Beta-amyloid deposition and neurofibrillary tangle formation in the olfactory bulb in ageing and Alzheimer's disease. *Neuropathol Appl Neurobiol* **25**, 481-491.

[6] Serby M, Larson P, Kalkstein D (1991) The nature and course of olfactory deficits in Alzheimer's disease. *Am J Psychiatry* **148**, 357-360.

[7] Tsuboi Y, Wszolek ZK, Graff-Radford NR, Cookson N, Dickson DW (2003) Tau pathology in the olfactory bulb correlates with Braak stage, Lewy body pathology and apolipoprotein epsilon4. *Neuropathol Appl Neurobiol* **29**, 503-510.

[8] De Santi S, de Leon MJ, Rusinek H, Convit A, Tarshish CY, Roche A, Tsui WH, Kandil E, Boppana M, Daisley K, Wang GJ, Schlyer D, Fowler J (2001) Hippocampal formation glucose metabolism and volume losses in MCI and AD. *Neurobiol Aging* **22**, 529-539.

[9] Dickerson BC, Goncharova I, Sullivan MP, Forchetti C, Wilson RS, Bennett DA, Beckett LA, deToledo-Morrell L (2001) MRI-derived entorhinal and hippocampal atrophy in incipient and very mild Alzheimer's disease. *Neurobiol Aging* **22**, 747-754.

[10] Killiany RJ, Hyman BT, Gomez-Isla T, Moss MB, Kikinis R, Jolesz F, Tanzi R, Jones K, Albert MS (2002) MRI measures of entorhinal cortex vs hippocampus in preclinical AD. *Neurology* **58**, 1188-1196.

[11] Krasuski JS, Alexander GE, Horwitz B, Daly EM, Murphy DG, Rapoport SI, Schapiro MB (1998) Volumes of medial temporal lobe structures in patients with Alzheimer's disease and mild cognitive impairment (and in healthy controls). *Biol Psychiatry* **43**, 60-68.

[12] Pantel J, Kratz B, Essig M, Schröder J (2003) Parahippocampal volume deficits in subjects with aging-associated cognitive decline. *Am J Psychiatry* **160**, 379-382.

[13] Abolmaali ND, Hietschold V, Vogl TJ, Huttenbrink KB, Hummel T (2002) MR evaluation in patients with isolated anosmia since birth or early childhood. *AJNR Am J Neuroradiol* **23**, 157-164.

[14] Rombaux P, Mouraux A, Bertrand B, Nicolas G, Duprez T, Hummel T (2006) Retronasal and orthonasal olfactory function in relation to olfactory bulb volume in patients with posttraumatic loss of smell. *Laryngoscope* **116**, 901-905.

[15] Turetsky BI, Moberg PJ, Yousem DM, Doty RL, Arnold SE, Gur RE (2000) Reduced olfactory bulb volume in patients with schizophrenia. *Am J Psychiatry* **157**, 828-830.

[16] Turetsky BI, Moberg PJ, Arnold SE, Doty RL, Gur RE (2003) Low olfactory bulb volume in first-degree relatives of patients with schizophrenia. *Am J Psychiatry* **160**, 703-708.

[17] Yousem DM, Geckle RJ, Bilker WB, Doty RL (1998) Olfactory bulb and tract and temporal lobe volumes. Normative data across decades. *Ann N Y Acad Sci* **855**, 546-555.

[18] Thomann PA, Dos Santos V, Toro P, Schönknecht P, Essig M, Schröder J (2007) Reduced olfactory bulb and tract volume in early Alzheimer's disease-A MRI study. *Neurobiol Aging*, doi:10.1016/j.neurobiolaging.2007.08.001

[19] Levy R (1994) Aging-associated cognitive decline. Working Party of the International Psychogeriatric Association in collaboration with the World Health Organization. *Int Psychogeriatr* **6**, 63-68.

[20] McKhann G, Drachman D, Folstein M, Katzman R, Price D, Stadlan EM (1984) Clinical diagnosis of Alzheimer's disease: report of the NINCDS-ADRDA Work Group under the auspices of Department of Health and Human Services Task Force on Alzheimer's Disease. *Neurology* **34**, 939-944.

[21] Folstein MF, Folstein SE, McHugh PR (1975) "Mini-mental state". A practical method for grading the cognitive state of patients for the clinician. *J Psychiatr Res* **12**, 189-198.

[22] Morris JC, Heyman A, Mohs RC, Hughes JP, van Belle G, Fillenbaum G, Mellits ED, Clark C (1989) The Consortium to Establish a Registry for Alzheimer's Disease (CERAD). Part I. Clinical and neuropsychological assessment of Alzheimer's disease. *Neurology* **39**, 1159-1165.

[23] Magnotta VA, Harris G, Andreasen NC, O'Leary DS, Yuh WT, Heckel D (2002) Structural MR image processing using the BRAINS2 toolbox. *Comput Med Imaging Graph* **26**, 251-264.

[24] Good CD, Johnsrude IS, Ashburner J, Henson RN, Friston KJ, Frackowiak RS (2001) A voxel-based morphometric study of ageing in 465 normal adult human brains. *Neuroimage* **14**, 21-36.

[25] Bottino CM, Castro CC, Gomes RL, Buchpiguel CA, Marchetti RL, Neto MR (2002) Volumetric MRI measurements can differentiate Alzheimer's disease, mild cognitive impairment, and normal aging. *Int Psychogeriatr* **14**, 59-72.

[26] Pennanen C, Kivipelto M, Tuomainen S, Hartikainen P, Hanninen T, Laakso MP, Hallikainen M, Vanhanen M, Nissinen A, Helkala EL, Vainio P, Vanninen R, Partanen K, Soininen H (2004) Hippocampus and entorhinal cortex in mild cognitive impairment and early AD. *Neurobiol Aging* **25**, 303-310.

[27] Wolf H, Hensel A, Kruggel F, Riedel-Heller SG, Arendt T, Wahlund LO, Gertz HJ (2004) Structural correlates of mild cognitive impairment. *Neurobiol Aging* **25**, 913-924.

[28] Sims KS, Williams RS (1990) The human amygdaloid complex: a cytologic and histochemical atlas using Nissl, myelin, acetylcholinesterase and nicotinamide adenine dinucleotide phosphate diaphorase staining. *Neuroscience* **36**, 449-472.

[29] Fujishiro H, Tsuboi Y, Lin WL, Uchikado H, Dickson DW (2008) Co-localization of tau and alpha-synuclein in the olfactory bulb in Alzheimer's disease with amygdala Lewy bodies. *Acta Neuropathol* **116**, 17-24.

[30] Nieuwenhuys R, Voogd J, van Huijzen C (1988) *The Human Central Nervous System*, Springer-Verlag, Berlin.

[31] Mesholam RI, Moberg PJ, Mahr RN, Doty RL (1998) Olfaction in neurodegenerative disease: a meta-analysis of olfactory functioning in Alzheimer's and Parkinson's diseases. *Arch Neurol* **55**, 84-90.

[32] Murphy C, Gilmore MM, Seery CS, Salmon DP, Lasker BR (1990) Olfactory thresholds are associated with degree of

dementia in Alzheimer's disease. *Neurobiol Aging* **11**, 465-469.

[33]   Peters JM, Hummel T, Kratzsch T, Lotsch J, Skarke C, Frölich L (2003) Olfactory function in mild cognitive impairment and Alzheimer's disease: an investigation using psychophysical and electrophysiological techniques. *Am J Psychiatry* **160**, 1995-2002.

[34]   Djordjevic J, Jones-Gotman M, De Sousa K, Chertkow H (2008) Olfaction in patients with mild cognitive impairment and Alzheimer's disease. *Neurobiol Aging* **29**, 693-706.

[35]   McCaffrey RJ, Duff K, Solomon GS (2000) Olfactory dysfunction discriminates probable Alzheimer's dementia from major depression: a cross-validation and extension. *J Neuropsychiatry Clin Neurosci* **12**, 29-33.

[36]   Devanand DP, Michaels-Marston KS, Liu X, Pelton GH, Padilla M, Marder K, Bell K, Stern Y, Mayeux R (2000) Olfactory deficits in patients with mild cognitive impairment predict Alzheimer's disease at follow-up. *Am J Psychiatry* **157**, 1399-1405.

[37]   Murphy C, Jernigan TL, Fennema-Notestine C (2003) Left hippocampal volume loss in Alzheimer's disease is reflected in performance on odor identification: a structural MRI study. *J Int Neuropsychol Soc* **9**, 459-471.

Presence of ApoE ε4 Allele Associated with Thinner Frontal Cortex in Middle Age

Christine Fennema-Notestine[a,b,*], Matthew S. Panizzon[a], Wesley R. Thompson[a], Chi-Hua Chen[a], Lisa T. Eyler[a,c], Bruce Fischl[d,e,f], Carol E. Franz[a], Michael D. Grant[g], Amy J. Jak[a,c], Terry L. Jernigan[a,b,h,i], Michael J. Lyons[g], Michael C. Neale[j], Larry J. Seidman[g], Ming T. Tsuang[a,k,l], Hong Xian[m], Anders M. Dale[b,n] and William S. Kremen[a,c,k]

[a]*Department of Psychiatry, University of California, San Diego, La Jolla, CA, USA*
[b]*Department of Radiology, University of California, San Diego, La Jolla, CA, USA*
[c]*Veterans' Administration San Diego Healthcare System, San Diego, CA, USA*
[d]*Department of Radiology, Massachusetts General Hospital, Boston, MA, USA*
[e]*Harvard Medical School, Boston, MA, USA*
[f]*Computer Science and AI Lab, Massachusetts Institute of Technology, Cambridge, MA, USA*
[g]*Department of Psychology, Boston University, Boston, MA, USA*
[h]*Department of Cognitive Science, University of California, San Diego, La Jolla, CA, USA*
[i]*Center for Human Development, University of California, San Diego, La Jolla, CA, USA*
[j]*Virginia Institute for Psychiatric and Behavioral Genetics, Virginia Commonwealth University School of Medicine, Richmond, VA, USA*
[k]*Center for Behavioral Genomics, University of California, San Diego, La Jolla, CA, USA*
[l]*Harvard Institute of Psychiatric Epidemiology and Genetics, Harvard Medical School and School of Public Health, Boston, MA, USA*
[m]*Department of Psychiatry, Washington University School of Medicine, St. Louis, MO, USA*
[n]*Department of Neurosciences, University of California, San Diego, La Jolla, CA, USA*

Abstract. The presence of an ApoE ε4 allele (ε4+) increases the risk of developing Alzheimer's disease (AD). Previous studies support an adverse relationship between ε4+ status and brain structure and function in mild cognitive impairment and AD; in contrast, the presence of an ε2 allele may be protective. Whether these findings reflect disease-related effects or pre-existing endophenotypes, however, remains unclear. The present study examined the influence of ApoE allele status on brain structure solely during middle-age in a large, national sample. Participants were 482 men, ages 51–59, from the Vietnam Era Twin Study of Aging (VETSA). T1-weighted images were used in volumetric segmentation and cortical surface reconstruction methods to measure regional volume and thickness. Primary linear mixed effects models predicted structural measures with ApoE status (ε3/3, ε2/3, ε3/4) and control variables for effects of site, non-independence of twin data, age, and average cranial vault or cortical thickness. Relative to the ε3/3 group, the ε3/4 group demonstrated significantly thinner cortex in superior frontal and left rostral and right caudal midfrontal regions; there were no significant effects of ε4 status on any temporal lobe measures.

*Correspondence to: Christine Fennema-Notestine, Ph.D. UCSD School of Medicine 9500 Gilman Dr #0738 La Jolla, CA 92093-0738 Tel.: 858 246 0605; Fax: 858 246 0556; E-mail: Fennema@UCSD.edu.

The ε2/3 group demonstrated significantly thicker right parahippocampal cortex relative to the ε3/3 group. The ApoE ε4 allele may influence cortical thickness in frontal areas, which are later developing regions thought to be more susceptible to the natural aging process. Previous conflicting findings for mesial temporal regions may be driven by the inclusion of older individuals, who may evidence preclinical manifestations of disease, and by unexamined moderators of ε4-related effects. The presence of the ε2 allele was related to thicker cortex, supporting a protective role. Ongoing follow-up of the VETSA sample may shed light on the potential for age- and disease-related mediation of the influence of ApoE allele status.

INTRODUCTION

The ApoE ε4 allele is studied within imaging genetics as the most common polymorphism associated with late-onset Alzheimer's disease (AD) [1–4]. ApoE is thought to play a role in lipoprotein transport and cell maintenance and repair, including amyloid clearance, and is bound to senile plaques and neurofibrillary tangles [5–7]. Of the three alleles (ε2, ε3, ε4), the ε3/3 pairing is the most common phenotype in the U.S. population (∼60%), while the presence of ε2 and ε4 alleles is less frequent [8]. There is an increased prevalence of the ε4 allele in disease populations relative to healthy controls [1, 4, 9–12], and individuals carrying at least one ε4 allele (ε4+) are at an increased risk for developing AD [13–15]. In contrast, the presence of an ε2 allele may impart protection from AD-related neurodegeneration [8, 15–21].

In combination with the risk conferred by ApoE allele status, neuroimaging biomarkers may improve the identification of individuals at risk for AD and the potential for successful intervention in the earliest stages. Studies in AD and mild cognitive impairment (MCI) often demonstrate more significant mesial temporal lobe (MTL) atrophy in ε4+ individuals relative to non-carriers [22–29]. In a positron emission tomography (PET) study using a marker of amyloid and tau proteins (FDDNP), ε4+ MCI demonstrated abnormally high binding in the MTL [30]. Neuropathological studies of ε4 carriers support earlier and greater amyloid deposition in AD, as well as in MCI and in older healthy individuals [20]. Further evidence of an earlier and faster rate of cognitive decline also has been demonstrated in MCI and AD ε4+ individuals [15]. These and other studies support strong disease-related effects within ε4+ MCI and AD individuals.

Studying individuals earlier in life, prior to the development of MCI or AD, is critical to understanding the influence of ApoE allele status. PET studies have shown glucose metabolism reductions in ε4+ late-middle-aged individuals with a positive family history for AD [31, 32] and an accelerated rate of decline in regional cerebral blood flow for ε4 carriers [33]. The affected areas overlap with AD-related regions supporting the potential for a pre-symptomatic endophenotype. Of particular interest, however, a recent PET FDDNP study [30] found higher amyloid and tau binding in frontal areas for ε4+ relative to ε4- healthy individuals, in contrast to an increased temporal lobe binding in the ε4+ MCI group [30]. Structural neuroimaging studies also have been somewhat inconsistent, with reports of smaller MTL structures, including the hippocampus [34–36] and entorhinal cortex [37, 38], in ε4+ carriers, alongside other reports of no significant ε4-related effect in these or other areas [24, 37, 39]. Studies beyond the MTL that have included younger-old and middle-aged individuals are varied, reporting thickening of small cortical areas [40], thinning in medial orbitofrontal areas [24], and lower gray matter density in small anterior frontal and temporal regions [36]. Several reports, however, have suggested that such effects may be driven by older individuals in the samples, rather than reflecting an early ε4-related endophenotype [35, 41].

Fewer studies have examined the potential protective influence of the ε2 allele, particularly in healthy individuals, in part due to the lower prevalence of this allele in the U.S. population. Previous work has provided neuropathological evidence for less cortical amyloid and fewer plaques and neurofibrillary tangles in ε2 carriers (ε2+) [16–18, but see 21]. In addition, ε2 carriers may evidence a reduced rate of cognitive decline [8, 15, 19–21] and fewer are diagnosed with AD [8]. Neuroimaging corroboration for such a protective effect is rarer. A recent study of older individuals reported larger cortical gray matter volume and smaller

ventricles in MCI and AD but found no significant effect related to the ε2 allele in healthy older individuals; the sample sizes for ε2 carriers, however, were quite small across all groups studied [42]. A study of adolescents suggested a tendency for thicker mesial temporal and medial orbitofrontal cortex in a larger ε2+ group [38]. An investigation of the ε2 allele in a large community sample may provide complementary insight into the potentially opposing influences of ApoE ε4 and ε2 alleles.

The present study examined the influence of ApoE allele status on brain structure solely during middle age in a national sample from the Vietnam Era Twin Study of Aging (VETSA). This cohort captures individuals in their 6th decade of life likely prior to the onset of AD or other age-related complications [43]. We examined *a priori* AD-related regions of interest (ROIs) as well as regions expected to be influenced by normal aging, which tend to follow an anterior–posterior gradient, exhibiting the greatest rates of decline in frontal areas [44, 45]. Relative to ε3/3 carriers, we expected the ε3/4 group to show the smallest and thinnest MTL areas, most affected in AD, and we also proposed that this group would demonstrate thinner frontal cortex, associated with normal aging. In contrast, the ε2/3 group may evidence larger, thicker MTL areas, supporting a potential protective effect. Continuous surface maps were also generated to explore the extent of effects without the constraints of predefined boundaries.

MATERIALS AND METHODS

Participants

Data were obtained in the first wave of VETSA, a longitudinal study of cognitive and brain aging beginning in midlife [46]. Participants were randomly sampled from over 3,300 Vietnam Era Twin (VET) Registry twin pairs with the constraint that they were in their 50s at the time of recruitment into VETSA. The VET Registry is a nationally distributed sample of male-male twin pairs who served in the U.S. military sometime between 1965 and 1975; descriptions of the composition and method of ascertainment have been reported elsewhere [47]. Importantly, these are Vietnam era, not necessarily Vietnam, veterans; the large majority did not serve in combat. In comparison to census data, VETSA participants are similar in demographic and health characteristics to American men

in their age range [48]. Aside from standard exclusion criterion for MRI studies (e.g., metal in the body), there were no additional eligibility requirements for selection into the MRI component.

Participants traveled either to Boston University or the University of California, San Diego (UCSD) for a series of physical, psychosocial, and neurocognitive assessments. Informed consent was obtained from all participants prior to data collection, and the scanning protocol was approved of by the Institutional Review Boards at UCSD, Boston University, and the Massachusetts General Hospital (MGH).

A subset of the 1237 VETSA participants underwent structural MRI, and the present non-twin analyses include data from 482 participants for whom neuroimaging data and APOE genotyping were adequate and available. The dataset included 205 twin pairs (119 monozygotic and 86 dizygotic twin pairs) and 72 unpaired individuals with an average age of 55.7 years (sd = 2.6; range 51–59). Participants in this MRI study were similar to the larger VETSA sample with respect to education (mean=13.8; sd=2.1), ethnicity (85.7% Caucasian), employment (75% employed full-time), and self-reported health status.

ApoE genotype was determined from blood samples using established methods [49, 50]. All genotypes were independently determined twice by laboratory personnel at the VA Puget Sound Healthcare System who were blind to the initial genotype and the identity of the co-twin. Of the 482 participants, 2 (0.4%) possessed a ε2/2 genotype, 67 (13.9%) ε2/3, 18 (3.7%) ε2/4, 288 (59.8%) ε3/3, 94 (19.5%) ε3/4, and 13 (2.7%) ε4/4 (Table 1). These rates are roughly equivalent to those found in the general population [14, 51]. Because the proportion of individuals with ε2/2, ε2/4, and ε4/4 parings were small, these cases were not included in the primary models, however, a secondary overall analyses comparing ε4+ and non-ε4 carriers was completed using all available data.

Participants studied for the primary model were classified as ε2/3, ε3/3, or ε3/4 (see Table 1). These groups did not differ on age (F=1.4, p>.05). General cognitive ability was assessed by the Armed Forces Qualification Test (AFQT), a well-validated test that also was given to VETSA participants in early adulthood [52]. The mean for the entire sample was 63.1 (sd=20.8); this AFQT score is slightly above the mean and would be comparable to an average IQ of approximately 105. The mean across the three primary groups was 63.2 (sd=20.6) and the means did not differ between these groups (Table 1; $F < 1.0$, $p > .05$).

Table 1

Participant characteristics. For all ApoE allele pairings, sample size, mean age in years, and mean Armed Forces Qualifications Test (AFQT) score are provided, along with the standard deviation (sd) and *range*. The primary model considered the first three groups (ε2/3, ε3/3, ε3/4) with sufficient power to examine influence on brain structure

	ε2/3	ε3/3	ε3/4	ε2/2	ε2/4	ε4/4
n	67	288	94	2	18	13
age	56.2 (2.5)	55.7 (2.6)	55.5 (2.8)	55.0 (4.2)	55.1 (2.5)	56.2 (2.6)
	52–59	*51–59*	*51–59*	*52–58*	*52–58*	*51–58*
AFQT (%)	63.2 (22.7)	62.8 (19.8)	64.4 (21.5)	71.5 (27.6)	55.0 (24.4)	70.9 (18.9)
	15–97	*4–95*	*15–98*	*52–91*	*14–94*	*28–89*

MR Image Acquisition

As described previously [53], images were acquired on 1.5 Tesla scanners (255 at UCSD; 227 at MGH). Sagittal T1-weighted MPRAGE sequences were employed with TI=1000ms, TE=3.31ms, TR=2730ms, flip angle=7degrees, slice thickness = 1.33 mm, voxel size $1.3 \times 1.0 \times 1.3$ mm. Raw DICOM MRI scans (two T1 volumes per case) were transferred to MGH for image processing. These raw data were reviewed for quality, registered, and averaged to improve signal-to-noise.

Image processing

As described elsewhere [53], we employed volumetric segmentation [54] and cortical surface reconstruction [55–57] methods based on the publicly available FreeSurfer software package (http://surfer. nmr.mgh.harvard.edu/fswiki; Version 3.0.1b). The 3D whole-brain segmentation procedure [54] uses a probabilistic atlas and applies a Bayesian classification rule to assign a neuroanatomical label to each voxel. The atlas consists of a manually-derived training set created by the Center for Morphometric Analysis (http://www. cma.mgh.harvard.edu/) from 20 unrelated, randomly selected VETSA participants. Use of this study-specific atlas produced more accurate measurements than more commonly used atlases [53]. Estimated total cranial vault (eTIV) volume was calculated to control for differences in head size for volumetric measures. Based on Buckner et al. [58], FreeSurfer provides an eTIV volume derived from the atlas scaling factor on the basis of the transformation of the full brain mask into atlas space. Although this estimate is not a direct volume, this eTIV measure has been shown to correlate well with other cranial vault volumes incorporating T2-weighted information, including manual tracings in controls and individuals with Alzheimer's Disease (r=0.93) [58] and multi-channel tissue segmentations [as in 44] in older controls and

individuals with Alzheimer's disease (r=0.87) [59]. The primary volumetric ROI was the hippocampus; exploratory ROIs included amygdala, caudate nucleus, putamen, nucleus accumbens, and thalamus.

The cortical surface was reconstructed to measure thickness at each surface location, or vertex [described in 53, 55, 56]. The explicit reconstruction of the cortical surface requires inhomogeneity corrections, creation of a normalized intensity image, and removal of non-brain. The resulting surface is covered with a polygonal tessellation and smoothed to reduce metric distortions. The gray/white boundary surface is deformed outwards to obtain a representation of the pial surface; the surface model is manually reviewed and edited for technical accuracy in alignment with standard, objective editing rules. Each individual surface is non-rigidly aligned to an atlas in a spherical surface-based coordinate system and divided into distinct ROIs [57], with each vertex assigned a neuroanatomical label [60], to estimate average thickness in each ROI. Primary cortical thickness ROIs included mesial temporal (entorhinal, parahippocampal); lateral temporal (inferior, middle, and superior temporal); and frontal (caudal and rostral middle; superior; inferior; orbitofrontal) cortex (Fig. 1). Exploratory ROIs included superior and inferior parietal, supramarginal, lingual, fusiform, cingulate, and precuneus cortex. Cortical thickness was also estimated over continuous maps on the surface with no predefined regional boundaries as described in Statistical Analysis; smoothing of volumes was done prior to the vertex-wise analyses using a 30 mm FWHM Gaussian kernel.

Statistical analysis

Although the study participants were twins, all analyses in this article are non-twin analyses. Derived ROI values (thickness in mm or volume in mm^3) were submitted to linear mixed effects models with fixed effects of site, ApoE allele status (ε2/3 and ε3/4 were compared to ε3/3), and age. Importantly, site was included
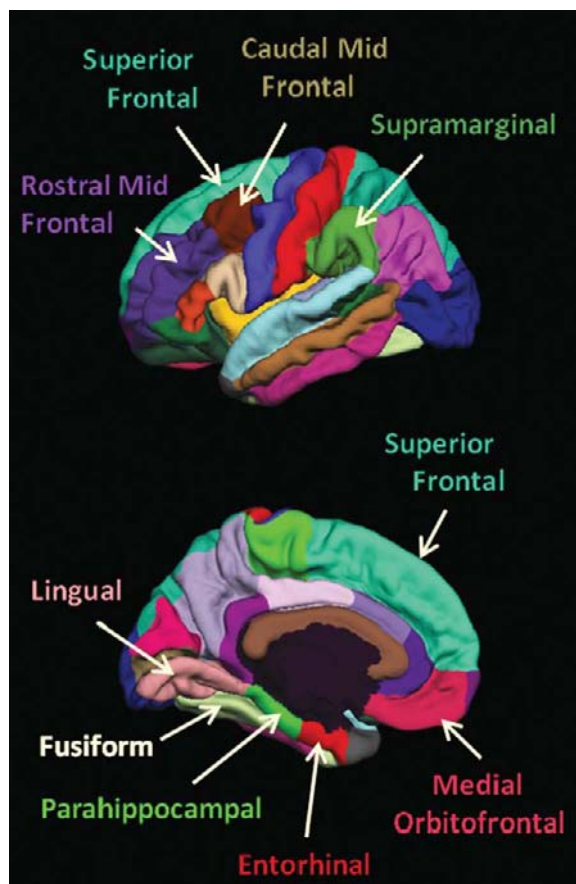
Fig. 1. Cortical region of interest parcellation (30). Primary ROIs include superior frontal (*teal*), rostral (*purple*) and caudal (*brown*) mid frontal, parahippocampal (*green*), entorhinal (*red*), and medial orbitofrontal (*rose*) cortex. Additional exploratory ROIs include fusiform (*yellow*), supramarginal (*olive green*), and lingual (*pink*) gyrus. *Top row:* lateral views; *bottom row:* medial views.

in the model to control for effects related to differences in scanner hardware, known to differentially influence morphometric measures of volume and thickness [e.g., 59, 61–63]. Because twins within pairs are not independent observations, it is necessary to adjust for this non-independence when performing non-twin analyses in a twin sample. Therefore, the "family ID" of each member of a twin pair was entered as a random effect in the model. Doing so adjusts the degrees of freedom and makes it more difficult to attain statistical significance. Finally, to adjust for individual differences in overall head size or thickness of the cortical ribbon, an additional fixed effect was included in each model: eTIV for volumetric measures and average cortical thickness for thickness measures.

Planned comparisons included ROIs implicated in AD: hippocampus, entorhinal cortex, parahippocampal cortex, and lateral temporal gyri; and regions susceptible to the effects of normal aging: superior frontal gyrus, middle frontal gyrus (rostral and caudal), inferior frontal (pars opercularis, pars orbitalis and pars triangularis), and orbitofrontal cortex (medial and lateral). Planned comparisons were limited to these predefined ROIs driven by prior work, and we employed an alpha level of 0.05. Effect sizes were calculated by ROI using Cohen's *d* and were based on estimated marginal means resulting from the full model. In general, a Cohen's *d* of 0.2–0.3 is considered a small, 0.5 a medium, and 0.8 a large effect size.

In a secondary analysis, the same model was modified to utilize the entire cohort of 482 participants to compare ε4+ (n=125) and non-ε4 (n=357) carriers, as has been done in some previous studies. That is, the variables for ApoE allele status were replaced by ApoE ε4 allele status. Given the small sample of homozygous ε4/4 genotype, a dose effect of ε4 (0, 1, or 2 alleles) was not examined due to insufficient power.

To further explore the statistical findings based on our *a priori* ROI analyses, the same model was implemented at each vertex, or point on the cortical surface, resulting in a continuous surface map of cortical thickness without the predefined constraints of ROI boundaries. The resulting map is exploratory in nature and provides guidance for future studies.

RESULTS

There was no significant effect of ApoE allele status on eTIV or average cortical thickness (all $t \leq 1.0$, $p > 0.05$). Relative to the ε3/3 group, the ε3/4 group demonstrated significantly thinner cortex in bilateral superior frontal, left rostral midfrontal, and right caudal midfrontal regions (Table 2; Fig. 2). Although the right rostral midfrontal and left caudal midfrontal ROIs tended to be thinner, these effects were not significant (Table 2). No temporal areas or any other frontal regions were significantly related to ε4 status. Analysis of the entorhinal cortex did not reveal any significant influence of ε4 status, although the variability of thickness in this area was larger than in other ROIs (Table 2). Exploratory cortical analyses suggested thicker fusiform cortex in the ε3/4 group (Table 2, bottom). Primary volumetric analyses did not reveal any significant effect of ε4 status on the hippocampus (Table 2). Exploratory volumetric analyses

Table 2

Effect of ApoE allele status by Regions of Interest. Controlling for other variables in the model, the estimated marginal mean (in mm for cortical thickness and in mm^3 for volumetric ROIs) and standard deviation (sd) are reported by ROI for each primary ApoE allele group. Based on results of the full statistical model, within which the ε3/4 and ε2/3 groups were compared to the ε3/3 group, the resultant t-value, level of significance, and the associated effect size (Cohen's d) are reported. Negative t-values reflect an effect thinner or smaller than the ε3/3 group; positive t-values reflect thicker or larger effects relative to the ε3/3 group

Region of Interest	Hemi-sphere	ε3/3 mean (sd)	ε3/4 mean (sd)	t value	d	ε2/3 mean (sd)	t value	d
Superior Frontal Gyrus	right	2.204 (0.080)	2.179 (0.087)	−2.80**	−0.30	2.202 (0.085)	<1[ns]	−0.02
	left	2.195 (0.084)	2.173 (0.091)	−2.42*	−0.26	2.189 (0.089)	<1[ns]	−0.07
Rostral Mid Frontal Gyrus	right	1.819 (0.080)	1.803 (0.090)	−1.73[ns]	−0.19	1.820 (0.088)	<1[ns]	0.01
	left	1.851 (0.075)	1.833 (0.085)	−1.95*	−0.21	1.859 (0.083)	<1[ns]	0.11
Caudal Mid Frontal Gyrus	right	2.052 (0.121)	2.018 (0.133)	−2.49*	−0.27	2.023 (0.129)	−1.80[ns]	−0.23
	left	2.042 (0.112)	2.028 (0.126)	−1.12[ns]	−0.12	2.029 (0.122)	<1[ns]	−0.11
Entorhinal Cortex	right	2.800 (0.385)	2.883 (0.426)	+1.89[ns]	0.20	2.816 (0.415)	<1[ns]	0.04
	left	2.553 (0.336)	2.574 (0.378)	<1[ns]	−0.06	2.628 (0.367)	+1.68[ns]	0.21
Hippocampal Volume	right	4216 (444)	4168 (479)	<1[ns]	−0.11	4289 (466)	+1.28[ns]	0.16
	left	3988 (399)	3954 (430)	<1[ns]	−0.08	4067 (419)	+1.54[ns]	0.19
Parahippocampal Gyrus	right	1.901 (0.242)	1.922 (0.266)	<1[ns]	−0.09	1.967 (0.259)	+2.10*	0.27
	left	1.900 (0.260)	1.894 (0.288)	<1[ns]	−0.02	1.916 (0.280)	<1[ns]	0.06
Medial Orbitofrontal	right	1.847 (0.159)	1.838 (0.175)	<1[ns]	−0.06	1.851 (0.170)	<1[ns]	0.02
	left	1.849 (0.156)	1.838 (0.175)	<1[ns]	−0.06	1.882 (0.170)	+1.59[ns]	0.20
Fusiform Gyrus	right	2.011 (0.101)	2.035 (0.114)	+2.04*	0.22	2.000 (0.110)	<1[ns]	−0.11
	left	1.975 (0.106)	2.000 (0.119)	+1.88[ns]	0.20	1.968 (0.115)	<1[ns]	−0.06
Putamen Volume	right	5002 (558)	4846 (582)	−2.60*	−0.27	5010 (567)	<1[ns]	0.01
	left	4942 (582)	4788 (598)	−2.50*	−0.26	4868 (582)	−1.04[ns]	−0.13
Supramarginal Gyrus	right	2.085 (0.110)	2.089 (0.124)	<1[ns]	0.04	2.054 (0.120)	−2.08*	−0.26
	left	2.071 (0.099)	2.076 (0.112)	<1[ns]	0.05	2.071 (0.109)	<1[ns]	0.00
Lingual Gyrus	right	1.703 (0.093)	1.715 (0.104)	+1.12[ns]	0.12	1.700 (0.101)	<1[ns]	−0.03
	left	1.654 (0.095)	1.655 (0.105)	<1[ns]	0.01	1.630 (0.102)	−1.97*	−0.25

**$p < 0.01$, *$p < 0.05$, ns = $p > 0.05$

suggested a significantly smaller putamen volume in ε4 carriers (Table 2, bottom).

In the secondary ROI analyses utilizing the entire 482 datasets, a comparison of all ε4+ with all non-ε4 carriers provided similar results. Given the significant pattern of effects in the ROI analyses, we reviewed the influence of ε4 allele status on the continuous cortical surface map to explore effects without the predefined constraints of ROI boundaries. Continuous maps of the cortical surface supported a broad distribution of thinner lateral and mesial superior frontal, and thicker fusiform cortex in the ε4+ relative to the non-ε4 group (Fig. 3). In the context of Fig. 1, Fig. 3 shows that some regional effects (e.g., left middle frontal area) fall across the confines of predefined ROIs. The thinnest areas (in orange/yellow) may lie across the intersection of a number of ROIs, to include the more lateral, inferior extent of the caudal midfrontal gyrus, posterior rostral midfrontal gyrus, posterior inferior frontal gyrus, and inferior portions of the pre-central gyrus. With respect to the unexpectedly thicker regions in the ε4+ group suggested by exploratory ROI analyses, posterior regions may be more broadly affected. This map provides guidance for future studies.

Relative to the ε3/3 group, our investigation of the ε2/3 group demonstrated significantly thicker right parahippocampal cortex (Table 2; Fig. 2) and non-significant tendencies towards thicker left entorhinal cortex, left medial orbitofrontal cortex, and hippocampal volumes (Table 2). Exploratory analyses suggested significantly thinner right supramarginal and left lingual gyri (Table 2, bottom).

DISCUSSION

This study of a large, community-dwelling sample provides a comprehensive view of the influence of ApoE allele status on brain structure in men. Few previous studies have captured such a broad description particularly within a solely middle-aged sample. The findings suggest that carriers of the ε4 allele on average have thinner frontal cortices in middle age, without direct evidence of any significant ε4 effect on MTL regions commonly affected in AD. These frontal effects were widespread, although the effect sizes were small, suggesting that studies with smaller sample sizes may not have sufficient power to reliably detect such
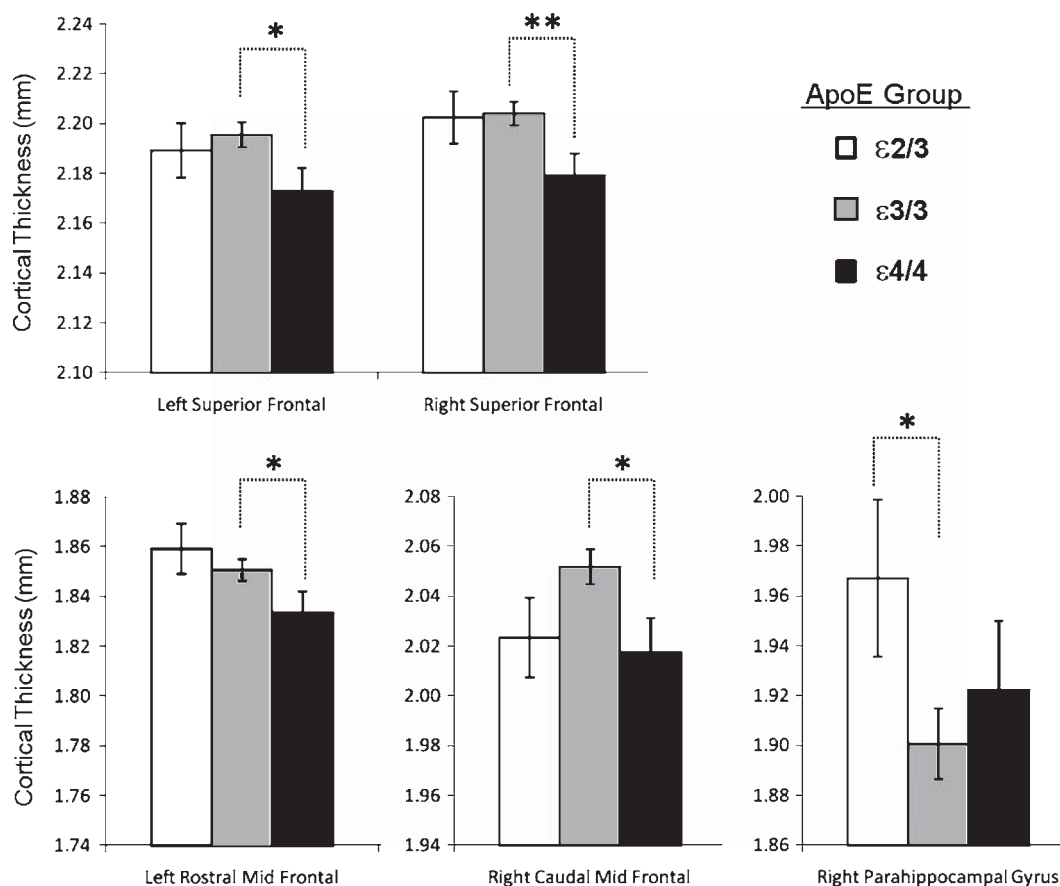
Fig. 2. Cortical thickness in ROIs with significant effects of ApoE allele status. Estimated marginal means (with standard error bars), controlling for all variables in the full model, are shown for cortical thickness (mm) in frontal and temporal ROIs that demonstrated a significant effect of ApoE allele status. Significance levels are reported in Table 2 and denoted in the graph with ** for p<.01 and * for p<.05.

effects. Exploratory analyses also suggested thicker fusiform cortex in ε4+ carriers, in line with a previous study [40]. Potential protective effects of the ε2/3 genotype were supported in part by thicker left parahippocampal cortex and broader MTL and medial orbitofrontal tendencies towards thicker cortex, relative to the ε3/3 group.

Our findings of ε4-related differences in superior and middle frontal cortical thickness are relatively unique and of interest in the context of normal aging. One cross-sectional study including middle-aged and older individuals suggested accelerated age-related thinning in ε4 carriers in the superior medial frontal gyrus; however, the majority of the participants were over the age of 60, limiting the inference of effects in middle age [40]. Within Shaw et al.'s study of children and adolescents [38], there were potential ε4 status effects in frontal regions, with continuous maps showing small areas of thinner orbitofrontal cortex in the

ε4+ group. While the present study does not show significant orbitofrontal ROI effects, the continuous surface maps (Fig. 3) further explore patterns without the predefined constraints of ROI boundaries, which may be relatively arbitrary with respect to the underlying cellular, functional, or developmental aspects of the brain. The maps support widespread frontal effects, and the potential influence on frontal cortex development into the adult age range may inform these regional differences.

The ε4-related effects on frontal cortical thickness are bolstered by findings from other modalities and disorders. Amyloid and tau binding PET studies in healthy individuals suggest that binding is higher for ε4+ carriers in frontal areas, as opposed to commonly reported increased temporal lobe binding in ε4+ MCI individuals [30]. In addition, ε4 status may influence dendritic density and complexity in the cortex [64], and may differentially influence cortical patterns of
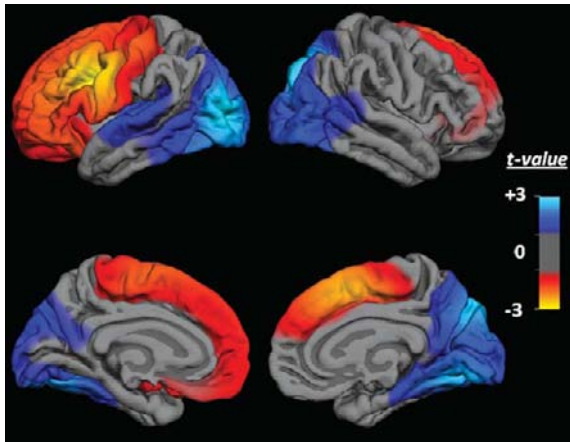
Fig. 3. Continuous surface maps of the estimated ApoE allele status *effect on cortical thickness.* Using the entire available sample (n=482), the *t*-statistic for the effect of carrying the ε4 allele, from the full statistical model, was applied vertex-wise on the pial surface. The color scale denotes effects for the ε4+ relative to the non-ε4 group as follows: thinner cortex in orange/yellow areas (larger negative *t*-values) and thicker cortex in areas with bright blue (cyan) (larger positive *t*-values). Both left (*left column*) and right (*right column*) hemispheres are presented.

thinning based on mediating factors. In a study of AD and frontotemporal dementia, cortical atrophy was greater in both ε4+ subgroups; however, the pattern of thinning in AD represented known neuropathological areas such as the mesial temporal lobe, whereas in frontotemporal dementia, the ε4+ group evidenced greater frontal atrophy [65]. The broad, frontal findings support the relationship between the ε4 allele and increased amyloid deposition in these areas with normal aging, although any progressive nature of such effects must be demonstrated in a longitudinal study, currently underway.

The lack of significant MTL ε4 related effects is not unexpected given conflicting previous reports and may reflect studies including a low proportion of individuals in a preclinical phase of AD and, importantly, other mediating influences on the impact of ε4 status, such as gender and hormones. While substantial support exists for ε4-related MTL effects in MCI and AD, findings in healthy individuals are inconsistent, even in older adults [23, 37, 39, 40, 66]. There is some evidence suggesting the influence of ε4 status on MTL structures in middle age [34] and in children and adolescents [38]; however, other studies including middle-aged individuals have not found the same effects [35, 40] or have found that effects across a broad age range were driven by individuals over 60 or 65 years of age [35]. Some of

these older individuals may demonstrate poor cognitive performance relative to their non-ε4 counterparts and some may be in the prodromal stages of AD. Indeed, a recent study of cognition suggests that family history of AD and ε4 status may be additive factors, and that, with the removal of individuals known to convert to AD, only individuals with both a positive family history of AD and ε4+ status demonstrate a more rapid cognitive decline [67]. The present sample represents individuals in their 6th decade of life, when few are likely to be affected by dementia, although we do not have data on family history at this time. In contrast, the unique study of children and adolescents (n=174 non-ε4, n=65 ε4+; 8–21 years) provides support for the thinner left entorhinal cortex for ε4+ individuals [38], although these effects were subtle and the variability in thickness was slightly larger within the ε4+ relative to the non-ε4 group, similar to the present study. These findings together support the hypothesis that additional factors likely mediate the influence of ε4 status on brain structure.

Other studies have demonstrated differences in ε4-related effects by gender and report potential mediating or moderating factors such as hormones. There may be an interaction between gender and ApoE ε4 status [68] such that, in general, females are more influenced by ε4 status than males. In MCI, female ε4+ carriers have a higher risk of developing AD than men of the same genotype [14]. A neuroimaging study reported that female, but not male, ε4+ carriers had significantly smaller hippocampal volumes relative to non-ε4 individuals; the authors suggested the potential for hormonal mediation of the influence of ε4 status [69]. It is possible, then, that in the present male sample, ε4-related MTL effects may be reduced and/or obscured by other factors. In fact, a study of VETSA participants revealed a significant interaction between testosterone and ε4 status indicating that ε4+ men who also had low levels of testosterone have smaller hippocampal volumes [70]. A similar interaction between ε4 status and cortisol levels or patterns also has been observed with respect to cognition in older adults [71].

The present study also included a larger sample, relative to published reports [e.g., 42], that allowed for a characterization of the influence of carrying an ε2 allele in middle-aged individuals. In contrast to ε4 status, the ε2 allele appears to have a subtle impact on thickness in MTL and medial orbitofrontal areas. The significantly thicker right parahippocampal cortex and broader tendencies for thicker cortex in these areas lend support to findings in adolescents [38] and corroborate the protec-

tive influence of ε2 demonstrated in neuropathological and cognitive studies [8, 15–21]. Exploratory analyses suggesting thinner right supramarginal and left lingual cortex are intriguing but require further replication.

The unique VETSA cohort provided significant power to examine the influence of ApoE allele status, although the study presents some limitations to generalizability. Because our sample was solely male and largely Caucasian, we cannot be certain of the generalizability of these findings to women or ethnic minorities. Furthermore, although the sample is quite similar in health and demographics to comparably-aged men in the U.S., a minority of them did experience varying amounts of combat exposure 35 years earlier. Thus, concerns might be raised as to the effect of combat exposure or possible posttraumatic stress disorder (PTSD) on the results. As of their mid-40s, 7.7% had a lifetime diagnosis of PTSD, slightly higher than the 5.0% prevalence for men nationally [72]. Importantly, this is unlikely to be create a confound in the present study because previous co-twin control findings indicate that smaller hippocampal volume may be a risk factor for PTSD, rather than a consequence [73]. Another potential limitation of our study is that, with T1-based image processing approaches, it is difficult to distinguish tentorium cerebelli from cortex in some mesial and inferior temporal regions. That is, while we have made every effort to separate cortical gray matter from tentorium, thickness estimates in these regions, such as the entorhinal cortex, may be more variable than in other areas. Such an increase in variability may result in less power to detect significant effects of ApoE allele status on thickness, although we would not expect differential effects across ApoE groups.

CONCLUSION

This study of middle-aged men suggests that the presence of the ApoE ε4 allele may influence cortical thickness in frontal areas, later developing regions thought to be more susceptible to natural aging. In contrast, previous conflicting findings of ε4 effects on MTL regions may be driven by the inclusion of older individuals who may evidence preclinical manifestations of neurodegenerative disease, and by moderators of ε4-realted effects, such as hormone levels. The finding of unexpectedly thicker fusiform cortex in the ε4+ group needs to be explored further and replicated. The examination of the ε2 allele supports a protective role, suggesting tendencies for thicker cor-

tex in some MTL and orbitofrontal areas, although some exploratory areas were thinner. Whether these ε2 and ε4 related findings reflect pre-existing endophenotypes or early neurodegeneration is not clear in these cross-sectional data. Ongoing follow-up studies of the VESTA sample may shed light on the potential for age- and disease-related mediation of the influence of ApoE allele status, as these participants enter the age range within which normal age-related neurodegeneration along with memory decline in ε4+ individuals may accelerate [43, 74].

REFERENCES

[1] Saunders AM, Strittmatter WJ, Schmechel D, George-Hyslop PH, Pericak-Vance MA, Joo SH, Rosi BL, Gusella JF, Crapper-MacLachlan DR, Alberts MJ, Hulette C, Crain B, Goldgaber D, Roses AD (1993) Association of apolipopro-

tein E allele epsilon 4 with late-onset familial and sporadic Alzheimer's disease. *Neurology* **43**, 1467-1472.

[2]   Bookheimer S, Burggren A (2009) APOE-4 genotype and neurophysiological vulnerability to Alzheimer's and cognitive aging. *Annu Rev Clin Psychol* **5**, 343-362.

[3]   Pericak-Vance MA, Bebout JL, Gaskell PC Jr, Yamaoka LH, Hung WY, Alberts MJ, Walker AP, Bartlett RJ, Haynes CA, Welsh KA, Earl NL, Heyman A, Clark CM, Roses AD (1991) Linkage studies in familial Alzheimer disease: evidence for chromosome 19 linkage. *Am J Hum Genet* **48**, 1034-1050.

[4]   Strittmatter WJ, Saunders AM, Schmechel D, Pericak-Vance M, Enghild J, Salvesen GS, Roses AD (1993) Apolipoprotein E: high-avidity binding to beta-amyloid and increased frequency of type 4 allele in late-onset familial Alzheimer disease. *Proc Natl Acad Sci U S A* **90**, 1977-1981.

[5]   Siest G, Pillot T, Regis-Bailly A, Leininger-Muller B, Steinmetz J, Galteau MM, Visvikis S (1995) Apolipoprotein E: an important gene and protein to follow in laboratory medicine. *Clin Chem* **41**, 1068-1086.

[6]   Mahley RW (1988) Apolipoprotein E: cholesterol transport protein with expanding role in cell biology. *Science* **240**, 622-630.

[7]   Schipper H.M. Apolipoprotein E: Implications for AD neurobiology, epidemiology and risk assessment. *Neurobiol Aging*. (In Press)

[8]   Corder EH, Saunders AM, Risch NJ, Strittmatter WJ, Schmechel DE, Gaskell PC, Rimmler JB, Locke PA, Conneally PM, Schmader KE, Small GW, Roses AD, Haines JL, Pericak-Vance MA (1994) Protective effect of apolipoprotein E type 2 allele for late onset Alzheimer disease. *Nat Genet* **7**, 180-184.

[9]   DeCarli C, Reed T, Miller BL, Wolf PA, Swan GE, Carmelli D (1999) Impact of apolipoprotein E epsilon4 and vascular disease on brain morphology in men from the NHLBI twin study. *Stroke* **30**, 1548-1553.

[10] Finch CE, Sapolsky RM (1999) The evolution of Alzheimer disease, the reproductive schedule, and apoE isoforms. *Neurobiol Aging* **20**, 407-428.

[11] Bleumink GS, van Duijn CM, Kingma JH, Witteman JC, Hofman A, Stricker BH (2004) Apolipoprotein E epsilon4 allele is associated with left ventricular systolic dysfunction. *Am Heart J* **147**, 685-689.

[12] Fazekas F, Enzinger C, Ropele S, Schmidt H, Schmidt R, Strasser-Fuchs S (2006) The impact of our genes: consequences of the apolipoprotein E polymorphism in Alzheimer disease and multiple sclerosis. *J Neurol Sci* **245**, 35-39.

[13] Corder EH, Saunders AM, Strittmatter WJ, Schmechel DE, Gaskell PC, Small GW, Roses AD, Haines JL, Pericak-Vance MA (1993) Gene dose of apolipoprotein E type 4 allele and the risk of Alzheimer's disease in late onset families. *Science* **261**, 921-923.

[14] Farrer LA, Cupples LA, Haines JL, Hyman B, Kukull WA, Mayeux R, Myers RH, Pericak-Vance MA, Risch N, van Duijn CM (1997) Effects of age, sex, and ethnicity on the association between apolipoprotein E genotype and Alzheimer disease. A meta-analysis. APOE and Alzheimer Disease Meta Analysis Consortium. *JAMA* **278**, 1349-1356.

[15] Martins CA, Oulhaj A, de Jager CA, Williams JH (2005) APOE alleles predict the rate of cognitive decline in Alzheimer disease: a nonlinear model. *Neurology* **65**, 1888-1893.

[16] Lippa CF, Smith TW, Saunders AM, Hulette C, Pulaski-Salo D, Roses AD (1997) Apolipoprotein E-epsilon 2 and

Alzheimer's disease: genotype influences pathologic phenotype. *Neurology* **48**, 515-519.

[17] Tiraboschi P, Hansen LA, Masliah E, Alford M, Thal LJ, Corey-Bloom J (2004) Impact of APOE genotype on neuropathologic and neurochemical markers of Alzheimer disease. *Neurology* **62**, 1977-1983.

[18] Oyama F, Shimada H, Oyama R, Ihara Y (1995) Apolipoprotein E genotype, Alzheimer's pathologies and related gene expression in the aged population. *Brain Res Mol Brain Res* **29**, 92-98.

[19] Blacker D, Lee H, Muzikansky A, Martin EC, Tanzi R, McArdle JJ, Moss M, Albert M (2007) Neuropsychological measures in normal individuals that predict subsequent cognitive decline. *Arch Neurol* **64**, 862-871.

[20] Baum L, Chen L, Ng HK, Pang CP (2000) Apolipoprotein E isoforms in Alzheimer's disease pathology and etiology. *Microsc Res Tech* **50**, 278-281.

[21] Berlau DJ, Corrada MM, Head E, Kawas CH (2009) APOE epsilon2 is associated with intact cognition but increased Alzheimer pathology in the oldest old. *Neurology* **72**, 829-834.

[22] Juottonen K, Lehtovirta M, Helisalmi S, Riekkinen PJ Sr., Soininen H (1998) Major decrease in the volume of the entorhinal cortex in patients with Alzheimer's disease carrying the apolipoprotein E epsilon4 allele. *J Neurol Neurosurg Psychiatry* **65**, 322-327.

[23] Schuff N, Woerner N, Boreta L, Kornfield T, Shaw LM, Trojanowski JQ, Thompson PM, Jack CR Jr., Weiner MW (2009) MRI of hippocampal volume loss in early Alzheimer's disease in relation to ApoE genotype and biomarkers. *Brain* **132**, 1067-1077.

[24] Liu Y, Paajanen T, Westman E, Zhang Y, Wahlund LO, Simmons A, Tunnard C, Sobow T, Proitsi P, Powell J, Mecocci P, Tsolaki M, Vellas B, Muehlboeck S, Evans A, Spenger C, Lovestone S, Soininen H (2010) APOE epsilon2 allele is associated with larger regional cortical thicknesses and volumes. *Dement Geriatr Cogn Disord* **30**, 229-237.

[25] Wolk DA, Dickerson BC (2010) Apolipoprotein E (APOE) genotype has dissociable effects on memory and attentional-executive network function in Alzheimer's disease. *Proc Natl Acad Sci U S A* **107**, 10256-10261.

[26] Farlow MR, He Y, Tekin S, Xu J, Lane R, Charles HC (2004) Impact of APOE in mild cognitive impairment. *Neurology* **63**, 1898-1901.

[27] Geroldi C, Pihlajamaki M, Laakso MP, DeCarli C, Beltramello A, Bianchetti A, Soininen H, Trabucchi M, Frisoni GB (1999) APOE-epsilon4 is associated with less frontal and more medial temporal lobe atrophy in AD. *Neurology* **53**, 1825-1832.

[28] Filippini N, Rao A, Wetten S, Gibson RA, Borrie M, Guzman D, Kertesz A, Loy-English I, Williams J, Nichols T, Whitcher B, Matthews PM (2009) Anatomically-distinct genetic associations of APOE epsilon4 allele load with regional cortical atrophy in Alzheimer's disease. *Neuroimage* **44**, 724-728.

[29] Hua X, Leow AD, Parikshak N, Lee S, Chiang MC, Toga AW, Jack CR Jr., Weiner MW, Thompson PM (2008) Tensor-based morphometry as a neuroimaging biomarker for Alzheimer's disease: an MRI study of 676 AD, MCI, and normal subjects. *Neuroimage* **43**, 458-469.

[30] Small GW, Siddarth P, Burggren AC, Kepe V, Ercoli LM, Miller KJ, Lavretsky H, Thompson PM, Cole GM, Huang SC, Phelps ME, Bookheimer SY, Barrio JR (2009) Influence of cognitive status, age, and APOE-4 genetic risk on brain

FDDNP positron-emission tomography imaging in persons without dementia. *Arch Gen Psychiatry* **66**, 81-87.

[31] Reiman EM, Caselli RJ, Yun LS, Chen K, Bandy D, Minoshima S, Thibodeau SN, Osborne D (1996) Preclinical evidence of Alzheimer's disease in persons homozygous for the epsilon 4 allele for apolipoprotein E. *N Engl J Med* **334**, 752-758.

[32] Reiman EM, Chen K, Alexander GE, Caselli RJ, Bandy D, Osborne D, Saunders AM, Hardy J (2005) Correlations between apolipoprotein E epsilon4 gene dose and brain-imaging measurements of regional hypometabolism. *Proc Natl Acad Sci U S A* **102**, 8299-8302.

[33] Thambisetty M, Beason-Held L, An Y, Kraut MA, Resnick SM (2010) APOE epsilon4 genotype and longitudinal changes in cerebral blood flow in normal aging. *Arch Neurol* **67**, 93-98.

[34] Plassman BL, Welsh-Bohmer KA, Bigler ED, Johnson SC, Anderson CV, Helms MJ, Saunders AM, Breitner JC (1997) Apolipoprotein E epsilon 4 allele and hippocampal volume in twins with normal cognition. *Neurology* **48**, 985-989.

[35] Mueller SG, Schuff N, Raptentsetsang S, Elman J, Weiner MW (2008) Selective effect of Apo e4 on CA3 and dentate in normal aging and Alzheimer's disease using high resolution MRI at 4 T. *Neuroimage* **42**, 42-48.

[36] Wishart HA, Saykin AJ, McAllister TW, Rabin LA, McDonald BC, Flashman LA, Roth RM, Mamourian AC, Tsongalis GJ, Rhodes CH (2006) Regional brain atrophy in cognitively intact adults with a single APOE epsilon4 allele. *Neurology* **67**, 1221-1224.

[37] Burggren AC, Zeineh MM, Ekstrom AD, Braskie MN, Thompson PM, Small GW, Bookheimer SY (2008) Reduced cortical thickness in hippocampal subregions among cognitively normal apolipoprotein E e4 carriers. *Neuroimage* **41**, 1177-1183.

[38] Shaw P, Lerch JP, Pruessner JC, Taylor KN, Rose AB, Greenstein D, Clasen L, Evans A, Rapoport JL, Giedd JN (2007) Cortical morphology in children and adolescents with different apolipoprotein E gene polymorphisms: an observational study. *Lancet Neurol* **6**, 494-500.

[39] Lemaitre H, Crivello F, Dufouil C, Grassiot B, Tzourio C, Alperovitch A, Mazoyer B (2005) No epsilon4 gene dose effect on hippocampal atrophy in a large MRI database of healthy elderly subjects. *Neuroimage* **24**, 1205-1213.

[40] Espeseth T, Westlye LT, Fjell AM, Walhovd KB, Rootwelt H, Reinvang I (2008) Accelerated age-related cortical thinning in healthy carriers of apolipoprotein E epsilon 4. *Neurobiol Aging* **29**, 329-340.

[41] Lind J, Larsson A, Persson J, Ingvar M, Nilsson LG, Backman L, Adolfsson R, Cruts M, Sleegers K, Van Broeckhoven C, Nyberg L (2006) Reduced hippocampal volume in non-demented carriers of the apolipoprotein E epsilon4: relation to chronological age and recognition memory. *Neurosci Lett* **396**, 23-27.

[42] Liu Y, Paajanen T, Westman E, Wahlund LO, Simmons A, Tunnard C, Sobow T, Proitsi P, Powell J, Mecocci P, Tsolaki M, Vellas B, Muehlboeck S, Evans A, Spenger C, Lovestone S, Soininen H (2010) Effect of APOE epsilon4 allele on cortical thicknesses and volumes: the AddNeuroMed study. *J Alzheimers Dis* **21**, 947-966.

[43] Caselli RJ, Dueck AC, Osborne D, Sabbagh MN, Connor DJ, Ahern GL, Baxter LC, Rapcsak SZ, Shi J, Woodruff BK, Locke DE, Snyder CH, Alexander GE, Rademakers R, Reiman EM (2009) Longitudinal modeling of age-related memory decline and the APOE epsilon4 effect. *N Engl J Med* **361**, 255-263.

[44] Jernigan TL, Archibald SL, Fennema-Notestine C, Gamst AC, Stout JC, Bonner J, Hesselink JR (2001) Effects of age on tissues and regions of the cerebrum and cerebellum. *Neurobiol Aging* **22**, 581-594.

[45] Thambisetty M, Wan J, Carass A, An Y, Prince JL, Resnick SM (2010) Longitudinal changes in cortical thickness associated with normal aging. *Neuroimage* **52**, 1215-1223.

[46] Kremen WS, Thompson-Brenner H, Leung YM, Grant MD, Franz CE, Eisen SA, Jacobson KC, Boake C, Lyons MJ (2006) Genes, environment, and time: the Vietnam Era Twin Study of Aging (VETSA). *Twin Res Hum Genet* **9**, 1009-1022.

[47] Goldberg J, Curran B, Vitek ME, Henderson WG, Boyko EJ (2002) The Vietnam Era Twin Registry. *Twin Res* **5**, 476-481.

[48] Centers for Disease Control and Prevention. Health data for all ages [online]. Available at: http://www.cdc.gov/nchs/hdi.htm. Accessed April 20, 2007

[49] Emi M, Wu LL, Robertson MA, Myers RL, Hegele RA, Williams RR, White R, Lalouel JM (1988) Genotyping and sequence analysis of apolipoprotein E isoforms. *Genomics* **3**, 373-379.

[50] Hixson JE, Vernier DT (1990) Restriction isotyping of human apolipoprotein E by gene amplification and cleavage with HhaI. *J Lipid Res* **31**, 545-548.

[51] Rebeck GW, Perls TT, West HL, Sodhi P, Lipsitz LA, Hyman BT (1994) Reduced apolipoprotein epsilon 4 allele frequency in the oldest old Alzheimer's patients and cognitively normal individuals. *Neurology* **44**, 1513-1516.

[52] Lyons MJ, York TP, Franz CE, Grant MD, Eaves LJ, Jacobson KC, Schaie KW, Panizzon MS, Boake C, Xian H, Toomey R, Eisen SA, Kremen WS (2009) Genes determine stability and the environment determines change in cognitive ability during 35 years of adulthood. *Psychol Sci* **20**, 1146-1152.

[53] Kremen WS, Prom-Wormley E, Panizzon MS, Eyler LT, Fischl B, Neale MC, Franz CE, Lyons MJ, Pacheco J, Perry ME, Stevens A, Schmitt JE, Grant MD, Seidman LJ, Thermenos HW, Tsuang MT, Eisen SA, Dale AM, Fennema-Notestine C (2010) Genetic and environmental influences on the size of specific brain regions in midlife: the VETSA MRI study. *Neuroimage* **49**, 1213-1223.

[54] Fischl B, Salat DH, Busa E, Albert M, Dieterich M, Haselgrove C, van der Kouwe A, Killiany R, Kennedy D, Klaveness S, Montillo A, Makris N, Rosen B, Dale AM (2002) Whole brain segmentation: automated labeling of neuroanatomical structures in the human brain. *Neuron* **33**, 341-355.

[55] Dale AM, Fischl B, Sereno MI (1999) Cortical surface-based analysis. *I. Segmentation and surface reconstruction. Neuroimage* **9**, 179-194.

[56] Fischl B, Sereno MI, Dale AM (1999) Cortical surface-based analysis. *II: Inflation, flattening, and a surface-based coordinate system. Neuroimage* **9**, 195-207.

[57] Fischl B, Van Der Kouwe A, Destrieux C, Halgren E, Segonne F, Salat DH, Busa E, Seidman LJ, Goldstein J, Kennedy D, Caviness V, Makris N, Rosen B, Dale AM (2004) Automatically parcellating the human cerebral cortex. *Cereb Cortex* **14**, 11-22.

[58] Buckner RL, Head D, Parker J, Fotenos AF, Marcus D, Morris JC, Snyder AZ (2004) A unified approach for morphometric and functional data analysis in young, old, and demented adults using automated atlas-based head size normalization: reliability and validation against manual measurement of total intracranial volume. *Neuroimage* **23**, 724-738.

[59] Fennema-Notestine C, Gamst AC, Quinn BT, Pacheco J, Jernigan TL, Thal L, Buckner R, Killiany R, Blacker D, Dale AM, Fischl B, Dickerson B, Gollub RL (2007) Feasibility of multi-site clinical structural neuroimaging studies of aging using legacy data. *Neuroinformatics* **5**, 235-245.

[60] Desikan RS, Segonne F, Fischl B, Quinn BT, Dickerson BC, Blacker D, Buckner RL, Dale AM, Maguire RP, Hyman BT, Albert MS, Killiany RJ (2006) An automated labeling system for subdividing the human cerebral cortex on MRI scans into gyral based regions of interest. *Neuroimage* **31**, 968-980.

[61] Barnes J, Ridgway GR, Bartlett J, Henley SM, Lehmann M, Hobbs N, Clarkson MJ, MacManus DG, Ourselin S, Fox NC (2010) Head size, age and gender adjustment in MRI studies: a necessary nuisance? *Neuroimage* **53**, 1244-1255.

[62] Han X, Jovicich J, Salat D, van der Kouwe A, Quinn B, Czanner S, Busa E, Pacheco J, Albert M, Killiany R, Maguire P, Rosas D, Makris N, Dale A, Dickerson B, Fischl B (2006) Reliability of MRI-derived measurements of human cerebral cortical thickness: The effects of field strength, scanner upgrade and manufacturer. *Neuroimage*

[63] Stonnington CM, Tan G, Kloppel S, Chu C, Draganski B, Jack CR Jr., Chen K, Ashburner J, Frackowiak RS (2008) Interpreting scan data acquired from multiple scanners: a study with Alzheimer's disease. *Neuroimage* **39**, 1180-1185.

[64] Dumanis SB, Tesoriero JA, Babus LW, Nguyen MT, Trotter JH, Ladu MJ, Weeber EJ, Turner RS, Xu B, Rebeck GW, Hoe HS (2009) ApoE4 decreases spine density and dendritic complexity in cortical neurons in vivo. *J Neurosci* **29**, 15317-15322.

[65] Agosta F, Vossel KA, Miller BL, Migliaccio R, Bonasera SJ, Filippi M, Boxer AL, Karydas A, Possin KL, Gorno-Tempini ML (2009) Apolipoprotein E epsilon4 is associated with disease-specific effects on brain atrophy in Alzheimer's disease and frontotemporal dementia. *Proc Natl Acad Sci U S A* **106**, 2018-2022.

[66] Cherbuin N, Leach LS, Christensen H, Anstey KJ (2007) Neuroimaging and APOE genotype: a systematic qualitative review. *Dement Geriatr Cogn Disord* **24**, 348-362.

[67] Hayden KM, Zandi PP, West NA, Tschanz JT, Norton MC, Corcoran C, Breitner JC, Welsh-Bohmer KA (2009) Effects of family history and apolipoprotein E epsilon4 status on cognitive decline in the absence of Alzheimer dementia: the Cache County Study. *Arch Neurol* **66**, 1378-1383.

[68] Rao VS, Cupples A, van Duijn CM, Kurz A, Green RC, Chui H, Duara R, Auerbach SA, Volicer L, Wells J, van Broeckhoven C, Growdon JH, Haines JL, Farrer LA (1996) Evidence for major gene inheritance of Alzheimer disease in families of patients with and without apolipoprotein E epsilon 4. *Am J Hum Genet* **59**, 664-675.

[69] Fleisher A, Grundman M, Jack CR Jr., Petersen RC, Taylor C, Kim HT, Schiller DH, Bagwell V, Sencakova D, Weiner MF, DeCarli C, DeKosky ST, van Dyck CH, Thal LJ (2005) Sex, apolipoprotein E epsilon 4 status, and hippocampal volume in mild cognitive impairment. *Arch Neurol* **62**, 953-957.

[70] Panizzon MS, Hauger R, Dale AM, Eaves LJ, Eyler LT, Fischl B, Fennema-Notestine C, Franz CE, Grant MD, Jak AJ, Jacobson KC, Lyons MJ, Mendoza SP, Neale MC, Prom-Wormley EC, Seidman LJ, Tsuang MT, Xian H, Kremen WS (2010) Testosterone modifies the effect of APOE genotype on hippocampal volume in middle-aged men. *Neurology* **75**, 874-880.

[71] Gerritsen L, Comijs HC, Deeg DJ, Penninx BW, Geerlings MI Salivary cortisol, APOE-varepsilon4 allele and cognitive decline in a prospective study of older persons. *Neurobiol Aging* (In Press)

[72] Kessler RC, Sonnega A, Bromet E, Hughes M, Nelson CB (1995) Posttraumatic stress disorder in the National Comorbidity Survey. *Arch Gen Psychiatry* **52**, 1048-1060.

[73] Gilbertson MW, Shenton ME, Ciszewski A, Kasai K, Lasko NB, Orr SP, Pitman RK (2002) Smaller hippocampal volume predicts pathologic vulnerability to psychological trauma. *Nat Neurosci* **5**, 1242-1247.

[74] Jernigan TL, Gamst AC (2005) Changes in volume with age–consistency and interpretation of observed effects. *Neurobiol Aging* **26**, 1271-1274; discussion 1275-1278.

Alzheimer's Disease and Dementia with Lewy Bodies can be Differentiated by High Resolution MR Imaging of the Hippocampus

Michael J. Firbank [a,*], Andrew M. Blamire [b], Andrew Teodorczuk [a], Dipayan Mitra [c], Emma Teper [a] and John T. O'Brien [a]

[a] *Institute for Ageing and Health, Newcastle University, Newcastle upon Tyne, UK*
[b] *Newcastle Magnetic Resonance Centre, Newcastle University, Newcastle upon Tyne, UK*
[c] *Department of Neuroradiology, Royal Victoria Infirmary, Newcastle upon Tyne, UK*

Abstract. The medial temporal lobe is affected early on in Alzheimer's disease (AD), and the presence of medial temporal atrophy can be used in the differential diagnosis of AD. However, the hippocampus has a complex structure, and subregions of the hippocampus are differentially affected in different dementia types. We used high resolution (0.3 mm in-plane) coronal 3T MR imaging of the medial temporal lobe in 16 subjects with Alzheimer's disease (AD), 16 with dementia with Lewy bodies (DLB) and 16 similarly aged healthy subjects to investigate differences in the hippocampus subregions. On the anterior section of the hippocampus body, regions of interest were manually drawn blind to diagnosis on the CA1, CA2 & CA3/4 subregions, and the width of the subiculum and entorhinal cortex was measured.

Controlling for intracranial volume, age and years of education, we found the subiculum thickness was significantly reduced in AD (2.03 ± 0.29 mm) compared to both control (2.37 ± 0.28 mm, $p = 0.008$) and DLB (2.35 ± 0.24 mm, $p = 0.001$) subjects. The area of CA1 was likewise reduced in AD compared to controls and DLB.

In the hippocampus images, a hypointense line is visible between CA1 and CA3/4. This line was significantly less distinct in AD, suggesting disease related changes to this region. Future studies should investigate whether subiculum thickness or the hypointense line could be a diagnostic feature to help discriminate AD from DLB.

Keywords: Alzheimer's disease, dementia with Lewy bodies, hippocampus, MRI, subiculum

INTRODUCTION

Alzheimer's disease (AD) is characterised by extensive tissue loss in the medial temporal lobe region, especially in the hippocampus and entorhinal cortex. However, the hippocampus has a complex anatomical structure, and is not uniformly affected in disease.

A number of MRI studies using T1 weighted imaging, and approximately isotropic 1 mm³ voxels, have shown that, along with the entorhinal cortex, atrophy in AD is largely confined to the CA1 and subiculum regions of the hippocampus [1, 2], consistent with the major site of pathology observed at autopsy [3]. However, these studies have not directly visualised subfields but relied on inferring the location of the subregions from the known anatomy of the hippocampus surface. Using a high in plane resolution coronal T2 weighted sequence at 4T, Mueller and colleagues have shown it is possible

---

*Correspondence to: Michael J. Firbank, Institute for Ageing and Health, Newcastle University, Wolfson Research Centre, Campus for Ageing and Vitality, Newcastle upon Tyne NE4 5PL. Tel.: +0191 248 1319; Fax: +0191 248 1301; E-mail: m.j.firbank@ncl.ac.uk.

to differentiate the hippocampal subregions directly in both control [4] and AD [5].

Previous MR imaging studies in dementia with Lewy bodies (DLB) have shown that the degree of hippocampal atrophy is less in DLB than in AD [6–8]. Using shape analysis on hippocampi manually traced from T1 weighted images, a study [9] also found less atrophy in DLB compared to AD. The distribution of atrophy was somewhat different, affecting more anterior regions in DLB, and posterior regions in AD, consistent with more CA2 and CA3 atrophy in DLB. Kenny [10] measured the entorhinal cortex using a region of interest on T1 weighted images, and found comparable atrophy in AD and DLB. Neuropathological studies have found Lewy body neurites preferentially in the CA2 and CA3 region [11, 12], though Harding [13] found no difference between control and DLB in any hippocampal subregion volume.

The purpose of this study was to investigate atrophy of the subfields of the anterior part of the body of the hippocampus, using high resolution coronal imaging of the medial temporal lobe. We hypothesised that there would be more atrophy of the CA1 and subiculum in AD, with more atrophy of the CA2 or CA3/4 region in DLB and that these changes may be helpful for differentiating AD from DLB.

MATERIALS AND METHODS

Subjects

We recruited 16 people with Alzheimer's disease and 16 with dementia with Lewy bodies, from clinical Old Age Psychiatry, Geriatric Medicine and Neurology Services. Sixteen healthy subjects of similar age were also recruited.

All subjects were aged over 60, and did not have contra-indications for MRI. Subjects with dementia had mild to moderate severity (MMSE > 10). All Alzheimer's disease subjects fulfilled criteria for probable AD according to NINCDS/ADRDA [14]. Dementia with Lewy body cases all met criteria for probable DLB according to the consensus criteria [15] (i.e. they met two or more of the core features of fluctuating cognition, visual hallucinations and parkinsonism). Nine of the DLB subjects had a ^{123}I-FP-CIT SPECT scan, all of whom demonstrated reduced dopamine transporter uptake in the basal ganglia. All diagnoses were made by consensus between two experienced clinicians, a method we have previously

validated against autopsy diagnosis [16]. Diagnoses were made independent of MRI scanning. Routine clinical workup for dementia included detailed physical, neurological and neuropsychiatric examinations, including screening blood tests and CT scan. Presence of diabetes and hypertension were determined through a combination of medical records, interview with subject, and examining medications. Additional assessments performed were of cognition (Cambridge Cognitive Examination (CAMCOG)) [17], mood (Cornell depression scale) [18], neuropsychiatric features (Neuropsychiatric inventory (NPI)) [19], clinical fluctuation (Clinical Assessment of Fluctuation scale) [20], memory (Rey auditory verbal learning test [21]) and motor features of parkinsonism (UPDRS subsection III) [22].

Exclusion criteria included severe concurrent illness (apart from dementia for patients), space occupying lesions on imaging, history of stroke and contraindications to MRI. In addition, controls had no history of psychiatric illnesses.

The study was approved by the local ethics committee, and all subjects gave signed informed consent for participation.

MRI acquisition

Subjects were scanned on a 3T MRI system (Intera Achieva scanner; Philips, Eindhoven, the Netherlands). Images acquired included a T1 weighted volumetric sequence covering the whole brain (MPRAGE, sagittal acquisition, slice thickness 1.2 mm, voxel size 1.15 × 1.15 mm; TR = 9.6 ms; TE 4.6 ms; flip angle = 8°; SENSE factor = 2).

We used a high resolution T2 weighted turbo spin echo coronal imaging sequence based on previous work at 4T [4]. Prior to commencing the study, we attempted to optimize the high resolution sequence using a range of TR (2500–5000 ms) and TE (19–80 ms) on a 42 year old volunteer. On the first 13 subjects we used the following sequence: turbo factor 15; 24 slices; slice thickness 2 mm, field of view 210 × 167; pixel resolution 0.41 × 0.52 mm; TR 2568 ms; TE 19 ms; flip angle 90°. This scan was repeated to collect 2 datasets – acquisition time = 2*2:50.

After the first 13 subjects (5 Control, 7 AD, 1 DLB) one of the high resolution acquisitions was replaced (see results for explanation of reasons) by 3 acquisitions of a sequence with the following parameters altered (12 slices; pixel resolution 0.27 × 0.35 mm; TR

3852 ms; 3 acquisitions – acquisition time = 3*2:07). The number of acquisitions was increased to maintain SNR in the face of smaller voxels. The first 13 subjects were not rescanned with the new sequence. Data were acquired using multiple acquisitions to allow correction of patient motion prior to averaging to increase signal to noise ratio. This approach was found to maintain highest resolution in pilot studies compared with direct averaging by the scanner. The coronal images were positioned for each subject so they were angled perpendicular to the main axis of the hippocampus. This was achieved by angling the image plane at 25° relative to a line joining the inferior aspect of the genu and splenium of the corpus callosum. This line is similarly oriented to the standard anterior-posterior commissure orientation. We have previously found this to be a reliable and repeatable method to give a good angulation in the temporal lobe.

MRI processing

We used the FLIRT image registration tool [23] (part of FSL http://www.fmrib.ox.ac.uk/fsl/) to register all the high resolution images from each subject together, and interpolate with linear interpolation to 0.27×0.27 mm resolution. A higher signal to noise ratio image was then created by summing together all the registered high resolution images. For the initial 13 subjects in which two datasets were collected, these datasets were averaged together. For the subsequent subjects where four datasets were collected, an image was produced by averaging all four images (three images with 0.27×0.35 mm resolution and one with 0.41×0.52 mm) together. This was found by visual inspection to optimise contrast to noise.

Regions of interest (ROI) were manually drawn on coronal T2 weighted images of the hippocampus subregions CA1,CA2 and CA3/4 according to the method of Mueller [4] starting on the slice on which the head of the hippocampus was no longer visible, and the 2 slices posterior to that. This method uses the hypointense line visible on the coronal T2 weighted images in the hippocampus to determine the boundary between CA1 and CA3/4 (see Fig. 1). All regions were drawn with the temporal lobe presented with its medial aspect on the right of the screen. Figure 1 depicts the regions. The external boundary of CA1 was drawn starting with a line perpendicular to the subiculum cortex surface where it meets the CA3/4 region, and following the boundary of the hippocampus round to the CA2 region. The hypointense line was used to differentiate CA3/4 from CA1, and from the inferior portion of CA2. The fimbria was excluded. The medial border of CA2 was positioned halfway laterally across the hippocampus,
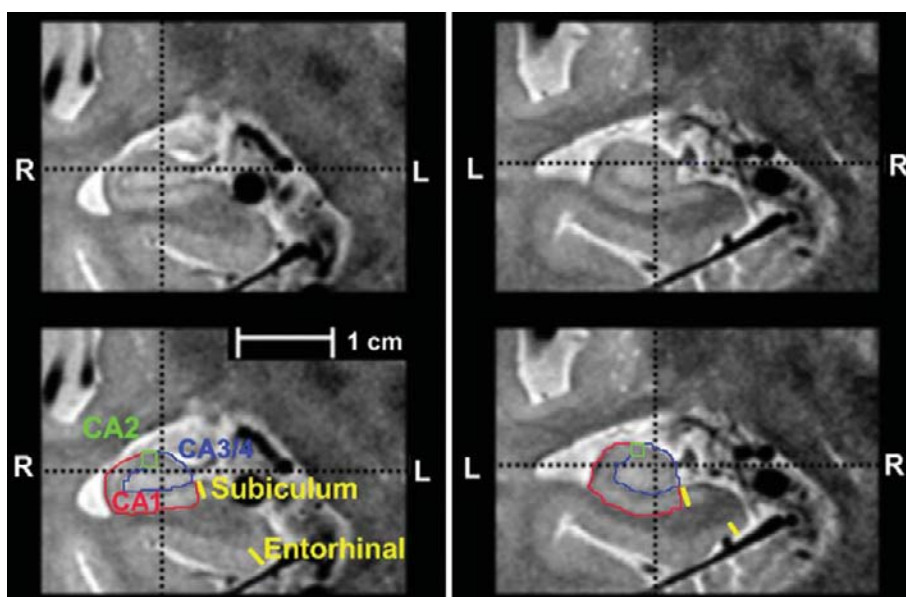
Fig. 1. Close up of hippocampi from one subject in the high resolution T2 weighted coronal sequence. (The left hippocampus has been flipped left-right so that the hippocampus has the same relative orientation). Bottom image shows the regions drawn CA1 (red) CA3/4 (blue) and CA2 (green). The thickness measurement of entorhinal cortex and subiculum is shown as a yellow line. (For reference to colour, see the online version of the image). R = right, and L = left.

measured from the superficial hippocampal sulcus. CA2 was then drawn as a square angled according to the superior surface of the hippocampus, whose height was determined by the distance between the hypointense line and the superior surface. We calculated the area of each ROI and then averaged values over the three slices on which they were defined to give an average area for each structure. An average hippocampus area was defined by summing together the values for CA1,CA2 & CA3/4. All regions were drawn using the freely available itk-snap package [24] (http://www.itksnap.org/pmwiki/pmwiki.php) by the same operator (MJF), blinded to diagnosis. Images were displayed with linear interpolation, and image display settings were determined by viewing the image intensity histogram – window levels were set from the width of the main bell-shaped histogram curve at approximately 10% of its height. This display setting enhanced the grey/white matter contrast.

Since the length of the subiculum and entorhinal cortex varied, and because it is known that thickness rather than area measurements are more consistent in these structures [25], we measured the thickness, rather than area, of the subiculum and entorhinal cortex. The imageJ (http://rsb.info.nih.gov/ij/index.html) image viewing package was used for distance measurement. This was performed by determining the length of a manually drawn line on the coronal images on three adjacent slices, and calculating the average length. The orientation of the line was drawn (by eye) perpendicular to the surface at the point of measurement. The subiculum thickness was measured on the same three slices as the CA1 region, where the medial border of the hippocampus joined the subiculum (see Fig. 1). The entorhinal cortex thickness was measured on the start-

ing slice of the CA1 measurement, and the two anterior slices. Position of entorhinal thickness measurement is also shown in Fig. 1. We also measured the thickness of the CA2 region on the same three slices as the region of interest was drawn, as a potentially more reliable measurement. Since we had no hypothesis regarding laterality, we averaged all left and right measurements.

Reliability was assessed by repeating the region drawing and distance measurement on 6 subjects (=12 hippocampi) chosen at random (2 control, 2 AD & 2 DLB) at least a month after initial region drawing. From these, we calculated intraclass correlation coefficient (ICC), percent difference, and (for region measurements) percent overlap. These were defined as

$$\text{Percent difference} = |V2 - V1|/(V2 + V1) \times 200$$

$$\text{Percent overlap} = (V1 \cap V2)/(V2 + V1) \times 200.$$

Where V1 is first measurement, V2 second measurement, and V1∩V2 the overlap between V1 and V2.

Reliability measures for the manual region drawing for repeat measurements on the 6 subjects are presented in Table 1, and are comparable with those of Mueller [4] showing that we can obtain good depiction of the internal structure of the hippocampus at 3T. Interrater reliability was assessed by a second trained observer (EJB) performing the analysis on the 6 cases, and results are also presented in Table 1. In order to compare the two different image protocols, on the 4 of these 6 subjects who had both coronal image sequences, we repeated the segmentations using just the lower resolution image (0.4 × 0.5 mm) and compared these to the segmentations performed on the averaged image

Table 1

Reliability measures of hippocampal area/thickness, performed on 6 subjects (12 medial temporal lobes). Final column is agreement between the image with resolution 0.41 × 0.52 mm and the average of four images (3 with resolution 0.27 × 0.36 mm and 1 with 0.41 × 0.52 mm), and these data are from the 4/6 of the subjects who had both sequences. Percent difference is absolute difference in area as percentage of average area, and percent overlap is area in common as a percentage of average area. Values are mean (95% Confidence interval)

	Within observer comparison			Between observer comparison			Initial vs. final sequence comparison		
	Percent difference	Percent overlap	ICC	Percent difference	Percent overlap	ICC	Percent difference	Percent overlap	ICC
CA1	7.7 (5–10)	90 (88–91)	0.98	16 (9–23)	76 (72–29)	0.91	5.2 (2–8)	81 (76–86)	0.98
CA2	24 (15–32)	68 (62–75)	0.62	20 (10–29)	34 (25–46)	0.23	20 (11–29)	59 (48–70)	0.20
CA3/4	7.3 (3–11)	90 (88–91)	0.95	22 (15–29)	79 (76–82)	0.80	13 (7–19)	84 (80–88)	0.74
Thicknesses:									
Entorhinal	13.2 (7–20)		0.72	11 (5–16)		0.78	13 (10–15)		0.68
Subiculum	8.0 (4–12)		0.84	11 (7–15)		0.78	10 (7–13)		0.90
CA2	7.0 (4–10)		0.74	19 (11–26)		0.57	12 (9–14)		0.72
Clarity			0.97			0.80			0.58

ICC = intraclass correlation coefficient.
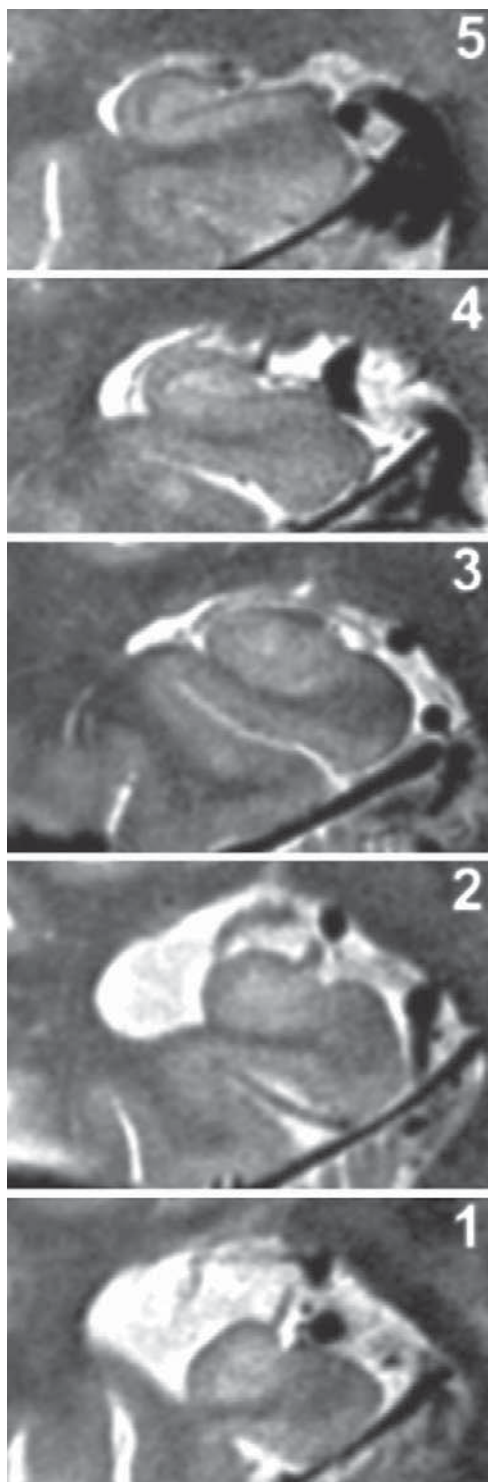
Fig. 2. Example hippocampi with visual rating for clearness. The visual rating is indicated in the top right of each hippocampus. The scale was based on the visibility of the dark line separating CA1 from CA3/4. Rating of 5 = line clearly visible on all slices; 3 = line partly visible; 1 = line not at all visible.

from all four acquisitions (lower resolution plus three higher resolution image). The comparison data are shown in the table. There is good agreement between measurements on the sequences, apart from the CA2 area.

As described above, we followed the method of Mueller et al. [4] which uses the location of the hypointense line in the hippocampus to determine the boundary between CA1 and CA2 & CA3/4 (see Fig. 1). Since we observed considerable variability in how clearly this line could be visualised between subjects, each hippocampus was assigned a score (1 to 5) according to how clearly the hippocampus internal structure was depicted throughout the 3 slices examined. On this scale, 5 = line clearly visualised throughout, 4 = most of the line clearly visualised, 3 = line semi clearly defined, 2 = line mostly not clearly defined, but recognisable, 1 = line not visualised at all (see Fig. 2 for example of each category). This was done at the same time as the region of interest drawing by the same investigator, again blinded to diagnosis. Reliability of the rating scale was assessed on the same cases as the hippocampus regions, and results are also presented in Table 1. The intrarater reliablility of the visual rating was also assessed separately on the first and second imaging sequences, and there was no significant difference in the visual rating reliability between imaging sequences.

We also obtained on all subjects a T1 weighted whole brain scan. We processed this scan to segment into grey and white matter and CSF using SPM 5 (http://www.fil.ion.ucl.ac.uk/spm/) from which the total intracranial volume (ICV) was determined by the sum of these three components. This was then used to control for differences in head size between individuals. We also used a previously validated automated segmentation technique [26] to determine the volume of left and right hippocampi from the T1 weighted image. This procedure uses the grey matter segmentation from SPM5, along with a standard hippocampus template to segment the hippocampus. The SPM grey/white matter & hippocampus segmentions were visually checked for any gross errors.

Statistics

We tested all variables for normality using the Kolmogorov Smirnov test. All apart from education, UPDRS and Rey scores were normally distributed. The Levene test was then used to compare homogeneity of variance, and, apart from MMSE, CAMCOG

and Fluctuation all had equal variances across groups. Education was dichotomised at 11 years (ie those who left school aged 16). Fisher's exact test was used to compare sex and post-16 education. We used ANOVA to compare normally distributed demographic factors and the Kruskal-Wallis test for the non-normally distributed variable between groups, followed by post hoc tests using Mann-Whitney, with a Bonferroni correction ($p = 0.05/3 = 0.016$) for multiple comparisons.

Since education varied between groups, it was included as a covariate in the analysis of the imaging data. Differences in hippocampal area between groups were examined with a three group ANCOVA with covariates of age, ICV and the binary variable of post-16 education, followed by Tukey post-hoc tests. To test the discriminant power, we used discriminant analysis with cross validation (leave one out). Wilks' Lambda test was used to assess the significance of the discriminant model. We investigated the relationship between memory function (Rey delayed recall and Rey total item score) and those hippocampus measurements which showed a group difference using a Spearman correlation within each group separately.

All p values quoted are two sided. Results were regarded as significant if $p < 0.05$. All statistical analysis was performed with Minitab 15 (Minitab inc, Pennsylvania, USA).

RESULTS

Subject and image characteristics

Demographic data is summarised in Table 2. There were no differences between groups in age or sex, presence of hypertension or diabetes, but the DLB subjects had fewer years of education than both control and AD subjects. Intracranial volumes did not differ between groups and there was no difference between AD and DLB groups in MMSE, CAMCOG, or duration of dementia. As would be expected, the UPDRS and NPI scores were higher in DLB subjects, as was the Rey delayed recall score – the latter indicative of better preserved memory function that is characteristic of DLB subjects.

Images were generally of good quality, with only one high resolution MR (from a DLB subject) not usable due to motion. However, early on in the study, we noticed that in those subjects with atrophied hippocampi, the hypointense band which divides CA1 from CA3/4 was not consistently visible. To try to improve visibility of substructures, after the first 13 subjects (5 Control, 7 AD, 1 DLB), we added a sequence with increased coronal resolution (from 24 coronal slices with resolution 0.4×0.5 to 12 slices with 0.27×0.35 resolution - see Fig. 3 for a compar-

Table 2
Subject demographics.

	Control $N = 16$	AD $N = 16$	DLB $N = 16$	
Age in years	76.3 (8.2) [61–93]	77.3 (8.9) [64–94]	81.0 (5.9) [70–88]	§$F = 1.6$; $p = 0.2$
Sex (Female : Male)	7 : 9	8 : 8	6 : 10	†$p = 0.9$
Education in years	11.5 [9–18]	10.5 [9–16]	9.0 [8–10] [b,c]	‡$H = 18$; $p = 0.001$
Education post 16 (Yes : No)	8 : 8	5 : 11	0 : 16 [b,c]	†$p = 0.004$
MMSE	29 [26–30]	21.5 [16–27] [a]	18 [15–27] [c]	‡$H = 31$; $p < 0.001$
Duration dementia (months)	–	40.4 (25) [6–72]	43.7 (24) [3–96]	$t = 0.16$; $p = 0.9$
UPDRS	2.0 [0–14]	5.5 [1–13] [a]	17.5 [9–33] [b,c]	‡$H = 32$; $p < 0.001$
CAMCOG	97 (3.5)	69 (11.4) [a]	67.4 (14.0) [c]	‡$H = 32$; $p < 0.001$
NPI total	–	8.5 (11.8)	24.1 (11.7) [b]	$t = 3.6$; $p = 0.001$
Rey total trials 1–5 (max 75)	42 [30–61]	21 [5–31] [a]	18 [4–36] [c]	‡$H = 31$; $p < 0.001$
Rey delayed recall (max 15)	8 [5–14]	0.0 [0–3] [a]	1.0 [0–8] [b,c]	‡$H = 35$; $p < 0.001$
Fluctuation score	0 [0] ($n = 4$)	0 [0–9]	7 [0–16] [b,c]	‡$H = 13$; $p = 0.002$
Hypertension Yes : No	7 : 9	6 : 10	6 : 10	†$p = 0.7$
Diabetes Yes : No	1 : 15	2 : 14	0 : 16	†$p = 0.3$
Intracranial volume (mL)	1504 (150)	1449 (159)	1472 (140)	§$F = 0.56$, $p = 0.6$

Values in the table are mean (SD) or median [range]; Post hoc $p < 0.05$ (a) AD vs Control; (b) DLB vs AD; (c) DLB vs Control; §ANOVA; †Fisher's exact test; ‡Kruskal-Wallis (H is the Kruskal-Wallis test statistic); MMSE = mini mental state exam; CAMCOG = Cambridge cognitive exam; UPDRS = Unified Parkinson's disease rating scale (subsection 3); NPI = Neuropsychiatric inventory; Rey = Rey auditory verbal learning test; Fluctuation score = Clinical Assessment of Fluctuation scale; Education post 16 and sex–Fisher's exact test; Post Hoc (Mann Whitney): Education: Con > DLB $p < 0.001$; AD > DLB $p = 0.001$; MMSE: Con > AD $p < 0.001$; Con > DLB $p < 0.001$; CAMCOG: Con > AD $p < 0.001$; Con > DLB $p < 0.001$; UPDRS Con < AD p = 0.008; Con < DLB $p < 0.001$; AD < DLB $p < 0.001$; Rey 1–5: Con > AD $p < 0.001$; Con > DLB $p < 0.001$; Rey delayed: Con > AD $p < 0.001$; Con > DLB $p < 0.001$; AD < DLB $p = 0.001$; Fluctuation: Con > DLB $p = 0.01$; AD > DLB $p = 0.006$.
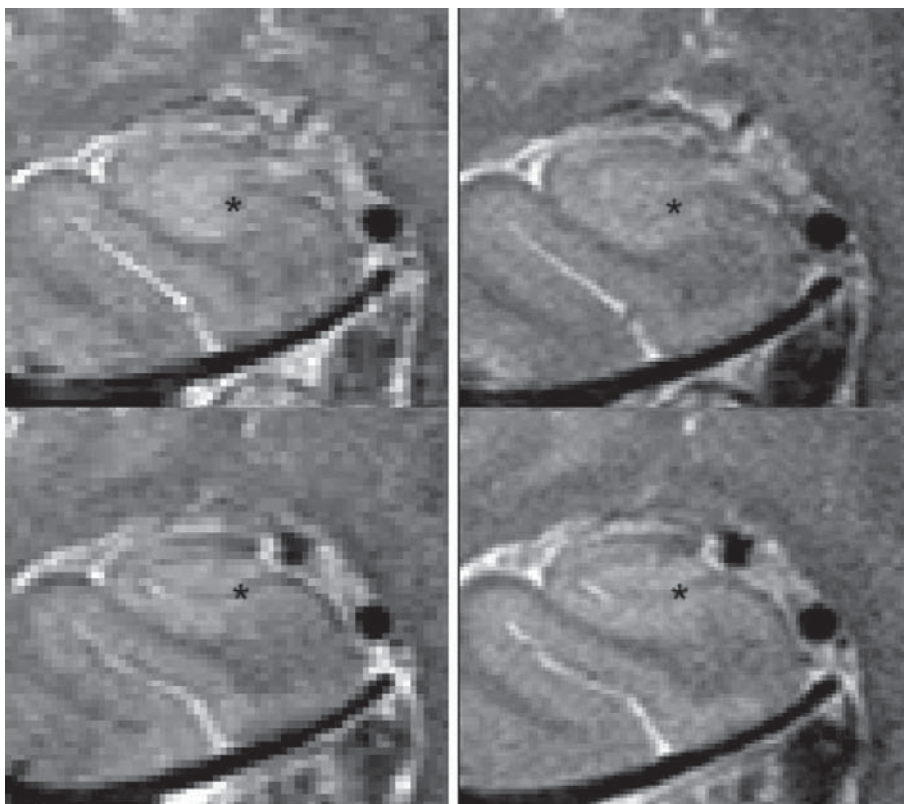
Fig. 3. Left column – hippocampus imaging in first 13 subjects (with resolution of 0.41×0.52 mm), right column – imaging used in subsequent subjects, with higher image resolution (0.27×0.35 mm). Note the hypointense line (indicated by an asterisk) in the hippocampus is more clearly depicted in the higher resolution image, allowing better definition of the subfield boundaries.

ison in a normal subject). There were no significant differences ($p > 0.2$) in any hippocampal measurements between images from the two sequences in any group.

Hippocampus measurements

Table 3 summarises the hippocampal measurements on the three groups in the 6 mm thick anterior portion of the hippocampus body that we examined. Controlling for age, ICV and post-16 education, we found the subiculum thickness was significantly reduced in AD compared to both control and DLB ($p < 0.01$). The area of CA1 was also reduced in AD relative to both control and DLB. Entorhinal cortex thickness was reduced in AD compared to controls, with DLB not being significantly different to either group. There was, however, no difference between any of the groups in CA2 or CA3/4. Table 3 also shows values from the automated segmentation of the whole hippocampus from the T1 weighted image. Both the AD and DLB groups had sig-

nificantly smaller hippocampi than the control group, and there was no difference between AD and DLB in hippocampal volume. Adding a binary variable of MRI sequence (0.4×0.5 mm vs 0.27×0.35 mm) to the ANCOVA model in Table 3 did not change the significance of any of the comparisons.

Visual rating

As mentioned above, we noticed that the definition of the hippocampus subregions was less clear in some scans, suggesting structural changes potentially relating to the underlying disease process. We therefore visually rated the clearness of the scan on a 1–5 scale for the three slices on which the hippocampus regions were drawn. Typical scan data illustrating hippocampi with each of the 5 scores are shown in Fig. 2. Figure 4 shows the relationship to hippocampal size and diagnostic group. In a general linear model, predictors of the visual rating were diagnosis ($F = 7.7$; $p = 0.002$), hippocampus area ($F = 11.9$; $p = 0.001$) but

Table 3

Comparison of hippocampal measurements in the three groups. Values quoted are the average of the left and right side measurements made on three adjacent image slices. The hippocampus volume is from automated segmentation of the T1 weighted MPRAGE sequence. ANCOVA differences between AD/control/DLB controlling for age, intracranial volume and post 16 education. All values are mean (SD) [95% Confidence interval].

	Control	AD	DLB	ANCOVA F; p
CA1 area mm^2	26.7 (3.1) [25–28]	22.6 (3.9) [21–25] [a,b]	23.8 (3.0) [22–25]	$F = 6.3$; $p = 0.004$
CA2 area mm^2	1.53 (0.31) [1.36–1.70]	1.45 (0.33) [1.27–1.62]	1.53 (0.38) [1.33–1.75]	$F = 0.1$; $p = 0.9$
CA2 thickness mm	1.36 (0.15) [1.28–1.43]	1.30 (0.19) [1.20–1.40]	1.32 (0.19) [1.21–1.42]	$F = 0.3$; $p = 0.7$
CA3/4 area mm^2	17.2 (2.2) [16.1–18.4]	15.5 (3.0) [13.9–17.1]	16.0 (2.4) [14.7–17.3]	$F = 1.4$; $p = 0.3$
Entorhinal thickness mm	2.25 (0.18) [2.16–2.35]	1.87 (0.24) [1.74–2.00] [a]	1.96 (0.27) [1.81–2.11]	$F = 9.9$; $p < 0.001$
Subiculum thickness mm	2.37 (0.28) [2.22–2.52]	2.03 (0.29) [1.87–2.18] [a,b]	2.35 (0.24) [2.22–2.48]	$F = 9.1$; $p = 0.001$
Hippocampus area mm^2	45.4 (5.2) [43–48]	39.5 (6.5) [36–43] [a]	41.3 (4.8) [39–44]	$F = 4.2$; $p = 0.022$
Subfield visual clarity	4.0 (0.9) [3.6–4.6]	2.4 (0.8) [1.9–2.8] [a,b]	3.3 (1.1) [2.7–3.9]	$F = 16$; $p < 0.001$
Hippocampus volume mm^3	2878 (333) [2700–3055]	2163 (551) [1870–2457] [a]	2078 (616) [1737–2419] [c]	$F = 8.6$; $p = 0.001$

Post hoc $p < 0.05$ (a) AD vs Control; (b) AD vs DLB; (c) DLB vs Control; Post hoc comparisons (Tukey); CA1 area: Control > AD $p = 0.007$; AD < DLB $p = 0.043$; Subiculum thickness: Control > AD $p = 0.006$; AD < DLB $p = 0.002$; Entorhinal thickness: Control > AD $p < 0.001$; Hippocampus area: Control > AD $p = 0.03$; Subfield clarity: Control > AD $p < 0.001$; AD < DLB $p < 0.001$; Hippocampus volume: Control > AD $p < 0.001$; Control > DLB $p = 0.01$.

not intracranial volume ($p = 0.4$) or imaging sequence (0.4×0.5 mm vs 0.27×0.35 mm: $F = 2.8$; $p = 0.1$).

Removing the 3 subjects (2 AD, 1 DLB) with the worst hippocampus clearness rating did not alter the significance of any of the findings.

Predictive diagnostic ability

To investigate the potential discriminating power of the hippocampal measurement, we performed a lin-
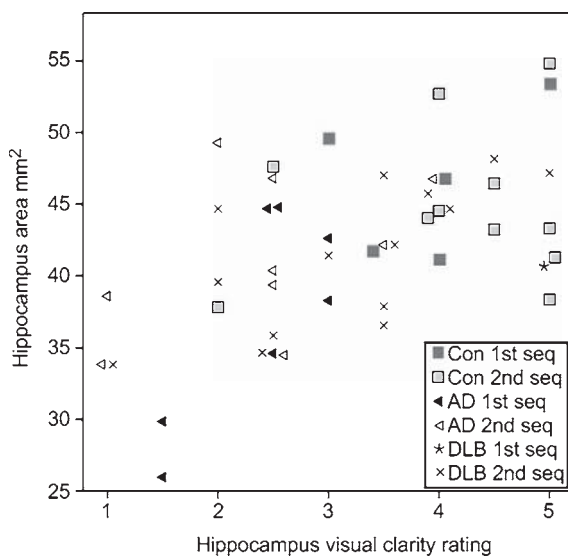
Fig. 4. Graph of average of left and right hippocampus visual clarity rating vs. average hippocampus area. Data acquired with the two different T2 weighted imaging protocols are shown (1st seq - resolution of 0.41×0.52 mm; 2nd seq - resolution of 0.27×0.35 mm).

ear regression to find the best predictors, with group (AD vs DLB) as the dependent variable, age, ICV and education as fixed covariates, and all of the hippocampal measurements added to the model in a stepwise fashion. This produced a model ($F = 12.3$; $p < 0.001$) in which subiculum thickness ($p = 0.005$), visual clearness ($p = 0.001$) and hippocampus volume ($p = 0.024$) independently predicted group membership. We then performed discriminant analysis with cross validation to estimate discriminating power with subiculum, clearness, and hippocampal volume to classify group (AD vs DLB). This correctly classified 81% (14 AD and 11 DLB; $p = 0.007$). Hippocampal volume by itself did not classify subjects above chance (61% correct; $p = 0.7$), while using just subiculum and clearness correctly classified 74% of subjects (11 AD and 12 DLB; $p = 0.005$), and either variable by itself performed almost as well: clearness 71% (12 AD & 10 DLB; $p = 0.015$) subiculum 71% (9 AD & 13 DLB; $p = 0.002$).

Memory function

To see if the hippocampus measurements related to memory function, we performed a Spearman correlation in each group of CA1, subiculum, entorhinal cortex, hippocampal area, hippocampus volume (from automated segmentation), and visual clearness against Rey delayed recall and Rey total items. In the DLB group, there were significant correlations between Rey delayed score and hippocampus area ($r = 0.7$; $p = 0.004$), hippocampus volume ($r = 0.8$; $p < 0.001$), CA1 area ($r = 0.7$; $p = 0.011$) and visual
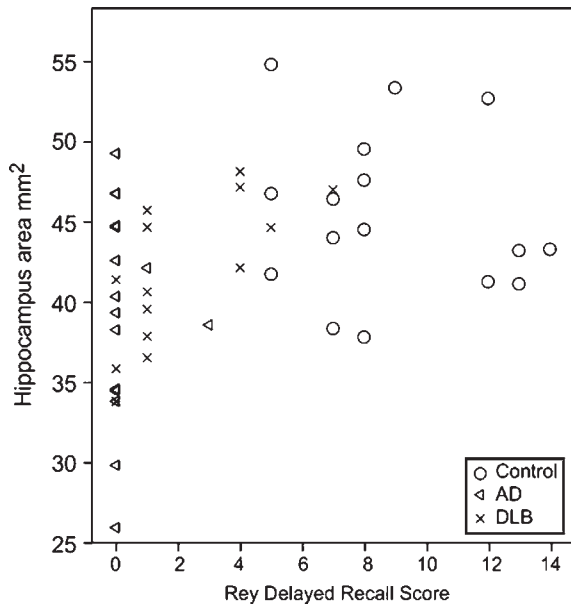
Fig. 5. Graph of average hippocampus area vs. Rey delayed memory score in the three groups.

clearness ($r = 0.6$ $p = 0.03$). There were no significant correlations in the AD or control group. Figure 5 shows the Rey delayed memory score plotted against average hippocampus area. As Fig. 5 shows, the lack of correlation in the AD group is due to floor effects in the memory test for that group.

Motor function

As expected, controlling for diagnosis, there were no significant correlations in the dementia group between UPDRS score and any of the hippocampus measures.

DISCUSSION

The main finding of the study was that on high field strength hippocampal MR imaging, in DLB, the subiculum and CA1 areas in the anterior portion of the hippocampus body were significantly less atrophied than in AD. The entorhinal cortex was smaller in AD, with DLB being intermediate between control and AD, whilst there was no difference in the CA2 and CA3/4 regions. These data add to previous studies in AD and DLB which assessed overall hippocampal atrophy [6–8] and further support the hypothesis that the medial temporal lobe is differentially affected in the two dementias.

Adachi, using high resolution coronal diffusion imaging of the hippocampus also observed CA1 and subiculum atrophy in AD, with no CA3/4 atrophy compared to control subjects. [27] Using a comparable coronal sequence to the one in this study at 4T, Mueller et al. [5] found CA1, CA2, entorhinal cortex and subiculum reduced in AD compared with controls, whilst the CA3/4 area was only reduced in those with the Apo e4 allele. Burggren, [25] in (asymptomatic) Apo e4 carriers using a similar imaging sequence, found only differences in entorhinal cortex and subiculum, not CA1, CA2 or CA3/4. They also found that thickness measurements were more reliable than area. We did not have information on Apo e status of our subjects, and hence could not investigate its relationship to hippocampus atrophy.

The majority of studies using T1 weighted imaging and subregions inferred from the hippocampus surface have also found CA1 and subiculum, but not CA2 or CA3/4 atrophy relative to controls. [1, 2, 28] The study of Sabattoli [9] with such a 1 mm^3 resolution T1 weighted sequence, found atrophy in DLB vs AD mostly confined to the head of the hippocampus, whereas the regions of greater atrophy in AD were largely in the tail, but also CA1 and subiculum of the hippocampal body. We found relatively little atrophy of the entorhinal and subiculum regions of DLB, whereas the total hippocampus volume measured from the T1 weighted images was of similar magnitude in AD and DLB. This suggests that either the body or tail of the hippocampus was smaller in DLB, which would be in keeping with Sabattoli's findings. [9] Most studies have found some degree of overall hippocampus atrophy in DLB [6–8] and Burton et al. found that medial temporal atrophy was a good predictor of postmortem diagnosis of Alzheimer's disease, but had only a modest relationship with tau pathology [29] suggesting that while some of the variability in hippocampal size may be due to AD pathology, other factors associated with volume loss need to be determined.

It is possible that our lack of significant difference in CA2 was due to the increased variability in measuring this structure, due to its small size, and difficulty discerning its boundaries within the hippocampus. However, in an attempt to increase reliability, we measured both area and thickness of the structure, and in neither case was there any indication of a significant difference between the groups. The high variability of the CA2 region both between raters, and within rater on the two different sequences used does limit the interpretation of our finding of no difference in

CA2 between groups. Unfortunately, we did not discover any means of reliably identifying CA2 medial and lateral borders. The entorhinal cortex measurement also had greater intra-rater variability, which may have made it more difficult to find differences between DLB and AD or control groups. We used the thickness rather than area of the subiculum and entorhinal cortex rather than area due to large variations in the length of these structures. Although this gave a more precise measurement, it does mean that we were not sensitive to changes in the overall shapes.

The CA1 region was differentiated from the CA3/4 region by determining the location of a hypointense line on the image. This line is likely to represent fibres in the hippocampal layers of stratum moleculare, stratum lacunosum and stratum radiatum [30, 31]. We found that the visibility of this line in the anterior portion of the hippocampus body varied considerably between cases, and was less clear in AD subjects and those with smaller hippocampi. This variable visibility either represents changes in the MR relaxation properties of these layers, or loss of the underlying tissue itself. In either case it potentially represents disease related changes in the internal structure of the hippocampus. A study by Kantarci [32] used diffusion weighted imaging and found that increased diffusivity in the hippocampus of MCI subjects predicted conversion to AD, indicating early loss or damage to neuronal bodies in the hippocampus. Hippocampal atrophy has been found to relate to changes in WM of the cingulum which connects the hippocampus to the posterior cingulate [33, 34] suggesting that breakdown of the white matter in and connecting the hippocampus is associated with atrophy, a notion supported by our findings.

We saw correlations in the DLB group between memory function and CA1 and overall hippocampus area, suggesting that hippocampal atrophy (possibly due to concomitant Alzheimer pathology) is related to worsening short term memory, as would be expected. We did not see any correlations in the Alzheimer group, probably due to floor effects – the maximum score on the Rey delayed test was 3/15 in the AD group (see Fig. 5). Due to the relatively small numbers in each group, these results should be considered tentative.

We found reasonable predictive ability of the subiculum thickness to distinguish AD from DLB, with 71% of cases correctly classified. In this study it was better than any other hippocampal measurement, including overall area or volume. In the revised international consensus criteria for clinical diagnosis of DLB [15] a visual rating of overall hippocampal atrophy can be used as a supportive feature for diagnosis. Possibly subiculum thickness could provide additional diagnostic information and further studies on larger numbers of subjects should investigate whether subiculum thickness provides a more specific diagnostic discriminator. This is important as another putative specific marker for AD, atrophy of the entorhinal cortex, did not differentiate between AD and DLB, similar to findings from a previous study using more standard 1.5T imaging [10]. Previous studies have found similar levels for discriminating AD from DLB on hippocampus volume. Data from Whitwell et al. [7] suggest a diagnostic accuracy of 65%, while Barber et al. [35] had an accuracy of 74% for DLB vs AD. However in our study, the hippocampus area and volume by themselves did not distinguish between AD and DLB, suggesting that the subiculum and visual rating might provide additional diagnostic information which is complementary to measurement of overall hippocampus atrophy. Scans using the dopamine transporter tracer FPCIT have been shown in a large multicentre study to have a very good (85%) accuracy for distinguishing DLB from non-DLB dementia [36]. However, MRI has the advantage that information can also be acquired in the same scanning session about other pathologies eg vascular.

Strengths of the study include high resolution hippocampus imaging, careful ROI measurements. The cohort was well defined, with all dementia subjects fulfilling criteria for either probable AD or probable DLB, using a clinical diagnostic method we have previously validated against postmortem findings and utilising dopaminergic imaging in 9 DLB subjects. Weaknesses are that only a 6 mm portion of the hippocampus body was examined, and (as noted by Mueller et al. [5]) the boundaries of CA2 are somewhat arbitrary. We used two different imaging protocols, as we tried to improve the image resolution during the study, and the initial 13 subjects were not rescanned. Although this is a potential confounder, we obtained good agreement between the area and thickness measurements made on the two sequences, and controlling for the type of sequence used in the analysis did not alter the results. Detection of hippocampal substructures requires sufficient in-plane resolution and image contrast between individual structures. Although our sequences were based largely on the study of Mueller et al. [4] which was performed at higher field (4 Tesla), we conducted preliminary investigations varying sequence parameters (TR and TE) and did not obtain any significant improvement in contrast.

An important limitation of the study was that the measurement of subiculum and entorhinal cortex was not validated by an established technique. Following Mueller et al., our working definition for the medial boundary of CA1 was to use the superficial hippocampal sulcus. Whilst this is a consistent and easily identified boundary, it does mean that the CA1 region will include some of the subiculum, and hence our CA1 findings will be slightly influenced by any subiculum changes.

We did not have autopsy confirmation of the diagnoses in the subjects, however we used a consensus clinical diagnosis, which we have previously shown to have good accuracy against autopsy.[16] In addition, all 9 of our DLB subjects who had dopamine transporter imaging had abnormal scans consistent with DLB as the diagnosis. It is quite possible that the DLB subjects had some degree of concomitant Alzheimer's pathology, which contributed to the hippocampus atrophy. A CT image was used as part of the clinical diagnosis, and this does have the potential to bias the sample towards AD having greater hippocampal atrophy. We do not feel this was a major issue, since the hippocampus volume did not differ between the AD and DLB groups. For the hippocampus volume measurement, we used an automated technique. This is not as accurate as the gold standard of manually tracing, (though much quicker) and may give incorrect results in subjects with abnormalities/severe atrophy. However, we have previously shown good reliability with this method in a dementia population [26] and feel the results should be representative.

The fact that we observed less clear definition of hippocampal structures in Alzheimer's disease was interesting in that it indicated internal breakdown of the hippocampus. But it also will have limited the accuracy of delimiting the subregions. However, the analysis did not change on excluding those with the least clear hippocampi. The subiculum thickness measurement was relatively clear on all subjects as its upper surface was the ventricle, and lower surface, the temporal lobe white matter, and it showed good intra-rater reliability (ICC was 0.8). If replicated in a larger study, the subiculum thickness could be a simply measured useful additional diagnostic feature of AD vs. DLB.

ACKNOWLEDGEMENTS

REFERENCES

[1] Chételat G, Fouquet M, Kalpouzos G, Denghien I, De la Sayette V, Viader F, Mézenge F, Landeau B, Baron JC, Eustache F, Desgranges B (2008) Three dimensional surface mapping of hippocampal atrophy progression from MCI to AD and over normal aging as assessed using voxel-based morphometry. *Neuropsychologia* **46**, 1721-1731.

[2] Frisoni GB, Sabattoli F, Lee AD, Dutton RA, Toga AW, Thompson PM (2006) In vivo neuropathology of the hippocampal formation in AD: A radial mapping MR-based study. *NeuroImage* **32**, 104-110.

[3] Rössler M, Zarski R, Bohl J, Ohm TG (2002) Stage-dependent and sector-specific neuronal loss in hippocampus during Alzheimer's disease. *Acta Neuropathol* **103**, 363-369.

[4] Mueller SG, Stables L, Du AT, Schuff N, Truran D, Cashdollar N, Weiner MW (2007) Measurement of hippocampal subfields and age-related changes with high resolution MRI at 4T. *Neurobiol Aging* **28**, 719-726.

[5] Mueller SG, Schuff N, Raptentsetsang S, Elman J, Weiner MW (2008) Selective effect of Apo e4 on CA3 and dentate in normal aging and Alzheimer's disease using high resolution MRI at 4T. *NeuroImage* **42**, 42-48.

[6] Tam CW, Burton EJ, McKeith IG, Burn DJ, O'Brien JT (2005) Temporal lobe atrophy on MRI in Parkinson disease with dementia: a comparison with Alzheimer disease and dementia with Lewy bodies. *Neurology* **64**, 861-865.

[7] Whitwell JL, Weigand SD, Shiung MM, Boeve BF, Ferman TJ, Smith GE, Knopman DS, Petersen RC, Benarroch EE, Josephs KA, Jack CR (2007) Focal atrophy in dementia with Lewy bodies on MRI: a distinct pattern from Alzheimer's disease. *Brain* **130**, 708-719.

[8] Barber R, Gholkar A, Scheltens P, Ballard C, McKeith IG, O'Brien JT (1999) Medial temporal lobe atrophy on MRI in dementia with Lewy bodies. *Neurology* **52**, 1153-1158.

[9] Sabattoli F, Boccardi M, Galluzzi S, Treves A, Thompson PM, Frisoni GB (2008) Hippocampal shape differences in dementia with Lewy bodies. *NeuroImage* **41**, 699-705.

[10] Kenny ER, Burton EJ, O'Brien JT (2008) A volumetric magnetic resonance imaging study of entorhinal cortex volume in dementia with Lewy bodies. *Dement Geriatr Cogn Disord* **26**, 218-225.

[11] Iseki E, Takayama N, Marui W, Ueda K, Kosaka K (2002) Relationship in the formation process between neurofibrillary tangles and Lewy bodies in the hippocampus of dementia with Lewy bodies brains. *J Neurol Sci* **195**, 85-91.

[12] Dickson DW, Ruan D, Crystal H, Mark MH, Davies P, Kress Y, Yen SH (1991) Hippocampal degeneration differentiates diffuse Lewy body disease (DLBD) from Alzheimer's disease - light and electron microscopic immunocytochemistry of CA2-3 neurites specific to DLBD. *Neurology* **41**, 1402-1409.

[13] Harding AJ, Lakay B, Halliday GM (2002) Selective hippocampal neuron loss in dementia with Lewy bodies. *Ann Neurol* **51**, 125-128.

[14] McKhann G, Drachman D, Folstein M, Katzman R, Price D, Stadlan EM (1984) Clinical diagnosis of Alzheimer's disease: Report of the NINCDS-ADRDA Work Group under the auspices of Department of Health and Human Services Task Force on Alzheimer's disease. *Neurology* **34**, 939-944.

[15] McKeith IG, Dickson DW, Lowe J, Emre M, O'Brien JT, Feldman H, Cummings J, Duda JE, Lippa C, Perry EK, Aarsland D, Arai H, Ballard CG, Boeve B, Burn DJ, Costa D, Del Ser T, Dubois B, Galasko D, Gauthier S, Goetz CG, Gomez-Tortosa E, Halliday G, Hansen LA, Hardy J, Iwatsubo T, Kalaria RN, Kaufer D, Kenny RA, Korczyn A, Kosaka K, Lee VM-Y, Lees A, Litvan I, Londos E, Lopez OL, Minoshima S, Mizuno Y, Molina JA, Mukaetova-Ladinska EB, Pasquier F, Perry RH, Schulz JB, Trojanowski JQ, Yamada M (2005) Diagnosis and management of dementia with Lewy bodies: Third report of the DLB consortium. *Neurology* **65**, 1863-1872.

[16] McKeith IG, Ballard CG, Perry RH, Ince PG, O'Brien JT, Neill D, Lowery K, Jaros E, Barber R, Thompson P, Swann A, Fairbairn AF, Perry EK (2000) Prospective validation of Consensus criteria for the diagnosis of dementia with Lewy bodies. *Neurology* **54**, 1050-1058.

[17] Roth M, Tym E, Mountjoy CQ, Huppert FA, Hendrie H, Verma S, Goddard R (1986) CAMDEX - A Standardised instrument for the diagnosis of mental disorder in the elderly with special reference to the early detection of dementia. *Br J Psychiatry* **149**, 698-709.

[18] Alexopoulos GS, Abrams RC, Young RC, Shamoian CA (1988) Cornell scale for depression in dementia. *Biol Psychiatry* **23**, 271-284.

[19] Cummings JL, Mega M, Gray K, Rosenberg-Thompson S, Carusi DA, Gornbein J (1994) The neuropsychiatric inventory: comprehensive assessment of psychopathology in dementia. *Neurology* **44**, 2308-2314.

[20] Walker MP, Ayre GA, Cummings JL, Wesnes K, McKeith IG, O'Brien JT, Ballard CG (2000) The clinician assessment of fluctuation and the one day fluctuation assessment scale. *Br J Psychiatry* **177**, 252-256.

[21] Rey A (1964) *L'examen Clinique en Psychologie*, Presses Universitaires de France, Paris.

[22] Fahn S, Elton R (1987) Members of the UPDRS development commitee. Unified Parkinson's disease rating scale *In Recent developments in Parkinson's disease*, Fahn S, Marsden CD, Calne DB, Goldstein M, eds. MacMillan Healthcare Information, Florham Park; NJ.

[23] Jenkinson M, Smith SM (2001) A global optimisation method for robust affine registration of brain images. *Med Image Anal* **5**, 143-156.

[24] Yushkevich PA, Piven J, Hazlett HC, Smith RG, Ho S, Gee JC, Gerig G (2006) User-guided 3D active contour segmentation of anatomical structures: significantly improved efficiency and reliability. *NeuroImage* **31**, 1116-1128.

[25] Burggren AC, Zeineh MM, Ekstrom AD, Braskie MN, Thompson PM, Small GW, Bookheimer SY (2008) Reduced cortical thickness in hippocampal subregions among cognitively normal apolipoprotein E e4 carriers. *NeuroImage* **41**, 1177-1183.

[26] Firbank MJ, Barber R, Burton EJ, O'Brien JT (2008) Validation of a fully automated hippocampal segmentation method on patients with dementia. *Hum Brain Mapp* **29**, 1442-1449.

[27] Adachi M, Kawakatsu S, Hosoya T, Otani K, Honma T, Shibata A, Sugai Y (2003) Morphology of the inner structure of the hippocampal formation in Alzheimer disease. *Am J Neuroradiol* **24**, 1575-1581.

[28] Wang L, Miller JP, Gado MH, McKeel DW, Rothermich M, Miller MI, Morris JC, Csernansky JG (2006) Abnormalities of hippocampal surface structure in very mild dementia of the Alzheimer type. *NeuroImage* **30**, 52-60.

[29] Burton EJ, Barber R, Mukaetova-Ladinska EB, Robson J, Perry RH, Jaros E, Kalaria RN, O'Brien JT (2009) Medial temporal lobe atrophy on MRI differentiates Alzheimer's disease from dementia with Lewy bodies and vascular cognitive impairment: a prospective study with pathological verification of diagnosis. *Brain* **132**, 195-203.

[30] Wieshmann UC, Symms MR, Mottershead JP, MacManus DG, Barker GJ, Tofts PS, Revesz T, Stevens JM, Shorvon SD (1999) Hippocampal layers on high resolution magnetic resonance images: real or imaginary? *J Anat* **195**, 131-135.

[31] Thomas BP, Welch EB, Blake D, Niederhauser BD, Whetsell WO, Anderson AW, Gore JC, Avison MJ, Creasy JL (2008) High resolution 7T MRI of the human hippocampus in vivo. *J Magn Reson Imaging* **28**, 1266-1272.

[32] Kantarci K, Petersen RC, Boeve BF, Knopman DS, Weigand SD, O'Brien PC, Shiung MM, Smith GE, Ivnik RJ, Tangalos EG, Jack CR (2005) DWI predicts future progression to Alzheimer disease in amnestic mild cognitive impairment. *Neurology* **64**, 902-904.

[33] Villain N, Desgranges B, Viader F, de la Sayette V, Mézenge F, Landeau B, Baron J-C, Eustache F, Chételat G (2008) Relationship between hippocampal atrophy, white matter disruption, and gray matter hypometabolism in Alzheimer's disease. *J Neurosci* **28**, 6174-6181.

[34] Xie S, Xiao JX, Wang YH, Wu HK, Gong GL, Jiang XX (2005) Evaluation of bilateral cingulum with tractography in patients with Alzheimer's disease. *Neuroreport* **16**, 1275-1278.

[35] Barber R, Ballard C, McKeith IG, Gholkar A, O'Brien JT (2000) MRI volumetric study of dementia with Lewy bodies. *Neurology* **54**, 1304-1309.

[36] McKeith I, O'Brien J, Walker Z, Tatsch K, Booij J, Darcourt J, Padovani A, Giubbini R, Bonuccelli U, Volterrani D, Holmes C, Kemp P, Tabet N, Meyer I, Reininger C (2007) Sensitivity and specificity of dopamine transporter imaging with I-123-FP-CIT SPECT in dementia with Lewy bodies: a phase III, multicentre study. *Lancet Neurol* **6**, 305-313.

Automated Volumetric Methods to Detect Alzheimer's Disease

Pedro Paulo de Magalhães Oliveira Jr.[a,d,*], Ricardo Nitrini[b], Geraldo Busatto[c], Carlos Buchpiguel[d], João Ricardo Sato[a] and Edson Amaro Jr.[a]

[a]*NIF - Neuroimagem Funcional, Departamento de Radiologia da Faculdade de Medicina do Hospital das Clínicas da Faculdade de Medicina da Universidade de São Paulo, São Paulo, Brazil*
[b]*Departamento de Neurologia da Faculdade de Medicina do Hospital das Clínicas da Faculdade de Medicina da Universidade de São Paulo, São Paulo, Brazil*
[c]*LIM21 - Instituto de Psiquiatria da Faculdade de Medicina do Hospital das Clínicas da Faculdade de Medicina da Universidade de São Paulo, São Paulo, Brazil*
[d]*Medicina Nuclear, Departamento de Radiologia da Faculdade de Medicina do Hospital das Clínicas da Faculdade de Medicina da Universidade de São Paulo, São Paulo, Brazil*
[d]*Netfilter Research, www.netfilter.com.br*

Abstract. We examine morphological changes in cortical thickness of patients with Alzheimer's disease (AD) using image analysis algorithms for brain structure segmentation in order to automatic detect AD patients using cortical and volumetric data. Cortical thickness of 14 AD patients was measured using FreeSurfer software package in T1 weighted MRI images and compared with 20 healthy subjects. An automated classifier based on Support Vector Machine (SVM) was applied over the volumetric measurements of subcortical and cortical structures to separate AD patients from controls. Besides the volumetric classification we noticed that the cortical thickness group analysis showed cortical thickness reduction in the superior temporal lobe, parahippocampal gyrus, and enthorhinal cortex in both hemispheres. We also found cortical thinning in the isthmus of cingulate gyrus and middle temporal gyrus at the right hemisphere, as well as a reduction of the cortical mantle in areas previously shown to be associated with AD. Automatic classification algorithms using SVM can be helpful to distinguish AD patients from healthy controls. Moreover, the same areas implicated in the pathogenesis of AD were the main parameters driving the classification algorithm. While the patient sample used in this study was relatively small, we expect that using a database of regional volumes derived from MRI scans of a large number of subjects will increase the SVM power of AD patient identification.

Keywords: Alzheimer's disease, FreeSurfer, magnetic resonance imaging, support vector machine, surface based methods

INTRODUCTION

Alzheimer's disease (AD) is the most prevalent cause of dementia in elderly people [1]. In the last two decades, the comprehension of the under-lying mechanisms of elderly dementia and AD have been enlightened by evidence emerging from different research fields, perhaps with more contribution arising from neuropathology, genetics [2], and neuroimaging [3] data.

Current literature from neuropathology and neuroimaging studies shows evidence that common changes can be found in AD patients, but unfortunately, these are neither specific nor diagnostic at an individual level. The most celebrated anatomical finding is

---

*Correspondence to: Pedro Paulo de Magalhães Oliveira Jr., Rua Dr. Enéas de Carvalho Aguiar, s/n, InRad – Instituto de Radiologia - Setor de RM, São Paulo – SP, CEP 05403-900, Brazil. Tel.: +55 11 3069 7919; E-mail: ppj@netfilter.com.br.

a volumetric reduction in the hippocampal formation and parahippocampal gyrus [4, 5]. However, in earlier stages of the disease, there is no evidence that this finding can be used as a diagnostic criterion. Rather, volumetric assessment of the hippocampal formation seems to be more specific at an individual level when analyzing temporal progression [6]. Imaging data can provide insights of how the disease progresses in time at each brain structure from a macroscopic viewpoint.

The high variability of AD phenotypes, a broad range of clinical presentations, and the role of cognitive reserve in disease progression are confounding factors in creating a generic neuroimaging criterion for AD diagnosis. A promising approach is to study groups of AD patients showing common patterns (old age, mild cognitive impairment, high education, apolipoprotein E (ApoE) $\varepsilon 4$ carriers, etc.) in order to access the power of specific techniques in differentiating patients from healthy volunteers—then proceed with further steps to design diagnostic tests that can be applied in all types of AD patients.

Some studies have explored artificial intelligence and machine learning methods to detect cerebral changes and discriminate normal aging from AD [7–11]. This marker (obtained from MRI data alone) is neither fully conclusive nor predictive of the outcome, in spite of the frequently reported correlation between cerebral atrophy and symptoms. Nevertheless, some studies showed that machine learning methods are a reliable tool for indicating the presence of probable AD, even compared to conventional radiological analysis [12].

However, new methods for early detection and early estimation of treatment outcome are needed [13] as specific treatment drugs for dementia aimed to delay the progression of disease (in terms of brain degeneration effects) [1, 14] are emerging on a daily basis. Perhaps the combination between surrogate markers (laboratory, genetic, and quantitative neuroimaging data) with automated classification algorithms may play an important role in detecting subtle changes preceding AD clinical manifestations.

Support vector machines (SVM) are a broad term to refer to a group of supervised learning methods that attempt to maximize the distance of a hyperplane or hypersurface separating two classes [15]. Machine learning techniques have been applied in several science fields, including neuroscience [16, 17]. SVM allows classification of both linear and non-linear separable data. It has been used to detect AD using

mostly voxel-based morphometry (VBM) and sometimes VBM with auxiliary data (ApoE $\varepsilon 4$ mutation, PET) [8, 10]. One study used SVM in conjunction with surface based analysis to separate AD patients from healthy controls [11], and another recent study used the same technique to classify AD using cortical parcelation data [18].

In this study, our aim is to: 1) use surface based morphometry techniques to study cortical thickness differences between healthy controls and AD patients; 2) use SVM classifiers based on parameters extracted from MR images to separate patients with AD from healthy controls; and 3) compare this multivariate method with a single variable classifier.

MATERIAL AND METHODS

Study groups

Fourteen patients with AD from an outpatient unit in the city of São Paulo, Brazil (Department of Psychiatry, University of São Paulo) were interviewed with the Cambridge Mental Disorders of the Elderly Examination (CAMDEX) [19]. All met NINDS/ADRDA criteria for probable AD [20]. They also passed screening laboratory examinations including complete blood count; liver, renal, and thyroid function tests; and Vitamin B12 and folate levels. The exclusion criteria included positive syphilis serology, a Hachinski Ischemic score ≥ 4, Parkinson's disease, non-neuroleptic induced Parkinson-like syndrome, hyperthyroidism, hyperparathyroidism, diabetes mellitus, other psychiatric disorders (schizophrenia, obsessive compulsive disorder), claustrophobia, chronic use of neuroleptics, and previous use of cholinesterase inhibitor. The same exclusion criteria were used to select a control group of normal elderly subjects ($n = 20$). They were free of symptoms suggestive of physical or mental disorder based on the CAMDEX interview, general medical questioning, and physical and neurological examination.

The overall severity of cognitive impairment was rated with the Mini-Mental State Examination (MMSE) [21]. The average MMSE in patients was 21.5 ± 2.27 and in the control group average MMSE was 27.9 ± 1.44. The average onset time of the symptoms in AD group was 22.5 ± 11.4 months. Further details are shown in Table 1.

Table 1
Clinical, demographic and neuropsychological characteristics of AD subjects ($n = 14$) and healthy controls ($n = 20$). Age ($p = 0.027$).

Code	Gender	Age	Diagnosis	Education (years)	Family History for AD	MMSE	Symptom Onset (months)
ALZ01	M	78	AD	17	N	24	28
ALZ02	F	77	AD	12	N	26	12
ALZ03	F	70	AD	4	N	19	24
ALZ04	M	68	AD	9	S	21	36
ALZ05	F	80	AD	4	N	20	12
ALZ06	M	74	AD	10	N	21	36
ALZ07	M	77	AD	4	N	22	24
ALZ08	F	76	AD	4	N	22	18
ALZ09	F	76	AD	8	N	21	18
ALZ10	F	74	AD	4	S	18	24
ALZ11	M	84	AD	7	N	24	8
ALZ12	F	79	AD	12	S	24	18
ALZ13	M	79	AD	9	N	21	10
ALZ14	M	75	AD	4	S	19	48
CTL01	F	80	CTL	8	N	28	N/A
CTL02	F	74	CTL	4	N	28	N/A
CTL03	F	75	CTL	15	N	27	N/A
CTL04	M	76	CTL	11	N	28	N/A
CTL05	M	76	CTL	4	N	26	N/A
CTL06	F	72	CTL	16	N	29	N/A
CTL07	F	70	CTL	5	N	26	N/A
CTL08	M	80	CTL	4	N	26	N/A
CTL09	F	68	CTL	8	N	29	N/A
CTL10	M	71	CTL	16	N	29	N/A
CTL11	M	75	CTL	8	N	27	N/A
CTL12	M	75	CTL	4	N	25	N/A
CTL13	M	68	CTL	11	N	30	N/A
CTL14	M	73	CTL	11	N	29	N/A
CTL15	M	75	CTL	4	N	27	N/A
CTL16	F	74	CTL	16	N	29	N/A
CTL17	F	75	CTL	15	N	29	N/A
CTL18	F	66	CTL	16	N	30	N/A
CTL19	F	66	CTL	15	N	29	N/A
CTL20	F	70	CTL	4	N	27	N/A

Summary			
	AGE	Education	MMSE
AD Patients	76.21 (SD 4.04)	7.71 (SD 4.07)	21.5 (SD 2.28)
Controls	72.95 (SD 4.03)	9.75 (SD 5.00)	27.9 (SD 1.45)

M – male F – female; AD –Alzheimer's disease, CTL - Control; N – Not present; Y – Present; N/A – Not applicable

MRI acquisition

Images were acquired using a 1.5 T GE Horizon LX 8.3 scanner (General Electric Medical Systems, Milwaukee). A series of contiguous 1.6 mm thick coronal images across the entire brain were acquired, using a T1-weighted fast field echo sequence (TE = 9 ms, TR = 27 ms, flip angle = 30º, field of view = 240 mm, 256 × 256 matrix), acquired perpendicular to the main temporal axis.

Image analysis

Cortical reconstruction and volumetric segmentation was performed with the FreeSurfer image analysis suite (version 4.3.0), which is documented and freely available for download online (http://surfer.nmr.mgh.harvard.edu/). The technical details of these procedures are described in previous publications [22–28]. Briefly, this processing includes removal of non-brain tissue using a hybrid

watershed/surface deformation procedure [29], automated Talairach transformation, segmentation of the subcortical white matter and deep gray matter volumetric structures (including hippocampus, amygdala, caudate, putamen, ventricles) [26, 27], intensity normalization [30], tessellation of the gray matter white matter boundary, automated topology correction [28, 31], and surface deformation following intensity gradients to optimally place the gray/white and gray/cerebrospinal fluid (CSF) borders at the location where the greatest shift in intensity defines the transition to the other tissue class [22, 23].

Once the cortical models are complete, a number of deformable procedures can be performed for further data processing and analysis including surface inflation [24]; registration to a spherical atlas which utilized individual cortical folding patterns to match cortical geometry across subjects [32]; parcellation of the cerebral cortex into units based on gyral and sulcal structure [25, 33]; and creation of a variety of surface based data including maps of curvature and sulcal depth.

This method uses both intensity and continuity information from the entire three dimensional MR volume in segmentation and deformation procedures to produce representations of cortical thickness, calculated as the closest distance from the gray/white boundary to the gray/CSF boundary at each vertex on the tessellated surface [22]. The maps are created using spatial intensity gradients across tissue classes and are therefore not simply reliant on absolute signal intensity. The maps produced are not restricted to the voxel resolution of the original data thus are capable of detecting submillimeter differences between groups. Procedures for the measurement of cortical thickness have been validated against histological analysis [34] and manual measurements [35, 36]. FreeSurfer morphometric procedures have been demonstrated to show good test-retest reliability across scanner manufacturers and across field strengths [37].

To verify the quality of the processed data, two of the authors (PPMOJ, EA) visually inspected and eventually manually corrected the segmentation for each individual. Only one individual required such intervention.

Statistical analysis

Step 1: The group analysis of cortical thickness was performed using mri_glmfit from FreeSurfer, using a general linear model over a common spherical coordinate system [32] to produce a surface map of cortical thickness difference comparing controls and AD patients. We do not use this step for classification but to visualize where the cortex of AD patients is thinner than controls.

Step 2: The volume measurement of cortical and subcortical structures obtained from FreeSurfer was used to train a multivariate classifier: a support vector machine (SVM) using a radial basis function (RBF) kernel [k $(x, x') = \exp (\gamma |x-x'|^2)$].

Cost and γ, for the RBF were estimated using the grid-search algorithm: pairs of (Cost, γ) are tried and the one producing the best cross-validation accuracy is chosen [38].

Step 3: The training step was used to detect and remove the volume structures not relevant to discriminate patients with AD from controls. This feature selection, over volumetric measures, was performed in a software developed by one of the authors [PPM] using LibSVM [38]. The software executes the following procedure:

1. To train SVM using all features: (Volume of 45 areas, each volume is a feature)
2. Compute cross validation leave-one-out accuracy for step 1.
3. From the 45 areas, eliminate the features whose F-Score is lower than 10% of the largest F-Score.
4. For each of all combination of the remaining areas execute:
    a. To train the SVM using only the subset of the combination's features
    b. Compute cross validation leave-one-out for step 3 a
    c. Save the feature subset if the value of 3 b is equal the value of step 2 and the number of features is smaller than previously obtained.

Step 4: A ROC curve for the volume of each individual brain structure was constructed to verify whether a multivariate classifier was needed.

RESULTS

The group analysis of cortical thickness among patients with AD and the healthy aged-matched control group showed areas of cortical reduction ($p < 0.01$, corrected for multiple comparisons with false discovery rate) in the superior temporal lobe, parahippocampal gyrus, and enthorrinal cortex in both hemispheres. In the right hemisphere, we also found the reduction in isthmus of cingulate gyrus and middle temporal gyrus.

In both hemispheres, there is a small area of cortical thinning in AD patients in superior frontal lobe (Fig. 1).

The volume from the 45 brain areas calculated with FreeSurfer automatic segmentation and volume estimation (Table 2) has been used as an input to train a SVM with RBF kernel ($\gamma = 0.0078125$ and Cost $= 8.0$). This technique produced a discriminating power of 88.2% [$CI_{95\%}$; 72.5%-96.7%] (Sensitivity $= 92.8\%$ [$CI_{95\%}$; 66.1%-99.8%], Specificity $= 85.0\%$ [$CI_{95\%}$; 62.1%-96.8%]) using cross validation with leave-one-out.

When analyzing the classification provided by each of the 45 areas alone, left and right hippocampi, as well as overall cortical thickness were the most relevant fea-
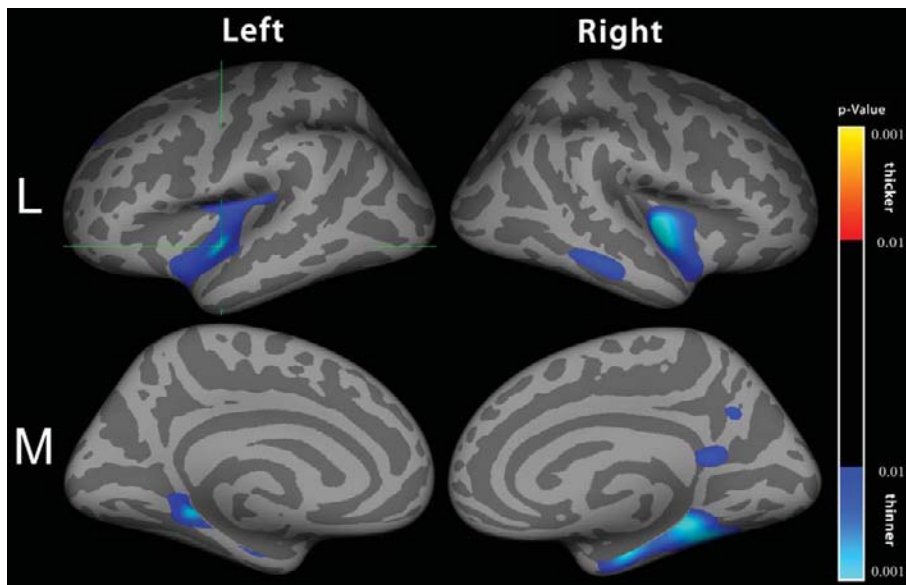
Fig. 1. Comparison of cortical thickness of patients with AD versus healthy elderly controls using age as a covariate. Left and right hemisphere of group analysis showing thinning in AD patients are displayed in Lateral (L) and Medial (M) views. Colors are mapped to p-values using the color scale attached.

Table 2
Volumetric Structures used in the SVM classification model

Right Cerebellum White Matter	Right Ventral Diencephalon
Right choroid plexus	Left Putamen
Left Amygdala	Left Cerebral White Matter
Left Cerebellum White Matter	Corpus Callosum Medial Anterior
Right Thalamus Proper	Right Putamen
Right Pallidum	Left Accumbens area
Left Ventral Diencephalon	Right Amygdala
Right Accumbens area	Left Thalamus Proper
Right Cerebral White Matter	Left Cerebellum Cortex
Corpus Callosum Medial Posterior	Left Lateral Ventricle
Right Lateral Ventricular Horn	Right Cerebellum Cortex
Corpus Callosum Central	Left vessel
Brain Stem	Left choroid plexus
Right Hippocampus	Left Caudate
Right Caudate	Left Lateral Ventricular Horn
Corpus Callosum Posterior	Left Cerebral Cortex
Corpus Callosum Anterior	Right Cerebral Cortex
Right Lateral Ventricle	Right vessel
Left Hippocampus	Optic Chiasm
Left Pallidum	4th Ventricle
3rd Ventricle	5th Ventricle
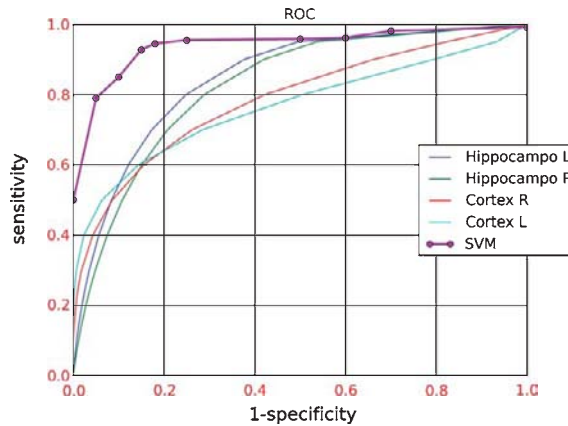
Fig. 2. ROC (receiver operating characteristic). Curve of the variables used in SVM classification showing that the multivariate classifier used has more accurate results than using any of the variables alone. SVM ROC has been created with distinct trainings using distinct weights in the cost function.

Table 3
Volumetric Structures useful to SVM prediction, ordered by importance in SVM model

Anatomic Region	Volume Patients (mm^3)	Volume Control (mm^3)
Right Lateral Ventricular Horn	1360 mm^3 $\pm$ 989	570 mm^3 $\pm$ 267
Left Hippocampus	2581 mm^3 $\pm$ 499	3271 mm^3 $\pm$ 452
Right Hippocampus	2862 mm^3 $\pm$ 615	3596 mm^3 $\pm$ 508
Left Cerebral Cortex	194093 mm^3 $\pm$ 14 x10^3	212592 mm^3 $\pm$ 19 x10^3
Right Cerebral Cortex	193095 mm^3 $\pm$ 12 x10^3	212620 mm^3 $\pm$ 19 x10^3
Corpus Callosum Posterior	1771 mm^3 $\pm$ 72.03	877 mm^3 $\pm$ 100
Corpus Callosum Anterior	596 mm^3 $\pm$ 87.42	751 mm^3 $\pm$ 122

tures, to classification using ROC areas. Nevertheless, SVM outperforms the classification produced from each feature alone (Fig. 2).

The feature selection in the SVM revealed areas relevant to discriminate AD patients and normal controls comprising anterior and posterior corpus callosum volume, left and right hippocampus, right lateral ventricular horn size, and right gray matter volume (Table 3).

The scatter plot matrix showing from this multidimensional data shows a variable power for each parameter contributing to the classification, as well as individual patients and groups produced (Fig. 3).

DISCUSSION

We show that a group of patients with AD compared to a matched population have a reduction in cortical thickness when analyzing MRI data using a surface based method. The cortical surface analysis findings in our AD sample replicate previous reports in the neuroimaging literature [4, 39–41]. The cortical thinning

in temporal, limbic, and enthorrinal cortex confirms the previous literature on cortical thickness analysis and surface based volumetric analysis of AD [40, 41]. In addition, the findings in AD with mild to moderate impairment or recent onset [4, 39] regarding cortical volume decrease occurring centered on medial temporal lobes, are confirmed in this study. However, our results have some differences from previous reports: parietal cortex did not show significant thinning in AD compared to controls, and the right brain hemisphere showed more alteration both in surface based and volumetric measurement techniques. We have also shown that the SVM analysis showed a good performance to classify AD patients and healthy controls as well in identifying anatomic structures that have a reduced volume in AD patients.

In imaging studies of AD, it is usual to find differences either metabolic or volumetric in parietal cortex [5]. We did not find evidence of a parietal cortex involvement, maybe due to the lack of statistical power. However, this finding is consistent with the hypothesis that in this particular group of older patients with recent onset, there is less involvement of the parietal
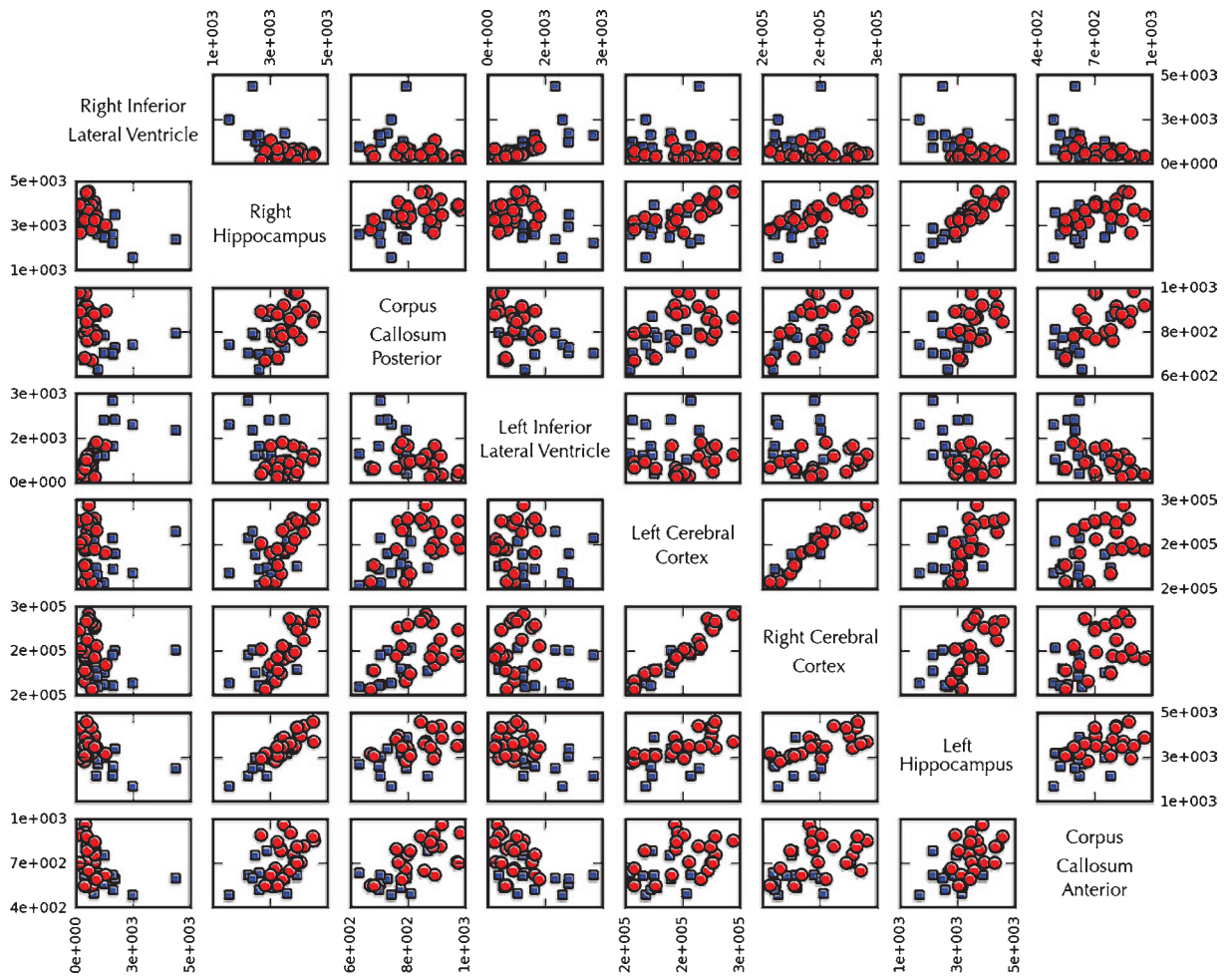
Fig. 3. Scatter plot matrix of the eight volumetric features used in SVM classification. This figure helps visualizing the multidimensional data used to classify between AD patients and healthy controls. Blue squares represent AD patients and red dots represent healthy controls. The volumes of brain structures are given in mm^3 (for black and white version). Scatter plot matrix of the eight volumetric features used in SVM classification. This figure helps visualizing the multidimensional data used to classify between AD patients and healthy controls. White squares represent AD patients and dark dots represent healthy controls. The volumes of brain structures are given in mm^3.

lobe. Other studies with groups with mild to moderate impairment [39] showed that the predominant differences are in the temporal lobe. A hypothesis is that these patients may have developed AD symptoms later in life simply because of particular disease mechanisms, which *per se* could induce to a more delayed progression with less cortex involvement.

The findings presented here reinforce the importance of image studies of AD in all subgroups. Previous reports have concentrated on findings from mild impairment [3, 39], but these actually may reflect changes specific to a subgroup of patients, and therefore the alterations at this initial phase can be difficult to detect if one only looks for a predetermined pattern.

Patients with recent symptoms, late or early onset, high or low education level, or positive ApoE4 mutation [41, 42] may provide distinct features to be pursued in order to discriminate mechanisms of AD damage in nervous system.

The differences between cortical thinning from right to left hemispheres are not easy to explain. One possible theory for these findings is that degeneration is distinct in the dominant hemisphere [43]. Another possible explanation is the progressive degeneration pattern affecting language in a later stage, after the usual initial compromise found in olfaction and memory. However, this finding requires further study to determine whether it is a constant feature of AD or an

artifact produced by the methodology used, data outliers, or a small sample. Further studies are required to analyze this effect properly.

We have also introduced the use of SVM as a trained classifier to detect AD based only in the volume of subcortical structures and cerebral cortex with data obtained using a surface based approach. Similar techniques have been also studied with voxel based morphometry (VBM) [9, 44], combining VBM with ApoE ε4 marker [10], with cortical thickness [11], using VBM with a cortical parcelation atlas [18], and combining VBM with PET data [45]. Most of the results presented here confirm the previous published papers regarding classification of AD patients using machine learning techniques [9–11, 44]. Also the classification accuracy in this present study is similar with the above mentioned publications, considering the sample size used. However, we noticed very interesting converging results emerging from a completely different image analysis approach, free from the formalisms of classic statistical assumptions, and with the power of providing patterns emerging from data behavior, without a priori constraints. We believe that our results help to add information related to the robustness of findings in specific cortical regions. If this marker is reproducible at an individual level, it represents another tool that is able to provide parameters to guide neurologists' decisions about when to start any available medical treatment.

One possible issue regarding the SVM results presented in this paper is whether they are novel results or lack originality compared to previously published studies. We believe the differences of our work to the cited papers are, among others:

  (i) Use of a surface based method software in order to generate automatically the measures.
 (ii) Use of subcortical structures volumes as a classifier feature.
(iii) Study cortical thickness difference between the two groups to ensure that the data is comparable with other cortical thickness studies.

The paper from Lerch and colleagues [11] indeed uses surface based methods, however, it relies on cortical thickness only as an input feature to the classifier while we used the volume of gray matter, white matter, and subcortical structures to train the SVM.

The results shown here were obtained with a very recent version of FreeSurfer, optimized to estimate the volumes of cortical and sub-cortical structures. This software is a freeware, has a sound reliability, and has

been used in many published articles [37]. We believe the SVM approach shown here can be used to compare classification performance in different populations and subtypes of the disease in multicentre studies.

Another point worth mentioning is that our findings are in the same line as results from recent neuropathological studies [46], pointing out that a diagnosis of AD is virtually impossible on a routine basis—thus making the search for a biomarker for AD very challenging. At the same time, clinical evaluation is a subjective estimate and prone to errors, not to mention that there is no clear-cut estimate of patient prognosis from a structured diagnostic criterion. SVM and other specialized statistical classification methods based on image are promising techniques to improve the diagnosis and monitor the progression of AD.

Another fair concern would be whether the age matching was adequate (Table 1). We believe this study would provide better evidence if the two groups had a better age matching. However using age as confound factor did not altered the results.

ACKNOWLEDGMENTS

REFERENCES

[1] Pangalos, MN, Schechter, LE, Hurko, O (2007) Drug development for cns disorders: strategies for balancing risk and reducing attrition. *Nat Rev Drug Discov* **6**, 521-532.

[2] McCarron MO, Nicoll JA, Stewart J, Ironside JW, Mann DM, Love S, Graham DI, Dewar D, (1999) The apolipoprotein E epsilon2 allele and the pathological features in cerebral amyloid angiopathy-related hemorrhage. *J Neuropathol Exp Neurol* **58**, 711-718.

[3] Dickerson BC, Bakkour A, Salat DH, Feczko E, Pacheco J, Greve DN, Grodstein F, Wright CI, Blacker D, Rosas HD, Sperling RA, Atri A, Growdon JH, Hyman BT, Morris JC, Fischl B, Buckner RL, (2009) The cortical signature of Alzheimer's disease: regionally specific cortical thinning relates to symptom severity in very mild to mild ad dementia and is detectable in asymptomatic amyloid-positive individuals. *Cereb Cortex* **19**, 497-510.

[4] Fox NC, Warrington EK, Freeborough PA, Hartikainen P, Kennedy AM, Stevens JM, Rossor MN, (1996) Presymptomatic hippocampal atrophy in Alzheimer's disease. A Longitudinal MRI Study. *Brain* **119(Pt 6)**, 2001-2007.

[5] Foundas AL, Leonard CM, Mahoney SM, Agee OF, Heilman KM, (1997) Atrophy of the hippocampus, parietal cortex, and insula in Alzheimer's disease: a volumetric magnetic resonance imaging study. *Neuropsychiatry Neuropsychol Behav Neurol* **10**, 81-89.

[6] Colliot O, Chetelat G, Chupin M, Desgranges B, Magnin B, Benali H, Dubois B, Garnero L, Eustache F, Lehericy S, (2008) Discrimination between Alzheimer disease, mild cognitive impairment, and normal aging by using automated segmentation of the hippocampus. *Radiology* **248**, 194-201.

[7] Thompson PM, Hayashi KM, Dutton RA, Chiang MC, Leow AD, Sowell ER, De Zubicaray G, Becker JT, Lopez OL, Aizenstein HJ, Toga AW, (2007) Tracking Alzheimer's disease. *Ann N Y Acad Sci* **1097**, 183-214.

[8] Fan Y, Batmanghelich N, Clark CM, Davatzikos C, (2008) Spatial patterns of brain atrophy in mci patients, identified via high-dimensional pattern classification, predict subsequent cognitive decline. *Neuroimage* **39**, 1731-1743.

[9] Kloppel S, Stonnington CM, Chu C, Draganski B, Scahill RI, Rohrer JD, Fox NC, Jack CR, Ashburner J, Frackowiak RS, (2008) Automatic classification of mr scans in Alzheimer's disease. *Brain* **131**, 681-689.

[10] Vemuri P, Gunter JL, Senjem ML, Whitwell JL, Kantarci K, Knopman DS, Boeve BF, Petersen RC, Jack CR, (2008) Alzheimer's disease diagnosis in individual subjects using structural MR images: validation studies. *Neuroimage* **39**, 1186-1197.

[11] Lerch JP, Pruessner J, Zijdenbos AP, Collins DL, Teipel SJ, Hampel H, Evans AC, (2008) Automated cortical thickness measurements from MRI can accurately separate Alzheimer's patients from normal elderly controls. *Neurobiol Aging* **29**, 23-30.

[12] Kloppel S, Stonnington CM, Barnes J, Chen F, Chu C, Good CD, Mader I, Mitchell LA, Patel AC, Roberts CC, Fox NC, Jack CR, Jr., Ashburner J, Frackowiak RS, (2008) Accuracy of dementia diagnosis: a direct comparison between radiologists and a computerized method. *Brain* **131**, 2969-2974.

[13] Tanaka Y, Hanyu H, Sakurai H, Shimizu S, Takasaki M, (2003) [Characteristics of MRI features in Alzheimer's disease patients predicting response to donepezil treatment]. *Nippon Ronen Igakkai Zasshi* **40**, 261-266.

[14] Ames D, Kaduszkiewicz H, van den Bussche H, Zimmermann T, Birks J, Ashby D, (2008) For debate: is the evidence for the efficacy of cholinesterase inhibitors in the symptomatic treatment of Alzheimer's disease convincing or not?. *Int Psychogeriatr* **20**, 259-292.

[15] Boser BE, Guyon IM, Vapnik VN, (1992) in *Proceedings of the fifth annual workshop on Computational learning theory* (ACM, Pittsburgh, Pennsylvania, United States).

[16] Fu CH, Mourao-Miranda J, Costafreda SG, Khanna A, Marquand AF, Williams SC, Brammer MJ, (2008) Pattern classification of sad facial processing: toward the development of neurobiological markers in depression. *Biol Psychiatry* **63**, 656-662.

[17] Marquand AF, Mourao-Miranda J, Brammer MJ, Cleare AJ, Fu CH, (2008) Neuroanatomy of verbal working memory as a diagnostic biomarker for depression. *Neuroreport* **19**, 1507-1511.

[18] Magnin B, Mesrob L, Kinkingnehun S, Pelegrini-Issac M, Colliot O, Sarazin M, Dubois B, Lehericy S, Benali H, (2009) Support vector machine-based classification of Alzheimer's disease from whole-brain anatomical MRI. *Neuroradiology* **51**, 73-83.

[19] Roth M, Tym E, Mountjoy CQ, Huppert FA, Hendrie H, Verma S, Goddard R, (1986) CAMDEX. A standardised instrument for the diagnosis of mental disorder in the elderly with special reference to the early detection of dementia. *Br J Psychiatry* **149**, 698-709.

[20] McKhann G, Drachman D, Folstein M, Katzman R, Price D, Stadlan EM, (1984) Clinical diagnosis of Alzheimer's disease: report of the NINCDS-ADRDA Work Group under the auspices of department of health and human services task force on Alzheimer's disease. *Neurology* **34**, 939-944.

[21] Folstein MF, Folstein SE, McHugh PR, (1975) "Mini-mental state". A practical method for grading the cognitive state of patients for the clinician. *J Psychiatr Res* **12**, 189-198.

[22] Fischl B, Dale AM, (2000) Measuring the thickness of the human cerebral cortex from magnetic resonance images. *Proc Natl Acad Sci U S A* **97**, 11050-11055.

[23] Dale AM, Fischl B, Sereno MI, (1999) Cortical surface-based analysis. I. segmentation and surface reconstruction. *Neuroimage* **9**, 179-194.

[24] Fischl B, Sereno MI, Dale AM, (1999) Cortical surface-based analysis. II: inflation, flattening, and a surface-based coordinate system. *Neuroimage* **9**, 195-207.

[25] Fischl B, van der Kouwe A, Destrieux C, Halgren E, Segonne F, Salat DH, Busa E, Seidman LJ, Goldstein J, Kennedy D, Caviness V, Makris N, Rosen B, Dale AM, (2004) Automatically parcellating the human cerebral cortex. *Cereb Cortex* **14**, 11-22.

[26] Fischl B, Salat DH, van der Kouwe AJ, Makris N, Segonne F, Quinn BT, Dale AM, (2004) Sequence-independent segmentation of magnetic resonance images. *Neuroimage* **23(Suppl 1)**, S69-S84.

[27] Fischl B, Salat DH, Busa E, Albert M, Dieterich M, Haselgrove C, van der Kouwe A, Killiany R, Kennedy D, Klaveness S, Montillo A, Makris N, Rosen B, Dale AM, (2002) Whole brain segmentation: automated labeling of neuroanatomical structures in the human brain. *Neuron* **33**, 341-355.

[28] Fischl B, Liu A, Dale AM, (2001) Automated manifold surgery: constructing geometrically accurate and topologically correct models of the human cerebral cortex. *IEEE Trans Med Imaging* **20**, 70-80.

[29] Segonne F, Dale AM, Busa E, Glessner M, Salat D, Hahn HK, Fischl B, (2004) A hybrid approach to the Skull stripping problem in MRI. *Neuroimage* **22**, 1060-1075.

[30] Sled JG, Zijdenbos AP, Evans AC, (1998) A nonparametric method for automatic correction of intensity nonuniformity in MRI data. *IEEE Trans Med Imaging* **17**, 87-97.

[31] Segonne F, Pacheco J, Fischl B, (2007) Geometrically accurate topology-correction of cortical surfaces using non-separating loops. *IEEE Trans Med Imaging* **26**, 518-529.

[32] Fischl B, Sereno MI, Tootell RB, Dale AM, (1999) High-resolution intersubject averaging and a coordinate system for the cortical surface. *Hum Brain Mapp* **8**, 272-284.

[33] Desikan RS, Segonne F, Fischl B, Quinn BT, Dickerson BC, Blacker D, Buckner RL, Dale AM, Maguire RP, Hyman BT, Albert MS, Killiany RJ, (2006) An automated labeling system for subdividing the human cerebral cortex on MRI scans into gyral based regions of interest. *Neuroimage* **31**, 968-980.

[34] Rosas HD, Liu AK, Hersch S, Glessner M, Ferrante RJ, Salat DH, van der Kouwe A, Jenkins BG, Dale AM, Fischl B, (2002) Regional and progressive thinning of the cortical ribbon in Huntington's disease. *Neurology* **58**, 695-701.

[35] Kuperberg GR, Broome MR, McGuire PK, David AS, Eddy M, Ozawa F, Goff D, West WC, Williams SC, van der Kouwe AJ, Salat DH, Dale AM, Fischl B, (2003) Regionally localized

thinning of the cerebral cortex in schizophrenia. *Arch Gen Psychiatry* **60**, 878-888.

[36] Salat DH, Buckner RL, Snyder AZ, Greve DN, Desikan RS, Busa E, Morris JC, Dale AM, Fischl B, (2004) Thinning of the cerebral cortex in aging. *Cereb Cortex* **14**, 721-730.

[37] Han X, Jovicich J, Salat D, van der Kouwe A, Quinn B, Czanner S, Busa E, Pacheco J, Albert M, Killiany R, Maguire P, Rosas D, Makris N, Dale A, Dickerson B, Fischl B, (2006) Reliability of MRI-derived measurements of human cerebral cortical thickness: the effects of field strength, scanner upgrade and manufacturer. *Neuroimage* **32**, 180-194.

[38] Chih-Chung C, Chih-Jen L. (2009) LIBSVM: a library for support vector machines, http://www.csie.ntu.edu.tw/~cjlin/libsvm, Accessed November 22, 2009

[39] Singh V, Chertkow H, Lerch JP, Evans AC, Dorr AE, Kabani NJ, (2006) Spatial patterns of cortical thinning in mild cognitive impairment and Alzheimer's disease. *Brain* **129**, 2885-2893.

[40] Du AT, Schuff N, Kramer JH, Rosen HJ, Gorno-Tempini ML, Rankin K, Miller BL, Weiner MW, (2007) Different regional patterns of cortical thinning in Alzheimer's disease and frontotemporal dementia. *Brain* **130**, 1159-1166.

[41] Desikan RS, Fischl B, Cabral HJ, Kemper TL, Guttmann CR, Blacker D, Hyman BT, Albert MS, Killiany RJ, (2008) MRI measures of temporoparietal regions show differential rates of atrophy during prodromal ad. *Neurology* **71**, 819-825.

[42] Jack CR, Shiung MM, Gunter JL, O'Brien PC, Weigand SD, Knopman DS, Boeve BF, Ivnik RJ, Smith GE, Cha RH, Tangalos EG, Petersen RC, (2004) Comparison of different mri brain atrophy rate measures with clinical disease progression in ad. *Neurology* **62**, 591-600.

[43] Likeman M, Anderson VM, Stevens JM, Waldman AD, Godbolt AK, Frost C, Rossor MN, Fox NC, (2005) Visual assessment of atrophy on magnetic resonance imaging in the diagnosis of pathologically confirmed young-onset dementias. *Arch Neurol* **62**, 1410-1415.

[44] Davatzikos C, Resnick SM, Wu X, Parmpi P, Clark CM, (2008) Individual patient diagnosis of AD and FTD via high-dimensional pattern classification of MRI. *Neuroimage* **41**, 1220-1227.

[45] Fan Y, Resnick SM, Wu X, Davatzikos C, (2008) Structural and functional biomarkers of prodromal Alzheimer's disease: a high-dimensional pattern classification study. *Neuroimage* **41**, 277-285.

[46] Funke SA, Birkmann E, Willbold D, (2009) Detection of amyloid-beta aggregates in body fluids: a suitable method for early diagnosis of Alzheimer's disease?. *Curr Alzheimer Res* **6**, 285-289.

Survey of Protocols for the Manual Segmentation of the Hippocampus: Preparatory Steps Towards a Joint EADC-ADNI Harmonized Protocol

Marina Boccardi[a], Rossana Ganzola[a], Martina Bocchetta[a], Michela Pievani[a], Alberto Redolfi[a], George Bartzokis[b], Richard Camicioli[c], John G. Csernansky[d], Mony J. de Leon[e], Leyla deToledo-Morrell[f], Ronald J. Killiany[g], Stéphane Lehéricy[h], Johannes Pantel[i], Jens C. Pruessner[j], H. Soininen[k], Craig Watson[l], Simon Duchesne[m], Clifford R. Jack Jr[n] and Giovanni B. Frisoni[a,*]

[a]*LENITEM (Laboratory of Epidemiology, Neuroimaging and Telemedicine) IRCCS – S. Giovanni di Dio – Fatebenefratelli Brescia, Italy*
[b]*Department of Psychiatry, David Geffen School of Medicine at UCLA, Los Angeles, CA, USA*
[c]*Department of Biomedical Engineering, Centre for Neuroscience, University of Alberta, Edmonton, AB, Canada*
[d]*Department of Psychiatry and Behavioral Sciences, Northwestern University Feinberg School of Medicine, Chicago, IL, USA*
[e]*Center for Brain Health, New York University School of Medicine, New York, NY, USA*
[f]*Department of Neurological Sciences, Rush University, Chicago, IL, USA*
[g]*Department of Anatomy and Neurobiology, Boston University School of Medicine, Boston, MA, USA*
[h]*Center for NeuroImaging Research - CENIR and Dept of Neuroradiology, Université Pierre et Marie Curie-Paris 6, Groupe Hospitalier Pitié-Salpêtrière, Paris, France*
[i]*Department of Psychiatry and Psychotherapy, University of Frankfurt/Main, Germany*
[j]*McGill Centre for Studies in Aging, Department of Psychiatry, McGill University, Montreal, Quebec, Canada*
[k]*Department of Neurology, University of Eastern Finland and Kuopio University Hospital, Kuopio, Finland*
[l]*Department of Neurology, Wayne State University School of Medicine, 8D-University Health Center, St. Antoine, Detroit, MI, USA*
[m]*Department of Radiology, Université Laval and Centre de Recherche Université Laval – Robert Giffard, Quebec City, Canada*
[n]*Department of Diagnostic Radiology, Mayo Clinic and Foundation, Rochester, MN, USA*

Abstract. Manual segmentation from magnetic resonance imaging (MR) is the gold standard for evaluating hippocampal atrophy in Alzheimer's disease (AD). Nonetheless, different segmentation protocols provide up to 2.5-fold volume differences. Here we surveyed the most frequently used segmentation protocols in the AD literature as a preliminary step for international harmonization. The anatomical landmarks (anteriormost and posteriormost slices, superior, inferior, medial, and lateral borders) were identified from 12 published protocols for hippocampal manual segmentation ([Abbreviation] first author, publication year:

---

*Correspondence to: Giovanni B. Frisoni, LENITEM, IRCCS S.Giovanni di Dio, via Pilastroni, 4, 25100 Brescia – Italy, Tel.: +39 030 3501361; Fax: +39 02 700435727; E-mail: gfrisoni@ fatebenefratelli.it.

[B] Bartzokis, 1998; [C] Convit, 1997; [dTM] deToledo-Morrell, 2004; [H] Haller, 1997; [J] Jack, 1994; [K] Killiany, 1993; [L] Lehericy, 1994; [M] Malykhin, 2007; [Pa] Pantel, 2000; [Pr] Pruessner, 2000; [S] Soininen, 1994; [W] Watson, 1992). The hippocampi of one healthy control and one AD patient taken from the 1.5T MR ADNI database were segmented by a single rater according to each protocol. The accuracy of the protocols' interpretation and translation into practice was checked with lead authors of protocols through individual interactive web conferences. Semantically harmonized landmarks and differences were then extracted, regarding: (a) the posteriormost slice, protocol [B] being the most restrictive, and [H, M, Pa, Pr, S] the most inclusive; (b) inclusion [C, dTM, J, L, M, Pr, W] or exclusion [B, H, K, Pa, S] of alveus/fimbria; (c) separation from the parahippocampal gyrus, [C] being the most restrictive, [B, dTM, H, J, Pa, S] the most inclusive. There were no substantial differences in the definition of the anteriormost slice. This survey will allow us to operationalize differences among protocols into tracing units, measure their impact on the repeatability and diagnostic accuracy of manual hippocampal segmentation, and finally develop a harmonized protocol.

INTRODUCTION

Hippocampal volumetry is a marker sensitive to disease state and progression in Alzheimer's disease (AD). The proposal for revised diagnostic criteria [1] posits that, even in the preclinical stages of the disease, the presence of hippocampal atrophy on magnetic resonance imaging (MR) is a marker suggestive of AD, the others being temporo-parietal hypometabolism on FDG PET, abnormal CSF tau and Abeta42 proteins, cerebral amyloidosis on molecular PET imaging. Currently, hippocampal volumetry is included as a secondary outcome measure in several clinical trials of disease modifying drugs to support the claim of disease modification [2].

Manual outlining on MR images by trained raters is presently the most accurate, validated and used procedure to measure hippocampal volumes [3–6], and the gold standard for the validation of automated segmentation algorithms [7–12]. However, a large number of protocols for the manual segmentation of the hippocampus is available and adopted in different fields of neuroscience research, including those investigating a variety of psychiatric and neurodegenerative conditions [13, 14]. These segmentation protocols differ in their definition of anatomical boundaries and tracing procedures, thus originating hippocampal volume estimates that cannot be straightforwardly compared. Indeed, the mean volume for a normal hippocampus can range from 2 to 5.3 cm^3 [14] across laboratories worldwide. Even if individual differences in head size are taken into account, this range is far too broad to

accept hippocampal volumetry as a valid marker for any neurological condition. Although these differences are in part caused by heterogeneities in image acquisition and preprocessing, heterogeneities in the landmark definitions are major contributors. Heterogeneity was found in the definition of the most rostral and most caudal slices, in the criteria for inclusion or exclusion of hippocampal white matter (alveus and fimbria), in the definition of boundary lines with adjacent anatomical structures [13, 14].

This heterogeneity prevents a direct comparison of the outcome of different studies, and slows down the transfer of the marker from the research laboratory to the clinical setting. Standard operational procedures (SOPs) are clearly required for manual hippocampal volumetry to be transferred to routine diagnostic settings and gain status as a surrogate outcome in clinical trials for disease modifying drugs. SOPs will promote the large use of hippocampal atrophy measurements for the early diagnosis of AD and allow the comparison of the effect of different drugs in clinical trials. Moreover, the automated approaches need to be validated using a gold standard, for a given clinical population. SOPs may represent the gold standard for the many automated algorithms aiming to extract hippocampal volume with minimal or no human input that are presently under development [15, 16].

The aim of this study is to survey a selection of the most popular protocols for hippocampal segmentation used in AD research, in order to extract commonalities and differences. Importantly, we sought explicit input from protocol authors to check for proper

understanding of their work. This survey is the first step of a larger project aiming to develop an internationally harmonized protocol for hippocampal segmentation.

MATERIALS AND METHODS

In this work we surveyed the landmark definitions provided for the manual segmentation of the hippocampus from MR images. A pilot survey was first carried out on 5 protocols belonging to the repertoire routinely used at LENITEM as tracing criteria, or for study purposes. The study design was then extended to a wider set of protocols including all of the most commonly used ones within the AD literature (see '*Selection of segmentation protocols*' below). Hippocampal manual segmentation was performed by a single tracer on the left hippocampus of two subjects based on each protocol (see '*Selection of scans for the prototypical tracings*', '*Image processing*', and '*Prototypical tracings*' sections below), and tracings were then checked for correctness with the lead authors of the protocols ('*Authors' check*') to obtain certified segmentations. We then extracted differences among protocols through the semantic harmonization of terms (see '*Extraction of similarities and differences*' below).

Selection of segmentation protocols

The pilot survey was carried out on five protocols routinely used in our laboratory for learning and as tracing criteria [17–21]. In the experimental phase, the selection was expanded to include all the most widely cited protocols in the AD literature (Table 1).

The protocols mentioned in the two available reviews on manual segmentation of the hippocampus were examined first [13,14]. Original protocols were drawn from the recent paper by Konrad and colleagues [13] and the review by Geuze and colleagues [14]. The review by Konrad and colleagues' included 71 protocols for hippocampal segmentation. Of these, 50 protocols provided an original description of landmarks for segmentation and were retained in the present survey, while the remaining 21 redirected the reader to previously published protocols and, thus, were excluded from this survey. All but one [22] of the protocols reviewed by Geuze and colleagues were included among these 50; the one that was not [22] was retained in the present survey.

Two of the 5 protocols of the pilot study [19,20] were not among those reviewed by Konrad and colleagues or

Geuze and colleagues, and were retained in the present survey.

In order to ascertain whether the 53 protocols retained in the present survey included all of the most cited protocols for hippocampal segmentation in the AD literature, we repeated the same search carried out by Konrad, using the key-words "Alzheimer*", "AD" or "dementia" instead of Konrad's "depression", "major depression" or "unipolar depression". This search lead to the inclusion of 3 more protocols [23–25] with a high rate of citations in the AD literature (Table 1), leading to a total of 56 protocols retained in the present survey.

To be selected for harmonization, protocols had to satisfy five criteria, considered in the following hierarchical order: i) Number of citations in the AD literature greater than 40. Literature citations of the 56 protocols were identified using the ISI Web of Science portal, and the keywords "(Alzheimer* OR dementia) AND hippo*" were used to compute citations only within the AD literature (Table 1, "Citation in the AD literature"). Papers with less than 40 citations on December 31, 2009 were excluded; ii) at least the head and body of the hippocampus were included in the segmentation; iii) adjacent structures such as the amygdala, the choroid plexus, and major portions of the parahippocampal cortex were excluded from the segmentation; iv) three-dimensional (3D) T1-weighted MR sequences with slice thickness smaller or equal to 3 mm were used; v) MR scans were acquired using a scanner with field strength greater than 1 Tesla; vi) the availability of a lead author to perform a one hour web-conference was required, to check the correctness of the tracings according to the specific protocol (Table 1, "Compliance with selection criteria").

Finally, we included 12 protocols (Table 1, First author, publication year, in alphabetical order): [B] Bartzokis, 1998 [21]; [C] Convit, 1997 [26]; [dTM] deToledo-Morrell, 2004 [23]; [H] Haller, 1997 [27]; [J] Jack, 1994 [17]; [K] Killiany, 1993 [24]; [L] Lehericy, 1994 [25]; [M] Malykhin, 2007 [20]; [Pa] Pantel, 2000 [19]; [Pr] Pruessner, 2000 [18]; [S] Soininen, 1994 [28]; [W] Watson, 1992 [29].

Selection of scans for the prototypical tracings

Tracings of the left hippocampus were carried out on images of one healthy control and one AD patient taken from the 3D T1-weighted structural ADNI dataset [74], following the landmarks of each of the 12 protocols. The accuracy of the application of the protocols as

Table 1
Surveyed protocols for hippocampal segmentation.

Protocol	Citations in the AD literature	Cited by Konrad and colleagues	Cited by Geuze and colleagues	Compliance with selection criteria	Inclusion stage	Selected for harmonization	Ref
Killiany, 1993	173	No	No	Satisfying criteria	Experimental	Yes	[24]
Convit, 1997	143	Yes	Yes	Satisfying criteria	Experimental	Yes	[26]
Watson, 1992	122	Yes	Yes	Satisfying criteria	Experimental	Yes	[30]
Soininen, 1994	118	Yes	Yes	Satisfying criteria	Experimental	Yes	[28]
Sheline, 1996	79	Yes	No	Author not available	Experimental	No	[31]
Lehericy, 1994	78	No	No	Satisfying criteria	Experimental	Yes	[25]
Pruessner, 2000	78	Yes	No	Satisfying criteria	Pilot	Yes	[18]
Bremner, 1995	53	Yes	Yes	Only hippocampal body included	Experimental	No	[32]
deToledo-Morrell, 2004	50	No	No	Satisfying criteria	Experimental	Yes	[23]
Haller, 1997	44	Yes	No	Satisfying criteria	Experimental	Yes	[27]
Cook, 1992	44	Yes	Yes	Plexus choroideus included	Experimental	No	[33]
Bigler, 1997	38	Yes	Yes	Less than 40 citations	Experimental	No	[34]
Shenton, 1992	33	Yes	Yes	Less than 40 citations	Experimental	No	[35]
MacQueen, 2003	30	Yes	No	Less than 40 citations	Experimental	No	[36]
Bogerts, 1993	30	No	Yes	Less than 40 citations	Experimental	No	[22]
Narr, 2004	25	Yes	No	Less than 40 citations	Experimental	No	[37]
Mervaala, 2000	21	Yes	No	Less than 40 citations	Experimental	No	[38]
Steffens, 2002	20	Yes	No	Less than 40 citations	Experimental	No	[39]
Jack, 1994	18	Yes	Yes	Satisfying criteria except citations number	Pilot	Yes	[17]
O'Brien, 2004	18	Yes	No	Less than 40 citations	Experimental	No	[40]
Ashtari, 1999	17	Yes	No	Less than 40 citations	Experimental	No	[41]
Bartzokis, 1993	17	Yes	Yes	Satisfying criteria except citations number (<40 in AD literature)	Pilot	Yes	[21]
Pantel, 2000	17	No	No	Satisfying criteria except citations number (<40 in AD literature)	Pilot	Yes	[19]
Zipursky, 1994	16	Yes	Yes	Less than 40 citations	Experimental	No	[42]
Giedd, 1996	16	Yes	Yes	Less than 40 citations	Experimental	No	[43]
Kates, 1997	16	Yes	No	Less than 40 citations	Experimental	No	[44]
Honeycutt, 1998	15	Yes	Yes	Less than 40 citations	Experimental	No	[45]
von Gunten, 2000	13	Yes	No	Less than 40 citations	Experimental	No	[46]
Vythilingam, 2004	10	Yes	No	Less than 40 citations	Experimental	No	[47]
Hastings, 2004	9	Yes	No	Less than 40 citations	Experimental	No	[48]
Niemann, 2000	9	Yes	No	Less than 40 citations	Experimental	No	[49]
Lobnig, 2006	7	Yes	No	Less than 40 citations	Experimental	No	[50]
Lloyd, 2004	6	Yes	No	Less than 40 citations	Experimental	No	[51]
Driessen, 2000	6	Yes	No	Less than 40 citations	Experimental	No	[52]
Barr, 1997	5	Yes	No	Less than 40 citations	Experimental	No	[53]
Neumeister, 2005	5	Yes	No	Less than 40 citations	Experimental	No	[54]
Caetano, 2004	5	Yes	No	Less than 40 citations	Experimental	No	[55]
Frodl, 2004	5	Yes	No	Less than 40 citations	Experimental	No	[56]
Rusch, 2001	4	Yes	No	Less than 40 citations	Experimental	No	[57]
Nakano, 2002	4	Yes	No	Less than 40 citations	Experimental	No	[58]
MacMillan, 2003	3	Yes	No	Less than 40 citations	Experimental	No	[59]
Yucel, 2007	3	Yes	No	Less than 40 citations	Experimental	No	[60]
Brambilla, 2003	3	Yes	No	Less than 40 citations	Experimental	No	[61]
Saylam, 2006	3	Yes	No	Less than 40 citations	Experimental	No	[62]

(*Continued*)

Table 1
(*Continued*)

Protocol	Citations in the AD literature	Cited by Konrad and colleagues	Cited by Geuze and colleagues	Compliance with selection criteria	Inclusion stage	Selected for harmonization	Ref
MacMaster & Kusumakar, 2004	2	Yes	No	Less than 40 citations	Experimental	No	[63]
Malykhin, 2007	2	No	No	Satisfying criteria except citations number (<40 in AD literature)	Pilot	Yes	[20]
Scott, 2004	2	Yes	No	Less than 40 citations	Experimental	No	[64]
Chen, 2004	2	Yes	No	Less than 40 citations	Experimental	No	[65]
Vermetten, 2006	1	Yes	No	Less than 40 citations	Experimental	No	[66]
Arango, 2003	1	Yes	No	Less than 40 citations	Experimental	No	[67]
Chang, 2005	1	Yes	No	Less than 40 citations	Experimental	No	[68]
Rosso, 2005	1	Yes	No	Less than 40 citations	Experimental	No	[69]
Xia, 2004	1	Yes	No	Less than 40 citations	Experimental	No	[70]
Frazier, 2005	1	Yes	No	Less than 40 citations	Experimental	No	[71]
Bossini, 2008	1	Yes	No	Less than 40 citations	Experimental	No	[72]
Starkman, 2007	0	Yes	No	Less than 40 citations	Experimental	No	[73]

Protocols are sorted in order of citation in the AD literature (first the most cited)

described in the manuscripts was checked with the pertinent lead author.

The AD patient (ID: 021_S_0642) was selected from those with moderate to severe medial temporal atrophy (MTA) (score of 3 on Scheltens's visual rating scale, ranging from 0 to 4) [75], was 85 years old, had MMSE score of 25/30, and Clinical Dementia Rating (CDR) of 1. The control (ID: 023_S_0058) was chosen for having minimum atrophy (score of 1 on Scheltens's visual rating scale). The control was 70 years of age, had a MMSE score of 30/30, a CDR of 0 [75].

Image processing

A combination of several freely available tools was used to prepare the raw MR ADNI images for manual segmentation. DICOM images were converted to Analyze/NIFTI format using the MRIcron software (V.8.0, http://www.cabiatl.com/mricro/). Prior to prototypical tracing, the 3D image was manually reoriented based on the requirement of the corresponding protocol. Seven of the protocols considered in this study required the reorientation of the image to the long axis of the hippocampus, 5 required aligning the image to the line which passes through the anterior and posterior commissures of the brain (AC-PC line). These reorientation steps were performed using the 3D-Slicer software (V.3.2, http://www.slicer.org/). All MR images were analyzed in native space.

Prototypical tracings

A single tracer (RG) segmented the left hippocampus of the two subjects according to each of the 12 protocols, after reorienting the image as required by each protocol. The intra-rater (0.94) and inter-rater (0.89) correlation coefficients of the tracer were computed previously, on a sample of 20 healthy controls, not including the ones examined for this study, and in comparison to another expert tracer within the laboratory [76]. The protocol used for computing the correlation coefficients was that by Pruessner and colleagues [18]. Tracings were performed using Multitracer (http://air.bmap.ucla.edu/MultiTracer/) developed at the Laboratory Of NeuroImaging (LONI) at UCLA (Los Angeles, USA), allowing simultaneous 3D navigation in the axial and sagittal planes (Fig. 1). Hippocampal boundaries based on each protocol were traced on approximately 20 1.2 mm thick coronal slices.

Authors' check

Hippocampal tracings were certified as compliant with the original protocols using a three-stage check procedure: check with the lead author of the protocol, trace editing, and final check.

A Power Point presentation was provided to the lead author showing native and segmented slices of
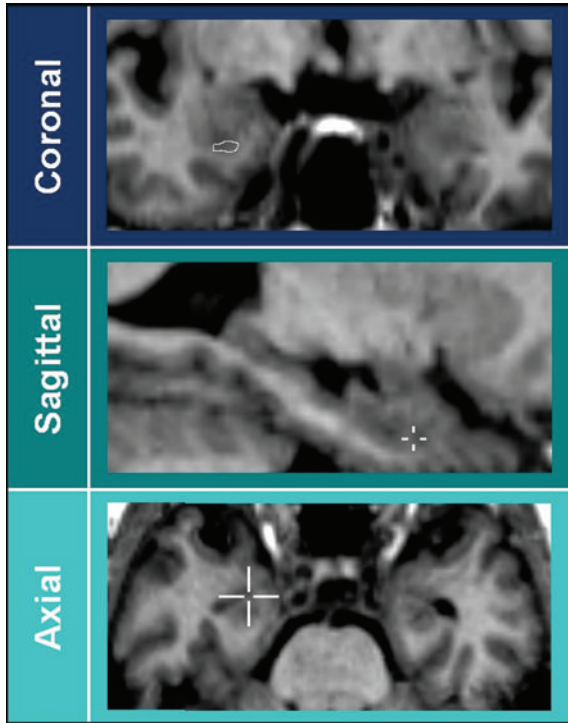
Fig. 1. Most anterior slice. Differences in the definition of the most anterior slice are overcome due to currently used software for 3D brain navigation. The visualization of the cursor position in 3D provides unequivocal information about its location in the amygdale or in the hippocampus, even if a single coronal section may not provide sufficiently clear information.

the two sample subjects. These slices were also paired with pictures of corresponding histological cuts, and text notes were added to describe tracings, landmarks and questions on unclear issues. Power Point presentations begun with a survey table, summarizing the explicit landmarks for that protocol, the main included and excluded structures, and other possibly specific key features of each protocol (Power Point presentations can be accessed at http://www.hippocampal-protocol.net/SOPs/investigatedprotocols.html). The lead author was asked to correct the survey table, examine the tracings, and take note of the unclear points that he/she would be asked to discuss subsequently. The appropriateness of our understanding of criteria was verified with the lead author at both the semantic and the practical levels, by means of individual teleconferences (TCs). TCs were carried out with a web-seminar system that allowed all participants to share the same desktop view, scroll the slides, control the cursor and carry out tracings on the same image viewed by all concurrently. TCs were recorded (available upon request),

to ensure information availability over time. The tracings were verified, and unclear points were elucidated, by working on the power point presentations and with the use of Multitracer when necessary. It should be noted that the correction stage included the update to advances in tracing method, such as the use of 3D visualization tools, or other changes occurring in the tracing methods over time. After the TC, the tracings were edited according to the author's input and re-sent to the author for further check. This procedure was iteratively repeated until the author was satisfied that tracings had been performed according to his/her original description. These presentations, including the final summary table and the final "certified" tracings, are available at http://www.hippocampal-protocol.net/SOPs/investigatedprotocols.html.

Extraction of similarities and differences

A compendium of the survey tables of all protocols was created, by reporting the features for each segmentation criterion as it was certified by the lead authors (http://www.hippocampal-protocol.net/SOPs/LINK_PAGE/anatomical-landmarks-certified-12.xls). A semantic harmonization of the features was necessary in order to ensure the correct comparison among these heterogeneous criteria, since the very same landmark was indeed named and described using different words in different protocols (http://www.hippocampal-protocol.net/SOPs/LINK_PAGE/harmonized-anatomical-landmarks-12.xls). This phase of the survey can also be considered as the first step in the operationalization of the differences among the examined protocols. By operationalization, we mean the process of reducing the variability among protocols into a finite number of differences, sufficiently well defined to lend themselves to quantitative investigation. In practice, the wide heterogeneity in landmarks would be reduced into a finite number of elementary tracing units, which could be measured and tested.

The harmonized definitions for each landmark were chosen by two of us (MB and RG) after having checked our comprehension in the teleconferences, based on the ability of definitions to unequivocally identify the landmark, and assuming that tracing would be carried out on coronal slices from rostral to caudal.

After the semantic harmonization, the extraction of differences among the author-certified protocols was carried out for each of the examined portion of the hippocampus where different criteria could be applied, i.e., most anterior and most posterior slices,

Table 2
General features of the 12 selected protocols

Protocol	Slice	Direction of tracing	MR Sequence	Validation Sample	Included Hippocampal tissue	Reproducibility measures
Bartzokis et al., 1998 [21]	coronal	from rostral to caudal	T1	healthy controls	Head, body, and tail until visualization of colliculi	5% error
Convit et al., 1997 [26]	coronal	from rostral to caudal	T1	AD	Head, body, and tail until visualization of crus/crura of fornix/ces in full profile	0.85 inter-rater reliability (ICC)
deToledo-Morrell et al., 2004 [23]	coronal	from rostral to caudal	T1	MCI	Head, body, and tail until visualization of crus/crura of fornix/ces in full profile	0.97 intra-rater and inter-rater reliability (ICC)
Haller et al., 1997 [27]	coronal, sagittal and axial	from caudal to rostral	T1	schizophrenia	Head, body, and whole tail	77.9% overlap of voxels
Jack et al., 1994 [17]	coronal	from caudal to rostral	T1	epilepsy	Head, body, and tail until visualization of crus/crura of fornix/ces in full profile	1.2% and 3.4% intra- and inter-observer variability (5% error with slices below a thickness of 3 mm)
Killiany et al., 1993 [24]	coronal	from rostral to caudal	T1	AD	Head, body, and tail until visualization of crus/crura of fornix/ces in full profile	0.91 and 0.92 intra- and inter-rater reliability (ICC)
Lehericy et al., 1994 [25]	coronal	from caudal to rostral	T1	AD	Head, body, and tail ntil visualization of crus/crura of fornix/ces in full profile	7% inter-rater relative error on volume [81]
Malykhin et al., 2007 [20]	coronal; sagittal at the level of the head	from the hippocampal body to the tail, then from the posterior part of head to its rostral part	T1	Parkinson's disease; depression	Head, body, and whole tail	0.86 and 0.96 intra- and inter-rater reliability (ICC)
Pantel et al., 2000 [19]	coronal	from rostral to caudal	T1 + T2	healthy controls	Head, body, and whole tail	intraclass $R = 0.78$
Pruessner et al., 2000 [18]	coronal	from caudal to rostral	T1	healthy controls	Head, body, and whole tail	0.92 and 0.99 intra- and inter-rater reliability (ICC)
Soininen et al., 1994 [28]	coronal	from rostral to caudal	T1	MCI	Head, body, and tail until visualization of crus/crura of fornix/ces in full profile	0.95 intra-rater reliability (ICC)
Watson et al., 1992 [29]	coronal	from rostral to caudal	T1	healthy controls	Head, body, and tail until visualization of crus/crura of fornix/ces in full profile	intra-rater score range between 0.88 and 0.99

superior border (i.e., inclusion or exclusion of alveus and fimbria), and medial border at the level of the body. Each different criterion adopted for each of these portions denotes a different definition of landmarks, which outline specific regions of hippocampal tissue. This means that, based on these criteria, well defined regions of hippocampal tissue can be isolated, and included or excluded in the segmentation of the hippocampus on MR images, depending on the adopted protocol. Therefore, this phase was also the basis for the operationalization of differences among protocols into a limited number of concrete and elementary segmentation units, to allow quantitative investigation in the next stage of this project.

The semantic harmonization and the extraction of similarities and differences also implied a hierarchy-based selection. Landmarks internal (e.g., alveus) or adjacent (e.g., CSF, parahippocampal white matter) to the hippocampus were considered as having higher value than those external to the hippocampus (i.e., pulvinar), and, whenever possible, were chosen for the definition and first operationalization stage, since these are invariant to the plane of orientation of the 3D MR images.

RESULTS

Protocols were uniform as to magnetic field strength of MR (1.5T) and reproducibility values. Moreover, they were uniform on use of 3D visualization, and in the exclusion of non-hippocampal tissue (amygdala, choroid plexus). Instead, differences could be detected in the direction of segmentation (i.e., rostral to caudal), as well as in the population used for validating the procedure (Table 2).

The survey tables for each protocol are available at: www.hippocampal-protocol.net. As illustrated in the summary survey table, following semantic harmonization of landmarks (http://www.hippocampal-protocol. net/SOPs/LINK_PAGE/harmonized-anatomical-land marks-12.xls), differences between the protocols that most likely had an impact on the volumetric estimates concerned heterogeneities in the definition of (a) the orientation of the images; (b) the most posterior slice; (c) the superior border; (d) the separation from the parahippocampal gyrus at the level of the subiculum, in the hippocampal body (Table 3). Heterogeneities in the definition of (e) the most anterior slice are not shown in Table 3 for reasons that will be explained below.

a) Plane of tracing. Seven of the protocols reoriented the images along the long axis of the hippocampus [17, 21, 23, 25, 26, 28, 29], and 5 used images oriented along the AC-PC line [18–20, 24, 27]. Among these, 3 are the most recently published protocols [18–20], consistently with a trend to taking advantage of the greater availability of AC-PC automatic registration algorithms [77–80], that min-

Table 3
Differences of anatomical landmarks among the 12 selected protocols, after semantic harmonization

a) Plane of tracing			
Axis of hippocampus [B, C, dTM, J, L, S, W]	AC-PC line [H, K, M, Pa, Pr]		
b) Most posterior slice			
Where inferior and superior colliculi are jointly visualized [B]	Where crus/crura of fornix/ces is/are visible in full profile [C, dTM, J, K, L, S, W]	Where gray matter is visible inferomedially to the trigone of the lateral ventricle [H, M, Pa, Pr]	
c) Superior border			
Lower border of alveus/fimbria [B, H, K, Pa, S]	Upper border of alveus/fimbria [C, dTM, J, L, M, Pr, W]		
d) Medial border at subiculum level			
vertical line from the CA to the WM of the parahippocampal gyrus [C]	Oblique line with same inclination of parahippocampal WM, connecting the inferior part of the subiculum to the quadrigeminal cistern [K, L, M, Pr, W]	Horizontal line from the highest medial point of the parahippocampal WM to the cistern [B, dTM, H]	Line outlining the contour of white matter of parahippocampal gyrus [J, Pa, S]

AC = anterior commissure; PC = posterior commissure; CA = cornu Ammonis; WM = white matter; [B] Bartzokis et al., 1998, [C] Convit et al.,1997, [dTM] deToledo-Morrell et al., 2004; [H] Haller et al., 1997, [J] Jack et al., 1994, [K] Killiany et al., 1993, [L] Lehericy et al., 1994, [M] Malykhin et al., 2007, [Pa] Pantel et al., 2000, [Pr] Pruessner et al., 2000, [S] Soininen et al., 1994, [W] Watson et al., 1992.
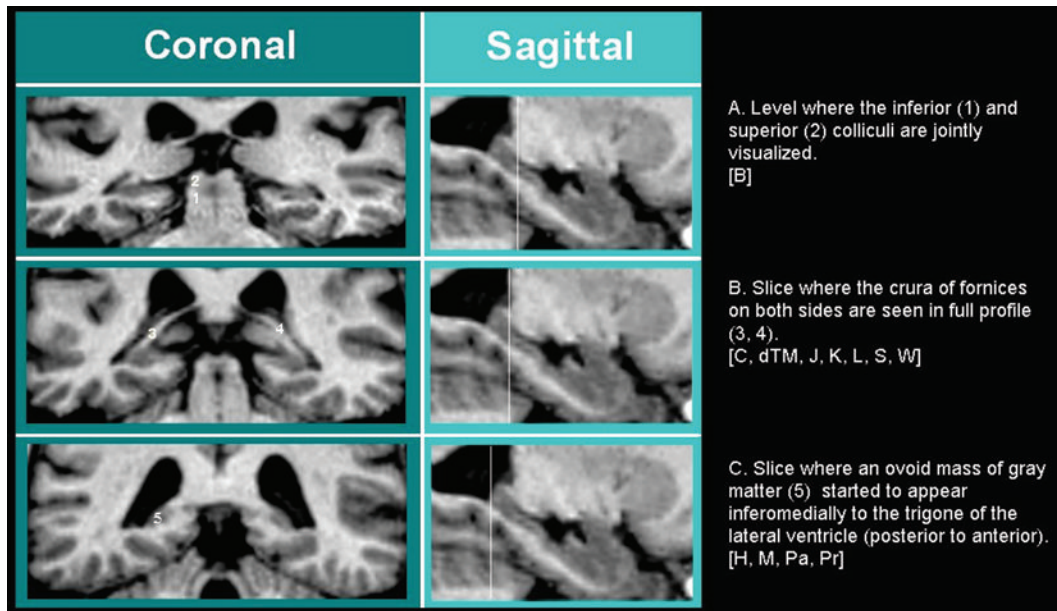
Fig. 2. Most posterior slice. The criterion in A) is followed by protocol [B], B) by protocols [C, dTM, J, K, L, S, W], C) by [H, M, Pa, Pr].

imize and facilitate human work in the preprocessing stages.

b) Definition of the most posterior slice. Important differences characterize the protocols as to the definition of the most posterior slice where hippocampal tissue is segmented. The most restrictive protocol stops tracing at the level where both the inferior and superior colliculi are visible (Table 3; Fig. 2A). Less restrictive protocols stop when the crus or both crura of the fornices are seen in full profile, these two criteria differing often by one single slice (Fig. 2B). The less restrictive ones trace as long as they can detect hippocampal gray matter on the coronal slices (Fig. 2 C), the only difference among these consisting in the attempt to exclude gray matter belonging to the vestigial hippocampal tissue of the Andrea Retzius and fasciolar gyri (see point *c*, *Definition of the superior border*).

c) Definition of the superior border. The definition of the superior border concerns the inclusion or exclusion of hippocampal white matter (i.e., alveus and fimbria) along the structure and, for most caudal slices, the inclusion or exclusion of the vestigial gray matter (i.e., fasciolar gyrus and Andrea Retzius gyrus) that extends dorso-medially (Fig. 3, last column).

Seven of the protocols included alveus and fimbria in the segmentation (Fig. 3, bottom line), and five excluded these white matter layers (Table 3; Fig. 3, 3rd line), at least whenever visible.

As to the vestigial gray matter located on the most caudal portion of the hippocampus, arbitrary linear demarcations are adopted to separate the uppermost tissue belonging to the fasciolar and Andrea Retzius gyri [Pr] (Fig. 3, last column), or a superior portion is limited, by excluding a little layer of gray matter below the cingulate gyrus and the isthmus of the cingulum [M]. As in the case of the most anterior slice, the separation from vestigial gray matter may benefit from the 3D visualization allowed by recent software.

d) Definition of the medial border. The definition of the medial border was not problematic for the head and tail. Instead, its definition differed through the protocols for the level of the body, where the subicular region of the hippocampus joins the entorhinal cortex within the parahippocampal gray matter.

Five different methods can be found across the 12 protocols to separate the hippocampal body from the adjacent parahippocampal gray matter (Table 3; Fig. 4). Arbitrary linear demarcations are adopted by most of them. The most restrictive protocol draws a vertical line from the most medial point of the cornu Ammonis (CA) gray matter, on the dorsal aspect of the hippocampus, down to the parahippocampal white matter (Fig. 4A). Less restrictive protocols use oblique lines with different angles. These oblique lines are drawn from the lowest point of the parahippocampal white matter, and proceed medially to the liquor of the

Fig. 3. Superior border. The superior border concerns the hippocampal white matter, i.e. the alveus and fimbria, that can be excluded [B, H, K, Pa, S] or included in different tracing protocols [C, dTM, J, L, M, Pr, W]. Additional criteria for separation of vestigial gray matter tissue in posterior-most slices are reported in [Pr] (last column). In the first line, histological pictures corresponding to the MRI slice of the same column are presented. Line II: MRI images without tracings. Lines III-IV: same MRI images with tracing example of exclusion (III) and inclusion (IV) of the hippocampal white matter.

cistern, with an angle of $45°$, or with a similar angle as the parahippocampal white matter below (Fig. 4B). Three protocols used a horizontal line connecting the highest point in the medial parahippocampal white matter to the CSF (Fig. 4 C). Finally, three protocols segment the hippocampal gray matter relying on the visible morphology determined by the white matter shape and possible gray matter signal (Fig. 4D).

e) Definition of the most anterior slice. Heterogeneities in the definition of the boundary with the amygdala were found (http://www.hippocampal-proto col.net/SOPs/LINK_PAGE/anatomical-landmarks-cer tified-12.xls), but these can be overcome due to the currently available software allowing 3D navigation (Fig. 1). This common approach allows direct visualization of the exact cursor location and of the tracing in different planes simultaneously; i.e., within the hippocampal head, within the amygdala, or in any neighboring or boundary region, the cursor can be seen from orthogonal visualization planes, where the spatial relationships among neighboring structures can be seen in different perspectives, thus providing additional complementary information. This possibility to visualize in 3D the position of

the cursor allows to disambiguate whether the gray matter belongs to the hippocampus or to the amygdala in the most anterior slice. Thus, for this slice, the definition of anatomical landmarks in the coronal plane, which may differ among protocols, and which is less reliable than the direct visualization in 3D, can be considered less relevant. The consequence of this approach was that the only difference that applied to the segmentation of the hippocampal head consisted in the inclusion or exclusion of the hippocampal white matter (alveus/fimbria) when visible, i.e. in the definition of its superior border (see point *c*).

DISCUSSION

In this work, we have extracted similarities and differences among 12 protocols for hippocampal segmentation widely used in the field of Alzheimer's disease, in order to capture the source of volume variability that can be ascribed to heterogeneity in landmark definition across protocols. This extraction is the basis for an operationalization procedure aiming to achieve a finite number of well-defined units
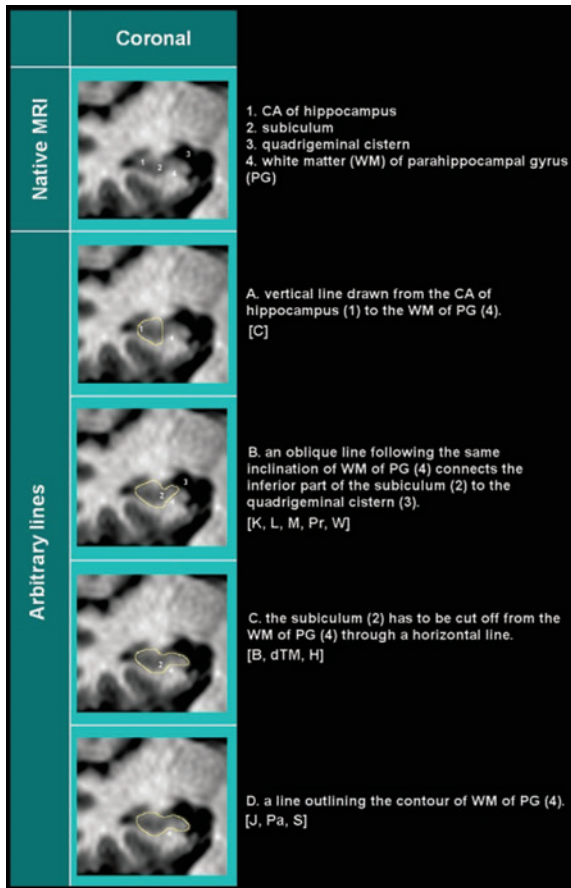
Fig. 4. Medial border. Five different methods are described across protocols to separate the subiculum, medially, from the rest of the parahippocampal gyrus. CA=cornu Ammonis; WM=white matter; PG=parahippocampal gyrus. The method in A is adopted by [C], that in B by [K, L, M, Pr, W], C by [B, dTM, H], D by [J, Pa, S].

representing differences among protocols, that enable the gathering of quantitative information on these differences. Quantitative investigation will assess their impact on re-trace reliability, and on the volume differences due to AD. This and other information will help a panel of experts to make evidence-based decisions about the specific features that should be included in a harmonized protocol, using a Delphi procedure, within an international project that is currently ongoing ("A harmonized protocol for hippocampal volumetry: an EADC-ADNI effort", Alzheimer's Association funding number 174022, www.hippocampal-protocol.net).

Heterogeneities across protocols

The main differences between protocols concerned the definition of the most caudal slice, of the medial border at the level of the hippocampal body, and the inclusion or exclusion of the alveus and fimbria. The definition of the most rostral slice was considered to be no longer relevant as current software packages for 3D visualization can clarify the anatomical localization of the cursor on the MR image. It is possible that this tool may also solve the separation of the vestigial fasciolar and Andrea-Retzius gyri. There is consensus that their exclusion from proper hippocampal tissue should be recommended, and care in excluding them was indeed used by two protocols [M, Pr]. Most of the protocols [B, C, dTM, J, K, L, S, W] did not trace any hippocampal tissue located caudal to the slice where the crus or both crura of the fornices could be seen in full profile. This led to an *a priori* exclusion of the vestigial hippocampal tissue, but also to sacrificing a large portion of the hippocampal tail, which may convey relevant information about AD [76].

Different arbitrary linear demarcations were used to trace the medial border, to separate hippocampal tissue from the rest of the parahippocampal gyrus, at the level of the subiculum. No anatomical details have ever been certified as valid landmarks for the tracing of this boundary [13]. The next stage of the project will evaluate whether arbitrary linear demarcations are more reliable than tracings based on the visual morphology apparent on the MR images.

Results in the context of the literature

Two reviews on protocols for hippocampal segmentation were previously carried out. The first [14], examining most cited protocols up to December 2003, provided an extensive description of heterogeneities in all components of tracing protocols, including image acquisition parameters, pre-processing procedures, landmark definitions, and provided recommendations to carry out optimal hippocampal segmentation. The second [13] focused mostly on landmark definitions. Although we extracted protocols from these reviews, we evaluated a much lower number of reports than those examined in the review by Konrad. Nonetheless, our results are similar to this larger review. Across the 71 protocols examined, Konrad found heterogeneities in the definition of the most anterior and most posterior slices, of the inferomedial border of hippocampal body, in the inclusion or exclusion of the alveus and fimbria, and on the use of arbitrary linear demarcations when anatomical detail provided by the imaging sequence was unclear [13]. All these sources of variance were

also detected among the 12 protocols examined in our study. This increases the confidence that, although our study was carried out on a limited number of protocols, they were representative of the variability of landmarks present in the literature on hippocampal segmentation, without missing anatomical landmark specifications that may affect a harmonization project. Furthermore, we obtained the authors' certification of appropriate comprehension and execution of the tracing. This is an important point because the complexity of the anatomical structure of the hippocampal formation requires clarification of protocol details from the expert protocol designers with first-hand tracing experience.

Study limitations

We adopted the criterion of selecting protocols widely used in the literature of AD although different selection criteria could have been used. Nevertheless, our results were entirely in line with the previous larger review.

Another possible limitation is the inclusion of both recent and older protocols. These may differ in landmark definition since the older protocols are based on the view of coronal slices. Moreover, our categorization of landmarks for these protocols includes subsequent modifications that the authors carried out in more recent years to benefit of more recent tools like the 3D visualization, and that we ascertained through the individual teleconferences. Other subsequent changes to protocols were dictated by focusing on different study targets than those expressed in the paper reporting the original protocols. One example is the desire (or lack thereof) to accurately segment adjacent regions, like the parahippocampal gyrus, that overlaps in part with hippocampal tissue from the point of view of its anatomical definition. Moreover, alternative criteria may be used by the same author, depending on image quality. For example, the medial border may be segmented following visible morphology or through arbitrary linear demarcations depending on visibility of any boundary on the MR slices [J], and the inclusion of alveus and fimbria could be an acceptable criterion if their exclusion was made difficult due to poor visibility or contrast [B, K, Pa]. In cases like these, we gave priority to the criterion that the author would adopt in cases where anatomical structures are fully visible, even though more than one criterion may be appropriately reported for the same author.

*The next steps towards the development
of a harmonized protocol*

The global project, described and updated on www.hippocampal-protocol.net, joins experts from the ADNI and EADC consortia, and other centres with advisory role. It is aimed to achieve and validate a homogeneous protocol, and implement its standard learning and use across laboratories. Standard hippocampal segmentation is indeed required in clinical trials and as a gold standard in the development and validation of more automated approaches to define hippocampal volumes, as they demonstrate utility. The development of a standard approach that relies on now commonly used T1-weighted high resolution images will allow a broader comparison across studies. The immediate next step of the project will be the completion of the operationalization of differences among protocols in order to model and quantify them. Information about differences in reliability, across different tracers, and in test re-test assessments will be provided for each of the relevant differences among protocols detected by this survey. Moreover, their value to inform on AD pathology will be computed on an adequate sample of representative patients with a diagnosis of AD. A panel of experts will then be provided with quantitative information that would support decisions on which features should be included in a harmonized protocol.

This effort is particularly relevant in light of the new diagnostic clinical and pre-clinical criteria for AD, which can be found at http://www.alz. org/research/diagnostic_criteria. In line with the 2007 research criteria by Dubois *et al.* [1], these criteria place emphasis on hippocampal volumetry, stating that, although not specific for this kind of disorder, this biomarker better correlates with disease progression than the more specific molecular biomarkers, such as the Abeta and Tau CSF concentration levels [1, 82]. A uniform method for the computation of hippocampal volume would improve AD diagnosis across laboratories, and hopefully provide a comparable hippocampal outcome measure in clinical trials for disease modifying drugs.

ACKNOWLEDGMENTS

REFERENCES

[1] Dubois B, Feldman HH, Jacova C, Dekosky ST, Barberger-Gateau P, Cummings J, Delacourte A, Galasko D, Gauthier S, Jicha G, Meguro K, rsquo O'brien J, Pasquier F, Robert P, Rossor M, Salloway S, Stern Y, Visser PJ, Scheltens P (2007) Research criteria for the diagnosis of Alzheimer's disease: revising the NINCDS-ADRDA criteria. *Lancet Neurol* **6**, 734-746.

[2] Gauthier S, Aisen PS, Ferris SH, Saumier D, Duong A, Haine D, Garceau D, Suhy J, Oh J, Lau W, Sampalis J (2009) Effect of tramiprosate in patients with mild-to-moderate Alzheimer's disease: exploratory analyses of the MRI subgroup of the Alphase study. *J Nutr Health Aging* **13**, 550-557.

[3] Rodionov R, Chupin M, Williams E, Hammers A, Kesavadas C, Lemieux L (2009) Evaluation of atlas-based segmentation of hippocampi in healthy humans. *Magn Reson Imaging* **27**, 1104-1109.

[4] Kennedy KM, Erickson KI, Rodrigue KM, Voss MW, Colcombe SJ, Kramer AF, Acker JD, Raz N (2009) Age-related differences in regional brain volumes: a comparison of optimized voxel-based morphometry to manual volumetry. *Neurobiol Aging* **30**, 1657-1676.

[5] Hasan KM, Pedraza O (2009) Improving the reliability of manual and automated methods for hippocampal and amygdala volume measurements. *Neuroimage* **48**, 497-498.

[6] Bosscher L, Scheltens P (2002) Functional imaging in dementia. *In Evidence-Based Dementia Practice,*,Qizilbash N, Schneider LS, Chui H, Tariot P, Brodaty H, Kaye J, Erkinjuntti T, eds. Blackwell, Oxford, UK, pp. 162-169.

[7] Duchesne S, Pruessner J, Collins DL (2002) Appearance-based segmentation of medial temporal lobe structures. *Neuroimage* **17**, 515-531.

[8] Barnes J, Foster J, Boyes RG, Pepple T, Moore EK, Schott JM, Frost C, Scahill RI, Fox NC (2008) A comparison of methods for the automated calculation of volumes and atrophy rates in the hippocampus. *Neuroimage* **40**, 1655-1671.

[9] Morra JH, Tu Z, Apostolova LG, Green AE, Avedissian C, Madsen SK, Parikshak N, Hua X, Toga AW, Jack CR,Jr. Weiner MW, Thompson PM, Alzheimer's Disease Neuroimaging, Initiative (2008) Validation of a fully automated 3D hippocampal segmentation method using subjects with Alzheimer's disease mild cognitive impairment, and elderly controls. *Neuroimage* **43**, 59-68.

[10] Brewer JB, Magda S, Airriess C, Smith ME (2009) Fully-automated quantification of regional brain volumes for improved detection of focal atrophy in Alzheimer disease. *AJNR Am J Neuroradiol* **30**, 578-580.

[11] Colliot O, Chetelat G, Chupin M, Desgranges B, Magnin B, Benali H, Dubois B, Garnero L, Eustache F, Lehericy S (2008) Discrimination between Alzheimer disease, mild cognitive impairment, and normal aging by using automated segmentation of the hippocampus. *Radiology* **248**, 194-201.

[12] Collins DL, Pruessner JC (2010) Towards accurate, automatic segmentation of the hippocampus and amygdala from MRI by augmenting ANIMAL with a template library and label fusion. *Neuroimage* **52**, 1355-1366.

[13] Konrad C, Ukas T, Nebel C, Arolt V, Toga AW, Narr KL (2009) Defining the human hippocampus in cerebral magnetic resonance images–an overview of current segmentation protocols. *Neuroimage* **47**, 1185-1195.

[14] Geuze E, Vermetten E, Bremner JD (2005) MR-based *in vivo* hippocampal volumetrics: 1. Review of methodologies currently employed. *Mol Psychiatry* **10**, 147-159.

[15] Frisoni GB, Fox NC, Jack CR Jr., Scheltens P, Thompson PM (2010) The clinical use of structural MRI in Alzheimer disease. *Nat Rev Neurol* **6**, 67-77.

[16] Frisoni GB, Jack CR (2010) Harmonization of magnetic resonance-based manual hippocampal segmentation: A mandatory step for wide clinical use. *Alzheimer's & Dementia*, in press.

[17] Jack CR Jr. (1994) MRI-based hippocampal volume measurements in epilepsy. *Epilepsia* **35**, S21-9.

[18] Pruessner JC, Li LM, Serles W, Pruessner M, Collins DL, Kabani N, Lupien S, Evans AC (2000) Volumetry of hippocampus and amygdala with high-resolution MRI and three-dimensional analysis software: minimizing the discrepancies between laboratories. *Cereb Cortex* **10**, 433-442.

[19] Pantel J, O'Leary DS, Cretsinger K, Bockholt HJ, Keefe H, Magnotta VA, Andreasen NC (2000) A new method for the *in vivo* volumetric measurement of the human hippocampus with high neuroanatomical accuracy. *Hippocampus* **10**, 752-758.

[20] Malykhin NV, Bouchard TP, Ogilvie CJ, Coupland NJ, Seres P, Camicioli R (2007) Three-dimensional volumetric analysis and reconstruction of amygdala and hippocampal head, body and tail. *Psychiatry Res* **155**, 155-165.

[21] Bartzokis G, Altshuler LL, Greider T, Curran J, Keen B, Dixon WJ (1998) Reliability of medial temporal lobe volume measurements using reformatted 3D images. *Psychiatry Res* **82**, 11-24.

[22] Bogerts B, Lieberman JA, Ashtari M, Bilder RM, Degreef G, Lerner G, Johns C, Masiar S (1993) Hippocampus-amygdala volumes and psychopathology in chronic schizophrenia. *Biol Psychiatry* **33**, 236-246.

[23] deToledo-Morrell L, Stoub TR, Bulgakova M, Wilson RS, Bennett DA, Leurgans S, Wuu J, Turner DA (2004) MRI-derived entorhinal volume is a good predictor of conversion from MCI to AD. *Neurobiol Aging* **25**, 1197-1203.

[24] Killiany RJ, Moss MB, Albert MS, Sandor T, Tieman J, Jolesz F (1993) Temporal lobe regions on magnetic resonance imaging identify patients with early Alzheimer's disease. *Arch Neurol* **50**, 949-954.

[25] Lehericy S, Baulac M, Chiras J, Pierot L, Martin N, Pillon B, Deweer B, Dubois B, Marsault C (1994) Amygdalohippocampal MR volume measurements in the early stages of Alzheimer disease. *AJNR Am J Neuroradiol* **15**, 929-937.

[26] Convit A, De Leon MJ, Tarshish C, De Santi S, Tsui W, Rusinek H, George A (1997) Specific hippocampal volume reductions in individuals at risk for Alzheimer's disease. *Neurobiol Aging* **18**, 131-138.

[27] Haller JW, Banerjee A, Christensen GE, Gado M, Joshi S, Miller MI, Sheline Y, Vannier MW, Csernansky JG (1997) Three-dimensional hippocampal MR morphometry with high-dimensional transformation of a neuroanatomic atlas. *Radiology* **202**, 504-510.

[28] Soininen HS, Partanen K, Pitkanen A, Vainio P, Hanninen T, Hallikainen M, Koivisto K, Riekkinen PJS (1994) Volumetric MRI analysis of the amygdala and the hippocampus in subjects with age-associated memory impairment: correlation to visual and verbal memory. *Neurology* **44**, 1660-1668.

[29] Watson C, Andermann F, Gloor P, Jones-Gotman M, Peters T, Evans A, Olivier A, Melanson D, Leroux G (1992) Anatomic basis of amygdaloid and hippocampal volume measurement by magnetic resonance imaging. *Neurology* **42**, 1743-1750.

[30] Watson C, Jack CR Jr., Cendes F (1997) Volumetric magnetic resonance imaging. Clinical applications and contributions to the understanding of temporal lobe epilepsy. *Arch Neurol* **54**, 1521-1531.

[31] Sheline YI, Wang PW, Gado MH, Csernansky JG, Vannier MW (1996) Hippocampal atrophy in recurrent major depression. *Proc Natl Acad Sci U S A* **93**, 3908-3913.

[32] Bremner JD, Randall P, Scott TM, Bronen RA, Seibyl JP, Southwick SM, Delaney RC, McCarthy G, Charney DS, Innis RB (1995) MRI-based measurement of hippocampal volume in patients with combat-related posttraumatic stress disorder. *Am J Psychiatry* **152**, 973-981.

[33] Cook MJ, Fish DR, Shorvon SD, Straughan K, Stevens JM (1992) Hippocampal volumetric and morphometric studies in frontal and temporal lobe epilepsy. *Brain* **115**, 1001-1015.

[34] Bigler ED, Blatter DD, Anderson CV, Johnson SC, Gale SD, Hopkins RO, Burnett B (1997) Hippocampal volume in normal aging and traumatic brain injury. *AJNR Am J Neuroradiol* **18**, 11-23.

[35] Shenton ME, Kikinis R, Jolesz FA, Pollak SD, LeMay M, Wible CG, Hokama H, Martin J, Metcalf D, Coleman M (1992) Abnormalities of the left temporal lobe and thought disorder in schizophrenia. A quantitative magnetic resonance imaging study. *N Engl J Med* **327**, 604-612.

[36] MacQueen GM, Campbell S, McEwen BS, Macdonald K, Amano S, Joffe RT, Nahmias C, Young LT (2003) Course of illness, hippocampal function, and hippocampal volume in major depression. *Proc Natl Acad Sci U S A* **100**, 1387-1392.

[37] Narr KL, Thompson PM, Szeszko P, Robinson D, Jang S, Woods RP, Kim S, Hayashi KM, Asunction D, Toga AW, Bilder RM (2004) Regional specificity of hippocampal volume reductions in first-episode schizophrenia. *Neuroimage* **21**, 1563-1575.

[38] Mervaala E, Fohr J, Kononen M, Valkonen-Korhonen M, Vainio P, Partanen K, Partanen J, Tiihonen J, Viinamaki H, Karjalainen AK, Lehtonen J (2000) Quantitative MRI of the hippocampus and amygdala in severe depression. *Psychol Med* **30**, 117-125.

[39] Steffens DC, Byrum CE, McQuoid DR, Greenberg DL, Payne ME, Blitchington TF, MacFall JR, Krishnan KR (2000) Hippocampal volume in geriatric depression. *Biol Psychiatry* **48**, 301-309.

[40] O'Brien JT, Lloyd A, McKeith I, Gholkar A, Ferrier N (2004) A longitudinal study of hippocampal volume, cortisol levels, and cognition in older depressed subjects. *Am J Psychiatry* **161**, 2081-2090.

[41] Ashtari M, Greenwald BS, Kramer-Ginsberg E, Hu J, Wu H, Patel M, Aupperle P, Pollack S (1999) Hippocampal/ amygdala volumes in geriatric depression. *Psychol Med* **29**, 629-638.

[42] Zipursky RB, Marsh L, Lim KO, DeMent S, Shear PK, Sullivan EV, Murphy GM, Csernansky JG, Pfefferbaum A (1994) Volumetric MRI assessment of temporal lobe structures in schizophrenia. *Biol Psychiatry* **35**, 501-516.

[43] Giedd JN, Vaituzis AC, Hamburger SD, Lange N, Rajapakse JC, Kaysen D, Vauss YC, Rapoport JL (1996) Quantitative MRI of the temporal lobe, amygdala, and hippocampus in normal human development: ages 4-18 years. *J Comp Neurol* **366**, 223-230.

[44] Kates WR, Abrams MT, Kaufmann WE, Breiter SN, Reiss AL (1997) Reliability and validity of MRI measurement of the amygdala and hippocampus in children with fragile X syndrome. *Psychiatry Res* **75**, 31-48.

[45] Honeycutt NA, Smith PD, Aylward E, Li Q, Chan M, Barta PE, Pearlson GD (1998) Mesial temporal lobe measurements on magnetic resonance imaging scans. *Psychiatry Res* **83**, 85-94.

[46] von Gunten A, Fox NC, Cipolotti L, Ron MA (2000) A volumetric study of hippocampus and amygdala in depressed patients with subjective memory problems. *J Neuropsychiatry Clin Neurosci* **12**, 493-498.

[47] Vythilingam M, Vermetten E, Anderson GM, Luckenbaugh D, Anderson ER, Snow J, Staib LH, Charney DS, Bremner JD (2004) Hippocampal volume, memory, and cortisol status in major depressive disorder: effects of treatment. *Biol Psychiatry* **56**, 101-112.

[48] Hastings RS, Parsey RV, Oquendo MA, Arango V, Mann JJ (2004) Volumetric analysis of the prefrontal cortex, amygdala, and hippocampus in major depression. *Neuropsychopharmacology* **29**, 952-959.

[49] Niemann K, Hammers A, Coenen VA, Thron A, Klosterkotter J (2000) Evidence of a smaller left hippocampus and left temporal horn in both patients with first episode schizophrenia and normal control subjects. *Psychiatry Res* **99**, 93-110.

[50] Lobnig BM, Kromeke O, Optenhostert-Porst C, Wolf OT (2006) Hippocampal volume and cognitive performance in long-standing Type 1 diabetic patients without macrovascular complications. *Diabet Med* **23**, 32-39.

[51] Lloyd AJ, Ferrier IN, Barber R, Gholkar A, Young AH, O'Brien JT (2004) Hippocampal volume change in depression: late- and early-onset illness compared. *Br J Psychiatry* **184**, 488-495.

[52] Driessen M, Herrmann J, Stahl K, Zwaan M, Meier S, Hill A, Osterheider M, Petersen D (2000) Magnetic resonance imaging volumes of the hippocampus and the amygdala in women with borderline personality disorder and early traumatization. *Arch Gen Psychiatry* **57**, 1115-1122.

[53] Barr WB, Ashtari M, Schaul N (1997) Bilateral reductions in hippocampal volume in adults with epilepsy and a history of febrile seizures. *J Neurol Neurosurg Psychiatry* **63**, 461-467.

[54] Neumeister A, Wood S, Bonne O, Nugent AC, Luckenbaugh DA, Young T, Bain EE, Charney DS, Drevets WC (2005) Reduced hippocampal volume in unmedicated, remitted patients with major depression versus control subjects. *Biol Psychiatry* **57**, 935-937.

[55] Caetano SC, Hatch JP, Brambilla P, Sassi RB, Nicoletti M, Mallinger AG, Frank E, Kupfer DJ, Keshavan MS, Soares JC (2004) Anatomical MRI study of hippocampus and amygdala in patients with current and remitted major depression. *Psychiatry Res* **132**, 141-147.

[56] Frodl T, Meisenzahl EM, Zill P, Baghai T, Rujescu D, Leinsinger G, Bottlender R, Schule C, Zwanzger P, Engel RR, Rupprecht R, Bondy B, Reiser M, Moller HJ (2004) Reduced hippocampal volumes associated with the long variant of

the serotonin transporter polymorphism in major depression. *Arch Gen Psychiatry* **61**, 177-183.

[57] Rusch BD, Abercrombie HC, Oakes TR, Schaefer SM, Davidson RJ (2001) Hippocampal morphometry in depressed patients and control subjects: relations to anxiety symptoms. *Biol Psychiatry* **50**, 960-964.

[58] Nakano T, Wenner M, Inagaki M, Kugaya A, Akechi T, Matsuoka Y, Sugahara Y, Imoto S, Murakami K, Uchitomi Y (2002) Relationship between distressing cancer-related recollections and hippocampal volume in cancer survivors. *Am J Psychiatry* **159**, 2087-2093.

[59] MacMillan S, Szeszko PR, Moore GJ, Madden R, Lorch E, Ivey J, Banerjee SP, Rosenberg DR (2003) Increased amygdala: hippocampal volume ratios associated with severity of anxiety in pediatric major depression. *J Child Adolesc Psychopharmacol* **13**, 65-73.

[60] Yucel K, Taylor VH, McKinnon MC, Macdonald K, Alda M, Young LT, MacQueen GM (2008) Bilateral hippocampal volume increase in patients with bipolar disorder and short-term lithium treatment. *Neuropsychopharmacology* **33**, 361-367.

[61] Brambilla P, Harenski K, Nicoletti M, Sassi RB, Mallinger AG, Frank E, Kupfer DJ, Keshavan MS, Soares JC (2003) MRI investigation of temporal lobe structures in bipolar patients. *J Psychiatr Res* **37**, 287-295.

[62] Saylam C, Ucerler H, Kitis O, Ozand E, Gonul AS (2006) Reduced hippocampal volume in drug-free depressed patients. *Surg Radiol Anat* **28**, 82-87.

[63] MacMaster FP, Kusumakar V (2004) Hippocampal volume in early onset depression. *BMC Me* **2**, 2.

[64] Scott TM, Tucker KL, Bhadelia A, Benjamin B, Patz S, Bhadelia R, Liebson E, Price LL, Griffith J, Rosenberg I, Folstein MF (2004) Homocysteine and B vitamins relate to brain volume and white-matter changes in geriatric patients with psychiatric disorders. *Am J Geriatr Psychiatry* **12**, 631-638.

[65] Chen BK, Sassi R, Axelson D, Hatch JP, Sanches M, Nicoletti M, Brambilla P, Keshavan MS, Ryan ND, Birmaher B, Soares JC (2004) Cross-sectional study of abnormal amygdala development in adolescents and young adults with bipolar disorder. *Biol Psychiatry* **56**, 399-405.

[66] Vermetten E, Schmahl C, Lindner S, Loewenstein RJ, Bremner JD (2006) Hippocampal and amygdalar volumes in dissociative identity disorder. *Am J Psychiatry* **163**, 630-636.

[67] Arango C, Breier A, McMahon R, Carpenter WT Jr., Buchanan RW (2003) The relationship of clozapine and haloperidol treatment response to prefrontal, hippocampal, and caudate brain volumes. *Am J Psychiatry* **160**, 1421-1427.

[68] Chang K, Karchemskiy A, Barnea-Goraly N, Garrett A, Simeonova DI, Reiss A (2005) Reduced amygdalar gray matter volume in familial pediatric bipolar disorder. *J Am Acad Child Adolesc Psychiatry* **44**, 565-573.

[69] Rosso IM, Cintron CM, Steingard RJ, Renshaw PF, Young AD, Yurgelun-Todd DA (2005) Amygdala and hippocampus volumes in pediatric major depression. *Biol Psychiatry* **57**, 21-26.

[70] Xia J, Chen J, Zhou Y, Zhang J, Yang B, Xia L, Wang C (2004) Volumetric MRI analysis of the amygdala and hippocampus in subjects with major depression. *J Huazhong Univ Sci Technolog Med Sci* **24**, 500-502, 506.

[71] Frazier JA, Chiu S, Breeze JL, Makris N, Lange N, Kennedy DN, Herbert MR, Bent EK, Koneru VK, Dieterich ME, Hodge

SM, Rauch SL, Grant PE, Cohen BM, Seidman LJ, Caviness VS, Biederman J (2005) Structural brain magnetic resonance imaging of limbic and thalamic volumes in pediatric bipolar disorder. *Am J Psychiatry* **162**, 1256-1265.

[72] Bossini L, Tavanti M, Calossi S, Lombardelli A, Polizzotto NR, Galli R, Vatti G, Pieraccini F, Castrogiovanni P (2008) Magnetic resonance imaging volumes of the hippocampus in drug-naive patients with post-traumatic stress disorder without comorbidity conditions. *J Psychiatr Res* **42**, 752-762.

[73] Starkman MN, Giordani B, Gebarski SS, Schteingart DE (2007) Improvement in mood and ideation associated with increase in right caudate volume. *J Affect Disord* **101**, 139-147.

[74] Jack CR Jr, Bernstein MA, Fox NC, Thompson P, Alexander G, Harvey D, Borowski B, Britson PJ, L Whitwell J, Ward C, Dale AM, Felmlee JP, Gunter JL, Hill DL, Killiany R, Schuff N, Fox-Bosetti S, Lin C, Studholme C, DeCarli CS, Krueger G, Ward HA, Metzger GJ, Scott KT, Mallozzi R, Blezek D, Levy J, Debbins JP, Fleisher AS, Albert M, Green R, Bartzokis G, Glover G, Mugler J, Weiner MW (2008) The Alzheimer's Disease Neuroimaging Initiative (ADNI): MRI methods. *J Magn Reson Imaging* **27**, 685-691.

[75] Scheltens P, Leys D, Barkhof F, Huglo D, Weinstein HC, Vermersch P, Kuiper M, Steinling M, Wolters EC, Valk J (1992) Atrophy of medial temporal lobes on MRI in "probable" Alzheimer's disease and normal ageing: diagnostic value and neuropsychological correlates. *J Neurol Neurosurg Psychiatry* **55**, 967-972.

[76] Frisoni GB, Ganzola R, Canu E, Rub U, Pizzini FB, Alessandrini F, Zoccatelli G, Beltramello A, Caltagirone C, Thompson PM (2008) Mapping local hippocampal changes in Alzheimer's disease and normal ageing with MRI at 3 Tesla. *Brain* **131**, 3266-3276.

[77] Pallavaram S, Yu H, Spooner J, D'Haese PF, Koyama T, Bodenheimer B, Konrad PE, Dawant BM (2007) Automated selection of anterior and posterior commissures based on a deformable atlas and its evaluation based on manual selections by neurosurgeons. *SPIE*.

[78] Carone DA, Benedict RH, Dwyer MG, Cookfair DL, Srinivasaraghavan B, Tjoa CW, Zivadinov R (2006) Semi-automatic brain region extraction (SABRE) reveals superior cortical and deep gray matter atrophy in MS. *Neuroimage* **29**, 505-514.

[79] Anbazhagan P, Carass A, Bazin PL, Prince JL (2006) Automatic estimation of midsagittal plane and AC-PC alignment based on non-rigid registration. *IEEE*.

[80] Han Y, Park HW (2003) Automatic Brain MR Image Registration Based on Talairach Reference System. *ICIP* **1**, I1097.

[81] Chupin M, Mukuna-Bantumbakulu AR, Hasboun D, Bardinet E, Baillet S, Kinkingnehun S, Lemieux L, Dubois B, Garnero L (2007) Anatomically constrained region deformation for the automated segmentation of the hippocampus and the amygdala: Method and validation on controls and patients with Alzheimer's disease. *Neuroimage* **34**, 996-1019.

[82] Dubois B, Feldman HH, Jacova C, Cummings JL, Dekosky ST, Barberger-Gateau P, Delacourte A, Frisoni G, Fox NC, Galasko D, Gauthier S, Hampel H, Jicha GA, Meguro K, O'Brien J, Pasquier F, Robert P, Rossor M, Salloway S, Sarazin M, de Souza LC, Stern Y, Visser PJ, Scheltens P (2010) Revising the definition of Alzheimer's disease: a new lexicon. *Lancet Neurol*.

This page intentionally left blank

Relationship Between CSF Biomarkers of Alzheimer's Disease and Rates of Regional Cortical Thinning in ADNI Data

Duygu Tosun[a,*], Norbert Schuff[a,b], Leslie M. Shaw[c], John Q. Trojanowski[c], Michael W. Weiner[a,b] and the Alzheimer's Disease NeuroImaging Initiative[1]

[a]*Center for Imaging of Neurodegenerative Diseases, Department of Veterans Affairs Medical Center, San Francisco, CA, USA*
[b]*Department of Radiology, University of California, San Francisco, CA, USA*
[c]*Department of Pathology and Laboratory Medicine, Medicine at the Hospital of the University of Pennsylvania, Philadelphia, PA, USA*

Abstract. Previously it was reported that Alzheimer's disease (AD) patients have reduced amyloid ($A\beta_{1-42}$) and elevated total tau (*t*-tau) and phosphorylated tau (*p*-tau$_{181p}$) in the cerebro-spinal fluid (CSF), suggesting that these same measures could be used to detect early AD pathology in healthy elderly (CN) and mild cognitive impairment (MCI). In this study, we tested the hypothesis that there would be an association among rates of regional brain atrophy, the CSF biomarkers $A\beta_{1-42}$, *t*-tau, and *p*-tau$_{181p}$ and ApoE $\varepsilon4$ status, and that the pattern of this association would be diagnosis specific. Our findings primarily showed that lower CSF $A\beta_{1-42}$ and higher tau concentrations were associated with increased rates of regional brain tissue loss and the patterns varied across the clinical groups. Taken together, these findings demonstrate that CSF biomarker concentrations are associated with the characteristic patterns of structural brain changes in CN and MCI that resemble to a large extent the pathology seen in AD. Therefore, the finding of faster progression of brain atrophy in the presence of lower $A\beta_{1-42}$ levels and higher *p*-tau levels supports the hypothesis that CSF $A\beta_{1-42}$ and tau are measures of early AD pathology. Moreover, the relationship among CSF biomarkers, ApoE $\varepsilon4$ status, and brain atrophy rates are regionally varying, supporting the view that the genetic predisposition of the brain to amyloid and tau mediated pathology is regional and disease stage specific.

Keywords: MRI, Alzheimer's disease, cerebrospinal fluid, biomarkers, cortical thickness, atrophy, ApoE

INTRODUCTION

There is an increasing body of evidence from *in vivo* imaging and post mortem studies indicating that Alzheimer's disease (AD) is associated with a sequence of pathophysiological events that can occur over a long period (approximately 20-years) before clinical symptoms become apparent [1]. A slow disease progression provides potentially a window for early interventions to reduce or even stop progression of AD. Histopathological studies showed that the hallmarks of the disease, Aβ-rich amyloid plaques and

neurofibrillary tangles formed by abnormal tau, precede neuron loss in presymptomatic AD patients [1]. Substantial accumulations of plaques and tangles in the brain can also be found in non-demented subjects with mild cognitive impairment (MCI), individuals at an increased risk of developing AD or other dementias [2–4]. Consistent with histopathological findings, cerebrospinal fluid (CSF) chemistry studies have pointed to alterations in CSF Aβ (in particular Aβ_{1-42}), total tau (t-tau) and phosphorylated tau (p-tau$_{181p}$) concentrations preceding clinical symptoms of AD [5]. In general, studies found that increased CSF t-tau and p-tau$_{181p}$ were associated with neuronal and axonal damage, whereas reduced CSF Aβ_{1-42}, the form of Aβ that most readily fibrillizes and deposits earliest in plaques, has been implicated to reflect higher amyloid plaque burden in the brain [6, 7]. However, the CSF measures are not easily interpretable because their origins are not exclusively brain derived and they provide no information about the regional spread of brain damage. Despite this, there is considerable agreement that measuring CSF Aβ_{1-42}, t-tau, and p-tau$_{181p}$ improves the diagnostic accuracy for AD [8].

Independent of biomarker studies, numerous structural MRI studies have shown a characteristic pattern of brain atrophy in AD and a similar pattern in MCI, affecting primarily regions in the parietotemporal lobe, including the hippocampus, which plays a central role in memory formation [9–22]. In addition, an increasing number of longitudinal MRI studies show that both AD and MCI are also associated with a regional pattern of increased rates of brain tissue loss compared to normal aging [23–29]. With the emerging findings of CSF biomarker and structural imaging alterations in AD, there is considerable interest in utilizing the CSF and MRI measures together to improve detection of early signs of AD, as well as, in unraveling relationships between CSF Aβ_{1-42}, t-tau, and p-tau$_{181p}$ and MRI measures of regional brain alterations. Recently it has been shown that the combination of CSF biomarkers and atrophy rates can provide better prediction of AD than either source of data alone [30–32]. However, whether relationships between brain atrophy rates and CSF biomarkers help further to improve predictions has not fully been explored.

Moreover, the role of the apolipoprotein E allele $\varepsilon 4$ (ApoE $\varepsilon 4$) gene, a major risk factor for AD, ought to be considered for a comprehensive evaluation. Presence of ApoE $\varepsilon 4$ is related to abnormal CSF biomarker concentrations [33, 34], as well as, to higher rates of brain atrophy [35–39]. The relationships among all

three factors, CSF biomarkers, ApoE $\varepsilon 4$, and rates of regional brain atrophy, might therefore provide important information about the vulnerability of the brain to AD. Our overall goal in this study was therefore to unravel the relationships among all three factors: brain atrophy rates, CSF biomarker concentrations, and presence of ApoE $\varepsilon 4$. Toward the goal of identifying an AD biomarker, it will be important to fully understand the relationship between CSF biomarker concentrations and brain degeneration, such as neuron loss, which is thought to underlie the clinical symptoms in AD [4, 5]. While CSF biomarkers relate to cumulative AD pathology in the brain as peripheral measures, MRI as an external tool elucidates the distribution of the AD related neurodegeneration (i.e., brain atrophy in terms of tissue loss and ventricular enlargement). However, relatively few MRI studies so far have reported correlations between CSF biomarkers and the pattern of brain atrophy or the rate of atrophy progression [37, 40–46]. Specifically, in healthy elderly individuals, it has been shown that low CSF levels of Aβ_{1-42} correlate with ventricular expansion and volumetric reductions in widespread brain areas [45]. In individuals with progressive MCI, low CSF Aβ_{1-42} concentration and high concentrations of CSF p-tau$_{181p}$ and t-tau are associated with higher subsequent rates of hippocampal atrophy [37, 40–42]. In AD patients, elevated CSF p-tau$_{181p}$ concentrations were associated with higher subsequent rates of hippocampal atrophy and medial temporal atrophy [40–43], while low CSF Aβ_{1-42} concentrations exhibited larger rates of medial temporal atrophy [43]. However, the majority of previous MRI studies in this context focused on hippocampal and temporal lobe atrophy and ventricular expansion in MCI and AD patients, while relatively little is known about relations between the CSF biomarker concentrations and atrophy rates of other regions throughout the brain. In addition, variations in these relationships across the spectrum of cognitive impairments have not been comprehensively studied for regions across the brain.

Our main goal in this study was to test the hypothesis that relations between CSF biomarkers (i.e., Aβ_{1-42}, t-tau, and p-tau$_{181p}$ concentrations) and rates of regional brain atrophy not only vary across brain regions but also across the cognitive spectrum, including healthy elderly individuals (CN), individuals with MCI, and AD patients. In particular we tested that (1) low Aβ_{1-42} and high t-tau and p-tau$_{181p}$ concentrations were associated with smaller absolute cortical thickness including parieto-temporal and prefrontal

cortical regions in CN, MCI, and AD, (2) low $A\beta_{1-42}$ and high t-tau and p-tau$_{181p}$ concentrations were associated with increased rates of regional brain atrophy including parieto-temporal, especially medial temporal, precuneus, and posterior cingulate cortical regions in CN, MCI, and AD, and (3) the patterns of association were group-specific. In addition, we tested whether abnormal CSF biomarker concentrations and ApoE $\varepsilon4$ status separately or together were associated with higher rates of brain atrophy.

COHORT AND METHODS

We examined the baseline cortical thickness and the rate of change in cortical thickness across the brain in CN, individuals with MCI, and AD patients. Structural magnetic resonance imaging (MRI) brain scans at multiple time points (four time point scans – baseline, 6, 12, and 24 months – for CN and AD subjects and five time point scans – baseline, 6, 12, 18, and 24 months – for individuals with MCI) were acquired at multiple Alzheimer's Disease Neuroimaging Initiative (ADNI) sites using 1.5 Tesla MRI scanners. Using FreeSurfer longitudinal processing framework, local cortical thickness throughout the entire cortex was automatically measured at each time point. In each diagnostic group separately, generalized linear mixed effect models followed by pair-wise maximum likelihood tests were performed to test: 1) if baseline CSF biomarker concentrations predict absolute local thickness at baseline; 2) if baseline CSF biomarker concentrations modulate the rates of brain atrophy (i.e., the rate of change in cortical thickness); and 3) if CSF biomarkers and ApoE $\varepsilon4$ modulate the rates of brain atrophy jointly or independently, after accounting for variations in age, sex, and education. Finally, we tested if the observed modulation effects of baseline CSF biomarkers on rates of atrophy differ among groups. The methodological details are explained herein.

Participants

The participants in this study were recruited through the ADNI, a longitudinal, multicenter study launched in 2003 by the National Institute on Aging (NIA), the National Institute of Biomedical Imaging and Bioengineering (NIBIB), the Food and Drug Administration (FDA), private pharmaceutical companies, and non-profit organizations, as a $60 million, 5-year public–private partnership to define biomarkers of early Alzheimer's disease for clinical trials

(http://www.adni-info.org). The Principal Investigator of this initiative is Michael W. Weiner, MD of the Veteran Affairs Medical Center and University of California in San Francisco.

Briefly, inclusion criteria for the CN group were Mini-Mental State Examination (MMSE) scores between 24 and 30, a Clinical Dementia Rating - Sum of Boxes (CDR-SB) score of 0, and lack of depression, MCI, or dementia. Inclusion criteria for the MCI group followed the Peterson criteria [47] for amnestic MCI, which required a subjective memory complaint, objective memory loss measured by education-adjusted Wechsler Memory Scale-Revised Logical Memory II scores, a CDR-SB of 0.5, absence of significant impairment in other cognitive domains, preserved activities of daily living, and an absence of dementia. AD participants met the National Institute for Neurological and Communicative Disorders and Stroke-Alzheimer's Disease and Related Disorder Association (NINDS/ADRDA) criteria for probable AD, had an MMSE between 18 and 26, and a CDR-SB of 0.5 to 1.0. Exclusion criteria included history of structural brain lesions or head trauma, significant neurological disease other than incipient AD, and use of psychotropic medications that could affect memory. The full details of the inclusion and exclusion criteria for the ADNI can be found at ht//www.adni-info.org. Written consent was obtained from all subjects participating in the study according to the Declaration of Helsinki (Br Med J 1991; 302 : 1194), and the study was approved by the institutional review board at each participating site.

The population in this study included ADNI subjects with valid test result for all three CSF biomarkers and successful longitudinal FreeSurfer processing of MR images from at least two time points. Overall, the study population was comprised of 77 CN, 119 MCI, and 53 AD subjects. Details of CSF biomarker concentration measurement and longitudinal structural MR image processing are described in the following sections. The demographic details of each group are given in Table 1.

Structural MRI acquisition

The participants underwent a standardized 1.5 Tesla MRI protocol (http://www.loni.ucla.edu/ADNI/Research/Cores/index.shtml), which included two T1-weighted MRI scans using a sagittal volumetric magnetization prepared rapid gradient echo (MP-RAGE) sequence with the following acquisition

Table 1
Demographic features of study groups

	CN	MCI	AD
N (baseline)	77	119	54
N follow-up (6, 12, 18, 24 months)	77, 76, 0, 63	119, 109, 96, 77	54, 53, 0, 31
Baseline age (years)	75 ± 5.0	74 ± 7.6	74 ± 8.0
Gender (F/M)	40/37	46/73	25/29
Baseline CSF $A\beta_{1-42}$ (pg/mL)	203 ± 51.8	165 ± 57.5	142 ± 39.7
Baseline CSF t-tau (pg/mL)	70 ± 29.5	101 ± 50.0	128 ± 53.1
Baseline CSF p-tau$_{181p}$ (pg/mL)	26 ± 15.0	35 ± 16.5	42 ± 16.8
ApoE $\varepsilon4$ status (3/4 – 4/4 carriers)	$18 - 0$	$50 - 13$	$25 - 11$
Education (years)	15.7 ± 2.9	15.7 ± 3.1	15.0 ± 2.8
Baseline CDR	0.0 ± 0.0	0.5 ± 0.0	0.72 ± 0.25
Baseline MMSE	29.1 ± 1.3	26.9 ± 2.7	23.5 ± 4.7

parameters: echo time (TE) of 4 ms, repetition time (TR) of 9 ms, flip angle of $8°$, acquisition matrix size of $256 \times 256 \times 166$ in the *x*-, *y*- and *z*-dimensions with a nominal voxel size of $0.94 \times 0.94 \times 1.2$ mm^3. Only one of the MPRAGE sets was used for analysis. The ADNI MRI quality control center at the Mayo Clinic selected the MP-RAGE image with higher quality and corrected for system-specific image artifacts, as described in [48].

CSF biomarker concentrations

CSF samples were obtained from 53% of ADNI participants, while the rest did not undergo lumbar puncture. The demographics of ADNI subjects with CSF samples are comparable with that in the full ADNI patient population (http://www.adni-info.org).

A small sample of CSF from the lower spine of each subject was collected at baseline by lumbar puncture in the morning after an overnight fast. Lumbar puncture was performed with a 20- or 24-gauge spinal needle as described in the ADNI procedures manual (ht//www.adni-info.org). In brief, CSF was collected into collection tubes provided to each site, then transferred into polypropylene transfer tubes followed by freezing on dry ice within 1 hour after collection, and shipped overnight to the ADNI Biomarker Core laboratory at the University of Pennsylvania Medical Center on dry ice. 0.5 mL aliquots were prepared from these samples after thawing for 1 hour at room temperature and gentle mixing. The aliquots were stored in bar code–labeled polypropylene vials at $-80°C$. $A\beta_{1-42}$, *t*-tau, and *p*-tau$_{181p}$ were measured in each aliquots using the multiplex xMAP Luminex platform (Luminex Corp, Austin, TX) with Innogenetics (INNO-BIA AlzBio3; Ghent, Belgium; for research use–only reagents) immunoassay kit–based reagents.

Full details of this combination of immunoassay reagents and analytical platform are provided elsewhere [49]. The ADNI baseline CSF samples were analyzed over a 14-day period and included test–retest analyses of 29 of the samples that further substantiated the analytical performance (r^2 values for comparison of initial test result with retest result of 0.98, 0.90, and 0.85 for *t*-tau, $A\beta_{1-42}$, and *p*-tau$_{181p}$, respectively for 29 randomly selected samples). Full details of ADNI baseline CSF biomarker measurements are provided elsewhere [7].

FreeSurfer longitudinal MR image processing

Automated cortical thickness measures were performed with FreeSurfer software package, version 4.4 (http://surfer.nmr.mgh.harvard.edu/fswiki). To reduce the confounding effect of intra-subject morphological variability, each subject's longitudinal data series was processed by FreeSurfer longitudinal workflow. The longitudinal workflow was designed to estimate brain morphometry measurements that were unbiased with respect to any time point. Instead of using information from a specific time point as a prior for other time points, a template image volume was created as an unbiased prior for all time points.

FreeSurfer longitudinal workflow consists of four stages: (1) processing of all time points individually with the cross-sectional workflow; (2) creation of a probabilistic template unbiased toward time points from all time points' cross-sectional data; (3) processing of unbiased template with the cross-sectional workflow; and finally (4) re-processing of each time point with the longitudinal workflow, which uses the unbiased template results as initial guess for the segmentation and surface reconstruction. For a full description of the FreeSurfer

processing steps, see [50, 51], and for a full description of the longitudinal workflow, see http://surfer.nmr.mgh.harvard.edu/fswiki/LongitudinalProcessing.

Vertex-based cortical thickness measurements were obtained as the distance between the reconstructed surface representations of the gray matter/white matter and white matter/CSF tissue interfaces [52]. Each cortical surface was spatially normalized to a template cortical surface using a non-rigid high-dimensional spherical averaging method to align cortical folding patterns. Subject cortical thickness maps were mapped onto the template surface based on this spatial normalization and then smoothed by a surface-based Gaussian blurring kernel with a standard deviation of 10 mm to remove noise-induced variations in the measurements.

The surface reconstruction results were visually examined for anatomical accuracy. Although the FreeSurfer software package allows for manual editing to correct registration and segmentation errors, given the large number of subjects in ADNI data set, only the data with accurate results from fully automated processing were used in the subsequent analysis in the interest of a practical total processing time and avoidance of reader bias. 74% of the MR images passed this quality control, 3% of the images failed the quality control completely, and remaining 23% of the images got partial pass on the quality control. Details of the quality control procedure are posted online at http://www.loni.ucla.edu/twiki/pub/ADNI/ADNIPostProc/UCS-FFreeSurferMethodsSummary.pdf.

According to our FreeSurfer quality control protocol, segmentation and pial surface estimates were checked globally and regionally in the coronal view for regions of overestimation/underestimation, inconsistency with the structural boundaries, or segmentation regions not accurately reflecting the underlying anatomy. The quality control procedure accounted only for gross errors; a gross error for these purposes was defined as an area of over/underestimation that was larger than the cursor, and which occurred on two or more slices. This was to account for inevitable small errors in segmentation such as those which may have been the result of partial voluming. Orientations other than the coronal view were used to confirm possible pial border and segmentation gross errors. Subjects with complete segmentation failure or gross errors throughout all brain regions were rated as complete failure and the ones with gross errors in one or more specific brain regions (i.e., temporal lobe regions, supe-

rior regions, occipital regions, and insula) were given partial pass rating. All the subjects with passing quality control rating were included in analyses presented in this work.

Statistical analyses

For each subject, variations in cortical thickness were modeled as a function of time starting with the baseline scan (time-point zero) in intervals of subsequent MRI scans in units of years. We employed a general linear mixed effects (GLME) model for analysis of the longitudinal data in which the response variable (i.e., cortical thickness) was regressed against the explanatory variables including time, baseline CSF biomarker concentration (i.e., $A\beta_{1-42}$, p-tau$_{181p}$, or t-tau), and the interaction between time and baseline CSF biomarker concentration to estimate the fixed effects in the group, separately from the random effects such as within subject variations in both baseline and longitudinal measures. This concept was used to test the primary hypothesis that variations in CSF biomarker concentrations modulate rates of brain atrophy (i.e., cortical thinning). The fixed effect model was formulated as follows:

$$V_{ij} = \beta_0 + \beta_{Years}\,T_{ij} + \beta_{CSFbio}\,B_{i0}$$
$$+ \beta_{Years:CSFbio}\,T_{ij}B_{i0} + \varepsilon_{ij}$$

Here, V_{ij} represents the size of a brain structure (cortical thickness) from subject i at time point j. Accordingly, T_{ij} indicates the time point of the individual MRI scan, B_{i0} represents individual CSF biomarker concentrations at baseline and ε_{ij} is the mixed effects error. Our goal was to test the significance of the coefficient $\beta_{Years:CSFbio}$ in explaining structural variations (i.e., the moderator) relative to the coefficients β_0, β_{Years}, and β_{CSFbio} and independent of random variations in brain structures at baseline and over time. For a significant interaction to occur, CSF biomarker concentration must modulate the relationship between time and the response variable (i.e., local cortical thickness). To determine if the addition of an interaction term ($\beta_{Years:CSFbio}$) between rates of brain atrophy and CSF biomarkers in the model significantly improves the explanatory power of regional variations in cortical thickness as a function of biomarkers, we compared pair-wise GLME models (i.e., with and without the $\beta_{Years:CSFbio}$ term), fitted by maximum likelihood (ML) via F-tests. These tests were performed separately for each group (i.e.,

CN, MCI, and AD). Similarly, to determine the significance of CSF biomarker effects on cortical thickness at baseline, the additive term β_{CSFbio} was assessed by pair-wise comparisons of GLME models with and without β_{CSFbio} term, followed by maximum likelihood (ML) via F-tests. Each CSF biomarker was centered on its population mean to reduce colinearity.

To assess if the effect of CSF biomarkers on rates of regional brain atrophy differ across groups (CN, MCI, and AD), we resampled the random effects residual of the fits by 100-fold bootstrap and evaluated differences in distributions by analysis of variance.

Finally, we tested the extent to which ApoE $\varepsilon4$ status contributes to higher brain atrophy rates independent of CSF biomarker concentrations (ApoE $\varepsilon4$ status + CSF biomarker) or via a synergistic interaction with the biomarkers (ApoE $\varepsilon4$ status *CSF biomarker). Again, pair-wise ML tests were performed between models with and without the interaction term (i.e. ApoE $\varepsilon4$ ×CSF biomarker) to determine the contribution of the interaction.

Age, gender, and education were included as covariates in each regression model described above. The GLME models and the corresponding pair-wise ML F-tests were evaluated at each surface vertex independently. All statistical analyses were computed using R (the R Project for Statistical Computing; www.r-project.org). To control for false positive findings given the large number of comparisons per brain map, we used the concept of a false discovery rate (FDR) at the level $q = 0.05$ [53]. For testing the a-priori hypotheses on associations between baseline CSF biomarker levels and the absolute cortical thickness as well as the rates of regional cortical atrophy, which comprised a limited number of planned tests, we used a per comparison error rate of $q = 0.05$ for each test to determine the probability that any one contrast, after passing FDR, is found by chance.

RESULTS

Effects of baseline CSF biomarker concentrations on absolute cortical thickness

Next, we report effects of CSF biomarker concentrations on absolute cortical thickness after accounting for variations in age, gender, and education across subjects. Figure 1 depicts the regional distribution of CSF $A\beta_{1-42}$ effects on absolute cortical thickness for CN based on the ML F-tests. In CN, lower baseline CSF $A\beta_{1-42}$ was associated with a thinner cortex in the bilat-
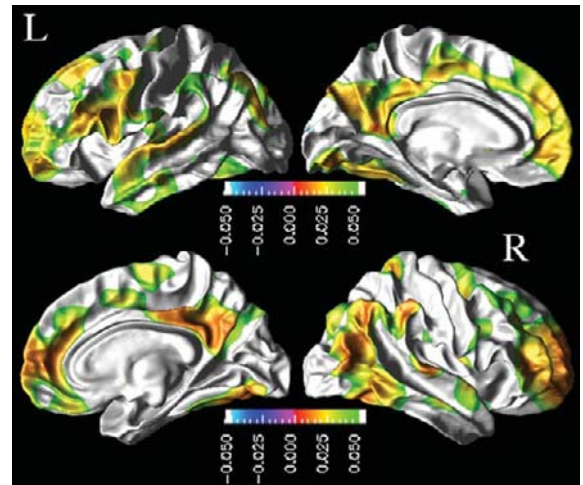
Fig. 1. Association between baseline CSF $A\beta_{1-42}$ concentrations and absolute cortical thickness in CN group: FDR corrected p-value maps at 0.05 level from pair-wise ML F-tests. Hot color (green to red) indicates an association between lower baseline CSF $A\beta_{1-42}$ and thinner cortex.

eral frontal pole, rostral-middle frontal, supramarginal, inferior parietal, middle temporal, inferior temporal, posterior cingulate, precuneus, and fusiform cortices, in the left superior frontal, pars opercularis, pars triangularis, and superior temporal cortices, and in the right superior parietal, medial orbito-frontal, and paracentral lobule cortices. In MCI and AD, no statistically significant association between the baseline CSF biomarker concentrations and the absolute cortical thickness measures were observed.

Neither t-tau nor p-tau$_{181p}$ showed significant association with absolute cortical thickness in CN, MCI, and AD groups.

Effects of baseline CSF biomarkers concentrations on the rates of regional cortical atrophy

Similarly, we report next the modulation effects of CSF biomarkers on the rates of cortical thinning after accounting for variations in age, gender, and education across subjects. Figure 2 depicts the regional distribution of a CSF $A\beta_{1-42}$ modulation effects on the rates of cortical thinning for MCI based on the ML F-tests. In MCI, lower concentrations of CSF $A\beta_{1-42}$ were associated with increased rates of cortical thinning throughout the cortex. The effects were statistically significant (FDR corrected; $p < 0.05$) in the bilateral inferior temporal and middle temporal cortices and in the left temporal pole, inferior parietal,
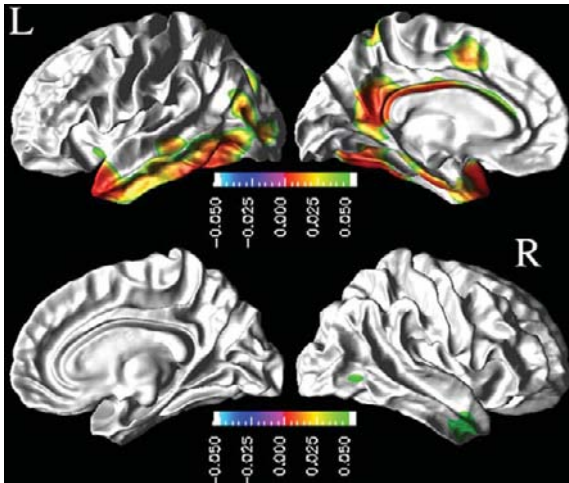
Fig. 2. Effects of baseline CSF Aβ$_{1\text{-}42}$ concentrations on the rate of cortical atrophy in MCI group: FDR corrected *p*-value map at 0.05 level from pair-wise ML *F*-tests. Hot color (green to red) indicates an association between lower concentrations of CSF Aβ$_{1\text{-}42}$ and increased rates of cortical thinning.

paracentral lobule, cingulate, isthmus cingulate, precuneus, entorhinal, and fusiform cortices.

Neither CN nor AD patients showed significant modulation effects of baseline CSF biomarkers on the cortical atrophy rates after correcting for multiple comparison.

In Fig. 3 are shown the regional distribution of CSF *p*-tau$_{181p}$ effects on the rates of cortical thin-
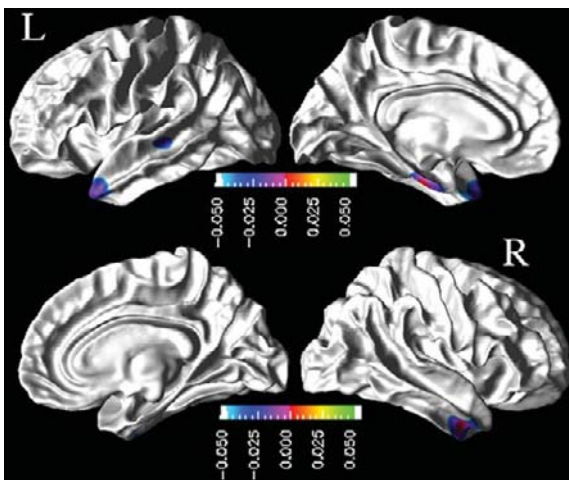
Fig. 3. Effects of baseline CSF *p*-tau$_{181p}$ concentrations on the rates of cortical atrophy in MCI group: FDR corrected *p*-value map at 0.05 level from pair-wise ML *F*-tests. Cold color (blue to purple) indicates an association between higher baseline CSF *p*-tau$_{181p}$ concentrations and higher rates of cortical thinning.
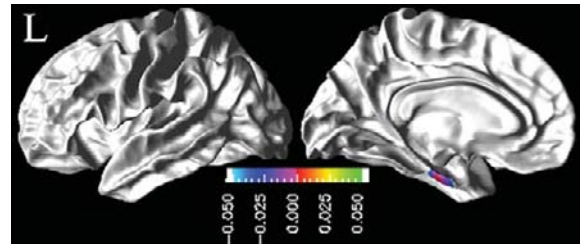
Fig. 4. Effects of baseline CSF *t*-tau concentrations on rate of cortical atrophy in MCI group: FDR corrected *p*-value map at 0.05 level from pair-wise ML *F*-tests. Cold color (blue to purple) indicates an association between higher baseline CSF *t*-tau concentrations and higher rates of cortical thinning.

ning for MCI. The results indicate that higher baseline CSF *p*-tau$_{181p}$ concentrations in MCI were associated with higher rates of cortical thinning, significantly in the left temporal pole, superior temporal sulcus, and entorhinal gyrus regions, and in the right inferior and middle temporal cortices. Similarly, higher baseline CSF *t*-tau concentrations were associated with higher cortical atrophy rates in the left entorhinal gyrus in MCI patients, as shown in Fig. 4.

Group differences in CSF biomarker effects on rates of cortical thinning

By bootstrapping the random effects residuals of the GLME fits with time and baseline CSF biomarker concentration interaction term, we tested if the estimates of the association between biomarkers and atrophy rates significantly differ across populations. Based on pairwise group comparison, we found that differences in the estimations between the groups were all significant ($p = 0.05$ level). This implies that the relationship among CSF biomarkers and brain atrophy rates was not only regionally specific but also varied across the clinical groups.

ApoE ε4 analyses

In our data set, presence of ApoE ε4 alleles correlated significantly with the CSF Aβ$_{1\text{-}42}$ concentrations ($r = -0.50$, $p < 10^{-5}$ in CN, $r = -0.49$, $p < 10^{-8}$ in MCI, and $r = -0.53$, $p < 10^{-5}$ in AD), after controlling for age. A partial correlation between presence of ApoE ε4 alleles and *p*-tau$_{181p}$ and *t*-tau after controlling for age was significant only in MCI group ($r = 0.34$ with $p < 10^{-3}$ and $r = 0.39$ with $p < 10^{-6}$, respectively).

Only in individuals with MCI, lower CSF Aβ$_{1\text{-}42}$ and ApoE ε4 together were associated with higher

rates of cortical thinning in temporoparietal cortex, including precuneus and posterior cingulate. CSF tau and ApoE $\varepsilon4$ together were associated with higher rates of cortical thinning in the entorhinal cortex, precuneus and temporal pole. In contrast, lower $A\beta_{1-42}$ alone explained higher rates of cortical thinning in left entorhinal, fusiform, inferior temporal, temporal pole, and parahippocampal cortices without a significant contribution from ApoE $\varepsilon4$. Similarly, higher CSF tau explained higher rates of cortical thinning in entorhinal cortex without a significant contribution from ApoE e4.

In no case did an interaction between ApoE $\varepsilon4$ status and CSF biomarker concentration (i.e. ApoE $\varepsilon4$ status $\times$ CSF biomarker) approach significance in predicting rate of cortical thinning.

DISCUSSION

We have three major findings: (1) In controls, an association between CSF $A\beta_{1-42}$ and baseline cortical thickness was observed prominently in regions that generally appear affected in AD. (2) In MCI subjects, lower CSF $A\beta_{1-42}$ and higher p-tau$_{181p}$ and t-tau concentrations were associated with higher rates of brain atrophy in regions of the temporal and parietal cortices implicated in AD pathology. (3) The relationship among CSF biomarkers, ApoE $\varepsilon4$ status and brain atrophy rates was regionally specific and varied across the clinical groups.

Our finding in controls, demonstrating that low baseline CSF $A\beta_{1-42}$ biomarker concentration is associated with thinner cortex predominantly in the inferior temporal, parietal, frontal, precuneus, and posterior cingulate cortices, provides evidence for a link between variations in peripheral CSF chemistry and regional brain size. Moreover, the result suggests that the link between CSF markers and regional brain size is already established in absence of any apparent clinical symptoms of cognitive deficits. A previous study in cognitively normal elderly also found an association between low levels of CSF $A\beta_{1-42}$ and smaller whole-brain volume [44]. It has been shown that in healthy elderly individuals, reduction in CSF $A\beta_{1-42}$ is a predictor of cognitive decline and development of AD [54–56]; therefore, the association between low baseline CSF $A\beta_{1-42}$ concentration and thin cortex in controls could reflect preclinical AD pathology. However, pathological conditions other than AD might also contribute to the relationship

between low CSF $A\beta_{1-42}$ concentration and cortical thinning.

In individuals with MCI, baseline cortical thickness measures had no significant association with CSF biomarker concentrations. This finding implies a dissociation between CSF biomarkers and their effects on the brain in individuals with MCI. The finding in MCI, showing that variations in CSF biomarker concentrations are associated with a characteristic pattern of altered rates of regional brain atrophy, similar to the pattern seen in AD, further supports the view that these relations reflect brain alterations presymptomatic to AD and could be useful for staging disease severity and assessing disease progression. Specifically, lower CSF $A\beta_{1-42}$ and increased CSF p-tau$_{181p}$ and t-tau concentrations in MCI were associated with higher atrophy rates involving primarily inferior and medial temporal, parietal, precuneus, and posterior cingulate cortices. Structural MRI studies in AD consistently revealed a pattern of neuroanatomic abnormalities that predominantly involves structures in the medial temporal cortex (i.e., hippocampus and the entorhinal cortex [9–14, 19, 23, 28, 29, 40]) where the early pathological changes are seen, then gradually extends to temporoparietal cortical areas [15–18, 24] as severity of AD progresses [15, 17, 25–27, 57]. Our finding that lower CSF $A\beta_{1-42}$ and higher CSF p-tau$_{181p}$ and t-tau concentrations were associated with higher atrophy rates of the temporal horn and inferior temporal lobe regions points to a selective vulnerability of these regions to AD pathology, consistent with histopathological findings. The finding that lower CSF $A\beta_{1-42}$ is associated with a characteristic pattern of brain atrophy in MCI that resembles the atrophy pattern seen in AD is encouraging for the use of CSF $A\beta_{1-42}$ as an early indicator of AD. Most importantly, elucidating the detrimental relationship between CSF biomarkers and rates of brain atrophy is of great interest to detect AD pathology in early stage, which is fundamental for an accurate early diagnosis of the disease, development of new treatment interventions, and evaluation of clinical trials in AD. The synergistic relationship between CSF biomarker and neurodegeneration patterns are of clinical interest as they may not only improve monitoring AD progression and evaluation of new AD therapies but also aid enrichment of clinical trial cohorts by identifying specific subsets of patients with MCI especially at high risk of developing AD [58–60]. Such a custom tailored cohort selection is desirable since drugs with disease-arresting effects have better efficacy in the preclinical and early phase of the

disease before the synaptic and neuronal loss become widespread [61].

The spatial extent of baseline CSF $A\beta_{1-42}$ modulation effects on brain atrophy observed in individuals with MCI is consistent with previous volumetric studies on patterns of increased atrophy rate in AD patients compared to elderly healthy controls [62]. In addition, a prior autopsy study on AD patients [63] reported neuritic plaques distributed throughout the cortex with the highest densities in the temporal and occipital lobes, while relatively lower plaque densities were found in the parietal lobe. This is consistent with our CSF $A\beta_{1-42}$ modulation effect findings in MCI. Compared to the prior autopsy study in AD patients [63], the spatial extents of CSF p-tau$_{181p}$ and t-tau modulation effects are consistent with the neurofibrillary tangle distributions in AD pathology. In particular, cortical regions surrounding entorhinal cortex were reported among the most severely affected areas by neurofibrillary tangles. However, since we do not know how many of the MCI subjects in this study will ultimately develop AD, we cannot determine the predictive value of CSF biomarker concentrations for AD. Another observation in the MCI group was the left hemisphere dominance of the CSF biomarkers' atrophy modulation effects. This observation is consistent with the asymmetric loss of GM (i.e., the left hemisphere atrophies faster than the right hemisphere) in AD [64] and yet again supporting the hypothesis that CSF $A\beta_{1-42}$, p-tau$_{181p}$, and t-tau are measures of early AD pathology.

A surprising finding in AD patients was that abnormal CSF biomarker levels were not significantly associated with rates of cortical thinning. Similarly, abnormal CSF biomarker levels in controls were also not significantly associated with rates of cortical thinning. It is also plausible that the finding in AD is the result of a complex relationship between advanced AD pathology in most cortical regions and peripheral biomarker concentration, while the finding in controls might reflect a threshold effect of minimum biomarker concentration on cortical thinning [45]. More studies are warranted to further investigate these issues.

Compared to CN and MCI groups, CSF biomarker concentrations have opposite modulation effects on rates of brain tissue volume change in AD. Specifically, we observed decreased rates of atrophy in the right posterior cingulate and precuneus cortices in the presence of higher concentrations of baseline CSF t-tau (relative to the CSF t-tau concentration distribution in AD group). Although not statistically significant, decelerative effects of CSF biomarker concentrations

on rates of cortical atrophy were observed in AD. One explanation of this finding could be the disease-stage specific effects of CSF biomarkers on brain atrophy. AD subjects with lower CSF $A\beta_{1-42}$ and higher CSF t-tau concentrations (relative to the biomarker concentration distributions in AD group) probably have advanced AD pathology where they reach a plateau in their rate of brain atrophy, which appears as a slower progression of the brain atrophy.

An interesting finding was that relations between the rate of brain atrophy and CSF biomarker concentrations varied across the CSF $A\beta_{1-42}$, p-tau$_{181p}$, and t-tau. This is not unexpected because it is known that amyloid plaques and tau containing tangles are distributed discordantly in brain at early stages of the disease. Specifically, the accumulation of amyloid plaques occurs in cortical regions whereas tangles appear in subcortical structures, predominantly involving the hippocampus [1, 63, 65]. Our findings reflect this pattern to some extent.

Finally, the finding of regional variations among CSF biomarkers, ApoE ε4 status, and brain atrophy rate relationships support the view that the genetic predisposition of the brain to amyloid and tau mediated pathology is region and disease stage specific. Interestingly, the most prominent region associated with CSF biomarker regardless of ApoE ε4 status in MCI included the entorhinal cortex, which is thought to be affected early by AD. Moreover, the effect of ApoE ε4 status on the relationships could be dose dependent [33, 34, 66].

Our findings in this study are largely consistent with several similar studies on relationships between CSF biomarkers and brain alterations in MCI and AD [40–42]. Specifically, increased concentrations of CSF p-tau$_{181p}$ are associated with higher subsequent rates of hippocampal atrophy in the progressive MCI and AD patients [40, 41] [42], of medial temporal atrophy in AD patients [43], of the temporal and parietal atrophy in MCI [46], and of right posterior ventricular horn expansion [67]. In contrast, low CSF $A\beta_{1-42}$ concentration exhibited an association with increased rate of left hippocampal atrophy in the progressive MCI patients [42, 46], of the medial temporal atrophy in AD [43], of the temporal and parietal atrophy in MCI [46], and of ventricular expansion [67]. Elevated CSF t-tau concentrations are associated with higher rates of hippocampal atrophy in stable MCI patients [42]. In controls, it has been shown that low CSF $A\beta_{1-42}$ concentration correlates with ventricular expansion and volumetric reductions in

widespread brain areas, including inferior temporal, inferior parietal, frontal, posterior cingulate, precuneus, caudate, and amygdala regions [45]. Fjell et al. reported generally larger effects of CSF biomarkers on brain tissue change than what we found on the same cohort [45, 46]. However, several methodological differences between our study and that by Fjell et al. complicate direct comparisons. For example, whereas Fjell et al. aimed to evaluate potentially accelerated rates between the first and second scan intervals while accepting mixed effects on rates, we aimed to separate random from fixed effects on rates in order to boost sensitivity while ignoring the possibility of accelerated rates. Since each approach has its estimation bias, the different findings are difficult to interpret.

The majority of previous MRI studies, except [45, 46], in this context focused on the hippocampal and temporal lobe atrophy and ventricular enlargement, while our approach was generalized by assessing various other brain regions. Based on this, we discovered that the association between CSF biomarkers and structural changes are regionally differential. Although this observation is not entirely surprising, given that the pathological processes of plaque and tangle formation, which CSF $A\beta_{1-42}$ and p-tau$_{181p}$ and t-tau indirectly represent, respectively. The finding of faster progression of brain atrophy in presence of lower baseline concentrations of $A\beta_{1-42}$ and higher concentrations of p-tau$_{181p}$/t-tau in MCI together with the similarities between the MCI pattern of CSF biomarker atrophy modulation effects and distribution of tangles and plaques in AD support the hypothesis that CSF biomarkers are measures of early AD pathology. MCI pattern of relations between rate of brain atrophy and CSF biomarker concentrations should be further explored to identify possible pre-symptomatic AD pathology. This finding also suggests a strategy for the potential use of biomarkers in clinical trials. CSF biomarker cut-offs to select fastest progressing cohorts could greatly improve the power of AD prevention trials on healthy elderly and MCI.

Several limitations of our study ought to be mentioned. First, MCI and AD subjects were diagnosed clinically; therefore other pathologies may have contributed to their symptoms and the relationships between CSF biomarkers and brain alterations may be unrelated to AD pathology. Another limitation is that CSF biomarkers, especially CSF $A\beta_{1-42}$, have been shown to be saturated and may not accurately reflect severity of brain amyloid deposition or plaque density in the later stages of the disease [8, 68]. Therefore,

structural brain changes may still occur secondarily to ongoing amyloid deposition or plaque accumulation. Restriction to linear, time-invariant brain atrophy rates is a technical limitation of our study. This is likely a gross simplification because the loss of brain tissue may be compounding and furthermore neurodegeneration in AD may be a dynamic process, which varies during disease progression. Therefore, models with nonlinear atrophy rate characteristics might lead to different results; however, such models are not always robust, given the limited number of serial MRI measurements and they also require careful validation. Finally, another technical limitation is that our study included fewer CN and AD subjects than MCI subjects despite expectations that power to detect atrophy will be higher for MCI than in CN and AD because of higher annual atrophy rates in MCI. Therefore, comparisons between CN and MCI as well as AD and MCI could be biased toward lower sensitivity to detect a change in CN and AD.

In summary, our findings demonstrate that alterations in CSF $A\beta_{1-42}$, p-tau$_{181p}$, and t-tau are each associated with characteristic patterns of structural brain changes (cross-sectionally or longitudinally) in CN and MCI that resembles to a large extent the pattern seen in AD pathology. Specifically, the finding of faster progression of brain atrophy in individuals with MCI in the presence of lower baseline CSF $A\beta_{1-42}$ and higher CSF tau levels supports the view that these CSF biomarkers reflect AD brain pathology. Since the CSF $A\beta_{1-42}$ and tau levels were also associated with a systematic pattern of regional brain atrophy rates that resembled the pattern known in AD, our findings further support the view that CSF $A\beta_{1-42}$ and tau reflect brain damage due to AD pathology. Overall, the findings imply that CSF $A\beta_{1-42}$ and tau taken together with MRI measures of rates of brain atrophy progression are promising candidates as biomarkers for early detection of AD.

DISCLOSURE STATEMENT

ACKNOWLEDGMENTS

REFERENCES

[1] Price JL, Morris JC (1999) Tangles and plaques in nondemented aging and ldquopreclinicalrdquo Alzheimer's disease. *Ann Neurol* **45**, 358-368.

[2] Aizenstein HJ, Nebes RD, Saxton JA, Price JC, Mathis CA, Tsopelas ND, Ziolko SK, James JA, Snitz BE, Houck PR, Bi W, Cohen AD, Lopresti BJ, DeKosky ST, Halligan EM, Klunk WE (2008) Frequent amyloid deposition without significant cognitive impairment among the elderly. *Arch Neurol* **65**, 1509-1517.

[3] Mintun MA, LaRossa GN, Sheline YI, Dence CS, Lee SY, Mach RH, Klunk WE, Mathis CA, DeKosky ST, Morris JC (2006) [11C]PIB in a nondemented population: Potential antecedent marker of Alzheimer disease. *Neurology* **67**, 446-452.

[4] Jack CR Jr, Lowe VJ, Weigand SD, Wiste HJ, Senjem ML, Knopman DS, Shiung MM, Gunter JL, Boeve BF, Kemp BJ, Weiner M, Petersen RC, the Alzheimer's Disease Neuroimaging, Initiative (2009) Serial PIB and MRI in normal, mild cognitive impairment and Alzheimer's disease: implications for sequence of pathological events in Alzheimer's disease. *Brain* **132**, 1355-1365.

[5] Fjell AM, Walhovd KB, Amlien I, Bjornerud A, Reinvang I, Gjerstad L, Cappelen T, Willoch F, Due-Tonnessen P, Grambaite R, Skinningsrud A, Stenset V, Fladby T (2008) Morphometric changes in the episodic memory network and tau pathologic features correlate with memory performance in patients with mild cognitive impairment. *AJNR Am J Neuroradiol* **29**, 1183-1189.

[6] Clark CM, Xie S, Chittams J, Ewbank D, Peskind E, Galasko D, Morris JC, McKeel DW Jr, Farlow M, Weitlauf SL, Quinn J, Kaye J, Knopman D, Arai H, Doody RS, DeCarli C, Leight S, Lee VM-Y, Trojanowski JQ (2003) Cerebrospinal fluid tau and β-amyloid: how well do these biomarkers reflect autopsy-confirmed dementia diagnoses? *Arch Neurol* **60**, 1696-1702.

[7] Shaw LM, Vanderstichele H, Knapik-Czajka M, Clark CM, Aisen PS, Petersen RC, Blennow K, Soares H, Simon A, Lewczuk P, Dean R, Siemers E, Potter W, Lee VM-Y, Trojanowski JQ, Initiative AsDN (2009) Cerebrospinal fluid biomarker signature in Alzheimer's disease neuroimaging initiative subjects. *Ann Neurol* **65**, 403-413.

[8] Andreasen N, Minthon L, Vanmechelen E, Vanderstichele H, Davidsson P, Winblad B, Blennow K (1999) Cerebrospinal fluid tau and A[beta]42 as predictors of development of Alzheimer's disease in patients with mild cognitive impairment. *Neurosci Lett* **273**, 5-8.

[9] Morra JH, Tu Z, Apostolova LG, Green AE, Avedissian C, Madsen SK, Parikshak N, Hua X, Toga AW, Jack CR,

Schuff N, Weiner MW, Thompson PM (2009) Automated 3D mapping of hippocampal atrophy and its clinical correlates in 400 subjects with Alzheimer's disease, mild cognitive impairment, and elderly controls. *Hum Brain Mapp* **30**, 2766-2788.

[10] Morra JH, Tu Z, Apostolova LG, Green AE, Avedissian C, Madsen SK, Parikshak N, Toga AW, Jack Jr CR, Schuff N, Weiner MW, Thompson PM (2009) Automated mapping of hippocampal atrophy in 1-year repeat MRI data from 490 subjects with Alzheimer's disease, mild cognitive impairment, and elderly controls. *NeuroImage* **45**, S3-S15-.

[11] deToledo-Morrell L, Stoub TR, Bulgakova M, Wilson RS, Bennett DA, Leurgans S, Wuu J, Turner DA (2004) MRI-derived entorhinal volume is a good predictor of conversion from MCI to AD. *Neurobiol Aging* **25**, 1197-1203.

[12] Schroeter ML, Stein T, Maslowski N, Neumann J (2009) Neural correlates of Alzheimer's disease and mild cognitive impairment: a systematic and quantitative meta-analysis involving 1351 patients. *NeuroImage* **47**, 1196-1206.

[13] Morra JH, Tu Z, Apostolova LG, Green AE, Avedissian C, Madsen SK, Parikshak N, Hua X, Toga AW, Jack Jr CR, Weiner MW, Thompson PM (2008) Validation of a fully automated 3D hippocampal segmentation method using subjects with Alzheimer's disease mild cognitive impairment, and elderly controls. *NeuroImage* **43**, 59-68.

[14] Thompson PM, Hayashi KM, de Zubicaray GI, Janke AL, Rose SE, Semple J, Hong MS, Herman DH, Gravano D, Doddrell DM, Toga AW (2004) Mapping hippocampal and ventricular change in Alzheimer disease. *NeuroImage* **22**, 1754-1766.

[15] Whitwell JL, Shiung MM, Przybelski SA, Weigand SD, Knopman DS, Boeve BF, Petersen RC, Jack CR Jr (2008) MRI patterns of atrophy associated with progression to AD in amnestic mild cognitive impairment. *Neurology* **70**, 512-520.

[16] Hua X, Leow AD, Lee S, Klunder AD, Toga AW, Lepore N, Chou Y-Y, Brun C, Chiang M-C, Barysheva M, Jack Jr CR, Bernstein MA, Britson PJ, Ward CP, Whitwell JL, Borowski B, Fleisher AS, Fox NC, Boyes RG, Barnes J, Harvey D, Kornak J, Schuff N, Boreta L, Alexander GE, Weiner MW, Thompson PM, the Alzheimer's Disease Neuroimaging I (2008) 3D characterization of brain atrophy in Alzheimer's disease and mild cognitive impairment using tensor-based morphometry. *NeuroImage* **41**, 19-34.

[17] Whitwell JL, Przybelski SA, Weigand SD, Knopman DS, Boeve BF, Petersen RC, Jack CR Jr (2007) 3D maps from multiple MRI illustrate changing atrophy patterns as subjects progress from mild cognitive impairment to Alzheimer's disease. *Brain* **130**, 1777-1786.

[18] Chetelat Ga, Baron J-C (2003) Early diagnosis of alzheimer's disease: contribution of structural neuroimaging. *NeuroImage* **18**, 525-541.

[19] Du AT, Schuff N, Amend D, Laakso MP, Hsu YY, Jagust WJ, Yaffe K, Kramer JH, Reed B, Norman D, Chui HC, Weiner MW (2001) Magnetic resonance imaging of the entorhinal cortex and hippocampus in mild cognitive impairment and Alzheimer's disease. *J Neurol Neurosurg Psychiatry* **71**, 441-447.

[20] Du AT, Schuff N, Laakso MP, Zhu XP, Jagust WJ, Yaffe K, Kramer JH, Miller BL, Reed BR, Norman D, Chui HC, Weiner MW (2002) Effects of subcortical ischemic vascular dementia and AD on entorhinal cortex and hippocampus. *Neurology* **58**, 1635-1641.

[21] Kramer JH, Schuff N, Reed BR, Mungas D, Du A-T, Rosen HJ, Jagust WJ, Miller BL, Weiner MW, Chui HC (2004) Hip-

pocampal volume and retention in Alzheimer's disease. *J Int Neuropsychol Soc* **10**, 639-643.

[22] Duarte A, Hayasaka S, Du A, Schuff N, Jahng G-H, Kramer J, Miller B, Weiner M (2006) Volumetric correlates of memory and executive function in normal elderly, mild cognitive impairment and Alzheimer's disease. *Neurosci Lett* **406**, 60-65.

[23] Stoub TR, Bulgakova M, Leurgans S, Bennett DA, Fleischman D, Turner DA, deToledo-Morrell L (2005) MRI predictors of risk of incident Alzheimer disease: a longitudinal study. *Neurology* **64**, 1520-1524.

[24] Desikan RS, Fischl B, Cabral HJ, Kemper TL, Guttmann CRG, Blacker D, Hyman BT, Albert MS, Killiany RJ (2008) MRI measures of temporoparietal regions show differential rates of atrophy during prodromal AD. *Neurology* **71**, 819-825.

[25] Jack CR Jr, Shiung MM, Gunter JL, O'Brien PC, Weigand SD, Knopman DS, Boeve BF, Ivnik RJ, Smith GE, Cha RH, Tangalos EG, Petersen RC (2004) Comparison of different MRI brain atrophy rate measures with clinical disease progression in AD. *Neurology* **62**, 591-600.

[26] Jack CR Jr, Shiung MM, Weigand SD, O'Brien PC, Gunter JL, Boeve BF, Knopman DS, Smith GE, Ivnik RJ, Tangalos EG, Petersen RC (2005) Brain atrophy rates predict subsequent clinical conversion in normal elderly and amnestic MCI. *Neurology* **65**, 1227-1231.

[27] Jack CR Jr, Weigand SD, Shiung MM, Przybelski SA, O'Brien PC, Gunter JL, Knopman DS, Boeve BF, Smith GE, Petersen RC (2008) Atrophy rates accelerate in amnestic mild cognitive impairment. *Neurology* **70**, 1740-1752.

[28] Du AT, Schuff N, Kramer JH, Ganzer S, Zhu XP, Jagust WJ, Miller BL, Reed BR, Mungas D, Yaffe K, Chui HC, Weiner MW (2004) Higher atrophy rate of entorhinal cortex than hippocampus in AD. *Neurology* **62**, 422-427.

[29] Du AT, Schuff N, Zhu XP, Jagust WJ, Miller BL, Reed BR, Kramer JH, Mungas D, Yaffe K, Chui HC, Weiner MW (2003) Atrophy rates of entorhinal cortex in AD and normal aging. *Neurology* **60**, 481-486.

[30] Brys M, Glodzik L, Mosconi L, Switalski R, De Santi S, Pirraglia E, Rich K, Kim BC, Mehta P, Zinkowski R, Pratico D, Wallin A, Zetterberg H, Tsui WH, Rusinek H, Blennow K, de Leon MJ (2009) Magnetic resonance imaging improves cerebrospinal fluid biomarkers in the early detection of Alzheimer's disease. *J Alzheimers Dis* **16**, 351-362.

[31] Vemuri P, Wiste HJ, Weigand SD, Shaw LM, Trojanowski JQ, Weiner MW, Knopman DS, Petersen RC, Jack CR Jr, On behalf of the Alzheimer's Disease Neuroimaging, Initiative (2009) MRI and CSF biomarkers in normal, MCI, and AD subjects: predicting future clinical change. *Neurology* **73**, 294-301.

[32] Vemuri P, Wiste HJ, Weigand SD, Shaw LM, Trojanowski JQ, Weiner MW, Knopman DS, Petersen RC, Jack CR Jr, On behalf of the Alzheimer's Disease Neuroimaging, Initiative (2009) MRI and CSF biomarkers in normal, MCI, and AD subjects: diagnostic discrimination and cognitive correlations. *Neurology* **73**, 287-293.

[33] Glodzik-Sobanska L, Pirraglia E, Brys M, de Santi S, Mosconi L, Rich KE, Switalski R, Louis LS, Sadowski MJ, Martiniuk F, Mehta P, Pratico D, Zinkowski RP, Blennow K, de Leon MJ (2009) The effects of normal aging and ApoE genotype on the levels of CSF biomarkers for Alzheimer's disease. *Neurobiol Aging* **30**, 672-681.

[34] Sunderland T, Mirza N, Putnam KT, Linker G, Bhupali D, Durham R, Soares H, Kimmel L, Friedman D, Bergeson

J, Csako G, Levy JA, Bartko JJ, Cohen RM (2004) Cerebrospinal fluid β-amyloid1-42 and tau in control subjects at risk for Alzheimer's disease: the effect of APOE ε4 allele. *Biol Psychiatry* **56**, 670-676.

[35] Basso M, Gelernter J, Yang J, MacAvoy MG, Varma P, Bronen RA, van Dyck CH (2006) Apolipoprotein E epsilon4 is associated with atrophy of the amygdala in Alzheimer's disease. *Neurobiol Aging* **27**, 1416-1424.

[36] Sluimer JD, Vrenken H, Blankenstein MA, Fox NC, Scheltens P, Barkhof F, van der Flier WM (2008) Whole-brain atrophy rate in Alzheimer disease: identifying fast progressors. *Neurology* **70**, 1836-1841.

[37] Schuff N, Woerner N, Boreta L, Kornfield T, Shaw LM, Trojanowski JQ, Thompson PM, Jack CR Jr, Weiner MW, Alzheimer's Disease Neuroimaging, Initiative (2009) MRI of hippocampal volume loss in early Alzheimer's disease in relation to ApoE genotype and biomarkers. *Brain* **132**, 1067-1077.

[38] Potkin SG, Guffanti G, Lakatos A, Turner JA, Kruggel F, Fallon JH, Saykin AJ, Orro A, Lupoli S, Salvi E, Weiner M, Macciardi F, for the Alzheimer's Disease Neuroimaging I (2009) Hippocampal atrophy as a quantitative trait in a genome-wide association study identifying novel susceptibility genes for Alzheimer's disease. *PLoS ONE* **4**, e6501.

[39] Fleisher A, Grundman M, Jack CR Jr, Petersen RC, Taylor C, Kim HT, Schiller DHB, Bagwell V, Sencakova D, Weiner MF, DeCarli C, DeKosky ST, van Dyck CH, Thal LJ, for the Alzheimer's Disease Cooperative, Study (2005) Sex, apolipoprotein E ε4 status, and hippocampal volume in mild cognitive impairment. *Arch Neurol* **62**, 953-957.

[40] Hampel H, Burger K, Pruessner JC, Zinkowski R, DeBernardis J, Kerkman D, Leinsinger G, Evans AC, Davies P, Moller H-J, Teipel SJ (2005) Correlation of cerebrospinal fluid levels of tau protein phosphorylated at threonine 231 with rates of hippocampal atrophy in Alzheimer disease. *Arch Neurol* **62**, 770-773.

[41] Henneman WJP, Vrenken H, Barnes J, Sluimer IC, Verwey NA, Blankenstein MA, Klein M, Fox NC, Scheltens P, Barkhof F, van der Flier WM (2009) Baseline CSF *p*-tau levels independently predict progression of hippocampal atrophy in Alzheimer disease. *Neurology* **73**, 935-940.

[42] Herukka S-K, Pennanen C, Soininen H, Pirttilä T (2008) CSF Aβ42, tau and phosphorylated tau correlate with medial temporal lobe atrophy. *J Alzheimers Dis* **14**, 51-57.

[43] Leow AD, Yanovsky I, Parikshak N, Hua X, Lee S, Toga AW, Jack CR Jr, Bernstein MA, Britson PJ, Gunter JL, Ward CP, Borowski B, Shaw LM, Trojanowski JQ, Fleisher AS, Harvey D, Kornak J, Schuff N, Alexander GE, Weiner MW, Thompson PM (2009) Alzheimer's Disease Neuroimaging Initiative: A one-year follow up study using tensor-based morphometry correlating degenerative rates, biomarkers and cognition. *NeuroImage* **45**, 645-655.

[44] Fagan AM, Head D, Shah AR, Marcus D, Mintun M, Morris JC, Holtzman DM (2009) Decreased cerebrospinal fluid A beta(42) correlates with brain atrophy in cognitively normal elderly. *Ann Neurol* **65**, 176-183.

[45] Fjell AM, Walhovd KB, Fennema-Notestine C, McEvoy LK, Hagler DJ, Holland D, Blennow K, Brewer JB, Dale AM, the Alzheimer's Disease Neuroimaging, Initiative (2010) Brain atrophy in healthy aging is related to CSF levels of Aβ1-42. *Cereb Cortex* **279**, 2069-2079.

[46] Fjell AM, Walhovd KB, Fennema-Notestine C, McEvoy LK, Hagler DJ, Holland D, Brewer JB, Dale AM, for the

Alzheimer's Disease Neuroimaging, Initiative (2010) CSF biomarkers in prediction of cerebral and clinical change in mild cognitive impairment and Alzheimer's disease. *J. Neurosci* **30**, 2088-2101.

[47] Petersen RC, Smith GE, Waring SC, Ivnik RJ, Tangalos EG, Kokmen E (1999) Mild cognitive impairment: clinical characterization and outcome. *Arch Neurol* **56**, 303-308.

[48] Jack CR, Bernstein MA, Fox NC, Thompson P, Alexander G, Harvey D, Borowski B, Britson PJ, Whitwell JL, Ward C, Dale AM, Felmlee JP, Gunter JL, Hill DLG, Killiany R, Schuff N, Fox-Bosetti S, Lin C, Studholme C, DeCarli CS, Krueger G, Ward HA, Metzger GJ, Scott KT, Mallozzi R, Blezek D, Levy J, Debbins JP, Fleisher AS, Albert M, Green R, Bartzokis G, Glover G, Mugler J, Weiner MW, Study A (2008) The Alzheimer's Disease Neuroimaging Initiative (ADNI): MRI methods. *J Magn Resonance Imag* **27**, 685-691.

[49] Olsson A, Vanderstichele H, Andreasen N, De Meyer G, Wallin A, Holmberg B, Rosengren L, Vanmechelen E, Blennow K (2005) Simultaneous measurement of {beta}-amyloid(1-42), total tau, and phosphorylated tau (Thr181) in cerebrospinal fluid by the xMAP technology. *Clin Chem* **51**, 336-345.

[50] Fischl B, Salat DH, Busa E, Albert M, Dieterich M, Haselgrove C, van der Kouwe A, Killiany R, Kennedy D, Klaveness S, Montillo A, Makris N, Rosen B, Dale AM (2002) Whole brain segmentation: automated labeling of neuroanatomical structures in the human brain. *Neuron* **33**, 341-355.

[51] Fischl B, van der Kouwe A, Destrieux C, Halgren E, Segonne F, Salat DH, Busa E, Seidman LJ, Goldstein J, Kennedy D, Caviness V, Makris N, Rosen B, Dale AM (2004) Automatically parcellating the human cerebral cortex. *Cereb. Cortex* **14**, 11-22.

[52] Fischl B, Dale AM (2000) Measuring the thickness of the human cerebral cortex from magnetic resonance images. *Proc Natl Acad Sci U S A* **97**, 11050-11055.

[53] Benjamini Y, Hochberg Y (1995) Controlling the false discovery rate: a practical and powerful approach to multiple testing. *J R Stat Soc Series B Stat Methodol* **57**, 289-300.

[54] Stomrud E, Hansson O, Blennow K, Minthon L, Londos E (2007) Cerebrospinal fluid biomarkers predict decline in subjective cognitive function over 3 years in healthy elderly. *Dement Geriatr Cogn Disord* **24**, 118-124.

[55] Skoog I, Davidsson P, Aevarsson ì, Vanderstichele H, Vanmechelen E, Blennow K (2003) Cerebrospinal Fluid β-Amyloid 42 Is Reduced before the Onset of Sporadic Dementia: A Population-Based Study in 85-Year-Olds. *Dement Geriatr Cogn Disord* **15**, 169-176.

[56] Leinonen V, Koivisto AM, Savolainen S, Rummukainen J, Tamminen JN, Tillgren T, Vainikka S, Pyykkö OT, Mälsä J, Fraunberg M, Pirttilä T, Jääskeläinen JE, Soininen H, Rinne J, Alafuzoff I (2010) Amyloid and tau proteins in cortical brain biopsy and Alzheimer's disease. *Ann Neurol* **68**, 446-453.

[57] DeCarli C, Frisoni GB, Clark CM, Harvey D, Grundman M, Petersen RC, Thal LJ, Jin S, Jack CR Jr, Scheltens P, for the Alzheimer's Disease Cooperative Study, Group (2007) Qualitative Estimates of Medial Temporal Atrophy as a Predictor of Progression From Mild Cognitive Impairment to Dementia. *Arch Neurol* **64**, 108-115.

[58] Blennow K, Hampel H (2003) CSF markers for incipient Alzheimer's disease. *Lancet Neurol* **2**, 605-613.

[59] Hampel H, Teipel SJ, Fuchsberger T, Andreasen N, Wiltfang J, Otto M, Shen Y, Dodel R, Du Y, Farlow M, Moller HJ, Blennow K, Buerger K (2003) Value of CSF β-amyloid1-42

and tau as predictors of Alzheimer's disease in patients with mild cognitive impairment. *Mol Psychiatry* **9**, 705-710.

[60] John HG (2001) Incorporating biomarkers into clinical drug trials in Alzheimer's disease. *J Alzheimers Dis* **3**, 287-292.

[61] Shaw LM, Korecka M, Clark CM, Lee VMY, Trojanowski JQ (2007) Biomarkers of neurodegeneration for diagnosis and monitoring therapeutics. *Nat Rev Drug Discov* **6**, 295-303.

[62] Scahill RI, Schott JM, Stevens JM, Rossor MN, Fox NC (2002) Mapping the evolution of regional atrophy in Alzheimer's disease: Unbiased analysis of fluid-registered serial MRI. *Proc Natl Acad Sci U S A* **99**, 4703-4707.

[63] Arnold SE, Hyman BT, Flory J, Damasio AR, Van Hoesen GW (1991) The topographical and neuroanatomical distribution of neurofibrillary tangles and neuritic plaques in the cerebral cortex of patients with Alzheimer's disease. *Cereb. Cortex* **1**, 103-116.

[64] Thompson PM, Hayashi KM, de Zubicaray G, Janke AL, Rose SE, Semple J, Herman D, Hong MS, Dittmer SS, Doddrell DM, Toga AW (2003) Dynamics of Gray Matter Loss in Alzheimer's Disease. *J. Neurosci* **23**, 994-1005.

[65] Braak H, Braak E. (1991) Neuropathological stageing of Alzheimer-related changes Acta Neuropathol 82, 239-259.

[66] Andersson C, Blennow K, Johansson SE, Almkvist O, Engfeldt P, Lindau M, Eriksdotter-Jonhagen M (2007) Differential CSF Biomarker Levels in APOE- e4-Positive and -Negative Patients with Memory Impairment. *Dement Geriatr Cogn Disord* **23**, 87-95.

[67] Chou Y-Y, Avedissian LeporÈN, Madsen C, Parikshak SK, Hua N, Shaw X, Trojanowski LM, Weiner JQ, Toga MW, Thompson AW, PM (2009) Mapping correlations between ventricular expansion and CSF amyloid and tau biomarkers in 240 subjects with Alzheimer's disease, mild cognitive impairment and elderly controls. *NeuroImage* **46**, 394-410.

[68] Stefani A, Martorana A, Bernardini S, Panella M, Mercati F, Orlacchio A, Pierantozzi M. (2006) CSF markers in Alzheimer disease patients are not related to the different degree of cognitive impairment. *J Neurol Sci* **251**, 124-128.

Quantitative Structural MRI and CSF Biomarkers in Early Diagnosis of Alzheimer's Disease

Miroslaw Brys[a,b,*], Lidia Glodzik[a], Lisa Mosconi[a], Remigiusz Switalski[a], Susan De Santi[a],
Elizabeth Pirraglia[a], Kenneth Rich[a], Byeong C. Kim[d], Pankaj Mehta[f], Ray Zinkowski[e],
Domenico Pratico[g], Anders Wallin[h], Henryk Zetterberg[h], Wai H. Tsui[a], Henry Rusinek[a],
Kaj Blennow[h] and Mony J. de Leon[a,c]

[a]*Center for Brain Health, New York University School of Medicine, New York, NY, USA*
[b]*Department of Neurology, New York University School of Medicine, New York, NY, USA*
[c]*Nathan Kline Institute, Orangeburg, NY, USA*
[d]*Chonnam National University Medical School, Gwangju, Korea*
[e]*Applied Neurosolutions, Vernon Hills, IL, USA*
[f]*Institute for Basic Research, Staten Island, NY, USA*
[g]*Department of Pharmacology, Temple University, Philadelphia, PA, USA*
[h]*University of Goeteborg, Goeteborg, Sweden*

Abstract. Combined utility of biomarkers in prediction of neurodegenerative diseases gains popularity, and is expected to become a future standard for early diagnosis, screening and monitoring of disease progression. This study investigated combined use of MRI and CSF biomarkers for prediction of pre-clinical Alzheimer's disease (AD). Forty-five subjects (21 controls (NL-NL), 16 stable mild cognitive impairment patients (MCI-MCI) and 8 MCI patients who declined to AD (MCI-AD)) received MRI and lumbar puncture at baseline and again after 2-years. CSF biomarkers included total and phosphorylated tau (T-tau, P-tau$_{231}$), amyloid beta Aβ_{42}/Aβ_{40} and isoprostane (IP). Structural MRI images were used to identify brain regions with differences of gray matter concentration (GMC) best distinguishing study groups and to calculate individual GMC values. Additionally, rate of medial temporal lobe (MTL) atrophy was examined using regional boundary shift (rBS) method. At baseline, for MRI, MCI-AD showed reduced GMC in MTL, and for CSF higher CSF T-tau, P-tau$_{231}$, IP and lower Aβ_{42}/Aβ_{40} as compared with MCI-MCI or NL-NL. Longitudinally, rBS-MTL atrophy was higher in MCI-AD than in either MCI-MCI or NL-NL, particularly in the left hemisphere. CSF data showed longitudinally greater increases of CSF IP in MCI-AD as compared with healthy controls. Combining baseline CSF-P-tau$_{231}$ and GMC-MTL significantly increased overall prediction accuracy of preclinical AD from 74 to 84% ($p_{step} < 0.05$). These results justify use of multiple modalities of biomarkers in the identification of memory clinic patients at increased risk for dementia.

Keywords: Brain atrophy, CSF biomarkers, Alzheimer's disease, early diagnosis

*Correspondence to: Miroslaw Brys, Center of Excellence on Brain Aging and Dementia, 145 E 32nd Street, New York, NY 10016, USA. Tel.:+1 212 263 7563; E-mail: miroslaw.brys@nyumc.org.

INTRODUCTION

As new Alzheimer's disease (AD) treatments become available, the diagnosis of AD at the Mild Cognitive Impairment (MCI) stage becomes particu-

larly important. Identification of suitable patients for early and high-risk treatments requires both high sensitivity and specificity. Recent data suggests that the combination of MRI and CSF modalities can improve preclinical diagnostic accuracy of AD [1–3].

MRI estimates of medial temporal lobe (MTL) atrophy are among the most sensitive predictors of decline from MCI to AD, although they are not specific to AD (for a review see [4]). Cerebrospinal fluid (CSF) biomarkers are both promising for early diagnosis and in the case of hyperphosphorylated tau (P-tau) and amyloid beta (Aβ), measurements afford AD pathological specificity [5, 6]. The most promising CSF biomarkers include: P-tau total tau (T-tau), $A\beta_{1-42}$ and $A\beta_{1-40}$, and isoprostanes (IP) (for a review see [7]). However, little is known of the combined utility of imaging and CSF biomarkers in the prediction and longitudinal course of the transitions between MCI and AD.

This longitudinal MRI and CSF study investigated the relationships of five CSF biomarkers for AD in combination with two automated MRI methods for assessing brain atrophy in three clinical groups: MCI who declined to AD (MCI-AD), stable MCI subjects (MCI-MCI), and clinically stable normal elderly controls (NL-NL). This study tested the hypothesis that the MRI and CSF biomarkers are complementary predictors of the decline from MCI to AD.

MATERIAL AND METHODS

Subjects

From a pool of 56 consecutive Alzheimer's disease research center patients and controls who completed a 2-year, 2-timepoint examination with CSF and MRI, 45 were selected (see below). The standardized longitudinal protocol included: history, physical, neurological, neuropsychological, and psychiatric evaluations, and clinical laboratory analysis including apolipoprotein E (APOE) genotyping. Subjects with at least one APOE ε4 allele were classified as "APOE4 carriers". All subjects signed IRB approved informed consent.

NL subjects were highly functioning individuals, defined as having a Clinical Dementia Rating (CDR [8]) score of 0, a Global Deterioration Scale (GDS [9]) score of 1 or 2 and a MMSE score ≥28. The diagnosis of MCI was based on: progressive cognitive (typically memory) complaints corroborated by an informant,

a CDR = 0.5, GDS score = 3 and clinically recognizable cognitive impairment without fulfilling either the DSM-IV [10] or NINCDS-ADRDA [11] criteria for dementia or AD. AD patients fulfilled the DSM-IV criteria for dementia and the NINCDS-ADRDA criteria for probable AD, and had GDS scores ≥4 and CDR ≥1.0.

Individuals with medical conditions or a history of significant conditions that affect brain structure or function (e.g. other neurodegenerative or metabolic diseases) were not enrolled in the study. Additionally, all subjects with MRI-based evidence of cortical infarctions or mass lesions as assessed with T1- and T2-weighted images at baseline were excluded. Eleven enrolled subjects from the total pool ($n = 56$) were excluded from the study: 9 subjects due to significant motion artifact on MRI preventing accurate brain measurements (6 NL and 3 MCI-MCI) and 2 MCI patients due to a change in clinical diagnosis at follow-up (1 NPH, 1 FTD).

Three study groups were created: a normal control group that remained normal (NL-NL: $n = 21$), an MCI patient group that did not deteriorate (MCI-MCI: $n = 16$); and an MCI patient group that declined to AD (MCI-AD: $n = 8$). The creation of the study groups was based solely on the clinical diagnosis and was blinded to all CSF, quantitative MRI, and APOE data.

MRI acquisitions

Images were acquired on a 1.5T GE Signa Imager scanner (General Electric, Milwaukee, USA). All subjects received a diagnostic and a research MRI study. The diagnostic study was used to satisfy the exclusion criteria and included 2 mm coronal T_2-weighted and contiguous 3 mm Fluid-attenuated Inversion-Recovery fast spin echo axial images. The research study was used for quantitative longitudinal measurements of brain atrophy and included a high-resolution T1-weighted 3D fast gradient-echo acquired in a coronal orientation which encompassed the entire brain without gap or wrap artifact (TR: 35 ms, TE: 9 ms, FA: 60°, FOV: 18×18 cm, matrix: 256×192), obtaining 124 coronal slices spanning the entire brain with a 1.7 mm section thickness.

The MR images were stripped of demographic information and were transferred to our central image data bank and satellite workstations for further processing. Image analysis was done using proprietary MIDAS software running on a UNIX operating system [12].

Image preprocessing

Voxel Based Morphometry (VBM) analysis

All T1-weighted MRI images were analyzed using Statistical Parametric Mapping (SPM'2, Wellcome Department of Cognitive Neurology, London, UK). Briefly, the method allows assessment of differences in gray matter concentrations (GMC) on a voxel-wise basis [13]. After correcting all T1 images for signal intensity distortions the MRI scans were realigned and spatially normalized to a reference MRI image in the standardized anatomical space and resliced with sinc interpolation to a final voxel size of $1.5 \times 1.5 \times 1.5$ mm. The normalized MRI scans were then segmented into gray matter (GM), white matter and CSF images, after removal of all non-brain voxels and after applying an image intensity non-uniformity correction [13]. The GM images were retained for analyses and re-normalized to a customized GM template by using the same normalization parameters described above. To preserve the volume of a particular tissue compartment within each voxel, the images were modulated by the Jacobian determinants derived from the spatial normalization, and smoothed using an 8-mm FWHM isotropic Gaussian kernel. Normalization for global differences in voxel intensity across scans was effected by inclusion of the global mean GM voxel value as a covariate, while preserving regional differences in GM intensity. Additionally, individual differential GMC images (follow-up GMC minus baseline GMC) were calculated for each study participant. In order to simplify the description of the VBM results, all local maxima within the medial temporal lobe (including hippocampus, parahippocampal gyrus, entorhinal cortex and amygdala) are collectively described as the "MTL".

Medial temporal lobe atrophy rate assessment

The longitudinal MTL atrophy rate, using the regional boundary shift (rBS) method [14] as described by Rusinek et al. was computed from the coregistered and intensity normalized MR images. The method extends the original whole-brain protocol of Fox et al. [15]. This protocol assesses the proportion of CSF and brain tissue per voxel over time and thus provides an atrophy measure. The atrophy rates were defined as the follow-up minus the baseline brain tissue volume, divided by the baseline volume and by the time interval between the two MRI scans (%/year) [16].

The rBS-MTL was assessed for the right and left MTL using standardized semi-automated ROIs using published protocols with intra-rater reliability >90% [14]. The rectangular solid-shaped bilateral MTL region of interest (ROI) was generated using the following criteria [14]. Horizontal and vertical box sizes were defined as 0.25 times the left-to-right and craniocaudal dimensions of the cranial cavity. The anterior plane was defined as 4.5 mm posterior to the frontal-temporal junction and the posterior plane was defined by the anterior crux of the fornix. The operator placed the MTL box on all coronal images in the anterior to posterior MTL range by manually selecting within each scan section centers of both hippocampi with a mouse click. These centers became the centers of the left and the right MTL boxes (see Fig. 1). The contents of the rBS-MTL ROI included nearly the entire hippocampus, and parts of the piriform lobe, entorhinal cortex, amygdala and parahippocampal gyrus. ROIs were drawn by single operator (M.B.) and independently verified by a co-author.

CSF collection and analysis

After an overnight fast, at 11:00 A.M. and on the same day the MRI scan, CSF was acquired using a 25-gauge Sprott lumbar puncture needle. Samples were centrifuged, aliquoted to polypropylene tubes and stored at $-80°C$. Assays were blinded to clinical data. Analysis of both baseline and follow-up samples was performed in the same batch assay without refreezing.
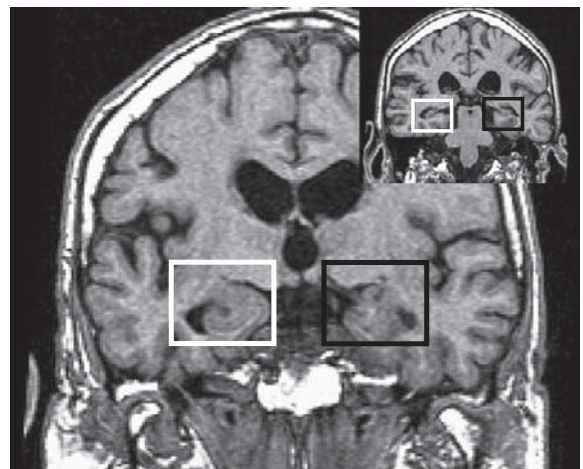
Fig. 1. Placement of right (white box) and left (black box) MTL ROIs on sinc interpolated, coronal T_1 MRI image cut to "pathological" angle (offset shows location of the ROI on one of the posterior slices).

A sandwich ELISA assay was used to detect tau phosphorylated at threonine 231 (P-tau$_{231}$) using tau-1 and CP-27 antibodies in the first step and P-tau$_{231}$-specific CP9 antibody in the second step [17]. CSF T-tau levels were determined using a commercially available INNOTEST hTAU antigen kit (Innogenetics®, Gent, Belgium). The CSF Aβ levels (Aβ$_{40}$ and Aβ$_{42}$) were measured using a monoclonal antibody 6E10 (specific to an epitope present on Aβ-16) and to rabbit antisera to Aβ$_{40}$ and Aβ$_{42}$ respectively, in a double antibody sandwich ELISA [18]. As some prior studies demonstrated that the Aβ$_{42}$/Aβ$_{40}$ ratio is superior to either the Aβ$_{42}$ or the Aβ$_{40}$ level in discriminating AD from NL or from other dementias [6], for predicting future MCI [19] or MCI transition to AD [20], the ratio was used in this study. CSF levels of isoprostanes (8,12-iso-iPF$_{2\alpha}$-VI) were assayed by negative ion chemical ionization gas chromatography/ mass spectrometry, after CSF samples were spiked with a fixed amount of internal standard (d4–8,12-iso-iPF2α-VI), extracted on a C^{18} cartridge column and purified by thin-layer chromatography [21].

STATISTICAL ANALYSIS

All results for the SPM analyses are presented in terms of clusters of significant differences in gray matter concentration (GMC) between study groups. The General Linear Model/univariate analysis with pair-wise post-hoc *t*-tests was used to test for GMC cross-sectional and longitudinal differences across study groups. Results were assessed over the whole-brain at a conservative $p < 0.001$ level, and uncorrected for multiple comparisons. Anatomical location of areas showing GMC effects was described using the Talairach and Tournoux coordinates [22].

Analysis of covariance (ANCOVA) with subsequent post-hoc Tukey tests was used to examine between-group differences in demographic data, rBS-MTL atrophy and CSF biomarker levels. Significant baseline effects were tested in binary logistic regression models as predictors of decline among MCI patients. Logistic regression prediction models were also used to characterize the incremental diagnostic classification properties of the best univariate CSF and MRI measures. *p* values <0.05 were considered significant. All analyses were performed with SPSS 12.0 (SPSS, Chicago, IL 2004).

RESULTS

The demographic data of the study participants are presented in Table 1. During the 2 years observation, 8 (33%) out of the 24 evaluable MCI subjects seen at baseline declined to AD and 16 retained the diagnosis of MCI. None of the 21 normal controls changed diagnostic group. There were no significant age, education, or length of observation period differences between the study groups (p's > 0.05; see Table 1). MCI-AD patients had lower MMSE scores than MCI-MCI patients at follow-up ($p < 0.05$) and against controls at both baseline and follow-up (p's < 0.01). MCI-AD patients had a higher prevalence of APOE4 carriers than either stable MCI or control (p's < 0.05). Both MCI-AD and control groups demonstrated a higher prevalence of females than MCI-MCI ($\chi^2 = 9.17$, $p < 0.05$). As previous brain studies show age effects [23], age (in addition to APOE genotype and gender) was controlled for in the subsequent analyses.

Voxel-based gray matter concentration results

Baseline effects

Univariate ANOVA over the 3 study groups at baseline showed several GMC clusters in the right

Table 1
Demographics of study participants

	NL-NL ($n = 21$)	MCI-MCI ($n = 16$)	MCI-AD ($n = 8$)
Age at baseline	65.0 ± 10.0	71.1 ± 6.9	70.3 ± 8.3
ApoE4 (carriers/non-carriers)	6/15	6/10	7/1[a]
Gender (males/females)	6/15	11/5[b]	1/7
Education [years]	15.0 ± 3.8	14.4 ± 3.6	12.3 ± 3.2
Observation period [years]	2.1 ± 0.7	1.7 ± 0.5	2.0 ± 0.5
MMSE score at baseline [points]	29.7 ± 0.5	28.4 ± 1.7	27.6 ± 1.9[c]
MMSE score at follow-up [points]	29.3 ± 1.1	28.9 ± 1.3	24.9 ± 2.7[c]

Values for continuous variables are Mean±SD; a - indicates value significantly different than in NL-NL and MCI-MCI groups; b - indicates value significantly different than NL-NL and MCI-AD groups; c - indicates value significantly different than in NL-NL group and MCI-MCI.

hemisphere (including MTL, superior, middle and inferior temporal gyri) and in the left (including MTL and posterior cingulate gyrus). Similarly, at follow-up the analysis detected clusters in the right (including MTL, superior and inferior temporal gyri) and in the left hemisphere (including MTL and posterior cingulate gyrus).

Post-hoc analysis showed that MCI-AD subjects as compared with MCI-MCI, at baseline demonstrated reduced GMC bilaterally in MTL and in right inferior temporal gyrus (for local maxima and Brodman areas see Table 2, Fig. 2). Similar effects were found at the follow-up.

Comparison of NL-NL with MCI-AD subjects at baseline showed bilateral MTL effects with superior and middle temporal gyri in the right hemisphere and inferior frontal and posterior cingulate gyri in the left hemisphere. Similar effects were found at follow-up (Table 2, Fig. 2).

No significant differences in GMC between NL-NL and MCI-MCI groups were detected at either baseline or follow-up.

Longitudinal

The between-group analysis of the differential GMC images (follow-up minus baseline) did not detect differences in GMC. Further, the unprotected paired-t-tests analyses within each study group also failed to reach statistical significance.

In summary, at baseline and follow-up for the VBM analyses, only the MTL showed consistent bilateral effects separating decliners from the other groups.

Longitudinal MRI rBS-determined atrophy rates

Given our hypothesized longitudinal MTL effects, the MTL region was specifically examined with the rBS method. After controlling for confounds, annualized atrophy rates for both the left ($F_{(2,36)} = 9.5$, $p < 0.001$) and right rBS-MTL ($F_{(2,36)} = 4.4$, $p < 0.05$) differed among three study groups (see Table 3 and Fig. 3). Post hoc analysis showed that atrophy rates in the left MTL were higher in MCI-AD patients than in either NL-NL or MCI-MCI (p's < 0.01). Atrophy rates in the right MTL were only higher in MCI-

Table 2
Voxel-based morphometry: local maxima and Brodman areas (BA) of clusters of significant baseline and follow-up differences in gray matter concentration between MCI-MCI and MCI-AD and between NL-NL and MCI-AD

Cluster extent (K_e)	Brain region	Coordinates (x, y, z)	z value	p
MCI-MCI vs. MCI-AD				
	Baseline			
1108	Right Inferior Temporal Gyrus, BA 20	(+35, −24, −33)	4.05	$p < 0.001$
	Right Parahippocampal Gyrus, Hippocampus	(+25, −15, −21)	3.73	$p < 0.001$
359	Left Parahippocampal Gyrus, BA 28	(−21, −20, −17)	4.36	$P < 0.001$
	Left Parahippocampal Gyrus, Hippocampus	(−26, −15, −20)	3.88	$p < 0.001$
	Follow-up			
1152	Right Inferior Temporal Gyrus, BA 20	(+41, −22, −28)	4.22	$p < 0.001$
	Right Parahippocampal Gyrus, Hippocampus	(+26, −13, −19)	4.00	$P < 0.001$
364	Left Parahippocampal Gyrus, BA 28	(−24, −18, −13)	4.18	$p < 0.001$
	Left Parahippocampal Gyrus, Hippocampus	(−24, −13, −16)	4.15	$p < 0.001$
NL-NL vs. MCI-AD				
	Baseline			
2978	Right Superior Temporal Gyrus, BA 38	(+42, +4, −17)	4.89	$p < 0.001$
	Right Middle Temporal Gyrus, BA 21	(+56 −20 −6)	3.89	$p < 0.001$
	Right Parahippocampal Gyrus, BA 28	(+17, −7, −14)	3.57	$p < 0.001$
	Right Parahippocampal Gyrus, Hippocampus	(+30, −12, +21)	3.36	$p < 0.001$
218	Left Parahippocampal Gyrus, BA 34	(−18, +4, −17)	4.87	$p < 0.001$
189	Left Inferior Frontal Gyrus, BA 47	(−38, +20, −6)	3.84	$p < 0.001$
357	Left Amygdala	(−24, −12, −12)	3.80	$p < 0.001$
109	Left Posterior Cingulate Gyrus, BA 31	(−5, −65, 16)	3.47	$p < 0.001$
2978	Right Superior Temporal Gyrus, BA 38	(+42, +4, −17)	4.89	$p < 0.001$
	Follow-up			
3612	Right Superior Temporal Gyrus, BA 38	(+41, +5, −13)	5.06	$p < 0.001$
138	Right Limbic Lobe, Uncus, BA 34	(+20, +2, −20)	4.26	$p < 0.001$
	Right Superior Temporal Gyrus, BA 22	(+48, −17, +6)	3.80	$P < 0.001$
280	Left Parahippocampal Gyrus, BA 34	(−23, +5, −17)	4.86	$P < 0.001$
794	Left Parahippocampal Gyrus BA 27	(−24, −30, −8)	3.51	$p < 0.001$
552	Left Posterior Cingulate Gyrus BA 30	(−5, −61, +13)	3.64	$P < 0.001$
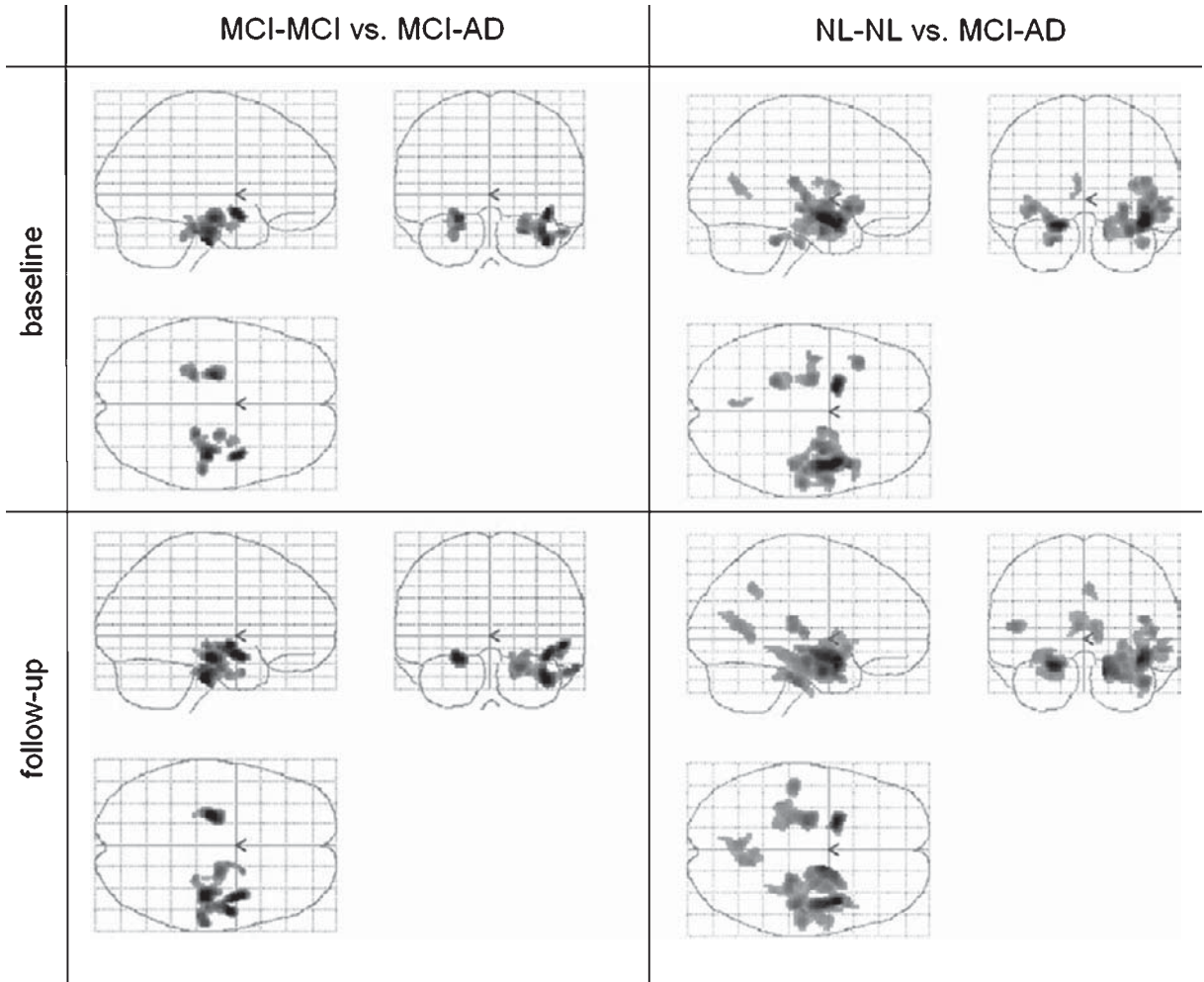
Fig. 2. Voxel-based morphometry results: clusters with significantly different GMC in MCI-MCI subjects vs. MCI-AD subjects (A) and NL-NL subjects vs. MCI-AD subjects (B) at baseline and at follow-up.

AD patients as compared with NL-NL ($p < 0.01$). For neither hemisphere were the annual MTL atrophy rates different between MCI-MCI patients and NL-NL ($p > 0.05$).

The rBS showed consistent longitudinal MTL effects distinguishing the decliners from the other groups.

CSF biomarkers analysis: baseline, follow-up and longitudinal results

Baseline data

Across all groups, there were significant baseline effects for all CSF analytes (see Table 3). The MCI-AD patients showed significantly higher values of T-tau, P-tau$_{231}$ and IP levels, and lower values of Aβ_{42}/Aβ_{40} ratio when compared with either MCI-MCI patients or with NL-NL (p's < 0.05; see Table 3). Similar significant effects were found at the follow-up with exception the Aβ_{42}/Aβ_{40} ratio (see Table 3). No differences were found between MCI-MCI and NL-NL subjects at baseline, or follow-up.

Longitudinal data

Analysis of longitudinal changes in CSF biomarker levels showed a trend for overall between-group differences for IP ($p = 0.07$; see Table 3). Exploratory post hoc analysis showed that a significantly greater increase in the IP level was found in MCI-AD patients as compared with NL-NL ($p < 0.01$). No other

Table 3
Baseline and follow-up measures of CSF biomarkers and annualized rates of change for CSF and MRI measures by diagnostic group

	NL-NL (n = 21)	MCI-MCI (n = 16)	MCI-AD (n = 8)	Overall group difference (ANCOVA)
Baseline measures				
T-tau level [pg/mL]	312 ± 126	398 ± 202	$643 \pm 147^{a,b}$	$p < 0.01$
P-tau$_{231}$ level [pg/ml]	15.1 ± 15.0	21.8 ± 26.5	$46.1 \pm 20.6^{a,b}$	$p < 0.01$
IP level [pg/mL]	31.5 ± 12.3	30.7 ± 12.2	$48.3 \pm 12.9^{a,b}$	$p < 0.01$
Ab$_{42}$/Ab$_{40}$ ratio*	12.1 ± 4.8	10.3 ± 3.4	$6.8 \pm 1.6^{a,b}$	$p < 0.01$
Follow-up measures				
T-tau level [pg/mL]	328 ± 156	429 ± 237	$659 \pm 184^{a,b}$	$p < 0.01$
P-tau$_{231}$ level [pg/mL]	14.6 ± 15.2	24.0 ± 27.5	$52.8 \pm 23.0^{a,b}$	$p < 0.01$
IP level [pg/mL]	34.6 ± 12.5	40.4 ± 26.3	$60.1 \pm 13.9^{a,b}$	$p < 0.05$
Ab$_{42}$/Ab$_{40}$ ratio*	11.3 ± 3.2	11.3 ± 3.1	8.3 ± 5.8	n.s.
Annualized measures				
rBS-MTL left [%]	0.53 ± 0.09	0.57 ± 0.14	$1.36 \pm 0.27^{a,b}$	$p < 0.01$
rBS-MTL right [%]	0.38 ± 0.11	0.76 ± 0.14	1.08 ± 0.14^{a}	$p < 0.05$
rBS-MTL left + right [%]	0.45 ± 0.08	0.67 ± 0.14	$1.22 \pm 0.19^{a,b}$	$p < 0.01$
T-tau rate of change [pg/mL/year]	$+16.29 \pm 16.3$	$+31.50 \pm 29.0$	$+16.13 \pm 62.1$	n.s.
P-tau$_{231}$ rate of change [pg/mL/year]	-0.54 ± 1.7	$+2.27 \pm 0.8$	$+6.67 \pm 2.2$	n.s.
IP rate of change [pg/mL/year]	$+3.10 \pm 1.7$	$+9.69 \pm 4.1$	$+11.88 \pm 2.0^{a}$	$p = 0.07$
Ab$_{42}$/Ab$_{40}$ ratio* rate of change	-0.81 ± 1.0	$+1.03 \pm 0.5$	$+1.57 \pm 1.7$	n.s.
MMSE rate of change [pts/year]	$+0.33 \pm 0.2$	$+0.50 \pm 0.4$	$-2.75 \pm 1.2^{a,b}$	$p < 0.01$

Values are Mean $\pm$ SD; a - value significantly different than in NL-NL group; b - value significantly different than in MCI-MCI group; * - the values of the aβ_{42}/aβ_{40} ratio are multiplied by 100, n.s. - not significant.

CSF biomarker showed longitudinal diagnostic group effects.

In summary, consistent baseline and follow-up effects were found in MCI-AD as compared with the other groups for T-tau, P-tau$_{231}$ and IP levels. Only IP showed a trend towards a longitudinal effect.

The Prediction of decline to AD

Univariate predictors

Logistic regression outcome models classifying MCI-MCI and MCI-AD subjects showed that at baseline, both right and left GMC-MTL values predicted MCI to AD decline with $\geq 74\%$ accuracy ($p < 0.01$, see Table 4). All baseline CSF measures discriminated the groups in the logistic regression models ($\geq 70\%$, $p < 0.05$, see Table 4).

Multivariate predictors

Multivariate CSF and MRI models were used to test for incremental prediction effects among the significant baseline measures (see Table 4). The results showed that adding the right GMC-MTL to baseline CSF P-tau$_{231}$ raised the overall prediction accuracy to 84% ($p_{step} < 0.05$). Addition of right GMC-MTL to baseline CSF IP levels increased the prediction accuracies to 78% ($p_{step} < 0.05$).

Longitudinal correlates of decline

Univariate correlates

Longitudinally, atrophy of the left MTL using the rBS method discriminated MCI-MCI from MCI-AD with 74% overall accuracy (p's < 0.01). The right rBS-MTL atrophy and longitudinal changes in CSF biomarkers levels were not significant group discriminators ($p > 0.05$). No longitudinal correlations were observed between the MRI and CSF biomarkers.

Multivariate correlates

Combining the rBS-MTL atrophy rate with the baseline IP level resulted in a significant increment in the correlation with decline ($p < 0.05$). Combining the rBS-MTL atrophy rate with the IP change did not result in a significant increment in the correlation with decline ($p > 0.05$).

Follow-up diagnostic classifications

All follow-up CSF measures with the exception of the AB$_{42/40}$ ratio discriminated the groups in the logistic regression models ($\geq 70\%$, $p < 0.05$). Similarly, both right and left GMC-MTL at follow-up discriminated the groups in the logistic regression models ($\geq 78\%$, $p < 0.05$).
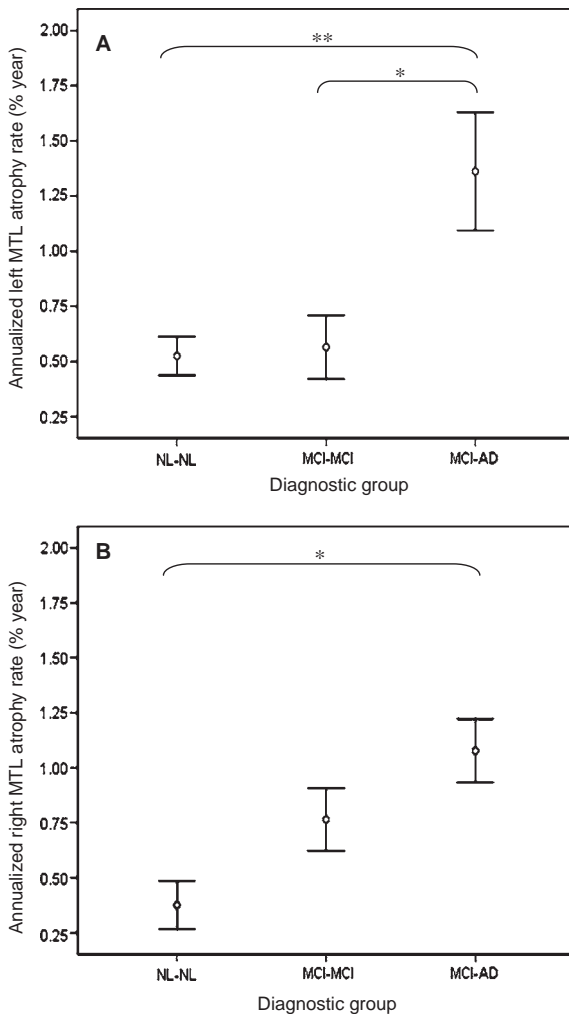
Fig. 3. rBS atrophy rates in the left (A) and right (B) MTL region for the three diagnostic outcome groups. The bars represent mean value $\pm$ SEM. One star indicates $p < 0.05$, two stars: $p < 0.001$.

DISCUSSION

This longitudinal study examined both CSF biomarkers and MRI measures of brain atrophy in the prediction and course of the MCI to AD conversion. We applied an automated regional boundary shift algorithm and voxel-based morphometry.

An important finding from our study was the observation that individually, GMC-MTL atrophy measure and CSF biomarkers for tauopathy are both useful in the separation of MCI-AD from both normal and non-declining MCI. Further, the combination of the baseline, AD-specific CSF P-tau$_{231}$ [5] with the base-

line MRI medial temporal lobe gray matter atrophy measure improved the prediction accuracy for the MCI to AD conversion from 74 to 84%. Although previous studies of from our lab [24;25] and of Bouwman et al. [1] demonstrated the added value of combining the CSF and MRI biomarkers in the diagnostic workup of MCI subjects, to our knowledge the present longitudinal study is the first to evaluate the conversion of MCI to AD using 2-timepoints to estimate CSF biomarker levels and quantitative measures of brain atrophy.

We previously showed that both longitudinal CSF and MRI measures in MCI-MCI correlate with psychometric progression and with each other [2, 26]. In the present study we observed the conversion of MCI to AD and demonstrated that MRI-MTL and CSF measures - while accurate and additive predictors of decline from MCI to AD are not related to each other either at cross-section or longitudinally.

MRI effects

Prior CT and MRI studies demonstrated that hippocampal atrophy (assessed either qualitatively or volumetrically) is one of the earliest features predicting among MCI patients future AD [26–28]. Similarly, our VBM analysis identified clusters of decreased MTL gray matter density in MCI patients who progressed to AD both at both timepoints. These results largely confirm previous findings of reduced MTL GMC in subjects with AD [29] and MCI [30]. One of the major findings of the study is that at an individual level, the GMC-MTL can serve as a valuable predictor of MCI to AD decline. Other studies suggest that MTL atrophy is likely due to neuronal loss [31] secondary to neurofibrillary tangle pathology which is toxic to neurons and known to affect the entorhinal cortex and hippocampus in pre-dementia [32] and even presymptomatic stages [33]. Another imaging study showed that other cortical regions (including lateral temporal and parietal lobes) were predictive of MCI to AD decline [34]. However, in that study the observation period was longer than ours and different image analysis procedures were used. In our study, when NL-NL were compared with MCI-AD, temporal and posterior cingulate and frontal cortical regions were also identified.

In our study, no longitudinal differences in GMC were detected, but we did detect differences in rBS-MTL atrophy rates between the groups. In our opinion, the most likely explanation of this finding refers to the pre-processing of the MRI images: the spatial normalization technique used with VBM renders

Table 4
Significant predictors of MCI to AD decline corrected for confounding measures

	AUC	Sensitivity [%]	Specificity [%]	Overall accuracy [%]	*p* for the step increase
Univariate predictors – MR measures					
GMC-MTL (right) at baseline	0.83	100	67	78	$p < 0.01$
GMC-MTL (left) at baseline	0.78	100	60	74	$p < 0.01$
rBS-MTL (left)	0.71	50	87	74	$P < 0.01$
rBS-MTL (right)	n/a	n/a	n/a	n/a	$P > 0.05$
Univariate predictors – CSF measures					
IP at baseline	0.75	63	80	74	$p < 0.01$
P-tau$_{231}$ at baseline	0.72	75	73	74	$p < 0.01$
aβ_{42}/aβ_{40} ratio at baseline	0.73	100	53	70	$p = 0.05$
T-tau at baseline	0.76	63	73	70	$p < 0.05$
Combined measures (CSF + MR)					
Baseline P-tau$_{231}$ + GMC-MTL (right)	0.85	100	73	84	$p < 0.05$
Baseline P-tau$_{231}$ + rBS-MTL (left)	0.78	50	100	84	$p < 0.05$
Baseline IP + GMC-MTL (right)	0.85	100	67	78	$p < 0.05$
Baseline IP + rBS-MTL (left)	0.85	75	87	78	$p < 0.05$

the technique less sensitive to detect subtle atrophy changes within subjects. In contrast, the rBS method works on individual, non-spatially-normalized scans and may be more sensitive to small atrophic changes. Another factor contributing to the different results yielded with the 2 techniques is that boundary shift method detects changes in CSF volume, while VBM detects changes in gray matter concentration.

Although both left and right rBS-MTL atrophy was greater in the MCI-AD than in controls, only left rBS-MTL differentiated MCI decliners from MCI non-decliners. Our right and left rBS-MTL atrophy rates are within the range reported by others (e.g. approximately 2–3%/year for the MTL structures) [35–37]. The high MTL atrophy rates among MCI-AD suggest that loss of brain tissue in this region is an important feature of AD distinguishing it from controls and stable MCI. The lack of difference in atrophy rates between controls and stable MCI subjects may be explained in several ways. First, MCI is a clinically defined concept and not a biologically defined early AD stage. Thus, the inhomogeneity of the diagnosis of MCI may be expected to differentially affect their atrophy rates. While it is likely that many of the MCI subjects have AD, an unknown fraction of this group is expected to progress to other types of dementia or even revert back to normal. It is also possible that heterogeneity in the NL-NL group accounts for some of the variance. The fact that the MCI-MCI group was also not different from controls with the CSF measures suggests that the subjects in fact did not have early AD or that it was below delectability thresholds.

Interestingly, left rBS-MTL atrophy was better correlated with the transition to AD than right rBS-MTL atrophy, which is consistent with our previous atrophy rate study [16] as well as with the studies of other authors [38, 39]. Similarly, left GMC-MTL (but not right) predicted AD in this study.

CSF effects

At baseline, all the CSF measures provided good prediction of incipient AD. The results are consistent with an extensive literature (see [40] for a review), including our previously published study [20]. The best predictions found were P-tau$_{231}$ and IP. The presence of pathological levels of P-tau$_{231}$, T-tau, IP and A$\beta_{42/40}$ ratio in MCI decliners points to the fact that changes in the CSF biochemical composition appear before the onset of clinically overt AD. Prior validation studies show that pathological CSF levels of biomarkers reflect AD pathology: amyloid plaques [41] neurofibrillary tangles [42] and oxidative damage to neuronal cell membranes [43].

We previously reported that only IP showed longitudinal effects [2, 20]. In this report, only IP levels showed a trend towards increasing over 2 years in association with the MCI-AD conversion as compared with NL subjects. Since IP is a marker of membrane lipid peroxidation and inflammation, these data continue to suggest that the increase of IP levels in cognitively deteriorating patients reflects progressive neuronal damage [21].

Additive effects

The observed additive effect of MRI and CSF biomarkers offers a potential diagnostic advance. We demonstrated that the combination of baseline levels of either P-tau$_{231}$ or IP with the right MTL GMC raised the prediction accuracy levels to $\geq 78\%$.

There are few published reports where both CSF biomarkers and MRI measures of brain atrophy were applied in diagnosis of AD. In a cross-sectional study by Schoonenboom et al., MTL atrophy was found to contribute to CSF measures of Aβ_{1-42} and P-Tau$_{181}$ in incrementing the diagnostic separation of AD and control subjects [3]. Our previous work demonstrated that the longitudinal reductions in the hippocampal volume were associated with progressive elevations in P-Tau$_{231}$ level and reductions in the Aβ_{42} [25]. Another study published by our group showed that in NL and MCI subjects, longitudinal increases in IsoP levels correlated with atrophy in both the left MTL and left inferior temporal gyrus regions [2].

There are several limitations of our study. First, the small sample size reduces statistical power and restricts detection of other effects. The results warrant a replication with a larger sample and perhaps testing in a community based random study predicting cognitive decline and AD. Second, in dementia centers the clinical diagnoses of AD correspond with the post-mortem diagnoses about 85% of the time [44] and in our study the diagnosis of AD was not confirmed with pathology. Third, the observed CSF data combined with MRI needs to be evaluated for AD diagnostic specificity with diverse patient groups at the MCI stage, as prior diagnostic specificity studies have not included MCI patients. It will be important to learn if other forms of dementia will be correctly discriminated at their MCI stages. Fourth, the generalizability of the study results is restricted because of known selection bias of a memory clinic population. Nevertheless, our results probably will generalize to other memory clinics as our observed 30% decline rate over two years for the MCI subjects is consistent other AD center studies [45].

CONCLUSION

The high diagnostic accuracy of both MRI-MTL and AD CSF biomarkers to identify incident AD from MCI patients is improved when both measurements are combined in a prediction model. These results provide support for including CSF and MRI biomarkers in the evaluation of memory clinic patients, a position advocated in recent reviews [46]. Our data suggest that in the near future, both imaging and biomarker identification of preclinical AD subjects will be a part of pharmacologic and non-pharmacologic treatment and prevention strategies.

REFERENCES

[1] Bouwman FH, Schoonenboom SN, van der Flier WM, van Elk EJ, Kok A, Barkhof F, Blankenstein MA, Scheltens (2007) CSF biomarkers and medial temporal lobe atrophy predict dementia in mild cognitive impairment. *Neurobiol Aging* **28**, 1070-1074.

[2] de Leon MJ, Mosconi L, Li J, De Santi S, Yao Y, Tsui WH, Pirraglia E, Rich K, Javier E, Brys M, Glodzik L, Switalski R, Saint Louis LA, Pratico D (2007) Longitudinal CSF isoprostane and MRI atrophy in the progression to AD. *J Neurol* **254**, 1666-1675.

[3] Schoonenboom NS, van der Flier WM, Blankenstein MA, Bouwman FH, Van Kamp GJ, Barkhof F, Scheltens P (2008) CSF and MRI markers independently contribute to the diagnosis of Alzheimer's disease. *Neurobiol Aging* **29**, 669-675.

[4] de Leon MJ, Golomb J, Convit A, De Santi S, McRae TD, George AE (1993) Measurement of medial temporal lobe atrophy in diagnosis of Alzheimer's disease. *Lancet* **341**, 125-126.

[5] Buerger K, Zinkowski R, Teipel SJ, Tapiola T, Arai H, Blennow K, Andreasen N, Hofmann-Kiefer K, DeBernardis J, Kerkman D, McCulloch C, Kohnken R, Padberg F, Pirttilä T , Schapiro MB, Rapoport SI, Möller HJ, Davies P, Hampel H (2002) Differential diagnosis of Alzheimer disease with cerebrospinal fluid levels of tau protein phosphorylated at Threonine 231. *Arch Neurol* **59**, 1267-1272.

[6] Lewczuk P, Esselmann H, Otto M, Maler JM, Henkel AW, Henkel MK, Eikenberg O, Antz C, Krause WR, Reulbach U, Kornhuber J, Wiltfang J (2004) Neurochemical diagnosis of Alzheimer's dementia by CSF A[beta]42, A[beta]42/A[beta]40 ratio and total tau. *Neurobiol Aging* **25**, 273-281.

[7] Blennow K, de Leon MJ, Zetterberg H (2006) Alzheimer's disease. *Lancet Neurol* **368**, 387-403.

[8] Morris JC (1993) The Clinical Dementia, Rating (CDR): Current version and scoring rules. *Neurol* **43**, 2412-2414.

[9] Reisberg B, Ferris SH, de Leon MJ, Crook T (1982) The Global Deterioration Scale for assessment of primary degenerative dementia. *Am J Psychiatry* **139**, 1136-1139.

[10] American Psychiatric Association (1994) *Diagnostic and Statistical Manual of Mental Disorders (Fourth Edition),* 4 edn., American Psychiatric Association, Washington, DC.

[11] McKhann G, Drachman D, Folstein M, Katzman R, Price D, Stadlan EM (1984) Clinical diagnosis of Alzheimer's disease: report of the NINCDS-ADRDA Work Group under the auspices of Department of Health and Human Services Task Force on Alzheimer's disease. *Neurol* **34**, 939-944.

[12] Tsui WH, Rusinek H, Van Gelder P, Lebedev S (2001) Analyzing multi-modality tomographic images and associated regions of interest with MIDAS. *Proc SPIE Med Imag: Imag Proc* **4322**, 1725-1734.

[13] Ashburner J, Friston KJ (2000) Voxel-based morphometry-the methods. *Neuroimage* **11**, 805-821.

[14] Rusinek H, De Santi S, Frid D, Tsui WH, Tarshish CY, Convit A, de Leon MJ (2003) Regional brain atrophy rate predicts future cognitive decline: 6-year longitudinal MR imaging study of normal aging. *Radiology* **229**, 691-696.

[15] Fox NC, Freeborough PA (1997) Brain atrophy progression measured from registered serial MRI: validation and application to Alzheimer's disease. *J Magn Reson Imag* **7**, 1069-1075.

[16] Rusinek H, Endo Y, De Santi S, Frid D, Tsui WH, Segal S, Convit A, de Leon MJ (2004) Atrophy rate in medial temporal lobe during progression of Alzheimer disease. *Neurol* **63**, 2354-2359.

[17] Kohnken R, Buerger K, Zinkowski R, Miller C, Kerkman D, DeBernardis J, Shen J, Moumlller HJ, Davies P, Hampel H (2000) Detection of tau phosphorylated at threonine 231 in cerebrospinal fluid of Alzheimer's disease patients. *Neurosci Lett* 187-190

[18] Mehta PD, Pirttila T, Mehta SP, Sersen EA, Aisen PS, Wisniewski HM (2000) Plasma and cerebrospinal fluid levels of amyloid beta proteins 1-40 and 1-42 in Alzheimer disease. *Arch Neurol* **57**, 100-105.

[19] Fagan AM, Roe CM, Xiong C, Mintun M, Morris JC, Holtzman DM (2007) Cerebrospinal fluid tau/beta-Amyloid42 ratio as a prediction of cognitive decline in nondemented older adults. *Arch Neurol* **64**, 343-349.

[20] Brys M, Pirraglia E, Rich K, Rolstad S, Mosconi L, Switalski R, Glodzik-Sobanska L, De Santi S, Zinkowski R, Mehta P, Pratico D, Saint Louis LA, Wallin A, Blennow K, de Leon MJ (2009) Prediction and longitudinal study of CSF biomarkers in mild cognitive impairment. *Neurobiol Aging* **30**, 682-690.

[21] Pratico D, Clark CM, Lee VM, Trojanowski JQ, Rokach J, Fitzgerald GA (2000) Increased 8,12-iso-iPF2alpha-VI in Alzheimer's disease: correlation of a noninvasive index of lipid peroxidation with disease severity. *Ann Neurol* **48**, 809-812.

[22] Talairach J, Tournoux P (1988) Co-Planar stereotaxic atlas of the human brain, Thieme, Stuttgart.

[23] Good CD, Johnsrude IS, Ashburner J, Henson RN, Friston KJ, Frackowiak RSJ (2001) A voxel-based morphometric study of ageing in 465 normal adult human brains. *Neuroimage* **14**, 21-36.

[24] de Leon MJ, Segal S, Tarshish CY, DeSanti S, Zinkowski R, Mehta PD, Convit A, Caraos C, Rusinek H, Tsui W, Saint Louis LA, DeBernardis J, Kerkman D, Qadri F, Gary A, Lesbre P, Wisniewski T, Poirier J, Davies P (2002) Longitudinal CSF tau load increases in mild cognitive impairment. *Neurosci Lett* **333**, 183-186.

[25] de Leon MJ, DeSanti S, Zinkowski R, Mehta PD, Pratico D, Segal S, Rusinek H, Li J, Tsui W, Saint Louis LA, Clark CM, Tarshish C, Li Y, Lair L, Javier E, Rich K, Lesbre P, Mosconi L, Reisberg B, Sadowski M, DeBernadis JF, Kerkman DJ, Hampel H, Wahlund LO, Davies P (2006) Longitudinal CSF and MRI biomarkers improve the diagnosis of mild cognitive impairment. *Neurobiol Aging* **27**, 394-401.

[26] Convit A, de Asis J, de Leon MJ, Tarshish C, De Santi S, Rusinek H (2000) Atrophy of the medial occipitotemporal, inferior, and middle temporal gyri in non-demented elderly predict decline to Alzheimer's disease. *Neurobiol Aging* **21**, 19-26.

[27] de Leon MJ, George AE, Stylopoulos LA, Smith G, Miller DC (1989) Early marker for Alzheimer's disease: the atrophic hippocampus. *Lancet* **2**, 672-673.

[28] Jack CR Jr, Shiung MM, Weigand SD, O'Brien PC, Gunter JL, Boeve BF, Knopman DS, Smith GE, Ivnik RJ, Tangalos EG, Petersen RC (2005) Brain atrophy rates predict subsequent clinical conversion in normal elderly and amnestic MCI. *Neurol* **65**, 1227-1231.

[29] Busatto GF, Garrido GE, Almeida OP, Castro CC, Camargo CH, Cid CG, Buchpiguel CA, Furuie S, Bottino CM (2003) A voxel-based morphometry study of temporal lobe gray matter reductions in Alzheimer's disease. *Neurobiol Aging* **24**, 221-231.

[30] Pennanen C, Testa C, Laakso MP, Hallikainen M, Helkala EL, Hänninen T, Kivipelto M, Könönen M, Nissinen A, Tervo S, Vanhanen M, Vanninen R, Frisoni GB, Soininen H (2005) A voxel based morphometry study on mild cognitive impairment. *J Neurol Neurosurg Psychiatry* **76**, 11-14.

[31] Bobinski M, Wegiel J, Wisniewski HM, Tarnawski M, Bobinski M, Reisberg B, De Leon MJ, Miller DC (1996) Neurofibrillary pathology - correlation with hippocampal formation atrophy in Alzheimer disease. *Neurobiol Aging* **17**, 909-919.

[32] Gómez-Isla T, Hollister R, West H, Mui S, Growdon JH, Petersen RC, Parisi JE, Hyman BT (1997) Neuronal loss correlates with but exceeds neurofibrillary tangles in Alzheimer's disease. *Ann Neurol* **41**, 17-24.

[33] Morris JC, Storandt M, McKeel DW Jr, Rubin EH, Price JL, Grant EA, Berg L (1996) Cerebral amyloid deposition and diffuse plaques in "normal" aging: evidence for presymptomatic and very mild Alzheimer's disease. *Neurol* **46**, 707-719.

[34] Karas G, Sluimer J, Goekoop R, van der Flier W, Rombouts SA, Vrenken H, Scheltens P, Fox N, Barkhof F (2008) Amnestic mild cognitive impairment: structural MR imaging findings predictive of conversion to Alzheimer disease. *AJNR* **29**, 944-949.

[35] Fox NC, Warrington EK, Freeborough PA, Hartikainen P, Kennedy AM, Stevens JM, Rossor MN (1996) Presymptomatic hippocampal atrophy in Alzheimer's disease: a longitudinal MRI study. *Brain* **119**, 2001-2007.

[36] Kaye JA, Swihart T, Howieson D, Dame A, Moore MM, Karnos T, Camicioli R, Ball M, Oken B, Sexton G (1997) Volume loss of the hippocampus and temporal lobe in healthy elderly persons destined to develop dementia. *Neurol* **48**, 1297-1304.

[37] Visser PJ, Scheltens P, Verhey FR, Schmand B, Launer LJ, Jolles J, Jonker C (1999) Medial temporal lobe atrophy and memory dysfunction as predictors for dementia in subjects with mild cognitive impairment. *J Neurol* **246**, 477-485.

[38] Thompson PM, Moussai J, Zohoori S, Goldkorn A, Khan AA, Mega MS, Small GW, Cummings JL, Toga AW (1998) Cortical variability and asymmetry in normal aging and Alzheimer's disease. *Cereb Cortex* **8**, 492-509.

[39] Thompson PM, Mega MS, Woods RP, Zoumalan CI, Lindshield CJ, Blanton RE, Moussai J, Holmes CJ, Cummings JL, Toga AW (2001) Cortical change in Alzheimer's disease detected with a disease-specific population-based brain atlas. *Cereb Cortex* **11**, 1-16.

[40] Brys M, Mosconi L, De Santi S, Rich KE, de Leon MJ (2006) CSF Biomarkers for mild cognitive impairment. *Aging Health* **2**, 111-121.

[41] DeMattos RB, Bales KR, Parsadanian M, O'Dell MA, Foss EM, Paul SM, Holtzman DM (2002) Plaque-associated disruption of CSF and plasma amyloid-beta (Abeta) equilibrium in a mouse model of Alzheimer's disease. *J Neurochem* **81**, 229-236.

[42] Augustinack JC, Schneider A, Mandelkow EM, Hyman BT (2002) Specific tau phosphorylation sites correlate with severity of neuronal cytopathology in Alzheimer's disease. *Acta Neuropathol* **103**, 26-35.

[43] Montine TJ, Markesbery WR, Morrow JD, Roberts LJ (1998) Cerebrospinal fluid F2-isoprostane levels are increased in Alzheimer's disease. *Ann Neurol* **44**, 410-413.

[44] Becker JT, Boller F, Lopez OL, Saxton J, McGonigle KL (1994) The natural history of Alzheimer's disease: description of study cohort and accuracy of diagnosis. *Arch Neurol* **51**, 585-594.

[45] Petersen RC, Smith GE, Waring SC, Ivnik RJ, Tangalos EG, Kokmen E (1999) Mild cognitive impairment: clinical characterization and outcome. *Arch Neurol* **56**, 303-308.

[46] Dubois B (2000) Prodromal Alzheimer's disease: a more useful concept than mild cognitive impairment. *Curr Opin Neurol* **13**, 367-369.

Ultra-High Field 7T MRI: A New Tool for Studying Alzheimer's Disease

Geoffrey A. Kerchner*
Department of Neurology and Neurological Sciences, Stanford Center for Memory Disorders,
Stanford University School of Medicine, Stanford, CA, USA

Abstract. Ultra-high field 7T MRI offers superior signal-to-noise and spatial resolution relative to any other noninvasive imaging technique. By revealing fine anatomical details of the living brain, 7T MRI allows neuroimaging researchers the opportunity to observe in patients disease-related structural changes previously apparent only on postmortem tissue analysis. Alzheimer's disease (AD) is a natural subject for this technology, and I review here two AD-related applications of 7T MRI: direct visualization of cortical plaques, and high resolution hippocampal imaging. I also discuss limitations of this technology as well as expected advances that are likely to establish 7T MRI as an increasingly important tool for the diagnosis and tracking of AD.

Keywords: magnetic resonance imaging (MRI), 7-Tesla (7T), hippocampus, CA1, beta-amyloid, Alzheimer's disease, biomarker

INTRODUCTION

Diagnosing Alzheimer's disease (AD) should be easy. The illness is defined by the presence cortical plaques and tangles in a patient with progressive dementia, and all that is needed, beyond a standard clinical assessment, is visualization of the requisite neuropathology.

The catch, of course, is that the neuropathological hallmarks of AD are too small to be seen noninvasively using conventional neuroimaging technology. For this reason, surrogate neuroimaging markers and other clinical data must be used instead. An abundance of such markers exist, enough to fill books (such as this one), yet each remains an imperfect substitute for histopathology.

Ultra-high field 7.0 Tesla (7T) MRI has made some headway towards addressing the problem of spatial resolution. These powerful magnets — about 140,000 times the strength of the earth's field — are manufactured by Siemens, Philips, and General Electric, and approximately 30 whole-body human 7T MRI scannersare currently deployed at research centers around the world. With enhanced signal-to-noise relative to 3T and lower field technologies, 7T MRI offers not only remarkable spatial resolution, but also the possibility of reduced scan time, greater tissue-type differentiation, and better spectroscopic resolution.

In this brief chapter, I will discuss two possible uses of 7T MRI in the diagnosis and tracking of AD: direct imaging of individual amyloid plaques, and visualization of hippocampal microstructure. I will discuss limitations of the technology and future directions. Although 7T MRI cannot replace a microscope, it does produce remarkable images and has the potential to provide novel ways to detect and track AD-related anatomical changes in the brains of patients.

VISUALIZING PLAQUES

Direct, noninvasive detection of neuropathology is an ultimate goal of structural neuroimaging in AD. Unlike amyloid imaging with positron emission tomography (PET), which offers a highly specific

---

*Correspondence to: Geoffrey A. Kerchner, MD, PhD, Assistant Professor of Neurology and Neurological Sciences, Department of Neurology and Neurological Sciences, Stanford Center for Memory Disorders, Stanford University School of Medicine, 300 Pasteur Drive, Room A343, MC5235, Stanford, CA 94305-5235, USA. Tel.: +1 650 723 2078; Fax: +1 650 723 7434; E-mail: kerchner@stanford.edu.

but low-resolution measure of brain amyloid burden [1], MRI offers the potential of visualizing individual plaques [2, 3].

Ultra-high field imaging of postmortem human brain tissue [4, 5] and *ex vivo* transgenic mouse brains [5–11] reveals cortical lesions that correspond histopathologically to amyloid plaques. Such images feature remarkable resolution, as high as 62.5 μm^3 [10], at the expense of image acquisition times typically in excess of 12 hours. By compromising a bit on spatial resolution, plaque detection has also been achieved in transgenic mice *in vivo*, both with [12–14] and without [6, 9, 11, 15–19] the use of a contrast-enhancing agent. One group has even reported the *in vivo* visualization of plaque-like structures in the parietal cortex of human patients with AD[20].

Plaques exhibit reduced T2 and T2* signal compared to surrounding cortex, and the source of that signal contrast is controversial. Iron deposition within plaques may be a cause of this reduced signal, and there is a correlation between T2* hypointensity and plaque iron content, determined by a histochemical stain, in both mice [6] and humans [5]. If iron deposition were indeed the main source of signal contrast, then T2*- and susceptibility-weighting should be superior to T2-weighting at detecting plaques. However, subsequent work in transgenic mice revealed similar T2 and T2* signal contrast characteristics, suggesting a more limited role for iron than previously envisioned [11]; instead, highly compact fibrillar amyloid may drive the reduction in T2 and T2* signal in mouse models of AD [5, 11]. By contrast, in humans, whose disease is fundamentally different than that in transgenic mice (amyloid plaques develop in the absence of mutant amyloid precursor protein overexpression), iron deposition may indeed be the major source of plaque signal contrast [5]. An imaging modality that identifies plaques as tiny foci of cortical iron accumulation is problematic for at least two reasons: First, tiny iron deposits occur not only in plaques, but also in areas of microhemorrhage and nonspecifically in other pathological or non-pathological cortical microstructures [21]. Second, the iron content of plaques is not necessarily uniform [6], and bias towards detecting plaques with higher iron loads is not necessarily pathologically relevant or desirable.

For these reasons, the intrinsic MRI signal contrast characteristics of cortical plaques relative to surrounding cortex may be insufficiently sensitive or specific. Several groups are working to develop contrast agents that cross the blood-brain-barrier and bind selectively to beta-amyloid [2, 10, 12, 13]. Such agents, which would offer the specificity of amyloid PET imaging at the resolution of ultra-high field MRI, are a promising way forward.

A robust method of visualizing amyloid plaques noninvasively in humans is a worthy goal. It would contribute to clinical diagnosis and to tracking the efficacy of anti-amyloid treatment strategies, and it would allow scientists to study how plaques develop and change longitudinally in the human brain. It is nevertheless germane to note that the presence of amyloid plaque pathology alone is not specific for AD [22], and eliminating the pathology in patients with AD is not clearly beneficial [23, 24]. Therefore, even if it is perfected, an ultra-high field MRI method of plaque visualization would still reveal only a part of the story. Neurofibrillary tau tangles more faithfully track clinical symptoms and brain atrophy in AD [25]; unfortunately, they are much smaller than plaques and almost surely beyond the detection limit of any current MRI technology.

HIGH RESOLUTION HIPPOCAMPAL IMAGING

The hippocampus is one of the earliest brain structures, after the entorhinal cortex, to exhibit neurofibrillary tangle pathology and atrophy [25]. For this reason, the hippocampus has long been a focus of AD neuroimaging [26].

The earliest AD-associated changes to the hippocampus are focal and subtle. As neurons of the entorhinal cortex become consumed by neurofibrillary pathology, still in the preclinical stages of the illness, the apical dendrites of CA1 pyramidal neurons — a target of the perforant pathway axons arising from dying neurons in the entorhinal cortex — are affected next [27–29]. Prior to the death of the CA1 neurons themselves, their tau-laden apical dendrites go on to become dilated and dystrophic, and the CA1 apical neuropil region involutes as the disease progresses [30, 31]. These same CA1 apical dendrites are where long term potentiation and other forms of synaptic plasticity have been investigated for decades [32]; synapses onto those dendrites are postulated to be a critical node for memory formation, the very cognitive modality that declines first in AD.

Fine details of hippocampal structure are evident *in vivo* using 7T MRI [33–35]. On oblique coronal slices showing the hippocampus in cross section, the technique permits not only the precise identification

of individual subfields by their morphological signatures, but also the visualization of individual strata within those subfields. My colleagues and I recently published a study using 7T MRI to reveal thinning of the CA1 apical neuropil in patients with early AD [33]. In that study, the hippocampal cell body layer appeared as a hyperintense band, and the neuropil was comparatively hypointense (Fig. 1). As would be predicted from the postmortem literature discussed above, thinning of the apical neuropil was more sensitive than thinning of the cell body layer or overall hippocampal volume reduction at distinguishing patients with AD from age-matched normal controls.
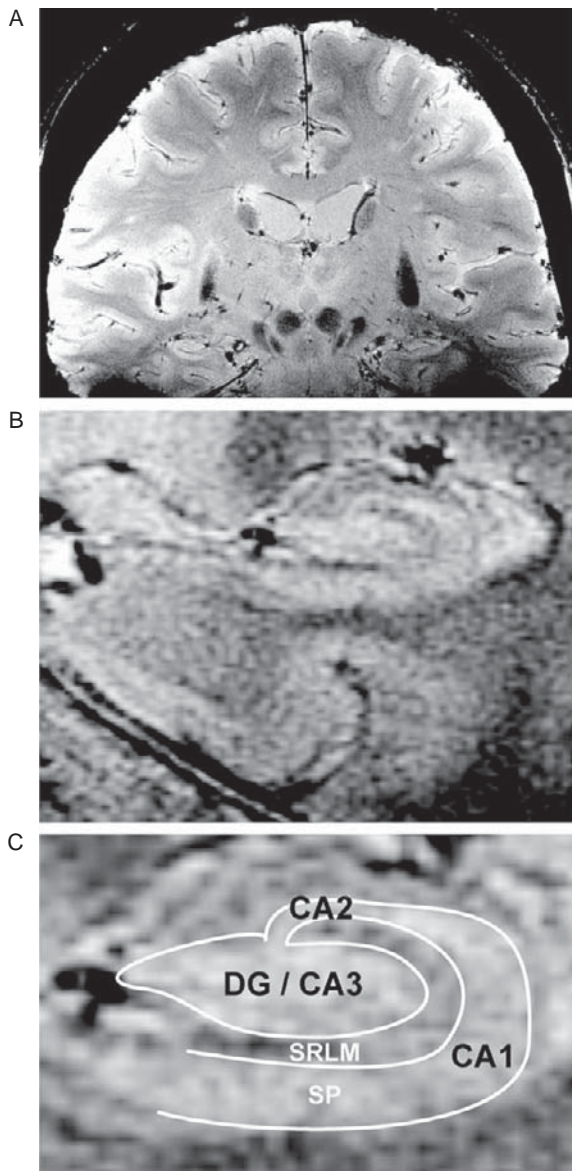
This study highlights an important concept, that by narrowing the focus of neuroimaging to the very specific microstructural features of the hippocampus known to be affected earliest in AD, sensitivity to the disease rises. Indeed, by the time macroscopic hippocampal atrophy becomes unambiguous by conventional imaging, clinical manifestations are similarly unambiguous, as patients already exhibit dementia and meet standard clinical criteria for AD [26]. Future work on high resolution hippocampal imaging should focus on individuals who are normal or who complain of mild cognitive impairment; after baseline imaging and longitudinal follow-up, the earliest structural markers of preclinical AD may become apparent. Meanwhile, the implementation of newer 7T MRI sequences, such as a T2-weighted fast spin echo sequence, may improve gray-white signal contrast within the hippocampus and speed the development of automated image analysis. Multi-echo 7T functional MRI shows promise at revealing laminar activation patterns in the cortex [36], and this technique may extend to the hippocampal laminae. Finally, 7T hippocampal imaging, combined with neuropsychological measures of memory performance, may permit the study of structural-functional correlations at a resolution not previously possible.

LIMITATIONS

A powerful magnetic field poses challenges along with benefits. Limiting the easy clinical implemen-

Fig. 1. High resolution 7T MRI of the Hippocampus. **A**. This oblique coronal brain slice, obtained from a patient with very mild AD (filling NINCDS-ADRDA criteria for probable AD by clinical consensus; Mini Mental State Exam 29/30; Clinical Dementia Rating score 0.5) is oriented orthogonal to the longitudinal axis of the hippocampus. The image was obtained on a 7T GE MRI system (General Electric, Waukesha, WI) equipped with an 8-channel phased-array receive head coil (Nova Medical Inc., Wilmington, MA). This 9.6 minute T2*-weighted gradient recalled echo sequence used a 1024×768 matrix over a 20×20 cm field of view, yielding an in-plane resolution of 0.195×0.260 mm on slices 2 mm thick; sequence parameters included T_E 15 ms, T_R 250 ms, flip angle $20°$, NEX 3. The image is presented in radiological orientation. In this unprocessed image, signal intensity varies from the periphery to the center of the image, and from left to right, reflecting radiofrequency field inhomogeneities and other factors (see text). **B**. Magnification of (A), focusing on the left medial temporal lobe. **C**. Further magnification of the left hippocampus, highlighting relevant anatomical features. CA1–3, cornus ammonis subfields; DG, dentate gyrus; SP, stratum pyramidale, or the cell body layer of hippocampal cortex; SRLM, stratum radiatum/stratum lacunosum-moleculare, or the apical neuropil. Thinning of the SRLM sensitively discriminates patients with AD from normal controls [33].

tation of 7T MRI is the fact that human dimensions are no longer a negligible fraction of the wavelength of radiofrequency radiation, leading to radiofrequency field (B_1) inhomogeneities that compromise image quality (Fig. 1). In addition, magnetic field (B_0) inhomogeneities produced by air/water interfaces or mineralization become amplified at 7T compared to lower field strengths. Higher energy absorption (measured by the specific absorption ratio, or SAR) constrains sequence development. And motion — even the pulsation of the brain during the cardiac cycle — limits spatial resolution.

To a large extent, apparent limitations of 7T MRI arise from the use of coils and other equipment that had been developed for lower field strengths. The development of new hardware and software optimized for an ultra-high field environment is a current priority of academic and industry groups. A navigator echo technique may reduce motion artifacts [37].

Fortunately, people — including specifically patients with AD — tolerate the experience of being in a 7T scanner [20, 33, 37, 38]. Some individuals report vertigo and nausea, especially during movement into and out of the scanner [35], and gradient noise is loud. However, these factors are not practically limiting, and as a general rule, patients who tolerate 3T scans have no difficulty with 7T MRI. No long term side effect of ultra-high field human imaging has been reported.

Finally, anyone concerned that scarce availability of 7T MRI will limit its practical use should look to the history of 3T MRI. It has been less than a decade since 3T magnets were approved by the FDA for clinical use, and they are now so widely deployed as to be considered the principal imaging workhorse at many hospitals and outpatient radiology centers.

CONCLUSIONS

Ultra-high field 7T MRI allows us to peer into the living human brain with stunning precision. It is likely that a method will be developed to visualize individual cortical plaques, probably with the assistance of a selective contrast-enhancing agent. And while individual neurofibrillary tangles may be too small, the consequence of neurofibrillary pathology, including early focal atrophy of the hippocampal neuropil, is detectable. While not providing an easy solution to the challenge of providing a definitive preclinical diagnosis of AD, 7T MRI has opened broad new avenues of neuroimaging research. The technology is being used

to study not only AD, but also epilepsy, multiple sclerosis, cerebrovascular disease, and other neurological conditions. It may be useful at informing the differential diagnosis of patients with age-related cognitive decline, detecting subtle structural correlates of vascular disease [39] and even Parkinson's disease [40]. And, in analogy to what has happened at 3T, structural imaging will become merely one arrow in a broadening quiver of 7T sequences, which is already starting to include diffusion tensor imaging, functional imaging, and spectroscopy. 7T MRI may not replace a microscope, but it is likely to uncover details of brain structure, connectivity, and function that are available with no other technology.

REFERENCES

[1]   Klunk WE, Engler H, Nordberg A, Wang Y, Blomqvist G, Holt DP, Bergstrom M, Savitcheva I, Huang GF, Estrada S, Ausen B, Debnath ML, Barletta J, Price JC, Sandell J, Lopresti BJ, Wall A, Koivisto P, Antoni G, Mathis CA, Langstrom B (2004) Imaging brain amyloid in Alzheimer's disease with Pittsburgh Compound-B. *Ann Neurol* **55**, 306-319.

[2]   Wengenack T, Jack C, Garwood M, Poduslo J (2008) MR Microimaging of amyloid plaques in Alzheimer's disease transgenic mice. *European Journal of Nuclear Medicine and Molecular Imaging* **35**, 82-88.

[3]   Jack CR, Marjanska M, Wengenack TM, Reyes DA, Curran GL, Lin J, Preboske GM, Poduslo JF, Garwood M (2007) Magnetic resonance imaging of Alzheimer's pathology in the brains of living transgenic mice: a new tool in Alzheimer's disease research. *The Neuroscientist* **13**, 38-48.

[4]   Benveniste H, Einstein G, Kim KR, Hulette C, Johnson GA (1999) Detection of neuritic plaques in Alzheimer's disease by magnetic resonance microscopy. *Proc Natl Acad Sci U S A* **96**, 14079-14084.

[5]   Meadowcroft MD, Connor JR, Smith MB, Yang QX (2009) MRI and histological analysis of beta-amyloid plaques in both human Alzheimer's disease and APP/PS1 transgenic mice. *J Magn Reson Imaging* **29**, 997-1007.

[6]   Jack CR, Garwood M, Wengenack TM, Borowski B, Curran GL, Lin J, Adriany G, Gröhn OHJ, Grimm R, Poduslo JF (2004) *In vivo* visualization of Alzheimer's amyloid plaques by magnetic resonance imaging in transgenic mice without a contrast agent. *Magn Reson Med* **52**, 1263-1271.

[7]   Zhang J, Yarowsky P, Gordon MN, Di Carlo G, Munireddy S, van Zijl PC, Mori S (2004) Detection of amyloid plaques in mouse models of Alzheimer's disease by magnetic resonance imaging. *Magn Reson Med* **51**, 452-457.

[8]   Lee S-P, Falangola MF, Nixon RA, Duff K, Helpern JA (2004) Visualization of β-amyloid plaques in a transgenic mouse model of Alzheimer's disease using MR microscopy without contrast reagents. *Magn Reson Med* **52**, 538-544.

[9]   Faber C, Zahneisen B, Tippmann F, Schroeder A, Fahrenholz F (2007) Gradient-echo and CRAZED imaging for minute detection of Alzheimer plaques in an APPV717I × ADAM10-dn mouse model. *Magn Reson Med* **57**, 696-703.

[10] Poduslo JF, Wengenack TM, Curran GL, Wisniewski T, Sigurdsson EM, Macura SI, Borowski BJ, Jack CR (2002)

Molecular targeting of Alzheimer's amyloid plaques for contrast-enhanced magnetic resonance imaging. *Neurobiol Dis* **11**, 315-329.

[11] Chamberlain R, Reyes D, Curran GL, Marjanska M, Wengenack TM, Poduslo JF, Garwood M, Jack CR (2009) Comparison of amyloid plaque contrast generated by T2-weighted, T2*-weighted, and susceptibility-weighted imaging methods in transgenic mouse models of Alzheimer's disease. *Magn Reson Med* **61**, 1158-1164.

[12] Wadghiri YZ, Sigurdsson EM, Sadowski M, Elliott JI, Li Y, Scholtzova H, Tang CY, Aguinaldo G, Pappolla M, Duff K, Wisniewski T, Turnbull DH (2003) Detection of Alzheimer's amyloid in transgenic mice using magnetic resonance microimaging. *Magn Reson Med* **50**, 293-302.

[13] Higuchi M, Iwata N, Matsuba Y, Sato K, Sasamoto K, Saido TC (2005) 19F and 1 H MRI detection of amyloid [beta] plaques *in vivo*. *Nat Neurosci* **8**, 527-533.

[14] Teipel SJ, Kaza E, Hadlich S, Bauer A, Brüning T, Plath A-S, Krohn M, Scheffler K, Walker LC, Lotze M, Pahnke J (2011) Automated detection of amyloid-β-related cortical and subcortical signal changes in a transgenic model of Alzheimer's disease using high-field MRI. *Journal of Alzheimer's Disease* **23**, 221-237.

[15] Borthakur A, Gur T, Wheaton AJ, Corbo M, Trojanowski JQ, Lee VMY, Reddy R (2006) *In vivo* measurement of plaque burden in a mouse model of Alzheimer's disease. *J Magn Reson Imaging* **24**, 1011-1017.

[16] Helpern JA, Lee SP, Falangola MF, Dyakin VV, Bogart A, Ardekani B, Duff K, Branch C, Wisniewski T, de Leon MJ, Wolf O, O'Shea J, Nixon RA (2004) MRI assessment of neuropathology in a transgenic mouse model of Alzheimer's disease. *Magn Reson Med* **51**, 794-798.

[17] Braakman N, Matysik J, van Duinen SG, Verbeek F, Schliebs R, de Groot HJM, Alia A (2006) Longitudinal assessment of Alzheimer's β-amyloid plaque development in transgenic mice monitored by *in vivo* magnetic resonance microimaging. *J Magn Reson Imaging* **24**, 530-536.

[18] Jack CR Jr, Wengenack TM, Reyes DA, Garwood M, Curran GL, Borowski BJ, Lin J, Preboske GM, Holasek SS, Adriany G, Poduslo JF (2005) *In vivo* magnetic resonance microimaging of individual amyloid plaques in Alzheimer's transgenic mice. *J Neurosci* **25**, 10041-10048.

[19] Vanhoutte G, Dewachter I, Borghgraef P, Van Leuven F, Van der Linden A (2005) Noninvasive *in vivo* MRI detection of neuritic plaques associated with iron in APP [V717I] transgenic mice, a model for Alzheimer's disease. *Magn Reson Med* **53**, 607-613.

[20] Nakada T, Matsuzawa H, Igarashi H, Kwee YFIL (2008) *In vivo* visualization of senile-plaque-like pathology in Alzheimer's disease patients by MR microscopy on a 7T system. *J Neuroimaging* **18**, 125-129.

[21] Dhenain M, Privat N, Duyckaerts C, Jacobs RE (2002) Senile plaques do not induce susceptibility effects in T2*-weighted MR microscopic images. *NMR Biomed* **15**, 197-203.

[22] Rabinovici GD, Jagust WJ (2009) Amyloid imaging in aging and dementia: Testing the amyloid hypothesis *in vivo*. *Behavioural Neurology* **21**, 117-128.

[23] Kerchner GA, Boxer AL (2010) Bapineuzumab. *Expert Opin Biol Ther* **10**, 1121-1130.

[24] Holmes C, Boche D, Wilkinson D, Yadegarfar G, Hopkins V, Bayer A, Jones RW, Bullock R, Love S, Neal JW, Zotova E, Nicoll JAR (2008) Long-term effects of Aβ42 immunisation in Alzheimer's disease: follow-up of a randomised, placebo-controlled phase I trial. *The Lancet* **372**, 216-223.

[25] Braak H, Alafuzoff I, Arzberger T, Kretzschmar H, Del Tredici K (2006) Staging of Alzheimer disease-associated neurofibrillary pathology using paraffin sections and immunocytochemistry. *Acta Neuropathol (Berl)* **112**, 389-404.

[26] Frisoni GB, Fox NC, Jack CR, Scheltens P, Thompson PM (2010) The clinical use of structural MRI in Alzheimer disease. *Nat Rev Neurol* **6**, 67-77.

[27] Braak E, Braak H (1997) Alzheimer's disease: transiently developing dendritic changes in pyramidal cells of sector CA1 of the Ammon's horn. *Acta Neuropathol* **93**, 323-325.

[28] Thal DR, Holzer M, Rub U, Waldmann G, Gunzel S, Zedlick D, Schober R (2000) Alzheimer-related tau-pathology in the perforant path target zone and in the hippocampal stratum oriens and radiatum correlates with onset and degree of dementia. *Exp Neurol* **163**, 98-110.

[29] Lace G, Savva GM, Forster G, de Silva R, Brayne C, Matthews FE, Barclay JJ, Dakin L, Ince PG, Wharton SB (2009) Hippocampal tau pathology is related to neuroanatomical connections: an ageing population-based study. *Brain* **132**, 1324-1334.

[30] Mizutani T, Kasahara M (1997) Hippocampal atrophy secondary to entorhinal cortical degeneration in Alzheimer-type dementia. *Neurosci Lett* **222**, 119-122.

[31] Scheff SW, Price DA, Schmitt FA, DeKosky ST, Mufson EJ (2007) Synaptic alterations in CA1 in mild Alzheimer disease and mild cognitive impairment. *Neurology* **68**, 1501-1508.

[32] Kerchner GA, Nicoll RA (2008) Silent synapses and the emergence of a postsynaptic mechanism for LTP. *Nat Rev Neurosci* **9**, 813-825.

[33] Kerchner GA, Hess CP, Hammond-Rosenbluth KE, Xu D, Rabinovici GD, Kelley DAC, Vigneron DB, Nelson SJ, Miller BL (2010) Hippocampal CA1 apical neuropil atrophy in mild Alzheimer disease visualized with 7-T MRI. *Neurology* **75**, 1381-1387.

[34] Thomas BP, Welch EB, Niederhauser BD, Whetsel WO, Anderson AW, Gore JC, Avison MJ, Creasy JL (2008) High-resolution 7T MRI of the human hippocampus *in vivo*. *J Magn Reson Imaging* **28**, 1266-1272.

[35] Theysohn JM, Kraff O, Maderwald S, Schlamann MU, de Greiff A, Forsting M, Ladd SC, Ladd ME, Gizewski ER (2009) The human hippocampus at 7 T–*in vivo* MRI. *Hippocampus* **19**, 1-7.

[36] Koopmans PJ, Barth M, Orzada S, Norris DG (2011) Multi-echo fMRI of the cortical laminae in humans at 7T. *Neuroimage* **56**, 1276-1285.

[37] Versluis MJ, Peeters JM, van Rooden S, van der Grond J, van Buchem MA, Webb AG, van Osch MJP (2010) Origin and reduction of motion and f0 artifacts in high resolution T2*-weighted magnetic resonance imaging: Application in Alzheimer's disease patients. *Neuroimage* **51**, 1082-1088.

[38] von Morze C, Kelley DAC, Shepherd TM, Banerjee S, Xu D, Hess CP (2010) Reduced field-of-view diffusion-weighted imaging of the brain at 7 T. *Magn Reson Imaging* **28**, 1541-1545.

[39] Theysohn JM, Kraff O, Maderwald S, Barth M, Ladd SC, Forsting M, Ladd ME, Gizewski ER (2011) 7 tesla MRI of microbleeds and white matter lesions as seen in vascular dementia. *J Magn Reson Imaging* **33**, 782-791.

[40] Eapen M, Zald DH, Gatenby JC, Ding Z, Gore JC (2011) Using high-resolution MR imaging at 7T to evaluate the anatomy of the midbrain dopaminergic system. *American Journal of Neuroradiology* **32**, 688-694.

This page intentionally left blank

Section 3
Imaging of Cerebral Blood Flow, Glucose Metabolism, Amyloid Plaques and Neurofibrillary Tangles in AD

This page intentionally left blank

Introduction

Section 3: Imaging of Cerebral Blood Flow, Glucose Metabolism, Amyloid Plaques and Neurofibrillary Tangles in AD

Ansgar J. Furst[a,b,c,*] and Osama Sabri[d]

[a]*War Related Illness and Injury Study Center, VA Palo Alto Health Care System, Palo Alto, CA, USA*
[b]*Department of Psychiatry and Behavioral Sciences, Stanford University School of Medicine, Stanford, CA, USA*
[c]*Department of Neurology and Neurological Sciences, Stanford University School of Medicine, Stanford, CA, USA*
[d]*Department of Nuclear Medicine, University of Leipzig, Leipzig, Germany*

The present section provides an overview of the progress that has been made in the past decades in imaging AD pathology using chiefly techniques developed in nuclear medicine such as positron emission tomography (PET) and single photon emission tomography (SPECT). Together with new approaches using also magnetic resonance imaging (MRI) these techniques have focused on the detection and quantification of cerebral hypoperfusion, glucose hypometabolism and the hallmark pathological features of the disease, amyloid plaques (A-beta) and neurofibrillary tangles (NFT).

A brief introductory review of existing imaging techniques in the context of AD diagnostics is provided in the chapter by Weih et al. [1]. This is followed by 3 chapters (Sedaghat et al., Allegret et al. & Bastin et al. [2–4]) illustrating the usefulness of imaging in detecting and exploring the neural correlates of cognitive deficits associated with AD pathology. Due to the failure of many clinical trials and the growing need for disease modifying drugs Reiman et al. (in Section 8 [5]) outlines the Alzheimer's Prevention Initiative (API), an ambitious plan to target populations that are genetically at high risk for developing AD close to their expected onset of the disease with new drugs using imaging as outcome measures. Similarly, Tzimopoulou et al. (in Section 8 [6]) makes the case for the specific utility of fluorodeoxyglucose (FDG) glucose imaging in multi-center clinical trials settings. The value of the more widely available SPECT in mild cognitive impairment and AD is discussed in Nobili et al. [7]. A comprehensive comparison of the utility of FDG vs. the to-date most widely studied amyloid tracer Pittsburgh-compound B (PIB) is provided in Mosconi et al. [8] followed by a detailed comparison of the uptake patterns of the two tracers in AD, specifically in Furst & Lal [9]. Further, the current knowledge and future research activities for the 18F-labeled β-amyloid-targeted PET tracer florbetaben are reviewed by Barthel & Sabri [10]. Austin et al. [11] discusses arterial spin labeling (ASL) a more recent MR-based alternative to measure hypoperfusion in AD. Finally the last 2 chapters of this section are focused on the challenges in imaging NFT pathology: Shin et al. [12] discusses this in the context of data of the only available compound capable of detecting both A-beta and NFT and points to the necessity for modification of current A-beta centered disease progression frameworks in order to accommodate these findings. In order to clearly distinguish the contributions of A-beta vs. NFT to AD pathology a tracer that is solely binding to NFT is urgently needed for future research. The specific difficulties in developing such an imaging agent are illustrated in the last chapter Jensen et al. [13].

*Correspondence to: E-mail: ajfurst@stanford.edu.

REFERENCES

[1]   Weih M, Degirmenci Ü, Kreil S, Suttner G, Schmidt D, Kornhuber J, Lewczuk P, Kuwert T (2011) Nuclear medicine diagnostic techniques in the era of pathophysiology-based CSF biomarkers for Alzheimer's disease. In *Handbook of Imaging the Alzheimer Brain*, Ashford JW et al., eds. IOS Press, Amsterdam, pp. 163-169.

[2]   Sedaghat F, Baloyannis SJ (2011) Unawareness of cognitive and behavioral deficits in Alzheimer's disease may be reflected by perfusion SPECT. In *Handbook of Imaging the Alzheimer Brain*, Ashford JW et al., eds. IOS Press, Amsterdam, pp. 171-177.

[3]   Alegret M, Vinyes-Junqué G, Boada M, Martínez-Lage P, Cuberas G, Espinosa A, Roca I, Hernández I, Valero S, Rosende-Roca M, Mauleón A, Becker JT, Tárraga L (2011) Brain perfusion and neuropsychological deficits in mild cognitive impairment and mild Alzheimer's disease. In *Handbook of Imaging the Alzheimer Brain*, Ashford JW et al., eds. IOS Press, Amsterdam, pp. 179-190.

[4]   Bastin C, Kerrouche N, Lekeu F, Adam S, Guillaume B, Lemaire C, Aerts J, d'Ydewalle G, Collette F, Salmon E (2011) Neural correlates of controlled memory processes in questionable Alzheimer's disease. In *Handbook of Imaging the Alzheimer Brain*, Ashford JW et al., eds. IOS Press, Amsterdam, pp. 191-204.

[5]   Reiman EM, Langbaum JBS, Fleisher AS, Caselli RJ, Chen K, Ayutyanont N, Quiroz YT, Kosik KS, Lopera F, Tariot PN (2011) Alzheimer's prevention initiative: A plan to accelerate the evaluation of presymptomatic treatments. In *Handbook of Imaging the Alzheimer Brain*, Ashford JW et al., eds. IOS Press, Amsterdam, pp. 589-597.

[6]   Tzimopoulou S, Cunningham VJ, Nichols TE, Searle G, Bird NP, Mistry P, Dixon IJ, Hallett WA, Whitcher B, Brown AP, Zvartau-Hind M, Lotay N, Lai RYK, Castiglia M, Jeter B, Matthews JC, Chen K, Bandy D, Reiman EM, Gold M, Rabiner EA, Matthews PM (2011) Validation and pilot application of [^{18}F]FDG-PET in evaluation of a metabolic therapy for Alzheimer's disease. In *Handbook of Imaging the Alzheimer Brain*, Ashford JW et al., eds. IOS Press, Amsterdam, pp. 627-642.

[7]   Nobili F, De Carli F, Frisoni GB, Portet F, Verhey F, Rodriguez G, Caroli A, Touchon J, Morbelli S, Guerra UP, Dessi B, Brugnolo A, Visser PJ (2011) The Value of SPECT in detecting Alzheimer-type neurodegeneration in mild cognitive impairment. In *Handbook of Imaging the Alzheimer Brain*, Ashford JW et al., eds. IOS Press, Amsterdam, pp. 205-217.

[8]   Mosconi L, Berti V, McHugh P, Pupi A, de Leon MJ (2011) A tale of two tracers: Glucose metabolism and amyloid positron emission tomography imaging in Alzheimer's disease. In *Handbook of Imaging the Alzheimer Brain*, Ashford JW et al., eds. IOS Press, Amsterdam, pp. 219-234.

[9]   Furst AJ, Lal RA (2011) Amyloid-β and glucose metabolism in Alzheimer's disease. In *Handbook of Imaging the Alzheimer Brain*, Ashford JW et al., eds. IOS Press, Amsterdam, pp. 235-246.

[10]   Barthel H, Sabri O (2011) Florbetaben to trace amyloid-β in the Alzheimer brain by means of PET. In *Handbook of Imaging the Alzheimer Brain*, Ashford JW et al., eds. IOS Press, Amsterdam, pp. 247-251.

[11]   Austin BP, Nair VA, Meier TB, Xu G, Rowley HA, Carlsson CM, Johnson SC, Prabhakaran V (2011) Effects of hypoperfusion in Alzheimer's disease. In *Handbook of Imaging the Alzheimer Brain*, Ashford JW et al., eds. IOS Press, Amsterdam, pp. 253-263.

[12]   Shin J, Kepe V, Barrio JR, Small GW (2011) The merits of FDDNP-PET imaging in Alzheimer's disease. In *Handbook of Imaging the Alzheimer Brain*, Ashford JW et al., eds. IOS Press, Amsterdam, pp. 265-275.

[13]   Jensen JR, Cisek K, Funk KE, Naphade S, Schafer KN, Kuret J (2011) Research towards tau imaging. In *Handbook of Imaging the Alzheimer Brain*, Ashford JW et al., eds. IOS Press, Amsterdam, pp. 277-287.

Nuclear Medicine Diagnostic Techniques in the Era of Pathophysiology-Based CSF Biomarkers for Alzheimer's Disease

Markus Weih[a,*], Ümüt Degirmenci[a], Sebastian Kreil[a], Gerald Suttner[a], Daniela Schmidt[b], Johannes Kornhuber[a], Piotr Lewczuk[a] and Torsten Kuwert[b]

[a]*Department for Psychiatry and Psychiatry, University of Erlangen-Nurenberg, Erlangen, Germany*
[b]*Clinic of Nuclear Medicine, University Hospital, University of Erlangen-Nurenberg, Erlangen, Germany*

Abstract. Nuclear medicine techniques were the first functional imaging techniques used to support the clinical diagnosis of Alzheimer's Disease (AD). Perfusion-SPECT allows registration of regional cerebral blood flow (rCBF) which is altered in a characteristic temporal-parietal pattern in AD. Numerous studies have shown the diagnostic value of reduced CBF and metabolic changes using perfusion-SPECT and FDG-PET in AD diagnosis as well as in differential diagnosis against frontotemporal dementia (FTD), dementia with Lewy-Bodies (DLB), and vascular cognitive disorders. This renders perfusion-SPECT an important piece of the puzzle (together with other diagnostic tests) by the clinician is often faced when making a final etiologic dementia diagnosis especially between AD and FTD. A similar diagnostic value can be expected when arterial spin labeling (ASL) MRI sequence is used, but the diagnostic value has yet to be confirmed in lager studies. Recently, more pathophysiology-based biomarkers in CSF and Amyloid-PET tracers have been developed that probably have a higher diagnostic accuracy than the more indirect rCBF changes seen in perfusion-SPECT. In the current review, we describe recent advances in AD biomarkers as well as improvements in the SPECT technique.

INTRODUCTION

Memory problems in elderly patients are common and can be due to a wide range of conditions. Alzheimer's disease (AD) accounts for a large amount of cases, especially when gradual onset and further cognitive problems like aphasia, apraxia or reduced activities of daily life are present. AD has originally been a pathologic diagnosis. The "golden standards" of AD are comprehensive clinical criteria (like NINCDS-ADRDA, DSM-IV or ICD-10). These criteria have been validated against pathology with a wide range of sensitivity (65–100%) and specificity (65–90%) [1]. Thus, during the last decades, imaging and cerebrospinal fluid (CSF) taps were then performed to rule out secondary memory disorders, e. g. due to intracranial mass or infection (like syphilis). As a first approach to in vivo AD imaging, single photon emission computed tomography (SPECT) with perfusion tracers was developed and validated approximately 25 years ago. Perfusion SPECT shows a characteristic (non-vascular) pattern in parietal-temporal cortical areas that indirectly reflect the underlying spatial distribution of neurofibrillary and Amyloid pathology. The coupling of neural activity and glucose metabolism to reduced

*Correspondence to: Markus Weih, Universitätsklinikum Erlangen, Psychiatrische und Psychotherapeutische Klinik, Schwabachanlage 6, 91054 Erlangen, Germany. Tel.: +09131 85 34262; Fax: +09131 85 36002; E-mail: markus.weih@uk-erlangen.de.; Website: www.psych.med.uni-erlangen.de.

Table 1
Nuclear medicine techniques vs. CSF biomarkers in AD

Method	FDG-PET	Perfusion-SPECT	CSF	Amyloid-PET
First publication	Farkas [14]	Launes [2]	Motter [38]	Klunk [26]
Year	1982	1991	1995	2004
Diagnostic accuracy	[15]	[3]	[18, 20]	[27]
Sensitivity	86% (CI: 76–93%)	66% (CI: 62–69%)	80–85%	85–100%
Specificity	86% (CI: 72–93%)	79%(CI: 75–83%)	85–90%	85–100%
Meta-analysis	Yes	Yes	Yes	No
Typical clinical setting	Academic centers	Greater hospitals	Theoretically everywhere	Academic centers
Equipment	Cycloton	Gamma-Camera	ELISA Reader	Zycloton
Cost estimation	>800 EUR	<300 EUR	<200 EUR	>800 EUR
Expertise for result interpretation	High	High	High	High
Treatment options if test positive	MCI: Negative AD: Positive	MCI: Negative AD: Positive DLB: Off-Label FTD: Negative	MCI: Negative AD: Positive	MCI: Negative AD: Positive

CI: 95% Confidence interval. MCI: Mild Cognitive Impairment.

regional cerebral blood flow (rCBF) allowed for the first time real albeit indirect "functional imaging" in neurodegenerative diseases using SPECT and later FDG-PET. More recently, advances in CSF protein assays and the development of specific Amyloid-binding Positron Emission Tomography (PET) tracers allowed direct and pathophysiology-based tests and imaging. Here we would like to review the diagnostic value, accuracy, advantages and disadvantages of perfusion SPECT in comparison to these more advanced CSF and PET biomarkers.

DIAGNOSTIC VALUE OF PERFUSION SPECT

During the last 20 years, numerous studies compared the diagnostic value of perfusion SPECT (mostly ^{99m}Tc-HMPAO) in AD vs. normal volunteers, patients without neurodegenerative dementia (like depression) or other forms of dementia like frontotemporal dementia (FTD), dementia with Lewy-Bodies (DLB) or vascular dementia [2]. Taken together these studies clearly showed added value of SPECT for or against a clinical diagnosis of AD. A comprehensive review of Dougall et al. [3] identified 389 publications on this issue. After exclusion of non-relevant studies using a methodology checklist the authors found 37 studies of clinical AD vs. healthy controls (comprising 1559 subjects) and 13 studies of AD vs. non-demented control patients (1082 patients). The case-control studies with AD patients vs. normal subjects were too het-

erogeneous to compare. The studies of clinical AD vs. non-demented patients showed pooled sensitivities/specificities of 66% and 79% respectively yielding a diagnostic odds ratio of 8.2 [3]. Since the Meta-Analysis was published, further studies, like that of Morinaga have largely confirmed these results and found a sensitivity of 82% [4]. Unfortunately specificity could not be determined in this study due to a lack of a control group. In our own data base, we found sensitivities of 48–60% [5] and a specificity of 77–100% [6]. Comparison of blinded SPECT vs. a pathologically confirmed diagnosis of dementia yielded SPECT sensitivity/specificity of 63–86% and 73–93% [7, 8]. Taken together these results suggest that SPECT has a sensitivity for AD that is most likely below the desired threshold of a valid biomarker, but a high specificity, making SPECT at least a useful diagnostic tool to rule out AD. In Table 1 the individual components of perfusion SPECT are displayed against other techniques.

DIAGNOSTIC VALUE OF PERFUSION MRI

More recently, advanced MRI sequences, originally used by clinicians to detect vascular perfusion defects surrounding the core of diffusion-impaired cerebral ischemia, have been employed as a diagnostic tool in dementia. The main technique is structural MRI, which is now the imaging method of choice in dementia. This offers the opportunity to perform structural and functional imagning in one session. ASL studies have shown that there is also compensatory hyperper-

fusion in AD and FTD [9]. The general principle is selective magnetic spin labeling of an arterial blood volume (arterial spin labeling, ASL), mostly the internal carotid artery at the level of the skull base, proximal to the cortical volumes of interest (for review, see Paiva [10]). This technique was first employed in AD and FTD patients by Johnson et al. 2005 [11]. The main finding in this pilot study was that the ASL technique confirmed the known perfusion deficits in the parietal but also other cortical areas. Hu et al. found a discriminatory value of hyperperfused vs. hypoperfused areas in AD and FTD using ASL MRI [9]. Du et al. were the first to perform a ROC analysis using this technique [12]. For FTD vs. control they found a sensitivity of 71%, a specificity of 76% and an AUC of 0.80. AD vs. control was not examined, but good separation (correct classification in 75%) between FTD and AD was found. Direct comparison of ASL perfusion MRI with ^{15}O-water PET in elderly subjects at risk for AD was performed by Xu et al. [13]. The authors found good overall and regional agreement of the two methods with correlation coefficients between 0.89 and 0.98 in gray matter. Taken together, ASL MRI opens the opportunity to measure lobar perfusion for differential diagnosis of FTD vs. AD during resp. after structural MRI in one session with a similar diagnostic value like perfusion SPECT, but more studies are needed.

COMPARISON OF PERFUSION SPECT AND FDG-PET

The standard radionuclide in clinical PET centers is FDG (^{18}F tagged to deoxyglucose). FDG has long been the traditional method to measure secondary glucose metabolism changes downstream the neurodegenerative process in AD. Since cerebral metabolism and blood flow are coupled, there is a similar pattern of regional disturbed glucose metabolic rates (rCMRGlu) in the temporal-parietal cortex, less in the prefrontal area as mentioned before. The first description appeared in 1982 by Farkas et al. [14]. Since then, many other groups have confirmed the diagnostic value of FDG-PET in AD. In a Meta-Analysis of 15 articles, Patwardhan et al. found a pooled sensitivity of 86% and a specificity of 86% [15]. Direct comparison of both techniques in the same population has been performed in the study of Moninaga [4]. In this single study from a memory clinic population the sensitivity of FDG-PET exceeded that of SPECT (93 vs. 82%).

DIAGNOSTIC VALUE OF CSF-BASED BIOMARKERS

Since the identification of Amyloid Precursor Protein (APP) in AD pathophysiology there have been numerous efforts to find appropriate APP-based CSF tests. However, initial assays measured total Amyloid peptide levels and were not specific enough. After the pioneering work of Motter et al. in 1995 [16] who found a specific reduction of beta-amyloid peptide-42 in CSF, these results were confirmed by many other groups. On average there is a reduction of beta-amyloid peptide-42 of app. 40–50%. The tests have a sensitivity and specificity of 85% or higher, dependent on the clinical setting. Other publications evaluated whether Tau-Pathology is also reflected in CSF changes. CSF levels of the microtubule-associated Tau Protein are typically increased (on average 2.5-fold) in AD and reflect neuronal damage [17]. Data from more than 35 single-center studies comprising more than 2500 AD patients and 1400 controls, meta-analyses and consensus papers [18] are now available. When the specificity is set to 90% (which is a desirable value for biomarkers) total-Tau has a sensitivity of app. 80% [19]). Hyperphosphorylation of Tau (at position Threonine 181, 231 and Serine 199) occurs solely in AD and is therefore theoretically a more specific biomarker. However, studies showed large differences in sensitivity and specificity. A meta-analysis of 51 single-center studies by Mitchell et al. [20] showed a pooled sensitivity of 78% and a specificity of 88% against patients without cognitive impairment. More recently, the different CSF markers have been combined [21] and the interpretation algorithms have been refined [22].

When evaluated in larger multicenter trials in patients with MCI, AD and nondemented patients or healthy subjects, the sensitivity of the combined CSF biomarkers (Amyloid peptide-42 – and Tau markers) to detect AD in MCI patients was then 85–95% and the specificity 72–83% [23, 24]. Other biomarkers like soluble APP are under investigation [25] and need to be validated. It turned out to be a that disadvantage that there are larger than expected interlaboratory discrepancies in CSF biomarker levels [23].

When CSF biomarkers are directly compared to SPECT or FDG-PET, like performed in the work done by Morinaga [4], the sensitivity of CSF exceeded SPECT (94 vs. 82%) and was similar to FDG-PET (93%). However, this interpretation is based on only one study without a control group. Further studies are needed for a better comparison of the two techniques.

COMBINED AMYLOID-AND TAU IMAGING

The Pittsburgh Compound-B (^{11}C - PiB) was the first of a new family of PET tracers that have shown to be of high diagnostic value in AD. Specific binding of brain Amyloid to PiB has been extensively studied in case-control studies and longitudinal observations since 2004 [26]. The area under the curve (AUC) in receiver operator characteristics (ROC) for PiB is around 0.8–0.9 and can be improved to 0.94 when the concept of reserve variables like education, brain volume, gender, physical health and medications are taken into account [27]. The main limitation for ^{11}C-based PET tracers is their short half-life (app. 20 minutes) which restricts their use to dedicated research sites with on-site cyclotrons and radiochemistry labs. ^{18}F –based tracers have a longer half-life (appr. 110 minutes). Since the landmark description of PiB, several papers have reported novel findings in other populations like elderly subjects without dementia [28] or mild dementia [29] which mainly confirmed the diagnostic value and confirmed this tracer as a main diagnostic tool for AD. The first ^{18}F tracer for AD was FDDNP and developed to recognize both plaques and tangles, opening the door for simultaneous Amyloid and Tangle (Tau) imaging. The AUC for global rating of the FDDNP-PET could be up to 1.0 for AD vs. control; 0.95 for MCI vs. control and 0.98 for AD vs. MCI. To our knowledge, PET tracers with specificity only for Tau-Protein are not known. Other studies with ^{18}F-PET markers like Flutemetamol (PiB with ^{18}F) are in phase II clinical studies [30]. Florbetapir (18F-AV-45) is the most widely studied ^{18}F Amyloid imaging agent [31] and could receive official approval as a diagnostic drug within next time by the US Food and Drug Administration (FDA) and other legislative authorities like the European Medicines Agency (EMA). Other compounds like Florbetaben (ClinicalTrial NCT01020838) are in phase III clinical studies. It is expected that the first ^{18}F Amyloid tracers will be approved within the next years.

These promising results suggest that Amyloid-PETs or combined Amyloid-Tau-PETs may have a diagnostic value superior to other imaging tools like perfusion-SPECT, FDG-PET or MRI biomarkers [32] in prevalent AD. Also, Amyloid-PET tracers have been studied in MCI as a tool for early diagnosis but the results need to be validated in independent studies. To date there is no Meta-Analysis about the diagnostic value of Amyloid-PET as a biomarker in AD, which makes direct comparison with other techniques difficult.

DIFFERENTIAL DIAGNOSIS: VASCULAR AND FRONTOTEMPORAL DEMENTIA, DEMENTIA WITH LEWY-BODIES

Although AD is the most prevalent dementia, several other neurodegenerative disorders have to be taken into account by the clinician. Vascular dementia is usually characterized by a past medical history with the presence of typical cardiovascular risk factors (like hypertension, diabetes, smoking, previous stroke, hyperlipidemia, coronary or peripheral artery disease), stepwise deterioration and vascular lesions on MRI or CT. Still, Perfusion SPECT has been used to discriminate vascular from primary neurodegenerative dementia. According to the Meta-Analysis of Dougall et al., the pooled weighted sensitivity and specificity against AD is 71% resp. 76% [3]. Using clinical features alone, the differential diagnosis of frontotemporal dementia (FTD) and Dementia with Lewy-Bodies (DLB) vs. AD is sometimes difficult. FTD is a heterogeneous disease and in contrast to AD no established specific and validated biomarkers are available. In the above mentioned review of Dougall from 2004 [3], the authors found a pooled sensitivity and specificity of SPECT for discriminating AD from FTD of 72% and 78%, respectively. The diagnostic odds ratio was 8.4 and is in the same range as that for AD vs. control. In pathologically confirmed FTD cases, McNeill et al. found a sensitivity of bilateral frontal lobe CBF reduction of 80% and a specificity of 81% vs. AD [33]. In a larger sample of FTD patients, Mendez et al. found a sensitivity/specificity of 91% and 75% and a negative predictive value of 90% [34]. These results suggest that SPECT provides useful additional information in discriminating AD from FTD. Since extracellular plaque deposition is more specific for AD and usually absent in FTD, Amyloid-PET will probably be of additional value in diagnostic workup of clinical difficult cases. Some patients with Dementia with Lewy bodies (DLB) have prominent cognitive deficits, but MRI usually shows not the characteristic global atrophy as seen in AD. Here several nuclear medicine techniques may be of advantage like assessment of occipital hypoperfusion alone [35] or in combination with MRI [36]. If symptoms of Parkinson's disease are predominant in DLB, Iodine-123 FP-CIT SPECT is of diagnostic value [37].

The characteristic sympathetic denervation in DLB can be assessed using Iodine-123-MIBG in a very specific manner [35]. Given the fact that SPECT scanners are available in many larger hospitals, the differential diagnosis of FTD and DLB against AD with SPECT is feasible and clinical relevant, since antidementive drugs like cholinesterase-inhibitors are unlikely to be of therapeutic benefit in FTD, but are approved for AD, Parkinson's disease dementia (PDD) and are beneficial in DLB (positive therapeutic studies, but off-label use).

TECHNICAL IMPROVEMENTS

The image acquisition technique in SPECT is prone to signal degradation due to different physical phenomena like depth-dependent blurring, photon attenuation and scattering. Technical limitations in the past made iterative image reconstruction necessary [39]. Traditionally, SPECT images are subjective, similar to other visualizing techniques like MRI or CT, inferring bias due to differences in expertise of image interpretation. Large improvements have been achieved in the past decade after the development of objective resp. semiquantitating software like the Minoshima package [40] or rapid statistical parametric mapping (SPM[41]). In recent years, coregistration of SPECT/PET and structural imaging has led to considerable advances. Hybrid SPECT/CT devices allow simultaneous registration of anatomy and function and take advantage of optimized, fast imaging reconstruction hard- and software. These advances now allow improved calibration and quantification of SPECT/PET images. The coregistration of SPECT/PET images with structural imaging and advances in automated anatomical labeling (AAL) opened the possibility to identify voxels of interest (VOI) which increases the originally limited spatial resolution of SPECT ultimately leading to better discrimination of AD patients. In addition, Pagani [42] as well as Merhof [43] have recently shown that rCBF patterns together with anatomical information can be subjected to principal component analysis (PCA) resp. multivariate analysis, which allows to draw further conclusion about disturbed functional connectivity between brain regions in dementia. Perfusion imaging using arterial spin labeling MRI (ASL-MRI) is a standard technique in cerebrovascular disease and has been applied to AD diagnosis and differential diagnosis to FTD with promising results [9, 44] but the exact diagnostic value parameters like sensitivity, specificity have to be delineated in detail in inde-

pendent studies. Imaging of neuroinflammation resp. cerebral macrophages using ^{11}C-(R)-PK11195 – PET is an other interesting finding already observed in 2001 [45] but recent studies showed limited sensitivity [46].

AREAS OF UNCERTAINTY

It is still unclear whether the "AD-pattern" in perfusion SPECT merely reflects cortical neurodegeneration or the secondary cholinergic deficit following degeneration of the basal nucleus of Meynert. Studies that both investigated CSF biomarkers and SPECT showed no correlation [6, 47]. Simultaneous registration of the cholinergic deficit (e. g. using Nicotinic 123I-5IA-85380 SPECT [48]) and perfusion SPECT or Amyloid-PET with perfusion SPECT could help to resolve this issue. In perfusion SPECT usually lobar hypoperfusion is registrated, but there are also hyperperfused areas. Possible underlying mechanisms are partial deafferentation or a cognitive reserve mechanism. It would be interesting to confirm these results in perfusion SPECT resp. to explore the diagnostic value of hyperperfusion in correlation to reserve variables.

CONCLUSIONS

Perfusion-SPECT and FDG-PET were the first method of "functional metabolic" brain imaging in Alzheimer's disease showing hypoperfusion in the temporal-parietal regions with the highest load with plaques and tangles in post mortem brains with AD. This has lead to a widespread use of perfusion SPECT and FDG-PET as a diagnostic tool in AD. Since specificity exceeds sensitivity the diagnostic value of perfusion SPECT to rule out AD usually is higher than to confirm it. However, accuracy of any diagnostic tool is critically dependent on disease severity and the population under investigation. In addition, perfusion SPECT is useful in discriminating vascular dementia, FTD and DLB in the absence of validated specific biomarkers for these conditions. More recently pathophysiology-based CSF-biomarkers, especially Beta-Amyloid peptide-42 and Tau protein have been investigated with a diagnostic accuracy that seems to be superior to perfusion SPECT and FDG-PET. In addition, due to their direct reflection of the underlying process, CSF biomarkers (alone or in combination) are also suited for early diagnosis, e.g. in patients with MCI, where the diagnostic value for SPECT is lower than in prevalent AD.

In contrast to CSF assays, PET biomarkers have the advantage of showing the anatomic distribution of pathology and were first available for amyloid plaques (^{11}C PiB). Now, there is development of longer-lasting ^{18}F PET tracers as well first evidence that plaques and tangles can be imaged with a single PET compound, but the results have to be confirmed in independent studies.

REFERENCES

[1] Knopman D, DeKosky S, Cummings J, Chui H, Corey-Bloom J, Relkin N, Small G, Miller B, Stevens J (2001) Practice parameter: diagnosis of dementia (an evidence-based review). Report of the Quality Standards Subcommittee of the American Academy of Neurology. *Neurology* **56**, 1143-1153.

[2] Launes J, Sulkava R, Erkinjuntti T, Nikkinen P, Lindroth L, Liewendahl K, Iivanainen M (1991) 99Tcm-HMPAO SPECT in suspected dementia. *Nucl Med Commun* **12**, 757-765.

[3] Dougall NJ, Bruggink S, Ebmeier KP (2004) Systematic review of the diagnostic accuracy of 99mTc-HMPAO-SPECT in dementia. *Am J Geriatr Psychiatry* **12**, 554-570.

[4] Morinaga A, Ono K, Ikeda T, Ikeda Y, Shima K, Noguchi-Shinohara M, Samuraki M, Yanase D, Yoshita M, Iwasa K, Mastunari I, Yamada M (2010) A comparison of the diagnostic sensitivity of MRI, CBF-SPECT, FDG-PET and cerebrospinal fluid biomarkers for detecting Alzheimer's disease in a memory clinic. *Dement Geriatr Cogn Disord* **30**, 285-292.

[5] Weih M, Krinninger M, Zimmermann R, Lewczuk P, Svitek J, Schaller G, Degirmenci U, Richter-Schmidinger T, Wiltfang J, Kuwert T, Kornhuber J, Schmidt D (2009) Sensitivität der neurochemischen Demenzdiagnostik im Liquor im Vergleich zur 99mTc-SPECT bei Alzheimer Demenz. *Fortschr Neurol Psychiatr* **77**, 407-411.

[6] Schmidt D, Zimmermann R, Lewczuk P, Schaller G, Degirmenci U, Kreil S, Wiltfang J, Kuwert T, Kornhuber J, Weih M (2010) Confirmation rate of blinded (99 m)Tc-SPECT compared to neurochemical dementia biomarkers in CSF in patients with Alzheimer disease. *J Neural Transm* **117**, 1111-1114.

[7] Bonte FJ, Weiner MF, Bigio EH, White CL 3rd (1997) Brain blood flow in the dementias: SPECT with histopathologic correlation in 54 patients. *Radiology* **202**, 793-797.

[8] Jagust W, Thisted R, Devous MD Sr, Van Heertum R, Mayberg H, Jobst K, Smith AD, Borys N (2001) SPECT perfusion imaging in the diagnosis of Alzheimer's disease: a clinical-pathologic study. *Neurology* **56**, 950-956.

[9] Hu WT, Wang Z, Lee VM, Trojanowski JQ, Detre JA, Grossman M (2010) Distinct cerebral perfusion patterns in FTLD and AD. *Neurology* **75**, 881-888.

[10] Paiva FF, Tannus A, Silva AC (2007) Measurement of cerebral perfusion territories using arterial spin labelling. *NMR Biomed* **20**, 633-642.

[11] Johnson NA, Jahng GH, Weiner MW, Miller BL, Chui HC, Jagust WJ, Gorno-Tempini ML, Schuff N (2005) Pattern of cerebral hypoperfusion in Alzheimer disease and mild cognitive impairment measured with arterial spin-labeling MR imaging: initial experience. *Radiology* **234**, 851-859.

[12] Du AT, Jahng GH, Hayasaka S, Kramer JH, Rosen HJ, Gorno-Tempini ML, Rankin KP, Miller BL, Weiner MW, Schuff N (2006) Hypoperfusion in frontotemporal dementia and Alzheimer disease by arterial spin labeling MRI. *Neurology* **67**, 1215-1220.

[13] Xu G, Rowley HA, Wu G, Alsop DC, Shankaranarayanan A, Dowling M, Christian BT, Oakes TR, Johnson SC (2010) Reliability and precision of pseudo-continuous arterial spin labeling perfusion MRI on 3.0 T and comparison with 15O-water PET in elderly subjects at risk for Alzheimer's disease. *NMR Biomed* **23**, 286-293.

[14] Farkas T, Ferris SH, Wolf AP, De Leon MJ, Christman DR, Reisberg B, Alavi A, Fowler JS, George AE, Reivich M (1982) ^{18}F-2-deoxy-2-fluoro-D-glucose as a tracer in the positron emission tomographic study of senile dementia. *Am J Psychiatry* **139**, 352-353.

[15] Patwardhan MB, McCrory DC, Matchar DB, Samsa GP, Rutschmann OT (2004) Alzheimer disease: operating characteristics of PET–a meta-analysis. *Radiology* **231**, 73-80.

[16] Motter R, Vigo-Pelfrey C, Kholodenko D, Barbour R, Johnson-Wood K, Galasko D, Chang L, Miller B, Clark C, Green R (1995) Reduction of beta-amyloid peptide42 in the cerebrospinal fluid of patients with Alzheimer's disease. *Ann Neurol* **38**, 643-648.

[17] Lewczuk P, Esselmann H, Bibl M, Beck G, Maler JM, Otto M, Kornhuber J, Wiltfang J (2004) Tau protein phosphorylated at threonine 181 in CSF as a neurochemical biomarker in Alzheimer's disease: original data and review of the literature. *J Mol Neurosci* **23**, 115-122.

[18] Wiltfang J, Lewczuk P, Riederer P, Grunblatt E, Hock C, Scheltens P, Hampel H, Vanderstichele H, Iqbal K, Galasko D, Lannfelt L, Otto M, Esselmann H, Henkel AW, Kornhuber J, Blennow K (2005) Consensus paper of the WFSBP Task Force on Biological Markers of Dementia: the role of CSF and blood analysis in the early and differential diagnosis of dementia. *World J Biol Psychiatry* **6**, 69-84.

[19] Blennow K, Hampel H (2003) CSF markers for incipient Alzheimer's disease. *Lancet Neurol* **2**, 605-613.

[20] Mitchell A (2009) CSF phosphorylated tau in the diagnosis and prognosis of mild cognitive impairment and Alzheimer's disease: a meta-analysis of 51 studies. *J Neurol Neurosurg Psychiatry* **80**, 966-975.

[21] Lewczuk P, Esselmann H, Otto M, Maler JM, Henkel AW, Henkel MK, Eikenberg O, Antz C, Krause WR, Reulbach U, Kornhuber J, Wiltfang J (2004) Neurochemical diagnosis of Alzheimer's dementia by CSF Abeta42, Abeta42/Abeta40 ratio and total tau. *Neurobiol Aging* **25**, 273-281.

[22] Lewczuk P, Zimmermann R, Wiltfang J, Kornhuber J (2009) Neurochemical dementia diagnostics: a simple algorithm for interpretation of the CSF biomarkers. *J Neural Transm* **116**, 1163-1167.

[23] Mattsson N, Zetterberg H, Hansson O, Andreasen N, Parnetti L, Jonsson M, Herukka S, van der Flier W, Blankenstein M, Ewers M, Rich K, Kaiser E, Verbeek M, Tsolaki M, Mulugeta E, Rosén E, Aarsland D, Visser P, Schröder J, Marcusson J, de Leon M, Hampel H, Scheltens P, Pirttilä T, Wallin A, Jönhagen M, Minthon L, Winblad B, Blennow K (2009) CSF biomarkers and incipient Alzheimer disease in patients with mild cognitive impairment. *JAMA* **302**, 385-393.

[24] Hansson O, Zetterberg H, Buchhave P, Londos E, Blennow K, Minthon L (2006) Association between CSF biomarkers and incipient Alzheimer's disease in patients with mild cognitive impairment: a follow-up study. *Lancet Neurol* **5**, 228-234.

[25] Lewczuk P, Kamrowski-Kruck H, Peters O, Heuser I, Jessen F, Popp J, Burger K, Hampel H, Frolich L, Wolf S, Prinz B, Jahn H, Luckhaus C, Perneczky R, Hull M, Schroder J, Kessler H, Pantel J, Gertz HJ, Klafki HW, Kolsch H, Reulbach U, Esselmann H, Maler JM, Bibl M, Kornhuber J, Wiltfang J (2010) Soluble amyloid precursor proteins in the cerebrospinal fluid as novel potential biomarkers of Alzheimer's disease: a multicenter study. *Mol Psychiatry* **15**, 138-145.

[26] Klunk W, Engler H, Nordberg A, Wang Y, Blomqvist G, Holt D, Bergström M, Savitcheva I, Huang G, Estrada S, Ausén B, Debnath M, Barletta J, Price J, Sandell J, Lopresti B, Wall A, Koivisto P, Antoni G, Mathis C, Långström B (2004) Imaging brain amyloid in Alzheimer's disease with Pittsburgh Compound-B. *Ann Neurol* **55**, 306-319.

[27] Roe C, Mintun M, Ghoshal N, Williams M, Grant E, Marcus D, Morris J (2010) Alzheimer disease identification using amyloid imaging and reserve variables: proof of concept. *Neurology* **75**, 42-48.

[28] Bourgeat P, Chetelat G, Villemagne VL, Fripp J, Raniga P, Pike K, Acosta O, Szoeke C, Ourselin S, Ames D, Ellis KA, Martins RN, Masters CL, Rowe CC, Salvado O (2010) Beta-amyloid burden in the temporal neocortex is related to hippocampal atrophy in elderly subjects without dementia. *Neurology* **74**, 121-127.

[29] Morris JC, Roe CM, Grant EA, Head D, Storandt M, Goate AM, Fagan AM, Holtzman DM, Mintun MA (2009) Pittsburgh compound B imaging and prediction of progression from cognitive normality to symptomatic Alzheimer disease. *Arch Neurol* **66**, 1469-1475.

[30] Vandenberghe R, Van Laere K, Ivanoiu A, Salmon E, Bastin C, Triau E, Hasselbalch S, Law I, Andersen A, Korner A, Minthon L, Garraux G, Nelissen N, Bormans G, Buckley C, Owenius R, Thurfjell L, Farrar G, Brooks DJ (2010) 18F-flutemetamol amyloid imaging in Alzheimer disease and mild cognitive impairment: a phase 2 trial. *Ann Neurol* **68**, 319-329.

[31] Vardy ER, Langheinrich T, Hinz R, Snowden JS, Gerhard A, Richardson AM, Neary D, Anton J, Brown GD, Herholz K (2010) POD14 Amyloid PET using 18F-AV-45 in Alzheimer's disease and frontotemporal dementia: first UK results. *J Neurol Neurosurg Psychiatry* **81**, e45.

[32] Small GW, Kepe V, Ercoli LM, Siddarth P, Bookheimer SY, Miller KJ, Lavretsky H, Burggren AC, Cole GM, Vinters HV, Thompson PM, Huang SC, Satyamurthy N, Phelps ME, Barrio JR (2006) PET of brain amyloid and tau in mild cognitive impairment. *N Engl J Med* **355**, 2652-2663.

[33] McNeill R, Sare GM, Manoharan M, Testa HJ, Mann DM, Neary D, Snowden JS, Varma AR (2007) Accuracy of single-photon emission computed tomography in differentiating frontotemporal dementia from Alzheimer's disease. *J Neurol Neurosurg Psychiatry* **78**, 350-355.

[34] Mendez MF, Shapira JS, McMurtray A, Licht E, Miller BL (2007) Accuracy of the clinical evaluation for frontotemporal dementia. *Arch Neurol* **64**, 830-835.

[35] Shimizu S, Hanyu H, Kanetaka H, Iwamoto T, Koizumi K, Abe K (2005) Differentiation of dementia with Lewy bodies from Alzheimer's disease using brain SPECT. *Dement Geriatr Cogn Disord* **20**, 25-30.

[36] Goto H, Ishii K, Uemura T, Miyamoto N, Yoshikawa T, Shimada K, Ohkawa S (2010) Differential diagnosis of dementia with Lewy bodies and Alzheimer disease using combined MR imaging and brain perfusion single-photon emission tomography. *AJNR Am J Neuroradiol* **31**, 720-725.

[37] Tissingh G, Booij J, Bergmans P, Winogrodzka A, Janssen AG, van Royen EA, Stoof JC, Wolters EC (1998) Iodine-123-N-omega-fluoropropyl-2beta-carbomethoxy-3beta-(4-iod ophenyl)tropane SPECT in healthy controls and early-stage, drug-naive Parkinson's disease. *J Nucl Med* **39**, 1143-1148.

[38] Motter R, Vigo-Pelfrey C, Kholodenko D, Barbour R, Johnson-Wood K, Galasko D, Chang L, Miller B, Clark C, Green R et al. (1995) Reduction of beta-amyloid peptide42 in the cerebrospinal fluid of patients with Alzheimer's disease. *Ann Neurol* **38**, 643-648.

[39] Zeintl J, Vija AH, Yahil A, Hornegger J, Kuwert T (2010) Quantitative accuracy of clinical 99mTc SPECT/CT using ordered-subset expectation maximization with 3-dimensional resolution recovery, attenuation, and scatter correction. *J Nucl Med* **51**, 921-928.

[40] Bartenstein P, Minoshima S, Hirsch C, Buch K, Willoch F, Mosch D, Schad D, Schwaiger M, Kurz A (1997) Quantitative assessment of cerebral blood flow in patients with Alzheimer's disease by SPECT. *J Nucl Med* **38**, 1095-1101.

[41] Signorini M, Paulesu E, Friston K, Perani D, Colleluori A, Lucignani G, Grassi F, Bettinardi V, Frackowiak RS, Fazio F (1999) Rapid assessment of regional cerebral metabolic abnormalities in single subjects with quantitative and non-quantitative [18F]FDG PET: A clinical validation of statistical parametric mapping. *Neuroimage* **9**, 63-80.

[42] Pagani M, Salmaso D, Rodriguez G, Nardo D, Nobili F (2009) Principal component analysis in mild and moderate Alzheimer's disease–a novel approach to clinical diagnosis. *Psychiatry Res* **173**, 8-14.

[43] Merhof D, Markiewicz PJ, Platsch G, Declerck J, Weih M, Kornhuber J, Kuwert T, Matthews JC, Herholz K (2010) Optimized data preprocessing for multivariate analysis applied to (99 m)Tc-ECD SPECT data sets of Alzheimer's patients and asymptomatic controls. *J Cereb Blood Flow Metab*.

[44] Luckhaus C, Cohnen M, Fluss MO, Janner M, Grass-Kapanke B, Teipel SJ, Grothe M, Hampel H, Peters O, Kornhuber J, Maier W, Supprian T, Gaebel W, Modder U, Wittsack HJ (2010) The relation of regional cerebral perfusion and atrophy in mild cognitive impairment (MCI) and early Alzheimer's dementia. *Psychiatry Res* **183**, 44-51.

[45] Cagnin A, Brooks DJ, Kennedy AM, Gunn RN, Myers R, Turkheimer FE, Jones T, Banati RB (2001) In-vivo measurement of activated microglia in dementia. *Lancet* **358**, 461-467.

[46] Wiley CA, Lopresti BJ, Venneti S, Price J, Klunk WE, DeKosky ST, Mathis CA (2009) Carbon 11-labeled Pittsburgh Compound B and carbon 11-labeled (R)-PK11195 positron emission tomographic imaging in Alzheimer disease. *Arch Neurol* **66**, 60-67.

[47] Tsolaki M, Sakka V, Gerasimou G, Dimacopoulos N, Chatzizisi O, Fountoulakis KN, Kyriazis G, Papanastasiou J, Kazis A (2001) Correlation of rCBF (SPECT), CSF tau, and cognitive function in patients with dementia of the Alzheimer's type, other types of dementia, and control subjects. *Am J Alzheimers Dis Other Dement* **16**, 21-31.

[48] Colloby SJ, Perry EK, Pakrasi S, Pimlott SL, Wyper DJ, McKeith IG, Williams ED, O'Brien JT (2010) Nicotinic 123I-5IA-85380 single photon emission computed tomography as a predictor of cognitive progression in Alzheimer's disease and dementia with Lewy bodies. *Am J Geriatr Psychiatry* **18**, 86-90.

This page intentionally left blank

Unawareness of Cognitive and Behavioral Deficits in Alzheimer's Disease may be reflected by Perfusion SPECT

Fereshteh Sedaghat[a,b,*] and Stavros J. Baloyannis[b]

[a]*Nuclear Medicine Research Center, Mashhad University of Medical Sciences, Mashhad, Iran*
[b]*1st Department of Neurology, Aristotle University of Thessaloniki, Thessaloniki, Greece*

Abstract. Unawareness of the disease or anosognosia is a common symptom among many neuropsychiatric patients and may affect the quality of life and treatment compliance in patients suffering from AD and make them to behave unsafely. Although generalized cognitive impairment may be a prerequisite for anosognosia in dementia, not all patients with cognitive impairment, present anosognosia. Deficit in regional cerebral blood flow (rCBF) can be seen in different brain regions in dementia with a typical posterior temporoparietal defect in patients with Alzheimer's disease. Although functional brain imaging methods such as single photon emission computed tomography (SPECT) have relatively limited spatial resolution, they offer the potential advantage of being able to assess functional connectivity patterns, associated with neural networks involved in awareness. We try to determine the brain regions that contributed to unawareness in patients with Alzheimer's disease, using SPECT. This study will focus on awareness deficits in cognitive and behavioral domains, rather than personality.

Keywords: Brain SPECT, Alzheimer, unawareness, right parietal, right prefrontal

INTRODUCTION

Unawareness of cognitive and functional deficit is a common symptom among many neuropsychiatric patients. Usually the frequency of the symptom increases with the progression of the disease. Different terms have been used to describe the phenomena as, lack of insight, unawareness of disease and anosognosia [1, 2].

Anosognosia comes from the Greek, nosos (illness) and gnosis (knowledge), a term named by the neurologist Joseph Babinski in 1914 [3] and is defined as a lack of awareness or denial of a neurologic defect or illness in general.

Regional cerebral blood flow (rCBF) impairment is seen in posterior temporoparietal regions of patients with AD [4].

We studied a group of AD, in mild and moderate stages of dementia as we hypothesized that a deficit in neuronal function, for instance potential pathological involvement of neural network in some regions, may contribute for unawareness in AD.

PATIENTS AND METHODS

Forty-two patients in mild or moderate stage of AD dementia based on NINCDS-ADRDA criteria, are included in the study. The Hachinski's ischemic score of 7 or more was used to exclude patients with vascular pathogenesis of dementia from primary neurodegener-

*Correspondence to: Fereshteh Sedaghat, MD, PhD, E-mail: fereshsedag@yahoo.com.

ative dementia and all the patients underwent CT scan and then if needed MRI and patients with stroke were excluded. Cornell Scale for Depression in Dementia (CSDD) was used to exclude patients with symptoms of depression. Clinical Dementia Rating (CDR) scale and Mini mental State exam (MMSE) were done for all the patients to determine the severity of dementia. MMSE score of ≥ 20 was considered as mild and MMSE score of 10–19 as moderate stage of dementia. The patients with a MMSE of 20–26 (cut-off scores for mild stage) underwent also Short performance test, Syndrom-Kurz Test (SKT) and frontal assessment battery (FAB) test. All the patients had undergone brain SPECT using HMPAO as one of our routine examinations for confirming different types of dementias. SPECT images of our patients showed bilateral posterior temporoparietal hypoperfusion with or without prefrontal hypoperfusion, which is the characteristic image for AD.

After clinical interviews (at least 2 visits) with patients and their relatives by the same interviewer for all the patients, the patients were divided into two groups:

I) Anosognosia: consisted of 22 patients (mean age 74 ± 7 y) (mean MMSE 18 ± 4) (9 mild stage, 13 moderate stage), who were not aware of their deficit in cognitive and/or functional domains, at least after two consecutive interviews.

II) No anosognosia: including 20 patients (mean age 73 ± 4 y) (mean MMSE 21 ± 4) (12 mild stage, 8 moderate), who had full awareness of their disorder in cognitive and also functional domains (Table 1).

The diagnosis of anosognosia was based on a non-structured interview with the patients and his/her relatives about their cognitive function and the instrumental activities of daily living and functional changes of the patient, in at least 2 consecutive visits which was confirmed by follow- up of the patients too. Any denial of cognitive or functional impairment in at least 2 consecutive visits of the patient was established as our cut-off decision for diagnosing anosognosia. Only the patients with spontaneous complaint or the ones, who agreed when questioned, were categorized in No-anosognosia group.

To compare the effect of severity of dementia in our results we also categorized the patients in four following subgroups:

a) Mild AD with Anosognosia, b) Moderate AD with Anosognosia c) Mild AD and No-anosognosia, d) Moderate AD and No-anosognosia

The patients had undergone brain SPECT after intravenously injection of 555 MBq of $^{99\,m}$Tc-HMPAO, in a quiet and bright room with patient's eyes opened. Each patient had an IV line at least 15 minutes before the injection of the agent.

Images were acquired after 45 minutes of injection using a single headed ADAC gamma camera equipped with a low-energy-high-resolution (LEHR) collimator. The patient was in a supine position with his head stabled with a special belt, if indicated. The total acquisition consisted of 120 projections acquired for 20 seconds into a 128×128-acquisition matrix. The count rate was more than 5 million for every image. The images were processed on a Sun Pegasys computer and were reconstructed with Butterworth filter back projection. Slices were generated parallel to the orbitomeatal line.

The attenuation correction based on Chang's method and reorientations were done on reconstructed brain images. The images were visually evaluated for their perfusion pattern and then a region of interest (ROI) accounting for blood flow (rCBF) was drawn above the whole cerebellum (CER) and ROIs with the size of 5×5 pixels were used to measure the mean count, in the following regions: right and left prefrontal cortex (RPF, LPF), frontal (RF, LF), superior parietal (RSP,LSP), inferior parietal (RIP, LIP), medial

Table 1

Mean age, MMSE score, number and gender of our patients in our four subgroups of Mild-AD-Anosognosia, Moderate-AD-Anosognosia, Mild-AD-No-anosognosia and Moderate-AD-No-anosognosia

	Subgroups data			
	Mild AD-Anosog ($N = 9$) ($M = 2, F = 7$) Mean $\pm$ SD	Mod-AD-Anosog($N = 13$) ($M = 7, F = 6$) Mean $\pm$ SD	Mild-AD-No-anosog ($N = 12$) ($M = 4, F = 8$) Mean $\pm$ SD	Mod-AD-No-anosog ($N = 8$) ($M = 2, F = 6$) Mean $\pm$ SD
Age	74 ± 5	73 ± 8	72 ± 4	74 ± 4
MMSE	22 ± 2	14 ± 2	24 ± 2	16 ± 2

Table 2
Significant correlation between MMSE and rCBF in right prefrontal, left frontal and medial temporal regions was found. No correlation of MMSE score with right inferior parietal perfusion was observed

Correlation		RPF	RF	RIP	RMT	LMT
MMSE	Pearson Correlation	0.230	0.086	0.261	0.476(**)	0.650(**)
	Sig. (2-tailed)	0.143	0.587	0.094	0.001	0.000
	N	42	42	42	42	42

** Correlation is significant at the 0.01 level.

and lateral temporal (RMT, RLT, LMT, LLT), occipital (RO, LO) and posterior cingulate gyros (PC). The coronal slices were used to study the temporal lobes and transverse slices for studying the other regions. Semiquantitative regional cerebral blood flow (rCBF) analysis using cortex to cerebellum ratio was done.

The results of CBF were compared in two groups of anosognosia and no-anosognosia and also were compared in our 4 subgroups of mild AD-Anosognosia with mild AD-No anosognosia and moderate AD-Anosognosia with moderate AD-No anosognosia to study the effect of severity of the disease in our results. The correlation between MMSE and CBF in these regions was studied in our patients too.

Data were analyzed using the Statistical Package for Social Sciences (SPSS for windows, version 15, Inc SPSS, 2006). Variables were tested for normality of distribution using the Kolmogorov-Smirnov test. T test for independent samples was used to compare the mean values and Pearson correlation for evaluating different correlations.

RESULTS

Anosognosia group significantly differed from No-anosognosia group in rCBF in right prefrontal ($P \leq 0.02$), right inferior parietal ($P \leq 0.00$), right ($P \leq 0.01$) and left medial temporal cortex ($P \leq 0.01$) and also in MMSE score ($P \leq 0.01$) (Fig. 1).

Mild-AD-Anosognosia (subgroup a) was compared with mild-AD-No-anosognosia (subgroup c) and statistically significant difference of mean rCBF, in right prefrontal ($p \leq 0.002$), right frontal ($p \leq 0.002$) and right inferior parietal ($p \leq 0.000$) regions was found. Also comparison was made between moderate-AD-Anosognosia (subgroup b) with Moderate AD-No-anosognosia (subgroup d) and statistically significant difference in rCBF only in right inferior parietal region ($p \leq 0.002$) was found (Fig. 2). There was a significant correlation between MMSE score and rCBF in medial temporal regions in our patients but not with right prefrontal, frontal and right inferior parietal regions (Fig. 3). Patients with mild AD differed significantly from moderate AD in rCBF of left frontal ($p \leq 0.01$), right and left prefrontal ($p \leq 0.001$, $p \leq 0.04$ respectively), right and left superior parietal($p \leq 0.04$), right and left medial ($p \leq 0.02$, $p \leq 0.00$) and lateral temporal($p \leq 0.02$, $p \leq 0.01$), left occipital ($p \leq 0.04$) and posterior cingulate ($p \leq 0.04$) regions.
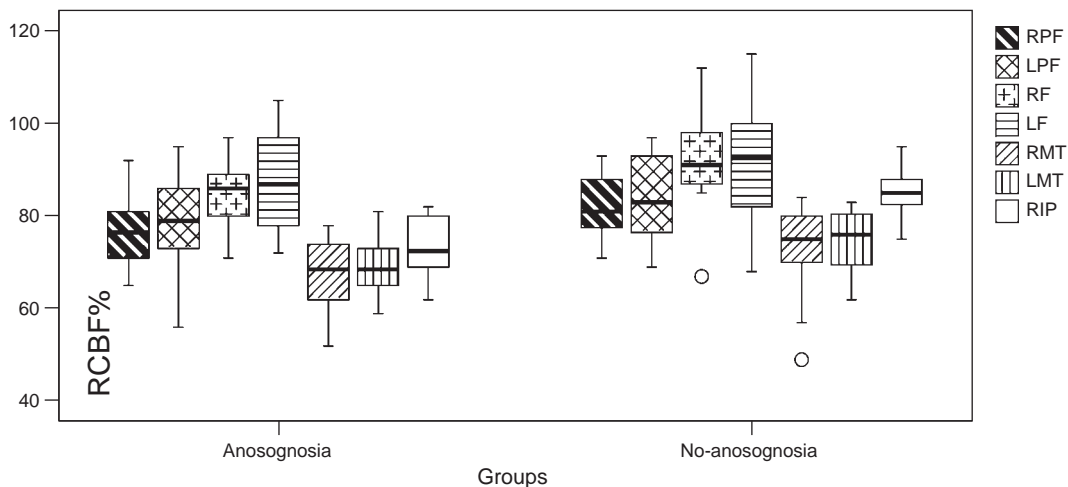
Fig. 1. Median, inter-quartile range and outliers for regional cerebral blood flow (rCBF%) in right and left prefrontal (RPF, LPF), right and left frontal (RF, LF),medial temporal (RMT, LMT) and right inferior parietal(RIP) regions in Anosognosia and No-anosognosia groups.
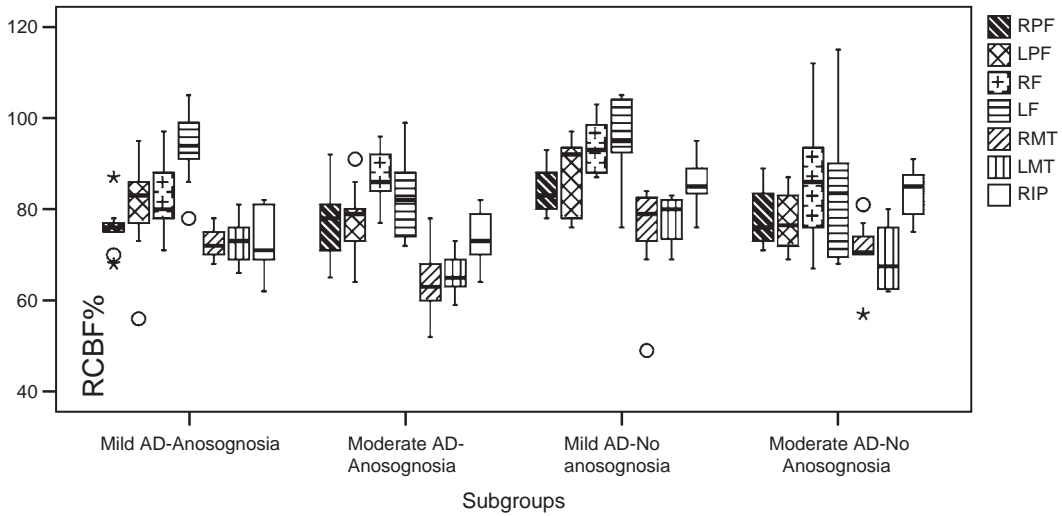
Fig. 2. Regional cerebral blood flow (rCBF%) in right and prefrontal (RPF, LPF), right and left frontal (RF, LF), medial temporal (RMT, LMT) and right inferior parietal(RIP) in our four subgroups of Mild-AD-Anosognosia, Moderate-AD-Anosognosia, Mild-AD-No-anosognosia and Moderate-AD-No-anosognosia. Box plots show median, inter-quartile range and outliers for rCBF% in these four groups. CBF in RIP dose not differ significantly regarding the severity of the disease but regarding the anosognosia status.
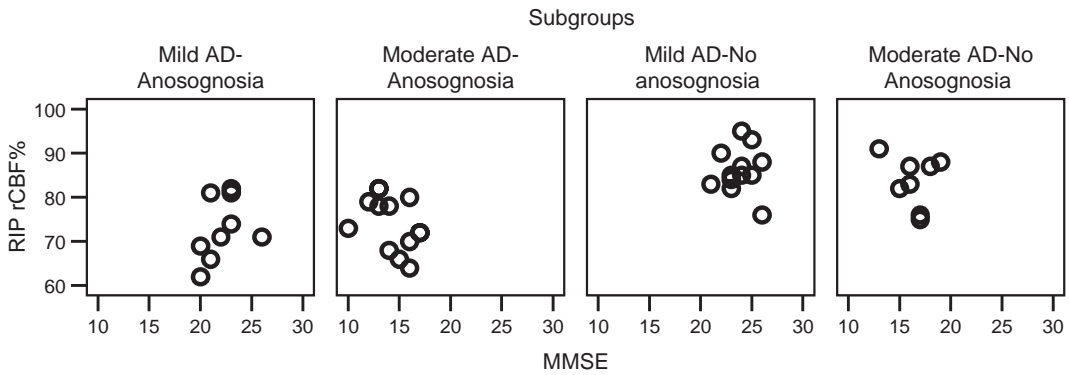
Fig. 3. Dots show the mean value of rCBF% in right inferior parietal (RIP) in correlation with mean MMSE score of our patients in four subgroups.

Groups didn't differ significantly with regard to age or educational level.

DISCUSSION

Specific patterns of hypoperfusion have been correlated with unawareness in AD in previous studies. A correlation of hypoperfusion in right frontal lobe with unawareness was found in AD by Reed et al. (1993) and Starkstein et al. (1995) [5, 6]. Derouesn et al. (1999) reported that awareness of the deficit was correlated with overall frontal rCBF [7]. In a study by Vogel et al. (2005) the ROIs were selected above

the frontal region in patients with mild AD and mild cognitive impairment (MCI), and they used a categorical four-point scale for anosognosia. They found a significant correlation between rCBF in right and left frontal gyros and unawareness [8]. Shibata et al. (2008) in a study using I-123-IMP and SPECT in patients with Alzheimer's disease reported a significant association between anosognosia and decreased perfusion in the orbitofrontal cortex and suggested that the orbitofrontal cortex specifically associates with anosognosia in AD [9].

In these studies bilateral frontal or only right frontal regions are considered to be associated with anosognosia in Alzheimer's disease which are partly

consistent with our results. Methodological differences and also the use of different groups of patients may be the main reasons for achieving different results. The advantage of our study is the measuring of rCBF in different regions of the brain, in mild and moderate stage of AD.

Ott et al. (1996) reported that impaired insight was correlated to right temporoparietal hypoperfusion [10]. A study which had done comparison between patients with frontotemporal dementia (FTD) and AD, reported that patients with AD seems to exhibit smaller but significant changes in personality. They are often more introverted and neurotic, less socially dominant and conscientious [11]. On the other hand, AD patients were found to be more markedly unaware of their cognitive and functional deficit in comparison with vascular dementia patients [12].

Still the etiology, clinical correlates, and prognostic value of anosognosia are unclear. Some authors have proposed that unawareness is part of a defensive mechanism that would protect demented patients from depressive feelings while other authors have proposed that anosognosia may result from dysfunction in specific brain areas [13].

Migliorelli et al. (2005) reported that patients with anosognosia showed significantly longer duration of illness, more severe cognitive impairments and deficits in activities of daily living, and higher mania and pathological laughing scores than AD patients without anosognosia and suggested that anosognosia in AD may be part of a specific neuropsychiatric syndrome [14].

Patients unaware of their cognitive deficits were more cognitively impaired, as measured by the Mini-Mental State Examination, and had a specific defect in frontal/executive functions. The presence of major depression, delusion and hallucination was reported to be more among patients who were unaware of their cognitive impairment than those who were aware [15]. Some authors suggest that anosognosia in Alzheimer's disease is not related to the degree of cognitive deterioration but results, at least in part, from frontal dysfunction [16]. A high discrepancy score between patient's and caregiver's assessment of cognitive functions has been related to impaired activity in the superior frontal sulcus and the parietal cortex in AD. It was assumed that anosognosia for cognitive deficits in AD could be partly explained by impaired metabolism in parts of networks subserving self-referential processes (e.g., the superior frontal sulcus) and also perspective-taking (e.g., the temporoparietal junction)

and hypothesized that these patients have impairment in the ability to see themselves with a third-person perspective (i.e., being able to see themselves as other people see them) [17].

Salmon E. et al. (2006) explored the neural substrate of anosognosia for cognitive impairment in Alzheimer's disease (AD), with 18F-2-fluoro-2-deoxy-D-glucose positron emission tomography (FDG-PET) and reported a decrease in brain metabolism in orbital prefrontal cortex and in medial temporal structures. They assume that medial temporal dysfunction may produce impairment in the mechanism of comparison between current information on cognition and personal knowledge. Also hypoactivity in orbitofrontal cortex may not allow AD patients to update the qualitative judgment associated with their impaired cognitive abilities. They found that discrepancy score between caregiver's and patient's evaluations, another measure of anosognosia, was negatively related to metabolic activity located in the temporoparietal junction, consistent with an impairment of self-referential processes and perspective taking in AD [18].

Some studies implicate parietal structures, particularly the inferior parietal region, in identifying self generated actions [19, 20]. Abu-Akel (2003) suggested that information about oneself is first perceived and represented in parietal structures. This information is then relayed to a limbic-paralimbic module, where it is rapidly evaluated for personal relevance and emotional meaning. At last this information is relayed to a prefrontal module, where executive function processes [21]. Marshal et al. (2004) found increased senile plaque density in right presubiculum region of AD patients with anosognosia, using histopathology of necropsy brain tissue of these patients and suggested that selective pathological involvement of this area contributes to awareness deficits in Alzheimer's disease [22].

However, quantification of anosognosia is difficult and there are detailed scales (questionnaire) which can be applied, but no gold standard for assessing awareness of the disease exists.

Vogel et al. (2004) believed that a short categorical rating is very useful in everyday clinical practice [23].

Several studies showed association between measures of dementia severity and decrease in cerebral perfusion and reported maximum correlation in temporal and parietal lobes [24–27]. Because of the concern that the severity of the disease could have contributed to cerebral hypoperfusion, we performed a comparison between mild and moderate stages separately and

observed that 'right inferior parietal region' was the common region which showed significant hypoperfusion in both our anosognosia subgroups. CBF differs also significantly in right prefrontal and right frontal regions in mild-AD-Anosognosia compared to mild-AD-No-anosognosia subgroup. This finding was not apparent in moderate subgroup of anosognosia. It is possible that in mild stage of AD without anosognosia, higher concentration of cortical synapses in prefrontal and frontal regions results in higher activity of these regions to be able to mask cognitive decline. This cognitive reserve may not be present in mild AD with anosognosia and also in moderate stage of dementia. This finding needs to be studied more. We also examined the correlation between MMSE score and rCBF. MMSE score had not a significant correlation with right inferior parietal, right prefrontal and frontal blood perfusion in our patients but significant correlation was shown with perfusion in medial temporal regions. Therefore this is another clue that shows right inferior parietal hypoperfusion is unlikely affected by MMSE score. Consequently our results show that, mean CBF reduction in medial temporal regions more likely is the subsequence of the severity of dementia. We studied also the patients based on the severity, independent of the anosognosia variable and found significant difference in right and left prefrontal, medial and lateral temporal, superior parietal, left occipital, left frontal and cingulate regions in mild compared to moderate AD. Ashford et al. (2000) studied AD patients using ^{99m}Tc-ethyl cysteinate dimer (ECD) and SPECT and had found a pronounced correlation of hypoperfusion in temporoparietal regions with the severity of the disease while prefrontal area perfusion showed less association with severity [24]. Regional cerebral glucose metabolism measured by positron emission tomography of 18F-2-fluoro-2-deoxy-D-glucose was studied longitudinally by Mielke et al. (1994) in 25 patients with probable AD and a significant decline was noted in the whole brain which was most pronounced in the temporoparietal, frontal, superior parietal and occipital association cortex [27]. They reported that the changes of regional cerebral glucose metabolism in temporoparietal, frontal and occipital association cortex were related to the change of the Mini Mental State Examination score. Consistent with these findings, rCBF deficit is associated with dementia severity. The disease heterogeneity, the relationship between specific neuropsychologic characteristics and brain perfusion defect and also variability of the measures may have effects in some controversies in the results

of these studies. Our findings also show that anosognosia is not an unusual finding in the mild stage of AD.

The main limitation of our study may be the use of a non-structured interview and low number of patients in different subgroups.

Based on our results we conclude that anosognosia may exist from the beginning stages of AD and may reflect functional impairment, radically in right inferior parietal region. Deficits of rCBF in this region may contribute to perspective- taking defects and seem to be independent of MMSE variable in our patients. Hypoperfusion in medial temporal regions seems to reflect more, the severity of the disease in our groups of patients. Right inferior parietal, prefrontal and frontal regions may be parts of a large circuit in self awareness.

REFERENCES

[1] Harwood DG, Sultzer DL, Wheatley MV (2000) Impaired insight in alzheimer disease: association with cognitive deficits, psychiatric symptoms, and behavioral disturbances. *Neuropsychiatry Neuropsychol Behav Neurol* **13**, 83-88.

[2] Starkstein SE, Chemerinski E, Sabe L, Kuzis G, Petracca G, Tesón A, Leiguarda (1997) Prospective longitudinal study of depression and anosognosia in Alzheimer's disease. *Br J Psychiatry* **171**, 47-52.

[3] Philippon J, Poirer J (2008). *Joseph Babinski A Biography*, Oxford University Press, US, pp. 205-207.

[4] Alavi A, Hirsch LJ (1991) Studies of central nervous system disorders with single photon emission computed tomography and positron emission tomography: evolution over the past 2 decades. *Semin Nucl Med* **21**, 58-81.

[5] Reed BR, Jagust WJ, Coulter L (1993) Anosognosia in Alzheimer's disease: relationships to depression, cognitive function, and cerebral perfusion. *J Clin Exp Neuropsychol* **15**, 231-244.

[6] Starkstein SE, Vazquez S, Migliorelli R, Teson A, Sabe L, Leiguarda R (1995) A single-photon emission computed tomographic study of anosognosia in Alzheimer's disease. *Arch Neurol* **52**, 415-420.

[7] Derouesn C, Thibault S, Lagha-Pierucci S, Baudouin-Madec V, Ancri D, Lacomblez L (1999) Decreased awareness of cognitive deficits in patients with mild dementia of the Alzheimer type. *Int J Geriatr Psychiatry* **14**, 1019-1030.

[8] Vogel A, Hasselbalch SG, Gade A, Ziebell M, Waldemar G (2005) Cognitive and functional neuroimaging correlate for anosognosia in mild cognitive impairment and Alzheimer's disease. *Int J Geriatr Psychiatry* **20**, 238-246.

[9] Shibata K, Narumoto J, Kitabayashi Y, Ushijima Y, Fukui K (2008) Correlation between anosognosia and regional cerebral blood flow in Alzheimer's disease. *Neurosci Lett* **435**, 7-10.

[10] Ott BR, Noto RB, Fogel BS (1996) Apathy and loss of insight in Alzheimer's disease: a spect imaging study. *J Neuropsychiatry Clin Neurosci* **8**, 41-46.

[11] Rankin KP, Baldwin E, Pace-Savitsky C, Kramer JH, Miller BL (2005) Self awareness and personality change in dementia. *J Neurol Neurosurg Psychiatry* **76**, 632-639.

[12] Marco Tamietto, Luca Latini Corazzini, Lorys Castelli, Giuliano, Geminiani (2004) Domain-specific anosognosia in Alzheimer disease and vascular dementia. *Brain Impairment* **5**, 187-197.

[13] Antoine C, Antoine P, Guermonprez P, Frigard B (2004) Awareness of deficits and anosognosia in Alzheimer's disease. *Encephale* **30**, 570-577.

[14] Migliorelli R, Tesón A, Sabe L, Petracca G, Petracchi M, Leiguarda R, Starkstein SE (1995) Anosognosia in Alzheimer's disease: a study of associated factors. *J Neuropsychiatry Clin Neurosci* **7**, 338-344.

[15] Lopez OL, Becker JT, Somsak D, Dew MA, DeKosky ST (1994) Awareness of cognitive deficits and anosognosia in probable Alzheimer's disease. *Eur Neurol* **34**, 277-282.

[16] Michon A, Deweer B, Pillon B, Agid Y, Dubois B (1994) Relation of anosognosia to frontal lobe dysfunction in Alzheimer's disease. *J Neurol Neurosurg Psychiatry* **57**, 805-809.

[17] Salmon E, Ruby P, Perani D, Kalbe E, Laureys S, Adam S, Collette F (2005) Two aspects of impaired consciousness in Alzheimer's disease. *Prog Brain Res* **150**, 287-298.

[18] Salmon E, Perani D, Herholz K, Marique P, Kalbe E, Holthoff V, Delbeuck X, Beuthien-Baumann B, Pelati O, Lespagnard S, Collette F, Garraux G (2006) Neural correlates of anosognosia for cognitive impairment in Alzheimer's disease. *Hum Brain Mapp* **27**, 588-597.

[19] Iacoboni M, Woods RP, Brass M, Bekkering H, Mazziotta JC, Rizzolatti G (1999) Cortical mechanisms of human imitation. *Science* **286**, 2526-2528.

[20] Vogeley K, Bussfeld P, Newen A, Herrmann S, Happ&eacute F, Falkai P, Maier W, Shah NJ, Fink GR, Zilles K (2001) Mind reading: neural mechanisms of theory of mind and self-perspective. *Neuroimage* **14**, 170-181.

[21] Abu-Akel A (2003) A neurobiological mapping of theory of mind. *Brain Res Brain Res Rev* **43**, 29-40.

[22] Marshall GA, Kaufer DI, Lopez OL, Rao GR, Hamilton RL, DeKosky ST (2004) Right prosubiculum amyloid plaque density correlates with anosognosia in Alzheimer's disease. *J Neurol Neurosurg Psychiatry* **75**, 1396-1400.

[23] Vogel A, Stokholm J, Gade A, Andersen BB, Hejl AM, Waldemar G (2004) Awareness of deficits in mild cognitive impairment and Alzheimer's disease: do mci patients have impaired insight? *Dement Geriatr Cogn Disord* **17**, 181-187.

[24] Ashford JW, Shih WJ, Coupal J, Shetty R, Schneider A, Cool C, Aleem A, Kiefer VH, Mendiondo MS, Schmitt FA (2000) Single spect measures of cerebral cortical perfusion reflect time-index estimation of dementia severity in Alzheimer's disease. *J Nucl Med* **41**, 57-64.

[25] Shih WJ, Ashford JW, Coupal JJ, Ryo YU, Stipp VV, Magoun SL, Gross K (1999) Consecutive brain spect surface three-dimensional displays show progression of cerebral cortical abnormalities in Alzheimer's disease. *Clin Nucl Med* **24**, 773-777.

[26] DeKosky ST, Shih WJ, Schmitt FA, Coupal J, Kirkpatrick C (1990) Assessing utility of single photon emission computed tomography (spect) scan in Alzheimer disease: correlation with cognitive severity. *Alzheimer Dis Assoc Disord* **4**, 14-23.

[27] Mielke R, Herholz K, Grond M, Kessler J, Heiss WD (1994) Clinical deterioration in probable Alzheimer's disease correlates with progressive metabolic impairment of association areas. *Dementia* **5**(1), 36-41.

This page intentionally left blank

Brain Perfusion and Neuropsychological Deficits in Mild Cognitive Impairment and Mild Alzheimer's Disease

Montserrat Alegret[a,*], Georgina Vinyes-Junqué[a], Mercè Boada[a,b], Pablo Martínez-Lage[a], Gemma Cuberas[c], Ana Espinosa[a], Isabel Roca[c], Isabel Hernández[a], Sergi Valero[a,d], Maitée Rosende-Roca[a], Ana Mauleón[a], James T. Becker[e,f,g] and Lluís Tárraga[a]

[a]*Fundació ACE. Institut Català de Neurociències Aplicades, Barcelona, Spain*
[b]*Hospital Universitari Vall d'Hebron -Institut de Recerca, Universitat Autònoma de Barcelona (VHIR-UAB), Spain*
[c]*Nuclear Medicine Department. Hospital Universitari Vall d'Hebron, Barcelona, Spain*
[d]*Psychiatry Department. Hospital Universitari Vall d'Hebron, Universitat Autònoma de Barcelona, Barcelona, Spain*
[e]*Department of Neurology, University of Pittsburgh School of Medicine. Pittsburgh, Pennsylvania, USA*
[f]*Department of Psychiatry, University of Pittsburgh School of Medicine. Pittsburgh, Pennsylvania, USA*
[g]*Department of Psychology, University of Pittsburgh School of Medicine. Pittsburgh, Pennsylvania, USA*

Abstract. Visuoperceptual processing is impaired early in the clinical course of Alzheimer's disease (AD). The 15-Objects test (15-OT), a visual discrimination task based on the Poppelreuter test consisting on 15 overlapping objects, detects such subtle performance deficits in Mild Cognitive Impairment (MCI) and mild AD. Single Photon Emission Tomography (SPECT) studies have reported reduced brain perfusion in temporal, parietal and prefrontal regions in early AD and MCI. The aim of the present study was to confirm the role of the 15-OT in the diagnosis of MCI and AD, and to investigate the brain perfusion correlates of visuoperceptual dysfunction in subjects with MCI, AD and normal aging. For this purpose, 42 AD, 42 MCI and 42 control subjects underwent a brain SPECT and separately completed the 15-OT. Results showed that the 15-OT performace was impaired in MCI and AD patients. In terms of SPECT scans, AD patients showed reduced perfusion in temporal-parietal regions, while MCI subjects had decreased perfusion in the middle and posterior cingulate. When MCI and AD groups were compared, a greater brain perfusion reduction was found in temporo-parietal regions in AD than MCI. In the whole sample, 15-OT performance was significantly correlated with clinical dementia rating scores, and with perfusion in the bilateral posterior cingulate and the right temporal pole, with no significant correlation in each separate group. Our findings suggest that the 15-OT performance provides a useful gradation of impairment from normal aging to AD, and it seems to be related to perfusion in the bilateral posterior cingulate and the right temporal pole.

Keywords: Alzheimer's disease, visuoperception, the 15-Objects test, mild cognitive impairment, brain SPECT, cerebral perfusion

INTRODUCTION

Structural and functional neuroimaging has focused on the early detection of Alzheimer's disease (AD), with a special interest in predicting conversion to dementia by those patients with Mild Cognitive Impairment (MCI) [1–9]. Functional brain imaging studies in

---
*Correspondence to: Montserrat Alegret, Fundació ACE. Institut Català de Neurociències Aplicades, Barcelona, Spain. E-mail: malegret@fundacioace.com.

mild AD have found significant hypometabolism and reduced cerebral blood flow in the medial temporal lobe, the temporal-parietal cortex, posterior cingulate, precuneus and dorsolateral frontal cortex [6, 10–19]. Similar changes have been found in subjects with MCI using Single-Photon Emission Computed Tomography (SPECT) [7, 14, 20, 21], and longitudinal studies have found hypoperfusion in the medial temporal lobe, the posterior cingulate gyrus and precuneus, and the parietal cortex and frontal cortex in MCI patients that later progressed to dementia [6–9].

Changes in brain *structure* sufficient to be detected by MRI usually follow changes in brain function and behavior (e.g., [22] Chételat et al., 2006), which may limit their utility in pre-symptomatic individuals. Thus, cognitive tests that challenge brain functionality may provide greater sensitivity in terms of predicting the change from MCI to AD [23]. For example, impaired performance on tests measuring visuoperception can be detected in patients with amnestic MCI, a condition that in many instances represents very early, prodromal AD [24–26], and these visuoperceptual deficits worsen with disease progression [26, 27].

Patients diagnosed of MCI [28, 29] have a global cognitive status and daily living activities relatively preserved. However, when they are exhaustively assessed it can be found memory and other cognitive impairments [24, 25, 30], such as visuoperceptual deficits [24, 25]. Poppelreuter type tests are the most frequently included in neuropsychological batteries to detect visuoperceptual deficits. In the clinical practice, however, their extremely simplicity (i.e., Poppelreuter test has only 5 overlapping figures) makes difficult to identify the incipient visuoperceptual deficits. More complex tests are required to detect the first visual discrimination signs in those patients that perform correctly on simple visual gnosis tests. One such measure, the 15-OT, is primarily a test of visuoperceptual function, but it also it also requires the ability to disentangle a simple visual form from a complex figure, as well as recognizing the whole of the figure and not confusing "parts". In order to successfully complete this task, individual patients must be able to perform visual attentional functions, executive abilities and to recognize the objects as objects.

In a previous study, Alegret et al. (2009) [25] reported that the 15-Objects Test (15-OT), a relatively complex test of visuoperceptual processing, detects subtle performance deficits in MCI and mild AD patients who otherwise perform normally on more simple measures of visual discrimination, such as the Poppelreuter test. These findings indicated that the 15-OT test is sensitive to the clinical progression of the visuoperceptual impairment associated with AD. However, in order to increase the clinical and research utility of the measure, it is important to understand the relationship between 15-OT performance and measures of brain function.

In this study the relationship between the 15-OT performance and brain perfusion (SPECT) was studied in mild AD and MCI patients. To the extent that the 15-OT is mainly a visuoperceptual task, we would predict that performance on the test would be related to perfusion in the temporo-parietal areas. Not only does the 15-OT involve visual perception [31], and thus require the parietal lobes, visual object identification has been found associated with posterior cingulate perfusion using SPECT [32]. We would thus expect that 15-OT performance would be related to cerebral perfusion along the occipito-temporo-parietal axis. This prediction is supported by the hypothesis that there is functional hierarchy in the occipital-temporal pathways in which neuronal properties shift from sensitivity to local object features to a more global and holistic representation (that is, the semantic processing) [33]. Moreover, we would expect that the pathological progression of AD from MCI would have an effect on brain perfusion in these critical regions.

The purpose of the present study was to confirm the role of the 15-OT in the diagnosis of MCI and mild AD, and to investigate the brain perfusion correlates of visuoperceptual dysfunction (as measured by the 15-OT) in subjects with MCI or AD.

METHODS

Subjects

We studied a sample of 148 subjects divided into three groups: 51 mild AD patients, 48 MCI subjects and 49 healthy elderly controls (EC). From this original sample, we selected 126 subjects, 42 subjects per group, with equivalent ages and educational level. Age, education and gender distribution were similar among the groups (see Table 1). All subjects were assessed in the Diagnostic Unit of *Fundació ACE* (Barcelona, Spain), and they received a comprehensive neurobehavioral evaluation as part of their diagnostic work-up.

The AD patients met the *National Institute of Neurological and Communicative Disorders and Stroke-Alzheimer's Disease and Related Disorders Association* (NINCDS/ADRDA) criteria for Probable

Table 1
Demographic characteristics of the participants

	EC	MCI	AD	Statistics	p
N	42	42	42		
Sex n (%) Male	33.3	31	26.2	0.528_1	0.768
Education (n (%))					
Middle/Elementary school	26.2	23.8	28.6		
High School/Associate degree	33.3	31	16.7	8.06_1	0.234
Bachelor's degree	23.8	11.9	16.7		
Less than 3 years	16.7	33.3	33.1		
Age in years (mean/SD)	74.7/4.4	76.8/4.3	76.4/4.5	2.73_2	0.069

EC: Elderly Controls; MCI: Mild Cognitive Impairment; AD: Alzheimer's disease; MMSE: Mini-Mental State Examination; 15-OT: The 15-Objects test; SD: Standard deviation; $_1$: $\mathcal{X}^2$;$_2$: F.

AD [34]. All AD patients had a clinical dementia rating (CDR) score of 1, indicating a mild degree of dementia. All AD patients were taking stable doses of acetylcholinesterase inhibitors (AChEIs) for at least 2 months prior to the study.

The MCI patients fulfilled Petersen's diagnostic criteria [28], including subjective memory complaints, normal general cognition, preserved performance in activities of daily living, absence of dementia and a measurable impairment in memory function, with or without deficit in other cognitive domains (MCI amnestic single domain or MCI amnestic multiple domain) [29]. All MCI subjects had a CDR rating of 0.5 and none were taking any dementia medication (i.e., AChEIs or memantine).

The control subjects included the patients' spouses, friends or relatives who agreed to participate. They had no cognitive complaints or other neurologic symptoms reported either by the participant or an informant, and there was no evidence by history of functional impairment due to declining cognition. All of the control subjects had Mini-Mental State Examination (MMSE) [35] scores of at least 26 (the lower limit of the normal range in the Spanish population older than 70 [36] Blesa et al., 2001), and normal performance on the neuropsychological battery (detailed elsewhere [25] and the RBANS visual memory subtest [37]). Although most of the control subjects did not have any CT or MRI, the subjects were considered as controls when the neurological and neuropsychological exams were normal.

For the whole sample, exclusion criteria were: age younger than 65 years, illiteracy, presence of moderate depressive symptoms (Geriatric Depression *Scale* ≥ 10) [38], major depression or other DSM-IV Axis-I psychiatric disorder (except for dementia), neurological disease (other than dementia), structural focal lesion on CT imaging (stroke or tumors, brain traumatic injury, moderate leukoaraiosis or more than one lacunae), history of alcohol or other substance abuse, severe visual abnormalities including glaucoma or cataracts, or significant aphasia.

Neuropsychological assessment

In the 15-OT [39], the subjects were shown a card with 15 overlapping line drawings of common objects (see Fig. 1). They were asked to say aloud the names of all of the objects that they could see on the card, and the number of correct responses was recorded. Subjects were allowed to take as much time as they needed to identify as many objects as they could. Errors or misidentifications were also recorded (that is, the incorrect interpretation of an object or the incorrect interpretation of a part of an object). To limit the influence of impaired naming, when subjects were unable to name an object that they had correctly identified (i.e., if they were able to define or describe the object), the answer was taken as correct (i.e., "To play tennis" instead of "A racquet").

As explained in a previous study [25], the 15-OT was developed by Pillon and coworkers (1989) [39] to assess the slowing of cognitive processing (measuring the time needed to complete the task) in Parkinson's disease (PD), and until our previous study it had only been used in patients with PD [39, 40, 41] and Huntington's disease [42, 43]. We were the first to use response accuracy of the 15-OT as a measure of performance, and we did so because of the lack of a similar visuoperceptual test to detect subtle changes in the mild stages of AD [25]. Although the 15-OT has not specifically been validated as a visuoperceptual test, it is based on the Poppelreuter paradigm which accurately explores visuoperceptive abilities [31].
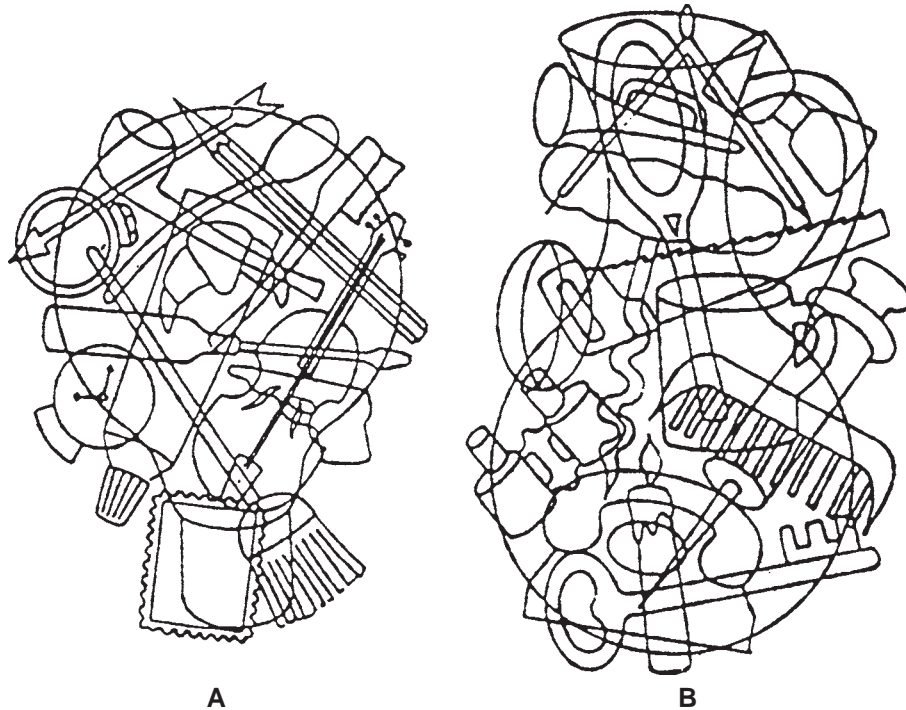
Fig. 1. The 15-Objects test.

The neuropsychological battery administered in the diagnostic procedure included tests sensitive to orientation, attention, verbal and visual memory, language, visual gnosis, praxis and executive functions: Temporal, Spatial and Personal Orientation; Digit span forwards and backwards, Block Design and Similarities subtests of Wechsler Adult Intelligence Scale-Third Edition (WAIS-III) [44]; The Word List Learning test from the Wechsler Memory Scale-Third Edition (WMS-III) [45]; the RBANS visual memory subtest [37]; Verbal comprehension (to correctly execute 2 simple, 2 semi-complex and 2 complex commands extracted from the ADAS-cog [46] and the Barcelona test battery [47]; The abbreviated Boston Naming Test with 15 items [48]; the Poppelreuter test [49]; the Luria's Clock test [50]; Ideomotor and Imitation praxis; the Automatic Inhibition subtest of the *Syndrom Kurtz Test* (SKT) [51]; Phonetic Verbal Fluency (words beginning with 'P' during one minute) [52]; Semantic Verbal Fluency ('animals' during one minute) [31] and the Spanish version of the Clock Test [53]. The Mini-Mental State Examination [35] (MMSE) was administered as a measure of global cognition. Moreover, depressive symptoms were assessed with the Geriatric Depression Scale [38].

Brain SPECT procedure

Within three weeks following the clinical assessment, a brain SPECT was performed. After lying supine in quiet surroundings, each subject received an intravenous injection of 740 MBq 99mTc-ECD (Neurolite®, Bristol-Myers Squibb). The SPECT acquisition began between 30 and 120 minutes after intravenous injection, in a double-headed gamma camera (Siemens e-Cam) equipped with low-energy, high-resolution collimators. The SPECT acquisition consisted in 30 seconds frames, 1 image / 3º, format 128×128. The studies were reconstructed using filtered back projection (Butterworth 0.4 – 0.5, cut off 7), without Chang attenuation correction.

Image VBM analysis

A voxel-level analysis was performed using Statistical Parametric Mapping (SPM5, using non-attenuation corrected studies), running on Matlab 7.2 (Mathworks Inc, Sherborn, MA). Images were initially converted from DICOM to Analyze format using MRIcro (http://www.mricro.com), and transferred to SPM5. The images were normalized to the Montreal

Neurological Institute atlas, and the dimensions of the resulting voxels were $3 \times 3 \times 3$ mm. Between-group analyses were performed using ANOVA with the proportional scaling normalization routine to control for individual variation in global brain perfusion. The SPM T maps were obtained using a cluster and voxel level threshold corrected for multiple comparisons using a False Discovery Rate (FDR of $p < 0.05$) [54] and were corregistered to the MRI T1 template from SPM to locate the cluster areas.

Region of interest (ROI) analyses were performed with those clusters that showed significant brain perfusion differences between controls and AD patients using the WFU-Pickatlas software toolbox (http://fMRi.wfubuc.edu/CMS/software). The PickAt-

las software toolbox [55, 56] provides a method for generating ROI masks based on the Talairach Daemon database [57, 58], using Brodmann areas, Lobes, Hemispheres, Anatomic Labels (gyral anatomy) and Tissue Type. The atlases have been extended to the vertex in the Montreal Neurological (MNI) space. Eigenvariates were extracted at the peak voxels for identified clusters using the Volume of Interest (VOI) tool within SPM5.

Statistical analysis

Statistical analysis of the clinical variables was performed using SPSS for Windows (version 15.0; SPSS Inc., Chicago, Ill). An analysis of variance (ANOVA)

Table 2
Neuropsychological performances of the study subjects

	EC	MCI	AD	F (2, 125)
N (male, female)	42 (14,28)	42 (13,29)	42 (11,31)	
15-OT correct answers	13.48 (1.33)	11.14 (2.10)	9.83 (1.96)	42.75[1,2,3]
15-OT errors	1.45 (1.21)	3.26 (1.93)	4.10 (1.34)	32.96[1,2,3]
Orientation				
Temporal	4.98 (0.15)	3.81 (1.23)	2.45 (1.48)	53.57[1,2,3]
Spatial	5.00 (0.00)	4.95 (0.22)	4.88 (0.33)	2.94
Personal	5.00 (0.00)	4.88 (0.33)	4.45 (0.74)	15.98[2,3]
Memory				
Learning Trial 1 WMS-III	4.79 (1.49)	3.07 (1.40)	2.55 (1.25)	29.96[1,2]
Trial 4 WMS-III	10.21 (1.37)	5.98 (1.60)	4.62 (1.19)	183.39[1,2,3]
Delayed Recall WMS-III	8.38 (2.02)	1.26 (1.40)	0.17 (0.66)	386.54[1,2,3]
Visual memory RBANS	7.62 (1.91)	3.12 (2.41)	1.00 (1.54)	121.24[1,2,3]
Digit Span Forward	7.86 (1.75)	7.21 (1.75)	6.76 (1.49)	4.58[2]
Digit Span Backwards	4.95 (1.77)	4.21 (1.51)	3.48 (1.40)	9.34[2]
Praxis				
Ideomotor	4.00 (0.00)	3.95 (0.22)	3.93 (0.26)	1.46
onstruction	3.88 (0.33)	3.14 (1.12)	2.55 (1.36)	17.47[1,2,3]
Imitation	3.95 (0.22)	3.36 (0.91)	2.43 (1.11)	35.49[1,2,3]
Language				
Comprehension	6.00 (0.00)	5.81 (0.40)	5.62 (0.66)	7.69[2]
Repetition	4.00 (0.00)	4.00 (0.00)	3.98 (0.15)	1.00
Visual Naming (15-BNT)	14.79 (0.52)	13.38 (1.68)	12.26 (2.32)	23.80[1,2,3]
Visual gnosis				
Poppelreuter test	9.83 (0.49)	9.19 (0.94)	8.83 (1.58)	8.95[1,2]
Luria's Clock test*	3.69 (0.52)	2.71 (0.92)	2.12 (1.06)	35.36[1,2,3]
Executive functions				
SKT errors	0.62 (1.01)	2.17 (2.58)	4.02 (5.45)	9.77[2]
Phonetic verbal fluency	14.64 (4.11)	11.19 (4.43)	11.43 (4.57)	8.16[1,2]
Semantic verbal fluency	18.19 (4.08)	11.81 (3.24)	10.83 (4.07)	46.01[1,2]
Abstract Reasoning	11.62 (1.64)	9.33 (2.75)	8.19 (2.37)	24.23[1,2]
Global cognition				
Clock Test[#]	6.90 (0.37)	5.45 (1.64)	4.76 (2.09)	20.90[1,2]
MMSE score	29.40 (0.94)	25.71 (1.99)	23.00 (2.20)	134.89[1,2,3]

EC: Elderly Controls; MCI: Mild Cognitive Impairment; AD: Alzheimer's disease. 15-OT: The 15-Objects test; WMS-III: Wechsler Memory Scale-III; 15-BNT: 15 items abreviated Boston Naming Test; SKT: Automatic Inhibition subtest of the *Syndrom Kurtz Test (number of errors)*; MMSE: Mini-Mental State Examination. [1] Significant differences between EC and MCI; [2] Significant differences between EC and AD; [3] Significant differences between MCI and AD.

and post-hoc analyses (Bonferroni) were used to compare sociodemographic, clinical and neuropsychological data between the three groups. Pearson's correlation tests were performed between the 15-OT scores and CDR, MMSE, neuropsychological tests and SPECT data. A linear multiple regression analysis, using the stepwise procedure, was performed to determine which neuropsychological tests were able to predict performance on the 15-OT. Moreover, a Component Analysis with Varimax rotation was carried out using the variables that correlated with the 15-OT in the case of clinical groups.

RESULTS

The scores of the subjects on the neuropsychological tests are shown in Table 2. Performance on the MMSE were progressively lower from EC to MCI and AD patients (see Table 2). The 15-OT performance was significantly different between groups. Scores of MCI and AD patients were significantly lower than those of controls, and the MCI subjects performed significantly better than the AD patients. In the whole sample, the 15-OT performance was significantly correlated with the CDR ($r = -0.63$; $p < 0.001$) and the MMSE ($r = 0.67$; $p < 0.001$) scores. As detailed in Table 3, the performance of the MCI and AD patients on the 15-OT was highly correlated with performance on the Poppelreuter test, and the measures of visual naming and phonetic verbal fluency.

The control group and patients (MCI and AD groups) differed on the relationship between the 15-OT and the other neuropsychological tests. The sense of the correlation values between the 15-OT and the other cognitive tests was the same in the three groups, but in the control group only the MMSE reached the significance. The other correlations were small. Probably, these results were partially determined by a ceiling effect in this group (table 3).

The variables related to visuoperception and language were introduced in the a linear regression analysis to examine the influence of semantic knowledge and visuoperceptual functions on the performance of the 15-OT. We also took into account the results of preliminary correlation analyses between the 15-OT and the neuropsychological tests. The stepwise linear multiple regression analysis (including the 15-BNT, phonetic and semantic verbal fluency, and Poppelreuter tests) executed on the clinical sample (MCI and AD) showed that only phonetic verbal flu-

ency ($\beta = 0.35$, $p = 0.0005$) and the Poppelreuter test ($\beta = 0.41$; $p = 0.0005$) were related to the 15-OT. Moreover, a Principal Component Analysis with Varimax rotation was carried out in the MCI and AD patients using the variables that correlated with the 15-OT (See Table 3). The best solution included three dimensions that explained 70.4% of the variance. The first dimension included high factor loadings for the Poppelreuter test (0.85), 15-OT (0.80) and BNT (0.67). The second factor included memory (0.88) and learning (0.79) and the third factor was constituted by phonetic (0.90) and semantic verbal fluencies (0.60).

Significant hypoperfusion was found in AD patients compared to controls in the temporal pole (bilaterally), the parahippocampal gyrus (right), middle and posterior cingulate (bilaterally), angular gyrus, supramarginal gyrus and inferior parietal lobe (right) (Fig. 2). Compared to MCI subjects, AD patients showed significant brain perfusion reduction in the same areas as the EC-AD comparison, except for bilateral middle and posterior cingulate. This latter structure was the only one found to be significantly hypoperfused in MCI compared to EC (Table 4).

The perfusion levels of the MCI patients fell between those of the EC and AD groups. The data from the eigenvariates for the five regions identified in the EC/AD contrast were entered into a MANCOVA, with age as a covariate. The overall model was significant (Hotellings $F(10, 234) = 110.3$, $p < 0.001$). The differences between all of the groups were significant in each of the five brain regions ($p < 0.001$) (see Fig. 3).

The correlation between 15-OT performance and perfusion in all 126 participants revealed that regions of the posterior cingulate and the pole of the right temporal lobe were significantly linked to succesful performance. The eigenvariates from these regions were significantly correlated ($p < 0.001$) with the 15-OT (temporal pole $r = 0.48$; posterior cingulate $r = 0.55$), the abbreviated 15-BNT (temporal pole $r = 0.40$; posterior cingulate $r = 0.46$), the Poppelreuter test (temporal pole $r = 0.34$; posterior cingulate $r = 0.37$) and the MMSE scores (temporal pole $r = 0.68$; posterior cingulate $r = 0.72$) even after adjusting for age. As shown graphically in Fig. 4, the performance on the 15-OT was more accurate among those MCI patients with higher eigenvariates in the posterior cingulate. However, no significant correlations were found in any of the individual groups. The EC and AD groups did not show statistically significant correlations likely due to ceiling and floor effects.

Table 3
Correlations between the scores obtained on the 15-OT and the main neuropsychological tests

	15-OT	Learning	Delayed recall	Poppelreuter	SKT time	Visual naming	Phonetic verbal fluency	Semantic verbal fluency	Abstract Reasoning	MMSE
15-OT	–	0.29	0.18	0.05	−0.24	0.26	0.23	0.12	0.20	0.54**
Learning	0.15	–	0.61**	0.05	−0.47**	0.25	0.20	0.47**	0.26	0.34*
	0.15									
Delayed Recall	0.09	0.39**	–	−0.01	−0.14	0.15	−0.08	0.25	0.17	0.25
	0.13	*0.21*								
Poppelreuter	0.49**	−0.00	0.09	–	0.08	0.14	−0.25	0.11	0.16	0.20
	*0.49**	*0.16*	*−0.18*							
SKT time	−0.37*	−0.23	0.04	−0.13	–	−0.33*	−0.42**	−0.53**	−0.053**	−0.09
	−0.01	*−0.10*	*0.13*	*−0.02*						
Visual Naming	0.41**	0.16	0.14	0.34*	−0.21	–	0.26	0.39*	0.36*	0.13
	*0.48**	*0.37*	*−0.09*	*0.66**	*−0.24*					
Phonetic verbal fluency	0.41**	0.33*	0.10	0.29	−0.46**	0.32*	–	0.49**	0.21	−0.01
	*0.53**	*0.17*	*0.49*	*0.20*	*−0.47**	*0.55**				
Semantic verbal fluency	0.18	0.11	0.18	0.12	−0.14	0.38*	0.18	–	0.26	0.20
	0.10	*0.20*	*−0.06*	*0.23*	*−0.23*	*0.42**	*0.41**			
Abstract Reasoning	0.49**	0.38*	0.19	0.35*	−0.39*	0.58**	0.56**	0.21	–	0.20
	0.16	*0.18*	*0.03*	*−0.06*	*−0.37*	*0.32*	*0.40**	*0.30*		
MMSE	0.37*	0.41**	0.30	0.19	−0.34*	0.28	0.26	0.36*	0.43**	–
	0.20	*0.27*	*0.22*	*0.23*	*−0.20*	*0.44**	*0.18*	*0.14*	*0.40**	

In the upper-right side are reported correlations obtained for the controls; in the lower-left side are correlations obtained for MCI and AD (*in italics*).; * $p < 0.05$; ** $p < 0.01$.; 15-OT: The 15-Objects test; SKT: Automatic Inhibition subtest of the *Syndrom Kurtz Test (time)*; MMSE: Mini-Mental State Examination.

Table 4
Brain areas showing significantly lower perfusion in mild AD and MCI patients compared to controls

Group comparison	Region	Cluster size (num.voxels)	Coordinates (X, Y, Z)	Z scores of maximum	*p* (FDR) Cluster	*p* (FDR) Voxel
AD < EC	Temporal pole and parahippocampal (R)	418	45 21 -21	5.52	0.0001	0.001
	Angular gyrus, parietal, supramarginalis (R)	200	45 -57 39	4.65	0.002	0.004
	Temporal pole (L)	86	-36 18 -27	4.02	0.055	0.015
	Middle and posterior cingulate (Bil)	73	0 -42 33	4.46	0.083	0.006
MCI < EC (ROI)	Middle and posterior cingulate (Bil)	63	-3 -42 36	4.33	0.022	0.004
AD < MCI (ROI)	Temporal pole and parahippocampal (R)	226	51 21 -9	4.16	0.014	0.005
	Angular gyrus, parietal, supramarginalis (R)	173	60 -51 24	3.94	0.013	0.011
	Temporal pole (L)	167	-51 21 -12	3.67	0.048	0.016

AD: Alzheimer's disease; EC: Elderly Controls; MCI: Mild Cognitive Impairment; ROI: Regions of interest; R: right; L: left; Bil: Bilateral.
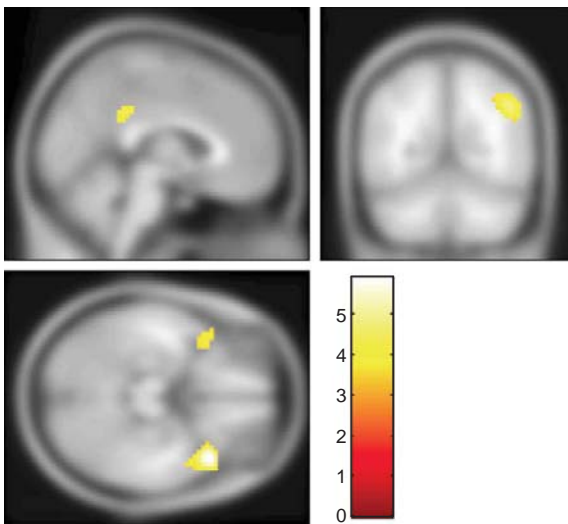
Fig. 2. The section rendering of the contrast between the EC and AD groups (SPECT images) projected onto the T1 template image from SPM5. The areas marked in yellow have significantly higher flow in the EC group compared to the AD patients (*FDR* = 0.05, extent threshold 100 voxels).

Fig. 3. The mean and standard deviations of the eigenvariates derived from the SPM5 analysis. The values were taken at the peak voxel, with an area including a sphere of 1 voxel radius. The standard deviation was taken from the MANCOVA (controlling for age) and is group-specific. The differences between all of the groups were significant in each of the five brain regions (*p* < 0.001).

DISCUSSION

The results of the present study confirm and extend our understanding of the neuropsychological deficits in MCI and AD, and their neuroanatomical correlates. We replicated our prior findings that performance on the 15-OT is progressively less accurate as subjects move from normal cognition through MCI to AD [25]. Second, we found that performance on the 15-OT was highly related to performance on the Poppelreuter test, and measures of visual naming and phonetic verbal fluency. The 15-OT was also linked to perfusion in the posterior cingulate and anterior temporal cor-

tices. Third, subjects with MCI showed decreased brain perfusion in the posterior cingulate that was between that of the EC and AD groups.

We interpret the pattern of correlations between 15-OT performance and both cerebral perfusion and neuropsychological tests, as reflecting two separate, but related, processes (that is, dementia severity and semantic networks). The first is related to overal dementia severity, and is reflected in the perfusion in the posterior cingulate gyrus. Alteration of the temporal-parietal cortex and posterior cingulate gyrus are strong predictors of conversion to AD from MCI [1, 59]. Longitudinal studies have reported brain perfusion reduction of the posterior cingulate gyrus and
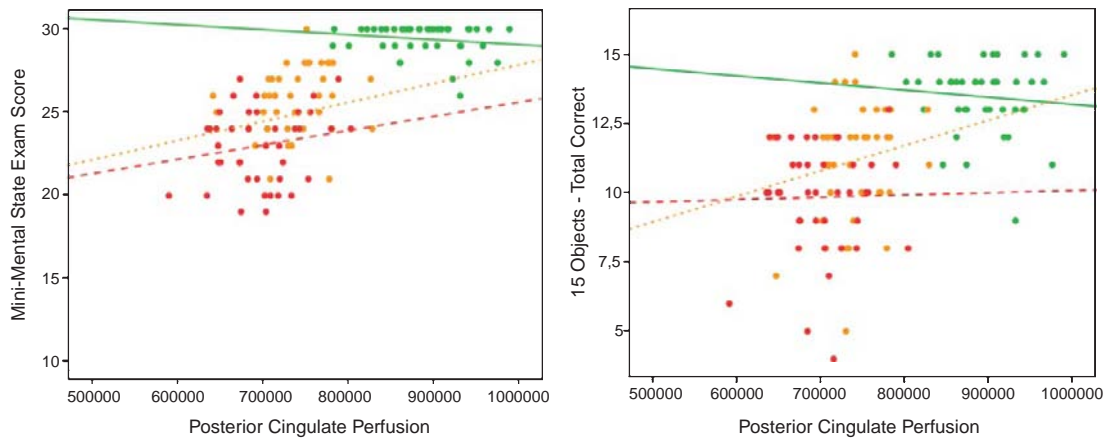
Fig. 4. Scatterplots of performance on the MMSE (left panel) and the 15-OT (right panel) as a function of the eigenvariate from the posterior cingulate gyrus region of interest. Each point represents a single subject in each group, and the lines represent the best-fit regression lines for each group. The green lines represent the EC group, the orange the MCI, and the red AD.

precuneus in those MCI subjects who converted to AD [6, 7, 60]. Further, the decreasing perfusion in the posterior cingulate may reflect alterations in the default mode network [60, 61] (which is down-regulated in AD. Thus, as posterior cingulate perfusion decreases with increasing severity of the degenerative process, performance on the 15-OT declines. Alternatively, visuoconstructional and visuoperceptual functions may be affected by decreased posterior cingulate perfusion [32]. In addition, we found that performances on the15-OT and another recognized visuoperceptual test (Poppelreuter) were highly related in MCI and AD patients. However, as the degree of atrophy and dysfunction in the posterior cingulate is related to severity of AD [62], we believe that the most parsimonious explanation of these findings is that they reveal the link between 15-OT performance and overall clinical state. In this regard, in our sample the 15-OT was found highly related to the CDR and MMSE scores, which reflects dementia severity.

In terms of the correlation between the 15-OT performances and the 15-BNT scores and the anterior temporal lobe perfusion, there is evidence that this part of the ventral processing stream [63] is involved in processing semantic information [64]. This part of the temporal lobe is generally not affected early in the course of AD and MCI [65], so perhaps the correlation reflects the demands of the 15-OT, in particular identifying objects from a field of overlapping visual information. Moreover, in our clinical sample, the Principal Components Analysis showed that the 15-OT was included in the same dimention than the visuop-

erceptual (Poppelreuter) and visual naming (15-BNT) tests.

Obviously, these interpretations of the data are speculative, and they must be tested with longitudinal data. If they are correct, we would predict that change in the 15-OT performance would be related to *change* in perfusion in the posterior cingulate and right temporal pole. As clinical disease becomes more severe, we might find that other brain regions are linked to performance, but our hypotheses require that we are able to predict performance change from these specific alterations in regional perfusion.

Scores on the 15-OT were abnormal in the MCI and AD patients, and the performance deficits were more severe in the AD group relative to the MCI group. Thus, this neuropsychological test provides a useful gradation of visuoperceptual impairment. These findings, in combination with other studies, strongly suggest that MCI may be early identified in elderly using an exhaustive assessment of cognitive functions rather than simply focusing on memory [24, 66–68].

Our SPECT findings are also consistent with previous studies using PET [15, 16, 18] and SPECT [6, 13, 17, 60]. The AD patients had significant hypoperfusion in the temporal lobes, in parietal cortex including the precuneus and angular gyrus, and cingulate. The reductions in perfusion may reflect cortical atrophy and the disconnection of these cerebral regions from the mesial temporal lobe [69].

There are several aspects of this study that need to be kept in mind when interpreting the data. First, the SPECT imaging was done with the subjects at rest

and the 15-OT data were obtained at a different time. As such, the correlations between the 15-OT and the SPECT have to be interpreted with caution. Second, we did not have anatomical MRI scans from these subjects. Consequently, although all of the data were spatially normalized to a standard template, we did not perform any atrophy correction. Thus, some of our results may have been related to focal regional atrophy and we cannot determine which structural changes can explain the functional ones. A major concern in the interpretation of the results of the SPECT studies in our healthy elderly control subjects is the absence of structural imaging. Normal cognitive performance could have occurred because of functional compensation despite morphological abnormalities.

In conclusion, our findings suggest that the 15-OT performance provides a useful gradation of impairment from normal aging to AD, and it seems to be related to perfusion in the bilateral posterior cingulate and the right temporal pole. Further longitudinal studies are needed to determine if those amnestic MCI subjects, even healthy elderly, with combined lower performances on the 15-OT and hypoperfusion in some cerebral areas have an increased risk of conversion to AD.

ACKNOWLEDGMENTS

REFERENCES

[1] Bell-McGinty S, Lopez OL, Meltzer CC, Scanlon JM, Whyte EM, DeKosky ST, Becker JT (2005) Differential cortical atrophy in subgroups of mild cognitive impairment. *Arc Neurol* **62**, 1393-1397.

[2] Devanand DP, Pradhaban G, Liu X, Khandji A, De Santi S, Segal S, Rusinek H, Pelton GH, Honig LS, Mayeux R, Stern Y, Tabert MH, de Leon MJ (2007) Hippocampal and entorhinal atrophy in mild cognitive impairment: prediction of Alzheimer disease. *Neurology* **68**, 828-836.

[3] Whitwell JL, Josephs KA, Murray ME, Kantarci K, Przybelski SA, Weigand SD, Vemuri P, Senjem ML, Parisi JE, Knopman DS, Boeve BF, Petersen RC, Dickson DW, Jack CR (2008) MRI correlates of neurofibrillary tangle pathology at autopsy: A voxel-based morphometry study. *Neurology* **71**, 743-749.

[4] Karas G, Sluimer J, Goekoop R, van der Flier W, Rombouts SARB, Vrenken H, Scheltens P, Fox N, Barkhof F (2008) Amnestic mild cognitive impairment: Structural MR Imaging findings predictive of conversion to Alzheimer disease. *AJNR Am J Neuroradiol* **29**, 944-949.

[5] Desikan RS, Cabral HJ, Fischl B, Guttmann CR, Blacker D, Hyman BT, Albert MS, Killiany RJ (2009) Temporoparietal MR imaging measures of atrophy in subjects with mild cognitive impairment that predict subsequent diagnosis of Alzheimer disease. *Am J Neuroradiol* **30**, 532-538.

[6] Matsuda H, Kitayama N, Ohnishi T, Asada T, Nakano S, Sakamoto S, Imabayashi E, Katoh A (2002) Longitudinal evaluation of both morphologic and functional changes in the same individuals with Alzheimer's disease. *J Nucl Med* **43**, 304-311.

[7] Hirao K, Ohnishi T, Hirata Y, Yamashita F, Mori T, Moriguchi Y, Matsuda H, Nemoto K, Imabayashi E, Yamada M, Iwamoto T, Arima K, Asada T (2005) The prediction of rapid conversion of Alzheimer's disease in mild cognitive impairment using regional cerebral blood flow SPECT. *Neuroimage* **28**, 1014-1021.

[8] Wolf H, Jelic V, Gertz HJ, Nordberg A, Julin P, Wahlund LO (2003) A critical discussion of the role of neuroimaging in mild cognitive impairment. *Acta Neurol Scand Suppl* **179**, 52-76.

[9] Nobili F, De Carli F, Frisoni GB, Portet F, Verhey F, Rodriguez G, Caroli A, Touchon J, Morbelli S, Guerra UP, Dessi B, Brugnolo A, Visser PJ (2009) SPECT predictors of cognitive decline and Alzheimer's disease in mild cognitive impairment. *J Alzheimers Dis* **17**, 761-772.

[10] Wang H, Golob E, Bert A, Nie K, Chu Y, Dick MB, Mandelkern M, Su MY (2009) Alterations in regional brain volume and individual MRI-Guided perfusion in normal control, stable mild cognitive impairment, and MCI-AD converter. *J Geriatr Psychiatry Neurol* **22**, 35-45.

[11] Nobili F, Salmaso D, Morbelli S, Girtler N, Piccardo A, Brugnolo A, Dessi B, Larsson SA, Rodriguez G, Pagani M (2008) Principal compent analysis of FDG PET in amnestic MCI. *Eur J Nucl Med Imaging* **35**, 2191-2202.

[12] Pearlson GD, Harris GJ, Powers RE, Barta PE, Camargo EE, Chase GA, Noga JT, Tune LE (1992) Quantitative changes in mesial temporal volume, regional cerebral blood flow, and cognition in Alzheimer's disease. *Arch Gen Psychiatry* **49**, 402-408.

[13] Encinas M, De Juan R, Marcos A, Gil P, Barabash A, Fernández C, De Hugarte C, Cabranes JA (2003) Regional cerebral blood flow assessed with 99mTc-ECD SPET as a marker of progression of mild cognitive impairment to Alzheimer's disease. *Eur J Nucl Med Mol Imaging* **30**, 1473-1480.

[14] Johnson KA, Jones K, Holman BL, Becker JA, Spiers PA, Satlin A, Albert MS (1998) Preclinical prediction of Alzheimer's disease using SPECT. *Neurology* **50**, 1563-1571.

[15] Minoshima S, Giordani B, Berent S, Frey KA, Foster NL, Kuhl DE (1997) Metabolic reduction in the posterior cingulate cortex in very early Alzheimer's disease. *Ann Neurol* **42**, 85-94.

[16] Ishii K, Sasaki M, Yamaji S, Kitagaki H, Mori E (1997) Demonstration of decreased posterior cingulated perfusion in mild Alzheimer's disease by means of $H_2^{15}O$ positron emission tomography. *Eur J Nucl Med* **24**, 670-673.

[17] Ashford JW, Shih WJ, Coupal J, Shetty R, Schneider A, Cool C, Aleem A, Kiefer VH, Mendiondo MS, Schmitt FA (2000) Single SPECT measures of cerebral cortical perfusion reflect time-index estimation of dementia severity in Alzheimer's disease. *J Nucl Med* **41**, 57-64.

[18] Ibañez V, Pietrini P, Alexander GE, Furey ML, Teichberg D, Rajapakse JC, Rapoport SI, Schapiro MB, Horwitz B (1998) Regional glucose metabolic abnormalities are not the results of atrophy in Alzheimer's disease. *Neurology* **50**, 1585-1593.

[19] Nestor PJ, Cine D, Fryer TD, Clarke J, Hodges JR (2003) The topography of metabolic deficits in posterior cortical atrophy (the visual variant of Alzheimer's disease) with FDG-PET. *J Neurol Neurosurg Psychiatry* **74**, 1521-1529.

[20] Kogure D, Matsuda H, Ohnishi T, Asada T, Uno M, Kunihiro T, Nakano S, Takasaki M (2000) Longitudinal evaluation of early Alzheimer's disease using brain perfusion SPECT. *J Nucl Med* **41**, 1155-1162.

[21] Nobili F, Frisoni GB, Portet F, Verhey F, Rodriguez G, Caroli A, Touchon J, Calvini P, Morbelli S, De Carli F, Guerra UP, Van de Pol LA, Visser PJ (2008) Brain SPECT in subtypes of mild cognitive impairment. Findings from the DESCRIPA multicenter study. *J Neurol* **255**, 1344-1353.

[22] Chételat G, Desgranges B, Eustache F (2006) [Brain profile of hypometabolism in early Alzheimer's disease: relationships with cognitive deficits and atrophy]. *Rev Neurol* **162**, 945-951.

[23] Fleischer AD, Sun S, Taylor C, Ward CP, Gamst AC, Petersen RC, Jack CR, Aisen RS, Thal LJ (2008) Volumetric MRI vs clinical predictors of Alzheimer disease in mild cognitive impairment. *Neurology* **70**, 191-199.

[24] Nordlund A, Rolstad S, Hellström P, Sjögren M, Hansen S, Wallin A (2005) The Goteborg MCI study: mild cognitive impairment is a heterogeneous condition. *J Neurol Neurosurg Psychiatry* **76**, 1485-1490.

[25] Alegret M, Boada-Rovira M, Vinyes-Junqué G, Valero S, Espinosa A, Hernández I, Modinos G, Rosende-Roca M, Mauleón A, Becker JT, Tárraga L (2009) Detection of visuoperceptual deficits in preclinical and mild Alzheimers disease. *J Clin Exp Neuropsychol* **31**, 860-867.

[26] Johnson DK, Storandt M, Morris JC, Calvin JE (2009) Longitudinal study of the transition from healthy aging to Alzheimer Disease. *Arch Neurol* **66**, 1254-1259.

[27] Paxton JL, Peavy GM, Jenkins C, Rice VA, Heindel WC, Salmon DP (2007) Deterioration of visual-perceptual organization in Alzheimer's disease. *Cortex* **43**, 967-975.

[28] Petersen RC, Smith GE, Waring SC, Ivnik RJ, Tangalos EG, Kokmen E (1999) Mild cognitive impairment. Clinical characterization and outcome. *Arch Neurol* **56**, 303-308.

[29] Petersen RC, Morris JC (2005) Mild cognitive impairment as a clinical entity and treatment target. *Arch Neurol* **62**, 1160-1163.

[30] Tales A, Haworth J, Nelson S, Snowden RJ, Wilcock G (2005) Abnormal visual search in mild cognitive impairment and Alzheimer's disease. *Neurocase* **11**, 80-84.

[31] Lezak MD, Howieson DB, Loring DW (2004). In *Neuropsychological Assessment* (4th ed), Oxford University Press, New York.

[32] Tippett WJ, Black SE (2008) Regional cerebral blood flow correlated of visuospatial tasks in Alzheimer's disease. *J Int Neuropsychol Soc* **14**, 1034-1045.

[33] Lerner Y, Hendler T, Ben-Bashat D, Harel M, Malach R (2001) A hierarchical axis of object processing stages in the human visual cortex. *Cereb Cortex* **11**, 287-297.

[34] McKhann G, Drachman D, Folstein M, Katzman R, Price D, Stadlan EM (1984) Clinical diagnosis of Alzheimer's disease: report of the NINCDS-ADRDA Work Group under the auspices of Department of Health and Human Services Task Force on Alzheimer's Disease. *Neurology* **34**, 939-|944.

[35] Folstein MF, Folstein SE, McHugh PR (1975) "Mini-Mental state". A practical method for grading the cognitive state of patients for the clinician. *J Psychiatr Res* **12**, 189-198.

[36] Blesa R, Pujol M, Aguilar M, Santacruz P, Bertran-Serra I, Hernández G, Sol JM, Peña-Casanova J, NORMACODEM Group (2001) Clinical validity of the 'mini-mental state' for Spanish speaking communities. *Neuropsychologia* **39**, 1150-1157.

[37] Randolph C, Tierney MC, Mohr E, Chase TN (1998) The Repeatable Battery for the Assessment of Neuropsychological Status (RBANS): Preliminary clinical validity. *J Clin Exp Neuropsychol* **20**, 310-319.

[38] Martínez de la Iglesia J, Onís Vilches MC, Dueñas Herrero R, Albert Colomer C, Aguado Taverné C, Luque Luque R (2002) Versión española del cuestionario de Yesavage abreviado (GDS) para el despistaje de depresión en mayores de 65 años: adaptación y validación. *MEDIFAM* **12**, 620-630.

[39] Pillon B, Dubois B, Bonnet AM, Esteguy M, Guimaraes J, Vigouret JM, Lhermitte F, Agid Y (1989) Cognitive slowing in Parkinson's disease fails to respond to levodopa treatment: The 15-objects test. *Neurology* **39**, 762-768.

[40] Leroy A, Michelet D, Mahieux F, Geni D, Defer G, Monfort JC, Degos JD, N'Guyen JP, Penschanski M, Cesaro P (1996) Neuropsychological testing of 5 patients with Parkinson's disease before and after neuron graft. *Revue Neurologique (Paris),* **152**, 158-164.

[41] Alegret M, Vendrell P, Junqué C, Valldeoriola F, Nobbe FA, Rumià J, Tolosa E (2000) Effects of unilateral posteroventral pallidotomy on 'on-off' cognitive fluctuations in Parkinson's disease. *Neuropsychologia* **38**, 628-633.

[42] Gómez-Ansón B, Alegret M, Muñoz E, Monté GC, Alayrach E, Sánchez A, Boada M, Tolosa E (2009) Prefrontal cortex volume reduction on MRI in preclinical Huntington's disease relates to visuomotor performance and CAG number. *Parkinsonism Relat Disord* **15**, 213-219.

[43] Gómez-Ansón B, Alegret M, Muñoz E, Sainz A, Monte GC, Tolosa E (2007) Decreased frontal choline and neuropsychological performance in preclinical Huntington disease. *Neurology* **68**, 906-910.

[44] Wechsler D (1997). In *WAIS-III. Wechsler Adult Intelligence Scale-Third Edition.* Technical manual. The Psychological Corporation, San Antonio, TX.

[45] Wechsler D (1997). In *WMS-III. Wechsler Memory Scale-Third Edition*. Administration and scoring manual. The Psychological Corporation, San Antonio, TX.

[46] Rosen WG, Mohs RC, Davis KL (1984) A new rating scale for Alzheimer's disease. *Am J Psychiatry* **141**, 1356-1364.

[47] Peña-Casanova J (1991). In *Programa Integrado de Exploración Neuropsicológica*. Test Barcelona [Integrated program of neuropsychological assessment. Barcelona Test], Masson, Barcelona.

[48] Kaplan EF, Goodglass H, Weintraub S (1983). In *The Boston Naming Test*, Lea & Febiger, Philadelphia.

[49] Della Sala S, Laiacona M, Trivelli C, Spinnler H (1995) Poppelreuter-Ghent overlapping figures test. Its sensitivity to age, and its clinical use. *Arch Clin Neuropsychol* **10**, 511-534.

[50] Golden CJ (1980) In reply to Adams "In search of Luria' s battery : A false start". *J Consult Clin Psychol* **48**, 517-521.

[51] Erzigkeit H (1989) The SKT: A short cognitive performance test as an instrument for the assessment of clinical efficacy of cognitive enhancers. In: Berenger M, Reisberg B, eds. Diagnosis and treatment of senile dementia. Berlin, Springer Verlag, 164-174.

[52] Artiola L, Hermosillo D, Heaton R, Pardee RE (1999). In *Manual de normas y procedimientos para la batería neuropsicológica en español. M*, Press Tucson, Arizona.

[53] Del Ser T, Sánchez F, García de Yébenes MJ, Otero A, Zunzunegui MV, Muñoz DG (2004) Versión española del Test de los 7 Minutos. Datos normativos de una muestra poblacional de ancianos de más de 70 años. *Neurología* **19**, 344-348.

[54] Genovese CR, Lazar NA, Nichols T (2002) Thresholding of statistical maps in functional neuroimaging using the false discovery rate. *Neuroimage* **15**, 870-878.

[55] Maldjian JA, Laurienti PJ, Burdette JH (2004) Precentral gyrus discrepancy in electronic versions of the Talairach atlas. *Neuroimage* **21**, 450-455.

[56] Maldjian JA, Laurienti PJ, Kraft RA, Burdette JH (2003) An automated method for neuroanatomic and cytoarchitectonic atlas-based interrogation of fMRI data sets. *Neuroimage* **19**, 1233-1239.

[57] Lancaster JL, Summerln JL, Rainey L, Freitas CS, Fox PT (1997) The Talairach Daemon, a database server for Talairach Atlas Labels. *Neuroimage* **5**, S633.

[58] Lancaster JL, Woldorff MG, Parsons LM, Liotti M, Freitas CS, Rainey L, Kochunov PV, Nickerson D, Mikiten SA, Fox PT (2000) Automated Talairach atlas labels for functional brain mapping. *Hum Brain Mapp* **10**, 120-131.

[59] Chételat G, Desgranges B, de la Sayette V, Viader F, Eustache F, Baron JC (2003) Mild cognitive impairment. Can FDG-PET predict who is to rapidly convert to Alzheimer's disease? *Neurology* **60**, 1374-1377.

[60] Okamura N, Arai H, Maruyama M, Higuchi M, Matsui T, Tanji H, Seki T, Hirai H, Chiba H, Itoh M, Sasaki H (2002) Combined analysis of CSF tau levels and [123]Iodoamphetamine SPECT in mild cognitive impairment: Implications for a novel predictor of Alzheimer's disease. *Am J Psychiatry* **159**, 474-476.

[61] Buckner RL, Andrews-Hanna JR, Schacter DL (2008) The brain's default network: anatomy, function, and relevance to disease. *Ann N Y Acad Sci* **1124**, 1-38.

[62] Raichle ME, Snyder AZ (2007) A default mode of brain function: a brief history of an evolving idea. *Neuroimage* **37**, 1083-1090.

[63] Mishkin M, Ungerleider LG (1982) Contribution of striate inputs to the visuospatial functions of parieto-preoccipital cortex in monkeys. *Behav Brain Res* **6**, 57-77.

[64] Mummery CJ, Patterson K, Price CJ, Ashburner J, Frackowiak RSJ, Hodges JR (2000) A voxel-based morphometry study of semantic dementia: relationship between temporal lobe atrophy and semantic memory. *Ann Neurol* **47**, 36-45.

[65] Braak H, Braak E (1991) Neuropathological stageing of Alzheimer-related changes. *Acta Neuropathol* **82**, 239-259.

[66] Beversdorf DQ, Ferguson JLW, Hillier A, Sharma UK, Nagaraja HN, Bornstein RA, Sharre DW (2007) Problem solving ability in patients with mild cognitive impairment. *Cogn Behav Neurol* **20**, 44-47.

[67] Traykov L, Raoux N, Latour F, Gallo L, Hanon O, Baudic S, Bayle C, Wenisch E, Remy P, Rigaud AS (2007) Executive functions deficit in mild cognitive impairment. *Cogn Behav Neurol* **20**, 219-224.

[68] Espinosa A, Alegret M, Boada M, Viñas G, Valero S, Martínez-Lage P, Peña-Casanova J, Becker JT, Wilson BA, Tarraga Ll (2009) Ecological assessment of executive functions in Mild Cognitive Impairment and mild Alzheimer's Disease. *J Int Neuropsychol Soc* **15**, 751-757.

[69] Matsuda H (2007) The role of neuroimaging in mild cognitive impairment. *Neuropathology* **27**, 570-577.

Neural Correlates of Controlled Memory Processes in Questionable Alzheimer's Disease

Christine Bastin[a,*], Nacer Kerrouche[b], Françoise Lekeu[a,c], Stéphane Adam[c,d], Bénédicte Guillaume[c], Christian Lemaire[a], Joël Aerts[a], Géry d'Ydewalle[e], Fabienne Collette[a,d] and Eric Salmon[a,c]

[a]*Cyclotron Research Center, University of Liège, Liège, Belgium*

[b]*Greyou Medical, Constantine, Algeria*

[c]*Memory Center, CHU Liège, Liège, Belgium*

[d]*Neuropsychology Unit, University of Liège, Liège, Belgium*

[e]*Department of Psychology, University of Leuven, Leuven, Belgium*

Abstract. Alzheimer's disease (AD) is characterized by a progressive loss of controlled cognitive processes (processes requiring mental effort and attentional resources), and functional neuroimaging at early stages of AD provides an opportunity to tease out the neural correlates of controlled processes. Controlled and automatic memory performance was assessed with the Process Dissociation Procedure in 50 patients diagnosed with questionable Alzheimer's disease (QAD). The patients' brain glucose metabolism was measured using FDG-PET. After a follow-up period of 36 months, 27 patients had converted to AD, while 23 remained stable. Both groups showed a similar decrease in controlled memory processes but preserved automatic processes at entry into the study, suggesting that impairment of controlled memory would not be specific for AD. Patients who subsequently converted to Alzheimer type dementia showed significantly decreased brain metabolism at baseline compared to stable QAD in associative cortices known to be involved in AD (the left precuneus, the right inferior parietal lobule and bilateral middle temporal cortex).Voxel-based cognitive and metabolic correlations showed that a decrease in controlled memory processes was preferentially correlated with lower activity in the dorsomedial prefrontal and posterior cingulate cortices in very early AD patients. The dorsomedial prefrontal cortex would play a role in controlled memory processes as they relate to reflective and monitoring processes, while the posterior cingulate cortex is involved in the controlled access to previously encoded episodes. In stable QAD patients, reduced controlled performance in verbal memory correlated with impaired activity in the left anterior hippocampal structure, which would alter the reactivation of associations created at encoding.

Keywords: Alzheimer's disease, neuroimaging, cognitive impairment, FDG, memory, controlled processes

INTRODUCTION

In Alzheimer's disease (AD), controlled processes – processes requiring mental effort and attentional resources [1] - are affected early in the course of the dis-

ease, whereas automatic processing is relatively preserved in the early stages [2]. Even before the diagnosis of AD, future demented patients already present a specific disruption of controlled processes [3, 4]. In the memory domain, AD patients typically show impairments in controlled, explicit memory tasks, such as recall or recognition tests [5]. In contrast, implicit (more automatic) memory tasks, such as priming, are better preserved, although contradictory results have

*Correspondence to: Christine Bastin, Cyclotron Research Center, University of Liège, Allée du 6 Août, B30, 4000, Liège, Belgium, Tel.: +32 4 366 23 27; Fax: +32 4 366 29 46; E-mail: Christine. Bastin@ulg.ac.be.

been reported [6]. The ambiguity of the findings concerning implicit memory in AD may stem from the contamination of priming tasks by the use of explicit memory strategies. To overcome this contamination problem, Jacoby developed a paradigm (the Process Dissociation Procedure) that allows one to estimate the separate contributions of controlled versus automatic processes within a single verbal memory task [7]. The distinction is made possible by a comparison of two conditions (inclusion and exclusion) of word-stem completion in which these processes operate in different ways. Typically, in the inclusion condition, both controlled and automatic processes lead to the retrieval of a studied item. In the exclusion condition, automatic and controlled processes work in opposition, with the former leading to an erroneous answer, and the latter helping to consciously avoid it. Mathematical equations (described in the Methods section below) applied to the data provide separate estimates of the contributions of controlled and automatic memory processes. With this procedure, Adam et al. [8] confirmed the significant deterioration of controlled processes and the integrity of automatic processes in early AD patients.

Functional imaging is well suited to examine the neural correlates of controlled memory processes, as estimated by the Process Dissociation Procedure, in AD. Previous studies of correlation between cerebral activity and recall or recognition performance in AD have related explicit memory processing to a network of frontal, posterior associative and limbic regions [9, 10] (see [11], for a review of PET studies in AD). This suggests that the memory deficit in AD is not exclusively associated with a specific dysfunction of the medial temporal region, although that structure plays a central role in episodic memory [12] and is affected early in the course of the disease [13].

In this context, the aim of the present study was to tease out the neural correlates of controlled memory processing in AD. To disentangle consciously controlled from automatic memory processes, we adopted the Process Dissociation Procedure with a word stem completion task [14]. Moreover, because it has been suggested that a deficit affecting the controlled aspects of cognition may represent an early indicator of dementia [4], the study focused on the very early stages of AD. More specifically, we selected patients who were clinically characterized by a cognitive dysfunction that did not significantly disrupt their activities of daily living. Although the patients did not meet the criteria for dementia, they might still be in a very

early stage of AD (questionable Alzheimer's disease or QAD [15]). It has been shown that many such patients progress to dementia in the following years [16, 17].

Therefore, the current study using the Process Dissociation Procedure examined whether QAD patients present the same profile of impaired controlled memory processes and preserved automatic memory processes as early AD patients [8]. Moreover, the patients were followed up for 36 months in order to identify those who converted to AD. This allowed us to retrospectively compare future converters and stable QAD patients with regard to their performance on controlled and automatic memory components.

Among the risk factors associated with conversion to dementia, the level of education has been put forward in the cognitive reserve hypothesis [18]. According to this hypothesis, individuals with a high level of education have a reduced risk of developing Alzheimer's disease, possibly because they can optimize the efficiency of brain networks so that the impact of brain pathology is limited on their cognitive performance. As most studies examined the influence of educational level on the onset of AD in community-base cohorts of elderly people [19, 20], little is known on the effect of cognitive reserve in the conversion of QAD to AD. Moreover, even when dementia is diagnosed, cognitive deterioration differs as a function of education, with low-educated AD patients presenting with greater memory and attention deficits than high-educated patients [20]. So, we examined the influence of education level on controlled and automatic memory processes in QAD as a function of the clinical outcome.

Finally, images of the patients' brain glucose metabolism were obtained with FDG-PET. Voxel-based cognitive-metabolic correlations were used to identify the regions where metabolism was positively correlated with controlled memory processes in the QAD patients who subsequently went on to develop AD and those who remained stable in the following 36 months. Such analyses should help us to better understand the cerebral modifications underlying the decline in controlled memory processes in QAD, and specifically to clarify whether the neural correlates of controlled processes in the early stages of AD still involve the medial temporal lobe, which is already quite affected in early AD [13] or include frontal and posterior associative regions, as previously suggested [11].

MATERIALS AND METHODS

Participants

The study included 50 QAD patients (28 women) who were referred by neurologists working in memory clinics. Their mean age was 69 years old ($SD = 7.6$). The patients had completed an average of 11.5 years of education ($SD = 4.0$, range 5–22). Patients were classified as having a high educational level if they achieved at least a short secondary school levels (9 years of education), whereas they were classified as having a low educational level if they had a primary school level or less (less than 9 years of education, cf. [20]). They were selected on the basis of general examination, neurological and neuropsychological assessments, laboratory evaluation and structural neuroimaging. No subject had mental retardation, less than 4 years of education, brain trauma, epilepsy, cancer, depression, any major systemic disease or any substance abuse.

On the Clinical Dementia Rating (CDR) scale, the patients were all at stage 0.5, corresponding to questionable dementia with impaired memory, but preserved everyday skills, activities and self-care [15]. The neuropsychological profile of the patients was also compatible with the criteria for amnestic mild cognitive impairment (aMCI) proposed by Petersen et al. [17, 21]: memory complaints confirmed by a relative, memory deficits for their age and education (that is, performance 1.5 standard deviations below the mean of matched controls on at least one memory test), possibly additional cognitive dysfunction in another non-memory domain (42 amnestic single-domain MCI and 8 amnestic multiple-domain MCI), relatively preserved general cognitive function, preserved activities of daily living, and no dementia. Structural neuroimaging showed mild atrophy or mild leukoaraiosis, at most. All patients had Mini Mental State Examination (MMSE) scores of 22 and over.

At inclusion, they performed the experimental task and underwent a positron emission tomography examination using (^{18}F)fluoro-2-deoxy-D-glucose (FDG-PET). Both the experimental task and the FDG-PET were performed on the same day. Every 6 months, the QAD patients were re-evaluated with a neuropsychological battery, either until conversion or until 36 months had elapsed.

At the end of a follow-up of 36 months, 27 patients converted to dementia, meeting the criteria for AD [22] and 23 remained stable QAD. Conversion was seen in 6 multiple-domain aMCI patients (75%) and 21 single-

domain aMCI patients (50%). On average, conversion occurred 14 months ($SD = 9.8$) after the initial testing. Interestingly, most conversions occurred within 6 months ($n = 11$, including 3 multiple-domain aMCI) and 12 months ($n = 8$, including 3 multiple-domain aMCI). Three patients converted after 18 months, 3 after 30 months and 2 after 36 months. The cumulative frequency of conversion over time fits tightly with an exponential function ($R = .99$, see Fig. 1).

Appropriate approval and procedures were used concerning human subjects. Indeed, according to the Declaration of Helsinki (BMJ, 1991; 302: 1194), all participants gave their written consent to participate to the study, which was approved by the ethics committee of the University Hospital of Liège.

The experimental task was also administered to 21 healthy controls, without cognitive problems, as confirmed by a normal score on the Mattis Dementia Rating Scale (DRS [23]). They had no psychiatric problems, they were free of medication that could affect cognitive functioning, and they reported being in good health. In considering demographic and clinical data as a function of follow-up diagnosis (Table 1), the 23 stable QAD patients were younger than the 27 patients who subsequently converted to AD and the controls, and the converters scored lower on the initial Mattis DRS and the MMSE than the stable QAD subjects and the controls. In contrast, there was no difference in terms of education between the three groups. Moreover, the stable QAD subjects and the AD converters did not differ on measures of executive function such as the Stroop test [24] and a verbal fluency test.
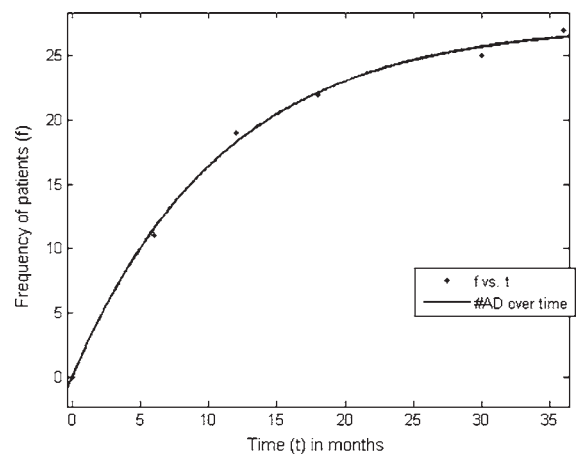
Fig. 1. Exponential conversion to AD over time in the AD converters group.

Table 1
Demographic and clinical data as a function of follow-up diagnosis

	AD converters	Stable QAD	Controls
Age	72.0 (5.9)*	67.1 (8.6)	71.7 (5.1)
Women/men	16/11	12/11	17/4
Education (years)	11.1 (3.8)	12.0 (4.2)	11.2 (3.05)
MMSE	25.5 (2.0)*	27.1 (1.6)	–
Mattis DRS[a]	131.5 (6.8)*	137.6 (5.2)	139.4 (2.3)
Stroop[b]	129.2 (82.8)	99.5 (58.3)	–
Verbal fluency[c]			
Phonological	18.6 (8.7)	18.3 (7.7)	–
Semantic	20.7 (6.3)	24.3 (8.4)	–

Note: Standard deviations appear in parentheses.
[a] Score available for 21 stable QAD patients, 23 AD converters and 20 controls.
[b] Time in seconds for interference condition minus time for naming condition.
[c] Number of words produced in 2 min, for letter P (phonological) and animals (semantic).
*Significant difference between groups, $p < .05$.

Experimental task

Participants were individually submitted to the French version of a stem completion task (described in details in Adam et al. [8]). The stimuli comprised 112 six-letter French words, for which the first three letters (stem) were all different. The task comprised two separate conditions (inclusion and exclusion). Condition order was counterbalanced across participants (half of them beginning with the inclusion condition).

Each condition involved the intermixed presentation of words and stems. Each word was presented on a computer screen for 3 s. Participants were asked to read the words aloud and to try and remember them. After a word had been encoded, the first three letters of this word appeared either immediately after presentation of the word (Lag 0), after three words (Lag 3) or after 12 words (Lag 12). During the retention interval, participants had to either encode new words or complete stems related to previously encoded words. The stems stayed on the screen until the participants gave an answer or for a maximum of 15 s. Participants had to complete them following two different sets of instructions according to the condition.

In the inclusion condition, participants had to complete the stem with a word that had been presented in the list. If they did not remember any such word, they were asked to complete the stem with the first six-letter word that came to mind. In the exclusion condition, participants were asked to avoid completing the stem with a previously studied word and to give a new six-letter word beginning with the same three letters.

Before the task started, participants were also informed that it would not always be possible to recall a previously seen word for some stems, because no corresponding word had actually been presented (baseline condition). In this case, they should give the first six-letter word that came to mind. The baseline condition gave the base-rate level of completion for stems (i.e. random probability of completing the stem with the chosen target word without having seen it).

Controlled and automatic processes can be assessed on the basis of the participants' performance in the two conditions. In the inclusion condition (I), participants were able to correctly complete a stem with a previously studied word because they consciously remembered it (C) or because it was the first word that came to mind automatically (A) without any recollection (1 – C). Thus, the probability of completing a stem with a previously presented word in the inclusion condition is formalized as $I = C + A(1 - C)$. By contrast, in the exclusion condition (E), participants might incorrectly complete the stem with a previously studied word because the word came automatically to mind (A) without any controlled memory of its prior appearance (1 – C). So, the probability of completing the stem with an old word in the exclusion condition is represented by $E = A(1 - C)$.

Given these two equations, an estimate of controlled processes is obtained by subtracting the proportion of exclusion trials completed with an old word from the proportion of inclusion trials completed with an old word: $C = I - E$. An estimate of automatic processes is computed by dividing the proportion of exclusion trials completed with a previously studied word by the estimated probability of a failure of controlled processes: $A = E / (1 - C)$.

PET acquisition method

PET images were acquired at entry only, in all patients, on a Siemens CTI 951 R 16/31 scanner during quiet wakefulness with eyes closed and ears unplugged after intravenous injection of 110 to 370 Mbq ^{18}F-2-fluoro-2-deoxy-D-glucose. Images of tracer distribution in the brain were used for analysis: scan start time was 30 min after tracer injection and scan duration was 20 min. Images were reconstructed using filtered backprojection including correction for measured attenuation and scatter using standard software.

Image processing

Using statistical parametric mapping (SPM5, Wellcome Department of Cognitive Neurology, London, UK), the PET data were subjected to an affine and non-

linear spatial normalization onto the SPM5 standard PET brain template. A mean image was then generated from all the resulting normalized images and smoothed using an 8-mm full-width at half-maximum isotropic Gaussian filter. This mean image served as a brain template specific to the patient group. Each PET image was then spatially normalized onto this group-specific brain template. Finally, images were smoothed with a 12-mm full-width at half-maximum filter.

Proportional scaling was used to control for individual variation in global ^{18}FDG uptake [25], as this is the best method in a scanner with a limited field of view, where the cerebellum is cut at different levels and cannot be taken as reference structure. To test hypotheses about region-specific effects, the parameters were estimated according to the general linear model at each voxel. The statistical analyses performed in SPM5 consisted of multiple regression analyses where individual PET images were entered as independent variable for each group (AD converters and stable QAD) and with the estimates of controlled memory processes (collapsed across Lags 3 and 12 to provide a single, more sensitive measure), age and MMSE score as covariates. Age and MMSE score served as nuisance variables because they differed between AD converters and stable QAD patients. In the AD converters group, time of conversion was also included as confounding variable. In order to isolate the metabolic correlates of controlled memory processes, linear contrasts were used to identify the brain regions where metabolism was positively correlated with controlled processes in each group. Clinical magnetic resonance imaging (MRI) had already been performed in most patients before their inclusion in the study, on a variety of machines, and we did not have the possibility of performing experimental structural MRI to correct the brain metabolism for atrophy in this population.

Based on the literature on functional neuroimaging of memory, specific brain coordinates associated with controlled memory processes were selected a priori for small volume correction (SVC) on whole brain statistical maps in SPM5. Interest in those areas was motivated by publications dealing with controlled retrieval from episodic memory and related concepts, such as retrieval success (i.e., retrieval of episodic information and explicit consciousness that information is old). Peak locations (in MNI coordinates) for areas associated with controlled and successful retrieval from memory were: (1) the medial temporal lobe, including the perirhinal cortex: –24 –16 –36 [26], the hippocampus: –15 –5 –25 [26], and the parahippocampal cortex: 21 –38 –14 [27]; (2) the left parietal cortex (BA 39/40): –39 –58 36 [28, 29]; (3) the posterior cingulate cortex: 0 –32 37 [30]; (4) the left anterior frontal cortex (BA 10/46): –35 52 11 [28, 31]; (5) the left inferior ventrolateral frontal cortex: –45 36 –2 (BA 45/47) and –47 16 26 (BA 44) [31]; and (6) the dorsomedial prefrontal cortex: –6 34 47 (BA 8 [30, 32].

We first searched for voxel-based correlation in the entire brain on SPM using a $p < .05$ (FWE-corrected for multiple comparisons) and a $p < .001$ (uncorrected). In the latter case, the SVC routine in SPM5 was subsequently used for confirmation, testing a priori hypotheses about brain coordinates of interest. Hypothesis-driven analyses were performed using a 10-mm sphere centred on the above-mentioned coordinates that corresponded to regions observed on the statistical parametric map at $p < .001$ uncorrected. The threshold of significance was set at $pSVC < .05$ corrected for multiple comparisons.

RESULTS

Behavioral data

Word stem completion

For the AD converters, the stable QAD patients and the control group, the proportions of stems completed with the target words in the baseline condition (new items), the inclusion condition (Lags 0, 3 and 12) and the exclusion condition (Lags 0, 3 and 12) are reported in Table 2.

First, analyses were performed on the probability of giving the target word when completing a stem even though this target word had not been seen earlier (i.e., new items). A 3 (Group: AD converters vs. stable QAD vs. controls) by 2 (Condition: inclusion vs. exclusion) analysis of variance (ANOVA) did not reveal any significant effect (all $ps > .31$). Thus, the probability of guessing was similar in all the groups and the same criterion was used to respond in both conditions.

Second, the proportion of completion of stems presented immediately after encoding of the corresponding word (Lag 0) was examined. There was no significant difference between the groups in either condition [inclusion: $F(2,68) = 0.85$, $p > .43$; exclusion: $F(2,68) = 1.42$, $p > .24$]. Thus, the patients were able to adequately follow the instructions, and so the estimates of controlled and automatic processes can be considered to be valid.

The proportion of stems completed with the target word in the inclusion condition was then analyzed

Table 2
Proportions of stems completed with target words as a function of condition (Inclusion versus Exclusion) and item type (new, Lag 0, Lag 3, Lag 12), and estimation of controlled and automatic processes in AD converters, stable QAD and controls

	AD converters		Stable QAD		Controls	
Inclusion New	.09 (.08)		.10 (.07)		.12 (.08)	
Exclusion New	.10 (.06)		.12 (.08)		.09 (.06)	
Inclusion Lag 0	.82 (.18)		.87 (.16)		.87 (.12)	
Exclusion Lag 0	.05 (.08)		.06 (.10)		.02 (.04)	
	Lag 3	Lag 12	Lag 3	Lag 12	Lag 3	Lag 12
Inclusion	.51 (.16)	.34 (.11)	.55 (.18)	.36 (.24)	.68 (.13)	.48 (.14)
Exclusion	.21 (.11)	.24 (.13)	.19 (.15)	.19 (.11)	.15 (.06)	.18 (.11)
Estimates of controlled processes	.30 (.20)	.10 (.19)	.36 (.22)	.20 (.27)	.54 (.14)	.30 (.18)
Estimates of automatic processes	.29 (.13)	.25 (.11)	.28 (.18)	.25 (.14)	.33 (.18)	.25 (.12)

Note: Standard deviations appear in parentheses

with Group (AD converters vs. stable QAD vs. controls) as between-subject variable and Lag (3 vs. 12) as within-subject variable. The results showed a main effect of Group, $F(2,68) = 7.82$, $MSE = 0.04$, $p < .01$. HSD Tukey test showed that the control group produced more target words than the QAD patients, but there was no difference between the AD converters and the stable QAD. The main effect of Lag was also significant, $F(1,68) = 94.69$, $MSE = 0.01$ $p < .01$. The completion score was better at Lag 3 than at Lag 12. Finally, the interaction was not significant, $F < 1$. In the exclusion condition, a 3 (Group) by 2 (Lag) ANOVA did not yield any significant result (all $ps > .09$).

Estimates of controlled and automatic processes

The estimates of controlled and automatic processes are shown in the lowest part of Table 2. Controlled process estimates underwent a two-way ANOVA (Group × Lag). The results revealed a main effect of Group, $F(2, 68) = 8.93$, $MSE = 0.06$, $p < .01$. Controlled processes were less efficient in the QAD patients than in the controls, with no difference between the two patient subgroups. There was also a main effect of Lag, $F(1,68) = 77.00$, $MSE = 0.01$, $p < .01$, showing a decrease in controlled processes as the retention interval increased (3 vs. 12). The Group by Lag interaction was not significant ($F < 1$). As for the estimates of automatic processes, a 3 (Group) by 2 (Lag) ANOVA showed a significant main effect of Lag, $F(1,68) = 5.03$, $MSE = 0.01$, $p < .05$. This effect showed that automatic processes were lower at Lag 12 than at Lag 3. Automatic processes did not differ between groups, and there was no interaction ($Fs < 1$).

Finally, as the women/men ratio differ between the patient group and the control group (56% of women in the patient group vs. 81% of women in the control group), the ANOVAs were also performed with gender as a between-subject variable. No difference as a function of gender was observed, and there was no significant interaction between gender and group.

Influence of the level of education on controlled and automatic processes

Among the AD converters, there were 20 patients with a high educational level (74%) and 7 patients with a low educational level. In the stable QAD group, there were 18 high-educated patients (78%) and 5 low-educated patients. There was no difference in the proportion of high- and low-educated patients between the groups (Chi-square = 0.12, $p > .72$). Given the small number of participants in some subgroups, between-group comparisons of controlled and automatic processes estimates were performed using non-parametric Mann-Whitney tests. The comparison of high-educated and low-educated patients in each group (converters and stable QAD) failed to reveal any significant difference on controlled and automatic estimates (all $ps > .14$). When the performance of each subgroup was compared with that of controls with the same educational level (4 controls with a low educational level and 17 controls with a high educational level), both the converters and the stable QAD with high educational level showed deficient controlled memory processes, $Z = -3.7$ and -1.9 respectively, $p < .05$, but preserved automatic memory processes, $Z = 0.09$ and 0.08 respectively, $p > .92$. The comparison of converters and stable QAD with low educational level ($n = 5$) versus controls ($n = 4$) failed to reach significance for controlled estimates, $Z = -1.6$, $p < .11$, and was not significant for automatic estimates, $Z = -0.2$ and 0.8 respectively, $p > .39$. However, given the very small number of participants included and the absence of difference in other comparisons, it certainly
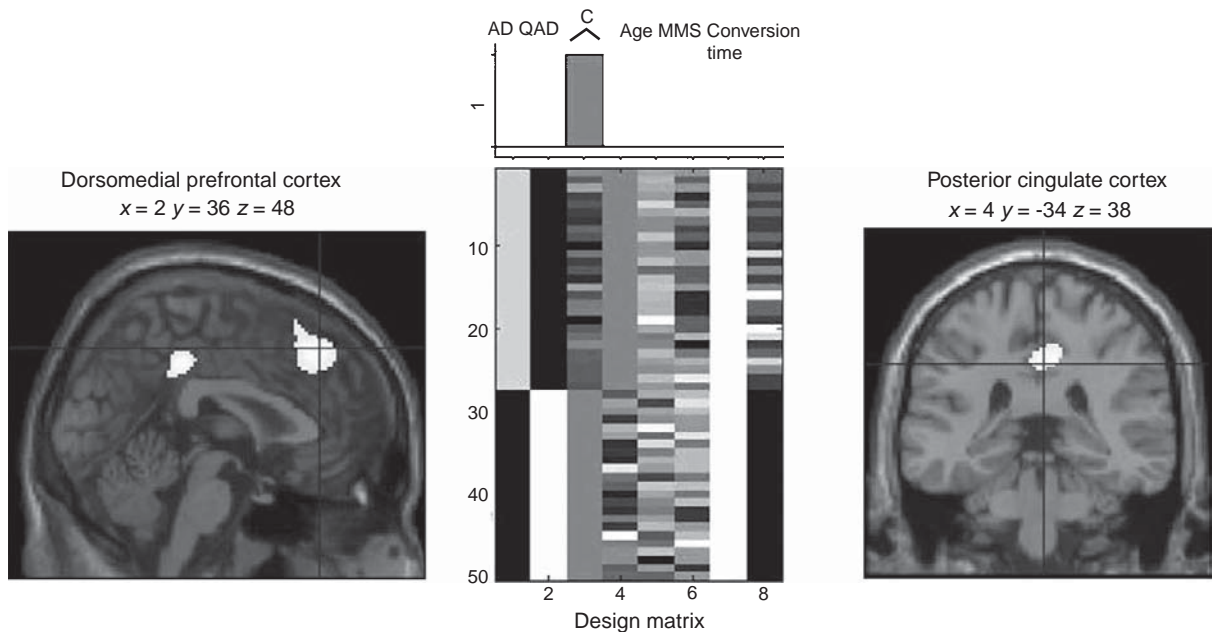
Fig. 2. Results of SPM5 analysis in the QAD patients who subsequently converted to AD: Positive correlation between metabolic activity of the dorsomedial prefrontal cortex and right posterior cingulate cortex and controlled memory processes (C) in the AD converters is displayed on a T1-weighted MRI, and the corresponding design matrix is shown.

is hazardous to conclude that low-educated patients had preserved controlled memory processes.

Metabolic data

Metabolic comparisons between converters and stable QAD

This comparison was performed in SPM5 taking age and MMSE score as confounding covariates. Patients who subsequently converted to Alzheimer type dementia showed significantly decreased brain metabolism at baseline compared to stable QAD ($p < .001$ uncorrected) in the left precuneus, the right inferior parietal lobule and bilateral middle temporal cortex. Such a distribution of impaired metabolism in associative cortices is classically observed in neuroimaging studies of AD patients [33, 34].

Cognitive and metabolic correlations

Voxel-based correlations were computed ($p < .05$ FWE-corrected and $p < .001$ uncorrected) for the AD converters and the stable QAD groups and SVC was further applied in specific brain coordinates associated with controlled and successful retrieval of information from episodic memory (*pSVC* FWE-corrected, voxel-level $< .05$).

When looking at the metabolic correlates of controlled memory processes at entry in the 27 patients who subsequently converted to AD (during the 36-month follow-up period), significant positive correlations were found in the right dorsal posterior cingulate cortex ($\sim$BA 31, MNI coordinates $x = 4$ $y = -34$ $z = 38$, *pSVC* corrected $< .05$) and the dorsomedial prefrontal cortex ($\sim$BA 8, MNI coordinates $x = 2$ $y = 36$ $z = 48$, p corrected for the entire brain $< .05$; see Fig. 2). This suggests that decreased activity in those dorsomedial and posteromedial regions is related to poorer controlled memory performances in very early AD patients.

In the 23 QAD patients who remained stable, lower scores of controlled memory processes were correlated with decreased metabolic activity in the left anterior medial temporal lobe (MTL), encompassing the hippocampus and the entorhinal cortex (MNI coordinates $x = -20$ $y = -6$ $z = -24$, *pSVC* corrected $< .05$, see Fig. 3).

DISCUSSION

This study aimed at examining the neural basis of controlled memory processes in the early stages of Alzheimer's disease. Controlled and automatic uses of
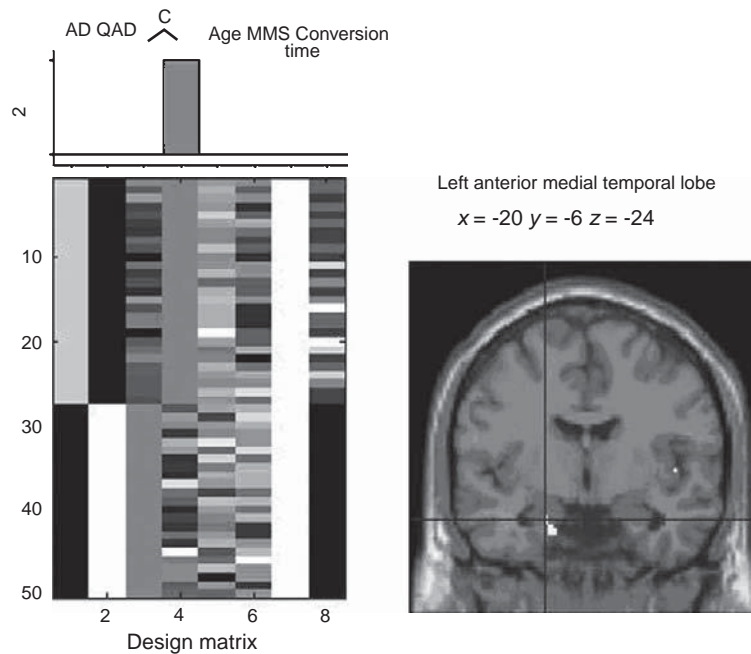
Fig. 3. Results of SPM5 analysis in the stable QAD patients: Positive correlation between metabolic activity of the left anterior medial temporal lobe and controlled memory processes (C) in the stable QAD is displayed on a T1-weighted MRI, and the design matrix is shown.

memory were isolated by means of the Process Dissociation Procedure and examined in a group of 50 QAD patients. After a follow-up period of 36 months, it was possible to compare the patients retrospectively as a function of the clinical outcome at the last neuropsychological testing (AD or stable QAD). The metabolic correlates of controlled memory processes in each subgroup were explored via FDG-PET images.

The main behavioural findings were that QAD patients showed impaired controlled memory processes, but preserved automatic processes. Moreover, the patients who subsequently converted to AD and those who remained stable could not be distinguished in terms of the severity of their controlled memory deficit at entry in the study. However, voxel-based cognitive and metabolic correlations suggested that the cerebral regions preferentially associated with controlled memory processes differed in the AD converters and the stable QAD patients.

At a clinical level, the follow-up of the patients with a neuropsychological battery confirmed that the diagnosis of QAD (or MCI) incorporates qualitatively different patients [16, 21]. It should be noted that the 50 patients analyzed in the study came from an original group of 59 QAD patients. Among the 9 patients who were not included in the analyses, five patients did not complete the follow-up, two converted to frontotemp-

ral dementia, one returned to the normal level and one was diagnosed with depression. Approximately 45% of the initial group progressed to AD in 3 years. This conversion rate is similar to what has previously been reported for follow-up periods of 36 to 48 months [35, 36]. Interestingly, most conversions to AD occurred within one year after entry into the study. Moreover, multiple-domain aMCI patients seemed to progressed to AD at a higher rate and earlier than single-domain aMCI patients, as previously reported [37]. A high level of education is known to delay the onset of Alzheimer's disease in community-based elderly people (e.g. [19]), but little is known on its influence on conversion in QAD populations. In the current study, there was no difference related to educational level between converters and stable QAD. It should be noted however that most patients were highly educated, and all but one passed the primary school diploma. Letenneur et al. [19] showed that the critical educational threshold is the achievement of the primary school diploma, as people who reached this threshold have a lower risk, independently of the number of years of education they completed afterwards. As almost all patients could be considered as high-education with regard to Letenneur et al.'s categorization, differences in educational level probably had a very limited impact, if any, on the progression to dementia in our sample.

Memory performances

At the behavioural level, QAD patients were characterized by a dissociation between impaired controlled memory processes and intact automatic processes. Even after the shortest retention interval (three intervening items), the patients found it difficult to consciously recall the previous occurrence of studied words. In contrast, when they failed to explicitly recall the studied word, the previous encounter with this word nevertheless influenced (primed) their response to the stem. So priming seems to be intact in QAD patients, at least when assessed by a word stem completion paradigm and when one uses a procedure that avoids contamination of implicit memory by explicit retrieval. This result extends to patients with QAD the dissociation between controlled and automatic processes previously observed in AD [8].

It is noteworthy that scores for controlled memory processes could not distinguish the patients who would develop dementia in the following 36 months from those who would not. At first sight, this finding somewhat contrasts with the idea that a deficit affecting controlled aspects of cognition represents an early indicator of dementia [4]. However, Fabrigoule et al. distinguished future converters from future normal participants, whereas our study compared two subgroups of cognitively impaired elderly participants. Thus, one could argue that stable QAD patients may eventually convert to AD later on. Moreover, we focused on the memory domain, while Fabrigoule et al. examined a general cognitive factor that incorporates controlled aspects of a variety of tasks. Actually, our results suggest that even if a deficit affecting particularly the controlled aspects of memory function is sensitive to early dementia, it may not be specific. In fact, such a deficit has been described in a number of other pathologies, such as depression [38], chronic pain [39] and hippocampal amnesia [40, 41].

Neural correlates of controlled processes in pre-dementia stages of Alzheimer's disease

Although the neural correlates of episodic memory were previously searched for in the AD literature [9, 10, 42–48], previous studies did not specifically assess controlled memory retrieval uncontaminated by automatic processes. Among the AD converters, we found that the poorer the controlled memory performance for cued retrieval, the lower the metabolism in the posterior cingulate cortex and in the dorsomedial prefrontal

cortex (BA 8). Thus, whereas important lesions of the medial temporal lobe are present very early in AD [13] and have sometimes been related to AD patients' impaired retrieval of information from episodic memory (e.g., Lekeu et al. [46]), the present study indicates that the deficit affecting controlled processes in episodic memory cannot be reduced to the prominent pathology of the hippocampal formation but is associated with a dysfunction of anterior and posterior medial cortical regions. This is also consistent with evidence that a relative dysfunction, at a pre-dementia stage, of medial frontal regions and posterior cingulate cortex is characteristic of future AD patients [33, 34, 49–51].

An association between controlled memory processes and the dorsomedial prefrontal cortex has been previously reported in the neuroimaging literature [52]. Activation of a nearby region has been reported in several fMRI studies of episodic memory, particularly when participants successfully recollected contextual information (during source or contextual memory [32, 53, 54] or for Remember versus Know responses [30]). Interestingly, a recent study showed that, in patients with mild AD, the proportion of correctly recollected words (as measured by Remember responses) correlated with metabolism in the frontal regions, including a dorsomedial prefrontal region very close to the one reported here [55]. The dorsomedial prefrontal cortex was also activated when normal participants elaborated on episodic memories and possible future episodic events [56]. Finally, in a PET study, D'Argembeau et al. [57] reported that the dorsomedial prefrontal cortex increased its activity when participants engaged in reflection about themselves, another person or society in contrast to at rest. They suggested that this region may play a role in the monitoring of personal or other persons' states or characteristics (e.g., considering one's own internal experience or understanding other people's mental states). Together, these neuroimaging data suggest that the dorsomedial prefrontal cortex plays a role in controlled memory processes as they relate to reflective and monitoring processes. These processes may be useful for monitoring the products of retrieval (including associated contextual information) and deciding whether the word generated in response to the stem has actually been studied.

The finding that the metabolic activity of the posterior cingulate cortex was positively correlated with successful use of controlled memory processes in the AD converters is in keeping with previous studies showing an involvement of this region in episodic memory performance of QAD patients [25, 58–60].

For example, Chételat et al. [25] found a relationship between verbal free recall performance in QAD and posterior cingulate glucose metabolism. Also, fMRI studies showed that MCI subjects activated the posterior cingulate cortex less than control participants during episodic memory retrieval [58, 60]. Moreover, the region found here corresponds to the locus of the posterior cingulate regions activated by recollection more than familiarity [30, 61], and by successful source retrieval [62]. Thus, the posterior cingulate cortex may play a role in the reactivation of previously encoded episodes.

Neural correlates of controlled processes in stable QAD

In the stable QAD patients, more efficient controlled memory processes were associated with higher metabolic activity in the anterior part of the left MTL, encompassing the hippocampus and entorhinal cortex. Previous imaging studies in healthy participants and in early AD suggested that the anterior hippocampal formation plays a role in reactivating associations created at encoding, allowing subjects to recollect the contextual details linked to items [26, 43, 63, 64]. The possibility that the left anterior medial temporal area is involved in associative retrieval is compatible with the demands of the present task, which consisted of cued recall in which a stem must reactivate an old word and potentially its associated context at encoding.

It should be considered that the anterior part of the parahippocampal region has also been associated with familiarity-based retrieval, that is, the feeling that a piece of information is old without any recollection of the context of encoding [65]. One cannot exclude a contribution of familiarity in the present task, because, in presence of a stem, a previously seen word may come automatically to mind and then be consciously judged as old because it feels familiar to the participant, although there is no recollection of contextual details. However, in fMRI studies of retrieval processes, familiarity is associated with deactivation, rather than activation, of the anterior medial temporal lobe. Yet, in the present study, a positive association was observed between anterior hippocampal/entorhinal metabolic activity and higher controlled memory performance.

Heterogeneity of metabolic correlations in QAD

The current findings of different brain correlates of controlled memory processes in AD converters and sta-

ble QAD may be interpreted in light of the dynamical brain changes over the course of mild cognitive impairment and early Alzheimer's disease. Early in the course of mild cognitive impairment, when dysfunction of the hippocampus and entorhinal cortex is still minimal, hyperactivation of the medial temporal lobe can be seen during a memory task performed in an fMRI scanner [66–68]. Regional cerebral blood flow measured with continuous arterial spin-labeling magnetic resonance imaging has also been found to be increased in the hippocampus and amygdala in MCI patients [69]. Increased activation/activity of the MTL may indicate that compensatory mechanisms are at work [69, 70]. Such compensatory processes may explain the relationship between MTL activity and controlled processes in some stable QAD patients. Indeed, patients with the highest MTL metabolism demonstrated better use of controlled memory processes. Hence, the stable QAD patients are at a sufficiently early stage, so that MTL activity can still support controlled memory processes.

When patients enter a more advanced stage of mild cognitive impairment, that follow-up revealed to be a very early AD stage, the medial temporal structures may be so damaged that they can no longer support memory processes, and then controlled memory processes are preferentially associated with other brain regions. In the present group of very early AD patients, controlled memory processes correlated with activity in the dorsomedial prefrontal and posterior cingulate cortices. This is consistent with the idea that MTL atrophy leads to some reorganization in brain functioning at the MCI stage of Alzheimer's disease. For instance, in QAD, the volume of right hippocampus and entorhinal cortex correlated negatively with perfusion in the medial and dorsolateral prefrontal cortex [71]. Increased perfusion of the prefrontal cortex has also been found in MCI who converted to AD within 2 years compared to controls and non-converters [72]. The results suggest that even at a very early AD stage, the MTL was too damaged to support memory processes and the much variable activity in dorsomedial prefrontal and posterior cingulate cortex was preferentially responsible for the variability in controlling the retrieval of information from episodic verbal memory.

Finally, it should be noted that the correlational approach used here underlined the existence of a continuum in the neuropsychological deficit demonstrated by the patients as well as in their functional brain damage. The analyses revealed that, within this functional continuum, there are two nodes, the variable activity of

which was more particularly associated with controlled memory processing: on the one hand, the medial temporal lobe in stable QAD patients, and on the other hand, the posterior cingulate/dorsomedial prefrontal regions in very early AD patients when damage to the MTL do no longer support individual performance in controlled processes.

Potential models of the neural correlates of controlled memory processes in dementia

It is interesting to note that the regions found to correlate with controlled memory processes in pre-dementia AD patients and stable QAD patients belong to the default network, a network of intrinsically correlated regions that activates during free-thinking in resting state and internally-focused tasks [73, 74]. The regions belong also to the core network which is involved in retrieving previous events and imagining future ones [56–75]. Previous studies have shown a disruption of the default network in Alzheimer's disease and mild cognitive impairment [76–82] and suggested a link with the memory deficit observed in the patients. The current data suggest that, within the default or core network, whose general function may be mental simulation or anticipating the future, the medial prefrontal cortex, the posterior cingulate cortex and the hippocampal formation are more specifically concerned with the controlled access to memory representations of personally experienced events. Recently, Jaffard et al. [83] proposed that, within the default network, the medial prefrontal cortex and the posterior cingulate cortex have a role in top-down inhibitory control, which serves to refrain from reacting automatically to events. Our results thus join them in relating these regions to the concept of controlled processes (see also [52]).

A concept closely related to that of control is consciousness. Although the distinctions conscious/unconscious and controlled/automatic are not interchangeable (i.e. controlled processes are not always conscious [84, 85]), Jacoby argued that the Process Dissociation Procedure applied to word stem completion distinguishes controlled and conscious reactivation of a memory trace from automatic and unconscious influence of memory on performance [14]. From this point of view, the current data can be related to the neuronal global workspace for conscious processing of information [86–88]. In this model, the neuronal global workspace constitutes a distributed neural system interconnected to distant cortical and subcortical processors specialized in the non-conscious processing of specific type of information. Via top-down mobilization, the neuronal global workspace can amplify information from a processor and make it experienced consciously and available to various processes, including memory, evaluation and verbal reports. In AD, the decrease in controlled processes of memories associated with a dysfunction of the medial frontal and posterior regions may represent an aspect of the dysfunction of the neuronal global workspace for conscious processing of information.

However, relating the neural correlates of controlled memory processes as measured by the Process Dissociation Procedure to theoretical models of consciousness is complicated by the ambiguous relationship between the concepts of consciousness and controlled processes. Moors [84] has proposed specific definitions of each concept. Thus, controlled processes refer to processes for which one has a goal (to engage the process or to stop it) and which end with the achievement of the desired effect. In contrast, consciousness refers to the availability of some content to a subjective feeling. In the present task, controlled completion of the stems with a studied word also involved awareness of its status as an old item. So the task did not allow assessing orthogonally controlled processes and consciousness. Formally, it is the distinction controlled/automatic that is put forward here, and the results suggest that, in very early AD, the dorsomedial prefrontal cortex and the posterior cingulate cortex are associated to top-down control over memory production.

ACKNOWLEDGMENTS

DISCLOSURE STATEMENT

There is no actual or potential conflict of interest for any author concerning this manuscript.

REFERENCES

[1] Schneider W, Shiffrin RM (1977) Controlled and automatic human information processing: I. Detection, search and attention. *Psychological Review* **84**, 1-66.

[2] Jorm AF (1986) Controlled and automatic information processing in senile dementia: A review. *Psychological Medicine* **16**, 77-88.

[3] Amieva H, Rouch-Leroyer I, Fabrigoule C, Dartigues JF (2000) Deterioration of controlled processes in the preclinical phase of dementia: A confirmatory analysis. *Dementia and Geriatric Cognitive Disorders* **11**, 46-52.

[4] Fabrigoule C, Rouch I, Taberly A, Letenneur L, Commenges D, Mazaux JM, Orgogozo JM, Dartigues JF (1998) Cognitive processes in preclinical phase of dementia. *Brain* **121**, 135-141.

[5] Collette F, Feyers D, Bastin C (2008) La maladie d'Alzheimer In *Neuropsychologie du vieillissement normal et pathologique,* Dujardin K, Lemaire P, eds. Masson, Paris pp. 105-122.

[6] Fleischman DA, Gabrieli JDE (1998) Repetition priming in normal aging and Alzheimer's disease: A review of findings and theories. *Psychology and Aging* **13**, 88-119.

[7] Jacoby LL (1991) A process dissociation framework : Separating automatic from intentional uses of memory. *Journal of Memory and Language* **30**, 513-541.

[8] Adam S, Van der Linden M, Collette F, Lemauvais L, Salmon E (2005) Further exploration of controlled and automatic memory processes in early Alzheimer's disease. *Neuropsychology* **19**, 420-427.

[9] Starr JM, Loeffler B, Abousleiman Y, Simonotto E, Marshall I, Goddard N, Wardlaw JM (2005) Episodic and semantic memory tasks activate different brain regions in Alzheimer disease. *Neurology* **65**, 266-269.

[10] Rémy F, Mirrashed F, Campbell B, Richter W (2005) Verbal episodic memory impairment in Alzheimer's disease: A combined structural and functional MRI study. *NeuroImage* **25**, 253-266.

[11] Salmon E, Lekeu F, Bastin C, Garraux G, Collette F (2008) Functional imaging of cognition in Alzheimer's disease using positron emission tomography. *Neuropsychologia* **46**, 1613-1623.

[12] Squire LR, Stark CEL, Clark RE (2004) The medial temporal lobe. *Annual Review of Neuroscience* **27**, 279-306.

[13] Braak H, Braak E (1991) Neuropathological stageing of Alzheimer-related changes. *Acta Neuropathologica* **82**, 239-259.

[14] Jacoby LL (2009) Memory, process-dissociation procedure In *The Oxford companion to consciousness*, Bayne T, Cleeremans A, Wilken P, eds. Oxford University Press, Oxford, 430-432.

[15] Morris JC (1993) The clinical dementia rating (CDR): Current version and scoring rules. *Neurology* **43**, 2412-2414.

[16] Petersen RC, Doody R, Kurz A, Mohs RC, Morris JC, Rabins PV, Ritchie K, Rossor M, Thal L, Winblad B (2001) Current concepts in Mild Cognitive Impairment. *Archives of Neurology* **58**, 1985-1992.

[17] Petersen RC, Negash S (2008) Mild Cognitive Impairment: An overview. *CNS Spectr* **13**, 45-53.

[18] Stern Y (2006) Cognitive reserve and Alzheimer disease. *Alzheimer Disease & Associated Disorders* **20**, 112-117.

[19] Letenneur L, Gilleron V, Commenges D, Helmer C, Orgogozo JM, Dartigues JF (1999) Are sex and educational level independent predictors of dementia and Alzheimer's disease? Incidence data from the PAQUID project. *Journal of Neurology, Neurosurgery & Psychiatry* **66**, 177-183.

[20] Le Carret N, Auriacombe S, Letenneur D, Bergua V, Dartigues JF, Fabrigoule C (2005) Influence of education on the pattern of cognitive deterioration in AD patients: The cognitive reserve hypothesis. *Brain and Cognition* **57**, 120-126.

[21] Petersen RC (2004) Mild cognitive impairment as a diagnostic entity. *Journal of Internal Medicine* **256**, 183-194.

[22] McKhann G, Drachman D, Folstein M, Katzman R, Price D, Stadlan EM (1984) Clinical diagnosis of Alzheimer's disease: report of the NINCDS-ADRDA Work Group under the auspices of Department of Health and Human Services Task Force on Alzheimer's Disease. *Neurology* **34**, 939-944.

[23] Mattis S (1973) Dementia Rating Scale; NFER-Nelson, Windsor, England.

[24] Stroop JR (1935) Studies of interference in serial verbal reactions. *Journal of Experimental Psychology* **18**, 643-662.

[25] Chételat G, Desgranges B, de la Sayette V, Viader F, Berkouk K, Landeau B, Lalevée C, Le Doze F, Dupuy B, Hannequin D, Baron J-C, Eustache F (2003) Dissociating atrophy and hypometabolism impact on episodic memory in mild cognitive impairment. *Brain* **126**, 1955-1967.

[26] Dobbins IG, Rice HJ, Wagner AD, Schacter DL (2003) Memory orientation and success: Separable neurocognitive components underlying episodic recognition. *Neuropsychologia* **41**, 318-333.

[27] Eldridge LL, Knowlton BJ, Furmanski CS, Bookheimer SY, Engel SA (2000) Remembering episodes : A selective role for the hippocampus during retrieval. *Nature Neuroscience* **3**, 1149-1152.

[28] Konishi S, Wheeler ME, Donaldson DI, Buckner RL (2000) Neural correlates of episodic retrieval success. *NeuroImage* **12**, 276-286.

[29] Wheeler MA, Buckner RL (2004) Functional-anatomic correlates of remembering and knowing. *NeuroImage* **21**, 1337-1349.

[30] Henson RNA, Rugg MD, Shallice T, Josephs O, Dolan RJ (1999) Recollection and familiarity in recognition memory: An event-related functional magnetic resonance imaging study. *The Journal of Neuroscience* **19**, 3962-3972.

[31] Velanova K, Jacoby LL, Wheeler MA, McAvoy MP, Petersen SE, Buckner RL (2003) Functional-anatomic correlates of sustained and transient processing components engaged during controlled retrieval. *The Journal of Neuroscience* **23**, 8460-8470.

[32] Dobbins IG, Foley H, Schacter DL, Wagner AD (2002) Executive control during episodic retrieval: Multiple prefrontal processes subserve source memory. *Neuron* **35**, 989-996.

[33] Chételat G, Eustache F, Viader F, De La Sayette V, Pélerin A, Mézenge F, Hannequin D, Dupuy B, Baron JC, Desgranges B (2005) FDG-PET measurement is more accurate than neuropsychological assessments to predict global cognitive deterioration in patients with mild cognitive impairment. *Neurocase* **11**, 14-25.

[34] Drzezga A, Lautenschlager N, Siebner H, Riemenschneider M, Willoch F, Minoshima S, Schwaiger M, Kurz A (2003) Cerebral metabolic changes accompanying conversion of mild cognitive impairment into Alzheimer's disease: A PET follow-up study. *European Journal of Nuclear Medicine and Molecular Imaging* **30**, 1104-1113.

[35] Bowen, Teri J, Kukull L, McCormick W, McCurry W, Larson SM, EB (1997) Progression to dementia in patients with isolated memory loss. *The Lancet* **349**, 763-765.

[36] Petersen RC, Smith GE, Ivnik RJ, Tangalos EG, Schaid DJ, Thibodeau SN, Kokmen E, Waring SC, Kurland LT (1995) Apolipoprotein E status as a predictor of the development of Alzheimer's disease in memory-impaired individuals. *JAMA* **273**, 1274-1278.

[37] Tabert MH, Manly JJ, Liu X, Pelton GH, Rosenblum S, Jacobs M, Zamora D, Goodkind M, Bell K, Stern Y, Devanand DP (2006) Neuropsychological prediction of conversion to Alzheimer disease in patients with mild cognitive impairment. *Archives of General Psychiatry* **63**, 916-924.

[38] Jerman F, Van der Linden M, Adam S, Ceschi G, Perroud A (2005) Controlled and automatic uses of memory in depressed patients: Effect of retention interval lengths. *Behaviour Research and Therapy* **43**, 681-690.

[39] Grisart JM, Van der Linden M (2001) Conscious and automatic uses of memory in chronic pain patients. *Pain* **94**, 305-313.

[40] Bastin C, Van der Linden M, Charnallet A, Denby C, Montaldi D, Roberts N, Mayes A (2004) Dissociation between recall and recognition memory performance in an amnesic patient with hippocampal damage following carbon monoxide poisoning. *Neurocase* **10**, 330-344.

[41] Turriziani P, Serra L, Fadda L, Caltagirone C, Carlesimo GA (2008) Recollection and familiarity in hippocampal amnesia. *Hippocampus* **18**, 469-480.

[42] Desgranges B, Baron JC, De La Sayette V, Petit-Tabou, MC, Benali K, Landeau B, Lechevalier B, Eustache F (1998) The neural substrates of memory systems impairment in Alzheimer's disease: A PET study of resting brain glucose utilization. *Brain* **121**, 611-631.

[43] Desgranges B, Baron JC, Giffard B, Chételat G, Lalevée C, Viader F, De La Sayette V, Eustache F (2002) The neural basis of intrusions in free recall and cued recall: A PET study in Alzheimer's disease. *NeuroImage* **17**, 1658-1664.

[44] Eustache F, Desgranges B, Giffard B, De La Sayette V, Baron JC (2001) Entorhinal cortex disruption causes memory deficit in early Alzheimer's disease as shown by PET. *NeuroReport* **12**, 683-685.

[45] Golby A, Silverberg G, Race E, Gabrieli S, O'Shea JO, Knierim K, Stebbins G, Gabrieli J (2005) Memory encoding in Alzheimer's disease: An fMRI study of explicit and implicit memory. *Brain* **128**, 773-787.

[46] Lekeu F, Van der Linden M, Chicherio C, Collette F, Degueldre C, Franck G, Moonen G, Salmon E (2003) Brain correlates of performance in a free/cued recall task with semantic encoding in Alzheimer disease. *Alzheimer Disease and Associated Disorders* **17**, 35-45.

[47] Sperling R (2007) Functional MRI studies of associative encoding in normal aging, mild cognitive impairment, and Alzheimer's disease. *Annals New York Academy of Sciences* **1097**, 146-155.

[48] Trivedi MA, Schmitz TW, Ries ML, Torgerson BM, Sager MA, Hermann BP, Asthana S, Johnson SC (2006) Reduced hippocampal activation during episodic encoding in middle-aged individuals at genetic risk of Alzheimer's disease: A cross-sectional study. *BMC Medicine* **4**, 1-14.

[49] Huang C, Wahlund LO, Svensson L, Winblad B, Julin P (2002) Cingulate cortex hypoperfusion predicts Alzheimer's disease in mild cognitive impairment. *BMC Neurology* **2**, 1-6.

[50] Johnson KA, Jones K, Holman BL, Becker JA, Spiers PA, Satlin A, Albert MS (1998) Preclinical prediction of Alzheimer's disease using SPECT. *Neurology* **50**, 1563-1571.

[51] Minoshima S, Giordani B, Berent S, Frey KA, Foster NL, Kuhl DE (1997) Metabolic reduction in the posterior cingulate cortex in very early Alzheimer's disease. *Annals of Neurology* **42**, 85-94.

[52] Vincent JL, Kahn I, Snyder AP, Raichle ME, Buckner RL (2008) Evidence for a frontoparietal control system revealed by instrinsic functional connectivity. *Journal of Neurophysiology* **100**, 3328-3342.

[53] Rugg MD, Henson RNA, Robb WGK (2003) Neural correlates of retrieval processing in the prefrontal cortex during recognition and exclusion tasks. *Neuropsychologia* **41**, 40-52.

[54] Simons JS, Owen AM, Fletcher PC, Burgess PW (2005) Anterior prefrontal cortex and the recollection of contextual information. *Neuropsychologia* **43**, 1774-1783.

[55] Rauchs G, Piolino P, Mézenge F, Landeau B, Lalevée C, Pélerin A, Viader F, De La Sayette V, Eustache F, Desgranges B (2007) Autonoetic consciousness in Alzheimer's disease: Neuropsychological and PET findings using an episodic learning and recognition task. *Neurobiology of Aging* **28**, 1410-1420.

[56] Addis DR, Wong AT, Schacter DL (2007) Remembering the past and imagining the future: Common and distinct neural substrates during event construction and elaboration. *Neuropsychologia* **45**, 1363-1377.

[57] D'Argembeau A, Collette F, Van der Linden M, Laureys S, Del Fiore G, Degueldre C, Luxen A, Salmon E (2005) Self-referential reflective activity and its relationship with rest: A PET study. *NeuroImage* **25**, 616-624.

[58] Johnson SC, Schmitz TW, Moritz CH, Meyerand MB, Rowley HA, Alexander AL, Hansen KW, Gleason CE, Carlsson CM, Ries ML, Asthana S, Chen K, Reiman EM, Alexander GE (2006) Activation of brain regions vulnerable to Alzheimer's disease: The effect of mild cognitive impairment. *Neurobiology of Aging* **27**, 1604-1612.

[59] Trivedi MA, Murphy CM, Goetz C, Shah RC, Gabrieli JDE, Whitfield-Gabrieli S, Turner DA, Stebbins GT (2008) fMRI activation changes during successful episodic memory encoding and recognition in amnestic mild cognitive impairment relative to cognitively healthy older adults. *Dementia and Geriatric Cognitive Disorders* **26**, 123-137.

[60] Ries ML, Schmitz TW, Kawahara TN, Togerson BM, Trivedi MA, Johnson SC (2006) Task-dependent posterior cingulate activation in mild cognitive impairment. *NeuroImage* **9**, 485-492.

[61] Woodruff CC, Johnson JD, Uncapher MR, Rugg MD (2005) Content-specificity of the neural correlates of recollection. *Neuropsychologia* **43**, 1022-1032.

[62] Lundstrom BN, Ingvar M, Petersson KM (2005) The role of precuneus and left inferior frontal cortex during source memory episodic retrieval. *NeuroImage* **27**, 824-834.

[63] Giovanello KS, Schnyer DM, Verfaellie M (2004) A critical role for the anterior hippocampus in relational memory: Evidence from an fMRI study comparing associative and item recognition. *Hippocampus* **14**, 5-8.

[64] Weis S, Specht K, Klaver P, Tendolkar I, Willmes K, Ruhlmann J, Elger CE, Fernandez G (2004) Process dissociation between contextual retrieval and item recognition. *NeuroReport* **15**, 2729-2733.

[65] Eichenbaum H, Yonelinas AP, Ranganath C (2007) The medial temporal lobe and recognition memory. *Annual Review of Neuroscience* **30**, 123-152.

[66] Dickerson BC, Salat DH, Greve DN, Chua EF, Rand-Giovannetti E, Rentz DM, Bertram L, Mullin K, Tanzi RE, Blacker D, Albert MS, Sperling RA (2005) Increased hippocampal activation in mild cognitive impairment compared to normal aging and AD. *Neurology* **65**, 404-411.

[67] Hämäläinen A, Pihlajamäki M, Tanila H, Hänninen T, Niskanen E, Tervo S, Karjalainen PA, Vanninen RL, Soininen H (2007) Increased fMRI responses during encoding in mild cognitive impairment. *Neurobiology of Aging* **28**, 1889-1903.

[68] Kircher TT, Weis S, Freymann K, Erb M, Jessen F, Grodd W, Heun R, Leube DT (2007) Hippocampal activation in patients with mild cognitive impairment is necessary for successful memory encoding. *Journal of Neurology, Neurosurgery, and Psychiatry* **78**, 812-818.

[69] Dai W, Lopez OL, Carmichael OT, Becker JT, Kuller LH, Gach HM (2009) Mild cognitive impairment and Alzheimer disease: Patterns of altered cerebral blood flow at MR imaging. *Radiology* **250**, 856-866.

[70] Dickerson BC, Sperling RA (2008) Functional abnormalities of the medial temporal lobe memory system in mild cognitive impairment and Alzheimer's disease: Insights from functional MRI studies. *Neuropsychologia* **46**, 1624-1635.

[71] Guedj E, Barbeau EJ, Didic M, Felician O, De Laforte C, Ranjeva J-P, Poncet M, Cozzone PJ, Mundler O, Ceccaldi M (2009) Effects of medial temporal lobe degeneration on brain perfusion in amnestic MCI of AD type: Deafferentation and functional compensation?. *European Journal of Nuclear Medicine and Molecular Imaging* **36**, 1101-1112.

[72] Huang C, Wahlund LO, Almkvist O, Elehu D, Svensson L, Jonsson T, Winblad B, Julin P (2003) Voxel- and VOI-based analysis of SPECT CBF in relation to clinical and psychological heterogeneity of mild cognitive impairment. *NeuroImage* **19**, 1137-1144.

[73] Buckner RL, Andrews-Hanna JR, Schacter DL (2008) The brain's default network. *Annals New York Academy of Sciences* **1124**, 1-38.

[74] Fox MD, Snyder AZ, Vincent JL, Corbetta M, Van Essen DC, Raichle ME (2005) The human brain is instrincisally organized into dynamic, anticorrelated functional networks. *Proc. Natl. Acad. Sci* **102**, 9673-9678.

[75] Schacter DL, Addis DR, Buckner RL (2008) Episodic simulation of future events: Concepts, data and applications. *Annals New York Academy of Sciences* **1124**, 39-60.

[76] Buckner RL, Sepulcre J, Talukdar T, Krienen FM, Liu H, Hedden T, Andrews-Hanna JR, Sperling RA, Johnson KA (2009) Cortical hubs revealed by intrinsic functional connectivity: Mapping, assessment of stability, and relation to Alzheimer's disease. *The Journal of Neuroscience* **29**, 1860-1873.

[77] Buckner RL, Snyder AZ, Shannon BJ, LaRossa G, Sachs R, Fotenos AF, Sheline YI, Klunk WE, Mathis CA, Morris JC, Mintun MA (2005) Molecular, structural, and functional characterization of Alzheimer's disease: Evidence for a relationship between default activity, amyloid, and memory. *The Journal of Neuroscience* **25**, 7709-7717.

[78] Greicius MD, Srivastava G, Reiss AL, Menon V (2004) Default-mode network activity distinguishs Alzheimer's disease from healthy aging: Evidence from functional MRI. *Proc. Natl. Acad. Sci* **101**, 4637-4642.

[79] Lustig C, Snyder AZ, Bhakta M, O'Brien KC, McAvoy M, Raichle ME, Morris JC, Buckner RL (2003) Functional deactivations: Change witha ge and dementia of the Alzheimer type. *Proc. Natl. Acad. Sci* **100**, 14504-14509.

[80] Rombouts SARB, Barkhof F, Goekoop R, Stam CJ, Scheltens P (2005) Altered resting state networks in mild cognitive impairment and mild Alzheimer's disease: An fMRI study. *Human Brain Mapping* **26**, 231-239.

[81] Sorg C, Riedl V, Mülhau M, Calhoun VD, Eichele T, Läer L, Drzezga A, Förstl H, Kurz A, Zimmer C, Wohlschläger AM (2007) Selective changes of resting-state networks in individuals at risk for Alzheimer's disease. *Proc. Natl. Acad. Sci* **104**, 18760-18765.

[82] Wang L, Zang Y, He Y, Liang M, Zhang X, Tian L, Wu T, Jiang T, Li K (2006) Changes in hippocampal connectivity in the early stages of Alzheimer's disease: Evidence from resting state fMRI. *NeuroImage* **31**, 496-504.

[83] Jaffard M, Longcamp M, Velay J-L, Anton J-L, Roth M, Nazarian B, Boulinguez P (2008) Proactive inhibitory control of movement assessed by event-related fMRI. *NeuroImage* **42**, 1196-1206.

[84] Moors A (2009)Automaticity In *The Oxford companion to consciousness*, Bayne T, Cleeremans A, Wilken P, eds; Oxford University Press, Oxford, pp. 91-94.

[85] Tzelgov J, Pinku G (2009) Cognitive control and consciousness In *The Oxford companion to consciousness*, Bayne T, Cleeremans A, Wilken P, eds. Oxford University Press, Oxford, pp. 139-140.

[86] Dehaene S, Naccache L (2001) Towards a cognitive neuroscience of consciousness: Basic evidence and a workspace framework. *Cognition* **79**, 1-37.

[87] Salmon E, Ruby P, Perani D, Kalbe E, Laureys S, Adam S, Collette F (2005) Two aspects of impaired consciousness in Alzheimer's disease In *Progress in brain research*, Laureys S, ed. Elsevier, Amsterdam, pp. 287-298.

[88] Dehaene S (2009) Neuronal global workspace In *The Oxford companion to consciousness*, Bayne T, Cleeremans A, Wilken P, eds. Oxford University Press, Oxford, pp. 466-469.

The Value of SPECT in Detecting Alzheimer-Type Neurodegeneration in Mild Cognitive Impairment

Flavio Nobili[a,*], Fabrizio De Carli[b], Giovanni B. Frisoni[c], Florence Portet[d], Frans Verhey[e], Guido Rodriguez[a], Anna Caroli[c,f], Jacques Touchon[d], Silvia Morbelli[g], Ugo P. Guerra[h], Barbara Dessi[a], Andrea Brugnolo[a] and Pieter Jelle Visser[e,i]

[a]*Clinical Neurophysiology Unit, Department of Neurosciences, Ophthalmology and Genetics, University of Genoa, Genoa, Italy*
[b]*Institute of Molecular Bioimaging and Physiology, National Research Council, Genoa, Italy*
[c]*LENITEM – Laboratory of Epidemiology Neuroimaging & Telemedicine, IRCCS San Giovanni di Dio Fatebenefratelli, Brescia, Italy*
[d]*Centre Memoire de Ressource et de Recherche, Service de Neurologie, CHU Guy de Chauliac, Montpellier, France*
[e]*Department of Psychiatry and Neuropsychology, University of Maastricht, Maastricht, The Netherlands*
[f]*Medical Imaging Unit, Biomedical Engineering Department, Mario Negri Institute, Bergamo, Italy*
[g]*Nuclear Medicine Unit, Department of Internal Medicine, University of Genoa, Genoa, Italy*
[h]*Nuclear Medicine Unit, Ospedali Riuniti of Bergamo, Bergamo, Italy*
[i]*Department of Neurology, VU University Medical Centre, Amsterdam, The Netherlands*

Abstract. Despite brain perfusion SPECT with technetium radiopharmaceuticals has not been formally included among the biomarkers for the early diagnosis of Alzheimer's disease (AD), its worldwide availability and the large literature evidence in AD and related disorders still make of it a valid alternative to FDG-PET, wherever the latter is unavailable. In this article, baseline brain SPECT has been evaluated in 80 subjects presenting with a cognitive complaint who have been followed for a mean of about two years, when twelve patients developed AD-dementia (AD-D), nineteen showed significant memory decline (D), and forty-three had normal cognition assessment (stable: S), while six patients dropped-out. Volumetric Regions of Interest (VROI) analysis was performed in six associative cortical areas in each hemisphere. ANOVA for repeated measures showed significant effects for both the group (S, D, and AD-D; $p < 0.004$) and VROI ($p < 0.0001$) factors, with significant group*region interaction ($p < 0.01$). At post-hoc comparison, hippocampal VROIs values were lower in AD-D than in D and S, while parietal VROIs values were lower in D and AD-D than in S. These four VROI significantly correlated with verbal delayed recall score at follow-up visit. Receiver operating characteristic (ROC) curves for the mean hippocampal VROI value showed 0.81 sensitivity with 0.86 specificity in separation of S + D from AD-D ($p < 0.0001$), and 0.69 sensitivity with 0.75 specificity in separation of S from D + AD-D ($p < 0.0002$). ROC curves for the mean parietal VROI value showed 0.62 sensitivity with 0.70 specificity in separation of S from D + AD-D ($p < 0.0002$). Baseline SPECT can support outcome prediction in subjects with MCI and assist clinicians in identifying MCI patients with biological signs of neurodegeneration of the AD-type in critical cortical areas.

Keywords: Subjective cognitive impairment, amnestic MCI, non-amnestic MCI, Alzheimer's disease, cognitive decline, brain SPECT

---

*Correspondence to: Flavio Nobili, Clinical Neurophysiology Unit, Department of Neurosciences, Ophthalmology and Genet-ics, Viale Benedetto XV, 6, University of Genoa, 16132 Genoa, Italy. Tel.: +39 010 3537568; Fax: +39 010 5556893; E-mail: flaviomariano.nobili@hsanmartino.it.

INTRODUCTION

There is a strong heterogeneity among non-demented subjects with cognitive complaints who access clinical evaluation. Secondary causes of cognitive impairment, such as systemic pathologies and drug abuse, should be ruled out. Detectable neurological and psychiatric diseases, mainly including cerebrovascular disease and depression, should be identified and treated. Even after these causes of cognitive disturbances are excluded, the underlying pathophysiological mechanisms remain to be clarified.

A part of these subjects does not actually show any objective impairment and are referred to as subjects with 'subjective memory complaints'. Some evidence points to a slightly increased risk to develop dementia in these subjects [1], which remains uncertain and considerably lower than in patients with objective cognitive deficit [2]. An objective cognitive deficit can be proven by neuropsychology, which also allows further classification into subjects with a memory deficit (amnestic Mild Cognitive Impairment, aMCI) and subjects with a deficit in other cognitive domains (non amnestic MCI, naMCI) [3]. These populations share a higher risk to develop dementia, but especially the former is prone to develop Alzheimer's disease (AD) [3, 4].

In the last years, efforts have been directed toward finding biomarkers of conversion to dementia in subjects with MCI. Some of these biomarkers have been established, such as medial temporal lobe (MTL) atrophy assessment at Magnetic Resonance Imaging (MRI), posterior temporal-parietal hypometabolism at Positron Emission Tomography (FDG-PET), and altered amyloid precursors and tau protein levels in cerebrospinal fluid, but they are supported by evidence mainly limited to subjects with aMCI [5]. Amyloid PET imaging is a new promising biomarker but, to date, amyloid tracers are not available on the market yet. These, as well as other potential biomarkers, have been poorly evaluated in subtypes of MCI other than aMCI, such as subjective memory complaints (SUBJ) and naMCI. According to the new proposed lexicon in AD, such biomarkers would allow the diagnosis of prodromal AD before dementia is clinically defined [6].

Brain perfusion Single Photon Emission Computed Tomography (SPECT) has been used for years in patients with cognitive disorders, yielding to the identification of topographic patterns of brain dysfunction in the main dementias [7]. In aMCI, perfusion SPECT has consistently replicated, although with a slightly lower accuracy, the main findings obtained with FDG-PET, showing hypoperfusion in the posterior temporal-parietal associative cortex, in the posterior cingulate-precuneus, and in the MTL [8–16]. The lower spatial resolution and sensitivity of SPECT as compared to FDG-PET is still counterbalanced by its wider availability and lower costs [17].

In a previous paper, baseline SPECT findings in different subtypes of MCI, classified according to their neuropsychological profile, were reported at their first access to memory evaluation units [16]. Superficial temporal hypoperfusion in both hemispheres was found both in aMCI and naMCI groups, while hippocampal hypoperfusion characterized aMCI and lateral frontal hypoperfusion characterized naMCI. On the other hand, no significant changes were observed in SUBJ in comparison to controls. While SPECT data in aMCI confirmed the results of previous SPECT studies, novel findings were reported both in naMCI and SUBJ subjects, highlighting new potentials of SPECT in the basal evaluation of subjects with subtypes of MCI.

Most of those subjects taking part in the baseline SPECT study has been followed-up through clinical and neuropsychological assessment for a mean of about two years. They were re-classified at the last follow-up visit into subjects without memory decline (*stable* = S), with memory decline but not demented (D), or with dementia of the Alzheimer type (AD-D). Baseline SPECT measures were re-considered according to this new grouping, in order to pick out prognostic differences of cerebral perfusion at baseline evaluation.

METHODS

Subjects

The 'DESCRIPA' multicenter study (http://www.descripa.eu/) is an EU-funded concerted action (5th framework program) undertaken by European dementia clinics in the frame of the European Alzheimer Disease Consortium (EADC; http://eadc.alzheimer-europe.org/). DESCRIPA is aimed to the development of screening guidelines and clinical criteria of predementia AD.

The inclusion criteria, detailed elsewhere [16, 18], basically included outpatients aged 55 years or older, newly referred for cognitive complaints but without dementia. All kinds of referrals were considered,

including self- or relative-referral, referral from general practitioner and from first-level neurological or geriatric clinics. Cognitive complaints mainly included memory complaints but they could also include difficulties in other cognitive domains, such as attention and orientation. All the secondary causes of cognitive impairment were excluded, as previously described [18]. Dementia at baseline was excluded by the clinical interviews with subjects and caregivers and by means of formal questionnaires assessing the basic and instrumental activities of daily living. At last, subjects were classified into those without any objective deficit (SUBJ) and those with an objective deficit, either in the memory domain (aMCI) or in non-memory domains (naMCI).

Perfusion SPECT was optional in the research protocol and SPECT results were not used to classify subjects. SPECT was performed at baseline in six DESCRIPA centers, but the present study concerns only the three centres using [99m]TC-ECD. After baseline visit, a yearly clinical-neuropsychological follow-up started. The study was approved by the local Medical Ethics Committee in each centre.

Definition of MCI subtypes

The baseline assessment has been detailed previously [18]. Briefly, all subjects underwent a standard battery of examinations, including clinical history, medical and neurological examinations, laboratory tests, functional evaluation using the Clinical Dementia Rating scale (CDR), rating scales for depression and neuropsychiatric symptoms, a neuropsychological test-battery, and structural neuroimaging. General cognition was assessed using the Mini-Mental State Examination (MMSE). Depression was assessed by the 15-item Geriatric Depression Scale or the Center for Epidemiologic Symptoms of Depression (CES-D) scale [19]. A depressive trait was defined according to the standard cut-off of each scale.

In each center, a battery of neuropsychological tests was performed to assess cognitive performance in the domains of memory, language, executive function and attention, and visuoconstruction. Raw scores were converted to age, education, and gender corrected Z-scores according to locally collected or published normative data and these Z-scores were used for further analysis, as described elsewhere [16, 18].

Baseline classification included 3 groups, on the basis of test performances in these cognitive domains. Impairment was defined as a Z-score of –1.5 or lower.

Subjects without impairment in any domain were classified as SUBJ. aMCI and naMCI were defined according to Petersen et al. [20]. The aMCI and naMCI subgroups were not subdivided into single or multiple domain subgroups in order to avoid groups with too few subjects to be analysed.

Due to variability among the neuropsychological protocols, the tests used to define MCI subtypes varied between centres, as detailed in the baseline SPECT paper [16]. This was due to the observational nature of the Descripa study, as approved by the European Commission, according to which each center should have used the routinely applied tests. In detail, the tests for memory were the learning measure and delayed recall measure of the Rey Auditory Verbal Learning test (1 centre), of the Buschke-Fuld Selective Reminding test (1 center), or of the Grober-Buschke test (1 center). The tests for language were 1-minute verbal fluency for animals (1 center), 2-minute verbal fluency for animals (1 center), or 1-minute verbal fluency for fruits, animals and car trades (1 center). Executive function and attention were assessed with the Trail Making Test part A and B (TMT A and B) in all centers. The tests for visuoconstruction were the copy subtest of the Rey-Osterrieth complex figure (2 centers) and the copy of figures from the Mental Deterioration Battery (1 center).

Follow-up examination

The 80 subjects started the yearly-based follow-up in the same way as the rest of the DESCRIPA population, undergoing the same clinical and neuropsychological assessment as at baseline. The last available follow-up visit was considered. This varied between 1 and 3 years. Five subjects dropped out before reaching the 1-year visit and were excluded. The remaining 75 subjects (93.7%) were classified as follows. Subjects with normal clinical and neuropsychological examinations were labelled as 'stable' (S) (mean follow-up time: 2.2 ± 0.7 years). Subjects with a Z score < 1.5 on the delayed recall measure of verbal episodic memory test were labelled as 'significant memory decline' (D) (mean follow-up time: 2.1 ± 0.9 years). Finally, subjects matching the NINCDS-ADRDA and the DSM-IVr criteria for AD were diagnosed as AD dementia (AD-D; diagnosis made 1.3 ± 0.5 years after the baseline visit, but all still followed for at least two years). One patient developed fronto-temporal dementia according to the current criteria [21] and was excluded from further analysis. Diagnoses were made

in each centre by a multidisciplinary team blinded for baseline (including SPECT) data.

SPECT acquisition and reconstruction

Subjects underwent ^{99m}Tc-ECD SPECT 0.1 ± 0.2 (mean $\pm$ SD) years after the baseline clinical assessment, according to the guidelines of the European Association of Nuclear Medicine [22]. About 1000 MBq of ^{99m}Tc-ECD were injected i.v. through a catheter while the subject was lying on a reclining chair, in a silent and dimly-lit room, eyes closed and ears unplugged, being unaware of injection. Thirty to ninety min after injection, image acquisition started for a time ranging from 20 to 35 min. Radius of rotation was < 15 cm. A 2-head camera, equipped with low-energy, high-resolution, parallel beam collimators, was employed in Brescia (Helix, Elscint) and in Genoa (Millenium VG, General Electric), and a 3-head camera, equipped with low-energy, ultra high-resolution, fan beam collimators, in Montpellier (Prism 3000, Picker).

Image reconstruction and post-processing procedures were undertaken in order to reduce inhomogeneity among centres [16]. Briefly, a 1-mm thick glass capillary was acquired in each centre and transmitted together with the subjects' scans to the elaboration centre in Genoa, where data reconstruction was performed. On the basis of the analysis on the capillary data, it could be concluded that the camera plus collimator performance was nicely comparable among the three centers in terms of spatial resolution. The number of acquired angular views was 120 in Brescia and Genoa and 90 in Montpellier. In principle, the 3-head gamma camera could generate data of better quality in comparison with the other 2 cameras, but the choice of acquiring only 90 projections in Montpellier generated images of quite comparable quality. The projections were reconstructed with the Ordered Subsets Expectation Maximization algorithm (8 iterations, 10 subsets) followed by 3D Gaussian postfiltering (FWHM = 9 mm). The projector-backprojector pair embedded in the iterative algorithm compensated for the camera spatial resolution and for attenuation [23, 24]. Attenuation was modelled to be uniform (linear attenuation coefficient = 0.10 cm^{-1}) inside the skull volume, which was automatically computed based on the head skin contour uptake. In this way, the peculiar anatomical features of each subject were accounted for. No scatter subtraction was performed. After inspecting some sample images,

the same value for the linear attenuation coefficient was judged to be applicable to the reconstruction of data from the three centres. Independently of the original pixel size on the detector, all images were reconstructed with an isotropic voxel side of 2.35 mm.

Volumetric Regions of Interest (VROI)

SPECT images were normalized in the Montreal Neurological Institute space using Statistical Parametric Mapping (SPM2). A study-specific ^{99m}Tc-ECD SPECT template, generated using both SPECT and MRI scans of a MCI group [25], was used. This allows for a better normalisation procedure, since both the deep and cortical hypoperfusion effects are taken into account. The following VROI were chosen in each hemisphere from the Pick atlas by a subroutine implemented on SPM2 [26]: hippocampus and para-hippocampal gyrus as taken together, posterior cingulate, precuneus, medium frontal gyrus, inferior parietal lobule and superior temporal gyrus (Fig. 1). The choice of these regions was based on previous SPECT and PET studies in subjects with MCI [8–11, 13, 15, 27–31]. The whole cerebellum was chosen for normalization of VROI counts.

Statistics

The following analyses used VROI values, corrected for age and center, since the statistical analysis on baseline data had already showed a significant effect of both these variables ($p < 0.05$). Vascular risk factors and other clinical features, such as the presence of treated thyroid disease and depression, as well as years of education were not considered because they did not show any effect on SPECT data in the analysis at baseline [16].

ANOVA for repeated measures was run on SPECT data of the 74 subjects, considering the three groups (S, D, AD-D) as between-subject source of variation, VROI as within-subject source of variation, and group*VROI interaction. SPECT data distribution within each region and group was preliminarily evaluated by Shapiro-Wilk statistic in order to detect deviations from the normal distribution and to apply suitable transformations. The same statistic was then applied to ANOVA residuals to check for fulfillment of basic assumptions.

Post-hoc analysis of between-group differences in each region was performed by applying the Duncan multiple range test. Moreover, correlation was assessed
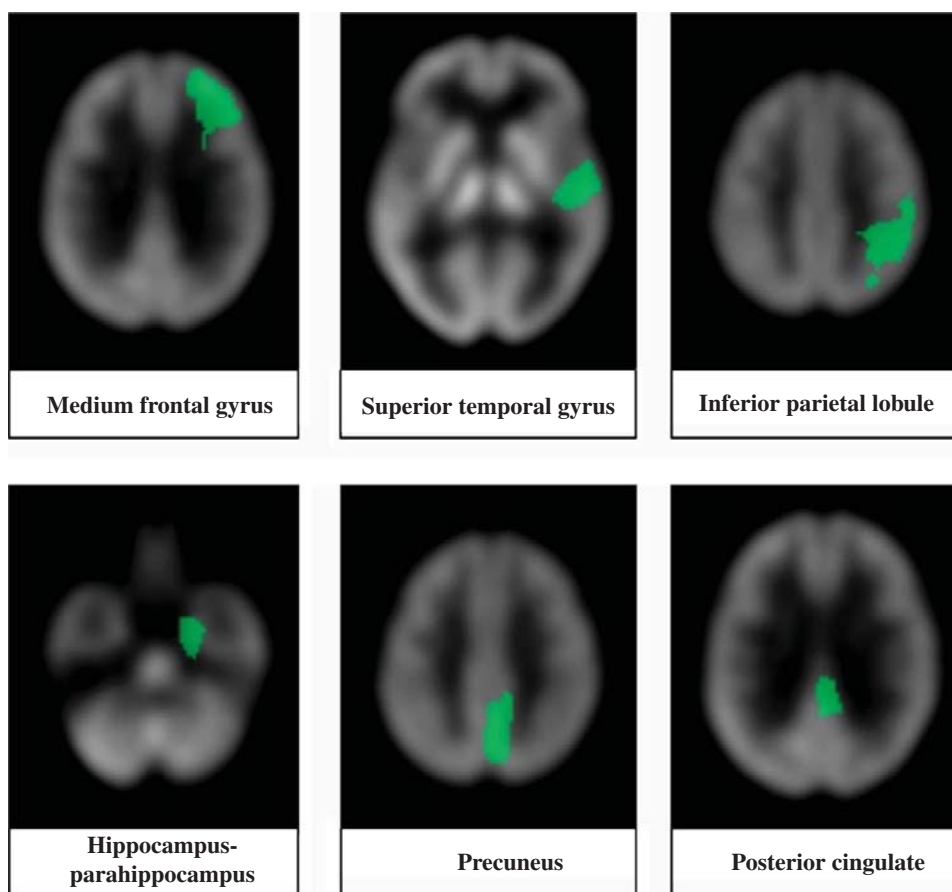
Fig. 1. Volumetric regions of interest (VROIs) are selected according to the Pick atlas, a sub-routine implemented in SPM, superimposed to transaxial sections of a ^{99m}Tc-ECD SPECT MCI-specific template. Example images of medium frontal gyrus, superior temporal gyrus, inferior parietal lobule, hippocampus and the para-hippocampal gyrus, precuneus and posterior cingulate are shown in the left hemisphere.

between those VROI that significantly differed among groups and the Z score of verbal episodic memory test (delayed recall) at follow-up. To this purpose, the product-moment correlation (Pearson) between each VROI and the Z score at the memory test was computed and suitably transformed into t-value in order to estimate the associated probability level.

Finally, the receiver operating characteristic (ROC) curves were computed for the VROI yielding significant differences among groups. ROC curves were computed in all subjects. Morever, since just one subject in the SUBJ group showed memory decline at follow-up (which might 'spuriously' increase the specificity in the whole sample of 74 subjects), ROC curves were also computed after eliminating the SUBJ group (i.e., naMCI + aMCI) and then in aMCI group only. For ROC curves, the area under curve (AUC) with the associated significance level, and the optimal

threshold of perfusion level, with associated sensitivity and specificity values, were computed. The optimal threshold was estimated by searching along the ROC curve for the point closest to (0, 1), i.e., the point yielding maximum sensitivity and specificity.

Statistical analyses were performed using the statistical package of SAS software (SAS/STAT, v.8.1, Copyright© 1999 SAS Institute Inc., Cary, NC, USA) and RocKit software (ROCKIT, Kurt Rossmann Laboratories for Radiologic Image Research, University of Chicago, Chicago, IL, USA).

RESULTS

According to baseline classification, there was no significant difference for age, years of education, CDR-Sum of Boxes (CDR-SB), vascular risk fac-

Table 1
Main characteristics of 74 patients observed at follow-up, according to follow-up classification

	All subjects (n = 74)	1. Stable (n = 43)	2. Decline (n = 19)	3. AD-D (n = 12)	Statistics Overall p value	Group comparisons
Baseline classification	**22 SUBJ**	**21 SUBJ**	**1 SUBJ**			
	16 naMCI	**13 naMCI**	**2 naMCI**	**1 naMCI**		
	36 aMCI	**9 aMCI**	**16 aMCI**	**11 aMCI**		
Age, years (SD)	72.1 (6.9)	71.0 (6.2)	75.0 (8.8)	71.6 (4.7)	n.s.	
Sex, n female (%)	41 (55)	24 (55.8)	10 (52.6)	7 (58.3)	n.s.	
Education, years (SD)	9.7 (4.4)	9.2 (4.3)	10.3 (3.6)	10.4 (5.9)	n.s.	
MMSE (SD)	27.4 (2.2)	28.7 (1.6)	26.2 (1.6)	24.7 (1.1)	$p < 0.01$	3 < 2 < 1
CDR-SB (SD)	1.6 (0.9)	1.2 (0.5)	1.7 (0.9)	2.6 (1.2)	$p < 0.01$	3 < 1,2
Hypertension, n (%)	39 (52.7)	25 (58)	10 (53)	4 (33)	n.s.	
Diabetes Mellitus, n (%)	2 (2.7)	1 (2)	1 (5)	0	n.s.	
Hypercholesterolemia, n (%)	33 (44.6)	22 (51)	6 (32)	5 (42)	n.s.	
Ischemic heart dis., n (%)	8 (10.8)	4 (9)	2 (11)	2 (17)	n.s.	
Thyroid disease, n (%)	10 (13.5)	5 (12)	4 (21)	1 (8)	n.s.	
Current smoking, n (%)	8 (10.8)	4 (9)	3 (16)	1 (8)	n.s.	
Depression, n (%)	19 (25.7)	11 (26)	3 (16)	5 (42)	$p < 0.05$	1,2 < 3
White matter hyperintensities	**(n = 50)**	**(n = 29)**	**(n = 12)**	**(n = 9)**		
ARWMC score (SD)*	5.75 (3.9)	6.2 (4.2)	4.7 (2.2)	5.7 (5.1)	n.s.	

One-way ANOVA was performed to test between-group differences for quantitative variables; the Fisher's exact test was applied to compare frequencies for categorical variables. The last column reports separation among groups when descriptive statistic indicates a significant difference. SUBJ = subjective cognitive complaints; naMCI = non amnestic Mild Cognitive Impairment; aMCI = amnestic Mild Cognitive Impairment; MMSE = Mini-Mental State Examination; CDR-SB = Clinical Dementia Rating scale – Sum of Boxes; ARWMC = Age-Related White Matter Changes scale. SD = standard deviation; AD = Alzheimer's disease. * Values recorded at baseline. The numbers in bold following white matter hyperintensity refer to the number of subjects in whom MRI data are available. Of the original 80 patients, five dropped-out during follow-up and one developed fronto-temporal dementia.

tors, depression, and white matter hyperintensity score among groups (Table 1, top). A prevalence of females was found in naMCI group, whereas the MMSE score was lower in aMCI group.

At follow-up visit, 21 out of 23 subjects with SUBJ had no memory impairment (S), one showed memory impairment (D) and one dropped-out. Thirteen out of the 17 naMCI subjects did not show memory impairment at follow-up (S), 2 showed memory impairment (D), one developed AD-D, and one dropped-out. Finally, 9 aMCI subjects no longer had memory decline (S), 16 showed again memory impairment (D), 11 developed AD-D, 1 FTD, and 3 dropped-out. Therefore, according to follow-up classification, there were 43 S subjects (21 from SUBJ, 13 from naMCI, 9 from aMCI), 19 D subjects (1 from SUBJ, 2 from naMCI, 16 from aMCI) and 12 AD-D patients (1 from naMCI, 11 from aMCI).

The main characteristics of these 74 subjects are shown in Table 2, according to follow-up classification. The MMSE score progressively declined from S to D and to AD-D groups, whereas the CDR-SB was significantly higher in AD-D group than in the other two groups.

Shapiro-Wilk statistic showed minor deviations from normal distribution (involving four region-group subsamples out of 36 at 0.05 probability level) which were balanced by data standardization at zero mean, followed by asymmetric power transform. No significant deviations from normal distribution were found by Shapiro-Wilk test applied to ANOVA residuals.

ANOVA for repeated measures on SPECT data showed a significant effect of region ($F = 170.9$, $p < 0.0001$), a significant effect of follow-up grouping ($F = 5.95$, $p < 0.004$), and a significant group*region interaction ($F = 2.66$, $p < 0.01$).

The post-hoc comparison between regions showed significantly hypoperfusion in the AD-D group versus the other two groups in the left ($F = 12.95$, $p < 0.0001$) and right ($F = 18.97$, $p < 0.0001$) hippocampus. Instead, significantly hypoperfusion was found in right ($F = 8.25$, $p < 0.0006$) and left ($F = 4.33$, $p < 0.02$) parietal lobules in both D and AD-D groups in comparison to S group. Finally, hypoperfusion ($F = 2.73$, $p = 0.07$, borderline significance) was found in the right posterior cingulate in AD-D group versus S group, while D group could not be distinguished from either AD-D or S (Fig. 2).
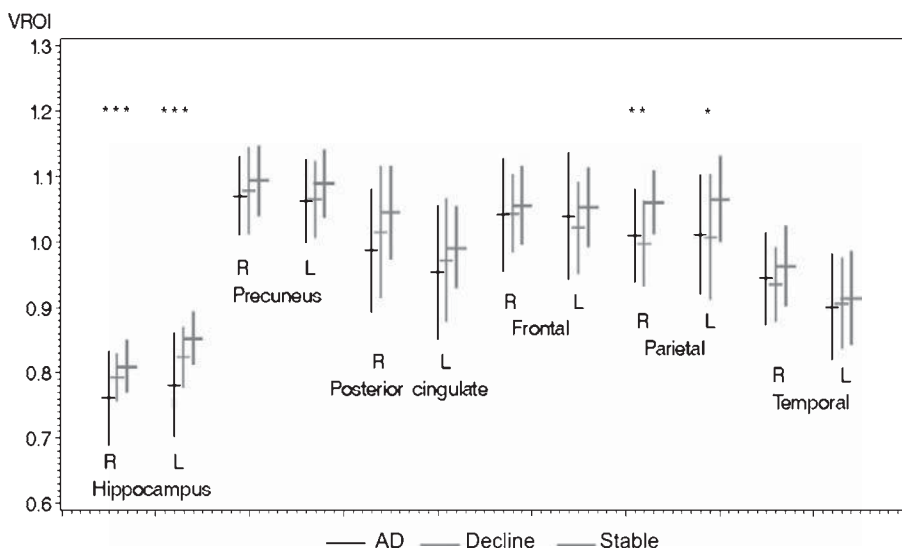
Fig. 2. Graphs of the mean (and standard errors) VROI values (y axis) for the three groups at follow-up (AD-D, D, and S). These mean VROI values have been obtained by averaging the individual mean VROI value, normalized on the cerebellum, of each patient belonging to the group. Data in AD-D (black lines), D (thin grey lines) and S (thick grey lines) are shown in this order. Significance levels (*: $p < 0.02$; **: $p < 0.001$; ***: $p < 0.0001$) refer to post-hoc Duncan's multiple range test, following repeated measures ANOVA.

Perfusion values and verbal delayed recall Z score at follow-up were directly correlated just in the same five regions that also yielded significant perfusional differences among groups, namely the left hippocampus ($r = 0.495$, $p < 0.0001$) (Fig. 3), right hippocampus ($r = 0.393$, $p < 0.0007$), right parietal lobule ($r = 0.424$,
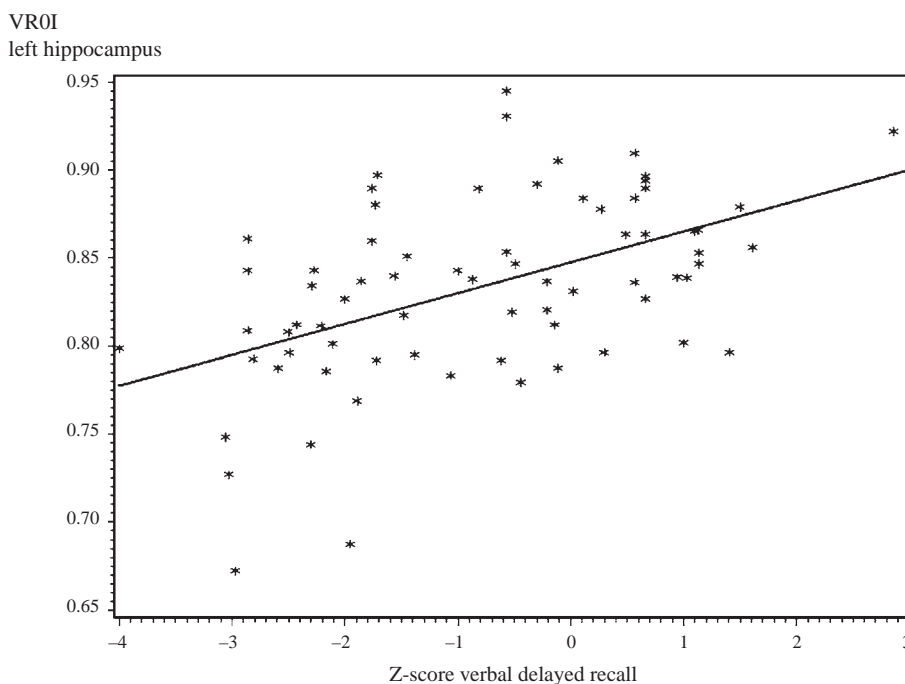
Fig. 3. Correlation between left hippocampal perfusion (normalised on mean cerebellar counts) and verbal memory test (delayed recall) Z scores at follow-up in the whole sample of 74 subjects. A highly significant correlation was found ($r = 0.495$, $p < 0.0001$).

$p < 0.0002$), left parietal lobule ($r = 0.307$, $p < 0.01$), and right posterior cingulate ($r = 0.268$, $p < 0.03$).

ROC curve analysis in the whole of subjects showed that both hippocampal (AUC = 0.77; $p < 0.0002$) and parietal (AUC = 0.72; $p < 0.0002$) relative perfusion (mean between the two sides) yielded moderate accuracy in separating S group from D + AD-D groups. The cut point for hippocampal perfusion was 0.81, with 69% sensitivity and 75% specificity (Fig. 4a). On the other hand, mean hippocampal perfusion yielded rather good accuracy (AUC = 0.90; $p < 0.0001$) in separating AD-D from D + S, while mean parietal perfusion did not. The cut point for hippocampal perfusion was 0.783, with 81% sensitivity and 86% specificity (Fig. 4b).

After eliminating the SUBJ group, ROC curve analysis showed better discrimination values achieved by mean hippocampal perfusion in separating either D + AD-D from S (AUC = 0.78, $p < 0.0001$; sensitivity 0.66 with 0.80 specificity; cut point 0.806) or AD-D from S + D (AUC = 0.89, $p < 0.0001$; sensitivity 0.82 with 0.83 specificity; cut point 0.788) than parietal perfusion.

When considering the aMCI group only, ROC curve analysis confirmed the good discrimination values of hippocampal perfusion in separating either D + AD-D from S (AUC = 0.84, $p < 0.0001$; sensitivity 0.76 with 0.75 specificity; cut point 0.813) or AD-D from S + D (AUC = 0.88, $p < 0.0001$; sensitivity 0.77 with 0.85 specificity; cut point 0.775).

DISCUSSION

The clinical-neuropsychological outcome of subjects deserves some epidemiological considerations. The 17.3% of all subjects developed dementia (all but one of the AD type), with an annual conversion rate of about 8%, which is slightly lower than that reported in epidemiological studies on the MCI population [3, 20], as a likely consequence of inclusion of twenty-two subjective cognitive impairment subjects. When computing the annual conversion rate just in the fifty-three MCI subjects, it is about 12% and increases to 17% if only the aMCI group is considered. Moreover, all but one of the AD-D patients come from the aMCI group, confirming that episodic verbal memory deficit is actually the most typical neuropsychological deficit in AD patients before dementia [5]. Looking at the aMCI group, the clinical outcome was almost equally distributed among S, D and converters to AD-
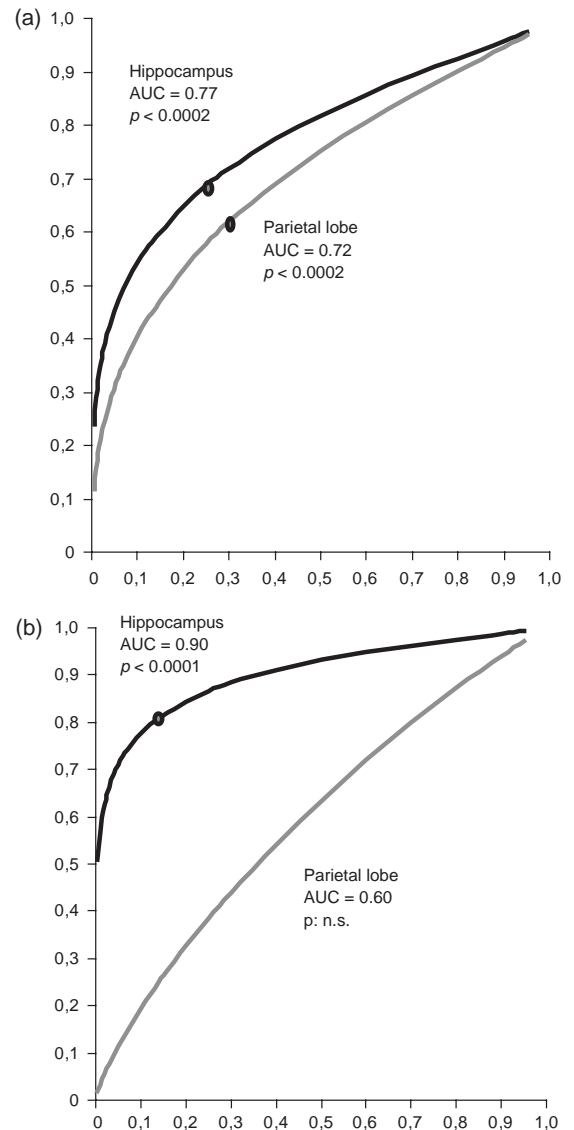
Fig. 4. (a) Receiver operating characteristic (ROC) curves for mean values of the two hippocampal VROI (black line) and of the two parietal VROIs (grey line) in the comparison between S versus AD-D + D. The two curves indicate a discrimination power significantly greater than random ($p < 0.0002$), reaching a sensitivity of 69% and a specificity of 75% for hippocampal VROI; a sensitivity of 62% and a specificity of 70% for parietal VROI. Chi-square statistic for the difference between the two ROC curves was $\chi^2 = 1.057$; p: not significant. (b) ROC curves for mean values of the two hippocampal VROI (black line) and of the two parietal VROIs (grey line) in the comparison between S + D and AD-D. Discrimination power of the hippocampus was highly significant ($p < 0.0001$), leading to 81% sensitivity with 86% specificity, while the parietal VROI did not yield significant results. Chi-square statistic for the difference between the two ROC curves was $\chi^2 = 9.3$; $p < 0.01$. AUC = area under curve. The threshold point with optimal sensitivity and specificity for hippocampal perfusion value was 0.81 in (a) and 0.783 in (b).

D, while just three out of the 16 subjects with naMCI showed further deterioration after two years (1 AD-D, 2 D), with a lower rate than aMCI. Indeed, it is known that a transient deficit in a non-memory domain can be the results of a variety of conditions, such as a depressive trait, low social-education environment, or inadequacy to the neuropsychological setting. Concerning these subjects, some of them still showed impairment in a non-memory domain at follow-up, but we choose to considered only memory decline as an outcome measure. By this choice, we wanted to focus on memory decline as the main hallmark of AD-D and, more generally, of dementia rather than on other domains which are too heterogeneous to be meaningfully analysed, given the limited number of subjects.

Baseline hippocampal perfusion progressively declined across S, D and AD-D (Fig. 2), significantly separated AD-D from the other two groups, especially left hippocampal perfusion, and was highly correlated with the delayed recall score at follow-up. Moreover, ROC curve analysis showed sensitivity and specificity values around or above 0.80, which are particularly high when considering that they were reached in the MCI stage. Moderate accuracy was also reached in separating S group from the other two groups. This figure is just a bit lower than accuracy reached by FDG-PET and supports the use of perfusion SPECT as a biomarker for AD in an aMCI population, wherever FDG-PET is unavailable or cannot be accessed due to logistic constraints.

Just belonging to the SUBJ group yielded the highest likelihood not to develop either D or AD-D at follow-up. This could vanish the utility of SPECT in these subjects and spuriously increase specificity of SPECT in the analysis of the whole sample. We therefore re-computed the ROC curves in naMCI and aMCI groups only, as well as in the aMCI group only, and the results were substantially confirmed. Irrespective of whether ROC curve analysis was conducted in the whole of subjects or in subgroups, the cut-points of about 0.81 in separating S from D + AD-D groups and of 0.78 in separating AD-D from S + D groups were consistently found, with a 'shadow' zone between these two values. By taking in mind that these values were obtained with ^{99m}Tc-ECD, they may serve as a starting point for further evaluation in larger samples of subjects. In fact, the procedure adopted in the present study (image normalization in the stereotactic space, application of VROI from a standardized atlas and normalization of VROI uptake values on cerebellar counts) might

be simple enough to be further evaluated and may represent a step forward in finding shared Standard Operational Procedures for brain SPECT imaging in AD and related conditions. This perspective could lead to apply SPECT in the clinical setting with greater confidence.

The finding related to hippocampal hypoperfusion raises the question about why hippocampal dysfunction has not been reported as an early marker of aMCI by a substantial portion of the SPECT/PET literature [8–10, 12, 14, 15], despite being largely expected on the basis of current knowledge on the pathophysiology of AD. This issue has been deeply discussed [32], pointing to the problems of low spatial resolution of first-generation SPECT/PET equipments. As a matter of fact, hippocampal dysfunction has been also reported by a voxel-based analysis (VBA) approach by more recent reports, employing both SPECT [11, 13, 33] and PET [27, 28] last-generation equipments. Even more important, the smoothing procedure needed by the software programs performing VBA, which is avoided by a VROI-based approach, may contribute to mask hippocampal dysfunction. In fact, it has been recently shown that VBA possibly fails to detect dysfunction within small brain structures, such as hippocampus, especially in MCI when functional changes are still of moderate extent [34, 35]. On the contrary, hippocampal dysfunction has been often reported by a VROI-based approach on both SPECT [36] and PET [31] data. Another consideration is that we merged together the hippocampus and the para-hippocampal gyrus within the same hippocampal VROI. Indeed, functional compensation has been recently shown by means of ^{99m}Tc-ECD SPECT in the hippocampal head (i.e., relative hyperperfusion), while functional depression (i.e., hypoperfusion) in the parahippocampal gyrus [37]. Thus, future works should take into account this compensation/depression mismatch in the MTL and choose to select just the parahippocampal gyrus which could be more sensitive than the whole hippocampal region. Furthermore, partial volume effect (PVE) correction was not performed in the present study, as well as in the majority of SPECT studies, thus hippocampal hypoperfusion likely represents a mixed of MTL atrophy and dysfunction. However, most studies in which PVE correction was performed, reported a relative independence of functional measurements from brain atrophy [38]. Nonetheless, in previous studies on normal elderly [35], correction for atrophy generally led to increased –rather than decreased- statistical val-

ues, improving the detection of significant functional alterations.

Baseline parietal perfusion levels, especially in the right hemisphere, significantly distinguished the S group from AD-D + D, and were similarly correlated with delayed recall score at follow-up, as hippocampal perfusion levels. ROC curve analysis showed a moderate accuracy in identifying S group from the other two groups, but no accuracy in identifying AD-D from the other two groups. Therefore, parietal perfusion levels seem similarly useful as hippocampal perfusion levels in predicting S at follow-up, but not useful to predict AD-D conversion. In fact, while hippocampal perfusion progressively reduced from S to AD, parietal perfusion dropped between S and D and then remained substantially constant in AD. An interpretation might be that the majority of D subjects are late converters, thus already showing SPECT signs of neurodegeneration. If this was the case, we should admit that up to the 80% of present aMCI subjects will develop AD in future years. This may be verified when the 5-year follow-up data will be available, but seems unlikely according to a recent pooled meta-analysis [39]. Alternatively, parietal perfusion levels would mainly reflect memory performances, as shown by the high correlation with the delayed recall score in our data and supported by experimental data [40], but they would not necessarily be a marker of AD conversion.

Perfusion reduction in the posterior cingulate just showed borderline statistical significance. Posterior cingulate hypoperfusion has been reported in some series of MCI subjects [9, 13, 15], but often hypoperfusion has been rather reported in the posterior parietal cortex and the hippocampal region [8, 10–12]. Notably, among SPECT studies, only those performed using ^{99m}Tc-HMPAO [9, 15] or ^{123}I-iodoamphetamine [13] disclosed posterior cingulate hypoperfusion, which has not, however, been reported by ^{99m}Tc-ECD studies [8, 12]. This may be correlated with the different distribution among tracers within the brain of both healthy subjects and AD patients [41].

However, posterior cingulate hypometabolism was found in a recent FDG-PET study in both aMCI patients converting to AD-D and aMCI patients not converters at 2-year follow-up [42]. Thus, it could be an early sign of memory deficit rather than a specific hallmark of AD conversion. Nestor et al. [43] have suggested that significant hypometabolism in the posterior cingulate is typical of all MCI patients, without a direct relationship to their future conversion. In a recent SPECT study, aMCI converters and nonconvert-

ers were found to share a common retrosplenial pattern of hypoperfusion [33], suggesting that retrosplenial cortex dysfunction could be the pathophysiological correlate of memory impairment, without being a biomarker of conversion to dementia. Although a 2-year follow-up may be still insufficient, the risk of AD conversion is at a maximum within the first few years following the diagnosis of aMCI, and then substantially decreases [39]. SPECT and FDG-PET long-term follow-up studies in stable aMCI are needed to show whether posterior cingulate dys-function is confirmed over time despite the lack of dementia or whether subjects with dys-function in this region convert to AD-type dementia over longer follow-up intervals.

In the previous study on baseline SPECT Descripa data, we found also bilateral temporal relative hypoperfusion in both aMCI and naMCI, and right frontal hypoperfusion in naMCI. None of these regions was shown to be predictive of 2-year outcome. Bilateral temporal as well as frontal hypoperfusion may indeed be revealed in hypertensive patients [44], in patients with vascular dementia [45] and in depression [46] without having a specific meaning as a marker of AD conversion. More recently, some FDG-PET studies have highlighted the relevance of lateral frontal cortex hypometabolism as one of the areas involved in the conversion pattern [26, 29] but it should be noted that FDG-PET is more sensitive to dysfunction than perfusion SPECT in patients with AD, especially in the frontal areas [47].

Methodological issues

In this study we had to face the problem of inhomogeneity of SPECT data coming from three different equipments. This issue has been analysed in ad-hoc investigations. In a methodological study, dealing with three different cameras, it was shown that the major source of variability was the physiological/pathological condition, accounting for about 17% of between-subject variability. The between-camera variability was slightly higher (about 8%) than the within-camera (about 5%) variability, when some compensation was applied during the reconstruction step (as in the present study), even by using different reconstruction protocols (either filtered back-projection or iterative) [48]. To minimize inhomogeneities, in the present study the reconstruction phase was centralized and the same protocol was used. We also avoided to apply VBA because we judged more prudent to use a VROI-based approach when managing data com-

ing from three different cameras. Despite the efforts done in SPECT reconstruction, some residual inhomogeneity at voxel level might persist, affecting VBA more likely than VROI-based analysis, as the latter minimizes such inhomogeneities by averaging across all voxels within the VROI. In fact, between-camera inhomogeneities seemed ininfluent when using a ROI-based approach in a FDG-PET study [49]. A second methodological aspect is the *a-priori* selection of VROI, which reduced the issue of multiple comparisons on the one hand, but that, on the other hand, prevented the detection of other possibly significant areas.

Some evidence in the literature suggests that AD patients with high education show more severe hypoperfusion than severity-matched patients with low education [50]. However, we did not correct SPECT data for the years of education because the groups were very similar as for educational level and the variable 'education' was not shown to significantly influence SPECT data using stepwise regression analysis, as detailed in a previous paper [18].

To conclude, baseline perfusion SPECT is an useful aid in the prediction of outcome in patients presenting with memory complaints, by integrating data coming from clinical and neuropsychological evaluations. Hippocampal hypoperfusion appears to play a major role in prediction of an AD neurogeneration pattern in patients with memory impairment.

ACKNOWLEDGMENTS

REFERENCES

[1] Mol ME, van Boxtel MP, Willems D, Jolles J (2006) Do subjective memory complaints predict cognitive dysfunction over time? A six-year follow-up of the Maastricht Aging Study. *Int J Geriatr Psychiatry* **21**, 432-441.

[2] Reisberg B, Gauthier S (2008) Current evidence for subjective cognitive impairment (SCI) as the pre-mild cognitive impairment (MCI) stage of subsequently manifest Alzheimer's disease. *Int Psychogeriatr* **20**, 1-16.

[3] Petersen RC (2004) Mild cognitive impairment as a diagnostic entity. *J Intern Med* **256**, 183-194.

[4] Visser PJ, Kester A, Jolles J, Verhey F (2006) Ten-year risk of dementia in subjects with mild cognitive impairment. *Neurology* **67**, 1201-1207.

[5] Dubois B, Feldman HH, Jacova C, DeKosky ST, Barberger-Gateau P, Cummings J, Delacourte A, Galasko D, Gauthier S, Jicha G, Meguro K, O'Brien J, Pasquier F, Robert P, Rossor M, Salloway S, Stern Y, Visser PJ, Scheltens P (2007) Research criteria for the diagnosis of Alzheimer's disease: revising the NINCDS-ADRDA criteria. *Lancet Neurol* **6**, 734-746.

[6] Matsuda H (2007) Role of neuroimaging in Alzheimer's disease, with emphasis on brain perfusion SPECT. *J Nucl Med* **48**, 1289-1300.

[7] Dubois B, Feldman HH, Jacova C, Cummings JL, Dekosky ST, Barberger-Gateau P, Delacourte A, Frisoni G, Fox NC, Galasko D, Gauthier S, Hampel H, Jicha GA, Meguro K, O'Brien J, Pasquier F, Robert P, Rossor M, Salloway S, Sarazin M, de Souza LC, Stern Y, Visser PJ, Scheltens P (2010) Revising the definition of Alzheimer's disease: a new lexicon. *Lancet Neurol* **9**, 1118-1127.

[8] Encinas M, De Juan R, Marcos A, Gil P, Barabash A, Fernandez C, De Ugarte C, Cabranes JA (2003) Regional cerebral blood flow assessed with 99 mTc-ECD SPET as a marker of progression of mild cognitive impairment to Alzheimer's disease. *Eur J Nucl Med Mol Imaging* **30**, 1473-1480.

[9] Huang C, Wahlund LO, Almkvist O, Elehu D, Svensson L, Jonsson T, Winblad B, Julin P (2003) Voxel- and VOI-based analysis of SPECT CBF in relation to clinical and psychological heterogeneity of mild cognitive impairment. *Neuroimage* **19**, 1137-1144.

[10] Høgh P, Madsen Sjö N, Gade A, Gade A, Waldemar G (2004) Temporal lobe hypoperfusion in isolated amnesia with slow onset: a single photon emission computer tomography study. *Dement Geriatr Cogn Disord* **18**, 15-23.

[11] Hirao K, Ohnishi T, Hirata Y, Yamashita F, Mori T, Moriguchi Y, Matsuda H, Nemoto K, Imabayashi E, Yamada M, Iwamoto T, Arima K, Asada T (2005) The prediction of rapid conversion to Alzheimer's disease in mild cognitive impairment using regional cerebral blood flow SPECT. *Neuroimage* **28**, 1014-1021.

[12] Borroni B, Anchisi D, Paghera B, Vicini B, Kerrouche N, Garibotto V, Terzi A, Vignolo LA, Di Luca M, Giubbini R, Padovani A, Perani D (2006) Combined 99mTc-ECD SPECT and neuropsychological studies in MCI for the assessment of conversion to AD. *Neurobiol Aging* **27**, 24-31.

[13] Ishiwata A, Sakayori O, Minoshima S, Mizumura S, Kitamura S, Katayama Y (2006) Preclinical evidence of Alzheimer changes in progressive mild cognitive impairment: a qualitative and quantitative SPECT study. *Acta Neurol Scand* **114**, 91-96.

[14] Guedj E, Barbeau EJ, Didic M, Felician O, de Laforte C, Ceccaldi M, Mundler O, Poncet M (2006) Identification of subgroups in amnestic mild cognitive impairment. *Neurology* **67**, 356-358.

[15] Johnson KA, Moran EK, Becker JA, Blacker D, Fischman AJ, Albert MS (2007) SPECT perfusion differences in mild cognitive impairment. *J Neurol Neurosurg Psychiatry* **78**, 240-247.

[16] Nobili F, Frisoni GB, Portet F, Verhey F, Rodriguez G, Caroli A, Touchon J, Calvini P, Morbelli S, De Carli F, Guerra UP, Van de Pol LA, Visser P-J (2008) Brain SPECT in subtypes of mild cognitive impairment: findings from the 'DESCRIPA' multicenter study. *J Neurol* **255**, 1344-1353.

[17] Pupi A, Nobili FM (2005) PET is better than perfusion SPECT for early diagnosis of Alzheimer's disease – against. *Eur J Nucl Med Mol Imaging* **32**, 1466-1472.

[18] Visser PJ, Verhey FR, Boada M, Bullock R, De Deyn PP, Frisoni GB, Frolich L, Hampel H, Jolles J, Jones R, Minthon L, Nobili F, Olde Rikkert M, Ousset PJ, Rigaud AS, Scheltens P, Soininen H, Spiru L, Touchon J, Tsolaki M, Vellas B, Wahlund LO, Wilcock G, Winblad B (2008) Development of screening guidelines and clinical criteria for predementia Alzheimer's disease. The DESCRIPA Study. *Neuroepidemiology* **30**, 254-265.

[19] Radloff LS (1977) The CES-D scale: a self-report depression scale for research in the general population. *Appl Psychol Measurem* **1**, 385-401.

[20] Petersen RC, Doody R, Kurz A, Mohs RC, Morris JC, Rabins PV, Ritchie K, Rossor M, Thal L, Winblad B (2001) Current concepts in mild cognitive impairment. *Arch Neurol* **58**, 1985-1992.

[21] Knopman DS, Boeve BF, Parisi JE, Dickson DW, Smith GE, Ivnik RJ, Josephs KA, Petersen RC (2005) Antemortem diagnosis of frontotemporal lobar degeneration. *Ann Neurol* **57**, 480-488.

[22] Tatsch K, Asenbaum S, Bartenstein P, Catafau A, Halldin C, Pilowsky LS, Pupi A (2002) European Association of Nuclear Medicine (2002) European Association of Nuclear Medicine procedure guidelines for brain perfusion SPECT using 99 mTc-labelled radiopharmaceuticals. *Eur J Nucl Med* **29**, BP36-BP42.

[23] Tsui BMW, Frey EC, Zhao X, Lalush DS, Johnston RE, McCartney WH (1994) The importance and implementation of accurate 3D compensation methods for quantitative SPECT. *Phys Med Biol* **39**, 509-530.

[24] Zeng GL, Hsieh Y-L, Gullberg GT (1994) A rotating and warping projector-backprojector pair for fan-beam and cone-beam iterative algorithms. *IEEE Trans Nucl Sci* **41**, 2807-2811.

[25] Caroli A, Testa C, Geroldi C, Nobili F, Guerra UP, Sonetti M, Frisoni GB (2007) Brain perfusion correlates of medial temporal lobe atrophy and white matter hyperintensities in mild cognitive impairment. *J Neurol* **254**, 1000-1008.

[26] Maldjian JA, Laurienti PJ, Kraft RA, Burdette JH (2003) An automated method for neuroanatomic and cytoarchitectonic atlas-based interrogation of fMRI data sets. *Neuroimage* **19**, 1233-1239.

[27] Drzezga A, Lautenschlager N, Siebner H, Riemenschneider M, Willoch F, Minoshima S, Schwaiger M, Kurz A (2003) Cerebral metabolic changes accompanying conversion of mild cognitive impairment into Alzheimer's disease: a PET follow-up study. *Eur J Nucl Med Mol Imaging* **30**, 1104-1113.

[28] Anchisi D, Borroni B, Franceschi M, Kerrouche N, Kalbe E, Beuthien-Beumann B, Cappa S, Lenz O, Ludecke S, Marcone A, Mielke R, Ortelli P, Padovani A, Pelati O, Pupi A, Scarpini E, Weisenbach S, Herholz K, Salmon E, Holthoff V, Sorbi S, Fazio F, Perani D (2005) Heterogeneity of brain glucose metabolism in mild cognitive impairment and clinical progression to Alzheimer disease. *Arch Neurol* **62**, 1728-1733.

[29] Chetelat G, Eustache F, Viader F, De La Sayette V, Pelerin A, Mezenge F, Hannequin D, Dupuy B, Baron JC, Desgranges B (2005) FDG-PET measurement is more accurate than neuropsychological assessments to predict global cognitive deterioration in patients with mild cognitive impairment. *Neurocase* **11**, 14-25.

[30] Drzezga A, Grimmer T, Riemenschneider M, Lautenschlager N, Siebner H, Alexopoulus P, Minoshima S, Schwaiger M, Kurz A (2005) Prediction of individual clinical outcome in MCI by means of genetic assessment and 18F-FDG PET. *J Nucl Med* **46**, 1625-163.

[31] Mosconi L, Tsui WH, De Santi S, Li J, Rusinek H, Convit A, Li Y, Boppana M, de Leon MJ (2005) Reduced hippocampal metabolism in MCI and AD: automated FDG-PET image analysis. *Neurology* **64**, 1860-1867.

[32] Mosconi L (2005) Brain glucose metabolism in the early and specific diagnosis of Alzheimer's disease. FDG-PET studies in MCI and AD. *Eur J Nucl Med Mol Imaging* **32**, 486-510.

[33] Caroli A, Testa C, Geroldi C, Nobili F, Barnden LR, Guerra UP, Sonetti M, Frisoni GB (2007) Cerebral perfusion correlates of conversion to Alzheimer's disease in amnestic mild cognitive impairment. *J Neurol* **254**, 1698-1707.

[34] de Leon MJ, Convit A, Wolf OT, Tarshish CY, DeSanti S, Rusinek H, Tsui W, Kandil E, Scherer AJ, Roche A, Imossi A, Thorn E, Bobinski M, Caraos C, Lesbre P, Schlyer D, Poirier J, Reisberg B, Fowler J (2001) Prediction of cognitive decline in normal elderly subjects with 2-[(18)F]fluoro-deoxy-D-glucose/positronemission tomography (FDG/PET). *Proc Natl Acad Sci U S A* **98**, 10966-10971.

[35] Nestor PJ, Fryer TD, Smielewski P, Hodges JR (2003) Limbic hypometabolism in Alzheimer's disease and mild cognitive impairment. *Ann Neurol* **54**, 343-351.

[36] Rodriguez G, Vitali P, Calvini P, Bordoni C, Girtler N, Taddei G, Mariani C, Nobili F (2000) Hippocampal hypoperfusion in mild Alzheimer's disease. *Psychiatry Res* **100**, 65-74.

[37] Ibáñez V, Pietrini P, Alexander GE, Furey ML, Teichberg D, Rajapakse JC, Rapoport SI, Schapiro MB, Horwitz B (1998) Regional glucose metabolic abnormalities are not the result of atrophy in Alzheimer's disease. *Neurology* **50**, 1585-1593.

[38] Caroli A, Geroldi C, Nobili F, Barnden LR, Guerra UP, Bonetti M, Frisoni GB (2010) Functional compensation in incipient Alzheimer's disease. *Neurobiol Aging* **31**, 387-397.

[39] Mitchell AJ, Shiri-Feshki M (2008) Temporal trends in the long term risk of progression of mild cognitive impairment: a pooled analysis. *J Neurol Neurosurg Psychiatry* **79**, 1386-1391.

[40] Cabeza R, Colcos F, Prince SE, Rice HJ, Weissman DH, Nyberg L (2003) Attention-related activity during episodic memory retrieval: a crossfunction fMRI study. *Neuropsychologia* **41**, 390-399.

[41] Koulibaly PM, Nobili F, Migneco O, Vitali P, Robert PH, Girtler N, Darcourt J, Rodriguez G (2003) 99mTc-HMPAO and 99mTc-ECD perform differently in typically hypoperfused areas in Alzheimer's disease. *Eur J Nucl Med Mol Imaging* **30**, 1009-1013.

[42] Morbelli S, Piccardo A, Villavecchia G, Dessi B, Brugnolo A, Piccini A, Caroli A, Frisoni G, Rodriguez G, Nobili F (2010) Mapping brain morphological and functional conversion patterns in amnestic MCI: a voxel-based MRI and FDG-PET study. *Eur J Nucl Med Mol Imaging* **37**, 36-45.

[43] Nestor PJ, Fryer TD, Smielewski P, Hodges JR (2003) Limbic hypometabolism in Alzheimer's disease and mild cognitive impairment. *Ann Neurol* **54**, 343-351.

[44] Rodriguez G, Arvigo F, Marenco S, Nobili F, Romano P, Sandini G, Rosadini G (1987) Regional cerebral blood flow in essential hypertension: data evaluation by a mapping system. *Stroke* **18**, 13-20.

[45] Kurz A, Riemenschneider M, Wallin A (2003) Potential biological markers for cerebrovascular disease. *Int Psychogeriatr* **15**(Suppl 1), 89-97.

[46] Smith DJ, Cavanagh JT (2005) The use of single photon emission computed tomography in depressive disorders. *Nucl Med Commun* **26**, 197-203.

[47] Messa C, Perani D, Lucignani G, Zenorini A, Zito F, Rizzo G, Grassi F, Del Sole A, Franceschi M, Gilardi MC, Fazio F

(1994) High-resolution technetium-99m-HMPAO SPECT in patients with probable Alzheimer's disease: comparison with fluorine-18-FDG PET. *J Nucl Med* **35**, 210-216.

[48] Koulibaly PM, Glabus MF, Eschner W (2003) Combining images from different clinical settings: technical issues. In: SPECT in dementia. Ebert D, Ebmeier KP, Kaschka WP, Rechlin T, eds. Advances in Biological Psychiatry, Karger, Bazel (Switzerland), Vol. 22, pp. 62-71.

[49] Herholz K, Perani D, Salmon E, Franck G, Fazio F, Heiss WD, Comar D (1993) Comparability of FDG PET studies in probable Alzheimer's disease. *J Nucl Med* **34**, 1460-1466.

[50] Hanyu H, Sato T, Shimizu S, Kanetaka H, Iwamoto T, Koizumi K (2008) The effect of education on rCBF changes in Alzheimer's disease: a longitudinal SPECT study. *Eur J Nucl Med Mol Imaging* **35**, 2182-2190.

This page intentionally left blank

A Tale of Two Tracers: Glucose Metabolism and Amyloid Positron Emission Tomography Imaging in Alzheimer's Disease

Lisa Mosconi[a,*], Valentina Berti[b], Pauline McHugh[a], Alberto Pupi[b] and Mony J. de Leon[a,c]

[a]*Department of Psychiatry, New York University School of Medicine, New York, NY, USA*
[b]*Department of Clinical Neurophysiology, Nuclear Medicine Unit, University of Florence, Italy*
[c]*Nathan Kline Institute, Orangeburg, NY, USA*

Abstract. The development of prevention therapies for Alzheimer's disease (AD) would greatly benefit from biomarkers that are sensitive to subtle brain changes occurring prior to the onset of clinical symptoms, when the potential for preservation of function is at the greatest. *In vivo* brain imaging is a promising tool for the early detection of AD through visualization of abnormalities in brain structure, function and histopathology. Currently, Positron Emission Tomography (PET) imaging with amyloid-beta (Aβ) tracers and 2-[^{18}F]fluoro-2-Deoxy-D-glucose (FDG) is largely utilized in the early and differential diagnosis of AD. Aβ PET tracers bind to Aβ plaques in brain, and provide an in vivo estimate of AD pathology. FDG-PET is used to measure glucose metabolism, a marker of brain activity. This paper reviews brain Aβ- and FDG-PET studies in AD patients as well as in non-demented individuals at risk for AD. We then discuss the potential of combining symptoms-sensitive FDG-PET measures with pathology-specific Aβ-PET to improve the early detection of AD.

Keywords: Positron Emission Tomography, cerebral metabolic rate of glucose (CMRglc), amyloid-beta, preclinical detection, normal aging

ABBREVIATIONS

^{18}F-FDG PET	2-[^{18}F]fluoro-2-Deoxy-D-glucose Positron Emission Tomography
AD	Alzheimer's disease
Aβ	amyloid beta
APP	amyloid precursor protein
ApoE	apolipoprotein E
CMRglc	cerebral metabolic rate of glucose
EOFAD	early onset familial AD
MRI	magnetic resonance imaging
MCI	mild cognitive impairment
Pittsburgh Compound-B, PIB	*N*-methyl-[^{11}C]2-(4′-methyla-minophenyl)-6-hydroxybenzo-thiazole

*Correspondence to: Lisa Mosconi, PhD, Department of Psychiatry, NYU School of Medicine, 145 East 32 nd ST, 5 th Floor, New York NY 10016. Tel.: +212 263 3255; Fax: +212 263 3279; E-mail: lisa.mosconi@nyumc.org.

INTRODUCTION

Alzheimer's disease (AD) is becoming an increasingly important reason for concern for healthcare and society. AD is the most common form of dementia, affecting approximately 1% of individuals 65 years of age, with the prevalence doubling every 5 years up to age 80, above which the prevalence exceeds

40% [1]. In 2007, there were more than 26.6 million people affected by AD in the world [2]. The prevalence of AD is estimated to be further increasing in the next few years, as the baby-boomers generation ages [3]. The main reason for increasing prevalence in AD is the lack of disease-modifying treatments. Once disease-modifying drugs become available, they will likely be most effective if administered early in the course of disease, before irreversible brain damage has occurred. Therefore, another major problem in AD is the lack of diagnostic markers, especially for the early stages of disease when clinical symptoms are not clearly expressed. Detection of preclinical pathological modifications in the brain is likely the key to identify individuals bound to develop AD.

Brain imaging, among other techniques, is a promising tool for the early detection of AD. Changes in brain histopathology, and consequently in its structure and function, are known to precede the clinical manifestations of disease by many years. These modifications can be visualized in vivo using brain imaging modalities. In chronological order, Computerized Tomography (CT) came first, followed by Magnetic Resonance (MR), and Positron Emission Tomography (PET) with functional tracers such as 2-[^{18}F]fluoro-2-Deoxy-D-glucose (FDG), and to a lesser extent with receptor ligands. Not yet 10 years ago, PET tracers for fibrillar amyloid-beta (Aβ), the principal constituent of AD senile plaques, have been developed, which made detection of AD pathology *in vivo* a reality. Presently, many AD clinical and research centers perform Aβ PET imaging, and an effort has been made in the United States to receive FDA approval for amyloid PET ligands in the diagnosis of AD and other dementias [4]. However, much remains to be learned about fibrillar Aβ as a biomarker for AD, especially at the early stages of disease. Prior to development of Aβ tracers, FDG was the most widely used PET tracer. FDG-PET was used to measure cerebral metabolic rates of glucose (CMRglc), a proxy for neuronal activity, in clinical AD patients and in at risk individuals. The present paper reviews FDG-PET findings in the early detection of AD, and discusses the value of performing FDG-PET with or without amyloid imaging.

Why we need brain imaging for the early detection of Alzheimer's disease

Alzheimer's disease (AD) is a neurodegenerative disorder with insidious onset and progressive declines in memory, attention and language [5]. Currently, the provisional diagnosis of AD remains based on clinical history, neurological examination, cognitive testing and structural neuroimaging, while the definitive diagnosis of AD is based on the postmortem detection of specific pathological lesions: Aß plaques in the extracellular space and blood vessels, intracellular neurofibrillary tangles (NFT), neuronal and synaptic loss in specific brain regions [6]. There are no tests for the definitive diagnosis of AD *in vivo*. Ironically, we ultimately define the disease with pathological criteria, but we have hardly any information in this regard during life. As a result, patients may be misdiagnosed with AD when in fact they have another dementia, or may be left undiagnosed [7]. The lack of standardized diagnostic tests for AD greatly limits the potential for an accurate diagnosis, and even more so, for early detection.

The problem is not what to measure, but how to measure it. Once the 'how' is resolved, the next question is when - how early in life can we detect clear-cut signs of an ongoing neurodegenerative process distinct from normal aging. Neurodegeneration in AD is estimated to begin 20–30 years before the clinical manifestations of disease become evident [8–11]. According to a popular theoretical model in AD, the "amyloid cascade hypothesis" [12], during this preclinical phase, Aβ plaques and NFT load increase, causing synapse loss and neuronal death. In light of recent findings that Aβ fibrils do not appear to be the main promoter of neuronal degeneration [12], the amyloid hypothesis was reformulated by stating that Aβ oligomers confer neurotoxicity to neurons by disrupting nerve signaling pathways in AD [13, 14].

While the causes of AD are being investigated, consensus exists as to where neurodegeneration strikes first in AD. The medial temporal lobes (MTL, i.e., hippocampus, transentorhinal/entorhinal cortex, and subiculum), which are critically involved in the neural control of memory functions, are most vulnerable to AD pathology [9, 11, 15–17]. The posterior cingulate, parieto-temporal and frontal cortices become affected later in the course of disease, in keeping with progression of clinical symptoms [9, 11, 15–17]. The local and distant effects of AD pathology on tissue physiology impair neuronal function in these vulnerable regions [18], causing cognitive impairment and dementia [19]. While post-mortem staging is based on cross-sectional detection of different patterns of anatomical involvement across subjects with different levels of dementia severity, longitudinal imaging studies enabled us to characterize the temporal progression

of these regional brain deficits in the same individual, as discussed below.

Why we have been using FDG-PET imaging

The early appearance of pathological lesions and the progressive nature of cognitive deterioration in AD indicate a great need for developing biological markers of disease, sensitive to early, longitudinal changes. Until 10 years ago, when Aβ PET imaging was developed, other technologies had to be used to measure surrogate markers of AD pathology. The most readily available techniques were Magnetic Resonance Imaging (MRI), which is used to measure structural tissue loss (i.e., atrophy), and FDG-PET to measure the functional effects of neuronal activity at the tissue level.

A growing list of observations has highlighted the importance of FDG-PET as a tool to distinguish AD from other dementias, predict and track decline from normal cognition to AD, and to identify individuals at risk for AD prior to the onset of cognitive symptoms. What we have learned from over 30 years of FDG-PET research in AD is that, first of all, AD is characterized by a specific regional pattern of CMRglc reductions. AD patients show consistent CMRglc deficits in the parieto-temporal areas [20, 21], posterior cingulate cortex (PCC) [22], and MTL [23]. As the disease progresses, frontal association cortices become involved, while cerebellum, striatum, basal ganglia, primary visual and sensorimotor cortices remain preserved [21, 23]. The extent and regional distribution of hypometabolism may vary across subjects, and hemispherical asymmetries are often noted [23, 24], especially at the early stages of AD. This *in vivo* pattern of hypometabolism is found in the vast majority of clinically diagnosed AD patients, and in over 85% pathologically confirmed AD cases [21].

CMRglc is highly correlated with clinical disabilities in dementia [25]. Clinical AD symptoms essentially never occur without CMRglc decreases, the extent of which is related to the severity of cognitive impairment [26–29]. Moreover, despite some overlap, the characteristic AD-pattern of CMRglc reductions yields high sensitivity in distinguishing AD from controls [30, 31], from other neurodegenerative dementias, such as frontotemporal (FTD) and lewy body dementia (DLB) [21, 31], and from cerebrovascular disease [32]. In a large multi-center study of NL, AD, FTD and DLB, individual FDG-PET scans were processed using automated voxel-based methods to generate disease-specific patterns of regional FDG uptake [31]. These standardized disease-specific PET patterns correctly classified 95% AD, 92% DLB, 94% FTD, and 94% NL [31]. The method yielded high discrimination accuracy in patients with mild dementia as well as moderate-to-severe dementia [31]. Altogether, these findings support the use of FDG-PET in the differential diagnosis of the major neurodegenerative dementing disorders.

Second, CMRglc reductions on FDG-PET precede the onset of AD symptoms in predisposed individuals, including both genetic and non genetic AD forms (Table 1). Presymptomatic persons carrying autosomal dominant genetic mutations associated with early onset familial AD (EOFAD, onset age < 65 yrs) show the typical AD pattern of hypometabolism compared to age-matched mutation non-carriers [33–35]. FDG-PET abnormalities were observed up to 13 years prior to the onset of symptoms in EOFAD subjects [35]. While findings in EOFAD may not apply to the more common forms of late-onset AD, studies of patients with Mild Cognitive Impairment (MCI) have reported similar evidence for presymptomatic CMRglc reductions. Among MCI patients, those presenting with more pronounced, or more AD-like, CMRglc reductions decline to AD at higher rates than those who do not show hypometabolism [22, 36–38]. CMRglc reductions in MCI predict future AD with 75%–100% accuracy [22, 36–41]. While early and late onset AD may or may not share a common pathology [12], FDG-PET studies have identified a similar outcome pattern of hypometabolism that appears to be a prodromal "metabolic signature" of AD independent of the age at onset of disease. More studies are needed to examine and compare the mechanisms underlying CMRglc reductions in the early and late onset AD.

A few FDG-PET showed an even earlier prediction capacity at the normal stages of cognition. By monitoring progression to MCI and AD among cognitively normal (NL) elderly, these studies showed that CMRglc reductions precede the onset of dementia by many years [42–45], and predict cognitive decline from NL cognition to MCI/AD with over 80% accuracy [42, 43]. The decliners to MCI and AD showed greater rates of CMRglc reductions as compared to the non-decliners [38, 42–45]. Progressive CMRglc reductions were observed years in advance of clinical symptoms in a clinico-pathological series of subjects followed with longitudinal *in vivo* FDG-PET scans from normal cognition to the clinical diagnosis and to post-mortem confirmation of AD [45].

Table 1
FDG- and PIB-PET findings in preclinical AD

At-risk group	Control group		FDG-PET findings vs controls	References	PIB-PET findings vs controls	References
Presymptomatic Early-onset Familial AD	Mutation non-carriers	Cross-sectional	• Whole brain hypometabolism • Parieto-temporal, PCC, frontal cortex, and MTL hypometabolism	33	• Higher PIB retention in striatum	71
		Longitudinal	• Greater CMRglc declines over time	33	N.A.	
NL decliners to MCI and to AD	Stable NL	Cross-sectional (baseline data predicts clinical change)	• MTL hypometabolism when NL	42	• Higher PIB retention in frontal, PCC/PRecuneus, temporal and parietal cortex	85–87
			• Parieto-temporal and PCC hypometabolism at time of decline to MCI/AD			
		Longitudinal	• Greater CMRglc declines over time	43	N.A.	
MCI decliners to AD	Stable MCI	Cross-sectional (baseline data predicts clinical change)	• Parieto-temporal, PCC and frontal cortex hypometabolism	22	• Higher PIB retention in PCC and frontal cortex	82–84
					• Higher cortical FDDNP binding	106
		Longitudinal	• Greater CMRglc declines over time	38	• Increases in cortical FDDNP binding	106
NL with Subjective Memory Complaints	NL without Subjective Memory Complaints	Cross-sectional	• Parieto-temporal and MTL hypometabolism	48	• No diffferences	102
		Longitudinal	N.A.		N.A.	
NL ApoE-4 carriers	NL ApoE-4 non-carriers	Cross-sectional	• Parieto-temporal, PCC, thalamus, and frontal cortex hypometabolism	49	• Higher PIB retention in frontal, temporal, PCC/precuneus, parietal cortex and basal ganglia	88
		Longitudinal	• Greater CMRglc declines over time	51, 52	N.A.	
NL Kibra CC carriers	NL Kibra CT and TT carriers	Cross-sectional	• PCC/Precuneus hypometabolism	55	N.A.	
		Longitudinal	N.A.	N.A.	N.A.	
NL with a 1 st degree family history of late onset AD	NL with negative family history of AD	Cross-sectional	• Parieto-temporal, PCC, frontal cortex, and MTL hypometabolism in NL with AD mothers as compared to those with AD fathers and to those with no parents with AD	56	• Higher PIB retention in frontal, temporal, PCC/precuneus, parietal cortex and striatum	89
		Longitudinal	• Greater CMRglc declines over time in NL with AD mothers as compared to those with AD fathers and to those with no parents with AD	57	N.A.	

CMRglc deficits resembling those in clinical AD patients have been observed in NL individuals at clinical or genetic risk for AD. With respect to AD risk established on clinical grounds, cognitively normal individuals with subjective memory complaints are regarded as a group at increased risk for dementia [46, 47]. On FDG-PET, middle-age to old normal individuals with subjective memory complaints showed CMRglc reductions in AD-vulnerable brain regions as compared to demographically matched individuals with no such complaints [48]. With respect to genetic risk factors for late-onset AD, many studies have shown that non-demented individuals carrying an Apolipoprotein E (ApoE) ε4 allele have CMRglc reductions as compared to ApoE ε4 non-carriers [49–53]. CMRglc deficits in NL ApoE ε4 carriers are progressive, correlate with reductions in cognitive performance [49, 52], and occur in young adulthood [53]. Likewise, NL carriers of the KIBRA CC haplotype, a risk factor for memory impairment in late life [54], showed CMRglc reductions as compared to low-risk KIBRA TT and CT carriers [55].

First degree relatives of AD patients also appear to be at high risk for late onset AD. In particular, a maternal history of AD was shown to affect brain metabolism in NL individuals [56, 57]. CMRglc deficits in AD-vulnerable regions were observed in NL with a maternal family history of AD as compared to those with a paternal history and those with no family history of AD (Fig. 1) [56]. Interestingly, NL children of AD fathers did not show CMRglc abnormalities [56]. Over a 2-year period, NL individuals with an AD mother showed progressive declines in regional CMRglc compared to those with no parents with AD as well as to those with an AD father [57]. The genetic mechanisms that underlie maternally inherited CMRglc reductions are under investigation [58]. More studies are needed to replicate these first reports and to identify the genetic factors involved in hypometabolism in preclinical AD.

Overall, the major strengths of FDG-PET in AD can be summarized as: high sensitivity to distinguish AD from controls and from other neurodegenerative diseases, and individuals at higher vs lower AD risk, and good quantitative and topographical correlation with clinical progression. However, a major limitation to most of the above FDG-PET studies is the absence of post-mortem data. Doubt remains as to whether clinical symptoms and CMRglc reductions are due to AD pathology or to other causes. Using clinical diagnosis as the gold-standard may lead to erroneously include patients with a dementia other than AD in the AD group, and viceversa. In asymptomatic subjects showing hypometabolism, CMRglc deficits may develop for reasons other than AD, and not all subjects showing hypometabolism will necessarily decline to AD. Here is where, in our opinion, imaging of AD pathology plays an essential role.

When FDG-PET alone is not enough, and the advent of amyloid PET tracers

Several PET tracers for Aβ plaques have been developed in the last few years. The best known
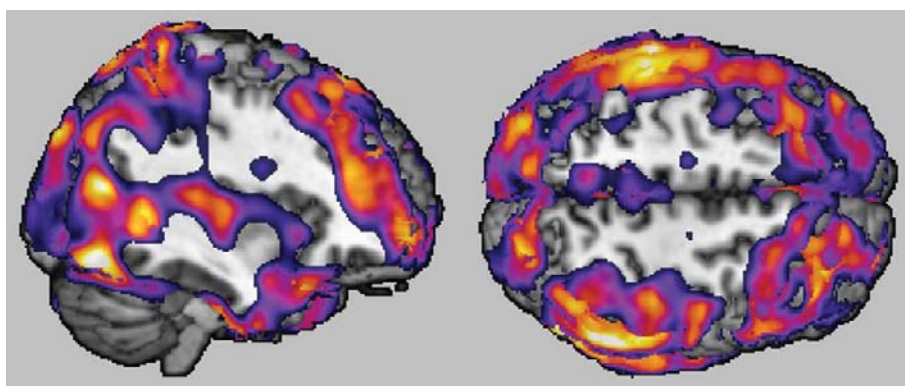
Fig. 1. Brain regions showing reduced CMRglc on FDG-PET in cognitively normal individuals with a maternal family history of AD (FHm) as compared to demographically matched subjects with a paternal family history (FHp) and with a negative family history of AD (FH-)[57]. Statistical parametric maps showing regions of hypometabolism in NL FHm are displayed on a purple-to-yellow color coded scale at $P < 0.001$. Figure shows the left lateral and superior views of a 3D volume-rendered MRI.

tracers are *N*-methyl-[^{11}C]2-(4′-methylaminophenyl)-6-hydroxybenzothiazole, aka Pittsburgh Compound-B (PIB) [59], 4-N-[^{11}C-methyl]amino-4′-hydroxystilbene (SB13) [60], 2-(1-96-(2-^{18}F-fluoroethyl)(methyl)amino)-2-naphthyl)ethyldene)malono nitrile (FDDNP) [61] and more recently the *trans*-4-(*N*-methyl-amino)-4′-2-[2-(2-[18F]fluoro-ethoxy)-ethoxy]-ethoxy-stilbene (BAY94-9172) [62]. Among these tracers, PIB is the most widely utilized and best characterized in terms of tracer kinetics, modeling, and analytic methods. PIB binds to fibrillar Aβ plaques with high affinity [63]. Several PIB-PET studies demonstrated significant PIB retention in AD patients as compared to controls, mostly in the frontal cortex, parieto-temporal, PCC/precuneus, occipital lobes, thalamus and striatum [63–67], consistent with the known pattern of Aβ plaques deposition observed at post-mortem. Significant PIB retention is found in over 90% clinically diagnosed AD patients, in as many as 60% of MCI [64–70] and 30% of NL elderly [67]. PIB-PET showed higher Aβ load in asymptomatic and symptomatic individuals carrying presinilin-1 (PSEN1) and APP mutations as compared to controls [71]. PIB retention was especially high in the striatum of mutation carriers as compared to controls and to sporadic AD patients [71]. These findings suggest that the striatum may be more affected in early onset AD, and the neocortex in the late onset AD forms. However, there is discordance between the striatal pattern seen on PIB imaging and the more severe cortical Aβ pathology found at post-mortem in early-onset AD [12], and PIB was shown to bind poorly to plaques in transgenic mice expressing many FAD mutations [72], although binding improved at higher specific activity [73]. It remains to be established whether PiB imaging may underestimate the extent of Aβ pathology in EOFAD.

Interestingly, subjects can be easily dichotomized as showing either significant (*PIB*+) or absent PIB retention (PIB-), but hardly show intermediate levels [64–70]. This could facilitate interpretation of PIB-PET scans for clinical use. The presence of a PIB + pattern has been shown to improve the differential diagnosis of AD from FTD and from Parkinson's disease [67, 74]. However, significant PIB retention is observed in DLB [64], and in patients with cerebral amyloid angiopathy (CAA) [75].

The impact of vascular amyloid on PIB signal is particularly relevant in view of using PIB, or other Aβ tracers, in the early detection of AD. A study showed that PIB is not specific for dense, classical plaques [76],

but rather binds to a family of amyloid substrates ranging from diffuse plaques to plaques in the vascular system (i.e., CAA) [77]. Vascular pathology is common in the elderly, and it is not known how much of the PIB retention observed in NL elderly is due to vascular Aβ deposits. Moreover, it is known from post-mortem studies that typical amyloid and NFT lesions are found in both demented and non-demented individuals [10, 11, 78–80]. Non-demented cases with substantial AD pathology are often described as a 'preclinical' AD group given the absence of cognitive abnormalities [10, 80]. This observation brings up the important, and often overlooked, discrepancy between AD-pathology and AD-dementia [81]. Those NL and MCI showing an AD-like PIB pattern (and therefore Aβ pathology) are conceivably at higher risk for developing AD-dementia as compared to individuals without brain Aβ pathology. However, having Aβ plaques does not equal to being at a 'pre-dementia stage', and the prognostic value of increased Aβ load on PET has to be established. Since Aβ imaging is a relatively new technique, there aren't enough published longitudinal PIB-PET studies to draw conclusions on its preclinical value in AD and the utility of this technique for early detection of AD pathology in non-demented individuals is less understood than with FDG (Table 1). A few studies in MCI have shown that, at baseline, those MCI who later declined to AD showed higher PIB retention as compared to the non-decliners [82–84]. Additionally, recent PiB-PET studies have shown that high PiB is a risk fator for longitudinal decline in cognitively NL elderly [85–87]. PiB-PET has also been shown to be of value for the early detection of amyloid pathology in elderly individuals with known risk factor for AD, such as those carrying the ApoE ε4 genotype and those with a maternal history of AD. Increased PIB retention in AD-vulnerable regions was observed in NL ApoE ε4 carriers compared to non-carriers [88], and in NL with a maternal history of AD compared to those with a paternal history and negative family histories [89]. Although the predictive value of PIB abnormalities in the asymptomatic ApoE ε4 carriers and adult children of AD-mothers is not known, PIB measures may be useful to discriminate NL individuals at higher vs lower risk for AD [88, 89].

Multi-tracer FDG and amyloid PET studies have begun to answer questions about the relationship between brain amyloidosis and activity *in vivo*. In AD patients, negative correlations between PiB retention and metabolism were reported by some studies [63, 90, 91], but not others 92–94], while positive correlations

were observed in MCI [95]. The few published multi-tracer studies in NL elderly reported generally absent correlations between Aβ and metabolism [95, 96]. Interestingly, Cohen et al. (2009) provided intriguing evidence that local elevations in glucose metabolism are associate with increased PiB retention at the MCI stage of AD, with the expected trend inversion occurring after the onset of dementia, suggesting that the relationship between amyloid, glucose metabolism and clinical status is quite complex [95].

In fact, while Aß deposition and metabolic impairments are likely co-occurring phenomena in the pathogenesis of AD, the causal and temporal relationship between these AD biomarkers remains to be clarified, and discrepancies in timing and regional distribution are to be expected, especially at the early stages of disease. Overall, the correlation between PIB retention and cognition does not appear to be as strong as with functional PET or structural MRI [97], consistent with the notion that Aβ plaques distribution does not necessarily correlate with clinical symptoms in AD [98]. While some PiB reports suggested a correlation between PiB binding and cognitive impairment in AD [99], most did not [63, 94, 96, 100, 101]. For instance, Jagust et al. (2009) showed that, in AD patients, Mini-Mental State Examination score was significantly correlated with FDG-PET but not with PIB-PET or CSF Abeta 1-42 [94]. Likewise, Furst et al. (2010) reported strong associations between glucose metabolism and cognitive measures in AD, and no correlations between regional and global PiB load and clinical status or metabolism [96]. Chetelat and colleagues showed that PiB load was strongly related to global and regional atrophy on MRI in subjects with subjective cognitive impairment (SCI) [102]. However, the correlation was not significant in MCI and AD patients, and direct comparison of patients with and without SCI showed reduced gray matter volumes in SCI but no significant differences in PiB retention [102].

Additionally, the few published longitudinal PIB-PET papers indicate a lack of progression of PIB uptake in NL, MCI and AD [90, 103, 104]. AD patients apparently reach a plateau in PIB retention, despite progression of their clinical symptoms and worsening of hypometabolism on FDG-PET [90]. Jack et al. [103] examined longitudinal PIB-PET in NL, MCI and AD and showed that the rate of PIB change did not differ by clinical group. The lack of longitudinal progression suggests that PIB deposition could be an early event during aging and disease. Otherwise, lack of change

suggests that PIB and similar tracers may not be the best option for longitudinal studies (discussed below), although amyloid tracers are obviously more suitable than FDG to test the effects of amyloid-based therapies. A recent paper by Rinne et al. (2010) showed that AD patients showed a reduced rate of PiB accumulation compared to placebo-treated patients over 78 weeks of treatment with Bapineuzumab, an antibody targeted against the N terminus of amyloid β that has been used as a passive immunotherapy [105].

In terms of capturing the effect of naturally occurring amyloid deposition, FDDNP appears to have an advantage over PIB [61]. FDDNP binds both Aß fibrils and NFT, and shows a cortical binding pattern similar to PIB, and additionally binds to the MTL [61, 106]. FDDNP uptake was highly correlated with scores on memory and global cognition [106]. Although limited by the small sample, longitudinal progression effects were reported for 3 non-demented subjects that deteriorated over 2 years, including one subject that declined from NL to MCI, and 2 MCI that converted to AD [106]. The major limitation to using FDDNP is the low specific to non-specific binding ratio of the tracer [61, 106] which may make these scans difficult to interpret for clinical use.

It is important to mention that, in order to be accepted in clinical practice, a tracer must be widely accessible. The key difference between carbon-11 and fluorine-18 radionuclides is their rate of decay or their decay 'half-life'. This physical parameter determines both how quickly the radiolabeled form disappears from the body and how far they can be distributed from the point of radiochemical production. The decay half-live of carbon-11 is approximately 20 min and that of fluorine-18 is approximately 110 min. Only a minority of PET centers world-wide have the on-site capability of producing high specific activity carbon-11-labeled products, and need to rely on external production of fluorine-18 radiotracers (such as FDG) by regional cyclotron facilities that distribute the radiotracers to local scanners. The approximately 110 min half-life of fluorine-18 allows distribution within a 2–4 h travel radius, whereas the 20 min half-life of carbon-11 does not. As such, PiB and other ^{11}C-ligands are not widely available, and several companies are now developing ^{18}F-amyloid ligands. Among these, for example, Florbetapir, Flutemetamol and Florbetaben are promising ^{18}F-labeled amyloid tracers that are being developed for clinical use [62, 107–110]. ^{18}F-Florbetapir has been validated against pathology showing 96% agreement between in vivo PET images and postmortem results

rated as positive or negative for β-amyloid [108]. Many other fluorinated tracers for amyloid PET are being developed, as reviewed elsewhere [110–112].

While PIB and FDG may have complementary diagnostic roles, recent studies have demonstrated that early time-point PIB frames are perfusion-dominated and correlate highly with FDG, suggesting that PiB could serve as a double source of information: PiB binding potential and cerebral blood flow [112, 113]. This procedure may reduce costs and burden for patients. However, as discussed above, PiB is not readily available to most PET centers, and the procedure is based on dynamic modeling, which requires an expert image analyst, and patients need to be in the scanner for 90 minutes, which may create discomfort and increase movement artifacts. It is nonetheless an interesting approach.

Using FDG-PET with or without amyloid imaging for the early detection of AD

Given the low specificity of FDG-PET for AD pathology, the addition of amyloid PET tracers may be useful in the early detection of AD. An effective strategy to increase the preclinical diagnostic accuracy would be to combine the sensitivity of FDG-PET with pathology-specific Aß measures.

For clinical purposes, amyloid-PET appears to be most useful to distinguish AD from non-amyloid dementias, such as FTD. Such capacity may prove particularly useful at the mild stages of dementia, when symptoms are not fully expressed, and FDG-PET scans may not show clear-cut regional metabolic abnormalities. Amyloid imaging would be suitable to rule out AD in the presence of a PIB- scan, since a demented patient without brain Aß can not have AD-dementia by definition. However, false negatives amyloid scans have been observed [114, 115]. On the other hand, if a patient with uncertain diagnosis is PIB+, it would not possible to distinguish between AD, DLB and CAA based on PiB scans alone.

Diagnosis of AD at early stages of dementia would also be problematic because many NL elderly with brain Aß deposits never develop dementia in life [116]. Amyloid imaging is necessary for the early detection of Aß pathology, but is not sufficient to make an early diagnosis of AD-dementia. Histology studies have shown that, among individuals with AD pathology, what differentiates demented from non-demented subjects is the presence of neuronal loss. In general, non-demented subjects with AD pathology

do not show neuronal loss at post mortem, while demented subjects with AD pathology show decreases in neuronal number and volume [116]. These findings indicate that neuronal degeneration is a stronger predictor of dementia than AD pathology [116]. Therefore, functional tracers like FDG-PET, whose signal correlates well with cognitive impairment, may be needed to appreciate the extent to which Aß is affecting brain function. Non-demented individuals showing increased Aß load and reduced CMRglc would be the ideal target population for prevention studies in AD (Fig. 2).

FDG-PET studies have shown preclinical CMRglc abnormalities in individuals in their 40's [53]. It is not known how early in the course of disease Aß depositions can be detected. Except for the known presence of amyloid deposits in young individuals with Down's syndrome [117, 118], Aß plaques are more prevalent in brains of individuals older than age 50 [119, 120]. It was hoped that Aß imaging would facilitate the study of the time course of amyloid deposition in brain. However, people appear to either have substantial brain Aß or not, and to remain relatively unchanged over time. This could be due to the fact that Aß deposition is a very early event in AD. Should this be the case, amyloid tracers may be more useful for longitudinal examination of younger individuals with minimal tracer uptake, who may still show progression effects. Otherwise, lack of effects could be due to technical issues, such as the intrinsically low spatial resolution of PET scanners, or to the fact that PIB uptake reflects the presence of Aß fibrils, but not fibrils' dimension or growth [121, 122].

The exact role played by Aß plaques in AD is not clear. Recent studies have shown that Aβ dimers and oligomers, not plaques, promote neuronal degeneration [12, 13, 123, 124]. Aβ plaques represent a fraction of total Aβ in the brain that has been condensed and neutralized, and no longer contributes to neurotoxicity [124]. Measurement of soluble Aβ is needed to correctly estimate risk for developing AD, but tracers for soluble Aß are not available. Measurement of fibrillar Aβ, as achieved with PET, could be seen in two opposing ways: either as an index of how much soluble Aβ the brain has been dealing with, and therefore as a sign of increased risk, or as an index of how well the brain has been getting rid of toxic Aβ, and therefore as a sign that the brain is strong enough to cope with the bad Aβ. The question of whether Aβ predisposes to AD-dementia will be answered once treatment against fibrillar Aß becomes available.
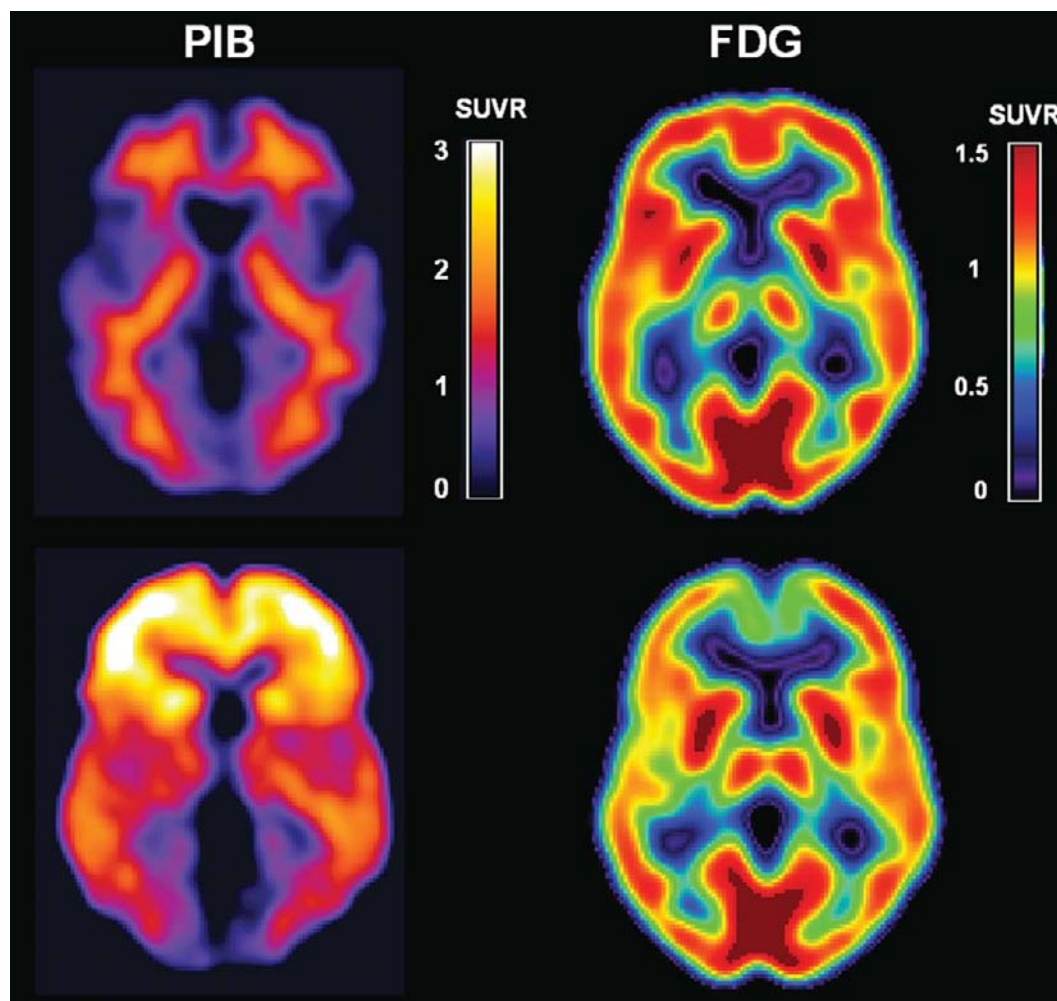
Fig. 2. Coregistered PIB and FDG-PET scans in 2 representative cognitively normal individuals at conceivably low risk for AD (top row: negative PIB and normal FDG uptake), and at high risk for AD (bottom row: positive PIB and reduced FDG uptake) based on PET imaging findings. Cerebral-to-cerebellar PIB Standardized Uptake Value ratios (SUVR) are displayed for each modality using a color coded scale.

Further research is required to clarify the relation of PiB retention to clinical impairment and to elucidate the influence of mediating factors. One of these potentially mediating factors is cognitive reserve (CR), which is a broad concept conferring a reduced susceptibility to impairment due to individual characteristics such as increased synaptic or neuronal capacity, greater efficiency engaging brain networks, or the use of alternative strategies [92, 125, 126]. There is evidence that highly educated AD patients show increased PIB uptake and lower CMRglc as compared to patients with low education, but with a similar degree of cognitive impairment [23, 92, 125, 126]. Interestingly, in NL elderly, CR significantly modified the relationship

between PiB uptake and neuropsychological test performance, such that at progressively higher levels of CR, increased amyloid deposition was less or not at all associated with poorer cognition [126]. Furthermore, Cohen et al. [95] showed negative correlations between amyloid load and metabolism in AD, whereas a positive correlation was found in MCI, although FDG uptake was not significantly reduced in MCI compared to controls. The Authors hypothesize that higher basal metabolism may retard the conversion from clinical MCI to AD, as a form of "brain reserve" such as developing cognitive impairment would require more Aβ deposition at higher levels of baseline metabolism [95]. Age at symptoms onset is known to influence

brain metabolism in AD [23, 24]. For instance, a large FDG-PET analysis of 120 AD patients by Kim et al. (2005) [24] showed that glucose hypometabolism was more severe and extended in those AD patients who developed symptoms before age 65 (early onset AD) than in those who were diagnosed after age 65 (late onset AD), although groups were comparable for overall dementia severity. The Authors suggest that the more severe hypometabolism observed in early onset relative to late onset patients of comparable dementia severity may reflect greater brain reserve in the younger early-onset group [24]. Overall, these results support the hypothesis that cognitive or brain reserve influences the association between Aβ pathology, metabolism and AD symptoms [23, 24, 92, 95, 125, 126].

It is also worth pointing out that, in the enthusiasm of being able to image Aβ *in vivo*, tau pathology has been somewhat neglected. Although the relationship between these two abnormal proteins in AD is not clear [98, 123], the diagnosis of AD remains based on the presence of both plaques, NFT, and neuronal loss with a specific neuroanatomy. Imaging NFT is particularly important as NFT progression follows the expected pattern of regional involvement based on clinical symptoms [11], and unlike Aβ plaques, NFT load correlates with cognitive impairment in AD [127]. In vivo imaging of NFT is still under development. Hopefully, continued technological progress will one day allow us to image all aspects of AD pathology *in vivo*, at proper microscopic resolution, without the need for invasive procedures.

Finally, structural CT and Magnetic resonance (MR) imaging has long been used in the diagnostic work up of AD to exclude alternative causes of dementia, such as brain tumor, subdural haematoma, and cerebrovascular disease such as cerebral infarcts and white-matter lesions. Volumetric MRI analysis shows that brain atrophy is an early event in AD and correlates with disease progression (for review see [128]). Studies that compared FDG to MRI showed that metabolic alterations precede atrophy in at risk individuals [35, 42, 129] and yield higher accuracy for differential diagnosis of AD from other dementias [23]. However, MRI is more readily accessible than FDG-PET, has higher anatomical resolution and does not require exposure to radioactive tracers. More studies are needed to establish with biomarker yields the highest positive and negative predictive value for detection of AD risk in yet asymptomatic individuals. For a recent review of MRI and PET studies in AD, please see [128, 130].

In conclusion, much research has been done with FDG-PET in AD since the first studies in the 1980's. Thanks to the technique's sensitivity to progression effects, FDG-PET is a prime candidate modality for detecting functional brain changes in early AD. Technical improvements, particularly the enhanced resolution of modern PET-CT and HRRT scanners, have led to increased anatomical accuracy. Nonetheless, there remains a great need to increase preclinical diagnostic specificity. It is possible that the combination of dementia-sensitive CMRglc with pathology-specific Aβ and NFT imaging would improve the early, differential diagnosis of AD. Since emerging evidence suggests that distinct patterns of change may be detected in each modality for patients and people at risk, an effective strategy may be to combine dementia-sensitive FDG-PET with pathology-specific Aß measures. For clinical purposes, we offer that a double-tracer approach will likely lead to the most accurate diagnosis. For example, FDG-PET is an FDA-approved test for the differential diagnosis of AD from FTD. However, while an abnormal FDG-PET scan may be used to determine the presence of a dementing disorder, oftentimes the picture is not clear-cut and diagnosis may remain uncertain. An additional positive finding on amyloid-PET would successfully distinguish AD from FTD, which typically has much less amyloid deposition and therefore is more likely to show a negative PiB scan.

On the other hand, PiB has limited value for differential diagnosis of AD from DLB and vascular pathology (i.e., congophylic amyloid angiopathy, CAA), as these patients may exhibit PiB uptake comparable to AD. In case of a PiB+ scan, FDG-PET evidence of occipito-parietal hypometabolism characteristic of DLB, or global hypometabolism typical of vascular disease would further improve discrimination. Additional validation studies are needed before Aβ PET imaging can enter into clinical practice, and more longitudinal studies are necessary to establish the limits and strengths of both tracers for early diagnosis of AD. Specific gaps in knowledge that are preventing immediate clinical application of amyloid-PET are:

– PiB positive scans are found in pathologies other than AD, including Parkinson's, DLB, CAA, etc, which limits the use of amyloid-PET for differential diagnosis. Nonetheless, amyloid-PET is of value for the discrimination of AD from non-amyloidogenic disorders such as FTD.

– PiB positive scans are found in up to 50% cognitively normal elderly, which prevents implementation of amyloid-PET imaging to discriminate AD from normal aging.

– More longitudinal studies with longer time to follow up are needed to establish whether amyloid load and glucose hypometabolism on PET are accurate predictors of future AD. At present, the few published longitudinal studies have been published provide encouraging evidence that these may be the case. However, these studies were performed in a research setting and results were based on detection of group differences. In order to validate PET imaging as a prognostic marker for AD: (1) The positive and negative predictive value of these tracers must be established based on examination of correspondence between individual scans and clinical outcome; and (2) research findings must be confirmed in community-based studies.

Once more multi-modality PET studies are available to clarify the incremental accuracy of FDG and amyloid-PET for differential diagnosis, we believe that most suspected AD patients will benefit from receiving both FDG and amyloid PET imaging. Likewise, we offer that accurate characterization of the extent and nature of brain damage in individual cases, based on converging evidence from different biomarkers, will likely play an important role in the prediction of subjects' clinical course. Other potential benefits include the selection of individualized treatment plans and screening of patients with more uniform underlying pathology for targeted research and drug trials. It is momentous that on April 19 th 2011, for the first time in 27 years, new criteria and guidelines for the diagnosis of AD have been published by three expert workgroups spearheaded by the Alzheimer's Association and the National Institute on Aging (NIA) of the National Institutes of Health (NIH). Along with ready-to-use clinical diagnostic criteria for AD and MCI due to AD, a research agenda was proposed for preclinical AD to expand the definition of Alzheimer's to include two new phases of the disease: (1) presymptomatic and (2) mildly symptomatic but pre-dementia, along with (3) dementia caused by Alzheimer's. This reflects current thinking that AD begins creating distinct and measurable changes in the brains of affected people years, perhaps decades, before memory and thinking symptoms are noticeable. However, the use of biomarkers in AD and MCI, let alone at pre-AD

states, was proposed as a research agenda only, and is not intended for application in clinical settings at this time. The early detection of AD is challenging, both mathematically and ethically, while disease-modifying treatments remain unavailable. There are several potential dangers of misdiagnosis using PET or any other biomarker in yet asymptomatic individuals. Even in a disease such as breast cancer, in which early detection may be indisputably linked to improved clinical outcome, there is considerable controversy about the methodology and ethics of providing genetic testing as a means of assessing the risk for eventual development of this disease. No data are currently available to provide insight into the policies and choices that would be made and the repercussions that may ensue if PET, or some other measure of the preclinical risk of AD, were to be used in asymptomatic individuals. For more discussion on this important issue, we recommend [128–130].

ACKNOWLEDGMENTS

REFERENCES

[1] Kukull WA, Higdon R, Bowen JD, McCormick WC, Teri L, Schellenberg GD, van Belle, Jolley, Larson EB (2002) Dementia and Alzheimer disease incidence: A prospective cohort study. *Arch Neurol* **59**, 1737-1746.

[2] Brookmeyer R, Johnson E, Ziegler-Graha K, Arrighi HM (2007) Forecasting the global burden of Alzheimer's disease. *Alzheimers Dementia* **3**, 186-191.

[3] Hebert LE, Scherr PA, Bienias JL, Bennett DA, Evans DA (2004) State-specific projections through 2025 of Alzheimer disease prevalence. *Neurolog* **62**, 1645.

[4] Talan J (2008) Neuroimaging tracers for AD detection not yet ready for prime time, FDA panel advises. *Neurol Today* **8**, 7-8.

[5] McKhann G, Drachman D, Folstein M, Katzman R, Price D, Stadlan EM (1984) Clinical diagnosis of Alzheimer's disease: report of the NINCDS-ADRDA work group under the auspices of department of health and human services task force on Alzheimer's disease. *Neurology* **34**, 939-944.

[6] Mirra SS, Heyman A, McKeel D, Sumi SM, Crain BJ, Brownlee LM, Fogel FS, Hughes JP, van Belle G, Berg L (1991) The consortium to establish a registry for Alzheimer's disease (CERAD). *Part II. Standardization of the Neuropathologic Assessment of Alzheimer's Disease. Neurology* **41**, 479-486.

[7] Hebert LE, Scherr PA, Bienias JL, Bennett DA, Evans DA (2003) Alzheimer disease in the US population: prevalence estimates using the 2000 census. *Arch Neurol* **60**, 1119-1122.

[8] Braak H, Braak E (1996) Development of Alzheimer-related neurofibrillary changes in the neocortex inversely recapitulates cortical myelogenesis. *Acta Neuropathol* **92**, 197-201.

[9] Delacourte A, David JP, Sergeant N, Buee L, Wattez A, Vermersch P, Ghozali F, Fallet-Bianco C, Pasquier F, Lebert F, Petit H, Di Menza C (1999) The biochemical pathway of neurofibrillary degeneration in aging and Alzheimer's disease. *Neurology* **52**, 1158-1165.

[10] Morris JC, Storandt M, McKeel DW, Rubin EH, Price JL, Grant EA, Berg L (1996) Cerebral amyloid deposition and diffuse plaques in "normal" aging: evidence for presymptomatic and very mild alzheiemer's disease. *Neurology* **46**, 707-719.

[11] Braak H, Braak E (1991) Neuropathological stageing of Alzheimer-related changes. *Acta Neuropathol* **8**, 239-259.

[12] Selkoe DJ (1997) Alzheimer's disease: genotypes, phenotype, and treatments. *Science* **275**, 630-631.

[13] Lambert MP, Barlow AK, Chromy BA, Edwards C, Freed R, Liosatos M, organ TE, Rozovsky I, Tronner B, Viola KL, Wals P, Zhang C, Finch CE, Krafft GA, Klein WL (1998) Diffusible, nonfibrillar ligands derived from abeta1-42 are potent central nervous system neurotoxins. *Proc Natl Acad Sci USA* **95**, 6448-6453.

[14] Lue LF, Kuo YM, Roher AE, Brachova L, Shen Y, Sue L, Beach T, Kurth JH, Rydel RE, Rogers J (1999) Soluble amyloid beta peptide concentration as a predictor of synaptic change in Alzheimer's disease. *Am J Pathol* **155**, 853-862.

[15] Arriagada PV, Marzloff K, Hyman BT (1992) Distribution of Alzheimer-type pathologic changes in nondemented elderly individuals matches the pattern in Alzheimer's disease. *Neurology* **42**, 1681-1688.

[16] Giannakopoulos P, Hof PR, Mottier S, Michel JP, Bouras C (1994) Neuropathological changes in the cerebral cortex of 1258 cases from a geriatric hospital: retrospective clinicopathological evaluation of a 10-year autopsy population. *Acta Neuropathol* **87**, 456-468.

[17] Ulrich J (1985) Alzheimer changes in nondemented patients younger than sixty-five: possible early stages of Alzheimer's disease and senile dementia of Alzheimer type. *Ann Neurol* **17**, 273-277.

[18] Morrison JH, Hof PR (1997) Life and death of neurons in the aging brain. *Science* **278**, 412-419.

[19] Hyman BT, Van Hoesen GW, Damasio AR, Barnes CL (1984) Alzheimer's disease: cell-specific pathology isolates the hippocampal formation. *Science* **225**, 1168-1170.

[20] Mazziotta JC, Phelps ME (1986) Positron Emission Tomography studies of the brain. In: Phelps ME, Mazziotta JC, Schelbert H, editors. Positron Emission Tomography & Autoradiography: Principles & Applications for the Brain & Heart. New York: Raven Press, pp. 493-579.

[21] Silverman DHS, Small GW, Chang CY, Lu CS, Kung de Aburto MA, Chen W, Czernin J, Rapoport SI, Pietrini P, Alexander GE, Schapiro MB, Jagust WJ, Hoffman JM, Welsh-Bohmer KA, Alavi A, Clark CM, Salmon E, de Leon MJ, Mielke R, Cummings JL, Kowell AP, Gambhir SS, Hoh CK, Phelps ME (2001) Positron emission tomography in evaluation of dementia: regional brain metabolism and long-term outcome. *JAMA* **286**, 2120-2127.

[22] Minoshima S, Giordani B, Berent S, Frey KA, Foster NL, Kuhl DE (1997) Metabolic reduction in the posterior cingulate cortex in very early Alzheimer's disease. *Ann Neurol* **42**, 85-94.

[23] Mosconi L (2005) Brain glucose metabolism in the early and specific diagnosis of Alzheimer's disease. *Eur J Nucl Med* **32**, 486-510.

[24] Kim EJ, Cho SS, Jeong Y, Park KC, Kang SJ, Kang E, Kim SE, Lee KH, Na DL (2005) Glucose metabolism in early onset versus late onset Alzheimer's disease: an SPM analysis of 120 patients. *Brain* **128**, 1790-1801.

[25] Blass JP (2002) Alzheimer's disease and Alzheimer's dementia: distinct but overlapping entities. *Neurobiol Aging* **23**, 1077-1084.

[26] Grady CL, Haxby JV, Schlageter NL, Berg G, Rapoport SI (1986) Stability of metabolic and neuropsychological asymmetries in dementia of the Alzheimer type. *Neurology* **36**, 1390-1392.

[27] Haxby JV, Grady CL, Koss E, Horwitz B, Heston L, Schapiro M, Friedland R, Rapoport SJ (1990) Longitudinal study of cerebral metabolic asymmetries and associated neuropsychological patterns in early dementia of the Alzheimer type. *Arch Neurol* **47**, 753-760.

[28] Desgranges B, Baron J-C, De La Sayette V, Petit-Taboue MC, Benali K, Landeau B, Lechevalier B, Eustache F (1998) The neural substrates of memory systems impairment in Alzheimer's disease a PET study of resting brain glucose utilization. *Brain* **121**, 611-631.

[29] Brown AM, Sheu RK, Mohs R, Haraoutunian V, Blass JP (2001) Correlation of the clinical severity of Alzheimer's disease with an aberration in mitochondrial DNA (mtDNA). *J Mol Neurosci* **16**, 41-48.

[30] Herholz K, Salmon E, Perani D, Baron JC, Holthoff V, Frölich L, Schönknecht P, Ito K, Mielke R, Kalbe E, Zündorf G, Delbeuck X, Pelati O, Anchisi D, Fazio F, Kerrouche N, Desgranges B, Eustache F, Beuthien-Baumann B, Menzel C, Schröder J, Kato T, Arahata Y, Henze M, Heiss WD (2002) Discrimination between Alzheimer dementia and controls by automated analysis of multicenter FDG PET. *Neuroimage* **17**, 302-316.

[31] Mosconi L, Tsui WH, Herholz K, Pupi A, Drzezga A, Lucignani G, Reiman EM, Holthoff V, Kalbe E, Sorbi S, Diehl-Schmid J, Perneczky R, Mariani C, Caselli R, Beuthien-Baumann B, Kurz A, Minoshima S, de Leon MJ (2008) Multi-center standardized FDG-PET diagnosis of mild cognitive impairment, Alzheimer's disease and other dementias. *J Nucl Med* **49**, 390-398.

[32] Szelies B, Mielke R, Herholz K, Heiss W-D (1994) Quantitative topographical EEG compared to FDG PET for classification of vascular and degenerative dementia. *Electroencephal Clin Neurophysiol* **91**, 131-139.

[33] Kennedy AM, Newman SK, Frackowiak RS, Cunningham VJ, Roques P, Stevens J, Neary D, Bruton CJ, Warrington EK, Rossor MN (1995) Chromosome 14 linked familial Alzheimer's disease. *A Clinico-Pathological Study of a Single Pedigree. Brain* **118**, 185-205.

[34] Kennedy AM, Frackowiak RSJ, Newman SK, Bloomfield PM, Seaward J, Roques P, Stevens J, Neary D, Bruton CJ, Warrington EK, Rossor MN (1995) Deficits in cerebral glucose metabolism demonstrated by positron emission tomography in individuals at risk of familial Alzheimer's disease. *Neurosci Lett* **186**, 17-20.

[35] Mosconi L, Sorbi S, de Leon MJ, Li Y, Nacmias B, Myoung PS, Tsui W, Bessi V, Fayyazz M, Caffarra P, Pupi A (2006) Hypometabolism exceeds atrophy in presymptomatic early-onset familial Alzheimer's disease. *J Nucl Med* **47**, 1778-1786.

[36] Chetelat G, Desgranges B, De La Sayette V, Viader F, Eustache F, Baron JC (2003) Mild cognitive impairment: can FDG-PET predict who is to rapidly convert to Alzheimer's disease?. *Neurology* **60**, 1374-1377.

[37] Mosconi L, Perani D, Sorbi S, Herholz K, Nacmias B, Holthoff V, Salmon E, Baron JC, Padovani A, Borroni B, Franceschi M, Bracco L, Pupi A (2004) Mci conversion to dementia and the apoe genotype: a prediction study with FDG-PET. *Neurology* **63**, 2332-2340.

[38] Drzezga A, Lautenschlager N, Siebner H, Riemenschneider M, Willoch F, Minoshima S, Schwaiger M, Kurz A (2003) Cerebral metabolic changes accompanying conversion of mild cognitive impairment into Alzheimer's disease: a PET follow-up study. *Eur J Nucl Med Mol Imaging* **30**, 1104-1113.

[39] Herholz K, Nordberg A, Salmon E, Perani D, Kessler J, Mielke R, Halber M, Jelic V, Almkvist O, Collette F, Alberoni M, Kennedy A, Hasselbalch S, Fazio F, Heiss WD (1999) Impairment of neocortical metabolism predicts progression in Alzheimer's disease. *Dement Geriatr Cog Dis* **10**, 494-504.

[40] Drzezga A, Grimmer T, Riemenschneider M, Lautenschlager N, Siebner H, Alexopoulus P, Minoshima S, Schwaiger M, Kurz A (2005) Prediction of individual outcome in MCI by means of genetic assessment and 18f-FDG PET. *J Nucl Med* **46**, 1625-1632.

[41] Anchisi D, Borroni B, Franceschi M, Kerrouche N, Kalbe E, Beuthien-Beumann B, Cappa S, Lenz O, Ludecke S, Marcone A, Mielke R, Ortelli P, Padovani A, Pelati O, Pupi A, Scarpini E, Weisenbach S, Herholz K, Salmon E, Holthoff V, Sorbi S, Fazio F, Perani D (2005) Heterogeneity of brain glucose metaboism in mild cognitive impairment and clinical progression to Alzheimer disease. *Arch Neurol* **62**, 1728-1733.

[42] de Leon MJ, Convit A, Wolf OT, Tarshish CY, De Santi S, Rusinek H, Tsui W, Kandil E, Scherer AJ, Roche A, Imossi A, Thorn E, Bobinski M, Caraos C, Lesbre P, Schlyer D, Poirier J, Reisberg B, Fowler J (2001) Prediction of cognitive decline in normal elderly subjects with 2-[18f]fluoro-2-deoxy-d-glucose/positron-emission tomography (FDG/PET). *Proc Natl Acad Sci USA* **98**, 10966-10971.

[43] Mosconi L, De Santi S, Li J, Tsui WH, Li Y, Boppana M, Laska E, Rusinek H, de Leon MJ (2008) Hippocampal hypometabolism predicts cognitive decline from normal aging. *Neurobiol Aging* **29**, 676-692.

[44] Jagust WJ, Gitcho A, Sun F, Kuczynski B, Mungas D, Haan M (2006) Brain imaging evidence of preclinical Alzheimer's disease in normal aging. *Ann Neurol* **59**, 673-681.

[45] Mosconi L, Mistur R, Switalski R, Tsui WH, Glodzik L, Brys M, Li Y, Pirraglia E, De Santi S, Reisberg B, Wisniewski T, de Leon MJ (2009) Longitudinal changes in brain glucose metabolism from normal cognition to pathologically verified Alzheimer's disease. *Eur J Nucl Med Mol Imaging* **36**, 811-822.

[46] Geerlings MI, Jonker C, Bouter LM, Ader HJ, Schmand B (1999) Association between memory complaints and incident Alzheimer's disease in elderly people with normal baseline cognition. *Am J Psychiat* **156**, 531-537.

[47] Reisberg B, Prichep L, Mosconi L, John ER, Glodzik-Sobanska L, Boksay I, Monteiro I, Torossian C, Vedvyas A, Ashraf N, Jamil IA, de Leon MJ (2008) The pre-mild cognitive impairment, subjective cognitive impairment stage of Alzheimer's disease. *Alzheimers Dementia* **4**, S98-S108.

[48] Mosconi L, De Santi S, Brys M, Tsui WH, Pirraglia E, Glodzik-Sobanska L, Rich KE, Switalski R, Mehta PD, Pratico D, Zinkowski R, Blennow K, de Leon MJ (2008) Hypometabolism and altered csf markers in normal apoe e4 carriers with subjective memory complaints. *Biol Psychiatry* **63**, 609-618.

[49] Small GW, Mazziotta JC, Collins MT, Baxter LR, Phelps ME, Mandelkern MA, Kaplan A, La Rue A, Adamson CF, Chang L (1995) Apolipoprotein e type 4 allele and cerebral glucose metabolism in relatives at risk for familial Alzheimer disease. *Jama* **273**, 942-947.

[50] Reiman EM, Caselli RJ, Yun LS, Chen K, Bandy D, Minoshima S, Thobodou SN, Osborne D (1996) Preclinical evidence of Alzheimer's disease in persons homozygous for the e4 allele for apolipoprotein e. *N Engl J Med* **334**, 752-758.

[51] Small GW, Ercoli LM, Silverman DHS, Huang SC, Komo S, Bookheimer S, Lavretsky H, Miller K, Siddarth P, Rasgon NL, Mazziotta JC, Saxena S, Wu HM, Mega MS, Cummings JL, Saunders AM, Pericak-Vance MA, Roses AD, Barrio JR, Phelps ME (2000) Cerebral metabolic and cognitive decline in persons at genetic risk for Alzheimer's disease. *Proc Natl Acad Sci USA* **97**, 6037-6042.

[52] Reiman EM, Caselli RJ, Chen K, Alexander GE, Bandy D, Frost J (2001) Declining brain activity in cognitively normal apolipoprotein e epsilon 4 heterozygotes: a foundation for using positron emission tomography to efficiently test treatments to prevent Alzheimer's disease. *Proc Natl Acad Sci USA* **98**, 3334-3339.

[53] Reiman EM, Chen K, Alexander GE, Caselli RJ, Bandy D, Osborne D, Saunders AM, Hardy J (2004) Functional brain abnormalities in young adults at genetic risk for late-onset Alzheimer's dementia. *Proc Natl Acad Sci USA* **10**, 284-289.

[54] Papassotiropoulos A, Stephan DA, Huentelman MJ, Hoerndli FJ, Craig DW, Pearson JV, Huynh KD, Brunner F, Corneveaux J, Osborne D, Wollmer MA, Aerni A, Coluccia D, Hänggi H, Mondadori CR, Buchmann A, Reiman EM, Caselli RJ, Henke K, de Quervain DJ (2006) Common kibra alleles are associated with human memory performance. *Science* **314**, 475-478.

[55] Corneveaux JJ, Liang WS, Reiman EM, Webster JA, Myers AJ, Zismann VL, Joshipura KD, Pearson JV, Hu-Lince D, Craig DW, Coon KD, Dunckley T, Bandy D, Lee W, Chen K, Beach TG, Mastroeni D, Grover A, Ravid R, Sando SB, Aasly JO, Heun R, Jessen F, Kölsch H, Rogers J, Hutton ML, Melquist S, Petersen RC, Alexander GE, Caselli RJ, Papassotiropoulos A, Stephan DA, Huentelman MK (2008) Evidence for an association between kibra and late-onset Alzheimer's disease. *Neurobiol Aging* Epub ahead of print.

[56] Mosconi L, Brys M, Switalski R, Mistur R, Glodzik L, Pirraglia E, Tsui WH, De Santi S, de Leon MJ (2007) Maternal family history of Alzheimer's disease predisposes to reduced brain glucose metabolism. *Proc Natl Acad Sci USA* **104**, 19067-19072.

[57] Mosconi L, Mistur R, Glodzik L, Pirraglia E, Tsui WH, De Santi S, de Leon MJ (2009) Declining brain glucose metabolism in normal individuals with a maternal history of Alzheimer's. *Neurology* **72**, 513-520.

[58] Mosconi L, Berti V, Swerdlow RH, Mistur R, Pupi A, Duara R, de Leon MJ. (2009) Maternal transmission of Alzheimer's disease: Prodromal metabolic phenotype and the search for genes. *Human Genom*, in press.

[59] Mathis CA, Bacskai BJ, Kajdasz ST, McLellan ME, Frosch MP, Hyman BT, Holt DP, Wang Y, Huang GF, Debnath ML,

Klunk WE (2002) A lipophilic thioflavin-t derivative for positron emission tomography (PET) imaging of amyloid in brain. *Bioorganic Med Chem Lett* **12**, 295-298.

[60] Ono M, Wilson A, Nobrega J, Westaway D, Verhoeff P, Zhuang ZP, Kung MP, Kung HF (2003) 11C-labeled stilbene derivatives as abeta-aggregate-specific PET imaging agents for Alzheimer's disease. *Nucl Med Biol* **30**, 565-571.

[61] Agdeppa ED, Kepe V, Liu J, Flores-Torres S, Satyamurthy N, Petric A, Cole GM, Small GW, Huang SC, Barrio JR (2001) Binding characteristics of radiofluorinated 6-dialkylamino-2-naphthylethylidene derivatives as positron emission tomography imaging probes for beta-amyloid plaques in Alzheimer's disease. *J Neurosci* **21**, 1-5.

[62] Rowe CC, Ackermann U, Browne W, Mulligan R, Pike KL, O'Keefe G, Tochon-Danguy H, Chan G, Berlangieri SU, Jones G, Dickinson-Rowe KL, Kung HP, Zhang W, Kung MP, Skovronsky D, Dyrks T, Holl G, Krause S, Friebe M, Lehman L, Lindemann S, Dinkelborg LM, Masters CL, Villemagne VL (2008) Imaging of amyloid beta in Alzheimer's disease with (18)F-BAY94-9172, a novel PET tracer: proof of mechanism. *Lancet Neurol* **7**, 129-135.

[63] Klunk WE, Engler H, Nordberg A, Wang Y, Blomqvist G, Holt DP, Bergström M, Savitcheva I, Huang GF, Estrada S, Ausén B, Debnath ML, Barletta J, Price JC, Sandell J, Lopresti BJ, Wall A, Koivisto P, Antoni G, Mathis CA, Långström B (2004) Imaging brain amyloid in Alzheimer's disease with Pittsburgh compound-B. *Ann Neurol* **55**, 306-319.

[64] Rowe CC, Ng S, Ackermann U, Gong SJ, Pike K, Savage G, Cowie TF, Dickinson KL, Maruff P, Darby D, Smith C, Woodward M, Merory J, Tochon-Danguy H, O'Keefe G, Klunk WE, Mathis CA, Price JC, Masters CL, Villemagne VL (2007) Imaging {beta}-amyloid burden in aging and dementia. *Neurology* **68**, 1718-1725.

[65] Kemppainen N, Aalto S, Wilson I, Nagren K, Någren K, Helin S, Brück A, Oikonen V, Kailajärvi M, Scheinin M, Viitanen M, Parkkola R, Rinne JO (2006) Voxel-based analysis of PET amyloid ligand [11C]PIB uptake in Alzheimer disease. *Neurology* **67**, 1575-1580.

[66] Pike KE, Savage G, Villemagne VL, Ng S, Moss SA, Maruff P, Mathis C, Klunk WE, Masters CL, Rowe CC (2007) Beta-amyloid imaging and memory in non-demented individuals: evidence for preclinical Alzheimer's disease. *Brain* **130**, 2837-2844.

[67] Mintun MA, LaRossa GN, Sheline YIM, Dence CSM, Lee SYP, Mach RHP, Klunk WE, Mathis CA, DeKosky ST, Morris JC (2006) [11C]PIB in a nondemented population: potential antecedent marker of Alzheimer disease. *Neurology* **67**, 446-452.

[68] Kemppainen NM, Aalto S, Wilson IA, Nagren K, Helin S, Bruck A, Oikonen V, Kailajärvi M, Scheinin M, Viitanen M, Parkkola R, Rinne JO (2007) Pet amyloid ligand [11C]PIB uptake is increased in mild cognitive impairment. *Neurology* **68**, 1603-1606.

[69] Li Y, Rinne JO, Mosconi L, Tsui W, Pirraglia E, Rusinek H, De Santi S, Kemppainen N, Nagren K, Kim BC, de Leon MJ (2008) Regional analysis of FDG and PIB-PET images in normal aging, mild cognitive impairment and Alzheimer's disease. *Eur J Nucl Med Mol Imaging* **35**, 2169-2181.

[70] Jack CR, Jr., Lowe VJ, Senjem ML, Weigand SD, Kemp BJ, Shiung MM, Knopman DS, Boeve BF, Klunk WE, Mathis CA, Petersen RC (2008) 11 C PIB and structural MRI provide complementary information in imaging of Alzheimer's disease and amnestic mild cognitive impairment. *Brain* **131**, 665-680.

[71] Klunk WE, Price JC, Mathis CA, Tsopelas ND, Lopresti BJ, Ziolko SK, Bi W, Hoge JA, Cohen AD, Ikonomovic MD, Saxton JA, Snitz BE, Pollen DA, Moonis M, Lippa CF, Swearer JM, Johnson KA, Rentz DM, Fischman AJ, Aizenstein HJ, DeKosky ST (2007) Amyloid deposition begins in the striatum of presenilin-1 mutation carriers from two unrelated pedigrees. *J Neurosci* **27**, 6174-6184.

[72] Klunk WE, Lopresti BJ, Ikonomovic MD, Lefterov IM, Koldamova RP, Abrahamson EE, Debnath ML, Holt DP, Huang GF, Shao L, DeKosky ST, Price JC, Mathis CA (2005) Binding of the positron emission tomography tracer Pittsburgh compound-B reflects the amount of amyloid-beta in Alzheimer's disease brain but not in transgenic mouse brain. *J Neurosci* **25**, 10598-10606.

[73] Willuweit A, Velden J, Godemann R, Manook A, Jetzek F, Tintrup H, Kauselmann G, Zevnik B, Henriksen G, Drzezga A, Pohlner J, Schoor M, Kemp JA, von der Kammer H (2009) Early-onset and robust amyloid pathology in a new homozygous mouse model of Alzheimer's disease. *PLOS One* **4**, 7931.

[74] Johansson A, Savitcheva I, Forsberg A, Engler H, Langstrom B, Nordberg A, Asmark H (2008) [(11)C]-PIB imaging in patients with parkinson's disease: preliminary results. *Parkinsonism Relat Disord* **14**, 345-347.

[75] Johnson KA, Gregas M, Becker JA, Kinnecom C, Salat DH, Moran EK, Smith EE, Rosand J, Rentz DM, Klunk WE, Mathis CA, Price JC, Dekosky ST, Fischman AJ, Greenberg SM (2007) Imaging of amyloid burden and distribution in cerebral amyloid angiopathy. *Ann Neurol* **62**, 229-234.

[76] Mathis CA, Wang Y, Klunk W (2004) Imaging [beta]-amyloid plaques and neurofibrillary tangles in the aging human brain. *Curr Pharm Design* **10**, 1469-1492.

[77] Lockhart A, Lamb JR, Osredkar T, Sue LI, Joyce JN, Ye L, Libri V, Leppert D, Beach TG (2007) PIB is a non-specific imaging marker of amyloid-beta (A{beta}) peptide-related cerebral amyloidosis. *Brain* **130**, 2607-2615.

[78] Crystal HA, Dickson D, Davies P, Masur D, Grober E, Lipton RB (2000) The relative frequency of "dementia of unknown etiology" increases with age and is nearly 50% in nonogenerians. *Arch Neurol* **57**, 713-719.

[79] Crystal H, Dickson D, Fuld P, Masur D, Scott R, Mehler M, Masdue J, Kawas C, Aronson M, wolfson L (1988) Clinico-pathologic studies in dementia: nondemented subjects with pathologically confirmed Alzheimer's disease. *Neurology* **38**, 1682-1687.

[80] Petersen RC, Doody R, Kurz A, Mohs RC, Morris JC, Rabins PV, Ritchie K, Rossor M, Thal L, Winblad B (2001) Current concepts in mild cognitive impairment. *Arch Neurol* **58**, 1985-1992.

[81] Blass JP (2002) Alzheimer's disease and Alzheimer's dementia: distinct but overlapping entities. *Neurobiol Aging* **23**, 1077-1084.

[82] Forsberg A, Engler H, Almkvist O, Blomqvist G, Hagman G, Wall A, Ringheim A, aring L, ngstr, ouml, m B, Nordberg A (2008) PET imaging of amyloid deposition in patients with mild cognitive impairment. *Neurobiol Aging* **29**, 1456-1465.

[83] Okello A, Koivunen J, Edison P, Archer HA, Turkheimer FE, Nagren K, Bullock R, Walker Z, Kennedy A, Fox NC, Rossor MN, Rinne JO, Brooks DJ (2009) Conversion of amyloid positive and negative MCI to AD over 3 years. An 11C-PIB PET study. *Neurology* **73**, 754-760.

[84] Wolk DA, Price JC, Saxton JA, Snitz BE, James JA, Lopez OL, Aizenstein HJ, Cohen AD, Weissfeld LA, Mathis CA, Klunk WE, De-Kosky ST (2009) Amyloid imaging in mild cognitive impairment subtypes. *Ann Neurol* **65**, 557-568.

[85] Mintun MA, Larossa GN, Sheline YI, Dence CS, Lee SY, Mach RH, Klunk WE, Mathis CA, DeKosky ST, Morris JC (2006) [11C]PIB in a nondemented population: potential antecedent marker of Alzheimer disease. *Neurology;* **67**, 446-452.

[86] Storandt M, Mintun MA, Head D, Morris JC (2009) Cognitive decline and brain volume loss as signatures of cerebral amyloid-beta peptide deposition identified with Pittsburgh compound B: cognitive decline associated with abeta deposition. *Arch Neurol* **66**, 1476-1481.

[87] Resnick SM, Sojkova J, Zhou Y, An Y, Ye W, Holt DP, Dannals RF, Mathis CA, Klunk WE, Ferrucci L, Kraut MA, Wong DF (2010) Longitudinal cognitive decline is associated with fibrillar amyloid-beta measured by [11C]PIB. *Neurology* **74**, 807-815.

[88] Reiman EM, Chen K, Liu X, Bandy D, Yu M, Lee W, Ayutyanont N, Keppler J, Reeder SA, Langbaum JB, Alexander GE, Klunk WE, Mathis CA, Price JC, Aizenstein HJ, DeKosky ST, Caselli RJ (2009) Fibrillar amyloid-beta burden in cognitively normal people at 3 levels of genetic risk for Alzheimer's disease. *Proc Natl Acad Sci USA* **106**, 6820-6825.

[89] Mosconi L, Rinne JO, Tsui WH, Berti V, Li Y, Wang H, Murray J, Scheinin N, Någren K, Williams S, Glodzik L, De Santi S, Vallabhajosula S, de Leon MJ (2010) Increased fibrillar amyloid-{beta} burden in normal individuals with a family history of late-onset Alzheimer's. *Proc Natl Acad Sci USA* **107**, 5949-5954.

[90] Engler H, Forsberg A, Almkvist O, Blomquist G, Larsson E, Savitcheva I, Wall A, Ringheim A, Långström B, Nordberg A (2006) Two-year follow-up of amyloid deposition in patients with Alzheimer's disease. *Brain* **129**, 2856-2866.

[91] Edison P, Archer HA, Hinz R, Hammers A, Pavese N, Tai YF, Hotton G, Cutler D, Fox N, Kennedy A, Rossor M, Brooks DJ (2007) Amyloid, hypometabolism, and cognition in Alzheimer disease: an [11C]PIB and [18F]FDG PET study. *Neurology* **68**, 501-508.

[92] Kemppainen NM, Aalto S, Karrasch M, Nagren K, Savisto N, Oikonen V, Vitanen M, Parkkola R, Rinne JO (2008) Cognitive reserve hypothesis: Pittsburgh compound B and fluorodeoxyglucose positron emission tomography in relation to education in mild Alzheimer's disease. *Arch Neurol* **63**, 112-118.

[93] Li Y, Rinne JO, Mosconi L, Pirraglia E, Rusinek H, DeSanti S, Kemppainen N, Någren K, Kim BC, Tsui W, de Leon MJ (2008) Regional analysis of FDG and PIB-PET images in normal aging, mild cognitive impairment, and Alzheimer's disease. *Eur J Nucl Med Mol Imaging* **35**, 2169-2181.

[94] Furst AJ, Rabinovici GD, Rostomian AH, Steed T, Alkalay A, Racine C, Miller BL, Jagust WJ (2010) Cognition, glucose metabolism and amyloid burden in Alzheimer's disease. *Neurobiol Aging* Epub ahead of print.

[95] Cohen AD, Price JC, Weissfeld LA, James J, Rosario BL, Bi W, Nebes RD, Saxton JA, Snitz BE, Aizenstein HA, Wolk DA, Dekosky ST, Mathis CA, Klunk WE (2009) Basal cerebral metabolism may modulate the cognitive effects of abeta in mild cognitive impairment: an example of brain reserve. *J Neurosci* **29**, 14770-14778.

[96] Jagust WJ, Landau SM, Shaw LM, Trojanowski JQ, Koeppe RA, Reiman EM, Foster NL, Petersen RC, Weiner MW, Price JC, Mathis CA; Alzheimer's Disease Neuroimaging Initiative.(2009) Relationships between biomarkers in aging and dementia. Neurology 73, 1193-1199.

[97] Jagust WJ (2009) Mapping brain beta-amyloid. *Curr Opin Neurol* **22**, 356-361.

[98] Mesulam MM (1999) Neuroplasticity failure in Alzheimer's disease: bridging the gap between plaques and tangles. *Neuron* **24**, 521-529.

[99] Mormino EC, Kluth JT, Madison CM, Rabinovici GD, Baker SL, Miller BL, Koeppe RA, Mathis CA, Weiner MW, Jagust WJ, Alzheimer's Disease Neuroimaging, Initiative (2009) Episodic memory loss is related to hippocampal-mediated beta-amyloid deposition in elderly subjects. *Brain* **132**, 1310-1323.

[100] Rowe CC, Ng S, Ackermann U, Gong SJ, Pike K, Savage G, Cowie TF, Dickinson KL, Maruff P, Darby D, Smith C, Woodward M, Merory J, Tochon-Danguy H, O'Keefe G, Klunk WE, Mathis CA, Price JC, Masters CL, Villemagne VL (2007) Imaging beta-amyloid burden in aging and dementia. *Neurology* **68**, 1718-1725.

[101] Pike KE, Savage G, Villemagne VL, Ng S, Moss SA, Maruff P, Mathis CA, Klunk WE, Masters CL, Rowe CC (2007) Beta-amyloid imaging and memory in non-demented individuals: evidence for preclinical Alzheimer's disease. *Brain* **130**, 2837-2844.

[102] Chételat G, Villemagne VL, Bourgeat P, Pike KE, Jones G, Ames D, Ellis KA, Szoeke C, Martins RN, O'Keefe GJ, Salvado O, Masters CL, Rowe CC, Australian Imaging Biomarkers, Lifestyle Research, Group (2010) Relationship between atrophy and beta-amyloid deposition in Alzheimer disease. *Ann Neurol* **67**, 317-324.

[103] Jack CR, Jr., Lowe VJ, Weigand SD, Wiste HJ, Senjem ML, Knopman DS, Shiung MM, Gunter JL, Boeve BF, Kemp BJ, Weiner M, Petersen RC (2009). In Alzheimer's Disease Neuroimaging Initiative, Serial PIB and MRI in normal, mild cognitive impairment and Alzheimer's disease: implications for sequence of pathological events in Alzheimer's disease. *Brain* **132**, 1355-65.

[104] Klunk WE, Mathis CA, Price JC, Lopresti BJ, DeKosky ST (2006) Two-year follow-up of amyloid deposition in patients with Alzheimer's disease. *Brain* **129**, 2805-2807.

[105] Rinne JO, Brooks DJ, Rossor MN, Fox NC, Bullock R, Klunk WE, Mathis CA, Blennow K, Barakos J, Okello AA, Rodriguez Martinez de Liano S, Liu E, Koller M, Gregg KM, Schenk D, Black R, Grundman M (2010) 11C-PIB PET assessment of change in fibrillar amyloid-beta load in patients with Alzheimer's disease treated with bapineuzumab: a phase 2, double-blind, placebo-controlled, ascending-dose study. *Lancet Neurol* **9**, 363-372.

[106] Small GW, Kepe V, Ercoli LM, Siddarth P, Bookheimer SY, Miller KJ, Lavretsky H, Burggren AC, Cole GM, Vinters HV, Thompson PM, Huang SC, Satyamurthy N, Phelps ME, Barrio JR (2006) PET of brain amyloid and tau in mild cognitive impairment. *N Engl J Med 355, 2652-2663,*.

[107] Vandenberghe R, Van Laere K, Ivanoiu A, Salmon E, Bastin C, Triau E, Hasselbalch S, Law I, Andersen A, Korner A, Minthon L, Garraux G, Nelissen N, Bormans G, Buckley C, Owenius R, Thurfjell L, Farrar G, Brooks DJ (2010) 18F-flutemetamol amyloid imaging in Alzheimer disease and mild cognitive impairment: a phase 2 trial. *Ann Neurol* **68**, 319-329.

[108] Clark CM, Schneider JA, Bedell BJ, Beach TG, Bilker WB, Mintun MA, Pontecorvo MJ, Hefti F, Carpenter AP, Flitter ML, Krautkramer MJ, Kung HF, Coleman RE, Doraiswamy PM, Fleisher AS, Sabbagh MN, Sadowsky CH, Reiman EP, Zehntner SP, Skovronsky DM, AV45-A07 Study, Group (2011) Use of florbetapir-PET for imaging beta-amyloid pathology. *Jama* **305**, 275-283.

[109] Barthel H, Gertz HJ, Dresel S, Peters O, Bartenstein P, Buerger K, Hiemeyer F, Wittemer-Rump SM, Seibyl J, Reininger C, Sabri O, for the Florbetaben Study, Group (2011) Cerebral amyloid-β PET with florbetaben ((18)F) in patients with Alzheimer's disease and healthy controls: a multicentre phase 2 diagnostic study. *Lancet Neurol* **10**, 424-435.

[110] Klunk WE, Mathis CA (2008) The future of amyloid-beta imaging: a tale of radionuclides and tracer proliferation. *Curr Opin Neurol* **21**, 683-687.

[111] Någren K, Halldin C, Rinne JO (2010) Radiopharmaceuticals for positron emission tomography investigations of Alzheimer's disease. *Eur J Nucl Med Mol Imaging* **37**, 1575-1593.

[112] Rostomian AH, Madison C, Rabinovici GD, Jagust WJ (2011) Early 11C-PIB frames and 18f-FDG PET measures are comparable: a study validated in a cohort of AD and FTLD patients. *J Nucl Med* **52**, 173-179.

[113] Meyer PT, Hellwig S, Amtage F, Rottenburger C, Sahm U, Reuland P, Weber WA, Hüll H (2011) Dual-biomarker imaging of regional cerebral amyloid load and neuronal activity in dementia with PET and 11C-labeled Pittsburgh compound B. *J Nucl Med* **52**, 393-400.

[114] Cairns NJ, Ikonomovic MD, Benzinger T, Storandt M, Fagan AM, Shah AR, Reinwald LT, Carter D, Felton A, Holtzman DM, Mintun MA, Klunk WE, Morris JC (2009) Absence of Pittsburgh compound B detection of cerebral amyloid beta in a patient with clinical, cognitive, and cerebrospinal fluid markers of Alzheimer disease: a case report. *Arch Neurol* **66**, 1557-1562.

[115] Rosen RF, Ciliax BJ, Wingo TS, Gearing M, Dooyema J, Lah JJ, Ghiso JA, LeVine H, 3rd, Walker LC (2010) Deficient high-affinity binding of Pittsburgh compound B in a case of Alzheimer's disease. *Acta Neuropathol* **119**, 221-233.

[116] Price JL, Ko AI, Wade MJ, Tsou SK, McKeel DW, Morris JC (2001) Neuron number in the entorhinal cortex and CA1 in preclinical Alzheimer disease. *Arch Neurol* **58**, 1395-1402.

[117] Masters CL, Simms G, Weinman NA, Multhaup G, McDonald B, Beyreuther K (1985) Amyloid plaque core protein in Alzheimer disease and Down Syndrome. *Proc Natl Acad Sci USA* **82**, 4245-4249.

[118] Isacson O, Seo H, Lin L, Albeck D, Granholm AC (2002) Alzheimer's disease and down's syndrome: roles of APP, trophic factors and ACH. *Trends Neurosci* **25**, 79-84.

[119] Price JL, Morris JC (1999) Tangles and plaques in nondemented aging and "preclinical" Alzheimer's disease. *Ann Neurol* **45**, 358-368.

[120] Davies L, Wolska B, Hilbich C, Multhaup G, Martins R, Simms G, Bayreuther K, Masters CL, (1988) A4 amyloid protein deposition and the diagnosis of Alzheimer's disease: prevalence in aged brains determined by immunocytochemistry compared with conventional neuropathologic techniques. *Neurology* **38**, 1688-1693.

[121] Shoghi-Jadid K, Barrio JR, Kepe V, Huang SC (2006) Exploring a mathematical model for the kinetics of beta-amyloid molecular imaging probes through a critical analysis of plaque pathology. *Mol Imaging Biol* **8**, 151-162.

[122] Shoghi-Jadid K, Barrio JR, Kepe V, Wu HM, Small GW, Phelps ME, Huang SC (2005) Imaging beta-amyloid fibrils in Alzheimer's disease: a critical analysis through simulation of amyloid fibril polymerization. *Nucl Med Biol* **32**, 337-351.

[123] Haass C, Selkoe D (2007) Soluble protein oligomers in neurodegeneration: lessons from the Alzheimer's amyloid beta-peptide. *Nat Rev Mol Cell Biol* **8**, 101-112.

[124] Hardy J, Selkoe DJ (2002) The amyloid hypothesis of Alzheimer's disease: progress and problems on the road to therapeutics. *Science* **297**, 353-356.

[125] Roe CM, Mintun MA, D'Angelo D, Xiong C, Grant EA, Morris JC (2008) Alzheimer disease and cognitive reserve: variation of education effect with carbon 11-labeled Pittsburgh compound B uptake. *Arch Neurol* **65**, 1467-1471.

[126] Rentz DM, Locascio JJ, Becker JA, Moran EK, Eng E, Buckner RL, Sperling RA, Johnson KA (2010) Cognition, reserve, and amyloid deposition in normal aging. *Ann Neurol* **67**, 353-364.

[127] Powell MR, Smith GE, Knopman DS, Parisi JE, Boeve BF, Petersen RC, Ivnik RJ (2006) Cognitive measures predict pathologic Alzheimer disease. *Arch Neurol* **63**, 865-868.

[128] Jack CR, Jr., Knopman DS, Jagust WJ, Shaw LM, Aisen PS, Weiner MW, Petersen RC, Trojanowski JQ (2010) Hypothetical model of dynamic biomarkers of the Alzheimer's pathological cascade. *Lancet Neurol* **9**, 119-128.

[129] De Santi S, de Leon MJ, Rusinek H, Convit A, Tarshish CY, Roche A, Tsui WH, Kandil E, Boppana M, Daisley K, Wang GJ, Schlyer D, Fowler J (2001) Hippocampal formation glucose metabolism and volume losses in MCI and AD. *Neurobiol Aging* **22**, 529-539.

[130] Frisoni GB, Fox NC, Jack CR, Jr., Scheltens P, Thompson PM (2010) The clinical use of structural MRI in Alzheimer disease. *Nat Rev Neurol* **6**, 67-77.

[131] DeKosky ST, Carrillo MC, Phelps C, Knopman D, Petersen RC, Frank R, Schenk D, Masterman D, Siemers ER, Cedarbaum JM, Gold M, Miller DS, Morimoto BH, Khachaturian AS, Mohs RC (2011) Revision of the criteria for Alzheimer's disease: a symposium. *Alzheimers Dement* **7**, 1-12.

[132] Britton GB, Rao KS (2011) Cognitive aging and early diagnosis challenges in Alzheimer's disease. *J Alzheimers Dis.* [Epub ahead of print]

[133] Mayeux R. (2010) Clinical practice. Early Alzheimer's disease. *N Engl J Med* **362**, 2194-2201.

Amyloid-β and Glucose Metabolism in Alzheimer's Disease

Ansgar J. Furst[a,b,c,*] and Rayhan A. Lal[d]

[a]*War Related Illness and Injury Study Center, VA Palo Alto Health Care System, Palo Alto, CA, USA*
[b]*Department of Psychiatry and Behavioral Sciences, Stanford University School of Medicine, Stanford, CA, USA*
[c]*Department of Neurology and Neurological Sciences, Stanford University School of Medicine, Stanford, CA, USA*
[d]*University of California at Davis, School of Medicine, Davis, CA, USA*

Abstract. This study used PET with the amyloid-β (Aβ) imaging agent [11]C Pittsburgh Compound-B (PIB) and the glucose metabolic tracer ^{18}F-fluorodeoxyglucose (FDG) to map the relationship of Aβ deposition to regional glucose metabolism in Alzheimer's disease (AD). Comparison of 13 AD patients' FDG scans with 11 healthy controls confirmed a typical temporo-parietal hypometabolic pattern in AD. In contrast, PIB distribution-volume-ratios showed a distinct pattern of specific tracer retention in fronto-temporo-parietal regions and striatum in AD with peaks in left frontal cortex, precuneus, temporal cortex, striatum and right posterior cingulate. There were no region-to-region or within region correlations between FDG and PIB uptake in PIB positive AD patients but when the impact of Aβ load on glucose metabolism was assessed via probabilistic maps, increased amyloid burden was coupled with decreased metabolism in temporo-parietal regions and the posterior cingulate. However, importantly, severe Aβ burden was not associated with comparable metabolic decreases in large parts of the frontal lobes, the striatum and the thalamus.

Keywords: Alzheimer's disease, amyloid plaques, amyloidosis, fluorodeoxyglucose, glucose metabolism, Pittsburgh compound-B

INTRODUCTION

Alzheimer's disease (AD) is a neurodegenerative disease with a distinct neuropathology involving extracellular neuritic amyloid-β (Aβ) plaques and intraneuronal neurofibrillary tangles (NFT) [1–3]. Triggered by findings that genetic defects in the amyloid-β protein precursor (AβPP) gene lead to over-production of Aβ and early-onset familial AD [4, 5], it has been suggested that Aβ is in fact the primary cause of AD [6]. According to this framework Aβ causes synaptic dysfunction, synapse loss, and neuronal death and eventuates in the formation of NFT. However, deposition of Aβ plaques correlate poorly both spatially and temporally with the occurrence of NFT [2, 3, 7]. While global insoluble Aβ plaque concentration does not seem to be a good predictor of dementia severity [8–10], recent evidence suggests that soluble Aβ oligomers play a central role in synaptic loss in AD [11] and soluble Aβ correlates with cognitive status [12]. Evidence from mouse models suggests, however, that Aβ plaques do disrupt the synchrony of converging neuronal inputs and therefore may influence network efficiency in AD [13, 14]. Clearly, while Aβ occupies a central role in the pathophysiology of AD, its relationship to both NFT and brain function is unclear.

The regional effects of Aβ deposition on brain function can be assessed by combining recently developed PET ligands that track Aβ deposition with measures of glucose metabolism using ^{18}F-fluorodeoxyglucose (FDG). In particular, [*N*-methyl-^{11}C]-2-(4'-methy-

*Correspondence to: Dr. Ansgar Furst, War Related Illness and Injury Study Center, VA Palo Alto Health Care System, 3801 Miranda Ave, Mailcode 151Y, Palo Alto, CA 94304-1290, USA. Tel.: +650 493 5000 1 1, x68652; E-mail: ajfurst@stanford.edu.

laminophenyl)-6-hydroxybenzothiazole, more commonly known as Pittsburgh Compound-B (PIB), specifically binds to fibrillar Aβ both *in vitro* [15] and *in vivo* [16] and has been used to study AD, normal aging, mild cognitive impairment (MCI), frontotemporal dementia (FTD) and other dementias [16–29]. The available evidence suggests that Aβ deposition while most prominent in frontal, parietal, temporal, posterior cingulate and striatal regions, does not exert uniform effects on brain function since regional hypometabolism appears to be limited to posterior cingulate and temporoparietal cortex.

Some authors [16, 30] using region-of-interest (ROI) analyses have reported negative correlations between Aβ load and glucose metabolism in temporal and parietal regions. These correlations included PIB negative healthy controls or PIB negative AD patients, however, and did not include effects of atrophy on the data. More recently, Cohen and colleagues [31] performed a detailed ROI and voxel-based analysis of the relationship between Aβ deposition and metabolism in PIB positive controls, MCI and AD patients which included atrophy correction. They reported a local negative correlation between FDG uptake and PIB retention in parietal and precuneus cortices of AD patients along with a more tenuous association with PIB uptake in the frontal cortex. However, the inverse correlation between FDG and PIB in AD has been challenged by several other groups. Li and colleagues [32] studied this relationship using an ROI approach combined with probabilistic gray matter masking and did not find any negative correlations. Similarly, Furst et al. [33] explored this question in the to-date largest AD cohort and did not find any inverse correlations using ROI and voxel-wise approaches with or without atrophy correction.

The current study aimed at investigating the relationship between Aβ deposition and glucose metabolism by comparing PIB and FDG scans in AD patients with β-amyloidosis contrasting traditional correlational approaches with Bayesian probabilistic modeling.

MATERIALS AND METHODS

Subject selection

Patients were recruited from an AD research cohort followed at the University of California San Francisco Memory and Aging Center (UCSF-MAC). The clinical evaluation included a history and physical examination by a neurologist, a structured caregiver interview administered by a nurse, and a comprehensive battery of neuropsychological tests. Patients' functional status was measured using the Clinical Dementia Rating Scale (CDR) [34]. Clinical diagnoses were assigned by consensus at a multidisciplinary conference using standard research criteria [35].

Patients were considered eligible for the study if they had a clinical diagnosis of probable AD, did not have significant co-morbid medical, neurological or psychiatric illness and had a PIB positive scan according to a previously established cut-off [36]. Two subjects were excluded from the final analysis due to technical reasons (motion artifact, incomplete study). Our final cohort consisted of 13 patients with probable AD (Table 1). Five subjects were included in a previously published series examining the utility of PIB-PET in differentiating between AD and frontotemporal lobar degeneration [20].

Eleven control subjects were recruited from the community by advertisement. All were free of significant medical illnesses and were not taking medications deemed to affect cognition. Control subjects were judged to be cognitively normal following an evaluation that included a medical history, functional, neurological and neuropsychological assessment.

The study was approved by the University of California at Berkeley Campus Committee for the Protection of Human Subjects and the University of California San Francisco Committee for Human Research.

Radiochemical synthesis

[11]C-PIB was synthesized at the Lawrence Berkeley National Laboratory's Biomedical Isotope Facility using a previously published protocol [37]. The final compound was injected at high specific activity (average 3369 mCi/μmol, range 1356–9461). ^{18}F-fluorodeoxyglucose was purchased from a commercial vendor (Eastern Isotopes, Sterling, VA).

Table 1
Group characteristics. P values correspond to comparisons between AD and controls

	AD	Control	*p*
n	13	11	
Age	63.9 (7.1)	72.6 (4.3)	< .01
Male/Female	6/7	5/6	ns
Education	15.9 (3.4)	18.1 (2.9)	ns
MMSE	20.0 (7.0)	29.4 (0.7)	< .01
CDR	0.9 (0.2)*	N/A	
PIB positive	13	0	

* - Data not available for one subject; AD = Alzheimer's disease; MMSE = Mini-Mental State Exam; CDR = clinical dementia rating; N/A – not available; ns = not statistically significant (*p* > 0.05).

Image acquisition

PET scans were performed at Lawrence Berkeley National Laboratory using a Siemens ECAT EXACT HR PET scanner in 3D acquisition mode. All 24 subjects underwent PET imaging with ^{11}C-PIB. Between 10–20 mCi of ^{11}C-PIB was injected as a bolus into an antecubital vein. Dynamic acquisition frames were obtained as follows: 4×15 s, 8×30 s, 9×60 s, 2×180 s, 8×300 s and 3×600 s, for a total of 90 min. The same subjects also underwent PET imaging with ^{18}F-FDG. ^{18}F-FDG imaging began a minimum of two hours following ^{11}C-PIB injection (six Carbon-11 half-lives). Six emission frames of 5 min each were acquired starting 30 minutes after injection of approximately 10 mCi of the tracer, with the patient resting quietly in a well lighted room with minimum ambient noise, and eyes and ears open during tracer uptake. Ten minute transmission scans for attenuation correction were obtained either immediately prior or following each ^{11}C-PIB and ^{18}F-FDG scan. PET data were reconstructed using an ordered subset expectation maximization algorithm with weighted attenuation. Images were smoothed with a 4 mm Gaussian kernel with scatter correction. All images were evaluated prior to analysis for patient motion and adequacy of statistical counts.

All patients underwent MRI scans on a 1.5-T Magnetom VISION system (Siemens Inc., Iselin, NJ) using a previously published protocol [38]. In patients with multiple MRIs, the MRI closest to the date of the PET scan was used for analysis. T1-weighted images for control subjects were collected on a 1.5T Magnetom Avanto System (Siemens Inc., Iselin, NJ) with a 12 channel head coil run in triple mode. Volumetric magnetization prepared rapid gradient echo (MP-RAGE) scans were collected on each subject (TR/TE/TI = 2.11 s/3.58 ms/1.1 s, flip angle = 15°), with 1 mm^3 voxel dimensions.

Image pre-processing for voxel-wise analysis in SPM2

Subjects' structural scans (T1-weighted MRIs) were manually reoriented to the anterior–posterior commissure plane and origins were set to the anterior commissure (AC). Structural images were segmented in SPM2 (http://www.fil.ion.ucl.ac.uk/spm) and the resulting gray and white matter images were added to form a brain mask. This mask was then applied to the original structural scan to effectively skull-strip the brain. The skull-stripped image was used to determine the spatial normalization parameters (SPM2 defaults) to warp the structural scan to the Ch2bet template, a high-resolution skull-stripped single-subject T1-weighted scan in Montreal Neurological Institute (MNI) space [39]. The resulting normalization parameters were then inverted and used to perform a reversed (backwards) MNI-to-native space normalization of two (MNI space) reference region templates that included the cerebellum and the pons. The cerebellar reference region was derived from the Ch2bet based Automated Anatomic Labeling (AAL) Atlas [40] and comprised the cerebellar cortex excluding peduncular white matter. The pons reference region was drawn directly onto the Ch2bet template. We reverse normalized the MNI space template reference regions into each subject's native-space in order to visually inspect and manually edit them if needed based on their original anatomy.

Origins were manually set to AC in all PET frames. ^{11}C-PIB frames 6-34 were coregistered and resliced with SPM2 PET realignment parameters using a mid-scan frame visually judged to best represent the subject's anatomy (usually number 17) as the reference frame. Frames 1–5 were coregistered separately to the mean ^{11}C-PIB image obtained from realignment, since these frames typically contain a paucity of anatomical information due to low tracer counts. ^{18}F-FDG scans were realigned with defaults and summed. In order to overlay the native-space reference regions obtained previously ^{11}C-PIB and ^{18}F-FDG scans were now coregistered to the structural scans. Since the pons has been previously shown to be preferable over the cerebellum as reference region in FDG imaging involving AD patients [41] ^{18}F-FDG scans were normalized to mean activity in the pons reference region. For ^{11}C-PIB, voxel-wise Distribution Volume Ratios (DVRs) were calculated using Logan graphical analysis [42], with the cerebellum reference region time-activity curve used as a reference tissue input function. The cerebellum was chosen as a reference region because it is relatively free of fibrillar plaques in AD [43], and results obtained with this analysis are similar to those derived from arterial input functions [16, 44, 45]. Kinetic parameters ($T = 35$–90 min, $k_2 = 0.15$ min^{-1}) were based on previously reported values [45]. DVRs and pons normalized ^{18}F-FDG scans (FDGs) were partial volume corrected for effects of cerebrospinal fluid (for details see 2.5.). The obtained *native-space* DVRs and FDGs were later used for a separate region-of-interest (ROI) analysis (see 2.6.). However, for

the purpose of voxel-wise analysis within SPM2 the images underwent an additional processing step in which the subjects' structural scans were *spatially normalized* to the SPM2 T1 template and the resulting normalization parameters were applied to the FDG and DVR volumes to allow group-wise comparisons within SPM2.

Partial volume correction of PET scans

Using MATLAB and SPM2, a 6 degree of freedom coregistration of the subject's PET scan to the structural scan was calculated, inverted and applied to the structural scan to bring it into the subject's native PET scan space. The structural scan was then segmented and gray and white matter combined to specify a brain mask. This binary brain mask was convolved with the specific point spread function of our scanner to estimate the fraction of brain matter in each region. The PET scan was then divided by this proportion to account for the spill out into non-brain regions. This one compartment model does not account for different uptake in white and gray matter regions [46-48].

Native space gray matter ROI analysis in FreeSurfer

Pre-processed native-space partial volume corrected DVRs and FDGs (see 2.5 & 2.6) were used for this analysis. In order to obtain optimized gray-matter only ROIs a separate stream of T1-weighted image processing and native space ROI labeling was implemented using the FreeSurfer software package (http://surfer.nmr.mgh.harvard.edu/), which has been described in detail elsewhere [49–53]. In brief, T1-weighted scans were resampled to 1 mm isotropic dimensions, intensity normalized, and skull stripped. A white matter-based segmentation procedure was performed, and subcortical structures were labeled based on a probabilistic atlas and voxel intensity values. The gray/white matter and pial surfaces were defined, and topology correction was applied to the reconstructed surfaces. Resulting outputs were visually confirmed and manual edits were performed when necessary. Finally, cortical ROIs were labeled along the reconstructed surface using a probabilistic atlas and each subject's surface geometry. An a priori set of FreeSurfer ROIs were overlaid on the coregistered native-space partial volume corrected DVR and FDG images and values were extracted from both PET modalities.

ROIs from association cortices and the striatum were selected since these regions have been shown to have high DVR values in AD [16, 21]. In our native space analysis, we sought to confirm differences in DVR counts between AD and controls, and also explore the relationship between PIB and FDG in brain regions vulnerable to Aβ pathology. Based on the available *a priori* set the following ROIs were used/defined: dorsolateral (dlFr = caudal and rostral middle frontal gyrus) and medialorbital (moFr) prefrontal cortex, anterior (aCin = rostral anterior cingulate) and posterior (pCin = isthmus cingulate) cingulate, parietal (Par = inferior parietal and supramarginal gyrus), temporal (Temp = middle & superior temporal gyrus), occipital cortex (Occi = cuneus and lingual gyrus), thalamus (Thal), caudate (Caud), putamen (Put) and precuneus (Pre). In an additional analysis partial correlations were computed between ROI counts in PIB vs. FDG scans from AD patients only controlling for age and education. We adopted a liberal $p < .05$ (omitting Bonferroni correction) in order to be able to pick up potential trends.

Voxel-wise analysis

First, two (one-tailed) independent sample comparisons were performed. One compared FDG scans in AD patients vs. controls and the other PIB DVR scans between the two groups. T-maps were thresholded at a false discovery corrected $t = 3.3$, $p < 0.05$ and $t = 3.1$, $p < 0.01$, respectively. We also computed average DVR images to demonstrate the specific retention pattern seen in AD patients compared to the non-specific tracer uptake in controls.

The second analysis investigated the impact of Aβ load (DVRs) on glucose metabolism (FDGs) in AD patients only. For this purpose all functional images were additionally intensity normalized by dividing each voxel in a given PET scan by the maximum value of that scan. We opted for intensity normalization rather than z-score transformation because the former results in images with a range from 0 to 1 instead of positive and negative values clustered around a zero mean. For FDG-PET scans, for example, values closer to 0 represent voxels that show the most severe hypometabolism whereas in PIB-PET scans this corresponds to areas with the lowest Aβ burden. Conversely, values approaching 1 stem from regions of highest metabolic activity and highest Aβ load for FDG- and PIB-PET scan, respectively. We hypothesized that if Aβ load is indeed detrimental to local

synaptic activity/integrity one would expect relatively increased DVR values to be accompanied by relatively decreased FDG values (DVR-FDG > .0). In order to test this hypothesis we created difference images subtracting FDGs of each patient from their DVR counterparts. In order to assess the strength of the hypothesized relationship on a continuous scale we opted for Bayesian posterior probability maps (PPMs) rather than standard t-maps since the former show exact probabilities for the research hypothesis rather than the null hypothesis. We further plotted the highest (95–100%) and lowest (0–5%) probabilities for DVR-FDG approaching 1 in regions of very high Aβ load (top 25% DVR counts in a given patient) while excluding white matter. The chosen probability thresholds are roughly equivalent to $p < 0.05$ and $p > 0.95$ in null-hypothesis testing. Note that this approach was preferred over running voxel-wise correlations since the latter can be problematic due to lack of degrees of freedom, false-discovery correction issues and the less straightforward interpretation of correlation coefficients.

Statistical analysis

Group differences in demographic and neuropsychological measures were examined using two-tailed independent sample t-tests. Dichotomous variables were analyzed using Fisher's Exact tests. Mean FDG ROI values were compared between groups using two-tailed independent sample t-tests with a Bonferroni corrected p of 0.0045 (0.05/11). An analogous analysis was carried out with the DVR ROI data. Statistical analyses were implemented in Statistica 6.0 software (StatSoft Inc., Tulsa, OK).

RESULTS

AD patients were significantly younger than controls (see Table 1). As expected patients scored significantly lower on the MMSE compared to controls. The two groups did not differ concerning, gender or years of education.

Native space mean ROI analyses of FDG uptake revealed a significant metabolic reduction in parietal cortex (−17%) in AD patients compared to controls (see Table 2). Reductions were also seen in precuneus (−16%), and posterior cingulate (−13%) although these were not significant after Bonferroni correction, and a trend was noted in temporal cortex (−10%). Mean PIB DVR values obtained in native space ROIs were significantly elevated everywhere except the thalamus (trend) when patients were compared with controls (see Table 3). The largest relative

Table 2
Comparison of FDG uptake in AD vs. Controls in selected brain regions

	dlFr	moFr	aCin	pCin	Par	Temp	Occi	Thal	Caud	Put	Pre
AD	1.19	1.06	0.90	0.87	0.98	1.02	1.10	0.97	0.94	1.00	0.93
	(0.15)	(0.15)	(0.13)	(0.13)	(0.14)	(0.14)	(0.12)	(0.16)	(0.12)	(0.16)	(0.11)
Con	1.27	1.00	0.88	1.00	1.18	1.13	1.16	1.00	0.99	0.99	1.11
	(0.16)	(0.18)	(0.19)	(0.18)	(0.15)	(0.14)	(0.20)	(0.15)	(0.18)	(0.18)	(0.17)
Decr*	−7	N/A	N/A	−13	**−17**	−10	−5	−3	−5	N/A	−16
p	0.19	0.38	0.82	0.05	**0.003**	0.08	0.40	0.63	0.43	0.88	0.005

* Relative decrease (%) of FDG uptake in AD when compared to controls. Bold figures indicate a significant effect at a corrected $p < 0.0045$.
dlFr = dorsolateral prefrontal cortex, moFr = medialorbital prefrontal cortex, aCin = anterior cingulate, pCin = posterior cingulate, Par = parietal cortex, Temp = temporal cortex, Occi = occipital cortex, Thal = thalamus, Caud = caudate, Put = putamen, Pre = precuneus.

Table 3
Comparison of PIB uptake (DVRs) in AD vs. controls in selected brain regions

	dlFr	moFr	aCin	pCin	Par	Temp	Occi	Thal	Caud	Put	Pre
AD	2.35	2.25	2.14	1.96	2.17	2.22	1.59	1.89	1.77	1.90	2.17
	(0.32)	(0.41)	(0.40)	(0.31)	(0.34)	(0.39)	(0.17)	(0.22)	(0.25)	(0.27)	(0.36)
Con	1.49	1.32	1.35	1.34	1.44	1.42	1.35	1.72	1.38	1.36	1.32
	(0.11)	(0.08)	(0.07)	(0.07)	(0.06)	(0.06)	(0.09)	(0.14)	(0.12)	(0.05)	(0.08)
Incr*	**58**	**70**	**58**	**46**	**51**	**56**	**18**	10	**28**	**40**	**64**
	3E–0	**2E–0**	**2E–0**	**2E–0**	**5E–0**	**8E–0**	**4E–0**	4E–0	**1E–0**	**1E–0**	**1E–0**
p	**8**	**7**	**6**	**6**	**7**	**7**	**4**	2	**4**	**6**	**7**

Relative increase (%) of PIB uptake in AD when compared to controls. Bold Fig.s indicate a significant effect at a corrected $p < 0.0045$.
dlFr = dorsolateral prefrontal cortex, moFr = medialorbital prefrontal cortex, aCin = anterior cingulate, pCin = posterior cingulate, Par = parietal cortex, Temp = temporal cortex, Occi=occipital cortex, Thal = thalamus, Caud = caudate, Put = putamen, Pre = precuneus

increases of PIB uptake were observed in medialorbital prefrontal cortex (+70%) and precuneus (+64%).

Voxel-wise comparison of FDG in AD patients and controls revealed significant ($p < .05$, FDR corrected) bilateral hypometabolism in angular gyrus, precuneus, posterior cingulate, and middle/inferior temporal cortex (see Fig. 1). Hypometabolism was most severe in the left angular gyrus. Group averaged DVRs showed a distinct pattern of specific PIB retention in AD whereas only low non-specific retention was observed in controls (Fig. 2). Map-wise t-tests ($p < 0.01$, FDR corrected) confirmed that PIB uptake was significantly higher in AD compared to controls (Fig. 4, A1 & 2) in bilateral precuneus, angular gyrus, anterior & posterior cingulate, superior and middle frontal, dorsolateral (BA 9 & 46) and ventrolateral (BA 44, 45, 47) prefrontal and orbitofrontal cortex, striatum, thalamus, middle and inferior temporal cortex, fusiform gyrus, calcarine and lingual gyrus. Peaks were located in left precuneus, right posterior cingulate, left middle & infe-

rior temporal cortex, left fusiform gyrus, left striatum, left orbitofrontal cortex, bilateral superior & middle frontal cortex.

Partial correlations between DVR and FDG ROI data of AD patients neither revealed any inverse correlations nor visible trends ($p > 0.10$). Whole-brain averaged intensity normalized DVRs and FDGs for AD patients only are shown in Fig. 3. Probability maps (PPMs) assessing the likelihood for a voxel with increased (top 25%) Aβ load (DVRs) to be accompanied by lowered glucose metabolism (FDGs) were computed and white matter was masked out. We then plotted the highest (95–100%) and lowest (0–5%) probabilities for the effect (Fig. 4, B1 & B2). High Aβ load was found to be coupled with reduced glucose metabolism in posterior cingulate, precuneus, angular gyrus, middle & inferior temporal cortex. Importantly, however, the same Aβ burden was *not* coupled with comparable metabolic reduction in large parts of superior & middle frontal cortex, orbitofrontal
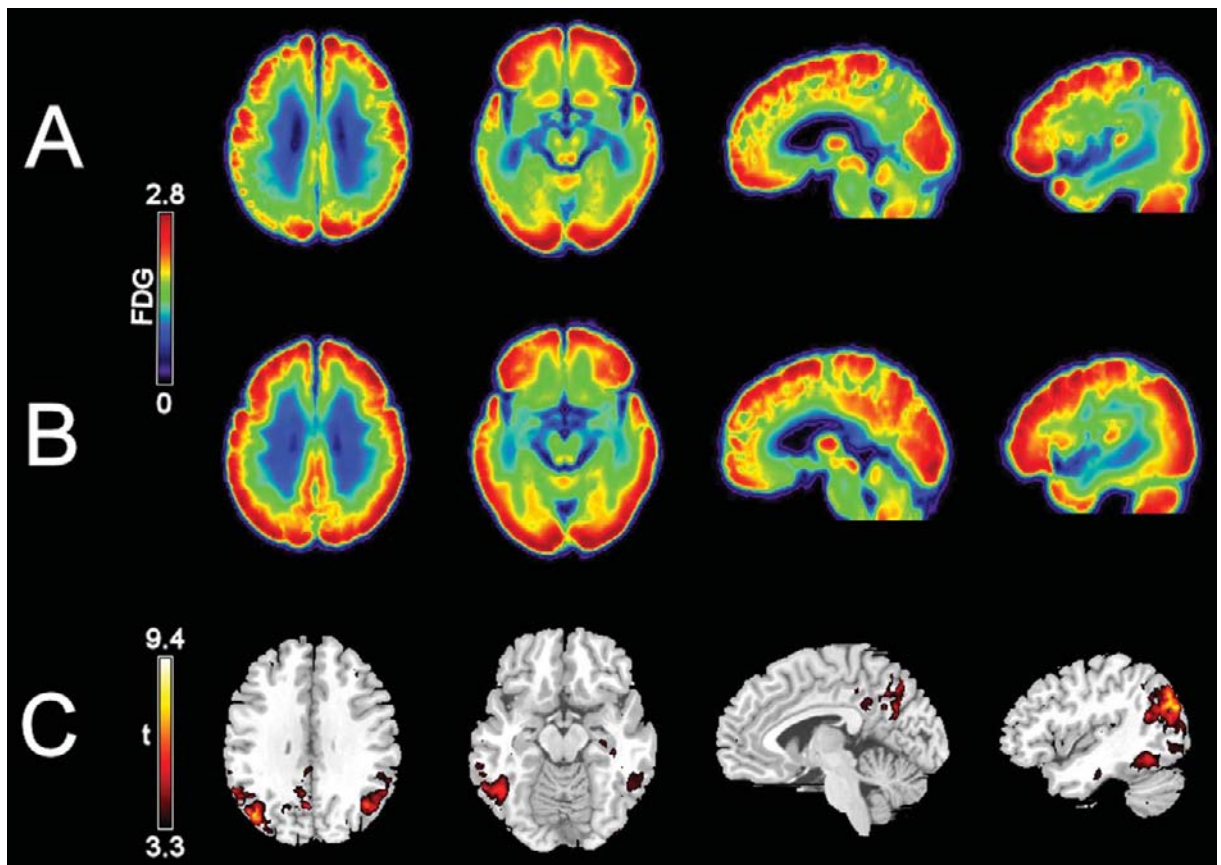
Fig. 1. FDG uptake in AD vs. controls. A) averaged FDG scans for 13 PIB + AD patients; B) averaged FDG scans for 11 PIB- controls; $C =$ one-tailed t-maps comparing FDG uptake in controls and AD patients (FDR corrected at $p < 0.05$). All figures are in neurological orientation.
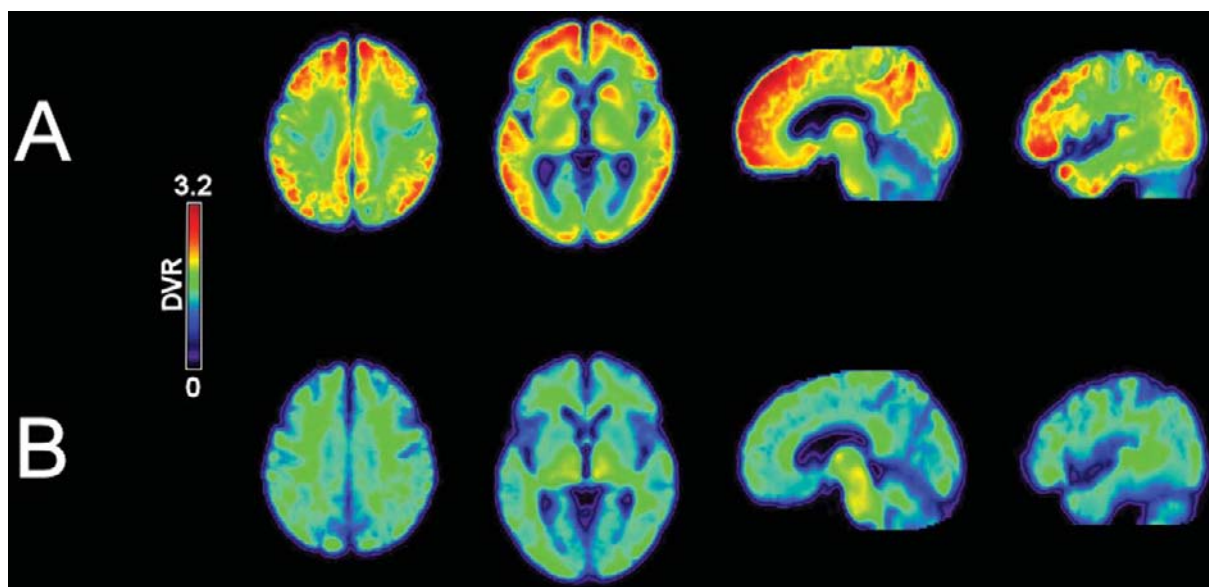
Fig. 2. PIB uptake (DVRs) in AD vs. controls. A) averaged DVR scans for AD patients; B) averaged DVR scans for controls.
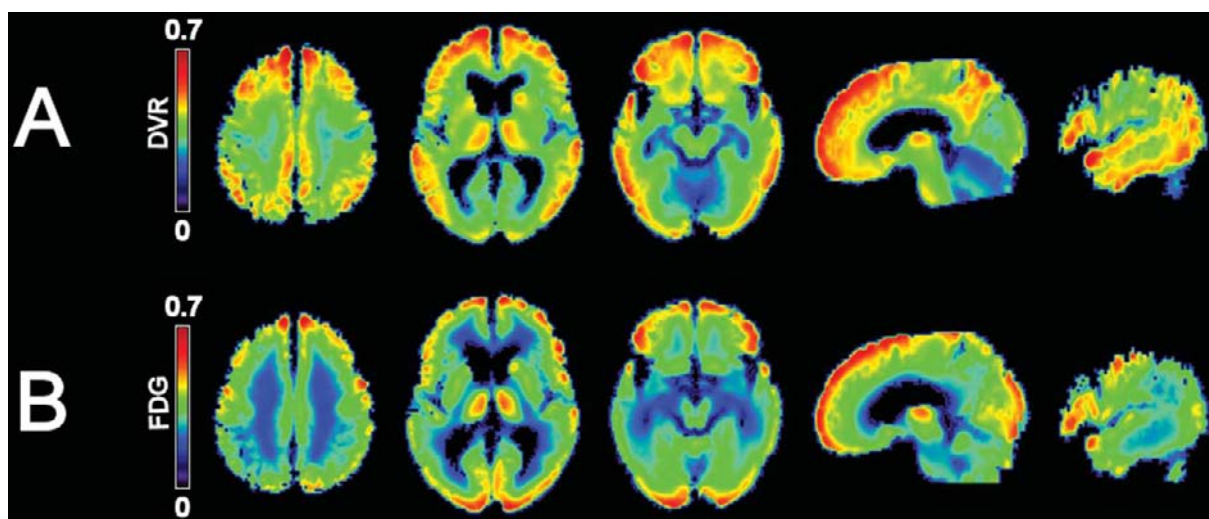
Fig. 3. Intensity normalized PIB and FDG images in AD only. A) averaged intensity normalized DVR volumes for AD patients only B) averaged intensity normalized FDG volumes for AD patients only.

& inferiofrontal cortex, striatum, thalamus, calcarine, lingual and inferior occipital lobes. Furthermore, as can be seen in Fig. 4 some of these regions had been identified earlier as showing maximal Aβ load when patients were compared with controls (A1 & A2). While high Aβ load seems to be consistently coupled with metabolic reduction in temporo-parietal (posterior) areas no comparable reduction can be seen in large frontal (anterior) regions and striatum in spite of very high levels of Aβ.

DISCUSSION

In this study we used atrophy corrected data to investigate the relationship between Aβ plaque load and glucose metabolism as measured by the radiotracers PIB and FDG and both voxel-wise and native space ROI approaches. Analysis of the FDG data confirmed a typical temporo-parietal hypometabolic pattern in AD [54, 55], while PIB DVRs illustrated a distinct pattern of specific PIB retention in fronto-
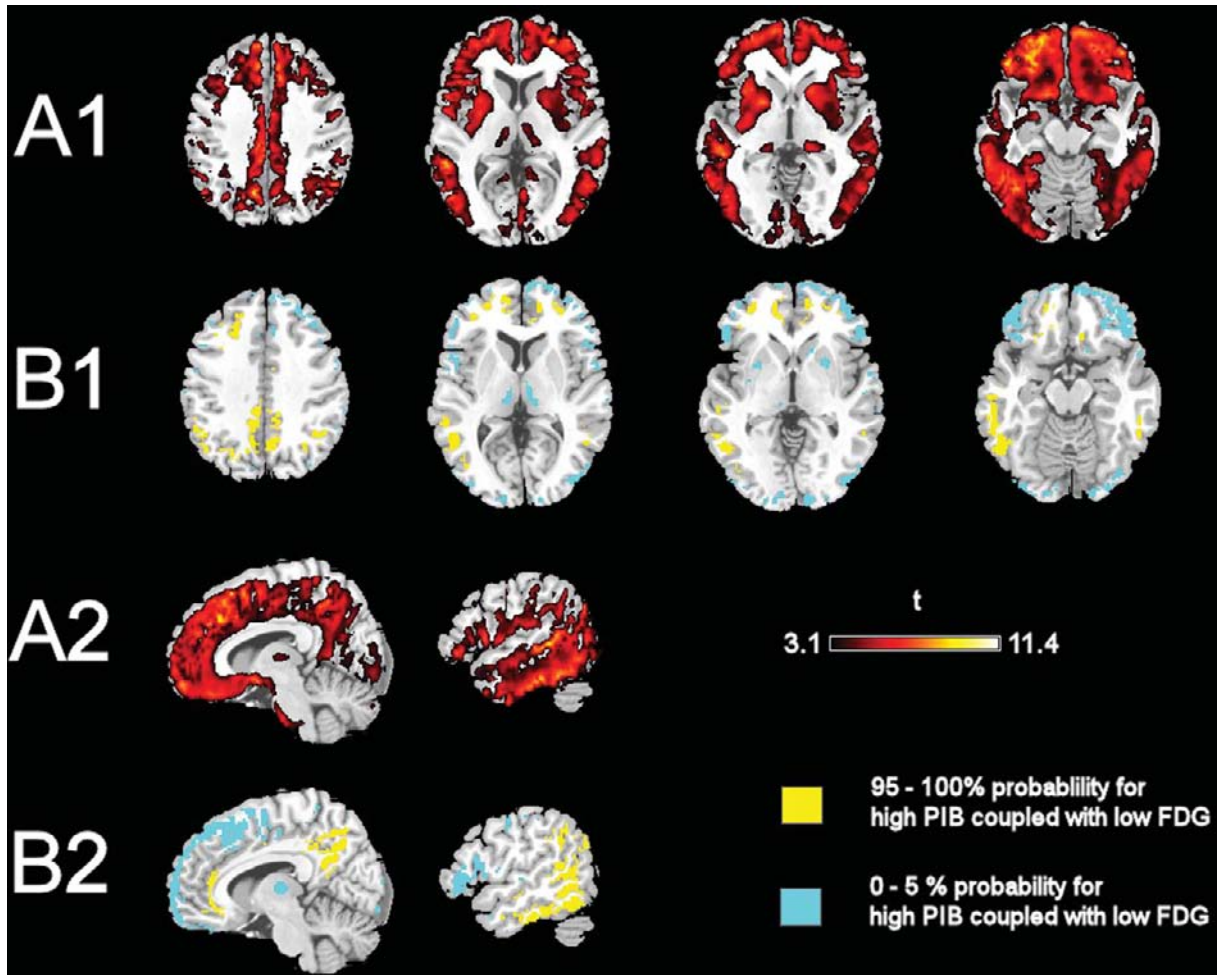
Fig. 4. Impact of severe Aβ load on glucose metabolism in AD only and comparison with peak Aβ regions in AD vs. controls. A1 & A2 = voxel-wise comparison of PIB uptake (DVRs) in AD patients (13) vs. controls (11). Thresholded at a corrected (FDR) $p < 0.01$. B1 & B2 = voxel-wise comparison of the 25% highest PIB counts and their spatially corresponding FDG counterparts in AD patients only. Bayesian posterior probability maps indicate regions where high Aβ load was coupled with lowered glucose metabolism and regions where high Aβ burden was not accompanied with a comparable metabolic reduction. Slice selection is the same as in A1 & A2.

temporo-parietal, precuneus, posterior cingulate, and striatal regions in AD and only weak non-specific PIB retention in white matter in controls [16]. Consistent with previously published data [32, 33, 56] we did not observe any region-to-region or within region effects between FDG and PIB in AD patients when using partial correlations. However, our voxel-wise analysis of PPMs showed that increased Aβ burden was found to coincide with decreased metabolism in temporo-parietal regions (including precuneus) and the posterior cingulate. However, severe Aβ plaque burden was not coupled with comparable metabolic decreases in large parts of the frontal lobes, the striatum and the thalamus.

These patterns of metabolic reduction and Aβ deposition are similar to those that have been reported in other studies [16, 18, 19, 30, 54, 55, 57–62]. Variations in the findings concerning which of these three regions is most hypometabolic are in part accounted by different ROI drawing methods, degrees of statistical thresholding and whether the data was partial volume corrected. However, the absence of relative metabolic reductions despite severe Aβ load (top 25% PIB counts) in frontal, striatal and thalamic regions compared to temporo-parietal regions is intriguing and needs to be considered in more detail.

While Cohen and colleagues [31] found in their analysis of PIB positive AD patients a negative correlation

between metabolism in the precuneus and PIB retention in the frontal regions we did not observe any such correlations in our ROI data. The discrepancy between their findings and the present data are unlikely due to differences in sample sizes with an $n = 14$ in their study vs. 13 in ours. Therefore lack of statistical power can be ruled out as an explanation particularly since studies with considerably larger Ns (34) also failed to find such a correlation [33]. As Cohen et al., our studies also applied atrophy correction to adjust for partial volume effects. However, interestingly the authors applied some arbitrary pre-thresholding of their PIB data (discarding all DVR values smaller than 0.75) which may account for the differences in the findings as it changes the variance and range of the underlying data.

In order to appreciate the key findings of the present paper it is important to consider the distinction between correlational approaches and the increased probabilities in terms of PPM as we report them here. PPMs are not directly comparable to correlations as we aimed at looking at the most severely affected regions of the brain across subjects in contrast to relating FDG and PIB in a continuous fashion. Our procedure involved intensity normalization which allows for direct comparison between modalities across subjects followed by thresholding to indentify the most severely affected regions in terms of Aβ load and hypometabolism. Obviously, this approach only looks at a subset of the data and is not suitable for looking at continuous effects. Nonetheless, our finding of relative metabolic sparing in anterior compared to posterior brain regions despite more pronounced Aβ burden in anterior vs. posterior regions is intriguing and has been noted before [32, 33].

Indeed, in a recent study using the triplet of the tracers 2-(1-{6-[(2-[18F]fluoroethyl)(methyl) amino]-2-naphthyl}ethylidene)malononitrile (FDDNP), PIB and FDG [63] presented an analysis that is very relevant to our findings. The authors compared the uptake in the three tracers in AD vs age-matched controls and found similar patterns for PIB and FDG together with the expected differential uptake of FDDNP illustrating the tracer's binding to both Aβ plaques and NFT. Importantly, when the authors produced a visual rendering of the overlap between the regions that were both most hypometabolic and showed the largest Aβ burden they found the same temporo-parietal pattern as we report it here. However, as in our data PIB uptake peaked in frontal (anterior) brain regions which were relatively spared in terms of metabolism.

As hypometabolism is related to synaptic integrity two other studies exploring the relationship between PIB uptake and gray matter densities should be considered here. Chetelat and colleagues [64] looked at this relationship across the diagnostic spectrum and did not find any correlations between PIB uptake and gray matter densities in controls, MCI or AD but only controls with subjective memory complaints. By contrast Frisoni et al. [65] found an anterior-posterior gradient of increasing atrophy in posterior brain regions in relation to PIB uptake when combining the data of a group of AD patients and controls. They reported a voxel-wise pattern that closely resembles the findings of our PPM analysis. Unfortunately, however, the authors did not report separate regressions for AD and controls, respectively.

Despite the fact that in AD Aβ load and hypometabolism seem to spatially coincide in multiple brain regions the lack of a direct correlation between the two measures is consistent with the finding that while FDG correlates reliably with measures of cognitive decline PIB does not [33, 56]. These reports are in line with longitudinal data on Aβ accumulation including the very first AD patient ever scanned with PIB [66] suggesting that Aβ levels remain relatively stable as cognitive functions deteriorate [23, 67].

Similarly longitudinal MRI but not PIB changes were found to be correlated with dementia severity in another study [29]. Consequently, there seems to be a growing consensus in the field that once AD pathology is fully present Aβ is no longer a driving factor of the continued cognitive decline [7, 29, 68].

The above suggests that ongoing clinical trials aimed at lowering Aβ levels in AD [69] may ultimately fail in improving the symptoms at such a late stage of the disease. Instead intervention at pre-symptomatic stages seems to be more promising.

ACKNOWLEDGEMENTS

DISCLOSURE STATEMENT

The authors have nothing to disclose.

REFERENCES

[1] Arnold SE, Hyman BT, Flory J, Damasio AR, Van Hoesen GW (1991) The topographical and neuroanatomical distribution of neurofibrillary tangles and neuritic plaques in the cerebral cortex of patients with Alzheimer's disease. *Cereb Cortex* **1**, 103-116.

[2] Braak H, Braak E (1991) Neuropathological stageing of Alzheimer-related changes. *Acta Neuropathol (Berl)* **82**, 239-259.

[3] Braak H, Braak E (1997) Diagnostic criteria for neuropathologic assessment of Alzheimer's disease. *Neurobiol. Aging* **18**, S85-S88.

[4] Goate A, Chartier-Harlin MC, Mullan M, Brown J, Crawford F, Fidani L, Giuffra L, Haynes A, Irving N, James L, et al. (1991) Segregation of a missense mutation in the amyloid precursor protein gene with familial Alzheimer's disease. *Nature* **349**, 704-706.

[5] Naruse S, Igarashi S, Kobayashi H, Aoki K, Inuzuka T, Kaneko K, Shimizu T, Iihara K, Kojima T, Miyatake, T et al. (1991) Mis-sense mutation Val—-Ile in exon 17 of amyloid precursor protein gene in Japanese familial Alzheimer's disease. *Lancet* **337**, 978-979.

[6] Hardy JA, Higgins GA (1992) Alzheimer's disease: the amyloid cascade hypothesis. *Science* **256**, 184-185.

[7] Ingelsson M, Fukumoto H, Newell KL, Growdon JH, Hedley-Whyte ET, Frosch MP, Albert MS, Hyman BT, Irizarry MC (2004) Early Abeta accumulation and progressive synaptic loss, gliosis, and tangle formation in AD brain. *Neurology* **62**, 925-931.

[8] Dickson DW, Crystal HA, Bevona C, Honer W, Vincent I, Davies P (1995) Correlations of synaptic and pathological markers with cognition of the elderly. *Neurobiol Aging* **16**, 285-298; discussion 298-304.

[9] Katzman R (1986) Alzheimer's disease. *N Engl J Med* **314**, 964-973.

[10] Terry RD, Masliah E, Salmon DP, Butters N, DeTeresa R, Hill R, Hansen LA, Katzman R (1991) Physical basis of cognitive alterations in Alzheimer's disease: synapse loss is the major correlate of cognitive impairment. *Ann Neurol* **30**, 572-580.

[11] Walsh DM, Selkoe DJ (2007) A beta oligomers - a decade of discovery. *J Neurochem* **101**, 1172-1184.

[12] Samuels SC, Silverman JM, Marin DB, Peskind ER, Younki SG, Greenberg DA, Schnur E, Santoro J, Davis KL (1999) CSF beta-amyloid, cognition, and APOE genotype in Alzheimer's disease. *Neurology* **52**, 547-551.

[13] Stern EA, Bacskai BJ, Hickey GA, Attenello FJ, Lombardo JA, Hyman BT (2004) Cortical synaptic integration in vivo is disrupted by amyloid-beta plaques. *J Neurosci* **24**, 4535-4540.

[14] Palop JJ, Chin J, Roberson ED, Wang J, Thwin MT, Bien-Ly N, Yoo J, Ho KO, Yu GQ, Kreitzer A, Finkbeiner S, Noebels JL, Mucke L (2007) Aberrant excitatory neuronal activity and compensatory remodeling of inhibitory hippocampal circuits in mouse models of Alzheimer's disease. *Neuron* **55**, 697-711.

[15] Klunk WE, Engler H, Nordberg A, Bacskai BJ, Wang Y, Price JC, Bergstrom M, Hyman BT, Langstrom B, Mathis CA (2003) Imaging the pathology of Alzheimer's disease: amyloid-imaging with positron emission tomography. *Neuroimaging Clin N Am* **13**, 781-789, ix.

[16] Klunk WE, Engler H, Nordberg A, Wang Y, Blomqvist G, Holt DP, Bergstrom M, Savitcheva I, Huang GF, Estrada S, Ausen B, Debnath ML, Barletta J, Price JC, Sandell J, Lopresti BJ, Wall A, Koivisto P, Antoni G, Mathis CA, Langstrom B (2004) Imaging brain amyloid in Alzheimer's disease with Pittsburgh Compound-B. *Ann Neurol* **55**, 306-319.

[17] Boxer AL, Rabinovici GD, Kepe V, Goldman J, Furst AJ, Huang SC, Baker SL, O'Neil JP, Chui H, Geschwind MD, Small GW, Barrio JR, Jagust W, Miller BL (2007) Amyloid imaging in distinguishing atypical prion disease from Alzheimer disease. *Neurology* **69**, 283-290.

[18] Forsberg A, Engler H, Almkvist O, Blomqvist G, Hagman G, Wall A, Ringheim A, Langstrom B, Nordberg A (2008) PET imaging of amyloid deposition in patients with mild cognitive impairment. *Neurobiol Aging* **29**, 1456-1465.

[19] Kemppainen NM, Aalto S, Wilson IA, Nagren K, Helin S, Bruck A, Oikonen V, Kailajarvi M, Scheinin M, Viitanen M, Parkkola R, Rinne JO (2006) Voxel-based analysis of PET amyloid ligand [11C]PIB uptake in Alzheimer disease. *Neurology* **67**, 1575-1580.

[20] Rabinovici GD, Furst AJ, O'Neil JP, Racine CA, Mormino EC, Baker SL, Chetty S, Patel P, Pagliaro TA, Klunk WE, Mathis CA, Rosen HJ, Miller BL, Jagust WJ (2007) 11C-PIB PET imaging in Alzheimer disease and frontotemporal lobar degeneration. *Neurology* **68**, 1205-1212.

[21] Rowe CC, Ng S, Ackermann U, Gong SJ, Pike K, Savage G, Cowie TF, Dickinson KL, Maruff P, Darby D, Smith C, Woodward M, Merory J, Tochon-Danguy H, O'Keefe G, Klunk WE, Mathis CA, Price JC, Masters CL, Villemagne VL (2007) Imaging beta-amyloid burden in aging and dementia. *Neurology* **68**, 1718-1725.

[22] Forsberg A, Almkvist O, Engler H, Wall A, Langstrom B, Nordberg A (2010) High PIB retention in Alzheimer's disease is an early event with complex relationship with CSF biomarkers and functional parameters. *Curr Alzheimer Res* **7**, 56-66.

[23] Koivunen J, Scheinin N, Virta JR, Aalto S, Vahlberg T, Nagren K, Helin S, Parkkola R, Viitanen M, Rinne JO (2011) Amyloid PET imaging in patients with mild cognitive impairment: a 2-year follow-up study. *Neurology* **76**, 1085-1090.

[24] Okello A, Koivunen J, Edison P, Archer HA, Turkheimer FE, Nagren K, Bullock R, Walker Z, Kennedy A, Fox NC, Rossor MN, Rinne JO, Brooks DJ (2009) Conversion of amyloid positive and negative MCI to AD over 3 years. An 11C-PIB PET study. *Neurology* **73**, 754-760.

[25] Villemagne VL, Pike KE, Chetelat G, Ellis KA, Mulligan RS, Bourgeat P, Ackermann U, Jones G, Szoeke C, Salvado O, Martins R, O'Keefe G, Mathis CA, Klunk WE, Ames D, Masters CL, Rowe CC (2011) Longitudinal assessment of Abeta and cognition in aging and Alzheimer disease. *Ann Neurol* **69**, 181-192.

[26] Wolk DA, Price JC, Saxton JA, Snitz BE, James JA, Lopez OL, Aizenstein HJ, Cohen AD, Weissfeld LA, Mathis CA, Klunk WE, DeKoskym ST (2009) Amyloid imaging in mild cognitive impairment subtypes. *Ann Neurol* **65**, 557-568.

[27] Rabinovici GD, Furst AJ, Alkalay A, Racine CA, O'Neil JP, Janabi M, Baker SL, Agarwal N, Bonasera SJ, Mormino EC, Weiner MW, Gorno-Tempini ML, Rosen HJ, Miller BL, Jagust WJ (2010) Increased metabolic vulnerability in early-onset Alzheimer's disease is not related to amyloid burden. *Brain* **133**, 512-528.

[28] Jack CR, Jr., Lowe VJ, Senjem ML, Weigand SD, Kemp BJ, Shiung MM, Knopman DS, Boeve BF, Klunk WE, Mathis CA, Petersen RC (2008) 11 C PiB and structural MRI provide complementary information in imaging of Alzheimer's disease and amnestic mild cognitive impairment. *Brain* **131**, 665-680.

[29] Jack CR, Jr., Lowe VJ, Weigand SD, Wiste HJ, Senjem ML, Knopman DS, Shiung MM, Gunter JL, Boeve BF, Kemp BJ, Weiner M, Petersen RC (2009) Serial PIB and MRI in normal, mild cognitive impairment and Alzheimer's disease: implications for sequence of pathological events in Alzheimer's disease. *Brain. 132(Pt 5)*, 1355-1365.

[30] Edison P, Archer HA, Hinz R, Hammers A, Pavese N, Tai YF, Hotton G, Cutler D, Fox N, Kennedy A, Rossor M, Brooks DJ (2007) Amyloid, hypometabolism, and cognition in Alzheimer disease: an [11C]PIB and [18F]FDG PET study. *Neurology* **68**, 501-508.

[31] Cohen AD, Price JC, Weissfeld LA, James J, Rosario BL, Bi W, Nebes RD, Saxton JA, Snitz BE, Aizenstein HA, Wolk DA, Dekosky ST, Mathis CA, Klunk WE (2009) Basal cerebral metabolism may modulate the cognitive effects of Abeta in mild cognitive impairment: an example of brain reserve. *J Neurosci* **29**, 14770-14778.

[32] Li Y, Rinne JO, Mosconi L, Pirraglia E, Rusinek H, DeSanti S, Kemppainen N, Nagren K, Kim BC, Tsui W, de Leon MJ (2008) Regional analysis of FDG and PIB-PET images in normal aging, mild cognitive impairment, and Alzheimer's disease. *Eur J Nucl Med Mol Imaging* **35**, 2169-2181.

[33] Furst AJ, Rabinovici GD, Rostomian AH, Steed T, Alkalay A, Racine C, Miller BL, Jagust WJ (2010) Cognition, glucose metabolism and amyloid burden in Alzheimer's disease. *Neurobiol Aging*, doi:10.1016/j.neurobiolaging.2010.03.011.

[34] Morris JC (1993) The Clinical Dementia Rating (CDR): current version and scoring rules. *Neurology* **43**, 2412-2414.

[35] McKhann G, Drachman D, Folstein M, Katzman R, Price D, Stadlan EM (1984) Clinical diagnosis of Alzheimer's disease: report of the NINCDS-ADRDA Work Group under the auspices of Department of Health and Human Services Task Force on Alzheimer's Disease. *Neurology* **34**, 939-944.

[36] Mormino EC, Kluth JT, Madison CM, Rabinovici GD, Baker SL, Miller BL, Koeppe RA, Mathis CA, Weiner MW, Jagust WJ (2009) Episodic memory loss is related to hippocampal-mediated beta-amyloid deposition in elderly subjects. *Brain* **132**, 1310-1323.

[37] Mathis CA, Wang Y, Holt DP, Huang GF, Debnath ML, Klunk WE (2003) Synthesis and evaluation of 11C-labeled 6-substituted 2-arylbenzothiazoles as amyloid imaging agents. *J Med Chem* **46**, 2740-2754.

[38] Du AT, Schuff N, Kramer JH, Rosen HJ, Gorno-Tempini ML, Rankin K, Miller BL, Weiner MW (2007) Different regional patterns of cortical thinning in Alzheimer's disease and frontotemporal dementia. *Brain* **130**, 1159-1166.

[39] Holmes CJ, Hoge R, Collins L, Woods R, Toga AW, Evans AC (1998) Enhancement of MR images using registration for signal averaging. *J Comput Assist Tomogr* **22**, 324-333.

[40] Tzourio-Mazoyer N, Landeau B, Papathanassiou D, Crivello F, Etard O, Delcroix N, Mazoyer B, Joliot M (2002) Automated anatomical labeling of activations in SPM using a macroscopic anatomical parcellation of the MNI MRI single-subject brain. *Neuroimage* **15**, 273-289.

[41] Minoshima S, Frey KA, Foster NL, Kuhl DE (1995) Preserved pontine glucose metabolism in Alzheimer disease: a reference region for functional brain image (PET) analysis. *J Comput Assist Tomogr* **19**, 541-547.

[42] Logan J, Fowler JS, Volkow ND, Wang GJ, Ding YS, Alexoff DL (1996) Distribution volume ratios without blood sampling from graphical analysis of PET data. *J Cereb Blood Flow Metab* **16**, 834-840.

[43] Joachim CL, Morris JH, Selkoe DJ (1989) Diffuse senile plaques occur commonly in the cerebellum in Alzheimer's disease. *Am J Pathol* **135**, 309-319.

[44] Lopresti BJ, Klunk WE, Mathis CA, Hoge JA, Ziolko SK, Lu X, Meltzer CC, Schimmel K, Tsopelas ND, DeKosky ST, Price JC (2005) Simplified quantification of Pittsburgh Compound B amyloid imaging PET studies: a comparative analysis. *J Nucl Med* **46**, 1959-1972.

[45] Price JC, Klunk WE, Lopresti BJ, Lu X, Hoge JA, Ziolko SK, Holt DP, Meltzer CC, DeKosky ST, Mathis CA (2005) Kinetic modeling of amyloid binding in humans using PET imaging and Pittsburgh Compound-B. *J Cereb Blood Flow Metab* **25**, 1528-1547.

[46] Meltzer CC, Kinahan PE, Greer PJ, Nichols TE, Comtat C, Cantwell MN, Lin MP, Price JC (1999) Comparative evaluation of MR-based partial-volume correction schemes for PET. *J Nucl Med* **40**, 2053-2065.

[47] Meltzer CC, Leal JP, Mayberg HS, Wagner HN, Jr., Frost JJ (1990) Correction of PET data for partial volume effects in human cerebral cortex by MR imaging. *J Comput Assist Tomogr* **14**, 561-570.

[48] Zaidi H, Ruest T, Schoenahl F, Montandon ML (2006) Comparative assessment of statistical brain MR image segmentation algorithms and their impact on partial volume correction in PET. *Neuroimage* **32**, 1591-1607.

[49] Dale AM, Fischl B, Sereno MI (1999) Cortical surface-based analysis. I. Segmentation and surface reconstruction. *Neuroimage* **9**, 179-194.

[50] Desikan RS, Segonne F, Fischl B, Quinn BT, Dickerson BC, Blacker D, Buckner RL, Dale AM, Maguire RP, Hyman BT, Albert MS, Killiany RJ (2006) An automated labeling system for subdividing the human cerebral cortex on MRI scans into gyral based regions of interest. *Neuroimage* **31**, 968-980.

[51] Fischl B, Liu A, Dale AM (2001) Automated manifold surgery: constructing geometrically accurate and topologically correct models of the human cerebral cortex. *IEEE Trans Med Imaging* **20**, 70-80.

[52] Fischl B, Salat DH, Busa E, Albert M, Dieterich M, Haselgrove C, van der Kouwe A, Killiany R, Kennedy D, Klaveness S, Montillo A, Makris N, Rosen B, Dale AM (2002) Whole brain segmentation: automated labeling of neuroanatomical structures in the human brain. *Neuron* **33**, 341-355.

[53] Segonne F, Dale AM, Busa E, Glessner M, Salat D, Hahn HK, Fischl B (2004) A hybrid approach to the skull stripping problem in MRI. *Neuroimage* **22**, 1060-1075.

[54] Herholz K, Salmon E, Perani D, Baron JC, Holthoff V, Frolich L, Schonknecht P, Ito K, Mielke R, Kalbe E, Zundorf G, Delbeuck X, Pelati O, Anchisi D, Fazio F, Kerrouche N, Desgranges B, Eustache F, Beuthien-Baumann B, Menzel C, Schroder J, Kato T, Arahata Y, Henze M, Heiss WD (2002) Discrimination between Alzheimer dementia and controls by automated analysis of multicenter FDG PET. *Neuroimage* **17**, 302-316.

[55] Minoshima S, Frey KA, Koeppe RA, Foster NL, Kuhl DE (1995) A diagnostic approach in Alzheimer's disease using three-dimensional stereotactic surface projections of fluorine-18-FDG PET. *J Nucl Med* **36**, 1238-1248.

[56] Kadir A, Almkvist O, Forsberg A, Wall A, Engler H, Langstrom B, Nordberg A (2010) Dynamic changes in PET amyloid and FDG imaging at different stages of Alzheimer's disease. *Neurobiol Aging*, doi:10.1016/j.neurobiolaging.2010.06.015

[57] Ziolko SK, Weissfeld LA, Klunk WE, Mathis CA, Hoge JA, Lopresti BJ, DeKosky ST, Price JC (2006) Evaluation of voxel-based methods for the statistical analysis of PIB PET amyloid imaging studies in Alzheimer's disease. *Neuroimage* **33**, 94-102.

[58] Heiss WD, Kessler J, Szelies B, Grond M, Fink G, Herholz K (1991) Positron emission tomography in the differential diagnosis of organic dementias. *J Neural Transm Suppl* **33**, 13-19.

[59] Heiss WD, Szelies B, Kessler J, Herholz K (1991) Abnormalities of energy metabolism in Alzheimer's disease studied with PET. *Ann N Y Acad Sci* **640**, 65-71.

[60] Herholz K, Perani D, Salmon E, Franck G, Fazio F, Heiss WD, Comar D (1993) Comparability of FDG PET studies in probable Alzheimer's disease. *J Nucl Med* **34**, 1460-1466.

[61] Ichimiya A, Herholz K, Mielke R, Kessler J, Slansky I, Heiss WD (1994) Difference of regional cerebral metabolic pattern between presenile and senile dementia of the Alzheimer type: a factor analytic study. *J Neurol Sci* **123**, 11-17.

[62] Klunk WE, Price JC, Mathis CA, Tsopelas ND, Lopresti BJ, Ziolko SK, Bi W, Hoge JA, Cohen AD, Ikonomovic MD, Saxton JA, Snitz BE, Pollen DA, Moonis M, Lippa CF, Swearer JM, Johnson KA, Rentz DM, Fischman AJ, Aizenstein HJ, DeKosky ST (2007) Amyloid deposition begins in the striatum of presenilin-1 mutation carriers from two unrelated pedigrees. *J Neurosci* **27**, 6174-6184.

[63] Shin J, Lee SY, Kim SJ, Kim SH, Cho SJ, Kim YB (2010) Voxel-based analysis of Alzheimer's disease PET imaging using a triplet of radiotracers: PIB, FDDNP, and FDG. *NeuroImage* **52**, 488-496.

[64] Chetelat G, Villemagne VL, Bourgeat P, Pike KE, Jones G, Ames D, Ellis KA, Szoeke C, Martins RN, O'Keefe GJ, Salvado O, Masters CL, Rowe CC (2010) Relationship between atrophy and beta-amyloid deposition in Alzheimer disease. *Ann Neurol* **67**, 317-324.

[65] Frisoni GB, Lorenzi M, Caroli A, Kemppainen N, Nagren K, Rinne JO (2009) In vivo mapping of amyloid toxicity in Alzheimer disease. *Neurology* **72**, 1504-1511.

[66] Kadir A, Marutle A, Gonzalez D, Scholl M, Almkvist O, Mousavi M, Mustafiz T, Darreh-Shori T, Nennesmo I, Nordberg A (2011) Positron emission tomography imaging and clinical progression in relation to molecular pathology in the first Pittsburgh Compound B positron emission tomography patient with Alzheimer's disease. *Brain* **134**, 301-317.

[67] Engler H, Forsberg A, Almkvist O, Blomquist G, Larsson E, Savitcheva I, Wall A, Ringheim A, Langstrom B, Nordberg A (2006) Two-year follow-up of amyloid deposition in patients with Alzheimer's disease. *Brain* **129**, 2856-2866.

[68] Jack CR, Jr., Knopman DS, Jagust WJ, Shaw LM, Aisen PS, Weiner MW, Petersen RC, Trojanowski JQ (2010) Hypothetical model of dynamic biomarkers of the Alzheimer's pathological cascade. *Lancet Neurol* **9**, 119-128.

[69] Rinne JO, Brooks DJ, Rossor MN, Fox NC, Bullock R, Klunk WE, Mathis CA, Blennow K, Barakos J, Okello AA, Rodriguez Martinez de Liano S, Liu E, Koller M, Gregg KM, Schenk D, Black R, Grundman M (2010) 11C-PiB PET assessment of change in fibrillar amyloid-beta load in patients with Alzheimer's disease treated with bapineuzumab: a phase 2, double-blind, placebo-controlled, ascending-dose study. *Lancet Neurol* **9**, 363-372.

Florbetaben to Trace Amyloid-β in the Alzheimer Brain by Means of PET

Henryk Barthel* and Osama Sabri
Department of Nuclear Medicine, University of Leipzig, Leipzig, Germany

Abstract. PET imaging of amyloid-β has recently emerged as a valuable biomarker to support the *in vivo* diagnosis of Alzheimer's disease (AD). So far, however, no tracer is available suitable for general clinical routine application. Florbetaben is a promising ^{18}F-labeled amyloid-β-targeted PET tracer currently in Phase2/3 clinical development. This review provides an overview on the current knowledge and future research activities on florbetaben. Recently, the first worldwide multi-center trial to test the diagnostic performance of amyloid-β PET in AD was conducted with this tracer. From this trial, a sensitivity and specificity of 80 and 91% in the discrimination between patients with probable AD and age-matched healthy controls was reported. Ongoing florbetaben PET trials deal with correlating the *in vivo* PET signal to *post mortem* histopathology evaluation, and with investigating the value of the tracer to predict progression to AD at the stage of mild cognitive impairment. The preclinical and clinical data currently available verify florbetaben as a safe and efficacious PET tracer suitable for detection of amyloid-β deposition in the brain. The results of the ongoing trials will contribute to current knowledge on the characteristics of florbetaben, and will help to determine the future potential of florbetaben PET imaging as a visual adjunct to supplement the routine clinical "AD diagnostic toolbox".

Keywords: Alzheimer's disease, amyloid-β, PET imaging, florbetaben

INTRODUCTION

In the Alzheimer's disease (AD) community, there is increasing understanding of the importance to incorporate biomarker information into the diagnostic work-up [1,2]. Amongst the different biomarker alternatives to support the *in vivo* AD diagnosis, positron emission tomography (PET) imaging of brain amyloid-β (Aβ) is particularly appealing as it permits direct non-invasive visualization and quantification of one of the two histological hallmarks of the disease. Amongst the different available Aβ-targeted PET tracers, [11C]PIB was so far most frequently used [3]. The short radioactive half life of the label (20 min), however, limits the use of this tracer to PET facilities with an on-site cyclotron. Therefore, there is currently intensive research to identify more stable Aβ-targeted PET tracers. In this overview, we describe florbetaben as a promising ^{18}F-labeled Aβ-PET tracer with favorable characteristics to potentially allow future routine use in the clinic to support AD diagnosis. We review the current knowledge on florbetaben as it was obtained from recent preclinical and clinical studies, and summarize future directions to develop this tracer.

PRECLINICAL DATA ON FLORBETABEN

Florbetaben ([^{18}F]BAY 94-9172, trans-4-(*N*-methyl-amino)-4′-2-[2-(2-^{18}F]fluoro-ethoxy)-ethoxy]-ethoxy-stilbene) is an polyethylene glycol stilbene derivative. The first radiosynthesis of this tracer including the radio-labelling of the non-radioactive precursor (BOC-Stilbenmesylate) with [18]F (the radioactive fluoride provided by an onsite cyclotron) followed

---
*Correspondence to: Dr. Henryk Barthel, Department of Nuclear Medicine, University of Leipzig, Liebigstraße 18, 04103 Leipzig, Germany. Tel.: +49 341 9718082; Fax: +49 341 9718069; E-mail: henryk.barthel@medizin.uni-leipzig.de.

by acid hydrolysis and semi-preparative HPLC for purification was described by Zhang et al. (2005) [4].

Florbetaben showed high binding affinity to synthetic $A\beta_{1-42}$ fibrils *in vitro* (inhibition of $[^{125}I]$IMPY binding: $IC_{50} = 146$ nM) and to human *post-mortem* AD brain homogenate (inhibition of $[^{125}I]$IMPY binding: $IC_{50} = 24$ nM). Fluorescence microscopy demonstrated that the non-radioactive drug substance does not bind to hyperphosphorylated tau deposits on FTD and AD brain tissue sections. Further, employing radioligand binding assays for the non-radioactive drug substance, a broad panel of animal and human receptors and transporters not related to $A\beta$ were tested: no significant binding of florbetaben was observed.

In NMRI mice, a high initial brain uptake of florbetaben was detected (4.77% ID/g at 2 min p.i.). Blood serum clearance in rats was rapid (3.1 l/h/kg) and bone uptake was low over a long time span (4.64% ID/g at 4 h p.i.).

The tracer's pre-clinical safety evaluation also showed favorable results. Further, in the extended single dose and repeated dose pre-clinical toxicity studies the non-radioactive drug substance was well tolerated, and the *in vitro* and *in vivo* genotoxicity assays performed did not reveal a mutagenic potential.

PREVIOUS CLINICAL DATA ON FLORBETABEN

Florbetaben was initially tested in Australia by Rowe et al. (2008) [5]. To provide proof of mechanism for the ability of florbetaben to image $A\beta$, 15 AD patients, 15 healthy controls (HCs) as well as five patients with frontotemporal lobe dementia (FTLD) underwent PET imaging. The visual and quantitative PET data obtained in this trail allowed discriminating the subject cohorts with high power: In visual PET data analysis, all AD patients were scored as positive for $A\beta$, 13 of the 15 HCs as $A\beta$-negative, and all FTLD patients as $A\beta$-negative. In quantitative analysis, neocortical tracer uptake was significantly higher for the AD patients as compared to the HCs (SUVR 2.0 ± 0.3 vs. 1.3 ± 0.2, $p < 0.0001$) [5].

Further to this first in man trial, O'Keefe and colleagues initially determined the human radiation exposure related to the application of florbetaben: By investigation three elderly healthy controls, the highest absorbed dose was found for the gall bladder. The effective dose was determined to be 14.7 ± 1.4 mSv/MBq [6] which translates to a radia-

tion exposure of 4.4 mSv in case of a standard activity of 300 MBq. This amount of radiation is similar to what subjects are routinely exposed to in case of other brain PET tracers, without radiation effect concerns.

OUR OWN CLINICAL EXPERIENCES WITH FLORBETABEN

Our group also performed a Phase 0 trial employing florbetaben, the results of which were recently published [7]. The primary aim of this trial was to investigate the diagnostic efficacy, pharmacokinetics, safety and tolerability of florbetaben in a European population. Further, various quantitative PET parameters were investigated for their potential to serve as surrogate markers of cognitive decline. Finally, we for the first time aimed at developing a compartment model for florbetaben suitable for obtaining outcome measures of the brain $A\beta$ concentration. In this trial, ten patients with probable AD and ten age-matched HCs were included. All subjects underwent dynamic PET imaging up to 4 h after tracer injection. The PET data were analyzed visually, by means of volumes of interest (VOIs), by a voxelwise analysis approach, as well as by full kinetic modeling. The kinetic PET data obtained in this trial showed that PET image analysis was optimal with regard to the group discrimination at a time-point of ~90 min p.i. Visual PET data analysis by three blinded reader discriminated well between AD patients and HCs: 9 of the 10 AD patients and 1 of the 10 HCs were scored as positive for $A\beta$ ($p = 0.001$). This was accomplished with high inter-reader agreement (weighted kappa = 0.88 to 0.94). With regard to the VOI analysis performed, the neocortical florbetaben uptake was significantly higher for the AD patients when compared to the HCs in frontal, lateral temporal, occipital, anterior and posterior cingulate, and parietal cortices ($p = 0.003$ to 0.010). Voxelwise analyses permitted determination of the individual brain volume affected by $A\beta$. Of interest, this new measure of the "whole brain $A\beta$ load" was – amongst all PET parameters compared – best correlated with the severity of cognitive deficits, following a non-linear regression curve [7]. The results of this European proof of mechanism Phase 0 trial provided further evidence for the efficacy and safety of florbetaben PET in detecting brain $A\beta$ and stimulated the tracer testing in a multi-center, multi-camera setting.

During the above mentioned trial, arterial blood samples were obtained from all subjects at differ-

ent time-points after florbetaben administration. From these blood samples, it was possible in a sub-study to determine the tracer metabolism over time. For that purpose, it was possible to establish a suitable HPLC method which revealed a rapid florbetaben metabolism with a half life of ∼6 min, without differences between AD patients and HCs [8].

Subsequent to the above Phase 0 proof of mechanism trials, two Phase 1 safety and dosimetry trials with florbetaben PET were performed in Caucasian and Japanese HCs and a multi-centre Phase 2 trial was conducted. The primary endpoints of the latter trial were the sensitivity and specificity of independent visual assessment of 90–110 min p.i. florbetaben PET images in discriminating AD patients from HCs. Secondary endpoints were related to alternative imaging time-points, optimized PET data analysis methods, quantitative PET data, radiotracer safety/tolerability, and the association between the PET data and APOE ε4 genotype. The results of this trial were recently published [9]. As part of this trial, florbetaben PET imaging was carried out in 18 centers in Australia, Germany,

Switzerland, and the USA. Altogether, 81 patients with mild to moderate probable AD (age ≥ 55 yrs, MMSE = 18–26, CDR = 0.5–2) and 69 age-matched HCs (MMSE ≥ 28, CDR = 0) were included. Florbetaben uptake in neocortical regions was visually scored by three independent blinded readers, and quantified using standardized uptake value ratios (SUVRs) determined from pre-established VOIs on the individual grey-matter-segmented PET/MRI data. Figure. 1 shows typical florbetaben PET images of an AD patient and a HC obtained in this trial. In the AD patient, the tracer was taken up by different neocortical brain regions. This was in contrast to the HC which only exhibited the typical white matter uptake pattern (Fig. 1).

The blinded read of the 90–110 min p.i. florbetaben PET data resulted in a sensitivity of 80% (95% CI 71–89%) and a specificity of 91% (95% CI 84–98%) in discriminating between the two subject cohorts, which was achieved with high inter-reader agreement. Of interest, a post-hoc modeling approach which is able to account for the imperfectness of the clini-
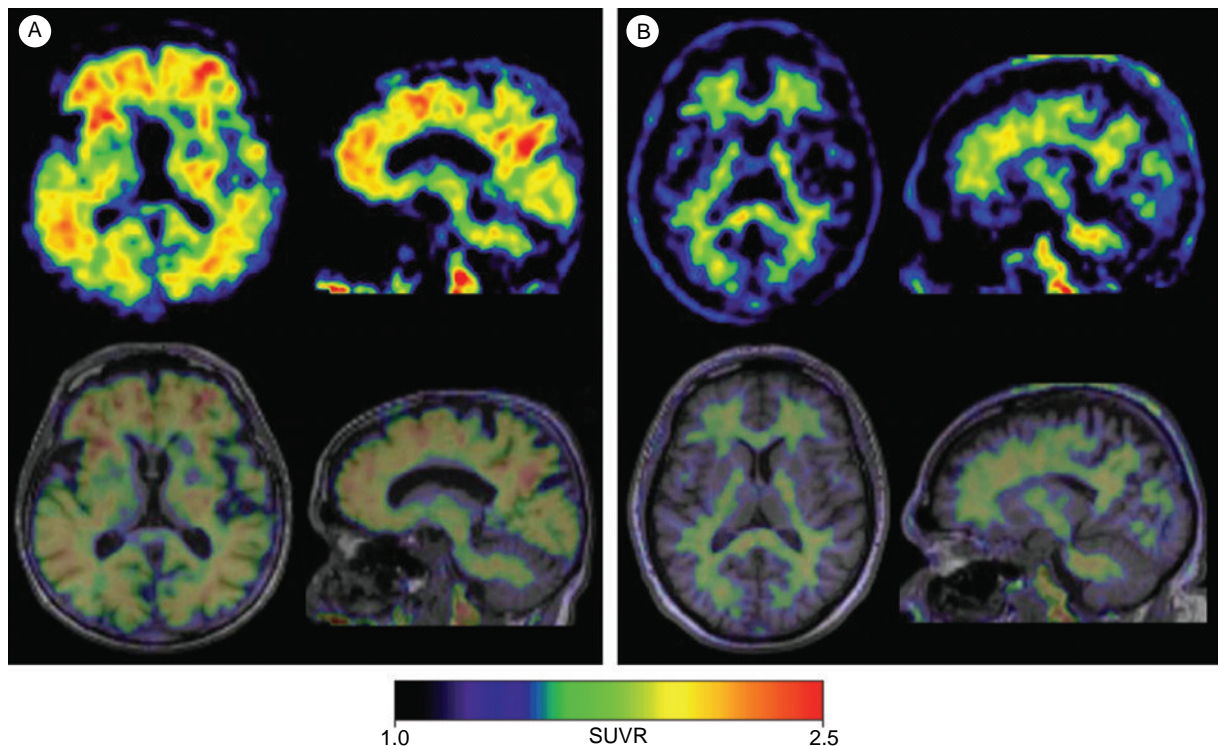
Fig. 1. Typical axial and sagittal florbetaben PET images (top) and co-registered PET/T1-weighted MR images (bottom) of an AD patient (A) and a HC (B). The PET images are 90–110 min p.i. standardized uptake value ratio (SUVR) data using the cerebellar cortex as reference region. Reprinted from *The Lancet Neurology*, volume 10, Barthel et al., Cerebral amyloid-β PET with florbetaben (^{18}F) in patients with Alzheimer's disease and healthy controls: a multicentre Phase 2 diagnostic study, pages 424–435, copyright 2011, with permission from Elsevier.

cal diagnosis as standard of truth (as compared to the diagnostic gold standard histopathology, clinical diagnosis owes a limited positive predictive value of 70–90% [10, 11]) resulted in adjusted sensitivity and specificity values for florbetaben of 96 and 97%, respectively. With regard to the PET image quantification, the SUVRs were significantly higher for the AD patients as compared to the HCs in different neocortical brain regions. Highest effect size for group discrimination was observed for the posterior cingulate (Cohen's $d = 1.49$). Figure 2 gives the composite and posterior cingulate SUVRs determined for the study population (Fig. 2).

A linear discriminant analysis of the quantitative PET data resulted in a sensitivity of 85% and a specificity of 91% for the discrimination between AD patients and HCs. For the association between the quantitative PET data and the cognition scores, we interestingly found significant correlation only for the AD patients, and only for neocortical brain regions (for instance lateral temporal SUVRs vs. word-list memory scores: $r = -0.33$, $p = 0.004$). For the relation between the florbetaben PET data and the APOE ε4 genotype, it was found that in AD patients with Aβ-positive (according to blinded read) PET scans APOE ε4 alleles were more frequent than in Aβ-negative AD patients. A similar tendency was observed for the HCs (Fig. 3).

Fig. 3. Comparison of *APOE* ε4 allele carrier rate between florbetaben PET-positive and PET-negative subjects, separately investigated for AD patients and HCs. Reprinted from *The Lancet Neurology*, volume 10, Barthel et al., Cerebral amyloid-β PET with florbetaben (^{18}F) in patients with Alzheimer's disease and healthy controls: a multicentre phase 2 diagnostic study, pages 424–435, copyright 2011, with permission from Elsevier.

During this trial, no safety or tolerability problems were observed for florbetaben PET imaging [9]. In conclusion, this largest and first global trial on a ^{18}F-labelled Aβ-targeted PET tracer provided evidence in a multi-center, multi-camera setting for the efficacy, safety and biological relevance of florbetaben PET. In a population representative for a clinical routine situation, the florbetaben PET data could be reliably assessed on a visual base, as well as quantified in an objective manner.

ONGOING STUDIES WITH FLORBETABEN

Presently, a dual-center Phase 2 trial assessing the efficacy of florbetaben PET in patients with Down syndrome (ClinicalTrials.gov Identifier: NCT00928304) has completed its recruiting phase. This study is aimed at providing additional evidence for the assumption that the tracer binds to brain Aβ. Further, a mono-center florbetaben trial in subjects with mild cognitive impairment is still active (NCT01138111). In this trial, the potential of the tracer to predict the conversion to AD is being examined. In addition, a pivotal, multi-center Phase 3 trial (NCT01020838) investigating the association between the *in vivo* florbetaben brain uptake and the *post mortem* brain Aβ deposition, as determined by histopathology is currently in the recruitment phase. Finally, a mono-center investigator

Fig. 2. Composite and posterior cingulate standardized uptake value ratios (SUVRs) 90–110 m min p.i. of florbetaben PET in AD patients and HCs. Box plots (median, 25 and 75% quartiles) with whiskers with maximum 1.5 inter-quartile range, as well as cut-off value (red dotted line) for maximum accuracy in group differentiation. Reprinted from *The Lancet Neurology*, volume 10, Barthel et al., Cerebral amyloid-β PET with florbetaben (^{18}F) in patients with Alzheimer's disease and healthy controls: a multicentre Phase 2 diagnostic study, pages 424–435, copyright 2011, with permission from Elsevier.

initiated trial (NCT01222351) is currently evaluating the association between the florbetaben brain uptake and Aβ plasma levels in elderly subjects. So far, florbetaben was not intra-individually compared with [^{11}C]PIB. Such comparison would allow determining similarities or differences with regard to the diagnostic accuracy of both tracers. Therefore, it should also be in the focus of the future research.

SUMMARY AND CONCLUSIONS

The preclinical and clinical data currently available verify florbetaben as a safe and efficacious PET tracer suitable for detection of Aβ deposition in the brain. The results of the ongoing trials will contribute to current knowledge on the characteristics of florbetaben, and will help to determine the future potential of florbetaben PET imaging as a visual adjunct to supplement the routine clinical "AD diagnostic toolbox".

FINANCIAL DISCLOSURE

REFERENCES

[1] Dubois B, Feldman HH, Jacova C, Dekosky ST, Barberger-Gateau P, Cummings J, Delacourte A, Galasko D, Gauthier S, Jicha G, Meguro K, O'Brien J, Pasquier F, Robert P, Rossor M, Salloway S, Stern Y, Visser PJ, Scheltens P (2007) Research criteria for the diagnosis of Alzheimer's disease: revising the NINCDS-ADRDA criteria. *Lancet Neurol* **6**, 734-746.

[2] Dubois B, Feldman HH, Jacova C, Cummings JL, Dekosky ST, Barberger-Gateau P, Delacourte A, Frisoni G, Fox NC, Galasko D, Gauthier S, Hampel H, Jicha GA, Meguro K, O'Brien J, Pasquier F, Robert P, Rossor M, Salloway S, Sarazin M, de Souza LC, Stern Y, Visser PJ, Scheltens P (2010) Revising the definition of Alzheimer's disease: a new lexicon. *Lancet Neurol* **9**, 1118-1127.

[3] Klunk WE, Engler H, Nordberg A, Wang Y, Blomqvist G, Holt DP, Bergström M, Savitcheva I, Huang GF, Estrada S, Ausén B, Debnath ML, Barletta J, Price JC, Sandell J, Lopresti BJ, Wall A, Koivisto P, Antoni G, Mathis CA, Långström B (2004) Imaging brain amyloid in Alzheimer's disease with Pittsburgh Compound-B. Ann Neurol **55**, 306-319.

[4] Zhang W, Oya S, Kung MP, Hou C, Maier DL, Kung HF (2005) F-18 Polyethyleneglycol stilbenes as PET imaging agents targeting Abeta aggregates in the brain. Nucl Med Biol **32**, 799-809.

[5] Rowe CC, Ackerman U, Browne W, Mulligan R, Pike KL, O'Keefe G, Tochon-Danguy H, Chan G, Berlangieri SU, Jones G, Dickinson-Rowe KL, Kung HP, Zhang W, Kung MP, Skovronsky D, Dyrks T, Holl G, Krause S, Friebe M, Lehman L, Lindemann S, Dinkelborg LM, Masters CL, Villemagne VL (2008) Imaging of amyloid beta in Alzheimer's disease with ^{18}F-BAY94-9172, a novel PET tracer: proof of mechanism. *Lancet Neurol* **7**, 129-135.

[6] O'Keefe GJ, Saunder TH, Ng S, Ackerman U, Tochon-Danguy HJ, Chan JG, Gong S, Dyrks T, Lindemann S, Holl G, Dinkelborg L, Villemagne V, Rowe CC (2009) Radiation dosimetry of beta-amyloid tracers 11C-PiB and ^{18}F-BAY94-9172. *J Nucl Med* **50**(2), 309-315.

[7] Barthel H, Luthardt J, Becker G, Patt M, Hammerstein E, Hartwig K, Eggers B, Sattler B, Schildan A, Hesse S., Meyer PM, Wolf H, Zimmermann T, Reischl J, Rohde B, Gertz HJ, Reininger C, Sabri O (2011) Individualized quantification of brain β-amyloid burden - Results of a proof of mechanism Phase 0 florbetaben PET trial in patients with Alzheimer's disease and healthy controls. *Eur J Nucl Med Mol Imaging*, May 6 [Epub ahead of print].

[8] Patt M, Schildan A, Barthel H, Becker G, Schultze-Mosgau MH, Rohde B, Reininger C, Sabri O (2010) Metabolite analysis of [18F]Florbetaben (BAY94-9172) in human subjects: A substudy within a proof of mechanism clinical trial. *J Radioanal Nucl Chem* **284**, 557-562.

[9] Barthel H, Gertz HJ, Dresel S, Peters O, Bartenstein P, Buerger K, Hiemeyer F, Wittemer-Rump SM, Seibyl J, Reininger C, Sabri O (2011) Cerebral amyloid-β PET with florbetaben (^{18}F) in patients with Alzheimer's disease and healthy controls: a multicentre phase 2 diagnostic study. *Lancet Neurology* **10**, 424-435.

[10] Kukull WA, Larson EB, Reifler BV, Lampe TH, Yerby MS, Hughes JP (1990) The validity of 3 clinical diagnostic criteria for Alzheimer's disease. *Neurology* **40**, 1364-1369.

[11] Jellinger K, Danielczyk W, Fischer P, Gabriel E (1990) Clinicopathological analysis of dementia disorders in the elderly. *J Neurol Sci* **95**, 239-258.

This page intentionally left blank

Effects of Hypoperfusion in Alzheimer's Disease

Benjamin P. Austin[a,b,c], Veena A. Nair[c], Timothy B. Meier[d], Guofan Xu[b], Howard A. Rowley[c,f], Cynthia M. Carlsson[b,e,f], Sterling C. Johnson[b,e,f] and Vivek Prabhakaran[c,d,*]

[a]*UW Cardiovascular Research Center, University of Wisconsin School of Medicine and Public Health, Madison, WI, USA*
[b]*Department of Veterans Affairs (VA) Geriatric Research, Education and Clinical Center (GRECC), Madison, WI, USA*
[c]*Department of Radiology, University of Wisconsin School of Medicine and Public Health, Madison, WI, USA*
[d]*Neuroscience Training Program, University of Wisconsin-Madison, Madison, WI, USA*
[e]*Department of Medicine, Division of Geriatrics and Gerontology, University of Wisconsin School of Medicine and Public Health, Madison, WI, USA*
[f]*Wisconsin Alzheimer's Disease Research Center, University of Wisconsin School of Medicine and Public Health, Madison, WI, USA*

Abstract. The role of hypoperfusion in Alzheimer's disease (AD) is a vital component to understanding the pathogenesis of this disease. Disrupted perfusion is not only evident throughout disease manifestation, it is also demonstrated during the pre-clinical phase of AD (i.e., mild cognitive impairment) as well as in cognitively healthy persons at high-risk for developing AD due to family history or genetic factors. Studies have used a variety of imaging modalities (e.g., SPECT, MRI, PET) to investigate AD, but with its recent technological advancements and non-invasive use of blood water as an endogenous tracer, arterial spin labeling (ASL) MRI has become an imaging technique of growing popularity. Through numerous ASL studies, it is now known that AD is associated with both global and regional cerebral hypoperfusion and that there is considerable overlap between the regions implicated in the disease state (consistently reported in precuneus/posterior cingulate and lateral parietal cortex) and those implicated in disease risk. Debate exists as to whether decreased blood flow in AD is a cause or consequence of the disease. Nonetheless, hypoperfusion in AD is associated with both structural and functional changes in the brain and offers a promising putative biomarker that could potentially identify AD in its pre-clinical state and be used to explore treatments to prevent, or at least slow, the progression of the disease. Finally, given that perfusion is a vascular phenomenon, we provide insights from a vascular lesion model (i.e., stroke) and illustrate the influence of disrupted perfusion on brain structure and function and, ultimately, cognition in AD.

Keywords: Alzheimer's disease, hypoperfusion, perfusion, stroke, mild cognitive impairment, ASL, MRI, vascular risk factors

*Correspondence to: Vivek Prabhakaran, MD, PhD, Department of Radiology, University of Wisconsin, School of Medicine and Public Health, 600 Highland Avenue, Madison, WI 53792-3252, USA. Tel.: +1 608 265 5269; Fax: +1 608 265 4152; E-mail: vprabhakaran@uwhealth.org.

INTRODUCTION

Alzheimer's disease (AD) is a neurodegenerative disorder characterized by gradual onset, progressive deterioration, and decreased regional cerebral blood flow (CBF) [1]. Indeed, vascular factors play a critical role in the pathogenesis of AD [2, 3], and it is

currently debated whether decreased CBF is a *cause* or a *consequence* of AD [1]. Perfusion deficiencies are present from the very early pre-clinical phases of AD (i.e., during mild cognitive impairment (MCI)) and persist well into the latest stages of the disease, demonstrating a pattern of increased hypoperfusion with disease development. This phenomenon, over time, yields catastrophic consequences on brain structure, function, and cognition, leaving the patient irreversibly impaired, especially in their memory faculties.

Although there is no cure for this devastating illness, identification of pre-symptomatic AD is necessary to explore treatments (pharmacological and non-pharmacological) that could potentially prevent or at least slow the progression of the disease. Thus, much research has been focused on identifying biomarkers associated with AD manifestation as well as biomarkers in individuals at high risk for developing AD. Among the most promising of these putative biomarkers are the well-documented abnormalities in CBF associated with AD and its development.

Investigating perfusion in AD, however, is no straightforward task, as decreased CBF is only one of many neuropathological characteristics associated with AD. Indeed, the co-occurrence of hypoperfusion, arterial plaques, neurofibrillary tangles, vascular amyloid deposits, atrophy, and stenosis complicate the investigation of any one neuropathological feature, and it becomes increasingly difficult to distinguish *cause* from *consequence*. Thus, in order to better understand the effects of perfusion disruption in AD, a vascular lesion model such as stroke that examines the simplest form of perfusion alteration can be examined in order to gain further insight.

The following review investigates the role of perfusion in the development of AD. After a brief review of the genetic and vascular risk factors associated with AD, we discuss 1) imaging methods used to measure perfusion, 2) the brain regions most frequently disrupted by hypoperfusion in both pre-clinical and progressive AD, 3) the effects of hypoperfusion on the structure and function of the brain in AD, and 4) the role of disrupted perfusion in aging and stroke and its relation to AD.

VASCULAR RISK FACTORS

The prevalence of late-onset AD, which accounts for approximately 97% of AD cases, is highly associated with the presence of the $\varepsilon4$ allele of the apolipoprotein

E (APOE) gene on chromosome 19. The presence of one copy of the $\varepsilon4$ allele, which is carried by about half of all patients with dementia [4], is reported to increase the likelihood of developing AD by fourfold while two copies of the $\varepsilon4$ allele may increase risk by ninefold [5]. This genetic factor (APOE4), however, is neither necessary nor sufficient to cause AD, and so it remains of critical importance to identify biomarkers associated with developing AD in high-risk groups.

Vascular factors are repeatedly implicated in the risk for developing AD [1]. Factors such as ischemic stroke, atherosclerosis, hypertension, diabetes, and cardiac disease have been reported to result in cerebrovascular disease and trigger AD pathology in older adults [6–9]. Hypercholesterolemia in midlife also can lead to AD and has been targeted as a potentially modifiable risk factor [10]. Animal studies suggest that amyloid-β deposition in the brain, a hallmark characteristic of AD, is stimulated by hypercholesterolemia [11] and may be modified with the use of lipid-lowering agents, such as statins [12]. A recent study in humans showed that simvastatin improved cognition in asymptomatic middle-aged adults with a parental history of AD without significantly changing CSF Aβ42 or total tau levels [13].

The vascular risk factors associated with AD, however, also play a fundamental role in the development of vascular dementia (VaD), which by current diagnostic criteria, is differentiated from AD by its vascular pathology and its abrupt clinical onset [1]. The diagnostic mutual exclusivity of these two dementias is further equivocated by evidence from epidemiological, neuropathological, clinical, pharmacological, and functional studies which report considerable overlap in the risk factors and pathological changes associated with AD and VaD [1]. In this light, recent AD studies have focused more on brain circulation abnormalities and have collectively found that such vascular factors, including hypoperfusion, are more commonly associated with AD than was previously thought [14].

MEASURING PERFUSION

In AD, perfusion (cerebral blood flow, cerebral blood volume (CBV)) has been measured using a number of different imaging modalities including magnetic resonance imaging (MRI), CT, single photon emission computed tomography (SPECT), and regional cerebral metabolism using 2-deoxy-2-[F-18]fluoro-D-glucose (FDG-PET). Perfusion in AD has also been

investigated using dynamic perfusion computed tomography and transcranial Doppler, but the incidence of such studies is far lower [14]. For the past two decades, SPECT and FDG-PET have served as the mainstream imaging techniques for perfusion and metabolism studies in AD, respectively [14]. SPECT, despite its relatively low spatial resolution ($\sim$1 cm), lends to a large number of applications [15–17], while FDG-PET, with higher sensitivity and spatial resolution than SPECT, is better able to measure regional cerebral metabolism in low perfusion areas [14]. These techniques, however, require the use of exogenous radioactive tracers and are more expensive than the more recently developed perfusion-weighted MRI (PW-MRI) techniques. PW-MRI, as an alternative to nuclear imaging techniques, offers the benefits of 1) economic efficiency (PET may require a cyclotron in proximity which is expensive to maintain), 2) accessibility (most hospitals now have at least one MRI system used for clinical practice but rarely have a cyclotron), and 3) higher spatial accuracy (MRI systems have a spatial resolution of up to 0.1 mm while PET systems are only capable of 5-mm resolution). Indeed, PW-MRI is a powerful and promising brain imaging technique and is currently being used by many researchers investigating perfusion in AD.

PW-MRI techniques can be divided into two categories based on the type of contrast agent used. Techniques that use an exogenous contrast tracer (such as dynamic contrast enhancement imaging and dynamic susceptibility contrast [DSC]) fall into the *dynamic perfusion imaging* subcategory, and techniques that use an endogenous contrast tracer fall into the *arterial spin labeling* (ASL) subcategory [14]. Currently, the AD perfusion literature is dominated by studies using DSC MRI [14], but many researchers are now migrating towards the use of ASL MRI because it is completely non-invasive and poses less risk for the patient. ASL measures CBF directly by using magnetically-labeled arterial blood water as an endogenous tracer [18]. In addition, ASL can be used to investigate blood flow associated with task performance by using a subtractive method similar to that used in blood oxygen level-dependent (BOLD) functional MRI (fMRI) studies. ASL, though equal in sensitivity as the BOLD signal for detecting task-induced changes in local brain function, provides more quantitative information and has been shown to be more robust than BOLD-fMRI with reduced intra- and inter-subject variability [19, 20]. ASL is further divided into sub-classes based on the labeling method (contin-

uous, pulsed, or velocity-dependent) and can quantify CBF in single slices or for the whole brain. With its many recent advancements, ASL is fast becoming a popular choice for AD researchers and is thus the modality of focus for the current review.

ARTERIAL SPIN LABELING

Numerous studies have used ASL perfusion MRI to investigate CBF in AD, MCI, and in individuals at high-risk for developing AD, i.e., those with a parental history of AD or with at least one copy of APOE4. While individuals with AD demonstrate a global decrease in blood flow (averaged 40%) compared to healthy controls [21], CBF reduction may be specific to certain regions of the brain. Indeed, research has shown that individuals with AD consistently demonstrate reduced CBF in regions of the precuneus and/or posterior cingulate and frequently in lateral parietal cortex [see 18 for a review]. Other regions associated with decreased CBF in AD compared to healthy controls include regions of the temporo-occipital and parieto-occipital association cortices [22] as well as bilateral inferior parietal regions [23], hippocampus and parahippocampal gyrus [21], and regions in the prefrontal cortex [24] including bilateral superior and middle frontal gyri [23]. Even in studies which include an atrophy correction for gray matter loss, individuals with AD persist at demonstrating reduced CBF in the right inferior parietal lobe extending into the bilateral posterior cingulate gyri, bilateral middle frontal gyri [23], posterior cingulate extending into the precuneus, inferior parietal cortex, left inferior lateral frontal and orbitofrontal cortex [25]. Also, perfusion measures have been shown to correlate with dementia severity in the parieto-occipital region [as measured by a subset of the Blessed Dementia Scale; 22] and parietal cortex along with the precuneus/posterior cingulate [as measured by the Mini-Mental State Examination; 24].

Interestingly, some studies report elevated blood flow in AD compared to healthy controls. Individuals with AD have been reported to demonstrate hyperperfusion, even after atrophy correction, in hippocampus, parahippocampal gyrus, temporal pole, superior temporal gyrus [26] and anterior cingulate [25, 26]. Hyperperfusion in the prefrontal cortex may serve as a compensation mechanism, especially in the early stages of disease [14]. As for hyperperfusion in the hippocampal regions, it should be noted that increased blood flow to this region is in

contrast to the previously discussed hypoperfusion [see 21 above]. Perhaps this discrepancy is attributable to differences in patient demographics as the study reporting hyperperfusion investigated individuals with AD of unspecified severity and a mean age of 75.6 ± 9.2 yrs [26] whereas the study reporting hypoperfusion investigated individuals with mild AD and a mean age 70.7 ± 8.7 yrs [21].

Studies of patients with MCI, a condition of memory impairment considered to be the clinical transition stage between normal aging and dementia [27, 28], provide insight into the prodromal phases of AD. Investigations of brain perfusion in individuals with MCI show that this group, in comparison to a healthy control group, demonstrates a reduction of CBF in the posterior cingulate with extension to the medial precuneus [atrophy corrected CBF; 25] as well as in right inferior parietal lobe (IPL) [23]. In the study by Johnson et al. [23], which compared individuals with AD and MCI to healthy controls, decreased perfusion in IPL was observed in both the AD and MCI groups but was more significantly reduced in the AD group. Compared to the MCI group, the AD group also demonstrated greater hypoperfusion in bilateral precuneus/posterior cingulate and bilateral inferior parietal lobe [23].

Hyperperfusion of certain brain regions has also been reported in MCI and other high-risk groups. MCI has been associated with increased blood flow in left hippocampus, right amygdala, and right basal ganglia compared to healthy controls [25]. Non-symptomatic high-risk groups also demonstrate hyperperfusion in the hippocampus; middle-aged (average 58.5 years) individuals with a parental history of AD and at least one copy of APOE4 showed an approximately 25% elevated blood flow in the hippocampus compared to non-high-risk subjects [29].

Recent studies suggest that MCI may be a clinically heterogeneous syndrome [30]. Chao et al. [31] examined this idea by investigating CBF differences in two groups of single-domain MCI patients - those with isolated memory impairments (amnestic MCI) and those with isolated executive dysfunction impairments (dysexecutive MCI). Both groups demonstrated hypoperfusion in posterior cingulate compared to healthy controls, but individuals with dysexecutive MCI had significantly lower perfusion in left middle frontal gyrus, left posterior cingulate, and left precuneus when compared to individuals with amnestic MCI [31]. In another study investigating CBF during rest and during a memory encoding task, amnestic

MCI patients demonstrated hypoperfusion in right precuneus and cuneus during the control state which extended to the posterior cingulate during task performance. Interestingly, healthy controls demonstrated a significant increase in perfusion in the parahippocampal gyrus when comparing task to baseline rest, but this increase was not observed in the MCI group. This suggests that individuals with amnestic MCI may lack the dynamic capability to modulate regional CBF in response to task demands [32]. In summary, research consistently demonstrates reduced CBF in posterior cingulate in MCI which could be a promising region for early detection [18].

PERFUSION AND STRUCTURAL CHANGES

The pathway leading to AD genesis is marked not only by CBF deficiency but also by structural changes observed in AD and MCI, which are debated by some to be a consequence of primary hypoperfusion (see [33] or [1] for an extensive review). Numerous studies have utilized voxel-based morphometry (VBM), a fully-automated technique that allows the quantifiable investigation of structures across the whole brain [34], to investigate atrophy in the brains of patients with AD and MCI. Collectively, these studies report numerous regions of cell death that are either specific to the pre-clinical phase (MCI), specific to disease manifestation, or that overlap both groups. Studies of patients with AD report atrophy of the entire hippocampus and regions of the temporal lobe, cingulum, precuneus, insular cortex, caudate nucleus, amygdala, entorhinal cortex, medial thalamus, and frontal cortex [35–39]. Studies of patients with MCI report atrophy of the parahippocampal gyrus and medial temporal lobe [40], entorhinal cortex and cingulum [41], and insula and thalamus [37].

Patients with MCI, especially of the amnestic type, can be divided longitudinally by those who progress to AD and those who do not, and these groups show differential atrophy. Studies show that over time, patients with amnestic MCI who eventually progress to AD demonstrate gray matter loss in the medial and inferior temporal lobes, the temporoparietal neocortex, posterior cingulate, precuneus, anterior cingulate, and frontal lobes compared to amnestic MCI patients who are clinically stable [42]. Atrophy, however, is not exclusive to memory-impaired MCI patients; brain volume changes are also observed in cognitively

healthy individuals. Studies report that individuals with a parental history of late-onset AD demonstrate decreased gray matter volume in precuneus, middle frontal, inferior frontal, and superior frontal gyri compared to individuals without a parental history of AD. Also, persons carrying the APOE4 allele have been reported to demonstrate decreased volume in hippocampus and amygdala compared to those without the APOE4 allele [43, 44].

Hypoperfusion may also lead to changes in cortical thickness as obtained from structural MRI scans. Cortical thickness measures are significant predictors of evolution to AD for subjects with MCI [45]. Carriers of the APOE4 allele, a demographic with reported decreased glucose metabolism in medial temporal and parietal lobes [46, 47], demonstrate accelerated cortical thinning in areas most vulnerable to aging (medial prefrontal and pericentral cortices) as well as in areas associated with AD and amyloid-aggregation (e.g., occipitotemporal and basal temporal cortices) [48]. Also, these carriers demonstrate significantly reduced cortical thickness in the entorhinal cortex when compared to non-carriers [49]. There is some evidence that the APOE4 allele has a stronger effect on cognitive decline in the earlier stages of AD and is less severe in the later stages [50].

PERFUSION AND FUNCTIONAL CHANGES

In addition to abnormal perfusion and structural changes, individuals with AD also demonstrate functional changes in the brain. Functional connectivity is the temporal dependence of neuronal activity patterns of anatomically separated brain regions [51, 52]. This phenomenon can be investigated using MRI BOLD signal which is collected during rest (i.e., the signal is not driven by task performance). Although resting functional connectivity, or resting fMRI, methodologies are relatively new compared to those developed in task-driven fMRI, research has already yielded significant findings in AD. Because of the network-wide changes demonstrated as a result of local structural changes, AD is considered to be a disconnection syndrome [53]. During rest, patients with AD demonstrate decreased functional connectivity in both the default mode network (DMN) and the dorsal visuo-spatial system. The default mode network describes a set of brain regions that demonstrate decreased activation during task performance [54–57], i.e., these regions demonstrate high BOLD activity and a high degree of intrinsic functional connectivity during rest and are "deactivated" during task- or stimulus-driven activity [58–62]. The regions of the DMN include both medial (anterior and posterior cortical midline regions such as the ventromedial prefrontal cortex, the dorsomedial prefrontal cortex, different parts of the anterior cingulate cortex, the posterior cingulate cortex and precuneus) and lateral brain regions (lateral parietal cortex and hippocampus) [59].

Functional connectivity in AD as measured by resting fMRI may vary with severity of symptoms. Zhang et al. [63] investigated resting activity in three separate AD groups – those with mild, moderate, and severe AD. Their results show that all three groups demonstrated dissociated functional connectivity between the posterior cingulate cortex (PCC) and a set of other regions including bilateral visual cortices, inferior temporal cortex, hippocampus, and especially medial prefrontal cortex and precuneus/cuneus. Interestingly, the disruption of these various networks involving PCC intensified with increasing severity of AD. It should also be noted that certain regions (extending from left lateralized frontoparietal regions and spreading to bilateral frontoparietal regions) demonstrated *increased* connectivity to PCC with increasing severity of AD [63].

PERFUSION IN AGING AND STROKE

Aging is the leading risk factor for the development of late-onset AD. Investigation of the normal aging brain and age-related changes in vasculature serves as a fundamental template on which to better understand the pathogenesis of AD and its effect on cognition. Evidence from aging and stroke studies suggest that chronic brain hypoperfusion (CBH) leads to tissue pathology and cognitive impairments that are characteristic of AD.

With normal aging, cerebral vasculature undergoes both structural and functional changes that may act as a catalyst for cerebrovascular diseases and subsequent cognitive deficits. For example, changes in vascular ultrastructure, vascular reactivity, resting cerebral blood flow (rCBF) and oxygen metabolism are all associated with age [64]. There is also evidence that aging, per se, in the absence of other risk factors, promotes thickening and stiffness of the arteries and increases the morbidity and mortality of myocardial infarction

and stroke [65, 66]. Perfusion studies have shown that in normal aging, uncomplicated by the presence of hypertension, diabetes, arteriosclerosis or dementia, there is evidence for decreased CBF, CBV, cerebral metabolic rate for oxygen (CMRO2), and glucose oxidation without significant change in oxygen extraction or blood brain barrier permeability [e.g., 67]. Also, these changes in CBF and CMRO2 have been found to be largely restricted to discrete brain regions presumed to be associated with cell loss [68].

Studies have documented that CBF decreases with age, either globally or in a region specific manner. In an ASL study, Bertsch et al. demonstrated an association between the age-dependent decline in global rCBF and performance in an attention task [69], but other studies suggest that declines in perfusion may be more region-specific. For example, brain regions critical to higher-cognition, such as the frontal cortex, the medial temporal lobe, and the cingulate gyrus display local age-related decreases in rCBF, even after controlling for partial volume effects [70, 71].

In addition to decreasing the volume of blood flow, age-related changes in cerebral vasculature can significantly alter the speed of blood flow during task performance. In a functional transcranial Doppler ultrasound study measuring cerebral blood flow velocities (BFV) in the ACA (anterior cerebral artery) and PCA (posterior cerebral artery), Sorond et al. found differences in BFV in healthy young and old adults during a word stem completion and a visual search task. In the younger subjects, greater activation was observed in the ACA than in the PCA territories during the word task, but older subjects did not show the same pattern. During the visual search task, however, both younger subjects and older subjects showed greater activation in PCA than in the ACA territories [72]. This suggests that blood flow to frontal areas may be altered in some cognitive tasks as part of the aging process.

Neurovascular and physiological changes associated with normal aging are often reflected in behavioral differences between the young and old. Studies show that older adults tend to display a general slowing in processing speed, a reduction in inhibitory control, and a general decline of attentional resources [73–75]. Models of neurocognitive aging based on neuroimaging studies suggest that during task performance, older adults recruit additional brain regions compared to younger adults due to the effects of age on brain integrity and function [76, 77].

The relationship between perfusion and cognition in older adults raises the question of whether hyperperfusion can serve as compensatory mechanism against the cognitive decline seen in normal aging. It is known that exercise promotes healthy cognitive aging [78]. Conversely, Mozolic et al. have recently demonstrated that cognitive training increases rCBF in the rostrolateral PFC in older adults, and that this increase in rCBF correlated with the increase in their attention task [79]. Interestingly, models of neurocognitive aging suggest that the PFC is the seat of compensatory recruitment in older adults [76, 77] and sometimes in MCI. In an fMRI study in which MCI patients were divided into two groups based on Mattis Dementia Rating Scale scores, higher-cognition MCI patients activated right ventrolateral and dorsolateral prefrontal cortex during verbal memory tasks while lower-cognition MCI patients and control subjects did not [80]. This suggests that PFC compensation is present at the beginning of the MCI continuum but eventually breaks down as the symptoms increase in severity. This is similar to the hypothesis that PFC hyperperfusion is compensatory in early stages of AD [14]. Another interesting connection between perfusion in normal aging and in AD was noted in a study by Lee et al. [81]. In this study, cognitively normal elderly individuals displayed cortical thinning and hypoperfusion, as measured by ASL, in patterns similar to those observed in AD.

Animal studies have shown that reduced CBF over long durations, or chronic brain hypoperfusion, leads to neurochemical, metabolic, anatomic [e.g., 33, 82, 83–89], and cognitive changes that are very similar to that observed in AD [90]. Aged rats that were subjected to 1–2 weeks of 2-vessel occlusion showed behavioral, physiological and anatomical changes. A significant finding was that the age of the animal together with the severity of CBH determined whether reperfusion could aid the animals to recover the CBF levels that existed prior to vessel occlusion. Based on evidence from rat CBH studies, de la Torre [85] suggests that aging combined with a vascular risk factor can lead to CBH which can, upon falling below a certain threshold (i.e., the critically attained threshold of cerebral hypoperfusion [CATCH]), trigger hemodynamic changes in the brain micro-circulature and impair optimal delivery of glucose and oxygen needed for normal brain cell function. Because glucose and oxygen are the crucial substrates in the production of tissue energy, metabolic energy deficits can trigger an intracellular biochemical cascade that effectively compromises brain cells and eventually leads to metabolic, cognitive and tissue pathology that characterize AD [91, 92].

There is strong evidence for hypoperfusion and the occurrence of brain ischemia and infarcts. Patients with severe arterial stenosis, or narrowing of the arteries, often show the presence of microemboli that fail to get washed out on account of reduced blood flow [93]. Hypoperfusion also leads to sub-optimal supply of nutrients to places that may be blocked by the emboli. It has been suggested that the degree of severity of stenosis is accompanied by differential rates of transient ischemic attacks (TIA; an episode of stroke-like symptoms lasting less than 24 hours) and strokes. Stroke patients in the acute and sub-acute phase show region specific hypoperfusion leading to cognitive deficits [94–96]. There is also evidence that chronic stroke patients show hypoperfusion associated with cognitive deficits although without accompanying structural infarcts as indicated by T1- or T2-weighted scans [97–99]. This suggests that functional areas receive enough blood supply so that tissue viability is sustained but not enough to support cognitive or neurological functioning [100]. Twenty to twenty-five percent of ischemic stroke patients go on to develop post-stroke dementia, especially in patients who are 55 years or older [101]. Patients with post-stroke dementia show changes in cerebral blood flow, white matter hyperintensities, and cortical thinning associated with varying degrees of cognitive impairments.

Although the evidence of a direct relationship between brain hypoperfusion and micro- or macro-structural changes leading to cognitive impairments is still forthcoming, recent studies suggest that the animal model of CBH proposed by de la Tore and colleagues [33] may very likely hold true in humans too. The thesis that CBH is a key determinant of eventual cognitive impairment is born out of studies that have demonstrated that reperfusion of hypoperfused but dysfunctional regions leads to better functional outcomes [e.g., 102]. We therefore suggest that compromised vasculature may be represented on a continuum with mild vasculopathy falling at one end of this continuum (such as the vascular changes seen with aging), followed by moderate vasculopathy (such as those seen in patients with TIA or MCI) and severe vasculopathy (as noted in patients with stroke, VaD, or AD) falling at the other end of this continuum (see Fig. 1). Chronic brain hypoperfusion may lead to micro- and macro-structural changes that are associated with cognitive impairments and dementia. However, the acuity of onset of these hypoperfusion changes contributes to the varying presentations of clinical disease in these population subsets.
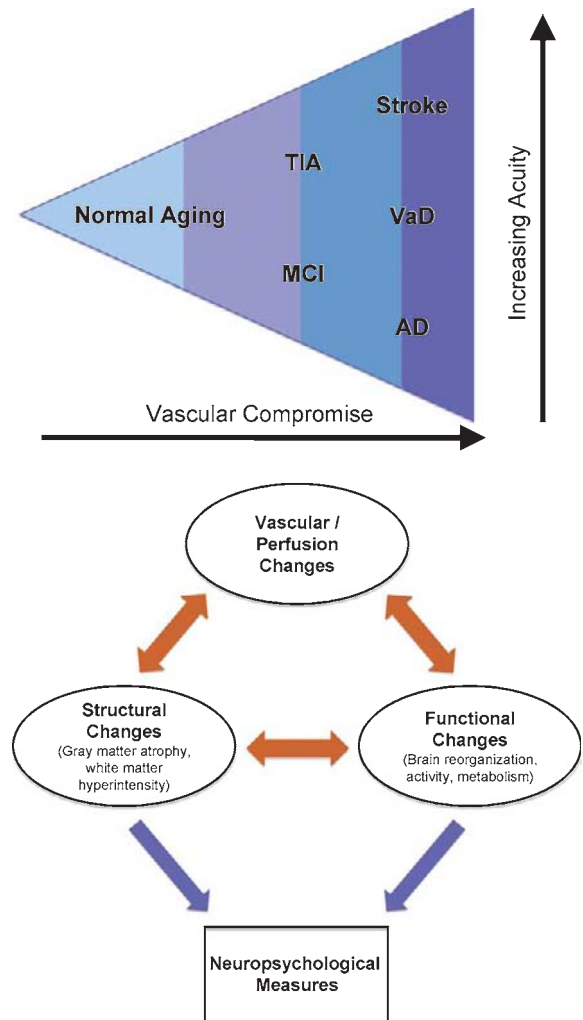
Fig. 1. Schematic figure of a perfusion model of chronic brain hypoperfusion (CBH) and micro- and macro-structural changes leading to behavioral deficits and cognitive impairment. The triangle represents a vasculature compromised in varying degrees with accompanying hemodynamic changes leading to CBH. Normal-aging, followed by TIA and MCI, followed by stroke, VaD, and AD in a graded fashion influence neural network reorganization in terms of increasing degree of vascular/perfusion changes as well as structural and functional mapping changes. These changes ultimately influence neuropsychological measures. AD, Alzheimer's disease; MCI, mild cognitive impairment; TIA, transient ischemic attack; VaD, vascular dementia.

CONCLUSION

Although much is known about the role of hypoperfusion in AD, the direct consequences of disrupted blood flow is obscured by the co-occurrence of other neuropathological features implicated in AD including, e.g., arterial plaques, neurofibrillary tangles,

vascular amyloid deposits, and cortical atrophy. Models of vascular lesion patients, however, provide a suitable model in which to investigate this phenomenon and help elucidate the effects of decreased perfusion on cognition in AD. With the development of more economically efficient and non-invasive imaging techniques, such as ASL MRI, researchers are now able to measure blood flow with unprecedented spatial accuracy and with minimal risk to the patient. Thus, it is hopeful that in the near future, scientists will be able to identify putative biomarkers in AD and develop treatments to prevent, or at least slow, the progression of this incurable disease.

REFERENCES

[1] Mazza M, Marano G, Traversi G, Bria P, Mazza S (2011) Primary cerebral blood flow deficiency and Alzheimer's disease: shadows and lights. *J Alzheimers Dis* **23**, 375-389.

[2] Dede DS, Yavuz B, Yavuz BB, Cankurtaran M, Halil M, Ulger Z, Cankurtaran ES, Aytemir K, Kabakci G, Ariogul S (2007) Assessment of endothelial function in Alzheimer's disease: is Alzheimer's disease a vascular disease? *J Am Geriatr Soc* **55**, 1613-1617.

[3] Zhu X, Smith MA, Honda K, Aliev G, Moreira PI, Nunomura A, Casadesus G, Harris PL, Siedlak SL, Perry G (2007) Vascular oxidative stress in Alzheimer disease. *J Neurol Sci* **257**, 240-246.

[4] Eschweiler GW, Leyhe T, Kloppel S, Hull M (2010) New developments in the diagnosis of dementia. *Dtsch Arztebl Int* **107**, 677-683.

[5] Carlsson CM, Gleason CE, Puglielli L, Asthana S (2009) Chapter 65. Dementia including Alzheimer's disease. In *Hazzard's Geriatric Medicine and Gerontology*, Halter JB, Ouslander JG, Tinetti ME, Studenski S, High KP, Asthana S, eds. McGraw-Hill Medical, New York, pp. 797-811.

[6] de la Torre JC (2009) Cerebrovascular and cardiovascular pathology in Alzheimer's disease. *Int Rev Neurobiol* **84**, 35-48.

[7] Morovic S, Jurasic MJ, Martinic Popovic I, Seric V, Lisak M, Demarin V (2009) Vascular characteristics of patients with dementia. *J Neurol Sci* **283**, 41-43.

[8] Skoog I, Gustafson D (2003) Hypertension, hypertension-clustering factors and Alzheimer's disease. *Neurol Res* **25**, 675-680.

[9] Viswanathan A, Rocca WA, Tzourio C (2009) Vascular risk factors and dementia: how to move forward? *Neurology* **72**, 368-374.

[10] Kivipelto M, Helkala EL, Laakso MP, Hanninen T, Hallikainen M, Alhainen K, Iivonen S, Mannermaa A, Tuomilehto J, Nissinen A, Soininen H (2002) Apolipoprotein E epsilon4 allele, elevated midlife total cholesterol level, and high midlife systolic blood pressure are independent risk factors for late-life Alzheimer disease. *Ann Intern Med* **137**, 149-155.

[11] Refolo LM, Malester B, LaFrancois J, Bryant-Thomas T, Wang R, Tint GS, Sambamurti K, Duff K, Pappolla MA (2000) Hypercholesterolemia accelerates the Alzheimer's amyloid pathology in a transgenic mouse model. *Neurobiol Dis* **7**, 321-331.

[12] Fassbender K, Simons M, Bergmann C, Stroick M, Lutjohann D, Keller P, Runz H, Kuhl S, Bertsch T, von Bergmann K, Hennerici M, Beyreuther K, Hartmann T (2001) Simvastatin strongly reduces levels of Alzheimer's disease beta-amyloid peptides Abeta 42 and Abeta 40 in vitro and in vivo. *Proc Natl Acad Sci U S A* **98**, 5856-5861.

[13] Carlsson CM, Gleason CE, Hess TM, Moreland KA, Blazel HM, Koscik RL, Schreiber NT, Johnson SC, Atwood CS, Puglielli L, Hermann BP, McBride PE, Stein JH, Sager MA, Asthana S (2008) Effects of simvastatin on cerebrospinal fluid biomarkers and cognition in middle-aged adults at risk for Alzheimer's disease. *J Alzheimers Dis* **13**, 187-197.

[14] Chen W, Song X, Beyea S, D'Arcy R, Zhang Y, Rockwood K (2011) Advances in perfusion magnetic resonance imaging in Alzheimer's disease. *Alzheimers Dement* **7**, 185-196.

[15] DeKosky ST, Shih WJ, Schmitt FA, Coupal J, Kirkpatrick C (1990) Assessing utility of single photon emission computed tomography (SPECT) scan in Alzheimer disease: correlation with cognitive severity. *Alzheimer Dis Assoc Disord* **4**, 14-23.

[16] Holman BL, Tumeh SS (1990) Single-photon emission computed tomography (SPECT). Applications and potential. *JAMA* **263**, 561-564.

[17] Wintermark M, Sesay M, Barbier E, Borbely K, Dillon WP, Eastwood JD, Glenn TC, Grandin CB, Pedraza S, Soustiel JF, Nariai T, Zaharchuk G, Caille JM, Dousset V, Yonas H (2005) Comparative overview of brain perfusion imaging techniques. *Stroke* **36**, e83-e99.

[18] Alsop DC, Dai W, Grossman M, Detre JA (2010) Arterial spin labeling blood flow MRI: its role in the early characterization of Alzheimer's disease. *J Alzheimers Dis* **20**, 871-880.

[19] Aguirre GK, Detre JA, Zarahn E, Alsop DC (2002) Experimental design and the relative sensitivity of BOLD and perfusion fMRI. *Neuroimage* **15**, 488-500.

[20] Tjandra T, Brooks JC, Figueiredo P, Wise R, Matthews PM, Tracey I (2005) Quantitative assessment of the reproducibility of functional activation measured with BOLD and MR perfusion imaging: implications for clinical trial design. *Neuroimage* **27**, 393-401.

[21] Asllani I, Habeck C, Scarmeas N, Borogovac A, Brown TR, Stern Y (2008) Multivariate and univariate analysis of continuous arterial spin labeling perfusion MRI in Alzheimer's disease. *J Cereb Blood Flow Metab* **28**, 725-736.

[22] Sandson TA, O'Connor M, Sperling RA, Edelman RR, Warach S (1996) Noninvasive perfusion MRI in Alzheimer's disease: a preliminary report. *Neurology* **47**, 1339-1342.

[23] Johnson NA, Jahng GH, Weiner MW, Miller BL, Chui HC, Jagust WJ, Gorno-Tempini ML, Schuff N (2005) Pattern of cerebral hypoperfusion in Alzheimer disease and mild cognitive impairment measured with arterial spin-labeling MR imaging: initial experience. *Radiology* **234**, 851-859.

[24] Alsop DC, Detre JA, Grossman M (2000) Assessment of cerebral blood flow in Alzheimer's disease by spin-labeled magnetic resonance imaging. *Ann Neurol* **47**, 93-100.

[25] Dai W, Lopez OL, Carmichael OT, Becker JT, Kuller LH, Gach HM (2009) Mild cognitive impairment and Alzheimer disease: patterns of altered cerebral blood flow at MR imaging. *Radiology* **250**, 856-866.

[26] Alsop DC, Casement M, de Bazelaire C, Fong T, Press DZ (2008) Hippocampal hyperperfusion in Alzheimer's disease. *Neuroimage* **42**, 1267-1274.

[27] Morris JC, Cummings J (2005) Mild cognitive impairment (MCI) represents early-stage Alzheimer's disease. *J Alzheimers Dis* **7**, 235-239; discussion 255-262.

[28] Rombouts SA, Barkhof F, Goekoop R, Stam CJ, Scheltens P (2005) Altered resting state networks in mild cognitive impairment and mild Alzheimer's disease: an fMRI study. *Hum Brain Mapp* **26**, 231-239.

[29] Fleisher AS, Podraza KM, Bangen KJ, Taylor C, Sherzai A, Sidhar K, Liu TT, Dale AM, Buxton RB (2009) Cerebral perfusion and oxygenation differences in Alzheimer's disease risk. *Neurobiol Aging* **30**, 1737-1748.

[30] Gauthier S, Reisberg B, Zaudig M, Petersen RC, Ritchie K, Broich K, Belleville S, Brodaty H, Bennett D, Chertkow H, Cummings JL, de Leon M, Feldman H, Ganguli M, Hampel H, Scheltens P, Tierney MC, Whitehouse P, Winblad B (2006) Mild cognitive impairment. *Lancet* **367**, 1262-1270.

[31] Chao LL, Pa J, Duarte A, Schuff N, Weiner MW, Kramer JH, Miller BL, Freeman KM, Johnson JK (2009) Patterns of cerebral hypoperfusion in amnestic and dysexecutive MCI. *Alzheimer Dis Assoc Disord* **23**, 245-252.

[32] Xu G, Antuono PG, Jones J, Xu Y, Wu G, Ward D, Li SJ (2007) Perfusion fMRI detects deficits in regional CBF during memory-encoding tasks in MCI subjects. *Neurology* **69**, 1650-1656.

[33] de la Torre JC (1999) Critical threshold cerebral hypoperfusion causes Alzheimer's disease? *Acta Neuropathol* **98**, 1-8.

[34] Kakeda S, Korogi Y (2010) The efficacy of a voxel-based morphometry on the analysis of imaging in schizophrenia, temporal lobe epilepsy, and Alzheimer's disease/mild cognitive impairment: a review. *Neuroradiology* **52**, 711-721.

[35] Busatto GF, Garrido GE, Almeida OP, Castro CC, Camargo CH, Cid CG, Buchpiguel CA, Furuie S, Bottino CM (2003) A voxel-based morphometry study of temporal lobe gray matter reductions in Alzheimer's disease. *Neurobiol Aging* **24**, 221-231.

[36] Frisoni GB, Testa C, Zorzan A, Sabattoli F, Beltramello A, Soininen H, Laakso MP (2002) Detection of grey matter loss in mild Alzheimer's disease with voxel based morphometry. *J Neurol Neurosurg Psychiatry* **73**, 657-664.

[37] Karas GB, Scheltens P, Rombouts SA, Visser PJ, van Schijndel RA, Fox NC, Barkhof F (2004) Global and local gray matter loss in mild cognitive impairment and Alzheimer's disease. *Neuroimage* **23**, 708-716.

[38] Hirata Y, Matsuda H, Nemoto K, Ohnishi T, Hirao K, Yamashita F, Asada T, Iwabuchi S, Samejima H (2005) Voxel-based morphometry to discriminate early Alzheimer's disease from controls. *Neurosci Lett* **382**, 269-274.

[39] Karas GB, Burton EJ, Rombouts SA, van Schijndel RA, O'Brien JT, Scheltens P, McKeith IG, Williams D, Ballard C, Barkhof F (2003) A comprehensive study of gray matter loss in patients with Alzheimer's disease using optimized voxel-based morphometry. *Neuroimage* **18**, 895-907.

[40] Visser PJ, Scheltens P, Verhey FR, Schmand B, Launer LJ, Jolles J, Jonker C (1999) Medial temporal lobe atrophy and memory dysfunction as predictors for dementia in subjects with mild cognitive impairment. *J Neurol* **246**, 477-485.

[41] Chetelat G, Desgranges B, De La Sayette V, Viader F, Eustache F, Baron JC (2002) Mapping gray matter loss with voxel-based morphometry in mild cognitive impairment. *Neuroreport* **13**, 1939-1943.

[42] Whitwell JL, Przybelski SA, Weigand SD, Knopman DS, Boeve BF, Petersen RC, Jack CR Jr (2007) 3D maps from multiple MRI illustrate changing atrophy patterns as subjects progress from mild cognitive impairment to Alzheimer's disease. *Brain* **130**, 1777-1786.

[43] Honea RA, Swerdlow RH, Vidoni ED, Goodwin J, Burns JM (2010) Reduced gray matter volume in normal adults with a maternal family history of Alzheimer disease. *Neurology* **74**, 113-120.

[44] Lu PH, Thompson PM, Leow A, Lee GJ, Lee A, Yanovsky I, Parikshak N, Khoo T, Wu S, Geschwind D, Bartzokis G (2011) Apolipoprotein E genotype is associated with temporal and hippocampal atrophy rates in healthy elderly adults: a tensor-based morphometry study. *J Alzheimers Dis* **23**, 433-442.

[45] Querbes O, Aubry F, Pariente J, Lotterie JA, Demonet JF, Duret V, Puel M, Berry I, Fort JC, Celsis P (2009) Early diagnosis of Alzheimer's disease using cortical thickness: impact of cognitive reserve. *Brain* **132**, 2036-2047.

[46] Reiman EM, Caselli RJ, Yun LS, Chen K, Bandy D, Minoshima S, Thibodeau SN, Osborne D (1996) Preclinical evidence of Alzheimer's disease in persons homozygous for the epsilon 4 allele for apolipoprotein E. *N Engl J Med* **334**, 752-758.

[47] Reiman EM, Chen K, Alexander GE, Caselli RJ, Bandy D, Osborne D, Saunders AM, Hardy J (2004) Functional brain abnormalities in young adults at genetic risk for late-onset Alzheimer's dementia. *Proc Natl Acad Sci U S A* **101**, 284-289.

[48] Espeseth T, Westlye LT, Fjell AM, Walhovd KB, Rootwelt H, Reinvang I (2008) Accelerated age-related cortical thinning in healthy carriers of apolipoprotein E epsilon 4. *Neurobiol Aging* **29**, 329-340.

[49] Burggren AC, Zeineh MM, Ekstrom AD, Braskie MN, Thompson PM, Small GW, Bookheimer SY (2008) Reduced cortical thickness in hippocampal subregions among cognitively normal apolipoprotein E e4 carriers. *Neuroimage* **41**, 1177-1183.

[50] Cosentino S, Scarmeas N, Helzner E, Glymour MM, Brandt J, Albert M, Blacker D, Stern Y (2008) APOE epsilon 4 allele predicts faster cognitive decline in mild Alzheimer disease. *Neurology* **70**, 1842-1849.

[51] Aertsen AM, Gerstein GL, Habib MK, Palm G (1989) Dynamics of neuronal firing correlation: modulation of "effective connectivity". *J Neurophysiol* **61**, 900-917.

[52] Friston KJ, Frith CD, Liddle PF, Frackowiak RS (1993) Functional connectivity: the principal-component analysis of large (PET) data sets. *J Cereb Blood Flow Metab* **13**, 5-14.

[53] Delbeuck X, Van der Linden M, Collette F (2003) Alzheimer's disease as a disconnection syndrome? *Neuropsychol Rev* **13**, 79-92.

[54] Broyd SJ, Demanuele C, Debener S, Helps SK, James CJ, Sonuga-Barke EJ (2009) Default-mode brain dysfunction in mental disorders: a systematic review. *Neurosci Biobehav Rev* **33**, 279-296.

[55] Buckner RL, Andrews-Hanna JR, Schacter DL (2008) The brain's default network: anatomy, function, and relevance to disease. *Ann N Y Acad Sci* **1124**, 1-38.

[56] Morcom AM, Fletcher PC (2007) Does the brain have a baseline? Why we should be resisting a rest. *Neuroimage* **37**, 1073-1082.

[57] Raichle ME, MacLeod AM, Snyder AZ, Powers WJ, Gusnard DA, Shulman GL (2001) A default mode of brain function. *Proc Natl Acad Sci U S A* **98**, 676-682.

[58] Beckmann CF, DeLuca M, Devlin JT, Smith SM (2005) Investigations into resting-state connectivity using independent component analysis. *Philos Trans R Soc Lond B Biol Sci* **360**, 1001-1013.

[59] Damoiseaux JS, Rombouts SA, Barkhof F, Scheltens P, Stam CJ, Smith SM, Beckmann CF (2006) Consistent resting-state networks across healthy subjects. *Proc Natl Acad Sci U S A* **103**, 13848-13853.

[60] Fox MD, Snyder AZ, Vincent JL, Corbetta M, Van Essen DC, Raichle ME (2005) The human brain is intrinsically organized into dynamic, anticorrelated functional networks. *Proc Natl Acad Sci U S A* **102**, 9673-9678.

[61] Fransson P (2005) Spontaneous low-frequency BOLD signal fluctuations: an fMRI investigation of the resting-state default mode of brain function hypothesis. *Hum Brain Mapp* **26**, 15-29.

[62] Greicius MD, Menon V (2004) Default-mode activity during a passive sensory task: uncoupled from deactivation but impacting activation. *J Cogn Neurosci* **16**, 1484-1492.

[63] Zhang HY, Wang SJ, Liu B, Ma ZL, Yang M, Zhang ZJ, Teng GJ (2010) Resting brain connectivity: changes during the progress of Alzheimer disease. *Radiology* **256**, 598-606.

[64] D'Esposito M, Jagust W, Gazzaley A (2009) Methodological and Conceptual Issues in the Study of the Aging Brain. In *Imaging the Aging Brain*, Jagust W, D'Esposito M, eds. Oxford University Press, New York, pp. 11-25.

[65] Lakatta EG, Levy D (2003) Arterial and cardiac aging: major shareholders in cardiovascular disease enterprises: Part II: the aging heart in health: links to heart disease. *Circulation* **107**, 346-354.

[66] Lakatta EG, Levy D (2003) Arterial and cardiac aging: major shareholders in cardiovascular disease enterprises: Part I: aging arteries: a "set up" for vascular disease. *Circulation* **107**, 139-146.

[67] Dastur DK (1985) Cerebral blood flow and metabolism in normal human aging, pathological aging, and senile dementia. *J Cereb Blood Flow Metab* **5**, 1-9.

[68] Stoquart-ElSankari S, Baledent O, Gondry-Jouet C, Makki M, Godefroy O, Meyer ME (2007) Aging effects on cerebral blood and cerebrospinal fluid flows. *J Cereb Blood Flow Metab* **27**, 1563-1572.

[69] Bertsch K, Hagemann D, Hermes M, Walter C, Khan R, Naumann E (2009) Resting cerebral blood flow, attention, and aging. *Brain Res* **1267**, 77-88.

[70] Asllani I, Habeck C, Borogovac A, Brown TR, Brickman AM, Stern Y (2009) Separating function from structure in perfusion imaging of the aging brain. *Hum Brain Mapp* **30**, 2927-2935.

[71] Beason-Held LL, Kraut MA, Resnick SM (2009) Stability of Default-Mode Network Activity. In The Aging Brain. *Brain Imaging Behav* **3**, 123-131.

[72] Sorond FA, Schnyer DM, Serrador JM, Milberg WP, Lipsitz LA (2008) Cerebral blood flow regulation during cognitive tasks: Effects of healthy aging. *Cortex* **44**, 179-184.

[73] Craik FI (1982) Aging and cognitive deficits: The role of attentional resources. In *Aging and Cognitive Processes*, Craik FI, Trehub D, eds. Plenum, New York, pp. 191-211.

[74] Hasher L, Stoltzfus ER, Zacks RT, Rypma B (1991) Age and inhibition. *J Exp Psychol Learn Mem Cogn* **17**, 163-169.

[75] Salthouse TA (1996) The processing-speed theory of adult age differences in cognition. *Psychol Rev* **103**, 403-428.

[76] Cabeza R (2002) Hemispheric asymmetry reduction in older adults: the HAROLD model. *Psychol Aging* **17**, 85-100.

[77] Park DC, Reuter-Lorenz P (2009) The adaptive brain: aging and neurocognitive scaffolding. *Annu Rev Psychol* **60**, 173-196.

[78] Rolland Y, Abellan van Kan G, Vellas B (2010) Healthy brain aging: role of exercise and physical activity. *Clin Geriatr Med* **26**, 75-87.

[79] Mozolic JL, Hayasaka S, Laurienti PJ (2010) A cognitive training intervention increases resting cerebral blood flow in healthy older adults. *Front Hum Neurosc* **4**, 16.

[80] Clement F, Belleville S (2010) Compensation and disease severity on the memory-related activations in mild cognitive impairment. *Biol Psychiatry* **68**, 894-902.

[81] Lee C, Lopez OL, Becker JT, Raji C, Dai W, Kuller LH, Gach HM (2009) Imaging cerebral blood flow in the cognitively normal aging brain with arterial spin labeling: implications for imaging of neurodegenerative disease. *J Neuroimag* **19**, 344-352.

[82] De Jong GI, Farkas E, Stienstra CM, Plass JR, Keijser JN, de la Torre JC, Luiten PG (1999) Cerebral hypoperfusion yields capillary damage in the hippocampal CA1 area that correlates with spatial memory impairment. *Neuroscience* **91**, 203-210.

[83] de la Torre JC (1997) Hemodynamic consequences of deformed microvessels in the brain in Alzheimer's disease. *Ann N Y Acad Sci* **826**, 75-91.

[84] de la Torre JC (2000a) Cerebral hypoperfusion, capillary degeneration, and development of Alzheimer disease. *Alzheimer Dis Assoc Disord* **14**(Suppl 1), S72-S81.

[85] de la Torre JC (2000b) Critically attained threshold of cerebral hypoperfusion: can it cause Alzheimer's disease? *Ann N Y Acad Sci* **903**, 424-436.

[86] de la Torre JC (2008) Pathophysiology of neuronal energy crisis in Alzheimer's disease. *Neurodegener Dis* **5**, 126-132.

[87] de la Torre JC, Fortin T, Park GA, Butler KS, Kozlowski P, Pappas BA, de Socarraz H, Saunders JK, Richard MT (1992a) Chronic cerebrovascular insufficiency induces dementia-like deficits in aged rats. *Brain Res* **582**, 186-195.

[88] de la Torre JC, Fortin T, Park GA, Saunders JK, Kozlowski P, Butler K, de Socarraz H, Pappas B, Richard M (1992b) Aged but not young rats develop metabolic, memory deficits after chronic brain ischaemia. *Neurol Res* **14**, 177-180.

[89] de la Torre JC, Stefano GB (2000) Evidence that Alzheimer's disease is a microvascular disorder: the role of constitutive nitric oxide. *Brain Res Brain Res Rev* **34**, 119-136.

[90] Lee JS, Im DS, An YS, Hong JM, Gwag BJ, Joo IS (2011) Chronic cerebral hypoperfusion in a mouse model of Alzheimer's disease: An additional contributing factor of cognitive impairment. *Neurosci Lett* **489**, 84-88.

[91] Kalaria RN (1997) (Blackwell Publishing Ltd), pp. 263-271

[92] Ongali B, Nicolakakis N, Lecrux C, Aboulkassim T, Rosa-Neto P, Papadopoulos P, Tong X-K, Hamel E (2010) Transgenic mice overexpressing APP and transforming growth factor-[beta]1 feature cognitive and vascular hallmarks of Alzheimer's disease. *Am J Pathol* **177**, 3071-3080.

[93] Caplan LR, Hennerici M (1998) Impaired clearance of emboli (Washout) is an important link between hypoperfusion, embolism, and ischemic stroke. *Arch Neurol* **55**, 1475-1482.

[94] Hillis AE, Wityk RJ, Barker PB, Beauchamp NJ, Gailloud P, Murphy K, Cooper O, Metter EJ (2002) Subcortical aphasia and neglect in acute stroke: the role of cortical hypoperfusion. *Brain* **125**, 1094-1104.

[95] Hillis AE, Wityk RJ, Beauchamp NJ, Ulatowski JA, Jacobs MA, Barker PB (2004) Perfusion-weighted MRI as a marker of response to treatment in acute and subacute stroke. *Neuroradiology* **46**, 31-39.

[96] Hillis AE, Wityk RJ, Tuffiash E, Beauchamp NJ, Jacobs MA, Barker PB, Selnes OA (2001) Hypoperfusion of Wernicke's area predicts severity of semantic deficit in acute stroke. *Ann Neurol* **50**, 561-566.

[97] Krakauer JW, Radoeva PD, Zarahn E, Wydra J, Lazar RM, Hirsch J, Marshall RS (2004) Hypoperfusion without stroke alters motor activation in the opposite hemisphere. *Ann Neurol* **56**, 796-802.

[98] Love T, Swinney D, Wong E, Buxton R (2002) Perfusion imaging and stroke: A more sensitive measure of the brain bases of cognitive deficits. *Aphasiology* **16**, 873-883.

[99] Prabhakaran V, Raman SP, Grunwald MR, Mahadevia A, Hussain N, Lu H, Van Zijl PC, Hillis AE (2007) Neural substrates of word generation during stroke recovery: the influence of cortical hypoperfusion. *Behav Neurol* **18**, 45-52.

[100] Brumm KP, Perthen JE, Liu TT, Haist F, Ayalon L, Love T (2010) An arterial spin labeling investigation of cerebral blood flow deficits in chronic stroke survivors. *Neuroimage* **51**, 995-1005.

[101] Leys D, Hénon H, Mackowiak-Cordoliani M-A, Pasquier F (2005) Poststroke dementia. *Lancet Neurol* **4**, 752-759.

[102] Hillis AE, Kane A, Tuffiash E, Ulatowski JA, Barker PB, Beauchamp NJ, Wityk RJ (2001) Reperfusion of specific brain regions by raising blood pressure restores selective language functions in subacute stroke. *Brain Lang* **79**, 495-510.

This page intentionally left blank

The Merits of FDDNP-PET Imaging in Alzheimer's Disease

Jonghan Shin[a,b,c], Vladimir Kepe[b], Jorge R. Barrio[b] and Gary W. Small[c,*]

[a]*Neuroscience Research Institute, Gachon University of Medicine and Science, Incheon, Republic of Korea*
[b]*Department of Molecular and Medical Pharmacology, The University of California, Los Angeles David Geffen School of Medicine, Los Angeles, CA, USA*
[c]*Department of Psychiatry and Biobehavioral Sciences and Semel Institute for Neuroscience and Human Behavior, The University of California, Los Angeles David Geffen School of Medicine, Los Angeles, CA, USA*

Abstract. 2-(1-{6-[(2-[fluorine-18]fluoroethyl)(methyl)amino]-2-naphthyl}-ethylidene)malononitrile (FDDNP) is the first positron emission tomography (PET) molecular imaging probe to visualize Alzheimer's disease (AD) pathology in living humans. The most unique features of FDDNP are that (1) it is the only currently available radiotracer to image neurofibrillary tangles, beside amyloid aggregates, in living humans; and (2) it is also the only radiotracer to visualize AD pathology in the hippocampal region of living humans. In this article, we discuss FDDNP's unique ability to image tau pathology in living humans. Emphasizing tau pathology imaging capability using FDDNP in AD, as well as other tauopathies, is timely and beneficial considering that (1) *post mortem* histopathological studies using human specimens have consistently demonstrated that neurofibrillary tangles, compared with amyloid plaques, are better correlated with the disease severity and neuronal death; and (2) recently reported clinical trial failures of disease-modifying drugs in development, based on the amyloid-cascade hypothesis, suggest that some of the basic assumptions of AD causality warrant reassessment and redirection.

INTRODUCTION

The first attempt to visualize Alzheimer's disease (AD) pathology in the brain of living humans using positron emission tomography (PET) was presented in preliminary form by Barrio and associates in 1999 [1], and the first full report of this work appeared in 2002 [2]. This radiotracer is 2-(1-{6-[(2-[F-18]fluoroethyl)(methyl)amino]-2-naphthyl}ethylidene)malononitrile (FDDNP)[3], which was demonstrated to be effective in the measurement of *in vivo* brain cortical accumulation of both amyloid plaques and neurofibrillary tangles in living subjects using PET [2, 4–8]. The

first carbon-11-labeled PET radiotracer intended for human *in vivo* amyloid-beta imaging known as Pittsburgh Compound-B (PIB) was presented in preliminary form in 2002, with the full report in 2004 (see [9] for review)[1].

After FDDNP and PIB appeared, results from human studies with at least five other amyloid-beta imaging PET probes have been reported (^{11}C-SB-13 [12]; ^{11}C-BF-227 [13], ^{18}F-BAY94-9172 (AV-1) [14], ^{18}F-Florbetapir (AV-45) [15], and ^{18}F-Flutemetamol [16]). The most unique feature of FDDNP is its ability for structural recognition of β-sheet aggregate conformations in neuroaggregates (e.g., β-amyloid, tau and prions) – like Congo Red and Thioflavin-T [17]. Moreover, it is the only imaging probe to allow the visualization of neurofibrillary tangles as well as

---

*Correspondence to: Gary W. Small, M.D., Department of Psychiatry and Biobehavioral Sciences and Semel Institute for Neuroscience and Human Behavior, The University of California, Los Angeles David Geffen School of Medicine, Los Angeles, CA 90095 6948, USA. Tel.: +310 825 0291; +Fax: 310 825 3910; E-mail: GSmall@mednet.ucla.edu

---

[1] Note that there are new data on the *in vivo* binding properties of PIB (see [10] and [11])

amyloid plaques in living humans. In addition, FDDNP is the only imaging probe which successfully visualizes AD pathology in the hippocampal region of living humans.

In this article, we discuss FDDNP's merits based on its unique ability to image tau pathology in living humans. While β-amyloid plaques and neurofibrillary tangles are two representative hallmarks of AD pathology, the amyloid cascade hypothesis, a widely proposed pathogenic mechanism for AD [18], has shifted the attention to β-amyloid aggregates in the assumption that tangle formation is a direct consequence of amyloid plaque formation. However, several lines of histopathological evidence demonstrate that neurofibrillary tangles antecede β-amyloid plaques in AD [19–23]. Moreover, *post mortem* histopathological determinations using human brain specimens have consistently demonstrated that neurofibrillary tangles, and not β-amyloid plaques, are best correlated with the severity of cognitive impairment (e.g., minimental state examination, MMSE) in normal aging, mild cognitive impairment (MCI), and patients with AD [24–27]. Finally, recently repeated clinical trial failures with disease-modifying drugs based on the amyloid cascade hypothesis cast significant doubts on the basic assumptions of AD causality [28]. Therefore, the potential benefits of tangle pathology imaging using FDDNP in AD and other tauopthies cannot be underestimated.

FDDNP VISUALIZES NEUROFIBRILLARY TANGLES BESIDES β-AMYLOID PLAQUES

Earlier *in vitro* studies initially suggested FDDNP binding to β-amyloid plaques and tangles and its potential for *in vivo* use [3]. Moreover, binding of FDDNP to brain β-amyloid aggregates in transgenic rat models (e.g., in a homozygous triple-transgenic rat model of AD [Tg478/Tg1116/Tg11587]) present excellent correlations (ELISA) with amyloid content [29]. Also, aged rhesus monkeys develop amyloid plaques without neurofibrillary tangles in the brain [30]. A recent study with FDDNP-PET imaging in aged adult male rhesus monkeys reported that brain regions known to have amyloid plaque deposition showed increased FDDNP uptake [31], yet no *post mortem* determination of β-amyloid load was performed in this study. These results support the conclusion that FDDNP binds to amyloid plaques in the brain *in vivo*. Similarly, several lines of evidence support FDDNP binding to tau aggre-

gates. First, the DDNP moiety co-crystallizes with tau segments (VQIVYK) and the structure of the crystal was resolved at atomic resolution [32]; FDDNP also labels cell transfected with tau constructs (SY5Y) and also labels tau aggregates in MAPT transgenic mice (G. Cole et al, personal communication). Also, in humans FDDNP accumulation in hippocampus has been correlated with abundant tau tangle accumulation in this area [5], consistent with FDDNP labeling of tau-containing protein aggregates in brain specimens of various neurodegenerative diseases [4, 17]. In living patients FDDNP-PET succeeded in showing a pattern of neurofibrillary tangle distribution in patients with frontotemporal dementia [33], a disease with abundant brain neurofibrillary tangles without significant β-amyloid plaque deposition in the brain [34]. Similarly, in progressive supranuclear palsy (PSP) – a neurodegenerative disease lacking amyloid and with various tau-positive abnormal aggregates. FDDNP-PET shows imaging patterns highly consistent with the presence of tau aggregation in subcortical structures (e.g., brain stem, caudate, putamen, thalamus) and cerebellum extending towards cortical structures with disease progression [35]. Moreover, a recent report of a positive association between FDDNP and CSF tau in AD [36] further supports the binding of FDDNP to tau.

Finally, FDDNP-PET results performed independently at three different sites agreed with the observation that medial temporal cortical FDDNP binding is consistently higher than neocortical FDDNP binding in AD [2, 5, 6]. Previous *post mortem* histological studies demonstrated that, in AD, β-amyloid-plaque deposition is high in neocortical regions but relatively lower in some medial temporal cortical substructures, e.g., hippocampus [37], even though it is high in entorhinal cortices [10, 38]. By contrast, tangle accumulation is high in the medial temporal cortex at all levels of cognitive impairment with subsequent neocortical increases with disease progression [37, 39]. Taken together, the available data on FDDNP *in vivo* binding patterns and neuropathology indicate that FDDNP is a sensitive *in vivo* marker for neurofibrillary tangles.

FDDNP BINDING MATCHES THE PATTERN OF BRAIN PATHOLOGY AND CLINICAL PROGRESSION IN AD

As noted above, *post mortem* histopathological determinations with human brain specimens have
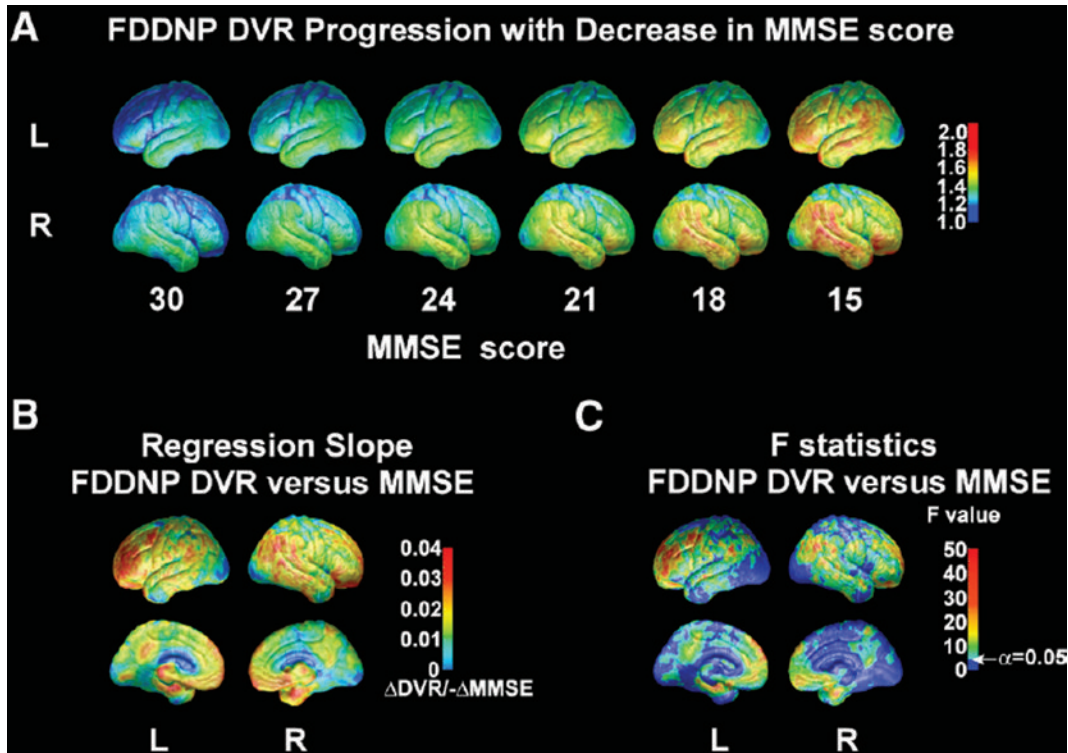
Fig. 1. Panel (A) shows a hemispheric surface map of FDDNP DVR progression/spread as mini-mental state examination (MMSE) scores decreases. We see a similar trend between the left side and the right side. There is a bit of signal in the left temporal lobe at a normal MMSE of 30 that increases in the temporal lobe and spreads to the parietal and frontal areas as MMSE drops. This DVR spreading mimics the pathology progression of beta-amyloid plaques and neurofibrillary tangles accumulation in Alzheimer's disease. Panel (B) shows the surface map of regression slope of FDDNP DVR increase per unit change of MMSE score. The higher the slope corresponds to a faster increase of the FDDNP DVR. The areas of highest slope (red) match areas of significant beta-amyloid plaques and neurofibrillary tangles in AD that include the lateral temporal, lateral frontal, anterior cingulate, medial temporal and posterior cingulate areas. Panel (C) shows a cortical surface map of F-statistics of the linear regression model between FDDNP DVR and MMSE. Areas that have a significant slope with $\alpha = 0.05$ are shown with colors above dark blue. It is important to note that lateral frontal, lateral temporal, medial temporal, anterior cingulate and posterior cingulate all have a significant slope, and all have been shown to be important in AD. Adapted and reprinted with permission from Protas et al., (2010) [Copyright (2010) Neuroimage]

consistently demonstrated that neurofibrillary tangles, compared with β-amyloid plaques, are better correlated with the severity of cognitive impairment (e.g., mini-mental state examination [MMSE] or clinical dementia rating [CDR] in normal aging, MCI, and patients with AD) [23–27, 40–44]. Consistent with these *post mortem* studies, FDDNP-PET imaging studies performed in normal aging, MCI, and patients with AD show significant correlations with MMSE scores [45, 46], while PET imaging studies using radiotracers (e.g., PIB and BF-227) thought to bind amyloid plaques without binding to tangles do not [47, 48].

In addition, FDDNP signal progression in AD matches the progressive accumulation of brain pathology described by Braak and Braak [37] (see Fig. 1). By contrast, PIB has not shown a progressive pattern as expected from autopsy data [37]. For example, MCI

patients show an 'on and off' PIB binding pattern that is either negative, that is similar to controls (which is difficult to explain since brain pathology deposition is generally present in MCI) or positive (i.e., similar to AD) [49–51]. Further, PIB binding in the precuneus has been found to be the highest of all cortical areas [52], yet autopsy studies have not found higher β-amyloid deposition in the precuneus compared with other cortical areas [10].

FDDNP-PET SHOWS SUPERIOR PERFORMANCE COMPARED WITH FDG-PET AND MRI

Imaging techniques, such as 2-deoxy-2-[18F]fluoro-D-glucose (FDG)-PET and structural magnetic

resonance imaging (MRI) have been investigated to classify normal aging, MCI, and patients with AD. Small et al. [5] found global FDDNP binding values to be more accurate than previously established sensitive measures for FDG-PET [53–55] or volumetric MRI measures [56–58] for diagnostic classification of subjects.

In these comparisons, values for FDDNP-PET global binding were more effective in discriminating among diagnostic groups than FDG-PET glucose metabolism in the posterior cingulate gyrus or parietal regions [53, 54] or MRI volumes of the medial temporal regions, which many clinicians currently rely upon for diagnostic confirmation of AD [57].

FDDNP BINDING IS RELATED TO NEURONAL LOSS IN THE HIPPOCAMPUS

Neurofibrillary tangle density correlates more strongly with neuronal death than does total plaque burden [59]. Large pyramidal neurons in the CA1 and subicular regions of the hippocampus, a part of the medial temporal lobe system supporting declarative memory, are among the most vulnerable neuronal populations affected in the earliest stages of the disease in a pattern that differs from that of normal aging, and is highest in entorhinal cortex and hippocampus CA1 region [60]. Although these large pyramidal neurons are glutamatergic in nature, they receive inhibitory serotonergic input from the dorsal raphe nucleus via the serotonin 1A (5-HT1A) receptors located on their axonal hillock. Hippocampal CA1 region and subiculum have the highest density of 5-HT1A receptors in the brain, Therefore, a decrease in 5-HT1A receptor densities in the same areas in AD can be demonstrated *in vivo* by using 4-[F-18]fluoro-N-{2-[1-(2-methoxyphenyl)piperazinyl]ethyl}-N-(2-pyridinyl)benzamide (MPPF) PET in patients and correlated with the hippocampal cellular pathology, which includes loss of glutamatergic pyramidal neurons in the CA1 field of hippocampus. Thus, MPPF-PET can provide a measure of hippocampal degeneration in AD, including pyramidal neuron loss in hippocampus [61].

To investigate the relationship between FDDNP binding and hippocampal degeneration, FDDNP-PET and MPPF-PET scans were performed, and hippocampal MPPF binding values were found to closely correlate with cortical increases in FDDNP binding. Moreover, they were also strongly correlated with the severity of cognitive decline in AD, as measured by MMSE scores [45, 61]. Particularly remarkable is that hippocampal 5-HT1A densities were found to be decreased in MCI subjects, making their assessment a possible target for early diagnosis of AD [61]. Densities of hippocampal 5-HT1A receptors at pre-clinical stages of AD are affected by two opposing processes: pyramidal neuron losses in CA1 and subiculum regions causing decreases in regional receptor density, but these decreases are counteracted by increased receptor expression on surviving pyramidal neurons. In contrast to our observations, Truchot and colleagues [62] initially reported increases in hippocampal 5-HT1A receptor density in their amnestic MCI population compared to controls measured by MPPF-PET and attributed it to compensatory mechanisms. In their subsequent paper [63] on measurement of 5-HT1A receptor densities with MPPF-PET, they observed decreased hippocampal 5-HT1A receptor densities in the amnestic MCI group compared to controls, similar to our results [61], and increased receptor density in several neocortical regions. When the disease reaches clinical stages, hippocampal pyramidal neuronal losses and volume loss in the CA1 region of the hippocampus and subiculum [64, 65] prevail over compensatory effects, and significantly decreased hippocampal 5-HT1A receptor densities have been observed in all studies [61–63]. The combined evaluation of FDDNP-PET (targeting tangles and plaques) with MPPF-PET (targeting serotonin 1A receptors as a marker of hippocampal degeneration) offers the opportunity for reliable, *non invasive* detection of both AD pathology and hippocampal neuronal loss.

By contrast, the relationship between PIB binding and hippocampal neuronal loss is controversial: While some studies found that global and regional atrophy were strongly related to PIB binding in subjects with subjective cognitive impairment, not such relationship has been found in patients with MCI or AD [66]. Other reports have found no associations detected between current PIB binding and regional brain volume decline trajectories in preceding years [67].

MULTITRACER PET IMAGING USING BOTH FDDNP AND PIB

Because of their different imaging characteristics, multitracer PET imaging using PIB and FDDNP in the same subjects may help visualize different aspects of AD development. To investigate this issue,
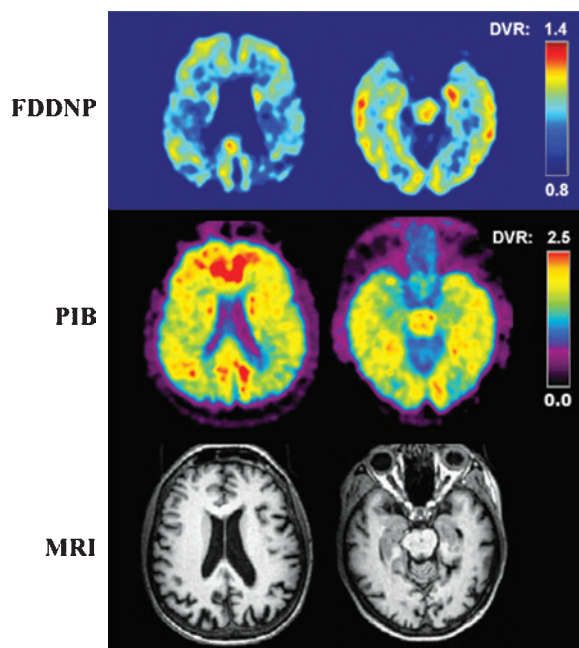
Fig. 2. Co-registered FDDNP-PET (upper panel), PIB-PET (middle panel), and MRI scans of a patient with Alzheimer's disease. Warmer colors (reds, yellows) indicate higher binding levels in PET scans. Images in the left column are at the level of the parietal lobe; images in the right column are at the level of the temporal lobe. Warmer colors (reds, yellows) indicate higher binding levels on PET scans.

Fig. 3. FDDNP minus PIB results (yellow blobs) in the same patients with AD as statistical parameter mapping (SPM) projections superimposed on a standardized magnetic resonance imaging brain template in the three orthogonal right sagittal (upper left), coronal (upper right), and axial (lower left) views ($p < 0.05$ (FWE); corrected, $k = 100$). Adapted and reprinted with permission from Shin et al., (2010) [Copyright (2010) Neuroimage].

multitracer PET imaging using FDDNP and PIB in the same subjects, with and without AD were performed [6].

Patients with AD have consistently shown low PIB but high FDDNP binding in the medial temporal cortex (limbic regions including hippocampus, parahippocampal areas, and entorhinal cortex), while both PIB and FDDNP binding are significantly increased in neocortical areas in AD compared with age matched controls (See Fig. 2). Consistent with these results, subtracted PET data (FDDNP minus PIB) acquired from the same patients with AD (analyzed using statistical parameter mapping software [8]) found that the medial temporal cortex was the most significant differential brain region in the voxel mapping (see Fig. 3).

Post mortem studies describing the hierarchical progression of tau lesions in normal aging and early stages of AD suggest that damage to the medial temporal cortex and association cortex would account for the memory and non-memory cognitive impairments, respectively [68]. Therefore, high FDDNP binding observed in the medial temporal cortex of patients with AD is consistent with the suggested relationship between the medial temporal tau pathology and memory impairment in AD.

MEDIAL TEMPORAL FDDNP BINDING IS RELATED TO EPISODIC MEMORY PERFORMANCE

Episodic memory impairment is one of the most prevalent cognitive deficits in patients with AD [69], and a subtle decline in episodic memory often occurs prior to the emergence of the full dementia syndrome in non-demented older adults who eventually develop AD [70].

The medial temporal cortex has been well-established as playing a central role in modulating episodic memory [71]. We found that medial temporal FDDNP uptake values in normal elderly subjects are correlated inversely with long delay recall scores in the CVLT ($r = -0.684$, $p = 0.029$), an instrument used to test episodic memory performance [6]. By contrast, medial temporal PIB binding does not show a statistically significant correlation with episodic memory performance [6]. These findings may suggest that episodic memory impairment in healthy control subjects might be related to the presence of intraneuronal neurofibrillary tangles in the medial temporal cortex.

Post mortem pathological evidence previously showed that neurofibrillary tangle density in the medial temporal cortex of cognitively normal elderly persons correlates with memory scores, whereas density of amyloid plaques in the same region does not [72, 73]. Determining the details of the connections between tau pathology and episodic memory impairment warrants further study, but it is expected that tangle formation may at least partly contribute to episodic memory deterioration via impairing electroencephalogram (EEG) theta rhythm [74–76].

FDDNP BINDING PATTERN IN THE BRAIN'S DEFAULT NETWORK

The concept of a default mode network – an interconnected set of brain regions (frontal, parietal, posterior cingulate, lateral, and medial temporal regions) that is active when the brain is in a resting state and deactivated during focused mental tasks – was first proposed in 2001 [77]. This concept rapidly became the target of hot research in AD, where such a default network appears disrupted, most prominently in the medial temporal cortex [78–80]. FDDNP binding patterns in patients with AD show significantly increased binding values in the entire default network, including the medial temporal cortex [5, 6], which points to the utility of FDDNP-PET in identifying the role of the default network in AD [81].

QUANTITATIVE ANALYSIS OF FDDNP-PET USING SUBCORTICAL WHITE MATTER AS REFERENCE REGION

There is imprecise information in the literature regarding non-specific white matter binding of FDDNP and other probes. Recently, Wong et al. [82] investigated this issue and found that for FDDNP, the ratio of white matter over cerebellum is 1.0, whereas for PIB the white matter/cerebellum ratio is 1.5; that ratio is even higher for imaging probes structurally related to trans-stilbenes (e.g., AV-45). Therefore, the cortex/cerebellum ratio for expressing a signal is misleading and the cortex/white matter ratio would better express the signal to noise ratio in adjacent tissues. High white matter signal produces a significant spillover effect of the signal to the cortical grey matter. It also adds to partial volume effects, which distort results, most particularly in AD when significant cortical atrophy is present. These effects can be com-

pensated to some extent by analytical approaches that use segmentation of grey and white matter based on MRI scans before quantitation of PET data to determine grey matter cortical binding of these tracers, yet the question of the origin of high white matter binding of these tracers still remains.

Because the white matter/cerebellum ratio for FDDNP uptake is 1.0 [82], subcortical white matter is a good alternative reference region to the cerebellum for analyzing FDDNP-PET data, particularly when the cerebellar region is affected by disease (e.g., in prion disease) [83]. Wong and colleagues [82] have shown that lower perfusion of white matter compared to grey matter does not present a problem for Logan graphical analysis for this tracer and that it does not increase inter-subject variability over that observed in analysis performed with the cerebellum as the reference region. In practice, both the subcortical white matter and the cerebellum should be used together to cross-validate the findings with different reference regions, especially when arterial input blood data are not available or blood sampling is not feasible due to practical clinical considerations. Comparison of both approaches was tested in 10 AD and 10 control subjects and results show very good correlations ([83], Supplementary Materials).

THE LIMITATIONS OF FDDNP-PET

One of the most frequently mentioned limitations of FDDNP is the small cortical signal difference between control and AD subjects [9]. The *in vivo* FDDNP binding differences between controls and AD patients are significantly lower (approx 10-15%) than those of PIB-PET (approx 80%) in some neocortical regions when the cerebellum is used as a reference [6]. That difference is reduced to about 25-30% for PIB-PET (vs 10-15% for FDDNP-PET) when the adjacent white matter region is used as a reference [82]. It also should be noted that in the medial temporal region, the cortical area with the earliest pathology deposition in AD, the FDDNP binding difference between controls and AD is much higher (approx 30%) compared with PIB-PET (approx 5%) which shows the lowest level of signal of all brain regions [6]. To demonstrate this characteristic between FDDNP-PET and PIB-PET, we show the differential PET image (FDDNP minus PIB) in Fig. 3, where PIB binding values are shown to be higher than FDDNP binding values in several neocortical regions and FDDNP binding values are higher than PIB binding values in the medial temporal cortical regions [10].

Unlike PIB-PET, which shows a single pattern of affected areas at all stages of AD progression, we have observed an increasing pattern of FDDNP cortical brain involvement with disease progression consistent with known pathological data at all levels of neurological impairment [46]. This may increase the difficulty in quantification of FDDNP-PET data if group separation (e.g., controls vs. AD) is intended, yet it more closely matches the stepwise evolution of pathology pattern in AD (see Fig. 1).

Another often mentioned critique of FDDNP is that it does not bind to β-amyloid plaques selectively. However, this argument is strongly biased by the influence of the amyloid cascade hypothesis which considers β-amyloid as causative of AD, in contrast to other criteria which attributes the disease to other factors (e.g., inflammation) and considers both neurofibrillary tangles and β-amyloid plaques as pathological diagnostic hallmarks of AD. In AD both pathologies are contributing to disease and thus binding to both Alzheimer's pathologies could be considered an advantage since evolution of these pathologies follows different time- and space-related patterns. Recent repeated failures in developing anti-amyloid drugs and vaccines cast doubts on the amyloid cascade hypothesis for which the ability of FDDNP to image both plaque and tangle would be considered favorably rather than an obstacle in AD diagnosis and drug treatment monitoring, particularly at the earliest stages involving the medial temporal lobe where PIB-PET shows no signal [84]. Therefore, even with the relatively low neocortical signal, FDDNP value as an imaging agent is enhanced by two important facts: (1) at present, it is the only clinically available *in vivo* imaging probe to visualize tau pathology in living humans; and (2) it is also the only radiotracer to visualize AD pathology in the hippocampal region of living humans, which is among the earliest affected brain region in AD.

THE POTENTIAL ADVANTAGE OF FDDNP-PET IN THE ASSESSMENT OF EARLY ALZHEIMER'S DISEASE AND/OR THOSE SUBJECTS AT RISK FOR AD

The amyloid cascade hypothesis assumes that amyloid plaque formation precedes neurofibrillary tangle formation [8]. Supporting evidence for the amyloid cascade hypothesis comes from early-onset familial AD cases caused by mutations in three different genes, amyloid precursor protein (*APP*) and presenilin-1 and -2 (*PS1* and *PS2*). However, less than 5 percent of all Alzheimer cases are early-onset familial AD. By contrast, human postmortem histopathology data suggest that the initial development of tangles might precede the development of amyloid plaques by at least two decades [20, 21]. The progression of tangle formation is stepwise and consistent from the entorhinal cortex, through the hippocampus, and into the isocortex [37]. Therefore, early detection of AD pathology in living humans at its onset before it spreads widely will contribute to the early, preclinical diagnosis of, and early treatments for, AD. If so, because of its sensitivity for tau aggregates, FDDNP-PET imaging would have an advantage in an early, preclinical diagnosis of AD, especially in imaging medial temporal cortex.

CONCLUSIONS

Previously well-established *post mortem* human data suggest that tau tangles are more accurate predictors than amyloid plaques in monitoring disease stages and cognitive performance in normal aging, MCI, and AD. Consistent with *post mortem* studies, FDDNP-PET imaging scans performed in normal aging, MCI, and patients with AD show significant correlations with MMSE scores, as well as MPPF-PET hippocampal neuronal loss measures, while other PET imaging probes purportedly designed to bind amyloid pathology do not. In addition, FDDNP signal progression in AD also matches the progressive accumulation of brain pathology described by *post mortem* histopathological studies. Furthermore, FDDNP is the only imaging probe to succeed in visualizing AD pathology in the medial temporal cortex (especially, in the hippocampus) of living humans, and thus the FDDNP binding in the medial temporal cortex is expected to associate with predominant tangle formation in the region, episodic memory impairment, the brain's default network, and early, preclinical diagnosis of AD. Therefore, FDDNP-PET, which can visualize neurofibrillary tangles in addition to amyloid plaques, provides unique information on AD brain pathology relevant to disease progression.

FINANCIAL DISCLOSURE

The University of California, Los Angeles, owns a U.S. patent (6,274,119) entitled "Methods for Labeling β-Amyloid Plaques and Neurofibrillary

Tangles," that uses the approach outlined in this article. Drs. Small and Barrio are among the inventors, have received royalties, and may receive royalties on future sales. Dr. Small reports having served as a consultant and/or having received lecture fees from Eisai, Forest, Medivation, Novartis, and Pfizer. Dr. Barrio reports having served as a consultant and having received lecture fees from Nihon Medi-Physics Co, Bristol-Meyer Squibb, PET-Net Pharmaceuticals, and Siemens.

REFERENCES

[1] Barrio JR, Huang SC, Cole GM, Satyamurthy N, Petric A, Phelps ME, Small G (1999) PET imaging of tangles and plaques in Alzheimer's disease with a highly hydrophilic probe. *J Labelled Comp Radiopharm* **42**, S194-S195.

[2] Shoghi-Jadid K, Small GW, Agdeppa ED, Kepe V, Ercoli LM, Siddarth P, Read S, Satyamurthy N, Petric A, Huang SC, Barrio JR (2002) Localization of neurofibrillary tangles and beta-amyloid plaques in the brains of living patients with Alzheimer disease. *Am J Geriatr Psychiatry* **10**, 24-35.

[3] Agdeppa ED, Kepe V, Liu J, Flores-Torres S, Satyamurthy N, Petric A, Cole GM, Small GW, Huang SC, Barrio JR (2001) Binding characteristics of radiofluorinated 6-dialkylamino-2-naphthylethylidene derivatives as positron emission tomography imaging probes for beta-amyloid plaques in Alzheimer's disease. *J Neurosci* **21**, RC189.

[4] Agdeppa ED, Kepe V, Liu J, Small GW, Huang SC, Petric A, Satyamurthy N, Barrio JR (2003) 2-Dialkylamino-6-acylmalononitrile substituted naphthalenes (DDNP analogs): novel diagnostic and therapeutic tools in Alzheimer's disease. *Mol Imaging Biol* **5**, 404-417.

[5] Small GW, Kepe V, Ercoli LM, Siddarth P, Bookheimer SY, Miller KJ, Lavretsky H, Burggren AC, Cole GM, Vinters HV, Thompson PM, Huang SC, Satyamurthy N, Phelps ME, Barrio JR (2006) PET of brain amyloid and tau in mild cognitive impairment. *N Engl J Med* **355**, 2652-2663.

[6] Shin J, Lee SY, Kim SH, Kim YB, Cho SJ (2008) Multitracer PET imaging of amyloid plaques and neurofibrillary tangles in Alzheimer's disease. *Neuroimage* **43**, 236-244.

[7] Tolboom N, Yaqub M, Van der Flier WM, Boellaard R, Luurtsema G, Windhorst AD, Barkhof F, Scheltens P, Lammertsma AA, van Berckel BN (2009) Detection of Alzheimer pathology *in vivo* using both 11C-PIB and 18F-FDDNP PET. *J Nucl Med* **50**, 191-197.

[8] Shin J, Lee SY, Kim SJ, Kim SH, Cho SJ, Kim YB (2010) Voxel-based analysis of Alzheimer's disease PET imaging using a triplet of radiotracers: PIB, FDDNP, and FDG. *Neuroimage* **52**, 488-496.

[9] Klunk WE, Mathis CA (2008) The future of amyloid-beta imaging: a tale of radionuclides and tracer proliferation. *Curr Opin Neurol* **21**, 683-687.

[10] Nelson PT, Abner EL, Scheff SW, Schmitt FA, Kryscio RJ, Jicha GA, Smith CD, Patel E, Markesbery WR (2009) Alzheimer's-type neuropathology in the precuneus is not increased relative to other areas of neocortex across a range of cognitive impairment. *Neurosci Lett* **450**, 336-339.

[11] Cole GB, Keum G, Liu J, Small GW, Satyamurthy N, Kepe V, Barrio JR (2010) Specific estrogen sulfotransferase (SULT1E1) substrates and molecular imaging probe candidates. *Proc Natl Acad Sci U S A* **107**, 6222-6227.

[12] Verhoeff NP, Wilson AA, Takeshita S, Trop L, Hussey D, Singh K, Kung HF, Kung MP, Houle S (2004) In-vivo imaging of Alzheimer disease beta-amyloid with [11C]SB-13 PET. *Am J Geriatr Psychiatry* **12**, 584-595.

[13] Kudo Y, Okamura N, Furumoto S, Tashiro M, Furukawa K, Maruyama M, Itoh M, Iwata R, Yanai K, Arai H (2007) 2-(2-[2-Dimethylaminothiazol-5-yl]ethenyl)-6- (2-[fluoro]ethoxy)benzoxazole: a novel PET agent for *in vivo* detection of dense amyloid plaques in Alzheimer's disease patients. *J Nucl Med* **48**, 553-561.

[14] Rowe CC, Ackerman U, Browne W, Mulligan R, Pike KL, O'Keefe G, Tochon-Danguy H, Chan G, Berlangieri SU, Jones G, Dickinson-Rowe KL, Kung HP, Zhang W, Kung MP, Skovronsky D, Dyrks T, Holl G, Krause S, Friebe M, Lehman L, Lindemann S, Dinkelborg LM, Masters CL, Villemagne VL (2008) Imaging of amyloid beta in Alzheimer's disease with 18F-BAY94-9172, a novel PET tracer: proof of mechanism. *Lancet Neurol* **7**, 129-135.

[15] Wong DF, Rosenberg PB, Zhou Y, Kumar A, Raymont V, Ravert HT, Dannals RF, Nandi A, Brasić JR, Ye W, Hilton J, Lyketsos C, Kung HF, Joshi AD, Skovronsky DM, Pontecorvo MJ (2010) In vivo imaging of amyloid deposition in Alzheimer disease using the radioligand 18F-AV-45 (florbetapir [corrected] F 18). *J Nucl Med* **51**, 913-920.

[16] Vandenberghe R, Van Laere K, Ivanoiu A, Salmon E, Bastin C, Triau E, Hasselbalch S, Law I, Andersen A, Korner A, Minthon L, Garraux G, Nelissen N, Bormans G, Buckley C, Owenius R, Thurfjell L, Farrar G, Brooks DJ (2010) 18F-flutemetamol amyloid imaging in Alzheimer disease and mild cognitive impairment: a phase 2 trial. *Ann Neurol* **68**, 319-329.

[17] Smid LM, Vovko TD, Popovic M, Petric A, Kepe V, Barrio JR, Vidmar G, Brejanac M (2006) The 2, 6-Disubstituted Naphthalene Derivative FDDNP Labels Amyloid-like Deposits Displaying Congo Red Birefringence. *Brain Pathology* **16**, 124-130.

[18] Hardy JA, Higgins GA (1992) Alzheimer's disease: the amyloid cascade hypothesis. *Science* **256**, 184-185.

[19] Ohm TG, Müller H, Braak H, Bohl J (1995) Close-meshed prevalence rates of different stages as a tool to uncover the rate of Alzheimer's disease-related neurofibrillary changes. *Neuroscience* **64**, 209-217.

[20] Braak H, Braak E (1997) Frequency of stages of Alzheimer-related lesions in different age categories. *Neurobiology of Aging* **18**, 351-357.

[21] Duyckaerts C, Hauw JJ (1997) Prevalence, incidence and duration of Braak's stages in the general population: can we know? *Neurobiol Aging* **18**, 362-369.

[22] Schönheit B, Zarski R, Ohm TG (2004) Spatial and temporal relationships between plaques and tangles in Alzheimer-pathology. *Neurobiol Aging* **25**, 697-711.

[23] Nelson PT, Braak H, Markesbery WR (2009) Neuropathology and cognitive impairment in Alzheimer disease: a complex but coherent relationship. *J Neuropathol Exp Neurol* **68**, 1-14.

[24] Green MS, Kaye JA, Ball MJ (2000) The Oregon brain aging study: neuropathology accompanying healthy aging in the oldest old. *Neurology* **54**, 105-113.

[25] Giannakopoulos P, Herrmann FR, Bussière T, Bouras C, Kövari E, Perl DP, Morrison JH, Gold G, Hof PR (2003)

Tangle and neuron numbers, but not amyloid load, predict cognitive status in Alzheimer's disease. *Neurology* **60**, 1495-1500.

[26] Chubb C, Inagaki Y, Sheu P, Cummings B, Wasserman A, Head E, Cotman C (2006) BioVision: an application for the automated image analysis of histological sections. *Neurobiol Aging* 27, 1462-1476.

[27] Duyckaerts C, Delatour B, Potier MC (2009) Classification and basic pathology of Alzheimer disease. *Acta Neuropathol* **118**, 5-36.

[28] Williams M (2009) Progress in Alzheimer's disease drug discovery: an update. *Curr Opin Investig Drugs* **10**, 23-34.

[29] Teng E, Kepe V, Frautschy SA, Liu J, Satyamurth N, Yang F, Chen PP, Jones MR, Huang SC, Flood DG, Trusko SP, Small GW, Cole GM, Barrio JR (2011) *In vivo* [F-18]FDDNP microPET imaging correlates with brain Aβ burden in a transgenic rat model of Alzheimer disease: Effects of aging, *in vivo* blockade, and anti-Aβ antibody treatment. *Neurobiol Disease.* [Epub ahead of print]

[30] Gearing M, Rebeck GW, Hyman BT, Tigges J, Mirra SS (1994) Neuropathology and apolipoprotein E profile of aged chimpanzees: implications for Alzheimer disease. *Proc Natl Acad Sci U S A* **91**, 9382-9386.

[31] Noda A, Murakami Y, Nishiyama S, Fukumoto D, Miyoshi S, Tsukada H, Nishimura S (2008) Amyloid imaging in aged and young macaques with [11C]PIB and [18F]FDDNP. *Synapse* **62**, 472-475.

[32] Landau M, Sawaya MR, Faull KF, Laganowsky A, Jiang L, Sievers SA, Liu J, Barrio JR, Eisenberg D (2011) Towards a Pharmacophore for Amyloid, PLOS Biol, in press.

[33] Small GW, Kepe V, Barrio JR (2006) Seeing is believing: neuroimaging adds to our understanding of cerebral pathology. *Curr Opin Psychiatry* **19**, 564-569.

[34] Cairns NJ, Bigio EH, Mackenzie IR, Neumann M, Lee VM, Hatanpaa KJ, White CL, 3rd, Schneider JA, Grinberg LT, Halliday G, Duyckaerts C, Lowe JS, Holm IE, Tolnay M, Okamoto K, Yokoo H, Murayama S, Woulfe J, Munoz DG, Dickson DW, Ince PG, Trojanowski JQ, Mann DM (2007) Consortium for frontotemporal lobar degeneration neuropathologic diagnostic and nosologic criteria for frontotemporal lobar degeneration: consensus of the Consortium for Frontotemporal Lobar Degeneration. *Acta Neuropathol* **114**, 5-22.

[35] Barrio JR, Bordelon Y, Small G, Kepe V Visualizing Tau Pathology in the Living Brain of Progressive Supranuclear Palsy. 10th International Conference on Alzheimer's and Parkinson's Diseases, Barcelona, Spain, March, 9-13.

[36] Tolboom N, van der Flier WM, Yaqub M, Boellaard R, Verwey NA, Blankenstein MA, Windhorst AD, Scheltens P, Lammertsma AA, van Berckel BN (2009) Relationship of cerebrospinal fluid markers to 11C-PiB and 18F-FDDNP binding. *J Nucl Med* **50**, 1464-1470.

[37] Braak H, Braak E (1991) Neuropathological staging of Alzheimer-related changes. *Acta Neuropathol* **82**, 239-259.

[38] Näslund J, Haroutunian V, Mohs R, Davis KL, Davies P, Greengard P, Buxbaum JD (2000) Correlation between elevated levels of amyloid beta-peptide in the brain and cognitive decline. *JAMA* **283**, 1571-1577.

[39] Arnold SE, Hyman BT, Flory J, Damasio AR, Van Hoesen GW (1991) The topographical and neuroanatomical distribution of neurofibrillary tangles and neuritic plaques in the cerebral cortex of patients with Alzheimer's disease. *Cereb Cortex* **1**, 103-116.

[40] Bierer LM, Hof PR, Purohit DP, Carlin L, Schmeidler J, Davis KL, Perl DP (1995) Neocortical neurofibrillary tangles correlate with dementia severity in Alzheimer's disease. *Arch Neurol* **52**, 81-88.

[41] Berg L, McKeel DW Jr, Miller JP, Storandt M, Rubin EH, Morris JC, Baty J, Coats M, Norton J, Goate AM, Price JL, Gearing M, Mirra SS, Saunders AM (1998) Clinicopathologic studies in cognitively healthy aging and Alzheimer's disease: relation of histologic markers to dementia severity, age, sex, and apolipoprotein E genotype. *Arch Neurol* **55**, 326-335.

[42] Giannakopoulos P, Hof PR, Michel JP, Guimon J, Bouras C (1997) Cerebral cortex pathology in aging and Alzheimer's disease: a quantitative survey of large hospital-based geriatric and psychiatric cohorts. *Brain Res Rev* **25**, 217-245.

[43] Jicha GA, Parisi JE, Dickson DW, Johnson K, Cha R, Ivnik RJ, Tangalos EG, Boeve BF, Knopman DS, Braak H, Petersen RC (2006) Neuropathologic outcome of mild cognitive impairment following progression to clinical dementia. *Arch Neurol* **63**, 674-681.

[44] Petersen RC, Parisi JE, Dickson DW, Johnson KA, Knopman DS, Boeve BF, Jicha GA, Ivnik RJ, Smith GE, Tangalos EG, Braak H, Kokmen E (2006) Neuropathologic features of amnestic mild cognitive impairment. *Arch Neurol* **63**, 665-672.

[45] Barrio JR, Kepe V, Satyamurthy N, Huang SC, Small G (2008) Amyloid and tau imaging, neuronal losses and function in mild cognitive impairment. *J Nutr Health Aging* **12**, 61S-65S.

[46] Protas HD, Huang SC, Kepe V, Hayashi K, Klunder A, Braskie MN, Ercoli L, Bookheimer S, Thompson PM, Small GW, Barrio JR (2010) FDDNP binding using MR derived cortical surface maps. *Neuroimage* **49**, 240-248.

[47] Jagust WJ, Landau SM, Shaw LM, Trojanowski JQ, Koeppe RA, Reiman EM, Foster NL, Petersen RC, Weiner MW, Price JC, Mathis CA (2009) Alzheimer's Disease Neuroimaging Initiative. Relationships between biomarkers in aging and dementia. *Neurology* **73**, 1193-1199.

[48] Waragai M, Okamura N, Furukawa K, Tashiro M, Furumoto S, Funaki Y, Kato M, Iwata R, Yanai K, Kudo Y, Arai H (2009) Comparison study of amyloid PET and voxel-based morphometry analysis in mild cognitive impairment and Alzheimer's disease. *J Neurol Sci* **285**, 100-108.

[49] Kemppainen NM, Aalto S, Wilson IA, Någren K, Helin S, Brück A, Oikonen V, Kailajärvi M, Scheinin M, Viitanen M, Parkkola R, Rinne JO (2007) PET amyloid ligand [11C]PIB uptake is increased in mild cognitive impairment. *Neurology* **68**, 1603-1606.

[50] Okello A, Koivunen J, Edison P, Archer HA, Turkheimer FE, Någren K, Bullock R, Walker Z, Kennedy A, Fox NC, Rossor MN, Rinne JO, Brooks DJ (2009) Conversion of amyloid positive and negative MCI to AD over 3 years: an 11C-PIB PET study. *Neurology* **73**, 754-760.

[51] Wolk DA, Price JC, Saxton JA, Snitz BE, James JA, Lopez OL, Aizenstein HJ, Cohen AD, Weissfeld LA, Mathis CA, Klunk WE, De-Kosky ST (2009) Amyloid imaging in mild cognitive impairment subtypes. *Ann Neurol* **65**, 557-568.

[52] Mintun MA, Larossa GN, Sheline YI, Dence CS, Lee SY, Mach RH, Klunk WE, Mathis CA, DeKosky ST, Morris JC (2006) [11C]PIB in a nondemented population: potential antecedent marker of Alzheimer disease. *Neurology* **67**, 446-452.

[53] Small GW, Ercoli LM, Silverman DHS, Huang SC, Komo S, Bookheimer SY, Lavretsky H, Miller K, Siddarth P, Rasgon NL, Mazziotta JC, Saxena S, Wu HM, Mega MS, Cummings JL, Saunders AM, Pericak-Vance MA, Roses AD, Barrio JR, Phelps ME (2000) Cerebral metabolic and cognitive decline in persons at genetic risk for Alzheimer's disease. *Proc Natl Acad Sci U S A* **97**, 6037-6042.

[54] Silverman DH, Small GW, Chang CY, Lu CS, Kung De Aburto MA, Chen W, Czernin J, Rapoport SI, Pietrini P, Alexander GE, Schapiro MB, Jagust WJ, Hoffman JM, Welsh-Bohmer KA, Alavi A, Clark CM, Salmon E, de Leon MJ, Mielke R, Cummings JL, Kowell AP, Gambhir SS, Hoh CK, Phelps ME (2001) Positron emission tomography in evaluation of dementia: regional brain metabolism and long-term clinical outcome. *JAMA* **286**, 2120-2127.

[55] Chetelat G, Desgranges B, de la Sayette V, Viader F, Eustache F, Baron JC (2003) Mild cognitive impairment: can FDG PET predict who is to rapidly convert to Alzheimer's disease?. *Neurology* **60**, 1374-1377.

[56] Thompson PM, Hayashi KM, De Zubicaray GI, Janke AL, Rose SE, Semple J, Hong MS, Herman DH, Gravano D, Doddrell DM, Toga AW (2004) Mapping hippocampal and ventricular change in Alzheimer disease. *Neuroimage* **22**, 1754-1766.

[57] Korf ES, Wahlund LO, Visser PJ, Scheltens P (2004) Medial temporal lobe atrophy on MRI predicts dementia in patients with mild cognitive impairment. *Neurology* **63**, 94-100.

[58] Stoub TR, Bulgakova M, Leurgans S, Bennett DA, Fleischman D, Turner DA, deToledo-Morrell L (2005) MRI predictors of risk of incident Alzheimer disease: a longitudinal study. *Neurology* **64**, 1520-1524.

[59] Gomez-Isla T, Price JL, McKeel DW JJr., Morris JC, Growdon JH, Hyman BT (1996) Profound loss of layer II entorhinal cortex neurons occurs in very mild Alzheimer's disease. *J Neurosci* **16**, 4491-4500.

[60] Hall H, Lundkvist C, Halldin C, Farde L, Pike VW, McCarron JA, Fletcher A, Cliffe IA, Barf T, Wikstrom H, Sedvall G (1997) Autoradiographic localization of 5-HT1A receptors in the postmortem human brain using [3H]WAY-100635 and [11C]WAY-100635. *Brain Res* **745**, 96-108.

[61] Kepe V, Barrio JR, Huang S-C, Ercoli L, Siddarth P, Shoghi-Jadid K, Cole GM, Satyamurthy N, Cummings JL, Small GW, Phelps M (2006) Serotonin 1A receptors in the living brain of Alzheimer's disease. *Proc Natl Acad Sci USA* **103**, 702-707.

[62] Truchot L, Costes SN, Zimmer L, Laurent B, Le Bars D, Thomas-Antérion C, Croisile B, Mercier B, Hermier M, Vighetto A, Krolak-Salmon P (2007) Up-regulation of hippocampal serotonin metabolism in mild cognitive impairment. *Neurology* **69**, 1012-1017.

[63] Truchot L, Costes N, Zimmer L, Laurent B, Le Bars D, Thomas-Antérion C, Mercier B, Hermier M, Vighetto A, Krolak-Salmon P (2008) A distinct [18F]MPPF PET profile in amnestic mild cognitive impairment compared to mild Alzheimer's disease. *Neuroimage* **40**, 1251-1256.

[64] Rössler M, Zarski R, Bohl J, Ohm TG (2002) Stage-dependent and sector-specific neuronal loss in hippocampus during Alzheimer's disease. *Acta Neuropathol* **103**, 363-369.

[65] Apostolova LG, Dinov ID, Dutton RA, Hayashi KM, Toga AW, Cummings JL, Thompson PM (2006) 3D comparison of hippocampal atrophy in amnestic mild cognitive impairment and Alzheimer's disease. *Brain* **129**, 2867-2873.

[66] Chételat G, Villemagne VL, Bourgeat P, Pike KE, Jones G, Ames D, Ellis KA, Szoeke C, Martins RN, O'Keefe GJ, Salvado O, Masters CL, Rowe CC (2010) Australian Imaging Biomarkers and Lifestyle Research Group. Relationship between atrophy and beta-amyloid deposition in Alzheimer disease. *Ann Neurol* **67**, 317-324.

[67] Driscoll I, Zhou Y, An Y, Sojkova J, Davatzikos C, Kraut MA, Ye W, Ferrucci L, Mathis CA, Klunk WE, Wong DF, Resnick SM (2010) Lack of association between (11)C-PiB and longitudinal brain atrophy in non-demented older individuals.Neurobiol Aging doi:10.1016/j. neurobiolaging.2009.12.008.

[68] Chetelat G, Baron JC (2003) Early diagnosis of Alzheimer's disease: contribution of structural neuroimaging. *Neuroimage* **18**, 525-541.

[69] Dubois B, Feldman HH, Jacova C, Dekosky ST, Barberger-Gateau P, Cummings J, Delacourte A, Galasko D, Gauthier S, Jicha G, Meguro K, O'brien J, Pasquier F, Robert P, Rossor M, Salloway S, Stern Y, Visser PJ, Scheltens P (2007) Research criteria for the diagnosis of Alzheimer's disease: revising the NINCDS-ADRDA criteria. *Lancet Neurol* **6**, 734-746.

[70] Lange KL, Bondi MW, Salmon DP, Galasko D, Delis DC, Thomas RG, Thal LJ (2002) Decline in verbal memory during preclinical Alzheimer's disease: examination of the effect of APOE genotype. *J Int Neuropsychol Soc* **8**, 943-955.

[71] Cohen NJ, Eichenbaum H (1993) Memory, Amnesia, and the Hippocampal System. *The MIT Press, Cambridge, MA*.

[72] Mitchell TW, Mufson EJ, Schneider JA, Cochran EJ, Nissanov J, Han LY, Bienias JL, Lee VM, Trojanowski JQ, Bennett DA, Arnold SE (2002) Parahippocampal tau pathology in healthy aging, mild cognitive impairment, and early Alzheimer's disease. *Ann Neurol* **51**, 182-189.

[73] Guillozet AL, Weintraub S, Mash DC, Mesulam MM (2003) Neurofibrillary tangles, amyloid, and memory in aging and mild cognitive impairment. *Arch Neurol* **60**, 729-736.

[74] Shin J, Kim D, Bianchi R, Wong RK, Shin HS (2005) Genetic dissection of thetarhythm heterogeneity in mice. *Proc Natl Acad Sci U S A* **102**, 18165-18170.

[75] Shin J, Gireesh G, Kim SW, Kim DS, Lee S, Kim YS, Watanabe M, Shin HS (2009) Phospholipase C b4 in the medial septum controls cholinergic theta oscillations and anxiety behaviors. *J. Neurosci* **29**, 15375-15385.

[76] Shin J (2010) Theta rhythm heterogeneity in humans. *Clin Neurophysiol* **121**, 456-457.

[77] Gusnard DA, Raichle ME (2001) Searching for a baseline: functional imaging and the resting human brain. *Nat Rev Neurosci* **2**, 685-694.

[78] Buckner RL, Snyder AZ, Shannon BJ, LaRossa G, Sachs R, Fotenos AF, Sheline YI, Klunk WE, Mathis CA, Morris JC, Mintun MA (2005) Molecular, structural, and functional characterization of Alzheimer's disease: evidence for a relationship between default activity, amyloid, and memory. *J Neurosci* **25**, 7709-7717.

[79] Buckner RL, Andrews-Hanna JR, Schacter DL (2008) The brain's default network: anatomy, function, and relevance to disease. *Ann N Y Acad Sci* **1124**, 1-38.

[80] Shin J, Tsui W, Li Y, Lee SY, Kim SJ, Cho SJ, Kim YB, de Leon MJ (2011) Resting-state glucose metabolism level is associated with the regional pattern of amyloid pathology in Alzheimer's disease. *Int J Alzheimers Dis* **2011**, 759780.

[81] Shin J, Kepe V, Small GW, Phelps ME, Barrio JR (2011) Multimodal Imaging of Alzheimer Pathophysiology in the Brain's Default Mode Network. *Int J Alzheimers Dis* **2011**, 687945.

[82] Wong KP, Wardak M, Shao W, Dahlbom M, Kepe V, Liu J, Satyamurthy N, Small GW, Barrio JR, Huang SC (2010) Quantitative analysis of [18F]FDDNP PET using subcortical white matter as reference region. *Eur J Nucl Med Mol Imaging* **37**, 575-588.

[83] Kepe V, Ghetti B, Farlow MR, Bresjanac M, Miller K, Huang SC, Wong KP, Murrell JR, Piccardo P, Epperson F, Repovš G, Smid LM, Petric A, Siddarth P, Liu J, Satyamurthy N, Small GW, Barrio JR (2010) PET of brain prion protein amyloid in Gerstmann–Sträussler–Scheinker disease. *Brain Pathol* **20**, 419-430.

[84] Shin J (2011) Towards development of drugs targeting both amyloid and tau pathologies of Alzheimer's disease. *Int J Geriatr Psychiatry* **26**, 546-548.

This page intentionally left blank

Research Towards Tau Imaging

Jordan R. Jensen, Katryna Cisek, Kristen E. Funk, Swati Naphade, Kelsey N. Schafer and Jeff Kuret*
*Department of Molecular and Cellular Biochemistry, The Ohio State University College of Medicine,
Columbus, OH, USA*

Abstract. Tau-bearing neurofibrillary lesions present a promising biomarker for premortem diagnosis and staging of Alzheimer's disease and certain forms of frontotemporal lobar degeneration by whole brain imaging methods. Although brain penetrating compounds capable of binding tau aggregates with high affinity have been disclosed for this purpose, the major barrier to progress remains the need for tau lesion binding selectivity relative to amyloid-beta plaques and other deposits of proteins in cross-beta-sheet conformation. Here we discuss challenges faced in the development of tau lesion-selective imaging agents, and recent preclinical advances in pursuit of this goal.

Keywords: Alzheimer's disease, frontotemporal lobar degeneration, tau, neurofibrillary tangle, paired helical filaments, biomarker

INTRODUCTION

Current methods for whole-brain imaging of dementia patients leverage positron emission tomography (PET) to capture the binding of radiolabeled compounds to lesions containing filamentous amyloid-β (Aβ) peptide. Radiolabeled PET compounds currently in advanced clinical trials for this purpose include the aminostyryl benzene molecules [^{18}F]BAY94-9172 and [^{18}F]Florbetapir, and the benzthiazole-aryl (BTA) compounds [^{11}C]PIB and [^{18}F]Flutemetamol [1–3]. Although Aβ-directed agents have high sensitivity for detection of AD [4], they have limited specificity, with ∼30% of normal controls and only a subset of MCI cases showing positive signal [4, 5]. In addition, Aβ levels plateau as disease progresses [6, 7], limiting utility of premortem Aβ detection for longitudinal assessment. Finally, Aβ-directed imaging agents cannot distinguish different forms of frontotemporal lobar degeneration (FTLD; [8]), which do not accumulate Aβ aggregates, from AD or from each other.

Selective radiotracers for tau-bearing neurofibrillary lesions could complement the established Aβ imaging signature in several ways. First, neurofibrillary lesions appear in large numbers at certain sites of predilection [9] decades before the onset of dementia in AD [10–12], potentially providing the means to detect disease at very early stages. When combined with emerging therapies for AD, direct *in situ* premortem diagnosis of tau has the potential to change the standard of care for this deadly disease. Second, unlike Aβ aggregates, tau aggregate load correlates with neurodegeneration [13, 14] and cognitive decline in AD [15–17], proving a potential surrogate marker for disease. Because of the well-established relationship between disease progression and spatial distribution of neurofibrillary pathology [10], tau-based imaging could help monitor the effectiveness of drug treatments over time [18, 19]. Finally, neurofibrillary lesions are found in ∼40% of FTLD cases (FTLD-tau) including Pick disease (PiD) [20], progressive supranuclear palsy (PSP) [21], and corticobasal degeneration (CBD) [22, 23]. These forms of FTLD differ in their spatial distribution of lesions [24]. For example, Pick bodies are most commonly found in the dentate gyrus of the hippocampus, amygdala, and frontal and temporal

---

*Correspondence to: J. Kuret, Ph.D., Professor, 1060 Carmack Rd, Columbus, OH 43210, USA. Tel.: +1 614 688 5899; Fax: +1 614 292 5379. E-mail: kuret.3@osu.edu.

neocortex [20], whereas CBD is characterized by frontal, parietal and striatal involvement. In contrast, PSP pathology is predominantly in the brainstem, cerebellum and basal ganglia, with relatively little cortical involvement [14, 23–25]. Tau-based diagnostic agents may aid the diagnosis of FTLD forms that are difficult to distinguish based solely on clinical presentation.

Despite their potential for premortem diagnosis and staging of dementing illnesses, no tau lesion-selective, radiolabeled imaging agents are in clinical trials. The purpose of this review is to explore design considerations for developing tau-directed radiotracers, and to assess recent progress made toward discovery of such agents since this area was last discussed [26].

PHARMACOKINETIC REQUIREMENTS FOR TAU-DIRECTED RADIOTRACERS

Tau-directed imaging agents must fulfill four principal criteria if they are to take full advantage of their diagnostic potential. First, like other contrast agents, they must rapidly cross the blood brain barrier (BBB) after intravenous injection while simultaneously being subject to rapid elimination, so that specific binding can be detected during the short lifetimes of the major PET radionuclides ^{11}C and [18]F [26–28]. Thus tau-directed radiotracers will likely resemble other imaging agents with respect to plasma protein binding affinity, hydrophobicity, molecular weight, and metabolic stability [27].

Second, for maximal sensitivity, tau imaging agents should be capable of engaging their target within cells undergoing neurofibrillary degeneration. This is because new intracellular lesions form throughout the course of AD [29] in parallel with ongoing cell death, which exposes appreciable amounts of tau aggregates (*i.e.*, "ghost" tangles) to the extracellular environment [30, 31]. The intracellular environment is crowded with macromolecules that slow molecular diffusion [32] and potentially increase binding affinities [33]. Recent findings with [^{11}C]rolipram, a ligand for phosphodiesterase 4 (PDE4), shows the feasibility of imaging intracellular targets [34]. Interestingly, [^{11}C]rolipram binds PDE4 with higher affinity *in vivo* than in tissue homogenates [33]. Although this observation has been attributed to phosphorylation differences, the effects of crowding on association rate constants could also contribute to higher target affinity. These data suggest that imaging of intracellular targets such as tau is feasible and may have the advantage of modestly

increased affinity relative to targets localized to extracellular spaces.

Third, tau-directed radiotracers must bind a target that varies in composition and post-translational modification, both in FTLD and AD [35]. Although encoded by a single gene, human tau is composed of six distinct splice variants that vary with respect to inclusion or exclusion of three alternatively spliced segments. One of these is located in the C-terminal region of tau that mediates self association and composes part of the filamentous core [36]. In addition to phosphorylation and glycosylation, new modifications, such as the acetylation of ε-amino groups of Lys residues, continue to be discovered [37]. Such heterogeneity may contribute to the differential binding affinity reported for certain quinoline-aryl and benzimidazole derivatives, which bind neurofibrillary lesions in AD tissue, but not the Pick bodies, globose tangles or glial pathology found in PiD and PSP [38]. Overall, tau presents a binding target that is more complex and heterogeneous than those associated with Aβ deposits.

Finally, successful radiotracers must bind tau aggregates with sufficient selectivity so that neuritic lesion spatial distribution is not masked or confounded by other lesions that appear in disease. In the case of AD, the major confounding lesions are plaques and other deposits composed of Aβ peptide. By late stage disease, in for example frontal cortex, insoluble Aβ accumulates to ∼3–4 nmol/g wet tissue [39, 40]. In contrast, insoluble tau levels range from only ∼0.2–1 nmol/g wet tissue [41, 42], although higher estimates have been reported [43]. Ideally, tau imaging agents should be able to selectively detect neurofibrillary lesions in the presence of up to ∼20 fold molar excess of insoluble Aβ, although lower levels of selectivity would suffice in brain regions where Aβ/tau ratios are lower (e.g., entorhinal cortex, [29, 44]).

At equilibrium, the ratio of specifically bound to free tracer in tissue is proportional to the binding potential (*BP*), which represents the ratio of receptor binding site density (B_{max} in concentration units) to the equilibrium dissociation constant (K_D, also in concentration units) [45]. B_{max} is directly proportional to the concentration of accessible protein protomers that accumulate in lesions and to the stoichiometry of radiotracer binding (*i.e.*, mol radiotracer/mol protein protomer). The latter has been found to vary among Aβ aggregate ligands, perhaps reflecting differential binding to heterogeneous sites [46]. The overall *BP* is the sum of contributions from Aβ plaques and neurofibrillary tangles [28]:

$$BP = \frac{B_{\max \cdot A\beta}}{K_{D \cdot A\beta}} + \frac{B_{\max \cdot tau}}{K_{D \cdot tau}}$$

Thus, were a contrast agent to bind with similar affinity and mol compound/mol protein protomer stoichiometry to both Aβ and tau aggregates, then the overall *BP* would be dominated by the Aβ term owing to the higher concentration of Aβ (and hence higher $B_{\max}$) relative to tau protomers in brain. Consistent with this prediction, Pittsburgh Compound B, which binds both Aβ and tau aggregates, yielded a stronger signal for the former over the latter when applied to AD brain sections [47]. The forgoing suggests that radiotracers capable of selectively binding tau aggregates in the presence of excess Aβ binding sites must be developed if the full potential of neurofibrillary lesion detection is to be realized, and that selectivity may be achieved through increases in relative binding affinity or $B_{\max}$.

PROGRESS TOWARD TAU IMAGING AGENTS

The first tau aggregate binding agents were identified on the basis of direct fluorescence in tissue, and include Thioflavin T (ThT) and its neutral benzothiazole derivatives [48], FDDNP [49], BF-168 [50], and X-34 [51, 52]. Binding to AD lesions was nonspecific under these conditions, and only FDDNP and neutral ThT derivatives such as PIB went on to be extensively characterized at radiotracer concentrations. [^{18}F]FDDNP-PET was found to be taken up weakly into AD brain relative to [^{11}C]PIB [53, 54], perhaps owing to its lower binding affinity for protein aggregates [55]. Nonetheless, post mortem neuropathological assessment of AD patients who previously received [^{18}F]FDDNP-PET scans confirmed that the FDDNP signal correlated with AD lesion distribution in certain brain regions [56]. To deconvolute the signal into its plaque and tangle constituents, Shin et al. has proposed that both PIB and FDDNP be employed sequentially in the same subject for visualization of total AD pathology, with the net difference between them used to selectively detect the neurofibrillary component [53, 57]. Successful application of this multitracer strategy depends on the binding characteristics of both PIB and FDDNP. PIB binds both plaques and tangles [47], which may limit the sensitivity of the multitracer approach. Furthermore, the evidence for FDDNP interaction with neurofibrillary

tangles remains indirect and circumstantial since direct binding of [^{3}H]FDDNP to neurofibrillary lesions in tissue sections has not been confirmed at radiotracer concentrations [55]. These data illustrate the need for new tau-directed imaging agents with better selectivity for neurofibrillary lesions.

New composition of matter that binds tau aggregates with high affinity while fostering rapid brain uptake has recently been disclosed in the patent literature. For example, Kemp et al. [58] identified certain benzothiazole, imidazothiazole, and pyrimidazole compounds that displaced primuline (present at 1 μM concentration), a fluorescent probe for cross-β-sheet structure, from binding to both authentic PHFs and to synthetic tau aggregates created in a proprietary transgenic mouse line expressing P301S/G335D tau. Chemical structures for the most potent primuline displacers ($AC_{50} < 0.1$ μM) along with compounds subjected to secondary assays are summarized in Table 1 . In addition to displacing primuline from PHFs, SK2033-30 directly stained tau lesions in sections prepared from transgenic mice. Frozen brain sections also stained with LS-T213, revealing a pattern consistent with tau-positive neurons. Moreover, both SK2033-30 and LS-T213 were able to stain tau filaments within murine 3T3 cells engineered to express full-length and truncated tau. In addition to having promising binding affinity, these compounds are taken up into brain with significant washout after 60 min, as demonstrated with [^{18}F]SKT04-137 in mice (4.0% injected dose/g tissue after 2 min, 1.4% injected dose/g tissue after 60 min). These data show the feasibility of identifying high-affinity ligands for tau filaments that react with the highly modified tau in authentic PHFs while retaining appropriate size and structure for brain penetrability. However, it is not clear what level of binding selectivity for tau lesions is available from these lead compounds.

Other recently disclosed tau binding agents include quinoline-aryl [59], benzoxazole [60], and other derivatives, which have been assessed on the basis of the fluorescence emitted when bound directly to lesions in brain sections (Table 2). Recent disclosures have emphasized the pan-selectivity of these compounds for lesions composed of different protein aggregates, including Aβ, tau, and α-synuclein [60]. But some members of these compound families, such as TSK-523, reportedly deliver up to 20-fold binding affinity selectivity for tau over Aβ aggregates [61]. These data show the feasibility of identifying ligands with at least an order of magnitude selectivity for tau over Aβ while maintaining brain permeability. Although high binding

Table 1
New neurofibrillary labels [58]. Potency (AC_{50}) was estimated in competition format against $1\,\mu M$ primuline

Name	Structure	AC_{50} (nM)
LS-T213		80
SKT03-107		30
SKT06-117		50
SKT05-163		30
SK2033-30		ND
^{18}F-SKT04-137		ND

selectivity was shown at histochemical concentrations ($>10\,\mu M$), it will be important to confirm selectivity at radiotracer concentrations (low nanomolar).
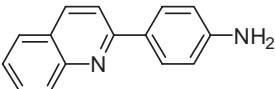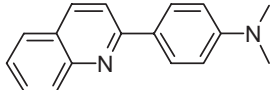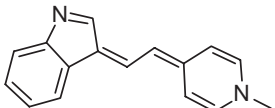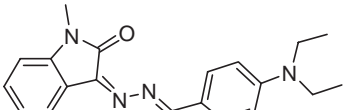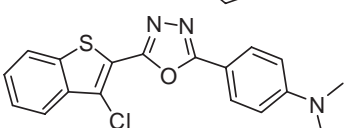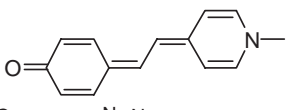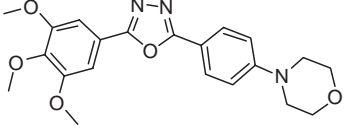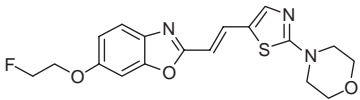
Finally, Rojo et al. [62] tested the ability of benzimidazole derivatives astemizole (a histamine H1 antagonist; Table 3) and lansoprazole (a proton pump inhibitor; Table 3) to directly bind filaments composed of Aβ peptide, heparin-induced recombinant tau protein, and authentic PHF isolated from AD brain *in vitro*. Although ^{3}H-astemizole bound with similar affinity to synthetic filaments composed of Aβ peptide and full-length, human, recombinant tau ($K_D \sim 2\,nM$ for each), B_{max} was >50-fold higher for tau (5.7 ± 0.4 pmol ^{3}H-astemizole/nmol tau) relative to Aβ (0.12 ± 0.002 pmol ^{3}H-astemizole/nmol Aβ). These data suggest that it may be possible to generate binding selectivity for tau relative to Aβ aggregates by leveraging differences in B_{max}.

Overall, tau ligands continue to be discovered using empirical methods, with little definitive information on binding selectivity relative to Aβ plaques at radiotracer concentrations. However, these studies show the feasibility of generating at least part of the selectivity needed for a useful tau-directed radiotracer, and that this selectivity can arise from differences in binding site density or affinity.

NEW LIGAND-BINDING MODELS FOR CROSS-β-SHEET AGGREGATES

Tau, Aβ, and other proteins that fibrillize in disease adopt parallel, in-register cross-β-sheet conformation [63]. On the basis of molecular dynamics simulations and direct binding studies, small molecules can bind sites created along the filament surface [64, 65].

Table 2
Recently disclosed neurofibrillary labels and their binding selectivity as determined on tissue sections by direct fluorescence at histochemical concentrations

Name	Structure	Lesions bound	Ref
BF-170		Tangles/Aβ Fibrils	[38, 59]
N-310		Tangles	[59]
THK-185		Tangles/Aβ plaques	[60]
THK-254		Tangles	[60]
THK-258		Tangles/Aβ plaques	[60]
THK-317		Tangles/Aβ plaques	[60]
THK-386		Tangles	[60]
THK-525		Aβ plaques	[60]

The search for selective protein-aggregate radiotracers would be greatly accelerated if their poses within binding sites were known. Although an atomic resolution structure has not yet been reported for any ligand in its bound state, two exciting new hypothetical models reported in the past year have potentially important implications for rational ligand discovery. Both models focus on ThT (Fig. 1A) , a fluorescent benzothiazole aryl used to detect tau, Aβ, and other amyloid fibrils owing to its Stokes shift upon binding [66]. Experimentally, ThT has been found to bind with its long axis parallel to the filament axis, presumably along filament channels [64, 67], similar to other amyloid-staining dyes [68, 69]. When assayed by circular dichroism spectroscopy, binding of ThT to some [70, 71], but not all [72] filament morphologies produces a Cotton effect, suggesting that its benzothia-

zole and benzaminic ring systems twist relative to each other by ∼35°. These observations set constraints that must be satisfied in structural models of ligand binding.

To create the first model, Rodriguez-Rodriguez et al. [73] solved the crystal structure of ThT, docked it onto a structure of the Aβ$_{42}$ protofilament determined by solid state NMR [74], and then refined its binding pose on mainchain atoms using a quantum mechanical method that was optimized for dispersion forces. The model predicts that ThT interacts directly with the β-sheet backbone of the Aβ protofibril, which is uniquely accessible in the wide channels created along the filament axis by Gly residues. The model, which we have arbitrarily placed into the context of Aβ protofibril residue Gly33 in Fig. 1B, rationalizes many experimental observations made on ligand binding to filamentous aggregates. First, it is consistent with

Table 3
Benzimidazole derivatives characterized on the basis of direct radioligand binding measurements [62]

Name	Structure
Astemizole	
Lansoprazole	

the planar geometry of most filament binding ligands (including those shown in Tables 1 and 2), and predicts that their ring systems interact with flat β-sheet surfaces through van der Waals dispersion forces. These forces, which are directly proportional to distance and contact surface area [75], arise owing to the high polarizability of ligands and of the β-sheet hydrogen-bonding network oriented parallel to the long axis of each filament. The hydrogen bonding network is inherent in cross-β-sheet structure and independent of

protomer packing geometry [63, 76, 77]. In fact, the forces generated by this network may help orient bound ligand so that its long axis is parallel with the filament axis. Second, the prediction that ThT binds to pleats formed by consecutive sheet α-carbon atoms (yielding a twisted ThT conformation with ∼40° dihedral angle; Fig. 1B) is consistent with the experimentally observed Cotton effect. It also rationalizes high ThT fluorescence yield in the bound state, which arises owing to restriction of torsional freedom [78, 79]. Third, the requirement for Gly as part of the filament core suggests that binding affinity depends on solvent accessibility to specific residues, which can vary with filament composition and morphology. For example, both Gly33 and Gly38 are fully exposed in the protofibrillar form of Aβ (Fig. 2A) [74, 80], but can have variable accessbility depending on how the protofibrils pack within mature filaments (Fig. 2B-D). Indeed, access to Gly33 and Gly38 is completely blocked in the model of Aβ$_{40}$ striated ribbons (characterized by two-fold symmetry [80]; Fig. 2B), only partially exposed at the ends of Aβ$_{40}$ filaments having twisted morphology (characterized by three-fold symmetry [81]; Fig. 2C), and completely exposed on only one face of the stacked protofilaments observed in mature Aβ$_{42}$ filaments [74] (Fig. 2D). Authentic AD-derived Aβ filaments adopt at least two additional morphologies,
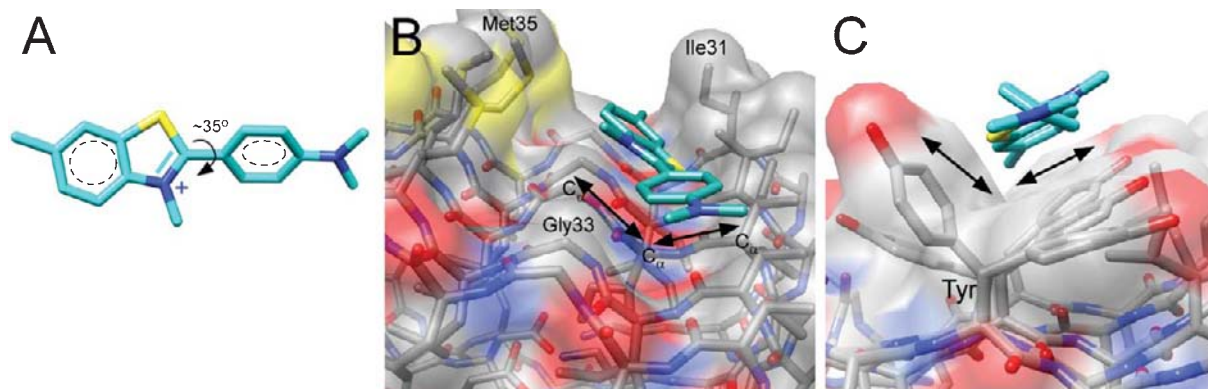
Fig. 1. Hypothetical ThT binding sites on cross-β-sheet binding targets, created using UCSF Chimera Alpha Version 1.5 (build 31329) software. (**A**) Model of ThT in which carbon, nitrogen, and sulfur atoms are colored cyan, blue, and yellow, respectively. The benzothiazole and benzaminic ring systems are depicted as being ∼35° out of plane with respect to each other. (**B**) Proposed binding mode of ThT, where protein backbone atoms are colored by heteroatom and overlaid with a transparent molecular surface area. To create this model, the quantum-refined binding pose B1 of Rodriguez-Rodriguez [73] was placed in the context of a channel on the Aβ protofilament [80] formed by Gly33 and flanked by the side chains of Ile31 and Met35. The proposed interaction is stabilized by strong dispersion effects between the ThT aromatic ring systems and the hydrogen-bonding network of backbone peptide bonds. The flat surfaces formed by the β-sheet pleats (*black arrows*) bind ThT such that the benzothiazole and benzaminic ring systems twist ∼40° with respect to each other. (**C**) ThT bound at the surface of the PSAM scaffold (adapted from [87]). This model represents an average ThT conformation obtained through a molecular dynamics simulation. In this binding mode, ThT interacts with protein in a shallow, hydrophobic groove formed by aromatic side chains (Tyr in this case). This binding mode can bind ThT in a twisted conformation (∼52° dihedral) to maximize van der Waals interactions between planar surfaces (*black arrows*).
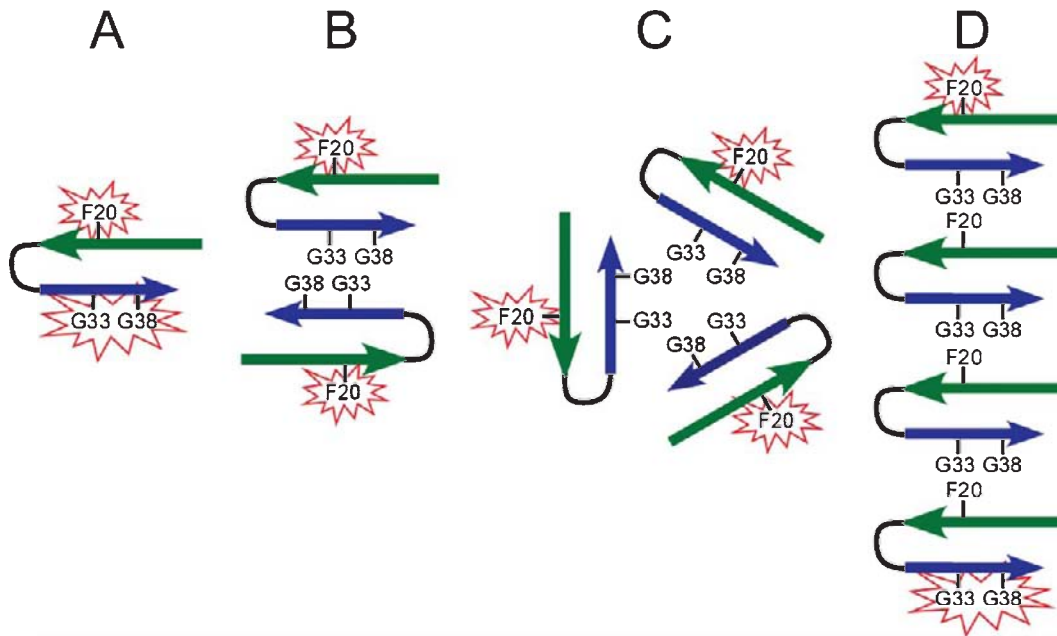
Fig. 2. Schematic representation of Aβ filament quaternary structure. **(A)** In Aβ protofibrils, putative ligand binding sites on β-sheet surfaces (*starbursts*) are exposed to solvent. These include Gly33 and Gly38, each of which creates wide channels for access to mainchain surfaces, and Phe20, which may interact with ligand much like Tyr in PSAM. **(B)** Striated ribbon conformation [80] having two-fold rotation symmetry maintains solvent exposure of residue F20, which can interact with ligands, but occludes Gly33 and Gly38, so that compounds cannot gain access to backbone atoms. **(C)** Twisted conformation [81] having three-fold rotation symmetry maintains solvent exposure of F20, but constrains access to Gly residues. **(D)** Stacked mature fibril [74] composed of four stacked protofibrils exposes both F20 and the Gly residues to solvent, but only at the limiting faces. These models illustrate how ligand accessibility to different binding sites can vary with aggregate quaternary structure.

both of which are distinct from synthetic striated and twisted packings [82], suggesting that additional binding site heterogeneity exists *in vivo*. These data point to a potential mechanism underlying the variable binding stoichiometries reported with certain small molecule ligands [46, 83], and also the failure of certain agents that bind synthetic filaments *in vitro* to bind authentic lesions *in situ* [84]. Finally, the model rationalizes the structure-activity relationship (SAR) for benzothiazole aryls (including PIB), which identified substituents at the para position as being favorable for high affinity binding, with meta and ortho substituents being unfavorable [85, 86]. The model predicts that these latter substitutents clash with the side chains of residues that line the channel wall (Fig. 1B). Importantly, this SAR was deduced at radiotracer concentrations. Overall, this model may be useful for identifying potential ligand binding sites on tau and other proteins that form cross-β-sheet structure, and for engineering binding selectivity among them.

In the other model, Wu et al. [87] propose a distinct binding mode where the ThT molecule interacts primarily with amino acid side chains that line filament channels rather than main chain atoms (Fig. 1C). This model was created *in silico* from ThT and a crystal structure of a synthetic protein scaffold (Peptide Self-Assembly Mimic; PSAM) that forms a single-layer cross-β-sheet. Although PSAM adopts antiparallel rather than parallel cross-β-sheet structure, the model nonetheless has implications for ligand binding to amyloid filaments. First, binding is dominated by the hydrophobic effect and by van der Waals interactions between the ThT ring moieties and the aromatic side chains of the PSAM scaffold, resulting in ThT orienting parallel with the filament axis, again consistent with experimental observation. In the case of PSAM, the aromatic residue is Tyr, but Phe or other aromatic amino acid residues could substitute in other proteins. Interestingly, amyloid fibrils composed of non-aromatic residues, such as Lys-$(Glu)_n$-Lys sequences, exhibit classic ThT fluo-

rescence, however, the quantum yield is an order of magnitude lower than for $A\beta_{40}$ [88]. This would suggest that side-chain-mediated binding permits torsional freedom, allowing the molecule to adjust its conformation with the dynamic motion of the side chains. Second, this binding mode can accommodate ThT binding in twisted conformation ($\sim 52°$ dihedral angle) [87] which is in agreement with the Cotton effect identified by circular dichroism studies performed at high micromolar concentrations of the dye [70, 71]. Finally, side-chain mediated binding is ideal for accomodating the high binding stoichiometry observed for some ligands at histochemical concentrations.

Together, the new binding models suggest that benzothiazole-aryl binding selectivity can be achieved through two distinct binding modes that are strongly influenced by side chain composition, and that rationalize differences in ligand affinity and stoichiometry observed with filaments of differing morphology and protein composition.

CONCLUSIONS

Tau-directed imaging agents hold promise for diagnosing and staging of AD and certain forms of FTLD. Advantages of the approach include very early detection of pathogenesis, differential diagnosis of AD and FTLD, resolution of FTLD subtypes, and the opportunity for longitudinal assessment. Disadvantages include the complexity of the target, which presents up to six tau isoforms in varying states of post-translational modification, and its low concentration relative to $A\beta$ aggregates, which provide a confounding source of off target binding sites. As a result, tau-directed imaging agents must deliver substantial binding selectivity if their diagnostic potential is to be realized. Although binding selectivity is not well understood, recently-developed models of ligand binding have the potential to complement current empirical methods and speed the discovery process.

ACKNOWLEDGEMENTS

REFERENCES

[1] Choi SR, Golding G, Zhuang Z, Zhang W, Lim N, Hefti F, Benedum TE, Kilbourn MR, Skovronsky D, Kung HF (2009) Preclinical properties of 18F-AV-45: a PET agent for Abeta plaques in the brain. *J Nucl Med* **50**, 1887-1894.

[2] Nelissen N, Van Laere K, Thurfjell L, Owenius R, Vandenbulcke M, Koole M, Bormans G, Brooks DJ, Vandenberghe R (2009) Phase 1 study of the Pittsburgh compound B derivative 18F-flutemetamol in healthy volunteers and patients with probable Alzheimer disease. *J Nucl Med* **50**, 1251-1259.

[3] Rowe CC, Ackerman U, Browne W, Mulligan R, Pike KL, O'Keefe G, Tochon-Danguy H, Chan G, Berlangieri SU, Jones G, Dickinson-Rowe KL, Kung HP, Zhang W, Kung MP, Skovronsky D, Dyrks T, Holl G, Krause S, Friebe M, Lehman L, Lindemann S, Dinkelborg LM, Masters CL, Villemagne VL (2008) Imaging of amyloid beta in Alzheimer's disease with 18F-BAY94-9172, a novel PET tracer: proof of mechanism. *Lancet Neurol* **7**, 129-135.

[4] Rowe CC, Ng S, Ackermann U, Gong SJ, Pike K, Savage G, Cowie TF, Dickinson KL, Maruff P, Darby D, Smith C, Woodward M, Merory J, Tochon-Danguy H, O'Keefe G, Klunk WE, Mathis CA, Price JC, Masters CL, Villemagne VL (2007) Imaging β-amyloid burden in aging and dementia. *Neurology* **68**, 1718-1725.

[5] Kemppainen NM, Aalto S, Wilson IA, Nagren K, Helin S, Bruck A, Oikonen V, Kailajarvi M, Scheinin M, Viitanen M, Parkkola R, Rinne JO (2007) PET amyloid ligand [^{11}C]PIB uptake is increased in mild cognitive impairment. *Neurology* **68**, 1603-1606.

[6] Engler H, Forsberg A, Almkvist O, Blomquist G, Larsson E, Savitcheva I, Wall A, Ringheim A, Langstrom B, Nordberg A (2006) Two-year follow-up of amyloid deposition in patients with Alzheimer's disease. *Brain* **129**, 2856-2866.

[7] Jack CR, JJr., Lowe VJ, Weigand SD, Wiste HJ, Senjem ML, Knopman DS, Shiung MM, Gunter JL, Boeve BF, Kemp BJ, Weiner M, Petersen RC (2009) Serial PIB and MRI in normal, mild cognitive impairment and Alzheimer's disease: implications for sequence of pathological events in Alzheimer's disease. *Brain* **132**, 1355-1365.

[8] Rabinovici GD, Miller BL (2010) Frontotemporal lobar degeneration: epidemiology, pathophysiology, diagnosis and management. *CNS Drugs* **24**, 375-398.

[9] Arriagada PV, Marzloff K, Hyman BT (1992) Distribution of Alzheimer-type pathologic changes in nondemented elderly individuals matches the pattern in Alzheimer's disease. *Neurology* **42**, 1681-1688.

[10] Braak H, Braak E (1991) Neuropathological stageing of Alzheimer-related changes. *Acta Neuropathol* **82**, 239-259.

[11] Duyckaerts C, Hauw JJ. (1997) Prevalence, incidence and duration of Braak's stages in the general population: can we know?. *Neurobiol Aging* **18**, 362-369; discussion 389-392.

[12] Morsch R, Simon W, Coleman PD (1999) Neurons may live for decades with neurofibrillary tangles. *J. Neuropathol. Exp. Neurol* **58**, 188-197.

[13] Gomez-Isla T, Price JL, McKeel DW, Jr., Morris JC, Growdon JH, Hyman BT (1996) Profound loss of layer II entorhinal cortex neurons occurs in very mild Alzheimer's disease. *J Neurosci* **16**, 4491-4500.

[14] Josephs KA, Whitwell JL, Dickson DW, Boeve BF, Knopman DS, Petersen RC, Parisi JE, Jack CR, Jr. (2008) Voxel-based morphometry in autopsy proven PSP and CBD. *Neurobiol Aging* **29**, 280-289.

[15] Ghoshal N, Garcia-Sierra F, Wuu J, Leurgans S, Bennett DA, Berry RW, Binder LI (2002) Tau conformational changes correspond to impairments of episodic memory in mild cognitive impairment and Alzheimer's disease. *Exp. Neurol* **177**, 475-493.

[16] Giannakopoulos P, Herrmann FR, Bussiere T, Bouras C, Kovari E, Perl DP, Morrison JH, Gold G, Hof PR (2003) Tangle and neuron numbers, but not amyloid load, predict cognitive status in Alzheimer's disease. *Neurology* **60**, 1495-1500.

[17] Royall DR, Palmer R, Mulroy AR, Polk MJ, Roman GC, David JP, Delacourte A (2002) Pathological determinants of the transition to clinical dementia in Alzheimer's disease. *Exp. Aging Res* **28**, 143-162.

[18] Coley N, Andrieu S, Delrieu J, Voisin T, Vellas B (2009) Biomarkers in Alzheimer's disease: not yet surrogate endpoints. *Ann N Y Acad Sci* **1180**, 119-124.

[19] Small GW, Bookheimer SY, Thompson PM, Cole GM, Huang SC, Kepe V, Barrio JR (2008) Current and future uses of neuroimaging for cognitively impaired patients. *Lancet Neurol* **7**, 161-172.

[20] Dickson DW (2001) Neuropathology of Pick's disease. *Neurology* **56**, S16-S20.

[21] Goedert M (2004) Tau protein and neurodegeneration. *Semin Cell Dev Biol* **15**, 45-49.

[22] Dickson DW, Bergeron C, Chin SS, Duyckaerts C, Horoupian D, Ikeda K, Jellinger K, Lantos PL, Lippa CF, Mirra SS, Tabaton M, Vonsattel JP, Wakabayashi K, Litvan I (2002) Office of Rare Diseases neuropathologic criteria for corticobasal degeneration. *J Neuropathol Exp Neurol* **61**, 935-946.

[23] Dickson DW (1999) Neuropathologic differentiation of progressive supranuclear palsy and corticobasal degeneration. *J Neurol* **246(Suppl. 2)**, II6-I15.

[24] Cairns NJ, Bigio EH, Mackenzie IR, Neumann M, Lee VM, Hatanpaa KJ, White CL, 3rd, Schneider JA, Grinberg LT, Halliday G, Duyckaerts C, Lowe JS, Holm IE, Tolnay M, Okamoto K, Yokoo H, Murayama S, Woulfe J, Munoz DG, Dickson DW, Ince PG, Trojanowski JQ, Mann DM (2007) Neuropathologic diagnostic and nosologic criteria for frontotemporal lobar degeneration: consensus of the Consortium for Frontotemporal Lobar Degeneration. *Acta Neuropathol* **114**, 5-22.

[25] Boxer AL, Geschwind MD, Belfor N, Gorno-Tempini ML, Schauer GF, Miller BL, Weiner MW, Rosen HJ (2006) Patterns of brain atrophy that differentiate corticobasal degeneration syndrome from progressive supranuclear palsy. *Arch Neurol* **63**, 81-86.

[26] Kim S, Jensen JR, Cisek K, Funk KE, Naphade S, Schafer K, Kuret J (2010) Imaging as a strategy for premortem diagnosis and staging of tauopathies. *Curr Alzheimer Res* **7**, 230-234.

[27] Guo Q, Brady M, Gunn RN (2009) A biomathematical modeling approach to central nervous system radioligand discovery and development. *J Nucl Med* **50**, 1715-1723.

[28] Laruelle M, Slifstein M, Huang Y (2003) Relationships between radiotracer properties and image quality in molecular imaging of the brain with positron emission tomography. *Mol Imaging Biol* **5**, 363-375.

[29] Braak H, Braak E (1997) Frequency of stages of Alzheimer-related lesions in different age categories. *Neurobiol Aging* **18**, 351-357.

[30] Bancher C, Brunner C, Lassmann H, Budka H, Jellinger K, Wiche G, Seitelberger F, Grundke-Iqbal I, Iqbal K, Wisniewski HM (1989) Accumulation of abnormally phos-phorylated tau precedes the formation of neurofibrillary tangles in Alzheimer's disease. *Brain Res* **477**, 90-99.

[31] Braak E, Braak H, Mandelkow EM (1994) A sequence of cytoskeleton changes related to the formation of neurofibrillary tangles and neuropil threads. *Acta Neuropathol* **87**, 554-567.

[32] Kao HP, Abney JR, Verkman AS (1993) Determinants of the translational mobility of a small solute in cell cytoplasm. *J Cell Biol* **120**, 175-184.

[33] Zhou HX, Rivas G, Minton AP (2008) Macromolecular crowding and confinement: biochemical, biophysical, and potential physiological consequences. *Annu Rev Biophys* **37**, 375-397.

[34] Itoh T, Abe K, Zoghbi SS, Inoue O, Hong J, Imaizumi M, Pike VW, Innis RB, Fujita M (2009) PET measurement of the in vivo affinity of ^{11}C-(R)-rolipram and the density of its target, phosphodiesterase-4, in the brains of conscious and anesthetized rats. *J Nucl Med* **50**, 749-756.

[35] Sergeant N, Bretteville A, Hamdane M, Caillet-Boudin ML, Grognet P, Bombois S, Blum D, Delacourte A, Pasquier F, Vanmechelen E, Schraen-Maschke S, Buee L (2008) Biochemistry of Tau in Alzheimer's disease and related neurological disorders. *Expert Rev Proteomics* **5**, 207-224.

[36] Novak M, Kabat J, Wischik CM (1993) Molecular characterization of the minimal protease resistant tau unit of the Alzheimer's disease paired helical filament. *EMBO J* **12**, 365-370.

[37] Min SW, Cho SH, Zhou Y, Schroeder S, Haroutunian V, Seeley WW, Huang EJ, Shen Y, Masliah E, Mukherjee C, Meyers D, Cole PA, Ott M, Gan L (2010) Acetylation of tau inhibits its degradation and contributes to tauopathy. *Neuron* **67**, 953-966.

[38] Okamura N, Suemoto T, Furumoto S, Suzuki M, Shimadzu H, Akatsu H, Yamamoto T, Fujiwara H, Nemoto M, Maruyama M, Arai H, Yanai K, Sawada T, Kudo Y (2005) Quinoline and benzimidazole derivatives: candidate probes for in vivo imaging of tau pathology in Alzheimer's disease. *J Neurosci* **25**, 10857-10862.

[39] Li R, Lindholm K, Yang LB, Yue X, Citron M, Yan R, Beach T, Sue L, Sabbagh M, Cai H, Wong P, Price D, Shen Y (2004) Amyloid beta peptide load is correlated with increased beta-secretase activity in sporadic Alzheimer's disease patients. *Proc Natl Acad Sci U S A* **101**, 3632-3637.

[40] Wang J, Dickson DW, Trojanowski JQ, Lee VM (1999) The levels of soluble versus insoluble brain Abeta distinguish Alzheimer's disease from normal and pathologic aging. *Exp Neurol* **158**, 328-337.

[41] Bramblett GT, Trojanowski JQ, Lee VM (1992) Regions with abundant neurofibrillary pathology in human brain exhibit a selective reduction in levels of binding-competent tau and accumulation of abnormal tau-isoforms (A68 proteins). *Lab Invest* **66**, 212-222.

[42] Greenberg SG, Davies P (1990) A preparation of Alzheimer paired helical filaments that displays distinct tau proteins by polyacrylamide gel electrophoresis. *Proc Natl Acad Sci U S A* **87**, 5827-5831.

[43] Khatoon S, Grundke-Iqbal I, Iqbal K (1992) Brain levels of microtubule-associated protein tau are elevated in Alzheimer's disease: a radioimmuno-slot-blot assay for nanograms of the protein. *J Neurochem* **59**, 750-753.

[44] Braak H. Del Tredici K. (2004) Alzheimer's disease: intraneuronal alterations precede insoluble amyloid-beta formation. *Neurobiol Aging* **25**, 713-718. discussion 743-716.

[45] Mintun MA, Raichle ME, Kilbourn MR, Wooten GF, Welch MJ (1984) A quantitative model for the in vivo assessment of drug binding sites with positron emission tomography. *Ann Neurol* **15**, 217-227.

[46] Lockhart A, Ye L, Judd DB, Merritt AT, Lowe PN, Morgenstern JL, Hong G, Gee AD, Brown J (2005) Evidence for the presence of three distinct binding sites for the thioflavin T class of Alzheimer's disease PET imaging agents on β-amyloid peptide fibrils. *J Biol Chem* **280**, 7677-7684.

[47] Lockhart A, Lamb JR, Osredkar T, Sue LI, Joyce JN, Ye L, Libri V, Leppert D, Beach TG (2007) PIB is a non-specific imaging marker of amyloid-beta (Abeta) peptide-related cerebral amyloidosis. *Brain* **130**, 2607-2615.

[48] Klunk WE, Wang Y, Huang GF, Debnath ML, Holt DP, Mathis CA (2001) Uncharged thioflavin-T derivatives bind to amyloid-beta protein with high affinity and readily enter the brain. *Life Sci* **69**, 1471-1484.

[49] Agdeppa ED, Kepe V, Liu J, Flores-Torres S, Satyamurthy N, Petric A, Cole GM, Small GW, Huang SC, Barrio JR (2001) Binding characteristics of radiofluorinated 6-dialkylamino-2-naphthylethylidene derivatives as positron emission tomography imaging probes for beta-amyloid plaques in Alzheimer's disease. *J Neurosci* **21**, RC189.

[50] Okamura N, Suemoto T, Shimadzu H, Suzuki M, Shiomitsu T, Akatsu H, Yamamoto T, Staufenbiel M, Yanai K, Arai H, Sasaki H, Kudo Y, Sawada T (2004) Styrylbenzoxazole derivatives for in vivo imaging of amyloid plaques in the brain. *J Neurosci* **24**, 2535-2541.

[51] Ikonomovic MD, Abrahamson EE, Isanski BA, Debnath ML, Mathis CA, Dekosky ST, Klunk WE (2006) X-34 labeling of abnormal protein aggregates during the progression of Alzheimer's disease. *Methods Enzymol* **412**, 123-144.

[52] Styren SD, Hamilton RL, Styren GC, Klunk WE (2000) X-34, a fluorescent derivative of Congo red: a novel histochemical stain for Alzheimer's disease pathology. *J Histochem Cytochem* **48**, 1223-1232.

[53] Shin J, Lee SY, Kim SH, Kim YB, Cho SJ (2008) Multitracer PET imaging of amyloid plaques and neurofibrillary tangles in Alzheimer's disease. *Neuroimage* **43**, 236-244.

[54] Tolboom N, Yaqub M, van der Flier WM, Boellaard R, Luurtsema G, Windhorst AD, Barkhof F, Scheltens P, Lammertsma AA, van Berckel BN (2009) Detection of Alzheimer pathology in vivo using both ¹¹C-PIB and 18F-FDDNP PET. *J Nucl Med* **50**, 191-197.

[55] Thompson PW, Ye L, Morgenstern JL, Sue L, Beach TG, Judd DJ, Shipley NJ, Libri V, Lockhart A (2009) Interaction of the amyloid imaging tracer FDDNP with hallmark Alzheimer's disease pathologies. *J Neurochem* **109**, 623-630.

[56] Small GW, Kepe V, Ercoli LM, Siddarth P, Bookheimer SY, Miller KJ, Lavretsky H, Burggren AC, Cole GM, Vinters HV, Thompson PM, Huang SC, Satyamurthy N, Phelps ME, Barrio JR (2006) PET of brain amyloid and tau in mild cognitive impairment. *N Engl J Med* **355**, 2652-2663.

[57] Shin J, Lee SY, Kim SJ, Kim SH, Cho SJ, Kim YB (2010) Voxel-based analysis of Alzheimer's disease PET imaging using a triplet of radiotracers: PIB, FDDNP, and FDG. *Neuroimage* **52**, 488-496.

[58] Kemp S, Storey L, Storey J, Rickard J, Harrington C, Wischik C. (2010) Ligands for aggregated tau molecules. *International Patent* 2010/034982

[59] Kudo Y, Susuki M, Suemoto T, Okamura N, Shiomitzu T, Shimazu H. (2006) Quinoline derivative as diagnostic probe for disease with tau protein accumulation. *U.S. Patent* 7,118,730

[60] Kudo Y, Furumoto S, Okamura N. (2010) Benzoxazole derivatives. *U.S. Patent Application* 2010/0021385

[61] Fodero-Tavoletti MT, Okamura N, Furumoto S, Mulligan RS, Connor AR, McLean CA, Cao D, Rigopoulos A, Cartwright GA, O'Keefe G, Gong S, Adlard PA, Barnham KJ, Rowe CC, Masters CL, Kudo Y, Cappai R, Yanai K, Villemagne VL (2011) ¹⁸F-THK523: a novel in vivo tau imaging ligand for Alzheimer's disease. *Brain* **134**, 1089-1100.

[62] Rojo LE, Alzate-Morales J, Saavedra IN, Davies P, Maccioni RB (2010) Selective interaction of lansoprazole and astemizole with tau polymers: potential new clinical use in diagnosis of Alzheimer's disease. *J Alzheimers Dis* **19**, 573-589.

[63] Nelson R, Sawaya MR, Balbirnie M, Madsen AO, Riekel C, Grothe R, Eisenberg D (2005) Structure of the cross-beta spine of amyloid-like fibrils. *Nature* **435**, 773-778.

[64] Wu C, Wang Z, Lei H, Duan Y, Bowers MT, Shea JE (2008) The binding of thioflavin T and its neutral analog BTA-1 to protofibrils of the Alzheimer's disease Abeta(16-22) peptide probed by molecular dynamics simulations. *J Mol Biol* **384**, 718-729.

[65] Wu C, Wang Z, Lei H, Zhang W, Duan Y (2007) Dual binding modes of Congo red to amyloid protofibril surface observed in molecular dynamics simulations. *J Am Chem Soc* **129**, 1225-1232.

[66] Vassar P, Culling C (1959) Fluorescent stains, with special reference to amyloid and connective tissues. *Arch Pathol* **68**, 487-498.

[67] Krebs MR, Bromley EH, Donald AM (2005) The binding of thioflavin-T to amyloid fibrils: localisation and implications. *J Struct Biol* **149**, 30-37.

[68] Cooper JH (1974) Selective Amyloid Staining as a Function of Amyloid Composition and Structure - Histochemical Analysis of Alkaline Congo Red, Standardized Toluidine Blue, and Iodine Methods. *Laboratory Investigation* **31**, 232-238.

[69] Glenner GG, Eanes ED, Bladen HA, Linke RP, Termine JD (1974) Beta-Pleated Sheet Fibrils - Comparison of Native Amyloid with Synthetic Protein Fibrils. *J Histochem Cytochem* **22**, 1141-1158.

[70] Dzwolak W, Pecul M (2005) Chiral bias of amyloid fibrils revealed by the twisted conformation of Thioflavin T: An induced circular dichroism/DFT study. *FEBS Lett* **579**, 6601-6603.

[71] Sabate R, Lascu I, Saupe SJ (2008) On the binding of Thioflavin-T to HET-s amyloid fibrils assembled at pH 2. *J Struct Biol* **162**, 387-396.

[72] Loksztejn A, Dzwolak W (2008) Chiral bifurcation in aggregating insulin: an induced circular dichroism study. *J Mol Biol* **379**, 9-16.

[73] Rodriguez-Rodriguez C, Rimola A, Rodriguez-Santiago L, Ugliengo P, Alvarez-Larena A, Gutierrez-de-Teran H, Sodupe M, Gonzalez-Duarte P (2010) Crystal structure of thioflavin-T and its binding to amyloid fibrils: insights at the molecular level. *Chem Commun* **46**, 1156-1158.

[74] Luhrs T, Ritter C, Adrian M, Riek-Loher D, Bohrmann B, Dobeli H, Schubert D, Riek R (2005) 3D structure of Alzheimer's amyloid-β(1-42) fibrils. *Proc Natl Acad Sci U S A* **102**, 17342-17347.

[75] Parsegian VA (2006) *Van der Waals forces: a handbook for biologists, chemists, engineers, and physicists*, Cambridge University Press, New York.

[76] Eisenberg D, Nelson R, Sawaya MR, Balbirnie M, Madsen A, Riekel C, Sambashivan S, Liu Y, Gingery M, Grothe R (2005) Structural studies of amyloid. *FEBS J* **272**, 78-79.

[77] Nelson R, Eisenberg D (2006) Recent atomic models of amyloid fibril structure. *Curr Opinion Struct Biol* **16**, 260-265.

[78] Friedhoff P, Schneider A, Mandelkow EM, Mandelkow E (1998) Rapid assembly of Alzheimer-like paired helical filaments from microtubule-associated protein tau monitored by fluorescence in solution. *Biochemistry* **37**, 10223-10230.

[79] Singh PK, Kumbhakar M, Pal H, Nath S (2010) Ultrafast Bond Twisting Dynamics in Amyloid Fibril Sensor. *J Phys Chem B* **114**, 2541-2546.

[80] Petkova AT, Yau WM, Tycko R (2006) Experimental constraints on quaternary structure in Alzheimer's beta-amyloid fibrils. *Biochemistry* **45**, 498-512.

[81] Paravastu AK, Leapman RD, Yau WM, Tycko R (2008) Molecular structural basis for polymorphism in Alzheimer's β-amyloid fibrils. *Proc Natl Acad Sci U S A* **105**, 18349-18354.

[82] Paravastu AK, Qahwash I, Leapman RD, Meredith SC, Tycko R (2009) Seeded growth of β-amyloid fibrils from Alzheimer's brain-derived fibrils produces a distinct fibril structure. *Proc Natl Acad Sci U S A* **106**, 7443-7448.

[83] Groenning M (2009) Binding mode of Thioflavin T and other molecular probes in the context of amyloid fibrils-current status. *J Chem Biol* **3**, 1-18.

[84] Ye L, Velasco A, Fraser G, Beach TG, Sue L, Osredkar T, Libri V, Spillantini MG, Goedert M, Lockhart A (2008) In vitro high affinity α-synuclein binding sites for the amyloid imaging agent PIB are not matched by binding to Lewy bodies in postmortem human brain. *J. Neurochem* **105**, 1428-1437.

[85] Kim MK, Choo IH, Lee HS, Woo JI, Chong Y (2007) 3D-QSAR of PET agents for imaging beta-amyloid in Alzheimer's disease. *B Kor Chem Soc* **28**, 1231-1234.

[86] Leuma Yona R, Mazeres S, Faller P, Gras E (2008) Thioflavin derivatives as markers for amyloid-beta fibrils: Insights into structural features important for high-affinity binding. *ChemMedChem* **3**, 63-66.

[87] Wu C, Biancalana M, Koide S, Shea JE (2009) Binding Modes of Thioflavin-T to the Single-Layer beta-Sheet of the Peptide Self-Assembly Mimics. *J Mol Biol* **394**, 627-633.

[88] Chen SM, Berthelier V, Hamilton JB, O'Nuallain B, Wetzel R (2002) Amyloid-like features of polyglutamine aggregates and their assembly kinetics. *Biochemistry* **41**, 7391-7399.

This page intentionally left blank

Section 4
Current Advances in Functional Magnetic Resonance Imaging for Detecting Alzheimer's Disease

This page intentionally left blank

Introduction

Section 4: Current Advances in Functional Magnetic Resonance Imaging for Detecting Alzheimer's Disease

Maheen M. Adamson*

Department of Veterans Affairs, Sierra-Pacific MIRECC and WRIISC Palo Alto, CA, USA
and Department of Psychiatry and Behavioral Sciences, Stanford University School of Medicine,
Stanford, CA, USA

Abstract. Functional Magnetic Resonance Imaging (fMRI) is widely used to study abnormalities of the medial temporal lobe (MTL) system in not only mild cognitive impairment (MCI) and Alzheimer's disease (AD) but also in Apolipoprotein Epsilon 4 (APOE ε4) carriers. Despite its limitations, new techniques involving fMRI have emerged that provide greater insights into the disruptions of the memory systems associated with AD, MCI and carrying the APOE ε4 genotype. This short review presents findings from recent fMRI studies and prepares the reader for the original research contributions in this chapter.

INTRODUCTION

Recent advances in imaging techniques have placed functional magnetic resonance imaging (fMRI) on the forefront for improving ways by which to identify individuals with very mild symptoms prior to dementia. Efforts are currently underway to revise the diagnostic criteria for Alzheimer's disease (AD) with the goal of diagnosis prior to not only dementia but also mild cognitive impairment (MCI). Such criteria will likely include results of monitoring the changes in functional brain activity particularly in the medial temporal lobe (MTL) as measured by fMRI. The MTL is the seat of episodic memory [1–3], including visuo-spatial memory [4], and the first site affected by AD [5]. Even at the preclinical stage, the hippocampus and the entorhinal and perirhinal cortices show AD-like pathology [6]. Many studies have provided evidence for neuronal changes that occur in the preclinical stage of AD and

fMRI may be a very useful technique to measure these changes in vivo. In the current article, we will review recent fMRI studies in MCI, AD and preclinical AD.

FUNCTIONAL MRI IN AD & MCI

Functional magnetic resonance imaging (fMRI) studies frequently focus on MTL subregions to capture activation patterns that are predictive of subsequent clinically significant decline [7] and predictive of progression from MCI to AD [8]. A number of fMRI studies have identified alteration in task-related blood-oxygen level dependent (BOLD) response in not only medial temporal lobe (MTL) area but also in frontal regions in AD patients compared to controls [9]. The use of a variety of tasks addressing MTL involvement in various memory systems has led to wide-ranging results in AD and MCI groups. For instance, both increased and decreased activations in temporal and frontal regions have been reported previously [10, 11] in mild AD patients. Some evidence also suggests that

---

*Correspondence to: Maheen M. Adamson, E-mail: madamson @stanford.edu.

decreased hippocampus activity during encoding may be associated with increased frontal activity in mild AD patients. The latter is consistent with the idea that due to atrophy-related changes in MTL, other areas are recruited to perform the tasks at hand.

Results from studies in MCI have been very inconsistent possibly due to the varying stages of dementia for the individuals at this stage. Decreased hippocampal activation, similar to AD patients, has been reported in MCI patients compared to controls during encoding [12] and retrieval [13, 14]. In contrast, several studies investigating memory encoding with face, objects and word stimuli, have found increased activation in MCI compared to controls [15–17]. As mentioned earlier, these differences are likely due to the difference in the wide-range of MCI subjects used based on the clinical dementia rating (CDR) in some studies. Other studies may use a more strict range allowing for very mild cases to be included in the study. In addition to level of clinical impairment, the type of fMRI task used and other methodological differences also make a difference in the interpretation of results obtained in each study.

Whether there is increase or decrease in hippocampus activation in MCI and/or AD, fMRI can detect changes in the brain regions responsible for different memory systems that are associated with preclinical symptoms of AD. More recently, studies of resting state (non-task related fMRI) have provided evidence for the "default mode" network, comprising of medial parietal/posterior cingulate cortex, along with medial frontal and lateral parietal regions. This network is active during rest or when individuals are not engaged in a task. During a task, these regions show deactivation [18]. This "default mode" network has been shown to be disrupted in AD by a number of recent studies [19–22]. Recently, Frings et al. [23], suggested that the lack of task-related deactivation in the precuneus, an important node in the "default mode" network, is due to connectivity disruption in MCI and AD patients and may not be atrophy related. Evidence also links regions with amyloid deposition in AD to areas involved in this "default mode" network [24].

FUNCTIONAL MRI IN APOE ε4 CARRIERS

Carriers of Apolipoprotein (APOE) ε4 are at an increased risk of developing late onset Alzheimer's disease (AD) [25–27]. Carrying at least one ε4 allele is a predictor of clinical progression from Mild Cognitive Impairment (MCI) to AD [28–31]. In cognitively normal populations, APOE ε4-related dif-

ferences in neuropsychological task performance have been detected before age 65 [32–35], although differences are typically modest [36]. The medial temporal lobe (MTL) is the seat of episodic memory [1–3], including visuo-spatial memory [4], and the first site affected by AD [5]. However, reports of APOE ε4-related differences in brain structure, particularly in the MTL, are not consistent [37]. This is especially the case in cross-sectional studies, which have alternately revealed smaller and no difference in hippocampal volumes in APOE ε4 carriers compared to non-carriers [32]. While it is possible that the impact of APOE ε4 on hippocampal volume changes over time will turn out to be larger or more consistent than single-time point assessments, more timely methods of assessing early indications of AD pathology are needed. Functional magnetic resonance imaging (fMRI) studies frequently focus on MTL subregions to capture activation patterns that are predictive of subsequent clinically significant decline [7] and predictive of progression from MCI to AD [8]. Studying APOE ε4-related hippocampal and MTL cortical activity differences during an episodic memory task may prove promising for evaluating the risk of AD associated with APOE ε4 genotype in cognitively normal older adults.

Results from recent fMRI studies using episodic memory paradigms, however, have not been consistent in evaluating the APOE ε4 risk for AD in cognitively normal older adults. Several studies followed the approach of measuring brain activity relative to fixation or rest periods. While an increase in MTL Blood Oxygen Level Dependent (BOLD) activity was reported in APOE ε4 carriers using word-pair [7,38] and verbal paired-associate tasks [39], a decrease was reported in APOE ε4 carriers during spatial learning [40] and semantic categorization [41]. No APOE ε4-related differences were reported during another paired-associate task [42]. Recently, Adamson et al. (43) reported that encoding-related activation during a perspective-dependent spatial memory task in the hippocampus was significantly lower in carriers than non-carriers. These results have implications for fMRI studies that investigate the default-mode network (DMN) in middle-aged to older APOE ε4 carriers to help evaluate AD risk in this otherwise cognitively normal population.

The DMN is altered in cognitively normal older APOE ε4 carriers similar to MCI and AD patients [44–48, 22]. Lustig et al. [21] reported that activation in medial parietal and posterior cingulate regions went from activation during a semantic judgment task to deactivation during fixation in young participants, but these regions were consistently activated in older

adults with Alzheimer's disease (AD). Pihlajamaki et al. [48] provides evidence for the disruption of DMN along the continuum from normal aging to APOE ε4 carriers to MCI and then AD. Recently, Fleisher et al. [45] reported no encoding-related activity differences in ε4 carriers compared to non-carriers during a novel face-name pair task. Encoding-associated deactivations in the medial and right lateral parietal cortex were greater in non-carriers, similar to findings in AD studies. Fleisher et al. [45] also did a resting-state DMN analysis which revealed nine regions in the prefrontal, orbital frontal, temporal and parietal lobes that were different between ε4 carriers and non-carriers. Adamson et al. (43) report APOE ε4 related differences (ε4 carriers < non-carriers) in the orbital frontal and temporal lobe areas during encoding when compared to a non-MTL based control task. These areas are included in the default mode network where resting state activity is reported to be different between carriers and non-carriers [45]. In addition, a previous study also reported the pattern of altered task-induced deactivations in APOE ε4 carriers to be similar with the DMN [46].

It is possible that the ε4-related difference in the previous studies is driven by preclinical atrophy in the hippocampus and surrounding areas. The underlying structural atrophy of these regions (hippocampal, surrounding MTL and orbital frontal lobe) may be the reason for the alteration in the DMN of ε4 carriers, MCI and AD as well as the reduction of encoding activity in APOE ε4 carriers compared to non-carriers in the Adamson et al. study [43] Previous studies have shown that although elderly ε4 carriers show some atrophy in the MTL, there is no global brain atrophy [49–51].

In conclusion, fMRI is a promising technique that provides novel insights into the disease-related changes of cognitive systems during the course of AD. Despite its limitations, ranging from symptom severity and differences in task performances, fMRI is a unique tool that can provide answers to a disease which, to this day, can only be definitely diagnosed via autopsy. Combined with other emerging and state-of-the-art techniques, like Diffusion Tensor Imaging (DTI), perfusion MRI and amyloid based imaging, multi-modal imaging is the likely candidate to decipher the puzzle behind the development of early AD.

REFERENCES

[1] Eichenbaum H (2000) A cortical-hippocampal system for declarative memory. *Nat Rev Neurosci* **1**, 41-50.

[2] Schacter DL, Wagner AD (1999) Medial temporal lobe activations in fMRI and PET studies of episodic encoding and retrieval. *Hippocampus* **9**, 7-24.

[3] Squire LR, Stark CE, Clark RE (2004) The medial temporal lobe. *Annu Rev Neurosci* **27**, 279-306.

[4] Burgess N, Maguire EA, O'Keefe J (2002) The human hippocampus and spatial and episodic memory. *Neuron* **35**, 625-641.

[5] Braak H, Braak E (1997) Diagnostic criteria for neuropathologic assessment of Alzheimer's disease. *Neurobiol Aging* **18(4 Suppl)**, S85-S88.

[6] Kordower JH, Chu Y, Stebbins GT, DeKosky ST, Cochran EJ, Bennett D et al. (2001) Loss and atrophy of layer II entorhinal cortex neurons in elderly people with mild cognitive impairment. *Ann Neurol* **49**, 202-213.

[7] Bookheimer SY, Strojwas MH, Cohen MS, Saunders AM, Pericak-Vance MA, Mazziotta JC et al. (2000) Patterns of brain activation in people at risk for Alzheimer's disease. *N Engl J Med* **343**, 450-456.

[8] Machulda MM, Ward HA, Borowski B, Gunter JL, Cha RH, O'Brien PC et al. (2003) Comparison of memory fMRI response among normal, MCI, and Alzheimer's patients. *Neurology* **61**, 500-506.

[9] Dickerson BC, Sperling RA (2008) Functional abnormalities of the medial temporal lobe memory system in mild cognitive impairment and Alzheimer's disease: insights from functional MRI studies. *Neuropsychologia* **46**, 1624-1635.

[10] Rombouts SA, Goekoop R, Stam CJ, Barkhof F, Scheltens P (2005) Delayed rather than decreased BOLD response as a marker for early Alzheimer's disease. *Neuroimage* **26**, 1078-1085.

[11] Sperling RA, Bates JF, Chua EF, Cocchiarella AJ, Rentz DM, Rosen BR et al. (2003) FMRI studies of associative encoding in young and elderly controls and mild Alzheimer's disease. *J Neurol Neurosurg Psychiatry* **74**, 44-50.

[12] Small SA, Perera GM, DeLaPaz R, Mayeux R, Stern Y (1999) Differential regional dysfunction of the hippocampal formation among elderly with memory decline and Alzheimer's disease. *Ann Neurol* **45**, 466-472.

[13] Johnson SC, Schmitz TW, Moritz CH, Meyerand ME, Rowley HA, Alexander AL et al. (2006) Activation of brain regions vulnerable to Alzheimer's disease: the effect of mild cognitive impairment. *Neurobiol Aging* **27**, 1604-1612.

[14] Petrella JR, Krishnan S, Slavin MJ, Tran TT, Murty L, Doraiswamy PM (2006) Mild cognitive impairment: evaluation with 4-T functional MR imaging. *Radiology* **240**, 177-186.

[15] Dickerson BC, Salat DH, Greve DN, Chua EF, Rand-Giovannetti E, Rentz DM et al. (2005) Increased hippocampal activation in mild cognitive impairment compared to normal aging and AD. *Neurology* **65**, 404-411.

[16] Hamalainen A, Pihlajamaki M, Tanila H, Hanninen T, Niskanen E, Tervo S et al. (2007) Increased fMRI responses during encoding in mild cognitive impairment. *Neurobiol Aging* **28**, 1889-1903.

[17] Kircher TT, Weis S, Freymann K, Erb M, Jessen F, Grodd W et al. (2007) Hippocampal activation in patients with mild cognitive impairment is necessary for successful memory encoding. *J Neurol Neurosurg Psychiatry* **78**, 812-818.

[18] Raichle ME, MacLeod AM, Snyder AZ, Powers WJ, Gusnard DA, Shulman GL (2001) A default mode of brain function. *Proc Natl Acad Sci U S A* **98**, 676-682.

[19] Celone KA, Calhoun VD, Dickerson BC, Atri A, Chua EF, Miller SL et al. (2006) Alterations in memory networks in mild cognitive impairment and Alzheimer's disease: an independent component analysis. *J Neurosci* **26**, 10222-10231.

[20] Greicius MD, Srivastava G, Reiss AL, Menon V (2004) Default-mode network activity distinguishes Alzheimer's dis-

ease from healthy aging: evidence from functional MRI. *Proc Natl Acad Sci US A* **101**, 4637-4642.

[21] Lustig C, Snyder AZ, Bhakta M, O'Brien KC, McAvoy M, Raichle ME et al. (2003) Functional deactivations: change with age and dementia of the Alzheimer type. *Proc Natl Acad Sci USA* **100**, 14504-14509.

[22] Rombouts SA, Barkhof F, Goekoop R, Stam CJ, Scheltens P (2005) Altered resting state networks in mild cognitive impairment and mild Alzheimer's disease: an fMRI study. *Hum Brain Mapp* **26**, 231-239.

[23] Frings L, Dressel K, Abel S, Saur D, Kummerer D, Mader I et al. (2010) Reduced precuneus deactivation during object naming in patients with mild cognitive impairment, Alzheimer's disease, and frontotemporal lobar degeneration. *Dement Geriatr Cogn Disord* **30**, 334-343.

[24] Buckner RL, Snyder AZ, Shannon BJ, LaRossa G, Sachs R, Fotenos AF et al. (2005) Molecular, structural, and functional characterization of Alzheimer's disease: evidence for a relationship between default activity, amyloid, and memory. *J Neurosci* **25**, 7709-7717.

[25] Corder EH, Saunders AM, Strittmatter WJ, Schmechel DE, Gaskell PC, Small GW et al. (1993) Gene dose of apolipoprotein E type 4 allele and the risk of Alzheimer's disease in late onset families. *Science* **261**, 921-923.

[26] Saunders AM, Schmader K, Breitner JC, Benson MD, Brown WT, Goldfarb L et al. (1993) Apolipoprotein E epsilon 4 allele distributions in late-onset Alzheimer's disease and in other amyloid-forming diseases. *Lancet* **342**, 710-711.

[27] Tanzi RE, Bertram L (2001) New frontiers in Alzheimer's disease genetics. *Neuron* **32**, 181-184.

[28] de Leon MJ, Mosconi L, Blennow K, DeSanti S, Zinkowski R, Mehta PD et al (2007) Imaging and CSF studies in the preclinical diagnosis of Alzheimer's disease. *Ann N YAcad Sci* **1097**, 114-145.

[29] DeCarli C, Miller BL, Swan GE, Reed T, Wolf PA, Carmelli D (2001) Cerebrovascular and brain morphologic correlates of mild cognitive impairment in the National Heart, Lung, and Blood Institute Twin Study. *Arch Neurol* **58**, 643-647.

[30] Landau SM, Harvey D, Madison CM, Koeppe RA, Reiman EM, Foster NL et al. (in press) Associations between cognitive, functional, and FDG-PET measures of decline in AD and MCI. *Neurobiol Aging*. doi:10.1016/j.neurobiolaging.2009.07.002

[31] Petersen RC, Smith GE, Ivnik RJ, Tangalos EG, Schaid DJ, Thibodeau SN et al. (1995) Apolipoprotein E status as a predictor of the development of Alzheimer's disease in memory-impaired individuals. *JAMA* **273**, 1274-1278.

[32] Adamson MM, Landy KM, Duong S, Fox-Bosetti S, Ashford JW, Murphy GM et al. (2010) Apolipoprotein E epsilon4 influences on episodic recall and brain structures in aging pilots. *Neurobiol Aging* **31**, 1059-1063.

[33] Blair CK, Folsom AR, Knopman DS, Bray MS, Mosley TH, Boerwinkle E (2005) APOE genotype and cognitive decline in a middle-aged cohort. *Neurology*, **64**, 268-276.

[34] Caselli RJ, Dueck AC, Osborne D, Sabbagh MN, Connor DJ, Ahern GL et al. (2009) Longitudinal modeling of age-related memory decline and the APOE epsilon4 effect. *N Engl J Med* **361**, 255-263.

[35] Kozauer NA, Mielke MM, Chan GK, Rebok GW, Lyketsos CG (2008) Apolipoprotein E genotype and lifetime cognitive decline. *Int Psychogeriatr* **20**, 109-123.

[36] Small BJ, Rosnick CB, Fratiglioni L, Backman L (2004) Apolipoprotein E and cognitive performance: a meta-analysis. *Psychol Aging* **19**, 592-600.

[37] Trachtenberg AJ, Filippini N, Mackay CE (in press) The effects of APOE-epsilon4 on the BOLD response. *Neurobiol Aging*. doi:10.1016/j.neurobiolaging.2010.03.009

[38] Fleisher A, Grundman M, Jack CR Jr, Petersen RC, Taylor C, Kim HT et al. (2005) Sex, apolipoprotein E epsilon 4 status, and hippocampal volume in mild cognitive impairment. *Arch Neurol* **62**, 953-957.

[39] Han SD, Houston WS, Jak AJ, Eyler LT, Nagel BJ, Fleisher AS et al. (2007) Verbal paired-associate learning by APOE genotype in non-demented older adults: fMRI evidence of a right hemispheric compensatory response. *Neurobiol Aging* **28**, 238-247.

[40] Borghesani PR, Johnson LC, Shelton AL, Peskind ER, Aylward EH, Schellenberg GD et al. (2008) Altered medial temporal lobe responses during visuospatial encoding in healthy APOE*4 carriers. *Neurobiol Aging* **29**, 981-991.

[41] Lind J, Larsson A, Persson J, Ingvar M, Nilsson LG, Backman L et al. (2006) Reduced hippocampal volume in non-demented carriers of the apolipoprotein E epsilon4: relation to chronological age and recognition memory. *Neurosci Lett* **396**, 23-27.

[42] Bassett SS, Yousem DM, Cristinzio C, Kusevic I, Yassa MA, Caffo BS et al. (2006) Familial risk for Alzheimer's disease alters fMRI activation patterns. *Brain* **129**, 1229-1239.

[43] Adamson MM, Hutchinson JB, Shelton A, Wagner AD, Taylor JL (in press) Reduced hippocampal activity during encoding in cognitively normal adults carrying the APOE ε4 allele. *Neuropsychologia*. doi:10.1016/j.neuropsychologia. 2011.04.022

[44] Filippini N, MacIntosh BJ, Hough MG, Goodwin GM, Frisoni GB, Smith SM et al. (2009) Distinct patterns of brain activity in young carriers of the APOE-epsilon4 allele. *Proc Natl Acad Sci U S A* **106**, 7209-7214.

[45] Fleisher AS, Sherzai A, Taylor C, Langbaum JB, Chen K, Buxton RB (2009) Resting-state BOLD networks versus task-associated functional MRI for distinguishing Alzheimer's disease risk groups. *Neuroimage* **47**, 1678-1690.

[46] Persson J, Lind J, Larsson A, Ingvar M, Sleegers K, Van Broeckhoven C et al. (2008) Altered deactivation in individuals with genetic risk for Alzheimer's disease. *Neuropsychologia* **46**, 1679-1687.

[47] Pihlajamaki M, O'Keefe K, Bertram L, Tanzi RE, Dickerson BC, Blacker D et al. (2010) Evidence of altered posteromedial cortical FMRI activity in subjects at risk for Alzheimer disease. *Alzheimer DisAssoc Disord* **24**, 28-36.

[48] Pihlajamaki M, Sperling RA (2009) Functional MRI assessment of task-induced deactivation of the default mode network in Alzheimer's disease and at-risk older individuals. *Behav Neurol* **21**, 77-91.

[49] den Heijer T, Oudkerk M, Launer LJ, van Duijn CM, Hofman A, Breteler MM (2002) Hippocampal, amygdalar, and global brain atrophy in different apolipoprotein E genotypes. *Neurology* **59**, 746-748.

[50] Geroldi C, Pihlajamaki M, Laakso MP, DeCarli C, Beltramello A, Bianchetti A et al. (1999) APOE- epsilon4 is associated with less frontal and more medial temporal lobe atrophy in AD. *Neurology* **53**, 1825-1832.

[51] Soininen H, Partanen K, Pitkanen A, Hallikainen M, Hanninen T, Helisalmi S et al. (1995) Decreased hippocampal volume asymmetry on MRIs in nondemented elderly subjects carrying the apolipoprotein E epsilon 4 allele. *Neurology* **45**, 391-392.

Combining MRI Modalities to Study Visual and Default-Mode Networks in a-MCI

Roser Sala-Llonch[a], Beatriz Bosch[b], Eider M. Arenaza-Urquijo[a], Lorena Rami[b], Núria Bargalló[c,d], Carme Junqué[a,d], José-Luis Molinuevo[b,c] and David Bartrés-Faz[a,d,*]

[a]*Department of Psychiatry and Clinical Psychobiology, Faculty of Medicine, University of Barcelona, Barcelona, Spain*
[b]*Alzheimer's Disease and Other Cognitive Disorders Unit, Neurology Service, Hospital Clínic de Barcelona, Barcelona, Spain*
[c]*Radiology Service, Hospital Clínic de Barcelona, Barcelona, Spain*
[d]*Institut d'Investigacions Biomèdiques August Pi i Sunyer (IDIBAPS), Barcelona, Spain*

Abstract. Patients with pure amnestic MCI (a-MCI) are reported to have cognitively preserved visual processing skills. However, functional and anatomical abnormalities and/or reorganizations might be already detectable in the brain networks that underlie these cognitive functions. To investigate this possibility, we conducted an integrated multi-modal MRI study using task-fMRI, high resolution structural MRI and Diffusion Tensor Imaging (DTI) in 15 a-MCI patients and 15 matched Healthy Elders (HE). Using fMRI data, we identified an Activation Task Related Pattern (ATRP), including areas related to complex visual processing, and a Deactivation Task Related Pattern (DTRP), or default-mode network (DMN). These two networks were further characterized regarding their structural properties (gray matter volumes and white matter pathways). Within the ATRP, we found increased fMRI responses for the a-MCI group in the frontal lobe, and greater involvement of ventral visual areas. However, there were no differences in ATRP-related white matter or gray matter measures. Regarding the DTRP, a-MCI showed spatial functional reorganizations in coincidence with those reported in DMN studies. Moreover, structural abnormalities in a-MCI patients were clearly found in the DTRP (reduced GM volumes and less fiber tract integrity). In summary, the work presented here highlights the importance of conducting integrated multi-modal MRI studies in early stages of dementia based on spared cognitive domains in order to identify incipient functional abnormalities in critical areas of the DMN and their precise anatomical substrates, possibly reflecting early neuroimaging biomarkers in dementia.

Keywords: Mild cognitive impairment, Alzheimer's disease, functional magnetic resonance, visual processing, structural magnetic resonance, diffusion MRI, tractography, default-mode network, compensation

INTRODUCTION

Mild cognitive impairment (MCI) defines a transitional state between normal ageing and dementia, being considered a prodromal stage of Alzheimer's disease (AD) [1], especially when presented in its amnestic subtype [2, 3]. MCI thus represents an ideal model for broadening our understanding of the early pathophysiology occurring in incipient AD. Recently, both structural and functional neuroimaging techniques have been extensively applied in order to characterize MCI cross-sectionally [4], and have identified a set of imaging biomarkers that have predictive value regarding future conversion or clinical stability in these patients [5, 6].

---
*Correspondence to: David Bartrés-Faz, Faculty of Medicine, Department of Psychiatry and Clinical Psychobiology, University of Barcelona, Casanova 143, 08036 Barcelona, Spain. E-mail: dbartres@ub.edu.

Functional magnetic resonance imaging (fMRI) measures the hemodynamic response or blood flow changes related to neural activity in the human brain. It is a well suited technique to investigate neural responses due to a specific action or external stimulus. Moreover, novel imaging analysis techniques allow the identification of brain systems or functional networks formed by spatially remote areas showing temporally correlated activity, a term commonly defined as functional connectivity. Furthermore, fMRI may be a particular sensitive technique to investigate whether early functional brain reorganizations can be detected prior to overt neuropsychological or structural brain abnormalities [7], and thus reveal subtle cerebral functional adaptations in preclinical dementia. In MCI patients, several fMRI studies have used learning and/or memory paradigms, a cognitive area which by definition is affected in MCI [8–14]. As regards other cognitive domains, a few independent fMRI reports have revealed abnormal patterns of brain activity in attentional and executive domains [15, 16] or in language processing [17]. In a recent study [18] the authors performed a combined study of language, memory, attention and empathy abilities in a cohort of a-MCI patients. Finally, a promising line of research has focused on the investigation of complex visual processing in MCI patients, given the well-characterized anatomy of the dorsal and ventral visual pathways and the fact that visuospatial and visuoperceptive functions are compromised in early AD. These investigations revealed preclinical functional reorganizations in high order visual areas supporting both visuospatial [19, 20] and visuoperceptive [20–23] processing among MCI and early AD. Furthermore, the fMRI-based study of complex visual functions in these patients provides clinically relevant evidence, as it has been demonstrated that patients who will convert to AD present increased brain responses with increasing task demands in areas related to visuospatial processing, probably reflecting reduced neuronal efficiency due to accumulating AD pathology [19].

In dementia, the optimal use of cerebral networks in terms of cognitive capability strongly depends on the integrity and precise spatio-temporal tuning of their functional and structural components [24]. In this regard, fMRI can be combined with structural brain information, including high-resolution 3D MRI which can be used to evaluate gray matter (GM) densities, and diffusion tensor MRI (DTI), a method that measures the microstructural characteristics of water diffusion, allowing the characterization of white matter (WM)

fiber tracts. However, in the study of complex visual functions in MCI, only Teipel and colleagues [22] have investigated system-specific associations between the functional connectivity of neural systems and their underlying morphological features. In their report, the authors observed more positive associations for MCI patients than for controls between GM volumes in regions of the ventral visual system and fusiform gyrus activity during a face-matching task, as well as negative correlations between this region and anatomical areas outside the ventral visual pathway. That study supported the notion that the functional segregation within the visual system is based on the distribution of cortical GM volumes in MCI patients. However, the investigation restricted the analysis of brain activity to a particular area based on an a priori hypothesis and did not consider structural connectivity as a further measure in the model.

The aim of the present study was to provide the first comprehensive characterization of a functional and structural cerebral network underlying complex visual processing in a-MCI patients. Our main objective was to determine whether network-related alterations in MCI appear even before clinical impairment in this cognitive domain can be detected. To conduct this study, we used three MRI modalities (fMRI, T1-structural, and Diffusion MRI) to perform an integrated analysis including functional BOLD analysis, GM volumetry and probabilistic tractography. Regarding the fMRI analysis, we will refer to functional connectivity as correlated BOLD activity during task-performance between separated brain areas. First, the study of task-activated regions allows the characterization of these visual processing related networks. Furthermore, the study of task-deactivations allows to investigate the brain's default-mode network (DMN, [25–28]), defined as a set of brain regions showing high levels of functional connectivity with core areas in the anterior/frontal and posterior midline structures as well as in the parietal regions. The DMN is significantly more activated during rest or passive sensory tasks than in cognitively demanding or goal-directed tasks and is known to be compromised in neurodegenerative disorders, including Alzheimer's Disease (AD), particularly in the posterior cingulate cortex (PCC), an area primarily affected by AD-associated alterations such as hypometabolism or elevated atrophy rate [28]. More recent studies of deactivations in the context of memory tasks [29] or resting state fMRI conditions [30, 31] have also noted dysfunction in this system in MCI, but the relationship between functional alterations and

their precise underlying structural brain correlates is still largely unknown in this condition.

Briefly, the main steps of the data analyses presented in this paper are as follows. First, we used Independent Component Analysis (ICA), and model-based fMRI analysis (FEAT) to explore the functional networks involved in the task and to find functional differences between groups. Importantly, regions showing both task-related activations and deactivations were identified, defining two different networks. Then, the spatial maps of the previous functional networks were thresholded and several ROIs defining isolated but functionally connected regions were extracted from them. Subsequently, these ROIs were used to evaluate structural characteristics of the networks such as gray matter volumes and network-related white matter pathways between pairs of ROI. We investigated differences in these measures as well as relationships between structure and functionality.

METHODS

Subjects

Thirty right-handed subjects aged over 65 were prospectively recruited from the Alzheimer's disease and other cognitive disorders unit at the Neurology Service of the Hospital Clinic in Barcelona. The sample comprised 15 healthy elders (HE) and 15 MCI patients. Patients with a clinical diagnosis of AD were not included because the study focused on identifying a brain network related to a preserved cognitive domain, which would have been more difficult to attain with demented patients. MCI patients were prospectively selected only if they presented the amnestic form of the disorder (a-MCI; single memory domain affected), defined by the fact that their remaining cognitive functions and activities of daily living were within the normal range. We used the Pfeffer Functional Activities Questionnaire (FAQ) [32] to assess patients' functional activities. The FAQ comprises 10 items, which evaluate a variety of Activities of Daily Living (ADL) and complex cognitive/social functions. We considered that ADL were impaired if the FAQ score was ≥ 3. All subjects scored <3 in the FAQ. Healthy individuals did not meet criteria for dementia and presented no cognitive complaints or scores below -1.5 SD on any neuropsychological test. Patients with a-MCI reported complaints of memory function and scores below -1.5 SD on an episodic memory test (long term retrieval test from the FCRST: Free and cued

selective reminding test). A comprehensive neuropsychological battery was administered to all subjects, including assessments of memory, frontal lobe 'executive' functions, language, gnosis and praxis tests [16]. Visuoperceptive-visuospatial functions were assessed by means of the Incomplete Letters and the Number location tests of the Visual Object and Space Perception Battery (VOSP, [33]). Additionally, the Perception Digital Test (PDT) was also administered to evaluate high order visual functions [34]. We verified that all a-MCI patients performed within normal limits in this test, which was adapted for use within the fMRI context (see below).

MRI acquisition

Subjects were examined on a 3T MRI scanner (Magnetom Trio Tim, Siemens Medical Systems, Germany). For the functional magnetic resonance image (fMRI) protocol, 225 T2*-weighted volumes were acquired during the task performance ($TR = 2000$ ms, $TE = 29$ ms, 36 slices per volume, slice thickness $= 3$ mm, distance factor $= 25\%$, $FOV = 240$ mm, matrix size $= 128 \times 128$). A high resolution 3D structural dataset (T1-weighted MP-RAGE, $TR = 2300$ ms, $TE = 2.98$ ms, 240 slices, $FOV = 256$ mm; matrix size $= 256 \times 256$; Slice thickness $= 1$ mm) was also acquired, followed by a Diffusion Weighted Imaging (DWI) protocol which consisted of an echoplanar imaging (EPI) sequence (30 directions, $TR = 5600$ ms, $TE = 89$ ms, 44 slices, slice thickness $= 2$ mm, distance factor $= 30$ %, $FOV = 250$ mm, matrix size $= 122 \times 122$). The DWI protocol also provided a T2-weighted volume (B0) which was used to exclude participants with evidence of cerebrovascular disease based on the evaluation of white matter hyperintensities. Specifically, a board-certified neuroradiologist (N.B) rated all images using the Fazekas scale [35]. Because of this, some WM abnormalities were observed in our sample, probably age-related, as all the participants rated 1-2 on this scale. No differences were observed between the two clinical groups [mean (SD) Fazekas scores were 1.13 (0.74) and 1.06 (0.59) for the HE and a-MCI groups respectively; $t = 0.27$, $p = 0.78$].

fMRI task

We used a block design paradigm consisting of three alternating conditions: orientated images, color squares and fixation. During the orientated images condition (active condition, duration: 20 seconds) subjects

were presented with four blurred images within each of the four quadrants of the screen. Three of the images were rotated 90, -90 and 180 degrees respectively, while the remaining one was randomly positioned in the correct orientation. After correct identification of the content of the images (i.e. visually decoding the picture to identify that it represented, for example, a landscape, an object or people) the subject was asked to answer whether the image that was correctly orientated was on the right or on the left side of the screen by pressing a right/left button. During the color squares task (control condition, duration: 20 seconds), four plain colored squares were presented in the same spatial arrangement as the images of the task stimuli, and the subject was asked to indicate whether the red square was on the right or the left side. As instructions were given to the subjects before the scanning session, no written instructions appeared on the screen during the task. The number of right/left responses was equivalent in the active and control conditions. Finally, a fixation block was also presented, consisting of a white cross on a black screen (duration: 10 seconds). The whole paradigm included 9 repetitions of the three conditions, with a total duration of 450 s, during this time, 250 volumes were acquired per subject. (Fig. 1).

MRI processing and analyses

All the procedures carried out in the analysis of the three MR modalities used and their inferences are shown in Fig. 2. The functional brain networks extracted from ICA analysis of fMRI data were used to guide GM volumetric and DTI analyses in order to define the anatomical parts of the network. Neuroimaging tools used in all the steps are part of the FSL software (Hhttp://www.fmrib.ox.ac.uk/fsl/H, [36]).

Functional MRI processing and analysis

First, each fMRI dataset was corrected for motion using MCFLIRT [37]. Then, non-brain voxels were removed using BET [38], spatial smoothing (Gaussian kernel of FWHM 8.0 mm) was applied, and the entire 4D dataset was normalized using the grand-mean intensity. High pass temporal filtering (sigma = 50 s) was applied to restrict for task-related temporal patterns, and 4D sets were finally registered to the MNI152 template using FLIRT [39]. After this preprocessing, fMRI analysis of the task was carried out using Tensorial Independent Component Analysis (TICA) [40] as implemented in MELODIC, part of FSL. MELODIC allows fMRI data to be broken down
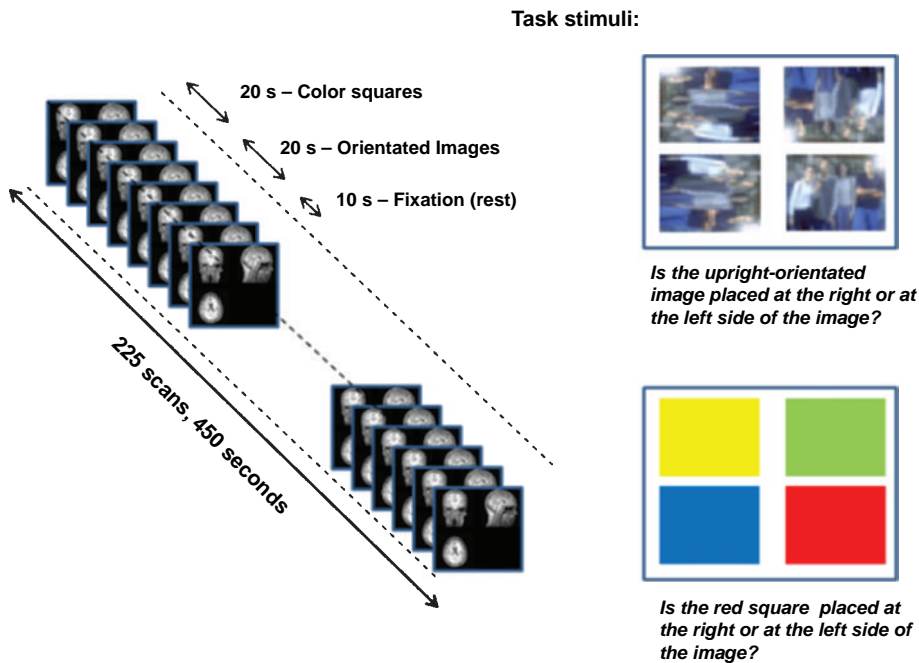
Task stimuli:

Fig. 1. Design of the fMRI task and stimuli used. Instructions were given to the subjects once, before the scanning session. See main text for full description of the task.
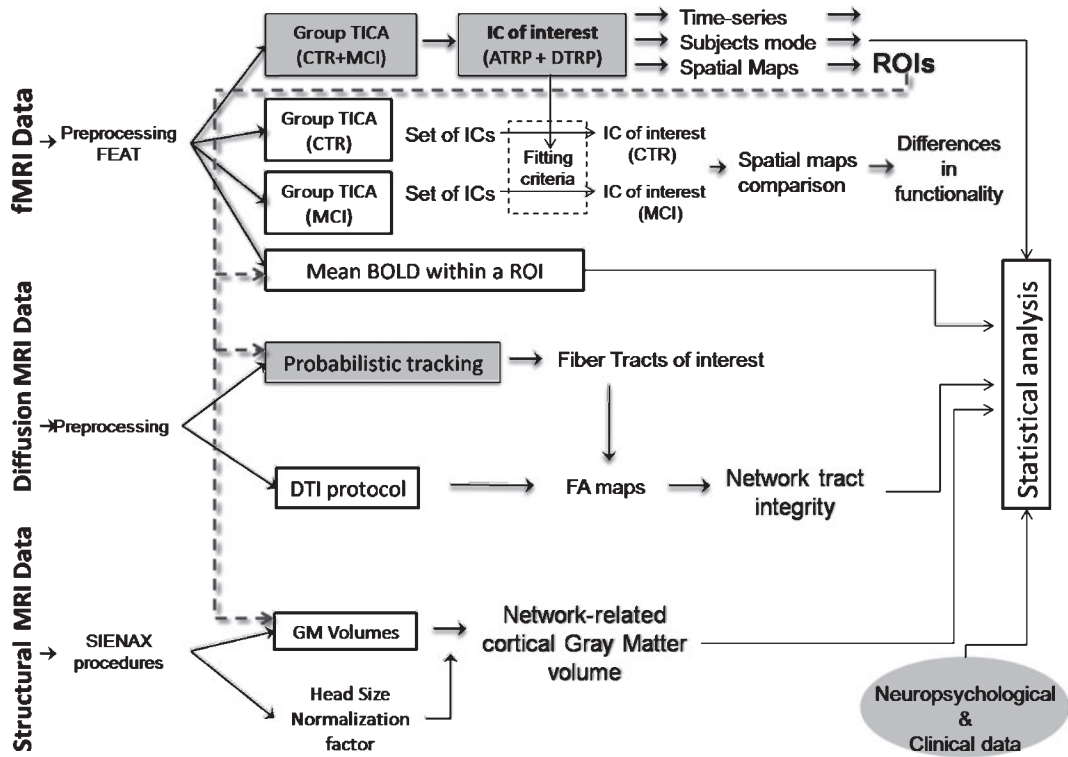
Fig. 2. Multi-modal MRI processing and analysis stream.

into three-dimensional sets of vectors which describe signal variation across the temporal domain (time-courses), the spatial domain (spatial maps), and the subject domain (subject modes). Spatial maps include regions of synchronous activations and deactivations, and subject modes reveal the strength of both these activations and deactivations; higher subject modes values indicate higher activations and higher deactivations of the positive and negative parts of an IC respectively. A simple Pearson correlation was performed on the rank-1 estimated time course and the task time-series model, in order to identify task-related components. Spatial maps of the IC of interest were thresholded using a Gaussian/gamma-mixture model and represented on the MNI standard template.

As shown in Fig. 2, group-TICA decompositions were performed at two levels. The first decomposition included data for all the subjects, with the specific aim of finding a common task-related region, a general lineal model (GLM) matrix was introduced in this analysis in order to determine if the components differed between groups. Then, a second analysis was performed separately for the two groups (HE and MCI)

in order to evaluate subtle differences in the spatial extent of the network.

The main task-related component was selected from the whole-group analysis, using information from both time-series analysis and subject modes. Then, to select the analog component in the separate ICAs, we used the spatial cross correlation value (fslcc in FSL).

The ROI definition process was derived from the thresholded spatial map of the selected component. Large (i.e. more than 50 voxels) isolated clusters in gray matter regions were separated into binary ROIs.

Finally, from the preprocessed fMRI data, a measure of the mean BOLD activity within the defined ROIs was extracted separately for each individual and each condition (i.e., task, control and fixation).

A model-driven analysis was also performed on the fMRI data using FEAT from FSL. FEAT preprocessing included head motion correction [37], brain extraction [38], spatial smoothing using a Gaussian kernel of 6 mm, and high-pass temporal filtering equivalent to 100 s. fMRI volumes were then registered to standard MNI space using FLIRT [39]. Time-series for each of the three conditions and their temporal deriva-

tives were used to model the data. The contrasts of interest were images > color squares, images > fixation and baseline (i.e., fixation > images + color squares). Higher level analysis was performed using FLAME [41] and a general linear model (GLM) matrix that included two groups (HE and a-MCI). We tested for group average and differences between groups. All the Z-statistics images were thresholded at $Z > 2.3$ and corrected for family-wise error with a significance level of $p < 0.05$.

Structural MRI analysis

Structural 3D-MPRAGE images were used to obtain gray matter volumes. Brain tissue volume, normalized for subject head size, was estimated with SIENAX [42]. In the first part of the SIENAX procedure, a volumetric scaling factor was obtained for each subject which referred to the relationship between the subject's head size and the MNI152 standard template. Next, tissue-type segmentation with partial volume estimation was carried out [43]. ROI Gray matter volumes were extracted from the tissue-type segmentation. More specifically, each subject's gray matter volume was masked using the pre-defined binary ROIs (from functional activation maps) and the resulting volumes were calculated. Finally they were normalized using the scaling factor, to account for head-size differences. A Voxel Based Morphometry (VBM) analysis was also performed on the gray matter maps, using tools available in FSL.

Diffusion MRI analysis

Diffusion MRI Images were analyzed using FDT (FMRIB's Diffusion Toolbox), a software tool for analysis of diffusion weighted images included in FSL [44–46]. Firstly, data were corrected for distortions caused by the eddy currents in the gradient coils and for simple head motion, using the B0 non-diffusion data as a reference volume. Then, Fractional Anisotropy (FA) maps from each subject were obtained using a Diffusion Tensor Model fit, and registered to MNI space, as in a recent study [47]. A probabilistic tractography algorithm was also applied to the diffusion images. For this purpose, in the first step, diffusion parameters were estimated using the BEDPOSTX tool from FSL, which computes a Bayesian estimation of the parameters (i.e. diffusion parameters and local fiber directions) using sampling techniques and a model of Crossing Fibers [44]. The density functions obtained were subsequently used to estimate connectivity between pairs of ROIs (seed ROI and end ROI) with the PROBTRACX tool from FSL. The entire probabilistic tracking procedure was carried out in each subject's anatomical space. Using the probabilistic tractography algorithm, we obtained individual maps for each pair of ROIs, where each voxel value indicated the probability of having fibers connecting the two regions. These maps were thresholded (at 2% of their maximum) in order to remove very-low probability fiber paths. Finally, the pathways obtained were visually inspected. Individual FA scores inside each pathway were then used to quantify and compare the integrity of the paths identified (Fig. 2).

Statistical analyses

Functional measurements (mean BOLD signal within each ROI and condition), ROI GM volumes and tract integrity (mean FA along the tracts-of interest) were introduced into SPSS v.16 (Statistical Package for Social Sciences, Chicago, II, USA). Between groups comparison were performed using two-tailed t-tests. Partial correlations were also undertaken to investigate the relationship between functional and structural components of the network and the relationship with cognitive performance within each group. In the partial correlation analysis, age, gender and task performance (when not evaluated) were included as covariates. Results were considered as statistically significant if they attained a p value < 0.05. When the analyses included multiple comparisons, Bonferroni correction was applied.

RESULTS

Table 1 summarizes the main characteristics of the sample groups, including demographic variables and cognitive measures. HE and a-MCI patients were comparable in age, gender distribution, global cognitive performance, language, and visuoperceptive-visuospatial functions. Educational levels were also similar between groups. In general, attentional / frontal lobe functions were also comparable, except for the Symbol Search test assessing speed of processing and working memory. Despite the statistical differences that emerged for this test between groups, none of the patients was clinically impaired in any of the above cognitive domains when analyzed individually. As expected, patients performed worse on both verbal and visual episodic memory tests. Task performance scores (correct responses and response times) inside the scanner were lost for a high number of subjects ($n = 6$) due

Table 1
Sample demographics and cognitive characteristics

	HE	a-MCI	*t*-test	*p* value
Age	75.20 (5.76)	74.33 (6.99)	0.91	0.37
Gender (women/men)	10/5	10/5	–	–
MMSE	27.67 (1.49)	25.50 (2.10)	3.31	<0.001
Education (years)	8.93 (4.6)	8.87 (4.0)	0.04	0.97
Memory functions				
Recall of Constructional Praxis CERAD	8.13 (2.10)	4.73 (2.40)	4.12	<0.0001
Free recall (FCSRT)	25.67 (5.76)	9.73 (5.21)	7.93	<0.0001
Long term retrieval (FCSRT)	8.47 (1.99)	0.60 (1.12)	13.3	<0.0001
Frontal functions				
Digit span (Inverse) (WAIS-III)	5.13 (1.88)	4.40 (1.68)	1.12	0.27
Symbol search (WAIS-III)	24.13 (10.09)	17.33 (5.51)	2.28	0.03
COWAT	24.80 (9.52)	23.53 (8.37)	0.38	0.70
Similarities (WAIS-III)	15.27 (4.57)	13.47 (3.46)	1.21	0.23
Language				
BNT	49.93 (5.39)	48.73 (4.26)	0.67	0.50
BDAE comprehension	14.93 (0.25)	14.87 (0.35)	0.59	0.55
Visuoperceptive / visuospatial functions				
Incomplete Letters VOSP	19.60 (1.92)	19.47 (0.92)	0.24	0.81
Number location VOSP	9.60 (0.63)	8.87 (1.64)	1.61	0.12
PDT score	14.07 (0.96)	13.60 (0.74)	1.49	0.15
Praxis				
Ideomotor praxis	5 (0)	5.40 (1.54)	1.00	0.32
Constructional praxis CERAD	9.47 (1.64)	9.60 (1.63)	2.22	0.82

HE: healthy elders, a-MCI: amnestic Mild Cognitive Impairment. MMSE: Mini-Mental State Examination. CERAD: Consortium to Establish a Registry for Alzheimer's Disease: Clinical and Neuropsychology Assessment. FCRST: Free and cued selective reminding test. VOSP: Visual Object and Space Perception Battery. *PDT* = Perception Digital Test. WAIS-III: Wechsler Adult Intelligence Scale III version. COWAT: Controlled Oral Word Association Test. BNT: Boston Naming Test. BDAE: Boston Diagnostic Aphasia Battery.

to technical problems. Therefore, the score on the clinical test administered to the subjects before the MRI session was used in all cases to measure individual performance.

Functional networks identified

The main task-related component was selected from the group T-ICA decomposition, including all the subjects (HE and a-MCI). Its timecourse fitted the task time series with Pearson's $r = 0.72$ ($p < 0.001$) and its fMRI signal was specific for the task scans ($t = 15.92$, $p < 0.001$ in the blurred images > coloured squares contrast). Other task-related components were found, but they were not considered in this study either because (i) they were not homogeneous throughout the whole sample (with very high subject modes in a few subjects, and very low or negative values in the others) or (ii) they did not form a consistent anatomical network (i.e., isolated regions located in the non-gray matter brain region).

This main task-related pattern comprised an Activation Task-Related Pattern (ATRP, Fig. 3A, red-yellow maps), and a Deactivation Task-Related Pattern (DTRP, Fig. 3A, blue maps). This component did not show differences between the two groups. The ATRP included areas whose activity was synchronously higher in the task scans (i.e., blurred images) and concomitantly lower in the control stimulus (i.e., square colours) or even lower in rest scans (Fig. 3B, red line). Conversely, regions in the DTRP were strongly deactivated during the task scans, with medium levels in the control scans and no deactivation at rest. The ATRP network included anterior and posterior areas of both hemispheres, with the posterior parts of the right hemisphere being the most clearly represented. In posterior regions the ATRP was formed bilaterally by parts of the primary (BA17) and secondary associative visual areas (BA18, BA19), temporoccipital and parietal regions. Ventrally, the posterior segments of the lingual and fusiform cortices (BA 18/19) were involved bilaterally, as was the inferior temporal gyrus (BA37). Dorsally and in the medial aspect of the occipital lobe, the cuneus (BA18/31) was also included in the ATRP network, as well as the superior occipital gyrus (BA19) bilaterally. Close to this latter region
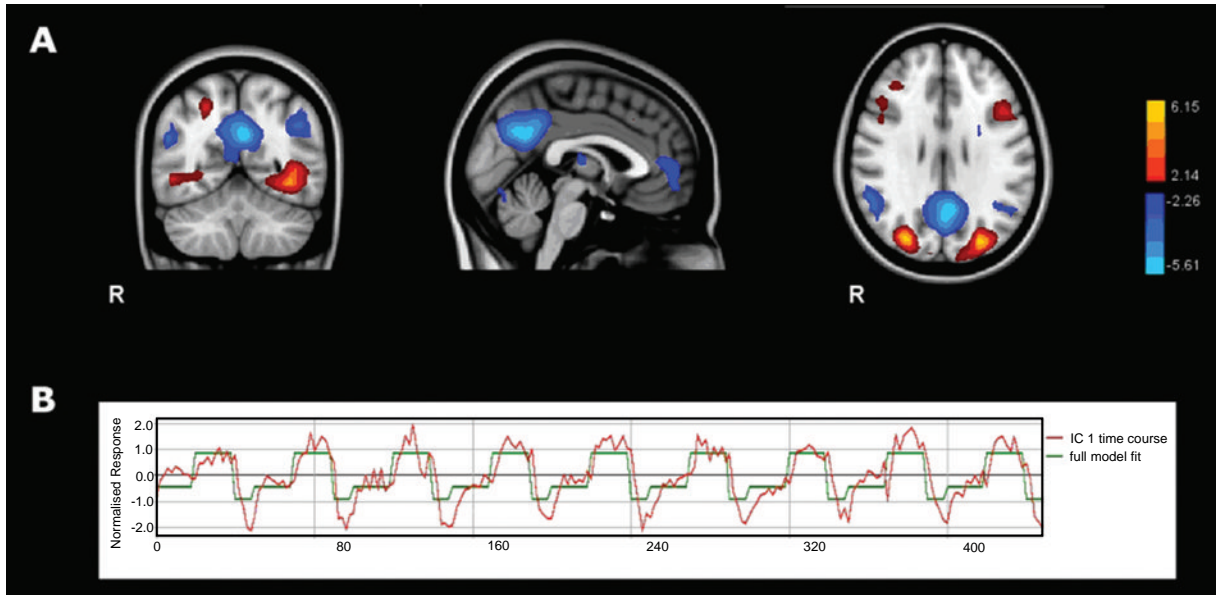
Fig. 3. (A) Spatial maps and (B) time-course of the main task-related component obtained from the whole group (HE and a-MCI subjects) TICA analysis. In (A), regions in red-yellow show the positive part of the component (task-activations) and regions in blue are the negative part (task-deactivations or rest-activations). In (B), red line shows the rank-1 approximation of the IC's temporal activation, and green line shows an idealized reference function of the task.

and in the right hemisphere, parts of the inferior (gyrus angularis BA39) and superior parietal lobe (BA7) were also included. In frontal regions the inferior and middle frontal gyri were involved (BA 44/45, 6 and 9). In the right hemisphere the functional network also included parts of the BA6 corresponding to the precentral gyrus.

The DTRP included medial and lateral cortical regions in close correspondence with those described as the Default Mode Network (DMN, [26, 28]). In medial prefrontal cortex regions, the anterior cingulate was involved (BA24 and BA32). In posterior areas the middle occipital (BA31) and parietal (BA7) precuneus, the posterior cingulate cortex (PCC, BA31, and BA23) and the retrosplenial cingulate cortex (BA29/30) were included. Finally, regions of the inferior parietal lobe (BA39 and BA40 of both hemispheres), and regions of the right superior temporal gyrus (BA41) also formed part of this network (see Figs 3 and 5).

fMRI differences of the main task-related network between HE and a-MCI patients

When HE and MCI groups were analyzed in separate ICAs, we found differences regarding the spatial extension of the main task-related component for both groups (see Methods for the procedures used in the selection of the component). Figure 4 shows the task-related component for each group (Fig. 4A and B) and inferences between them (Fig. 4C). For ease of presentation, activation and deactivation regions from a single IC were split into separate figures. Here we see that the spatial map of the ATRP comprised occipital regions that were more ventrally orientated in the MCI group than in HE. The differential areas were found in the middle occipital gyrus, fusiform and lingual cortices (BA17/18/19), with the occipital fusiform cortex being the region that showed the largest differences between groups, extending to the anterior fusiform (temporal) among MCI. In contrast, among HE, increased activity was found in the cuneal cortex, the middle occipital gyrus (BA19), and the inferior (BA39) and superior parietal lobe (BA7). Finally, in anterior regions we found a large cluster of increased activation among HE in the inferior frontal gyrus (BA6/BA46). However, in nearby areas a-MCI also exhibited a stronger fMRI signal (inferior frontal gyrus and precentral gyrus (BA6/9). Smaller clusters of differences were further observed in the orbital cortex (BA13/BA47) where HE showed increased activations, and in the postcentral and precentral sulcus (BA2/3/4), subgenual cortex (BA25/32) and frontal pole, where the fMRI signal was higher in a-MCI than in HE.

The spatial extension of the DTRP also differed between groups. First, the posteromedial area was
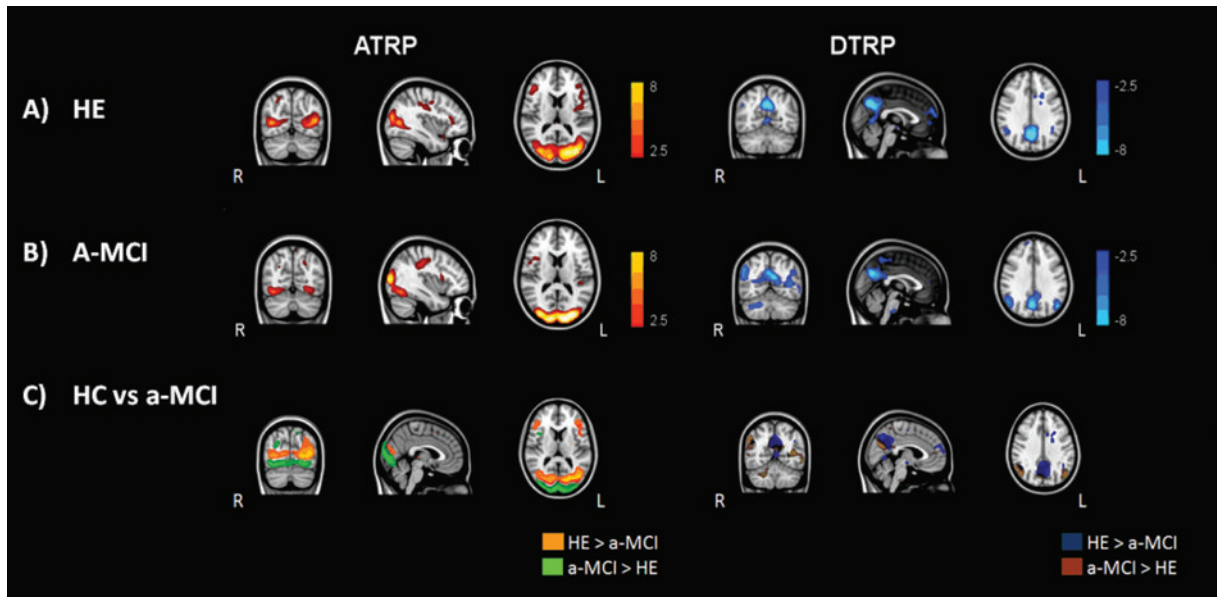
Fig. 4. Spatial Maps for the ATRP and DTRP corresponding to the main task-related component for the HE group (A) and the a-MCI group (B), and inferences (spatial difference) between these maps (C).

larger for the HE group in the precuneus (BA7) and PPC (BA31 and BA 29/30) cortices. Conversely, in a-MCI the extension was bigger in inferior parietal lobes including the angular gyrus (BA39) bilaterally and the supramarginal gyri in the right hemisphere (BA40).

Model-driven analysis of functional data

Results from FEAT analysis gave spatial patterns of brain activated areas during the task that had a high similarity with the ATRP described above (Fig. 5). Group average maps from HE and a-MCI (one sample t-test, $p < 0.05$ corrected) showed greater extend of activations for a-MCI than for HE, especially in the ventral visual pathway and in left frontal areas for both images > color and images > fixation contrasts. This result was further confirmed by the between group statistics: a-MCI showed areas of task-related hyper-activation with respect to the HE group in the superior, middle and Inferior frontal gyrus, the anterior cingulate gyrus (BA32, 6) and the frontal pole (BA9) in the images > fixation contrast. Regarding the baseline condition, despite no group-average maps survived the significance threshold, a-MCI showed a deficit of activation with respect to the HE group in an area placed on the superior frontal gyrus and the anterior cingulate gyrus (BA6, 24).

Gray matter volumes within the identified functional networks

Several ROIs were defined on the basis of the functional results reported (see Methods and Fig. 2 for the methodology used). First, four isolated regions were identified within the ATRP, two in posterior brain areas (posterior right and posterior left) and two in the anterior part (anterior right and anterior left). Furthermore, three ROIs were defined from DTRP areas (henceforth the anterior cingulate ROI, posteromedial ROI and bilateral inferior parietal ROIs). Note that in the case of the DTRP, the two inferior parietal regions (bilaterally) were considered as a single ROI.

Gray matter volumes were measured within each ROI. Group differences are shown in Table 2 and Fig. 8. Gray matter volumes in areas of the DTRP showed statistically significant differences, mainly due to differences in the posteromedial ROI (precuneus/PCC).

Moreover, a standard whole-brain VBM analysis was also performed to compare gray matter from both groups. Results from this analysis are not shown, but they corroborated the previous literature on MCI patients (being the main differences in regions in the temporal lobes, such as the hippocampus and parahippocampus, lingual gyrus and temporal fusiform, $p < 0.01$, FWE corrected).
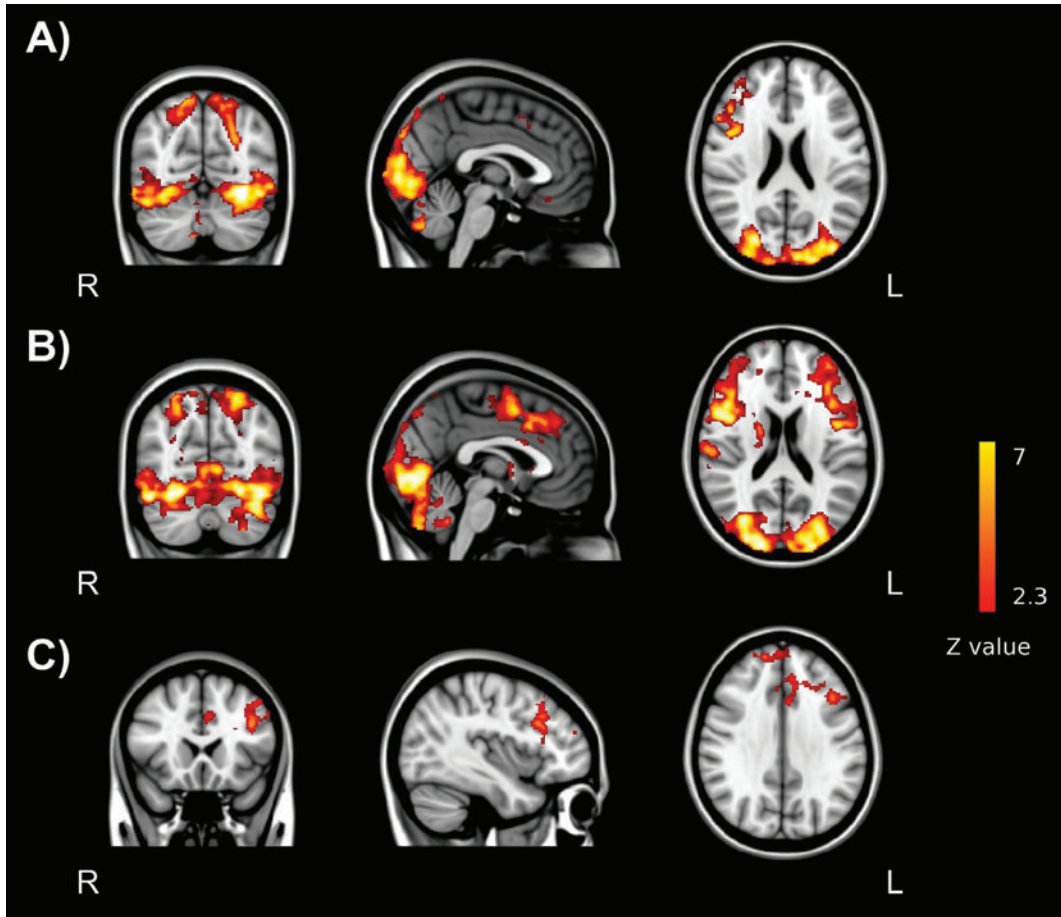
Fig. 5. Results from the model-based analysis of fMRI data when comparing the presentation of orientated images and the fixation periods. A) average map for the HE group (one-sample t-test, $p < 0.05$ FWE corrected), B) average map for the a-MCI group (one-sample t-test, $p < 0.05$ FWE corrected), and C) difference maps (student's t-test, $p < 0.05$ FWE corrected).

White matter connectivity

White matter fiber tracts were identified using probabilistic tractography as described previously. Results can be seen in Figs 6 and 7. Figure 6 contains a three-dimensional representation of cortical areas and fiber pathways connecting them (pathways are averaged across all the subjects). In Fig. 7, average connectivity maps for each group are represented separately on an FA template.

In the ATRP, fronto-occipital connectivity was analyzed separately for each hemisphere (using its posterior ROI and anterior ROI as seed regions), and interhemispheric connectivity was analyzed between both the two anterior and the two posterior ROIs.

Fiber tracking results indicated that the main paths connecting ATRP regions were the superior longitudinal fasciculus bilaterally, the right inferior longitudinal fasciculus, and the right inferior fronto-occipital fasciculus. Moreover, the splenium and the genu of the corpus callosum provided inter-hemispheric connectivity.

As regards the identification of white matter fiber tracts connecting DTRP areas, the cingulum bundle bilaterally was clearly identified as the major component connecting the posteromedial ROI with the anterior cingulate. Furthermore, DTRP-related structural connectivity was also found in the right inferior fronto-occipital fasciculus, the inferior longitudinal fasciculus bilaterally and, finally, in the splenium of the

Table 2
Gray Matter and FA measurements within the ATRP and DTRP areas

	HE	a-MCI	*t*-test	*p* value
ATRP measures				
GM volumes (mm^3)	31564 (2876)	29576 (3627)	1.70	0.11
Left posterior areas	15894 (1720)	14816 (1970)	1.59	0.12
Left anterior areas	1581 (125)	1523 (160)	1.09	0.28
Right posterior areas	11343 (1306)	10596 (1610)	1.39	0.17
Right anterior areas	2746 (304)	2639 (257)	1.04	0.31
FA scores				
Left longitudinal tracts	0.445 (0.038)	0.427 (0.041)	1.23	0.22
Right longitudinal tracts	0.410 (0.031)	0.386 (0.031)	2.07	0.05
Anterior CC	0.399 (0.084)	0.391 (0.037)	0.35	0.73
Posterior CC	0.460 (0.057)	0.439 (0.067)	0.92	0.36
DTRP measures				
GM volumes (mm^3)	15240 (1079)	14112 (1564)	2.30	0.03
Posteromedial area	6897 (649)	6195 (1050)	2.20	0.04
Bilateral parietal areas	6477 (710)	6059 (783)	1.52	0.13
Anterior cingulate	1891 (203)	1797 (216)	0.61	0.55
FA scores				
Cingulum bundle	0.396 (0.032)	0.369 (0.025)	2.54	0.017
Posterior interhemispheric tracts	0.397 (0.038)	0.371 (0.034)	2.0	0.06
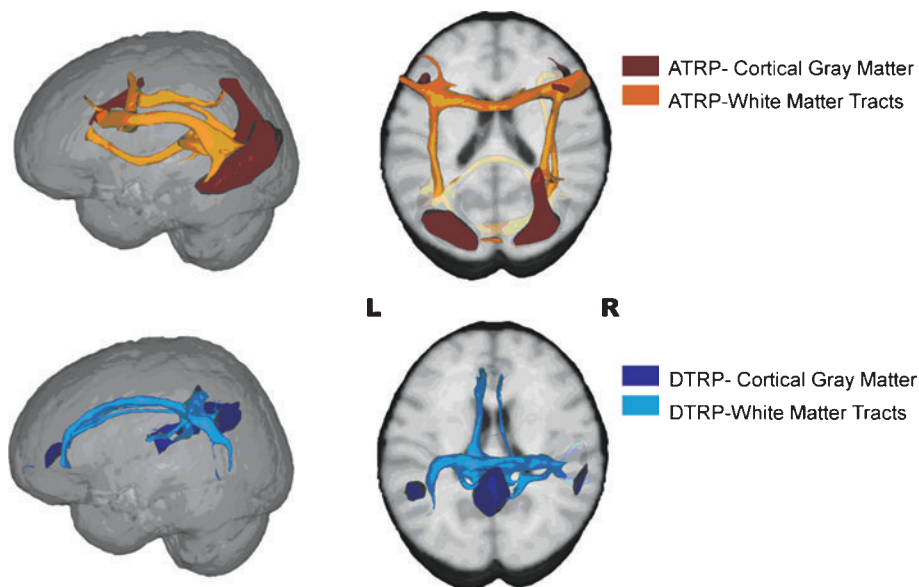
Fig. 6. Three dimensional representation of the structural brain network subserving the main task-related ICA pattern in healthy elders and a-MCI patients. A complete description of all the cortical areas and white matter connectivity paths shown in the figure is given in the main text.

corpus callosum connecting posteromedial and bilateral inferior parietal ROIs.

Moreover, FA values were used to quantify fiber integrity within each pathway. Comparisons of these results showed significant differences between groups only in DTRP related pathways, due mainly to differences in the tracts of the cingulum bundle (see Table 2 and Fig. 8).

Correlations between structural measures, functional activation and task performance

Task/rest activations: As expected, there was a high correlation between the mean BOLD signal in ATRP regions during task performance and in DTRP regions during rest periods for the HE and a-MCI groups ($r = 0.83$, $p < 0.001$).
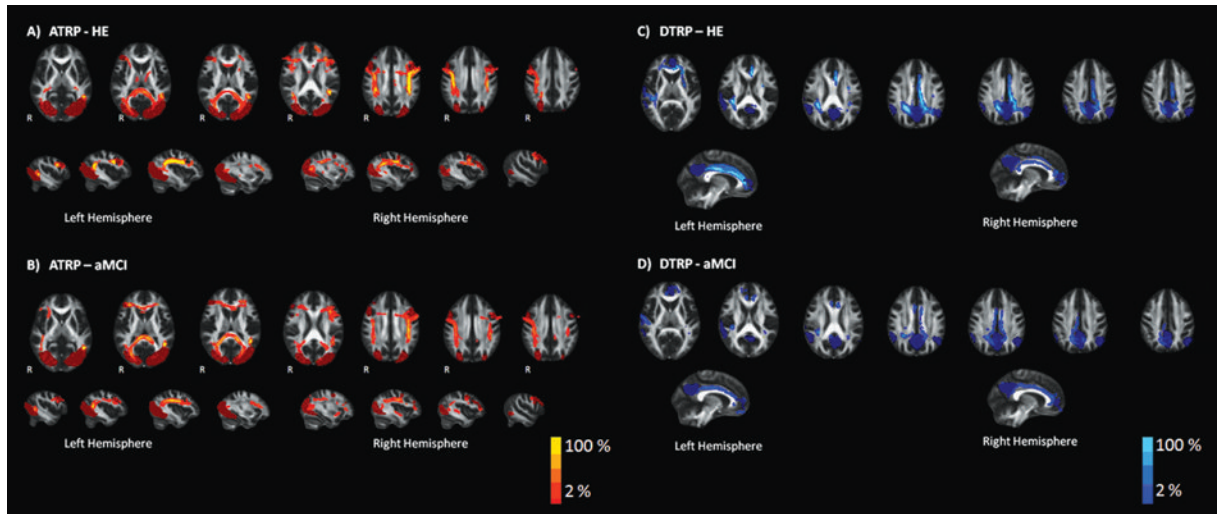
Fig. 7. Mean probabilistic maps reflecting white matter connectivity in both ATRP (A and B) and DTRP (C and D) and for the two groups (HE and a-MCI) separately.

Activation and task performance: Mean BOLD signal measured in the posteromedial ROI of the DTRP during rest (rest-DTRP activation) correlated positively with task performance only in the HE group ($r = 0.72$, $p = 0.03$, corrected). No relationships with the PDT score and task-ATRP activations or rest-DTRP activation were found in the a-MCI group.

Structure and task performance: No relationships were found in the HE group between main task-related pattern structural measures and task performance. Moreover, for the a-MCI group, two significant correlations were found, both concerning DTRP-related measures. Task performance correlated positively with both DTRP gray matter volumes ($r = 0.60$, $p = 0.04$, uncorrected) and mean FA within the longitudinal medial tracts of the DTRP ($r = 0.62$, $p = 0.03$, uncorrected). However, these two latter results did not survive correction for multiple comparisons.

Function and structure: When the mean BOLD signal was measured individually in all the ROIs defined, only the signal measured in the two ROIs formed by bilateral parietal regions of the DTRP (BA 39/40) showed negative correlations with its underlying GM volumes in the a-MCI group ($r = -0.73$, $p = 0.011$).

DISCUSSION

To our knowledge, this is the first MRI-based study in MCI patients to characterize the GM and WM anatomical components of a task related cognitive cerebral network. Several main findings emerge from our multi-modal MRI study. First, using both data-driven and model-driven analysis of fMRI data, we identified two major anatomo-functional networks related to the processing of the visual task. The Activation Task-Related Pattern network (ATRP) was identified by virtue of higher activity mainly in occipital, temporal and parietal areas, and to a lesser extent in frontal regions, and the Deactivation Task-Related Pattern network (DTRP) comprised areas anatomically comparable to the DMN in which increased activity was observed during passive processing. In the ARTP network, a-MCI exhibited functional reorganizations reflected by an increase in the fMRI signal in frontal areas, and greater extension of activations in ventral occipital areas compared to healthy elders in the context of comparable GM atrophy and WM fiber integrity. In DTRP regions, patients presented deactivation deficits in posteromedial and frontal areas and increased deactivation in lateral parietal regions. a-MCI patients showed GM atrophy in the regions underlying the DTRP network, particularly in the precuneus and PCC, as well as reduced white matter integrity in structural pathways connecting DTRP areas, specifically in the cingulate bundles. Finally, relationships between structure, function and performance were found only in DTRP-related measures; in the HE group, activation of the PCC during rest was correlated with task performance, and among
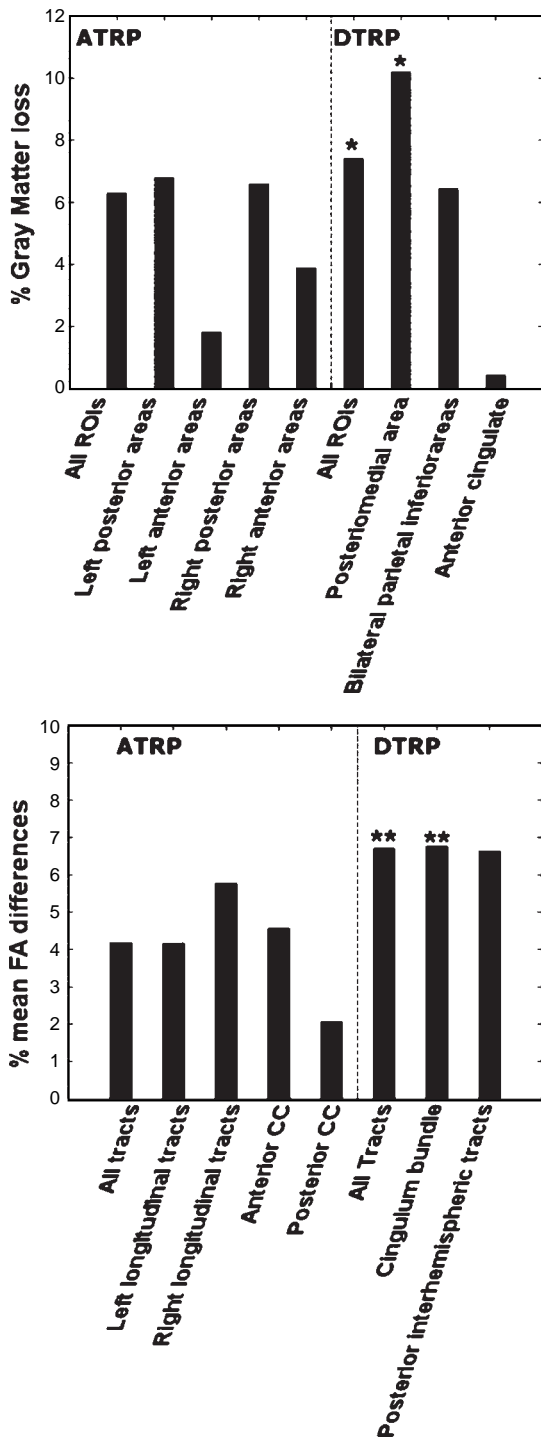
Fig. 8. Percentages of mean Gray Matter and tract-related FA loss for the MCI group relative to the HE group. An extended description of the anatomical cortical regions included in each ROI, and fiber tracts considered in each connectivity pathway is given in the main text. *$p < 0.05$ in the HE vs a-MCI t-test, and ** $p < 0.02$ in the HE vs a-MCI t-test.

patients, the structural measures of the DTRP network correlated with task performance. Nonetheless, this latter result should be considered with caution, since it did not survive multiple comparison correction.

Our findings for the ATRP revealed that regions activated during the processing of complex visual pictures mainly span primary and lateral extrastriate regions, the posterior parts of the temporal lobes (temporo-occipital) and the superior and inferior parietal cortices. Overall, this pattern of activation is consistent with previous PET and fMRI studies of brain activity associated with face and object recognition, spatial localization [48–51] and visuospatial attention [52]. Hence, topographic analysis of the ATRP network suggests that our task incorporates both visuoperceptive components of the ventral visual stream (identification of the blurred images) and the visuospatial function related to the dorsal visual system (selecting the image in a given position in space). Moreover, and especially in the right hemisphere, areas of the dorsolateral prefrontal cortex including the inferior prefrontal (BA45) and dorsal premotor (BA6) cortices were also found to be part of the network. The involvement of these regions also corroborates the findings of Bokde et al. [21] in MCI patients using a visuoperceptive task and functional connectivity analyses, and those of Vannini et al. [19] who used a visuospatial task based on an angle discrimination test in MCI. In our study the observation of frontal lobe activity supports the idea that it includes both visual systems, as the prefrontal cortex is the principal area of integration of visual information from the ventral and dorsal pathways [53].

The probabilistic tractography analysis identified WM tracts connecting ATRP cortical sites compatible with anatomical descriptions of the superior longitudinal fasciculus dorsally and the inferior longitudinal and fronto-occipital fasciculi ventrally. In general, the identification of these major bundles corroborates a recent study in young healthy subjects which identified WM tracts based on fMRI activations during a visuospatial attention task [54]. The convergence between the two sets of findings provides methodological support for the idea that the pathways identified in our studies among HE and MCI correspond to the actual anatomical connections between dorsolateral and posterior functional brain areas. The fact that in our study superior longitudinal fasciculi were identified bilaterally, whereas inferior longitudinal and inferior fronto-occipital fasciculi were only located in the right

hemisphere, may suggest a stronger load of the task in the dorsal than in the ventral pathway.

Regarding group comparisons for the ATRP functionality, our results were obtained from both ICA and FEAT analyses. Despite the fact that ICA performed in the whole-sample revealed a spatial pattern that was common for both groups, the construction of average-group maps (both using separate ICA and FEAT) showed higher activity in the a-MCI group in ventral visual cortices, as well as in frontal and prefrontal regions. Previous studies [23, 54] have reported increased activations in AD in the fusiform gyrus during visuospatial processing and reduced activations in areas of the dorsal stream. These findings build on previous fMRI studies of visuospatial [19, 20] and visuoperceptive [20, 21] functions in MCI, showing that patients tend to use alternative networks during complex visual processing. One possible explanation may be that a-MCI patients use distinct functional strategies, as it has already been observed by Bokde et al. [23]. Alternatively, the increased activation in ventral pathway may reflect the use of the same functional strategy as in HE (albeit used less efficiently) and the need to recruit additional resources as a compensatory mechanism. The neuropathological damage present in MCI [56–59] may account for the existence of these functional compensatory mechanisms. Moreover, the task-related frontal hyperactivation found in the a-MCI group would also support the use of compensatory mechanisms in these patients that has already been described in other studies [20, 23].

Concerning the comparison of the anatomical components of the ATRP, GM volumes and fiber tract FA measures did not reveal significant differences between a-MCI and healthy elders. In our study, the morphological characteristics of the ATRP did not correlate with task performance or fMRI changes. However, as functional differences were found, these results are in line with previous fMRI reports that showed functional reorganizations preceding marked MRI-detectable brain atrophy, a finding already demonstrated in studies of at-risk dementia populations [4, 7, 60, 61]. The lack of structure-function associations of our study is at variance with those of Teipel and colleagues [22] in MCI, who found relationship between brain activity and the underlying GM volumes. The differences between the results are probably due to distinct methodological approaches (region-based vs whole-brain analyses) and may also be related to different levels of task-demands. Furthermore, a study by Gold et al. [62] also reported differential fMRI patterns in

the fusiform gyrus between a-MCI and healthy elders, accompanied by preserved underlying anatomy (but GM atrophy in the medial temporal lobe was observed in a whole-brain VBM analysis). In summary, although our study shows that a-MCI patients recruit a differential pattern of brain activity; these functional changes do not seem to correspond to clearly detectable damage in GM and WM regions of this network.

Using an ICA approach – a powerful tool to find spatio-temporally independent brain networks – we were able to identify, in addition to the main task-activation areas, the task-deactivation network which closely matched the anatomical regions of the DMN [26, 27]. However the DMN was more difficult to identify in the model-driven analysis, probably due to the limitations of the GLM-based analysis as regards the characteristics of the fMRI-signal [63]. Within this pattern, we observed a high correlation between rest-related activation and task performance in the HE group, which was in concordance with previous studies of DMN activity and its relationship with task outcome [64, 65]. In contrast, such correlations could not be observed for the functional components of the ATRP in any of the studied groups. On the other hand, the associations regarding the posterior DMN could reflect either a system already affected by the ageing process [66] and/or a system that correlates with cognitive function in a more general way [28], and thus being more sensitive to a broader range of subtle behavioral differences. This relationship (DMN and task performance) was not found in a-MCI, probably due to the atrophy - in DTRP areas in this group. Furthermore, from the separate ICAs approach, in the DTRP network, a-MCI exhibited deficits mainly in posteromedial structures, including the PCC and the precuneus. These observations have been already reported in fMRI studies on memory tasks [4, 14, 29, 67, 68] and in resting-fMRI studies [4, 31, 69, 70]. A further observation was that besides exhibiting disruption of posteromedial deactivations, the opposite pattern was observed in lateral inferior parietal areas. These latter findings are in agreement with those of Qi et al. [31], who reported areas of greater signal in parietal regions in the context of reduced PCC activity, and are also comparable with those of Bai et al. [69]. These neocortical activations have been associated to compensatory responses related to memory process. Our study also provides the direct observation that higher task-related deactivation in inferior parietal regions appears to be in response to greater GM atrophy, as negative correlations between GM volumes and brain activity were observed only for

the a-MCI group in these particular regions. Furthermore, from the FEAT analysis, we obtained that a-MCI patients showed less collaboration of the frontal lobe in the DMN (as obtained with the baseline condition). This result is in concordance with previous literature [4].

The presence of both significant GM atrophy and reduced microstructural WM damage in DRTP regions in our patients was one of the principal findings of our investigation. Brain atrophy in a-MCI patients, as well as functional abnormalities in DMN-related regions have been separately reported in the literature (see [4] for a review). However, to our knowledge, only two previous reports were specifically designed to investigate the relationship between structural changes and functional resting-state networks in a-MCI; these studies included voxel-based morphometry analyses and were restricted to GM measures [69, 70]. In one of those studies, GM atrophy in patients did not overlap with the functional resting networks identified, including the DMN [69]; however, they also found GM atrophy in the PPC/precuneus area. As discussed above, here DTRP structural alterations emerged in the context of an anatomically preserved main-task (i.e. ATRP) brain network. Furthermore, we observed a correlation between structural DTRP-related measures (GM volume and mean FA within the cingulum) and task performance, suggesting that structural alterations in the DMN already have an impact on cognitive variation in a-MCI. However, these latter results did not survive correction for multiple comparisons and thus need to be considered very cautiously. Taken together, these observations emphasize the need to consider not only the functionality but also the structure of the DMN-related regions as early markers of neurodegeneration in preclinical dementia, a notion that in general is compatible with the progressive convergence of functional, molecular and structural damage in this area in established AD patients reported by Buckner and colleagues [28, 71]. More specifically, the clinical relevance of functional and structural alterations in these posteromedial regions in a-MCI has been reported in separate recent findings revealing focal gray matter atrophy in the posterior cingulate region (BA 29/30 and BA 23 retrosplenial cortex [72], as well as regional metabolic dysfunctions [73, 74] and fMRI deactivation alterations [68] in a-MCI patients with confirmed conversion to dementia.

Finally, in our study we identified major WM fiber bundles connecting DTRP cortical areas. In spite of the methodological differences in DTI sequence

acquisition and processing, these results corroborate recent resting-state fMRI findings that the connectivity of functional networks including the DMN is generally supported by direct structural connectivity, as proved by the identification of the same main bundles, such as the cingulum [75, 76] the superior fronto-occipital fasciculus and the genu of the corpus callosum [77]. Anatomically, a-MCI patients showed significant FA reductions in medial tracts compatible with the anatomical characterization of the cingulate bundle. In our previous DTI study using a voxel-wise DTI analysis, we observed mean FA reductions among a-MCI in all regions where AD patients showed alterations, including parts of this pathway [46]. Overall, cingulate bundle involvement based on FA measures has been demonstrated in recent DTI literature in MCI [4, 78–82]. The novelty of our study, besides being one of the few investigations of MCI to include tractography, is that we demonstrate microstructural damage of this bundle and posterior GM-associated regions and do not isolate them on the basis of an anatomical label, but as part of the anatomy integrated within functional deactivation areas during task performance.

In summary, the results of the present study provide novel information that should be useful for a better understanding of the functional and structural brain characteristics in MCI as a prodromal condition of AD. First, our study confirms previous findings indicating that the investigation of the visual system using fMRI provides useful information reflecting early changes in this condition. Importantly, they extend former knowledge demonstrating that brain dysfunctions, mainly in the dorsal pathway and probably reflecting compensatory mechanisms, can be evidenced at the stages where clinical compromise of visuoperceptive and visuospatial functions is excluded. This latter observation reinforces the idea that fMRI information may be considered as a potential biological marker of prodromal AD. Second, like some of the cortical areas of the visual system, the DMN especially in its posteromedial part exhibited functional abnormalities. Further, in our analytical approach from the fMRI information we were able to observe cortical atrophy as an anatomical substrate of these deactivation deficits. In the same comprehensive analyses, white matter compromise was evidenced in the cingulate bundle, a main fiber pathway conforming part of the structural network of the DMN, as identified in previous studies. Thus, a second and most relevant implication derived from our study is that it supports the use of ICA-based, multimodal MRI investigation as a particularly sen-

sitive approach to illuminate the breakdown of the anatomofunctional components of the DMN in early AD, differentiating them from healthy aging. Finally it is also interesting to note at a practical level that since the cognitive task adapted to the fMRI was clinically spared in all patients, our multimodal study represents an heuristic approach to investigate the functional and structural status of relevant brain networks in prodromal stages of AD reducing common problems associated with complex tasks such as very poor execution levels, or inability to understand or perform the task in a proportion of patients.

ACKNOWLEDGMENTS

REFERENCES

[1] Petersen RC, Doody R, Kurz A, Mohs RC, Morris JC, Rabins PV, Ritchie K, Rossor M, Thal L, Winblad B (2001) Current concepts in mild cognitive impairment. *Arch Neurol* **58**, 1985-1992.

[2] Morris JC, Storandt M, Miller JP, McKeel DW, Price JL, Rubin EH, Berg L (2001) Mild cognitive impairment represents early-stage Alzheimer disease. *Arch Neurol* **58**, 397-405.

[3] Lopez OL, Kuller LH, Becker JT, Dulberg C, Sweet RA, Gach HM, Dekosky ST (2007) Incidence of dementia in mild cognitive impairment in the cardiovascular health study cognition study. *Arch Neurol* **64**, 416-420.

[4] Pihlajamäki M, Jauhiainen AM, Saninen H (2009) Structural and functional MRI in mild cognitive impairment. *Curr Alzheimer Res* **6**, 179-185.

[5] Hampel H, Burger K, Teipel SJ, Bokde AL, Zetterberg H, Blennow K (2008) Core candidate neurochemical and imaging biomarkers of Alzheimer's disease. *Alzheimers Dement* **4**, 38-48.

[6] Ries ML, Carlsson CM, Rowley HA, Sager MA, Gleason CE, Asthana S, Johnson SC (2008) Magnetic resonance imaging characterization of brain structure and function in mild cognitive impairment: a review. *J Am Geriatr Soc* **56**, 920-934.

[7] Bookheimer SY, Strojwas MH, Cohen MS, Saunders AM, Pericak-Vance MA, Mazziotta JC, Small GW (2000) Patterns of brain activation in people at risk for Alzheimer's disease. *N Engl J Med* **343**, 450-456.

[8] Woodard JL, Seidenberg M, Nielson KA, Antuono P, Guidotti L, Durgerian S, Zhang Q, Lancaster M, Hantke N, Butts A, Rao SM (2009) Semantic memory activation in amnestic mild cognitive impairment. *Brain* **132**, 2068-2078.

[9] Bai F, Zhang Z, Watson DR, Yu H, Shi Y, Yuan Y, Zang Y, Zhu C, Qian Y (2009) Abnormal functional connectivity of hippocampus during episodic memory retrieval processing network in amnestic mild cognitive impairment. *Biol Psychiatry* **65**, 951-958.

[10] Dickerson BC, Salat DH, Bates JF, Atiya M, Killiany RJ, Greve DN, Dale AM, Stern CE, Blacker D, Albert MS, Sperling RA (2004) Medial temporal lobe function and structure in mild cognitive impairment. *Ann Neurol* **56**, 27-35.

[11] Dickerson BC, Salat DH, Greve DN, Chua EF, Rand-Giovannetti E, Rentz DM, Bertram L, Mullin K, Tanzi RE, Blacker D, Albert MS, Sperling RA (2005) Increased hippocampal activation in mild cognitive impairment compared to normal aging and AD. *Neurology* **65**, 404-411.

[12] Machulda MM, Ward HA, Borowski B, Gunter JL, Cha RH, O'Brien PC, Petersen RC, Boeve BF, Knopman D, Tang-Wai DF, Ivnik RJ, Smith GE, Tangalos EG, Jack CR Jr (2003) Comparison of memory fMRI response among normal, MCI, and Alzheimer's patients. *Neurology* **61**, 500-506.

[13] Machulda MM, Senjem ML, Weigand SD, Smith GE, Ivnik RJ, Boeve BF, Knopman DS, Petersen RC, Jack CR (2009) Functional magnetic resonance imaging changes in amnestic and nonamnestic mild cognitive impairment during encoding and recognition tasks. *J Int Neuropsychol Soc* **15**, 372-382.

[14] Celone KA, Calhoun VD, Dickerson BC, Atri A, Chua EF, Miller SL, DePeau K, Rentz DM, Selkoe DJ, Blacker D, Albert MS, Sperling RA (2006) Alterations in memory networks in mild cognitive impairment and Alzheimer's disease: an independent component analysis. *J Neurosci* **26**, 10222-10231.

[15] Dannhauser TM, Walker Z, Stevens T, Lee L, Seal M, Shergill SS (2005) The functional anatomy of divided attention in amnestic mild cognitive impairment. *Brain* **128**, 1418-1427.

[16] Rosano C, Aizenstein HJ, Cochran JL, Saxton JA, De Kosky ST, Newman AB, Kuller LH, Lopez OL, Carter CS (2005) Event-related functional magnetic resonance imaging investigation of executive control in very old individuals with mild cognitive impairment. *Biol Psychiatry* **57**, 761-767.

[17] Bosch B, Bartres-Faz D, Rami L, Arenaza-Urquijo EM, Fernandez-Espejo D, Junque C, Sole-Padulles C, Sanchez-Valle R, Bargallo N, Falcon C, Molinuevo JL (2010) Cognitive reserve modulates task-induced activations and deactivations in healthy elders, amnestic mild cognitive impairment and mild Alzheimer's disease. *Cortex* **46**, 451-461.

[18] Lenzi D, Serra L, Perri R, Pantano P, Lenzi GL, Paulesu E, Caltagirone C, Bozzali M, Macaluso E (2009) Single domain amnestic MCI: A multiple cognitive domains fMRI investigation. *Neurobiol Aging*.

[19] Vannini P, Almkvist O, Dierks T, Lehmann C, Wahlund LO (2007) Reduced neuronal efficacy in progressive mild cognitive impairment: a prospective fMRI study on visuospatial processing. *Psychiatry Res* **156**, 43-57.

[20] Bokde AL, Lopez-Bayo P, Born C, Dong W, Meindl T, Leinsinger G, Teipel SJ, Faltraco F, Reiser M, Moller HJ, Hampel H (2008) Functional abnormalities of the visual processing system in subjects with mild cognitive impairment: an fMRI study. *Psychiatry Res* **163**, 248-259.

[21] Bokde AL, Lopez-Bayo P, Meindl T, Pechler S, Born C, Faltraco F, Teipel SJ, Moller HJ, Hampel H (2006) Functional connectivity of the fusiform gyrus during a face-matching task in subjects with mild cognitive impairment. *Brain* **129**, 1113-1124.

[22] Teipel SJ, Bokde AL, Born C, Meindl T, Reiser M, Moller HJ, Hampel H (2007) Morphological substrate of face matching

in healthy ageing and mild cognitive impairment: a combined MRI-fMRI study. *Brain* **130**, 1745-1758.

[23] Bokde AL, Lopez-Bayo P, Born C, Ewers M, Meindl T, Teipel SJ, Faltraco F, Reiser MF, Moller HJ, Hampel H (2010) Alzheimer disease: functional abnormalities in the dorsal visual pathway. *Radiology* **254**, 219-226.

[24] Bokde AL, Ewers M, Hampel H (2009) Assessing neuronal networks: Understanding Alzheimer's disease. *Prog Neurobiol* **89**, 125-133.

[25] Shulman GL, Corbetta M, Buckner RL, Raichle ME, Fiez JA, Miezin FM, Petersen SE (1997) Top-down modulation of early sensory cortex. *Cereb Cortex* **7**, 193-206.

[26] Raichle ME, MacLeod AM, Snyder AZ, Powers WJ, Gusnard DA, Shulman GL (2001) A default mode of brain function. *Proc Natl Acad Sci USA* **98**, 676-682.

[27] Greicius MD, Krasnow B, Reiss AL, Menon V (2003) Functional connectivity in the resting brain: a network analysis of the default mode hypothesis. *Proc Natl Acad Sci USA* **100**, 253-258.

[28] Buckner RL, Andrews-Hanna JR, Schacter DL (2008) The brain's default network: anatomy, function, and relevance to disease. *Ann N Y Acad Sci* **1124**, 1-38.

[29] Pihlajamaki M, DePeau KM, Blacker D, Sperling RA (2008) Impaired medial temporal repetition suppression is related to failure of parietal deactivation in Alzheimer disease. *Am J Geriatr Psychiatry* **16**, 283-292.

[30] Rombouts SA, Damoiseaux JS, Goekoop R, Barkhof F, Scheltens P, Smith SM, Beckmann CF (2009) Model-free group analysis shows altered BOLD FMRI networks in dementia. *Hum Brain Mapp* **30**, 256-266.

[31] Qi Z, Wu X, Wang Z, Zhang N, Dong H, Yao L, Li K (2010) Impairment and compensation coexist in amnestic MCI default mode network. *Neuroimage* **50**, 48-55.

[32] Pfeffer RI, Kurosaki TT, Harrah CH Jr, Chance JM, Filos S (1982) Measurement of functional activities in older adults in the community. *J Gerontol* **37**, 323-329.

[33] Warrington EK, James M (1991) A new test of object decision: 2D silhouettes featuring a minimal view. *Cortex* **27**, 370-383.

[34] Rami L, Serradell M, Bosch B, Villar A, Molinuevo JL (2007) Perception Digital Test (PDT) for the assessment of incipient visual disorder in initial Alzheimer's disease. *Neurologia* **22**, 342-347.

[35] Fazekas F, Chawluk JB, Alavi A, Hurtig HI, Zimmerman RA (1987) MR signal abnormalities at 1.5 T in Alzheimer's dementia and normal aging. *Am J Roentgenol* **149**, 351-356.

[36] Smith SM, Jenkinson M, Woolrich MW, Beckmann CF, Behrens TE, Johansen-Berg H, Bannister PR, De Luca M, Drobnjak I, Flitney DE, Niazy RK, Saunders J, Vickers J, Zhang Y, De Stefano N, Brady JM, Matthews PM (2004) Advances in functional and structural MR image analysis and implementation as FSL. *Neuroimage* **23**(1), S208-S219.

[37] Jenkinson M, Bannister P, Brady M, Smith S (2002) Improved optimization for the robust and accurate linear registration and motion correction of brain images. *Neuroimage* **17**, 825-841.

[38] Smith SM (2002) Fast robust automated brain extraction. *Hum Brain Mapp* **17**, 143-155.

[39] Jenkinson M, Smith S (2001) A global optimisation method for robust affine registration of brain images. *Med Image Anal* **5**, 143-156.

[40] Beckmann CF, Smith SM (2005) Tensorial extensions of independent component analysis for multisubject FMRI analysis. *Neuroimage* **25**, 294-311.

[41] Beckmann CF, Jenkinson M, Smith SM (2003) General multi-level linear modeling for group analysis in FMRI. *Neuroimage* **20**, 1052-1063.

[42] Smith SM, De Stefano N, Jenkinson M, Matthews PM (2001) Normalized accurate measurement of longitudinal brain change. *J Comput Assist Tomogr* **25**, 466-475.

[43] Zhang Y, Brady M, Smith S (2001) Segmentation of brain MR images through a hidden Markov random field model and the expectation-maximization algorithm. *IEEE Trans Med Imaging* **20**, 45-57.

[44] Behrens TE, Berg HJ, Jbabdi S, Rushworth MF, Woolrich MW (2007) Probabilistic diffusion tractography with multiple fibre orientations: What can we gain? *Neuroimage* **34**, 144-155.

[45] Behrens TE, Johansen-Berg H, Woolrich MW, Smith SM, Wheeler-Kingshott CA, Boulby PA, Barker GJ, Sillery EL, Sheehan K, Ciccarelli O, Thompson AJ, Brady JM, Matthews PM (2003) Non-invasive mapping of connections between human thalamus and cortex using diffusion imaging. *Nat Neurosci* **6**, 750-757.

[46] Behrens TE, Woolrich MW, Jenkinson M, Johansen-Berg H, Nunes RG, Clare S, Matthews PM, Brady JM, Smith SM (2003) Characterization and propagation of uncertainty in diffusion-weighted MR imaging. *Magn Reson Med* **50**, 1077-1088.

[47] Bosch B, Arenaza-Urquijo EM, Rami L, Sala-Llonch R, Junque C, Sole-Padulles C, Peña-Gómez C, Bargallo N, Molinuevo JL, Bartres-Faz D (2010) Multiple DTI index analysis in normal aging, amnestic MCI and AD. Relationship with neuropsychological performance. *Neurobiol Aging*.

[48] Haxby JV, Grady CL, Horwitz B, Ungerleider LG, Mishkin M, Carson RE, Herscovitch P, Schapiro MB, Rapoport SI (1991) Dissociation of object and spatial visual processing pathways in human extrastriate cortex. *Proc Natl Acad Sci USA* **88**, 1621-1625.

[49] Haxby JV, Horwitz B, Ungerleider LG, Maisog JM, Pietrini P, Grady CL (1994) The functional organization of human extrastriate cortex: a PET-rCBF study of selective attention to faces and locations. *J Neurosci* **14**, 6336-6353.

[50] Clark VP, Keil K, Maisog JM, Courtney S, Ungerleider LG, Haxby JV (1996) Functional magnetic resonance imaging of human visual cortex during face matching: a comparison with positron emission tomography. *Neuroimage* **4**, 1-15.

[51] Grill-Spector K (2003) The neural basis of object perception. *Curr Opin Neurobiol* **13**, 159-166.

[52] Corbetta M, Miezin FM, Shulman GL, Petersen SE (1993) A PET study of visuospatial attention. *J Neurosci* **13**, 1202-1226.

[53] Ungerleider LG, Courtney SM, Haxby JV (1998) A neural system for human visual working memory. *Proc Natl Acad Sci USA* **95**, 883-890.

[54] Umarova RM, Saur D, Schnell S, Kaller CP, Vry MS, Glauche V, Rijntjes M, Hennig J, Kiselev V, Weiller C (2010) Structural connectivity for visuospatial attention: significance of ventral pathways. *Cereb Cortex* **20**, 121-129.

[55] Prvulovic D, Hubl D, Sack AT, Melillo L, Maurer K, Frolich L, Lanfermann H, Zanella FE, Goebel R, Linden DE, Dierks T (2002) Functional imaging of visuospatial processing in Alzheimer's disease. *Neuroimage* **17**, 1403-1414.

[56] Markesbery WR, Schmitt FA, Kryscio RJ, Davis DG, Smith CD, Wekstein DR (2006) Neuropathologic substrate of mild cognitive impairment. *Arch Neurol* **63**, 38-46.

[57] Bennett DA, Schneider JA, Bienias JL, Evans DA, Wilson RS (2005) Mild cognitive impairment is related to Alzheimer

disease pathology and cerebral infarctions. *Neurology* **64**, 834-841.

[58] Saito Y, Murayama S (2007) Neuropathology of mild cognitive impairment. *Neuropathology* **27**, 578-584.

[59] Schneider JA, Arvanitakis Z, Leurgans SE, Bennett DA (2009) The neuropathology of probable Alzheimer disease and mild cognitive impairment. *Ann Neurol* **66**, 200-208.

[60] Smith CD, Andersen AH, Kryscio RJ, Schmitt FA, Kindy MS, Blonder LX, Avison MJ (1999) Altered brain activation in cognitively intact individuals at high risk for Alzheimer's disease. *Neurology* **53**, 1391-1396.

[61] Bartres-Faz D, Serra-Grabulosa JM, Sun FT, Sole-Padulles C, Rami L, Molinuevo JL, Bosch B, Mercader JM, Bargallo N, Falcon C, Vendrell P, Junque C, D'Esposito M (2008) Functional connectivity of the hippocampus in elderly with mild memory dysfunction carrying the APOE epsilon4 allele. *Neurobiol Aging* **29**, 1644-1653.

[62] Gold BT, Jiang Y, Jicha GA, Smith CD (2010) Functional response in ventral temporal cortex differentiates mild cognitive impairment from normal aging. *Hum Brain Mapp* **31**, 1249-1259.

[63] Monti MM (18) (2011) Statistical analysis of fMRI time-series: a critical review of the GLM approach. *Front Hum Neurosci* **5**, 28.

[64] Persson J, Lustig C, Nelson JK, Reuter-Lorenz PA (2007) Age differences in deactivation: a link to cognitive control? *J Cogn Neurosci* **19**, 1021-1032.

[65] Park DC, Polk TA, Hebrank AC, Jenkins LJ (2010) Age differences in default mode activity on easy and difficult spatial judgment tasks. *Front Hum Neurosci* **3**, 75.

[66] Damoiseaux JS, Greicius MD (2009) Greater than the sum of its parts: a review of studies combining structural connectivity and resting-state functional connectivity. *Brain Struct Funct* **213**, 525-533.

[67] Lustig C, Snyder AZ, Bhakta M, O'Brien KC, McAvoy M, Raichle ME, Morris JC, Buckner RL (2003) Functional deactivations: change with age and dementia of the Alzheimer type. *Proc Natl Acad Sci USA* **100**, 14504-14509.

[68] Petrella JR, Prince SE, Wang L, Hellegers C, Doraiswamy PM (2007) Prognostic value of posteromedial cortex deactivation in mild cognitive impairment. *PLoS One* **2**, e1104.

[69] Sorg C, Riedl V, Muhlau M, Calhoun VD, Eichele T, Laer L, Drzezga A, Forstl H, Kurz A, Zimmer C, Wohlschlager AM (2007) Selective changes of resting-state networks in individuals at risk for Alzheimer's disease. *Proc Natl Acad Sci USA* **104**, 18760-18765.

[70] Bai F, Zhang Z, Yu H, Shi Y, Yuan Y, Zhu W, Zhang X, Qian Y (2008) Default-mode network activity distinguishes amnestic type mild cognitive impairment from healthy aging: a combined structural and resting-state functional MRI study. *Neurosci Lett* **438**, 111-115.

[71] Buckner RL, Snyder AZ, Shannon BJ, LaRossa G, Sachs R, Fotenos AF, Sheline YI, Klunk WE, Mathis CA, Morris JC, Mintun MA (2005) Molecular, structural, and functional characterization of Alzheimer's disease: evidence for a relationship between default activity, amyloid, and memory. *J Neurosci* **25**, 7709-7717.

[72] Pengas G, Hodges JR, Watson P, Nestor PJ (2010) Focal posterior cingulate atrophy in incipient Alzheimer's disease. *Neurobiol Aging* **31**, 25-33.

[73] Chetelat G, Desgranges B, de la Sayette V, Viader F, Eustache F, Baron JC (2003) Mild cognitive impairment: Can FDG-PET predict who is to rapidly convert to Alzheimer's disease? *Neurology* **60**, 1374-1377.

[74] Anchisi D, Borroni B, Franceschi M, Kerrouche N, Kalbe E, Beuthien-Beumann B, Cappa S, Lenz O, Ludecke S, Marcone A, Mielke R, Ortelli P, Padovani A, Pelati O, Pupi A, Scarpini E, Weisenbach S, Herholz K, Salmon E, Holthoff V, Sorbi S, Fazio F, Perani D (2005) Heterogeneity of brain glucose metabolism in mild cognitive impairment and clinical progression to Alzheimer disease. *Arch Neurol* **62**, 1728-1733.

[75] Van den Heuvel M, Mandl R, Luigjes J, Hulshoff Pol H (2008) Microstructural organization of the cingulum tract and the level of default mode functional connectivity. *J Neurosci* **28**, 10844-10851.

[76] Greicius MD, Supekar K, Menon V, Dougherty RF (2009) Resting-state functional connectivity reflects structural connectivity in the default mode network. *Cereb Cortex* **19**, 72-78.

[77] Van den Heuvel MP, Mandl RC, Kahn RS, Hulshoff Pol HE (2009) Functionally linked resting-state networks reflect the underlying structural connectivity architecture of the human brain. *Hum Brain Mapp* **30**, 3127-3141.

[78] Fellgiebel A, Muller MJ, Wille P, Dellani PR, Scheurich A, Schmidt LG, Stoeter P (2005) Color-coded diffusion-tensor-imaging of posterior cingulate fiber tracts in mild cognitive impairment. *Neurobiol Aging* **26**, 1193-1198.

[79] Zhang Y, Schuff N, Jahng GH, Bayne W, Mori S, Schad L, Mueller S, Du AT, Kramer JH, Yaffe K, Chui H, Jagust WJ, Miller BL, Weiner MW (2007) Diffusion tensor imaging of cingulum fibers in mild cognitive impairment and Alzheimer disease. *Neurology* **68**, 13-19.

[80] Bai F, Zhang Z, Watson DR, Yu H, Shi Y, Yuan Y, Qian Y, Jia J (2009) Abnormal integrity of association fiber tracts in amnestic mild cognitive impairment. *J Neurol Sci* **278**, 102-106.

[81] Chua TC, Wen W, Chen X, Kochan N, Slavin MJ, Trollor JN, Brodaty H, Sachdev PS (2009) Diffusion tensor imaging of the posterior cingulate is a useful biomarker of mild cognitive impairment. *Am J Geriatr Psychiatry* **17**, 602-613.

[82] Kiuchi K, Morikawa M, Taoka T, Nagashima T, Yamauchi T, Makinodan M, Norimoto K, Hashimoto K, Kosaka J, Inoue Y, Inoue M, Kichikawa K, Kishimoto T (2009) Abnormalities of the uncinate fasciculus and posterior cingulate fasciculus in mild cognitive impairment and early Alzheimer's disease: a diffusion tensor tractography study. *Brain Res* **1287**, 184-191.

Verbal Working Memory in Amnestic Mild Cognitive Impaired Subjects: An fMRI Study

Arun L.W. Bokde[a,*], Michaela Karmann[b], Christine Born[c], Stefan J. Teipel[d], Muamer Omerovic[b], Michael Ewers[e], Thomas Frodl[f], Eva Meisenzahl[b], Maximilian Reiser[c], Hans-Jürgen Möller[b] and Harald Hampel[f]

[a]*Cognitive Systems Group, Discipline of Psychiatry, School of Medicine and Trinity College Institute of Neuroscience, Trinity College Dublin, Dublin, Ireland*

[b]*Department of Psychiatry and Psychotherapy, Ludwig-Maximilian University, Munich, Germany*

[c]*Institute for Clinical Radiology, Ludwig-Maximilian University, Munich, Germany*

[d]*Department of Psychiatry, University of Rostock, Rostock, Germany*

[e]*Department of Radiology, University of California - San Francisco, San Francisco, CA, USA*

[f]*Department of Psychiatry, Psychosomatic Medicine and Psychotherapy, Goethe University, Frankfurt, Germany*

Abstract. Memory impairments are a core symptom of Alzheimer's disease (AD) and amnestic Mild Cognitive Impaired (aMCI) subjects are a high risk group for conversion to AD. Working memory (WM) is the ability to hold information in memory while performing another mental operation, which is a key cognitive domain for higher cognition and is impaired in MCI subjects. The objective of this study was to delineate the differences in brain activation between amnestic MCI and age-matched healthy controls (HC) supporting verbal working memory. It was a delay match to sample task and functional magnetic resonance imaging (fMRI) was used to measure brain activation. Group differences were calculated using Analysis of Covariance (ANCOVA) with statistical significance at $p < 0.05$ corrected for multiple comparisons. Both groups activated a wide network in the posterior and frontal areas of the brain. There was higher activation in the parietal and frontal lobes in the aMCI compared to the HC during the delay phase. There were no areas in the HC that activated higher than the MCI subjects. Response time in the HC group was correlated to activation in left hippocampus during encoding phase and to the parietal and frontal areas during the recall phase. In the MCI group response time was correlated to the inferior and middle temporal gyrii during encoding, the middle frontal gyrus during the maintenance phase, and hippocampus during recall phase. The activation differences between groups may reflect compensatory mechanisms within the MCI group for the effects of the putative AD neuropathology.

Keywords: Alzheimer's disease, brain compensation, dorsolateral prefrontal cortex, dementia, neurodegeneration

INTRODUCTION

Alzheimer's disease (AD) is one of the most common psychiatric disorders in older subjects and the first clinical symptoms are in the memory domain. One of the high risk groups for Alzheimer's disease are sub-jects with Mild Cognitive Impairment (MCI) [1], a group that has cognitive impairments in memory or in other domains but the severity of impairment does not meet the criteria for AD. Within the MCI group there are various subgroups, with the amnestic Mild Cognitive Impairment (aMCI) group characterized by a single memory disorder [2]. This group is at higher risk for converting to AD compared to healthy subjects and other MCI subtypes such as non-amnestic MCI [2–7].

---

*Correspondence to: Arun Bokde, PhD, Discipline of Psychiatry, School of Medicine and Trinity College Institute of Neuroscience, Lloyd Building, room 4.55, Dublin 2, Ireland. Tel.: +353 1 896 4104; Fax: +353 1 896 3183; E-mail: Arun.Bokde@tcd.ie.

Working memory (WM), the ability to hold information in memory while performing another mental operation [8–10], is a key cognitive domain important for higher cognition and is impaired in MCI subjects [11] and AD patients [12]. WM tasks recruit a network of regions that include bilateral frontal and parietal regions, as well as the cingulate cortex, and cerebellum in young healthy subjects [13–19] and older healthy subjects [17, 20–25]. WM has also been investigated in MCI and AD patients with both groups recruiting alternate networks compared to the HC. For example using the n-back WM task in MCI subjects Goekoop and colleagues [26] found a network of activation that included the bilateral parietal lobes and prefrontal cortex with the extent of activation increasing in the 2-back compared to 1-back WM task. Another study that examined a verbal 0-, 1-, and 2-back WM tasks found that the MCI had reduced activation compared to HC bilaterally in the parietal and frontal regions [27]. A recent study found that aMCI and HC in a 2-back WM task using visually presented emotional stimuli activated a wide network including bilaterally the parietal and frontal lobes with a group by emotion interaction effect in the left cuneus, where the HC group had lower activation for the positive valence stimuli compared to the neutral valence stimuli [28]. The aMCI group revealed a signal increase in the right precuneus for negative compared to neutral valence stimuli.

The alterations in brain activation described previously in the MCI and AD groups reflect compensatory mechanisms in the brain. The level of compensation may be an index of disease progression, for example, Celone and colleagues found that a mild MCI group compensated with higher activation in the hippocampus but in the more advanced MCI group the activation in the hippocampus decreased compared to the mild MCI [29]. Disease severity can also be quantified by measurement of the hippocampal volume, for example there was increased recruitment of the posterior hippocampus and fusiform gyrus in the MCI compared to the HC during an associate encoding task, with the increased recruitment linearly correlated to the atrophy of the hippocampus in the MCI group [30]. In an encoding task with visual stimuli, the aMCI subjects had higher activation in right parahippocampal gyrus compared to HC and those that showed the greatest activation in this region within the aMCI group, had the greater cognitive decline within the following 2.5 years [31]. Compensatory mechanisms have been found not only in memory but also in a visual perception task in MCI subjects [32]. In addition in a study of AD patients

there was increased recruitment of frontal lobe regions for performance of short term tasks and the recruitment of frontal regions was associated with performance of the task [33-34].

To further investigate the brain compensatory mechanisms in MCI subjects, we used a delay-match-to-sample (DMTS) working memory task with verbal stimuli. We hypothesized that the aMCI group would have higher activation, reflecting a compensatory mechanism compared to the HC group. The design of the DMTS task allowed for quantification of the different phases of the working memory task.

METHODS

Subjects

There were 5 males and 3 females in the HC group and 6 males and 2 females in the MCI group, with an average age $\pm$ standard deviation of 66.6 ± 3.9 (age range 60 to 71) and 70.8 ± 5.3 (age range 63 to 76) in the HC and MCI subjects, respectively (neuropsychological profiles in Table 1). All subjects were right handed. The MCI subjects were recruited from a specialized memory problems unit at a university hospital. The clinical assessment included detailed medical history, neurological and neuropsychological examinations, and laboratory tests (routine hematology and biochemistry screen, thyroid function tests). Major systemic, psychiatric, or neurological illnesses were carefully investigated and excluded in all subjects by clinical and neurological examinations, blood testing (complete blood count, sedimentation rate, electrolytes, glucose, blood urea nitrogen, creatinine, liver-associated enzymes, cholesterol, high-density lipoprotein, triglycerides, antinuclear antibodies, rheumatoid factor, HIV, serum B12, folate, thyroid function tests, and urine analysis), and psychiatric examination. Subjects were excluded if they had cortical infarction, subcortical vascular disease, space-occupying lesions, depression, and any other psychiatric or neurological disease. FLAIR and T2 weighted scans were utilized to rule out vascular pathology (clinical judgment by radiologist).

The diagnostic criteria [35, 36] were (a) memory impairment for the age and education of the subject, (b) memory impairment was corroborated by a close family member, (c) relatively preserved cognition outside of memory domain for age (fulfilled by the various subtests in the Consortium to establish a Registry for Alzheimer's Disease battery (CERAD) [37],

Table 1
Average CERAD results for HC and MCI subjects

Group	MMSE [0–30]	Word List Memory [0–30]	Word List Recall [0–10]	Verbal List Recognition [0–10]	Verbal Fluency [0–24]	Boston Naming [0–15]	Constructional Praxis [0–11]
HC	30 ± 0	23 ± 3.0	8.5 ± 1.2	10 ± 0	19.8 ± 2.8	14.6 ± 0.5	10.6 ± 0.7
MCI	**26.6 ± 1.3**	**15.9 ± 3.2**	**3.8 ± 2.6**	**8.1 ± 2.2**	18.5 ± 3.2	14.2 ± 0.9	11 ± 0.0

Median values in the MCI subjects that are bolded are statistically significant different from the HC group, using t-tests (df = 14), significance at the $p < 0.05$ level, no correction for multiple comparisons. The values in brackets indicate the range of possible scores (if applicable).

(d) no impairment in activities of daily living, (e) no dementia. Clinical judgment was utilized to determine whether there was impairment in activities of daily living. The patients were systematically evaluated for the presence of affective symptoms, particularly depression and if any symptoms appeared that might have indicated the possibility of depression the subject was evaluated with a Hamilton Test (21 item version) and any subject with a score higher than 7 was excluded; none of the MCI subjects had depression. The threshold for determining a cognitive impairment was 1.5 standard deviation below the age norms [38, 39] in the CERAD neuropsychological test battery. The diagnosis of the MCI subjects was established through consensus among the responsible psychiatric consultants (SJT, MO and HH).

The HC were recruited from the community, did not have an active neurological or psychiatric illness, or an illness that could affect cognitive function, and were independently functioning members of the community. The HC did not complain about cognitive problems, and there was no evidence of cognitive deficits as measured by neuropsychological testing using the CERAD [37]. If there was possible presence of depression, the Hamilton Test (21 item version) was performed and any subject with a score higher than 7 was excluded.

All subjects gave written informed consent to participate in the study after the study was explained to them. The study was performed in accordance with the Declaration of Helsinki and the Ethics Committee of the Faculty of Medicine at Ludwig-Maximilian University approved the study.

Stimuli and tasks

The WM task was composed of an encoding phase, a delay phase, and a recall phase (see Fig. 1). The encoding phase was 4 seconds long and 5 capital letters were presented. The maintenance phase was 6 seconds long and a fixation cross was presented in the center of
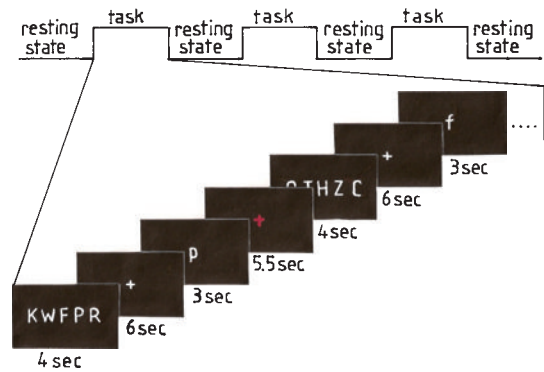
Fig. 1. Schematic of the working memory task. Each run had three blocks where the working memory task was performed and four blocks where the subjects fixated on a fixation point. Within each block there were 3 trials of the working memory task.

the screen. After 6 seconds one single lower case letter appeared, for which the subjects were to decide if it was among the 5 letters they had seen in the encoding phase. The subject indicated a positive answer by pressing a button in the right hand with the right index finger and a negative answer by pressing a button in the left hand with the left index finger. No vowels were included among the letters utilized so as to minimize the probability that the subjects would encode the letters as a word or pseudoword.

Each subject performed three runs of the working memory task. Each run contained 3 blocks of working memory (50 seconds per block) and each block had 3 trials. Each subject performed 27 trials. The working memory trials alternated with four resting state blocks (20 seconds per block). Before each block, the subjects saw a short instruction for 10 seconds.

The task was explained to the subjects using examples on paper and once understood they were shown a short demonstration version of the task on a computer. The stimuli were presented using VAPP [40]. The participants were told to respond as fast as possible to the probe.

Scanning

The imaging sequence was an interleaved T2* weighted echoplanar (EPI) sequence with 28 axial slices (4 mm slice thickness and slice gap = 1 mm, repetition time (TR) = 3.60 s, echo time (TE) = 60 ms, flip angle = 90°, field of view = 240 mm, matrix = 64 × 64) and 87 volumes acquired per run (each volume was measured in 2.8 sec with 0.8 sec gap between volumes) on a 1.5 Tesla Siemens Magneton Vision scanner (Erlangen, Germany). For anatomical reference in each subject a high resolution T1-weighted 3D Magnetization Prepared Rapid Gradient Echo (MPRAGE) structural image was acquired (TR = 11.4 ms, TE = 4.4 ms, flip angle = 8°, FOV = 270 mm, matrix = 224 × 256, Rect. FOV = 7/8, Effective Thickness = 1.25 mm).

Data analysis

The data was analyzed on an Intel Pentium III computer (San Jose, California, USA) running Linux (Red Hat version 7.0, Red Hat Inc, Raleigh, North Carolina, USA) using AFNI [41] and FSL [42].

The initial step was to delete the first 4 volumes of each scan to remove the initial T1 magnetic transients. The remaining data were corrected for the timing differences between each slice using Fourier interpolation and then corrected for motion effects (6-parameter rigid body) (programs utilized were within the AFNI software package unless specifically noted). The structural images were utilized to convert the EPI data from native space to Montreal Neurological Institute/International Consortium for Brain Mapping 152 standard (MNI/ICBM) space. To accomplish this, the structural images were first edited of the non-brain tissue using BET from the FSL software package. The EPI images were co-registered to the MPRAGE image (6 parameter rigid body), and the MPRAGE image was registered to the MNI/ICBM template (12 parameter affine) using FLIRT from the FSL package. The transformation matrices were utilized to convert the EPI data from native to MNI/ICBM stereotaxic space. The data were smoothed (Gaussian filter at full width at half maximum = 6 × 6 × 6 mm) and high pass filtered with a cutoff at (1/100) Hz.

The event related design of the task allowed us to match the performance between the two groups. The activation maps and comparison were based on the trials that were successfully encoded and the subjects were matched for performance. In addition, not only were the activation maps and comparisons based only on the successfully encoded trials, but also the same number of trials was included in the regressor for calculation of the activation maps. For example, if an MCI subject responded correctly to 7 trials in a run and a HC to 8 trials in the run, the regressor for the "correct trials" included 7 trials in the MCI and 7 trials in the HC group. The additional correct trial in the HC group was modeled by another regressor. Thus in this way, the activation maps in both groups included the same number of correct trials in both groups and the correct response rate was matched.

Each run for each subject was analyzed using a fixed effects general linear model using AFNI. Each model was composed of the regressor modeling the encoding phase, the delay phase, and the matching phase. These three regressors were for the correctly performed trials and not-correctly performed trials for a total of 6 regressors. If needed there were additional regressors (one for each phase) for the correctly performed working memory trials that were not required for performance matching with the subject in the other group (see previous paragraph). There were additional regressors for the instruction before each block, and the fixation period between blocks. The regressors were square wave-forms (on-off) which were convolved with a standard double gamma hemodynamic response function.

The group activation statistical analyses maps were based on a random effects model with a voxel wise threshold of $p < 0.01$ and was corrected for multiple comparisons at the $p < 0.05$ level using Monte Carlo simulations. The models for obtaining the activation maps of the functional tasks compared to the control task was the one sample t-test. To compare the activation between groups an analysis of covariance (ANCOVA) was utilized with group membership as the random variable and age as covariate.

A conjunction overlay was performed to delineate area of common activation in the HC and MCI groups. The individual activation analysis maps (for each phase of the WM task) of each group were thresholded at a voxel level of $p < 0.01$ and corrected to $p < 0.05$.

In addition, it was examined if performance (response time) in each group was linearly associated with brain activation in the three phases of the working memory task. Thus a linear regression model was utilized with performance as independent variable and brain activation as dependent variable. Statistical significance was tested using a t-test, with voxel level significance at $p < 0.01$ and cluster level at $p < 0.05$ level.

Structural data was analysed with FSL-VBM, a voxel-based morphometry style analysis [43, 44] carried out with FSL tools [42]. First, structural images were brain-extracted using BET [45]. Next, tissue-type segmentation was carried out using FAST4 [46]. The resulting grey-matter partial volume images were then aligned to MNI152 standard space using the affine registration tool FLIRT [47, 48], followed optionally by nonlinear registration using FNIRT, which uses a b-spline representation of the registration warp field [49]. The resulting images were averaged to create a study-specific template, to which the native grey matter images were then non-linearly re-registered. The registered partial volume images were then modulated (to correct for local expansion or contraction) by dividing by the Jacobian of the warp field. The modulated segmented images were then smoothed with an isotropic Gaussian kernel with a sigma of 6 mm. Finally, voxelwise GLM was applied using parametric testing, correcting for multiple comparisons across space.

The Talairach and Tournoux template [50] was used as reference for locating the activation in the brain. The MNI/ICBM coordinates were converted to the Talairach and Tournoux coordinates using a non-linear transformation developed by M. Brett for transforming coordinate location between both stereotaxic spaces (http://www.mrc-cbu.cam.ac.uk/Imaging/mnispace.html).

RESULTS

Neuropsychological and behavioral performance

There were statistically significant differences in the mean scores between both groups in the following sub-tests of the CERAD: MMSE, word list memory, word list recall, word list recognition (see Table 1, t-test, df = 14, $p < 0.05$, uncorrected for multiple comparisons). In the sub-tests of verbal fluency, naming and constructional praxis of the CERAD there were no statistically significant differences.

The average response time (RT) of the included correct trials was 1.61 ± 0.39 s and 1.83 ± 0.54 s in the HC and MCI, respectively (see Table 2). There was not a statistically significant difference in the RT between groups. In addition, the overall correct response of every subject in both groups and the overall response time for the correct trials are included in Table 2. In the MCI subjects the response time of the correct trials included in the activation analysis were not linearly

Table 2
Performance in the working memory task in the HC and MCI groups. The response time of the included correct trials included in analysis, the overall correct rate and the overall response rate (all correct trials)

Subject	Working memory response time (included trials in analysis) (sec)	Overall working memory correct rate (percent)	Overall working memory response time (sec)
HC Group			
1	1.97 ± 0.29	89	1.65 ± 0.46
2	1.84 ± 0.35	85	1.92 ± 0.37
3	1.76 ± 0.38	70	1.85 ± 0.36
4	1.53 ± 0.40	96	1.46 ± 0.48
5	1.51 ± 0.40	93	1.76 ± 0.38
6	1.39 ± 0.56	96	1.50 ± 0.32
7	1.46 ± 0.47	93	1.48 ± 0.46
8	1.42 ± 0.25	85	1.41 ± 0.25
Median	1.61 ± 0.39	88 ± 9	1.63 ± 0.39
MCI Group			
1	1.41 ± 0.29	63	2.58 ± 1.44
2	3.59 ± 0.95	74	3.59 ± 0.95
3	1.61 ± 0.45	93	1.62 ± 0.45
4	1.71 ± 0.28	93	1.70 ± 0.31
5	1.35 ± 0.21	70	1.54 ± 0.34
6	1.50 ± 0.51	74	1.45 ± 0.45
7	1.50 ± 0.32	93	1.61 ± 0.36
8	2.01 ± 1.36	89	2.01 ± 1.37
Median	1.83 ± 0.54	81 ± 12	2.01 ± 0.71

correlated (Pearson's correlation coefficient) to word list memory performance of the CERAD. The overall performance (correct response rate) in the WM task in the MCI group showed a trend to significance ($p = 0.06$) to the word list memory score from the CERAD. In the HC group similar tests were performed and no statistically significant correlations were found.

Common activation in the healthy control and mild cognitive impairment groups

The activation for the three different phases activated a wide network of regions primarily in the parietal and frontal lobes. In Fig. 2 and 3 the areas of common activation within each group are detailed. In the HC the regions activated in all three phases of the task were bilaterally in the ventrolateral frontal cortex (VLPFC), left dorsolateral prefrontal cortex (DLPFC), and bilateral inferior parietal cortex. The activation across all phases of the WM task varies and present a dynamic picture of regions activated only during one or two phases of the task. As with the HC, the MCI group had a dynamic recruitment of various regions of the brain during the task, with the pattern different from
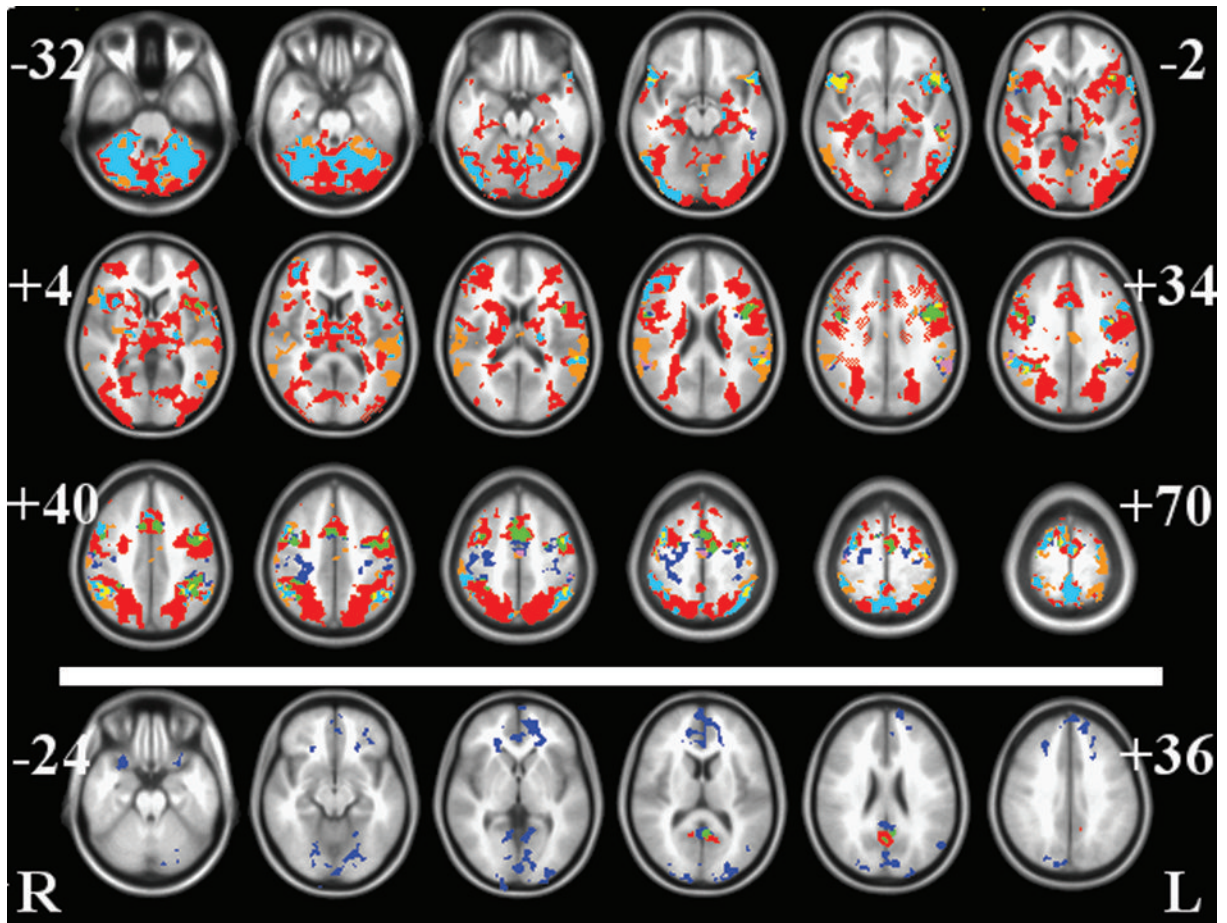
Fig. 2. The activation pattern in the HC subjects during the three phases of the WM task. The different colors at each voxel indicate which WM phase or phases had significant activation in the voxel. The numbers on the images indicate the z axis (inferior-superior) relative to the anterior commissure – posterior commissure plane in the ICBM/MNI stereotaxic brain. The upper part of the image (top 3 rows) are the positiveactivation and last row are the areas deactivated. Color legend: RED, encoding; BLUE, maintenance; TAN, recall; GREEN, encoding and maintenance; CYAN, encoding and recall; VIOLET, maintenance and recall; YELLOW, all three phases.

the HC. In the MCI group, there was no region that was recruited during all three phases of the task.

In addition a conjunction overlay was performed to delineate common activation areas in the HC and MCI groups, which was detailed in Table 3. This table shows areas of common activation across the two groups.

Differences in activation among differences phases of working memory task

In each group the differences in activation between each of the phases of the WM task was computed (Tables 4 and 5). In the HC group we found that there was higher activation in the maintenance phase compared to encoding and recall, as well as differences (higher and lower) in activation between encoding and recall. The areas of greater activation during maintenance compared to encoding or recall are located in visual areas (occipital and temporal lobes) and in the frontal lobe areas. The differences in encoding and recall were located in the visual areas (occipital lobes) and frontal lobe regions.

In the MCI group we found that there were regions with statistically significant higher activation during the maintenance phase compared to recall phase (as with the HC group), brain regions with greater activation in encoding compared to recall (as with HC group), and regions with higher activation during encoding compared to maintenance (different from HC group).
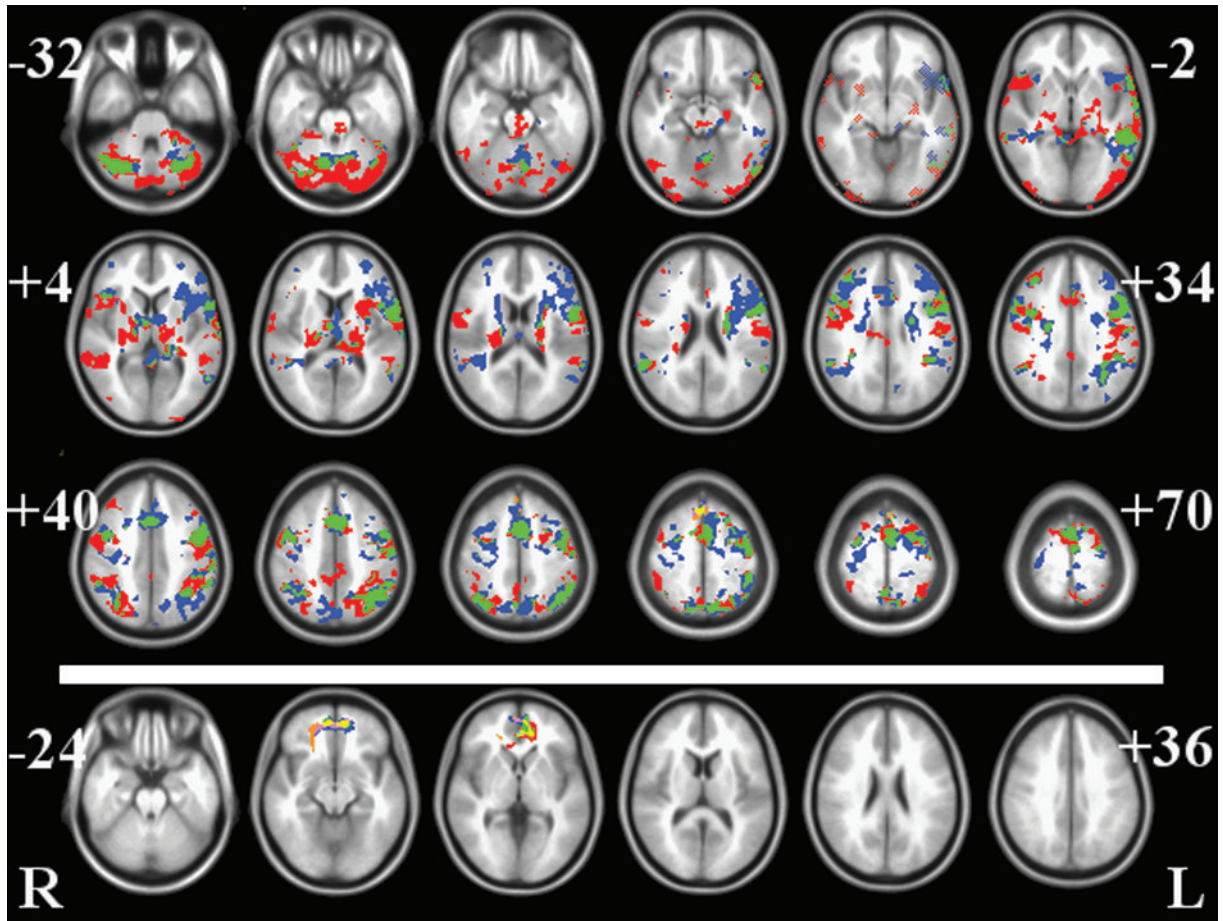
Fig. 3. The activation pattern in the MCI subjects during the three phases of the working memory task. See Fig. 1 for image details.

Differences in activation between groups

During the encoding phase there were statistically significant differences in activation between the HC and the MCI groups in temporal and frontal lobes and cerebellum (Table 6).

During the maintenance phase, there was a wide network of regions with statistically significant higher activation in MCI compared to HC (Table 7, Fig. 4). There was no higher activation in the HC compared to the MCI group. The peaks of activation in the anterior cingulate and inferior frontal gyrus (Figs. 5 and 6) in both groups show that the the estimated hemodynamic response function with confidence intervals are different between groups.

During the recall phase of the task, there was significantly higher activation in the HC compared to the MCI (Table 8).

Linear association of task performance with brain activation

In the HC group, there was statistically significant linear association between brain activation during encoding phase and recall phase and response time. In the MCI group, the linear association was found in all 3 phases of the task. See Fig. 7 for more details.

Structural differences between groups

The was statistically significantly decreased grey matter density in the MCI compared to the HC ($p < 0.05$ corrected) bilaterally in medial and lateral temporal lobes, hippocampus, fusiform gyrus, parahippocampal gyrus, cuneus, and medial frontal gyrus. Examination of the areas of differences in grey matter density between the HC and MCI group did not overlap with

Table 3

Regions of overlapping statistically significant activation in the MCI and HC groups in the (a) encoding, (b) maintenance phases of the WM task. There are no areas of overlapping statistically significant activation in the recall phase of the WM task so the areas of activation are detailed in (c) for HC and (d) for MCI

Region	Side	Volume	BA	X	Y	Z	T-score
(a) Encoding							
Inferior Occipital Gyrus	R	1912	18	36	−88	−7	7.53
Lingual Gyrus			*18*	*26*	*−97*	*−4*	*6.81*
Cerebellum	R	42440		18	−63	−20	15.64
Fusiform Gyrus	*L*		*19*	*−50*	*−71*	*−12*	*13.04*
Inferior Frontal Gyrus	R	2624	47	46	15	−4	11.20
Superior Temporal Gyrus	*R*		*38*	*57*	*13*	*−6*	*6.03*
Superior Temporal Gyrus	L	1312	22	−65	−21	1	8.14
Middle Temporal Gyrus	*L*		*21*	*−61*	*−39*	*2*	*6.46*
Thalamus	R	4552		24	−23	14	13.27
	R	*4552*		*2*	*−11*	*12*	*7.48*
Inferior Parietal Lobule	L	23792	40	−40	−50	50	10.43
	R			46	−44	54	9.07
Middle Frontal Gyrus	R	9192	6	28	1	53	12.74
			51	*2*	*40*	*8.18*	
Medial Frontal Gyrus	L	10592	6	−4	11	57	10.5
				−6	*−3*	*61*	*8.62*
Middle Frontal Gyrus	L	25528	9	−51	13	34	11.85
Precentral Gyrus			*4*	*−48*	*−11*	*50*	*9.94*
(b) Maintenance							
Precentral Gyrus	L	4664	6	−50	4	37	14.58
Middle Frontal Gyrus			*6*	*−42*	*2*	*50*	*7.05*
Superior Frontal Gyrus	L	4368	6	−4	6	48	9.45
Medial Frontal Gyrus	*R*		*32*	*2*	*8*	*46*	*6.72*
Superior Parietal Lobule	L	1680	7	−38	−56	49	8.57
Inferior Parietal Lobule	*L*		*40*	*−36*	*−54*	*41*	*5.26*
Inferior Parietal Lobule	R	1024	40	36	−56	45	5.78
Precentral Gyrus	R	1016	4	40	−17	56	4.87
(c) Recall in HC							
Cerebellum	L	156760		−24	−67	−25	9.85
	R			26	−62	−28	8.09
Middle Occipital Gyrus	*R*		*37*	*56*	*−62*	*08*	*6.63*
Superior Temporal Gyrus	*R*		*22*	*60*	*−48*	*16*	*6.55*
Inferior Parietal Lobule	*R*		*40*	*52*	*−44*	*38*	*6.10*
Supramarginal Gyrus	*L*		*40*	*−60*	*−46*	*30*	*7.83*
Superior Temporal Gyrus	*L*		*22*	*−54*	*−38*	*12*	*6.66*
Superior Frontal Gyrus	L	5688	38	−48	19	−11	5.92
Hippocampus	L	2720		−2	−2	−7	5.45
Thalamus	R	2640		−20	16	4	5.26
Cingulate Gyrus	L	2184	23	−4	−18	30	6.93
Cingulate Gyrus	R	1072	24	2	17	27	5.17
Middle Frontal Gyrus	L	2240	9	−53	13	31	6.08
Precentral Gyrus	L	1616	6	−40	−1	28	5.23
Precentral Gyrus	L	3200	6	−38	−10	63	6.37
Middle Frontal Gyrus	R	3968	47	22	36	−9	−7.31
Putamen	R	1016		26	9	−7	−6.61
(d) Recall in aMCI							
Medial Frontal Gyrus	L	4664	6	2	23	55	5.13
Anterior Cingulate	R	6840	10	6	40	−7	−5.84
Medial Frontal Gyrus	*L*		*10*	*−8*	*49*	*5*	*−5.22*
Middle Temporal Gyrus	R	992	21	40	6	32	−4.74

The volume is in micro Liters. Italicized values represent subpeaks of significant clusters. The T-score refers to the Student's *t*-value (df = 7); a *t* value of 5.41 is at the *p* = 0.0005 significance level.

Table 4

Statistical comparison of activation levels between the different phases of the WM task in the HC group (a) maintenance greater than encoding; (b) encoding greater than recall; (c) recall greater encoding; (d) maintenance greater than recall

Region	Side	Volume	BA	X	Y	Z	T-score
(a) Maintenance greater Encoding							
Precentral Gyrus	L	23760	6	−46	−10	32	11.01
Inferior Frontal Gyrus	L		9	−55	13	25	7.19
Anterior Cingulate	L		33	−6	20	19	6.71
Precuneus	L	247752	7	−26	−65	29	9.90
Precuneus	R		7	32	−75	46	7.31
Cuneus	R		23	2	−77	12	7.82
Inferior Occipital Gyrus	L		18	−36	−88	−7	7.67
Hippocampus	R			34	22	−12	6.79
Middle Temporal Gyrus	R	1336	22	44	−30	−2	6.76
Middle Frontal Gyrus	R	3664	6	30	3	59	6.30
(b)Encoding greater Recall							
Transverse Temporal Gyrus	R	8632	41	48	−19	10	6.35
Inferior Parietal Lobule			40	65	−33	31	4.85
Transverse Temporal Gyrus	L	3392		−53	−25	10	6.48
Middle Temporal Gyrus	R	2008	38	46	14	−39	4.94
Superior Temporal Gyrus	L	3133	22	−61	−57	19	6.81
(c)Recall greater Encoding							
Middle Temporal Gyrus	L	1064	21	−61	−27	−2	5.20
Parahippocampal Gyrus	L	1296	20	−36	−18	−16	4.09
Precuneus	L	15712	7	−24	−68	35	8.73
Superior Parietal Lobule			7	−28	−56	42	7.90
Superior Parietal Lobule	R	17560	7	30	−60	51	8.56
Inferior Parietal Lobule			40	42	−42	45	6.49
Putamen	R	2336		24	11	−4	10.59
Putamen	L	3872		−24	10	−4	8.22
Middle Occipital Gyrus	L	2304	19	−42	−68	−8	8.58
	R	4320	18	32	−89	1	7.06
	L	6136	18	−40	−85	4	6.74
Middle Frontal Gyrus	L	17560	6	−26	−3	50	8.56
Inferior Frontal Gyrus			44	−51	1	17	7.21
Middle Frontal Gyrus	L	3528	46	−42	26	19	7.44
Medial Frontal Gyrus	L	3552	6	−4	5	51	9.08
Cerebellum		2136		20	−77	−23	4.92
		2944		48	−52	−33	5.64
		1008		34	−61	−46	4.38
(d) Maintenance greater Recall							
Superior Temporal Gyrus	R	1336	38	55	15	−9	4.77
Inferior Parietal Lobule	R	2528	40	51	−52	41	6.58
Cingulate Gyrus	R	1328	23	2	−12	30	5.70
Postcentral Gyrus	R	1472	1	30	−33	70	5.34
	L	7024	5	−22	−45	70	5.08
Middle Occipital Gyrus	L	2704	19	−32	−91	10	5.78
Inferior Frontal Gyrus	R	1632	45	57	20	21	5.03
	L	2504	47	−50	21	−13	5.16
Superior Frontal Gyrus	L	1752	9	−16	50	34	4.17
Anterior Cingulate Gyrus	L	1638	24	0	33	8	6.40
Cerebellum	L	36256		−24	−57	−21	9.09
	R			30	−51	−18	5.88
Lingual Gyrus	R		18	2	−84	−8	5.34

The cluster volume is in micro Liters. Italicized values represent subpeaks of significant clusters. The T-score refers to the Student's *t*-value (df = 7); a *t* value of 5.41 is at the *p* = 0.0005 significance level.

Table 5
Statistical comparison of activation levels between the different phases of the WM task in the MCI group (a) encoding greater than maintenance; (b) encoding greater than recall; (c) maintenance greater than recall. Other contrasts such as recall greatr than maintenance are not included as no statistically differences were found

Region	Side	Volume	BA	X	Y	Z	T-score
(a) Encoding greater Maintenance							
Superior Temporal Gyrus	R	1466	22	52	−39	6	5.20
Putamen	R	1360		29	−17	3	5.16
Precentral Gyrus	R	1712	6	56	0	39	6.82
	L	2800	6	−56	−8	37	7.69
	R	1592	6	54	−6	30	5.33
Postcentral Gyrus	L	1064	3	−60	−10	22	5.01
Middle Occipital Gyrus	L	3224	18	−38	−89	4	8.47
Cerebellum	L	24384		−10	−75	−28	10.14
Inferior Occipital Gyrus	*L*		*18*	*−28*	*−90*	*−7*	*7.57*
Cuneus	*R*		*18*	*26*	*−97*	*−2*	*7.39*
(b) Encoding greater Recall							
Superior Temporal Gyrus	R	1168	21	66	−18	−2	5.50
Medial Frontal Gyrus	L	7326	6	0	10	47	8.06
Precentral Gyrus	R	8408	6	53	0	35	10.06
	L	15936	6	−53	−10	36	11.37
Inferior Frontal Gyrus	L	2848	45	−58	12	22	5.89
Putamen	R	2200		28	−10	4	5.91
Cerebellum	L	91144		−34	−69	−20	12.65
Fusiform Gyrus	*L*		*37*	*−36*	*−44*	*−18*	*8.22*
Cerebellum	*R*			*30*	*−69*	*−20*	*7.39*
Cuneus	*L*		*31*	*−24*	*−72*	*28*	*7.39*
Cerebellum	L	1136		−2	−64	−32	5.17
(c) Maintenance greater Recall							
Middle Temporal Gyrus	L	1056	22	−32	−58	18	5.41
Lingual Gyrus	L	1616	18	−6	−80	−13	5.20
Cerebellum	L	1296		−6	−82	−24	5.65

The cluster volume is in micro Liters. Italicized values represent subpeaks of significant clusters. The T-score refers to the Student's *t*-value (df = 7); a *t* value of 5.41 is at the *p* = 0.0005 significance level.

Table 6
Statistically significant higher activation peaks in the encoding phase (a) for MCI compared to HC and (b) for HC compared to MCI

Region	Side	Volume	BA	X	Y	Z	T-score
(a)							
Middle Temporal Gyrus	R	992	22	63	−37	6	5.22
Cerebellum	L	976		−42	−71	−18	4.61
(b)							
Middle Frontal Gyrus	R	1472	10	36	38	16	4.90
Anterior Cingulate	L	1176	32	−12	41	−4	4.98

The cluster volume is in micro Liters. The T-score refers to the Student's *t*-value (df = 14); a *t* value of 4.14 is at the *p* = 0.0005 significance level.

Table 7
Statistically significant clusters of higher activation in MCI compared to HC during the maintenance phase

Region	Side	Volume	BA	X	Y	Z	T-score
Lingual Gyrus	L	1232	18	−16	−70	0	5.66
Fusiform Gyrus	L	1192	19	−36	−69	−13	4.82
Superior Temporal Gyrus	L	912	39	−54	−61	20	4.28
Superior Temporal Gyrus	L	12096	22	−57	10	1	7.26
Precuneus	L	1136	7	−18	−54	47	5.01
		5680	7	−6	−62	51	5.49
Posterior Cingulate Gyrus	R	2760	29	6	−44	8	5.56
Inferior Frontal Gyrus	L	2456	45	−30	28	6	6.25
Middle Frontal Gyrus	L	3360	10	−38	38	22	5.06
Superior Frontal Gyrus	R	1016	6	6	28	54	6.39
Anterior Cingulate Gyrus	L	2472	32	−8	18	42	6.39
Medial Frontal Gyrus	L	2400	6	−8	5	55	5.72
	L	1144	6	−2	−26	69	5.51
	R	4296	9	22	32	26	5.13
Caudate	L	2040		0	2	7	4.85
Cerebellum	R	1816		28	−71	−27	5.53

The cluster volume is in micro Liters. The T-score refers to the Student's *t*-value (df = 14); a *t* value of 4.14 is at the *p* = 0.0005 significance level.

the activation differences between groups in the three phases of the WM task.

Single aMCI activation

One of the aMCI subjects had a 63% performance on the task and as exploratory step we examined the activation pattern of the correctly performed and correctly performed trials during the encoding and recall
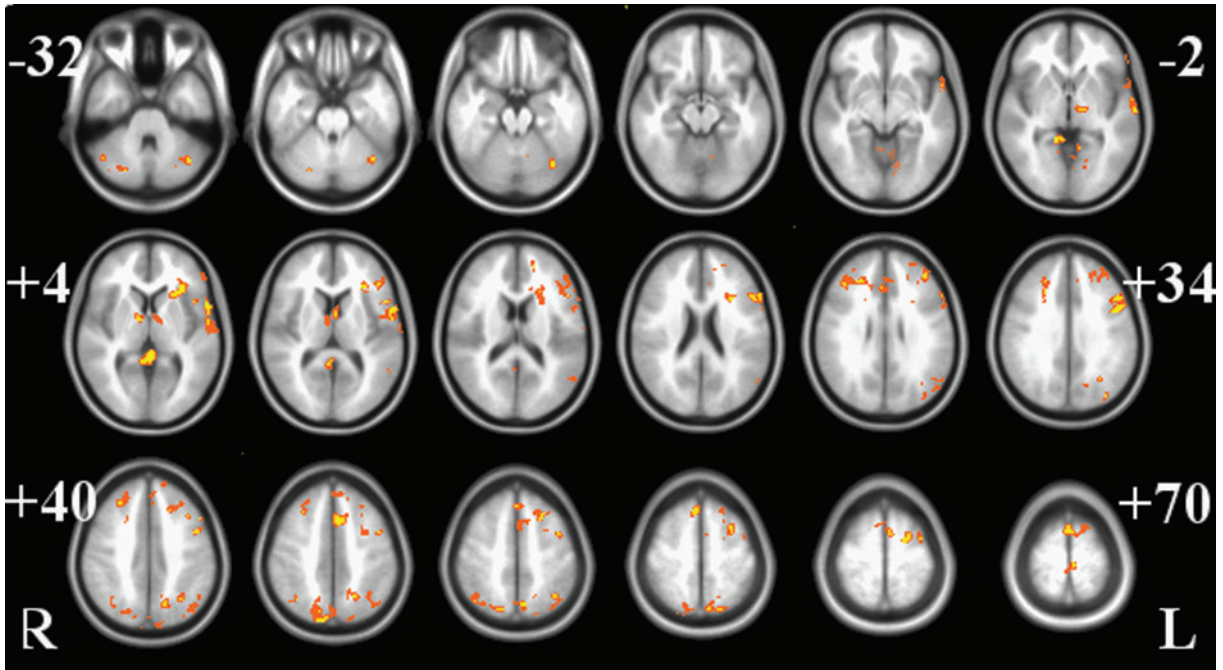
Fig. 4. The pattern of greater activation in the MCI subjects compared to the HC subjects in the areas where either group had positive activation during the maintenance phase.
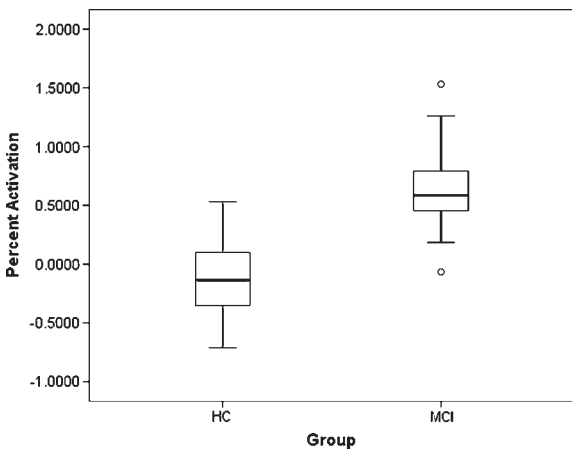
Fig. 5. The percent increase activation in the MCI and HC groups at the maxima of differences between groups in the left anterior cingulate gyrus (−8, 18, 42).
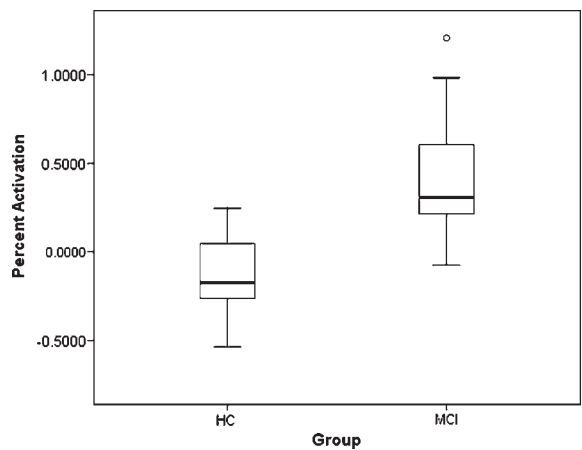
Fig. 6. The percent increase activation in the MCI and HC groups at the maxima of differences between groups in the left inferior frontal gyrus (−30, 28, 6).

phases. We found that for the correctly performed trials (Fig. 8) we had activation bilaterally on the hippocampus (encoding). In the recall phase we found right hippocampus activation dominating the activation pattern. In both phases, for the incorrectly performed trials we found no statistically significant activation (significance level at $p < 0.05$, no cluster correction).

DISCUSSION

In this study we have identified the regions that are activated in DMTS design of the WM task in older HC and MCI subjects. The results have shown that there is not a single network activated through the three different phases of the WM. The HC group had a "core" set of

Table 8
Statistically significant clusters of higher activation in HC compared to MCI during the recall phase

Region	Side	Volume	BA	X	Y	Z	T-score
Cuneus	L	2408	18	−12	−74	26	4.27
Superior Temporal Gyrus	L	1320	22	−44	−21	5	4.50
Precuneus	L	920	7	−6	−63	60	3.87
Medial Frontal Gyrus	R	1192	6	2	−13	52	5.85
Cerebellum	L	6296		−30	−69	120	4.65
	R	1744		4	−49	−18	4.59

The cluster volume is in micro Liters. The T-score refers to the Student's t-value (df = 14); a t value of 4.14 is at the $p = 0.0005$ significance level.

regions that were active through the entire task whereas the MCI group did not recruit a set of regions activated through all three phases of the WM task. There were differences in activation between both groups in all three phases, with the largest differences during the delay phase. The response time was found to be linearly associated to different areas of the brain in both groups, with the hippocampus associated with performance level in both groups but in different phases of the task.

The two groups of subjects were matched based on performance so that the alterations were not due to differences in performance between groups. The present results suggest that even when behavioral performance between groups does not differ, the neural systems that support performance may not be the same (see some previous studies supporting such a view such as [22, 25, 34]. The differences in activation pattern that we found may occur when the optimal or ideal network (as defined by the HC) is compromised by disease. In the case of the MCI group, the putative lesion or lesions that define a subject as having MCI, may be "partial" in the sense that the ideal network for the cognitive task is only partially damaged. Thus this could lead to mild changes in performance that may go undetected unless brain imaging techniques are utilized to measure altered brain activation during performance of a cognitive task.

The first novel contribution from this study was that the networks supporting WM in MCI subjects were altered in all phases of the task compared to the HC group. In the initial analysis step, the conjunction analysis showed the areas of common activation in both groups within the encoding and maintenance phase of the task which included the ventral and dorsolateral prefrontal cortices (VLPFC and DLPFC), inferior

parietal regions, and visual processing areas in occipital and temporal lobes. These areas have been shown to be activated in WM tasks in young subjects [13, 18, 51–57] and remain as part of the network supporting memory function in older HC and MCI subjects. The alterations in activation between the two groups (shown in Tables 6–8) were primarily located in temporal and frontal lobe areas. The largest difference between groups were during the maintenance phase with the MCI group requiring greater neural resources to maintain the information during the delay compared to the HC group. The greater demand of resources in the MCI group were located bilaterally in frontal areas and left hemispheric temporal lobe regions. The regions of the temporal lobe are associated with the visual processing of the stimuli (fusiform gyrus and lingual gyrus) and the superior temporal gyrus are areas associated with language processing [58–61] whereas the frontal lobe regions have been shown to be involved in both language and working memory tasks [13, 16, 18, 51–57, 62–63]. Studies that have examined normal aging processes in working memory found that bilateral frontal lobe activaiotn in older subjects was associated with performance – hence the increased activation could be interpreted as a compensatory process [17, 20, 22, 23] An alternative explanation for the differences in activation may be that the MCI group are using an alternative strategy – one possibility is that the MCI subjects are utilizing the visual spatial characteristics of the stimuli to perform the task and not attend to the actual letters in the stimuli.

The HC group activated a "core" set of regions, that is, the regions activated over the three phases of the WM task (indicated by yellow in Fig. 2) while the MCI group did not. The activation of the core regions found in the present study was consistent with previous studies, showing activation in inferior parietal areas, DLPFC, and language areas in the temporal lobe [26–28] to be key regions for verbal WM. The DLPFC is recruited for executive components of a task [64] and this region is also thought responsible for initiating the controlled processing of verbal working memory material [65, 66]. Prefrontal regions and inferior parietal regions have been previously identified as part of a network for maintaining the neural representation of the stimuli during the maintenance phase [13, 18, 51–57]. Parietal regions, with the highest extent during the encoding phase, reflect the stores affected by the working memory updating process [19, 67]. The areas that we found activated in all three phases may be due to (a) maintenance processes that are activate
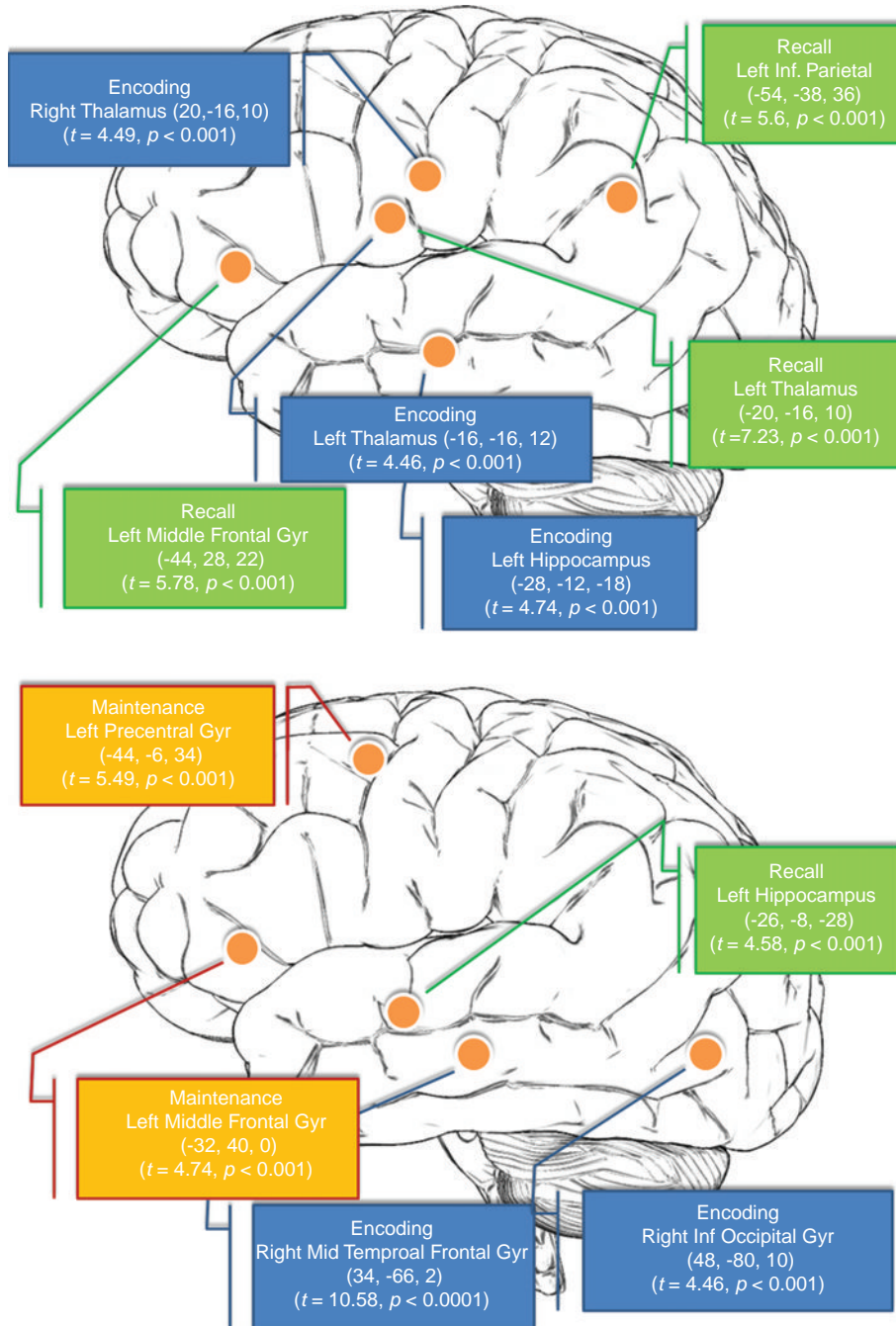
Fig. 7. Cartoon illustration of regions in the HC (upper image) and MCI group (lower image) where activation was linearly associated with response time. Regions with blue tag are during encoding phase, with orange tag during the delay phase, and with green tag during recall phase of task.

during encoding and recall phases or (b) these regions mediated computational processes that are common in all three phases such as phonological processing and access to long term memory. Previous studies that examined WM obtained the average activation pattern across all phases of the WM task or the n-back design was utilized, which did not allow for a separation of the different components of the task [26–28, 68].
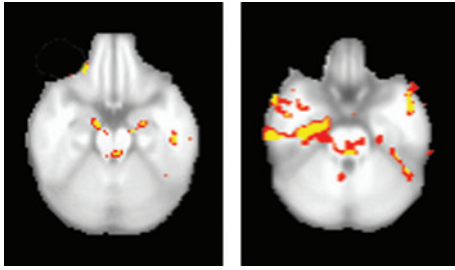
Fig. 8. Activation pattern of a single aMCI subject during the encoding (left image) and recall (right image) phase with 63% correct performance. There was no statistically significant activation for the incorrectly perfomed trials. Image is in MNI space, $z = -22$ mm, with left image being right hand side of the brain.

Task performance in the HC was linearly positively associated to activation in the left hippocampus and bilaterally the thalami during encoding and to the left inferior parietal region and middle frontal gyrus during recall. Thus for the HC group, the encoding and recall phases are critical for performance while the maintenance phase did not seem to play a role in performance. Greater activation of the hippocampus during encoding may indicate stronger representations of the memory trace and thus lead to more efficient retrieval in the later phase of the WM task. In addition, the inferior and middle frontal areas during recall are key areas for maintaining information in working memory but also support executive function during working memory. The positive association with thalamus activation in both phases may indicate greater interaction among the regions activated in the HC, that is, increased or stronger connectivity among the regions of the network may lead to greater performance. This issue would need further investigation to address.

We demonstrated in this study that the MCI use alternative regions to subserve performance of a WM task. Thus performance was positively associated with activation in regions not found in HC in all three phases. Grady and colleagues [34] were the first to find that performance was correlated to a compensatory network in an AD patient group during a semantic and episodic task. The linear correlation of response time to brain activation in regions of the right occipital-temporal lobes could indicate that the MCI subjects are performing the task as a visual-spatial task instead of a language task. Visual spatial tasks generally recruit regions in the right hemisphere but it is not a consistent finding [9, 69–71] and the differences in activation between the two groups may be due to different task strategies being used by the groups.

Within each group there were differences in activation among the different phases of the WM task. Even though there were many regions of common activation (see Figs. 2 and 3) the different phases of the task require activation of different regions among the three phases of the WM task. The differences are likely due to the different processes active in the working memory task and also due to compensatory mechanisms – see for example [9] for review of the processes active in WM. Given the significant activation in the prefrontal cortex in the MCI group during the WM task it may be that there is impairment in executive and attentional resources in the MCI group.

As an exploratory step we examined the activation pattern in correctly and incorrectly performed trials in one aMCI subject with a correct performance of 63%. We found in this subject that the activation pattern for the correctly performed trials in the encoding and recall phases had significant activation in hippocampus. Examination of the activation for the incorrectly performed trials showed no significant activation pattern – possible reasons for this may have been that subjects were not attending to the task during the trials, or may have had many different strategies that did not work. Another possibility is that there may have been confusion on the part of the participant about the task. This would need further investigation in a new study to make more definite statements.

We examined the grey matter (GM) density differences between groups using VBM. In the MCI group we found statistically significantly decreased GM density differences compared to the HC, particularly in medial temporal areas. Our two groups showed similar structural differences as shown by previous studies [72, 73]. Visual examination of the fMRI and VBM results showed that the differences between the MCI and HC groups were in different regions for the two modalities. A more detailed analysis integrating the two modalities is necessary, such as performed by Oakes and colleagues [74], to make statements about the possible interaction between brain activation and GM density.

A limitation of the current study is the small numbers of HC and MCI subjects. It would be useful to reproduce the study with a larger cohort. In addition, acceptance and rejection of the probes during the recall phase lead to different processes and activation pattern [75, 76] and it was not controlled for in this study. It would be of interest in a follow up study to examine these differences due to memory impairments. In addition, in the current analysis it was assumed that the hemodynamic response function (HRF) was well modeled

across subjects and across groups. A study by Rombouts and colleagues showed that there can be variation in the delay or shape of the HRF [77] and found that from 7 regressors used to model the variance in delay and shape of the HRF, 2 of the regressors were statistically significant between HC and MCI in the visual cortex. One of the possible interpretations is that it indicates differences in the vascular coupling between MCI and HC groups or that it may be another measure of the effects of AD related neuropathology in the brain. Examination of these effects could potentially be used as an additional neuroimaging-based marker for discriminating between HC and patients groups.

A limitation in the study to be aware of is that in delay match to sample designs, particularly with short delay phases as in the current study, part of the activation that is due to the encoding processes may appear as activation in the delay phase because the encoding phase is short. One approach around this limitation is to have a long delay phase (for example 30 seconds) and model the activation in the delay phase with two different regressors. One regressor would model the first part of the delay phase (i.e. first 10 seconds) and the other regressor the last part of the delay phase (i.e. the later 20 seconds). Thus the activation modeled by the second regressor would be taken as the activation during the delay phase as it is unlikely to have activation due to encoding processes. Another approach would be to orthogonalize the regressors but then the challenge is that interpretation of the results can be difficult as the shape of the orthogonal regressors may not reflect the cognitive processes one wishes to investigate. Related to the previous limitation is that the time between trials (5.5 sec) in the task may not be sufficient to separate the activation in the recall phase from the encoding phase in the following trial. The time between trials should have been longer.

Even though the MCI group has a high risk of converting to AD, not all subjects will convert to dementia as some may remain stable in this domain or may even revert to normal cognitive domain [3, 35, 78–81]. The MCI group is likely to have subjects that will not convert to AD and thus it would be valuable to follow-up this group of subjects and see how the composition of the group develops.

This has been the first study that has examined working memory in MCI subjects using a event related design. A next possible step for examining working memory would be examining the effective connectivity differences between groups and doing longitudinal follow-up studies.

ACKNOWLEDGMENTS

REFERENCES

[1] Winblad B, Palmer K, Kivipelto M, Jelic V, Fratiglioni L, Wahlund LO, Nordberg A, Backman L, Albert M, Almkvist O, Arai H, Basun H, Blennow K, de Leon M, DeCarli C, Erkinjuntti T, Giacobini E, Graff C, Hardy J, Jack C, Jorm A, Ritchie K, van Duijn C, Visser P, Petersen RC (2004) Mild cognitive impairment–beyond controversies, towards a consensus: report of the international working group on mild cognitive impairment. *J Intern Med* **256**, 240-246.

[2] Petersen RC, Doody R, Kurz A, Mohs RC, Morris JC, Rabins PV, Ritchie K, Rossor M, Thal L, Winblad B (2001) Current concepts in mild cognitive impairment. *Arch Neurol* **58**, 1985-1992.

[3] Larrieu S, Letenneur L, Orgogozo JM, Fabrigoule C, Amieva H, Le Carret N, Barberger-Gateau P, Dartigues JF (2002) Incidence and outcome of mild cognitive impairment in a population-based prospective cohort. *Neurology* **59**, 1594-1599.

[4] Amieva H, Letenneur L, Dartigues JF, Rouch-Leroyer I, Sourgen C, D'Alchee-Biree F, Dib M, Barberger-Gateau P, Orgogozo JM, Fabrigoule C (2004) Annual rate and predictors of conversion to dementia in subjects presenting mild cognitive impairment criteria defined according to a population-based study. *Dement Geriatr Cogn Disord* **18**, 87-93.

[5] Tervo S, Kivipelto M, Hanninen T, Vanhanen M, Hallikainen M, Mannermaa A, Soininen H (2004) Incidence and risk factors for mild cognitive impairment: a population-based three-year follow-up study of cognitively healthy elderly subjects. *Dement Geriatr Cogn Disord* **17**, 196-203.

[6] Tabert MH, Manly JJ, Liu X, Pelton GH, Rosenblum S, Jacobs M, Zamora D, Goodkind M, Bell K, Stern Y, Devanand DP (2006) Neuropsychological prediction of conversion to Alzheimer disease in patients with mild cognitive impairment. *Arch Gen Psychiatry* **63**, 916-924.

[7] Ishikawa T, Ikeda M, Matsumoto N, Shigenobu K, Brayne C, Tanabe H (2006) A longitudinal study regarding conversion from mild memory impairment to dementia in a Japanese community. *Int J Geriatr Psychiatry* **21**, 134-139.

[8] Baddeley A (1997) *Human Memory*, Psychology Press,. East Sussex,.

[9]   Wager TD, Smith EE (2003) Neuroimaging studies of working memory: a meta-analysis. *Cogn Affect Behav Neurosci* **3**, 255-274.

[10] Smith EE, Jonides J (1998) Neuroimaging analyses of human working memory. *Proc Natl Acad Sci U S A* **95**, 12061-12068.

[11] Economou A, Papageorgiou SG, Karageorgiou C, Vassilopoulos D (2007) Nonepisodic memory deficits in amnestic MCI. *Cogn Behav Neurol* **20**, 99-106.

[12] Kensinger EA, Shearer DK, Locascio JJ, Growdon JH, Corkin S (2003) Working memory in mild Alzheimer's disease and early Parkinson's disease. *Neuropsychology* **17**, 230-239.

[13] Courtney SM, Ungerleider LG, Keil K, Haxby JV (1997) Transient and sustained activity in a distributed neural system for human working memory. *Nature* **386**, 608-611.

[14] Ungerleider LG, Courtney SM, Haxby JV (1998) A neural system for human visual working memory. *Proc Natl Acad Sci U S A* **95**, 883-890.

[15] Nystrom LE, Braver TS, Sabb FW, Delgado MR, Noll DC, Cohen JD (2000) Working memory for letters, shapes, and locations: fMRI evidence against stimulus-based regional organization in human prefrontal cortex. *Neuroimage* **11**, 424-446.

[16] Smith EE, Jonides J, Marshuetz C, Koeppe RA (1998) Components of verbal working memory: evidence from neuroimaging. *Proc Natl Acad Sci U S A* **95**, 876-882.

[17] Jonides J, Marshuetz C, Smith EE, Reuter-Lorenz PA, Koeppe RA, Hartley A (2000) Age differences in behavior and PET activation reveal differences in interference resolution in verbal working memory. *J Cogn Neurosci* **12**, 188-196.

[18] Jonides J, Schumacher E, Smith E, Lauber E, Awh E (1997) Verbal working memory load affects regional brain activation as measured by PET. *J Cogn Neurosci* **9**, 462-473.

[19] Jonides J, Schumacher EH, Smith EE, Koeppe RA, Awh E, Reuter-Lorenz PA, Marshuetz C, Willis CR (1998) The role of parietal cortex in verbal working memory. *J Neurosci* **18**, 5026-5034.

[20] Grady CL, Yu H, Alain C (2008) Age-related differences in brain activity underlying working memory for spatial and nonspatial auditory information. *Cereb Cortex* **18**, 189-199.

[21] Grady CL, McIntosh AR, Bookstein F, Horwitz B, Rapoport SI, Haxby JV (1998) Age-related changes in regional cerebral blood flow during working memory for faces. *Neuroimage* **8**, 409-425.

[22] Smith EE, Geva A, Jonides J, Miller A, Reuter-Lorenz P, Koeppe RA (2001) The neural basis of task-switching in working memory: effects of performance and aging. *Proc Natl Acad Sci U S A* **98**, 2095-2100.

[23] Reuter-Lorenz PA, Jonides J, Smith EE, Hartley A, Miller A, Marshuetz C, Koeppe RA (2000) Age differences in the frontal lateralization of verbal and spatial working memory revealed by PET. *J Cogn Neurosci* **12**, 174-187.

[24] Gazzaley A, Cooney JW, Rissman J, D'Esposito M (2005) Top-down suppression deficit underlies working memory impairment in normal aging. *Nat Neurosci* **8**, 1298-1300.

[25] Gazzaley A, Sheridan MA, Cooney JW, D'Esposito M (2007) Age-related deficits in component processes of working memory. *Neuropsychology* **21**, 532-539.

[26] Goekoop R, Rombouts SA, Jonker C, Hibbel A, Knol DL, Truyen L, Barkhof F, Scheltens P (2004) Challenging the cholinergic system in mild cognitive impairment: a pharmacological fMRI study. *Neuroimage* **23**, 1450-1459.

[27] Saykin AJ, Wishart HA, Rabin LA, Flashman LA, McHugh TL, Mamourian AC, Santulli RB (2004) Cholinergic enhance-
ment of frontal lobe activity in mild cognitive impairment. *Brain* **127**, 1574-1583.

[28] Dohnel K, Sommer M, Ibach B, Rothmayr C, Meinhardt J, Hajak G (2007) Neural correlates of emotional working memory in patients with mild cognitive impairment. *Neuropsychologia* **46**, 37-48.

[29] Celone KA, Calhoun VD, Dickerson BC, Atri A, Chua EF, Miller SL, DePeau K, Rentz DM, Selkoe DJ, Blacker D, Albert MS, Sperling RA (2006) Alterations in memory networks in mild cognitive impairment and Alzheimer's disease: an independent component analysis. *J Neurosci* **26**, 10222-10231.

[30] Hamalainen A, Pihlajamaki M, Tanila H, Hanninen T, Niskanen E, Tervo S, Karjalainen PA, Vanninen RL, Soininen H (2007) Increased fMRI responses during encoding in mild cognitive impairment. *Neurobiol Aging* **28**, 1889-1903.

[31] Dickerson BC, Salat DH, Bates JF, Atiya M, Killiany RJ, Greve DN, Dale AM, Stern CE, Blacker D, Albert MS, Sperling RA (2004) Medial temporal lobe function and structure in mild cognitive impairment. *Ann Neurol* **56**, 27-35.

[32] Bokde ALW, Lopez-Bayo P, Born C, Dong W, Meindl T, Leinsinger G, Teipel SJ, Faltraco F, Reiser M, Möller H-J, Hampel H (2008) Functional abnormalities of the visual processing system in subjects with mild cognitive impairment: an fMRI study. *Psychiatr Res: Neuroimaging* **163**, 248-259.

[33] Rosenbaum RS, Furey ML, Horwitz B, Grady CL (2008) Altered connectivity among emotion-related brain regions during short-term memory in Alzheimer's disease. *Neurobiol Aging* **31**, 780-786.

[34] Grady CL, McIntosh AR, Beig S, Keightley ML, Burian H, Black SE (2003) Evidence from functional neuroimaging of a compensatory prefrontal network in Alzheimer's disease. *J Neurosci* **23**, 986-993.

[35] Petersen RC, Smith GE, Waring SC, Ivnik RJ, Tangalos EG, Kokmen E (1999) Mild cognitive impairment: clinical characterization and outcome. *Arch Neurol* **56**, 303-308.

[36] Petersen RC, Stevens JC, Ganguli M, Tangalos EG, Cummings JL, DeKosky ST (2001) Practice parameter: early detection of dementia: mild cognitive impairment (an evidence-based review): Report of the Quality Standards Subcommittee of the American Academy of Neurology. *Neurology* **56**, 1133-1142.

[37] Morris JC, Heyman A, Mohs RC, Hughes JP, van Belle G, Fillenbaum G, Mellits ED, Clark C (1989) The Consortium to Establish a Registry for Alzheimer's Disease (CERAD). Part I. Clinical and neuropsychological assessment of Alzheimer's disease. *Neurology* **39**, 1159-1165.

[38] Berres M, Monsch AU, Bernasconi F, Thalmann B, Stahelin HB (2000) Normal ranges of neuropsychological tests for the diagnosis of Alzheimer's disease. *Stud Health Technol Inform* **77**, 195-199.

[39] Welsh KA, Butters N, Mohs RC, Beekly D, Edland S, Fillenbaum G, Heyman A (1994) The Consortium to Establish a Registry for Alzheimer's Disease (CERAD). Part V. A normative study of the neuropsychological battery. *Neurology* **44**, 609-614.

[40] Gray T, Kiehl K (2002) Visual and Auditory Presentation Package. http://nrc-iol.org/vapp/index.htm - accessed March 2011.

[41] Cox RW (1996) AFNI: software for analysis and visualization of functional magnetic resonance neuroimages. *Comput Biomed Res* **29**, 162-173.

[42] Smith AD, Jenkinson M, Woolrich MW, Beckmann CF, Behrens TE, Johansen-Berg H, Bannister PR, De Luca M,

Drobnjak I, Flitney DE, Niazy R, Saunders J, Vickers J, Zhang Y, De Stefano N, Brady JM, Matthews PM (2004) Advances in funcitonal and structural MR image analysis and implementation as FSL. *Neuroimage* **23**, 208-219.

[43] Ashburner J, Friston KJ (2000) Voxel-based morphometry–the methods. *Neuroimage* **11**, 805-821.

[44] Good CD, Johnsrude IS, Ashburner J, Henson RN, Friston KJ, Frackowiak RS (2001) A voxel-based morphometric study of ageing in 465 normal adult human brains. *Neuroimage* **14**, 21-36.

[45] Smith SM (2002) Fast robust automated brain extraction. *Hum Brain Mapp* **17**, 143-155.

[46] Zhang Y, Brady M, Smith S (2001) Segmentation of brain MR images through a hidden Markov random field model and the expectation-maximization algorithm. *IEEE Trans Med Imaging* **20**, 45-57.

[47] Jenkinson M, Bannister P, Brady M, Smith S (2002) Improved optimization for the robust and accurate linear registration and motion correction of brain images. *Neuroimage* **17**, 825-841.

[48] Jenkinson M, Smith S (2001) A global optimisation method for robust affine registration of brain images. *Med Image Anal* **5**, 143-156.

[49] Rueckert D, Sonoda LI, Hayes C, Hill DL, Leach MO, Hawkes DJ (1999) Nonrigid registration using free-form deformations: application to breast MR images. *IEEE Trans Med Imaging* **18**, 712-721.

[50] Talaraich J, Tournoux P (1988) *Co-Planar stereotaxic atlas of the human brain*, Thieme Medical, New York.

[51] Courtney SM, Ungerleider LG, Keil K, Haxby JV (1996) Object and spatial visual working memory activate separate neural systems in human cortex. *Cereb Cortex* **6**, 39-49.

[52] Braver TS, Cohen JD, Nystrom LE, Jonides J, Smith EE, Noll DC (1997) A parametric study of prefrontal cortex involvement in human working memory. *Neuroimage* **5**, 49-62.

[53] Klingberg T, O'Sullivan BT, Roland PE (1997) Bilateral activation of fronto-parietal networks by incrementing demand in a working memory task. *Cereb Cortex* **7**, 465-471.

[54] Courtney SM, Petit L, Haxby JV, Ungerleider LG (1998) The role of prefrontal cortex in working memory: examining the contents of consciousness. *Philos Trans R Soc Lond B Biol Sci* **353**, 1819-1828.

[55] Petit L, Courtney SM, Ungerleider LG, Haxby JV (1998) Sustained activity in the medial wall during working memory delays. *J Neurosci* **18**, 9429-9437.

[56] Rypma B, D'Esposito M (1999) The roles of prefrontal brain regions in components of working memory: effects of memory load and individual differences. *Proc Natl Acad Sci U S A* **96**, 6558-6563.

[57] Fiebach CJ, Rissman J, D'Esposito M (2006) Modulation of inferotemporal cortex activation during verbal working memory maintenance. *Neuron* **51**, 251-261.

[58] Rotte M (2005) Age-related differences in the areas of Broca and Wernicke using functional magnetic resonance imaging. *Age Ageing* **34**, 609-613.

[59] Binder JR, Frost JA, Hammeke TA, Cox RW, Rao SM, Prieto T (1997) Human brain language areas identified by functional magnetic resonance imaging. *J Neurosci* **17**, 353-362.

[60] Tagamets MA, Novick JM, Chalmers ML, Friedman RB (2000) A parametric approach to orthographic processing in the brain: an fMRI study. *J Cogn Neurosci* **12**, 281-297.

[61] Bokde AL, Tagamets MA, Friedman RB, Horwitz B (2001) Functional interactions of the inferior frontal cortex during the processing of words and word-like stimuli. *Neuron* **30**, 609-617.

[62] Cohen JD, Perlstein WM, Braver TS, Nystrom LE, Noll DC, Jonides J, Smith EE (1997) Temporal dynamics of brain activation during a working memory task. *Nature* **386**, 604-608.

[63] Honey GD, Fu CH, Kim J, Brammer MJ, Croudace TJ, Suckling J, Pich EM, Williams SC, Bullmore ET (2002) Effects of verbal working memory load on corticocortical connectivity modeled by path analysis of functional magnetic resonance imaging data. *Neuroimage* **17**, 573-582.

[64] Hautzel H, Mottaghy FM, Schmidt D, Zemb M, Shah NJ, Muller-Gartner HW, Krause BJ (2002) Topographic segregation and convergence of verbal, object, shape and spatial working memory in humans. *Neurosci Lett* **323**, 156-160.

[65] Park DC, Lautenschlager G, Hedden T, Davidson NS, Smith AD, Smith PK (2002) Models of visuospatial and verbal memory across the adult life span. *Psychol Aging* **17**, 299-320.

[66] Whitwell JL, Sampson EL, Watt HC, Harvey RJ, Rossor MN, Fox NC (2005) A volumetric magnetic resonance imaging study of the amygdala in frontotemporal lobar degeneration and Alzheimer's disease. *Dement Geriatr Cogn Disord* **20**, 238-244.

[67] Schumacher EH, Lauber E, Awh E, Jonides J, Smith EE, Koeppe RA (1996) PET evidence for an amodal verbal working memory system. *Neuroimage* **3**, 79-88.

[68] Rombouts SA, Barkhof F, Van Meel CS, Scheltens P (2002) Alterations in brain activation during cholinergic enhancement with rivastigmine in Alzheimer's disease. *J Neurol Neurosurg Psychiatry* **73**, 665-671.

[69] Haxby JV, Grady CL, Koss E, Horwitz B, Heston L, Schapiro M, Friedland RP, Rapoport SI (1990) Longitudinal study of cerebral metabolic asymmetries and associated neuropsychological patterns in early dementia of the Alzheimer type. *Arch Neurol* **47**, 753-760.

[70] Yeh YY, Kuo BC, Liu HL (2007) The neural correlates of attention orienting in visuospatial working memory for detecting feature and conjunction changes. *Brain Res* **1130**, 146-157.

[71] Fink GR, Dolan RJ, Halligan PW, Marshall JC, Frith CD (1997) Space-based and object-based visual attention: shared and specific neural domains. *Brain* **120**, 2013-2028.

[72] Karas GB, Scheltens P, Rombouts SA, Visser PJ, van Schijndel RA, Fox NC, Barkhof F (2004) Global and local gray matter loss in mild cognitive impairment and Alzheimer's disease. *Neuroimage* **23**, 708-716.

[73] Teipel SJ, Born C, Ewers M, Bokde AL, Reiser MF, Moller HJ, Hampel H (2007) Multivariate deformation-based analysis of brain atrophy to predict Alzheimer's disease in mild cognitive impairment. *Neuroimage* **38**, 13-24.

[74] Oakes TR, Fox AS, Johnstone T, Chung MK, Kalin N, Davidson RJ (2007) Integrating VBM into the General Linear Model with voxelwise anatomical covariates. *Neuroimage* **34**, 500-508.

[75] Jonides J, Smith EE, Marshuetz C, Koeppe RA, Reuter-Lorenz PA (1998) Inhibition in verbal working memory revealed by brain activation. *Proc Natl Acad Sci U S A* **95**, 8410-8413.

[76] Nelson JK, Reuter-Lorenz PA, Sylvester CY, Jonides J, Smith EE (2003) Dissociable neural mechanisms underlying response-based and familiarity-based conflict in working memory. *Proc Natl Acad Sci U S A* **100**, 11171-11175.

[77] Rombouts SA, Goekoop R, Stam CJ, Barkhof F, Scheltens P (2005) Delayed rather than decreased BOLD response as a marker for early Alzheimer's disease. *Neuroimage* **26**, 1078-1085.

[78] Fisk JD, Merry HR, Rockwood K (2003) Variations in case definition affect prevalence but not outcomes of mild cognitive impairment. *Neurology* **61**, 1179-1184.

[79] Artero S, Tierney MC, Touchon J, Ritchie K (2003) Prediction of transition from cognitive impairment to senile dementia: a prospective, longitudinal study. *Acta Psychiatr Scand* **107**, 390-393.

[80] Lopez OL, Jagust WJ, DeKosky ST, Becker JT, Fitzpatrick A, Dulberg C, Breitner J, Lyketsos C, Jones B, Kawas C, Carlson M, Kuller LH (2003) Prevalence and classification of mild cognitive impairment in the cardiovascular health study cognition study: part 1. *Arch Neurol* **60**, 1385-1389.

[81] Visser PJ, Kester A, Jolles J, Verhey F (2006) Ten-year risk of dementia in subjects with mild cognitive impairment. *Neurology* **67**, 1201-1207.

331

Disease Tracking Markers for Alzheimer's Disease at the Prodromal (MCI) Stage

Valeria Drago[a], Claudio Babiloni[b], David Bartrés-Faz[c], Anna Caroli[a,e], Beatriz Bosch[c], Tilman Hensch[d], Mira Didic[f], Hans-Wolfgang Klafki[g], Michela Pievani[a], Jorge Jovicich[h], Luca Venturi[a], Philipp Spitzer[g], Fabrizio Vecchio[i], Peter Schoenknecht[d], Jans Wiltfang[g], Alberto Redolfi[a], Gianluigi Forloni[j], Olivier Blin[k], Elaine Irving[l], Ceri Davis[l], Hans-goran Hårdemark[m] and Giovanni B. Frisoni[a,*]

[a]*LENITEM Laboratory of Epidemiology, Neuroimaging and Telemedicine, IRCCS "San Giovanni di Dio – Fatebenefratelli", Brescia, Italy*
[b]*Department of Biomedical Sciences, University of Foggia, Foggia, Italy*
[c]*Institut d'Investigació Biomèdiques August Pi i Sunyer (IDIBAPS), Barcelona, Departament de Psiquiatria i Psicobiologia Clínica, Facutat de Medicina, Universitat de Barcelona, and Alzheimer's disease and other cognitive disorders unit, Neurology Service, Hospital Clínic de Barcelona, Barcelona, Spain*
[d]*Department of Psychiatry, University of Leipzig, Leipzig, Germany*
[e]*Medical Imaging Unit, Biomedical Engineering Department, Mario Negri, Institute for Pharmacological Research, Bergamo*
[f]*Service de Neurologie et de Neuropsychologie, Pôle de neurosciences cliniques, Assistance Publique des Hôpitaux de Marseille, Hôpitaux de la Timone, CMRR PACA Ouest & INSERM U751, Faculté de Médecine, Université de la Méditerranée, Marseille, France*
[g]*Department of Psychiatry and Psychotherapy, University of Duisburg-Essen, LVR-Klinikum, Essen, Germany*
[h]*Functional NeuroImaging Laboratory, Center for Mind Brain Sciences, University of Trento*
[i]*A.Fa.R., Dip. Neurosci. Osp. FBF, Isola Tiberina, Rome, Italy*
[j]*Istituto di Ricerche Farmacologiche "Mario Negri"*
[k]*Clinical Investigation Centre (CIC-UPCET) and Department of Clinical Pharmacology, UMR-CNRS, 6193 Institute of Cognitive Neurosciences, CHU, Timone, Marseille, France*
[l]*Neurosciences CEDD, GlaxoSmithKline, Harlow, Essex, UK*
[m]*AstraZencea R&D Clinical Neuroscience Therapy Area SE-151 85 Södertälje, Sweden*

Abstract. Older persons with Mild Cognitive Impairment (MCI) feature neurobiological Alzheimer's Disease (AD) in 50% to 70% of the cases and develop dementia within the next 5 to 7 years. Current evidence suggests that biochemical, neuroimaging, electrophysiological, and neuropsychological markers can track the disease over time since the MCI stage (also called prodromal AD). The amount of evidence supporting their validity is of variable strength. We have reviewed the current literature and categorized evidence of validity into three classes: Class A, availability of multiple serial studies; Class B a single serial study or multiple cross sectional studies of patients with increasing disease severity from MCI to probable AD; and class C, multiple

*Correspondence to: Giovani B. Frisoni, Via Pilastroni 1, 25125, Brescia, Italy. Tel.: +39 030 35011; Fax: +39 030 348255; E-mail: gfrisoni@fatebenefratelli.it.

cross sectional studies of patients in the dementia stage, not including the MCI stage. Several Class A studies suggest that episodic memory and semantic fluency are the most reliable neuropsychological markers of progression. Hippocampal atrophy, ventricular volume and whole brain atrophy are structural MRI markers with class A evidence. Resting-state fMRI and connectivity, and diffusion MR markers in the medial temporal white matter (parahippocampus and posterior cingulum) and hippocampus are promising but require further validation. Change in amyloid load in MCI patients warrant further investigations, e.g. over longer period of time, to assess its value as marker of disease progression. Several spectral markers of resting state EEG rhythms that might reflect neurodegenerative processes in the prodromal stage of AD (EEG power density, functional coupling, spectral coherence, and synchronization) suffer from lack of appropriately designed studies. Although serial studies on late event-related potentials (ERPs) in healthy elders or MCI patients are inconclusive, others tracking disease progression and effects of cholinesterase inhibiting drugs in AD, and cross-sectional including MCI or predicting development of AD offer preliminary evidence of validity as a marker of disease progression from the MCI stage. CSF Markers, such as $A\beta_{1-42}$, *t*-tau and *p*-tau are valuable markers which support the clinical diagnosis of Alzheimer´s disease. However, these markers are not sensitive to disease progression and cannot be used to monitor the severity of Alzheimer´s disease. For Isoprostane F2 some evidence exists that its increase correlates with the progression and the severity of AD.

INTRODUCTION

There is considerable evidence to support the concept that Alzheimer's disease (AD) has a long preclinical period [1]. For example, some of the biochemical changes that precede the clinical onset of AD may be present up to 20 years before the onset of this dementia [1–3]. Thus there are many people who already have pathological alterations of AD several decades before the clinical onset of the sign and symptoms.

Recently much of the literature has been directed to patients with prodromal AD (Mild Cognitive Impairment (MCI). MCI is often a precursor to Alzheimer's dementia and the annual rate of development of AD for patients with MCI is 10 to 15% [4, 5]. Some individuals, however, do not show progression of symptoms and do not develop dementia. Some even improve and these individuals who do not progress or even show improvement do not have AD. While it is important to search for treatable causes of AD, it is important to track patients with MCI who will progress and develop dementia and those who will not in order to study what are the most sensible markers to disease progression.

A "marker of disease progression" is a marker sensitive to cognitive deterioration, thus a marker that can be used to track the progression of the disease or the effectiveness of a disease modifying drug. A "marker of disease state" can be used to diagnose AD in patients with MCI, i.e. to predict which patients with MCI will progress to dementia and those who will not. Although a marker of disease state might also be a sensitive marker of disease progression, in this review we will

focus on studies on markers of disease progression. Although we are aware that some of the markers of disease progression are also good markers of disease state, the literature regarding markers of disease state has been neglected since it was not within the scope of this review.

Currently available evidence from longitudinal and cross sectional clinical studies suggest that markers such as neuropsychological tests, neuroimaging, including structural magnetic resonance imaging (MRI), diffusion tensor imaging (DTI), functional MRI (fMRI), spectroscopy, positron emission tomography (PET), EEG, event-related potentials (ERP), as well as cerebrospinal fluid (CSF) analysis may be sensitive to cognitive deterioration. The evidence of these markers validity and sensitivity is variable, with some markers being supported by rigorous serial studies, and others merely suggestive based on cross sectional observations. For these latter markers there is a need for additional validation that these biomarkers track disease progression.

The aim of this paper is to review the studies that have been conducted in the past 10 years (2000–2010) using neuropsychological tests, neuroimaging, neurophysiological and biochemical markers of disease progression in patients with MCI. This review will identify the markers that have the greatest evidence for being valid markers of disease progression as well as those that have received less support and those that might be the most promising.

Validity has been assessed identifying studies showing parallel changes between the candidate

Table 1
Categorization of markers of disease progression based on literature evidence of validity

Class A	Validity demonstrated by multiple serial studies
Class B	Validity demonstrated by a single serial study or multiple cross sectional studies of patients at different severity stages including MCI
Class C	Validity demonstrated by multiple cross sectional studies of patients at different severity stages, but not including MCI (studies on AD patients at the dementia stage only)

"progression" marker and some measure of clinical deterioration (e.g. Mini Mental State Evalutation).

The related topic of reliability addresses whether repeated measurements or assessments provide a consistent result given the same initial circumstances. Clearly, after identifying candidate markers on the basis of group studies, it will be necessary to assess the reliability of such validated markers by testing their ability to predictively classify individual subjects.

We decided to focus on modalities used in the context of the "PHARMA-COG" project*. Recently the EU Council of Ministers for Health underlined the importance of generating novel therapeutic agents both for symptomatic and disease modifying treatment of Alzheimer's disease (AD). Bringing together European experts in technologies fully translatable from animal to human, experts in translational medicine, drug discovery and mathematical modelling, "PHARMA-COG" proposes to accelerate this validation using a 'MATRIX' approach i.e. conducting parallel experiments in animals and human using a comprehensive and standardised battery of behavioural, neurophysiological, morphological/functional imaging, and biochemical endpoints to: develop models with greater predictive capacity for the clinics, develop and validate translatable pharmacodynamic markers to support dose selection, develop challenge models to support early hint of efficacy studies, identify and validate of markers of disease progression.

In this review we have categorized these markers into three classes of decreasing strength of evidence, as illustrated in Table 1.

NEUROPSYCHOLOGY

The neuropathological changes of Alzheimer's dementia (AD) appear well before the disease becomes clinically apparent. At the prodromic stage of the disease (MCI), there are often subtle cognitive signs; however there are currently no reliable and validated diagnostic neuropsychological test results that are able to track progression to AD.

One of the first and most common cognitive domains to be affected in individuals that have been diagnosed with a Mild Cognitive Impairment (MCI) is episodic memory. Impaired episodic memory in AD is caused by neuropathological changes that result in dysfunction of the mesial temporal lobe. Neurofibrillary tangles, related to the clinical signs of AD [6], first appear in the mesial temporal lobe [7], sequentially affecting the entorhinal cortex and the hippocampus. Recently, there has also been evidence for a relationship between episodic memory loss and hippocampal-mediated beta-amyloid deposition in elderly subjects and in AD [8]. In addition to atrophy of the medial temporal lobes that accounts for these patients' amnestic disorder, areas of polymodal cortex such as the frontal and parietal lobes can be involved even early in AD [9]. Dysfunction of these regions may impair cognitive functions such as verbal and semantic fluency.

Class A markers

In our review of the literature, we did find several studies that systematically examined the course of episodic memory changes in patients affected by MCI [10–13]. Although the authors of these studies used different tests to assess learning and episodic memory and their follow up intervals were different (from 1.5 up to 6 years), the majority of them indicate a decline of learning and episodic memory in individuals affected by MCI, providing converging evidence for considering declining episodic memory as a good marker of disease progression.

Another neuropsychological marker that has been widely investigated in longitudinal studies of individuals affected by MCI is working memory. Backman [10] and Bennett [13] used the digit span backward and forward, the alpha span as well as digit ordering to assess working memory. These studies used a group of healthy controls who eventually developed AD during the course of the study and a group of MCI and healthy elderly controls respectively. These studies did not find that a temporal change in working memory performances was a useful marker of progression.

Semantic fluency has also been thought to be a potential marker of disease progression. In order to produce as many words as possible that come from the same semantic category the subject needs to have a good retrieval strategy, which may be an executive

Table 2
Neuropsychological markers of disease progression based on literature evidence of validity

Marker	N of subject and diagnosis	Time B-FU[1]	Results	References
CLASS A				
Learning and memory	*MCI 15;* HC 105	3 years	Stable	Bäckman et al., 2001
	33 HC; 22 sMCI[2]; 95 dMCI; *47 Converters*	4 years	Decline	Albert et al., 2007
	20AD; *40 MCI;* 40 HC	1 year	Decline	Leow et al., 2009
	211 MCI; 587 HC	6 years	Decline	Bennett et al., 2002
Working Memory	*211 MCI*; 587 HC	6 years	Stable	Bennett et al., 2002
	MCI 15; HC 105	3 years	Stable	Bäckman et al., 2001
Semantic Fluency	96HC; *21MCI*; 122AD	1 year	Decline	Clark et al., 2009
	211 MCI; 587 HC	6 years	Decline	Bennett et al., 2002
CLASS B				
Global Cognitive Performances (CDR and MMSE)	20 AD, *40 MCI,* 40 HC	1 year	Increase (CDR), Decline (MMSE)	Leow et al., 2009
Visual Memory	19 HC, 12 QD[3] stable, *9 QD deter.*, 16 AD	2 years	decline	Fowler et al., 2002
Logical Memory	20 AD, *40 MCI,* 40 HC	1 year	Decline	Leow et al., 2009
Visuospatial Abilities	*211 MCI*, 587 HC	6 years	Decline	Bennett et al., 2002
	15AD, 31 MCI, 27 HC	NA	Decline (*MCI* < HC)	Economou et al., 2007
Letter Fluency	230 CDR = 0 (non demented), 152 CDR = 0.5 (incipient and very mild), 137 CDR = 1 (mild)	18 years	Decline	Storandt et al., 2002
	HC, MCI, AD	NA	Stable	Dudas et al., 2005
Processing Speed	*211 MCI*, 587 HC	6 years	decline	Bennett et al., 2002
	15AD, 31 MCI, 27 HC	NA	Decline (*MCI* < HC; *AD* < MCI)	Economou et al., 2007
Picture naming	230 CDR = 0 (non demented), 152 CDR = 0.5 (incipient and very mild), 137 CDR = 1 (mild)	18 years	Decline	Storandt et al., 2002
Clock drawing	36 HC, *18 MCI*, 24 AD	1 year	Stable	De Jager, 2004
CLASS C				
Anosognosia (Discrepancy between the patients and caregivers' estimation of impairments)	79 MCI, 82 AD	NA	AD < MCI each compared to their caregiver's assessment	Kalbe, et al., 2005
Stroop Test (Response Inhibition)	22 MCI, 33 AD	NA	Decline	Kramer et al., 2006
Trail Making Test (Set shifting)	22 MCI, 33 AD	NA	Decline	Kramer et al., 2006
Design Fluency	22 MCI, 33 AD	NA	Decline	Kramer et al., 2006
Emotional Expression	13 HC, 30 AD	NA	Decline	Allender, 1989
Emotional Comunication	20 HC, 27 probable AD: 8 Mild, 8 Moderate, 11 Severe	NA	Decline	Testa et al., 2001
Ideational, ideomotor and conceptual Apraxia	22 AD, 10 HC	NA	Decline	Derouesnè et al., 2000.
	15 AD, 18 HC	NA	Decline	Mozaz et al., 2006
	12 AD, 21 HC	NA	Decline	Schwartz et al., 2000

[1]Time B-FU: Time Baseline-Follow up; [2]sMCI: Stable MCI; dMCI: Decliners MCI; [3]QD: Questionable Dementia.

function and thus dependent upon the frontal lobe as well as semantic knowledge about categories. Patients affected by AD have more difficulty with category fluency than letter fluency [14] and this impairment is usually attributed to a breakdown in semantic knowledge about categories [15]. In our review, however, we could not find longitudinal studies indicating a decline in semantic fluency in subjects affected by MCI [16, 13].

Class B markers

As part of the AD Neuroimaging Initiative, in a longitudinal study of 12 months Leow et al. [12] compared

the anatomical distribution of structural changes, in 20 patients with AD, 40 healthy elderly controls, and 40 individuals with MCI. Each individual's longitudinal change was mapped (Jacobian map) using an unbiased registration technique, and spatially normalized to a geometrically-centered average image based on healthy controls. A voxelwise statistical analysis revealed regional differences in atrophy rates, and these differences were correlated with clinical measures and biomarkers. For clinical measures, longitudinal assessments of temporal lobe atrophy were significantly correlated with progression of cognitive impairment in the MCI group, including an increase over time in the Clinical Dementia Rating (CDR) scores, a decrease over time of the participants scores on the Mini-Mental State Examination (MMSE) and a progressive performance decline on the immediate memory portion of the Wechler Memory Scale's Logical Memory test. A lower score on the delayed Logical Memory test also correlated with a greater rate of temporal lobe atrophy.

This longitudinal study was the only one that we were able to find using global cognitive performances as a marker of disease progression. For this reason this marker has been listed as Class B evidence.

Using a computerized neuropsychological assessment, the CANTAB (Cambridge Neuropsychological Test Automated Battery), Fowler et al. [17], found a longitudinal decline in spatial short term memory and a visual recognition memory task over 6, 12, 18 and 24 months in a subgroup of patients with questionable dementia at baseline who declined over the 2 years follow-up. This is the only longitudinal study assessing visual memory as a potential marker of disease progression in patients affected by MCI.

A common way to assess visuospatial abilities in patients who are being evaluated for dementia is using the Judgement of Line Orientation (JOLO). Patients with dementia frequently perform poorly on this test [18], many receiving scores much below the 18 point cut-off.

We did find one cross sectional and one longitudinal study that assessed visuospatial abilities in patients with MCI. In the longitudinal study by Bennett et al. [13], individuals affected by MCI showed a decline in visuospatial abilities, as measured by the JOLO, and Standard Progressive Matrices. The cross sectional study performed by Economou et al. [19], compared the performance of participants with AD, MCI and Healthy Controls on the JOLO and found that the participants with MCI performed more poorly than did the healthy controls.

Reduced capacity to generate words that start with a specific letter (letter fluency) has been associated with a wide variety dementing diseases, although the patients' performance on these assessments tends to vary [20]. Letter fluency was found to be abnormal in a single longitudinal study that was investigating patients with incipient and mild dementia (CDR = 0.5) who were followed for 18 years [21]. In contrast, in a cross sectional study, performed by Dudas et al. [22], which compared letter fluency in subjects with, MCI and AD to that of healthy controls did not reveal any differences in these groups verbal fluency.

One of the most commonly used tests to assess patients for the cognitive disorders associated with dementia is to have patients name series of pictures and frequently the Boston Naming test is used for this purpose. Performance on this is test appears to be a sensitive indicator of both the presence and the degree of cognitive deterioration. Patients with AD have both lexical retrieval and semantic deficits [23] and therefore, often demonstrate impaired picture naming. Patients with AD tend to name supra-ordinate category instead of the target word [24]. We did find a longitudinal study which indicated that even with mild dementia (CDR = 0.5) there is a decline in picture naming as assessed by the BNT in subjects with incipient and very mild dementia (CDR = 0.5) [21].

The digit symbol test, which assesses processing speed, is extremely sensitive and specific test in detecting the presence of dementia, being one of the first tests to demonstrate a decline and with little overlap with the performance of healthy controls subjects on this test. Performance on this test also declines rapidly as these patient's disease progresses [25]. Bennett et al. [13] followed a group of individuals affected by MCI over 6 years and did find a decline in this test over time. The same results were also found in a cross sectional study by Economou et al. [19] who studied and compared participants with MCI, AD and healthy controls.

A longitudinal study assessing clock drawing in MCI, AD, and healthy controls did not indicate a decline of the performances over time.

Class C

Anosognosia was also assessed in a single cross sectional study comparing patients with MCI and AD and their caregivers. The authors indicated a discrepancy between the patients with AD and caregivers in their estimation of impairment Patients with MCI, however did not show this difference [26].

Response inhibition, using the Stroop test, in individuals affected by MCI was assessed in a cross sectional study [27]. The results of this study indicated that patients with AD performed more poorly than those with MCI. In this same study set shifting abilities were assessed using the Trail making test (TMT) as well as Design fluency. The results of the study indicate that AD patients perform worse than healthy controls. We are not aware, however, of any serial study examining response inhibition, set shifting or design fluency in patients affected by MCI.

Patients with AD may have disorders of emotional communication [28, 29]. These investigators compared healthy controls and AD's abilities to express and comprehend emotional prosody. Their results indicated that patients with AD were impaired.

These emotional communication disorders, as well as abulia, might be responsible for the impression that patients with AD are apathetic. In addition, many emotional experiences are induced by perceiving stimuli and understanding situations. Thus, patients with AD might also appear apathetic because they do not understand the circumstances that normally induce emotions.

Several cross sectional study that compared healthy controls to AD patients on apraxia indicate a worse performance of AD compared to healthy controls [30–32].

Conclusions

The utility of neuropsychological tests as markers for disease progression needs to be tested with further serial studies. Current data suggests that episodic memory and semantic fluency are the most reliable neuropsychological markers of disease progression.

STRUCTURAL MRI

Recently, there have been remarkable advances in the application of the neuroimaging to the study of MCI, providing information about those brain structures which are most likely to reveal changes in patients with MCI. Volumetric MR techniques provide the most sensitive indices of brain alteration in MCI and inform us how we can classify individuals into diagnostic categories. The two main MR analysis techniques employed in these studies are the region of interest (ROI) methods and more automated methods such as voxel based morphometry (VBM).

Medial temporal lobe (MTL) structures have long been known to play a critical role in episodic memory, and some of the earliest changes seen in AD are found in this region [33]. Therefore many volumetric studies of MCI measured hand traced regions of interest (ROI's) of specific MTL structures, such as the hippocampus and the entorhinal cortex [34–43]. The pattern of AD pathology is, however, complex and evolves as the disease progresses. Whereas AD starts mainly in the hippocampus and entorhinal cortex, these pathological changes subsequently develop throughout most of the temporal lobes and the posterior cingulate cortex. These are the changes associated with impaired episodic memory. Subsequently, pathological changes involve neocortex; especially the cortex in the temporal, parietal, and prefrontal regions and it is damage to these regions that induces language deficits (e.g., anomia), apraxia, visuospatial deficits as well as executive disorders.

The sensitivity of a marker to track disease progression depends on several factors, including the rate of change during the disease stage of interest, the precision of the measurements, and its statistical effect size. Markers that have plateaued or have not yet changed (ceiling and floor effects, respectively) are likely to be poor markers of progression [44]. The available evidence suggests that structural markers fulfil many of these sensitivity requirements and are therefore, good candidates for monitoring disease progression.

Alzheimer's dementia (AD) is associated with progressive accumulation of beta amyloid - Aβ and hyperphosphorylated tau and this accumulation leads to progressive synaptic, neuronal, and axonal damage. Following the pathological staging scheme proposed by Braak and Braak [45], neurofibrillary tangles first occur in the entorhinal cortex and hippocampus (transentorhinal stages I and II), before spreading out into the amygdale and basolateral temporal lobe (limbic stages III and IV) and then into the isocortical association areas (isocortical stages V and VI). The same pattern of progression can be identified by MRI-based assays for atrophic changes. Rates of change in a number of structural measures including volumes of the whole brain, the entorhinal cortex hippocampus, and temporal lobe as well as ventricular enlargement, correlate closely with changes in cognitive performance, supporting their validity as markers of disease progression.

From MCI to well into the moderate dementia stage of AD, structural markers are sensitive to disease progression and appear to be even more sensitive to change than are markers of Aβ deposition (PIB-PET or CSF). Case control and longitudinal studies

employing a number of MR analysis techniques have substantially augmented our knowledge about volumetric brain changes that characterize MCI and predict development of AD [46].

Several studies have been conducted with patients who have MCI examining structural changes over time. Some of these studies use within group comparisons rather than a between group comparisons at different times thereby providing a correlation between structural atrophy and cognitive performances. We included these serial studies in Class A. Additionally, not all individuals with MCI subsequently develop AD, and individuals with MCI who do develop AD vary in their rate of clinical progression [47]. Therefore, there are several serial studies that have examined the accuracy with which volumetric MRI measures predict those MCI participants who will progress to AD (progressive MCI: pMCI) versus those MCI who show functional stability (stable MCI: sMCI) over the time to follow up [35, 48], whereas others focused on volumetric MRI changes in pMCI versus sMCI over time [49]. We did not focus our review on predictors of progression rather on markers of change dividing them according to the criteria mentioned in the introduction's section.

Class A markers

Whole brain atrophy rate; isocortical association areas atrophy

Studies conducting analysis of the whole brain indicate that faster atrophy in pMCI occurs in wide-spread cortical regions [50]. Jack et al. [50] measured rate of brain atrophy from serial MRI with corresponding clinical changes in normal elderly subjects, patients with MCI and patients with probable AD. The annualized changes in volume of four structures were measured from the serial MRI studies including: hippocampus, entorhinal cortex, whole brain, and ventricles. Rates of change on several cognitive tests and rating scales were also assessed. Subjects who were classified as normal or MCI at baseline could either remain stable or could convert to a lower functioning group. Patients with AD were dichotomized into those with slow versus fast progression. The atrophy rates for these four structures were greater among MCI subjects who converted to AD than MCI subjects who remained stable. The atrophy rate was also greater for patients with AD who were progressing rapidly than those who progressed slowly. Among MCI subjects, correlation were calculated between change in MRI and change in performance on four cognitive tests/rating scales the Mini

Mental State Examination (MMSE), Dementia Rating Scale (DRS), Logical Memory II (LM II) (%) and CDR sum of boxes. Significant correlations were seen for the hippocampal rate of atrophy with the change in DRS, and atrophy of the entorhinal cortex correlated with the change in CDR sum of boxes. With one exception, both the whole brain and ventricular rate measures were correlated with the changes on all these rating scales.

Additionally, Sluimer et al. [51] determined whole brain atrophy rate in MCI and Alzheimer's dementia (AD) and its association with cognitive decline. Two magnetic resonance images were acquired with an average interval of 1.8 years + 0.7. Whole brain atrophy was strongly associated with cognitive decline in the participants with AD and MCI, but healthy controls and subjects affected by subjective memory complaints did not show this atrophy.

A serial study was also conducted comparing atrophy changes in participants with MCI with healthy controls. In this study the subjects were 138 non-demented individuals have been followed annually for up to 10 consecutive years, but 18 of these participants were diagnosed with MCI. This MCI group showed accelerated changes compared to healthy controls in whole brain volume, ventricular CSF, temporal gray matter, as well as the orbitofrontal and temporal association cortices, including the hippocampus [52].

McDonald et al. [53] evaluated the spatial pattern and regional rates of neocortical atrophy from normal aging to early AD. Annual atrophy rate were derived by calculating percent cortical volume loss between baseline images and images taken 12 months after the baseline images. Planned comparisons were used to evaluate the change of atrophy rates across levels of disease severity. The score on the Clinical Dementia Rating scale (CDR) was used to divide the study sample into groups reflecting degree of impairment. In patients with MCI with CDR scores of 0.5–1 annual atrophy rates were greatest in medial temporal, middle and inferior lateral temporal, inferior parietal, and posterior cingulate gyrus. With increased impairment (MCI-CDR- 1.5–2.5) atrophy spread to parietal, frontal and lateral occipital cortex, followed by anterior cingulate cortex. Analysis of regional trajectories revealed increasing rates of atrophy across all neocortical regions with clinical impairment. However, increase in atrophy rates were greater in early disease within medial temporal cortex, whereas increases in atrophy rates were greater at later stages in prefrontal, parietal, posterior temporal, and cingulate cortex.

Table 3
Structural MR markers of disease progression based on literature evidence of validity

	N subjects and diagnosis	Time B-FU	Results	Technical notes	References
CLASS A					
Whole Brain (WB) Atrophy	*HC55; MCI 41; AD 64*	1 to 5 years	Increased of atrophy in converters	Manual tracing	Jack 2004
	HC 10; MCI 45; AD 65	1.8 years + 0.7	WBA associated with MMSE change in AD and MCI	Autom Structural Image Eval. SIENA or SIENAX	Sluimer et al., 2008
	HC 120; MCI 18	10 years	Accelerated atrophy changes in MCI compared to healthy controls	VBM using RAVENS approach	Driscoll et al., 2009
	AD 99; MCI 235; C 131	1 year	WBA associated with MMSE, ADAS-cog changes in MCI and AD.	Software MIDAS used for WB and ventr. semi automated segmentation.	Evans et al., 2010
	aMCI progr 46; aMCI Stab 23; HC 46	3 years	Changes in Brain volume over time	TIV measured by manual tracing. WB ventr atrophy rates measured with BSI.	Jack et al., 2008
	C 137; MCI 105 (CDR-SB = 0.5–1.0); MCI 126 (CDR-SB = 1.5–2.5); Mild AD 104 (CDR-SB > 2.5)	1 year	Early disease: Increased atrophy rates (AR) in MTL. Later stages: Increases AR in PFC, PL, post. Temp., cingul. cortex.	FreeSurfer 3.02 software	McDonald et al., 2009
	88 HC; Very Mild dem; Mild dem.; Mod	Mean of 2.04 years (+1.42 SD)	Tot brain volume loss increased in Mild and Mod dem. vs HC. MMSE correlated with brain volume loss.	MR image analysis was performed utilizing the program REGION.	Kaye et al., 2005
Ventricles Volume (VV)	*aMCI progr 46; aMCI Stab 23; HC 46*	3 years	Changes in ventricular expansion over time	TIV measured manually. WB and ventr. atrophy measured with BSI	Jack et al., 2008
	79 HC (37 developed MCI)	Up to 15 years	Rates of VV expansion greater in those who developed MCI.	Standardized semi automated segmentation technique.	Carlson et al., 2008
	AD 99; MCI 235; C 131	1 year	Association between ventricular expansion and MMSE and ADAS-cog changes in MCI and AD.	Software MIDAS used for WB and ventr. semi automated segmentation.	Evans et al. 2010
	88 HC; Very Mild dem; Mild dem.; Mod	Mean of 2.04 years (+1.42 SD)	VV increased in Very Mild and Mild dem vs HC, and in Mod dem vs HC and Mild dem. MMSE corr with VV increase.	MR image analysis was performed utilizing the program REGION.	Kaye et al., 2005
	C 152; MCI 247; AD105	NA	Increase VV AD > MCI > HC	Semi automated software to assess VV.	Nestor 2008
	HC 104; MCI 29; Dementia 12	NA	AD < MCI < C	Change rate in lateral ventricle-to-brain ratio (VBR) using automated ventricular and WB volume estimation.	Carmichael et al., 2007
	HC 55; MCI 41; AD 64	1 to 5 years	Increased of atrophy in converters (either HC or MCI and fast AD progr)	Manual tracing	Jack 2004
	HC 120; MCI 18	10 years	Accelerated VV enlargement in MCI vs HC	VBM using RAVENS approach	Driscoll et al., 2009
Hippo Atrophy (HA)	*518 HC (50 developed dementia; 36 out of 50 AD)*	10 years	Increased in HA correlated with decline in delayed memory recall.	Automated segmentation procedures	Den Heijer et al., 2010
	20 MCI (conv and stable)	3 years	Increase HA of conv MCI vs stable MCI	3 D Computational modelling tech.	Apostolova et al., 2006

Table 3
(*Continued*)

	N subjects and diagnosis	Time B-FU	Results	Technical notes	References
	88 HC; Very Mild dem; Mild dem.; Mod	Mean of 2.04 years (+1.42 SD)	HA in Mild dem > HC	MR image analysis using the program REGION.	Kaye et al., 2005
	58 C; 43 MCI; 28 AD	3 + 1 years	Increase HA over time of cMCI vs sMCI	Manual tracing	Jack 2000
	HC 55; MCI 41; AD 64	1 to 5 years	Increased of HA in conv (either HC or MCI and fast AD progr)	Manual tracing	Jack 2004
	58 MCI(19 conv); 20 C	2 years	Conv MCI had the highest annual decline rates in cognition and HVvs stable *MCI* and *HC*	Manual tracing	Wang et al., 2009
	33 MCI	3 years	Increased HA vs HC	VBM	Withwell et al., 2009
	35 HC; 23 MCI (11 conv.);14 AD	6 years	Increased rate of HA and the enthorinal cortex for the cMCI and AD vs HC.	Manual tracing	Stoub et al., 2010
	97 AD; 245 MCI; 148 HC	1 year	HA correlated with baseline and changes in MMSE and global sum of boxes CDR scores	Automated segmentation method based on AdaBoost to create 3D hippocampal surface model	Morra et al., 2009
	18 MCI	18 months	Greater Gray matter loss in conv. vs non conv in hippoc area, ITG, MTG, post cyngulate and precuneus	Modified VBM procedure specially designed for longitudinal studies	Chételat et al. 2005
CLASS B					
Cortical Thinning	pMCI 15, SMCI 45,	7 years	pMCI > sMCI Reduced Cortical thickness	Automatic computational surface method	Julkunen et al., 2009
	HC 34, MCI 62, AD 42	NA	AD > MCI > C	automated MRI-based analysis techniques in order to determine the pattern of cortical thinning	Singh 2006
Substantia Innominata (SI) Atrophy	HC 12, AD 13	NA	AD > C	Automated technique of image regression analysis, implemented through code written in Matlab 5.3, to the analysis of proton density weighted structural MRI of the basal forebrain. This technique allows searching a large portion of the substantia innominata for signal changes.	Teipel et al., 2005
	26 aMCI, 46 HC, 12 AD	NA	AD > MCI > C Correlation between performance in the word list recall (CERAD subtest) and SI volume in AD patients	Manually tracement using a custom made segmentation program	Muth., et al., 2010
	HC 27, MCI 33, AD 19	NA	AD < MCI; AD < C; MCI = C	SI volumes were traced on three consecutive gapless 1 mm thick coronal slices.	George et al., 2010 (ahead of print)

WBA: Whole Brain Atrophy; VBM: Voxel Based Morphometry; TIV: Total Intracranial Volume; BSI: Boundary Shift Integral; MTL: Medial Temporal lobe; PFC: Pre-Frontal Cortex; PL: Parietal lobe.

Spatial patterns of brain atrophy as detected in neuroimaging (SPARE A Index) has been tested as a means early detection or index of suspicion for diseases such as AD. This method uses sophisticated pattern analysis algorithms that are trained to identify patterns of normal or abnormal structure and function [54] which are used for classification at the individual level. This approach considers all brain regions jointly and identifies a minimal set of regions whose volumes jointly maximally differentiate between the two groups (normal control versus patients with AD) on the basis of an individual scan. For a classifier constructed from the healthy controls and AD groups, a positive index implies AD like brain and negative index implies controls like brain. Davatzikos et al. [54] investigated whether differences in spatial pattern of brain atrophy could be detected in cognitively healthy controls versus patients with MCI and whether these patterns are associated with cognitive decline. Images from the Alzheimer's Disease Neuroimaging Initiative (ADNI) dataset were used to construct a pattern classifier that recognized spatial patterns of brain atrophy which best distinguish AD patients from cognitive normal control subjects and MCI participants in the Baltimore Longitudinal Study of Aging (BLSA) neuroimaging study. The degree to which AD like patterns were present in control and MCI subjects was evaluated serially in relation to cognitive performance. The oldest control participants showed progressively increasing AD like pattern of atrophy, and individuals with these patterns had reduced cognitive performance. MCI was associated with steeper longitudinal increases of AD like pattern of atrophy, which separated them from the cognitively normal control subjects.

Ventricular volume

A series of cross sectional studies have examined changes in ventricular volumes comparing people with MCI, AD and healthy controls. All studies reported that the AD group had greater ventricular enlargement compared to both subjects with MCI and healthy controls. In addition, the participants with MCI had a greater rate of ventricular enlargement compared to healthy controls. We report here three studies looking at this phenomenon using three different techniques to assess ventricular volume, such as a semi automated software [55], an automated ventricular extraction approach [56], and a voxel based morphometry using RAVENS approach [52].

A longitudinal study has also been performed by Jack et al. [57] with 46 subjects who had MCI and progressed to AD (progressive MCI: pMCI), 23 participants who had sMCI (stable MCI) without progression to dementia and 46 healthy controls. All subjects including in this study had three or more serial MRI scans within 3 years from their initial scan when they had MCI or were control subjects and a final MRI when they were either diagnosed with AD, sMCI or a normal control.

Rate of brain shrinkage and ventricular expansion were measured across all available MRI scans in each subject and the results indicated that rate of atrophy accelerate as individuals progressed from amnesic MCI (aMCI) to typical late onset AD. In pMCI the change in pre to post diagnostic scan rate of ventricular expansion was $1.7\,cm^3$/year and acceleration in brain shrinkage was $5.3\,cm^3$/year. Brain volume declined and ventricular volume increased in all the three groups with age. The rate of atrophy was greater in younger than older subjects with aMCI who progressed to AD and the rate was also less in subjects with aMCI who did not progress (stable MCI: sMCI) that in those who did progress (progressive MCI: pMCI). The authors did not find that the rates of atrophy varied as a function of age in 70-to 90 years' old cognitively normal subjects.

A similar study was performed by Evans et al. [58], who assessed the relationships between anatomic changes of the whole brain and ventricular volume, as determined by MRI, with change in cognitive scores in participants with AD, MCI and healthy controls. Their results indicated that brain atrophy rates and ventricular enlargement differed between groups and in subjects with MCI and AD these atrophic changes were associated with lowering of the scores on the MMSE. In the subjects with MCI both of these anatomic measures were also associated with scores on the ADAS-cog and on Trails B in MCI. For the participants with AD, their ventricular expansion was associated with scores on the ADAS-cog. Additionally brain atrophy and ventricular expansion were higher in MCI subjects who progressed to AD within 12 months of follow up, compared with MCI subjects who remained stable. The authors conclude that whole brain atrophy rates and ventricular enlargement tracked disease progression and psychological decline, demonstrating their relevance as biomarkers.

Carlson et al. [59], investigated a group of 79 healthy elderly subjects for up to 15 consecutive years with standardized clinical evaluations and volumetric brain MRI assessments of ventricular volume. During the study period, 37 subjects developed MCI. Their results indicated that the annual rate of expansion of ven-

tricular volume were greater in those who developed cognitive impairment during follow-up than those participants who did not.

Hippocampal atrophy

Longitudinal studies have examined the relationship between brain atrophy rates and progression from MCI to AD. Most such studies collect MRI data and conduct coincident clinical /neuropsychological assessment at two time points spaced several years apart. Several studies have reported a relatively low hippocampal atrophy rate ranging from 1.0–2.2%/year for healthy controls, to 2.5–4.3%/year in subjects with MCI and 2.8–4.0%/year for participants with mild AD [49, 60, 61]. Most studies indicate that hippocampus shows higher annual rates of atrophy in pMCI than sMCI [49, 50, 62–64]. Estimates of annualized hippocampal atrophy in pMCI are generally about 3.7%, for sMCI estimates are about 2.5–2.8% [49, 63].

Withwell et al. [64] followed 33 MCI subjects over 3 years. Voxel based morphometry was used to assess patterns of grey matter atrophy. The pattern of grey matter atrophy involved primarily the medial temporal lobes, including the amygdale, anterior hippocampus, entorhinal cortex and fusiform gyrus. Subsequently the atrophy developed in more posterior regions, such as the parietal lobe and later with the development from MCI to AD, atrophy developed in the temporoparietal association cortex and the frontal lobes.

Chételat et al. [62] used voxel based morphometry to map structural changes associated with rapid development of AD in MCI. Eighteen amnesic MCI patients were followed-up for a predefined fixed period of 18 months and development of AD was judged according to NINCDS-ADRDA criteria. Each patient underwent a high resolution T1-weighted volume MRI scan both at entry in the study and 18 months later. To map gray matter loss from baseline to follow up assessment, the authors used a modified voxel-based morphometry (VBM) procedure specially designed for longitudinal studies. Regions of significant gray matter (GM) loss over the 18 months follow up period common to both converters and non-converters included the temporal neocortex, parahippocampal cortex, orbitofrontal and inferior parietal areas and the left thalamus. However, there was significantly greater GM loss in converters relative to non-converters in the hippocampal areas, inferior and middle temporal gyrus, posterior cingulate gyrus and precuneus [62].

Another longitudinal volumetric MRI analysis of 155 subjects has been performed by Kaye et al. [65]

to determine if rates and location of brain volume loss associated with AD are phase specific, occurring prior to clinical onset and/or at a later stage. Subjects were divided by Clinical Dementia Rating (CDR) scale into stages of normal (CDR = 0 at baseline and CDR = 0 at follow ups), very mild (CDR = 0 at baseline and CDR = 0.5 at follow up or CDR 0.5 at baseline and at follow up) Mild (CDR = 0.5 at baseline and CDR = 1 at follow up or CDR = 1.0 at baseline and follow up) and Moderate dementia (CDR = 1.0 at baseline and CDR = 2.0 at follow ups or CDR = 2.0 at baseline and CDR = 2.0 at follow up). Subjects were followed for a mean of 2.04 (+1.42 SD) years within a clinical stage. The authors measured the volume of supratentorial intracranial cavity, total brain, frontal lobe, temporal lobe, and parieto-occipital lobar region, basal ganglia-thalamic region, ventricular CSF, parahippocampal gyrus, and hippocampal body. Although they did find a cross sectional difference in hippocampal volume between the participants with mild dementia (CDR 0.5 to 1.0 or CDR 1.0 at baseline and follow up) and healthy controls (CDR = 0 at baseline and follow up), the rates of changes were not significantly accelerating. The authors attempt to explain these findings by assuming that the hippocampus might undergo a relatively constant slow atrophy several years before the onset of clinical detected cognitive changes [34, 66].

In the next clinical transition stage to mild impairment (Mild group) the rates of both ventricular enlargement and total brain volume loss were greater than the normal group. In the later stage of dementia (Moderate group) in addition to the ventricles and total brain, the temporal lobe and basal ganglia-thalamic regions increased in the rate of atrophy when compared to the normal group and ventricular enlargement was significantly greater than the very mild group as well. Rates of global cognitive decline, measured by rate of annual MMSE change, correlated with brain volume loss and ventricular volume increase.

Stoub et al. [67] studied three groups of elderly participants following them with yearly high resolution MRI scans over 6 years. At baseline participants consisted of 35 healthy controls, 33 MCI, and 14 AD. Eleven patients affected by aMCI developed AD during the course of the study and 9 healthy controls declined in cognitive functions. Longitudinal analysis showed that the rate of the entorhinal cortex and hippocampus for the stable healthy controls differed significantly from MCI participants who converted

to AD and the AD group. Additionally longitudinal decreases in hippocampal and entorhinal volume were related to longitudinal decline in declarative memory performance.

Wang et al. [68] investigated 58 subjects with aMCI and 20 normal aging elderly controls. All the participants underwent an annual neuropsychological assessment and MRI. Annual decline in neuropsychological test score, hippocampal and amygdala volumes were calculated. Nineteen MCI converted to AD during the course of the study (2 years). The annual hippocampal atrophy rate was correlated with a decline in memory test score. Compared to subjects with sMCI and normal aging, those with pMCI had the highest annual decline rates in cognition and hippocampal volume, but no differences in the amygdala volume were found.

Morra et al. [69] mapped the 3D profile of hippocampal degeneration over time in 490 subjects scanned twice with brain MRI over a 1 year interval. There were 97 participants who had AD, 148 were healthy control subjects and 245 who demonstrated MCI. The authors used a validated automated segmentation method, to create 3D hippocampal surface models in all 980 scans. Hippocampal volume loss rates increased with clinical deterioration (healthy controls 0.66%/year; MCI 3.12%/year; AD 5.59%/year) and correlated with both baseline and interval changes in MMSE scores and CDR sum of boxes scores. Converters from MCI to AD showed faster atrophy than non-converters.

Den Heijer et al. [70] used sequential MRI as a biomarker of disease process in healthy individuals. The authors examined 581 elderly participants taken from the population based Rotterdam Scan Study. A MRI was performed at baseline in 1995–1996 that was repeated in 1999–2000 (in 244 persons) and in 2006 (in 185 persons). All participants were free of dementia at baseline and followed over time for cognitive decline and dementia. These subjects had 4 repeated neuropsychological tests at the research center over a 10 years period. During this time 50 people developed dementia with 36 having AD. In addition to learning that a decline in hippocampal volume predicted the onset of clinical dementia, in those people who remained free of dementia during the entire follow up period, they found that decline in hippocampal volume paralleled and preceded a specific decline in delayed recall of words and those who had a faster decline of hippocampal volume also had a significant faster decline in delayed memory recall.

Class B markers

Cortical thinning pattern

Cortical thinning patterns have been investigated cross-sectionally by Singh et al. [71]. The authors compared patients affected by AD, MCI and healthy controls. Their results indicated a greater cortical thinning in AD compared to MCI as well as greater thinning in MCI than in healthy controls.

Julkunen et al. [72] also analyzed the cortical thickness in pMCI and sMCI subjects. These investigators followed 60 participants with MCI for 7 years in order to examine the differences in cortical thickness between those participants with progressive versus those with stable MCI. When compared to the sMCI subjects, the pMCI group displayed significantly reduced cortical thickness bilaterally, in the superior and middle frontal gyri, the superior, middle and inferior temporal, the fusiform gyrus and parahippocampal regions. In the pMCI participants the cingulate and retrosplenial cortices, as well as the right precuneal and paracentral regions were also atrophic.

Substantia innominata

The substantia innominata (SI) contains the nucleus basalis of Maynert, which provides the major cholinergic innervations to the entire cortical mantle and the amygdale as well as the medial septal and diagonal band of Broca, which supply cholinergic innovation to the hippocampus. Degeneration of nucleus basalis neurons correlates with cognitive decline in AD. George et al. [73] investigated 27 healthy controls, 33 MCI and 19 AD participants comparing their SI volumes. Their results indicated that SI volume was significantly reduced in AD group compared to MCI and normal control participants; however the healthy controls and MCI participants did not differ from each other.

Muth et al. [74] recently performed a study examining the volume loss of the cholinergic basal forebrain region (substantia innominata) between healthy controls, and subjects with MCI and AD. Their results indicated the volume of SI to be significantly different between groups in that healthy controls had the largest SI volumes, followed by aMCI and then the AD patients. In vivo quantification of these changes might be of use as a novel neuroimaging marker of cholinergic neurodegeneration in AD.

The authors ended their manuscript suggesting that the use of SI volume may serve as a surrogate marker for the monitoring of cholinergic neurodegeneration during the course of dementing diseases.

Conclusions

Up to date hippocampal atrophy, ventricular volume and whole brain atrophy are the structural MRI markers to have the greatest class A evidence to be good markers of disease progression.

RESTING STATE FMRI

Alzheimer's dementia is characterized by severe synaptic/neuronal dysfunction and selective neuronal loss [75]. Early on, misfolded proteins aggregate within small, selectively vulnerable neuron populations that reside in specific brain regions [76]. Synapses falter, and damage develops in new regions accompanied by increasing clinical deficits [75]. Often, later-affected regions bear known anatomical connections with the sites of earlier injury [77]. Based on neuropathology [78], neuroimaging [79, 80] and evidence from transgenic animal models [81], it has been suggested that neurodegeneration may relate to neural network dysfunction [79, 82].

Resting-state fMRI provides an indirect marker of neuronal activity by measuring the spontaneous low-frequency (<0.08–0.1 Hz) fluctuations in the blood oxygen level dependent (BOLD) signal [83]. This technique allows the investigation of brain activity within spatially distinct, functionally related group of cortical and subcortical regions [84–86]. Networks relevant to AD are (i) the default mode network (DMN), a set of regions which comprises the posterior cingulate cortex (PCC), the hippocampus, the medial temporal cortex, the parietal lobule, and the medial prefrontal cortex (mPFC); (ii) the working memory network (WMN); and (iii) the attention/executive network. The DMN is relevant to AD because the areas that comprise this network overlap with the regions that are selectively affected by this disease [87]. The networks that mediate working memory and attention are relevant because of the forms of cognitive deficits which characterize AD patients.

The characterization of human brain's intrinsic functional networks from resting-state BOLD fMRI data therefore has the potential of defining functional connectivity markers that may follow the progression in neurodegenerative diseases, such as AD.

Currently there is only a little evidence that the markers of resting state activity are sensitive to disease progression. A progressive reduction of brain activity and connectivity in the regions of the DMN (namely the hippocampus and PCC) seems the most consistent finding among studies. These changes, however, have never been investigated by *ad hoc* serial studies. Furthermore, currently other networks have been not been fully investigated.

Class A markers

There are no serial studies which have investigated resting-state brain activity.

Class B markers

Reduced activity in the DMN is the most consistent marker among studies [88–92]. These studies showed significant reductions of resting-state activity in MCI within the hippocampus, PCC/precuneus and medial prefrontal cortex.

Class C markers

There is little evidence that brain activity of other functional networks could provide markers of disease progression: a single cross-sectional study carried on MCI subjects showed reduced activity in the attention/executive network [92]. Currently there is no published study that has investigated the WMN. Other potential markers for disease progression could be drawn by measures of increased activity/connectivity between parietal and frontal regions [93–95]. These studies were carried out on AD patients only and suggest that patients may rely on increased prefrontal connectivity to compensate for reduced temporal connectivity. A new class of functional markers might in the future be obtained by measures of network small-worldness [96, 97].

Conclusions

The utility of resting-state activity and connectivity as markers for disease progression still needs to be tested with longitudinal studies. Current data suggests that resting-state activity may be a useful marker for the diagnosis [80].

DIFFUSION TENSOR IMAGING

As mentioned earlier AD is characterized by the deposition of two toxic proteins which target specific neuronal populations [75]. AD pathology spreads following a well established pattern [78] and the damage is accompanied by worsening of specific clinical deficits [75]. Given that later-affected regions bear

Table 4
fMRI markers of disease progression based on literature evidence of validity.

Marker	N subjects & diagnosis	Time B-FU	Results	Technical notes	References
CLASS B					
DMN activity	41 HC; 28 MCI; 18 AD	NA	Reduced mPFC: $AD < MCI < HC$ precuneus: $AD < HC, MCI < HC$	Single site, 1.5T study $Voxel = 3 \times 3 \times 5\,mm^3$ $TE = 60\,ms$ Axial orientation	Rombouts et al., 2005
DMN activity (HP synchrony)	9 HC, 5 MCI 10 AD	NA	Reduced $(AD < MCI < HC)$	Single site 1.5T study $Voxel = 3.75 \times 3.75 \times 7\,mm^3$ $TR = 2\,s$, 6 min Sagital orientation	Li et al., 2002
CLASS C					
Attention/executive network activity	16 HC, 24 aMCI	NA	Reduced	Single site, 1.5T $Voxel = 3.125 \times 3.125 \times 4\,mm^3$ $TR = 3\,s$, 4 min Axial ACPC orientation	Sorg et al., 2007
Small world properties (clustering coefficient)	18 HC, 21 mild AD	NA	Reduced	Single site, 3T study $Voxel = 3.75 \times 3.75 \times 4\,mm^3$ $TR = 2\,s$, 6 min Axial ACPC orientation	Supekar et al., 2008
Activity in frontal and parietal regions (connectivity between prefrontal-parietal)	13 HC, 13 mild AD	NA	Reduced	Single site, 1.5T $Voxel = 3.75 \times 3.75 \times 4mm^3$ $TR = 2\,s$, 6 min Axial ACPC orientation	Wang, et al. 2007
Activity in frontal and parietal regions (frontal/prefrontal)	18 HC, 21 mild AD	NA	Increased	Single site, 3T study $Voxel = 3.75 \times 3.75 \times 4mm^3$ $TR = 2\,s$, 6 min Axial ACPC orientation	Supekar et al., 2008
Activity in frontal and parietal regions (connectivity with PCC)	16 HC, 16 mild AD	NA	Increased	Single site, 1.5T $Voxel = 3.75 \times 3.75 \times 6mm^3$ $TR = 3\,s$, 5–6.27 min	Zhang et al., 2009
Activity in frontal and parietal regions (connectivity with HP)	14 HC, 14 mild AD	NA	Increased	Single site, 1.5T $Voxel = 3.75 \times 3.75 \times 4mm^3$ $TR = 2\,s$, 6 min Axial ACPC orientation	Wang et al., 2006

AD: Alzheimer's disease; aMCI: amnestic mild cognitive impairment; HC: healthy controls; DMN: default mode network; HP: hippocampus; PCC:poster cingulate cortex; ACPC: Anterior Commissure, Poterior Commissure.

known anatomical connections with the sites of earlier injury [77], the structural integrity of white matter (WM) tracts connecting these regions is thought to play some role in the progression of this disease. It has been posited that cognitive deficits may be related to the disruption of functionally relevant tracts [98–100]. The disruption of the parahippocampus, which contain a tract that connects the posterior cingulate-retrosplenial cortex (PCC/RSC) with the hippocampus, is thought to be responsible for the dissociation between functional/metabolic changes (which affect mainly the PCC/RSC) and structural abnormalities (which affect primary the hippocampus and temporal lobe) found in AD [80]. Post-mortem studies have shown WM changes in AD in the form of atrophy, myelin attenuation, axonal loss, or reactive gliosis [101, 102], but specific WM tracts have not been thoroughly investigated.

Diffusion Tensor Imaging (DTI) is a non-conventional MRI technique that allows the investigation of the integrity of WM tracts *in vivo* [103]. This technique, by measuring the movement of water molecules within tissues, is sensitive to tissue changes in pathological conditions. Commonly, two indexes are obtained from DTI: mean diffusivity (MD), which is a measure of overall water diffusion, and fractional anisotropy (FA), which is a measure of overall tissue integrity [104]. Two additional measures of WM damage can be obtained from DTI: axial (DA) and radial (DR) diffusivity. DA and DR seem more specific markers than MD/FA of axonal loss and myelin damage [105], but to date these markers has not been used extensively. Commonly used methods for DTI analysis are ROI-based analyses; tractography and automated tract analysis.

Currently, there is some evidence from cross-sectional studies carried out on MCI patients that DTI changes in the medial temporal lobe WM could provide markers sensitive to disease progression. Specifically, DTI changes in the parahippocampal WM tract and in the hippocampus seem the most promising markers. Another tract connecting to the temporal lobe, the posterior cingulum, provide some evidence of sensitivity in the detection of disease, whereas less specific markers such as temporal lobe WM provide low evidence. There is some evidence that diffusivity changes in the frontal WM follow disease progression. Specific cortico-cortical association tracts (inferior and superior longitudinal fasciculus, inferior fronto-occipital fasciculus) are promising markers because of their association with cognitive functions however currently there are a paucity of studies assessing this possible biomarker. The genu and splenium of the corpus callosum, and motor cortex tracts do not seem valid markers of disease progression. Longitudinal changes in DA and DR indexes may provide more specific disease markers in the future, but currently these markers have only been investigated in a limited number of cross-sectional studies [106–110].

Class A markers

Unfortunately, all the candidate markers have been investigated on cross-sectional studies except for a single longitudinal study [111], thus none of the markers satisfy criteria for inclusion in Class A.

Class B markers

(1) Multiple cross-sectional studies have consistently shown DTI changes (reduced FA or increased MD) in the parahippocampal tract [112–115] and in the hippocampus [116–119] of MCI subjects. As these tracts are located in key regions of AD pathology (medial temporal lobe), they are good candidate markers to track disease progression.

(2) DTI changes in the posterior cingulum have been reported quite consistently in the majority [110, 113, 114, 120–123] but not all the studies [111, 112, 116]. Compared to the above markers, the posterior cingulum has the advantage that measurement of this structure is more reliable than that of the parahippocampal tract.

(3) One longitudinal study [111] and some cross-sectional studies [114, 119], but not all [116,

118, 124–126], reported a progressive decline in the frontal WM in MCI subjects. The changes in the frontal WM may therefore be valid candidate markers of disease progression.

(4) DTI changes in the fornix have been reported inconsistently among studies [108, 110–112]. This tract is relevant to AD as it is part of the limbic system; however its assessment suffers from major technical limitations due to CSF contamination [127].

(5) FA reduction and MD increases in the temporal lobe WM have been widely investigated but findings are inconsistent among studies: some studies reported significant changes [106, 114, 118] whereas several others showed no difference [116, 119, 124, 125, 128, 129]. It is likely that investigating more specific tracts connecting to the temporal lobe may provide more accurate markers of disease progression. Indeed, studies generally showed changes in the uncinate fasciculus [108, 110, 112], in the inferior [110, 119] and superior [108, 110, 119, 121] longitudinal fasciculus, and in the inferior fronto-occipital fasciculus [108, 110, 121].

(6) There is very low evidence that MD or FA changes in the splenium [119, 125] and genu [120, 121, 128] of the corpus callosum, and corticospinal tract [118, 119] may be markers for disease progression. The majority of the studies indeed reported no change in the splenium [111–113, 118, 124, 126] and genu [112, 113, 118, 119, 124–126, 130] of the corpus callosum, or in the CST [111, 113, 123].

(7) There is increasing evidence that DA and DR may be more sensitive to WM changes than MD and FA, especially in the temporal lobe WM.

(8) Diffusivity changes in the cerebellum [112], thalamus [114], entorhinal cortex [114], and subventricular zone [131] have been investigated by single studies.

Class C markers

Future DTI markers may be obtained by analysis of WM tracts shape and deformation [132].

Conclusions

DTI changes in the WM tracts of the medial temporal lobe (parahippocampus and posterior cingulum) and hippocampus seem promising markers for disease

Table 5
DTI markers of disease progression based on literature evidence of validity

Marker	N subjects and diagnosis	Time between baseline and follow-up	Results	Technical notes	References
Class B					
PARAHIP-POCAMPUS (FA)	HC 19, MCI 27, AD 17	NA	Reduced (MCI<C; AD<C)	1.5T, 8-channel coil, (1.72 × 1.72 × 5)mm³, TE/TR = 98/5000 ms, 1b0, b = 1000, 30 dir, 2 : 53 min	Liu et al., Neurob Aging 2009
(FA, MD)	HC 18, MCI 17, AD 17	NA	Reduced FA (MCI<C; AD<C) Increased MD (MCI>C; AD>C)	1.5T, IR-EPI, TE/TR/TI = 100/6000/2000 ms, (2.34 × 2.34 × 5)mm³, 1b0, b = 1000, 6 dir,	Zhang et al., Neurology 2007
(FA)	HC 17, aMCI 17	NA	Reduced	1.5T, (1.8 × 1.8 × 2.5)mm³, TE/TR = 106/6000 ms, 16b0, b = 1100, 44 dir, 8 min	Rose et al., JNNP 2006
(FA)	HC 10, MCI 10, AD 10	NA	Reduced (MCI<C; AD<C)	1.5T, 6 dir, TE/TR = 87/2000 ms, (3.3 × 2.5 × 2.5)mm³,1b0, b = 1200	Kalus et al., Neuroimage 2006
HIPPOCAMPUS (MD: ADC)	HC 55, MCI 19, AD 21	NA	Increased (MCI>C; AD>C)	1.5T, FLAIR-DTI, 3 dir, 1b0, b = 1000; TR/TE = 9999/93 ms; 5 mm coronal	Kantarci et al., Radiology 2001
(FA, MD)	HC 18, aMCI 18	NA	Reduced FA Increased MD	1.5T, 6 dir, TE/TR = 100/8000 ms, (1.8 × 1.8 × 5)mm³,1b0, b = 900	Muller et al., Neuroimage 2005
(MD)	HC 10, MCI 14, AD 19	NA	Increased (MCI>C; AD>C)	1.5T, 6 dir, NA = 4, TE/TR = 100/8000 ms, (1.8 × 1.8 × 5)mm³,1b0, b = 900	Fellgiebel et al., Dem Geriatr Cogn Dis 2004
(FA, MD)	HC, MCI 11	NA	Reduced FA Increased MD	1.5T, 25 dir, TE/TR = 78/10000 ms, (2 × 2 × 4)mm³,1b0, b = 1000	Cho et al., J Korean Med Sci 2008
POSTERIOR CINGULUM (FA)	HC 25, aMCI 25, AD 25	3 M	Longitudinal: unchanged Cross-sectional: unchanged (AD<C at baseline and follow-up)	3T, 6-channel RF coil, TE/TR = 80/7000 ms; 32 dir, b=700, 5 b0=33; (2.2 × 2.2 × 2.2)mm³;SENSE=2.5; ACPC, NA=2, 7 min	Mielke et al., Neuroimage 2009
(FA, DA, DR)	HC 26, MCI/SCI-tau- 12, MCI/SCI-tau + 35	NA	Unchanged DA Reduced FA: MCI-tau+<C, MCI-tau+<MCI-tau- Increased DR: MCI-tau+>C, MCI-tau+>MCI-tau- FA and DR correlated with CSF-tau levels	Scan1 : 1.5T, (1.8 × 1.8 × 5)mm³, TE/TR = 131/4300 ms, 2b0, b = 1100, 12 dir, Scan2: 1.5T, (1.2 × 1.2 × 3)mm³, TE/TR = 117/6100 ms, 5b0, b=750, 12 dir,	Stenset et al., Neurob Aging 2009
(FA)	HC 19, MCI 27, AD 17	NA	Unchanged (AD<C; AD<MCI)	1.5T, 8-channel coil, (1.72 × 1.72 × 5)mm³, TE/TR = 98/5000 ms, 1b0, b = 1000, 30 dir, 2 : 53 min	Liu et al., Neurob Aging 2009
(FA)	HC 22, aMCI 22	NA	Reduced FA correlated with MMSE	1.5T, EPI (AC-PC plane), TE/TR = 81.2/10000 ms, (1.88 × 1.88 × 4)mm³,1b0, b = 1000, 25 dir,	Bai et al., J Neurol Sci 2009
(MD: ADC)	HC 55, MCI 19, AD 21	NA	Unchanged (AD>C)	1.5T, FLAIR-DTI, 3 dir, 1b0, b = 1000; TR/TE = 9999/93 ms; 5 mm coronal	Kantarci et al., Radiology 2001
(FA, MD)	HC 21, aMCI 17, AD 25	NA	Reduced FA (aMCI<C; AD<C) Increased MD (aMCI>C; AD>C)	1.5T, 6 dir, NA = 4, TE/TR = 100/8000 ms, (1.8 × 1.8 × 5)mm³,1b0, b = 900	Fellgiebel et al., Neurob Aging 2005
(FA, MD)	HC 18, MCI 17, AD 17	NA	Reduced FA (AD<MCI<C) Increased MD (AD>MCI>C)	1.5T, IR-EPI, TE/TR/TI = 100/6000/2000 ms, (2.34 × 2.34 × 5)mm³,1b0, b = 1000, 6 dir,	Zhang et al., Neurology 2007
(FA)	HC 17, aMCI 17	NA	Reduced	1.5T, (1.8 × 1.8 × 2.5)mm³, TE/TR = 106/6000 ms, 16b0, b = 1100, 44 dir, 8 min	Rose et al., JNNP 2006

Region (measures)	Groups	Field	Findings	Acquisition parameters	Reference
(FA, MD: ADC)	HC 16, MCI 16, AD 17	NA	Reduced FA (MCI<C; AD<C)	1.5T, b=1000, 6 dir, (1.8 × 1.8 × 3)mm³, NA=6, TE/TR=85/4900 ms,	Kiuchi et al., *Brain Res* 2009
(FA, MD, DA, DR)	HC 15, aMCI 16, AD 15	NA	Increased ADC (MCI>C; AD>C) Increased MD, DR (*aMCI*>C, AD>C) Unchanged FA (AD<C) Unchanged DA (AD>C)	3T, (1.22 × 1.22 × 2)mm³, TE/TR=89/5600 ms, 30 dir, 1b0	Bosch et al., *Neurob Aging* 2010
FRONTAL WM (FA)	HC 25, aMCI 25, AD 25	3 M	Reduced	3T, 6-channel RF coil, TE/TR=80/7000 ms; 32 dir, b=700, 5 b0=33; (2.2 × 2.2 × 2.2)mm³;SENSE=2.5; ACPC, NA=2, 7 min	Mielke et al., *Neuroimage* 2009
(MD: ADC)	HC 55, MCI 19, AD 21	NA	Unchanged	1.5T, FLAIR-DTI, 3 dir, 1b0, b=1000; TR/TE=9999/93 ms; 5 mm coronal	Kantarci et al., *Radiology* 2001
(MD)	HC 17, aMCI 17	NA	Increased	1.5T, (1.8 × 1.8 × 2.5)mm³, TE/TR=106/6000 ms, 16b0, b=1100, 44 dir, 8 min	Rose et al., *JNNP* 2006
(FA, MD: ADC)	HC 19, MCI 16, AD 15	NA	Unchanged	1.5T, 8-channel coil, GRAPPA (AF=3, 10 averages, b=1000, 6 dir, TE/TR=71/6000 ms, 1.8 × 1.8.3.6mm³, 7 : 44 min	Stahl et al., *Radiology* 2007
(FA)	HC 18, MCI 15, AD 14	NA	Unchanged	1.5T, 1b0, b=1000, 32 dir, TE/TR=92/7895 ms, 5 : 00 min	Ukmar et al., *Radiol Med* 2008
(FA, MD)	HC 10, MCI 14, AD 19	NA	Unchanged	1.5T, 6 dir, NA=4, TE/TR=100/8000 ms, (1.8 × 1.8 × 5)mm³, 1b0, b=900	Fellgiebel et al., *Dem Geriatr Cogn Dis* 2004
(FA, MD)	HC 11, MCI 11	NA	Increased MD Unchanged FA	1.5T, 25 dir, TE/TR=78/10000 ms, (2 × 2 × 4)mm³, 1b0, b=1000	Cho et al., *J Korean Med Sci* 2008
(MD)	HC 20, aMCI 10, AD 30	NA	Unchanged (AD>C)	1.5T, 25 dir; b=1000; NEX=2;ACPC; 1 b0; (1.875 × 1.875 × 5)mm³, 5 min40 sec	Chen et al., *Psych Res* 2009
FORNIX (FA)	HC 25, MCI1 (CDR-*SB* <1) 12, MCI2 (CDR-*SB* >1.5) 13, AD 25	3 M	Longitudinal: unchanged Cross-sectional: reduced (MCI2<C at follow-up; AD<C at baseline and follow-up)	3T, 6-channel RF coil, TE/TR=80/7000 ms; 32 dir, b=700, 5 b0=33; (2.2 × 2.2 × 2.2)mm³;SENSE=2.5; ACPC, NA=2; 7 min	Mielke et al., *Neuroimage* 2009
(FA)	HC 19, MCI 27, AD 17	NA	Unchanged (AD<C; AD<MCI)	1.5T, 8-channel coil, (1.72 × 1.72 × 5)mm³, TE/TR=98/5000 ms, 1b0, b=1000, 30 dir, 2 : 53 min	Liu et al., *Neurob Aging* 2009
(FA, MD, DA, DR)	HC 15, aMCI 19, AD 25	NA	Unchanged MD, DA Unchanged DR (*aMCI*>C, AD>C) Increased DR (*aMCI*>C, AD>C)	1.5T, PGSE-EPI (1.88 × 1.88 × 2.5)mm³, TE/TR=95/6500 ms, 1b0, b=1000, 12 dir, 8 averages	Pievani et al., *Hum Brain Map* 2010
(FA, MD, DA, DR)	HC 15, aMCI 16, AD 15	NA	Increased MD (*aMCI*>C, AD>C)	3T, (1.22 × 1.22 × 2)mm³, TE/TR=89/5600 ms, 30 dir, 1b0	Bosch et al., *Neurob Aging* 2010
TEMPORAL WM (MD: ADC, temporal stem)	HC 55, MCI 19, AD 21	NA	Unchanged (AD>C)	1.5T, FLAIR-DTI, 3 dir, 1b0, b=1000; TR/TE=9999/93 ms; 5 mm coronal	Kantarci et al., *Radiology* 2001
(FA)	HC 17, aMCI 17	NA	Reduced	1.5T, (1.8 × 1.8 × 2.5)mm³, TE/TR=106/6000 ms, 16b0, b=1100, 44 dir, 8 min	Rose et al., *JNNP* 2006
(FA, MD: ADC)	HC 19, MCI 16, AD 15	NA	Unchanged	1.5T, 8-channel coil, GRAPPA (AF=3, 10 averages, b=1000, 6 dir, TE/TR=71/6000 ms, 1.8 × 1.8.3.6mm³, 7 : 44 min	Stahl et al., *Radiology* 2007
(FA)	HC 18, MCI 15, AD 14	NA	Unchanged	1.5T, 1b0, b=1000, 32 dir, TE/TR=92/7895 ms, 5 : 00 min	Ukmar et al., *Radiol Med* 2008

Table 5
(*Continued*)

Marker	N of subjects and diagnosis	Time between baseline and follow-up	Results	Technical notes	References
(MD)	HC 10, MCI 14, AD 19	NA	Increased (MCI>C; AD>C)	1.5T, 6 dir, NA=4, TE/TR = 100/8000 ms, (1.8 × 1.8 × 5)mm³, 1b0, b=900	Fellgiebel et al., *Dem Geriatr Cogn Dis* 2004
(FA)	HC 16, aMCI 13, AD 11	NA	Unchanged	1.5T; 25 dir; b=1000; NEX=2;ACPC; 1 b0; (1.875 × 1.875 × 5)mm³, 5 min40 sec	Chen et al., *HBM* 2009
(FA, DA, DR)	HC 8, MCI 11, AD 6	NA	Reduced FA (AD<MCI<C) Reduced DA (MCI<C; AD<C) Unchanged DR (AD>C)	1.5T,12 dir, 2b0, b=1000, 7:06 min, (1.875 × 1.875 × 3)mm³, TE/TR = 109/8000 ms,	Huang et al., *AJNR* 2007
(FA, MD)	HC 11, MCI 11	NA	Unchanged	1.5T, 25 dir, TE/TR = 78/10000 ms, (2 × 2 × 4)mm³,1b0, b = 1000	Cho et al., *J Korean Med Sci* 2008
(FA)	HC 8, MCI 8, AD 16	NA	Unchanged (AD<C)	1.5T, TE/TR = 86/8500 ms, 23mm³ ,60 dir, b = 700, 10b0,	Damoiseaux et al., *HBM* 2009
UNCINATE (FA)	HC 19, MCI 27, AD 17	NA	Reduced (AD<MCI<C)	1.5T, 8-channel coil, (1.72 × 1.72 × 5)mm³, TE/TR = 98/5000 ms, 1b0, b = 1000, 30 dir, 2 :53 min	Liu et al., *Neurob Aging* 2009
(FA, MD, DA, DR)	HC 15, aMCI 19, AD 25	NA	Increased DA (aMCI>C, AD>C) Unchanged FA Unchanged MD (AD>C) Unchanged DR	1.5T, PGSE-EPI (1.88 × 1.88 × 2.5)mm³, TE/TR = 95/6500 ms, 1b0, b = 1000, 12 dir, 8 averages	Pievani et al., *Hum Brain Map* 2010
(FA and MD: ADC)	HC 16, MCI 16, AD 17	NA	Unchanged FA (AD<C) Unchanged MD (AD>C)	1.5T, b=1000, 6 dir, (1.8 × 1.8 × 3)mm³, NA=6, TE/TR = 85/4990ms	Kiuchi et al., *Brain Res* 2009
(FA, MD, DA, DR)	HC 15, aMCI 16, AD 15	NA	Increased MD (aMCI>C, AD>C) Increased DR (aMCI>C, AD>C) Unchanged FA (AD<C) Unchanged DA (AD>C)	3T, (1.22 × 1.22 × 2)mm³, TE/TR = 89/5600 ms, 30 dir, 1b0	Bosch et al., *Neurob Aging* 2010
SUPERIOR LONGITUDINAL FASCICULUS (FA)	HC 22, aMCI 22	NA	Reduced Correlated with TMT A and B	1.5T, EPI (AC-PC plane), TE/TR = 81.2/10000 ms, (1.88 × 1.88 × 4)mm³, 1b0, b = 1000, 25 dir,	Bai et al., *J Neurol Sci* 2009
(FA, MD, DA, DR)	HC 15, aMCI 19, AD 25	NA	Increased DA (aMCI>C, AD>C) Unchanged FA Unchanged MD (AD>C) Unchanged DR	1.5T, PGSE-EPI (1.88 × 1.88 × 2.5)mm³, TE/TR = 95/6500 ms, 1b0, b = 1000, 12 dir, 8 averages	Pievani et al., *Hum Brain Map* 2010
(FA, MD, DA, DR)	HC 15, aMCI 16, AD 15	NA	Increased MD (aMCI>C, AD>C) Increased DR (aMCI>C, AD>C) Unchanged FA (AD<C) Unchanged DA (AD>C)	3T, (1.22 × 1.22 × 2)mm³, TE/TR = 89/5600 ms, 30 dir, 1b0	Bosch et al., *Neurob Aging* 2010
(FA, MD)	HC 11, MCI 11	NA	Reduced FA Increased MD	1.5T, 25 dir, TE/TR = 78/10000 ms, (2 × 2 × 4)mm³,1b0, b = 1000	Cho et al., *J Korean Med Sci* 2008
INFERIOR LONGITUDINAL FASCICULUS (FA, MD, DA, DR)	HC 15, aMCI 19, AD 25	NA	Unchanged MD (AD>C) Unchanged DA, DR (AD>C)	1.5T, PGSE-EPI (1.88 × 1.88 × 2.5)mm³, TE/TR = 95/6500 ms, 1b0, b = 1000, 12 dir, 8 averages	Pievani et al., *Hum Brain Map* 2010

Region (Marker)	Sample	Follow-up	Results	Acquisition	Reference
(FA, MD, DA, DR)	HC 15, aMCI 16, AD 15	NA	Increased DR (aMCI>C, AD>C); Unchanged FA (AD<C); Unchanged DA (AD>C); Unchanged MD (AD>C)	3T, $(1.22 \times 1.22 \times 2)$mm^3, TE/TR = 89/5600 ms, 30 dir, 1b0	Bosch et al., Neurob Aging 2010
(FA, MD)	HC 11, MCI 11	NA	Reduced FA; Increased MD	1.5T, 25 dir, TE/TR = 78/10000 ms, $(2 \times 2 \times 4)$mm^3, 1b0, b=1000	Cho et al., J Korean Med Sci 2008
INFERIOR FRONTO OCCIPITAL (FA, DA, DR)	HC 15, aMCI 19, AD 25	NA	Increased DA (aMCI>C, AD>C); Unchanged FA, MD; Unchanged DR	1.5T, PGSE-EPI $(1.88 \times 1.88 \times 2.5)$mm^3, TE/TR = 95/6500 ms, 1b0, b=1000, 12 dir, 8 averages	Pievani et al., Hum Brain Map 2010
(FA)	HC 22, aMCI 22	NA	Reduced	1.5T, EPI (AC-PC plane), TE/TR = 81.2/10000 ms, $(1.88 \times 1.88 \times 4)$mm^3, 1b0, b=1000, 25 dir,	Bai et al., J Neurol Sci 2009
(FA, MD, DA, DR)	HC 15, aMCI 16, AD 15	NA	Increased MD (aMCI>C, AD>C); Increased DR (aMCI>C, AD>C); Unchanged FA (AD<C); Unchanged DA (AD>C)	3T, $(1.22 \times 1.22 \times 2)$mm^3, TE/TR = 89/5600 ms, 30 dir, 1b0	Bosch et al., Neurob Aging 2010
SPLENIUM OF CC (FA)	HC 25, aMCI 25, AD 25	3 M	Longitudinal: unchanged Cross-sectional: unchanged (AD<aMCI at baseline)	3T, 6-channel RF coil, TE/TR = 80/7000 ms; 32 dir, b=700, 5 b0=33; $(2.2 \times 2.2 \times 2.2)$mm^3;SENSE = 2.5; ACPC, NA = 2, 7 min	Mielke et al., Neuroimage 2009
(FA)	HC 19, MCI 27, AD 17	NA	Unchanged (AD<C; AD<MCI)	1.5T, 8-channel coil, $(1.72 \times 1.72 \times 5)$mm^3, TE/TR = 98/5000 ms, 1b0, b=1000, 30 dir, 2 : 53 min	Liu et al., Neurob Aging 2009
(FA, MD)	HC 18, MCI 17, AD 17	NA	Unchanged FA (AD<C; AD<MCI); Unchanged MD	1.5T, IR-EPI, TE/TR/TI = 100/6000/2000 ms, $(2.34 \times 2.34 \times 5)$mm^3, 1b0, b=1000, 6 dir,	Zhang et al., Neurology 2007
(FA, MD: ADC)	HC 19, MCI 16, AD 15	NA	Unchanged FA (AD<MCI); Unchanged MD	1.5T, 8-channel coil, GRAPPA (AF=3), 10 averages, b=1000, 6 dir, TE/TR = 71/6000 ms, $1.8 \times 1.8.3.6$mm^3, 7 : 44 min	Stahl et al., Radiology 2007
(FA)	HC 18, MCI 15, AD 14	NA	Reduced (MCI<C; AD<C)	1.5T, 1b0, b=1000, 32 dir, TE/TR = 92/7895 ms, 5 : 00 min	Ukmar et al., Radiol Med 2008
(FA, MD)	HC 10, MCI 14, AD 19	NA	Unchanged	1.5T, 6 dir, NA=4, TE/TR = 100/8000 ms, $(1.8 \times 1.8 \times 5)$mm^3,1b0, b=900	Fellgiebel et al., Dem Geriatr Cogn Dis 2004
(FA, MD)	HC 11, MCI 11	NA	Reduced FA; Increased MD	1.5T, 25 dir, TE/TR = 78/10000 ms, $(2 \times 2 \times 4)$mm^3, 1b0, b=1000	Cho et al., J Korean Med Sci 2008
(FA, MD)	HC 20, aMCI 10, AD 30	NA	Unchanged FA (AD<C); Unchanged MD (AD>C)	1.5T, 25 dir; b=1000; NEX = 2;ACPC; 1 b0; $(1.875 \times 1.875 \times 5)$mm^3, 5 min40 sec	Chen et al., Psych Res 2009
GENU OF CC (FA, DA, DR)	HC 26, MCI/SCI tau- 12, MCI/SCI tau+ 35	NA	Reduced FA (MCI/SCI tau+<C); Increased DR (MCI/SCI tau+>C); Unchanged DA	Scan1 :1.5T, $(1.8 \times 1.8 \times 5)$mm^3, TE/TR = 131/4300 ms, 2b0, b=1100, 12 dir, Scan2 :1.5T, $(1.2 \times 1.2 \times 3)$mm^3, TE/TR = 117/6100 ms, 5b0, b=750, 12 dir,	Stenset et al., Neurob Aging 2009
(FA, DA, DR)	HC 40, MCI 38, AD 38	NA	Unchanged (FA: AD<C, DR: AD>C)	3T, $(1.8 \times 1.8 \times 1.8)$mm^3, TE/TR = 89/8500 ms, 6b0, b=1000, 30dir, 3 averages	Di Paola et al., Neurology 2010
(FA)	HC 19, MCI 27, AD 17	NA	Unchanged (AD<C; AD<MCI)	1.5T, 8-channel coil, $(1.72 \times 1.72 \times 5)$mm^3, TE/TR = 98/5000 ms, 1b0, b=1000, 30 dir, 2 : 53 min	Liu et al., Neurob Aging 2009

Table 5
(*Continued*)

Marker	N of subjects and diagnosis	Time between baseline and follow-up	Results	Technical notes	References
(FA)	HC 22, aMCI 22	NA	Reduced	1.5T, EPI (AC-PC plane), TE/TR = 81.2/10000 ms, (1.88 × 1.88 × 4)mm³, 1b0, b=1000, 25 dir,	Bai et al., *J Neurol Sci* 2009
(FA, MD)	HC 18, MCI 17, AD 17	NA	Unchanged	1.5T, IR-EPI, TE/TR/TI= 100/6000/2000 ms, (2.34 × 2.34 × 5)mm³, 1b0, b=1000, 6 dir,	Zhang et al., *Neurology* 2007
(FA, MD: ADC)	HC 19, MCI 16, AD 15	NA	Unchanged	1.5T, 8-channel coil, GRAPPA (AF=3), 10 averages, b=1000, 6 dir, TE/TR = 71/6000 ms, 1.8 × 1.8.3.6mm³, 7 : 44 min	Stahl et al., *Radiology* 2007
(FA)	HC 18, MCI 15, AD 14	NA	Unchanged (AD<C)	1.5T, 1b0, b=1000, 32 dir, TE/TR = 92/7895 ms, 5 : 00 min	Ukmar et al., *Radiol Med* 2008
(FA, MD)	HC 10, MCI 14, AD 19	NA	Unchanged	1.5T, 6 dir, NA =4, TE/TR = 100/8000 ms, (1.8 × 1.8 × 5)mm³, 1b0, b=900	Fellgiebel et al., *Dem Geriatr Cogn Dis* 2004
(FA, MD)	HC 16, aMCI 13, AD 11	NA	Unchanged FA (AD<C) Increased MD (MCI>C; AD>C)	1.5T, 25 dir; b=1000; NEX =2;ACPC; 1 b0; (1.875 × 1.875 × 5)mm³, 5 min40 sec	Cho et al., *J Korean Med Sci* 2008
(FA, MD)	HC 11, MCI 11	NA	Unchanged	1.5T, 25 dir, TE/TR =78/10000 ms, (2 × 2 ×4)mm³,1b0, b=1000	Cho et al., *J Korean Med Sci* 2008
(FA, MD)	HC 20, aMCI 10, AD 30	NA	Unchanged (AD>C)	1.5T, 25 dir; b=1000; NEX =2;ACPC; 1 b0; (1.875 × 1.875 × 5)mm³, 5 min40 sec	Chen et al., *Psych Res* 2009
CORTICOSPINAL TRACT (FA, cerebral peduncles)	HC 25, aMCI 25, AD 25	3 M	Unchanged	3T, 6-channel RF coil, TE/TR =80/7000ms; 32 dir, b=700, 5 b0=33; (2.2 × 2.2 × 2.2)mm³;SENSE =2.5; ACPC, NA =2, 7 min	Mielke et al., *Neuroimage* 2009
(FA, MD, internal capsule)	HC, MCI 17, AD 17	NA	Unchanged	1.5T, IR-EPI, TE/TR/TI= 100/6000/2000 ms, (2.34 × 2.34 × 5)mm³, 1b0, b=1000, 6 dir,	Zhang et al., *Neurology* 2007
(FA, MD: ADC)	HC 16, MCI 16, AD 17	NA	Unchanged	1.5T, b=1000, 6 dir, (1.8 × 1.8 × 3)mm³, NA =6, TE/TR = 85/4900ms	Kiuchi et al., *Brain Res* 2009
(FA, MD centrum semiovale)	HC 10, MCI 14, AD 19	NA	Unchanged FA Increased MD (MCI>C; AD>C)	1.5T, 6 dir, NA =4, TE/TR = 100/8000 ms, (1.8 × 1.8 × 5)mm³, 1b0, b=900	Fellgiebel et al., *Dem Geriatr Cogn Dis* 2004
(FA, MD internal capsule)	HC 11, MCI 11	NA	Reduced FA Increased MD	1.5T, 25 dir, TE/TR = 78/10000 ms, (2 × 2 ×4)mm³,1b0, b=1000	Cho et al., *J Korean Med Sci* 2008
CEREBELLUM (FA)	HC 19, MCI 27, AD 17	NA	Reduced (AD<MCI<C)	1.5T, 8-channel coil, (1.72 × 1.72 × 5)mm³, TE/TR = 98/5000 ms, 1b0, b=1000, 30 dir, 2 : 53 min	Liu et al., *Neurob Aging* 2009
Entorhinal cortex (MD)	HC 17, aMCI 17	NA	Increased	1.5T, (1.8 × 1.8 × 2.5)mm³, TE/TR =106/6000 ms, 16b0, b=1100, 44 dir, 8 min	Rose et al., *JNNP* 2006
Thalamus (MD)	HC 17, aMCI 17	NA	Increased	1.5T, (1.8 × 1.8 × 2.5)mm³, TE/TR =106/6000 ms, 16b0, b=1100, 44 dir, 8 min	Rose et al., *JNNP* 2006
Subventricular zone (MD)	HC 30, aMCI 30, AD 30	NA	Increased (AD>aMCI>C)	3T, TE/TR = 89/500 ms; (1.5 × 1.5 × 2)mm³, 2b0, b=1000, 12 dir, 3averages	Cherubini et al., *Neurosci Lett* 2010
CLASS C					
Cingulum shape (MD)	HC 19, AD 13	NA	Shape compression	3T, SENSE with reduction *fctor* =2.5, TE/TR =71/6112 ms; (2.2 × 2.2 × 2.2)mm³, 60 slices parallel to AC-PC, 5b0, b=700, 30	Qiu et al., *Plos One* 2010

progression. Given the technical difficulties related to parahippocampal assessment, the posterior cingulum and hippocampus may be the best candidate marker to track the disease. Their validity however needs to be confirmed by serial studies.

BETA-AMYLOID POSITRON EMISSION TOMOGRAPHY (PET) IMAGING

A definite diagnosis of Alzheimer's dementia (AD) is based on post-mortem identification of extracellular beta- amyloid plaques and intraneuronal fibrillary tangles. Formation of neuritic plaques by beta-amyloid deposits is thought to play a major role in the pathophysiology of AD, and several therapeutic agents intended to remove or prevent the build-up of beta-amyloid deposits are currently in clinical development. Recent development of positron emission tomography (PET) ligands for detection of beta amyloid in patients has provided a new potential for the diagnosis of AD during lifetime. In addition, this imaging method may allow investigators and clinicians to monitor disease progression or regression with new treatments. When searching for a biological marker of AD amyloid imaging could hopefully replace invasive procedures such as lumbar puncture. There is very active research investigating molecules labelled with radioactive isotopes that might enter the brain, bind selectively to β-amyloid, be visualised with PET scanners and analysed with PET imaging tools, enabling in vivo quantification of beta-amyloid plaque load in AD [133, 134].

Currently, the compound at the most advanced stage of validation is the Pittsburgh compound B (PIB), a carbon-11-labelled benzothiazole derivative, which has been recently shown to provide information as reliable as CSF Aβ 42 [135]. More than 3000 subjects at 40 centers have been examined with C11-PIB [136]. From quantitative image evaluation a cut-off and simplified rating of PIB-negative vs PIB-positive has been developed to facilitate the use of PIB as a diagnostic marker for the presence of AD [137]. As C11-PIB availability is limited by the need for an on-site cyclotron, a (18)F-labeled PIB derivative named (18)F-flutemetamol has recently been developed; (18)F-Flutemetamol was shown to perform similarly to the (11)C-PIB parent molecule within the same cohort of AD, MCI patients and normal control subjects, with potentially much wider accessibility for clinical and research use [138].

Another promising radioligand applicable to imaging beta-amyloid plaques in living human brains with PET is [(18)F]FDDNP. The results using this technique has been found to be strongly correlated with cognitive performance, especially in regions deteriorating earliest in AD, suggesting the potential utility of [(18)F]FDDNP for early diagnosis [139]. The advantage of this compound is that it binds to both plaques and tangles [140].

More recently, new F-18-labeled Abeta ligands have been identified. The first one is (18)F-BAY94-9172 (Florbetaben), whose binding was reported to match the reported post-mortem distribution of Abeta plaques in AD [141]; (18)F-GE067 was recently tested on a cohort of healthy elderly human subjects [142]; 18F-AV-45 (Florbetapir) was found to accumulate in cortical regions expected to be high in Aβ deposition [143], was shown to be correlated with the presence and density of β-amyloid at histopathology [144] and was shown to be easily synthetized under GMP-compliant conditions, with potentially wide availability for routine clinical use [145, 146]; AZD4694 was recently characterized [147] and preliminarily validated in two small clinical cohorts [148, 149]. Other F18-amyloid imaging radioligands are under development, currently at a preclinical validation step [150, 151] and could potentially facilitate integration of beta amyloid imaging into clinical practice.

Amyloid imaging as marker of disease progression. A number of markers based on amyloid PET imaging have been used to track the progression of Alzheimer's disease. Longitudinal studies with repeated amyloid PET scanning are limited, and only two of them involved MCI patients [152, 153]. The other studies have been cross-sectional.

Class A marker

Global index

Most amyloid imaging studies use a global index of radioligand uptake. In these studies there is not a single global index, but rather a variety of different indexes have been reported. Most of them are computed as global cortical standardized uptake value ratios (SUVR) with averages on a specific set of regions (e.g., weighted average of prefrontal, orbitofrontal, parietal, temporal, anterior cingulate and posterior cingulate/precuneus ratio values [152], average of the area-weighted mean for frontal, superior parietal, lateral temporal, lateral occipital and anterior and

posterior cingulated [141, 153, 154], volume-weighted average of frontal, parietal, temporal cortices, medial-temporal lobe and posterior cingulate gyrus, average of the medial frontal, lateral frontal, temporal, parietal cortices and the posterior cingulate gyrus [155], and overall cortical average [143]. Other indexes are computed from the relative distribution volume (DVR) images, as average DVR in parietal, medial temporal, lateral temporal, posterior cingulate and frontal regions [156] or overall average DVR. There is a longitudinal study by Jack and colleagues assessing the global index change in MCI [152]. These investigators reported that the annual change in global PIB retention in patients with MCI did not differ from the change observed in NC, although small was greater than zero among all subjects. Another study shows that 2-years change in PIB retention in AD was not significantly different from the change in NC [155]. Recently, a large longitudinal study showed that Aβ deposition increases slowly and continuously from cognitive normality to moderately severe AD [153].

Cross-sectional studies have revealed that global cortical PIB binding in MCI is significantly higher than in NC, and significantly lower than in AD [154, 157]. Contradictory results, however, were reported when using the FDDNP radioligand to assess global cortical binding in MCI. Whereas in one study binding was found to be significantly different from both AD and NC [156], in another study binding in MCI was not different from either AD or NC [157]. A recent study involving the novel radioligand AV-45 showed significant differences between AD and NC [143].

Class B marker

Mean uptake in single ROIs (frontal cortex/parietal cortex/temporal cortex/posterior cingulate and precuneus)

Several cross-sectional studies involving participants with MCI analyzed the mean uptake in single ROIs. For each of the following ROIs – frontal cortex, parietal cortex, temporal cortex, posterior cingulate and precuneus, mean uptake in MCI was found to be significantly higher in participants with MCI than in NC (for both PIB [158, 159] and FDDNP [156]), and mean uptake in subjects with MCI was found to be significantly lower than in patients with AD (for both PIB [158] and FDDNP [156]). In those regions, mean AV-45 uptake in NC was significantly lower than in AD [143].

Class C marker

Mean uptake in single ROIs (anterior cingulate/putamen/caudate/striatum/occipital cortex)

There is a single study showing that PIB uptake in putamen and caudate in MCI is significantly higher than in NC [159]. Two other studies showed that PIB uptake in the caudate [155] and striatum [160] in NC was significant lower than in patients with AD.

There is a single cross sectional study showing that PIB uptake in the occipital cortex of patients with AD is significantly higher than in NC [160]. There is also a single study showing that FDDNP uptake in the medial temporal lobe in patients with MCI is significantly higher than in NC [156, 161]. Another recent study showed that FDDNP uptake in the medial temporal lobe in NC is significant lower than in AD [140]. The same study, in which both PIB-PET and FDDNP-PET were performed, shows that FDDNP uptake is significant lower in NC than in AD both in inferior temporal and visual cortex [140], suggesting that FDDNP could be more sensitive than PIB for investigating AD-related regional pathology.

Conclusion

In vivo imaging with beta amyloid PET-ligands provides clinicians and investigators the ability to visualize, localize (in specific regions) and quantify brain beta amyloid deposition in relation to disease severity.

Longitudinal change of beta amyloid load in MCI patients has been first addressed using an amyloid PET ligand in a study showing no significant increase in beta-amyloid burden during one year. However, several cross-sectional studies have indicated that beta amyloid load generally is lower in MCI patients as compared to AD patients, and higher in MCI patients as compared to healthy controls, suggesting the need for further investigations. A recent longitudinal study over longer (2 to 3 years) period of time showed that Aβ deposition increases slowly and continuously from cognitive normality to moderate Alzheimer's disease, providing first evidence to the potential value of change in beta amyloid load as a marker of disease progression.

RESTING EEG

Since its introduction by Hans Berger in 1924, the electroencephalogram (EEG) has been viewed with great enthusiasm as the only methodology allowing a direct, on-line view of the "brain at work" [162].

Table 6
PET markers of disease progression based on literature evidence of validity

Marker	Ligand	N subjects and diagnosis	Time B-FU	Results	References
Class A					
Global index	11C-PIB	106 HC, 65 MCI, 35 AD	20 ± 3 months, 3 years (subgroup)	PIB uptake increases slowly and continuously from NC to moderately severe AD	Villemagne et al., 2011
	11C-PIB	21 HC, 32aMCI, 8 AD	Mean of 1 year	The annual change in global PIB retention did not differ by clinical group	Jack et al., 2009
	11C-PIB	32 HC, 33 MCI, 31 AD	Cross-sectional study	neocortical PIB binding NC < MCI < AD	Pike et al., 2007
Class B					
Uptake in the frontal cortex	11C-PIB	6 HC, 21 MCI, 27 AD	Cross-sectional study	PIB retention: MCI < AD	Forsberg et al., 2008
	11C-PIB	14 HC, 13 aMCI	Cross-sectional study	[11C]PIB uptake: MCI > NC	Kemppainen et al., 2007
Uptake in the parietal cortex	11C-PIB	6 HC, 21 MCI, 27 AD	Cross-sectional study	PIB retention: MCI < AD in the parietal cortex	Forsberg et al., 2008
	11C-PIB	14 HC, 13 aMCI	Cross-sectional study	[11C]PIB uptake: MCI > NC in parietal cortex (voxel-based analysis). [11C]PIB uptake: MCI > NC in parietal cortex (ROI-based analysis)	Kemppainen et al., 2007
Uptake in the temporal (or lateral temporal) cortex	11C-PIB	6 HC, 21 MCI, 27 AD	Cross-sectional study	Lower PIB retention: MCI < AD in temporal cortex. The MCI group showed no significant difference compared to the NC.	Forsberg et al., 2008
	11C-PIB	14 HC, 13 aMCI	Cross-sectional study	Higher [11C]PIB uptake: MCI > NC in temporal cortex (voxel-based analysis). Increased [11C]PIB uptake: MCI > NC in lateral temporal cortex (ROI-based analysis)	Kemppainen et al., 2007
Uptake in the Posterior cingulate/precuneus	11C-PIB	6 HC, 21 MCI, 27 AD	Cross-sectional study	Lower PIB retention: MCI < AD in posterior cingulum.	Forsberg et al., 2008
	11C-PIB	14 HC, 13 aMCI	Cross-sectional study	Higher [11C]PIB uptake: MCI > NC in posterior cingulate, showing the main difference (voxel-based analysis. Increased [11C]PIB uptake in posterior cingulated: MCI > NC	Kemppainen et al., 2007

Analysis of the EEG offers appreciable promise as a means to characterize significant deviations from the 'natural' aging found in Alzheimer and other dementias [163]. From the 1970s and 1980s with the introduction of structural imaging technologies such as computer assisted tomography (CAT) and magnetic resonance imaging (MRI), these newer methods produced non-invasive views of *in vivo* brain anatomy with considerable resolution that contributed to their clinical and therefore economic utility. Over the course of the following two decades, development of regional metabolic-perfusion methods such as positron emission tomography (PET), single photon emission computed tomography (SPECT), and the ability to map oxygen consumption and regional blood flow in specific neural locations with functional magnetic resonance imaging (fMRI) have reduced the role of electroencephalography in basic and clinical stud-

ies. However, these functional brain imaging methods with their high spatial resolution for anatomical details are relatively limited in their temporal resolution when measuring functional brain activation (seconds to minutes). Thus, these neuroimaging techniques cannot discriminate in series or parallel activation of different relays within a distributed network [164]. As these imaging methods were being developed, similar advances were being made for EEG measures in part because neuroelectric signals can track information processing with millisecond precision, and may measure natural brain aging as well as help to discriminate normal aging from neurodegeneration [165, 166].

In recent years, increasing attention has been paid to the application of quantitative EEG (qEEG) and/or event-related potentials (ERPs) as useful clinical markers of early disease or progression [167]. In large part,

this was made possible as a result of recent improvements in the ease of use of technological advances and in access to sufficient computing power with the development of algorithms that permit rapid processing and interpretation of complex raw datasets. In addition, recent technological advances include a reduction in the size (and portability) of EEG amplifiers as well as the development of high-density array nets that do not require skin abrasion to place electrodes with low impedance.

This section briefly reviews the alterations in resting EEG that are associated with normal and pathological brain aging. For the sake of brevity, the methods used to extract these EEG markers will not be reviewed; however, people who are interested in these methodological approaches can review references 168–187.

Resting state EEG rhythms typically change with aging, with gradual modifications in spectral power profile including a decrease in amplitude and a decrease of alpha (8–13 Hz) activity with global "slowing" of the background EEG, and an increase in power in the slower delta (2–4 Hz) and theta (4–8 Hz) frequency ranges [188–191]. A recent study in a large sample of healthy subjects ($N = 215$, 18–85 years) confirmed an age-dependent power decrement of low-frequency alpha rhythms (8–10.5 Hz) in parietal, occipital, and temporal regions, as well as a decrease of occipital delta power [192].

There is also an extensive literature which reports changes in quantitative electroencephalogram with clinical deterioration in progressive dementia, including longitudinal studies which have demonstrated EEG differences between those patients with pMCI and sMCI.

Class A markers

There have been several studies using resting state EEGs (with eyes closed) that assessed at baseline people who were healthy elderly or patients with MCI and AD. These studies can be found in Table 1. Most of them assessed changes in the EEG as people had cognitive deterioration and also attempted to determine the changes in the baseline EEG, such as power density and coherence that may be able to predict a cognitive decline. Some EEG studies addressed the issue of linear EEG markers that change in line with cognitive status of MCI subjects along the period from "baseline" to "follow up" recordings. In the participants with MCI, the markers of disease progression included an increase in the power of theta and delta activity in the temporal and occipital lobes as well as the reduction of beta power in the temporal and occipital lobes [193]. AD patients were characterized by an increase in the power of theta and delta activity and by the reduction of alpha and beta activity in the parieto-occipital lobes [194]. Furthermore, half of the AD patients showed an increase in the power of theta and delta activity in a temporal-occipital lead [195].

Class B and C markers

Other "cross-sectional" studies have compared markers of resting state EEG rhythms between Healthy controls, MCI and AD subjects, and have correlated these markers to subjects' cognitive status ("Class B markers"). Luckhaus and colleagues have shown that alpha power was lower in AD than MCI subjects and was correlated to cognitive status in these subjects as a whole [196]. A study by Huang and colleagues has evaluated the use of dipole sources of resting state EEG power for the differentiation of MCI from mild AD. Dipole sources of alpha and beta power were shifted more anteriorly in AD patients compared to both the control and MCI subjects [197]. Abnormalities of resting state EEG rhythms in AD patients obtained from conventional spectral analysis and nonlinear dynamical methods have been previously reviewed [198].

A study by Babiloni and colleagues has demonstrated that cortical sources of posterior occipital delta and low frequency alpha power have an intermediate magnitude in MCI subjects compared to mild AD and Healthy controls subjects, the mild AD subjects showing the highest delta power and the lowest alpha power [199]. These sources were both linearly and nonlinearly (linear, exponential, logarithmic, and power) correlated with subjects' global cognitive level as revealed by the MMSE. As a methodological remark, it is remarked that source estaimation was performed by the popular software low resolution brain electromagnetic tomography (LORETA), which can be downloaded from Internet (http://www.uzh.ch/keyinst/loreta.htm) and ensures replicability of the results by independent groups.

It has been reported that the posterior (LORETA) sources of low frequency alpha power are strictly related to a well known neuroanatomic marker of neurodegeneration such as atrophy of hippocampus [200]. Specifically, it has been shown that posterior low frequency alpha sources were maximum in MCI with larger hippocampal volume, intermediate in MCI with

smaller hippocampal volume, and low in AD patients. Furthermore, the power of these sources was linearly and non-linearly correlated with the normalized hippocampal volume.

Other EEG markers of interest were those related to functional coupling of resting state EEG rhythms. It has been shown that the global linear functional coupling as revealed by total spectral coherence at low frequency alpha rhythms was highest in the healthy controls, intermediate in the MCI subjects with low cholinergic damage (i.e. a structural marker of AD), and lowest in the MCI subjects with high cholinergic damage [201]. Furthermore, these coherence values were negatively correlated to (moderate to high) cholinergic lesion across the MCI subjects.

Another study has evaluated fronto-parietal coupling of resting EEG rhythms by an index capturing linear and non-linear dimension of this coupling, namely the so called 'synchronization likelihood' [202]. It has been shown that synchronization likelihood progressively decreased from healthy controls subjects, to those with MCI, and then to those subjects with mild AD subjects at midline (Fz-Pz) and right (F4-P4) fronto-parietal electrodes. The same was true for the likelihood of delta synchronization at the right fronto-parietal electrodes (F4-P4). For these EEG bands, the synchronization likelihood correlated with global cognitive status as measured by the MMSE.

Spectral coherence and synchronization likelihood do not allow the determination of the directional flux of information in the fronto-parietal coupling of resting state EEG rhythms. This dimension can be explored by a technique called direct transfer function (DTF) [203]. It has been shown that parietal to frontal direction of the information flux (DTF) within functional coupling of alpha and beta rhythms is stronger in healthy controls than in MCI and/or AD subjects. Noteworthy, such a direction of the fronto-parietal functional coupling is relatively preserved in aMCI subjects in whom the cognitive decline is mainly explained by extent of white-matter vascular disease [204]. Indeed, fronto-parietal functional coupling of EEG rhythms was higher in magnitude in the healthy controls than in MCI subjects, and the coupling was higher at theta, alpha, and low frequency beta in MCI subjects with a higher than lower extent of vascular disease.

There are a lot of cross-sectional studies addressing the comparison of markers of resting state EEG rhythms between AD and healthy control subjects, which did not include MCI subjects. For sake of brevity, here we just mentioned that by Babiloni and colleagues showing a decline of (LORETA) sources of posterior low frequency alpha power in mild AD subjects when compared to very mild AD subjects [205]. Of note, these sources characterized the whole group of AD subjects with respect to both subjects with cerebrovascular dementia and healthy control subjects [205]. This result is of interest since sources of alpha power are supposed to be an extremely sensitive EEG marker for the progression of MCI to dementia.

Conclusion

The results reviewed in the present article suggest that several spectral markers of resting state EEG rhythms might reflect neurodegenerative processes in the preclinical and clinical stages of AD. Among these markers, we include LORETA sources of EEG power density and functional coupling of scalp EEG rhythms such as spectral coherence, DTF, and synchronization. Unfortunately, this remarkably rich literature suffers from the lack of integration of the various EEG markers for the evaluation of physiological brain aging and discrimination from abnormal scenarios heralding neurodegenerative dementia.

EVENT RELATED POTENTIALS

Long latency event-related potentials (ERPs) are extensively used in analyzing cognitive processes. The P3, a positive peak around 300 ms after a relevant event, is the most often analyzed component in this context. The P3 is typically elicited by an oddball paradigm [206], in which patients with AD usually show increased P3 latencies and – less consistently – reduced amplitudes. Other components, preceding or following the P3, such as the N2 negativity, are also associated with memory and attentional processes, and have also been analyzed in studies on MCI and AD [207].

The alterations of the P3 component in AD and MCI may be caused by several reasons (for references see 208): Brain areas affected in AD contribute to the P3 generation, and the P3 is related to cognitive processes, which are impaired in AD. In addition, the P3 is under cholinergic modulation. Patients with AD have degeneration of their basal forebrain and with this degeneration there is a reduction of the production of acetylcholine. Anticholinergic drugs lead to an increase in P3 latency and a decrease of P3 amplitude, which is partially reversed by cholinesterase inhibiting drugs [209]. In patients with AD, cholinesterase

Table 7
EEG markers of disease progression based on literature evidence of validity

Marker	N subject and diagnosis	Time B-FU	Results	References
Class A				
Delta, theta, and beta power (scalp)	27 MCI, 15 AD, 16 HC	21 months	In MCI subjects, the main disease progression markers were the increment of temporal and temporo-occipital slow EEG power (relative delta and theta) and the reduction of temporal and temporo-occipital beta power	Jelic V, et al., 2000
Delta, theta, alpha and beta power (scalp)	40 AD and 40 HC	30 months	AD patients were characterized by an increase in the power of theta and delta activity and by the reduction of alpha and beta activity in the parieto-occipital lobes	Coben et al., 1985
Delta, theta (scalp)	24 AD	12 months	Half of the AD patients were characterized by an increase in the power of theta and delta activity in a temporal-occipital lead	Soininen et al., 1989
Class B				
Delta power (scalp)	88 MCI	Cross-sectional study	Alpha power was lower in AD than MCI subjects and was correlated to cognitive status in these subjects as a whole	Luckhaus C, et al., 2008
Alpha power (distributed sources)	155 MCI, 193 AD, 126 HC	Cross-sectional study	Distributed (LORETA) sources of posterior occipital delta and alpha power have an intermediate magnitude in MCI subjects compared to mild AD and HC subjects, the mild AD subjects showing the highest delta power and the lowest alpha power. These sources were both linearly and nonlinearly (linear, exponential, logarithmic, and power) correlated with subjects' global cognitive level as revealed by mini mental state examination score	Babiloni C, et al., 2006
Alpha power (distributed sources)	60 HC, 88 MCI, 35 AD	Cross-sectional study	Distributed (LORETA) sources of posterior alpha power are strictly related to a well known neuroanatomic marker of neurodegeneration such as atrophy of hippocampus. Specifically, it has been shown that posterior alpha sources were maximum in MCI subjects with larger hippocampal volume, intermediate in MCI subjects with smaller hippocampal volume, and low in AD patients.	Babiloni C, et al., 2009
Theta, alpha power, and beta power (dipole sources)	38 AD, 31 MCI, 24 HC	Cross-sectional study	Dipole sources of alpha and beta power shifted more anteriorly in AD patients compared to both the healthy controls and MCI subjects. Compared to stable MCI, MCI converted to AD had a more anterior localization of dipole sources of theta, alpha and beta power (baseline antero-posterior dipole localization of alpha power predicted clinical follow up).	Huang C, et al., 2000

Alpha and beta directed transfer function (DTF)	64 HC, 69 MCI, 73 AD	Cross-sectional study	Parietal to frontal direction of the information flux within EEG functional coupling was stronger in HC than in MCI and/or AD subjects, namely for alpha and beta rhythms.	Babiloni C, et al., 2009
Theta, alpha and beta DTF	40 HC, 78 MCI	Cross-sectional study	Directionality of fronto-parietal functional coupling of EEG rhythms was estimated by directed transfer function software. Fronto-parietal functional coupling of EEG rhythms was higher in magnitude in the HC than in the MCI subjects. More interestingly, that coupling was higher at theta, alpha1, alpha2, and beta1 in MCI V + (high vascular load) than in MCI V- group (low vascular load).	Babiloni C, et al., 2008
Alpha coherence	28 HC, 57 MCI	Cross-sectional study	The global EEG linear functional coupling as revealed by total spectral coherence at low frequency alpha rhythms was highest in the normal control, intermediate in the MCI subjects with low cholinergic damage (i.e. a structural marker of AD), and lowest in the MCI subjects with high cholinergic damage. Furthermore, these coherence values were negatively correlated to (moderate to high) cholinergic lesion across the MCI subjects.	Babiloni C, et al., 2010
Delta and alpha synchronization likelihood	69 HC, 88 MCI, 109 AD	Cross-sectional study	Synchronization likelihood of alpha rhythms progressively decreased across normal subjects, MCI, and mild AD subjects at midline (Fz-Pz) and right (F4-P4) fronto-parietal electrodes. The same was true for the delta synchronization likelihood at right fronto-parietal electrodes (F4-P4). For these EEG bands, the synchronization likelihood correlated with global cognitive status as measured by the Mini Mental State Evaluation.	Babiloni C, et al., 2006
Class C				
Alpha power (distributed sources)	48 AD, 20 VaD, 38 HC	Cross-sectional study	Decline of distributed (LORETA) sources of alpha power is specific in mild AD subjects when compared to very mild AD subjects. These sources have also collectively characterized AD subjects with respect to subjects with cerebrovascular dementia and to normal control subjects	Babiloni C, et al., 2004

inhibiting drugs resulted in a shortening of P3 latency and increase in P3 amplitude; and in some of these studies an association was reported between improvement in cognitive test scores and reduction of P3 latencies [210–216].

Since cortical neuronal functioning is directly reflected by EEG [217], deteriorations on the synaptic level should be visible in ERPs at very early stages of disease even before pathology is reflected in disrupted cognitive functions. This assumption is supported by a recent study by Golob et al. [218], which assessed ERPs in 26 subjects with a family history of Familial Alzheimer disease (FAD): The still asymptomatic 15 FAD mutations carriers, when compared to 11 participants who were not carriers, showed longer latencies of several components, including the N2 and P3 components. These electrophysiological alterations were observed about ten years before estimated dementia onset. Similarly, cohorts carrying genetic risks for AD showed increased P3 and N2 latencies in one study [219], and only increased N2 latency in another study [220]. Furthermore, different ERP components, including the P50, N2 and P3, were able to longitudinally predict cognitive decline [220] and conversion from MCI to AD [207, 221–224].

Sensitivity to track disease progression

Class A markers

Longitudinal studies starting with MCI or healthy subjects

Only three studies have been conducted that longitudinally followed patients with MCI or elderly subjects who were still healthy (see Table 8). These studies do not primarily focus on the assessment of disease progression and therefore only comprise one or two follow-up examinations.

Applying an oddball paradigm, all three studies cross-sectionally found increased P3 latencies in AD patients; and two of the studies [207, 225] also demonstrated increased latencies in MCI compared with healthy controls (HCs). Longitudinally, the study by Lai et al. [225] demonstrated higher mean P3 latencies at follow up after one year within both patient groups (MCI and AD), whereas the HCs did not show a significant increase. As neither conversion from MCI to AD, nor significant changes in cognitive test scores were reported within the follow-up, Lai et al. concluded that the P3 latency may be more sensitive to track disease progression than the cognitive tests.

The second study by Papaliagkas [207] also reported a significant mean increase of the P3 latency between baseline and 14-months follow up. However, there was no control group at follow-up. Therefore, it is not possible to separate the disease-associated latency increase in the MCI patients from the normal age-related increase. Recently, a further analysis of a subgroup of this study has been published: Papaliagkas et al. [226] analyzed a subsample of 22 MCI patients, which could be re-assessed at a second follow-up. The difference of the P3 latencies between baseline and the first 14-months follow-up was not significant, but the latencies at the second 23-months follow-up were significantly increased compared with 14-months follow-up and baseline. The authors argue that the observed increases were higher than the age-related increase in healthy subjects of an independent study.

In the third study by Gironell et al. [222], three ERP recordings were done in outpatients with subjective memory complaints, immediately after the first clinical evaluation (T0) and approximately at 12 (T1) and 24 months (T2). The ERPs at T0, T1 and T2 were only analyzed for the final diagnostic groups at T2, which comprised 28 AD and 30 MCI patients. The P3 latency was significantly higher for the T2-AD group throughout the study, supporting the role of the P3 latency as an early predictor of AD. However, there were no differences between the participants with MCI and HC in P3 parameters throughout this entire study. Some limitations have to be considered when interpreting this study with regard to tracking disease progression: As the study was designed to assess the predictive power of P3 in subjects with memory complaints, the analysis of group differences is only retrospectively based on the final diagnoses at T2. There may have been AD subjects at T2 who might have had MCI at T1, but no data are given about the P3 latencies of these possible T1-MCI subjects. A further limitation is that the authors do not provide clear data on their participants' consumption of anticholinesterase medications. These medications reduce the latency of P3 and thus the use of these medications could result in false negative results. Data on other psychotropic medications at T0 are, however, given, revealing that in the MCI group (as classified at T2) a substantial proportion of participants (33%) used benzodiazepines. This class of drugs is not only known to produce cognitive impairments but also an increase of the P3 latency [227]. In addition, in this report no data are given about changes in medications throughout the study. Overall, these three longitudinal studies do support the potential predictive

Table 8
ERP markers of disease progression based on literature evidence of validity

Marker	N subject and diagnosis	Time B-FU	Results	References
Class A				
ERPs (Oddball task)	91 MCI (54 re-examined at follow-up), 5 converted to AD, 30 HC	14 months (T0, T14)	P3 latency increase, P3 and N2 amplitude decrease	Papaliagkas et al., 2008
ERPs (Oddball task)	22 MCI (subsample of Papaliagkas et al., 2008), 3 converted to AD, 30 HC	23 months (T0, T14, T23)	P3 latency increase, N2 amplitude decrease	Papaliagkas et al., in press (subsample of Papaliagkas et al., 2008)
ERPs (Oddball task)	18 MCI, 20 AD, 14 HC	12 months (T0, T12)	P3 latency increase (in AD and, at Pz, in MCI)	Lai et al., 2010
P3 (Oddball task)	116 outpatients with subjective memory complaints At the end of follow-up (T24): 30 MCI, 28 AD, 6 other types of dementia, 30 cases of normal cognition, 22 "lost".	24 months (T0, T12, T24)	P3 latency in patients with stable MCI at T24: no difference nor increase with time compared with healthy controls	Gironell et al., 2005

power and cross-sectional diagnostic value of ERPs, but unfortunately only give limited information about the ability of ERPs to track disease progression.

In addition to the longitudinal studies assessing healthy participants or patients with MCI, there are also longitudinal observations in patients with AD. Within AD, P3 latencies increased in parallel with cognitive deterioration [214, 228–231].

Class B and C markers

Most cross-sectional studies that assessed ERPs in MCI reported higher P3 latencies in patients with MCI compared with HCs [223, 235–237]. However, the P3 latency increase did not reach significance level in one study [237] and reached significance in another study only for the Pz electrode position [238]. It is noteworthy that an increased P3 latency was found in MCI patients of even those studies, in which a substantial proportion of patients were treated with cholinesterase inhibiting drugs at the time of EEG recording [223, 234]. Four cross-sectional studies included patients with AD in addition to MCI and HCs. In these studies, the P3 latencies of MCI patients were *numerically* in between that of AD patients and HCs (with the exception of one singular finding at one electrode position in one study) [238]. However, the *post-hoc* comparisons between all three groups (AD vs. MCI vs. HCs) did not always reach statistical significance. Some of the studies suffer from methodological limitations, such as small sample sizes, insufficient control of psychotropic drug effects and inadequate matching. For example, the study by Bennys et al. [235] was not well matched according to sex and age leading to more

males and younger subjects in the HCs than the MCI group [235].

Several cross-sectional studies on ERPs in patients with AD have already been reviewed elsewhere [206, 233, 239]. These cross-sectional studies show that patients with AD have increased P3 latencies compared with HCs, and some [232] but not all [222], studies reported a correlation between P3 latency and cognitive tests.

Conclusions

Late ERPs may very well be a sensitive marker that either normal people or patients with MCI will progress to AD. So far, however, there are only three serial studies starting with healthy elderly or MCI patients that are unfortunately characterized by few follow-ups and methodological limitations. Nonetheless, studies tracking disease progression within AD, cross-sectional studies including MCI, studies predicting conversion to AD, and studies tracking effects of cholinesterase inhibiting drugs, further support the assumption that late ERPs might be a good marker for disease progression from the earliest stages.

There are several attractive aspects for using ERPs as a marker. Recording ERPs is relatively inexpensive and noninvasive procedure, with almost no side-effects. ERPs can be performed quickly and can be performed with mobile equipment. Thus, additional well controlled longitudinal studies are warranted.

Cross-sectional studies, such as those that compare MCI with HCs, can be influenced by substantial variance due to the high inter-individual variability of the P3, irrespective of any disease state. Whereas P3

latencies recorded at different times are relatively stable within an individual, different individuals often have different latencies suggesting that P3 variability is trait-like. Therefore, variance of P3 should present no problem for within person-designs, such as tracking disease progression or effects of drugs and future studies should try to reduce the error variance of the late ERPs [233] in order to further improve their diagnostic power. In addition, the use of drugs that cause increase or decrease of P3 latencies should be better controlled in these studies.

Further research should also be performed to help clarify which testing paradigm (e.g., odd ball, cognitive tests) [224, 240, 241] and which ERP component (or which combination of ERP components) is most sensitive or predictive of disease onset, disease progression, or disease regression with treatment. Alternative methods, such as source localization analyses [208, 242, 243], should also be assessed for reliability and validity as well as sensitivity and specificity.

CSF

Amyloid plaques, tau pathology, neuro-inflammation, oxidative stress, astrogliosis and synaptic and neuronal losses are typical neuropathological findings in AD. To find markers useful to support the clinical diagnosis and to monitor disease progression and possibly therapeutic effects in clinical trials all these different pathological processes have to be considered. Examination of the cerebral spinal fluid for beta amyloid peptides and tau proteins may provide information about the pathological processes occurring in the brain.

Class A markers

The concentration of soluble beta-amyloid (1–42) ($A\beta_{1-42}$) is selectively reduced in the CSF of individuals affected by AD. The inverse correlation between CSFAβ42 and *in vivo* amyloid imaging load [244, 245] suggests that the selective reduction of Aβ42 in CSF in AD is a direct biomarker of Aβ deposition in human brain and presumably reflects the preferential deposition of Aβ42. This decrease is already present in early stages of the disease. Several longitudinal studies have shown that CSF levels of $A\beta_{x-40}$ and $A\beta_{1-42}$ are stable during disease progression. Coefficients of variation (CVs) around 8% were reported between baseline and follow-up measurement [246]. Consequently, no correlations with the severity of the disease have been found [247]. (See table) [248–251].

CSF-biomarkers that may be related to the abnormal hyperphosphorylation tau protein are phospho-tau181 and phospho-tau231. The concentration of both of these markers is increased in CSF early in the course of the disease. Also some studies reported increasing phospho-tau levels in very early stages of AD, most authors of longitudinal studies concluded that phospho-tau181 as well as phospho-tau231 remain stable throughout the course of the disease. Correlations of phospho-tau levels in CSF with the severity of the disease were not conclusively observed (see table)

Tau protein in CSF is believed to be related the rate of axonal and neuronal degeneration. Although there is some conflicting data, most longitudinal studies report conclusively increased total-tau concentrations in CSF, even in the early stages. During further progression of the disease, CSF total-tau remains elevated but stable [247]. Total-tau measurements at baseline and follow-up are highly correlated with each other [246]. The reported CVs were around 8% [246].

In accordance with the postulate that tau in CSF is related to neuronal degeneration, Hesse et al. observed elevated total-tau levels in CSF after stroke. The CSF tau levels were correlated with the infarct area and normalized within five months after the initial event [252]. Thus, elevated tau levels are not pathognomic of AD [253].

In regard to treatment, Gilman et al. [254] reported reduced CSF total-tau levels in immunization responders in the first abeta immunisation trial. The stability over time and the sensitivity to CNS consolidation makes this marker especially interesting for the monitoring of neurodegeneration during the therapy with disease modifying drugs.

A well established marker representing oxidative stress is the F2 isoprostane. Longitudinal studies report evidence, that isoprostanes increase early in AD and correlate with disease duration and severity. [255–258]. Furthermore, the concentration of isoprostane can be reduced by application of Vitamin C or tocopherol, two antioxidative vitamins [258] (see table)

Class C markers

Gliosis of the affected brain areas is another typical finding in the brains of patients with AD. Following neuronal cell death, astroglia becomes activated to form a scar. S-100B and GFAP are believed to reflect astrocyte activity. In cross sectional studies it is reported that S-100B in CSF [259] is normal in AD,

Table 9
CSF markers of disease progression based on literature evidence of validity

Marker	N subjects and diagnosis	Time B-FU	Results	References
Class A				
CSF - $A\beta_{1-42}$	21 HC, 22 converter, 43 sMCI	2 years	stable	Brys 2009
CSF $A\beta_{1-40}$				
CSF total-tau				
CSF phospho-tau				
CSF F2-isoprostane			increase	
CSF $A\beta_{1-42}$	17 HC, 83 MCI	2 years	stable	Zetterberg 2007
CSF total-tau				
CSF phospho-tau				
CSF $A\beta_{1-42}$	9 HC, 7 MCI	2 years	stable	de Leon 2006
CSF $A\beta_{1-40}$				
CSF phospho-tau				
CSF F2-isoprostane	9 HC, 7 MCI	2 years	increase	de Leon 2006
CSF $A\beta_{1-42}$	10 HC; 8 MCI	1 year	stable	de Leon 2002
CSF $A\beta_{1-40}$				
CSF phospho-tau	10 HC, 8 MCI	1 year	increase	de Leon 2002
CSF $A\beta_{1-42}$	17 HC, 38 MCI, 50 AD	21 months	increase	Bouwman 2007
CSF total-tau				
CSF phospho-tau			stable	
CSF total-tau	9 MCI, 18 AD, 9 OD	14 months	stable	Blomberg 1996
CSF total-tau	40 early MCI	34 months	stable	Andersson 2008
CSF phospho-tau	40 early MCI	34 months	increase	Andersson 2008
CSF F2-isoprostane	11 HC, 6 MCI	2 years	increase	de Leon 2007
Class B				
Class C				
CSF GFAP	14 HC,18 AD, 22 CJD		No corr. With MMSE	Jesse, 2009
CSF GFAP	8 HC, 27 AD		increase	Fukujama, 2001
CSF S100B	14 HC,18 AD, 22 CJD		stable	Jesse, 2009
CSF IL-1	9 HC, 8 AD	6 years	No corr. With MMSE	Lanzrein, 1998
CSF IL-1	9 HC, 8 AD	6 years	No corr. With MMSE	Lanzrein, 1998
CSF IL-1 receptor antagonist	9 HC, 8 AD	6 years	No corr. With MMSE	Lanzrein, 1998
CSF soluble IL-2 receptor	20 HC, 42 AD		no corr. With MMSE	Engelborghs, 1999
CSF IL-1β	MS, MID, AD		increase	Cacabelos 1991
CSF IL-1β	20 HC, 42 AD		no corr. With MMSE	Engelborghs, 1999
CSF IL-6	9 HC, 8 AD	6 years	No corr. With MMSE	Lanzrein, 1998
CSF IL-6	24 HC, 41 AD		No corr. With MMSE	Kalman, 1997
CSF IL-6	27 AD		No corr. With MMSE	Sun, 2003
CSF IL-6	20 HC, 42 AD		no corr. With MMSE	Engelborghs, 1999
CSF soluble IL-6 receptor	20HC, 41 AD		No corr. With MMSE	Hampel, 1998
CSF IL10	25 HC, 30 AD		no corr. With MMSE	Rota, 2006
CSF IL-10	20 HC, 42 AD		no corr. With MMSE	Engelborghs, 1999
CSF IL12	25 HC, 30 AD		no corr. With MMSE	Rota, 2006
CSF IL-12	20 HC, 42 AD		no corr. With MMSE	Engelborghs, 1999
CSF TNFα	9 HC, 8 AD	6 years	No corr. With MMSE	Lanzrein, 1998
CSF TNFα	27 HC; 23 AD, 15 OD, 11 depress		no corr. With MMSE	Blasko, 2006
CSF sTNF-receptors I and II	9 HC, 8 AD	6 years	No corr. With MMSE	Lanzrein, 1998
CSF α1-antichymotrypsin	9 HC, 8 AD	6 years	No corr. With MMSE	Lanzrein, 1998
CSF α1-antichymotrypsin	141 AD		No corr. With MMSE	Sun, 2003
CSF α1-antitrypsin	136 AD		No corr. With MMSE	Sun, 2003
CSF MCP-1	27 HC; 23 AD, 15 OD, 11 depress		Weak corr. With MMSE	Blasko, 2006
CSF MCP-1	136 AD		No corr. With MMSE	Sun, 2003
CSF oxLDL	132 AD		No corr. With MMSE	Sun, 2003

Table 9
(*Continued*)

Marker	N subjects and diagnosis	Time B-FU	Results	References
CSF TGF 1β	27 HC; 23 AD, 15 OD, 11 depress		no corr. With MMSE	Blasko, 2006
CSF TGF1β	25 HC, 30 AD		Weak corr. With MMSE	Rota, 2006
CSF IFN-γ	20 HC, 42 AD		no corr. With MMSE	Engelborghs, 1999
CSF neopterin	20 HC, 42 AD		no corr. With MMSE	Engelborghs, 1999
CSF BDNF, FGF-2, GDNF, VEGF, HGF	27 HC; 23 AD, 15 OD, 11 depress		no corr. With MMSE	Blasko, 2006
CSF MIP-1α	27 HC; 23 AD, 15 OD, 11 depress		no corr. With MMSE	Blasko, 2006

AD: Alzheimer's disease; HD: Healthy controls; QD: Questionable Dementia (Defined by Berg 1985)** Questionable dementia (CDR = 0.5); sMCI: stable MCI: participants with MCI whose CDR-SB score did not differ between the first and last evaluation; dMCI: decliners MCI: participant with MCI whose CDR-SB score declined between the first and last evaluation; converters: participants who received a clinical diagnosis of AD during the follow up period; CJD: Creutzfeld Jacobs disease; OD: other dementias.

whereas several authors report a significant increase in CSF GFAP concentration in AD patients. [259, 260]. Fukujama et al. [260] reported an increase in CSF GFAP concentrations related to the severity of dementia whereas Jesse and his colleagues found no correlation with disease progression. In a longitudinal study, Crols et al. [261] observed increasing GFAP concentrations in the acute stage of encephalitis which normalized in patients who recovered. In one patient, who died from herpes encephalitis GFAP remained elevated [261]. This may point to GFAP as a general marker for astrocyte activation and possibly gliosis.

Several CSF-markers reflecting the neuro-inflammatory processes of AD are discussed as biomarkers. So far there is only cross-sectional data from AD patients in different stages of the disease available. For none of these proteins does conclusive data exist that there is a correlation with these markers and the severity of the disease. [262–269]

In summary the available data shows, that $A\beta_{1-42}$, t-tau and p-tau are valuable markers which support the clinical diagnosis of Alzheimer's disease. However, these markers are not sensitive to disease progression and cannot be used to monitor the severity of Alzheimer's disease. The reason may be that all three markers change already in the preclinical stage of AD and then remain stable in the later stages when patients seek medical help [3]. For Isoprostane F2 some evidence exists that its increase correlates with the progression and the severity of AD.

ACKNOWLEDGMENTS

REFERENCES

[1] Grady CL, Haxby JV, Horwitz B, Sundaram M, Berg G, Schapiro M, Friedland RP, Rapoport SI (1988) Longitudinal study of the early neuropsychological and cerebral metabolic changes in dementia of the Alzheimer type. *J Clin Exp Neuropsychol* **10**, 576-596.

[2] Morris JC, Price AL (2001) Pathologic correlates of nondemented aging, mild cognitive impairment, and early-stage Alzheimer's disease. *J Mol Neurosci* **17**, 101-118.

[3] Jack CR Jr, Wiste HJ, Vemuri P, Weigand SD, Senjem ML, Zeng G, Bernstein MA, Gunter JL, Pankratz VS, Aisen PS, Weiner MW, Petersen RC, Shaw LM, Trojanowski JQ, Knopman DS (2010) Alzheimer's Disease Neuroimaging Initiative. Brain beta-amyloid measures and magnetic resonance imaging atrophy both predict time-to-progression from mild cognitive impairment to Alzheimer's disease. *Brain* **133**, 3336-3348.

[4] Petersen RC, Doody R, Kurz A, Mohs RC, Morris JC, Rabins PV, Ritchie K, Rossor M, Thal L, Winblad B (2001) Current concepts in mild cognitive impairment. *Arch Neurol* **58**, 1985-1992.

[5] Blennow K, Hampel H (2003) CSF markers for incipient Alzheimer's disease. *Lancet Neurol* **2**, 605-613.

[6] Arriagada PV, Marzloff K, Hyman BT (1992) Distribution of Alzheimer-type pathologic changes in nondemented elderly individuals matches the pattern in Alzheimer's disease. *Neurology* **42**, 1681-1688.

[7] Braak H, Braak E (1991) Demonstration of amyloid deposits and neurofibrillary changes in whole brain sections. *Brain Pathol* **1**, 213-216.

[8] Mormino EC, Kluth JT, Madison CM, Rabinovici GD, Baker SL, Miller BL, Koeppe RA, Mathis CA, Weiner MW, Jagust WJ, Alzheimer's Disease Neuroimaging, Initiative (2009) Episodic memory loss is related to hippocampal-mediated beta-amyloid deposition in elderly subjects. *Brain* **132**, 1310-1323.

[9] Wenk GL (2003) Neuropathologic changes in Alzheimer's disease. *J Clin Psychiatry* **64(9)**, 7-10.

[10] Backman L, Small BJ, Fratiglioni L (2001) Stability of the preclinical episodic memory deficit in Alzheimer's disease. *Brain* **124**, 96-102.

[11] Albert M, Blacker D, Moss MB, Tanzi R, McArdle JJ (2007) Longitudinal change in cognitive performance among individuals with mild cognitive impairment. *Neuropsychology* **21**, 158-169.

[12] Leow AD, Yanovsky I, Parikshak N, Hua X, Lee S, Toga AW, Jack CR Jr, Bernstein MA, Britson PJ, Gunter JL, Ward CP, Borowski B, Shaw LM, Trojanowski JQ, Fleisher AS, Harvey D, Kornak J, Schuff N, Alexander GE, Weiner MW, Thompson PM, Alzheimer's Disease Neuroimaging, Initiative (2009) Alzheimer's disease neuroimaging initiative: a one-year follow up study using tensor-based morphometry correlating degenerative rates, biomarkers and cognition. *Neuroimage* **45**, 645-655.

[13] Bennett DA, Wilson RS, Schneider JA, Evans DA, Beckett LA, Aggarwall NT, Barnes LL, Fox JH, Bach J (2002) Natural history of mild cognitive impairment in older persons. *Neurology* **59**, 198-205.

[14] Fama R, Sullivan EV, Shear PK, Marsh L, Fama R, Lim KO, Yesavage JA, Tinklenberg JR, Pfefferbaum A (1998) Fluency performance patterns in Alzheimer's disease and Parkinson's disease. *Clin Neuropsychologist* **12**, 487-499.

[15] Monsch AU, Bondi MW, Butters N, Paulsen JS, Salmon DP, Brugger P, Swenson MR (1994) A comparison of category and letter fluency in Alzheimer's disease. *Neuropsychology* **8**, 25-30.

[16] Clark LJ, Gatz M, Zheng L, Yu-Ling Chen, McCleary C, Mack WJ (2009) Longitudinal verbal fluency in normal aging, preclinical, and prevalent Alzheimer's disease. *Am J Alzheimers Dis Other Dement* **24**, 461-468.

[17] Fowler KS, Saling MM, Conway EL, Semple JM, Louis WJ (2002) Paired associate performance in early detection of DAT. *J Int Neuropsychol Soc* **8**, 58-71.

[18] Ska B, Poissant A, Joanette Y (1990) Line orientation judgment in normal elderly and subjects with dementia of Alzheimer's type. *J Clin Exp Neuropsychol* **12**, 695-702.

[19] Economou A, Papageorgiou SG, Karageorgiou C, Vassilopoulos D (2007) Non episodic memory deficits in amnestic MCI. *Cogn Behav Neurol* **20**, 99-106.

[20] Tröster AI, Fields JA, Testa JA, Paul RH, Blanco CR, Hames KA, Salmon DP, Beatty WW (1998) Cortical and subcortical influences on clustering and switching in the performance of verbal fluency tasks. *Neuropsychologia* **36**, 295-304.

[21] Storandt M, Grant EA, Miller PJ, Morris JC (2002) Rates of progression in mild cognitive impairment and early Alzheimer's disease. *Neurology* **59**, 1035-1041.

[22] Dudas RB, Clague F, Thompson SA, Graham KS, Hodges JR (2005) Episodic and semantic memory in mild cognitive impairment. *Neuropsychologia* **43**, 1266-1276.

[23] Laine M, Vuorinen E, Rinne JO (1997) Picture naming deficits in vascular dementia and Alzheimer's disease. *J Clin Exp Neuropsychol* **19**, 126-140.

[24] Lukatela K, Malloy P, Jenkins M, Cohen R (1998) The naming deficit in early Alzheimer's and Vascular dementia. *Neuropsychology* **12**, 565-572.

[25] Lezak MD, Howieson DB, Loring DW (2004) *Neuropsychological assessment*, 4th Edition, Oxford, p. 369.

[26] Kalbe E, Salmon E, Perani D, Holthoff V, Sorbi S, Elsner A, Weisenbach S, Brand M, Lenz O, Kessler J, Luedecke S, Ortelli P, Herholz K (2005) Anosognosia in very mild Alzheimer's disease but not in mild cognitive impairment. *Dement Geriatr Cogn Disord* **19**, 349-356.

[27] Kramer JH, Nelson A, Johnson JK, Yaffe K, Glenn S, Rosen HJ, Miller BL (2006) Multiple cognitive deficits in amnestic mild cognitive impairment. *Dement Geriatr Cogn Disord* **22**, 306-311.

[28] Allender J, Kaszniak AW (1989) Processing of emotional cues in patients with dementia of the Alzheimer's type. *Int J Neurosci* **46**, 147-155.

[29] Testa JA, Beatty WW, Gleason BA, Orbelo BA, Ross ED (2001) Impaired affective prosody in AD. *Neurology* **57**, 1475-1481.

[30] Derouesné C, Lagha-Pierucci S, Thibault S, Baudouin-Madec V, Lacomblez L (2000) Apraxic disturbances in patients with mild to moderate Alzheimer's disease. *Neuropsychologia* **38**, 1760-1769.

[31] Mozaz M, Garaigordobil M, Gonzalez Rothi LJ, Anderson J, Crucian GP, Heilman KM (2006) Posture recognition in Alzheimer's disease. *Brain Cogn* **62**, 241-245.

[32] Schwartz RL, Adair JC, Raymer AM, Williamson DJ, Crosson B, Rothi LJ, Nadeau SE, Heilman KM (2000) Conceptual apraxia in probable Alzheimer's disease as demonstrated by the Florida Action Recall Test. *J Int Neuropsychol Soc* **6**, 265-270.

[33] Braak H, Braak E, Bohl J (1993) Staging of Alzheimer-related cortical destruction. *Eur Neurol* **33**, 403-408.

[34] Kaye JA, Swihart T, Howieson D, Dame A, Moore MM, Karnos T, Camicioli R, Ball M, Oken B, Sexton G (1997) Volume loss of the hippocampus and temporal lobe in healthy elderly persons destined to develop dementia. *Neurology* **48**, 1297-1304.

[35] Jack CR Jr, Petersen RC, Xu YC, O'Brien PC, Smith GE, Ivnik RJ, Boeve BF, Waring SC, Tangalos EG, Kokmen E (1999) Prediction of AD with MRI-based hippocampal volume in mild cognitive impairment. *Neurology* **52**, 1397-1403.

[36] Convit A, de Asis J, de Leon MJ, Tarshish CY, De Santi S, Rusinek H (2000) Atrophy of the medial occipitotemporal, inferior, and middle temporal gyri in non-demented elderly predict decline to Alzheimer's disease. *Neurobiol Aging* **21**, 19-26.

[37] Killiany RJ, Gomez-Isla T, Moss M, Kikinis R, Sandor T, Jolesz F, Tanzi R, Jones K, Hyman BT, Albert MS (2000) Use of structural magnetic resonance imaging to predict who will get Alzheimer's disease. *Ann Neurol* **47**, 430-439.

[38] Dickerson BC, Goncharova I, Sullivan MP, Forchetti C, Wilson RS, Bennett DA, Beckett LA, deToledo-Morrell L (2001) MRI-derived entorhinal and hippocampal atrophy in incipient and very mild Alzheimer's disease. *Neurobiol Aging* **22**, 747-754.

[39] Chételat G, Desgranges B, De La Sayette V, Viader F, Eustache F, Baron JC (2002) Mapping gray matter loss with voxel-based morphometry in mild cognitive impairment. *Neuroreport* **13**, 1939-1943.

[40] Visser PJ, Verhey FR, Hofman PA, Scheltens P, Jolles J (2002) Medial temporal lobe atrophy predicts Alzheimer's disease in patients with minor cognitive impairment. *J Neurol Neurosurg Psychiatry* **72**, 491-497.

[41] Stoub TR, Bulgakova M, Leurgans S, Bennett DA, Fleischman D, Turner DA, deToledo-Morrell L (2005) MRI predictors of risk of incident Alzheimer disease: a longitudinal study. *Neurology* **64**, 1520-1524.

[42] de Leon MJ, DeSanti S, Zinkowski R, Mehta PD, Pratico D, Segal S, Rusinek H, Li J, Tsui W, Saint Louis LA, Clark CM, Tarshish C, Li Y, Lair L, Javier E, Rich K, Lesbre P, Mosconi L, Reisberg B, Sadowski M, DeBernadis JF, Kerkman DJ, Hampel H, Wahlund LO, Davies P (2006) Longitudinal CSF

and MRI biomarkers improve the diagnosis of mild cognitive impairment. *Neurobiol Aging* **27**, 394-401.

[43] Csernansky JG, Wang L, Swank J, Miller JP, Gado M, Mc Keel D, Miller MI, Morris JC (2005) Preclinical detection of Alzheimer's disease: hippocampal shape and volume predict dementia onset in the elderly. *Neuroimage* **25**, 783-792.

[44] Frisoni GB, Fox NC, Jack CR Jr, Scheltens P, Thompson PM (2010) The clinical use of structural MRI in Alzheimer disease. *Nat Rev Neurol* **6**, 67-77.

[45] Braak H, Braak E (1996) Development of Alzheimer-related neurofibrillary changes in the neocortex inversely recapitulates cortical myelogenesis. *Acta Neuropathol* **92**, 197-201.

[46] Ries ML, Carlsson CM, Rowley HA, Sager MA, Gleason CE, Asthana S, Johnson SC (2008) Magnetic resonance imaging characterization of brain structure and function in mild cognitive impairment: a review. *J Am Geriatr Soc* **56**, 920-934.

[47] Alexopoulos P, Grimmer T, Perneczky R, Domes G, Kurz A (2006) Progression to dementia in clinical subtypes of mild cognitive impairment. *Dement Geriatr Cogn Disord* **22**, 27-34.

[48] Jack CR Jr, Shiung MM, Weigand SD, O'Brien PC, Gunter JL, Boeve BF, Knopman DS, Smith GE, Ivnik RJ, Tangalos EG, Petersen RC (2005) Brain atrophy rates predict subsequent clinical conversion in normal elderly and amnestic MCI. *Neurology* **65**, 1227-1231.

[49] Jack CR Jr, Petersen RC, Xu Y, O'Brien PC, Smith GE, Ivnik RJ, Boeve BF, Tangalos EG, Kokmen E (2000) Rates of hippocampal atrophy correlate with change in clinical status in aging and AD. *Neurology* **55**, 484-489.

[50] Jack CR Jr, Shiung MM, Gunter JL, O'Brien PC, Weigand SD, Knopman DS, Boeve BF, Ivnik RJ, Smith GE, Cha RH, Tangalos EG, Petersen RC (2004) Comparison of different MRI brain atrophy rate measures with clinical disease progression in AD. *Neurology* **62**, 591-600.

[51] Sluimer JD, van der Flier WM, Karas GB, Fox NC, Scheltens P, Barkhof F, Vrenken H (2008) Whole-brain atrophy rate and cognitive decline: longitudinal MR study of memory clinic patients. *Radiology* **248**, 590-598.

[52] Driscoll I, Davatzikos C, An Y, Wu X, Shen D, Kraut M, Resnick SM (2009) Longitudinal pattern of regional brain volume change differentiates normal aging from MCI. *Neurology* **72**, 1906-1913.

[53] McDonald CR Jr, McEvoy LK, Gharapetian L, Fennema-Notestine C, Hagler DJ Jr, Holland D, Koyama A, Brewer JB, Dale AM (2009) Regional rates of neocortical atrophy from normal aging to early Alzheimer disease. Alzheimer's Disease Neuroimaging Initiative. *Neurology* **73**, 457-465.

[54] Davatzikos C, Xu F, An Y, Fan Y, Resnick SM (2009) Longitudinal progression of Alzheimer's-like patterns of atrophy in normal older adults: the SPARE-AD index. *Brain* **132**, 2026-2035.

[55] Nestor SM, Rupsingh R, Borrie M, Smith M, Accomazzi V, Wells JL, Fogarty J, Bartha R, Alzheimer's Disease Neuroimaging, Initiative (2008) Ventricular enlargement as a possible measure of Alzheimer's disease progression validated using the Alzheimer's disease neuroimaging initiative database. *Brain* **131**, 2443-2454.

[56] Carmichael OT, Kuller LH, Lopez OL, Thompson PM, Dutton RA, Lu A, Lee SE, Lee JY, Aizenstein HJ, Meltzer CC, Liu Y, Toga AW, Becker JT (2007) Cerebral ventricular changes associated with transitions between normal cognitive function, mild cognitive impairment, and dementia. *Alzheimer Dis Assoc Disord* **21**, 14-24.

[57] Jack CR Jr, Weigand SD, Shiung MM, Przybelski SA, O'Brien PC, Gunter JL, Knopman DS, Boeve BF, Smith GE, Petersen RC (2008) Atrophy rates accelerate in amnestic mild cognitive impairment. *Neurology* **70**, 1740-1752.

[58] Evans MC, Barnes J, Nielsen C, Kim LG, Clegg SL, Blair M, Leung KK, Douiri A, Boyes RG, Ourselin S, Fox NC, Alzheimer's Disease Neuroimaging, Initiative (2010) Volume changes in Alzheimer's disease and mild cognitive impairment: cognitive associations. *Eur Radiol* **20**, 674-682.

[59] Carlson NE, Moore MM, Dame A, Howieson D, Silbert LC, Quinn JF, Kaye JA (2008) Trajectories of brain loss in aging and the development of cognitive impairment. *Neurology* **70**, 828-833.

[60] Jack CR Jr, Petersen RC, Xu Y, O'Brien PC, Smith GE, Ivnik RJ, Tangalos EG, Kokmen E (1998) Rate of medial temporal lobe atrophy in typical aging and Alzheimer's disease. *Neurology* **51**, 993-999.

[61] Laakso MP, Frisoni GB, Könönen M, Mikkonen M, Beltramello A, Geroldi C, Bianchetti A, Trabucchi M, Soininen H, Aronen HJ (2000) Hippocampus and entorhinal cortex in frontotemporal dementia and Alzheimer's disease: a morphometric MRI study. *Biol Psychiatry* **47**, 1056-1063.

[62] Chételat G, Landeau B, Eustache F, Mézenge F, Viader F, de la Sayette V, Desgranges B, Baron JC (2005) Using voxel-based morphometry to map the structural changes associated with rapid conversion in MCI: a longitudinal MRI study. *Neuroimage* **27**, 934-946.

[63] Apostolova LG, Dutton RA, Dinov ID, Hayashi KM, Toga AW, Cummings JL, Thompson PM (2006) Conversion of mild cognitive impairment to Alzheimer disease predicted by hippocampal atrophy maps. *Arch Neurol* **63**, 693-699.

[64] Whitwell JL, Przybelski SA, Weigand SD, Knopman DS, Boeve BF, Petersen RC, Jack CR Jr (2007) 3D maps from multiple MRI illustrate changing atrophy patterns as subjects progress from mild cognitive impairment to Alzheimer's disease. *Brain* **130**, 1777-1786.

[65] Kaye JA, Moore MM, Dame A, Quinn J, Camicioli R, Howieson D, Corbridge E, Care B, Nesbit G, Sexton G (2005) Asynchronous regional brain volume losses in presymptomatic to moderate AD. *J Alzheimers Dis* **8**, 51-56.

[66] Marquis S, Moore MM, Howieson DB, Sexton G, Payami H, Kaye JA, Camicioli R (2002) Independent predictors of cognitive decline in healthy elderly persons. *Arch Neurol* **59**, 601-606.

[67] Stoub TR, Rogalski EJ, Leurgans S, Bennett DA, deToledo-Morrell L (Aging) (2010) Rate of entorhinal and hippocampal atrophy in incipient and mild AD: relation to memory function. *Neurobiol Aging* **31**, 1089-1098.

[68] Wang L, Goldstein FC, Veledar E, Levey AI, Lah JJ, Meltzer CC, Holder CA, Mao H (2009) Alterations in cortical thickness and white matter integrity in mild cognitive impairment measured by whole-brain cortical thickness mapping and diffusion tensor imaging. *AJNR Am J Neuroradiol* **30**, 893-899.

[69] Morra JH, Tu Z, Apostolova LG, Green AE, Avedissian C, Madsen SK, Parikshak N, Hua X, Toga AW, Jack CR Jr, Schuff N, Weiner MW, Thompson PM, Alzheimer's Disease Neuroimaging Initiative (2009) Automated 3D mapping of hippocampal atrophy and its clinical correlates in 400 subjects with Alzheimer's disease, mild cognitive impairment, and elderly controls. *Hum Brain Mapp* **30**, 2766-2788.

[70] den Heijer T, van der Lijn F, Koudstaal PJ, Hofman A, van der Lugt A, Krestin GP, Niessen WJ, Breteler MM (2010)

A 10-year follow-up of hippocampal volume on magnetic resonance imaging in early dementia and cognitive decline. *Brain* **133**, 1163-1172.

[71] Singh V, Chertkow H, Lerch JP, Evans AC, Dorr AE, Kabani NJ (2006) Spatial patterns of cortical thinning in mild cognitive impairment and Alzheimer's disease. *Brain* **129**, 2885-2893.

[72] Julkunen V, Niskanen E, Muehlboeck S, Pihlajamäki M, Könönen M, Hallikainen M, Kivipelto M, Tervo S, Vanninen R, Evans A, Soininen H (2009) Cortical thickness analysis to detect progressive mild cognitive impairment: a reference to Alzheimer's disease. *Dement Geriatr Cogn Disord* **28**, 404-412.

[73] George S, Mufson EJ, Leurgans S, Shah RC, Ferrari C, Detoledo-Morrell L. (Epub ahead of print) MRI-based volumetric measurement of the substantia innominata in amnestic MCI and mild AD. *Neurobiol Aging*

[74] Muth K, Schönmeyer R, Matura S, Haenschel C, Schröder J, Pantel J (2010) Mild cognitive impairment in the elderly is associated with volume loss of the cholinergic basal forebrain region. *Biol Psychiatry* **67**, 588-591.

[75] Selkoe DJ (2002) Alzheimer's disease is a synaptic failure. *Science* **298**, 789-791.

[76] Hyman BT, Damasio AR, Van Hoesen GW, Barnes CL (1984) Alzheimer's disease: cell-specific pathology isolates the hippocampal formation. *Science* **225**, 1168-1170.

[77] Seeley WW, Crawford RK, Zhou J, Miller BL, Greicius MD (2009) Neurodegenerative Diseases Target Large-Scale Human Brain Networks. *Neuron* **62**, 42-52.

[78] Braak H, Braak E (1991) Neuropathological staging of Alzheimerrelated changes. *Acta Neuropathol. (Berl.)* **82**, 239-259.

[79] Buckner RL, Snyder AZ, Shannon BJ, LaRossa G, Sachs R, Fotenos AF, Sheline YI, Klunk WE, Mathis CA, Morris JC, Mintun MA (2005) Molecular, structural, and functional characterization of Alzheimer's disease: evidence for a relationship between default activity, amyloid, and memory. *J Neurosci* **25**, 7709-7717.

[80] Greicius MD, Srivastava G, Reiss AL, Menon V (2004) Default-mode network activity distinguishes Alzheimer's disease from healthy aging: evidence from functional MRI. *Proc Natl Acad Sci U S A* **101**, 4637-4642.

[81] Palop JJ, Chin J, Roberson ED, Wang J, Thwin MT, Bien-Ly N, Yoo J, Ho KO, Yu GQ, Kreitzer A et al. (2007) Aberrant excitatory neuronal activity and compensatory remodeling of inhibitory hippocampal circuits in mouse models of Alzheimer's disease. *Neuron* **55**, 697-711.

[82] Palop JJ, Chin J, Mucke L (2006) A network dysfunction perspective on neurodegenerative diseases. *Nature* **443**, 768-773.

[83] Peltier SJ, Noll DC (2002) T(2)(*) dependence of low frequency functional connectivity. *Neuroimage* **16**, 985-992.

[84] Fox MD, Raichle ME (2007) Spontaneous fluctuations in brain activity observed with functional magnetic resonance imaging. *Nat Rev Neurosci* **8**, 700-711.

[85] Greicius MD, Krasnow B, Reiss AL, Menon V (2003) Functional connectivity in the resting brain: a network analysis of the default mode hypothesis. *Proc Natl Acad Sci U S A* **100**, 253-258.

[86] Beckmann CF, DeLuca M, Devlin JT, Smith SM (2005) Investigations into resting-state connectivity using independent component analysis. *Philos Trans R Soc Lond B Biol Sci* **360**, 1001-1013.

[87] Buckner RL, Andrews-Hanna JR, Schacter DL (2008) The brain's default network: anatomy, function, and relevance to disease. *Ann N Y Acad Sci* **1124**, 1-38.

[88] Rombouts SA, Barkhof F, Goekoop R, Stam CJ, Scheltens P (2005) Altered resting state networks in mild cognitive impairment and mild Alzheimer's disease: an fMRI study. *Hum Brain Mapp* **26**, 231-239.

[89] Qi Z, Wu X, Wang Z, Zhang N, Dong H, Yao L, Li K (2010) Impairment and compensation coexist in amnestic MCI default mode network. *Neuroimage* **50**, 48-55.

[90] Gili T, Cercignani M, Serra L, Perri R, Giove F, Maraviglia B, Caltagirone C, Bozzali M (2011) Regional brain atrophy and functional disconnection across Alzheimer's disease evolution. *J Neurol Neurosurg Psychiatry* **82**, 58-66.

[91] Li SJ, Li Z, Wu G, Zhang MJ, Franczak M, Antuono PG (2002) Alzheimer disease: evaluation of a functional MR imaging index as a marker. *Radiology* **225**, 253-259.

[92] Sorg C, Riedl V, Mühlau M, Calhoun VD, Eichele T, Läer L, Drzezga A, Förstl H, Kurz A, Zimmer C, Wohlschläger AM (2007) Selective changes of resting-state networks in individuals at risk for Alzheimer's disease. *Proc Natl Acad Sci U S A* **104**, 18760-18765.

[93] Wang L, Zang Y, He Y, Liang M, Zhang X, Tian L, Wu T, Jiang T, Li K (2006) Changes in hippocampal connectivity in the early stages of Alzheimer's disease: evidence from resting state fMRI. *NeuroImage* **31**, 496-504.

[94] Wang K, Liang M, Wang L, Tian L, Zhang X, Li K, Jiang T (2007) Altered functional connectivity in early Alzheimer's disease: a resting-state fMRI study. *Hum Brain Mapp* **28**, 967-978.

[95] Zhang HY, Wang SJ, Xing J, Liu B, Ma ZL, Yang M, Zhang ZJ, Teng GJ (2009) Detection of PCC functional connectivity characteristics in resting-state fMRI in mild Alzheimer's disease. *Behav Brain Res* **197**, 103-108.

[96] Supekar K, Menon V, Rubin D, Musen M, Greicius MD (2008) Network analysis of intrinsic functional brain connectivity in Alzheimer's disease. *PLoS Comput Biol* **4**, e1000100.

[97] Sanz-Arigita EJ, Schoonheim MM, Damoiseaux JS, Rombouts SA, Maris E, Barkhof F, Scheltens P, Stam CJ (2010) Loss of 'small-world' networks in Alzheimer's disease: graph analysis of FMRI resting-state functional connectivity. *PLoS One* **5**, e13788.

[98] Fellgiebel A, Schermuly I, Gerhard A, Keller I, Albrecht J, Weibrich C, Müller MJ, Stoeter P (2008) Functional relevant loss of long association fibre tracts integrity in early Alzheimer's disease. *Neuropsychologia* **46**, 1698-1706.

[99] Kavcic V, Ni H, Zhu T, Zhong J, Duffy CJ (2008) White matter integrity linked to functional impairments in aging and elderly Alzheimer's disease. *Alzheimers Dement* **4**, 381-389.

[100] Delbeuck X, Van der Linden M, Collette F (2003) Alzheimer's disease as a disconnection syndrome? *Neuropsychol Rev* **13**, 79-92.

[101] Englund E, Brun A, Alling C (1988) White matter changes in dementia of Alzheimer's type. Biochemical and neuropathological correlates. *Brain* **111**, 1425-1439.

[102] Bronge L, Bogdanovic N, Wahlund LO (2002) Postmortem MRI and histopathology of white matter changes in Alzheimer brains. A quantitative, comparative study. *Dement Geriatr Cogn Disord* **13**, 205-212.

[103] Basser PJ, Mattiello J, LeBihan D (1994) MR diffusion tensor spectroscopy and imaging. *Biophys J* **66**, 259-267.

[104] Beaulieu C (2002) The basis of anisotropic water diffusion in the nervous system - a technical review. *NMR Biomed* **15**, 435-55.

[105] Pierpaoli C, Barnett A, Pajevic S, Chen R, Penix LR, Virta A, Basser P (2001) Water diffusion changes in Wallerian degeneration and their dependence on white matter architecture. *Neuroimage* **13**, 1174-1185.

[106] Huang J, Friedland RP, Auchus AP (2007) Diffusion tensor imaging of normal-appearing white matter in mild cognitive impairment and early Alzheimer disease: preliminary evidence of axonal degeneration in the temporal lobe. *Am J Neuroradiol* **28**, 1943-1948.

[107] Salat DH, Tuch DS, van der Kouwe AJ, Greve DN, Pappu V, Lee SY, Hevelone ND, Zaleta AK, Growdon JH, Corkin S, Fischl B, Rosas HD (2010) White matter pathology isolates the hippocampal formation in Alzheimer's disease. *Neurobiol Aging* **31**, 244-256.

[108] Pievani M, Agosta F, Pagani E, Canu E, Sala S, Absinta M, Geroldi C, Ganzola R, Frisoni GB, Filippi M (2010) Assessment of white matter tract damage in mild cognitive impairment and Alzheimer's disease. *Hum Brain Mapp* **31**, 1862-1875.

[109] Acosta-Cabronero J, Williams GB, Pengas G, Nestor PJ (2010) Absolute diffusivities define the landscape of white matter degeneration in Alzheimer's disease. *Brain* **133**, 529-539.

[110] Bosch B, Arenaza-Urquijo EM, Rami L, Sala-Llonch R, Junqué C, Solé-Padullés C, Peña-Gómez C, Bargalló N, Molinuevo JL, Bartrés-Faz D (2010) Multiple DTI index analysis in normal aging, amnestic MCI and AD. Relationship with neuropsychological performance. *Neurobiol Aging*. doi:10.1016/j.neurobiolaging.2010.02.004

[111] Mielke MM, Kozauer NA, Chan KC, George M, Toroney J, Zerrate M, Bandeen-Roche K, Wang MC, Vanzijl P, Pekar JJ, Mori S, Lyketsos CG, Albert M (2009) Regionally-specific diffusion tensor imaging in mild cognitive impairment and Alzheimer's disease. *Neuroimage* **46**, 47-55.

[112] Liu Y, Spulber G, Lehtimäki KK, ouml K, Könönen M, Hallikainen I, Gröhn H, Kivipelto M, Hallikainen M, Vanninen R, Soininen H (2009) Diffusion tensor imaging and Tract-Based Spatial Statistics in Alzheimer's disease and mild cognitive impairment. *Neurobiol Aging*. doi:10.1016/j.neurobiolaging.2009.10.006

[113] Zhang Y, Schuff N, Jahng GH, Bayne W, Mori S, Schad L, Mueller S, Du AT, Kramer JH, Yaffe K, Chui H, Jagust WJ, Miller BL, Weiner MW (2007) Diffusion tensor imaging of cingulum fibers in mild cognitive impairment and Alzheimer disease. *Neurology* **68**, 13-19.

[114] Rose SE, McMahon KL, Janke AL, O'Dowd B, de Zubicaray G, Strudwick MW, Chalk JB (2006) Diffusion indices on magnetic resonance imaging and neuropsychological performance in amnestic mild cognitive impairment. *J Neurol Neurosurg Psychiatry* **77**, 1122-1128.

[115] Kalus P, Slotboom J, Gallinat J, Mahlberg R, Cattapan-Ludewig K, Wiest R, Nyffeler T, Buri C, Federspiel A, Kunz D, Schroth G, Kiefer C (2006) Examining the gateway to the limbic system with diffusion tensor imaging: the perforant pathway in dementia. *Neuroimage* **30**, 713-720.

[116] Kantarci K, Jack CR Jr, Xu YC, Campeau NG, O'Brien PC, Smith GE, Ivnik RJ, Boeve BF, Kokmen E, Tangalos EG, Petersen RC (2001) Mild cognitive impairment and Alzheimer disease: regional diffusivity of water. *Radiology* **219**, 101-107.

[117] Müller MJ, Greverus D, Dellani PR, Weibrich C, Wille PR, Scheurich A, Stoeter P, Fellgiebel A (2005) Functional implications of hippocampal volume and diffusivity in mild cognitive impairment. *Neuroimage* **28**, 1033-1042.

[118] Fellgiebel A, Wille P, Müller MJ, Winterer G, Scheurich A, Vucurevic G, Schmidt LG, Stoeter P (2004) Ultrastructural hippocampal and white matter alterations in mild cognitive impairment: a diffusion tensor imaging study. *Dement Geriatr Cogn Disord* **18**, 101-108.

[119] Cho H, Yang DW, Shon YM, Kim BS, Kim YI, Choi YB, Lee KS, Shim YS, Yoon B, Kim W, Ahn KJ (2008) Abnormal integrity of corticocortical tracts in mild cognitive impairment: a diffusion tensor imaging study. *J Korean Med Sci* **23**, 477-483.

[120] Stenset V, Bjørnerud A, Fjell AM, Walhovd KB, Hofoss D, Tønnessen P, Gjerstad L, Fladby T (2011) Cingulum fiber diffusivity and CSF T-tau in patients with subjective and mild cognitive impairment. *Neurobiol Aging* **32**, 581-589.

[121] Bai F, Zhang Z, Watson DR, Yu H, Shi Y, Yuan Y, Qian Y, Jia J (2009) Abnormal integrity of association fiber tracts in amnestic mild cognitive impairment. *J Neurol Sci* **278**, 102-106.

[122] Fellgiebel A, Müller MJ, Wille P, Dellani PR, Scheurich A, Schmidt LG, Stoeter P (2005) Color-coded diffusion-tensor-imaging of posterior cingulate fiber tracts in mild cognitive impairment. *Neurobiol Aging* **26**, 1193-1198.

[123] Kiuchi K, Morikawa M, Taoka T, Nagashima T, Yamauchi T, Makinodan M, Norimoto K, Hashimoto K, Kosaka J, Inoue Y, Inoue M, Kichikawa K, Kishimoto T (2009) Abnormalities of the uncinate fasciculus and posterior cingulate fasciculus in mild cognitive impairment and early Alzheimer's disease: a diffusion tensor tractography study. *Brain Res* **1287**, 184-191.

[124] Stahl R, Dietrich O, Teipel SJ, Hampel H, Reiser MF, Schoenberg SO (2007) White matter damage in Alzheimer disease and mild cognitive impairment: assessment with diffusion-tensor MR imaging and parallel imaging techniques. *Radiology* **243**, 483-492.

[125] Ukmar M, Makuc E, Onor ML, Garbin G, Trevisiol M, Cova MA (2008) Evaluation of white matter damage in patients with Alzheimer's disease and in patients with mild cognitive impairment by using diffusion tensor imaging. *Radiol Med* **113**, 915-922.

[126] Chen TF, Lin CC, Chen YF, Liu HM, Hua MS, Huang YC, Chiu MJ (2009) Diffusion tensor changes in patients with amnesic mild cognitive impairment and various dementias. *Psychiatry Res* **173**, 15-21.

[127] Concha L, Gross DW, Beaulieu C (2005) Diffusion tensor tractography of the limbic system. *AJNR Am J Neuroradiol* **26**, 2267-2274.

[128] Chen TF, Chen YF, Cheng TW, Hua MS, Liu HM, Chiu MJ (2009) Executive dysfunction and periventricular diffusion tensor changes in amnesic mild cognitive impairment and early Alzheimer's disease. *Hum Brain Mapp* **30**, 3826-3836.

[129] Damoiseaux JS, Smith SM, Witter MP, Sanz-Arigita EJ, Barkhof F, Scheltens P, Stam CJ, Zarei M, Rombouts SA (2009) White matter tract integrity in aging and Alzheimer's disease. *Hum Brain Mapp* **30**, 1051-1059.

[130] Di Paola M, Di Iulio F, Cherubini A, Blundo C, Casini AR, Sancesario G, Passafiume D, Caltagirone C, Spalletta G (2010) When, where, and how the corpus callosum changes in MCI and AD: a multimodal MRI study. *Neurology* **74**, 1136-1142.

[131] Cherubini A, Spoletini I, Péran P, Luccichenti G, Di Paola M, Sancesario G, Gianni W, Giubilei F, Bossù P, Sabatini U, Caltagirone C, Spalletta G (2010) A multimodal MRI investigation of the subventricular zone in mild cognitive impairment and Alzheimer's disease patients. *Neurosci Lett* **469**, 214-218.

[132] Qiu A, Oishi K, Miller MI, Lyketsos CG, Mori S, Albert M (2010) Surface-based analysis on shape and fractional anisotropy of white matter tracts in Alzheimer's disease. *PLoS One* **5**, e9811.

[133] Nordberg A (2008) Amyloid plaque imaging in vivo: current achievement and future prospects. *Eur J Nucl Med Mol Imaging* **35**, 846-850.

[134] Villemagne VL, Fodero-Tavoletti MT, Pike KE, Cappai R, Masters CL, Rowe CC (2008) The ART of Loss: Aβ Imaging in the Evaluation of Alzheimer's Disease and other Dementias. *Mol Neurobiol* **38**, 1-15.

[135] Jagust WJ, Landau SM, Shaw LM, Trojanowski JQ, Koeppe RA, Reiman EM, Foster NL, Petersen RC, Weiner MW, Price JC, Mathis CA (2009) Alzheimer's Disease Neuroimaging Initiative. Relationships between biomarkers in aging and dementia. *Neurology* **73**, 1193-1199.

[136] Klunk WE, Mathis CA (2008) The future of amyloid-beta imaging: a tale of radionuclides and tracer proliferation. *Curr Opin Neurol* **21**, 683-687.

[137] Lopresti BJ, Klunk WE, Matthis CA, Hoge JA, Ziolko SK, Lu X, Meltzer CC, Schimmel K, Tsopelas ND, DeKosky ST, Price JC (2005) Simplified quantification of Pittsburg compound B amyloid imaging PET studies: a comparative study. *J Nucl Med* **46**, 1959-1972.

[138] Vandenberghe R, Van Laere K, Ivanoiu A, Salmon E, Bastin C, Triau E, Hasselbalch S, Law I, Andersen A, Korner A, Minthon L, Garraux G, Nelissen N, Bormans G, Buckley C, Owenius R, Thurfjell L, Farrar G, Brooks DJ (2010) 18F-flutemetamol amyloid imaging in Alzheimer disease and mild cognitive impairment: a phase 2 trial. *Ann Neurol* **68**, 319-329.

[139] Braskie MN, Klunder AD, Hayashi KM, Protas H, Kepe V, Miller KJ, Huang SC, Barrio JR, Ercoli LM, Siddarth P, Satyamurthy N, Liu J, Toga AW, Bookheimer SY, Small GW, Thompson PM (2010) Plaque and tangle imaging and cognition in normal aging and Alzheimer's disease. *Neurobiol Aging* **31**, 1669-1678.

[140] Shin J, Lee SY, Kim SJ, Kim SH, Cho SJ, Kim YB (2010) Voxel-based analysis of Alzheimer's disease PET imaging using a triplet of radiotracers: PIB, FDDNP, and FDG. *NeuroImage* **52**, 488-496.

[141] Rowe CC, Ackerman U, Browne W, Mulligan R, Pike KL, O'Keefe G, Tochon-Danguy H, Chan G, Berlangieri SU, Jones G, Dickinson-Rowe KL, Kung HP, Zhang W, Kung MP, Skovronsky D, Dyrks T, Holl G, Krause S, Friebe M, Lehman L, Lindemann S, Dinkelborg LM, Masters CL, Villemagne VL (2008) Imaging of amyloid [beta] in Alzheimer's disease with 18F-BAY94-9172, a novel PET tracer: proof of mechanism. *Lancet Neurology* **7**, 129-135.

[142] Koole M, Lewis DM, Buckley C, Nelissen N, Vandenbulcke M, Brooks DJ, Vandenberghe R, Van Laere K (2009) Whole-Body Biodistribution and Radiation Dosimetry of 18F-GE067: A Radioligand for In Vivo Brain Amyloid Imaging. *J Nucl Med* **50**, 818-822.

[143] Wong DF, Rosenberg PB, Zhou Y, Kumar A, Raymont V, Ravert HT, Dannals RF, Nandi A, Brasić JR, Ye W, Hilton J, Lyketsos C, Kung HF, Joshi AD, Skovronsky DM, Pontecorvo MJ (2010) In vivo imaging of amyloid deposition in Alzheimer disease using the radioligand 18F-AV-45 (flobetapir F 18). *J Nucl Med* **51**, 913-920.

[144] Clark CM, Schneider JA, Bedell BJ, Beach TG, Bilker WB, Mintun MA, Pontecorvo MJ, Hefti F, Carpenter AP, Flitter ML, Krautkramer MJ, Kung HF, Coleman RE, Doraiswamy PM, Fleisher AS, Sabbagh MN, Sadowsky CH, Reiman PE, Zehntner SP, Skovronsky DM (2011) AV45-A07 Study Group. Use of florbetapir-PET for imaging beta-amyloid pathology. *JAMA* **305**, 275-283.

[145] Yao CH, Lin KJ, Weng CC, Hsiao IT, Ting YS, Yen TC, Jan TR, Skovronsky D, Kung MP, Wey SP (2010) GMP-compliant automated synthesis of [(18)F]AV-45 (Florbetapir F 18) for imaging beta-amyloid plaques in human brain. *Appl Radiat Isot* **68**, 2293-2297.

[146] Liu Y, Zhu L, Plössl K, Choi SR, Qiao H, Sun X, Li S, Zha Z, Kung HF (2010) Optimization of automated radiosynthesis of [18F]AV-45: a new PET imaging agent for Alzheimer's disease. *Nucl Med Biol* **37**, 917-925.

[147] Juréus A, Swahn BM, Sandell J, Jeppsson F, Johnson AE, Johnström P, Neelissen JA, Sunnemark D, Farde L, Svensson SP (2010) Characterization of AZD4694, a novel fluorinated Abeta plaque neuroimaging PET radioligand. *J Neurochem* **114**, 784-794.

[148] Cselényi Z, Jönhagen ME, Forsberg A, Halldin C, Julin P, Schou M, Johnström P, Varnäs K, Svensson S, Farde L (2010) Clinical validation of [18F]AZD4694, a novel amyloid-specific PET radioligand. 11th International Geneva/Springfield Symposium on Advances in Alzheimer Therapy Geneva, Switzerland.

[149] Reiman E (2010) (18F)AZD4694 Amyloid PET studies in presymptomatic and Alzheimer disease patients. 11th International Geneva/Springfield Symposium on Advances in Alzheimer Therapy Geneva, Switzerland.

[150] Wey SP, Weng CC, Lin KJ, Yao CH, Yen TC, Kung HF, Skovronsky D, Kung MP (2009) Validation of an 18F-labeled biphenylalkyne as a positron emission tomography imaging agent for beta-amyloid plaques. *Nucl Med Biol* **36**, 411-417.

[151] Serdons K, Verduyckt T, Vanderghinste D, Cleynhens J, Borghgraef P, Vermaelen P, Terwinghe C, Van Leuven F, Van Laere K, Kung H, Bormans G, Verbruggen A (2009) Synthesis of 18F-labelled 2-(4′-fluorophenyl)-1,3-benzothiazole and evaluation as amyloid imaging agent in comparison with [11C]PIB. *Bioorg Med Chem Lett* **19**, 602-605.

[152] Jack CR, Lowe VJ, Weigand SD, Wiste HJ, Senjem ML, Knopman DS, Shiung MM, Gunter JL, Boeve BF, Kemp BJ, Weiner M, Petersen RC, Alzheimer's Disease Neuroimaging, Initiative (2009) Serial PIB and MRI in normal, mild cognitive impairment and Alzheimer's disease: implications for sequence of pathological events in Alzheimer's disease. *Brain* **132**, 1355-1365.

[153] Villemagne VL, Pike KE, Chételat G, Ellis KA, Mulligan RS, Bourgeat P, Ackermann U, Jones G, Szoeke C, Salvado O, Martins R, O'Keefe G, Mathis CA, Klunk WE, Ames D, Masters CL, Rowe CC (2011) Longitudinal assessment of Aβ and cognition in aging and Alzheimer disease. *Ann Neurol* **69**, 181-192.

[154] Pike KE, Savage G, Villemagne VL, Ng S, Moss SA, Maruff P, Mathis CA, Klunk WE, Masters CL, Rowe CC (2007) β-amyloid imaging and memory in non-demented individuals: evidence for preclinical Alzheimer's disease. *Brain* **130**, 2837-2844.

[155] Scheinin NM, Aalto S, Koikkalainen J, Lötjönen J, Karrasch M, Kemppainen N, Viitanen M, Någren K, Helin S, Scheinin M, Rinne JO (2009) Follow-up of [11C]PIB uptake and brain volume in patients with Alzheimer disease and controls. *Neurology* **73**, 1186-1192.

[156] Small GW, Kepe V, Ercoli LM, Siddarth P, Bookheimer SY, Miller KJ, Lavretsky H, Burggren AC, Cole GM, Vinters HV, Thompson PM, Huang SC, Satyamurthy N, Phelps ME, Barrio JR (2006) PET of brain amyloid and tau in mild cognitive impairment. *N Engl J Med* **355**, 2652-2663.

[157] Tolboom N, Yaqub M, van der Flier WM, Boellaard R, Luurtsema G, Windhorst AD, Barkhof F, Scheltens P, Lammertsma AA, van Berckel BN (2009) Detection of Alzheimer pathology in vivo using both 11C-PIB and 18F-FDDNP PET. *J Nucl Med* **50**, 191-197.

[158] Forsberg A, Engler H, Almkvist O, Blomquist G, Hagman G, Wall A, Ringheim A, aring L, A, Långström B, Nordberg A (2008) Pet imaging of amyloid deposition in patients with mild cognitive impairment. *Neurobiol Aging* **29**, 1456-1465.

[159] Kemppainen NM, Aalto S, Wilson IA, Någren K, Helin S, Brück A, Oikonen V, Kailajärvi M, Scheinin M, Viitanen M, Parkkola R, Rinne JO (2007) PET amyloid ligand [11C]PIB uptake is increased in mild cognitive impairment. *Neurology* **68**, 1603-1606.

[160] Engler H, Forsberg A, Almkvist O, Blomquist G, Larsson E, Savitcheva I, Wall A, Ringheim A, Långström B, Nordberg A (2006) Two year follow-up of amyloid deposition in patients with Alzheimer's disease. *Brain* **129**, 2856-2866.

[161] Small GW, Kepe V, Ercoli LM, Siddarth P, Bookheimer SY, Miller KJ, Lavretsky H, Burggren AC, Cole GM, Vinters HV, Thompson PM, Huang SC, Satyamurthy N, Phelps ME, Barrio JR (2006) PET of brain amyloid and tau in mild cognitive impairment. *N Engl J Med* **355**, 2652-2663.

[162] Berger H (1929) Über das Elektroenkephalogramm des Menschen. *Archiv für Psychiatrie und Nervenkrankheiten* **87**, 527-570.

[163] Berger H (1938) Das Elektroenkephalogramm des Menschen. Halle an der Saale, Buchdruckerei des Waisenhauses. *Nova acta Leopoldina Neue Folge* **6(38)**.

[164] Rossini PM, Dal Forno G (2004) Integrated technology for evaluation of brain function and neural plasticity. *Phys Med Rehabil Clin N Am* **15**, 263-306.

[165] Celesia GG, Kaufman D, Cone S (1987) Effects of age and sex on pattern electroretinograms and visual evoked potentials. *Electroencephalogr Clin Neurophysiol* **68**, 161-171.

[166] Rossini PM (2009) Implications of brain plasticity to brain-machine interfaces operation a potential paradox? *Int Rev Neurobiol* **86**, 81-90.

[167] Rossini PM, Rossi S, Babiloni C, Polich J (2007) Clinical neurophysiology of aging brain: from normal aging to neurodegeneration. *Prog Neurobiol* **83**, 375-400.

[168] Nunez PL (2000) Toward a quantitative description of large-scale neocortical dynamic function and EEG. *Behav Brain Sci* **23**, 371-398.

[169] Babiloni F, Carducci F, Cincotti F, Del Gratta C, Pizzella V, Romani GL, Rossini PM, Tecchio F, Babiloni C (2001) Linear inverse source estimate of combined EEG and MEG data related to voluntary movements. *Hum Brain Mapp* **14**, 197-209.

[170] Babiloni F, Babiloni C, Fattorini L, Carducci F, Onorati P, Urbano A (1995) Performances of surface Laplacian estimators: a study of simulated and real scalp potential distributions. *Brain Topogr* **8**, 35-45.

[171] Babiloni F, Babiloni C, Carducci F, Fattorini L, Onorati P, Urbano A (1996) Spline Laplacian estimate of EEG potentials over a realistic magnetic resonance-constructed scalp surface model. *Electroencephalogr Clin Neurophysiol* **98**, 363-373.

[172] Babiloni F, Babiloni C, Carducci F, Cincotti F, Rossini PM (2003) 'The stone of madness' and the search for the cortical sources of brain diseases with non-invasive EEG techniques. *Clin Neurophysiol* **114**, 1775-1780.

[173] Nunez PL, Srinivasan R (2006). In *Electric Fields of the Brain: The Neurophysics of EEG*, Oxford University Press, New York, USA.

[174] Nunez PL (1995). In *Neocortical Dynamics and Human EEG Rhythms*, Oxford University Press, New York, USA.

[175] Kaminski MJ, Blinowska KJ (1991) A new method of the description of the information flow in the structures. *Biol Cybern* **65**, 203-210.

[176] Kaminski MJ, Blinowska KJ, Szclenberger W (1997) Topographic analysis of coherence and propagation of EEG activity during sleep and wakefulness. *Electroencephalogr Clin Neurophysiol* **102**, 216-227.

[177] Korzeniewska A, Kasicki S, Kaminski M, Blinowska KJ (1997) Information flow between hippocampus and related structures during various types of rat's behavior. *J Neurosci Methods* **73**, 49-60.

[178] Mima T, Matsuoka T, Hallett M (2000) Functional coupling of human right and left cortical motor areas demonstrated with partial coherence analysis. *Neurosci Lett* **287**, 93-96.

[179] Babiloni C, Vecchio F, Babiloni F, Brunelli GA, Carducci F, Cincotti F, Pizzella V, Romani GL, Tecchio FT, Rossini PM (2004) Coupling between "hand" primary sensorimotor cortex and lower limb muscles after ulnar nerve surgical transfer in paraplegia. *Behav Neurosci* **118**, 214-222.

[180] Babiloni C, Babiloni F, Carducci F, Cincotti F, Vecchio F, Cola B, Rossi S, Miniussi C, Rossini PM (2004) Functional frontoparietal connectivity during short-term memory as revealed by high-resolution EEG coherence analysis. *Behav Neurosci* **118**, 687-697.

[181] Pascual-Marqui RD, Michel CM, Lehmann D (1994) Low resolution electromagnetic tomography: a new method for localizing electrical activity in the brain. *Int J Psychophysiol* **18**, 49-65.

[182] Pascual-Marquiì RD, Lehmann D, Koenig T, Kochi K, Merlo MC, Hell D, Koukkou M (1999) Low resolution brain electromagnetic tomography (LORETA) functional imaging in acute, neurolepticnaive, first-episode, productive schizophrenia. *Psychiatry Res* **90**, 169-179.

[183] Pascual-Marqui RD, Esslen M, Kochi K, Lehmann D (2002) Functional imaging with low resolution brain electromagnetic tomography (LORETA): a review. *Methods Find Exp Clin Pharmacol* **24**, 91-95.

[184] Isotani T, Tanaka H, Lehmann D, Pascual-Marqui RD, Kochi K, Saito N, Yagyu T, Kinoshita T, Sasada K (2001) Source localization of EEG activity during hypnotically induced anxiety and relaxation. *Int J Psychophysiol* **41**, 143-153.

[185] Mientus S, Gallinat J, Wuebben Y, Pascual-Marqui RD, Mulert C, Frick K, Dorn H, HerrmannWM, Winterer G (2002) Cortical hypoactivation during resting EEG in schizophrenics but not in depressives and schizotypal subjects as revealed by low resolution electromagnetic tomography (LORETA). *Psychiatry Res* **116**, 95-111.

[186] Babiloni C, Binetti G, Cassetta E, Cerboneschi D, Dal Forno G, Del Percio C, Ferreri F, Ferri R, Lanuzza B, Miniussi C,

Moretti DV, Nobili F, Pascual-Marqui RD, Rodriguez G, Romani GL, Salinari S, Tecchio F, Vitali P, Zanetti O, Zappasodi F, Rossini PM (2004) Mapping distributed sources of cortical rhythms in mild Alzheimer's disease. A multicentric EEG study. *Neuroimage* **22**, 57-67.

[187] Saletu M, Anderer P, Saletu-Zyhlarz GM, Mandl M, Arnold O, Zeitlhofer J, Saletu B (2004) EEG-tomographic studies with LORETA on vigilance differences between narcolepsy patients and controls and subsequent double-blind, placebo-controlled studies with modafinil. *J Neurol* **251**, 1354-1363.

[188] Dujardin K, Bourriez JL, Guieu JD (1994) Event-related desynchronization (ERD) patterns during verbal memory tasks: effect of age. *Int J Psychophysiol* **16**, 17-27.

[189] Dujardin K, Bourriez JL, Guieu JD (1995) Event-related desynchronization (ERD) patterns during memory processes: effects of aging and task difficulty. *Electroencephalogr Clin Neurophysiol* **96**, 169-182.

[190] Klass DW, Brenner RP (1995) Electroencephalography of the elderly. *J Clin Neurophysiol* **12**, 116-131.

[191] Klimesch W (1999) EEG alpha and theta oscillations reflect cognitive and memory performance: a review and analysis. *Brain Res Rev* **29**, 169-195.

[192] Babiloni C, Binetti G, Cassarono A, Dal Forno G, Del Percio C, Ferreri F, Ferri R, Frisoni G, Galderisi S, Hirata K, Lanuzza B, Miniassi C, Mucci A, Nobili F, Rodriguez G, Romani GL, Rossigni PM (2006) Sources of cortical rhythms in adults during physiological aging: a multicentric EEG study. *Hum Brain Mapp* **27**, 162-172.

[193] Jelic V, Johansson SE, Almkvist O, Shigeta M, Julin P, Nordberg A, Winblad B, Wahlund LO (2000) Quantitative electroencephalography in mild cognitive impairment: longitudinal changes and possible prediction of Alzheimer's disease. *Neurobiol Aging* **21**, 533-540.

[194] Coben LA, Danziger W, Storandt M (1985) A longitudinal EEG study of mild senile dementia of Alzheimer type: changes at 1 year and at 2.5 years. *Electroencephalogr Clin Neurophysiol* **61**, 101-112.

[195] Soininen H, Partanen J, Laulumaa V, Helkala EL, Laakso M, Riekkinen PJ (1989) Longitudinal EEG spectral analysis in early stage of Alzheimer's disease. *Electroencephalogr Clin Neurophysiol* **72**, 290-297.

[196] Luckhaus C, Grass-Kapanke B, Blaeser I, Ihl R, Supprian T, Winterer G, Zielasek J, Brinkmeyer J (2008) Quantitative EEG in progressing vs stable mild cognitive impairment (MCI): results of a 1-year follow-up study. *Int J Geriatr Psychiatry* **23**, 1148-1155.

[197] Huang C, Wahlund L, Dierks T, Julin P, Winblad B, Jelic V (2000) Discrimination of Alzheimer's disease and mild cognitive impairment by equivalent EEG sources: a cross-sectional and longitudinal study. *Clin Neurophysiol* **111**, 1961-1967.

[198] Jeong J (2004) EEG dynamics in patients with Alzheimer's disease. *Clin Neurophysiol* **115**, 1490-1505.

[199] Babiloni C, Binetti G, Cassetta E, Dal Forno G, Del Percio C, Ferreri F, Ferri R, Frisoni G, Hirata K, Lanuzza B, Miniussi C, Moretti DV, Nobili F, Rodriguez G, Romani GL, Salinari S, Rossini PM (2006) Sources of cortical rhythms change as a function of cognitive impairment in pathological aging: a multicenter study. *Clin Neurophysiol* **117**, 252-268.

[200] Babiloni C, Frisoni GB, Pievani M, Vecchio F, Lizio R, Buttiglione M, Geroldi C, Fracassi C, Eusebi F, Ferri R, Rossini PM (2009) Hippocampal volume and cortical sources of EEG alpha rhythms in mild cognitive impairment and Alzheimer disease. *Neuroimage* **44**, 123-135.

[201] Babiloni C, Frisoni GB, Vecchio F, Pievani M, Geroldi C, De Carli C, Ferri R, Vernieri F, Lizio R, Rossini PM (2010) Global functional coupling of resting EEG rhythms is related to white-matter lesions along the cholinergic tracts in subjects with amnesic mild cognitive impairment. *J Alzheimers Dis* **19**, 859-871.

[202] Babiloni C, Ferri R, Binetti G, Cassarino A, Dal Forno G, Ercolani M, Ferreri F, Frisoni GB, Lanuzza B, Miniussi C, Nobili F, Rodriguez G, Rundo F, Stam CJ, Musha T, Vecchio F, Rossini PM (2006) Fronto-parietal coupling of brain rhythms in mild cognitive impairment: a multicentric EEG study. *Brain Res Bull* **69**, 63-73.

[203] Babiloni C, Ferri R, Binetti G, Vecchio F, Frisoni GB, Lanuzza B, Miniussi C, Nobili F, Rodriguez G, Rundo F, Cassarino A, Infarinato F, Cassetta E, Salinari S, Eusebi F, Rossini PM (2009) Directionality of EEG synchronization in Alzheimer's disease subjects. *Neurobiol Aging* **30**, 93-102.

[204] Babiloni C, Frisoni GB, Pievani M, Vecchio F, Infarinato F, Geroldi C, Salinari S, Ferri R, Fracassi C, Eusebi F, Rossini PM (2008) White matter vascular lesions are related to parietal-to-frontal coupling of EEG rhythms in mild cognitive impairment. *Hum Brain Mapp* **29**, 1355-1367.

[205] Babiloni C, Binetti G, Cassetta E, Cerboneschi D, Dal Forno G, Del Percio C, Ferreri F, Ferri R, Lanuzza B, Miniussi C, Moretti DV, Nobili F, Pascual-Marqui RD, Rodriguez G, Romani GL, Salinari S, Tecchio F, Vitali P, Zanetti O, Zappasodi F, Rossini PM (2004) Mapping distributed sources of cortical rhythms in mild Alzheimer's disease. A multicentric EEG study. *Neuroimage* **22**, 57-67.

[206] Polich J, Corey-Bloom J (2005) Alzheimer's disease and P300: review and evaluation of task and modality. *Curr Alzheimer Res* **2**, 515-525.

[207] Papaliagkas V, Kimiskidis V, Tsolaki M, Anogianakis G (2008) Usefulness of event-related potentials in the assessment of mild cognitive impairment. *BMC Neurosci* **9**, 107.

[208] Pogarell O, Mulert C, Hegerl U (2006) Event related potentials and fMRI in neuropsychopharmacology. *Clin EEG Neurosci* **37**, 99-107.

[209] Meador KJ, Loring DW, Davis HC, Sethi KD, Patel BR, Adams RJ, Hammond EJ (1989) Cholinergic and serotonergic effects on the P3 potential and recent memory. *J Clin Exp Neuropsychol* **11**, 252-260.

[210] Katada E, Sato K, Sawaki A, Dohi Y, Ueda R, Ojika K (2003) Long-term effects of donepezil on P300 auditory event-related potentials in patients with Alzheimer's disease. *J Geriatr Psychiatry Neurol* **16**, 39-43.

[211] Neshige R, Barrett G, Shibasaki H (1988) Auditory long latency event-related potentials in Alzheimer's disease and multi-infarct dementia. *J Neurol Neurosurg Psychiatry* **51**, 1120-1125.

[212] Onofrj M, Thomas A, Luciano AL, Iacono D, Di Rollo A, D'Andreamatteo G, Di Iorio A (2002) Donepezil versus vitamin E in Alzheimer's disease: Part 2: mild versus moderate-severe Alzheimer's disease. *Clin Neuropharmacol* **25**, 207-215.

[213] Reeves RR, Struve FA, Patrick G, Booker JG, Nave DW (1999) The effects of donepezil on the P300 auditory and visual cognitive evoked potentials of patients with Alzheimer's disease. *Am J Geriatr Psychiatry* **7**, 349-352.

[214] Thomas A, Iacono D, Bonanni L, D'Andreamatteo G, Onofrj M (2001) Donepezil, rivastigmine, and vitamin E in Alzheimer disease: a combined P300 event-related potentials/neuropsychologic evaluation over 6 months. *Clin Neuropharmacol* **24**, 31-42.

[215] Werber AE, Klein C, Rabey JM (2001) Evaluation of cholinergic treatment in demented patients by P300 evoked related potentials. *Neurol Neurochir Pol* **35**, 37-43.

[216] Werber EA, Gandelman-Marton R, Klein C, Rabey JM (2003) The clinical use of P300 event related potentials for the evaluation of cholinesterase inhibitors treatment in demented patients. *J Neural Transm* **110**, 659-669.

[217] Hegerl U, Möller HJ (1997) Electroencephalography as a diagnostic instrument in Alzheimer's disease: reviews and perspectives. *Int Psychogeriatr* **9**, 237-246.

[218] Golob EJ, Ringman JM, Irimajiri R, Bright S, Schaffer B, Medina LD, Starr A (2009) Cortical event-related potentials in preclinical familial Alzheimer disease. *Neurology* **73**, 1649-1655.

[219] Green J, Levey AI (1999) Event-related potential changes in groups at increased risk for Alzheimer disease. *Arch Neurol* **56**, 1398-1403.

[220] Espeseth T, Rootwelt H, Reinvang I (2009) Apolipoprotein E modulates auditory event-related potentials in healthy aging. *Neurosci Lett* **459**, 91-95.

[221] Chapman RM, McCrary JW, Gardner MN, Sandoval TC, Guillily MD, Reilly LA, Degrush E (2009) Brain ERP components predict which individuals progress to Alzheimer's disease and which do not. *Neurobiol Aging*. doi:10.1016/j.neurobiolaging.2009.11.010

[222] Gironell A, Garcia-Sanchez C, Estevez-Gonzalez A, Boltes A, Kulisevsky J (2005) Usefulness of p300 in subjective memory complaints: a prospective study. *J Clin Neurophysiol* **22**, 279-284.

[223] Golob EJ, Irimajiri R, Starr A (2007) Auditory cortical activity in amnestic mild cognitive impairment: relationship to subtype and conversion to dementia. *Brain* **130**, 740-752.

[224] Olichney JM, Taylor JR, Gatherwright J, Salmon DP, Bressler AJ, Kutas M, Iragui-Madoz VJ (2008) Patients with MCI and N400 or P600 abnormalities are at very high risk for conversion to dementia. *Neurology* **70**, 1763-1770.

[225] Lai CL, Lin RT, Liou LM, Liu CK (2010) The role of event-related potentials in cognitive decline in Alzheimer's disease. *Clin Neurophysiol* **121**, 194-199.

[226] Papaliagkas, VT, Kimiskidis, VK, Tsolaki, MN, Anogianakis G. Cognitive event-related potentials: Longitudinal changes in mild cognitive impairment. *Clin. Neurophysiol.* doi:10.1016/j.clinph.2010.12.036

[227] Ray PG, Meador KJ, Loring DW (1992) Diazepam effects on the P3 event-related potential. *J Clin Psychopharmacol* **12**, 415-419.

[228] Ball SS, Marsh JT, Schubarth G, Brown WS, Strandburg R (1989) Longitudinal P300 latency changes in Alzheimer's disease. *J Gerontol* **44**, M195-M200.

[229] Onofrj M, Gambi D, Del Re ML, Fulgente T, Bazzano S, Colamartino P, Malatesta G (1991) Mapping of event-related potentials to auditory and visual odd-ball paradigms in patients affected by different forms of dementia. *Eur Neurol* **31**, 259-269.

[230] St Clair D, Blackburn I, Blackwood D, Tyrer G (1988) Measuring the course of Alzheimer's disease. A longitudinal study of neuropsychological function and changes in P3 event-related potential. *Br J Psychiatry* **152**, 48-54.

[231] Swanwick GR, Rowan MJ, Coen RF, Lawlor BA, Coakley D (1997) Measuring cognitive deterioration in Alzheimer's disease. *Br J Psychiatr* **170**, 580.

[232] Polich J, Ehlers CL, Otis S, Mandell AJ, Bloom FE (1986) P300 latency reflects the degree of cognitive decline in dementing illness. *Electroencephalogr Clin Neurophysiol* **63**, 138-144.

[233] Polich J, Herbst KL (2000) P300 as a clinical assay: rationale, evaluation, and findings. *Int J Psychophysiol* **38**, 3-19.

[234] Golob EJ, Johnson JK, Starr A (2002) Auditory event-related potentials during target detection are abnormal in mild cognitive impairment. *Clin Neurophysiol* **113**, 151-161.

[235] Bennys K, Portet F, Touchon J, Rondouin G (2007) Diagnostic value of event-related evoked potentials N200 and P300 subcomponents in early diagnosis of Alzheimer's disease and mild cognitive impairment. *J Clin Neurophysiol* **24**, 405-412.

[236] Li X, Shao X, Wang N, Wang T, Chen G, Zhou H (2010) Correlation of auditory event-related potentials and magnetic resonance spectroscopy measures in mild cognitive impairment. *Brain Res* **1346**, 204-212.

[237] Frodl T, Hampel H, Juckel G, Bürger K, Padberg F, Engel RR, Möller HJ, Hegerl U (2002) Value of event-related P300 subcomponents in the clinical diagnosis of mild cognitive impairment and Alzheimer's Disease. *Psychophysiology* **39**, 175-181.

[238] van Deursen JA, Vuurman EF, Smits LL, Verhey FR, Riedel WJ (2009) Response speed, contingent negative variation and P300 in Alzheimer's disease and MCI. *Brain Cogn* **69**, 592-599.

[239] Olichney JM, Hillert DG (2004) Clinical applications of cognitive event-related potentials in Alzheimer's disease. *Phys Med Rehabil Clin N Am* **15**, 205-233.

[240] Missonnier P, Deiber MP, Gold G, Herrmann FR, Millet P, Michon A, Fazio-Costa L, Ibañez V, Giannakopoulos P (2007) Working memory load-related electroencephalographic parameters can differentiate progressive from stable mild cognitive impairment. *Neuroscience* **150**, 346-356.

[241] Rossini PM, Rossi S, Babiloni C, Polich J (2007) Clinical neurophysiology of aging brain: from normal aging to neurodegeneration. *Prog Neurobiol* **83**, 375-400.

[242] Hegerl U, Frodl-Bauch T (1997) Dipole source analysis of P300 component of the auditory evoked potential: a methodological advance? *Psychiatry Res* **74**, 109-118.

[243] Juckel G, Clotz F, Frodl T, Kawohl W, Hampel H, Pogarell O, Hegerl U (2008) Diagnostic usefulness of cognitive auditory event-related p300 subcomponents in patients with Alzheimers disease? *J Clin Neurophysiol* **25**, 147-152.

[244] Fagan AM, Mintun MA, Mach RH, Lee SY, Dence CS, Shah AR, LaRossa GN, Spinner ML, Klunk WE, Mathis CA, DeKosky ST, Morris JC, Holtzman DM (2006) Inverse relation between in vivo amyloid imaging load and cerebrospinal fluid Abeta42 in humans. *Ann Neurol* **59**, 512-519.

[245] Grimmer T, Riemenschneider M, Förstl H, Henriksen G, Klunk WE, Mathis CA, Shiga T, Wester HJ, Kurz A, Drzezga A (2009) Beta amyloid in Alzheimer's disease: increased deposition in brain is reflected in reduced concentration in cerebrospinal fluid. *Biol Psychiatry* **65**, 927-934.

[246] Zetterberg H, Pedersen M, Lind K, Svensson M, Rolstad S, Eckerström C, Syversen S, Mattsson UB, Ysander C, Mattsson N, Nordlund A, Vanderstichele H, Vanmechelen E, Jonsson M, Edman A, Blennow K, Wallin A (2007) Intra-individual stability of CSF biomarkers for Alzheimer's disease over two years. *J Alzheimers Dis* **12**, 255-260.

[247] Zhou B, Teramukai S, Yoshimura K, Fukushima M (2009) Validity of cerebrospinal fluid biomarkers as endpoints in early-phase clinical trials for Alzheimer's disease. *J Alzheimers Dis* **18**, 89-102.

[248] Andersson C, Blennow K, Almkvist O, Andreasen N, Engfeldt P, Johansson SE, Lindau M, Eriksdotter-Jönhagen M (2008) Increasing CSF phospho-tau levels during cognitive decline and progression to dementia. *Neurobiol Aging* **29**, 1466-1473.

[249] Blomberg M, Jensen M, Basun H, Lannfelt L, Wahlund LO (1996) Increasing cerebrospinal fluid tau levels in a subgroup of Alzheimer patients with apolipoprotein E allele epsilon 4 during 14 months follow-up. *Neurosci Lett* **214**, 163-166.

[250] Bouwman FH, van der Flier WM, Schoonenboom NS, van Elk EJ, Kok A, Rijmen F, Blankenstein MA, Scheltens P (2007) Longitudinal changes of CSF biomarkers in memory clinic patients. *Neurology* **69**, 1006-1011.

[251] de Leon MJ, Segal S, Tarshish CY, DeSanti S, Zinkowski R, Mehta PD, Convit A, Caraos C, Rusinek H, Tsui W, Saint Louis LA, DeBernardis J, Kerkman D, Qadri F, Gary A, Lesbre P, Wisniewski T, Poirier J, Davies P (2002) Longitudinal cerebrospinal fluid tau load increases in mild cognitive impairment. *Neurosci Lett* **333**, 183-186.

[252] Hesse C, Rosengren L, Andreasen N, Davidsson P, Vanderstichele H, Vanmechelen E, Blennow K (2001) Transient increase in total tau but not phospho-tau in human cerebrospinal fluid after acute stroke. *Neurosci Lett* **297**, 187-190.

[253] Zemlan FP, Rosenberg WS, Luebbe PA, Campbell TA, Dean GE, Weiner NE, Cohen JA, Rudick RA, Woo D (1999) Quantification of axonal damage in traumatic brain injury: affinity purification and characterization of cerebrospinal fluid tau proteins. *J Neurochem* **72**, 741-750.

[254] Gilman S, Koller M, Black RS, Jenkins L, Griffith SG, Fox NC, Eisner L, Kirby L, Rovira MB, Forette F, Orgogozo JM (2005) Clinical effects of Abeta immunization (AN1792) in patients with AD in an interrupted trial. *Neurology* **64**, 1553-1562.

[255] Brys M, Pirraglia E, Rich K, Rolstad S, Mosconi L, Switalski R, Glodzik-Sobanska L, De Santi S, Zinkowski R, Mehta P, Pratico D, Saint Louis LA, Wallin A, Blennow K, de Leon MJ (2009) Prediction and longitudinal study of CSF biomarkers in mild cognitive impairment. *Neurobiol Aging* **30**, 682-690.

[256] de Leon MJ, DeSanti S, Zinkowski R, Mehta PD, Pratico D, Segal S, Rusinek H, Li J, Tsui W, Saint Louis LA, Clark CM, Tarshish C, Li Y, Lair L, Javier E, Rich K, Lesbre P, Mosconi L, Reisberg B, Sadowski M, DeBernadis JF, Kerkman DJ, Hampel H, Wahlund LO, Davies P (2006) Longitudinal CSF and MRI biomarkers improve the diagnosis of mild cognitive impairment. *Neurobiol Aging* **27**, 394-401.

[257] de Leon MJ, Mosconi L, Li J, De Santi S, Yao Y, Tsui WH, Pirraglia E, Rich K, Javier E, Brys M, Glodzik L, Switalski R, Saint Louis LA, Pratico D (2007) Longitudinal CSF isoprostane and MRI atrophy in the progression to AD. *J Neurol* **254**, 1666-1675.

[258] Quinn JF, Montine KS, Moore M, Morrow JD, Kaye JA, Montine TJ (2004) Suppression of longitudinal increase in CSF F2-isoprostanes in Alzheimer's disease. *J Alzheimers Dis* **6**, 93-97.

[259] Jesse S, Steinacker P, Cepek L, von Arnim CA, Tumani H, Lehnert S, Kretzschmar HA, Baier M, Otto M (2009) Glial fibrillary acidic protein and protein S-100B: different concentration pattern of glial proteins in cerebrospinal fluid of patients with Alzheimer's disease and Creutzfeldt-Jakob disease. *J Alzheimers Dis* **17**, 541-551.

[260] Fukuyama R, Izumoto T, Fushiki S (2001) The cerebrospinal fluid level of glial fibrillary acidic protein is increased in cerebrospinal fluid from Alzheimer's disease patients and correlates with severity of dementia. *Eur Neurol* **46**, 35-38.

[261] Crols R, Saerens J, Noppe M, Lowenthal A (1986) Increased GFAp levels in CSF as a marker of organicity in patients with Alzheimer's disease and other types of irreversible chronic organic brain syndrome. *J Neurol* **233**, 157-160.

[262] Blasko I, Lederer W, Oberbauer H, Walch T, Kemmler G, Hinterhuber H, Marksteiner J, Humpel C (2006) Measurement of thirteen biological markers in CSF of patients with Alzheimer's disease and other dementias. *Dement Geriatr Cogn Disord* **21**, 9-15.

[263] Cacabelos R, Barquero M, García P, Alvarez XA, Varela de Seijas E (1991) Cerebrospinal fluid interleukin-1 beta (IL-1 beta) in Alzheimer's disease and neurological disorders. *Methods Find Exp Clin Pharmacol* **13**, 455-458.

[264] Hampel H, Sunderland T, Kötter HU, Schneider C, Teipel SJ, Padberg F, Dukoff R, Levy J, Möller HJ (1998) Decreased soluble interleukin-6 receptor in cerebrospinal fluid of patients with Alzheimer's disease. *Brain Res* **780**, 356-359.

[265] Rota E, Bellone G, Rocca P, Bergamasco B, Emanuelli G, Ferrero P (2006) Increased intrathecal TGF-beta1, but not IL-12, IFN-gamma and IL-10 levels in Alzheimer's disease patients. *Neurol Sci* **27**, 33-39.

[266] Sun YX, Minthon L, Wallmark A, Warkentin S, Blennow K, Janciauskiene S (2003) Inflammatory markers in matched plasma and cerebrospinal fluid from patients with Alzheimer's disease. *Dement Geriatr Cogn Disord* **16**, 136-144.

[267] Engelborghs S, De Brabander M, De Crée J, D'Hooge R, Geerts H, Verhaegen H, De Deyn PP (1999) Unchanged levels of interleukins, neopterin, interferon-gamma and tumor necrosis factor-alpha in cerebrospinal fluid of patients with dementia of the Alzheimer type. *Neurochem Int* **34**, 523-530.

[268] Kálmán J, Juhász A, Laird G, Dickens P, Járdánházy T, Rimanóczy A, Boncz I, Parry-Jones WL, Janka Z (1997) Serum interleukin-6 levels correlate with the severity of dementia in Down syndrome and in Alzheimer's disease. *Acta Neurol Scand* **96**, 236-240.

[269] Lanzrein AS, Johnston CM, Perry VH, Jobst KA, King EM, Smith AD (1998) Longitudinal study of inflammatory factors in serum, cerebrospinal fluid, and brain tissue in Alzheimer disease: interleukin-1beta, interleukin-6, interleukin-1 receptor antagonist, tumor necrosis factor-alpha, the soluble tumor necrosis factor receptors I and II, and alpha1-antichymotrypsin. *Alzheimer Dis Assoc Disord* **12**, 215-227.

This page intentionally left blank

Section 5
Electromagnetic Brain Mapping: EEG, EP, ERP, and their Magnetic Equivalents

This page intentionally left blank

Introduction

Section 5: Electromagnetic Brain Mapping

Kerry L. Coburn[a,*], John Olichney[b] and J. Wesson Ashford[c]

[a]*Mercer University School of Medicine, Macon, GA, USA*
[b]*University of California, Davis; Department of Neurology, Sacramento CA, USA*
[c]*War Related Illness and Injury Study Center Veterans Affairs Palo Alto Health Care System, Palo Alto,
CA, and Clinical Professor (Affiliated) Department of Psychiatry and Behavioral Sciences,
Stanford University School of Medicine, Stanford, CA, USA*

Although studies of brain electrical activity have a long history in psychiatry and neurology, the advent of quantitative electroencephalography (qEEG) systems in the 1980 s introduced topographic mapping ("brain mapping") as a display option. This important development brought EEG and related techniques squarely into the domain of neuroimaging. Onto a standardized head or brain template (or more recently onto the subject's own brain MRI) could be mapped the raw voltages of EEGs, averaged voltages of Evoked Potentials (EPs) and Event-related Potentials (ERPs), frequency domain measurements of EEG amplitude and power deriving from fast Fourier transformations (FFTs), results of inferential statistical tests such as significance probability mapping (SPM), and a wide range of other quantitative data. Simultaneously the technique of magnetoencephalography (MEG), recording magnetic instead of voltage fields produced by brain activity, made its debut, introducing magnetic counterparts to EEGs, EPs, and ERPs. Application of these new techniques to dementia in general and Alzheimer's disease (AD) in particular was rapid.

There are two broad paradigms for studying brain electrical activity. In one, the EEG/MEG eavesdrops on the resting or idling brain while the subject sits quietly with his eyes open or closed. Verdoorn et al. in this volume present a vivid example of the use of the resting MEG to investigate AD. The other paradigm, subsuming EPs, ERPs and their magnetic equivalents, actively interrogates brain systems using external stimuli. In EP studies auditory, visual, or other stimuli are used to drive the brain's sensory systems producing a sensory evoked potential containing a series of waves (components) corresponding to stages of cortical information processing. ERP studies elaborate on this framework by requiring the subject to perform a specific cognitive task related to the stimuli. The most common such task is the auditory oddball, in which the subject is instructed to ignore one class of stimuli (e.g., low pitch tones) but to respond to a second class of stimuli (e.g., high pitch tones). The brain responds with an ERP containing the familiar auditory sensory components followed by one or more new components (e.g., N200, P300) reflecting the additional information processing related to the cognitive task.

In many ways EEG offers an ideal method for assessing brain function. Its exquisite temporal resolution can track brain activity in the millisecond time domain characteristic of neuronal activity in the cortical substrate. It is entirely noninvasive and employs no ionizing radiation. It records both excitatory and inhibitory signals directly rather than secondary hemodynamic processes. It also is inexpensive. MEG offers these same advantages, although MEG systems are not in widespread clinical use due to their size and the necessity of supercooling their superconducting sensors with liquid helium. In contrast, EEG systems are abundant and in many cases portable.

Another important advantage is that normative databases are available for EEG, allowing statistical comparison of a patient's brain activity with that of age-matched controls. The use of quantitative tech-

---

*Correspondence to: Kerry L. Coburn, Mercer University School of Medicine, Macon, GA 31207, USA. E-mail: coburn_kl@mercer.edu.

niques and inferential statistics moves EEG analysis from the realm of qualitative clinical impressions into the realm of quantitative empirical assessment. Such comparison with healthy controls yields information about the degree of abnormality of the patient's brain activity recorded by each electrode. Some databases additionally offer comparison with known clinical conditions, allowing a statistically based multivariate "best fit" classification that can aid clinical diagnosis. EEG's poor spatial resolution is being overcome by the use of increasingly dense electrode arrays, from 20 a decade ago to as many as 256 today. MEG, in addition to having a theoretically better spatial resolution than EEG, has experienced a similar increase in the number of sensors.

It has long been known that the typical EEG in Alzheimer's disease contains increased slow activity in the theta (4–8 Hz) frequency range and decreased fast activity in the beta (13–24 Hz) range over the broad regions of the temporal and parietal lobes sustaining high levels of tissue damage from the disease [1, 2]. More localized cortical damage resulting from strokes produces more focal theta, and in principle it should be possible to use this to identify individuals suffering from vascular dementia [3]. In practice however, this has been difficult to achieve using traditional univariate analysis techniques. Applications of multivariate techniques have shown more promise.

Quantitative EEG studies applying multivariate analysis to dementia have been reviewed extensively [4, 5]. Well-replicated studies have shown repeatedly that individual AD subjects and matched healthy controls can be classified into their appropriate groups on the basis of multivariate EEG analysis alone with accuracies as high as 80–90%. Furthermore, individual AD subjects could be discriminated from their nondemented depressed, alcoholic, or delirious, counterparts, and within the dementias AD subjects could be separated from those suffering from vascular or fronto-temporal dementia. However, such studies were performed using patients with established diagnoses and usually did not attempt to identify subjects in the earliest stages of a dementing process.

More recent work, reviewed in the Bablioni et al. and Moretti et al. chapters in this volume, greatly refines our understanding of the earliest frequency domain EEG changes in dementia. Subjects suffering from Minimal Cognitive Impairment (MCI) were found to display several promising EEG markers. The markers not only distinguish between groups of MCI subjects and matched groups of healthy controls, but

also between MCI sub-groups that will remain in MCI, progress to AD, or progress to non-AD dementia. It will be interesting to see whether these EEG markers can be used to accurately classify individual subjects. If so, they could be employed as diagnostic aids and perhaps more importantly in a prognostic capacity. Additionally, the markers could serve as surrogate measures of disease progression, greatly aiding the development of new therapies.

The frequency domain changes seen in the EEG are paralleled by MEG changes. Verdoorn et al. in this volume document MEG differences between groups of AD patients and healthy controls, and additionally find several MEG markers that change over time in parallel with neuropsychological changes to track disease progression. As with EEG, the critical question is whether MEG markers derived from groups of subjects can be applied to individuals. If so, they offer great potential for early phase development of novel treatments.

Pritchard et al. [6] developed a new nonlinear mathematical method of analyzing EEG activity based on deterministic chaos theory, and derived a measure of brain activity they termed dimensional complexity. They then used dimensional complexity to study AD and found that not only did this measure reliably distinguish between groups of AD patients and groups of matched healthy controls [7, 8], but it also could reliably classify individuals as belonging to either of these two groups [2]. Direct comparison between standard frequency analysis and a combination of frequency analysis and dimensional complexity clearly showed the superiority of the combined technique. The use of nonlinear dynamic analysis has been limited by the availability of computational power. Indeed, those early studies required collaboration with the Supercomputer Computations Research Institute at Florida State University. But in the two decades since those seminal studies rapid increases in computational power have allowed the analyses to be run on desktop computers, and nonlinear analysis has occupied a minor but important role in EEG research. The Bablioni et al. chapter in this volume reviews some recent nonlinear dynamic findings regarding AD (e.g., the sparing of resting state posterior alpha EEG rhythms in AD patients with more severe ischemic changes in the white-matter).

Because AD involves widespread brain pathology and marked deterioration of cognitive functions one might expect changes in both EPs and ERPs, and both are seen. For example, the visual EP in response to a

diffuse light flash contains a P2 component that has been found consistently to be delayed in groups of AD patients [1, 9, 10, 12, 13]. This delay probably reflects damage to the cholinergic neurons in visual association areas of the cortex. Similarly, the ERP produced by AD victims during the oddball task typically contains a delayed P300 component, probably reflecting the additional processing time necessary for the damaged higher-order association areas of the cortex to perform the cognitive task. The amplitude of the P300 component is often found to be diminished in AD, presumably reflecting a reduced population of cortical pyramidal neurons involved in the cognitive oddball task. Unfortunately, neither the latency increase nor the amplitude decrease is sufficiently reliable to be of clinical value when assessing individual patients. In an effort to extract a more reliable P300 signal from the background noise Ashford et al. in this volume compute power and energy measures from the recorded P300 voltage record. Both derived measures appear to track age- and AD-related changes more closely than does the traditional voltage wave. In this volume, Olichney et al. review prior ERP studies of AD, including P300 studies of attention and N400 studies of linguistic processing. Importantly, ERP studies can be designed to be sensitive to the cardinal features of AD. In this regard, recent work by Olichney and colleagues suggests that a Late Positive Component important for memory processes, sometimes termed the P600, may be particularly sensitive to the earliest stage of synaptic dysfunction during the 'Pre-clinical' (MCI) stage of AD. Olichney et al. [14] have demonstrated that two late ERP components (N400 and P600) are also promising in their ability to predict outcome in MCI. As with the EEG markers proposed by Bablioni et al, an important question is whether ERP markers can accurately classify individual subjects during the MCI stage or even earlier. Recently proposed research criteria for Pre-clinical AD [15] (Sperling et al, in press) divided this entity into 3 stages based on the presence/absence of very mild cognitive deficits and synaptic dysfunction. We believe that this volume illustrates several applications of the EEG, ERP and MEG techniques to characterize synaptic/neuronal function and their earliest derailments in AD. Further research and validation of these measures are needed to test their clinical utility, cost-effectiveness and to determine which information is most complimentary to the results from other imaging modalities (e.g., MRI, PET) and other AD biomarkers.

REFERENCES

[1]   Coburn K, Parks R, Pritchard W (1993a) Electrophysiological indexes of cortical deterioration and cognitive impairment in dementia. In: *Neuropsychology of Alzheimer's Disease and Other Dementias*. Parks R.W, Zec R.F, Wilson R.S. eds, New York: Oxford University Press, pp. 511-533.

[2]   Pritchard W, Duke D, Coburn K, Moore N, Tucker K, Hostetler R, Jann M (1994) EEG-based, neural-net predictive classification of Alzheimer's disease versus control subjects is augmented by non-linear EEG measures. *Electroencephalog Clin Neurophysiol* **91**, 118-130.

[3]   Parks R, Zec R, Kuhn M, Vicari S, Feldman E, Coburn K, Ashford J, Crockett D, Moreno M, Rashid A (1991) Electrocortical mapping, MRI, and neuropsychological measures: Evidence of Alzheimer's disease in the presence of vascular lesions. *Arch Clin Neuropsychol* **6**, 393-408.

[4]   Boutros N, Coburn K (2006) Electroencephalography in neuropsychiatry (Neuropsychiatry Special Report). *Psychiat Times* **23**(4), 34, 39-40.

[5]   Coburn K, Lauterbach E, Boutros N, Black K, Arciniegas D, Coffey C (2006) The value of quantitative electroencephalography in clinical psychiatry. *J Neuropsychiat Clin Neurosci* **18**, 460-500.

[6]   Pritchard W, Duke D, Coburn K (1991a) Dimensional analysis of topographic EEG: Some methodological considerations. In: *Measuring Chaos in the Human Brain*. Singapore: D Duke, W Pritchard eds, World Scientific Press, pp. 181-198.

[7]   Pritchard W, Duke D, Coburn K (1991b) Altered EEG dynamical responsivity associated with normal aging and probable Alzheimer's disease. *Dementia* **2**, 102-105.

[8]   Pritchard W, Duke D, Coburn K, Robinson J (1992) Nonlinear dynamical EEG analysis applied to nicotine psychopharmacology and Alzheimer's disease. In: *The Biology of Nicotine*. P Lippiello et al. eds, New York: Raven Press, pp. 195-214.

[9]   Coburn K, Ashford J, Moreno M (1991) Visual evoked potentials in dementia: Selective delay of flash P2 in probable Alzheimer's disease. *J Neuropsychiat Clin Neurosci* **3**, 431-435.

[10]   Coburn K, Ashford J, Moreno M (1993b) Delayed late component of visual global field power in probable Alzheimer's disease. *J Geriat Psychiat Neurol* **6**, 72-77.

[11]   Coburn K, Arruda J, Estes K, Amoss R (2003) Diagnostic utility of VEP changes in Alzheimer's Disease. *J Neuropsychiat Clin Neurosci* **15**, 175-179.

[12]   Moore N, Tucker K, Jann M, Hostetler R, Coburn K (1995) Flash P2 delay in primary degenerative dementia of the Alzheimer type. *Prog Neuropsychopharmacol Biol Psychiat* **19**, 403-410.

[13]   Moore N, Tucker K, Khairy N, Coburn K (1996) Flash P2 visual evoked response delay may be a marker of cognitive dysfunction in healthy elderly volunteers. *Int Psychogeriat* **8**, 549-559.

[14]   Olichney JM, Taylor JR, Gatherwright J, Salmon DP, Bressler AJ, Kutas M, Iragui-Madoz VJ (2008) Patients with MCI and N400 or P600 abnormalities are at very high risk for conversion to dementia. *Neurology* **6**, 1763-1770.

[15]   Sperling RA, Aisen PS, Beckett LA, Bennett DA, Craft S, Fagan AM et al. (2011) Toward defining the preclinical stages of Alzheimer's disease: Recommendations from the National Institute on Aging and the Alzheimer's Association workgroup. *Alzheimers Dement* doi:10.1016/j.jalz.2011.03.003.

This page intentionally left blank

EEG Changes are Specifically Associated with Atrophy in Amydala and Hippocampus in Subjects with Mild Cognitive Impairment

Davide V. Moretti*, Orazio Zanetti, Giuliano Binetti and Giovanni B. Frisoni
IRCCS S. Giovanni di Dio Fatebenefratelli, Brescia, Italy

Abstract. We evaluated the association between amygdalo-hippocampal complex (AHC) atrophy and two EEG markers of cognitive decline: increase of theta/gamma and increase of alpha3/alpha2 relative power ratio. Seventy-nine subjects with mild cognitive impairment (MCI) underwent EEG recording and MRI scan.. Three groups of AHC growing atrophy were obtained. The groups were characterized by the performance to cognitive tests and theta/gamma and alpha3/alpha2 relative power ratio. AHC atrophy is associated with memory deficits as well as with increase of theta/gamma and alpha3/alpha2 ratio. Moreover, when the amygdalar and hippocampal volume are separately considered, within AHC, the increase of theta/gamma ratio is best associated with amygdalar atrophy whereas alpha3/alpha2 ratio is best associated with hippocampal atrophy. AHC atrophy is associated with memory deficits and EEG markers of cognitive decline. So far, these EEG markers could have a prospective value in differential diagnosis between MCI who will convert in in Alzheimer's disease (AD), MCI converting in non-AD dementias and MCI non-converters. The alterations of the functional connections, inducing global network pathological changes, in the whole AHC could better explain MCI state.

Keywords: Mild cognitive impairment, electroencephalography, theta rhythm, gamma rhythm, cognitive tests, amygdalo-hippocampal complex

INTRODUCTION

The last decade has seen a surge in research in biomarkers for Alzheimer disease (AD) and other dementia disorders [1]. With predictions of 1 in 4 persons ultimately developing the disease, disorders causing dementia have become one of the major health concerns in aging societies. Impending costs to society and individuals, as well as the enormous and increasing market potential to industry, make this an extremely important field in which the stakes, pres-

sure, and expectations are high to develop better means to establish presence of disease, monitor progression, and make a diagnosis. In that arena, it is of the utmost importance that biomarkers in a prodromal stage of disease, commonly referred as mild cognitive impairment (MCI) are evaluated in a valid and rigorous way in order to obtain an early diagnosis [2]. A biomarker must be validated in the population and clinical setting for which the biomarker is intended.[5] A diagnostic marker for AD would typically be used to distinguish between individuals with cognitive problems who have AD-type pathology and those who do not, or, in the case of early diagnosis, to predict which of the cognitively healthy persons might develop cognitive decline over time. Furthermore, biomarkers must be identified that can be obtained relatively easily and with

*Correspondence to: Vito Davide Moretti, MD, PhD, IRCCS 'San Giovanni di Dio – FBF', 4, Pilastroni road, 25125 – Brescia, Italy. Tel.: +39 0303501597; Fax: +39 0303533513; E-mail: davide.moretti@afar.it.

minimal invasiveness. Previous longitudinal studies showed that changes in a patient's EEG might have prognostic value with regard to the future progression of the illness [3–5]. Our group is developing by many years an MCI observational project, in which EEG activity is studied, together with other variables, to detect specific neuroelectric biomarkers able to identify prodromal stage of AD. In other words, our aim is to look at EEG markers in subjects with the so-called mild cognitive impairment state who are at major risk to develop the AD or other dementias. Moreover, the collected studies on this "prodromal road" may helps us to understand neurophysiological mechanism of the disease and the association of the modification of EEG rhythms with MRI morphostructural features in MCI subjects. Overall, the bulk of evidence our group have produced, confirming recent functional studies [6, 7], shows that the EEG changes of rhythmicity occurs in a non-linear way respect to the decourse of disease. In particular we found that some EEG markers are associated to the hippocampal atrophy but the EEG modifications are non-proportionally to the hippocampal atrophy itself [8, 9]. Moreover, the functional connectivity in MCI with hippocampal atrophy is increased whereas in MCI with vascular lesions is impaired [10], determining a state of oversynchronization. Of note, recent studies using animal models suggest that beta-amyloid deposits can act to trigger oversynchronization with epileptiform activity and that this abnormal neuronal activity might also contribute to cognitive decline [11]. The present study adds another step towards understanding the complex relationship between EEG phenotype and AD pathology. As a final result, the modifications of theta/gamma and alpha3/alpha2 ratio are associated with specific anatomical structure atrophy of amygdale and hippocampus.

Mild cognitive impairment (MCI) refers to the transitional state between the cognitive changes of normal aging and very early dementia [12]. Patients with MCI, who are at high risk of developing Alzheimer disease [AD; 13], have smaller hippocampal and amygdalar volumes than healthy elderly people [14, 15]. Medial temporal lobe (MTL) structures, in particular the amygdala and hippocampus, show atrophy in the early stages of AD and are potential markers for detecting pre-clinical AD [16–18]. Moreover, a recent study has demonstrated that atrophy of the hippocampus and amygdala on MRI in cognitively intact elderly people predicts dementia, in particular of Alzheimer type, during a 6-year follow-up [19].

Interactions between amygdala and hippocampus are particularly important for memory formation, for attention [20, 21] and for production of theta and gamma rhythmic activity [22, 23]. Amygdala lesions attenuate hippocampal synaptic plasticity and block the memory-enhancing effects of direct hippocampal stimulation [24, 25]. Further, behavioral stress as well as stimulation of the amygdala interferes with synaptic plasticity in the hippocampal formation [26–28]. This interaction appears to be bidirectional, given that tetanic stimulation of hippocampal efferent fibers can induce long-term potentiation in the lateral amygdala [LA; 29] which is the major input station of sensory signals of the amygdala to the CA1 area of the hippocampus [30]. Associative memories involves both the LA and the dorsal hippocampus and a lesion of the area reduces the retrieval of associative tasks [31]. The LA/CA1 network system seems to be well suited to rhythmically oscillate at theta frequencies: the basolateral amygdaloid complex receives synaptic inputs from the hippocampus [32], where theta waves have been observed [33], and from the anterior thalamic nuclei, which could transfer hippocampal theta rhythms to the amygdala [34, 35]. On the whole, the amygdalo-hippocampal network is a strictly coupled functional complex. As a consequence, the atrophy of the amygdalo-hyppocampal complex (AHC) has to be related with both cognitive deficits and modifications in brain oscillatory activity.

Recent works showed that in subjects with MCI is present an increase of theta relative power [36–38], a decrease of gamma relative power [36, 37] as well as an increase of high alpha as compared to low alpha band [37, 38]. As a working hypothesis, EEG markers like theta/gamma and alpha3/alpha2 power ratio could show modifications proportional to the AHC atrophy. In the present study the association between AHC atrophy and two EEG markers of cognitive decline (increase of theta/gamma and increase of alpha3/alpha2 relative power ratio) was investigated in subjects with MCI.

MATERIALS AND METHODS

Subjects

For the present study, 79 subjects with MCI were recruited from the memory Clinic of the Scientific Institute for Research and Care (*IRCCS*) of Alzheimer's and psychiatric diseases 'Fatebenefratelli' in Brescia, Italy. All experimental protocols

had been approved by the local Ethics Committee. Informed consent was obtained from all participants or their caregivers, according to the Code of Ethics of the World Medical Association (Declaration of Helsinki).

Diagnostic criteria

Patients were taken from a prospective project on the natural history of MCI. The project was aimed to study the natural history of non-demented persons with apparently primary cognitive deficits, i.e., deficits not due to psychic (anxiety, depression) or physical (hypothyroidism, vit. B12 and folate deficiency, uncontrolled heart disease, uncontrolled diabetes) conditions. Patients were rated with a series of standardized diagnostic and severity instruments, including the Mini-Mental State Examination [MMSE; 39], the Clinical Dementia Rating Scale [CDRS; 40], the Hachinski Ischemic Scale [HIS; 41] and the Instrumental and Basic Activities of Daily Living [IADL, BADL, 42]. In addition, patients underwent diagnostic neuroimaging procedures (magnetic resonance imaging, MRI), and laboratory testing to rule out other causes of cognitive impairment. These inclusion and exclusion criteria for MCI were based on previous seminal studies [43–49]. Inclusion criteria of the study were all of the following: (i) complaint by the patient, or report by a relative or the general practitioner, of memory or other cognitive disturbances; (ii) Mini-Mental State Examination (MMSE) score of 24 to 27/30, or MMSE of 28 and higher plus low performance (score of 2–6 or higher) on the clock drawing test [50]; (iii) sparing of instrumental and basic activities of daily living or functional impairment steadily due to causes other than cognitive impairment, such as physical impairments, sensory loss, gait or balance disturbances. Exclusion criteria were any one of the following: (i) patients aged 90 years and older; (ii) history of depression or juvenile-onset psychosis; (iii) history or neurological signs of major stroke; (iv) other psychiatric diseases, epilepsy, drug addiction, alcohol dependence; (v) use of psychoactive drugs, including acetylcholinesterase inhibitors or other drugs enhancing brain cognitive functions; and (vi) current or previous uncontrolled or complicated systemic diseases (including diabetes mellitus), or traumatic brain injuries. All patients underwent: (i) semi-structured interview with the patient and – whenever possible – with another informant (usually, the patient's spouse or a child of the patient) by a geriatrician or neu-

rologist; (ii) physical and neurological examinations; (iii) performance-based tests of physical function, gait and balance; (iv) neuropsychological battery assessing verbal and non-verbal memory, attention and executive functions [Trail Making Test B-A; Clock Drawing Test; 50, 51], abstract thinking [Raven matrices; 52], frontal functions [Inverted Motor Learning; 53]; language [Phonological and Semantic fluency; Token test; 54], and apraxia and visuo-constructional abilities [Rey figure copy; 55]; (v) assessment of depressive symptoms by means of the Center for Epidemiologic Studies Depression Scale [CES-D; 56]. Inclusion and exclusion criteria were homogeneous with previous works [36–38, 49]. As the aim of our study was to evaluate the specific association between AHC atrophy with both EEG markers and cognitive decline, we did not consider the clinical subtype of MCI, *i.e.*, amnesic, non-amnesic or multiple domains.

EEG recordings

All recordings were obtained in the morning with subjects resting comfortably. Vigilance was continuously monitored in order to avoid drowsiness.

The EEG activity was recorded continuously from 19 sites by using electrodes set in an elastic cap (Electro-Cap International, Inc.) and positioned according to the 10–20 International system (Fp1, Fp2, F7, F3, Fz, F4, F8, T3, C3, Cz, C4, T4, T5, P3, Pz, P4, T6, O1, O2). The ground electrode was placed in front of Fz. The left and right mastoids served as reference for all electrodes. The recordings were used off-line to re-reference the scalp recordings to the common average. Data were recorded with a band-pass filter of 0.3–70 Hz, and digitized at a sampling rate of 250 Hz (BrainAmp, BrainProducts, Germany). Electrodes-skin impedance was set below 5 kΩ. Horizontal and vertical eye movements were detected by recording the electrooculogram (EOG). The recording lasted 5 minutes, with subjects with closed eyes. Longer recordings would have reduced the variability of the data, but they would also have increased the possibility of slowing of EEG oscillations due to reduced vigilance and arousal. EEG data were then analyzed and fragmented off-line in consecutive epochs of 2 seconds, with a frequency resolution of 0.5 Hz. The average number of epochs analyzed was 140 ranging from 130 to150. The EEG epochs with ocular, muscular and other types of artifacts were discarded.

Analysis of individual frequency bands

A digital FFT-based power spectrum analysis (Welch technique, Hanning windowing function, no phase shift) computed – ranging from 2 to 45 Hz – the power density of EEG rhythms with a 0.5 Hz frequency resolution. Methods are exposed in detail elsewhere [36–38, 57]. Briefly, two anchor frequencies were selected according to literature guidelines [58], that is, the theta/alpha transition frequency (TF) and the individual alpha frequency (IAF) peak. Based on TF and IAF, we estimated the following frequency band range for each subject: delta, theta, low alpha band (alpha1 and alpha2), and high alpha band (alpha3). Moreover, individual beta and gamma frequencies were computed. Three frequency peaks were detected in the frequency range from the individual alpha 3 frequency band and 45 Hz. These peaks were named beta1 peak (IBF 1), beta2 peak (IBF 2) and gamma peak (IGF). Based on peaks, the frequency ranges were determined. Beta1 ranges from alpha 3 to the lower spectral power value between beta1 and beta2 peak; beta2 frequency ranges from beta 1 to the lower spectral power value between beta2 and gamma peak; gamma frequency ranges from beta 2 to 45 Hz, which is the end of the range considered. The mean frequency range computed in MCI subjects considered as a whole are: delta 2.9–4.9 Hz; theta 4.9–6.9 Hz; alpha1 6.9–8.9 Hz; alpha2 8.9–10.9 Hz; alpha3 10.9–12–9 Hz; beta1 12.9–19.2 Hz; beta2 19.2–32.4; gamma 32.4–45. In the frequency bands determined in this way, the relative power spectra for each subject were computed. The relative power density for each frequency band was computed as the ratio between the absolute power and the mean power spectra from 2 to 45 Hz. The relative band power at each band was defined as the mean of the relative band power for each frequency bin within that band. Finally, the theta/gamma and alpha3/alpha2 relative power ratio were computed and analyzed. The analysis of other frequencies was not in the scope of this study.

MRI scans

MRI scans were acquired with a 1.0 Tesla Philips Gyroscan at the Neuroradiology Unit of the Città di Brescia hospital, Brescia. The following sequences were used to measure hippocampal and amygdalar volumes: a high-resolution gradient echo T1-weighted sagittal 3D sequence (TR = 20 ms, TE = 5 ms, flip angle = 30°, field of view = 220 mm, acquisition matrix = 256 × 256, slice thickness = 1.3 mm), and a fluid-attenuated inversion recovery (FLAIR) sequence (TR = 5000 ms, TE = 100 ms, flip angle = 90°, field of view = 230 mm, acquisition matrix = 256 × 256, slice thickness = 5 mm). Hippocampal, amygdalar and white matter hyperintensities (WMHs) volumes were obtained for each subject. The hippocampal and amygdalar boundaries were manually traced on each hemisphere by a single tracer with the software program DISPLAY (McGill University, Montreal, Canada) on contiguous 1.5 mm slices in the coronal plane. The amygdala is an olive-shaped mass of gray matter located in the superomedial part of the temporal lobe, partly superior and anterior to the hippocampus. The starting point for amygdala tracing was at the level where it is separated from the entorhinal cortex by intrarhinal sulcus, or tentorial indentation, which forms a marked indent at the site of the inferior border of the amygdala. The uncinate fasciculus, at the level of basolateral nuclei groups, was considered as the anterior-lateral border. The amygdalo-striatal transition area, which is located between lateral amygdaloid nucleus and ventral putamen, was considered as the posterior-lateral border. The posterior end of amygdaloid nucleus was defined as the point where gray matter starts to appear superior to the alveolus and laterally to the hippocampus. If the alveolus was not visible, the inferior horn of the lateral ventricle was employed as border [48]. The starting point for hippocampus tracing was defined as the hippocampal head when it first appears below the amygdala, the alveus defining the superior and anterior border of the hippocampus. The fimbria was included in the hippocampal body, while the grey matter rostral to the fimbria was excluded. The hippocampal tail was traced until it was visible as an oval shape located caudally and medially to the trigone of the lateral ventricles [36, 37]. The intraclass correlation coefficients were 0.95 for the hippocampus and 0.83 for the amygdala.

White matter hyperintensities (WMHs) were automatically segmented on the FLAIR sequences by using previously described algorithms [36, 37]. Briefly, the procedure includes (i) filtering of FLAIR images to exclude radiofrequency inhomogeneities, (ii) segmentation of brain tissue from cerebrospinal fluid, (iii) modelling of brain intensity histogram as a gaussian distribution and (iv) classification of the voxels whose intensities were ≥3.5 SDs above the mean as WMHs [36, 37]. Total WMHs volume was computed by counting the number of voxels segmented as WMHs and multiplying by the voxel size (5 mm^3). To correct

for individual differences in head size, hippocampal, amygdalar and WMHs volumes were normalized to the total intracranial volume (TIV), obtained by manually tracing with DISPLAY the entire intracranial cavity on 7 mm thick coronal slices of the T1 weighted images. Both manual and automated methods user here have advantages and disadvantages. Manual segmentation of the hippocampus and amygdala is currently considered the gold standard technique for the measurement of such complex structures. The main disadvantages of manual tracing are that it is operator dependent and time consuming. Conversely, automated techniques are more reliable and less time-consuming, but may be less accurate when dealing with structures without clearly identifiable borders. This however is not the case for WMHs which appear as hyperintense on FLAIR sequences.

Left and right hippocampal as well as amygdalar volumes were estimated and summed to obtain a total volume (individual) of both anatomical structures. In turn, total amygdalar and hippocampal volume were summed obtaining the whole AHC volume. AHC (whole) volume has been divided in tertiles obtaining three groups. In each group hippocampal and amygdalar volume (within AHC) has been computed. The last volumes were compared with the previous obtained individual (hippocampal and amygdalar) volumes.

Statistical analysis and data management

The analysis of variance (ANOVA) has been applied as statistical tool. At first, any significant differences among groups in demographic variables, i.e., age, education, MMSE score, and morphostructural characterics, i.e., AHC, hippocampal, amygdalar and white matter hyperintensities (WMHs) volume were evaluated (Table 1). Greenhouse-Geisser correction and Mauchley's sphericity test were applied to all ANOVAs. In order to avoid a confounding effect, ANOVAs were carried out using age, education, MMSE score, and WMHs as covariates. Duncan's test was used for post-hoc comparisons. For all statistical tests the significance level was set at $p < 0.05$.

Preliminarily, ANOVA was performed in order to verify 1) the difference of AHC volume among groups; 2) the difference of hippocampal and amygdalar volume within AHC among groups; 3) the difference of hippocampal and amygdalar volume individually considered among groups; 4) NPS impairment based on ACH atrophy.

Moreover, as a control analysis, in order to detect if difference in EEG markers was linked to significant difference in volume measurements, the volume of hippocampus within AHC was compared with the hippocampal volume individually considered, as well as the amygdalar volume within AHC was compared with the amygdalar volume individually considered. This control analysis was performed through a paired *t*-test.

Subsequently, ANOVA was performed in order to check differences in theta/gamma and alpha3/alpha2 relative power ratio in the three groups ordered by decreasing tertile values of the whole AHC volume. In each ANOVA, group was the independent variable, the frequency ratios was the dependent variable and

Table 1
Mean values±standard deviation of sociodemographic characteristics, MMSE scores

	MCI cohort	Group 1	Group 2	Group 3	*p* value (ANOVA)
Number of subjects (f/m)	79 (42/37)	27 (14/13)	27 (15/12)	25 (13/12)	
Age (years)	69.2 ± 2.3	66.8 ± 6.8	69.4 ± 8.7	71.5 ± 6.9	0.1
Education (years)	7.7 ± 0.8	8.3 ± 4.5	6.7 ± 3.1	8.2 ± 4.6	0.2
MMSE	27.1 ± 0.4	27.5 ± 1.5	27.4 ± 1.5	26.6 ± 1.8	0.1
Total AHC volume	6965.3 ± 1248.8	8151.2 ± 436.4	7082.7 ± 266.9	5661.8 ± 720.4	0.00001
AHC-hippocampal volume (mm^3)	4891.7 ± 902.6	5771.6 ± 361.1	4935.6 ± 380.9	3967.9 ± 650.3	0.00001
AHC-amygdalar volume (mm^3)	2073.5 ± 348.7	2379.6 ± 321.3	2147.1 ± 301.3	1693.9 ± 288.5	0.0001
Individual hippocampal volume (mm^3)	4889.8 ± 962.4	5809.6 ± 314.2	4969.4 ± 257.6	3890.1 ± 551.4	0.00001
Individual amygdalar volume (mm^3)	2071.7 ± 446.4	2514.4 ± 259.5	2079.2 ± 122.8	1621.6 ± 185.2	0.0001
White matter hyperintensities (mm^3)	3.8 ± 0.5	3.2 ± 2.8	4.2 ± 3.8	4.1 ± 3.6	0.7
t-Test hippocampus (*p* values)		0.4	0.5	0.1	
t-Test amygdala (*p* values)		0.03	0.2	0.1	

Mean values±standard deviation of sociodemographic characteristics, MMSE scores, white matter hyperintensities, hippocampal and amygdalar volume measurements. Hippocampal and amygdalar volumes are referred to the whole amygdalo-hippocampal complex (AHC) and singularly considered (individual). The *t*-test refers to AHC vs individual volume in each group.

age, education, MMSE score, and WMHs was used as covariates. Duncan's test was used for post-hoc comparisons. For all statistical tests the significance level was set at $p < 0.05$.

In order to check closer association with EEG markers, hippocampal volume, and amygdalar volume within AHC were analyzed separately. A control analysis was carried out also on the individual hippocampal and amygdalar volumes based on decreasing tertile values for homogeneity with the main analysis.

RESULTS

Table 1 summarizes the ANOVA results of demographic variables, i.e., age, education, MMSE score, and morphostructural characteristics, i.e., hippocampal, amygdalar and white matter hyperintensities volume in the whole MCI cohort as well as in the three subgroups in study. Hippocampal and aymgdalar volumes are considered as parts of the whole AHC volume as well as individually considered. Significant statistical results were found in hippocampal and amygdalar volume both within the AHC (respectively, $F_{2,76} = 92.74$; $p < 0.00001$ and $F_{2,76} = 33.82$; $p < 0.00001$) and individually considered (respectively, $F_{2,76} = 157.27$; $p < 0.00001$ and $F_{2,76} = 132.5$; $p < 0.00001$). The global AHC volume also showed significant results ($F_{2,76} = 159.27$; $p < 0.00001$). Duncan's post-hoc test showed a significant increase ($p < 0.01$) in all comparisons. The paired *t*-test showed significant difference between the volume of ACH-amygdala vs amygdalar volume individually considered in the first group ($p < 0.03$). The amygdalar volume difference in the other groups (respectively $p = 0.2$ and 0.1) as well as the difference in the volume of AHC-hippocampus vs individual hippocampus ($p = 0.4$ in the first, $p = 0.5$ in the second and $p = 0.1$ in the third group) was not statistically significant.

Table 2 summarizes the ANOVA results of the memory NPS tests score. The analysis revealed significant main effect Group in Babcock test ($F_{2,76} = 2.76$; $p < 0.03$), Rey word list immediate recall ($F_{2,76} = 4.80$; $p < 0.01$), Rey word list delayed recall ($F_{2,76} = 6.26$; $p < 0.003$) and Rey figure recall ($F_{2,76} = 5.20$; $p < 0.007$). Duncan's post-hoc test showed a significant decrease of performance (lower scores) as the AHC volume decreases (all p's < 0.05), with the only exception of the post-hoc test in the Babcock test between the first and the second group ($p = 0.2$). The ANOVA results in other NPS test did not show significant results.

Table 3 shows the results of theta/gamma and alpha3/alpha2 ratio in the groups based on the decrease of whole AHC volume as well as, within the same group, the decrease of hippocampal and amygdalar volumes separately considered. ANOVA shows results towards significance when amygdalo-ippocampal volume is considered globally both in theta/gamma ($F_{2,76} = 2.77$; $p < 0.06$) and alpha3/alpha2 ratio ($F_{2,76} = 2.71$; $p < 0.07$). When amygdalar and hippocampal volumes were considered separately, ANOVA results revealed significant main effect Group, respectively, in theta/gamma ratio analysis ($F_{2,76} = 3.46$; $p < 0.03$) for amygdalar and alpha3/alpha2 ratio for hippocampal ($F_{2,76} = 3.38$; $p < 0.03$) decreasing volume. The ANOVA did not show significant results in theta/gamma ratio when considering hippocampal volume ($F_{2,76} = 0.3$; $p < 0.7$) and in alpha3/alpha2 ratio when considering amygdalar volume ($F_{2,76} = 1.46$; $p < 0.2$). The control analysis (individual volumes) did not show any significant result neither for hippocampal (theta/gamma, $F_{2,76} = 0.3$; $p < 0.7$; alpha3/alpha2, $F_{2,76} = 2.15$; $p < 0.1$) nor for amygdalar volume (theta/gamma, $F_{2,76} = 0.76$; $p < 0.4$; alpha3/alpha2, $F_{2,76} = 2.15$; $p < 0.1$).

DISCUSSION

The main result of the present study is that AHC atrophy is associated with the increase of theta/gamma and

Table 2
Mean values±standard deviation and cut off of NPS scores

NPS TEST	Group1	Group2	Group3	CUT-OFF	*p* value (ANOVA)
Babcock	10.5 ± 3.8	10.5 ± 3.5	7.8 ± 4.1	8	0.02
Rey list immediate recall	45.1 ± 8.7	39.5 ± 11.2	34.7 ± 10.2	28.52	0.002
Rey list delayed recall	10.1 ± 3.5	7.9 ± 3.4	6.2 ± 3.9	4.68	0.001
Rey figure recall	17.2 ± 6.7	14.2 ± 6.3	10.5 ± 5.7	9.47	0.001

Mean values ± standard deviation and cut off of NPS scores. In red the test with ANOVA statistical significant difference.

Table 3
Relative power band ratios in amygdalo-hippocampal complex (AHC)

Hippocampal + amygdalar volume	theta/gamma ratio (μv^2)	p value	alpha3/alpha2 ratio (μv^2)	p value
Group 1	1.40 ± 0.35	0.06	1.05 ± 0.11	0.07
Group 2	1.43 ± 0.35		1.11 ± 0.14	
Group 3	1.47 ± 0.44		1.12 ± 0.16	
AHC-hippocampal volume				
Group 1	1.39 ± 0.27	0.7	1.04 ± 0.11	0.03
Group 2	1.48 ± 0.45		1.11 ± 0.15	
Group 3	1.43 ± 0.41		1.12 ± 0.14	
AHC-amygdalar volume				
Group 1	1.36 ± 0.37	0.03	1.04 ± 0.13	0.2
Group 2	1.44 ± 0.36		1.12 ± 0.16	
Group 3	1.49 ± 0.39		1.09 ± 0.11	
Individual hippocampal volume				
Group 1	1.39 ± 0.27	0.7	1.04 ± 0.11	0.1
Group 2	1.48 ± 0.45		1.07 ± 0.15	
Group 3	1.43 ± 0.40		1.10 ± 0.14	
Individual amygdalar volume				
Group 1	1.39 ± 0.37	0.1	1.04 ± 0.13	0.4
Group 2	1.43 ± 0.36		1.12 ± 0.16	
Group 3	1.46 ± 0.39		1.09 ± 0.11	

Relative power band ratios in amygdalo-hippocampal complex (AHC), hippocampal and amygdalar atrophy. Hippocampal and amygdalar volumes are referred to the whole amygdalo-hippocampal complex (AHC) and singularly considered (individual).

alpha3/alpha2 ratio and with cognitive decline. Moreover, when the amygdalar and hippocampal volume are separately considered, within AHC, the increase of theta/gamma ratio is best associated with amygdalar atrophy whereas alpha3/alpha2 ratio is best associated with hippocampal atrophy. The volumes of hippocampal and amygdala among the groups within AHC are different from those of hippocampus and amygdala individually considered. The differences are significant only in the amygdala volume of the group with minor atrophy, but it could be due to the sample size. On the other hand, it should be considered that small volumetric difference could give rise to major changes in brain rhythmicity. On the whole, the results support the idea that AHC is not simply the summation of two separate structures. Rather, it suggests that AHC is a definite structural and functional network confirming previous studies showing that atrophy of both amygdala and hippocampus in cognitively intact elderly people could predict dementia [12, 19, 59].

Theta/gamma and alpha3/alpha2 ratio: possible relationship with AHC and physiological meaning

A large body of literature has previously demonstrated that subjects with cognitive decline show an increase of theta relative power [36–38], a decrease of gamma relative power [38, 39] as well as an increase of high alpha as compared to low alpha band [38]. On the whole theta/gamma ratio and alpha3/alpha2 ratio could be considered reliable EEG markers of cognitive decline.

The amygdalo-hippocampal network is a key structure in the generation of theta rhythm. More specifically, theta synchronization is increased between LA and CA1 region of hippocampus during long-term memory retrieval [34, 35], during period of intense arousal [34], or during the maintenance of vigilance to negative stimuli [50]. So far, the theta synchronization induced by the amygdala is deeply involved in both memory and endogenous attentional mechanism. Our results shows that amygdala volume reduction is mainly associated to the theta synchronization. It is possible that the loss of GABA inhibitory process, triggered by the hippocampal atrophy, could determine the decrease of gamma rhythm generation as well as the amygdala excitation mechanism [61, 62].

The increase of alpha3/alpha2 ratio is associated with the hippocampal formation within the AHC, confirming previous results of our group showing that the increase of high alpha is related to hippocampal atrophy in MCI patients [37]. In the present study our

results extend those previous findings, clearly showing that AHC atrophy is more correlated with EEG markers and cognitive performance than the hippocampus alone. Moreover, present results specify the possible anatomical correlation of EEG markers with the single structure within AHC. The increase of high alpha synchronization has been found in internally-cued mechanisms of attention, associated with inhibitory top-down processes [63], acting as filter to irrelevant information. This filter activity could be carried out by hippocampus. Indeed, a recent work has demonstrated that the mossy fiber (MF) pathway of the hippocampus, connecting the dentate gyrus to the auto-associative CA3 network, is controlled by a feed-forward circuit combining disynaptic inhibition with monosynaptic excitation. Analysis of the MF associated circuit revealed that it could act as a highpass filter [64].

Theta/gamma and alpha3/alpha2 ratio: possible interactions at system level

In a previous work [37] we proposed that hippocampal atrophy is linked to memory and attention disfunction. In the present work a picture emerge in which the AHC atrophy (more specifically than hippocampal atrophy alone) determines a dysregulation of inhibitory mechanisms probably inducing an overactivity of amygdalo-hippocampal network associated with alterations in memory and attention circuits along AHC-thalamic-cingulate pathways. Of note, the amygdala is intimately involved in the anatomo-physiological anterior pathways of attention through its connections with anterior cingulated cortex, anteroventral, anteromedial and pulvinar thalamic nuclei [65].The loss of inhibitory mechanism at hippocampal level, associated with a decrease in gamma power, impairs the filter function of hippocampus. Indeed, the integrity of CA3-CA1 interplay, coordinated by gamma oscillations, is crucial for hippocampal activity [62]. The increase in cortico-subcortical inputs to AHC determines an increase of memory retrieval effort in long-term memory system and dysregulation of divided attention, in particular when multiple stimuli have to be processed [66–68], inducing behavioural dysfunction as well as subsequent memory deficits. The exchange of information between memory and attentive systems has been associated with theta synchronization and upper alpha band desynchronization [69, 70]. The increase of high alpha power found in our results could represent the need of

a selection process on the ongoing information generating more cortical inhibitory mechanism [63].

GENERAL REMARKS

The main scope of our project is to detect EEG biomarkers useful in individual patients. Indeed, the results at group level, although interesting, are not yet helpful for the diagnostic/prognostic aims. In this view, the main results of our project is that two specific EEG markers could be considered reliable markers of cognitive decline: theta/gamma ratio and alpha3/alpha2 ratio. Indeed, these markers have been associated with memory decline in psychometric tests and with hippocampal atrophy [8, 9]. The results of the present study are important for understanding of the peculiarity of EEG rhythms changes in a clinical setting. Of note, in another study of our group it was showed that the increase of theta/gamma ratio is linked to MCI subjects who convert in non-AD dementia whereas the increase of alpha3/alpha2 ratio is associated with MCI subject who convert to AD [71]. We should to strengthen that the claim that a risk factor can be used as a biomarker requires much more substantiation and evaluation than the mere presence of an association. A significant and strong relation with the outcome is a prerequisite, not a guarantee, for a biomarker. For a predictive biomarker, the question is not just whether that factor relates to the outcome of the disease but what its incremental contribution is in predicting who will get the disease and when. In this view, the EEG tool has many advantages. It is the less invasive and cheapest among the neuroscience techniques. The EEG has very good reliability given that about one century of experience have increased the skills of a lot of scientists in performing it. On the whole, the EEG allows the collection of a big amount of data, helpful for analysis and a possible widespread application as a diagnostic/prognostic test.

CONCLUSION

The increase of theta/gamma and alpha3/alpha2 ratio is associated with AHC atrophy and with cognitive decline. The vulnerability and damage of the connections within AHC could affect reconsolidation of long-term memory and give rise to memory deficits, attentive disorders and behavioural symptoms. The increase of theta/gamma and alpha3/alpha2 ratio could be a promising tool for diagnostic and neurophysiological research purposes.

REFERENCES

[1] Clark CM, Schneider JA, Bedell BJ, Beach TG, Bilker WB, Mintun MA, Pontecorvo MJ, Hefti F, Carpenter AP, Flitter ML, Krautkramer MJ, Kung HF, Coleman RE, Doraiswamy PM, Fleisher AS, Sabbagh MN, Sadowsky CH, Reiman EM, Zehntner SP Skovronsky DM; AV45-A07 Study Group (2011). Use of florbetapir-PET for imaging-amyloid pathology. *JAMA* **305**, 275-283.

[2] Yaffe K, Weston A, Graff-Radford NR, Satterfield S, Simonsick EM, Younkin SG, Younkin LH, Kuller L, Ayonayon HN, Ding J, Harris TB (2011) Association of plasma-amyloid level and cognitive reserve with subsequent cognitive decline. *JAMA* **305**, 261-266.

[3] Jonkman EJ (1997) The role of the electroencephalogram in the diagnosis of dementia of the Alzheimer type: an attempt at technology assessment. *Neurophysiol Clin* **27**, 211-219.

[4] Jeong J (2004) EEG dynamics in patients with Alzheimer's disease. *Clin Neurophysiol* **115**, 1490-1505.

[5] de Waal H, Stam CJ, Blankenstein MA, Pijnenburg YA, Scheltens P, van der Flier WM (2011) EEG abnormalities in early and late onset Alzheimer's disease: understanding heterogeneity. *J Neurol Neurosurg Psychiatry* **82**, 67-71.

[6] Dickerson BC, Salat DH, Bates JF, Atiya M, Killiany RJ, Greve DN, Dale AM, Stern CE, Blacker D, Albert MS, Sperling RA (2004) Medial temporal lobe function and structure in mild cognitive impairment. *Ann Neurol* **56**, 27-35.

[7] Dickerson BC, Salat DH, Greve DN, Chua EF, Rand-Giovannetti E, Rentz DM, Bertram L, Mullin K, Tanzi RE, Blacker D, Albert MS, Sperling RA (2005) Increased hippocampal activation in midl cognitive impairment compared to normal aging and AD. *Neurology* **65**, 404-411.

[8] Moretti DV, Miniussi C, Frisoni GB, Geroldi C, Zanetti O, Binetti G, Rossini PM (2007) Hippocampal atrophy and EEG markers in subjects with mild cognitive impairment. *Clin Neurophysiol* **118**, 2716-2729.

[9] Moretti DV, Fracassi C, Pievani M, Geroldi C, Binetti G, Zanetti O, Sosta K, Rossini PM, Frisoni GB (2009) Increase of theta/gamma ratio is associated with memory impairment. *Clin Neurophysiol* **120**, 295-303.

[10] Moretti DV, Frisoni GB, Pievani M, Rosini S, Geroldi C, Binetti G, Rossini PM (2008) Cerebrovascular disease and hippocampal atrophy are differently linked to functional coupling of brain areas: an EEG coherence study in MCI subjects. *J Alzheimers Dis* **14**, 285-299.

[11] Palop JJ, Chin J, Roberson ED, Wang J, Thwin MT, Bien-Ly N, Yoo J, Ho KO, Yu GQ, Kreitzer A, Finkbeiner S, Noebels JL, Mucke L (2007) Aberrant excitatory neuronal activity and compensatory remodeling of inhibitory hippocampal circuits in mouse models of Alzheimer's disease. *Neuron* **55**, 697-711.

[12] Petersen RC, Negash S (2008) Mild cognitive impairment: an overview. *CNS Spectr* **13**, 45-53.

[13] DeCarli C (2003) Mild cognitive impairment: prevalence, prognosis, aetiology, and treatment. *Lancet Neurol* **2**, 15-21.

[14] Jack CR Jr, Petersen RC, Xu YC, Waring SC, O'Brien PC, Tangalos EG, Smith GE, Ivnik RJ, Kokmen E (1997) Medial temporal atrophy on MRI in normal aging and very mild Alzheimer's disease. *Neurology* **49**, 786-794.

[15] Du AT, Schuff N, Amend D, Laakso MP, Hsu YY, Jagust WJ, Yaffe K, Kramer JH, Reed B, Norman D, Chui HC, Weiner MW (2001) Magnetic resonance imaging of the entorhinal cortex and hippocampus in mild cognitive impairment and Alzheimer's disease. *J Neurol Neurosurg Psychiatry* **71**, 441-447.

[16] Bobinski M, de Leon MJ, Convit A, De Santi S, Wegiel J, Tarshish CY, Saint Louis LA, Wisniewski HM (1999) MRI of entorhinal cortex in mild Alzheimer's disease. *Lancet* **353**, 38-40.

[17] Golebiowski M, Barcikowska M, Pfeffer A (1999) Magnetic resonance imaging-based hippocampal volumetry in patients with dementia of the Alzheimer type. *Dement Geriatr Cogn Disord* **10**, 284-288.

[18] Laakso MP, Lehtovirta M, Partanen K, Riekkinen PJ, Soininen H (2000) Hippocampus in Alzheimer's disease: a 3-year follow-up MRI study. *Biol Psychiatry* **47**, 557-561.

[19] den Heijer T, Geerlings MI, Hoebeek FE, Hofman A, Koudstaal PJ, Breteler MM (2006) Use of hippocampal and amygdalar volumes on magnetic resonance imaging to predict dementia in cognitively intact elderly people. *Arch Gen Psychiatry* **63**, 57-62.

[20] Cahill, L (2000) Neurobiological mechanisms of emotionally influenced, long-term memory. *Prog Brain Res* **126**, 29-37.

[21] Cahill L, McGaugh JL (1998) Mechanisms of emotional arousal and lasting declarative memory. *Trends Neurosci* **7**, 294-299.

[22] Paré D, Collins DR (2000) Neuronal correlates of fear in the lateral amygdala: multiple extracellular recordings in conscious cats. *J Neurosci* **20**, 2701-2710.

[23] Paré D, Collins DR, Pelletier JG (2002) Amygdala oscillations and the consolidation of emotional memories. *Trends Cogn Sci* **6**, 306-314.

[24] Packard MG, Cahill L, McGaugh JL (1994) Amygdala modulation of hippocampal-dependent and caudate nucleus-dependent memory processes. *Proc Natl Acad Sci U S A* **91**, 8477-8481.

[25] Ikegaya Y, Saito H, Abe K (1994) Attenuated hippocampal long-term potentiation in basolateral amygdala-lesioned rats. *Brain Res* **656**, 157-164.

[26] Ikegaya Y, Abe K, Saito H, Nishiyama N (1995) Medial amygdala enhances synaptic transmission and synaptic plasticity in the dentate gyrus of rats in vivo. *J Neurophysiol* **74**, 2201-2203.

[27] Akirav I, Richter-Levin G (1999) Priming stimulation in the basolateral amygdala modulates synaptic plasticity in the rat dentate gyrus. *Neurosci Lett* **270**, 83-86.

[28] Frey S, Bergado-Rosado J, Seidenbecher T, Pape HC, Frey JU (2001) Reinforcement of early long-term potentiation (early-LTP) in dentate gyrus by stimulation of the basolateral amygdala: heterosynaptic induction mechanisms of late-LTP. *J Neurosci* **10**, 3697-3703.

[29] Maren S, Fanselow MS (1995) Synaptic plasticity in the basolateral amygdala induced by hippocampal formation stimulation in vivo. *J Neurosci* **15**, 7548-7564.

[30] Pitkänen A, Pikkarainen M, Nurminen N, Ylinen A (2000) Reciprocal connections between the amygdala and the hippocampal formation, perirhinal cortex, and postrhinal cortex in rat. A review. *Ann N Y Acad Sci* **911**, 369-391.

[31] Maren S, Aharonov G, Fanselow MS (1997) Neurotoxic lesions of the dorsal hippocampus and Pavlovian fear conditioning in rats. *Behav Brain Res* 88, 261-274.

[32] Willingham DB (1997) Systems of memory in the human brain. *Neuron* **18**, 5-8.

[33] Buzsáki G (2002) Theta oscillations in the hippocampus. *Neuron* **33**, 325-340.

[34] Seidenbecher T, Laxmi TR, Stork O, Pape HC (2003) Amygdalar and hippocampal theta rhythm synchronization during fear memory retrieval. *Science* **301**, 846-850.

[35] Narayanan RT, Seidenbecher T, Sangha S, Stork O, Pape HC (2007) Theta resynchronization during reconsolidation of remote contextual fear memory. *Neuroreport* **18**, 1107-1111.

[36] Moretti DV, Miniussi C, Frisoni GB, Zanetti O, Binetti G, Geroldi C, Galluzzi S, Rossini PM (2007) Vascular damage and EEG markers in subjects with mild cognitive impairment. *Clin Neurophysiol* **118**, 1866-1876.

[37] Moretti DV, Pievani M, Fracassi C, Geroldi C, Calabria M, DeCarli C, Rossini PM (2008) Brain vascular damage of cholinergic pathways and E.E.G. Markers in mild cognitive impairment. *J Alzheimers Dis* **15**, 357-372.

[38] Stam CJ, van der Made Y, Pijnenburg YA, Scheltens P (2003) EEG synchronization in mild cognitive impairment and Alzheimer's disease. *Acta Neurol Scand* **108**, 90-96.

[39] Folstein MF, Folstein SE, McHugh PR (1975) 'Mini mental state': a practical method for grading the cognitive state of patients for clinician. *J Psychiatr Res* **12**, 189-198.

[40] Hughes CP, Berg L, Danziger WL, Cohen LA, Martin RL (1982) A new clinical rating scale for the staging of dementia. *Br J Psychiatry* **140**, 1225-1230.

[41] Rosen WG, Terry RD, Fuld PA, Katzman R, Peck A (1980) Pathological verification of ischemic score in differentiation of dementias. *Ann Neurol* **7**, 486-488.

[42] Lawton MP, Brodie EM (1969) Assessment of older people: self maintaining and instrumental activity of daily living. *J Gerontol* **9**, 179-186.

[43] Albert M, Smith LA, Scherr PA, Taylor JO, Evans DA, Funkenstein HH (1991) Use of brief cognitive tests to identify individuals in the community with clinically diagnosed Alzheimer's disease. *Int J Neurosci* **57**, 167-178.

[44] Petersen RC, Doody R, Kurz A, Mohs RC, Morris JC, Rabins PV, Ritchie K, Rossor M, Thal L, Winblad B (2001) Current concepts in mild cognitive impairment. *Arch Neurol* **58**, 1985-1992.

[45] Petersen RC, Smith GE, Ivnik RJ, Tangalos EG, Schaid SN, Thibodeau SN, Kokmen E, Waring SC, Kurland LT (1995) Apolipoprotein E status as a predictor of the development of Alzheimer's disease in memoryimpaired individuals. *J Am Med Assoc* **273**, 1274-1278.

[46] Petersen RC, Smith GE, Waring SC, Ivnik RJ, Kokmen E, Tangelos EG (1997) Aging, memory, and mild cognitive impairment. *Int Psychogeriatr* **9**, 65-69.

[47] Portet F, Ousset P J, Visser P J, Frisoni G B, Nobili F, Scheltens Ph, Vellas B, Touchon J. and the MCI Working Group of the European Consortium on Alzheimer's Disease (EADC, 2006) Mild cognitive impairment (MCI) in medical practice: a critical review of the concept and new diagnostic procedure. Report of the MCI Working Group of the European Consortium on Alzheimer's Disease. *J Neurol Neurosurg Psychiatry* **77**, 714-718.

[48] Geroldi C, Rossi R, Calvagna C, Testa C, Bresciani L, Binetti G, Zanetti O, Frisoni GB (2006) Medial temporal atrophy but not memory deficit predicts progression to dementia in patients with mild cognitive impairment. *J Neurol. Neurosurg Psychiatry* **77**, 1219-1222.

[49] Dubois B, Feldman HH, Jacova C, Dekosky ST, Barberger-Gateau P, Cummings J, Delacourte A, Galasko D, Gauthier S, Jicha G, Meguro K, O'brien J, Pasquier F, Robert P, Rossor M, Salloway S, Stern Y, Visser PJ, Scheltens P (2007) Research criteria for the diagnosis of Alzheimer's disease: revising the NINCDS-ADRDA criteria. *Lancet Neurol* **8**, 734-746.

[50] Shulman KI (2000) Clock-drawing: is it the ideal cognitive screening test? *Int J Geriatr Psychiatry* **15**, 548-561.

[51] Amodio P, Wenin H, Del Piccolo F, Mapelli D, Montagnese S, Pellegrini A, Musto C, Gatta A, Umiltà C (2002) Variability of trail making test, symbol digit test and line trait test in normal people. A normative study taking into account age-dependent decline and sociobiological variables. *Aging Clin Exp Res* **14**, 117-131.

[52] Basso A, Capitani E, Laiacona M (1987) Raven's coloured progressive matrices: normative values on 305 adult normal controls. *Funct Neurol* **2**, 189-194.

[53] Spinnler H, Tognoni G (1987) Standardizzazione e taratura italiana di test neuropsicologici. *Ital J Neurol Sci* **6**, 1-120.

[54] Carlesimo GA, Caltagirone C, Gainotti G (1996) The Mental Deterioration Battery: normative data, diagnostic reliability and qualitative analyses of cognitive impairment. The Group for the Standardization of the Mental Deterioration Battery. *Eur Neurol* **36**, 378-384.

[55] Caffarra P, Vezzadini G, Dieci F, Zonato F, Venneri A (2002) Rey-Osterrieth complex figure: normative values in an Italian population sample. *Neurol Sci* **22**, 443-447.

[56] Radloff LS (1977) The CES-D scale: A self-report depression scale for research in the general population. *Appl Psychol Meas* **1**, 385-401.

[57] Moretti DV, Babiloni C, Binetti G, Cassetta E, Dal Forno G, Ferreri F, Ferri R, Lanuzza B, Miniussi C, Nobili F, Rodriguez G, Salinari S, Rossini PM (2004) Individual analysis of EEG frequency and band power in mild Alzheimer's disease. *Clin Neurophysiol* **115**, 299-308.

[58] Klimesch W (1999) EEG alpha and theta oscillations reflect cognitive and memory performance: a review and analysis. *Brain Res Rev* **29**, 169-195.

[59] Sperling R (2007) Functional MRI studies of associative encoding in normal aging, mild cognitive impairment, and Alzheimer's disease. *Ann N Y Acad Sci* **1097**, 146-155.

[60] Garolera M, Coppola R, Muñoz KE, Elvevåg B, Carver FW, Weinberger DR, Goldberg TE (2007) Amygdala activation in affective priming: a magnetoencephalogram study. *Neuroreport* **18**, 1449-1453.

[61] Bragin A, Jando G, Nadasdy Z, Hetke J, Wise K, Buzsaki G (1995) Gamma (40–100 Hz) oscillation in the hippocampus of the behaving rat. *J Neurosci* **15**, 47-60.

[62] Montgomery SM, Buzsaki G (2007) Gamma oscillations dynamically couple hippocampal CA3 and CA1 regions during memory task performance. *Proc Natl Acad Sci U S A* **104**, 14495-14500.

[63] Klimesch W, Sauseng P, Hanslmayr S (2007) EEG alpha oscillations: The inhibition timing hypothesis. *Brain Res Rev* **53**, 63-88.

[64] Zalay OC, Bardakjian BL (2006) Simulated mossy fiber associated feedforward circuit functioning as a highpass filter. *Conf Proc IEEE Eng Med Biol Soc* **1**, 4979-4982.

[65] Young KA, Holcomb LA, Bonkale WL, Hicks PB, Yazdani U, German DC (2007) 5HTTLPR polymorphism and enlargement of the pulvinar: unlocking the backdoor to the limbic system. *Biol Psychiatry* **61**, 813-818.

[66] Johannsen P, Jacobsen J, Bruhn P, Gjedde A (1999) Cortical responses to sustained and divided attention in Alzheimer's disease. *Neuroimage* **10**, 269-281.

[67] Tales A, Haworth J, Nelson S, Snowden RJ, Wilcock G (2005) Abnormal visual search in mild cognitive impairment and Alzheimer's disease. *Neurocase* **11**, 80-84.

[68] Tales A, Snowden RJ, Haworth J, Wilcock G (2005) Abnormal spatial and non-spatial cueing effects in mild cognitive impairment and Alzheimer's disease. *Neurocase* **11**, 85-92.

[69] Sauseng P, Klimesch W, Gruber W, Doppelmayr M, Stadler W, Schabus M (2002) The interplay between theta and alpha oscillations in the human electroencephalogram reflects the transfer of information between memory systems. *Neurosci Lett* **324**, 121-124.

[70] Sauseng P, Klimesch W, Doppelmayr M, Hanslmayr S, Schabus M, Gruber WR (2004) Theta coupling in the human electroencephalogram during a working memory task. *Neurosci Lett* **354**, 123-126.

[71] Moretti DV, Frisoni GB, Fracassi C, Pievani M, Geroldi C, Binetti G, Rossini PM, Zanetti O (2011) MCI patients' EEGs show group differences between those who progress and those who do not progress to AD. *Neurobiol Aging* **32**, 563-571.

This page intentionally left blank

Resting State Cortical Rhythms in Mild Cognitive Impairment and Alzheimer's Disease: Electroencephalographic Evidence

Claudio Babiloni[a,b,*], Fabrizio Vecchio[c], Roberta Lizio[d], Raffaele Ferri[e], Guido Rodriguez[f],
Nicola Marzano[g], Giovanni B. Frisoni[h] and Paolo M. Rossini[b,i]

[a]*Department of Biomedical Sciences, University of Foggia, Foggia, Italy*

[b]*Casa di Cura San Raffaele Cassino, Cassino, Italy*

[c]*A.Fa.R., Dip. Neurosci. Osp. FBF, Isola Tiberina, Rome, Italy*

[d]*IRCCS San Raffaele Pisana, Rome, Italy*

[e]*Department of Neurology, Oasi Institute for Research on Mental Retardation and Brain Aging (IRCCS), Troina, Italy*

[f]*Clinical Neurophysiology, Department of Endocrinological and Metabolic Sciences, University of Genoa, Genoa, Italy*

[g]*IRCCS "SDN", Naples, Italy*

[h]*IRCCS "S. Giovanni di Dio-F.B.F.", Brescia, Italy*

[i]*Neurology Catholic University "Sacro Cuore" Rome, Rome, Italy*

Abstract. Physiological brain aging is characterized by a combination of synaptic pruning, loss of cortico-cortical connections and neuronal apoptosis that provoke age-dependent decline of cognitive functions. Neural/synaptic redundancy and plastic remodeling of brain networking, also secondary to mental and physical training, promotes maintenance of brain activity in healthy elderly for everyday life and fully productive affective and intellectual capabilities. Unfortunately, in pathological situations, aging triggers neurodegenerative processes that impact on cognition, like Alzheimer's disease (AD). Oscillatory electromagnetic brain activity is a hallmark of neuronal network function in various brain regions. Modern neurophysiological techniques including digital electroencephalography (EEG) allow non-invasive analysis of cortico-cortical connectivity and neuronal synchronization of firing, and coherence of brain rhythmic oscillations at various frequencies. The present review of field EEG literature suggests that discrimination between physiological and pathological brain aging clearly emerges at the group level, with some promising result on the informative value of EEG markers at the individual level. Integrated approaches utilizing neurophysiological techniques together with biological markers and structural and functional imaging are promising for large-scale, low-cost, widely available on the territory and non-invasive screening of at-risk populations.

Keywords: Consciousness, electroencephalography (EEG), persistent vegetative state, Alzheimer's disease.

INTRODUCTION

Several decades ago, electroencephalogram (EEG) was introduced to allow a direct, on-line view of human "brain at work" in physiological and pathological conditions [1]. Indeed, EEG is a direct correlate of brain function, and it reflects CNS dysfunction including the characterization of significant deviations from the 'natural' aging such as Alzheimer's disease (AD) and other dementias [2]. Starting from the 1970 s, EEG was progressively supplanted for clinical applications on diagnosis of abnormal brain aging. This happen first with the introduction of structural imaging tech-

*Correspondence to: Claudio Babiloni, Department of Biomedical Sciences, University of Foggia, Viale Pinto 7, Foggia I-71100, Italy. Tel.: +39 0881 713276; Fax:+39 0881 711716; E-mail: c.babiloni@unifg.it.

nologies such as computer assisted tomography (CAT) and magnetic resonance imaging (MRI), and then with the development of regional metabolic-perfusion methods such as positron emission tomography (PET), single photon emission computed tomography (SPECT), and the ability to map oxygen consumption and regional blood flow in specific neural locations with functional magnetic resonance imaging (fMRI). These new techniques produce relatively non-invasive views of "in vivo" brain anatomy with high spatial resolution (millimeters to few centimeters) when compared to standard EEG (several centimeters). However, these functional brain imaging methods are relatively limited in their temporal resolution when measuring functional brain activation (seconds to minutes) compared to EEG (milliseconds) and cannot discriminate the activation and the temporal hierarchy of different relays within a distributed network either in series or in parallel [3]. It should be noted that high temporal resolution of EEG is crucial for the study of an emerging property of brain activity, namely the spontaneous and event-related oscillatory activity at different frequencies ranging at 1–4 Hz (delta), 4–8 Hz (theta), 8–13 Hz (alpha), 13–30 Hz (beta), and >30 Hz (gamma). Each of these frequencies conveys peculiar physiological information on brain functional state during sleep and wake periods.

Recently, greater attention has been focused on the application of quantitative EEG (qEEG) and/or event-related potentials (ERPs) as suitable clinical markers of early stage of disease or its progression [4–6]. It has been reported that a positive ERP peaking 600 ms after the zerotime of stimuli to be encoded (P600) was reduced in patients with AD and mild cognitive impairment (MCI), particularly in those MCI patients who subsequently converted to AD [7, 8]. Furthermore, a positive ERP peaking 300 ms after the zerotime of oddball stimuli (P300) was reduced in amplitude in AD patients [5, 9], even during its early stages [10]. However, recording of ERPs requires a peculiar set up between the stimulation device and EEG machine, about 40–60 minutes of time for the examination in the patient, and technicians able to carry out engaging experimental conditions. In this regard, recording of resting state eyes closed EEG rhythms represents a fully standardized procedure much easier and rapid that does not require stimulation devices and is not prone to anxiety for task performance or to fatigue.

There is a vivid scientific debate about the physiological generation of sleep and resting state or spontaneous on-going EEG rhythms in the cerebral cortex, high-voltage, slow oscillatory potentials being observed in isolated, large slabs of neocortical tissue [11–13]. A certain consensus is reached on the following physiological model. During slow-wave sleep, corticofugal slow oscillations (<1 Hz) are effective in grouping thalamic-generated delta rhythms (1–4 Hz) and spindling activity (7–14 Hz) [14]. In this condition, delta rhythms would dominate EEG oscillations, while alpha rhythms (about 8–12 Hz) would be suppressed. In the case of endogenous or exogenous arousing stimuli, spindles, high- and low-frequency components of the delta rhythms are blocked by the inhibition of reticulo-thalamic (7–14 Hz), thalamo-cortical (1–4 Hz), and intracortical (<1 Hz) oscillators. These rhythms are replaced by fast oscillations in the range of beta (14–30 Hz) and gamma frequencies (>30 Hz) [14, 15]. In the wake resting state condition, alpha rhythms would dominate the human EEG oscillatory activity, while delta rhythms would be quite low in amplitude in physiological conditions [16–18].

In line with the above model, fluctuation of wake resting state EEG rhythms is supposed to reflect the continuous transitions between synchronization (i.e. reduced arousal) and desynchronization (i.e. increased arousal) of pyramidal cortical neurons at alpha rhythms together with an increased synchronization of relevant neural populations at operating beta/gamma rhythms spanning 14–40 Hz or higher frequencies [18]. Along the temporal flux of the resting state condition, these transitions may be mainly regulated by the fluctuating activity of cholinergic basal forebrain neurons projecting to hippocampus, large cortical regions, and reticular thalamus as well as by thalamocortical projections [11, 19, 20].

The present review outlines the impact of EEG techniques for the measurement of physiological and pathological brain aging. Its major goal is to highlight the emerging neurophysiological findings important to determine whether these techniques provide sufficient innovative and potentially useful information for the assessment of normal aging and AD, both at the group- and at the single-subject levels

ADVANCED EEG TECHNIQUES

Advanced EEG analysis techniques can illustrate changes in specific rhythms oscillating at various frequencies over time, provide quantitative measure-

ments of individual rhythms and reduce the effects of volume currents from far-field generators [21, 22]. Hence, EEG signals generated from extracerebral sources (e.g., electrocardiogram, electromyogram, electroretinogram, eye movements etc.) can be isolated from those produced by the brain, providing a direct measure of the recorded neuroelectric signals mainly generated in brain areas adjacent to the exploring electrode [22]. EEG coherence or synchronicity of rhythmic signals from separate electrodes, in different frequency bands, generated in different cortical areas, can also be measured providing a faithful reflection of "*whether, where and for how long*" separate neuronal assemblies work together.

The high resolution EEG technique has markedly enhanced the spatial resolution of the conventional EEG from about 6–9 cm to 2–3 cm by the use of spatial enhancement methods such as Laplacian transformation with a regularized 3D spline function. This method reduces the low spatial EEG frequencies contributed by volume conduction and eliminates electrode reference influence [23–26]. Compared to other linear or nonlinear modelling analysis techniques of cortical sources of EEG–MEG, surface Laplacian estimation provides a rough representation of the neural currents without an explicit model of the generators (i.e., shape, number, location) by using a model of the head as a volume conductor [23, 24]. However, surface Laplacian methods cannot disentangle the activity of two spatially separated but extremely adjacent cortical zones such as primary somatosensory and motor areas that are contiguous across the central sulcus or deep cortical sources in secondary somatosensory and insular cortices. Surface Laplacian estimation is also unreliable when computed at the borders of the recording electrodes grid (i.e., temporo-parietal electrodes). Its maxima often overlie cortical sources of EEG potentials, since the influence of tangential relative to radial oriented generators is greater [23, 24, 27].

Spectral coherence analysis indexes the temporal synchronization of two EEG time series among electrodes in the frequency domain and permits characterization of linear functional cortico–cortical connectivity. EEG spectral coherence is a normalized measure of the coupling between two electroencephalographic signals at any given frequency [28, 29]. It is commonly interpreted as an index of functional coupling [30, 31], mutual information exchange [28], functional co-ordination [32], and integrity of cortical neural pathways [33]. Its basic theoretical assumption

is that when the activity of two cortical areas is functionally coordinated, the EEG rhythms of these cortical areas show linear correlation and high spectral coherence. In general, decreased coherence reflects reduced linear functional connections and information transfer (i.e., functional uncoupling or unbinding) among cortical areas or modulation of common areas by a third region. In contrast, coherence increase is interpreted as augmented linear functional connections and information transfer (i.e., functional coupling or binding), which reflects the interaction of different cortical structures for a given task. It has been repeatedly demonstrated that perceptive, cognitive, and motor processes are associated with enhanced EEG spectral coherence [34–37], as a function of the extension and type of the neural networks engaged [18, 38]. Finally, the direction of the information flow within the EEG rhythms between pairs of electrodes can be estimated by a directed transfer function (DTF) [39–44].

There are different methods to solve the non-invasive localization of the neuronal generators responsible for measured EEG phenomena (i.e. the source reconstruction of the electromagnetic brain scalp signals). Low-resolution electromagnetic tomography algorithm (LORETA) software, which can be freely downloaded by Internet (http://www.unizh.ch/keyinst/NewLORETA/LORETA01.htm), has been successfully used in recent EEG studies on pathological brain aging [45–50]. LORETA computes 3D linear solutions (LORETA solutions) for the EEG inverse problem within a 3-shell spherical head model including scalp, skull, and brain compartments [51–53]. LORETA solutions consisted of voxel z-current density values able to predict EEG spectral power density at scalp electrodes As it is a reference-free method of EEG analysis, one can obtain the same LORETA source distribution for EEG data referenced to any reference electrode including common average. Furthermore, it can be also used from data collected by low spatial sampling (e.g., 19 electrodes) when cortical sources are estimated from resting EEG rhythms [54–57]. A normalization of the data was obtained by normalizing the LORETA current density at each voxel with the power density averaged across all frequencies (0.5–45 Hz) and across all voxels of the brain volume. After the normalization, the solutions lost the original physical dimension and were represented by an arbitrary unit scale. This procedure reduced inter-subjects variability and was used in previous EEG studies [46–50].

RESTING STATE EEG RHYTHMS AND PHYSIOLOGICAL AGING

Resting state eyes closed cortical EEG rhythms typically change across physiological aging, with gradual modifications in profile and magnitude of the spectra power spectrum. It was observed a marked amplitude decrease of alpha (8–13 Hz) and a global "slowing" of the background EEG, which increases in power and spatial distribution in the slower delta (1–4 Hz) and theta (4–8 Hz) rhythms [58–61]. A recent study in a large sample of healthy subjects ($N = 215$, 18–85 years) confirmed an age-dependent power decrement of posterior low-frequency alpha (alpha 1; 8–10.5 Hz) and delta rhythms [62]. Aging effects on parieto-occipital alpha rhythms presumably reflect the activity of dominant oscillatory neural network in the resting awaken brain. This activity is modulated by thalamo–cortical and cortico–cortical interactions facilitating/inhibiting the transmission of sensorimotor information and the retrieval of semantic information from cortical storage [17, 18, 63].

In the condition of awaken rest, low-frequency alpha rhythms (about 8–10 Hz) would be mainly related to subject's global attentional readiness [16, 64–67]. Noteworthy, there is consensus that alpha rhythms represent the dominant resting oscillations of the adult, awaken human brain [16, 61, 64–67] and have been linked to intelligent quotient, memory, and cognition [61]. Whereas high-frequency alpha rhythms (about 10–12 Hz) reflect the oscillation of specific neural systems for the elaboration of sensorimotor or semantic information [60, 64, 65]. Over the course of "natural" aging, the power decrease of the occipital alpha rhythms might be associated with changes in the cholinergic basal forebrain system function, which sustains the excitatory activity in the cholinergic brainstem pathway [68].

Neuroelectric output does not scale linearly with inputs received. Therefore, that assessment of nonlinear EEG interactions is important, as this method can provide information on the strength, direction and topography of the interdependencies. Spatial organization of non-linear interactions between different brain regions has been investigated to compare anterior-posterior intra-hemispheric and left–right inter-hemispheric interactions across physiological aging. Differences were found in the rates of interdependencies between the left pre-frontal and the right parietal regions between young and elderly, suggesting that the aging brain engages the right parietal region to assist the pre-frontal cortex [69].

RESTING STATE EEG RHYTHMS AND AD

Dementia is one of the most frequent chronic diseases of the elderly and it is characterized by loss of intellectual and behavioral abilities that interfere with daily functioning. Dementia incidence tends to increase with age affecting over 30% of people after age 85 [70, 71]. The elderly are the fastest growing segment of the population. Consequently, social costs for managing dementia are expected to rise becoming an important social problem. Furthermore, dementia profoundly affects the caregivers and family dynamics and relationships. AD is the most common cause of dementia in geriatric patients.

Important neuropathological features indicating AD include brain cortical and subcortical atrophy leading to ventricular enlargements primarily due to neuronal loss in the temporal and parietal structures. Among the primary markers of AD, microscopic signs including neurofibrillary tangles (intracellular aggregates of tau protein filaments) and amyloid plaques (extracellular aggregates of amyloid beta-peptides) that are dispersed throughout the cerebral cortex and basal ganglia, particularly concentrated in the hippocampus, entorhinal cortex, and post-central parietal neocortex [72]. Tangles are mainly found in hippocampal and parahippocampal limbic structures, whereas amyloid plaques are largely diffuse throughout the cortex [73]. A neurophysiological hallmark of brain aging is a progressive impairment of use-dependent synaptic plasticity and of synaptic connectivity between neurons and its association with the degree of dementia [74]. In the aging brain –including the AD ones during pre-clinical conditions- plastic compensatory remodeling guarantees functional maintenance, so that the neuronal and synaptic death can occur in the absence of symptoms for an unknown period of time that might last years or even decades. This mechanism of "cognitive or brain reserve" motivates the use of instrumental markers of AD in association to standard assessment of cognitive functions with "paper and pencil" neuropsychological batteries.

When compared to the resting state EEG rhythms of healthy normal elderly (Nold) subjects, AD patients showed an amplitude increase of widespread delta and theta sources and an amplitude decrease of posterior alpha (8–13 Hz) and/or beta (13–30 Hz)

sources [45, 55, 56, 76–78]. The observation of these abnormalities of the EEG rhythms could allow discrimination among different dementia diagnoses, for instance a marked decline of posterior slow-frequency alpha power shows peculiar features in mild AD subjects when compared to cerebrovascular dementia, fronto-temporal dementia and normal elderly subjects with similar cognitive impairment. Furthermore, pathological increased amplitude of the theta sources characterized cerebro-vascular dementia patients [56].

These EEG abnormalities have been associated with altered regional cerebral blood flow/metabolism and with impaired global cognitive function as evaluated by mini mental state evaluation (MMSE) [77, 79–81].

Of note, early stages of AD (even preclinical) are typically associated to slowing down of resting occipital alpha rhythms, namely a decrease of the individual alpha frequency (IAF) peak in power density [82]. The IAF peak, defined as the frequency associated to the strongest EEG power at the extended alpha range [61], should be always taken into account in EEG studies in AD subjects, since power changes in theta and alpha bands might be dependent phenomena. Furthermore, the conventional partition of EEG power into many conventional frequency bands allows the comparison of the results with those of most of the field studies but may prevent the separation of independent EEG rhythms or sources.

Despite the evidence of abnormal cortical rhythms in MCI and AD subjects, EEG analysis alone is unable to allow a diagnosis of disease. Additional biological parameters are needed for this purpose. In this regard, several studies have shown a strict relationship between genetic risk factors such as Apolipoprotein E ε 4 genotype (Apo-E ε 4) and late-onset AD. Apo-E ε 4 has been found to affect EEG rhythms in AD patients; it is associated with abnormalities of resting state EEG rhythms in AD [83–86] with relatively specific EEG measures. Compared to AD patients with ε2 and ε3, AD patients with ε4 showed higher theta and lower beta spectral power [85]. Furthermore, the AD ApoE ε4 carriers patients were characterized by higher theta power and lower beta power at baseline, whereas they were characterized by higher delta power and lower alpha power at 3 years at follow-up [84]. Moreover, AD patients with ApoE ε4 has been related to selective decrease in functional cortico–cortical connectivity, which was suggested by the reduction of right and left temporoparietal, right temporofrontal, and left occipitoparietal

alpha EEG coherence [83]. Thus, genetic risk factors for AD are combined with relatively specific EEG measures.

EEG power per se does not capture one of the main features of AD, namely the impairment of functional neural connectivity. This parameter –however- can be fruitfully approached by coherence measurements. It has been in fact reported that AD patients present a reduced linear coupling of resting state EEG rhythms among cortical regions, as revealed by spectral EEG coherence [33, 83, 87–90], suggesting a linear temporal synchronicity of coupled EEG rhythms from simultaneously engaged neural sources. Such findings imply that functional coupling of cortical rhythms at certain frequency bands might be interesting features of AD, and that abnormality of cortical EEG coherence may be a fine-grained marker of AD, which is supposed to reflect a disease of cerebral networks subserving global cognition. It could be speculated that this impaired pattern of EEG functional coupling is modulated by cholinergic systems, and that a decrease of cortical EEG coherence is characterized by defective basal forebrain cholinergic inputs to cortex and hippocampus [91].

Most EEG studies of AD have reported a prominent decrease of alpha band coherence [33, 74, 83, 86–90, 92–94]. This result also has been found to be associated with ApoE genetic risk, which is hypothesized to be mediated by cholinergic deficit [95]. However, delta and theta band coherence changes in AD are not homogeneous, as some studies demonstrate contradictory results with either a decrease or an increase of slow-band EEG coherence [33, 90, 92, 96]. These conflicting results might be due to the use of coherence markers from single electrode pairs rather than for the "total coherence" as obtained averaging the EEG spectral coherence across all combinations of electrode pairs. The latter may better take into account frequency band-by-frequency band the global impairment of brain networks and cognition along the AD process, which is supposed to be a disease affecting the functional integration within cerebral neural networks supporting cognition. In a recent study [97] the results show that the delta total coherence is higher in the AD than in the MCI and in the MCI than in the Nold group. Furthermore, the low-frequency alpha total coherence is lower in the AD group than in the MCI and Nold groups. This evidence confirms that the functional coupling of resting EEG rhythms is progressively abnormal in amnesic MCI and AD subjects.

To improve the functional coupling evaluation, EEG and MEG data have been analyzed with procedures inspired by the theory of nonlinear dynamics, which provide a measure of signal dynamic coordination [98]. It is shown that AD patients generate a nonlinearly defined dimensional "complexity" of the EEG, which is a measure of signal dynamic coordination. The AD patients have significantly lower dimensional complexity of EEG than age-approximated non-demented controls. This may be associated with deficient information processing in the brain injured by AD. Brain rhythms loose the usual modulation in complexity as observed by eyes-open versus eyes-close comparisons, as a reflection of neuronal death, deficiency in neurotransmission, and/or loss of connectivity in local neuronal networks [99, 100]. Non-linear analysis has also been used to model brain flexibility in information processing, defined as the capability to affect state of information processing from identical initial conditions. AD patients show a decrease in information processing flexibility, such that decrease of EEG complexity in AD might be attributable to decreased nonlinear dynamics that are associated with cognitive decline. Among the techniques for nonlinear brain dynamics evaluation, synchronization likelihood combines sensitivity to linear and nonlinear functional coupling of EEG/MEG rhythms [98]. This measure has been shown to be significantly decreased at alpha and low beta bands when comparing AD to MCI and/or Nold subjects [35, 101–103].

In addition to the cortico–cortical uncoupling progression, a decrease of synaptic coupling is likely to contribute to reducing selective EEG coherence for faster rhythms, as observed in healthy humans by transient use of a cholinergic synaptic blocker like scopolamine [104]. Animal models suggest that acetylcholine loss produces a decrease of high-frequency EEG couplings and an increase of slow-frequency couplings [105]. Loss or a significant drop in EEG synchronization in faster rhythms has also been correlated with decreased MMSE scores in MCI and AD patients [98]. Linear and non-linear EEG analyses improve classification accuracy of AD compared to unaffected controls, and these methods correlate with disease severity [35, 98, 102].

Few studies have assessed EEG measures over the course of dementia progression. A significant increase of delta and theta power in conjunction with decrease of alpha and beta power over a period of 30 months from diagnosis have been found [106]. The length of the follow-up is of paramount importance and indicates the reason for a lack of findings over a 12-month period [107]. The major question in this context is: "Which is the physiological mechanism at the basis of abnormal resting brain rhythms in MCI and AD?" Abnormality of resting EEG rhythms may originate from impairment in the cholinergic neural projections from basal forebrain, which is a pivotal aspect of AD [20]. Resting EEG alpha power is decreased from experimental damage to this cholinergic pathway [108]. Furthermore, the cholinergic basal forebrain has been found to be responsive to the treatment with cholinesterase inhibitors more for AD than other dementias [109]. Conversely, brainstem cholinergic innervations of the thalamus are relatively spared in AD patients [20]. Long-term (1 year) treatments of acetylcholinesterase inhibitors (AChEI) demonstrate less temporal and occipital alpha reduction for responders compared to non-responders and a combined effect on delta and low alpha [47, 110]. Hence, increasing cholinergic tone was related to restoring temporal and occipital alpha rhythms in responders. Brain cholinergic systems also appear to improve primarily cerebral blood flow with a functional impact on attention and memory functions [111].

RESTING STATE EEG RHYTHMS AND MILD COGNITIVE IMPAIRMENT (MCI)

Assessing pre-clinical dementia is of keen interest as a clinical research issue, since MCI often precedes loss of autonomy in daily life. As the selective cognitive impairments characteristic of MCI are primarily memory-related and not severe enough to exceed standard clinical criteria for AD, their prodromal qualities do not greatly impair daily functioning but can be reliably identified by refined clinical and neuropsychological evaluation. Consistent MCI symptoms 3–5 years following their identification either remain stable or decrease in 30–50% of the cases, whereas the remaining cases progress toward a frank AD condition or, less frequently, to other dementias. The amnesic MCI condition has often been considered a precursor of AD, despite the fact that not all the MCI patients develop the AD. Epidemiological and clinical follow-up studies confirm that MCI reflects a transition state towards mild AD and prompts the idea that early identification of MCI patients can facilitate rehabilitative or pharmacological interventions to slow down the disease progression [112–114].

Figs 1–3 show the results of a re-analysis of resting state eyes closed EEG data of our Italian Consortium.
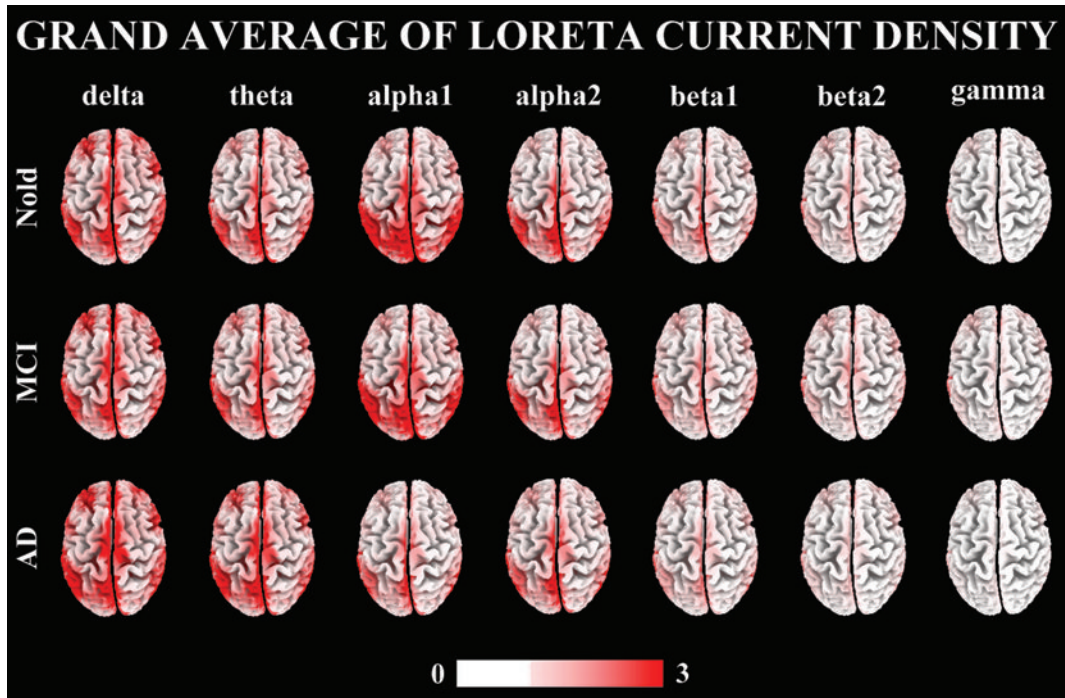
Fig. 1. Grand average of low resolution brain electromagnetic source tomography (LORETA) solutions (i.e., normalized relative current density at the cortical voxels) modeling the distributed EEG sources for delta, theta, alpha 1, alpha 2, beta 1 (13–20 Hz), and beta 2 (20–30 Hz) bands in normal elderly (Nold), mild cognitive impairment (MCI) and mild Alzheimer's disease (AD) groups. The left side of the maps (top view) corresponds to the left hemisphere. Legend: LORETA, low-resolution brain electromagnetic tomography.
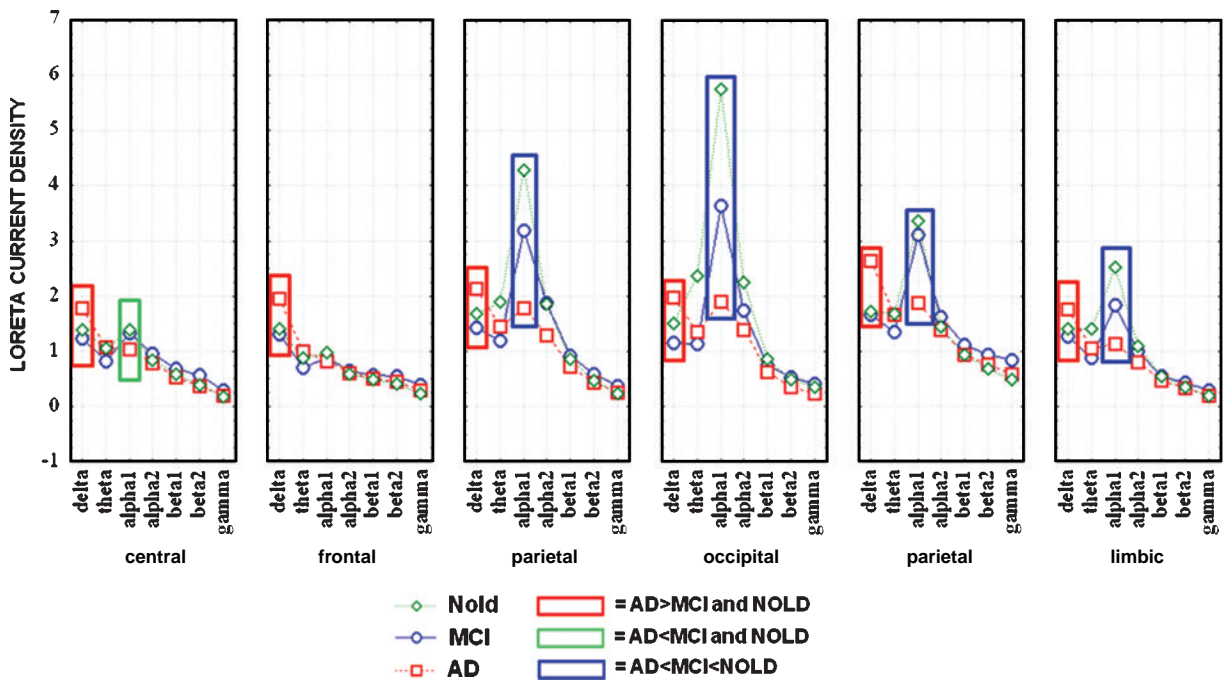
Fig. 2. Statistical ANOVA interaction (F(60,8010)=10.16; $p < 0.0001$) among the factors Group (Nold, MCI, AD), Band (delta, theta, alpha 1, alpha 2, beta 1, beta 2, gamma), and regions of interest (frontal, central, parietal, occipital, temporal, limbic).

CORRELATION BETWEEN MMSE AND CORTICAL RHYTHMS
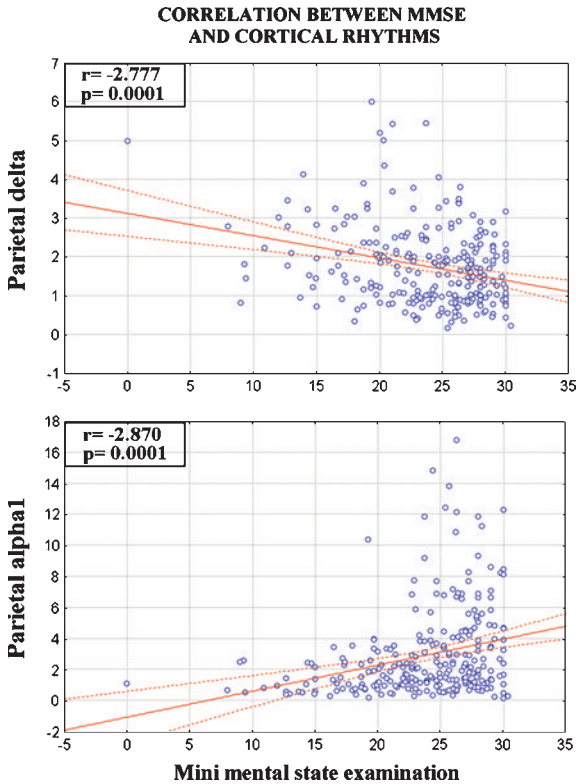
Fig. 3. Scatterplots of LORETA solutions for the delta and alpha 1 parietal rhythms and MMSE values in all subjects. Statistical values of linear correlation were obtained by Pearson test ($p < 0.005$)

Table 1
Demographic and clinical data of healthy elderly (Nold), amnesic mild cognitive impairment (MCI), and Alzheimer (AD) subjects

	Subjects (N)	Gender (M/F)	Age (years)	MMSE	IAF (Hz)
Nold	56	29/27	$73.4 \pm (0.9)$	$27.7 \pm (0.2$ SE$)$	$9.2 \pm (0.2)$
MCI	106	36/70	$70.0 \pm (0.7)$	$25.9 \pm (0.2$ SE$)$	$9.4 \pm (0.1)$
AD	108	35/73	$71.3 \pm (0.8)$	$19.8 \pm (0.5$ SE$)$	$8.7 \pm (0.1)$

For this re-analysis, we selected 56 Nold, 106 amnesic MCI, and 108 AD subjects with paired age, gender, and education (Table 1). Fig. 1 maps the grand average of (LORETA) cortical sources of these rhythms in the three groups. Fig. 2 plots the power of these sources collapsed for cortical lobar regions of interest. It can be observed an intermediate magnitude of low-frequency alpha rhythms (8–10.5 Hz) in parietal, occipital, and limbic areas in MCI compared to mild AD and Nold subjects, according to original evidence reported in a previous study [48]. Noteworthy, the spectral magnitude of some delta and alpha sources was correlated with MMSE scores across Nold, MCI, and AD sub-

jects as a whole group. Fig. 3 plots these correlations for delta and low-frequency sources in parietal lobe. There was a negative correlation of the MMSE score and delta sources, as well as a positive correlation of the MMSE score and low-frequency alpha sources. This suggests that EEG evidence of alpha power decreases in AD and MCI compared to normal subjects in relation to global cognition. These results agree with a bulk of previous evidence [75, 83, 94, 115–117]. It can be speculated that the relative spectral magnitude decrease of posterior low-frequency alpha sources in MCI may be related to an initial selective impairment of the cholinergic basal forebrain, which could induce a sustained increase of the excitatory activity in the cholinergic brainstem pathway [68, 104, 105]. Studies using transcranial magnetic stimulation (TMS) have shown that the motor cortex of AD patients is reorganized and hyperexcitable, and that such hyperexcitability even may offer clues for the differential diagnosis from other dementias in which the cholinergic deficit is not predominant [117–119]. As a consequence, the increased excitability of thalamocortical connections would unselectively desynchronize the resting alpha rhythms and enhance the cortical excitability. Hence, changes of low-frequency alpha power in MCI and mild AD suggest a progressive impairment of the thalamo–cortical and cortico–cortical systems that govern visual attention. This hypothesis is consistent with clinical findings of increasing deficits of visuo-spatial abilities in MCI and mild AD [120]. In the same vein, limbic sources imply a progressive impairment of thalamo–cortical and cortico–cortical systems regulating attention tone for memory functions.

Decreases in cortico–thalamic modulation and increase of slow EEG rhythms have been found to correlate to progressive cortical hypoperfusion in AD [81, 121]. Abnormal delta and alpha sources in the posterior brain regions could therefore index the progressive decline of cognitive visuo-spatial functions across MCI and mild AD, thereby supporting a transition between these conditions [112–114]. An intriguing aspect includes the peculiar magnitude increase of the parieto-occipital high-frequency alpha sources (alpha 2, 10.5–13 Hz) in MCI compared to mild AD and normal elderly [48]. Furthermore, prospective studies have demonstrated that increased delta/theta activity, decreased alpha and beta, and slowed mean frequency may be predictors of progression from MCI to dementia [75, 94]. These findings imply that neuroelectric indices could be developed for the preclinical assessment of dementia, as their acquisition are inexpensive,

easily implemented, entirely non-invasive and very well suited for large-scale screening and follow-up of at-risk populations.

The hypothesis of some strict relationships between brain activity in MCI and AD subjects implies the prediction of similar features of resting state EEG rhythm in MCI and AD subjects as a function of genetic risk factors. A corollary hypothesis is that the presence of ApoE ε4 affects sources of resting EEG rhythms in both MCI and AD was assessed in 89 MCI with 34.8% ε4 incidence and 103 AD with 50.4% ε4 incidence [122]. Alpha 1 and 2 sources in occipital, temporal, and limbic areas were of lower amplitude in subjects carrying the ApoE ε4 allele. For AD homozygous for ApoE ε4 allele, abnormal temporo-parietal and occipitoparietal EEG or MEG rhythms were found [83, 98]. However, in addition to ApoE ε4 allele, another important genetic risk factor for late-onset AD is haplotype B of CST3 (the gene coding for cystatin C—a neurotrophic protein), which was investigated to establish eventual links with cortical rhythmicity [123]. EEG measures were obtained from 84 MCI with 42% B haplotype and 65 AD with 40% B haplotype. Slow alpha (from parietal, occipital, temporal areas) and fast alpha (from occipital areas) power were statistically lower in CST3 B carriers. A trend was observed for occipital delta power sources as stronger in CST3 B carriers than in non-carriers for both MCI and AD patients.

Association between the presence and amount of hippocampal atrophy in AD and MCI subjects and changes in sources of posterior slow rhythms have been observed by EEG and whole-head MEG [19, 124, 125]. Less known is the relationships between impairment of white matter and slow rhythms across the continuum from MCI to AD. This issue has been addressed with EEG assessments in MCI ($N = 34$) and AD ($N = 65$) cases [46]. Delta activity was related to the amount of cortical atrophy revealed by MRI voxel-to-voxel volumetry of lobar brain volume (white and gray matter), such that as delta power increased brain volume decreased. Thus, changes in brain structure and function could be found for MCI and AD patients.

As life expectancy and elderly populations in Western countries are increasing, the incidence of MCI that may predict AD or vascular dementia is rising. Cognitive impairment associated with MCI or AD is combined with decreased power and coherence in the alpha/beta band, at least at the group level. This observation suggests the occurrence of a functional disconnection among cortical areas, since both power and coherence in the delta and theta bands increase with

cortical deafferentiation from subcortical structures [126]. However, the extent to which features of neuro-electric activity can be used to predict the conversion from MCI to AD in single subjects is as yet unclear. In a seminal EEG study, a multiple logistic regression of theta power (3.5–7.5 Hz), mean frequency, and interhemispheric coherence have been able to predict decline from MCI to AD at long term with an overall predictive accuracy of about 90% [127]. Furthermore, spectral EEG coherence or other EEG features have shown to contribute to the discrimination of Nold from mild AD with 89–45% of success, from MCI to AD with 92–78% of success, and the conversion of MCI subjects to AD with 87–60% of success [75, 90, 94, 128–133]. These findings are encouraging for future development of this prognostic and perhaps diagnostic approach [134].

Rossini et al. (2006) [117] have investigated whether combined analysis of EEG power and coherence provide early and reliable discrimination of MCI subjects who will convert to AD after a relatively brief follow-up. Cortical connectivity using spectral coherence measures and LORETA was evaluated to characterize EEG sources at baseline in 69 MCI cases that were reassessed clinically after about 14 months. At follow-up, 45 subjects were classified as stable MCI (MCI Stable), whereas the remaining 24 had converted to AD (MCI Converted). Results showed that at baseline, fronto-parietal midline coherence as well as delta (temporal), theta (parietal, occipital and temporal), and low-frequency alpha (central, parietal, occipital, temporal, limbic) sources were stronger in MCI Converted than MCI Stable subjects. Cox regression modeling showed low midline coherence and weak temporal source was associated with 10% annual rate AD conversion, while this rate increased up to 40% and 60% when strong temporal delta source and high midline gamma coherence were observed, respectively. This outcome indicates that quantitative EEG is able to predict with a good approximation MCI progression to AD in the short run.

CONCLUSIONS

The present review highlights the use of modern EEG techniques that report assessment of physiological and pathological brain aging. Application of these techniques allows the quantification of the power and functional coupling of resting state eyes closed EEG rhythms at scalp electrodes and mathematical corti-

cal sources. The results reviewed in the present article suggest that these quantitative indexes of resting state EEG rhythms might reflect neurodegenerative processes along preclinical and clinical stages of AD, at least at group level. Furthermore, independent genetic risk factors were related to specific features of these EEG rhythms. Unfortunately, this remarkable literature suffers from the partial lack of integration of various EEG techniques such as analysis of power density and functional coupling (i.e. spectral coherence, directed transfer function) within a unique frame of goal-directed test for evaluation of physiological brain aging and discrimination from abnormal scenarios heralding neurodegeneration. In the near future, systematic evaluation of AD and other dementing disorders compared to normal aging using refined and integrated EEG techniques will help to integrate these methodologies and improve diagnostic utility. If this approach can provide clinically useful information at the individual level, such methods should prompt design of an instrument widely available for large-scale population-based screening studies.

REFERENCES

[1] Berger HU (1929) ber das Elektroenkephalogramm des Menschen. *Archiv für Psychiatrie und Nervenkrankheiten* **87**, 527-570.

[2] Berger H (1938) Das Elektroenkephalogramm des Menschen. Halle an der Saale. *Buchdruckerei des Waisenhause* volume 6, No. 38 of Nova acta Leopoldina. Neue Folge.

[3] Rossini PM, Dal Forno G (2004) Integrated technology for evaluation of brain function and neural plasticity. *Phys Med Rehabil Clin N Am* **15**, 263-306.

[4] Celesia GG, Kaufman D, Cone S (1987) Effects of age and sex on pattern electroretinograms and visual evoked potentials. Electroencephalogr. *Clin Neurophysiol* **68**, 161-171.

[5] Rossini PM, Rossi S, Babiloni C, Polich J (2007) Clinical neurophysiology of aging brain: from normal aging to neurodegeneration. *Prog Neurobiol Epub 2007 Aug 8. Review* **83**, 375-400.

[6] Rossini PM (2009) Implications of brain plasticity to brain-machine interfaces operation a potential paradox? *Int Rev Neurobiol* **86**, 81-90. Review.

[7] Olichney JM, Morris SK, Ochoa C, Salmon DP, Thal LJ, Kutas M, Iragui VJ (2002) Abnormal verbal event related potentials in mild cognitive impairment and incipient Alzheimer's disease. *J Neurol Neurosur Ps* **73**, 377-384.

[8] Olichney JM, Iragui VJ, Salmon DP, Riggins BR, Morris SK, Kutas M (2006) Absent event-related potential (ERP) word repetition effects in mild Alzheimer's disease. *Clin Neurophysiol* **117**, 1319-1330.

[9] Wesson Ashford J, Kerry L Coburn(2011) The Topography of P300 Energy Loss in Aging and Alzheimer's Disease. *This volume*.

[10] Polich J, Corey-Bloom J (2005) Alzheimer's disease and P300: review and evaluation of task and modality. *Curr Alzheimer Res* **2**, 515-525.

[11] Steriade M, McCormick DA, Sejnowski TJ (1993) Thalamocortical oscillations in the sleeping and aroused brain. *Science* **262**, 679-85. Review.

[12] Achermann P,Borb eacute; ly AA (1997) Low-frequency (<1Hz) oscillations in the human sleep electroencephalogram. *Neuroscience* **81**, 213-222.

[13] Timofeev I, Grenier F, Bazhenov M, Sejnowski TJ, Steriade M (2000) Origin of slow cortical oscillations in deafferented cortical slabs. *Cereb Cortex* **10**, 1185-1199.

[14] Steriade M (2003) The corticothalamic system in sleep. *Front Biosci* **8**, d878-d899.

[15] Steriade M, Contreras D, Amzica F, Timofeev I (1996) Synchronization of fast (30-40Hz) spontaneous oscillations in intrathalamic and thalamocortical networks. *J Neurosci* **6**, 2788-2808.

[16] Steriade M, Llinas RR (1988) The functional states of the thalamus and the associated neuronal interplay. *Physiol Rev* **68**, 649-742.

[17] Brunia CH (1999) Neural aspects of anticipatory behavior. *Acta Psychol (Amst)* **101**, 213-242.

[18] Pfurtscheller G, Lopes da Silva FH (1999) Event-related EEG/MEG synchronization and desynchronization: basic principles. *Clin Neurophysiol* **110**, 1842-1857. Review.

[19] Helkala EL, Hanninen T, Hallikainen M, Kononen M, Laakso MP, Hartikainen P, Soininen H, Partanen J, Partanen K, Vainio P, Riekkinen Sr P (1996) Slow-wave activity in the spectral analysis of the electroencephalogram and volumes of hippocampus in subgroups of Alzheimer's disease patients. *Behav Neurosci* **110**, 1235-1243.

[20] Mesulam M (2004) The cholinergic lesion of Alzheimer's disease: pivotal factor or side show?. *Learn Mem* **11**, 13-19.

[21] Nunez PL (2000) Toward a quantitative description of large-scale neocortical dynamic function and EEG. *Behav Brain Sci* **23**, 371-398. discussion.

[22] Babiloni F, Carducci F, Cincotti F, Del Gratta C, Pizzella V, Romani GL, Rossini PM, Tecchio F, Babiloni C (2001) Linear inverse source estimate of combined EEG and MEG data related to voluntary movements. *Hum Brain Mapp* **14**, 197-209.

[23] Babiloni F, Babiloni C, Fattorini L, Carducci F, Onorati P, Urbano A (1995) Performances of surface Laplacian estimators: a study of simulated and real scalp potential distributions. *Brain Topogr* **8**, 35-45.

[24] Babiloni F, Babiloni C, Carducci F, Fattorini L, Onorati P, Urbano A (1996) Spline Laplacian estimate of EEG potentials over a realistic magnetic resonance-constructed scalp surface model. Electroencephalogr. *Clin Neurophysiol* **98**, 363-373.

[25] Babiloni F, Babiloni C, Carducci F, Cincotti F, Rossini PM (2003) 'The stone of madness' and the search for the cortical sources of brain diseases with non-invasive EEG techniques. *Clin Neurophysiol* **114**, 1775-1780.

[26] Nunez PL, Srinivasan R (2006) *Electric Fields of the Brain: The Neurophysics of EEG*,Oxford University Press, New York, USA.

[27] Nunez PL (1995) *Neocortical Dynamics and Human EEG Rhythms*,Oxford University Press, New York.

[28] Rappelsberger P, Petsche H (1988) Probability mapping: power and coherence analyses of cognitive processes. *Brain Topography* **1**, 46-54.

[29] Andrew C, Pfurtscheller G (1996) Event-related coherence as a tool for studying dynamic interaction of brain regions. *Electroencephalography and Clinical Neurophysiology* **98**, 144-148.

[30] Gerloff C, Richard J, Hadley J, Schulman AE, Honda M, Hallett M (1998) Functional coupling and regional activation of human cortical motor areas during simple, internally paced and externally paced finger movements. *Brain* **121**, 1513-1531.

[31] Thatcher RW, Krause PJ, Hrybyk M (1986) Cortico-cortical associations and EEG coherence: a two-compartmental model. Electroencephalogr. *Clin Neurophysiol* **64**, 123-143.

[32] Gevins A, Smith ME, Leong H, McEvoy L, Whitfield S, Du R, Rush G (1998) Monitoring working memory load during computer-based tasks with EEG pattern recognition methods. *Hum Factors* **40**, 79-91.

[33] Locatelli T, Cursi M, Liberati D, Franceschi M, Comi G (1998) EEG coherence in Alzheimer's disease. Electroencephalogr. *Clin Neurophysiol* **106**, 229-237.

[34] Sauseng P, Klimesch W, Schabus M, Doppelmayr M (2005) Fronto-parietal EEG coherence in theta and upper alpha reflect central executive functions of working memory. *Int J Psychophysiol* **57**, 97-103.

[35] Babiloni C, Ferri R, Binetti G, Cassarino A, Forno GD, Ercolani M, Ferreri F, Frisoni GB, Lanuzza B, Miniussi C, Nobili F, Rodriguez G, Rundo F, Stam CJ, Musha T, Vecchio F, Rossini PM (2006) Fronto-parietal coupling of brain rhythms in mild cognitive impairment: a multicentric EEG study. *Brain Res Bull* **69**, 63-73.

[36] Vecchio F, Babiloni C, Ferreri F, Curcio G, Fini R, Del Percio C, Rossini PM (2007) Mobile phone emission modulates interhemispheric functional coupling of EEG alpha rhythms. *Eur J Neurosci* **25**, 1908-1913.

[37] Vecchio F, Babiloni C, Ferreri F, Buffo P, Cibelli G, Curcio G, van Dijkman S, Melgari JM, Giambattistelli F, Rossini PM (2009) Mobile phone emission modulates interhemispheric functional coupling of EEG alpha rhythms in elderly compared to young subjects. *Clin Neurophysiol* **121**, 163-171.

[38] von Stein A, Sarnthein J (2000) Different frequencies for different scales of cortical integration: from local gamma to long range alpha/theta synchronization. *Int J Psychophysiol* **38**, 301-313. Review.

[39] Kaminski MJ, Blinowska KJ (1991) A new method of the description of the information flow in the structures. *Biol Cybern* **65**, 203-210.

[40] Kaminski MJ, Blinowska KJ, Szclenberger W (1997) Topographic analysis of coherence and propagation of EEG activity during sleep and wakefulness. Electroencephalogr. *Clin Neurophysiol* **102**, 216-227.

[41] Korzeniewska A, Kasicki S, Kaminski M, Blinowska KJ (1997) Information flow between hippocampus and related structures during various types of rat's behavior. *J Neurosci Methods* **73**, 49-60.

[42] Mima T, Matsuoka T, Hallett M (2000) Functional coupling of human right and left cortical motor areas demonstrated with partial coherence analysis. *Neurosci Lett* **287**, 93-96.

[43] Babiloni C, Vecchio F, Babiloni F, Brunelli GA, Carducci F, Cincotti F, Pizzella V, Romani GL, Tecchio FT, Rossini PM (2004) Coupling between "hand" primary sensorimotor cortex and lower limb muscles after ulnar nerve surgical transfer in paraplegia. *Behav Neurosci* **118**, 214-222.

[44] Babiloni C, Babiloni F, Carducci F, Cincotti F, Vecchio F, Cola B, Rossi S, Miniussi C, Rossini PM (2004) Functional frontoparietal connectivity during short-term memory as revealed by high-resolution EEG coherence analysis. *Behav Neurosci* **118**, 687-697.

[45] Dierks T, Jelic V, Pascual-Marqui RD, Wahlund L, Julin P, Linden DE, Maurer K, Winblad B, Nordberg A (2000) Spatial pattern of cerebral glucose metabolism (PET) correlates with localization of intracerebral EEG-generators in Alzheimer's disease. *Clin Neurophysiol* **111**, 1817-1824.

[46] Babiloni C, Frisoni G, Steriade M, Bresciani L, Binetti G, Del Percio C, Geroldi C, Miniussi C, Nobili F, Rodriguez G, Zappasodi F, Carfagna T, Rossini PM (2006) Frontal white matter volume and delta EEG sources negatively correlate in awake subjects with mild cognitive impairment and Alzheimer's disease. *Clin Neurophysiol* **117**, 1113-1129.

[47] Babiloni C, Cassetta E, Dal Forno G, Del Percio C, Ferreri F, Ferri R, Lanuzza B, Miniussi C, Moretti DV, Nobili F, Pascual-Marqui RD, Rodriguez G, Luca Romani G, Salinari S, Zanetti O, Rossini PM (2006) Donepezil effects on sources of cortical rhythms in mild Alzheimer's disease: responders vs. non-responders. *Neuroimage* **31**, 1650-1665.

[48] Babiloni C, Binetti G, Cassetta E, Dal Forno G, Del Percio C, Ferreri F, Ferri R, Frisoni G, Hirata K, Lanuzza B, Miniussi C, Moretti DV, Nobili F, Rodriguez G, Romani GL, Salinari S, Rossini PM (2006) Sources of cortical rhythms change as a function of cognitive impairment in pathological aging: a multicenter study. *Clin Neurophysiol* **117**, 252-268.

[49] Babiloni C, Lizio R, Vecchio F, Frisoni GB, Pievani M, Geroldi C, Claudia F, Ferri R, Lanuzza B, Rossini PM (2010) Reactivity of cortical alpha rhythms to eye opening in mild cognitive impairment and Alzheimer's disease: an EEG study. *J Alzheimers Dis* **22**, 1047-1064.

[50] Babiloni C, Frisoni GB, Vecchio F, Lizio R, Pievani M, Cristina G, Fracassi C, Vernieri F, Rodriguez G, Nobili F, Ferri R, Rossini PM (2010) Stability of clinical condition in mild cognitive impairment is related to cortical sources of alpha rhythms: An electroencephalographic study. *Hum Brain Mapp*.

[51] Pascual-Marqui RD, Michel CM, Lehmann D (1994) Low resolution electromagnetic tomography: a new method for localizing electrical activity in the brain. *Int J Psychophysiol* **18**, 49-65.

[52] Pascual-Marquiì RD, Lehmann D, Koenig T, Kochi K, Merlo MC, Hell D, Koukkou M (1999) Low resolution brain electromagnetic tomography (LORETA) functional imaging in acute, neurolepticnaive, first-episode, productive schizophrenia. *Psychiatry Res* **90**, 169-179.

[53] Pascual-Marqui RD, Esslen M, Kochi K, Lehmann D (2002) Functional imaging with low resolution brain electromagnetic tomography (LORETA): a review. Methods Find Exp. *Clin Pharmacol* **24**, 91-95.

[54] Isotani T, Tanaka H, Lehmann D, Pascual-Marqui RD, Kochi K, Saito N, Yagyu T, Kinoshita T, Sasada K (2001) Source localization of EEG activity during hypnotically induced anxiety and relaxation. *Int J Psychophysiol* **41**, 143-153.

[55] Mientus S, Gallinat J, Wuebben Y, Pascual-Marqui RD, Mulert C, Frick K, Dorn H, HerrmannWM, Winterer G (2002) Cortical hypoactivation during resting EEG in schizophrenics but not in depressives and schizotypal subjects as revealed by low resolution electromagnetic tomography (LORETA). *Psychiatry Res* **116**, 95-111.

[56] Babiloni C, Binetti G, Cassetta E, Cerboneschi D, Dal Forno G, Del Percio C, Ferreri F, Ferri R, Lanuzza B, Miniussi C, Moretti DV, Nobili F, Pascual-Marqui RD, Rodriguez G,

Romani GL, Salinari S, Tecchio F, Vitali P, Zanetti O, Zappasodi F, Rossini PM (2004) Mapping distributed sources of cortical rhythms in mild Alzheimer's disease. A multicentric EEG study. *Neuroimage* **22**, 57-67.

[57] Saletu M, Anderer P, Saletu-Zyhlarz GM, Mandl M, Arnold O, Zeitlhofer J, Saletu B (2004) EEG-tomographic studies with LORETA on vigilance differences between narcolepsy patients and controls and subsequent double-blind, placebo-controlled studies with modafinil. *J Neurol* **251**, 1354-1363.

[58] Dujardin K, Bourriez JL, Guieu JD (1994) Event-related desynchronization (ERD) patterns during verbal memory tasks: effect of age, int. *J Psychophysiol* **16**, 17-27.

[59] Dujardin K, Bourriez JL, Guieu JD (1995) Event-related desynchronization (ERD) patterns during memory processes: effects of aging and task difficulty. Electroencephalogr. *Clin Neurophysiol* **96**, 169-182.

[60] Klass DW, Brenner RP (1995) Electroencephalography of the elderly. *J Clin Neurophysiol* **12**, 116-131.

[61] Klimesch W (1999) EEG alpha and theta oscillations reflect cognitive and memory performance: a review and analysis. *Brain Research Reviews* **29**, 169-195.

[62] Babiloni C, Binetti G, Cassarono A, Dal Forno G, Del Percio C, Ferreri F, Ferri R, Frisoni G, Galderisi S, Hirata K, Lanuzza B, Miniassi C, Mucci A, Nobili F, Rodriguez G, Romani GL, Rossigni PM (2006) Sources of cortical rhythms in adults during physiological aging: a multicentric EEG study. *Hum Brain Mapp* **27**, 162-172.

[63] Steriade M, Llinas RR (1998) The functional states of the thalamus and the associated neuronal interplay. *Physiol Rev* **68**, 649-742.

[64] Klimesch W (1996) Memory processes, brain oscillations and EEG synchronization. *Int J Psychophysiol* **24**, 61-100.

[65] Klimesch W (1997) EEG-alpha rhythms and memory processes. *Int J Psychophysiol* **26**, 319-340.

[66] Klimesch W, Doppelmayr M, Russegger H, Pachinger T, Schwaiger J (1998) Induced alpha band power changes in the human EEG and attention. *Neurosci Lett* **244**, 73-76.

[67] Rossini PM, Desiato MT, Lavaroni F, Caramia MD (1991) Brain excitability and electroencephalographic activation: non-invasive evaluation in healthy humans via transcranial magnetic stimulation. *Brain Res* **13567**, 111-119.

[68] Sarter M, Bruno JP (1998) Cortical acetylcholine, reality distortion, schizophrenia, and Lewy body dementia: too much or too little cortical acetylcholine? *Brain Cogn* **38**, 297-316.

[69] Terry JR, Anderson C, Horne JA (2004) Nonlinear analysis of EEG during NREM sleep reveals changes in functional connectivity due to natural aging. *Hum Brain Mapp* **23**, 73-84.

[70] Vicioso BA (2002) Dementia: when is it not Alzheimer disease? *Am J Med Sci* **324**, 84-95.

[71] Graves AB, Kukull WA (1994) The epidemiology of dementia. In: Morris JC, ed. *Handbook of Dementing Illnesses*, 23-69.

[72] Iqbal K, Alonso Adel C, El-Akkad E, Gong CX, Haque N, Khatoon S, Pei JJ, Tsujio I, Wang JZ, Grundke-Iqbal I (2002) Significance and mechanism of Alzheimer neurofibrillary degeneration and therapeutic targets to inhibit this lesion. *J Mol Neurosci* **19**, 95-99.

[73] Goedert M, Spillantini MG (2006) A century of Alzheimer's disease. *Science* **314**, 777-781.

[74] Cook IA, Leuchter AF (1996) Synaptic dysfunction in Alzheimer's disease: clinical assessment using quantitative EEG. *Behav Brain Res* **78**, 15-23.

[75] Huang C, Wahlund L, Dierks T, Julin P, Winblad B, Jelic V (2000) Discrimination of Alzheimer's disease and mild cognitive impairment by equivalent EEG sources: a cross-sectional and longitudinal study. *Clin Neurophysiol* **111**, 1961-1967.

[76] Ponomareva NV, Selesneva ND, Jarikov GA (2003) EEG alterations in subjects at high familial risk for Alzheimer's disease. *Neuropsychobiology* **48**, 152-159.

[77] Jeong J (2004) EEG dynamics in patients with Alzheimer's disease. *Clin Neurophysiol* **115**, 1490-1505.

[78] Prichep LS (2005) Use of normative databases and statistical methods in demonstrating clinical utility of QEEG: importance and cautions. *Clin EEG Neurosci* **36**, 82-87.

[79] Sloan EP, Fenton GW, Kennedy NS, MacLennan JM (1995) Electroencephalography and single photon emission computed tomography in dementia: a comparative study. *Psychol Med* **25**, 631-638.

[80] Rodriguez G, Vitali P, Nobili F (1998) Long-term effects of boxing and judochoking techniques on brain function. *Ital J Neurol Sci* **19**, 367-372.

[81] Rodriguez G, Nobili F, Copello F, Vitali P, Gianelli MV, Taddei G, Catsafados E, Mariani G (1999) 9mTc-HMPAO regional cerebral blood flow and quantitative electroencephalography in Alzheimer's disease: a correlative study. *J Nucl Med* **40**, 522-529.

[82] Moretti DV, Babiloni C, Binetti G, Cassetta E, Dal Forno G, Ferreric F, Ferri R, Lanuzza B, Miniassi C, Nobili F, Rodriguez G, Salinari S, Rossigni PM (2004) Individual analysis of EEG frequency and band power in mild Alzheimer's disease. *Clin Neurophysiol* **115**, 299-308.

[83] Jelic V, Julin P, Shigeta M, Nordberg A, Lannfelt L, Winblad B, Wahlund LO (1997) Apolipoprotein E epsilon4 allele decreases functional connectivity in Alzheimer's disease as measured by EEG coherence. *J Neurol Neurosurg Psychiatry* **63**, 59-65.

[84] Lehtovirta M, Partanen J, Kononen M, Hiltunen J, Helisalmi S, Hartikainen P, Riekkinen Sr.P, Soininen H (2000) A longitudinal quantitative EEG study of Alzheimer's disease: relation to apolipoprotein E polymorphism. *Dement Geriatr Cogn Disord* **11**, 29-35.

[85] Lehtovirta M, Partanen J, Kononen M, Soininen H, Helisalmi S, Mannermaa A, Ryynanen M, Hartikainen P, Riekkinen Sr P (1996) Spectral analysis of EEG in Alzheimer's disease: relation to apolipoprotein. *E polymorphism Neurobiol Aging* **17**, 523-526.

[86] Almkvist O, Jelic V, Amberla K, Hellstrom-Lindahl E, Meurling L, Nordberg A (2001) Responder characteristics to a single oral dose of cholinesterase inhibitor: a double-blind placebo-controlled study with tacrine in Alzheimer patients. Dement. *Geriatr Cogn Disord* **12**, 22-32.

[87] Wada Y, Nanbu Y, Kikuchi M, Koshino Y, Hashimoto T, Yamaguchi N (1998) Abnormal functional connectivity in Alzheimer's disease: intrahemispheric EEG coherence during rest and photic stimulation. *Eur Arch Psychiatry Clin Neurosci* **248**, 203-208.

[88] Wada Y, Nanbu Y, Koshino Y, Yamaguchi N, Hashimoto T (1998) Reduced interhemispheric EEG coherence in Alzheimer disease: analysis during rest and photic stimulation. *Alzheimer Dis Assoc Disord* **12**, 175-181.

[89] Knott V, Mohr E, Mahoney C, Ilivitsky V (2000) Electroencephalographic coherence in Alzheimer's disease: comparisons with a control group and population norms. *J Geriatr Psychiatry Neurol* **13**, 1-8.

[90] Adler G, Brassen S, Jajcevic A (2003) EEG coherence in Alzheimer's dementia. *J Neural Transm* **9**, 1051-1058.

[91] Stam CJ, Jones BF, Manshanden I, van Cappellen van Walsum AM, Montez T, Verbunt JP, de Munck JC, van Dijk BW, Berendse HW, Scheltens P (2006) Magnetoencephalographic evaluation of resting-state functional connectivity in Alzheimer's disease. *Neuroimage* **32**, 1335-1344.

[92] Leuchter AF, Spar JE, Walter DO, Weiner H (1987) Electroencephalographic spectra and coherence in the diagnosis of Alzheimer's-type and multi-infarct dementia. A pilot study. *Arch Gen Psychiatry* **44**, 993-998.

[93] Leuchter AF, Newton TF, Cook IA, Walter DO, Rosenberg-Thompson S, Lachenbruch PA (1992) Changes in brain functional connectivity in Alzheimer-type and multi-infarct dementia. *Brain* **115**, 1543-1561.

[94] Jelic V, Johansson SE, Almkvist O, Shigeta M, Julin P, Nordberg A, Winblad B, Wahlund LO (2000) Quantitative electroencephalography in mild cognitive impairment: longitudinal changes and possible prediction of Alzheimer's disease. *Neurobiol* **21**, 533-540.

[95] Jelic V, Shigeta M, Julin P, Almkvist O, Winblad B, Wahlund LO (1996) Quantitative electroencephalography power and coherence in Alzheimer's disease and mild cognitive impairment. *Dementia* **7**, 314-323.

[96] Brunovsky M, Matousek M, Edman A, Cervena K, Krajca V (2003) Objective assessment of the degree of dementia by means of EEG. *Neuropsychobiology* **48**, 19-26.

[97] Babiloni C, Frisoni G, Vecchio F, Lizio R, Pievani M, Geroldi C, Fracassi C, Vernieri F, Ursini F, Rodriguez G, Nobili F, Salinari S, Van Dijkman S, Ferri R, Rossini M (2009) Global Functional Coupling of Resting EEG Rhythms is Abnormal in Mild Cognitive Impairment and Alzheimer's Disease: A Multicenter EEG Study. *Journal of Psychophysiology* **23**, 224-234.

[98] Stam CJ (2005) Nonlinear dynamical analysis of EEG and MEG: review of an emerging field. *Clin Neurophysiol* **116**, 2266-2301.

[99] Besthorn C, Sattel H, Geiger-Kabisch C, Zerfass R, Forstl H (1995) Parameters of EEG dimensional complexity in Alzheimer's disease. Electroencephalogr. *Clin Neurophysiol* **95**, 84-89.

[100] Jeong J, Kim SY, Han SH (1998) Non-linear dynamical analysis of the EEG in Alzheimer's disease with optimal embedding dimension. Electroencephalogr. *Clin Neurophysiol* **106**, 220-228.

[101] Stam CJ, van Cappellen van Walsum AM, Pijnenburg YA, Berendse HW, de Munck JC, Scheltens P, van Dijk BW (2002) Generalized synchronization of MEG recordings in Alzheimer's disease: evidence for involvement of the gamma band. *J Clin Neurophysiol* **19**, 562-574.

[102] Babiloni C, Ferri R, Moretti DV, Strambi A, Binetti G, Dal Forno G, Erreri F, Lanuzza B, Bonato C, Nobili F, Rodriguez G, Salinari S, Passero S, Rocchi R, Stam CJ, Rossini PM (2004) Abnormal frontoparietal coupling of brain rhythms in mild Alzheimer's disease: a multicentric EEG study. *Eur J Neurosci* **19**, 2583-2590.

[103] Pijnenburg YA, v d Made Y, van Cappellen van Walsum AM, Knol DL, Scheltens P, Stam CJ (2004) EEG synchronization likelihood in mild cognitive impairment and Alzheimer's disease during a working memory task. *Clin Neurophysiol* **115**, 1332-1339.

[104] Kikuchi M, Wada Y, Koshino Y, Nanbu Y, Hashimoto T (2000) Effects of scopolamine on interhemispheric EEG coherence in healthy subjects: analysis during rest and photic stimulation. *Clin Electroencephalogr* **31**, 109-115.

[105] Villa AE, Tetko IV, Dutoit P, Vantini G (2000) Non-linear corticocortical interactions modulated by cholinergic afferences from the rat basal forebrain. *Biosystems* **58**, 219-228.

[106] Coben LA, Danziger W, Storandt M (1985) A longitudinal EEG study of mild senile dementia of Alzheimer type: changes at 1 year and at 2.5 years. Electroencephalogr. *Clin Neurophysiol* **61**, 101-112.

[107] Soininen H, Partanen J, Laulumaa, Helkala EL, Laakso M, Riekkinen PJ (1989) Longitudinal EEG spectral analysis in early stage of Alzheimer's disease. Electroencephalogr. *Clin Neurophysiol* **72**, 290-297.

[108] Holschneider DP, Leuchter AF, Scremin OU, Treiman DM, Walton NY (1998) Effects of cholinergic deafferentation and NGF on brain electrical coherence. *Brain Res Bull* **45**, 531-541.

[109] Tanaka Y, Hanyu H, Sakurai H, Takasaki M, Abe K (2003) Atrophy of the substantia innominata on magnetic resonance imaging predicts response to donepezil treatment in Alzheimer's disease patients. *Dement Geriatr Cogn Disord* **16**, 119-125.

[110] Rodriguez G, Vitali P, De Leo C, De Carli F, Girtler N, Nobili F (2002) Quantitative EEG changes in Alzheimer patients during long-term donepezil therapy. *Neuropsychobiology* **46**, 49-56.

[111] Classen JA, Jansen RW (2006) Cholinergically mediated augmentation of cerebral perfusion in Alzheimer's disease and related cognitive disorders: the cholinergic-vascular hypothesis. *J Gerontol A: Biol Sci Med Sci* **61**, 267-271.

[112] Winblad B, Palmer K, Kivipelto M, Jelic V, Fratiglioni L, Wahlund L.O. Nordberg A, Backman L, Albert M, Almkvist O, Arai H, Basun H, Blennow K, de Leon M DeCarli C, Erkinjuntti T, Giacobini E, Graff C, Hardy J, Jack C, Jorm A, Ritchie K, van Duijn C, Visser P, Petersen RC (2004) Mild cognitive impairment—beyond controversies, towards a consensus: report of the International Working Group on Mild Cognitive Impairment. *J Intern Med* **256**, 240-246.

[113] Gauthier S, Reisberg B, Zaudig M, Petersen RC, Ritchie K, Broich K, Belleville S, Brodaty H, Bennett D, Chertkow H, Cummings JL, De Leon M, Feldman H, Ganguli M, Hampel H, Scheltens P, Tierney MC, Whitehouse P, Winblad B (2006) International Psychogeriatric Association Expert Conference on mild cognitive impairment. Mild cognitive impairment. *Lancet* **367**, 1262-1270.

[114] Portet F, Ousset PJ, Visser PJ, Frisoni GB, Nobili F, Scheltens P, Vellas B, Touchon J (2006) MCI Working Group of the European Consortium on Alzheimer's Disease (EADC). Mild cognitive impairment (MCI) in medical practice: a critical review of the concept and new diagnostic procedure. Report of the MCI Working Group of the European Consortium on Alzheimer's Disease. *J Neurol Neurosurg Psychiatry* **77**, 714-718.

[115] Grunwald M, Busse F, Hensel A, Kruggel F, Riedel-Heller S, Wolf H, Arendt T, Gertz HJ (2001) Correlation between cortical theta activity and hippocampal volumes in health,

mild cognitive impairment, and mild dementia. *J Clin Neurophysiol* **18**, 178-184.

[116] Kwak YT (2006) Quantitative EEG findings in different stages of Alzheimer's disease. *J Clin Neurophysiol* **23**, 456-461.

[117] Rossini PM, Del Percio C, Pasqualetti P, Cassetta E, Binetti G, Dal Forno F, Ferreri F, Frisoni G, Chiovenda P, Miniussi C, Parisi L, Tombini M, Vecchio F, Babiloni C (2006) Conversion from mild cognitive impairment to Alzheimer's disease is predicted by sources and coherence of brain electroencephalography rhythms. *Neuroscience* **143**, 793-803.

[118] Ferreri F, Pauri F, Pasqualetti P, Fini R, Dal Forno G, Rossini PM (2003) Motor cortex excitability in Alzheimer's disease: a transcranial magnetic stimulation study. *Ann Neurol* **53**, 102-108.

[119] Ferreri F, Pasqualetti P, Määttä S, Ponzo D, Guerra A, Bressi F, Chiovenda P, Del Duca M, Giambattistelli F, Ursini F, Tombini M, Vernieri F, Rossini PM (2011) Motor cortex excitability in Alzheimer's disease: a transcranial magnetic stimulation follow-up study. *Neurosci Lett* **492**, 94-98.

[120] Arnaiz E, Almkvist O (2003) Neuropsychological features of mild cognitive impairment and preclinical Alzheimer's disease. *Acta Neurol Scand Suppl* **179**, 34-41.

[121] Rodriguez G, Vitali P, Canfora M, Calvini P, Girtler N, De Leo C, Piccardo A, Nobili F (2004) Quantitative EEG and perfusional single photon emission computed tomography correlation during long-term donepezil therapy in Alzheimer's disease. *Clin Neurophysiol* **115**, 39-49.

[122] Babiloni C, Benussi L, Binetti G, Cassetta E, Dal Forno G, Del Percio C, Ferreri F, Ferri R, Frisoni G, Ghidoni R, Miniussi C, Rodriguez G, Romani GL, Squitti R, Ventriglia MC, Rossini PM (2006e) Apolipoprotein E and alpha brain rhythms in mild cognitive impairment: a multicentric electroencephalogram study. *Ann Neurol* **59**, 323-334.

[123] Babiloni C, Benussi L, Binetti G, Bosco P, Busonero G, Cesaretti S, Dal Forno G, Del Percio C, Ferri R, Frisoni G, Ghidoni R, Rodriguez G, Squitti R, Rossini PM (2006f) Genotype (cystatin C) and EEG phenotype in Alzheimer disease and mild cognitive impairment: a multicentric study. *Neuroimage* **29**, 948-964.

[124] Fernandez A, Arrazola J, Maestu F, Amo C, Gil-Gregorio P, Wienbruch C, Ortiz T (2003) Correlations of hippocampal atrophy and focal lowfrequency magnetic activity in Alzheimer disease: volumetric MR imagingmagnetoencephalographic study. *AJNR Am J Neuroradiol* **24**, 481-487.

[125] Wolf H, Jelic V, Gertz HJ, Nordberg A, Julin P, Wahlund LO (2003) A critical discussion of the role of neuroimaging in mild cognitive impairment. *Acta Neurol Scand Suppl* **179**, 52-76.

[126] Spiegel A, Tonner PH, Renna M (2006) Altered states of consciousness: processed EEG in mental disease. *Best Pract Res Clin Anaesthesiol* **20**, 57-67.

[127] Prichep LS, John ER, Ferris SH, Rausch L, Fang Z, Cancro R, Torossian C, Reisberg B (2006) Prediction of longitudinal cognitive decline in normal elderly with subjective complaints using electrophysiological imaging. *Neurobiol* 27, 471-481. *Nerve* **21**, 1209-1215.

[128] Nuwer M (1997) Assessment of digital EEG, quantitative EEG and brain mapping: report of the American Clinical Neurophysiology Society. *Neurology* **49**, 277-292.

[129] Claus JJ, Strijers RL, Jonkman EJ, Ongerboer de Visser BW, Jonker C, Walstra GJ, Scheltens P, van Gool WA (1999) The diagnostic value of electroencephalography in mild senile Alzheimer's disease. *Clin Neurophysiol* **110**, 825-832.

[130] Bennys K, Rondouin G, Vergnes C, Touchon J (2001) Diagnostic value of quantitative EEG in Alzheimer disease. *Neurophysiol Clin* **31**, 153-160.

[131] Brassen S, Braus DF, Weber-Fahr W, Tost H, Moritz S, Adler G (2004) Late-onset depression with mild cognitive deficits: electrophysiological evidences for a preclinical dementia syndrome. *Dement Geriatr Cogn Disord* **218**, 271-277.

[132] Lehmann C, Koenig T, Jelic V, Prichep L, John RE, Wahlund LO, Dodge Y, Dierks T (2007) Application and comparison of classification algorithms for recognition of Alzheimer's disease in electrical brain activity (EEG). *J Neurosci Methods* **161**, 342-350.

[133] Missonnier P, Gold G, Herrmann FR, Fazio-Costa L, Michel JP, Deiber MP, Michon A, Giannakopoulos P (2006) Decreased theta event-related synchronization during working memory activation is associated with progressive mild cognitive impairment. *Dement Geriatr Cogn Disord* **22**, 250-259.

[134] Buscema M, Rossini P, Babiloni C, Grossi E (2007) The IFAST model, a novel parallel nonlinear EEG analysis technique, distinguishes mild cognitive impairment and Alzheimer's disease patients with high degree of accuracy. *Artif Intell Med* **40**, 127-41.

Working Memory Electroencephalographic Patterns in Subtypes of Amnestic Mild Cognitive Impairment

Marie-Pierre Deiber[a,b,*], Vicente Ibáñez[b], Gabriel Gold[c] and Panteleimon Giannakopoulos[d,e]

[a]*INSERM U1039, Faculty of Medicine, La Tronche, France*
[b]*Clinical Neurophysiology and Neuroimaging Unit, Division of Neuropsychiatry, Department of Psychiatry, University Hospitals of Geneva, Chêne-Bourg, Switzerland*
[c]*Department of Rehabilitation and Geriatrics, University Hospitals of Geneva, Thônex, Switzerland*
[d]*Division of Geriatric Psychiatry, Department of Psychiatry, University Hospitals of Geneva, Chêne-Bourg, Switzerland*
[e]*Division of Old Age Psychiatry, University Hospitals of Lausanne, Prilly, Switzerland*

Abstract. Amnestic mild cognitive impairment (aMCI) is characterized by memory deficits alone (single-domain, sd-aMCI) or associated with other cognitive disabilities (multi-domain, md-aMCI). Conversion rates to dementia are greater in multi- than in single-domain aMCI, but it remains unclear whether md-aMCI is a mere progression of sd-aMCI or represents a distinct clinical entity. Electroencephalography (EEG) is an easily accessible modality particularly powerful to investigate the functional activation of neocortical circuits. Sensitive attention- and working memory-related EEG indices have been identified in MCI, providing valuable insight on the underlying cerebral alterations. The present study examined the patterns of EEG activity during the encoding and retrieval phases of working memory in md- and sd-aMCI, with the purpose to identify early differences in neural activation between the two subtypes. Continuous EEG was recorded in 43 aMCI patients, whose 16 sd-aMCI and 27 md-aMCI, and 36 age-matched controls (EC) during delayed match-to-sample tasks for face and letter stimuli. At encoding, attended stimuli elicited parietal alpha (8–12 Hz) power decrease (desynchronization), whereas distracting stimuli were associated with alpha power increase (synchronization) over right central sites. No difference was observed in parietal alpha desynchronization among the three groups, suggesting similar attention-related activation of cortical circuits. For attended faces, the alpha synchronization underlying suppression of distracting letters was reduced in both aMCI subgroups, but more severely in md-aMCI cases that differed significantly from EC. At retrieval, the early N250r recognition effect was significantly reduced for faces in md-aMCI as compared to both sd-aMCI and EC. The results suggest the differential alteration of working memory cerebral processes for

*Correspondence to: Marie-Pierre Deiber, PhD, INSERM U1039, Faculty of Medicine, Bâtiment Jean Roger, 38700 La Tronche, France; Clinical Neurophysiology and Neuroimaging Unit, Division of Neuropsychiatry, Department of Psychiatry, University Hospitals of Geneva, Chemin du Petit-Bel-Air 2, 1225 Chêne-Bourg, Switzerland. Tel.: +41 22 305 53 82; Fax: +41 22 305 53 50. E-mail: Marie.P.DeiberIbanez@hcuge.ch.

faces in the two aMCI subtypes. Whereas a progressive impairment of the cerebral activity related to distracter suppression at encoding is already present in sd-aMCI, md-aMCI is characterized by a specific deterioration of face covert recognition process at retrieval.

INTRODUCTION

The concept of MCI assumes that there is a continuum between normal aging and dementia, and designates a heterogeneous condition that includes individuals presenting cognitive impairment in memory and/or other domains but preserved daily life activities and absence of dementia [1]. Clinical characterization further subdivides MCI into amnestic type (aMCI), presenting mainly memory deficits, and non-amnestic type (na-MCI), presenting impairment in non-memory cognitive domains. Amnestic MCI is the most likely to convert to clinically overt Alzheimer's Disease (AD) with an annual rate of 10–15% [2, 3]. The number of affected cognitive functions has been used to further differentiate single domain aMCI (sd-aMCI) with isolated memory impairment from multiple domain aMCI (md-aMCI) showing additional deficits in language, executive functions, or visuospatial abilities [3]. Recent studies suggest that conversion rates to AD are considerably greater for md-aMCI compared to sd-aMCI [4–7]. The psychophysical, structural, and functional imaging characteristics of sd-aMCI and md-aMCI are currently explored, in search for possible differences in the expression of the underlying AD pathology. For instance, a more severe total, but not hippocampal brain atrophy in md-aMCI as compared to sd-aMCI was observed [8]. However, a study using PIB amyloid imaging did not evidence significant differences in the proportion of amyloid-positive patients as a function of the aMCI subtype [9]. Moreover, a larger activation of cerebral networks associated with preserved cognitive functions was even described in sd-aMCI patients compared to controls, pointing to the presence of compensation mechanisms [10]. To date, no formal differentiation between the aMCI subtypes has been evidenced.

Whether the md-aMCI subtype represents a natural progression of sd-aMCI or involves specific pathological processes remains an open question. In front of the inherent heterogeneity of the MCI construct and the limitation of the neuropsychological instruments, the need for an objective evaluation of underlying cerebral pathology appears as a prerequisite for addressing this issue. Among in-vivo investigating tools of the brain, electroencephalography (EEG) represents a widely available, non-invasive and low-cost procedure able to depict dynamic information on brain function with high temporal resolution, particularly suitable to capture subtle alteration in the instant activation of neural generators before the occurrence of significant brain damage in MCI. Early EEG studies focusing on cross-sectional quantitative differences between healthy controls, MCI and AD cases have reported controversial observations, mainly due to the substantial overlap in the quantitative EEG parameters between controls and MCI ([11] for review). In contrast, analysis of the EEG signal in response to controlled events represents a powerful tool for investigating the functional activation of neocortical circuits. Event-related potentials (ERPs), typically recorded by event-locked averaging of the EEG, are made of various components designed by their polarity (N for negative, P for positive) and mean latency of occurrence after event presentation ([12] for review). In parallel, event-related oscillatory activities are obtained by power analysis of the EEG signal, displaying specific response patterns according to the frequency band and the nature of the event ([13] for review). Several EEG contributions in healthy subjects have reported the reactivity of cerebral oscillatory activity to various cognitive attention and memory tasks, especially in the theta, alpha and beta frequency ranges [14–17]. Of particular interest in this context is the distinction between frontal and parietal theta activities in relation to selective attention and working memory load, respectively [18]. In MCI, cognitive activation designs have provided various ERP markers of altered brain function, mostly endogenous components reacting to the cognitive content of the task, such as the P200, N200, P300, N400 or P600 components [19–26]. In working memory tasks, an ERP index of memory load proved to efficiently predict rapid cognitive deterioration in MCI cases [27]. In MCI patients having later deteriorated, the reduction of frontal theta activity as compared to stable cases and elderly controls suggested the presence of early deficits in selective attention networks [28]. Furthermore, combination of event-related indices and beta

activity collected during working memory tasks proved to efficiently predict MCI deterioration [29].

Relatively few studies have used EEG indices to specifically investigate aMCI cases [30–32], and none of them have directly compared the two aMCI subtypes. While episodic memory impairment is a central feature in aMCI, working memory, which refers to the ability to hold and manipulate incoming information for short time periods, may also be affected in this condition [33–36]. Since it refers to short-term processing, working memory is easily accessible to experimental implementation and has proved useful in the evaluation of related processes, i.e., selective attention, manipulation and rehearsal of information, retrieval and central executive functions [37]. Some behavioral studies have suggested that the focusing of attention, a key component of successful working memory, is altered in MCI [38, 39]. Further behavioral data have reported more severe working memory deficits in multi- than single-domain MCI patients [34]. Despite these observations, potential functional differences in memory processes in aMCI have not been examined, although they could represent basic distinctive features of cerebral dysfunction. The present chapter describes an EEG study designed to investigate whether EEG responses can discriminate md-aMCI from sd-aMCI and age-matched controls during working memory performance [40]. In order to disentangle the different processes of memory activation, the delayed-match-to-sample (DMS) experimental task was adopted, which typically contains three phases: encoding ("stimulus"), maintenance ("retention"), and retrieval ("probe") [41]. The encoding phase included face and letter stimuli that were alternatively attended or ignored according to task instruction. Thus, processes of selective attention for task-relevant stimuli as well as suppression of task-irrelevant stimuli were independently evaluated, both processes being susceptible to cognitive deterioration [28, 39, 42, 43]. Letter and face stimuli permitted the evaluation of verbal and non-verbal memory, known to be highly sensitive to cognitive decline ([44] for review). Among non-verbal material, faces represent complex visual stimuli with high social and emotional significance, which recognition is impaired in AD but appears to be preserved in aMCI [45–47]. Such findings underline the need for closer examination of the functional substrates of face recognition, in search for potential cerebral alteration preceding behavioral impact.

The event-related EEG analysis was performed in the encoding and retrieval phases of the DMS task, using formerly identified sensitive electrophysiological markers. In the encoding phase, selective attention processes were examined using the alpha (8–12 Hz) oscillatory activity time-locked to stimulus onset. A decrease in alpha power, or desynchronization (ERD), is commonly observed in cerebral regions actively engaged in the task ([15] for review), while recent evidence suggests that alpha power increase, or synchronization (ERS), can be concomitantly recorded in disengaged regions, allowing functional inhibition necessary for optimal information processing ([48] for review). Deiber and colleagues recently explored the ERPs as well as the alpha activity during the encoding phase of the same DMS task in healthy young and elderly subjects [49]. They showed that alpha activity at encoding depended on whether the stimulus had to be attended or ignored, and that the activity related to suppression of ignored stimuli was altered with age, in correspondence with increased age-related distractibility [50–52]. In the retrieval phase, ERPs elicited by the probe stimuli were examined. The 'N250r' component has been consistently identified in the DMS task, larger in amplitude for attended stimuli previously stored in short-term memory [53]. This repetition-sensitive N250r, particularly pronounced for faces, is thought to represent an early index of covert recognition preceding active recollection processes [54–56]. The rationale for examining early covert processes was that they are less susceptible to be affected by potential compensatory mechanisms that may occult subtle differences between aMCI subtypes.

MATERIALS AND METHODS

Inclusion procedure

Seventy-nine right-handed elderly subjects (64.7 ± 5.9 years; 46 women) were recruited using announcements in local newspapers. All individuals were screened with the Mini Mental State Examination (MMSE) [57], the Lawton's Instrumental Activities of Daily Living (IADL) [58], and the Hospital Anxiety and Depression Scale (HAD) [59]. In addition, extensive neuropsychological testing was performed, including attention (Wechsler Adult Intelligence Scale-Revised, WAIS-R, Code [60], Trail Making Test A [61]), working memory (verbal: Digit Span Forward [62], visuo-spatial: Corsi Block Tapping [63]), episodic memory (verbal: Buschke

Double Memory Test 48 items [64], visual: Shapes [65]), executive functions (Trail Making Test B [61], verbal fluency [66], Wisconsin Card Sorting Test [67]), language (Boston Naming [68]), visual gnosis (Ghent Overlapping Figures [69]) and praxis (ideomotor [70], reflexive [71], and constructional [72]). Subjects were also evaluated with the Clinical Dementia Rating scale (CDR) [73], and only CDR 0 cases with scores within 1.5 standard deviations of the age appropriate mean in all tests were included in the control group (EC), made of 36 individuals (64.7 ± 6.6 years; 24 women). Participants having a CDR score of 0.5 but no dementia, and a score more than 1.5 standard deviations below the age appropriate mean in any of the above tests, were diagnosed as possible MCI [74]. Among these cases, single domain amnestic MCI (decreased performance in the Buschke Double Memory Test 48 items) were distinguished from multi-domain amnestic MCI (decreased performance in the Buschke Double Memory Test 48 items and either the Trail Making test or the Corsi Block Tapping test) [75]. These patients were reviewed independently by two highly experienced clinicians blinded to each other's findings and were included in the respective MCI groups only if both clinicians concurred on the diagnosis. The final sample included 16 single domain amnestic MCI (sd-aMCI, 65.8 ± 5.4 years, 7 women), and 27 multi-domain amnestic MCI (md-aMCI, 64 ± 5.3 years, 15 women) (Table 1).

All EC and aMCI participants had normal or corrected-to-normal visual acuity, and none reported a history of major medical disorders (cancer, cardiac illness), sustained head injury, psychiatric or neurological disorders, and alcohol or drug abuse. Subjects with regular use of psychotropics, stimulants and ß-blockers were excluded because of the potential effects of these drugs on cerebral activity. Informed written consent was obtained from all participants included in the study. The study was approved by the Ethical Committee of the University Hospitals of Geneva, and was in line with the Helsinki Declaration.

Experimental design

Three blockwise-interleaved delayed-match-to-sample (DMS) tasks were used in which visual information was held constant while the task demands were manipulated [49, 76]. The participants, comfortably seated, watched a computer-controlled display screen at a distance of 80 cm. In each task, they viewed series of four images, two faces and two letters, presented in a randomized order (Fig. 1). Each image was presented for 1000 ms with a 600 ms blank-screen inter-stimulus interval. The tasks differed on the basis of the instruction informing the participants on how to process the stimuli: (A1) Face task: Remember Faces and Ignore Letters, (A2) Letter task: Remember Letters and Ignore Faces, and (A3) Passive task: Passive View of both Faces and Letters, with no attempt to remember or evaluate them. The attention status was conceptualized as follows: for A1 and A2 memory conditions, attention is required for one stimulus category ("Attend"), the irrelevant stimulus category being ignored ("Ignore") (e.g., faces are selectively attended in task A1, and ignored in task A2); in task A3, no attention is devoted to neither stimulus category ("Passive"). Images were followed by a 1200 ms delay period, after which a fifth stimulus (probe) was presented until the subjects responded or for a maximum of 2800 ms. In the memory tasks (A1, A2), the probe was a face or a letter (depending upon the condition), and participants were required to report whether it matched (target) or not (lure) one of the previously presented, relevant stimuli. In the Passive task (A3), an arrow was presented as probe and the subjects were required to indicate its direction. A 2000 ms inter-trial interval followed either the response or the 2800 ms response-window. In all tasks, the subjects' response consisted in pressing a button with the right or left index finger (memory tasks: target or lure, Passive task: right or left arrow direction). Targets and lures, as well as right and left arrow directions, occurred with equal probability. Images of faces and letters were embedded in a 50% random noise grey rectangular background patch subtending approximately $6° \times 7°$ of visual angle. Sixty

Table 1
Demographic and clinical data

Variables	EC	sd-aMCI	md-aMCI
Age (years)	64.7 ± 6.6	65.8 ± 5.4	64.0 ± 5.3
Gender (f/m)	24/12	7/9	15/12
Education[a]	2.0 ± 0.8	2.4 ± 0.6	1.9 ± 0.7
MMSE	29.0 ± 0.8	28.2 ± 1.5	27.7 ± 1.9
IADL	8.4 ± 1.0	8.6 ± 0.7	8.5 ± 1.0
HAD anxiety	6.0 ± 2.4	5.3 ± 3.5	6.1 ± 3.4
HAD depression	2.6 ± 1.9	1.8 ± 1.8	2.3 ± 1.8

Data are presented as mean $\pm$ SD. EC: elderly controls ($N = 36$); sd-aMCI: single-domain amnestic MCI ($N = 16$); md-aMCI: multi-domain amnestic MCI ($N = 27$). [a]Education levels, 1: $\leq$9 years, 2: 10 to 12 years, 3: >12 years; MMSE: Mini-Mental State Examination; IADL: Lawton's Instrumental Activities of Daily Living; HAD: Hospital Anxiety and Depression Scale (cut off is 8 for both anxiety and depression).
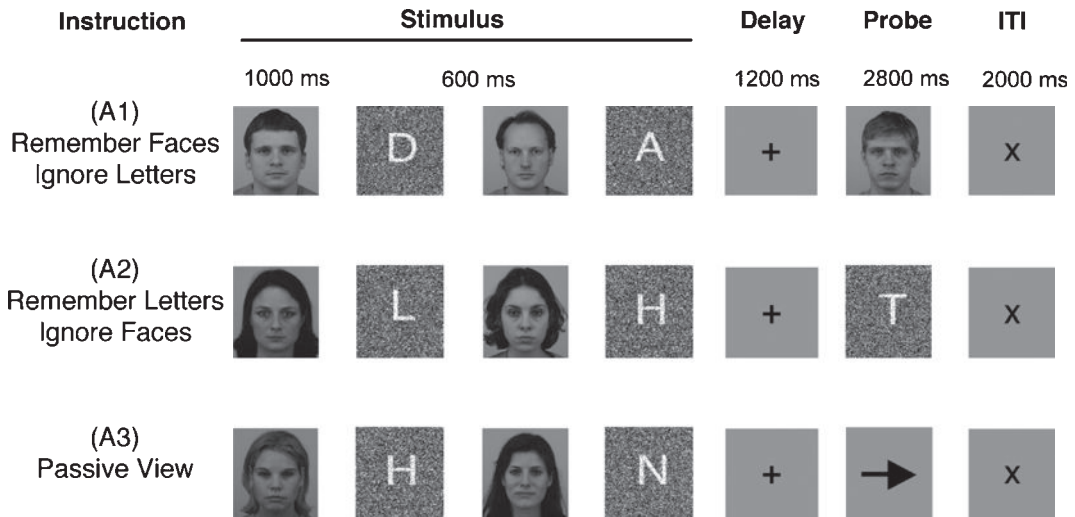
Fig. 1. Experimental design. In each trial, 2 faces and 2 letters are presented in a randomized order. Tasks differ in the instructions given at the beginning of each run and in the response requirements. In the response period (Probe), a face (A1) or a letter (A2) is presented, and subjects must report with a button press whether the stimulus matched one of the previously presented stimuli. In the passive task (A3), subjects make a button press indicating the direction of the arrow.

digitized grayscale images of male (30) and female (30) faces of neutral expressions were selected from the Karolinska Directed Emotional Faces set [77], the gender of the face stimuli used within each trial being held constant. Twenty letter images were used, made of Arial font white letters with 10% grey noise. Each task consisted of 36 trials (72 face and 72 letter stimuli) and lasted approximately 5.5 min. Twenty out of the 72 face images were repeated once within a run, while letters were repeated on average 3.6 times per run. The order of task presentation was randomized across participants. A short training session on the Face task preceded the session, so that each participant got familiar with the task requirements.

Data acquisition and processing

Continuous EEG was recorded using 30 surface electrodes mounted on a cap (NeuroScan Quick Cap) and referenced to the linked earlobes. Electrode impedances were kept below 5 kΩ. Electrophysiological signals were sampled at 1000 Hz with lower cutoff at 0.05 Hz and upper cutoff at 200 Hz (DC amplifiers and software by NeuroScan, USA). The electrooculogram was recorded using two pairs of bipolar electrodes in both vertical and horizontal directions. Visual stimuli and button presses were automatically documented with markers in the continuous EEG file, which were used off-line to segment the contin-

uous EEG data into epochs time-locked to stimulus onset.

Reaction time (RT) was measured as the time interval between probe onset and response button press. Accuracy was defined as the percentage of correct responses. Raw EEG data were re-referenced to the average reference off-line. Ocular artifacts were removed using singular value decomposition (NeuroScan software). The EEG was segmented into epochs of 1000 ms time-locked on stimulus onset and epochs of 1200 ms starting 200 ms before probe onset for encoding and retrieval analysis, respectively. The epochs were automatically scanned for contamination by muscular or electrode artifacts, and the remaining trials were inspected visually to control for residual minor artifacts.

Encoding

The power of the signal in the alpha frequency range was obtained using the frequency extraction module of Brain Vision Analyzer software between 7.5 and 12.5 Hz. Within each task and for each trial, the power from stimulus onset to offset (1000 ms) corresponded to the power in the active state (A), whereas the average power during the 500 ms preceding the trial was selected as the reference period power (R). The percentage of power change over baseline was calculated using the traditional formula: $\%ERD/ERS = (A–R)/R \times$

100. Thus, negative percentage values correspond to a decrease in power, or desynchronization (ERD), and positive percentage values to a power increase, or synchronization (ERS) [13]. Deiber et al. previously demonstrated that alpha ERD associated to attended stimuli displayed a parietal distribution with right lateralization for faces (P4) and left lateralization for letters (P7), whereas alpha ERS associated to ignored and passively viewed stimuli culminated in the right central region (C4) [49]. The alpha %ERD/ERS time course was measured between 200 and 1000 ms in 10 ms time-windows over the electrodes showing maximal alpha responses, i.e, right parietal (P4) for attended faces, left parietal (P7) for attended letters, and right central (C4) for both faces and letters in Ignore and Passive status.

Retrieval

ERPs were obtained by averaging the EEG signal within 1000 ms after probe onset, with a 200-ms pre-probe baseline, for correct-response trials only. They were band-pass filtered between 0.5 and 30 Hz (-48 dB/octave) using a zero-phase shift digital filter. To examine the effects of stimulus repetition on ERPs at retrieval, the waveforms for faces/letters that matched a face/letter in the encoding set (target ERPs) were compared to the waveforms for faces/letters that did not match any of the faces/letters in the encoding set (lure ERPs). A target minus lure difference waveform was obtained for each Face and Letter task, which revealed the N250r component as an increased negativity over the right central region in the latency range between 230 and 350 ms. N250r amplitude was measured on the culmination electrodes identified in the grand average target minus lure difference waveform (FC4, C4, CP4).

Statistical analysis

Demographic (age, gender, education) and neuropsychological scores were compared among the three groups using the Kruskal-Wallis non-parametric test, with Bonferroni correction for multiple group comparisons. The distribution of performance values was normalized using cubic transformation. RT as well as normalized performance values were compared using a two-way repeated measures ANCOVA with Task (Face, Letter, Passive) as within-subject and Group (EC, sd-aMCI, md-aMCI) as between-subject factors, while controlling for age, gender and education. Post-hoc analysis used paired t-tests with

Bonferroni correction for multiple comparisons. In the encoding phase, for each stimulus category and attention status, the effect of group was tested on alpha %ERD/ERS within each 10 ms-time window using a one-way repeated measures ANCOVA with control for age, gender and education. To partially correct for multiple comparisons, data were considered reliable only when at least 5 consecutive time-windows (50 ms) were significant ($p < 0.05$). In the retrieval phase, the N250r amplitude values were entered into a two-way repeated-measures ANCOVA, with Stimulus category (Face, Letter) as within-subject and Group (EC, sd-aMCI, md-aMCI) as between-subject factors, while controlling for age, gender and education. Post-hoc analysis used paired t-tests with Bonferroni correction for multiple comparisons.

RESULTS

Clinical and neuropsychological data (Tables 1 and 2)

Age, gender and education did not differ significantly between the three groups. IADL and HAD

Table 2
Neuropsychological data

Variables	EC	sd-aMCI	md-aMCI
Attention			
WAIS-R; Code	64.8 ± 13.4	62.2 ± 10.8	56.2 ± 12.6
Trail Making Test A (s)	37.0 ± 9.8	35.6 ± 9.1	46.9 ± 15.6
Working memory			
Verbal (Digit)	6.8 ± 2.0	7.0 ± 2.4	6.0 ± 1.5
Visuo-spatial (Corsi)	5.6 ± 1.4	5.6 ± 1.5	4.7 ± 1.6
Episodic memory			
Verbal (Buschke 48)			
Immediate recall (IR)	42.7 ± 3.6	35.9 ± 8.3	36.1 ± 5.2
Differed cued recall (DR)	29.7 ± 4.9	17.9 ± 4.2	23.0 ± 5.1
Intrusions	2.6 ± 2.2	3.6 ± 3.0	4.3 ± 2.8
Visual (Shapes)	11.8 ± 0.4	11.6 ± 0.8	10.9 ± 1.5
Executive functions			
Trail Making Test B (s)	59.0 ± 17.6	57.9 ± 17.5	89.3 ± 44.9
Verbal Fluency	24.2 ± 6.8	20.5 ± 6.0	22.5 ± 6.6
WCST	5.3 ± 1.5	5.4 ± 1.2	4.4 ± 2.0
Language (Boston)	19.6 ± 0.8	19.1 ± 0.8	19.1 ± 0.9
Visual gnosis (Ghent)	5.0 ± 0.0	5.0 ± 0.0	5.0 ± 0.0
Standardized praxis			
Ideomotor	29.3 ± 1.2	28.1 ± 3.2	28.3 ± 1.9
Reflexive	7.5 ± 0.8	7.6 ± 0.5	7.0 ± 0.9
Constructional	10.6 ± 1.7	11.0 ± 0.0	10.6 ± 0.7

Data are presented as mean ± SD. EC: elderly controls; sd-aMCI: single-domain amnestic MCI; md-aMCI: multi-domain amnestic MCI. WAIS-R: Wechsler Adult Intelligence Scale - Revised; WCST: Wisconsin Card Sorting Test, number of completed categories (/6); Ideomotor praxis: transitive and intransitive (/30).

scores were also comparable among groups. EC had a significantly higher MMSE than md-aMCI ($p < 0.005$), and significantly higher Buschke immediate recall (IR) and differed cued-recall (DR) scores than both sd-aMCI (IR: $p < 0.005$, DR: $p < 0.0001$) and md-aMCI (IR, DR: $p < 0.0001$). Md-aMCI were slower than both EC and sd-aMCI in the Trail Making Test A ($p < 0.01$) and B ($p < 0.001$).

Behavioral data

Figure 2 displays the mean reaction time and performance for each task and group. There was a significant task effect on RTs ($F_{(2,72)} = 102.8$, $p < 0.0001$), with longest RTs for Face followed by Letter and Passive tasks (Face > Passive: $t = 21.84$, $p < 0.005$; Face > Letter: $t = 8.43$, $p < 0.005$; Letter > Passive: $t = 21.94$, $p < 0.005$). Main effects of group ($F_{(2,72)} = 5.78$, $p < 0.001$) and task ($F_{(2,72)} = 98.4$, $p < 0.001$) were observed on performance. Md-aMCI was the worst performing group, with significantly poorer overall performance than EC ($t = 3.06$, $p < 0.005$). In terms of performance, the Face task was significantly harder that the Letter and Passive tasks (Face < Letter: $t = 9.8$, $p < 0.005$; Face < Passive: $t = 13.63$, $p < 0.005$; Letter < Passive: $t = 5.95$, $p < 0.005$). Additionally, there was an interaction between group and task ($F_{(4,72)} = 2.79$, $p < 0.05$), with md-aMCI performing significantly worse than EC in the Face task only ($t = 3.19$, $p < 0.01$). No effects of age, gender and education were observed on RT and performance.

Electrophysiological data at encoding: alpha %ERD/ERS

Figure 3A shows the time course of alpha power for each group, stimulus category and attention status, on electrodes with maximal alpha responses. After 200 ms, attended stimuli elicited an alpha ERD on parietal electrodes, maximal on right and left hemisphere for face and letter, respectively. Ignored stimuli were accompanied by a sustained alpha ERS culminating on right central electrode for both stimulus categories. A main effect of group was observed only for ignored letters, starting at 230 and ending at 360 ms ($F_{(2,72)}$ range = 3.27 to 4.64, $p < 0.05$). Whereas both aMCI subgroups showed reduced alpha ERS as compared to EC, this reduction was significant only in md-aMCI (t range = 2.43 to 2.84, $p < 0.05$). There was also a trend for reduced alpha ERS between 260 and
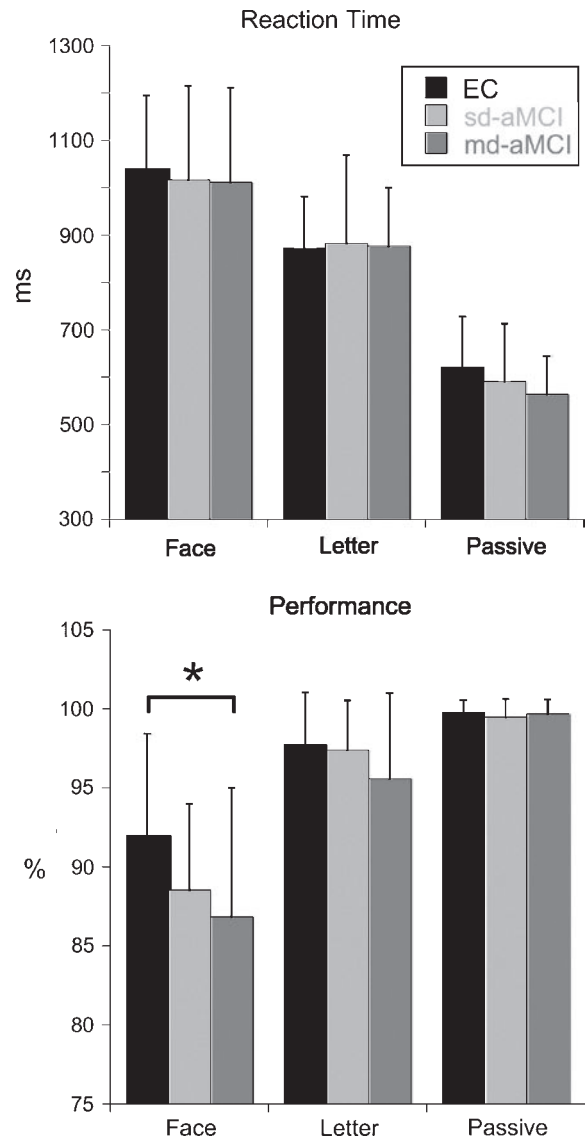
Fig. 2. Mean reaction time (ms) and performance (% of correct response) for each task and group, with standard deviations. EC: elderly controls ($N = 36$); sd-aMCI: single-domain amnestic MCI ($N = 16$); md-aMCI: multi-domain amnestic MCI ($N = 27$). Face performance is significantly worse in md-aMCI as compared to EC (*: $p < 0.01$).

330 ms in md-aMCI compared to EC when ignoring faces ($p < 0.07$). The topographic distribution of alpha power for ignored letters reveals the marked reduction of alpha ERS on right central region in md-aMCI as compared to EC, and the intermediate reduction level for sd-aMCI (Fig. 3B). No effects of age, gender and education were observed on alpha %ERD/ERS.
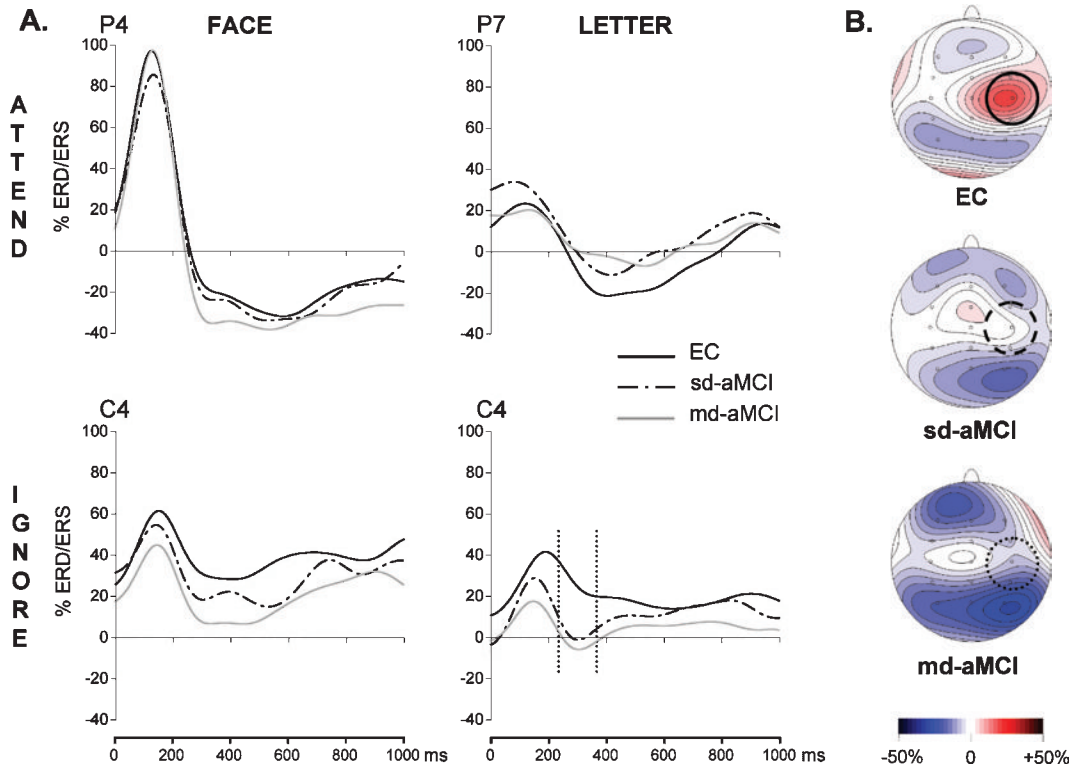
Fig. 3. **A**. Grand average alpha %ERD/ERS for face and letter stimuli in Attend (upper row) and Ignore (bottom row) attention status in the 3 groups. Data are presented at electrodes showing largest alpha responses. After 200 ms the Attend status is associated with a parietal alpha ERD (negative values), and the Ignore status with a sustained central alpha ERS (positive values). The alpha ERS to ignored letters is significantly smaller in md-aMCI compared to EC between 230 and 360 ms (dotted lines). **B**. Topographic distribution of alpha %ERD/ERS for ignored letters in the 3 groups, average between 230 to 360 ms after stimulus onset. Blue colors for ERD, red colors for ERS. Compared to controls (solid circle), the right central ERS is reduced in sd-aMCI (dashed circle) and negligible in md-aMCI (dotted circle).

Electrophysiological data at retrieval: target vs. lure ERPs

Figures 4 and 5 show the grand average waveforms to target and lure probes within each group for face and letter, respectively. P1 and N1 early visual ERP components were recorded at occipital sites, while the N170 component culminated over the right occipito-temporal region and was larger for face than letter stimuli, in agreement with the well described face-sensitivity of the N170 ([78] for review). There was no significant difference on these components across groups. Subtracting lure from target ERPs revealed a N250r component with right centro-parietal distribution. The N250r was markedly reduced in md-aMCI for faces (Fig. 4), whereas it was similar among groups for letters (Fig. 5). Main effects of group ($F_{(2,72)} = 8.36$, $p < 0.001$) and stimulus category ($F_{(1,72)} = 6.95$, $p < 0.05$) were observed on N250r

amplitude. N250r for faces was significantly reduced in md-aMCI as compared to EC ($t = 3.40$, $p < 0.005$) and sd-aMCI ($t = 3.48$, $p < 0.005$), whereas no significant difference was observed across groups for letters. N250r for faces was larger than for letters ($t = 2.92$, $p < 0.05$). No effects of age, gender and education were observed on N250r.

DISCUSSION

The present data revealed distinct patterns of EEG responses in aMCI subtypes during working memory tasks. Unlike sd-aMCI cases who display moderate EEG activity alteration confined to encoding, md-aMCI show significant alteration of EEG patterns that concerns both the encoding and retrieval phases of the memory process. These results pointed out the sensitivity of electrophysiological indices to detect early

ERPs to FACE probes

A.

EC   sd-aMCI   md-aMCI

O2

N1

P1

target
lure
target - lure

P8

N170

2 µV

100 ms

CP4

N250r   N250r   ?

C4

N250r   N250r   ?

B.

-2 µV   0   +2 µV

Fig. 4. **A**. Grand average ERPs to target (solid line) and lure (dotted line) face probes, and difference waves between target and lure (gray line). The N250r repetition effect signaled on difference waves over CP4 and C4 electrodes in EC and md-aMCI (dashed line) is negligible in md-aMCI (dotted line). **B**. Topographic distribution of N250r repetition effect for faces at latency of peak amplitude in the 3 groups. N250r displays a right centro-parietal distribution in both EC and sd-aMCI, and is not detectable in md-aMCI (dotted circle).
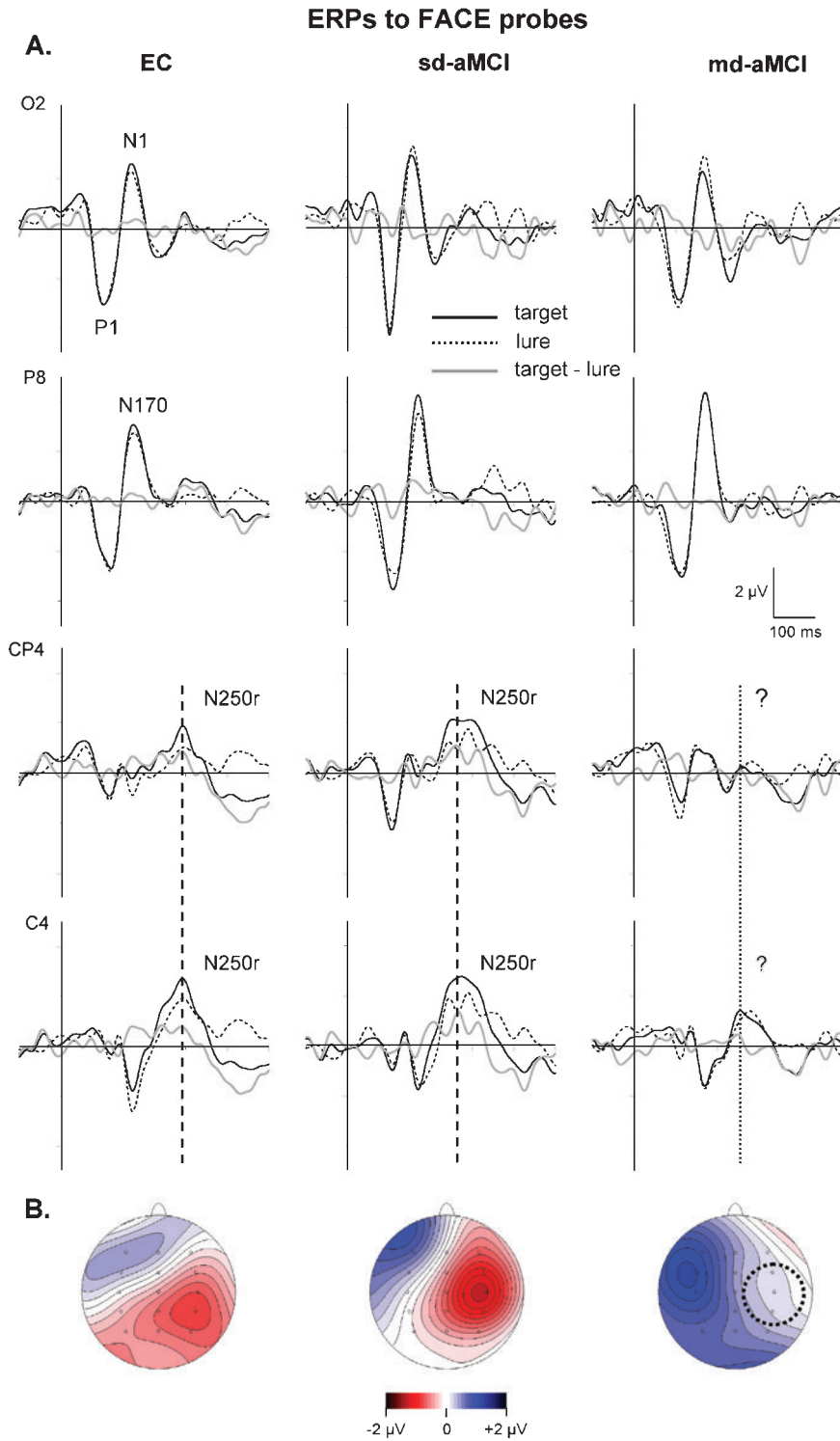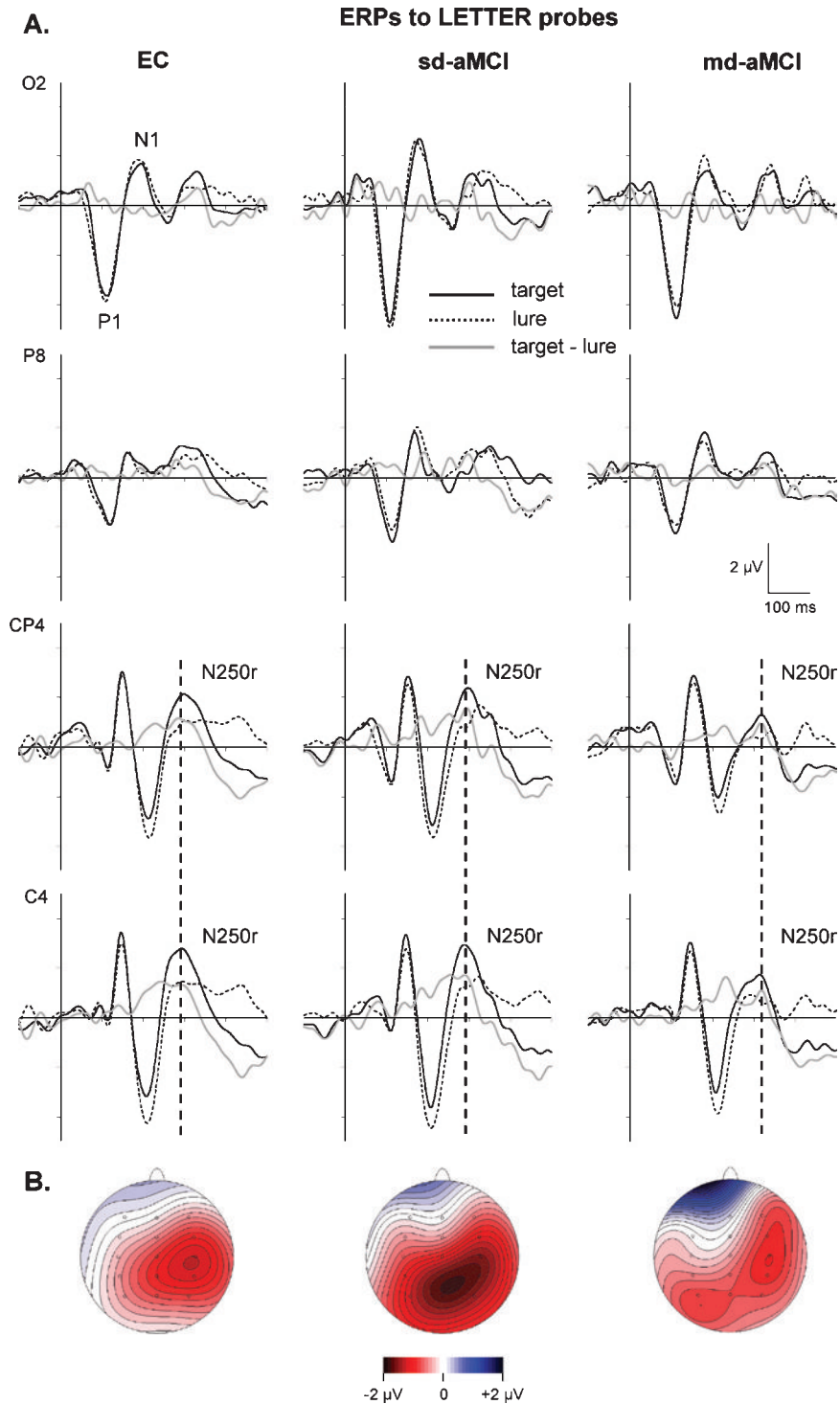
Fig. 5. **A.** Grand average ERPs to target (solid line) and lure (dotted line) letter probes, and difference waves between target and lure (gray line). The N250r repetition effect signaled on difference waves over CP4 and C4 electrodes is similar in the 3 groups (dashed line). **B**. Topographic distribution of N250r repetition effect for letters at latency of peak amplitude in the 3 groups.

functional differences in short-term memory processes between subtypes of aMCI.

Encoding

The observation on alpha ERD/ERS confirmed the patterns of alpha activity according to the top-down control of attention carried by the instruction that were recently described in healthy elderly controls [49]. Attended stimuli were associated with a bilateral parietal alpha ERD showing stimulus-specific lateralization tendency, i.e., predominant right and left distribution for faces and letters, respectively. Such posterior alpha desynchronization reflects selective attentional activation in dedicated cerebral areas [13, 15]. Intervening distracting stimuli that had to be ignored were associated with right predominant central alpha ERS, suggesting a role of this region in the top-down mechanism of distracter suppression. Indeed, alpha ERS, corresponding to an increase in alpha power, is thought to reflect the functional inhibition of task-irrelevant regions necessary to allocate resources to task-relevant regions [48, 79–82].

The similar parietal alpha ERD observed in the three diagnostic groups supported the preservation of cerebral processes relative to selective visual attention in aMCI. There is an ongoing discussion about the attentional processes that are altered in MCI patients. Whereas alteration of selective attention was proposed [38, 39], the most severe difficulties were often observed in disengaging and shifting attention, as well as in inhibiting competing responses [42, 43, 83, 84]. Deiber and colleagues recently reported that stable MCI patients showed similar frontal induced theta activity as controls at inclusion, suggesting the preservation of cortical circuits involved in selective attentional processes [18, 28]. They also observed spared attention-related alpha activity in elderly as compared to young healthy individuals [49]. The comparable posterior alpha activity in aMCI and controls reported here is concordant with these findings. However, MCI cases that deteriorate at one-year follow-up displayed decreased frontal induced theta activity at inclusion, suggesting early deficits in selective attention networks in progressive MCI [28]. Taken together, these results indicate that the cerebral activity underlying selective attention is preserved independently of age and mild cognitive decline, but may undergo early significant alteration in rapidly evolving cognitive impairment.

The reduction of alpha ERS to ignored stimuli in md-aMCI compared to controls suggested altered suppression activity for distracters in this subgroup [49]. Although such deficit was observed in both face and letter tasks, it was only significant in the most difficult face task, in which the participants had to suppress irrelevant letters. Interestingly, in the same task, md-aMCI displayed significantly worst performances compared to controls. These findings are consistent with most attention studies in MCI and early AD reporting an association between cognitive impairment and enhanced vulnerability to interferences [42, 85, 86]. In line with the data in md-aMCI cases, an age-related reduction of alpha ERS to distracting letters was recently evidenced [49], supporting the vulnerability of top-down suppression mechanisms even in normal brain aging [50–52, 87]. Sd-aMCI showed alpha ERS values closer to md-aMCI than to controls, but not significantly different from either groups. Such intermediate alpha ERS pattern supports the idea of a continuum in the susceptibility of top-down inhibition mechanisms from young to healthy elderly and sd-aMCI, the md-aMCI displaying the highest vulnerability of related cortical circuits.

Retrieval

The subtraction of lure ERPs from target ERPs did not reveal any significant difference before 250 ms in any of the diagnostic group. This observation supports previous findings reporting preserved sensory processing in MCI and AD, as indexed by unaltered cortical ERPs before 185–200 ms [19, 88, 89]. The N200 component is among the initial ERP whose latency delay has been described as potentially predictive of cognitive deterioration in MCI patients [26, 29]. Concerning early cognitive components, the N250r is a negative deflection consistently described for immediate face repetitions [90, 91]. It refers to a relatively more negative ERP for repeated (target) as compared to unrepeated (lure) faces, typically peaking between 230 and 330 ms over right parieto-temporal sites. The N250r, also observed for other visual stimuli such as letters and words [56, 92–94], is thought to reflect the covert repetition-sensitive activation of stored representations for recognition. The present data revealed a larger N250r for faces than letters, consistent with the well-established sensitivity for face recognition of this component [55]. Importantly, a significant group effect was evidenced on the N250r, with md-aMCI showing smaller N250r amplitude for faces than both

sd-aMCI and control subjects. This result suggests that the brain process of matching face information to short-term representations is specifically altered in md-aMCI subgroup, supporting distinct functional vulnerability among the two aMCI subtypes. Parallel observations indicate that retrieval processes are particularly sensitive to cognitive decline. The memory "storage" C250 component, analogous to the N250r, was recently shown to be among the ERP components predicting MCI individuals who deteriorate versus those who remain stable, supporting its discriminating power for MCI conversion to AD [19]. Regarding face processing, neuropsychological studies have documented the absence of deficit in face recognition in aMCI compared to AD patients [45, 47]. The present results reveal early deficits in the activation of neural generators involved in covert face recognition in md-aMCI patients, and suggest distinctive underlying functional characteristics between the two aMCI subgroups at retrieval.

Single versus multi-domain aMCI

Very few studies have specifically addressed the potential disparities in cognitive activation between single- and multi-domain aMCI subgroups. In a visual search task, behavioral measures of visual attention and intraindividual variability showed significant differences in attention between md-aMCI (but not sd-aMCI) and controls, with decrements in controlled processing and shifting efficacy, albeit preserved attentional distribution [95]. Such visual attention impairment could be expected to affect encoding processing in md-aMCI. The present data confirm this hypothesis and reveal for the first time to our knowledge a differential alteration of working memory-related cerebral processes for faces in aMCI subtypes. Compared to controls md-aMCI were more severely impaired than sd-aMCI in respect to brain activation related to distracter inhibition at encoding. Such activation was moderately altered in sd-aMCI, supporting the idea of a progressive worsening in the cerebral control of interfering stimuli with increasing severity of cognitive deficits. Contrasting with this continuum between sd- and md-aMCI at encoding, only md-aMCI displayed a vulnerability of cortical circuits involved in covert face recognition at retrieval. This qualitative difference implies that md-aMCI are exposed not only to the progressive damage of neural generators already affected in sd-aMCI during the encoding phase of working memory, but also to spe-

cific pathological processes relative to covert face recognition.

REFERENCES

[1] Petersen RC (2004) Mild cognitive impairment as a diagnostic entity. *J Intern Med* **256**, 183-194.

[2] Mariani E, Monastero R, Mecocci P (2007) Mild cognitive impairment: a systematic review. *J Alzheimers Dis* **12**, 23-35.

[3] Petersen RC, Negash S (2008) Mild cognitive impairment: an overview. *CNS Spectr* **13**, 45-53.

[4] Alexopoulos P, Grimmer T, Perneczky R, Domes G, Kurz A (2006) Progression to dementia in clinical subtypes of mild cognitive impairment. *Dement Geriatr Cogn Disord* **22**, 27-34.

[5] Forlenza OV, Diniz BS, Nunes PV, Memoria CM, Yassuda MS, Gattaz WF (2009) Diagnostic transitions in mild cognitive impairment subtypes. *Int Psychogeriatr* **21**, 1088-1095.

[6] Rasquin SM, Lodder J, Visser PJ, Lousberg R, Verhey FR (2005) Predictive accuracy of MCI subtypes for Alzheimer's disease and vascular dementia in subjects with mild cognitive impairment: a 2-year follow-up study. *Dement Geriatr Cogn Disord* **19**, 113-119.

[7] Tabert MH, Manly JJ, Liu X, Pelton GH, Rosenblum S, Jacobs M, Zamora D, Goodkind M, Bell K, Stern Y, Devanand DP (2006) Neuropsychological prediction of conversion to Alzheimer disease in patients with mild cognitive impairment. *Arch Gen Psychiatry* **63**, 916-924.

[8] He J, Farias S, Martinez O, Reed B, Mungas D, Decarli C (2009) Differences in brain volume, hippocampal volume, cerebrovascular risk factors, and apolipoprotein E4 among mild cognitive impairment subtypes. *Arch Neurol* **66**, 1393-1399.

[9] Wolk DA, Price JC, Saxton JA, Snitz BE, James JA, Lopez OL, Aizenstein HJ, Cohen AD, Weissfeld LA, Mathis CA, Klunk WE, De-Kosky ST (2009) Amyloid imaging in mild cognitive impairment subtypes. *Ann Neurol* **65**, 557-568.

[10] Lenzi D, Serra L, Perri R, Pantano P, Lenzi GL, Paulesu E, Caltagirone C, Bozzali M, Macaluso E (2009) Single domain amnestic MCI: A multiple cognitive domains fMRI investigation. *Neurobiol Aging*. doi:10.1016/j.neurobiolaging.2009.09.006

[11] Giannakopoulos P, Missonnier P, Kovari E, Gold G, Michon A (2009) Electrophysiological markers of rapid cognitive decline in mild cognitive impairment. *Front Neurol Neurosci* **24**, 39-46.

[12] Picton TW, Lins OG, Scherg M (1995) The recording and analysis of event-related potentials. In *Handbook of Neuropsychology, Section 14: Event-Related Brain Potentials and Cognition*, Johnson R, ed. Elsevier, Amsterdam, pp. 3-73.

[13] Pfurtscheller G, Lopes da Silva FH (1999) Event-related EEG/MEG synchronization and desynchronization: basic principles. *Clin Neurophysiol* **110**, 1842-1857.

[14] Jensen O, Gelfand J, Kounios J, Lisman JE (2002) Oscillations in the alpha band (9-12 Hz) increase with memory load during retention in a short-term memory task. *Cereb Cortex* **12**, 877-882.

[15] Klimesch W (1999) EEG alpha and theta oscillations reflect cognitive and memory performance: a review and analysis. *Brain Res Rev* **29**, 169-195.

[16] Raghavachari S, Kahana MJ, Rizzuto DS, Caplan JB, Kirschen MP, Bourgeois B, Madsen JR, Lisman JE (2001) Gating of human theta oscillations by a working memory task. *J Neurosci* **21**, 3175-3183.

[17] Tallon-Baudry C, Bertrand O, Fischer C (2001) Oscillatory synchrony between human extrastriate areas during visual short-term memory maintenance. *J Neurosci* **21**, RC177.

[18] Deiber MP, Missonnier P, Bertrand O, Gold G, Fazio-Costa L, Ibáñez V, Giannakopoulos P (2007) Distinction between perceptual and attentional processing in working memory tasks: a study of phase-locked and induced oscillatory brain dynamics. *J Cogn Neurosci* **19**, 158-172.

[19] Chapman RM, McCrary JW, Gardner MN, Sandoval TC, Guillily MD, Reilly LA, Degrush E (2009) Brain ERP components predict which individuals progress to Alzheimer's disease and which do not. *Neurobiol Aging*,. doi:10.1016/j.neurobiolaging.2009.11.010

[20] Chapman RM, Nowlis GH, McCrary JW, Chapman JA, Sandoval TC, Guillily MD, Gardner MN, Reilly LA (2007) Brain event-related potentials: Diagnosing early-stage Alzheimer's disease. *Neurobiol Aging* **28**, 194-201.

[21] Ford JM, Askari N, Mathalon DH, Menon V, Gabrieli JD, Tinklenberg JR, Yesavage J (2001) Event-related brain potential evidence of spared knowledge in Alzheimer's disease. *Psychol Aging* **16**, 161-176.

[22] Gironell A, Garcia-Sanchez C, Estevez-Gonzalez A, Boltes A, Kulisevsky J (2005) Usefulness of P300 in subjective memory complaints: a prospective study. *J Clin Neurophysiol* **22**, 279-284.

[23] Golob EJ, Starr A (2000) Effects of stimulus sequence on event-related potentials and reaction time during target detection in Alzheimer's disease. *Clin Neurophysiol* **111**, 1438-1449.

[24] Olichney JM, Hillert DG (2004) Clinical applications of cognitive event-related potentials in Alzheimer's disease. *Phys Med Rehabil Clin N Am* **15**, 205-233.

[25] Olichney JM, Taylor JR, Gatherwright J, Salmon DP, Bressler AJ, Kutas M, Iragui-Madoz VJ (2008) Patients with MCI and N400 or P600 abnormalities are at very high risk for conversion to dementia. *Neurology* **70**, 1763-1770.

[26] Papaliagkas V, Kimiskidis V, Tsolaki M, Anogianakis G (2008) Usefulness of event-related potentials in the assessment of mild cognitive impairment. *BMC Neurosci* **9**, 107.

[27] Missonnier P, Gold G, Fazio-Costa L, Michel JP, Mulligan R, Michon A, Ibáñez V, Giannakopoulos P (2005) Early event-related potential changes during working memory activation predict rapid decline in mild cognitive impairment. *J Gerontol A Biol Sci Med Sci* **60**, 660-666.

[28] Deiber MP, Ibáñez V, Missonnier P, Herrmann F, Fazio-Costa L, Gold G, Giannakopoulos P (2009) Abnormal-induced theta activity supports early directed-attention network deficits in progressive MCI. *Neurobiol Aging* **30**, 1444-1452.

[29] Missonnier P, Deiber MP, Gold G, Herrmann FR, Millet P, Michon A, Fazio-Costa L, Ibáñez V, Giannakopoulos P (2007) Working memory load-related electroencephalographic parameters can differentiate progressive from stable mild cognitive impairment. *Neuroscience* **150**, 346-356.

[30] Golob EJ, Irimajiri R, Starr A (2007) Auditory cortical activity in amnestic mild cognitive impairment: relationship to subtype and conversion to dementia. *Brain* **130**, 740-752.

[31] Teipel SJ, Pogarell O, Meindl T, Dietrich O, Sydykova D, Hunklinger U, Georgii B, Mulert C, Reiser MF, Moller HJ, Hampel H (2009) Regional networks underlying interhemispheric connectivity: an EEG and DTI study in healthy ageing and amnestic mild cognitive impairment. *Hum Brain Mapp* **30**, 2098-2119.

[32] van der Hiele K, Vein AA, Kramer CGS, Reijntjes RHAM, van Buchem MA, Westendorp RGJ, Bollen ELEM, van Dijk JG, Middelkoop HAM (2007) Memory activation enhances EEG abnormality in mild cognitive impairment. *Neurobiol Aging* **28**, 85-90.

[33] Bokde AL, Karmann M, Born C, Teipel SJ, Omerovic M, Ewers M, Frodl T, Meisenzahl E, Reiser M, Moller HJ, Hampel H (2010) Altered brain activation during a verbal working memory task in subjects with amnestic mild cognitive impairment. *J Alzheimers Dis* **21**, 103-118.

[34] Brandt J, Aretouli E, Neijstrom E, Samek J, Manning K, Albert MS, Bandeen-Roche K (2009) Selectivity of executive function deficits in mild cognitive impairment. *Neuropsychology* **23**, 607-618.

[35] Economou A, Papageorgiou SG, Karageorgiou C, Vassilopoulos D (2007) Nonepisodic memory deficits in amnestic MCI. *Cogn Behav Neurol* **20**, 99-106.

[36] Kessels RP, Meulenbroek O, Fernandez G, Olde Rikkert MG (2010) Spatial working memory in aging and mild cognitive impairment: effects of task load and contextual cueing. *Neuropsychol Dev Cogn B Aging Neuropsychol Cogn* **17**, 556-574.

[37] Baddeley A (1992) Working memory. *Science* **255**, 556-559.

[38] Alescio-Lautier B, Michel BF, Herrera C, Elahmadi A, Chambon C, Touzet C, Paban V (2007) Visual and visuospatial short-term memory in mild cognitive impairment and Alzheimer disease: Role of attention. *Neuropsychologia* **45**, 1948-1960.

[39] Levinoff EJ, Saumier D, Chertkow H (2005) Focused attention deficits in patients with Alzheimer's disease and mild cognitive impairment. *Brain Cogn* **57**, 127-130.

[40] Deiber MP, Ibáñez V, Herrmann F, Rodriguez C, Emch J, Missonnier P, Millet P, Gold G, Giannakopoulos P (2011) Face short-term memory-related electroencephalographic patterns can differentiate multi- versus single-domain amnestic mild cognitive impairment. *J Alzheimers Dis* in press.

[41] Habeck C, Rakitin BC, Moeller J, Scarmeas N, Zarahn E, Brown T, Stern Y (2005) An event-related fMRI study of the neural networks underlying the encoding, maintenance, and retrieval phase in a delayed-match-to-sample task. *Brain Res Cogn Brain Res* **23**, 207-220.

[42] Amieva H, Phillips LH, Della Sala S, Henry JD (2004) Inhibitory functioning in Alzheimer's disease. *Brain* **127**, 949-964.

[43] Perry RJ, Hodges JR (1999) Attention and executive deficits in Alzheimer's disease: a critical review. *Brain* **122**, 383-404.

[44] Chetelat G, Eustache F, Viader F, De La Sayette V, Pelerin A, Mezenge F, Hannequin D, Dupuy B, Baron JC, Desgranges B (2005) FDG-PET measurement is more accurate

than neuropsychological assessments to predict global cognitive deterioration in patients with mild cognitive impairment. *Neurocase* **11**, 14-25.

[45] Bediou B, Ryff I, Mercier B, Milliery M, Henaff MA, D'Amato T, Bonnefoy M, Vighetto A, Krolak-Salmon P (2009) Impaired social cognition in mild Alzheimer disease. *J Geriatr Psychiatry Neurol* **22**, 130-140.

[46] Holdnack JA, Delis DC (2004) Parsing the recognition memory components of the WMS-III face memory subtest: normative data and clinical findings in dementia groups. *J Clin Exp Neuropsychol* **26**, 459-483.

[47] Seelye AM, Howieson DB, Wild KV, Moore MM, Kaye JA (2009) Wechsler Memory Scale-III Faces test performance in patients with mild cognitive impairment and mild Alzheimer's disease. *J Clin Exp Neuropsychol* **31**, 682-688.

[48] Jensen O, Mazaheri A (2010) Shaping functional architecture by oscillatory alpha activity: gating by inhibition. *Front Hum Neurosci* **4**, 186.

[49] Deiber MP, Rodriguez C, Jaques D, Missonnier P, Emch J, Millet P, Gold G, Giannakopoulos P, Ibáñez V (2010) Aging effects on selective attention-related electroencephalographic patterns during face encoding. *Neuroscience* **171**, 173-186.

[50] Commodari E, Guarnera M (2008) Attention and aging. *Aging Clin Exp Res* **20**, 578-584.

[51] Fabiani M, Low KA, Wee E, Sable JJ, Gratton G (2006) Reduced suppression or labile memory? Mechanisms of inefficient filtering of irrelevant information in older adults. *J Cogn Neurosci* **18**, 637-650.

[52] Kane MJ, Hasher L, Stoltzfus ER, Zacks RT, Connelly SL (1994) Inhibitory attentional mechanisms and aging. *Psychol Aging* **9**, 103-112.

[53] Chapman RM, McCrary JW, Chapman JA (1978) Short-term memory: the "storage" component of human brain responses predicts recall. *Science* **202**, 1211-1214.

[54] Boehm SG, Paller KA (2006) Do I know you? Insights into memory for faces from brain potentials. *Clin EEG Neurosci* **37**, 322-329.

[55] Schweinberger SR, Burton AM (2003) Covert recognition and the neural system for face processing. *Cortex* **39**, 9-30.

[56] Schweinberger SR, Pickering EC, Burton AM, Kaufmann JM (2002) Human brain potential correlates of repetition priming in face and name recognition. *Neuropsychologia* **40**, 2057-2073.

[57] Folstein MF, Folstein SE, McHugh PR (1975) "Mini-mental state". A practical method for grading the cognitive state of patients for the clinician. *J Psychiatr Res* **12**, 189-198.

[58] Barberger-Gateau P, Chaslerie A, Dartigues JF, Commenges D, Gagnon M, Salamon R (1992) Health measures correlates in a French elderly community population: the PAQUID study. *J Gerontol* **47**, S88-S95.

[59] Zigmond AS, Snaith RP (1983) The hospital anxiety and depression scale. *Acta Psychiatr Scand* **67**, 361-370.

[60] Wechsler D (1981) *Adult Intelligence Scale, Revised (WAIS-R)*, The Psychological Corporation, San Antonio.

[61] Reitan RM (1958) Validity of the Trail Making Test as an indicator of organic brain damage. *Percept Mot Skills* **8**, 271-276.

[62] Wechsler D (1955) *Manual for the Wechsler Adult Intelligence Scale*, The Psychological Corporation, New York.

[63] Milner B (1971) Interhemispheric differences in the localization of psychological processes in man. *Br Med Bull* **27**, 272-277.

[64] Buschke H, Sliwinski MJ, Kuslansky G, Lipton RB (1997) Diagnosis of early dementia by the Double Memory Test: encoding specificity improves diagnostic sensitivity and specificity. *Neurology* **48**, 989-997.

[65] Baddeley AD, Emslie H, Nimmo-Smith I (1994). In *The Doors and People Test: a test of visual and verbal recall and recognition*, Bury St Edmunds: Thames Valley Test Company, England.

[66] Borkowski JG, Benton AL, Spreen O (1967) Word fluency and brain damage. *Neuropsychologia* **5**, 135-140.

[67] Heaton RK (1981) *Wisconsing Card Sorting Test Manual, Odessa*, Fla: Psychological Assessment Resources.

[68] Kaplan EF, Goodglass H, Weintraub S (1983) *The Boston Naming Test*, Lea and Febiger, Philadelphia.

[69] Ghent L (1956) Perception of overlapping and embedded figures by children of different ages. *Am J Psychol* **69**, 575-587.

[70] Schnider A, Hanlon RE, Alexander DN, Benson DF (1997) Ideomotor apraxia: behavioral dimensions and neuroanatomical basis. *Brain Lang* **58**, 125-136.

[71] Poeck K (1985) Clues to the Nature of Disruption to Limb Praxis. In *Neuropsychological Studies of Apraxia and Related Disorders*, Roy EA, ed. Elsevier, Amsterdam, pp. 99-109.

[72] Welsh KA, Butters N, Mohs RC, Beekly D, Edland S, Fillenbaum G, Heyman A (1994) The Consortium to Establish a Registry for Alzheimer's Disease (CERAD). Part V. A normative study of the neuropsychological battery. *Neurology* **44**, 609-614.

[73] Hughes CP, Berg L, Danziger WL, Coben LA, Martin RL (1982) A new clinical scale for the staging of dementia. *Br J Psychiatry* **140**, 566-572.

[74] Petersen RC, Doody R, Kurz A, Mohs RC, Morris JC, Rabins PV, Ritchie K, Rossor M, Thal L, Winblad B (2001) Current concepts in mild cognitive impairment. *Arch Neurol* **58**, 1985-1992.

[75] Petersen RC, Morris JC (2005) Mild cognitive impairment as a clinical entity and treatment target. *Arch Neurol* **62**, 1160-1163.

[76] Gazzaley A, Cooney JW, McEvoy K, Knight RT, D'Esposito M (2005) Top-down enhancement and suppression of the magnitude and speed of neural activity. *J Cogn Neurosci* **17**, 507-517.

[77] Lundqvist D, Flykt A, Ohman A. (1998) The Karolinska Directed Emotional Faces - KDEF, CD ROM from Department of Clinical Neuroscience, Psychology section, Karolinska Institutet, ISBN 91-630-7164-9

[78] Rossion B, Jacques C (2008) Does physical interstimulus variance account for early electrophysiological face sensitive responses in the human brain. Ten lessons on the N170. *Neuroimage* **39**, 1959-1979.

[79] Freunberger R, Fellinger R, Sauseng P, Gruber W, Klimesch W (2009) Dissociation between phase-locked and nonphase-locked alpha oscillations in a working memory task. *Hum Brain Mapp* **30**, 3417-3425.

[80] Kelly SP, Lalor EC, Reilly RB, Foxe JJ (2006) Increases in alpha oscillatory power reflect an active retinotopic mechanism for distracter suppression during sustained visuospatial attention. *J Neurophysiol* **95**, 3844-3851.

[81] Klimesch W, Sauseng P, Hanslmayr S (2007) EEG alpha oscillations: The inhibition-timing hypothesis. *Brain Res Rev* **53**, 63-88.

[82] Toscani M, Marzi T, Righi S, Viggiano MP, Baldassi S (2010) Alpha waves: a neural signature of visual suppression. *Exp Brain Res* **207**, 213-219.

[83] Foldi NS, Lobosco JJ, Schaefer LA (2002) The effect of attentional dysfunction in Alzheimer's disease: theoretical and practical implications. *Semin Speech Lang* **23**, 139-150.

[84] Tales A, Snowden RJ, Haworth J, Wilcock G (2005) Abnormal spatial and non-spatial cueing effects in mild cognitive impairment and Alzheimer's disease. *Neurocase* **11**, 85-92.

[85] Perry RJ, Hodges JR (2000) Relationship between functional and neuropsychological performance in early Alzheimer disease. *Alzheimer Dis Assoc Disord* **14**, 1-10.

[86] Zamarian L, Stadelmann E, Nurk HC, Gamboz N, Marksteiner J, Delazer M (2007) Effects of age and mild cognitive impairment on direct and indirect access to arithmetic knowledge. *Neuropsychologia* **45**, 1511-1521.

[87] Vallesi A, Stuss DT, McIntosh AR, Picton TW (2009) Age-related differences in processing irrelevant information: evidence from event-related potentials. *Neuropsychologia* **47**, 577-586.

[88] Bennys K, Portet F, Touchon J, Rondouin G (2007) Diagnostic value of event-related evoked potentials N200 and P300 subcomponents in early diagnosis of Alzheimer's disease and mild cognitive impairment. *J Clin Neurophysiol* **24**, 405-412.

[89] Lai CL, Lin RT, Liou LM, Liu CK (2010) The role of event-related potentials in cognitive decline in Alzheimer's disease. *Clin Neurophysiol* **121**, 194-199.

[90] Schweinberger SR, Huddy V, Burton AM (2004) N250r: a face-selective brain response to stimulus repetitions. *Neuroreport* **15**, 1501-1505.

[91] Schweinberger SR, Pickering EC, Jentzsch I, Burton AM, Kaufmann JM (2002) Event-related brain potential evidence for a response of inferior temporal cortex to familiar face repetitions. *Brain Res Cogn Brain Res* **14**, 398-409.

[92] Carreiras M, Gillon-Dowens M, Vergara M, Perea M (2009) Are vowels and consonants processed differently? Event-related potential evidence with a delayed letter paradigm. *J Cogn Neurosci* **21**, 275-288.

[93] Dunabeitia JA, Molinaro N, Laka I, Estevez A, Carreiras M (2009) N250 effects for letter transpositions depend on lexicality: 'casual' or 'causal'? *Neuroreport* **20**, 381-387.

[94] Zhang XL, Begleiter H, Porjesz B, Litke A (1997) Visual object priming differs from visual word priming: an ERP study. *Electroencephalogr Clin Neurophysiol* **102**, 200-215.

[95] McLaughlin PM, Borrie MJ, Murtha SJ (2010) Shifting efficacy, distribution of attention and controlled processing in two subtypes of mild cognitive impairment: response time performance and intraindividual variability on a visual search task. *Neurocase* **16**, 408-417.

This page intentionally left blank

Cognitive Event-Related Potentials: Biomarkers of Synaptic Dysfunction Across the Stages of Alzheimer's Disease

John M. Olichney[a,b,*], Jin-Chen Yang[a,b], Jason Taylor[c] and Marta Kutas[d,e]

[a]*Department of Neurology, University of California, Davis, CA, USA*
[b]*Center for Mind and Brain, University of California, Davis, CA, USA*
[c]*MRC Cognition and Brain Sciences Unit, Cambridge, UK*
[d]*Department of Cognitive Science, University of California, San Diego, CA, USA*
[e]*Department of Neurosciences, University of California, San Diego, CA, USA*

Abstract. Cognitive event-related brain potential (ERP) studies of decision-making and attention, language, and memory impairments in Alzheimer's disease (AD) and mild cognitive impairment (MCI) are reviewed. Circumscribed lesions of the medial temporal lobe (MTL), as may be the case in individuals with amnestic MCI, generally produce altered plasticity of the late positive P600 component, with relative sparing of earlier sensory ERP components. However, as the neuropathology of AD extends to neocortical association areas, abnormalities of the P300 and N400 (and perhaps even P50) become more common. Critically, ERP studies of individuals at risk for AD may reveal neurophysiological changes prior to clinical deficits, which could advance the early detection and diagnosis of "presymptomatic AD".

Keywords: Alzheimer's disease (AD), mild cognitive impairment (MCI), synaptic dysfunction, preclinical AD, event-related potentials (ERP), P300, N400, P600, Late Positive Component (LPC), EEG

INTRODUCTION/OVERVIEW

This article offers a concise overview of the scientific literature on several event-related brain potential (ERP) components with demonstrated sensitivity to Alzheimer's disease (AD). These components include the N200, P300, N400, and P600 (or LPC for late positive component), each of which taps different aspects of perceptual and/or cognitive processing. ERPs provide a flexible and powerful technique, with superb temporal resolution, which can be used to probe subtle, sometimes 'subclinical', abnormalities of cognition. Despite over 30 years of ERP research since the initial

P300 studies, the full potential of cognitive ERPs for diagnosing and/or treating AD patients has yet to be realized. In this era of rapidly evolving brain imaging techniques, non-invasive electrophysiological data are increasingly important in advancing our understanding of the *what* and *where* of cognition. Understanding the mechanisms by which AD causes an unraveling of many key cognitive processes, far broader than memory processes alone, is finally within the reach of cognitive neuroscientists.

COGNITIVE EVENT-RELATED POTENTIALS (ERPS)

Cognitive ERPs provide a powerful, non-invasive, tool for studying the brain's synaptic function. ERPs

---

*Correspondence to: Prof. John M. Olichney, M.D., Center for Mind and Brain, 267 Cousteau Place, Davis, CA 95618, USA. Fax: +1 530 297 4000; E-mail: jmolichney@ucdavis.edu.

are an instantaneous reflection of the summated post-synaptic excitatory (EPSPs) and inhibitory (IPSPs) membrane potentials, primarily of pyramidal cells in the neocortex [1–3]. The temporal immediacy of ERPs is especially advantageous in the study of memory, given that memory encoding and retrieval processes can be very fast, and in light of the evidence that the temporal encoding of information may be important if not essential for synaptic plasticity [4, 5]. Because ERPs (like Magnetoencephalography or MEG) reflect the precise timing and temporal patterns of neuronal activity, they are very useful in quantifying the timing and sequence of the various stages or aspects of cognitive processing, more generally. In broad stroke, evoked potential (EP) and ERP research have shown that early brain responses (e.g., the visual N1) generally reflect the sensory input characteristics, while later responses are relatively more dependent on the mental operations performed on the stimuli as well as on non-sensory factors such as predictability, higher perceptual and semantic features. It is these slower, later, so-called endogenous components that have shown particular sensitivity to Alzheimer's disease (AD), a disease with predilection for the medial temporal lobes and higher association neocortical regions [6, 7].

AD AND SYNAPTIC DYSFUNCTION

In recent years, several investigators have suggested that AD may be primarily a disorder of the synapse and synaptic plasticity [8–10]. Several transgenic animal models of AD, for instance, have revealed prominent inhibition of long-term potentiation (LTP) and/or reduced synaptic transmission before the appearance of extensive AD pathology (amyloid plaques and neurofibrillary changes) or neuron loss [11, 12]. As a consequence, much of the current basic research focuses on the mechanisms of synaptic dysfunction in AD and its relationship to Aβ oligomers [13]. Selkoe [9], for example, made a substantive change in his model of AD pathogenesis, when he suggested that the earliest changes in synaptic function may be due to soluble forms of Aβ and precede the appearance of any extracellular amyloid deposits. Clinico-neuropathologic studies, likewise, have implicated the synapse as a primary mediator of dementia severity. Terry et al. [14], for example, found that nearly 90% of the variance in dementia severity could be accounted for by the density of pre-synaptic ter-

minals in mid-frontal cortex. Electron microscopy of cortical biopsies in early- to mid-stage AD shows a 30% decrease in synaptic density and a 25% decrease in synapses/ neuron [15]. Bertoni-Freddari et al. [16] reported a large increase in the proportion of deafferented synapses on hippocampal neurons from autopsied AD cases. In short, it is reasonable to conceive of AD as a diffuse deafferentation syndrome, in which both the neocortex and hippocampus have lost a critical proportion of their normal inputs [17]. Accordingly, cognitive ERPs may provide a highly sensitive biomarker for AD.

MIDDLE-LATENCY ERP COMPONENTS IN AD DEMENTIA (P50, N100, P200 AND N200)

In general, EP and ERP studies in AD have shown normal latency and amplitude of the early "sensory" components (e.g., visual and auditory N1 or N100). In 1987, Goodin and Aminoff [18] reported normal auditory N100 and P200 latencies in AD in response to frequent, standard (i.e., non- target) tones in a classic auditory "oddball" P300 paradigm (see also section on P300 studies of AD below). This finding was despite the fact that their AD patient group was severely impaired (6 of 22 AD patients were too severe to be tested with the mini-mental state exam (MMSE)). N100 and P200 latencies were also found to be relatively insensitive to normal aging, but sensitive to subcortical dementias such as Huntington's or Parkinson's disease [19].

Delayed P200 latency to pattern reversal or to flash stimuli in AD has been reported in some (e.g., [20, 21]) but not other studies (e.g., [22]). A delayed flash P200 has been suggested as useful in distinguishing AD from other dementias, particularly when normal flash P100 and pattern reversal P100 s are present [23, 24]. Martinelli et al. [20] also found delayed visual P200 in AD, using pattern visual evoked potentials. Furthermore, they reported that P200 amplitude over the right posterior scalp correlated with visuospatial abilities. However, Saitoh [25] used a visual target P300 paradigm, and found normal P100, N100, and P200 components in AD.

Most investigations of verbal stimuli – spoken [26] or written [27] also have found normal (amplitude and latency) N100 and P200 components in mild AD patients. In response to non-verbal, auditory tones, Golob and Starr [28] found robust P50 potentials (also termed the auditory P1) in mild AD, which were sig-

nificantly enlarged compared to healthy elderly. One caveat for this result is that reduced slow-negative "readiness potentials" in AD also resulted in slightly more positive pre-stimulus baseline voltage in the AD group.

N200

Rather consistent abnormalities in auditory N200 latency have been reported in AD [19, 29, 30]. The N200 is the earliest ERP component which consistently differentiates target from non-target stimuli in an "oddball" task, and immediately precedes the P300 discussed below. It is also sensitive to normal aging, becoming smaller and slower with age [31] at a rate nearly as fast as the slowing of P300 latency [19] (e.g., estimated at 0.74 ms/year, in comparison to 1.15 ms/year for the P300). Duffy et al. [32, 33] have shown that visual motion-elicited ERPs may help identify a subtype of AD. AD patients with low ability to detect random dot motion also showed large decrease in their N200 amplitude response to optic flow with nearly absent N200 in response to radial motion of coherent dots. The authors interpreted this finding as implicating greater neuropathology in the extrastriate visual cortex of this subgroup.

In sum, later components, such as the N200 and P300 (discussed below) have shown better sensitivity to dementia than early sensory components, albeit poor specificity in differentiating among the various dementias.

P300: OVERVIEW

The P300 (or 'P3b') component is a scalp positivity elicited by low-probability task-relevant stimuli during stimulus classification tasks in auditory, visual, and somatosensory modalities. In the canonical P300-eliciting experiment, the "auditory oddball" task, participants are asked to detect (by counting or button press) a low-probability "target" (e.g., high-pitched) tone embedded in a stream of "standard" (e.g., low-pitched) tones. The target tones normally elicit a large scalp positivity which peaks ∼300 ms post-stimulus onset and is maximal over midline centroparietal electrode sites (unlike the frontally distributed 'P3a' elicited by task-irrelevant stimuli, e.g., dog barking). The standard tones typically do not elicit a P300 (although see Squires et al. [34] for demonstration that standards may also occasionally elicit some P300

activity). This pattern of results (P300 s to target tones only) is dependent on attention. The P300 has been extensively studied and well characterized in both normal and neurologically-impaired populations. P300 latency is variable, and generally increases with the complexity of the stimulus evaluation and decisional processes demanded by the task. P300 amplitude and latency are modulated by a variety of factors-subjective probability, stimulus saliency, availability of attentional resources [35] —and it appears to be generated by a distributed network of neural regions—inferotemporal, perirhinal, prefrontal, cingulate, superior temporal and parietal cortices, as well as the hippocampus [36, 37] —suggesting that P300 may index a heterogeneous set of cognitive processes. On the other hand, studies of patients with damage to the temporo-parietal junction have found that the auditory (although not visual) P300 response is eliminated [38], suggesting that this neocortical region may be critical in generation or propagation of the scalp P300 (in the auditory modality). In general, the P3b amplitude has proven more sensitive to sensory-perceptual than response selection and execution factors, in contrast to reaction time measures which are sensitive to both, It is generally agreed that when a stimulus elicits a P300 component, it is reasonable to assume that the stimulus has been encoded into working memory. This is generally consistent with the hypotheses that P300 reflects processes involved in updating of working memory [39], or the processes of stimulus categorization [40].

P300 IN ALZHEIMER'S DISEASE

With normal aging, the latency of the auditory P300 increases ∼1–2 ms/year [19, 41]. In AD, an even greater latency increase (∼2 standard deviations above the mean of normal older individuals) is commonly reported, and some studies have found that P300 latency may be useful to differentiate between AD pathology and other disorders (e.g., depression, schizophrenia [42, 43]), although others have not [44, 45]. The clinical utility of P300 latency measures is generally enhanced in combination with standard neuropsychological tests. Goodin [46], for example, found that in cases of equivocal dementia (50% pretest probability), those with concurrent P300 latency delay showed a greater likelihood of having a dementing illness (estimated at 90%). One study found change in P300 latency was more sensitive to disease progression (over 1 year) than either the Cognitive Abilities Screen-

ing Instruments (CASI) or MMSE in both AD and MCI [47]. P300 amplitude also appears to be reduced in AD, although P300 amplitude reductions are also seen in several other neurological and psychiatric disorders (e.g., vascular dementia, schizophrenia). In summary, the literature indicates that auditory P300 measures show moderate correlations with mini-mental status exam (MMSE) scores [45, 48] and have greater sensitivity to more advanced stages of dementia.

Factors that appear to affect the clinical utility of P300 include the methodology used — especially with respect to attentional and memory-load demands — and the dementia severity of the patient group (see detailed review in Olichney and Hillert [49]). Abnormal P300 latencies are more likely to be reported in more complex tasks (e.g., counting) relative to simple target-detection tasks. It is interesting to note, however, that this effect is not simply due to task difficulty *per se*; Polich and Pitzer [50], for example, reported that increasing the difficulty of sensory discriminations actually decreased the discriminative sensitivity of P300 latency and amplitude measures. Although the P300 response has been most commonly studied in the auditory modality, studies using visual [50] and olfactory [51] stimuli have reported greater sensitivity to AD pathology. Morgan and Murphy [51] investigated olfactory event-related potentials (OERPs) and found delayed P200 and P300 latencies, which were significantly correlated with AD dementia severity and had a stronger (92%) value in differentiating AD from normal aging group than auditory P300 measures.

N400: OVERVIEW

The N400 is a scalp negativity elicited in response to potentially meaningful stimuli that peaks 400 ms post-stimulus over bilateral posterior channels. The N400 is typically larger over the right hemisphere for visual words, but sometimes shows a slight left-hemisphere bias for spoken words [52, 53]. Intracranial recordings have consistently found N400-like potentials in the anterior fusiform and parahippocampal gyri bilaterally [54, 55]; other candidate N400 generators include the superior temporal sulcus, and posterior parietal and ventral prefrontal cortices [56]. N400 amplitude is sensitive to the semantic congruity of the eliciting stimulus with the (preceding) context, being smaller in a congruous context (e.g., a coherent sentence, a single related word) than incongruous one. N400 amplitude is

also reduced by stimulus repetition (reviewed in a later section). The effect of semantic congruity on N400 amplitude (the "N400 effect") has been interpreted to reflect the reduction in processing effort needed to access the meaning of a stimulus, given a coherent predictable context [57, 58], i.e., "contextual integration" (though see Kutas & Federmeier [59] for an alternative account in terms of semantic memory activation).

N400 IN ALZHEIMER'S DISEASE

The presence or absence and amplitude of the N400 have been used to evaluate the integrity of semantic memory in Alzheimer's disease. Language dysfunction is evident relatively early in the course of AD, patients often presenting with word-finding difficulties and poor performance on tests of letter and category fluency [60]. The latter is especially suggestive of a breakdown of semantic memory [61]. Indeed, behavioral studies (e.g., the triadic word task) have found evidence that semantic associations are progressively degraded in AD [62]. Nonetheless, it continues to be a matter of debate whether the semantic impairment in AD is primarily a deficit in retrieving information from an intact memory store, or a degradation of the representations themselves [63].

The N400 response to written words is sensitive to normal aging: N400 latency increases at ~2 ms/year and N400 amplitude decreases at ~0.07 μV/year across the adult lifespan [64, 65]. From ERP studies of semantic memory (reviewed below), it is apparent that the N400 is usually abnormal in AD, typically reduced in amplitude and delayed in latency beyond that seen in normal aging. The progressive flattening of the N400 may be a manifestation of failing N400 generators. Quantitative measures of N400 latency may provide an accurate metric of dementia stage and progression. Using multiple linear regression analyses, Iragui and colleagues [66] found that neuropsychological test scores could explain >80% of the variance ($R = 0.90$) in the N400 latency (fractional area latency of the difference wave contrasting incongruous and congruous endings to statements defining opposites).

N400: SEMANTIC CONGRUITY EFFECTS IN AD

Investigations of the N400 congruity effect in sentence processing have generally found abnormalities in AD. For example, Ford et al. [67] found that

the N400 expectancy/congruity effect to sentence-terminal words in speech was significantly reduced (though still greater than zero) in AD relative to age-matched controls. Revonsuo et al. [26] likewise reported a reduced N400 congruity effect in speech in AD patients. In that study, no overt response was required of the participants—they were simply told and periodically reminded to attend to the sentences—so the results are unlikely to be 'contaminated' by the P300 component, known to be delayed in AD. In an early study by Hamberger et al. [68], the N400 to visually presented sentence-ending words was modulated by expectancy and semantic relation to virtually the same extent in AD patients as in young controls. Older controls showed a different pattern of N400 and RT effects, which the authors attributed to a response strategy, although N400 amplitudes in the older controls and AD patients were not reliably different.

Studies using minimal semantic contexts to elicit an N400 effect have generally found that the effect to be diminished in AD. In a study by Schwartz et al. [69], participants heard a category name, then saw a word, and judged whether the word belonged to the named category (e.g., "animal" – 'cow'). The N400 effect — small negativity elicited by congruous relative to incongruous target words — was both smaller and delayed in AD patients relative to age-matched controls. Iragui et al. [66] observed similar results. In that study, participants listened to short statements that defined a category (e.g., "a type of flower") or an antonymic relation (e.g., "the opposite of tall"), and then saw a word that was either congruous or incongruous with the preceding statement; their task was to judge the congruity of the statement and target word. The N400 effect was significantly reduced and delayed in AD patients relative to controls. Reduced N400 effects in AD also have been found with pictorial stimuli used as primes for lexical targets [27], as targets following lexical primes [70], and as both prime and target [71–73].

Despite the preponderance of evidence suggesting that the N400 response is abnormal in amplitude and/or latency in AD, some of these studies have nonetheless found evidence of normal semantic network structure in AD. Hamberger et al. [68], for example, found that AD patients' N400 response followed the expected amplitude gradient across sentence ending types: unrelated-nonsense > unrelated-sense > related-sense > best completion. Schwartz et al. [69] compared the N400 effect for target words primed by superordinate and subordinate category labels and found

that, in both AD patients and controls, the effect was larger for subordinate labels. Furthermore, two studies found evidence that anomia in AD may be independent of the integrity of the semantic system. Auchterlonie et al. [70] observed that the N400 congruity effect for pictures primed by words was similarly diminished for pictures, whether or not they were later named correctly. Ford et al. [27] also noted a dissociation between naming behavior and N400 response, albeit the opposite one: AD patients showed small but significant N400 congruity effects for word targets whether primed by named or unnamed pictures. One possible explanation for this apparent discrepancy is that the semantic information contained in pictures may provide a more powerful connection to the representations still present in the long-term memory of AD patients than do written words.

SUMMARY: N400 SEMANTIC CONGRUITY EFFECTS IN AD

Most ERP studies of semantic processing in AD have shown smaller and later N400 congruity effects. At the same time, AD patients have been found to show a normal gradient of N400 congruity effects over different levels of category hierarchy and expectancy, suggesting that the functional organization of semantic memory is relatively preserved in mild AD. Furthermore, ERP evidence has been used to argue that anomia in AD is not simply attributable to impaired semantic processing. Thus, there appear to be an independent deficit in the retrieval of semantic information. The N400 component may provide a useful biomarker for monitoring the stages of disease progression in AD.

LATE POSITIVE COMPONENT (LPC/P600): OVERVIEW

Many ERP studies in normal subjects have identified a Late Positive Component (LPC), sometimes called the P600, which appears to be important in the mediation of both memory encoding and retrieval processes. Subsequently recalled or recognized words generally have larger late positivities than non-recalled words [74, 75] and the size of this difference (often called "Dm" in the ERP literature) be reduced by "directed forgetting" instructions [76]. Intracranial studies in the human hippocampus have recapitulated the "Dm" effect of scalp ERPs [77], with larger positivities to

words subsequently recalled [78]. The scalp P600, or 'LPC', is a late positivity with a centro-posterior maximum, which peaks 600 ms post-stimulus onset. Intracranial studies also identified putative P600 generators in the parahippocampal gyrus, many paralimbic cortical areas (e.g., temporal pole, rhinal & perirhinal cortex, posterior cingulate) and in multimodal association (e.g., ventrolateral prefrontal, lateral temporal cortex) [37, 56]. Intracranial depth recordings have shown that very large (>200mV) P600-like potentials are generated in the human hippocampus (HC) but it is unclear to what extent these potentials propagate to the scalp [37].

N400/P600: QUANTITATIVE MEASURES OF REPETITION EFFECTS IN ALZHEIMER'S DISEASE

The neuropathology of AD affects the medial temporal lobes early in the course of the disease, and deficits of episodic memory are usually the earliest presenting symptom. One might thus expect ERP word-repetition effects in AD to resemble those of medial-temporal amnesics. Studies of ERP word-repetition effects in AD, however, have produced a complex pattern of results.

Using a continuous semantic judgment task (button-press required for 'animal' names) with incidental repetition of non-targets ('non-animal' words were repeated; average lag: 30 sec) in AD, Friedman et al. [79] reported preserved late (700–1000 ms) repetition effects in most (6 of 10) mild AD patients. These authors attributed the residual repetition effects to relatively preserved implicit memory processes in AD. Rugg et al. [80] used a similar continuous task with incidental repetition at somewhat shorter lags (average: 6–21 sec) and found ERP repetition effects (300–400 and 400–700 ms) in AD that were statistically indistinguishable from those in controls, although a trend for a smaller repetition effect with longer lags was noted. In contrast, Tendolkar et al. [81] employing an explicit word-list memory task and a longer inter-item lag (∼5 minutes), found very different results. In that study, controls exhibited a large repetition positivity for correctly recognized old items in both early (300–600 ms) and late (700–900 ms) latency windows. This effect was further enhanced for items for which source memory was also correctly retrieved (words had been displayed in one of two colors) from 600–900 ms, supporting a link

between late positivity (P600) and conscious retrieval processes. In AD patients, no late repetition effect was present, and an effect in early latency windows (300–500 ms) showed a distinctly frontal distribution. The authors attributed this frontal old/new effect to familiarity [82]. Furthermore, patients' source memory was at chance, suggesting that their above-chance recognition performance (62%) was due to a sense of familiarity (or another such implicit process) and not to recollection of the study event. Using a continuous lexical decision task with incidental repetition at long lags (>90 items or >7.5 minutes), Schnyer et al. [83] likewise found a repetition positivity from 300 to 650 ms in controls, but no discernible effect in AD patients.

A study in our laboratory [84] applied a word repetition paradigm with semantically congruous and incongruous words (details described in [85]) to patients with mild AD. Normal elderly demonstrated large decrement in P600 amplitude to repeated, relative to new, congruous words, and the amplitude of this change correlated strongly with verbal memory performance [85]. Thus, we believe this P600 word repetition effect is a measure of the updating of working memory with the content of long-term memory. With efficient learning of category exemplars, this updating is not necessary for repeated target stimuli. As we had observed in patients with chronic amnesia, patients with mild AD had markedly reduced P600 word-repetition effects (statistically 'absent' when analyzed across all scalp channels). Unlike chronic amnesia, patients with mild AD also showed significant diminution of the N400 word-repetition effect. Thus, both the P600 and N400 repetition effects were 'lacking' in the AD group [84]. The loss of the N400 repetition effect may correspond to abnormal semantic/conceptual priming, as has been found in several behavioral studies of mild AD [86]. Furthermore, when 10th percentile (in normal elderly) cutoffs for the P600 and N400 word-repetition effects were applied, all 11 mild AD patients were correctly classified as abnormal on one or both measures (sensitivity: 100%; specificity: 82%), suggesting that this paradigm has promise for use in the diagnosis or early detection of AD.

FMRI STUDIES OF WORD REPETITION IN AD

The word repetition paradigm described above has been adapted for functional Magnetic Resonance

Imaging (fMRI) studies, in order to identify the neural generators underlying the P600 word repetition effect. Normal elderly showed activation to New > Old congruous words in a distributed network of putative P600 generators, including bilateral cingulate and fusiform gyri, left medial temporal lobe (LMTL), and left inferior frontal gyri (IFG) [87]. Furthermore, significant correlations were present between the magnitude of New–Old activation in these regions and subsequent memory performance, implicating this neural circuit as critical for successful verbal memory encoding. In contrast, a group of mild AD patients showed weak or absent response to New-Old congruous word contrast, with only one such significant cluster (IFG) in the entire left hemisphere [88].

EEG OSCILLATORY ABNORMALITIES IN AD

Event-related dysynchronization/synchronization (ERD/ERS), the time-locked change in power of EEG frequency band (i.e., delta, theta, alpha, beta, and gamma) activities [89], also has been employed to explore cognitive and non-cognitive neural processing in AD. In a finger movement task, for example, AD was found to show increased centromedial beta ERD during movement and increased ipsilateral rolandic beta ERS in the post-movement period, with abnormal frontal preponderance of both activities [90]. Diminished ERD in 7–17 Hz frequency over temporal area has been observed in the AD group during retrieval of a Sternberg memory task [91]. Another study using a two-back working memory paradigm found reduced beta ERS at parietal sites of AD patients [92]. Event-related oscillation analysis also has been used to evaluate the outcome of cholinesterase inhibitor treatment on AD. Both treated and untreated AD patients exhibited lower delta activity, while theta response was sensitive to the treatment with a reduction after cholinesterase inhibitor therapy [93, 94].

ERPS IN MILD COGNITIVE IMPAIRMENT (MCI)

In a 5 year follow-up study, Golob and colleagues [95] demonstrated that both P50 amplitude and P300 latency, elicited in an auditory oddball task, increase with mild cognitive impairment (MCI). P50 amplitude predicted progression from MCI to AD, and

differentiated amnestic MCI subtype from MCI with other cognitive impairments beyond memory deficit [96, 97]. Several studies have found N200 and P300 abnormalities in MCI, with some results suggesting that amplitude or latency of N200 may have stronger value in discriminating MCI patients from normal control [98–100]. However, Phillips et al. [101], using the Sternberg working memory task, found no difference in either the P300 or N200 in MCI compared with controls (but their mild AD group had reduced P300 amplitude). In a sample of amnestic mild cognitive impairment (aMCI), ERP components reflecting familiarity and retrieval monitoring were preserved for picture, but not for word recognition [102].

N400/P600: REPETITION EFFECTS IN MILD COGNITIVE IMPAIRMENT

Another study in our laboratory used the congruous/incongruous word repetition paradigm to evaluate N400 and P600 repetition effects in MCI [103]. In MCI, as in controls, target words that followed congruous category statements elicited a positive shift in N400 amplitude relative to incongruous pairings, but this effect (incongruous vs. congruous word voltage difference) was delayed in MCI. The N400 repetition effect—initial vs. repeated incongruous pairings—was likewise present but delayed in MCI. The P600 repetition effect—initial vs. repeated congruous pairings—was not significantly different from zero in the MCI grand average.

Longitudinal follow-up with annual ERP assessments [104] demonstrated that the N400 repetition effect is diminished and spatially restricted at baseline (Year 1) in MCI patients who convert to dementia within the next 3 years ("MCI converters", see Fig. 1., 3rd column). One year later, when most of these patients were still in the MCI stage, the converter group on average showed an absence of the N400 repetition effect (right side of Fig. 1.). The P600 repetition effect also proved very sensitive to MCI converters, with no statistically significant repetition effects at either year 1 or year 2. It is noteworthy that abnormalities of either the P600 or N400 repetition effect at baseline in MCI carried a poor prognosis, with approximately 88% risk of conversion to AD within 3 years, compared to a 11–27% risk in those MCI cases with normal ERP repetition effects.

Incongruous Word Repetition Effect

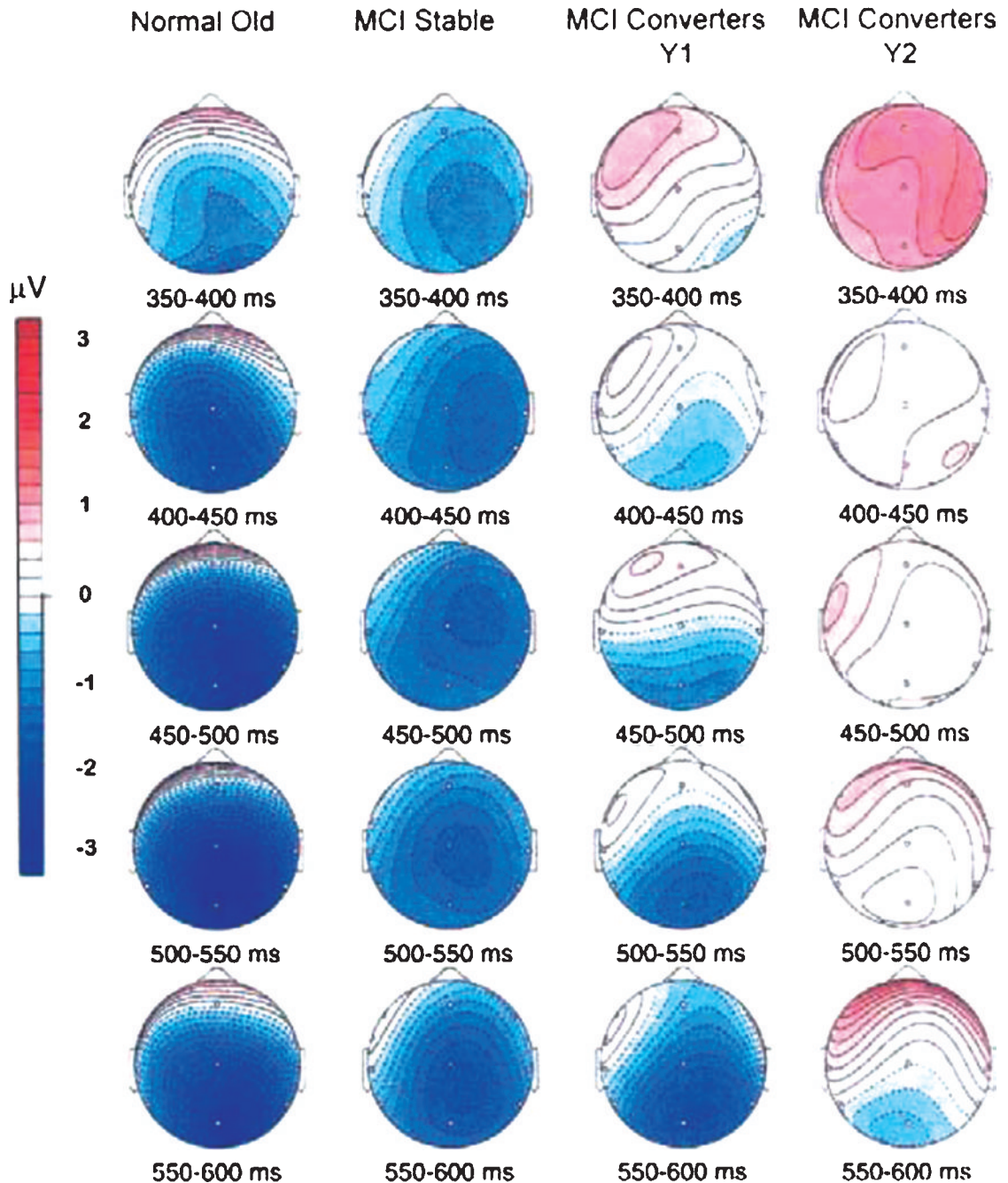## Spline Topography Maps
(New – Repeated, 50 ms epochs)

Fig. 1. Spherical spline topographic maps illustrate the incongruous word repetition effect (ERPs to new minus old semantically incongruous words) in consecutive 50 msec epochs for normal old (left) and MCI stable (left middle) groups at year 1, and MCI converters at year 1 (right middle) and year 2 (right).

SUMMARY: N400/P600 REPETITION EFFECTS

Recent work dissociating N400 and P600 repetition effects has found that MTL amnesics, whose ability to encode events into long term memory is compromised, show intact N400 but impaired P600 effects. This pattern of findings supports an association between implicit and explicit processes and N400 and P600, respectively. In AD, both N400 and P600 repetition effects are severely diminished. In MCI, the presence of either reduced N400 or P600 repetition effects appears very promising as a potentially useful biomarker for those individuals at highest risk for subsequent conversion to AD dementia.

PRECLINICAL AD

In this era of sensitive biomarkers to amyloid deposition (e.g., PiB-PET and CSF A-beta amyloid levels), many elderly persons now have AD-related changes detected many years prior to observable cognitive symptoms, i.e. in the 'preclinical AD' stage. While brain amyloid is necessary for the diagnosis of AD, it may not suffice to produce cognitive decline in some elderly persons. As noted above, neuropathologic studies have implicated the synapse as the primary mediator of dementia severity in AD, with >80% of the variance in severity accounted for by the density of pre-synaptic terminals in mid-frontal cortex [14]. Transgenic animals often show inhibition of LTP and/or reduced synaptic transmission prior to the appearance of amyloid plaques and neurofibrillary changes [12]. This highlights the need for more accurate biomarkers for AD, especially biomarkers sensitive to emerging memory failure (pre-'MCI'). Therefore, recently proposed research criteria for Preclinical AD [105] divide this entity into 3 stages, based on the presence of symptoms and evidence of synaptic dysfunction (or neurodegeneration). Elevated CSF phospho-tau is one such marker of synaptic dysfunction. To date, neither EEG nor ERP markers have been incorporated into these criteria. Non-invasive cost-effective measures of synaptic dysfunction, as can be provided by ERPs and EEG, however, could potentially be very useful for the earlier diagnosis staging of AD. In short, there is a pressing need for improved electrophysiological markers of impaired synaptic plasticity and memory. One important application for such a marker would be to aid in the differentiation of Preclinical AD, perhaps while still in the asymptomatic stage, from normal aging.

EEG/ERP ABNORMALITIES IN PRECLINICAL AD

A rich literature has shown that EEG and ERPs can both be very sensitive tools for measuring brain aging. Prichep and colleagues [106], for example, applied quantitative EEG (QEEG) to elderly persons with symptomatic memory complaints ("Reisberg FAST stage 2") and found that certain QEEG abnormalities (e.g., increased theta power, slowed mean background frequency, changes in covariance among centro-parietal regions) were strongly predictive of subsequent cognitive decline over the next 7 years (logistic regression models achieved a predictive accuracy of 90%). ERPs likewise have shown promise in their sensitivity to preclinical stages of AD. Several ERP studies have reported various sensitivities in those at increased genetic risk for AD. Boutros and colleagues [107], for example, reported increased P50 and P300 amplitudes in a small group of normal subjects genetically at-risk for AD (first degree relatives of autopsy confirmed AD cases; mean age 53 yr old). Green and colleagues [108] reported delayed N200 and P300 latencies in a similarly-aged group of apolipoprotein E4 (the most common genetic risk factor for AD) carriers with a positive family history of AD. Murphy et al. [109] presented names of odors previously encoded (targets) or not (foils) to carriers of ApoE4, and found significantly longer P300 latencies in the ApoE4 carriers, consistent with prior reports of olfactory odor recognition memory impairment in ApoE4 carriers [110]. Golob et al. [111] examined familial AD (FAD) carriers (mean age = 34) with presenilin-1 (*PSEN1*) or amyloid precursor protein (*APP*) mutations with an auditory oddball task and obtained delayed ERP components including N100, P200, N200 and P300 in this group with familial AD while most were in the asymptomatic (CDR = 0) stage. Bobes and colleagues [74] observed that asymptomatic carriers of E280A PS-1 mutation have a parietal distribution of N400 congruity effect elicited by picture-pairs while normal elderly show a central maximum.

Recent retrospective review of all our "normal" elderly controls, followed longitudinally by a NIH-funded ADRC or ADC, identified 7 cases who were most probably in the early stages of Preclinical AD at the time of their ERP recordings. All entered as nor-
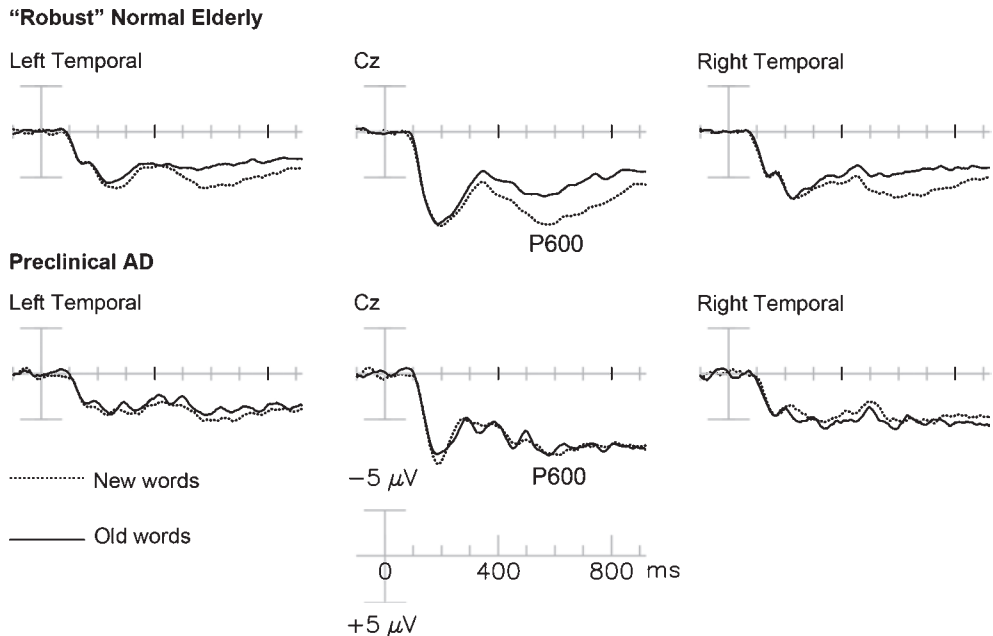
"Robust" Normal Elderly

Fig. 2. Grand average ERPs to initial (dash line) and repeated (solid line) presentation of congruous words in "robust" normal elderly (RNE) (top row) and Preclinical AD patients (bottom).

mal controls and continued to perform within normal limits on an annually administered extensive neuropsychological test battery. In the years following the ERPs, however, these cases showed cognitive decline (to AD or MCI, $n = 6$) or had AD pathology verified at autopsy ($n = 4$, mean Braak stage = 3.0). Compared to 12 "robust" normal elderly (RNE) participants (top row in Fig. 2), all of whom remained cognitively normal (average follow-up = 9.1 years) with longitudinal neuropsychological testing, the Preclinical AD group had significantly smaller P600 repetition effects (mean amplitude of RNE = 3.28 μV; Pre-AD = 0.10 ± 0.89 μV) [112]. The consistently abnormal (reduced or absent) P600 effects seen in this small Preclinical AD group shows the great promise which ERP biomarkers such as the P600 have for the detection of the earliest stages of synaptic dysfunction.

CONCLUSIONS

We reviewed several abnormalities in the cognitive ERPs of AD patients. Early, sensory-evoked, obligatory potentials (e.g., N100) are typically normal in AD (though see work on P50) whereas potentials starting around 200 ms and beyond are more consistently abnormal even in the earliest stages of AD and MCI.

This pattern of ERP findings is consistent with the neuropathology of AD. Predilection sites in early AD include the medial temporal lobe, other limbic areas, and multimodal association cortices with relative sparing of unimodal sensory cortex. Late endogenous components in known paradigms can be useful for assessing specific hypotheses about the change in cognitive processes in AD, MCI, and amnestic patients. A P300 paradigm, for example, can be very useful in detecting a disorder of attention or in quantifying the effects of drugs which improve attention, such as the cholinesterase inhibitors. For the early diagnosis of AD or other memory disorders, a word repetition paradigm (typically eliciting N400 and P600 modulations) with an explicit recognition task or one that fosters associative learning would be recommended. As discussed above, the N400 has potential use in tracking AD progression. Last but not least, the sensitivities of a number of ERP components have great promise in the detection and quantification of synaptic dysfunction in the presymptomatic stages of Alzheimer's disease.

ACKNOWLEDGMENTS

to thank the UC Davis ADC and Center for Mind and Brain.

REFERENCES

[1] Nunez PL (1990) Physical principles and neurophysiological mechanisms underlying event-related potentials. In: J.W. Rohrbaugh, R. Parasuraman, R. Johnson Jr. eds, Event-related brain potentials, Oxford University Press, New York, pp. 19-36.

[2] [2] Nunez PL, Srinivasan R (2006) Oxford University Press, Electric fields of the brain: the neurophysics of EEG (2nd Ed.). New York, pp. 163-166.

[3] Wood CC, Allison T (1981) Interpretation of evoked potentials: a neurophysiological perspective. *Can J Psychol* **35**, 113-135.

[4] Ang CW, Carlson GC, Coulter DA (2005) Hippocampal ca1 circuitry dynamically gates direct cortical inputs preferentially at theta frequencies. *J Neurosci* **25**, 9567-9580.

[5] Schack B, Weiss S (2005) Quantification of phase synchronization phenomena and their importance for verbal memory processes. *Biol Cybern* **92**, 275-287.

[6] Braak H, Braak E (1991) Neuropathological stageing of Alzheimer-related changes. *Acta Neuropathol* **82**, 239-259.

[7] Katada E, Sato K, Ojika K, Ueda R (2004) Cognitive event-related potentials: useful clinical information in Alzheimer's disease. *Curr Alzheimer Res* **1**, 63-69.

[8] Mesulam MM (1999) Neuroplasticity failure in Alzheimer's disease: bridging the gap between plaques and tangles. *Neuron* **24**, 521-529.

[9] Selkoe DJ (2002) Alzheimer's disease is a synaptic failure. *Science* **298**, 789-791.

[10] Lacor PN, Buniel MC, Chang L, Fernandez SJ, Gong Y, Viola KL, Lambert MP, Velasco PT, Bigio EH, Finch CE, Krafft GA, Klein WL (2004) Synaptic targeting by Alzheimer's-related amyloid beta oligomers. *J Neurosci* **24**, 10191-10200.

[11] Moechars D, Dewachter I, Lorent K, et al. (1999) Early phenotypic changes in transgenic mice that overexpress different mutants of amyloid precursor protein in brain. *J Biol Chem* **274**, 6483-6492.

[12] Rowan MJ, Klyubin I, Cullen WK, Anwyl R (2003) Synaptic plasticity in animal models of early Alzheimer's disease. *Philos Trans R Soc Lond B Biol Sci* **358**, 821-828.

[13] Walsh D, Klyubin I, Fadeeva J, Cullen W, Anwyl R, Wolfe M, et al. (2002) Naturally secreted oligomers of amyloid beta protein potently inhibit hippocampal long-term potentiation *in vivo*. *Nature* **416**, 536-539.

[14] Terry RD, Masliah E, Salmon DP, Butters N, DeTeresa R, Hill R, Hansen LA, Katzman R (1991) Physical basis of cognitive alterations in Alzheimer's disease: synapse loss is the major correlate of cognitive impairment. *Ann Neurol* **30**, 572-580.

[15] Davies CA, Mann DM, Sumpter PQ, Yates PO (1987) A quantitative morphometric analysis of the neuronal and synaptic content of the frontal and temporal cortex in patients with Alzheimer's disease. *J Neurol Sci* **78**, 151-164.

[16] Bertoni-Freddari C, Fattoretti P, Delfino A, Solazzi M, Giorgetti B, Ulrich J, Meier-Ruge W (2002) Deafferentative synaptopathology in physiological aging and Alzheimer's disease. *Ann N Y Acad Sci* **977**, 322-326.

[17] Hyman BT, Van Hoesen GW, Damasio AR, Barnes CL (1984) Alzheimer's disease: cell-specific pathology isolates the hippocampal formation. *Science* **225**, 1168-1170.

[18] Goodin DS, Aminoff MJ (1987) Electrophysiological differences between demented and nondemented patients with parkinson's disease. *Ann Neurol* **21**, 90-94.

[19] Goodin DS, Aminoff MJ (1986) Electrophysiological differences between subtypes of dementia. *Brain* **109**, 1103-1113.

[20] Martinelli V, Locatelli T, Comi G, Lia C, Alberoni M, Bressi S, Rovaris M, Franceschi M, Canal N (1996) Pattern visual evoked potential mapping in Alzheimer's disease: correlations with visuospatial impairment. *Dementia* **7**, 63-68.

[21] Swanwick GR, Rowan MJ, Coen RF, Coakley D, Lawlor BA (1999) Prognostic value of electrophysiological markers in Alzheimer's disease. *Am J Geriatr Psychiatry* **7**, 335-338.

[22] Ruessmann K, Beneicke U (1991) P2 latency of the flash visual evoked potential in dementia. *Int J Neurosci* **56**, 273-276.

[23] Moore NC (1997) Visual evoked responses in Alzheimer's disease: a review. *Clin Electroencephalogr* **28**, 137-142.

[24] Philpot MP, Amin D, Levy R (1990) Visual evoked potentials in Alzheimer's disease: correlations with age and severity. *Electroencephalogr Clin Neurophysiol* **77**, 323-329.

[25] Saitoh E, Adachi-Usami E, Mizota A, Fujimoto N (2001) Comparison of visual evoked potentials in patients with psychogenic visual disturbance and malingering. *J Pediatr Ophthalmol Strabismus* **38**, 21-26.

[26] Revonsuo A, Portin R, Juottonen K, Rinne JO (1998) Semantic processing of spoken words in Alzheimer's disease: an electrophysiological study. *J Cogn Neurosci* **10**, 408-420.

[27] Ford JM, Askari N, Mathalon DH, Menon V, Gabrieli JD, Tinklenberg JR, Yesavage J (2001) Event-related brain potential evidence of spared knowledge in Alzheimer's disease. *Psychol Aging* **16**, 161-176.

[28] Golob EJ, Starr A (2000) Effects of stimulus sequence on event-related potentials and reaction time during target detection in Alzheimer's disease. *Clin Neurophysiol* **111**, 1438-1449.

[29] Takeda M, Tachibana H, Sugita M (1993) Multimodal evoked potentials in patients with dementia. *Nippon Ronen Igakkai Zasshi* **30**, 1058-1067.

[30] Yokoyama Y, Nakashima K, Shimoyama R, Urakami K, Takahashi K (1995) Distribution of event-related potentials in patients with dementia. *Electromyogr Clin Neurophysiol* **35**, 431-437.

[31] Iragui VJ, Kutas M, Mitchiner MR, Hillyard SA (1993) Effects of aging on event-related brain potentials and reaction times in an auditory oddball task. *Psychophysiology* **30**, 10-22.

[32] Fernandez R, Kavcic V, Duffy CJ (2007) Neurophysiologic analyses of low- and high-level visual processing in Alzheimer disease. *Neurology* **68**, 2066-2076.

[33] Kavcic V, Fernandez R, Logan D, Duffy CJ (2006) Neurophysiological and perceptual correlates of navigational impairment in Alzheimer's disease. *Brain* **129**, 736-746.

[34] Squires K, Wickens C, Squires NK, Donchin E (1976) The effect of stimulus sequence on the waveform of the cortical event-related potential. *Science* **193**, 1142-1146.

[35] Johnson R, Jr. (1986) A triarchic model of p300 amplitude. *Psychophysiology* **23**, 367-384.

[36] Halgren E, Marinkovic K, Chauvel P (1998) Generators of the late cognitive potentials in auditory and visual odd-

ball tasks. *Electroencephalogr Clin Neurophysiol* **106**, 156-164.

[37] Guillem F, Rougier A, Claverie B (1999) Short- and long-delay intracranial erp repetition effects dissociate memory systems in the human brain. *J Cogn Neurosci* **11**, 437-458.

[38] Yamaguchi S, Knight RT (1992) Effects of temporal-parietal lesions on the somatosensory p3 to lower limb stimulation. *Electroencephalogr Clin Neurophysiol* **84**, 139-148.

[39] Donchin E, Coles MGH (1988) Is the p300 component a manifestation of context updating? *Behav Brain Sci* **11**, 357-374.

[40] Kok A (2001) On the utility of p3 amplitude as a measure of processing capacity. *Psychophysiology* **38**, 557-577.

[41] Ford JM, Pfefferbaum A (1985) Age-related changes in event-related potentials. *Advances in Psychophysiology* **1**, 301-339.

[42] Squires KC, Chippendale TJ, Wrege KS, Goodin DS, Starr A (1980) Electrophysiological assessment of mental function in aging and dementia. In Poon L (ed). Aging in the 1980s. American Psychology Association, Washington, DC, pp. 125-134.

[43] Gordon E, Kraiuhin C, Harris A, Meares R, Howson A (1986) The differential diagnosis of dementia using p300 latency. *Biological Psychiatry* **21**, 1123-1132.

[44] Pfefferbaum A, Wenegrat BG, Ford JM, Roth WT, Kopell BS (1984) Clinical application of the p3 component of event-related potentials ii: dementia, depression and schizophrenia. *Electroencephalogr Clin Neurophysiol* **59**, 104-124.

[45] Patterson JV, Michalewski HJ, Starr A (1988) Latency variability of the components of auditory event-related potentials to infrequent stimuli in aging, Alzheimer-type dementia, and depression. *Electroencephalogr Clin Neurophysiol* **71**, 450-460.

[46] Goodin DS (1990) Clinical utility of long latency 'cognitive' event-related potentials (p3): the pros. *Electroencephalogr Clin Neurophysiol* **76**, 2-5.

[47] Lai CL, Lin RT, Liou LM, Liu CK (2010) The role of event-related potentials in cognitive decline in Alzheimer's disease. *Clin Neurophysiol* **121**, 194-199.

[48] Tanaka F, Kachi T, Yamada T, Sobue G (1998) Auditory and visual event-related potentials and flash visual evoked potentials in Alzheimer's disease: correlations with mini-mental state examination and raven's coloured progressive matrices. *J Neurol Sci* **156**, 83-88.

[49] Olichney JM, Hillert DG (2004) Clinical applications of cognitive event-related potentials in Alzheimer's disease. *Phys Med Rehabil Clin N Am* **15**, 205-233.

[50] Polich J, Pitzer A (1999) P300 and Alzheimer's disease: odd-ball task difficulty and modality effects. *Electroencephalogr Clin Neurophysiol Suppl* **50**, 281-287.

[51] Morgan CD, Murphy C (2002) Olfactory event-related potentials in Alzheimer's disease. *J Int Neuropsychol Soc* **8**, 753-763.

[52] Kutas M, Hillyard SA (1980) Reading senseless sentences: brain potentials reflect semantic incongruity. *Science* **207**, 203-205.

[53] Kutas M, Neville HJ, Holcomb PJ (1987) A preliminary comparison of the n400 response to semantic anomalies during reading, listening and signing. *Electroencephalogr Clin Neurophysiol Suppl* **39**, 325-330.

[54] McCarthy G, Nobre AC, Bentin S, et al. (1995) Language-related field potentials in the anterior-medial temporal lobe:

1. Intracranial distribution and neural generators. J Neurosci **15**, 1080-1089.

[55] Nobre AC, Allison T, McCarthy G (1994) Word recognition in the human inferior temporal lobe. *Nature* **372**, 260-263.

[56] Halgren E, Baudena P, Heit G, Clarke J, Marinkovic K, Clarke M (1994) Spaciotemporal stages in face and word processing 1 . Depth Recorded Potentials in Human Occipital and Parietal Lobes. J Physiol Paris **88**, 1-150.

[57] Kutas M, Van Petten C (1988) Event-related brain potential studies of language. In: Ackles PK, Jennings JR, Coles MGH (eds), Advances in Psychophysiology, vol.3. JAI Press, Greenwich, CT, pp. 139-187.

[58] Osterhout l, Holcomb pj (1995) Event-related potentials and language comprehension Rugg M.D. Coles MGH. Electrophysiology of Mind: Event-related Brain Potentials and Cognition Oxford, UK Oxford University Press, 171-215.

[59] Kutas M, Federmeier KD (2011) Thirty years and counting: finding meaning in the n400 component of the event-related brain potential (erp). *Annu Rev Psychol* **62**, 621-647.

[60] Monsch AU, Bondi MW, Butters N, Salmon DP, Katzman R, Thal LJ (1992) Comparisons of verbal fluency tasks in the detection of dementia of the Alzheimer type. *Arch Neurol* **49**, 1253-1258.

[61] Salmon DP, Butters N, Chan AS (1999) The deterioration of semantic memory in Alzheimer's disease. *Can J Exp Psychol* **53**, 108-117.

[62] Chan AS, Butters N, Salmon DP (1997) The deterioration of semantic networks in patients with Alzheimer's disease: a cross-sectional study. *Neuropsychologia* **35**, 241-248.

[63] Ober BA, Shenaut GK. (1995) Semantic priming in Alzheimer's disease: meta analysis and theoretical evaluation. in: Allen PA, Bashore TR (eds). Advances in Psychology: Age Differences in Word and Language Processing. Elsevier, Amsterdam, pp. 247-271.

[64] King J, Kutas M. (1995) Do the waves begin to waver? ERP studies of language processing in the elderly. In: Allen PA, Bashore TR (eds). Advances in Psychology: Age Differences in Word and Language Processing. Amsterdam: Elsevier, pp. 314-344.

[65] Kutas M, Iragui V (1998) The n400 in a semantic categorization task across 6 decades. *Electroencephalogr Clin Neurophysiol* **108**, 456-471.

[66] Iragui V, Kutas M, Salmon DP (1996) Event-related brain potentials during semantic categorization in normal aging and senile dementia of the Alzheimer's type. *Electroencephalog Clin Neurophysiol* **100**, 392-406.

[67] Ford JM, Woodward SH, Sullivan EV, Isaacks BG, Tinklenberg JR, Yesavage JA, Roth WT (1996) N400 evidence of abnormal responses to speech in Alzheimer's disease. *Electroencephalogr Clin Neurophysiol* **99**, 235-246.

[68] Hamberger MJ, Friedman D, Ritter W, Rosen J (1995) Event-related potential and behavioral correlates of semantic processing in Alzheimer's patients and normal controls. *Brain Lang* **48**, 33-68.

[69] Schwartz TJ, Kutas M, Butters N, et al. (1996) Electrophysiological insights into the nature of the semantic deficit in Alzheimer's disease. *Neuropsychologia* **34**, 827-841.

[70] Auchterlonie S, Phillips PA, Chertkow H (2002) Behavioral and electrical brain measures of semantic priming in patients with Alzheimer's disease: implications for access failure versus deterioration hypotheses. *Brain Cogn* **48**, 264-267.

[71] Castañeda M, Ostrosky-Solís F, Pérez M, Bobes MA, Rangel LE (1997) Erp assessment of semantic memory in Alzheimer's disease. *Int J Psychophysiol* **27**, 201-214.

[72] Ostrosky-Solís F, Castañeda M, Pérez M, Castillo G, Bobes MA (1998) Cognitive brain activity in Alzheimer's disease: electrophysiological response during picture semantic categorization. *J Int Neuropsychol Soc* **4**, 415-425.

[73] Bobes MA, García YF, Lopera F, Quiroz YT, Galán L, Vega M, Trujillo N, Valdes-Sosa M, Valdes-Sosa P (2010) Erp generator anomalies in presymptomatic carriers of the Alzheimer's disease e280a ps-1 mutation. *Hum Brain Mapp* **31**, 247-265.

[74] Mangels JA, Picton TW, Craik FIM (1996) Neurophysiological (erp) correlates of encoding and retrieval from verbal episodic memory. *(Abstract) Soc Neurosci Abs* **22**, 1450.

[75] Paller KA, Kutas M, Mayes AR (1987) Neural correlates of encoding in an incidental learning paradigm. *Electroencephalogr Clin Neurophysiol* **67**, 360-371.

[76] Paller KA (1990) Recall and stem-completion priming have different electrophysiological correlates and are modified differentially by directed forgetting. *J Exp Psychol Learn Mem Cogn* **16**, 1021-1032.

[77] Paller KA, McCarthy G, Wood CC (1988) Erps predictive of subsequent recall and recognition performance. *Biol Psychol* **26**, 269-276.

[78] Fernandez G, Effern A, Grunwald T, Pezer N, Lehnertz K, Dumpelmann M (1999) Real-time tracking of memory formation in the human rhinal cortex and hippocampus. *Science* **285**, 1582-1585.

[79] Friedman D, Hamberger M, Stern Y, Marder K (1992) Event-related potentials (erps) during repetition priming in Alzheimer's patients and young and older controls. *J Clin Exp Neuropsychol* **14**, 448-462.

[80] Rugg MD, Pearl S, Walker P, Roberts RC, Holdstock JS (1994) Word repetition effects on event-related potentials in healthy young and old subjects, and in patients with Alzheimer-type dementia. *Neuropsychologia* **32**, 381-398.

[81] Tendolkar I, Schoenfeld A, Golz G, Fernandez G, Kuhl KP, Ferszt R, Heinze HJ (1999) Neural correlates of recognition memory with and without recollection in patients with Alzheimer's disease and healthy controls. *Neurosci Lett* **263**, 45-48.

[82] Rugg MD, Mark RE, Walla P, Schloerscheidt AM, Birch CS, Allan K (1998) Dissociation of the neural correlates of implicit and explicit memory. *Nature* **392**, 595-598.

[83] Schnyer DM, Allen JJ, Kaszniak AW, Forster KI (1999) An event-related potential examination of masked and unmasked repetition priming in Alzheimer's disease: implications for theories of implicit memory. *Neuropsychology* **13**, 323-337.

[84] Olichney JM, Riggins BR, Morris SK, Salmon DP, Kutas M, Iragui VJ (2002) Reduced effects of word repetition on the n400 and lpc event-related potentials are common in mild Alzheimer's disease and mild cognitive impairment converters. *Neurology* **58**, A216.

[85] Olichney JM, Van Petten C, Paller K, Salmon DP, Iragui VJ, Kutas M (2000) Word repetition in amnesia: electrophysiological measures of impaired and spared memory. *Brain* **123**, 1948-1963.

[86] Keane M, Gabrieli J, Fennema A, et al. (1991) Evidence for a dissociation between perceptual and conceptual priming in Alzheimer's disease. *Behav Neurosci* **105**, 326-342.

[87] Olichney JM, Taylor JR, Hillert DG, Chan SH, Salmon DP, Gatherwright J, Iragui VJ, Kutas M (2010) Fmri congruous word repetition effects reflect memory variability in normal elderly. *Neurobiol Aging* **31**, 1975-1990.

[88] Olichney JM, Taylor JR, Chan S, Yang JC, Stringfellow A, Hillert DG, Simmons AL, Salmon DP, Iragui-Madoz V, Kutas M (2010) Fmri responses to words repeated in a congruous semantic context are abnormal in mild Alzheimer's disease. *Neuropsychologia* **48**, 2476-2487.

[89] Pfurtscheller G, Lopes da Silva FH (1999) Event-related eeg/meg synchronization and desynchronization: basic principles. *Clin Neurophysiol* **110**, 1842-1857.

[90] Babiloni C, Babiloni F, Carducci F, Cincotti F, Del Percio C, De Pino G, Maestrini S, Priori A, Tisei P, Zanetti O, Rossini PM (2000) Movement-related electroencephalographic reactivity in Alzheimer disease. *Neuroimage* **12**, 139-146.

[91] Karrasch M, Laine M, Rinne JO, Rapinoja P, Sinervä E, Krause CM (2006) Brain oscillatory responses to an auditory-verbal working memory task in mild cognitive impairment and Alzheimer's disease. *Int J Psychophysiol* **59**, 168-178.

[92] Missonnier P, Deiber MP, Gold G, Herrmann FR, Millet P, Michon A, Fazio-Costa L, Ibañez V, Giannakopoulos P (2007) Working memory load-related electroencephalographic parameters can differentiate progressive from stable mild cognitive impairment. *Neuroscience* **150**, 346-356.

[93] Yener G, Güntekin B, Başar E (2008) Event-related delta oscillatory responses of Alzheimer patients. *Eur J Neurol* **15**, 540-547.

[94] Yener GG, Güntekin B, Tülay E, Başar E (2009) A comparative analysis of sensory visual evoked oscillations with visual cognitive event related oscillations in Alzheimer's disease. *Neurosci Lett* **462**, 193-197.

[95] Golob EJ, Irimajiri R, Starr A (2007) Auditory cortical activity in amnestic mild cognitive impairment: relationship to subtype and conversion to dementia. *Brain* **130**, 740-752.

[96] Golob EJ, Johnson JK, Starr A (2001) Auditory event-related potentials during target detection are abnormal in mild cognitive impairment. *Clin Neurophysiol* **113**, 151-161.

[97] Irimajiri R, Michalewski HJ, Golob EJ, Starr A (2007) Cholinesterase inhibitors affect brain potentials in amnestic mild cognitive impairment. *Brain Res* **1145**, 108-116.

[98] Papaliagkas VT, Kimiskidis VK, Tsolaki MN, Anogianakis G (2011) Cognitive event-related potentials: Longitudinal changes in mild cognitive impairment. *Clin Neurophysiol*. [Epub ahead of print]

[99] Papaliagkas V, Kimiskidis V, Tsolaki M, Anogianakis G (5) (2008) Usefulness of event-related potentials in the assessment of mild cognitive impairment. *BMC Neurosci* **9**, 107.

[100] Bennys K, Portet F, Touchon J, Rondouin G (2007) Diagnostic value of event-related evoked potentials n200 and p300 subcomponents in early diagnosis of Alzheimer's disease and mild cognitive impairment. *J Clin Neurophysiol* **24**, 405-412.

[101] Phillips NA, Chertkow H, Leblanc MM, Pim H, Murtha S (2004) Functional and anatomical memory indices in patients with or at risk for Alzheimer's disease. *J Int Neuropsychol Soc* **10**, 200-210.

[102] Ally BA, McKeever JD, Waring JD, Budson AE (2009) Preserved frontal memorial processing for pictures in patients with mild cognitive impairment. *Neuropsychologia* **47**, 2044-2055.

[103] Olichney JM, Morris SK, Ochoa C, Salmon DP, Thal LJ, Kutas M, Iragui VJ (2002) Abnormal verbal event-related potentials in mild cognitive impairment and incipient ad. *J Neurol Neurosurg Psychiatry* **73**, 377-384.

[104] Olichney JM, Taylor JR, Gatherwright J, Salmon DP, Bressler AJ, Kutas M, Iragui-Madoz VJ (2008) Patients with mci and n400 or p600 abnormalities are at very high risk for conversion to dementia. *Neurology* **6**, 1763-1770.

[105] Sperling R, Beckett L, Bennett D, et al. CRITERIA FOR PRECLINICAL ALZHEIMER'S DISEASE (2010) http://www.alz.org/research/diagnostic_criteria/preclinical_recommendations.pdf

[106] Prichep LS, John ER, Ferris SH, Rausch L, Fang Z, Cancro R, Torossian C, Reisberg B (2006) Prediction of longitudinal cognitive decline in normal elderly with subjective complaints using electrophysiological imaging. *Neurobiol Aging* **27**, 471-481.

[107] Boutros N, Torello MW, Burns EM, Wu SS, Nasrallah HA (1995) Evoked potentials in subjects at risk for Alzheimer's disease. *Psychiatry Res* **57**, 57-63.

[108] Green J, Levey AI (1999) Event-related potential changes in groups at increased risk for Alzheimer disease. *Arch Neurol* **56**, 1398-1403.

[109] Murphy C, Solomon ES, Haase L, Wang M, Morgan CD (2009) Olfaction in aging and Alzheimer's disease: event-related potentials to a cross-modal odor-recognition memory task discriminate apoe epsilon4 + and apoe epsilon 4- individuals. *Ann N Y Acad Sci* **1170**, 647-657.

[110] Gilbert PE, Murphy C (2004) The effect of the apoe epsilon4 allele on recognition memory for olfactory and visual stimuli in patients with pathologically confirmed Alzheimer's disease, probable Alzheimer's disease, and healthy elderly controls. *J Clin Exp Neuropsychol* **26**, 779-794.

[111] Golob EJ, Ringman JM, Irimajiri R, Bright S, Schaffer B, Medina LD, Starr A (2009) Cortical event-related potentials in preclinical familial Alzheimer disease. *Neurology* **73**, 1649-1655.

[112] Olichney JM, Pak J, Salmon DP, Yang JC, Gahagan T, Nowacki R, Hansen L, Galasko D, Kutas M, Iragui-Madoz VJ (2011) ERP studies of Preclinical Alzheimer's Disease (AD): P600 abnormalities are common in elderly persons who later develop MCI or AD pathology. *(Abstract) Neurology Suppl* **76**, A233.

P300 Energy Loss in Aging and Alzheimer's Disease

J. Wesson Ashford[a,e,*], Kerry L. Coburn[b], Terrence L. Rose[c] and Peter J. Bayley[d,e]

[a]*War Related Illness and Injury Study Center, VA Palo Alto Health Care System, Palo Alto, CA, USA*

[b]*Department of Psychiatry and Behavioral Sciences, Mercer University School of Medicine, GA, USA*

[c]*Multivariate Measurement Technology Corporation, Sherman, CT, USA*

[d]*VA Palo Alto Health Care System, Palo Alto, CA, USA*

[e]*Department of Psychiatry and Behavioral Sciences, Stanford University, Palo Alto, CA, USA*

Abstract. The amplitude of the event-related potential P300 component is sensitive to aging and Alzheimer's disease (AD). Using a standard 20-electrode configuration, the P300 was measured during an "oddball" task in 14 young normal individuals (YN: 21–41 years), 11 elderly normal individuals (EN: 61–80 years), and 23 probable AD patients (AD: 63–93 years; NINCDS-ADRDA criteria). P300 latencies and amplitudes were measured at PZ. Additionally, algorithmic calculations were made from spline plots across the 11 central electrodes for P300 peak voltage latency and total field energy. The measured versus calculated latencies were in general agreement. Furthermore, the measured P300 voltage amplitude was closely related to the calculated total field energy. P300 voltage latency was significantly prolonged in the elderly, but not more so in AD patients (average latency [ms ± SD]; YN, 315 ± 21; EN, 364 ± 48 and AD, 361 ± 56). P300 amplitude showed the expected pattern of change from young to elderly to AD (average voltage [uV ± SD]; YN, 13 ± 5.1; EN, 8.3 ± 2.8; and AD, 4.9 ± 3.3). Summing the squares of each wave (an indication of power: $P = V^2 R$) showed the expected change with age more strongly than the P300 amplitude (average ± SD; YN, 44,397 ± 32,386; EN, 9,996 ± 7,018; and AD, 3,347 ± 2,971). Mini-Mental State Exam scores showed no relationship to P300 latency and minimal relationship to amplitude. Results suggest that the P300 is not obliterated in early AD, but is barely discernable in late AD. The approaches to calculating the P300 described here are potentially useful for measuring specific neural systems affected by aging and AD.

Keywords: Aging, Alzheimer's disease, dementia, event-related potentials, P300, P3a, P3b

INTRODUCTION

The P300 event-related potential (ERP) component represents an electrophysiological response of the brain to a stimulus which is unexpected or "surprising". This component is characterized by a positive voltage wave, occurring about 300 msecs after the stimulus onset in young individuals, and somewhat independent of stimulus modality or detail. The P300 phenomenon is widely studied due to the probability that it reflects an information processing cascade in which both attentional and memory processes are engaged [1–3]. Furthermore, the P300 has a particular relevance to Alzheimer's disease (AD) due to the profound memory impairments which occur early in the course of the disease and form the most prominent hallmark of this disorder [4].

The characteristics of the P300 are usually considered in terms of amplitude and latency. Using these indices, numerous studies have shown that P300 latency increases with age (1.0 to 2.0 msec/year; [5, 6]). In addition, studies suggest that the P300 latency is further increased in dementia [7–10] and is delayed in proportion to the severity of the dementia. P300 amplitude decreases with age and often becomes so small in

---

*Correspondence to: J. Wesson Ashford M.D., Ph.D., VA Palo Alto Health Care System, 3801 Miranda Avenue, Mailcode 151Y, Palo Alto, CA 94304-1290, USA. Tel.: +650 852 3287; Fax: +650 852 3297; E-mail: ashford@stanford.edu.

elderly demented patients that it is difficult to measure [11]. However, it is recognized that task demands and other methodological factors can blur the distinction between the P300 changes in normal aging, mild dementia [12], and severe dementia [13, 14].

There is considerable controversy over the utility of the P300 as a diagnostic tool for AD. Some studies advocate the use of P300 as a reliable marker for AD [15]. A P300 abnormality is observed in demented patients in proportion to the degree of dementia [13, 14]. However, similar abnormalities are also observed in age matched controls [13, 14]. Further, P300 changes are found to be non-specific with regard to the etiology of dementia [16] or even diverse cognitive changes, as in schizophrenia [17]. For example, in schizophrenia (dementia praecox, clearly a form of impairment of cognitive functioning), the P300 amplitude is decreased without a change in latency [17, 18]. Because of the variability and uncertainty of P300 measurements in demented patients, a clear relationship between the P300 and dementia severity is not always apparent [13, 14]. In view of these inconsistent findings, it is now generally accepted that the most robust difference between AD and control groups is a reduction in P300 amplitude in the AD group, while latency is a less robust measure (for review see [11]).

One potential difficulty in measuring the P300 in AD patients is the change in waves that occur temporally before the P300, which may interfere with the P300 generation and delay its activity independently of any pathology directly impacting the P300 [19]. When resolving this issue, topographic specificity may be a key factor to consider [20]. Topographic specificity of the P300 can be divided into two components: the P3a and the P3b. These components are observed in healthy controls using various experimental designs which evoke ERPs which vary in scalp topography. To illustrate these differences, three different task designs can be considered; a "standard 3-item discrimination design", a "novelty design", and a "no-go design". Using a "standard 3-item discrimination design" (e.g., [21]) subjects press a button whenever an infrequent target (small circle) is detected in a series of standard stimuli (larger circle). Infrequently presented distracter patterns (checkerboard) are also presented. The checkerboard elicits the P3a component which has a frontal/central maximum, whereas the small circle elicits a P3b component with a bilateral parietal maximum. Peak latency is shorter over the frontal (P3a) and longer over the parietal electrode sites (P3b). The so-called "novelty P300" design produces a

different pattern of results and is found when perceptually novel unexpected distracters (e.g., dog bark, color forms, etc.) occur in a series of more expected stimuli (e.g., tones, letters of the alphabet, etc.). Under these conditions, a frontal/central P300 is elicited with a relatively short peak latency that habituates rapidly [22, 23]. This potential is interpreted as reflecting frontal lobe activity related to the hippocampus [24, 25]. It is observed across modalities [26, 27] and populations ([28–31]. Consistent with the novelty interpretation, novelty P300 decreases in amplitude with repeated stimulus presentations suggesting that it may be more directly related to the orienting response than the P3b [23, 32–34]. Finally, an oddball design can be used in which an infrequent distracter is similar to the target and makes the discrimination between distracter and target more difficult. Under these conditions the distracter elicits the so called "No-Go" P300. Under these conditions, subjects do not respond to the infrequent distracter and only respond to the targets [35, 36]. The P300 from this type of distracter has maximum amplitude over central/parietal areas [37, 38]. The topographic distribution is somewhat more central than the parietal P300 from the target stimulus. The "no-go" P300 has been linked to response inhibition mechanisms, although this hypothesis is debated [39–42].

The P3a, novelty P300, and no-go P300 pattern of results reviewed here are suggested to be variants of the same ERP (see [1] for review). The P3a is considered to be related to focused attention and working memory and is elicited around the vertex as a reflection of some orienting response and subsequent medial frontal inhibitory neural processes involving dopaminergic modulation. In contrast, the P3b is considered to be related to updating of the neural representation of a stimulus, memory operation, and subsequent inhibitory processes following the target and is elicited in parietal regions bilaterally and is mainly generated by temporal-parietal cortex involving noradrenergic modulation.

When selecting a task capable of discriminating between the P300 generated by AD patients and controls, discrimination will obviously depend on the magnitude of the latency and the amplitude in each group. Amplitude has been suggested to be modulated by global level of arousal, such that the higher the arousal level, the higher the P300 (both P3a and P3b). When task conditions are relatively undemanding (such as when using an easy discrimination as with the standard oddball stimuli), P3b amplitude following

target presentation is suggested to be an index of attentional resources. Under these conditions, the amplitude of P3b is relatively large, and the peak latency is relatively short. In contrast, when demands for attentional resources increase, the P3b amplitude is smaller and the peak latency is longer due to the extra processing of intervening non-target events which engage attention [43]. The P300 can therefore be manipulated in terms of its latency and amplitude. At issue is whether the P3a or P3b component of the P300 produces a better discrimination of age-related and AD-related changes. One suggestion which is supported by empirical data [14] is that an oddball task with a simple discrimination shows the best discrimination between normal elderly and AD patients. One advantage of this task is that it is relatively easy and makes minimal demands on attentional resources. A second advantage is that an easy task would produce higher performance in the AD group, which in turn would produce more EEG epochs to be used for the averaging procedure.

The present study examined the effects of AD on P300 with regard to age, behavioral performance, and dementia severity as measured by the Mini-Mental State Exam (MMSE) [44] using a standard auditory oddball design. In order to determine the topographic distribution of the P300 impairment, recordings were made from 20 scalp leads. The P3b component of the P300 relates to underlying memory performance and has a posterior parietal distribution, which corresponds to the well-known posterior-temporal/inferior parietal distribution of Alzheimer pathology (particularly neurofibrillary changes and decrease of blood flow and metabolism). Therefore, a measure was developed for assessing the amplitude of the P300 in a relevant topographic distribution. Accordingly, this study used potentials from 11 electrodes at posterior locations anterior to the occipital leads for calculating "total field energy". The hypothesis was that global field energy measurements would account for a larger proportion of the age-related and dementia-related changes associated with the P300 than the conventional latency and amplitude measurements.

MATERIALS AND METHODS

Subjects

Older subjects were recruited from the patient population presenting with memory problems and dementia symptoms to the Southern Illinois University Regional Alzheimer Disease Assistance Center in Springfield,

IL, and from a normal elderly population volunteering through the Center for Dementia Research (between 1987 and 1990). Of 47 serial patients meeting DSM-III-R criteria for dementia, 23 were further diagnosed as probable AD (mean age $\pm$ SD = 74.7 $\pm$ 7.7 years; mean symptom duration $\pm$ SD = 4 $\pm$ 3 years; mean MMSE score $\pm$ SD = 16.6 $\pm$ 7.3) [27] on the basis of NINCDS-ADRDA criteria [45] and included in the study. Eight of the 47 patients were diagnosed as unlikely AD (mean age $\pm$ SD = 71 $\pm$ 11 years; mean symptom duration $\pm$ SD = 5 $\pm$ 6 years; mean MMSE score $\pm$ SD = 25.6 $\pm$ 4.2) and were excluded from the study. The remaining 16 of the 47 patients met criteria for possible AD and were excluded from this report due to diagnostic uncertainties. Eleven elderly normal (EN) controls (mean age $\pm$ SD = 69.3 $\pm$ 6.3 years; mean MMSE score $\pm$ SD = 28.8 $\pm$ 1.7, note all >27 except one with MMSE = 24), spouses of dementia patients, had medical histories free from psychiatric and neurologic illnesses and showed no evidence of dementia. Thirteen young normal (YN) controls were medical staff or wives (mean age $\pm$ SD = 28.3 $\pm$ 6.2 years, range: 21 to 41 years). All subjects were free from medications having notable effects on the cholinergic system, including nonprescription antihistamines, for at least 2 weeks prior to recording (note that these recordings occurred prior to the availability of cholinesterase inhibitor medications for the treatment of dementia). Visual Evoked Potential (VEP) recordings from patients and global field power (GFP) analyses were performed blind to clinical diagnosis. Previous studies of these patients had found a selective flash P2 delay in the mandibular-referenced voltage records of the probable AD group [19] and that the GFP peak corresponding to the late P2 component of the flash VEP is delayed in the probable AD group but not in the demented unlikely AD group [46].

Auditory oddball recording

EEG recordings were made using 20 active scalp electrodes of the International 10–20 System (plus Fpz as inactive ground) referenced to linked mandibles. (This recording reference allowed comparison to a large normative database for clinical purposes.) Individual low-noise tin electrodes were applied with collodion, all electrode locations were recorded and confirmed to be within 3 mm of their target positions, and all impedances were kept below 1.6 kOhm. Additional electro-oculogram, electrocardiogram, and submental electromyogram electrodes were used for

artifact monitoring. The recording instrument was a Bio-logic Brain Atlas III with a parallel Grass model 6 electroencephalograph (EEG) for artifact monitoring.

Auditory oddball task and ERP analysis

In a darkened room, subjects were instructed to count rare tones in an auditory oddball task. Performance on the auditory oddball task was recorded as the percentage of target items identified as oddball tones. Data were recorded between 0 and 512 msecs after the stimulus onset. To achieve an unbiased estimate of P300 latency and GFP, potentials were referenced to a virtual average reference [46]. Re-referenced bins were

then subtracted (rare-frequent) and 3-point smoothed 40 times to achieve an effective low-pass filter. Topographic display with a spline program [47] indicated that young individuals had relatively less positivity during the P300 epoch over the frontal or anterior temporal electrodes compared to posterior regions (Fig. 1A). Therefore, the estimated potentials at the 11 central electrodes (F3, Fz, F4, C3, Cz, C4, P3, Pz, P4, T3, T4; International 10–20 System) based on the spline program (Fig. 1), were squared (preserving sign) transforming potential (voltage) into an index of power (assuming constant resistance at all electrodes: $P = V^2 R$, units related to watts). The power indices from all 11 electrodes were added (if positive, thus
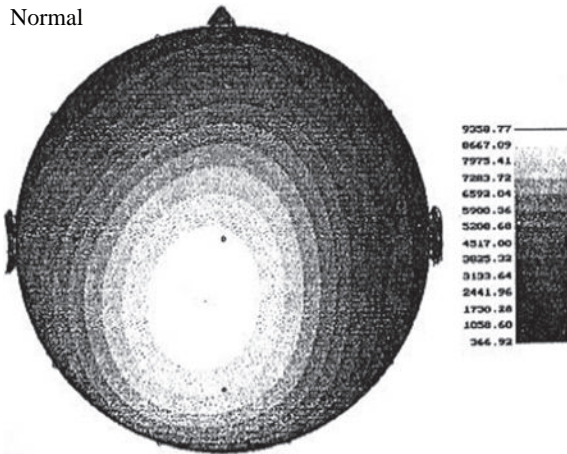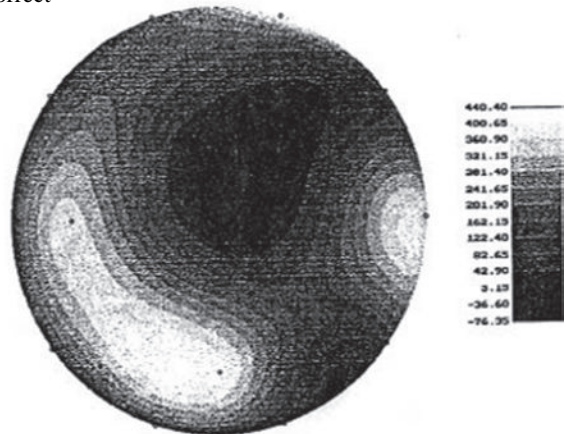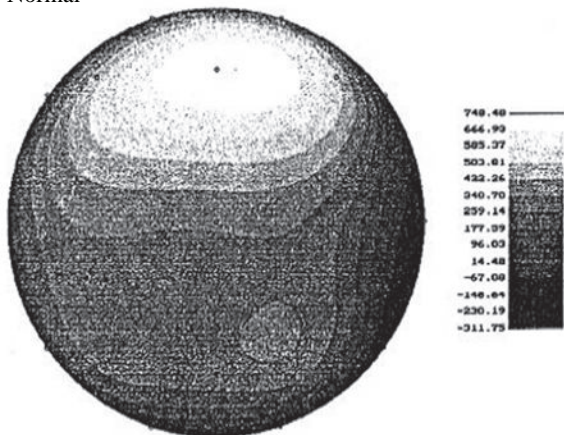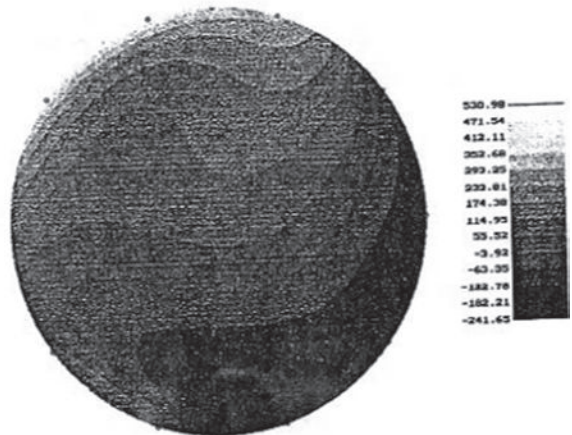
Fig. 1. Topographic distribution of P300 total field energy made from averaging of repeated stimulus presentations in an auditory oddball task in; (A) young normal adults ($n = 14$), (B) elderly normal adults ($n = 11$), (C) patients diagnosed with probably Alzheimer's disease ($n = 10$) who scored >75% on the oddball task, and (D) patients diagnosed with probably Alzheimer's disease ($n = 13$) who scored <75% on the oddball task. Spline plot data was measured across 11 central electrodes.

removing negative voltages), to give an index of field power. The maximum value in the 290 to 490 msec range was designated as the P300 peak power latency. The latencies at 15% of the estimated P300 peak power amplitude, before and after the peak were found (rising and falling) and the power values from these points were summed (essentially integrating the area under the curve produced by the P300 wave), yielding an index of P300 total field energy (units related to watt-hours, but not absolute given uncertainties in tissue factors including skull and scalp). For the oddball paradigm, there were 20% rare tones, and the task was run until 50 artifact-free rare-tone trials were recorded, providing 50 rare, target tone responses and approximately 200 frequent tone responses. The responses were averaged to visualize specific ERPs.

Analysis

There was considerable variability in all aspects of the P300 component, including latency, amplitude, sharpness of focus, total energy, scalp location of peak energy, and general topography. The purpose of this study was to evaluate the relationship between P300 peak voltage latency, amplitude, peak power latency, and P300 total field energy with respect to age and dementia diagnosis, including auditory-oddball task performance and the MMSE index of dementia severity. Statistical tests included one-way analysis of variance (ANOVA). Significant effects were further characterized using follow-up t-tests. Two-tailed levels of 0.05 were used in all tests.

RESULTS

Task performance

YNs and ENs had close to perfect performance on the auditory oddball task. Of 23 probable AD patients, there were 10 mild to moderately demented individuals (mean MMSE $\pm$ SD = 22.1 $\pm$ 3.6, range = 18–28) who scored >75% correct on the task. There were 13 probable AD patients (mean MMSE $\pm$ SD = 12.4 $\pm$ 6.5, range 1–23), who scored less than 75% correct on the task. A score of less than 75% suggests that the individual with these scores may not have been adequately attending to the oddball task. Consequently, subjects were grouped according to whether they scored above or below 75% correct on the oddball task. A t-test for groups with unequal variances showed the MMSE scores of the two AD groups were significantly differ-

ent ($t(18) = 4.55$, $p < 0.0005$). However, initial analyses revealed that none of the observed mean differences between the two AD groups on the P300 parameters were statistically significant. For this reason the two AD groups were combined for most subsequent analyses.

P300 Measurements

Latency

Two measures of P300 latency were examined. Peak voltage latency reflects the traditional measure of latency used in prior studies. Means ($\pm$SD) for the three groups on this measure were 315 $\pm$ 21 ms in the YN group, 364 $\pm$ 48 ms in the EN group, and 361 $\pm$ 56 ms in the AD group. A one-way ANOVA indicated a significant main effect of group ($F(2,44) = 4.67$, $p < 0.05$). The two elderly groups (EN and AD) did not differ reliably from each other but the young participants had shorter latencies than the elderly normal participants ($t(32) < 1$, ns, and $t(22) = -3.33$, $p < 0.005$, respectively) (Fig. 2A).

The calculated measure, peak power latency, was also examined. Mean scores ($\pm$SD) on this measure were 331 $\pm$ 38 ms in YN, 371 $\pm$ 41 ms in EN, and 378 $\pm$ 69 ms in the AD group. Thus, this measure of latency of the peak of the field power was prolonged in the elderly (Fig. 2B), but not further prolonged in the AD group. An ANOVA revealed a marginally significant main effect of group ($F(2,44) = 2.99$, $p = 0.06$).

Amplitude and energy measures

The peak voltage amplitude measure showed effects of both age and dementia. Young participants displayed the greatest amplitude (13.0 + 5.1 uV) followed by those in the EN group (8.3 + 2.8 uV), and then the AD participants (4.9 + 3.3 uV). A significant effect of group was revealed in the ANOVA ($F(2,44) = 18.96$, $p < 0.0001$), and post-hoc tests showed the mean difference between the YN and EN groups to be significant ($t(22) = 2.73$, $p < 0.05$) (Fig. 2C), as well as that between the EN and AD groups ($t(32) = 2.92$, $p < 0.01$). This order is the expected pattern of deterioration from young to elderly to dementia.

Rather than examining only the amount of peak energy, the total field energy (summing the squares of each wave across its duration and expanse) variable reflects the total amount of energy of the P300 waveform, again showing the expected amplitude pattern even more strongly. As with peak ampli-
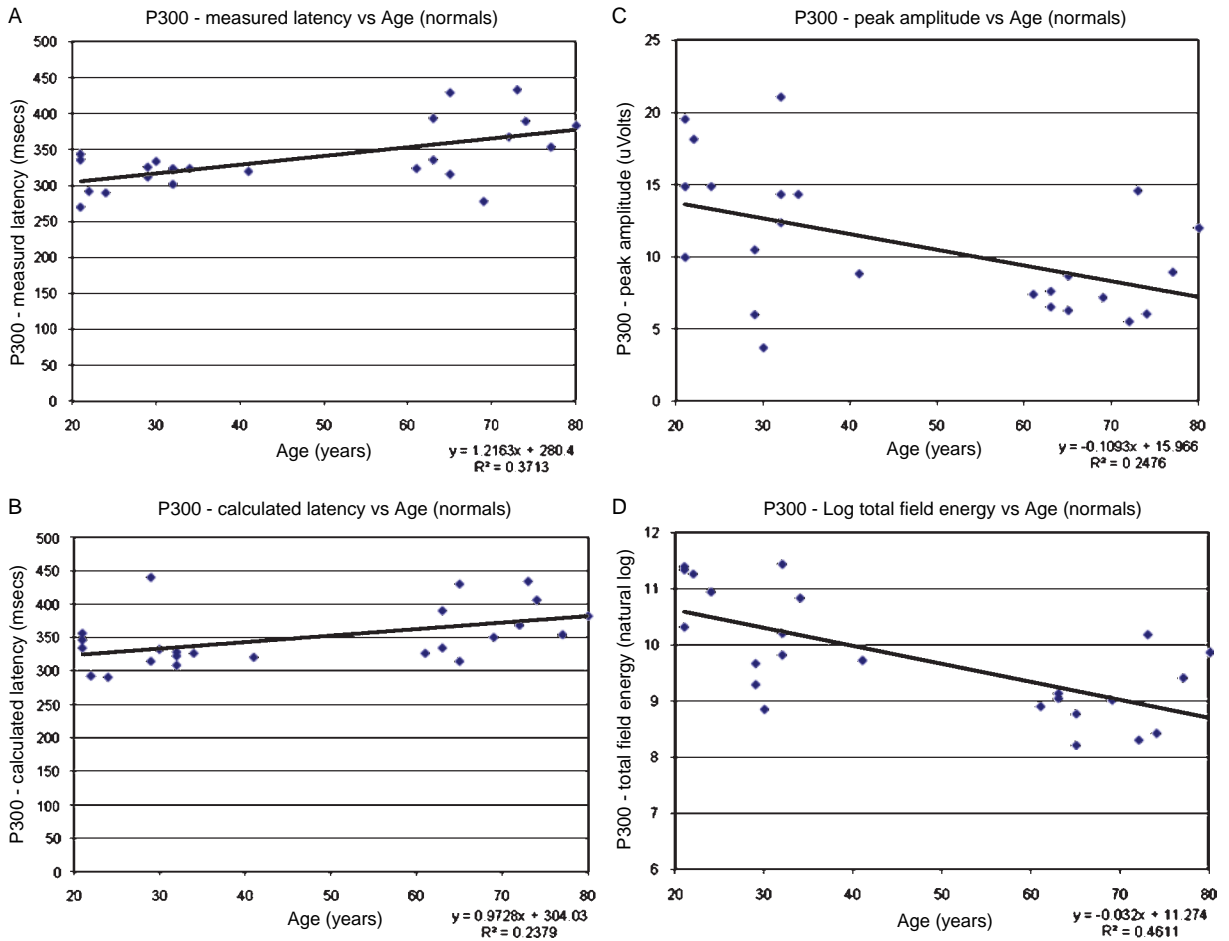
Fig. 2. P300 waveform as a function of age in young normal adults ($n = 14$) and elderly normal adults ($n = 11$); (A) P300 measured latency, (B) P300 calculated latency, (C) P300 peak amplitude, (D) Log total field energy.

tude, mean scores ($\pm$SD) on this measure were greatest for the YN group ($44,397 + 32,286$) followed by the EN group ($9,996 + 7,018$) and, finally, the AD group ($3,347 + 2,971$) (Fig. 2D). For AD patients with MMSE scores >20, mean total field energy ($\pm$SD) was $3,223 \pm 3,357$; with MMSE scores 10–20, $3,719 \pm 3,259$; and with MMS < 10, power = $2,327 \pm 1,210$, indicating that the P300 is not obliterated early in AD, but is barely discernable in late AD (Fig. 1).

Unlike the peak amplitude measure, variances on total field energy revealed large departures from homogeneity of variance across groups, and a graph of this variable against age showed the relationship to be non-linear. The ratio of the largest to smallest variance was 118, a very large value. Therefore, in order to more adequately equate the variances across groups

and transform the scores to ones more linearly related to age, a natural logarithmic transform was applied to the original scores, (a transformation supported by the Gompertz Law of Aging). This transformation reduced the ratio of largest to smallest variance to 4.0 and provided a more linear relationship to age. Mean values ($\pm$SD) on the transformed scores were $10.4 + 0.88$, $9.0 + 0.62$, and $7.6 + 1.24$ for the YN, EN and AD groups, respectively.

An ANOVA of the log transformed total field energy scores revealed a highly significant main effect of group ($F(2,44) = 31.91$. $p < 0.0001$). A t-test contrasting the YN and EN groups was highly significant ($t(22 = 4.34$, $p < 0.0005$), as was the contrast between the EN and AD groups ($t(32) = 3.67$, $p < 0.001$). Thus, both age and dementia were associated with reductions in total field energy.

DISCUSSION

The results from this study replicate the numerous studies that have shown that the latency of the P300 phenomenon increases with age. Our results also show a corresponding decrease in P300 amplitude with increasing age, especially when calculated using spline interpolations and deriving total field energy. While the spline plots appear to show that the P300 peak shifts forward with age, an analysis of energy amplitudes across the scalp shows that this effect was in fact due to a decline in energy in posterior regions relative to anterior regions. Presumably the latency reflects the time course of activity responsible for recognizing the improbability of the stimulus, while the amplitude represents the size of the ascending volley of neuronal activity and the capacity of neuronal systems to respond to that volley. Thus, the P300 latency prolongation with aging indicates that P300-related processing slows with age, while the energy decrease associated with the P300, about 75% from the young to the elderly in this sample, is associated with a decline in the posterior cortex more than the frontal cortex (comparing spline plots and field potentials). The shift in latency from normal elderly to dementia is not apparent in our data, although the P300 in the AD group was generated with significantly less energy relative to the normal elderly group. The finding of no shift in latency in the AD group relative to controls is at variance with many other studies which have used an auditory oddball task (for review, see [11]). This may be due to the fact that unlike our study, participants in most of the previous studies were required to perform an overt motor response, thus allowing averaging of the EEG epochs relative to correct performance. Furthermore, the requirement for making an overt motor response might better probe some attentional processes associated with the selection of the motor response and sensorimotor integration. The topography of the small potentials seen in several probable AD patients indicates severe disruption of the physiological mechanisms generating the P300. However, since the rare tones still elicited more energy than the common tones in the 300 to 500 msec range, some residual P300 activity seems to be present, even in the severely demented AD patients.

This study further shows that the latency of the P300 peak field power increases with age, just as has been extensively reported for voltage peak latencies in many prior studies [4, 8–10, 25]. Furthermore, the amplitude of the total field energy decreased with age, by as much as 75%, and is consistent with prior reports of a decrease of P300 peak voltage amplitude with age. The P300 total field energy decreased further in the AD group even in mildly demented individuals. Further, in several of these demented individuals, the P300 activity is so small that measurement of the latency, field potentials, and total field energy becomes uncertain. A substantial difference between normal elderly and the mildly demented AD patients is present even though the patients could perform the oddball task with substantially correct performance, so the difference in the P300 parameters between these groups was not specifically related to task performance. Furthermore, without removing patients with unclear P300 events [9], neither task performance nor severity of dementia corresponded to a robust difference in P300 amplitude or latency compared to normal elderly subjects.

The major decline in P300 total field energy in the elderly seems to be located posteriorly, though there is also evidence for a loss of frontal activity with aging and age-associated memory impairment [6]. While others have suggested that the P300 vector moves forward with age [12], the data from the present sample indicate that the apparent shift is actually due to a selective loss of energy over the posterior temporal-parietal regions (Fig. 1A,B). In the more mildly demented patients (MMSE >20 and/or >75% correct on the auditory oddball task), the distribution of the P300 energy seems to reflect a loss of energy centrally, represented as a black hole (Fig. 1C) and essentially no P300 in the more impaired patients (Fig. 1D). This finding is consistent with the observation of large reductions of P300 amplitude in the parietal region for AD patients [48]. The topographical distribution found in the present study is similar to that seen in patients with hippocampal damage [25]. This pattern of loss is consistent with the pathological data which indicate that AD-related neurofibrillary changes occur in the entorhinal cortex and hippocampus very early in the course of the disease, and soon extend to the posterior-temporal and inferior parietal regions [49]. This pattern is reflected in AD patients by reduced blood flow and metabolism in the posterior temporal and parietal regions [50]. Thus, the pattern of loss of P300 energy over the posterior cortical regions is consistent with the distribution of neuronal disturbance seen in the brains of AD patients.

The P300 generation likely occurs in a sequence of at least two steps. First, a brain region or dedicated distributed system sensitive to "unexpected occurrences" must determine that an unusual event has occurred [6]. The temporo-parietal junction appears to be impor-

tant in such detections [27]. There is also evidence that the prefrontal cortex plays a role [51], likely as an attention system to guide processing in cortical regions more involved in the processing of incoming sensory information [52]. The initiating system must in turn activate the neurons responsible for synchronizing and generating the P300 component. That activation likely involves a signal through critical ascending brain systems, such as the cholinergic nucleus basalis of Meynert [53], the noradrenergic system projecting rostrally from the locus coeruleus [54], or the serotonergic raphe neurons [55]. All three systems project to the hippocampus and diffusely to the cortex and are affected by age and AD pathology. Which system is involved in the generation of any given P300 event may depend on internal sets or task demands. However, as discussed above, these neural systems whose activity appears to involve generating the P300 are associated with the slowing and amplitude reduction shown in this study to be associated with aging and AD.

An important issue is exactly which brain regions generate the actual P300 component observed on the scalp. Cortically projecting axons cause potential changes in a substantial proportion of radially oriented dendrites of cortical pyramidal neurons, leading to the voltage changes observed on the scalp [56]. The location of the major field generators has been suggested to be temporal lobe structures, possibly including the hippocampus [57, 58], or frontal and temporo-parietal structures [51]. Alternatively, multiple brain structures may be activated diffusely [52, 59–61]. The loss of P300 over a particular large cortical region may suggest either that the medial temporal lobe structures are not suitably activated to generate a scalp voltage or that cortical generators in diffuse areas are dysfunctional.

Simultaneous activation of numerous brain structures, which the P300 may be reflecting, would support concurrent activation of diffusely spread neural networks [52, 62] and parallel distributed processing [63]. Synchronous activation would provide a mechanism for permitting long-term potentiation-type memory mechanisms, which is the specific type of memory function that is most disrupted by AD [4]. The loss of P300 energy across a specific scalp region would suggest that the neuronal ensembles responsible for generating that energy were dysfunctional and have a reduced capacity to store new information. The basis for that dysfunction could lie at any of the steps leading to the generation of the P300, including both loss of cortically projecting brainstem neurons (cholinergic, noradrenergic, or serotonergic) or loss of the synapses involved in generating the dendritic dipoles, in the medial temporal lobe or neocortex [64–67]. Accordingly, a large amount of P300 energy loss occurs across the posterior scalp in normal elderly, and the dementia associated with AD appears to develop after that loss progresses beyond a critical threshold.

It should be noted that the current study used a measure of global field power (GFP) which was based on squaring the output of up to 11 electrodes showing positive P300. This method is different from the standard index in which GFP is calculated by squaring the output of all electrodes, regardless of whether they are positive or negative. In the standard calculation, both positive and negative polarities assume positive values according to the view that the activity of generators are indifferently associated with positive or negative scalp voltages. The assumption is that the underlying pattern of cortical sources can generate both positive and negative components of the voltage at scalp level as a function of their orientation with respect to the scalp surface. However, there is no ideal electrode montage for computing GFP, and virtually all ERP studies use limited electrode montages centered on Pz or Cz. The current findings based on a subset of 11 electrodes suggest that the modified GFP analysis may be more sensitive to the effects of age and AD than the standard array. However, this conclusion awaits further investigation using broader samples with regard to both the aging and dementia severity spectra.

One of the major difficulties in the AD field is the distinction of normal aging from AD. Our data suggest that most of the P300 energy loss occurs during the course of aging, while the scalp distribution of P300 energy loss in early dementia associated with AD is different from normal aging. However, an important issue in the AD field that has recently emerged is the association of the APOE genotype with the risk of developing AD [68]. More specifically, the association between the APOE genotype and early reductions in CSF Aβ and Aβ levels in fronto-corical regions is potentially related to the P300 changes [69, 70]. Our data suggest a need to study the P300 waveform in relation to APOE genotype and to investigate the involvement of attention mechanisms. Recent evidence indicates that P300 voltages are significantly decreased in amplitude and increased in latency in individuals with a family history of AD [71] and for ApoE-ε4 carriers compared to non-carriers [72].

The P300 is an electrophysiological phenomenon that is relevant to the study of dementia and AD. For example, longitudinal monitoring of P300 could reveal

pathology-specific changes. Future understanding of AD and its progression may be gained by studying P300 effects using higher density electrode arrays and other brain imaging techniques across the spectrum of normal aging and AD with regard to specific genetic factors, particularly APOE genotype.

ACKNOWLEDGMENTS

REFERENCES

[1] Polich J (2007) Updating P300: an integrative theory of P3a and P3b. *Clin Neurophysiol* **118**, 2128-2148.

[2] Fabiani M, Karis D, Donchin E (1986) P300 and recall in an incidental memory paradigm. *Psychophysiology* **23**, 298-308.

[3] Paller KA, Zola-Morgan S, Squire LR, Hillyard SA (1988) P3-like brain waves in normal monkeys and in monkeys with medial temporal lesions. *Behav Neurosci* **102**, 714-725.

[4] Ashford JW (2008) Screening for memory disorder, dementia, and Alzheimer's disease. *Aging Health* **4**, 399-432.

[5] Miller GA, Bashore TR, Farwell LA, Donchin E (1987) Research in geriatric psychophysiology. *Annu Rev Gerontol Geriatr* **7**, 1-27.

[6] Anderer P, Saletu B, Semlitsch HV, Pascual-Marqui RD (2003) Non-invasive localization of P300 sources in normal aging and age-associated memory impairment. *Neurobiol Aging* **24**, 463-479.

[7] Goodin DS, Squires KC, Starr A (1978) Long latency event-related components of the auditory evoked potential in dementia. *Brain* **101**, 635-648.

[8] Ball SS, Marsh JT, Schubarth G, Brown WS, Strandburg R (1989) Longitudinal P300 latency changes in Alzheimer's disease. *J Gerontol* **44**, M195-M200.

[9] Marsh JT, Schubarth G, Brown WS, Riege W, Strandburg R, Dorsey D, Maltese A, Kuhl D (1990) PET and P300 relationships in early Alzheimer's disease. *Neurobiol Aging* **11**, 471-476.

[10] Ally BA, Jones GE, Cole JA, Budson AE (2006) The P300 component in patients with Alzheimer's disease and their biological children. *Biol Psychol* **72**, 180-187.

[11] Rossini PM, Rossi S, Babiloni C, Polich J (2007) Clinical neurophysiology of aging brain: from normal aging to neurodegeneration. *Prog Neurobiol* **83**, 375-400.

[12] Ford JM, Duncan-Johnson CC, Pfefferbaum A, Kopell BS (1982) Expectancy for events in old age: stimulus sequence effects on P300 and reaction time. *J Gerontol* **37**, 696-704.

[13] Polich J, Ehlers CL, Otis S, Mandell AJ, Bloom FE (1986) P300 latency reflects the degree of cognitive decline in dementing illness. *Electroencephalogr Clin Neurophysiol* **63**, 138-144.

[14] Polich J, Corey-Bloom J (2005) Alzheimer's disease and P300: review and evaluation of task and modality. *Curr Alzheimer Res* **2**, 515-525.

[15] Frodl T, Hampel H, Juckel G, Burger K, Padberg F, Engel RR, Moller HJ, Hegerl U (2002) Value of event-related P300 subcomponents in the clinical diagnosis of mild cognitive impairment and Alzheimer's Disease. *Psychophysiology* **39**, 175-181.

[16] Ortiz T, Martin Loeches M, Miguel F, Abdad EV, Puente AE (1994) P300 latency and amplitude in the diagnosis of dementia. *J Clin Psychol* **50**, 381-388.

[17] Roth WT, Pfefferbaum A, Horvath TB, Berger PA, Kopell BS (1980) P3 reduction in auditory evoked potentials of schizophrenics. *Electroencephalogr Clin Neurophysiol* **49**, 497-505.

[18] Pritchard WS (1981) Psychophysiology of P300. *Psychol Bull* **89**, 506-540.

[19] Coburn KL, Ashford JW, Moreno MA (1991) Visual evoked potentials in dementia: selective delay of flash P2 in probable Alzheimer's disease. *J Neuropsychiatry Clin Neurosci* **3**, 431-435.

[20] Jordan SE, Nowacki R, Nuwer M (1989) Computerized electroencephalography in the evaluation of early dementia. *Brain Topogr* **1**, 271-282.

[21] Conroy MA, J.P (2007) Normative variation of P3a and P3b from a large sample (N = 120): gender, topography, and response time. *J Psychophysiol* **21**, 22-32.

[22] Courchesne E, Hillyard SA, Galambos R (1975) Stimulus novelty, task relevance and the visual evoked potential in man. *Electroencephalogr Clin Neurophysiol* **39**, 131-143.

[23] Knight RT (1984) Decreased response to novel stimuli after prefrontal lesions in man. *Electroencephalogr Clin Neurophysiol* **59**, 9-20.

[24] Grunwald T, Lehnertz K, Heinze HJ, Helmstaedter C, Elger CE (1998) Verbal novelty detection within the human hippocampus proper. *Proc Natl Acad Sci U S A* **95**, 3193-3197.

[25] Knight R (1996) Contribution of human hippocampal region to novelty detection. *Nature* **383**, 256-259.

[26] Fabiani M, Friedman D, Cheng JC (1998) Individual differences in P3 scalp distribution in older adults, and their relationship to frontal lobe function. *Psychophysiology* **35**, 698-708.

[27] Yamaguchi S, Knight RT (1991) Anterior and posterior association cortex contributions to the somatosensory P300. *J Neurosci* **11**, 2039-2054.

[28] Friedman D, Simpson GV (1994) ERP amplitude and scalp distribution to target and novel events: effects of temporal order in young, middle-aged and older adults. *Brain Res Cogn Brain Res* **2**, 49-63.

[29] Friedman D, Kazmerski VA, Cycowicz YM (1998) Effects of aging on the novelty P3 during attend and ignore oddball tasks. *Psychophysiology* **35**, 508-520.

[30] Knight RT (1987) Aging decreases auditory event-related potentials to unexpected stimuli in humans. *Neurobiol Aging* **8**, 109-113.

[31] Yamaguchi S, Tsuchiya H, Yamagata S, Toyoda G, Kobayashi S (2000) Event-related brain potentials in response to novel sounds in dementia. *Clin Neurophysiol* **111**, 195-203.

[32] Kok A (2001) On the utility of P3 amplitude as a measure of processing capacity. *Psychophysiology* **38**, 557-577.

[33] Riggins BR, Polich J (2002) Habituation of P3a from visual stimuli. *Kor J Think Prob Solving* **12**, 71-81.

[34] Rushby JA, Barry RJ, Doherty RJ (2005) Separation of the components of the late positive complex in an ERP dishabituation paradigm. *Clin Neurophysiol* **116**, 2363-2380.

[35] Kok A (1986) Effects of degradation of visual stimulation on components of the event-related potential (ERP) in go/nogo reaction tasks. *Biol Psychol* **23**, 21-38.

[36] Pfefferbaum A, Ford JM, Weller BJ, Kopell BS (1985) ERPs to response production and inhibition. *Electroencephalogr Clin Neurophysiol* **60**, 423-434.

[37] Falkenstein M, Hoormann J, Hohnsbein J (1999) ERP components in Go/Nogo tasks and their relation to inhibition. *Acta Psychol (Amst)* **101**, 267-291.

[38] Katayama J, Polich J (1996) P300 from one-, two-, and three-stimulus auditory paradigms. *Int J Psychophysiol* **23**, 33-40.

[39] Azizian A, Freitas AL, Watson TD, Squires NK (2006) Electrophysiological correlates of categorization: P300 amplitude as index of target similarity. *Biol Psychol* **71**, 278-288.

[40] Eimer M (1993) Spatial cueing, sensory gating and selective response preparation: an ERP study on visuo-spatial orienting. *Electroencephalogr Clin Neurophysiol* **88**, 408-420.

[41] Falkenstein M, Hoormann J, Christ S, Hohnsbein J (2000) ERP components on reaction errors and their functional significance: a tutorial. *Biol Psychol Aging* **51**, 87-107.

[42] Salisbury DF, Griggs CB, Shenton ME, McCarley RW (2004) The NoGo P300 'anteriorization' effect and response inhibition. *Clin Neurophysiol* **115**, 1550-1558.

[43] Donchin E, Karis D, Bashore TR, Coles MGH, Gratton G (1986) Cognitive psychophysiology: systems, processes, and applications. *In Psychophysiology: systems, processes, and applications*, Coles M, Donchin E, Porges S, eds. The Guilford Press, New York, pp. 244-267.

[44] Folstein MF, Folstein SE, McHugh PR (1975) "Mini-mental state". A practical method for grading the cognitive state of patients for the clinician. *J Psychiatric Res* **12**, 189-198.

[45] McKhann G, Drachman D, Folstein M, Katzman R, Price D, Stadlan EM (1984) Clinical diagnosis of Alzheimer's disease: report of the NINCDS-ADRDA work group under the auspices of department of health and human services task force on Alzheimer's disease. *Neurology* **34**, 939-944.

[46] Coburn KL, Ashford JW, Moreno MA (1993) Delayed late component of visual global field power in probable Alzheimer's disease. *J Geriatr Psychiatry Neurol* **6**, 72-77.

[47] Perrin F, Pernier J, Bertrand O, Echallier JF (1989) Spherical splines for scalp potential and current density mapping. *Electroencephalogr Clin Neurophysiol* **72**, 184-187.

[48] Holt LE, Raine A, Pa G, Schneider LS, Henderson VW, Pollock VE (1995) P300 topography in Alzheimer's disease. *Psychophysiology* **32**, 257-265.

[49] Braak H, Braak E (1996) Evolution of the neuropathology of Alzheimer's disease. *Acta Neurol Scand Suppl* **165**, 3-12.

[50] Ashford JW, Shih WJ, Coupal J, Shetty R, Schneider A, Cool C, Aleem A, Kiefer VH, Mendiondo MS, Schmitt FA (2000) Single SPECT measures of cerebral cortical perfusion reflect time-index estimation of dementia severity in Alzheimer's disease. *J Nucl Med* **41**, 57-64.

[51] Yamaguchi S, Hale LA, D'Esposito M, Knight RT (2004) Rapid prefrontal-hippocampal habituation to novel events. *J Neurosci* **24**, 5356-5363.

[52] Ashford JW, Coburn KL, Fuster JM (1998) Functional Cognitive Networks in Primates In *Fundamentals of Neural Networks: Neuropsychology and Cognitive Neuroscience*, Parks RW, Levine DS, eds. The MIT Press, Cambridge, Mass.

[53] Callaway E, Halliday R, Naylor H (1992) Cholinergic activity and constraints on information processing. *Biol Psychol* **33**, 1-22.

[54] Swick D, Pineda JA, Foote SL (1994) Effects of systemic clonidine on auditory event-related potentials in squirrel monkeys. *Brain Res Bull* **33**, 79-86.

[55] Ito J, Yamao S, Fukuda H, Mimori Y, Nakamura S (1990) The P300 event-related potentials in dementia of the Alzheimer type. Correlations between P300 and monoamine metabolites. *Electroencephalogr Clin Neurophysiol* **77**, 174-178.

[56] Elul R (1971) The genesis of the EEG. *Int Rev Neurobiol* **15**, 227-272.

[57] Halgren E, Squires NK, Wilson CL, Rohrbaugh JW, Babb TL, Crandall PH (1980) Endogenous potentials generated in the human hippocampal formation and amygdala by infrequent events. *Science* **210**, 803-805.

[58] McCarthy G, Wood CC, Williamson PD, Spencer DD (1989) Task-dependent field potentials in human hippocampal formation. *J Neurosci* **9**, 4253-4268.

[59] Ashford JW, Fuster JM (1985) Occipital and inferotemporal responses to visual signals in the monkey. *Exp Neurol* **90**, 444-466.

[60] Coburn KL, Ashford JW, Fuster JM (1990) Visual response latencies in temporal lobe structures as a function of stimulus information load. *Behav Neurosci* **104**, 62-73.

[61] Gevins AS, Doyle JC, Cutillo BA, Schaffer RE, Tannehill RS, Ghannam JH, Gilcrease VA, Yeager CL (1981) Electrical potentials in human brain during cognition: new method reveals dynamic patterns of correlation. *Science* **213**, 918-922.

[62] Murdock BB (1993) TODAM2: a model for the storage and retrieval of item, associative, and serial-order information. *Psychol Rev* **100**, 183-203.

[63] McClelland JL, RD the PDP Research Group, (1986) *Parallel Distributed Processing: Explorations in the Microstructure of Cognition, Vol. 2: Psychological and Biological Models*, MIT Press, Cambridge, MA.

[64] Terry RD (2000) Cell death or synaptic loss in Alzheimer disease. *J Neuropathol Exp Neurol* **59**, 1118-1119.

[65] Terry RD, Katzman R (2001) Life span and synapses: will there be a primary senile dementia?. *Neurobiol Aging* **22**, 347-348. discussion 353-344.

[66] Terry RD (2006) Alzheimer's disease and the aging brain. *J Geriatr Psychiatry Neurol* **19**, 125-128.

[67] Scheff SW, Price DA, Schmitt FA, Scheff MA, Mufson EJ (2011) Synaptic loss in the inferior temporal gyrus in mild cognitive impairment and Alzheimer's disease. *J Alzheimers Dis* **24**, 547-557.

[68] Raber J, Huang Y, Ashford JW (2004) ApoE genotype accounts for the vast majority of AD risk and AD pathology. *Neurobiol Aging* **25**, 641-650.

[69] Morris JC, Roe CM, Xiong C, Fagan AM, Goate AM, Holtzman DM, Mintun MA (2010) APOE predicts amyloid-beta but not tau Alzheimer pathology in cognitively normal aging. *Ann Neurol* **67**, 122-131.

[70] Jack CR Jr, Knopman DS, Jagust WJ, Shaw LM, Aisen PS, Weiner MW, Petersen RC, Trojanowski JQ (2010) Hypothetical model of dynamic biomarkers of the Alzheimer's pathological cascade. *Lancet Neurol* **9**, 119-128.

[71] Green J, Levey AI (1999) Event-related potential changes in groups at increased risk for Alzheimer disease. *Arch Neurol* **56**, 1398-1403.

[72] Irimajiri R, Golob EJ, Starr A (2010) ApoE genotype and abnormal auditory cortical potentials in healthy older females. *Neurobiol Aging* **31**, 1799-1804.

Evaluation and Tracking of Alzheimer's Disease Severity Using Resting-State Magnetoencephalography

Todd A. Verdoorn[a,*], J. Riley McCarten[b], David B. Arcienegas[c], Richard Golden[d], Leslie Moldauer[e], Apostolos Georgopoulos[b], Scott Lewis[b], Michael Cassano[a] and Laura Hemmy[b], William Orr[f] and Donald C. Rojas[c]

[a]*Orasi Medical, Inc., Minneapolis, MN, USA*

[b]*Geriatric Research and Education Clinic and Brain Sciences Center, Minneapolis VA Medical Center, Minneapolis, MN, USA*

[c]*Neurobehavioral Disorders Program, Department of Psychiatry, University of Colorado School of Medicine, Denver, CO, USA*

[d]*Noran Neurology Clinic, Minneapolis, MN, USA*

[e]*Radiant Research, Denver, CO, USA*

[f]*Orr and Associates Memory and Geriatric Behavioral Clinic, Mendota Heights, MN, USA*

Abstract. We have conducted multicenter clinical studies in which brain function was evaluated with brief, resting-state magnetoencephalography (MEG) scans. A study cohort of 117 AD patients and 123 elderly cognitively normal volunteers was recruited from community neurology clinics in Denver, Colorado and Minneapolis, Minnesota. Each subject was evaluated through neurological examination, medical history, and a modest battery of standard neuropsychological tests. Brain function was measured by a one-minute, resting-state, eyes-open MEG scan. Cross-sectional analysis of MEG scans revealed global changes in the distribution of relative spectral power (centroid frequency of healthy subjects $= 8.24 \pm 0.2$ Hz and AD patients $= 6.78 \pm 0.25$ Hz) indicative of generalized slowing of brain signaling. Functional connectivity patterns were measured using the synchronous neural interactions (SNI) test, which showed a global increase in the strength of functional connectivity (cO^2 value of healthy subjects $= 0.059 \pm 0.0007$ versus AD patients $= 0.066 \pm 0.001$) associated with AD. The largest magnitude disease-associated changes were localized to sensors near posterior and lateral cortical regions. Part of the cohort (31 AD and 46 cognitively normal) was evaluated in an identical fashion approximately 10 months after the first assessments. Follow-up scans revealed multiple MEG scan features that correlated significantly with changes in neuropsychological test scores. Linear combinations of these MEG scan features generated an accurate multivariate model of disease progression over 10 months. Our results demonstrate the utility of brief resting-state tests based on MEG. The non-invasive, rapid and convenient nature of these scans offers a new tool for translational AD research and early phase development of novel treatments for AD.

Keywords: Alzheimer's disease, magnetoencephalography, electrophysiology, biomarkers

INTRODUCTION

Recent advances in detecting Alzheimer's disease (AD) with fluid and imaging biomarkers are changing conceptions about the fundamental disease processes

*Correspondence to: Todd A. Verdoorn, Chief Scientific Officer, Orasi Medical, Inc., 6465 Wayzata Blvd, Suite 810, Minneapolis, MN 55426, USA. Tel.: +763 405 2210; E-mail: todd.verdoorn@orasimedical.com.

and definitions. New recommendations about disease stages and associated diagnostic criteria [1–4] now emphasize the importance of measuring a variety of endpoints including temporal lobe atrophy, amyloid plaque, brain function and levels of A-β and phosphorylated tau in CSF. These recommendations also include new diagnostic entities representing very early, even preclinical states of AD. These improved biomarkers and diagnostic recommendations should not only improve patient care, but also facilitate the evaluation of novel treatments for the disease. Recent work based on the Alzheimer's Disease Neuroimaging Initiative (ADNI) suggests ways in which imaging biomarkers can improve the statistical power of AD clinical trials, especially later stage Phase III studies [5, 6]. Moreover, the clear definition of preclinical AD included in the recommendations also may support testing of disease modifying treatments much earlier in the disease process. So far, imaging and CSF biomarkers have found only sporadic use in clinical trials, and in some cases their use in this setting has generated unanticipated results [7, 8]. Adoption of AD biomarkers in clinical trials requires they track disease severity with high fidelity and can be conveniently applied during all phases of the drug development cycle, areas where the current options fall short. MR-based measurements of brain atrophy have shown reliable correlations with cognitive decline over the course of 12 months [5, 9], but recent hypotheses suggest that brain atrophy occurs quite late in the disease process [10]. Trials that use atrophy as an endpoint most often require long treatment times (one year at a minimum), and multicenter imaging studies likely need better alignment and standardization between MR instruments. Finally, all standard endpoints, including neuropsychological testing, are time-consuming, expensive, invasive and poorly tolerated by fragile, elderly patient populations. Thus, further work is needed to identify and develop additional AD biomarkers, especially patient-friendly measures that track disease severity over short periods of time.

One promising alternative is high-resolution measurement of electrophysiological function using standard electroencephalography (EEG) or magnetoencephalography (MEG). Deficits in brain function associated with AD have been routinely observed when measuring potentials generated by sensory stimuli [11, 12] as well as resting-state EEG recordings, leading to a well-established view that slowing of brain function and loss of high frequency rhythmicity are hallmarks of AD functional pathology (see [13, 14] for review). Sig-

nificant correlations between EEG scan features and neuropsychological testing also have been observed [15], and such EEG scans have shown good ability to predict conversion to AD [16]. Application of MEG, with its theoretically finer spatial resolution has produced very similar findings with respect to the distribution of high and low frequency brain signaling [17, 18]. However, other neurological and psychiatric disorders are associated with brain function slowing [19, 20] suggesting that more refined measurements may be needed to identify changes that are specific for particular diseases.

Assessment of functional connectivity may provide the additional information needed to improve the specificity and utility of electrophysiological recordings. Non-electrophysiological measures of functional connectivity such as fMRI [21] and diffusion tensor imaging [22, 23] have detected pathological changes in communication networks in AD patients. However, such measurements are either static reflections of structure (diffusion tensor imaging) or quite slow compared to the synaptic currents that underlie the signals (fMRI). Both MEG and EEG are able to measure signals in the millisecond time range, but MEG is better suited for evaluating functional connectivity because signals are measured without the reference electrode that introduces spurious connectivity measures in EEG recordings. Importantly, recent work indicates that resting-state MEG scans can detect changes in functional connectivity in AD [24], and these changes are consistent with a more random network architecture that could underlie impaired cognition [25]. High-resolution assessment of functional connectivity may complement other functional measurements and help implement improved tools for diagnosing and tracking the disease.

Technologies available for measuring functional connectivity and brain communication networks (including fMRI) rely on quantifying correlations between spatially separated sensors or brain regions. Detecting correlated activity is outwardly straightforward and involves measuring the degree of relatedness of signal pairs over a particular time period under consideration. One possible confound in most approaches is the unknown contribution of correlations within a single time series (autocorrelations) to the calculation of correlation across two time series (cross-correlations). Since cross-correlations represent the critical values for measuring functional connectivity, attempts to limit the influence of autocorrelations could provide novel insight into communication networks.

Georgopoulos and colleagues [24, 26, 27] have developed a data processing methodology for resting-state MEG scans that implements a functional connectivity measure in which autocorrelations are removed with a prewhitening step prior to calculation of cross-correlations. Application of this technology, called the synchronous neural interactions (SNI) test, has revealed a network of correlated activity that is stable across a large group of healthy control subjects [27]. Moreover, the properties of the network change in unique ways in patients suffering from a variety of neurological and psychiatric disorders, allowing preliminary multi-group classification based on resting-state MEG scans [24]. The SNI test has more recently been used to accurately classify a relatively large population of patients with post-traumatic stress disorder compared to healthy volunteers [28]. In addition to providing robust, quantitative empirical data on brain function in health and disease, the SNI test is simple, quick, non-invasive and very patient-friendly. Since there are no complex tasks it is reasonable to assume that the SNI test measures fundamental functional properties and not simply motivational state, the ability to accurately complete the task or follow directions. It is therefore, ideally suited for use in controlled settings such as clinical trials where patient compliance and retention are critically important.

Despite the growing evidence that human electrophysiology may have diagnostic utility for AD, EEG and MEG are still not widely used in the search for new AD treatments. Most electrophysiology studies include relatively small groups of subjects (often between 20–30 subject per group), each using different data processing and analysis techniques. Most processing methods include a manual review step that is difficult to standardize and therefore difficult to use in multicenter clinical studies. The research presented here was designed to identify, implement and verify a standardized data processing and analysis method that could provide a robust MEG-based endpoint to support the development of new AD treatments. To accomplish this we have identified a single measure to capture information about the distribution of relative spectral power, the frequency centroid. This is complemented by the SNI test, which is a novel method for evaluating functional connectivity that requires only one minute of input data. Another critical goal of this work was to identify specific changes in resting-state MEG scans that were associated with AD, and begin to determine how these MEG scan features track with disease severity both cross-sectionally and longitudi-

nally. We have found that our approach for combining the frequency centroid and SNI measurements is capable of tracking disease progression longitudinally in a manner that could be beneficially applied to clinical development programs. Once fully established and validated, such tests could eventually find wider use in normal clinical practice.

METHODS

Subjects

Subjects were recruited during the course of two clinical studies, which originally included a total of 279 study volunteers. The clinical studies were sponsored by the Brain Sciences Center (BSC) at the Minneapolis VA Medical Center and Orasi Medical, Inc. The study sponsored by Orasi included clinical sites and MEG centers in two cities: Minneapolis, MN (Noran Neurology Clinic, Orr Consulting Psychiatric Recovery, Minneapolis VA Medical Center-GRECC) and Denver, CO (Radiant Research, University of Colorado – Denver). The BSC study involved a single clinical site and MEG center at the Minneapolis VA Medical Center. The Orasi-sponsored study was a multicenter, exploratory cohort study designed to identify patterns of functional activity associated with AD. The design of the BSC study has been described previously [24]. Clinical studies were conducted in accordance with the Declaration of Helsinki of 1975 and were approved by the Western Institutional Review Board as well as Institutional Review Boards at participating medical centers and clinics. All subjects were recruited from the community through their neurology clinic or through community advertising. Recruitment focused on subjects with a previous diagnosis of AD or healthy status. Twenty-four subjects were enrolled in the AD group, but did not meet DSM-IV-TR criteria for Dementia of Alzheimer's Type (see below). It is likely that at least some of these subjects could be classified as having Mild Cognitive Impairment [29], and although they were scanned and evaluated in the studies, their results are not reported here. There also were 19 subjects that were excluded because their MEG scans were not of acceptable quality. Table 1 summarizes the demographics of the remaining study subjects ($n = 240$) separated according to the particular study or geographic location. On average the AD patients were somewhat older than the healthy control group and there were relatively more males in the AD group compared to the healthy controls. Eighty subjects from

Table 1
Subject demographics

	Age	% Female	MMSE	ADAS (SOB)	CDR (SOB)
Minneapolis cohort*					
Healthy ($n = 81$)	66.2 ± 1.7	56.8	29.0 ± 0.1	N/A	N/A
DAT ($n = 84$)	76.4 ± 0.8	40.5	19.7 ± 0.7	22.5 ± 1.4	6.8 ± 0.5
Denver cohort					
Healthy ($n = 16$)	67.8 ± 2.4	62.5	28.2 ± 0.3	N/A	N/A
DAT ($n = 15$)	75.9 ± 2.7	40.0	16.1 ± 2.2	27.5 ± 3.4	7.1 ± 1.0
BSC study cohort					
Healthy ($n = 34$)	72.6 ± 1.3	23.5	N/A	N/A	N/A
DAT ($n = 32$)	76.6 ± 1.3	3.2	21.9 ± 0.7	N/A	N/A

*Table values represent the *mean* $\pm$ SEM values for each of the demographic and severity measures. N/A = data not collected.

Table 2
Longitudinal cohort demographics

	Age	% Female	MMSE	ADAS (SOB)	CDR (SOB)
Healthy longitudinal cohort ($n = 46$)*					
Scan 1	71.8 ± 1.1	52.2	28.8 ± 0.17	N/A	N/A
Scan 2	72.9 ± 1.2	52.2	28.8 ± 0.18	N/A	N/A
AD longitudinal cohort ($n = 31$)					
Scan 1	74.4 ± 1.1	54.8	20.5 ± 1.3	21.0 ± 2.6	5.8 ± 0.75
Scan 2	75.2 ± 1.2	54.8	19.3 ± 1.4	27.5 ± 3.4	7.4 ± 0.84

*Table values represent the mean $\pm$ SEM values for each of the demographic and severity measures. N/A = data not collected.

the original Orasi Minneapolis cohort were invited to participate in a longitudinal follow-up approximately 10 months after the first tests. A total of 31 AD patients and 46 healthy subjects joined the longitudinal component of the study and were evaluated identically to that of the original assessments. The demographics of the longitudinal cohort are summarized in Table 2.

Clinical evaluation

Study investigators at each clinical site were responsible for evaluating the subjects and confirming either their pre-existing diagnosis or healthy status. The evaluation of subjects included neurological examination and review of medical history and records. All subjects from the Orasi-sponsored study were evaluated with the Mini-Mental State Examination (MMSE) to assess cognitive functioning at the time of screening, and the Modified Hachinski Scale [30] to evaluate the potential for vascular dementia. Subjects who scored higher than a 4 on the Hachinski Scale were excluded from participation. The AD subjects in the Orasi-sponsored study also were assessed using the Alzheimer's Disease Assessment Scale – Cognitive Subscale (ADAS-Cog), and the Clinician Dementia Rating (CDR) to further establish disease severity. The BSC study used a slightly different strategy to evalu-

ate study participants. The MMSE was administered only to the AD group, and they were not tested with the CDR or ADAS-Cog. However, an extensive set of neuropsychological and neurological tests were conducted to confirm disease or healthy status. Based on their clinical evaluations, study investigators generated a diagnosis for each subject: either 1) healthy; or 2) Dementia of Alzheimer's Type (DAT). Subjects also were classified according to the NINCDS-ADRDA criteria for probable and possible AD or mild cognitive impairment (MCI) [24] but these secondary classifications were not used to define formal group assignments. Subjects not considered healthy, but who also did not meet DSM-IV-TR criteria for DAT were evaluated, but their results are not reported here. Subjects in the longitudinal component of the study were evaluated in an identical manner approximately 10 months after first evaluation (mean time difference = 9.8 ± 0.2 months).

MEG scan

Subjects underwent a single MEG scan session using WH3600 Gradiometer Instruments Manufactured by 4D Neuroimaging (San Diego, CA) located either at the University of Colorado – Denver MEG Center or the Minneapolis VA Medical Center. Once the subject was situated properly in the scanner MEG data col-

lection was initiated. Subjects were instructed to close their eyes for approximately 30 seconds to prepare for the eyes open fixation task. Subjects then were asked to open their eyes and gaze at a white dot projected on a video screen located 60 cm in front of their eyes at an angle allowing the subject to comfortably gaze straight ahead. MEG data collection was stopped after completion of the series, which consisted of 120 seconds of MEG data collection. During the scan both subjects and recordings were observed for evidence of excessive eye, head or body movement and scans contaminated by such artifacts were rejected. The MEG scan operator was instructed to collect multiple scan series to replace rejected series or if otherwise deemed necessary according to the operator's judgment. In most cases 2–3 scan series were completed for each subject. Prior to digitization by the MEG instrument at 1071 Hz data from each of the 248 sensors was low-pass filtered at 400 Hz to avoid aliasing.

Data processing

MEG scan data including all associated acquisition and instrument setting information was sent to Orasi Medical over the internet using Orasi's secure web browser interface. The time-series from each sensor were evaluated for quality automatically by measuring the wideband absolute variance (0.1–400 Hz), the low frequency variance (0.1–1 Hz) and whether prewhitened time series were stationary. In some cases, visual inspection was conducted to verify the results of automated quality tests. Any visual inspection was done by individuals who were blind to the subject's clinical diagnosis. Data from sensors that showed any variance greater than 5 standard deviations away from the mean (higher or lower) or those generated prewhitened time series that were not formally stationary (homogeneous mean and variance across the entire time series) were excluded from analysis. In most cases multiple scan series were available and if overall quality did not differ between them, the first series was used. Otherwise the scan series with the fewest excluded sensors was used. Because data from 43 frontal sensors were most likely to fall outside of quality criteria, we chose to exclude those sensors from the analysis in all subjects. In addition, 19 subjects (8 healthy and 11 AD, 7% of subjects tested) were excluded from MEG analysis because of overall poor scan quality (all sensors met exclusion criteria). These quality control procedures resulted in a relatively homogeneous data set in which neither the wideband absolute variance nor low fre-

quency variance differed significantly between study groups at any sensor. Subsequent analysis was conducted using sixty seconds of high-quality, contiguous, eyes-open data.

An important analytical strategy for this study was to identify a minimal set of MEG-scan parameters that could broadly characterize functional pathology associated with AD, while being robust, reliable and amenable to standardization. Therefore, the centroid frequency was used to measure the distribution of relative spectral power and zero-lag cross-correlations (e.g. the SNI test) quantified functional connectivity. The fundamental increment of analyzed data, referred to as an individual "feature", was either a single sensor for centroid frequency (205 sensors total) or a single sensor-pair for the cross-correlation analysis ($[205 \times 204]/2 = 20910$ measures of functional connectivity). In a conservative attempt to characterize differences between groups, global values (e.g. one value per subject per data type, described below) were subjected to initial statistical tests followed by a more detailed analysis based on individual features or distance-based subgroups (see below).

To evaluate the distribution of spectral power in the MEG time series, power spectral density plots were generated from the entire one-minute of eyes-open raw data over the 0.1–50 Hz frequency range using fast Fourier transform. To characterize the spectral power distribution, we calculated the centroid frequency, which is defined as the frequency at which the spectral power in high and low frequencies is balanced. The centroid frequency was calculated for each sensor from the area under the power spectral density function from 1 to 50 Hz (Fig. 1A). Relative power also was calculated for each of 5 standard frequency bands (delta: 0.5–3 Hz, theta: 3–8 Hz, alpha: 8–13 Hz, beta: 13–30 Hz, gamma: 30–50 Hz). Global values for each measurement were generated by averaging the power spectra of all sensors and using the averaged power spectra to calculate centroid frequency or band-specific relative spectral power.

Functional connectivity was assessed by a variant of the SNI test developed by Georgopoulos and coworkers [24, 26, 27]. Sixty-second time series were down sampled by a factor of 10 and digitally filtered at 50 Hz. The resulting time series were prewhitened by a single differencing step followed by fitting to an autoregressive moving average (ARMA) model and taking the residuals. The parameters used for prewhitening were optimized through iterative testing that attempted to identify the minimal differencing and lowest order
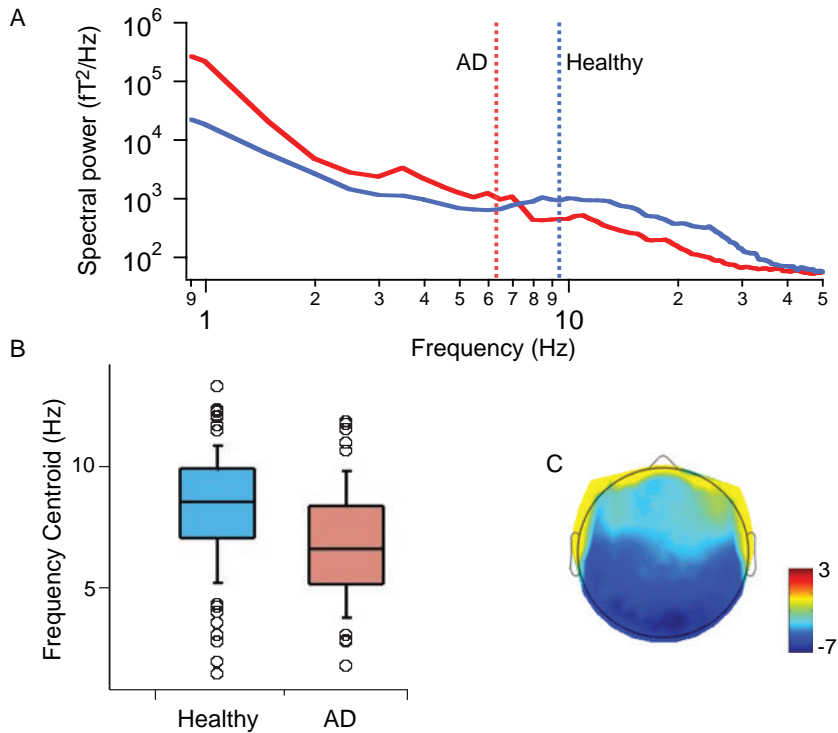
Fig. 1. Resting-state MEG scans reveal significant differences in the distribution of spectral power between AD and elderly, cognitively healthy volunteers. A) Shown is a power spectral density plot (averaged across all sensors) for a single AD patient (red) and a single cognitively healthy subject (blue). The dotted lines represent the centroid frequencies calculated for each of those subjects. Increased power in lower frequencies and decreased power in higher frequencies result in a marked leftward shift of the centroid frequency in AD patients. B) Shown are box-and-whisker plots of global centroid frequency for 123 cognitively healthy and 117 AD patients. The boxes represent the 25–75% confidence intervals, the error bars represent the 95% confidence intervals and each open circle represents subjects outside of the 95% confidence interval. C) The heat map illustrates the localization and direction of the most significant differences in centroid frequency. Standard *t*-tests were conducted for each sensor in the array and the T-value for each sensor is plotted in this heat map based on the color calibration bar on the right. Blue represents values that were lower in AD compared to healthy controls and warmer colors denotes were the values were higher in the AD group.

AR models needed to suppress autocorrelations to an asymptotic level. For these scans first-order differencing combined with an AR order of 5 was found to be optimal; and all data was prewhitened with these model parameters. The level and direction of correlation between every pair of sensors ($n = 20910$ sensor pairs) was calculated from the AR residuals at time lags ranging from -100 to $+100$ ms. Our analysis focused on the instantaneous or zero-lag correlation (cO) value and did not use statistical partialling of the cO values These cO values include information about both direction (positive or negative) and magnitude of correlated activity. In most cases a direct comparison of magnitude was more informative and relevant for connectivity analysis. Therefore, all group comparisons and severity analyses used the square of the cO value (cO^2), which represents the percentage of

variance that is common to the two time series. A global connectivity value was calculated for each subject by averaging the cO^2 values for all sensor pairs in the array. Distance-based functional connectivity measures were calculated as the mean of all cO^2 values of sensor groups defined by a range of physical distances between sensors (see Fig. 2B for average sensor distances for each group). Comparisons with neuropsychological test scores and longitudinal models of severity change also used cO^2 values.

Two general mapping methods were used to show the spatial distribution of MEG scan features that differ between groups or are correlated to neuropsychological test scores. Colorized heat maps were constructed to delineate the array location of notable features. Specific colors correspond to either the T statistic for group differences or the Pearson R value for correlations.
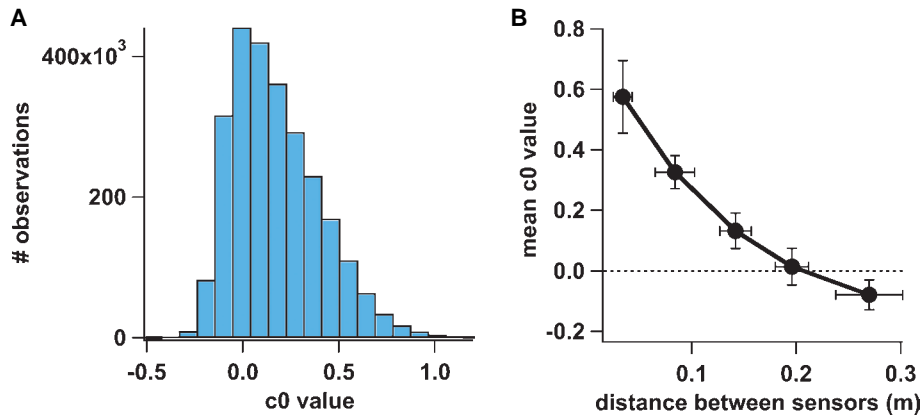
Fig. 2. The magnitude and direction of cO values varies regularly with the distance between sensors. A) Shown is the distribution of all cO values from all sensor pairs and all cognitively healthy subjects (bin width = 0.1). Each subject scan generated 20910 cO values ($n = 123$ subjects in the cognitively healthy group). B) The network of cO values was divided into five groups based on the distance between the sensor pairs. Individual cO values within each distance group were averaged for each subject followed by averaging across subjects. The markers represent the average of these distance-group cO values plotted as a function of average distance between sensors. Y error bars represent the standard deviation across the cognitively healthy group for each of the five distance groups and the X error bars represent the standard deviation of the distances within each group.

These values were calculated for each sensor or sensor pair and mapped according to the location of the sensors in the MEG array. For SNI functional connectivity measures the results for each sensor represented the average values of the connections between that sensor and all other sensors in the array. Lines drawn between the relevant pair of sensors also were used to denote features of particular interest (e.g. sensor pairs that showed the most significant differences or strongest correlation with test scores).

Statistical analysis

Group differences in global and distance-based features were evaluated using a Multivariate Analysis of Variance (MANOVA) with age and MEG study site as covariates to control for possible age- or site-related confounds. Bonferroni corrected p values were reported to account for multiple comparisons. To investigate group differences at the level of single data features, standard, two-group t-tests comparing each feature, and in most cases the resulting T statistic was used to denote magnitude and direction of group differences. For these surveys of all sensors or pairs (e.g. Table 3) the p values reported were not corrected for multiple comparisons. Relationships between MEG scan features and neuropsychological test scores (MMSE, ADAS-Cog, CDR) were quantified by calculating Pearson correlation coefficients

Table 3
Scan features that differed significantly across groups

	Proportion of significant features[1]	Minimum p value[2]	T score range[3]
cO^2	0.38	1.4×10^{-7}	–4.1–5.4
Centroid	0.62	5.3×10^{-10}	–7.4– –1.2
Delta band	0.20	0.006	–2.8–2.0
Theta band	0.94	5×10^{-9}	0.12–6.1
Alpha band	0.13	0.003	–2.4–3.0
Beta band	0.42	1.6×10^{-7}	–5.4–1.7
Gamma band	0.16	0.001	–3.3–2.3

[1]Individual data features (20910 total sensor pairs for cO^2 values and 205 sensors for centroid frequency) measures were subjected to a t-test evaluating the difference between the cognitively healthy and the AD groups. The column reports the proportion of those features that were significantly different ($p < 0.05$) between study groups based on the t-test ($n = 117$ AD and 123 healthy); [2]The minimum p-value (not Bonferroni corrected) for the individual feature that was most significantly different between study groups (t-test); [3]The range of T values in the MEG scan features based on t-tests.

between sensor or sensor-pair level MEG scan features and the individual test scores. For the MMSE this was done for both groups combined as well as for the AD group separately. For the ADAS-Cog and CDR this analysis was conducted for the AD group only. To produce and compare preliminary models of disease severity change we employed a multivariate linear regression approach [31]. MEG features that were strongly correlated with changes in the ADAS-Cog were used to construct models. A jack-knife cross-validation approach was used to characterize the

models. Models were built using data from 30 (n – 1) subjects and then applied to the one subject not used for model calculation. This process was repeated so that each subject was left out and tested against a data model built from the rest of subjects to generate the results shown in Fig. 6. The sum of squared differences between estimated and actual ADAS-Cog changes were used to compare models based on goodness-of-fit.

RESULTS

Global spectral power

To confirm and extend previous observations that spectral power of electrophysiology recordings shifts to lower frequencies in AD, we analyzed the 60-second MEG scan data after transforming the time series into power spectral density functions using fast Fourier transform. We focused on a single value to characterize the distribution, the frequency centroid, which represents the frequency where spectral power is balanced over a particular frequency range (Fig. 1A). The global frequency centroid value was significantly lower in the AD group compared to the cognitively healthy group (AD $= 6.78 \pm 0.25$ Hz; healthy $= 8.24 \pm 0.20$ Hz, $p < 0.0001$, $F = 24.2$, MANOVA, Fig. 1B). Age and site were included in the MANOVA as covariates and neither variable altered the disease group differences. Frequency centroid values measured in the two MEG instruments did not differ significantly (cognitive healthy group Minneapolis average $= 8.20 \pm 0.20$ Hz, $n = 107$; Denver average $= 8.66 \pm 0.53$, $n = 16$, $p = 0.41$, t-test). To place these observations in context with other methods for evaluating spectral power, we also evaluated the effect of AD on the relative spectral power in each of five frequency bands often used in standard quantitative EEG or MEG analysis (Table 3). We observed a substantial increase in theta band relative power (0.15 ± 0.007 for AD, $n = 117$, and 0.11 ± 0.005 for cognitively healthy, $n = 123$, $F = 24.02$, $p < 0.0001$, MANOVA) and a more modest reduction in beta band relative spectral power that did not quite reach statistical significance (0.15 ± 0.008 for AD and 0.17 ± 0.008 for healthy, $F = 3.54$, $p = 0.06$, MANOVA). The shift to slower frequencies in the AD group was widely distributed across the sensor array (Fig. 1 C) with the sensors nearest posterior brain regions showing the most marked group differences. T-tests of data from individual sensors revealed that the frequency centroid values measured in over half of them differed

significantly between groups with an even greater proportion of sensors showing group differences in theta band relative power (Table 3).

Global functional connectivity

The cO values represent the weights and signs of the connections among a dense network formed by the sensor array in the MEG instrument [24]. They ranged from -0.5 to 1.1 and were distributed as shown in Fig. 2A. The magnitude and sign of cO values varied regularly with the distance between pairs of sensors (Fig. 2B). Neighboring sensors showed relatively strong positive correlations whereas negative correlations were more prominent between pairs of sensors that were distant. Although the distribution of global cO values (e.g. mean cO value of all sensors measured for each subject) differed significantly between groups (0.14 ± 0.004 for AD, $n = 117$, and 0.12 ± 0.004 for cognitively healthy, $n = 123$, $F = 14.0$, $p = 0.0002$, MANOVA), we focused on comparing cO^2 values, which measure only the strength of synchronous activity and not the sign of the correlation. The strength of correlated brain activity measured by global cO^2 values increased significantly in the AD group (average $= 0.066 \pm 0.001$, $n = 117$) compared to the cognitively healthy group (average $= 0.059 \pm 0.0007$, $n = 123$, $F = 11.4$, $p = 0.0009$, MANOVA, Fig. 3). Age and MEG study site were included as covariates in the MANOVA and did not impact the evaluation of disease group differences, The average global cO^2 value measured in the healthy group in Minneapolis was 0.059 ± 0.0008 ($n = 107$) and the average global cO^2 value measured in the healthy group in Denver was 0.060 ± 0.0002 ($n = 16$, $p = 0.87$, t-test).

Distribution of functional changes

The results of global analysis demonstrate that there are widespread differences between the AD and healthy groups in spectral power and functional connectivity and these are not likely due to statistical anomalies associated with multiple comparisons or other complex, multivariate analysis approaches. Having established the group differences at the global level, we examined how specific, individual features vary with disease to provide additional insight into the nature of functional changes wrought by AD. T-tests conducted on sensor-level (frequency domain)
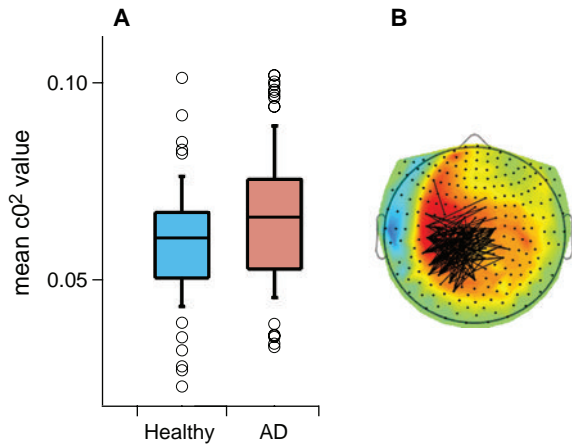
Fig. 3. Global cO^2 values were significantly higher in AD patients compared to the cognitively healthy group. A) The box and whisker plot illustrates the differing distribution of global average cO^2 values in the two study groups. The boxes represent the 25–75% confidence intervals, the error bars represent the 95% confidence intervals and each open circle represents subjects outside of the 95% confidence interval. B) The heat map represents the spatial distribution of group differences. T-values were calculated for each sensor pair with standard *t*-tests and mapped on the head plot according to magnitude and direction (see color calibration bar). Blue represents values that were lower in AD compared to healthy controls and warmer colors denote where the values were higher in the AD group. The superimposed lines represent the 100 cO^2 values that were most significantly different between the study groups.

or sensor pair-level (functional connectivity) features identified numerous differences between study groups (see Table 3). Robust differences in functional connectivity were observed among sensors located bilaterally over temporal regions of the cortex reaching into more frontal regions (Fig. 3), whereas AD-associated changes in centroid frequency were seen in sensors located more posterior, over occipital and parietal regions of the cortex (Fig. 1).

An analysis of functional connectivity based on sensor distance offered additional useful insights into AD functional pathology (Fig. 4). AD patients showed increased functional connectivity among short and intra-regional sensor pairs over large parts of the sensor array. By contrast, the strength of correlation between distant sensors was significantly lower in the AD group, especially between pairs of sensors in the left parietal and right frontal regions.

Relationship between MEG features and neuropsychological tests

Based on the marked differences between cognitively healthy and AD groups, we anticipated that a number of MEG features would change in concert with
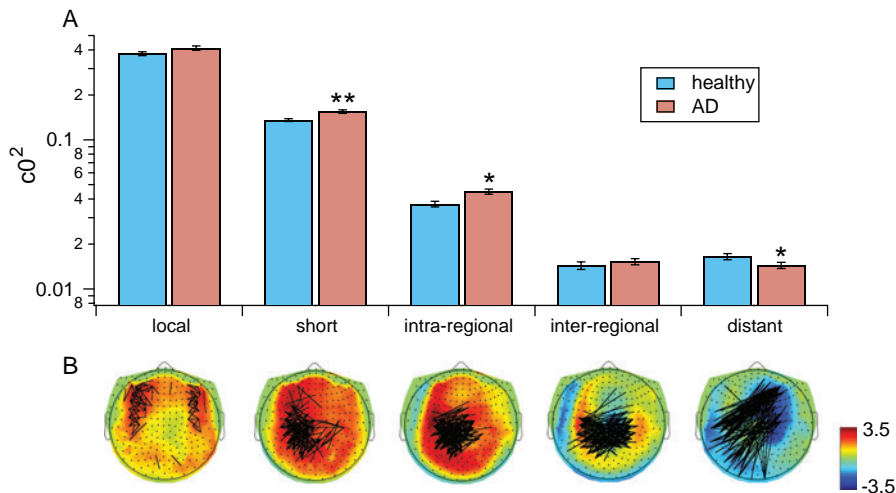
Fig. 4. AD patients show increased functional connectivity between nearby sensors and decreased connectivity between distant sensors. A) Bars represent the *mean* ± SEM cO^2 value (representing strength of correlated activity) for each of five sets of sensor pairs defined by the distance between them (see Fig. 1 for average distance in each group; *$p < 0.01$; **$p < 0.001$). B) Heat maps represent the T-values calculated from standard *t*-tests conducted on each sensor pair. For each map only those pairs within the corresponding distance group are mapped. Blue represents values that were lower in AD compared to healthy controls and warmer colors denote where the values were higher in the AD group. Superimposed on the heat maps are line maps illustrating the 100 sensor pairs within each distance set that showed the most significant differences between study groups ($p < 0.05$ for all plotted lines).

Table 4
Relationship to neuropsychological testing

	ADAS-Cog Prop[1]	R range[2]	CDR Prop	R range	MMSE Prop	R range
Cross sectional[3]						
cO^2	0.07	–0.37– –0.33	0.08	–0.36– –0.30	0.02	–0.32– –0.33
Centroid	1.0	–0.58– –0.25	0.60	–0.44– –0.09	0.89	0.16–0.49
Longitudinal[4]						
cO^2	0.12	–0.67– –0.79	0.10	–0.62– –0.62	0.10	–0.52– –0.53
Centroid	0.13	–0.43– –0.01	0.23	–0.47– –0.18	0.16	–0.47– –0.27

[1]The proportion of individual MEG scan features (20910 total sensor pairs for cO^2 values and 205 sensors for centroid frequency) that showed statistically significant correlations between the indicated neuropsychological test and MEG scan feature; [2]The range of Pearson correlation coefficient values (R value) calculated for individual MEG scan features and neuropsychological test scores; [3]Cross-sectional correlation values across the AD group ($n = 99$ with complete neuropsychological test scores); [4]Correlations between change in neuropsychological test score and change in MEG scan features measured longitudinally by two scans conducted approximately 10 months apart ($n = 31$ AD patients).

disease severity defined by neuropsychological test scores. The majority of subjects in both groups completed the MMSE ($n = 97$ healthy and 131 AD). AD patients also were evaluated with the ADAS-Cog and CDR. Many individual scan features correlated significantly with the MMSE when subjects from both groups were analyzed together. Thus, cross-sectional analysis of the entire cohort ($n = 228$) showed that 100% of sensors generated centroid frequency values that were significantly correlated with the MMSE score, with a range of Pearson *r*-values of 0.21 to 0.5. For functional connectivity, 22% of the sensor pairs generated cO^2 values that were significantly correlated with the MMSE score, and the range of Pearson *r*-values in both study groups was -0.29–0.21. Because of the previously described functional differences between groups, it was not particularly surprising that such correlations were observed.

It was more informative to identify MEG scan features that correlated with neuropsychological test scores within the AD cohort only. Table 4 summarizes the extent of such correlations for both cross-sectional (n varies by test) and longitudinal ($n = 31$) measurements. A substantial majority of sensors generated centroid frequency values that correlated significantly with the MMSE, ADAS-Cog and CDR whereas a relatively modest proportion of sensor pairs generated cO^2 values with significant cross-sectional correlations. A larger proportion of cO^2 features showed significant correlations between the change in test scores and the change in MEG features measured longitudinally. MEG features that showed strong longitudinal relationships with the ADAS-Cog and the CDR were localized to posterior temporal and parietal regions, and there was marked spatial overlap between strongly corre-
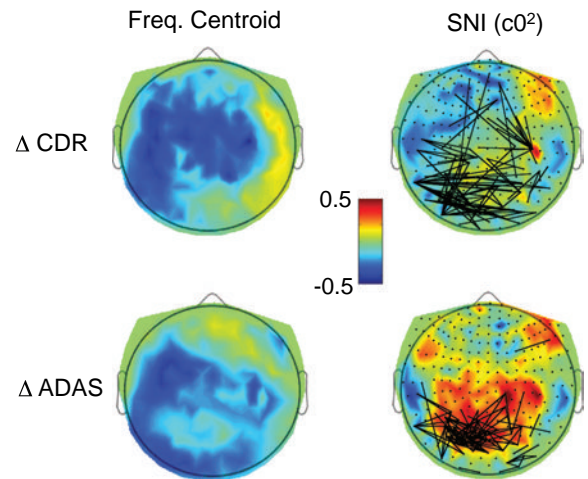
Fig. 5. Longitudinal changes in MEG scan features show robust correlations with changes in neuropsychological measures of disease severity. Shown are heat maps of Pearson R values for correlations between changes in the CDR (top row) or ADAS-Cog (bottom row) and frequency centroid values (left column) or cO^2 values (right column). Blue represents stronger negative correlations between MEG scan features and CDR or ADAS-cog whereas red represents stronger positive correlations. Superimposed on the heat maps for the cO^2 values are line maps of the 100 most highly correlated sensor pairs.

lated frequency domain and SNI features (Fig. 5). Notably, there also was substantial spatial overlap between highly correlated MEG features and those that differed significantly between groups.

Multivariate modeling of longitudinal severity change

The strong relationship between MEG features and the ADAS-Cog allowed us to develop preliminary
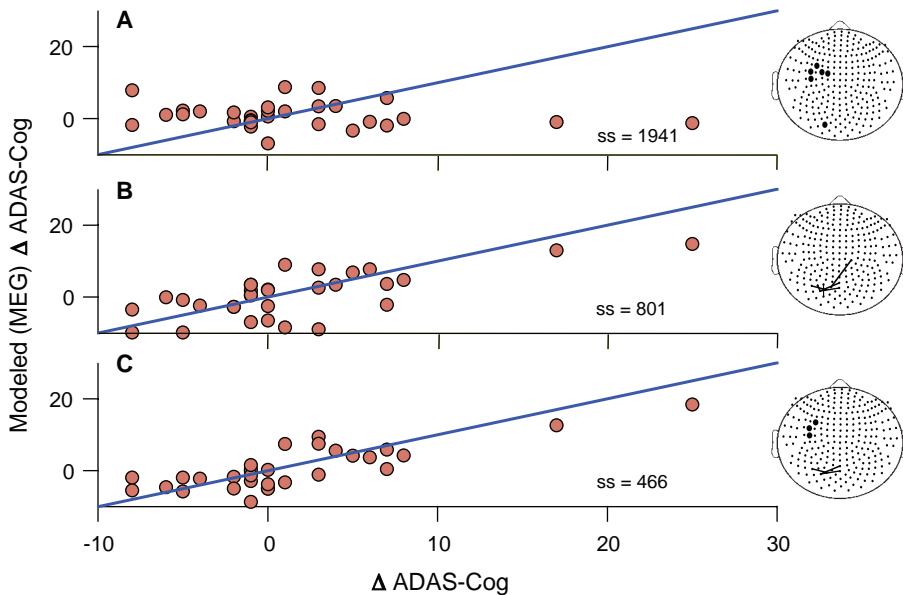
Fig. 6. MEG features measured longitudinally include information that accurately tracks changes in ADAS-Cog performance. Each plot shows the output of preliminary, linear models of disease severity change that include sets of MEG scan features. Each point represents the results from a single AD patient tested twice over the course of approximately 10 months. The X-axis represent the measured change in the ADAS-Cog score and the Y-axis represents the output of linear regression model including 6 MEG features for either cO^2 values alone (A), frequency centroid values alone (B) or a combination of cO^2 values and frequency centroid values (C). The blue lines represent the points where the modeled values and the actual values correspond exactly (slope = 1). The maps on the right depict the individual features that were used as input for each modeling exercise. The large dots represent the sensor that generated the input centroid frequency values and the lines represent the sensor pairs that contributed the cO^2 values.

models of severity change based on linear combinations of MEG features (Fig. 6). Models were based on either functional connectivity features alone (Fig. 6A), spectral power features alone (Fig. 6B) or a combination of the two (Fig. 6 C). In each case, the 6 features that correlated most significantly to the longitudinal change in the ADAS-Cog were used to estimate a multivariate linear regression model [26]. The model that optimally tracked actual ADAS-Cog change consisted of 3 cO^2 values and 3 centroid frequency measures. This particular model strongly tracked the actual change in ADAS-Cog scores observed in the 31 AD patients. The output of this model also correlated significantly with the change in the CDR ($r = 0.50$) and the change in the MMSE ($r = 0.38$, not shown). None of the data features used in the AD severity model differed between the 2 scans in the cognitively healthy group ($n = 46$). Although jack-knife cross validation was used to generate the model output, this remains a relatively small population, and we anticipate further model building efforts based on greater numbers of subjects will be needed. Importantly, validation of a final model will require formal, blinded

testing. Nonetheless, this analysis demonstrates that brief, resting-state MEG scans are potentially capable of tracking changes in disease severity using modest numbers of features, and that combinations of SNI-based functional connectivity measures and frequency centroid data resulted in models with the best fit.

DISCUSSION

We report here the combined outcome of two, exploratory case-controlled studies in which previously diagnosed AD patients and cognitively healthy volunteers were recruited from the community and evaluated with standard clinical assessments and resting-state MEG scans. Most subjects were scanned a single time, but a subset was scanned twice separated by approximately 10 months. The major goals of this study were: 1) to test the hypothesis that a brief, resting state MEG scan generates sufficient information to detect the functional pathology of AD; 2) to implement automated data processing methods that help standardize data analysis and support broad use of

MEG technology for evaluating AD; and 3) to identify data features that are altered by AD and change in concert with disease severity measures based on neuropsychological tests.. The results indicated that brief resting-state MEG scans of AD patients and cognitively healthy volunteers showed significantly different properties. Brain rhythms appeared to slow resulting in a significant reduction in the centroid frequency of the power spectra. Underlying the change in centroid frequency was a widespread increase in theta band (3–8 Hz) and a decrease in beta band (13–30 Hz) relative spectral power in sensors nearest to parietal and temporal regions. Functional connectivity measured by the SNI test showed a significant increase in global zero-lag cross-correlation values (global cO and cO^2) in AD patients compared to cognitively healthy volunteers. Detailed analysis revealed that AD was associated with increased strength of correlation between nearby sensors and decreased strength of correlation between distant pairs. The largest magnitude AD-associated changes were found in lateral and posterior sensors nearest to the parietal and temporal regions that are generally considered to be critical areas for AD pathology. A substantial number of MEG scan features measured in AD patients correlated significantly with the MMSE, ADAS-Cog, or CDR values measured at single time points, and these also were located largely in lateral or posterior sensors. Importantly, there were a substantial number of features that changed in concert with the changes in neuropsychological test scores during the 10-month interval between study assessments.

It was possible to develop multivariate models of MEG scan features that tracked changes in disease severity measured longitudinally by the ADAS-Cog. The results suggest that optimal models for tracking severity will require information from both centroid frequency and SNI analyses. Similar multivariate approaches have been applied to resting-state EEG scans [16, 32, 33] supporting the idea that the extent of disease progression can be determined through high-resolution measures of brain electrophysiology. Notably, we used very simple linear models and attempted to track changes in the ADAS-Cog, which also has known limitations and significant variability. More robust MEG-based models may arise from analyses that include specific ADAS-Cog or CDR components, combinations of multiple neuropsychological test scores, or incorporation of other disease-specific information. Non-linear modeling techniques or inclusion of additional MEG scan features may also provide critical improvements. Nonetheless, these results represent a promising start to our ongoing work to identify, improve and validate better tools for tracking the progression of AD.

Subject volunteers were recruited based on a previous diagnosis of AD or a self-reported healthy status. Medical evaluations of subjects based on examination and/or review of medical records were conducted in sufficient detail to confirm the AD diagnosis based on DSM-IV-TR (Dementia of Alzheimer's Type) criteria or generally healthy status. It is possible that a modest proportion of subjects were misclassified by this process, especially within the cognitively healthy group. However, based on MMSE scores it seems likely that the large majority of healthy volunteers were generally free of AD or were in a very early state. In fact, there were a number of cognitively normal subjects that showed MEG scans features more similar to the AD group, which may indicate the presence of early functional impairment. Further longitudinal follow-up of these subjects maybe particularly informative. It is worth noting that inadvertent inclusion of functionally impaired individuals in the cognitively healthy group would have the effect of spuriously dampening the observed disease-based differences compared to the actual effect of the disease. The AD group was not evaluated with MRI or other diagnostic tools as part of the study, but in many cases such technologies were used in the patient's original diagnostic work-up to confirm the diagnosis of AD. There is also a potential for some of the subjects to have dementia from diseases other than AD, but the studies included specific exclusions for all significant, non-AD neurological and psychiatric conditions. In an attempt to rule out one very common non-AD cause of dementia, all subjects in the Orasi-sponsored study were evaluated with the Hachinski Modified Ischemia Scale [30] and excluded if their Hachinski scores exceeded 4.

Although the study examined differences between disease states, it is possible that some features of the MEG scans were affected by prescription medications taken by the subjects. Since most other major neurological and psychiatric disorders were specifically excluded from the study, none of the subjects were known to be taking major neuroactive medications at the time of the study including antipsychotics and anticonvulsants. However, the majority of AD patients were on stable doses of cholinesterase inhibitors and a few also were taking memantine. Some subjects in both study groups were taking antidepressant medications, but those with known substance or alcohol abuse were

specifically excluded from the study. Ad hoc analysis of the MEG scan data suggested there were no obvious effects of medication state on the MEG scan (not shown), but these analyses cannot substitute for formal testing of drug effect with placebo-controlled studies. Therefore, it is possible that some of the MEG features identified here were confounded by the effect of medications, particularly cholinesterase inhibitors in the AD subjects.

Functional connectivity was evaluated by a variant of the SNI test first developed by Georgopoulos [21, 22]. This time series based approach uses prewhitening to reduce the influence of autocorrelations in the calculation of sensor pair cross-correlations. We have optimized specific data processing steps (filtering, AR order, etc) to generate robust measures of correlated activity that could be applied reliably across the widest number of subjects regardless of MEG instrument. We made every attempt to reduce or eliminate the impact of movement artifacts (e.g. eye blinks, head movement etc.) on the results. However, undetected artifacts still may have altered some of the results presented here. It also is possible that the cO and cO^2 values reported here were modestly influenced common signal sources that may or may not be derived from brain electrical activity. However, common sources cannot fully explain the differences between disease groups or the relationships between MEG scans and neuropsychological test scores as it is unlikely that external common sources would differ systematically between groups. There are a wide variety of methods for measuring brain rhythmicity and functional connectivity using MEG or EEG data. Each has particular advantages and it is possible that even more robust information could be gleaned by using alternative data processing or analysis approaches. For example, Stam [34, 35] has proposed that the effect of common sources can be mitigated by applying specialized techniques to assess functional connectivity from MEG or EEG scans. Even within the general context of the SNI test there remains substantial information embedded in the lagged (e.g. non time 0) correlations, which may provide richer, more useful information.

Importantly, the results reported here were based on data from two different MEG instruments and MEG scans separated by a significant amount of time (scan time range = approximately 4 years). Although it is possible to identify minor differences between instruments (based on empty room scans, for example), the main parameters used to define AD functional pathology did not differ between instruments, and disease differences observed in each instrument were essentially the same. Separate analysis of subject data from each instrument revealed nearly identical differences between groups with some variation in statistical significance between differing group sizes. The robust nature of the data features combined with the standardized method for processing and analyzing the scans demonstrates that use of resting-state MEG scans in multicenter trials is clearly feasible.

The slowing of cortical rhythms observed here is consistent with the results of multiple studies using EEG [13, 15, 16, 33, 36–40] and MEG [17, 18, 24, 41]. Similar to the results reported here, previous MEG studies have shown that the most marked slowing is found in temporal and occipital regions [17]. Both MEG and EEG have detected a loss of signal complexity in scans of AD patients [34, 40], and changes in functional connectivity have been widely observed. Increased spectral power in delta and theta frequency bands together with decreased power in beta and gamma bands have been routinely observed in human electrophysiology studies. Similarly, cortical responses to sensory stimulation also are delayed in AD patients compared to healthy controls [11, 42]. Despite the reproducibility of these findings, there is evidence that this may not be specific to AD. For example, patients with Parkinson's disease also show generalized slowing of cortical rhythms very similar to that seen in AD patients [43]. Better specificity may come from improved spatial localization of changes or alternative data analysis techniques. Compared to EEG, MEG is theoretically capable of measuring cortical sources with higher spatial resolution, and therefore, may more readily differentiate among disease states. Further work will be required to fully determine the relative utility of MEG and EEG in differentiating neurological disorders. Interestingly, our results were obtained using an eyes-open scan task, while many of the previous studies using EEG have employed an eye-closed condition [13, 14]. The advantages and disadvantages of each approach are not entirely clear, but future work directly comparing the eyes-open and eyes-closed scans may provide additional insights into the pathophysiology of AD.

Electrophysiology data provides a rich source of functional connectivity information that may prove critical for tracking AD and other neurological and psychiatric disorders [29, 34]. Although changes in connectivity have been identified using EEG [39], MEG does not employ a common reference electrode and is less susceptible to tissue-associated volume

conduction of signals, both of which can cloud interpretation of correlated activity [44]. In contrast to the method used here, which measures correlated activity across a wide range of frequencies, previous work in this area has focused on techniques that rely on frequency domain transformations of the MEG time series [45]. Thus, functional connectivity measures derived from these analyses are specific for particular frequency bands. Stam et al. [46], using linear (coherence) and nonlinear (synchronization likelihood) measures of connectivity observed that AD subjects showed decreased long distance connectivity in the alpha and beta bands, with an increased connectivity between local sensor pairs in the theta, beta and gamma bands. Similar findings also were observed in a separate study [45] in which connectivity was assessed by mean square coherence methods. These results show that electrophysiology detects the results of disturbed communication networks in AD. In fact, resting-state scans from either MEG [25], or EEG [39] analyzed with graph theoretical approaches suggest that functional networks in AD patients have a more random structure than those in matched healthy volunteers. Notably, resting-state fMRI, which measures communication over much longer time frames, also has detected similar disruption of communication networks in AD [21, 47], and diffusion tensor imaging has detected structural evidence of degradation in white matter tracts [22]. Thus independently derived evidence using a variety of technologies clearly supports the idea that changes in functional communication networks represent a critical pathological feature of AD that could be used to evaluate AD patients in experimental and clinical settings.

It is not surprising that the substantial structural damage caused by AD would manifest itself in disruptions of normal electrical activity, however we do not yet understand the relationship between neuronal loss and brain electrophysiology in sufficient detail to fully explain the electrophysiology observations in terms of damage to specific structures. More generally, it is possible that increased synchronous activity between neighboring brain regions (e.g. cO^2 values between nearby sensors) represents an attempt by the brain to work around the loss of longer distance lines of communication. Additionally, changes to resting state synchronous communication may result from degradation of communication pathways that maintain rhythmic signaling between cortex and sub cortical structures. Llinas and colleagues have proposed a pathological process called thalamocortical dysrhythmia [48] that is hypothesized to explain the electrophysiological consequences of a variety of brain pathologies.

Recent improvements in diagnostic technology for AD have provided the rationale for redefining the criteria for AD and associated conditions [1–4]. The new criteria rely heavily on PET imaging to detect plaque [49] or CSF measures of A-beta and tau [5], especially to support detection of "preclinical" disease processes. Thus, dysregulation of amyloid processing and plaque accumulation are proposed to be a very early manifestation of AD according to a recent theoretical model of disease progression [10]. Biomarkers that underpin the progression model suggest that measurable cognitive decline and pathological brain atrophy occur largely in the later stages of the disease. This framework currently does not include biomarker tools capable of tracking progression during the period between plaque accumulation and detectable atrophy or cognitive dysfunction. The results presented here, as well as other observations, suggest that high-resolution measures based on resting-state MEG scans may generate additional information to help track changes in disease severity. Resting-state electrophysiology has identified features that are significantly correlated with neuropsychological measures of cognitive function in both cross-sectional [11, 17, 39, 41, 46], and longitudinal settings [38]. EEG scans also have detected disturbed function at earlier stages of the disease process in patients diagnosed with MCI [50]. There is growing evidence from both MEG and fMRI studies indicating that evaluation of functional connectivity offers hope for detecting pathology that may be otherwise difficult to characterize [51]. The default mode network defined by fMRI studies represents a robust and consistent feature [52] that has been shown to be disturbed in AD [53] and MCI [54]. MEG studies using the SNI approach have demonstrated that functional connectivity patterns are consistent across healthy subjects [27] and show disease-specific changes [24, 28, 55]. These observations along with the current results support the idea that brief, resting-state MEG scans contain information that may help track changes in AD severity more accurately and perhaps earlier in the disease process.

The results presented here represent the first step in qualifying and validating a robust diagnostic tool for AD. We have demonstrated that data from multiple instruments can be readily combined and that the results can generalize across a patient population that is substantially larger than most previous

MEG or EEG studies. Further work is being conducted to confirm and extend these findings including additional study cohorts and MEG instruments, as well as continued longitudinal follow-up of the current patient population. Blinded testing of diagnostic accuracy also is planned to rigorously prove the utility of MEG scans and the analysis algorithms that support the tool. The goal of this effort will be to develop a new AD biomarker that provides information about disease severity and progression to aid in development and testing of novel treatments and eventually in routine clinical practice. These promising early observations suggest that brief, resting-state MEG scans may offer some advantages over available biomarker tools. Unlike PET imaging and CSF-based biomarkers, MEG is completely non-invasive, requiring no injections or needles. MEG scans also are faster, requiring significantly less scanner time than structural MRI. The outcome of this study demonstrates the potential utility of resting-state MEG scans in clinical trials for experimental AD treatments. The patient-friendly nature of the scan acquisition facilitates recruitment and retention, and the scan clearly generates data relevant to known AD pathology. Moreover, the use of combined frequency domain and functional connectivity results can generate sufficient information to track modest changes in severity that are currently measured by neuropsychological tests. The objective and quantitative nature of MEG may be particularly amenable to supporting early stage proof-of-concept trials in which short time-in-study and modest subject numbers are critical.

ACKNOWLEDGMENTS

REFERENCES

[1] Jack CR Jr, Albert M, Knopman DS, McKhann GM, Sperling RA, Carrillo MC, Thies B, Phelps CH (2011) Introduction to revised criteria for the diagnosis of Alzheimer's disease: National Institute on Aging and the Alzheimer's Association Workgroup. *Alzheimers Dement* **7**, 257-262.

[2] Sperling RA, Aisen PS, Beckett LA, Bennett DA, Craft S, Fagan AM, Iwatsubo T, Jack CR, Kaye J, Montine TJ, Park DC, Reiman EM, Rowe CC, Siemers E, Stern Y, Yaffe K, Carrillo MC, Thies B, Morrison-Bogorad M, Wagster MV, Phelps CH (2011) Toward defining the preclinical stages of Alzheimer's disease: Recommendations from the National Institute on Aging and the Alzheimer's Association Workgroup. *Alzheimers Dement* **7**, 280-292.

[3] Albert MS, Dekosky ST, Dickson D, Dubois B, Feldman HH, Fox NC, Gamst A, Holtzman DM, Jagust WJ, Petersen RC, Snyder PJ, Carrillo MC, Thies B, Phelps CH (2011) The diagnosis of mild cognitive impairment due to Alzheimer's disease: Recommendations from the National Institute on Aging and Alzheimer's Association Workgroup. *Alzheimers Dement* **7**, 270-279.

[4] McKhann GM, Knopman DS, Chertkow H, Hyman BT, Jack CR Jr, Kawas CH, Klunk WE, Koroshetz WJ, Manly JJ, Mayeux R, Mohs RC, Morris JC, Rossor MN, Scheltens P, Carillo MC, Thies B, Weintraub S, Phelps CH (2011) The diagnosis of dementia due to Alzheimer's disease: Recommendations from the National Institute on Aging and the Alzheimer's Association Workgroup. *Alzheimers Dement* **7**, 263-269.

[5] Vemuri P, Wiste HJ, Weigand SD, Knopman DS, Trojanowski JQ, Shaw LM, Bernstein MA, Aisen PS, Weiner M, Petersen RC, Jack CR (2010) Serial MRI and CSF biomarkers in normal aging, MCI, and AD. *Neurology* **75**, 143-151.

[6] Fleisher AS, Donohue M, Chen K, Brewer JB, Aisen PS (2009) Applications of neuroimaging to disease-modification trials in Alzheimer's disease. *Behav Neurol* **21**, 129-136.

[7] Saumier D, Aisen PS, Gauthier S, Vellas B, Ferris SH, Duong A, Suhy J, Oh J, Lau W, Garceau D, Haine D, Sampalis J (2009) Lessons learned in the use of volumetric mri in therapeutic trials in Alzheimer's disease: the Alzhemed (tramiprosate) experience. *J Nutr Health Aging* **13**, 370-372.

[8] Vellas B, Black R, Thai LJ, Fox NC, Daniels M, McLennan G, Tompkins C, Leibman C, Pomfret M, Grundman M (2009) Long-term follow-up of patients immunized with AN1792: reduced functional decline in antibody responders. *Curr Alzheimer Res* **6**, 144-151.

[9] Jack CR, Wiste HJ, Vemuri P, Weigand SD, Senjem ML, Zeng G, Bernstein MA, Gunter JL, Pankratz VS, Aisen PS, Weiner MW, Petersen RC, Shaw LM, Trojanowski JQ, Knopman DS (2010) Brain beta-amyloid measures and magnetic resonance imaging atrophy both predict time-to-progression from mild cognitive impairment to Alzheimer's disease. *Brain* **133**, 3336-3348.

[10] Jack CR, Knopman DS, Jagust WJ, Shaw LM, Aisen PS, Weiner MW, Petersen RC, Trojanowski JQ (2010) Hypothetical model of dynamic biomarkers of the Alzheimer's pathological cascade. *Lancet Neurol* **9**, 119-128.

[11] Lai CL, Lin RT, Liou LM, Liu CK (2010) The role of event-related potentials in cognitive decline in Alzheimer's disease. *Clin Neurophysiol* **121**, 194-199.

[12] Szelies B, Mielke R, Grond M, Heiss WD (1995) P300 in Alzheimer's disease: relationships to dementia severity and glucose metabolism. *J Neurol Sci* **130**, 77-81.

[13] Jeong J (2004) EEG dynamics in patients with Alzheimer's disease. *Clin Neurophysiol* **115**, 1490-1505.

[14] Rossini PM, Rossi S, Babiloni C, Polich J (2007) Clinical neurophysiology of aging brain: from normal aging to neurodegeneration. *Prog Neurobiol* **83**, 375-400.

[15] Babiloni C, Cassetta E, Binetti G, Tombini M, Del Percio C, Ferreri F, Ferri R, Frisoni G, Lanuzza B, Nobili F, Parisi L, Rodriguez G, Frigerio L, Gurzi M, Prestia A, Vernieri F, Eusebi F, Rossini PM (2007) Resting EEG sources correlate with attentional span in mild cognitive impairment and Alzheimer's disease. *Eur. J. Neurosci* **25**, 3742-3757.

[16] Buscema M, Grossi E, Capriotti M, Babiloni C, Rossini P (2010) The I.F.A.S.T. model allows the prediction of conversion to Alzheimer disease in patients with mild cognitive impairment with high degree of accuracy. *Curr Alzheimer Res* **7**, 173-187.

[17] de Haan W, Stam CJ, Jones BF, Zuiderwijk IM, van Dijk BW, Scheltens P (2008) Resting-state oscillatory brain dynamics in Alzheimer disease. *J Clin Neurophysiol* **25**, 187-193.

[18] Criado JR, Amo C, Quint P, Kurelowech L, Otis SM (2006) Using magnetoencephalography to study patterns of brain magnetic activity in Alzheimer's disease. *Am J Alzheimers Dis Other Demen* **21**, 416-423.

[19] Kähkönen S, Yamashita H, Rytsälä H, Suominen K, Ahveninen J, Isometsa E (2007) Dysfunction in early auditory processing in major depressive disorder revealed by combined MEG and EEC. *J Psychiatry Neurosci* **32**, 316-322.

[20] Rutter L, Carver FW, Holroyd T, Nadar SR, Mitchell-Francis J, Apud J, Weinberger DR, Coppola R (2009) Magnetoencephalographic gamma power reduction in patients with schizophrenia during resting condition. *Hum Brain Mapp* **30**, 3254-3264.

[21] Supekar K, Menon V, Rubin D, Musen M, Greicius MD (2008) Network analysis of intrinsic functional brain connectivity in Alzheimer's disease. *PLoS Comput. Biol* **4**, el000l00.

[22] Zarei M, Patenaude B, Damoiseaux J, Morgese C, Smith S, Matthews PM, Barkhof F, Rombouts S, Sanz-Arigita E, Jenkinson M (2010) Combining shape and connectivity analysis: an MRI study of thalamic degeneration in Alzheimer's disease. *Neurolmage* **49**, 1-8.

[23] Sexton CE, Kalu UG, Filippini N, Mackay CE, Ebmeier KP (2010) A meta-analysis of diffusion tensor imaging in mild cognitive impairment and Alzheimer's disease. *Neurobiol Aging*.

[24] Georgopoulos AP, Karageorgiou E, Leuthold AC, Lewis SM, Lynch JK, Alonso AA, Aslam Z, Carpenter AF, Georgopoulos A, Hemmy LS, Koutlas IG, Langheim FJP, McCarten JR, McPherson SE, Pardo JV, Pardo PJ, Parry GJ, Rottunda SJ, Segal BM, Sponheim SR, Stanwyck JJ, Stephane M, Westermeyer JJ (2007) Synchronous neural interactions assessed by magnetoencephalography: a functional biomarker for brain disorders. *J Neural Eng* **4**, 349-355.

[25] Stam CJ, de Haan W, Daffertshofer A, Jones BF, Manshanden I, van Cappellen van Walsum AM, Montez T, Verbunt JPA, de Munck JC, van Dijk BW, Berendse HW, Scheltens P (2009) Graph theoretical analysis of magnetoencephalographic functional connectivity in Alzheimer's disease. *Brain* **132**, 213-224.

[26] Leuthold AC, Langheim FJP, Lewis SM, Georgopoulos AP (2005) Time series analysis of magnetoencephalographic data during copying. *Exp Brain Res* **164**, 411-422.

[27] Langheim FJP, Leuthold AC, Georgopoulos AP (2006) Synchronous dynamic brain networks revealed by magnetoencephalography. *Proc Natl Acad Sci U.S.A* **103**, 455-459.

[28] Georgopoulos AP, Tan H-RM, Lewis SM, Leuthold AC, Winskowski AM, Lynch JK, Engdahl B (2010) The synchronous neural interactions test as a functional neuromarker for post-traumatic stress disorder (PTSD): a robust classification method based on the bootstrap. *J Neural Eng* **7**, 16011.

[29] Petersen RC, Stevens JC, Ganguli M, Tangalos EG, Cummings JL, DeKosky ST (2001) Practice parameter: early detection of dementia: mild cognitive impairment (an evidence-based review). Report of the Quality Standards Subcommittee of the American Academy of Neurology. *Neurology* **56**, 1133-1142.

[30] Hachinski VC, Iliff LD, Zilhka E, Du Boulay GH, McAllister VL, Marshall J, Russell RW, Symon L (1975) Cerebral blood flow in dementia. *Arch Neurol* **32**, 632-637.

[31] Lattin J, Carroll D, Green P (2002) In *Analyzing Multivariate Data (with CD-ROM)*, Duxbury Press.

[32] Lehmann C, Koenig T, Jelic V, Prichep L, John RE, Wahlund L-O, Dodge Y, Dierks T (2007) Application and comparison of classification algorithms for recognition of Alzheimer's disease in electrical brain activity (EEG). *J Neurosci Methods* **161**, 342-350.

[33] Snaedal J, Johannesson GH, Gudmundsson TE, Gudmundsson S, Pajdak TH, Johnsen K (2010) The use of EEG in Alzheimer's disease, with and without scopolamine – a pilot study. *Clin Neurophysiol* **121**, 836-841.

[34] Stam CJ (2010) Use of magnetoencephalography (MEG) to study functional brain networks in neurodegenerative disorders. *J Neurol Sci* **289**, 128-134.

[35] Stam CJ, Nolte G, Daffertshofer A (2007) Phase lag index: assessment of functional connectivity from multi channel EEG and MEG with diminished bias from common sources. *Hum Brain Mapp* **28**, 1178-1193.

[36] Babiloni C, Bosco P, Ghidoni R, Del Percio C, Squitti R, Binetti G, Benussi L, Ferri R, Frisoni G, Lanuzza B, Cassetta E, Anello G, Gurzi M, Bartesaghi S, Lizio R, Tombini M, Rossini PM (2007) Homocysteine and electroencephalographic rhythms in Alzheimer disease: a multicentric study. *Neuroscience* **145**, 942-954.

[37] Babiloni C, Squitti R, Del Percio C, Cassetta E, Ventriglia MC, Ferreri F, Tombini M, Frisoni G, Binetti G, Gurzi M, Salinari S, Zappasodi F, Rossini PM (2007) Free copper and resting temporal EEG rhythms correlate across healthy, mild cognitive impairment, and Alzheimer's disease subjects. *Clin Neurophysiol* **118**, 1244-1260.

[38] Coben LA, Danziger W, Storandt M (1985) A longitudinal EEG study of mild senile dementia of Alzheimer type: changes at 1 year and at 2.5 years. *Electroencephalogr Clin Neurophysiol* **61**, 101-112.

[39] de Haan W, Pijnenburg Y, Strijers R, van der Made Y, van der Flier W, Scheltens P, Stam C (2009) Functional neural network analysis in frontotemporal dementia and Alzheimer's disease using EEG and graph theory. *BMC Neuroscience* **10**, 101.

[40] Mizuno T, Takahashi T, Cho RY, Kikuchi M, Murata T, Takahashi K, Wada Y (2010) Assessment of EEG dynamical complexity in Alzheimer's disease using multiscale entropy. *Clin Neurophysiol* **121**, 1438-1446.

[41] Fernández A, Hornero R, Gómez C, Turrero A, Gil-Gregorio P, Matías-Santos J, Ortiz T (2010) Complexity analysis of spontaneous brain activity in Alzheimer disease and mild cognitive impairment: an MEG study. *Alzheimer Dis Assoc Disord* **24**, 182-189.

[42] Golob EJ, Ringman JM, Irimajiri R, Bright S, Schaffer B, Medina LD, Starr A (2009) Cortical event-related potentials in preclinical familial Alzheimer disease. *Neurology* **73**, 1649-1655.

[43] Bosboom JLW, Staffers D, Stam CJ, van Dijk BW, Verbunt J, Berendse HW, Wolters EC (2006) Resting state oscillatory brain dynamics in Parkinson's disease: an MEG study. *Clin Neurophysiol* **117**, 2521-2531.

[44] Srinivasan R, Winter WR, Ding J, Nunez PL (2007) EEG and MEG coherence: measures of functional connectivity at distinct spatial scales of neocortical dynamics. *J Neurosci Methods* **166**, 41-52.

[45] Alonso JF, Poza J, Mañanas MA, Romero S, Fernández A, Hornero R (2010) MEG connectivity analysis in patients with Alzheimer's disease using cross mutual information and spectral coherence. *Ann Biomed Eng* **39**, 524-536.

[46] Stam C, Jones B, Manshanden I, Vancappellenvanwalsum A, Montez T, Verbunt J, Demunck J, Vandijk B, Berendse H, Scheltens P (2006) Magnetoencephalographic evaluation of resting-state functional connectivity in Alzheimer's disease. *Neurolmage* **32**, 1335-1344.

[47] Zhang H-Y, Wang S-J, Liu B, Ma Z-L, Yang M, Zhang Z-J, Teng G-J (2010) Resting brain connectivity: changes during the progress of Alzheimer disease. *Radiology* **256**, 598-606.

[48] Llinās RR, Ribary U, Jeanmonod D, Kronberg E, Mitra PP (1999) Thalamocortical dysrhythmia: a neurological and neuropsychiatric syndrome characterized by magnetoencephalography. *Proc Natl Acad Sci USA* **96**, 15222-15227.

[49] Klunk WE, Engler H, Nordberg A, Wang Y, Blomqvist G, Holt DP, Bergström M, Savitcheva I, Huang G-feng, Estrada S, Ausén B, Debnath ML, Barletta J, Price JC, Sandell J, Lopresti BJ, Wall A, Koivisto P, Antoni G, Mathis CA, Långström B (2004) Imaging brain amyloid in Alzheimer's disease with pittsburgh compound-B. *Ann Neurol* **55**, 306-319.

[50] Cantero JL, Atienza M, Cruz-Vadell A, Suarez-Gonzalez A, Gil-Neciga E (2009) Increased synchronization and decreased neural complexity underlie thalamocortical oscillatory dynamics in mild cognitive impairment. *Neuroimage* **46**, 938-948.

[51] Uhlhaas PJ, Singer W (2006) Neural synchrony in brain disorders: relevance for cognitive dysfunctions and pathophysiology. *Neuron* **52**, 155-168.

[52] Raichle ME, MacLeod AM, Snyder AZ, Powers WJ, Gusnard DA, Shulman GL (2001) A default mode of brain function. *Proc Natl Acad Sci USA* **98**, 676-682.

[53] Greicius MD, Srivastava G, Reiss AL, Menon V (2004) Default-mode network activity distinguishes Alzheimer's disease from healthy aging: evidence from functional MRI. *Proc Natl Acad Sri USA* **101**, 4637-4642.

[54] Rombouts SARB, Barkhof F, Goekoop R, Stam CJ, Scheltens P (2005) Altered resting state networks in mild cognitive impairment and mild Alzheimer's disease: an fMRI study. *Hum Brain Mapp* **26**, 231-239.

[55] Engdahl B, Leuthold AC, Tan H-RM, Lewis SM, Winskowski AM, Dikel TN, Georgopoulos AP (2010) Post-traumatic stress disorder: a right temporal lobe syndrome? *J Neural Eng* **7**, 066005.

This page intentionally left blank

Section 6
Diffusion Tensor Imaging

This page intentionally left blank

Introduction

Section 6: Diffusion Tensor Imaging

Norbert Schuff*
University of California and Veterans Affairs Medical Center, San Francisco, CA, USA

For many years, Alzheimer's disease (AD) has been considered primarily a disorder of the hippocampus and cortex, i.e. gray matter. Nowadays, a broader view prevails in which white matter also plays a critical role in the disease process. The changing view arose to a large part from brain studies using diffusion tensor imaging (DTI), a variant of MRI, which provides a unique contrast for the assessment of white matter. DTI captures the microstructural architecture of tissue by measuring the systematic directionality of water diffusion. The degree of diffusion directionality is usually expressed as fractional anisotropy (FA), which ranges theoretically from zero for isotropic diffusion to unity for diffusion exclusively along one direction [1]. It is now well established that FA is sensitive to changes in white matter integrity [2], although the biological underpinnings of FA alterations are often not known in detail. Information from DTI can also be used for mapping fiber tracts and for studies of brain connectivity using the concept of tractography [3]. DTI has become the method of choice for studying alterations in white matter in normal aging as well as in a variety of neurological diseases. In AD research alone, roughly 100 articles have been published in the past decade with a growing number of new reports appearing now every year.

The articles in this section of the handbooks represent the status of current DTI research in AD and mild cognitive impairment (MCI) and highlight the characteristics of white matter damage associated with AD. The article by Fellgiebel focuses on DTI studies of the hippocampus and associated limbic

structures, which have received particular attention in AD research because of their critical role in memory processing and function. Several findings suggest that DTI-based indices of microstructural integrity of limbic structures might outperform conventional measures of macrostructural volume loss as predictor of AD. The diagnostic utility of DTI in direct comparison to that of brain atrophy for AD is taken up directly in the article by Friese et al. The feasibility of DTI as a biomarker for AD in clinical research settings and pharmacological trials is also discussed. Another perspective on using DTI and structural MRI together is presented in the article by Canu and colleagues, who aimed to identify the extent to which microstructural alterations and macrostructural atrophy provide independent information to the characterization of AD pathology in a small group of diagnosed AD patients and healthy elderly controls. Their findings further expand the understanding of the topography of pathological changes in AD that can be captured with various MRI methods. The value of DTI for predicting cognitive decline from MCI toward dementia is investigated in the article by Haller et al, using fractional anisotropy as primary summary measure of DTI. The value of various other summary measures of DTI is addressed in the article by He et al. The different DTI measures are outlined and the sensitivity and interpretation of each measure is discussed in the context of detecting AD at an early stage. The potential translation of DTI research into clinical practice is critically examined in the article by Oshi et al. In addition, principles of DTI are reviewed and strategies for investigating white matter alterations are described. In the article by Teipel et al., DTI is used to study associations between white matter integrity and education in the context of AD and brain reserve capacity. Finally, in the article by Yassa, a high resolution DTI method is

---

*Correspondence to: Norbert Schuff, VA Medical Center, 4150 Clement Street, 114M San Francisco, CA 94121, USA. E-mail: Norbert.Schuff@va.gov.

reviewed to map the intricate structure of the perforant pathway, a connectional route linking the entorhinal cortex to the hippocampal formation and a target of early AD pathology. This method presents novel and exciting opportunities but technical challenges remain. Taken together, the articles in this section demonstrate consistently that anisotropic diffusion of water in brain tissue measured by DTI is a highly sensitive probe to assess subtle disease processes in AD, not normally seen with conventional MRI contrast mechanisms. DTI holds great promise to become a useful clinical tool for early AD detection.

REFERENCES

[1] Pierpaoli C, Basser PJ (1996) Toward a quantitative assessment of diffusion anisotropy. *Magn Reson Med* **36**, 893-906.

[2] Beaulieu C (2002) The basis of anisotropic water diffusion in the nervous system – a technical review. *NMR Biomed* **15**, 435-455.

[3] Basser PJ, Pajevic S, Pierpaoli C, Duda J, Aldroubi A (2000) In vivo fiber tractography using DT-MRI data. *Magn Reson Med* **44**, 625-632.

Diffusion Tensor Imaging of the Hippocampus in MCI and Early Alzheimer's Disease

Andreas Fellgiebel* and Igor Yakushev
Department of Psychiatry and Psychotherapy, University Medical Center Mainz, Mainz, Germany

Abstract. The hippocampus is among the first brain structures to be affected by Alzheimer's disease (AD) pathology. Microstructural alterations within this region have been quantified *in vivo* using diffusion tensor imaging (DTI), a relatively novel MRI-based technique for mapping diffusion properties of water. Existing evidence indicates that DTI-derived mean diffusivity (MD) of the anterior hippocampus is more predictive than ordinary volumetric indices of the degree of episodic memory impairment in patients with early AD. Thus, altered MD of the (anterior) hippocampus might be highly indicative of hippocampal dysfunction, thereby potentially qualifying this measure as a candidate marker for monitoring progression of AD. Longitudinal studies are needed to confirm this concept. DTI-based assessment of hippocampal microstructure might be also of value for early AD diagnosis and for predicting the course of cognitive decline in subjects at risk for Alzheimer's dementia. Mean diffusivity as microstructural and volume as macrostructural index of hippocampal integrity seem to reflect different, albeit overlapping, aspects of the neurodegenerative process. In contrast, fractional anisotropy is less efficient for quantifying microstructural integrity of the diseased hippocampus in the clinical context. Development of automatic algorithms, providing MD measurements of the hippocampus for routine use, is a task for future studies.

Keywords: DTI, mild cognitive impairment, dementia, memory, multi-modal, longitudinal axis, biomarker, atrophy, microstructural, diffusivity

There is strong empirical evidence that the hippocampus plays an essential role in memory encoding and retrieving [1]. The hippocampus is among the first brain structures to be affected by Alzheimer's disease (AD) pathology [2], consistent with the observation that deficits in episodic memory are among the first clinical signs of AD [3]. Consequently, the hippocampus and associated limbic structures have been the focus of particular attention in AD research. The occurrence of global and regional volume reduction in the hippocampus has been a consistent finding of structural MR studies of AD patients, as well as in subjects with mild cognitive impairment (MCI), who run a risk for transition to AD. Less is known about concomitant microstructural alterations of the AD hippocampus. With the advent of diffusion tensor imaging (DTI), a relatively novel MRI-based technique for mapping diffusion properties of water in a constrained compartment, it is now possible to measure microstructural alterations in the living brain. DTI measures the random motion of water molecules, which is typically quantified as the mean diffusivity (MD) and fractional anisotropy (FA). The MD is a measure of randomized mean water diffusion [4]. As any neurodegenerative

*Correspondence to: Dr. Andreas Fellgiebel, Department of Psychiatry and Psychotherapy, University Medical Center Mainz, Untere Zahlbacher Str. 8, 55131 Mainz, Germany. Tel.: +49 (0) 6131 176786, Fax:+49 6131 176690, E-mail: fellgiebel@psychiatrie.klinik.uni-mainz.de.

process is accompanied by a progressive loss of the barriers restricting water molecule motion in cellular compartments (e.g. neuronal loss), DTI sensitively reveals degeneration of brain tissue through pathologically elevated MD [4]. In highly structured tissues such as bundles of myelinated fibres, the motion of water molecules is particularly restricted, with a relative preference for the diffusion along the axial fibre direction (anisotropic diffusion). The degree of this motion directionality, or anisotropy, is reported as fractional anisotropy (FA), an index of primarily white matter integrity [5], which can decline in neurodegenerative disease.

MICROSTRUCTURAL ALTERATIONS OF THE HIPPOCAMPUS IN MCI

To explore early, potentially AD-related, changes in the hippocampal microstructural integrity and their functional relevance, we investigated subjects with amnestic MCI. DTI-derived diffusivity as well as MRI-based volumetric measurements of the hippocampus [6] were obtained from 18 patients with MCI (mean age of 67.3 ± 8.7 years) and 18 age- and gender-matched healthy controls. Episodic memory performance was assessed with the delayed verbal recall test (DVRT) and the visual-constructive memory function test of the CERAD test battery [7]. Microstructural (MD, FA) and volumetric indices of the hippocampus were derived using a region-of-interest (ROI) analysis. The MCI patient group had a significantly smaller mean volume of the left hippocampus (-11%, $p = 0.025$) and significantly increased MD in the left ($+11\%$, $p = 0.002$) as well as right hippocampus ($+12\%$, $p = 0.022$). The left hippocampus volume ($r = 0.35$; $p = 0.03$) and MD ($r = -0.55$; $p < 0.0005$) both correlated with verbal memory function (DVRT). Multiple regression analyses revealed left hippocampal MD to be the strongest predictor of verbal episodic memory performance, explaining 25 % of DVRT variance ($p = 0.009$) in the patient group. No such a correlation was observed in the control group. Regression analyses using FA instead of MD values revealed similar but less pronounced correlations.

Increased hippocampal MD, which we found to be the most sensitive predictor of impaired memory function, might be explained by the occurrence of increased intercellular spaces and elevated extracellular water content, which might arise due to degenerative neuronal loss and Wallerian degeneration. The results of

our study suggested that microstructural alterations of the hippocampus in MCI patients are more sensitive to early and functionally relevant degenerative changes than are "macrostructural" findings of hippocampal atrophy. Neither in MCI patients nor controls were DTI measures and volumes significantly correlated ($p > 0.10$ for all correlation coefficients), suggesting that the two measures reveal different, albeit overlapping, pathological changes [8, 9].

DIFFUSIVITY OF THE HIPPOCAMPUS FOR THE PREDICTION OF DEMENTIA

In a further DTI study, we aimed to establish whether microstructural indices of hippocampal integrity can predict transition to Alzheimer's dementia in subjects with MCI. Thirteen MCI subjects were followed-up by clinical assessment over a mean period of 1,5 years [10]. MCI patients who converted to dementia (6 of 13) during the observation period proved to have had significantly elevated left hippocampal MD at baseline compared to those MCI patients who remained clinically stable. Notably, this finding is in agreement with an independent study by Kantarci and colleagues, who also reported increased baseline hippocampal diffusivity as a predictor of conversion to dementia in MCI patients [11].

DIFFUSIVITY OF THE ANTERIOR HIPPOCAMPUS IN EARLY ALZHEIMER'S DISEASE

Intracellular aggregates of the cytoskeletal tau protein are one of the hallmarks of AD. There is evidence from autopsy and imaging studies that tau deposition in AD occurs in a temporal sequence following the neuronal connectivity of the affected brain regions [12–14]. Specifically, tau deposition starts from layer II of the entorhinal cortex and spreads via the perforant path to the lateral entorhinal cortex, CA1/subiculum border and the distal apical dendrites of CA1 neurons in the stratum lacunosum-moleculare [13]. The perforant path, one of the first structures to be affected in AD, projects primarily to the anterior part of the hippocampus, thus constituting the multimodal sensory input from the entorhinal cortex [14, 15]. Its ventral afferent portion is restricted to approximately 30% of the anterior denate gyrus, which is located within the hippocampal head [16].
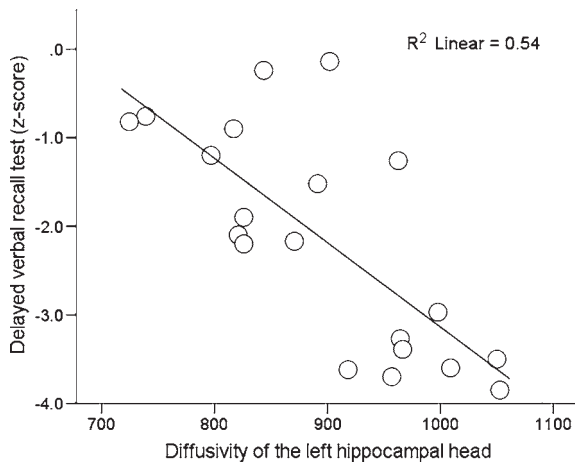
Fig. 1. Left anterior hippocampal diffusivity and verbal memory in early Alzheimer's disease. Left anterior hippocampal mean diffusivity (MD) correlates significantly with performance on the delayed verbal recall task in patients with early Alzheimer's disease ($n = 20$) [22].

This anatomical distinction of the hippocampal head, or anterior hippocampus, might underline the functional differentiation along the longitudinal axis of the hippocampus [16, 17]. This concept, initially based on animal data, has later been supported from the results of human studies of neuroanatomy [16], electrophysiology[18], genetics, and functional neuroimaging. Concerning the latter approach, functional MRI has revealed specific activation of the anterior hippocampus in the process of associative memory storage [19]. Subsequently, a multimodal imaging study documented a primary involvement of the anterior hippocampus in the performance of episodic memory [20]. Recently, a specific role of the anterior hippocampal formation in successful memory encoding has been highlighted [21].

Inspired by this evidence, we examined specifically the anterior and posterior hippocampal microstructure and volume in 20 patients with early AD (MMSE 25.7 ± 1.7) and 18 healthy control subjects by DTI and structural MRI [22]. Using an ROI analysis, we obtained volumetric and diffusivity measures of the hippocampal head and body-tail sections, as well as of the whole hippocampus. All volumetric measures and also diffusivity measurements of the hippocampus head were significantly ($p < 0.01$) different in the AD group as compared to the control group. In patients, increased left hippocampus head diffusivity had a significant negative correlation with performance on DVRT ($r = -0.74$, $p = 0.0002$) (Fig. 1) and with the

CERAD global score. In contrast, no correlation was noted for the body-tail section. Stepwise regression analyses revealed that increased left hippocampus head diffusivity was the only predictor for performance on DVRT ($R^2 = 52\%$, $p < 0.0005$). These findings suggest that anterior hippocampal diffusivity is more closely predictive of impaired verbal episodic memory function in AD than are other regional or global structural measures. Our data support in general the hypothesis of functional differentiation along the main axis of the hippocampus, and more specifically indicate a particular role of the anterior hippocampus in episodic memory deficits of AD. Thus, we propose that regional diffusivity measurements are a highly sensitive indicator of functionally relevant degenerative alterations of the hippocampus.

HIPPOCAMPAL MICROSTRUCTURE, GLUCOSE METABOLISM, AND FUNCTION IN EARLY AD

Consistent with the imaging-based findings of abnormal microstructural integrity, reduced synaptic activity/density of the hippocampus is commonly observed in studies of early AD. The relationship between these two classes of pathophysiological phenomena remains elusive. Furthermore, it has been unclear which measure is more related to the AD symptom of episodic memory impairment. In a multimodal imaging study, we obtained positron emission tomography with [(18)F]fluorodeoxyglucose (FDG-PET) and also DTI measurements in the same study group of patients with early AD. By this means we sought to investigate associations between diffusivity and metabolic indices of the hippocampal subdivisions, also in relation to the individual extent of episodic memory impairment [23]. In an intermodality correlation analysis, glucose metabolism as assessed by FDG-PET was strongly associated with diffusivity only in left anterior hippocampal division ($r = -0.81$, $p < 0.05$ Bonferroni-corrected for multiple tests) (Fig. 2). Performance on DVRT significantly correlated with left anterior ($r = -0.80$, $p < 0.05$) and total ($r = -0.72$, $p < 0.05$) hippocampal diffusivity, while the correlation with anterior hippocampal FDG uptake did not reach our predefined level of statistical significance ($r = 0.52$, n.s.). We concluded that diffusivity measurements specifically of the anterior hippocampus might be a sensitive marker of early hippocampal dysfunction as reflected in impaired energy metabolism,
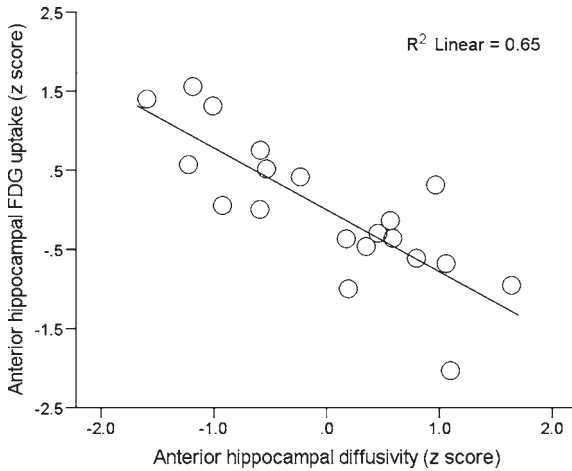
Fig. 2. Anterior hippocampal diffusivity and glucose metabolism. Left anterior hippocampal mean diffusivity (MD) correlates significantly with relative FDG uptake in the left anterior hippocampus in patients with early Alzheimer's disease ($n = 20$). Z scores are standardized residuals after effects of age, gender, education, and, for FDG uptake, volume had been regressed out.

and also cognitive symptoms. As mentioned above, this neurobiological distinction of the anterior hippocampus might be related to the disruption of the perforant path, which is known to occur early in the course of AD [24].

The great clinical relevance of degenerative alterations within the hippocampus in AD, and especially the alterations of the perforant path, is also supported by further neuroimaging studies, which showed a sig-

nificant correlation between volume of the perforant pathway zone and memory performance in patients with MCI and AD [25, 26]. Moreover, our findings concerning the anterior hippocampus are corroborated by a recent study comparing DTI in hippocampal subdivisions of AD patients, patients with idiopathic normal pressure hydrocephalus, and normal controls. The authors found maximum diffusivity increases within the hippocampal head in AD patients compared to the other two subject groups [27].

ASSOCIATION OF HIPPOCAMPAL DIFFUSIVITY AND CEREBRAL GLUCOSE METABOLISM

In contrast to structural imaging studies, functional imaging with FDG-PET and single photon emission tomography (SPECT) blood flow studies have revealed the posterior cingulate cortex (PCC) to be the most common site of the earliest metabolic and perfusion deficits in AD. The most prevalent hypothesis to explain this discrepancy is that hypometabolism/hypoperfusion of the PCC arises as a remote 'downstream' effect of AD-specific neuronal damage to the hippocampal formation, in the manner of a functional denervation. To investigate effects of hippocampal damage (as assessed by DTI) on regional glucose metabolism (as measured by FDG-PET), we performed a voxel-based multimodal imaging study in a well-characterized previously studied group of patients with early AD [28]. The major
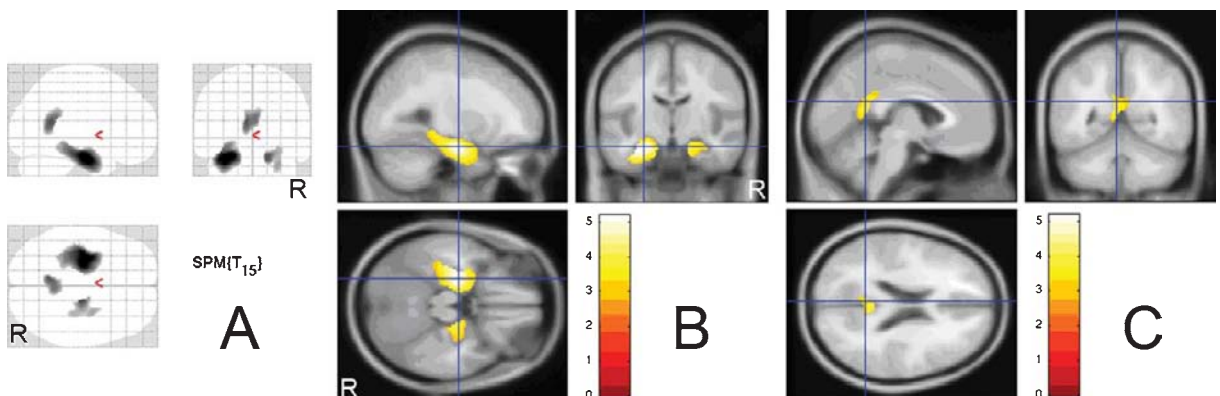
Fig. 3. Association between anterior hippocampal diffusivity and cerebral FDG uptake in early Alzheimer's disease. SPM results of the partial (corrected for age, sex, and education) negative correlation of left anterior hippocampal diffusivity with whole-brain relative FDG uptake in a sample of 20 patients with early Alzheimer's disease. Correlated regions are indicated as dark clusters projected onto glass brain (for viewing all significant findings) (A) and as color-coded clusters projected onto sections of a standard MRI template (B, C). Cross-bars indicate the location of significant voxel clusters in the hippocampus (B) and posterior cingulate (C). Applied thresholds are $p < 0.005$ uncorrected for multiple comparisons and $k > 30$ voxels. R – right, L – left.

finding of that study was that anterior hippocampal diffusivity correlated negatively with relative FDG uptake in the hippocampus, parahippocampal gyrus, and the PCC, i.e. the major components of hippocampal output pathways (Fig. 3). These structures also constitute critical nodes of the Papez circuit, which has an established role in the formation and retrieval of episodic memory. The functional relevance of this microstructural-metabolic association was supported by the findings of a significant negative correlation between relative FDG uptake in precisely the above-mentioned regions and individual performance on the DVRT. We concluded that our data support the diaschisis hypothesis described above, implicating a dysfunction of structures along the hippocampal output pathways as a significant contributor to the genesis of episodic memory impairment in AD.

SUMMARY AND PERSPECTIVES

There is increasing evidence that the differential assessment of hippocampal structure and function is particularly sensitive for making an early AD diagnosis and for predicting the course of cognitive decline in normal aging and in subjects at risk for developing AD. In summary, our findings suggest that altered diffusivity (MD) of the (anterior) hippocampus is highly indicative of hippocampal dysfunction, thereby potentially qualifying this measure as a candidate marker for monitoring progression of AD. The neurobiological distinction of the anterior division of the hippocampus might be relevant to the disruption of the perforant path that is known to occur early in the course of AD. In contrast, FA seems to be less efficient for quantifying microstructural integrity of the diseased hippocampus. Furthermore, our data indicate that the DTI-based index of diffusivity as a marker of microstructural integrity outperforms conventional volumetric, or macrostructural, measurements of the hippocampus as a predictor of AD. In view of the rather modest sample sizes in our studies [6, 22] these conclusions should be viewed with some caution.

In order to serve as a reliable marker of (early) AD, diffusivity measurements of the hippocampus should be performed in an automated and reproducible fashion. Thus, implementation of such methods for routine use is a task for future studies, based on our promising early results. Furthermore, longitudinal DTI studies of the hippocampus have not yet been conducted. They would be necessary to determine if the progressive

anterior hippocampal degeneration is related to declining episodic memory performance as occurs in patients with early AD and in subjects at risk for AD. Finally, assessment of the network of hippocampal/anterior hippocampal connections, e.g., by fiber tractography, should be used to test the prevailing assumptions about structural connectivity in the failing brain.

ACKNOWLEDGMENTS

REFERENCES

[1] Squire LR (1992) Memory and the hippocampus: a synthesis from findings with rats, monkeys, and humans. *Psychol Rev* **99**, 195-231.

[2] Braak H, Braak E (1991) Neuropathological stageing of Alzheimer-related changes. *Acta Neuropathol* **82**, 239-259.

[3] Jacobs DM, Sano M, Dooneief G, Marder K, Bell KL, Stern Y (1995) Neuropsychological detection and characterization of preclinical Alzheimer's disease. *Neurology* **45**, 957-962.

[4] Basser PJ, Pierpaoli C (1996) Microstructural and physiological features of tissues elucidated by quantitative-diffusion-tensor MRI. *J Magn Reson B* **111**, 209-219.

[5] Pierpaoli C, Jezzard P, Basser PJ, Barnett A, Di Chiro G (1996) Diffusion tensor MR imaging of the human brain. *Radiology* **201**, 637-648.

[6] Müller MJ, Greverus D, Dellani PR, Weibrich C, Wille PR, Scheurich A, Stoeter P, Fellgiebel A (2005) Functional implications of hippocampal volume and diffusivity in mild cognitive impairment. *Neuroimage* **28**, 1033-1042.

[7] Welsh KA, Butters N, Mohs RC, Beekly D, Edland S, Fillenbaum G, Heyman A (1994) The Consortium to Establish a Registry for Alzheimer's Disease (CERAD). Part V. A normative study of the neuropsychological battery. *Neurology* **44**, 609-614.

[8] Canu E, McLaren DG, Fitzgerald ME, Bendlin BB, Zoccatelli G, Alessandrini F, Pizzini FB, Ricciardi GK, Beltramello A, Johnson SC, Frisoni GB (2010) Microstructural diffusion changes are independent of macrostructural volume loss in moderate to severe Alzheimer's disease. *J Alzheimers Dis* **19**, 963-976.

[9] Cherubini A, Peran P, Spoletini I, Di Paola M, Di Iulio F, Hagberg GE, Sancesario G, Gianni W, Bossu P, Caltagirone C, Sabatini U, Spalletta G (2010) Combined volumetry and DTI in subcortical structures of mild cognitive impairment and Alzheimer's disease patients. *J Alzheimers Dis* **19**, 1273-1282.

[10] Fellgiebel A, Dellani PR, Greverus D, Scheurich A, Stoeter P, Müller MJ (2006) Predicting conversion to dementia in mild cognitive impairment by volumetric and diffusivity measurements of the hippocampus. *Psychiatry Res* **146**, 283-287.

[11] Kantarci K, Petersen RC, Boeve BF, Knopman DS, Weigand SD, O'Brien PC, Shiung MM, Smith GE, Ivnik RJ, Tangalos EG, Jack CR, Jr. (2005) DWI predicts future progression to Alzheimer disease in amnestic mild cognitive impairment. *Neurology* **64**, 902-904.

[12] Braak H, Alafuzoff I, Arzberger T, Kretzschmar H, Del Tredici K (2006) Staging of Alzheimer disease-associated neurofibrillary pathology using paraffin sections and immunocytochemistry. *Acta Neuropathol* **112**, 389-404.

[13] Lace G, Savva GM, Forster G, de Silva R, Brayne C, Matthews FE, Barclay JJ, Dakin L, Ince PG, Wharton SB (2009) Hippocampal tau pathology is related to neuroanatomical connections: an ageing population-based study. *Brain* **132**, 1324-1334.

[14] Kerchner GA, Hess CP, Hammond-Rosenbluth KE, Xu D, Rabinovici GD, Kelley DA, Vigneron DB, Nelson SJ, Miller BL (2010) Hippocampal CA1 apical neuropil atrophy in mild Alzheimer disease visualized with 7-T MRI. *Neurology* **75**, 1381-1387.

[15] Yassa MA, Muftuler LT, Stark CE (2010) Ultrahigh-resolution microstructural diffusion tensor imaging reveals perforant path degradation in aged humans in vivo. *Proc Natl Acad Sci U S A* **107**, 12687-12691.

[16] Witter MP (2007) The perforant path: projections from the entorhinal cortex to the dentate gyrus. *Prog Brain Res* **163**, 43-61.

[17] Yakushev I, Fellgiebel A (2011) Horizontal versus longitudinal axis of the hippocampus: metabolic differentiation as measured with high-resolution PET/MRI. *J Nucl Med* **52**, 329.

[18] Paller KA, McCarthy G (2002) Field potentials in the human hippocampus during the encoding and recognition of visual stimuli. *Hippocampus* **12**, 415-420.

[19] Schacter DL, Wagner AD (1999) Medial temporal lobe activations in fMRI and PET studies of episodic encoding and retrieval. *Hippocampus* **9**, 7-24.

[20] Chetelat G, Desgranges B, de la Sayette V, Viader F, Berkouk K, Landeau B, Lalevee C, Le Doze F, Dupuy B, Hannequin D, Baron JC, Eustache F (2003) Dissociating atrophy and hypometabolism impact on episodic memory in mild cognitive impairment. *Brain* **126**, 1955-1967.

[21] Chua EF, Schacter DL, Rand-Giovannetti E, Sperling RA (2007) Evidence for a specific role of the anterior hippocampal region in successful associative encoding. *Hippocampus* **17**, 1071-1080.

[22] Yakushev I, Müller MJ, Lorscheider M, Schermuly I, Weibrich C, Dellani PR, Hammers A, Stoeter P, Fellgiebel A (2010) Increased hippocampal head diffusivity predicts impaired episodic memory performance in early Alzheimer's disease. *Neuropsychologia* **48**, 1447-1453.

[23] Yakushev I, Gerhard A, Müller MJ, Lorscheider M, Schermuly I, Weibrich C, Hammers A, Stoeter P, Schreckenberger M, Fellgiebel A (2011) Relationships between hippocampal microstructure, metabolism, and function in early Alzheimer's disease. *Brain Structure and Function*, in press; DOI 10.1007/s00429-011-0302-4.

[24] Hyman BT, Van Hoesen GW, Kromer LJ, Damasio AR (1986) Perforant pathway changes and the memory impairment of Alzheimer's disease. *Ann Neurol* **20**, 472-481.

[25] Kalus P, Slotboom J, Gallinat J, Mahlberg R, Cattapan-Ludewig K, Wiest R, Nyffeler T, Buri C, Federspiel A, Kunz D, Schroth G, Kiefer C (2000) Examining the gateway to the limbic system with diffusion tensor imaging: the perforant pathway in dementia. *Neuroimage* **30**, 713-720.

[26] Stoub TR, deToledo-Morrell L, Stebbins GT, Leurgans S, Bennett DA, Shah RC (2006) Hippocampal disconnection contributes to memory dysfunction in individuals at risk for Alzheimer's disease. *Proc Natl Acad Sci U S A* **103**, 10041-10045.

[27] Hong YJ, Yoon B, Shim YS, Cho AH, Lim SC, Ahn KJ, Yang DW (2010) Differences in microstructural alterations of the hippocampus in alzheimer disease and idiopathic normal pressure hydrocephalus: a diffusion tensor imaging study. *AJNR Am J Neurorad* **31**, 1867-1872.

[28] Fellgiebel A, Müller MJ, Schermuly I, Stoeter P, Gerhard A, Yakushev I (2010) Relationships between hippocampal microstructural alterations and regional brain metabolism in early Alzheimer's disease: A combined DTI-PET study. *Alzheimer's & Dementia: The Journal of the Alzheimer's Association* **6**, 104-105.

Detection of Alzheimer's Disease with Diffusion Tensor Imaging and Deformation-Based Morphometry

Uwe Friese[a,b,*], Thomas Meindl[c], Sabine C. Herpertz[d], Maximilian F. Reiser[c],
Harald Hampel[e,f] and Stefan J. Teipel[g,b]

[a]*Institute of Psychology, University of Osnabrueck, Osnabrueck, Germany*

[b]*Department of Psychiatry, University of Rostock, Rostock, Germany*

[c]*Department of Radiology, University of Munich, Munich, Germany*

[d]*Department of General Psychiatry, University of Heidelberg, Heidelberg, Germany*

[e]*Discipline of Psychiatry, School of Medicine & Trinity College Institute of Neuroscience (TICN),
Laboratory of Neuroimaging & Biomarker Research, The Adelaide and Meath Hospital
incorporating the National Children´s Hospital (AMNCH), Trinity College, University of Dublin,
Dublin, Ireland*

[f]*Alzheimer Memorial Center, Department of Psychiatry, University of Munich, Munich, Germany*

[g]*Deutsches Zentrum für neurodegenerative Erkrankungen (DZNE), Bonn, Germany*

Abstract. Novel MRI based acquisition and analysis techniques are increasingly used as biomarkers to discriminate between Alzheimer's disease and normal aging. Evaluating the diagnostic utility of the various approaches in use is difficult though because of significant methodological differences between studies. In this research we directly compare the diagnostic utility of deformation-based morphometry (DBM) and diffusion tensor imaging (DTI) with data derived from the same group of patients with probable AD and healthy control participants. DBM was used to assess regional relative volume reductions in patients compared to controls. Distributed cortical atrophy effects were found in frontal, parietal, and temporal regions. As DTI measures, mean diffusivity and fractional anisotropy were employed to index white matter integrity. The results also point to widespread decline of white matter integrity in frontal, parieto-occipital, and temporal regions in AD. Concerning diagnostic utility, we found that the discrimination performance was best for maps of mean diffusivity and DBM. In a logistic regression model a combination of modalities reached a classification accuracy of AUC = 0.86 after leave-one-out cross-validation. We discuss the results with regard to the feasibility of current MRI based biomarkers for future applications in clinical research settings.

Keywords: Alzheimer´s disease, biomarker, MRI

INTRODUCTION

In recent years, considerable progress has been made to establish biomarkers for AD based on magnetic resonance imaging (MRI). On the one hand, processing methods and statistical procedures have been developed which can be applied to entire brain scans at once without requiring major manual user input. Early MR-based techniques to quantify structural brain changes in AD were mostly based on time-consuming and error-prone manual volumetry of key brain structures which show volume decline during the progression of AD. The hippocampus or the enthorinal cortex

---

*Correspondence to: Uwe Friese, University of Osnabrueck, Institute of Psychology, Seminarstrasse 20, D-49074 Osnabrueck, Germany. Tel.: +49(0)541/969 6213; Fax: +49(0)541/969 4470; E-mail: uwe.friese@uni-osnabrueck.de.

have been typical target structures in these studies [1–3]. In contrast, more recent approaches aim at minimizing manual user input and try to establish semi-automated analyses on the whole brain volumes (see [4] for a comprehensive overview). This makes it possible to quantify and describe widespread patterns of macroscopic changes across the whole brain instead of changes in a restricted number of preselected regions. Further advances are related to the modality of MR measurement, i.e., to the question what is actually measured. While traditional T1-weighted MRI images can be used to estimate volume changes, novel techniques like diffusion tensor imaging (DTI) also allow inferences about more subtle structural changes. In this research, we directly compare two relatively new and potentially complementing approaches with respect to their capability to distinguish between patients with AD and healthy control subjects. We characterize macroscopic morphological changes with deformation-based morphometry (DBM) based on T1-weighted MRI, and we employ DTI to find indications for deterioration of white brain matter integrity. Our analyses are based on standard multivariate statistics applied to the whole brain volumes.

The basic idea of DBM is to map individual brain scans to a "standard" brain and to use the parameters of the necessary deformations as information about relative volume differences. In other words, if a certain region of the original brain scan needs to be enlarged to map the respective region of the standard, this might be viewed as evidence for atrophy in the corresponding areas of the original brain. In DBM, the warping of individual brain scans into a standard space provides information about relative reduction of brain volume with high spatial resolution, and the algorithm preserves the intensities of voxels during the transformation [5]. Hence, the normalized brain images are almost identical, and the information of interest (regional volume change relative to the standard) must be derived from the so called deformation fields. These contain information about the positional difference between every voxel of the source brain and the reference brain. The deformation fields can be transformed into images which then constiue the input for statistical analyses. Whereas DBM is usually based on T1-weighted MR scans, DTI is an advancement of diffusion weighted imaging. Diffusion weighted imaging allows to estimate the rate of water diffusion within each voxel. With DTI, diffusion weighted images are acquired in multiple spatial orientations to characterize the diffusion in three dimensional space (diffusion

tensor ellipsoid). Depending on properties of the surrounding, diffusion is more or less restricted, i.e., this space can be shaped more like a sphere (isotropic diffusion) or rather like a cigar (anisotropic diffusion). There is evidence that the diffusion of water molecules in white brain matter is biased in the direction of the fibers and is thus anisotropic [6]. The impairment of fibers then, as it supposedly occurs in AD [7, 8], leads to more unconstrained, isotropic diffusion as a consequence of progressive neurodegeneration [9]. Therefore, DTI measures can be assumed to reveal fibre tract integrity. DTI scans and deformation fields derived with DBM can be analyzed with various statistical procedures to detect patterns of degenerative changes in the whole brain without hypothesis-driven manual selection of regions of interest [10–12].

From the clinical perspective, it is important to know how these different approaches compare with respect to their ability to differentiate between the brains of healthy controls and brains of AD patients. Usually, studies focus on one specific MRI modality or technique which compromises the evaluation of the various approaches. Often, studies differ with respect to several factors which can seriously affect the comparability of results. For instance, the diagnostic criteria to define subject samples, scanner equipment, image processing, and statistical analyses are usually not uniform across studies. For a reliable comparison it would be necessary to study the different modalities (DBM vs. DTI) within the same group of patients and controls. The objectives of the current study were to establish which method discriminates with the highest accuracy between the two groups (AD vs. control), and to evaluate if a combination of modalities may further increase diagnostic utility. To these aims we applied DBM and DTI to the brain scans of the same sample of patients with AD and healthy control participants. We followed a multivariate statistical analysis approach which has been demonstrated to successfully reveal brain atrophy and decrease of white matter integrity in AD patients as compared to healthy control patients [11, 12] and which has also been applied to the analysis of PET data [13, 14].

METHODS

Participants

MRI and DTI data were obtained from 21 patients with clinically probable AD and 20 healthy control

	AD patients	Healthy controls
Mean age in years (SE)	76 (1.61)	67 (1.64)
Sex (female/male)	12/9	9/11
Mean MMSE score (SE)	22.9 (0.64)	29 (0.15)

participants. Neuropsychological testing included the Mini Mental State Examination (MMSE) [15] and the CERAD battery [16]. AD patients fulfilled the criteria of the National Institute of Neurological Communicative Disorders and Stroke and the Alzheimer Disease and Related Disorders Association (NINCDS-ADRDA) criteria for clinically probable AD [17]. Healthy control participants reported no cognitive deficits and performed within one standard deviation from the age- and education-adjusted means of the neuropsychological tests applied. Table 1 depicts sample characteristics and average MMSE scores of the participant groups. There was no significant difference between groups with respect to sex distribution (Pearson $\chi^2 = 0.61$, $df = 1$, $p = 0.54$). AD patients were significantly older than controls ($t_{39} = 3.98$, $p < 0.01$) and obtained lower MMSE scores ($t_{39} = 9.04$, $p < 0.01$).

All participants volunteered and gave written informed consent. The study was approved by the institutional review board.

MRI acquisition

MRI acquisitions of the brain were conducted with a 3.0 Tesla scanner with parallel imaging capabilities (Magnetom TRIO, Siemens, Erlangen, Germany), maximum gradient strength: 45 mT/m, maximum slew rate: 200 T/m/s, 12 element head coil. Participants were scanned in a single session without changing their position in the scanner. The following sequences were used: for anatomical reference, a sagittal high-resolution 3-dimensional gradient-echo sequence was performed (magnetization prepared rapid gradient echo MPRAGE, field-of-view $256\,mm \times 240\,mm$, spatial resolution $0.8 \times 0.8 \times 1.2\,mm^3$, repetition time 14 ms, echo time 7.61 ms, flip angle $20°$, number of slices 160). To identify white matter lesions a 2-dimensional T2-weighted sequence was performed (fluid attenuation inversion recovery FLAIR, field-of-view 230 mm, repetition time 9000 ms, echo time 117 ms, voxel size $0.9 \times 0.9 \times 5.0\,mm$, TA 3.20 minutes, flip angle $180°$, number of slices 28, acceleration

factor 2). These images were only used to ensure that subjects had no more than three subcortical white matter hyperintensities exceeding 10 mm diameter. Diffusion-weighted imaging was performed with an echo-planar-imaging sequence (field-of-view 256 mm, repetition time 9300 ms, echo time 102 ms, voxel size $2 \times 2 \times 2\,mm^3$, 4 repeated acquisitions, $b\text{-value}_1 = 0$, $b\text{-value}_2 = 1000$, 12 directions, slice thickness 2 mm, 64 slices, no overlap).

MRI data processing

The processing of MRI data to derive DBM-based brain maps was implemented with SPM2 (Wellcome Department of Imaging Neuroscience, London, UK, http://www.fil.ion.ucl.ac.uk/spm/) in Matlab 7 (Mathworks, Natwick). Processing of DTI data was performed with FSL and the FMRIB's Diffusion Toolbox FDT (http://fmrib.ox.ac.uk/fsl/). The detailed procedure has been described elsewhere [11, 12], and only the major processing steps are summarized in the following. First, a group specific template was created by averaging the individual anatomical images after low-dimensional normalization to the standard MNI-152 template. One good quality MRI scan of a healthy control subject then was normalized to this anatomical average image using high-dimensional normalization with symmetric priors [18] resulting in a pre-template image. The MRI scan in native space of the same subject was then normalized to this pre-template image using high-dimensional normalization to produce the final group specific template. The individual anatomical scans in standard space (after low-dimensional normalization) were normalized to the anatomical template using high-dimensional image warping [18]. These normalized images were resliced to a final isotropic voxel size of $1.0\,mm^3$. Next, for the DBM analysis we derived Jacobian determinant maps from the voxel-based transformation tensors. These Jacobian maps contain information about regional volumetric atrophy or hypertrophy effects, i.e., each voxel value denotes a shrinkage or expansion of the source voxel with respect to the reference brain. The Jacobian determinant maps were masked for gray and white brain matter excluding CSF spaces (subsequently called BRAIN maps), and we additionally created corresponding maps for CSF spaces (CSF maps). The masks were obtained by segmenting the template image into gray and white matter and CSF spaces using SPM2. We took the logarithm of the

masked maps of the Jacobian determinants [19] and then applied a 10 mm full width at half maximum isotropic Gaussian kernel. For the DTI analysis we employed fractional anisotropy (FA) and mean diffusivity (MD) as measures of white matter integrity [20]. FA values indicate the directionality of the diffusion movement, ranging from 0 (isotropy) to 1 (anisotropy). The MD values inform about the overall diffusivity of a tissue. After applying corrections for eddy currents and head-motion to the images of the diffusion-weighted sequence, diffusion tensors were calculated, and maps of FA- and MD-values were produced. FA- and MD maps were restricted to white matter only by using a white matter mask derived from the segmentation of the template image. Thus, the output of the data processing step were:

- BRAIN-maps: DBM images indicating atrophy or hypertrophy in gray and white brain matter.
- CSF-maps: DBM images indicating enlargement or reduction of CSF spaces.
- FA-maps: DTI images indicating white matter integrity with respect to the directionality of diffusion (isotropy vs. anisotropy).
- MD-maps: DTI images indicating integrity with respect to the overall diffusivity within white matter.

Statistical analysis

For the statistical analysis we followed an approach which is based on standard multivariate statistical procedures (PCA, MANCOVA, CVA; [13, 14]). A key advantage of this multivariate approach, in contrast to mass univariate analyses, is that the former considers all voxels from the entire brain volume at once. This is a particularly useful feature considering the propagation of AD pathology in distributed brain systems or networks. It also allows to characterize, summarize, and compare distributed patterns in the volumes, instead of making voxel-by-voxel comparisons. This analysis has been demonstrated to reveal effects of atrophy and decrease of fibre tract integrity in AD patients [11, 12]. The analysis sequence includes:

1. Principal component analysis (PCA) to reduce the dimensionality of FA-, MD-, BRAIN-, and CSF-maps (separately for each modality).
2. Multiple multivariate analyses of covariance (MANCOVA) for each modality using the principle components from step 1 as dependent variables to reveal general differences between

the data of AD patients and control participants (effect of diagnosis).
3. Canonical variate analyses (CVA), again with principle components as input, to illustrate the spatial distribution of atrophy effects and effects of decreased fibre tract integrity.
4. Receiver operating characteristic curves (ROC) and to assess the diagnostic utility of the different modalities (based on the principal component scores of the components which showed the highest correlations with diagnosis).
5. Logistic regression analysis to evaluate the diagnostic utility of combinations of modalities.

In the context of statistical analyses of neuroimaging data a major problem is that the number of dependent variables (usually the number of voxels in the order of tens or hundreds of thousands) greatly exceeds the number of observations (i.e., scans). One way to deal with this problem is to find a limited number of patterns within the original data—which, if combined, closely approximate the original data—and to perform the statistics on these patterns. PCA is frequently applied to simplify complex and correlated data as it exists in neuroimaging. The procedure can be viewed as projecting the original images into a new space in which the so called principal components represent the axes of an orthogonal coordinate system with fewer dimensions than the original data. The principal components can also be interpreted as images with the first image explaining the largest amount of variance in the original data. Subsequent images then represent orthogonal components of the residual variance of the original data. Here, we determined the eigenvectors, also called eigenimages, and the associated eigenvalues of the covariance matrices of each modality (FA-, MD-, BRAIN-, and CSF-maps) by means of singular value decomposition. The resulting eigenvectors are the principal components, and the eigenvalues correspond to the amount of variance in the data explained by these components. In our analysis we only used eigenimages associated with an eigenvalue greater than unity. The expression of a principal component in each scan is called the principal component score and represents the projection of the scan in the new space. After reducing the dimensionality of the original data we used MANOVAs to test on a global level if there were differences between AD patients and controls. The significance of the overall effect diagnosis (AD vs. controls) was tested through the ratio between the covariance matrix of the effect to the error covariance

matrix under the null hypothesis, known as Wilk's lambda. Under the null hypothesis, the values of Wilk's lambda can be transformed and tested for significance using the CHI^2-distribution with the degrees of freedom equal to the product of the number of eigenimages with a corresponding eigenvalue greater than unity and the rank of the design matrix [13]. To illustrate the nature of significant effects with respect to spatial topography, CVA was performed. CVA finds the eigenvectors that are maximally correlated with the explanatory variables. In our case, CVA identifies the principal component that best discriminates between AD patients and controls. To this end, we identified canonical images such that the variance ratio between the effect of interest and the total error sum of squares was maximized. Each canonical image has an associated canonical value that corresponds to a variance ratio and can be compared to an F distribution with nominator degrees of freedom equal to the rank of the design matrix and denominator degrees of freedom equal to the degrees of freedom of the error term. The canonical images with canonical values exceeding the critical *F*-value threshold for $p < 0.05$ characterize the differences in the respective parameter maps of AD patients versus controls. We verified whether positive or negative loadings in the canonical images represent decreased white matter integrity and atrophy by conducting directed *t*-tests with the respective maps of AD patients and healthy controls (data not shown).

Note that in this multivariate approach the statistical inference is about the whole image volume. An advantage this approach is that it allows to characterize rather complex pattern across the entire brain volume by single scalar values. These, in turn, can be subjected to further statistical analyses to assess the diagnostic utility of the input modalities.

To determine the diagnostic utility of individual FA-, MD-, BRAIN-, and CSF-maps we identified the principal component that was significantly associated with diagnosis (AD vs. controls) by correlating the principal component scores of each scan with diagnosis. The scores from the principal component that was significantly correlated with diagnosis were entered in ROC-analyses as result variable. Diagnosis served as the state variable, and the estimated area under the curve (AUC) was chosen as a measure of discrimination accuracy. A logistic regression analysis with diagnosis (HC vs. AD) as dichotomous outcome measure was conducted. The principal component scores of DBM-Brain, DTI-MD, and DTI-FA maps, as well as patient age were used as predictor variables to estimate

the classification performance of the combination of modalities. The validity of the results was evaluated with leave-one-out cross validation. This was done by conducting 41 logistic regression analyses, specified as described above, leaving out data from one subject per iteration. The predicted values of the left-out subjects were later on used as result variable in another ROC-analyses to estimate cross-validated discrimination accuracy.

To summarize the output of the analysis steps: (Note that all but the last step are done modality by modality.)

- Principal components represent the original scans (as linear combinations).
- Principal component scores indicate to what extent a principal component is expressed in a given scan.
- MANOVA tests for global differences between data from AD patients and controls.
- CVA identifies the principal component that best discriminates between AD patients and controls (canonical image).
- Area under the curve (AUC) indices describe the discrimination accuracy of FA-, MD-, BRAIN-, and CSF-maps.
- Logistic regression establishes which combinations of modalities enhance discrimination performance (with leave-one-out cross validation).

RESULTS

Multivariate analysis

See Table 2 for details on the main statistical results. Applying principal component analysis reduced the dimensionality of the data of FA-, MD-, CSF-, and BRAIN-maps to between 8 (CSF) and 12 (FA, MD) eigenimages with eigenvalues greater than one. Separate MANOVAs revealed that the overall effect of diagnosis (AD vs. control) was significant for all dependent variables (FA, MD, CSF, BRAIN) with $p < 0.01$. Moreover, canonical variate analyses allowed us to identify the components which accounted for the effects of diagnosis. For each modality there was exactly one canonical image significantly associated with diagnosis ($p < 0.01$ for FA, MD, CSF, and BRAIN).

Figure 1 shows effects of atrophy or decrease of fibre tract integrity in AD patients in comparison to healthy controls as they were revealed by the different

Table 2
Results of the statistical analyses

	DTI		DBM	
	FA	MD	CSF	BRAIN
MANCOVA				
Number of eigenvectors	12	12	8	11
Wilk´sΛ	39.04	50.54	36.52	34.85
[a]p	<0.01	<0.01	<0.01	<0.01
Canonical variate analysis				
Canonical value	−88.23	−141.37	−71.71	−71.37
[b]p	<0.01	<0.01	<0.01	<0.01
[c]Correlation with diagnosis				
r	0.37	0.60	0.54	0.61
p	0.02	<0.01	<0.01	<0.01
ROC-analysis				
Area under curve, AUC	0.75	0.88	0.82	0.85
Standard errors	0.08	0.06	0.07	0.01
[d]Sensitivity/Specificity	0.86/0.65	0.86/0.95	0.81/0.80	0.90/0.70

Abbreviations: FA = fractional anisotropy, MD = mean diffusivity, CSF = deformations fields masked to show effects within CSF = spaces, BRAIN = deformations fields masked to show effects within white and gray matter (excluding CSF spaces); [a]CHI^2-test with df = number of eigenvectors; [b]F-test with numerator df = 39 and denominator df = 2; [c]Correlation of principal component scores of each scan with diagnosis; [d]Maximum of the average sensitivity/specificity coordinate pairs of the respective ROC-curve.

modalities. We projected the loadings of the canonical image which characterized atrophy effects or decrease of fibre tract integrity into voxel space. In detail, FA-maps show regions in which the fractional anisotropy was lower for AD patients than for controls, MD maps show areas in which mean diffusivity was higher for AD patients than for controls. CSF deformation maps depict areas with a widening of CSF-spaces in AD patients in comparison to controls. In BRAIN-deformations maps regions are shown which were atrophic in AD patients compared to controls. For purposes of clarity we only depict voxels with values above the 80th percentile. In addition, anatomical labels associated with peak values, are presented in Table 3 for DTI-data (FA and MD) and in Table 4 for DBM-data (CSF and BRAIN). Peak values were defined as local maxima exceeding the 99th percentile with a distance of at least 10 mm to other local maxima.

Figure 1, Tables 3 and 4 reveal that for FA, MD, and BRAIN differential spatial patterns of atrophy or decrease of fibre tract integrity were found. Regional effects were widespread over cortical and subcortical areas. Summarizing the regional patterns, it is noticeable that the corpus callosum and the anterior cingulate cortex were the regions in which atrophic effects or decrease of fibre tract integrity were found consistently with FA, MD, and BRAIN maps (see Fig. 2 for an overlay of effects). FA maps furthermore revealed

decreased white matter integrity in parieto-occipital regions (precuneus, cuneus), in the prefrontal lobe, and in the basal ganglia (lentiform nucleus). MD maps also indicate effects in parieto-occipital areas, in the frontal lobe (e.g., middle frontal gyrus and precentral gyrus) and in the basal ganglia, as well as in the medial temporal lobe (parahippocampal gyrus). The DBM-analysis in gray and white matter resulted in broad atrophy effects in frontal, parietal, and temporal regions. Subcortical structures (lentiform nucleus and thalamus) were also found to be affected. In contrast to the DTI measures, no effects were found in occipital regions. The CSF-maps illustrate wider CSF-spaces in AD patients along the third ventricle, the inter-hemispheric fissure, and the left sylvian fissure.

For each modality there was one principal component which was significantly correlated with diagnosis. The correlation coefficients ranged from $r = 0.37$ (FA) to $r = 0.61$ (BRAIN). To assess the diagnostic utility of the different modalities we performed ROC-analyses on the scores of the principal components which were correlated with diagnosis. We estimated the area under the curve (AUC) for each modality as measures of discrimination accuracy, and conducted pairwise comparisons between modalities (Table 3). Statistical tests were based on a procedure which builds on the correspondence of the AUC and the Wilcoxon statistic, and which accounts for the correlated nature of different

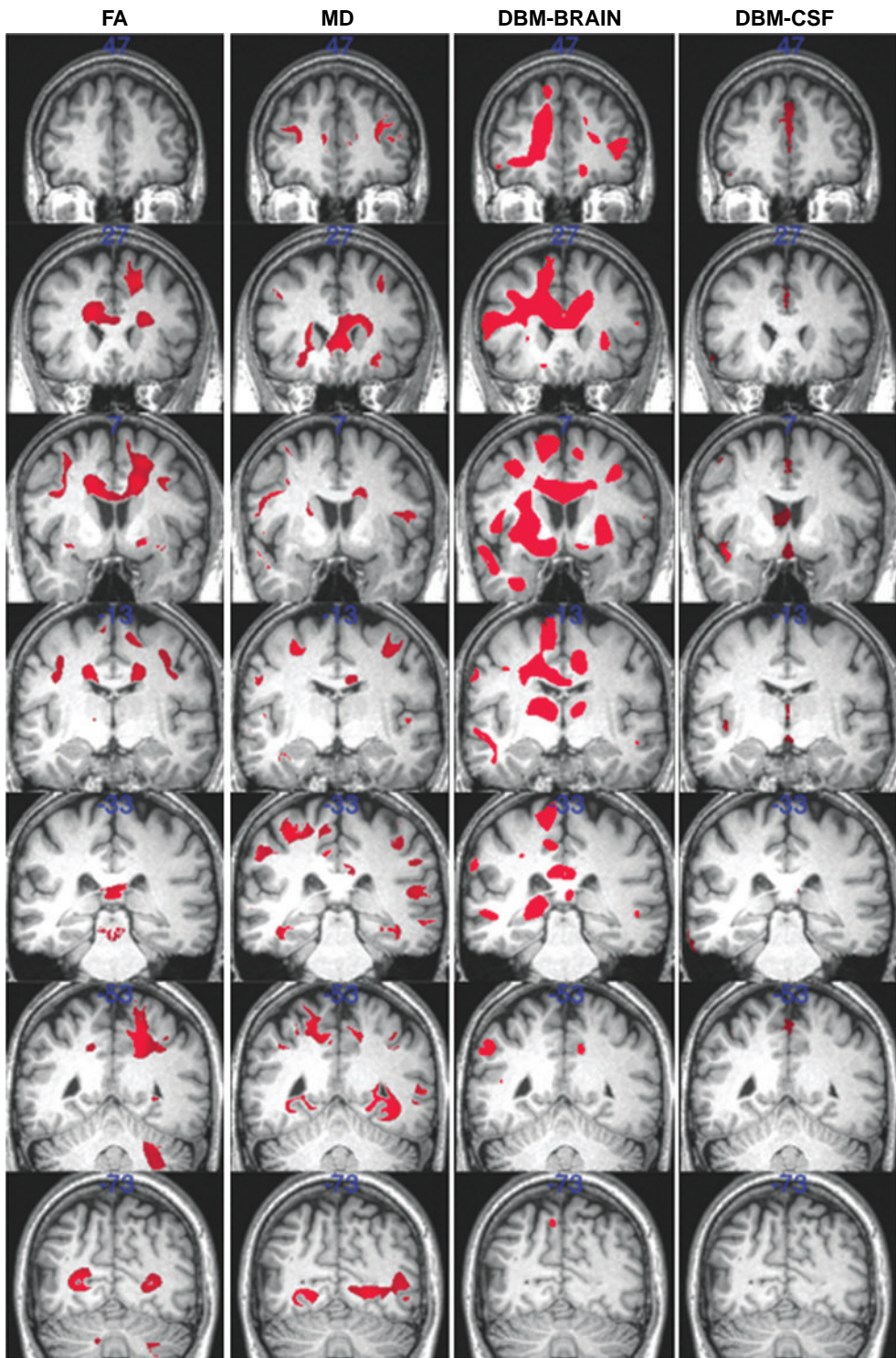Fig. 1. Spatial distribution of atrophy effects revealed by diffusion tensor imaging (FA, MD) and deformation-based morphometry (BRAIN, CSF). Components of canonical images which reflect atrophy effects were projected into voxel space. Only voxel-values above the 80th percentile on the respective canonical image were overlaid on coronal slices of a normalized anatomical image according to neurological convention (left is left).

Table 3
FA and MD peak loadings on the canonical images

Region	Side	x,y,z
Fractional anisotropy FA		
Precentral gyrus	L	−42, −1, 25
Superior frontal gyrus	R	20, 19, 41
Precuneus	R	16, −53, 35
Precuneus	R	16, −52, 44
Cuneus	L	−25, −73, 8
Anterior cingulate gyrus	R	13, −2, 49
Lentiform nucleus	R	23, 3, −9
Mean diffusivity MD		
Middle frontal gyrus	L	−55, 4, 41
Middle frontal gyrus	L	−45, 38, 23
Middle frontal gyrus	L	−43, 13, 33
Precentral gyrus	L	−30, −9, 48
Middle frontal gyrus	L	−28, −2, 50
Medial frontal gyrus	L	−12, 59, 10
Middle frontal gyrus	R	23, 53, 19
Inferior frontal gyrus	R	33, 32, −12
Middle frontal gyrus	R	37, 46, 15
Middle frontal gyrus	R	44, 42, 11
Inferior frontal gyrus	R	45, 17, 4
Postcentral gyrus	L	−62, −27, 39
Postcentral gyrus	L	−40, −27, 47
Lingual gyrus	L	−28, −71, 0
Middle occipital gyrus	L	−27, −97, 14
Cuneus	L	−5, −86, 29
Cuneus	R	3, 86, 28
Anterior cingulate gyrus	L	−3, 37, 0
Posterior cingulate gyrus	L	−12, −43, 42
Posterior cingulate gyrus	L	−7, −29, 40
Parahippocampal	R	28, −56, 2
Caudate	L	−21, 17, 8
Putame0n	L	−18, 18, −3
Caudate	R	19, 20, 7

Note: Effects reflecting decrease of fractional anisotropy (negative component of canonical image) and increase of diffusivity (positive component of canonical image) in white matter of AD patients as compared to healthy control participants. Shown are characteristics of voxels with peak loadings on the canonical image above the 99 th percentile. Anatomical labels refer to nearest gray matter as reported by the talairach daemon client [44].

Table 4
DBM peak loadings on the canonical images

Region	Side	x,y,z
BRAIN-mask		
Inferior frontal gyrus	L	−53, 29, 15
Precentral gyrus	L	−39, 16, 40
Superior frontal gyrus	L	−15, 37, 41
Superior frontal gyrus	L	−14, 13, 53
Precentral gyrus	R	35, 10, 37
Middle temporal gyrus	L	−55, 7, −16
Supramarginal gyrus	L	−58, −48, 36
Posterior cingulate gyrus	L	−20, −10, 36
Anterior cingulate gyrus	L	−17, 24, 29
Anterior cingulate gyrus	L	−17, 44, 11
Anterior cingulate gyrus	L	−12, 26, 16
Claustrum	L	−30, 14, −2
Lentiform nucleus	L	−27, 7, 2
Thalamus	L	−25, −34, 4
Sub-lobar	L	−11, 10, −11
Lentiform nucleus	R	25, 15, −1
CSF-mask		
Superior temporal gyrus	L	−50, 11, −12
Superior temporal gyrus	L	−47, 0, −14

Note: Effects reflecting atrophy in AD patients as compared to healthy control participants. Two different masks were used: The BRAIN mask images included white and gray matter and the CSF-mask images included only CSF-spaces. Shown are characteristics of voxels with peak loadings on the canonical image above the 99 th percentile.

AUCs which are derived from the same subjects [21]. Numerically, AUC was found to be lowest for FA (0.75) and highest for MD (0.88). The aforementioned statistical test revealed that the comparison between FA and MD showed a tendency towards significance ($p = 0.09$). No other pair of AUC-values was associated with $p < 0.10$. XY-plots in Fig. 3 a–c illustrate pairwise comparisons of the discrimination abilities of the pc-scores from different modalities (DBM-CSF pc-scores were not included because of high correlation with DBM-Brain scores; $r = 0.85$). As AD patients were significantly older than participants of the control group we additionally analyzed the data with age as covariate. This did not have an impact on any of the statistical inferences mentioned above. In particular, the analysis of discrimination accuracy resulted in identical ROC-values, and the patterns of atrophy or decrease of fibre tract integrity in the different modalities were not altered substantially. Therefore, we do not present the results of these analyses as they do not lead to different conclusions regarding the main objective of this study.

Supplementing the results of the ROC-analyses we conducted a logistic regression analysis with diagnosis as dependent variable. The pc-scores based on DBM-Brain, DTI-MD, and DTI-FA maps as well as age served as predictor variables. The overall fit of this logistic regression model was significant ($p < 0.01$, $\chi^2 = 35.2$, Nagelkerke's $R^2 = 0.77$; Hoshmer-Lemeshow test $p = 0.26$). The contributions of both DTI predictors were significant (MD: $p = 0.04$; FA: $p = 0.03$) whereas age and DBM-Brain scores were not significant contributors ($p > 0.1$). Performing an ROC-analysis with the predicted probabilities of this model resulted in AUC = 0.95, sensitivity = 1, specificity = 0.95. After leave-one-out cross-validation these values dropped to AUC = 0.86, sensitivity = 0.85, specificity = 0.85 (Fig. 3 d).
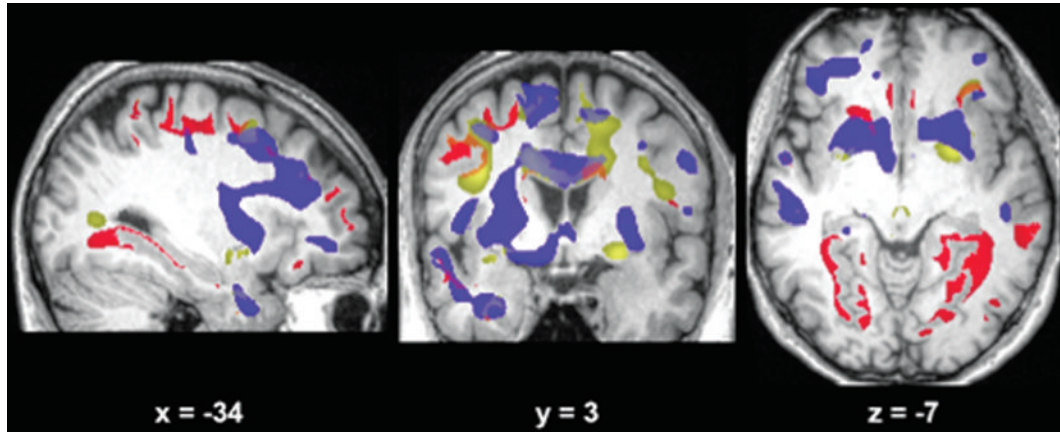
Fig. 2. Overlay of FA-maps (yellow), MD-maps (red), and DBM BRAIN-maps (blue). Notice the overlap of decreased white matter integrity and atrophy in the corpus callosum (coronal slice). MD-maps in the sagittal and horizontal sections illustrate widespread decrease of fibre tracts integrity reaching from the occipital cortex into the temporal lobe.
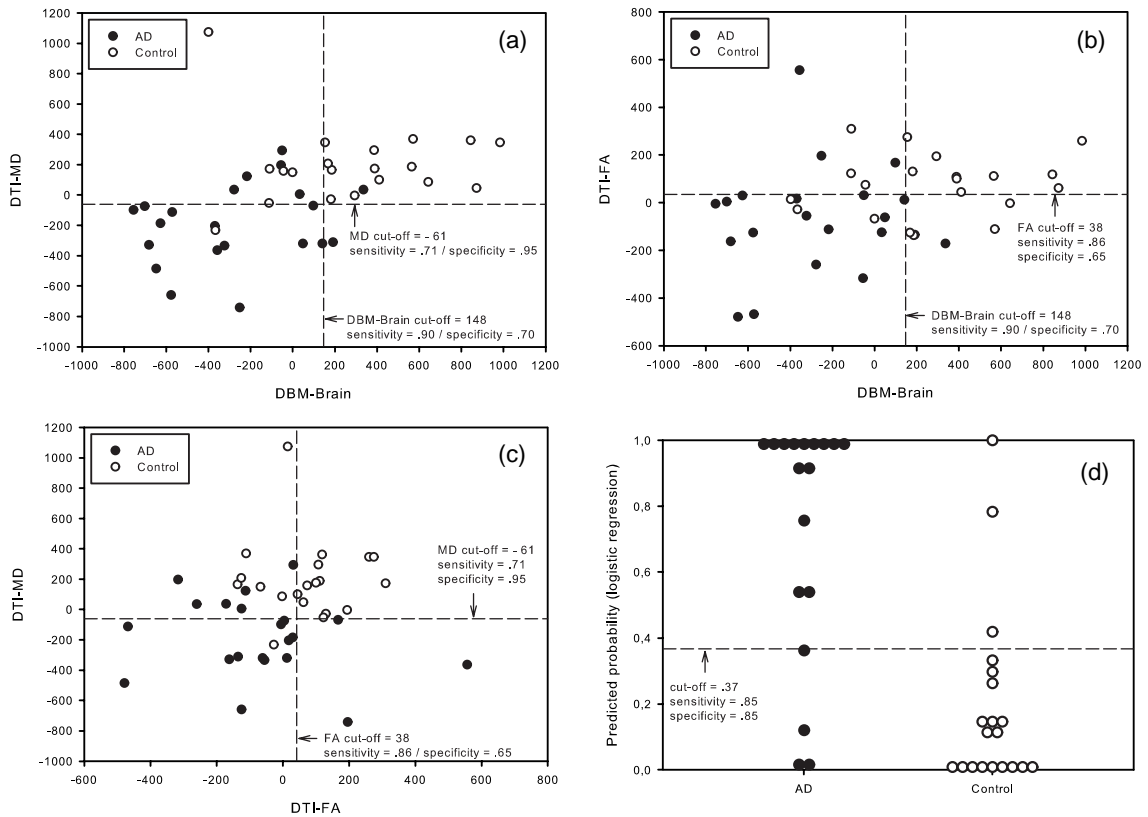
Fig. 3. XY plots of pc-scores from different modalities for AD patients (solid circles) and healthy controls (open circles): (a) DBM-Brain versus DTI-MD, (b) DBM-Brain versus DTI-FA, (c) DTI-FA versus DTI-MD. Panel (d) illustrates group separation based on the predicted probability values of the logistic regression model after leave-one out cross validation. Dashed lines indicate cut-off values determined by maximizing the average of sensitivity and specificity values of the respective ROC-curve.

DISCUSSION

In this study we investigated the diagnostic utility of DBM- and DTI-based measures for the discrimination between patients with AD and healthy controls. We used a multivariate analysis approach to determine significant patterns of atrophy or decrease of white matter integrity throughout the whole brain as reflected by DBM-maps (in gray and white brain matter and in CSF spaces) as well as FA-maps and MD-maps. For individual modalities, highest accuracy was found with MD maps (AUC = 0.88) and DBM-maps in gray and white matter (AUC = 0.85). The ability of FA to reveal directionality did not result in better diagnostic utility (AUC = 0.75). Combining modalities by means of a logistic regression, we found that only FA-maps and MD-maps were significant contributors to group separation. Cross validated discrimination accuracy was associated with AUC = 0.86.

It is important to note that the discrimination accuracies for DBM- and DTI-measures presented here were derived from the same group of AD patients and controls and can be readily compared to each other. On the first glance, the finding that overall DTI did not perform better than DBM in discriminating AD patients and controls seems to suggest that the measurement of decreased white matter integrity by DTI adds no further useful information for the separation of the groups than the assessment of atrophy effects by DBM. In particular, the discrimination accuracy of FA-maps (AUC = 0.75) was even slightly lower to that of DBM-based maps and MD-maps. On the other hand, direct comparisons of the discrimination performance of FA, MD, and DBM (Fig. 3 a–c) suggest that combining modalities should lead to better sensitivity/specificity. Correspondingly, the logistic regression analysis indicated that FA and MD both contributed significantly to the classification when modalities were combined in one model. Hence, FA maps and MD maps can complement one another for achieving better group separation. The question in how far changes of FA and MD in white matter represent different neurodegenerative processes has been addressed lately in a study on normal aging [22]. It was proposed that concordant changes of FA and MD might indicate demyelination and axonal loss, and that discordant changes (FA decrease without MD changes) might indicate Wallerian degeneration. Hence, for increasing diagnostic utility it may be advantageous to combine FA and MD for capturing different aspects of white matter damages in Alzheimer's disease.

Our finding of relatively high discrimination accuracy of individual MD-maps is a consistent replication of the results of a former study [12] where similar discrimination accuracy with DBM-maps in gray and white brain matter was found in an independent sample of AD patients and healthy controls (AUC = 0.87 in that study vs. AUC = 0.88 reported here). The finding that DBM was not a significant contributor in the logistic regression model should not be overrated because the classification performance of the model was very high, and the algorithm sequentially picks out the predictor which explains most of the (remaining) variance. As we calculated the predictors separately in each modality, multicollinearity could have impacted the estimated contributions of predictors. In the few studies combining DTI and morphometry measures to increase diagnostic utility an inconclusive picture is drawn. DTI was found to be more sensitive than hippocampal volumetry for separating between patients suffering from mild cognitive impairment (MCI) and healthy controls [23]. A logistic regression model with left hippocampal MD and left hippocampus volume reached a classification accuracy of 86%. Moreover, hippocampal diffusivity was a better predictor than hippocampal volumetry for the conversion from MCI to AD [24]. Comparable classification accuracies were reported for DTI indices (FA and apparent diffusion coefficients, ADC) and cortical thickness in various regions of interest [25]. While individual AUCs were in the range of 0.78 (superior temporal cortex thickness) to 0.86 (left temporal ADC), the combination of DTI and morphometry led to a maximal AUC = 0.98 for FA plus cortical thickness in the left temporal region.

All of the aforementioned studies used region of interest approaches. In addition, the reported diagnostic accuracies are likely to overestimate the true capability of the respective method to distinguish between the diagnostic groups because no cross validation procedures were implemented. In contrast, our multivariate analysis approach takes changes across the entire brain volume into account which, on the one hand, might increase sensitivity and, on the other hand, avoids the need for manual, hypothesis-driven selection of regions of interest. Furthermore, we applied leave-one-out validation to obtain less biased estimates of discrimination accuracy. Additional indirect evidence for the validity of our procedure comes from a study in which the same multivariate analysis was applied to morphometry data from AD patients, MCI patients, and healthy controls [12]. There, the principal component solution used to discriminate between

AD and controls was applied to the data from MCI patients (an independent sample) to predict conversion to AD. It was found that the method allowed to discriminate between converters and non-converters with an accuracy of 80%.

The patterns of structural changes which were found in white brain matter of AD patients were considerably different for FA, MD, and BRAIN maps, reflecting the differential aspects of the structural changes reflected by these modalities. Overlap of effects across FA, MD, and BRAIN maps occurred, for example, in the body of the corpus callosum and in the anterior cingulum. This is consistent with the abundant evidence that these structures are affected in AD [9, 26–30]. The pattern of brain tissue loss revealed by DBM in the present study largely corresponds to known sites of atrophy in AD in the frontal, parietal and temporal regions as well as in basal ganglia and also in the thalamus [12, 31, 32]. Many of the regions with decreased white matter integrity we found with FA- and MD-maps constitute intracortical projections from and to atrophic regions. For instance, the increase of diffusivity in the parahippocampal white matter might indicate damage to fibers connecting the hippocampus formation and enthorinal cortex with the posterior cingulate. These regions are typically affected relatively early in AD and have been demonstrated to be functionally connected [33]. Although occipital regions such as the cuneus are typically not among the most affected in AD, decreased white matter integrity and also atrophy in this area have been demonstrated [11, 12, 34]. This is compatible with our DTI results showing decreased FA and increased MD spreading over occipital, parietal, and temporal regions (see Fig. 2). With respect to the proposal that entire networks of areas are affected in AD [35, 36], these findings are not surprising since long association fibre tracts (superior longitudinal fasciculus, inferior fronto-occipital fasciculus) connect occipital visual processing areas and parietal, frontal, and temporal lobes [37, 38].

Several limitations of this study should be mentioned: Firstly, due to the rather small sample size, independent replications of the results are demanded to further validate the methods used. Additionally, although we did not observe significant direct influences of subject age as a covariate in our analyses, a closer match between patient and control group with respect to age would further increase validity. Based on our data it is not possible to rule out completely potential differential age effects on DTI and DBM measures. Concerning sample size and corresponding power to reveal robust effects our study cannot compete with approaches such as the multi-center Alzheimer's Disease Neuroimaging Initiative (ADNI; [39]) which provides the opportunity to study MRI data from much larger samples (e.g., [40, 41]). However, no multimodal MRI data are available for ADNI or other multi-center initiatives so far. Therefore, the development of new methods has to proceed with single center data first where the findings then guide the selection of innovative acquisitions for future multicenter studies. One reason being the still relatively high amount of data processing—a second limitation of the present study concerning immediate practical implications.

Clearly, an application of most likely all recently proposed MRI-based biomarkers in daily clinical use is not reasonable to date. This technical problem could be reduced to considerable degree, e.g., by extending existing analysis software as our approach builds on popular standard statistical procedures. We believe that a future application in a research context, for instance as a surrogate endpoint in clinical trials, would be conceivable. Basically, clinical application would be build on the principle component (PC) solution acquired from a larger reference population. Technically, one would estimate the PC-scores of the individual patient using the reference data. This can be seen as projecting the individual patient's data (e.g., FA-values) into a coordinate system in which the principle components of the reference data constitute the axes. The estimated PC-score on the axis which had been shown to distinguish best between the diagnostic groups could be compared to the respective cut-off value. In this regard, the PC-score would be used as a diagnostic marker.

Of course, as we have already pointed out, additional data is needed for validation. Foremost this includes the evaluation in other patient groups—particularly with MCI. As a next step it must to be shown if a multivariate analysis of DTI and DBM measures might improve early diagnosis of AD in predementia stages when atrophy effects are less distinctive than in the current study. As DTI has been shown to reveal damage to cortical projection fibers which are particularly affected in early stages of the disease [38, 42, 43], our method might be suited particularly well to differentiate between converters and non-converters.

In summary, we have demonstrated that multivariate analyses of mean diffusivity maps in white matter and deformation-based morphometry maps in brain matter (excluding CSF spaces) are equally accurate in distinguishing between patients with Alzheimer's disease and healthy controls. FA-maps were less effective for

group separation. The combination of modalities in a logistic regression model resulted in a classification accuracy of AUC = 0.86 after leave-one-out cross-validation. Future studies should reveal if multivariate analyses of DTI and DBM measures can improve early diagnosis of AD in predemedia stages when atrophic changes are less distinct than in manifest AD.

ACKNOWLEDGMENTS

REFERENCES

[1]   Jack CR, Petersen RC, O'Brien PC, Tangalos EG (1992) MR-based hippocampal volumetry in the diagnosis of Alzheimer's disease. *Neurology* **42**, 183-188.

[2]   Busatto GF, Garrido GE, Almeida OP, Castro CC, Camargo CH, Cid CG, Buchpiguel CA, Furuie S, Bottino CM (2003) A voxel-based morphometry study of temporal lobe gray matter reductions in Alzheimer's disease. *Neurobiol Aging* **24**, 221-231.

[3]   Krasuski JS, Alexander GE, Horwitz B, Daly EM, Murphy DG, Rapoport SI, Schapiro MB (1998) Volumes of medial temporal lobe structures in patients with Alzheimer's disease and mild cognitive impairment (and in healthy controls). *Biol Psychiatry* **43**, 60-68.

[4]   Teipel SJ, Meindl T, Grinberg L, Heinsen H, Hampel H (2008) Novel MRI techniques in the assessment of dementia. *Eur J Nucl Med Mol Imaging* **35 suppl 1**, S58-S69.

[5]   Ashburner J, Hutton C, Frackowiak R, Johnsrude I, Price C, Friston K (1998) Identifying global anatomical differences: deformation-based morphometry. *Hum Brain Mapp* **6**, 348-357.

[6]   Basser PJ, Mattiello J, LeBihan D (1994) MR diffusion tensor spectroscopy and imaging. *Biophys J* **66**, 259-267.

[7]   Su JH, Cummings BJ, Cotman CW (1993) Identification and distribution of axonal dystrophic neurites in Alzheimer's disease. *Brain Res* **625**, 228-237.

[8]   Brun A, Englund E (1986) A white matter disorder in dementia of the Alzheimer type: a pathoanatomical study. *Ann Neurol* **19**, 253-262.

[9]   Head D, Buckner RL, Shimony JS, Williams LE, Akbudak E, Conturo TE, McAvoy M, Morris JC, Snyder AZ (2004) Differential vulnerability of anterior white matter in nondemented

aging with minimal acceleration in dementia of the Alzheimer type: evidence from diffusion tensor imaging. *Cereb Cortex* **14**, 410-423.

[10] Davatzikos C, Fan Y, Wu X, Shen D, Resnick SM (2008) Detection of prodromal Alzheimer's disease via pattern classification of mri. *Neurobiol Aging* **29**, 514-523.

[11] Teipel SJ, Stahl R, Dietrich O, Schoenberg SO, Perneczky R, Bokde AL, Reiser MF, Moller HJ, Hampel H (2007) Multivariate network analysis of fiber tract integrity in Alzheimer's disease. *Neuroimage* **34**, 985-995.

[12] Teipel SJ, Born C, Ewers M, Bokde AL, Reiser MF, Moller HJ, Hampel H (2007) Multivariate deformation-based analysis of brain atrophy to predict Alzheimer's disease in mild cognitive impairment. *Neuroimage* **38**, 13-24.

[13] Friston KJ, Poline JP, Holmes AP, Frith C, Frackowiak RSJ (1996) A multivariate analysis of pet activation studies. *Hum Brain Map* **4**, 140-151.

[14] Zuendorf G, Kerrouche N, Herholz K, Baron JC (2003) Efficient principal component analysis for multivariate 3D voxel-based mapping of brain functional imaging data sets as applied to FDG-PET and normal aging. *Hum Brain Mapp* **18**, 13-21.

[15] Folstein MF, Folstein SE, McHugh PR (1975) Mini-mental-state: a practical method for grading the cognitive state of patients for the clinician. *J Psychiatr Res* **12**, 189-198.

[16] Morris JC, Heyman A, Mohs RC, Hughes JP, van Belle G, Fillenbaum G, Mellits ED, Clark C (1989) The consortium to establish a registry for Alzheimer's disease (CERAD). Part I. Clinical and neuropsychological assessment of Alzheimer's disease. *Neurology* **39**, 1159-1165.

[17] McKhann G, Drachman D, Folstein M, Katzman R, Price D, Stadlan EM (1984) Clinical diagnosis of Alzheimer's disease: report of the NINCDS-ADRDA Work Group under the auspices of the Department of Health and Human Services Task Force on Alzheimer's disease. *Neurology* **34**, 939-944.

[18] Ashburner J, Andersson JL, Friston KJ (1999) High-dimensional image registration using symmetric priors. *Neuroimage* **9**, 619-628.

[19] Scahill RI, Schott JM, Stevens JM, Rossor MN, Fox NC (2002) Mapping the evolution of regional atrophy in Alzheimer's disease: unbiased analysis of fluid-registered serial MRI. *Proc Natl Acad Sci U S A* **99**, 4703-4707.

[20] Sullivan EV, Pfefferbaum A (2003) Diffusion tensor imaging in normal aging and neuropsychiatric disorders. *Eur J Radiol* **45**, 244-255.

[21] Hanley JA, McNeil BJ (1983) A method of comparing the areas under receiver operating characteristics curves derived from the same cases. *Radiology* **148**, 839-843.

[22] Zhang Y, Du AT, Hayasaka S, Jahng GH, Hlavin J, Zhan W, Weiner MW, Schuff N (2010) Patterns of age-related water diffusion changes in human brain by concordance and discordance analysis. *Neurobiol Aging* **31**, 1991-2001.

[23] Muller MJ, Greverus D, Weibrich C, Dellani PR, Scheurich A, Stoeter P, Fellgiebel A (2007) Diagnostic utility of hippocampal size and mean diffusivity in amnestic MCI. *Neurobiol Aging* **28**, 398-403.

[24] Fellgiebel A, Dellani PR, Greverus D, Scheurich A, Stoeter P, Muller MJ (2006) Predicting conversion to dementia in mild cognitive impairment by volumetric and diffusivity measurements of the hippocampus. *Psychiatry Res* **146**, 283-287.

[25] Wang L, Goldstein FC, Veledar E, Levey AI, Lah JJ, Meltzer CC, Holder CA, Mao H (2009) Alterations in cortical thickness and white matter integrity in mild cognitive impairment

measured by whole-brain cortical thickness mapping and diffusion tensor imaging. *AJNR Am J Neuroradiol* **30**, 893-899.

[26] Hampel H, Teipel SJ, Alexander GE, Horwitz B, Teichberg D, Schapiro MB, Rapoport SI (1998) Corpus callosum atrophy is a possible indicator of region- and cell type-specific neuronal degeneration in Alzheimer disease: a magnetic resonance imaging analysis. *Arch Neurol* **55**, 193-198.

[27] Sydykova D, Stahl R, Dietrich O, Ewers M, Reiser MF, Schoenberg SO, Moller HJ, Hampel H, Teipel SJ (2007) Fiber connections between the cerebral cortex and the corpus callosum in Alzheimer's disease: a diffusion tensor imaging and voxel-based morphometry study. *Cereb Cortex* **17**, 2276-2282.

[28] Zhang Y, Schuff N, Jahng GH, Bayne W, Mori S, Schad L, Mueller S, Du AT, Kramer JH, Yaffe K, Chui H, Jagust WJ, Miller BL, Weiner MW (2007) Diffusion tensor imaging of cingulum fibers in mild cognitive impairment and Alzheimer disease. *Neurology* **68**, 13-19.

[29] Teipel SJ, Bayer W, Alexander GE, Bokde AL, Zebuhr Y, Teichberg D, Muller-Spahn F, Schapiro MB, Moller HJ, Rapoport SI, Hampel H (2003) Regional pattern of hippocampus and corpus callosum atrophy in Alzheimer's disease in relation to dementia severity: evidence for early neocortical degeneration. *Neurobiol Aging* **24**, 85-94.

[30] Bozzali M, Falini A, Franceschi M, Cercignani M, Zuffi M, Scotti G, Comi G, Filippi M (2002) White matter damage in Alzheimer's disease assessed *in vivo* using diffusion tensor magnetic resonance imaging. *J Neurol Neurosurg Psychiatry* **72**, 742-746.

[31] Baron JC, Chetelat G, Desgranges B, Perchey G, Landeau B, de la Sayette V, Eustache F (2001) *In vivo* mapping of gray matter loss with voxel-based morphometry in mild Alzheimer's disease. *Neuroimage* **14**, 298-309.

[32] Frisoni GB, Testa C, Zorzan A, Sabattoli F, Beltramello A, Soininen H, Laakso MP (2002) Detection of grey matter loss in mild Alzheimer's disease with voxel based morphometry. *J Neurol Neurosurg Psychiatry* **73**, 657-664.

[33] Firbank MJ, Blamire AM, Krishnan MS, Teodorczuk A, English P, Gholkar A, Harrison R, O'Brien JT (2007) Atrophy is associated with posterior cingulate white matter disruption in dementia with Lewy bodies and Alzheimer's disease. *Neuroimage* **36**, 1-7.

[34] Kinkingnehun S, Sarazin M, Lehericy S, Guichart-Gomez E, Hergueta T, Dubois B (2008) VBM anticipates the rate of progression of Alzheimer disease: a 3-year longitudinal study. *Neurology* **70**, 2201-2211.

[35] De LaCoste M-C, White C (1993) The role of cortical connectivity in Alzheimer's disease pathogenesis: a review and model system. *Neurobiology of Aging* **14**, 1-16.

[36] Delacourte A, David JP, Sergeant N, Buee L, Wattez A, Vermersch P, Ghozali F, Fallet-Bianco C, Pasquier F, Lebert F, Petit H, Di Menza C (1999) The biochemical pathway of neurofibrillary degeneration in aging and Alzheimer's disease. *Neurology* **52**, 1158-1165.

[37] Catani M, Jones DK, Donato R, Ffytche DH (2003) Occipitotemporal connections in the human brain. *Brain* **126**, 2093-2107.

[38] Fellgiebel A, Schermuly I, Gerhard A, Keller I, Albrecht J, Weibrich C, Muller MJ, Stoeter P (2008) Functional relevant loss of long association fibre tracts integrity in early Alzheimer's disease. *Neuropsychologia* **46**, 1698-1706.

[39] Mueller SG, Weiner MW, Thal LJ, Petersen RC, Jack CR, Jagust W, Trojanowski JQ, Toga AW, Beckett L (2005) Ways toward an early diagnosis in Alzheimer's disease: the Alzheimer's Disease Neuroimaging Initiative (ADNI). *Alzheimers Dement* **1**, 55-66.

[40] Hua X, Leow AD, Parikshak N, Lee S, Chiang MC, Toga AW, Jack CRJ, Weiner MW, Thompson PM (2008) Tensor-based morphometry as a neuroimaging biomarker for Alzheimer's disease: an MRI study of 676 AD, MCI, and normal subjects. *Neuroimage* **43**, 458-469.

[41] Misra C, Fan Y, Davatzikos C (2009) Baseline and longitudinal patterns of brain atrophy in MCI patients, and their use in prediction of short-term conversion to AD: results from ADNI. *Neuroimage* **44**, 1415-1422.

[42] Kantarci K, Jack CR, Jr, Xu YC, Campeau NG, O'Brien PC, Smith GE, Ivnik RJ, Boeve BF, Kokmen E, Tangalos EG, Petersen RC (2001) Mild cognitive impairment and Alzheimer disease: regional diffusivity of water. *Radiology* **219**, 101-107.

[43] Fellgiebel A, Wille P, Muller MJ, Winterer G, Scheurich A, Vucurevic G, Schmidt LG, Stoeter P (2004) Ultrastructural hippocampal and white matter alterations in mild cognitive impairment: a diffusion tensor imaging study. *Dement Geriatr Cogn Disord* **18**, 101-108.

[44] Lancaster JL, Woldorff MG, Parsons LM, Liotti M, Freitas CS, Rainey L, Kochunov PV, Nickerson D, Mikiten SA, Fox PT (2000) Automated talairach atlas labels for functional brain mapping. *Hum Brain Mapp* **10**, 120-131.

This page intentionally left blank

Mapping the Structural Brain Changes in Alzheimer's Disease: The Independent Contribution of Two Imaging Modalities

Elisa Canu[a,1], Donald G. McLaren[b,c,d], Michele E. Fitzgerald[b,d], Barbara B. Bendlin[b,d], Giada Zoccatelli[e], Franco Alessandrini[e], Francesca B. Pizzini[e], Giuseppe K. Ricciardi[e], Alberto Beltramello[e], Sterling C. Johnson[b,d] and Giovanni B. Frisoni[a*]

[a]*LENITEM - Laboratory of Epidemiology Neuroimaging and Telemedicine, IRCCS Centro San Giovanni di Dio FBF, The National Centre for Research and Care of Alzheimer's and Mental Diseases, Brescia, Italy*
[b]*Geriatric Research Education and Clinical Center, William S. Middleton Memorial Veteran's Hospital, Madison, WI, USA*
[c]*Neuroscience Training Program, University of Wisconsin, Madison, WI, USA*
[d]*Wisconsin Alzheimer's Disease Research Center, Department of Medicine, University of Wisconsin, Madison, WI, USA*
[e]*Service of Neuroradiology, Ospedale Maggiore, Borgo Trento, Verona, Italy*

Abstract. The macrostructural atrophy of Alzheimer's disease (AD) has been fully described. Current literature reports that also microstructural alterations occur in AD since the early stages. However, whether the microstructural changes offer unique information independent from macrostructural atrophy is unclear. Aim of this study is to define the independent contribution of macrostructural atrophy and microstructural alterations on AD pathology. The study involved 17 moderate to severe AD patients and 13 healthy controls. All participants underwent conventional and non conventional MRI (respectively, T1-weighted and diffusion-weighted MR scanning). We processed the images in order to obtain gray and white matter volumes to assess macrostructural atrophy, and fractional anisotropy and mean diffusivity to assess the microstructural damage. Analyses of covariance between patients and controls were performed to investigate microstructural tissue damage independent of macrostructural tissue loss, and viceversa, voxel by voxel. We observed microstructural differences, independent of macrostructural atrophy, between patients and controls in temporal and retrosplenial regions, as well as in thalamus, corticopontine tracts, striatum and precentral gyrus. Volumetric differences, independent of microstructural alterations, were observed mainly in the entorhinal cortex, posterior cingulum, and splenium. Measures of microstructural damage provide unique information not obtainable with volumetric mapping in regions known to be pivotal in AD as well as in others thought to be spared. This work expands the understanding of the topography of pathological changes in AD that can be captured with imaging techniques.

Keywords: Diffusion Tensor Imaging (DTI), Alzheimer's disease (AD), Microstructure, Fractional Anisotropy (FA), Mean Diffusivity (MD).

---

[1] current address: Neuroimaging Research Unit, Institute of Experimental Neurology, Division of Neuroscience, Scientific Institute and University Ospedale San Raffaele, Milan, Italy.

*Correspondence to: Giovanni B. Frisoni, LENITEM - Laboratory of Epidemiology, Neuroimaging and Telemedicine, IRCCS San Giovanni di Dio – FBF, Via Pilastroni 4, 25125 – Brescia, Italy. Tel.: +39 0303501361; Fax: +39 02 700435727; E-mail: gfrisoni@fatebenefratelli.it.

INTRODUCTION

Although Alzheimer's disease (AD) has been often described as a disease of the gray matter (GM), white matter (WM) alterations are also commonly observed [1–4] at the early stages of the disease as well as in preclinical conditions. Whether these alterations are explained by a primary WM damage, or as a

degeneration secondary to GM loss (or both) is currently unknown and requires further research [5]. Microstructural investigations with diffusion tensor imaging (DTI) offer a promising approach to improve our understanding of WM, but also GM, changes in disease detection and progression [6, 7]. At the microscopic level, brain parenchymal structures have distinct boundaries, including axons membranes and myelin sheaths, which constrain the diffusion of water molecules along boundaries rather than across them [8]. Fractional anisotropy (FA) and mean diffusivity (MD) are two quantitative indices of diffusion reflecting the integrity of the brain tissue [9, 10]. Alterations in the microstructure environment, as happens in neurodegenerative processes, such as small vessel alterations, demyelination of axonal structures, degradation of microtubules, loss of axonal structure and possibly gliosis reduce directional diffusion and thus reduce FA [11–13]. Increased MD results from decreased tissue density reflecting cell loss of both neurons and glia [11, 14].

In AD, a number of studies using diffusivity indices have been carried out using specific region-of-interest (ROI) analyses [15–21] or whole brain voxel-wise methods [22–24]. However, the meaning of changes in FA or MD must be interpreted cautiously because diffusivity changes may be influenced by GM and WM atrophy [25]. For instance, although these indices are considered to be measures of tissue microstructure, it is currently unknown how they are related to WM volume [25]. Moreover, the relationship between FA and volume may not be consistent across the lifespan [26, 27], due to changes in cell and tissue complexity at different stages of development and aging [28], and this relationship may be altered further by neurodegenerative disease. Thus, the situation is more complicated in presence of tissue atrophy. A study by Hugenschmidt and colleagues [29] used a recently published method [30] to detect FA changes over WM and GM volume loss in 66 healthy adults across a broad age span. They observed that regions exhibiting decrease in FA in middle age were the same areas that exhibit volume loss in older age, suggesting that microstructural FA changes may precede and predict volume loss. They also found age-related decreases in FA in atrophy-spared regions, suggesting FA provides unique information.

Isolating the contribution of microstructural damage in AD will likely improve models of disease progression, be important for early diagnosis and for monitoring the efficacy of treatments. The purpose of the present study is to determine whether AD patients show microstructural changes that are not explained by GM and WM volume loss in areas specific to AD. In the light of previous data on healthy people [29], we hypothesized that AD patients compared to healthy controls would exhibit separable microstructural (FA and MD indices) and macrostructural changes (GM and WM volume loss) that each provides unique information about the disease.

METHODS

Participants

Seventeen patients with moderate to severe probable AD, diagnosed according to NINCDS-ADRDA criteria [31] at the IRCCS Centro S. Giovanni di Dio Fatebenefratelli (Brescia, Italy) and 13 healthy volunteers participated in the study. The participant or primary caregiver provided written informed consent. All patients with a Clinical Dementia Rating of 2 or greater [32], were included in this study. Additionally, disease severity was assessed with the Mini Mental State Examination (MMSE) [33]. Healthy volunteers were mostly patients' non-consanguineous relatives of similar age. Exclusion criteria included history of transient ischemic attack (TIA) or stroke, WM hyperintensities and lesions, head trauma, alcohol or substance abuse, corticosteroid therapy, recent weight loss, or a modified Hachinski ischemic scale score greater than 4 [34]. Standardized history taking, behavioral and functional assessments, physical and neurological examinations, and a comprehensive neuropsychological battery were carried out for all the participants. There was no difference in age between groups, however they differed in gender, years of education and MMSE score (Table 1). The study was approved by the Ethics Committee of the Centre in accordance with the Declaration of Helsinki.

MRI acquisition

Images were acquired on a Siemens (Erlangen, Germany) 3 Tesla Allegra scanner at the Neuroradiology Unit of the Ospedale Maggiore Borgo Trento, Verona, Italy, with a standard head coil. High resolution T1-weighted scans were acquired with a 3D sagittal magnetization prepared rapid gradient echo and diffusion-weighted images were acquired in 30 directions. These MRI sequences were acquired totally in about 12 minutes.

Table 1
Demographic characteristics of Alzheimer's disease (AD) patients and healthy controls.

	AD (*n* = 17)	Controls (*n* = 13)	*P-value*
Age, years [range]	76.7 ± 6.4 [66–87]	72.6 ± 6.6 [65–82]	0.097
Gender, female	14 (82%)	6 (46%)	0.038
Education, years [range]	5.5 ± 2.2 [3–13]	9.2 ± 3.2 [5–13]	0.001
Mini Mental State Exam [range]	14.1 ± 3.7 [8–21]	28.9 ± 0.9 [27–30]	<0.0005

Numbers denote means ± SD [range] or n (%).

Imaging post-processing

T1-weighted MR and DTI images were processed in order to be perfectly aligned each other. This was necessary for running the statistical analyses where macrostructural and microstructural tissues were analyzed together voxel by voxel. Thus, in each voxel we could be able to assess macrostructural tissue differences independent from microstructural tissue differences (and viceversa) between patients and controls.

In the following session, we briefly described the procedure from the imaging processing to the imaging analysis.

Voxel-based morphometry (VBM)

T1-weighted MR scans were processed with Statistical Parametric Mapping software http://www.fil.ion.ucl.ac.uk/spm (SPM5, University College London, London, UK) using the following supervised protocol (see also Graph 1, beginning at the top left): (i) T1-weighted images were segmented using the VBM5 toolbox [a modified version of unified VBM, http://dbm.neuro.uni-jena.de/vbm/vbm5-for-spm5/;35] to produce gray matter (GM), white matter (WM) and cerebrospinal fluid (CSF) tissues in a common space (MNI space); (ii) tissue segmentations were averaged across participants and smoothed with an 8 mm FWHM Gaussian filter to create prior probability maps representative of the sample; (iii) a customized T1-weighted template was created by applying the transformations produced in step (i) to the native space T1-weighted images, averaged across participants, and smoothed with an 8 mm FWHM Gaussian filter; (iv) Original T1-weighted images were segmented a second time using the custom priors to obtain new segmentation and parameters of the common space normalization. Segmenting the images one more time with the customized T1-weighted template created at the step (iii) is critical when atrophy is present in at least one group (in this case in AD). This further step improves the segmentation since, compared to the default template of SPM5 used at the first segmentation (i), the customized T1-weighted template is more representative of the sample. The remaining process stream uses the fast diffeomorphic image registration algorithm developed by Ashburner and colleagues as implemented in the Diffeomorphic Anatomical Registration using Exponentiated Lie Algebra (DARTEL) toolbox [36]. The parameters created in DARTEL provided a more accurate spatial normalization: they improved the alignment within subjects and benefit the alignment between modalities once the DTI images are included in the procedure. Briefly using DARTEL, (v) T1-weighted images were rigidly aligned (using the rigid –body component of the normalization parameters from step (iv)) and segmented one more time into GM and WM (using the segmentation parameters from step (iv)) and resampled to 1.5 mm isotropic voxels. vi) GM and WM segments were simultaneously coregistered using the fast diffeomorphic image registration algorithm [35]; and (vii) the flow fields were then applied to the rigidly-aligned segments to warp them to the common DARTEL space and then modulated using the Jacobian determinants. Modulation scales the final GM and WM images by the amount of contraction required to warp the images to the template. The final result is GM and WM volume maps for each participant, where the total amount of GM and WM remains the same as in the original images. Note that the parameters created in DARTEL provided a more accurate spatial normalization: they improve the alignment within subjects and benefit the alignment between modalities once the DTI images are included in the procedure. (viii) Prior to the statistical computations, the images were brought back to the MNI common space according to a well defined procedure [37] and smoothed with an 8 mm FWHM Gaussian filter.

Fractional anisotropy and mean diffusivity

FA and MD measures were calculated with the following procedures in FSL [http://www.fmrib.ox.ac.uk/fsl/fdt/index.html, 38]: (1) image distortions in the DTI data caused by eddy currents were cor-
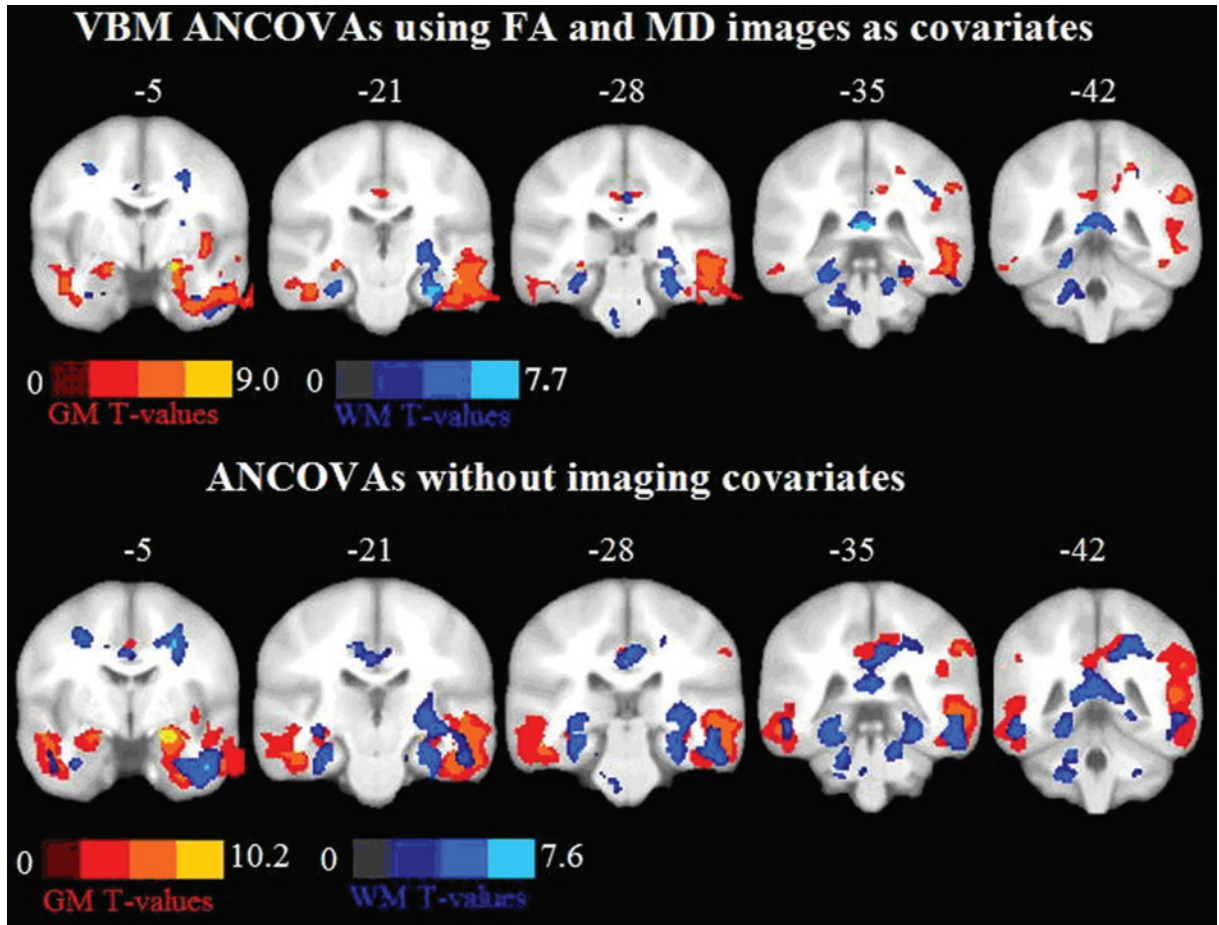
Fig. 1. Coronal slices from $Y = -5$ to $Y = -42$ showing regions with gray matter (GM, 'warm' colors) and white matter loss (WM, 'cold' colors) in Alzheimer's disease (AD) patients compared to controls. The image shows Biolgical Pattern Matching (BPM) analyses of covariance (ANCOVAs) using fractional anisotropy and mean diffusivity (MD) images as covariates and ANCOVAs without imaging covariates. Contrasts are shown at $p < 0.001$ uncorrected in at least 50 edge connected voxels. Color bars denote t-values.

rected; (2) estimation of diffusion tensors was achieved using DTIFIT; (3) three-dimensional maps of FA and MD images were computed from the tensors from step (2).

In order to employ GM and WM volume as covariates in the analyses of the DTI measurements, it was necessary to align the FA and MD maps with the T1-weighted images normalized using DARTEL. To do this we used the following procedure (see also Graph 1, beginning at the top right): (a) the non-diffusion-weighted images were normalized to the MNI T2 template in SPM5; (b) a custom FA template was created by normalizing the FA images using the normalization parameters from step (a), averaging them and smoothing them with an 8 mm FWHM Gaussian filter; (c) the cus-

tom FA template was normalized to the custom T1-weighted template (VBM step (iii)) in FLIRT [http://www.fmrib.ox.ac.uk/fsl/flirt/index.html, 39]; (d) native space FA and MD images were normalized to the custom FA template (from step (c)); (e) the normalization parameters from step (d) were multiplied by the inverse transformation parameters for the second T1-weighted segmentation (VBM step (iv)) and applied to both the FA and MD images; (f) FA and MD images were rigidly aligned and resampled to the same voxel size as T1 weighted images using the rigid-body component of the transformations produced in VBM step (iv); (g) warped using flow fields from DARTEL (VBM step (vi)), but not modulated. (h) As with the VBM, the FA and MD images were brought back to the common MNI space and smoothed with
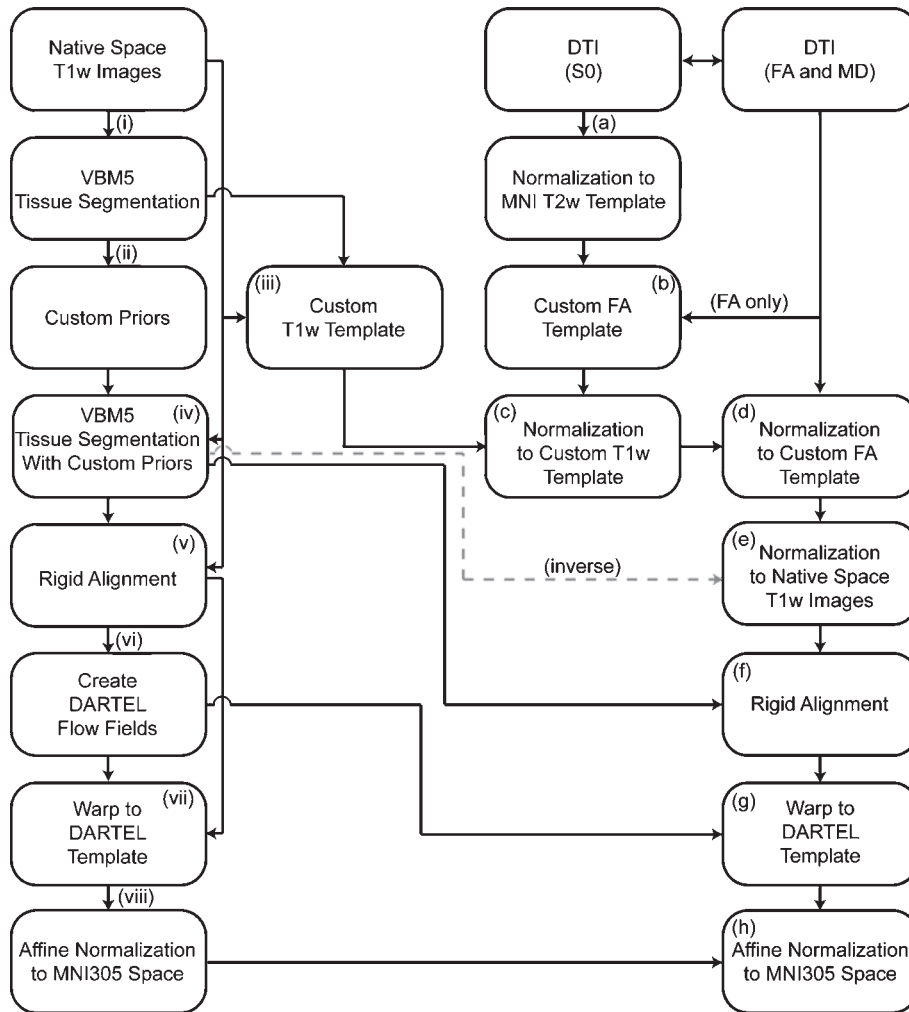
Graph 1. A diagrammatic representation of the image processing streams. The text provides a full description of the image processing stream with Roman Numerals detailing T1-weighted processing and letters detailing Diffusion Tensor Imaging processing. Abbreviations: T1 w, T1-weighted; T2 w, T2-weighted; DTI, Diffusion Tensor Imaging; S0, DTI with no diffusion weighting; MNI, Montreal Neurological Institute; DARTEL, Diffeomorphic Anatomical Registration Through Exponentiated Lie Algebra; FA, Fractional Anisotropy; MD, Mean Diffusivity; VBM5, Voxel-Based Morphometry Toolbox 5.

an 8 mm FWHM Gaussian filter similar to the strategy employed by Hugenschmidt and colleagues [29].

Masking to exclude the CSF

To exclude the CSF contamination from the results, a mask was created based on previously published CSF levels for MD [9]. For each participant's normalized and unsmoothed MD image, a mask of voxels with values less than 0.00283 mm^2/sec (2 standard deviations below the CSF mean) was created. A group mask was computed as the intersection of all participant masks.

This mask has been applied after the smoothing and used through all statistical analyses.

Statistical analysis

Voxel-wise analyses were performed in order to test for group differences on GM, WM, FA, and MD regardless of the effect of the other imaging modalities. Next, voxel-wise analyses were performed using microstructural variables as voxel-wise covariates for macrostructural (GM and WM volume) group differences. Similarly, macrostructural variables (GM

and WM volume) were used as voxel-wise covariates for microstructural (FA and MD) group differences. The Biological Parametric Mapping (BPM) toolbox implemented in SPM5 [30] was used. In all analyses, statistical maps were threshold at $p < 0.001$ uncorrected in at least 50 edge connected voxels and total intracranial volume (TIV) and age were included in the models as non imaging covariates. For all analyses CSF voxels were excluded by using the aforementioned mask.

Macrostructural analyses (GM and WM)

VBM analyses without imaging covariates

Two analyses of covariance (ANCOVAs) were computed in SPM5 to assess GM and WM differences between AD patients and controls. GM and WM images were added in two separated models as dependent variables with the group (AD and HC) as independent factor. This approach tests for locations where volume loss may be also affected from FA and MD microstructure alterations.

VBM analyses with imaging covariates (using Biological Parametric Mapping-BPM)

Two ANCOVAs, one for GM and the other for WM, were computed using the BPM toolbox to assess macrostructural differences between AD patients and controls. GM and WM images were entered as dependent variables in two separate models with the group (AD and HC) as independent factor. FA and MD maps were included in both models as imaging covariates. This approach tests for locations where the group (AD or control) is explaining unique variance in the volume that is not accounted for by FA or MD microstructure measures.

Microstructural analyses (FA and MD)

DTI analyses without imaging covariates

We performed two ANCOVAs to assess the differences in FA and MD between AD patients and controls without using the imaging covariates. FA and MD images were added in two separated models as dependent variables with the group (AD and HC) as independent factor.

DTI analyses with imaging covariates (using BPM)

Two ANCOVAs, one for MD and the other for FA, were computed using the BPM toolbox to assess MD and FA differences between AD patients and controls. FA and MD images were entered as dependent variables in two separate models with the group (AD and HC) as independent factor. GM and WM segmented maps were included in both models as imaging covariates. This approach tests for locations where the group (AD or control) is explaining unique variance in DTI measures that is not accounted for by volume loss.

VBM/DTI combination

To assess the overlap in VBM and DTI group differences, we identified the total volume loss (derived from the combination of the T-maps of both GM and WM analysis without imaging covariates) and microstructural damage (derived from the combination of the T-maps of both FA and MD analysis without imaging covariates). Thus, we created the combination map included areas with either volume loss or microstructural damage. From this map, we observed regions that had volume loss only, microstructural damage only, and volume loss with microstructural damage.

Sociodemographic analyses

ANOVA and chi-squared tests were performed to analyze the sociodemographic and clinical features (Table 1).

RESULTS

Macrostructural analyses (GM and WM)

VBM analyses without imaging covariates

The AD group showed less GM than controls in the medial temporal lobe including the hippocampi, prefrontal cortex, frontal lobe, posterior cingulate cortex and cerebellum bilaterally, and in the right parietal lobe and insula (Fig. 1, 'warm' colors). Additionally, the AD group showed less WM than controls in the body, genu and splenium of the corpus callosum, in the left retrosplenial region and right superior parietal lobe, posterior cingulate and prefrontal region, in the cingulum, frontal lobe, occipital and temporal lobe, and cerebellar hemispheres (Fig. 1, 'cold' colors). No regions showed less GM or WM in the controls compared to AD patients.

VBM analyses with imaging covariates (using BPM)

After controlling for microstructural changes with BPM we found GM atrophy in AD compared to controls in the inferior temporal lobe bilaterally and in left posterior cingulate (Fig. 1, 'warm' colors); in WM in the splenium of corpus callosum, in the right inferior temporal lobe, in the entorhinal region and cerebellum bilaterally (Fig. 1, 'cold' colors). These were regions where AD group is explaining unique variance in the volume that is not accounted for by FA or MD microstructure measures.

Microstructural analysis (MD and FA)

DTI analyses without images covariates

Using an ANCOVA without GM and WM as imaging covariates, we found that AD brains had significant higher MD compared to controls in the hippocampal and parahippocampal regions, in temporal, superior parietal and medial frontal lobe bilaterally, in the right insula, internal capsule, thalamus, posterior cingulate cortex, occipital lobe, prefrontal and frontal lobe, inferior frontal gyrus and precentral gyrus, in the left caudate nucleus and anterior internal capsule,
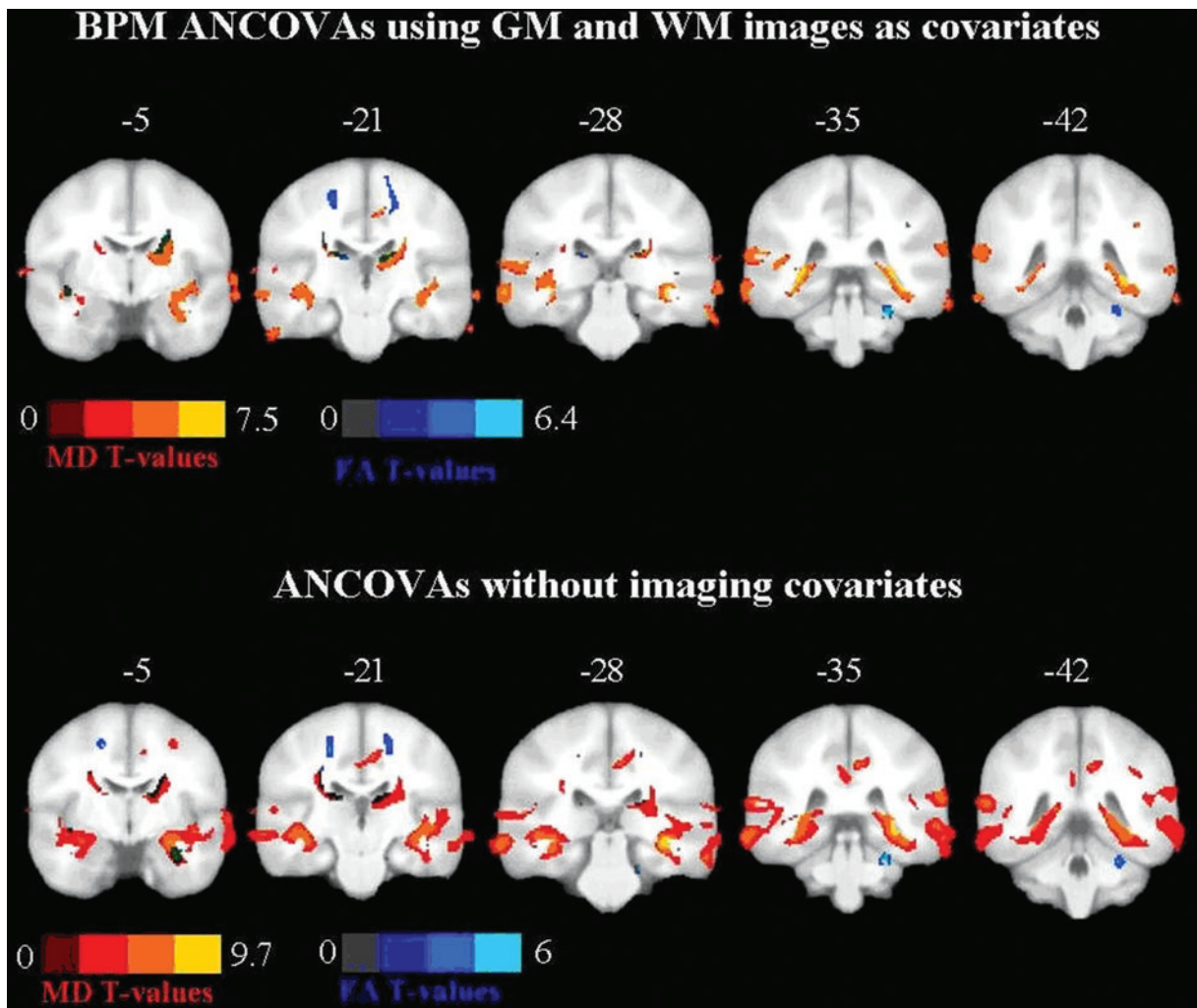
Fig. 2. Coronal slices from $Y = -5$ to $Y = -42$ showing regions with higher mean diffusivity (MD) values ('warm' colors) and lower fractional anisotropy (FA) values ('cold' colors) in Alzheimer's disease (AD) patients compared to controls. The image shows Biolgical Pattern Matching (BPM) analyses of covariance (ANCOVAs) using gray matter (GM) and white matter (WM) images as covariates and ANCOVAs without imaging covariates. Darkened green indicates areas with both FA and MD changes. Contrasts are shown at $p < 0.001$ uncorrected in at least 50 edge connected voxels. Color bars denote t-values.

in the cingulum and corpus callosum (Fig. 2, 'warm' colors).

A significant reduction in FA in AD brains was found in the anterior cingulate, caudate and parietal lobe bilaterally, in right hippocampus, cerebral peduncle, thalamus and occipital lobe, in the left putamen and medial temporal lobe (Fig. 2, 'cold' colors).

DTI analyses with images covariates (using BPM)

Using an ANCOVA with GM and WM volume as imaging covariates, we found that AD brains had significantly higher MD, indicating damage, in the parahippocampal regions, parietal lobe and precentral gyrus, internal capsule and caudate bilaterally, in the right thalamus, occipital lobe, in the body of cingulum and in the left medial frontal lobe including white matter tracts such as fornix, corona radiata, thalamic, corticopontine and corticospinal radiation (Fig. 2, 'warm' colors).

Reduced FA values, indicating damage, were found in the right cerebral peduncle and posterior limb of the internal capsule, in the thalamus and parietal lobe bilaterally, and in the left medial temporal lobe and striatum. The following tracts pass through those regions: the anterior commissure, superior corona radiata, thalamic, cortico-pontine and corticospinal radiation (Fig. 2, 'cold' colors). These were regions where AD group is explaining unique variance in DTI measures that is not accounted for by volume loss.

No regions showed a significant decrease in MD or increase in FA in AD patients compared to controls.

VBM/DTI combination

The combination of the VBM and the DTI results reveals regions that show both atrophy and microstructrual damage (Fig. 3, green color); however, there are regions that show microstructural damage but not significant atrophy (Fig. 3, blue color); and, finally, there are regions with atrophy but not significant microstructural changes (Fig. 3, red color).

DISCUSSION

In the present work we differentiated microstructural damage from GM and WM volume loss in patients with moderate to severe AD. We observed atrophy-independent group differences in both MD and FA, indicative of microstructural damage beyond that explained by gross GM and WM volume loss in AD.
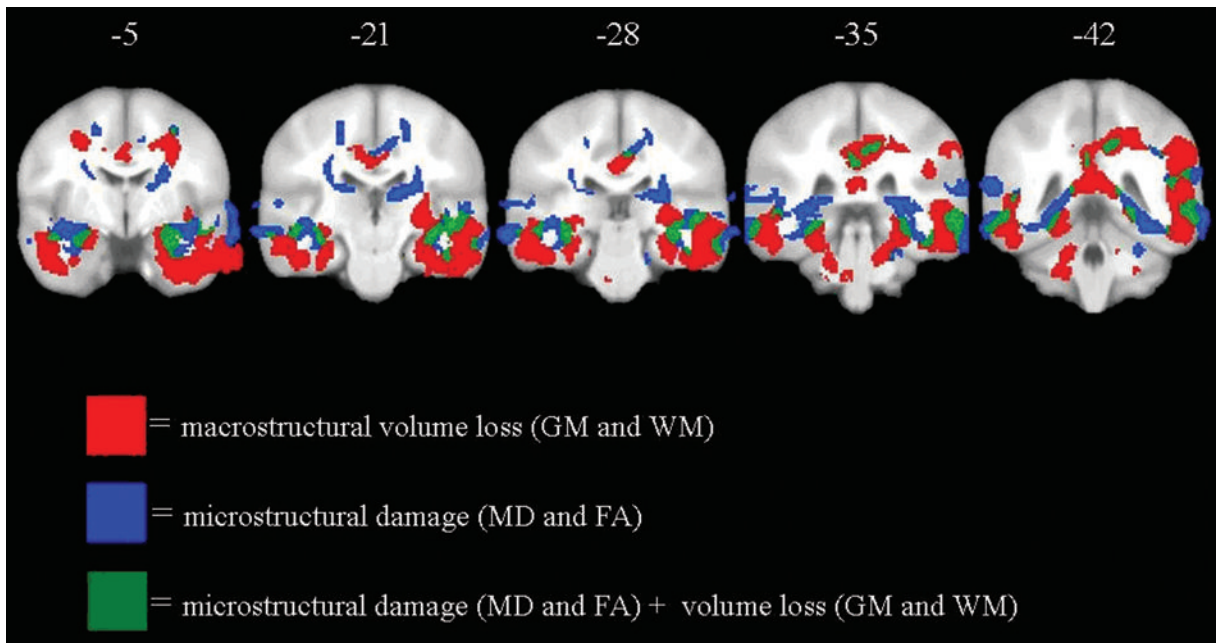

Fig. 3. Coronal slices from $Y = -5$ to $Y = -42$ showing areas with macrostructural volume loss only (gray matter-GM or white matter-WM, red); microstructural damage only (mean diffusivity-MD and fractional anisotropy-FA, blue); and the combination of macrostructural and microstructural changes (green).

Regions affected included the medial temporal and retrosplenial regions as well as the anterior commissure, corona radiata, internal capsule, thalamus and thalamo-cortical projections, corticopontine tracts, cerebral peduncle, striatum and precentral gyrus. Finally, volumetric differences independent of microstructural changes were observed in the entorhinal cortex, inferior temporal lobe, posterior cingulate, splenium and cerebellum.

Microstructural changes in late stage AD

In the present work, without controlling for GM and WM volume loss, we observed that our results would confirm previous findings on altered diffusion changes in AD. The comparison of FA and MD between patients and controls without GM and WM maps as imaging covariates, produced results that closely resembled other DTI studies in AD. Specifically, we observed higher MD in AD group in the hippocampi and parahippocampal regions [6, 18, 21, 23], internal capsule [23, 24], cingulum and posterior cingulate cortex [6, 23, 40], medial temporal lobe and temporal pole [16, 18, 21, 23], parietal [6, 16, 21, 23] and frontal lobe [16, 23], including the inferior and medial frontal gyrus [23]. Confirming previous studies we observed lower anisotropy in AD compared to controls in parahippocampal regions [41, 42], putamen [43], thalamus [23, 41], cerebral peduncle [24], cingulum [22, 40, 44, 45], temporal [16, 18, 21, 24, 41, 45], frontal lobe [16, 22, 23, 41, 45] and occipital lobe [41, 45].

Using the same BPM method in a normal sample with a broad age range, a previous study [29] showed that regions with decreased FA in the middle age were the same regions that exhibit volume loss in old age. In the light of those findings, regions in our sample showing microstructural alterations in AD may be predictive of future atrophy with further disease progression. While this hypothesis can only be evaluated with longitudinal follow-up, several recent studies provide supporting evidence. First, some of the regions where we found microstructural alterations independent of macrostructural volume loss, such as internal capsule, middle cerebellar peduncle, striatum, thalamus, motor cortex (precentral region), corticopontine and talamo-cortical projections, are involved in movement control. This is consistent with the notion that advanced AD patients are more likely to show motor deficits in disease stages more severe than that of the patients in the present study [24, 46]. Second, the presence of amyloid depositions and neurofibrillar tangles has been found in the striatum of moderate AD [47],

in the primary motor cortex of severe AD [48] and in early onset AD [49, 50] which may cause white matter changes in input and output projection fibers. Third, higher iron levels, known to be associated to neurodegeneration [51, 52], have been found in the striatum of moderate AD compared to controls [53]. Moreover, pathological changes in the motor system regions have been reported in AD mainly related to the severity of the disease [54]. In the light of the mentioned literature, this study shows that changes in AD, in terms of low FA and high MD values, may suggest where the atrophy could occur during the late stages of the disease. If this is true, since it has been not proven by this study, knowledge of regions at-risk for atrophy could provide valuable insight into the optimal treatment of patients when appropriate drugs are available and for monitoring the efficacy of the treatment itself.

Regions with volume loss but not microstructural changes: why?

Without controlling for FA and MD changes, as we expected based on several previous VBM studies (for a detailed review see [55]), we found GM volume loss in regions known to be pivotal in AD such as the hippocampus, medial temporal lobe, posterior cingulate cortex and parietal lobe. Recently, using VBM, WM volume loss has been observed in AD in regions relevant for the anatomical connection through the brain as the corpus callosum [56], the parahipppocampal areas [57] and the cingulum bundle [58], which are the same regions we observed in the present study.

Moreover, we found some regions of atrophy without significant microstrucural differences, a finding that has several possible explanations. First, the relation between gross volume and DTI indices may not be linear [59, 60]. The relationship between FA and WM differs over the life-span [26, 27]. FA is related to the microstructure of WM and only some properties may affect volume such as the degree of myelination and axonal degeneration [61]. Moreover, FA reflects a complex and dense cytoskeleton of axons composed of microtubules containing cellular organelles (mitochondria and vesicles); in general the cellular microstructure of tissue influences the overall mobility of diffusing molecules by providing different barriers (intracellular and extracellular) [8], which are in turn affected by age and AD [28]. Second, the image modalities used in this study differed in voxel resolution and this may have affected sensitivity to group differences in favor of the higher resolution T1 w modality. Third, morphometry findings included regions where

DTI acqusition was poor such as in the inferior temporal lobe and cerebellum where inhomogeneity artifact can result in a significant signal dropout with an echoplanar acquisition such as that used to collect the diffusion-weighted images. Future studies will benefit from the use of less suceptibility-prone sequences and higher resolution DTI acquisition protocols. The latter will also assist in detecting microstructural alterations in regions where the number of crossing fiber tracts is high, such as the centrum semiovale.

Potential issues occurring when combining different modalities

Recently, the use of the multi-modality imaging has been largely adopted in order to better understand the neurobiology of several diseases *in vivo*. However, several limitations need to be considered carefully in order to avoid misleading interpretation of the findings. First, some imaging modalities, such as DTI, are more prone to distortions and artifacts than others. Second, different imaging modalities may have different spatial resolutions (as usually occurs with DTI or functional MRI compared to T1 images). As a consequence, co-registering and normalizing different imaging modalities is one of the most common source of confound.

The pathophysiology of alterations of diffusion in AD

In AD, a number of studies suggest that diffusion changes in the WM could reflect Wallerian degeneration and be secondary to cortical pathology [62]. According to this hypothesis, the amyloid β (Aβ) deposits around the neuronal cells and/or the neurofibrillary tangles in the body of the cells lead to the degeneration of axons and myelin (secondary degeneration). However, a primary damage of WM tissue can not be excluded. In fact, Aβ deposits have been found near the vessels in the WM in AD [63] and recently it has been demonstrated that Aβ peptides are cytotoxic to oligodendrocytes in vitro [64]. A neuropathologic study [65] established the phases of Aβ deposition in AD cases. They also observed that the Aβ deposition correlated with the presence and the phases of the neurofibrillar tangles. Thus, tau may also provide a mechanism pathogenesis of white matter in AD. The role of tau has recently gained credibility for the apparently successful phase II trial of an anti-tau drug (Claude M. Wischik. "Tau aggregation inhibitor (TAI) therapy with remberTM arrests disease progression in mild and moderate Alzheimer's disease over 50 weeks", ICAD, Chicago 2008). Tau protein binds to the microtubules for the integrity and stabilization of the cytoskeleton and for axonal transport [66]. With the disease, the axonal cytoskeleton can be perturbated [67] and axonal transport becomes disrupted [67]. Thus, the functional failure of tau due to hyperphosphorylation may be result in changes in FA. This hypothesis is supported by data from the present study, indicating that the largest areas of alteration of diffusion map to regions known to be affected by tangle pathology [68].

Limitations

Some limitations of the present study need to be discussed. The main limitation is that the significance threshold was uncorrected for multiple comparisons and this might have led to false positive results. The sample size was small and a replication of the method in a larger sample is needed for avoiding power-related issues. Second, the two imaging modalities we used differ in resolution. Although, the images are rigid aligned each other, the original resolution could still affect the results in order of false negative/positive findings. Future studies should taking into account this possible issue. Third, groups of MCI and mild AD could add information on the progression of these microstructural alterations. Finally, the impact of these alterations requires longitudinal follow-up. The longitudinal component is critical in evaluating the hypothesis that future volume loss occurs in regions with altered diffusion which was generated by the present study.

tion and progression of the study. Finally, we wish to thank the patients and their families for their persisting and admirable collaboration.

REFERENCES

[1] Bartzokis G, Cummings JL, Sultzer D, Henderson VW, Nuechterlein KH, Mintz J (2003) White matter structural integrity in healthy aging adults and patients with Alzheimer disease: a magnetic resonance imaging study. *Arch Neurol* **60**, 393-398.

[2] Bowen BC, Barker WW, Loewenstein DA, Sheldon J, Duara R (1990) MR signal abnormalities in memory disorder and dementia. *AJNR Am J Neuroradiol* **11**, 283-290.

[3] Scheltens P, Barkhof F, Leys D, Wolters EC, Ravid R, Kamphorst W (1995) Histopathologic correlates of white matter changes on MRI in Alzheimer's disease and normal aging. *Neurology* **45**, 883-888.

[4] Vermersch P, Roche J, Hamon M, Daems-Monpeurt C, Pruvo JP, Dewailly P, Petit H (1996) White matter magnetic resonance imaging hyperintensity in Alzheimer's disease: correlations with corpus callosum atrophy. *J Neurol* **243**, 231-234.

[5] Zhang Y, Schuff N, Du AT, Rosen HJ, Kramer JH, Gorno-Tempini ML, Miller BL, Weiner MW (2009) White matter damage in frontotemporal dementia and Alzheimer's disease measured by diffusion MRI. *Brain* **132**, 2579-2592.

[6] Kantarci K, Jack CR Jr, Xu YC, Campeau NG, O'Brien PC, Smith GE, Ivnik RJ, Boeve BF, Kokmen E, Tangalos EG, Petersen RC (2001) Mild cognitive impairment and Alzheimer disease: regional diffusivity of water. *Radiology* **219**, 101-107.

[7] Rose SE, McMahon KL, Janke AL, O'Dowd B, de Zubicaray G, Strudwick MW, Chalk JB (2006) Diffusion indices on magnetic resonance imaging and neuropsychological performance in amnestic mild cognitive impairment. *J Neurol Neurosurg Psychiatry* **77**, 1122-1128.

[8] Beaulieu C (2002) The basis of anisotropic water diffusion in the nervous system - a technical review. *NMR Biomed* **15**, 435-455.

[9] Basser PJ, Pierpaoli C (1996) Microstructural and physiological features of tissues elucidated by quantitative-diffusion-tensor MRI. *J Magn Reson B* **111**, 209-219.

[10] Pierpaoli C, Jezzard P, Basser PJ, Barnett A, Di Chiro G (1996) Diffusion tensor MR imaging of the human brain. *Radiology* **201**, 637-648.

[11] Bronge L, Bogdanovic N, Wahlund LO (2002) Post-mortem MRI and histopathology of white matter changes in Alzheimer brains. A quantitative, comparative study. *Dement Geriatr Cogn Disord* **13**, 205-212.

[12] Englund E (1998) Neuropathology of white matter changes in Alzheimer's disease and vascular dementia. *Dement Geriatr Cogn Disord* **9(Suppl 1)**, 6-12.

[13] Moseley M (2002) Diffusion tensor imaging and aging - a review. *NMR Biomed* **15**, 553-560.

[14] Kantarci K, Petersen RC, Boeve BF, Knopman DS, Weigand SD, O'Brien PC, Shiung MM, Smith GE, Ivnik RJ, Tangalos EG, Jack CR Jr (2005) DWI predicts future progression to Alzheimer disease in amnestic mild cognitive impairment. *Neurology* **64**, 902-904.

[15] Allen G, Barnard H, McColl R, Hester AL, Fields JA, Weiner MF, Ringe WK, Lipton AM, Brooker M, McDonald E, Rubin CD, Cullum CM (2007) Reduced hippocampal functional connectivity in Alzheimer disease. *Arch Neurol* **64**, 1482-1487.

[16] Bozzali M, Falini A, Franceschi M, Cercignani M, Zuffi M, Scotti G, Comi G, Filippi M (2002) White matter damage in Alzheimer's disease assessed in vivo using diffusion tensor magnetic resonance imaging. *J Neurol Neurosurg Psychiatry* **72**, 742-746.

[17] Choi SJ, Lim KO, Monteiro I, Reisberg B (2005) Diffusion tensor imaging of frontal white matter microstructure in early Alzheimer's disease: a preliminary study. *J Geriatr Psychiatry Neurol* **18**, 12-19.

[18] Hanyu H, Sakurai H, Iwamoto T, Takasaki M, Shindo H, Abe K (1998) Diffusion-weighted MR imaging of the hippocampus and temporal white matter in Alzheimer's disease. *J Neurol Sci* **156**, 195-200.

[19] Naggara O, Oppenheim C, Rieu D, Raoux N, Rodrigo S, Dalla Barba G, Meder JF (2006) Diffusion tensor imaging in early Alzheimer's disease. *Psychiatry Res* **146**, 243-249.

[20] Sandson TA, Felician O, Edelman RR, Warach S (1999) Diffusion-weighted magnetic resonance imaging in Alzheimer's disease. *Dement Geriatr Cogn Disord* **10**, 166-171.

[21] Fellgiebel A, Wille P, Muller MJ, Winterer G, Scheurich A, Vucurevic G, Schmidt LG, Stoeter P (2004) Ultrastructural hippocampal and white matter alterations in mild cognitive impairment: a diffusion tensor imaging study. *Dement Geriatr Cogn Disord* **18**, 101-108.

[22] Medina D, DeToledo-Morrell L, Urresta F, Gabrieli JD, Moseley M, Fleischman D, Bennett DA, Leurgans S, Turner DA, Stebbins GT (2006) White matter changes in mild cognitive impairment and AD: A diffusion tensor imaging study. *Neurobiol Aging* **27**, 663-672.

[23] Rose SE, Janke AL, Chalk JB (2008) Gray and white matter changes in Alzheimer's disease: a diffusion tensor imaging study. *J Magn Reson Imaging* **27**, 20-26.

[24] Xie S, Xiao JX, Gong GL, Zang YF, Wang YH, Wu HK, Jiang XX (2006) Voxel-based detection of white matter abnormalities in mild Alzheimer disease. *Neurology* **66**, 1845-1849.

[25] Salat DH, Tuch DS, Hevelone ND, Fischl B, Corkin S, Rosas HD, Dale AM (2005) Age-related changes in prefrontal white matter measured by diffusion tensor imaging. *Ann N Y Acad Sci* **1064**, 37-49.

[26] Abe O, Yamasue H, Aoki S, Suga M, Yamada H, Kasai K, Masutani Y, Kato N, Ohtomo K (2008) Aging in the CNS: comparison of gray/white matter volume and diffusion tensor data. *Neurobiol Aging* **29**, 102-116.

[27] Fjell AM, Westlye LT, Greve DN, Fischl B, Benner T, van der Kouwe AJ, Salat D, Bjornerud A, Due-Tonnessen P, Walhovd KB (2008) The relationship between diffusion tensor imaging and volumetry as measures of white matter properties. *Neuroimage* **42**, 1654-1668.

[28] Hayakawa N, Kato H, Araki T (2007) Age-related changes of astorocytes, oligodendrocytes and microglia in the mouse hippocampal CA1 sector. *Mech Ageing Dev* **128**, 311-316.

[29] Hugenschmidt CE, Peiffer AM, Kraft RA, Casanova R, Deibler AR, Burdette JH, Maldjian JA, Laurienti PJ (2008) Relating imaging indices of white matter integrity and volume in healthy older adults. *Cereb Cortex* **18**, 433-442.

[30] Casanova R, Srikanth R, Baer A, Laurienti PJ, Burdette JH, Hayasaka S, Flowers L, Wood F, Maldjian JA (2007) Biological parametric mapping: A statistical toolbox for multimodality brain image analysis. *Neuroimage* **34**, 137-143.

[31] McKhann G, Drachman D, Folstein M, Katzman R, Price D, Stadlan EM (1984) Clinical diagnosis of Alzheimer's dis-

ease: report of the NINCDS-ADRDA Work Group under the auspices of Department of Health and Human Services Task Force on Alzheimer's Disease. *Neurology* **34**, 939-944.

[32] Morris JC (1993) The Clinical Dementia Rating (CDR): current version and scoring rules. *Neurology* **43**, 2412-2414.

[33] Folstein MF, Folstein SE, McHugh PR (1975) "Mini-mental state"A practical method for grading the cognitive state of patients for the clinician. *J Psychiatr Res* **12**, 189-198.

[34] Rosen WG, Terry RD, Fuld PA, Katzman R, Peck A (1980) Pathological verification of ischemic score in differentiation of dementias. *Ann Neurol* **7**, 486-488.

[35] Ashburner J, Friston KJ (2005) Unified segmentation. *Neuroimage* **26**, 839-851.

[36] Ashburner J (2007) A fast diffeomorphic image registration algorithm. *Neuroimage* **38**, 95-113.

[37] McLaren DG, Kosmatka KJ, Kastman EK, Bendlin BB, Johnson SC Rhesus macaque brain morphometry: a methodological comparison of voxel-wise approaches. *Methods* **50**, 157-165.

[38] Behrens TE, Woolrich MW, Jenkinson M, Johansen-Berg H, Nunes RG, Clare S, Matthews PM, Brady JM, Smith SM (2003) Characterization and propagation of uncertainty in diffusion-weighted MR imaging. *Magn Reson Med* **50**, 1077-1088.

[39] Jenkinson M, Smith S (2001) A global optimisation method for robust affine registration of brain images. *Med Image Anal* **5**, 143-156.

[40] Fellgiebel A, Muller MJ, Wille P, Dellani PR, Scheurich A, Schmidt LG, Stoeter P (2005) Color-coded diffusion-tensor-imaging of posterior cingulate fiber tracts in mild cognitive impairment. *Neurobiol Aging* **26**, 1193-1198.

[41] Salat DH, Tuch DS, van der Kouwe AJ, Greve DN, Pappu V, Lee SY, Hevelone ND, Zaleta AK, Growdon JH, Corkin S, Fischl B, Rosas HD (2008) White matter pathology isolates the hippocampal formation in Alzheimer's disease. *Neurobiol Aging*.

[42] Zhang Y, Schuff N, Jahng GH, Bayne W, Mori S, Schad L, Mueller S, Du AT, Kramer JH, Yaffe K, Chui H, Jagust WJ, Miller BL, Weiner MW (2007) Diffusion tensor imaging of cingulum fibers in mild cognitive impairment and Alzheimer disease. *Neurology* **68**, 13-19.

[43] Camara E, Bodammer N, Rodriguez-Fornells A, Tempelmann C (2007) Age-related water diffusion changes in human brain: a voxel-based approach. *Neuroimage* **34**, 1588-1599.

[44] Rose SE, Chen F, Chalk JB, Zelaya FO, Strugnell WE, Benson M, Semple J, Doddrell DM (2000) Loss of connectivity in Alzheimer's disease: an evaluation of white matter tract integrity with colour coded MR diffusion tensor imaging. *J Neurol Neurosurg Psychiatry* **69**, 528-530.

[45] Teipel SJ, Stahl R, Dietrich O, Schoenberg SO, Perneczky R, Bokde AL, Reiser MF, Moller HJ, Hampel H (2007) Multivariate network analysis of fiber tract integrity in Alzheimer's disease. *Neuroimage* **34**, 985-995.

[46] Honig LS, Mayeux R (2001) Natural history of Alzheimer's disease. *Aging (Milano)* **13**, 171-182.

[47] Braak H, Braak E (1990) Alzheimer's disease: striatal amyloid deposits and neurofibrillary changes. *J Neuropathol Exp Neurol* **49**, 215-224.

[48] Suva D, Favre I, Kraftsik R, Esteban M, Lobrinus A, Miklossy J (1999) Primary motor cortex involvement in Alzheimer disease. *J Neuropathol Exp Neurol* **58**, 1125-1134.

[49] Golaz J, Bouras C, Hof PR (1992) Motor cortex involvement in presenile dementia: report of a case. *J Geriatr Psychiatry Neurol* **5**, 85-92.

[50] Jagust WJ, Davies P, Tiller-Borcich JK, Reed BR (1990) Focal Alzheimer's disease. *Neurology* **40**, 14-19.

[51] Zecca L, Youdim MB, Riederer P, Connor JR, Crichton RR (2004) Iron, brain ageing and neurodegenerative disorders. *Nat Rev Neurosci* **5**, 863-873.

[52] Loeffler DA, Connor JR, Juneau PL, Snyder BS, Kanaley L, DeMaggio AJ, Nguyen H, Brickman CM, LeWitt PA (1995) Transferrin and iron in normal, Alzheimer's disease, and Parkinson's disease brain regions. *J Neurochem* **65**, 710-724.

[53] Bartzokis G, Sultzer D, Mintz J, Holt LE, Marx P, Phelan CK, Marder SR (1994) In vivo evaluation of brain iron in Alzheimer's disease and normal subjects using MRI. *Biol Psychiatry* **35**, 480-487.

[54] Frisoni GB, Prestia A, Rasser PE, Bonetti M, Thompson PM (2009) In vivo mapping of incremental cortical atrophy from incipient to overt Alzheimer's disease. *J Neurol* **256**, 916-924.

[55] Busatto GF, Diniz BS, Zanetti MV (2008) Voxel-based morphometry in Alzheimer's disease. *Expert Rev Neurother* **8**, 1691-1702.

[56] Chaim TM, Duran FL, Uchida RR, Perico CA, de Castro CC, Busatto GF (2007) Volumetric reduction of the corpus callosum in Alzheimer's disease in vivo as assessed with voxel-based morphometry. *Psychiatry Res* **154**, 59-68.

[57] Stoub TR, deToledo-Morrell L, Stebbins GT, Leurgans S, Bennett DA, Shah RC (2006) Hippocampal disconnection contributes to memory dysfunction in individuals at risk for Alzheimer's disease. *Proc Natl Acad Sci U S A* **103**, 10041-10045.

[58] Villain N, Desgranges B, Viader F, de la Sayette V, Mezenge F, Landeau B, Baron JC, Eustache F, Chetelat G (2008) Relationships between hippocampal atrophy, white matter disruption, and gray matter hypometabolism in Alzheimer's disease. *J Neurosci* **28**, 6174-6181.

[59] Peters A, Moss MB, Sethares C (2000) Effects of aging on myelinated nerve fibers in monkey primary visual cortex. *J Comp Neurol* **419**, 364-376.

[60] Peters A, Sethares C (2002) Aging and the myelinated fibers in prefrontal cortex and corpus callosum of the monkey. *J Comp Neurol* **442**, 277-291.

[61] Wozniak JR, Lim KO (2006) Advances in white matter imaging: a review of in vivo magnetic resonance methodologies and their applicability to the study of development and aging. *Neurosci Biobehav Rev* **30**, 762-774.

[62] Brun A, Gustafson L, Englund E (1990) Subcortical pathology of Alzheimer's disease. *Adv Neurol* **51**, 73-77.

[63] Iwamoto N, Nishiyama E, Ohwada J, Arai H (1997) Distribution of amyloid deposits in the cerebral white matter of the Alzheimer's disease brain: relationship to blood vessels. *Acta Neuropathol* **93**, 334-340.

[64] Xu J, Chen S, Ahmed SH, Chen H, Ku G, Goldberg MP, Hsu CY (2001) Amyloid-beta peptides are cytotoxic to oligodendrocytes. *J Neurosci* **21**, RC118.

[65] Thal DR, Rub U, Orantes M, Braak H (2002) Phases of A beta-deposition in the human brain and its relevance for the development of AD. *Neurology* **58**, 1791-1800.

[66] Higuchi M, Lee VM, Trojanowski JQ (2002) Tau and axonopathy in neurodegenerative disorders. *Neuromolecular Med* **2**, 131-150.

[67] Lee VM, Daughenbaugh R, Trojanowski JQ (1994) Microtubule stabilizing drugs for the treatment of Alzheimer's disease. *Neurobiol Aging* **15(Suppl 2)**, S87-S89.

[68] Braak H, Braak E, Bohl J (1993) Staging of Alzheimer-related cortical destruction. *Eur Neurol* **33**, 403-408.

Diffusion Tensor Imaging (DTI) Based Individual Prediction of Cognitive Decline in Mild Cognitive Impairment Using a Support Vector Machine Analysis

Sven Haller[a,*], Duy Nguyen[a], Cristelle Rodriguez[b], Joan Emch[b], Gabriel Gold[c], Andreas Bartsch[d], Karl O. Lovblad[a] and Panteleimon Giannakopoulos[b,e]

[a]*Service Neuro-diagnostique et Neuro-interventionnel DISIM, University Hospitals of Geneva, Geneva, Switzerland*
[b]*Division of Geriatric Psychiatry, Department of Psychiatry, University Hospitals of Geneva and Faculty of Medicine, University of Geneva, Geneva, Switzerland*
[c]*Department of Rehabilitation and Geriatrics, University Hospitals of Geneva, and Faculty of Medicine, University of Geneva, Geneva, Switzerland*
[d]*Department of Neuroradiology, University Hospital of Heidelberg, Heidelberg, Germany*
[e]*Division of Old Age Psychiatry (PG), University of Lausanne School of Medicine, Lausanne, Switzerland*

Abstract. The aim of this study was to predict further cognitive decline in mild cognitive impairment (MCI) using an individual level support vector machine (SVM) classification analysis of white matter derived from diffusion tensor imaging (DTI).

Thirty-five healthy controls (HC) and 67 MCI subjects had DTI at baseline. MCI subjects were neuropsychologically followed for after one year and categorized into 40 stable (sMCI; 9 single domain amnestic, 7 single domain frontal, 24 multiple domain) and 27 progressive (pMCI; 7 single domain amnestic, 4 single domain frontal, 16 multiple domain). Fractional anisotropy (FA), longitudinal (LD), radial (RD) and mean (MD) diffusivity were assessed using Tract-Based Spatial Statistics (TBSS). Statistical analyses included both group comparisons and individual classification using SVM using 10 fold cross validation.

FA was significantly higher in HC compared to MCI in a distributed network including the ventral part of the corpus callosum, right temporal and frontal pathways. There were no significant group-level differences between sMCI versus pMCI or between MCI subtypes after correction for multiple comparisons. SVM analysis allowed for an individual classification with accuracies up to 91.4% (HC versus MCI) and 98.4% (sMCI versus pMCI). When considering the MCI subgroups separately, the minimum SVM classification accuracy for stable versus progressive cognitive decline was 97.5% in the multiple domain MCI group.

SVM analysis of DTI data provided highly accurate individual prediction of cognitive decline in MCI regardless of MCI subtype, indicating that this method may become an easily applicable tool for early individual detection of MCI subjects evolving to dementia.

Keywords: MCI, TBSS, SVM, FA, DTI

*Correspondence to: Dr. Sven Haller, M.Sc., Service Neuro-diagnostique et Neuro-interventionnel DISIM, Hôpitaux Universitaires de Genève, Rue Gabrielle Perret-Gentil 4, 1211 Genève 14, Switzerland. Tel.: +41 (0) 22 37 23311; Fax: +41 (0) 22 37 27072; E-mail: sven.haller@hcuge.ch.

ABBREVIATIONS

DTI	diffusion tensor imaging
FA	fractional anisotropy
GM	grey matter

HC	healthy control
LD	longitudinal diffusivity
MCI	mild cognitive impairment
MD	mean diffusivity
MRI	magnetic resonance imaging
MVPA	multi vector pattern analysis
pMCI	progressive MCI
RBF	radial basis function
RD	radial diffusivity
ROI	region of interest
sMCI	stable MCI
SMO	sequential minimal optimization
SVM	support vector machine
TBSS	tract-based spatial statistics
WM	white matter

INTRODUCTION

Mild cognitive impairment (MCI) was originally conceived as a functionally non-disabling amnestic disorder that has been later on expanded to include essentially any form of cognitive complaint [1]. The effect of an intervention on the conversion rate from MCI to AD has become a paradigm for assessing possible neurobiological modifiers early in the course of the disease. Although there are currently no proven disease-modifying treatments for Alzheimer disease (AD), several promising candidates are to date evaluated (for review see [2, 3]). However, recent studies pointed to the limited performance of some of these curative strategies in patients with clinically overt dementia [4, 5]. Not all MCI evolve to AD or decline at identical rates and a significant proportion of cases remain stable for several years or even improve (for review see [6]). Based on this observation, several research groups attempted to identify structural neuroimaging markers that could predict at baseline the subsequent cognitive decline within this diagnostic category. The most common approach that has been taken up in previous investigations consisted on group comparisons of grey matter (GM) volumes based on magnetic resonance imaging (MRI) in restricted cortical areas such as the hippocampus or entorhinal cortex (for review see [7]). As a complement to region of interest (ROI)-based volumetry, several studies implemented either semi-manual volume segmentation (for example [8, 9]), or automatic voxel-based morphom-

etry (VBM) [10] providing an analysis of the GM concentration across the entire brain (for example [11–16]). A series of voxel-based morphometric studies revealed volume differences between MCI and controls mainly distributed within the precuneus and cingulate gyrus (for review see [17]). More recently, multivariate models such as principal component analysis, structural equation modeling and support vector machine (SVM) [18] were used to provide individual risk scores for MCI conversion to AD on the basis of GM VBM data [17, 19–22].

Despite the fact that cortico-cortical disconnection is thought to be a main determinant of clinically overt dementia (for review see [23]), only a few studies explored the structural changes occurring in white matter (WM) in MCI. Diffusion tensor imaging (DTI) is a MRI technique that allows for the interrogation of the microstructural integrity of white matter. Fractional anisotropy (FA) is estimated from diffusion tensor imaging (DTI) [24] and correlates with the integrity of white matter fiber bundles [25]. Earlier studies on DTI FA in MCI can be separated into three main categories: ROI-based [26–37], voxel-based [38–41] and recently introduced Tract-Based Spatial Statistics (TBSS), an improved voxel-based technique [42–44]. These contributions documented the presence of reduced FA primarily in white matter tracts with homogeneously oriented fibers (i.e. genu or splenium of the corpus callosum, superior longitudinal fasciculus, cingulus) and more rarely in frontal, parietal and temporal white matter. However, other studies led to negative data challenging this point of view (for review see [45]).

To date and unlike the recent GM-focusing reports, there are no longitudinal studies addressing the utility of the DTI as an assessment tool for individual prediction of MCI rapid cognitive decline. We report here the results of a DTI-TBSS analysis in 35 HC and 67 MCI individuals who were neuropsychologically followed-up after one year (2 drop-outs at follow-up). The present data reveal that the assessment of white matter tract changes at baseline provides a highly accurate discrimination between cases that remain cognitively stable (sMCI) and those which displayed progressive cognitive deficits at follow-up (pMCI). Despite the known morphometric differences between MCI subtypes (amnestic, frontal and multiple domain), we deliberately included all MCI subtypes because a potentially clinically useful individual classifier should correctly discriminate sMCI versus pMCI regardless of MCI subtype.

METHODS AND MATERIALS

Subjects

After formal approval of the local Ethics Committee, informed written consent was obtained from all participants prior to inclusion in this study. Both MCI and healthy controls (HC), with a high school degree or equivalent, were recruited in Geneva and Lausanne counties through advertisements in local newspapers. All participants had normal or corrected-to-normal visual acuity, and none reported a history of sustained head injury, or neurological or psychiatric disorders. All participants with regular use of psychotropics, stimulants and β-blockers as well as those with severe physical illness that precludes the participation in either phase of the project were excluded.

All individuals were first screened with the Mini Mental State Examination (MMSE) [46]. The neuropsychological assessment included the MMSE orientation items, memory Digit Span Forward [47], Corsi Block-Tapping Test [48], Buschke double memory test [49], Shapes test [50], Verbal Fluency test [51] Trail Making test part B [52], Wisconsin Card Sort test (WCST, [53]), Boston Naming test [54], tests of ideomotor [55], reflexive [56] and constructional praxis [57], and Ghent Overlapping Figure test [58]. Attention was assessed with the WAIS-R, Code [59] and Trail Making Test part A [52]. Global cognitive function was assessed with the Clinical Dementia Rating scale (CDR, [60]). Cases with CDR 0 and test scores compatible with the age appropriate mean in all tests were classified as HC ($n = 35$, 26 women, mean age 63.7 ± 5.1 years).

Subjects with MMSE scores between 25 and 28 were considered as possible MCI cases. Subsequently, these cases underwent an additional clinical evaluation, which included the Hospital Anxiety and Depression Scale (HAD, [61]) and Lawton's Instrumental Activities of Daily Living (IADL, [62]). Depressive co-morbidity was excluded on the basis of a Hospital Anxiety and Depression Scale score consistently equal or more than 8. All individuals having a test score more than 1.5 SD below the age and education level adjusted mean in any of the above tests and a CDR score of 0.5 but no dementia, were diagnosed as possible MCI [63]. Among these cases, 16 had single domain amnestic MCI. All of them displayed decreased performances in the Buschke Double Memory Test and at least in one among the Shapes test,

Digit Span Forward test, and Corsi Block Tapping test. Eleven cases had single domain frontal MCI. All of them displayed decreased performances in the Trail Making test B and/or in WCST test. The remaining 40 cases had multiple domain MCI characterized by impaired performances in the Verbal Fluency test, Trail Making test, and WCST test as well as in one among the Shapes test, Corsi Block Tapping test, and Digit Span Forward test [64]. Two highly experienced clinicians blinded to each other's findings reviewed these cases independently. Subjects were only included in the MCI group if both clinicians concurred on this diagnosis.

The final sample included 67 MCI cases (38 women, mean age: 65.0 ± 5.1 years), which underwent a detailed neuropsychological follow-up evaluation 1 year after inclusion using the same neuropsychological battery. Upon follow-up, subjects were considered to have progressed and were included in the pMCI group if: (1) they exhibited a significant deterioration (defined as ≥ 1.0 SD compared to inclusion values) in one memory test and at least one among the other neuropsychological tests, and (2) they showed clinically deterioration based on the review of all the neuropsychological tests by an independent physician highly experienced in cognitive disorders who was blinded to the scope of the study. Subjects were considered stable and included in the sMCI group if (1) they exhibited no or marginal changes in their neuropsychological performances upon follow-up (test result improved or decreased <1.0 SD compared to inclusion values), and (2) they were considered to be clinically stable by the independent physician who reviewed the neuropsychological data.

MR imaging

MR imaging was performed at baseline on a 3.0 T clinical routine whole body scanner (Magnetom Trio, Siemens, Erlangen, Germany). We used a standard DTI sequence: 12 diffusion directions isotropically distributed on a sphere, 1 B0 image with no diffusion weighting, $128 \times 128 \times 64$ matrix, $1.8 \times 1.8 \times 2.0$ mm voxel size, echo time TE 76 ms, repetition time TR 7800 ms, 1 average. Additional sequences (T1 w, T2 w, FLAIR) were acquired and analyzed to exclude brain pathology such as ischemic stroke, subdural hematomas or space-occupying lesions. In particular, white matter lesions were analyzed according to the Fazekas score [65].

Statistical analysis

Demographic and clinical data

Demographic and clinical characteristics, neuropsychological values as well as the Fazekas score at baseline were compared between groups HC, pMCI and sMCI using non-parametric Kruskal-Wallis group test and pair-wise post test if overall $p < 0.05$ using Dunn's Multiple Comparison test. Cognitive changes over time within the pMCI and sMCI groups were assessed using the Wilcoxon matched-pairs signed-ranks test.

DTI TBSS FA analysis

Pre-processing of the FA data was carried out using standard procedure of TBSS (Tract-Based Spatial Statistics) including Eddy current and distortion correction, as described in detail before [66, 67] in the FSL software package [68]. In principle, TBSS projects all subjects' FA data onto a mean FA tract skeleton using non-linear registration. The tract skeleton is the basis for voxel-wise cross-subject statistics and reduces potential misregistrations as the source for false-positive or -negative analysis results. The other DTI derived parameters longitudinal (LD), radial (RD) and mean (MD) diffusivity were analyzed in the same way using spatial transformation parameters that were estimated in the initial FA analysis. For MCI versus HC comparisons, we performed a voxel-wise statistical analysis with correction for multiple comparisons implementing threshold-free cluster enhancement (TFCE) considering fully corrected *p*-values <0.05 as significant [69]. Age and gender were used as covariates in the analyses. We used the JHU ICBM white matter tractography atlas, which is distributed in the FSL package, for anatomic labeling of the supra-threshold voxels. For sMCI versus pMCI comparisons, there were no supra-threshold voxels after TCFE correction at *p* corrected <0.05.

SVM individual classification analysis

The individual classification was analyzed in the WEKA software package (http://www.cs.waikato.ac.nz/ml/weka, Version 3.6.1). This freely available tool is highly flexible and versatile, and includes for example numerous classifiers not only from the SVM type but also for example J48 as an example for a tree classifier [70]. After conversion of the pre-processed DTI FA data in a WEKA compatible data format, separate analyses were performed for the differences between HC and MCI as well as within the MCI group (sMCI

versus pMCI). We additionally performed the analysis between stable versus progressive cognitive decline separately in each MCI subgroup. All TBSS preprocessed 149 259 voxels were taken into account. The analysis included two steps. In a first step, we performed a feature selection. The rationale behind this step is that not all voxels discriminate between groups. On the one hand, inclusion of non-discriminative voxels results in overlapping features (or voxels), which reduces the accuracy of the classification. On the other hand, exclusion of discriminative features also reduces the accuracy of the classification. To identify the optimum number of voxels, we used the feature selection algorithm "Relieff" [71]. In principle, this method chooses features (or voxel) that most distinguish between classes. These are known as the relevant features. At each step of an iterative process, an instance x is chosen at random from the dataset and the weight for each feature is updated according to the distance of x to its Nearmiss and NearHit. For each comparison, we selected the top 100, 250, 500, 750 and 1000 features implementing 10 fold cross validation. The second step consisted of the "actual" classification analyses for each comparison using the SVM algorithm "sequential minimal optimization" SMO [72] (distributed in the WEKA package) with a radial basis function (RBF) kernel [73]. We chose the commonly used RBF kernel, which nonlinearly maps samples into a higher dimensional space. Unlike linear kernels, RBF can handle the case when the relation between class labels and attributes is nonlinear. There are two parameters while using RBF kernels: C and GAMMA. GAMMA represents the width of the radial basis function, and C represents the error/trade-off parameter that adjusts the importance of the separation error in the creation of the separation surface. It is not known beforehand which parameters are best for a given analysis. Consequently, we determined the optimal values of these two constants using a grid search with C between 0.01 and 1.00 and GAMMA iteratively explored from the value of 0.01 to 0.09. We used a ten fold cross validation technique, which divided the data into 10 parts. Nine parts were used for training, and one part for testing. This was done 10 times, such that each part was once used for testing. We repeated this whole procedure 10 times to further reduce variation related to data selection. We present the average accuracy of 10 repetitions of 10 fold cross validations for the best parameter settings. For technical reasons, the reported sensitivity and specificity values are only based only on single repetitions using 10 fold cross validation.

RESULTS

Clinical data

Demographic and clinical characteristics did not differ at inclusion between groups (Table 1). Two MCI cases were lost upon follow-up, which took place one year after baseline assessment (range 1.03 ± 0.17 years). The progressive MCI (pMCI) group consisted of twenty-seven (40.3%) cases showing significant deterioration in MMSE ($p < 0.001$), executive functions (Verbal Fluency test, $p < 0.05$), working memory (Digit Span Forward test, $p < 0.05$) and episodic memory (Shapes test $p < 0.05$). This group included 7 single domain amnestic, 4 single domain frontal, and 16 multiple domain MCI cases. In seven among the pMCI cases, the clinical diagnosis of dementia was made according to the DSM-IV criteria. The remaining 40 cases (59.7%) showed no significant changes in cognitive functions (stable MCI, sMCI; 9 single domain amnestic, 7 single domain frontal, 24 multiple domain). The sMCI showed a significant improvement from inclusion to follow-up in executive functions (Verbal Fluency test and Trail Making test B, $p < 0.05$), attention (Trail Making test A, $p < 0.05$), episodic memory (Buschke double memory test, CR imm $p < 0.05$ and CR tot $p < 0.005$), probably related to re-test learning (Table 2). Compared to baseline assessment, this group displayed decreased performances only in one test of executive functions (Verbal Fluency test, $p < 0.05$).

TBSS group differences

There were significantly lower FA values in MCI cases compared to HC in a large distributed network, most pronounced in the ventral part of the corpus callosum and the right temporal and frontal WM pathways including the inferior longitudinal and uncinate fasciculi, and the parahippocampal white matter. Additional structures involved were the internal and external capsule, predominantly on the right, the superior and middle cerebellar peduncle, predominantly on the left, and the cerebellar white matter bilaterally. There was no supra-threshold difference in LD, RD or MD between HC and MCI cases. The inverse comparison of MCI versus HC also yielded no supra-threshold voxels (see Fig. 1, Table 3). The FA differences between HC and MCI cases persisted when adjusting for age and gender. No additional structures with significant group differences were identified in these multivariate models. The comparison between sMCI versus pMCI yielded no supra-threshold differences (FA, LD, RD and MD) after TFCE correction for multiple comparisons. There were no significant differences in Fazekas scores between groups (HC 0.97 ± 0.82, sMCI 0.95 ± 0.78, pMCI 1.18 ± 0.88). In particular, this was the case in all areas where significant FA group differences were identified in our TBSS analysis.

SVM individual classification analysis

The best individual classification accuracies based on DTI FA were 91.4% for the distinction between MCI and HC and 98.4% for that between sMCI and pMCI (see Table 4). Considering one SVM classifier for all MCI subgroups, the classification accuracy per subgroup were >97% in multiple domain MCI, >99% in single domain frontal and >99% in single domain amnestic MCI. These results were replicated when using three separate SVMs for the three MCI subtypes. The spatial distribution of the most discriminative voxels of the SVM analysis is illustrated in Fig. 2.

DISCUSSION

White matter track changes are widely present in the brain of MCI individuals and affect both homogeneously distributed fibers within the corpus callosum and longitudinal fasciculus as well as axons in the parahippocampal white matter known to be particularly vulnerable in the course of the neurodegenerative

Table 1
Demographic and clinical characteristics of EC, sMCI, pMCI and AD cases at inclusion

Variable	HC ($n = 35$)	sMCI ($n = 40$)	pMCI ($n = 27$)	Group differences
Age (years)	63.7 ± 5.1	65.4 ± 5.4	64.4 ± 4.6	0.1979
Gender (f/m)	26/9	23/17	15/12	0.2196
Education*	2.1 ± 0.8	1.9 ± 0.8	2 ± 0.7	0.8182
MMSE[¶]	28.9 ± 1.0	28.1 ± 1.2	28.1 ± 2.2	0.0517
IADL[†]	8.4 ± 0.7	8.3 ± 1.1	8.4 ± 0.7	0.9956
HAD[‡] (anxiety)	5 ± 2.3	5.2 ± 3.2	6.2 ± 3.2	0.4335
HAD[‡] (depression)	1.9 ± 1.8	2 ± 2.2	2.2 ± 1.8	0.6307

Data are presented as mean $\pm$ SD. * Education levels from 1 to 3; [¶] MMSE, Mini-mental state examination; [†] Lawton's instrumental activities of daily living score; [‡] Hospital anxiety and depression scales (cut off of 8 for both anxiety and depression). There were no significant differences in demographic and clinical variables between HC, sMCI and pMCI cases.

Table 2
Neuropsychological data for sMCI and pMCI cases at inclusion and follow-up

Variables	sMCI ($n = 40$)			pMCI ($n = 27$)		
	Inclusion	Follow-up	p	Inclusion	Follow-up	p
Global assessment						
MMSE	28.1 ± 1.2	28.1 ± 1.3	0.8747	**28.1 ± 2.2**	**26.7 ± 2.1**	**0.0004**
Executive functions						
Verbal Fluency	**22.1 ± 6.7**	**20.6 ± 7.6**	**0.0209**	*22.2 ± 6.0*	*19.3 ± 6.3*	**0.0219**
Trail Making Test B (sec)	*78.4 ± 32.9*	*66.6 ± 23.6*	*0.0120*	81.8 ± 41.0	77.4 ± 28.3	0.5213
WCST	4.5 ± 2.0	5.2 ± 1.5	0.0618	4.5 ± 1.9	4.4±.21	0.3828
Language abilities						
Boston Naming Test	19.1 ± 0.8	19.2 ± 1.2	0.8655	19.4 ± 0.9	19.0 ± 1.4	0.1531
Standardized praxis						
Ideomotor praxis transitive	9.2 ± 1.1	9.2 ± 1.1	0.4168	9.6 ± 0.6	9.1 ± 1.1	0.0637
Ideomotor praxis intransitive	19.0 ± 1.9	19.2 ± 1.3	0.8403	19.0 ± 1.2	18.8 ± 1.3	0.2017
Reflexive praxis	7.2 ± 1.0	7.1 ± 1.0	0.7100	7.1 ± 0.9	7.0 ± 1.1	0.4605
Constructive praxis	10.7 ± 0.8	10.8 ± 0.5	0.3008	10.8 ± 0.6	10.6 ± 0.7	0.1250
Gnosis						
Ghent Overlapping Figures Test	5.0 ± 0.0	5.0 + 0.0	NA	5.0 ± 0.0	5.0 + 0.0	NA
Attention						
Code	55.5 ± 12.7	55.5 ± 13.1	0.9303	55.3 ± 14.0	55.6 ± 14.7	0.4040
Trail Making Test A (sec)	*44.5 ± 17.0*	*38.9 ± 11.4*	*0.0350*	46.9 ± 13.4	42.7 ± 15.1	0.0665
Working Memory						
Digit Span Forward	6.7 ± 2.0	6.8 ± 1.7	0.7018	**6.4 ± 1.8**	**5.8 ± 1.5**	**0.0245**
Corsi Blocks	4.9 ± 1.4	4.9 ± 1.3	0.8798	4.9 ± 1.9	4.7 ± 1.5	0.2596
Episodic Memory						
Buschke double memory test (48 items)						
Recognition	47.9 ± 0.4	48.0 ± 0.2	0.5000	48.0 ± 0.0	47.9 ± 0.4	NA
CR immediate	*38.1 ± 5.5*	*39.9 ± 4.4*	*0.0169*	38.4 ± 6.6	39.8 ± 4.9	0.1180
CR total	*22.6 ± 5.5*	*24.6 ± 5.1*	*0.0050*	22.6 ± 5.3	23.3 ± 6.4	0.4547
Intrusions	3.7 ± 3.1	3.7 ± 3.1	0.9210	4.1 ± 4.0	4.9 ± 4.2	0.1203
Shapes Test	11.3 ± 1.3	11.4 ± 1.6	0.1361	**11.4 ± 1.1**	**10.7 ± 1.8**	**0.0302**

Data are presented as mean ± SD. MMSE, Mini-mental state examination; Verbal Fluency; Trail Making Test B; WSCT, Wisconsin Card Sort Test; Boston Naming Test; Ideomotor praxis transitive; Ideomotor praxis intransitive; Constructive praxis, CERAD, Consortium to Establish a Registry for Alzheimer's disease; Ghent Overlapping Figures Test; Code, WAIS-R, Wechsler adult intelligence scale, revised; Trail Making Test A; Digit Span Forward; Corsi Blocks, Corsi Block Tapping Test; Buschke double memory test (48 items): Rec, Recognition; CR imm, Cued Recall immediate; CR tot, Cued Recall total; Intr, Intrusions; Shapes Test: LTR shapes, long term recall shapes. Italic characters were used for significant improvement of performances; bold characters indicate significant neuropsychological decline.

process. Most importantly, they reveal that the automatic assessment of white matter integrity using DTI-TBSS provide a highly accurate tool for the prediction of rapid cognitive deterioration in MCI. We were able to discriminate sMCI from pMCI with an accuracy of up to 98%.

Group analysis

As a first step, a group level analysis was performed to identify the spatial distribution of differences in white matter between MCI versus controls, and between sMCI and pMCI. Overall, the regional distribution of observed decrease in FA in MCI compared to controls confirms the vulnerability of interhemispheric and intrahemispheric corticocortical connections in MCI as already described by Lee and collaborators

[41]. As in most recent ROI and voxel-based DTI studies, white matter tracts with homogeneously oriented fibers in the ventral part of corpus callosum display a significant decrease of FA in MCI compared to HC cases [33, 34, 36, 37, 74, 75]. This area concentrates the main interhemispheric long association fibers that originate primarily from large pyramidal neurons known to be prone to NFT formation (for review see [23]). Interestingly, our data show that among fibers with intermediate anisotropy, temporal and frontal white matter pathways, i.e. the right uncinate and inferior longitudinal fasciculi involved in memory performances [76] display the more pronounced loss of FA in MCI cases [77]. To date, only three TBSS studies attempted to explore DTI patterns in limited series of MCI cases [42–44]. The study by Damoiseaux et al. [43] focused on AD cases and included only 8 MCI cases with-
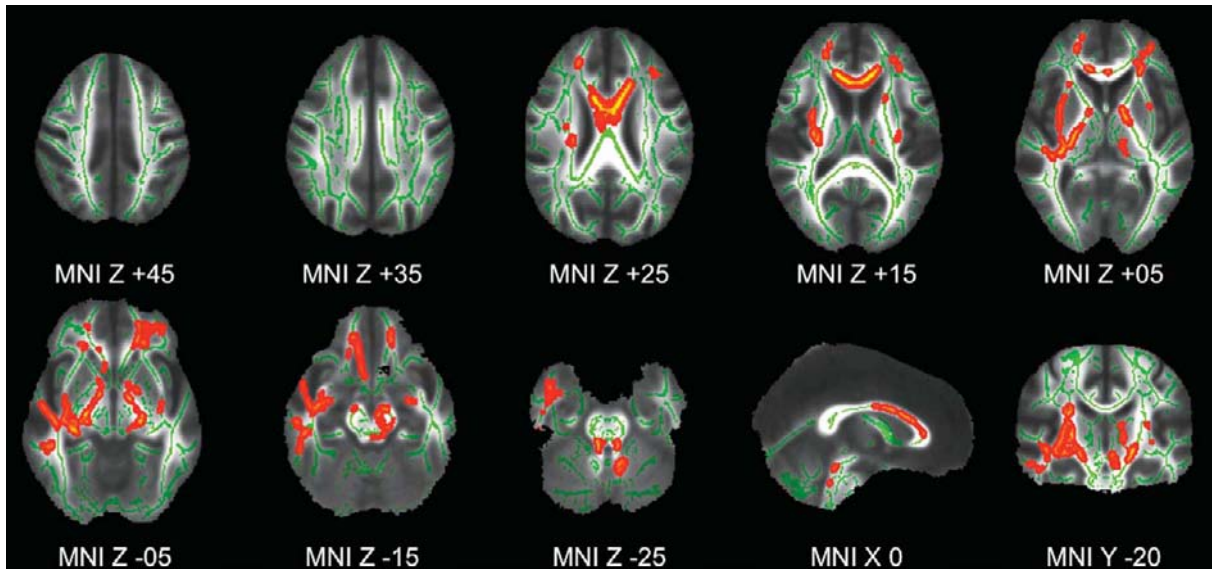
Fig. 1. Tract-Based Spatial Statistics (TBSS) analysis between healthy controls (HC) and mild cognitive impairment (MCI). HC subjects had significantly higher FA in a distributed network, most pronounced in the ventral part of the corpus callosum and the right temporal and frontal WM pathways in the parahippocampal white matterincluding the inferior longitudinal and uncinate fasciculi (red-yellow indicates level of significance). The inverse comparison of MCI versus HC yielded no supra-threshold differences. Axial, mid-saggital and coronal slices at the indicated position in MNI (Montreal Neurological Institute) standard space coordinates (radiological convention with right hemisphere on left hand side). Grey: mean FA value, green: average skeleton, red: HC > MCI Threshold-Free Cluster Enhancement (TFCE) corrected for multiple comparisons at $p < 0.05$. Supra-threshold voxels were enlarged using TBSS fill (part of FSL) for illustrative purposes.

out definite conclusions. Liu and collaborators [42] analyzed 27 MCI cases and detected significant FA decreases in the same corticocortical circuits. As some previous ROI and voxel-based studies, these authors reported additional FA decreases in the parahippocampal white matter and cingulum [27, 31, 32, 38, 75]. An FA decrease in these areas was also found for suprathreshold voxels in our larger MCI series, yet it was less pronounced than that of the ventral part of the corpus callosum and front-temporal WM pathways.

In agreement with the recent study of Bosch and colleagues [44], our data indicate that FA is a more sensitive DTI parameter than longitudinal (LD), radial (RD) or mean (MD) diffusivity for the distinction between MCI and HC cases. Another recent TBSS study assessing the same diffusion parameters in clinically overt AD cases compared to HC led to opposite results [78]. The few available recent investigations on the different diffusion parameters in normal aging, MCI and AD [44, 78–81] demonstrated regional differences in the distribution of significant changes in the different diffusion parameters FA, LD, RD and MD. These available studies are partially controversial. For example in a study of MCI and AD subjects

FA was closer related to the cognitive profile than LD or RD. In contrast, another study in AD showed stronger differences in LD, RD and MD as compared to FA, suggesting that FA is the least sensitive diffusion parameter [78]. This discordance implies that the sensitivity of the different diffusion parameters may vary substantially as a function of the disease severity. Research using these different diffusion indices is still at an early stage, as is our understanding of the relevance of LD and RD changes in terms of myelin or axonal damage. For example, wallerian degeneration suggested by increased mean diffusivity without significant changes in FA may take place only in advanced stages of the degenerative process. Future work is needed to determine the evolution of changes of these different diffusion parameters in aging, MCI and AD, and to improve our understanding how axonal and myelin changes are related to possibly specific patterns of these different diffusion parameters.

SVM individual classification analysis

As a second step, an individual level classification analysis was performed in order to obtain individual

Table 3

List of supra-threshold clusters (TFCE corrected at $p < 0.05$) for the comparison of MCI versus HC in univariate models. DTI FA: Controls versus MCI. Controls > MCI

No	Voxels	Max p-value	MAX X	MAX Y	MAX Z	COG X	COG Y	COG Z	Side	Anatomic structure
1	2917	0.97	38	−4	−23	32	−12	−4	Right	Uncinate fasciculus
									Right	Inferior longitudinal fasciculus
									Right	Corticospinal tract
									Right	Inferior fronto-occipital fasciculus
									Right	Anterior thalamic radiation
									Right	Superior longitudinal fasciculus
2	1772	0.97	−9	28	11	−1	16	20	Bilateral	Corpus callosum
									Bilateral	Forceps minor
									Bilateral	Cingulum
3	1525	0.95	−11	−42	−36	−12	−23	−13	Left	Uncinate fasciculus
									Left	Anterior thalamic radiation
									Left	Corticospinal tract
									Bilateral	Cerebellum
4	753	0.96	−14	36	−15	−24	40	−2	Left	Inferior Fronto-occipital fasciculus
									Left	Uncinate fasciculus
									Left	Anterior thalamic radiation
									Left	Forceps minor
5	363	0.95	49	−30	−15	50	−32	−13	Right	Inferior longitudinal fasciculus
									Right	Superior longitudinal fasciculus
6	316	0.95	21	43	13	20	46	13	Right	Forceps minor
7	167	0.96	7	23	−19	8	24	−16	Right	Uncinate fasciculus
8	165	0.95	9	41	−19	16	34	−11	Right	Uncinate fasciculus
									Right	Inferior fronto-occipital fasciculus
9	75	0.95	−31	31	22	−34	27	27	Left	Anterior thalamic radiation
									Left	Frontal
10	60	0.95	16	44	−12	18	45	−9	Right	Uncinate fasciculus
									Right	Inferior fronto-occipital fasciculus
11	58	0.95	−12	0	−10	−14	1	−7	Left	Corticospinal tract
									Left	Anterior thalamic radiation
12	53	0.95	−31	31	13	−31	35	18	Left	Anterior thalamic radiation
									Left	Frontal
13	45	0.95	7	16	−10	7	18	−8	Right	Forceps minor
									Right	Cingulum
14	42	0.95	−31	−18	7	−31	−16	12	Left	Superior longitudinal fasciculus
									Left	Corticospinal tract
15	22	0.95	−34	−9	−7	−34	−8	−3	Left	Inferior fronto-occipital fasciculus
16	13	0.95	−20	48	7	−19	48	9	Left	Forceps minor
17	12	0.95	−32	4	4	−31	6	6	Left	Uncinate fasciculus
18	9	0.95	−32	−13	−6	−33	−13	−5	Left	Inferior fronto-occipital fasciculus
19	5	0.95	−32	−21	0	−32	−21	0	Left	Inferior fronto-occipital fasciculus
20	4	0.95	59	−25	−11	59	−25	−11	Right	Superior longitudinal fasciculus
21	1	0.95	11	27	−13	11	27	−13	Right	Uncinate fasciculus
									Right	Forceps minor
22	1	0.95	5	8	−15	5	8	−15	Right	Frontobasal

Cluster index, number of supra-threshold voxels in cluster, maximum p-value, location of maximum p-value per cluster in MNI standard space (X, Y, Z) and centre of gravity of the cluster in NMI standard space (X, Y, Z).

discrimination between HC and MCI and most importantly between sMCI and pMCI. This classification analysis represents a fundamental change in paradigm compared to the established group level analyses, aiming to identify patterns of DTI changes, which may eventually contribute to the diagnosis of an individual patient in a clinical context. We adopted a complex methodology including a processing chain of TBSS

pre-processing of DTI FA data, feature selection of the most discriminative voxels, and subsequent SVM classification [17]. The classification accuracy of over 98% for stable versus progressive MCI in our series implies that on average across the 10 repetitions of the 10 fold cross validation, only one subject was incorrectly classified regardless of MCI subgroup. In the present study, the performance of the SVM classifi-

Table 4
Individual SVM classification based on DTI FA TBSS

Features (voxels)	HC vs MCI			sMCI vs pMCI		
	Accuracy (%)	Sensitivity (%)	Specificity (%)	Accuracy (%)	Sensitivity (%)	Specificity (%)
100	87.82	89.65	88.00	92.48	90.47	95.12
250	90.05	93.10	89.33	95.24	97.50	96.30
500	**91.36**	**90.32**	**90.41**	96.76	97.50	96.30
750	90.34	92.86	88.15	**98.38**	**97.56**	**100.00**
1000	84.22	95.00	80.95	95.9	93.02	100.00

Accuracy, sensitivity and specificity values for individual classifications using a SVM classifier. Note that the accuracy is calculated as average accuracy of 10 repetitions using 10 fold cross validation. For technical reasons, the sensitivity and specificity values are calculated on the basis of single repetitions using 10 fold cross validation. The different rows represent the number of features that were selected using a "Relieff" feature selection procedure (also using 10 fold cross validation). The optimum number of features is highlighted with bold characters. The highest accuracy for HC versus MCI was 91.36% using 500 features (voxels). The highest accuracy for sMCI versus pMCI was 98.38% using 750 features (voxels).
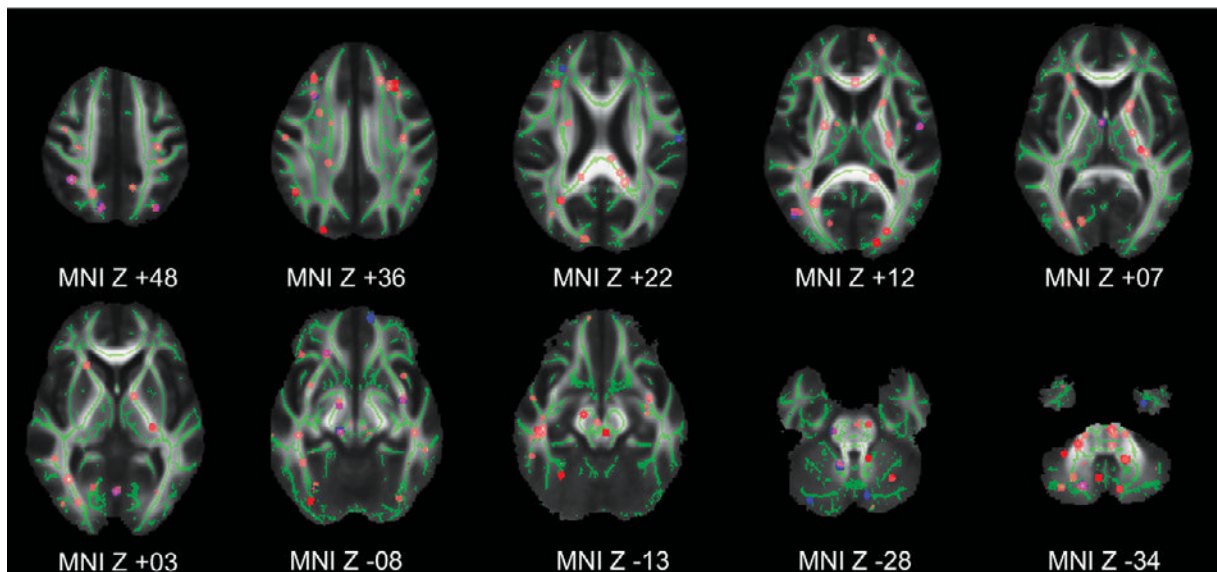

Fig. 2. Spatial distribution of the group level TBSS and the individual level SVM analyses for stable versus progressive MCI. There were no TFCE corrected supra-threshold voxels for the TBSS group analysis. The TBSS group level comparison of sMCI > pMCI (red) and pMCI > sMCI (blue) is displayed for illustrative purposes at an uncorrected threshold of $p < 0.001$. Additionally, the most discriminative voxels for the individual level SVM analysis identified using a feature selection are superimposed in pink. Despite the fundamentally different methods and considering the higher number of voxels for the SVM analysis (hence not all SVM voxels may have a corresponding TBSS voxel), there is a good overlap between the voxels for the group level TBSS and the individual level SVM analyses. Grey: mean FA value, green: average skeleton, radiological convention. Supra-threshold voxels were again enlarged using TBSS fill (part of FSL) for illustrative purposes.

cation for the different MCI subgroups was assessed using two different methods. The first possibility is to train only one SVM classifier with all MCI subgroups, and assess the performance of this classifier for each MCI subgroup separately. In our data, only one sMCI subject (multiple domain) was falsely classified as pMCI. This led to classification accuracy of over 97% for multiple domain MCI and a nearly perfect classification for single domain amnestic and single

domain frontal MCI. The second possibility is to use three separate SVM classifiers for the three different MCI subgroups. These results confirmed the extremely high accuracy values in multiple domain MCI subject (97.5%) and nearly perfect classification of single amnestic and single frontal cases. These separate SVM analyses for the MCI subgroups should however be considered with caution given the small sample sizes in particular for single domain amnestic and frontal

MCI subgroups. With respect to future clinical applications, our data suggest that one SVM classifier may be sufficient to discriminate stable versus progressive cases even if the neuropsychological profile of MCI subgroups is unknown at the time of SVM analysis.

Two previous studies successfully applied a SVM classifier to discriminate AD versus HC, with accuracies of 89% [19] and 94.5% [22]. More relevant in the context of the present investigation are three recent contributions that classified stable versus progressive MCI with accuracies of 75% [17], 81.5% [21] and 85% [20]. Unlike the present investigation that assessed WM tract changes, all of these studies were based on voxel-based morphometry (VBM) [10] analyses of grey matter (GM) concentration derived from T1 w images. In comparison to these data, our WM-based classification accuracies tend to be slightly higher based on the DTI FA data. This suggests that the disruption of axonal integrity might be a key determinant of subsequent cognitive decline in MCI. Supporting this possibility, two recent investigations in spinocerebellar ataxia and Friedreich ataxia [82, 83] showed a higher sensitivity of DTI TBSS compared to GM VBM in the early stages of the degenerative process. Similarly, a recent study assessing GM VBM and WM TBSS in early primary progressive multiple sclerosis pointed to the need of longitudinal studies to determine whether the GM atrophy precedes or follows the WM damage [84]. The presented SVM analysis of DTI TBSS data is not intended to replace, but to complement the previous classification studies, including SVM studies on GM VBM data. Future work is needed to develop methods to combine GM VBM and WM DTI analyses to obtain higher accuracy rates and more robust classification results.

At first glance, it might appear counterintuitive that the SVM individual classification was very successful in discriminating stable versus progressive MCI despite the absence of TFCE corrected supra-threshold differences for the corresponding TBSS group comparison. This can however be readily explained by the major conceptual differences of these techniques. For the group comparison, a *t*-value is computed for each voxel that is subsequently corrected to take into account the multiple comparisons of over 150000 voxels. Increasing the number of considered voxels augments the effect of multiple comparison correction. In the individual SVM analysis, the most discriminative voxels are selected using a feature selection algorithm. The number of additional, not selected voxels is thus irrelevant in this context. Moreover, the SVM analysis results in a single parameter per subject taking into account all included voxels without multiple comparison biases. Finally, the higher classification accuracy for the comparison of sMCI versus pMCI in relation to comparison of HC versus MCI can be explained by the more homogeneous group composition for the first comparison (considering only sMCI or pMCI). Combining all MCI subjects for the second comparison of HC versus MCI results in a more heterogeneous MCI group. The more homogeneous the group composition, the better the SVM classifier can differentiate between groups.

In other words, classification analyses combine specific patterns of differences to classify individual subjects. A specific pattern of multiple voxels might very well discriminate between groups, even though each individual voxel considered separately does not yield a significant difference at the group level. The spatial distribution of the discriminative voxels (Fig. 2) is thus of limited importance for the classification analyses. In fact, the spatial distribution of the most discriminative voxels is methodologically fundamentally different from the much more established spatial distribution of group-level analyses. This might be more evident in the example of face recognition. Due to variability between subjects, no feature of the face might show a significant difference in the group analysis. In contrast, the combination of e.g. lateral eyebrow, tip of the nose and chin may identify an individual face. Once again, this does not necessarily imply that these features are also significantly different at the group level analysis.

Limitations

Three limitations should be taken into account when interpreting the present data. First, in order to preserve statistical power, we did not perform separate analyses of our TBSS DTI data according to MCI subtypes. We cannot thus exclude that the patterns of TBSS comparisons between HC and MCI may be different in single domain amnestic, single domain frontal and multiple domain MCI [32, 75]. Second, the best classification data were obtained with nonlinear (RBF-kernel) SVM that does not provide an easy to interpret weight vector to identify the most discriminative brain areas. Third, the very high accuracy rates of individual classification exceeded our expectations. These values were obtained by a well established ten-fold cross validation where nine parts are used for training and the remaining part is used for testing the classifier [17]. Even though this

cross validation approach is a standard method in the field of machine learning/multi voxel pattern analysis and appropriate for the number of subjects of our study, the present results seem to be too optimistic, probably related to some degree of over-fitting of the data. Additional validation in larger independent datasets, which should be ideally acquired on different MR scanners, is warranted to confirm the present findings.

Conclusions

In the light of our observations, the DTI FA may become an applicable and clinically useful tool for the individual classification of stable versus progressive MCI. The high proportion of subject who already undergo brain MRI for dementia suspicion in routine clinical settings in combination with the short measurement time of DTI and potentially almost automatic post-processing of the data imply a potential benefit and clinical practicability of this objective and individual classifier which is universally applicable to single domain amnestic, single domain frontal and multiple domain MCI cases.

DISCLOSURE

No conflicts of interest.

ACKNOWLEDGMENTS

REFERENCES

[1] Petersen RC (2004) Mild cognitive impairment as a diagnostic entity. *J Intern Med* **256**, 183-194.

[2] Nitsch RM, Hock C (2008) Targeting beta-amyloid pathology in Alzheimer's disease with Abeta immunotherapy. *Neurotherapeutics* **5**, 415-420.

[3] Duara R, Barker W, Loewenstein D, Bain L (2009) The basis for disease-modifying treatments for Alzheimer's disease: the Sixth Annual Mild Cognitive Impairment Symposium. *Alzheimers Dement* **5**, 66-74.

[4] Holmes C, Boche D, Wilkinson D, Yadegarfar G, Hopkins V, Bayer A, Jones RW, Bullock R, Love S, Neal JW, Zotova E, Nicoll JA (2008) Long-term effects of Abeta42 immunisation in Alzheimer's disease: follow-up of a randomised, placebo-controlled phase I trial. *Lancet* **372**, 216-223.

[5] Lannfelt L, Blennow K, Zetterberg H, Batsman S, Ames D, Harrison J, Masters CL, Targum S, Bush AI, Murdoch R,

Wilson J, Ritchie CW (2008) Safety, efficacy, and biomarker findings of PBT2 in targeting Abeta as a modifying therapy for Alzheimer's disease: a phase IIa, double-blind, randomised, placebo-controlled trial. *Lancet Neurol* **7**, 779-786.

[6] Petersen RC, Negash S (2008) Mild cognitive impairment: an overview. *CNS Spectr* **13**, 45-53.

[7] Ferreira LK, Diniz BS, Forlenza OV, Busatto GF, Zanetti MV (2009) Neurostructural predictors of Alzheimer's disease: a meta-analysis of VBM studies. *Neurobiol Aging*, Epub ahead of print.

[8] Apostolova LG, Dinov ID, Dutton RA, Hayashi KM, Toga AW, Cummings JL, Thompson PM (2006) 3D comparison of hippocampal atrophy in amnestic mild cognitive impairment and Alzheimer's disease. *Brain* **129**, 2867-2873.

[9] Henneman WJ, Sluimer JD, Barnes J, van der Flier WM, Sluimer IC, Fox NC, Scheltens P, Vrenken H, Barkhof F (2009) Hippocampal atrophy rates in Alzheimer disease: added value over whole brain volume measures. *Neurology* **72**, 999-1007.

[10] Ashburner J, Friston KJ (2000) Voxel-based morphometry – the methods. *Neuroimage* **11**, 805-821.

[11] Scahill RI, Schott JM, Stevens JM, Rossor MN, Fox NC (2002) Mapping the evolution of regional atrophy in Alzheimer's disease: unbiased analysis of fluid-registered serial MRI. *Proc Natl Acad Sci U S A* **99**, 4703-4707.

[12] Karas GB, Burton EJ, Rombouts SA, van Schijndel RA, O'Brien JT, Scheltens P, McKeith IG, Williams D, Ballard C, Barkhof F (2003) A comprehensive study of gray matter loss in patients with Alzheimer's disease using optimized voxel-based morphometry. *Neuroimage* **18**, 895-907.

[13] Karas GB, Scheltens P, Rombouts SA, Visser PJ, van Schijndel RA, Fox NC, Barkhof F (2004) Global and local gray matter loss in mild cognitive impairment and Alzheimer's disease. *Neuroimage* **23**, 708-716.

[14] Karas G, Sluimer J, Goekoop R, van der Flier W, Rombouts SA, Vrenken H, Scheltens P, Fox N, Barkhof F (2008) Amnestic mild cognitive impairment: structural MR imaging findings predictive of conversion to Alzheimer disease. *AJNR Am J Neuroradiol* **29**, 944-949.

[15] Chupin M, Gerardin E, Cuingnet R, Boutet C, Lemieux L, Lehericy S, Benali H, Garnero L, Colliot O (2009) Fully automatic hippocampus segmentation and classification in Alzheimer's disease and mild cognitive impairment applied on data from ADNI. *Hippocampus* **19**, 579-587.

[16] Holland D, Brewer JB, Hagler DJ, Fenema-Notestine C, Dale AM, Weiner M, Thal L, Petersen R, Jack CRJ, Jagust W, Trojanowki J, Toga AW, Beckett L, Green RC, Gamst A, Potter WZ, Montine T, Anders D, Bernstein M, Felmlee J, Fox N, Thompson P, Schuff N, Alexander G, Bandy D, Koeppe RA, Foster N, Reiman EM, Chen K, Shaw L, Lee VM, Korecka M, Crawford K, Neu S, Harvey D, Kornak J, Kachaturian Z, Frank R, Snyder PJ, Molchan S, Kaye J, Vorobik R, Quinn J, Schneider L, Pawluczyk S, Spann B, Fleisher AS, Vanderswag H, Heidebrink JL, Lord JL, Johnson K, Doody RS, Villanueva-Meyer J, Chowdhury M, Stern Y, Honig LS, Bell KL, Morris JC, Mintun MA, Schneider S, Marson D, Griffith R, Badger B, Grossman H, Tang C, Stern J, Detoledo-Morrell L, Shah RC, Bach J, Duara R, Isaacson R, Strauman S, Albert MS, Pedroso J, Toroney J, Rusinek H, de Leon MJ, De Santi SM, Doraiswamy PM, Petrella JR, Aiello M, Clark CM, Pham C, Nunez J, Smith CD, Given CAn, Hardy P, Dekosky ST, Oakley M, Simpson DM, Ismail MS, Porsteinsson A, McCallum C, Cramer SC, Mulnard RA, McAdams-Ortiz C, Diaz-Arrastia R, Martin-Cook K, Devous

M, Levey AI, Lah JJ, Cellar JS, Burns JM, Anderson HS, Laubinger MM, Bartzokis G, Silverman DH, Lu PH, Fletcher R, Parfitt F, Johnson H, Farlow M, Herring S, Hake AM, van Dyck CH, Macavoy MG, Bifano LA, Chertkow H, Bergman H, Hosein C, Black S, Graham S, Caldwell C, Feldman H, Assaly M, Hsiung GY, Kertesz A, Rogers J, Trost D, Bernick C, Gitelman D, Johnson N, Mesulam M, Sadowsky C, Villena T, Mesner S, Aisen PS, Johnson KB, Behan KE, Sperling RA, Rentz DM, Johnson KA, Rosen A, Tinklenberg J, Ashford W, Sabbagh M, Connor D, Obradov S, Killiany R, Norbash A, Obisesan TO, Jayam-Truth A, Wang P, Auchus AP, Huang J, Friedland RP, Decarli C, Fletcher E, Carmichael O, Kittur S, Mirje S, Johnson SC, Borrie M, Lee TY, Asthana S, Carlsson CM, Potkin SG, Highum D, Preda A, Nguyen D, Tariot PN, Hendin BA, Scharre DW, Kataki M, Beversdorf DQ, Zimmerman EA, Celmins D, Brown AD, Gandy S, Marenberg ME, Rovner BW, Pearlson G, Blank K, Anderson K, Saykin AJ, Santulli RB, Pare N, Williamson JD, Sink KM, Potter H, Ashok Raj B, Giordano A, Ott BR, Wu CK, Cohen R, Wilks KL, Safirstein BE (2009) Subregional neuroanatomical change as a biomarker for Alzheimer's disease. *Proc Natl Acad Sci U S A* **106**, 20 954-20 959.

[17] Plant C, Teipel SJ, Oswald A, Bohm C, Meindl T, Mourao-Miranda J, Bokde AW, Hampel H, Ewers M (2010) Automated detection of brain atrophy patterns based on MRI for the prediction of Alzheimer's disease. *Neuroimage* **50**, 162-174.

[18] Noble WS (2006) What is a support vector machine? *Nat Biotechnol* **24**, 1565-1567.

[19] Kloppel S, Stonnington CM, Chu C, Draganski B, Scahill RI, Rohrer JD, Fox NC, Jack CRJ, Ashburner J, Frackowiak RS (2008) Automatic classification of MR scans in Alzheimer's disease. *Brain* **131**, 681-689.

[20] Fan Y, Batmanghelich N, Clark CM, Davatzikos C (2008) Spatial patterns of brain atrophy in MCI patients, identified via high-dimensional pattern classification, predict subsequent cognitive decline. *Neuroimage* **39**, 1731-1743.

[21] Misra C, Fan Y, Davatzikos C (2009) Baseline and longitudinal patterns of brain atrophy in MCI patients, and their use in prediction of short-term conversion to AD: results from ADNI. *Neuroimage* **44**, 1415-1422.

[22] Magnin B, Mesrob L, Kinkingnehun S, Pelegrini-Issac M, Colliot O, Sarazin M, Dubois B, Lehericy S, Benali H (2009) Support vector machine-based classification of Alzheimer's disease from whole-brain anatomical MRI. *Neuroradiology* **51**, 73-83.

[23] Morrison JH, Hof PR (2007) Life and death of neurons in the aging cerebral cortex. *Int Rev Neurobiol* **81**, 41-57.

[24] Le Bihan D, Mangin JF, Poupon C, Clark CA, Pappata S, Molko N, Chabriat H (2001) Diffusion tensor imaging: concepts and applications. *J Magn Reson Imaging* **13**, 534-546.

[25] Thomalla G, Glauche V, Koch MA, Beaulieu C, Weiller C, Röther J (2004) Diffusion tensor imaging detects early Wallerian degeneration of the pyramidal tract after ischemic stroke. *Neuroimage* **22**, 1767-1774.

[26] Fellgiebel A, Muller MJ, Wille P, Dellani PR, Scheurich A, Schmidt LG, Stoeter P (2005) Color-coded diffusion-tensor-imaging of posterior cingulate fiber tracts in mild cognitive impairment. *Neurobiol Aging* **26**, 1193-1198.

[27] Muller MJ, Greverus D, Weibrich C, Dellani PR, Scheurich A, Stoeter P, Fellgiebel A (2007) Diagnostic utility of hippocampal size and mean diffusivity in amnestic MCI. *Neurobiol Aging* **28**, 398-403.

[28] Huang J, Friedland RP, Auchus AP (2007) Diffusion tensor imaging of normal-appearing white matter in mild cognitive impairment and early Alzheimer disease: preliminary evidence of axonal degeneration in the temporal lobe. *AJNR Am J Neuroradiol* **28**, 1943-1948.

[29] Zhang Y, Schuff N, Jahng GH, Bayne W, Mori S, Schad L, Mueller S, Du AT, Kramer JH, Yaffe K, Chui H, Jagust WJ, Miller BL, Weiner MW (2007) Diffusion tensor imaging of cingulum fibers in mild cognitive impairment and Alzheimer disease. *Neurology* **68**, 13-19.

[30] Stahl R, Dietrich O, Teipel SJ, Hampel H, Reiser MF, Schoenberg SO (2007) White matter damage in Alzheimer disease and mild cognitive impairment: assessment with diffusion-tensor MR imaging and parallel imaging techniques. *Radiology* **243**, 483-492.

[31] Choo IH, Lee DY, Oh JS, Lee JS, Lee DS, Song IC, Youn JC, Kim SG, Kim KW, Jhoo JH, Woo JI (2010) Posterior cingulate cortex atrophy and regional cingulum disruption in mild cognitive impairment and Alzheimer's disease. *Neurobiol Aging* **31**, 772-779.

[32] Shim YS, Yoon B, Shon YM, Ahn KJ, Yang DW (2008) Difference of the hippocampal and white matter microalterations in MCI patients according to the severity of subcortical vascular changes: neuropsychological correlates of diffusion tensor imaging. *Clin Neurol Neurosurg* **110**, 552-561.

[33] Ukmar M, Makuc E, Onor ML, Garbin G, Trevisiol M, Cova MA (2008) Evaluation of white matter damage in patients with Alzheimer's disease and in patients with mild cognitive impairment by using diffusion tensor imaging. *Radiol Med* **113**, 915-922.

[34] Walhovd KB, Fjell AM, Amlien I, Grambaite R, Stenset V, Bjornerud A, Reinvang I, Gjerstad L, Cappelen T, Due-Tonnessen P, Fladby T (2009) Multimodal imaging in mild cognitive impairment: metabolism, morphometry and diffusion of the temporal-parietal memory network. *Neuroimage* **45**, 215-223.

[35] Stenset V, Bjornerud A, Fjell AM, Walhovd KB, Hofoss D, Due-Tonnessen P, Gjerstad L, Fladby T (2011) Cingulum fiber diffusivity and CSF T-tau in patients with subjective and mild cognitive impairment. *Neurobiol Aging* **32**, 581-589.

[36] Mielke MM, Kozauer NA, Chan KC, George M, Toroney J, Zerrate M, Bandeen-Roche K, Wang MC, Vanzijl P, Pekar JJ, Mori S, Lyketsos CG, Albert M (2009) Regionally-specific diffusion tensor imaging in mild cognitive impairment and Alzheimer's disease. *Neuroimage* **46**, 47-55.

[37] Grambaite R, Stenset V, Reinvang I, Walhovd KB, Fjell AM, Fladby T (2010) White matter diffusivity predicts memory in patients with subjective and mild cognitive impairment and normal CSF total tau levels. *J Int Neuropsychol Soc* **16**, 58-69.

[38] Rose SE, McMahon KL, Janke AL, O'Dowd B, de Zubicaray G, Strudwick MW, Chalk JB (2006) Diffusion indices on magnetic resonance imaging and neuropsychological performance in amnestic mild cognitive impairment. *J Neurol Neurosurg Psychiatry* **77**, 1122-1128.

[39] Medina D, DeToledo-Morrell L, Urresta F, Gabrieli JD, Moseley M, Fleischman D, Bennett DA, Leurgans S, Turner DA, Stebbins GT (2006) White matter changes in mild cognitive impairment and AD: a diffusion tensor imaging study. *Neurobiol Aging* **27**, 663-672.

[40] Xie S, Xiao JX, Gong GL, Zang YF, Wang YH, Wu HK, Jiang XX (2006) Voxel-based detection of white matter abnormalities in mild Alzheimer disease. *Neurology* **66**, 1845-1849.

[41] Lee DY, Fletcher E, Martinez O, Ortega M, Zozulya N, Kim J, Tran J, Buonocore M, Carmichael O, DeCarli C (2009)

Regional pattern of white matter microstructural changes in normal aging, MCI, and AD. *Neurology* **73**, 1722-1728.

[42] Liu Y, Spulber G, Lehtimaki KK, Kononen M, Hallikainen I, Grohn H, Kivipelto M, Hallikainen M, Vanninen R, Soininen H (2009) Diffusion tensor imaging and Tract-Based Spatial Statistics in Alzheimer's disease and mild cognitive impairment. *Neurobiol Aging*, Epub ahead of print.

[43] Damoiseaux JS, Smith SM, Witter MP, Sanz-Arigita EJ, Barkhof F, Scheltens P, Stam CJ, Zarei M, Rombouts SA (2009) White matter tract integrity in aging and Alzheimer's disease. *Hum Brain Mapp* **30**, 1051-1059.

[44] Bosch B, Arenaza-Urquijo EM, Rami L, Sala-Llonch R, Junque C, Sole-Padulles C, Pena-Gomez C, Bargallo N, Molinuevo JL, Bartres-Faz D (2010) Multiple DTI index analysis in normal aging, amnestic MCI and AD. Relationship with neuropsychological performance. *Neurobiol Aging*, Epub ahead of print.

[45] Stebbins GT, Murphy CM (2009) Diffusion tensor imaging in Alzheimer's disease and mild cognitive impairment. *Behav Neurol* **21**, 39-49.

[46] Folstein MF, Folstein SE, McHugh PR (1975) "Mini-mental state". A practical method for grading the cognitive state of patients for the clinician. *J Psychiatr Res* **12**, 189-198.

[47] Wechsler D (1955) Manual for the Wechsler Adult Intelligence Scale. Psychological Corporation, New York.

[48] Milner B (1971) Interhemispheric differences in the localization of psychological processes in man. *Br Med Bull* **27**, 272-277.

[49] Buschke H, Sliwinski MJ, Kuslansky G, Lipton RB (1997) Diagnosis of early dementia by the Double Memory Test: encoding specificity improves diagnostic sensitivity and specificity. *Neurology* **48**, 989-997.

[50] Baddley A, Emslie H, Nimmo-Smith I (1994) Doors and people. A test of visual and verbal recall and recognition. *Bury St Edmunds* **20**, 1-20.

[51] Borkowski JG, Benton AL, Spreen O (1967) Word fluency and brain damage. *Neuropsychologia* **5**, 135-140.

[52] Reitan RM (1958) Validity of the Trail Making Test as an indicator of organic brain damage. *Percept Mot Skills* **8**, 271-276.

[53] Heaton RK (1981) *Wisconsing Card Sorting Test Manual*, Psychological Assessment Resources Inc, Odessa.

[54] Kaplan EF, Goodglass H, Weintraub S (1983) The Boston naming test (2nd edition). Lea & Febiger, Philadelphia.

[55] Schnider A, Hanlon RE, Alexander DN, Benson DF (1997) Ideomotor apraxia: behavioral dimensions and neuroanatomical basis. *Brain Lang* **58**, 125-136.

[56] Poeck K, *Clues to the Nature of Disruption to Limb Praxis*, EA Roy, ed. Amsterdam, North-Holland, 1985, pp. 99-109

[57] Welsh KA, Butters N, Mohs RC, Beekly D, Edland S, Fillenbaum G, Heyman A (1994) The Consortium to Establish a Registry for Alzheimer's Disease (CERAD). Part V. A normative study of the neuropsychological battery. *Neurology* **44**, 609-614.

[58] Ghent L (1956) Perception of overlapping and embedded figures by children of different ages. *Am J Psychol* **69**, 575-587.

[59] Wechsler D (1981). *Adult Intelligence Scale, Revised (WAIS-R)*, Psychological Corporation, San Antonio.

[60] Hughes CP, Berg L, Danziger WL, Coben LA, Martin RL (1982) A new clinical scale for the staging of dementia. *Br J Psychiatry* **140**, 566-572.

[61] Zigmond AS, Snaith RP (1983) The hospital anxiety and depression scale. *Acta Psychiatr Scand* **67**, 361-370.

[62] Barberger-Gateau P, Commenges D, Gagnon M, Letenneur L, Sauvel C, Dartigues JF (1992) Instrumental activities of daily living as a screening tool for cognitive impairment and dementia in elderly community dwellers. *J Am Geriatr Soc* **40**, 1129-1134.

[63] Petersen RC, Doody R, Kurz A, Mohs RC, Morris JC, Rabins PV, Ritchie K, Rossor M, Thal L, Winblad B (2001) Current concepts in mild cognitive impairment. *Arch Neurol* **58**, 1985-1992.

[64] Petersen RC, Morris JC (2005) Mild cognitive impairment as a clinical entity and treatment target. *Arch Neurol* **62**, 1160-3; discussion 1167.

[65] Fazekas F, Chawluk JB, Alavi A, Hurtig HI, Zimmerman RA (1987) MR signal abnormalities at 1.5 T in Alzheimer's dementia and normal aging. *AJR Am J Roentgenol* **149**, 351-356.

[66] Smith SM, Jenkinson M, Johansen-Berg H, Rueckert D, Nichols TE, Mackay CE, Watkins KE, Ciccarelli O, Cader MZ, Matthews PM, Behrens TE (2006) Tract-based spatial statistics: voxelwise analysis of multi-subject diffusion data. *Neuroimage* **31**, 1487-1505.

[67] Smith SM, Johansen-Berg H, Jenkinson M, Rueckert D, Nichols TE, Miller KL, Robson MD, Jones DK, Klein JC, Bartsch AJ, Behrens TE (2007) Acquisition and voxelwise analysis of multi-subject diffusion data with tract-based spatial statistics. *Nat Protoc* **2**, 499-503.

[68] Smith SM, Jenkinson M, Woolrich MW, Beckmann CF, Behrens TE, Johansen-Berg H, Bannister PR, De Luca M, Drobnjak I, Flitney DE, Niazy RK, Saunders J, Vickers J, Zhang Y, De Stefano N, Brady JM, Matthews PM (2004) Advances in functional and structural MR image analysis and implementation as FSL. *Neuroimage* **23**(Suppl. 1), S208-S19.

[69] Smith SM, Nichols TE (2009) Threshold-free cluster enhancement: addressing problems of smoothing, threshold dependence and localisation in cluster inference. *Neuroimage* **44**, 83-98.

[70] Frank E, Hall M, Trigg L, Holmes G, Witten IH (2004) Data mining in bioinformatics using Weka. *Bioinformatics* **20**, 2479-2481.

[71] Kononenko I, Šimec E, Robnik-Šikonja M (1997) Overcoming the myopia of inductive learning algorithms with RELIEFF. *Applied Intelligence* **7**, 39-55.

[72] Platt J (1999) Sequential minimal optimization: a fast algorithm for training support vector machines. *Advances in Kernel Methods-Support Vector Learning* **208**, 1-21.

[73] Scholkopf B, Sung KK, Burges CJC, Girosi F, Niyogi P, Poggio T, Vapnik V (1997) Comparing support vector machines with Gaussian kernels to radialbasis function classifiers. *IEEE Transactions on Signal Processing* **45**, 2758-2765.

[74] Wang L, Goldstein FC, Veledar E, Levey AI, Lah JJ, Meltzer CC, Holder CA, Mao H (2009) Alterations in cortical thickness and white matter integrity in mild cognitive impairment measured by whole-brain cortical thickness mapping and diffusion tensor imaging. *AJNR Am J Neuroradiol* **30**, 893-899.

[75] Chua TC, Wen W, Chen X, Kochan N, Slavin MJ, Trollor JN, Brodaty H, Sachdev PS (2009) Diffusion tensor imaging of the posterior cingulate is a useful biomarker of mild cognitive impairment. *Am J Geriatr Psychiatry* **17**, 602-613.

[76] Sasson E, Doniger GM, Pasternak O, Assaf Y (2010) Structural correlates of memory performance with diffusion tensor imaging. *Neuroimage*, **50**, 1231-1242.

[77] Kiuchi K, Morikawa M, Taoka T, Nagashima T, Yamauchi T, Makinodan M, Norimoto K, Hashimoto K, Kosaka J, Inoue Y, Inoue M, Kichikawa K, Kishimoto T (2009) Abnormalities of

the uncinate fasciculus and posterior cingulate fasciculus in mild cognitive impairment and early Alzheimer's disease: a diffusion tensor tractography study. *Brain Res* **1287**, 184-191.

[78] Acosta-Cabronero J, Williams GB, Pengas G, Nestor PJ (2010) Absolute diffusivities define the landscape of white matter degeneration in Alzheimer's disease. *Brain* **133**, 529-539.

[79] Zhang Y, Du AT, Hayasaka S, Jahng GH, Hlavin J, Zhan W, Weiner MW, Schuff N (2010) Patterns of age-related water diffusion changes in human brain by concordance and discordance analysis. *Neurobiol Aging* **31**, 1991-2001.

[80] Pievani M, Agosta F, Pagani E, Canu E, Sala S, Absinta M, Geroldi C, Ganzola R, Frisoni GB, Filippi M (2010) Assessment of white matter tract damage in mild cognitive impairment and Alzheimer's disease. *Hum Brain Mapp* **31**, 1862-1875.

[81] Salat DH, Tuch DS, van der Kouwe AJ, Greve DN, Pappu V, Lee SY, Hevelone ND, Zaleta AK, Growdon JH, Corkin S, Fischl B, Rosas HD (2010) White matter pathology isolates the hippocampal formation in Alzheimer's disease. *Neurobiol Aging* **31**, 244-256.

[82] Della Nave R, Ginestroni A, Tessa C, Salvatore E, De Grandis D, Plasmati R, Salvi F, De Michele G, Dotti MT, Piacentini S, Mascalchi M (2008) Brain white matter damage in SCA1 and SCA2. An *in vivo* study using voxel-based morphometry, histogram analysis of mean diffusivity and tract-based spatial statistics. *Neuroimage* **43**, 10-19.

[83] Della Nave R, Ginestroni A, Tessa C, Salvatore E, Bartolomei I, Salvi F, Dotti MT, De Michele G, Piacentini S, Mascalchi M (2008) Brain white matter tracts degeneration in Friedreich ataxia. An *in vivo* MRI study using tract-based spatial statistics and voxel-based morphometry. *Neuroimage* **40**, 19-25.

[84] Bodini B, Khaleeli Z, Cercignani M, Miller DH, Thompson AJ, Ciccarelli O (2009) Exploring the relationship between white matter and gray matter damage in early primary progressive multiple sclerosis: an *in vivo* study with TBSS and VBM. *Hum Brain Mapp* **30**, 2852-2861.

Multiple Diffusion Indices Reveals White Matter Degeneration in Alzheimer's Disease and Mild Cognitive Impairment: A Tract-Based Spatial Statistics Study

Ni Shu [a,1], Zhiqun Wang [b,1], Zhigang Qi [b], Kuncheng Li [b,c,*] and Yong He [a,*]

[a] *State Key Laboratory of Cognitive Neuroscience and Learning, Beijing Normal University, Beijing, China*

[b] *Department of Radiology, Xuanwu Hospital of Capital Medical University, Beijing, China*

[c] *Key Laboratory for Neurodegenerative Diseases (Capital Medical University), Ministry of Education, Beijing, China*

Abstract. Alzheimer's disease (AD) is a progressive neurodegenerative disease involving the decline of memory and other cognitive functions. Mild cognitive impairment (MCI) represents a transition phase between normal aging and early AD. The degeneration patterns of the white matter across the brain in AD and MCI remain largely unclear. Here we used diffusion tensor imaging and tract-based spatial statistics (TBSS) to investigate white matter changes in multiple diffusion indices (e.g., fractional anisotropy, axial, radial and mean diffusivities) in both AD and MCI patients. Compared with the normal controls, the AD patients had reduced fractional anisotropy and increased axial, radial and mean diffusivities in widespread white matter structures, including the corpus callosum and the white matter of lateral temporal cortex, the posterior cingulate cortex/precuneus and the fronto-parietal regions. Similar white matter regions with reduced anisotropy were also found in MCI patients but with a much less extent than in AD. Between the AD and MCI groups, there were significant differences in the axial and mean diffusivities of the white matter tracts adjacent to the posterior cingulate cortex/precuneus without anisotropy changes. Taken together, our findings based upon multiple diffusion indices (FA, axial, radial and mean diffusivities) suggest distinct degeneration behaviors of the white matter in AD and MCI.

Keywords: Connectivity, axial diffusivity, radial diffusivity, DTI, TBSS

INTRODUCTION

Alzheimer's disease (AD) is the most common degenerative dementia in the elderly and is characterized as a progressive neurodegenerative disease involving the decline of memory and other cognitive functions [1]. Mild cognitive impairment (MCI) is defined as memory impairment in the setting of normal general cognitive function without dementia [2]. In particular, the amnestic subtype of MCI is considered

---

[1]These authors contributed equally to this work.

*Correspondence to: Yong He, Ph.D, State Key Laboratory of Cognitive Neuroscience and Learning, Beijing Normal University, Beijing 100875, China. Tel.: +86 10 5880 2036; E-mail: yong.he@bnu.edu.cn and Kuncheng Li, M.D., Department of Radiology, Xuanwu Hospital of Capital Medical University, Beijing 100053, China. Tel.: +86 10 8319 8376; E-mail: likuncheng@xwh.ccmu.edu.cn.

as a transition phase between normal aging and AD [2]. In the past decade, advanced magnetic resonance imaging (MRI) approaches have been extensively used for the assessment of brain structural and functional alterations in patients with AD and MCI [3–7], which are important for our understanding the neuropathological mechanisms of the diseases.

Diffusion tensor imaging is an advanced MRI technique for evaluating the white matter integrity and anatomical connectivity *in vivo* [8, 9], and has been increasingly employed to investigate the diffusion changes of the white matter in AD and MCI (for reviews, see [10, 11]). Fractional anisotropy (FA) and mean diffusivity (MD) are two important diffusion metrics for the analysis of DTI data: the former reflects the degree of directionality of cellular structures (i.e., structural integrity) within the fiber tracts by measuring anisotropic water diffusion [12, 13], while the latter measures diffusion in the noncolinear direction or free diffusion [13]. To date, these two diffusion metrics have been widely used to assess white matter changes in brain diseases [14–16]; however, it should be noted that they are not sufficient to reflect pathological changes in white matter at a microstructural level [17, 18]. Recently, two other metrics of water movement, parallel (axial diffusivity, λ_1) and perpendicular (radial diffusivity, λ_{23}) to the primary diffusion direction have been proposed to capture the neural bases of diffusion changes in white matter tracts [5, 17, 19–21]. Studies including histological verification have put forth the notion that alterations in axial and radial diffusivities may reflect specific changes in the axon and myelin, respectively [22, 23].

The vast majority of previous DTI studies in AD and MCI patients have concentrated on FA and/or MD changes without consideration of the component eigenvalues [10]. Notably, there is a lack of empirical biological evidence that FA changes necessarily capture the full extent of white matter changes in AD and MCI patients. By using multiple diffusion indices (FA, MD, λ_1 and λ_{23}), Huang et al. investigated MCI- and AD-related changes exclusively in the white matter of the temporal lobe [24]. More recently, Acosta-Cabronero et al. utilized these diffusion indices to examine white matter degeneration in the whole brain in early AD patients and found that the use of diffusivity metrics (i.e., λ_1, λ_{23}, and MD) generated more sensitive results than FA [5].

To give a comprehensive view of the degeneration patterns of the white matter in AD and MCI patients, we used the newly developed tract-based spatial statistics (TBSS) method and multiple diffusion indices (FA, MD, λ_1 and λ_{23}) to systematically study AD- and MCI-associated changes in white matter tracts across the whole brain. The TBSS method is a fully automated whole-brain analysis technique that uses voxel-wise statistics on diffusion indices but simultaneously minimizes the effects of misalignment using a conventional voxel-based analysis method [25]. For voxel-based DTI analysis in degenerative diseases such as AD and MCI, atrophy will lead to systematic misalignment to the template for the patients. To circumvent this problem, the TBSS method extracts each subject's white matter skeleton (i.e., the center of all major tracts "common" to all subjects) from the normalized FA images, minimizing the effect of atrophy-induced misregistration. In recent years, TBSS has been widely used to study FA changes in cerebral white matter in AD and MCI patients [5, 20, 26–31]. Although a few studies have investigated alterations of other diffusion metrics (i.e., axial, radial and mean diffusivities) across the brain in AD and MCI, the results were under debate (we will return this issue in Discussion section) [5, 20, 30, 31]. Therefore, a comprehensive analysis of multiple diffusion indices for describing the white matter degeneration patterns in AD and MCI patients was necessary.

MATERIAL AND METHODS

Participants

This study included 52 right-handed subjects (16 AD patients, 17 MCI patients and 19 healthy elderly controls) who gave written informed consent. The AD and MCI patients were recruited from those who had consulted a memory clinic for memory complaints at Xuanwu Hospital, Beijing, China. The healthy elderly controls (HC) were recruited from the local community by advertisements. This study was approved by the Medical Research Ethics Committee of Xuanwu Hospital.

The diagnosis of AD fulfilled the Diagnostic and Statistical Manual of Mental Disorders 4th Edition criteria for dementia [32] and the National Institute of Neurological and Communicative Disorders and Stroke/Alzheimer Disease and Related Disorders Association (NINCDS-ADRDA) criteria for possible or probable AD [1]. The subjects were also assessed using the Clinical Dementia Rating (CDR) score [33] (6 patients with CDR = 1 and 10 patients with CDR = 0.5).

Participants with MCI had memory impairment but did not meet the criteria for dementia. The criteria used for the identification and classification of subjects with MCI [34] were the following: (1) impaired memory performance on a normalized objective verbal memory delayed-recall test; (2) a recent history of symptomatic worsening in memory; (3) normal or near-normal performance on global cognitive tests, including a Mini-Mental State Examination (MMSE) score >24, and on activities described in a daily living scale; (4) a global rating of 0.5 on the CDR Scale, with a score of at least 0.5 on the memory domain; and (5) the absence of dementia. All MCI subjects are amnestic MCI (aMCI). The inclusion criteria for the healthy elderly controls were as follows: (1) no neurological or psychiatric disorders such as stroke, depression, or epilepsy; (2) no neurological deficiencies such as visual or hearing loss; (3) no abnormal findings such as infarction or focal lesions on conventional brain magnetic resonance imaging; (4) no cognitive complaints; (5) an MMSE score of 28 or higher; and (6) a CDR score of 0. Notably, the AD and MCI patients exhibited extensive periventricular or deep white matter hyperintensities (WMHs). Here, the presences of WMHs were not considered as exclusive criteria for the MCI and AD patients.

Clinical and demographic data for the participants are shown in Table 1 . There were no significant differences among the three groups in terms of gender, age, or years of education, but the MMSE scores were significantly different ($P < 0.01$) among the groups.

Image acquisition

DTI was performed using a 3.0 T Siemens Trio MR system with a standard head coil. Head motion was minimized with restraining foam pads provided by the manufacturer. Diffusion-weighted images were acquired using a single-shot echo planar imaging (EPI) sequence. An Integral Parallel Acquisition Technique (iPAT) was used with an accelerate factor of 2 as acquisition time and image distortion from susceptibility artifacts can be reduced by the iPAT method. The diffusion sensitizing gradients were applied along 12 non-linear directions ($b = 1000 \, \text{s/mm}^2$), together with an acquisition without diffusion weighting ($b = 0 \, \text{s/mm}^2$) (average = 4). The imaging parameters were 30 continuous axial slices with a slice thickness of 5 mm and no gap, FOV = 256 mm × 256 mm, TR/TE = 6000/85 ms, and acquisition matrix = 128 × 128. The reconstruction matrix was 256 × 256, resulting in an in-plane resolution of 1 mm × 1 mm.

Data preprocessing

Three steps were undertaken during preprocessing. First, eddy current distortions and motion artifacts in the DTI dataset were corrected by applying affine alignment of each diffusion-weighted image to the $b = 0$ image using FMRIB's Diffusion Toolbox (FDT) (FSL 4.1.4; www.fmrib.ox.ac.uk/fsl). The first volume of the diffusion data without a gradient applied (i.e., the $b = 0$ image) was then used to generate a binary brain mask using the Brain Extraction Tool. DTIfit was used to independently fit the diffusion tensor to each voxel. The output of DTIfit yielded voxel-wise maps of FA, MD, axial diffusivity (λ_1) and radial diffusivity (λ_{23}) for each subject. Finally, the FA, MD and λ_{23} of each voxel were calculated according to the following formulas:

$$FA = \frac{\sqrt{(\lambda_1 - \lambda_2)^2 + (\lambda_1 - \lambda_3)^2 + (\lambda_2 - \lambda_3)^2}}{\sqrt{2(\lambda_1^2 + \lambda_2^2 + \lambda_3^2)}}$$
$$MD = \frac{\lambda_1 + \lambda_2 + \lambda_3}{3}$$
$$\lambda_{23} = \frac{\lambda_2 + \lambda_3}{2}$$

Tract-based spatial statistics (TBSS)

Tract-based spatial statistics of FA, MD, λ_1 and λ_{23} images were carried out using TBSS in the FMRIB software library (FSL 4.1.4; www.fmrib.ox.ac.uk/fsl; for a detailed description of the methods, see [25]). The steps of the TBSS analyses in our study were as follows:

1. The FA image of each subject was aligned to a pre-identified target FA image (FMRIB58_FA)

Table 1
Characteristics of the AD and MCI patients and healthy controls

Characteristics	AD	MCI	Controls	P values
N (M/F)	16 (9/7)	17 (8/9)	19 (7/12)	0.52[a]
Age (years)	72.6 ± 6.3	71.5 ± 6.7	69.9 ± 6.2	0.45[*]
Education (years)	10.1 ± 3.4	9.9 ± 3.5	10.2 ± 4.0	0.98[*]
MMSE	18.7 ± 3.1	26.5 ± 1.0	28.6 ± 0.7	<0.01[*]

MMSE: Mini-Mental Status Examination; Plus-minus values are mean ± S.D.

[a]The *P* value for gender distribution in the three groups was obtained using a Chi-square test.

[*]The *P* values were obtained by one-way analysis of variance tests.

by non-linear registrations.

2. All of the aligned FA images were transformed into the MNI152 template (1 mm × 1 mm × 1 mm) by affine registrations.
3. The mean FA image and its skeleton (mean FA skeleton) were created from all subjects.
4. Individual subjects' FA images were projected onto the skeleton.
5. Voxel-wise statistics across subjects were calculated for each point on the common skeleton.

Data for MD, λ_1 and λ_{23} were also generated by applying the above FA transformations to the additional diffusivity maps and projecting them onto the skeleton using identical projection vectors to those inferred from the original FA data.

Statistical analyses

We first calculated the mean diffusion indices (FA, MD, λ_1 and λ_{23}) in the whole-brain white matter skeleton for each subject. We then performed two-sample t-tests to compare the mean diffusion indices between any two groups: MCI versus HC, early AD versus HC, and early AD versus MCI.

Voxel-wise statistics in TBSS were carried out using a permutation-based inference tool for nonparametric statistical thresholding ("randomize," part of FSL, see [25]). In this study, voxel-wise group comparisons were performed using non-parametric, two-sample t-tests in: MCI versus HC, early AD versus HC, and early AD versus MCI. The mean FA skeleton was used as a mask (thresholded at a mean FA value of 0.2), and the number of permutations was set to 5,000. The significance threshold for between-group differences was set at $P < 0.05$ (FWE corrected for multiple comparisons) using the threshold-free cluster enhancement (TFCE) option in the "randomize" permutation-testing tool in FSL [35].

RESULTS

Mean diffusion indices of white matter skeletons

Two-sample t-tests showed that the AD patients had significantly lower fractional anisotropy (FA, $P = 0.02$), higher mean diffusivity (MD, $P = 0.002$), higher axial diffusivity (λ_1, $P = 0.02$) and higher radial diffusivity, (λ_{23}, $P = 0.002$) in their white matter skeletons than the healthy controls. In MCI no significant differences were observed for any diffusion indices with neither AD nor healthy controls ($P < 0.05$) (Table 2).

TBSS analyses between groups

Early AD versus HC

The TBSS analyses revealed that the AD patients had significantly reduced FA in widespread brain regions compared with the controls, including the white matter of the lateral temporo-parietal regions, the posterior cingulate cortex/precuneus (PCC/PCu), the fronto-parietal regions and the whole corpus callosum (Fig. 1). The results for increased diffusivities (MD, λ_1 and λ_{23}) were broadly concordant with those for reduced FA. The radial (λ_{23}) and mean diffusivity (MD) changes were slightly more extensive than those for axial diffusivity (λ_1). There were no white matter tracts that showed increased FA or decreased diffusivities (MD, λ_1 and λ_{23}) in the AD patients compared to the controls.

MCI versus HC

The MCI subjects had significantly reduced FA in the white matter of the PCC/PCu and inferior frontal cortex in the left hemisphere compared to the controls (Fig. 2). There were no white matter tracts that showed increased FA in the MCI patients. There were also no significant differences in the absolute diffusivities (MD, λ_1 and λ_{23}) between MCI and HC groups.

Table 2
Mean diffusion indices of white matter skeletons for each group

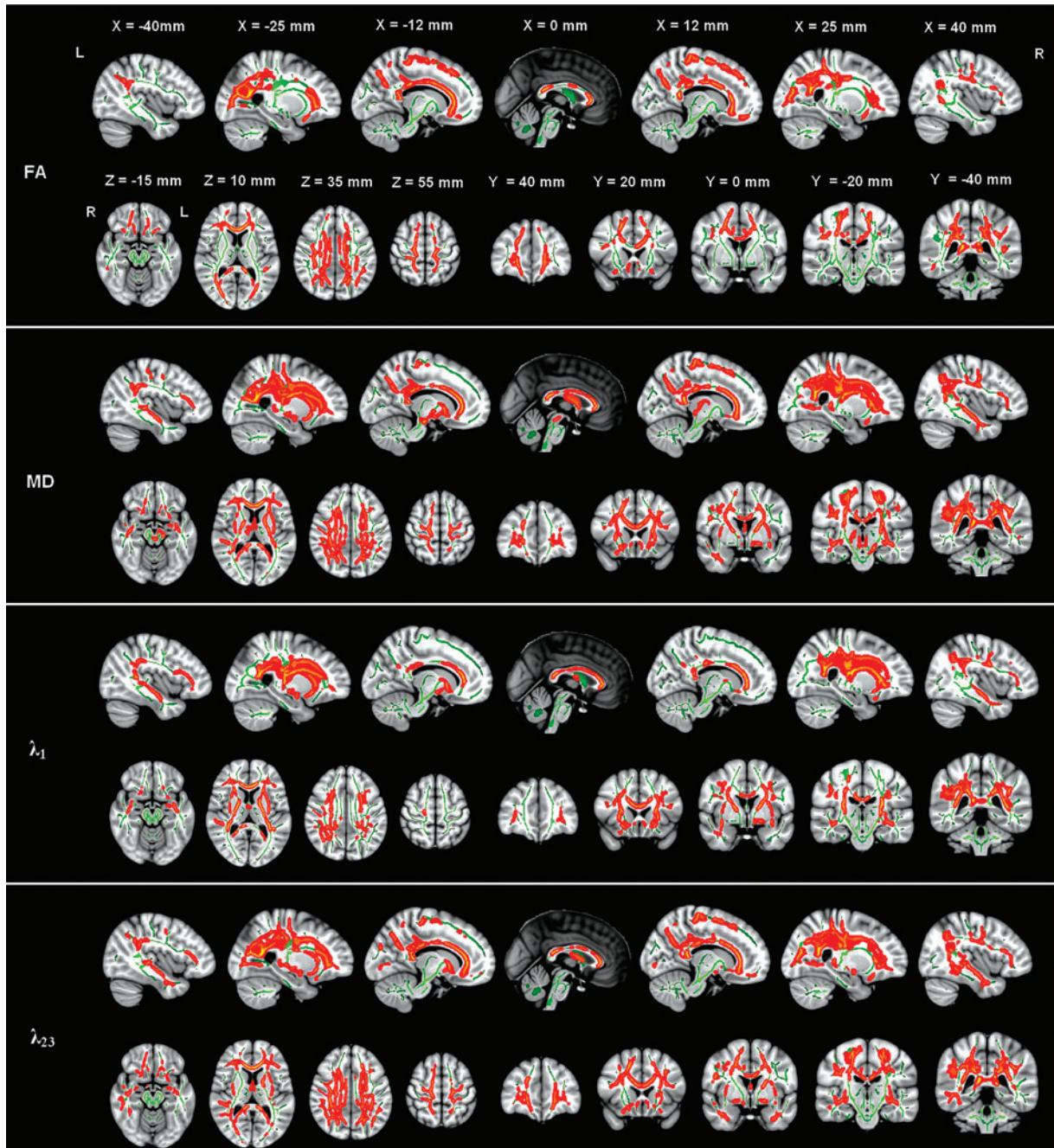| | AD | MCI | HC | P values | | |
				AD vs. HC	MCI vs. HC	AD vs. MCI
FA	0.39 ± 0.02	0.40 ± 0.02	0.41 ± 0.02	0.023^*	0.11	0.48
MD ($\times 10^{-3}$ mm^2/s)	0.81 ± 0.04	0.79 ± 0.03	0.78 ± 0.04	0.002^*	0.13	0.053
λ_1 ($\times 10^{-3}$ mm^2/s)	1.17 ± 0.04	1.15 ± 0.03	1.14 ± 0.04	0.011^*	0.37	0.067
λ_{23} ($\times 10^{-3}$ mm^2/s)	0.63 ± 0.04	0.60 ± 0.03	0.58 ± 0.04	0.002^*	0.094	0.072

*Significant group differences at $P < 0.05$.

Fig. 1. TBSS results of the diffusion indices between the AD and HC groups. Green represents the mean white matter skeleton of all subjects; red represents the regions with reduced FA (1st row), increased MD (2nd row), increased λ_1 (3rd row) and increased λ_{23} (4th row) in the early AD patients. The TBSS results for increased FA or decreased diffusivities (MD, λ_1 and λ_{23}) in the early AD patients did not show any statistically significant differences at $P < 0.05$ (FWE corrected for multiple comparisons).

Early AD versus MCI

There were no significant differences found in FA between the AD and MCI patients; however, we observed that the AD patients had increased MD in bilateral temporo-parietal regions, bilateral PCC/PCu, and the genu and splenium of the corpus callosum com-
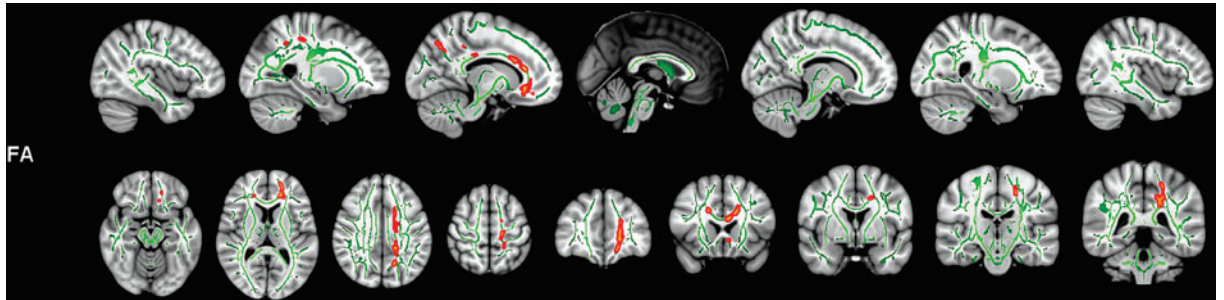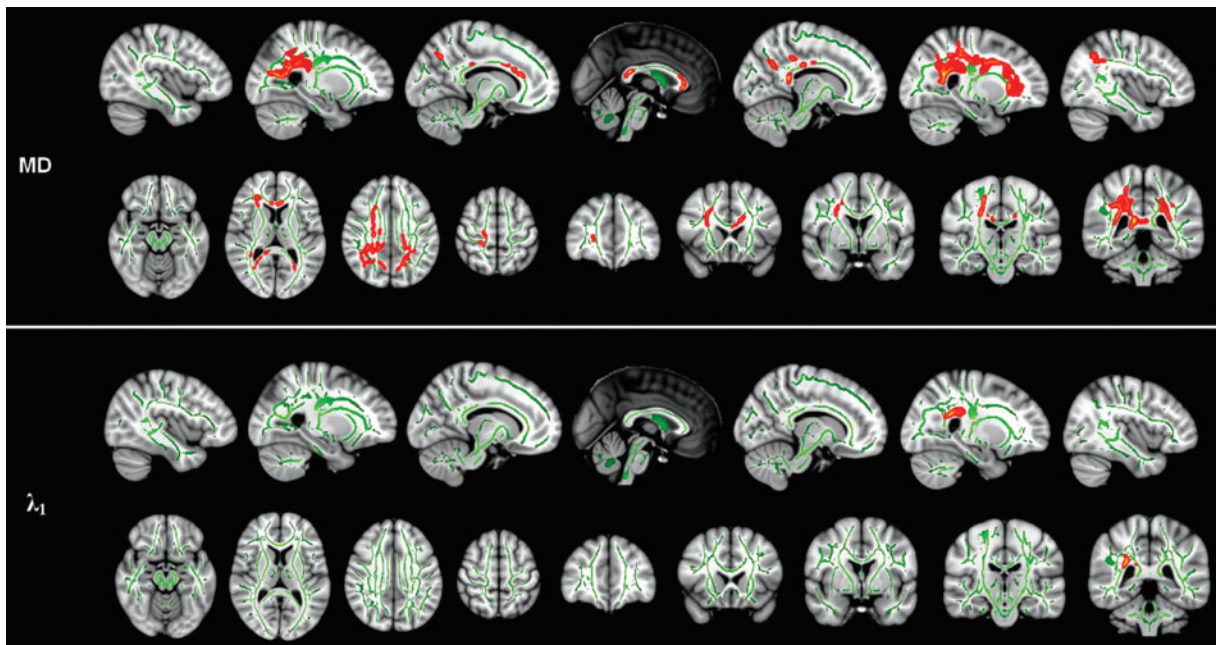
Fig. 2. TBSS results of the diffusion indices between the MCI and HC groups. Green represents the mean white matter skeleton of all subjects; red represents the regions with reduced FA in the MCI subjects. The TBSS results for increased FA or increased/decreased diffusivities (MD, λ_1 and λ_{23}) in the MCI subjects did not show any statistically significant differences at $P < 0.05$ (FWE corrected for multiple comparisons).

Fig. 3. TBSS results of the diffusion indices between the AD and MCI groups. Green represents the mean white matter skeleton of all subjects; red represents the regions with increased MD and increased λ_1 in the early AD patients. The TBSS results for increased/decreased FA or decreased diffusivities (MD, λ_1 and λ_{23}) in the early AD patients did not show any statistically significant differences at $P < 0.05$ (FWE corrected for multiple comparisons).

pared to the MCI patients (Fig. 3). Only one cluster located in the white matter adjacent to the PCC/PCu showed increased axial diffusivity (λ_1) in the AD patients. There were no significant differences in the radial diffusivities (λ_{23}) between AD and MCI groups.

DISCUSSION

In this study, we determined global maps of the white matter changes in AD and MCI patients by measuring fractional anisotropy (FA), mean diffusivity (MD), axial diffusivity (λ_1) and radial diffusivity (λ_{23}) across the brain, offering a comprehensive view of the landscape of white matter degeneration in AD and MCI. Compared with the healthy elderly controls, the AD patients exhibited significantly reduced FA and increased axial, radial and mean diffusivities in widespread white matter regions. Some regions with reduced FA were observed in the MCI patients as compared to the controls. Moreover, between the AD and

MCI groups, there were significant differences in the diffusivity metrics (i.e., MD and λ_1) in several white matter regions without FA changes. Taken together, these data provide empirical evidence for degenerative changes in widespread white matter structures in AD and MCI patients. The findings suggest distinct degeneration behaviors of the white matter in AD and MCI.

Distributed white matter regions with diffusion changes in AD and MCI

AD versus HC

We identified AD-related abnormalities in widespread white matter regions, including lateral temporoparietal regions, PCC/PCu and the fronto-parietal cortex. And reduced FA involved most of the white matter pathways, including bilateral superior longitudinal fasciculus, inferior longitudinal fasciculus, uncinate fasciculus, cingulum bundles, corticospinal tracts and corpus callosum. Most of these affected tracts have been reported in previous DTI studies in AD using regions of interest (ROI)-based or conventional voxel-based methods [16, 24, 36–39] and were found to be related to the cognitive dysfunctions in patients with AD [27, 30, 40, 41]. Furthermore, our finding are also parallel to the findings from recent TBSS studies in AD [5, 20, 26–30]. Specifically, one TBSS study reported diffusion abnormalities in the "default-mode" network (DMN)-related white matter structures, particularly in posterior components including the PCC/PCu, lateral temporo-parietal regions and the splenium of corpus callosum [5]. Another TBSS study found decreased FA only in the left temporal lobe [28]. Several other studies revealed FA reduction in many white matter tracts, such as uncinate fasciculus, superior longitudinal fasciculus, inferior longitudinal fasciculus, cingulum bundles and corpus callosum [20, 26, 27, 30]. The differences between the results of these TBSS studies could be due to different samples of AD or imaging parameters employed. However, it is worthy to note that they have consistently demonstrated widespread abnormalities of many white matter regions in AD patients, especially in the posterior areas.

MCI versus HC

In the MCI patients, we found that the regions with reduced FA were mainly located in the white matter of the PCC/PCu and inferior frontal cortex in the left hemisphere, to a less extent than in AD patients. For MCI subjects, the structural and functional abnormal-

ities in the posteromedial cortical circuit (e.g., the medial temporal lobe and PCC/PCu), which represents the prodromal changes of AD, have been consistently reported [3, 42–44]. Several DTI studies also demonstrated that the posterior cingulum, especially on the left, were affected in MCI when compared to controls [16, 39, 45], which provides support for our asymmetric findings. Considering recent TBSS studies in MCI [26–28, 30], the discrepancies among different studies need to be paid attention. First, two TBSS studies did not show significant differences in FA between MCI and healthy controls [28, 30]. In contrast, Serra and colleagues found that MCI patients had reduced FA in the anterior part of the right anterior thalamic radiation [27]. Additionally, Liu and colleague found decreased FA in the right parahippocampal white matter, bilateral uncinate fasciculus and tracts in the brain stem and cerebellum with an uncorrected threshold [26]. In our study, the white matter regions with FA changes in MCI are located in the PCC/PCu and inferior frontal cortex of the left hemisphere. The discrepancies between these studies could be attributable to different data samples, imaging parameters or the heterogeneous groups of subjects (converters and non-converters).

AD versus MCI

Between the AD and MCI groups, the regions with the most significant differences were located in the white matter adjacent to the PCC/PCu, which is a critical node in the human brain networks [46–48]. Many studies have consistently demonstrated that this region shows structural and functional abnormalities in AD and MCI patients [42, 49–53]. Moreover, between MCI and AD patients structural and functional differences in the PCC have been also reported [16, 26, 39, 54]. A DTI study suggested that the fractional anisotropy of the PCC can significantly improve the distinction of MCI and AD patients from healthy elderly subjects [39]. Taken together, our results imply that the PCC/PCu is a key region affected by AD and MCI, suggesting that the structural characteristics of this region could be useful for early detection and monitoring of disease progression. Furthermore, we found that no regions showed significant differences in FA between AD and MCI, which was consistent with the findings of two previous TBSS studies [28, 30].

Neural substrates of diffusion changes

In this study, we used four diffusion indices (FA, MD, λ_1 and λ_{23}) to investigate diffusion changes in

the white matter in AD and MCI patients, generating a comprehensive view of the landscape of white matter tract degeneration. Compared with the healthy controls, the AD patients showed significantly reduced FA and increased MD, λ_1 and λ_{23} in many brain regions, consistent with the findings of recent TBSS studies in AD [5, 30]. These changes in diffusion indices may underlie micro-structural changes in the white matter. Many studies on neurological diseases and disorders have observed regional reductions in anisotropy, and some researchers have proposed that the primary determinant of anisotropy is the packing density of axons within a voxel [12, 55]. Axonal packing density encompasses a variety of microstructural level variables (e.g., degree of myelination, axonal diameters, and extracellular space). Therefore, similar FA reductions may not be interpreted in the same way depending on the changes in the individual eigenvalues. Decreased axial diffusivity may reflect axonal loss or damage [21, 22, 56] and increased radial diffusivity may suggest demyelination and a loss of myelin integrity [19, 57]. More severe decreases in axonal packing density (e.g., from a greater loss of myelin or axons) would lead to a global increase in extracellular water, resulting in larger radial diffusivity increases and subsequent axial diffusivity increases [5, 18].

In AD patients, we found some regions with increased radial diffusivity, but no changes in axial diffusivity, such as white matter of the fronto-parietal regions (superior longitudinal fasciculus) and PCC/PCu (cingulum bundles). This pattern of diffusion changes has been reported by several recent TBSS studies in AD, normal aging and multiple sclerosis [18, 26, 30, 58]. In animal literatures the changes in radial diffusivity is related to myelin deficient or myelin loss [19, 57]. Thus, the abnormalities in white matter observed here might reflect alterations of integrity of myelin, which was in accordance with retrogenesis through mechanisms outlined by Bartzokis et al. [59]. On the other hand, some regions were found to have increased axial diffusivity, but no changes in radial diffusivity, such as the internal capsule and some regions around the cerebral ventricles. The interpretation of axial diffusivity variations is controversial in pathological conditions because both increases and decreases have been reported [5, 18, 30]. The underlying mechanisms may be related to axonal damages and fiber re-organization. In the present study, we noticed that AD and MCI patients exhibited a more extensive periventricular WMHs compared to controls. The findings of increased axial diffusivity, without changes in

radial diffusivity around the cerebral ventricles are possibly related to the occurrence of WMHs in the patients group. Additionally, other regions showed isotropic changes in axial and radial diffusivities, including white matter of the lateral temporal cortex and the corpus callosum. According to the previous studies, we speculated that these increases in both axial and radial diffusivity may be due to atrophy of the gray matter and an increase in the extracellular space, which could be due to a greater loss of myelin or axons from neurodegenerative processes or microvascular pathology [10]. However, it should be noted that the correspondence between axon and myelin damages and tensor diffusivities is still controversial with the current resolution of DTI sequences. Thus, we can not resolve histopathological implications in axial versus radial diffusivity changes and clinical correlations in the diseases.

Compared to FA, more sensitive results were obtained by using absolute diffusivity metrics (MD, λ_1 and λ_{23}) in the AD patients. For example, we identified the white matter of the lateral temporal cortex as having increased axial, radial and mean diffusivities, but no changes in FA. FA was inherently less sensitive in this situation because the axial and radial diffusivities changed in the same direction. Therefore, the analysis of component eigenvalues were necessary to capture the full extent of white matter changes [5]. Furthermore, the biological processes were not the same across different stages of the disease. We found that the most significant change between the healthy elderly and MCI groups was decreased FA in the white matter of the left hemisphere, while the most significant changes between the MCI and AD groups were increased axial and mean diffusivities in posterior white matter regions. Differences in the effects on glia, mechanisms of axonal degeneration, inflammatory responses and even the rate of degeneration could all give rise to different tensor behavior in different disease stages. Therefore, exploring the component eigenvalues of the tensor would be advantageous in studying all degenerative diseases rather than assuming that a single metric (such as FA) is sufficiently sensitive to different pathological states.

Methodological issues

Several methodological issues need to be addressed. First, we used a 5-mm slice thickness for the DTI data. In the TBSS analyses, the DTI data were converted into MNI space with an isotropic resolution of

1 mm × 1 mm × 1 mm. A previous study has shown that the non-isotropic voxel dimensions can underestimate the FA in areas with crossing fibers [60]. It may additionally confound the calculation of all diffusion indices, especially given the procedure for TBSS to reslice the low resolution voxels to 1 mm isotropic data in the present study. Therefore, diffusion changes less than 5 mm in the z-axis direction cannot be reliably evaluated due to the resolution limit, especially when evaluating small tracts such as the fornix. Based on the results of this study, all of the clusters with diffusion changes in the early AD and MCI patients were more than 5 mm in length, and this might minimize the limitations of slice thickness. To deal with the "fiber crossing" problem, several recent studies have proposed advanced imaging techniques, such as diffusion spectral imaging [61, 62] or high angular resolution diffusion imaging with Q-ball reconstruction of multiple fiber orientations [63, 64]. Therefore, future studies with improved data quality and advanced imaging techniques are needed to further validate our findings. Second, in this cross-sectional DTI study, all MCI participants were identified with aMCI according to the criteria: an isolated memory impairment with no neuropsychological evidence of any additional cognitive deficits. According to Petersen's criteria [65], these features may be considered as a prodromal state of AD. A large body of literature indicates that this subtype tends to progress to AD at a rate of 10% to 15% per year [34]. Thus, the longitudinal follow-up study would be important to identify the aMCI subjects who will convert to AD. It would be helpful to evaluate the preclinical abnormalities in AD and explore the changing patterns of white matter between converters and non-converters.

In summary, by using TBSS analyses, we generated a global map of the white matter changes in AD and MCI patients by measuring anisotropy and diffusivity changes across the brain. Compared with healthy elderly controls, the AD patients showed significantly reduced anisotropy and increased axial, radial and mean diffusivities in distributed white matter regions, particularly in the white matter of the posterior cingulate cortex/precuneus, lateral temporal cortex and the fronto-parietal cortex, in addition to the interhemispheric connections. In MCI, we found white matter changes in similar regions but with much less extent than in AD. Moreover, our findings suggest distinct degeneration behaviors of the white matter in AD and MCI. In future, the follow-up studies are necessary to determine the clinical values of the various DTI indices to predict AD or longitudinal DTI measurements.

REFERENCES

[1] McKhann G, Drachman D, Folstein M, Katzman R, Price D, Stadlan EM (1984) Clinical diagnosis of Alzheimer's disease: report of the NINCDS-ADRDA Work Group under the auspices of Department of Health and Human Services Task Force on Alzheimer's Disease. *Neurology* **34**, 939-944.

[2] Petersen RC, Stevens JC, Ganguli M, Tangalos EG, Cummings JL, DeKosky ST (2001) Practice parameter: early detection of dementia: mild cognitive impairment (an evidence-based review). Report of the Quality Standards Subcommittee of the American Academy of Neurology. *Neurology* **56**, 1133-1142.

[3] Pihlajamaki M, Jauhiainen AM, Soininen H (2009) Structural and functional MRI in mild cognitive impairment. *Curr Alzheimer Res* **6**, 179-185.

[4] Buckner RL, Snyder AZ, Shannon BJ, LaRossa G, Sachs R, Fotenos AF, Sheline YI, Klunk WE, Mathis CA, Morris JC, Mintun MA (2005) Molecular, structural, and functional characterization of Alzheimer's disease: evidence for a relationship between default activity, amyloid, and memory. *J Neurosci* **25**, 7709-7717.

[5] Acosta-Cabronero J, Williams GB, Pengas G, Nestor PJ (2010) Absolute diffusivities define the landscape of white matter degeneration in Alzheimer's disease. *Brain* **133**, 529-539.

[6] He Y, Chen Z, Gong G, Evans A (2009) Neuronal networks in Alzheimer's disease. *Neuroscientist* **15**, 333-350.

[7] Scola E, Bozzali M, Agosta F, Magnani G, Franceschi M, Sormani MP, Cercignani M, Pagani E, Falautano M, Filippi M, Falini A (2010) A diffusion tensor MRI study of patients with MCI and AD with a 2-year clinical follow-up. *J Neurol Neurosurg Psychiatry* **81**, 798-805.

[8] Basser PJ, Mattiello J, LeBihan D (1994) MR diffusion tensor spectroscopy and imaging. *Biophys J* **66**, 259-267.

[9] Basser PJ, Pajevic S, Pierpaoli C, Duda J, Aldroubi A (2000) *In vivo* fiber tractography using DT-MRI data. *Magn Reson Med* **44**, 625-632.

[10] Chua TC, Wen W, Slavin MJ, Sachdev PS (2008) Diffusion tensor imaging in mild cognitive impairment and Alzheimer's disease: a review. *Curr Opin Neurol* **21**, 83-92.

[11] Bozzali M, Cherubini A (2007) Diffusion tensor MRI to investigate dementias: a brief review. *Magn Reson Imaging* **25**, 969-977.

[12] Pierpaoli C, Basser PJ (1996) Toward a quantitative assessment of diffusion anisotropy. *Magn Reson Med* **36**, 893-906.

[13] Le Bihan D, Mangin JF, Poupon C, Clark CA, Pappata S, Molko N, Chabriat H (2001) Diffusion tensor imaging: concepts and applications. *J Magn Reson Imaging* **13**, 534-546.

[14] Kanaan RA, Kim JS, Kaufmann WE, Pearlson GD, Barker GJ, McGuire PK (2005) Diffusion tensor imaging in schizophrenia. *Biol Psychiatry* **58**, 921-929.

[15] Schneiderman JS, Buchsbaum MS, Haznedar MM, Hazlett EA, Brickman AM, Shihabuddin L, Brand JG, Torosjan Y, Newmark RE, Canfield EL, Tang C, Aronowitz J, Paul-Odouard R, Hof PR (2009) Age and diffusion tensor anisotropy in adolescent and adult patients with schizophrenia. *Neuroimage* **45**, 662-671.

[16] Medina D, DeToledo-Morrell L, Urresta F, Gabrieli JD, Moseley M, Fleischman D, Bennett DA, Leurgans S, Turner DA, Stebbins GT (2006) White matter changes in mild cognitive impairment and AD: A diffusion tensor imaging study. *Neurobiol Aging* **27**, 663-672.

[17] Hasan KM (2006) Diffusion tensor eigenvalues or both mean diffusivity and fractional anisotropy are required in quantitative clinical diffusion tensor MR reports: fractional anisotropy alone is not sufficient. *Radiology* **239**, 611-612; author reply 612-613.

[18] Bennett IJ, Madden DJ, Vaidya CJ, Howard DV, Howard JH, Jr. (2010) Age-related differences in multiple measures of white matter integrity: A diffusion tensor imaging study of healthy aging. *Hum Brain Mapp* **31**, 378-390.

[19] Song SK, Sun SW, Ramsbottom MJ, Chang C, Russell J, Cross AH (2002) Dysmyelination revealed through MRI as increased radial (but unchanged axial) diffusion of water. *Neuroimage* **17**, 1429-1436.

[20] Stricker NH, Schweinsburg BC, Delano-Wood L, Wierenga CE, Bangen KJ, Haaland KY, Frank LR, Salmon DP, Bondi MW (2009) Decreased white matter integrity in late-myelinating fiber pathways in Alzheimer's disease supports retrogenesis. *Neuroimage* **45**, 10-16.

[21] Pierpaoli C, Barnett A, Pajevic S, Chen R, Penix LR, Virta A, Basser P (2001) Water diffusion changes in Wallerian degeneration and their dependence on white matter architecture. *Neuroimage* **13**, 1174-1185.

[22] Song SK, Sun SW, Ju WK, Lin SJ, Cross AH, Neufeld AH (2003) Diffusion tensor imaging detects and differentiates axon and myelin degeneration in mouse optic nerve after retinal ischemia. *Neuroimage* **20**, 1714-1722.

[23] Sun SW, Liang HF, Trinkaus K, Cross AH, Armstrong RC, Song SK (2006) Noninvasive detection of cuprizone induced axonal damage and demyelination in the mouse corpus callosum. *Magn Reson Med* **55**, 302-308.

[24] Huang J, Friedland RP, Auchus AP (2007) Diffusion tensor imaging of normal-appearing white matter in mild cognitive impairment and early Alzheimer disease: preliminary evidence of axonal degeneration in the temporal lobe. *AJNR Am J Neuroradiol* **28**, 1943-1948.

[25] Smith SM, Jenkinson M, Johansen-Berg H, Rueckert D, Nichols TE, Mackay CE, Watkins KE, Ciccarelli O, Cader MZ, Matthews PM, Behrens TE (2006) Tract-based spatial statistics: voxelwise analysis of multi-subject diffusion data. *Neuroimage* **31**, 1487-1505.

[26] Liu Y, Spulber G, Lehtimaki KK, Kononen M, Hallikainen I, Grohn H, Kivipelto M, Hallikainen M, Vanninen R, Soininen H (2009) Diffusion tensor imaging and Tract-based spatial statistics in Alzheimer's disease and mild cognitive impairment. *Neurobiol Aging*. doi:10.1016/j.neurobiolaging.2009.10.006.

[27] Serra L, Cercignani M, Lenzi D, Perri R, Fadda L, Caltagirone C, Macaluso E, Bozzali M (2010) Grey and white matter changes at different stages of Alzheimer's disease. *J Alzheimers Dis* **19**, 147-159.

[28] Damoiseaux JS, Smith SM, Witter MP, Sanz-Arigita EJ, Barkhof F, Scheltens P, Stam CJ, Zarei M, Rombouts SA (2009) White matter tract integrity in aging and Alzheimer's disease. *Hum Brain Mapp* **30**, 1051-1059.

[29] Smith CD, Chebrolu H, Andersen AH, Powell DA, Lovell MA, Xiong S, Gold BT (2010) White matter diffusion alterations in normal women at risk of Alzheimer's disease. *Neurobiol Aging* **31**, 1122-1131.

[30] Bosch B, Arenaza-Urquijo EM, Rami L, Sala-Llonch R, Junque C, Sole-Padulles C, Pena-Gomez C, Bargallo N, Molinuevo JL, Bartres-Faz D (2010) Multiple DTI index analysis in normal aging, amnestic MCI and AD. Relationship with neuropsychological performance. *Neurobiol Aging*. doi:10.1016/j.neurobiolaging.2010.02.004.

[31] Agosta F, Pievani M, Sala S, Geroldi C, Galluzzi S, Frisoni GB, Filippi M (2011) White matter damage in Alzheimer disease and its relationship to gray matter atrophy. *Radiology* **258**, 853-863.

[32] American Psychiatric Association (1994) (Am. Psychiatric Assoc. Press, Washongton, DC).

[33] Morris JC (1993) The Clinical Dementia Rating (CDR): current version and scoring rules. *Neurology* **43**, 2412-2414.

[34] Petersen RC, Smith GE, Waring SC, Ivnik RJ, Tangalos EG, Kokmen E (1999) Mild cognitive impairment: clinical characterization and outcome. *Arch Neurol* **56**, 303-308.

[35] Smith SM, Nichols TE (2009) Threshold-free cluster enhancement: addressing problems of smoothing, threshold dependence and localisation in cluster inference. *Neuroimage* **44**, 83-98.

[36] Bozzali M, Falini A, Franceschi M, Cercignani M, Zuffi M, Scotti G, Comi G, Filippi M (2002) White matter damage in Alzheimer's disease assessed *in vivo* using diffusion tensor magnetic resonance imaging. *J Neurol Neurosurg Psychiatry* **72**, 742-746.

[37] Xie S, Xiao JX, Gong GL, Zang YF, Wang YH, Wu HK, Jiang TZ (2006) Voxel-based detection of white matter abnormalities in mild Alzheimer disease. *Neurology* **66**, 1845-1849.

[38] Rose SE, Chen F, Chalk JB, Zelaya FO, Strugnell WE, Benson M, Semple J, Doddrell DM (2000) Loss of connectivity in Alzheimer's disease: an evaluation of white matter tract integrity with colour coded MR diffusion tensor imaging. *J Neurol Neurosurg Psychiatry* **69**, 528-530.

[39] Zhang Y, Schuff N, Jahng GH, Bayne W, Mori S, Schad L, Mueller S, Du AT, Kramer JH, Yaffe K, Chui H, Jagust WJ, Miller BL, Weiner MW (2007) Diffusion tensor imaging of cingulum fibers in mild cognitive impairment and Alzheimer disease. *Neurology* **68**, 13-19.

[40] Xie S, Xiao JX, Wang YH, Wu HK, Gong GL, Jiang XX (2005) Evaluation of bilateral cingulum with tractography in patients with Alzheimer's disease. *Neuroreport* **16**, 1275-1278.

[41] Huang J, Auchus AP (2007) Diffusion tensor imaging of normal appearing white matter and its correlation with cognitive functioning in mild cognitive impairment and Alzheimer's disease. *Ann N Y Acad Sci* **1097**, 259-264.

[42] Sorg C, Riedl V, Muhlau M, Calhoun VD, Eichele T, Laer L, Drzezga A, Forstl H, Kurz A, Zimmer C, Wohlschlager AM (2007) Selective changes of resting-state networks in individ-

uals at risk for Alzheimer's disease. *Proc Natl Acad Sci U S A* **104**, 18760-18765.

[43] Nestor PJ, Fryer TD, Smielewski P, Hodges JR (2003) Limbic hypometabolism in Alzheimer's disease and mild cognitive impairment. *Ann Neurol* **54**, 343-351.

[44] Qi Z, Wu X, Wang Z, Zhang N, Dong H, Yao L, Li K (2010) Impairment and compensation coexist in amnestic MCI default mode network. *Neuroimage* **50**, 48-55.

[45] Fellgiebel A, Muller MJ, Wille P, Dellani PR, Scheurich A, Schmidt LG, Stoeter P (2005) Color-coded diffusion-tensor-imaging of posterior cingulate fiber tracts in mild cognitive impairment. *Neurobiol Aging* **26**, 1193-1198.

[46] Hagmann P, Cammoun L, Gigandet X, Meuli R, Honey CJ, Wedeen VJ, Sporns O (2008) Mapping the structural core of human cerebral cortex. *PLoS Biol* **6**, e159.

[47] Bullmore E, Sporns O (2009) Complex brain networks: graph theoretical analysis of structural and functional systems. *Nat Rev Neurosci* **10**, 186-198.

[48] Gong G, He Y, Concha L, Lebel C, Gross DW, Evans AC, Beaulieu C (2009) Mapping anatomical connectivity patterns of human cerebral cortex using *in vivo* diffusion tensor imaging tractography. *Cereb Cortex* **19**, 524-536.

[49] He Y, Chen Z, Evans A (2008) Structural insights into aberrant topological patterns of large-scale cortical networks in Alzheimer's disease. *J Neurosci* **28**, 4756-4766.

[50] Lerch JP, Pruessner JC, Zijdenbos A, Hampel H, Teipel SJ, Evans AC (2005) Focal decline of cortical thickness in Alzheimer's disease identified by computational neuroanatomy. *Cereb Cortex* **15**, 995-1001.

[51] Singh V, Chertkow H, Lerch JP, Evans AC, Dorr AE, Kabani NJ (2006) Spatial patterns of cortical thinning in mild cognitive impairment and Alzheimer's disease. *Brain* **129**, 2885-2893.

[52] Greicius MD, Srivastava G, Reiss AL, Menon V (2004) Default-mode network activity distinguishes Alzheimer's disease from healthy aging: evidence from functional MRI. *Proc Natl Acad Sci U S A* **101**, 4637-4642.

[53] He Y, Wang L, Zang Y, Tian L, Zhang X, Li K, Jiang T (2007) Regional coherence changes in the early stages of Alzheimer's disease: a combined structural and resting-state functional MRI study. *Neuroimage* **35**, 488-500.

[54] Morbelli S, Piccardo A, Villavecchia G, Dessi B, Brugnolo A, Piccini A, Caroli A, Frisoni G, Rodriguez G, Nobili F (2010)

Mapping brain morphological and functional conversion patterns in amnestic MCI: a voxel-based MRI and FDG-PET study. *Eur J Nucl Med Mol Imaging* **37**, 36-45.

[55] Beaulieu C (2002) The basis of anisotropic water diffusion in the nervous system - a technical review. *NMR Biomed* **15**, 435-455.

[56] Beaulieu C, Does MD, Snyder RE, Allen PS (1996) Changes in water diffusion due to wallerian degeneration in peripheral nerve. *Magn Reson Med* **36**, 627-631.

[57] Song SK, Yoshino J, Le TQ, Lin SJ, Sun SW, Cross AH, Armstrong RC (2005) Demyelination increases radial diffusivity in corpus callosum of mouse brain. *Neuroimage* **26**, 132-140.

[58] Roosendaal SD, Geurts JJ, Vrenken H, Hulst HE, Cover KS, Castelijns JA, Pouwels PJ, Barkhof F (2009) Regional DTI differences in multiple sclerosis patients. *Neuroimage* **44**, 1397-1403.

[59] Bartzokis G (2004) Age-related myelin breakdown: a developmental model of cognitive decline and Alzheimer's disease. *Neurobiol Aging* **25**, 5-18; author reply 49-62.

[60] Oouchi H, Yamada K, Sakai K, Kizu O, Kubota T, Ito H, Nishimura T (2007) Diffusion anisotropy measurement of brain white matter is affected by voxel size: underestimation occurs in areas with crossing fibers. *AJNR Am J Neuroradiol* **28**, 1102-1106.

[61] Wedeen VJ, Hagmann P, Tseng WY, Reese TG, Weisskoff RM (2005) Mapping complex tissue architecture with diffusion spectrum magnetic resonance imaging. *Magn Reson Med* **54**, 1377-1386.

[62] Wedeen VJ, Wang RP, Schmahmann JD, Benner T, Tseng WY, Dai G, Pandya DN, Hagmann P, D'Arceuil H, de Crespigny AJ (2008) Diffusion spectrum magnetic resonance imaging (DSI) tractography of crossing fibers. *Neuroimage* **41**, 1267-1277.

[63] Tuch DS (2004) Q-ball imaging. *Magn Reson Med* **52**, 1358-1372.

[64] Hess CP, Mukherjee P, Han ET, Xu D, Vigneron DB (2006) Q-ball reconstruction of multimodal fiber orientations using the spherical harmonic basis. *Magn Reson Med* **56**, 104-117.

[65] Petersen RC, Doody R, Kurz A, Mohs RC, Morris JC, Rabins PV, Ritchie K, Rossor M, Thal L, Winblad B (2001) Current concepts in mild cognitive impairment. *Arch Neurol* **58**, 1985-1992.

This page intentionally left blank

DTI Analyses and Clinical Applications in Alzheimer's Disease

Kenichi Oishi[a,*], Michelle M. Mielke[b], Marilyn Albert[c], Constantine G. Lyketsos[b] and Susumu Mori[a,d]

[a]*The Russell H. Morgan Department of Radiology and Radiological Science, School of Medicine, The Johns Hopkins University Baltimore, MD, USA*
[b]*Department of Psychiatry and Behavioral Sciences, School of Medicine, The Johns Hopkins University, Baltimore, MD, USA*
[c]*Department of Neurology, School of Medicine, The Johns Hopkins University, Baltimore, MD, USA*
[d]*F.M. Kirby Research Center for Functional Brain Imaging, Kennedy Krieger Institute, Baltimore, MD, USA*

Abstract. DTI is one of the most effective MR tools for the investigation of the brain anatomy. In addition to the gray matter, histopathological studies indicate that white matter is also a good target for both the early diagnosis of AD and for monitoring disease progression, which motivates us to use DTI to study AD patients *in vivo*. There are already a large amount of studies reporting significant differences between AD patients and controls, as well as to predict progression of disease in symptomatic non-demented individuals. Application of these findings in clinical practice remains to be demonstrated.

Keywords: Alzheimer's disease, mild cognitive impairment, white matter, diffusion tensor imaging, clinical application

INTRODUCTION: WHAT IS DTI?

Diffusion Tensor Imaging (DTI) is one of the MRI techniques that can measure the thermal motion of water molecules. Water molecules move randomly in all directions if there is no structure that prevents their free motion; this probability distribution is isotropic. In the brain, there are many structures that restrict the free motion of water molecules, such as tightly packed axons [1, 2], that alter the magnitude and shape of the probability distribution. For example, water molecules in white matter tend to diffuse more easily along axonal bundles, leading to anisotropic diffusion. On the other hand, the gray matter often does not have a clear structural alignment, leading to a more isotropic diffusion.

We can use this water diffusion property as a probe to infer the brain anatomy. In DTI, we quantify the diffusion property by fitting the measured water diffusion to a simple tensor model with a 3×3 symmetric matrix. In this way, we can quantitatively describe the diffusion properties using eigenvalues (λ_1, λ_2, and λ_3, describing the extent of anisotropy) and eigenvectors, (v_1, v_2, and v_3, describing the orientation of anisotropy).

Once a tensor is calculated in each pixel, several contrasts can be generated. For example, we can measure the mean diffusivity (MD), which is the average of three eigenvalues: $(\lambda_1 + \lambda_2 + \lambda_3)/3$, indicating the magnitude of overall water diffusion in each pixel (Fig. 1C). We can also measure the degree of diffusion anisotropy. One of the most widely used metrics of diffusion anisotropy is "fractional anisotropy (FA)," which is [3, 4] (Fig. 1D):

$$FA = \sqrt{\frac{1}{2}} \frac{\sqrt{((\lambda_1 - \lambda_2)^2 + (\lambda_2 - \lambda_3)^2 + (\lambda_3 - \lambda_1)^2)}}{\sqrt{\lambda_1{}^2 + \lambda_2{}^2 + \lambda_3{}^2}}$$

---

*Correspondence to: Kenichi Oishi, MD, PhD, The Russell H. Morgan Department of Radiology and Radiological Science, The Johns Hopkins University School of Medicine, 217 Traylor Building, 720 Rutland Avenue, Baltimore, MD 21205, USA. Work: 410 502 3553; E-mail: koishi@mri.jhu.edu.

This is a convenient index because it is scaled from 0 (isotropic) – 1 (anisotropic). If diffusion is isotropic ($\lambda_1 = \lambda_2 = \lambda_3$), this measure becomes 0. An FA close to 1 indicates high diffusion anisotropy. In addition to these scalar measures, we can also visualize orientation information. A color-coded orientation map of the first eigenvector (v_1) [5, 6] is one method to visualize orientation information, in which red (R), green (G), and blue (B) colors are assigned to right-left, anterior-posterior, and superior-inferior orientations, respectively. in Fig. 1, images created from DTI measurements are compared with conventional MR images. In conventional MRI (Fig. 1A and B), the white matter area looks homogeneous. However, the color-coded orientation map in Fig. 1E contains various colors in the white matter area, which represent the orientation of aligned structures.

DTI is a powerful method by which to identify specific fiber bundles that are affected by diseases. Various pathological conditions alter DTI-derived parameters and we can three-dimensionally map the area(s) that show such alterations. The other important feature of DTI is the ability to parcellate white matter structures. Using the images shown in Fig. 1E, we can identify and study the degeneration of specific white matter structures, such as the cingulum (Fig. 1F). It should be emphasized that, in imaging studies, we can investigate the anatomy of a specific structure only when it is discretely identifiable. Because of the capability to provide detailed anatomical information about the white matter, DTI could be one of the most effective MR tools for the investigation of the white matter anatomy. Although the use of DTI is not restricted to studies of the white matter, the majority of DTI stud-
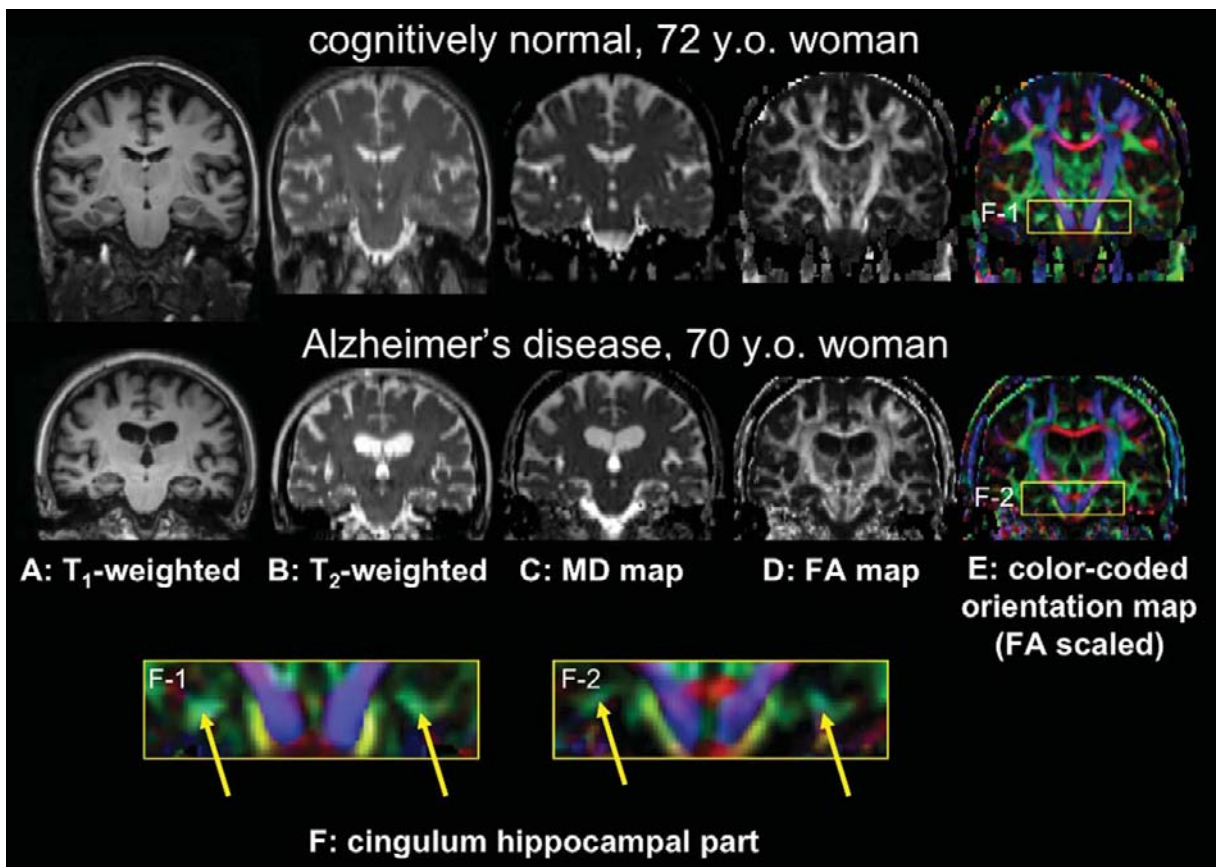

Fig. 1. Comparison of conventional T1- (A) and T2- (B) weighted images, and DTI-derived mean diffusivity (MD) (C), fractional anisotropy (FA) (D), and color-coded orientation (E) maps of cognitively normal 72-year-old woman (upper row) and 70-year-old woman with Alzheimer's disease. The areas surrounded by yellow rectangles in (E) are magnified and shown in (F) [left (F-1): from the cognitively normal woman; right (F-2): the Alzheimer's disease patient]. The yellow arrows indicate the cingulum hippocampal part.

ies are related to the normal or diseased anatomy of the white matter. However, directional information derived from DTI is less useful for investigating gray matter structures, except for several fiber-rich gray matter structures [7–12] and the fetal cortex, with the columnar structures showing clear directionality [13]. For the gray matter analysis, MD is often used to quantify the effects of various diseases.

Although DTI meets the requirements of many basic and clinical research purposes, the two main limitations should be noted. First, water diffusion is an INDIRECT indicator of the underlying neuroanatomy, and there are numerous microscopic structures that may affect the diffusion. Therefore, different histopathological conditions may result in similar alterations of DTI-derived parameters. Second, the diffusion process (1–10 μm during the 20–100 ms of diffusion time) is averaged over a large voxel volume, with typically 2–3 mm resolution. This leads to the sensitivity of DTI to macroscopic configuration of fiber bundles, such as the mixture of multiple fiber populations with different fiber orientations in a voxel or partial volume effects. Therefore, we cannot immediately conclude whether the source of changes in diffusion lies in cellular level structures or is due to the macroscopic reorganization of fiber structures. There have been several attempts to ameliorate the latter limitation (thus reducing the impact of the macroscopic averaging effect). For example, we can increase the total number of voxels within the brain(= increased image resolution). We can also extract more parameters from each voxel(= increased intra-voxel information) by using sophisticated non-tensor diffusion analysis methods rather than using a simple tensor approach [14–21]. The application of these new approaches to AD studies could be an important future research endeavor.

Recent technological advancements in both hardware (machine) and software (scan sequence) have greatly facilitated the use of DTI, and broadened the applications much more than was previously possible. The typical scan time required to gather whole brain DTI data using a 3 T scanner is only approximately 5 min, with 30 gradient axes and 2–3 mm cubic resolution. The short scanning time is very important because AD patients have difficulty remembering and following instructions during the scan, and thus, scanning in as short a time as possible is optimal. MRI scanners, equipped with devices for parallel imaging techniques, which are required to gather less-distorted DTI, are now widely available. In addition, modern clinical MRI scanners are equipped with DTI calculation tools, and the calculated images can be visualized in a filmless image-reading system. Thus, it may be possible for the clinician to utilize DTI-derived images as part of the diagnostic evaluation.

WHAT IS THE POTENTIAL OF DTI TO EVALUATE THE AD BRAIN?

Researchers have long been focused on the cortical pathology of Alzheimer's disease (AD), and have primarily used conventional MRI to characterize that pathology. Indeed, the most important pathologic features of AD are the senile plaques and the neurofibrillary tangles found in the cortex, as well as the cortical neuron loss. For instance, the loss of layer III and layer V large pyramidal neurons is seen in cortical association areas [22] and the loss of layer II pyramidal neurons is seen in the entorhinal cortex [23]. Loss of neurons in these areas results in GM atrophy that can be measured on conventional MR images [24, 25]. DTI has also identified altered water diffusivity in the GM. Increased MD was consistently found in the areas with the neurofibrillary pathology of AD [10, 26–30], such as the hippocampus, the entorhinal cortex, the parahippocampal gyrus, the temporo-parietal association cortex, and the posterior cingulate gyrus. Although the exact cause of these changes in DTI measurements are difficult to identify, the fact that the degree of MD increase is more evident in the areas with GM atrophy [26] suggest that neuronal loss [31] is one of the reasons. In addition, several studies indicate that the addition of MD measurements to GM morphometry in the hippocampus and parahippocampal gyrus improved the ability to distinguish an AD group from a control group [26, 28], which suggests the possibility of the existence of additional pathologies sensitively detected by DTI over conventional MRI.

In addition to the GM pathology, increasing evidence shows that neuronal degeneration begins in the neuronal periphery, such as in the axons and dendrites [32–35]. White matter atrophy also could be an indirect indicator of nerve cell loss, since the volume of the cell body is much smaller than its myelinated fiber [36]. Consistently, pathological studies have revealed various types of white matter alterations in AD, such as altered myelin and oligodendrocytes, axonal degeneration, and vascular pathologies [37–39]. Therefore, white matter seems to be a good target for both the early diagnosis of AD and for monitoring disease

progression, which motivates us to use DTI to study AD patients *in vivo*. Indeed, DTI has identified WM alterations in many WM tracts and superficially located WM areas. A meta-analysis of 41 DTI studies, published from 2002 to 2010 [40], indicates that the white matter abnormality of AD is widespread through the entire WM area. The limbic fibers, in particular, which have a direct connection to the medial temporal lobe, were repeatedly reported as the vulnerable WM structures [29, 41–49]. WM damage quantified by DTI has been correlated with atrophy in the anatomically connected GM areas in AD patients, but the correlation was not clear in patients with amnestic MCI in most of the WM tracts [50]. These findings suggest that primary WM damage that precedes GM atrophy may possibly exists in the pre-diagnostic phase of AD, but the WM damage seen in clinically diagnosed AD patients may reflect secondary degenerative processes after neuronal loss. An attempt to identify the earliest DTI-detectable WM abnormality using an AD mouse model identified a reduced first eigenvalue (l_1, parallel diffusion) in the WM, suggesting that the earliest anatomical change is axonal damage [51]. However, in contrast to this finding, an increased first eigenvalue, as well as increased MD, is often found in *in vivo* DTI scans of human AD patients [48, 52, 53]. Again, we would like to emphasize that, because of the oversimplification of the anatomical information during the multiple steps of DTI acquisition and calculation, interpretation of the DTI-derived parameters is not straightforward. DTI is useful for localizing and quantifying the anatomical abnormalities, but apparently not adequate to investigate the histopathological background of the diseases.

STRATEGIES TO INVESTIGATE THE PATHOLOGICAL FEATURES OF AD USING DTI

There are many important questions we want to answer through DTI analysis of AD. For example, what are the AD-specific features that can be observed with DTI? Can these features be observed in persons with mild cognitive impairment, thought to be the earliest symptomatic stage of AD, or even in the pre-symptomatic phase? How does DTI reflect or predict the progression of AD? Are there correlations between DTI and cognitive functions? To answer these questions, the quantification of DTI parameters is the first important step.

Several issues arise when we quantify DTI results. First, regions of interest (ROI) should be defined to measure DTI-derived parameters, such as FA or MD. The smallest ROI we can define is a single voxel, and the maximum ROI is the whole brain. The localization information is maximized when the smallest ROI (single voxel) is adopted, but the statistical power is lost because of the low signal-to-noise ratio and the difficulty of identifying the corresponding voxel across subjects. The statistical power is maximized when the size and shape of the ROI exactly follow pathological locations. If we have an *a priori* hypothesis about the locations of the pathologic tissues, we could pre-define the size and shape of ROIs according to the hypothesis. If we hypothesize that the pathology is seen in specific fiber tracts, we can use tractography to draw ROIs (tract-specific analysis, see, eg. [54, 55]). ROI-based DTI analyses have been widely used for AD studies and have successfully identified reduced FA or increased MD, or both, within the splenium of the corpus callosum [47, 56–59], the cingulum bundle [11, 27, 42, 60–62], and the fornix [43, 44]. However, this approach is hypothesis-dependent, and the majority of the brain area remains unexamined, which makes it difficult to evaluate the localization specificity.

Second, we need to decide whether we should explore the whole brain or limited areas of the brain. Whole brain analysis is ideal for evaluating the regional specificity of the findings. However, drawing a number of ROIs manually that would cover the whole brain is a tremendous effort. Thus, automated method, such as those based on image normalization (transformation), are typically used. After transforming images to a common template space (atlas), we can even quantify the image at the voxel level (voxel-based analysis). Although image normalization has been widely used to analyze conventional MRI contrasts, the transformation of DTI poses a unique challenge. DTI data consists of tensor fields (as opposed to scalar fields for conventional MRI), and white matter tracts revealed by the tensor field must be registered after normalization [63, 64]. To avoid false-positive and false-negative findings, the accuracy of the registration is a crucial requirement. Accuracy is especially critical when dealing with small structures, string-like structures, and sheet-like structures, which are often found in the white matter. In these structures, only a few pixel gaps between the subject and template image will cause significant missregistration.

Various non-linear transformation methods have been proposed for DTI analyses, such as tensor-to-

tensor matching [65–69], scalar measures matching [69, 70], or other DTI-derived information, as well as some combination of these methods [71–75]. Transformation methods based on non-DTI contrasts have also been applied to transform DTI, with high registration accuracy [64, 76].

To perform whole brain analysis with no *a priori* hypothesis, voxel-based analysis is one of the most widely used approaches [29, 52, 77–79]. Fig. 2A is an example of such an analysis, designed to find brain areas with AD-specific white matter alterations. This analysis indicates significant FA reduction in the fornix, the splenium of the corpus callosum, as well as several small areas in the superficial white matter in the frontal lobe. Although this result seems to be consistent with previous ROI-based investigations, we must interpret the results with great caution, since this approach tends to miss the widely distributed regions that show only small changes in the parameters [80]. One of the attempts to overcome such limitations is to apply multivariate models [81], such principal component analysis (PCA) [78] or canonical correlation analysis (CCA) [82], which have already been applied to DTI analysis of AD. Other methods include voxel grouping. For example, if we hypothesize that the white matter pathology of AD is tract-specific or structure-specific, especially in the early stages, we may apply tract-based voxel grouping, such as Tract-Based Spatial Statistics (TBSS) [83], or structure-based voxel grouping, such as atlas-based analysis (ABA) [84]. Indeed, TBSS has already revealed important findings, such as deteriorations in the limbic fibers, the fronto-occipital fasciculi, the inferior longitudinal fasciculi, and the forceps major, even in the early-symptomatic patients or in participants at high risk for developing AD [45, 53, 85–90]. ABA is a method that uses a set of pre-defined ROIs, called a parcellation map (Fig. 3), which covers the entire brain, in the atlas space. The parcellation map can be overlaid on the images normalized to the atlas space to measure DTI-derived parameters (eg., FA or MD) in each ROI (parcel), or can be transformed to each image to measure DTI-derived parameters as well as the volumes of each ROI. One additional feature that sets the ABA apart from TBSS is that ABA provides morphometric (volume) information about brain atrophy in the volume of each parcel. Our initial results from ABA (Fig. 2B) indicate a higher sensitivity for ABA in detecting changes in FA, especially in the areas with widely distributed small FA reductions, compared to the voxel-based analysis. The drawback of this approach is that if the region is limited in the small portion of the structure (parcel), the effect is diluted and sensitivity is decreased.
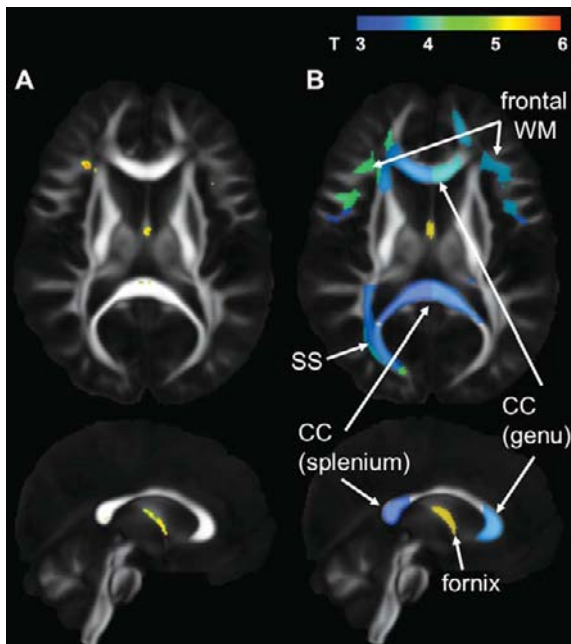

Fig. 2. Statistical group comparison of FA after image normalization. Nineteen patients with Alzheimer's disease and 22 age-matched cognitively normal participants were compared, and the areas with significance (*t*-test, $p < 0.05$ after correction for multiple comparisons using a false discovery rate) were shown with color scaling overlaid on the averaged FA map (A): Results from voxel-based analysis. (B): Results from atlas-based analysis. See Fig. 3. for the parcellation map used in this atlas-based analysis. CC, corpus callosum; SS, sagittal stratum; WM, white matter.

APPLICATION OF DTI TO AD RESEARCH AND CLINICAL PRACTICE

In the previous section, we discussed the detection of AD-specific pathology using DTI. There are already a large amount of studies reporting structure-specific brain abnormalities even in the very early stages of AD. In this section, we would like to discuss the application of DTI to studies of AD from the following two points of views.

Functional correlation

One of the important questions after the identification and quantification of structure-specific brain abnormalities is whether the degree of abnormalities correlates with cognitive functions. For example, even
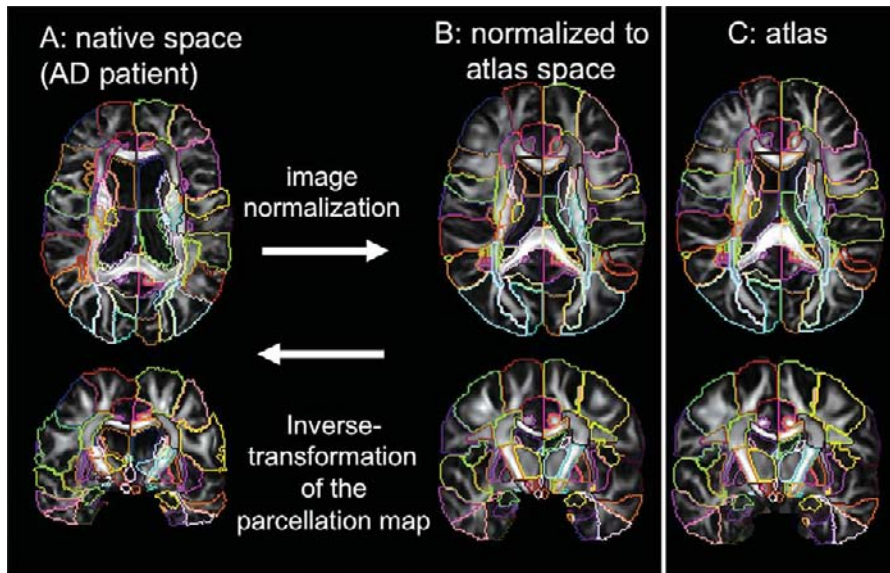
Fig. 3. Atlas-based analysis. The original FA map from a patient with Alzheimer's disease (A) was normalized to the atlas space (B). The atlas used as the template is shown in (C). After image normalization, pre-defined three-dimensional ROIs (color-contours, called a parcellation map) in the atlas space enables researchers to measure the FA value of each parcel. This parcellation map can be inversely transformed to the original space to measure the volume of each parcel, as well as to measure the FA value of each parcel without normalization-related artifacts (eg., effects of interpolation after normalization).

if we find reduced FA in a specific brain area, if the observed FA reduction does not correlate with the cognitive decline, the finding is not valuable as a marker to visualize the disease progression or to see the effects of therapeutic interventions. Research has identified the disruption of global WM [56], the frontal WM [91], or specific WM tracts, including the fornix, the cingulum, the cingulate WM, the genu and splenium of the corpus callosum, and the perforant pathway, which are related to global cognitive decline [44, 47, 92, 93]. Less is known about the tract or structure-specific contribution of cognitive domains, although several researchers have discovered a contribution by the temporal lobe WM [94, 95] and the posterior cingulate WM [10] to delayed recall, the frontal WM to executive function [95], and the posterior part of the corpus callosum to verbal fluency and figural memory [96]. However, the localization specificity of these findings has not been established, since these studies are based on a limited number of ROIs selected by an *a priori* hypothesis. Unfortunately, the anatomical background of the behavioral and psychiatric symptoms of AD, which are the most challenging and distressing effects of the disease, has not been fully explored.

Clinical application

AD studies typically adopt cognitively normal participants as a control group to identify AD-specific features. However, in the clinical situation, identification of AD-specific DTI markers would be of great value to differentiate it from other neurodegenerative dementias, such as frontotemporal dementia (FTD) and dementia with Lewy bodies (DLB). There are studies reporting more prominent DTI-detectable WM damage, especially in the frontal WM and the genu of the corpus callosum, in FTD than in AD [52, 82]. Although DTI findings about the DLB are controversial [26, 28, 97, 98], elevated MD without atrophy in the amygdala was proposed as a potential marker to differentiate DLB from AD [26]. However, the sensitivity and the specificity of the DTI-based indices to differentiate AD from these neurodegenerative dementias is still not established.

In summary, many of the scientific findings, to date, are not readily transferrable to clinical practice, even though the findings are important for understanding of the pathology of AD. A multi-center research project, seeking imaging biomarkers for AD, the Alzheimer's

Disease Neuroimaging Initiative (ADNI, ADNI-GO) [99], and the upcoming ADNI-2, did not adopt DTI as a core protocol because of the uncertain long-term test-retest precision, questionable relevance to clinical trials, and absence of an established calibration method [100], all of which should be thoroughly investigated before clinical application.

CONCLUSIONS

DTI measures have been used to demonstrate significant differences between AD patients and controls, as well as to predict progression of disease in symptomatic non-demented individuals. Application of these findings in clinical practice remains to be demonstrated.

ACKNOWLEDGMENTS

REFERENCES

[1] Beaulieu C, Allen PS (1994) Determinants of anisotropic water diffusion in nerves. *Magn Reson Med* **31**, 394-400.

[2] Moseley ME, Cohen Y, Kucharczyk J, Mintorovitch J, Asgari HS, Wendland MF, Tsuruda J, Norman D (1990) Diffusion-weighted MR imaging of anisotropic water diffusion in cat central nervous system. *Radiology* **176**, 439-445.

[3] Pierpaoli C, Basser PJ (1996) Toward a quantitative assessment of diffusion anisotropy. *Magn Reson Med* **36**, 893-906.

[4] Pierpaoli C, Jezzard, P, Basser PJ, Barnett A, Di Chiro G (1996) Diffusion tensor MR imaging of human brain. *Radiology* **201**, 637-648.

[5] Makris N, Worth AJ, Sorensen AG, Papadimitriou GM, Wu O, Reese TG, Wedeen VJ, Davis TL, Stakes JW, Caviness VS, Kaplan E, Rosen BR, Pandya DN, Kennedy DN (1997) Morphometry of in vivo human white matter association pathways with diffusion-weighted magnetic resonance imaging. *Ann Neurol* **42**, 951-962.

[6] Pajevic S, Pierpaoli C (1999) Color schemes to represent the orientation of anisotropic tissues from diffusion tensor data: application to white matter fiber tract mapping in the human brain. *Magn Reson Med* **42**, 526-540.

[7] Unrath A, Klose U, Grodd W, Ludolph AC, Kassubek J (2008) Directional colour encoding of the human thalamus by diffusion tensor imaging. *Neurosci Lett* **434**, 322-327.

[8] Duan Y, Li X, Xi Y (2007) Thalamus segmentation from diffusion tensor magnetic resonance imaging. *Int J Biomed Imagin* **2007**, 90216.

[9] Wakana S, Nagae-Poetscher LM, Jiang H, van Zijl P, Golay X, Mori S (2005) Macroscopic orientation component analysis of brain white matter and thalamus based on diffusion tensor imaging. *Magn Reson Med* **53**, 649-657.

[10] Fellgiebel A, Wille P, Muller MJ, Winterer G, Scheurich A, Vucurevic G, Schmidt LG, Stoeter P (2004) Ultrastructural hippocampal and white matter alterations in mild cognitive impairment: a diffusion tensor imaging study. *Dement Geriatr Cogn Disord* **18**, 101-108.

[11] Takahashi S, Yonezawa H, Takahashi J, Kudo M, Inoue T, Tohgi H (2002) Selective reduction of diffusion anisotropy in white matter of Alzheimer disease brains measured by 3.0 Tesla magnetic resonance imaging. *Neurosci Lett* **332**, 45-48.

[12] Solano-Castiella E, Anwander A, Lohmann G, Weiss M, Docherty C, Geyer S, Reimer E, Friederici AD, Turner R (2010) Diffusion tensor imaging segments the human amygdala in vivo. *Neuroimage* **49**, 2958-2965.

[13] Huang H, Xue R, Zhang J, Ren T, Richards LJ, Yarowsky P, Miller MI, Mori S (2009) Anatomical characterization of human fetal brain development with diffusion tensor magnetic resonance imaging. *J Neurosci* **29**, 4263-4273.

[14] Tuch DS, Reese TG, Wiegell MR, Wedeen VJ (2003) Diffusion MRI of complex neural architecture. *Neuron* **40**, 885-895.

[15] Tuch DS, Reese TG, Wiegell MR, Makris N, Belliveau JW, Wedeen VJ (2002) High angular resolution diffusion imaging reveals intravoxel white matter fiber heterogeneity. *Magn Reson Med* **48**, 577-582.

[16] Wedeen VJ, Hagmann P, Tseng WY, Reese TG, Weisskoff RM (2005) Mapping complex tissue architecture with diffusion spectrum magnetic resonance imaging. *Magn Reson Med* **54**, 1377-1386.

[17] Wiegell M, Larsson H, Wedeen V (2000) Fiber crossing in human brain depicted with diffusion tensor MR imaging. *Radiology* **217**, 897-903.

[18] Alexander DC, Barker GJ, Arridge SR (2002) Detection and modeling of non-Gaussian apparent diffusion coefficient profiles in human brain data. *Magn Reson Med* **48**, 331-340.

[19] Tournier JD, Calamante F, Gadian DG, Connelly A (2004) Direct estimation of the fiber orientation density function from diffusion-weighted MRI data using spherical deconvolution. *Neuroimage* **23**, 1176-1185.

[20] Frank LR (2001) Anisotropy in high angular resolution diffusion-weighted MRI. *Magn Reson Med* **45**, 935-939.

[21] Frank LR (2002) Characterization of anisotropy in high angular resolution diffusion-weighted MRI. *Magn Reson Med* **47**, 1083-1099.

[22] Pearson RC, Esiri MM, Hiorns RW, Wilcock GK, Powell TP (1985) Anatomical correlates of the distribution of the pathological changes in the neocortex in Alzheimer disease. *Proc Natl Acad Sci U S A* **82**, 4531-4534.

[23] Gomez-Isla T, Price JL, McKeel DW Jr, Morris JC, Growdon JH, Hyman BT (1996) Profound loss of layer II entorhinal cortex neurons occurs in very mild Alzheimer's disease. *J Neurosci* **16**, 4491-4500.

[24] Smith AD (2002) Imaging the progression of Alzheimer pathology through the brain. *Proc Natl Acad Sci U S A* **99**, 4135-4137.

[25] Stout JC, Jernigan TL, Archibald SL, Salmon DP (1996) Association of dementia severity with cortical gray matter and abnormal white matter volumes in dementia of the Alzheimer type. *Arch Neurol* **53**, 742-749.

[26] Kantarci K, Avula R, Senjem ML, Samikoglu AR, Zhang B, Weigand SD, Przybelski SA, Edmonson HA, Vemuri P, Knopman DS, Ferman TJ, Boeve BF, Petersen RC, Jack CR, Jr (2010) Dementia with Lewy bodies and Alzheimer disease: neurodegenerative patterns characterized by DTI. *Neurology* **74**, 1814-1821.

[27] Fellgiebel A, Muller MJ, Wille P, Dellani PR, Scheurich A, Schmidt LG, Stoeter P (2005) Color-coded diffusion-tensor-imaging of posterior cingulate fiber tracts in mild cognitive impairment. *Neurobiol Aging* **26**, 1193-1198.

[28] Firbank MJ, Blamire AM, Krishnan MS, Teodorczuk A, English P, Gholkar A, Harrison RM, O'Brien JT (2007) Diffusion tensor imaging in dementia with Lewy bodies and Alzheimer's disease. *Psychiatry Res* **155**, 135-145.

[29] Medina D, DeToledo-Morrell L, Urresta F, Gabrieli JD, Moseley M, Fleischman D, Bennett DA, Leurgans S, Turner DA, Stebbins GT (2006) White matter changes in mild cognitive impairment and AD: A diffusion tensor imaging study. *Neurobiol Aging* **27**, 663-672.

[30] Rose SE, Janke AL, Chalk JB (2008) Gray and white matter changes in Alzheimer's disease: a diffusion tensor imaging study. *J Magn Reson Imaging* **27**, 20-26.

[31] Bobinski M, de Leon MJ, Wegiel J, Desanti S, Convit A, Saint Louis LA, Rusinek H, Wisniewski HM (2000) The histological validation of post mortem magnetic resonance imaging-determined hippocampal volume in Alzheimer's disease. *Neuroscience* **95**, 721-725.

[32] Chevalier-Larsen E, Holzbaur EL (2006) Axonal transport and neurodegenerative disease. *Biochim Biophys Acta* **1762**, 1094-1108.

[33] Stokin GB, Lillo C, Falzone TL, Brusch RG, Rockenstein E, Mount SL, Raman R, Davies P, Masliah E, Williams DS, Goldstein LS (2005) Axonopathy and transport deficits early in the pathogenesis of Alzheimer's disease. *Science* **307**, 1282-1288.

[34] Gunawardena S, Goldstein LS (2001) Disruption of axonal transport and neuronal viability by amyloid precursor protein mutations in Drosophila. *Neuron* **32**, 389-401.

[35] Pigino G, Morfini G, Pelsman A, Mattson MP, Brady ST, Busciglio J (2003) Alzheimer's presenilin 1 mutations impair kinesin-based axonal transport. *J Neurosci* **23**, 4499-4508.

[36] Meier-Ruge W, Ulrich J, Bruhlmann M, Meier E (1992) Age-related white matter atrophy in the human brain. *Ann N Y Acad Sci* **673**, 260-269.

[37] Brun A, Englund E (1986) A white matter disorder in dementia of the Alzheimer type: a pathoanatomical study. *Ann Neurol* **19**, 253-262.

[38] Englund E, Brun A, Alling C (1988) White matter changes in dementia of Alzheimer's type. *Biochemical and neuropathological correlates Brain* **111 Pt(6)**, 1425-1439.

[39] Sjobeck M, Haglund M, Englund E (2005) Decreasing myelin density reflected increasing white matter pathology in Alzheimer's disease–a neuropathological study. *Int J Geriatr Psychiatry* **20**, 919-926.

[40] Sexton CE, Kalu UG, Filippini N, Mackay CE, Ebmeier KP (2010) A meta-analysis of diffusion tensor imaging in mild cognitive impairment and Alzheimer's disease. *Neurobiol Aging*, Epub ahead of print.

[41] Zhou Y, Dougherty JH, Jr, Hubner KF, Bai B, Cannon RL, Hutson RK (2008) Abnormal connectivity in the posterior cingulate and hippocampus in early Alzheimer's disease and mild cognitive impairment. *Alzheimers Dement* **4**, 265-270.

[42] Zhang Y, Schuff N, Jahng GH, Bayne W, Mori S, Schad L, Mueller S, Du AT, Kramer JH, Yaffe K, Chui H, Jagust WJ, Miller BL, Weiner MW (2007) Diffusion tensor imaging of cingulum fibers in mild cognitive impairment and Alzheimer disease. *Neurology* **68**, 13-19.

[43] Ringman JM, O'Neill J, Geschwind D, Medina L, Apostolova LG, Rodriguez Y, Schaffer B, Varpetian A, Tseng B, Ortiz F, Fitten J, Cummings JL, Bartzokis G (2007) Diffusion tensor imaging in preclinical and presymptomatic carriers of familial Alzheimer's disease mutations. *Brain* **130**, 1767-1776.

[44] Mielke MM, Kozauer NA, Chan KC, George M, Toroney J, Zerrate M, Bandeen-Roche K, Wang MC, Vanzijl P, Pekar JJ, Mori S, Lyketsos CG, Albert M (2009) Regionally-specific diffusion tensor imaging in mild cognitive impairment and Alzheimer's disease. *Neuroimage* **46**, 47-55.

[45] Damoiseaux JS, Smith SM, Witter MP, Sanz-Arigita EJ, Barkhof F, Scheltens P, Stam CJ, Zarei M, Rombouts SA (2009) White matter tract integrity in aging and Alzheimer's disease. *Hum Brain Mapp* **30**, 1051-1059.

[46] Kantarci K, Jack CR, Jr, Xu YC, Campeau NG, O'Brien PC, Smith GE, Ivnik RJ, Boeve BF, Kokmen E, Tangalos EG, Petersen RC (2001) Mild cognitive impairment and Alzheimer disease: regional diffusivity of water. *Radiology* **219**, 101-107.

[47] Rose SE, Chen F, Chalk JB, Zelaya FO, Strugnell WE, Benson M, Semple J, Doddrell DM (2000) Loss of connectivity in Alzheimer's disease: an evaluation of white matter tract integrity with colour coded MR diffusion tensor imaging. *J Neurol Neurosurg Psychiatry* **69**, 528-530.

[48] Salat DH, Tuch DS, van der Kouwe AJ, Greve DN, Pappu V, Lee SY, Hevelone ND, Zaleta AK, Growdon JH, Corkin S, Fischl B, Rosas HD (2010) White matter pathology isolates the hippocampal formation in Alzheimer's disease. *Neurobiol Aging* **31**, 244-256.

[49] Stahl R, Dietrich O, Teipel SJ, Hampel H, Reiser MF, Schoenberg SO (2007) White matter damage in Alzheimer disease and mild cognitive impairment: assessment with diffusion-tensor MR imaging and parallel imaging techniques. *Radiology* **243**, 483-492.

[50] Agosta F, Pievani M, Sala S, Geroldi C, Galluzzi S, Frisoni GB, Filippi M (2011) White matter damage in Alzheimer disease and its relationship to gray matter atrophy. *Radiology* **258**, 853-863.

[51] Sun SW, Song SK, Harms MP, Lin SJ, Holtzman DM, Merchant KM, Kotyk JJ (2005) Detection of age-dependent brain injury in a mouse model of brain amyloidosis associated with Alzheimer's disease using magnetic resonance diffusion tensor imaging. *Exp Neurol* **191**, 77-85.

[52] Zhang Y, Schuff N, Du AT, Rosen HJ, Kramer JH, Gorno-Tempini ML, Miller BL, Weiner MW (2009) White matter damage in frontotemporal dementia and Alzheimer's disease measured by diffusion MRI. *Brain* **132**, 2579-2592.

[53] Acosta-Cabronero J, Williams GB, Pengas G, Nestor PJ (2010) Absolute diffusivities define the landscape of white matter degeneration in Alzheimer's disease. *Brain* **133**, 529-539.

[54] Pagani E, Filippi M, Rocca MA, Horsfield MA (2005) A method for obtaining tract-specific diffusion tensor MRI

measurements in the presence of disease: application to patients with clinically isolated syndromes suggestive of multiple sclerosis. *Neuroimage* **26**, 258-265.

[55] Xue R, van Zijl PC, Crain BJ, Solaiyappan M, Mori S (1999) In vivo three-dimensional reconstruction of rat brain axonal projections by diffusion tensor imaging. *Magn Reson Med* **42**, 1123-1127.

[56] Bozzali M, Falini A, Franceschi M, Cercignani M, Zuffi M, Scotti G, Comi G, Filippi M (2002) White matter damage in Alzheimer's disease assessed *in vivo* using diffusion tensor magnetic resonance imaging. *J Neurol Neurosurg Psychiatry* **72**, 742-746.

[57] Duan JH, Wang HQ, Xu J, Lin X, Chen SQ, Kang Z, Yao ZB (2006) White matter damage of patients with Alzheimer's disease correlated with the decreased cognitive function. *Surg Radiol Anat* **28**, 150-156.

[58] Naggara O, Oppenheim C, Rieu D, Raoux N, Rodrigo S, Dalla Barba G, Meder JF (2006) Diffusion tensor imaging in early Alzheimer's disease. *Psychiatry Res* **146**, 243-249.

[59] Sydykova D, Stahl R, Dietrich O, Ewers M, Reiser MF, Schoenberg SO, Moller HJ, Hampel H, Teipel SJ (2007) Fiber connections between the cerebral cortex and the corpus callosum in Alzheimer's disease: a diffusion tensor imaging and voxel-based morphometry study. *Cereb Cortex* **17**, 2276-2282.

[60] Cho H, Yang DW, Shon YM, Kim BS, Kim YI, Choi YB, Lee KS, Shim YS, Yoon B, Kim W, Ahn KJ (2008) Abnormal integrity of corticocortical tracts in mild cognitive impairment: a diffusion tensor imaging study. *J Korean Med Sci* **23**, 477-483.

[61] Ding B, Chen KM, Ling HW, Zhang H, Chai WM, Li X, Wang T (2008) Diffusion tensor imaging correlates with proton magnetic resonance spectroscopy in posterior cingulate region of patients with Alzheimer's disease. *Dement Geriatr Cogn Disord* **25**, 218-225.

[62] Fellgiebel A, Schermuly I, Gerhard A, Keller I, Albrecht J, Weibrich C, Muller MJ, Stoeter P (2008) Functional relevant loss of long association fibre tracts integrity in early Alzheimer's disease *Neuropsychologia* 46, 1698-1706

[63] Alexander DC, Pierpaoli C, Basser PJ, Gee JC (2001) Spatial transformations of diffusion tensor magnetic resonance images. *IEEE Trans Med Imaging* **20**, 1131-1139.

[64] Xu D, Mori S, Shen D, van Zijl PC, Davatzikos C (2003) Spatial normalization of diffusion tensor fields. *Magn Reson Med* **50**, 175-182.

[65] Zhang H, Yushkevich PA, Alexander DC, Gee JC (2006) Deformable registration of diffusion tensor MR images with explicit orientation optimization. *Med Image Anal* **10**, 764-785.

[66] Cao Y, Miller MI, Mori S, Winslow RL, Younes L (2006) Diffeomorphic Matching of Diffusion Tensor Images. *Proc IEEE Comput Soc Conf Comput Vis Pattern Recogni* **2006**, 67.

[67] Yeo BT, Vercauteren T, Fillard P, Peyrat JM, Pennec X, Golland P, Ayache N, Clatz O (2009) DT-REFinD: diffusion tensor registration with exact finite-strain differential. *IEEE Trans Med Imaging* **28**, 1914-1928.

[68] Ruiz-Alzola J, Westin CF, Warfield SK, Alberola C, Maier S, Kikinis R (2002) Nonrigid registration of 3D tensor medical data. *Med Image Anal* **6**, 143-161.

[69] Park HJ, Kubicki M, Shenton ME, Guimond A, McCarley RW, Maier SE, Kikinis R, Jolesz FA, Westin CF (2003) Spatial normalization of diffusion tensor MRI using multiple channels. *Neuroimage* **20**, 1995-2009.

[70] Ceritoglu C, Oishi K, Li X, Chou MC, Younes L, Albert M, Lyketsos C, van Zijl PC, Miller MI, Mori S (2009) Multi-contrast large deformation diffeomorphic metric mapping for diffusion tensor imaging. *Neuroimage* **47**, 618-627.

[71] Ziyan U, Sabuncu MR, O'Donnell LJ, Westin CF (2007) Nonlinear registration of diffusion MR images based on fiber bundles. *Med Image Comput Comput Assist Interv* **10**, 351-358.

[72] Van Hecke W, Leemans A, D'Agostino E, De Backer S, Vandervliet E, Parizel PM, Sijbers J (2007) Nonrigid coregistration of diffusion tensor images using a viscous fluid model and mutual information. *IEEE Trans Med Imaging* **26**, 1598-1612.

[73] Chiang MC, Leow AD, Klunder AD, Dutton RA, Barysheva M, Rose SE, McMahon KL, de Zubicaray GI, Toga AW, Thompson PM (2008) Fluid registration of diffusion tensor images using information theory. *IEEE Trans Med Imaging* **27**, 442-456.

[74] Xue Z, Li H, Guo L, Wong ST (2010) A local fast marching-based diffusion tensor image registration algorithm by simultaneously considering spatial deformation and tensor orientation. *Neuroimage* **52**, 119-130.

[75] Li H, Xue Z, Guo L, Wong ST (2009) Simultaneous consideration of spatial deformation and tensor orientation in diffusion tensor image registration using local fast marching patterns. *Inf Process Med Imaging* **21**, 63-75.

[76] Zollei L, Stevens A, Huber K, Kakunoori S, Fischl B (2010) Improved tractography alignment using combined volumetric and surface registration. *Neuroimage* **51**, 206-213.

[77] Xie S, Xiao JX, Gong GL, Zang YF, Wang YH, Wu HK, Jiang XX (2006) Voxel-based detection of white matter abnormalities in mild Alzheimer disease. *Neurology* **66**, 1845-1849.

[78] Teipel SJ, Stahl R, Dietrich O, Schoenberg SO, Perneczky R, Bokde AL, Reiser MF, Moller HJ, Hampel H (2007) Multivariate network analysis of fiber tract integrity in Alzheimer's disease. *Neuroimage* **34**, 985-995.

[79] Head D, Buckner RL, Shimony JS, Williams LE, Akbudak E, Conturo TE, McAvoy M, Morris JC, Snyder AZ (2004) Differential vulnerability of anterior white matter in nondemented aging with minimal acceleration in dementia of the Alzheimer type: evidence from diffusion tensor imaging. *Cereb Cortex* **14**, 410-423.

[80] Davatzikos C (2004) Why voxel-based morphometric analysis should be used with great caution when characterizing group differences. *Neuroimage* **23**, 17-20.

[81] Ashburner J, Kloppel S (2011) Multivariate models of inter-subject anatomical variability. *Neuroimage* **56**, 422-439.

[82] Avants BB, Cook PA, Ungar L, Gee JC, Grossman M (2010) Dementia induces correlated reductions in white matter integrity and cortical thickness: a multivariate neuroimaging study with sparse canonical correlation analysis. *Neuroimage* **50**, 1004-1016.

[83] Smith SM, Jenkinson M, Johansen-Berg H, Rueckert D, Nichols TE, Mackay CE, Watkins KE, Ciccarelli O, Cader MZ, Matthews PM, Behrens TE (2006) Tract-based spatial statistics: voxelwise analysis of multi-subject diffusion data. *Neuroimage* **31**, 1487-1505.

[84] Oishi K, Faria A, Jiang H, Li X, Akhter K, Zhang J, Hsu JT, Miller MI, van Zijl PC, Albert M, Lyketsos CG, Woods R, Toga AW, Pike GB, Rosa-Neto P, Evans A, Mazziotta J,

Mori S (2009) Atlas-based whole brain white matter analysis using large deformation diffeomorphic metric mapping: application to normal elderly and Alzheimer's disease participantstlas. *Neuroimage* **46**, 486-499.

[85] Bosch B, Arenaza-Urquijo EM, Rami L, Sala-Llonch R, Junque C, Sole-Padulles C, Pena-Gomez C, Bargallo N, Molinuevo JL, Bartres-Faz D (2010) Multiple DTI index analysis in normal aging, amnestic MCI and AD. Relationship with neuropsychological performance. *Neurobiol Aging*, Epub ahead of print.

[86] Liu Y, Spulber G, Lehtimaki KK, Kononen M, Hallikainen I, Grohn H, Kivipelto M, Hallikainen M, Vanninen R, Soininen H (2009) Diffusion tensor imaging and Tract-Based Spatial Statistics in Alzheimer's disease and mild cognitive impairment. *Neurobiol Aging*, Epub ahead of print.

[87] Zarei M, Damoiseaux JS, Morgese C, Beckmann CF, Smith SM, Matthews PM, Scheltens P, Rombouts SA, Barkhof F (2009) Regional white matter integrity differentiates between vascular dementia and Alzheimer disease. *Stroke* **40**, 773-779.

[88] Stricker NH, Schweinsburg BC, Delano-Wood L, Wierenga CE, Bangen KJ, Haaland KY, Frank LR, Salmon DP, Bondi MW (2009) Decreased white matter integrity in late-myelinating fiber pathways in Alzheimer's disease supports retrogenesis. *Neuroimage* **45**, 10-16.

[89] Honea RA, Vidoni E, Harsha A, Burns JM (2009) Impact of APOE on the healthy aging brain: a voxel-based MRI and DTI study. *J Alzheimers Dis* **18**, 553-564.

[90] Smith CD, Chebrolu H, Andersen AH, Powell DA, Lovell MA, Xiong S, Gold BT (2010) White matter diffusion alterations in normal women at risk of Alzheimer's disease. *Neurobiol Aging* **31**, 1122-1131.

[91] Ukmar M, Makuc E, Onor ML, Garbin G, Trevisiol M, Cova MA (2008) Evaluation of white matter damage in patients with Alzheimer's disease and in patients with mild cognitive impairment by using diffusion tensor imaging. *Radiol Med(Torino)* **113**, 915-922.

[92] Yoshiura T, Mihara F, Ogomori K, Tanaka A, Kaneko K, Masuda K (2002) Diffusion tensor in posterior cingulate gyrus: correlation with cognitive decline in Alzheimer's disease. *Neuroreport* **13**, 2299-2302.

[93] Kalus P, Slotboom J, Gallinat J, Mahlberg R, Cattapan-Ludewig K, Wiest R, Nyffeler T, Buri C, Federspiel A, Kunz D, Schroth G, Kiefer C (2006) Examining the gateway to the limbic system with diffusion tensor imaging: the perforant pathway in dementia. *Neuroimage* **30**, 713-720.

[94] Goldstein FC, Mao H, Wang L, Ni C, Lah JJ, Levey AI (2009) White matter integrity and episodic memory performance in mild cognitive impairment: a diffusion tensor imaging study. *Brain Imaging Behav* **3**, 132-141.

[95] Huang J, Auchus AP (2007) Diffusion tensor imaging of normal appearing white matter and its correlation with cognitive functioning in mild cognitive impairment and Alzheimer's disease. *Ann N Y Acad Sci* **1097**, 259-264.

[96] Kavcic V, Ni H, Zhu T, Zhong J, Duffy CJ (2008) White matter integrity linked to functional impairments in aging and early Alzheimer's disease. *Alzheimers Dement* **4**, 381-389.

[97] Bozzali M, Falini A, Cercignani M, Baglio F, Farina E, Alberoni M, Vezzulli P, Olivotto F, Mantovani F, Shallice T, Scotti G, Canal N, Nemni R (2005) Brain tissue damage in dementia with Lewy bodies: an *in vivo* diffusion tensor MRI study. *Brain* **128**, 1595-1604.

[98] Ota M, Sato N, Ogawa M, Murata M, Kuno S, Kida J, Asada T (2009) Degeneration of dementia with Lewy bodies measured by diffusion tensor imaging. *NMR Biomed* **22**, 280-284.

[99] Mueller SG, Weiner MW, Thal LJ, Petersen RC, Jack CR, Jagust W, Trojanowski JQ, Toga AW, Beckett L (2005) Ways toward an early diagnosis in Alzheimer's disease: the Alzheimer's Disease Neuroimaging Initiative (ADNI). *Alzheimers Dement* **1**, 55-66.

[100] Jack CR, Jr, Bernstein MA, Borowski BJ, Gunter JL, Fox NC, Thompson PM, Schuff N, Krueger G, Killiany RJ, Decarli CS, Dale AM, Carmichael OW, Tosun D, Weiner MW (2010) Update on the magnetic resonance imaging core of the Alzheimer's disease neuroimaging initiative. *Alzheimers Dement* **6**, 212-220.

White Matter Microstructure in Relation to Education in Aging and Alzheimer's Disease

Stefan J. Teipel [a,b,*], Thomas Meindl [c], Maximilian Wagner [d], Thomas Kohl [d], Katharina Bürger [e], Maximilian F. Reiser [c], Sabine Herpertz [f], Hans-Jürgen Möller [d] and Harald Hampel [g]

[a]*Department of Psychiatry, University Rostock, Rostock, Germany*
[b]*DZNE, German Center for Neurodegenerative Disorders, Rostock, Germany*
[c]*Department of Clinical Radiology, University Hospitals – Grosshadern, Ludwig-Maximilian University, Munich, Germany*
[d]*Department of Psychiatry, Ludwig-Maximilian University, Munich, Germany*
[e]*ISD, Institute for Stroke and Dementia Research, Ludwig-Maximilian University, Munich, Germany*
[f]*Department of Psychiatry, University Heidelberg, Heidelberg, Germany*
[g]*Department of Psychiatry, University Frankfurt, Frankfurt, Germany*

Abstract. The reduced risk of dementia in high-educated individuals has been suggested to reflect brain reserve capacity. In the present study we determined the association between integrity of white matter microstructure and education separately in twenty-one patients with clinically probable Alzheimer's disease (AD) and 18 healthy elderly subjects. We used fractional anisotropy derived from high-resolution diffusion-tensor weighted imaging at 3 Tesla as *in vivo* marker of white matter microstructure. Based on multivariate network analysis, more years of education were associated with reduced white matter integrity of medial temporal lobe areas and association fiber tracts when age, gender and dementia severity had been controlled for ($p < 0.001$). In controls, higher education was associated with greater white matter integrity in medial temporal lobe areas and association fiber tracts ($p < 0.001$). In multiple regression models, education was the main factor accounting for fiber tract integrity even when occupation was taken into account. Reduced fiber tract integrity with higher education at the same level of cognitive impairment in AD patients and higher fiber tract integrity with higher education in similar white matter areas in cognitively healthy controls agrees with the hypothesis that white matter microstructure may contribute to brain reserve capacity in humans. A better understanding of the neurobiological basis of reserve capacity will be of high relevance for designing future studies on cognitive intervention approaches to prevent dementia in at risk subjects.

Keywords: Brain reserve capacity, cortical connectivity, education, Alzheimer's disease, aging, DTI

INTRODUCTION

Many epidemiological studies suggest a protective effect of higher education for the onset of dementia in elderly subjects [1–4]. Only few studies have shown no association of dementia with education [5]. Education may provide brain reserve against neurodegeneration [6]. Brain reserve capacity is defined as the ability of the brain to compensate for progressive lesions and to maintain normal cognitive function [6]. Consistently, patients with Alzheimer's disease (AD) with more years of education exhibit more functional [7, 8] or structural brain lesions [9] in imaging studies at a comparable level of dementia severity compared to patients with lower education. Reduced glucose consumption in predilection sites of AD with higher education has also been described in amnestic MCI patients who later

converted into AD [10]. It is not clear whether this represents a direct effect of education or if this effect is mediated by the effect of education on general health status [11] or occupational achievement [12]. Education is a risk factor of AD that is potentially accessible to intervention. Important risk factors for AD that are not accessible to intervention include age, female gender and ApoE4 genotype [13, 14].

Diffusion tensor imaging (DTI) allows determining the integrity of subcortical fiber tracts in the living human brain [15]. Fractional anisotropy (FA), derived from DTI, is sensitive towards subcortical fiber changes with brain maturation [16, 17] as well as towards fiber degeneration in AD [18–29]. Therefore, FA provides an interesting *in vivo* marker to determine the association between education and brain structure in aging and AD.

In the present study, we investigated whether fiber tract integrity was associated with years of education in patients with AD using observer independent multivariate analysis [29]. We hypothesized that AD patients with more years of education would present a higher degree of fiber degeneration in regional predilection sites of AD pathology compared to patients with less years of education when we controlled for dementia severity, age and gender. This would indicate that patients with higher education could maintain similar cognitive function compared to patients with lower education despite more severe impairment of fiber tract integrity. If the effect of education on brain reserve capacity was mediated by white matter microstructure one would expect that white matter microstructure was increased with higher education in healthy control subjects. We tested this hypothesis in a group of healthy elderly subjects controlling for established risk factors of AD including, age, gender and ApoE4 genoytpe. We used a multiple regression model to determine whether the effects of education on fiber tract integrity were dependent on occupational achievement.

SUBJECTS AND METHODS

Subjects

We examined 21 patients with the clinical diagnosis of probable AD (mean age: 76.1 (SD 7.4) years, ranging from 58 to 87 years, 12 women) according to NINCDS-ADRDA criteria [30]. For comparison, we investigated 18 cognitively healthy elderly subjects (mean age: 66.2 (SD 7.3) years, ranging between 56 to 83 years, 8 women). The AD and control groups dif-

fered significantly in age (*t*-test: $p = 0.001$, $T = -4.20$, 37 degrees of freedom), but showed a similar gender distribution ($Chi^2 = 0.63$, 1 degree of freedom, $p = 0.43$). The Mini-Mental-Status Examination (MMSE) was used to assess the degree of overall cognitive impairment [31] Groups differed significantly in MMSE scores, with 22.9 (SD 3.0, ranging from 17 to 29) points in AD and 29.1 (SD 0.6, ranging from 28 to 30) points in control subjects ($p < 0.001$, Mann-Whitney U = 8.5). Years of education were significantly different between AD patients and controls ($p < 0.03$, $T = 2.4$, 37 degrees of freedom) with 11.0 (SD 1.9, ranging from 8 to 18) years in AD patients and 13.2 (SD 3.7, ranging from 8 to 20) years in controls.

Years of education were assessed as years attending school plus years of apprenticeship, technical school, college and university. Occupation was determined as the most recent occupation or the last occupation before retirement. We used a modification of the Hollingshead occupational rating scale [32, 33]. This scale has 9 categories of occupational status ranging from unlearned worker to high level academic professions or senior manager level. As the number of subjects in our study was small and the range of professions limited, we collapsed the 9 dimensions into 4, leaving the category of unlearned worker (coded as 1), combining categories 2 to 4 (coded as 2), 5 to 7 (coded as 3) and 8 to 9 (coded as 4).

The clinical assessment included detailed medical history, clinical, psychiatric, neurological and neuropsychological examinations (CERAD battery [34], Clock-drawing-test [35], trail-making test [36]), and laboratory tests (complete blood count, electrolytes, glucose, blood urea nitrogen, creatinine, liver-associated enzymes, cholesterol, HDL, triglycerides, serum B12, folate, thyroid function tests, coagulation, serum iron).

Additionally, ApoE4 genotyping was available in 17 of the 21 AD patients and in all control subjects, with 7 AD patients and 7 controls carrying at least one ApoE4 allele.

Selection of subjects included a semiquantitative rating of T2-weighted MRI scans [37]. Only subjects were included who had no subcortical white matter hyperintensities exceeding 10 mm in diameter or 3 in number.

All patients and controls were only examined if they gave their written informed consent. The study was approved by the institutional review board of the Medical Faculty of the University of Munich.

MRI acquisition

MRI acquisitions of the brain were conducted with a 3.0 Tesla scanner with parallel imaging capabilities (Magnetom TRIO, Siemens, Erlangen, Germany), maximum gradient strength: 45 mT/m, maximum slew rate: 200 T/m/s, 12 element head coil.

Subjects were scanned in a single session without changing their position in the scanner. The following sequences were used: for anatomical reference, a sagittal high-resolution 3-dimensional gradient-echo sequence was performed (magnetization prepared rapid gradient echo MPRAGE, field-of-view 250 mm, spatial resolution $0.8 \times 0.8 \times 0.8$ mm^3, repetition time 14 ms, echo time 7.61 ms, flip angle 20^0, number of slices 160). To identify white matter lesions a 2-dimensional T2-weighted sequence was performed (fluid attenuation inversion recovery FLAIR, field-of-view 230 mm, repetition time 9000 ms, echo time 117 ms, voxel size $0.9 \times 0.9 \times 5.0$ mm, TA 3:20 minutes, flip angle 180^0, number of slices 28, acceleration factor 2).

Diffusion-weighted imaging was performed with an echo-planar-imaging sequence. (field-of-view 256 mm, repetition time 9300 ms, echo time 102 ms, voxel size $2.0 \times 2.0 \times 2.0$ mm^3, 4 repeated acquisitions, b-value $1 = 0$, b-value $2 = 1000$, 12 directions, noise level 10, slice thickness 2.0 mm, 64 slices, no overlap).

DTI data processing

Pre-processing

DTI data were preprocessed using the DTI toolbox of the FSL software (http://www.fmrib.ox.ac.uk/fsl/written mainly by members of the Analysis Group, FMRIB, Oxford, UK. Version 3.2). After correcting for susceptibility artifacts [38], from the 12 gradient directions we derived a 12×12-tensor to extract eigenvalues and eigenvectors to determine fractional anisotropy maps [29].

The processing was implemented within Matlab 7.6 (MathWorks, Natwick, Mass.) through Statistical Parametric Mapping [39, 40] (SPM 2, Wellcome Department of Imaging Neuroscience, London; available at http://www.fil.ion.ucl.ac.uk/spm), as described in a previous study [29].

In brief, we used low-dimensional normalization with a set of nonlinear basis functions [41, 42] and high-dimensional normalization with symmetric priors [43] to normalize the anatomical MPRAGE scans into standard space. The normalization parameters were sequentially applied to FA maps that had been spatially coregistered using affine transformation to the anatomical MPRAGE scans in native space. This procedure resulted in FA maps projected into standard space.

Statistical analysis

Spatial effects of education

Voxels from outside the white matter were removed from the spatially normalized FA maps by means of a mask derived from the white matter maps of the anatomical MPRAGE scans [44]. The masked FA maps were smoothed with a 12-mm FWHM Gaussian kernel. Images were scaled to the same mean value and standard deviation using a voxel-wise z-transformation.

The multivariate approach followed three subsequent steps that will only briefly be described in the following section. For further details we refer to [29] and [45].

First, the high-dimensionally normalized FA maps were subjected to principal component analysis within the AD and control groups.

Secondly, we determined the significance of the hypothesized effect of education on FA values using multivariate analysis of covariance (MANCOVA). We employed a linear model with years of education as independent factor, controlling for MMSE score, age and gender in the AD patients and for age, gender and ApoE4 genotype in the control group, and the principal components from the FA maps as multivariate dependent variable.

Thirdly, we characterized the spatial distribution of these effects using canonical variate analysis in terms of the canonical vector that best captured the effect of education. To this end, we defined canonical images in the observation space such that the variance ratio between the effect of interest and the total error sum of squares was maximized. Each canonical image has an associated canonical value that serves to estimate whether a particular canonical image is important. The canonical value can be compared to an F distribution with denominator degrees of freedom equal to the rank of the matrix of the effect of interest and nominator degrees of freedom equal to the number of scans minus the rank of the design matrix (=degrees of freedom of the error term). We considered a canonical image important if its canonical value exceeded the critical F threshold for $p < 0.05$.

Calculations were carried out using an algorithm written in MATLAB v. 7.6 (Mathworks, Newton, MA).
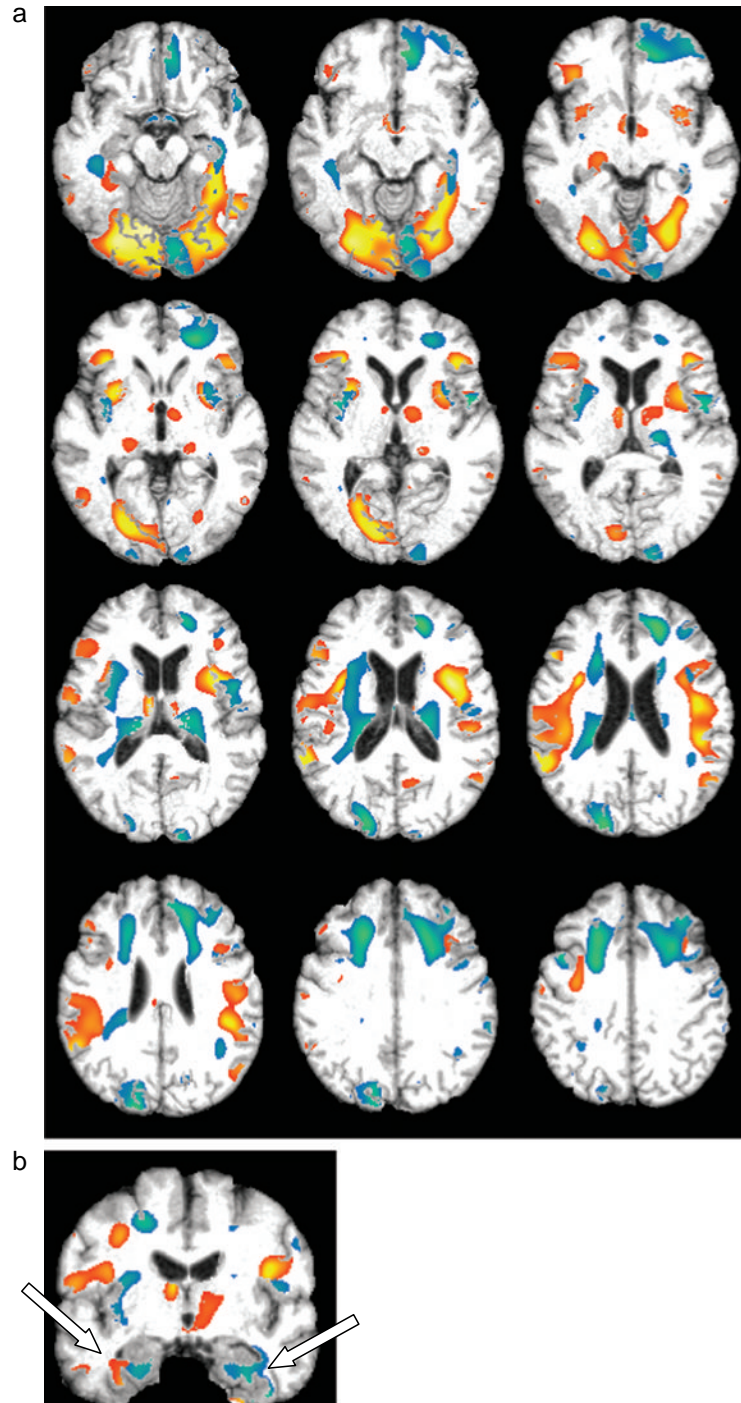
Fig. 1. Effect of education on FA values. The component of the second canonical image of the AD patients (red colors) representing lower FA values with more years of education after controlling for age, gender, and MMSE score, and the component of the second canonical image of the controls (blue colors) representing higher FA values with more years of education after controlling for age, gender, and ApoE4 genotype, are shown. The components of the FA maps in voxel space are projected on the rendered axial sections (Fig. 1a), and on a coronal slice through the medial temporal lobe at Talairach-Tournoux coordinate $y = -12$ (Fig. 1b) of the T1-weighted template brain. Axial sections go from ventral at Talairach-Tournoux coordinate $z = -17$ to dorsal at $z = 38$, sections are 5 mm apart. Right of image is right of brain (view from posterior in the coronal section, from superior in the axial section). The white arrows point to the right and left parahippocampal gyrus on the coronal slice.

Effects of education controlled for occupation

To find the principal component that was significantly associated with years of education, we correlated the principal component scores of each scan with education. The scores from the principal component that were significantly correlated with education represented scalar markers for the effect of education on FA maps for each subject. Multiple regression models were applied with the principal component scores as dependent variables and age, gender, MMSE score (in the AD patients), education and occupation as independent variables. In the first step all independent variables were forced into the model, in subsequent steps those variables were removed that did not significantly contribute to the fit of the model according to the overall F-test.

Robustness measures

To assess the stability of our multivariate solution, we followed an approach suggested by Zuendorf et al. [46]. First, we tested the data set for potential outliers, using Hotellings T^2 test [47], a multivariate generalization of Students t-test. T^2 gives a measure of the distance of a vector from a vector whose elements represent the means of a multivariate normal distribution. In our case, it was given by

$$T^2 = \sqrt{(n-1)}y^T \bullet y$$

with n = number of subjects, y = a column vector of PC scores belonging to one subject whose elements are divided by the square root of the corresponding eigenvalues.

The T^2 statistics is related to the F-distribution by:

$$F_{n-p}^p = \frac{(n-p)}{p(n-1)}T^2$$

with n = number of subjects and p = number of of principal component scores used for the test.

Additionally, we carried out repeated MANCOVAs based on seven subsets of 18 scans each after randomly removing three different scans each time from the full data set in the AD patients and based on 6 subsets of 15 scans each after randomly removing three different scans each time from the full data set in the controls. The resulting overall effects of the MANCOVAs were compared to the Chi^2 distribution for $p < 0.001$ at 7 df in AD patients and at 6 df in controls.

Identification of voxel with peak loading

The 98th percentile was used as threshold for voxel with highest positive or negative loading on the canonical image. The Talairach-Tournoux coordinates [48] of these voxel were determined using in-house software written in C. The program produces a listing of all local maxima and minima of the canonical image with each local peak at least 1 cm away from neighboring peaks.

RESULTS

Effects of education in AD patients

We assessed the significance of the effect of education with a design matrix having 21 rows (one for each scan) and 5 columns, one for the effect of education, and one each for the effects of the intercept, MMSE scores, age and gender. The data were reduced to the first 7 eigenvectors having eigenvalues greater than unity. The resulting matrix was subject to MANCOVA. Wilk's lambda after transformation corresponded to $\chi^2 = 36.2$ with 7 degrees of freedom, $p < 0.001$. The effect of education was almost completely accounted for by the second canonical image. The canonical value was 272.2 and was larger than the threshold $F_1^{16} = 246$ for $p < 0.05$. We divided the canonical image in one image containing only voxels with high positive loadings (positive components) and one image containing only voxels with high negative loadings (negative components) on the canonical image.

Subsequently, we considered only the negative components representing a decline of FA associated with more years of education. Figure 1 shows the negative components of the second canonical image projected onto the T1-weighted MRI template in standard space (in red). The 80th percentile threshold was used to show only the most relevant features. Table 1 shows the Talairach-Tournoux coordinates of the voxel with the highest negative loadings on the canonical image lying above the 98th percentile. The canonical image compromised medial temporal lobes (including fusiform gyrus, parahippocampal gyrus and hippocampus), subcortical white matter of insula cortex, as well as lateral temporal, occipital, frontal and parietal lobes white matter. Additionally, the canonical image compromised white matter of the posterior lobe of the cerebellum.

When we used the sum score from the CERAD battery based on z-score transformation of each subtest according to [49] instead of the MMSE score to con-

Table 1
Voxel with positive peak loadings on the second canonical image in AD patients, representing lower fractional anisotropy with higher education

Region	Side	Coordinates (mm)		
		x	y	z
Inferior frontal gyrus	L	−38	26	−1
		−37	4	18
Superior temporal gyrus	L	−61	−50	21
Lingual gyrus	L	−16	−83	5
Cerebellum	L	−4	−86	−24
		−11	−74	−12
		−31	−78	−15
Insula	R	35	3	15
Inferior temporal gyrus	R	30	−14	−35
Inferior parietal lobule	R	45	−35	24
Lingual gyrus	R	23	−71	−6
Fusiform gyrus	R	36	−33	−17
		47	−60	−18
Cerebellum	R	37	−80	−16
		55	−64	−20

Voxel with positive loading above the 98th percentile. Brain regions are indicated by Talairach and Tournoux coordinates, x, y and z [48]: x = the medial to lateral distance relative to midline (positive = right hemisphere); y = the anterior to posterior distance relative to the anterior commissure (positive = anterior); z = superior to inferior distance relative to the anterior commissure -posterior commissure line (positive = superior). R/L = right/left.

trol for cognitive impairment, the significance of the results and the spatial distribution of the effects were unchanged (Fig. 2). Inclusion of ApoE4 genotype as covariate in the analysis of the effect of education on FA in the subset of 17 AD patients where ApoE4 was available did not alter the significance or spatial distribution of effects (data not shown).

Effects of education in the controls

We assessed the significance of the effect of education with a design matrix having 18 rows (one for each scan) and 5 columns, one for the effect of education, and one each for the effects of the intercept, ApoE4 genotype, age and gender. The data were reduced to the first 7 eigenvectors having eigenvalues greater than unity. The resulting matrix was subject to MANCOVA. Wilk's lambda after transformation corresponded to Chi2 = 39.5 with 7 degrees of freedom, $p < 0.001$. The effect of education was almost completely accounted for by the second canonical image. The canonical value was 820.0 and was larger than the threshold $F_1^{13} = 243$ for $p < 0.05$. We divided the canonical image in one image containing only voxels with high positive loadings (positive components) and one image containing only voxels with high negative loadings (negative components) on the canonical image.

Subsequently, we considered only the negative components representing a higher FA associated with more years of education (Fig. 1 (blue) and Table 2). The canonical image compromised medial temporal lobes (including fusiform gyrus, parahippocampal gyrus and uncus), subcortical white matter of insula, middle and medial frontal cortex, as well as lateral temporal, parietal and occipital lobes white matter. Additionally, the canonical image compromised white matter of the pons and thalamus.

Effect of education relative to occupation

In the AD patients, the third and the 17th principal components, in the controls the fourth principal component were significantly correlated with education (Fig. 3). Within the AD group, occupation was only significantly correlated with the scores for the 17th principal component, within the control group occupation was significantly correlated with the scores for the 4th principal component (Fig. 3).

After stepwise backward selection only education remained in the model for both principal component scores in the AD group ($F_{19}^1 = 4.7$, $p < 0.05$ for the third, $F_9^1 = 11.0$, $p < 0.005$ for the 17th principal component) and for the 4th principal component in the healthy control group ($F_{16}^1 = 11.7$, $p < 0.003$).

Robustness measures

Hotelling's T^2 test demonstrated the absence of outliers at the $p = 0.25$ level (suggesting a low type II error of erroneously assuming no outliers in the data) both in the AD patients and in the controls (Fig. 4). Repeated MANCOVAs based on seven subsets of 18 scans each in AD patients and six subsets of 15 scans each in the controls, respectively, showed that the effect of education controlling for dementia severity, age and gender were above the critical threshold for all subsets of the data (Fig. 5).

DISCUSSION

We assessed the association between years of education and subcortical fiber tract integrity in patients with AD. The study is based on a large body of evidence that years of education impacted the age of onset and rate of progression of dementia in elderly subjects. Fiber tract integrity in characteristic predilection sites of AD
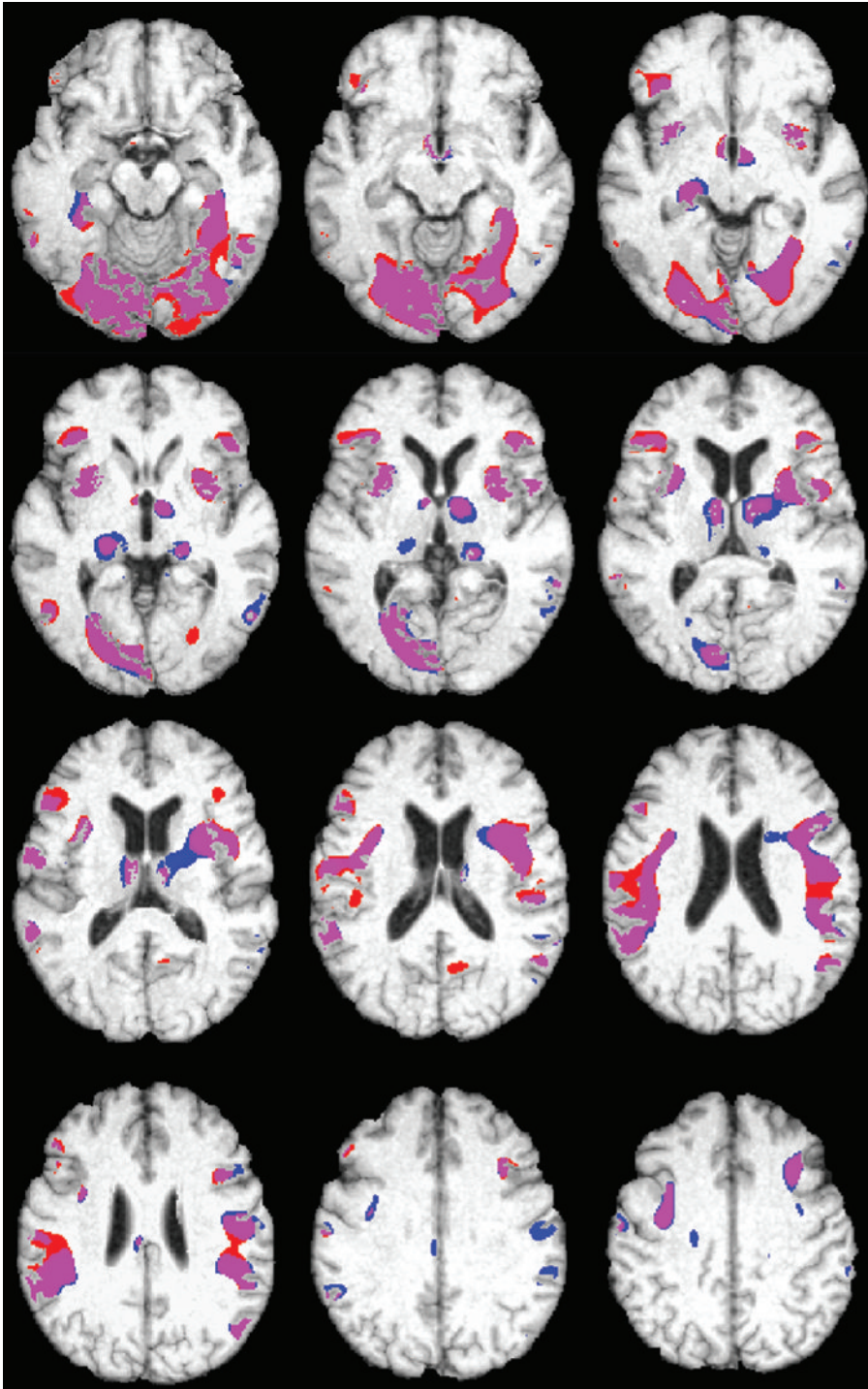
Fig. 2. Effect of education on FA values controlling for MMSE score or CERAD sum score. The negative components of the second canonical image controlling for MSME score (red) or controlling for CERAD sum score (blue) are shown, representing lower FA values with more years of education after controlling for age, gender, and cognitive impairment. Overlapping areas are in pink. The effects are projected on the rendered axial sections of the T1-weighted template brain. Axial sections go from ventral at Talairach-Tournoux coordinate $z = -17$ to dorsal at $z = 38$, sections are 5 mm apart. Right of image is right of brain (view from superior in the axial sections). Please note that controlling for MSME score or for CERAD score leads to nearly identical spatial pattern, compare also Fig. 1.

Table 2
Voxel with positive peak loadings on the second canonical image in controls, representing higher fractional anisotropy with higher education

Region	Side	Coordinates (mm)		
		x	y	z
Middle frontal gyrus	L	−24	5	37
		−24	23	30
		−26	−10	44
		−49	10	34
Insula	L	−42	−1	1
Superior temporal gyrus	L	−30	6	−30
Postcentral gyrus	L	−33	−34	54
Fusiform gyrus	L	−50	−28	−25
Precuneus	L	−8	−55	50
Cuneus	L	−20	−89	25
Corpus callosum	L	−24	17	19
Thalamus	L	−18	−26	15
Projecting on fasc. occipito-frontalis	L	−27	−32	21
Pons	L	−6	−19	−36
Middle frontal gyrus	R	32	38	34
Medial frontal gyrus	R	2	45	−12
		16	39	17
Anterior cingulate	R	20	20	29
Cingulate gyrus	R	10	13	42
Uncus	R	30	−7	−32
Parahippocampal gyrus	R	21	41	−5
		36	−20	−18
		10	−9	−29
Superior temporal gyrus	R	47	1	0
Fusiform gyrus	R	40	−12	−38
Inferior parietal lobule	R	36	−30	41
Middle occipital gyrus	R	10	−98	16
Lingual gyrus	R	7	−84	−9
		9	−102	−9
Fornix	R	1	−16	17
Thalamus	R	15	−23	10

Voxel with negative loading above the 98th percentile. Brain regions are indicated by Talairach and Tournoux coordinates, x, y and z [48]: x = the medial to lateral distance relative to midline (positive = right hemisphere); y = the anterior to posterior distance relative to the anterior commissure (positive = anterior); z = superior to inferior distance relative to the anterior commissure -posterior commissure line (positive = superior). R/L = right/left.
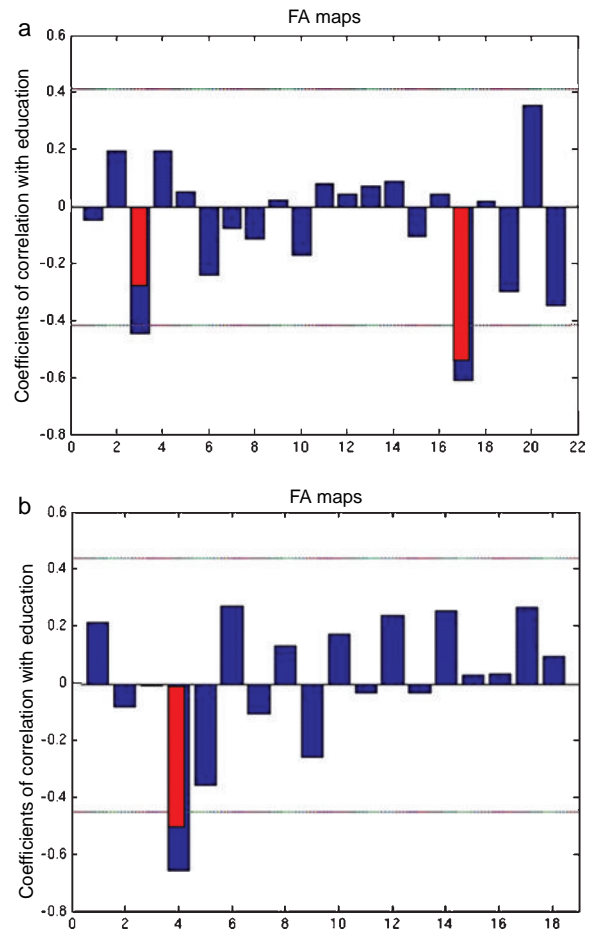

Fig. 3. Correlation between principal component scores and education. The third and 17th principal components of the FA maps of the AD patients (upper row) and the 4th principal component of the FA maps of the controls (lower row) are correlated with education at the level of $p < 0.05$. Vertical lines indicate the threshold for the correlation coefficient at $p < 0.05$. Red bars indicate the correlation coefficients between occupation and those principal component scores that were significantly associated with education.

was more impaired with higher education (controlled for dementia severity, age and gender). In a multiple regression model education, not occupation was the main predictor of fiber tract integrity. In a group of healthy elderly subjects, after controlling for age, gender and ApoE4 genotype as major risk factors of AD, we found that higher education was associated with higher fiber tract integrity in several brain areas, including areas that showed reduced fiber tract integrity with higher education in AD.

Fractional anisotropy was more reduced in fiber tracts of parietal, temporal and occipital lobes, including fusiform and parahippocampal gyrus, with more

years of education. These fiber tracts have previously been found to be involved in AD in independent samples [18–29], suggesting that the FA reductions in our sample reflect lesions to predilection sites of AD.

The finding of increased lesion load in patients with higher education is in line with positron emission tomography (PET) studies showing reduced parieto-temporal cortical metabolism in AD [7] and MCI [10] and increased frontal lobe amyloid binding [8] in AD patients with higher compared to patients with lower education at the same level of dementia severity. In an MRI-based study, AD patients with higher education showed more ventricular enlargement compared
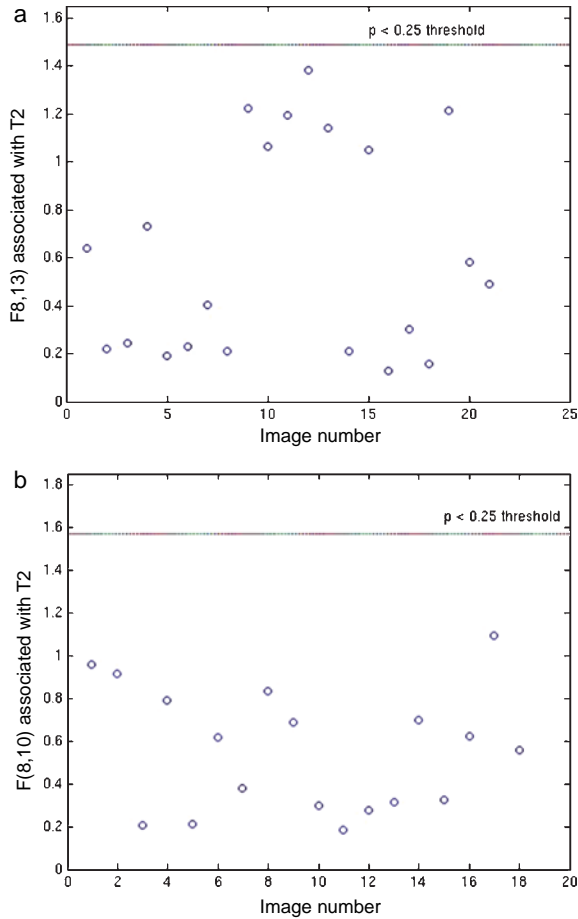
Fig. 4. Hotelling T^2-test for the first 8 principal components. Hotelling T^2-test for the first 8 principal component scores showing no outliers at $p = 0.25$ for the AD patients (Fig. 4a) and the controls (Fig. 4b).
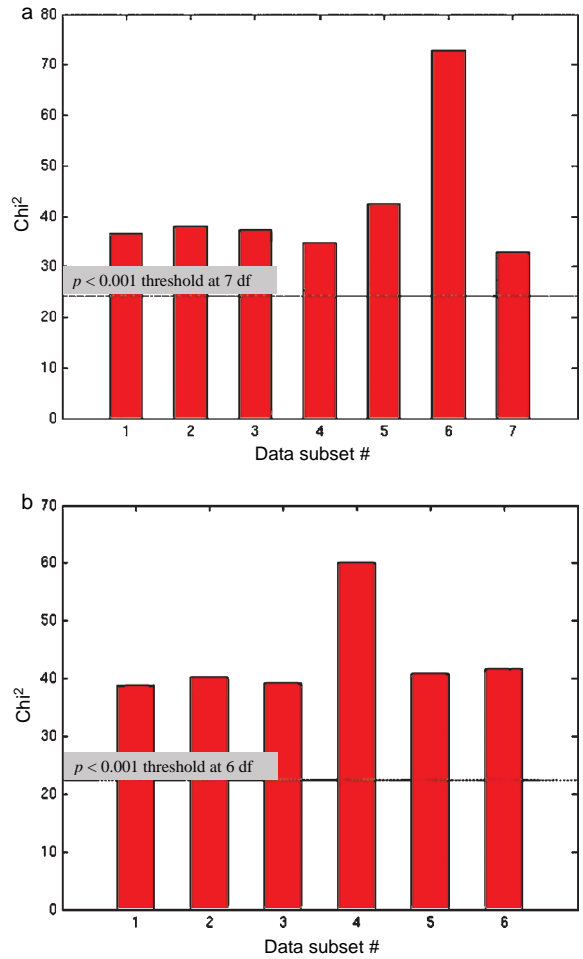

Fig. 5. Wilk's lambda for subsets of the data, randomly leaving out 3 different scans each. Distribution of Wilk's lambda after transformation corresponding to Chi^2 at 7 (Fig. 5a) or 6 (Fig. 5b) df derived from subsets of the data after randomly removing 3 different scans each from the entire data set of the AD patients (Fig. 5a) or controls (Fig. 5b).

to patients with lower education after controlling for dementia severity [9]. Our findings are also in line with a more recent study on DTI changes with measures of cognitive reserve determined from a composite score of verbal intelligence, education and leisure activities [50]. In this later study, FA was reduced with higher cognitive reserve in late myelinating fibers, including corticocortical associative fasciculi and commissural fibers, in amnestic MCI patients [50]. These observations suggest that patients with higher education maintain a comparable level of cognitive function despite more severe structural and functional brain lesions.

In a synthesis of three large clinical and neuropathological cohort studies, longer years of education were associated with higher brain weight and reduced risk

of dementia largely independently of the severity of pathology [51]. These findings support the notion that education may be a surrogate marker for mechanisms of functional reserve capacity that may mitigate the effects of neurodegeneration on cognitive performance.

Our study provides first evidence for education related differences in the fiber tract integrity that may underlie differences in brain reserve capacity. DTI is a sensitive technique to assess mechanisms of brain maturation [16, 17]. The neuron populations that mature later during brain development are the earliest affected by characteristic AD neuropathology [52]. Environmental factors influence the formation and myelination

of axons during early childhood and adolescence [53]. Brain maturation may even proceed into the fifth decade of life [54]. It is tempting to assume that the changes in FA reflect the more severe changes to originally stronger myelinated and more richly connected fiber tracts in patients with higher education that are required to induce the same level of dementia in these patients. This interpretation would agree with the finding that some of the brain areas regions that were negatively associated with education in the AD group were positively associated with education in the healthy control group, including medial temporal lobe areas (entorhinal cortex and hippocampus), fusiform gyrus, insula, superior temporal gyrus and lingual gyrus. These areas belong to typical predilection sites of AD pathology and seem to have higher fiber tract integrity with higher education in cognitively healthy elderly subjects after controlling for major risk factors of AD. The spatial pattern, however, additionally involved pons and posterior cingulate gyrus white matter, suggesting that the effect of education was not specific to predilection sites of AD in healthy elderly controls. Given the age range of the healthy control subjects, we can not exclude the possibility that some of these subject harbor preclinical AD. Therefore, to further address the question whether education contributes to fiber tract integrity one will have to study a group of young healthy subjects (adolescence to early adulthood) comparing fiber tract integrity in higher and lower educated subjects.

However, the association between education and onset of dementia and severity of underlying structural and functional brain lesions is likely more complex. A young person's educational achievement is influenced by their innate intelligence, as well as environmental factors, such as their parents' educational and socioeconomic background, and available schooling. In turn, education influences the subsequent occupation, environment and the likelihood for continued mentally and physically healthy and stimulating activities (such as continuous learning, exercise and nutrition). All these factors in themselves may contribute to neurogenesis, and the organization, myelination and maintenance of subcortical fiber tracts over the lifetime. Complexity of occupational work lowered the risk of dementia in monozygotic twin pairs discordant for AD [12], where complexity of work was related to educational achievement. We used linear multiple regression models to determine whether the effect of education was mediated by occupation. Interestingly, education was the main predictor of fiber tract integrity.

We would, however, need larger samples to allow for cross validation of these effects. Therefore, education still serves as an adjunct for the overall concept of brain reserve capacity. Within this conceptual framework, our findings suggest that the integrity of subcortical fiber tracts underlies brain reserve capacity.

One could argue that the association between education and dementia is accounted for by an ascertainment bias: higher education could raise skills of subjects to score higher on diagnostic tests [55]. However, in an earlier study subjects with higher education showed higher rates of decline in cognitive performance compared to lower educated subjects [56]. This observation would be unlikely, if performance in cognitive tests was mainly determined by educational background once patients got demented.

Years of education in our sample were similar to those in a previous study on the association between education levels and cortical glucose consumption in a memory clinic sample of 96 AD patients [7], suggesting that our subjects represent a typical memory clinics sample.

Although the number of scans was small in comparison to the dimensionality of the imaging data, Hotellings T^2 statistic suggested that the DTI data represented a homogeneous data set and that the significance of the multivariate solution remained stable across different subsets of the data.

We had excluded AD patients with evidence for significant cerebrovasuclar disease based on the rating of white matter hyperintensities, to be able to study the association of education and white matter microstructure in predominant neurodegenerative disease. Inclusion of patients with extended white matter changes would be required to further study the association between education and cerebrovascular disease as a measure of vascular reserve capacity.

In summary, our findings agree with the hypothesis that education contributes directly to brain reserve capacity. They complement earlier findings on the structural and functional basis of reserve capacity of the human brain by providing insight into integrity of subcortical fiber tracts. The maturation of cerebral fiber tracts is known to proceed at least into early adulthood if not even into higher age. Our findings support a close association between mechanisms of brain maturation and plasticity. First cognitive intervention studies have shown effects on cortical metabolism and cognitive performance in AD and MCI, suggesting a potential role of brain reserve capacity for the prevention or treatment of AD [57]. Therefore, our data should stim-

ulate further research on the dynamic basis of brain reserve capacity to help in the design of interventions to strengthen individual brain reserve capacity in order to prevent the initiation and progression of pathological mechanisms in AD.

ACKNOWLEDGEMENT

REFERENCES

[1] Ampuero I, Ros R, Royuela A, Abraira V, del Ser T, Garcia-Ribas G, Garcia de Yebenes J (2008) Risk factors for dementia of Alzheimer type and aging-associated cognitive decline in a Spanish population based sample, and in brains with pathology confirmed Alzheimer's disease. *J Alzheimers Dis* **14**, 179-191.

[2] McDowell I, Xi G, Lindsay J, Tierney M (2007) Mapping the connections between education and dementia. *J Clin Exp Neuropsychol* **29**, 127-141.

[3] Chin AV, O'Connell H, Kirby M, Denihan A, Bruce I, Walsh JB, Coakley D, Lawlor BA, Cunningham C (2006) Co-morbid and socio-demographic factors associated with cognitive performance in an elderly community dwelling Irish population. *Int J Geriatr Psychiatry* **21**, 1150-1155.

[4] Katzman R (1993) Education and the prevalence of dementia and Alzheimer's disease. *Neurology* **43**, 13-20.

[5] Cobb JL, Wolf PA, Au R, White R, D'Agostino RB (1995) The effect of education on the incidence of dementia and Alzheimer's disease in the Framingham Study. *Neurology* **45**, 1707-1712.

[6] Stern Y, Alexander GE, Prohovnik I, Stricks L, Link B, Lennon MC, Mayeux R (1995) Relationship between lifetime occupation and parietal flow: implications for a reserve against Alzheimer's disease pathology. *Neurology* **45**, 55-60.

[7] Perneczky R, Drzezga A, Diehl-Schmid J, Schmid G, Wohlschlager A, Kars S, Grimmer T, Wagenpfeil S, Monsch A, Kurz A (2006) Schooling mediates brain reserve in Alzheimer's disease: findings of fluoro-deoxy-glucose-positron emission tomography. *J Neurol Neurosurg Psychiatry* **77**, 1060-1063.

[8] Kemppainen NM, Aalto S, Karrasch M, Nagren K, Savisto N, Oikonen V, Viitanen M, Parkkola R, Rinne JO (2008) Cognitive reserve hypothesis: Pittsburgh Compound B and fluorodeoxyglucose positron emission tomography in relation to education in mild Alzheimer's disease. *Ann Neurol* **63**, 112-118.

[9] Kidron D, Black SE, Stanchev P, Buck B, Szalai JP, Parker J, Szekely C, Bronskill MJ (1997) Quantitative MR volumetry in Alzheimer's disease. Topographic markers and the effects of sex and education. *Neurology* **49**, 1504-1512.

[10] Garibotto V, Borroni B, Kalbe E, Herholz K, Salmon E, Holtoff V, Sorbi S, Cappa SF, Padovani A, Fazio F, Perani D (2008) Education and occupation as proxies for reserve in aMCI converters and AD: FDG-PET evidence. *Neurology* **71**, 1342-1349.

[11] Del Ser T, Hachinski V, Merskey H, Munoz DG (1999) An autopsy-verified study of the effect of education on degenerative dementia. *Brain* **122**(Pt 12), 2309-2319.

[12] Andel R, Crowe M, Pedersen NL, Mortimer J, Crimmins E, Johansson B, Gatz M (2005) Complexity of work and risk of Alzheimer's disease: a population-based study of Swedish twins. *J Gerontol B Psychol Sci Soc Sci* **60**, P251-P258.

[13] Gao S, Hendrie HC, Hall KS, Hui S (1998) The relationships between age, sex, and the incidence of dementia and Alzheimer disease: a meta-analysis. *Arch Gen Psychiatry* **55**, 809-815.

[14] Slooter AJ, Cruts M, Kalmijn S, Hofman A, Breteler MM, Van Broeckhoven C, van Duijn CM (1998) Risk estimates of dementia by apolipoprotein E genotypes from a population-based incidence study: the Rotterdam Study. *Arch Neurol* **55**, 964-968.

[15] Beaulieu C (2002) The basis of anisotropic water diffusion in the nervous system – a technical review. *NMR Biomed* **15**, 435-455.

[16] Lebel C, Walker L, Leemans A, Phillips L, Beaulieu C (2008) Microstructural maturation of the human brain from childhood to adulthood. *Neuroimage* **40**, 1044-1055.

[17] Huppi PS, Dubois J (2006) Diffusion tensor imaging of brain development. *Semin Fetal Neonatal Med* **11**, 489-497.

[18] Stahl R, Dietrich O, Teipel SJ, Hampel H, Reiser MF, Schoenberg SO (2007) White matter damage in Alzheimer's disease and in mild cognitive impairment: assessment with diffusion tensor MRI using parallel imaging techniques. *Radiology* **243**, 483-492.

[19] Bozzali M, Falini A, Franceschi M, Cercignani M, Zuffi M, Scotti G, Comi G, Filippi M (2002) White matter damage in Alzheimer's disease assessed *in vivo* using diffusion tensor magnetic resonance imaging. *J Neurol Neurosurg Psychiatry* **72**, 742-746.

[20] Fellgiebel A, Wille P, Muller MJ, Winterer G, Scheurich A, Vucurevic G, Schmidt LG, Stoeter P (2004) Ultrastructural hippocampal and white matter alterations in mild cognitive impairment: a diffusion tensor imaging study. *Dement Geriatr Cogn Disord* **18**, 101-108.

[21] Head D, Buckner RL, Shimony JS, Williams LE, Akbudak E, Conturo TE, McAvoy M, Morris JC, Snyder AZ (2004) Differential vulnerability of anterior white matter in nondemented aging with minimal acceleration in dementia of the Alzheimer type: evidence from diffusion tensor imaging. *Cereb Cortex* **14**, 410-423.

[22] Rose SE, Chen F, Chalk JB, Zelaya FO, Strugnell WE, Benson M, Semple J, Doddrell DM (2000) Loss of connectivity in Alzheimer's disease: an evaluation of white matter tract integrity with colour coded MR diffusion tensor imaging. *J Neurol Neurosurg Psychiatry* **69**, 528-530.

[23] Takahashi S, Yonezawa H, Takahashi J, Kudo M, Inoue T, Tohgi H (2002) Selective reduction of diffusion anisotropy in white matter of Alzheimer disease brains measured by 3.0 Tesla magnetic resonance imaging. *Neurosci Lett* **332**, 45-48.

[24] Yoshiura T, Mihara F, Ogomori K, Tanaka A, Kaneko K, Masuda K (2002) Diffusion tensor in posterior cingulate gyrus: correlation with cognitive decline in Alzheimer's disease. *Neuroreport* **13**, 2299-2302.

[25] Fellgiebel A, Muller MJ, Wille P, Dellani PR, Scheurich A, Schmidt LG, Stoeter P (2005) Color-coded diffusion-tensor-imaging of posterior cingulate fiber tracts in mild cognitive impairment. *Neurobiol Aging* **26**, 1193-1198.

[26] Müller MJ, Greverus D, Dellani PR, Weibrich C, Wille PR, Scheurich A, Stoeter P, Fellgiebel A (2005) Functional implications of hippocampal volume and diffusivity in mild cognitive impairment. *Neuroimage* **28**, 1033-1042.

[27] Naggara O, Oppenheim C, Rieu D, Raoux N, Rodrigo S, Dalla Barba G, Meder JF (2006) Diffusion tensor imaging in early Alzheimer's disease. *Psychiatry Res* **146**, 243-249.

[28] Medina D, Detoledo-Morrell L, Urresta F, Gabrieli JD, Moseley M, Fleischman D, Bennett DA, Leurgans S, Turner DA, Stebbins GT (2006) White matter changes in mild cognitive impairment and AD: a diffusion tensor imaging study. *Neurobiol Aging* **27**, 663-672.

[29] Teipel SJ, Stahl R, Dietrich O, Schoenberg SO, Perneczky R, Bokde AL, Reiser MF, Moller HJ, Hampel H (2007) Multivariate network analysis of fiber tract integrity in Alzheimer's disease. *Neuroimage* **34**, 985-995.

[30] McKhann G, Drachman D, Folstein M, Katzman R, Price D, Stadlan EM (1984) Clinical diagnosis of Alzheimer's disease: report of the NINCDS-ADRDA Work Group under the auspices of the Department of Health and Human Services Task Force on Alzheimer's disease. *Neurology* **34**, 939-944.

[31] Folstein MF, Folstein SE, McHugh PR (1975) Mini-mental-state: a practical method for grading the cognitive state of patients for the clinician. *J Psychiatr Res* **12**, 189-198.

[32] Hollingshead AB (1975) *Four factor index of social status*, Department of Sociology, Yale University New Haven, CT.

[33] Davis J, Smith T, Hodge R, Nakao K, Treas J (1991) Occupational prestige ratings from the 1989 general social survey. *Inter-university Consortium for Political and Social Research, Ann Arbor, MI.*

[34] Berres M, Monsch AU, Bernasconi F, Thalmann B, Stahelin HB (2000) Normal ranges of neuropsychological tests for the diagnosis of Alzheimer's disease. *Stud Health Technol Inform* **77**, 195-199.

[35] Shulman KI, Shedletsky R, Silver IL (1986) The challenge of time: Clock drawing and cognitive function in the elderly. *Int J Geriatr Psychiatry* **1**, 135-140.

[36] Chen P, Ratcliff G, Belle SH, Cauley JA, DeKosky ST, Ganguli M (2000) Cognitive tests that best discriminate between presymptomatic AD and those who remain nondemented. *Neurology* **55**, 1847-1853.

[37] Scheltens P, Barkhof F, Leys D, Pruvo JP, Nauta JJP, Vermersch P, Steinling M, Valk J (1993) A semiquantitative rating scale for the assessment of signal hyperintensities on magnetic resonance imaging. *J Neurol Sci* **114**, 7-12.

[38] Mangin JF, Poupon C, Clark C, Le Bihan D, Bloch I (2002) Distortion correction and robust tensor estimation for MR diffusion imaging. *Med Image Anal* **6**, 191-198.

[39] Friston K, Holmes AP, Worsley K, Poline J-B, Frith CD, Frackowiak RSJ (1995) Statistical parametric maps in functional imaging: a general linear approach. *Hum Brain Mapp* **2**, 189-210.

[40] Friston K, Ashburner J, Frith CD, Poline J-B, Heather JD, Frackowiak RSJ (1995) Spatial registration and normalization of images. *Hum Brain Mapp* **2**, 165-189.

[41] Ashburner J, Friston KJ (2000) Voxel-based morphometry-the methods. *Neuroimage* **11**, 805-821.

[42] Ashburner J, Neelin P, Collins DL, Evans A, Friston K (1997) Incorporating prior knowledge into image registration. *Neuroimage* **6**, 344-352.

[43] Ashburner J, Andersson JL, Friston KJ (1999) High-dimensional image registration using symmetric priors. *Neuroimage* **9**, 619-628.

[44] Ashburner J, Friston K (1997) Multimodal image coregistration and partitioning – a unified framework. *Neuroimage* **6**, 209-217.

[45] Friston KJ, Poline JP, Holmes AP, Frith C, Frackowiak RSJ (1996) A multivariate analysis of PET activation studies. *Hum Brain Map* **4**, 140-151.

[46] Zuendorf G, Kerrouche N, Herholz K, Baron JC (2003) Efficient principal component analysis for multivariate 3D voxel-based mapping of brain functional imaging data sets as applied to FDG-PET and normal aging. *Hum Brain Mapp* **18**, 13-21.

[47] Hotelling H (1931) A generalization of Student's ratio. *Ann Math Stat* **2**, 360-378.

[48] Talairach J, Tournoux P (1988) *Co-Planar Stereotaxic Atlas of the Human Brain*, Thieme, New York.

[49] Chandler MJ, Lacritz LH, Hynan LS, Barnard HD, Allen G, Deschner M, Weiner MF, Cullum CM (2005) A total score for the CERAD neuropsychological battery. *Neurology* **65**, 102-106.

[50] Arenaza-Urquijo EM, Bosch B, Sala-Llonch R, Sole-Padulles C, Junque C, Fernandez-Espejo D, Bargallo N, Rami L, Molinuevo JL, Bartres-Faz D (2011) Specific anatomic associations between white matter integrity and cognitive reserve in normal and cognitively impaired elders. *Am J Geriatr Psychiatry* **19**, 33-42.

[51] Brayne C, Ince PG, Keage HA, McKeith IG, Matthews FE, Polvikoski T, Sulkava R (2011) Education, the brain and dementia: neuroprotection or compensation? *Brain* **133**, 2210-2216.

[52] Arendt T (2000) Alzheimer's disease as a loss of differentiation control in a subset of neurons that retain immature features in the adult brain. *Neurobiol Aging* **21**, 783-796.

[53] Levitt P (2003) Structural and functional maturation of the developing primate brain. *J Pediatr* **143**, S35-S45.

[54] Bartzokis G, Beckson M, Lu PH, Nuechterlein KH, Edwards N, Mintz J (2001) Age-related changes in frontal and temporal lobe volumes in men: a magnetic resonance imaging study. *Arch Gen Psychiatry* **58**, 461-465.

[55] O'Connor DW, Pollitt PA, Treasure FP (1991) The influence of education and social class on the diagnosis of dementia in a community population. *Psychol Med* **21**, 219-224.

[56] Bruandet A, Richard F, Bombois S, Maurage CA, Masse I, Amouyel P, Pasquier F (2008) Cognitive decline and survival in Alzheimer's disease according to education level. *Dement Geriatr Cogn Disord* **25**, 74-80.

[57] Förster S, Buschert V, Buchholz H, Teipel S, Friese U, Zach C, la Fougere C, Rominger A, Hampel H, Bartenstein P, Bürger K (2011) Effects of a 6-month cognitive intervention program on brain metabolism in amnestic MCI and mild Alzheimer´s disease. *J Alzheimer Dis* in press.

Searching for Novel Biomarkers Using High Resolution Diffusion Tensor Imaging

Michael A. Yassa*

Psychological and Brain Sciences, Johns Hopkins University, Baltimore, MD, USA

Abstract. Diffusion tensor imaging is capable of resolving large fiber bundles (e.g. the corpus callosum) and has been quite informative in understanding the overall structural connectivity of the brain. Recent data has shown that traditional resolution limitations can be exceeded in humans in vivo to submillimeter resolution. This chapter discusses these new techniques, and specific applications to small pathways such as the perforant path in the medial temporal lobe. High-resolution diffusion tensor imaging is a promising new tool that can be used to discover novel biomarkers for Alzheimer's disease and other disorders. It allows for a much more detailed investigation of brain white matter than previously possible, perhaps offering clues into the first signs of synaptic deterioration that may precede frank neuronl loss. Although these methods are still in their infancy and many challenges have to be overcome before they can be used in a clinical fashion, results so far have been promising. Challenges and future directions are discussed in detail.

Keywords: Hippocampus, perforant path, diffusion tensor imaging, biomarkers, Alzheimer's disease, aging, entorhinal cortex

OVERVIEW OF DTI AND ITS APPLICATIONS TO ALZHEIMER'S DISEASE

Diffusion tensor imaging (DTI) is based on the principle that water molecules are constantly in motion. Although this motion is typically random, organized structures such as axons or dendrites constrain the mobility of water molecules making it less random. For example, water will diffuse more readily along the principal axis of an axon than perpendicular to it, thus its motion becomes more directional or anisotropic. In a broad sense, DTI attempts to quantify diffusion anisotropy in a meaningful way. The pioneering work of Basser and colleagues [1–4] first introduced a rigorous formulation of anisotropy in the diffusion tensor. Since the mid-nineties, DTI has evolved through many stages of development.

It is now possible to sample water movement in hundreds of directions (high-angular resolution diffusion imaging or HARDI) whereas original DTI studies only required six directions, the minimum number of directions required to estimate a diffusion tensor. Methods to account for fiber crossing, bending and twisting such as Q-ball imaging [5] and diffusion spectrum imaging (DSI) [6, 7] have been developed. Various sophisticated fiber-tracking techniques have now become commonplace tools in neuroimaging laboratories for mapping white matter connectivity [8–12].

Diffusion signals capture microstructural properties of white matter that cannot otherwise be captured on traditional structural MRI scans. For example, diffusion anisotropy is increased in regions of high axonal coherence, robust myelination, and tight packing and decreased in areas where white matter is not as organized [1, 4, 13]. Given the method's increased sensitivity to microscopic changes in white matter, it has remarkable promise for detecting white matter abnormalities otherwise invisible to traditional structural MRI methods [14]. This makes it an especially attractive technology to use for investigating white matter

*Correspondence to: Michael A. Yassa, Department of Psychological and Brain Sciences, Johns Hopkins University 3400 N. Charles St. Ames 216A, Baltimore, MD 21218-2686, USA. Tel.: +1 (410) 516 0202; Fax: +1 (410) 516 4478; E-mail: yassa@jhu.edu.

changes in aging as well as Alzheimer's disease (AD) and its prodromal state, mild cognitive impairment (MCI).

Studies of the aging brain using DTI have generally found decreased fractional anisotropy (FA) and increased mean diffusivity (MD) in frontal white matter, the anterior cingulum, the fornix, and the corpus callosum (c.f. [15]). These changes in anisotropy and diffusivity are generally attributed to fiber degeneration and demyelination with increasing age. On the other hand, diffusion imaging studies of MCI and AD patients have observed decreased anisotropy throughout the brain but most notably in the temporal lobes (see recent reviews [15] and [16]).

A large body of research has indicated that the medial temporal lobes (MTL), and in particular the hippocampus and entorhinal cortex, are the first to deteriorate in the course of AD [17–19]. Several studies have used DTI to investigate the MTL in particular in MCI and AD. For example, Fellgiebel and colleagues [20] observed decreased FA and increased MD in the left hippocampus in AD patients compared to controls. Mielke et al. [21] noted in AD patients decreased FA in the fornix and cingulum, the two major fiber bundles that connect the limbic lobes to the rest of the brain. They also observed less dramatic changes in individuals with MCI, suggesting that these microstructural alterations likely vary along a spectrum from MCI to AD.

Changes in parahippocampal white matter have been observed in AD patients using DTI, e.g. [22]. A recent study by Choo et al. [23] reported a dissociation within cingulum fibers that may distinguish MCI from AD. They observed decreased FA in parahippocampal cingulum fibers in individuals with MCI and decreased FA in posterior cingulate cingulum fibers in AD patients. This may indicate that there is a topological pattern of white matter degeneration that manifests at the early stages of AD with the parahippocampal white matter being the site of the earliest changes.

THE NEED FOR HIGH-RESOLUTION DTI OF THE MEDIAL TEMPORAL LOBE

Although traditional DTI has been helpful in evaluating the state of MTL white matter in general, it remains largely unable to distinguish among the many fiber pathways in the region. Very few attempts have been made to use DTI to investigate smaller pathways within the medial temporal lobe. Aside from the

work I will discuss shortly, only one previous study attempted to quantify diffusion signals in the perforant path region in vivo. Kalus et al. [24] found reductions in intervoxel coherence in the perforant path zone in individuals with MCI compared to controls, possibly indicating synaptic loss in the region. However, since there are many crossing fibers in this region, it was not possible to uniquely attribute these signal losses to the perforant path itself.

High-resolution DTI offers a means to identify microstructural signals that can be uniquely attributed to individual fiber bundles. The increased resolution allows us to conduct a more detailed investigation where the contribution of each individual fiber bundle to an image voxel is magnified. As is the case with almost any imaging technique, increasing resolution is a substantial challenge. First, it is almost impossible to increase the resolution without sacrificing signal-to-noise ratio (SNR). Multiple averages are necessary to match traditional SNR levels. Second, one would need to apply parallel imaging techniques such as SENSE [25, 26] in order to reduce scan time to a clinically applicable range (~1 hr).

Third, the microstructural anatomical features reflected in high-resolution diffusion signals need to be adequately investigated. For example, at high resolution, white matter is not the only tissue in which anisotropic diffusion can be observed. Pyramidal cells have long apical dendrites, which also demonstrate remarkable anisotropy on high-resolution rodent DTI scans [27–29]. Thus, diffusion indices at high-resolution must be validated either by relating them to other structural and functional measures, to a relevant behavioral outcome, or to histological features.

If all of the above challenges can be addressed, one key question is the extent to which resolution can/must be enhanced. Here, it is important to keep in mind that the required resolution to resolve a small pathway like the perforant path may be different from the maximum resolution that can be achieved in a clinically practical scan time. The physiological limitation in diffusion imaging is imposed by water molecules. Thus, unlike functional MRI where optimal resolutions range around 1–1.5 mm (the approximate size of the capillary bed giving rise to the BOLD signal), the theoretical limitation on resolution in DTI is far smaller and is quite likely in the nanometer range. Our experiments with this technique in humans in vivo suggest that a resolution of ~0.5 mm sufficiently samples signals from small regions within the hippocampus and can index anisotropic diffusion in pyramidal dendrites as well as
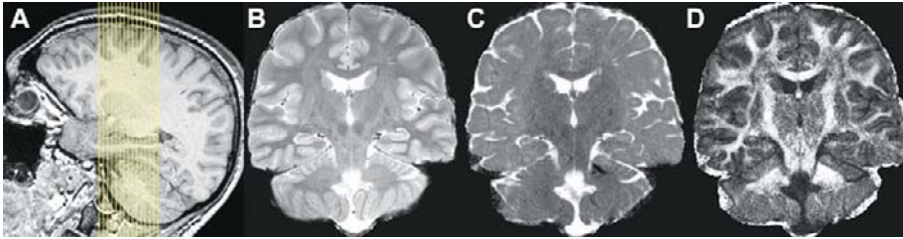
Fig. 1. (A) Slice placement and field of view for high-resolution DTI scan, (B) High-resolution T2-weighted FSE scan acquired in the same geometry as the DTI scan, (C) single subject sample MD image based on 12 averages, and (D) single subject sample FA image based on 12 averages. B, C, and D are from the same subject. Alignment of C and D with B shows the limited effects of distortions on the region of interest.

small fiber pathways [30]. It is also a sequence that can be performed in under forty minutes (twelve scans) and thus can be applied in a clinical setting.

HIGH-RESOLUTION DTI AND THE PERFORANT PATH

A novel high-resolution DTI sequence was recently introduced by Yassa et al. [30]. It is a 32-direction, limited field of view (FOV) scanning protocol at 0.66 mm x 0.66 mm in-plane, with a slice thickness of 3 mm. This is a sequence optimized for the MTL with the high-resolution plane corresponding to the coronal plane perpendicular to the principal axis of the hippocampus (Fig. 1A). Our choice of this plane was guided by tracer studies in primate tissue [31] suggesting that the coronal sections are the ones where the perforant path can be evaluated easily.

The technical details of this sequence were published in [30] and are shown here in Table 1. Fig. 1B shows an in-plane T2 Fast Spin Echo scan acquired in the same resolution as the diffusion images for regis-

tration. Fig. 1C shows a sample mean diffusivity (MD) and Fig. 1D shows a sample fractional anisotropy (FA) image.

This sequence can be easily adapted to any Philips 3.0 Tesla scanner or any scanner that can make use of parallel imaging techniques (e.g. SENSE and GRAPPA). We used this sequence in order to visualize and quantify the perforant path (Fig. 2A) and assess its integrity in a sample of young and older adults. We developed a simple assessment method that calculated the magnitude of the diffusion signal along the canonical orientation of the perforant path. This quantity (Eq. 1 in [30]) was evaluated along the entire bank of the entorhinal cortex giving rise to a Gaussian-like curve that captured the perforant path from its most medial extent to its most lateral. This signal was operationalized as area-under-the-curve (AUC), which showed a significant difference between young and aged adults (Fig. 2B).

To ascertain that this difference was unique to the perforant path, we conducted the same measurements in another hippocampal pathway, the temporoalvear pathway, which does not seem to degrade substantially with aging [32]. We found no evidence for a group difference in this "control" pathway suggesting that the perforant path findings are not evidence for global white matter differences between groups. We also found a strong relationship in the older adults between our measure of perforant path integrity and scores on the Rey Auditory Verbal Learning Test (RAVLT), a memory measure that is sensitive to hippocampal deficits (Fig. 2C), suggesting that this diffusion signal has a valid neurobiological basis. No other relationships with neuropsychological measures of intelligence, working memory, attention and executive function were found, strongly suggesting that perforant path deficits have specific functional implications to hippocampal-dependent memory.

Table 1
High-resolution DTI Scan Parameters

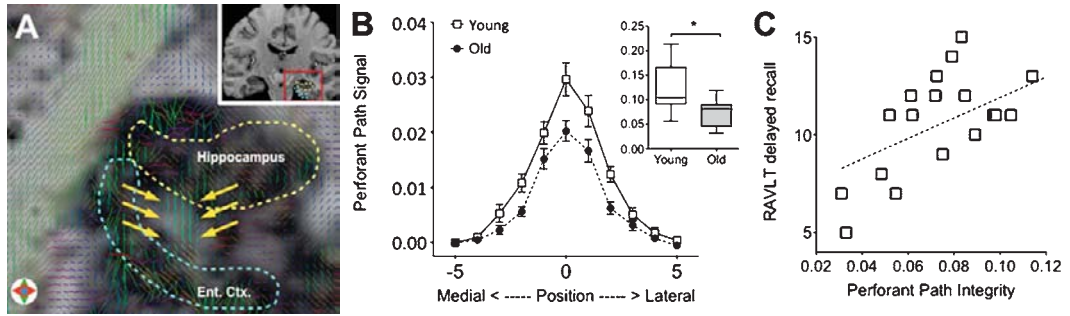| Parameter	Value
FOV	170×170
Matrix size	256×256
Voxel size	0.664×0.664 mm
Slice thickness	3 mm (1 mm gap)
Number of slices	15
TR/TE	2,717 ms/67 ms
Flip angle	90°
SENSE factor	2.5
b-value	1,200 s/mm^2
Directions	32
Averages	12

Fig. 2. (A) Tensor visualization of the perforant path (indicated by yellow arrows) overlaid on a FA map. After Yassa et al., PNAS 2010; 107(28):12687-91, Fig. 1D, reprinted with permission. (B) comparison of perforant path diffusion signal in young vs. old showing a significant difference in area under the curve. After Yassa et al., PNAS 2010; 107(28):12687-91, Fig. 3, reprinted with permission, (C) correlation between perforant path integrity (operationalized as area under the curve) and delayed verbal recall in older adults. Adapted from Yassa et al., PNAS 2010; 107(28):12687-91 with permission.
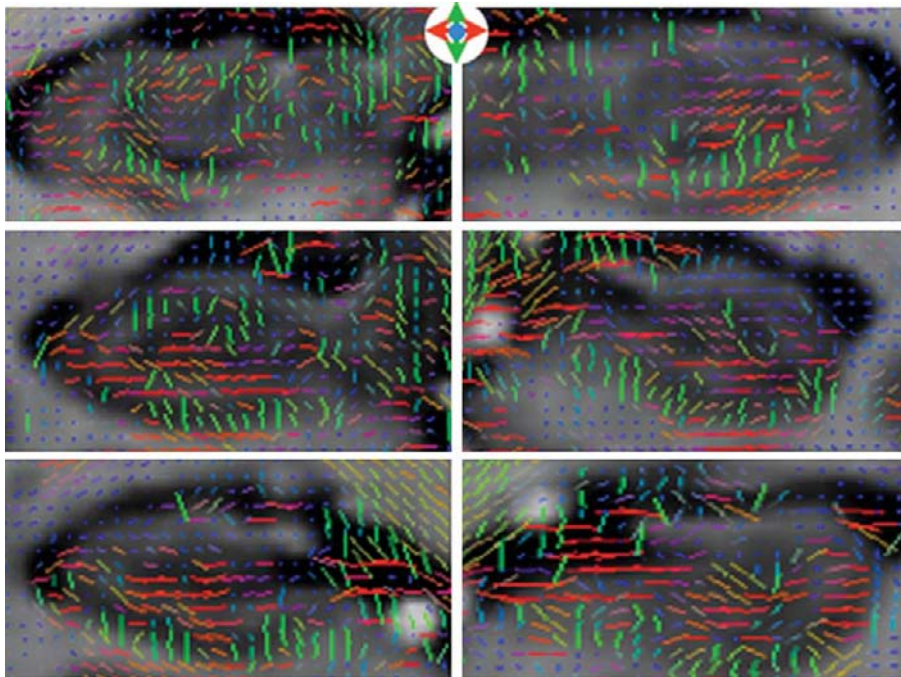

Fig. 3. Hippocampal gray matter anisotropy. Note the change in tensor orientation from green (superior-inferior) to red (left-right) consistent with the changing orientation of the pyramidal cells in the folded hippocampal sheet. After Yassa et al., PNAS 2010; 107(28):12687-91, Fig. S2, reprinted with permission.

In addition, we showed that high-resolution DTI is sensitive to hippocampal diffusion signals likely arising from pyramidal dendrites, although we did not formally assess dendritic integrity in this study (Fig. 3). This investigation requires the parcellation of gray and white matter compartments inside the hippocampus using a combination of structural images and FA maps with the additional delineation of subfields. Pre-

liminary data suggest that dendritic integrity can be assessed at the subfield level (Yassa M. and Stark C. unpublished data).

Overall, the results of this high-resolution DTI investigation in humans in vivo have been quite promising. They demonstrate that: (1) high-resolution DTI is possible in humans in clinically applicable scan durations (45–60 minutes), (2) high-resolution diffu-
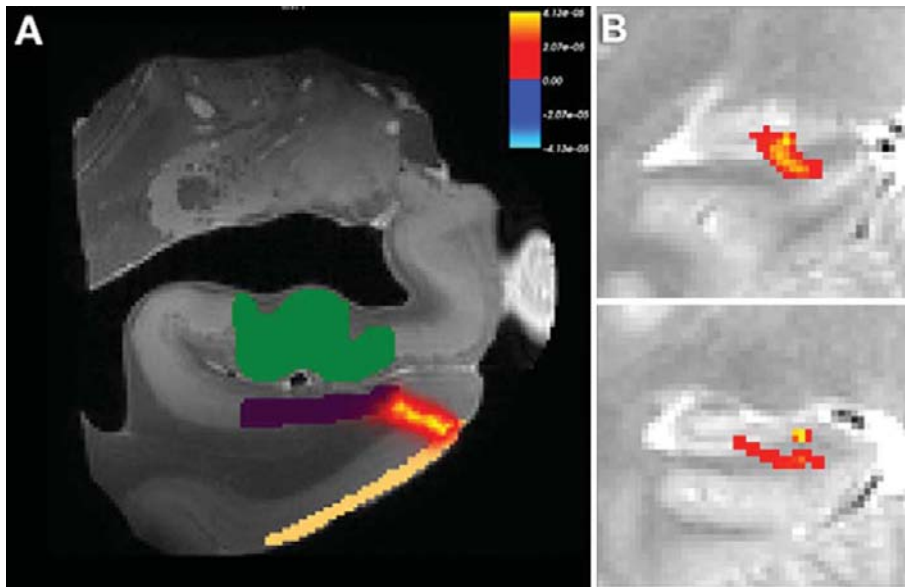
Fig. 4. (A) Probabilistic tractography of the perforant path in ex vivo human tissue. After Augustinack et al., Frontiers in Human Neuroscience, 2010; 4(42),1-13 reprinted with author's permission. (B) Sample probabilistic tractography of the perforant path in a human subject in vivo. In both cases, the perforant path clearly originates in the entorhinal cortex and terminates in the hippocampus. Both studies are consistent in terms of the location and approximate size of the perforant path.

sion signals have the key advantage of being able to evaluate small diffuse pathways such as the perforant path as well as dendritic diffusion signals, and (3) high-resolution diffusion measures are associated with behavioral measures dependent on the integrity of the pathway or region in question.

RELATIONSHIP OF HIGH-RESOLUTION DIFFUSION INDICES TO HISTOLOGICAL FEATURES

A critical issue with diffusion imaging especially in the absence of frank pathology (e.g. stroke or lesion) is the validity of the signal. For example, what does it mean to have decreased fractional anisotropy? Is there a neurobiological basis for FA group differences? Although there have not been many formal investigations of the microstructural anatomical features that may give rise to differences in diffusion signals, recent work has provided some promising results.

For example, Pych and colleagues [33] used DTI microimaging to show that the size of the hippocampal dendritic compartment was tightly coupled to fractional anisotropy in a mouse model of AD. In fact, their initial experiments and the work by Mori and

others [27–29] partly inspired our attempt to use in vivo high-resolution DTI to attempt to visualize and quantify pyramidal dendrites in the hippocampus.

A recent investigation [34] used high-resolution DTI to visualize the perforant pathway in ex vivo human tissue. The authors used probabilistic tractography to map the perforant pathway from the entorhinal cortex to the hippocampus (Fig. 3A). We have also conducted a similar investigation using FSL's bedpostX and probtrackX and found remarkably similar results (Fig. 3B). The authors validated the *ex vivo* tractography results using histology (Luxol Fast Blue myelin stain) which stained the perforant path in the same locations identified by the diffusion signals.

These studies were a necessary first step towards validation. However, other potential relationships between diffusion signals and synaptic markers remain to be investigated. For example, work by Smith et al. [35] suggests that synaptophysin immunoreactivity at the entorhinal-dentate perforant path synapse is reduced in aged rodents with spatial learning impairments. It would be interesting to see how well diffusion measures correlate with presynaptic markers such as synaptophysin. In addition, if these diffusion measures can be used to track dendritic changes, validation using dendritic markers such as synaptopodin and MAP2

may also be informative. These validation efforts can be conducted in animal models and can significantly inform neuroimaging efforts in the human.

ISOLATING BIOMARKERS FOR ALZHEIMER'S DISEASE

A logical question is whether high-resolution DTI can be used to identify early biomarkers for Alzheimer's disease. AD biomarker discovery is one of the most active areas of research. Converging evidence across studies suggests that about a third of cognitively normal older adults have many of the traditional biomarker signatures present in AD, such as cortical amyloid binding [36–38] and cerebrospinal fluid-derived Aβ42 and phosphorylated tau [39, 40]. The above is also true for histopathological features (i.e., senile plaques and neurofibrillary tangles) identified upon autopsy [41]. There is an emerging consensus that these markers in nondemented adults represent a preclinical form of AD [37, 38, 41]. However, determining which cognitively normal individuals will ultimately develop AD remains a significant challenge.

There is an increasing need to develop biomarkers that reflect neural changes at the earliest stages of the disease in order to correctly target susceptible individuals. It is unlikely that any single biomarker will be 100% predictive. However, we can attempt to develop a "biomarker profile" that combines the most predictive probes in order to determine who will convert to AD with greater confidence.

High-resolution DTI of the hippocampus may offer novel contributions to this endeavor. One potential biomarker may be perforant path integrity. We have shown that perforant path integrity is coupled to behavioral performance on a hippocampus-dependent verbal learning test [30]. Although this investigation was conducted in nondemented older adults, the same approach can be applied to the earliest stages of dementia.

While AD affects the entire brain, the hippocampus and entorhinal cortex are the sites of the earliest pathological changes. It is possible that perforant path degradation is one of the earliest pathological features in the MTL that precedes frank cellular loss. Such a measure, if combined with other biomarkers, can increase our diagnostic accuracy and can also be used as an outcome measure to evaluate the efficacy of therapeutic interventions. Furthermore, since perforant path integrity is related to performance on a memory test, it is likely that it is part of a mechanistic dysfunction. If

so, then intervention at this level may rescue memory deficits.

The terrain for Alzheimer's disease biomarker discovery using high-resolution DTI is largely uncharted. This method presents novel and exciting opportunities. Unlike other structural and functional imaging methods high-resolution DTI could provide important insights into fiber/synaptic and dendritic integrity, making it possible to address numerous questions that could not previously be addressed.

REMAINING TECHNICAL CHALLENGES AND FUTURE DIRECTIONS

Although the first high-resolution DTI experiments have been largely successful, it is important to note that the technique is still in its infant stages. There are many challenges that remain to be addressed. For example, the use of single shot echoplanar imaging (ssEPI) is associated with geometric distortions (stretching and shearing) caused by local eddy currents in the gradient coils. We have avoided this problem largely by acquiring a small FOV around the medial temporal lobe. However, in order to more directly ameliorate this problem, multishot sequences can be used. These sequences are far more robust against distortion effects, however they are much more susceptible to motion artifacts. As a result, about 30–40% of all scans might be discarded due to motion effects.

Even if the subject holds perfectly still, the brain's pulsatile motion can potentially induce artifacts. One way to address this is the use of cardiac or respiratory gating, which can compensate for pulsatile motion [42]. Of course, this comes at the cost of increasing scan time, but there may be a suitable tradeoff that can be reached. It is worthy of note that the effect of physiological noise on high-resolution scans is much higher than traditional resolution scans, since smaller voxels are more likely to be affected than larger voxels (where the same shifts are less likely to affect whole voxels).

Our current scan time is under an hour. However, in order to make this type of scan more clinically applicable, reducing this time to under a half hour is an important future direction. We are currently experimenting with increasing parallel imaging factors to achieve this goal. One additional benefit of decreasing the scan time is that scan fidelity would remain high as smaller amounts of motion correction have to be applied to the data before tensor solving.

Although our current in-plane resolution is relatively high, the thru-plane resolution is still on par with traditional DTI, thus leading to partial volume contamination. Despite the fact the hippocampus is a relatively straight structure that largely conforms to the plane of slice acquisition, it still does exhibit some inter-individual variation and bends upwards towards the tail. Thus, an important future goal in increasing our scan resolution is to use isotropic voxels and perhaps achieve a 0.5 mm isotropic resolution. This can be made possible by scanning at higher field strengths. As 7.0 Tesla magnets are becoming more commonplace across institutions in the country, this endeavor is becoming more feasible. Adapting the sequence we created for the 3.0 T scanner to 7.0 T should not be difficult but will requires additional pulse sequence programming to optimize it for the higher-strength magnet.

Another significant challenge is that the SNR in individual scans is still quite low and thus multiple averages are required in order to generate reasonable scalar maps. Although averaging may help with SNR, the low SNR in individual scans can induce a bias in the diffusion images that depends on the scan orientation and the gradients employed. We used a slightly higher b-value than is typical for traditional DTI (1200 s/mm^2) to attempt to increase the individual scan SNR. It is possible that even higher b-values can be used, although this has to be balanced against the choice of voxel resolution, angular resolution, SNR and clinically feasible times. This compromise is unfortunately far from trivial.

The MTL and in particular the perforant path regions contain many crossing fibers. A fundamental flaw in the diffusion tensor model is that it assumes a single ellipsoid with a single orientation in each voxel, thus it is unable to capture physiological features of white matter tracts such as fiber crossing, bending and twisting. Other evolving methods may offer some promise in resolving these characteristics. For example, Q-ball imaging [5], a high-angular resolution diffusion imaging (HARDI) technique, uses a mathematical alternative to the tensor model that employs probability distributions and vector math to model anisotropy. By collecting high-angular resolution data (e.g., 256 directions) it is possible to identify several crossing tracts per voxel.

More recently, several methods to extract super-resolution features from diffusion data have been developed. One such method, Spatial HARDI [43] uses spatial information in a Bayesian framework to constrain the reconstruction of raw diffusion MRI data. This spatial regularization scheme when applied to spherical harmonic q-ball imaging improves SNR and better identification of crossing fibers leading to more accurate tractography. Another method, track-density imaging (TDI; [44]) uses post-processing methods based on diffusion MRI fiber-tracking to increase spatial resolution beyond the limitations of the single voxel. Each technique is not without its own challenges and limitations, however, using multiple techniques to arrive at similar conclusions is an essential component of neuroscientific inquiry.

Another significant challenge for using diffusion methods to investigate the integrity of the medial temporal lobe in Alzheimer's disease is that this region undergoes substantial structural changes that could have profound effect on diffusion indices. For example, a decrease in fractional anisotropy could be caused by a decrease in white matter integrity or regional atrophy. It is likely that diffusion-based methods will be more helpful in elucidating subtle changes early in the course of the disease and not late. Comparison of these high-resolution methods with traditional DTI methods for investigating aging and AD is also necessary.

Aside from the technical challenges, much remains to be done to validate the measures and indices we are currently using. This can be done using cross-species investigations with histological validation. Augustinack et al., [34] and others have already initiated this important work. However, scanning an animal model in vivo and following up the scans with detailed histological analyses of pre- and post-synaptic integrity will also be necessary to determine the meaning of high-resolution diffusion signals.

In summary, high-resolution DTI and the application to perforant path imaging demonstrates the power and promise of diffusion imaging at high resolutions. Together with other functional and structural imaging tools, diffusion imaging may provide important clues and help discover novel biomarkers that can be used for diagnosis and intervention in Alzheimer's disease and other brain disorders.

REFERENCES

[1] Basser PJ (1995) Inferring microstructural features and the physiological state of tissues from diffusion-weighted images. *NMR Biomed* **8**, 333-344.

[2] Basser PJ, Mattiello J, LeBihan D (1994) MR diffusion tensor spectroscopy and imaging. *Biophys J* **66**, 259-267.

[3] Basser PJ, Mattiello J, LeBihan D (1994) Estimation of the effective self-diffusion tensor from the NMR spin echo. *J Magn Reson B* **103**, 247-254.

[4] Pierpaoli C, Jezzard P, Basser PJ, Barnett A, Di Chiro G (1996) Diffusion tensor MR imaging of the human brain. *Radiolog* **201**, 637.

[5] Tuch DS (2004) Q-ball imaging. *Magn Reson Med* **52**, 1358-1372.

[6] Wedeen VJ, Hagmann P, Tseng WY, Reese TG, Weisskoff RM (2005) Mapping complex tissue architecture with diffusion spectrum magnetic resonance imaging. *Magn Reson Med* **54**, 1377-1386.

[7] Wedeen VJ, Wang RP, Schmahmann JD, Benner T, Tseng WY, Dai G, Pandya DN, Hagmann P, D'Arceuil H, de Crespigny AJ (2008) Diffusion spectrum magnetic resonance imaging (DSI) tractography of crossing fibers. *Neuroimage* **41**, 1267-1277.

[8] Mori S, van Zijl PC (2002) Fiber tracking: principles and strategies - a technical review. *NMR Biomed* **15**, 468-480.

[9] Behrens TE, Berg HJ, Jbabdi S, Rushworth MF, Woolrich MW (2007) Probabilistic diffusion tractography with multiple fibre orientations: what can we gain? *Neuroimage* **34**, 144-155.

[10] Tournier JD, Calamante F, King MD, Gadian DG, Connelly A (2002) Limitations and requirements of diffusion tensor fiber tracking: an assessment using simulations. *Magn Reson Med* **47**, 701-708.

[11] Berman JI, Chung S, Mukherjee P, Hess CP, Han ET, Henry RG (2008) Probabilistic streamline q-ball tractography using the residual bootstrap. *Neuroimage* **39**, 215-222.

[12] Iturria-Medina Y, Canales-Rodriguez EJ, Melie-Garcia L, Valdes-Hernandez PA, Martinez-Montes E, Aleman-Gomez Y, Sanchez-Bornot JM (2007) Characterizing brain anatomical connections using diffusion weighted MRI and graph theory. *Neuroimage* **36**, 645-660.

[13] Pierpaoli C and Basser PJ (1996) Toward a quantitative assessment of diffusion anisotropy. *Magn Reson Med* **36**, 893-906.

[14] Taylor WD, Hsu E, Krishnan KR, MacFall JR (2004) Diffusion tensor imaging: background, potential, and utility in psychiatric research. *Biol Psychiatry* **55**, 201-207.

[15] Chua TC, Wen W, Slavin MJ, Sachdev PS (2008) Diffusion tensor imaging in mild cognitive impairment and Alzheimer's disease: a review. *Curr Opin Neurol* **21**, 83-92.

[16] Stebbins GT, Murphy CM (2009) Diffusion tensor imaging in Alzheimer's disease and mild cognitive impairment. *Behav Neurol* **21**, 39-49.

[17] West MJ, Coleman PD, Flood DG, Troncoso JC (1994) Differences in the pattern of hippocampal neuronal loss in normal ageing and Alzheimer's disease. *Lancet* **344**, 769-772.

[18] Gomez-Isla T, Price JL, McKeel DWJ, Morris JC, Growdon JH, Hyman BT (1996) Profound loss of layer ii entorhinal cortex neurons occurs in very mild Alzheimer's disease. *J Neurosci* **16**, 4491-4500.

[19] Scheff SW, Price DA, Schmitt FA, Mufson EJ (2006) Hippocampal synaptic loss in early Alzheimer's disease and mild cognitive impairment. *Neurobiol Aging* **27**, 1372-1384.

[20] Fellgiebel A, Wille P, Muller MJ, Winterer G, Scheurich A, Vucurevic G, Schmidt LG, Stoeter P (2004) Ultrastructural hippocampal and white matter alterations in mild cognitive impairment: a diffusion tensor imaging study. *Dement Geriatr Cogn Disord* **18**, 101-108.

[21] Mielke MM, Kozauer NA, Chan KC, George M, Toroney J, Zerrate M, Bandeen-Roche K, Wang MC, Vanzijl P, Pekar JJ, Mori S, Lyketsos CG, Albert M (2009) Regionally-specific diffusion tensor imaging in mild cognitive impairment and Alzheimer's disease. *Neuroimage* **46**, 47-55.

[22] Salat DH, Tuch DS, van der Kouwe AJ, Greve DN, Pappu V, Lee SY, Hevelone ND, Zaleta AK, Growdon JH, Corkin S, Fischl B, Rosas HD (2010) White matter pathology isolates the hippocampal formation in Alzheimer's disease. *Neurobiol Aging* **31**, 244-256.

[23] Choo IH, Lee DY, Oh JS, Lee JS, Lee DS, Song IC, Youn JC, Kim SG, Kim KW, Jhoo JH, Woo JI (2010) Posterior cingulate cortex atrophy and regional cingulum disruption in mild cognitive impairment and Alzheimer's disease. *Neurobiol Aging* **31**, 772-779.

[24] Kalus P, Slotboom J, Gallinat J, Mahlberg R, Cattapan-Ludewig K, Wiest R, Nyffeler T, Buri C, Federspiel A, Kunz D, Schroth G, Kiefer C (2006) Examining the gateway to the limbic system with diffusion tensor imaging: the perforant pathway in dementia. *Neuroimage* **30**, 713-720.

[25] Jaermann T, Crelier G, Pruessmann KP, Golay X, Netsch T, van Muiswinkel AM, Mori S, van Zijl PC, Valavanis A, Kollias S, Boesiger P (2004) SENSE-DTI at 3 t. *Magn Reson Med* **51**, 230-236.

[26] Pruessmann KP, Weiger M, Scheidegger MB, Boesiger P (1999) SENSE: sensitivity encoding for fast MRI. *Magn Reson Med* **42**, 952-962.

[27] Zhang J, Miller MI, Plachez C, Richards LJ, Yarowsky P, van Zijl P, Mori S (2005) Mapping postnatal mouse brain development with diffusion tensor microimaging. *Neuroimage* **26**, 1042-1051.

[28] Zhang J, Richards LJ, Yarowsky P, Huang H, van Zijl PC and Mori S (2003) Three-dimensional anatomical characterization of the developing mouse brain by diffusion tensor microimaging. *Neuroimage* **20**, 1639-1648.

[29] Zhang J, van Zijl PC, Mori S (2002) Three-dimensional diffusion tensor magnetic resonance microimaging of adult mouse brain and hippocampus. *Neuroimage* **15**, 892-901.

[30] Yassa MA, Muftuler LT, Stark CE (2010) Ultrahigh-resolution microstructural diffusion tensor imaging reveals perforant path degradation in aged humans in vivo. *Proc Natl Acad Sci U S A* **107**, 12687-12691.

[31] Witter MP (2007) The perforant path: projections from the entorhinal cortex to the dentate gyrus. *Prog Brain Res* **163**, 43-61.

[32] Wilson IA, Gallagher M, Eichenbaum H, Tanila H (2006) Neurocognitive aging: prior memories hinder new hippocampal encoding. *Trends Neurosci* **29**, 662-670.

[33] Pych JC, Venkatasubramanian PN, Faulkner J, Wyrwicz A (2008) IC-P2-161: Decreased hippocampal fractional anisotropy in Tg2576 Alzheimer's disease model mice may reflect a reduction in dendrites. *Alzheimer's and Dementia* **4**, T71-T72.

[34] Augustinack JC, Helmer K, Huber KE, Kakunoori S, Zollei L, Fischl B (2010) Direct visualization of the perforant pathway in the human brain with *ex vivo* diffusion tensor imaging. *Front Hum Neurosci* **4**, 42.

[35] Smith TD, Adams MM, Gallagher M, Morrison JH, Rapp PR (2000) Circuit-specific alterations in hippocampal synaptophysin immunoreactivity predict spatial learning impairment in aged rats. *J Neurosci* **20**, 6587-6593.

[36] Aizenstein HJ, Nebes RD, Saxton JA, Price JC, Mathis CA, Tsopelas ND, Ziolko SK, James JA, Snitz BE, Houck PR,

Bi W, Cohen AD, Lopresti BJ, DeKosky ST, Halligan EM, Klunk WE (2008) Frequent amyloid deposition without significant cognitive impairment among the elderly. *Arch Neurol* **65**, 1509-1517.

[37] Pike KE, Savage G, Villemagne VL, Ng S, Moss SA, Maruff P, Mathis CA, Klunk WE, Masters CL, Rowe CC (2007) Beta-amyloid imaging and memory in non-demented individuals: evidence for preclinical Alzheimer's disease. *Brain* **130**, 2837-2844.

[38] Villemagne VL, Pike KE, Darby D, Maruff P, Savage G, Ng S, Ackermann U, Cowie TF, Currie J, Chan SG, Jones G, Tochon-Danguy H, O'Keefe G, Masters CL, Rowe CC (2008) Abeta deposits in older non-demented individuals with cognitive decline are indicative of preclinical Alzheimer's disease. *Neuropsychologia* **46**, 1688-1697.

[39] De Meyer G, Shapiro F, Vanderstichele H, Vanmechelen E, Engelborghs S, De Deyn PP, Coart E, Hansson O, Minthon L, Zetterberg H, Blennow K, Shaw L, Trojanowski JQ (2010) Diagnosis-independent Alzheimer disease biomarker signature in cognitively normal elderly people. *Arch Neurol* **67**, 949-956.

[40] Fagan AM, Roe CM, Xiong C, Mintun MA, Morris JC, Holtzman DM (2007) Cerebrospinal fluid tau/beta-amyloid(42) ratio as a prediction of cognitive decline in nondemented older adults. *Arch Neurol* **64**, 343-349.

[41] Price JL, McKeel DWJ, Buckles VD, Roe CM, Xiong C, Grundman M, Hansen LA, Petersen RC, Parisi JE, Dickson DW, Smith CD, Davis DG, Schmitt FA, Markesbery WR, Kaye J, Kurlan R, Hulette C, Kurland BF, Higdon R, Kukull W, Morris JC (2009) Neuropathology of nondemented aging: presumptive evidence for preclinical Alzheimer disease. *Neurobiol Aging* **30**, 1026-1036.

[42] Chung S, Courcot B, Sdika M, Moffat K, Rae C, Henry RG (2010) Bootstrap quantification of cardiac pulsation artifact in DTI. *Neuroimage* **49**, 631-640.

[43] Raj A, Hess C, Mukherjee P (2011) Spatial HARDI: improved visualization of complex white matter architecture with bayesian spatial regularization. *Neuroimage* **54**, 396-409.

[44] Calamante F, Tournier JD, Jackson GD, Connelly A (2010) Track-density imaging (TDI): super-resolution white matter imaging using whole-brain track-density mapping. *Neuroimage* **53**, 1233-1243.

This page intentionally left blank

Section 7
Magenetic Resonance Spectroscopy

This page intentionally left blank

Introduction

Section 7: Magnetic Resonance Spectroscopy

Daniel Spielman
Department of Psychiatry and Behavioral Sciences, Stanford University, Stanford, CA, USA

The profound morphological changes that occur in the human brain in normal aging and neurodegenerative diseases have molecular, neurochemical, and cellular underpinnings as well as behavioral concomitants. Magnetic Resonance Spectroscopy (MRS) and Spectroscopic Imaging (MRSI) provides one of the few noninvasive *in vivo* investigative tools for deriving knowledge about the physiological processes of normal aging and the pathophysiological ones by which Alzheimer's disease (AD) causes dementia. As shown in the representative spectrum depicted in Fig. 1, proton MRS (^{1}H-MRS) permits visualization of a variety of markers of cellular integrity and function, including those of living neurons (N-acetyl compounds comprising mainly N-acetyl aspartate [NAA] and with contributions also from other N-acetyl compounds, especially N-acetyl aspartyl glutamate), glia (myo-Inositol [mI]), high-energy metabolic products (creatine [Cr]), cell membrane synthesis or degradation (choline [Cho]), plus less well resolved amino acids, including glutamate and glutamine). Table 1 contains a brief overview of the MR characteristics and bio-chemical roles of the most prominent MRS-detectable metabolites.

A large number of *in vivo* studies have been conducted documenting changes associated with AD, mild cognitive impairment (MCI), and other dementias [1–8]. These studies range from single voxel acquisitions, in which data are acquired from a single targeted volume of tissue, to multi-voxel MRSI studies acquiring spectroscopic data from an array of voxels allowing the assessment of both spectral and spatial variations. Reduced NAA (or NAA/Cr ratios) and elevated mI (or mI/Cr ratios) have been the most consistent findings with respect to AD. Similar, though somewhat smaller effects, seen in individuals with MCI suggest that MRS may also have a predictive role in identifying early stage disease. However, to date, there have been no published studies of ^{1}H-MRS in combination with confirmed diagnosis as assessed by histopathology at autopsy.

A summary of the current literature demonstrates MRSI is a powerful approach for addressing questions about the neurobiology and neurochemistry of
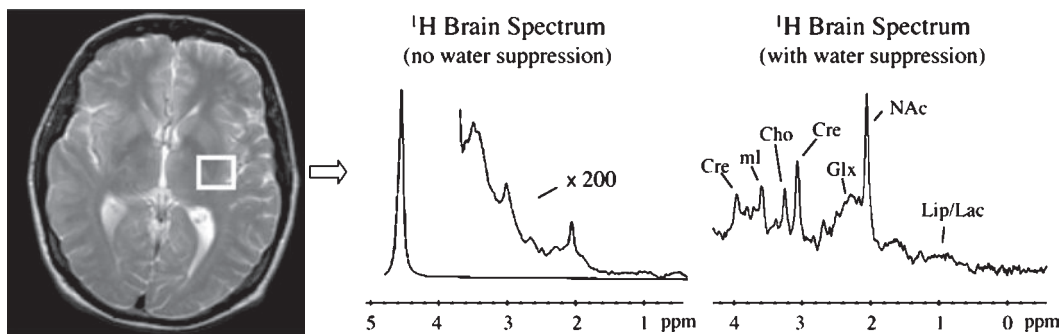

Fig. 1. Typical human adult 1H Brain spectrum.

Table 1
Commonly observed proton metabolites and their corresponding biochemical roles

Compound	Chemical shift	Biochemical role
N-acetyl aspartate (NAA)	2.0 ppm	NAA is only present in living neurons and is thus commonly used as a marker of neuronal density and viability (i.e. it is absent when neurons die or are absent). Note, the *in vivo* 2.0 ppm peak, while primarily comprised of NAA, actually contains contributions from several other N-acetyl compounds. For this reason the peak is sometimes labeled "NA" or "NAc".
Creatine (Cre)	3.0, 3.9	The Cre peak reflects the total creatine stores in cells (hence the common notation tCr), and plays a primary role in maintaining the energy storage systems in cells. Cre levels tend to stay relatively stable in a variety of conditions and is thus often used as an internal standard for comparison to other metabolites. There are actual two peaks due to creatine, one at 3.0 and the other at 3.9 ppm (although the later peak is often lost due to water suppression).
Choline (Cho)	3.2	The bulk of the *in vivo* Cho peak comes from constituents of phospholipid metabolism of cell membranes. It has thus been used as a marker for cellular proliferation and density.
myo-Inositol (mI)	3.6	The biochemical role of myo-Inositol is not fully understood, though some have suggested in may be used as a glial cell marker. mI levels are relatively high in neonates, and it has also been observed to be elevated in Alzheimer's disease (along with decreased NAA).
Glutamine + Glutamate (Glx)	2.1–2.5	Glutamate is an excitatory neurotransmitter that play a critical role in the action of nerve cells in the brain. Glutamine plays a role in regulating neurotransmitter activities as well as in detoxification processes. These two metabolites resonate very close together and often cannot be separated at fields < 3T (hence the common notation Glx to refer to the sum of these peaks).
Lipids (Lip)	0.9–1.4	Lipids, while common in many tissues in the body, are generally not MRS-detectable in the brain (lipids found in the brain are generally tightly bound and exhibit very short T_2 relaxation times). Elevated lipids in the brain may reflect necrosis and cellular breakdown products. These signals can also obscure the measurement of lactate.
Lactate (Lac)	1.3	The signal due to lactate, which actually consists of two closely spaced peaks called a doublet, is an indicator of anaerobic metabolism. Normal brain tissue typically contains very low levels of lactate, and elevated lactate is usually an indicator of ischemia or hypoxia.

the living human brain in health and disease and suggests that the MRS observable changes in AD are not merely an exaggeration of those seen in normal aging. The method is a safe, noninvasive technique ideal for longitudinal study, the essential design for characterizing aging and disease progression. Characterization of NAA, Cr, Cho, and mI, in particular, may provide a diagnostic tool, a monitor of disease progression, and insight into mechanisms of treatment response. Published data thus support the use of ^{1}H-MRS as an important adjunct to the clinical evaluation and diagnosis of dementia. The value of ^{1}H-MRS has been especially noteworthy for monitoring disease progression and identifying group effects for drug trials. However, the most valuable studies use MRS in conjunction with other imaging tools, such as structural MRI, tissue segmentation and volumetric analysis, fMRI, and diffusion tensor imaging (DTI), in order to provide a multi-parametric assessment of brain tissue structure, function, and integrity. With the increasing availability of high field scanners, which yield MRS studies with improved signal-to-noise ratios and increased spectral separation, the role of ^{1}H-MRS in the study of aging and dementia is anticipated to grow in the future.

REFERENCES

[1] Griffith HR, Stewart CC, den Hollander JA (2009) Proton magnetic resonance spectroscopy in dementias and mild cognitive impairment. *Int Rev Neurobiol* **84**, 105-131.

[2] Jessen F, et al. (2009) A multicenter (1)H-MRS study of the medial temporal lobe in AD and MCI. *Neurology* **72**, 1735-1740.

[3] Schott JM, et al. Short echo time proton magnetic resonance spectroscopy in Alzheimer's disease: a longitudinal multiple time point study. *Brain* **133**, 3315-3322.

[4] Siger M, et al. (2009) Regional myo-inositol concentration in mild cognitive impairment using 1H magnetic resonance spectroscopic imaging. *Alzheimer Dis Assoc Disord* **23**, 57-62.

[5] Adalsteinsson E, et al. (2000) Longitudinal decline of the neuronal marker N-acetyl aspartate in Alzheimer's disease. *Lancet* **355**, 1696-1697.

[6] Kantarci K (2007) 1H magnetic resonance spectroscopy in dementia. *Br J Radiol* **80**, S146-S152.

[7] Martin WR (2007) MR spectroscopy in neurodegenerative disease. *Mol Imaging Biol* **9**, 196-203.

[8] Mueller SG, Schuff N, Weiner MW (2006) Evaluation of treatment effects in Alzheimer's and other neurodegenerative diseases by MRI and MRS. *NMR Biomed* **19**, 655-668.

Magnetic Resonance Spectroscopic Imaging Detects Metabolic Changes within the Medial Temporal Lobe in aMCI

Mira Didic[a,*], Jean Philippe Ranjeva[b], Emmanuel J. Barbeau[c], Sylviane Confort-Gouny[b], Olivier Felician[a], Yann Le Fur[b], Eve Tramoni[a], Julien Mancini[d], Michel Poncet[a], Patrick J Cozzone[b] and Mathieu Ceccaldi[a]

[a]*Service de Neurologie et de Neuropsychologie, Pôle de neurosciences cliniques, Assistance Publique des Hôpitaux de Marseille, Hôpitaux de la Timone, CMRR PACA Ouest & INSERM U751, Faculté de Médecine, Université de la Méditerranée, Marseille, France*
[b]*Centre d'Exploration Métabolique par Résonance Magnétique (UMR CNRS 6612), Université de la Méditerranée, Marseille, France*
[c]*Université de Toulouse, UPS, Centre de Recherche Cerveau et Cognition & CNRS, CerCo, Toulouse, France*
[d]*Université Aix-Marseille, Faculté de Médecine, Laboratoire d'Enseignement et de Recherche sur le Traitement de l'Information Médicale (LERTIM, EA 3283), Marseille & Service de Santé Publique et d'Information Médicale (SSPIM), Assistance Publique des Hôpitaux de Marseille, Hôpitaux de la Timone, Marseille, France*

Abstract. There is a critical need for reliable diagnosis of Alzheimer's Disease (AD) at an early stage, as disease modifying agents are being developed, likely to be most efficient when lesions are minimal. Using Magnetic Resonance Spectroscopy (MRS), reflecting metabolic change, the NAA/mIno-ratio has been shown to be reduced in AD and to be associated with the severity of AD pathology on postmortem brain tissue. However, it is not clear if this ratio is reduced in the early stages of AD, especially within the mesial temporal lobe (MTL), where tau pathology first develops in AD. Within the MTL, neurofibrillary tangles, related to clinical signs, first affect the anterior subhippocampal cortex, then the hippocampus during the limbic stage. In the monkey, experimental studies show that the sub-hippocampal cortex is crucial for visual recognition memory (VRM). We previously found that aMCI-patients that are impaired on a VRM task have features of early AD. We assessed metabolic changes by measuring NAA/mIno-ratios within the MTL of patients with amnestic MCI (aMCI), at risk for AD, using MRS Imaging. The MTL was sampled at different levels in order to evaluate its subcomponents. The NAA/mIno-ratio was reduced in the MTL of aMCI patients. However, while these ratios in aMCI-patients with normal VRM did not differ from controls, the subgroup of aMCI patients with impaired VRM scores had reduced MTL NAA/mIno ratios. Moreover, VRM performance was correlated with NAA/mIno levels within the anterior MTL. In addition, clinical follow-up data suggests that patients with impaired VRM are more likely to develop probable AD and MCI converters were found to have metabolic changes in the MTL at baseline in

*Correspondence to: Mira Didic, MD, PhD, Service de Neurologie et Neuropsychologie, CHU la Timone, 264, rue Saint Pierre, 13385 Marseille Cedex 5, France. Tel.: +33 4 91 38 59 28; Fax: +04 91 38 49 22; E-mail: mira.didic@ap-hm.fr.

comparison with controls. This confirms that MRS may be useful for the detection of AD at the predementia stage of the disease and that NAA/mIno could be considered as a further biomarker of AD. Moreover, taking into account the cognitive profile is crucial in order to select aMCI patients at very high risk for AD. Finally, this study supports the role of anterior MTL structures in VRM.

INTRODUCTION

A reliable diagnosis at the predementia stage of Alzheimer's Disease (AD) becomes critical as disease modifying agents are being developed. These agents are likely to be most efficient when lesions are minimal and patients are independent in daily life. In AD, neurofibrillary tangles (NFT), related to clinical signs of the disease, initially develop in the mesial temporal lobe (MTL). Regional pathologic metabolic change can be assessed using Magnetic Resonance Spectroscopy (MRS). Several MRS studies report changes in metabolic patterns in AD at the stage of dementia, with neuronal loss or dysfunction reflected by a decrease in N-acetylaspartate (NAA) levels [1], and glial cell activation indicated by increased myo-Inositol (mIno) levels [2–4]. Combining the NAA/mIno ratio has been reported to improve diagnostic accuracy in AD [2]. In addition, the ante-mortem NAA/mIno ratio was found to be associated with severity of AD pathology on postmortem brain tissue [5].

Metabolic changes in patients with mild cognitive impairment (MCI), patients who are independent in daily life, while at risk to develop AD, have also been reported using MRS. Many studies assessed easily accessible brain regions, such as the posterior cingular cortex [5–7] or paratrigonal white matter [8]. MRS studies focusing on the MTL, a brain region that is less accessible to neuroimaging techniques, but where tau pathology first appears in AD, have been less conclusive. That a decrease of the concentration of NAA in the hippocampus can be detected in patients with MCI using MRS was recently reported by Watanabe et al. [9]. Other studies also report metabolic changes mainly concerning NAA levels in voxels that measure metabolites within the MTL in patients with MCI [3, 10, 11]. However, one study reported no metabolic change [12].

In AD, neurofibrillary tangles (NFT) in the MTL develop in a sequential manner, initially affecting the anterior subhippocampal cortex (transentorhinal, entorhinal and perirhinal cortex) before reaching the hippocampus [13, 14]. Although the difficulty of identifying boundaries of the entorhinal and perirhinal cortex, as well as the inter-personal variability of these anterior subhippocampal structures make it more difficult to assess than the hippocampus using neuroimaging techniques, potential non-invasive diagnostic tools that could reliably detect change of the subhippocampal region are currently receiving increasing interest. Using MRI, several studies demonstrated atrophy of the entorhinal cortex in predementia AD [15–20]. However, the assessment of metabolic changes within the anterior subhippocampal region using MRS is a technical challenge related to the size and the topography of the MTL leading to frequent artifacts.

In order to contribute to early diagnosis of AD, our group developed a delayed matching to sample task for human patients based on tasks used in experimental animals in order to evaluate visual recognition memory (VRM) and assess the function of the anterior subhippocampal cortex, the DMS48. In previous studies, we reported that patients failing on the DMS48 had both clinical [21] and neuroimaging features [22, 23] of patients with early AD.

We conducted a multi-voxel study in aMCI-patients using MRSI (Magnetic Resonance Spectroscopy Imaging), in order to assess NAA/mIno-ratios in subregions within the MTL, including anterior subhippocampal structures where NFT first develop in AD, in patients with aMCI. This study was also designed to determine if impaired VRM in aMCI patients is associated with changes of the NAA/mIno-ratio within the MTL.

MATERIALS AND METHODS

Twenty eight patients with single domain amnestic MCI [24], defined by a memory complaint, a performance of more than 1.5 SD below the mean of matched control subjects on delayed free recall of a
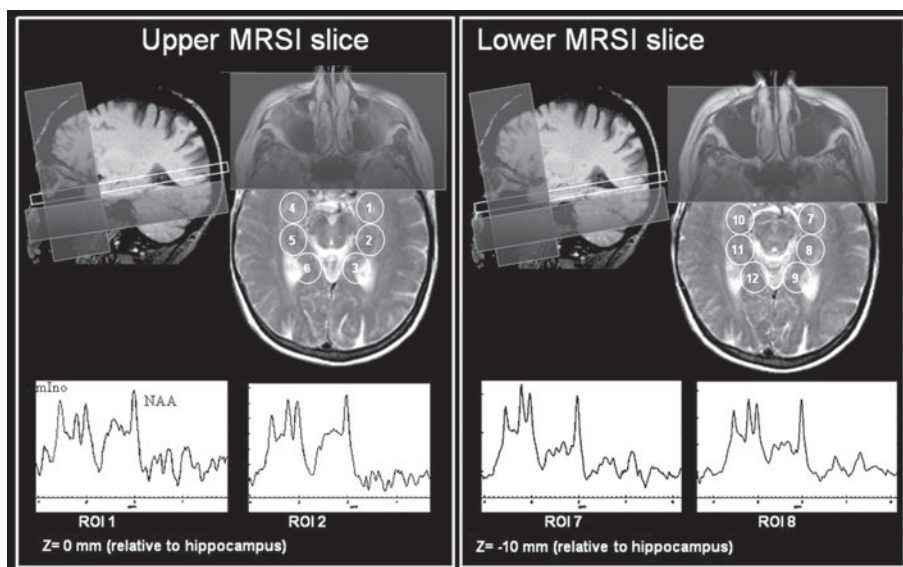
Fig. 1. MRSI slices acquired to sample medial temporal lobe structures in aMCI patients and controls. Schematic representation of the MRSI ROIs including real point spread function. The gray shade represents the saturation bands used to limit fat bone contamination. The first MRSI slice was centered on the hippocampus to sample the amygdala and the head of the hippocampus (ROIs 1 and 4), the body of hippocampus (ROIs 2 and 5) and the tail of the hippocampus (ROIs 3 and 6). The second MRSI slice was contiguous to the first and positioned just below in order to sample perirhinal/entorhinal cortices and part of the head of the hippocampus (ROIs 7 and 10), the medial parahippocampal cortex and part of the body of the hippocampus (ROIs 8 and 11), the posterior parahippocampal cortex and part of the tail of the hippocampus (ROI 9 and 12).

verbal memory task, intact activities of daily living and no impairment in other cognitive domains, included into the Marseilles memory study (Mms), were studied. 28 consecutively enrolled control subjects with normal cognitive functions and no history of systemic, mental and neurological disorder were also included. Both, patients and controls underwent a full neuropsychological evaluation followed by MRSI exploration.

Visual recognition memory was assessed using the DMS48 (delayed matching to sample – 48 items; downloadable for research purposes at http://www.cerco.ups-tlse.fr/~DMS48) [21], a VRM test directly derived from tasks used in animal studies [25]. In the DMS48, stimuli to be learned consist of 48 color drawings. Recognition is evaluated after a 3 minutes delay following the interfering task, and delayed recognition one hour later. Results reported in the present study are percentages of correct recognitions after the one-hour delay. A detailed description of the inclusion and exclusion criteria, as well as the procedure of used in the DMS48 is provided elsewhere [26].

aMCI-patients were then subdivided into two groups, according to their performance on the DMS48,

defining the cut-off of impaired performance at 1.5 SD below the mean of age matched controls [21].

In order to evaluate outcome, 22 patients were assessed clinically 6 years after the inclusion into the study. Two patients died before the 6 year follow-up due to acute diseases that were unrelated to their memory dysfunction.

MRSI

MR explorations were performed on a 1.5T MR scanner after inclusion into the study (Magnetom Vision Plus system, Siemens, Erlangen, Germany). The spectroscopic examination consisted of two 2D-MRSI slices acquired in the axial bihippocampal plane (Fig. 1) at two levels: the first slice was centered on the hippocampal formation (10 mm thickness) and the second was contiguous to the first but located 10 mm below including anterior subhippocampal tissue (Figure 1). MRSI acquisitions consisted in home-designed Hamming shape acquisition–weighted, inversion recovery (IR) 2D-SE pulse sequences (TI/TE/TR=150ms/22ms/1500ms; slice thickness 10 mm; FOV = 240 mm, 21 x 21 encod-

ing steps leading to 524 free induction decays; acquired in 11 min 27 s) with outer volume suppression scheme [27, 28]. There were 5 repetitions at the center of the k-space. The signal to noise ratio was 22,5 +/- 6.9. Full and widths at half maximum of the peak™fs height (FWHM) were 6.3 +/- 2.7 Hz. The IR scheme was used in order to minimize the contribution of fat scalp in the spectra. All radiofrequency pulses were optimized and generated using the Matpulse software [29]. The spatial resolution was defined as the width of the spatial response function at 64% of maximum voxel volume of 5.7 ml [30, 31]. Due to the pseudo circular spatial k sampling, voxel shape was cylindrical, resulting in an effective resolution of 22 mm of diameter. The water/lipid suppression scheme was implemented according to Tkac et al. [32] with outer volume saturation and chemical selection saturation scheme to suppress scalp fat and water signals, respectively. Automatic (mapshim) and manual shimming was performed on the water signal in the slice of interest. Measurement was conducted after optimization (frequency and pulse intensity) of the water suppression scheme.

Regions of interest (ROIs) for spectroscopic analyses within the MTL were delineated in ROIs in the bi-hippocampal plane at two levels. The first slice was centered on the hippocampal formation because of evidence for metabolic change in this area from studies in AD [1, 12] and MCI [3, 10] using MRSI and because NFT in the hippocampal formation have been reported in patients with AD at the stage of MCI [33]. Because of evidence for an antero-posterior gradient in the distribution of NFT within the hippocampus, NFT first appearing in the CA1 subfield [34] most represented in the hippocampal head and a differential implication of the anterior and the posterior hippocampus in declarative memory [35], as well as within MTL networks [36], several ROIs were placed along its long axis (Figure 1). The second MRSI slice was contiguous to the first and positioned just below in order to sample metabolites in the perirhinal/entorhinal cortices because of evidence for neurofibrillary tangles in transentorhinal, perirhinal and entorhinal cortex in Braak and Braak's stage I of AD [13, 14] and these anterior subhippocampal areas are involved in VRM [23, 25, 37, 38]. For comparative reasons, we also sampled the medial parahippocampal cortex and the parahippocampal cortex, since these regions are not involved in VRM [39, 40] while being implicated in a posterior MTL network [36] (Figure 1). However, because of the technical challenge related to the assess-

ment of the anterior subhippocampal areas and the parahippocampal gyrus with MRSI due to its small size and neighboring structures causing artifacts, all ROIs of the second MRSI slice included some additional signal from the hippocampal formation.

The metabolic ratio NAA/mIno was determined because of evidence for a high diagnostic accuracy using this ratio in AD [2] and the association of NAA/mIno ratio with Braak and Braak stages in a correlative neuropathological study [5], as well as correlations of cognitive measures reflecting disease severity with this ratio [1, 3].

RESULTS

12 aMCI-patients had normal DMS48 scores (DMS+), while performance on the DMS48 was impaired in 16 patients (DMS-). Demographical and clinical data is displayed in Table 1. Patients with aMCI were significantly older than controls. As expected, aMCI patients differed significantly from controls on the Mini Mental State Examination (MMSE), a global assessment of cognitive function and all tasks evaluating memory.

The aMCI-patient subgroup with impaired performance on the DMS48 (DMS-) did not differ from that of controls concerning age. MMSE differed from controls, as expected. However, the aMCI subgroup with normal performance on the DMS48 (DMS+) was significantly older than controls. MMSE differed from controls for both subgroups. The two subgroups of aMCI-patients did not differ concerning age or gender. MMSE did not differ between the subgroups either.

Amongst the 22 patients available for clinical follow-up, 11 patients fulfilled NINCDS-ADRDA criteria for AD [41]. 6 of the patients still fulfilled criteria for MCI (Table 2). 5 patients, although still complaining of memory loss, regained normal scores on tasks evaluating memory. Below cut-off performance on the DMS48 at baseline (i.e., 1.5 SD below the mean of controls) predicted conversion to AD at 6 year with a sensitivity of 81.8 %, and a specificity of 81.8 %.

Compared with controls and controlling for age, we found a decreased NAA/mIno ratio in patients with aMCI in the right body of the hippocampus (Table 3). However, only the subgroup of aMCI-patients with impaired VRM showed a decrease in NAA/mIno in the right hippocampal body and in the region containing the left head of the hippocampus and the amygdala, as well as in the region containing the left anterior sub-

Table 1
Demographic and neuropsychological data of patients and controls at the time of scan

	Controls	aMCI	aMCI subgroup DMS48+	aMCI subgroup DMS48−
N	28	28	12	16
Women/men	13/15	16/12	7/5	9/7
Age in years	63.3 (7.2)	69.3 (8.6)*	72.1 (9.1)*	67.3 (7.8)
MMSE	28.9 (1.0)	27.4 (1.4) *	27.7 (1.7)*	27.2 (1.2)*
Assessment of memory				
DMS48 (max = 100%)	98% (3%)	87% (10%)*	95% (3%)*	82% (9%)*[a]
Delayed free recall of words (max = 16)	13.1 (1.7)	5.3 (3.1)*	6.8 (2.5)*	4.2 (3.1)*[a]
Cueing efficiency (max = 100%)	89% (22%)	74% (22%)*	86% (12%)	66% (24%)*[a]
Intrusions during recall	0.8 (1.2)	4.3 (5.2) *	1.8 (2.1)	8.2 (8.5)[a]
Assessment of executive functions				
WMS-III digit span scaled score	10.6 (3.2)	9.4 (2.9)	9.7 (3.1)	9.1 (2.7)
Verbal fluency "P" in 2 mn	26.9 (7.1)	17.4 (4.7) *	19.5 (4.5)*	15.8 (6.2) *[a]
Verbal fluency repetition	0.37 (0.69)	0.61 (0.96)	1.17 (1.19)*	0.19 (0.40)
MCST– categories (max = 6)	n/a	4.8 (1.2)	4.8 (1.4)	4.7 (1.0)
MCST – errors	n/a	19.39 (12.1)	21.5 (12.8)	17.8 (11.6)
Picture naming (max = 80)	79.7 (0.6)	79.3 (1.3)	78.7 (1.8)	79.6 (0.9)

Mean, SD in brackets. n/a: not available. *$p < 0.05$ relative to controls; [a] $p < 0.05$ aMCI succeeding on the DMS48 relative to MCI failing on the DMS48. DMS48+: aMCI subgroup with normal performance on the DMS48. DMS48-: aMCI subgroup with impaired performance on the DMS48. MCST: Modified Card Sorting Test.

Table 2
Follow-up data on conversion 6 years after the inclusion into the study

	aMCI subgroup DMS48+	aMCI subgroup DMS48−
N	12	16
Converters	2	9
Non-converters	9	2
Follow-up scheduled	0	4

Converters: patients with probable AD fulfilling NINCDS-ADRDA criteria for AD (McKhann et al. 1984). Non-converters: patient not fulfilling NINCDS-ADRDA criteria for AD (McKhann et al. 1984). DMS48 +: aMCI subgroup with normal performance on the DMS48. DMS48−: aMCI subgroup with impaired performance on the DMS48.

Moreover, a correlation between performance on the DMS48 and NAA/mIno-ratios was observed the ROI containing anterior subhippocampal cortex on both the left and the right side, as well as for the left anterior hippocampus.

In addition, aMCI patients who later developed AD (aMCI converters) were found to have decreased NAA/mIno-ratios in the region that contains the left head of the hippocampus and the amygdala as well as the right body of the hippocampus when compared to a group of age matched controls (Table 4).

DISCUSSION

We found that it is possible to detect reduced NAA/mIno levels, associated with AD pathology, within the MTL in patients with aMCI using MRSI. Moreover, when performance on a VRM memory task

hippocampal cortex, compared with controls (Table 3). By contrast, aMCI-patients with normal performance on the VRM task showed no significant difference of NAA/mIno levels relative to controls (Table 3).

Table 3
NAA/mIno-ratios in the aMCI-group, as well as aMCI-subgroups

		Controls ($n = 28$)	all aMCI ($n = 28$)	aMCI DMS− ($n = 16$)	aMCI DMS+ ($n = 12$)
#	Location				
ROI 1	L amygdala/head of HF	1.60 (0.72)	1.3 (0.56)	1.25 (0.28) **	1.58 (0.78)
ROI 5	R body of HF	2.48 (0.50)	2.16 (0.49) *	2.07 (0.49) **	2.29 (0.48)
ROI 7	L PC–ER cortices	1.74 (0.40)	1.53 (0.33)	1.48 (0.30) **	1.63 (0.41)

Mean, SD in brackets. Only results for regions with NAA/mIno-ratios that differ significantly across groups/subgroups are reported.; DMS48+: aMCI subgroup with normal performance on the DMS48. DMS48-: aMCI subgroup with impaired performance on the DMS48. L = left, R = right, EC = entorhinal cortex, PC = perirhinal cortex, HF = hippocampal formation, ROI = region of interest.; * Significantly different from controls using ANOVA with group and age and as variables.; * * Significantly different from controls (Mann-Whitney U test).

Table 4
MCI-converters compared to controls

		Controls (n = 14)	aMCI converters (n = 11)	p*
	Age	70.14 (4.38)	73.55 (4.59)	ns
ROI 1	L amygdala/ head of HF	1.74 (0.99)	1.16 (0.23)	< 0.05
ROI 5	R body of HF	2.61 (0.50)	2.13 (0.40)	< 0.05

Converters: patients with probable AD fulfilling NINCDS-ADRDA criteria for AD (McKhann et al. 1984). Mean, SD in brackets. The control group for this comparison consisted of a subset of controls that were matched for age with the aMCI converters. Only results for regions with NAA/mIno-ratios that differ significantly across groups/subgroups are reported. L = left, R = right, EC = entorhinal cortex, PC = perirhinal cortex, HF = hippocampal formation, ROI = region of interest. * Mann-Whitney U test.

was taken into account, metabolic change in several regions of the MTL was only found in a subgroup of aMCI patients failing on this task designed to assess the function of the anterior subhippocampal region, where tau pathology first appears in AD. NAA/mIno levels were also reduced in the MTL of aMCI-patients who later developed AD. In addition, performance on the DMS48 was correlated with the NAA/mIno ratio of anterior MTL structures, confirming that the anterior MTL is involved in VRM.

NAA/mIno levels are reduced in the MTL of aMCI patients

Metabolic change within the MTL has inconsistently been reported in patients with MCI using MRSI. Watanabe et al. [9] recently demonstrated that a decrease of the absolute concentration of NAA can be detected using MRS in the hippocampus bilaterally in patients with MCI. Assessing MTL structures, NAA related metabolic changes were also reported by other groups [3, 10], but a recent multicenter study found no metabolic change in the MTL of MCI patients [12]. This was partly attributed to a selection bias, suggesting that the low threshold in the inclusion criteria might have led to the inclusion of a large proportion of patients without underlying degenerative disease Our findings confirm that metabolic changes can be detected in the MTL as early as the stage of single domain amnestic MCI (or in cognitively impaired but not-demented patients), as previously reported for NAA [9, 11]. Moreover, these changes were also found in aMCI patients who later developed probable AD.

Metabolic changes on MRSI in the aMCI subgroup failing on the DMS48

Patient selection using appropriate neuropsychological tasks also appears to be crucial. When aMCI-patients were separated into subgroups on the basis on their performance on a VRM-task, metabolic change in several regions of the MTL was only found in the aMCI subgroup with impaired VRM, compared to controls. In this subgroup, reduced NAA/mIno levels were detected in the left anterior hippocampus and a region that contains the anterior subhippocampal region, where NFT first appear in AD. If metabolic change had been restricted to this lower region containing anterior subhippocampal metabolites, this could have been in favor of specific subhippocampal changes. However, because of the overlap with signal emerging from the hippocampal formation in this region of interest, and since reduced NAA/mIno levels were also found in the adjacent region sampling the head of the hippocampus, it is uncertain whether these changes are related to the anterior subhippocampal region only. Further MRSI studies using higher magnetic fields, with a better spatial resolution, may be able to identify metabolic changes related to neuropathological lesions in the entorhinal and perirhinal cortex more reliably. Within the hippocampus, reduced NAA/mIno ratios within the left head and the right body could be related to neuropathological change in the CA1 field of the hippocampus, where changes have been described in the early stages of AD in both neuropathological [34] and neuroimaging studies [42]. As expected, there was no reduction of the NAA/mIno ratio in the tail of the hippocampus and the posterior parahippocampal gyrus. No metabolic anomalies were found in the aMCI subgroup succeeding on the VRM task compared with controls. Although this subgroup was significantly older than the controls, age is unlikely to account for the present findings, since pathological changes would be expected to increase with age. Also, there was no correlation of metabolic ratios with age. Distinct metabolic patterns in the two subgroups of aMCI-patients could not be explained by a difference in severity of cognitive decline, since mean MMSE scores did not differ either.

Metabolic AD-related changes

It is likely that reduced NAA/mIno ratios in the present study are AD related, since not only aMCI-patients with impaired VRM, but also those who later

developed AD had reduced NAA/mIno levels. This is consistent with the NAA/mIno ratio being associated with severity of AD pathology on postmortem brain tissue [5]. Decreased NAA is a marker of neuronal dysfunction or axonal injury, due to impaired mitochondrial metabolism, while elevated mIno levels are associated with glial activation [2]. In AD, a decrease of NAA combined with an increase in mIno is thought to reflect neuronal loss combined with replacement through gliosis. In line with the findings of the present study, reductions of the NAA ratio or of NAA/Cr levels have previously been reported in MCI-patients who later declined to AD [43–45] and in patients with probable AD [1–3, 10, 12]. Increased mIno has been reported in the white matter of patients with MCI and AD [8, 46, 47]. This is in line with the suggestion that NAA/mIno ratios [5] or NAA measures [12] could be additional biomarker candidates for AD.

Performance on the DMS48 is associated with NAA/mIno levels in an anterior MTL network

The association of performance on the VRM memory task with NAA/mIno levels supports the role of anterior MTL structures in VRM. Performance on a VRM task was correlated with NAA/mIno in the MTL lobes, with both, the region containing metabolites from the anterior subhippocampal cortex and the anterior hippocampal formation. A functional relationship between NAA/mIno ratios or the NAA/Cr-ratio with cognitive function or disease severity is supported by several studies [1, 2, 48]. It is possible that this is related to the fact that the neural basis of the impairment on the VRM-task in aMCI patients implicates an anterior MTL network that includes both the perirhinal cortex and the anterior hippocampus, as recently suggested by a study using resting state functional MRI [36]. That no correlation was found in the posterior parahippocampal gyrus and more posterior structures within the hippocampal formation is consistent with studies using experimental animals [39] and patients with focal lesions suggesting that the posterior MTL is not involved in VRM [40].

The assessment of visual recognition memory contributes to the diagnosis of AD in patients with aMCI

Metabolic changes in the MTL of aMCI patients failing on the DMS48 confirms previous findings that suggested that aMCI patients with impaired VRM may be at particularly high risk for AD [21–23]. On SPECT, Guedj and collaborators [22] found hypoperfusion in the MTL, the posterior cingulate and the temporo-parietal cortices in a subgroup of aMCI patients with impaired VRM, a profile that is commonly found in early AD [49, 50]. Using Voxel Based Morphometry, aMCI-patients who fail on the VRM-task have been found to display gray matter loss in the MTL and temporo-parietal cortex [23], an imaging profile also reported in early AD [51–53]. Although not specifically investigated, a number of studies report deficits on tasks evaluating visual recognition memory in patients with AD [54], including the earliest stages of AD and patients with MCI [55–59].

Clinical follow-up for 22 patients who have been followed over 6 years indicates that assessing VRM using the DMS48 can identify early AD in patients with aMCI with a sensibility and specificity of both 81.8%. Considering the small group of subjects, the predictive value appears high. This adds to neuropsychological and imaging findings that suggest that these patients may be those who will ultimately develop AD. However, this should be confirmed in studies with larger numbers of subjects, CSF assessing biomarkers for AD, as well as amyloid PET or neuropathological data that could provide additional evidence for AD pathology in these patients, since the combined use of these measures is most likely to predict AD in patients with aMCI [60].

The conversion rate in the present study of about 40% over the 6 year follow-up does appear low and the proportion of aMCI patients who did not convert to AD during the 6 year follow-up of 40% relatively high. However, conversion rates vary considerably across studies. Several studies found that patients with MCI do not develop dementia even after a long clinical follow-up [61]. The etiology of the memory dysfunction of the non-converters of the present study remains to be determined and is likely to be heterogeneous. Some patients in this group may still convert to AD after the 6 year follow-up, since the inclusion of patients with single domain amnestic MCI may lead to an overrepresentation of patients with AD due to focal mesial temporal lobe dysfunction with a slow rate of cognitive decline [62, 63]. In some patients, minor depression could be responsible for the memory disorder, while others may suffer from hippocampal sclerosis. In addition, despite our attempts to exclude patients with cardiovascular disease, it is also possible that some patients may have minor microvascular change.

Taken together, the findings of the present study indicate that it appears crucial to integrate the type of memory impairment in early diagnosis of AD, as previously suggested [64]. In addition, early diagnosis of AD should not only take into account changes concerning the hippocampus, but also those resulting from dysfunction of the subhippocampal region. Neuropsychological tasks designed to evaluate brain areas where degenerative change causes dysfunction could be considered as biomarkers reflecting neural dysfunction on a clinical level. In this context, assessing the function of the subhippocampal region through VRM may critically contribute to early diagnosis of AD.

CONCLUSIONS

It is possible to detect metabolic changes, likely to be related to AD pathology, within the MTL in patients with aMCI using Magnetic Resonance Spectroscopy. However, further MRSI studies using higher magnetic fields, with a better spatial resolution, should be conducted in order to identify metabolic changes related to neuropathological lesions in the entorhinal and perirhinal cortex, where tau pathology first appears, more reliably. Moreover, patient selection in a heterogeneous patient group as aMCI, using appropriate neuropsychological tasks, is crucial. This is consistent with previous findings that suggest that aMCI patients with impaired VRM are at particularly high risk for AD.

ACKNOWLEDGMENTS

REFERENCES

[1] Jessen F, Block W, Träber F, Keller E, Flacke S, Papassotiropoulos A, Lamerichs R, Heun R, Schild HH (2000) Proton MR spectroscopy detects a relative decrease of N-acetylaspartate in the medial temporal lobe of patients with AD. *Neurology* **55**, 684-688.

[2] Valenzuela MJ, Sachdev P (2001) Magnetic resonance spectroscopy in AD. *Neurology* **13**(56), 592-598.

[3] Chantal S, Braun CM, Bouchard RW, Labelle M, Boulanger Y (2004) Similar ^{1}H magnetic resonance spectroscopic metabolic pattern in the medial temporal lobes of patients with mild cognitive impairment and Alzheimer disease. *Brain Res* **1003**, 26-35.

[4] Kantarci K, Petersen RC, Boeve BF, Knopman DS, Tang-Wai DF, O'Brien PC, Weigand SD, Edland SD, Smith GE, Ivnik RJ, Ferman TJ, Tangalos EG, Jack CR, Jr (2004) MR spectroscopy in common dementias. *Neurology* **63**, 1393-1398.

[5] Kantarci K, Knopman DS, Dickson DW, Parisi JE, Whitwell JL, Weigand SD, Josephs KA, Boeve BF, Petersen RC, Jack CR Jr(2008) Alzheimer disease: postmortem neuropathologic correlates of antemortem ^{1}H MR spectroscopy metabolite measurements. *Radiology* **248**, 210-212.

[6] Kantarci K, Jack CR, Jr, Xu YC, Campeau NG, O'Brien PC, Smith GE, Ivnik RJ, Boeve BF, Kokmen E, Tangalos EG, Petersen RC (2000) Regional metabolic patterns in mild cognitive impairment and Alzheimer's disease: a ^{1}H MRS study. *Neurology* **55**, 210-217.

[7] Kantarci K, Weigand SD, Petersen RC, Boeve BF, Knopman DS, Gunter J, Reyes D, Shiung M, O'Brien PC, Smith GE, Ivnik RJ, Tangalos EG, Jack CR, Jr (2007) Longitudinal ^{1}H MRS changes in mild cognitive impairment and Alzheimer's disease. *Neurobiol Aging* **28**, 1330-1339.

[8] Catani M, Cherubini A, Howard R, Tarducci R, Pelliccioli GP, Piccirilli M, Gobbi G, Senin U, Mecocci P (2001) (1)H-MR spectroscopy differentiates mild cognitive impairment from normal brain aging. *Neuroreport* **12**, 2315-2317.

[9] Watanabe T, Shiino A, Akiguchi I (2010) Absolute quantification in proton magnetic resonance spectroscopy is useful to differentiate amnesic mild cognitive impairment from Alzheimer's disease and healthy aging. *Dement Geriatr Cogn Disord* **30**, 71-77.

[10] Ackl N, Ising M, Schreiber YA, Atiya M, Sonntag A, Auer DP (2005) Hippocampal metabolic abnormalities in mild cognitive impairment and Alzheimer's disease. *Neurosci Lett* **384**, 23-28.

[11] Chao LL, Schuff N, Kramer JH, Du AT, Capizzano AA, O'Neill J, Wolkowitz OM, Jagust WJ, Chui HC, Miller BL, Yaffe K, Weiner MW (2005) Reduced medial temporal lobe N-acetylaspartate in cognitively impaired but nondemented patients. *Neurology* **64**, 282-289.

[12] Jessen F, Gür O, Block W, Ende G, Fr, ouml, lich L, Hammen T, Wiltfang J, Kucinski T, Jahn H, Heun R, Maier W, ouml K, lsch H, Kornhuber J, Träber F (2009) A multicenter (1)H-MRS study of the medial temporal lobe in AD and MCI. *Neurology* **72**, 1735-1740.

[13] Braak H, Braak E (1991) Neuropathological staging of Alzheimer-related changes. *Acta Neuropathol* **82**, 239-259.

[14] Delacourte A, David JP, Sergeant N, Buee L, Wattez A, Vermersch P, Ghozali F, Fallet-Bianco C, Pasquier F, Lebert F, Petit H, Di Menza C (1999) The biochemical pathway of neurofibrillary degeneration in aging and Alzheimer's disease. *Neurology* **52**, 1158-1165.

[15] Xu Y, Jack CR, Jr, O'Brien PC, Kokmen E, Smith GE, Ivnik RJ, Boeve BF, Tangalos RG, Petersen RC (2000) Usefulness of MRI measures of entorhinal cortex versus hippocampus in AD. *Neurology* **54**, 1760-1767.

[16] Killiany, RJ (2009) Temporoparietal MRI measures of atrophy in subjects with mild cognitive impairment that predict subsequent diagnosis of Alzheimer's disease. *Am J Neuroradiol* **30**, 532-538.

[17] Du AT, Schuff N, Amend D, Laakso MP, Hsu YY, Jagust WJ, Yaffe K, Kramer JH, Reed B, Norman D, Chui HC, Weiner MW (2001) Magnetic resonance imaging of the entorhinal cortex and hippocampus in mild cognitive impairment and Alzheimer's disease. *J Neurol Neurosurg Psychiatry* **71**, 441-447.

[18] Dickerson BC, Goncharova I, Sullivan MP, Forchetti C, Wilson RS, Bennett DA, Beckett LA, deToledo-Morrell L (2001) MRI-derived entorhinal and hippocampal atrophy in incipient and very mild Alzheimer's disease. *Neurobiol Aging* **22**, 747-754.

[19] Stoub TR, Bulgakova M, Leurgans S, Bennett DA, Fleischman D, Turner DA, deToledo-Morrell L (2005) MRI predictors of risk of incident Alzheimer disease: a longitudinal study. *Neurology* **64**, 1520-1524.

[20] DeToledo-Morrell L, Stoub TR, Bulgakova M, Wilson RS, Bennett DA, Leurgans S, Wuu J, Turner DA (2004) MRI-derived entorhinal volume is a good predictor of conversion from MCI to AD. *Neurobiol Aging* **25**, 1197-1203.

[21] Barbeau E, Didic M, Tramoni E, Felician O, Joubert S, Sontheimer A, Ceccaldi M, Poncet M (2004) Evaluation of visual recognition memory in MCI patients. *Neurology* **62**, 1317-1322.

[22] Guedj E, Barbeau EJ, Didic M, Felician O, de Laforte C, Ceccaldi M, Mundler O, Poncet M (2006) Identification of subgroups in amnestic mild cognitive impairment. *Neurology* **67**, 356-358.

[23] Barbeau EJ, Ranjeva JP, Didic M, Confort-Gouny S, Felician O, Soulier E, Cozzone PJ, Ceccaldi M, Poncet M (2008) Profile of memory impairment and gray matter loss in Mild Cognitive Impairment. *Neuropsychologia* **46**, 1009-1019.

[24] Petersen RC, Doody R, Kurz A, Mohs RC, Morris JC, Rabins PV, Ritchie K, Rossor M, Thal L, Winblad B (2001) Current concepts in mild cognitive impairment. *Arch Neurol* **58**, 1985-1992.

[25] Meunier M, Bachevalier J, Mishkin M, Murray EA (1993) Effects on visual recognition of combined and separate ablations of the entorhinal and perirhinal cortex in rhesus monkeys. *J Neurosci* **13**, 5418-5432.

[26] Didic M, Ranjeva JP, Barbeau EJ, Confort-Gouny S, Le Fur Y, Felician O, Poncet M, Ceccaldi M, Cozzone PJ (2010) Impaired visual recognition memory in amnestic MCI is associated with mesial temporal metabolic changes on MRSI. *J Alzheimer's Dis* **22**, 1269-1279.

[27] Galanaud D, Le Fur Y, Nicoli F, Denis B, Confort-Gouny S, Ranjeva JP, Viout P, Pelletier J, Cozzone PJ (2001) Regional metabolite levels of the normal posterior fossa studied by proton chemical shift imaging. *MAGMA* **13**, 127-133.

[28] Guye M, Ranjeva JP, Le Fur Y, Bartolomei F, Confort-Gouny S, Regis J, Chauvel P, Cozzone PJ (2005) ^{1}H-MRS imaging in intractable frontal lobe epilepsies characterized by depth electrode recording. *Neuroimage* **26**, 1174-1183.

[29] Matson GB (1994) An integrated program for amplitude-modulated RF pulse generation and re-mapping with shaped gradients. *Magn Reson Imaging* **12**, 1205-1225.

[30] Weidensteiner C, Lanz T, Horn M, Neubauer S, Haase A, von Kienlin M (2000) Three-dimensional (13)C-spectroscopic imaging in the isolated infarcted rat heart. *J Magn Reson* **143**, 17-23.

[31] von Kienlin M, Ziegler A, Le Fur Y, Rubin C, Decorps M, Rémy C (2000) 2D-spatial/2D-spectral spectroscopic imaging of intracerebral gliomas in rat brain. *Magn Reson Med* **43**, 211-219.

[32] Tkac I, Starcuk Z, Choi IY, Gruetter R (1999) In vivo ^{1}H NMR Spectroscopy of rat brain at 1 ms echo time. *Magn Reson Med* **41**, 649-656.

[33] Bennett DA, Schneider Bienias JA, JL, Evans DA, Wilson RS (2005) Mild cognitive impairment is related to Alzheimer disease pathology and cerebral infarctions. *Neurology* **64**, 834-841.

[34] Bobinski M, de Leon MJ, Tarnawski M, Wegiel J, Reisberg B, Miller DC, Wisniewski HM (1998) Neuronal and volume loss in CA1 of the hippocampal formation uniquely predicts duration and severity of Alzheimer disease. *Brain Res* **805**, 267-269.

[35] Lepage M, Habib R, Tulving E (1998) Hippocampal PET activations of memory encoding and retrieval: the HIPER model. *Hippocampus* **8**, 313-322.

[36] Kahn I, Jessica R, Andrews-Hanna, Justin L, Vincent, Abraham Z, Snyder, Randy L, Buckner (2008) Distinct cortical anatomy linked to subregions of the medial temporal lobe revealed by intrinsic functional connectivity. *J Neurophysiol* **100**, 129-139.

[37] Mayes AR, Holdstock JS, Isaac CL, Hunkin NM, Roberts N (2002) Relative sparing of item recognition memory in a patient with adult-onset damage limited to the hippocampus. *Hippocampus* **12**, 325-340.

[38] Barbeau EJ, Felician O, Joubert S, Sontheimer A, Ceccaldi M, Poncet M (2005) Preserved visual recognition memory in an amnesic patient with hippocampal lesions. *Hippocampus* **15**, 587-596.

[39] Mishkin M, Suzuki WA, Gadian DG, Vargha-Khadem F (1997) Hierarchical organization of cognitive memory. *Philos Trans R Soc Lond B Biol Sci* **352**, 1461-1486.

[40] Mayes AR, Montaldi D, Migo E (2007) Associative memory and the medial temporal lobes. *TRENDS in Cognitive Sciences* **3**, 126-135.

[41] McKhann G, Drachman D, Folstein M, Katzman R, Price D, Stadlan EM (1984) Clinical diagnosis of Alzheimer's disease: report of the NINCDS-ADRDA. Work Group under the auspices of Department of Health and Human Services Task Force on Alzheimers disease Neurology **34**, 939-944.

[42] Chetelat G, Fouquet M, Kalpouzos G, Denghien I, De la Sayette V, Viader F, Mézenge F, Landeau aB, Baron JC, Eustache F, Desgranges F (2008) Three-dimensional surface mapping of hippocampal atrophy progression from MCI to AD and over normal aging as assessed using voxel-based morphometry. *Neuropsychologia* **46**, 1721-1731.

[43] Modrego PJ, Fayed N, Pina MA (2005) Conversion from mild cognitive impairment to probable Alzheimer's disease predicted by brain magnetic resonance spectroscopy. *Am J Psychiatry* **162**(4), 667-675.

[44] Metastasio A, Rinaldi P, Tarducci R, Mariani E, Feliziani FT, Cherubini A, Pelliccioli GP, Gobbi G, Senin U, Mecocci P (2006) Conversion of MCI to dementia: Role of proton magnetic resonance spectroscopy. *Neurobiol Aging* **27**, 926-932.

[45] Fayed N, Dávila J, Oliveros A, Castillo J, Medrano JJ (2008) Utility of different MR modalities in mild cognitive impairment and its use as a predictor of conversion to probable dementia. *Acad Radiol* **15**, 1089-1098.

[46] Salvan AM, Ceccaldi M, Confort-Gouny S, Milandre C, Cozzone PJ, Vion-Dury J (1998) Correlation between cognitive status and cerebral inositol in Alzheimer-type dementia. *J Neurol* **245**, 686-688.

[47] Siger M, Schuff N, Zhu X, Miller BL, Weiner MW (2008) Regional myo- inositol concentration in mild cognitive

impairment using ^{1}H magnetic resonance spectroscopic imaging. *Alzheimer Dis Assoc Disord* **23**, 57-62.

[48] Rose SE, De Zubicaray G, Wang D, Galloway GJ, Chalk JB, Eagle SC, Semple J, Dodrell DM (1999) A ^{1}H MRS study of probable Alzheimer's disease and normal aging: implications for longitudinal monitoring of dementia progression. *Magn Reson Imaging* **17**, 291-299.

[49] Borroni B, Anchisi D, Paghera B, Vicini B, Kerrouche N, Garibotto V, Terzi A, Vignolo LA, Di Luca M, Giubbini R, Padovani A, Perani D (2006) Combined 99mTc-ECD SPECT and neuropsychological studies in MCI for the assessment of conversion to AD. *Neurobiol Aging* **27**, 24-31.

[50] Nobili F, De Carli F, Frisoni GB, Portet F, Verhey F, Rodriguez G, Caroli A, Touchon J, Morbelli S, Guerra UP, Dessi B, Brugnolo A, Visser PJ (2009) SPECT predictors of cognitive decline and Alzheimer's disease in mild cognitive impairment. *J Alzheimers Dis* **4**, 761-772.

[51] Karas GB, Scheltens P, Rombouts SA, Visser PJ, van Schijndel RA, Fox NC, Barkhof F (2004) Gobal and local gray matter loss in mild cognitive impairment and Alzheimer's disease. *Neuroimage* **23**, 708-716.

[52] Desikan RS, Cabral HJ, Fischl B, Guttmann G, Blacker D, Hyman BT, Albert MS, Killiany RJ (2009) Temporoparietal MRI measures of atrophy in subjects with mild cognitive impairment that predict subsequent diagnosis of Alzheimer's disease. *Am J Neuroradiol* **30**, 532-538.

[53] McDonald CR, McEvoy LK, Gharapetian L, Fennema-Notestine C, Hagler DJ, Jr, Holland D, Koyama A, Brewer JB, Dale AM (2009) Alzheimer's Disease Neuroimaging and Initiative Regional rates of neocortical atrophy from normal aging to early Alzheimer disease. *Neurology* **73**, 457-465.

[54] Tierney MC, Black SE, Szalai JP, et al. (2001) Recognition memory and verbal fluency differentiate probable Alzheimer disease from subcortical ischemic vascular dementia. *Arch Neurol* **58**, 1654-1659.

[55] Greene JD, Baddeley AD, Hodges JR (1996) Analysis of the episodic memory deficit in early Alzheimers disease: evidence from the doors and people test. *Neuropsychologia* **34**, 537-551.

[56] Fox NC, Warrington EK, Seiffer AL, Agnew SK, Rossor MN (1998) Presymptomatic cognitive deficits in individuals at risk of familial Alzheimer's disease. *A longitudinal prospective study. Brain* **121**, 1631-1639.

[57] Fowler KS, Saling MM, Conway EL, Semple JM, Louis WJ (2002) Paired associate performance in the early detection of DAT. *J Int Neuropsychol Soc* **8**, 58-71.

[58] Small BJ, Herlitz A, Fratiglioni L, Almkvist O, Bäckman L (1997) Cognitive predictors of incidental Alzheimer's disease: A prospective longitudinal study. *Neuropsychology* **11**, 413-420.

[59] Wolk DA, Signoff ED, Dekosky ST (2008) Recollection and familiarity in amnestic mild cognitive impairment: a global decline in recognition memory. *Neuropsychologia* **46**, 1965-1978.

[60] Mariani E, Monastero R, Mecocci P (2007) Mild cognitive impairment: a systematic review. *J Alzheimers Dis* **12**, 23-35.

[61] Mitchell AJ, Shiri-Feshki M (2009) Rate of progression of mild cognitive impairment to dementia–meta-analysis of 41 robust inception cohort studies. *Acta Psychiatr Scand* **119**, 252-265.

[62] Butters MA, Lopez OL, Becker JT (1996) Focal temporal lobe dysfunction in probable Alzheimer's disease predicts a slow rate of cognitive decline. *Neurology* **46**, 687-692.

[63] Didic M, Ali Cherif A, Gambarelli D, Poncet M, Boudouresques J (1998) A permanent pure amnestic syndrome of insidious onset related to Alzheimer's disease. *Ann Neurol* **43**, 526-530.

[64] Dubois B, Feldman HH, Jacova C, Dekosky ST, Barberger-Gateau P, Cummings J, Delacourte A, Galasko D, Gauthier S, Jicha G, Meguro K, O'Brien J, Pasquier F, Robert P, Rossor M, Salloway S, Stern Y, Visser PJ, Scheltens P (2007) Research criteria for the diagnosis of Alzheimer's disease: revising the NINCDS-ADRDA criteria. *Lancet Neurol* **6**(8), 734-746.

Magnetic Resonance Imaging and Magnetic Resonance Spectroscopy for Detection of Early Alzheimer's Disease

Eric Westman [b,c,*], Lars-Olof Wahlund [a], Catherine Foy [b], Michaela Poppe [b], Allison Cooper [b], Declan Murphy [b], Christian Spenger [d], Simon Lovestone [b] and Andrew Simmons [b,c]

[a]*Department of Neurobiology, Care Sciences and Society, Section of Clinical Geriatrics, Karolinska Institutet, Karolinska University Hospital, Huddinge, Stockholm, Sweden*
[b]*NIHR Specialist Biomedical Research Centre for Mental Health at the South London and Maudsley NHS Foundation Trust and King's College London and the MRC Centre for Neurodegeneration, Kings College London, Institute of Psychiatry, London, UK*
[c]*Department of Neuroimaging, Kings College London, Institute of Psychiatry, London, UK*
[d]*Department of Clinical Science, Intervention and Technology, Karolinska Institutet, Stockholm, Sweden*

Abstract. Alzheimer's disease is the most common form of neurodegenerative disorder and early detection is of great importance if new therapies are to be effectively administered. We have investigated whether the discrimination between early Alzheimer's disease (AD) and elderly healthy control subjects can be improved by adding magnetic resonance spectroscopy (MRS) measures to magnetic resonance imaging (MRI) measures.

In this study 30 AD patients and 36 control subjects were included. High resolution T1-weighted axial magnetic resonance images were obtained from each subject. Automated regional volume segmentation and cortical thickness measures were determined for the images. ^{1}H MRS was acquired from the hippocampus and LCModel was used for metabolic quantification. Altogether, this yielded 58 different volumetric, cortical thickness and metabolite ratio variables which were used for multivariate analysis to distinguish between subjects with AD and Healthy controls. Combining MRI and MRS measures resulted in a sensitivity of 97% and a specificity of 94% compared to using MRI or MRS measures alone (sensitivity: 87%, 76%, specificity: 86%, 83% respectively). Adding the MRS measures to the MRI measures more than doubled the positive likelihood ratio from 6 to 17.

Adding MRS measures to a multivariate analysis of MRI measures resulted in significantly better classification than using MRI measures alone. The method shows strong potential for discriminating between Alzheimer's disease and controls.

Keywords: MRS, MRI, OPLS, AD, multivariate analysis

INTRODUCTION

Multivariate analysis provides the opportunity to analyze many variables simultaneously and observe inherent patterns in the data. Methods like principal component analysis (PCA), Partial least square to latent structures (PLS) and orthogonal PLS (OPLS) are efficient, robust and validated tools for modelling complex biological data [1].

Alzheimer's disease (AD) is one of the most common forms of neurodegenerative disorders. The clinical symptoms of AD include gradual loss of cognitive functions and AD is largely a disorder of the

*Correspondence to: Eric Westman, PhD, Karolinska Universitetssjukhuset, Novum, Plan 4, 141 86 Stockholm, Sweden. Tel.: ++46 73 655 5179; Fax: ++46 8 517 761 11. E-mail: eric.westman@ki.se.

elderly with a small percentage of non-age-related AD cases being familial and secondary to specific gene mutations.

Magnetic resonance imaging (MRI) is a non-invasive method which has been widely studied for early detection and diagnosis of AD [2–4]. In particular early changes in hippocampus and entorhinal cortex have been demonstrated using MRI [5–9]. These early changes are consistent with the underlying pathology of AD but it is not yet clear which measures are most useful for early diagnosis [2]. Due to the complexity of this disorder measures of single structures from MRI are probably not sufficient for accurate diagnosis at the early stages of the disease. The most common way of describing the spread of atrophy in AD is according to the neurofibrillary tangle spread described by Braak and Braak [10]. It has also been proposed that the pattern of atrophy can progress in other ways, where the hippocampus and entorhinal cortex are not as affected [11]. By combining different measures of atrophy using multivariate methods we might gain a better understanding of the natural history of the disease.

Magnetic resonance spectroscopy (^{1}H-MRS) provides useful information on the neurochemical profile of different neurodegenerative diseases [12, 13] from defined target volumes *in vivo*. The metabolites measured represent different aspects of the pathological processes in AD [13]. Examples of measurable metabolites are N-acetylaspartate (NAA), a marker for neuronal density and/or function, myo-inositol (mI), a marker for astrogliosis and/or osmotic stress and choline (Cho), a marker for cell membrane turnover and degradation [14]. Brain metabolites are sensitive to pathological processes in neurodegenerative disorders such as AD [13].

Other MR modalities which can be used for the study of AD include diffusion MRI which measures microstructural changes in white matter [15], functional MRI which measures brain function using BOLD contrast [16], arterial spin labelling which measures the perfusion of blood [17] and MR-relaxometry which characterizes $T1$ and $T2$ relaxation times of tissue [18].

McEvoy et al. have previously shown with a largely automated image analysis pipeline that using multiple MRI measurements of regional volumes and regional cortical surface measurements in combination with multivariate analysis is useful in distinguishing between subjects with Alzheimer's disease and healthy controls [19]. This indicates that a combination of different MRI measures may prove to be more useful than hippocampal or entorhinal cortex measures alone for early detection of Alzheimer's disease. The use of automated measures may in particular have advantages when it comes to widespread uptake in either clinical or research practice. Several other studies have utilized different multivariate techniques including OPLS to analyze MR-data [20–26]. Alzheimer's disease is a complex disorder and one biomarker is probably not enough to establish a correct diagnosis. Therefore we wanted to investigate the potential of combining different MRI measures (i.e. regional volumes and regional cortical thickness measures) with MRS measures. OPLS was chosen to analyze the large number of variables generated from the different MR-modalities. The aim of this study was to investigate whether adding MRS measures to a battery of automated structural MRI measures would further improve the ability to distinguish patients with AD from healthy controls using multivariate data analysis.

MATERIAL AND METHODS

Study data and inclusion and diagnostic criteria

Thirty patients with Alzheimer's disease and 36 healthy volunteers were included in this study who had both MRI and hippocampal MRS. Table 1 gives the demographics of the study cohort. The study population was derived from a largely community-based population of subjects with AD and healthy elderly people [Alzheimer's Research Trust (ART) cohort] [27]. Community or nursing home resident cases with NINCDS-ADRDA (The National Institute of Neurological and Communicative Disorders and Stroke - the Alzheimer's disease and related Disorders Association) probable-AD were identified from secondary care

Table 1
Subject characteristics

Variable	AD	CONTROL
Number	30	36
Gender (female/male)	15/15	22/14
Mean age (SD)	77,3 (5,0)	76,5 (5,1)
Mean MMSE (SD)	23,1 (3,6)	29,4 (0,7)
Mean GDS (SD)	4,0 (0,7)	–
Mean duration of disease (years; SD)	4,3 (2,3)	–
Mean years of education (years; SD)	11,2 (3,1)	11,7 (3,2)

Data are represented as average ± standard deviation. AD = Alzheimer's Disease, CONTROL = healthy controls, MMSE = Mini Mental State Examination and GDS = Global Dementia Scale.

services for elderly people with dementia. In addition to a clinical diagnosis, subjects were assessed with a standardised assessment protocol including informant interview for diagnosis, MMSE and Global Dementia Scale (GDS) assessments for severity. Healthy volunteers were recruited from non-related members of the patient's families, caregiver's relatives or social centres for the elderly. The inclusion and exclusion criteria were as follows.

Alzheimer's disease

Inclusion criteria: (1) ADRDA/NINCDS and DSM-IV criteria for probable Alzheimer's disease. (2) Mini Mental State Examination score range between 12 and 28. (3) Age 65 years or above. *Exclusion criteria*: (1) Significant neurological or psychiatric illness other than Alzheimer's disease. (2) Significant unstable systematic illness or organ failure.

Controls

Inclusion criteria: (1) Mini Mental State Examination score >26. (2) Geriatric Depression Scale score less than or equal to 5. (3) Age 65 years or above. (4) Medication stable. (5) Good general health. *Exclusion criteria*: (1) Meet the DSM-IV criteria for Dementia. (2) Significant neurological or psychiatric illness other than Alzheimer's disease. (3) Significant unstable systematic illness or organ failure.

Although additional subjects had MRI only the cohort considered here did not differ statistically from the larger cohort. MRI and MRS measures were not a part of the clinical evaluation and therefore did not influence the diagnostic decision. This study was approved by the South London and Maudsley NHS Trust research ethics committee.

MRI and MRS acquisition

Subjects were scanned using a 1.5 Tesla, GE NV/i Signa MR system (General Electric, Milwaukee, WI, USA) at the Maudsley Hospital, London. 3D T1-weighted volume images were acquired in the axial plane with 1.5-mm contiguous sections using acquisition parameters chosen using a contrast simulation tool [28]. Repetition time (TR) was 13.8 ms, inversion time (TI 450 ms, echo time (TE) 2.8 ms, and the flip angle was 20° with one data average and a $256 \times 256 \times 124$ voxel matrix. Acquisition time was 6 min, 27 s. [1]H-

MRS voxels of interest measuring $20 \times 20 \times 15 \text{ mm}^3$ (6 mL) were defined in standard locations in the left and right hippocampi using previously published methods [29]. We chose hippocampal regions of interest as this is one of the earliest sites of change in Alzheimer's disease. The anterior extent of the voxel was defined as the coronal slice where the amygdala disappeared, with the posterior extent 20 mm from this (Fig. 1A). The hippocampal volume of interest contained both grey and white matter and included the parahippocampal gyrus and the posterior portion of the amygdala. A point resolved spectroscopy (PRESS) pulse sequence (TE 35 ms, TR 1500 ms, 256 data averages and 2048 points) with automated shimming and water suppression and excellent reproducibility [30] was used to obtain spectra from each voxel after CHESS water suppression with high signal to noise ratio and clearly resolved NAA, Cho, mI and Cr + PCr peaks among other metabolites. Not all subjects had spectral data from both left and right hippocampus. No significant differences were found in the metabolic content between the right and the left side of hippocampus. Therefore, we averaged the metabolic ratios from the left and right hippocampus from the subjects which had data from both hemispheres.

MRI data analysis

Freesurfer (version 5.0.0), a highly automated structural MRI image processing pipeline was utilised for data analysis. The pipeline produces regional cortical thickness and volumetric measures. Cortical reconstruction and volumetric segmentation includes removal of non-brain tissue using a hybrid watershed/surface deformation procedure [31], automated Talairach transformation, segmentation of the subcortical white matter and deep grey matter volumetric structures (including hippocampus, amygdala, caudate, putamen, ventricles) [31–33] intensity normalization [34], tessellation of the grey matter white matter boundary, automated topology correction [35, 36], and surface deformation following intensity gradients to optimally place the grey/white and grey/cerebrospinal fluid borders at the location where the greatest shift in intensity defines the transition to the other tissue class [37–39]. Once the cortical models are complete, registration to a spherical atlas takes place which utilizes individual cortical folding patterns to match cortical geometry across subjects [40]. This is followed by parcellation of the cerebral
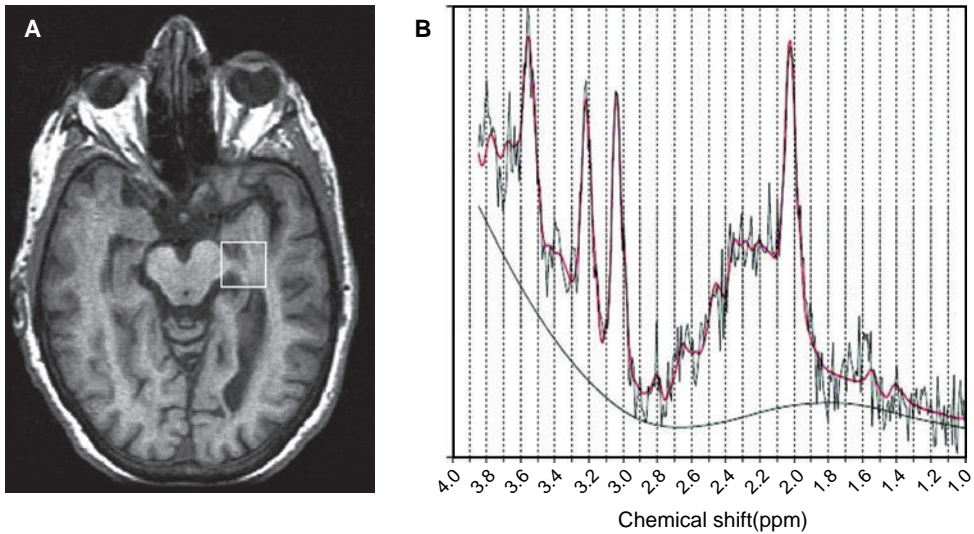
Fig. 1. (A) Representative axial T1-weighted magnetic resonance image of an AD patient illustrating the location of 1H-MRS voxel in the left hippocampus (B) Representative spectrum and model fit from LCModel output.

cortex into units based on gyral and sulcal structure [41, 42]. Fig. 2A and B show representations of ROIs included as candidate input variables in the multivariate OPLS model. All volumetric measures from each subject were normalized by the subject's intracranial volume. This segmentation approach has previously been used for neuropsychological-image analysis [43, 44], imaging-genetic analysis [45–47] and biomarker discovery [48, 49].

MRS data analysis

The software package LCModel (http://www.s-provencher.com) [50, 51] was used for the analysis of the spectra. Fig. 1B shows a representative LCModel output, a spectrum with the model fit. The LCModel algorithm applies linear combinations of individual metabolite signals to calculate the best fit of the experimental spectra to the model spectra. In this case, a basis set of alanine, aspartate, creatine, gamma-aminobutyric acid (GABA), glutamine, glutamate, glycerophosphocholine, mI, lactate, NAA, N-acetyl-aspartylglutamate (NAAg), scyllo-inositol, and taurine, together with a baseline function were used for analysis. As expected, many of the metabolite peaks included in the LC-model did not reach statistical significance when fitted; however those for

NAA, mI, $Cr + PCr$ and Cho did reach significant for all spectra. Metabolite concentration ratios relative to creatine + phosphocreatine $(Cr + PCr)$ were calculated as applied by others [52, 53]. To ensure that differences in tissue composition did not account for metabolite differences between subject groups, we segmented the 3-D T1 weighted volume using SPM (Statistical Parametric Mapping) software (http://www.fil.ion.bpmf.ac.uk/spm) to determine the percentage of grey and white matter and CSF composition within each MRS voxel. The metabolite concentrations reported by LCModel were divided by the fractional content of brain tissue (p[GM] + p[WM], where p[GM] and p[WM] represent the percentage of grey matter and white matter in the voxel, respectively) to correct for the relative proportion of cerebrospinal fluid (CSF) in the MRS voxel (mean(SD) for AD = 0.10(0.04) and for controls = 0.16(0.07), $p = 7.2e$-6). The fraction p[GM] was calculated for each subject to investigate if there were any significant differences in gray content between AD patients and control subjects in the MRS voxels. No significant differences were observed (mean(SD) for AD = 0.62(0.07) and for controls = 0.65(0.06), $p = 0.60$). The metabolite ratios included in the study were: *myo*-inositol (mI/Cr + PCr), choline-containing compounds (Cho/Cr + PCr) and N-acetylaspartate + N-acetylaspartylglutamate (NAA + NAAG/Cr + PCr).
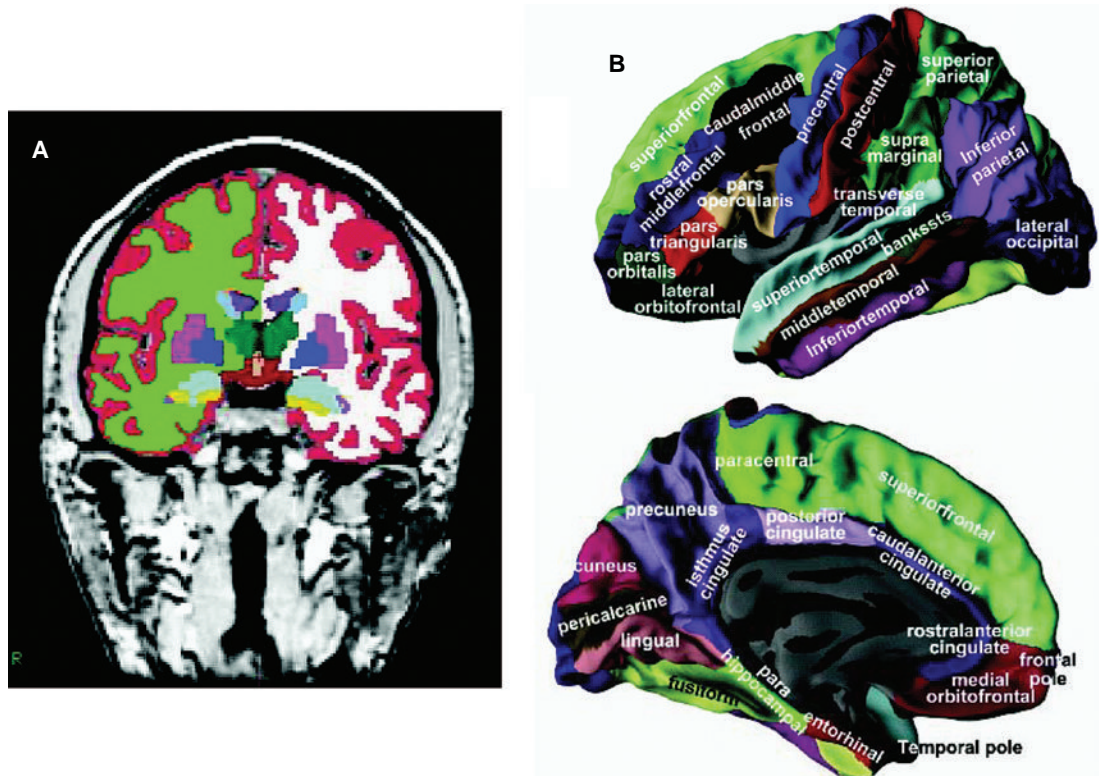
Fig. 2. Representations of ROIs included as candidate input variables in the multivariate OPLS model. (A) Regional volumes. (B) Regional cortical thickness measures.

Multivariate data analysis

MRI measures were analyzed using orthogonal partial least squares to latent structures (OPLS) [1, 24, 54–56], a supervised multivariate data analysis method included in the software package SIMCA (Umetrics AB, Umea, Sweden). A very similar method, partial least squares to latent structures (PLS) has previously been used in several studies to analyze MR-data [23, 25, 26, 57, 58]. OPLS and PLS are very similar methods and when performed, give the same predictive accuracy. The advantage of OPLS compared to PLS is that the model created to compare groups is rotated. This means that the information related to class separation is found in the first component of the model, the predictive component. The other orthogonal components in the model, if any, relate to variation in the data not connected to class separation. Focusing the information related to class separation on the first component makes data interpretation easier [1].

Pre-processing was performed using mean centring and unit variance scaling. Mean centring improves the interpretability of the data, by subtracting the variable average from the data. By doing so the data set is repositioned around the origin. Large variance variables are more likely to be expressed in modeling than low variance variables. Consequently, unit variance scaling was selected to scale the data appropriately. This scaling method calculates the standard deviation of each variable. The inverse standard deviation is used as a scaling weight for each MR-measure.

The results from the OPLS analysis are visualized in a scatter plot by plotting the predictive component, which contains the information related to class separation. Components are vectors, which are linear combinations of partial vectors and are dominated by the input variables (x). The first and second components are by definition orthogonal to each other and span the projection plane of the points. Each point in the scatter plot represents one individual subject.

The predictive component receives a $Q^2(Y)$ value that describes its statistical significance for separating groups. $Q^2(Y)$ values >0.05 are regarded as statistically significant and a model with a $Q^2(Y)$ value >0.5 is regarded as good [59].

$$Q^2(Y) = 1 - PRESS/SSY$$

PRESS (predictive residual sum of squares) = $\Sigma(y_{actual} - y_{predicted})^2$ and SSY is the total variation of the Y matrix after scaling and mean centring [59]. $Q^2(Y)$ is the fraction of the total variation of the Ys (expected class values) that can be predicted by a component according to cross validation (CV). Cross validation is a statistical method for validating a predictive model which involves building a number of parallel models. These models differ from each other by leaving out a part of the data set each time. The data omitted is then predicted by the respective model. In this study we used seven fold cross-validation, which means that 1/7th of the data is omitted for each cross-validation round. Data is omitted once and only once. Variables were plotted according to their importance for the separation of groups. The plot shows the MRI measures and their corresponding jack-knifed confidence intervals. Jack-knifing is used to estimate the bias and standard error. Measures with confidence intervals that include zero have low reliability [1]. Covariance is plotted on the y-axis.

$$Cov(t, Xi) = t^T X_i / (N - 1)$$

Where t is the transpose of the score vector t in the OPLS model, i is the centered variable in the data matrix X and N is the number of variables [1]. A measure with high covariance is more likely to have an impact on group separation than a variable with low covariance. MRI and MRS measures below zero in the scatter plot have lower values in controls compared to AD subjects, while MRI and MRS measures above zero are higher in controls compared to AD subjects in the model.

Altogether 58 variables were used for OPLS analysis. No feature selection was performed, meaning all measured variables were included in the analysis. Three OPLS models were created. The first model contained MRS measures, the second model contained MRI measures and the third model combined both MRI and MRS measures. OPLS has previously been used to combine measures from different techniques [54, 56].

Models containing age, gender and education were also created to test if there were any significant differences between the groups in these measures. Finally we also investigated whether age, gender and education would increase the predictive power of the models using them as x-variables. As the models demonstrated no effect of age, gender and education these were excluded from further analysis.

The sensitivity and the specificity were calculated from the cross-validated prediction values received from the OPLS models. Finally, the positive likelihood ratios (LR+ = sensitivity/(100-specificity)) were calculated. A positive likelihood ratio between 5-10 increases the diagnostic value in a moderate way, while a value above 10 significantly increases the diagnostic value of the test [60].

RESULTS

Subject cohort

Sixty-six subjects were included in this study: 30 AD patients and 36 controls as detailed in Table 1. The gender distribution was equal for the AD subjects, but there were more females than males within the control group. Neuropsychological test results did not differ between females and males and gender differences were accounted for by dividing each regional volume by the subjects' intracranial volume. There were no significant differences between the two groups regarding age and education. As expected, the mean MMSE scores were significantly higher for the control group than the AD group. To measure the disease severity of the AD group the Global Dementia Scale was used. The mean value for the group was 4, which corresponds to mild dementia. Finally the mean disease duration of the AD subjects was 4 years.

OPLS modelling and quality

Three models were created, the first using MRS measures, the second using MRI measures and the third model using both MRI and MRS measures. The first model (MRS measures) resulted in one predictive component. The model accounted for 59% of the variance of the original data ($R^2(X)$) and its' cross validated predictability, $Q^2(Y) = 31\%$. The second model (MRI measures) resulted in one predictive component and one orthogonal component. For this model $R^2(X) = 59\%$ and the cross validated predictability, $Q^2(Y) = 57\%$. The third model (MRI + MRS) resulted in one predictive component and two orthogonal

components. $R^2(X) = 62\%$ and its' cross validated predictability, $Q^2(Y) = 67\%$.

Cross validated scatter plots

Figure 3A shows the separation between AD and controls using MRS measures. This resulted in a sensitivity of 76% and specificity of 83%. In the model containing automated regional volume measures and regional cortical thickness measures a sensitivity of 87% and a specificity of 86% was found (Fig. 3B). The third model (MRI + MRS) had the highest prediction accuracy (Fig. 3C) yielding a sensitivity of 97% and a specificity of 94%. The positive likelihood ratio more than doubled from 6 to 17 when the MRI and MRS measures were combined (Table 2). This significant improvement in diagnostic accuracy can also be observed in the increase of $Q^2(Y)$ described above.
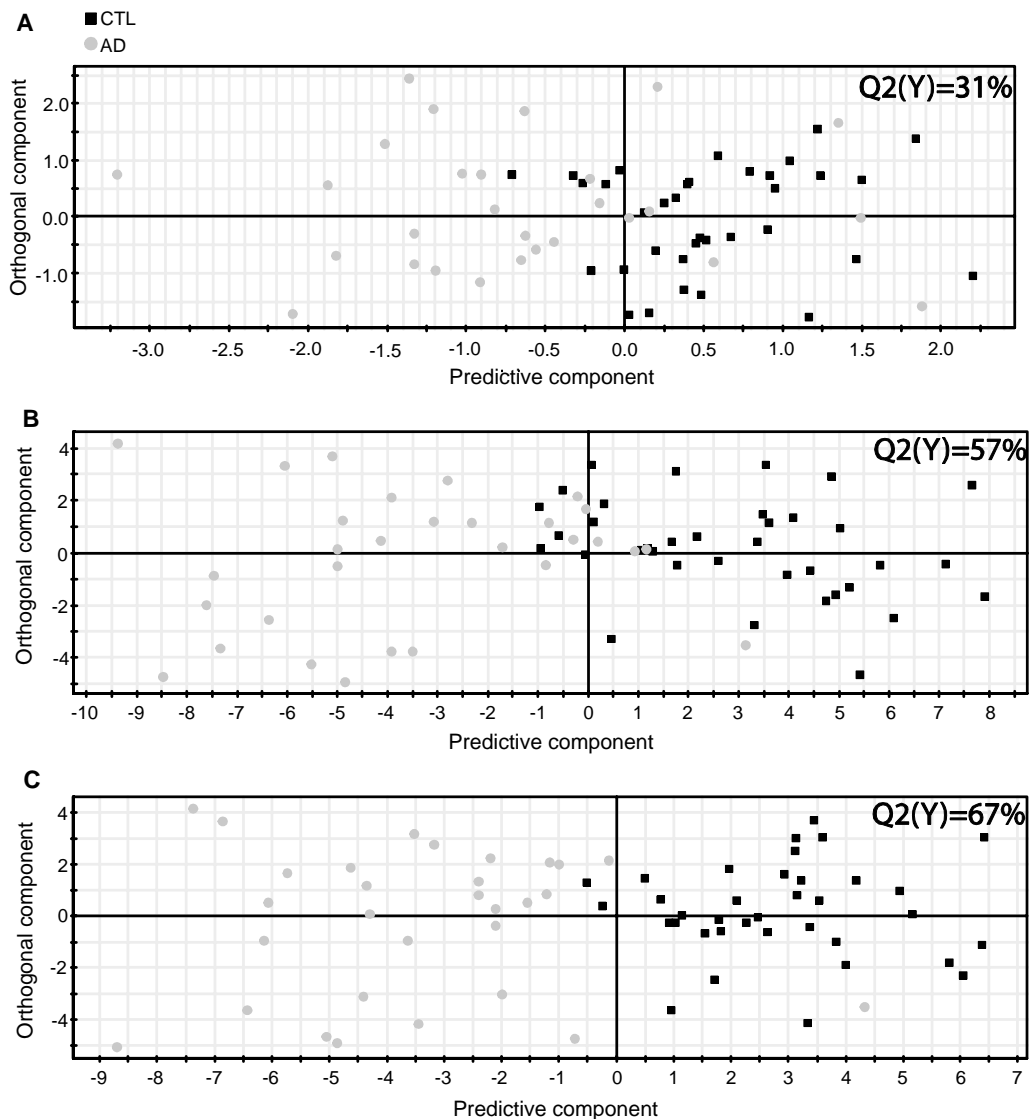
Fig. 3. OPLS cross validated score plots (A) MRS measures (B) MRI Measures (C) The combination of MRI and MRS measures. The scatter plots visualise group separation and the predictability of the three different AD vs. controls models. Each grey circle represents an AD subjects and each black square a control subject. Control subjects to the left of zero and AD subjects to the right of zero are falsely predicted. $Q^2(Y) > 0.05$ (statistically significant model) and $Q^2(Y) > 0.5$ (good model).

Table 2
Sensitivity/specificity and positive Likelihood Ratio (LR+)

	AD vs. CONTROL			
	Sensitivity	Specificity	LR+	$Q^2(Y)$
MRS measures	76% (59–88)	83% (71–94)	5 (2–10)	0.31
MRI measures	87% (70–95)	86% (71–94)	6 (3–14)	0.57
MRI + MRS measures	97% (83–99)	94% (82–98)	17 (5–67)	0.67

MRI = magnetic resonance imaging, MRS = magnetic resonance spectroscopy, AD = Alzheimer's disease, CONTROL = healthy controls, LR+ = likelihood ratio = sensitivity/(1-specificity), confidence intervals for the sensitivity, specificity and LR+ within parenthesis, $Q^2(Y) > 0.05$ (statistically significant model), $Q^2(Y) > 0.5$ (good model) and $Q^2(Y) > 0.7$ (excellent model).

Variables responsible for separation

Figure 4 illustrates the importance of the different variables in the model containing both MRI and MRS measures. Medial, lateral temporal lobe structures and isthmus cingulate as well as parietal and orbitofrontal regions were important for the separation between the two groups. The most important spectroscopic measure was NAA/Cr + PCr.

DISCUSSION

Modern technology can allow high resolution MR images to be acquired in relatively short period of time which are suitable for making large numbers of mea-

sures from. However it can be more challenging to study large numbers of patients due to cost and time constraints. Classical analysis methods such as multiple linear regression and analysis of variance assume statistical independence between variables and that the variables are highly relevant to the research question in hand [59]. The assumption that variables are statistically independent is not true when the number of variables exceeds the number of observations. Multivariate data analysis methods such as OPLS provide the opportunity to analyze many variables simultaneously. Unlike traditional methods, multivariate projection methods can also handle missing data and are robust to noise in both X and Y [59].

The OPLS method has previously been successfully applied by others to a wide range of data types [1, 54]. Bylesjö et al. have shown that OPLS can be used to combine different types of omics data. They showed that the systematic variation from two analytical platforms could be combined and separated from the systematic variation specific to each analytical platform [54]. This illustrates one of the advantages of OPLS, that it divides the systematic variation within the data set into two parts, one correlated with Y and one uncorrelated with Y, making data interpretation easier [1]. We have also recently used OPLS to analyze data from a large multi-center study (AddNeuroMed) using only structural MRI data as input variables [24].
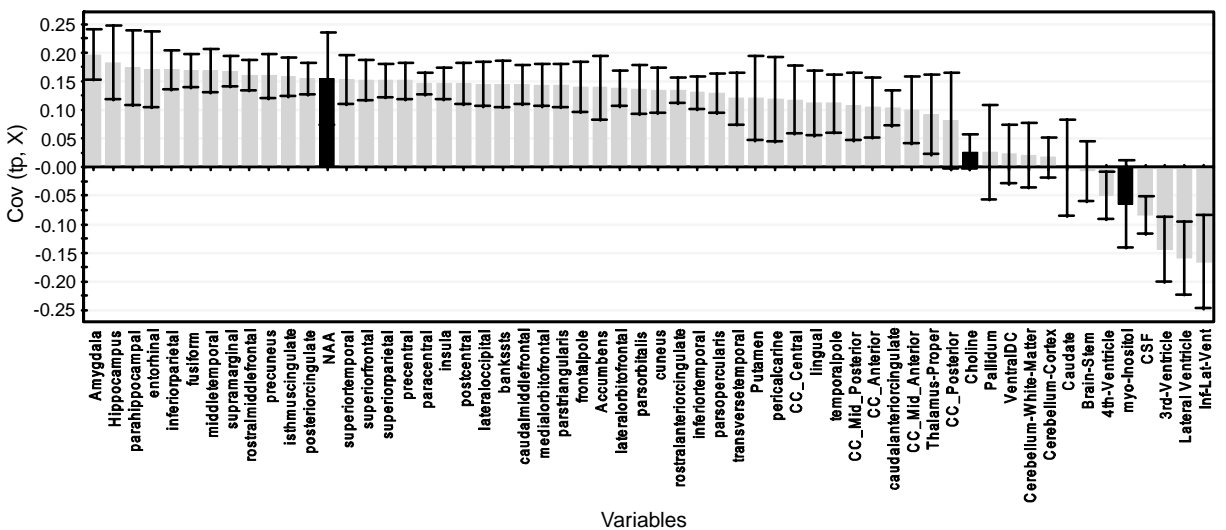

Fig. 4. MRI and MRS measures of importance for the separation between AD and controls. Measures above zero have a larger value in controls compared to AD and measures below zero have a lower value in controls compared to AD. A measure with high covariance is more likely to have an impact on group separation than a measure with low covariance. Measures with jack knifed confidence intervals that include zero have low reliability. Measures in black are metabolite ratios and those in grey are regional volumes and cortical thickness measures.

Model predictability

This study was designed to investigate the feasibility of discriminating between AD and controls using OPLS as a tool combining MRI measures with MRS measures. Several studies have used hippocampal or entorhinal cortex measures for classification between AD and controls with a high degree of accuracy (80%–90%) [5–8, 61–65]. Other prior studies have shown up to 100% accuracy when discriminating between AD and controls but these studies either had very small sample size [66], included more severely impaired AD groups [8, 66, 67] or did not use fully cross-validated results [8, 20, 67, 68]. If cross-validation is not used it can create an optimistic bias in classification accuracy [69, 70]. McEvoy et al. used linear discriminant analysis (LDA) on quantitative structural neuroimaging measures of regional MRI volumes and regional cortical thicknesses to distinguish between Alzheimer's disease and healthy controls [19]. They obtained a sensitivity of 83%, a specificity of 93% and a positive likelihood ratio of 12 when comparing the two groups. By combining automated regional volumes and cortical thickness measures we found a sensitivity of 87% and specificity of 86% in the current study using the multivariate OPLS technique resulting in a positive likelihood ratio of 6. We found a higher sensitivity but a lower specificity than McEvoy et al. for MRI measures alone which is reflected in the lower positive likelihood ratio. In another study Vemuri et al. used support vector machines (SVM) to classify subjects with probable AD from controls [71]. Including ApoE in their analysis they received a sensitivity of 88%, a specificity of 90% resulting in a positive likelihood ratio of +9. As before, we received a higher sensitivity and a lower specificity. Both the studies described above (Vemuri et al. and McEvoy et al.) are multi centre studies including larger cohorts of subjects, which may be the reason for the lower sensitivity values. Different centres can have slightly different inclusion criteria for AD patients, resulting in a more heterogeneous group. Several other studies have used SVM for discriminating between AD and controls with similar results to ours [21, 22, 72]. PLS, which is a similar method to OPLS, has also been utilized with success for the analysis of MR, PET and MEG data [23, 57].

We compared the discriminant ability of structural MRI analyses with those of MRS and to the combination of MRI and MRS. The model containing only MRS measures gave a sensitivity of 76% and specificity of 83% (LR+ = 5); somewhat less effective in discriminating AD from controls than the structural MRI analyses. The addition of MRS measures to the MRI measures improved the discrimination, however, resulting in a sensitivity of 97% and specificity of 94% which gave a positive likelihood ratio of 17, better than that of McEvoy et al. The sensitivity and specificity of combined measures was greater than either MRI or MRS alone, with a more than doubling of the likelihood ratio. This significant improvement in diagnostic accuracy can also be observed in the increase of $Q^2(Y)$ (Table 2). We have previously also used OPLS to distinguish between AD and controls using another automated pipeline combined with manual hippocampal volumes [24].

The OPLS multivariate method has previously been used to discriminate been groups successfully in other fields of research. Wiklund et al. used gas chromatography coupled mass spectroscopy data to differentiate between two transgenic poplar lines and wild type [1]. Another study combined data from two different platforms (2D-DIEGE proteomic and ^{1}H-NMR metabolic data) to analyse blood plasma from mice with a prostate cancer xenograft and matched controls [56]. This study demonstrated that data from different analytical platforms can be successfully combined and gives us a better understanding of in vivo model systems.

MR-measures of importance

McEvoy et al. found that atrophy in medial and lateral temporal, isthmus cingulate and orbitofrontal areas aided the discrimination of control subjects from subjects with AD [19]. We also found that these regions were of importance for the cohort investigated in this study (Fig. 4). This demonstrates that the results can be reproduced and that the automated pipeline analysis methods used in both studies are robust. Decreased levels of NAA/Cr + PCr were observed in AD compared to controls and adding the spectroscopic measures increased the prediction accuracy. Kantarci et al. demonstrated that combining MRI with MRS improves the ability to identify patients with prodromal dementia [73]. Other studies have also shown that the combination of NAA and structural MRI improves the classification accuracy [74, 75]. This indicates the potential value of adding MR spectroscopic measures to volumetric measures in the diagnosis of AD and other neurodegerative disorders. Metabolic changes have previously been detected in presymptomatic mutation carriers years before expected onset

[76] which demonstrates the potential use of MRS. It is possible that metabolite ratios provide less information about how individual metabolites change than metabolite concentrations. However, ratios are not susceptible to CSF partial volume effect and may represent more sensitive biomarkers of disease [77]. While we studied hippocampal MRS it would be interesting to apply the same technique to other regions of interest including the anterior cingulate using either single voxel MRS or magnetic resonance spectroscopic imaging (MRSI). A possible explanation for the added value of MRS to MRI is that they reflect different aspects of pathological processes, brain atrophy and metabolic changes. In AD, molecular neuropathology is thought to precede structural brain changes by several years and the neurodegeneration is estimated to start 20–30 years before the clinical diagnosis is given [78]. These factors may play a role in explaining why these methods in combination improve the diagnostic outcome.

Conclusion

Quantitative MRI and MRS measurements in combination can improve the accuracy of discriminating patient with early Alzheimer's disease from normally cognitive elderly subjects over and above that of MRI measures and multivariate analysis alone. The multivariate method applied here (OPLS) provides the opportunity to analyze all of the MRI and MRS measures simultaneously, allowing the building of robust OPLS models for the prediction of disease demonstrating high sensitivity and specificity. Combining the automated MRS measures with MRI measures more than doubled the positive likelihood ratio from 6 to 17 which highlights the importance of MRS measures as a valuable complement to MRI in the diagnosis of Alzheimer's disease. A potential limitation of the current study is that the analysis technique was applied to a moderately sized MRI study with subjects recruited from a single site. Further, studies are warranted including those focusing on patients with mild cognitive impairment, patients with other types of dementia, longitudinal data and external test data sets to validate the robustness of the models. Applying this approach to typical clinical populations including mixed pathology and unclear clinical presentation would be of particular interest. Ultimately, pathologically confirmed data sets are needed to determine the applicability of the method described. However the improvement in discrimination when adding the MRS measures led to a clear and large improvement in

the positive likelihood ratio. We chose a hippocampal region of interest for MRS since this is a particularly relevant area for AD and can be measured in a clinically realistic time. It would be of scientific interest in future to use the same approach described here for MR spectroscopic imaging or multiple single voxel MRS measures, though this may not be realistic for routine clinical imaging. To conclude, combining global and regional measures of atrophy with MRS measures significantly improves the classification accuracy when distinguishing between AD patients and healthy controls. Since all measures can be acquired with fully automated methods it makes them attractive for further use.

ACKNOWLEDGEMENTS

REFERENCES

[1] Wiklund S, Johansson E, Sjostrom L, Mellerowicz EJ, Edlund U, Shockcor JP, Gottfries J, Moritz T, Trygg J (2008) Visualization of GC/TOF-MS-based metabolomics data for identification of biochemically interesting compounds using OPLS class models. *Anal Chem* **80**, 115-122.

[2] O'Brien JT (2007) Role of imaging techniques in the diagnosis of dementia. *Br J Radiol* **80 Spec No 2**, S71-S77.

[3] Ries ML, Carlsson CM, Rowley HA, Sager MA, Gleason CE, Asthana S, Johnson SC (2008) Magnetic resonance imaging characterization of brain structure and function in mild cognitive impairment: a review. *J Am Geriatr Soc* **56**, 920-934.

[4] Scahill RI, Fox NC (2007) Longitudinal imaging in dementia. *Br J Radiol* **80** Spec No 2, S92-S98.

[5] Fox NC, Warrington EK, Freeborough PA, Hartikainen P, Kennedy AM, Stevens JM, Rossor MN (1996) Presymptomatic hippocampal atrophy in Alzheimer's disease. A longitudinal MRI study. *Brain* **119(Pt 6)**, 2001-2007.

[6] Jack CR Jr, Petersen RC, O'Brien PC, Tangalos EG (1992) MR-based hippocampal volumetry in the diagnosis of Alzheimer's disease. *Neurology* **42**, 183-188.

[7] Jack CR Jr, Petersen RC, Xu YC, Waring SC, O'Brien PC, Tangalos EG, Smith GE, Ivnik RJ, Kokmen E (1997) Medial temporal atrophy on MRI in normal aging and very mild Alzheimer's disease. *Neurology* **49**, 786-794.

[8] Juottonen K, Laakso MP, Partanen K, Soininen H (1999) Comparative MR analysis of the entorhinal cortex and

hippocampus in diagnosing Alzheimer disease. *AJNR Am J Neuroradiol* **20**, 139-144.

[9] Xu Y, Jack CR Jr, O'Brien PC, Kokmen E, Smith GE, Ivnik RJ, Boeve BF, Tangalos RG, Petersen RC (2000) Usefulness of MRI measures of entorhinal cortex versus hippocampus in AD. *Neurology* **54**, 1760-1767.

[10] Braak H, Braak E (1991) Neuropathological stageing of Alzheimer-related changes. *Acta Neuropathologica* **82**, 239-259.

[11] Shiino A, Watanabe T, Maeda K, Kotani E, Akiguchi I, Matsuda M (2006) Four subgroups of Alzheimer's disease based on patterns of atrophy using VBM and a unique pattern for early onset disease. *Neuroimage* **33**, 17-26.

[12] Firbank MJ, Harrison RM, O'Brien JT (2002) A comprehensive review of proton magnetic resonance spectroscopy studies in dementia and Parkinson's disease. *Dement Geriatr Cogn Disord* **14**, 64-76.

[13] Kantarci K (2007) 1 H magnetic resonance spectroscopy in dementia. *Br J Radiol* **80 Spec No 2**, S146-S152.

[14] Soares DP, Law M (2009) Magnetic resonance spectroscopy of the brain: review of metabolites and clinical applications. *Clin Radiol* **64**, 12-21.

[15] Douaud G, Jbabdi S, Behrens TEJ, Menke RA, Gass A, Monsch AU, Rao A, Whitcher B, Kindlmann G, Matthews PM, Smith S (2011) DTI measures in crossing-fibre areas: Increased diffusion anisotropy reveals early white matter alteration in MCI and mild Alzheimer's disease. *Neuroimage* **55**, 880-890.

[16] Sperling RA, Dickerson BC, Pihlajamaki M, Vannini P, LaViolette PS, Vitolo OV, Hedden T, Becker JA, Rentz DM, Selkoe DJ, Johnson KA (2010) Functional alterations in memory networks in early Alzheimer's disease. *Neuromolecular Med* **12**, 27-43.

[17] Chen W, Song X, Beyea S, D'Arcy R, Zhang Y, Rockwood K (2011) Advances in perfusion magnetic resonance imaging in Alzheimer's disease. *Alzheimer's and Dementia* **7**, 185-196.

[18] Deoni SC, Peters TM, Rutt BK (2005) High-resolution T1 and T2 mapping of the brain in a clinically acceptable time with DESPOT1 and DESPOT2. *Magn Reson Med* **53**, 237-241.

[19] McEvoy LK, Fennema-Notestine C, Roddey JC, Hagler JDJ Jr, Holland D, Karow DS, Pung CJ, Brewer JB, Dale AM (2009) Alzheimer disease: Quantitative structural neuroimaging for detection and prediction of clinical and structural changes in mild cognitive impairment. *Radiology* **251**, 195-205.

[20] Fan Y, Batmanghelich N, Clark CM, Davatzikos C (2008) Spatial patterns of brain atrophy in MCI patients, identified via high-dimensional pattern classification, predict subsequent cognitive decline. *Neuroimage* **39**, 1731-1743.

[21] Kloppel S, Stonnington CM, Barnes J, Chen F, Chu C, Good CD, Mader I, Mitchell LA, Patel AC, Roberts CC, Fox NC, Jack CR Jr, Ashburner J, Frackowiak RS (2008) Accuracy of dementia diagnosis: A direct comparison between radiologists and a computerized method. *Brain* **131**, 2969-2974.

[22] Kloppel S, Stonnington CM, Chu C, Draganski B, Scahill RI, Rohrer JD, Fox NC, Jack CR Jr, Ashburner J, Frackowiak RSJ (2008) Automatic classification of MR scans in Alzheimer's disease. *Brain* **131**, 681-689.

[23] McIntosh AR, Lobaugh NJ (2004) Partial least squares analysis of neuroimaging data: Applications and advances. *Neuroimage* **23**, S250-S263.

[24] Westman E, Simmons A, Zhang Y, Muehlboeck J, Tunnard C, Liu Y, Collins L, Evans A, Mecocci P, Vellas B, Tsolaki M, Kłoszewska I, Soininen H, Lovestone S, Spenger C, Wahlund L, consortium. ftA (2011) Multivariate analysis of MRI data for Alzheimer's disease, mild cognitive impairment and healthy controls. *Neuroimage* **54**, 1178-1187.

[25] Westman E, Spenger C, Oberg J, Reyer H, Pahnke J, Wahlund LO (2009) *In vivo* 1 H-magnetic resonance spectroscopy can detect metabolic changes in APP/PS1 mice after donepezil treatment. *BMC Neurosci* **10**, 33.

[26] Westman E, Spenger C, Wahlund L-O, Lavebratt C (2007) Carbamazepine treatment recovered low N-acetylaspartate+N-acetylaspartylglutamate (tNAA) levels in the megencephaly mouse BALB/cByJ-Kv1.1 mceph/mceph. *Neurobiology of Disease* **26**, 221-228.

[27] Hye A, Lynham S, Thambisetty M, Causevic M, Campbell J, Byers HL, Hooper C, Rijsdijk F, Tabrizi SJ, Banner S, Shaw CE, Foy C, Poppe M, Archer N, Hamilton G, Powell J, Brown RG, Sham P, Ward M, Lovestone S (2006) Proteome-based plasma biomarkers for Alzheimer's disease. *Brain* **129**, 3042-3050.

[28] Simmons A, Arridge SR, Barker GJ, Williams SCR (1996) Simulation of MRI cluster plots and application to neurological segmentation. *Magnetic Resonance Imaging* **14**, 73-92.

[29] Robertson DMWM, van Amelsvoort TM, Daly EB, Simmons AP, Whitehead MM, Morris RGP, Murphy KCM, Murphy DGMM (2001) Effects of estrogen replacement therapy on human brain aging: An *in vivo* ^{1}H MRS study. *Neurology* **57**, 2114-2117.

[30] Simmons A, Smail M, Moore E, Williams SCR (1998) Serial precision of metabolite peak area ratios and water referenced metabolite peak areas in proton MR spectroscopy of the human brain. *Magnetic Resonance Imaging* **16**, 319-330.

[31] Segonne F, Dale AM, Busa E, Glessner M, Salat D, Hahn HK, Fischl B (2004) A hybrid approach to the skull stripping problem in MRI. *Neuroimage* **22**, 1060-1075.

[32] Fischl B, Salat DH, Busa E, Albert M, Dieterich M, Haselgrove C, van der Kouwe A, Killiany R, Kennedy D, Klaveness S, Montillo A, Makris N, Rosen B, Dale AM (2002) Whole brain segmentation: automated labeling of neuroanatomical structures in the human brain. *Neuron* **33**, 341-355.

[33] Fischl B, Salat DH, van der Kouwe AJ, Makris N, Segonne F, Quinn BT, Dale AM (2004) Sequence-independent segmentation of magnetic resonance images. *Neuroimage* **23 Suppl 1**, S69-S84.

[34] Sled JG, Zijdenbos AP, Evans AC (1998) A nonparametric method for automatic correction of intensity nonuniformity in MRI data. *IEEE Trans Med Imaging* **17**, 87-97.

[35] Fischl B, Liu A, Dale AM (2001) Automated manifold surgery: constructing geometrically accurate and topologically correct models of the human cerebral cortex. *IEEE Trans Med Imaging* **20**, 70-80.

[36] Segonne F, Pacheco J, Fischl B (2007) Geometrically accurate topology-correction of cortical surfaces using nonseparating loops. *IEEE Trans Med Imaging* **26**, 518-529.

[37] Dale AM, Fischl B, Sereno MI (1999) Cortical surface-based analysis. I. Segmentation and surface reconstruction. *Neuroimage* **9**, 179-194.

[38] Dale AM, Sereno MI (1993) Improved localizadon of cortical activity by combining EEG and MEG with MRI cortical sur-

face reconstruction: A linear approach. *Journal of Cognitive Neuroscience* **5**, 162-176.

[39] Fischl B, Dale AM (2000) Measuring the thickness of the human cerebral cortex from magnetic resonance images. *Proc Natl Acad Sci U S A* **97**, 11050-11055.

[40] Fischl B, Sereno MI, Tootell RB, Dale AM (1999) High-resolution intersubject averaging and a coordinate system for the cortical surface. *Hum Brain Mapp* **8**, 272-284.

[41] Desikan RS, Ségonne F, Fischl B, Quinn BT, Dickerson BC, Blacker D, Buckner RL, Dale AM, Maguire RP, Hyman BT, Albert MS, Killiany RJ (2006) An automated labeling system for subdividing the human cerebral cortex on MRI scans into gyral based regions of interest. *NeuroImage* **31**, 968-980.

[42] Fischl B, van der Kouwe A, Destrieux C, Halgren E, Segonne F, Salat DH, Busa E, Seidman LJ, Goldstein J, Kennedy D, Caviness V, Makris N, Rosen B, Dale AM (2004) Automatically parcellating the human cerebral cortex. *Cereb Cortex* **14**, 11-22.

[43] Liu Y, Paajanen T, Zhang Y, Westman E, Wahlund L-O, Simmons A, Tunnard C, Sobow T, Mecocci P, Tsolaki M, Vellas B, Muehlboeck S, Evans A, Spenger C, Lovestone S, Soininen H (2009) Combination analysis of neuropsychological tests and structural MRI measures in differentiating AD, MCI and control groups-The AddNeuroMed study. *Neurobiol Aging*. In press, Corrected Proof.

[44] Liu Y, Paajanen T, Zhang Y, Westman E, Wahlund L-O, Simmons A, Tunnard C, Sobow T, Mecocci P, Tsolaki M, Vellas B, Muehlboeck S, Evans A, Spenger C, Lovestone S, Soininen H (2010) Analysis of regional MRI volumes and thicknesses as predictors of conversion from mild cognitive impairment to Alzheimer's disease. *Neurobiology of Aging* **31**, 1375-1385.

[45] Furney SJ, Simmons A, Breen G, Pedroso I, Lunnon K, Proitsi P, Hodges A, Powell J, Wahlund LO, Kloszewska I, Mecocci P, Soininen H, Tsolaki M, Vellas B, Spenger C, Lathrop M, Shen L, Kim S, Saykin AJ, Weiner MW, Lovestone S (2010) Genome-wide association with MRI atrophy measures as a quantitative trait locus for Alzheimer's disease. *Mol Psychiatry* 2010 Nov 30. [Epub ahead of print]

[46] Liu Y, Paajanen T, Westman E, Wahlund LO, Simmons A, Tunnard C, Sobow T, Proitsi P, Powell J, Mecocci P, Tsolaki M, Vellas B, Muehlboeck S, Evans A, Spenger C, Lovestone S, Soininen H (2010) Effect of APOE epsilon4 allele on cortical thicknesses and volumes: the Add Neuro Med study. *J Alzheimers Dis* **21**, 947-966.

[47] Liu Y, Paajanen T, Westman E, Zhang Y, Wahlund LO, Simmons A, Tunnard C, Sobow T, Proitsi P, Powell J, Mecocci P, Tsolaki M, Vellas B, Muehlboeck S, Evans A, Spenger C, Lovestone S, Soininen H (2010) APOE epsilon2 allele is associated with larger regional cortical thicknesses and volumes. *Dement Geriatr Cogn Disord* **30**, 229-237.

[48] Thambisetty M, Hye A, Foy C, Daly E, Glover A, Cooper A, Simmons A, Murphy D, Lovestone S (2008) Proteome-based identification of plasma proteins associated with hippocampal metabolism in early Alzheimer's disease. *J Neurol* **255**, 1712-1720.

[49] Thambisetty M, Simmons A, Velayudhan L, Hye A, Campbell J, Zhang Y, Wahlund LO, Westman E, Kinsey A, Guntert A, Proitsi P, Powell J, Causevic M, Killick R, Lunnon K, Lynham S, Broadstock M, Choudhry F, Howlett DR, Williams RJ, Sharp SI, Mitchelmore C, Tunnard C, Leung R, Foy C, O'Brien D, Breen G, Furney SJ, Ward M, Kloszewska I, Mecocci P, Soininen H, Tsolaki M, Vellas B, Hodges A, Murphy DG, Parkins S, Richardson JC, Resnick SM, Ferrucci L, Wong DF, Zhou Y, Muehlboeck S, Evans A,

Francis PT, Spenger C, Lovestone S (2010) Association of plasma clusterin concentration with severity, pathology, and progression in Alzheimer disease. *Arch Gen Psychiatry* **67**, 739-748.

[50] Provencher SW (1993) Estimation of metabolite concentrations from localized *in vivo* proton NMR spectra. *Magn Reson Med* **30**, 672-679.

[51] Provencher SW (2001) Automatic quantitation of localized *in vivo* ^{1}H spectra with LCModel. *NMR Biomed* **14**, 260-264.

[52] Ackl N, Ising M, Schreiber YA, Atiya M, Sonntag A, Auer DP (2005) Hippocampal metabolic abnormalities in mild cognitive impairment and Alzheimer's disease. *Neurosci Lett* **384**, 23-28.

[53] Westman E, Spenger C, Wahlund LO, Lavebratt C (2007) Carbamazepine treatment recovered low N-acetylaspartate+N-acetylaspartylglutamate (tNAA) levels in the megencephaly mouse BALB/cByJ-Kv1.1(mceph/mceph). *Neurobiol Dis* **26**, 221-228.

[54] Bylesjo M, Eriksson D, Kusano M, Moritz T, Trygg J (2007) Data integration in plant biology: the O2PLS method for combined modeling of transcript and metabolite data. *Plant J* **52**, 1181-1191.

[55] Johan Trygg SW (2002) Orthogonal projections to latent structures (O-PLS). *Journal of Chemometrics* **16**, 119-128.

[56] Rantalainen M, Cloarec O, Beckonert O, Wilson ID, Jackson D, Tonge R, Rowlinson R, Rayner S, Nickson J, Wilkinson RW, Mills JD, Trygg J, Nicholson JK, Holmes E (2006) Statistically integrated metabonomic-proteomic studies on a human prostate cancer xenograft model in mice. *J Proteome Res* **5**, 2642-2655.

[57] Levine B, Kovacevic N, Nica EI, Cheung G, Gao F, Schwartz ML, Black SE (2008) The Toronto traumatic brain injury study: Injury severity and quantified MRI. *Neurology* **70**, 771-778.

[58] Oberg J, Spenger C, Wang FH, Andersson A, Westman E, Skoglund P, Sunnemark D, Norinder U, Klason T, Wahlund LO, Lindberg M (2008) Age related changes in brain metabolites observed by (1)H MRS in APP/PS1 mice. *Neurobiol Aging* **29**, 1423-1433.

[59] Eriksson L, Johansson E, Kettaneh-Wold N, Trygg J, Wiksröm C, Wold S (2006) *Multi- and Megavariate Data Analysis (Part I -Basics and Principals and Applications)*, Umetrics AB, Umeå.

[60] Qizilbash S, Chui, Tariot, Brodaty, Kaye, Erkinjuntti (2002) (Blackwell Publishing, Oxford), 20-23.

[61] Killiany RJ, Moss MB, Albert MS, Sandor T, Tieman J, Jolesz F (1993) Temporal lobe regions on magnetic resonance imaging identify patients with early Alzheimer's disease. *Arch Neurol* **50**, 949-954.

[62] Laakso MP, Partanen K, Riekkinen P, Lehtovirta M, Helkala EL, Hallikainen M, Hanninen T, Vainio P, Soininen H (1996) Hippocampal volumes in Alzheimer's disease, Parkinson's disease with and without dementia, and in vascular dementia: An MRI study. *Neurology* **46**, 678-681.

[63] Laakso MP, Soininen H, Partanen K, Lehtovirta M, Hallikainen M, Hanninen T, Helkala EL, Vainio P, Riekkinen PJ Sr (1998) MRI of the hippocampus in Alzheimer's disease: sensitivity, specificity, and analysis of the incorrectly classified subjects. *Neurobiol Aging* **19**, 23-31.

[64] Lehericy S, Baulac M, Chiras J, Pierot L, Martin N, Pillon B, Deweer B, Dubois B, Marsault C (1994) Amygdalo-hippocampal MR volume measurements in the early stages of Alzheimer disease. *AJNR Am J Neuroradiol* **15**, 929-937.

[65] Seab JP, Jagust WJ, Wong ST, Roos MS, Reed BR, Budinger TF (1988) Quantitative NMR measurements of hippocampal atrophy in Alzheimer's disease. *Magn Reson Med* **8**, 200-208.

[66] Lerch JP, Pruessner J, Zijdenbos AP, Collins DL, Teipel SJ, Hampel H, Evans AC (2008) Automated cortical thickness measurements from MRI can accurately separate Alzheimer's patients from normal elderly controls. *Neurobiol Aging* **29**, 23-30.

[67] Callen DJ, Black SE, Gao F, Caldwell CB, Szalai JP (2001) Beyond the hippocampus: MRI volumetry confirms widespread limbic atrophy in AD. *Neurology* **57**, 1669-1674.

[68] Killiany RJ, Hyman BT, Gomez-Isla T, Moss MB, Kikinis R, Jolesz F, Tanzi R, Jones K, Albert MS (2002) MRI measures of entorhinal cortex vs hippocampus in preclinical AD. *Neurology* **58**, 1188-1196.

[69] Schulerud H, Albregtsen F (2004) Many are called, but few are chosen. Feature selection and error estimation in high dimensional spaces. *Comput Methods Programs Biomed* **73**, 91-99.

[70] Simon Spycher MNJG (2004) Comparison of different classification methods applied to a mode of toxic action data set. *QSAR & Combinatorial Science* **23**, 779-791.

[71] Vemuri P, Gunter JL, Senjem ML, Whitwell JL, Kantarci K, Knopman DS, Boeve BF, Petersen RC, Jack CR Jr (2008) Alzheimer's disease diagnosis in individual subjects using structural MR images: validation studies. *Neuroimage* **39**, 1186-1197.

[72] Plant C, Teipel SJ, Oswald A, Böhm C, Meindl T, Mourao-Miranda J, Bokde AW, Hampel H, Ewers M (2009) Automated detection of brain atrophy patterns based on MRI for the prediction of Alzheimer's disease. *Neuroimage* **50**, 162-174.

[73] Kantarci K, Weigand SD, Przybelski SA, Shiung MM, Whitwell JL, Negash S, Knopman DS, Boeve BF, O'Brien PC, Petersen RC, Jack CR Jr (2009) Risk of dementia in MCI: Combined effect of cerebrovascular disease, volumetric MRI, and 1 H MRS. *Neurology* **72**, 1519-1525.

[74] Jessen F, Traeber F, Freymann N, Maier W, Schild HH, Heun R, Block W (2005) A Comparative Study of the Different N-Acetylaspartate Measures of the Medial Temporal Lobe in Alzheimerâ€™s Disease. *Dementia and Geriatric Cognitive Disorders* **20**, 178-183.

[75] Schuff N, Capizzano AA, Du AT, Amend DL, O'Neill J, Norman D, Kramer J, Jagust W, Miller B, Wolkowitz OM, Yaffe K, Weiner MW (2002) Selective reduction of N-acetylaspartate in medial temporal and parietal lobes in AD. *Neurology* **58**, 928-935.

[76] Godbolt AK, Waldman AD, MacManus DG, Schott JM, Frost C, Cipolotti L, Fox NC, Rossor MN (2006) MRS shows abnormalities before symptoms in familial Alzheimer disease. *Neurology* **66**, 718-722.

[77] Bartha R, Smith M, Rupsingh R, Rylett J, Wells JL, Borrie MJ (2008) High field (1)H MRS of the hippocampus after donepezil treatment in Alzheimer disease. *Prog Neuropsychopharmacol Biol Psychiatry* **32**, 786-793.

[78] Blennow K, de Leon MJ, Zetterberg H (2006) Alzheimer's disease. *The Lancet* **368**, 387-403.

This page intentionally left blank

Section 8

Longitudinal Neuroimaging Measures: Windows into Progression of Disease and Potential Endpoints for Clinical Trials

This page intentionally left blank

Introduction

Section 8: Longitudinal Neuroimaging Measures: Windows into Progression of Disease and Potential Endpoints for Clinical Trials

Steve D. Edland*

Department of Neuroscience, Department of Family Preventive Medicine Division of Biostatistics, University of California, San Diego, La Jolla, CA, USA

This section explores the application of longitudinal imaging measures to studies of aging and Alzheimer's disease (AD). Imaging allows highly focused assessment of specific aspects of disease effects, and many imaging measures are remarkably precise relative to clinical measures. For these reasons imaging measures hold great potential to characterize the natural history of disease and as endpoints for clinical trials. In the first chapter of this Section, Reiman et al. [1] explore the potential promise of imaging measures as endpoints for clinical trials and outline plans for large scale intervention trials. Feasibility is illustrated by four pilot clinical trials with novel interventions and imaging endpoints (Chapters 2 through 5). Ashford et al. [2] use magnetic resonance spectroscopy to assess the impact of memantine on mild to moderate AD. Förster et al. [3] use FDG-PET and Rosen et al. [4] use fMRI to assess the impact of cognitive interventions on brain function in early AD. Tzimopoulou et al. [5] describe a multicenter clinical trial using FDG-PET to assess the impact of rosiglitazone on metabolism in AD. The next two chapters review additional imaging measures. Olichney et al. [8] reviews accumulating data on the response of event related brain potential (ERP) measurements to the progressive stages of AD, and Zhang et al. [7] describe the application of

an MRI-based global atrophy and brain lesion index to AD. Finally, Ard and Edland [8] review statistical considerations relevant to planning clinical trials with imaging endpoints, and summarize the potential dramatic improvement in efficiency of clinical trial using those endpoints. Collectively, the chapters of this section suggest that longitudinal neuroimaging methods hold great promise to advance our understanding of AD and discover treatments for modifying the course of disease.

REFERENCES

[1] Reiman EM, Langbaum. J, Fleisher AS, Caselli RJ, Chen K, Ayutyanont N, Quiroz YT, Kosik KS, Lopera F, Tariot PN. (2011) Alzheimer's prevention initiative: A plan to accelerate the evaluation of presymptomatic treatments. In *Handbook of Imaging the Alzheimer Brain*, Ashford JW et al., eds. IOS Press, Amsterdam, pp. 589-597.

[2] Förster S, Buschert VC, Teipel SJ, Friese U, Buchholz HG, Drzezga A, Hampel H, Bartenstein P, Buerger K (2011) Effects of a 6-month cognitive intervention on brain metabolism in patients with amnestic MCI and mild Alzheimer´s disease. In *Handbook of Imaging the Alzheimer Brain*, Ashford JW et al., eds. IOS Press, Amsterdam, pp. 605-616.

[3] Rosen AC, Sugiura L, Kramer JH, Whitfield-Grabieli S, Gabrieli JD (2011) Cognitive training changes hippocampal function in mild cognitive impairment: A pilot study. In *Handbook of Imaging the Alzheimer Brain*, Ashford JW et al., eds. IOS Press, Amsterdam, pp. 617-625.

*Correspondence to: Steve Edland, E-mail: sedland@ucsd.edu.

[4] Ashford JW, Adamsin MM, Beale T, La D, Hernandez B, Noda A, Rosen A, O'Hara R, Fairchild JK, Spielman D, Yesavage JA (2011) MR spectroscopy for assessment of memantine treatment in mild to moderate Alzheimer's disease. In *Handbook of Imaging the Alzheimer Brain*, Ashford JW et al., eds. IOS Press, Amsterdam, pp. 599-604.

[5] Tzimopoulou S, Cunningham VJ, Nichols TE, Searle G, Bird NP, Mistry P, Dixon IJ, Hallett WA, Whitcher B, Brown AP, Zvartau-Hind M, Lotay N, Lai RYK, Castiglia M, Jeter B, Matthews JC, Chen K, Bandy D, Reiman EM, Gold M, Rabiner EA, Mathews PM (2011) Validation and pilot application of [^{18}F]FDG-PET in evaluation of a metabolic therapy for Alzheimer's disease. In *Handbook of Imaging the Alzheimer Brain*, Ashford JW et al., eds. IOS Press, Amsterdam, pp. 627-642.

[6] Olichney JM, Yang JC, Taylor J, Kutas M (2011) Cognitive event-related potentials: biomarkers of synaptic dysfunction across the stages of Alzheimer's disease. In *Handbook of Imaging the Alzheimer Brain*, Ashford JW et al., eds. IOS Press, Amsterdam, pp. 421-434.

[7] Zhang N, Song X, Zhang Y, Chen W, D'Arcy RCN, Darvesh S, Fisk JD, Rockwood K (2011) MRI brain atrophy and lesion index to assess the progression of structural changes in Alzheimer's disease, mild cognitive impairment, and normal aging: A follow-up study. In *Handbook of Imaging the Alzheimer Brain*, Ashford JW et al., eds. IOS Press, Amsterdam, pp. 643-651.

[8] Ard MC, Edland SD (2011) Power calculations for clinical trials in Alzheimer's disease. In *Handbook of Imaging the Alzheimer Brain*, Ashford JW et al., eds. IOS Press, Amsterdam, pp. 653-661.

Alzheimer's Prevention Initiative: A Plan to Accelerate the Evaluation of Presymptomatic Treatments

Eric M. Reiman[a,b,c,d,*], Jessica B.S. Langbaum[a,d], Adam S. Fleisher[a,d,e,f], Richard J. Caselli[d,g], Kewei Chen[a,d,h], Napatkamon Ayutyanont[a,d], Yakeel T. Quiroz[i], Kenneth S. Kosik[j], Francisco Lopera[k] and Pierre N. Tariot[a,b,d,f]

[a]*Banner Alzheimer's Institute, Phoenix, AZ, USA*
[b]*Department of Psychiatry, University of Arizona, Tucson, AZ, USA*
[c]*Neurogenomics Division, Translational Genomics Research Institute, Phoenix, AZ, USA*
[d]*Arizona Alzheimer's Consortium, Phoenix, AZ, USA*
[e]*Department of Neurosciences, University of CA, San Diego, CA, USA*
[f]*Alzheimer's Disease Cooperative Study (ADCS), San Diego, CA, USA*
[g]*Department of Neurology, Mayo Clinic Arizona, Scottsdale, AZ, USA*
[h]*Department of Mathematics and Statistics, Arizona State University, Tempe, AZ, USA*
[i]*Department of Psychology, Center for Memory and Brain, Boston University, MA, USA*
[j]*Neuroscience Research Institute, Department of Molecular Cellular Developmental Biology, University of California, Santa Barbara, CA, USA*
[k]*Neuroscience Group, University of Antioquia, Medellin, Colombia*

Abstract. There is an urgent need to find effective presymptomatic Alzheimer's disease (AD) treatments that reduce the risk of AD symptoms or prevent them completely. It currently takes too many healthy people, too much money and too many years to evaluate the range of promising presymptomatic treatments using clinical endpoints. We have used brain imaging and other measurements to track some of the earliest changes associated with the predisposition to AD. We have proposed the Alzheimer's Prevention Initiative (API) to evaluate investigational amyloid-modifying treatments in healthy people who, based on their age and genetic background, are at the highest imminent risk of developing symptomatic AD using brain imaging, cerebrospinal fluid (CSF), and cognitive endpoints. In one trial, we propose to study AD-causing *presenilin 1* [*PS1*] mutation carriers from the world's largest early-onset AD kindred in Antioquia, Colombia, close to their estimated average age at clinical onset. In another trial, we propose to study *apolipoprotein E* (*APOE*) *ε4* homozygotes (and possibly heterozygotes) close to their estimated average age at clinical onset. The API has several goals: 1) to evaluate investigational AD-modifying treatments sooner than otherwise possible; 2) to determine the extent to which the treatment's brain imaging and other biomarker effects predict a clinical benefit—

*Correspondence to: Dr. Reiman, Banner Alzheimer's Institute, 901 E. Willetta St., Phoenix, 85006, AZ, USA; Tel.: +602 839 6999; Fax: +602 839 6523; E-mail: eric.reiman@banner health.com.

information needed to help qualify biomarker endpoints for use in pivotal prevention trials; 3) to provide a better test of the amyloid hypothesis than clinical trials in symptomatic patients, when these treatments may be too little too late to exert their most profound effect; 4) to establish AD prevention registries needed to support these and other presymptomatic AD trials; and 5) to give those individuals at highest imminent risk of AD symptoms access to the most promising investigational treatments in clinical trials.

INTRODUCTION

In this article, we note the urgent need to find effective presymptomatic Alzheimer's disease (AD) treatments, which we define as an intervention intended to postpone the onset, reduce the risk of, or completely prevent AD symptoms. We suggest that the greatest roadblock to the development of effective presymptomatic treatments may be the scientific means and financial incentives needed to evaluate the range of promising treatments. We briefly summarize relevant findings from our longitudinal study of cognitively normal people at three levels of risk for late-onset AD, which led us to propose how brain imaging and other biomarkers could be used to rapidly evaluate presymptomatic treatments in proof-of-concept clinical trials. We note the need for humility when it comes to predicting how these biomarkers will respond to AD-slowing treatments in clinical trials and point out that regulatory agencies are unlikely to approve a presymptomatic treatment based solely on biomarker endpoints until evidence is provided to show that a presymptomatic treatment's biomarker effects are reasonably likely to predict a clinical benefit. Finally, we describe our Alzheimer's Prevention Initiative (API), in which we intend to evaluate investigational amyloid-modifying treatments in cognitively normal people who, based on their age and genetic background, are at the highest imminent risk for symptomatic AD. The API is intended to evaluate treatments sooner than otherwise possible, to provide a better test of the amyloid hypothesis, to provide the evidence needed to show that an AD-modifying treatment's biomarker effects are reasonably likely to predict a clinical benefit, and give individuals at the highest imminent risk of symptomatic AD access to promising treatments in prevention trials.

"PRESYMPTOMATIC (OR PRECLINICAL) AD TREATMENTS:" A PROPOSED DEFINITION

We have recently defined *presymptomatic* (or *preclinical*) *AD treatments*" as those interventions that are initiated before apparent cognitive decline and are intended to reduce the chance of developing AD-related symptoms [1]. The proposed term refers to an intervention whether it is started before or after biological evidence of the underlying disease (which may be hard to define), and whether it postpones the onset, partially reduces the risk of, or completely prevents symptomatic AD. We have introduced this term based on the United States Food and Drug Administration's (FDA's) stated view that it would not approve a treatment for the "prevention" of AD unless trials were able to demonstrate that a treatment prevented the onset of symptoms for the rest of a person's life, an impractically high hurdle to overcome. We believe that it will be easier to show that an intervention meets our proposed criterion as a presymptomatic or preclinical AD treatment and support regulatory agency approval. Our definition is also consistent with the research criteria for "preclinical AD treatment" recently proposed by a working group for the National Institute on Aging (NIA) and Alzheimer's Association [2].

BACKGROUND

Alzheimer's disease is an unacceptable problem due to the toll it takes on patients and family caregivers, and the current and project financial impact on society [3, 4]. A large number of healthy lifestyle interventions have been suggested but not yet proven to postpone the onset and reduce risk the risk of developing AD symptoms [5–12]. An even modestly effective

therapy could have a significant public health benefit. For instance, a treatment that postponed the onset of AD symptoms by only five years without increasing life-expectancy might be able to reduce the number of clinically affected patients by half [4]. Meantime, a growing number of investigational disease-modifying treatments are in preclinical and clinical development [13], including but not limited to a large number of medication and immunization therapies intended to interfere with the production and accumulation of certain amyloid-β (Aβ) species. If, as many but not all researchers believe, the amyloid hypothesis is correct [14], if the treatment is targeting the Aβ species critically involved in the predisposition to symptomatic AD, if it is sufficiently safe and well tolerated, and if it is started sufficiently early, it might be possible to substantially reduce the risk of symptomatic AD and maybe even prevent it completely.

Unfortunately, it takes too many healthy people, too much money, and too many years—longer than a drug product's patent life—to evaluate presymptomatic treatments using clinical endpoints. For instance, in order to determine whether cholesterol-lowering, blood pressure-lowering or hormonal treatments reduced the risk of symptomatic AD if they were started in middle-age, when epidemiological studies suggest that they may have their most profound effect, nearly 50,000 healthy middle-aged research participants would be needed for a two-year placebo-controlled randomized clinical trial (RCT), such that a sufficient number of people developed symptomatic AD to detect a significant treatment effect. While there have been a small number of large, time-consuming prevention trials in older people [15–18], a new paradigm is needed to evaluate the range of presymptomatic treatments.

We believe that brain imaging or other biomarker measurements of AD are needed to rapidly evaluate presymptomatic treatments without having to study thousands of healthy volunteers or wait many years to characterize and compare clinical endpoints in the investigational and placebo treatment groups. Brain imaging and other biomarker methods continue to be further developed and used to detect and track changes associated with the clinical progression of AD, and several of these methods have been used to detect and track similar changes in the presymptomatic stages of AD [19–34]. Based on findings from the AD Neuroimaging Initiative (ADNI) and other longitudinal studies, researchers have established standardized procedures for the acquisition of brain imaging data and biological samples, to provide common data sets that have helped researchers further develop, test and compare their data analysis methods, and to provide sample size estimates for the use of biomarker endpoints and enrichment strategies for clinical trials, particularly in patients in the symptomatic stages of AD [35]. To date, the best established biomarkers of AD are fluorodeoxyglucose positron emission tomography (FDG PET) measurements of decline in the regional cerebral metabolic rate for glucose (rCMRgl), volumetric magnetic resonance imaging (MRI) measurements of regional or whole brain shrinkage, PET measurements of fibrillar amyloid-β (Aβ) burden, and low cerebrospinal fluid (CSF) $A\beta_{42}$ levels, alone or in combination with high CSF total tau or phospho-tau levels [24, 1].

As noted below, we have suggested that biomarker endpoints could be used in proof-of-concept RCTs to rapidly evaluate presymptomatic treatments in cognitively normal people at increased risk for AD, and we have provided preliminary sample sizes estimates for some of these trials [36, 20]. Unfortunately industry partners are unlikely to provide financial support for these studies until the biomarker endpoints are qualified for use in pivotal trials. While the field needs the scientific means (i.e., biomarker endpoints) to rapidly evaluate presymptomatic treatments, it also needs the right financial incentive (i.e., regulatory agency qualification of the biomarker endpoints for use in the accelerated approval of presymptomatic AD treatments).

Regulatory agencies are unlikely to provide accelerated approval for a presymptomatic treatment based solely on biomarker (i.e., surrogate marker) endpoints without additional evidence to show that a treatment's biomarker effects are "reasonably likely" to predict a clinical benefit [37–41]. We believe that each of the most promising biomarker measurements should be included in clinical trials of AD-modifying treatments in order to show the extent to which an AD-modifying treatment moves the biomarkers, the extent to which the treatment moves the biomarkers in the right direction, and the extent to which a treatment's biomarker effects predict a clinical benefit [24, 1].

Regulatory agencies may require evidence from presympomatic AD trials themselves to demonstrate the presymptomatic AD treatment's biomarker effects are reasonably likely to predict a clinical benefit. On one hand, biomarkers are needed to evaluate presymptomatic treatments in a rapid and cost-effective way.

On the other hand, clinically proven treatments are needed to help qualify biomarkers for use as reasonably likely surrogate endpoints. Among other things, the API is intended to help resolve this apparent catch-22. We propose to characterize and compare the effects of an amyloid-modifying treatment on FDG PET, volumetric MRI, fibrillar amyloid PET and CSF endpoints in cognitively normal people who, based on their age and genetic background, are at the highest imminent risk of symptomatic AD. If, after two years, the treatment fails to move one or more of the biomarkers in the right direction, the Data Safety Monitoring Board (DSMB) would declare futility and the research participants would be eligible to participate in another trial. If, however, the treatment does have the predicted biomarker effects, the trial would be continued long enough to detect an effect on pre-specified cognitive endpoints.

Before we describe the API in more detail, we briefly summarize relevant biomarker and cognitive findings from our ongoing longitudinal study of cognitively normal people with two copies, one copy and no copies of the *apolipoprotein E (APOE) ε4* allele, the major late-onset AD susceptibility gene [42].

PRELIMINARY FINDINGS

In 1994, we initiated a longitudinal brain imaging study of cognitively normal, initially late-middle-aged, cognitively normal *APOE ε4* homozygotes, heterozygotes, and non-carriers, reflecting three levels of genetic risk for late-onset AD, who were initially matched for their gender, age and educational level. Our subjects are followed every two years using FDG PET, volumetric MRI, and a battery of neuropsychological and clinical tests. In the last few years, they have begun to be following using fibrillar amyloid-β (Aβ) PET measurements, additional MRI measurements, and additional cognitive assessments; their DNA has been used to provide genome-wide association data, and they have begun to provide serum and plasma samples for use in ongoing and future analyses; and most recently, some have begun to provide CSF samples.

Of particular relevance to the API, we have demonstrated associations between *APOE ε4* gene dose (i.e., three levels of genetic risk for AD) and a) baseline reductions and longitudinal declines in FDG PET measurements of the regional cerebral metabolic rate for glucose (rCMRgl) [19–22, 43–51], b) longitudinal declines in volumetric MRI measurements of whole brain shrinkage [52–45], c) PET measurements of the magnitude and spatial extent of fibrillar amyloid burden [23], and d) cross-sectional and longitudinal measurements of the decline in long-term verbal memory [55–62]. Based on our findings, we have estimated the number of cognitively normal late-middle-aged *APOE ε4* homozygotes or heterozygotes needed to evaluate presymptomatic AD treatments using the FDG PET, volumetric MRI and cognitive endpoints, and we developed voxel-based image-analysis algorithms with improved power to detect and track AD while addressing the Type I error associated with multiple regional comparisons [36, 63]. Meantime our amyloid PET findings suggest that fibrillar Aβ burden is "on the way up" in cognitively normal *APOE ε4* homozygotes and heterozygotes in their 50 s and 60 s (before fibrillar amyloid levels reaches the plateau observed in symptomatic patients [64]), that it will be possible to evaluate the differential effects of amyloid-modifying treatments in those carriers with more or less fibrillar Aβ (in case a presymptomatic treatment in normal people with significant Aβ burden is too little too late), and that it will be possible to assess the ability of these treatments to slow down further fibrillar Aβ deposition.

THE ALZHEIMER'S PREVENTION INITIATIVE (API)

The API proposes to evaluate investigational amyloid-modifying treatments in healthy people who, based on their age and genetic background, are at the highest imminent risk of developing AD symptoms using brain imaging, cerebrospinal fluid (CSF), and cognitive endpoints [1]. This complements the newly established criteria for preclinical AD [2], as well as other presymptomatic/preclinical AD treatment trials proposed by the Dominantly Inherited Alzheimer's Network (DIAN) [65], the AD Cooperative Study (ADCS), and others [66, 67].

The API has several goals: 1) to evaluate investigational AD-modifying treatments sooner than otherwise possible; 2) to determine the extent to which the treatment's effects on brain imaging and other biomarkers predicts a clinical benefit—information needed to help qualify biomarker endpoints for use in pivotal prevention trials; 3) to provide a better test of the amyloid hypothesis than clinical trials in symptomatic patients, when these treatments may be too little too late to exert their most profound effect; 4) to establish AD

prevention registries needed to support these and other presymptomatic AD trials; and 5) to give those individuals at highest imminent risk of AD symptoms access to the most promising investigational treatments in clinical trials.

In one trial, we propose to study cognitively normal AD-causing *presenilin 1* [PS1] *E280A* mutation carriers, at least 35 years of age (i.e., within 10 years of the carriers' estimated median age at clinical onset), from the world's largest early-onset AD kindred, located in Antioquia, Colombia [1]. This extraordinary kindred, which has been followed for more than 20 years by Dr. Francisco Lopera and his colleagues, and includes about 5,000 people [33, 68–83], with a sufficient number of presymptomatic carriers in the targeted age group to make it possible to relate a treatment's effects on both biomarker and clinical endpoints within 2–5 years. In the proposed trial, *PS1* mutation carriers would be randomized to active treatment or placebo, non-carriers would be assigned to placebo, and genetic test findings would not be disclosed to the family members simply because they are participating in this trial [84]. In the other trial, we propose to study cognitively normal 60–80 year-old *APOE ε4* homozygotes (and possibly heterozygotes), close to their estimated median age of clinical onset [1]. Including heterozygotes would depend on the safety and tolerability data for the chosen treatment, but would allow for both an increase in the available samples and an increase in the generalizablity of our findings [85, 86].

For each subject group, we have proposed to conduct a 24 months double-blind, randomized, placebo-controlled trial using fibrillar amyloid PET, FDG PET, volumetric MRI, CSF, and cognitive endpoints [1]. Biological fluids and other MRI measurements would be used to permit exploratory studies. If after two years, the treatment is not associated with predicted effects on one or more of the biomarkers, the DSMB would declare futility, the trial would be discontinued, and the participants would be eligible to participate in a trial of the next most promising AD-modifying treatment. If, however, the treatment is associated with predicted biomarker effects, the trial would be continued to assess effects on our compound cognitive endpoint.

To support these and other presymptomatic AD trials, we plan to establish two AD prevention registries. We aim to enroll 2,000 members of the *PS1 E280A* kindred (along with DNA samples, *PS1 E280A* mutation testing and baseline cognitive assessments), about one-third of whom are projected to be mutation carri-

ers, into the Colombian Registry by 2012. We aim to enroll several hundred thousand individuals in the US-based Alzheimer's Prevention Registry, some of whom will be invited to provide saliva samples for DNA acquisition and *APOE* screening. In anticipation of the Colombian trial, we have begun to acquire and analyze brain imaging and CSF samples in the *PS1* mutation carriers and non-carriers, a cyclotron/radiochemistry facility is being installed, and we have used data from the ongoing longitudinal study to estimate the sample sizes needed to detect a clinical effect using a composite cognitive endpoint.

While we believe that there is an opportunity to advance the evaluation of presymptomatic AD treatments, there is a responsibility to get it right. In October 2009, we hosted a meeting of 40 scientific advisors to get their input and help us to refine our proposal. In January 2010, we hosted a meeting with industry representatives to get their input and further refine our proposal [86]. In January 2011, we again met with industry representatives, academic advisors, and FDA and European Medicines Agency (EMA) officials, who provided thoughtful and encouraging feedback [85]. We have been communicating with pharmaceutical company leaders to explore their interest, the availability and timing of the most promising amyloid-modifying treatments, and to explore the scientific and logistical issues needed to prepare for our proposed trials. Selection of the drug will be made with the assistance of an independent academic advisory board, input from the affected kindred regarding potential benefits versus known adverse effects and previous use in human subjects, and will depend on factors such as target engagement, preclinical and clinical safety and tolerability data, dosing information, availability of the drug product, and in-kind industry support. We have proposed a mix of industry, philanthropic and federal funding, and we have indicated our intent to release the data to the public after the study is completed to help advance the use of biomarker and cognitive enrichment strategies and endpoints in future presymptomatic AD trials.

The proposed API treatment trials will help further develop the biomarker endpoints needed to evaluate a range of presymptomatic AD treatments, and will provide critically needed evidence to support the use of biomarker endpoints in the accelerated approval of presymptomatic AD treatments (i.e., to suggest that a treatment's biomarker effects may be reasonably likely to predict a clinical benefit in these or other populations). We believe that by helping to determine the extent to which the best established brain imaging and

CSF biomarkers of AD budge in response to treatment, the extent to which they move in the predicted direction, and the extent to which the treatment's biomarker effects are associated with subsequent clinical benefit will help provide regulatory agencies the evidence they need to begin to consider approving presymptomatic treatments solely on biomarker endpoints in future trials. Moreover, these presymptomatic treatment trials will not only provide a better test of the amyloid hypothesis than clinical trials using the same treatment in symptomatic AD patient, but will also provide research participants at the highest imminent risk of symptomatic AD access to the most promising and suitable investigational treatments sooner than otherwise possible.

ACKNOWLEDGMENTS

REFERENCES

[1] Reiman EM, Langbaum JBS, Tariot PN (2010) Alzheimer's Prevention Initiative: a proposal to evaluate presymptomatic treatments as quickly as possible. *Biomark Med* **4**, 3-14.

[2] Sperling RA, Aisen PS, Beckett LA, Bennett DA, Craft S, Fagan AM, Iwatsubo T, Jack CR, Kaye J, Montine TJ, Park DC, Reiman EM, Rowe CC, Siemers E, Stern Y, Yaffe K, Carrillo MC, Thies B, Morrison-Bogorad M, Wagster MV, Phelps CH (2011) Toward defining the preclinical stages of Alzheimer's disease: recommendations from the national institute on aging and the Alzheimer's association workgroup. *Alzheimers Dement* **7**, 280-292.

[3] Alzheimer's Association (2011) Alzheimer's disease facts and figures. *Alzheimers Dement* **7**, 208-244

[4] Brookmeyer R, Gray S, Kawas C (1998) Projections of Alzheimer's disease in the United States and the public health impact of delaying disease onset. *Am J Public Health* **88**, 1337-1342.

[5] Lautenschlager NT, Cox KL, Flicker L, Foster JK, van Bockxmeer FM, Xiao J, Greenop KR, Almeida OP (2008) Effect of physical activity on cognitive function in older adults at risk for Alzheimer disease: a randomized trial. *JAMA* **300**, 1027-1037.

[6] Wang HX, Karp A, Winblad B, Fratiglioni L (2002) Late-life engagement in social and leisure activities is associated with a decreased risk of dementia: a longitudinal study from the Kungsholmen project. *Am J Epidemiol* **155**, 1081-1087.

[7] Scarmeas N, Luchsinger JA, Schupf N, Brickman AM, Cosentino S, Tang MX, Stern Y (2009) Physical activity, diet, and risk of Alzheimer disease. *JAMA* **302**, 627-637.

[8] Haag MDM, Hofman A, Koudstaal PJ, Stricker BHC, Breteler MMB (2009) Statins are associated with a reduced risk of Alzheimer disease regardless of lipophilicity. *The Rotterdam Study. J Neurol Neurosurg Psychiatry* **80**, 13-17.

[9] Peila R, White LR, Masaki K, Petrovitch H, Launer LJ (2006) Reducing the risk of dementia: efficacy of long-term treatment of hypertension. *Stroke* **37**, 1165-1170.

[10] Szekely CA, Green RC, Breitner JCS, Ostbye T, Beiser AS, Corrada MM, Dodge HH, Ganguli M, Kawas CH, Kuller LH, Psaty BM, Resnick SM, Wolf PA, Zonderman AB, Welsh-Bohmer KA, Zandi PP (2008) No advantage of Aβ42-lowering NSAIDs for prevention of Alzheimer dementia in six pooled cohort studies. *Neurology* **70**, 2291-2298.

[11] Zandi PP, Anthony JC, Khachaturian AS, Stone SV, Gustafson D, Tschanz JT, Norton MC, Welsh-Bohmer KA, Breitner JC (2004) Reduced risk of Alzheimer disease in users of antioxidant vitamin supplements: the cache county study. *Arch Neurol* **61**, 82-88.

[12] Ball K, Berch DB, Helmers KF, Jobe JB, Leveck MD, Marsiske M, Morris JN, Rebok GW, Smith DM, Tennstedt SL, Unverzagt FW, Willis SL (2002) Effects of cognitive training interventions with older adults: a randomized controlled trial. *JAMA* **288**, 2271-2281.

[13] Kramp VP, Herrling P (2011) List of drugs in development for neurodegenerative diseases: update June 2010. *Neurodegener Dis* **8**, 44-94.

[14] Hardy J, Selkoe DJ (2002) The amyloid hypothesis of Alzheimer's disease: progress and problems on the road to therapeutics. *Science* **297**, 353-356.

[15] DeKosky ST, Williamson JD, Fitzpatrick AL, Kronmal RA, Ives DG, Saxton JA, Lopez OL, Burke G, Carlson MC, Fried LP, Kuller LH, Robbins JA, Tracy RP, Woolard NF, Dunn L, Snitz BE, Nahin RL, Furberg CD (2008) For the ginkgo evaluation of memory (GEM) study investigators, Ginkgo biloba for prevention of dementia: a randomized controlled trial. *JAMA* **300**, 2253-2262.

[16] ADAPT Research Group (2008) Cognitive function over time in the Alzheimer's Disease Anti-Inflammatory Prevention Trial (ADAPT): results of a randomized, controlled trial of naproxen and celecoxib. *Arch Neurol* **65**, 896-905.

[17] Shumaker SA, Legault C, Rapp SR, Thal L, Wallace RB, Ockene JK, Hendrix SL, Jones BN, III, Assaf AR, Jackson RD, Kotchen JM, Wassertheil-Smoller S, Wactawski-Wende J (2003) Estrogen plus progestin and the incidence of dementia and mild cognitive impairment in postmenopausal women: the women's health initiative memory study: a randomized controlled trial. *JAMA* **289**, 2651-2662.

[18] Shumaker SA, Legault C, Kuller L, Rapp SR, Thal L, Lane DS, Fillit H, Stefanick ML, Hendrix SL, Lewis CE, Masaki K, Coker LH (2004) Conjugated equine estrogens and incidence of probable dementia and mild cognitive impairment in postmenopausal women: women's health initiative memory study. *JAMA* **291**, 2947-2958.

[19] Reiman EM, Caselli RJ, Yun LS, Chen K, Bandy D, Minoshima S, Thibodeau SN, Osborne D (1996) Preclinical evidence of Alzheimer's disease in persons homozygous for the ε4 allele for apolipoprotein E. *N Engl J Med* **334**, 752-758.

[20] Reiman EM, Caselli RJ, Chen K, Alexander GE, Bandy D, Frost J (2001) Declining brain activity in cognitively normal apolipoprotein E ε4 heterozygotes: A foundation for using

positron emission tomography to efficiently test treatments to prevent Alzheimer's disease. *Proc Natl Acad Sci U S A* **98**, 3334-3339.

[21] Reiman EM, Chen K, Alexander GE, Caselli RJ, Bandy D, Osborne D, Saunders AM, Hardy J (2004) Functional brain abnormalities in young adults at genetic risk for late-onset Alzheimer's dementia. *Proc Natl Acad Sci U S A* **101**, 284-289.

[22] Reiman EM, Chen K, Alexander GE, Caselli RJ, Bandy D, Osborne D, Saunders AM, Hardy J (2005) Correlations between apolipoprotein E ε4 gene dose and brain-imaging measurements of regional hypometabolism. *Proc Natl Acad Sci U S A* **102**, 8299-8302.

[23] Reiman EM, Chen K, Liu X, Bandy D, Yu M, Lee W, Ayutyanont N, Keppler J, Reeder SA, Langbaum JBS, Alexander GE, Klunk WE, Mathis CA, Price JC, Aizenstein HJ, DeKosky ST, Caselli RJ (2009) Fibrillar amyloid-β burden in cognitively normal people at three levels of genetic risk for Alzheimer's disease. *Proc Natl Acad Sci U S A* **106**, 6820-6825.

[24] Reiman EM, Langbaum JBS (2009) Brain imaging in the evaluation of putative Alzheimer's disease slowing, risk-reducing and prevention therapies. In: *Imaging the Aging Brain*. Jagust WJ, D'Esposito M (Eds.). Oxford University Press, New York, pp. 319-350.

[25] Fox NC, Warrington EK, Freeborough PA, Hartikainen P, Kennedy AM, Stevens JM, Rossor MN (1996) Presymptomatic hippocampal atrophy in Alzheimer's disease. *A longitudinal MRI study. Brain* **119**, 2001-2007.

[26] Mosconi L, Sorbi S, de Leon MJ, Li Y, Nacmias B, Myoung PS, Tsui W, Ginestroni A, Bessi V, Fayyazz M, Caffarra P, Pupi A (2006) Hypometabolism exceeds atrophy in presymptomatic early-onset familial Alzheimer's disease. *J Nucl Med* **47**, 1778-1786.

[27] Bookheimer SY, Strojwas MH, Cohen MS, Saunders AM, Pericak-Vance MA, Mazziotta JC, Small GW (2000) Patterns of brain activation in people at risk for Alzheimer's disease. *N Engl J Med* **343**, 450-456.

[28] Burggren AC, Zeineh MM, Ekstrom AD, Braskie MN, Thompson PM, Small GW, Bookheimer SY (2008) Reduced cortical thickness in hippocampal subregions among cognitively normal apolipoprotein E ε4 carriers. *Neuroimage* **41**, 1177-1183.

[29] Small GW, Mazziotta JC, Collins MT, Baxter LR, Phelps ME, Mandelkern MA, Kaplan A, La Rue A, Adamson CF, Chang L (1995) Apolipoprotein E type 4 allele and cerebral glucose metabolism in relatives at risk for familial Alzheimer disease. *JAMA* **273**, 942-947.

[30] Small GW, Ercoli LM, Silverman DH, Huang SC, Komo S, Bookheimer SY, Lavretsky H, Miller K, Siddarth P, Rasgon NL, Mazziotta JC, Saxena S, Wu HM, Mega MS, Cummings JL, Saunders AM, Pericak-Vance MA, Roses AD, Barrio JR, Phelps ME (2000) Cerebral metabolic and cognitive decline in persons at genetic risk for Alzheimer's disease. *Proc Natl Acad Sci U S A* **97**, 6037-6042.

[31] Small GW, Komo S, La RA, Saxena S, Phelps ME, Mazziotta JC, Saunders AM, Haines JL, Pericak-Vance MA, Roses AD (1996) Early detection of Alzheimer's disease by combining apolipoprotein E and neuroimaging. *Ann N Y Acad Sci* **802**, 70-78.

[32] Fagan AM, Roe CM, Xiong C, Mintun MA, Morris JC, Holtzman DM (2007) Cerebrospinal fluid tau/β-amyloid42 ratio as a prediction of cognitive decline in nondemented older adults. *Arch Neurol* **64**, 343-349.

[33] Johnson KA, Lopera F, Jones K, Becker A, Sperling R, Hilson J, Londono J, Siegert I, Arcos M, Moreno S, Madrigal L, Ossa J, Pineda N, Ardila A, Roselli M, Albert MS, Kosik KS, Rios A (2001) Presenilin-1-associated abnormalities in regional cerebral perfusion. *Neurology* **56**, 1545-1551.

[34] Valla J, Yaari R, Wolf AB, Kusne Y, Beach TG, Roher AE, Corneveaux JJ, Huentelman MJ, Caselli RJ, Reiman EM (2010) Reduced posterior cingulate mitochondrial activity in expired young adult carriers of the APOE epsilon4 allele, the major late-onset Alzheimer's susceptibility gene. *J Alzheimers Dis* **22**, 307-313.

[35] Beckett LA, Harvey DJ, Gamst A, Donohue M, Kornak J, Zhang H, Kuo JH (2010) The Alzheimer's Disease Neuroimaging Initiative: annual change in biomarkers and clinical outcomes. *Alzheimers Dement* **6**, 257-264.

[36] Chen K, Langbaum JBS, Fleisher AS, Ayutyanont N, Reschke C, Lee W, Liu X, Bandy D, Alexander GE, Thompson PM, Foster NL, Harvey DJ, de Leon MJ, Koeppe RA, Jagust WJ, Weiner MW, Reiman EM (2010) The Alzheimer's Disease Neuroimaging, Initiative Twelve-month metabolic declines in probable Alzheimer's disease and amnestic mild cognitive impairment assessed using an empirically pre-defined statistical region-of-interest: Findings from the Alzheimer's disease neuroimaging initiative. *Neuroimage* **51**, 654-664.

[37] Prentice RL (1989) Surrogate endpoints in clinical trials: definition and operational criteria. *Stat Med* **8**, 431-440.

[38] Fleming TR, DeMets DL (1996) Surrogate end points in clinical trials: are we being misled? *Ann Intern Med* **125**, 605-613.

[39] Biomarkers Definitions Working, Group (2001) Biomarkers and surrogate endpoints: preferred definitions and conceptual framework. *Clin Pharmacol Ther* **69**, 89-95.

[40] Katz R (2004) Biomarkers and surrogate markers: an FDA perspective. *NeuroRx* **1**, 189-195.

[41] Broich K (2007) Outcome measures in clinical trials on medicinal products for the treatment of dementia: a European regulatory perspective. *Int Psychogeriatr* **19**, 509-524.

[42] Corder EH, Saunders AM, Strittmatter WJ, Schmechel DE, Gaskell PC, Small GW, Roses AD, Haines JL, Pericak-Vance MA (1993) Gene dose of apolipoprotein E type 4 allele and the risk of Alzheimer's disease in late onset families. *Science* **261**, 921-923.

[43] Langbaum JB, Chen K, Caselli RJ, Lee W, Reschke C, Bandy D, Alexander GE, Burns CM, Kaszniak AW, Reeder SA, Corneveaux JJ, Allen AN, Pruzin J, Huentelman MJ, Fleisher AS, Reiman EM (2010) Hypometabolism in Alzheimer-affected brain regions in cognitively healthy Latino individuals carrying the apolipoprotein E epsilon4 allele. *Arch Neurol* **67**, 462-468.

[44] Reiman EM, Caselli RJ, Alexander GE, Chen K (2001) Tracking the decline in cerebral glucose metablolism in persons and laboratory animals at genetic risk for Alzheimer's disease. *Clin Neurosci Res* **1**, 194-206.

[45] Chen K, Reiman EM, Alexander GE, Caselli RJ, Bandy D (2006) Using partial-least squares to demonstrate a correlation between combined PET/MRI scores and apolipoprotein E ε4 gene dose. *Alzheimers Dement* **2**, S672-S673

[46] Chen K, Reiman EM, Huan Z, Caselli RJ, Bandy D, Ayutyanont N, Alexander GE (2009) Linking functional and structural brain images with multivariate network analyses: A novel application of the partial least square method. *Neuroimage* **47**, 602-610.

[47] Corneveaux JJ, Liang WS, Reiman EM, Webster JA, Myers AJ, Zismann VL, Joshipura KD, Pearson JV, Hu-Lince D,

Craig DW, Coon KD, Dunckley T, Bandy D, Lee W, Chen K, Beach TG, Mastroeni D, Grover A, Ravid R, Sando SB, Aasly JO, Heun R, Jessen F, Kolsch H, Rogers J, Hutton ML, Melquist S, Petersen RC, Alexander GE, Caselli RJ, Papassotiropoulos A, Stephan DA, Huentelman MJ (2010) Evidence for an association between KIBRA and late-onset Alzheimer's disease. *Neurobiol Aging* **31**, 901-909.

[48] Reiman EM, Webster JA, Myers AJ, Hardy J, Dunckley T, Zismann VL, Joshipura KD, Pearson JV, Hu-Lince D, Huentelman MJ, Craig DW, Coon KD, Liang WS, Herbert RH, Beach T, Rohrer KC, Zhao AS, Leung D, Bryden L, Marlowe L, Kaleem M, Mastroeni D, Grover A, Heward CB, Ravid R, Rogers J, Hutton ML, Melquist S, Petersen RC, Alexander GE, Caselli RJ, Kukull W, Papassotiropoulos A, Stephan DA (2007) GAB2 alleles modify Alzheimer's risk in APOE ε4 carriers. *Neuron* **54**, 713-720.

[49] Liang WS, Chen K, Lee W, Sidhar K, Corneveaux JJ, Allen AN, Myers A, Villa S, Meechoovet B, Pruzin J, Bandy D, Fleisher AS, Langbaum JB, Huentelman MJ, Jensen K, Dunckley T, Caselli RJ, Kaib S, Reiman EM (2011) Association between GAB2 haplotype and higher glucose metabolism in Alzheimer's disease-affected brain regions in cognitively normal APOEepsilon4 carriers. *Neuroimage* **54**, 1896-1902.

[50] Reiman EM, Chen K, Caselli RJ, Alexander GE, Bandy D, Adamson JL, Lee W, Cannon A, Stephan EA, Stephan DA, Papassotiropoulos A (2008) Cholesterol-related genetic risk scores are associated with hypometabolism in Alzheimer's-affected brain regions. *Neuroimage* **40**, 1214-1221.

[51] Reiman EM, Chen K, Langbaum JB, Lee W, Reschke C, Bandy D, Alexander GE, Caselli RJ (2010) Higher serum total cholesterol levels in late middle age are associated with glucose hypometabolism in brain regions affected by Alzheimer's disease and normal aging. *Neuroimage* **49**, 169-176.

[52] Alexander GE, Chen K, Reiman EM, Caselli RJ, Lewis D, Bandy D, Prouty A (2002) Longitudinal declines of gray matter in cognitively normal apolipoprotein E ε4 homozygotes and heterozygotes evaluated by voxel-based MRI morphometry. *Neurobiol Aging* **23**, s363.

[53] Chen K, Reiman EM, Alexander GE, Caselli RJ, Gerkin R, Bandy D, Domb A, Osborne D, Fox N, Crum WR, Saunders AM, Hardy J (2007) Correlations between apolipoprotein E ε4 gene dose and whole brain atrophy rates. *Am. J Psychiatry* **164**, 916-921.

[54] Chen K, Reiman EM, Alexander GE, Bandy D, Renaut R, Crum WR, Fox NC, Rossor MN (2004) An automated algorithm for the computation of brain volume change from sequential MRIs using an iterative principal component analysis and its evaluation for the assessment of whole-brain atrophy rates in patients with probable Alzheimer's disease. *Neuroimage* **22**, 134-143.

[55] Caselli RJ, Hentz JG, Osborne D, Snyder CH, Alexander GE, Reiman EM (2006) Presymptomatic longitudinal decline in frontally mediated cognitive skills and memory in cognitively normal late middle aged APOE ε4 carriers. *Alzheimers Dement* **2**, S292.

[56] Caselli RJ, Reiman EM, Osborne D, Hentz JG, Baxter LC, Hernandez JL, Alexander GG (2004) Longitudinal changes in cognition and behavior in asymptomatic carriers of the APOE ε4 allele. *Neurology* **62**, 1990-1995.

[57] Caselli RJ, Osborne D, Reiman EM, Hentz JG, Barbieri CJ, Saunders AM, Hardy J, Graff-Radford NR, Hall GR, Alexander GE (2001) Preclinical cognitive decline in late

middle-aged asymptomatic apolipoprotein E-ε4/4 homozygotes: a replication study. *J Neurol Sci* **189**, 93-98.

[58] Caselli RJ, Graff-Radford NR, Reiman EM, Weaver A, Osborne D, Lucas J, Uecker A, Thibodeau SN (1999) Preclinical memory decline in cognitively normal apolipoprotein E-ε4 homozygotes. *Neurology* **53**, 201-207.

[59] Caselli RJ, Reiman EM, Locke DE, Hutton ML, Hentz JG, Hoffman-Snyder C, Woodruff BK, Alexander GE, Osborne D (2007) Cognitive domain decline in healthy Apolipoprotein E ε4 homozygotes before the diagnosis of Mild Cognitive Impairment. *Arch Neurol* **64**, 1306-1311.

[60] Caselli RJ, Chen K, Lee W, Alexander GE, Reiman EM (2008) Correlating cerebral hypometabolism with future memory decline in subsequent converters to amnestic pre-mild cognitive impairment. *Arch Neurol* **65**, 1231-1236.

[61] Caselli RJ, Dueck AC, Osborne D, Sabbagh MN, Connor DJ, Ahern GL, Baxter LC, Rapcsak SZ, Shi J, Woodruff BK, Locke DEC, Hoffman-Snyder C, Alexander GE, Rademakers R, Reiman EM (2009) Longitudinal modeling of age-related memory decline and the APOE ε4 effect. *N Engl J Med* **361**, 255-263.

[62] Caselli RJ, Dueck AC, Locke DE, Sabbagh MN, Ahern GL, Rapcsak SZ, Baxter LC, Yaari R, Woodruff BK, Hoffman-Snyder C, Rademakers R, Findley S, Reiman EM (2011) Cerebrovascular risk factors and preclinical memory decline in healthy APOE ε4 homozygotes. *Neurology* **76**, 1078-1084.

[63] Chen K, Ayutyanont N, Langbaum JBS, Fleisher AS, Reschke C, Lee W, Liu X, Bandy D, Alexander GE, Thompson PM, Shaw L, Trojanowski JQ, Jack CR Jr, Landau SM, Foster NL, Harvey DJ, Weiner MW, Koeppe RA, Jagust WJ, Reiman EM (2011) Alzheimer's Disease Neuroimaging Initiative. Characterizing Alzheimer's disease using a hypometabolic convergence index. *Neuroimage* **56**, 52-60.

[64] Klunk WE, Mathis CA, Price JC, Lopresti BJ, DeKosky ST (2006) Two-year follow-up of amyloid deposition in patients with Alzheimer's disease. *Brain* **129**, 2805-2807.

[65] Bateman RJ, Aisen PS, De Strooper B, Fox NC, Lemere CA, Ringman JM, Salloway S, Sperling RA, Windisch M, Xiong C (2011) Autosomal-dominant Alzheimer's disease: a review and proposal for the prevention of Alzheimer's disease. *Alzheimers Res. Ther* **3**, 1.

[66] Aisen PS, Andrieu S, Sampaio C, Carrillo M, Khachaturian ZS, Dubois B, Feldman HH, Petersen RC, Siemers E, Doody RS, Hendrix SB, Grundman M, Schneider LS, Schindler RJ, Salmon E, Potter WZ, Thomas RG, Salmon D, Donohue M, Bednar MM, Touchon J, Vellas B (2011) Report of the task force on designing clinical trials in early (predementia) AD. *Neurology* **76**, 280-286.

[67] Khachaturian ZS, Barnes D, Einstein R, Johnson S, Lee V, Roses A, Sager MA, Shankle WR, Snyder PJ, Petersen RC, Schellenberg G, Trojanowski J, Aisen P, Albert MS, Breitner JCS, Buckholtz N, Carrillo M, Ferris S, Greenberg BD, Grundman M, Khachaturian AS, Kuller LH, Lopez OL, Maruff P, Mohs RC, Morrison-Bogorad M, Phelps C, Reiman E, Sabbagh M, Sano M, Schneider LS, Siemers E, Tariot P, Touchon J, Vellas B, Bain LJ (2010) Developing a national strategy to prevent dementia: Leon Thal Symposium 2009. *Alzheimers Dement* **6**, 89-97.

[68] Acosta-Baena N, Sepulveda-Falla D, Lopera-Gomez CM, Jaramillo-Elorza MC, Moreno S, Aguirre-Acevedo DC, Saldarriaga A, Lopera F (2011) Pre-dementia clinical stages in presenilin 1 E280A familial early-onset Alzheimer's disease: a retrospective cohort study. *Lancet Neurol* **10**, 213-220.

[69] Arango-Lasprilla JC, Cuetos F, Valencia C, Uribe C, Lopera F (2007) Cognitive changes in the preclinical phase of familial Alzheimer's disease. *J Clin Exp Neuropsychol* **29**, 892-900.

[70] Arango Lasprilla JC, Iglesias J, Lopera F (2003) Neuropsychological study of familial Alzheimer's disease caused by mutation E280A in the presenilin 1 gene. *Am J Alzheimers Dis Other Demen* **18**, 137-146.

[71] Ardila A, Lopera F, Rosselli M, Moreno S, Madrigal L, Arango-Lasprilla JC, Arcos M, Murcia C, Arango-Viana JC, Ossa J, Goate A, Kosik KS (2000) Neuropsychological profile of a large kindred with familial Alzheimer's disease caused by the E280A single presenilin-1 mutation. *Arch Clin Neuropsychol* **15**, 515-528.

[72] Lopera F, Ardilla A, Martinez A, Madrigal L, Arango-Viana JC, Lemere CA, Arango-Lasprilla JC, Hincapie L, Arcos-Burgos M, Ossa JE, Behrens IM, Norton J, Lendon C, Goate AM, Ruiz-Linares A, Rosselli M, Kosik KS (1997) Clinical features of early-onset Alzheimer disease in a large kindred with an E280A presenilin-1 mutation. *JAMA* **277**, 793-799.

[73] Rosselli MC, Ardila AC, Moreno SC, Standish VC, Arango-Lasprilla JC, Tirado VM, Ossa JM, Goate AM, Kosik KS, Lopera F (2000) Cognitive decline in patients with familial Alzheimer's disease associated with E280a presenilin-1 mutation: a longitudinal study. *J Clin Exp Neuropsychol* **22**, 483-495.

[74] Quiroz YT, Budson AE, Celone K, Ruiz A, Newmark R, Castrillon G, Lopera F, Stern CE (2010) Hippocampal hyperactivation in presymptomatic familial Alzheimer's disease. *Ann Neurol* **68**, 865-875.

[75] Bobes MA, Garcia YF, Lopera F, Quiroz YT, Galan L, Vega M, Trujillo N, Valdes-Sosa M, Valdes-Sosa P (2010) ERP generator anomalies in presymptomatic carriers of the Alzheimer's disease E280A PS-1 mutation. *Hum Brain Mapp* **31**, 247-265.

[76] Cuetos F, Arango-Lasprilla JC, Uribe C, Valencia C, Lopera F (2007) Linguistic changes in verbal expression: a preclinical marker of Alzheimer's disease. *J Int Neuropsychol Soc* **13**, 433-439.

[77] Dorfman VB, Pasquini L, Riudavets M, Lopez-Costa JJ, Villegas A, Troncoso JC, Lopera F, Castano EM, Morelli L (2010) Differential cerebral deposition of IDE and NEP in sporadic and familial Alzheimer's disease. *Neurobiol Aging* **31**, 1743-1757.

[78] Gomez-Isla T, Growdon WB, McNamara MJ, Nochlin D, Bird TD, Arango JC, Lopera F, Kosik KS, Lantos PL, Cairns NJ, Hyman BT (1999) The impact of different presenilin 1 and-presenilin 2 mutations on amyloid deposition, neurofibrillary changes and neuronal loss in the familial Alzheimer's disease brain: evidence for other phenotype-modifying factors. *Brain* **122 (Pt 9)**, 1709-1719.

[79] Lemere CA, Lopera F, Kosik KS, Lendon CL, Ossa J, Saido TC, Yamaguchi H, Ruiz A, Martinez A, Madrigal L, Hincapie L, Arango JC, Anthony DC, Koo EH, Goate AM, Selkoe DJ, Arango JC (1996) The E280A presenilin 1 Alzheimer mutation produces increased A beta 42 deposition and severe cerebellar pathology. *Nat Med* **2**, 1146-1150.

[80] Lendon CL, Martinez A, Behrens IM, Kosik KS, Madrigal L, Norton J, Neuman R, Myers A, Busfield F, Wragg M, Arcos M, Arango Viana JC, Ossa J, Ruiz A, Goate AM, Lopera F (1997) E280A PS-1 mutation causes Alzheimer's disease but age of onset is not modified by ApoE alleles. *Hum Mutat* **10**, 186-195.

[81] Mejia S, Giraldo M, Pineda D, Ardila A, Lopera F (2003) Nongenetic factors as modifiers of the age of onset of familial Alzheimer's disease. *Int Psychogeriatr* **15**, 337-349.

[82] Parra MA, Sala SD, Abrahams S, Logie RH, Mendez LG, Lopera F (2011) Specific deficit of colour-colour short-term memory binding in sporadic and familial Alzheimer's disease. *Neuropsychologia*. doi:10.1016/j.neuropsychologia.2011.03.022

[83] Parra MA, Abrahams S, Logie RH, Mendez LG, Lopera F, Della SS (2010) Visual short-term memory binding deficits in familial Alzheimer's disease. *Brain* **133**, 2702-2713.

[84] Kosik KS, Lopera F (2008) Genetic testing must recognize impact of bad news on recipient. *Nature* **454**, 158-159.

[85] Strobel, G. (2011) Alzheimer's Prevention Intiative: a six part series. *Alzheimer Research Forum*, http://www.alzforum.org/new/detail.asp?id=2720, Accessed March 15, 2011.

[86] Strobel, G. (2010) Phoenix: Vision of shared prevention trials lures pharma to table. *Alzheimer Research Forum*, http://www.alzforum.org/new/detail.asp?id=2374, Accessed February 25, 2010

This page intentionally left blank

MR Spectroscopy for Assessment of Memantine Treatment in Mild to Moderate Alzheimer Dementia

J.W. Ashford[a,b,*], M. Adamson[a,b], T. Beale[b], D. La[a], B. Hernandez[b], A. Noda[b], A. Rosen[b,c], R. O'Hara[b,c], J. K. Fairchild[b,c], D. Spielman[b] and J.A. Yesavage[b,c]

[a]*War Related Illness and Injury Study Center, VA Palo Alto Health Care System, Palo Alto, CA, USA*
[b]*Department of Psychiatry and Behavioral Sciences, Stanford University, Stanford, CA, USA*
[c]*Department of Veterans Affairs and Sierra-Pacific MIRECC, Palo Alto, CA, USA*

Abstract. *Objectives:* Magnetic Resonance Spectroscopy (MRS) may provide a precise and reliable assessment of the extent and severity of neural tissue loss caused by various diseases. In particular, the N-Acetyl Aspartate (NAA) and Creatine (Cr) ratio has been found to be an indicator of the degree of neuronal loss in Alzheimer's disease (AD). Memantine is thought to benefit the AD brain by stabilizing the NMDA receptors on neurons in turn reducing excitotoxicity. Despite its effectiveness in treating moderate to severe AD, memantine has not had similar success in the treatment of mildly demented AD patients. The objective of this study was to test whether memantine would slow or prevent the loss of neurons in mild to moderate AD patients. *Methods:* A double-blind placebo-controlled study was designed to measure the effect of a year-long course of memantine in patients with a probable AD diagnosis with mild to moderate dementia. The primary outcome measure was stipulated to be change in MRS NAA/Cr ratio in inferior parietal cortex in memantine relative to the placebo treatment condition. The secondary outcome measures were changes in cognitive and function scale scores. *Results:* This pilot study failed to demonstrate a benefit of memantine on the primary outcome measure, the inferior parietal NAA/Cr ratio, or the secondary outcome measures. *Conclusions:* More studies are needed to determine the effect of memantine on regions of the brain significantly affected by AD pathology.

Keywords: Alzheimer disease, dementia, magnetic resonance spectroscopy, memantine, cognition, N-acetylaspartate, creatine

INTRODUCTION

Cognitive and functional measures are accepted surrogate markers of Alzheimer's disease (AD) severity. However, neuroimaging techniques, such as Magnetic Resonance Spectroscopy (MRS), can provide a more direct, precise, and reliable assessment of AD-related damage to brain tissue [1]. MRS measures neurochemicals, such as N-Acetyl Aspartate (NAA) and Creatine (Cr), and the NAA/Cr ratio reflects neural tissue volume. These neurochemical measurements are indicators of neuronal loss in AD, and clinical diagnosis of AD and frontotemporal lobar degeneration (FTLD) [2–4]. These measurements are additionally used to assess the efficacy of AD medication trials [5, 6] and correlate with the severity of neurofibrillary pathology and fibrillary tau density after death [5, 7].

While cholinesterase inhibitors are the most well established medications in AD treatment, memantine

---

has been effective in the treatment of moderate to severe AD [8]. Memantine works by stabilizing the NMDA receptors in neurons of the cerebrum thus reducing excitotoxicity. Memantine's utility in treating moderate to severe AD has not been consistent in studies of patients with mild AD using standard cognitive and functional measures to assess cognitive decline [9]. However, neuroimaging techniques are a more direct measure of AD pathology, and thus, more likely to demonstrate the effect, if any, that memantine has on the AD pathological progression.

We examined the effect of a year-long course of memantine in patients with a diagnosis of probable AD with mild dementia. Specifically, we hypothesized:

1) Memantine would result in less reduction of the NAA/Cr ratio in mild AD patients taking the drug for one year relative to patients taking placebo.
2) Slowing of the neuronal loss would correspond to a smaller decline in cognitive function in the treatment group.

METHOD

Patients

Mild to moderately demented patients with a probable AD diagnosis and their caregivers were recruited and consented. The Stanford University IRB approved the use of human subjects for this study. The clinical trials database at Stanford University has the records of this study, and this database is linked to "clinicaltrials.gov" with the "unique protocol ID" 95722. Patients had to be in stable health and able to comply with all procedures. Patients were excluded for Parkinson's disease, any MRI contraindications, certain neurologic or psychiatric conditions (e.g., seizures, clinically significant stroke, head trauma, major psychiatric disorder) or other medical or laboratory findings or medications rendering them unsuitable for an investigational trial.

Seventeen patients met screening criteria initially, but four patients were excluded during the treatment phase due to defibrillator implant, eyeliner tattoo, severe medical illness unrelated to the study, and diagnosis change to corticobasilar degeneration. Of the 13 eligible and randomized patients scanned at the baseline and study termination, 7 on memantine, 6 on placebo, 3 patients assigned memantine were eliminated from analysis due to their inability to comply with treatment. Accordingly, 10 patients (4 on meman-

tine, 6 on placebo) completed the study, having the repeat scans an average of 54 weeks after baseline (Table 1).

Study procedures

Patients underwent a medical history review and physical and neurological exam, laboratory tests, and cognitive assessment at the screening visit. Soon after, patients had a baseline evaluation including the MRS scan, symptom review, and neuropsychiatric measures. Patients were randomized to memantine or placebo arms by the un-blinded pharmacist and study medication was dispensed.

To assess possible safety concerns, health status, and medication compliance, brief treatment visits were performed at months 1, 3, 6 and 9 and telephone checks were done six weeks after each visit.

The final visit procedures repeated those done at screening and baseline, including MRS scan, medical and laboratory evaluation, and cognitive and clinical assessment.

MRS

Images were acquired on a 3T Excite GE MRI scanner. On a sagital scout scan, the AC-PC (anterior commissure–posterior commissure) line was determined to position a horizontal scan 1 cm above the AC-PC line. Three spectroscopic data sets were obtained from 2 x 2 x 2 cm voxels in the left cerebral cortex, inferior parietal, posterior cingulate, and occipital (Figure 1 shows the location of inferior parietal region, placed in a far lateral position just behind the insula to maximize inclusion of cortex in the voxel), using a spin-echo series of TR/TE 2000/35 msec with each preselected region of interest for point-resolved spectroscopy (PRESS). Data processing was performed using the fully automated PROBE/SV quantification tool (General Electric Medical System, Milwaukee, WI). During the second scanning session (1 year later) voxel positions were selected with reference to the structural scans from the first data acquisition.

Each of the five spectral areas associated with NAA, Cr, Choline (Cho), myoinositol (mI), and H_2O was quantified by Marquardt Levenworth curve fitting over that line region. Before curve fitting, line widths were normalized, and a Lorentzian-to-Gaussian transformation was performed. Cr was designated as the reference moiety. Data were analyzed as metabolite (NAA, Cho, and mI) to Cr ratio. This convention minimizes errors

Table 1
Descriptive statistics on demographic and cognitive measures at baseline ($n = 13$), and primary (NAA/Cr) and secondary (ADAS-Cog) measures at baseline and year 1 ($n = 10$). Mean $\pm$ sd unless otherwise noted.

		Memantine [1] ($n = 7$)	Placebo ($n = 6$)
Age (years)		76.5 ± 9.6	75.4 ± 6.3
Education (years)		15.4 ± 3.4	13.2 ± 1.7
Gender		14% female	67% female
Race			
White		71%	67%
Asian		29%	33%
Ethnicity			
Hispanic or Latino		14%	0%
Donepezil[2]		7 (86%)	6 (67%)
MMSE[3]		19.9 ± 4.8	21.8 ± 3.1
Verbal Fluency[4]		10.3 ± 6.6	12.2 ± 2.1
ADAS-Cog[5]		41.5 ± 10.2	49.2 ± 8.4
ADL[6]		56.9 ± 16.7	68.2 ± 5.1
NAA/Cr[7]	Time	Memantine ($n = 4$[8])	Placebo ($n = 6$)
	Baseline	1.47 ± 0.11	1.38 ± 0.10
	Year 1	1.62 ± 0.14	1.41 ± 0.10
ADAS-Cog	Baseline	44.67 ± 10.30	49.17 ± 8.37
	Year 1	45.75 ± 7.99	50.39 ± 8.88

[1]Memantine: During the course of the study, subjects were supplied with either memantine tablets or placebo provided by the sponsor (Forest Laboratories). After the screening visit, the pharmacist randomized subjects into one of two groups: Treatment (T; target dose 10mg memantine), or control (C; matching placebo), balancing the order of selection. Subjects were titrated from 5 mg medication or placebo tablets each morning with increments of 5 mg every week to reach 10 mg tablets twice per day at the third week. Subjects and all study staff, except the pharmacist were blind to treatment group.

[2]Subjects were already on donepezil at time of entry into the study.

[3]The Mini Mental State Exam.

[4]Verbal fluency assessed by animal naming in one min.

[5]Alzheimer's Disease Assessment Scale, Cognitive portion, ADAS-Cog [10].

[6]ADL: Activities of Daily Living-ADCS ADL.

[7]NAA/Cr ratio: Scans were obtained on a 3T GE Signa Excite magnet at the Lucas Center of Stanford University. Magnetic resonance spectra were obtained from three voxels, each $2 \times 2 \times 2$ cm, with GE scanning sequence. See Fig. 1 for detail on anatomical location of left inferior parietal lobe reported in this study. Magnetic resonance spectra were initially processed using the GE Signa Excite software, which provided peak measurements for each chemical, including NAA (n-acetyl aspartate), Cr (creatine), and MI (myo-inositol). MRS is able to measure neurochemicals, such as NAA and Cr, and it is this NAA/Cr ratio that has been found to be an indicator of the degree of loss of neural tissue in AD [5].

[8]Three subjects could not tolerate the study medication; two discontinued the study pills entirely and the third took a reduced dose but pill-count monitoring showed subject remained non-compliant with protocol.

arising from changes in magnetic field homogeneity and tissue volume. NAA measurements were additionally examined as NAA/Cho ratios, to test for possible alterations in the Cr peak as an internal reference. Histograms were computed only from the brain image voxels contained in the spectroscopic box. No correction was made for partial volume effects because all patients had at least 95% brain tissue in voxels of interest.

Statistical analysis

The primary efficacy measure was the change from the baseline to the final study visit in the MRS NAA/Cr ratio of the inferior parietal region. The secondary efficacy measure was change from the baseline to the final study visit in the ADAS-cog [10] measure.

Upon completion of the final visit of the last subject and prior to breaking the blind, analyses were conducted on the MRS measures with respect to cognitive/functional measures both in the 13 baseline and 10 final visit scans (see Table 2). Follow-up analyses were done on the 10 patients who completed the study.

RESULTS

Table 1 shows the mean and standard deviations in treatment ($n = 4$) and placebo ($n = 6$) patients at base-
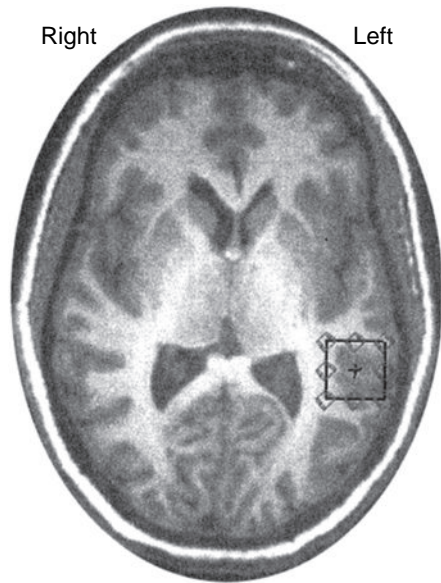
Right   Left

Fig. 1. MRS scans were performed on a 3 Tesla GE Signa Excite magnet. Voxels were 2x2x2 cm, with centers chosen on a plane 1 cm superior to the plane through the anterior-posterior commissure line, and to include as much gray matter as possible and as little CSF as possible. Three voxels were selected in the Left hemisphere, an inferior parietal voxel, placed as far laterally as possible, behind the sylvian sulcus (shown), an occipital voxel, as posterior as possible, just lateral to the inter-hemispheric sulcus, and a posterior-cingulate voxel, anterior to the occipital cortex and behind the corpus callosum, just lateral to the inter-hemispheric sulcus.

line and follow-up for both primary and secondary outcome measures. First, the placebo and treatment groups' inferior parietal region NAA/Cr ratio did not differ significantly at baseline (treatment group $M = 1.47 \pm 0.11$; placebo group $M = 1.38 \pm 0.10$;

$p > .1$) or follow-up (treatment group $M = 1.62 \pm 0.14$; placebo group $M = 1.41 \pm 0.10$; $p = .09$). Second, the two groups' ADAS-cog scores also did not differ significantly at baseline (treatment group $M = 44.67 \pm 10.30$; placebo group $M = 49.17 \pm 8.37$; $p > .1$) or follow up (treatment group $M = 45.75 \pm 7.99$; placebo group $M = 50.39 \pm 8.88$; $p > .1$). As shown in Table 2, baseline NAA/Cr ratio correlated only with verbal fluency (animal naming in one minute) and age. Baseline ADAS-cog, while not correlated with age or baseline NAA/Cr ratio, did show a robust correlation with the Mini-Mental State Exam (MMSE), MMSE-extended [11], verbal fluency, and Activities of Daily Living (ADL) measures.

Over the one year treatment course, change in NAA/Cr ratio was significantly correlated with change in ADAS-cog scores ($p < 0.001$) in all patients that completed the follow-up study ($n = 10$). However, there was no significant benefit for the group treated with memantine relative to the group treated with placebo with respect to either the NAA/Cr ratios or ADAS-cog scores. The change in the memantine group was not significantly different from the change in the placebo group ($p = .09$).

DISCUSSION

This pilot study failed to demonstrate a benefit of memantine on the primary outcome measure, the inferior parietal NAA/Cr ratio, thus not supporting the hypothesis that memantine protects a region of the brain significantly affected by AD pathology. The secondary cognitive and functional measures also did not provide any evidence for benefit from the memantine

Table 2
Correlation Matrix of demographic, MRI and cognitive measures at baseline, $n = 13$

	NAA/Cr	ADAS cog	MMSE	MMSE extended	Verbal fluency	ADAS word recall	ADL	Age	Education	NAA/Cr change	ADAS cog change
NAA/Cr	1.00	0.31	0.44	0.40	0.57*	0.07	0.46	−0.71**	0.10	−0.26	0.04
ADAS-cog		1.00	0.73**	0.82**	0.66*	0.54	0.59*	−0.46	−0.10	0.05	0.07
MMSE			1.00	0.92**	0.30	0.46	0.38	−0.23	0.22	0.18	0.30
MMSE ext				1.00	0.48	0.62*	0.51	−0.36	0.21	0.33	0.37
FAS					1.00	0.29	0.53	−0.60*	−0.12	−0.11	0.03
ADAS-word						1.00	0.39	−0.15	−0.16	0.34	0.42
ADL							1.00	−0.81**	−0.16	0.08	0.29
Age								1.00	0.11	0.14	0.02
Education									1.00	0.50	0.32
NAA/Cr change[1]										1.00	0.74**
ADAS cog change[2]											1.00

*$p < 0.05$ **$p < 0.01$.
[1]The change in NAA/Cr ratio at was calculated as the mean difference between baseline and follow-up.
[2]The change in ADAS-cog measure was calculated as the mean difference between baseline and follow-up.

intervention in this mild dementia group. However, there was a trend towards a benefit approaching significance, so a positive effect cannot be ruled out.

In this group of patients, the NAA/Cr ratio did correspond with one functional measure (verbal fluency), and its change over time corresponded to the change in the ADAS-Cog. These observations confirm that the measurements of the NAA/Cr ratio in this study did reflect the functional changes over time associated with these AD patients.

There are several possible reasons for the lack of treatment effect of memantine in this study. First, mildly demented patients may be at a stage of the disease that while devastating to the medial temporal lobe, is only beginning to manifest adverse effects in the posterior temporal and inferior parietal convexities of the cortex [12]. Therefore, at this stage of the disease, memantine's benefit may not be observable in the inferior parietal cortex or on measures of general cognition. MRS analysis of medial cortical structures, such as the hippocampus [13], may show benefit from memantine treatment. Second, more specific and sensitive measures of episodic memory dysfunction, the type of memory selectively affected early in AD [14], might be required to demonstrate the benefits of memantine on cognitive and functional measures. Finally, memantine is able to improve cognitive and behavioral function in moderately and severely demented patients by modulating noise at the NMDA receptor, which is severely dysfunctional later in the disease. Because the NMDA receptor might not be substantially impacted at the mild AD stage, it is possible that memantine does not exert influence in slowing down the underlying disease process earlier in the course of the disease.

The results from the present study may have shown an effect of memantine if there was a greater number of patients. However, a larger sample similar in dementia severity range to the current study [6] did not find any significant NAA/Cr ratio differences in memantine and donepezil groups over a six month period. Also consistent with results of the current study, the change in the NAA/Cr ratio was significantly correlated with the change in the ADAS-cog measure.

Recent studies have used sophisticated statistical and neuroimaging methods to enhance the sensitivity and specificity of MRS in diagnosing early AD [15]. Examination of effects with respect to APOE genotype may resolve specific population responses to treatment [16]. It is essential to continue the exploration of treatment options in studies utilizing biomarkers as well as cognitive and functional assessments targeting the early disease process in mild AD population to establish the biological effects of interventions against AD.

STUDY FUNDING

DISCLOSURES

Dr. Yesavage received an honorarium from Forest Research Institute prior to the proposal of this study. He has no other financial conflicts.

None of the other authors have or have had any financial involvement with Forest Companies.

Between 2003 and 2007, Dr. Ashford received honoraria from Janssen Pharmaceuticals for giving talks supporting the use of galantamine for the treatment of Alzeimer's disease.

None of the other authors have any disclosures to make.

REFERENCES

[1] Vemuri P, Wiste HJ, Weigand SD, Shaw LM, Trojanowski JQ, Weiner MW, Knopman DS, Petersen RC, Jack CR Jr (2009) MRI and CSF biomarkers in normal, MCI, and AD subjects: diagnostic discrimination and cognitive correlations. *Neurology* **73**, 287-293.

[2] Ernst T, Chang L, Melchor R, Mehringer CM (1997) Frontotemporal dementia and early Alzheimer disease: differentiation with frontal lobe H-1 MR spectroscopy. *Radiology* **203**, 829-836.

[3] Kantarci K, Petersen RC, Boeve BF, Knopman DS, Tang-Wai DF, O'Brien PC, Weigand SD, Edland SD, Smith GE, Ivnik RJ, Ferman TJ, Tangalos EG, Jack CR Jr (2004) 1H MR spectroscopy incommon dementias. *Neurology* **63**, 1393-1398.

[4] Kantarci K (2007) 1H magnetic resonance spectroscopy in dementia. *Br J Radiol 80 Spec No* **2**, S146-S152

[5] Kantarci K, Petersen RC, Przybelski SA, Weigand SD, Shiung MM, Whitwell JL, Negash S, Ivnik RJ, Boeve BF, Knopman DS, Smith GE, Jack CR Jr (2008) Hippocampal volumes, proton magnetic resonance spectroscopy metabolites, and cerebrovascular disease in mild cognitive impairment subtypes. *Arch Neurol* **65**, 1621-1628.

[6] Modrego PJ, Fayed N, Errea JM, Rios C, Pina MA, Sarasa M (2010) Memantine versus donepezil in mild to moderate Alzheimer's disease: a randomized trial with magnetic resonance spectroscopy. *Eur J Neurol* **17**, 405-412.

[7] Murray ME, Dickson DW, Jack CR, Kantarci K (2009) Aberrant tau pathology underlies H-1 MR spectroscopic alterations in Alzheimer's disease. *Neurology* **72**, A173-A174.

[8] Clerici F, Vanacore N, Elia A, Spila-Alegiani S, Pomati S, Da Cas R, Raschetti R, Mariani C (2009) Memantine in moderately-severe-to-severe Alzheimer's disease: a postmarketing surveillance study. *Drugs Aging* **26**, 321-332.

[9]   Porsteinsson AP, Grossberg GT, Mintzer J, Olin JT (2008) Memantine treatment in patients with mild to moderate Alzheimer's disease already receiving a cholinesterase inhibitor: a randomized, double-blind, placebo-controlled trial. *Curr Alzheimer Res* **5**, 83-89.

[10] Rosen WG, Mohs RC, Davis KL (1984) A new rating scale for Alzheimer's disease. *Am J Psychiatry* **141**, 1356-1364.

[11] Ashford JW, Kumar V, Barringer M, Becker M, Bice J, Ryan N, Vicari S (1992) Assessing Alzheimer severity with a global clinical scale. *Int Psychogeriatr* **4**, 55-74.

[12] Braak H, Braak E (1996) Evolution of the neuropathology of Alzheimer's disease. *Acta Neurol Scand Suppl* **165**, 3-12.

[13] Jessen F, Gur O, Block W, Ende G, Frolich L, Hammen T, Wiltfang J, Kucinski T, Jahn H, Heun R, Maier W, Kolsch H, Kornhuber J, Traber F (2009) A multicenter (1)H-MRS study

of the medial temporal lobe in AD and MCI. *Neurology* **72**, 1735-1740.

[14] Ashford JW, Shan M, Butler S, Rajasekar A, Schmitt FA (1995) Temporal quantification of Alzheimer's disease severity: 'time index' model. *Dementia* **6**, 269-280.

[15] Westman E, Wahlund L-O, Foy C, Poppe M, Cooper A, Murphy D, Spenger C, Lovestone S, Simmons A (in press) Combining MRI and MRS to distinguish between Alzheimer's disease and healthy controls. *Journal of Alzheimer's Disease*

[16] Kaufer D, Gandy S (2009) APOE {epsilon}4 and bapineuzumab: Infusing pharmacogenomics into Alzheimer disease therapeutics. *Neurology* **73**, 2052-2053.

Effects of a 6-Month Cognitive Intervention on Brain Metabolism in Patients with Amnestic MCI and Mild Alzheimer's Disease

Stefan Förster[a,i,*], Verena C. Buschert[b], Stefan J. Teipel[c,d], Uwe Friese[c,g], Hans-Georg Buchholz[f], Alexander Drzezga[i], Harald Hampel[e], Peter Bartenstein[a] and Katharina Buerger[b,h]

[a]*Department of Nuclear Medicine, Ludwig-Maximilian University, Munich, Germany*
[b]*Dementia Research Section and Memory Clinic, Alzheimer Memorial Center and Geriatric Psychiatry Branch, Department of Psychiatry Ludwig-Maximilian University, Munich, Germany*
[c]*Department of Psychiatry, University Rostock, Rostock, Germany*
[d]*DZNE, German Center for Neurodegenerative Disorders, Rostock, Germany*
[e]*Discipline of Psychiatry, School of Medicine & Trinity College Institute of Neuroscience (TCIN), Laboratory of Neuroimaging and Biomarker Research, Trinity College, University of Dublin, Dublin; The Adelaide and Meath Hospital Incorporating the National Children's Hospital (AMiNCH), Ireland*
[f]*Department of Nuclear Medicine, University Mainz, Mainz, Germany*
[g]*Institute of Psychology, University of Osnabrueck, Osnabrueck, Germany*
[h]*Institute for Stroke and Dementia Research, Klinikum Großhadern, Ludwig-Maximilian University, Munich, Germany*
[i]*Department of Nuclear Medicine, Technische Universität München, Munich, Germany*

Abstract. The effect of cognitive intervention on brain metabolism in AD is largely unexplored. Therefore, we aimed to investigate cognitive parameters and [18]FDG PET to test for effects of a cognitive intervention in patients with aMCI or mild AD.

Patients with aMCI ($N = 24$) or mild AD ($N = 15$) were randomly assigned either to cognitive intervention groups (IGs), receiving weekly sessions of group-based multicomponent cognitive intervention, or active control groups (CGs), receiving pencil-paper exercises for self-study. We obtained resting-state FDG-PET scans and neuropsychological testing at baseline and after six-months. Normalized FDG-PET images were analyzed using voxel-based SPM5 approaches to determine longitudinal changes, group-by-time interactions and correlations with neuropsychological outcome parameters. Primary global cognitive outcome was determined by analyses of covariance with MMSE and ADAS-cog scores as dependent measures.

Both, aMCI and AD subgroups of CGs showed widespread bilateral cortical declines in FDG uptake, while the AD subgroup of IGs showed discrete decline or rather no decline in case of the aMCI subgroup. Group by time analyses revealed strongest attenuation of metabolic decline in the aMCI subgroup of the IGs, involving left anterior temporal pole and anterior cingulate gyrus. However, correlation analyses revealed only weak non-significant associations between increased FDG uptake and improvement in primary or secondary outcome parameters. Concurrently, there was significant improvement in global cognitive status in the aMCI subgroup of the IGs.

*Correspondence to: Stefan Förster, MD; Klinik und Poliklinik für Nuklearmedizin, TU München; Ismaninger Str. 22, 81675 München, Germany. Tel.: +49 89 4140 2965; Fax: +49 89 4140 4950; E-mail: stefan-foerster@gmx.de.

A six-month cognitive intervention imparted cognitive benefits in patients with aMCI, which were concurrent with an attenuated decline of glucose metabolism in cortical regions affected by neurodegenerative AD.

INTRODUCTION

Cognitive intervention for patients with Alzheimer's Disease (AD) is considered an important contribution to the treatment of AD [1]. Specifically designed cognitive interventions can improve memory performance and can even attenuate the risk of future cognitive decline in non-demented elderly subjects [2, 3]. Beneficial effects of interventions on cognitive decline are reported in subjects with preclinical cognitive impairment (see review [4]) or mild-to-moderate stages of dementia (see meta-analyses [5, 6]).

Effective cognitive interventions might conceivably impart their effects through altered cerebral metabolism. The rate of cerebral glucose consumption can be assessed in positron emission tomography (PET) studies recording the uptake of the stable glucose analogue [^{18}F]fluorodeoxyglucose (FDG); the PET-FDG technique has been extensively used for studying the pathophysiology of neuropsychiatric and neurodegenerative disorders, including AD (see review [7]). FDG-PET recordings obtained at rest are a sensitive indicator of perturbed brain metabolism, and may reveal very early cerebrometabolic changes preceding the onset of clinical AD symptoms [8]. Voxel-wise mapping of FDG uptake is amenable for the longitudinal assessment of brain functional changes in dementia, and may more sensitively detect treatment-response than do commonly-used instruments for cognitive testing, such as the Mini Mental State Examination (MMSE) and the Alzheimer's Disease Assessment Scale - cognitive subscale, total score (ADAS-cog) [9]. However, the effect of cognitive intervention on cerebral metabolism in AD is largely unexplored. There are only two published studies investigating the effects of cognitive intervention on brain metabolism. In an early study, FDG-PET was obtained in a visual stimulus activation paradigm with AD patients, and the effects of an unspecified cognitive training of six months duration and a pharmacological intervention were tested [10]; the combined treatment proved to be superior to cognitive training alone. More recently, participation in 14-day long healthy lifestyle program consisting of a combination of mental and physical exercise, stress reduction, and healthy diet was associated with significant short-term benefits in cognitive function and cerebral FDG uptake in elderly non-demented subjects [11].

In the present study, we tested the hypothesis that a newly-developed multicomponent cognitive intervention [12] applied in a randomized controlled trial would lead to cognitive and non-cognitive benefits and mitigate against declining brain metabolism in patients with amnestic MCI or mild AD. To test this hypothesis, we examined global cognitive (MMSE- and ADAS-cog. scores) and additionally non-cognitive parameters, such as mood (Montgomery Asberg Depression Rating Scale, MADRS), which are deemed to be important for cognitive performance [13]. We used FDG-PET to map the pattern of declining cerebral glucose metabolism during six months (between baseline and follow-up scans) in a well-characterized sample of aMCI and mild AD patients, participating in a parallel group randomized controlled trial with two treatment arms, (i) specific cognitive intervention and (ii) an active control condition. Prior to the start of the study, a multicomponent cognitive intervention for patients with aMCI and patients with mild AD was conceptualized aiming at capabilities and needs of patients in different stages of AD [12]. In order to gain more direct insights into the functional-anatomical substrate of neuronal function along with cognitive improvement, voxel-based bidirectional SPM patient-group-by-time interaction analyses (later referred to as "difference of differences" analyses), measuring baseline to follow-up PET metabolic differences between the patient groups and treatment arms, were applied.

MATERIALS AND METHODS

Subjects

We screened 43 patients at the Dementia Research Section and Memory Clinic of the Alzheimer Memorial Center and Geriatric Psychiatry Branch, Department of Psychiatry, Ludwig-Maximilian University, Munich, from March to August 2007. In the

screening, we conducted a comprehensive clinical and neuropsychological assessment, in order to support the research diagnosis of either aMCI or mild AD. Participants with aMCI had a memory complaint and performed at least 1.5 SD below the average level of persons of a similar age and education on at least one of three memory tests of the Consortium to Establish a Registry for Alzheimer's Disease (CERAD) neuropsychological test-battery (Morris, et al., 1989) (immediate and/or delayed recall and/or recognition). Their cognitive difficulties had no significant repercussions on their functional independence, as assessed through clinical interviews with the patients and caregivers. Hence, they did not fulfil criteria for mild stages of clinically probable AD [14]. Neither of the patient (groups) had major physical illness, other mental disorder (i.e. major depression) or disability which could have affected participation. Thirty-nine patients, meeting stringent inclusion criteria, were included. For details please see [12].

Routine laboratory testing of all included patients consisted of full blood cell count, blood glucose, thyroid function tests, serum Vitamin B12 and folic acid levels as well as cerebrospinal fluid protein and Apo-E genotype testing; there were no major abnormalities at baseline. Each patient underwent structural magnetic resonance imaging (MRI) for detection of brain anatomical abnormalities; according to the Schelten´s scale [15] patients with structural lesions visible in the T2-weighted MR scans exceeding 10 mm in diameter, including white matter hyperintensities, were excluded from the study. According to the declaration of Helsinki approval of the local ethics commission (of the Ludwig-Maximilian University, Munich), and the German Radiation Safety Committee (BfS) was obtained prior to starting the study.

Design

Effects of a six-month cognitive intervention program on brain glucose metabolism were assessed in 36 patients with either aMCI ($N = 21$) or mild AD ($N = 15$) syndrome. The trial design is shown in Fig. 1.

Briefly, patients were randomly assigned to either a cognitive intervention treatment arm (IG) or active control condition treatment arm (CG), resulting in 9 aMCI patients and 8 AD patients for the mixed intervention groups (IGs), as well as 12 aMCI patients and 7 AD patients for the mixed control groups (CGs). During a six month period members of the IGs received
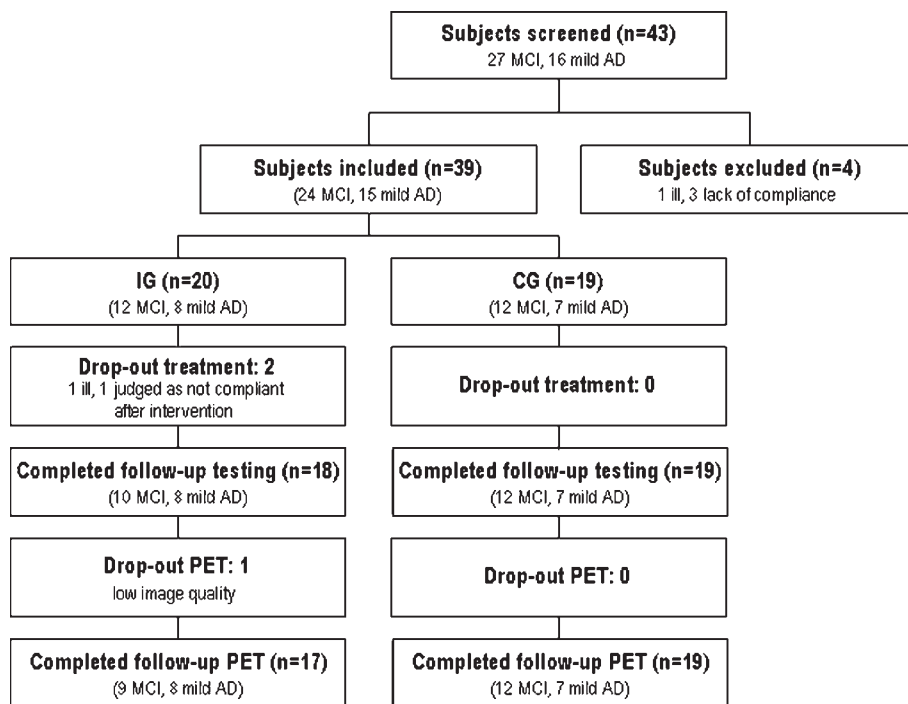

Fig. 1. Trial design. aMCI = amnestic mild cognitive impairment; AD = Alzheimer's Disease; IG = intervention treatment arm; CG = control condition treatment arm.

weekly sessions of 120-minutes group-based cognitive intervention, whereas the CGs participants met monthly and received pencil and paper exercises for self-study. The cognitive intervention was based on the theory of cognitive reserve [16] and was tailored to the cognitive and functional requirements of aMCI and mild AD patients according to the theory of Retrogenesis, as a theoretical basis for the selection of specific training tasks [17]. It focussed particularly on global cognitive functioning but addressed also non-cognitive domains, e.g. mood and quality of life, that are thought to be impaired in aMCI and frank AD [13]. On the supposition that MCI resides within the cognitive continuum from normal aging to AD [18], differences between the intervention for MCI and for mild AD corresponded rather to a quantitative than a qualitative distinction [12]. In contrast to the tailored cognitive intervention, the CGs sessions focussed on exercises of isolated, sustained attention, which is supposed to be largely unimpaired, at least in mild AD [19].

The colleagues who conducted neuropsychological testing sessions and PET-scanning were blinded to subject classification and treatment plan; an instructor uninvolved in these steps administered the IGs and CGs sessions.

PET imaging

Baseline and six-months follow-up FDG-PET scans of 36 patients were performed successfully. All patients had fasted for at least six hours prior to FDG-PET. Recordings were made using a Philips Allegro PET scanner with a 128×128 pixel matrix (pixel size 2 mm), an axial field of view of 180 mm and a full width at half maximum (FWHM) resolution of 5.5 mm. Patients were asked to recline on the scanner bed, resting quietly with their eyes covered and their ears occluded. Each patient's head was positioned within the aperture of the tomograph, and comfortably immobilized using a foam cushion. At 20 minutes after injection of FDG (mean 200 MBq, i.v.), an attenuation scan was obtained with a rotating $[^{137}Cs]$ point source. A dynamic emission recording consisting of five six-minute frames was obtained in the interval 30 to 60 minutes following the FDG injection. After visual inspection to exclude frames with unacceptable head motion, attenuation-corrected frames were summed into a single frame, and final images were reconstructed iteratively using a three-dimensional row action maximum likelihood algorithm (3D-RAMLA).

Cognitive data analysis

Prior to the screening-phase, the study was registered in a public trials registry (www.clinicaltrials.gov; ID: NCT00544856). Primary outcome was evaluated separately for aMCI and AD patients by comparing change in the global cognitive parameters (MMSE score [20] and Alzheimer's Disease Assessment Scale – total score of the cognitive subscale (ADAS-cog) [21]) in the cognitive intervention treatment arm versus change in the control condition treatment arm tested by the time (progression) by arm interaction term in a two-factor ANOVA. Further information regarding secondary outcome measures, not relevant for the present study, and the neuropsychological data analyses is described elsewhere [12].

PET data analysis

SPM5 routines (Wellcome Department of Cognitive Neurology, London, UK) implemented in MATLAB (version 7.1) were used to perform basic image processing and voxel-based statistical analysis. All PET scans were spatially normalized using default transformation parameters to the SPM5 standard PET brain template in the Montreal Neurological Institute (MNI) space. Normalized images were composed of a $79 \times 95 \times 69$ matrix, with $2 \times 2 \times 2$ mm voxel size. These images were then smoothed using an isotropic Gaussian kernel (12 mm FWHM), which accommodates inter-individual anatomical variability, and thus improves the sensitivity of the statistical analysis [22]. FDG uptake scaling was performed using the reference cluster approach as described in detail by Yakushev et al. [23]. Briefly, with this approach regional FDG uptake is normalized to that measured in brain regions defined *a posteriori* to be unaffected, relative to the results in a non-demented control group. This *a posteriori* method was shown to be more sensitive than the global mean approach in detecting disease-related metabolic disturbances in mild-to-moderate stages of neurodegenerative disorders [24, 25], especially in studies on dementia [23, 26, 27], [28]. For these comparisons we made use of previously obtained FDG-PET data from 11 healthy elderly subjects (5 female; mean age 59.0 ± 10.9 years), who were non-complainers, had an MMSE score above 28, had no signs of microangiopathy on MRI, no history of neurological- or major psychiatric diseases and did not receive any psychoactive medication [27]. The latter elderly control subjects had been examined in a resting-

state on the same scanner and with image processing according to the identical protocol as for the patients.

First of all, in order to characterize our patients neurobiological status at baseline, we compared baseline regional FDG uptake between all patients and nondemented controls, using an unpaired t-test.

Then for evaluation of longitudinal changes in FDG uptake we performed within-group comparisons (in both the AD and aMCI subgroups of the IGs and the CGs) between baseline and end-of-study PET scans using paired t-tests. For a more specific evaluation of neurobiological intervention effects we elected to use a voxel-based bidirectional patient-group-by-time interactions design, referred to as "difference of differences" analysis, which assessed the differences in extent of metabolic changes between both the AD and aMCI subgroups of the IGs and the CGs between the initial scan and the end-of-study scan. We considered a statistical threshold of $p < 0.001$ uncorrected and a threshold for minimum spatial extent of 30 contiguous voxels for anatomical reporting of significant changes in FDG uptake. Foci of significant changes were automatically assigned by the SPM software to the coordinate system of the MNI space, and then converted to Talairach and Tournoux coordinates [29] for identification of the Brodmann areas and anatomic designations.

In order to link the clinical neuropsychological outcome with the neurobiological PET findings we performed additional correlation analyses between changes in FDG uptake in brain regions, which had showed the highest metabolic effects, and changes in primary and secondary outcome parameters in aMCI patients. Using a ROI-based approach (MARSBAR toolbox implemented in SPM5), we extracted normalized baseline and follow-up FDG uptake values and performed correlation analyses between FDG uptake changes and the respective changes in neuropsychological test scores.

RESULTS

Of the 43 patients meeting initial inclusion criteria, 39 were randomly assigned to IG- or CG treatment arms, with exclusion of one patient due to concurrent physical illness, and three patients due to lack of compliance (less than 50% presence at the intervention sessions). Of these 39 patients, two aMCI patients dropped out from the IG arm because of new concurrent physical illness, or lack of compli-

Table 1
Demographic data of IGs and CGs subjects ($n = 36$)

	Igs	CGs	t-Test
Number	17	19	
AD	8	7	
aMCI	9	12	
Age (SD)	74.5 (8.6)	72.0 (7.1)	n.s.
in yrs. min–max	53.2–88.6	62.4–83.7	
Gender f / m	7/10	9/10	
Apo E4 allele (at least one)	12	11	
MMSE min–max	26.4 (2.4) 22–30	26.1 (1.6) 23–29	n.s.
Education (SD) in yrs. min–max	12.2 (3.4) 8–17	13.4 (4.1) 11–21.5	n.s.

aMCI = amnestic mild cognitive impairment; AD = mild Alzheimer's Disease; IGs = cognitive intervention groups; CGs = active control groups; min–max = ranges of scores; SD = standard deviation.
*t-Test results refer to post-hoc comparisons testing the differences of means in the adjacent columns

ance. Thirty-seven participants completed the study, with elimination of one aMCI patient from the IG arm due to poor PET image quality. Concurrent with the randomization process there was good matching between IG- and CG patient groups (IGs and CGs) for degree of cognitive impairment, education, age, gender, and for Apo-E genotype. All mild AD patients and one aMCI patient in the IG arm were on antidementia medication (acetylcholinesterase inhibitor and/or Memantine) at stable doses since at least since three months prior to study start and throughout the intervention/control condition until study end. Table 1 shows baseline demographic and clinical characteristics of all patients included in the PET data analysis.

Neuropsychological cognitive outcome

To detect intervention-related effects of the stage-specific cognitive intervention in the respective patient groups, we conducted a series of ANCOVAs with treatment (intervention treatment arm, IG, versus control treatment arm, CG), and progression (baseline versus end-of-study) as independent variables separately for AD and aMCI patients. The primary outcome measures MMSE and ADAS-cog scores served as dependent measures. Furthermore, we entered educational level (years of schooling) and patients' age as covariates into the analysis.

Table 2

Change from baseline in measures of efficacy in the cognitive intervention subgroups (IG$_{AD}$; IG$_{MCI}$) and in the active control subgroups (CG$_{AD}$; CG$_{MCI}$) regarding MMSE and ADAS-cog; standard deviation in ()

Target-variate	Timepoint	aMCI			AD		
		IG$_{MCI}$	CG$_{MCI}$	ANCOVA**	IG$_{AD}$	CG$_{AD}$	ANCOVA**
ADAS-cog	Baseline min–max	8.8 (3.1) 3–13	9.8 (4.3) 5–19	Interaction Treatment and Progression ($F_{1,17} = 4.7$, $p = .045$, $\eta 2 = .22$)	12.1 (5.3) 6–21	16.4 (4.8) 13–23	Treatment ($F_{1,11} = 4.4$, $p = .06$, $\eta 2 = .282$)
	Study end	7.4 (3.2)	11.7 (5.6)		11.4 (6.0)	16.4 (4.9)	
t-Test*		n.s.	$t(11) = 2.8$, $p = .02$		n.s.	n.s.	
MMSE	Baseline min–max	28.1 (1.6) 25–30	26.8 (1.5) 24–29	Interaction Treatment and Progression ($F_{1,17} = 4.3$, $p = .05$, $\eta 2 = .21$) Main Effect Treatment ($F_{1,17} = 6.8$, $p = 0.02$, $\eta 2 = .29$)	24.5 (1.6) 22–27	25.3 (1.5) 23–27	n.s.
	Study end	28.3 (1.2)	26.0 (1.3)	25.0 (2.7)	24.4 (2.4)		
t-Test*		n.s	$t(11) = 2.8$, $p = .02$		n.s.	n.s.	

aMCI = amnestic mild cognitive impairment; AD = mild Alzheimer's Disease; ADAS-cog = Alzheimer's Disease Assessment Scale; MMSE = Mini Mental State Examination; IGs = cognitive intervention groups; CGs = active control groups.;
*t-Test results refer to post-hoc comparisons testing the differences of means in the adjacent rows and columns.; **ANCOVA: univariate analysis of covariance; reported effects refer to the interaction between treatment and progression which reflects whether a change of the dependent variables from baseline to follow-up is quantitatively different in the two treatment arms.

For AD patients, only the treatment factor approached significance for ADAS-cog scores ($F_{1,11} = 4.4$, $p = .06$, $\eta^2 = .282$). For aMCI patients, we determined a marginally significant interaction effect between treatment and progression for ADAS-cog ($F_{1,17} = 4.7$, $p = .045$) and for MMSE ($F_{1,17} = 4.3$, $p = .05$). Furthermore, the analysis revealed a main effect for treatment regarding MMSE ($F_{1,17} = 6.8$, $p < .01$). Post-hoc t-tests suggest that interaction effects between treatment and progression occurred mainly due to performance decline in the CG$_{MCI}$. See Table 2 for details.

FDG-PET data

All patients relative to elderly non-demented controls showed reduced brain FDG uptake at baseline, mainly in the bilateral temporo-occipital association cortex (left worse than right), left temporal cortex, bilateral posterior cingulate cortices and precuneus, as well as in left prefrontal cortex (Fig. 2).

MCI subgroups of the CGs and of the IGs (CG$_{MCI}$ and IG$_{MCI}$) showed similar baseline patterns of reduced brain FDG uptake, involving parieto-temporal cortex, posterior cingulate cortex, precuneus and prefrontal cortex (Fig. 3). We omit reporting anatomical coordinates, since this finding matches the typical anatomical distribution of AD-associated changes [30-32].
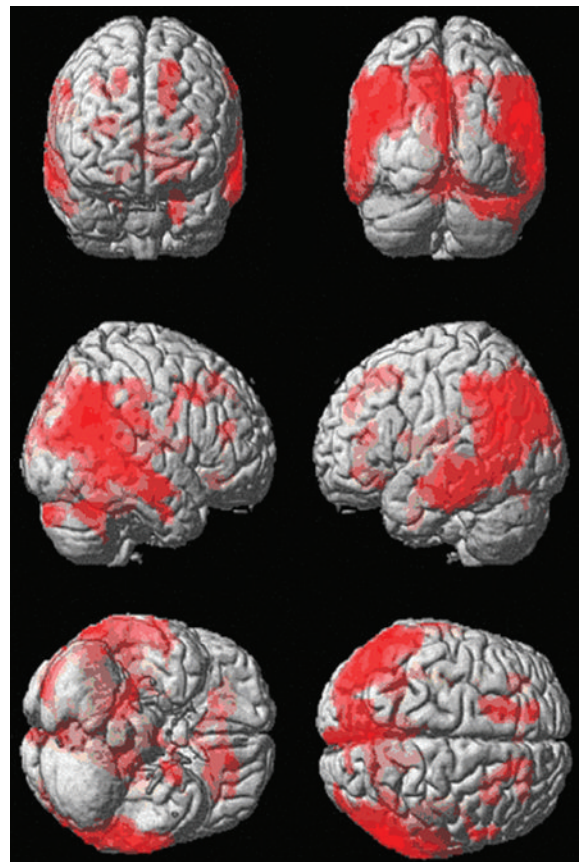

Fig. 2. Baseline pattern of reduced FDG uptake in all patients ($n = 36$) as compared to non-demented elderly controls ($n = 11$); ($P < 0.005$ uncorrected).
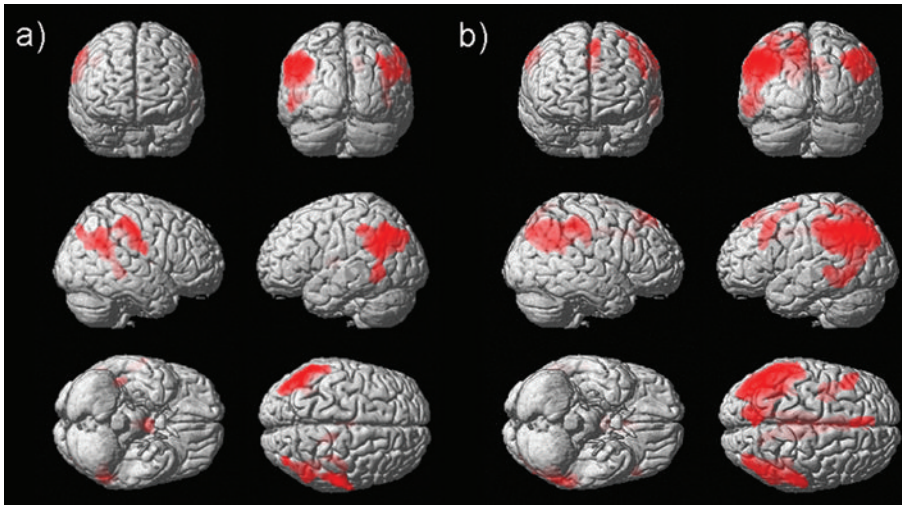
Fig. 3. Baseline patterns of reduced FDG uptake in a) IG_{MCI} ($n = 9$) and in b) CG_{MCI} ($n = 12$), as compared to non-demented elderly controls ($n = 11$); ($P < 0.005$ uncorrected).

There were no significant differences in baseline brain FDG uptake between the respective CGs- and IGs.

After six months, the AD subgroup of CGs (CG_{AD}) showed widespread bilateral declines in FDG uptake in parieto-temporal and parieto-occipital cortices as well as in left prefrontal cortex, while the AD subgroup of IGs (IG_{AD}) showed minor decline in FDG uptake in two single clusters located in the lingual gyrus and the left inferior temporal gyrus.

The CG_{MCI} showed widespread bilateral occipito-temporal (right more then left), parietal and prefrontal decline in FDG uptake, while the IG_{MCI} showed no decline in FDG uptake (Fig. 4).

"Difference of differences" analyses revealed strongest attenuated decline in FDG uptake in the subgroup of aMCI patients in the IGs (IG_{MCI}) in bi-hemispheric cortical areas, including bilateral temporal, prefrontal- and anterior cingulate cortex (Fig. 5 a). Clusters with main peaks surviving the $p < 0.001$ (unc.) threshold were located in the left anterior temporal pole and the left anterior cingulate gyrus (Table 4, Fig. 6).

The subgroup of AD patients in the IGs (IG_{AD}) revealed a more restricted attenuated decline in FDG uptake in the right temporal- and posterior cingulate cortex (Fig. 5 b), while none of these clusters survived the $p < 0.001$ (unc.) threshold.

Correlation analyses between changes in normalized FDG uptake (in those brain regions which had showed the highest metabolic attenuation) and changes in neuropsychological outcome parameters, revealed a single significant correlation for total MADRS score in the IG_{MCI} (Pearsons correlation coefficient: $r = -0.61$; $p = 0.039$ one-tailed), such that an increase in FDG uptake in the left anterior cingulate- and anterior temporal pole was associated with a decrease in total MADRS score. However, after eliminating the cognition-related MADRS item (concentration), which had primarily contributed to the total MADRS score, only a weak non-significant correlation remained (Pearsons correlation coefficient $r = -0.398$; $p = 0.144$ one-tailed). Detailed longitudinal outcome of secondary neuropsychological outcome parameters (i.e. MADRS, Trail Making Test, etc.) is described elsewhere [12].

DISCUSSION

We used FDG-PET to map effects of a newly developed multicomponent cognitive intervention on brain energy metabolism in patients with aMCI and mild AD. Upon entering the study, participants were randomly assigned to intervention (IGs) or active control groups (CGs). In both CGs, significant decline of FDG uptake in AD-typical brain areas during a relatively brief period of six months, confirmed that resting-state FDG-PET is a sensitive marker of disease progression [33]. Participation in the cognitive intervention program imparted cognitive benefits in the aMCI sub-
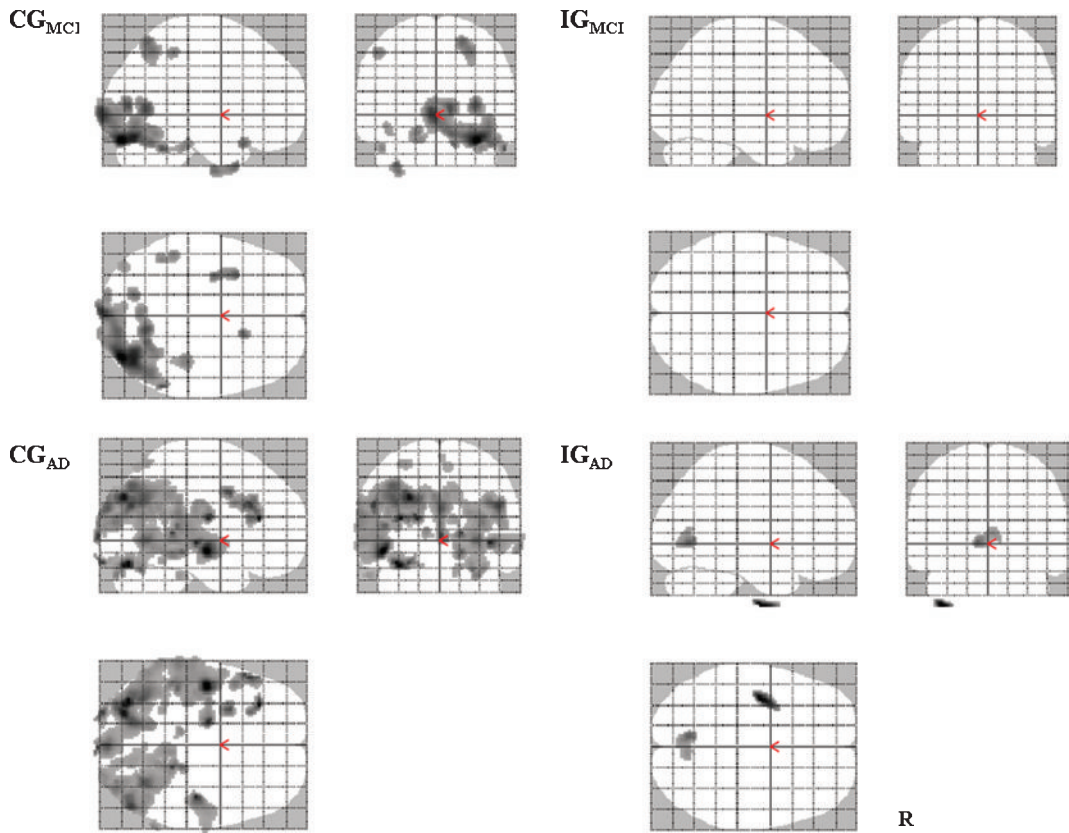
Fig. 4. Relative decline of brain FDG uptake in aMCI and AD- CGs and IGs after six months; ($p < 0.005$ uncorrected).
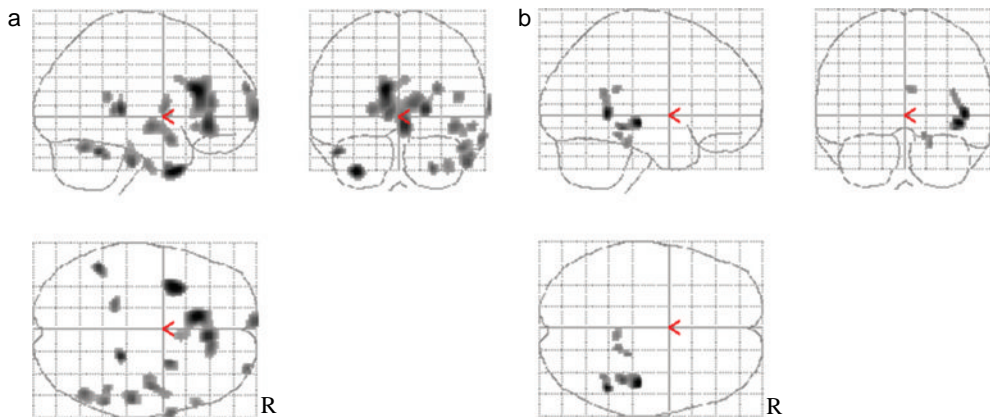

Fig. 5. Attenuated decline of brain FDG uptake after six months a) in the IG_{MCI} relative to the CG_{MCI}, b) in the IG_{AD} relative to the CG_{AD}; ($p < 0.005$ uncorrected).

group, which were reflected by an attenuated decline in cerebral FDG uptake relative to that seen in the respective active control group.

Upon entry in the study, the whole sample of patients had significantly reduced FDG uptake relative to a group of non-demented elderly control subjects.

Table 3
Regions of significantly attenuated decline in brain FDG uptake after six months in the IG$_{MCI}$ relative to the CG$_{MCI}$

Location		Talairach and Tournoux			Peak z-value	P uncorr.	Cluster extension
	BA	x	y	z			
L, Ant. Temporal Pole	38	−32	10	−42	3.39	0.000	152
L, Ant. Cingulate Gyrus	32	−10	28	20	3.37	0.000	1036

Cluster extension represents the number of contiguous voxels surpassing the threshold of $p < 0.001$. Bold markings delineate a cluster and the peak z-value within the cluster. Associated anatomic structures are indicated, along with designations of Brodman area (BA); R = right, L = left.

Main differences were seen in brain regions typically impaired in AD, including the bilateral temporo-occipital association cortices, left temporal cortex, bilateral posterior cingulate cortices and precuneus, as well as in left prefrontal cortex (Fig. 2). This pattern confirms previous FDG-PET results in aMCI or mild to moderately diseased AD patients [31, 34, 35], suggesting that our stringent clinical inclusion criteria were effective in selecting a representative patient sample. Demographics indicated that the patient groups had similar education background, Apolipoprotein E4 allele status and similar baseline cognitive function, as assessed by MMSE and ADAS-cog scores at onset of the intervention.

Longitudinal FDG-PET evaluation in both CGs (AD and aMCI) after six-months revealed widespread bilateral decline in metabolism throughout AD-typical cortical areas (Fig. 4), consistent with the progression of the clinical scores of cognitive function (MMSE and ADAS-cog). Peaks in the declining FDG uptake overlapped with the pattern of hypometabolism at baseline relative to FDG uptake in the non-demented control group, consistent with an on-going disease process during only six months, as reported in previous PET studies with one-year follow-up [9, 35]. In those one-year follow-up studies, FDG uptake was normalized to the global mean value, which we have shown to result in spurious detection of metabolic changes, which arise from bias due to undetected but real declines in metabolism [36]. Instead, we normalized regional FDG uptake to that measured in brain regions defined a posteriori to be unaffected, relative to the results in the non-demented elderly control group [23]. The a posteriori method is more sensitive than the global mean approach in detecting disease-related metabolic disturbances in mild-to-moderate stages of neurodegenerative disorders [24, 25], especially in studies on dementia [23, 26–28].

In contrast to the widespread six month declines in FDG uptake seen in both CG$_{AD}$ and CD$_{MCI}$ (Fig. 4), we saw in the IG$_{AD}$ discrete decline with two single significant clusters located in the lingual gyrus and the left inferior temporal gyrus, while the IG$_{MCI}$ showed no decline at all (Fig. 4). The latter finding strongly suggests positive effects of the cognitive intervention program on brain energy metabolism in the MCI subgroup. The relative preservation of normalized FDG uptake during six months especially in the IG$_{MCI}$ concurs with our clinical findings showing a significant change in global cognitive status, which seemed to be
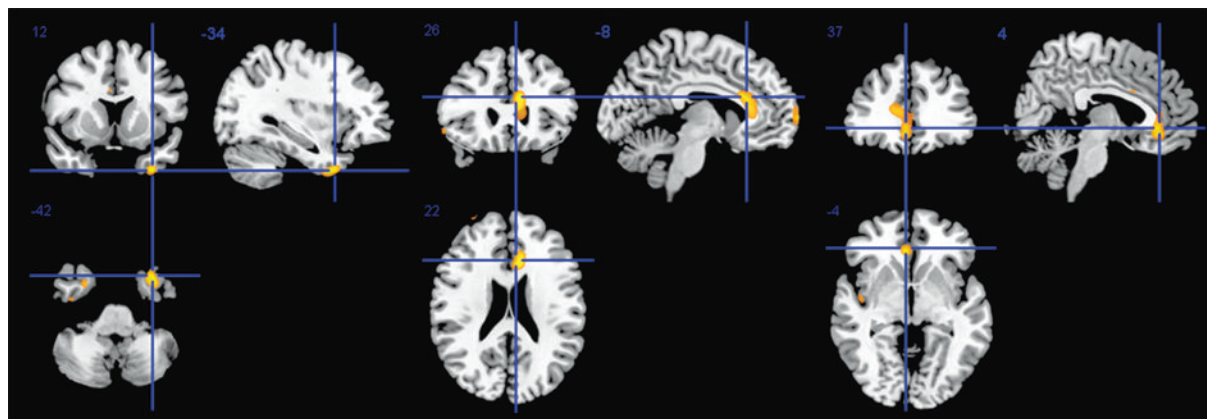

Fig. 6. Overlay image on transaxial slices of an averaged MRI data set of 152 healthy subjects, showing peak clusters of attenuated decline of brain FDG uptake after six months in the left anterior cingulate cortex and the left anterior temporal pole in the IG$_{MCI}$ relative to the CG$_{MCI}$. Radiological convention (Left is Right); set at >30 contiguous voxels passing the significance threshold $p < 0.005$ uncorrected.

driven by performance stabilisation in the IG$_{MCI}$, contrasted with declining performance in the CG$_{MCI}$ (see Table 2). Given the progressive nature of AD and its prodromal stage aMCI, the present suggestion of cognitive stabilization may emerge as a beneficial effect of the cognitive intervention.

In order to test more objectively for time-dependent effects of the cognitive intervention on brain metabolism, we made bidirectionally contrasted "difference of differences" analyses of the FDG-PET results in the aMCI and AD subgroups of the IGs and CGs. These SPM-based approaches revealed attenuated metabolic decline during six months of cognitive intervention mainly in the IG$_{MCI}$ subgroup. Instead, at the same statistical threshold the opposite contrasts revealed no attenuation of declining metabolism in the CG$_{MCI}$ relative to the IG$_{MCI}$ (or the respective AD subgroups), supporting the real presence of an attenuating effect on FDG decline in aMCI patients which had received the cognitive interventions.

The effect of attenuated metabolic decline was more widespread and pronounced in the IG$_{MCI}$ than in the IG$_{AD}$ (Fig. 5 a,b), which is in line with the results from the clinical cognitive parameters (MMSE, ADAS-cog.), showing significant changes only in the aMCI subgroup (Table 2). As mentioned before, changes in clinical cognitive parameters seemed to be attributed primarily to cognitive decline in the CG$_{MCI}$, raising the question about whether there were a greater percentage of aMCI subjects with prodromal AD in the control group who may have deteriorated over the 6 month follow-up. This possibility can be denied. Group comparisons of IG$_{MCI}$ and CG$_{MCI}$ relative to elderly non-demented control subjects at baseline, revealed for both MCI subgroups a similar distributional pattern of FDG hypometabolism, involving AD-typical brain regions (see Fig. 3). The latter finding strongly suggests an inclusion of aMCI patients in a preclinical AD stage and is in line with our stringent MCI-diagnosis inclusion criteria. Furthermore, a number-needed-to treat (NNT) analysis in the aMCI subpopulation indicated effectiveness of the cognitive intervention, as improvement by means of 4-point change on ADAS-cog occurred only in the IG$_{MCI}$, whereas cognitive decline appeared in both IG- and CG$_{MCI}$ [12].

In the aMCI subgroup we were able to map the peak areas of metabolic attenuation to the left anterior temporal pole and anterior cingulate cortex (ACC). The latter structure belongs to the fronto-limbic network and is well-known for its role in emotional and motivational control [37] as well as in attentional pro-

cessing [38], [39], [40]. To explore if mood-related effects might have lead to the observed PET effects, we performed an additional correlation analysis between the changes in normalized FDG uptake in the left anterior cingulate- as well as left anterior temporal pole, and the changes in MADRS score in the IG$_{MCI}$. This analysis revealed a single significant correlation for total MADRS score in the IG$_{MCI}$, such that an increase in FDG uptake in the left anterior cingulate- and superior temporal gyrus was associated with a decrease in total MADRS score. However, after eliminating the cognition-related MADRS item (concentration), which had primarily contributed to the total MADRS score [12], only a weak, non-significant correlation remained. Therefore, mood-specific effects might not have led to the observed attenuating effects on brain metabolism. However, we cannot rule out that cognition-related mood stimulating effects (i.e. increased concentration) of the intervention might have to some extent contributed to the observed PET effects.

Probably due to the limited patient number and the restricted variance of clinical scores in this relatively short time period of six months, correlation analyses between FDG uptake changes and performance changes in the global cognitive domains (MMSE, ADAS cog) did not show any significant correlation (data not shown).

We feel that the specific linkage between neuropsychological and neurobiological outcome remains to be established in future studies in larger patient populations.

Overall, our findings strongly suggest a positive short-term effect of the cognitive intervention program on brain energy metabolism in aMCI patients, which may manifest in cognitive benefits. We modelled our study on an earlier FDG-PET follow-up study investigating effects of a 14-day healthy longevity lifestyle program on cognition and cerebral energy metabolism in a group of non-demented subjects with mild age-related memory complaints [11]. In that study, the intervention group had after two weeks a 5% relative decrease in normalized FDG uptake in the left dorsolateral prefrontal cortex, which the authors interpreted to reveal an effect of training on cognitive efficiency of a brain region involved in working memory. Unlike in that study, we selected patients with objective cognitive impairment, suggesting that our findings of attenuated declines relate to moderation of a pathological process. In the only other FDG-PET study of cognitive training in AD patients [10], there was a six-month decline in resting-state cerebral glucose metabolism,

most notably in the temporo-parietal region, in a group of AD patients who had only received social support. In that study, FDG-PET changes evoked by a visual recognition task served as an indicator of therapeutic efficacy in AD. The AD patients who had received cognitive training with and without pharmacological treatment had a more distinct pattern of FDG activations after six months, whereas the subgroup with both interventions showed some improvement in cognitive performance, as measured by the MMSE. Despite diverse conceptual and methodological differences between that and the present studies, there is agreement that FDG-PET can detect effects of intervention on cerebral metabolism during six months progression of impaired cognition.

LIMITATIONS

The relatively small number of participants in this study limits its statistical power. Furthermore, this study design reveals only group differences in FDG uptake and cognitive scores, which may however be offset by the benefits of the prospective setting, in which the groups were well-matched for demographics and baseline metabolism. Direct result comparisons between the AD and MCI subgroups might be confounded by differences in the intervention design and should be interpreted with caution.

We allowed a more permissive statistical threshold of $p < 0.005$ (uncorrected) for the visualisation of PET results. However, application of the same permissive threshold for the respective negative SPM t-contrasts did not bear any significant results, which would have indicated an increased risk of false positive results.

ACKNOWLEDGMENTS

FINANCIAL DISCLOSURES

REFERENCES

[1] Buschert V, Bokde AL, Hampel H (2010) Cognitive intervention in Alzheimer disease. *Nat Rev Neurol* **6**, 508-517.

[2] Valenzuela M, Sachdev P (2009) Can cognitive exercise prevent the onset of dementia? Systematic review of randomized clinical trials with longitudinal follow-up. *Am J Geriatr Psychiatry* **17**, 179-187.

[3] Valenzuela MJ, Sachdev P (2006) Brain reserve, dementia: a systematic review. *Psychol Med* **36**, 441-454.

[4] Belleville S (2008) Cognitive training for persons with mild cognitive impairment. *Int Psychogeriatr* **20**, 57-66.

[5] Sitzer DI, Twamley EW, Jeste DV (2006) Cognitive training in Alzheimer's disease: a meta-analysis of the literature. *Acta Psychiatr Scand* **114**, 75-90.

[6] Olazaran J, Reisberg B, Clare L, Cruz I, Pena-Casanova J, Del Ser T, Woods B, Beck C, Auer S, Lai C, Spector A, Fazio S, Bond J, Kivipelto M, Brodaty H, Rojo JM, Collins H, Teri L, Mittelman M, Orrell M, Feldman HH, Muniz R (2010) Nonpharmacological therapies in Alzheimer's disease: A systematic review of efficacy. *Dement Geriatr Cogn Disord* **30**, 161-178.

[7] Herholz K (2003) PET studies in dementia. *Ann Nucl Med* **17**, 79-89.

[8] Reiman EM, Caselli RJ, Yun LS, Chen K, Bandy D, Minoshima S, Thibodeau SN, Osborne D (1996) Preclinical evidence of Alzheimer's disease in persons homozygous for the epsilon 4 allele for apolipoprotein E. *N Engl J Med* **334**, 752-758.

[9] Alexander GE, Chen K, Pietrini P, Rapoport SI, Reiman EM (2002) Longitudinal PET Evaluation of Cerebral Metabolic Decline in Dementia: A Potential Outcome Measure in Alzheimer's Disease Treatment Studies. *Am J Psychiatry* **159**, 738-745.

[10] Heiss WD, Kessler J, Slansky I, Mielke R, Szelies B, Herholz K (1993) Activation PET as an instrument to determine therapeutic efficacy in Alzheimer's disease. *Ann N Y Acad Sci* **695**, 327-331.

[11] Small GW, Silverman DH, Siddarth P, Ercoli LM, Miller KJ, Lavretsky H, Wright BC, Bookheimer SY, Barrio JR, Phelps ME (2006) Effects of a 14-day healthy longevity lifestyle program on cognition and brain function. *Am J Geriatr Psychiatry* **14**, 538-545.

[12] Buschert VC, Friese U, Teipel SJ, Schneider P, Merensky W, Rujescu D, Moller HJ, Hampel H, Buerger K (2011) Effects of a newly developed cognitive intervention in amnestic mild cognitive impairment and mild Alzheimer's disease:. A Pilot Study. *J Alzheimers Dis*, doi10.3233/JAD-2011-100999.

[13] Lachman ME, Weaver SL, Bandura M, Elliott E, Lewkowicz CJ (1992) Improving memory and control belief through cognitive restructuring and self-generated strategies. *J Gerontol* **47**, P293-P299.

[14] McKhann G, Drachman D, Folstein M, Katzman R, Price D, Stadlan EM (1984) Clinical diagnosis of Alzheimer's disease: report of the NINCDS-ADRDA Work Group under the auspices of Department of Health and Human Services Task Force on Alzheimer's Disease. *Neurology* **34**, 939-944.

[15] Scheltens P, Barkhof F, Leys D, Pruvo JP, Nauta JJ, Vermersch P, Steinling M, Valk J (1993) A semiquantative rating scale for the assessment of signal hyperintensities on magnetic resonance imaging. *J Neurol Sci* **114**, 7-12.

[16] Stern Y (2006) Cognitive reserve and Alzheimer disease. *Alzheimer Dis Assoc Disord* **20**, 112-117.

[17] Reisberg B, Franssen EH, Hasan SM, Monteiro I, Boksay I, Souren LE, Kenowsky S, Auer SR, Elahi S, Kluger A (1999) Retrogenesis: clinical, physiologic, and pathologic mechanisms in brain aging, Alzheimer's and other dementing processes. *Eur Arch Psychiatry Clin Neurosci* **249**(3), 28-36.

[18] Petersen RC, Smith GE, Waring SC, Ivnik RJ, Tangalos EG, Kokmen E (1999) Mild cognitive impairment: clinical characterization and outcome. *Arch Neurol* **56**, 303-308.

[19] Perry RJ, Hodges JR (1999) Attention and executive deficits in Alzheimer's disease. A critical review. Brain **122**(3), 383-404.

[20] Folstein M, Folstein S, McHugh P (1975) "Mini Mental State" A practical method for grading the cognitive state of patients for the clinician. *J Psychiatric Res* **12**, 189-198.

[21] Rosen WG, Mohs RC, Davis KL (1984) A new rating scale for Alzheimer's disease. *Am J Psychiatry* **141**, 1356-1364.

[22] Friston KJ, Frith CD, Liddle PF, Frackowiak RS (1991) Comparing functional (PET) images: the assessment of significant change. *J Cereb Blood Flow Metab* **11**, 690-699.

[23] Yakushev I, Hammers A, Fellgiebel A, Schmidtmann I, Scheurich A, Buchholz HG, Peters J, Bartenstein P, Lieb K, Schreckenberger M (2009) SPM-based count normalization provides excellent discrimination of mild Alzheimer's disease and amnestic mild cognitive impairment from healthy aging. *Neuroimage* **44**, 43-50.

[24] Borghammer P, Aanerud J, Gjedde A (2009) Data-driven intensity normalization of PET group comparison studies is superior to global mean normalization. *Neuroimage* **46**, 981-988.

[25] Borghammer P, Cumming P, Aanerud J, Forster S, Gjedde A (2009) Subcortical elevation of metabolism in Parkinson's disease - A critical reappraisal in the context of global mean normalization. *Neuroimage* **47**, 1514-1521.

[26] Yakushev I, Landvogt C, Buchholz HG, Fellgiebel A, Hammers A, Scheurich A, Schmidtmann I, Gerhard A, Schreckenberger M, Bartenstein P (2008) Choice of reference area in studies of Alzheimer's disease using positron emission tomography with fluorodeoxyglucose-F18 . *Psychiatry Res* **164**, 143-153.

[27] Forster S, Teipel S, Zach C, Rominger A, Cumming P, Fougere CL, Yakushev I, Haslbeck M, Hampel H, Bartenstein P, Burger K (2010) FDG-PET mapping the brain substrates of visuo-constructive processing in Alzheimer s disease. *J Psychiatr Res* **44**, 462-469.

[28] Forster S, Vaitl A, Teipel SJ, Yakushev I, Mustafa M, la Fougere C, Rominger A, Cumming P, Bartenstein P, Hampel H, Hummel T, Buerger K, Hundt W, Steinbach S (2010) Functional representation of olfactory impairment in early Alzheimer's disease. *J Alzheimers Dis* **22**, 581-591.

[29] Lancaster JL, Woldorff MG, Parsons LM, Liotti M, Freitas CS, Rainey L, Kochunov PV, Nickerson D, Mikiten SA, Fox PT (2000) Automated Talairach atlas labels for functional brain mapping. *Hum Brain Mapp* **10**, 120-131.

[30] Ishii K, Willoch F, Minoshima S, Drzezga A, Ficaro EP, Cross DJ, Kuhl DE, Schwaiger M (2001) Statistical brain mapping of 18F-FDG PET in Alzheimer's disease: validation of anatomic standardization for atrophied brains. *J Nucl Med* **42**, 548-557.

[31] Minoshima S, Giordani B, Berent S, Frey KA, Foster NL, Kuhl DE (1997) Metabolic reduction in the posterior cingulate cortex in very early Alzheimer's disease. *Ann Neurol* **42**, 85-94.

[32] Drzezga A, Riemenschneider M, Strassner B, Grimmer T, Peller M, Knoll A, Wagenpfeil S, Minoshima S, Schwaiger M, Kurz A (2005) Cerebral glucose metabolism in patients with AD and different APOE genotypes. *Neurology* **64**, 102-107.

[33] Förster S, Grimmer T, Miederer I, Henriksen G, Yousefi BH, Graner P, Wester HJ, Förstl H, Kurz A, Dickerson BC, Bartenstein P, Drzezga A (2011) Regional expansion of hypometabolism in AD follows amyloid-deposition with temporal delay. *Biological Psychiatry (in press)*.

[34] Minoshima S, Frey KA, Koeppe RA, Foster NL, Kuhl DE (1995) A diagnostic approach in Alzheimer's disease using three-dimensional stereotactic surface projections of fluorine-18-FDG PET. *J Nucl Med* **36**, 1238-1248.

[35] Drzezga A, Lautenschlager N, Siebner H, Riemenschneider M, Willoch F, Minoshima S, Schwaiger M, Kurz A (2003) Cerebral metabolic changes accompanying conversion of mild cognitive impairment into Alzheimer's disease: a PET follow-up study. *Eur J Nucl Med Mol Imaging* **30**, 1104-1113.

[36] Borghammer P, Jonsdottir KY, Cumming P, Ostergaard K, Vang K, Ashkanian M, Vafaee M, Iversen P, Gjedde A (2008) Normalization in PET group comparison studies – the importance of a valid reference region. *Neuroimage* **40**, 529-540.

[37] Wagner G, Koch K, Schachtzabel C, Schultz CC, Sauer H, Schlosser RG (2011) Structural brain alterations in patients with major depressive disorder and high risk for suicide: Evidence for a distinct neurobiological entity? *Neuroimage* **54**, 1607-1614.

[38] Haupt S, Axmacher N, Cohen MX, Elger CE, Fell J (2009) Activation of the caudal anterior cingulate cortex due to task-related interference in an auditory Stroop paradigm. *Hum Brain Mapp* **30**, 3043-3056.

[39] Crottaz-Herbette S, Menon V (2006) Where and when the anterior cingulate cortex modulates attentional response: combined fMRI and ERP evidence. *J Cogn Neurosci* **18**, 766-780.

[40] Margulies DS, Kelly AM, Uddin LQ, Biswal BB, Castellanos FX, Milham MP (2007) Mapping the functional connectivity of anterior cingulate cortex. *Neuroimage* **37**, 579-588.

Cognitive Training Changes Hippocampal Function in Mild Cognitive Impairment: A Pilot Study

Allyson C. Rosen[a,b,c,*], Lisa Sugiura[a,c], Joel H. Kramer[d], Susan Whitfield-Gabrieli[c,e] and John D. Gabrieli[c,e]

[a]*Department of Psychiatry, Stanford University, Stanford, CA, USA*
[b]*Palo Alto Veterans Affairs Health Care System, Palo Alto, CA, USA*
[c]*Department of Psychology, Stanford University, Stanford, CA, USA*
[d]*Memory and Aging Center, UCSF Medical Center, San Francisco, CA, USA*
[e]*Department of Brain and Cognitive Sciences, MIT, Cambridge, MA, USA*

Abstract. A randomized pilot experiment examined the neural substrates of response to cognitive training in participants with mild cognitive impairment (MCI). Participants performed exercises previously demonstrated to improve verbal memory and an active control group performed other computer activities. An auditory-verbal fMRI task was conducted before and after the two-month training program. Verbal memory scores improved significantly and left hippocampal activation increased significantly in the experimental group (gains in 5 of 6 participants) relative to the control group (reductions in all 6 participants). Results suggest that the hippocampus in MCI may retain sufficient neuroplasticity to benefit from cognitive training.

Keywords: MRI, dementia, cognition, MCI, mild cognitive impairment, fMRI, functional MRI, cognitive training, hippocampus, medial temporal lobe

INTRODUCTION

A fundamental goal in research on Alzheimer's disease (AD) is to intervene early in the progression from healthy aging to AD so that conversion to AD can be significantly slowed or prevented. Mild cognitive impairment (MCI) describes the transitional state in conversion from healthy aging to dementia in which there is cognitive (typically memory) dysfunction but not functional disability [3]. Early intervention may be important because brain changes leading to AD occur years before the diagnosis of AD [4, 5], by which time pathology is so severe that treatment is difficult. Epidemiologic studies suggest that enriching mental activity may moderate the trajectory of the disease because healthy older adults who participate in a variety of social and cognitive activities are less likely to develop MCI and less likely to progress to dementia [6–9]. Although some of these studies were prospective and longitudinal [e.g. 7, 8, 10], the strongest evidence supporting the claim that mental activity slows disease progression would be a randomized intervention study that alters both the key cognitive disability and the neural system affected early in AD. There have been several cognitive training programs for MCI participants [e.g. for a review see 11], but none has examined brain changes in a randomized intervention study.

*Correspondence to: Allyson C. Rosen, Ph.D., Palo Alto VA Medical Center, 3801 Miranda Ave (151Y), Palo Alto, CA 94304-1207, USA. Tel.: (650) 279 3949; Fax: (650) 852 3297; E-mail: rosena@psych.stanford.edu.

Medial temporal lobe (MTL) regions, including the hippocampus, are most commonly affected in MCI and early AD [4, 12, 13]. These MTL regions are essential [14, 15] for consciously recollected memory [16, 17]. Demonstrating both memory improvements and changes in the functioning of the MTL would thus provide evidence that it is possible for interventions to alter the brain system most affected by MCI and AD.

The cognitive training program from Posit Science involved adaptive games aimed at enhancing the speed and accuracy of auditory verbal processing [18–20], and has been demonstrated to improve memory performance in healthy elderly and MCI participants [1, 2, 18, 21]. Although the mechanism by which perceptual training could enhance MTL function is unknown, any influence of training on explicit or declarative memory likely involves MTL function.

Here, we examined the influence of this cognitive training program on memory ability and brain function in MCI participants in a random assignment design with an active control group. For the neuroimaging study, twelve participants with MCI (6 experimental, 6 active control) were recruited from a larger clinical trial of MCI [21], and fMRI researchers were blind to the assigned treatment conditions. An incidental repetition (versus novelty) fMRI paradigm was used because such a paradigm reveals impaired MTL function in AD [22], and is easy for memory-impaired participants to perform. AD participants exhibit reduced MTL differences between novel and repeated items [22], which indicates that MTL injury in AD reduces the typically greater MTL response for novel than repeated items during encoding. We used an auditory-verbal repetition paradigm to relate to the auditory-verbal nature of the training program. Because we were examining memory for verbal material, we expected any difference to be left-lateralized [23–25]; verbal memory has been associated with left hippocampal volume both in healthy aging and in mild AD [26, 27].

METHODS

Participants and procedure

Twelve participants provided informed consent as approved by institutional review boards at UCSF and Stanford University (neuropsychological data in Table 1). Diagnosis of MCI has been described previously [28] and was made by the Memory and Aging Center at UCSF according to recommendations of an international consensus committee [29]. Participants had to show evidence of cognitive decline based on patient and informant report. In addition, they had to be nondemented by DSM IV criteria and show no to minimal impairment in complex daily activities. Participants on acetylcholinesterase inhibitors were eligible, but only if they had been on a steady dose for at least two months. The two groups did not differ significantly on age or mental status (MMSE). The control group had significantly more years of education, but all participants had completed at least a college education.

Participants were randomly assigned to experimental or control groups. The randomization sequence was blinded from research personnel who enrolled participants or who administered cognitive tests. Participants were told that the purpose of the study was to compare the effects of two computer-based cognitive training programs.

Cognitive training was performed in participants' homes on study-provided computers. Participants were contacted weekly to make sure they were progressing through the training and to solve problems if necessary related to computer difficulties and issues of compliance. The experimental group completed a computer-based, cognitive training program developed by Posit Science Corporation (San Francisco, CA). The program involved 7 exercises designed to improve processing speed and accuracy in auditory processing: (1) determine whether 2 sounds were sweeping upward or downward; (2) identify a target syllable when it interrupted a repeated, similar sounding syllable; (3) distinguish between 2 similar sounds (e.g., "bo" and "do"); (4) match sounds on a spatial grid; (5) distinguish between 2 similar sounding words (e.g., "rake" and "lake"); (6) follow a series of instructions that increased in complexity; and (7) identify the picture that corresponded to the sentence. Each exercise employed adaptive tracking methods to continuously adjust task difficulty based on performance. Participants used the program for 100 minutes per day, 5 days per week until either achievement of asymptotic performance levels over a several day period or completion of 80% of the training material in a given exercise. Progress was monitored automatically through weekly electronic data upload. The control group performed 3 types of computer-based activities to control for the time intensity of the intervention and to keep participants "blind" as to their group assignment. Specifically, participants were given weekly "assignments" that involved listening to audio books, reading online newspapers, and playing a visuospatially oriented computer

Table 1
Baseline demographic and neuropsychological data and fMRI accuracy and reaction times

| | Experimental | | | | Control | | | | | |
	Mean Raw	SD	Mean SS	SD	Mean Raw	SD	Mean SS	SD	p (raw)	p (SS)
Age	70.67	(10.58)			78.00	(7.92)			0.20	
Education	16.67	(0.82)			18.33	(1.51)			0.04	
MMSE	29.33	(1.21)			27.83	(2.32)			0.19	
RBANS at baseline										
List learning	20.50	(2.59)	84	(13)	21.83	(3.25)	88	(12)	0.45	0.51
Story memory	14.17	(3.87)	88	(14)	15.17	(3.19)	92	(11)	0.64	0.59
Figure copy	19.17	(0.75)	110	(6)	17.83	(2.48)	102	(16)	0.24	0.27
Line orientation	17.17	(2.48)	103	(11)	17.50	(1.87)	106	(10)	0.80	0.59
Picture naming	9.83	(0.41)	107	(9)	9.83	(0.41)	109	(5)	1.00	0.60
Semantic fluency	15.83	(3.76)	90	(14)	15.50	(5.05)	91	(18)	0.90	0.93
Digit span (forward)	10.00	(2.28)	99	(14)	11.50	(2.88)	112	(19)	0.34	0.19
Coding	36.33	(4.13)	90	(8)	34.17	(5.42)	94	(15)	0.45	0.48
List recall	1.33	(1.21)	79	(15)	1.17	(2.86)	77	(13)	0.90	0.87
List recognition	16.33	(1.37)	66	(17)	16.00	(2.45)	68	(27)	0.78	0.92
Story recall	4.67	(3.08)	78	(26)	7.17	(3.25)	93	(15)	0.20	0.21
Figure recall	6.83	(7.03)	81	(26)	9.17	(7.68)	84	(27)	0.60	0.79
Index Scores										
Imediate memory			80	(6)			92	(9)		0.02
Visual constructional functioning			111	(14)			107	(17)		0.72
Language			94	(9)			97	(13)		0.66
Attention			94	(10)			104	(18)		0.23
Delayed memory			66	(13)			77	(22)		0.32
Total			85	(8)			94	(13)		0.18
Sum of index scores	443.83	(33.1)			477.33	(48.45)			0.19	
fMRI										
Visit 1										
Accuracy (percent)	90.43	(7.46)			91.83	(5.35)			0.74	
Novel reaction time (ms)	1072.48	(116.93)			1110.41	(253.14)			0.79	
Repeated reaction time (ms)	830.43	(100)			750.84	(110.44)			0.28	
Novelty effect (ms)	242.05	(33.05)			359.57	(199.44)			0.29	
Visit 2										
Accuracy (percent)	91.84	(6.27)			88.27	(8.15)			0.52	
Novel reaction time (ms)	1098.44	(102.8)			1157.57	(185.41)			0.75	
Repeated reaction time (ms)	699.53	(42.59)			716.48	(80.49)			0.87	
Novelty effect (ms)	398.91	(99.67)			441.08	(146.27)			0.76	

Note. Top of the table displays demographic and baseline neuropsychological test data (RBANS) for all subtests and index scores. Standard scores (SS) are displayed next to the raw subtest scores and these characterize relative strengths and weaknesses of the participant. Normative data were made available by the test author after the publication of the measure (Randolph, 2002, Test Supplement)[1]. Data from both pre and post functional MRI task sessions are displayed on the bottom of the graph including accuracy and reaction time.

game (Myst) for 30 minutes each, for a total of 90 minutes per day, 5 days per week. Progress was monitored through self-report. Training lasted an average of two months across participants. In the beginning of the training, there was a slight difference between the groups in the way time on the task was structured before the regular-length sessions (100 minutes) began. Training for the experimental group lasted 100 minutes per session for 24 sessions; the length gradually increased (20 minutes on the first day, 40 the second, 60, 80, then 100 on day five) for a total of 2200 minutes of training. In order to equate training time in the control group and adjust for the graded onset in the experimental group, training for the control group was 90 minutes per day for 24 sessions; the training session length was fixed for a total of 2160 minutes of training.

MEASURES

Neuropsychological evaluation

The RBANS [Repeatable Battery for the Assessment of Neuropsychological Status, 30] was admin-

---

[1] There was one participant in the experimental group who had a history of temporal lobe epilepsy; however, the clinical staff deemed that the illness was well controlled for a number of years and the current memory decline was of recent onset and unlikely to be due to the progression of the seizure disorder.

istered to evaluate whether training enhanced memory ability. There were two parallel forms of this measure and because the person conducting the assessments was blind to the group status of participants, Form A was used at time 1 and Form B was used at time 2. Because patients with MCI typically have poor memory, we used the immediate subtests rather than delayed memory subtests to avoid floor effects. Immediate memory scores for list learning (sum of word list learning trials) and story recall were averaged for each session (hereafter referred to as the RBANS memory score). Participants were impaired on memory tests, but the control group scored higher than the experimental group on some measures (Table 1). There were no group differences in the delay between pre- and post-testing ($M = 72$ days, $SD = 26$, $p = 0.13$) or the delay between the end of training and post-testing ($M = 10$ days, $SD = 7$, $p = 0.44$).

Functional neuroimaging evaluation

Participants underwent fMRI sessions before and within 2 ½ weeks after finishing training. Each session began with practice outside the MRI in which the participants performed several trials in which they were exposed to the repeated stimuli. Data were collected on a 3 Tesla GE Signa scanner using a spiral [31] acquisition sequence (TR 3000 ms, TE = 30 ms; flip angle = 70, FOV = 24 cm; 64 × 64 matrix; 3.75 mm in-plane resolution, 22 contiguous, axial, 5 mm slices, number of excitations = 1). In order to achieve improved data collection within the MTL, a spiral in/out sequence was used [32]. Clustered acquisition was applied such that the scanner remained silent when the words were presented, over the first 1500 ms of the TR, and the images were collected during the second 1500 ms in each of two 7 minute 21 second runs (data from the first 9 seconds were not collected to allow the MR signal to stabilize) (Fig. 1).

Word stimuli consisted of abstract and concrete, auditorily presented nouns that were equalized for volume. Parallel but different word lists were used pre- and post-training, each list consisting of 96 words for the novel condition, and 2 words (one abstract and one concrete) in the repeated condition. The forms were equated for frequency, concreteness, and numbers of syllables [33]. Words were classified as abstract if their concreteness ratings were less than 400 and concrete if their concreteness ratings were greater than 500. Words that had more than one meaning but sounded identical (e.g. pair, pare, pear) were excluded even if
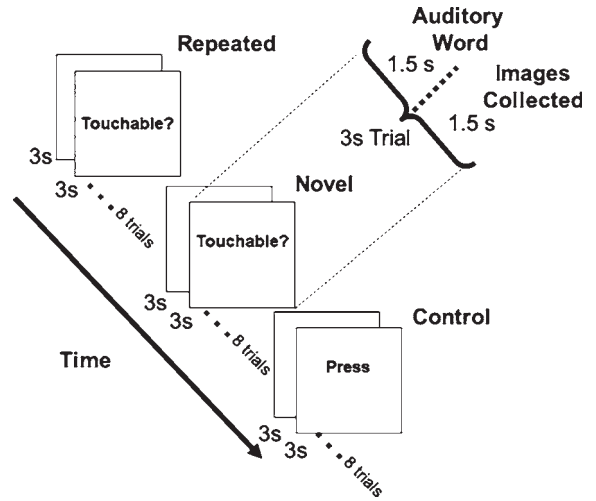
Fig. 1. The design of the experiment was that words were presented during periods when the MRI was silent so that participants could hear them. The instructions were displayed visually and word stimuli were presented auditorily.

both words resulted in the same response (e.g., son, sun). Because the neuroimaging researchers were blind to group assignment, the two lists were presented in a fixed order for pre- and post-testing. Because the study design involved the use of blocked trials, the ratio of abstract to concrete words was 1 : 4 so that for each block most nouns were concrete but there were enough "catch" (i.e., abstract word) trials that participants needed to attend and make decisions about each word.

Participants heard a series of auditorily presented words and performed a right index finger keypress to indicate whether or not each word was "touchable" (concrete). A blocked design was used with 3 conditions cycling 6 times in a pseudorandom order (novel, repeated, sensorimotor control). Trials lasted 3 seconds and there were 8 words in each 24-sec block. In novel blocks, 8 words were presented once only. In repeated blocks, there were 2 words, one abstract (2 times per block) and one concrete (presented 6 times per block) that were presented repeatedly in all repeated blocks. In the sensorimotor control periods, participants pressed the keypress in response to the auditorily presented command "press". During the repeated and novel word conditions, the visual command "Touchable?" was displayed, and during the sensorimotor control condition the command "Press" was displayed (Fig. 1).

Functional MRI data were analyzed using SPM2 (Wellcome Department of Cognitive Neurology, London, UK; SPM2) implemented in MATLAB (Version 6.5.1 Mathworks, Inc., Sherborn, MA). Functional images were motion corrected, normalized into a common stereotactic space (template from Montreal Neurological Institute) and spatially smoothed with a Gaussian filter (FWHM 6 mm). A model (a box-car reference function, corresponding to the time course of the novel, repeated, and control conditions convolved with an estimate of the hemodynamic response function) was fit to the fMRI time series data from each participant. Contrast images consisting of a weighted linear combination of parameter estimates at each voxel for the comparison of interest, the novelty effect (i.e., novel-repeated word judgments) were computed for each participant. Within-group and between-group random effects analyses were conducted on these contrast images. A mask of the left hippocampus was generated using the Wake Forest University pickatlas [http://www.fmri.wfubmc.edu/cms/software#Pick Atlas, 34, 35]. This mask was applied to perform a small volume correction in the left hippocampus ($p < 0.05$, family wise error corrected). In order to explore whether any other region in the brain showed a significant change due to treatment, we also performed a more liberal whole-brain analysis, $p < 0.001$, uncorrected, spatial threshold 5 voxels.

ANALYSES

The effect of training was examined in both the neuropsychological and fMRI data by submitting each to a mixed design ANOVA that tested for an interaction of time (pre- and post-training as a repeated measure) and group (experimental and control groups as a between subjects measure). Significant differences were interrogated with post-hoc t tests. We hypothesized that the experimental group would show a greater increase in RBANS immediate auditory verbal memory scores than the control group. This prediction was based on a prior finding of training-induced gains in healthy older people [1, 2], and a trend towards gains in MCI patients [21]. In the fMRI analysis, we hypothesized that the experimental group would demonstrate a greater increase in fMRI activation (novel > repeated conditions) than the control group. We also examined, via correlation analyses, whether there was any relation between changes in activation and either changes in RBANS scores.

RESULTS

Training progress in experimental participants

All participants in the experimental group made progress in the training program as measured by improved performance on training tasks from the beginning to the end of the program; improvements varied across participants from 43% to 100% of the stimulus content ($M = 78.8\%$, SD = 26.2).

Neuropsychological change

The experimental group (pre-training $M = 17.3$, $SD = 1.9$; post-training $M = 20.0$, $SD = 3.3$) showed a greater gain in performance than the control group (pre-training $M = 18.5$, $SD = 2.9$; post-training=17.4, $SD = 4.1$; $F (1,10) = 4.76$, $p = 0.054$) (no main effect of group or session). This trend toward an interaction reflected significantly greater gain in memory performance in the experimental group ($M = 2.67, SD = 3.16$) than in the control group, who declined ($M = -1.08$, $SD = 2.78$) in performance across sessions. Because there was reason to expect based on previous studies that the experimental group would have an advantage over the control group, a one-tailed test of change scores was performed (t (10) $= 2.61$, $p < .027$, Cohen's $d = 1.38$) (Fig. 2).

Brain function change

In the a priori region of interest in left hippocampus, there was a significant interaction between group, session, and activation in left anterior hippocampus (peak Talairach coordinates -32, -13, -19) (Fig. 2). This reflected a small but consistent gain in activation in this region in the experimental group (5/6 participants exhibiting post-treatment gains in activation) and a larger and consistent loss of activation in the control group (6/6 participants exhibiting post-treatment declines in activation). Exploratory whole-brain analysis revealed a significant interaction between group, session, and activation only in virtually the same location (peak Talairach coordinates -30, -14, -21). Pre-post changes in left hippocampal activation across all participants tended to correlate positively with pre-post changes in RBANS memory scores ($r = 0.49$, $p = 0.10$, Cohen's $d = 1.14$). Functional MRI pre-testing occurred an average of 4 days away from cognitive testing ($SD = 11$), and there were no differences between the groups in this delay ($p = 0.17$).
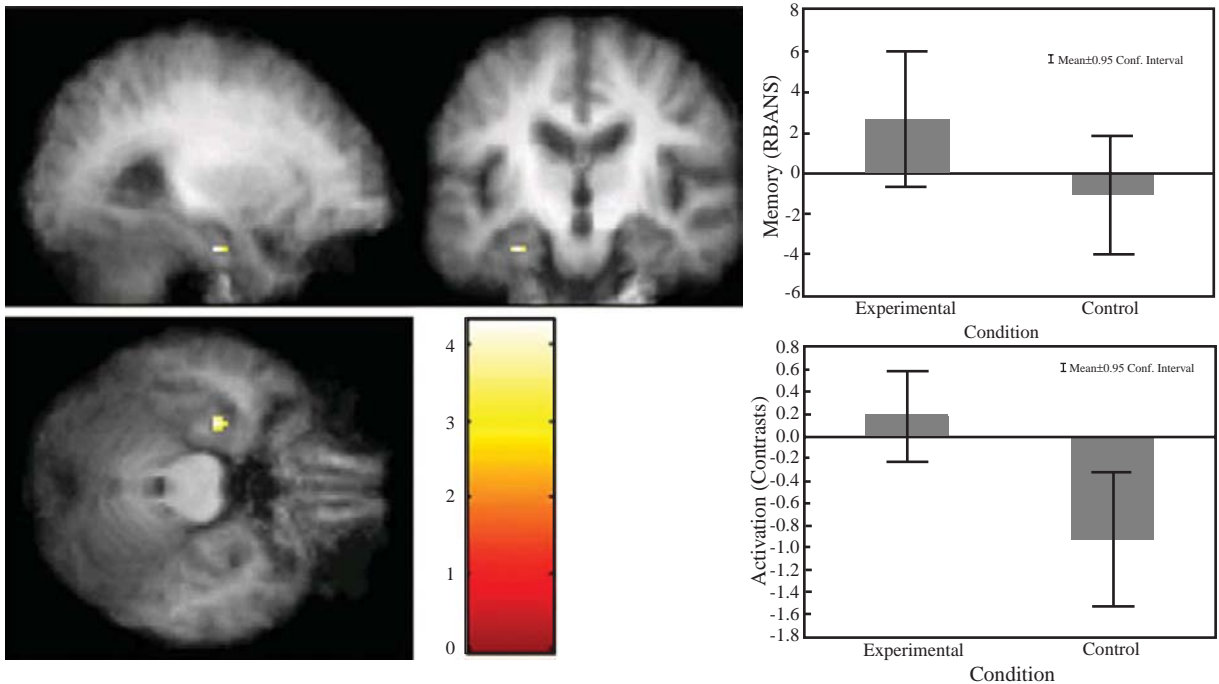
Fig. 2. Brain and behavioral differences between experimental and control groups before versus after intervention. The left panel depicts the location in left hippocampus that showed a significant interaction between group and intervention, such that the experimental group showed increased activation and the control group showed decreased activation for novel relative to repeated words after intervention (shown in bottom right panel). Top right panel shows changes in memory performance before versus after intervention, with a gain in memory performance for the experimental group and a loss in memory performance for the control group. Bars in histograms depict 95% confidence intervals.

Functional MRI post-testing occurred an average of 2 days away from the cognitive testing ($SD = 5$), and there was no difference between the groups in this delay ($p = 0.73$).

Behavioral effects in the MRI

Behavioral data from the scanner were lost on two participants from the experimental group during pretraining due to equipment error, and this left 4 experimental and 6 control subjects with complete behavioral data. Behavioral data were available from all 12 participants after training. There was no significant difference between the groups for either session with respect to accuracy (means in Table 1). An ANOVA of reaction times on the 10 participants with complete data comparing session (pre-, post-training), repetition (novel, repeated), and group (experimental, control) failed to detect any group differences, but responses were faster for repeated ($M = 746.8$, $SD = 90.3$) than novel words ($M = 1120.5$, $SD = 168.2$) (main effect of repetition ($F (1, 8) = 66.14$, $p < .001$),

and there was an interaction between session and repetition ($F (1, 8) = 14.62$, $p < .005$). The interaction reflected a growth of the advantage for repeated relative to novel words from pre-training ($M = 301$ ms, $SD = 162$) to post-training ($M = 420$ ms, $SD = 133$). Importantly, there was neither a main effect nor an interaction with group, which means that any activation differences between groups cannot be accounted for by response-time or accuracy differences between groups.

DISCUSSION

In a random-assignment, active-placebo experiment with MCI participants, cognitive training positively affected memory ability and memory-related left hippocampal function. The small number of participants in the study warrants a conservative interpretation of the findings. In regards to MTL activation, the benefit for the experimental group appeared to reflect less of the continuing decline that was expected in MCI and was evident in the MCI control group. The hippocam-

pal changes in function were, however, consistent at a single-patient level: There was virtually no overlap in pre-post activation changes between the experimental group (with 5/6 participants showing increased activation) and the control group (with all 6 participants showing decreased activation and with all decreases larger than the single decrease in the experimental group). Thus, these findings suggest that despite presumed injury to the hippocampus in MCI that typically leads to AD, the hippocampus in MCI retains sufficient neuroplasticity to benefit from cognitive remediation

The behavioral and imaging findings are consistent with and extend previous work in older adults and participants at risk for dementia showing that mental activity is associated with brain plasticity. MTL chemistry was modified by prolonged cognitive training in a study of healthy older adults that demonstrated changes in hippocampus using MR spectroscopy [36]. A longitudinal study found that self-reported histories of higher life-span cognitive activity were associated with a reduced rate of hippocampal volume atrophy [37]. A small cohort of older adults (8 experimental, 9 control) with memory difficulty performed a variety of healthy lifestyle changes over the course of 2 weeks, including performing "brain teasers" and verbal mnemonic memory training [38]. Improved verbal fluency was associated with decreased dorsolateral prefrontal metabolism, but there was no improvement in verbal memory.

Cognitive training in the present study appeared to enhance hippocampal function despite the fact that the training focused on auditory-verbal perception rather than memory per se. The finding that increased hippocampal activation was associated with better memory performance on neuropsychological testing is consistent with correlational evidence that increased hippocampal fMRI activation in MCI participants is compensatory [39]. Although it is expected that a gain, or reduced loss of, memory function in MCI would be associated with MTL plasticity, it is unknown as to why this training program was associated with MTL functional plasticity and not functional plasticity in auditory neocortex. Both frontal and hippocampal regions, as opposed to inferior parietal, superior temporal, and anterior cingulate regions, have exhibited upregulation in choline acetyletransferase activity in MCI relative to healthy older adults, and thus both regions may be particularly amenable to intervention [40]. Also, although MTL functional plasticity was observed, that plasticity could reflect a functional benefit of primary, structural plasticity in other brain regions; however, in this study only MTL plasticity was robust enough to detect with fMRI.

A question of interest is what psychological and neural mechanisms translate training that focuses on auditory perception to gains in auditory memory and hippocampal function. One possibility is suggested by animal studies of neuroplasticity showing that degraded brain processing of perceptual inputs can degrade the quality of mental representations, and that perceptual training can improve the accuracy of higher order mental representations [18, 41]. Improved auditory representations of the words heard in the scanner may have enhanced experience-dependent plasticity. Several studies of aging have shown surprisingly strong correlations between basic sensory and memory declines (e.g. [42]). These could reflect a shared mechanism that is related to performance on both sensory and memory tests, such as attention. Alternatively, it may be that improved perceptual processing enhances memory performance in that modality. Some studies have found, for example, that cataract surgery improving vision also improves broader cognition [43]. We did not observe training-related alterations of activation in auditory temporal-lobe regions that could mediate perceptual training, but this may reflect the limited sample size.

There were several limitations to the current study beyond the small sample. The study was conducted prior to current MCI subtyping so it is uncertain how many participants would now be classified as amnestic-MCI. The baseline test scores suggest that the majority of the participants had significant memory dysfunction, with low standardized scores on delayed tests of memory, but average scores on visual construction, language, and attention indices (Table 1). Overall, this would be consistent with an amnestic-MCI subtype. The present study was not designed to examine the duration of benefits from cognitive training. In healthy adults, gains achieved via cognitive training were sustained over a 3-month no-contact period [1]. In the present study, imaging occurred days to weeks after training was completed, so benefits do not appear to end immediately after training. It seems likely, however, that benefits from a cognitive training program in the face of a degenerative brain disease would not last long without continued application (as would be the case with physical exercise or medications). We attempted to match exact time spent training between the groups, but the control group self-reported their training times (in contrast automatic data downloading for the experimental group) so that training times of

the control group may be less accurate. Future studies should automatically track training times in all conditions.

Because of the relatively small group of participants, subtle individual differences may have an impact on our results and we address these differences here. One participant in the study had chronic, well controlled, temporal lobe epilepsy, but this participant's memory performance and activation pattern were typical for the treatment group and did not alter the overall outcomes. Also, the control group was slightly but significantly better educated than the experimental group. It is not possible to know the impact of this difference in education on the failure of the control group to benefit from training because so few studies of cognitive training in MCI have been conducted. A previous meta-analysis of 19 studies (30 training groups) comparing healthy older adults above and below 14 years of education (a median split) failed to find an effect of education on cognitive training outcome [44]. Education has also been found to be unrelated to disease progression in dementia, but is related to relatively higher cognitive functioning [45]. Thus, the available evidence suggests that the small but significant difference in education between the two groups is unlikely to account for the findings.

With the caveats noted above, however, the present findings report that cognitive training in a random-assignment, double-blinded, active-placebo design was associated with less loss of memory ability and growth of hippocampal activation in MCI. These findings ought to motivate larger studies to more definitively determine whether such cognitive training can slow memory loss and functional hippocampal degeneration and extend a higher quality of life in MCI.

ACKNOWLEDGMENTS

DISCLOSURE STATEMENT

REFERENCES

[1] Mahncke HW, Connor BB, Appelman J, Ahsanuddin ON, Hardy JL, Wood RA, Joyce NM, Boniske T, Atkins SM, Merzenich MM (2006) Memory enhancement in healthy older adults using a brain plasticity-based training program: a randomized, controlled study. *Proc Natl Acad Sci U S A* **103**, 12523-12528.

[2] Smith GE, Housen P, Yaffe K, Ruff R, Kennison RF, Mahncke HW, Zelinski EM (2009) A cognitive training program based on principles of brain plasticity: results from the Improvement in Memory with Plasticity-based Adaptive Cognitive Training (IMPACT) study. *J Am Geriatr Soc* **57**, 594-603.

[3] Petersen RC (2007) Mild Cognitive Impairment. *Continuum Lifelong Learning in Neurology* **13**, 15-38.

[4] Kordower JH, Chu Y, Stebbins GT, DeKosky ST, Cochran EJ, Bennett D, Mufson EJ (2001) Loss and atrophy of layer II entorhinal cortex neurons in elderly people with mild cognitive impairment. *Ann Neurol* **49**, 202-213.

[5] de Leon MJ, Convit A, Wolf OT, Tarshish CY, Desanti S, Rusinek H, Tsui W, Kandil E, Scherer AJ, Roche A, Imossi A, Thorn E, Bobinski M, Caraos C, Lesbre P, Schlyer D, Poirier J, Reisberg B, Fowler J (2001) Prediction of cognitive decline in normal elderly subjects with 2-[18F]fkyiri-2-deoxy-D-glucose/positron-emission tomography (FDG/PET). *Proceedings of the National Academy of Sciences of the United States of America* **98**, 10966-10971.

[6] Verghese J, Lipton RB, Katz MJ, Hall CB, Derby CA, Kuslansky G, Ambrose AF, Sliwinski M, Buschke H (2003) Leisure activities and the risk of dementia in the elderly. *New England Journal of Medicine* **348**, 2508-2516.

[7] Verghese J, LeValley A, Derby C, Kuslansky G, Katz M, Hall C, Buschke H, Lipton RB (2006) Leisure activities and the risk of amnestic mild cognitive impairment in the elderly. *Neurology* **66**, 821-827.

[8] Wilson RS, Mendes de Leon CF, Barnes LL, Schneider JA, Bienias JL, Evans DA, Bennett DA (2002) Participation in cognitively stimulating activities and risk of incident Alzheimer disease. *JAMA* **287**, 742-748.

[9] Fratiglioni L, Paillard-Borg S, Winblad B (2004) An active and socially integrated lifestyle in late life might protect against dementia. *Lancet Neurology* **3**, 343-353.

[10] Wang JYJ (2006) Leisure activity and risk of cognitive impairment: the Chongqing aging study. *Neurology* **66**, 911-913.

[11] Belleville S (2008) Cognitive training for persons with mild cognitive impairment. *Int Psychogeriatr* **20**, 57-66.

[12] Braak H, Braak E (1996) Evolution of the neuropathology of Alzheimer's disease. *Acta Neurol Scand Suppl* **165**, 3-12.

[13] Scheff SW, Price DA, Schmitt FA, Mufson EJ (2006) Hippocampal synaptic loss in early Alzheimer's disease and mild cognitive impairment. *Neurobiology of Aging* **27**, 1372-1384.

[14] Rempel-Clower NL, Zola SM, Squire LR, Amaral DG (1996) Three cases of enduring memory impairment after bilateral damage limited to the hippocampal formation. *Journal of Neuroscience* **16**, 5233-5255.

[15] Scoville WB, Milner B (1957) Loss of recent memory after bilateral hippocampus leasions. *Journal of Neurology, Neurosurgery, and Psychiatry* **20**, 11-21.

[16] Tulving E (2002) Episodic memory: from mind to brain. *Annual Review of Psychology* **53**, 1-25.

[17] Cohen NJ, Squire LR (1981) Retrograde amnesia and remote memory impairment. *Neuropsychologia* **19**, 337-356.

[18] Mahncke HW, Bronstone A, Merzenich MM (2006) Brain plasticity and functional losses in the aged: scientific bases for a novel intervention. *Prog Brain Res* **157**, 81-109.

[19] Ahissar E, Nagarajan S, Ahissar M, Protopapas A, Mahncke H, Merzenich MM (2001) Speech comprehension is correlated with temporal response patterns recorded from auditory cortex. *Proc Natl Acad Sci U S A* **98**, 13367-13372.

[20] Tallal P, Miller SL, Bedi G, Byma G, Wang X, Nagarajan SS, Schreiner C, Jenkins WM, Merzenich MM (1996) Language comprehension in language-learning impaired children improved with acoustically modified speech. *Science* **271**, 81-84.

[21] Barnes DEPM, Yaffe KM, Belfor NP, Jagust WJM, DeCarli CM, Reed BRM, Kramer JHP (2009) Computer-based Cognitive Training for Mild Cognitive Impairment: Results from a Pilot Randomized, Controlled Trial. *Alzheimer Disease & Associated Disorders* **23**, 205-210.

[22] Golby A, Silverberg G, Race E, Gabrieli S, O'Shea J, Knierim K, Stebbins G, Gabrieli J (2005) Memory encoding in Alzheimer's disease: an fMRI study of explicit and implicit memory. *Brain* **128**, 773-787.

[23] Kelley WM, Miezin FM, McDermott KB, Buckner RL, Raichle ME, Cohen NJ, Ollinger JM, Akbudak E, Conturo TE, Snyder AZ, Petersen SE (1998) Hemispheric specialization in human dorsal frontal cortex and medial temporal lobe for verbal and nonverbal memory encoding. *Neuron* **20**, 927-936.

[24] Golby AJ, Poldrack RA, Brewer JB, Spencer D, Desmond JE, Aron AP, Gabrieli JDE (2001) Material-specific lateralization in the medial temporal lobe and prefrontal cortex during memory encoding. *Brain* **124**, 1841-1854.

[25] Saykin AJ, Johnson SC, Flashman LA, McAllister TW, Sparling M, Darcey TM, Moritz CH, Guerin SJ, Weaver J, Mamourian A (1999) Functional differentiation of medial temporal and frontal regions involved in processing novel and familiar words: an fMRI study. *Brain* **122**, 1963-1971.

[26] deToledo-Morrell L, Dickerson B, Sullivan MP, Spanovic C, Wilson R, Bennett DA (2000) Hemispheric differences in hippocampal volume predict verbal and spatial memory performance in patients with Alzheimer's disease. *Hippocampus* **10**, 136-142.

[27] Rosen AC, Prull MW, Gabrieli JD, Stoub T, O'Hara R, Friedman L, Yesavage JA, Detoledo-Morrell L (2003) Differential associations between entorhinal and hippocampal volumes and memory performance in older adults. *Behav Neurosci* **117**, 1150-1160.

[28] Kramer JH, Nelson A, Johnson JK, Yaffe K, Glenn S, Rosen HJ, Miller BL (2006) Multiple cognitive deficits in amnestic mild cognitive impairment. *Dement Geriatr Cogn Disord* **22**, 306-311.

[29] Winblad B, Palmer K, Kivipelto M, Jelic V, Fratiglioni L, Wahlund LO, Nordberg A, Bäckman L, Albert M, Almkvist O, Arai H, Basun H, Blennow K, de Leon M, DeCarli C,

Erkinjuntti T, Giacobini E, Graff C, Hardy J, Jack C, Jorm A, Ritchie K, van Duijn C, Visser P, & Petersen RC (2004). Mild cognitive impairment–beyond controversies, towards a consensus: report of the International Working Group on Mild Cognitive Impairment. *Journal of Internal Medicine* **256**, 240-246.

[30] Randolph C, Tierney MC, Mohr E, Chase TN (1998) The Repeatable Battery for the Assessment of Neuropsychological Status (RBANS): preliminary clinical validity. *J Clin Exp Neuropsychol* **20**, 310-319.

[31] Glover GH, Lai S (1995) Self-navigated spiral fMRI: interleavedversus single-shot. *Magnetic Resonance Imaging* **39**, 361-368.

[32] Glover GH, Law CS (2001) Spiral-in/out BOLD fMRI for increased SNR and reduced susceptibility artifacts. *Magn Reson Med* **46**, 515-522.

[33] Coltheart M (1981) The MRC Psycholinguistic Database. *Quarterly Journal of Experimental Psychology* **33A**, 497-505.

[34] Lancaster JL, Woldorff MG, Parsons LM, Liotti M, Freitas CS, Rainey L, Kochunov PV, Nickerson D, Mikiten SA, Fox PT (2000) Automated Talairach atlas labels for functional brain mapping. *Human Brain Mapping* **10**, 120-131.

[35] Maldjian JA, Laurienti PJ, Kraft RA, Burdette JH (2003) An automated method for neuroanatomic and cytoarchitectonic atlas-based interrogation of fMRI data sets. *Neuroimage* 1233-1239.

[36] Valenzuela MJ (2003) Memory training alters hippocampal neurochemistry in healthy elderly. *Neuroreport* **14**, 1333-1337.

[37] Valenzuela MJ, Sachdev P, Wen W, Chen X, Brodaty H (2008) Lifespan mental activity predicts diminished rate of hippocampal atrophy. *PLoS One* **3**, e2598.

[38] Small GW, Silverman DH, Siddarth P, Ercoli LM, Miller KJ, Lavretsky H, Wright BC, Bookheimer SY, Barrio JR, Phelps ME (2006) Effects of a 14-day healthy longevity lifestyle program on cognition and brain function. *American Journal of Geriatric Psychiatry* **14**, 538-545.

[39] Dickerson BC, Sperling RA (2008) Functional abnormalities of the medial temporal lobe memory system in mild cognitive impairment and Alzheimer's disease: insights from functional MRI studies. *Neuropsychologia* **46**, 1624-1635.

[40] DeKosky ST, Ikonomovic MD, Styren SD, Beckett L, Wisniewski S, Bennett DA, Cochran EJ, Kordower JH, Mufson EJ (2002) Upregulation of choline acetyltransferase activity in hippocampus and frontal cortex of elderly subjects with mild cognitive impairment. *Ann Neurol* **51**, 145-155.

[41] Allard T, Clark SA, Jenkins WM, Merzenich MM (1991) Reorganization of somatosensory area 3b representations in adult owl monkeys after digital syndactyly. *J Neurophysiol* **66**, 1048-1058.

[42] Lindenberger U, Baltes PB (1994) Sensory functioning and Intelligence in Old Age: A Strong Connection 1057. *Psychology and Aging* **9**, 339-355.

[43] Tamura H, Tsukamoto H, Mukai S, Kato T, Minamoto A, Ohno Y, Yamashita H, Mishima HK (2004) Improvement in cognitive impairment after cataract surgery in elderly patients. *Journal of Cataract & Refractive Surgery* **30**, 598-602.

[44] Verhaeghen P, Marcoen A, Goossens L (1992) Improving memory performance in the aged through mnemonic training: a meta-analytic study. *Psychol Aging* **7**, 242-251.

[45] Wilson RS, Hebert LE, Scherr PA, Barnes LL, de Leon CFM, Evans DA (2009) Educational attainment and cognitive decline in old age. *Neurology* **72**, 460-465.

This page intentionally left blank

Validation and Pilot Application of [^{18}F]FDG-PET in Evaluation of a Metabolic Therapy for Alzheimer's Disease

Sofia Tzimopoulou [a], Vincent J. Cunningham [a], Thomas E. Nichols [b], Graham Searle [a], Nick P. Bird [c], Prafull Mistry [c], Ian J. Dixon [c], William A. Hallett [a], Brandon Whitcher [a], Andrew P. Brown [a], Marina Zvartau-Hind [d], Narinder Lotay [d], Robert Y.K. Lai [e], Mary Castiglia [f], Barbara Jeter [f], Julian C. Matthews [g], Kewei Chen [h,j,l], Dan Bandy [h,l], Eric M. Reiman [i,k,l], Michael Gold [f], Eugenii A. Rabiner [a,m] and Paul M. Matthews [a,m,*]

[a]*GlaxoSmithKline, Clinical Imaging Centre, Hammersmith Hospital, London, UK*

[b]*Department of Statistics & Warwick Manufacturing Group, University of Warwick, Coventry, UK*

[c]*GlaxoSmithKline, Discovery Biometrics, Harlow, UK*

[d]*GlaxoSmithKline, Neurosciences Medicine Development Centre, London, UK*

[e]*Glaxosmithkline, Neurosciences Discovery Medicine, Harlow, UK*

[f]*GlaxoSmithKline, Neurosciences Medicine Development Centre, Research Triangle Park, NC, USA*

[g]*School of Cancer and Enabling Sciences, Wolfson Molecular Imaging Centre, University of Manchester, Manchester, UK*

[h]*Banner Alzheimer's Institute, and Positron Emission Tomography Centre, Banner Good Samaritan Medical Centre, Phoenix, AZ, USA*

[i]*Department of Psychiatry, University of Arizona, Phoenix, AZ, USA*

[j]*Department of Mathematics and Statistics, Arizona State University, Tempe, AZ, USA*

[k]*Neurogenomics Division, Translational Genomics Research Institute, Phoenix, AZ, USA*

[l]*Arizona Alzheimer's Consortium, Phoenix, AZ, USA*

[m]*Department of Clinical Neuroscience, Imperial College, London, UK*

Abstract. Here we describe methods for application of quantitative fluorodeoxyglucose positron emission tomography ([^{18}F]FDG-PET) measures of brain glucose metabolism in multi-centre clinical trials for Alzheimer's disease. We validated methods and demonstrated their use in the context of a treatment trial with the PPARγ agonist Rosiglitazone XR versus placebo in mild to moderate AD patients. Novel quantitative indices related to the combined forward rate constant for [^{18}F]FDG uptake (K_i^{index}) and to the rate of cerebral glucose utilization (CMR_{glu}^{index}) were applied. Active treatment was associated with a sustained but not statistically significant trend from the first month for higher mean values in both. However, neither these nor another analytical approach recently validated using data from the Alzheimer's Disease Neuroimaging Initiative suggested that active treatment decreased the progression of decline in brain glucose metabolism. Rates of brain atrophy were similar between active

*Correspondence to: Professor P.M. Matthews, GSK Clinical Imaging Centre, Hammersmith Hospital, DuCane Road, London W12 0NN, UK. Tel.: +44 208 008 6036; Fax: +44 208 008 6491. E-mail: paul.m.matthews@gsk.com.

and placebo groups and measures of cognition also did not demonstrate clear group differences. Our study demonstrates the feasibility of using [¹⁸F]FDG-PET as part of a multi-centre therapeutics trial and describes new measures that can be employed. It suggests that Rosiglitazone is associated with an early increase in whole brain glucose utilisation, but not with any biological or clinical evidence for slowing progression over the period of study in the selected patient group.

INTRODUCTION

Alzheimer's disease (AD) is a progressive neurodegenerative disorder characterised neuropathologically by amyloid plaques, neurofibrillary tangles and neuronal and synaptic loss [1]. A unifying explanation for the aetiology and mechanisms of neurodegeneration in sporadic AD has not yet been established. Abnormal glucose metabolism accompanying systemic disorders such as diabetes mellitus has been proposed to play a contributory role [2].

Positron emission tomography (PET) with 2-fluoro-2-deoxy-D-glucose ([¹⁸F]FDG), demonstrates impairment of cerebral glucose metabolism that precedes clinical expression and worsens with the progression of AD. Characteristic and progressive reductions in glucose metabolism relative to healthy, age-matched controls have been reported for the parietal, temporal, frontal and posterior cingulate cortices in patients with mild to moderate AD [3–10]. Similar changes can be found in brains of people at risk for both familial and sporadic forms of AD prior to the onset of dementia, in pre-symptomatic carriers of the mutations that cause early onset familial AD [11] and in clinically normal carriers of the ε4 allele of the apolipoprotein E gene (APOE4), which predisposes to developing late onset sporadic AD [12–17]. The observed PET changes can be attributed to a reduction in glucose metabolism, the density or activity of terminal neuronal fields or peri-synaptic glial cells, or a combination of these mechanisms.

Post-mortem studies have shown that AD patients have reductions in posterior cingulate cortical mitochondrial activity [18] and reduced neuronal expression of most of the nuclear genes encoding electron transport chain genes and mitochondrial translocases [19]. More recently, genetic evidence has suggested that a variable length poly-T polymorphism of the translocase of outer mitochondrial membrane 40 homolog (TOMM40) gene, just upstream of the APOE gene on chromosome 18, accounts for the earlier age of presentation of late-onset AD in carriers and non-carriers of the ApoE ε4 allele, long considered the major late-onset AD susceptibility gene [20].

While these findings establish a rationale for the association between regional reduction of cerebral glucose metabolism and AD, it is not clear whether abnormalities of glucose metabolism are a cause or a consequence of the core pathology of AD. Abnormalities of glucose metabolism could contribute to the genesis of the disease. There is indirect evidence that abnormal insulin function or insulin resistance contribute to AD pathology. AD patients have lower cerebrospinal fluid (CSF) insulin concentrations, elevated plasma insulin concentrations and reduced CSF:plasma insulin ratios when compared with healthy controls [21]. Insulin is transported into the brain by a saturable, unidirectional process [22] and its uptake is modulated in diabetic mice [23]. Hippocampal and other medial temporal regions that support episodic memory encoding and retrieval that are affected by the earliest neurofibrillary pathology in AD express insulin receptors and insulin sensitive glucose transporters (GLUT4 and GLUT8) [24–26]. Rodents treated with intrathecal streptozotocin (which desensitises brain insulin receptors) develop cognitive impairment [27, 28]. Infusion of insulin while maintaining plasma glucose levels constant (glucose "clamp") was associated with an acute, short-term cognitive improvement in patients with AD, while infusion of glucose with constant plasma levels of insulin (insulin "clamp") did not have the same effect [29]. Together, these findings suggest that treatments augmenting brain insulin receptor function could improve cognition in patients with AD.

Rosiglitazone (RSG) is a peroxisome proliferator activated receptor gamma (PPAR-γ) agonist which has been shown to ameliorate insulin resistance in patients with type II diabetes mellitus [30, 31]. The insulin sensitizing action of PPAR-γ agonists leads to induction of transcription of several genes involved

in glucose and lipid metabolism including those that code for the insulin sensitive glucose transporter GLUT4 [32]. Chronic use of PPAR-γ agonists also increases the expression of GLUT1 [33], the primary, insulin-insensitive glucose transporter of the blood-brain barrier.

Tg2576 mice, a common preclinical model for AD with impaired learning, showed better spatial learning and memory abilities, similar to control wild-type mice, when administered rosiglitazone during behavioural testing [34]. A randomised, double blind study of memory and cognition with rosiglitazone or glyburine as add-on therapy to metformin in type II diabetes patients reported cognitive benefits with rosiglitazone [35]. A placebo controlled, double blind study of 6 months showed improvements in cognitive function in mild AD patients treated with rosiglitazone [36]. Post-hoc analysis of a 24 week, placebo controlled, double blind study showed that mild-to-moderate AD patients who did not carry APOE ε4 allele exhibited cognitive and functional improvement after 24 weeks of treatment with RSG extended release tablets (RSG-XR) (8 mg) [37].

[^{18}F]FDG-PET has been proposed as an end-point for clinical trials in AD [3] because it offers pharmacodynamic measures related to brain glucose metabolism, which can be related directly to synaptic function. Estimates of rates of change and measurement variance suggest that [^{18}F]FDG-PET could provide substantially higher sensitivity for detecting treatment effects than the clinical measures used conventionally in proof-of-concept studies [3, 13]. Recent work has validated an approach for optimising the sensitivity of longitudinal [^{18}F]FDG-PET observations based on the prior empirical definition of a single cortical grey matter region of interest showing maximum change with untreated progression of disease in datasets from the Alzheimer's Disease Neuroimaging Initiative (ADNI) [10], but this has yet to be applied in the context of a therapeutic trial. Other novel measures also are possible.

Here we describe validation of novel measures of brain FDG uptake suitable for use in a multi-centre trial. We also apply an alternative recently well-described measure [10] to distinguish the kinds of results that are available from different methods. Both are used in the contract of a a double blind, placebo controlled, multi-centre study of the effects of a 12 months course of RSG on the rate of decrease of cerebral glucose metabolism (CMR_{glu}) and cognitive performance in patients with mild to moderate AD.

MATERIALS AND METHODS

Study design

This was a 12 months, parallel group, double blind study with subjects randomised to receive either RSG in the form of extended release (XR) or matched placebo. The study was conducted at 14 centers in 3 countries including 2 Canadian sites, 4 sites in the United Kingdom, and 8 sites in the United States.

Subjects in the active group were dosed with RSG-XR 4 mg daily for the first month increasing to 8 mg daily for the remaining 11 months of the study. Subjects underwent 4 PET scans (baseline, 1 month, 6 months and 12 months) and 3 MRI scans (baseline, 6 months and 12 months) for PET registration and brain volumetric analysis. Clinical behavioural scales were evaluated at baseline, 1, 6 and 12 months. The 1 month scans were acquired to test for acute medication effects on brain imaging measurements independent of an AD-slowing effect. A sub-group of patients consented to APOE genotyping.

Recognising the novelty of FDG PET as an outcome measure in AD treatment trials, this study was intended as a hypothesis generating study and thus was powered on feasibility rather than formal statistical considerations. The primary outcome was 12-month cerebral glucose metabolic rate changes in brain regions preferentially affected by AD in the RSG-XR relative to placebo groups.

Subjects

Eligible subjects included males and females between 50–85 years of age who met the National Institute of Neurological and Communicative Diseases and Stroke/Alzheimer's Disease and Related Disorders Association criteria for mild to moderate probable AD [40], had a Mini-Mental State Examination (MMSE) [41] score between 16-26 at screening, and had a dedicated caregiver who was willing to attend all visits, oversee compliance with protocol-specified procedures and study drug use and provide ongoing reports on the subject's status. Patients living alone or in a nursing home were not eligible. Subjects with historical, physical or laboratory evidence of other neurological or non-neurological medical conditions that might influence the outcome or analysis of the PET results were excluded. Thus, patients with history of type I or type II diabetes mellitus or fasting plasma glucose level >126mg/dL or HbA1c >6.2%, as well

Table 1
PET study population demographics

A. Subjects who completed the baseline and 1 month PET scans

	Placebo, $N = 38$	RSG-XR, $N = 38$	Total, $N = 76$
Age (yrs) [Mean, Range]	69.9 (52, 84)	72.2 (53, 85)	71.1 (52, 85)
Gender [N (%)]			
Female	18 (47.4%)	17 (44.7%)	35 (46.1%)
Male	20 (52.6%)	21 (55.3%)	41 (53.9%)
Ethnicity			
White	36 (94.7%)	36 (94.7%)	72 (94.7%)
Non-white	2 (5.3%)	2 (5.3%)	4 (5.3%)
Height (cm) [Mean ± SD*]	169.18 ± 11.49	168.61 ± 10.81	168.89 ± 11.09
Weight (kg) [Mean ± SD]	73.26 ± 15.51	74.73 ± 16.12	74.0 ± 15.73
BMI (kg.m^2) [Mean ± SD]	25.45 ± 3.77	26.15 ± 4.12	25.8 ± 3.94

B. Subjects who completed the 12 months PET scans

	Placebo, $N = 29$	RSG-XR, $N = 31$	Total, $N = 60$
Age (yrs) [Mean, Range]	69.6 (52, 83)	71.9 (53, 85)	70.8 (52, 85)
Gender [N (%)]			
Female	15 (51.7%)	13 (41.9%)	28 (46.7%)
Male	14 (48.3%)	18 (58.1%)	32 (53.3%)
Ethnicity			
White	28 (96.6%)	29 (93.5%)	57 (95.0%)
Non-white	1 (3.4%)	2 (6.5%)	3 (5.0%)
Height (cm) [Mean ± SD*]	168.48 ± 10.38	169.71 ± 10.67	169.12 ± 10.46
Weight (kg) [Mean ± SD]	70.44 ± 11.56	76.38 ± 15.76	73.51 ± 14.10
BMI (kg.m^2) [Mean ± SD]	24.82 ± 3.62	26.42 ± 4.01	25.65 ± 3.90

*SD = standard deviation.

as patients on medications expected to directly affect glucose metabolism were excluded from participation.

Eighty subjects meeting these selection criteria were randomised equally to the active treatment (RSG-XR) and placebo arms of the study. Subjects in the active group were treated with RSG-XR 4 mg daily for the first month and then with 8 mg daily for the remaining 11 months of the study. 76 subjects completed baseline and 1 month scans (38 placebo, 38 RSG-XR), 70 (35 placebo, 35 RSG-XR) subjects completed the 6 month scan and 60 (29 placebo, 31 RSG-XR) completed the 12 months scan. The placebo and treatment groups were well-matched for age, gender, ethnicity and body habitus (Table 1A). Of the 80 randomised patients, 59 consented to APOE genotyping. Thirty nine of those consenting carried at least one APOE ε4 allele (24 placebo, 15 RSG-XR) (APOE4+) and 20 patients did not (6 placebo, 14 RSG- XR) (APOE4-).

Cognitive testing

MMSE

The MMSE [41] was performed by a qualified rater to screen subjects for dementia severity. Scores range from 0–30, with lower scores indicating greater cognitive impairment; scores between 16–26 were used to select subjects with mild-to-moderate severity.

ADAS-Cog

The ADAS-Cog was performed by a qualified rater, who monitored cognitive performance throughout the study. If the score for more than one question was missing, a total score was not imputed.

CIBIC+

CIBIC+ assessments were performed by an independent investigator who was not involved in any other aspect of subject care or assessment and who did not have access to other subject data for the study.

Imaging

PET scanning

Each subject had [18F]FDG-PET scans at baseline and at 1, 6 and 12 months after initiation of treatment. Subjects were requested to abstain from food and drink from the night before the day of the scan. However, scans were performed on patients who reported that

they did not fast if their plasma glucose was <7 mmol/L just before the time of radiotracer administration. The scanning protocol consisted of 34 frames, starting pre-injection through 60 minutes post-injection (see Supplementary Material). Venous samples were drawn at 10, 17.5, 25, 45 and 60 minutes post injection for plasma [^{18}F]FDG and glucose.

MRI scanning

MRI scans were performed at baseline and at 6 and 12 months after initiation of treatment. 3D T1 sequences were selected for measurements of brain atrophy and co-registration of PET images. Software corrections to normalise geometric distortions across sites were made based on data from scanning of a standard phantom across at each site. Acceptable reproducibility of brain structural measures was demonstrated with two serial 3D T1W scans (independently reviewed) of a human volunteer at each site before the start of patient scanning.

Data processing and analysis

Image reconstruction and pre-processing

Three-dimensional re-projection (3DRP) or Fourier re-binning (FORE), combined with two dimensional (2D) reconstruction or 3D ordinary Poisson ordered-subsets expectation maximization (OP-OSEM), were used for image reconstruction [1--3]. All sites were instructed to apply dead time correction, randoms correction, normalisation, geometric correction, measured attenuation correction, scatter correction, axial and transaxial ramp filters. In contrast to the image pre-processing procedures subsequently developed in ADNI [4], this study did not smooth the images acquired on different imaging systems to a common spatial resolution.

Dynamic PET images were corrected for frame-wise subject head motion and registered to the corresponding MRI via rigid body registration, with normalised mutual information as cost function. The brain volume was extracted from the whole head MRI and segmented to generate a grey matter map. The MNI152 template [5] and corresponding anatomical human brain atlas [6] were nonlinearly warped onto each subject's MRI brain image. The warped atlas was then applied in conjunction with the grey matter map to the PET dynamic in order to generate time activity curves (TACs) for the grey matter in the regions of interest (ROIs). TACs were obtained for global

grey matter and the following bilateral ROIs: posterior cingulate gyrus, parietal lobe, posterior temporal lobe, frontal lobe, cerebellum and medial temporal lobe (consisting of hippocampus, amygdala, medial anterior temporal lobe and parahippocampal ambiens gyrus). All rigid body image registrations, nonlinear warps and MRI segmentation were performed using SPM5b [http://www.fil.ion.ucl.ac.uk/spm]. The brain extraction process was performed with FSL3.3.5 [http://www.fmrib.ox.ac.uk/fsl].

The results of brain image extraction and segmentation were quality checked by visual inspection. PET motion correction, PET-MRI co-registration, atlas warp to subject's MRI and subsequent PET alignment and grey mask images were also checked by visual inspection. Image quality control (QC) failures after blinded review included scans with unavailable scan and/or blood data in the measurement interval, scans with faults at FDG injection (infiltration) or PET acquisition and scans associated with incorrect blood data. Five subjects were excluded from the subsequent analysis due to unacceptable image or data quality at the baseline. Additional QC failures at individual timepoints of 1, 6 and 12 months included 1, 1 and 2 scans respectively.

Data processing and analysis

The [^{18}F]FDG-PET and MRI images were stored, processed and analyzed by GSK investigators at the GSK Clinical Imaging Centre, Hammersmith Hospital, London, UK, as described below. Additional information on image acquisition, reconstruction, pre-processing and analysis methods is provided in the Supplementary Material.

PET data

Since arterial sampling to define the input function for each subject and allow conventional kinetic analysis for measurement of CMR_{glu} from [^{18}F] FDG-PET was not considered feasible for a multi-centre, AD protocol, we used two novel methods that were applied after common initial processing steps. The primary analysis was performed using a method based on principles of kinetic modelling (see 2.5.1.a). After the study was completed, we added a secondary analysis using a recently proposed alternative analytical method based on an empirically pre-defined statistical region-of-interest derived from the Alzheimer's Disease Neuroimaging Initiative.

Analysis based on principles of kinetic modelling. Conventionally, the cerebral metabolic rate for glucose, CMR_{glu}, would be estimated from dynamic [^{18}F]FDG-PET scans as

$$CMR_{glu} = K_i \frac{c_p^{glu}}{LC}$$

where K_i is the combined forward rate constant for [^{18}F]FDG, c_p^{glu} is the concentration of native glucose in plasma and LC (the so-called "lumped constant") accounts for the kinetic differences between native glucose and the deoxy analogue. However, in the present study protocol it was not considered practical to obtain arterial blood samples. In order to take into account the delivery of [^{18}F]FDG to the tissue and the concentration of native glucose in plasma without a direct measure of the arterial input function we therefore defined a pragmatic index of the combined forward rate constant as:

$$K_i^{index} = \frac{c_t^*}{c_p^* \times t}$$

where c_t^* is the average concentration of radioactivity in the tissue over the last 30 minutes of the 60 minute scan calculated as the frame average time activity curve of the last 6 frames of the PET dynamic, c_p^* is the average plasma radioactivity calculated from the venous blood samples collected within the last 30 minutes of the scan and $t = 45$ minutes. A corresponding index for the metabolic rate for glucose was then calculated as

$$CMR_{glu}^{index} = K_i^{index} \times c_p^{glu}$$

With these mathematical formulations, drug effects arising from changes in systemic plasma glucose concentration (reflected in c_p^{glu} changes) can be considered in addition to those arising from increased transport or phosphorylation of FDG (K_i^{index} changes).

The analytical approach is described further and data supporting its validation are provided in the original report. Results were obtained for grey matter globally and for the following bilateral ROIs: posterior cingulate gyrus, posterior temporal lobe, parietal lobe, frontal lobe, cerebellum and medial temporal lobe (consisting of amygdala, hippocampus, medial anterior temporal lobe and parahippocampal ambiens gyrus).

Analysis based on an empirically pre-defined statistical region-of-interest derived from the Alzheimer's Disease Neuroimaging Initiative (ADNI). While the analysis described above permitted us to characterize the effects of treatment group, time and their interaction on quantitative PET measurements in anatomically-based ROIs, the statistical power of the approach may be limited by inter-scanner variation in absolute measurements, insensitivity to change within ROIs that may not optimally conform to cluster of voxels most characteristically associated with twelve-month changes in subjects with probable AD and by an inflated Type I error due to the simultaneous search over multiple regions (the multiple comparisons problem). For these reasons, we also used a complementary approach (developed recently using data from ADNI) that may provide improved statistical power for evaluation of treatment effects in multi-centre AD treatment trials [10].

For this new approach, a pair of empirically predefined ROIs was created based on an analysis of a separate dataset of 69 mild probable AD patients from ADNI's training data for brain glucose metabolism. A "spared ROI" consisting of the cluster of voxels associated with 12-month *increases* ($p = 0.0005$) in [^{18}F]FDG uptake (clearly distinguishing them from those voxels associated with regions in which there is progression of neuropathology) and a second, "statistical ROI" (sROI) including voxels that showed the most significant decrease ($p = 0.0005$) were defined. These two pre-defined ROIs then were applied to each image of interest and a single outcome was computed as the ratio of relative glucose metabolism, sROI/"spared"ROI. Application of this *a priori* defined outcome has been found to improve statistical power and, as a single hypothesis, is not subject to loss of power from multiple comparisons when applied in independent data sets [10].

In application of this approach for the current study, we refer to the normalised ratio sROI/"spared" ROI as CMR_{ratio} and characterized 12-month declines in the placebo and RSG- XR groups for this single endpoint. While pre-processing of the image data in the present study was similar to the method as described originally, one difference was that a fixed 8 mm smoothing kernel was used instead of a site-specific kernel size used to obtain common empirically-determined resolution. This could result in less power to detect treatment effects [10].

A voxel-wise analysis of 12 months change in the entire dataset of parametric CMR_{glu}^{index} images from the current study also was performed to re-assess the "face validity" of the sROI.

MRI data

Estimates of changes in the normalised brain volume (NBV) (cubic millimetres) were obtained using SIENAX [38, 39], which is part of the FSL software package [http://www.fmrib.ox.ac.uk/fsl]. All structural MRI data were visually inspected both before and after applying brain segmentation procedures. Reasons for excluding a scan from the analysis included insufficient contrast-to-noise, segmentation failure, insufficient alignment between scans or differing acquisition parameters between scans. 3 subjects were excluded from analysis due to unacceptable quality of the baseline scan. In addition, the number of scans excluded for the 6 and 12 months were 5 and 2 respectively.

Statistical analyses

The difference between RSG-XR and placebo change from baseline was tested for statistical significance in the regional and global CMR_{glu}^{index}, K_i^{index}, as well as in CMR_{ratio}, NBV and clinical scale measures across the four evaluation time-points.

A separate mixed effects model for repeated measures (MMRM) implemented in SAS 9.1 [http://www.sas.com] was fitted to the primary endpoint of change from baseline for each ROI and grey matter. Point estimates and 95% confidence intervals (CI) for the difference were produced. The terms fitted in the MMRM included the fixed categorical terms of treatment, visit, treatment × visit interaction, and the fixed continuous covariates of baseline, baseline × visit interaction and repeated term visit. All p-values presented are for two sided alternatives. The estimates for the absolute change from baseline were re-expressed in percentage form and the differences between groups were expressed as a difference in percentage points.

Similar analyses were undertaken for the MRI data and the clinical scales.

RESULTS

76/80 subjects that enrolled in the study completed the PET baseline and 1 month scans (38 placebo, 38 RSG-XR). The subjects were well matched in terms of baseline MMSE scores (placebo 20.7, CI (19.8, 21.7), RSG-XR 20.9, CI (19.7, 22.1)) and demographic characteristics (Table 1A). 70/80 and 60/80 of the enrolled subjects completed visits up to the 6 and 12 months PET time points. The demographic characteristics of the study populations were still well matched at 12 months (Table 1B).

Testing for treatment effects on brain glucose metabolism in AD with a kinetic-modelling based analysis

For the primary analysis, mean values of CMR_{glu}^{index} and K_i^{index} in subjects receiving a 12 months course of RSG-XR were contrasted with those receiving placebo for the pre-determined, anatomically-defined cortical ROIs and for a global cerebral grey matter ROI. Baseline CMR_{glu}^{index} and K_i^{index} were not significantly different, but the placebo group had mean raw total grey matter values approximately 5.2% higher than the RSG-XR group for CMR_{glu}^{index} (44.7 μg cm^{-3} min^{-1} placebo; 42.5 μg cm^{-3} min^{-1} RSG-XR) and 7.7% higher for the mean raw K_i^{index} (53.1 10^{-3} mL cm^{-3} min^{-1} placebo; 49.3 10^{-3} mL cm^{-3} min^{-1} RSG-XR).

Following an approximately 4.7% decrease for the placebo group and a 1.5% *increase* for the RSG-XR treated group over the first month, the mean raw CMR_{glu}^{index} estimates were similar between the two subject groups (42.8 μg cm^{-3} min^{-1} placebo; 43.6 μg cm^{-3} min^{-1} RSG-XR). The mean raw K_i^{index} estimates also were similar at 1 month (50.0 10^{-3} mL cm^{-3} min^{-1} placebo; 51.8 10^{-3} mL cm^{-3} min^{-1} RSG-XR), reflecting a similar approximately 5.1% decrease in the placebo measures and a 3.1% *increase* in the RSG treated group. However, group differences in changes from baseline in neither of the indices achieved statistical significance ($p = 0.23$ for CMR_{glu}^{index}; $p = 0.14$ for K_i^{index}, both uncorrected for multiple comparisons).

Both placebo and RSG-XR groups showed decreases in CMR_{glu}^{index} over the full 12 months of observation (Fig. 1) (Table 2). Similar relative changes were seen for K_i^{index} in both groups (Fig. 2) (Table 3). Although there was a consistently smaller total decrease from baseline at each timepoint in the RSG-XR group, the difference in decline relative to the placebo group at best suggests no more than a trend (*p*-
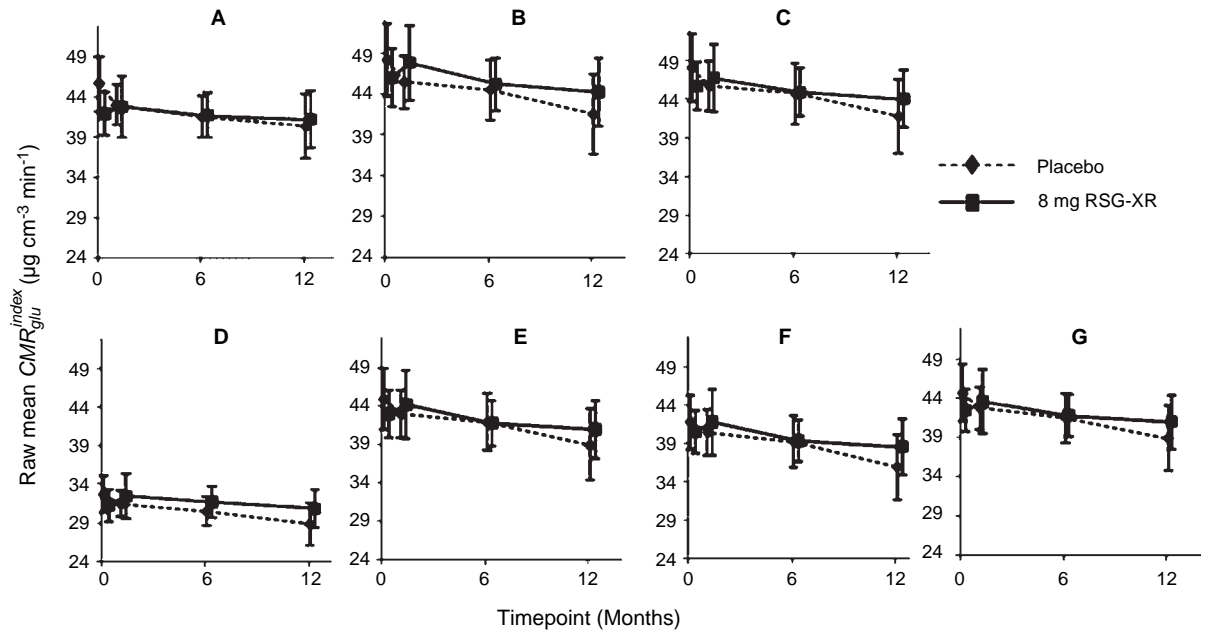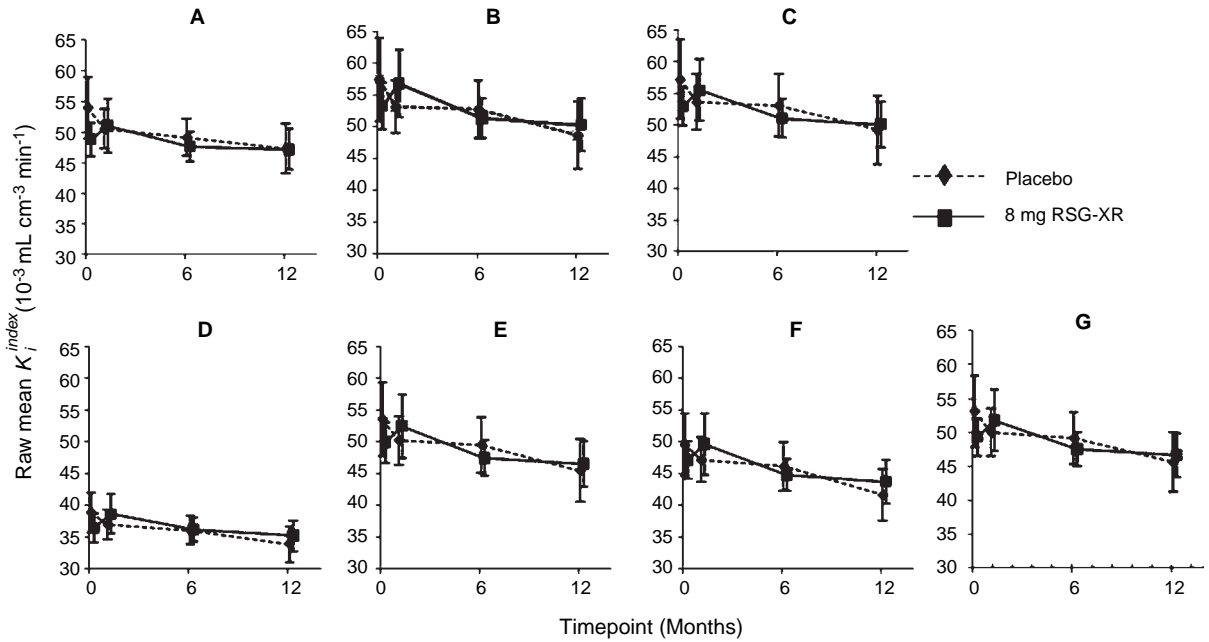
Fig. 1. Progression of decreases in mean raw values of CMR_{glu}^{index} over 12 months (95% confidence intervals shown) by anatomically pre-specified regions of interest (A. Cerebellum, B. Posterior cingulate Gyrus, C. Frontal lobe, D. Medial temporal lobe, E. Parietal lobe, F. Posterior temporal lobe, G. Global grey matter).

Table 2
CMR_{glu}^{index} (μg cm^{-3} min^{-1}), adjusted 12 months mean change from baseline in ROIs and global grey matter with CI (95%) and p-values (uncorrected)

	RSG-XR	Placebo	Difference (RSG-XR-Placebo)	Difference CI (95%)	Difference p-value
ROI					
Post cing gyrus	−2.480 (−5.3%)	−6.369 (−13.5%)	3.889 (8.3%)	(−0.844, 8.622)	0.11
Med temp lobe	−1.591 (−5.0%)	−4.020 (−12.5%)	2.431 (7.6%)	(−0.856, 5.716)	0.14
Parietal lobe	−3.296 (−7.5%)	−6.331 (−14.3%)	3.036 (6.9%)	(−1.276, 7.349)	0.16
Post temp lobe	−3.056 (−7.4%)	−5.853 (−14.2%)	2.798 (6.8%)	(−1.047, 6.642)	0.15
Cerebellum	−1.593 (−3.7%)	−4.567 (−10.5%)	2.976 (6.8%)	(−1.660, 7.609)	0.20
Frontal lobe	−3.267 (−6.9%)	−6.436 (−13.7%)	3.169 (6.7%)	(−1.536, 7.873)	0.18
Global grey matter	**−2.758 (−6.3%)**	**−5.724 (−13.1%)**	**2.964 (6.8%)**	**(−1.296, 7.224)**	**0.17**

Percentage change from baseline is given in parentheses. Abbreviations: CI, confidence interval; Cing, cingulate; ROI, region of interest; RSG, rosiglitazone; Temp, temporal; Post, posterior; Med, medial.

values for the group differences in regional CMR_{glu}^{index} changes over the 12 months ranged between 0.11 and 0.20).

In order to address directly any potentially confounding contributions of an acute medication-related effect on PET measurements unrelated to changes in disease progression, we also characterized and compared rates of change of [^{18}F]FDG-PET measures between the 1 and 12 months follow-up scans for the two treatment groups. Rates of decline for the placebo and RSG-XR groups were almost identical for

CMR_{glu}^{index} between the 1 and 12 months observations (−3.982 μg cm^{-3} min^{-1} [9.1%] decrease for placebo-treated and −3.556 μg cm^{-3} min^{-1} decrease [8.1%] for RSG-XR treated subjects between the 1 and 12 months visits).

In an exploratory pharmacogenetic analysis, we characterized and compared grey matter ROI PET changes in the APOE4 carrier and non-carrier subgroups (Table 4). Over the full 12 months of the study, there was smaller mean decrease in CMR_{glu}^{index} in the *APOE4−* (3.2%) than in the *APOE4+* (6.2%)

Fig. 2. Progression of decreases in mean raw values of K_i^{index} over 12 months (95% confidence intervals shown) by anatomically pre-specified regions (A. Cerebellum, B. Posterior cingulate gyrus, C. Frontal lobe, D. Medial temporal lobe, E. Parietal lobe, F. Posterior temporal lobe, G. Global grey matter).

Table 3
K_i^{index} (10^{-3} mL cm^{-3} min^{-1}), adjusted 12 months mean change from baseline in ROIs and global grey matter with CI (95%) and p-values (uncorrected)

	RSG-XR	Placebo	Difference (RSG-XR-Placebo)	Difference CI(95%)	*p*-value
ROI					
Post cing gyrus	−3.662 (−6.6%)	−7.789 (−14.1%)	4.127 (7.5%)	(−1.611, 9.864)	0.16
Post temp lobe	−4.276 (−8.9%)	−7.236 (−15.0%)	2.962 (6.1%)	(−1.636, 7.558)	0.20
Med temp lobe	−2.416 (−6.4%)	−4.511 (−12.0%)	2.096 (5.6%)	(−1.704, 5.898)	0.27
Parietal lobe	−4.736 (−9.2%)	−7.620 (−14.7%)	2.884 (5.6%)	(−2.356, 8.124)	0.28
Frontal lobe	−4.580 (−8.3%)	−7.524 (−13.6%)	2.942 (5.3%)	(−2.876, 8.760)	0.32
Cerebellum	−2.842 (−5.6%)	−4.793 (−9.4%)	1.953 (3.8%)	(−3.387, 7.291)	0.47
Global grey matter	**−4.058 (−7.9%)**	**−6.687 (−13.1%)**	**2.629 (5.1%)**	**(−2.491, 7.749)**	**0.31**

Percentage change from baseline is given in parentheses. Abbreviations: CI, confidence interval; Cing, cingulate; ROI, region of interest; RSG, rosiglitazone; Temp, temporal; Post, posterior; Med, medial.

Table 4
Adjusted 12 months mean change from baseline in global grey matter for CMR_{glu}^{index} (µg cm^{-3} min^{-1}) or the CMR_{ratio} (a unitless ratio) with CI (95%) and *p*-values (uncorrected), for the subgroup of patients consenting to APOE4 genotyping

APOE4 status	Index	RSG-XR	Placebo	Difference (RSG-XR-Placebo)	Difference CI (95%)	Difference *p*-value
Negative	CMR_{glu}^{index}	−1.413 (−3.2%)	−4.873 (−11%)	3.462 (7.8%)	(−6.551, 13.473)	0.49
	CMR_{ratio}	−0.0562 (−5.0%)	−0.0145 (−1.3%)	−0.0417 (−3.7%)	(−0.0880, 0.0047)	0.08
Positive	CMR_{glu}^{index}	−2.753 (−6.2%)	−4.184 (−9.5%)	1.429 (3.2%)	(−4.873, 7.731)	0.65
	CMR_{ratio}	−0.0344 (−3.1%)	−0.0689 (−6.1%)	0.0345 (3.1%)	(0.0060, 0.0629)	0.02

Percentage change from baseline is given in parentheses. Abbreviations: CI, confidence interval; RSG, rosiglitazone.

group for the RSG-XR group in contrast to similar declines for the placebo group (11% APOE4−, 9.5% APOE4+), but in neither genetic subgroup did the difference between active and placebo groups achieve statistical significance or show a meaningful trend (APOE4- difference between subgroups =
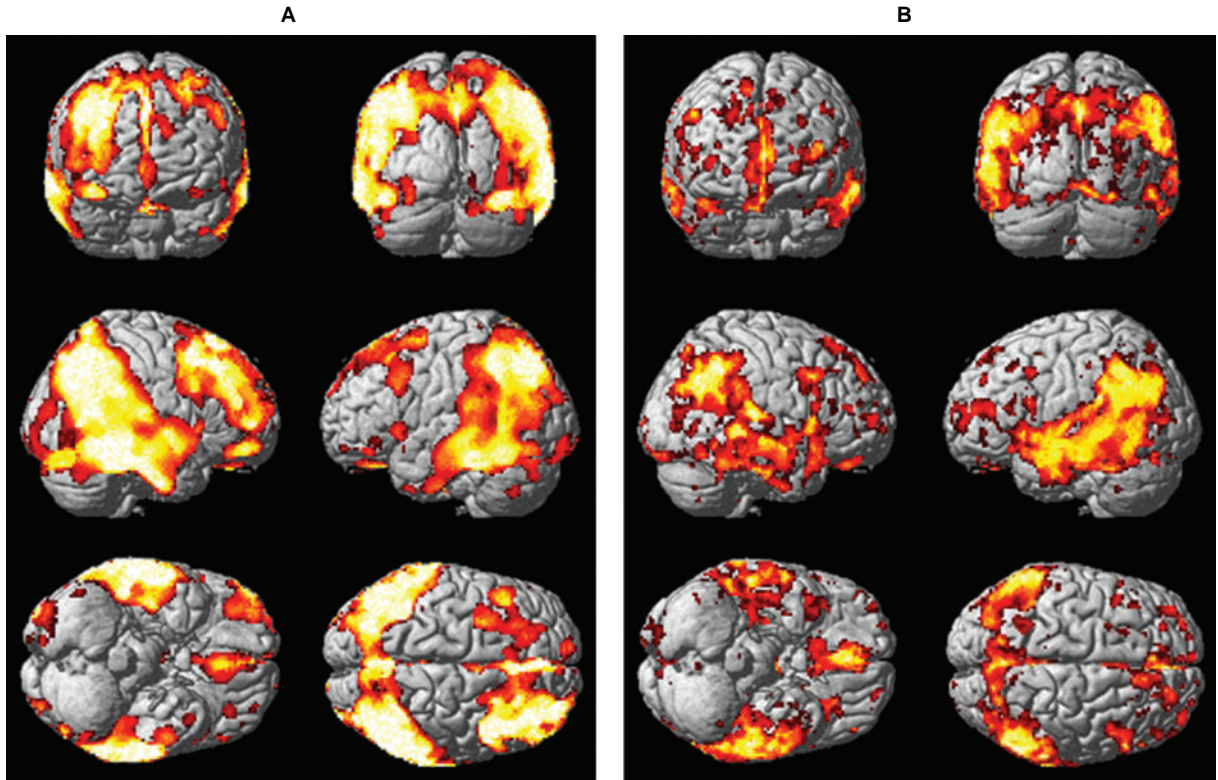
Fig. 3. Rendering of location of voxels with significant decrease in glucose metabolism (red) overlaid on surface of reference brain (grey). Figure A shows voxels significant for 12 months change in CMR_{glu}^{index}, $p < 0.0005$ uncorrected. Figure B shows voxels significant for 12 months change in ADNI training sample, $p < 0.0005$ uncorrected.

3.462 μg cm^{-3} min^{-1}, $p = 0.49$; APOE4+ difference between subgroups = 1.429 μg cm^{-3} min^{-1}, $p = 0.65$). The analysis was limited by small sample sizes and placebo subject imbalance in the two genetic subgroups.

Testing for treatment effects on brain glucose metabolism in AD with an empirically pre-defined statistical region-of-interest derived from the Alzheimer's Disease Neuroimaging Initiative (ADNI)

We first assessed the "face validity" of the sROI derived from the ADNI cohort for our study population. Voxel-wise analysis of the combined placebo and active groups in our study confirmed significant 12-month declines in regional CMR_{glu}^{index} (Fig. 3A) in an anatomical distribution similar to the ADNI patients [10] (Fig. 3B). Overlap between the thresholded masks was identified in regions including the precuneus and in the posterior cingulate, posterior temporal, and parietal cortices, which all have been described previously as showing decreases in CMR_{glu} with the progression of AD [5, 7].

We then characterized and compared sROI/spared ROI (CMR_{ratio}) declines in the RSG-XR and placebo groups. Rates of decline in the CMR_{ratio} for the placebo and RSG-XR groups were similar between the baseline and 12 months observations (-0.0465 (-4.2%) RSG-XR; -0.0602 (-5.4%) placebo; difference between groups 0.0137 (1.2%), CI (-0.0061, 0.0335), $p = 0.17$).

Unlike either CMR_{glu}^{index} or K_i^{index}, the mean raw baseline CMR_{ratio} value for the RSG-XR group (1.12) was minimally different from that for the placebo group (1.09). Similar changes in CMR_{ratio} were observed over the first month for both groups with no evidence for a short-term increase in brain glucose metabolism in the RSG-XR-treated subjects (one month decrease from baseline: -0.0060 (-0.5%) placebo; -0.0075 (-0.7%) RSG-XR; difference between groups -0.0015 (-0.2%), CI (-0.0147, 0.0117), $p = 0.82$).
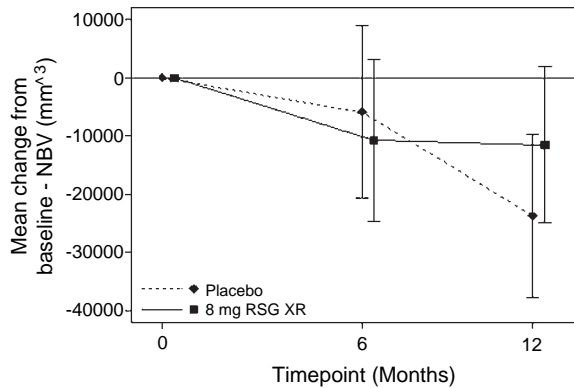
Fig. 4. Adjusted mean change from baseline in normalized brain volume (NBV) (95% confidence intervals shown).

Measures of the mean decrease in CMR_{ratio} from baseline at 6 months showed smaller mean declines in the RSG-XR group relative to placebo, but group differences did not approach statistical significance (−0.0298 (−2.7%) placebo; −0.0254 (−2.3%) RSG-XR; difference between groups 0.0044 (0.4%), CI (−0.0097, 0.0185), $p = 0.54$).

Overall, the mean CMR_{ratio} change over all time points was smaller for the RSG-XR group than for the placebo group, but the differences again failed to suggest even a trend favouring the active treatment group over the 12 months of observation from baseline (change, −0.0265(−2.4%) RSG-XR; −0.0320(−2.9%) placebo; difference between groups, 0.0055 (0.5%), CI (−0.0072, 0.0183), $p = 0.39$].

Exploratory pharmacogenetic analysis of the subgroup consenting to APOE genotyping demonstrated a smaller decrease in CMR_{ratio} from baseline over the full 12 months of the study in the RSG-XR group relative to placebo treatment for APOE4+ subjects (difference between groups in change from baseline 0.0345, $p = 0.02$) (Table 4). There was a trend for a larger decrease from baseline in the APOE4− subgroup subjects treated with RSG-XR relative to placebo (difference between groups in change from baseline −0.0417, $p = 0.08$).

6- and 12-month decreases in whole brain volume

Whole brain volume changes were assessed at baseline, 6 and 12 months for the two treatment groups. A progressive decrease in brain volume over the study period was measured for both groups (Fig. 4). Although the mean decrease in brain volume was lower for the RSG-XR group than for placebo-treated subjects at 12 months, the difference was neither statistically significant nor did it approach a level suggesting any trend (Table 5). Absence of a treatment effect on whole brain volume measured using SIENAX was confirmed in a separate analysis of the baseline and 12 months data with SIENA (data not shown).

Clinical outcome measures

The probable AD patients in the two treatment groups did not differ substantially in their baseline ADAS-Cog scores (placebo mean 19.4, CI (16.9, 21.9); RSG-XR mean 21.3, CI (18.9, 23.7)). Both ADAS-Cog and CIBIC+ measured progressive decreases in performance from baseline over the 12 months of the study for both treatment groups (Table 6). The ADAS-Cog results favoured placebo (difference between RSG-XR and placebo groups of 2.18 points) and the CIBIC+ results favoured the RSG-XR group (difference between RSG-XR and placebo groups of 0.1 points), but differences for neither test reached statistical significance.

Exploratory pharmacogenetic analysis did not show a significant treatment difference or meaningful trend in either genetically-defined subgroup (Table 6).

Plasma glucose

There were no consistent or significant differences in plasma glucose levels between the two groups at any of the time points. The mean glucose concentrations (CI 95%) were $0.859 \pm 0.033\,\text{mg mL}^{-1}$ (baseline) and $0.855 \pm 0.050\,\text{mg mL}^{-1}$ (12 months) for the placebo group and $0.861 \pm 0.033\,\text{mg mL}^{-1}$

Table 5

Normalised brain volume (NBV) (mm^3), adjusted mean change from baseline with CI (95%) and p-values (uncorrected)

Timepoint (months)	RSG-XR	Placebo	Difference (RSG-XR-Placebo)	Difference CI (95%)	Difference p-value
6	−10792 (−0.8%)	−5821 (−0.4%)	−4972 (−0.4%)	(−25516, 15573)	0.63
12	−11567 (−0.8%)	−23790 (−1.7%)	12223 (0.9%)	(−7450, 31897)	0.22

Percentage change from baseline is given in parentheses. Abbreviations: CI, confidence interval; RSG, rosiglitazone.

Table 6
Twelve month change from baseline in clinical scales for the total study group and for APOE4 allele subgroups (95%) and *p*-values (uncorrected)

Clinical scale/ patient group	RSG-XR	Placebo	Difference (RSG-XR-Placebo)	Difference CI (95%)	Difference *p*-value
Total group					
ADAS-Cog	7.62	5.44	2.18	(−1.68, 6.04)	0.26
CIBIC+	4.86	4.96	−0.10	(−0.70, 0.49)	0.74
APOE4− patients					
ADAS-Cog	10.26	7.5	2.76	(−5.01, 10.53)	0.48
CIBIC+	5.04	5.43	−0.39	(−1.71, 0.93)	0.56
APOE4+ patients					
ADAS-Cog	5.06	4.05	1.01	(−4.23, 6.26)	0.70
CIBIC+	4.62	4.65	−0.03	(−0.92, 0.85)	0.94

with CI Percentage change from baseline is given in parentheses. Abbreviations: CI, confidence interval; RSG, rosiglitazone.

(baseline) and 0.878 ± 0.039 mg mL^{-1} (12 months) for the RSG-XR group.

DISCUSSION

Multiple independent observations have shown that AD is associated with progressive reductions of oxidative metabolism of glucose in the brain [3–10] and both epidemiological and preclinical studies together suggest that impairment of insulin signalling and glucose metabolism could contribute to the genesis or progression of AD [2]. Here we have evaluated new measures for quantitative assessment of brain FDG uptake using PET that are applicable to multiple centre trials. We have done this while also evaluating a novel therapeutic hypothesis. Pilot studies have suggested that treatment with rosiglitazone, an insulin sensitising PPARγ agonist, improves cognition in AD [36] (but that effect could be limited to APOE4- subjects [37]).

The primary method of analysis proposed here is based on tracer kinetic principles with venous blood samples and is a straightforward extension of established methods. An advantage of the method is that it allows estimates for both K_i and CMR_{glu} to be extracted. These measures should be sensitive to global as well as to regional changes in brain metabolism. Limitations arise from the loss of statistical power with multiple comparisons (as several ROIs are assessed simultaneously) and any variance introduced from detection differences between scanners [47].

We therefore also employed an alternative method recently validated using data from ADNI patients undergoing serial [18F]FDG-PET assessments [10]. This method both employs a single, pre-specified ROI (sROI) selected to optimise power to detect a therapeutic effect and normalises individual subject level data using a second ROI not expected to show significant disease-related changes. Acceptable overlap of the sROI with the region of greatest change for subjects in the current study demonstrated "face validity" for its application to this population. However, a limitation is that the method is not sensitive to effects of any intervention that leads to similar changes across all regions of the brain (due to the notmalisation involved). This method was developed after the initiation of this study and is complementary to the primary approach in this work.

While data only suggested a trend for a therapeutic response, the increases in mean K_i^{index} and CMR_{glu}^{index} from the first month of treatment suggest early and sustained effects of RSG XR to enhance cerebral glucose metabolism in AD patients. However, there was no evidence from [18F]FDG-PET, MRI or clinical measures for slowing of the progression of disease over the 12 months of observation. This outcome is consistent with the results of completed Phase III randomised controlled trials using clinical endpoints in larger samples of probable AD patients [44–46].

Our results highlight the value of employing complementary analytical approaches. Relative trends for changes over time were similar for CMR_{glu}^{index} and K_i^{index} and CMR_{ratio} measures except over the first month of treatment, which we hypothesise to reflect short-term metabolic effects of RSG-XR treatment apparently independently of secondary effects on rates of progressive neurodegeneration. The differences in trends for CMR_{glu}^{index} and K_i^{index} relative to CMR_{ratio} that were observed over the first month are to be expected if RSG-XR has similar effects on glucose metabolism across the entire brain: CMR_{ratio} normal-

isation demonstrates relative changes in CMR_{glu} with respect to a reference region that is less affected by the disease, while CMR_{glu}^{index} and K_i^{index} should be sensitive to uniform global changes in glucose transport and phosphorylation. The relative increase in CMR_{glu}^{index} approached a trend to an increase over the first month, suggesting a possible short-term effect of RSG-XR to partially reverse impairments of brain glucose metabolism in AD. This evidence suggesting reversible components of pathologically reduced abnormal brain metabolism in AD is important to test further in future studies.

The exploratory pharmacogenetic elements of this study were not consistent between analyses using the two PET analytical approaches, but confidence in either specific outcome is limited because of the limited study power. A smaller change in the CMR_{ratio} was found for the group of APOE4+ subjects treated with RSG-XR. However, this direction of effect is opposite to that suggested by earlier clinical data [37]. More consistent with the latter, the mean decrease in CMR_{glu}^{index} was lower in the APOE4− patients on active treatment, although the result did not approach statistical significance. Further post-hoc analyses exploring possible drug effects for patients with specific genotypes E3/3 relative to E3/4 showed similarly negative results. We believe that discrepancies are due to the small sample sizes of the exploratory pharmacogenetic analyses and the unexpected subject imbalance in the placebo treated group. While the small numbers prevent any strong pharmacogenetic inference, these results overall give confidence that genetic heterogeneity between the study active treatment and placebo populations is not masking a large treatment effect.

While the primary objectives of our methods and pilot applications related to FDG PET, we also applied volumetric MRI as an additional, secondary outcome measure. Whole brain atrophy measured from serial MRI scanning has become a well-established tool in Alzheimer's disease research [48]. Neuronal dystrophy and loss together likely contribute most to the decrease in brain volume with disease progression. The SIENA software used in our study as a measure of changes in brain volume over time is robust enough to be applied even to data coming from different MRI scanners (and thus having differences in contrast [49]). Although the absolute estimates are different, the relative loss of volume assessed by SIENA is correlated with that measured using other methods [50]. Previous work (albeit using a different image analysis algorithm) suggests that a study with 40 patients per treatment arm (as in

the current study) should be able to detect a 40% or greater change in the rate of neurodegeneration over 12 months [51]. As neither a significant difference nor a trend was found, we conclude that it is unlikely that RSG-XR has a large effect on neurodegeneration in patients with mild-to-moderate, probable AD over the course of a year.

A major outcome from the current work relates to the piloting of more robust methods for PET in multi-centre therapeutic studies. There also were important pharmacological outcomes, although we recognise their limitations. As indicated above, the most significant limitation is the small number of subjects overall and the even smaller number of subjects included in the post-hoc pharmacogenetic analyses. We also were limited by not having applied current state of the art image-standardization and quality-assurance methods for the PET data acquisition (which were set out after initiation of our study [10]). Nonetheless, the lack of even a trend to a difference in rates of changes between treated and placebo groups in the PET quantitative indices after the first month and in the other study end points for the study duration, argues that RSG-XR treatment does not have a major effect on neurodegeneration in AD over the observed treatment period.

Further confidence in our conclusion derives from the consistency of conclusions from the two different methods applied to analysis. Patient selection differences between this and previous trials also could account for differences in outcomes between this PET study and the earlier small clinical study [36]. Patients in the study of Watson et al. had a higher median MMSE, but these investigators also suggested that there was no evidence for differences in cognitive responses between patients with established AD and MCI. However, well-powered, randomised, controlled trials of RSG-XR also have failed to find evidence for slowing of the clinical progression of AD [44–46]. A final limitation of our study arises from the fact that RSG is a substrate for P-glycoprotein [52]. Our study does not rule out possible effects of highly CNS penetrant PPARγ agonist on rates of neurodegeneration.

An intriguing element of our work outside of the methods evaluation has been its role in testing a novel metabolic hypothesis for the treatment of AD [2]. While failing to demonstrate an effect of RSG-XR on neurodegeneration, our results suggest partial reversibility of deficits in brain glucose metabolism in Alzheimer's disease. The concept that there are reversible components even with established

disease should motivate future work using more CNS-penetrant metabolic modulators, potentially applied in patients for longer periods and at even earlier stages in the disease. Preclinical results continue to suggest that metabolic modulation could alter progression or even reverse neuropathological change in AD [53]. The consistency of the negative Phase III clinical trials of RSG-XR [44–46] with results reported here provides new evidence supporting use of [^{18}F]FDG-PET and MRI measurements in exploratory Phase II studies to screen out treatments unlikely to show clinical efficacy in follow-on Phase III studies. We believe that our work has demonstrated feasibility and anticipate that future trials of new treatments directed at slowing the progression of AD will benefit from the inclusion of multiple imaging (and other) biomarkers able to add value as specific, mechanistic tests of therapeutic hypotheses.

DECLARATION OF INTERESTS

ACKNOWLEDGMENTS

REFERENCES

[1] Mirra SS, Hyman BT (2002) Ageing and dementia in *Greenfield's Neuropathology*, ed. Graham, D. I. L. P. L. London: Arnold, pp. 195-271.

[2] Craft S (2009) The role of metabolic disorders in Alzheimer disease and vascular dementia: two roads converged. *Arch Neurol* **66**, 300-305.

[3] Alexander GE, Chen K, Pietrini P, Rapoport SI, Reiman EM (2002) Longitudinal PET evaluation of cerebral metabolic decline in dementia: a potential outcome measure in Alzheimer's disease treatment studies. *Am J Psychiatry* **159**, 738-745.

[4] Edison P, Archer HA, Hinz R, Hammers A, Pavese N, Tai YF, Hotton G, Cutler D, Fox N, Kennedy A, Rossor M, Brooks DJ (2007) Amyloid, hypometabolism, and cognition in Alzheimer disease: an [11C]PIB and [18F]FDG PET study. *Neurology* **68**, 501-508.

[5] Herholz K, Carter SF, Jones M (2007) Positron emission tomography imaging in dementia. *Br J Radiol* **80 Spec No 2**, S160-S167.

[6] Hirono N, Hashimoto M, Ishii K, Kazui H, Mori E (2004) One-year change in cerebral glucose metabolism in patients with Alzheimer's disease. *J Neuropsychiatry Clin Neurosci* **16**, 488-492.

[7] Langbaum JB, Chen K, Lee W, Reschke C, Bandy D, Fleisher AS, Alexander GE, Foster NL, Weiner MW, Koeppe RA, Jagust WJ, Reiman EM (2009) Categorical and correlational analyses of baseline fluorodeoxyglucose positron emission tomography images from the Alzheimer's Disease Neuroimaging Initiative (ADNI). *Neuroimage* **45**, 1107-1116.

[8] Piert M, Koeppe RA, Giordani B, Berent S, Kuhl DE (1996) Diminished glucose transport and phosphorylation in Alzheimer's disease determined by dynamic FDG-PET. *J Nucl Med* **37**, 201-208.

[9] Smith GS, de Leon MJ, George AE, Kluger A, Volkow ND, McRae T, Golomb J, Ferris SH, Reisberg B, Ciaravino J, La Regina ME (1992) Topography of cross-sectional and longitudinal glucose metabolic deficits in Alzheimer's disease. Pathophysiologic implications. *Arch Neurol* **49**, 1142-1150.

[10] Chen K, Langbaum JBS, Fleisher AS, Reschke BS, Lee W, Xiaofen L, Napatkamon A, Bandy D, Alexander GE, Thompson PM, Foster NL, Harvey DJ, de Leon MJ, Koeppe RA, Jagust WJ, Weiner MW, Reiman EM (2010) Twelve month metabolic declines in probable Alzheimer's disease and amnestic mild cognitive impairment assesed using an empirically pre-defined statistical region-of-interest: findings from the Alzheimer's disease neuroimaging initiative. *Neuroimage* **51**, 654-664.

[11] Rossor MN, Kennedy AM, Frackowiak RS (1996) Clinical and neuroimaging features of familial Alzheimer's disease. *Ann N Y Acad Sci* **777**, 49-56.

[12] Reiman EM, Caselli RJ, Yun LS, Chen K, Bandy D, Minoshima S, Thibodeau SN, Osborne D (1996) Preclinical evidence of Alzheimer's disease in persons homozygous for the epsilon 4 allele for apolipoprotein E. *N Engl J Med* **334**, 752-758.

[13] Reiman EM, Caselli RJ, Chen K, Alexander GE, Bandy D, Frost J (2001) Declining brain activity in cognitively normal apolipoprotein E epsilon 4 heterozygotes: A foundation for using positron emission tomography to efficiently test treatments to prevent Alzheimer's disease. *Proc Natl Acad Sci U S A* **98**, 3334-3339.

[14] Reiman EM, Chen K, Alexander GE, Caselli RJ, Bandy D, Osborne D, Saunders AM, Hardy J (2004) Functional brain abnormalities in young adults at genetic risk for late-onset Alzheimer's dementia. *Proc Natl Acad Sci U S A* **101**, 284-289.

[15] Reiman EM, Chen K, Alexander GE, Caselli RJ, Bandy D, Osborne D, Saunders AM, Hardy J (2005) Correlations between apolipoprotein E epsilon4 gene dose and brain-imaging measurements of regional hypometabolism. *Proc Natl Acad Sci U S A* **102**, 8299-8302.

[16] Small GW, Mazziotta JC, Collins MT, Baxter LR, Phelps ME, Mandelkern MA, Kaplan A, La R A, Adamson CF, Chang L, Guze BH, Corder EH, Saunders AM, Haines JL, Pericak-Vance MA, Roses AD (1995) Apolipoprotein E type 4 allele and cerebral glucose metabolism in relatives at risk for familial Alzheimer disease. *JAMA* **273**, 942-947.

[17] Small GW, Ercoli LM, Silverman DH, Huang SC, Komo S, Bookheimer SY, Lavretsky H, Miller K, Siddarth P, Rasgon NL, Mazziota JC, Saxena S, Wu HM, Mega MS, Cummings JL, Saunders AM, Pericak-Vance MA, Roses, AD, Barrio JR, Phelps ME (2000) Cerebral metabolic and cognitive decline in persons at genetic risk for Alzheimer's disease. *Proc Natl Acad Sci U S A* **97**, 6037-6042.

[18] Valla J, Berndt JD, Gonzalez-Lima F (2001) Energy hypometabolism in posterior cingulate cortex of Alzheimer's patients: superficial laminar cytochrome oxidase associated with disease duration. *J Neurosci* **21**, 4923-4930.

[19] Liang WS, Reiman EM, Valla J, Dunckley T, Beach TG, Grover A, Niedzielko TL, Schneider LE, Mastroeni D, Caselli R, Kukull W, Morris JC, Hulette CM, Schmechel D, Rogers J, Stephan DA (2008) Alzheimer's disease is associated with reduced expression of energy metabolism genes in posterior cingulate neurons. *Proc Natl Acad Sci U S A* **105**, 4441-4446.

[20] Roses AD, Lutz MW, Mrine-Madsen H, Saunders AM, Crenshaw DG, Sundseth SS, Huentelman MJ, Welsh-Bohmer KA, Reiman EM (2009) A TOMM40 variable-length polymorphism predicts the age of late-onset Alzheimer's disease. *Pharmacogenomics J.* **10**(2010), 375-384.

[21] Craft S, Peskind E, Schwartz MW, Schellenberg GD, Raskind M, Porte D Jr. (1998) Cerebrospinal fluid and plasma insulin levels in Alzheimer's disease: relationship to severity of dementia and apolipoprotein E genotype. *Neurology* **50**, 164-168.

[22] Banks WA, Jaspan JB, Huang W, Kastin AJ (1997) Transport of insulin across the blood-brain barrier: saturability at euglycemic doses of insulin. *Peptides* **18**, 1423-1429.

[23] Banks WA, Jaspan JB, Kastin AJ (1997) Effect of diabetes mellitus on the permeability of the blood-brain barrier to insulin. *Peptides* **18**, 1577-1584.

[24] Apelt J, Mehlhorn G, Schliebs R (1999) Insulin-sensitive GLUT4 glucose transporters are colocalized with GLUT3-expressing cells and demonstrate a chemically distinct neuron-specific localization in rat brain. *J Neurosci Res* **57**, 693-705.

[25] Reagan LP, Gorovits N, Hoskin EK, Alves SE, Katz EB, Grillo CA, Piroli GG, McEwen BS, Charron MJ (2001) Localization and regulation of GLUTx1 glucose transporter in the hippocampus of streptozotocin diabetic rats. *Proc Natl Acad Sci U S A* **98**, 2820-2825.

[26] Unger JW, Livingston JN, Moss AM (1991) Insulin receptors in the central nervous system: localization, signalling mechanisms and functional aspects. *Prog Neurobiol* **36**, 343-362.

[27] Biessels GJ, Kamal A, Ramakers GM, Urban IJ, Spruijt BM, Erkelens DW, Gispen WH (1996) Place learning and hippocampal synaptic plasticity in streptozotocin-induced diabetic rats. *Diabetes* **45**, 1259-1266.

[28] Lannert H, Hoyer S (1998) Intracerebroventricular administration of streptozotocin causes long-term diminutions in learning and memory abilities and in cerebral energy metabolism in adult rats. *Behav Neurosci* **112**, 1199-1208.

[29] Craft S, Asthana S, Newcomer JW, Wilkinson CW, Matos IT, Baker LD, Cherrier M, Lofgreen C, Latendresse S, Petrova A, Plymate S, Raskind M, Grimwood K, Veith RC (1999) Enhancement of memory in Alzheimer disease with insulin and somatostatin, but not glucose. *Arch Gen Psychiatry* **56**, 1135-1140.

[30] Adams M, Montague CT, Prins JB, Holder JC, Smith SA, Sanders L, Digby JE, Sewter CP, Lazar MA, Chatterjee VK, O'Rahilly S (1997) Activators of peroxisome proliferator-activated receptor gamma have depot-specific effects on human preadipocyte differentiation. *J Clin Invest* **100**, 3149-3153.

[31] Lehmann JM, Moore LB, Smith-Oliver TA, Wilkison WO, Willson TM, Kliewer SA (1995) An antidiabetic thiazolidinedione is a high affinity ligand for peroxisome proliferator-activated receptor gamma (PPAR gamma). *J Biol Chem* **270**, 12953-12956.

[32] *The art of drug synthesis,* John Wiley & Sons (2007).

[33] Nugent C, Prins JB, Whitehead JP, Savage D, Wentworth JM, Chatterjee VK, O'Rahilly S (2001) Potentiation of glucose uptake in 3 T3-L1 adipocytes by PPAR gamma agonists is maintained in cells expressing a PPAR gamma dominant-negative mutant: evidence for selectivity in the downstream responses to PPAR gamma activation. *Mol Endocrinol* **15**, 1729-1738.

[34] Pedersen WA, McMillan PJ, Kulstad JJ, Leverenz JB, Craft S, Haynatzki GR (2006) Rosiglitazone attenuates learning and

memory deficits in Tg2576 Alzheimer mice. *Exp Neurol* **199**, 265-273.

[35]   Ryan CM, Freed MI, Rood JA, Cobitz AR, Waterhouse BR, Strachan MW (2006) Improving metabolic control leads to better working memory in adults with type 2 diabetes. *Diabetes Care* **29**, 345-351.

[36]   Watson GS, Cholerton BA, Reger MA, Baker LD, Plymate SR, Asthana S, Fishel MA, Kulstad JJ, Green PS, Cook DG, Kahn SE, Keeling ML (2005) Preserved cognition in patients with early Alzheimer disease and amnestic mild cognitive impairment during treatment with rosiglitazone: a preliminary study. *Am J Geriatr Psychiatry* **13**, 950-958.

[37]   Risner ME, Saunders AM, Altman JF, Ormandy GC, Craft S, Foley IM, Zvartau-Hind ME, Hosford DA, Roses AD (2006) Efficacy of rosiglitazone in a genetically defined population with mild-to-moderate Alzheimer's disease. *Pharmacogenomics J* **6**, 246-254.

[38]   Smith SM, Zhang Y, Jenkinson M, Chen J, Matthews PM, Federico A, De SN (2002) Accurate, robust, and automated longitudinal and cross-sectional brain change analysis. *Neuroimage* **17**, 479-489.

[39]   Smith SM, Jenkinson M, Woolrich MW, Beckmann CF, Behrens TE, Johansen-Berg H, Bannister PR, De LM, Drobnjak I, Flitney DE, Niazy RK, Saunders J, Vickers J, Zhang Y, De Stefano N, Brady JM, Matthews PM (2004) Advances in functional and structural MR image analysis and implementation as FSL. *Neuroimage* **23 Suppl 1**, S208-S219.

[40]   McKhann G, Drachman D, Folstein M, Katzman R, Price D, Stadlan EM (1984) Clinical diagnosis of Alzheimer's disease: report of the NINCDS-ADRDA Work Group under the auspices of Department of Health and Human Services Task Force on Alzheimer's disease. *Neurology* **34**, 939-944.

[41]   Folstein MF, Folstein SE, McHugh PR (1975) Mini-Mental State A practical method for grading the cognitive state of patients for the clinician. *Journal of Psychiatric Research* **12**, 189-198.

[42]   Rosen WG, Mohs RC, Davis KL (1984) A new rating scale for Alzheimer's disease. Am J Psychiatry. *Am J Psychiatry* **141**, 1356-1364.

[43]   Schneider LS, Olin JT, Doody RS, Clark CM, Morris JC, Reisberg B, Schmitt FA, Grundman M, Thomas RG, Ferris SH (1997) Validity and reliability of the Alzheimer's disease cooperative study-clinical global impression of change. The Alzheimer's disease cooperative study. *Alzheimer Dis Assoc Disord* **11 Suppl 2**, S22-S32.

[44]   Alderton C, Zvartau-Hind M, Ritchie S, Saunders A, Craft S, Landreth G, Linnamagi U, Sawchak S, Gold M (2009) Secondary endpoint and responder analyses in a study of rosiglitazone XR in APOE4-stratified subjects with mild-to-moderate Alzheimer's disease. *Alzheimer's and Dementia Journal* **5**, S-254.

[45]   Gold M, Zvartau-Hind ME, Ritchie S, Saunders AM, Craft S, Landreth G, Linnamaegi U, Sawchak K (2009) Effects of rosiglitazone as monotherapy in APE4-stratified subjects with mild-to-moderate Alzheimer's disease. *Alzheimer's and Dementia Journal* **5**, S-86.

[46]   Harrington C, Sawchak S, Chiang C, Davies J, Saunders A, Irizarry M, Zvartau-Hind M, van Dyke C, Gold M (2009) Effects of rosiglitazone extended release as adjunctive therapy with acetylcholinesterase inhibitors on cognition in APOE4-stratified subjects with mild-to-moderate Alzheimer's disease. *Alzheimer's and Dementia Journal* **5**, Se17.

[47]   Westerterp M, Pruim J, Oyen W, Hoekstra O, Paans A, Visser E, van LJ, Sloof G, Boellaard R (2007) Quantification of FDG PET studies using standardised uptake values in multicentre trials: effects of image reconstruction, resolution and ROI definition parameters. *Eur J Nucl Med Mol Imaging* **34**, 392-404.

[48]   Ridha BH, Barnes J, Bartlett JW, Godbolt A, Pepple T, Rossor MN, Fox NC (2006) Tracking atrophy progression in familial Alzheimer's disease: a serial MRI study. *Lancet Neurol* **5**, 828-834.

[49]   Jasperse B, Valsasina P, Neacsu V, Knol DL, De SN, Enzinger C, Smith SM, Ropele S, Korteweg T, Giorgio A, Anderson V, Polman CH, Filippi M, Miller DH, Rovaris M, Barkhof F, Vrenken H (2007) Intercenter agreement of brain atrophy measurement in multiple sclerosis patients using manually-edited SIENA and SIENAX. *J Magn Reson Imaging* **26**, 881-885.

[50]   Stevenson VL, Smith SM, Matthews PM, Miller DH, Thompson AJ (2002) Monitoring disease activity and progression in primary progressive multiple sclerosis using MRI: sub-voxel registration to identify lesion changes and to detect cerebral atrophy. *J Neurol* **249**, 171-177.

[51]   Fox NC, Cousens S, Scahill R, Harvey RJ, Rossor MN (2000) Using serial registered brain magnetic resonance imaging to measure disease progression in Alzheimer disease: power calculations and estimates of sample size to detect treatment effects. *Arch Neurol* **57**, 339-344.

[52]   Festuccia WT, Oztezcan S, Laplante M, Berthiaume M, Michel C, Dohgu S, Denis RG, Brito MN, Brito NA, Miller DS et al. (2008) Peroxisome proliferator-activated receptor-gamma-mediated positive energy balance in the rat is associated with reduced sympathetic drive to adipose tissues and thyroid status. *Endocrinology* **149**, 2121-2130.

[53]   Escribano L, Simon AM, Gimeno E, Cuadrado-Tejedor M, de Maturana RL, Garcia-Osta A, Ricobaraza A, Perez-Mediavilla A, Rio JD, Frechilla D (2010) Rosiglitazone rescues memory impairment in Alzheimer's transgenic mice: mechanisms involving a reduced amyloid and tau pathology. *Neuropsychopharmacology* **35**, 1593-1604.

An MRI Brain Atrophy and Lesion Index to Assess the Progression of Structural Changes in Alzheimer's Disease, Mild Cognitive Impairment, and Normal Aging: A Follow-Up Study

Ningnannan Zhang[a,b], Xiaowei Song[a,c,*], Yunting Zhang[b], Wei Chen[a,b], Ryan C.N. D'Arcy[a,d], Sultan Darvesh[e,f], John D. Fisk[e,g], Kenneth Rockwood[c,e,*] and Alzheimer's disease Neuroimaging Initiative[1]

[a]*National Research Council Canada Institute for Biodiagnostics (Atlantic), Halifax, NS, Canada*
[b]*Department of Radiology of the General Hospital, Tianjin Medical University, Tianjin, China*
[c]*Division of Geriatric Medicine, Department of Medicine, Dalhousie University, Halifax, NS, Canada*
[d]*Departments of Radiology and Neuroscience, Dalhousie University, Halifax, NS, Canada*
[e]*Centre for Health Care of the Elderly, QEII Health Sciences Centre, Halifax, NS, Canada*
[f]*Departments of Medicine (Neurology) and Anatomy and Neurobiology, Dalhousie University, Halifax, NS, Canada*
[g]*Departments of Psychiatry, Dalhousie University, Halifax, NS, Canada*

Abstract. *Background*:   A brain atrophy and lesion index (BALI) based on high-field magnetic resonance imaging (MRI) has recently been validated to evaluate structural changes in the aging brain. The present study investigated the two-year progression of brain structural deficits in people with Alzheimer's disease (AD) and mild cognitive impairment (MCI), and in healthy control older adults (HC) using the BALI rating.

*Correspondence to: Xiaowei Song, PhD, MSCS, National Research Council Canada, Institute for Biodiagnostics (Atlantic), Neuroimaging Research Laboratory, Suite 3900, 1796 Summer Street, Halifax, NS B3H 3A7, Canada. Tel.: +(902) 4731876; Fax: +(902) 4731851; E-mail: Xiaowei.Song@nrc.ca. Kenneth Rockwood, MD, FRCPC, Divisions of Geriatric Medicine and Neurology, Department of Medicine, Dalhousie University 1421-5955 Veterans Memorial Lane, Halifax, NS, Canada, B3H 2E1. Tel.: +(902) 473 4886; Fax: +(902) 473 1050; E-mail: Kenneth.Rockwood@dal.ca.

Methods: T1-weighted high-resolution anatomical imaging data using 3 Tesla MRI at baseline (AD = 39, MCI = 82, HC = 58) and at 24-months were obtained from the Alzheimer's disease Neuroimaging Initiative database. Lesions in various brain structures, including the infratentorial and basal ganglia areas, and the periventricular and deep white matter and global atrophy, were evaluated and combined into the BALI scale.

Results: Mean progression of brain deficits over two years was evident in all diagnostic groups ($p < 0.001$) and was statistically greater in MCI-AD converters than in the non-converters ($p = 0.044$). An increase in the BALI score was significantly associated with cognitive test scores ($p = 0.008$ for the Mini-Mental State Examination MMSE and $p = 0.013$ for the Alzheimer's Disease Assessment Scale-Cognitive Subscale ADAS-cog) in a model that adjusted for age, sex, and education.

Conclusion: The BALI rating quantified the progression of brain deficits over two years, which is associated with cognitive decline. BALI ratings may be used to help summarize AD-associated structural variations.

Keywords: Alzheimer's disease, aging, atrophy, cognition, lesion, visual scale

INTRODUCTION

Brain structural changes in older adults are commonly revealed on magnetic resonance imaging (MRI) [1] and such changes in otherwise healthy individuals commonly are related to reduced information processing speed and decreased executive capability [2]. Compared with age-associated changes in healthy individuals, brain structural changes in Alzheimer's disease (AD) can involve more profound gray matter atrophy and white matter deficits [3, 4]. These are often concordant with β-amyloid accumulation and/or chronic ischemia and small vessel disease, and are related to worse intellectual function [4, 5]. Reflecting how often more than one pathological disease process is commonly present in older adults, many brain structural changes do not present in isolation, but commonly are associated with each other [6–8].

The importance of considering all types of brain deficits in combination so as to better understand disease expression is increasingly recognized. This requires evaluation of structural changes of the whole brain and their cumulative effect. Even so, the overall impact of multiple brain structural changes on cognition in aging and in AD remains poorly understood, and in this context the evaluation of longitudinal change is paramount. Previous studies have attempted to quantify presumed pathological changes in several localized regions [9] and many have used visual rating scales [3, 10–12] based on T2-weighted imaging or proton density imaging that are sensitive to white matter lesions. More recently, high-field strength MRI (i.e., 3T and higher), using high-resolution T1-weighted imaging has also allowed for visualization of brain abnormalities in greater detail [13, 14]. To capture the range of relevant structural changes, a semi-quantitative brain atrophy and lesion index (BALI) based on high-field MRI has been developed [15]. The BALI approach adapts existing visual rating scales and summarizes various common types of brain structural changes in the aging brain in both supratentorial and infratentorial regions [15]. To date, BALI ratings have been validated using several independent datasets and been found to be useful in describing global structural variability [15]. Even so, it is not yet understood whether this tool can be used to evaluate the progression of brain structural changes and their relation to cognitive decline, a topic of considerable clinical and research interest [16–18].

The objectives of the present study were to investigate the progression of brain structural changes using BALI in people with AD, people with mild cognitive impairment (MCI), and a matched group of otherwise healthy control subjects (HC), and; to examine the relationship between BALI change and cognitive change. To accomplish these objectives, anatomical imaging data from the Alzheimer's Disease Neuroimaging Initiative were evaluated. A BALI score was constructed for each subject based on T1-weighted MRI at baseline and at 24-months follow-up.

SUBJECTS AND METHODS

Subjects

Data used for the present analysis were obtained from the Alzheimer's Disease Neuroimaging Initiative (ADNI) [19]. The ADNI was launched in 2003 by public organizations, private pharmaceutical companies, and non-profit organizations. The primary goal of ADNI has been to test serial neuroimaging and other

biological markers in the progression of MCI and early AD in order to aid in more effective treatments [19]. Subjects have been recruited non-randomly from over 50 sites across the U.S.A. and Canada, with a goal of recruiting 800 adults, including 200 cognitively normal older individuals, 400 people with MCI, and 200 people with early AD and to follow them for 2–3 years [19–21].

Before making them available for public access, all study scans were checked for quality control, so that subjects with structural abnormalities and/or having an image with common scan artifacts were not included in the dataset. The present analysis is restricted to all the data from subjects who had 3T MRI (about 20% of the total sample) at both baseline and two-year follow-up (AD = 39; MCI = 82; HC = 58 from 30 sites

at baseline). At the 24-months follow-up, 13 AD, 29 MCI, and 12 HC subjects had dropped out, were lost to follow-up, or had poor quality images. The high resolution (1.2 mm thickness) 3D T1WI using a MP-RAGE sequence were evaluated to generate BALI scores [20]. The quality of all images downloaded from ADNI website was satisfactory and therefore no further selection criteria were imposed for the present analyses.

Imaging evaluation and scoring

Aging-associated changes in the BALI include ratings of the severity of hypointensities in the infratentorial (IT), deep white matter (DWM), periventricular (PV) and basal ganglia (BG) (Table 1). Ratings were also used to reflect gray matter lesions and the extent

Table 1
Rating schema of the brain atrophy and lesion index

Category	Description	Rating					
		0	1	2	3	4	5
GM-SV	lesions in grey matter and small vessels	absence	punctuate foci in grey matter or multiple small vessels in subcortical areas	beginning of confluent foci in grey matter or diffuse small vessels in subcortical areas	large confluent lesions in grey matter	–	–
PV	lesions in periventricular regions	absence	"caps" or pencil-thin lining	smooth "halo"	periventricular abnormal signal intensities extending into the deep white matter	–	–
BG	lesions in basal ganglia and surronding areas	absence	one focal lesion	more than one focal lesions	large confluent lesions	–	–
IT	lesions in infratentorial regions	absence	one focal lesion	more than one focal lesions	large confluent lesions	–	–
DWM	lesions in deep white matter	absence	punctuate foci	beginning of confluent foci	large confluent areas	large confluent white matter areas involving all cerebral lobes	complete confluent white matter disease
GA	global atrophy	no atrophy	mild atrophy	moderate atrophy	severe atrophy	most severe atrophy presetned especially in the medial temporal lobes	most severe atrophy presented in the medial temporal and cerebral cortex
other lesions	neoplasm, trauma, deformation	nothing	any one kind	any two kinds	more than two kinds	–	–

of dilatation of small vessels (i.e., small and well-margined symmetric hypointensities; GM-SV) and global atrophy (GA). An "other lesions" category was included to allow for ratings of neoplasm, trauma, and deformity. The grading scheme followed the BALI construction [15] to adapt existing rating scores that address localized structural changes [3, 10–12] (Table 1). Specifically, a scale was assigned for each category based on the severity of deficits, with higher scores indicating greater severity (Fig. 1). To the existing DWM rating, scores of "4" and "5" were added, to describe large confluent WM areas involving all cerebral lobes and complete confluent lesions. Similarly, two more levels (i.e., 4 and 5) were included to evaluate progression of global atrophy, where "4" indicated most severe atrophy present, especially in the medial temporal lobes, and "5" indicated the most severe atrophy present in the medial temporal and cerebral cortex (Table 1).

At each time point, the scans were reviewed separately and the total BALI scores were calculated by summarizing the ratings of all seven categories. Ratings were completed independently by two trained radiologists. Baseline and follow-up images were rated in random order, with the raters blind to demographic data, diagnosis, scan time, and cognitive test results. Inter-rater correlation coefficients (ICC) for BALI total scores were evaluated on a randomly selected sample of 20% of subjects in each diagnostic group at both baseline and follow-up.

Clinical tests

Clinical tests and ratings of cognitive functioning at both baseline and follow-up were obtained from the ADNI clinical dataset. These included the Clinical Dementia Rating scale (CDR) and scores on the Mini-Mental State Examination (MMSE) and the Alzheimer's Disease Assessment Scale – cognitive subscale (ADAS-cog). The ADNI protocol required two initial visits. The first was a screening visit (at which time MMSE and CDR testing were performed), followed by a baseline visit (at which time the ADAS-cog and other clinical tests were performed). The 3T MRI scans were to be performed within 42 days after the screening visit and within 14 days of the baseline visit. The follow-up scans were designed to be completed within 14 days of the 24 months follow-up visit (at which time clinical tests including the ADAS-cog, MMSE, and CDR were performed) [21]. For this study sample, the baseline MMSE and CDR were completed

on average 40.2 ± 19.2 days ahead of the 3T MRI scans, while the ADAS-cog was completed 5.6 ± 10.7 days ahead of the MRIs. Follow-up cognitive testing was conducted on average 2.6 ± 10.3 days ahead of the MRI scans.

Diagnostic categorization of the subjects and classification of conversion between diagnostic groups were both made by the ADNI site physicians in accordance with the criteria of the National Institute of Neurologic and Communicative Disorders and Stroke/Alzheimer's Disease and Related Disorders Association (NINCDS/ADRDA), and were reviewed by ADNI clinical monitors [21]. Analyses involving follow-up data have taken into account information about disease conversion for diagnostic categorization.

Statistical analyses

Demographic characteristics across diagnostic group were examined using Kruskal-Wallis nonparametric tests for interval data and Chi-Square tests for ordinal data. A general linear model of repeated measures with unbalanced design was used to test the differences in the BALI total score and the cognitive testing scores, with time as within-subject factor and diagnostic-categorization as the between subject factor. All multivariate analyses were adjusted for age, sex, and education level. The main effects of time and diagnosis and their interactions were tested. Relationships between BALI scores at baseline and at follow-up were tested using correlation analyses. The effect of the BALI on cognitive testing scales was evaluated using multivariate linear regression analysis, adjusted for age, sex, education level. Similarly, multivariate linear regression analysis was used to examine the association between the change scores (i. e., follow-up - baseline) of the BALI and the cognitive tests. All analyses were performed using SPSS© 15.0 software package and codes developed using Matlab© R2007. Significance level was set at $p < 0.05$.

RESULTS

In general, demographic characteristics were similar across diagnostic groups. Subjects with MCI were more likely to be men ($p = 0.002$; Table 2), otherwise there were no statistical differences in age ($p = 0.37$) or in education ($p = 0.84$), although subjects in the MCI group appeared to be slightly younger, especially the non-converters (Table 2). As expected, a significant difference in cognitive ratings and performance

Score Category	0	1	2	3
IT (%) example	1.6 / 0.8	2.4 / 2.4	83.2 / 84.0	12.8 / 12.8
BG (%) example	0 / 0	0.8 / 0.8	88.8 / 80.8	10.4 / 18.4
DWM (%) example	2.4 / 5.6	34.4 / 23.2	32.8 / 36.8	23.2 / 26.4
PV (%) example	0.8 / 4.8	38.4 / 32.8	41.6 / 28.8	19.2 / 33.6
GM -SV (%) example	12.0 / 10.4	72.0 / 76.0	16.0 / 12.8	0 / 0.8
GA (%) example	12.8 / 0.8	42.4 / 33.6	27.2 / 37.6	17.6 / 28.0

Fig. 1. Example images showing subscore ratings for each category. White arrows indicate where the deficits are located. Percentage of subjects having each score at baseline and at two-year follow-up were given (i.e., baseline/follow-up).

was evident at baseline and at follow-up among the diagnostic groups even when adjusted for age, sex, and education level. (F = 99.1 for MMSE, F = 92.1 for ADAS-cog; $p_s < 0.001$). There was no significant time by diagnosis interaction associated with the two-year decline ($p > 0.05$), despite the noted differences in the timing of administration of the ADAS-Cog and MMSE in relation to the MRI. Note that in this subsample of

Table 2
Characteristics of the subjects in different diagnostic groups

Group		Alzheimer's disease	Mild cognitive impairment		Health control	$p*$
			Conversion	Stable		
Sample size	baseline	39			58	
	follow-up	26	31	22	46	
Female (%)	baseline	59.0	29.0	40.9	62.1	0.002
Education (years)	baseline	14.7 ± 2.4	15.7 ± 2.7	14.9 ± 2.8	15.4 ± 2.7	0.844
Age (years)	baseline	75.7 ± 9.4	74.2 ± 8.2	72.9 ± 7.0	76.0 ± 5.1	0.369
MMSE (/30)	baseline	23.0 ± 2.1	26.4 ± 1.8	27.6 ± 2.0	29.3 ± 0.9	0.001
	follow-up	18.3 ± 6.1	22.8 ± 3.6	27.9 ± 2.6	29.1 ± 1.1	<0.001
ADAS-cog (/70)	baseline	18.6 ± 6.8	13.8 ± 3.4	9.1 ± 4.0	5.3 ± 2.5	<0.001
	follow-up	27.8 ± 12.7	17.0 ± 6.5	10.2 ± 4.6	5.6 ± 2.7	<0.001
#CDR (0–3)	baseline	$0.7 \pm 0.2 (0.5)$	$0.5 \pm 0.0 (0.5)$	$0.5 \pm 0.0 (0.5)$	$0(0)$	<0.001
	follow-up	$1.2 \pm 0.6 (1)$	$0.8 \pm 0.3 (1)$	$0.5 \pm 0.1 (0.5)$	$0 \pm 0.1 (0)$	<0.001
BALI (/25)	baseline	11.2 ± 3.1	10.7 ± 2.8	9.5 ± 2.6	9.9 ± 2.4	0.072
	follow-up	12.4 ± 2.7	12.0 ± 2.7	9.9 ± 2.1	11.0 ± 2.4	0.001

Note: Data are presented as mean ± standard deviate, otherwise as indicated. AD: Alzheimer's disease. MCI: Mild Cognitive Impairment. HC: healthy control subjects. MMSE: Mini-Mental Status Examination. ADAS-cog: Alzheimer's Disease Assessment Scale-cognitive subscale. CDR: Clinical Dementia Rating. BALI: Brain Atrophy and Lesion Index. $p*$: Diagnostic group differences were examined using uni-variate Kruskal-Wallis nonparametric tests for interval data and Chi-Square tests for ordinal data. For the baseline comparisons, means of the AD, pooled MCI, and HC groups were compared. For the follow-up data, means of the pooled AD and converter MCI, non-converter MCI, and HC groups were compared. # Median value is presented in brackets.

people with 3T scans, none of the AD patients were re-classified as having MCI; likewise, only one of the healthy controls progressed to a diagnosis of MCI. Within the MCI group, most (31/53) had progressed to a diagnosis of AD by follow-up (Table 2).

The overall inter-rater agreement rate for BALI ratings was high (ICC = 90.8%). Brain structural deficits were common in all groups (Table 2) and on average increased (showed worsening) in each diagnostic group. This worsening of scores over time, with significant differences between diagnostic groups persisted when the analyses were adjusted for age, sex, and education ($F_{time} = 49.1$, $p < 0.001$; $F_{diagnosis} = 3.62$, $p = 0.030$) but without a significant time-diagnosis interaction. Note that whereas subjects with AD and MCI-AD converters showed the highest BALI values, the mean difference in BALI between the non-converters and health controls was not statistically significant ($p > 0.05$). Overall, the MCI-AD converter group showed a greater increase in the BALI (i.e., more brain structural deficits) than did MCI non-converters. The BALI scores at baseline and follow-up were highly correlated ($r^2 = 0.78$, $p < 0.01$), although a few MCI non-converters and HC subjects showed a decrease in BALI over the two-year period. The maximum BALI

score at baseline was 16 (0.64 of the total score) and 18 (0.72) at follow-up, showing no ceiling effect, despite average disease progression.

Given mean worsening in both structure (BALI scores) and function (MMSE, ADAS-Cog) the relationship between the two is of interest. The BALI score was significantly related both to MMSE at baseline (regression coefficient B = −0.310; $t = −2.71$; $p = 0.008$) and at follow-up (B = −0.725; $t = −3.5$; $p = 0.001$) and to ADAS-cog at baseline (B = 0.612; $t = 2.521$; $p = 0.013$) and at follow-up (B = 1.26; $t = 3.02$; $p = 0.003$), in a multivariable linear regression adjusted for age, sex and education. The change in BALI between baseline and follow-up was also associated with the change in MMSE (i.e., ΔMMSE; B = −0.226; $t = −2.176$; $p = 0.031$). By contrast, change in the BALI was not significantly associated with the change in the ADAS-cog ($p = 0.25$). Of the 30 MCI subjects who showed a worsening in MMSE (i.e., $MMSE_{(follow-up-baseline)} < 0$), 25 (83%) also showed a worsening in BALI (i.e., $BALI_{follow-up-baseline} > 0$); the BALI scores of the remaining 5 people did not change. Similarly, of the 23 MCI people who showed a stable or improved MMSE, 15 (66%) had a stable or improved BALI ($X^2 = 14.2$, $p = 0.007$).

DISCUSSION

In this secondary analysis of 3T MRI data, several common types of brain structural changes in AD, MCI and healthy controls could be quantified in a Brain Atrophy and Lesion Index (BALI) score, to evaluate overall brain deficits and their relationship to cognitive function. Over two years, people in each diagnostic group, on average, experienced increasing atrophy and more structural brain lesions. Cognitive test scores worsened in the AD group, and in most people with MCI, but were relatively stable in healthy controls and in a minority with MCI. In AD and in the people with MCI who by two years had progressed to AD, structural brain changes as indicated by the BALI score, and brain function as measured by the MMSE deteriorated in parallel. The accumulation of brain structural deficits in association with cognitive decline corresponds to lessons from large prospective neuropathological studies [6, 7] and supports the use of BALI to quantify whole brain changes in AD, MCI and normal aging [15].

It is of clear clinical and public health significance to understand the relationships between structural brain changes and changes in cognitive functioning as they occur in the development of AD, recognizing that AD involves multiple brain changes, including atrophy, white matter lesions, and vascular changes [8, 22]. Methods of collectively studying the cumulative impact of these many structural deficits have been sought [6, 7] and BALI ratings appear to fill this need. In particular, the BALI rating is easily accessible because it can be based on T1-weighted high-resolution imaging, the most routinely acquired sequence in MRI investigations. While many studies seek to establish the relationship between specific cognitive abilities and specific types of brain deficits, most cognitive tasks require the integrated functioning of a variety of neural networks. BALI ratings can serve to describe global structural status in a manner that allows for global cognitive dysfunction to be related to the accumulation of brain structural deficits.

Here, people with AD and those with MCI who progressed to AD showed both cognitive and structural decline. The BALI allows us to demonstrate the association between brain structural changes and cognitive decline using a cumulative index. Similar findings have been reported in earlier studies that were typically based on individual structural measures [18]. For example, recent serial MRI studies have suggested hippocampal atrophy or ventricular enlargement is predic-tive of cognitive decline and/or AD conversion [9, 16, 17, 23]. The rate of change of white matter damage has also been used to predict cognitive decline [18, 27]. It is also worth noting that while most people in the study sample had stable or greater brain deficits over two years, a small number of stable MCI and HC subjects did have a decreased BALI. Whereas, most people with brain structural worsening also had cognitive worsening, some did show improved cognitive test scores, possibly in keeping with the concept of cognitive reserve [28]. Importantly however, of those who converted to AD, none showed an improvement in BALI.

Our data must be interpreted with caution. Rating scales have inherently low precision with respect to volumetric measurements. For example, voxel/volume-base morphography can often reveal quantitative atrophy changes of about 1% per year [9], whereas with BALI a minimum increment of any domain including atrophy is one point. In other words, assigning a precise value using a rating scale may not be as easy as visualizing an apparent deficit. Even so, in practice, valid visual rating scales are particularly beneficial and welcome in clinical settings when evaluation time is a concern [29]. The scoring system utilized in this study has been adapted from existing rating scales and been validated by previous research [15]. Furthermore, the relatively high inter-rater reliability suggests that the BALI ratings can be consistently performed by different raters with training of the method.

To now construction of the BALI has not considered the assignment of relative weights to different BALI components, even though these clearly can affect cognition differently (e.g. medial temporal atrophy [30]). The algorithms for determining appropriate weights for BALI components are yet to be established. There may in fact be inherent benefit to a scale without weights, as weights for individual BALI items may vary across datasets, targeted outcome measures, follow-up durations, and study focus. In short, while weighting might improve prediction in a given dataset, it can impair generalizability. This needs to be evaluated.

Several other caveats also apply to our study; among these the fact that cognitive evaluations were limited to the MMSE, ADAS-cog, and CDR. Both MMSE and ADAS-cog can have ceiling effects with HC and MCI subjects that make sensitivity to change an issue for longitudinal studies. The number of people in whom the CDR increased (indicating worsening cognition and function) and/or converted to AD over two years was also relatively low, further limiting the sensitivity

to detect the association between cognitive decline and brain deficit progression. Here, in the subjects limited to those with 3T data, only one healthy control progressed to MCI or AD. In addition, while the time difference between MRI scans and the cognitive assessments were within a few days for all of the follow-up tests and for the baseline ADAS-cog, baseline MMSE and CDR were completed approximately 40 days in advance of the baseline imaging acquisition. Clearly it would have been preferable to have baseline clinical testing that was closer in time to the initial MRI scan. Lastly, we lack the knowledge of treatment effects in the AD and MCI groups, and therefore cannot identify whether any improvement in cognition and/or brain structure was related to treatment. Despite these limitations, the overall brain deficits as measured by BALI were related to the global cognitive assessment scales used in this study, at both baseline and follow-up. In the future, large-scale serial MRI research involving multiple follow-ups over longer terms and more detailed clinical assessments would be particularly valuable. Better understanding the relationships between structural and functional changes can help improve clinical management and preclinical strategies for AD [31].

In summary, the present study suggests that significant brain changes and cognitive changes can occur within two years in people with MCI and AD and in otherwise healthy elderly people. The BALI provides a readily available means to evaluate brain structural changes and their relation to cognitive decline as well as conversion to AD from MCI.

ACKNOWLEDGMENTS

REFERENCES

[1] Drayer BP (1988) Imaging of the aging brain. Part I. Normal findings. *Radiology* **166**, 785-796.

[2] Brickman AM, Zimmerman ME, Paul RH, Grieve SM, Tate DF, Cohen RA, Williams LM, Clark CR, Gordon E (2006) Regional white matter and neuropsychological functioning across the adult lifespan. *Biological Psychiatry* **60**, 444-453.

[3] Duara R, Loewenstein DA, Potter E, Appel J, Greig MT, Urs R, Shen Q, Raj A, Small B, Barker W, Schofield E, Wu Y, Potter H (2008) Medial temporal lobe atrophy on MRI scans and the diagnosis of Alzheimer disease. *Neurology* **71**, 1986-1992.

[4] Brickman AM, Muraskin J, Zimmerman ME (2009) Structural neuroimaging in Alzhheimer's disease: do white matter hyperintensities matter? *Dialogues Clin Neurosci* **11**, 181-190.

[5] Black S, Gao F, Bilbao J (2009) Understanding white matter disease: imaging-pathological correlations in vascular cognitive impairment. *Stroke* **40**, S48-S52.

[6] Savva GM, Wharton SB, Ince PG, Forster G, Matthews FE, Brayne C, Medical Research Council Cognitive Function,

Ageing, Study (2009) Age, neuropathology, and dementia. *N Engl J Med* **360**, 2302-2309.

[7] White L (2009) Brain lesions at autopsy in older Japanese-American men as related to cognitive impairment and dementia in the final years of life: a summary report from the Honolulu-Asia aging study. *J Alzheimers Dis* **18**, 713-725.

[8] Capizzano AA, Acion L, Bekinschtein T, Furman M, Gomila H, Martínez A, Mizrahi R, Starkstein SE (2004) White matter hyperintensities are significantly associated with cortical atrophy in Alzheimer's disease. *J Neurol Neurosurg Psychiatry* **75**, 822-827.

[9] Jack CR Jr, Shiung MM, Gunter JL, O'Brien PC, Weigand SD, Knopman DS, Boeve BF, Ivnik RJ, Smith GE, Cha RH, Tangalos EG, Petersen RC (2004) Comparison of different MRI brain atrophy rate measures with clinical disease progression in AD. *Neurology* **62**, 591-600.

[10] Kapeller P, Barber R, Vermeulen J, Adèr H, Scheltens P, Freidl W, Almkvist O, Moretti M, del Ser T, Vaghfeldt P, Enzinger C, Barkhof F, Inzitari D, Erkinjunti T, Schmidt R, Fazekas F (2003) European Task Force of Age Related White Matter Changes, Visual rating of age-related white matter changes on magnetic resonance imaging: scale comparison, interrater agreement, and correlations with quantitative measurements. *Stroke* **34**, 441-445.

[11] Wahlund LO, Barkhof F, Fazekas F, Bronge L, Augustin M, Sjögren M, Wallin A, Ader H, Leys D, Pantoni L, Pasquier F, Erkinjuntti T, Scheltens P (2001) European Task Force on Age-Related White Matter Changes, A new rating scale for age-related white matter changes applicable to MRI and CT. *Stroke* **32**, 1318-1322.

[12] Scheltens P, Barkhof F, Leys D, Pruvo JP, Nauta JJ, Vermersch P, Steinling M, Valk J (1993) A semiquantitative rating scale for the assessment of signal hyperintensities on magnetic resonance imaging. *J Neurol Sci* **114**, 7-12.

[13] Alvarez-Linera J (2008) 3T MRI: advances in brain imaging. *Eur J Radiol* **67**, 415-426.

[14] Duyn JH (2010) Study of brain anatomy with high-field MRI: recent progress. *Magn Reson Imaging* **28**, 1210-1215.

[15] Chen W, Song X, Zhang Y, Darvesh S, Zhang N, D'Arcy RC, Black S, Rockwood K (2010) An MRI-based semiquantitative index for the evaluation of brain atrophy and lesions in Alzheimer's disease, mild cognitive impairment and normal aging. *Dement Geriatr Cogn Disord* **30**, 121-130.

[16] den Heijer T, van der Lijn F, Koudstaal PJ, Hofman A, van der Lugt A, Krestin GP, Niessen WJ, Breteler MM (2010) A 10-year follow-up of hippocampal volume on magnetic resonance imaging in early dementia and cognitive decline. *Brain* **133**, 1163-1172.

[17] Whitwell JL, Przybelski SA, Weigand SD, Knopman DS, Boeve BF, Petersen RC, Jack CR Jr (2007) 3D maps from multiple MRI illustrate changing atrophy patterns as subjects progress from mild cognitive impairment to Alzheimer's disease. *Brain* **130**, 1777-1786.

[18] Silbert LC, Howieson DB, Dodge H, Kaye JA (2009) Cognitive impairment risk: white matter hyperintensity progression matters. *Neurology* **73**, 120-125.

[19] Werner MW, Aisen PS, Jack CR Jr, Jagust WJ, Trojanowski JQ, Shaw L, Saykin AJ, Morris JC, Cairns N, Beckett LA, Toga A, Green R, Walter S, Soares H, Snyder P, Siemers E, Potter W, Cole PE, Schmidt M (2010) Alzheimer's Disease Neuroimaging Initiative, The Alzheimer's disease

neuroimaging initiative: progress report and future plans. *Alzheimer's Dement* **6**, 201-211.

[20] Jack CR Jr, Bernstein MA, Fox NC, Thompson P, Alexander G, Harvey D, Borowski B, Britson PJ, Whitwell JL, Ward C, Dale AM, Felmlee JP, Gunter JL, Hill DL, Killiany R, Schuff N, Fox-Bosetti S, Lin C, Studholme C, DeCarli CS, Krueger G, Ward HA, Metzger GJ, Scott KT, Mallozzi R, Blezek D, Levy J, Debbins JP, Fleisher AS, Albert M, Green R, Bartzokis G, Glover G, Mugler J, Weiner MW (2008) The Alzheimer's Disease Neuroimaging Initiative (ADNI): MRI methods. *J Magn Reson Imaging* **27**, 685-691.

[21] ADNI General Procedures Manual, http://www.loni.ucla.edu/research/protocols/clinical-protocols/ADNI General Procedures Manual.pdf.

[22] van der Flier WM, Middelkoop HA, Weverling-Rijnsburger AW, Admiraal-Behloul F, Spilt A, Bollen EL, Westendorp RG, van Buchem MA (2004) Interaction of medial temporal lobe atrophy and white matter hyperintensities in AD. *Neurology* **62**, 1862-1864.

[23] Sean MN, Raul R, Michael B, Smith M, Accomazzi V, Wells JL, Fogarty J, Bartha R (2008) Alzheimer's Disease Neuroimaging Initiative, Ventricular enlargement as a possible measure of Alzheimer's disease progression validated using the Alzheimer's disease neuroimaging initiative database. *Brain* **131**, 2443-2454.

[24] Driscoll I, Davatzikos C, An Y, Wu X, Shen D, Kraut M, Resnick SM (2009) Longitudinal pattern of regional brain volume change differentiates normal aging from MCI. *Neurology* **72**, 1906-1913.

[25] Ezekiel F, Chao L, Kornak J, Du AT, Cardenas V, Truran D, Jagust W, Chui H, Miller B, Yaffe K, Schuff N, Weiner M (2004) Comparisons between global and focal brain atrophy rates in normal aging and Alzheimer disease: Boundary Shift Integral versus tracing of the entorhinal cortex and hippocampus. *Alzheimer Dis Assoc Disord* **18**, 196-201.

[26] DeCarli C, Fletcher E, Ramey V, Harvey D, Jagust WJ (2005) Anatomical Mapping of White Matter Hyperintensities (WMH). Exploring the relationships between periventricular WMH, deep WMH, and total WMH burden. *Stroke* **36**, 50-55.

[27] Brickman AM, Honig LS, Scarmeas N, Tatarina O, Sanders L, Albert MS, Brandt J, Blacker D, Stern Y (2008) Measuring cerebral atrophy and white matter hyperintensity burden to predict the rate of cognitive decline in Alzheimer disease. *Archives of neurology* **65**, 1202-208.

[28] Stern Y (2009) Cognitive reserve. *Neuropsychologia* **47**, 2015-2028.

[29] Gouw AA, van der Flier WM, van Straaten EC, Pantoni L, Bastos-Leite AJ, Inzitari D, Erkinjuntti T, Wahlund LO, Ryberg C, Schmidt R, Fazekas F, Scheltens P, Barkhof F; LADIS study group (2008) Reliability and sensitivity of visual scales versus volumetry for evaluating white matter hyperintensity progression. *Cerebrovasc Dis* **25**, 247-253.

[30] Enzinger C, Fazekas F, Matthews PM, Ropele S, Schmidt H, Smith S, Schmidt R (2005) Risk factors for progression of brain atrophy in aging: six-year follow-up of normal subjects. *Neurology* **24**, 1704-1711.

[31] Frisoni GB, Fox NC, Jack CR Jr, Scheltens P, Thompson PM (2010) The clinical use of structural MRI in Alzheimer disease. *Nat Rev Neurol* **6**, 67-77.

This page intentionally left blank

Power Calculations for Clinical Trials in Alzheimer's Disease

M. Colin Ard[a] and Steven D. Edland[a,b,*]

[a]*Department of Neuroscience, University of California, San Diego, La Jolla, CA, USA*

[b]*Department of Family Preventive Medicine Division of Biostatistics, University of California, San Diego, La Jolla, CA, USA*

Abstract. The Alzheimer research community is actively pursuing novel biomarker and other biologic measures to characterize disease progression or to use as outcome measures in clinical trials. One product of these efforts has been a large literature reporting power calculations and estimates of sample size for planning future clinical trials and cohort studies with longitudinal rate of change outcome measures. Sample size estimates reported in this literature vary greatly depending on a variety of factors, including the statistical methods and model assumptions used in their calculation. We review this literature and suggest standards for reporting power calculation results. Regardless of the statistical methods used, studies consistently find that volumetric neuroimaging measures of regions of interest, such as hippocampal volume, outperform global cognitive scales traditionally used in clinical treatment trials in terms of the number of subjects required to detect a fixed percentage slowing of the rate of change observed in demented and cognitively impaired populations. However, statistical methods, model assumptions, and parameter estimates used in power calculations are often not reported in sufficient detail to be of maximum utility. We review the factors that influence sample size estimates, and discuss outstanding issues relevant to planning longitudinal studies of Alzheimer's disease.

Keywords: Sample size, clinical trials, Alzheimer's disease, biostatistics

INTRODUCTION

There is increasing interest in the potential utility of biomarkers as outcomes in clinical trials. For example, the joint industry/NIH funded Alzheimer's Disease Neuroimaging Initiative (ADNI) was created expressly to investigate cerebrospinal fluid and volumetric neuroimaging measurements as diagnostic biomarkers of early Alzheimer's disease (AD) and as potential endpoints for monitoring clinical trial treatment effects [1]. ADNI has recruited and followed longitudinally approximately 200 AD cases, 400 mild cognitively

impaired (MCI), and 200 age-matched cognitively normal controls [2]. Additional novel biomarker endpoints, including MR spectroscopy [3] and FDG-PET [4] have been proposed and are being actively pursued. The hope is that biomarkers will allow monitoring of treatment effects at earlier stages of disease, before traditional cognitive and functional endpoints are measurable. It is also becoming apparent that biomarker measurements, particularly volumetric neuroimaging measures, are substantially more precise than traditional cognitive and functional measures, to the point that clinical trials using volumetric neuroimaging measures may be possible with a tenth or less of the sample size of current trials. Freely accessible ADNI data has provided a natural laboratory for exploring these issues. While this literature has consistently described the relative improvement in statistical power

---

*Correspondence to: Steven D. Edland, PhD, Associate Professor of Biostatistics, Associate Professor of Neuroscience, University of California, San Diego 9500 Gilman Dr. M/C 0948, La Jolla, CA 92093-0948. Tel.: +858 677 1550; Fax: +858 622 5845. E-mail: sedland@ucsd.edu.

of imaging outcomes relative to cognitive outcomes, there is little consistency across reports in estimated sample size requirements for each particular outcome measure. To characterize these discrepancies, we have reviewed the ADNI power calculation publications with an eye to the influence of statistical methods on sample size projections.

LITERATURE REVIEW METHODS

Articles were identified based on a search of published papers listed on the ADNI website (adniinfo. org /Scientists /ADNIScientistsHome/ADNIPublicatio ns.aspx) as of February 4, 2011. All papers containing search terms "power" or "sample size" were reviewed for reported sample size calculations by one of the authors (MCA). Of 143 papers searched, 17 contained abstractable reports of previously unpublished analytic sample size calculations [5–21]. These papers report required sample size for a future clinical trial to observe a stated treatment effect, with the magnitude of the treatment effect described in terms of percentage slowing of disease progression relative to placebo. An additional six papers reported on sample sizes required for various analyses (e.g., detection of correlations, differences between dementia types, or the presence of atrophy) using a non-analytic sample-reduction method in which subjects were randomly discarded from the pilot data set until it was no longer possible to reject the hypotheses in question [22–27]. The remaining search hits were all due to papers reporting retrospective power calculations, papers that only reported relative gains in sample sizes, and papers that cited previously published estimates.

Among the 17 papers that presented prospective analytic calculations, most reported sample size required to detect a 25% reduction in the observed rate of change with 80% power. To facilitate comparisons across publications, sample size estimates based on a different percentage reduction were recalculated to a 25% reduction using the formula $n_{25} = (k/25)^2 n_k$, where k equals the percentage used in the original report. Sample size estimates for power other than 80% (typically 90%) were standardized to 80% using the formula $n_{0.8} = (z_{\alpha/2} + z_{0.2})^2 n_p/(z_{\alpha/2} + z_{1-p})^2$, where in this case the subscript p indicates the power of the trial expressed as a probability. The characterization of effect size as a fixed percent reduction in observed rate of change is useful for comparing power calculations across studies, but is not intended to serve as a model for research

practice. In practice, effect sizes used in trial design should always be determined based on the plausibility and clinical significance of the hypothetical outcomes under consideration [28].

RESULTS

Tables 1 and 2 summarize reported sample size estimates for trials in AD and MCI. Table 1 summarizes estimates of sample size required to detect a 25% reduction in mean rate of decline on the standard cognitive outcome for AD treatment trials, the AD Assessement Scale - Cognitive Subscale (ADAS-Cog) [29]; Table 2 summarizes estimates of sample size required to detect a 25% reduction in atrophy rate for a likely MRI outcome, hippocampal volume. Reported sample size estimates for each measure are widely divergent. The differences in estimates may be explained by a number of factors, which we review in sequence below.

Trial design

Trial design, i.e. the length of the trial and the frequency of assessment, has a direct influence on statistical power. All other things being equal, longer trials, and to a lesser extent trials with finer assessment intervals, result in more precise estimates of rate of decline per arm and require fewer subjects to detect treatment effects. For example, Hua et al. [13] report a 6-fold decrease in required sample size for a 2-year compared to a 6-month long AD treatment trial using change on ADAS-Cog as the outcome variable (Table 1). Relatively noisy outcome measures, such as global cognitive scales represented here by the ADAS-Cog, experience more gain in precision and power by increased trial length or assessment frequency compared to relatively less noisy outcome measures such as volumetric imaging. For example, using change in hippocampal volume as the outcome measure, Hua et al. report only a 36% increase in sample size required for a 6-month compared to 2-year trial (Table 2). The influence of trial design on statistical power varies with different analysis plans. Within limits, longer trials and increased sampling frequency are associated with improved power for trials designed to detect changes in trajectory of disease under treatment, although there are diminishing returns with longer trials as dropout rates increase and linearity assumptions implicit in most statistical analysis plans become less tenable.

Table 1
Sample size required to detect a 25% reduction in annual rate of change for ADAS-Cog scores in AD and
MCI (80% power and two-sided $\alpha = 0.05$)

Paper	Trial design	AD		MCI	
	Yrs (#Obs)	ROC	n/arm	ROC	n/arm
Aisen et al. (2010)[a]	1(n.s.)	4.3	407	1.1	4099
Beckett et al. (2010)[a]	2(5)	4.37	–	1.05	375
Chen et al. (2010)[a]	1(2)	3.8	[353, 505][b]	1.0	[4026, 4219][b]
Fleisher et al. (2009)[a]	1(n.s.)	n.s.	[474, 612][c]	–	–
	2(n.s.)[d]	–	–	n.s.	854
Ho et al. (2010)[a]	1(2)	3.29	583	2.43	1183
Holland et al. (2009)[e]	1(3)	4.08	624	1.19	4167
	2(5)	4.84	324	1.44	1232
Hua et al. (2010)[a]	0.5(2)	n.s.	1371	n.s.	16645
	1(2)	n.s.	483	n.s.	8212
	1.5(2)	–	–	n.s.	1381
	2(2)	n.s.	215	n.s.	1013
Landau et al. (2009)[f]	1(3)	3.8	312	1.0	2175
McEvoy et al. (2010)[e]	2(5)	–	–	1.47	978
Nestor et al. (2008)[a, d]	0.5(2)	4.8	769	1.2	9500+
Schuff et al. (2009)[d, g]	0.5(2)	n.s.	557	n.s.	3484
	1(2)	n.s.	609	n.s.	6985
	1(3)	n.s.	426	n.s.	6241

Yrs (#Obs) = length of trial in years (number of evenly spaced observations); ROC = annual rate-of-change;
n.s. = not specified; – = not applicable (scenario not investigated in the manuscript). Superscripts: [a] analysis
plan or longitudinal statistical model not fully specified; [b] ranges reflect different values for nested subsets
of the data; [c] range reflects values from two cited reports; [d] N/arm in table adjusted from values reported
in manuscript to reflect 25% effect size and 80% power, see Methods for details; [e] linear mixed effects
model with random slopes and intercepts assumed; [f] model assumptions alternatively cited as linear mixed
effects with random-intercepts only and linear mixed effects with random slopes and intercepts; [g] random-
intercepts only model assumed.

Trials designed to detect acute, symptomatic treatment effects are unlikely to benefit from longer observation or increased frequency of sampling.

Magnitude of effect size

Effect size, the minimum treatment effect a trial is powered to detect, directly influences sample size requirements. For the power calculations reviewed here, the effect size is calculated as a percentage of the assumed mean rate of decline under the placebo condition. The various ADNI power calculation papers used different estimates of the placebo rate of decline in their calculations, and this explains to some degree the differences in required sample size reported. For example, for MCI treatment trials using the ADAS-Cog as the endpoint (Table 1), effects sizes used for power calculations range from 25% of 2.1 points per year [10] to 25% of 1.0 points per year [8, 14]. The sample size estimate in the former (1183 for a 1-year trial) is substantively smaller than the sample size estimates in the latter (4000+ and 2175 for a 1-year trial). Several papers did not report the effect size powered for [9, 13, 19], and we can only speculate on the extent to which

differences in sample size projections reported in these papers are attributable to differences in assumed effect size. However, in general, when defining effect size as a percentage reduction in mean rate of decline, a smaller assumed mean rate of decline under the null hypothesis translates to smaller effects sizes powered for and larger required sample size.

Target population of planned clinical trial

A critical factor when setting the effect size for power calculations is the issue of defining the target population of the planned future clinical trial. For the most part the power calculations reviewed here used estimates of mean rate of decline within the ADNI cohorts as the assumed trajectory of disease under the placebo condition. The implicit assumption is that subjects recruited in future trials will look much like the subjects recruited into the ADNI cohort study, a reasonable assumption given that the ADNI recruitment network and methods parallel those used by many multicenter trials [5]. The differences in effect size (Tables 1 and 2) used by the various studies may follow in part from random variability in data obtained

Table 2
Sample size required to detect a 25% reduction in annual rate of hippocampal atrophy in AD and MCI
(80% power and two-sided $\alpha = 0.05$)

Paper	Trial design	AD		MCI	
	Yrs (#Obs)	Atrophy rate	n/arm	Atrophy rate	n/arm
Aisen et al. (2010) [a]	1(n.s.)	n.s.	99	n.s.	208
Beckett et al. (2010)[a]	1(n.s.)	(116 mm^3)	–	(80 mm^3)	202
Holland et al. (2009)[b]	1(3)	3.42%	111	2.10%	235
	2(5)	3.28%	67	1.96%	179
Hua et al. (2010)[a]	0.5(2)	n.s.	114	n.s.	143
	1(2)	n.s.	68	n.s.	125
	1.5(2)	n.s.	–	n.s.	117
	2(2)	n.s.	84	n.s.	103
Leung et al. (2010)[a]	1(2)[c1]	4.57%	78	2.86%	196
	1(2)[c2]	4.58%	170	3.68%	285
McEvoy et al. (2010)[b]	2(5)	–	–	1.93%	186
Schuff et al. (2009)[d,e]	0.5(2)	3.3% (53.5 mm^3)	346	2.0% (37.7 mm^3)	709
	1(2)	4.4% (72.0 mm^3)	189	2.6% (47.5 mm^3)	522
	1(3)	n.s.	191	n.s.	503
Wolz et al. (2009)[a]	1(2)	3.85%	67	2.34%	206
	2(3)[f]	3.37%	46	2.25%	121
Yushekevich et al. (2010)[a]	1(2)	–	–	2.04%	220[g]

Yrs (#Obs) = length of trial in years (number of evenly spaced observations); Atrophy Rate reported as % change/year, or when indicated in parenthesis, reported in units of (mm^3/year); n.s. = not specified; −= not applicable (scenario not reported in the manuscript). Superscripts: [a] analysis plan or longitudinal statistical model not fully specified; [b] linear mixed effects model with random slopes and intercepts assumed; [c1] measurement by multiple-atlas propagation and segmentation-hippocampal boundary shift integral (MAPS-HBSI); [c2] measurement by Surgical Navigation Technologies; [d] random-intercepts only model assumed; [e] N/arm in table adjusted from values reported in manuscript to reflect 25% effect size and 80% power, see Methods for details; [f] Atrophy rates adjusted to % change/year, rates in original manuscript given as % change/2 years; [g] N/arm in table calculated directly from MCI atrophy rate, N/arm presented in original manuscript was for disease-specific treatment effect adjusted for normal age-related atrophy.

when the ADNI data were accessioned. Differences in effect size may also follow from differences in statistical methods used to calculate mean rate of decline, or differences in inclusion/exclusion criteria applied to the ADNI sample prior to estimation.

Regarding the effect of varying inclusion criteria, McEvoy et al. [17] describe the effect of inclusion criteria intended to enrich the study population for subjects more likely to have the underlying neurodegenerative process that is the target of most planned therapies. For example, restricting recruitment to MCI subjects with baseline MRI atrophy patterns consistent with AD resulted in a cohort with mean trajectory of decline on the ADAS-Cog of 2.3 points per year compared to a mean decline of 1.5 points per year in the unrestricted cohort; sample size requirements correspondingly dropped by over one-half using this inclusion criterion, from 978 per arm to 458 per arm [17]. Similarly, restricting recruitment to subjects with the APOE $\varepsilon 4$ risk allele increased the mean rate of ADAS-Cog decline to 1.7 points per year and reduced the required sample size to 774 persons per arm [17]. A limitation of trials with restrictive inclusion criteria

is that findings only generalize to the subpopulation examined.

Statistical analysis plan and assumptions

Power calculations are specific to the analysis plan of the planned trial. Sample size formulas for two-group comparisons under normality assumptions are of the form:

$$n/arm = 2(z_{1-\alpha/2} + z_{1-\beta})^2 \sigma_d^2 / \Delta^2 \qquad (1)$$

where Δ is the treatment effect size under the alternative, σ_d^2 is the within group variance of the outcome measure being compared across treatments, and $z_{1-\alpha/2}$ and $z_{1-\beta}$ are the usual quantiles of the standard normal distribution, with α equal to the type I error rate of a two-sided test, typically set to 0.05, and $(1 - \beta)$ equal to the power of the trial, typically set to 0.8 or 0.9. Treatment effect Δ and variance σ_d^2 are defined in terms of the outcome measure to be used in the planned trial. For example, for a trial with two observations per subject and outcome measure of change from baseline to followup, Δ is the change in the

treatment group minus the change in placebo, and σ_d^2 is the variance of change scores (e.g., Meinart [30], equation 9.14). In this example σ_d^2 can be estimated as the variance of change from baseline to follow-up observed in two-wave pilot data of comparable duration to the planned trial. For a trial with multiple observations per subject and outcome measure of least squares slope of longitudinal trajectories, Δ is the difference in expected slopes in treatment versus placebo and σ_d^2 is the within arm variance of least squares slopes [31]. In this example σ_d^2 can be estimated from the variance of least squares slopes observed in pilot data of comparable design to the planned trial. These are examples of two-stage "summary measures" analyses which require only the assumption that summary measures (i.e., change scores or least squares slopes) are independent, identically distributed asymptotically normal random variables. Several of the ADNI power calculation papers (Tables 1 and 2) use summary measures power formulas, although the exact statistical analysis and model assumptions used were not always stated in complete detail.

Several of the power calculation papers used formally parameterized longitudinal models and analysis plans as the basis of their power calculations. For example, McEvoy et al. [17] based power calculations on a linear mixed effects model analysis assuming longitudinal trajectories of decline are linear within subject and that the distribution of slopes and intercepts describing these trajectories is bivariate normal. Sample size requirements given this assumed model have been derived [32]. For a balanced design (with all subjects observed at the same time points), the required sample size per arm is:

$$n/arm = 2(z_{1-\alpha/2} + z_{1-\beta})^2$$
$$\times \left(\sigma_b^2 + \sigma_e^2/\Sigma(t_i - \bar{t})^2\right)/\Delta^2 \qquad (2)$$

where σ_b^2 and σ_e^2 are parameters of the linear mixed effects model, and $\Sigma(t_i - \bar{t})^2$ is the "design term", where t_i indexes the times at which measures are made and $\bar{t}$ is the mean of the times. For example, for a 12 months trial with observations at baseline, month 6 and month 12, $\Sigma(t_i - \bar{t})^2$ in units of years equals $(0 - 0.5)^2 + (0.5 - 0.5)^2 + (1 - 0.5)^2 = 0.5$. Here Δ is the difference in mean rate of decline in treatment versus control, and the parameters σ_b^2 and σ_e^2 from the mixed effects model are the person to person variability in random slopes and the residual error variance of model [32]. σ_b^2 and σ_e^2 can be estimated by fitting a lin-

ear mixed effects model to pilot data representative of the trial's target population. For balanced design pilot data, estimates by formula (2) are algebraically identical to estimates by the power formula for a summary measures analysis comparing the mean of least squares slopes of treatment to the mean of least squares slopes of controls (e.g. [33]).

An alternative mixed effects model power formula is:

$$n/arm = 2(z_{1-\alpha/2} + z_{1-\beta})^2 \left(\sigma_e^2/\Sigma(t_i - \bar{t})^2\right)/\Delta^2 \qquad (3)$$

This formula is appropriate assuming a mixed effects model in which the subjects have random intercepts but identical rates of decline within arm (or equivalently, a marginal model with compound symmetric covariance structure [34]). Formula (2) results in smaller sample size projections, but can be anti-conservative when the common within arm rate of decline assumption does not hold. Formulas (1), (2), and (3) assume equal sample size per arm. Some trials use unequal allocation ratios to increase the likelihood of assignment to the active treatment arm and make the trial more attractive to study participants (e.g., [35]). Unequal allocation trials are slightly less efficient and require a modest adjustment in total sample size [36].

Several of the papers reviewed here reported sample sizes using formula (3), either in lieu of [19], or in addition to [11, 17], formula (2). Sample size estimates derived using the random-intercepts model and formula (3) were generally smaller than estimates using the mixed effects model with random intercepts and random slopes and formula (2). Taken together these observations underscore the importance of model selection when powering trials.

Differences in the image processing methods

For volumetric imaging outcomes in particular, sample size estimates can vary depending on the method of image analysis used. Image processing can be based on manual tracings [33], semi-automated methods and fully automated methods (e.g., [17]). Even though each of these methods is measuring the same structure, they may have different signal-to-noise properties depending on the relative precision of the methods. For example, Leung et al. [16], calculated hippocampal volume change by two different image processing methods and calculated samples size requirements for each outcome measure. While both methods led to sample size estimates that were considerably smaller

than estimates typical of global cognitive measures like the ADAS-Cog, they found that required sample size for the more efficient image processing method was between 32–54% smaller than the less efficient method (see Table 2). Characterizing the relative performance of various imaging technologies and processing techniques [10, 12, 13, 15, 16, 21, 23, 24], will be an important outcome of the ADNI exercise.

DISCUSSION

The results above suggest that the wide divergence of sample size estimates calculated from ADNI data can be explained by multiple factors beyond differences in trial design and target population, including differences in power calculation algorithms used, and, for neuroimaging outcomes, differences in the signal-to-noise profile of the different image processing algorithms. Additional factors relevant to power calculations for AD trials, and general recommendations for improved reporting of power calculations, are discussed below.

Sensitivity analysis

The validity of a power calculation is dependent in large part upon the accuracy of the (assumed known) parameter values used in its calculation. In practice these values are almost always calculated from pilot data, as is the case in the ADNI papers reviewed here, and hence contain some degree of random variability. The practical consequence of this randomness is potentially significant, especially when the pilot study used for parameter estimation is small. Several of the reviewed papers reported statistical tests or confidence intervals to characterize the variability inherent in sample size estimates ([10, 11, 13, 15–17, 21, 26, 27], see also [6]). For example, McEvoy et al. [17] used a bootstrap procedure to calculate 95% confidence intervals around sample size estimates based on ADNI data. They found that even with the relatively large ADNI pilot data set these confidence intervals can be large [17], demonstrating the importance of confidence interval calculation as a sensitivity analysis when powering trials.

Treatment target (disease-specific versus non-disease specific)

Some age-related cognitive decline and brain atrophy is experienced even within cognitively normal

elderly. This is potentially relevant to the design of trials, as treatments that target the Alzheimer neurodegenerative process specifically may have no effect on non-Alzheimer related decline, and non-Alzheimer related decline may comprise a substantial fraction of the total decline that the sample size calculations described in Tables 1 and 2 are powered to detect. ADNI includes an age-matched, cognitively normal healthy control cohort from which the potential influence of non-treatment responsive age-associated decline can be estimated. We illustrate this with sample power calculations for hypothetical trials of MCI subjects powered to detect a 50% slowing of disease progression as measured by various neuroimaging measures (Tables 3 and 4 , adapted from [32]).

Table 3 summarizes estimated sample size requirements assuming a treatment that is effective at slowing both disease-specific atrophy and non-disease-specific age-associated atrophy. Table 3 is analogous to estimates summarized in Table 2 except that effect size is set to 50% slowing of progression. Power calculations are by formula (2) with parameter estimation using longitudinal ADNI data [32]. Ventricular volume was the most efficient outcome measure under this scenario, requiring an estimated 83 subjects per arm to detect a difference in rate of atrophy equal to one half the rate of atrophy observed in the ADNI pilot data. Mid-temporal cortical thinning, whole brain atrophy, and right hippocampal atrophy were slightly less efficient as potential endpoints (Table 3).

Table 4 summarizes samples size requirements to detect a 50% slowing of disease-specific atrophy, where disease-specific atrophy is defined as the atrophy experienced by MCI subjects that is above and beyond the atrophy experienced by age-matched cognitively normal ADNI subjects, and the effect size Δ is calculated as 50% of the difference between the normal and MCI rate of atrophy. For trials powered to detect a

Table 3
Sample size required to detect a 50% slowing of overall atrophy (trial of 12 months, with observation at 0, 6 and 12 months, equal allocation to arms, and 90% power)

Outcome variable	MCI mean slope	σ_b^2	σ_e^2	n/arm
Whole brain[a]	−3345	1613	2168	90
Ventricles[a]	1975	1033	1183	83
Left hippocampus[a]	−34.118	27.974	15.943	115
Right hippocampus[a]	−34.188	28.952	19.432	93
Left mid-temporal cortex[b]	−0.022	0.006	0.013	84
Right mid-temporal cortex[b]	−0.020	0.012	0.013	94

[a] volume in mm^3; [b] cortical thickness in mm.

Table 4
Sample size required to detect a 50% slowing of disease-specific atrophy, defined as atrophy above and beyond that experienced by age-matched non-impaired elderly (trial of 12 months, with observation at 0, 6 and 12 months, equal allocation to arms, and 90% power)

Outcome variable	Non-impaired annual decline	Disease specific annual decline	σ_b^2	σ_3^2	n/arm
Whole brain[a]	−1724	−1625	1613	2168	384
Ventricles[a]	1201	772	1033	1183	544
Left hippocampus[a]	−17.141	−16.977	27.974	15.943	376
Right hippocampus[a]	−16.427	−17.761	28.952	19.432	425
Left mid-temporal cortex[b]	−0.009	−0.013	0.006	0.013	252
Right mid-temporal cortex[b]	−0.009	−0.011	0.012	0.013	319

[a] volume in mm^3; [b] cortical thickness in mm.

slowing of disease-specific atrophy (Table 4), middle temporal cortical thinning was the most statistically efficient outcome measure, requiring 252 (left mid-temporal cortex) to 319 (right mid-temporal cortex) subjects per arm to detect a difference in rate of atrophy equal to one half the rate attributable specifically to the Alzheimer degenerative process. Ventricular volume, the most efficient outcome for detecting non-disease-specific atrophy (Table 3), was the least efficient volumetric outcome for detecting Alzheimer's disease-specific atrophy (Table 4).

Which sample size algorithm is most appropriate for a given trial? Table 3 is appropriate for treatments presumed to target both non-specific age-associated atrophy and Alzheimer's disease-associated atrophy. Table 4 is appropriate for treatments presumed to target only Alzheimer's disease-associated atrophy. Table 4 is conservative if you presume that some age-associated atrophy observed in cognitively intact elderly is due to a preclinical Alzheimer's disease neurodegenerative process, in which case sample sizes intermediate between Tables 3 and 4 would be sufficient. Further examples and discussion of this issue can be found in references [8, 11, 15–17, 21, 32].

Minimum reporting standards for power calculations

As noted above, a number of the ADNI publications did not report the magnitude of treatment effect being powered or did not explicitly state the statistical analysis plan upon which power calculations were based. We suggest that, as a minimum standard for reporting power calculation findings, these two items be reported. Estimates of minimum sample size requirements are of little utility to readers if the algorithm used for power calculations and the methods for calculating parameter estimates used in those calculations

are not reported. Furthermore, if the power calculation formula and parameter estimates are published (e.g., McEvoy et al. [17]), then outside investigators can use this information to inform sample size calculations for alternative designs (e.g., longer trials or trials with greater sampling frequency) or alternative treatment effect sizes.

Additional considerations

Consideration of several additional issues can greatly improve the value of power calculation reports. Power calculation estimates are valid only if implicit model assumptions are true. Pilot data (e.g., ADNI data) can be used to test these implicit assumptions, and describing diagnostics to justify the proposed analysis plan and power calculation algorithm would greatly improve power calculation reports. As discussed above, parameters used in power calculations are estimated with some uncertainty, and a sensitivity analysis (reporting confidence intervals around sample size estimates) is also an important qualification of power calculation findings. Detailed descriptions of the cognitive and demographic characteristics of the pilot data increases the utility of power calculation reports as well. Covariate adjustment was not discussed in this review, but may be a means of improving the efficiency of clinical trials and deserves further consideration [9]. Finally, we have also not addressed pragmatic issues such as adjusting sample size calculations to accommodate study subject dropout or loss to follow-up [13], which may vary as a function of the research protocol requirements of the various measurement methods.

CONCLUSIONS

We emphasize that we have focused exclusively on statistical issues in comparing published ADNI power

calculation papers. A number of issues beyond statistical considerations are critical to planning clinical trials. Not the least of these is establishing the relative feasibility and practical significance of a given percentage slowing of progression on cognitive versus proposed volumetric imaging measures. The current Food and Drug Administration standard for approving Alzheimer treatments is demonstrated effectiveness in slowing of cognitive and functional decline. The utility of neuroimaging outcomes, e.g., to demonstrate biological effect in phase 2 trials, or, ultimately, the acceptance of these biomarker measures as outcome measures for phase 3 trials, is yet to be established [37]. Nonetheless, the papers reviewed here consistently demonstrate the potential utility of these outcomes from the statistical efficiency perspective. The increased statistical efficiency translates to shorter trials with substantially smaller sample sizes, meaning more drugs could be effectively tested for the same cost in terms of dollars and human subject burden. Shorter, smaller trials may also be amenable to adaptive trial designs, which would open new avenues for potential gain in trial efficiency.

ACKNOWLEDGEMENTS

REFERENCES

[1]   Mueller SG, Weiner MW, Thal LJ, Petersen RC, Jack CR, Jagust W, Trojanowski JQ, Toga AW, Beckett L (2005) Ways toward an early diagnosis in Alzheimer's disease: the Alzheimer's Disease Neuroimaging Initiative (ADNI). *Alzheimers Dement* **1**, 55-66.

[2]   Weiner MW, Aisen PS, Jack CR Jr, Jagust WJ, Trojanowski JQ, Shaw L, Saykin AJ, Morris JC, Cairns N, Beckett LA, Toga A, Green R, Walter S, Soares H, Snyder P, Siemers E, Potter W, Cole PE, Schmidt M (2010) The Alzheimer's disease neuroimaging initiative: progress report and future plans. *Alzheimers Dement* **6**, 202-211.

[3]   Ashford JW, Adamson M, Beale T, La D, Hernandez B, Noda A, Rosen A, O'Hara R, Fairchild JK, Spielman D, Yesavage JA (2011) MR spectroscopy for assessment of memantine treatment in mild to moderate Alzheimer dementia. In *Handbook of Imaging the Alzheimer Brain*, Ashford JW et al., eds. IOS Press, Amsterdam, pp. 599-604.

[4]   Förster S, Buschert VC, Buchholz HG, Teipel SJ, Friese U, Zach C, a Fougere C, Rominger A, Drzezga A, Hampel H, Bartenstein P and Buerger K (2011) Effects of a 6-month cognitive intervention program on brain metabolism in amnestic MCI and mild Alzheimer´s disease. In *Handbook of Imaging the Alzheimer Brain*, Ashford JW et al., eds. IOS Press, Amsterdam, pp. 605-616.

[5]   Aisen PS, Petersen RC, Donohue MC, Gamst A, Raman R, Thomas RG, Walter S, Trojanowski JQ, Shaw LM, Beckett LA, Jack CR Jr, Jagust W, Toga AW, Saykin AJ, Morris JC, Green RC, Weiner MW (2010) Clinical Core of the Alzheimer's disease neuroimaging initiative: progress and plans. *Alzheimers Dement* **6**, 239-246.

[6]   Beckett LA, Harvey DJ, Gamst A, Donohue M, Kornak J, Zhang H, Kuo JH (2010) The Alzheimer's disease neuroimaging initiative: Annual change in biomarkers and clinical outcomes. *Alzheimers Dement* **6**, 257-264.

[7]   Carrillo MC, Sanders CA, Katz RG (2009) Maximizing the Alzheimer's disease neuroimaging initiative II. *Alzheimers Dement* **5**, 271-275.

[8]   Chen K, Langbaum JB, Fleisher AS, Ayutyanont N, Reschke C, Lee W, Liu X, Bandy D, Alexander GE, Thompson PM, Foster NL, Harvey DJ, de Leon MJ, Koeppe RA, Jagust WJ, Weiner MW, Reiman EM (2010) Twelve-month metabolic declines in probable Alzheimer's disease and amnestic mild cognitive impairment assessed using an empirically pre-defined statistical region-of-interest: findings from the Alzheimer's Disease Neuroimaging Initiative. *Neuroimage* **51**, 654-664.

[9]   Fleisher AS, Donohue M, Chen K, Brewer JB, Aisen PS (2009) Applications of neuroimaging to disease-modification trials in Alzheimer's disease. *Behav Neurol* **21**, 129-136.

[10] Ho AJ, Hua X, Lee S, Leow AD, Yanovsky I, Gutman B, Dinov ID, Lepore N, Stein JL, Toga AW, Jack CR Jr, Bernstein MA, Reiman EM, Harvey DJ, Kornak J, Schuff N, Alexander GE, Weiner MW, Thompson PM (2010) Comparing 3 T and 1.5 T MRI for tracking Alzheimer's disease progression with tensor-based morphometry. *Hum Brain Mapp* **31**, 499-514.

[11] Holland D, Brewer JB, Hagler DJ, Fennema-Notestine C, Dale AM (2009) Subregional neuroanatomical change as a biomarker for Alzheimer's disease. *Proc Natl Acad Sci U S A* **106**, 20954-20959.

[12] Hua X, Lee S, Yanovsky I, Leow AD, Chou YY, Ho AJ, Gutman B, Toga AW, Jack CR Jr, Bernstein MA, Reiman EM, Harvey DJ, Kornak J, Schuff N, Alexander GE, Weiner MW, Thompson PM (2009) Optimizing power to track brain degeneration in Alzheimer's disease and mild cognitive impairment with tensor-based morphometry: an ADNI study of 515 subjects. *Neuroimage* **48**, 668-681.

[13] Hua X, Lee S, Hibar DP, Yanovsky I, Leow AD, Toga AW, Jack CR Jr, Bernstein MA, Reiman EM, Harvey DJ, Kornak J, Schuff N, Alexander GE, Weiner MW, Thompson PM (2010) Mapping Alzheimer's disease progression in 1309 MRI scans: power estimates for different inter-scan intervals. *Neuroimage* **51**, 63-75.

[14] Landau SM, Harvey D, Madison CM, Koeppe RA, Reiman EM, Foster NL, Weiner MW, Jagust WJ (2009) Associations between cognitive, functional, and FDG-PET measures of decline in AD and MCI. *Neurobiol Aging*. doi:10.1016/j.neurobiolaging.2009.07.002

[15] Leung KK, Clarkson MJ, Bartlett JW, Clegg S, Jack CR Jr, Weiner MW, Fox NC, Ourselin S (2010) Robust atrophy rate measurement in Alzheimer's disease using multi-site serial MRI: tissue-specific intensity normalization and parameter selection. *Neuroimage* **50**, 516-523.

[16] Leung KK, Barnes J, Ridgway GR, Bartlett JW, Clarkson MJ, Macdonald K, Schuff N, Fox NC, Ourselin S (2010) Automated cross-sectional and longitudinal hippocampal volume

measurement in mild cognitive impairment and Alzheimer's disease. *Neuroimage* **51**, 1345-1359.

[17] McEvoy LK, Edland SD, Holland D, Hagler DJ Jr, Roddey JC, Fennema-Notestine C, Salmon DP, Koyama AK, Aisen PS, Brewer JB, Dale AM (2010) Neuroimaging enrichment strategy for secondary prevention trials in Alzheimer disease. *Alzheimer Dis Assoc Disord* **24**, 269-277.

[18] Nestor SM, Rupsingh R, Borrie M, Smith M, Accomazzi V, Wells JL, Fogarty J, Bartha R (2008) Ventricular enlargement as a possible measure of Alzheimer's disease progression validated using the Alzheimer's disease neuroimaging initiative database. *Brain* **131**, 2443-2454.

[19] Schuff N, Woerner N, Boreta L, Kornfield T, Shaw LM, Trojanowski JQ, Thompson PM, Jack CR Jr, Weiner MW (2009) MRI of hippocampal volume loss in early Alzheimer's disease in relation to ApoE genotype and biomarkers. *Brain* **132**, 1067-1077.

[20] Wolz R, Heckemann RA, Aljabar P, Hajnal JV, Hammers A, Lotjonen J, Rueckert D (2010) Measurement of hippocampal atrophy using 4D graph-cut segmentation: application to ADNI. *Neuroimage* **52**, 109-118.

[21] Yushkevich PA, Avants BB, Das SR, Pluta J, Altinay M, Craige C (2010) Bias in estimation of hippocampal atrophy using deformation-based morphometry arises from asymmetric global normalization: an illustration in ADNI 3 T MRI data. *Neuroimage* **50**, 434-445.

[22] Chou YY, Lepore N, Avedissian C, Madsen SK, Parikshak N, Hua X, Shaw LM, Trojanowski JQ, Weiner MW, Toga AW, Thompson PM (2009) Mapping correlations between ventricular expansion and CSF amyloid and tau biomarkers in 240 subjects with Alzheimer's disease, mild cognitive impairment and elderly controls. *Neuroimage* **46**, 394-410.

[23] Ho AJ, Stein JL, Hua X, Lee S, Hibar DP, Leow AD, Dinov ID, Toga AW, Saykin AJ, Shen L, Foroud T, Pankratz N, Huentelman MJ, Craig DW, Gerber JD, Allen AN, Corneveaux JJ, Stephan DA, DeCarli CS, DeChairo BM, Potkin SG, Jack CR Jr, Weiner MW, Raji CA, Lopez OL, Becker JT, Carmichael OT, Thompson PM (2010) A commonly carried allele of the obesity-related FTO gene is associated with reduced brain volume in the healthy elderly. *Proc Natl Acad Sci U S A* **107**, 8404-8409.

[24] Hua X, Leow AD, Lee S, Klunder AD, Toga AW, Lepore N, Chou YY, Brun C, Chiang MC, Barysheva M, Jack CR Jr, Bernstein MA, Britson PJ, Ward CP, Whitwell JL, Borowski B, Fleisher AS, Fox NC, Boyes RG, Barnes J, Harvey D, Kornak J, Schuff N, Boreta L, Alexander GE, Weiner MW, Thompson PM (2008) Alzheimer's Disease Neuroimaging I. 3D characterization of brain atrophy in Alzheimer's disease and mild cognitive impairment using tensor-based morphometry. *Neuroimage* **41**, 19-34.

[25] Morra JH, Tu Z, Apostolova LG, Green AE, Avedissian C, Madsen SK, Parikshak N, Hua X, Toga AW, Jack CR Jr,

Schuff N, Weiner MW, Thompson PM (2009) Automated 3D mapping of hippocampal atrophy and its clinical correlates in 400 subjects with Alzheimer's disease, mild cognitive impairment, and elderly controls. *Hum Brain Mapp* **30**, 2766-2788.

[26] Stein JL, Hua X, Lee S, Ho AJ, Leow AD, Toga AW, Saykin AJ, Shen L, Foroud T, Pankratz N, Huentelman MJ, Craig DW, Gerber JD, Allen AN, Corneveaux JJ, Dechairo BM, Potkin SG, Weiner MW, Thompson P (2010) Voxelwise genome-wide association study (vGWAS). *Neuroimage* **53**, 1160-1174.

[27] Stein JL, Hua X, Morra JH, Lee S, Hibar DP, Ho AJ, Leow AD, Toga AW, Sul JH, Kang HM, Eskin E, Saykin AJ, Shen L, Foroud T, Pankratz N, Huentelman MJ, Craig DW, Gerber JD, Allen AN, Corneveaux JJ, Stephan DA, Webster J, DeChairo BM, Potkin SG, Jack CR Jr, Weiner MW, Thompson PM (2010) Genome-wide analysis reveals novel genes influencing temporal lobe structure with relevance to neurodegeneration in Alzheimer's disease. *Neuroimage* **51**, 542-554.

[28] Kraemer HC, Mintz J, Noda A, Tinklenberg J, Yesavage JA (2006) Caution regarding the use of pilot studies to guide power calculations for study proposals. *Arch Gen Psychiatry* **63**, 484-489.

[29] Rosen WG, Mohs RC, Davis KL (1984) A new rating scale for Alzheimer's disease. *Am J Psychiatry* **141**, 1356-1364.

[30] Meinert CL (1986). In *Clinical Trials Design, Conduct and Analysis*, p. 84, Oxford University Press, Inc, New York.

[31] Schlesselman JJ (1973) Planning a longitudinal study: II. *Frequency of measurement and study duration. J Chron Dis* **26**, 561-570.

[32] Edland SD (2009) Which MRI measure is best for Alzheimer's disease prevention trials: Statistical considerations of power and sample size. *2009 Joint Stat Meeting Proceedings*. 4996-4999.

[33] Jack CR Jr, Shiung MM, Gunter JL, O'Brien PC, Weigand SD, Knopman DS, Boeve BF, Ivnik RJ, Smith GE, Cha RH, Tangalos EG, Petersen RC (2004) Comparison of different MRI brain atrophy rate measures with clinical disease progression in AD. *Neurology* **62**, 591-600.

[34] Diggle P, Heagerty P, Liang K-Y, Zeger S (2002). In *Analysis of Longitudinal Data*, 2nd ed., Oxford University Press, Oxford.

[35] Aisen PS, Schneider LS, Sano M, Diaz-Arrastia R, van Dyck CH, Weiner MF, Bottiglieri T, Jin S, Stokes KT, Thomas RG, Thal LJ (2008) High-dose B vitamin supplementation and cognitive decline in Alzheimer disease: a randomized controlled trial. *JAMA* **300**, 1774-1783.

[36] Vozdolska R, Sano M, Aisen P, Edland SD (2009) The net effect of alternative allocation ratios on recruitment time and trial cost. *Clinical Trials* **6**, 126-132.

[37] Aisen PS, Andrieu S, Sampaio C, Carrillo M, Khachaturian ZS et al. (2011) Report of the task force on designing clinical trials in early (predementia) AD. *Neurol* **76**, 280-286.

This page intentionally left blank

Section 9
Vascular Changes in the Brain Causing Dementia and Contributing to Alzheimer's Disease

This page intentionally left blank

Introduction

Section 9: Vascular Co-morbidity and Alzheimer's Disease

Sandra Black and Allyson Rosen*

Since the first description of dementia related to senile plaques and neurofibrillary changes by Alzheimer in 1907, there has been vacillation between thinking that most cognitive impairment in older individuals was related either to primary neurodegenerative disease or vascular insults. In the last few decades, there has been development of criteria for Alzheimer's dementia and its underlying pathology and multi-infarct/vascular dementia, with the recognition that many elders harbor both conditions. Accordingly, while AD and vascular dementia have long been viewed as separate disorders, there is now a growing appreciation that vascular insults are an important comorbidity that contribute to disability in AD. Furthermore, these comorbid disorders may attack the same neural systems.

Knopman and Roberts describe various pathological processes that comprise the major vascular risk factors and review how they relate to AD, including hypertension, diabetes, hypercholesterolemia and obesity. They also comment on population autopsy evidence suggesting that infarcts may be additive to AD pathology and accelerate its clinical expression as dementia. Quantifying ischemic lesions visible as hyperintensities on proton density/T2 weighted or FLAIR MRI provides an important means to study and understand, in vivo, the potential independent effects of covert infarcts in the deep nuclei and white matter lesions on cognition and expression of dementia in AD. Gao et al. compare the sensitivity and utility of the major methods for quantifying these lesions. They test how well three expert rating scales, varying in complex-

ity, compared to the results of automated, volumetric quantification in group classification of AD versus elderly controls, and in correlation to cognitive abilities. They find the scales to be highly correlated with each other and with the volumetrics, but the most complex rating scale and the continuous volumetric measures better predict cognitive function in different domains. Finally, Bernardi et al. describe a form of early onset, familial AD in which an amyloid-β protein precursor (AβPP A713T) genetic mutation is associated with strokes, cerebral amyloid angiopathy and AD pathology. This is important as it hints at mechanisms whereby AD and cerebrovascular disease may interact, as opposed to just being additive to each other. This possible interaction may be occurring at the level of the microvasculature with capillary obliteration by amyloid deposition and toxicity, causing ischemia and oxidative stress that may further drive the amyloid cascade and tau hyperphosophorylation. Furthermore, periarteriolar deposition of amyloid-β_{1-40}, may interfere with amyloid clearance, now thought to be a major mechanism resulting in parenchymal amyloid accumulation in sporadic AD. This can lead to microbleeds and macrohemorrhages and also infarction as described in the A713T mutation family reported by Bernardi et al., illustrating that AD is under-recognized as a risk factor and direct cause of stroke. The chapters in this section clearly describe some of key issues in the relationship between vascular and parenchymal disease in the context of dementia and its relationship with brain degeneration in the elderly and particularly AD.

*Correspondence to: Allyson Rosen, E-mail: rosena@psych. stanford.edu.

This page intentionally left blank

Impact of Vascular Risk Factors on Brain Structure

David S. Knopman[a,b,*] and Rosebud Roberts[b,c]

[a]*Department of Neurology, Mayo Clinic, Rochester, MN, USA*
[b]*Department of Mayo Clinic Alzheimer's Disease Research Center, Rochester, MN, USA*
[c]*Division of Epidemiology, Department of Health Sciences Research, Mayo Clinic, Rochester, MN, USA*

Abstract. The major vascular risk factors such as diabetes and impaired glycemic control, hypertension, obesity and hyper- or dyslipidemia have been associated both with Alzheimer's disease and vascular dementia. The purpose of this review is to consider how vascular risk factors impact the expression of cognitive impairment in the elderly. The review will focus on how vascular risk factors are associated with changes in brain imaging and neuropathological changes. Midlife diabetes mellitus, hypertension and obesity are the most important vascular risk factors on the basis of their prevalence and associations with late-life cognitive impairment. The basis for their relationships to changes in brain integrity could either be through microvascular brain disease, Alzheimer pathology or both. Midlife vascular risk factors represent potentially modifiable conditions that could mitigate disease in the future.

Keywords: Vascular risk factors, stroke, dementia, vascular dementia, cognitive impairment, diabetes, hypertension, obesity, hyperlipidemia

INTRODUCTION

Stroke and cerebrovascular disease play important roles in late-life cognitive decline, but their relationship to Alzheimer's Disease (AD), the most commonly diagnosed etiology of late-life cognitive impairment and dementia, has been enigmatic. Up until recently, the pathophysiologies of the two conditions have been regarded as distinct. However, "vascular" risk factors have also been shown to be associated with AD, further blurring the distinction between cerebrovascular and Alzheimer-type clinical diagnoses. The purpose of this review is to first consider the context in which cognitive impairment of vascular origin is diagnosed, place it in the context of clinical and pathological AD, and then to consider the evidence for the role of major vascular risk factors in late-life cognitive (after age 65 years) impairment. This is an area of growing interest because treatment of vascular risk factors, already important in their own right, would gain increased urgency for prevention of late-life cognitive impairment.

TERMINOLOGY

In order to avoid confusion, some conventions for terminology should be clarified. Clinical diagnoses and pathological diagnoses must have unique designations because of the lack of perfect correspondence between the two. Hereafter, whenever we refer to Alzheimer's disease, we will specify whether we mean clinically diagnosed dementia due to AD (AD*c) or pathologically-defined AD (AD*p) based on the presence of neuritic plaques and neurofibrillary tangles in isocortex. The term "vascular dementia" (VaD) will

---

*Correspondence to: Dr. DS Knopman, Department of Neurology, College of Medicine, Mayo Clinic, 200 First Street SW, Rochester, MN 55905, USA. Tel.: +507 538 1038; Fax: +507 538 6012; E-mail: knopman@mayo.edu.

refer to a clinical diagnosis of dementia in which CVD is presumed to be the etiology, whereas cerebrovascular pathology (CVP) refers to the pathologically observed processes of infarction and ischemia. The combination and possible interactions of CVP and AD*p are ultimately of the most interest. The label "Alzheimer's disease with cerebrovascular disease" [1] captures the overlap between the two, but doesn't do it in a very artful way. This review will focus on these two etiologies of cognitive impairment and their combination.

CEREBROVASCULAR DISEASE CAUSES COGNITIVE IMPAIRMENT

Stroke is one of the most common neurological diseases of advancing age. Strokes cause cognitive and motor impairments both acutely and persistently. Survivors of stroke have a far higher rate of incident dementia than age-matched peers [2–5]. A history of stroke at any point in the past is a risk factor for the development of cognitive impairment [6, 7], MCI [8] and dementia [9, 10]. MR imaging in population-based cohorts of elderly individuals has shown that 20% or more have clinically silent infarcts [11]. The burden of imaging-detectable cerebral infarction is even larger than clinically overt stroke [10]. Prospective observational studies show that numbers of lacunar infarcts are associated with risk for future cognitive impairment and dementia [12, 13]. There is evidence that the burden of macrovascular [14] as well as microvascular pathology independently accounts for cognitive impairment [15–17], even after taking AD*p into account.

Despite this wealth of observation, CVP as a cause of cognitive impairment may still be under-appreciated for several reasons. It has been very difficult – both in life with imaging and at autopsy neuropathologically – to quantitate the burden of CVP. There is no validated scheme for assigning different grades to CVP burden though progress is being made [16, 18, 19] in developing pathological ratings that reflect increasing burden of CVP pathology. Not only is there the problem of properly accounting for the role of small but strategically placed infarcts versus the total burden of ischemic pathology, but quantitating microscopic evidence of infarction is prohibitively labor-intensive and therefore, most neuropathological examinations use only qualitative estimates of CVP. There is a nagging concern that current neuropathological methods may tend to undercount ischemic lesions. Analyses that attempt clinical-pathological correlations with CVP, AD*p and their overlap are inherently more complex and require larger numbers of subjects than ones that look at AD*p alone.

WHERE VASCULAR DISEASE FITS IN THE ALZHEIMER PATHOLOGICAL CASCADE

To talk about CVP and dementia, it is necessary to put AD*p in perspective. While the focus of this review is to highlight why AD*p cannot be considered in isolation from CVP, AD*p is nonetheless a major neuropathologic process in late-life dementia [18, 20]. The loss of neurons, synapses, dendrites, axons in heteromodal association isocortices is the proximate cause of cognitive impairment from AD*p [18]. Neurodegeneration in AD*p is closely linked to the formation of neurofibrillary tangles (NFT) in neurons in heteromodal isocortex [21–23]. Modulators of the AD*p neurodegenerative cascade that could have either genetic or environmental bases affect the rate of accumulation of brain pathology or the time when the pathological changes express themselves clinically.

CVP could modulate the appearance of cognitive impairment in conjunction with AD*p by one of several mechanisms. If a certain volume of cortical or subcortical grey matter undergoes infarction, there will be a reduction in intact brain volume, loss of synapses and reduced connectivity between remaining neurons, and hence brain reserve. An increasing burden of CVP would either accelerate the appearance of cognitive impairment or increase its severity at a particular level of AD*p. There is substantial evidence that as the burden of CVP increases, the abundance of AD*p will be less, for a given severity of dementia [14, 17, 24–29]. The interaction of CVP and AD*p might account for the generally lower burden of AD*p for a given level of cognitive impairment after age 75–80 yrs [18]. There appears to be no interactive effect on dementia severity between the burden of cerebral infarcts and the amount of AD*p [19, 30]. Conceivably, microscopic CVP could accelerate the neurodegenerative process in the AD*p cascade, but there is no direct evidence that such an interactive mechanistic pathway exists.

CLINICAL-PATHOLOGICAL CORRELATIONS

Postmortem studies of patients dying with dementia that have compared clinical diagnoses with neu-

ropathological findings have shown that the clinical diagnosis of VaD is very insensitive for predicting CVP [31–33], and furthermore, AD*c is often associated with some degree of CVP [17, 34]. Problems with the diagnosis of VaD raise questions about the validity of the diagnosis, particularly when neuroimaging is not available. The clinical mis-recognition of CVP pathology in dementia patients has major implications for understanding the role vascular risk factors in the epidemiology of dementia. The presence of CVP in AD*c means that epidemiological studies that claim to study observations on risk factors for AD*c are actually targeting a dementing illness that includes some element of CVP. In other words, when an epidemiological study asserts that a risk factor is "associated with AD," that really means "associations with a dementing illness that mostly includes persons with AD*p and some amount of CVP", Conversely, factors reported to be associated with VaD may not be as specific for a dementing illness due only to CVP. An "association with VaD" means that the associations are with persons who have a higher burden of CVP but probably have coexistent AD*p. Therefore, in the absence of information about underlying pathology, investigations of risk factors using epidemiologic methods are limited in their inferences about the underlying dementia etiology.

VASCULAR RISK FACTORS (VRF)

A number of mid-life risk factors that have been traditionally viewed as causing vascular disease including the components of the metabolic syndrome –diabetes and impaired glycemic control, hypertension, hyper- or dyslipidemia and obesity – are associated with an increased incidence of cognitive impairment and dementia. This review focusses on individual vascular risk factors and their impact on structural changes on imaging and neuropathology.

DIABETES MELLITUS

Diabetes mellitus (DM) is a common condition from middle age and beyond. By age 65 about 20% of the population carries a diagnosis of DM, mainly type 2 diabetes [35, 36]. DM affects the kidney, heart, peripheral nerves and retina, in addition to the brain.

Alterations in midlife glycemic control and DM almost certainly have greater consequences for cognitive function than late-onset DM presumably because of the longer duration of exposure, although a more metabolically aggressive disease might also occur at younger ages. A meta-analysis [37] observed that the magnitude of risks for dementia were generally higher when DM was diagnosed at midlife versus later life.

The evidence linking DM to late-life cognitive impairment includes its associations with cognitive decline in middle age [6, 38–42], cognitive decline in later life, mild cognitive impairment [43, 44], AD*c [45–53] and VaD [45, 54–56]. In general, associations have been stronger for VaD than for AD*c. Not all studies show an association between dementia and DM [57], however, perhaps because of the age when DM was ascertained.

The nature of the cognitive deficits associated with DM provides some clues as to DM's brain targets. DM is associated with impairment of both amnestic and non-amnestic cognitive functions, but the association with non-amnestic dysfunction has been shown to be of greater magnitude [43, 44]. Less amnestic and greater non-amnestic cognitive dysfunction would be more consistent with involvement of white matter pathways, basal ganglia or thalamus, which in turn are loci expected to undergo infarction as a result of CVP.

DM is associated with structural brain changes that can be detected on imaging [58–62]. In a metaanalysis, the major changes on imaging associated with DM were brain atrophy, lacunar infarcts and to a less extent, white matter hyperintensities [63]. In the Atherosclerosis Risk in Communities (ARIC) study that included persons in late middle age (50–73 yr), there was a 4 to 7% increased risk of ventricular enlargement for each 10 mg/dL of fasting blood sugar elevation [58]. In the Cardiovascular Health Study (CHS), DM was associated with brain atrophy only in women. The CHS population was 65 and older [64]. Perhaps the less consistent associations in the CHS are a result of the older age of the subjects.

Neuropathological studies of diabetics also show an increased number of brain microinfarcts and lacunar infarcts compared to non-diabetics [65–69]. Several studies have shown that diabetics with dementia have a lower burden of β-amyloid pathology [65–67]. Diabetics also appear to have an increased numbers of neuritic plaques [50, 70]. In one of the studies, APOE e4 carriage was needed to show the association [50].

DM could cause also brain injury through non-CVP mechanisms. Hyperglycemia and impaired control of insulin homeostasis might have a direct effect on brain β-amyloidosis [71–74]. Insulin degrading enzyme (IDE), an enzyme that is involved in insulin trafficking,

is also a key enzyme that degrades β-amyloid. With increases in peripheral insulin levels in midlife in type 2 diabetics, brain insulin levels could be raised [75]. Insulin might compete with β-amyloid for binding to IDE; thus, elevated insulin levels would lead to decreased β-amyloid clearance, and raised β-amyloid levels in the brain.

Because most patients with DM are treated with either oral hypoglycemic agents or insulin, it may be very difficult to determine whether treatments alter clinical-pathological correlations in DM. Severity of DM is more likely to be associated with the use of insulin, whereas hyperglycemia that doesn't exceed 125 mg/dL might not be treated with medication at all. Since more severe DM will almost always be treated with insulin, the unique contributions of DM severity and insulin use to structural and neuropathological changes may not be resolvable. With insulin use, the impact of DM severity versus episodes of hypoglycemia must also be considered in evaluating dementia risk.

Based on imaging and neuropathological evidence, microvascular disease is a very strong candidate mechanism to account for the impact of DM on late-life cognitive impairment. DM as a microvascular disease could influence the course of AD*p by *decreasing* the threshold at which AD*p produces clinical effects, even if DM itself had no direct impact on AD*p-mediated neurodegeneration. If this were the case, then for a given level of cognitive impairment, persons with diabetes should have *less* AD*p, which in fact has been observed [65, 66]. An alternative hypothesis is that the metabolic or ischemic injury caused by DM *facilitates* β-amyloid pathology, tau pathology or both. In this alternative model, DM would be associated with *more* AD*p. The evidence so far does not support this latter model.

HYPERTENSION

Hypertension (HT) affects a majority of middle-aged and elderly populations [35]. While there are various ways to represent abnormal BP such as history of hypertension, systolic BP, diastolic BP, pulse pressure or mean arterial pressure, most of the data we will cite simply used either history of hypertension, systolic BP or diastolic BP. HT is a well-known major risk factor for ischemic heart disease, peripheral vascular disease, chronic kidney disease and CVP, via both ischemic and hemorrhagic mechanisms. HT in midlife

is associated with later life cognitive impairment and dementia [76–78]. Associations are generally stronger for VaD than AD*c [79–84].

Interpretation of the effects of HT in later life is confounded by the rising prevalence of *hypo*tension in late-life. In late-life both HT and hypotension may cause brain injury. Orthostatic hypotension becomes common with advancing age, and hypotension is also deleterious to the brain [85–87]. Even among normotensives, there may be an admixture of borderline hypertensives and hypotensives, making it quite difficult to identify the deleterious effects of HT in the very elderly. Several studies have failed to show an association of HT with poor cognition when assessed in late-life [85, 86, 88–91].

Different classes of antihypertensive medications have shown associations with lower rates of dementia in observational studies [92–94]. Similarly, clinical trials have demonstrated that treatment of persons with HT with several classes of antihypertensive medications reduces the incidence of dementia [95–98]. It is not clear which class or classes of antihypertensive provides the greatest protective effects for the brain. Duration of antihypertensive therapy also has an impact on associations of hypertension with dementia; especially in younger persons, those on antihypertensive therapies for longer periods of time had reduced rates of incident dementia [99]. Because therapy has an impact on blood pressure measurements themselves and also appears to impact cognitive function, naturalistic observations with either imaging or neuropathology are confounded by treatment.

In imaging studies involving both middle-aged and elderly persons, HT is more closely associated with white matter hyperintensities (WMH) than atrophy [58, 59, 100–106]. HT is the most consistent correlate of excess burden of WMH [104, 106, 107]. In the cross-sectional findings of the ARIC study, HT was not associated with increased ventricular volume, but there were strong associations with increasing burden of WMH [58]. In the longitudinal assessments of the ARIC cohort, systolic BP measured cumulatively over 14 years was strongly associated with progression of WMH. BP measurements from early years of follow-up showed stronger associations with WMH burden than later ones [108].

The effects of systolic versus diastolic BP on brain structure may differ. In elderly subjects (age 72 ± 7 yrs) from the Rotterdam Scan study, systolic blood pressure was not associated with brain atrophy. However, diastolic BP exhibited a J-shaped relationship to

brain atrophy. Subjects with high and low diastolic BP had greater brain atrophy than subjects with diastolic BPs in the 65–74 mmHg range. In addition, in a subset of subjects with BPs measured 20 years earlier, those with elevated diastolic BPs in midlife but who were not treated had greater brain atrophy than non-hypertensives. Subjects with elevated diastolic BP in midlife who were treated did not show any brain volume loss compared to non-hypertensives. Both elevated systolic and elevated diastolic BP were associated with WMH burden. The association between 20-year change in diastolic blood pressure and subcortical WMH was also J-shaped, indicating that both declines and elevations in BP over time were related to increasing burdens of WMH [109].

Several studies have found that midlife hypertension was associated with greater burdens of NFT and neuritic plaques in late life [110, 111], but medication effects make interpretation complex. Neuropathological studies that have compared subjects with and without antihypertensive medications have shown that medicated patients had either less cognitive impairment or less AD pathology than the un-medicated hypertensive peers [111]. Persons receiving antihypertensive therapy had less AD*p than normotensives.

Despite the likelihood that the effects of HT on the brain are microvascular and are similar to that seen in other microvascular beds such as in the heart or kidney, the neuropathological evidence suggests that HT has direct effects on AD*p that are independent of infarction. These findings suggest that HT could alter β-amyloid or abnormal tau production or clearance. A final speculation is that of reverse causality: AD*p in brainstem structures [21] might promote HT.

OBESITY

Rising levels of obesity across all age groups is a major public health issue. Obesity is usually defined by body mass index (BMI), but abdominal girth has been shown to have greater predictive ability for disease outcomes such as heart disease [112]. Obesity in midlife has been associated with later life cognitive impairment [113–115]. This association persists even when DM, HT and hyperlipidemia are included in the analytic models. The observation suggests that midlife obesity is associated with cognitive impairment in some ways that are unique from the other related risk factors. Similarly, obesity could promote microvascular disease by mechanisms that are distinct from DM

and HT. Various circulating factors released by adipose tissue could play a role, perhaps by promoting inflammation. Increased fat mass, particularly visceral fat, elevates blood levels of inflammatory cytokines such as TNFα and IL6. Elevations of circulating levels of these factors could alter endothelial function, which in turn could lead to insulin resistance [116]. Leptin, a hormone released by adipose tissue, regulates lean body mass, complements insulin action in the peripheral circulation, decreases brain β secretase levels, and modulates β-amyloid turnover. In obesity, chronically elevated leptin levels result in leptin resistance and an inability to regulate weight. In the late-life, consistent with the decreased BMI that occurs prior to dementia, leptin levels decrease and are inversely associated with dementia [117]. Similarly, adiponectin, a complement related protein produced by adipose tissue, is a risk factor for coronary heart disease. The associations with dementia are yet to be determined.

Studies that have examined weight, body-mass index or other measures of adiposity in late-life have found either no association with dementia, or a protective effect [118–121]. Obesity may appear to be a protective factor for impaired cognitive function in late-life because of the competing effects of the associations of weight loss with illnesses such as cancer. Furthermore, some studies have shown that persons destined to develop dementia lose weight in the few years preceding the diagnosis. Persons with dementia are highly likely to be thinner than non-demented peers [118–121]. It is uncertain whether reverse causality could also be acting here, whereby subtle cognitive or behavioral changes that occurred prior to dementia altered dietary habits.

There were no significant associations between elevated BMI and structural brain changes in either ARIC [58] or an earlier analysis of the CHS [64] cohort. A more recent study of a smaller number of CHS participants (mean age = 77 yrs) observed reductions in grey matter volume in persons with high BMI ($>30 kg/m^2$), even after controlling for DM [122]. In younger persons there also is an association of obesity with reduced brain volume [123–125]. To our knowledge, there are no neuropathological studies that have assessed the role of midlife obesity on neuropathology in late-life. Because late-life obesity appears to be protective for dementia, understanding the competing forces of midlife and late-life obesity may be very difficult.

Whether obesity plays an independent role in the genesis of dementia, AD*p or CVP, separate from DM

and HT is not clear. Midlife obesity, to the extent that it promotes DM and HT, has adverse effects on the brain, regardless of whether these effects are direct or indirect.

HYPERLIPIDEMIA

The relationship between elevated lipid levels and dementia is uncertain, as many studies fail to show associations between elevated LDL cholesterol or triglycerides and dementia, cognitive impairment or abnormalities on brain imaging. A few studies have shown that midlife hypercholesterolemia was associated with later life MCI or dementia [84, 126, 127]. In contrast, the Framingham study failed to observe an association between midlife cholesterol levels and AD [128]. The ARIC study involving, mainly middle aged subjects, found that elevated LDL-C was not associated with cognitive impairment [6]. When lipid levels are measured in later life, the association is even more uncertain [129]. Elevated levels of total cholesterol were protective of dementia in late-life [130]. Low levels of cholesterol were associated with dementia [131, 132], as well as a number of serious systemic diseases, in particular cancer and malnutrition, so that an admixture of persons with high and low cholesterol in epidemiological studies may obscure true associations between high cholesterol levels and dementia in late-life. Once again, processes that lower lipid levels and potential survival biases compete with hyperlipidemia and confound analyses.

Although hypercholesterolemia is a potent risk factor for cardiac disease, its impact on cerebrovascular disease has been inconsistent. In neither Northern Manhattan Study [133], ARIC [134] nor CHS [11] was there an association between HDL-C or LDL-C and either clinical strokes or infarctions on imaging. Why elevated cholesterol is not as strongly linked to cerebrovascular disease as it is to cardiovascular disease is a mystery that is beyond the scope of this essay.

Cholesterol or triglyceride level have not been associated with larger ventricular size or increased white matter hyperintensities in the ARIC cohort [58]. In the CHS cohort, high HDL and low LDL levels were associated with progression of WMH [105]. A few studies that investigated the relationship between lipid levels in late life and neuropathology have claimed associations between neuritic plaques and elevated HDL-C [135] or total cholesterol and LDL-C levels [136]. There are no studies of midlife lipid levels and neuropathology.

Given the biphasic nature of the relationship between lipids and dementia, it may be midlife levels of HDL-C or LDL-C that are most relevant.

It is not clear at this point what specific role hyperlipidemia plays in the development of dementia, AD*p and CVP. Because of the multiple demonstrations of either neutral or protective effects of hyperlipidemia on cognition and brain structure, this risk factor does not offer many insights into the mechanisms of cognitive impairment.

VRF AND SOCIOECONOMIC STATUS

Late-life dementia due to AD*p is strongly associated with educational attainment, occupation and socioeconomic status (SES) [137, 138]. CVP and VRF are also moderately strongly associated with SES [139, 140]. DM, HT, obesity, and heart disease itself are all more likely in persons of low educational attainment, the usual proxy for SES. Persons of lower SES are more likely to have a poor diet, to be overweight, to smoke, and to be sedentary, all of which contribute to higher burdens of VRF. Perhaps, VRFs are associated with cognitive impairment because they stand for an array of dysfunctional health behaviors that are more important than the VRFs themselves. It seems likely that dysfunctional health behaviors in persons with lower education or lower SES promote DM, HT, and obesity. The description of the associations of low intelligence test scores in childhood with late-life VaD rather than AD*c [141] in a Scottish cohort suggests that the impact of low education and low SES on brain integrity might actually begin in childhood. It is possible that SES shares variance with brain reserve, and as a consequence different levels of brain reserve have an impact on the threshold for the appearance of dementia for a given level of AD*p or CVP.

CONCLUSIONS

VRFs, when present in midlife, exert a consistent deleterious effect on late-life cognition and dementia. For DM, HT and obesity parallel effects on subclinical infarction, cognition and brain structure support their distinct roles in the pathogenesis of late-life cognitive impairment. These disorders might either promote microvascular disease, AD*p or both. In contrast, while midlife hyperlipidemia may be associated with late-life cognitive impairment, hyperlipidemia

does not seem to alter brain structure and is not clearly associated with an increased risk of stroke. The dissociation raises some doubts on how relevant hyperlipidemia is for cognitive impairment. In later life, the role of the VRFs is much more complex. For all four conditions when measured in late-life, their associations with cognitive impairment are either attenuated, neutral or reversed. The inverse of three of them – hypotension, low cholesterol and triglyceride levels and cachexia – are associated with serious systemic illnesses that worsen survival. The relationship of SES to VRF implies that the genesis of VRFs has its roots in childhood social class, education and culture.

The evidence from imaging studies suggests that treatment of VRFs in persons who already have late-life cognitive impairment may be too late to be curative, but there still could be lesser clinically important benefits. Treatment of VRFs in persons with both AD*c and VaD should be considered because of the etiological overlap of AD*p and CVP in both.

However, VRF can be treated in midlife, and that should be grounds for optimism. Public health initiatives to treat the VRFs in midlife are already well-justified on the grounds of preventing cardiovascular disease. Despite the cardiovascular imperatives, rates of effective treatment of DM, HT, obesity and hyperlipidemia are rather low [35, 36]. Perhaps fear of cognitive impairment would spur more aggressive attempts to treat VRF in midlife.

DISCLOSURES

DSK serves on a Data Safety Monitoring Board for Lilly Pharmaceuticals, and is an investigator for clinical trials sponsored by Elan Pharmaceuticals, Forest Pharmaceuticals and Baxter Healthcare. He is an associate editor of Neurology, and receives compensation for editorial activities. The other authors have no relationships to disclose.

SUPPORT

REFERENCES

[1] Roman GC, Tatemichi TK, Erkinjuntti T, Cummings JL, Masdeu JC, Garcia JH, Amaducci L, Orgogozo JM, Brun A, Hofman A et al. (1993) Vascular dementia: diagnostic criteria for research studies. Report of the NINDS-AIREN International Workshop. *Neurology* **43**, 250-260.

[2] Henon H, Durieu I, Guerouaou D, Lebert F, Pasquier F, Leys D (2001) Poststroke dementia: incidence and relationship to prestroke cognitive decline. *Neurology* **57**, 1216-1222.

[3] Kokmen E, Whisnant JP, O'Fallon WM, Chu CP, Beard CM (1996) Dementia after ischemic stroke: a population-based study in Rochester, Minnesota (1960–1984). *Neurology* **46**, 154-159.

[4] Pohjasvaara T, Mantyla R, Salonen O, Aronen HJ, Ylikoski R, Hietanen M, Kaste M, Erkinjuntti T (2000) MRI correlates of dementia after first clinical ischemic stroke. *J Neurol Sci* **181**, 111-117.

[5] Tatemichi TK, Desmond DW, Stern Y, Paik M, Sano M, Bagiella E (1994) Cognitive impairment after stroke: frequency, patterns, and relationship to functional abilities. *J Neurol Neurosurg Psychiatry* **57**, 202-207.

[6] Knopman D, Boland LL, Mosley T, Howard G, Liao D, Szklo M, McGovern P, Folsom AR (2001) Cardiovascular risk factors and cognitive decline in middle-aged adults. *Neurology* **56**, 42-48.

[7] Kuller LH, Shemanski L, Manolio T, Haan M, Fried L, Bryan N, Burke GL, Tracy R, Bhadelia R (1998) Relationship between ApoE, MRI findings, and cognitive function in the cardiovascular health study. *Stroke* **29**, 388-398.

[8] Knopman DS, Roberts RO, Geda YE, Boeve BF, Pankratz VS, Cha RH, Tangalos EG, Ivnik RJ, Petersen RC (2009) Association of prior stroke with cognitive function and cognitive impairment: A population-based study. *Arch Neurol* **66**, 614-619.

[9] Reitz C, Luchsinger JA, Tang MX, Manly J, Mayeux R (2006) Stroke and memory performance in elderly persons without dementia. *Arch Neurol* **63**, 571-576.

[10] Kuller LH, Lopez OL, Jagust WJ, Becker JT, Dekosky ST, Lyketsos C, Kawas C, Breitner JC, Fitzpatrick A, Dulberg C (2005) Determinants of vascular dementia in the Cardiovascular Health Cognition Study. *Neurology* **64**, 1548-1552.

[11] Longstreth WT Jr, Bernick C, Manolio TA, Bryan N, Jungreis CA, Price TR (1998) Lacunar infarcts defined by magnetic resonance imaging of 3660 elderly people: the Cardiovascular Health Study. *Arch Neurol* **55**, 1217-1225.

[12] Longstreth WT Jr, Dulberg C, Manolio TA, Lewis MR, Beauchamp NJ, O'Leary D, Carr J, Furberg CD (2002) Incidence, manifestations, and predictors of brain infarcts defined by serial cranial magnetic resonance imaging in the elderly: the Cardiovascular Health Study. *Stroke* **33**, 2376-2382.

[13] Vermeer SE, Prins ND, den Heijer T, Hofman A, Koudstaal PJ, Breteler MM (2003) Silent brain infarcts and the risk of dementia and cognitive decline. *N Engl J Med* **348**, 1215-1222.

[14] Troncoso JC, Zonderman AB, Resnick SM, Crain B, Pletnikova O, O'Brien RJ (2008) Effect of infarcts on dementia in the Baltimore longitudinal study of aging. *Ann Neurol* **64**, 168-176.

[15] Giannakopoulos P, Gold G, Kovari E, von Gunten A, Imhof A, Bouras C, Hof PR (2007) Assessing the cognitive impact of Alzheimer disease pathology and vascular burden in the

aging brain: the Geneva experience. *Acta Neuropathol* **113**, 1-12.

[16] White L, Petrovitch H, Hardman J, Nelson J, Davis DG, Ross GW, Masaki K, Launer L, Markesbery WR (2002) Cerebrovascular pathology and dementia in autopsied Honolulu-Asia Aging Study participants. *Ann N Y Acad Sci* **977**, 9-23.

[17] Schneider JA, Boyle PA, Arvanitakis Z, Bienias JL, Bennett DA (2007) Subcortical infarcts, Alzheimer's disease pathology, and memory function in older persons. *Ann Neurol* **62**, 59-66.

[18] Savva GM, Wharton SB, Ince PG, Forster G, Matthews FE, Brayne C (2009) Age, neuropathology, and dementia. *N Engl J Med* **360**, 2302-2309.

[19] Chui HC, Zarow C, Mack WJ, Ellis WG, Zheng L, Jagust WJ, Mungas D, Reed BR, Kramer JH, Decarli CC, Weiner MW, Vinters HV (2006) Cognitive impact of subcortical vascular and Alzheimer's disease pathology. *Ann Neurol* **60**, 677-687.

[20] Schneider JA, Arvanitakis Z, Bang W, Bennett DA (2007) Mixed brain pathologies account for most dementia cases in community-dwelling older persons. *Neurology* **69**, 2197-2204.

[21] Braak H, Braak E (1991) Neuropathological staging of Alzheimer-related changes. *Acta Neuropathol (Berl)* **82**, 239-259.

[22] Delacourte A, David JP, Sergeant N, Buee L, Wattez A, Vermersch P, Ghozali F, Fallet-Bianco C, Pasquier F, Lebert F, Petit H, Di Menza C (1999) The biochemical pathway of neurofibrillary degeneration in aging and Alzheimer's disease. *Neurology* **52**, 1158-1165.

[23] Giannakopoulos P, Herrmann FR, Bussiere T, Bouras C, Kovari E, Perl DP, Morrison JH, Gold G, Hof PR (2003) Tangle and neuron numbers, but not amyloid load, predict cognitive status in Alzheimer's disease. *Neurology* **60**, 1495-1500.

[24] Nagy Z, Esiri MM, Jobst KA, Morris JH, King EM, Mc Donald B, Joachim C, Litchfield S, Barnetson L, Smith AD (1997) The effects of additional pathology on the cognitive deficit in Alzheimer disease. *J Neuropathol Exp Neurol* **56**, 165-170.

[25] Snowdon DA, Greiner LH, Mortimer JA, Riley KP, Greiner PA, Markesbery WR (1997) Brain infarction and the clinical expression of Alzheimer disease. The Nun Study. *JAMA* **277**, 813-817.

[26] Heyman A, Fillenbaum GG, Welsh-Bohmer KA, Gearing M, Mirra SS, Mohs RC, Peterson BL, Pieper CF (1998) Cerebral infarcts in patients with autopsy-proven Alzheimer's disease: CERAD, part XVIII. Consortium to Establish a Registry for Alzheimer's Disease. *Neurology* **51**, 159-162.

[27] Esiri MM, Nagy Z, Smith MZ, Barnetson L, Smith AD (1999) Cerebrovascular disease and threshold for dementia in the early stages of Alzheimer's disease. *Lancet* **354**, 919-920.

[28] Riekse RG, Leverenz JB, McCormick W, Bowen JD, Teri L, Nochlin D, Simpson K, Eugenio C, Larson EB, Tsuang D (2004) Effect of vascular lesions on cognition in Alzheimer's disease: a community-based study. *J Am Geriatr Soc* **52**, 1442-1448.

[29] Zekry D, Duyckaerts C, Moulias R, Belmin J, Geoffre C, Herrmann F, Hauw JJ (2002) Degenerative and vascular lesions of the brain have synergistic effects in dementia of the elderly. *Acta Neuropathol* **103**, 481-487.

[30] Schneider JA, Wilson RS, Bienias JL, Evans DA, Bennett DA (2004) Cerebral infarctions and the likelihood of dementia from Alzheimer disease pathology. *Neurology* **62**, 1148-1155.

[31] Wetterling T, Kanitz RD, Borgis KJ (1996) Comparison of different diagnostic criteria for vascular dementia (ADDTC, DSM-IV, ICD-10, NINDS-AIREN). *Stroke* **27**, 30-36.

[32] Pohjasvaara T, Mantyla R, Ylikoski R, Kaste M, Erkinjuntti T (2000) Comparison of different clinical criteria. (DSM-III, ADDTC, ICD-10, NINDS-AIREN, DSM-IV) for the diagnosis of vascular dementia. *Stroke* **31**, 2952-2957.

[33] Gold G, Giannakopoulos P, Montes-Paixao C, Jr., Herrmann FR, Mulligan R, Michel JP, Bouras C (1997) Sensitivity and specificity of newly proposed clinical criteria for possible vascular dementia. *Neurology* **49**, 690-694.

[34] Sonnen JA, Larson EB, Crane PK, Haneuse S, Li G, Schellenberg GD, Craft S, Leverenz JB, Montine TJ (2007) Pathological correlates of dementia in a longitudinal, population-based sample of aging. *Ann Neurol* **62**, 406-413.

[35] Lloyd-Jones DM, Evans JC, Levy D (2005) Hypertension in adults across the age spectrum: current outcomes and control in the community. *JAMA* **294**, 466-472.

[36] Molenaar EA, Hwang SJ, Vasan RS, Grobbee DE, Meigs JB, D'Agostino RB, Sr., Levy D, Fox CS (2008) Burden and rates of treatment and control of cardiovascular disease risk factors in obesity: the Framingham Heart Study. *Diabetes Care* **31**, 1367-1372.

[37] Kloppenborg RP, van den Berg E, Kappelle LJ, Biessels GJ (2008) Diabetes and other vascular risk factors for dementia: which factor matters most? A systematic review. *Eur J Pharmacol* **585**, 97-108.

[38] Haan MN, Shemanski L, Jagust WJ, Manolio TA, Kuller L (1999) The role of APOE epsilon4 in modulating effects of other risk factors for cognitive decline in elderly persons. *JAMA* **282**, 40-46.

[39] Elias PK, Elias MF, D'Agostino RB, Cupples LA, Wilson PW, Silbershatz H, Wolf PA (1997) NIDDM and blood pressure as risk factors for poor cognitive performance. The Framingham Study. *Diabetes Care* **20**, 1388-1395.

[40] Kalmijn S, Feskens EJ, Launer LJ, Stijnen T, Kromhout D (1995) Glucose intolerance, hyperinsulinaemia and cognitive function in a general population of elderly men. *Diabetologia* **38**, 1096-1102.

[41] Yaffe K, Blackwell T, Kanaya AM, Davidowitz N, Barrett-Connor E, Krueger K (2004) Diabetes, impaired fasting glucose, and development of cognitive impairment in older women. *Neurology* **63**, 658-663.

[42] Saczynski JS, Jonsdottir MK, Garcia ME, Jonsson PV, Peila R, Eiriksdottir G, Olafsdottir E, Harris TB, Gudnason V, Launer LJ (2008) Cognitive impairment: an increasingly important complication of type 2 diabetes: the age, gene/environment susceptibility–Reykjavik study. *Am J Epidemiol* **168**, 1132-1139.

[43] Roberts RO, Geda YE, Knopman DS, Christianson TJ, Pankratz VS, Boeve BF, Vella A, Rocca WA, Petersen RC (2008) Association of duration and severity of diabetes mellitus with mild cognitive impairment. *Arch Neurol* **65**, 1066-1073.

[44] Luchsinger JA, Reitz C, Patel B, Tang MX, Manly JJ, Mayeux R (2007) Relation of diabetes to mild cognitive impairment. *Arch Neurol* **64**, 570-575.

[45] Ott A, Stolk RP, Hofman A, van Harskamp F, Grobbee DE, Breteler MM (1996) Association of diabetes mellitus

and dementia: the Rotterdam Study. *Diabetologia* **39**, 1392-1397.

[46] Ott A, Stolk RP, van Harskamp F, Pols HA, Hofman A, Breteler MM (1999) Diabetes mellitus and the risk of dementia: The Rotterdam Study. *Neurology* **53**, 1937-1942.

[47] Luchsinger JA, Tang MX, Shea S, Mayeux R (2004) Hyperinsulinemia and risk of Alzheimer disease. *Neurology* **63**, 1187-1192.

[48] Luchsinger JA, Tang MX, Stern Y, Shea S, Mayeux R (2001) Diabetes mellitus and risk of Alzheimer's disease and dementia with stroke in a multiethnic cohort. *Am J Epidemiol* **154**, 635-641.

[49] Arvanitakis Z, Wilson RS, Bienias JL, Evans DA, Bennett DA (2004) Diabetes mellitus and risk of Alzheimer disease and decline in cognitive function. *Arch Neurol* **61**, 661-666.

[50] Peila R, Rodriguez BL, Launer LJ (2002) Type 2 diabetes, APOE gene, and the risk for dementia and related pathologies: The Honolulu-Asia Aging Study. *Diabetes* **51**, 1256-1262.

[51] Peila R, Rodriguez BL, White LR, Launer LJ (2004) Fasting insulin and incident dementia in an elderly population of Japanese-American men. *Neurology* **63**, 228-233.

[52] Xu WL, Qiu CX, Wahlin A, Winblad B, Fratiglioni L (2004) Diabetes mellitus and risk of dementia in the Kungsholmen project: a 6-year follow-up study. *Neurology* **63**, 1181-1186.

[53] Schnaider Beeri M, Goldbourt U, Silverman JM, Noy S, Schmeidler J, Ravona-Springer R, Sverdlick A, Davidson M (2004) Diabetes mellitus in midlife and the risk of dementia three decades later. *Neurology* **63**, 1902-1907.

[54] Curb JD, Rodriguez BL, Abbott RD, Petrovitch H, Ross GW, Masaki KH, Foley D, Blanchette PL, Harris T, Chen R, White LR (1999) Longitudinal association of vascular and Alzheimer's dementias, diabetes, and glucose tolerance. *Neurology* **52**, 971-975.

[55] Leibson CL, Rocca WA, Hanson VA, Cha R, Kokmen E, O'Brien PC, Palumbo PJ (1997) Risk of dementia among persons with diabetes mellitus: a population- based cohort study. *Am J Epidemiol* **145**, 301-308.

[56] MacKnight C, Rockwood K, Awalt E, McDowell I (2002) Diabetes mellitus and the risk of dementia, Alzheimer's disease and vascular cognitive impairment in the Canadian Study of Health and Aging. *Dement Geriatr Cogn Disord* **14**, 77-83.

[57] Akomolafe A, Beiser A, Meigs JB, Au R, Green RC, Farrer LA, Wolf PA, Seshadri S (2006) Diabetes mellitus and risk of developing Alzheimer disease: results from the Framingham study. *Arch Neurol* **63**, 1551-1555.

[58] Knopman DS, Mosley TH, Catellier DJ, Sharrett AR (2005) Cardiovascular risk factors and cerebral atrophy in a middle-aged cohort. *Neurology* **65**, 876-881.

[59] Knopman DS, Mosley TH Jr, Bailey KR, Jack CR Jr, Schwartz GL, Turner ST (2008) Associations of microalbuminuria with brain atrophy and white matter hyperintensities in hypertensive sibships. *J Neurol Sci* **271**, 53-60.

[60] Enzinger C, Fazekas F, Matthews PM, Ropele S, Schmidt H, Smith S, Schmidt R (2005) Risk factors for progression of brain atrophy in aging: six-year follow-up of normal subjects. *Neurology* **64**, 1704-1711.

[61] Schmidt R, Launer LJ, Nilsson LG, Pajak A, Sans S, Berger K, Breteler MM, De Ridder M, Dufouil C, Fuhrer R, Giampaoli S, Hofman A (2004) Magnetic Resonance Imaging of the Brain in Diabetes: The Cardiovascular Determinants of Dementia (CASCADE) Study. *Diabetes* **53**, 687-692.

[62] den Heijer T, Vermeer SE, van Dijk EJ, Prins ND, Koudstaal PJ, Hofman A, Breteler MM (2003) Type 2 diabetes and atrophy of medial temporal lobe structures on brain MRI. *Diabetologia* **46**, 1604-1610.

[63] van Harten B, de Leeuw FE, Weinstein HC, Scheltens P, Biessels GJ (2006) Brain imaging in patients with diabetes: a systematic review. *Diabetes Care* **29**, 2539-2548.

[64] Longstreth WT Jr, Arnold AM, Manolio TA, Burke GL, Bryan N, Jungreis CA, O'Leary D, Enright PL, Fried L (2000) Clinical correlates of ventricular and sulcal size on cranial magnetic resonance imaging of 3,301 elderly people. The Cardiovascular Health Study. Collaborative Research Group. *Neuroepidemiology* **19**, 30-42.

[65] Sonnen JA, Larson EB, Brickell K, Crane PK, Woltjer R, Montine TJ, Craft S (2009) Different patterns of cerebral injury in dementia with or without diabetes. *Arch Neurol* **66**, 315-322.

[66] Beeri MS, Silverman JM, Davis KL, Marin D, Grossman HZ, Schmeidler J, Purohit DP, Perl DP, Davidson M, Mohs RC, Haroutunian V (2005) Type 2 diabetes is negatively associated with Alzheimer's disease neuropathology. *J Gerontol A Biol Sci Med Sci* **60**, 471-475.

[67] Arvanitakis Z, Schneider JA, Wilson RS, Li Y, Arnold SE, Wang Z, Bennett DA (2006) Diabetes is related to cerebral infarction but not to AD pathology in older persons. *Neurology* **67**, 1960-1965.

[68] Korf ES, White LR, Scheltens P, Launer LJ (2006) Brain aging in very old men with type 2 diabetes: the Honolulu-Asia Aging Study. *Diabetes Care* **29**, 2268-2274.

[69] Ahtiluoto S, Polvikoski T, Peltonen M, Solomon A, Tuomilehto J, Winblad B, Sulkava R, Kivipelto M (2010) Diabetes, Alzheimer disease, and vascular dementia. A population-based neuropathologic study. *Neurology*.

[70] Matsuzaki T, Sasaki K, Tanizaki Y, Hata J, Fujimi K, Matsui Y, Sekita A, Suzuki SO, Kanba S, Kiyohara Y, Iwaki T (2010) Insulin resistance is associated with the pathology of Alzheimer disease: the Hisayama study. *Neurology* **75**, 764-770.

[71] Craft S (2005) Insulin resistance syndrome and Alzheimer's disease: age- and obesity-related effects on memory, amyloid, and inflammation. *Neurobiol Aging* **26**(Suppl 1), 65-69.

[72] Craft S, Peskind E, Schwartz MW, Schellenberg GD, Raskind M, Porte D Jr (1998) Cerebrospinal fluid and plasma insulin levels in Alzheimer's disease: relationship to severity of dementia and apolipoprotein E genotype. *Neurology* **50**, 164-168.

[73] Craft S, Watson GS (2004) Insulin and neurodegenerative disease: shared and specific mechanisms. *Lancet Neurol* **3**, 169-178.

[74] Ronnemaa E, Zethelius B, Sundelof J, Sundstrom J, Degerman-Gunnarsson M, Berne C, Lannfelt L, Kilander L (2008) Impaired insulin secretion increases the risk of Alzheimer disease. *Neurology* **71**, 1065-1071.

[75] Watson GS, Peskind ER, Asthana S, Purganan K, Wait C, Chapman D, Schwartz MW, Plymate S, Craft S (2003) Insulin increases CSF Abeta42 levels in normal older adults. *Neurology* **60**, 1899-1903.

[76] Elias MF, Wolf PA, D'Agostino RB, Cobb J, White LR (1993) Untreated blood pressure level is inversely related to cognitive functioning: the Framingham Study. *Am J Epidemiol* **138**, 353-364.

[77] Carmelli D, Swan GE, Reed T, Miller B, Wolf PA, Jarvik GP, Schellenberg GD (1998) Midlife cardiovascular risk

factors, ApoE, and cognitive decline in elderly male twins. *Neurology* **50**, 1580-1585.

[78] Launer LJ, Masaki K, Petrovitch H, Foley D, Havlik RJ (1995) The association between midlife blood pressure levels and late-life cognitive function. The Honolulu-Asia Aging Study. *JAMA* **274**, 1846-1851.

[79] Luchsinger JA, Reitz C, Honig LS, Tang MX, Shea S, Mayeux R (2005) Aggregation of vascular risk factors and risk of incident Alzheimer disease. *Neurology* **65**, 545-551.

[80] Whitmer RA, Sidney S, Selby J, Johnston SC, Yaffe K (2005) Midlife cardiovascular risk factors and risk of dementia in late life. *Neurology* **64**, 277-281.

[81] Hebert R, Lindsay J, Verreault R, Rockwood K, Hill G, Dubois MF (2000) Vascular dementia : incidence and risk factors in the Canadian study of health and aging. *Stroke* **31**, 1487-1493.

[82] Skoog I, Lernfelt B, Landahl S, Palmertz B, Andreasson LA, Nilsson L, Persson G, Oden A, Svanborg A (1996) 15-year longitudinal study of blood pressure and dementia. *Lancet* **347**, 1141-1145.

[83] Kivipelto M, Ngandu T, Fratiglioni L, Viitanen M, Kareholt I, Winblad B, Helkala EL, Tuomilehto J, Soininen H, Nissinen A (2005) Obesity and vascular risk factors at midlife and the risk of dementia and Alzheimer disease. *Arch Neurol* **62**, 1556-1560.

[84] Kivipelto M, Helkala EL, Laakso MP, Hanninen T, Hallikainen M, Alhainen K, Soininen H, Tuomilehto J, Nissinen A (2001) Midlife vascular risk factors and Alzheimer's disease in later life: longitudinal, population based study. *BMJ* **322**, 1447-1451.

[85] Guo Z, Viitanen M, Winblad B, Fratiglioni L (1999) Low blood pressure and incidence of dementia in a very old sample: dependent on initial cognition. *J Am Geriatr Soc* **47**, 723-726.

[86] Verghese J, Lipton RB, Hall CB, Kuslansky G, Katz MJ (2003) Low blood pressure and the risk of dementia in very old individuals. *Neurology* **61**, 1667-1672.

[87] Ruitenberg A, Skoog I, Ott A, Aevarsson O, Witteman JC, Lernfelt B, van Harskamp F, Hofman A, Breteler MM (2001) Blood pressure and risk of dementia: results from the Rotterdam study and the Gothenburg H-70 Study. *Dement Geriatr Cogn Disord* **12**, 33-39.

[88] Johnson KC, Margolis KL, Espeland MA, Colenda CC, Fillit H, Manson JE, Masaki KH, Mouton CP, Prineas R, Robinson JG, Wassertheil-Smoller S (2008) A prospective study of the effect of hypertension and baseline blood pressure on cognitive decline and dementia in postmenopausal women: the Women's Health Initiative Memory Study. *J Am Geriatr Soc* **56**, 1449-1458.

[89] Posner HB, Tang MX, Luchsinger J, Lantigua R, Stern Y, Mayeux R (2002) The relationship of hypertension in the elderly to AD, vascular dementia, and cognitive function. *Neurology* **58**, 1175-1181.

[90] Obisesan TO, Obisesan OA, Martins S, Alamgir L, Bond V, Maxwell C, Gillum RF (2008) High blood pressure, hypertension, and high pulse pressure are associated with poorer cognitive function in persons aged 60 and older: the Third National Health and Nutrition Examination Survey. *J Am Geriatr Soc* **56**, 501-509.

[91] Morris MC, Scherr PA, Hebert LE, Glynn RJ, Bennett DA, Evans DA (2001) Association of incident Alzheimer disease and blood pressure measured from 13 years before to 2 years after diagnosis in a large community study. *Arch Neurol* **58**, 1640-1646.

[92] in't Veld BA, Ruitenberg A, Hofman A, Stricker BH, Breteler MM (2001) Antihypertensive drugs and incidence of dementia: the Rotterdam Study. *Neurobiol Aging* **22**, 407-412.

[93] Guo Z, Fratiglioni L, Zhu L, Fastbom J, Winblad B, Viitanen M (1999) Occurrence and progression of dementia in a community population aged 75 years and older: relationship of antihypertensive medication use. *Arch Neurol* **56**, 991-996.

[94] Khachaturian AS, Zandi PP, Lyketsos CG, Hayden KM, Skoog I, Norton MC, Tschanz JT, Mayer LS, Welsh-Bohmer KA, Breitner JC (2006) Antihypertensive medication use and incident Alzheimer disease: the Cache County Study. *Arch Neurol* **63**, 686-692.

[95] Hanon O, Forette F (2005) Treatment of hypertension and prevention of dementia. *Alzheimer's & Dementia: Journal of the Alzheimer's Association* **1**, 30-37.

[96] Forette F, Seux ML, Staessen JA, Thijs L, Birkenhager WH, Babarskiene MR, Babeanu S, Bossini A, Gil-Extremera B, Girerd X, Laks T, Lilov E, Moisseyev V, Tuomilehto J, Vanhanen H, Webster J, Yodfat Y, Fagard R (1998) Prevention of dementia in randomised double-blind placebo-controlled Systolic Hypertension in Europe (Syst-Eur) trial. *Lancet* **352**, 1347-1351.

[97] Tzourio C, Anderson C, Chapman N, Woodward M, Neal B, MacMahon S, Chalmers J (2003) Effects of blood pressure lowering with perindopril and indapamide therapy on dementia and cognitive decline in patients with cerebrovascular disease. *Arch Intern Med* **163**, 1069-1075.

[98] Bosch J, Yusuf S, Pogue J, Sleight P, Lonn E, Rangoonwala B, Davies R, Ostergren J, Probstfield J (2002) Use of ramipril in preventing stroke: double blind randomised trial. *BMJ* **324**, 699-702.

[99] Haag MDM, Hofman A, Koudstaal PJ, Breteler MM, Stricker BH (2009) Duration of antihypertensive drug use and risk of dementia, a prospective cohort study. *Neurology* **72**, 1727-1734.

[100] Veldink JH, Scheltens P, Jonker C, Launer LJ (1998) Progression of cerebral white matter hyperintensities on MRI is related to diastolic blood pressure. *Neurology* **51**, 319-320.

[101] DeCarli C, Murphy DG, Tranh M, Grady CL, Haxby JV, Gillette JA, Salerno JA, Gonzales-Aviles A, Horwitz B, Rapoport SI et al. (1995) The effect of white matter hyperintensity volume on brain structure, cognitive performance, and cerebral metabolism of glucose in 51 healthy adults. *Neurology* **45**, 2077-2084.

[102] Swan GE, DeCarli C, Miller BL, Reed T, Wolf PA, Jack LM, Carmelli D (1998) Association of midlife blood pressure to late-life cognitive decline and brain morphology. *Neurology* **51**, 986-993.

[103] Dufouil C, de Kersaint-Gilly A, Besancon V, Levy C, Auffray E, Brunnereau L, Alperovitch A, Tzourio C (2001) Longitudinal study of blood pressure and white matter hyperintensities: The EVA MRI Cohort. *Neurology* **56**, 921-926.

[104] van Dijk EJ, Breteler MM, Schmidt R, Berger K, Nilsson LG, Oudkerk M, Pajak A, Sans S, de Ridder M, Dufouil C, Fuhrer R, Giampaoli S, Launer LJ, Hofman A (2004) The association between blood pressure, hypertension, and cerebral white matter lesions: cardiovascular determinants of dementia study. *Hypertension* **44**, 625-630.

[105] Longstreth WT Jr, Arnold AM, Beauchamp NJ Jr, Manolio TA, Lefkowitz D, Jungreis C, Hirsch CH, O'Leary DH, Furberg CD (2005) Incidence, manifestations, and predictors of worsening white matter on serial cranial magnetic

resonance imaging in the elderly: the Cardiovascular Health Study. *Stroke* **36**, 56-61.

[106] Liao D, Cooper L, Cai J, Toole J, Bryan N, Burke G, Shahar E, Nieto J, Mosley T, Heiss G (1997) The prevalence and severity of white matter lesions, their relationship with age, ethnicity, gender, and cardiovascular disease risk factors: the ARIC Study. *Neuroepidemiology* **16**, 149-162.

[107] Longstreth WT Jr, Manolio TA, Arnold A, Burke GL, Bryan N, Jungreis CA, Enright PL, O'Leary D, Fried L (1996) Clinical correlates of white matter findings on cranial magnetic resonance imaging of 3301 elderly people. *The Cardiovascular Health Study. Stroke* **27**, 1274-1282.

[108] Gottesman RF, Coresh J, Catellier DJ, Sharrett AR, Rose KM, Coker LH, Shibata DK, Knopman DS, Jack CR, Mosley TH (2010) Blood pressure and white matter disease progression in a biethnic cohort: the Atherosclerosis Risk in Communities (ARIC) Study. *Stroke* **41**, 3-8.

[109] de Leeuw FE, de Groot JC, Oudkerk M, Witteman JC, Hofman A, van Gijn J, Breteler MM (1999) A follow-up study of blood pressure and cerebral white matter lesions. *Ann Neurol* **46**, 827-833.

[110] Petrovitch H, White LR, Izmirilian G, Ross GW, Havlik RJ, Markesbery W, Nelson J, Davis DG, Hardman J, Foley DJ, Launer LJ (2000) Midlife blood pressure and neuritic plaques, neurofibrillary tangles, and brain weight at death: the HAAS. *Honolulu-Asia aging Study. Neurobiol Aging* **21**, 57-62.

[111] Hoffman LB, Schmeidler J, Lesser GT, Beeri MS, Purohit DP, Grossman HT, Haroutunian V (2009) Less Alzheimer disease neuropathology in medicated hypertensive than nonhypertensive persons. *Neurology* **72**, 1720-1726.

[112] Kannel WB, Cupples LA, Ramaswami R, Stokes J, 3rd, Kreger BE, Higgins M (1991) Regional obesity and risk of cardiovascular disease; the Framingham Study. *J Clin Epidemiol* **44**, 183-190.

[113] Whitmer RA, Gustafson DR, Barrett-Connor E, Haan MN, Gunderson EP, Yaffe K (2008) Central obesity and increased risk of dementia more than three decades later. *Neurology* **71**, 1057-1064.

[114] Whitmer RA, Gunderson EP, Barrett-Connor E, Quesenberry CP Jr, Yaffe K (2005) Obesity in middle age and future risk of dementia: a 27 year longitudinal population based study. *BMJ* **330**, 1360-1364.

[115] Gustafson D, Rothenberg E, Blennow K, Steen B, Skoog I (2003) An 18-year follow-up of overweight and risk of Alzheimer disease. *Arch Intern Med* **163**, 1524-1528.

[116] Meigs JB, Hu FB, Rifai N, Manson JE (2004) Biomarkers of endothelial dysfunction and risk of type 2 diabetes mellitus. *JAMA* **291**, 1978-1986.

[117] Tezapsidis N, Johnston JM, Smith MA, Ashford JW, Casadesus G, Robakis NK, Wolozin B, Perry G, Zhu X, Greco SJ, Sarkar S (2009) Leptin: a novel therapeutic strategy for Alzheimer's disease. *J Alzheimers Dis* **16**, 731-740.

[118] Knopman DS, Edland SD, Cha RH, Petersen RC, Rocca WA (2007) Incident dementia in women is preceded by weight loss by at least a decade. *Neurology* **69**, 739-746.

[119] Buchman AS, Wilson RS, Bienias JL, Shah RC, Evans DA, Bennett DA (2005) Change in body mass index and risk of incident Alzheimer disease. *Neurology* **65**, 892-897.

[120] Stewart R, Masaki K, Xue QL, Peila R, Petrovitch H, White LR, Launer LJ (2005) A 32-year prospective study of change in body weight and incident dementia: the honolulu-Asia aging study. *Arch Neurol* **62**, 55-60.

[121] Nourhashemi F, Deschamps V, Larrieu S, Letenneur L, Dartigues JF, Barberger-Gateau P (2003) Body mass index and incidence of dementia: the PAQUID study. *Neurology* **60**, 117-119.

[122] Raji CA, Ho AJ, Parikshak NN, Becker JT, Lopez OL, Kuller LH, Hua X, Leow AD, Toga AW, Thompson PM (2009) Brain structure and obesity. *Hum Brain Mapp* epub ahead of print.

[123] Taki Y, Kinomura S, Sato K, Inoue K, Goto R, Okada K, Uchida S, Kawashima R, Fukuda H (2008) Relationship between body mass index and gray matter volume in 1,428 healthy individuals. *Obesity (Silver Spring)* **16**, 119-124.

[124] Pannacciulli N, Del Parigi A, Chen K, Le DS, Reiman EM, Tataranni PA (2006) Brain abnormalities in human obesity: a voxel-based morphometric study. *Neuroimage* **31**, 1419-1425.

[125] Debette S, Beiser A, Hoffmann U, Decarli C, O'Donnell CJ, Massaro JM, Au R, Himali JJ, Wolf PA, Fox CS, Seshadri S (2010) Visceral fat is associated with lower brain volume in healthy middle-aged adults. *Ann Neurol* **68**, 136-144.

[126] Kivipelto M, Helkala EL, Hanninen T, Laakso MP, Hallikainen M, Alhainen K, Soininen H, Tuomilehto J, Nissinen A (2001) Midlife vascular risk factors and late-life mild cognitive impairment: A population-based study. *Neurology* **56**, 1683-1689.

[127] Dufouil C, Richard F, Fievet N, Dartigues JF, Ritchie K, Tzourio C, Amouyel P, Alperovitch A (2005) APOE genotype, cholesterol level, lipid-lowering treatment, and dementia: The Three-City Study. *Neurology* **64**, 1531-1538.

[128] Tan ZS, Seshadri S, Beiser A, Wilson PW, Kiel DP, Tocco M, D'Agostino RB, Wolf PA (2003) Plasma total cholesterol level as a risk factor for Alzheimer disease: the Framingham Study. *Arch Intern Med* **163**, 1053-1057.

[129] Li G, Shofer JB, Kukull WA, Peskind ER, Tsuang DW, Breitner JC, McCormick W, Bowen JD, Teri L, Schellenberg GD, Larson EB (2005) Serum cholesterol and risk of Alzheimer disease: a community-based cohort study. *Neurology* **65**, 1045-1050.

[130] Mielke MM, Zandi PP, Sjogren M, Gustafson D, Ostling S, Steen B, Skoog I (2005) High total cholesterol levels in late life associated with a reduced risk of dementia. *Neurology* **64**, 1689-1695.

[131] Solomon A, Kareholt I, Ngandu T, Winblad B, Nissinen A, Tuomilehto J, Soininen H, Kivipelto M (2007) Serum cholesterol changes after midlife and late-life cognition: twenty-one-year follow-up study. *Neurology* **68**, 751-756.

[132] Romas SN, Tang MX, Berglund L, Mayeux R (1999) APOE genotype, plasma lipids, lipoproteins, and AD in community elderly. *Neurology* **53**, 517-521.

[133] Willey JZ, Xu Q, Boden-Albala B, Paik MC, Moon YP, Sacco RL, Elkind MS (2009) Lipid profile components and risk of ischemic stroke: the Northern Manhattan Study (NOMAS). *Arch Neurol* **66**, 1400-1406.

[134] Chambless LE, Shahar E, Sharrett AR, Heiss G, Wijnberg L, Paton CC, Sorlie P, Toole JF (1996) Association of transient ischemic attack/stroke symptoms assessed by standardized questionnaire and algorithm with cerebrovascular risk factors and carotid artery wall thickness. The ARIC Study, 1987-1989. *Am J Epidemiol* **144**, 857-866.

[135] Launer LJ, White LR, Petrovitch H, Ross GW, Curb JD (2001) Cholesterol and neuropathologic markers of AD: a population-based autopsy study. *Neurology* **57**, 1447-1452.

[136] Lesser GT, Haroutunian V, Purohit DP, Schnaider Beeri M, Schmeidler J, Honkanen L, Neufeld R, Libow LS (2009)

Serum lipids are related to Alzheimer's pathology in nursing home residents. *Dement Geriatr Cogn Disord* **27**, 42-49.

[137] Stern Y, Gurland B, Tatemichi TK, Tang MX, Wilder D, Mayeux R (1994) Influence of education and occupation on the incidence of Alzheimer's disease. *JAMA* **271**, 1004-1010.

[138] Evans DA, Hebert LE, Beckett LA, Scherr PA, Albert MS, Chown MJ, Pilgrim DM, Taylor JO (1997) Education and other measures of socioeconomic status and risk of incident Alzheimer disease in a defined population of older persons. *Arch Neurol* **54**, 1399-1405.

[139] Avendano M, Kawachi I, Van Lenthe F, Boshuizen HC, Mackenbach JP, Van den Bos GA, Fay ME, Berkman LF (2006) Socioeconomic status and stroke incidence in the US elderly: the role of risk factors in the EPESE study. *Stroke* **37**, 1368-1373.

[140] Kanjilal S, Gregg EW, Cheng YJ, Zhang P, Nelson DE, Mensah G, Beckles GL (2006) Socioeconomic status and trends in disparities in 4 major risk factors for cardiovascular disease among US adults, 1971-2002. *Arch Intern Med* **166**, 2348-2355.

[141] McGurn B, Deary IJ, Starr JM (2008) Childhood cognitive ability and risk of late-onset Alzheimer and vascular dementia. *Neurology* **71**, 1051-1056.

Complexity of MRI White Matter Hyperintensity Assessments in Relation to Cognition in Aging and Dementia from the Sunnybrook Dementia Study

Fu-qiang Gao[a,*], Richard H. Swartz[a,b,c], Philip Scheltens[e], Farrell S. Leibovitch[a], Alex Kiss[b,d], Kie Honjo[a] and Sandra E. Black[a,b,c]

[a]*LC Campbell Cognitive Neurology Research Unit, Heart and Stroke Foundation Centre for Stroke Recovery, University of Toronto, Toronto, ON, Canada*
[b]*Brain Sciences Research Program, Sunnybrook Research Institute, University of Toronto, Toronto, ON, Canada*
[c]*Institute of Medical Science, Department of Medicine (Neurology), University of Toronto, Toronto, ON, Canada*
[d]*Department of Health Policy, Management and Evaluation, University of Toronto, Toronto, ON, Canada*
[e]*Neurology, Alzheimer Center,Vrije Universiteit Medical Center, Amsterdam, the Netherlands*

Abstract. *Purpose*: Quantification methods for white matter hyperintensities (WMH) on Magnetic Resonance Imaging are heterogeneous, deterring their application. This study compared three WMH rating scales, varying in complexity, and a volumetric method, to evaluate trade-offs between complexity and clinical utility in differentiating dementia subgroups and in correlating with cognition.

Methods: WMH were rated using the Fazekas, Age-Related White Matter Changes (ARWMC) and Scheltens scales, and segmented by computational volumetry in 108 patients with Alzheimer's Disease (AD), 23 with Mild Cognitive Impairment (MCI) and 34 normal controls (NC). Global and hippocampal atrophy, age and education, were accounted for in correlations of WMH with cognitive domains.

Results: Intra- and inter-rater reliability were high (intraclass correlation coefficients = 0.88–0.97) across rating scales. WMH scores of all scales were highly correlated with volumes (Spearman $r = 0.78$–0.90, $Ps < 0.001$), as well as with each other (Spearman $r = 0.86$–0.91, $Ps < 0.001$). The Fazekas scale showed significant separation between AD, MCI and NC using non-parametric analysis, while the ARWMC and Scheltens' scales, and WMH volumes demonstrated significant correlations (standardized $\beta = -0.19$ to -0.24, $Ps < 0.05$) with cognitive domain scores using multivariate regression analysis, controlling for age, education, global and hippocampal atrophy in patients with AD.

*Correspondence to: Fuqiang Gao, MD, Cognitive Neurology, Sunnybrook Health Sciences Centre, 2075 Bayview Avenue, M4N 3M5, Toronto, ON, Canada, Tel.: +416 480 4551; Fax: +416 480 4552; E-mail: fgao@sri.utoronto.ca.

Conclusions:　　This study suggests that the degree of complexity of WMH rating scales did not affect validation against WMH volumes, but did vary in validation against cognition. The simplest scale performed best in separating cognitive subgroups, but the more complex scales and quantification correlated better with cognitive measures, especially executive function. Hence the best choice of scale depends on the particular application.

INTRODUCTION

White matter hyperintensities (WMH) on brain T2 and proton density (PD) weighted or fluid-attenuated inversion recovery (FLAIR) magnetic resonance images (MRI) are frequent in the elderly [1, 2]. Although the etiology of WMH is not entirely known, WMH are often thought to be induced by small vessel disease and to potentially disrupt cortical-subcortical networks. The degree of WMH varies considerably across individuals from a single focus to extensive involvement of the subcortical white matter. The extent of WMH increases from normal aging to mild cognitive impairment and to dementia [3, 4, 5], and WMH burden negatively correlates with cognitive performance in both healthy elderly and demented groups [4, 6]. However, the correlation between WMH and cognition has been inconsistent across studies. Some studies suggested WMH load must reach a threshold before neurobehavioral signs become manifest [7, 8] or must involve a strategic location [9, 10]. Others comment that WMH have little impact on cognition, especially when taking into account other factors such as hippocampal or general cerebral atrophy [11, 12].

Heterogeneity of quantifying methods of WMH could contribute to these inconsistent findings [13, 14]. Varied rating scales and direct volume measurement have been used in the assessment of WMH. Although computer-assisted quantitative volumetric measures of WMH are more objective and precise than the rating scales, they are technically more demanding and time-consuming. In comparison, WMH visual rating scales are relatively quicker and easier to perform even on the scans from varied modalities or qualities, and are more commonly used in clinical and even research settings. However, the specialized rating scales vary greatly in the degree of complexity in regard to morphology, size, number and anatomical distribution of WMH, which leads to a variable range across scales. How discrepancies between the various rating scales affect reliability or validity of the scales has not been well-investigated, though it is expected that a scale with smaller range

may have restriction for correlating with WMH volumes or with cognitive measures. It is also unclear how to determine which scales should be chosen for studies in varied clinical and research settings. In particular, it would be useful to know which scale would be the most suitable for measuring WMH in relation to cognitive status and neuropsychological measures.

In this study, three commonly used rating scales, differing in degree of complexity, were compared to WMH volumetry in a population of normal elderly, mild cognitive impairment (MCI) and Alzheimer's Disease (AD) subjects with mild to moderate dementia. We used T2/PD MR images for rating and volumetry of WMH, as these pulse sequences are sensitive in detecting WMH than FLAIR, especially in the thalamus, and have been in use since the beginning of our on-going longitudinal study of aging and dementia. We also investigated how complexity of WMH quantification techniques would affect differentiation between cognitive subgroups and correlations with neuropsychological test scores. We hypothesized that the more comprehensive a scale is, the better it will correlate with WMH volume and neuropsychological performance, as well as distinguish dementia participants from normal controls.

METHODS

Participants

Participants ($n = 165$) were recruited from the Sunnybrook Dementia Study, an ongoing observational neuroimaging study of aging and dementia being conducted at Sunnybrook Health Sciences Centre, an affiliated teaching hospital of the University of Toronto.

All subjects were eligible consecutive participants in this longitudinal study described previously [10], and included 34 healthy elderly controls (NC), 23 patients with MCI, and 108 possible (confined to those with subcortical ischemic vasculopathy) and probable AD. All patients, who had to be fluent in English,

underwent a standard neurological examination, routine biochemical screening, standardized MRI and cognitive testing. Participants were excluded if the MRI and neuropsychological testing were separated *by* > 10 weeks, or MRI was technically inadequate for volumetric analysis. Possible secondary causes of dementia and concomitant neurological or psychiatric illnesses were exclusionary for both controls and patients. For purposes of this study, which focused on incidental WMH, possible AD with lacunar infarcts was also exclusionary.

Dementia was defined significant decline in memory and at least one additional domain of cognitive functioning, sufficient to interfere with occupational or social function using Diagnostic Statistical Manual for Mental Disorders-fourth edition criteria [15]. Possible and Probable AD met the National Institute of Neurological and Communicative Diseases and Stroke/Alzheimer's Disease and Related Disorders Association clinical criteria [16]. Individuals with cognitive impairment not meeting criteria for dementia were designated as MCI according to the Petersen criteria [17], included: 1) a subjective memory complaint; 2) relatively normal general cognition; 3) normal activities of daily living; 4) an objective memory impairment (e.g. performance ≥1.5 standard deviations below that of age, gender, and education-matched peers). The normal participants were community-dwelling volunteers with no history of psychiatric or neurological diseases or evidence of impairment on cognitive testing. The protocol was reviewed and approved by the institutional research ethics board, and informed consent was obtained from all participants or their substitute decision-makers.

All participants underwent cognitive testing of multiple domains. Mini-Mental State Examination (MMSE) [18] and the Mattis Dementia Rating Scale (DRS) total score [19] were used to measure global cognitive function. The California Verbal Learning Task (CVLT) (the total acquisition score for the trials 1–5 on this 16 word list learning test) [20] was used to assess learning. Picture naming on the 30-item Boston Naming Test (BNT) [21] provided a language measure. Wisconsin Card Sorting Test (WCST) total correct [22] and phonemic verbal fluency (FAS) [23] were included as measures of executive function.

MRI methods

Imaging was performed on a GE 1.5 Tesla MR magnet (Signa, General Electric Medical Systems, Mil-

waukee, WI), using a standardized protocol including T2/PD-weighted sequences (TR/TE/*NEX* = 3000/30-80/0.5, field of view = 20 × 20 cm, matrix = 256 × 192, slice thickness = 3 mm, scan time = 11.5 minutes) and a T1-weighted 3D volumetric spoiled gradient echo sequence (TR/TE/*NEX* = 5/35/1, flip angle = 35°, matrix = 256 × 192, and slice thickness = 1.2 mm for a total 124 axial slices. Scan time = 10.5 minutes).

Imaging analysis

WMH were scored using three different rating scales: A) Fazekas et al. [24] B) Age-related White Matter Change (ARWMC) [25] and C) Scheltens et al. [26] on axial T2/PD-weighted MR images. Briefly, the original Fazekas scale rates periventricular WMH (0–3 points) and deep white matter hyperintensities (0–3 points) with a maximal score of 6. The ARWMC scale rates the degree of white matter changes (0–3 points) in 5 regions of frontal, parieto-occipital, temporal, infratentorial areas and the basal ganglia. Left and right hemisphere WMH are rated separately and added for a maximal score of 30. The Scheltens' scale rates overall (including both hemispheres) periventricular WMH (0–6 points), deep WMH in the frontal, parietal, temporal and occipital regions (0–24 points), the basal ganglia including the putamen, globus pallidus, caudate, thalamus and internal/external capsule (0–30 points), and infratentorial areas including the midbrain, pon, medulla and cerebellum (0–24 points). The maximal score is 84.

WMH volumetry was performed using previously published techniques [10, 27, 28]. WMH were extracted from the T2/PD MRI. Briefly, using a standardized protocol, trained observers selected "seed" training voxels representative of brain, cerebrospinal fluid (CSF) and hyperintensities on interleaved T2/PD images. Using a *k*-nearest neighbours algorithm [29], a fully segmented image was produced to classify supratentorial tissues into brain parenchyma, CSF and WMH. Further, WMH that were connected to lateral ventricle were assigned to the periventricular WMH automatically, WMH in the basal ganglia and thalamus were manually labeled as basal ganglia/thalamic WMH, and WMH not labeled as the periventricular or basal ganglia WMH were assigned to the deep WMH compartment. Infratentorial WMH were not included in the volume quantification, similar to the Fazekas' scale. For comparison purposes, therefore, the WMH scores for the infratentorial regions rated

in the ARWMC and Scheltens' scales were excluded from the analysis. Whole brain and total intracranial volumes were obtained using the volumetric protocol [10]. A general brain atrophy index was calculated as the ratio of the whole brain volume (total brain parenchyma) to the total intracranial capacity (total brain parenchyma and CSF volumes). Medial temporal lobe atrophy was measured (by FG) as previously described by using the thinnest medial temporal lobe width on axial T1 images parallel to the long axis of the hippocampus [30].

MR volumetry was done by R.H.S., Fazekas and ARWMC WMH were scored by F.G. The Scheltens WMH rating was performed by its originator, P.S. All raters were blinded to any clinical information. Intra-rater reliability for the three rating scales was tested by F.G., and inter-rater reliability was tested by K.H. and F.G. for Fazekas and ARWMC scales, and by P.S. and F.G. for the Scheltens scale on 20 subjects with a representative range of WMH.

Statistical analysis

One-way analysis of variance (ANOVA) with post-hoc least square difference test was performed to examine differences in age, education and neuropsychological testing scores between NC, MCI and AD groups. Sex frequency differences between groups were examined by Chi-square test. Non-parametric Mann-Whitney analysis was used to test differences between Fazekas, ARWMC, Scheltens' WMH scores, and WMH volumes in the three cognitive subgroups, because of the non-normal distributions of these WMH measurements.

Spearman rank correlation was used to test the relationship between WMH scores and WMH volumes. Linear regression analyses were used to determine the correlation of WMH load with cognitive performance after controlling for age, education, medial temporal and global brain atrophy in the three groups separately. To examine for a possible threshold effect of WMH on cognition, analysis of covariance (ANCOVA), controlling for age, education, medial temporal and global brain atrophy, was used to compare neuropsychological performance in the three subgroups with varying degree of WMH, which were categorized into tertiles of total WMH.

Intra-rater and inter-rater reliability for the three rating scales was tested using intraclass correlation coefficients analysis.

RESULTS

Demographic characteristics and cognitive measures

The differences between age, sex, education and cognitive measures across groups are given in Table 1. Age was significantly different between the three cognitive groups driven by the difference between NC and AD ($p = 0.002$) in post-hoc comparison. (See Table 1).

Intraobserver agreement of WMH rating scales and volumetry

Intraclass correlation coefficients of intrarater agreement were 0.95 (ARWMC scale), 0.96 (Fazekas scale), 0.97 (Scheltens scale), and 0.99 (volume measurement). Interrater agreements were 0.88 (Fazekas), 0.94 (ARWMC), and 0.89 (Scheltens).

Correlations between WMH rating scores and WMH volumes

Spearman correlation coefficients between the WMH rating scores of each scale and WMH volumes, and the scores between the three rating scales can be seen in Table 2. Scatterplots for the total Fazekas, ARWMC and Scheltens scores with WMH volume showed different 'ceiling' effects of the non-linear distributions, which were better described in quadratic models indicated by higher R^2 (See Fig. 1A–C). This was most obvious for the Fazekas scale (R^2 of linear vs quadratic model: 0.77 vs 0.88) (See Figure 1A) and least for the ARWMC scale (R^2 of linear vs quadratic model: 0.85 vs 0.87) (See Fig. 1B).

In addition, total WMH scores of all three rating scales and total WMH volumes negatively correlated with the general brain atrophy ($r = -0.35$ to -0.45, all $p < 0.01$) and medial temporal lobe atrophy ($r = -0.37$ to -0.43, all $p < 0.01$).

Differences of WMH scores and WMH volumes across groups

Table 3 shows the differences between the main cognitive sub-groups in MRI measurements of WMH rating scores, WMH volumes, general cerebral atrophy and medial temporal atrophy. In general, the AD group had significantly more WMH than the NC group, measured by all techniques with regard to both global and regional WMH burden. AD group also had more

Table 1
Comparison of demographic and neuropsychological test scores between cognitive subgroups

	NC ($n = 34$)	MCI ($n = 23$)	AD ($n = 108$)	F	p-values
Sex, men/women	14/20	13/10	55/53	1.48[a]	0.447
Age, years	66.6 (8.6)	70.2 (6.8)	72.2 (10.2)	4.50	0.012 [2]
Education, years	14.5 (2.7)	14.3 (3.2)	13.6 (3.7)	1.27	0.283
MMSE	28.6 (1.3)	27.3 (2.4)	22.2 (4.7)	41.39	<0.001[2,3]
DRS	140.6 (2.8)	135.7 (6.7)	114.8 (14.2)	76.77	<0.001[2,3]
CVLT	50.8 (8.1)	35.3 (10.6)	18.9 (9.4)	160.60	<0.001[1,2,3]
FAS	47.8 (16.6)	40.7 (12.0)	26.7 (13.0)	34.94	<0.001[2,3]
WCST	46.8 (13.0)	44.3 (10.9)	33.9 (9.9)	21.65	<0.001[2,3]
BNT	28.3 (1.9)	25.8 (3.7)	19.4 (6.8)	34.95	<0.001[2,3]

Data are presented as mean (standard deviation) unless otherwise indicated. One-way ANOVA was used to test differences for age, education and neuropsychological test scores, and x^2 was used to test sex difference ($a =$ Chi-square value). Significant differences (all $Ps < 0.01$) between groups from the post hoc tests: [1]NC vs MCI, [2]NC vs AD, [3]MCI vs AD. Abbreviations: AD, Alzheimer's disease; BNT, the Boston Naming Test; CVLT, the California Verbal Learning Task, total scores of Trials 1–5; DRS, the Mattis Dementia Rating Scale, total scores; FAS, FAS verbal fluency; MCI, mild cognitive impairment; MMSE, Mini-Mental State Examination; NC, normal controls; WCST: Wisconsin Card Sorting Test (total correct).

Table 2
Correlations between WMH scores and WMH volumes, and between scores of WMH rating scales

	Fazekas vs volume	ARWMC vs volume	Scheltens vs volume	Fazekas vs ARWMC	ARWMC vs Scheltens	Scheltens vs Fazekas
Total	0.82**	0.80**	0.78**	0.87**	0.91**	0.86**
PV	0.73**	n/a	0.68**	n/a	n/a	0.71**
DWM	0.74**	n/a	0.78**	n/a	n/a	0.54**
BG	n/a	0.52**	0.28**	n/a	0.52**	n/a

Data are presented as the Spearman correlation coefficients. * Correlation is significant at the 0.05 level; ** Correlation is significant at the 0.01 level. n/a: data are not available. Abbreviations: ARWMC, Age-related White Matter Change scale; BG, basal ganglia WMH; DWM, deep white matter hyperintensities; PV, periventricular WMH.

WMH burden than the MCI in some measures from the Fazekas and Scheltens scales. The Fazekas total and periventricular scores were the only rating scores that showed significant differences between NC and MCI, and BG WMH volume was the only volumetric measure to show a statistically significant difference between NC and MCI.

Note that patients with AD are significantly older than NCs in the overall sample (see Table 1). The differences between NC and AD were re-examined in an age-matched subsample of NC ($n = 34$, age $= 66.6 \pm 8.6$) and AD ($n = 56$, age $= 67.0 \pm 10.9$). Mann-Whitney U test demonstrated that the differences of global and regional WMH burden between age-matched NC and AD groups ($t_{2,88} = -0.20$, $p = 0.84$) remained across all rating scales and volumetry (all $p < 0.01$).

Correlations of WMH with cognitive performance

The relationship between WMH measures and cognition in the NC, MCI, and AD was analyzed after adjusting for age, education, medial temporal and global brain atrophy in linear regression analysis. The standardized β was used to represent relationships, as the square root of the standardized β represent the percentage of variance in the dependent variable accounted for by the independent variable. In the AD group, the overall and basal ganglia ARWMC scores, and the Scheltens periventricular WMH scores correlated with the Boston Naming Test (standardized β $= -0.21$ to -0.23, all $p < 0.05$). The total, periventricular and deep WMH volumes were also significantly related to the Boston Naming Test (standardized β $= -0.19$ to -0.24, all $p < 0.05$). The basal ganglia WMH volume was significantly related to FAS (standardized β $= -0.20$, $p < .05$) and WCST (standardized β$=-0.25$, $p < 0.01$). In the MCI group, there were no significant correlations between WMH measures and cognitive measures. In the NC group, the total ARWMC score was significantly related to WCST (standardized β $= -0.52$, $p < 0.05$). The Scheltens total, periventricular and deep WMH scores were also significantly correlated with WCST (standardized
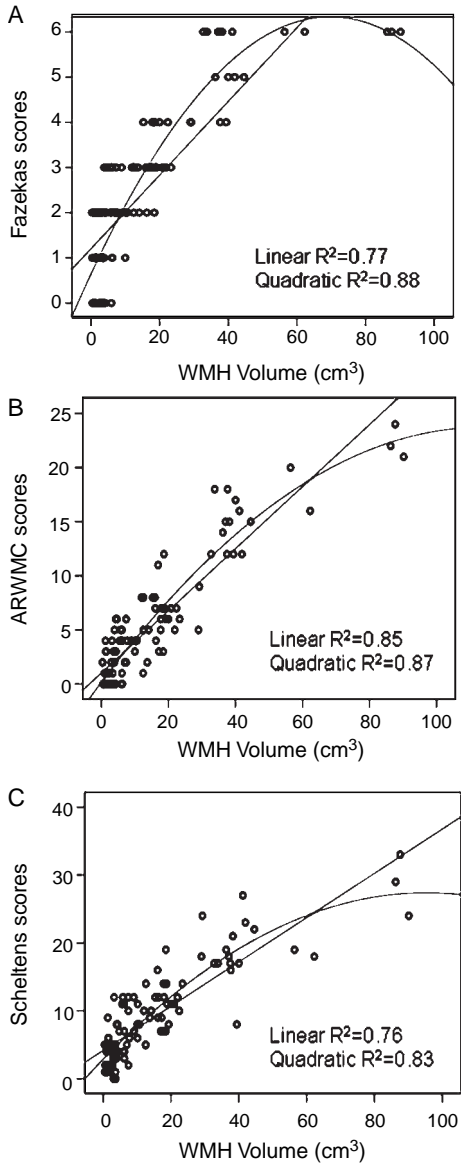
Fig. 1. Scatter plots showing the correlations between the overall WMH rating scores (y-axes) and total WMH volumes (x-axes). Each marker represents one subject. They show that quadratic regression models (curved fit lines) are better than linear regression models (straight fit lines) for the correlations between Fazekas score vs volume (A), ARWMC score vs volume (B) and Scheltens score vs volume (C), indicating 'ceiling' effects of the rating scores in reflecting increases of the WMH volumes.

$\beta = -0.51$ to -0.54, all $p < 0.005$). The Fazekas WMH scores did not negatively correlate with cognitive performance in the NC, MCI and AD groups.

To address possible threshold effects on cognition, the total WMH volume or rating score was divided into tertiles to categorize by severity for each quantification technique, and compared using ANCOVA covarying for age, education, medial temporal and global brain atrophy. Boston Naming Test and CVLT scores were significantly lower in the upper 3rd tertile ($n = 37$) of the WMH volume ($>16\,\mathrm{cm}^3$) compared to the 1st ($n = 32$) or 2nd ($n = 39$) tertile group ($p < 0.05$) in the AD groups. Visual rating scales did not show significant differences between the severity groups of WMH in the AD group. No significant differences were found from the rating scales and volumetry in this analysis in NC and MCI groups.

DISCUSSION

Correlations between the Fazekas, ARWMC and Scheltens' WMH rating scores and WMH volumes in this memory clinic sample did not reveal the expected hierarchy of correlations. That is, the more complex scale did not correlate better with WMH volumetry, taken as the gold standard. Rather, the total WMH rating scores of the three scales with different degree of complexity were all highly correlated with WMH volumes. However, the three rating scales had more ceiling effects compared to the WMH volume, consistent with a previous report [31]. This was greatest for the simple Fazekas scale compared to the more complex scales (Fig. 1). The smaller the range of a rating scale, the more limited it may be for correlating with cognitive measures in comparison to WMH volumetry. In sub-regional analyses of the deep nuclei, size of the correlation between the scales and volumes was lower for the basal ganglia compared to correlations for the periventricular and deep white matter regions. A major reason for this may be that the anatomical region of the basal ganglia is not consistently defined using the visual rating scales and the volumetric measures. For example, if a hyperintense lesion crossed the boundary between basal ganglia and deep white matter, it could be assigned to the basal ganglia by one method and to the deep white matter by the other. Nevertheless, this 'head-to-head' comparative study showed that the complexity of the rating scales had little impact on the strength of their correlations with semi-automatic WMH volumes using a recognized intensity thresholding technique. The present study also showed consistent, good inter- and intra-rater agreement of all WMH rating scales regardless of complexity of the method, in keeping with reports from the LADIS (Leukoaraiosis And Disability) and other studies [31, 33].

Table 3
Comparison of WMH scores, volumes and quantitative atrophy measurements between diagnostic subgroups

		NC (*n* = 34)	MCI (*n* = 23)	AD (*n* = 108)	*p*-values
Fazekas scores	Total	1.2 (1.0)	2.0 (1.6)	2.6 (1.4)	<0.001[1,2,3]
	PV	0.6 (0.7)	1.0 (0.8)	1.5 (0.8)	<0.001[1,2,3]
	DWM	0.6 (0.6)	1.0 (1.0)	1.2 (0.8)	0.001[2]
ARWMC scores	Total	2.4 (2.8)	4.4 (5.4)	5.3 (4.6)	0.002[2]
	DWM	2.2 (2.5)	3.6 (4.4)	4.4 (3.9)	0.005[2]
	BG	0.2 (0.6)	0.7 (1.4)	0.9 (1.4)	0.019[2]
Scheltens scores	Total	5.4 (4.5)	7.6 (6.7)	9.9 (6.6)	0.001[2]
	PV	2.1 (1.7)	2.3 (1.7)	3.2 (1.4)	<0.001[2,3]
	DWM	3.2 (3.2)	4.9 (5.3)	5.9 (4.9)	0.010[2]
	BG	0.2 (0.9)	0.3 (0.8)	0.9 (1.8)	0.021[2]
WMH volume (cm^3)	Total	3.64 (2.99)	10.82 (14.33)	12.58 (12.18)	<0.001[2]
	PV	3.37 (2.77)	10.08 (13.83)	11.68 (11.55)	<0.001[2]
	DWM	0.21 (0.27)	0.54 (0.76)	0.63 (0.89)	0.004[2]
	BG	0.07 (0.11)	0.20 (0.25)	0.27 (0.61)	0.003[1,2]
Brain atrophy index*		0.73 (0.03)	0.70 (0.04)	0.67 (0.04)	<0.001[1,2,3]
Medial temporal atrophy**		13.10 (2.10)	10.10 (3.70)	7.10 (4.30)	<0.001[1,2,3]

Nonparametric Kruskal-Wallis analysis was used for group differences in WMH score and WMH volume, and Mann-Whitney U test was used to test differences between groups. ANOVA was used to examine group differences for the atrophy measures. Data are presented as mean (standard deviation). Significant differences between groups [1]NC vs MCI, [2]NC vs AD, [3]MCI vs AD. *Brain atrophy index = total brain volume/total intracranial capacity; **Medial temporal *atrophy* = the thinnest medial temporal width in mm. Abbreviations: AD, Alzheimer's disease; ARWMC, Age-related White Matter Change scale; BG, basal ganglia; DWM, deep white matter; MCI, mild cognitive impairment; NC, normal controls; PV: periventricular.

WMH burden has been reported to be higher in AD than in controls in previous studies using different quantification techniques [3–5]. However, it has been unclear whether simpler or more complex rating scales would better distinguish between NC and AD, or dementia subgroups. Our study illustrated that AD patients did show significantly more WMH than the NC across all techniques. Since covariation for age was not possible in non-parametric analysis, we can not rule out that this difference was related to the older age of the patients with AD. In an age-matched subsample of our AD subjects, however, it remained statistically significant, suggesting that WMH differed by group membership and not by age alone. Ironically, the simple 'Fazekas' scale was the only measurement that differentiated MCI and NC. Although this was difficult to explain and contradictory to a previous report [31], a simple scale may better categorize the severity of WMH, and be more useful for quickly screening for brain-behavior studies.

Associations of WMH with neuropsychological data have been found across different methods in previous studies on validity of visual rating scales and quantitative WMH volumetry [32, 33]. It was argued that the gain using a more complex rating scale or more sensitive volumetric methods over a simple rating scale for WMH, may not be justified [33]. However, these studies used non-disabled, community-based subjects with limited cognitive evaluations. The current study included subjects with MCI and AD from a typical specialist memory clinic in an academic setting, allowing evaluation across a broader spectrum of cognitive deficits. Also a more detailed cognitive assessment was administered. In this context, as predicted, the complex rating scales with the larger range correlated better with cognition than did the simple scale. This suggests caution in settling for the simpler, quicker scales if the study goal is brain-behavior relationships. For example, based on the findings from this study, to study difficulties in language related to word finding (e.g. BNT), it would be better to use a more complex rating scale or volumetric measurement. To study executive functioning, volumetric analysis of WMH in the basal ganglia may be the most sensitive. Although the associations were modest, WMH still accounted for significant variance in the dependent variables after controlling for age, education, medial temporal and global cerebral atrophy in multivariate regression analysis, estimated by standardized β. As WMH in certain areas may be more correlated with executive functioning, an advantage of the complex scales is that they facilitate such sub-analyses.

Given the relatively small sample size of sub-groups, this study had limited ability to validate the WMH scales with neuropsychological performance in the sub-groups of NC and MCI subgroups.

It is generally agreed that linear correlations between WMH and cognitive measures are not robust. Some studies have argued that this may be partially due to a threshold effect, which means a significant accumulation of WMH is necessary before cognitive deficit becomes apparent [7, 8]. In this study, we re-classified the total volume into three categories based on tertile divisions. In so doing, we did find that subjects with the highest severity of WMH volume, e.g. the 3rd tertile, which *was* >16 cm^3 and approximately 1% of intracranial volume, had significantly lower performance on certain cognitive domains such as CVLT and BNT on ANCOVA, after adjusting for age, education, medial temporal and global brain atrophy in patients with AD. However, when we did this with the three WMH rating scales, we did not find the same result, illustrating some advantage of quantitative volumetry over rating scales. This difference might be explained by the ceiling effect of the rating scales compared to the threshold effect of the continuous WMH volumetric measure. Under the threshold effect, the lesion volume must reach a significant amount before symptom or cognitive decline manifests [7, 8]. However, the WMH rating score may no longer increase with increases in WMH volume beyond a certain threshold once the highest ordinate value is reached (i.e. the ceiling effect illustrated in Fig. 1). This may potentially make rating scales less sensitive in correlation with cognitive data.

Acquisition and segmentation techniques that facilitate volumetric measure of all tissue compartments are still the preferred approach to properly probe brain-behavior correlations [28, 37–39]. They may also be more reliable for longitudinal studies [40]. The advantage of the rating scales is that they can be performed by trained observers on scans obtained clinically, as long as they include a T2 weighted or FLAIR sequence, using standardized protocols, preferably compliant with the Vascular Cognitive Impairment Harmonization Criteria [35], and exemplified in the protocol for the Alzheimer's Disease Neuroimaging Initiative (ADNI) [36]. Processing pipelines have been developed by various groups to better measure WMH, as exemplified by our group's comprehensive pipeline for accurate removal of head-from-brain, tissue segmentation parcellation, and detailed lesion analysis subtyped as lacunar or incidental deep white or periventricular hyperintensities, based on 3DT1 and PD/T2 at 1.5T or at 3T (adding on a FLAIR) as well [28, 37–39]. This multifeature semiautomatic approach requires editing by a trained observer and averages 1.5 hours per scan. The Fazekas scale can be done in 5 minutes.

In conclusion, this study illustrated that rating scales have good concurrent and face validity and correlate well with quantitative WMH volumetry. The results suggest that the degree of complexity of WMH rating scales did not adversely affect correlations with WMH volume but that they may be less useful in correlations with cognition. The simplest scale performed best in separating cognitive subgroups, but the more complex ratings correlated better with cognition, especially executive function in the subjects with AD. This study suggests that the best choice of scale depends not only on the dataset and time available, but also on the goal of the study, i.e. the particular application. Hence the best choice of scale depends not only on convenience on the particular application, but the setting and questions being asked.

DISCLOSURE

SOURCES OF FUNDING

REFERENCES

[1] Kertesz A, Black SE, Tokar G, Benke T, Carr T, Nicholson L (1988) Periventricular and subcortical hyperintensities on magnetic resonance imaging: 'rims, caps, and unidentified bright objects'. *Arch Neurol* **45**, 404-408.

[2] de Leeuw FE, de Groot JC, Achten E, Oudkerk M, Ramos LM, Heijboer R, Hofman A, Jolles J, van Gijn J, Breteler MM (2001) Prevalence of cerebral white matter lesions in elderly people: a population based magnetic resonance imaging study. The Rotterdam Scan Study. *J Neurol Neurosurg Psychiatry* **70**, 9-14.

[3] Barber R, Scheltens P, Gholkar A, Ballard C, McKeith I, Ince P, Perry R, O'Brien J (1999) White matter lesions on magnetic resonance imaging in dementia with Lewy bodies, Alzheimer's disease, vascular dementia, and normal aging. *J Neurol Neurosurg Psychiatry* **67**, 66-72.

[4] Burns JM, Church JA, Johnson DK, Xiong C, Marcus D, Fotenos AF, Snyder AZ, Morris JC, Buckner RL (2005) White matter lesions are prevalent but differentially related with cognition in aging and early Alzheimer disease. *Arch Neurol* **62**, 1870-1876.

[5] Yoshita M, Fletcher E, Harvey D, Ortega M, Martinez O, Mungas DM, Reed BR, DeCarli CS (2006) Extent and distribution of white matter hyperintensities in normal aging, MCI, and AD. *Neurology* **67**, 2192-2198.

[6] Schmidt R, Fazekas F, Offenbacher H, Dusek T, Zach E, Reinhart B, Grieshofer P, Freidl W, Eber B, Schumacher M (1993) Neuropsychologic correlates of MRI white matter hyperintensities: a study of 150 normal volunteers. *Neurology* **43**, 2490-2494.

[7] Boone KB, Miller BL, Lesser IM, Mehringer CM, Hill-Gutierrez E, Goldberg MA, Berman NG (1992) Neuropsychological correlates of white-matter lesions in healthy elderly subjects. *A threshold effect. Arch Neurol* **49**, 549-554.

[8] DeCarli C, Murphy DG, Tranh M, Grady CL, Haxby JV, Gillette JA, Salerno JA, Gonzales-Aviles A, Horwitz B, Rapoport SI (1995) The effect of white matter hyperintensity volume on brain structure, cognitive performance, and cerebral metabolism of glucose in 51 healthy adults. *Neurology* **45**, 2077-2084.

[9] Damian MS, Schilling G, Bachmann G, Simon C, Stöppler S, Dorndorf W (1994) White matter lesions and cognitive deficits: relevance of lesion pattern? *Acta Neurol. Scand* **90**, 430-436.

[10] Swartz RH, Stuss DT, Gao F, Black SE (2008) Independent cognitive effects of atrophy and diffuse subcortical and thalamico-cortical cerebrovascular disease in dementia. *Stroke* **39**, 822-830.

[11] Inzitari D (2000) Age-related white matter changes and cognitive impairment (editorial). *Ann Neurol* **47**, 141-142.

[12] Bigler ED, Kerr B, Victoroff J, Tate DF, Breitner JC (2002) White matter lesions, quantitative magnetic resonance imaging, and dementia. *Alzheimer Dis Assoc Disord* **16**, 161-170.

[13] Pantoni L, Simoni M, Pracucci G, Schmidt R, Barkhof F, Inzitari D (2002) Visual rating scales for age-related white matter changes (leukoaraiosis): can the heterogeneity be reduced?. *Stroke* **33**, 2827-2833.

[14] Kapeller P, Barber R, Vermeulen RJ, Adèr H, Scheltens P, Freidl W, Almkvist O, Moretti M, del Ser T, Vaghfeldt P, Enzinger C, Barkhof F, Inzitari D, Erkinjunti T, Schmidt R, Fazekas F (2003) Visual rating of age-related white matter changes on magnetic resonance imaging: scale comparison, interrater agreement, and correlations with quantitative measurements. *Stroke* **34**, 441-445.

[15] American Psychiatric Association (1994) Diagnostic and statistical manual of mental disorders. 4 ed. Washington DC: American Psychiatric Association;

[16] McKhann G, Drachman D, Folstein M, Katzman R, Price D, Stadlan EM (1984) Clinical diagnosis of Alzheimer's disease: Report of the NINCDS- ADRDA Work Group under the auspices of department of health and human services task force on Alzheimer's disease. *Neurology* **34**, 939-944.

[17] Petersen RC, Smith GE, Waring SC, Ivnik RJ, Tangalos EG, Kokmen E (1999) Mild cognitive impairment: clinical characterization and outcome. *Arch. Neurol* **56**, 303-308.

[18] Folstein MF, Folstein SE, McHugh PR (1975) "Mini Mental State" A practical method for grading the cognitive state of patients for the clinician. *J Psychiatr Res* **12**, 189-198.

[19] Mattis S. (1976) Mental status examination for organic mental syndrome in the elderly patient. In: Bellak L. Karasu TB, (eds). *Geriatric psychiatry: A handbook for psychiatrists and primary care physicians*. Grune & Stratton, New York, pp. 77-121.

[20] California Verbal Learning Test: Adult Version (1987). San Antonio, Texas. The Psychological Corporation.

[21] Kaplan EF, Goodglass H, Weintraub S (1978). In *The Boston Naming Test*, Lea and Febiger, Boston.

[22] Lezak MD (1983). In *Neuropsychological assessment*, Oxford University Press, New York.

[23] Heaton RK (1981). *Wisconsin Card Sorting Test Manual*, Psychological Assessment Resources, Odessa, Fla.

[24] Fazekas F (1987). MR signal abnormalities at 1.5 T in Alzheimer's dementia and normal aging. *AJNR* **8**, 421-426.

[25] Wahlund LO, Barkhof F, Fazekas F, Bronge L, Augustin M, Sjögren M, Wallin A, Ader H, Leys D, Pantoni L, Pasquier F, Erkinjuntti T, Scheltens P (2001) A new rating scale for age-related white matter changes applicable to MRI and CT. *Stroke* **32**, 1318-1322.

[26] Scheltens P, Barkhof F, Leys D, Pruvo JP, Nauta JJ, Vermersch P, Steinling M, Valk J (1993) A semiquantitative rating scale for the assessment of signal hyperintensities on magnetic resonance imaging. *J Neurol Sci* **114**, 7-12.

[27] Swartz RH, Black SE, Feinstein A, Rockel C, Sela G, Gao FQ, Caldwell CB, Bronskill MJ (2002) Utility of simultaneous brain. CSF and hyperintensity quantification in dementia. *Psychiatry Res* **116**(**1–2**), 83-93.

[28] Kovacevic N, Lobaugh NJ, Bronskill MJ, Levine B, Feinstein A, Black SE (2002) A robust method for extraction and automatic segmentation of brain images. *Neuroimage* **17**, 1087-1100.

[29] Kikinis R, Shenton ME, Gerig G, Martin J, Anderson M, Metcalf M, Guttman CR, McCarley RW, Lorenson W, Cline H, Jolesz FA (1992) Routine quantitative analysis of brain and cerebrospinal fluid spaces with MR imaging. *Journal of Magnetic Resonance Imaging* **2**, 619-629.

[30] Gao FQ, Black SE, Leibovitch FS, Callen DJ, Lobaugh NJ, Szalai JP (2003) A reliable MR measurement of medial temporal lobe width from the Sunnybrook dementia study. *Neurobiol Aging* **24**, 49-56.

[31] van Straaten EC, Fazekas F, Rostrup E, Scheltens P, Schmidt R, Pantoni L, Inzitari D, Waldemar G, Erkinjuntti T, Mäntylä R, Wahlund LO, Barkhof F (2006) LADIS Grou. Impact of white matter hyperintensities scoring method on correlations with clinical data: the LADIS study. *Stroke* **37**, 836-840.

[32] Sachdev P, Cathcart S, Shnier R, Wen W, Brodaty H (1999) Reliability and validity of ratings of signal hyperintensities on MRI by visual inspection and computerised measurement. *Psychiatry Res* **20**(**92**), 103-115.

[33] Gouw AA, Van der Flier WM, van Straaten EC, Barkhof F, Ferro JM, Baezner H, Pantoni L, Inzitari D, Erkinjuntti T, Wahlund LO, Waldemar G, Schmidt R, Fazekas F, Scheltens P (2006) LADIS Study Group. Simple versus complex assessment of white matter hyperintensities in relation to physical performance and cognition: the LADIS study. *J Neurol* **253**, 1189-1196.

[34] Mungas D, Jagust WJ, Reed BR, Kramer JH, Weiner MW, Schuff N, Norman D, Mack WJ, Willis L, Chui HC (2001) MRI predictors of cognition in subcortical ischemic vascular disease and Alzheimer's disease. *Neurology* **57**, 2229-2235.

[35] Hachinski V, Iadecola C, Petersen RC, Breteler MM, Nyenhuis DL, Black SE, Powers WJ, DeCarli C, Merino JG, Kalaria RN, Vinters HV, Holtzman DM, Rosenberg GA, Wallin A, Dichgans M, Marler JR, Leblanc GG (2006) National institute of neurological disorders and stroke–canadian stroke network vascular cognitive impairment harmonization standards. *Stroke* **37**, 2220-2241.

[36] Jack CR Jr, Bernstein MA, Fox NC, Thompson P, Alexander G, Harvey D, Borowski B, Britson PJ, Whitwell JL, Ward C, Dale AM, Felmlee JP, Gunter JL, Hill DL, Killiany R,

Schuff N, Fox-Bosetti S, Lin C, Studholme C, DeCarli CS, Krueger G, Ward HA, Metzger GJ, Scott KT, Mallozzi R, Blezek D, Levy J, Debbins JP, Fleisher AS, Albert M, Green R, Bartzokis G, Glover G, Mugler J, Weiner MW (2008) The Alzheimer's Disease Neuroimaging Initiative (ADNI): MRI methods. *J Magn Reson Imaging* **27**, 685-691.

[37] Dade LA, Gao FQ, Kovacevic N, Roy P, Rockel C, O'Toole CM, Lobaugh NJ, Feinstein A, Levine B, Black SE (2004) Semiautomatic brain region extraction: a method of parcellating brain regions from structural magnetic resonance images. *Neuroimage* **22**, 1492-1502.

[38] Ramirez J, Gibson E, Quddus A, Lobaugh NJ, Feinstein A, Levine B, Scott CJ, Levy-Cooperman N, Gao FQ, Black SE (2011) Lesion Explorer: A comprehensive segmentation and parcellation package to obtain regional volumetrics for subcortical hyperintensities and intracranial tissue. *Neuroimage* **22**, 1123-1133.

[39] Gibson E, Gao F, Black SE, Lobaugh NJ (2010) Automatic segmentation of white matter hyperintensities in the elderly using FLAIR images at 3T. *J Magn Reson Imaging* **31**, 1311-1322.

[40] Prins ND, van Straaten EC, van Dijk EJ, Simoni M, van Schijndel RA, Vrooman HA, Koudstaal PJ, Scheltens P, Breteler MM, Barkhof F (2004) Measuring progression of cerebral white matter lesions on MRI: visual rating and volumetrics. *Neurology* **62**, 1533-1539.

Late Onset Alzheimer's Disease with Cerebrovascular Lesions as a Distinctive Phenotype of the AβPP A713T Mutation in Southern Italy

Livia Bernardi[1], Silvana Geracitano[1], Rosanna Colao, Gianfranco Puccio, Maura Gallo, Maria Anfossi, Francesca Frangipane, Sabrina A.M. Curcio, Maria Mirabelli, Carmine Tomaino, Elena Conidi, Franca Vasso, Nicoletta Smirne, Raffaele Maletta and Amalia C. Bruni*
Regional Neurogenetic Centre, ASP Catanzaro, Lamezia Terme (CZ), Italy

Abstract. The amyloid-β protein precursor (AβPP) gene located at chromosome 21 q21 was the first gene identified in which mutations cause autosomal dominant early-onset Alzheimer's disease (ADEOAD). However, a majority of mutations within the AβPP gene can cause also inherited forms of diseases such as Alzheimer's disease (AD) associated with cerebral amyloid angiopathy (CAA), cerebral haemorrhage, or both defining AD-AβPP related as a complex disease. We previously studied a large family in which neuropathology showed CAA, stroke and AD lesions due to the AβPP A713T mutation whose phenotype presented with clinical AD and subcortical ischemic lesions at Magnetic Resonance Imaging. Aim of this clinical and molecular study was to search AβPP gene mutations in 59 patients affected by AD with cerebrovascular lesions (CVLs) presenting a family history of dementia. Analysis of AβPP gene evidenced that three out of these 59 affected subjects carried the A713T mutation unusually presenting with late onset. Pathogenicity of this mutation was confirmed and the clinical AD phenotype with CVLs seems to be a distinctive feature at least in the southern Italian population. Moreover, being prevalence of this mutation worldwide very low, we assessed the possibility that a common founder among patients carrying the AβPP A713T mutation could exist in southern Italy. Molecular findings here provided, evidence that mutated patients are related and share a putative common ancestor. Identification of the A713T mutation in patients with this specific phenotype suggests that genetic epidemiology in large cohorts of familial late onset AD with CVLs would increase the probability of identifying AβPP mutations still underestimated.

Keywords: Alzheimer's disease, cerebrovascular lesions, white matter lesions, vascular risk factors, AβPP A713T mutation, amyloid-β

---

[1] These authors contributed equally to this work.

*Correspondence to: Dr. A.C. Bruni, Centro Regionale di Neurogenetica, Azienda Sanitaria Provinciale Catanzaro, Viale A. Perugini, 88046 Lamezia Terme (CZ), Italy. Tel.: +39 0968 208080; Fax: +39 0968 208032; E-mail: bruni@arn.it.

INTRODUCTION

Several studies indicate that Alzheimer's disease (AD) is frequently associated with multiple cerebrovascular lesions (CVLs) in cognitively impaired patients [1]. AD and vascular dementia (VaD) share some features which often occur together [2] mak-

ing differential diagnosis difficult and problematic in determining which disease plays the major role [3]. Furthermore, vascular risk factors (VRFs), such as diabetes mellitus, hypertension, hypercholesterolemia, smoking and atrial fibrillation may also affect cognitive functions since they are associated with the occurrence of VaD and also AD, even though conflicting results are still reported [4].

Neuropathological data from AD cases indicate that there is considerable overlap between cerebrovascular pathology and different degrees of vascular lesions such as cerebral amyloid angiopathy (CAA), microvascular degeneration and infarcts [5]. Current data indicate that CAA [6], the autosomal dominant early-onset Alzheimer's disease (ADEOAD) [7, 8] and hereditary cerebral haemorrhage with amyloidosis (HCHWA) [9] can be caused by mutations in the amyloid-β protein precursor (AβPP) gene. We have previously reported that the AβPP A713T mutation is associated with AD and subcortical ischemic lesions at Magnetic Resonance Imaging (MRI) in a large family (T. family) in which neuropathology exhibited CAA, stroke and AD lesions [10].

The aim of this study was to investigate mutations in the AβPP gene in a group of patients affected by AD with CVLs and a family history of dementia.

PATIENTS AND METHODS

Recruitment and selection of participants

Fifty nine consecutive unrelated subjects affected by AD with CVLs (42 females and 17 males; average age at onset 67.7 ± 7.9 years, range 46–84 years) were selected from a group of 1120 demented outpatients recruited from 1995 to 2005 at the Regional Neurogenetic Centre (southern Italy).

Inclusion criteria were a family history of dementia and a neuroradiological evidence of white matter lesions (WML) at MRI or white matter hypodensities at Computed Tomography (CT), evaluated according to the Wahlund scale [11], applicable to rate white matter lesions at both MRI and CT. The following scores were assigned to white matter lesions: 0, no lesions; 1, focal lesions; 2, beginning confluence of lesions; 3, diffuse involvement of the entire region [11].

To compare the APOE E4 allele frequency between the group of patients and controls, 319 age-matched, unrelated, cognitively healthy subjects (mean age $66.6 + 7.4$; MMSE 26 ± 3.7) were recruited from the same population.

The frequency of VRFs in the patient group was compared to another control group constituted by subjects from general population aged over 65 from the same ethnic and geographic background as reported in previous epidemiological studies [12].

Informed written consent was obtained from all the individuals participating in the study or from their legal guardians.

Clinical assessment

All patients underwent a detailed clinical assessment comprising medical history, physical and routine laboratory examinations, including serum folate, vitamin B12, thyroid function and syphilis serology.

VRFs such as hypertension, hypertrygliceridemia, hypercholesterolemia, cardiopathy and diabetes were also systematically evaluated. Family history and genealogical data were obtained over at least three generations.

The neuropsychological evaluation was performed by the Mental Deterioration Battery [13] including MMSE, 15 Rey's words Test and 15 Rey's words recall Test, Corsi Span, Babcock story, Token test, Phonological verbal fluency, Semantic verbal fluency, Drawing Copy and Drawing copy with hallmarks, Attentive Matrices, Raven Progressive Matrices and Winsconsin Card Sorting Test. A standardized behavioral assessment was performed.

The NINCDS-ADRDA [14], Mc Keith [15], Lund-Manchester group criteria [16] and NINDS-AIREN criteria [17] were used to make differential diagnosis. No cases with past history of psychiatric illnesses such as schizophrenia, major depression or bipolar disorder were identified and patients were considered affected by AD according to DSM-IV (Diagnostic and Statistical Manual of Mental Disorders) criteria [18].

Hachinski score was measured [19] in each case, to differentiate vascular dementia from degenerative forms of the dementia.

MRI and CT were obtained in 34 and 25 patients, respectively.

Genetic screening

Genomic DNA was extracted from blood buffy-coats using standard phenol-chloroform procedures. Coding exons (3–12) of Presenilin 1 (PSEN1) and Presenilin 2 (PSEN2) genes and exons 15–18 (exons with highest mutation frequency) of the AβPP gene were

amplified using specific primers previously described [7, 20, 21]. Sequencing was performed in both directions using the Big Dye kit (Perkin Elmer) and an ABI310 automated sequencer.

Apoliprotein E (APOE) genotype, H1/H2 Microtubule associated protein tau (MAPT) haplotypes and Prion protein (PRNP) Met129Val polymorphism were assessed as previously reported [22–24].

To determine whether the AβPP A713T mutation had been inherited from a common ancestor, haplotype analysis on the only one affected subject per family (CAR patient, GIG patient, PAO patient and T. Family proband) was performed. Five adjacent microsatellite markers, from the p-telomeric end, D21S1256, D21S221, D21S1268, DSi16 and D21S1253, as previously reported for the AβPP V717L (located on the same exon, gene and chromosome of the AβPP A713T mutation) [25] were selected. Each marker was amplified by PCR with one fluorescent labelled primer using standard conditions for microsatellites. The PCR products were assessed on the ABI Prism Genetic Analyzer (Applied Biosystems) and analyzed with Genescan version 3.0 and Genotyper software version 2.1.

Statistical analyses

Significant differences ($p < 0.05$) in APOE E4 allele frequency between the patient group and the control group of 319 cognitively healthy subjects were evaluated and compared using the chi-square test.

Significant differences ($p < 0.05$) in frequency of VRFs between the patient group and the control group reported in previous epidemiological studies [12] were evaluated and compared using the chi-square test.

To investigate the association between the APOE E4 allele and VRFs in patients, the Spearman rank correlation test was performed assuming the presence of at least one APOE E4 allele and the presence of a single specific risk factor or presence of at least one risk factor or presence of more than one risk factor. All statistical analyses were performed using SPSS 11.5.

RESULTS

Sequencing of exon 17 of the AβPP gene revealed the previously reported A713T heterozygous mutation (275329 G > A, Genebank accession number D87675.1) [10, 26] in three of 59 (5%) unrelated patients (AβPP plus patients), 2 females and 1 male, age of onset 72–82 years. None of the previously reported, nor novel PSEN1 and PSEN2 mutations were detected in any of the patients.

CAR patient

A farmer aged 72 years at onset presented symptoms of memory loss, loss of interest in daily living activities, temporal and sometimes spatial disorientation. His medical history was unremarkable except for hypertension. His father as well as his paternal uncle died with a clinical picture of dementia. One brother died at age 65 following a stroke. One sister had epileptic seizures and died at age 30 (Fig. 1A). At age 74 years the patient was moriatic, presented with environmental dependence syndrome, insight was absent. Neurological examination evidenced grasping and palmo-mental reflexes. Neuropsychological assessment revealed a MMSE of 16.7; impairment of long term verbal memory (*Babcock story 6* nv 12.15 ds 3.09) and of short term spatial memory (*Corsi test* 2 nv 4.35 ds 0.84); difficulties with verbal abstract reasoning, abstract thinking and critical judgment (he was untestable); and reduction of verbal fluency (*phonemic verbal fluency* 14.4 nv > 17.35). MRI flair sequences showed bilateral small WML in the subcortical periventricular area. SPECT imaging showed hypoperfusion of bilateral parieto-temporal lobes with prominent frontal and cerebellar hypoperfusion in the left hemisphere.

Memory impairment, critical thinking and attention deficits worsened together with dressing apraxia and, occasionally prosopoagnosia and episodes of urinary incontinence.

Three years later the patient was bedridden with severe rigidity of all limbs. Death occurred at age 77.

GIG patient

A housewife aged 84 years was examined because of behavioral and cognitive deterioration with onset following a car accident which occurred two years prior to the examination. Family history reported that her living brother showed memory disturbances and her sister had episodes of stroke; her mother died with dementia characterized by memory disturbances and delusions (Fig. 1B). Personal history included hypertension since the age of 54 and several Transient Ischemic Attacks occurred from the age of 64 years. During hospitaliza-
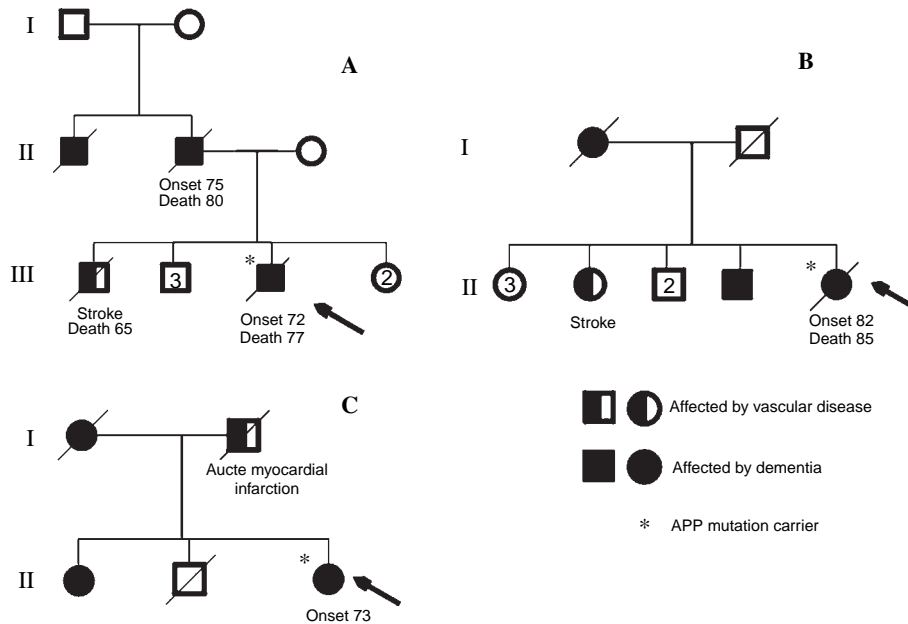
Fig. 1. A, B, C: pedigrees of CAR, GIG, PAO families. Probands are indicated with an arrow.

tion following the car accident the woman developed delirium with loss of consciousness. confusion, and spatio-temporal disorientation.

At home, the clinical picture of dementia became evident. The patient was unaware, manifested memory loss, she was unable to dress and to recognize relatives; progressively, apathy and loss of interest in doing housework, spatial and temporal disorientation worsened.

Neuropsychological evaluation at age 84 years revealed a MMSE = 14.5; memory disturbances (*Rey's words short term 24.2 nv 28.53; Rey's words long term 0; Babcock story 0; Corsi test 2 nv 4.35 ds 0.84*) difficulties with verbal abstract reasoning, abstract thinking and critical judgement (*Attentive Matrices 26.25 nv 31; Raven's Progressives Matrices 12 nv 18.96*), apraxia (*drawing copy untestable*) and reduction of verbal fluency (*she was untestable*). Blood chemistry investigations were normal. CT scan revealed temporo-parietal atrophy, periventricular white matter hypodensities. Echo-Doppler of cerebral arteries showed diffuse atheromatosis.

Cognitive functions became severely impaired, she developed lack of personal hygiene, motor impersistence, stereotypies, agitation, sundowning, sleep disturbances and urinary incontinence. She was placed in a nursing home and died at age 85 years.

PAO patient

Female at age 73 years manifested symptoms of a progressive cognitive deterioration. Family history showed that the patient's mother died with a clinical picture of dementia and presented prominent memory disturbances and one sister exhibited memory and behavioral disorders (Fig. 1C).

The medical history revealed that at age 68 years the patient presented with ischemic heart disease, hypertension, elevated serum cholesterol and triglyceride levels. Subsequently, insidious changes of mood and personality, memory loss and delusions together with irritability and sleep disturbances were noticed by family members. Neurological examination was normal, she presented with severe cognitive impairment. (MMSE 8.7) MRI showed bilateral temporo-parietal cortical atrophy associated with WML. Over time, in addition to worsening of cognitive functions, the patient developed aggressiveness, agitation, and bad language. Insight was absent. She is still alive. Clinic

Table 1
Summary of clinical, demographic and genetic characteristics of AβPP plus patients

Patient/ Gender	Family history of vascular disease	VRFs	Age at onset (years)	Current age or age at death* (years)	Insight	Symptoms at onset	First evaluation	Hachinski score	APOE	PRNP	APLO TAU
CAR/M	+	Hypertension	72	77*	No	Memory loss, spatial and temporal disoriented	MMSE 16.7; CDR 2; ADL 4/6; IADL 3/8	6	3/3	M/V	H1H2
GIG/F	+	Hypertension	82	85*	No	Delirium	MMSE 14.5; CDR 2; ADL 4/6; IADL 1/8	6	3/3	M/M	H1H2
PAO/F	+	Hypertension, ischemic heart disease, Hyper-cholestrolemia, Hyper-trygliceridemia.	73	77	No	Memory loss, insidious chenge of mood and personality, delusion	MMSE 8.7; CDR 3; ADL 5/6; IADL 2/8	5	2/3	M/M	H2H2

and genetic characteristics of AβPP plus patients are summarized in Table1.

Characteristics of patients without AβPP mutation (AβPP negative)

Characteristics of patients without the AβPP mutation (AβPP negative) are summarized in Table 2 and Table 3.

VRFs were differently represented in the AβPP negative group: 36% (20 patients) were completely free, 39% (22 patients) presented with only one VRF and 25% (14 patients) showed two or more. However, no correlation was found between the APOE E4 allele and the number of VRFs (data not shown).

APOE E4 allele frequency was however, significantly different ($p = 0.000$) between AβPP negative patients compared to the group of 319 cognitively healthy controls (data not shown).

The prevalence of VRFs was not significantly different when compared to general population aged over 65 from the same ethnic and geographic background, as already reported in previous epidemiological studies [12] (data not shown).

Haplotype analysis

A common shared DNA haplotype was identified among patients carriers of the AβPP A713T mutation thus suggesting that this mutation occurred in a putative common ancestor (Table 4). It is remarkable that PAO patient showed an allelic pattern for the D21S1256 marker different from that of the other patients. This microsatellite marker is the marker most distant from the AβPP gene and it is possible that a

Table 2
Summary of clinical and neuroradiological characteristics of AβPP negative patients

Variable	Mean value ± SD or %, (No.)
MMSE	14.6 ± 6.3 (55)
ADL	4.7 + 1.7 (52)
IADL	3.2 + 2.3 (52)
CDR	1.6 + 0.9 (56)
Hachinski score	3.3 + 2.4 (56)
Memory loss	96% (54)
Dis.space/time	45% (25)
Apathy	43% (24)
Depression	30% (17)
Apraxia	36% (20)
Aphasia	21% (12)
Other symptoms	<16%
WML rate	1–2 (Wahlund scale)

Table 3
Vascular and genetic risk factors of AβPP negative patients

Variable	% (No.)
Family history of vascular diseases	39% (22)
Family history of cerebrovascular disease	29% (16)
Hypertension	39% (22)
Hypertriglyceridemia	9% (5)
Hypercholesterolemia	38% (20)
Cardiopathy	16% (9)
Diabetes	14% (8)
APOE E4 allele carriers	54% (30)

Table 4
Haplotype analysis of the four patients with the AβPP A713T mutation

Marker	Position[1] on chromosome	Affected subjects			
		CAR patient	GIG patient	PAO patient	T. family proband
D21S1256(*)	18 244 527	*1*, 4	*1*, 1	2, 4	*1*, 6
D21S221(*)	25 686 727	*2, 1*	*2, 1*	*2, 1*	*2, 1*
D21S1268(*)	26 113 710	*1*, 1	*1*, 1	*1*, 2	*1*, 1
A713T	26 185 966	A, G	A, G	A, G	A, G
DSi16(*)	26 190 618	*1, 2*	*1, 2*	*1, 1*	*1*, 2
D21S1253(*)	26 356 282	*1*, 2	*1*, 4	*1*, 2	*1*, 5

*Microsatellite markers used in a previous study [25]. Bold and italic represent shared alleles.; [1]Distance (bp) from the p-telomeric end.

single recombination event has occurred in this region. Unfortunately, we cannot estimate the exact number of generations separating them from the putative common founder because of the limited number of available family members.

DISCUSSION

We investigated AβPP gene mutations in a selected group of 59 patients exhibiting both AD and cerebrovascular lesions. The relationship between AD and vascular lesions is currently under debate [1] and the model offered by AβPP gene mutations which produce either pure AD or HCHAW or CAA could be an interesting starting-point for better understanding this field. Almost all patients studied presented clear symptoms of AD at onset although apathy and depression were also evident as it occurs in Subcortical Ischemic Vascular Dementia (SIVD) [27]. However, a clear and complete dysexecutive syndrome, as expected in SIVD, was absent.

The VRFs were widely represented in the group of AβPP negative patients, although not significantly different from the control group of the general population as reported in previous epidemiological studies [12]; moreover, when comparing the group of AβPP negative patients with the 319 cognitively healthy controls, the APOE E4 allele strongly correlated with AD. In contrast with another study, where an interaction between APOE E4 allele, hypertension and WMLs was reported [28], we did not observed a similar interaction in these patients.

We detected AβPP A713T in three patients (AβPP plus) apparently unrelated at least over three generations. All patients presented with the same symptoms at onset: memory loss, absence of insight, behavioral and personality changes, mainly apathy. Interestingly,

hypertension, widely recognized as the most important risk factor for WML in the population [29], was ascertained in all AβPP plus patients in contrast to the previously reported T. family where neuropathology clearly demonstrated that the WML were due to CAA [10].

Whether in AβPP plus, WML were due to hypertension or CAA or both, could not be determined since neuropathology was not available. In these patients, WML seemed to correlate with onset rather than with hypertension [30].

It is of note that AβPP plus presented with a clear late onset ranging from 72 to 82 years and a short duration (3–5 years) while in the T. family onset was earlier (range 52–68 years) and disease duration ranged from 3 to 14 years. We assessed the possibility that specific genetic modifiers of age at onset in dementia [31–33], could explain this variability. However, neither the MAPT haplotypes, nor the PRNP polymorphism accounted for the differences (Table 1) and the only one APOE E2 allele did not correlate with the later onset. Variability of age at onset is widely recognized as an important biological feature which probably depends on other genetic and environmental factors. In our cases, it is also possible that a large span of onset for the AβPP A713T mutation could exist and that, by chance, we are observing the two extremes of the same probability distribution.

Although AβPP plus patients show some phenotypic variability when compared to the T. family, we tested the hypothesis that a common ancestor, linking all apparently unrelated cases, exists since they belong to a genetically isolated area (Calabria region) in which a founder effect has been confirmed for several other AD gene mutations [34] and illnesses [35]. Despite a genealogical reconstruction was not possible, a common shared DNA haplotype was identified among patients carrying the AβPP A713T mutation
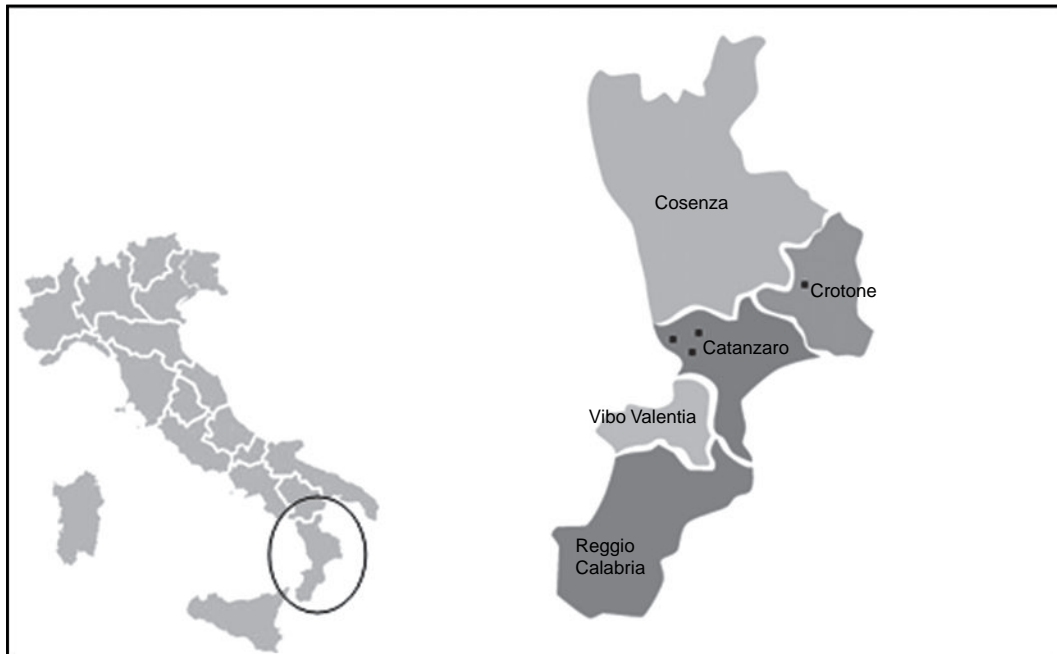
Fig. 2. On the left: geographic map showing Italy with the Calabria region highlighted. On the right: geographic map indicating the location of the Province relative to the Calabria region; ■ symbol indicates the countries of origin of the four patients carrying the AβPP A713T mutation. The name of the countries are not reported to protect family confidentiality.

thus suggesting that this mutation segregates from a putative common ancestor.

The prevalence of the AβPP A713T mutation worldwide is very low, while it was found to be 5% in this study. Except for the T. family [10] and the patients of the present study, only one paper reports the mutation in one patient having early onset FAD of unknown origin and with amyloid angiopathy restricted, however, to a few meningeal and parenchymal blood vessels [26]. Although neuropathology in this study was not performed, we speculate that the pathological features could be the same as those already described in the T. family, since both groups of the AβPP A713T patients descend from a common putative ancestor, share the AβPP genotype, clinical characteristics and geographic background (Fig. 2).

The neuropathological differences between the two previous papers [10, 26] could be due to different genetic backgrounds and/or environmental factors possibly acting in concert in apparently unrelated populations.

We speculate that the AβPP A713T mutation could act as the AβPP A692 G mutation identified in patients with haemorrhage, dementia or both, leading to an increased secretion of both amyloid β_{142} and amyloid β_{140} as demonstrated *in vitro* [36] and also compatible with the increased risk of AD pathology and vascular amyloid deposition observed in humans [37].

Finally, it is possible that the AβPP mutation frequency has been underestimated: almost all reported AβPP mutations were associated with early onset [38] while the identification of our late onset patients suggests that further epidemiological studies using large cohorts of familial late onset AD with CVLs could increase the probability of detecting AβPP mutations.

ACKNOWLEDGMENTS

1) DGRST n° 4/2760-P/I.9.ab, 2007; 2) RFPS-2006-7-334858, 2006.

REFERENCES

[1] Jellinger KA (2008) The pathology of "vascular dementia": a critical update. *J Alzheimers Dis* **14**, 107-123.

[2] de la Torre JC (2002) Alzheimer disease as a vascular disorder: nosological evidence. *Stroke* **33**, 1152-1162.

[3] Du AT, Schuff N, Laakso MP, Zhu XP, Jagust WJ, Yaffe K, Kramer JH, Miller BL, Reed BR, Norman D, Chui HC, Weiner MW (2002) Effects of subcortical ischemic vascular dementia and ad on entorhinal cortex and hippocampus. *Neurology* **58**, 1635-1641.

[4] Duron E, Hanon O (2008) Vascular risk factors, cognitive decline. and dementia. *Vasc Health Risk Manag* **4**, 363-381.

[5] Kalaria, R.N., Ballard, C (1999) Overlap between pathology of Alzheimer disease and vascular dementia. *Alzheimer Dis Assoc Disord* **13** (Suppl 3) , S115-S123.

[6] Obici L, Demarchi A, de Rosa G, Bellotti V, Marciano S, Donadei S, Arbustini E, Palladini G, Diegoli M, Genovese E, Ferrari G, Coverlizza S, Merlini G (2005) A novel abetapp mutation exclusively associated with cerebral amyloid angiopathy. *Ann Neurol* **58**, 639-644.

[7] Goate A, Chartier-Harlin MC, Mullan M, Brown J, Crawford F, Fidani L, Giuffra L, Haynes A, Irving N, James L (1991) Segregation of a missense mutation in the amyloid precursor protein gene with familial Alzheimer's disease. *Nature* **349**, 704-706.

[8] Hendriks L, Van Broeckhoven C (1996) A beta A4 amyloid precursor protein gene and Alzheimer's disease. *Eur J Biochem* **237**, 6-15.

[9] Maat-Schieman ML, van Duinen SG, Bornebroek M, Haan J, Roos RA (1996) Hereditary cerebral hemorrhage with amyloidosis-Dutch type (HCHWA-D): II – A review of histopathological aspects. *Brain Pathol* **6**, 115-120.

[10] Rossi G, Giaccone G, Maletta R, Morbin M, Capobianco R, Mangieri M, Giovagnoli AR, Bizzi A, Tomaino C, Perri M, Di Natale M, Tagliavini F, Bugiani O, Bruni AC (2004) A family with Alzheimer disease and strokes associated with A713 t mutation of the APP gene. *Neurology* **63**, 910-912.

[11] Wahlund LO, Barkhof F, Fazekas F, Bronge L, Augustin M, Sjogren M, Wallin A, Ader H, Leys D, Pantoni L, Pasquier F, Erkinjuntti T, Scheltens P, European (2001) Task force on age-related white matter changes. A new rating scale for age-related white matter changes applicable to MRI and CT. *Stroke* **32**, 1318-1322.

[12] www.cuore.iss.it/fat_rischio/regioni/calabria/calabria.html.

[13] Carlesimo GA, Caltagirone C, Gainotti G (1996) The mental deterioration battery: normative data, diagnostic reliability and qualitative analyses of cognitive impairment. The group for the standardization of the mental deterioration battery. *Eur Neurol* **36**, 378-384.

[14] McKhann G, Drachman D, Folstein M, Katzman R, Price D, Stadlan EM (1984) Clinical diagnosis of Alzheimer disease: report of the INCDS-ADRDA work group under the auspices of department of health and human services task force on Alzheimer's disease. *Neurology* **34**, 939-944.

[15] McKeith IG, Galasko D, Kosaka K, Perry EK, Dickson DW, Hansen LA, Salmon DP, Lowe J, Mirra SS, Byrne EJ, Lennox

G, Quinn NP, Edwardson JA, Ince PG, Bergeron C, Burns A, Miller BL, Lovestone S, Collerton D, Jansen EN, Ballard C, de Vos RA, Wilcock GK, Jellinger KA, Perry RH (1996) Consensus guidelines international workshop for the clinical and pathological diagnosis of dementia with lewy body disease (DLB): report of the consortium on dlb. *Neurology* **47**, 1113-1124.

[16] Brun A, Englund B, Gustafson L, Passant U, Mann DMA, Neary D, Snowden JS (1994) Consensus statement: clinical and neuropathological criteria for frontotemporal dementia. *J Neurol Neurosurg Psychiatry* **57**, 416-418.

[17] Roman GC, Tatemichi TK, Erkinjuntti T, Cummings JL, Masdeu JC, Garcia JH, Amaducci L, Orgogozo JM, Brun A, Hofman A (1993) Vascular dementia; diagnostic criteria for research studies. report of the NINCSDS-AIREN international work group. *Neurology* **43**, 250-260.

[18] American Psychiatric Association. AP., Diagnostic and Statistical Manual of Mental Disorders, Fourth Edition (DSM-IV), Washington, DC: American Psychiatric Association; 1994.

[19] Hachinski VC, Iliff LD, Zilhka E, Du Boulay GH, McAllister VL, Marshall J, Russell RW, Symon L (1975) Cerebral blood flow in dementia. *Arch Neurol* **32**, 632-637.

[20] Hutton M, Busfield F, Wragg M, Crook R, Perez-Tur J, Clark RF, Prihar G, Talbot C, Phillips H, Wright K, Baker M, Lendon C, Duff K, Martinez A, Houlden H, Nichols A, Karran E, Roberts G, Roques P, Rossor M, Venter JC, Adams MD, Cline RT, Phillips CA, Goate A, A (1996) Complete analysis of the presenilin 1 gene in early onset Alzheimer's disease. *Neuroreport* **7**, 801-805.

[21] Cruts M, van Duijn CM, Backhovens H, Van den Broeck M, Wehnert A, Serneels S, Sherrington R, Hutton M, Hardy J, St George-Hyslop PH, Hofman A, Van Broeckhoven C (1998) Estimation of the genetic contribution of presenilin 1 and 2 mutations in a population-based study of presenile Alzheimer disease. *Hum Mol Genet* **7**, 43-51.

[22] Hixson G, Vernier D (1990) Restriction isotyping of human apolipoprotein e by gene amplification and cleavage with HhaI. *J Lipid Res* **31**, 545-548.

[23] Bernardi L, Maletta RG, Tomaino C, Smirne N, Di Natale M, Perri M, Longo T, Colao R, Curcio SA, Puccio G, Mirabelli M, Kawarai T, Rogaeva E, P, St George Hyslop H, Passarino G, De Benedictis G, Bruni AC (2006) The effects of APOE and tau gene variability on risk of frontotemporal dementia. *Neurobiol Aging* **27**, 702-709.

[24] Combarros O, M. Sánchez-Guerra J, Llorca A, Alvarez-Arcaya J, Berciano N, Peña C, Fern andez-Viadero (2000) Polymorphism at codon 129 of the prion protein gene is not associated with sporadic AD. *Neurology* **55**, 593-595.

[25] Finckh U, Kuschel C, Anagnostouli M, Patsouris E, Pantes GV, Gatzonis S, Kapaki E, Davaki P, Lamszus K, Stavrou D, Gal A (2005) Novel mutations and repeated findings of mutations in familial Alzheimer disease. *Neurogenetics* **6**, 85-89.

[26] Armstrong J, Boada M, Rey MJ, Vidal N, Ferrer I (2004) Familial Alzheimer disease associated with A713 t mutation in APP. *Neurosci Lett* **370**, 241-243.

[27] Roman GC, Erkinjuntti T, Wallin A, Pantoni L, Chui HC (2002) Subcortical ischaemic vascular dementia. *Lancet Neurol* **1**, 426-436.

[28] de Leeuw FE, Richard F, de Groot JC, van Duijn CM, Hofman A, Van Gijn J, Breteler MM (2004) Interaction between hypertension, APOE, and cerebral white matter lesions. *Stroke* **35**, 1057-1060.

[29] de Leeuw FE, de Groot JC, Oudkerk M, Witteman JC, Hofman A, van Gijn J, Breteler MM (1999) A follow-up study of blood pressure and cerebral white matter lesions. *Ann Neurol* **46**, 827-833.

[30] de Leeuw FE, de Groot JC, Achten E, Oudkerk M, Ramos LM, Heijboer R, Hofman A, Jolles J, van Gijn J, Breteler MM (2001) Prevalence of cerebral white matter lesions in elderly people: a population based magnetic resonance imaging study. the Rotterdam scan study. *J Neurol Neurosurg Psychiatry* **70**, 9-14.

[31] Laws SM, Perneczky R, Drzezga A, Diehl-Schmid J, Ibach B, auml JB, uml T, Eisele HF, ouml, rstl A, Kurz M, Riemenschneider (2007) Association of the tau haplotype H2 with age at onset and functional alterations of glucose utilization in frontotemporal dementia. *Am J Psychiatry* **164**, 1577-1584.

[32] Pastor P, Roe CM, Villegas A, Bedoya G, Chakraverty S, Garciacute G, Tirado V , Norton J S Riacuteos, Martiacutenez M, Kosik KS, Lopera F, Goate AM, (2003) Apolipoprotein E epsilon4 modifies Alzheimer's disease onset in an E280A PS1 kindred. *Ann Neurol* **54**, 163-169.

[33] Mead S, Webb TE, Campbell TA, Beck J, Linehan JM, Rutherfoord S, Joiner S, Wadsworth JD, Heckmann J, Wroe S, Doey L, King A, Collinge J (2007) Inherited prion disease with 5-OPRI: phenotype modification by repeat length and codon 129 . *Neurology* **69**, 730-738.

[34] Sherrington R, Rogaev EI, Liang Y, Rogaeva EA, Levesque G, Ikeda M, Chi H, Lin C, Li G, Holman K, et al. (1995) Cloning of a gene bearing missense mutations in early-onset familial Alzheimer's disease. *Nature* **375**, 754-760.

[35] Heyer E, Toupance B, Perri C, De Vito O, Foncin JF, Bruni AC (2003) Manic depressive illness in a founder population. *Eur J Hum Genet* **11**, 597-602.

[36] De Jonghe C, Zehr C, Yager D, Prada CM, Younkin S, Hendriks L, Van Broeckhoven C, Eckman CB (1998) Flemish and Dutch mutations in amyloid beta precursor protein have different effects on amyloid beta secretion. *Neurobiol Dis* **4**, 281-286.

[37] Roks G, Van Harskamp F, De Koning I, Cruts M, De Jonghe C, Kumar-Singh S, Tibben A, Tanghe H, Niermeijer MF, Hofman A, Van Swieten JC, Van Broeckhoven C, Van Duijn CM (2000) Presentation of amyloidosis in carriers of the codon 692 mutation in the amyloid precursor protein gene (APP692). *Brain* **123**, 2130-2140.

[38] http://www.molgen.ua.ac.be/ADMutations

This page intentionally left blank

Section 10
Neuroimaging in the Context of Alzheimer's Disease

This page intentionally left blank

Introduction

Section 10: Neuroimaging in the Context of Alzheimer's Disease

Allyson C. Rosen and David Kennedy

The purpose of this section is to place the individual neuroimaging techniques in the larger context of how they can relate to one another and to the care and evaluation of patients with Alzheimer's disease (AD). The first article by Smith in this section briefly summarizes the current status of the use of neuroimaging techniques in the context of early diagnosis of AD. As with most technologies, within the next few years many of the limitations we may admit to in this volume will likely have been addressed. However, it is essential that anyone using these techniques be aware of these limitations and appropriate uses.

One current direction of development is to automate quantification of pathology. There are substantial advances being directed to make imaging techniques previously utilized only in select labs available to anyone with a computer and the resources to implement the analysis programs. Hippocampal volume decline is one of the most consistently reported imaging findings in AD so that a logical first approach in examining this process of using imaging in diagnostic decision making is to use hippocampal volume to discriminate diagnostic status between two obviously different populations, AD versus normal elderly. As with many techniques that extend clinical work, Mak et al. begin with an expert manually defining hippocampal volume as the

gold standard. They compare these results to some of the most commonly used, automated, approaches. A more extensive comparison of hippocampal volumetric techniques is also described in Boccardi et al. earlier in this volume.

Another fruitful approach is to compare a given structure using different imaging modalities, and this is particularly useful with respect to white matter regions. Di Paola, Spalletta, and Caltagirone review approaches to describing the integrity of the corpus callosum, a structure whose degeneration in AD is increasingly being studied, particularly in the context of vascular disease and AD [e.g., 1]. The authors compare information from high resolution T1 images and diffusion methods to study Wallerian degeneration. Wallerian degeneration, or anterograde degeneration, is a process that occurs when an axon degenerates after damage disconnects it from a cell body. The importance of connectivity between brain regions is a direction in which the field of neuroimaging is moving and this article relates connectivity to the degenerative process of AD. Chapter 6 discusses DTI more fully.

Whereas many investigators compare various sources of clinical information with respect to diagnostic sensitivity and specificity, classification and support vector machine learning offer a way of integrating existing information to improve the accuracy of diagnosis. We finish the section with two papers on these techniques. The tutorial by Haller et al. introduces classification in the context of discriminating MCI from

---

*Correspondence to: Allyson C. Rosen, E-mail: rosena@psych.stanford.edu.

AD patients. The paper by Furney et al. provides an example of how this method can be applied to predicting conversion of MCI to AD and includes both CSF biomarkers and MRI.

The ultimate question a clinician needs to answer is how information from imaging can enhance clinical management. Neuroimaging of individual patients in everyday clinical care will not be useful unless it can improve what a clinician can do without it. Traditionally structural imaging and FDG-PET contribute to AD diagnosis by facilitating exclusion of alternative etiologies. This handbook describes several instances where imaging information has the potential to provide convergent information supporting early diagnosis. Examples of potentially useful techniques include ligands for amyloid and tau, pathognomonic patterns of FDG-PET hypometabolism (Chapter 3), and gross hippocampal volume loss (Chapter 2). Looking to the near future, of all the roles in clinical care, imaging is likely to have the biggest impact on early diagnosis and will be most helpful when combined with other sources of converging information [2, 3]. This has been the focus of most articles in this section. Classification techniques are a way of formalizing the process of integrating multiple sources of information including biomarkers, genetic risk and other information. Ultimately the incremental value of early detection may be less dependent on the accuracy and sensitivity than whether there is a change in care as a result of early detection (i.e., treatment or avoidance of risk) to make it cost-effective.

Even if imaging data are not applied to the management of individual patients, they have the potential to assist in evaluating other components of care and diagnosis. To the extent that imaging can more sensitively measure brain integrity than existing techniques, novel treatments may not be abandoned because beneficial effects of treatments are not detectable. For example Chapter 8 applies imaging to evaluate the efficacy of pharmacologic and non-pharmacologic treatments. For investigators interested in conducting clinical research the chapter by Edland on power calculations will be extremely valuable. Therefore, to the extent neuroimaging can serve to detect the effects of treatments in the development pipeline, it can make early detection cost effective since treatments will be available.

An alternative to using neuroimaging in diagnosis and evaluation of treatments is to assist in clinical decisions that limit the autonomy of patients in order to protect them from harm; however, this is unlikely to be feasible any time soon. One good example of a likely candidate for this use comes from the difficult clinical decision as to whether patients can manage their own financial affairs. This capacity in MCI patients has been related to angular gyrus volume, a region previously demonstrated to be important in math ability [4]. This brain-behavior association may someday be used in the context of an early warning such that patients with a faster rate of change in this region may need special protections and monitoring to avoid financial predators who seek to exploit a developing vulnerability. In contrast, using neuroimaging to decide which MCI patients should lose driving rights is problematic. The processes and neural substrates of unsafe driving in AD are not well understood. Functional imaging studies that relate behavioral dysfunction to brain activation have the potential to indicate which brain regions underlie driving deficits; however, assessing driving in the MRI may not be comparable to assessing it in real life. In the typical MRI environment patients cannot talk or move a driving wheel but instead respond with minimal movement by pressing buttons. Remembering response mapping (e.g. left hand is yes and right hand is no) creates a dual task for patients that distorts and increases the complexity of the process an imager intends to study. The antisaccade task described by Kaufman et al. in this section is an example of a task which is simpler for patients and which can be used as a measure of executive control. For example it is possible to assess whether the patient moves their gaze in a manner that suggests appropriate attention to traffic and street signs without requiring an artificial response modality. This interface has only been possible in the past few years due to innovations that made these devices MR compatible. Ultimately, however, there would need to be strong data to suggest imaging provided better prediction of driving safety than a road test.

The variety of neuroimaging techniques in all modalities have great allure with respect to their potential to improve diagnosis and care, and anyone who seeks to perform research with neuroimaging data has multiple new tools and resources to facilitate this work. The Alzheimer's Disease Neuroimaging Initiative (ADNI) and affiliated initiatives (European and Japanese ADNI's) have provided clinicians and imagers with acquisition protocols that are standardized across sites. The benefit is that there can be multi-site collaborations to increase statistical power and facilitate cross-site generalizability. Several investigators in this book have benefitted from these

initiatives. Because neuroimaging data are large, complex, and diverse, there need to be a broad array of tools available to analyze them. The Neuroimaging Informatics Tools and Resources Clearinghouse (http://www.nitrc.org/) is a site from NIH which makes available neuroimaging software packages from a variety of modalities. There are reviews which advise all potential neuroimagers about the strengths and limitations of different software packages. For those clinicians who do not have resources to acquire their own data, there are multiple publically available datasets. The ADNI data have been made available to researchers around the world and now there are MRI protocols for spectroscopy (Chapter 7), diffusion tensor imaging (Chapter 6), and arterial spin labeling (Austin et al., Chapter 3) so this initiative is moving with the speed of innovation. In addition there are neuropsychological and biomarker data so that imaging data can be interpreted in context. Ultimately the prospects for neuroimaging to enhance clinical care are

bright as researchers collaborate and clinicians become informed about innovations and advances.

REFERENCES

[1] Lee DY, Fletcher E, Martinez O, Zozulya N, Kim J, Tran J, Buonocore M, Carmichael O, DeCarli C (2010) Vascular and degenerative processes differentially affect regional interhemispheric connections in normal aging, mild cognitive impairment, and Alzheimer disease. *Stroke* **41**, 1791-1797.

[2] Rosen AC, Bokde ALW, Pearl A, Yesavage JA (2002) Ethical, and practical issues in applying functional imaging to the clinical management of Alzheimer's disease. *Brain Cogn* **50**, 498-519.

[3] Illes J, Rosen A, Greicius M, Racine E (2007) Prospects for prediction: ethics analysis of neuroimaging in Alzheimer's disease. *Ann N Y Acad Sci* **1097**, 278-295.

[4] Griffith HR, Stewart CC, Stoeckel LE, Okonkwo OC, den Hollander JA, Martin RC, Belue K, Copeland JN, Harrell LE, Brockington JC, Clark DG, Marson DC (2010) Magnetic resonance imaging volume of the angular gyri predicts financial skill deficits in people with amnestic mild cognitive impairment. *J Am Geriatr Soc* **58**, 265-274.

This page intentionally left blank

Imaging in Alzheimer's Disease and Its Pre-States

Charles D. Smith[a,b,*]
[a]*Alzheimer's Disease Center, Sanders-Brown Center on Aging, Lexington, KY, USA*
[b]*Department of Neurology, Magnetic Resonance Imaging and Spectroscopy Center, Chandler Medical Center, University of Kentucky, KY, USA*

Abstract. This review uses an image-indexed framework for describing findings at key points during the course of Alzheimer's disease (AD), emphasizing recent contributions to the literature. Modalities considered include morphometric, diffusion tensor, and functional magnetic resonance imaging, resting and functional metabolic imaging and amyloid-label positron emission tomography. The major focus is on the AD pre-states (normal but high future AD risk, and mild cognitive impairment - MCI), and transition from MCI to mild AD. Imaging results relevant to the conduct of future prevention and early intervention trials are emphasized.

Keywords: Review, human, mild cognitive impairment, Alzheimer's disease, magnetic resonance imaging, diffusion tensor imaging, functional imaging, positron emission tomography, FDG, PIB, computed tomography, morphometry, prediction

INTRODUCTION

This review updates a previous paper by integrating new findings from this rapidly developing field [1], noting relationships between brain imaging and study group performance at key points along the course of Alzheimer's disease (AD). *Course* includes: (1) the state preceding clinical symptoms when AD neuropathology is nonetheless present, (2) symptomatic pre-states in the absence of dementia, and (3) later stage, clinically diagnosed AD. Many of the new imaging findings come from the landmark Alzheimer's Disease Neuroimaging Initiative (ADNI), a large-scale multi-center trial in AD [2, 3]. Although topics of great interest and importance, co-morbid illness and blood or cerebrospinal fluid biomarkers [4] are not considered here in order to maintain the AD-brain imaging focus. Likewise clinical neuroradiology, e.g., the use of imag-

ing to diagnose or to follow individual patients in the routine care of dementing disorders, is not reviewed in this article.

To provide a common clinical reference, brain function and cognitive performance is classified into 'Cognitive Independence' levels (Fig. 1) [5–7]. Relationships between levels and the clinical dementia rating scale (CDR) [8], global deterioration scale (GDS) [9], and clinical diagnosis [10] are provided in accompanying Table 1, keyed by letter to Fig. 1. The important issue of thresholds between levels and how best to determine them has recently been discussed [11]. Braak stage ranges given in Table 1 should be interpreted only as general guides because overlap is common [12–16].

The image-indexed framework for this article is illustrated in Fig. 2. In this conceptual model, the earliest Alzheimer's disease neuropathology (ADN; Fig. 2B; nominal age range 55–65 years) occurs in middle adulthood, accompanied by "compensatory" imaging functional changes (Fig. 2C) but unaccompanied by brain volume loss on imaging (Fig. 2C) or by
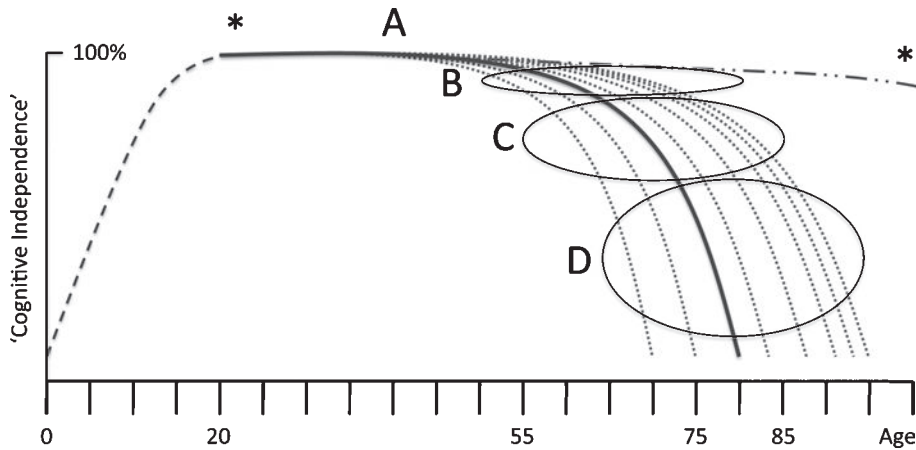
Fig. 1. Trajectories of cognitive independence over the lifespan, with normal cognition and function set arbitrarily at 100%. Cognitive independence increases during childhood and adolescence (—), reaching a plateau in early adulthood (—) followed by a slight decline after age 55 years in normal persons (•• - ••; trajectory A denoted by asterisks). Decline in cognitive independence due to late-onset AD is indicated by a solid central line, surrounded by dotted lines curving downward from this plateau indicating variability in onset age and rate. The rate of decline is shown as greater with earlier onset of symptoms, and trajectories are drawn closer together with later onset, denoting increased incidence of AD with age. Levels of cognitive independence within each trajectory are denoted by capital letters A to D. Approximate ranges in measures of cognitive performance, behavior and associated AD pathology corresponding to these letters are provided in Table 1.

Table 1
Correspondence between levels of cognitive independence and the CDR, GDS, Braak stage, and clinical diagnosis for the schema depicted in Fig. 1

Cognitive independence level	Global CDR	GDS	Braak stage	Clinical diagnosis	Description
A	0	1	0–3	Normal	Normal cognition and function consistent with trajectory A (Between asterisks)
B	0.5	2–3	2–4	MCI	Mild but definite memory decline, but independent function preserved (Trajectories B)
C	0.5–1	4–5	3–5	Mild AD	Mild impairment in more than one cognitive domain; decline in function ascribed to this impairment (Trajectories C)
D	2–3	6–7	4–6	Mod-Severe AD	Moderate to severe cognitive and functional impairments (Trajectories D)

Capital letters in the first column and descriptions in the last column refer to the same letters in Fig. 1.

diminished cognitive performance (Fig. 2A) [17]. With increasing age and ADN (nominal age range 65–75 years), compensatory functional changes are accompanied by early regional brain atrophy, likely associated with amyloid accumulation. Subsequent early symptoms of cognitive impairment represent a critical point beyond which functional alterations, brain atrophy, and cognitive performance continually worsen (nominal age in this diagram 75 years [17]). Functional losses in addition to compensations, increasing atrophy, and diminished cognitive performance ensue in diagnosed AD.

IMAGING MODALITIES

Figure 3 illustrates the imaging modalities discussed in this article, their approximate spatial resolution (volume of tissue yielding a single measurement), and the measures obtained from each. Structural techniques using CT [18–21] and MRI [22–32] measure sizes, shapes and densities of regional brain structures that typically index tissue losses or atrophies. Recent advances in structural MRI analysis include automated regional labeling [33–40], measurement of important cortical surface features (e.g., regional corti-
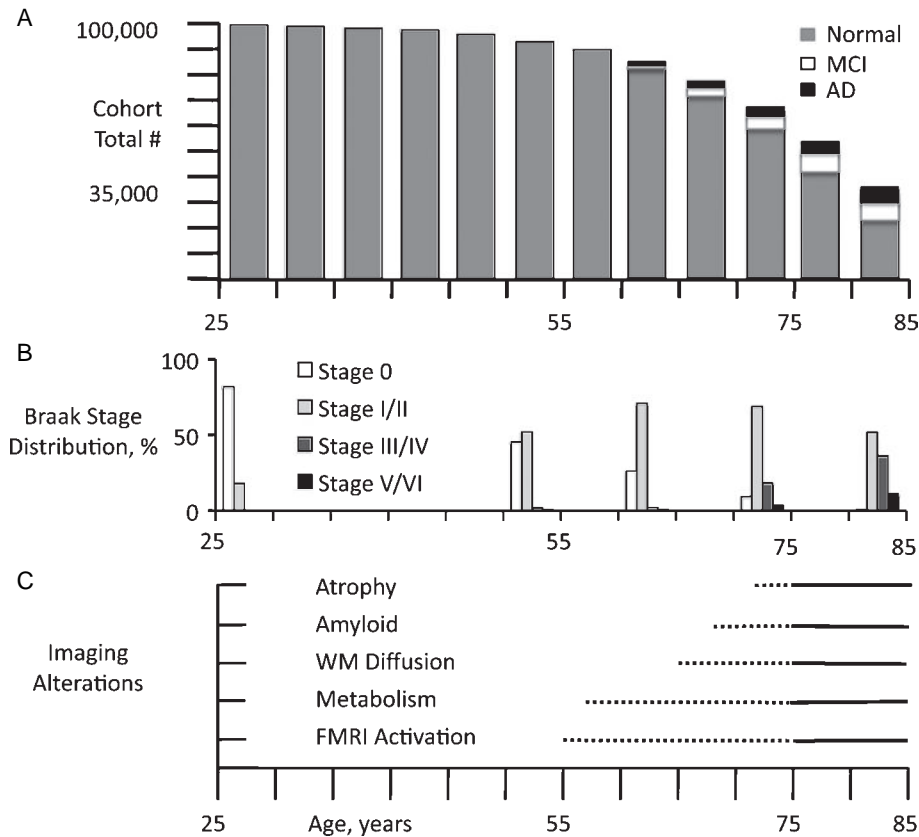
Fig. 2. Image-indexed framework. A: Illustration of a statistical cohort of 100,000 persons beginning at age 25 years, with bar height representing the expected remaining population at each 5-year interval to age 85 based on the US census [324]. Each bar divided into proportionate parts representing the expected number of persons with AD (black) or MCI (white), or who remain normal (grey), based on US population model estimates [325]. The incidence of MCI and AD, and overall death rate accelerate after age 55. B: Percentage of Braak stages over the same age range based on Braak [13, 326]. C: Conceptual diagram of the appearance of different image features by modality and age in a theoretical cohort of persons who develop symptoms of AD at age 75 years, based on results in the current literature reviewed in this paper. Dotted lines represent the variable appearance in individuals of the first detectible image changes within each modality, some of which may precede symptoms by decades. Solid lines represent the more certain appearance of alterations near the time symptoms appear (within a few years). The character and distribution of image alterations may change over time, e.g., in FMRI activation, a subtlety not captured in this simplified diagram.

cal thickness [41, 42]), and measurement of brain and hippocampal shape [43–45] and volume change over months to years [46, 47].

Local water diffusion is measured using MRI, and gives information concerning local white matter integrity (diffusion tensor imaging; DTI; [48]). Because water can diffuse in any direction, a map of the rate of diffusion in different directions within a voxel can provide summary metrics for underlying white matter structure, and with further specialized processing, dissection of short and long-range fiber tracks [49–56].

Functional imaging in the resting state measures physiologic parameters such as regional blood flow or glucose utilization (positron emission tomogra-

phy; PET [57]), resting state cortical connectivity (functional MRI or PET), or extent of tracer binding by cerebral neuritic amyloid plaques (e.g., ^{11}C-PIB [58–60]). Activation functional studies using MRI or PET indirectly localize brain regions that increase or decrease their relative synaptic activity during the performance of specific cognitive tasks [61–65]. Template standardization of image space allows images from different modalities such as PET and MRI to be visualized and compared quantitatively across modalities (image fusion) [66–68]. Strengths of linkages between brain regions at rest or during a task can be modeled using network analysis techniques [69–71].

Brain amyloid binding in AD has been most thoroughly studied using the ^{11}C-labelled tracer Pittsburgh
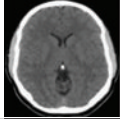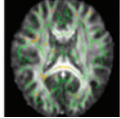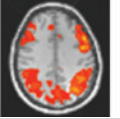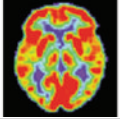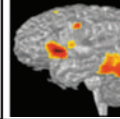
Modality	CT	MRI			PET	
		Structural	DTI	fMRI	Resting	Functional
Photon Energy, keV	40-140	0.5×10^{-9}			300-800	
Resolution, mm	0.5	1	5	10	2-5	5-10
Unit Type	Radiodensity	Signal S_v	S_v Tensor	$\Delta S/S_v$	Rate R_v	$\Delta R/R_v$
Measurements:	Voxel Electron Density; Medial Temporal Width; Ventricle-Brain Ratio; Volume Percent CSF	Voxel Volume: GM, WM, CSF; Tissue Density; Shape Metrics (hippocampus); Volume Change (within subject); Cortical Thickness	Fractional Anisotropy; Mean Diffusivity; Spatial Coherence; Spatial Connectivity	Regional Activation; Functional Connectivity	Glucose Uptake (^{18}FDG); Blood Flow (^{15}O); Amyloid Binding (^{11}C-PIB)	Regional Activation; Functional Connectivity

Fig. 3. Imaging modalities discussed in this article, illustrating the energy associated with each modality, spatial resolution, measurement units, and typical quantitative measurements made from each.

compound B, a hydroxylated derivative of thioflavin-T [72–75]. Current methods of amyloid binding quantitation include grey matter parcellated template registration from anatomic MRI to remove nonspecific binding in white matter and counts from cerebrospinal regions [76], partial volume correction to model and diminish effects of unwanted tissues in single voxels [77], and use of a common region as a nonspecific binding reference (cerebellar hemispheric grey matter or pons). Division of target by reference measures of central tendency yield a standardized uptake value [ratio] (SUV[R]) for each grey matter region, whereas dynamic modeling of time activity curves yields an estimate of the distribution volume ratio (DVR), a parameter directly related to the ligand binding potential [78]. A United States Food and Drug Administration advisory panel has recently approved an ^{18}F-amyloid binding agent florbetapir (AV-45) for clinical use that overcomes logistical and cost disadvantages of ^{11}C-PIB [79, 80]. There is no shortage of other agents in development for the numerous medical facilities that can use ^{18}F but not ^{11}C imaging ligands [81–86]. An ^{18}F agent, FDDNP, has demonstrated similar findings to ^{11}C-PIB in MCI despite a different affinity profile that includes neurofibrillary tangles in addition to amyloid [87, 88]. A recent potentially important finding deserving further study is that some focal amyloid accumulations are co-localized with microbleeds; these might be an unrecognized contribution to cortical pathology in AD [89]. These studies are an important recent development because, unlike indirect measures such as focal atrophies or network activation patterns, amyloid binding directly measures the distribution and extent of a known component of AD neuropathology. Thus amyloid imaging has strong theoretical appeal.

Brain imaging is a direct observation of the organ of interest, low-risk and repeatable, with a spatial resolution of millimeters to centimeters, and can provide dynamic measurements of brain structure and function with a time resolution ranging from seconds to years (Fig. 3; [90–97]). Imaging of the human brain continues to yield insights into Alzheimer's disease that could not be obtained in other ways, e.g., by medical and psychometric examination during life or by neuropathologic examination at death.

IMAGING DURING THE COURSE OF AD

Here moderate to severe AD serves as an anchor because the fewest assumptions in the image-indexed model are needed. At the end of the discussion the focus will be presymptomatic alterations, and on the future progress needed in order to use imaging to predict future AD in normally performing persons in AD prevention trials.

Moderate-severe AD (Figure 1D)

This is the classical stage defining AD as a cause of 'senile dementia' by Beljahow, Fuller, Alzheimer, and others using clinicopathologic correlation [98]. Early CT studies confirmed *in vivo* the generalized cerebral atrophy known from pathologic study of AD [99]. Because of the known pattern of typical early neuropathologic involvement of the medial temporal lobe

in AD, the focus of structural CT and MRI studies has been on the temporal lobe, particularly its medial limbic components. Decreased medial temporal width by CT in life, indicating atrophy, correlates with increased intensity of post mortem neurofibrillary and plaque pathology [18, 100].

Resting [18]FDG-PET studies demonstrate globally deceased glucose metabolism compared to normal, but the most marked glucose uptake decreases occur in the posterior cingulate region and in lateral parietal and temporal neocortex, sometimes asymmetrically, with variable decreases in other regions [101–104]. These findings conform well to a deficit model of moderate to severe AD: synaptic and neuronal losses result in tissue atrophy and decreased glucose uptake, parallel to the observed pattern and degree of overall clinical behavioral and cognitive decline. Furthermore, regional atrophy and decreased metabolism occur in a pattern consistent with the distribution and intensity of neuropathology in AD [100, 105–109].

Recent studies have identified factors that may index cerebral reserve, e.g., higher educational attainment, that have been associated with greater atrophy and metabolic decrements at a given clinical and behavioral stage of AD [110–113]. If atrophy and diminished glucose metabolism progress in parallel with pathology [114], then regional cerebral volume and metabolism could represent an indirect measure of cerebral reserve in AD [115]. Structural imaging studies may be interpreted alternatively as demonstrating that relatively increased regional volumes confer a reserve resistance to AD pathology [116].

Functional studies in AD generally have involved less impaired subjects because cooperation to hold still and to follow task paradigms is required. This cooperation often cannot be achieved in moderate-severe clinical stages of the illness. Moderate-severe AD patients have demonstrated reduced functional activation during passive tasks, e.g. in the visual or auditory systems in the few PET studies performed [117–120]. Moderate AD subjects have shown both reduced parietal activation (deficit) and enhanced prefrontal activation (possible compensation or release from inhibition) on an fMRI visually guided saccade task [121].

Mild AD (Figure 1C)

Anatomic MRI

Recent structural studies in early AD using whole-brain MRI volumetric techniques have demonstrated reduced volumes, interpreted as early atrophy, in the medial temporal, cingulate and precuneus regions, and in the inferolateral temporal and parietal neocortex [122–126]. The magnitude of volume reduction is less than in more advanced AD stages, but clearly distinguishable from asymptomatic normal subjects. Grey matter loss is progressive through the arbitrary clinical divisions between mild, moderate and severe AD [127]. Normalized cortical thickness measurements have yielded similar findings of reduction in AD [128]. High-order structural descriptions of the hippocampus have differentiated AD from normal [129, 130]. Shape features may prove more sensitive to structural change than simple volume information [131].

A recent pattern-classification approach has been used to capture in a single index the similarity between a canonical pattern and magnitude of structural change in AD versus an extracted pattern from a single subject scan [132, 133]. Scan pattern classification scores have also been used to predict performance on standardized cognitive tests in AD, e.g., the auditory verbal learning test (AVLT) [134]. Standardized pattern classification data reduction methods combined with more automated and robust extraction of salient anatomic features such as the hippocampus [135–137] are likely to emerge as the key methods for structural MRI analysis in the future [138].

White matter characterization

The available studies of diffusion tensor imaging (DTI) in mild AD are difficult to compare because a consensus on the best acquisition protocols, tensor metrics, and statistical analytical techniques has not yet emerged. Nor has the pathophysiology of DTI alterations in AD been well defined, a major weakness of this approach. Altered diffusion metrics most likely represent loss of white matter integrity as a secondary consequence of cortical abnormalities in AD (via alterations in projecting axons). However, increased appreciation of molecular interactions between axonal fibers and ensheathing oligodendroglial myelin raise the possibility of a primary neurodegenerative pathophysiology of AD white matter apart from Wallerian degeneration [139, 140]. Some variability between reported DTI studies in AD may be explained by different patient characteristics, e.g., disease severity, image characteristics such as presence of periventricular white matter hyperintensities [141], and by differences in analytical techniques (particularly region-of-interest versus voxel-based approaches).

Region-of-interest based fractional anisotropy (FA) and related measures appear to show the most consistent reductions in AD within large fiber bundles

of the temporal stem [142], splenium of the corpus callosum [141, 143–145] and other regions with high baseline anisotropy [146], cingulate bundle, particularly the posterior portion [141, 144, 147], and deep white matter of the frontal, parietal and temporal lobes [145, 148, 149], sparing the occipital lobe white matter. Decreasing regional FA in callosal white matter correlates generally with decreasing grey matter volume in association cortical regions, suggesting that altered FA may be reporting on degeneration in cortical neurons that contribute long-range projection fibers to the corpus callosum [150]. Connectivity analyses using DTI tractography have recently demonstrated that small-world topology, a property of functioning tuned complex networks, is preserved in AD, but that efficiency metrics such as shortest path length and nodal efficiency were reduced in AD [151].

Mean diffusivity (MD) derived from the DTI voxel tensor may be increased in overlapping regions demonstrating decreased FA in AD [145, 152]. However, other regions, particularly juxtacortical white matter and grey matter in the posterior cingulate gyrus, hippocampus, amygdala and parahippocampal gyrus, have shown MD increases in the absence of FA decreases in some studies [145, 147, 152]. Other paired FA and MD measurements have demonstrated decreased FA and increased radial diffusivity (indicating myelin alteration) in the parahippocampal gyrus and decreased FA in precuneus, both regions undergoing the earliest functional and pathologic change in AD [153]. It appears likely that the underlying pathobiology of alterations in FA differs importantly from that of MD, and therefore potentially useful distinctions could be made between these and other diffusion tensor metrics [153, 154]. DTI metrics may in future be able to further distinguish between alterations in myelination, fiber packing density and axonal integrity; more basic research is needed to clarify this point.

Functional imaging

Resting [18]FDG-PET studies demonstrate decreased glucose uptake in the posterior cingulate region and in lateral parietal and temporal neocortex [155]. A recent analysis of the PET data proposes a potentially useful hypometabolism index that captures in a single parameter the similarity between a canonical regional hypometabolism pattern expected in AD and an individual scan [156]. Functional PET has demonstrated relatively preserved activation patterns in mild AD, in contrast to markedly reduced activation in more advanced cases [157]. Glucose uptake in both temporal lobes was reduced during a serial learning task in mild AD patients [158]. Diminished functional connectivity between frontal and posterior cortex has been observed in early AD [70].

Functional MRI studies in mild AD have demonstrated three basic trends: (1) decreased hippocampal region activation, particularly on tasks of encoding and memory [159–163], (2) increased extent or intensity of activation in neocortical brain regions normally recruited by a given task, e.g., frontal region during semantic access [164] and (2) new regions of activation not seen during the task in comparison subjects [164, 165]. A heuristic interpretation of these findings is that increased or alternate processing within other brain regions in early AD compensates declining function in the medial temporal lobes.

An important theory emerging in the last decade is the existence of an adult "default network" –a complex of brain regions active (in "default mode") when the brain is not engaged in an attention-focusing task [166–168]. The anatomic components of the network include superior frontal and medial frontal gyrus (Brodmann areas BA 8, 9, 10, & 11), precuneus/posterior cingulate cortex (BA 23 & 31), middle and superior temporal gyri (BA 21 & 39) and parietal cortex (BA 39 & 40) [169].

Virtually any task needing active concentration results in deactivation of the default network; a failure of this normal deactivation, in parallel with decreased medial temporal activation, is associated with decreased cognitive performance in AD [165, 170–173]. It has been theorized that increased activity within the default network in AD due to reduced deactivation is associated with increased amyloid deposition within the network itself [174].

Amyloid imaging

Several studies with amyloid binding tracers have demonstrated three basic results in AD. Firstly, elevations in measures of amyloid burden, such as the mean cortical binding potential (MCBP), is strongly associated with clinical AD (>95%), and AD is only rarely seen in the absence of elevation [175]. Secondly, the cortical regions with the greatest amyloid burden generally match the pattern of amyloid plaque density known from neuropathologic studies in AD [176]. Although this general burden-plaque relationship appears to hold, correlation of regional ^{11}C-PIB binding with Consortium to Establish a Registry for Alzheimer's Disease neuritic plaque scores was recently found to be quite variable [177]. Thirdly, the

change in amyloid burden shows a minimal increase within that pattern despite clear worsening of AD clinical symptoms over the same time period [178, 179]. Amyloid accumulation rates (percent of baseline) in AD are on the order of 3–5% annually, and are greater in AD than in normal brain (1.3–3.8%) [179, 180].

PIB retention has been characterized as normal-like (minimal) or AD-like (increased retention in subcortical white matter, frontal lobe -particularly the middle frontal gyrus, posterior cingulate cortex, and inferolateral parietal and temporal lobes [181–185]. The correlation between regional PET binding and MRI brain atrophy measures appears complicated, however [182]. In frontal regions amyloid burden is high but not strongly related to atrophy (except perhaps in medial orbitofrontal cortex [186]). In regions of relatively low binding such as the medial temporal lobes, atrophy is significant but correlation with local binding has been variably reported [182, 187]. In parietal and temporal lobes increased binding correlates with regional atrophy in some studies [182], and in some subregions such as the posterior cingulate, with remote hippocampal atrophy.

Overall atrophy rates are correlated with overall amyloid burden [188]. Including measures of atrophy together with other clinical variables, e.g., education and medication, improves the classification accuracy between AD and normal using binding (MCBP) to 94% in a recent study [189]. Amyloid burden is greater in persons with higher education when matched on cognitive performance, further justifying the use of demographic and clinical values in interpreting amyloid binding studies [190, 191].

Mild cognitive impairment (MCI; Figure 1B)

MCI is defined as a mild but definite decline from previous cognitive ability, confirmed by a reliable observer, and substantiated by deficits on neurocognitive testing [5, 192–200]. Here we focus on amnestic MCI, the memory-dominant subtype most likely associated with ADN. There are two basic imaging issues in MCI: (1) detecting differences between MCI and normal, and between MCI and AD, and (2) predicting decline to dementia in persons with MCI.

MCI: detecting differences

Structural MRI studies have shown decreased size of the hippocampal formation in MCI, by rating techniques [201] and in both region-of-interest [202–205] and voxel-based volumetric studies [126, 206–209].

Studies are mixed regarding the presence of more global grey matter reductions in MCI, e.g., in frontal and parietal regions [125, 210]. Older adults who have memory complaints but do not meet formal criteria for MCI may nonetheless show similar grey matter reductions [211].

Diffusion tensor studies in MCI have in general demonstrated alterations (increased ADC and MD, and decreased FA) similar to those seen in mild AD but more restricted to the cingulum bundle [212, 213], parietal white matter and callosal splenium [214, 215], parietal and temporal white matter [216] and hippocampal region [217]. Mean diffusivity increases have been found in entorhinal and posterior occipital-parietal cortex in MCI [218].

Functional MRI studies in MCI have demonstrated increased medial temporal activation during memory tasks, in contrast to reduced activation consistently observed in mild AD [165, 219–221]. Medial temporal activation is greater during individually successful memory trials than during failed trials [222]. A period of increased medial temporal activation may be characteristic of compensation in memory-impaired MCI subjects, which gives way to decreased activation in the same region on memory tasks in the transition to mild AD as memory performance worsens [223].

Functional connectivity between posterior cingulate cortex (PCC), medial temporal lobe, and inferior parietal lobe is decreased in MCI, suggesting disruption of connections between these regions by the characteristic early accumulation of AD-type neuropathology in these areas [71, 224]. The specific neural circuitry underlying these functional connections is not yet known. Default network deactivation is decreased during focused memory tasks in MCI similar to the findings in mild AD [165, 225, 226].

It has been known for some time that amyloid plaque accumulation occurs in very mildly impaired older persons and in those classified as amnestic MCI [227]. A consistent finding is that PIB retention in MCI is intermediate in overall extent and intensity compared to the pattern in AD [182, 228], and is increased in apolipoprotein epslilon-4 allele (APOE4) carriers [229]. However a surprising finding has been that memory performance does not appear to correlate with global measures of cortical binding in MCI if hippocampal atrophy is taken into account [230, 231]. In contrast, regional binding in temporal neocortex has been correlated with memory performance in MCI independent of any influence of medial temporal volume [232]. From a classification perspective, amyloid

imaging offers an important compliment to structural and functional imaging information from the same MCI patients [182, 184].

MCI: conversion to AD

Structural and functional imaging may help predict future decline to AD dementia in MCI patients [233]. This transition is termed "conversion" [234]. Rates of global atrophy and ventricular expansion are higher in MCI converters [235]. Hippocampal atrophy was shown to predict AD in MCI patients with an odds ratio of 0.69, independent of psychometric scores or apolipoprotein-E genotype [236]. Studies using visual rating scales for medial temporal atrophy have yielded similar results [237, 238]. Reduced volumes in entorhinal cortex [239, 240], hippocampus [241–243] and lateral temporo-parietal cortex [244] have been predictive in subsequent studies. Normalized cortical thickness measurements demonstrate similar results [128]. Medial temporal mean diffusivity on DTI [245] has also been used to predict conversion from MCI to AD.

Sophisticated deformation analysis combining multiple brain regions into structural principal components predicted conversion from MCI to AD with 80% accuracy in a recent study [246]. This approach preserves geometrical registration information, roughly equivalent to shape, not captured in a single volume metric. Temporal lobe atrophy at baseline scan correlated with subsequent conversion from MCI to AD in the ADNI study [32, 126]. A baseline Jacobian volume metric in the inferomedial temporal lobe of MCI patients correlated with subsequent increase in the CDR sum of boxes over time, and in this sense was predictive of decline to AD.

A classifier built on a pattern of decreased grey matter volume in the anterior hippocampus, amygdala, posterior cingulate region, temporal lobe and insular cortex, and orbitofrontal cortex (together with other grey matter, white matter and CSF regions or cluster) distinguished MCI converters from MCI non-converters to AD with 70–80% accuracy [32]. Follow-up was an average 15 months, suggesting that persons with MCI who will convert within this interval after their baselines can have lower baseline tissue volumes in specific regions [247]. A classifier approach was used previously [248] with similar results. Prediction of MCI conversion to AD using the SPARE-AD pattern matching score (cited above under "Mild AD") was improved when combined with cerebrospinal fluid marker values for beta-amyloid and tau

[132], a result supported by a second similar study [249]. An approach using multikernal learning (MKL) that combines pattern similarity measures across imaging modalities has shown promise in predicting MCI conversion to AD [250].

Longitudinally-determined grey matter losses over time in the hippocampal region, inferior and middle temporal gyrus, posterior cingulate, and precuneus, are greater in AD converters relative to non-converters [251–253]. Brain atrophy, measured by rates of ventricular enlargement, and declines in whole brain and regional hippocampal volume, also predict conversion [254, 255]. Incorporation of gender and age reduced variability in brain atrophy rate estimation in a recent tensor based morphometry study of the ADNI cohort [256]. Changes in cortical thickness over 12 months also predicted conversion with 82% accuracy in a recent study [257].

Functional predictors of significant decline or frank conversion to AD in MCI have included decreased blood flow [258–260](SPECT studies) and decreased fluorodeoxyglucose uptake [261–264] in the cingulate and medial temporal regions [265], and in the temporoparietal region [266, 267]. Increased fMRI hippocampal activation [221] and decreased deactivation of the default network [268] has also been found predictive for conversion. Loss of hippocampal activation during an associative memory task was associated with cognitive decline in subjects with a baseline mild impairment (CDR 0.5) [269].

Recent studies have suggested increased ^{11}C-PIB binding in MCI subjects who later declined to dementia [270, 271]. Thus amyloid binding levels may prove useful in predicting decline in MCI, but it is uncertain what best predictive model will emerge when data from other imaging modalities, cerebrospinal fluid analytes, genetic results, cognitive performance and other clinical variables are included. Ideally, a small group of independent image predictors can be found that optimally balance cost, patient safety and convenience, and measurement reliability, repeatability and validity.

Presymptomatic AD (Figures 1A and 2C)

This section refers to imaging techniques that characterize the brain in normal subjects with the goal of predicting which normal subjects will develop MCI (cf. Figs. 1 and 2). If future MCI can be predicted with reasonable accuracy in normal subjects, interventions are possible that could slow the progress of ADN or enhance intrinsic brain compensatory

mechanisms, thereby delaying clinically symptomatic disease. Much work needs to be done to answer the key questions in this important field [272].

The basic assumptions are that: (1) underlying ADN accumulates in many normal persons years before any cognitive symptoms or measurable declines in cognitive testing occur, (2) the brain has intrinsic neural mechanisms that compensate for injury due to AD pathology at all stages of its accumulation, e.g. by synaptic remodeling, (3) the human brain has inborn, developmental and learned sources of cerebral reserve that may offset the cognitive effects of injury, or, inversely, specific liabilities to the effects of ADN, and (4) involutional age-related erosion of brain reserve and the presence of co-morbid brain pathologies is a fact of life in brain aging [17].

It is now well established that well-characterized, longitudinally followed cognitively normal persons undergo brain volume losses with age, emphasizing the need for carefully age-matched controls in cross-sectional structural studies [273–275]. However, as of now, only longitudinal studies can identify normal individuals from a cross-section who will later develop MCI or AD. Grey matter volume reductions with age are generalized, without the relatively selective regional medial temporal, lateral temporal and parietal reductions characteristic of AD. Selective volume reduction with age also occurs in the deep frontal white matter and genu of the corpus callosum [276, 277] (Fig. 4 A–C).

Annual rates of ventricular expansion have shown an increase in normal aged subjects who received a clinical diagnosis of MCI within an average of 2.3 years [278]. Normal subjects with a maternal history

of AD have demonstrated decreased cortical volumes compared to subjects with a paternal AD history or no family AD history [279].

Because the earliest ADN involves entorhinal cortex, amygdala, hippocampus and other medial temporal structures, early atrophy in these regions could predict normal subjects who will later develop MCI or AD [280–283]. Decreased grey matter density in the medial temporal and dorsolateral frontal lobes has been described in normal apolipoprotein epsilon-4 (APOE4) allele carriers at increased risk for AD [284]. Medial temporal atrophy also predicted decline on tests of delayed memory in normal subjects imaged at baseline and followed for 3.8 years [285]. An unexpected and significant finding in the ADNI study was that temporal lobe atrophy predicted subsequent cognitive decline even in the baseline cognitively normal participants in that study [126]. It has since been found that rate of atrophy in medial temporal structures in these subjects was associated with cognitive decline assessed by logical memory and AVLT tests [286].

A longitudinal general community study of 511 non-demented subjects demonstrated that reduced global, hippocampal and amygdalar volumes at baseline were predictive of dementia within average 6 years [287], with rate of volume change serving as an independent predictor [288]. Another recent study on 136 longitudinally-followed normal subjects undergoing a baseline structural scan demonstrated that volume in a combined region identified from these scans using VBM (anteromedial temporal and left parietal grey matter; Fig. 5A) predicted MCI within five years with 76% accuracy. Predictive accuracy increased to 87% by combining volume in the combined region with a
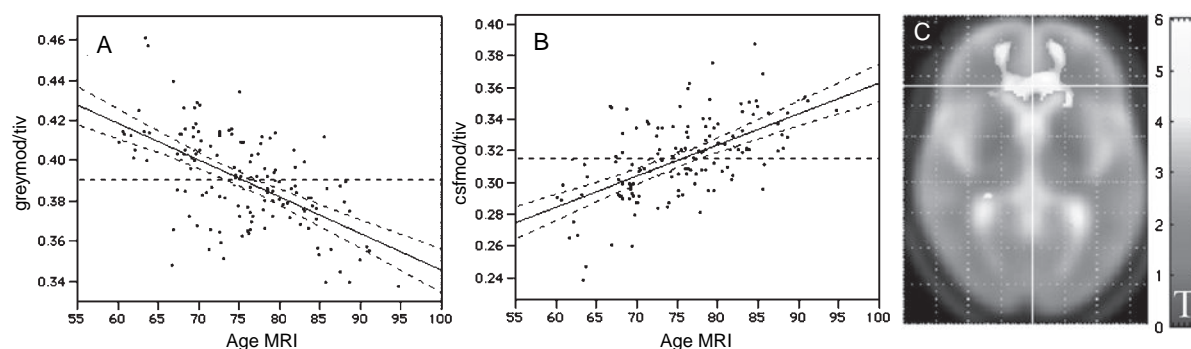

Fig. 4. Brain imaging alterations in normal aging. Based on a longitudinally followed cohort of 146 subjects analyzed by voxel-based morphometry [276]. Subjects who showed cognitive decline within 5 years of imaging were excluded. A: Whole brain grey matter normalized by total intracranial volume (*y*-axis; note scale origin is not at 0) decreases with age at scan (*x*-axis). There was no selective regional loss of limbic grey matter volume with age in this study. B: Normalized CSF volume increases with age. C: Focal loss of white matter volume in the callosal genu and forceps region with age; map is shown as *t*-value for the negative age correlation
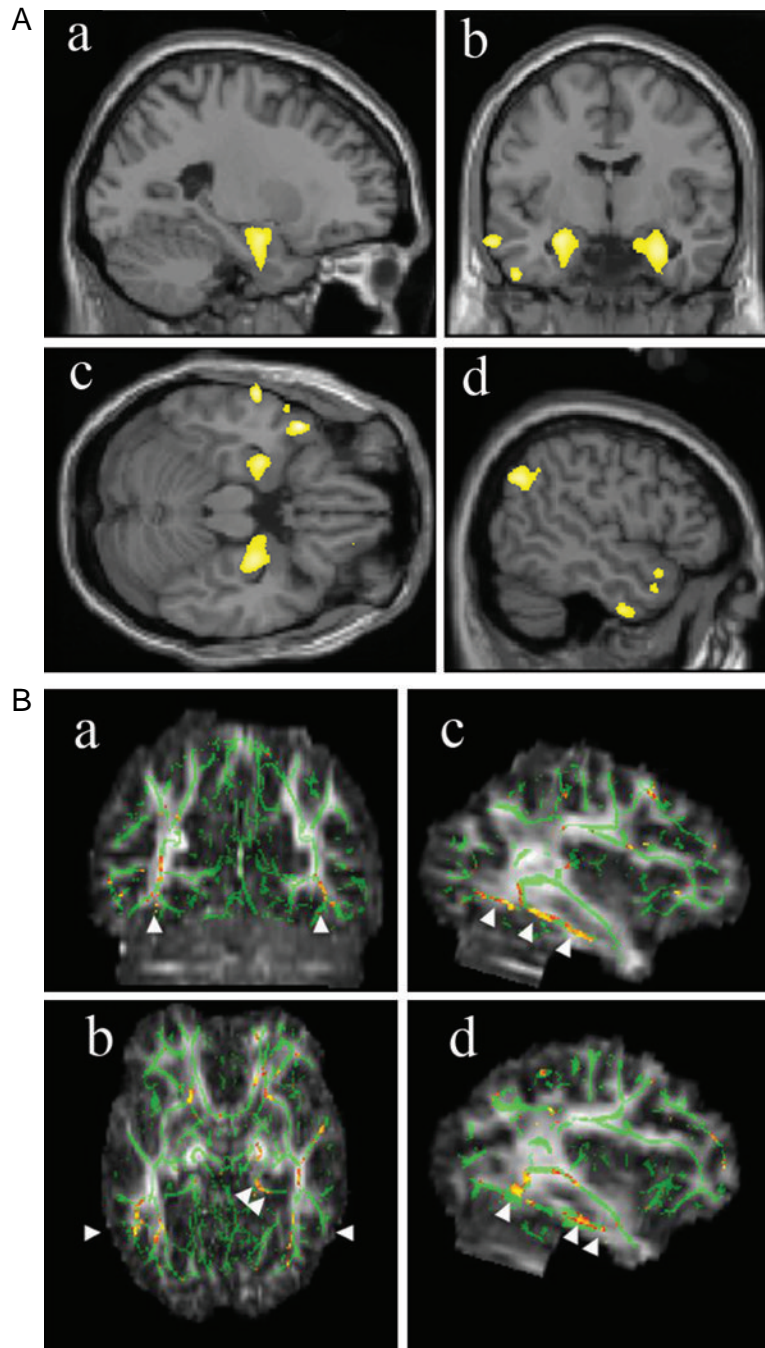
Fig. 5. Brain imaging alterations in cognitively normal persons at risk of MCI or AD. A: Grey Matter. Volume in a region identified by retrospective classification of baseline scans in normal subjects showing a region of significantly reduced volume at baseline in those who later developed MCI (yellow-white color scale). Views: a,d- sagittal; b- coronal; c- axial. Prediction accuracy of volume within this brain region alone was 76%, and 87% when combined with psychometric data [327]. B: White Matter. Linear red-yellow regions in the inferior temporal lobe white matter (white arrowheads) denote decreased FA in normal middle-aged women at high risk of AD. Green areas represent regions of no change. These areas of decreased white matter integrity may represent early injury related to AD pathology [291]. Views: a- coronal; b- axial; c,d- sagittal. C: Voxelwise negative correlation between amyloid burden in normal subjects with elevated global ^{11}C-PIB binding and hippocampal volume ($r = -0.6$, $p = 0.02$ using inferior temporal region). This relationship was not seen in subjects with MCI or AD, or in other brain regions outside of the inferomedial temporal lobe and parieto-occipital junction [322]. Views: a- sagittal; b- coronal; c- axial.
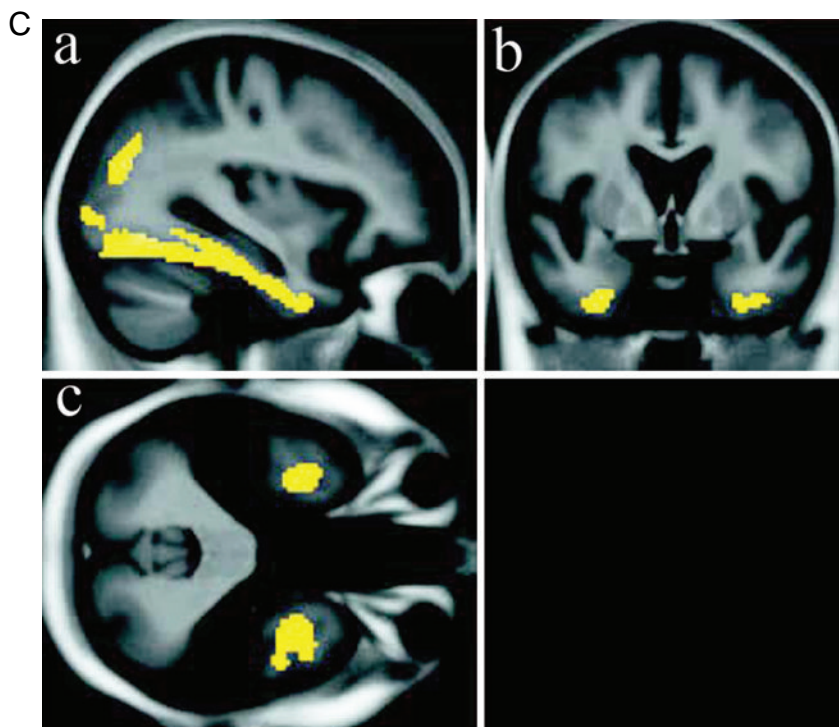
Fig. 5. (*Continued*)

cognitive measure, raw Wechsler Memory Scale score [289, 290]. Further three-year follow-up of these subjects revealed that the volume in the region depicted in Fig. 5A continued to predict conversion from normal to MCI or AD up to 8.3 years following scanning with 81% accuracy (unpublished data).

Diffusion-based MRI studies to predict MCI or dementia in normal persons are in their early phases. Normal middle-aged women at risk for MCI or AD by virtue of family history and APOE4 allele demonstrate diminished FA in the cingulum bundle, callosal splenium, and inferior temporo-occipital fasciculus [291] (Fig. 5B). Elderly cognitively normal APOE4 carriers demonstrate similar alterations in the medial temporal region [292]. Asymptomatic carriers of autosomal dominant mutations causative of AD show decreased white matter FA, notably in the fornix and perforant pathway [293].

Entorhinal glucose metabolism was shown to predict subsequent cognitive decline over three years in normal aged subjects [294], and decreased resting glucose metabolism in the left angular, mid temporal, and mid frontal gyri predicted decline on a global cognitive measure, the Mini Mental State Examination [285]. Baseline medial temporal glucose uptake in 77 nor-

mal subjects predicted decline to MCI (71% accuracy) or AD (81% accuracy) over 7.2 years mean follow-up [295].

Decreased PET resting glucose metabolism in posterior cingulate and parietal cortex has been demonstrated in normal subjects at increased risk of early-onset AD due to presenilin [296] or amyloid precursor protein (APP) mutations [297], and in subjects with a family history of late-onset AD and at least one APOE4 allele [298–300] or with a maternal AD history [301]. A pattern of decreased glucose utilization in normal subjects similar to that seen in AD but with additional involved areas in frontal lobe has been observed in insulin-resistant elderly (mean age 74.4 years [302]), and in mid-life in association with total cholesterol levels [303]. These latter findings suggest that metabolic factors may influence both the aging and AD phenotypes.

Active functional MRI results predicting MCI or AD in normal subjects have not been entirely consistent. Some studies have demonstrated decreased ventral temporal regions during picture naming in normal high-risk (APOE4 carrier) subjects [304], and in medial temporal regions during episodic memory encoding [305]. Paradoxically increased semantic

memory activation to familiar names in normal high-AD risk subjects was seen in the frontal lobes, temporo-parietal junction and precuneus, and interpreted to suggest a compensatory response in these normal elders [306]. Increased hippocampal activation has been seen in healthy young (average age 34 years) presenillin-1 (PS1) mutation carriers during a paired associates learning task, suggesting that functional alterations can precede symptoms by years in this illness [307]. However, the median age of onset for the earliest detectable decline in memory performance is 35 years in PS1 carriers [308], suggesting caution in comparing these finding with late-onset AD.

Other functional MRI studies in normal subjects have demonstrated increased parietal activation associated with working memory and verbal fluency tasks [309, 310], increased posterolateral temporal activation during visual learning [311] and increased medial temporal activation during episodic memory encoding [312] or encoding and recall [313]. Increased activation in high AD risk persons may be specific for memory tasks and not other equally demanding tasks [314]. Differences in the age of subjects, AD risk factors considered, cognitive paradigms performed during imaging, depth of cognitive testing, and methods of acquisition and analyses may explain some differences in results between fMRI studies.

The role of ^{11}C-PIB uptake for presymptomatic detection is not yet established but appears promising. Amyloid burden is increased in normal persons with a family history of AD, particularly if the mother was affected [315], and is increased with APOE4 allele dose [316]. Elevated PIB binding predicted decline and correlates inversely with memory change scores in initially normal elderly [231, 317–321]. Inferior temporal lobe neocortical binding and hippocampal atrophy are strongly correlated in cognitively normal subjects with elevated global PIB retention, but not in MCI or AD subjects, suggesting this relationship is only observable early in the disease process (Fig. 5C; [186, 322]).

SUMMARY AND FUTURE DIRECTIONS

Approximately half of normal persons harbor Braak stage I-II neurofibrillary pathology by age 55 years (Fig. 2B). The earliest documented imaging changes (Fig. 2C) in normal subjects at risk of late-onset AD occur in the temporal and parietal lobes in resting PET and in fMRI studies, when subjects are in their early to mid 50's. Presymptomatic white matter DTI changes

in the parietal and temporal lobes may appear at least as early as the late 50's. Decreased glucose uptake and decreased regional volume in the temporal lobe is predictive of later MCI or dementia in normal subjects in their 70's. Normal individuals with increased global amyloid burden demonstrate strong correlation between regional amyloid burden in the inferolateral temporal lobe and hippocampal atrophy.

MCI is characterized by: (1) baseline and accelerating ventricular enlargement and volume decreases in the medial temporal region, (2) decreased glucose uptake in the posterior cingulate, parietal and temporal lobes, and (3) increased FA in the cingulum bundle, callosal splenium and parietal and temporal white matter. Activation on fMRI memory tasks is increased relative to normal subjects, both in medial temporal lobe and in dorsolateral prefrontal areas. Transition from MCI to AD is best predicted in those MCI subjects with the greatest volume and glucose uptake decreases, and with the greatest rates of change in these measures. Increased memory task activation in the medial temporal lobe during fMRI also appears to be lost at this conversion, but activation may increase in extratemporal sites, e.g., the frontal lobe during memory or other tasks. Amyloid binding is increased in MCI subjects who transition to AD.

Mild AD is associated with continued ventricular enlargement and limbic atrophy, together with more widespread neocortical volume losses, particularly in the inferolateral parietal and temporal lobes and precuneus, and in the cingulate gyrus. The general pattern of imaging changes across the full course of AD is consistent with the spatial and temporal evolution of underlying pathology as currently understood. However, the detailed correlation is far from perfect: there is a range of neuropathologic and imaging features associated with a given clinical stage of AD (Fig. 2).

Better imaging characterization of ADN, e.g., labeling of abnormal tau material in addition to amyloid may provide valuable new insights, particularly with regard to any rapid accelerations of the AD neuropatholgic process near the onset of symptoms. Rapid acceleration could signal entry into a downward brain injury spiral that could prove particularly difficult to reverse, particularly with single agents. We also need imaging techniques that can help measure compensatory changes or components of cerebral reserve that confer resistance to the effects of aging, AD, and co-morbid pathologies.

The challenge for imaging is therefore to detect effects of early AD-related pathologic injury and its

compensations in normal subjects, taking into account modifying factors of cerebral reserve, aging and co-morbid pathologies. Imaging does not have to do this difficult job by itself. Multiple imaging modalities, e.g., structural, functional and pathology-tagging imaging modes can potentially be combined with demographic, psychometric, genetic and blood/CSF neurochemical data to form a comprehensive predictive model with improved sensitivity and specificity compared to single biomarker measurements alone. The age at which amyloid accumulation begins and the time course of this accumulation are critical in determining the timing of interventions targeted toward preventing this accumulation. These tools are urgently needed in the near term to improve the efficiency and to shorten the duration of cumbersome, slow clinical AD prevention trials [323].

CONFLICT OF INTEREST

The author has no financial or ethical conflict of interest with regard to the content of this manuscript.

ACKNOWLEDGMENTS

REFERENCES

[1] Smith CD (2010) Neuroimaging through the course of Alzheimer's disease. *J Alzheimers Dis* **19**, 273-290.

[2] Fleisher AS, Donohue M, Chen K, Brewer JB, Aisen PS, Alzheimer's Disease Neuroimaging I (2009) Applications of neuroimaging to disease-modification trials in Alzheimer's disease. *Behav Neurol* **21**, 129-136.

[3] Weiner MW, Aisen PS, Jack CR Jr, Jagust WJ, Trojanowski JQ, Shaw L, Saykin AJ, Morris JC, Cairns N, Beckett LA, Toga A, Green R, Walter S, Soares H, Snyder P, Siemers E, Potter W, Cole PE, Schmidt M, Alzheimer's Disease Neuroimaging I (2010) The Alzheimer's disease neuroimaging initiative: progress report and future plans. *Alzheimers Dement* **6**, 202-211, e207.

[4] Zhang D, Wang Y, Zhou L, Yuan H, Shen D, the Alzheimer rsquo s Disease Neuroimaging, I (2011) Multimodal classification of Alzheimer's disease and mild cognitive impairment. *Neuroimage* (in press).

[5] Petersen RC, Smith GE, Waring SC, Ivnik RJ, Tangalos EG, Kokmen E (1999) Mild cognitive impairment: clinical characterization and outcome. *Arch Neurol* **56**, 303-308.

[6] Knopman DS, Boeve BF, Petersen RC (2003) Essentials of the proper diagnoses of mild cognitive impairment, dementia, and major subtypes of dementia. *Mayo Clin Proc* **78**, 1290-1308.

[7] Kelley BJ, Petersen RC (2007) Alzheimer's disease and mild cognitive impairment. *Neurol Clin* **25**, 577-609.

[8] Morris JC (1997) Clinical dementia rating: a reliable and valid diagnostic and staging measure for dementia of the Alzheimer type. *Int Psychogeriatr* **9(Suppl 1)**, 173-176.

[9] Reisberg B, Ferris SF, deLeon MJ, Crook T (1988) The global deterioration scale (GDS). *Psychopharmacol Bull* **24**, 661-663.

[10] Small GW, Rabins PV, Barry PP, Buckholtz NS, DeKosky ST, Ferris SH, Finkel SI, Gwyther LP, Khachaturian ZS, Lebowitz BD, McRae TD, Morris JC, Oakley F, Schneider LS, Streim JE, Sunderland T, Teri LA, Tune LE (1997) Diagnosis and treatment of Alzheimer disease and related disorders. Consensus statement of the American Association for Geriatric Psychiatry, the Alzheimer's Association, and the American Geriatrics Society. *JAMA* **278**, 1363-1371.

[11] Seshadri S, Beiser A, Au R, Wolf PA, Evans DA, Wilson RS, Petersen RC, Knopman DS, Rocca WA, Kawas CH, Corrada MM, Plassman BL, Langa KM, Chui HC (2011) Operationalizing diagnostic criteria for Alzheimer's disease and other age-related cognitive impairment-Part 2. *Alzheimers Dement* **7**, 35-52.

[12] Braak H, Braak E (1991) Neuropathological staging of Alzheimer related changes. *Acta Neuropathol (Berl)* **82**, 239-259.

[13] Braak H, Braak E (1997) Frequency of stages of Alzheimer-related lesions of different age categories. *Neurobiol Aging* **18**, 351-357.

[14] Knopman DS, Parisi JE, Salviati A, Floriach-Robert M, Boeve BF, Ivnik RJ, Smith GE, Dickson DW, Johnson KA, Petersen LE, McDonald WC, Braak H, Petersen RC (2003) Neuropathology of cognitively normal elderly. *J Neuropathol Exp Neurol* **62**, 1087-1095.

[15] Petersen RC, Parisi JE, Dickson DW, Johnson KA, Knopman DS, Boeve BF, Jicha GA, Ivnik RJ, Smith GE, Tangalos EG, Braak H, Kokmen E (2006) Neuropathologic features of amnestic mild cognitive impairment. *Arch Neurol* **63**, 665-672.

[16] Jicha GA, Abner EL, Schmitt FA, Kryscio RJ, Riley KP, Cooper GE, Stiles N, Mendiondo MS, Smith CD, Van Eldik LJ, Nelson PT (2011) Preclinical AD Workgroup staging: pathological correlates and potential challenges. *Neurobiol Aging*. In Press.

[17] Smith CD (2007) Mild cognitive impairment is too late: The case for presymtomatic detection and treatment for Alzheimer's disease. *Cognitive Sciences* **3**, 127-177.

[18] Jobst KA, Smith AD, Szatmari M, Molyneux A, Esiri ME, King E, Smith A, Jaskowski A, McDonald B, Wald N (1992) Detection in life of confirmed Alzheimer's disease using a simple measurement of medial temporal lobe atrophy by computed tomography. *Lancet* **340**, 1179-1183.

[19] Smith AD, Jobst KA (1996) Use of structural imaging to study the progression of Alzheimer's disease. *Br Med Bull* **52**, 575-586.

[20] Victoroff J, Mack WJ, Grafton ST, Schreiber SS, Chui HC (1994) A method to improve interrater reliability of visual

inspection of brain MRI scans in dementia. *Neurology* **44**, 2267-2276.

[21] Kak AC, Slaney M (2001) *Principles of computerized Tomographic Imaging*, SIAM, Philadelphia.

[22] Jack CR Jr, Petersen RC, O'Brien PC, Tangalos EG (1992) MR-based hippocampal volumetry in the diagnosis of Alzheimer's disease. *Neurology* **42**, 183-188.

[23] Jack CR Jr, Petersen RC, Xu YC, O'Brien PC, Smith GE, Ivnik RJ, Boeve BF, Waring SC, Tangalos EG, Kokmen E (1999) Prediction of AD with MRI-based hippocampal volume in mild cognitive impairment. *Neurology* **52**, 1397-1403.

[24] Ashburner J, Friston KJ (2000) Voxel-based morphometry– the methods. *Neuroimage* **11**, 805-821.

[25] Zhang Y, Brady M, Smith S (2001) Segmentation of brain MR images through a hidden Markov random field model and the expectation maximization algorithm. *IEEE Trans on Medical Imaging* **29**, 45-57.

[26] Jack CR Jr, Shiung MM, Gunter JL, O'Brien PC, Weigand SD, Knopman DS, Boeve BF, Ivnik RJ, Smith GE, Cha RH, Tangalos EG, Petersen RC (2004) Comparison of different MRI brain atrophy rate measures with clinical disease progression in AD. *Neurology* **62**, 591-600.

[27] Mitchell DG, Cohen MS (2004) *MRI Principles* Saunders Philadelphia.

[28] Glodzik-Sobanska L, Rusinek H, Mosconi L, Li Y, Zhan J, de Santi S, Convit A, Rich K, Brys M, de Leon MJ (2005) The role of quantitative structural imaging in the early diagnosis of Alzheimer's disease. *Neuroimaging Clin N Am* **15**, 803-826.

[29] Ramani A, Jensen JH, Helpern JA (2006) Quantitative MR imaging in Alzheimer disease. *Radiology* **241**, 26-44.

[30] Leow AD, Klunder AD, Jack CR Jr, Toga AW, Dale AM, Bernstein MA, Britson PJ, Gunter JL, Ward CP, Whitwell JL, Borowski BJ, Fleisher AS, Fox NC, Harvey D, Kornak J, Schuff N, Studholme C, Alexander GE, Weiner MW, Thompson PM (2006) Longitudinal stability of MRI for mapping brain change using tensor-based morphometry. *Neuroimage* **31**, 627-640.

[31] Leow A, Yanovsky I, Chiang M, Lee A, Klunder A, Lu A, Becker J, Davis S, Toga A, Thompson P (2007) Statistical properties of Jacobian maps and inverse-consistent deformations in non-linear image registration. *IEEE Trans Med Imaging*, 822-832.

[32] Hua X, Leow AD, Lee S, Klunder AD, Toga AW, Lepore N, Chou YY, Brun C, Chiang MC, Barysheva M, Jack CR Jr, Bernstein MA, Britson PJ, Ward CP, Whitwell JL, Borowski B, Fleisher AS, Fox NC, Boyes RG, Barnes J, Harvey D, Kornak J, Schuff N, Boreta L, Alexander GE, Weiner MW, Thompson PM, Alzheimer's Disease Neuroimaging I (2008) 3D characterization of brain atrophy in Alzheimer's disease and mild cognitive impairment using tensor-based morphometry. *Neuroimage* **41**, 19-34.

[33] Talairach J, Tournoux P (1988) Co-Planar Stereotaxic Atlas of the Human Brain, Thieme Medical Publishers, New York.

[34] Tzourio-Mazoyer N, Landeau B, Papathanassiou D, Crivello F, Etard O, Delcroix N, Mazoyer B, Joliot M (2002) Automated anatomical labeling of activations in SPM using a macroscopic anatomical parcellation of the MNI MRI single-subject brain. *Neuroimage* **15**, 273-289.

[35] Dade LA, Gao FQ, Kovacevic N, Roy P, Rockel C, O'Toole CM, Lobaugh NJ, Feinstein A, Levine B, Black SE (2004) Semiautomatic brain region extraction: a method of par-

cellating brain regions from structural magnetic resonance images. *Neuroimage* **22**, 1492-1502.

[36] Farrow TF, Thiyagesh SN, Wilkinson ID, Parks RW, Ingram L, Woodruff PW (2007) Fronto-temporal-lobe atrophy in early-stage Alzheimer's disease identified using an improved detection methodology. *Psychiatry Res* **155**, 11-19.

[37] Walters NB, Eickhoff SB, Schleicher A, Zilles K, Amunts K, Egan GF, Watson JD (2007) Observer-independent analysis of high-resolution MR images of the human cerebral cortex: in vivo delineation of cortical areas. *Hum Brain Mapp* **28**, 1-8.

[38] Li G, Guo L, Nie J, Liu T (2009) Automatic cortical sulcal parcellation based on surface principal direction flow field tracking. *Neuroimage* **46**, 923-937.

[39] Destrieux C, Fischl B, Dale A, Halgren E (2010) Automatic parcellation of human cortical gyri and sulci using standard anatomical nomenclature. *Neuroimage* **53**, 1-15. Epub 2010 Jun 2012.

[40] Lotjonen J, Wolz R, Koikkalainen J, Julkunen V, Thurfjell L, Lundqvist R, Waldemar G, Soininen H, Rueckert D (2011) Fast and robust extraction of hippocampus from MR images for diagnostics of Alzheimer's disease. *Neuroimag* **31**, 31.

[41] Fischl B, Dale AM (2000) Measuring the thickness of the human cerebral cortex from magnetic resonance images. *Proc Natl Acad Sci U S A* **97**, 11050-11055.

[42] Salat DH, Buckner RL, Snyder AZ, Greve DN, Desikan RS, Busa E, Morris JC, Dale AM, Fischl B (2004) Thinning of the cerebral cortex in aging. *Cereb Cortex* **14**, 721-730.

[43] Small SA (2003) Measuring correlates of brain metabolism with high-resolution MRI: a promising approach for diagnosing Alzheimer disease and mapping its course. *Alzheimer Dis Assoc Disord* **17**, 154-161.

[44] Brun C, Lepore N, Pennec X, Chou YY, Lee AD, Barysheva M, de Zubicaray G, Meredith M, McMahon K, Wright MJ, Toga AW, Thompson PM (2008) A tensor-based morphometry study of genetic influences on brain structure using a new fluid registration method. *Med Image Comput Comput Assist Interv Int Conf Med Image Comput Comput Assist Interv* **11**, 914-921.

[45] Studholme C, Drapaca C, Iordanova B, Cardenas V (2006) Deformation-based mapping of volume change from serial brain MRI in the presence of local tissue contrast change. *IEEE Trans Med Imaging* **25**, 626-639.

[46] Fox NC, Cousens S, Scahill R, Harvey RJ, Rossor MN (2000) Using serial registered brain magnetic resonance imaging to measure disease progression in Alzheimer disease: power calculations and estimates of sample size to detect treatment effects. *Arch Neurol* **57**, 339-344.

[47] Fox NC, Freeborough PA (1997) Brain atrophy progression measured from registered serial MRI: validation and application to Alzheimer's disease. *J Magn Reson Imaging* **7**, 1069-1075.

[48] Conturo TE, McKinstry RC, Aronovitz JA, Neil JJ (1995) Diffusion MRI: precision, accuracy and flow effects. *NMR Biomed* **8**, 307-332.

[49] Douek P, Turner R, Pekar J, Patronas N, Le Bihan D (1991) MR color mapping of myelin fiber orientation. *J Comput Assist Tomogr* **15**, 923-929.

[50] Conturo TE, Lori NF, Cull TS, Akbudak E, Snyder AZ, Shimony JS, McKinstry RC, Burton H, Raichle ME (1999) Tracking neuronal fiber pathways in the living human brain. *Proc Natl Acad Sci U S A* **96**, 10422-10427.

[51] Poupon C, Clark CA, Frouin V, Regis J, Bloch I, Le Bihan D, Mangin J (2000) Regularization of diffusion-based direction maps for the tracking of brain white matter fascicles. *Neuroimage* **12**, 184-195.

[52] Pfefferbaum A, Sullivan EV, Hedehus M, Lim KO, Adalsteinsson E, Moseley M (2000) Age-related decline in brain white matter anisotropy measured with spatially corrected echo-planar diffusion tensor imaging. *Magn Reson Med* **44**, 259-268.

[53] Le Bihan D, Mangin JF, Poupon C, Clark CA, Pappata S, Molko N, Chabriat H (2001) Diffusion tensor imaging: concepts and applications. *J Magn Reson Imaging* **13**, 534-546.

[54] Lori NF, Akbudak E, Shimony JS, Cull TS, Snyder AZ, Guillory RK, Conturo TE (2002) Diffusion tensor fiber tracking of human brain connectivity: aquisition methods, reliability analysis and biological results. *NMR Biomed* **15**, 494-515.

[55] Shimony JS, Snyder AZ, Conturo TE, Corbetta M (2004) The study of neural connectivity using diffusion tensor tracking. *Cortex* **40**, 213-215.

[56] Smith SM, Jenkinson M, Johansen-Berg H, Rueckert D, Nichols TE, Mackay CE, Watkins KE, Ciccarelli O, Cader MZ, Matthews PM, Behrens TE (2006) Tract-based spatial statistics: voxelwise analysis of multi-subject diffusion data. *Neuroimage* **31**, 1487-1505.

[57] Phelps ME, Mazziotta JC (1985) Positron emission tomography: human brain function and biochemistry. *Science* **228**, 799-809.

[58] Wang Y, Klunk WE, Debnath ML, Huang GF, Holt DP, Shao L, Mathis CA (2004) Development of a PET/SPECT agent for amyloid imaging in Alzheimer's disease. *J Mol Neurosci* **24**, 55-62.

[59] Verhoeff NP, Wilson AA, Takeshita S, Trop L, Hussey D, Singh K, Kung HF, Kung MP, Houle S (2004) In-vivo imaging of Alzheimer disease beta-amyloid with [11C]SB-13 PET. *Am J Geriatr Psychiatry* **12**, 584-595.

[60] Cai L, Liow JS, Zoghbi SS, Cuevas J, Baetas C, Hong J, Shetty HU, Seneca NM, Brown AK, Gladding R, Temme SS, Herman MM, Innis RB, Pike VW (2008) Synthesis and evaluation of N-methyl and S-methyl 11C-labeled 6-methylthio-2-(4'-N,N-dimethylamino)phenylimidazo[1,2-a]pyridines as radioligands for imaging beta-amyloid plaques in Alzheimer's disease. *J Med Chem* **51**, 148-158.

[61] Turner R, Howseman A, Rees GE, Josephs O, Friston K (1998) Functional magnetic resonance imaging of the human brain: data acquisition and analysis. *Exp Brain Res* **123**, 5-12.

[62] Dickerson BC (2007) Advances in functional magnetic resonance imaging: technology and clinical applications. *Neurotherapeutics* **4**, 360-370.

[63] Schlund MW, Rosales-Ruiz J, Vaidya M, Glenn SS, Staff D (2008) Experience-dependent plasticity: differential changes in activation associated with repeated reinforcement. *Neuroscience* **155**, 17-23.

[64] Amaro E Jr, Barker GJ (2006) Study design in fMRI: basic principles. *Brain Cogn* **60**, 220-232.

[65] Buckner RL (1998) Event-related fMRI and the hemodynamic response. *Hum Brain Mapp* **6**, 373-377.

[66] Fox PT, Woldorff MG (1994) Integrating human brain maps. *Curr Opin Neurobiol* **4**, 151-156.

[67] Shekhar R, Zagrodsky V, Castro-Pareja CR, Walimbe V, Jagadeesh JM (2003) High-speed registration of three- and four-dimensional medical images by using voxel similarity. *Radiographics* **23**, 1673-1681.

[68] Cizek J, Herholz K, Vollmar S, Schrader R, Klein J, Heiss WD (2004) Fast and robust registration of PET and MR images of human brain. *Neuroimage* **22**, 434-442.

[69] Becker JT, Mintun MA, Aleva K, Wiseman MB, Nichols T, DeKosky ST (1996) Alterations in functional neuroanatomical connectivity in Alzheimer's disease. Positron emission tomography of auditory verbal short-term memory. *Ann N.Y.Acad Sci* **777**, 239-242.

[70] Grady CL, Furey ML, Pietrini P, Horwitz B, Rapoport SI (2001) Altered brain functional connectivity and impaired short-term memory in Alzheimer's disease. *Brain* **124**, 739-756.

[71] Zhou Y, Dougherty JH Jr, Hubner KF, Bai B, Cannon RL, Hutson RK (2008) Abnormal connectivity in the posterior cingulate and hippocampus in early Alzheimer's disease and mild cognitive impairment. *Alzheimers Dement* **4**, 265-270.

[72] Mathis CA, Wang Y, Holt DP, Huang GF, Debnath ML, Klunk WE (2003) Synthesis and evaluation of 11C-labeled 6-substituted 2-arylbenzothiazoles as amyloid imaging agents. *J Med Chem* **46**, 2740-2754.

[73] Klunk WE, Engler H, Nordberg A, Wang Y, Blomqvist G, Holt DP, Bergstrom M, Savitcheva I, Huang GF, Estrada S, Ausen B, Debnath ML, Barletta J, Price JC, Sandell J, Lopresti BJ, Wall A, Koivisto P, Antoni G, Mathis CA, Langstrom B (2004) Imaging brain amyloid in Alzheimer's disease with Pittsburgh Compound-B. *Ann Neurol* **55**, 306-319.

[74] Price JC, Klunk WE, Lopresti BJ, Lu X, Hoge JA, Ziolko SK, Holt DP, Meltzer CC, DeKosky ST, Mathis CA (2005) Kinetic modeling of amyloid binding in humans using PET imaging and Pittsburgh Compound-B. *J Cereb Blood Flow Metab* **25**, 1528-1547.

[75] Lopresti BJ, Klunk WE, Mathis CA, Hoge JA, Ziolko SK, Lu X, Meltzer CC, Schimmel K, Tsopelas ND, DeKosky ST, Price JC (2005) Simplified quantification of Pittsburgh Compound B amyloid imaging PET studies: a comparative analysis. *J Nucl Med* **46**, 1959-1972.

[76] Sun FT, Schriber RA, Greenia JM, He J, Gitcho A, Jagust WJ (2007) Automated template-based PET region of interest analyses in the aging brain. *Neuroimage* **34**, 608-617.

[77] Thomas BA, Erlandsson K, Modat M, Thurfjell L, Vandenberghe R, Ourselin S, Hutton BF (2011) The importance of appropriate partial volume correction for PET quantification in Alzheimer's disease. *Eur J Nucl Med Mol Imaging* Epub 2011/02/22.

[78] Zhou Y, Endres CJ, Brasic JR, Huang SC, Wong DF (2003) Linear regression with spatial constraint to generate parametric images of ligand-receptor dynamic PET studies with a simplified reference tissue model. *Neuroimage* **18**, 975-989.

[79] Clark CM, Schneider JA, Bedell BJ, Beach TG, Bilker WB, Mintun MA, Pontecorvo MJ, Hefti F, Carpenter AP, Flitter ML, Krautkramer MJ, Kung HF, Coleman RE, Doraiswamy PM, Fleisher AS, Sabbagh MN, Sadowsky CH, Reiman PE, Zehntner SP, Skovronsky DM, Group AAS (2011) Use of florbetapir-PET for imaging beta-amyloid pathology. *JAMA* **305**, 275-283.

[80] Wong DF, Rosenberg PB, Zhou Y, Kumar A, Raymont V, Ravert HT, Dannals RF, Nandi A, Brasic JR, Ye W, Hilton J, Lyketsos C, Kung HF, Joshi AD, Skovronsky DM, Pontecorvo MJ (2010) *In vivo* imaging of amyloid deposition in Alzheimer disease using the radioligand 18F-AV-45 (florbetapir [corrected] F 18). *J Nucl Med* **51**, 913-920.

[81] Cheng Y, Ono M, Kimura H, Kagawa S, Nishii R, Saji H (2010) A novel 18F-labeled pyridyl benzofuran derivative for imaging of beta-amyloid plaques in Alzheimer's brains. *Bioorg Med Chem Lett* **20**, 6141-6144.

[82] Jureus A, Swahn BM, Sandell J, Jeppsson F, Johnson AE, Johnstrom P, Neelissen JA, Sunnemark D, Farde L, Svensson SP (2010) Characterization of AZD4694, a novel fluorinated Abeta plaque neuroimaging PET radioligand. *J Neurochem* **114**, 784-794.

[83] Neumaier B, Deisenhofer S, Sommer C, Solbach C, Reske SN, Mottaghy F (2010) Synthesis and evaluation of 18F-fluoroethylated benzothiazole derivatives for *in vivo* imaging of amyloid plaques in Alzheimer's disease. *Appl Radiat Isot* **68**, 1066-1072.

[84] Kung HF, Choi SR, Qu W, Zhang W, Skovronsky D (2010) 18F stilbenes and styrylpyridines for PET imaging of A beta plaques in Alzheimer's disease: a miniperspective. *J Med Chem* **53**, 933-941.

[85] Ono M, Watanabe R, Kawashima H, Cheng Y, Kimura H, Watanabe H, Haratake M, Saji H, Nakayama M (2009) Fluoro-pegylated chalcones as positron emission tomography probes for in vivo imaging of beta-amyloid plaques in Alzheimer's disease. *J Med Chem* **52**, 6394-6401.

[86] O'Keefe GJ, Saunder TH, Ng S, Ackerman U, Tochon-Danguy HJ, Chan JG, Gong S, Dyrks T, Lindemann S, Holl G, Dinkelborg L, Villemagne V, Rowe CC (2009) Radiation dosimetry of beta-amyloid tracers 11C-PiB and 18F-BAY94-9172. *J Nucl Med* **50**, 309-315.

[87] Barrio JR, Kepe V, Satyamurthy N, Huang SC, Small G (2008) Amyloid and tau imaging, neuronal losses and function in mild cognitive impairment. *J Nutr Health Aging* **12**, S61-S65.

[88] Tolboom N, Yaqub M, van der Flier WM, Boellaard R, Luurtsema G, Windhorst AD, Barkhof F, Scheltens P, Lammertsma AA, van Berckel BN (2009) Detection of Alzheimer Pathology *in vivo* using both 11C-PIB and 18F-FDDNP PET. *J Nucl Med* **50**, 191-197.

[89] Dierksen GA, Skehan ME, Khan MA, Jeng J, Nandigam RN, Becker JA, Kumar A, Neal KL, Betensky RA, Frosch MP, Rosand J, Johnson KA, Viswanathan A, Salat DH, Greenberg SM (2010) Spatial relation between microbleeds and amyloid deposits in amyloid angiopathy. *Ann Neurol* **68**, 545-548.

[90] Sullivan EV, Pfefferbaum A (2007) Neuroradiological characterization of normal adult ageing. *Br J Radiol* **80(2)**, S99-S108.

[91] Ciccarelli O, Catani M, Johansen-Berg H, Clark C, Thompson A (2008) Diffusion-based tractography in neurological disorders: concepts, applications, and future developments. *Lancet Neurol* **7**, 715-727.

[92] Ciumas C, Montavont A, Ryvlin P (2008) Magnetic resonance imaging in clinical trials. *Curr Opin Neurol* **21**, 431-436.

[93] Dolan RJ (2008) Neuroimaging of cognition: past, present, and future. *Neuron* **60**, 496-502.

[94] Holdsworth SJ, Bammer R (2008) Magnetic resonance imaging techniques: fMRI, DWI, and PWI. *Semin Neurol* **28**, 395-406.

[95] Hyder F (2009) Dynamic imaging of brain function. *Methods Mol Biol* **489**, 3-21.

[96] Sossi V (2007) Cutting-edge brain imaging with positron emission tomography. *Neuroimaging Clin N Am* **17**, 427-440.

[97] Stufflebeam SM, Rosen BR (2007) Mapping cognitive function. *Neuroimaging Clin N Am* **17**, 469-484.

[98] Berchtold NC, Cotman CW (1998) Evolution in the conceptualization of dementia and Alzheimer's disease: Greco-Roman period to the 1960s. *Neurobiol Aging* **19**, 173-189.

[99] Brun A, Englund E (1986) Brain changes in dementia of Alzheimer's type relevant to new imaging diagnostic methods. *Prog Neuropsychopharmacol Biol Psychiatry* **10**, 297-308.

[100] Nagy Z, Hindley NJ, Braak H, Braak E, Yilmazer-Hanke DM, Schultz C, Barnetson L, Jobst KA, Smith AD (1999) Relationship between clinical and radiological diagnostic criteria for Alzheimer's disease and the extent of neuropathology as reflected by 'stages': a prospective study. *Dement Geriatr Cogn Disord* **10**, 109-114.

[101] Foster NL, Chase TN, Fedio P, Patronas NJ, Brooks RA, Di Chiro G (1983) Alzheimer's disease: focal cortical changes shown by positron emission tomography. *Neurology* **33**, 961-965.

[102] McGeer PL, Kamo H, Harrop R, Li DK, Tuokko H, McGeer EG, Adam MJ, Ammann W, Beattie BL, Calne DB (1986) Positron emission tomography in patients with clinically diagnosed Alzheimer's disease. *Can Med Assoc J* **134**, 597-607.

[103] Minoshima S, Frey KA, Koeppe RA, Foster NL, Kuhl DE (1995) A diagnostic approach in Alzheimer's disease using three-dimensional stereotactic surface projections of fluorine-18-FDG PET. *J Nucl Med* **36**, 1238-1248.

[104] Foster NL, Heidebrink JL, Clark CM, Jagust WJ, Arnold SE, Barbas NR, DeCarli CS, Turner RS, Koeppe RA, Higdon R, Minoshima S (2007) FDG-PET improves accuracy in distinguishing frontotemporal dementia and Alzheimer's disease. *Brain* **130**, 2616-2635.

[105] Davis PC, Gearing M, Gray L, Mirra SS, Morris JC, Edland SD, Lin T, Heyman A (1995) The CERAD experience, Part VIII: Neuroimaging-neuropathology correlates of temporal lobe changes in Alzheimer's disease. *Neurology* **45**, 178-179.

[106] Nagy Z, Jobst KA, Esiri MM, Morris JH, King EM, MacDonald B, Litchfield S, Barnetson L, Smith AD (1996) Hippocampal pathology reflects memory deficit and brain imaging measurements in Alzheimer's disease: clinicopathologic correlations using three sets of pathologic diagnostic criteria. *Dementia* **7**, 76-81.

[107] Jack CR Jr, Dickson DW, Parisi JE, Xu YC, Cha RH, O'Brien PC, Edland SD, Smith GE, Boeve BF, Tangalos EG, Kokmen E, Petersen RC (2002) Antemortem MRI findings correlate with hippocampal neuropathology in typical aging and dementia. *Neurology* **58**, 750-757.

[108] Csernansky JG, Hamstra J, Wang L, McKeel D, Price JL, Gado M, Morris JC (2004) Correlations between antemortem hippocampal volume and postmortem neuropathology in AD subjects. *Alzheimer Dis Assoc Disord* **18**, 190-195.

[109] Mortimer JA, Gosche KM, Riley KP, Markesbery WR, Snowdon DA (2004) Delayed recall, hippocampal volume and Alzheimer neuropathology: findings from the Nun Study. *Neurology* **62**, 428-432.

[110] Alexander GE, Furey ML, Grady CL, Pietrini P, Brady DR, Mentis MJ, Schapiro MB (1997) Association of premorbid intellectual function with cerebral metabolism in Alzheimer's disease: implications for the cognitive reserve hypothesis. *Am J Psychiatry* **154**, 165-172.

[111] Stern Y, Alexander GE, Prohovnik I, Stricks L, Lennon MC, Mayeux R (1995) Relationship between lifetime occupation and parietal flow: implications for a reserve against Alzheimer's disease pathology. *Neurology* **45**, 55-60.

[112] Stern Y, Alexander GE, Prohovnik I, Mayeux R (1992) Inverse relationship between education and parietotemporal perfusion deficit in Alzheimer's disease. *Ann Neurol* **32**, 371-375.

[113] Scarmeas N, Zarahn E, Anderson KE, Habeck CG, Hilton J, Flynn J, Marder KS, Bell KL, Sackeim HA, Van Heertum RL, Moeller JR, Stern Y (2003) Association of life activities with cerebral blood flow in Alzheimer disease: implications for the cognitive reserve hypothesis. *Arch Neurol* **60**, 359-365.

[114] Smith AD (2002) Imaging the progression of Alzheimer pathology through the brain. *Proc Natl Acad Sci U S A* **99**, 4135-4137.

[115] Stern Y, Moeller JR, Anderson KE, Luber B, Zubin NR, DiMauro AA, Park A, Campbell CE, Marder K, Bell K, Van Heertum R, Sackeim HA (2000) Different brain networks mediate task performance in normal aging and AD: defining compensation. *Neurology* **55**, 1291-1297.

[116] Erten-Lyons D, Woltjer RL, Dodge H, Nixon R, Vorobik R, Calvert JF, Leahy M, Montine T, Kaye J (2009) Factors associated with resistance to dementia despite high Alzheimer disease pathology. *Neurology* **72**, 354-360.

[117] Kessler J, Herholz K, Grond M, Heiss WD (1991) Impaired metabolic activation in Alzheimer's disease: a PET study during continuous visual recognition. *Neuropsychologia* **29**, 229-243.

[118] Mentis MJ, Alexander GE, Krasuski J, Pietrini P, Furey ML, Schapiro MB, Rapoport SI (1998) Increasing required neural response to expose abnormal brain function in mild versus moderate or severe Alzheimer's disease: PET study using parametric visual stimulation. *Am J Psychiatry* **155**, 785-794.

[119] Pietrini P, Furey ML, Alexander GE, Mentis MJ, Dani A, Guazzelli M, Rapoport SI, Schapiro MB (1999) Association between brain functional failure and dementia severity in Alzheimer's disease: resting versus stimulation PET study. *Am J Psychiatry* **156**, 470-473.

[120] Pietrini P, Alexander GE, Furey ML, Dani A, Mentis MJ, Horwitz B, Guazzelli M, Shapiro MB, Rapoport SI (2000) Cerebral metabolic response to passive audiovisual stimulation in patients with Alzheimer's disease and healthy volunteers assessed by PET. *J Nucl Med* **41**, 575-583.

[121] Thulborn KR, Martin C, Voyvodic JT (2000) Functional MR imaging using a visually guided saccade paradigm for comparing activation patterns in patients with probable Alzheimer's disease and in cognitively able elderly volunteers. *AJNR Am J Neuroradiol* **21**, 524-531.

[122] Krasuski JS, Alexander GE, Horwitz B, Daly EM, Murphy DG, Rapoport SI, Schapiro MB (1998) Volumes of medial temporal lobe structures in patients with Alzheimer's disease and mild cognitive impairment (and in healthy controls). *Biol Psychiatry* **43**, 60-68.

[123] Thompson PM, Mega MS, Woods RP, Zoumalan CI, Lindshield CJ, Blanton RE, Moussai J, Holmes CJ, Cummings JL, Toga AW (2001) Cortical change in Alzheimer's disease detected with a disease-specific population-based brain atlas. *Cereb Cortex* **11**, 1-16.

[124] Hirata Y, Matsuda H, Nemoto K, Ohnishi T, Hirao K, Yamashita F, Asada T, Iwabuchi S, Samejima H (2005) Voxel-based morphometry to discriminate early Alzheimer's disease from controls. *Neurosci Lett* **382**, 269-274.

[125] Apostolova LG, Steiner CA, Akopyan GG, Dutton RA, Hayashi KM, Toga AW, Cummings JL, Thompson PM (2007) Three-dimensional gray matter atrophy mapping in

mild cognitive impairment and mild Alzheimer disease. *Arch Neurol* **64**, 1489-1495.

[126] Hua X, Leow AD, Parikshak N, Lee S, Chiang MC, Toga AW, Jack CR Jr, Weiner MW, Thompson PM (2008) Tensor-based morphometry as a neuroimaging biomarker for Alzheimer's disease: An MRI study of 676 AD, MCI, and normal subjects. *Neuroimage* **43**, 458-469.

[127] Thompson PM, Hayashi KM, de Zubicaray G, Janke AL, Rose SE, Semple J, Herman D, Hong MS, Dittmer SS, Doddrell DM, Toga AW (2003) Dynamics of gray matter loss in Alzheimer's disease. *J Neurosci* **23**, 994-1005.

[128] Querbes O, Aubry F, Pariente J, Lotterie JA, Demonet JF, Duret V, Puel M, Berry I, Fort JC, Celsis P, Alzheimer's Disease Neuroimaging I (2009) Early diagnosis of Alzheimer's disease using cortical thickness: impact of cognitive reserve. *Brain* **132**, 2036-2047.

[129] Csernansky JG, Wang L, Swank J, Miller JP, Gado M, Mc Keel D, Miller MI, Morris JC (2005) Preclinical detection of Alzheimer's disease: hippocampal shape and volume predict dementia onset in the elderly. *Neuroimage* **25**, 783-792.

[130] Scher AI, Xu Y, Korf ES, White LR, Scheltens P, Toga AW, Thompson PM, Hartley SW, Witter MP, Valentino DJ, Launer LJ (2007) Hippocampal shape analysis in Alzheimer's disease: a population-based study. *Neuroimage* **36**, 8-18.

[131] Park H, Seo J, Adni (2011) Application of multidimensional scaling to quantify shape in Alzheimer's disease and its correlation with Mini Mental State Examination: a feasibility study. *J Neurosci Methods* **194**, 380-385.

[132] Davatzikos C, Bhatt P, Shaw LM, Batmanghelich KN, Trojanowski JQ (2010) Prediction of MCI to AD conversion, via MRI, CSF biomarkers, and pattern classification. *Neurobiol Aging* Epub 2010/06/29.

[133] Davatzikos C, Xu F, An Y, Fan Y, Resnick SM (2009) Longitudinal progression of Alzheimer's-like patterns of atrophy in normal older adults: the SPARE-AD index. *Brain* **132**, 2026-2035.

[134] Stonnington CM, Chu C, Kloppel S, Jack CR Jr, Ashburner J, Frackowiak RS, Alzheimer Disease Neuroimaging I (2010) Predicting clinical scores from magnetic resonance scans in Alzheimer's disease. *Neuroimage* **51**, 1405-1413.

[135] Chupin M, Gerardin E, Cuingnet R, Boutet C, Lemieux L, Lehericy S, Benali H, Garnero L, Colliot O, Alzheimer's Disease Neuroimaging I (2009) Fully automatic hippocampus segmentation and classification in Alzheimer's disease and mild cognitive impairment applied on data from ADNI. *Hippocampus* **19**, 579-587.

[136] Leung KK, Barnes J, Ridgway GR, Bartlett JW, Clarkson MJ, Macdonald K, Schuff N, Fox NC, Ourselin S, Alzheimer's Disease Neuroimaging I (2010) Automated cross-sectional and longitudinal hippocampal volume measurement in mild cognitive impairment and Alzheimer's disease. *Neuroimage* **51**, 1345-1359.

[137] Lotjonen J, Wolz R, Koikkalainen J, Julkunen V, Thurfjell L, Lundqvist R, Waldemar G, Soininen H, Rueckert D, The Alzheimer's Disease Neuroimaging I (2011) Fast and robust extraction of hippocampus from MR images for diagnostics of Alzheimer's disease. *Neuroimage* (in press).

[138] Cuingnet R, Gerardin E, Tessieras J, Auzias G, Lehericy S, Habert MO, Chupin M, Benali H, Colliot O, The Alzheimer's Disease Neuroimaging I (2011) Automatic classification of patients with Alzheimer's disease from structural MRI: A comparison of ten methods using the ADNI database. *Neuroimage* **56**, 766-781.

[139] Bartzokis G (2009) Alzheimer's disease as homeostatic responses to age-related myelin breakdown. *Neurobiol Aging* (in press).

[140] Alix JJ, Domingues AM (2011) White matter synapses: form, function, and dysfunction. *Neurology* **76**, 397-404.

[141] Takahashi S, Yonezawa H, Takahashi J, Kudo M, Inoue T, Tohgi H (2002) Selective reduction of diffusion anisotropy in white matter of Alzheimer disease brains measured by 3.0 Tesla magnetic resonance imaging. *Neurosci Lett* **332**, 45-48.

[142] Hanyu H, Sakurai H, Iwamoto T, Takasaki M, Shindo H, Abe K (1998) Diffusion-weighted MR imaging of the hippocampus and temporal white matter in Alzheimer's disease. *J Neurol Sci* **156**, 195-200.

[143] Sandson TA, Felician O, Edelman RR, Warach S (1999) Diffusion-weighted magnetic resonance imaging in Alzheimer's disease. *Dement Geriatr Cogn Disord* **10**, 166-171.

[144] Rose SE, Chen F, Chalk JB, Zelaya FO, Strugnell WE, Benson M, Semple J, Doddrell DM (2000) Loss of connectivity in Alzheimer's disease: an evaluation of white matter tract integrity with colour coded MR diffusion tensor imaging. *J Neurol Neurosurg Psychiatry* **69**, 528-530.

[145] Naggara O, Oppenheim C, Rieu D, Raoux N, Rodrigo S, Dalla Barba G, Meder JF (2006) Diffusion tensor imaging in early Alzheimer's disease. *Psychiatry Res* **146**, 243-249.

[146] Lee DY, Fletcher E, Martinez O, Ortega M, Zozulya N, Kim J, Tran J, Buonocore M, Carmichael O, DeCarli C (2009) Regional pattern of white matter microstructural changes in normal aging, MCI, and AD. *Neurology* **73**, 1722-1728.

[147] Yoshiura T, Mihara F, Ogomori K, Tanaka A, Kaneko K, Masuda K (2002) Diffusion tensor in posterior cingulate gyrus: correlation with cognitive decline in Alzheimer's disease. *Neuroreport* **13**, 2299-2302.

[148] Bozzali M, Falini A, Franceschi M, Cercignani M, Zuffi M, Scotti G, Comi G, Filippi M (2002) White matter damage in Alzheimer's disease assessed *in vivo* using diffusion tensor magnetic resonance imaging. *J Neurol Neurosurg Psychiatry* **72**, 742-746.

[149] Duan JH, Wang HQ, Xu J, Lin X, Chen SQ, Kang Z, Yao ZB (2006) White matter damage of patients with Alzheimer's disease correlated with the decreased cognitive function. *Surg Radiol Anat* **28**, 150-156.

[150] Sydykova D, Stahl R, Dietrich O, Ewers M, Reiser MF, Schoenberg SO, Moller HJ, Hampel H, Teipel SJ (2007) Fiber connections between the cerebral cortex and the corpus callosum in Alzheimer's disease: a diffusion tensor imaging and voxel-based morphometry study. *Cereb Cortex* **17**, 2276-2282.

[151] Lo CY, Wang PN, Chou KH, Wang J, He Y, Lin CP (2010) Diffusion tensor tractography reveals abnormal topological organization in structural cortical networks in Alzheimer's disease. *J Neurosci* **30**, 16876-16885.

[152] Rose SE, Janke AL, Chalk JB (2008) Gray and white matter changes in Alzheimer's disease: a diffusion tensor imaging study. *J Magn Reson Imaging* **27**, 20-26.

[153] Salat DH, Tuch DS, van der Kouwe AJ, Greve DN, Pappu V, Lee SY, Hevelone ND, Zaleta AK, Growdon JH, Corkin S, Fischl B, Rosas HD (2010) White matter pathology isolates the hippocampal formation in Alzheimer's disease. *Neurobiol Aging* **31**, 244-256.

[154] Conturo TE, Williams DL, Smith CD, Gultepe E, Akbudak E, Minshew NJ (2008) Neuronal fiber pathway abnormalities in autism: an initial MRI diffusion tensor tracking study

of hippocampo-fusiform and amygdalo-fusiform pathways. *J Int Neuropsychol Soc* **14**, 933-946.

[155] Langbaum JB, Chen K, Lee W, Reschke C, Bandy D, Fleisher AS, Alexander GE, Foster NL, Weiner MW, Koeppe RA, Jagust WJ, Reiman EM, Alzheimer's Disease Neuroimaging I (2009) Categorical and correlational analyses of baseline fluorodeoxyglucose positron emission tomography images from the Alzheimer's Disease Neuroimaging Initiative (ADNI). *Neuroimage* **45**, 1107-1116.

[156] Chen K, Ayutyanont N, Langbaum JB, Fleisher AS, Reschke C, Lee W, Liu X, Bandy D, Alexander GE, Thompson PM, Shaw L, Trojanowski JQ, Jack CR Jr, Landau SM, Foster NL, Harvey DJ, Weiner MW, Koeppe RA, Jagust WJ, Reiman EM, Alzheimer's Disease Neuroimaging I (2011) Characterizing Alzheimer's disease using a hypometabolic convergence index. *Neuroimage* Epub 2011/02/01.

[157] Rapoport SI (1999) In vivo PET imaging and postmortem studies suggest potentially reversible and irreversible stages of brain metabolic failure in Alzheimer's disease. *Eur Arch Psychiatry Clin Neurosci* **249**, 46-55.

[158] Schroder J, Buchsbaum MS, Shihabuddin L, Tang C, Wei TC, Spiegel-Cohen J, Hazlett EA, Abel L, Luu-Hsia C, Ciaravolo TM, Marin D, Davis KL (2001) Patterns of cortical activity and memory performance in Alzheimer's disease. *Biol Psychiatry* **49**, 426-436.

[159] Sperling RA, Bates JF, Chua EF, Cocchiarella AJ, Rentz DM, Rosen BR, Schacter DL, Albert MS (2003) fMRI studies of associative encoding in young and elderly controls and mild Alzheimer's disease. *J Neurol Neurosurg Psychiatry* **74**, 44-50.

[160] Diamond EL, Miller S, Dickerson BC, Atri A, DePeau K, Fenstermacher E, Pihlajamaki M, Celone K, Salisbury S, Gregas M, Rentz D, Sperling RA (2007) Relationship of fMRI activation to clinical trial memory measures in Alzheimer disease. *Neurology* **69**, 1331-1341.

[161] Kato T, Knopman D, Liu H (2001) Dissociation of regional activation in mild AD during visual encoding: a functional MRI study. *Neurology* **57**, 812-816.

[162] Small SA, Nava AS, Perera GM, Delapaz R, Stern Y (2000) Evaluating the function of hippocampal subregions with high-resolution MRI in Alzheimer's disease and aging. *Microsc Res Tech* **51**, 101-108.

[163] Rombouts SA, Barkhof F, Veltman DJ, Machielsen WC, Witter MP, Bierlaagh MA, Lazeron RH, Valk J, Scheltens P (2000) Functional MR imaging in Alzheimer's disease during memory encoding. *AJNR Am J Neuroradiol* **21**, 1869-1875.

[164] Saykin AJ, Flashman LA, Frutiger SA, Johnson SC, Mamourian AC, Moritz CH, O'Jile JR, Riordan HJ, Santulli RB, Smith CA, Weaver JB (1999) Neuroanatomic substrates of semantic memory impairment in Alzheimer's disease: patterns of functional MRI activation. *Journal of the International Neuropsychological Society* **5**, 377-392.

[165] Celone KA, Calhoun VD, Dickerson BC, Atri A, Chua EF, Miller SL, DePeau K, Rentz DM, Selkoe DJ, Blacker D, Albert MS, Sperling RA (2006) Alterations in memory networks in mild cognitive impairment and Alzheimer's disease: an independent component analysis. *J Neurosci* **26**, 10222-10231.

[166] Fair DA, Cohen AL, Dosenbach NU, Church JA, Miezin FM, Barch DM, Raichle ME, Petersen SE, Schlaggar BL (2008) The maturing architecture of the brain's default network. *Proc Natl Acad Sci U S A* **105**, 4028-4032.

[167] Raichle ME, MacLeod AM, Snyder AZ, Powers WJ, Gusnard DA, Shulman GL (2001) A default mode of brain function. *Proc Natl Acad Sci U S A* **98**, 676-682.

[168] Raichle ME, Snyder AZ (2007) A default mode of brain function: a brief history of an evolving idea. *Neuroimage* **37**, 1083-1090 Disscussion 1097-1089.

[169] van den Heuvel M, Mandl R, Luigjes J, Hulshoff Pol H (2008) Microstructural organization of the cingulum tract and the level of default mode functional connectivity. *J Neurosci* **28**, 10844-10851.

[170] Greicius MD, Srivastava G, Reiss AL, Menon V (2004) Default-mode network activity distinguishes Alzheimer's disease from healthy aging: evidence from functional MRI. *Proc Natl Acad Sci U S A* **101**, 4637-4642.

[171] Rombouts SA, Barkhof F, Goekoop R, Stam CJ, Scheltens P (2005) Altered resting state networks in mild cognitive impairment and mild Alzheimer's disease: an fMRI study. *Hum Brain Mapp* **26**, 231-239.

[172] Rombouts SA, Damoiseaux JS, Goekoop R, Barkhof F, Scheltens P, Smith SM, Beckmann CF (2009) Model-free group analysis shows altered BOLD FMRI networks in dementia. *Hum Brain Mapp* **30**, 256-266.

[173] Wermke M, Sorg C, Wohlschlager AM, Drzezga A (2008) A new integrative model of cerebral activation, deactivation and default mode function in Alzheimer's disease. *Eur J Nucl Med Mol Imaging* **35**(1), S12-S24.

[174] Buckner RL, Snyder AZ, Shannon BJ, LaRossa G, Sachs R, Fotenos AF, Sheline YI, Klunk WE, Mathis CA, Morris JC, Mintun MA (2005) Molecular, structural, and functional characterization of Alzheimer's disease: evidence for a relationship between default activity, amyloid, and memory. *J Neurosci* **25**, 7709-7717.

[175] Cairns NJ, Ikonomovic MD, Benzinger T, Storandt M, Fagan AM, Shah AR, Reinwald LT, Carter D, Felton A, Holtzman DM, Mintun MA, Klunk WE, Morris JC (2009) Absence of Pittsburgh compound B detection of cerebral amyloid beta in a patient with clinical, cognitive, and cerebrospinal fluid markers of Alzheimer disease: a case report. *Arch Neurol* **66**, 1557-1562.

[176] Rowe CC, Ng S, Ackermann U, Gong SJ, Pike K, Savage G, Cowie TF, Dickinson KL, Maruff P, Darby D, Smith C, Woodward M, Merory J, Tochon-Danguy H, O'Keefe G, Klunk WE, Mathis CA, Price JC, Masters CL, Villemagne VL (2007) Imaging beta-amyloid burden in aging and dementia. *Neurology* **68**, 1718-1725.

[177] Sojkova J, Driscoll I, Iacono D, Zhou Y, Codispoti KE, Kraut MA, Ferrucci L, Pletnikova O, Mathis CA, Klunk WE, O'Brien RJ, Wong DF, Troncoso JC, Resnick SM (2011) In vivo fibrillar beta-amyloid detected using [11C]PiB positron emission tomography and neuropathologic assessment in older adults. *Arch Neurol* **68**, 232-240.

[178] Scheinin NM, Aalto S, Koikkalainen J, Lotjonen J, Karrasch M, Kemppainen N, Viitanen M, Nagren K, Helin S, Scheinin M, Rinne JO (2009) Follow-up of [11C]PIB uptake and brain volume in patients with Alzheimer disease and controls. *Neurology* **73**, 1186-1192.

[179] Villemagne VL, Pike KE, Chetelat G, Ellis KA, Mulligan RS, Bourgeat P, Ackermann U, Jones G, Szoeke C, Salvado O, Martins R, O'Keefe G, Mathis CA, Klunk WE, Ames D, Masters CL, Rowe CC (2011) Longitudinal assessment of Abeta and cognition in aging and Alzheimer disease. *Ann Neurol* **69**, 181-192.

[180] Jack CR Jr, Lowe VJ, Weigand SD, Wiste HJ, Senjem ML, Knopman DS, Shiung MM, Gunter JL, Boeve BF, Kemp

BJ, Weiner M, Petersen RC, Alzheimer's Disease Neuroimaging I (2009) Serial PIB and MRI in normal, mild cognitive impairment and Alzheimer's disease: implications for sequence of pathological events in Alzheimer's disease. *Brain* **132**, 1355-1365.

[181] Li Y, Rinne JO, Mosconi L, Pirraglia E, Rusinek H, DeSanti S, Kemppainen N, Nagren K, Kim BC, Tsui W, de Leon MJ (2008) Regional analysis of FDG and PIB-PET images in normal aging, mild cognitive impairment, and Alzheimer's disease. *Eur J Nucl Med Mol Imaging* **35**, 2169-2181.

[182] Jack CR Jr, Lowe VJ, Senjem ML, Weigand SD, Kemp BJ, Shiung MM, Knopman DS, Boeve BF, Klunk WE, Mathis CA, Petersen RC (2008) 11C PiB and structural MRI provide complementary information in imaging of Alzheimer's disease and amnestic mild cognitive impairment. *Brain* **131**, 665-680.

[183] Forsberg A, Engler H, Almkvist O, Blomquist G, Hagman G, Wall A, Ringheim A, Langstrom B, Nordberg A (2008) PET imaging of amyloid deposition in patients with mild cognitive impairment. *Neurobiol Aging* **29**, 1456-1465.

[184] Raji CA, Becker JT, Tsopelas ND, Price JC, Mathis CA, Saxton JA, Lopresti BJ, Hoge JA, Ziolko SK, DeKosky ST, Klunk WE (2008) Characterizing regional correlation, laterality and symmetry of amyloid deposition in mild cognitive impairment and Alzheimer's disease with Pittsburgh Compound B. *J Neurosci Methods* **172**, 277-282.

[185] Kemppainen NM, Aalto S, Wilson IA, Nagren K, Helin S, Bruck A, Oikonen V, Kailajarvi M, Scheinin M, Viitanen M, Parkkola R, Rinne JO (2007) PET amyloid ligand [11C]PIB uptake is increased in mild cognitive impairment. *Neurology* **68**, 1603-1606.

[186] Chetelat G, Villemagne VL, Bourgeat P, Pike KE, Jones G, Ames D, Ellis KA, Szoeke C, Martins RN, O'Keefe GJ, Salvado O, Masters CL, Rowe CC, Australian Imaging B, Lifestyle Research G (2010) Relationship between atrophy and beta-amyloid deposition in Alzheimer disease. *Ann Neurol* **67**, 317-324.

[187] Frisoni GB, Lorenzi M, Caroli A, Kemppainen N, Nagren K, Rinne JO (2009) In vivo mapping of amyloid toxicity in Alzheimer disease. *Neurology* **72**, 1504-1511.

[188] Archer HA, Edison P, Brooks DJ, Barnes J, Frost C, Yeatman T, Fox NC, Rossor MN (2006) Amyloid load and cerebral atrophy in Alzheimer's disease: an 11C-PIB positron emission tomography study. *Ann Neurol* **60**, 145-147.

[189] Roe CM, Mintun MA, Ghoshal N, Williams MM, Grant EA, Marcus DS, Morris JC (2010) Alzheimer disease identification using amyloid imaging and reserve variables: proof of concept. *Neurology* **75**, 42-48.

[190] Kemppainen NM, Aalto S, Karrasch M, Nagren K, Savisto N, Oikonen V, Viitanen M, Parkkola R, Rinne JO (2008) Cognitive reserve hypothesis: Pittsburgh Compound B and fluorodeoxyglucose positron emission tomography in relation to education in mild Alzheimer's disease. *Ann Neurol* **63**, 112-118.

[191] Rentz DM, Locascio JJ, Becker JA, Moran EK, Eng E, Buckner RL, Sperling RA, Johnson KA (2010) Cognition, reserve, and amyloid deposition in normal aging. *Ann Neurol* **67**, 353-364.

[192] Flicker C, Ferris SH, Reisberg B (1991) Mild cognitive impairment in the elderly: predictors of dementia. *Neurology* **41**, 1006-1009.

[193] Almkvist O, Basun H, Backman L, Herlitz A, Lannfelt L, Small B, Viitanen M, Wahlund LO, Winblad B (1998)

Mild cognitive impairment–an early stage of Alzheimer's disease? *J Neural Transm. Suppl* **54**, 21-29.

[194] Celsis P (2000) Age-related cognitive decline, mild cognitive impairment or preclinical Alzheimer's disease?. *Ann Med* **32**, 6-14.

[195] Petersen RC, Doody R, Kurz A, Mohs RC, Morris JC, Rabins PV, Ritchie K, Rossor M, Thal L, Winblad B (2001) Current concepts in mild cognitive impairment. *Arch Neurol* **58**, 1985-1992.

[196] Winblad B, Palmer K, Kivipelto M, Jelic V, Fratiglioni L, Wahlund LO, Nordberg A, Backman L, Albert M, Almkvist O, Arai H, Basun H, Blennow K, de Leon M, DeCarli C, Erkinjuntti T, Giacobini E, Graff C, Hardy J, Jack C, Jorm A, Ritchie K, van Duijn C, Visser P, Petersen RC (2004) Mild cognitive impairment–beyond controversies, towards a consensus: report of the International Working Group on Mild Cognitive Impairment. *J Intern Med* **256**, 240-246.

[197] Morris JC (2005) Mild cognitive impairment and preclinical Alzheimer's disease. *Geriatrics* **60** (Suppl.), 9-14.

[198] Gauthier S, Reisberg B, Zaudig M, Petersen RC, Ritchie K, Broich K, Belleville S, Brodaty H, Bennett D, Chertkow H, Cummings JL, de Leon M, Feldman H, Ganguli M, Hampel H, Scheltens P, Tierney MC, Whitehouse P, Winblad B (2006) Mild cognitive impairment. *Lancet* **367**, 1262-1270.

[199] Morris JC (2006) Mild cognitive impairment is early-stage Alzheimer disease: time to revise diagnostic criteria. *Arch Neurol* **63**, 15-16.

[200] Petersen RC, Roberts RO, Knopman DS, Boeve BF, Geda YE, Ivnik RJ, Smith GE, Jack CR Jr, (2009) Mild cognitive impairment: ten years later. *Arch Neurol* **66**, 1447-1455.

[201] Golomb J, de Leon MJ, Kluger A, George AE, Tarshish C, Ferris SH (1993) Hippocampal atrophy in normal aging. An association with recent memory impairment. *Arch. Neurol* **50**, 967-973.

[202] Grundman M, Sencakova D, Jack CR, Jr., Petersen RC, Kim HT, Schultz A, Weiner MF, DeCarli C, DeKosky ST, van Dyck C, Thomas RG, Thal LJ (2002) Brain MRI hippocampal volume and prediction of clinical status in a mild cognitive impairment trial. *J Mol Neurosci* **19**, 23-27.

[203] Pantel J, Kratz B, Essig M, Schroder J (2003) Parahippocampal volume deficits in subjects with aging-associated cognitive decline. *American Journal of Psychiatry* **160**, 379-382.

[204] Dickerson BC, Salat DH, Bates JF, Atiya M, Killiany RJ, Greve DN, Dale AM, Stern CE, Blacker D, Albert MS, Sperling RA (2004) Medial temporal lobe function and structure in mild cognitive impairment. *Ann Neurol* **56**, 27-35.

[205] Jack CR Jr, Petersen RC, Xu YC, Waring SC, O'Brien PC, Tangalos EG, Smith GE, Ivnik RJ, Kokmen E (1997) Medial temporal atrophy on MRI in normal aging and very mild Alzheimer's disease. *Neurology* **49**, 786-794.

[206] Chetelat G, Desgranges B, De La Sayette V, Viader F, Eustache F, Baron JC (2002) Mapping gray matter loss with voxel-based morphometry in mild cognitive impairment. *Neuroreport* **13**, 1939-1943.

[207] Karas GB, Scheltens P, Rombouts SA, Visser PJ, van Schijndel RA, Fox NC, Barkhof F (2004) Global and local gray matter loss in mild cognitive impairment and Alzheimer's disease. *Neuroimage* **23**, 708-716.

[208] Pennanen C, Testa C, Laakso MP, Hallikainen M, Helkala EL, Hanninen T, Kivipelto M, Kononen M, Nissinen A, Tervo S, Vanhanen M, Vanninen R, Frisoni GB, Soininen H (2005) A voxel based morphometry study on mild cognitive impairment. *J Neurol Neurosurg Psychiatry* **76**, 11-14.

[209] Becker JT, Davis SW, Hayashi KM, Meltzer CC, Toga AW, Lopez OL, Thompson PM (2006) Three-dimensional patterns of hippocampal atrophy in mild cognitive impairment. *Arch Neurol* **63**, 97-101.

[210] Duarte A, Hayasaka S, Du A, Schuff N, Jahng GH, Kramer J, Miller B, Weiner M (2006) Volumetric correlates of memory and executive function in normal elderly, mild cognitive impairment and Alzheimer's disease. *Neurosci Lett* **406**, 60-65.

[211] Saykin AJ, Wishart HA, Rabin LA, Santulli RB, Flashman LA, West JD, McHugh TL, Mamourian AC (2006) Older adults with cognitive complaints show brain atrophy similar to that of amnestic MCI. *Neurology* **67**, 834-842.

[212] Zhang Y, Schuff N, Jahng GH, Bayne W, Mori S, Schad L, Mueller S, Du AT, Kramer JH, Yaffe K, Chui H, Jagust WJ, Miller BL, Weiner MW (2007) Diffusion tensor imaging of cingulum fibers in mild cognitive impairment and Alzheimer disease. *Neurology* **68**, 13-19.

[213] Fellgiebel A, Muller MJ, Wille P, Dellani PR, Scheurich A, Schmidt LG, Stoeter P (2005) Color-coded diffusion-tensor-imaging of posterior cingulate fiber tracts in mild cognitive impairment. *Neurobiol Aging* **26**, 1193-1198.

[214] Stahl R, Dietrich O, Teipel SJ, Hampel H, Reiser MF, Schoenberg SO (2007) White matter damage in Alzheimer disease and mild cognitive impairment: assessment with diffusion-tensor MR imaging and parallel imaging techniques. *Radiology* **243**, 483-492.

[215] Medina D, DeToledo-Morrell L, Urresta F, Gabrieli JD, Moseley M, Fleischman D, Bennett DA, Leurgans S, Turner DA, Stebbins GT (2006) White matter changes in mild cognitive impairment and AD: A diffusion tensor imaging study. *Neurobiol Aging* **27**, 663-672.

[216] Huang J, Friedland RP, Auchus AP (2007) Diffusion tensor imaging of normal-appearing white matter in mild cognitive impairment and early Alzheimer disease: preliminary evidence of axonal degeneration in the temporal lobe. *AJNR Am J Neuroradiol* **28**, 1943-1948.

[217] Kantarci K, Jack CR, Jr., Xu YC, Campeau NG, O'Brien PC, Smith GE, Ivnik RJ, Boeve BF, Kokmen E, Tangalos EG, Petersen RC (2001) Mild cognitive impairment and Alzheimer disease: regional diffusivity of water. *Radiology* **219**, 101-107.

[218] Rose SE, McMahon KL, Janke AL, O'Dowd B, de Zubicaray G, Strudwick MW, Chalk JB (2006) Diffusion indices on magnetic resonance imaging and neuropsychological performance in amnestic mild cognitive impairment. *J Neurol Neurosurg Psychiatry* **77**, 1122-1128.

[219] Dickerson BC, Salat DH, Greve DN, Chua EF, Rand-Giovannetti E, Rentz DM, Bertram L, Mullin K, Tanzi RE, Blacker D, Albert MS, Sperling RA (2005) Increased hippocampal activation in mild cognitive impairment compared to normal aging and AD. *Neurology* **65**, 404-411.

[220] Hamalainen A, Pihlajamaki M, Tanila H, Hanninen T, Niskanen E, Tervo S, Karjalainen PA, Vanninen RL, Soininen H (2007) Increased fMRI responses during encoding in mild cognitive impairment. *Neurobiol Aging* **28**, 1889-1903.

[221] Miller SL, Fenstermacher E, Bates J, Blacker D, Sperling RA, Dickerson BC (2008) Hippocampal activation in adults with mild cognitive impairment predicts subsequent cognitive decline. *J Neurol Neurosurg Psychiatry* **79**, 630-635.

[222] Kircher TT, Weis S, Freymann K, Erb M, Jessen F, Grodd W, Heun R, Leube DT (2007) Hippocampal activation in patients with mild cognitive impairment is necessary for suc-

cessful memory encoding. *J Neurol Neurosurg Psychiatry* **78**, 812-818.

[223] Sperling R (2007) Functional MRI studies of associative encoding in normal aging, mild cognitive impairment, and Alzheimer's disease. *Ann N Y Acad Sci* **1097**, 146-155.

[224] Bokde AL, Lopez-Bayo P, Meindl T, Pechler S, Born C, Faltraco F, Teipel SJ, Moller HJ, Hampel H (2006) Functional connectivity of the fusiform gyrus during a face-matching task in subjects with mild cognitive impairment. *Brain* **129**, 1113-1124.

[225] Petrella JR, Wang L, Krishnan S, Slavin MJ, Prince SE, Tran TT, Doraiswamy PM (2007) Cortical deactivation in mild cognitive impairment: high-field-strength functional MR imaging. *Radiology* **245**, 224-235.

[226] Bai F, Zhang Z, Yu H, Shi Y, Yuan Y, Zhu W, Zhang X, Qian Y (2008) Default-mode network activity distinguishes amnestic type mild cognitive impairment from healthy aging: a combined structural and resting-state functional MRI study. *Neurosci Lett* **438**, 111-115.

[227] Morris JC, Storandt M, McKeel DW Jr, Rubin EH, Price JL, Grant EA, Berg L (1996) Cerebral amyloid deposition and diffuse plaques in "normal" aging: Evidence for presymptomatic and very mild Alzheimer's disease. *Neurology* **46**, 707-719.

[228] Apostolova LG, Hwang KS, Andrawis JP, Green AE, Babakchanian S, Morra JH, Cummings JL, Toga AW, Trojanowski JQ, Shaw LM, Jack CR Jr, Petersen RC, Aisen PS, Jagust WJ, Koeppe RA, Mathis CA, Weiner MW, Thompson PM, Alzheimer's Disease Neuroimaging I (2010) 3D PIB and CSF biomarker associations with hippocampal atrophy in ADNI subjects. *Neurobiol Aging* **31**, 1284-1303.

[229] Rowe CC, Ellis KA, Rimajova M, Bourgeat P, Pike KE, Jones G, Fripp J, Tochon-Danguy H, Morandeau L, O'Keefe G, Price R, Raniga P, Robins P, Acosta O, Lenzo N, Szoeke C, Salvado O, Head R, Martins R, Masters CL, Ames D, Villemagne VL (2010) Amyloid imaging results from the Australian Imaging, Biomarkers and Lifestyle (AIBL) study of aging. *Neurobiol Aging* **31**, 1275-1283.

[230] Jagust WJ, Landau SM, Shaw LM, Trojanowski JQ, Koeppe RA, Reiman EM, Foster NL, Petersen RC, Weiner MW, Price JC, Mathis CA, Alzheimer's Disease Neuroimaging I (2009) Relationships between biomarkers in aging and dementia. *Neurology* **73**, 1193-1199.

[231] Mormino EC, Kluth JT, Madison CM, Rabinovici GD, Baker SL, Miller BL, Koeppe RA, Mathis CA, Weiner MW, Jagust WJ (2009) Episodic memory loss is related to hippocampal-mediated {beta}-amyloid deposition in elderly subjects. *Brain* **132**, 1310-1323.

[232] Chetelat G, Villemagne VL, Pike KE, Ellis KA, Bourgeat P, Jones G, O'Keefe GJ, Salvado O, Szoeke C, Martins RN, Ames D, Masters CL, Rowe CC, the Australian Imaging B, Lifestyle Study of ageing Research G (2011) Independent contribution of temporal beta-amyloid deposition to memory decline in the pre-dementia phase of Alzheimer's disease. *Brain* **134**, 798-807.

[233] Risacher SL, Saykin AJ, West JD, Shen L, Firpi HA, McDonald BC, Alzheimer's Disease Neuroimaging I (2009) Baseline MRI predictors of conversion from MCI to probable AD in the ADNI cohort. *Curr Alzheimer Res* **6**, 347-361.

[234] Petersen RC (2006) Conversion. *Neurology* **67**, S12-S13.

[235] Evans MC, Barnes J, Nielsen C, Kim LG, Clegg SL, Blair M, Leung KK, Douiri A, Boyes RG, Ourselin S, Fox NC, Alzheimer's Disease Neuroimaging I (2010) Volume

changes in Alzheimer's disease and mild cognitive impairment: cognitive associations. *Eur Radiol* **20**, 674-682.

[236] Jack CR, Petersen RC, Xu YC, O'Brien PC, Smith GE, Ivnik RJ, Boeve BF, Waring SC, Tangalos EG, Kokmen E (1999) Predicition of AD with MRI-based hippocampal volume in mild cognitive impairmnet. *Neurology* **52**, 1397-1403.

[237] Geroldi C, Rossi R, Calvagna C, Testa C, Bresciani L, Binetti G, Zanetti O, Frisoni GB (2006) Medial temporal atrophy but not memory deficit predicts progression to dementia in patients with mild cognitive impairment. *J Neurol Neurosurg Psychiatry* **77**, 1219-1222.

[238] Duara R, Loewenstein DA, Potter E, Appel J, Greig MT, Urs R, Shen Q, Raj A, Small B, Barker W, Schofield E, Wu Y, Potter H (2008) Medial temporal lobe atrophy on MRI scans and the diagnosis of Alzheimer disease. *Neurology* **71**, 1986-1992.

[239] deToledo-Morrell L, Stoub TR, Bulgakova M, Wilson RS, Bennett DA, Leurgans S, Wuu J, Turner DA (2004) MRI-derived entorhinal volume is a good predictor of conversion from MCI to AD. *Neurobiol Aging* **25**, 1197-1203.

[240] Tapiola T, Pennanen C, Tapiola M, Tervo S, Kivipelto M, Hanninen T, Pihlajamaki M, Laakso MP, Hallikainen M, Hamalainen A, Vanhanen M, Helkala EL, Vanninen R, Nissinen A, Rossi R, Frisoni GB, Soininen H (2008) MRI of hippocampus and entorhinal cortex in mild cognitive impairment: a follow-up study. *Neurobiol Aging* **29**, 31-38.

[241] Apostolova LG, Dutton RA, Dinov ID, Hayashi KM, Toga AW, Cummings JL, Thompson PM (2006) Conversion of mild cognitive impairment to Alzheimer disease predicted by hippocampal atrophy maps. *Arch Neurol* **63**, 693-699.

[242] Devanand DP, Pradhaban G, Liu X, Khandji A, De Santi S, Segal S, Rusinek H, Pelton GH, Honig LS, Mayeux R, Stern Y, Tabert MH, de Leon MJ (2007) Hippocampal and entorhinal atrophy in mild cognitive impairment: prediction of Alzheimer disease. *Neurology* **68**, 828-836.

[243] Eckerstrom C, Olsson E, Borga M, Ekholm S, Ribbelin S, Rolstad S, Starck G, Edman A, Wallin A, Malmgren H (2008) Small baseline volume of left hippocampus is associated with subsequent conversion of MCI into dementia: the Goteborg MCI study. *J Neurol Sci* **272**, 48-59.

[244] Karas G, Sluimer J, Goekoop R, van der Flier W, Rombouts SA, Vrenken H, Scheltens P, Fox N, Barkhof F (2008) Amnestic mild cognitive impairment: structural MR imaging findings predictive of conversion to Alzheimer disease. *AJNR Am J Neuroradiol* **29**, 944-949.

[245] Fellgiebel A, Dellani PR, Greverus D, Scheurich A, Stoeter P, Muller MJ (2006) Predicting conversion to dementia in mild cognitive impairment by volumetric and diffusivity measurements of the hippocampus. *Psychiatry Res* **146**, 283-287.

[246] Teipel SJ, Born C, Ewers M, Bokde AL, Reiser MF, Moller HJ, Hampel H (2007) Multivariate deformation-based analysis of brain atrophy to predict Alzheimer's disease in mild cognitive impairment. *Neuroimage* **38**, 13-24.

[247] Misra C, Fan Y, Davatzikos C (2009) Baseline and longitudinal patterns of brain atrophy in MCI patients, and their use in prediction of short-term conversion to AD: results from ADNI. *Neuroimage* **44**, 1415-1422.

[248] Duchesne S, Bocti C, De Sousa K, Frisoni GB, Chertkow H, Collins DL (2010) Amnestic MCI future clinical status prediction using baseline MRI features. *Neurobiol Aging* **31**, 1606-1617.

[249] Ewers M, Walsh C, Trojanowski JQ, Shaw LM, Petersen RC, Jack CR Jr, Feldman HH, Bokde AL, Alexander GE, Schel-

tens P, Vellas B, Dubois B, Weiner M, Hampel H, North American Alzheimer's Disease Neuroimaging I (2010) Prediction of conversion from mild cognitive impairment to Alzheimer's disease dementia based upon biomarkers and neuropsychological test performance. *Neurobiol Aging* Epub 2010/12/17.

[250] Hinrichs C, Singh V, Xu G, Johnson SC, The Alzheimers Disease Neuroimaging I (2011) Predictive markers for AD in a multi-modality framework: An analysis of MCI progression in the ADNI population. *Neuroimage* **55**, 574-589.

[251] Chetelat G, Landeau B, Eustache F, Mezenge F, Viader F, de la Sayette V, Desgranges B, Baron JC (2005) Using voxel-based morphometry to map the structural changes associated with rapid conversion in MCI: a longitudinal MRI study. *Neuroimage* **27**, 934-946.

[252] Chetelat G, Fouquet M, Kalpouzos G, Denghien I, De la Sayette V, Viader F, Mezenge F, Landeau B, Baron JC, Eustache F, Desgranges B (2008) Three-dimensional surface mapping of hippocampal atrophy progression from MCI to AD and over normal aging as assessed using voxel-based morphometry. *Neuropsychologia* **46**, 1721-1731.

[253] Risacher SL, Shen L, West JD, Kim S, McDonald BC, Beckett LA, Harvey DJ, Jack CR Jr, Weiner MW, Saykin AJ, Alzheimer's Disease Neuroimaging I (2010) Longitudinal MRI atrophy biomarkers: relationship to conversion in the ADNI cohort. *Neurobiol Aging* **31**, 1401-1418.

[254] Jack CR Jr, Shiung MM, Weigand SD, O'Brien PC, Gunter JL, Boeve BF, Knopman DS, Smith GE, Ivnik RJ, Tangalos EG, Petersen RC (2005) Brain atrophy rates predict subsequent clinical conversion in normal elderly and amnestic MCI. *Neurology* **65**, 1227-1231.

[255] Spulber G, Niskanen E, Macdonald S, Smilovici O, Chen K, Reiman EM, Jauhiainen AM, Hallikainen M, Tervo S, Wahlund LO, Vanninen R, Kivipelto M, Soininen H (2010) Whole brain atrophy rate predicts progression from MCI to Alzheimer's disease. *Neurobiol Aging* **31**, 1601-1605.

[256] Hua X, Hibar DP, Lee S, Toga AW, Jack CR, Jr., Weiner MW, Thompson PM, Alzheimer's Disease Neuroimaging I (2010) Sex and age differences in atrophic rates: an ADNI study with n = 1368 MRI scans. *Neurobiol Aging* **31**, 1463-1480.

[257] Li Y, Wang Y, Wu G, Shi F, Zhou L, Lin W, Shen D, The Alzheimer's Disease Neuroimaging I (2011) Discriminant analysis of longitudinal cortical thickness changes in Alzheimer's disease using dynamic and network features. *Neurobiol Aging* (in press).

[258] Huang C, Wahlund LO, Svensson L, Winblad B, Julin P (2002) Cingulate cortex hypoperfusion predicts Alzheimer's disease in mild cognitive impairment. *BMC Neuro* **2**, 9.

[259] Borroni B, Anchisi D, Paghera B, Vicini B, Kerrouche N, Garibotto V, Terzi A, Vignolo LA, Di Luca M, Giubbini R, Padovani A, Perani D (2006) Combined 99mTc-ECD SPECT and neuropsychological studies in MCI for the assessment of conversion to AD. *Neurobiol Aging* **27**, 24-31.

[260] Caroli A, Testa C, Geroldi C, Nobili F, Barnden LR, Guerra UP, Bonetti M, Frisoni GB (2007) Cerebral perfusion correlates of conversion to Alzheimer's disease in amnestic mild cognitive impairment. *J Neurol* **254**, 1698-1707.

[261] Drzezga A, Lautenschlager N, Siebner H, Riemenschneider M, Willoch F, Minoshima S, Schwaiger M, Kurz A (2003) Cerebral metabolic changes accompanying conversion of mild cognitive impairment into Alzheimer's disease: a PET follow-up study. *Eur J Nucl Med Mol Imaging* **30**, 1104-1113.

[262] Drzezga A, Grimmer T, Riemenschneider M, Lautenschlager N, Siebner H, Alexopoulus P, Minoshima S, Schwaiger M, Kurz A (2005) Prediction of individual clinical outcome in MCI by means of genetic assessment and (18)F-FDG PET. *J Nucl Med* **46**, 1625-1632.

[263] Mosconi L, Perani D, Sorbi S, Herholz K, Nacmias B, Holthoff V, Salmon E, Baron JC, De Cristofaro MT, Padovani A, Borroni B, Franceschi M, Bracco L, Pupi A (2004) MCI conversion to dementia and the APOE genotype: a prediction study with FDG-PET. *Neurology* **63**, 2332-2340.

[264] Landau SM, Harvey D, Madison CM, Koeppe RA, Reiman EM, Foster NL, Weiner MW, Jagust WJ, the Alzheimer's Disease Neuroimaging I (2011) Associations between cognitive, functional, and FDG-PET measures of decline in AD and MCI. *Neurobiol Aging* **32**, 1207-1218.

[265] Yuan Y, Gu ZX, Wei WS (2009) Fluorodeoxyglucose-Positron-Emission Tomography, Single-Photon Emission Tomography, and Structural MR Imaging for Prediction of Rapid Conversion to Alzheimer Disease in Patients with Mild Cognitive Impairment: A Meta-Analysis. *AJNR Am J Neuroradiol* **30**, 404-410.

[266] Chetelat G, Desgranges B, de la Sayette V, Viader F, Eustache F, Baron JC (2003) Mild cognitive impairment: Can FDG-PET predict who is to rapidly convert to Alzheimer's disease? *Neurology* **60**, 1374-1377.

[267] Chetelat G, Eustache F, Viader F, De La Sayette V, Pelerin A, Mezenge F, Hannequin D, Dupuy B, Baron JC, Desgranges B (2005) FDG-PET measurement is more accurate than neuropsychological assessments to predict global cognitive deterioration in patients with mild cognitive impairment. *Neurocase* **11**, 14-25.

[268] Petrella JR, Prince SE, Wang L, Hellegers C, Doraiswamy PM (2007) Prognostic value of posteromedial cortex deactivation in mild cognitive impairment. *PLoS ONE* **2**, e1104.

[269] O'Brien JL, O'Keefe KM, LaViolette PS, DeLuca AN, Blacker D, Dickerson BC, Sperling RA (2010) Longitudinal fMRI in elderly reveals loss of hippocampal activation with clinical decline. *Neurology* **74**, 1969-1976.

[270] Villemagne VL, Pike KE, Darby D, Maruff P, Savage G, Ng S, Ackermann U, Cowie TF, Currie J, Chan SG, Jones G, Tochon-Danguy H, O'Keefe G, Masters CL, Rowe CC (2008) Abeta deposits in older non-demented individuals with cognitive decline are indicative of preclinical Alzheimer's disease. *Neuropsychologia* **46**, 1688-1697.

[271] Okello A, Koivunen J, Edison P, Archer HA, Turkheimer FE, Nagren K, Bullock R, Walker Z, Kennedy A, Fox NC, Rossor MN, Rinne JO, Brooks DJ (2009) Conversion of amyloid positive and negative MCI to AD over 3 years: an 11C-PIB PET study. *Neurology* **73**, 754-760.

[272] Kohannim O, Hua X, Hibar DP, Lee S, Chou YY, Toga AW, Jack CR Jr, Weiner MW, Thompson PM, Alzheimer's Disease Neuroimaging I (2010) Boosting power for clinical trials using classifiers based on multiple biomarkers. *Neurobiol Aging* **31**, 1429-1442.

[273] Good CD, Johnsrude IS, Ashburner J, Henson RN, Friston KJ, Frackowiak RS (2001) A voxel-based morphometric study of ageing in 465 normal adult human brains. *Neuroimage* **14**, 21-36.

[274] Taki Y, Goto R, Evans A, Zijdenbos A, Neelin P, Lerch J, Sato K, Ono S, Kinomura S, Nakagawa M, Sugiura M, Watanabe J, Kawashima R, Fukuda H (2004) Voxel-based morphometry of human brain with age and cerebrovascular risk factors. *Neurobiol Aging* **25**, 455-463.

[275] Fotenos AF, Snyder AZ, Girton LE, Morris JC, Buckner RL (2005) Normative estimates of cross-sectional and longitudinal brain volume decline in aging and AD. *Neurology* **64**, 1032-1039.

[276] Smith CD, Chebrolu H, Wekstein DR, Schmitt FA, Markesbery WR (2007) Age and gender effects on human brain anatomy: a voxel-based morphometric study in healthy elderly. *Neurobiol Aging* **28**, 1075-1087.

[277] Wu YC, Field AS, Whalen PJ, Alexander AL (2011) Age- and gender-related changes in the normal human brain using hybrid diffusion imaging (HYDI). *Neuroimage* **54**, 1840-1853.

[278] Carlson NE, Moore MM, Dame A, Howieson D, Silbert LC, Quinn JF, Kaye JA (2008) Trajectories of brain loss in aging and the development of cognitive impairment. *Neurology* **70**, 828-833.

[279] Honea RA, Swerdlow RH, Vidoni ED, Burns JM (2011) Progressive regional atrophy in normal adults with a maternal history of Alzheimer disease. *Neurology* **76**, 822-829.

[280] Kaye JA, Swihart T, Howieson D, Dame A, Moore MM, Karnos T, Camicioli R, Ball M, Oken B, Sexton G (1997) Volume loss of the hippocampus and temporal lobe in healthy elderly persons destined to develop dementia. *Neurology* **48**, 1297-1304.

[281] Jack CR, Jr., Shiung MM, Weigand SD, OrsquoBrien PC, Gunter JL, Boeve BF, Knopman DS, Smith GE, Ivnik RJ, Tangalos EG, Petersen RC, Jack CR Jr, Shiung MM, Gunter JL, OrsquoBrien PC, Weigand SD, Knopman DS, Boeve BF, Ivnik RJ, Smith GE, Cha RH, Tangalos EG, Petersen RC (2005) Brain atrophy rates predict subsequent clinical conversion in normal elderly and amnestic MCI Comparison of different MRI brain atrophy rate measures with clinical disease progression in AD. *Neurology* **65**, 1227-1231.

[282] Adak S, Illouz K, Gorman W, Tandon R, Zimmerman EA, Guariglia R, Moore MM, Kaye JA (2004) Predicting the rate of cognitive decline in aging and early Alzheimer disease. *Neurology* **63**, 108-114.

[283] Apostolova LG, Mosconi L, Thompson PM, Green AE, Hwang KS, Ramirez A, Mistur R, Tsui WH, de Leon MJ (2010) Subregional hippocampal atrophy predicts Alzheimer's dementia in the cognitively normal. *Neurobiol Aging* **31**, 1077-1088.

[284] Wishart HA, Saykin AJ, McAllister TW, Rabin LA, McDonald BC, Flashman LA, Roth RM, Mamourian AC, Tsongalis GJ, Rhodes CH (2006) Regional brain atrophy in cognitively intact adults with a single APOE epsilon4 allele. *Neurology* **67**, 1221-1224.

[285] Jagust W, Gitcho A, Sun F, Kuczynski B, Mungas D, Haan M (2006) Brain imaging evidence of preclinical Alzheimer's disease in normal aging. *Ann Neurol* **59**, 673-681.

[286] Murphy EA, Holland D, Donohue M, McEvoy LK, Hagler DJ, Dale AM, Brewer JB, Alzheimer's Disease Neuroimaging I (2010) Six-month atrophy in MTL structures is associated with subsequent memory decline in elderly controls. *Neuroimage* **53**, 1310-1317.

[287] den Heijer T, Geerlings MI, Hoebeek FE, Hofman A, Koudstaal PJ, Breteler MM (2006) Use of hippocampal and amygdalar volumes on magnetic resonance imaging to predict dementia in cognitively intact elderly people. *Arch Gen Psychiatry* **63**, 57-62.

[288] den Heijer T, van der Lijn F, Koudstaal PJ, Hofman A, van der Lugt A, Krestin GP, Niessen WJ, Breteler MM (2010) A 10-year follow-up of hippocampal volume on magnetic resonance imaging in early dementia and cognitive decline. *Brain* **133**, 1163-1172.

[289] Smith CD, Chebrolu H, Wekstein DR, Schmitt FA, Jicha GA, Cooper G, Markesbery WR (2007) Brain structural alterations before mild cognitive impairment. *Neurology* **68**, 1268-1273.

[290] Smith CD, Chebrolu H, Markesbery WR, Liu J (2008) Improved Predictive Model for Presymptomatic Mild Cognitive Impairment and Alzheimer's Disease. *Neurological Research*. (In Press).

[291] Smith CD, Chebrolu H, Andersen AH, Powell DA, Lovell MA, Xiong S, Gold BT (2010) White matter diffusion alterations in normal women at risk of Alzheimer's disease. *Neurobiol Aging* **31**, 1122-1131.

[292] Nierenberg J, Pomara N, Hoptman MJ, Sidtis JJ, Ardekani BA, Lim KO (2005) Abnormal white matter integrity in healthy apolipoprotein E epsilon4 carriers. *Neuroreport* **16**, 1369-1372.

[293] Ringman JM, O'Neill J, Geschwind D, Medina L, Apostolova LG, Rodriguez Y, Schaffer B, Varpetian A, Tseng B, Ortiz F, Fitten J, Cummings JL, Bartzokis G (2007) Diffusion tensor imaging in preclinical and presymptomatic carriers of familial Alzheimer's disease mutations. *Brain* **130**, 1767-1776.

[294] de Leon MJ, Convit A, Wolf OT, Tarshish CY, DeSanti S, Rusinek H, Tsui W, Kandil E, Scherer AJ, Roche A, Imossi A, Thorn E, Bobinski M, Caraos C, Lesbre P, Schlyer D, Poirier J, Reisberg B, Fowler J (2001) Prediction of cognitive decline in normal elderly subjects with 2-[(18)F]fluoro-2-deoxy-D-glucose/poitron-emission tomography (FDG/PET). *Proc Natl Acad Sci U S A* **98**, 10966-10971.

[295] Mosconi L, De Santi S, Li J, Tsui WH, Li Y, Boppana M, Laska E, Rusinek H, de Leon MJ (2008) Hippocampal hypometabolism predicts cognitive decline from normal aging. *Neurobiol Aging* **29**, 676-692.

[296] Johnson KA, Lopera F, Jones K, Becker A, Sperling R, Hilson J, Londono J, Siegert I, Arcos M, Moreno S, Madrigal L, Ossa J, Pineda N, Ardila A, Roselli M, Albert MS, Kosik KS, Rios A (2001) Presenilin-1-associated abnormalities in regional cerebral perfusion. *Neurology* **56**, 1545-1551.

[297] Stefanova E, Nilsson A, Andersson J, Axelman K, Langstrom B, Viitanen M, Lannfelt L, Nordberg A (2002) In ICAD, Kyoto, Japan, p. 1743.

[298] Small GW, Ercoli LM, Silverman DH, Huang SC, Komo S, Bookheimer SY, Lavretsky H, Miller K, Siddarth P, Rasgon NL, Mazziotta JC, Saxena S, Wu HM, Mega MS, Cummings JL, Saunders AM, Pericak-Vance MA, Roses AD, Barrio JR, Phelps ME (2000) Cerebral metabolic and cognitive decline in persons at genetic risk for Alzheimer's disease. *Proc Natl Acad Sci U S A* **97**, 6037-6042.

[299] Reiman EM, Caselli RJ, Yun LS, Chen K, Bandy D, Minoshima S, Thibodeau SN, Osborne D (1996) Preclinical evidence of Alzheimer's disease in persons homozygous for the epsilon 4 allele for apolipoprotein E. *N Engl J Med* **334**, 752-758.

[300] Langbaum JB, Chen K, Caselli RJ, Lee W, Reschke C, Bandy D, Alexander GE, Burns CM, Kaszniak AW, Reeder SA, Corneveaux JJ, Allen AN, Pruzin J, Huentelman MJ, Fleisher AS, Reiman EM (2010) Hypometabolism in Alzheimer-affected brain regions in cognitively healthy Latino individuals carrying the apolipoprotein E epsilon4 allele. *Arch Neurol* **67**, 462-468.

[301] Mosconi L, Berti V, Swerdlow RH, Pupi A, Duara R, de Leon M (2010) Maternal transmission of Alzheimer's disease: prodromal metabolic phenotype and the search for genes. *Hum Genomics* **4**, 170-193.

[302] Baker LD, Cross DJ, Minoshima S, Belongia D, Watson GS, Craft S (2011) Insulin resistance and Alzheimer-like reductions in regional cerebral glucose metabolism for cognitively normal adults with prediabetes or early type 2 diabetes. *Arch Neurol* **68**, 51-57.

[303] Reiman EM, Chen K, Langbaum JB, Lee W, Reschke C, Bandy D, Alexander GE, Caselli RJ (2010) Higher serum total cholesterol levels in late middle age are associated with glucose hypometabolism in brain regions affected by Alzheimer's disease and normal aging. *Neuroimage* **49**, 169-176.

[304] Smith CD, Andersen AH, Kryscio RJ, Schmitt FA, Kindy MS, Blonder LX, Avison MJ (1999) Altered Brain Activation in Normal Subjects at Risk for Alzheimer's Disease. *Neurology* **54**, 1391-1396.

[305] Trivedi MA, Schmitz TW, Ries ML, Torgerson BM, Sager MA, Hermann BP, Asthana S, Johnson SC (2006) Reduced hippocampal activation during episodic encoding in middle-aged individuals at genetic risk of Alzheimer's disease: a cross-sectional study. *BMC Me* **4**, 1.

[306] Seidenberg M, Guidotti L, Nielson KA, Woodard JL, Durgerian S, Antuono P, Zhang Q, Rao SM (2009) Semantic memory activation in individuals at risk for developing Alzheimer disease. *Neurology* **73**, 612-620.

[307] Quiroz YT, Budson AE, Celone K, Ruiz A, Newmark R, Castrillon G, Lopera F, Stern CE (2010) Hippocampal hyperactivation in presymptomatic familial Alzheimer's disease. *Ann Neurol* **68**, 865-875.

[308] Acosta-Baena N, Sepulveda-Falla D, Lopera-Gomez CM, Jaramillo-Elorza MC, Moreno S, Aguirre-Acevedo DC, Saldarriaga A, Lopera F (2011) Pre-dementia clinical stages in presenilin 1 E280A familial early-onset Alzheimer's disease: a retrospective cohort study. *Lancet Neurol* **10**, 213-220.

[309] Smith CD, Andersen AH, Kryscio RJ, Schmitt FA, Kindy MS, Blonder LX, Avison MJ (2002) Women at risk for AD show increased parietal activation during a fluency task. *Neurology* **58**, 1197-1202.

[310] Wishart HA, Saykin AJ, Rabin LA, Santulli RB, Flashman LA, Guerin SJ, Mamourian AC, Belloni DR, Rhodes CH, McAllister TW (2006) Increased brain activation during working memory in cognitively intact adults with the APOE epsilon4 allele. *American Journal of Psychiatry* **163**, 1603-1610.

[311] Bondi MW, Houston WS, Eyler LT, Brown GG (2005) fMRI evidence of compensatory mechanisms in older adults at genetic risk for Alzheimer disease. *Neurology* **64**, 501-508.

[312] Fleisher AS, Houston WS, Eyler LT, Frye S, Jenkins C, Thal LJ, Bondi MW (2005) Identification of Alzheimer disease risk by functional magnetic resonance imaging. *Arch Neurol* **62**, 1881-1888.

[313] Bookheimer SY, Strojwas MH, Cohen MS, Saunders AM, Pericak-Vance MA, Mazziotta JC, Small GW (2000) Patterns of brain activation in people at risk for Alzheimer's disease. *N Engl J Med* **343**, 450-456.

[314] Burggren AC, Small GW, Sabb FW, Bookheimer SY (2002) Specificity of brain activation patterns in people at genetic risk for Alzheimer disease. *Am J Geriatr Psychiatry* **10**, 44-51.

[315] Mosconi L, Rinne JO, Tsui WH, Berti V, Li Y, Wang H, Murray J, Scheinin N, Nagren K, Williams S, Glodzik L, De Santi S, Vallabhajosula S, de Leon MJ (2010) Increased fibrillar amyloid-{beta} burden in normal individuals with a family history of late-onset Alzheimer's. *Proc Natl Acad Sci U S A* **107**, 5949-5954.

[316] Reiman EM, Chen K, Liu X, Bandy D, Yu M, Lee W, Ayutyanont N, Keppler J, Reeder SA, Langbaum JB, Alexander GE, Klunk WE, Mathis CA, Price JC, Aizenstein HJ, DeKosky ST, Caselli RJ (2009) Fibrillar amyloid-beta burden in cognitively normal people at 3 levels of genetic risk for Alzheimer's disease. *Proc Natl Acad Sci U S A* **106**, 6820-6825.

[317] Small GW, Siddarth P, Burggren AC, Kepe V, Ercoli LM, Miller KJ, Lavretsky H, Thompson PM, Cole GM, Huang SC, Phelps ME, Bookheimer SY, Barrio JR (2009) Influence of cognitive status, age, and APOE-4 genetic risk on brain FDDNP positron-emission tomography imaging in persons without dementia. *Arch Gen Psychiatry* **66**, 81-87.

[318] Small GW, Kepe V, Ercoli LM, Siddarth P, Bookheimer SY, Miller KJ, Lavretsky H, Burggren AC, Cole GM, Vinters HV, Thompson PM, Huang SC, Satyamurthy N, Phelps ME, Barrio JR (2006) PET of brain amyloid and tau in mild cognitive impairment. *N Engl J Med* **355**, 2652-2663.

[319] Morris JC, Roe CM, Grant EA, Head D, Storandt M, Goate AM, Fagan AM, Holtzman DM, Mintun MA (2009) Pittsburgh compound B imaging and prediction of progression from cognitive normality to symptomatic Alzheimer disease. *Arch Neurol* **66**, 1469-1475.

[320] Storandt M, Mintun MA, Head D, Morris JC (2009) Cognitive decline and brain volume loss as signatures of cerebral amyloid-beta peptide deposition identified with Pittsburgh compound B: cognitive decline associated with Abeta deposition. *Arch Neurol* **66**, 1476-1481.

[321] Resnick SM, Sojkova J, Zhou Y, An Y, Ye W, Holt DP, Dannals RF, Mathis CA, Klunk WE, Ferrucci L, Kraut MA, Wong DF (2010) Longitudinal cognitive decline is associated with fibrillar amyloid-beta measured by [11C]PiB. *Neurology* **74**, 807-815.

[322] Bourgeat P, Chetelat G, Villemagne VL, Fripp J, Raniga P, Pike K, Acosta O, Szoeke C, Ourselin S, Ames D, Ellis KA, Martins RN, Masters CL, Rowe CC, Salvado O, Group AR (2010) Beta-amyloid burden in the temporal neocortex is related to hippocampal atrophy in elderly subjects without dementia. *Neurology* **74**, 121-127.

[323] Cummings JL, Doody R, Clark C (2007) Disease-modifying therapies for Alzheimer disease: challenges to early intervention. *Neurology* **69**, 1622-1634.

[324] Hoyert DL, Heron MP, Murphy SL, Kung H-C (2006) Deaths: Final Data for 2003. *National Vital Statistics Reports* **54**, 23-24.

[325] Yesavage JA, O'Hara R, Kraemer H, Noda A, Taylor JL, Ferris S, Gely-Nargeot MC, Rosen A, Friedman L, Sheikh J, Derouesne C (2002) Modeling the prevalence and incidence of Alzheimer's disease and mild cognitive impairment. *J Psychiatr Res* **36**, 281-286.

[326] Ohm TG, Muller H, Braak H, Bohl J (1995) Close-meshed prevalence rates of different stages as a tool to uncover the rate of Alzheimer's disease-related neurofibrillary changes. *Neuroscience* **64**, 209-217.

[327] Smith CD, Chebrolu H, Wekstein DR, Schmitt FA, Markesbery WR (2007) Age and gender effects on human brain anatomy: A voxel-based morphometric study in healthy elderly. *Neurobiol Aging* **28**, 1075-1087.

729

Discriminating Alzheimer's Patients from Cognitively Normal Older Adults Based on Hippocampal Volumes - Voxel-Based Morphometry with DARTEL and Standard Registration Versus Manual Volumetry

Henry Ka-Fung Mak[a,e,f,*], Zhipeng Zhang[a], Kelvin Kai-Wing Yau[b], Linda Zhang[a], Queenie Chan[c] and Leung-Wing Chu[d,e,f]

[a]*Department of Diagnostic Radiology, Li Ka Shing Faculty of Medicine, The University of Hong Kong, Hong Kong, China*

[b]*Department of Management Sciences, City University of Hong Kong, Hong Kong, China*

[c]*Philips Healthcare, Hong Kong, Hong Kong, China*

[d]*Division of Geriatric Medicine, Department of Medicine, Queen Mary Hospital, Hong Kong, Hong Kong, China*

[e]*Alzheimer's Disease Research Network, The University of Hong Kong, Hong Kong, China*

[f]*Research Centre of Heart, Brain, Hormone & Healthy Aging, Li Ka Shing Faculty of Medicine, The University of Hong Kong, Hong Kong, China*

Abstract. Hippocampal atrophy on Magnetic Resonance Imaging (MRI) has been increasingly used as a supportive feature for the diagnosis of Alzheimer's patients. We attempt to compare voxel-based morphometry (VBM) with DARTEL and standard registration versus manual hippocampal volumetry in discriminating Alzheimer's disease (AD) patients from cognitively normal older adults.

Participants were 20 cognitively normal elderly subjects and 19 AD patients who met the criteria of probable AD according to NINCDS-ADRDA. High resolution T1-weighted (T1W) 3D volumetric Fast Field Echo sequence was obtained using 3.0-Tesla scanner. Bilateral manual hippocampal volumetry (ANALYZE 7.0 software) and VBM hippocampal region-of-interests (using hippocampal masks MARINA) were generated with DARTEL and standard registration (Statistical Parametric Mapping SPM5 software). Normalization with total intracranial volumes was employed for both methods.

All normalized hippocampal measurements showed significant reduction (20–30%; $p < 0.001$) in AD compared to controls. Logistic regression analysis also showed significant effects (odds ratios ranged from 88.2% to 94.0%) of all normalized measurements in predicting AD incidence after adjusting for age, gender, and education. The overall prediction accuracies of manual RH and LH volumes, standard RH-ROI and LH-ROI VBM, DARTEL RH-ROI and LH-ROI VBM were 87.2%, 84.6%, 87.2%, 76.9%, 87.2%, and 87.2%, respectively. VBM with DARTEL and standard registration have similarly high efficacies as manual hippocampal volumetry in discriminating AD from cognitively normal elderly adults.

---

*Correspondence to: Henry Ka-Fung Mak, Department of Diagnostic Radiology, Li Ka Shing Faculty of Medicine, The University of Hong Kong, Hong Kong, China. E-mail: makkf@hkucc.hku.hk.

INTRODUCTION

Structural magnetic resonance imaging (MRI) has been increasingly used to aid the diagnosis of AD and other forms of dementia [1]. Numerous cross-sectional studies found that AD patients have a reduction in the volumes of medial temporal structures such as the entorhinal cortex and the hippocampus [1, 2]. Total brain and regional atrophy rates by MRI were also found to be predictors for disease progression in AD and mild cognitive impairment (MCI) by previous longitudinal studies [3]. In the new research criteria proposed by Dubois et al. [4], presence of medial temporal lobe atrophy evidenced on MRI based on qualitative rating or quantitative volumetry of regions-of-interest (ROIs) was a supportive feature for the diagnosis of probable AD,

Due to rapid developments in computer science, computational neuroanatomy has gained widespread acceptance in neuroscience. A large variety of methods have been specifically developed for cross-sectional and longitudinal studies of normal aging, AD and MCI in the past decade [5]. One of these methods, Ashburner and Friston's voxel-based morphometry (VBM) [6], has been extensively used as an imaging biomarker to study regional grey matter loss [7–12]. Unlike deformation-based morphometry which deals with macroscopic differences in brain shape, VBM examines local composition of brain tissue after macroscopic differences have been discounted [13]. The merits of VBM include greater sensitivity for localizing small scale regional differences in grey or white matter and easier implementation within capabilities of most research units.

One major limitation of VBM is that imperfectly registered MR images to a common template can lead to false estimates [14]. The major objection is that VBM is sensitive to systematic shape differences attributable to misregistration from the spatial normalization step [15]. The introduction of DARTEL, based on a more sophisticated registration model [16], is a promising approach to solve this problem.

Recently, DARTEL has been employed as an image processing tool of computer based diagnostic image analysis in clinical practice [17]. Since SPM5 is a popular research tool [18], validated use of VBM with DARTEL registration is expected to expedite future AD research such as MCI conversion [12] and drug trials.

In the current study, we compare the accuracy of hippocampal-ROI VBM (with DARTEL and standard registration) to manual hippocampal volumetry in discriminating AD and cognitively normal elderly adults.

MATERIALS AND METHODS

Subjects

Participants in this retrospective study consisted of 20 elderly healthy control (HC) subjects without cognitive impairment (17 females, 3 males) and 20 AD patients (14 females, 5 males) who met the criteria for Alzheimer's disease. One AD patient was excluded as a final clinical diagnosis of cerebral amyloid angiopathy was made based on MRI findings (diffuse microbleeds in the grey-white junction of cerebral hemispheres on T2-weighted images, confirmed by susceptibility-weighted imaging). This was a nested case-control sample of an on-going local cohort study on aging and dementia, and details on clinical inclusion and exclusion criteria, baseline and neuropsychological assessments of participants were published previously [19]. The inclusion criteria included age 55 years or over and the availability of an informant. The exclusion criteria included cancer within 5 years, active infection, end-stage renal or other organ failure, non-ambulatory, depression by DSM-IV criteria, deafness and other communication barriers, and other neurological diseases such as epilepsy, psychiatric disorders or other types of dementia. A detailed medical history and mini-mental-state examination (MMSE) score (at time of MRI scanning) for global cognitive ability was obtained from all participants. A diagnosis of probable AD was made using criteria from the NINCDS-ADRDA [20]. Demographic data are shown in Table 1. It was worthy tomention that one of the controls was an outlier and had a MMSE score of 24.

Informed consent was obtained from all subjects who participated in the study, and Institutional Review Board approval from the Board of Ethics was obtained

	Gender	Age (years)			Education (years)			MMSE		
	n (Female/Male)	M	SD	Range	M	SD	Range	M	SD	Range
HC	20 (17/3)	71.3	6.8	59–85	5.0	4.2	0–12	28.3	1.9	24–30
AD	19 (14/5)	78.8	9.0	70–95	5.6	4.9	0–16	16.6	4.8	9–24
p-value	0.451	0.005*			0.666			<0.001*		

*denotes significance at 5% level, M- mean, SD- standard deviation.

prior to commencement of the study. The subjects and controls were scanned in an interleaved fashion within a period of 3.5 months. No scanner recalibration or upgrade was implemented during this period [21].

MRI scanning protocol

All MRI examinations were performed using a 3.0 Tesla scanner (Achieva, Philips Healthcare, The Netherlands). For MRI volumetric studies, a standardized T1-weighted 3D volumetric Fast Field Echo sequence was employed, i.e., TR/TE = 7.0 ms/3.2 ms, flip angle $8°$, voxel size = $1 \times 1 \times 1$ mm^3, FOV = 256 mm, 165 contiguous slices. Axial T2-weighted fast spin-echo images (TR/TE = 3000 ms/80 ms, flip angle $90°$, slice thickness 5 mm, ETL 16) were obtained to exclude structural abnormalities.

Image processing

Manual hippocampal volumetry

T1-weighted coronal images reconstructed as 1.5 mm slices perpendicular to the long axis of the hippocampus were measured. The boundaries of both hippocampi were traced manually as described by Jack et al. [22], by a neuroradiologist (HKM) who was blinded to subject identity and their volumes determined by ANALYZE 7.0 software (Mayo Clinic Foundation, Rochester, MN). To test inter-rater reliability, another radiologist (ZZ) performed the same procedure independently eight months later. The inter-rater agreement on the volumetric measures between the two observers was very high, with Pearson correlation of 0.974 ($p < 0.001$) and 0.957 ($p < 0.001$) for right and left hippocampus respectively.

Only the hippocampal rather than the entorhinal cortex volume was evaluated in the current study since a previous study had demonstrated similar discriminating values of both measurements and the former was preferred because of clarity of boundaries [22].

Normalization with total intracranial volume (TIV) was done. Manual total intracranial volume (mTIV)

was measured on the sagittal images by tracing the contour of the inner skull vault [23].

VBM

Preprocessing [24]. Data were preprocessed using the VBM5.1 toolbox (C. Gaser, structural Brain Imaging Group, Department of Psychiatry, University of Jena; http://dbm.neuro.uni-jena.de/vbm/) within an SPM5 environment (Wellcome Department of Imaging Neuroscience Group, London, UK; http://www.fil.ion.ucl.ac.uk/spm) on the Matlab v7.8 (MathWorks, Natrick, MA) platform. Segmentation was performed using the default parameters in VBM5.1 with Hidden Markov Random Field Model. Tissue probability image sets for native space white matter (WM), grey matter (GM), and cerebrospinal fluid (CSF) components were saved for later DARTEL analysis. Segmented images were normalized to the ICBM-152 template (Montreal Neurological Institute), and Jacobian modulation was applied to compensate for the effect of spatial normalization and to restore the original absolute GM volume in the segmented GM images. These normalized and modulated images were then smoothed with a 12 mm Full-Width at Half-Maximum (FWHM) smoothing kernel for final statistical analysis.

ROI analysis using hippocampal masks (MARINA) in standard VBM [24, 25]. Masks for both hippocampi were created with the MARINA software (Masks for Region of Interest Analysis, v0.61, B. Walter, Giessen, Germany). Mean volumes of the right hippocampus (RH) and left hippocampus (LH) on the segmented, normalized, modulated and smoothed GM images for each subject were calculated based on the hippocampal masks.

ROI analysis using adapted hippocampal masks (MARINA) and DARTEL [16, 25]. The above native GM images were imported into DARTEL, an alternative method of normalization in SPM5. With iterative bias field correction, a study-specific GM template was

created in the DARTEL toolbox, and flow fields that described the spatial deformations for normalizing the individual images to a study specific template were also acquired. With the flow fields, native GM images were warped and modulated in DARTEL. The warped and modulated GM images were smoothed with a 12 mm FWHM smoothing kernel. The hippocampal masks created in the MARINA software were spatially normalized to the study-specific template by using the normalization parameters generated by spatial normalization of the GM template in SPM5 to the study-specific template. With the adapted hippocampal masks, the mean volumes of RH and LH for each subject were calculated in these warped, modulated and smoothed GM images.

Bilateral hippocampal-ROIs, either with VBM-standard or VBM-DARTEL (as discussed above in 2 b and 2 c) were normalized with TIV. Automatic TIV (aTIV) is the sum of the masked modulated GM, WM and CSF maps generated according to a previously published procedure [26].

A comparison of the two VBM templates with mask overlay is shown in Fig. 1.

Statistical analysis

Data were first normalized pertaining to the respective measurements before conducting data analysis. Manually-drawn RH and LH volumes (in cubic mm) were normalized according to the corresponding manual TIV [22]. Likewise, RH and LH-ROI VBM with standard and DARTEL registrations were normalized according to the corresponding measure of automatic TIV [26].

The manually-drawn RH and LH volumes, and the RH and LH-ROI VBM with both standard and DARTEL registration of all study groups were compared using a 2-sample *t*-test. To further assess the mean difference of the volumetric measures between the HC and AD groups, a multiple regression analysis was conducted to adjust for the effect of age.

Logistic regression analysis was applied to assess the effects of manual hippocampal volumetry and hippocampal-ROI VBM (with standard or DARTEL registration) on AD incidence and predict their diagnostic accuracy, after adjusting for age, gender, and education. Prediction accuracy, sensitivity, specificity and area under Receiver Operating Characteristic (ROC) curves were reported. A baseline model with only age, gender and education being included as explanatory variables in the logistic regression analysis was also considered to find out the extra-predictive power of each of the volumetric measures.

All statistical analyses were conducted using SPSS Statistics 17.0. Level of significance was set at 0.05. Relevant 95% confidence intervals (95% CI) were reported where appropriate.

RESULTS

Demographic characteristics

Table 1 gives the demographic characteristics of the HC and AD groups respectively: female proportion = 0.85 and 0.75; mean age (in years) = 71.3 and 78.8; mean number of years of education = 5.0 and 5.6; mean MMSE score = 28.3 and 16.6. No significant difference in gender proportion ($p = 0.451$) and mean education level ($p = 0.666$) between the two groups was found. However, the mean age of the AD group is significantly higher than that of the HC group ($p = 0.005$). Mean MMSE score of the AD group is significantly lower than the HC group ($p < 0.001$). Given the significant difference in mean age between the two groups, age effect is included as a covariate for adjustment in subsequent regression analyses.
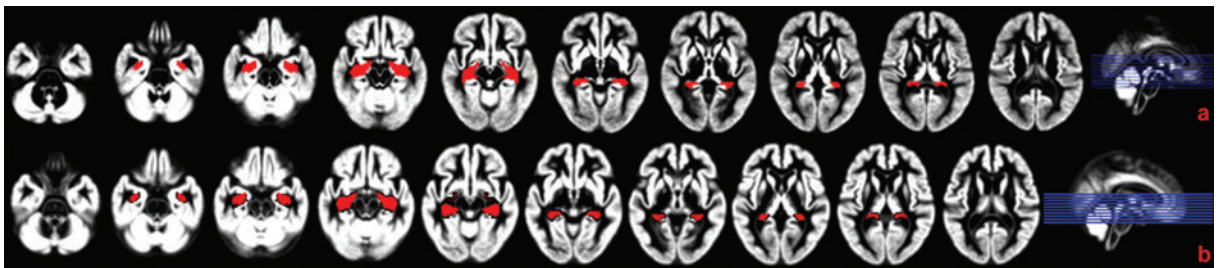

Fig. 1. Comparison between a) a DARTEL template with mask overlay, and b) standard VBM images with mask overlay.

Volumetric analysis

Table 2 compares the normalized RH and LH volumes, obtained manually and via ROI VBM, of the two study groups. All normalized measurements showed significant differences between AD and normal elderly subjects at a 5% level of significance. In particular, there is a significant reduction (20–30%, $p < 0.001$) in these normalized measurements when comparing AD patients to normal elderly subjects. Power analysis showed that the minimum mean difference for obtaining 80% power is: 22.3 and 20.8 for manual RH and LH volumes, 18.8 and 23.4 for standard RH and LH-ROI VBM, 22.9 and 22.5 for DARTEL RH and LH-ROI VBM, respectively. Given the observed mean differences in Table 2, the power to detect such observed mean differences was over 98% in all cases. To take into consideration the age difference between the two groups, the mean difference of the volumetric measures between the HC and AD groups was further assessed via a multiple regression analysis, using age as a covariate for adjustment. The adjusted mean difference of the volumetric measure between the two groups is given in the last column of Table 2. The mean differences between HC and AD were consistent and significant regardless of age adjustment.

Table 2
Descriptive measures and 2-sample t-test results of normalized RH and LH volumes (manual and VBM) comparing the AD and HC groups

Volumetric analysis method (Normalized)	Subjects	Mean	95% Confidence Interval	*t*-statistic	*p*-value (df = 37)	Mean (HC – AD) 95% Confidence interval	Age adjusted Mean (HC – AD) 95% confidence interval
Manual RH (per mTIV) ($\times 10^4$)	HC	153.9	(145.0, 162.8)	6.23*	<0.001	49.7	44.4
	AD	104.2	(89.8, 118.6)			(33.5, 65.8)	(26.6, 62.2)
Manual LH (per mTIV) ($\times 10^4$)	HC	151.9	(143.9, 159.8)	5.91*	<0.001	43.9	38.8
	AD	108.0	(94.4, 121.6)			(28.9, 59.0)	(22.2, 55.4)
Standard RH (per aTIV) ($\times 10^8$)	HC	188.3	(177.7, 198.8)	5.01*	<0.001	33.6	32.7
	AD	154.7	(145.5, 163.9)			(20.0, 47.2)	(17.4, 48.1)
Standard LH (per aTIV) ($\times 10^8$)	HC	204.9	(194.3, 215.4)	4.21*	<0.001	35.2	32.5
	AD	169.6	(155.5, 183.8)			(18.3, 52.2)	(13.4, 51.5)
DARTEL RH (per aTIV) ($\times 10^8$)	HC	224.0	(210.8, 237.1)	5.91*	<0.001	48.4	45.2
	AD	175.5	(164.6, 186.4)			(31.8, 65.0)	(26.6, 63.9)
DARTEL LH (per aTIV) ($\times 10^8$)	HC	212.1	(199.1, 225.0)	5.67*	<0.001	45.6	40.6
	AD	166.5	(155.9, 177.1)			(29.3, 61.9)	(22.5, 58.6)

*denotes significance at 5% level, mTIV was measured by manual tracing of the contour of the inner table [22], aTIV was the sum of the masked modulated GM, WM and CSF maps generated by SPM5 [26].

Table 3
Logistic regression analysis of normalized RH and LH volumes (manual and VBM) in predicting AD, after adjusting for age, gender, and education

Volumetric analysis method (Normalized)	Odds ratio (*p*-value)	95% Confidence interval	Prediction accuracy	Sensitivity	Specificity	Area under ROC curves
Baseline model (no volumetric measure)[†]	NA	NA	71.8%	73.7%	70.0%	0.77
Manual RH (per mTIV) ($\times 10^4$)	0.91* (0.003)	(0.86, 0.97)	87.2%	89.5%	85.0%	0.94
Manual LH (per mTIV) ($\times 10^4$)	0.89* (0.008)	(0.81, 0.97)	84.6%	78.9%	90.0%	0.93
Standard RH (per aTIV) ($\times 10^8$)	0.90* (0.002)	(0.84, 0.96)	87.2%	84.2%	90.0%	0.95
Standard LH (per aTIV) ($\times 10^8$)	0.94* (0.007)	(0.90, 0.98)	76.9%	73.7%	80.0%	0.87
DARTEL RH (per aTIV) ($\times 10^8$)	0.89* (0.006)	(0.82, 0.97)	87.2%	84.2%	90.0%	0.95
DARTEL LH (per aTIV) ($\times 10^8$)	0.88* (0.007)	(0.83, 0.97)	87.2%	89.5%	85.0%	0.95

[†]Baseline model only includes age, gender and education as explanatory variables in the logistic regression analysis, *denotes significance at 5% level
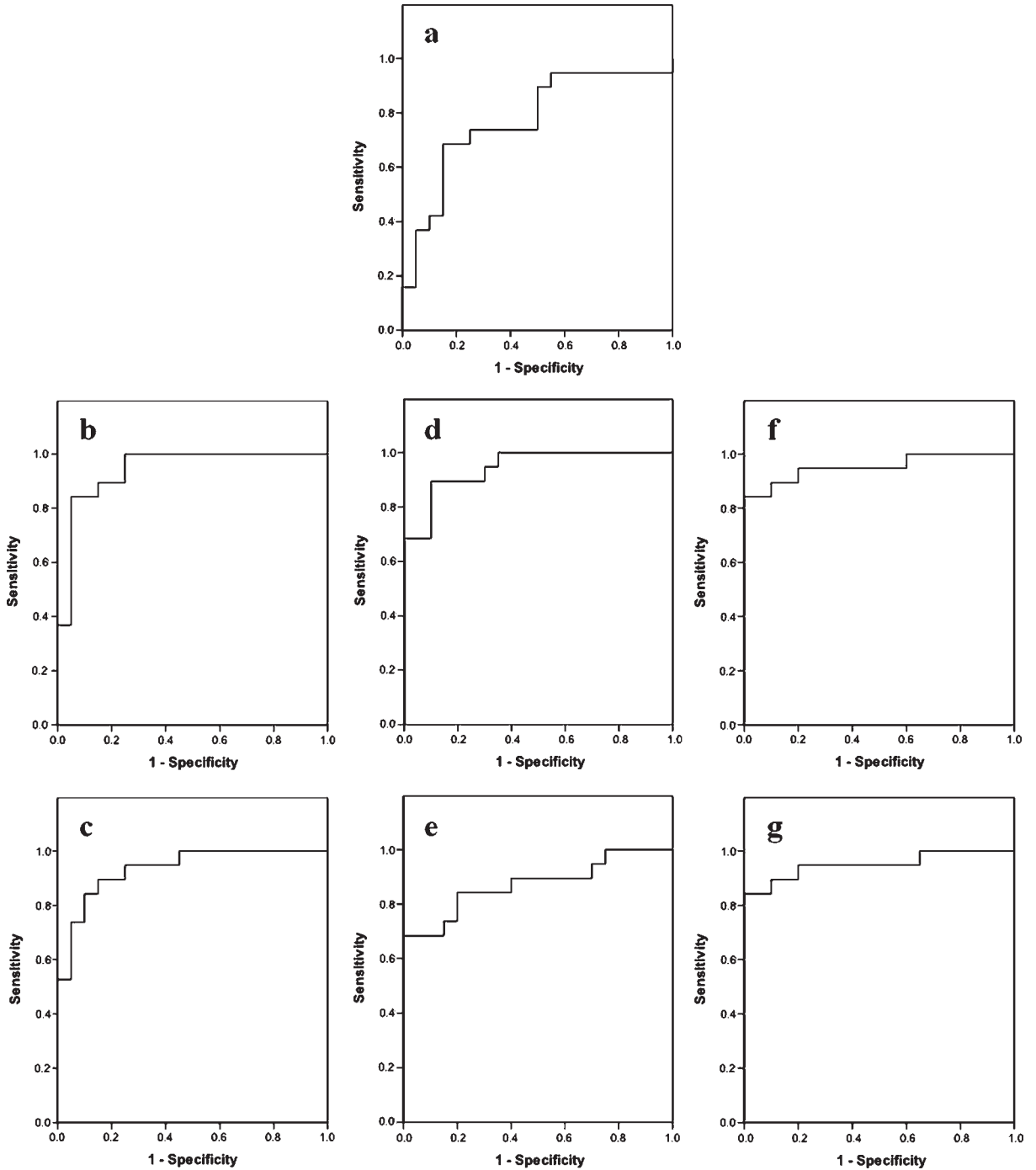
Fig. 2. ROC curves for the various logistic regression models. (a) Baseline model (Area under ROC = 77.1%); (b) Manual RH (per mTIV) (Area under ROC = 94.2%); (c) Manual LH (per mTIV) (Area under ROC = 93.4%); (d) Standard RH (per aTIV) (Area under ROC = 94.5%); (e) Standard LH (per aTIV) (Area under ROC = 87.4%); (f) DARTEL RH (per aTIV) (Area under ROC = 95.3%); (g) DARTEL LH (per aTIV) (Area under ROC = 95.0%).

Logistic regression analysis

In Table 3, logistic regression analysis results showed significant effects (odds ratios ranged from 88.2 to 94.0%) of all the normalized measurements in predicting AD incidence after adjusting for age, gender, and education. The overall prediction accuracies were 87.2% and 84.6% for manual RH and LH volumes, 87.2% and 76.9% for standard RH and LH-ROI VBM, and 87.2% and 87.2% for DARTEL RH and LH-ROI VBM, respectively. Table 3 also shows the accuracy, sensitivity, specificity and ROC of the various volumetric measures. The ROC results for intergroup discrimination show areas under the curve of 0.94 and 0.93 for manual RH and LH, 0.95 and 0.87 for standard RH and LH-ROI VBM, 0.95 and 0.95 for DARTEL RH and LH-ROI VBM, respectively. For comparison purposes, baseline model results were also included. The baseline model (with only age, gender and education being included as explanatory variables in the logistic regression analysis) gave a prediction accuracy of 71.8% and an area under the ROC curve of 0.77. The extra effect of the volumetric measures in prediction accuracy as well as in ROC is clearly demonstrated in Table 3 and Fig. 2. As MMSE has been taken as one of the main criteria for AD classification, it is not appropriate to include this variable back as an independent variable in the logistic regression analysis.

DISCUSSION

VBM with DARTEL registration showed similarly high accuracy as standard registration and manual volumetry in discriminating AD and cognitively normal elderly adults, albeit without significant improvement.

All of the VBM hippocampal measures in the current study achieved similar prediction accuracies (87.2%) to manual hippocampal volumetry, except standard LH-ROI VBM (76.9%). In our ROC analysis, areas under the curve were slightly higher for VBM with DARTEL registration than for manual hippocampal volumetry and VBM with standard registration.

Our results showed no significant improvement of DARTEL over standard registration in ROI-based VBM studies, in contradistinction to the study by Bergouignan et al. [25] Although both studies employed a similar DARTEL registration technique, the disease groups were very different. In their study on depression, the patients were much younger (33.2 years with age range of 20 to 49 versus 78.8 years with

age range of 70 to 95 in our AD subjects), thereby facilitating registration as patient brains were grossly comparable to controls.

Our hippocampal-ROI VBM with DARTEL registration compared favorably with new automated software for hippocampal volumetry. Colliot et al. [26] evaluated automated hippocampal volumetry in discriminating between AD, MCI, and normal aging. Their software performed rapid segmentation of the amygdalo-hippocampal complex and achieved accuracy, sensitivity, and specificity of 84%, 84%, and 84%, respectively, for classification between AD patients and controls. This automated software (SACHA) was again employed in the study by Bergouignan et al. [25], which revealed equal sensitivity to VBM-DARTEL in detecting hippocampal differences in depressed patients.

A word of caution should be made in the use of these 'semi-automatic' or 'automatic' software packages. For example, although much of the processing and analysis is automated in SPM, many methodological decisions remain such as the templates to use for normalization, the level and type of correction to use and threshold for statistical map display, as well as the choice of appropriate smoothing kernel size [21, 27]. As in current study, adoption of additional techniques such as DARTEL for registration and MARINA mask for ROI selection could be time-consuming and skill-demanding.

For example, in manual volumetry, the duration for tracing the hippocampus was about 20 minutes for each subject (or control) by either observer. For group analysis using VBM, the standard SPM5 software was set to run overnight to perform segmentation and normalization. The custom template was created by the DARTEL toolbox after another overnight run. Finally, the hippocampal ROIs were obtained using hippocampal masks in standard VBM and DARTEL, which required additional processing time of two hours each.

There are few studies on the comparison of volumetry at different field strengths. Using a cohort of 10 patients with intractable medial temporal lobe epilepsy, Scorzin et al. [28] determined that manual hippocampal and amygdalar volumetry did not differ between 1.5 T and 3 T and could be used interchangeably. VBM analyses showed satisfying inter-scanner volume quantification but not consistent enough to be deemed interchangeable. The better image quality at 3.0 T might be offset by a higher susceptibility for artifacts, resulting in geometric shift and signal loss. The study results (at 1.5 T) by Klauschen et al., also

hinted a higher contribution of noise than intensity-homogeneity to the image-quality-related instability of SPM5 [29]. The issue becomes interesting at 3 T MR imaging in which intensity-inhomogeneity is more pronounced, and future systematic studies will be necessary for further investigation.

In reality, manual volumetry by clinical experts is the most reliable, validated and used procedure and represents the current gold standard. In the literature, different segmentation protocols have been used for manual hippocampal volumetry [30]. Multi-national efforts for standardization of hippocampal volumetry will certainly pave the way for structural MRI to be widely accepted as Alzheimer's disease biomarker.

CONCLUSION

Hippocampal-ROI VBM with DARTEL registration (in SPM5) has a similarly high efficacy compared to standard registration and manual hippocampal volumetry in discriminating AD from cognitively normal elderly adults. Future research should be conducted to validate this technique in patients with MCI and other neurodegenerative diseases to broaden its clinical applications.

REFERENCES

[1] Scheltens P, Fox N, Barkhof F, De Carli, C (2002) Structural magnetic resonance imaging in the practical assessment of dementia: beyond exclusion. *Lancet Neurol* **1**, 13-21.

[2] Glodzik-Sobanska L, Rusinek H, Mosconi L, Li Y, Zhan J, de Santi S, Convit A, Rich K, Brys M, de Leon MJ (2005) The role of quantitative structural imaging in the early diagnosis of Alzheimer's disease. *Neuroimag Clin N Am* **15**, 803-826.

[3] Ramani A, Jensen JH, Helpern JA (2006) Quantitative MR imaging in Alzheimer disease. *Radiology* **241**, 26-44.

[4] Dubois B, Feldman HH, Jacova C, DeKosky ST, Barberger-Gateau P, Cummings J, Delacourte A, Galasko D, Gauthier S, Jicha G, Meguro K, O'Brien J, Pasquier F, Robert P, Rossor M, Salloway S, Stern Y, Visser PJ, Scheltens P (2007) Research criteria for the diagnosis of Alzheimer's disease: revising the NINCDS-ADRDA criteria. *Lancet Neurol* **6**, 734-746.

[5] Ashburner J, Csernansky JG, Davatzikos C, Fox NC, Frisoni GB, Thompson PM (2003) Computer-aided imaging to assess brain structure in healthy and diseased brains. *Lancet Neurol* **2**, 79-88.

[6] Ashburner J, Friston KJ (2000) Voxel-based morphometry – the methods. *Neuroimage* **11**, 805-821.

[7] Baron JC, Chetelat G, Desgranges B, Perchey G, Landeau B, de La Sayette V, Eustache F (2001) In vivo mapping of gray matter loss with voxel-based morphometry in mild Alzheimer's disease. *Neuroimage* **14**, 298-309.

[8] Good CD, Johnsrude IS, Ashburner J, Henson RNA, Friston KJ, Frackowiak RSJ (2001) A voxel-based morphometric study of ageing in 465 normal adult human brains. *Neuroimage* **14**, 21-36.

[9] Frisoni GB, Testa C, Zorzan A, Sabattoli F, Beltramello A, Soininen H, Laakso MP (2002) Detection of grey matter loss in mild Alzheimer's disease with voxel-based morphometry. *J Neurol Neurosurg Psychiatry* **73**, 657-664.

[10] Karas GB, Burton EJ, Rombouts SARB, van Schijndel RA, O'Brien JT, Scheltens P, McKeith IG, Williams D, Ballard C, Barkhof F (2003) A comprehensive study of gray matter loss in patients with Alzheimer's disease using optimized voxel-based morphometry. *Neuroimage* **18**, 895-907.

[11] Whitwell JL, Przybelski SA, Weigand SD, Knopman DS, Boeve BF, Petersen RC, Jack CR (2007) 3D maps from multiple MRI illustrate changing atrophy patterns as subjects progress from mild cognitive impairment to Alzheimer's disease. *Brain* **130**, 1777-1786.

[12] Risacher SL, Saykin AJ, West JD, Shen L, Firpi HA, McDonald BC (2009) The Alzheimer's disease Neuroimaging and Initiative. Baseline mri predictors of conversion from MCI to probable AD in the ADNI cohort. *Curr Alzheimer Res* **6**, 347-361.

[13] Mechelli A, Price CJ, Friston KJ, Ashburner J (2005) Voxel-based morphometry of the human brain: methods and applications. *Curr Med Imaging Rev* **1**, 1-9.

[14] Bookstein FL (2001) Voxel-based morphometry should not be used with imperfectly registered images. *Neuroimage* **14**, 1454-1462.

[15] Ashburner J, Friston KJ (2001) Why voxel-based morphometry should be used. *Neuroimage* **14**, 1238-1243.

[16] Ashburner J (2007) A fast diffeomorphic image registration algorithm. *Neuroimage* **38**, 95-113.

[17] Kloppel S, Stonnington CM, Chu C, Draganski B, Scahill RI, Rohrer JD, Fox NC, Jack CR, Ashburner J, Frackowiak RSJ (2008) Automatic classification of MR scans in Alzheimer's disease. *Brain* **131**, 681-689.

[18] Ashburner J (2009) Computational anatomy with the SPM software. *Magn Reson Imaging* **27**, 1163-1174.

[19] Chu LW, Tam S, Lee PWH, Wong RLC, Yik PY, Tsui W, Song Y, Cheung BMY, Morley JE, Lam KSL (2008) Bioavailable testosterone is associated with a reduced risk of amnestic mild cognitive impairment in older men. *Clin Endocrinol* **68**, 589-598.

[20] McKhann G, Drachman D, Folstein M, Katzman R, Price D, Stadlan EM (1984) Clinical diagnosis of Alzheimer's disease: report of the NINCDS-ADRDA work group under the auspices of department of health and human services task force on Alzheimer's disease. *Neurology* **34**, 939-944.

[21] Ridgway GR, Henley SMD, Rohrer JD, Scahill RI, Warren JD, Fox NC (2008) Ten simple rules for reporting voxel-based morphometry studies. *Neuroimage* **40**, 1429-1435.

[22] Xu Y, Jack CR, Jr, O'Brien PC, Kokmen E, Smith GE, Ivnik RJ, Boeve BF, Tangalos RG, Petersen RC (2000) Usefulness of MRI measures of entorhinal cortex versus hippocampus in AD. *Neurology* **54**, 1760-1767.

[23] Jack CR, Jr, Petersen RC, O'Brien PC, Tangalos EG (1992) MR-based hippocampal volumetry in the diagnosis of Alzheimer's disease. *Neurology* **42**, 183-188.

[24] Ashburner J, Friston KJ (2005) Unified segmentation. *Neuroimage* **26**, 839-851.

[25] Bergouignan L, Chupin M, Czechowska Y, Kinkingnehun S, Lemogne C, Le Bastard G, Lepage M, Garnero L,

Colliot O, Fossati P (2009) Can voxel-based morphometry, manual segmentation and automated segmentation equally detect hippocampal volume differences in acute depression? *Neuroimage* **45**, 29-37.

[26] Colliot O, Chetelat G, Chupin M, Desgranges B, Magnin B, Benali H, Dubois B, Garnero L, Eustache F, Lehericy S (2008) Discrimination between Alzheimer's disease, mild cognitive impairment and normal aging by using automated segmentation of the hippocampus. *Radiology* **248**, 194-201.

[27] Henley SMD, Ridgway GR, Scahill RI, Kloppel S, Tabrizi SJ, Fox NC, Kassubek J (2010) For the EHDN imaging working group (2010) Pitfalls in the use of voxel-based morphometry as a biomarker: examples from Huntington disease. *AJNR Am J Neuroradiol* **31**, 711-719.

[28] Scorzin JE, Kaaden S, Quesada CM, Muller CA, Fimmers R, Urbach H, Schramm J (2008) Volume determination of amygdala and hippocampus at 1.5 and 3.0 t MRI in temporal lobe epilepsy. *Epilepsy Res* **82**, 29-37.

[29] Klauschen F, Goldman A, Barra V, Meyer-Lindenberg A, Lundervold A (2009) Evaluation of automated brain MR image segmentation and volumetry methods. *Hum Brain Mapp* **30**, 1310-1327.

[30] Boccardi M, Gonzalo R, Duchesne S, Redolfi A, Bartzokis G, Csernansky J, de Leon M, Killiani R, Lehericy S, Malykhin N, Pantel J, Pruessner J, Soininen H, Jack CR, Jr, Frisoni GB (2010) Survey of segmentation protocols for manual hippocampal volumetry: preparatory phase for an EADC-ADNI harmonization protocol. *Alzheimer's & Dementia: The Journal of the Alzheimer's Association* **6**(4), S58-S59.

This page intentionally left blank

Structural MRI Investigation of Neuroanatomy of Corpus Callosum in Alzheimer's Disease and Mild Cognitive Impairment

Margherita Di Paola[a,b,*], Gianfranco Spalletta[a] and Carlo Caltagirone[a,c]

[a]*Clinical and Behavioural Neurology, IRCCS Santa Lucia Foundation, Rome, Italy*
[b]*Department of Internal Medicine and Public Health, University of L'Aquila, Coppito, Italy*
[c]*Department of Neuroscience and Memory Clinic, "Tor Vergata" University of Rome, Rome, Italy*

Abstract. The corpus callosum (CC), which connects the two cerebral hemispheres, is the largest white matter fiber bundle in the human brain. This structure presents a peculiar myelination pattern: it has small diameter fibers, located in the genu, which myelinate much later in normal development, and large diameter fibers of the splenium, which myelinate early in development. Although AD mainly compromise cerebral gray matter structure, there is evidence that white matter may also be involved in the pathology. To illustrate callosal white matter changes in AD pathology, we summarize "*in vivo*" MRI imaging studies in humans, focusing on region of interest (ROI), voxel-based morphometry (VBM), diffusion-weighted imaging (DWI) and diffusion tensor imaging (DTI) techniques. Results from the literature showed that changes in the anterior (genu and anterior body) as well as in the posterior (isthmus and splenum) portions of the CC might already be present in the early stages of AD. The spatial (in anterior and posterior callosal subregions) and the temporal (in the early stage of AD) presence of the CC changes support the hypothesis that two mechanisms, Wallerian degeneration and myelin breakdown, might be responsible for the region-specific changes detected in AD patients. Wallerian degeneration affects the posterior CC subregion, which receives axons directly from those brain areas (temporo-parietal lobe regions) primarily affected by the AD pathology. Instead, the myelin breakdown process affects the later-myelinating CC subregion and explains the earlier involvement of the genu in CC atrophy.

Keywords: Corpus callosum, Alzheimer's disease, mild cognitive impairment, region of interest, voxel-based morphometry, diffusion-weighted imaging, diffuse tensor imaging

INTRODUCTION

Although research in the field of Alzheimer's Disease (AD) has basically focused on gray matter (GM) degeneration, a number of investigations have also

documented a general white matter (WM) pathology associated with AD [1–6]. The corpus callosum (CC) has been implicated in this process [7–21]. In particular, it has been suggested that callosal atrophy in AD is the anatomical correlate of Wallerian degeneration of commissural nerve fibers. Thus, it might occur as a consequence of the death of projecting pyramidal cells in layer III of the neocortex and might reflect the pattern of neocortical neurodegeneration and the resulting cognitive dysfunction [13, 22–26].

*Correspondence to: Margherita Di Paola, IRCCS Santa Lucia Foundation, Via Ardeatina 306, 00179 Rome, Italy. Tel.: +39 06 515 01215; Fax: +39 06 51501213; E-mail: m.dipaola@hsantalucia.it.

Unfortunately, in spite of the plethora of studies on callosal changes in AD, results are unclear. Although it is commonly accepted that in AD patients, CC atrophy is mainly located in the anterior (genu and anterior body) and posterior (isthmus and splenium) subregions, it is less clear whether this finding is consistent in the different stages of AD pathology and across different methods.

In fact, the main result mentioned above, that is atrophy mainly in the callosal anterior and posterior subregions, comes from studies of AD groups that included patients in different illness stages, ranging from mild to severe dementia [7, 8, 10–12, 14–19, 23–25, 27–43] and sometimes selected using different diagnostic criteria [10, 14].

Furthermore, it has been found that different methods can produce different results. With regard to the region of interest (ROI) studies, for example, it has been shown that the earlier findings relied on manually tracing the CC and on the common callosal parcellation schemes (i.e, according to Witelson [19, 44]; Weis [45–47]; or Hampel [11, 18]) have generated some controversy regarding the assumed topography of callosal fibers [48]. In fact, in a previous study, we demonstrated that pre-defining callosal regions can give rise to misleading results [7]. This is also true for the voxel-based morphometry (VBM) technique. Senjem et al. [49] found that changes in the image processing chain of VBM noticeably influenced the results of intergroup morphometric comparisons. For example, the so-called "Optimized VBM" produced different results from those obtained with standard VBM.

Diffuse tensor imaging (DTI) studies have also produced different results. The vast majority of DTI studies are calculated as the diffusion parameters mean diffusivity (MD), which is a measure of the average motion of water molecules, independent of tissue directionality, and fractional anisotropy (FA), which measures the directionality of water diffusion. The pathological process of AD should alter both MD and FA values in the direction of lesser restriction on the movement of water and, therefore, with an increase in diffusivity (MD) and a decrease in anisotropy (FA). Nevertheless, in anatomically well-oriented structures, such as the CC, these two parameters seem to remain in the normal range. Thus, many DTI studies conclude that in the CC there is no difference between AD patients and healthy controls (HC).

Two main open questions motivated the present review: (i) how early callosal atrophy occurs in AD and whether the callosal changes involving the anterior and the posterior subregions can already be detected in mild AD and amnesic MCI; and (ii) which magnetic resonance imaging (MRI) techniques are most useful for detecting callosal changes. Therefore, this review is focused on exploring how the CC changes in the different stages of AD and in MCI (i.e. in the preclinical stage of dementia and in the group at highest risk for developing dementia)[50–52], and which measurements have been applied to study these modifications *in vivo*.

MATERIAL AND METHODS

A detailed search of the literature was conducted. For our purposes, the database was selected using PubMed Services to research the following keywords: corpus callosum, white matter, Alzheimer's disease, mild cognitive impairment, region of interest, voxel-based morphometry, diffusion-weighted imaging and diffusion tensor imaging. In examining research results, we paid attention to the clinical features of the patient groups to classify results obtained evaluating heterogeneous groups of patients (i.e. AD and/or MCI patients with different illness severity) separately from those obtained studying homogeneous groups of patients (i.e. only mild AD or only amnesic MCI). This was done to keep separated data in which the presence of more severe patients (e.g., severe AD) could bias results and to investigate whether a specific pattern of callosal degeneration was associated with different illness stages (from amnesic MCI to mild, moderate and severe AD). Thus, using the MRI modality as a starting point we reviewed an extensive body of literature focusing mainly on structural neuroimaging (i.e ROI and VBM) and quantitative parametric mapping (i.e. DWI and DTI).

Initially, 55 studies were selected as potential candidates for the present review. Studies were included if they: (1) were brain structural MRI studies published from January 1997 to March 2011, (2) compared AD or MCI patients with a HC group, and (3) were published in the English language. We also hand-searched relevant journals and inspected the bibliographies of all major articles to find other relevant publications. Historically important and conceptually related articles were included as well. One study was excluded from the review [53] because it did not compare AD patients with a HC group. Concerning the nomenclature of the CC subregions, to be consistent across studies we refer to the different subregions of the CC as follows: ros-
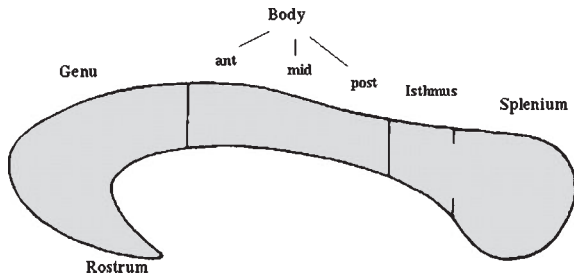
Fig. 1. Schematic view of corpus callosum for nomenclature. The image shows the different subregions of the CC regardless of splitting method and callosal fiber topography.

trum, genu, body (split into anterior, mid and posterior) isthmus and splenium (see Fig. 1 for a schematic view).

REGION OF INTEREST STUDIES

Early morphometric MRI studies of the CC in AD quantified atrophic changes using ROI analysis.

In general, to perform a ROI analysis a high spatial resolution 3D brain sequence has to be acquired with an isotropic voxel (e.g. $1 \times 1 \times 1$ mm^3) so that all three orthogonal planes can be inspected. This procedure also facilitates identification of anatomical landmarks for selection of the ROI. To obtain a better identification of the CC ROI, each MRI brain volume is usually positioned along the anterior-posterior commissure line. This is particularly important for obtaining a reliable measure of the CC, because it is sampled from its most medial part on a 1 mm thick slice. Each ROI is identified by its landmarks and manually mapped. Then the voxels belonging to the ROI are colored to show the volume of the CC in mm^3. According to the model used, an automatic procedure is applied to split the CC. To determine the size of the CC, several methodologies have been proposed for measuring its midsagittal surface area and regional divisions. In Fig. 2, we report the most frequently used methods. Finally, to reduce inter-individual variability in gross brain size, different reference measures, such as forebrain volume, cranial capacity, cross-sectional cerebral area or normalization of the MRI brain volumes into the Talairach proportional stereotaxic space, are used either as a ratio [54, 55] or as a covariate in the statistical model [56, 57]. In this way, gross brain size differences are ruled out.

ROI analysis is considered a robust, well-validated technique. However, it requires operator skills to define the boundaries of the structures to be investigated. Fur-

thermore, it is time consuming, because the researcher has to draw the ROI manually, and allows studying only a limited number of anatomical regions chosen *a priori*.

Numerous ROI studies have investigated callosal changes in AD patients [7, 10–12, 14–19, 24, 25, 27, 28, 31, 38, 42, 43]. Overall, these studies report a reduction of the total callosal area, specifically of the rostrum, genu, anterior body, isthmus and splenium of the CC. It should be noted that the vast majority of these studies included AD patients at different illness stage, ranging from mild to severe dementia (hereafter called AD "all stages"). Only a few studies investigated patients with fewer heterogeneous clinical features, such as those affected by mild or moderate AD, and they reported discrepant results. More specifically, while some studies on mild AD found atrophy in the posterior callosal subregions (isthmus and splenium) [9, 11, 13, 19], others found no atrophy in callosal regions [45, 58].

As far as we know, there is only one study [59] on moderate AD patients that describes a reduction of the anterior body, mid body and isthmus in AD patients compared with HC.

Likewise, inconsistent results have been reported in studies on subjects with MCI. In a study on amnesic MCI, Wang et al. [9] found atrophy in posterior subregions (isthmus and splenium). Yet, another research group [46] found no callosal changes when patients with amnesic MCI were compared with HC. By contrast, Thomann et al. [10] reported a reduction in the anterior subregion (rostrum, genu, anterior body) of the CC in a group of MCI patients with different cognitive subtypes (amnesic and multi-domain amnesic (hereafter called MCI "all subtypes") using the ROI approach. Finally, Hallam et al. [43] reported no differences between a mild ambiguous group (i.e. with a cognitive profile similar to that of multi-domain MCI) and HC.

Recently, our group [21] applied a well-validated structural analysis technique, that is, the computational mesh-based method, to map callosal thickness [60–63] and to study the CC changes in three distinct homogeneous groups of patients with mild AD, severe AD and amnesic MCI compared with HC. The main finding of our study was reduced thickness in the callosal genu, anterior body and splenium in severe AD patients compared with HC. The callosal reductions in the milder and pre-clinical stages of AD appeared to be less pronounced (i.e., they were more restricted spatially). When mild AD patients were compared with
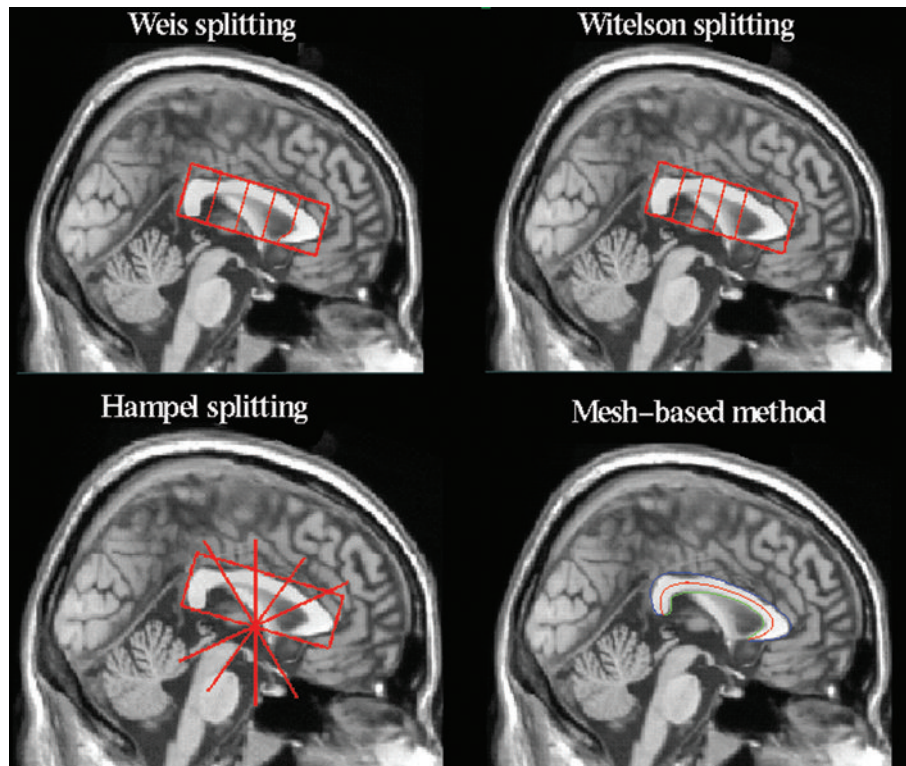
Fig. 2. Different corpus callosum manual tracing. In Weis splitting, the midsagittal slice of the CC is split into five distinct sectors of equal size along a line joining the most anterior and posterior points of the genu and splenium respectively. Subregions are the following: CC1 = rostrum and genu, CC2 = rostral body, CC3 = midbody, CC4 = isthmus, CC5 = splenium. In Witelson splitting, the midsagittal slice of the CC is split into five distinct sectors of different percentages: 33%, 17%, 17%, 13%, 20% respectively. The subregions are: CC1 = rostrum, genu and anterior body, CC2 = midbody, CC3 = caudal body, CC4 = isthmus, CC5 = splenium. In Hampel splitting, the midsagittal slice of CC is split into five distinct sectors of equal percentage (36%) along a line joining the most anterior and posterior points of genu and splenium respectively. The subregions are: CC1 = rostrum, CC2 = anterior truncus, CC3 = middle truncus, CC4 = posterior truncus, CC5 = splenium. In the Mesh-based method, there is no splitting. Upper and lower callosal boundaries are manually outlined in the midsagittal section. Then, the spatial average from 100 equidistant surface points representing the upper and lower boundaries is calculated. The result is a new midline segment (the spatial average), also consisting of 100 equidistant points. Finally, the midline segment is quantified, so that it corresponds to CC thickness.

HC, we observed reduced callosal thickness within the callosal anterior third, as well as at the border between the anterior third and the anterior body. When amnesic MCI patients were compared with HC, reduced callosal thickness was found in the callosal posterior body and within the splenium near the callosal posterior end. Nevertheless, group differences between mild AD and amnesic MCI subjects and HC were slight and not confirmed by permutation testing. (see Table 1 for technical details of the study).

VOXEL-BASED MORPHOMETRY STUDIES

After the ROI studies, a new imaging technique, VBM, has been adopted to examine CC changes [64]. VBM has been increasingly used to investigate differences in brain morphology among groups. Indeed, it provides an estimate of inter-group differences in GM and WM density and/or volume on a voxelwise basis in a standardized space. The VBM protocol has been somewhat changed in the last few years to improve the preprocessing steps. In its previous version, called the "Optimized VBM" protocol, running in the framework of Statistical Parametric Mapping (SPM99, SPM2, Wellcome Department of Imaging Neuroscience, University College London, London, UK), a customized GM template is created and subsequently used to normalize all structural images to the stereotaxic MNI space. To create the customized GM template, all images (patients and controls) are first spatially normalized (12-parameter affine and $6 \times 8 \times 5$ basis functions) using the standard MNI

Table 1
ROI studies of CC

Study (year)	Sample	MMSE mean ± SD (range)	MRI acquisition	ROI method	Positive findings	Negative findings
Kaufer et al. (1997)	-17 AD -16 FTD -12 HC	17.3 ± 6.4 (2–27) n.r. 29.4 ± 0.9 (27–30)	1.5 T magnet. A T1-weighted volumetric scan (slice thickness = 5 mm)	Radial splitting in 4 subregions: the two anterior sectors (CC-I), three anterior body sectors (CC-2), three posterior body sectors (CC-3), and the two posterior sectors (CC-4)	Regional decreases of CC in AD patients compared with HC were most prominent in CC-1. Regional decreases were seen to a lesser extent in the two middle CC regions (CC-2 and CC-3).	There were no significant differences in total CC area in AD patients compared with HC.
Lyoo et al. (1997)	-162 AD: n 49 AD n 47 AD n 33 AD n 33 AD -28 MID -36 HC	16.1 ± 6.4 (n.a.): n.a. ± n.a. (≥21) n.a. ± n.a. (20–16) n.a. ± n.a. (15–11) n.a. ± n.a. (≤10) n.r. 28.9 ± 1.3 (n.a.)	1.5 T magnet. A T1-weighted volumetric scan (slice thickness = 5 mm)	Witelson splitting	All regional areas of CC were smaller in all AD patients compared with HC. Atrophy only in the posterior body, isthmus and splenium of CC in a subgroup of mild AD (n 49 MMSE ≥21).	
Black et al. (2000)	-23 AD -17 HC	18.1 ± 5.4 (n.a.) 28.2 ± 1.8 (n.a.)	1.5 T magnet. A T1-weighted volumetric scan (slice thickness = 1.2 mm)	Witelson splitting	Reduction of total callosal area in AD patients compared with HC. Reduction of CC1 (genu) CC3 (anterior body) CC4 (posterior body) and CC5 (splenium) in AD patients compared with HC.	
Tomaiuolo et al. (2007)	-17 AD -17 HC	n.a. ± n.a. (<24) n.a. ± n.a. (>28)	1.5 T magnet. A T1-weighted volumetric scan (slice thickness = 1 × 1 × 1 mm)	Witelson splitting	Reduction of total callosal area in AD patients compared with HC. Reduction in rostrum, genu, anterior body, isthmus and splenium of CC in AD patients compared with HC.	
Hampel et al. (1998)	-14 AD: n 4 AD mild n 4 AD moderate n 6 AD severe -22 HC	11.4 ± 8.6 (n.a.): n.a. ± n.a. (≥20) n.a. ± n.a. (<20–≥10) n.a. ± n.a. (<10) 29.8 ± 0.4 (n.a.)	Two MRI sequences: -0.5 T magnet. A T1-weighted volumetric scan (slice thickness = 2.5 mm) -0.5 T magnet. A T1-weighted volumetric scan (slice thickness = 2 mm)	Hampel splitting	Absolute mean total callosal area was smaller in AD patients compared with HC. Reduction in the most rostral C1 (rostrum) and the most occipital C5 (splenium) subregions of CC in AD patients compared with HC.	

Table 1
(*Continued*)

Study (year)	Sample	MMSE mean ± SD (range)	MRI acquisition	ROI method	Positive findings	Negative findings
Teipel et al. (1998)	-20 AD: n 7 AD mild n 5 AD moderate n 8 AD severe -21 HC	12.2 ± 10.2 (n.a.): n.a. ± n.a. (≥20) n.a. ± n.a. (<20–≥10) n.a. ± n.a. (<10) 29.7 ± 0.5 (n.a.)	0.5 T magnet. A T1-weighted volumetric scan (slice thickness = 2 mm)	Hampel splitting	Absolute mean total callosal area was smaller in AD patients compared with HC. Reduction of most rostral C1 and C2 (rostrum and anterior body) and of most caudal C5 (splenium) subregions of CC in AD patients compared with HC.	
Teipel et al. (1999)	-12 AD: n 3 AD mild n 5 AD moderate n 4 AD severe -15 HC	12.5 ± 10.0 (n.a.): n.a. ± n.a. (>20) n.a. ± n.a. (<20–≥10) n.a. ± n.a. (<10) 29.7 ± 0.5 (n.a.)	Two MRI sequences: -0.5 T magnet. A T1-weighted volumetric scan (slice thickness = 2.5 mm); -0.5 T magnet. A T1-weighted volumetric scan (slice thickness = 2 mm)	Hampel splitting	Absolute mean total callosal area was smaller in AD patients compared with HC. Reduction in most rostral C1 and C2 (rostrum and anterior body) and in most occipital C5 (splenium) subregions of CC in AD patients compared with HC.	
Teipel et al. (2002)	-21 AD: n 9 AD mild n 10 AD moderate n 2 AD severe -10 HC	17.4 ± 6.7 (1–28): n.a. ± n.a. (≥20) n.a. ± n.a. (≥10–<20) n.a. ± n.a. (<10) 29.8 ± 0.4 (29–30)	0.5 T magnet. A T1-weighted volumetric scan (slice thickness = 2 mm)	Hampel splitting	Cross-sectional study results: i) absolute mean total callosal area was smaller in AD patients compared with HC; ii) atrophy in rostrum and genu (C1) and isthmus and splenium (C5) of CC in AD patients compared with HC. Longitudinal study results: percentage rates of change in total CC and callosal subregion, rostrum and genu (C1) and isthmus and splenium (C5) of CC in AD patients compared with HC (analysis performed on a subgroup of AD matched with HC for observation time).	
Teipel et al. (2003)	-27 AD: n 9 AD mild n 9 AD moderate n 9 AD severe -28 HC	13.4 ± 8.8 (0–27): n.a. ± n.a. (≥20) n.a. ± n.a. (<20–≥10) n.a. ± n.a. (<10) 29.8 ± 0.4 (29–30)	0.5 T magnet. A T1-weighted volumetric scan (slice thickness = 2 mm)	Hampel splitting	Total callosal size was smaller in AD patients compared with HC. Atrophy in rostrum and genu (C1) and isthmus and splenium (C5) of CC in AD patients compared with HC.	

Study	Sample	Age	MRI	Method	Findings
Pantel et al. (1998)	-32 AD -17 VD -13 HC	163 ± 6.4 (n.a.) n.r. 29.3 ± 0.8 (n.a.)	1.5 T magnet. A T1-weighted volumetric scan (slice thickness = 1.2 × 1.2 × 1.5 mm)	Weis splitting Five mid-sagittal slices of CC were used.	Atrophy in splenium of CC was present even in mild AD patients compared with HC. Total size of CC and the most rostral part of CC (C1 = genu and rostrum; C2 = rostral body) were significantly smaller in AD patients compared with HC
Pantel et al. (1999)	-38 AD -20 HC	16.6 ± 6.9 (n.a.) 29.2 ± 0.6 (n.a.)	1.5 T magnet. A T1-weighted volumetric scan (slice thickness = 1.2 × 1.2 × 1.5 mm)	Weis splitting. Three slices of CC were used.	Total size of CC and the five measured regional subsections of CC (rostrum and genu, anterior body, mid body, isthmus and splenium) were significantly smaller in AD patients compared with HC.
Ortiz Alonso et al. (2000)	-23 AD -24 HC	16.9 ± 2.4 (n.a.) 29.0 ± 0.9 (n.a.)	1.5 T magnet. A T1-weighted volumetric scan (slice thickness = 1 mm)	Weis splitting	Reduction of CC2 (anterior body), CC3 (mid body) and CC4 (isthmus) in AD patients compared with HC.
Hensel et al. (2002)	-23 AD -27 questionable dementia patients -33 HC	22.0 ± 1.8 (n.a.) 26.0 ± 1.8 (n.a.) 28.9 ± 0.8 (n.a.)	1.5 T magnet. A T1-weighted volumetric scan (slice thickness = 0.9 × 0.9 × 1.5 mm)	Weis splitting	Reduction of total callosal size in AD patients compared with HC. No statistically significant differences were found between patients with questionable dementia and any other group.
Hensel et al. (2004)	-12 AD: n 9 AD mild n 3 AD moderate -2 FTD -12 HC	23 ± 2.1 (20–26): n.a n.a n.r. 28.5 ± 1.3 (25–30)	Three MRI sequences and tomography: -1.5 T magnet. A T1-weighted volumetric scan (slice thickness = 0.9 × 0.9 × 1.5 mm) -1.5 T magnet. A T1-weighted volumetric scan (slice thickness = 0.9 × 0.9 × 1 mm) -3 T magnet. A T1-weighted volumetric scan (slice thickness = 1.5 mm)	Weis splitting	No CC segment was particularly atrophied in AD patients compared with HC. No specific subregion atrophy in CC in AD patients compared with HC.

Table 1
(*Continued*)

Study (year)	Sample	MMSE mean ± SD (range)	MRI acquisition	ROI method	Positive findings	Negative findings
Wiltshire et al. (2005)	-16 AD -24 PD -25 PDD -27 HC	21.0 ± 8.2 (n.a.) n.r. n.r. 29.0 ± 1.2 (n.a.)	Two MRI sequences: -1.5 T magnet. A T1-weighted volumetric scan (slice thickness = 5 mm) -1.5 T magnet. A T1-weighted volumetric scan (slice thickness = 5 mm).	Weis splitting	Total callosal area was reduced in AD patients compared with HC.	
Hensel et al. (2005)	-35 questionable dementia patients -39 HC	26.2 ± 1.8 (n.a.) 28.9 ± 1.1 (n.a.)	1.5 T magnet. A T1-weighted volumetric scan (slice thickness = 0.9 × 0.9 × 1.5 mm)	Weis splitting		No specific callosal subregion atrophy in questionable dementia patients compared with HC.
Thomann et al. (2006)	-10 AD -21 MCI "all subtypes" -21 HC	19.2 ± 3.8 (n.a.) n.a. n.a.	1.5 T magnet. A T1-weighted volumetric scan (slice thickness = 0.98 × 0.98 × 1.8 mm)	Weis splitting	Total callosal area was reduced in AD and MCI patients compared with HC. Reduction in rostral subregions C1 (rostrum and genu), C2 (anterior body) and C3 (midbody) of CC in AD patients compared with HC. Reduction in rostral subregions C1 (rostrum and genu) and C2 (anterior body) of CC in MCI patients compared with HC.	
Wang PI et al. (2006)	-22 AD -28 amnesic MCI -28 subjective cognitive complaints -50 HC	24.6 ± 2.7 (n.a.) 27.3 ± 2.2 (n.a.) 28.9 ± 1.1 (n.a.) 29.1 ± 1.2 (n.a.)	1.5 T magnet. A T1-weighted volumetric scan (slice thickness = 1.5 mm)	Weis splitting	Reduction in total callosal area in each group (AD, MCI and subjective cognitive complaints subjects) compared with HC. Reduction in posterior subregions C4 (isthmus) and C5 (splenium) in AD patients compared with HC. Reduction in posterior subregion C5 (splenium) in MCI and subjective cognitive complaints subjects compared with HC.	
Li et al. (2008)	-19 AD -20 HC	18.9 ± 3.9 (n.a.) 29.5 ± 0.9 (n.a.)	1.5 T magnet. A T1-weighted volumetric scan (slice thickness = 1.8 mm)	Weis splitting	Reduction in all five subregions of CC (rostrum and genu, anterior body, mid body, isthmus and splenium) in AD patients compared with HC.	

Study	Subjects	Age	MRI	Methodology	Results
Thompson et al. (1998)	-10 AD -10 HC	19.7 ± 5.7 (n.a.) 28.8 ± 1.0 (n.a.)	1.5 T magnet. A T1-weighted volumetric scan (slice thickness = 1 mm)	Midsagittal slice of CC was split into 5 distinct sectors of equal percentage (20%) along a line joining the most anterior and posterior points of genu and splenium respectively [129, 130]	Reduction in posterior "midbody" (corresponding mainly to the isthmus) of CC in AD patients compared with HC.
Hanyu et al. (1999a)	-23 AD: n 6 AD n 13 AD n 4 AD -16 HC	n.a.: n.a. ± n.a. (≥21) n.a. ± n.a. (20–11) n.a. ± n.a. (≤10) n.a. ± n.a. (<28)	1.5 T magnet. A T2-weighted image (section thickness 8 mm)	CC was split into four parts of equal size: anterior portion (rostrum and genu), middle portion (body) and posterior portion (isthmus and splenium) of CC.	Total callosal area was reduced in AD patients compared with HC. Atrophy of posterior subregions (isthmus and splenium) of CC in AD patients compared with HC.
Yamauchi et al. (2000)	-16 AD -11 FTD -9 PSP -23 HC	19 ± 5 (n.a.) n.r. n.r. 29 ± 1 (n.a.)	1.5 T magnet. A T1-weighted volumetric scan (slice thickness = 3 mm)	CC was split into four parts of equal size: anterior (rostrum), middle-anterior, middle-posterior, and posterior (splenium).	Total callosal area was smaller in AD patients compared with HC. Reduction of the posterior quarter area (splenium) in AD patients compared with HC.
Wang H. et al. (2006)	-13 amnesic MCI -13 HC	n.a. n.a.	1.5 T magnet. A T1-weighted volumetric scan (slice thickness = 1.5 mm)	Manual tracing of ROI of whole CC in midsagittal section.	No callosal atrophy in MCI patients compared with HC.
Hallam et al. (2008)	-78 AD -28 MA -55 VD -20 HC	17.3 ± 6.8 (n.a.) 25.9 ± 1.7 (n.a.) n.r. 28.2 ± 2.1 (n.a.)	0.5 T magnet. A T1-weighted 3-D volumetric scan (slice thickness = 5 mm)	The methodology derived 99 callosal widths based on an algorithm that divided each dorsal and ventral CC perimeter into 100 equidistant points and connected the corresponding numbered points between the dorsal and ventral surfaces of the CC. Subregions of CC were then identified by a factor analysis of these widths.	The sum of the widths in AD group was significantly smaller than that of HC when controlling for age. CC of AD group was smaller than that of HC in both anterior (W2–12 and W13–14) and posterior (W75-88 and W89-95) CC regions, with preservation of the midbody. No CC regional differences between MA group and controls, but a trend for the region (W2–12) to be smaller in this patient group (p = 0.05). No significant CC regional differences between patient groups after correcting for multiple comparisons.
Zarei et al. (2009)	-16 AD mild -13 VaD -22 HC	22.9 ± 3.2 (n.a.) n.r. 28.7 ± 1.4 (n.a.)	1.5 T magnet. A T1-weighted volumetric scan (slice thickness = 1 × 1.5 × 1 mm)	Probabilistic tractography to parcel the CC into 7 subregions according to its connectivity with major cerebral cortex: prefrontal cortical region, M1, S1, premotor cortical region, posterior parietal cortical region, temporal, occipital cortical region.	No significant difference in total CC volume or in volume of CC subregions in AD patients compared with HC.

Table 1
(Continued)

Study (year)	Sample	MMSE mean ± SD (range)	MRI acquisition	ROI method	Positive findings	Negative findings
Di Paola et al. (2010a)	-30 AD: n 10 AD severe n 20 AD mild -20 amnesic MCI -20 HC	n.a.: 10.7 ± 3.7 (n.a.) 22.0 ± 2.5 (n.a.) 27.1 ± 2.5 (n.a.) 29.1 ± 0.9 (n.a.)	3 T magnet. A T1-weighted volumetric scan (slice thickness = 1 × 1 × 1 mm)	Mesh-based method: upper and lower callosal boundaries in midsagittal section of each brain were manually outlined. Then callosal upper and lower sections were redigitized to obtain 100 equidistant points. The spatial average from the 100 equidistant surface points representing the upper and lower boundaries was calculated resulting in a new midline segment, also consisting of 100 equidistant points. Finally, distances between 100 corresponding surface points between midline segment and upper and lower boundaries were quantified in mm.	Reduction in the splenium, anterior body and anterior third of CC in severe AD patients compared with HC.	No significant difference in CC in mild AD and amnesic MCI patients compared with HC.

Studies are grouped by the splitting method used. AD = Alzheimer's Disease; CC = corpus callosum; MA = mild ambiguous (patients with cognitive problems not severe enough for diagnosis of dementia [43]. They seem to be similar to MCI "all subtypes". MCI = Mild Cognitive Impairment MID = multi-infarct dementia; HC = healthy controls; FTD = frontotemporal dementia; PD = Parkinson's Disease; PDD = PD with dementia; PSP = progressive supranuclear palsy. Questionable dementia patients are subjects typically suffering from mild forgetfulness. They are fully oriented and have no or slight impairment in social functions. They do not meet ICD-10 dementia criteria [45], and have a score of 0.5 in the Clinical Dementia Rating Scale (CDR) [58]. MMSE = Mini Mental Status Examination; mean (standard deviation). VD = Vascular Dementia; n.a. = data not available in the article; n.r. = data available in the article for different pathology, therefore not reported.

template in SPM99 or SPM2. Then each normalized image is segmented into GM, WM and cerebrospinal fluid (CSF). The normalized and segmented GM images are smoothed (isotropic kernel, usually with a FWHM between 8 and 12 mm) and averaged to create the customized GM template. Then all the original MR images in native space are segmented into GM, WM and CSF. The GM and the WM images are normalized to the customized GM template and the deformation parameters obtained from this are applied to all original images. This provides optimally normalized whole-brain images, which are segmented again into GM, WM and CSF. Finally, all GM and WM images are modulated or not (to assess the absolute amount or concentration of a region of tissue [34] and smoothed with an FWHM kernel (the smoothing conforms the data more closely to the Gaussian field model underlying the statistical procedures used for making inferences about regionally specific effects). Smoothing also has the effect of rendering the data more normally distributed (by the central limit theorem). The intensity of the smoothed data in each voxel is a locally weighted

average of GM density from a region of surrounding voxels. The size of the region is defined by the size of the smoothing kernel [64].

Although the current procedure is somewhat different from the original one, the logic of image pre-processing is the same. Briefly, in the unified segmentation step [65], implemented in the framework of Statistical Parametric Mapping (SPM5, Wellcome Department of Imaging Neuroscience, University College London, London, UK), images are normalized and segmented into GM and WM partitions and into CSF. For each subject, normalized segmented GM and WM are modulated or not and smoothed with a Gaussian Kernel (FWHM). In Fig. 3, we show a flow chart of Optimized VBM image processing.

Compared with ROI analysis, VBM analysis has the advantage of being a spatially specific and unbiased method for analyzing MR images. It is completely operator independent and provides a quantitative measure of the regional GM and WM volume or density at a voxel scale throughout the whole brain without choosing any *a priori* ROI [34, 64].
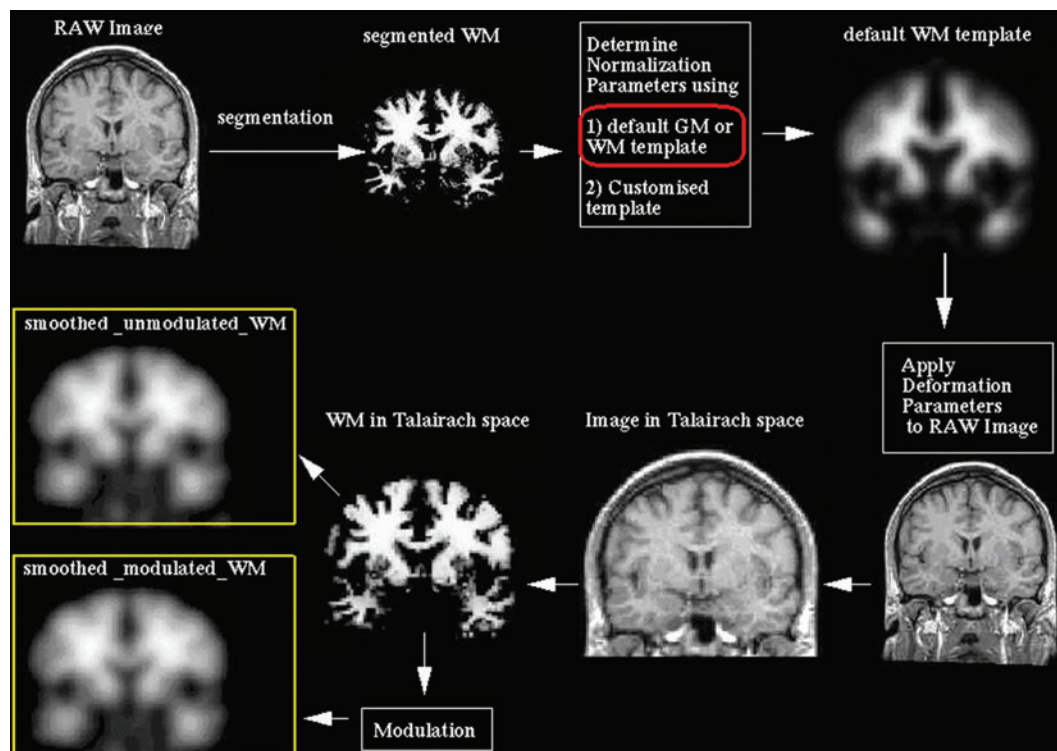
Fig. 3. Optimized Voxel-based Morphometry pipeline. Image shows the spatial processing steps of optimized VBM and the two resulting analyses. Templates used for normalization (gray matter or white matter) are indicated in red and the two analyses are indicated in yellow. Both affine and nonlinear basis function normalization are used in the technique.

The first VBM study on WM in moderate AD [66] reported the presence of diffuse atrophy within the CC but did not mention its specific location. Later works on AD "all stages" groups (more precisely on mild to moderate patients) reported conflicting results. Thomann et al. [10] found a significant loss of callosal volume in the anterior portion of the CC (rostrum, genu and anterior body). Chaim et al. [8] reported a reduction in almost all subregions of the CC (genu, anterior and posterior body, isthmus, splenium), but mainly in the left hemisphere. Li et al. [42] found a reduction limited to the posterior CC subregions (isthmus and splenium), and, in agreement with Chaim et al. [8], prevalently on the left side of the CC. More recently Guo et al. [67] reported volume reduction exclusively in the anterior portion of CC (rostrum, genu and anterior body) in AD patients

We found only one VBM study [10] on callosal changes in MCI. However, it did not report differences in the CC in MCI subjects compared with HC.

In our study [20], we applied the VBM technique to study CC changes in patients with mild AD, severe AD and amnesic MCI. We found atrophy in severe AD, specifically in the genu, anterior body and splenium of the CC. Patients with Mild AD presented a reduction in both the anterior and posterior CC and those with amnesic MCI only in the anterior CC. Nevertheless, the results obtained on patients with mild AD and amnesic MCI were not supported by statistical correction for multiple comparisons. Then, we replicated the study on a larger sample of patients with mild AD and amnesic MCI [21] and found a significant WM density reduction in the genu and splenium of the CC in patients with Mild AD. In patients with amnesic MCI compared with HC, we found a reduction only in the genu of the CC (see Table 2 for technical details of the study).

DIFFUSION-WEIGHTED IMAGING (DWI) AND DIFFUSION TENSOR IMAGING (DTI) STUDIES

Diffusion imaging is a non-invasive MR technique adopted to study aspects of WM anatomy. It uses local water diffusion in the tissues as the starting point. Although the determinants of water diffusion in WM tissues are still not completely understood, there is general agreement that the physicochemical properties of the tissue (e.g. viscosity and temperature) as well as its structural components (macromolecules, membranes,

and intracellular organelles) can substantially affect water diffusivity. In other words, diffusivity of water depends primarily on the presence of microscopic structural barriers in tissues that can alter the random motion of water molecules. Membranes of cell bodies, axons and myelin sheaths randomly impede the movement of water in the brain tissue, facilitating diffusion of water molecules preferentially along their main direction. Such preferentially oriented diffusion is called anisotropic diffusion. DWI is a one-dimensional technique, that is, it is used to measure the projection of all molecular displacements along one direction at a time. Therefore, it is sufficient to apply diffusion gradients along only one direction. As DTI is a three-dimensional technique, diffusion gradients must be applied along at least six noncollinear, non-coplanar directions in order to obtain enough information to estimate the six independent elements of the diffusion tensor (D) (in [68]).

In general, apparent diffusion coefficient (ADC), MD and FA have been used as the main diffusivity parameters. Although ADC measures the magnitude of water diffusion, it only provides a measure of the displacement of molecules in one direction; MD is a measure of the average motion of water molecules, independent of tissue directionality; and FA measures the directionality of water diffusion (see Fig. 4).

ADC, MD and FA may be altered by changes caused by the pathological process of AD. Pathological disruption of cell membranes and loss of myelin and axonal processes should lessen the restrictions on water movement. Therefore, the diffusivity measured with ADC or with MD should increase. Furthermore, the loss of tissue organization should also cause a decrease in anisotropy (FA). It is assumed that reduced water diffusion parallel to axonal tracts or FA is indicative of axonal degeneration and that increased water diffusion perpendicular to axonal tracts or MD is associated with changes in water content, disruption and partial breakdown of tissue cytoarchitecture [69, 70], sclerosis [71] or demyelinating processes [72–75]. Recently, Choi et al. [76] began investigating other measures of diffusion, such as radial diffusivity (DR) and axial diffusivity (DA), to determine whether differences in anisotropy are caused by diffusion perpendicular or parallel to the WM fibers, respectively. The assumption, arising out of experiments on animal models, is that significantly reduced DR in WM without differences in DA might represent specifically compromised integrity of myelin in the absence of axonal structural irregularities.

Table 2
VBM studies of CC

Study (year)	Sample	MMSE mean ± SD (range)	MRI acquisition	VBM method	Positive findings	Negative findings
Good et al. (2002)	-10 AD -10 SD -10 HC	21.2 ± 5.0 (n.a.) n.r. 29.8 ± 0.4 (n.a.)	1.5 T magnet. A T1-weighted volumetric scan (slice thickness = 1.5 mm)	Optimized VBM using custom template, with SPM99	Presence of diffuse white matter atrophy within CC in AD patients compared with HC (however, the finding was not detailed to ascertain the location of peak foci of CC atrophy).	
Thomann et al. (2006)	-10 AD -21 MCI "all subtypes" -21 HC	19.2 ± 3.8 (n.a.) n.a. n.a	1.5 T magnet. A T1-weighted volumetric scan (slice thickness = 0.98 × 0.98 × 1.8 mm)	Standard VBM with SPM99	Reduction of CC volume in posterior part of C1 (genu) and anterior part of C2 (anterior body) in AD patients compared with HC.	No difference in CC in MCI patients compared with HC.
Chaim et al. (2007)	-14 AD: n 11 AD n 3 AD -14 HC	20.7 ± 3.1 (n.a.): n.a. ± n.a. (≤20) n.a. ± n.a. (18–14) 29.1 ± 0.5 (n.a.)	1.5 T magnet. A T1-weighted volumetric scan (slice thickness = 1.2 × 1.2 × 1.2 mm)	Optimized VBM using custom template, with SPM2. Analysis restricted to VOI of CC	Reduction of CC volume in rostral portion of left genu, in anterior and posterior portions of left and right CC body and in left splenium and isthmus in AD patients compared with HC.	
Li et al. (2008)	-19 AD -20 HC	18.9 ± 3.9 (n.a.) 29.5 ± 0.9 (n.a.)	1.5 T magnet. A T1-weighted volumetric scan (slice thickness = 1.8 mm)	Optimized VBM using custom template, with SPM99	Reduction of CC volume in left isthmus and splenium in AD patients compared with HC.	
Di Paola et al. (2010a)	-30 AD: n 10 severe AD n 20 mild AD -20 amnesic MCI -20 HC	n.a.: 10.7 ± 3.7 (n.a.) 22.0 ± 2.5 (n.a.) 27.1 ± 2.5 (n.a.) 29.1 ± 0.9	3 T magnet. A T1-weighted 3-D MDFET volumetric scan (slice thickness = 1 × 1 × 1 mm)	VBM with unified segmentation algorithm in SPM5. Analysis restricted to VOI of CC.	Reduction of CC density in genu, anterior body and splenium of CC was found in severe AD patients compared with HC.	No CC difference in mild AD patients compared with HC. No CC difference in amnesic MCI patients compared with HC.
Di Paola et al. (2010b)	-38 AD -38 amnesic MCI -40 HC	22.6 ± 2.9 (n.a.) 27.0 ± 2.0 (n.a.) 29.2 ± 1.2 (n.a.)	3 T magnet. A T1-weighted volumetric scan (slice thickness = 1 × 1 × 1 mm)	VBM-DARTEL. Analysis restricted to VOI of entire CC.	Reduction of CC density in genu and splenium of CC in mild AD patients compared with HC. Reduction of CC density in genu in Amnesic MCI patients compared with HC.	
Guo et al. (2010)	-13 AD -14 HC	18.5 ± 3.5 (12–23) 28.5 ± 0.6 (27–29)	3 T magnet. A T1-weighted 3-D MPRAGE volumetric scan (slice thickness = 0.5 × 0.5 × 1 mm)	Optimized VBM using custom template, with SPM2.	Reduction of CC volume in rostrum, genu and anterior body of CC in AD patients compared with HC.	

The studies are presented in chronological order by publishing date; AD = Alzheimer's Disease ; CC = corpus callosum; HC = healthy controls; MCI = Mild Cognitive Impairment; MMSE = Mini Mental Status Examination; mean (standard deviation); SD = semantic dementia; VBM = Voxel-Based Morphometry; VOI = volume of interest; n.a. = data not available in the article; n.r. = data available in the article for different pathology, therefore not reported.
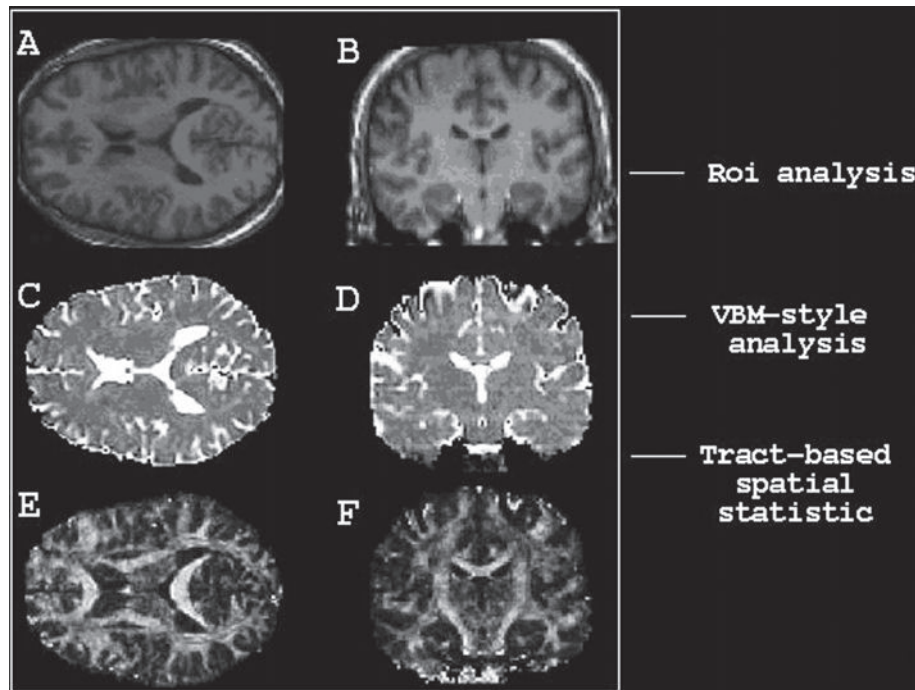
Fig. 4. Diffusion tensor-based images. A and B show axial (horizontal) and coronal T1-weighted anatomical images. C and D trace ADC maps (mean diffusivity) of the same slices shown in A and B. E and F are fractional anisotropy maps showing high contrast between gray and white matter. Once the mean diffusivity and fractional anisotropy maps are calculated, there are three approaches for post processing: manual ROI, VBM-style analysis [64] and tract-based spatial statistics (TBSS) [125].

With respect to structural MRI (ROI and VBM), DWI and DTI techniques have the advantage of being very sensitive in detecting microstructural abnormalities not revealed by other volumetric measures [28, 77]. In fact, structural MRI techniques, which reflect macrostructural changes, may not be sensitive to the degeneration of myelin and axons in the WM microstructure [28, 46]. On the contrary, DWI and DTI parameters have been applied in CC studies and have demonstrated much greater sensitivity in revealing the WM degeneration in AD than conventional MRI imaging techniques [69, 72, 78].

DWI studies on AD "all stages" patients [30, 33] report no significant group differences in measurements of the anisotropy index (AI) - calculated by dividing the ADC perpendicular to the prominent callosal fiber direction by the ADC parallel to the predominant fiber direction of the CC - within the genu and splenium of the CC. On the other hand, Hanyu et al. [28, 29] using the same index (that the Authors called ADC ratio) found a decrease in the anterior (rostrum and genu) and posterior (isthmus and splenium)

CC of AD "all stages" patients. Also, Wang et al., and Ray et al., [46, 79] found a higher ADC in the CC of patients with amnesic MCI than in HC.

DTI studies on AD "all stages" patients [32, 35, 36, 39, 41, 80–83] basically found changes in the anterior (genu) and posterior (splenium) subregions of the CC in AD patients compared with HC. More specifically, Rose et al. [32] found a value reduction in the splenium of AD patients but not in HC. They used lattice index (LI) as a measure of anisotropy. LI is an intervoxel measurement of diffusion anisotropy that exploits information about the orientation coherence of the eigenvectors of diffusion tensor in adjacent voxels to improve the estimate of diffusion anisotropy within a reference voxel. It is especially immune to background noise in the DW images and provides a quantitative, robust measurement of diffusion anisotropy [84].

The other studies [35, 36, 39, 41, 80, 81] that measured MD and/or FA can be separated into those which found mainly an increase of MD and/or a decrease of FA in the posterior subregion (splenium) of the CC

in AD [35, 36, 41, 80, 81] and those which reported an increase in MD or a decrease in FA in the anterior subregions (genu and anterior body) of CC in AD compared with HC [35, 39]. It is very difficult to summarize the general picture of these results because other studies on AD "all stages" [23, 37, 40, 76] reported no significant differences in MD or FA in the anterior and posterior CC when the patient group was compared with HC. Stahl et al. [40] also measured ADC and relative anisotropy and found no differences between AD patients and HC. Furthermore, the findings of studies on more homogeneous patients, such as those with mild AD, are discrepant. For example, Xie et al. [85] found a decrease of FA in the genu and left anterior body of the CC, whereas Ulkmar et al. [86] found a decrease of FA in the genu and splenium of the CC. Other studies [87–90] found no differences in the CC in patients with mild AD.

Finally Lee et al. [82] found a decreased FA values in all the CC regions (with the greatest group differences at the level of genu and splenium) in AD subjects compared with HC. Agosta et al. [83], who also collected DR and DA parameters, reported increased MD and DA in rostrum, body and splenium of CC in AD subjects compared with HC; and increased DR in rostrum and splenium of CC in AD subjects compared with HC.

At present, the DTI study results on MCI patients can be divided into two groups: (1) DTI studies on both amnesic and MCI "all subtypes" [23, 40, 41, 87, 88, 91] that found no differences in MD and/or in FA in the CC compared with HC; and (2) the most recent studies, which reported differences between patients and HC. One study on MCI "all subtypes" [92] found a significant change in MD and FA in the genu and the splenium of the CC in patients compared with HC. On the opposite, Lee et al., [82] did not find any significant differences of regional CC FA values in MCI "all subtypes" when compared with HC. Moreover, studies on amnesic MCI [86, 89, 93] mainly found a decreased FA and/or increased MD value in the splenium of the CC. Wang et al., [94] also reported a decreased FA value in the genu and the splenium and increased ADC in the genu of the CC (see Table 3 for technical details of the study). In our study [21], we found reduced FA in the genu and anterior body of the CC, increased DA in the body and in the posterior subregions of the CC and increased DR in the entire CC in patients with mild AD compared with HC. We found no significant differences in the CC in patients with amnesic MCI compared with HC.

More recently Agosta et al, [83] reported increased DA values in the rostrum, body and splenium of CC in amnesic MCI compared with HC, with no significant differences in MD, FA, and DR.

DISCUSSION

The purpose of this chapter was to summarize CC changes in patients with AD and MCI with regard to different illness stage and the measurements used to calculate the modifications. Regardless of the technique used (i.e. ROI, VBM, DWI or DTI), the main result in AD patients across all studies when severity of illness was not taken into consideration (AD "all stages") was primarily a change in the anterior (genu and anterior body) and posterior (isthmus and splenium) regions of the CC (see Table 4). This finding is less consistent when patients are separated into more homogeneous groups (e.g. mild AD and amnesic MCI). Indeed, some studies reported changes in the anterior subregion (e.g. [20, 46, 85]some in the posterior subregion [20, 86, 94] and some found no callosal changes [40, 88, 95]. This inconsistence in results may be the consequence of reduced sample size of studies considering discrete diagnostic categories of different clinical severity. But, whatever the reason, little is known about how early callosal atrophy occurs in AD and whether this change is already detectable in patients at higher risk of developing the disease, such as those with amnesic MCI [51] (see Table 4).

Region-specific callosal reduction

In summary, callosal atrophy in AD "all stages" affects the posterior and anterior subregions and spares the body of the CC. Therefore, the CC atrophy found in AD "all stages" groups corresponds with previously reported cortical areas considered to be involved in AD pathology [96]. The posterior subregion (splenium and isthmus) subserves two-thirds of the higher-order processing areas of the lateral temporal and parietal lobe, which, together with the mesial temporal structures [97], are primarily involved in cortical AD degeneration [96, 98, 99]. This could interfere with functioning of the posterior cortical memory networks, which subserve episodic memory operations and are impaired early in AD patients [100]. On the other hand, the anterior portion (genu and anterior body) is responsible for the inter-hemispheric connection between the prefrontal association cortices [90, 101, 102], that is,

Table 3
DWI and DTI studies of CC

Study (year)	Sample	MMSE mean ± SD (range)	MRI acquisition	Method	Positive findings	Negative findings
DWI studies						
Sandson et al. (1999)	-10 AD -11 HC	n.a. n.a.	1.5 T magnet; three-direction diffusion-weighted sequences obtained with EPI technique; slice thickness 7 mm, no interslice gap	ROIs were manually drawn on T2-weighted images, using characteristic landmarks and standard atlantes and were transferred onto the corresponding ADC maps. ROIs were placed in the genu and splenium. ROIs were of varying sizes (10–15 pixels).	Although AI was higher in splenium of CC in AD group compared with HC, this finding was not significant.	No difference was found in AI in genu of CC in AD patients compared with HC.
Hanyu et al. (1999a)	-23 AD: n 6 AD n 13 AD n 4 AD -16 HC	n.a.: n.a. ± n.a. (≥21) n.a. ± n.a. (20–11) n.a. ± n.a. (≤10) n.a. ± n.a. (<28)	1.5 T magnet; two-direction diffusion-weighted sequences obtained with EPI technique; slice thickness 8 mm with interslice gap	ROIs were manually drawn on T2-weighted reversed images; ROIs were placed in the genu and splenium. ROIs were of varying sizes (10–15 pixels) were placed in the anterior portion (rostrum and genu), in middle portion (body) and in posterior portion (isthmus and splenium) of CC. Circular ROIs were of varying sizes (4–6 mm in diameter).	ADC was higher in anterior (rostrum and genu) and posterior (isthmus and splenium) subregions of CC in AD patients compared with HC.	
Hanyu et al. (1999b)	-10 AD 14 VDBT -20 HC	13.4 ± 4.3 (n.a.) n.r. 29.3 ± 0.9 (n.a.)	1.5 T magnet; two-direction diffusion-weighted sequences obtained with EPI technique; slice thickness 8 mm with interslice gap	ROIs were manually drawn on T2-weighted images; ROIs were placed in genu and splenium of CC. Circular ROIs were of varying sizes (4–6 mm in diameter).	ADC in genu and splenium of CC were significantly higher in AD patients compared with HC.	
Bozzao et al. (2001)	-18 probable AD -16 Po/Pr AD -15 HC	17.1 ± 3.1 (n.a.) 27.2 ± 2.2 (n.a.) 29.4 ± 1.2 (n.a.)	1.5 T magnet; three-direction diffusion-weighted sequences obtained with EPI technique; slice thickness 6 mm with interslice gap	ROIs were drawn manually on ADC maps; they were placed in genu and splenium of CC and were of fixed size (50 pixel).		Measurements of AI within genu and splenium of CC did not disclose any significant group difference.
Wang H et al. (2006)	-13 amnesic MCI -13 HC	n.a. n.a	1.5 T magnet; three-direction diffusion-weighted sequences obtained with EPI technique; slice thickness 6 mm with interslice gap	ROIs were defined manually on T1- weighted images. Then T1- weighted images were coregistered to the DWI images. The transformation matrices obtained were used to map each ROI onto ADC maps; ROIs included the whole CC in midsagittal section.	ADC was increased in CC in MCI patients compared with HC.	
Ray et al. (2006)	-13 amnesic MCI -13 HC	26.8 ± 2.6 (n.a.) 28.6 ± 0.8 (n.a.)	1.5 T magnet; three-direction diffusion-weighted sequences obtained with EPI technique; slice thickness 6 mm with interslice gap	ROIs were defined manually on the T1- weighted image. Then T1- weighted images first coregistered to the ADC maps; so the ROIs could be mapped onto the ADC maps; ROIs included the whole CC in midsagittal section.	ADC was higher in the CC in MCI patients compared with HC	

DTI studies

Study	Subjects	Age	Technique	ROI method	Results
Rose et al. (2000)	-11 AD -9 HC	n.a. ± n.a. (6–21) n.a. ± n.a. (>28)	1.5 T magnet; six-direction diffusion-weighted sequences obtained with EPI technique; slice thickness 5 mm with interslice gap	The lattice index (LI) was used as a quantitative measure of anisotropy in DTI; ROI was manually traced in splenium of CC using color coding map to identify the region. Size of ROI n.a.	LI of splenium of CC was less in AD patients than in HC. Also, in a subgroup of AD patients with mild to moderate probable AD (MMSE 17–21), LI of splenium was less than in HC.
Bozzali et al. (2002)	-16 AD -10 HC	n.a. ± n.a. (9.3–25.4) median 19.4 n.a. ± n.a. (26.8–30.7) median 28.6	1.5 T magnet; eight-direction diffusion-weighted sequences obtained with EPI technique; slice thickness 5 mm with interslice gap	ROIs were sampled manually on three consecutive slices in genu and splenium of CC. Rectangular ROI of variable size (range = 11.4–46.7 mm^2) (the exact ROI size used for CC is n.a.).	MD was higher and FA lower in CC of AD patients compared with HC.
Takahashi et al. (2002)	-10 AD -10 HC	19.0 ± 3.2 (n.a.) n.a.	3 T magnet; six-direction diffusion-weighted sequences obtained with EPI technique; slice thickness 6 mm with interslice gap	ROIs were defined manually on anatomical T2-weighted image. ROIs were placed in anterior (genu) and posterior portion (splenium) of CC; size of ROIs for CC: 25 mm^2 for anterior and posterior CC.	Reduction in FA values in posterior portion (splenium) of CC in AD patients compared with HC.
Head et al. (2004)	-25 AD -25 non demented older adults -25 younger HC	22.9 ± 4.7 (15–30) 28.9 ± 1.2 (26–30) n.a.	1.5 T magnet; four + three-direction diffusion-weighted sequences obtained with EPI technique:. slice thickness 4 mm, no interslice gap	ROIs were manually outlined on the anisotropy image of each subject. ROIs of anterior (genu and rostrum) and posterior CC (splenium) consisted of 21 slices of CC.	Decreased FA in anterior and posterior CC in AD patients compared with younger adults (aging effect) Increased MD in callosal regions (anterior and posterior) in AD patients and non demented older adults compared with younger adults. No significant difference in MD and FA in anterior and posterior CC in AD patients compared with non demented older adults.
Fellgiebel et al. (2004)	-19 AD -14 amnesic MCI -10 HC	18.3 ± 4.8 (n.a.) 24.6 ± 2.7 (n.a.) 24.6 ± 1.3 (n.a.)	1.5 T magnet; six-direction diffusion-weighted sequences obtained with EPI technique; slice thickness 5 mm, no interslice gap	ROIs were defined manually on the anatomical T2-weighted image ($b = 0$ s/mm^2) and then transferred to FA and MD index maps. ROIs were of varying sizes (15–25 pixels) in genu and splenium of CC.	No difference in FA or MD were found in CC of AD and MCI patients compared with HC. No differences were found between MCI and AD patients regarding MD and FA values when the two groups were compared.
Sugihara et al. (2004)	-20 probable AD -20 VD -10 HC	n.a. n.a. n.a	1.5 T magnet; six non collinear direction diffusion-weighted sequences obtained with EPI technique; slice thickness 5 mm with interslice gap	ROIs in genu and splenium of CC were placed in T2-weighted image. ROIs of fixed size (6 pixels).	No differences in FA in AD patients compared with HC.

Table 3
(*Continued*)

Study (year)	Sample	MMSE mean ± SD (range)	MRI acquisition	Method	Positive findings	Negative findings
Choi et al. (2005)	-10 AD -10 HC	25.2 ± 2.5 (19–27) 29.5 ± 1.1 (27–30)	1.5 T magnet; six-direction diffusion-weighted sequences obtained with EPI technique; slice thickness n.a.	ROIs were defined manually on anatomical T2-weighted image ($b = 0$) of DTI data so that coregistration between different image acquisition methods was no longer necessary. Small-sized (area = 11.4 mm^2) circular ROIs were placed in genu and splenium of CC.		No differences in FA, MD, DR and DA within genu and splenium of CC in AD patients compared with HC.
Duan et al. (2006)	-16 AD -12 HC	13 ± n.a. (8–22) 28 ± n.a. (27–30)	1.5 T magnet; twenty-five-direction diffusion-weighted sequences obtained with EPI technique; slice thickness 5 mm, no interslice gap	Circular ROIs (of 20–40 mm^2) were placed in genu and splenium of CC. The genu and splenium of CC were sampled at the slices of the optic chiasm and anterior part of the inferior colliculus, respectively.	Decreased FA and increased MD were found in splenium of CC in AD patients compared with HC.	No differences were found in FA and MD in genu of CC in AD patients compared with HC.
Medina et al. (2006)	-14 AD -16 amnesic MCI -21 HC	24.5 ± 1.9 (n.a.) 26.9 ± 2.1 (n.a.) 29.3 ± 0.7 (n.a.)	1.5 T magnet; six-direction diffusion-weighted sequences obtained with EPI technique; slice thickness 6 mm, no interslice gap	Voxel-based analysis: the T2 images were spatially normalized to a standard T2 template in SPM99. Parameters from this transformation were then applied to the DTI images and statistical maps were created for DW and FA values. To limit the analysis to DW and FA values in white matter, an individual subject mask volumes were created, which were used to exclude voxels of no interest. The individual white matter masks were then applied to individual subject DW and FA maps. Group differences in voxel level DTI values were assessed using these individual, masked DW and FA maps.		No differences were found in FA or in MD in CC in AD and MCI patients compared with HC.
Naggara et al. (2006)	-12 AD -12 HC	27 ± 2.7 (20–30) 29.8 ± 0.4 (20–30)	1.5 T magnet; twenty five-direction diffusion-weighted sequences obtained with EPI technique; slice thickness 5 mm, no interslice gap	ROIs were defined manually on the anatomical T2-weighted image ($b = 0$) and then transferred onto MD and FA maps. Circular ROIs of variable sizes (mean: 40 mm^2) were placed in genu and splenium of CC.	Decreased FA and increased MD were found in splenium of CC in AD patients compared with HC.	No differences were found in genu of CC in AD patients compared with HC.

Study	Subjects	Age	MRI technique	Analysis	Results
Xie et al. (2006)	-13 AD -16 HC	21.1 ± n.a (19–24) n.a. ± n.a. (>27)	1.5 T magnet; thirteen-direction diffusion-weighted sequences obtained with EPI technique; slice thickness 4 mm, no interslice gap	Voxel-based analysis: the *b0* images of all control subjects and patients were normalized to the standard EPI template of SPM2. Then the FA maps were normalized by applying the normalization parameters determined from the normalization of the *b0* images. Because misregistration of FA maps can lead to falsepositive results, a mask was used to exclude those clusters of no interest (FA no more than 0.3).	Decreased FA in genu and left anterior body of CC was found in AD patients compared with HC.
Rose et al. (2006)	-17 amnesic MCI -17 HC	26.1 ± 2.2 (n.a.) 28.2 ± 1.2 (n.a.)	1.5 T magnet; optimized diffusion tensor sequence; slice thickness 2.5 mm with interslice gap	Voxel-based analysis: the *b0* images were normalized to the to the Montreal Neurological Institute template known as the ICBM152 to enable voxel-by-voxel statistical analysis of diffusivity indices between groups. Then the FA and MD maps were normalized by applying the normalization parameters determined from the normalization of the *b0* images. A value of t.4.095 was considered to be significant ($p = 0.001$). Voxels from the FA and MD maps with t.4.096 were automatically extracted and classified as a ROI when >20 voxels were contiguous.	No differences in FA and/or MD in CC were found in MCI patients compared with HC.
Stahl et al. (2007)	-15 AD -15 amnesic MCI -19 HC	n.a. ± n.a. (15–29) median 25 n.a. ± n.a. (23–29) median 27 n.a. ± n.a. (27–30) median 30	1.5 T magnet; six-direction diffusion-weighted sequences obtained with EPI technique; use of an 8-channel phased-array head coil and parallel imaging; slice thickness n.a.	ROIs were defined manually on the anatomical T2-weighted image ($b = 0$ s/mm²) and then transferred to the ADC, FA and RA maps. ROI placement approach (12–30 pixel size depending on the anatomical region) for genu and splenium of CC.	ADC increased and FA and RA decreased in splenium of CC in patients with AD compared with MCI patients.
Teipel et al. (2007)	-15 AD -14 HC	20.3 ± 4.6 (17–28) 28.8 ± 1.0 (27–30)	1.5 T magnet; six-direction diffusion-weighted sequences obtained with EPI technique; use of an 8-channel phased-array head coil and parallel imaging; slice thickness 3.6 mm, no interslice gap	Voxel-based analysis: normalization of FA maps to an anatomical template, resulting in FA maps projected into a standard space (i.e. a whole-brain voxel-based analytic method was used).	Decreased FA in anterior (genu) CC in AD patients compared with HC. No difference in ADC, FA and/or in RA in genu and splenium of CC in AD and MCI compared with HC.

Table 3
(*Continued*)

Study (year)	Sample	MMSE mean ± SD (range)	MRI acquisition	Method	Positive findings	Negative findings
Zhang et al. (2007)	-17 AD -17 MCI "all subtypes" -18 HC	22.1 ± 4.0 (n.a.) 27.9 ± 2.0 (n.a.) 29.5 ± 0.8 (n.a.)	1.5 T magnet; six-direction diffusion-weighted sequences obtained with EPI technique; slice thickness 5 mm, no interslice gap	ROI in the genu and splenium of CC; color maps to aid ROI placements; fixed-sized ROIs (from 4×4 mm² to 6×9 mm²).	Decreased FA in splenium of CC in AD patients compared with HC. Decreased FA in splenium of CC in AD patients compared with MCI.	No difference in FA in genu and splenium in MCI patients compared with HC. No difference in MD in CC in AD and MCI patients compared with HC and compared with one other.
Damoiseaux et al. (2008)	-16 AD -8 amnesic MCI -8 HC young -22 HC old	22.9 ± 3.2 (n.a.) 25.9 ± 2.6 (n.a.) 29.5 ± 0.5 (n.a.) 28.7 ± 1.4 (n.a.)	1.5 T magnet; sixty diffusion directions and 10 images with no diffusion weighting sequences obtained with EPI technique. Slice thickness 2 mm, no interslice gap	Analysis of FA data was carried out using TBSS on the whole WM.		No difference in FA in CC in either AD or MCI patients compared with HC.
Shim et al. (2008)	-40 multi-domain amnesic MCI: n 21 nvMCI n 19 vMCI -17 HC	n.a.: 24.5* ± 2.5 (n.a.) 25.3* ± 3.0 (n.a.) 28.7* ± 1.1 (n.a.)	1.5 T magnet; twenty five-direction diffusion-weighted sequences obtained with EPI technique; slice thickness 5 mm, no interslice gap	Manual tracing of ROI; all ROIs were placed on each MR image using a standardized placement procedure with atlas-based rules for morphological landmarks. They were placed on the *b*0 images and then superimposed over the identical slices on the FA and MD maps; sized ROI for CC: 25 mm³ for genu and splenium.	Decreased FA and increased MD values in genu and splenium of CC in both types of MCI patients compared with HC.	
Ukmar et al. (2008)	-14 mild AD -15 amnesic MCI -18 HC	23.4 ± 2.8 (n.a.) 28.9 ± 0.8 (n.a.) 29.9 ± 0.2 (n.a.)	1.5 T magnet; thirty-two directions diffusion-weighted sequences obtained with EPI technique; slice thickness 2 mm with interslice gap	Manual placement of 0.8-cm² of ROI's allowed measuring fractional anisotropy in the white matter of genu and splenium of CC.	Decreased FA in genu and splenium of CC in AD patients compared with HC. Decreased FA in splenium of CC in MCI patients compared with HC.	
Cho et al. (2008)	-11 amnesic MCI -11 HC	24.9* ± 2.4 (n.a.) 28.7 ± 0.8 (n.a.)	1.5 T magnet; twenty five directions diffusion-weighted sequences obtained with EPI technique; slice thickness 4 mm, no interslice gap	A standardized placement procedure was used to place spherical ROI's using atlas-based rules with morphological landmarks by taken from Mori et al. [127] for each MRI. The voxel size of the ROI was determined as 7 μL voxel for the body of the CC; it was 25 μL voxel for genu and splenium of the CC.	Decreased FA in splenium of CC in MCI patients compared with HC. Increased MD in splenium of CC in MCI patients compared with HC.	

Study	Groups	Age	Technique	Analysis	Results
Parente et al. (2008)	-15 possible AD -20 probable AD -25 amnesic MCI -16 HC	24.5 ± 0.5 (n.a.) 18.3 ± 5.1 (n.a.) 28.0 ± 1.1 (n.a.) 29.4 ± 0.9 (n.a.)	1.5 T magnet; six orthogonal directions diffusion-weighted sequences obtained with EPI technique; slice thickness 5 mm with interslice gap	Manual placement of 5 pixel circular ROI in splenium of CC.	Decreased FA in splenium of CC in MCI and probable AD patients compared with HC. No difference in FA in possible AD patients compared with HC.
Zarei et al. (2009)	-16 mild AD -13 VaD -22 HC	22.9 ± 3.2 (n.a.) n.r. 28.7 ± 1.4 (n.a.)	1.5 T magnet; sixty diffusion directions diffusion-weighted sequences obtained with EPI technique; slice thickness 2 mm, no interslice gap	Analysis of FA data was carried out using TBSS. CC was divided into 7 subregions: prefrontal cortical (PFC), premotor cortical, M1, S1, posterior parietal cortical, temporal cortical, and occipital cortical.	no difference in FA between AD patients and HC.
Wang L. et al. (2009)	-10 amnesic MCI -10 HC	26.4 ± 2.2 (n.a.) 29.7 ± 0.5 (n.a.)	3 T magnet; sixteen directions diffusion-weighted sequences obtained with EPI technique; slice thickness 2 mm; no interslice gap	Analysis of FA and ADC maps was carried out using FSL. ROIs were sampled manually on five consecutive slices in genu and splenium of CC.	Decreased FA in genu and splenium of CC in amnesic MCI patients. Increased ADC in genu of CC in amnesic MCI patients.
Di Paola et al. (2010b)	-38 AD -38 amnesic MCI -40 HC	22.6 ± 2.9 (n.a.) 27.0 ± 2.0 (n.a.) 29.2 ± 1.2 (n.a.)	3 T magnet; thirty diffusion directions diffusion-weighted sequences obtained with EPI technique. slice tickness 1.8 mm, no interslice gap.	Analysis of FA, DR and DA data was carried out using TBSS on the whole CC.	Decreased FA in genu and anterior body of CC; increased DA in body and posterior subregion of CC; and increased DR in the entire CC in mild AD subjects compared with HC. No difference in FA, DR or DA between amnesic MCI patients and HC.
Lee et al. (2010)	-47 AD, -77 MCI, -107 HC	20.0 ± 5.6 (n.a.) 25.2 ± 4.1 (n.a.) 27.9 ± 2.3 (n.a.)	1.5 T magnet; six diffusion directions diffusion-weighted sequences obtained with EPI technique.	Analysis of FA maps was carried out. CC ROI was sampled manually on mid-sagittal and 4 adjacent sagittal slices (2 right and 2 left slices to the mid-sagittal one; 1 slice thickness 0.938 mm) CC was divided into 4 subregion ROIs: CC I = rostrum, genu and anterior body; CC II = mid and posterior body; CC III = istmus; CC IV = splenium according to a recently proposed CC subdivision based on cytoarchitectonic cortical topography and advanced diffusion tensor imaging tractography [131]	Decreased FA values in all the CC regions (with the greatest group differences at the level of genu and splenium) in AD subjects compared with HC; Decreased FA in the CC II, CC III, and CC IV in AD when compared with MCI. No significant differences of regional CC FA values in MCI when compared with HC.

Table 3
(*Continued*)

Study (year)	Sample	MMSE mean ± SD (range)	MRI acquisition	Method	Positive findings	Negative findings
Agosta et al. (2011)	-23 AD -15 amnesic MCI -15 HC	14.0 ± 11.9 (n.a.) 25.8 ± 0.9 (n.a.) 28.8 ± 1.5 (n.a.)	1.5 T magnet; 12 noncollinear directions diffusion weighted sequences obtained with EPI technique; slice 2.5 mm thickness, no interslice gap.	Analysis of MD, FA, DR and DA data was carried out using TBSS.	Increased MD and DA in rostrum, body and splenium of CC in AD subject compared with HC; increased DR in rostrum and splenium of CC in AD subject compared with HC; Increased in DA values in the rostrum, body and splenium of CC amnesic MCI compared with HC.	No significant differences in MD, FA, and DR were found in patients with amnesic MCI compared with HC.

The studies are presented in chronological order by publishing date; AD = Alzheimer's Disease; ADC = apparent diffusion coefficient (i.e. magnitude of water diffusion); AI = anisotropy index; CC = corpus callosum; DA = axial diffusivity; DR = radial diffusivity; EPI = echo planar imaging sequence; FA = fractional anisotropy; HC = healthy controls; LI = lattice index; MCI = Mild Cognitive Impairment; MCI " all subtypes" = amnesic MCI and multiple-domain (both amnesic and/or non amnesic MCI; MD = mean diffusivity; MMSE = Mini Mental Status Examination; mean (standard deviation); nvMCI = non-vascular mild cognitive impairment; Po/Pr = Possible/Probable; RA = relative anisotropy; ROI = region of interest; TBSS = tract-based spatial statistics; VDBT = vascular dementia of the Binswanger type; vMCI = vascular mild cognitive impairment; n.a. = data not available in the article; n.r. = data available in the article for different pathology, therefore not reported; * = Korean Mini Mental State Examination [132].

Table 4
Summary of ROI, VBM, DWI and DTI studies of patients with Alzheimer's disease and mild cognitive impairment since 1997 showing corpus callosum changes

Patients	Techniques	Studies	Total CC Area	Anterior CC	Body			Posterior CC
					A	M	P	
AD "all stages"	ROI	Lyoo et al. (1997)		+	+	+	+	+
		Hampel et al. (1998)	+	+				+
		Teipel et al. (1998)	+	+	+			+
		Thompson et al. (1998)						+
		Pantel et al. (1998)	+	+	+			
		Hanyu et al. (1999b)	+					+
		Teipel et al. (1999)	+	+	+			+
		Pantel et al. (1999)	+	+	+	+		+
		Yamauchi et al. (2000)	+					+
		Black et al. (2000)	+	+	+		+	+
		Teipel et al. (2002)	+	+				+
		Teipel et al. (2003)	+	+				+
		Hensel et al. (2004)						
		Thomann et al. (2006)	+	+	+	+		
		Tomaiuolo et al. (2007)	+	+	+			+
		Li et al. (2008)		+	+	+		+
		Hallem et al. (2008)	+	+				+
	VBM	Good et al. (2002)	+					
		Thomann et al. (2006)		+	+			
		Chaim et al. (2007)		+	+		+	+
		Li et al. (2008)						+
		Guo et al. (2010)		+	+			
	DWI	Sandson et al. (1999)						
		Hanyu et al. (1999a)		+				+
		Hanyu et al. (1999b)		+				+
		Bozzao et al. (2001)						
	DTI	Rose et al. (2000)						+
		Bozzali et al. (2002)		+				+
		Takahashi et al. (2002)						+
		Head et al. (2004)						
		Fellgiebel et al. (2004)						
		Sugihara et al. (2004)						
		Duan et al. (2006)						+
		Stahl et al. (2007)						
		Teipel et al. (2007)		+				
		Zhang et al. (2007)						+
		Lee at al. (2010)		+	+	+	+	+
		Agosta et al. (2011)		+	+	+	+	+
Severe AD	ROI	Di Paola et al. (2010a)		+	+			+
	VBM	Di Paola et al. (2010a)		+	+			+
	DTI	Parente et al. (2008)						+
Moderate AD	ROI	Ortiz Alonso (2000)			+	+		+
Mild AD	ROI	Lyoo et al. (1997)					+	+
		Hensel et al. (2002)	+					
		Teipel et al. (2003)						+
		Hensel et al. (2005)						
		Wang PJ et al. (2006)	+					+
		Zarei et al. (2009)						
		Di Paola et al. (2010a)						

Table 4
(*Continued*)

| Patients | Techniques | Studies | Total CC Area | Anterior CC | Body | | | Posterior CC |
					A	M	P	
	VBM	Di Paola et al. (2010a)						
		Di Paola et al. (2010b)		+				+
	DWI	Bozzao et al. (2001)						
	DTI	Choi et al. (2005)						
		Medina et al. (2006)						
		Naggara et al. (2006)						+
		Xie et al. (2006)		+	+			
		Damoiseaux et al. (2008)						
		Ulkmar et al. (2008)						+
		Parente et al. (2008)						
		Zarei et al. (2009)						
		Di Paola et al. (2010b)	+	+				+
MCI "all subtypes"	ROI	Thomann et al. (2006)	+	+	+			
		Hallem et al. (2008)						
	VBM	Thomann et al. (2006)						
	DTI	Zhang et al. (2007)						
		Shim et al. (2008)		+				+
		Lee et al. (2010)						
Amnesic MCI	ROI	Wang H et al. (2006)	+					+
		Wang PJ et al. (2006)						
		Di Paola et al. (2010a)						
	VBM	Di Paola et al. (2010a)						
		Di Paola et al. (2010b)		+				
	DWI	Wang PJ et al. (2006)	+					
		Ray et al. (2006)	+					
	DTI	Fellgiebel et al. (2004)						
		Medina et al. (2006)						
		Rose et al. (2006)						
		Stahl et al. (2007)						
		Damoiseaux et al. (2008)						
		Ulkmar et al. (2008)						+
		Cho et al. (2008)						+
		Parente et al. (2008)						+
		Wang L et al. (2009)		+				+
		Di Paola et al. (2010b)						
		Agosta et al. (2011)		+	+	+		+

AD = Alzheimer's Disease; CC = corpus callosum; MA = mild ambiguous (similar to MCI); MCI = Mild Cognitive Impairment; Anterior CC = rostrum and genu; Body (A = anterior; M = mid; P = posterior body); Posterior CC = isthmus and splenium.

the regions involved in the later stages of AD pathology evolution [96, 98, 99]. These cortices are also implicated in monitoring information in working memory and in the active retrieval of information from posterior cortical association areas [103–105]. Thus, the volume reduction in these brain regions could account for general deficits in executive functions and attention in AD.

Finally, the body of the CC is most involved in motor and somato-sensory functions, which are usually spared in AD patients.

Possible underlying mechanisms

The basic assumption is that callosal atrophy in AD is the anatomical correlate of Wallerian degeneration of commissural nerve fibers. Therefore, it might show the same pattern of neocortical neurodegeneration. Based on the Wallerian degeneration hypothesis and on the AD neuronal degeneration pattern [106, 107], the posterior CC subregions should be involved in the earlier stages of the disease and the anterior CC subregions only in the later stages.

Nevertheless, several studies [20, 85, 92] found that a reduction in the genu of the CC was already present in the early and preclinical stages of AD.

It has been recently suggested that myelin breakdown is an important component of the illness process in AD [73, 108, 109]. According to this hypothesis, late-mylenating fibers should be more susceptible to myelin breakdown. The susceptibility of this subset of axons to myelin breakdown [110–113] may constitute an alternative mechanism through which the progression of cortical AD pathology occurs in the direction opposite to myelination [96], that is, the fibers that myelinate first in development are the last to be affected by AD and those that myelinate much later in normal development are the first to be affected by the AD degenerative process [73, 109].

The CC contains late-myelinating fibers in the genu [101, 102] and early-myelinating fibers in the splenium. Thus, it seems plausible to affirm that both Wallerian degeneration and myelin breakdown mechanisms are responsible for the region-specific illness effects. In this view, Wallerian degeneration affects the posterior CC subregion that receives axons directly from those brain areas (temporo-parietal lobe regions) that are primarily affected by AD pathology. Differently, the myelin breakdown process might affect the later-myelinating CC subregion, causing changes in the genu of the CC already in the early stage of the disease.

We tested the hypothesis that both Wallerian degeneration and myelin breakdown might be responsible for the region-specific callosal change detected in the mild AD patients in our VBM and DTI study [21]. We followed the assumption, arising out of experiments on animal models, that a reduction in DR might signify a loss of myelin integrity and that a reduction of DA might implicate axonal damage expected with Wallerian degeneration [72, 74, 75]. Our results [21] suggest that both of these mechanisms affecting the callosal WM are present. Indeed, we found atrophy in posterior and anterior subregions of the CC already in the early stage of AD (mild AD) and in amnesic MCI (see VBM data). However, the atrophy seemed to be due to different factors (see DTI data). In the anterior CC, we found loss of the preference of water diffusion in fiber direction (decreased FA) and major diffusion in the direction perpendicular to the CC fibers (increased DR). A change in DR not mirrored by a similar change in DA (such as that observed in the anterior portion of the CC) would most probably be caused by specific damage to the myelin sheaths that restrict DR. Thus,

these changes suggest a loss of myelin integrity, possibly due to a myelin breakdown mechanism. In the posterior CC subregion, we found an increase in water diffusion in the direction of the fibers (increased DA, no difference in FA). These changes suggest widespread tissue damage leading to a generalized increase in extracellular space due, for example, to the axonal atrophy expected with Wallerian degeneration.

Discrepancies with previous findings

The controversial results concerning regional atrophy of the CC are most likely due to the methods adopted across studies, such as the different criteria used to select patients, the different stages of illness considered and the different number of participants. Regarding the criteria used to select patients, here we report only a few examples. Thomann et al. [10] defined MCI patients according to the Aging-associated Cognitive Decline (AACD) criteria [114], which have been demonstrated to capture a larger group of patients than the MCI criteria [50, 51]. They also included people with cognitive impairment of a non-amnesic nature [115] and assigned the diagnosis of MCI with higher probability [116]. Therefore, this MCI group [10] was clearly more heterogeneous than groups in other studies. Yamauchi et al. [14] studied AD with early onset, which is considered a peculiar type of AD. In fact, it has been shown that AD patients with early onset have a typical and different topographical pattern of brain atrophy than patients with late onset AD, with possible consequences on CC subregion changes during the course of AD [117, 118].

Furthermore, the different degree of AD severity in some previous samples may also have been responsible for discrepant results. Many studies included AD patients with different degrees of pathology, for example, from mild to severe [7, 14, 15] or from mild to moderate [8, 10, 42] (see Tables 1–3). Thus, results may have been biased by the presence of subjects at different illness stages.

We have to consider that the vast majority of studies are cross-sectional, comparing AD patients and controls. Thus, anatomical changes described in AD patients could have existed prior to the onset of the illness and considered as a risk factor in AD. To solve this issue, in the near future follow-up investigations are strongly required in order to clarify how CC changes longitudinally in preclinical and clinical AD.

Limitations of the techniques

In early studies, the CC was manually traced (ROI studies) and segmented according to common parcellation schemes, that is, according to Witelson [44]; or Hampel [18] (see Table 1 and Fig. 2). These callosal segmentation methods have generated controversy with respect to the assumed topography of the callosal fiber [48]. In a previous study [7], we demonstrated that the pre-definition of callosal regions can give rise to erroneous results. To overcome these limits, some studies investigated callosal morphology using ROI analysis, which does not involve traditional parcellation [20, 43, 46], or applying an automated technique, such as VBM [8, 10, 20, 66], which completely eliminates the manual tracing step.

Nevertheless, the VBM technique also has limitations. One limitation is related to the variety of options available for implementing the VBM [49, 119]. Senjem et al. [49] found that 1) changes in the image processing chain of the VBM noticeably influenced the results of inter-group morphometric comparisons; 2) optimized VBM, using custom template and prior images, improved the plausibility of inter-group comparisons, presumably due to improved segmentation and spatial normalization. Thus, optimized VBM produces different results from those obtained with standard VBM. Prior to Senjem et al. [49], other authors had already pointed out the importance of spatial normalization, emphasizing that imperfect spatial normalization may affect the validity of VBM results [64, 120, 121].

There may be several reasons for the discrepant findings in DWI and DTI studies. First, the anisotropy indices from DWI are estimated from ADCs in three orthogonal directions, resulting in rotationally variant measurements that might differ if patients' heads are not the same size and oriented in the same way [122]. Thus, results are influenced by the different head positions of the subjects. DTI studies represent a step forward in this direction, because the scalar quantities associated with diffusion tensor (D) are invariant with respect to rotation of the coordinate system and, therefore, independent of the laboratory reference frame in which D is measured (i.e., they have the same value irrespective of the relative orientation of the "laboratory" and "fiber" frames of reference) [123]. Another aspect that can in part explain the variability in the results of DWI and DTI studies is how accurate the studies are in determining the location of changes. The latter can be inferred basically from ROI analyses [40, 41, 92], voxel-wise comparisons [32, 85,

87] or projecting diffusion values onto a tract-based template (TBSS) [88]. These approaches, however, all make assumptions about the correspondence of tract locations across subjects [124].

Moreover, with respect to the ROI analyses (the ones most frequently adopted in the DTI studies we reviewed; see Table 3), variability of results can be accounted for by the size and the placement of the ROIs across studies. As the placement of the ROIs is operator-dependent, care must be taken to place the ROIs only in WM areas to avoid partial volume effects through cerebrospinal fluid spaces. This is because intravoxel fiber incoherence diminishes the measured FA value. Thus, large ROIs are more likely to include other tissue than just WM, diminishing the FA value. Furthermore, the number of ROIs simultaneously examined in the studies and the difference in sample size (fixed vs variable) can influence results.

Furthermore, the VBM-style approach in DTI studies presents problems related to image registration and smoothing [125]. The first aspect can be generally expressed as the confidence we have that any given standard space voxel contains data from the same part of the same WM tract in each and every subject. A second problem with VBM-style analyses regards the standard practice of spatially smoothing data before computing voxelwise statistics. In fact, the amount of smoothing can greatly affect the final results, but there is no principled way of deciding how much smoothing is the "correct" amount [126]. Smoothing also increases effective partial voluming, a problem with VBM-style approaches particularly when applied to data such as FA. The use of TBSS [88, 90] seems to overcome the limitations due to alignment of FA images from multiple subjects and to the arbitrariness of choosing the degree of spatial smoothing. TBSS solves these issues by means of carefully tuned nonlinear registration followed by projection onto an alignment-invariant tract representation (the "mean FA skeleton") with no spatial smoothing. This projection step removes the effect of cross-subject spatial variability that remains after the non-linear registration.

New possibilities in the research of WM callosal anatomy arise from the use of DTI in conjunction with fiber tractography. DTI-based tractography provides unique access to *in vivo* information about the topography of callosal fibers [48, 127]. The technique allows to reconstruct the topographic arrangement of transcallosal fiber tracts projecting into specific cortical areas. Basically two ROIs are drawn, one is the

entire CC and the other is each cortical area of projection. Then, a fiber tracking software is used to compute a 3D trajectory between the two ROIs. In both studies cited [48, 127] the streamline fiber tracking method was based on fiber assignment by continuous tracking (FACT) [128]. The track trajectories follow the principal eigenvectors (the principal orientation of the fiber tract within the white matter). When the 3D fiber track trajectory enters a neighboring voxel, the fiber track's direction is altered to match the direction of the new voxel's primary eigenvector. The 3D fiber track is allowed to continue from voxel to voxel until it enters a region of FA less than 0.02, turns an angle greater than $50°$ between two consecutive voxels, or exits the brain.

Thus, DTI-based tractography is able to give information about the anatomical parcellation and cortical connectivity of CC subregions. This aspect is of great interest especially for those neurodegenerative disorders that affect the transcallosal connectivity.

However, DTI-based tractography has its own limits: it is prone to noise, partial volume effects and crossing fibers and to image resolution. Thus, future works would substantially benefit from DTI-based tractography especially if the limits of the technique will be improved with a better spatial resolution of DTI acquisitions, a greater number of diffusion-encoding gradients and a more adequate representation of orientational distributions.

CONCLUSIONS

Overall, the data suggest that studying the CC contributes to understanding the mechanisms underlying the progression of white matter changes in AD and to expanding knowledge of its role in cerebral cognitive functioning. For this purpose, the application of different MRI techniques (e.g., traditional structural MRI and DTI) is crucial, because the measurement of more parameters can offer a clearer picture of the WM changes in AD.

REFERENCES

[1] Hua X, Leow AD, Parikshak N, Lee S, Chiang MC, Toga AW, Jack CR Jr, Weiner MW, Thompson PM (2008) Tensor-based morphometry as a neuroimaging biomarker for Alzheimer's disease: an MRI study of 676 AD, MCI, and normal subjects. *Neuroimage* **43**, 458-469.

[2] Hua X, Leow AD, Lee S, Klunder AD, Toga AW, Lepore N, Chou YY, Brun C, Chiang MC, Barysheva M, Jack CR Jr, Bernstein MA, Britson PJ, Ward CP, Whitwell JL, Borowski B, Fleisher AS, Fox NC, Boyes RG, Barnes J, Harvey D, Kornak J, Schuff N, Boreta L, Alexander GE, Weiner MW, Thompson PM, Alzheimer's Disease Neuroimaging I (2008) 3D characterization of brain atrophy in Alzheimer's disease and mild cognitive impairment using tensor-based morphometry. *Neuroimage* **41**, 19-34.

[3] Bronge L, Bogdanovic N, Wahlund LO (2002) Postmortem MRI and histopathology of white matter changes in Alzheimer brains. A quantitative, comparative study. *Dement Geriatr Cogn Disord* **13**, 205-212.

[4] Smith CD, Snowdon DA, Wang H, Markesbery WR (2000) White matter volumes and periventricular white matter hyperintensities in aging and dementia. *Neurology* **54**, 838-842.

[5] Scheltens P, Barkhof F, Leys D, Wolters EC, Ravid R, Kamphorst W (1995) Histopathologic correlates of white matter changes on MRI in Alzheimer's disease and normal aging. *Neurology* **45**, 883-888.

[6] Brun A, Englund E (1986) A white matter disorder in dementia of the Alzheimer type: a pathoanatomical study. *Ann Neurol* **19**, 253-262.

[7] Tomaiuolo F, Scapin M, Di Paola M, Le Nezet P, Fadda L, Musicco M, Caltagirone C, Collins DL (2007) Gross anatomy of the corpus callosum in Alzheimer's disease: regions of degeneration and their neuropsychological correlates. *Dement Geriatr Cogn Disord* **23**, 96-103.

[8] Chaim TM, Duran FL, Uchida RR, Perico CA, de Castro CC, Busatto GF (2007) Volumetric reduction of the corpus callosum in Alzheimer's disease *in vivo* as assessed with voxel-based morphometry. *Psychiatry Res* **154**, 59-68.

[9] Wang PJ, Saykin AJ, Flashman LA, Wishart HA, Rabin LA, Santulli RB, McHugh TL, MacDonald JW, Mamourian AC (2006b) Regionally specific atrophy of the corpus callosum in AD, MCI and cognitive complaints. *Neurobiol Aging* **27**, 1613-1617.

[10] Thomann PA, Wustenberg T, Pantel J, Essig M, Schroder J (2006) Structural changes of the corpus callosum in mild cognitive impairment and Alzheimer's disease. *Dement Geriatr Cogn Disord* **21**, 215-220.

[11] Teipel SJ, Bayer W, Alexander GE, Bokde AL, Zebuhr Y, Teichberg D, Muller-Spahn F, Schapiro MB, Moller HJ, Rapoport SI, Hampel H (2003) Regional pattern of hippocampus and corpus callosum atrophy in Alzheimer's disease in relation to dementia severity: evidence for early neocortical degeneration. *Neurobiol Aging* **24**, 85-94.

[12] Teipel SJ, Bayer W, Alexander GE, Zebuhr Y, Teichberg D, Kulic L, Schapiro MB, Moller HJ, Rapoport SI, Hampel H (2002) Progression of corpus callosum atrophy in Alzheimer disease. *Arch Neurol* **59**, 243-248.

[13] Hampel H, Teipel SJ, Alexander GE, Pogarell O, Rapoport SI, Moller HJ (2002) *In vivo* imaging of region and cell type specific neocortical neurodegeneration in Alzheimer's disease. Perspectives of MRI derived corpus callosum measurement for mapping disease progression and effects of therapy. Evidence from studies with MRI, EEG and PET. *J Neural Transm* **109**, 837-855.

[14] Yamauchi H, Fukuyama H, Nagahama Y, Katsumi Y, Hayashi T, Oyanagi C, Konishi J, Shio H (2000) Comparison of the pattern of atrophy of the corpus callosum in frontotemporal dementia, progressive supranuclear palsy, and Alzheimer's disease. *J Neurol Neurosurg Psychiatry* **69**, 623-629.

[15] Teipel SJ, Hampel H, Pietrini P, Alexander GE, Horwitz B, Daley E, Moller HJ, Schapiro MB, Rapoport SI (1999)

Region-specific corpus callosum atrophy correlates with the regional pattern of cortical glucose metabolism in Alzheimer disease. *Arch Neurol* **56**, 467-473.

[16] Thompson PM, Moussai J, Zohoori S, Goldkorn A, Khan AA, Mega MS, Small GW, Cummings JL, Toga AW (1998) Cortical variability and asymmetry in normal aging and Alzheimer's disease. *Cereb Cortex* **8**, 492-509.

[17] Teipel SJ, Hampel H, Alexander GE, Schapiro MB, Horwitz B, Teichberg D, Daley E, Hippius H, Moller HJ, Rapoport SI (1998) Dissociation between corpus callosum atrophy and white matter pathology in Alzheimer's disease. *Neurology* **51**, 1381-1385.

[18] Hampel H, Teipel SJ, Alexander GE, Horwitz B, Teichberg D, Schapiro MB, Rapoport SI (1998) Corpus callosum atrophy is a possible indicator of region- and cell type-specific neuronal degeneration in Alzheimer disease: a magnetic resonance imaging analysis. *Arch Neurol* **55**, 193-198.

[19] Lyoo IK, Satlin A, Lee CK, Renshaw PF (1997) Regional atrophy of the corpus callosum in subjects with Alzheimer's disease and multi-infarct dementia. *Psychiatry Res* **74**, 63-72.

[20] Di Paola M, Luders E, Di Iulio F, Varsi AE, Sancesario G, Passafiume D, Thompson PM, Caltagirone C, Toga AW, Spalletta G (2010a) Callosal atrophy in mild cognitive impairment and Alzheimer's disease: Different effects in different stages. *Neuroimage* **49**, 141-149. [Epub 2009 Jul 2028]

[21] Di Paola M, Di Iulio F, Cherubini A, Blundo C, Casini AR, Sancesario G, Passafiume D, Caltagirone C, Spalletta G (2010b) When, where and how corpus callosal changes in preclinical and clinical AD using multimodal MRI at 3 Tesla. *Neurology* **74**, 1136-1142.

[22] Tomimoto H, Lin JX, Matsuo A, Ihara M, Ohtani R, Shibata M, Miki Y, Shibasaki H (2004) Different mechanisms of corpus callosum atrophy in Alzheimer's disease and vascular dementia. *J Neurol* **251**, 398-406.

[23] Fellgiebel A, Wille P, Muller MJ, Winterer G, Scheurich A, Vucurevic G, Schmidt LG, Stoeter P (2004) Ultrastructural hippocampal and white matter alterations in mild cognitive impairment: a diffusion tensor imaging study. *Dement Geriatr Cogn Disord* **18**, 101-108.

[24] Pantel J, Schroder J, Essig M, Minakaran R, Schad LR, Friedlinger M, Jauss M, Knopp MV (1998) Corpus callosum in Alzheimer's disease and vascular dementia–a quantitative magnetic resonance study. *J Neural Transm Suppl* **54**, 129-136.

[25] Pantel J, Schroder J, Jauss M, Essig M, Minakaran R, Schonknecht P, Schneider G, Schad LR, Knopp MV (1999) Topography of callosal atrophy reflects distribution of regional cerebral volume reduction in Alzheimer's disease. *Psychiatry Res* **90**, 181-192.

[26] Leys D, Pruvo JP, Parent M, Vermersch P, Soetaert G, Steinling M, Delacourte A, Defossez A, Rapoport A, Clarisse J et al. (1991) Could Wallerian degeneration contribute to "leuko-araiosis" in subjects free of any vascular disorder? *J Neurol Neurosurg Psychiatry* **54**, 46-50.

[27] Kaufer DI, Miller BL, Itti L, Fairbanks LA, Li J, Fishman J, Kushi J, Cummings JL (1997) Midline cerebral morphometry distinguishes frontotemporal dementia and Alzheimer's disease. *Neurology* **48**, 978-985.

[28] Hanyu H, Asano T, Sakurai H, Imon Y, Iwamoto T, Takasaki M, Shindo H, Abe K (1999a) Diffusion-weighted and magnetization transfer imaging of the corpus callosum in Alzheimer's disease. *J Neurol Sci* **167**, 37-44.

[29] Hanyu H, Imon Y, Sakurai H, Iwamoto T, Takasaki M, Shindo H, Kakizaki D, Abe K (1999b) Regional differences in diffusion abnormality in cerebral white matter lesions in patients with vascular dementia of the Binswanger type and Alzheimer's disease. *Eur J Neurol* **6**, 195-203.

[30] Sandson TA, Felician O, Edelman RR, Warach S (1999) Diffusion-weighted magnetic resonance imaging in Alzheimer's disease. *Dement Geriatr Cogn Disord* **10**, 166-171.

[31] Black SE, Moffat SD, Yu DC, Parker J, Stanchev P, Bronskill M (2000) Callosal atrophy correlates with temporal lobe volume and mental status in Alzheimer's disease. *Can J Neurol Sci* **27**, 204-209.

[32] Rose SE, Chen F, Chalk JB, Zelaya FO, Strugnell WE, Benson M, Semple J, Doddrell DM (2000) Loss of connectivity in Alzheimer's disease: an evaluation of white matter tract integrity with colour coded MR diffusion tensor imaging. *J Neurol Neurosurg Psychiatry* **69**, 528-530.

[33] Bozzao A, Floris R, Baviera ME, Apruzzese A, Simonetti G (2001) Diffusion and perfusion MR imaging in cases of Alzheimer's disease: correlations with cortical atrophy and lesion load. *AJNR Am J Neuroradiol* **22**, 1030-1036.

[34] Good CD, Johnsrude IS, Ashburner J, Henson RN, Friston KJ, Frackowiak RS (2001) A voxel-based morphometric study of ageing in 465 normal adult human brains. *Neuroimage* **14**, 21-36.

[35] Bozzali M, Falini A, Franceschi M, Cercignani M, Zuffi M, Scotti G, Comi G, Filippi M (2002) White matter damage in Alzheimer's disease assessed *in vivo* using diffusion tensor magnetic resonance imaging. *J Neurol Neurosurg Psychiatry* **72**, 742-746.

[36] Takahashi S, Yonezawa H, Takahashi J, Kudo M, Inoue T, Tohgi H (2002) Selective reduction of diffusion anisotropy in white matter of Alzheimer disease brains measured by 3.0 Tesla magnetic resonance imaging. *Neurosci Lett* **332**, 45-48.

[37] Head D, Buckner RL, Shimony JS, Williams LE, Akbudak E, Conturo TE, McAvoy M, Morris JC, Snyder AZ (2004) Differential vulnerability of anterior white matter in nondemented aging with minimal acceleration in dementia of the Alzheimer type: evidence from diffusion tensor imaging. *Cereb Cortex* **14**, 410-423.

[38] Wiltshire K, Foster S, Kaye JA, Small BJ, Camicioli R (2005) Corpus callosum in neurodegenerative diseases: findings in Parkinson's disease. *Dement Geriatr Cogn Disord* **20**, 345-351.

[39] Teipel SJ, Stahl R, Dietrich O, Schoenberg SO, Perneczky R, Bokde AL, Reiser MF, Moller HJ, Hampel H (2007) Multivariate network analysis of fiber tract integrity in Alzheimer's disease. *Neuroimage* **34**, 985-995.

[40] Stahl R, Dietrich O, Teipel SJ, Hampel H, Reiser MF, Schoenberg SO (2007) White matter damage in Alzheimer disease and mild cognitive impairment: assessment with diffusion-tensor MR imaging and parallel imaging techniques. *Radiology* **243**, 483-492.

[41] Zhang Y, Schuff N, Jahng GH, Bayne W, Mori S, Schad L, Mueller S, Du AT, Kramer JH, Yaffe K, Chui H, Jagust WJ, Miller BL, Weiner MW (2007) Diffusion tensor imaging of cingulum fibers in mild cognitive impairment and Alzheimer disease. *Neurology* **68**, 13-19.

[42] Li S, Pu F, Shi F, Xie S, Wang Y, Jiang T (2008) Regional white matter decreases in Alzheimer's disease using optimized voxel-based morphometry. *Acta Radiol* **49**, 84-90.

[43] Hallam BJ, Brown WS, Ross C, Buckwalter JG, Bigler ED, Tschanz JT, Norton MC, Welsh-Bohmer KA, Breitner JC (2008) Regional atrophy of the corpus callosum in dementia. *J Int Neuropsychol Soc* **14**, 414-423.

[44] Witelson SF (1989) Hand and sex differences in the isthmus and genu of the human corpus callosum. *A postmortem morphological study. Brain* **112(Pt 3)**, 799-835.

[45] Hensel A, Wolf H, Kruggel F, Riedel-Heller SG, Nikolaus C, Arendt T, Gertz HJ (2002) Morphometry of the corpus callosum in patients with questionable and mild dementia. *J Neurol Neurosurg Psychiatry* **73**, 59-61.

[46] Wang H, Su MY (2006) Regional pattern of increased water diffusivity in hippocampus and corpus callosum in mild cognitive impairment. *Dement Geriatr Cogn Disord* **22**, 223-229.

[47] Weis S, Jellinger K, Wenger E (1991) Morphometry of the corpus callosum in normal aging and Alzheimer's disease. *J Neural Transm Suppl* **33**, 35-38.

[48] Hofer S, Frahm J (2006) Topography of the human corpus callosum revisited–comprehensive fiber tractography using diffusion tensor magnetic resonance imaging. *Neuroimage* **32**, 989-994.

[49] Senjem ML, Gunter JL, Shiung MM, Petersen RC, Jack CR Jr, (2005) Comparison of different methodological implementations of voxel-based morphometry in neurodegenerative disease. *Neuroimage* **26**, 600-608.

[50] Petersen RC, Smith GE, Waring SC, Ivnik RJ, Tangalos EG, Kokmen E (1999) Mild cognitive impairment: clinical characterization and outcome. *Arch Neurol* **56**, 303-308.

[51] Petersen RC (2004) Mild cognitive impairment as a diagnostic entity. *J Intern Med* **256**, 183-194.

[52] Lopez OL, Kuller LH, Becker JT, Dulberg C, Sweet RA, Gach HM, Dekosky ST (2007) Incidence of dementia in mild cognitive impairment in the cardiovascular health study cognition study. *Arch Neurol* **64**, 416-420.

[53] Sydykova D, Stahl R, Dietrich O, Ewers M, Reiser MF, Schoenberg SO, Moller HJ, Hampel H, Teipel SJ (2007) Fiber connections between the cerebral cortex and the corpus callosum in Alzheimer's disease: a diffusion tensor imaging and voxel-based morphometry study. *Cereb Cortex* **17**, 2276-2282.

[54] Jancke L, Staiger JF, Schlaug G, Huang Y, Steinmetz H (1997) The relationship between corpus callosum size and forebrain volume. *Cereb Cortex* **7**, 48-56.

[55] Jancke L, Preis S, Steinmetz H (1999) The relation between forebrain volume and midsagittal size of the corpus callosum in children. *Neuroreport* **10**, 2981-2985.

[56] Wang PP, Doherty S, Hesselink JR, Bellugi U (1992) Callosal morphology concurs with neurobehavioral and neuropathological findings in two neurodevelopmental disorders. *Arch Neurol* **49**, 407-411.

[57] Schmitt JE, Eliez S, Warsofsky IS, Bellugi U, Reiss AL (2001) Corpus callosum morphology of Williams syndrome: relation to genetics and behavior. *Dev Med Child Neurol* **43**, 155-159.

[58] Hensel A, Wolf H, Busse A, Arendt T, Gertz HJ (2005) Association between global brain volume and the rate of cognitive change in elderly humans without dementia. *Dement Geriatr Cogn Disord* **19**, 213-221.

[59] Ortiz Alonso T, Martinez Castillo E, Fernandez Lucas A, Arrazola Garcia J, Maestu Unturbe F, Lopez-Ibor JJ (2000) Callosal atrophy and associated electromyographic

responses in Alzheimer's disease and aging. *Electromyogr Clin Neurophysiol* **40**, 465-475.

[60] Luders E, Narr KL, Zaidel E, Thompson PM, Jancke L, Toga AW (2006) Parasagittal asymmetries of the corpus callosum. *Cereb Cortex* **16**, 346-354.

[61] Thompson PM, MacDonald D, Mega MS, Holmes CJ, Evans AC, Toga AW (1997) Detection and mapping of abnormal brain structure with a probabilistic atlas of cortical surfaces. *J Comput Assist Tomogr* **21**, 567-581.

[62] Thompson PM, Schwartz C, Lin RT, Khan AA, Toga AW (1996a) Three-dimensional statistical analysis of sulcal variability in the human brain. *J Neurosci* **16**, 4261-4274.

[63] Thompson PM, Schwartz C, Toga AW (1996b) High-resolution random mesh algorithms for creating a probabilistic 3D surface atlas of the human brain. *Neuroimage* **3**, 19-34.

[64] Ashburner J, Friston KJ (2000) Voxel-based morphometry–the methods. *Neuroimage* **11**, 805-821.

[65] Ashburner J, Friston KJ (2005) Unified segmentation. *Neuroimage* **26**, 839-851.

[66] Good CD, Scahill RI, Fox NC, Ashburner J, Friston KJ, Chan D, Crum WR, Rossor MN, Frackowiak RS (2002) Automatic differentiation of anatomical patterns in the human brain: validation with studies of degenerative dementias. *Neuroimage* **17**, 29-46.

[67] Guo X, Wang Z, Li K, Li Z, Qi Z, Jin Z, Yao L, Chen K (2010) Voxel-based assessment of gray and white matter volumes in Alzheimer's disease. *Neurosci Lett* **468**, 146-150.

[68] Basser PJ, Jones DK (2002) Diffusion-tensor MRI: theory, experimental design and data analysis - a technical review. *NMR Biomed* **15**, 456-467.

[69] Neil J, Miller J, Mukherjee P, Huppi PS (2002) Diffusion tensor imaging of normal and injured developing human brain - a technical review. *NMR Biomed* **15**, 543-552.

[70] Beaulieu C (2002) The basis of anisotropic water diffusion in the nervous system - a technical review. *NMR Biomed* **15**, 435-455.

[71] Assaf BA, Mohamed FB, Abou-Khaled KJ, Williams JM, Yazeji MS, Haselgrove J, Faro SH (2003) Diffusion tensor imaging of the hippocampal formation in temporal lobe epilepsy. *AJNR Am J Neuroradiol* **24**, 1857-1862.

[72] Sun SW, Song SK, Harms MP, Lin SJ, Holtzman DM, Merchant KM, Kotyk JJ (2005) Detection of age-dependent brain injury in a mouse model of brain amyloidosis associated with Alzheimer's disease using magnetic resonance diffusion tensor imaging. *Exp Neurol* **191**, 77-85.

[73] Bartzokis G (2004a) Age-related myelin breakdown: a developmental model of cognitive decline and Alzheimer's disease. *Neurobiol Aging* **25**, 5-18; author reply 49-62.

[74] Song SK, Sun SW, Ju WK, Lin SJ, Cross AH, Neufeld AH (2003) Diffusion tensor imaging detects and differentiates axon and myelin degeneration in mouse optic nerve after retinal ischemia. *Neuroimage* **20**, 1714-1722.

[75] Song SK, Sun SW, Ramsbottom MJ, Chang C, Russell J, Cross AH (2002) Dysmyelination revealed through MRI as increased radial (but unchanged axial) diffusion of water. *Neuroimage* **17**, 1429-1436.

[76] Choi SJ, Lim KO, Monteiro I, Reisberg B (2005) Diffusion tensor imaging of frontal white matter microstructure in early Alzheimer's disease: a preliminary study. *J Geriatr Psychiatry Neurol* **18**, 12-19.

[77] Muller MJ, Greverus D, Dellani PR, Weibrich C, Wille PR, Scheurich A, Stoeter P, Fellgiebel A (2005) Functional

implications of hippocampal volume and diffusivity in mild cognitive impairment. *Neuroimage* **28**, 1033-1042.

[78] Sundgren PC, Dong Q, Gomez-Hassan D, Mukherji SK, Maly P, Welsh R (2004) Diffusion tensor imaging of the brain: review of clinical applications. *Neuroradiology* **46**, 339-350.

[79] Ray KM, Wang H, Chu Y, Chen YF, Bert A, Hasso AN, Su MY (2006) Mild cognitive impairment: apparent diffusion coefficient in regional gray matter and white matter structures. *Radiology* **241**, 197-205.

[80] Naggara O, Oppenheim C, Rieu D, Raoux N, Rodrigo S, Dalla Barba G, Meder JF (2006) Diffusion tensor imaging in early Alzheimer's disease. *Psychiatry Res* **146**, 243-249.

[81] Duan JH, Wang HQ, Xu J, Lin X, Chen SQ, Kang Z, Yao ZB (2006) White matter damage of patients with Alzheimer's disease correlated with the decreased cognitive function. *Surg Radiol Anat* **28**, 150-156.

[82] Lee DY, Fletcher E, Martinez O, Zozulya N, Kim J, Tran J, Buonocore M, Carmichael O, DeCarli C (2010) Vascular and degenerative processes differentially affect regional interhemispheric connections in normal aging, mild cognitive impairment, and Alzheimer disease. *Stroke* **41**, 1791-1797.

[83] Agosta F, Pievani M, Sala S, Geroldi C, Galluzzi S, Frisoni GB, Filippi M (2010) White matter damage in Alzheimer disease and its relationship to gray matter atrophy. *Radiology* **258**, 853-863.

[84] Pierpaoli C, Basser PJ (1996) Toward a quantitative assessment of diffusion anisotropy. *Magn Reson Med* **36**, 893-906.

[85] Xie S, Xiao JX, Gong GL, Zang YF, Wang YH, Wu HK, Jiang XX (2006) Voxel-based detection of white matter abnormalities in mild Alzheimer disease. *Neurology* **66**, 1845-1849.

[86] Ukmar M, Makuc E, Onor ML, Garbin G, Trevisiol M, Cova MA (2008) Evaluation of white matter damage in patients with Alzheimer's disease and in patients with mild cognitive impairment by using diffusion tensor imaging. *Radiol Med* **113**, 915-922.

[87] Medina D, DeToledo-Morrell L, Urresta F, Gabrieli JD, Moseley M, Fleischman D, Bennett DA, Leurgans S, Turner DA, Stebbins GT (2006) White matter changes in mild cognitive impairment and AD: a diffusion tensor imaging study. *Neurobiol Aging* **27**, 663-672.

[88] Damoiseaux JS, Smith SM, Witter MP, Sanz-Arigita EJ, Barkhof F, Scheltens P, Stam CJ, Zarei M, Rombouts SA (2009) White matter tract integrity in aging and Alzheimer's disease. *Hum Brain Mapp* **30**, 1051-1059.

[89] Parente DB, Gasparetto EL, da Cruz LC, Jr., Domingues RC, Baptista AC, Carvalho AC, Domingues RC (2008) Potential role of diffusion tensor MRI in the differential diagnosis of mild cognitive impairment and Alzheimer's disease. *AJR Am J Roentgenol* **190**, 1369-1374.

[90] Zarei M, Johansen-Berg H, Smith S, Ciccarelli O, Thompson AJ, Matthews PM (2006) Functional anatomy of interhemispheric cortical connections in the human brain. *J Anat* **209**, 311-320.

[91] Rose SE, McMahon KL, Janke AL, O'Dowd B, de Zubicaray G, Strudwick MW, Chalk JB (2006) Diffusion indices on magnetic resonance imaging and neuropsychological performance in amnestic mild cognitive impairment. *J Neurol Neurosurg Psychiatry* **77**, 1122-1128.

[92] Shim YS, Yoon B, Shon YM, Ahn KJ, Yang DW (2008) Difference of the hippocampal and white matter microalterations in MCI patients according to the severity of

subcortical vascular changes: neuropsychological correlates of diffusion tensor imaging. *Clin Neurol Neurosurg* **110**, 552-561.

[93] Cho H, Yang DW, Shon YM, Kim BS, Kim YI, Choi YB, Lee KS, Shim YS, Yoon B, Kim W, Ahn KJ (2008) Abnormal integrity of corticocortical tracts in mild cognitive impairment: a diffusion tensor imaging study. *J Korean Med Sci* **23**, 477-483.

[94] Wang L, Goldstein FC, Veledar E, Levey AI, Lah JJ, Meltzer CC, Holder CA, Mao H (2009) Alterations in cortical thickness and white matter integrity in mild cognitive impairment measured by whole-brain cortical thickness mapping and diffusion tensor imaging. *AJNR Am J Neuroradiol* **30**, 893-899.

[95] Zarei M, Damoiseaux JS, Morgese C, Beckmann CF, Smith SM, Matthews PM, Scheltens P, Rombouts SA, Barkhof F (2009) Regional white matter integrity differentiates between vascular dementia and Alzheimer disease. *Stroke* **40**, 773-779.

[96] Braak H, Braak E (1997a) Frequency of stages of Alzheimer-related lesions in different age categories. *Neurobiol Aging* **18**, 351-357.

[97] Schmahmann J, Pandya D (2006) *Fiber Pathways of the Brain*, Oxford Universiy Press, New York.

[98] Thompson PM, Hayashi KM, de Zubicaray G, Janke AL, Rose SE, Semple J, Herman D, Hong MS, Dittmer SS, Doddrell DM, Toga AW (2003) Dynamics of gray matter loss in Alzheimer's disease. *J Neurosci* **23**, 994-1005.

[99] Braak H, Braak E (1991) Neuropathological stageing of Alzheimer-related changes. *Acta Neuropathol* **82**, 239-259.

[100] Galton CJ, Patterson K, Xuereb JH, Hodges JR (2000) Atypical and typical presentations of Alzheimer's disease: a clinical, neuropsychological, neuroimaging and pathological study of 13 cases. *Brain* **123(pt3)**, 484-498.

[101] Aboitiz F, Rodriguez E, Olivares R, Zaidel E (1996) Age-related changes in fibre composition of the human corpus callosum: sex differences. *Neuroreport* **7**, 1761-1764.

[102] Aboitiz F, Scheibel AB, Fisher RS, Zaidel E (1992) Fiber composition of the human corpus callosum. *Brain Res* **598**, 143-153.

[103] Petrides M (2005) Lateral prefrontal cortex: architectonic and functional organization. *Philos Trans R Soc Lond B Biol Sci* **360**, 781-795.

[104] Petrides M (2002) The mid-ventrolateral prefrontal cortex and active mnemonic retrieval. *Neurobiol Learn Mem* **78**, 528-538.

[105] Petrides M (1996) Specialized systems for the processing of mnemonic information within the primate frontal cortex. *Philos Trans R Soc Lond B Biol Sci* **351**, 1455-1461; discussion 1461-1452.

[106] Brun A, Englund E (2002) Regional pattern of degeneration in Alzheimer's disease: neuronal loss and histopathological grading. *Histopathology* **41**, 40-55.

[107] Brun A, Englund E (1981) Regional pattern of degeneration in Alzheimer's disease: neuronal loss and histopathological grading. *Histopathology* **5**, 549-564.

[108] Bartzokis G, Cummings JL, Sultzer D, Henderson VW, Nuechterlein KH, Mintz J (2003) White matter structural integrity in healthy aging adults and patients with Alzheimer disease: a magnetic resonance imaging study. *Arch Neurol* **60**, 393-398.

[109] Bartzokis G, Sultzer D, Lu PH, Nuechterlein KH, Mintz J, Cummings JL (2004b) Heterogeneous age-related break-

down of white matter structural integrity: implications for cortical "disconnection" in aging and Alzheimer's disease. *Neurobiol Aging* **25**, 843-851.

[110] Nieuwenhuys R (1999) Structure and organization of fibre systems. In *The central nervous system of vertebrates*, Nieuwenhuys R, Ten Donkelaar HJ, Nicholson C, eds. Springer Berlin Heidelberg New york Tokyo pp. 113-157.

[111] Tang Y, Nyengaard JR, Pakkenberg B, Gundersen HJ (1997) Age-induced white matter changes in the human brain: a stereological investigation. *Neurobiol Aging* **18**, 609-615.

[112] Hildebrand C, Remahl S, Persson H, Bjartmar C (1993) Myelinated nerve fibres in the CNS. *Prog Neurobiol* **40**, 319-384.

[113] Meier-Ruge W, Ulrich J, Bruhlmann M, Meier E (1992) Age-related white matter atrophy in the human brain. *Ann N Y Acad Sci* **673**, 260-269.

[114] Levy R (1994) Aging-associated cognitive decline. Working party of the international psychogeriatric association in collaboration with the world health organization. *Int Psychogeriatr* **6**, 63-68.

[115] Richards M, Touchon J, Ledesert B, Richie K (1999) Cognitive decline in ageing: are AAMI and AACD distinct entities?. *Int J Geriatr Psychiatry* **14**, 534-540.

[116] Busse A, Bischkopf J, Riedel-Heller SG, Angermeyer MC (2003) Mild cognitive impairment: prevalence and incidence according to different diagnostic criteria. Results of the Leipzig Longitudinal Study of the Aged (LEILA75+). *Br J Psychiatry* **182**, 449-454.

[117] Frisoni GB, Pievani M, Testa C, Sabattoli F, Bresciani L, Bonetti M, Beltramello A, Hayashi KM, Toga AW, Thompson PM (2007) The topography of grey matter involvement in early and late onset Alzheimer's disease. *Brain* **130**, 720-730.

[118] Karas G, Scheltens P, Rombouts S, van Schijndel R, Klein M, Jones B, van der Flier W, Vrenken H, Barkhof F (2007) Precuneus atrophy in early-onset Alzheimer's disease: a morphometric structural MRI study. *Neuroradiology* **49**, 967-976.

[119] Keller SS, Wilke M, Wieshmann UC, Sluming VA, Roberts N (2004) Comparison of standard and optimized voxel-based morphometry for analysis of brain changes associated with temporal lobe epilepsy. *Neuroimage* **23**, 860-868.

[120] Bookstein FL (2001) "Voxel-based morphometry" should not be used with imperfectly registered images. *Neuroimage* **14**, 1454-1462.

[121] Salmond CH, Ashburner J, Vargha-Khadem F, Connelly A, Gadian DG, Friston KJ (2002) The precision of anatomical

normalization in the medial temporal lobe using spatial basis functions. *Neuroimage* **17**, 507-512.

[122] Kantarci K, Jack CR Jr, Xu YC, Campeau NG, O'Brien PC, Smith GE, Ivnik RJ, Boeve BF, Kokmen E, Tangalos EG, Petersen RC (2001) Mild cognitive impairment and Alzheimer disease: regional diffusivity of water. *Radiology* **219**, 101-107.

[123] Basser PJ, Mattiello J, LeBihan D (1994) MR diffusion tensor spectroscopy and imaging. *Biophys J* **66**, 259-267.

[124] Johansen-Berg H, Behrens TE (2006) Just pretty pictures? What diffusion tractography can add in clinical neuroscience. *Curr Opin Neurol* **19**, 379-385.

[125] Smith SM, Jenkinson M, Johansen-Berg H, Rueckert D, Nichols TE, Mackay CE, Watkins KE, Ciccarelli O, Cader MZ, Matthews PM, Behrens TE (2006) Tract-based spatial statistics: voxelwise analysis of multi-subject diffusion data. *Neuroimage* **31**, 1487-1505.

[126] Jones DK, Symms MR, Cercignani M, Howard RJ (2005) The effect of filter size on VBM analyses of DT-MRI data. *Neuroimage* **26**, 546-554.

[127] Huang H, Zhang J, Jiang H, Wakana S, Poetscher L, Miller MI, van Zijl PC, Hillis AE, Wytik R, Mori S (2005) DTI tractography based parcellation of white matter: application to the mid-sagittal morphology of corpus callosum. *Neuroimage* **26**, 195-205.

[128] Mori S, Crain BJ, Chacko VP, van Zijl PC (1999) Three-dimensional tracking of axonal projections in the brain by magnetic resonance imaging. *Ann Neurol* **45**, 265-269.

[129] Duara R, Kushch A, Gross-Glenn K, Barker WW, Jallad B, Pascal S, Loewenstein DA, Sheldon J, Rabin M, Levin B, et al. (1991) Neuroanatomic differences between dyslexic and normal readers on magnetic resonance imaging scans. *Arch Neurol* **48**, 410-416.

[130] Larsen JP, Höien T, Ödegaard H (1992) Magnetic resonance imaging of the corpus callosum in developmental dyslexia. *Cognitive Neuropsychology* **9**, 123-134.

[131] Chao YP, Cho KH, Yeh CH, Chou KH, Chen JH, Lin CP (2009) Probabilistic topography of human corpus callosum using cytoarchitectural parcellation and high angular resolution diffusion imaging tractography. *Hum Brain Mapp* **30**, 3172-3187.

[132] Kang YW, Na DL, Hahn SH (1997) A validity study on the Korean Mini-Mental State Examination (K-MMSE) in dementia patients. *J. Korean Neurol Assoc* **15**, 300-308.

This page intentionally left blank

Using an Eye Movement Task to Detect Frontal Lobe Dysfunction in Alzheimer's Disease

Liam D. Kaufman[a,b,*], Jay Pratt[c], Brian Levine[c,d] and Sandra E. Black[a,b,d]
[a]*LC Campbell Cognitive Research Unit, Division of Neurology, Department of Medicine, Sunnybrook Research Institute, Sunnybrook Health Sciences Centre, University of Toronto, Toronto, Canada*
[b]*Institute of Medical Science, University of Toronto, Toronto, Canada*
[c]*Department of Psychology, University of Toronto, Toronto, Canada*
[d]*Rotman Research Institute, Baycrest University of Toronto, Toronto, Canada*

Abstract. The number of people living with Alzheimer's Disease (AD), the number one cause of Dementia, is projected to increase dramatically over the next few decades, making the search for treatments and tools to measure the progression of AD increasingly urgent. The antisaccade task, a hands- and language-free measure of inhibitory control, has been utilized in AD as a potential diagnostic test. In the antisaccade task, a participant is told to inhibit a reflexive (or automatic), visually-guided saccade (rapid eye-movement) to a peripheral target, and to make an "antisaccade" in the opposite direction to a non-existent target. While antisaccades do not appear to differentiate AD from healthy aging better than measures of episodic memory, they may still be beneficial. Specifically antisaccades may provide not only a functional index of the Dorsolateral Prefrontal Cortex (DLPFC), which is damaged in the later stages of AD, but also a tool for monitoring the progression of Alzheimer's Disease.

Keywords: Alzheimer's disease, antisaccades, dorsolateral prefrontal cortex, dementia

INTRODUCTION

Alzheimer's disease (AD), characterized by gradual, progressive loss of episodic memory (autobiographical memory for events), is the most common single cause of dementia affecting four million Americans, and is quickly becoming one of the "most burdensome health conditions worldwide" [1]. In the next two decades, the number of individuals diagnosed with AD will nearly double in North America and Europe, while in Asia it will nearly quadruple [1]. As new pharmaceuticals are developed to treat and possibly prevent AD, early diagnosis and disease treatment monitoring will become increasingly important. Currently used NINCDS-ADRDA (National Institute of Neurological and Communicative Disorders and Stroke – Alzheimer's Disease and Related Disorders Association) diagnostic criteria, and the newly proposed criteria [2] both include deficits in episodic memory as the core diagnostic feature of AD. Although decline in episodic memory is central to typical AD, an understanding of additional deficits associated with AD may aid in tracking the progression of AD and monitoring the effectiveness of treatments. Once such deficit that has been noted in patients with AD is difficulty exerting flexible control over prepotent saccades dur-

*Correspondence to: Liam D. Kaufman, LC Campbell Cognitive Research Unit, Division of Neurology, Department of Medicine, Sunnybrook Research Institute, Sunnybrook Health Sciences Centre, Room A421-2075 Bayview Avenue, M4N 3M5, University of Toronto, Toronto, Canada. Tel.: +416 480 4551; Fax: +416 480 4552; E-mail: liam.kaufman@gmail.com.

Table 1
Studies investigating antisaccade performance in Alzheimer's disease

	N	Control age	N	Patient age	Diagnostic criteria	MMSE	PL	PA	AL	AE
Fletcher et al. (1986)	11	69 (6.5)	13	69 (6.1)	"Clinical Diagnosis"	18.3 (4.1)	ND*	Hypo	NA	74% GT
Currie et al. (1991)	180	41 (18)	30	67 (8)	NINCDS-ADRDA	NA	NA	NA	NA	>30% GT
Abel et al. (2002)	11	67.4 (5.4)	11	73.1 (9.4)	NINCDS-ADRDA	20.6 (7.6)	ND	NA	NA	75.6% GT
Shafiq-Antonacci et al. (2003)	245	62.8 (8.6)	35	70.9 (9.4)	NINCDS-ADRDA	17.1 (7.4)	GT	Hypo	GT	55.9% (32.7) ND
Crawford et al. (2005)	18	75.2 (3.8)	18	77.8 (4.8)	NINCDS+DSM IV	20.9 (4.3)	ND	ND	ND	53.4% (23.6) GT
Mosimann et al. (2005)	24	75.3 (5.8)	22	78.1 (6.8)	NINCDS-ADRDA	17.9 (4.7)	ND	ND	ND	80% (42) GT
Boxer et al. (2006)	20	64.4 (7.2)	18	58.4 (7.2)	NINCDS-ADRDA	18.7 (8.5)	ND	ND	ND	60% GT
Garbutt et al. (2008)	27	65 (1.5)	28	59.8 (1.4)	NINCDS-ADRDA	19.5 (5.3)	GT	ND	GT	75% GT

MMSE = Minimental Status Exam, PL = Prosaccade Latency, PA = Prosaccade Amplitude, AL = Antisaccade Latency, few studies included antisaccade amplitude, thus it was omitted from the present table, AE=Antisaccade Errors, ND = No difference, GT = Greater than, Hypo = Hypometric, NA = not applicable.

ing the antisaccade task (Table 1) [3–10]. A saccade is a rapid eye movement to a specific target that includes prepotent saccades that are reflexive and often made in response to a suddenly appearing visual stimulus. Results from antisaccade studies indicate that the task may have potential for monitoring progression, specifically the emergence of dorsofrontal functional deficits in AD, as well as monitoring new treatments

The antisaccade task

In the antisaccade task, a participant is told to inhibit a reflexive (or automatic), visually-guided saccade to a peripheral target, and to make an "antisaccade" in the opposite direction to a non-existent target (Fig. 1) [11]. Thus, the antisaccade task probes one's ability to exert flexible control by overcoming the prepotent reflexive saccade response. If the participant fails to inhibit the reflexive saccade and makes a saccade towards the peripheral target, this constitutes an antisaccade (i.e., inhibition) error. The task has been widely adopted in some clinical disorders because of several advantages over other cognitive tests: it does not require a verbal or manual response and is well tolerated in patients with dementia, including AD, and Frontotemporal Degeneration (FTD) [8]. Furthermore, patients are often unaware of their mistakes and rarely, if ever, become frustrated. Although the task relies on making a parsimonious response - a saccade, it provides multiple and easily quantifiable metrics. For instance, both errors that are later corrected and those that remain uncorrected can be quantified, as can amplitude (saccade distance), and latencies (time between stimulus presentation and saccade completion). Corrected antisaccade errors consists of trials in which a participant first made a prosaccade, when they should have made

an antisaccade, but then quickly follow-up with a correct antisaccade.

Recently, the neural correlates of the task have become better understood [12]. An absence of verbal or manual responses enables the antisaccade task to be used in neuroimaging environments, such as magnetoencephelography (MEG) and functional magnetic resonance imaging (fMRI), which do not tolerate movement well. Consequently non-human primates can be studied using the antisaccade task, providing a model for understanding its neural correlates [12]. The relative simplicity of the antisaccade task has enabled children, adolescents, adults and the elderly to complete the task, which has also provided developmental data [13].

Developmental changes

The frontal lobes undergo rapid changes from childhood to adolescence, followed by gradual changes during later adulthood as the later evolved structures such as the frontal lobes gradually become fully myelinated. Children under 10 years of age have great difficulty performing the antisaccade task, making more errors in direction than adults [13, 14]. Between the ages of 10 and 15 antisaccade performance improves dramatically and continues to improve into early adulthood. The reduction in antisaccade error rates appears to closely mirror structural changes that occur from childhood to adulthood. For example, volumetric imaging has shown that between the ages of 8 and 22, total white matter volume increases linearly with age [15]. In the frontal lobes, grey matter shows a non-linear increase over time, with a peak volume around the age of 12, followed by a gradual decline presumed to relate to synaptic
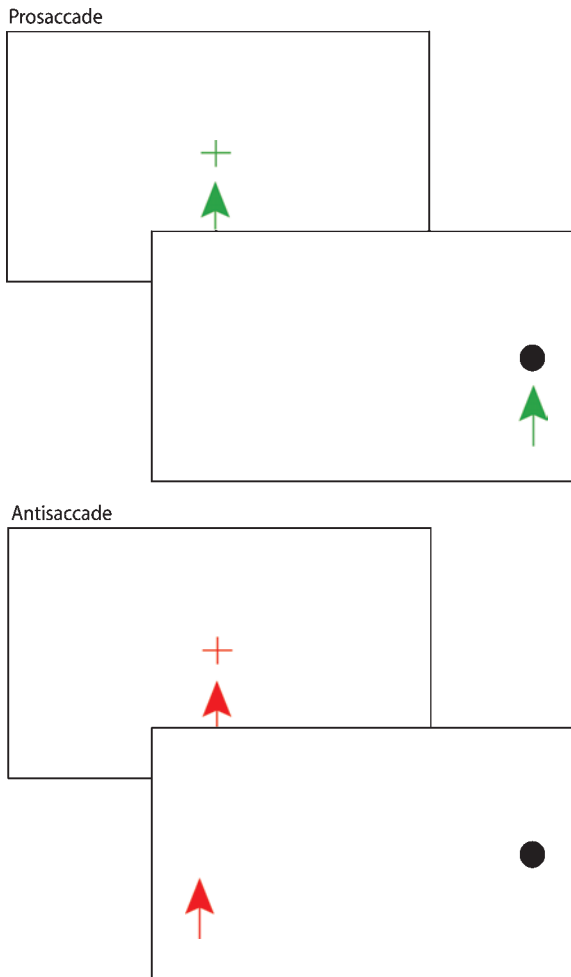
Fig. 1. The arrows denotes where participant is suppose to be looking. During the Prosaccade task they fixate on the cross, then make a saccade to the peripheral target. During the Antisaccade task they fixate on the cross but then look away from the peripheral target.

extermination [15]. In addition to volumetric indices of structure, diffusion tensor imaging (DTI) has revealed that white matter microstructural integrity and myelination, increases in the frontal lobes from childhood to adulthood [16].

During older adulthood, aging is associated with a general decline in grey matter volume [17] and a reduction in white matter microstructure integrity [18]: a gradual reversal of developmental changes. Studies of antisaccade performance from young adulthood onwards have reported either a non-significant upward trend in error rates [4, 7, 12, 19] or a significant increase in error rates with aging [13, 20, 21]. Furthermore, fMRI has revealed a compensatory shift in antisaccade related activation between young adults

and older adults indicative of functional differences between young and older adults [19].

Functional imaging studies

Developmental and aging studies indicate a relationship between frontal lobe function and inhibitory failure in the antisaccade task. Functional neuroimaging techniques such as positron emission tomography (PET) and fMRI have provided more specific information on neural substrates, implicating specific regions within the frontal lobes for successful antisaccade generation. In the simplest imaging experiments using either PET or fMRI, blocks of antisaccades were compared to prosaccades, and revealed greater activation for antisaccades in the frontal eye fields and the superior parietal lobule, when compared with prosaccades [22, 23]. Early functional imaging studies led to conflicting views on the involvement of the dorsolateral prefrontal cortex (DLPFC): some found activation in the right DLPFC [24, 25], while others did not [22, 26]. However, block designs have many shortcomings for analysing antisaccade related activity. Block designs do not allow temporal differentiation between the components of an antisaccade such as: 1) inhibiting a prosaccade, 2) generating an antisaccade and 3) making a retrosaccade back to the central fixation. There is the potential that activation could either be nullified or enhanced by a negative or a positive response respectively, from one of the other components. Furthermore it is difficult to tease apart the effect of antisaccade directional errors, reduced latencies and hypometric responses on the blood oxygen level dependent (BOLD) signal. Event-related designs, in which each antisaccade event is temporally spaced, and later averaged, have been used to overcome these problems.

Using an event-related design, the BOLD response associated with either preparation or with the motor phase of an antisaccade can be compared. When the BOLD response during these two phases was examined, it was discovered that increases in BOLD signal in the right DLPFC and bilateral frontal eye fields, associated with antisaccades, were actually due to preparation and not action [24]. These findings were confirmed in a combined electroencephalography (EEG)/MEG study which also found more activity in the medial aspects of the frontal eye fields, supplementary eye fields and prefrontal cortex during the planning phase of an antisaccade [27]. Finally, during the retrosaccade, when the participant makes a saccade back to the center, there is actually a negative

bold response [28], suggesting a mechanism by which retrosaccade activity may have cancelled out positive DLPFC BOLD signal in some block designs.

Comparison between successful antisaccades and antisaccade errors has also revealed some important details. For instance, fMRI and EEG have demonstrated increased BOLD signal and increased negative potentials, respectively, in the DLPFC during correct antisaccades when compared with incorrect [29, 30]. When Ford and colleagues compared correct antisaccades with correct prosaccades, they found greater activity in the anterior cingulate cortex, left DLPFC, bilateral frontal eye fields, pre-supplementary eye fields and parietal areas [30]. When they compared correct to incorrect antisaccades, they found a greater BOLD response in the right DLPFC, anterior cingulate cortex and pre-supplementary eye fields. Thus, the left DLPFC shows greater activity for antisaccades compared with prosaccades, and the right DLPFC exhibits greater activity for correct than incorrect antisaccades. The differences between right and left DLPFC activation reported by Ford and colleagues parallel the localization of two of the three frontal processes described by Stuss and Alexander [31], task setting and task monitoring. The antisaccade task requires greater task-set demands than the prosaccade task, which may explain the greater left DLPFC activation for antisaccades relative to prosaccades. In contrast to task setting, involving the left DLPFC, Stuss and Alexander [31] reported an association between damage of the right lateral dorsalfrontal regions and impairments in task monitoring. Greater right DLPFC activation for correct antisaccades, relative to incorrect antisaccades, may reflect increased in task monitoring related to successful antisaccade performance.

Focal lesion studies

The involvement of the DLPFC in antisaccades can be inferred indirectly from functional neuroimaging studies, but data from patients with focal lesions provide more direct evidence that its integrity is necessary for making correct antisaccades. Lesions affecting either the left or right mid-DLPFC are consistently associated with increased error rates [32–34]. For example, Pierrot-Deseilligny and colleagues examined patients with lesions that affected either the posterior parietal cortex, the frontal eye fields, supplementary motor area or the DLPFC [33]. They found that patients with lesions in the right or left DLPFC made more directional errors than controls or patients with lesions

in the frontal eye fields or supplementary motor area. In a recent study, patients with lesions resulting from infarcts were separated into two groups: those whose antisaccade performance was in the same range as normal controls and those who were outside that range [34]. Lesion analysis showed that damage in the high error group primarily involved areas in either the right or left dorsofrontal cortex that have efferent connections through the anterior limb of the internal capsule with the superior colliculi. Specifically the mid-DLPFC, which has efferent connections through the anterior limb of the anterior capsule into the superior colliculi, was the only area that was damaged in each patient in the high error group. Although Ploner and colleagues did not conduct significance tests on latency differences between the two groups, the high error group showed longer latencies than the low error group. Amplitude was not reported [34].

Gaymard and colleagues observed that a patient with a small focal lesion affecting the connections between the DLPFC and superior colliculi made more directional errors than controls, but had normal latency and amplitude [35]. A subsequent study that examined 30 patients with subcortical lesions found that only those with damage to the anterior limb of the internal capsule, the genu or the most anterior portion of the posterior limb of the internal capsule had high error rates. In contrast, those not considered impaired on the task had no damage to those regions; rather, their damage involved the posterior limb of the internal capsule and parts of the thalamus and basal ganglia [36]. Both groups of patients showed similar latencies and amplitude during the prosaccade task, but latency and amplitude were not reported for the antisaccade task.

The fact that there is some understanding about the neural correlates of the antisaccade task coupled with its other advantages make the antisaccade task an attractive measure of inhibitory control and executive function. Given that lesion and functional imaging evidence both support a critical role of the DLPFC in the antisaccade task, the task may also provide a useful index of DLPFC integrity in the dementias, such as AD.

Differentiating Alzheimer's disease from healthy aging

Patients with AD make significantly more antisaccade errors than controls (Table 1) and also leave many more of their errors uncorrected [9]. During the prosaccade task (Fig. 1), patients with AD perform mostly

within normal range (Table 1), emphasizing that errors in the antisaccade task are made in the absence of any impairment in visually-guided saccades. Despite the fact that AD patients make significantly more antisaccade errors than age-matched controls, antisaccades have limited diagnostic potential in differentiating patients from age-matched controls. Shafiq-Antonacci and colleagues [6] found that although robust differences between some patients with AD and controls exist, the antisaccade task had only a modest sensitivity and specificity and concluded that "antisaccade performance cannot identify AD in individual cases". In support of this conclusion, results from the most optimistic studies indicate that the task can only differentiate 40% of patients with AD from age-matched controls (Table 2) [6–8]. Moreover, groups of patients with AD show a much larger variance in the percentage of antisaccade errors relative to age-matched controls [3, 5, 6], emphasizing that some patients are either not significantly impaired or are not impaired at all. Relative to tests of episodic memory, antisaccades offer little utility for the detection of AD; they may, however, be an index of DLPFC involvement and thus useful for monitoring emergence of DLPFC deficits, progression over time and possibly response to treatment in AD. Unfortunately previous studies have not been longitudinal in nature, making it impossible to conclude if all patients with AD eventually develop antisaccade performance deficits and whether their performance degrades over time.

Antisaccade errors and dorsolateral prefrontal pathology in AD

Declines in hippocampal volume and episodic memory appear to be the earliest brain-behaviour correlations in AD, mirroring the development of AD pathology [2]. Progression and topographical distribution of neuropathology in AD has been categorized

Table 2
Power analysis and differentiation capabilities of the antisaccade task in Alzheimer's disease

	Control errors (SD)	AD Errors (SD)	Mean difference	Cohen's d*
Shafiq-Antonacci et al.	31.44 (15.36)	55.88 (32.74)	24.44	0.96
Crawford et al.	18.4 (13.4)	53.4 (23.6)	35	1.83
Mosimann et al.	25 (38)	80 (42)	55	1.37

Only studies which provided both mean and standard deviation (SD) values were included in this table; *Cohen's d = (Mean$_{AD}$ − Mean$_{Con}$)/SQRT((SD$^2_{AD}$ + SD$^2_{CON}$)/2).

into six stages, in which AD neurofibrillary tangles first appear in the medial temporal lobes, then gradually move into temporal-parietal association cortices and finally the frontal regions [37]. The DLPFC, critical for antisaccades, is thought to be relatively free of tangle pathology during the early phases of the disease, though paradoxically, PET labelling suggests the presence of pathology even in preclinical stages of the disease [38]. Therefore patients with early AD, who may have little or no dorsolateral frontal pathology, may show little to no impairment on the antisaccade task. The mini-mental status exam (MMSE), a general measure of cognition, shows a strong correlation with antisaccade error rates: as MMSE scores decline and dementia worsens, patients make more errors [4–6, 9]. However, Boxer and colleagues [9], examined a subgroup of patients with mild AD, who had MMSE scores greater than 22 out of 30, and found that they did not make significantly more errors than controls, suggesting antisaccade impairments may not arise in the early stages of the disease. An absence of antisaccade impairments in patients with mild AD, followed by a gradual increase in errors with dementia severity, as indexed by the MMSE, suggests that the task may provide information on not only the progression of the disease but also the progression and magnitude of DLPFC functional impairment.

Barriers in adopting the antisaccade task as a probe of DLPFC function

The validity of using the antisaccade task as a measure of executive function and inhibitory control in patients with AD is supported by its correlation with other measures of executive function [7, 9]. However, before the antisaccade task can be used as a clinical index of DLPFC function in AD, there are several issues that require further clarification. First, the relationship between dementia severity and antisaccade performance is based on cross-sectional between-subject data, not longitudinal within-subject data. Second, the proposed relationship between DLPFC pathology and increased error rates in AD is largely based on indirect inference and would benefit further from confirmatory structural and functional neuroimaging. Third, a successful antisaccade consists of several underlying processes, such as inhibition of a prepotent saccade and generation of a voluntary saccade, and impairment in any of the subprocesses may result in increased error rates, obfuscating potential brain behaviour relationships. Furthermore, despite the

potential testing convenience provided by clinical versions of the antisaccade task, which will be discussed shortly, typical saccade measurement relies on costly eye-monitoring equipment not available in most clinical environments, potentially deterring widespread clinical adoption.

Finally, each study in Table 1 has utilized slightly different temporal (gap, step or overlap) and spatial variants (angle of peripheral target offset) of the antisaccade task, which complicates direct comparison. The three main temporal variants of the antisaccade task, the gap, step and overlap refer to the temporal characteristics between the central fixation point and the peripheral target. The gap variant, used by Boxer and colleagues [7], typically includes a temporal gap of 200 ms between the disappearance of the central fixation point and the appearance of the peripheral target. In the overlap condition, the fixation target overlaps temporally with the peripheral target, while the step variant is a compromise between the overlap and gap variants, in which the central fixation point disappears simultaneously with the appearance of the peripheral target. Additionally, many studies fail to explicitly report the parameters they have used, making direct comparison difficult. Despite the variation and opacity in reported antisaccade parameters, the overall findings from the previously mentioned studies are consonant with each other: patients with AD make significantly more errors than controls.

The antisaccade task as an index of severity

The relationship between MMSE scores and antisaccade error rates supports the notion that error rates may mirror disease progression, but are 1) based on cross-sectional comparisons, and 2) under-represent those in the earliest stages of AD. Most existing studies have focused on patients in the moderate to severe stages of AD (see Table 1), which may exaggerate differences between AD and controls and may strengthen the correlation between MMSE scores and error rates. For instance patients on the lowest end of the MMSE spectrum tend to make 100% uncorrected errors making it difficult to infer whether directions were even understood or remembered. An emphasis on mild to moderate patients may reduce the likelihood of including patients who fail to understand the task and could enhance the understanding of the relationship between antisaccade performance and severity of dementia. Secondly, patients in the earlier stages of AD show greater heterogeneity in neuropsychologi-

cal impairment. For instance, some AD patients have been categorized as "frontal variant AD" as they not only perform significantly worse on frontal tasks, than average AD patients, but also show greater frontal atrophy [39]. Inclusion of only a small number of mild AD patients may have failed to capture variations in frontal deficits potentially underestimating error rates in mild AD.

Neuroimaging and dementia

The relationship between AD neurofibrillary tangle pathology distribution and antisaccade deficits is largely based on an assumption that those who are less demented, and make fewer errors, may have less pathology in the DLPFC. Boxer and colleagues [9] used voxel-based morphometry to examine the association between brain atrophy and antisaccade performance in patients with AD and those with frontotemporal degeneration (FTD). They found that the volume of an area located ventrally to the right frontal eye fields was correlated with correct responses, while supplementary eye fields volume was correlated with antisaccade latency. Although these findings reinforce the relationship between the dorsofrontal cortex and antisaccade performance, they failed to find a relationship between antisaccade performance with either DLPFC or frontal eye field volumes, which, as stated earlier, are regions critical for inhibition of prosaccades and generation of antisaccades respectively. By including both FTD and AD patients in a single group, despite the heterogeneity in the distribution and type of pathology within FTD and AD [40, 41], Boxer and colleagues may have prevented detection of correlations between structure and performance [9]. For instance, high variability in antisaccade performance, coupled with the low sensitivity of antisaccades [6] indicates many patients are unimpaired and may lack sufficient DLPFC pathology and atrophy, thus eliminating any significant correlations between structure and function. Furthermore, Boxer and colleagues corrected for MMSE scores, which are strongly correlated with error rates in AD; controlling for MMSE scores may have inadvertently eliminated any relationship between error rates and DLPFC or frontal eye field volumes. Utilizing methodology from antisaccade focal lesion studies [34], future investigations should divide patients with AD into two groups: 1) those whose percentage of errors fall within normal range and 2) those who make significantly more errors than normal. Such a division would be of interest in the middle stage of

disease, as error rates would be common in moderate to severe-stage disease. On the milder cases however, grouping patients by the differences in error rates could reveal whether this correlates with regional differences in atrophy, perfusion or white matter integrity in areas believed to be critical for antisaccade performance. Furthermore, could differences between high and low error AD patients could be correlated with neuropsychological deficits in executive function, more specifically with inhibitory control? Ultimately such a design would strengthen brain behaviour correlations by reducing the heterogeneity of performance and presumably pathology distribution within AD groups.

Diffusion tensor imaging, a technique for examining white matter tissue microstructure, has revealed differences in patients with AD relative to controls. Specifically, the superior longitudinal fasciculus, a bundle of fibers that connects posterior and frontal regions of the brain and also includes connections to the DLPFC, was reported to show a decrease in the Fractional Anisotropy (FA) [41]. FA is a measure of white matter cohesion and integrity, so a decrease is indicative of underlying structural aberrations that may elucidate brain-behaviour correlations. Correlating error rates and diffusion tensor metrics such as FA would provide insight into the potential role white matter injury may have on antisaccade performance in AD.

Functional imaging techniques such as single photon emission computerized tomography (SPECT), a semi-quantitative measure of regional cerebral blood flow and fMRI have provided important insights into the relationship between memory and brain function in AD and may provide further insight into antisaccade errors. Using SPECT, Garrido and colleagues found that patients with AD showed decreased cerebral blood flow in the left medial temporal lobes, relative to controls during a verbal recognition memory task [43]. Likewise Grady and colleagues used fMRI to study compensatory frontal network activity during memory tasks in mild AD [44]. The relationship found between functional aberrations and poor memory might be mirrored in a relationship between increased antisaccade errors and abnormal DLPFC activation patterns. For instance, fMRI and positron emission tomography have revealed decreases in activation in the anterior cingulate and DLPFC in Schizophrenia, a psychopathology associated with increased antisaccade errors [45]. Thus, antisaccade imaging studies conducted in healthy adults and other patient groups, such as Schizophrenia, could provide an experimental

framework that could be repeated in AD. Functional imaging results coupled with structural neuroimaging, in AD, could provide more direct *in vivo* evidence for a correlation between DLPFC changes and increased error rates.

Fractionation of processes in the antisaccade task

The antisaccade task is comprised of multiple sub-processes that contribute to a successful execution [12]. A participant must be able to fixate on the central fixation point, then inhibit a reflexive saccade, invert the saccade vector to a non-existent target and make a voluntary saccade in the direction of the updated vector. In addition to the processes directly related to the task, there are secondary processes that are also critical for successful antisaccades. For instance, a patient must be able to understand and remember the task's directions and vigilantly attend to the task. According to the accumulator model, the process that reaches threshold first, either the antisaccade or the erroneous prosaccade, determines which behaviour is initiated [12]. For instance, if the antisaccade process reaches threshold before an erroneous prosaccade, an antisaccade is carried out. Deficits in any of the above-mentioned processes could result in a slowing of the antisaccade process, increasing the chance that an erroneous prosaccade is generated. In determining whether antisaccade errors in AD result from inhibitory deficits and ultimately DLPFC dysfunction, it will be critical to fractionate the underlying sub-processes to insure other components impaired in AD, such as memory, are not contributing significantly to antisaccade errors.

Fractioning the antisaccade task: inhibition control

Fractionation of inhibition from the other processes can be accomplished through additional saccade task manipulations. Two tasks which focus on inhibition are: 1) the no-go task, in which the participant maintains fixation while peripheral targets appear, and 2) the go no-go task, in which the participant must fixate during some trials (no-go trials) and make saccades during other trials (go trials). No-go and go no-go tasks are easier than the antisaccade tasks because they do not require a vector inversion or volitional generation of a saccade: they simply require inhibition in a proportion of the trials. Crawford and co-workers found that patients with AD made significantly more inhibition errors on both tasks, when compared with controls, suggesting that inhibitory deficits, not deficits in vec-

tor inversion or volitional control, may be the greatest contributor to antisaccade errors in AD [7].

Fractioning the antisaccade task: fixation

Typical antisaccade coding schemes require a participant to fixate centrally for at least 200 ms prior to a successful antisaccade; trials that fail to meet this requirement are eliminated from analysis [6]. Reported fixation deficits in patients with AD [3] may result in greater numbers of eliminated trials in the AD group, resulting in fewer analyzable trials. Presenting a static image with several targets and asking the participant to maintain fixation on a single target for a specified time provides a parsimonious method for testing fixation. The task could be repeated using different static images and different fixation points.

Fractioning the antisaccade task: vector inversion

Successful antisaccades require a vector inversion: the prosaccade vector must be inverted to a saccade in the opposite direction towards a non-existent target, a visuospatial process which imaging and lesion studies have suggested is mediated by the posterior parietal cortex [46, 47]. Although not typically the presenting symptom, spatial and visuomotor deficits are often detectable in the mild to moderate stages of AD [47–50]. Correlations of performance of antisaccade tasks have been reported with two visuospatial tasks: fig. copying with correct antisaccades [9] and spatial span with uncorrected errors [7]. Despite these correlations of visuospatial deficits with antisaccade errors, it is unclear if they are contributing factors to the increased error rates present in AD. For instance, error rates are significantly elevated during the no-go task, which only includes the inhibitory component of the antisaccade task, not the visuospatial component.

Fractioning the antisaccade task: voluntary saccades

A voluntary saccade to a non-existent target differs both neurologically and in difficulty from the reflexive saccades generated in the prosaccade task. While the frontal eye fields are involved in generating voluntary saccades, a region in the parietal lobes is implicated in generating reflexive visually guided saccades [12]. When patients with frontal eye field focal lesions make antisaccades, they typically show longer antisaccade latency and depending on the study error rates remain normal [51] or are elevated [52]. In contrast, patients with AD do not consistently show longer latencies, but do consistently make more errors.

Furthermore, the frontal eye fields are one of the last regions to be affected by AD tangle pathology making it further unlikely that voluntary saccade generation is impaired or is the cause of increased error rates in AD.

Memory, understanding and Attention

A failure to make correct antisaccades could result from deficits in memory, understanding, and/or attention. Despite significant impairments in each of those domains in AD, studies have posited that those impairments do not contribute to increased errors because of two factors. First, when performance on an antisaccade block is divided into two halves, performance is stable between the two halves; indicating patients are not progressively forgetting task instructions [7]. Second, patients usually generate at least one correct antisaccade, or one corrected antisaccade, a reaction not seen in prosaccades. This suggests that patients remembered the task well enough to make at least one antisaccade [3]. However, just as inhibitory control is considered impaired in patients with DLPFC lesions, despite generating a few correct responses, patients with AD may still make errors due to poor short-term memory. Neuropsychological indices of memory, such as verbal episodic memory [9] and memory quotient [4], correlate with antisaccade performance, suggesting that impairments in memory may partly contribute to antisaccade errors. Perhaps the most pertinent question is whether patients not only remember and understand the task's instructions immediately before the task begins, but also once it has ended. A patient's understanding of the task is often determined by having the patient either point to where they are suppose to look, or verbal repetition of the instructions [7]. Repeating these steps after the task is completed would not only test memory but would also test a patient's understanding of the task, but this has yet to be reported in any published study.

Although deficits in attention have been documented in patients with AD [53], their effect on antisaccade performance has not been explored. If impairments in memory, understanding or attention lead to increased errors, there would be little utility in using the antisaccade task as a measure of disease progression as memory or other cognitive tasks would suffice. If either impairments in memory, understanding or attention contribute to increased error rates, a link between the DLPFC, inhibitory control and error rates in AD would be difficult to infer. Thus, excluding these processes and behavioural domains as major contributors to anti-

saccade error rates should remain a priority for future studies.

Task sequence

Statistical analysis of antisaccade data has primarily relied on univariate models that assume performance on a single trial is independent from other trials. For example, these models assume that performance on a trial $(n+1)$ is in no way affected by the previous trial (n). However, this assumption appears false, as data from normal controls indicates performance on a current trial is influenced by the direction of the previous trial, relative to the direction of the current trial [54–56]. For instance, if a peripheral target appears on the left side for two trials in a row, the second trial would be categorized as "same" and would be associated with fewer errors than a "different" trial (a trial preceding by a trial of a different direction, i.e. left then right) [54]. However, this effect may not be consistent across age and patient groups, potentially confounding differences between patients with AD and elderly controls.

Clinical adaptation

Although clinical variations of the antisaccade task are easy to administer, typical antisaccade experiments use sophisticated eye-tracking labs that are often costly to establish, lack portability and use techniques that require calibration, making the task clinically less appealing. In an effort to avoid these shortcomings, Currie and colleagues developed a clinical version of the antisaccade task that uses the clinician's nose as the central fixation and fingers as the peripheral targets [4]. Although the clinical variant yielded slightly lower error rates than the laboratory version, scores were highly correlated with those generated in the laboratory version ($r = 0.921$). The clinical version is also a component of the HIV Dementia scale that has been validated in both patients with HIV [57] and patients with subcortical vascular cognitive impairment [58]. The clinical variant of the antisaccade task provides a parsimonious method for testing and overcomes the shortcomings of the laboratory version. However, it is unclear how difficult it is for a clinician to remember a sequence of 10 to 20 trials while keeping track of how many trials have been administered and how many errors a patient has made. The clinical version, in its present form, limits the clinician to record only errors in direction, neglecting other metrics such as uncorrected errors, fixation errors, errors of omission, latency and amplitude partly because of the cognitive load of administering the task, but also because latency and amplitude can only be reliably recorded with eye-tracking equipment. Although the reliability of the clinical version, between different clinical centers, has not been tested, the laboratory version has been tested in patients with schizophrenia, revealing that the task can be carried out reliably in different centers [59].

Non-Alzheimer's dementia

The majority of studies examining antisaccade performance in patients with dementia have focused on Alzheimer's disease. However, antisaccade performance has been examined in other types of dementia (Table 3) [9, 10, 61–63]. A pattern of inhibitory impairment, as measured by antisaccade errors, seems to mirror the distribution of pathology in frontotemporal dementia, semantic dementia and progressive non-fluent aphasia. Frontotemporal dementia and progressive non-fluent aphasia, characterized by deficits in behavioural regulation and non-fluent speech respectively are both associated with pathology in the frontal lobes [60]. In contrast, the core diagnostic feature of semantic dementia is a deficit in word comprehension and it is associated with pathology in the anterior temporal lobes. The difference in the presence of frontal pathology between these groups is mirrored by their performance on the antisaccade task: frontotemporal dementia and progressive aphasia are associated with high antisaccade error rates, while semantic dementia is not [9]. Interestingly, all three of these groups correct more errors than patients with AD [9, 10].

Although Corticobasal Syndrome and Progressive Supranuclear Palsy are primarily characterized by motor impairments such as asymmetric extrapyramidal signs and vertical gaze palsy respectively, they are also associated with frontal deficits [64]. The clinical criteria for diagnosis of Progressive Supranuclear Palsy is highly predictive of autopsy findings, whereas Corticobasal Syndrome is less specific and can be associated with either corticobasal degeneration, progressive supranuclear palsy pathology, both overlapping [40] or even the tau negative ubiquitin positive pathology [65]. Patients with Corticobasal Syndrome and controls made an equal number of errors on the antisaccade task, while patients with Progressive Supranuclear Palsy made significantly more errors than controls [61, 62]. However, when patients with CBD completed a

Table 3
Studies investigating antisaccade performance in non-Alzheimer's dementia

	N	Control age	N	Patient age	Diagnostic criteria	MMSE	PL	PA	AL	AE
FTD										
Meyniel et al. (2005)[59]	10	68 (9)	23	67 (9)	Lund-Manchester	26.1 (2.8)	GT	NA	GT	63% GT
Boxer et al. (2006)[9]	20	64.4 (7.2)	14	59.9 (5.6)	Neary et al. (1998)	25.7 (3.7)	ND	ND	ND	60% GT
Garbutt et al. (2008)[10]	27	65 (1.5)	24	57.4 (1.7)	Neary et al. (1998)	23.5 (7.5)	NA	Hypo	ND	~55% GT
PNFA										
Boxer et al. (2006)[9]	20	64.4 (7.2)	7	65.7 (7.9)	Neary et al. (1998)	23.1 (5.3)	ND	ND	ND	~70% GT
Garbutt et al. (2008)[10]	27	65 (1.5)	6	64.5 (3.0)	Neary et al. (1998)	25.2 (3.5)	ND	ND	ND	~52% GT
SD										
Boxer et al. (2006)[9]	20	64.4 (7.2)	10	60.3	Neary et al. (1998)	20.1 (7.6)	ND	ND	ND	~25% ND
Garbutt et al. (2008)[10]	27	65 (1.5)	19	60.3 (1.3)	Neary et al. (1998)	21.7 (7.3)	ND	ND	ND	~28% ND
PSP										
Vidaihet et al. (1994)[60]	12	63.9 (8.3)	10	62.5 (5.5)	NA	NA	ND	Hypo	NA	~ 73.5 GT
Meyniel et al. (2005)[59]	10	68 (9)	14	70 (6)	Litvan's	28.6 (2.0)	ND	NA	GT	70% GT
Rivaud-Pechoux (2007)[61]	10	64 (9)	12	66 (9.9)	Litvan's	NA	ND	NA	GT	GT
Garbutt et al. (2008)[10]	27	65 (1.5)	10	65.5 (1.3)	Litvan et al. (1996)	26.8 (2.6)	GT	NA	NA	~92% GT
CBD										
Vidaihet et al. (1994)[60]	12	63.9 (8.3)	10	66.5 (6.8)	NA	NA	GT	ND	NA	~ 37.5 ND
Rivaud-Pechoux (2007)[61]	10	64 (9)	8	76 (5.4)	Litvan's 1997	NA	GT	NA	GT	ND
Garbutt et al. (2008)[10]	27	65 (1.5)	15	62.7 (2.0)	Several methods	19.8 (7.7)	GT	Hypo	NA	~75% GT

MMSE = Minimental Status Exam, PL = Prosaccade Latency, PA = Prosaccade Amplitude, AL = Antisaccade Latency, few studies included antisaccade amplitude, thus it was omitted from the present table, AE = Antisaccade Errors, ND = No difference, GT = Greater than, Hypo = Hypometric, NA = not applicable.

mixed block of prosaccades and antisaccades, they made many more errors than controls compared with patients with PSP who showed no difference between mixed and non-mixed blocks [63]. Differences in antisaccade performance between the two groups may provide information to help distinguish these diseases.

DISCUSSION

Pressure to increase the diagnostic accuracy for dementia, and specifically Alzheimer's disease is mounting due to the availability of new potential treatments. In the early stages, when the drugs will be the most effective, it is unlikely that the antisaccade task will provide greater diagnostic utility than existing tests for AD. However, in addition to its potential role as a probe of dorsolateral function and as a test to monitor treatment response, it may aid in differentiating other forms of dementia.

CONCLUSION

The neural correlates of antisaccades continue to be mapped and reported using a variety of neuroimaging techniques providing further insights into brain-behaviour correlations of this simple task. Antisaccades provide a well tolerated, language-free and hands-free neuropsychological probe that may not only help those with AD, but could be especially helpful in testing patients with expressive language problems or motor deficits, such as those with Progressive Aphasia and Amyotrophic Lateral Sclerosis.

Despite having limited utility in differentiating individuals with AD from normal aging, the available evidence indicates that the task may provide insight into frontal lobe function and an index of DLPFC pathology in AD. The potential utility of the antisaccade task as a neuropsychological probe of DLPFC and ultimately for progression and for treatment monitoring appears promising but requires further investigation. The relationship between the DLPFC, inhibitory control and errors rates in AD requires exclusion of other potential contributors, such as memory impairments, and would benefit from converging evidence from multiple neuroimaging modalities. This overview has outlined future avenues of research for testing the link between inhibitory deficits and DLPFC changes in patients with AD.

REFERENCES

[1] Ferri CP, Prince M, Brayne C, Brodaty H, Fratiglioni L, Ganguli M (2005) Global prevalence of dementia: a Delphi consensus study. *Lancet* **366**, 2112-2117.

[2] Dubois B, Feldman HH, Jacova C, Dekosky ST, Barberger-Gateau P, Cummings J et al. (2007) Research criteria for the diagnosis of Alzheimer's disease: revising the NINCDS-ADRDA criteria. *Lancet Neurol* **6**, 734-746.

[3] Fletcher WA, Sharpe JA (1986) Saccadic eye movement dysfunction in Alzheimer's disease. *Ann Neurol* **20**, 464-471.

[4] Currie J, Ramsden B, McArthur C, Maruff P (1991) Validation of a clinical antisaccadic eye movement test in the assessment of dementia. *Arch Neurol* **48**, 644-648.

[5] Abel LA, Unverzagt F, Yee RD (2002) Effects of stimulus predictability and interstimulus gap on saccades in Alzheimer's disease. *Dement Geriatr Cogn Disord* **13**, 235-243.

[6] Shafiq-Antonacci R, Maruff P, Masters C, Currie J (2003) Spectrum of saccade system function in Alzheimer disease. *Arch Neurol* **60**, 1272-1278.

[7] Crawford TJ, Higham S, Renvoize T, Patel J, Dale M, Suriya A et al. (2005) Inhibitory control of saccadic eye movements and cognitive impairment in Alzheimer's disease. *Biol Psychiatry* **57**, 1052-1060.

[8] Mosimann UP, Muri RM, Burn DJ, Felblinger J, O'Brien JT, McKeith IG (2005) Saccadic eye movement changes in Parkinson's disease dementia and dementia with Lewy bodies. *Brain* **128**, 1267-1276.

[9] Boxer AL, Garbutt S, Rankin KP, Hellmuth J, Neuhaus J, Miller BL, et al. (2006) Medial versus lateral frontal lobe contributions to voluntary saccade control as revealed by the study of patients with frontal lobe degeneration. *J Neurosci* **26**, 6354-6363.

[10] Garbutt S, Matlin A, Hellmuth J, Schenk AK, Johnson JK, et al. (2008) Oculomotor function in frontotemporal lobar degeneration, related disorders and Alzheimer's disease. *Brain* **131**, 1268-1281.

[11] Hallett PE (1978) Primary and secondary saccades to goals defined by instructions. *Vision Res* **18**, 1279-1296.

[12] Munoz DP, Everling S (2004) Look away: the anti-saccade task and the voluntary control of eye movement. *Nat Rev Neurosci* **5**, 218-228.

[13] Klein C, Foerster F, Hartnegg K, Fischer B (2005) Lifespan development of pro- and anti-saccades: multiple regression models for point estimates. *Brain Res Dev Brain Res* **160**, 113-123.

[14] Munoz DP, Broughton JR, Goldring JE, Armstrong IT (1998) Age-related performance of human subjects on saccadic eye movement tasks. *Exp Brain Res* **121**, 391-400.

[15] Giedd JN, Blumenthal J, Jeffries NO, Castellanos FX, Liu H, Zijdenbos A et al. (1999) Brain development during childhood and adolescence: a longitudinal MRI study. *Nat Neurosci* **2**, 861-863.

[16] Barnea-Goraly N, Menon V, Eckert M, Tamm L, Bammer R, Karchemskiy A et al. (2005) White matter development during childhood and adolescence: a cross-sectional diffusion tensor imaging study. *Cereb Cortex* **15**, 1848-1854.

[17] Good CD, Johnsrude IS, Ashburner J, Henson RN, Friston KJ, Frackowiak RS (2001) A voxel-based morphometric study of ageing in 465 normal adult human brains. *Neuroimage* **14**, 21-36.

[18] Pfefferbaum A, Sullivan EV (2003) Increased brain white matter diffusivity in normal adult aging: relationship to anisotropy and partial voluming. *Magn Reson Med* **49**, 953-961.

[19] Raemaekers M, Vink M, van den Heuvel MP, Kahn RS, Ramsey NF (2006) Effects of aging on BOLD fMRI during prosaccades and antisaccades. *J Cogn Neurosci* **18**, 594-603.

[20] Abel LA, Douglas J (2007) Effects of age on latency and error generation in internally mediated saccades. *Neurobiol Aging* **28**, 627-637.

[21] Olincy A, Ross RG, Youngd DA, Freedman R (1997) Age diminishes performance on an antisaccade eye movement task. *Neurobiol Aging* **18**, 483-489.

[22] Kimmig H, Greenlee MW, Gondan M, Schira M, Kassubek J, Mergner T (2001) Relationship between saccadic eye movements and cortical activity as measured by fMRI: quantitative and qualitative aspects. *Exp Brain Res* **141**, 184-194.

[23] O'Driscoll GA, Alpert NM, Matthysse SW, Levy DL, Rauch SL, Holzman PS (1995) Functional neuroanatomy of antisaccade eye movements investigated with positron emission tomography. *Proc Natl Acad Sci U S A* **92**, 925-929.

[24] DeSouza JF, Menon RS, Everling S (2003) Preparatory set associated with pro-saccades and anti-saccades in humans investigated with event-related FMRI. *J Neurophysiol* **89**, 1016-1023.

[25] McDowell JE, Clementz BA (2001) Behavioral and brain imaging studies of saccadic performance in schizophrenia. *Biol Psychol* **57**, 5-22.

[26] Connolly JD, Goodale MA, Desouza JF, Menon RS, Vilis T (2000) A comparison of frontoparietal fMRI activation during anti-saccades and anti-pointing. *J Neurophysiol* **84**, 1645-1655.

[27] McDowell JE, Kissler JM, Berg P, Dyckman KA, Gao Y, Rockstroh B et al. (2005) Electroencephalography/magnetoencephalography study of cortical activities preceding prosaccades and antisaccades. *Neuroreport* **16**, 663-668.

[28] Raemaekers M, Vink M, van den Heuvel MP, Kahn RS, Ramsey NF (2005) Brain activation related to retrosaccades in saccade experiments. *Neuroreport* **16**, 1043-1047.

[29] Everling S, Spantekow A, Krappmann P, Flohr H (1998) Event-related potentials associated with correct and incorrect responses in a cued antisaccade task. *Exp Brain Res* **118**, 27-34.

[30] Ford KA, Goltz HC, Brown MR, Everling S (2005) Neural processes associated with antisaccade task performance investigated with event-related FMRI. *J Neurophysiol* **94**, 429-440.

[31] Stuss DT, Alexander MP (2007) Is there a dysexecutive syndrome? *Philos Trans R Soc Lond B Biol Sci* **362**, 901-915.

[32] Guitton D, Buchtel HA, Douglas RM (1985) Frontal lobe lesions in man cause difficulties in suppressing reflexive glances and in generating goal-directed saccades. *Experimental Brain Research* **58**, 455-472.

[33] Pierrot-Deseilligny C, Rivaud S, Gaymard B, Agid Y (1991) Cortical control of reflexive visually-guided saccades. *Brain* **114**, 1473-1485.

[34] Ploner CJ, Gaymard BM, Rivaud-Pechoux S, Pierrot-Deseilligny C (2005) The prefrontal substrate of reflexive saccade inhibition in humans. *Biol Psychiatry* **57**, 1159-1165.

[35] Gaymard B, Francois C, Ploner CJ, Condy C, Rivaud-Pechoux S (2003) A direct prefrontotectal tract against distractibility in the human brain. *Ann Neurol* **53**, 542-545.

[36] Condy C, Rivaud-Pechoux S, Ostendorf F, Ploner CJ, Gaymard B (2004) Neural substrate of antisaccades: role of subcortical structures. *Neurology* **63**, 1571-1578.

[37] Braak H, Braak E (1991) Neuropathological stageing of Alzheimer-related changes. *Acta Neuropathol (Berl)* **82**, 239-259.

[38] Pike KE, Savage G, Villemagne VL, Ng S, Moss SA et al. (2007) Beta-amyloid imaging and memory in non-demented individuals: evidence for preclinical Alzheimer's disease. *Brain* **130**, 2837-2844.

[39] Johnson JK, Head E, Kim R, Starr A, Cotman CW (1999) Clinical and pathological evidence for a frontal variant of Alzheimer disease. *Arch Neurol* **56**, 1233-1239.

[40] Josephs KA, Petersen RC, Knopman DS, Boeve BF, Whitwell JL, Duffy JR et al. (2006) Clinicopathologic analysis of frontotemporal and corticobasal degenerations and PSP. *Neurology* **66**, 41-48.

[41] Snowden J, Neary D, Mann D (2007) Frontotemporal lobar degeneration: clinical and pathological relationships. *Acta Neuropathol (Berl)* **114**, 31-38.

[42] Medina D, DeToledo-Morrell L, Urresta F, Gabrieli JD, Moseley M, Fleischman D et al. (2006) White matter changes in mild cognitive impairment and AD: A diffusion tensor imaging study. *Neurobiol Aging* **27**, 663-672.

[43] Garrido GEJ, Furuie SS, Buchpiguel CA, Bottino CMC, Almeida P, Cid CG et al. (2002) Relation between medial temporal atrophy and functional brain activity during memory processing in Alzheimer's disease: a combined MRI and SPECT study. *J Neurol Neurosurg Psychiatry* **73**, 508-516.

[44] Grady CL, McIntosh AR, Beig S, Keightley ML, Burian H, Black SE (2003) Evidence from functional neuroimaging of a compensatory prefrontal network in Alzheimer's disease. *J of Neuroscience* **23**, 986-993.

[45] Hutton SB, Ettinger U (2006) The antisaccade task as a research tool in psychopathology: a critical review. *Psychophysiology* **43**, 302-313.

[46] Medendorp WP, Goltz HC, Vilis T (2005) Remapping the remembered target location for anti-saccades in human posterior parietal cortex. *J Neurophysiol* **94**, 734-740.

[47] Nyffeler T, Rivaud-Pechoux S, Pierrot-Deseilligny C, Diallo R, Gaymard B (2007) Visual vector inversion in the posterior parietal cortex. *Neuroreport* **18**, 917-920.

[48] Buck BH, Black SE, Behrmann M, Caldwell C, Bronskill MJ (1997) Spatial- and object-based attentional deficits in Alzheimer's disease. Relationship to HMPAO-SPECT measures of parietal perfusion. *Brain* **120**, 1229-1244.

[49] Cummings JL, Cole G (2002) Alzheimer disease. *JAMA* **287**, 2335-2338.

[50] Tippett WJ, Sergio LE (2006) Visuomotor integration is impaired in early stage Alzheimer's disease. *Brain Res* **1102**, 92-102.

[51] Gaymard B, Ploner CJ, Rivaud-Pechoux S, Pierrot-Deseilligny C (1999) The frontal eye field is involved in spatial short-term memory but not in reflexive saccade inhibition. *Experimental Brain Research* **129**, 288-301.

[52] Machado L, Rafal RD (2004) Control of fixation and saccades during an anti-saccade task: an investigation in humans with chronic lesions of oculomotor cortex. *Exp Brain Res* **156**, 55-63.

[53] Perry RJ, Hodges JR (1999) Attention and executive deficits in Alzheimer's disease. A critical review. Brain **122**, 383-404.

[54] Barton JJ, Goff DC, Manoach DS (2006) The inter-trial effects of stimulus and saccadic direction on prosaccades and anti-saccades, in controls and schizophrenia patients. *Exp Brain Res* **174**, 487-1498.

[55] Reuter B, Philipp AM, Kathmann N (2006) Effects of switching between leftward and rightward pro- and antisaccades. *Biol psychol* **72**, 88-95.

[56] Tatler BW, Hutton SB (2007) Trial by trial effects in the antisaccade task. *Exp brain res* **179**, 387-396.

[57] Power C, Selnes OA, Grim JA, McArthur JC (1995) HIV dementia scale: a rapid screening test. *J Acquir Immune Defic Syndr Hum Retrovirol* **8**, 273-278.

[58] van Harten B, Courant MN, Scheltens P, Weinstein HC (2004) Validation of the HIV dementia scale in an elderly cohort of patients with subcortical cognitive impairment caused by subcortical ischaemic vascular disease or a normal pressure hydrocephalus. *Dement Geriatr Cogn Disord* **18**, 109-114.

[59] Radant AD, Dobie DJ, Calkins ME, Olincy A, Braff DL, Cadenhead KS et al. (2007) Successful multi-site measurement of antisaccade performance deficits in schizophrenia. *Schizophr Res* **89**, 320-329.

[60] Neary D, Snowden JS, Gustafson L, Passant U, Stuss D, Black S et al. (1998) Frontotemporal lobar degeneration: a consensus on clinical diagnostic criteria. *Neurology* **51**, 1546-1554.

[61] Meyniel C, Rivaud-Pechoux S, Damier P, Gaymard B (2005) Saccade impairments in patients with fronto-temporal dementia. *J Neurol Neurosurg Psychiatry* **76**, 1581-1584.

[62] Vidailhet M, Rivaud S, Gouider-Khouja N, Pillon B, Bonnet AM, Gaymard B et al. (1994) Eye movements in parkinsonian syndromes. *Ann Neurol* **35**, 420-426.

[63] Rivaud-Pechoux S, Vidailhet M, Brandel JP, Gaymard B (2007) Mixing pro- and antisaccades in patients with parkinsonian syndromes. *Brain* **130**, 256-264.

[64] Kertesz A, Martinez-Lage P, Davidson W, Munoz DG (2000) The corticobasal degeneration syndrome overlaps progressive aphasia and frontotemporal dementia. *Neurology* **55**, 1368-1375.

[65] Masellis M, Momeni P, Meschino W, Heffner R, Elder J et al. (2006) Novel splicing mutation in the progranulin gene causing familial corticobasal syndrome. *Brain* **129**, 3115-3123.

Principles of Classification Analyses in Mild Cognitive Impairment (MCI) and Alzheimer Disease

Sven Haller[a,*], Karl O. Lovblad[a] and Panteleimon Giannakopoulos[b,c]

[a]*Service neuro-diagnostique et neuro-interventionnel DISIM, University Hospitals of Geneva, Geneva, Switzerland*
[b]*Division of Geriatric Psychiatry, Department of Psychiatry, University Hospitals of Geneva and Faculty of Medicine, Division of General Psychiatry, University of Geneva, Geneva, Switzerland*
[c]*Division of Old Age Psychiatry (PG), University of Lausanne School of Medicine, Lausanne, Switzerland*

Abstract. The majority of advanced neuroimaging studies implement group level analyses contrasting a group of patients versus a group of controls, or two groups of patients. Such analyses may identify for example changes in grey matter in specific regions associated with a given disease. Although such group investigations provided key contributions to the understanding of the pathological process surrounding a wide range of diseases, they are of limited utility at an individual level. Recently, there is a trend towards individual classification analyses, representing a fundamental shift of the research paradigm. In contrast to group comparisons, these latter studies do not provide insights on vulnerable brain areas but may allow for an early (and ideally preclinical) identification of at risk individuals in routine clinical setting. One currently very popular method in this domain are support vector machines (SVM), yet this method is only one of many available methods in the field of individual classification analyses. The current manuscript reviews the fundamental properties and features of such individual level classification analyses in neurodegenerative diseases.

Keywords: SVM (support vector machine), MVPA (multi voxel pattern analysis), artificial intelligence, machine learning, individual classification

INTRODUCTION

Advanced neuroimaging studies are based on the assumption that a given disease is associated with systematic changes in brain structure (morphometry) or function. The most frequently applied structural techniques in the domain of grey matter are voxel based morphometry (VBM) assessing grey matter concentration [1] and cortical thickness analysis [2]. In the

domain of white matter, there are several techniques including tract based spatial statistics (TBSS) analysis [3]. In the domain of functional MRI (fMRI), there are many techniques with general linear model analyses [4] of blood oxygenation level dependent (BOLD) functional magnetic resonance imaging (fMRI) [5]. Besides the classic type of fMRI, there are an increasing number of emerging techniques, notably resting state fMRI [6].

GROUP LEVEL ANALYSES

Regardless of the method, the common principle of most of theses studies are group level comparisons

---

*Correspondence to: Dr. Sven Haller, M.Sc., Service neuro-diagnostique et neuro-interventionnel DISIM, Hôpitaux Universitaires de Genève, Rue Gabrielle Perret-Gentil 4, 1211 Genève 14, Switzerland. Tel.: +41 (0) 22 37 23311; Fax: +41 (0) 22 37 27072; E-mail: sven.haller@hcuge.ch.

between patients and controls, or between two or more groups of patients. This standard type of data analysis is not discussed in detail here (see for example a VBM meta-analyses in MCI/Alzheimer disease [7]).

Pros

Group level analyses identify specific vulnerable regions that display structural or functional alterations associated with a given disease or condition.

Cons

While such analyses are highly contributive from a scientific perspective, the results cannot be transferred to the clinical early diagnosis of an individual at risk subject of patient.

INDIVIDUAL LEVEL CLASSIFICATION ANALYSES

Only recently, individual classification analyses are increasingly popular, representing a fundamental shift in research paradigm. Such analyses aim to individually classify healthy controls versus mild cognitive impairment cases. This fundamental difference can be illustrated in the example of recognition of female and male face images. The group level analysis between females and males might for example identify the nose as a region with significant differences between groups since on average women might have smaller noses than men. It is however not necessarily the case that the same region also provides a good discrimination between groups for a classification analysis. Assuming between subject variations in the morphometry of the nose, some males might for example have a nose, which is more similar to the average female nose, hence causing a false classification at the individual level. The best classification accuracy of an individual might be for example obtained by a specific pattern of different parts of the entire picture (called features in the domain of classification analyses), such as a combination of eyebrow, chin and lid. Individual classification analyses thus aim to identify patterns, which allow discriminating between groups, yet it is in general difficult to interpret the spatial distribution of the most discriminative features.

In the context of MCI, it is important to note that not all MCI evolve to Alzheimer disease (AD) or decline at identical rates and a significant proportion of cases
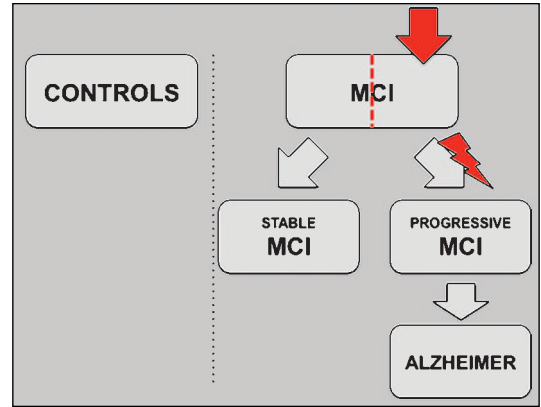
Fig. 1. The current concept is that not all MCI subjects will progress to Alzheimer disease. A classification analysis therefore must be able to detect MCI individuals at risk for cognitive decline in order to establish appropriate preventive strategies.

remain stable for several years or even improve (for review see [8]). The classification analysis must therefore be able to detect individual MCI cases who will eventually progress in order to start early curative treatments or to select at risk subjects for pharmaceutical trials (see Fig. 1).

Pros

Individual classification analyses are optimized to achieve a classification at the individual level, which might eventually be used for the early detection of at risk individuals in clinical settings.

Cons

The exact location of the discriminative regions is less relevant, and in particular less evidently interpretable. Also, the result of the analysis is the accuracy (and sensitivity/specificity) of a given classifier to predict the clinical outcome. Subsequently, there is no (at least not directly) statistical t or p value allowing for acceptance or rejection of an *a priori* hypothesis.

SUPPORT VECTOR MACHINE CLASSIFIERS

A classifier is a specific analysis method, which aims to classify data into two or more different groups. The currently most frequently implemented type of classifier in neuroimaging is support vector machines (SVM)
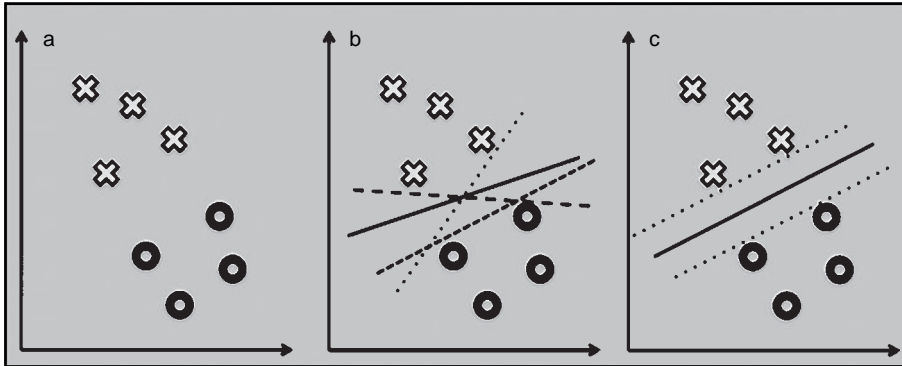
Fig. 2. The basic principle of a support vector machine (SVM) to discriminate between the two groups, represented by x and o (a). Of all possible solutions (multiple lines in b), the SVM identifies the optimum separation line between groups (c).

[9]. This type of classifier originates from multi vector pattern analyses (MVPA), a domain of machine learning or artificial intelligence. Considering the fact that SVM analyses were simply transferred yet not specifically developed for neuroimaging data, the results of this SVM method in neuroimaging are remarkable. In the domain of Alzheimer disease (AD), SVMs were first applied to grey matter data after standard VBM processing, discriminating AD versus controls with accuracies of 89% [10] and 94.5% [11]. Equivalently, SVM classification of grey matter VBM preprocessed data discriminated stable versus progressive MCI with accuracies of 75% [12], 81.5% [13] and 85% [14]. The equivalent SVM classification was also successfully applied to diffusion tensor imaging (DTI) data of white matter pre-processed in TBSS to discriminate stable versus progressive MCI based on fractional anisotropy (FA) with accuracies over 95% [15]. Moreover, the SVM analysis of susceptibility weighted imaging (SWI) assessing iron deposition also discriminated stable versus progressive MCI with a lower sensitivity of up to 85% [16].

The basic principle of a SVM classification analysis for a very simple case of only 2 groups (represented by "x" and "o") and 2 features can be illustrated on an x-y plot (Fig. 2a). In this simple example, there are unlimited possibilities to discriminate the between these two groups, indicated by the different lines in Fig. 2b. The strength of the SVM classifier is that this method detects the line, which best discriminates between groups (Fig. 2c). In a more complex example of three features, the line would become a plane. In higher number of features, this separating plane would be a super plane or hyper plane.

SMVs are only one type of classifier. A continuously increasing number of classifiers exist. Depending on their properties, the different classifiers are more or less suited for a given classification task and data structure.

FEATURE SELECTION ALGORITHMS

In order to perform a classification analysis, neuroimaging data are typically pre-processed with the established tools to obtain for example a spatial registration of each individual brain into a common standard space. The VBM pre-processing of grey matter typically results to data with about 200 000 voxels, while TBSS pre-processing of white matter data typically includes about 100 000 voxels. It is evident that not all voxels, or features in the terminology of classification analyses, will discriminate equally well between groups. Included non-discriminative voxel require unnecessary computation resources, and may even decrease the classification accuracy because the non-discriminative features generate overlapping point clouds.

The aim of feature selection algorithms consequently is to rank the features according to their discrimination between groups, and to include in the actual classification analysis only the most discriminative features/voxels. Similar to the classifiers discussed above, multiple algorithms exist. For example the RELIEFF algorithm [17] was successfully applied to MRI data [15, 16] yet depending on the type of data, other feature selection algorithms might be more adapted in other clinical settings.

CROSS VALIDATION

Classification analyses are typically performed in two steps. In a first step, a given type of classifier is trained using a *training* dataset. In a second step, the accuracy (and sensitivity/specificity) of this classifier is tested in another *test* dataset.

In practice, the number of available datasets is typically limited. Thus, cross validation techniques are often applied. The basic principle is to divide the data in for example 10 parts. Nine parts are used for training; the remaining part is then used for testing. This procedure is repeated ten times, until each data was used once for testing and nine times for training. This method limits the arbitrary variation of estimated accuracy (and sensitivity/specificity) rates related to randomly selecting a given set of training and test data. Its disadvantage is that the resulting accuracy (and sensitivity/specificity) rates are usually too optimistic because both training and testing data are very homogeneous and originate from the same pool. For instance in MCI, a classifier must be able to deal with training data acquired on one or more different MRI machines and be able to generalize the classification to other data acquired on different MRI machines. Also, the patient population itself might vary when generalizing a given trained classifier to other test data acquired in different institutions and countries.

PERSPECTIVES

Suppport vector machines, the currently most frequently used type of classifier in neuroimaging data, originates from multi vector pattern analysis (MVPA), a branch of machine learning or artificial intelligence, as discussed above.

Spatial information

The probably most evident point for further improvement of SVM classifiers is the integration of spatial information. SVM consider each voxel value as independent feature. This is however incomplete, because the pre-processed MRI data have a high degree of spatial interdependence since adjacent voxels are more likely to show similar behaviour between study groups than distant voxels. For example, the normal variation of cortical thickness is up to 15% between subjects even in healthy controls [18]. It was shown in the domain of psychosis, that the within-subject cortical asymmetry has less variability. The comparison of within-subject cortical asymmetry thus resulted in a higher sensitivity than the direct comparison of the cortical thickness per se [19]. The available spatial information in the pre-processed MRI data might be implemented in future modifications of SVMs (or related classifiers) to further improve the classification accuracy and make the classification more robust when exploring data acquired on various MRI scanners and patient populations.

Multi domain classification

The currently available studies successfully, yet separately, analyzed grey matter (T1w data and VBM pre-processing) [10–14], white matter (DTI data and TBSS pre-processing) [15] and iron deposition (SWI data and TBSS-derived pre-processing) [16]. The same principle of single-domain classification (however with a different methodology in detail) also discriminated AD, MCI and controls based on resting state functional MRI [20].

It is quite reasonable to assume that a combined classification analysis of multiple structural and functional neuroimaging modalities in combination with other modalities such as electroencephalography (EEG), laboratory parameters such as cerebro-spinal fluid analysis, neuropsychology etc. may further increase the accuracy and robustness of classification analyses. The combination of these different modalities is however not trivial. One possibility is to directly integrate all features into one "super classifier" (see Fig. 3). The different modalities may have different properties, and consequently different types of classifiers might be best suited for the different modalities. Consequently, it might be beneficial having separate classifiers for each modality at a first level, and to combine the output of these different classifiers into another classifier at the second level. One key issue to address is how to combine and weight the individual classifiers. First multimodal classification studies show promising results and have indeed increased classification accuracy when for example combining MRI, PET and CSF data as compared to separate classification of each modality [21]. Further optimization of combined multimodal classifications will be subject of current and future research.
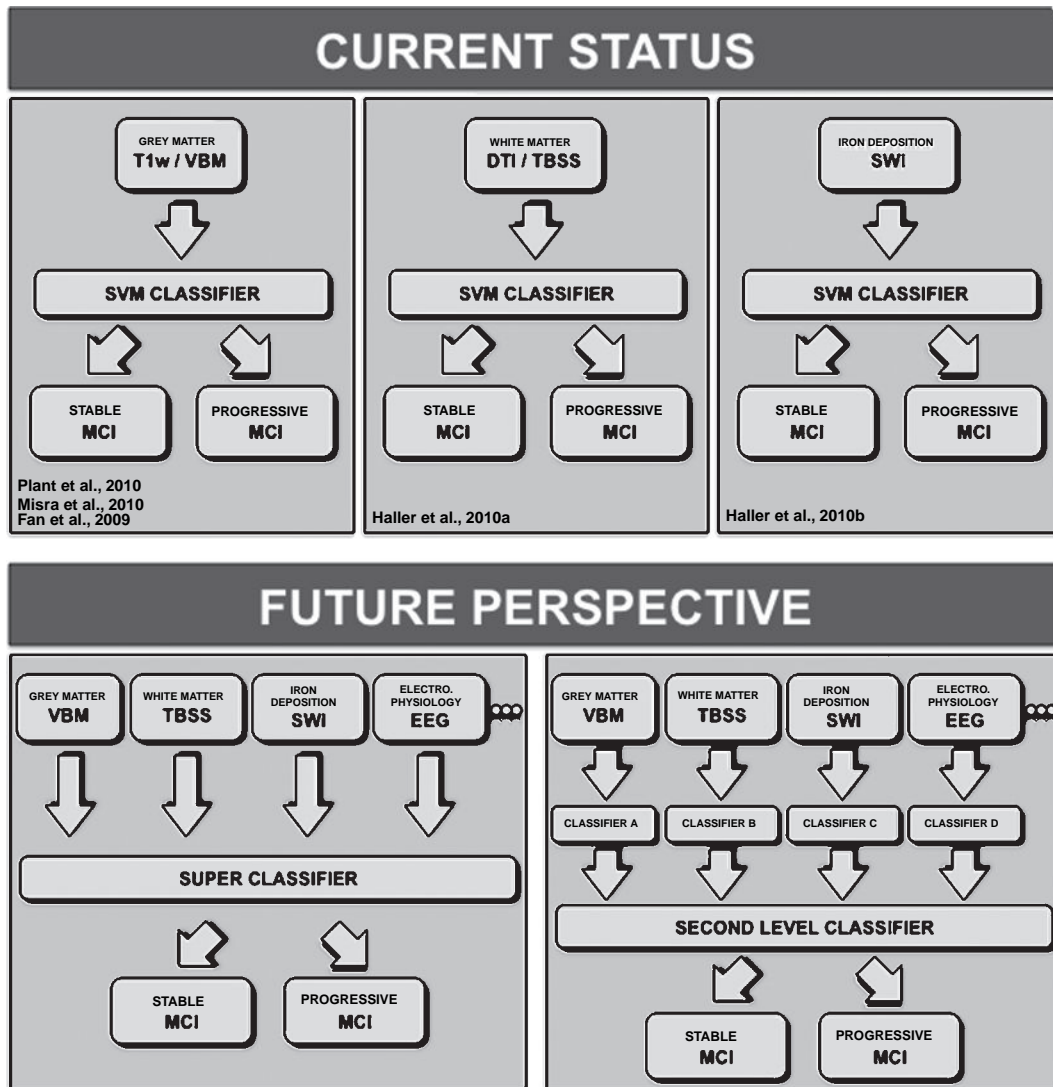
Fig. 3. The current status of classification analyses, which successfully implemented grey matter (T1w VBM), white matter (DTI TBSS) and iron deposition (SWI TBSS derived pre-processing) data. Current and future studies may try to integrate classification of multiple modalities in order to further improve classification accuracy and robustness. The way to integrate multiple modalities is however not trivial. On the one hand, it is possible to directly integrate each modality into a single "super classifier". On the other hand, different modalities might have different properties, hence different types of classifiers might be best suited for the different modalities. An alternative approach might be to have separate classifiers for each modality at a first level, and to integrate the output of these classifiers into a separate classifier on the second level.

CONCLUSIONS

Classification analyses represent a recent fundamental shift of focus away from the established group level analyses and aim to provide an individual detection of early and ideally preclinical stages of a disease. Recent classification analyses successfully discriminated stable versus progressive MCI based on grey matter T1w, white matter DTI or iron deposition SWI data. Current and future research will address the non-trivial combination of multiple modalities, including neurophysiology, laboratory parameters and neuropsychology into a single classification analysis aiming to further improve classification accuracy and robustness.

DISCLOSURE

No conflicts of interest.

ACKNOWLEDGMENTS

REFERENCES

[1] Ashburner J, Friston KJ (2000) Voxel-based morphometry–the methods. *Neuroimage* **11**, 805-821.

[2] Fischl B, Dale AM (2000) Measuring the thickness of the human cerebral cortex from magnetic resonance images. *Proc Natl Acad Sci USA* **97**, 11050-11055.

[3] Smith SM, Jenkinson M, Johansen-Berg H, Rueckert D, Nichols TE, Mackay CE, Watkins KE, Ciccarelli O, Cader MZ, Matthews PM, Behrens TE (2006) Tract-based spatial statistics: voxelwise analysis of multi-subject diffusion data. *Neuroimage* **31**, 1487-1505.

[4] Friston KJ, Holmes AP, Worsley KJ, Poline JB, Frith CD, Frackowiak RSJ (1995) Statistical parametric maps in functional imaging: a general linear approach. *Hum Brain Mapp*, 189-210.

[5] Ogawa S, Tank DW, Menon R, Ellermann JM, Kim SG, Merkle H, Ugurbil K (1992) Intrinsic signal changes accompanying sensory stimulation: functional brain mapping with magnetic resonance imaging. *Proc Natl Acad Sci U S A* **89**, 5951-5955.

[6] Biswal B, Yetkin FZ, Haughton VM, Hyde JS (1995) Functional connectivity in the motor cortex of resting human brain using echo-planar MRI. *Magn Reson Med* **34**, 537-541.

[7] Ferreira LK, Diniz BS, Forlenza OV, Busatto GF, Zanetti MV (2009) Neurostructural predictors of Alzheimer's disease: a meta-analysis of vbm studies. *Neurobiol Aging* [Epub ahead of print].

[8] Petersen RC, Negash S (2008) Mild cognitive impairment: an overview. *CNS Spectr* **13**, 45-53.

[9] Noble WS (2006) What is a support vector machine? *Nat Biotechnol* **24**, 1565-1567.

[10] Kloppel S, Stonnington CM, Chu C, Draganski B, Scahill RI, Rohrer JD, Fox NC, Jack CRJ, Ashburner J, Frackowiak RS (2008) Automatic classification of MR scans in Alzheimer's disease. *Brain* **131**, 681-689.

[11] Magnin B, Mesrob L, Kinkingnehun S, Pelegrini-Issac M, Colliot O, Sarazin M, Dubois B, Lehericy S, Benali H (2009) Support vector machine-based classification of Alzheimer's disease from whole-brain anatomical MRI. *Neuroradiology* **51**, 73-83.

[12] Plant C, Teipel SJ, Oswald A, Bohm C, Meindl T, Mourao-Miranda J, Bokde AW, Hampel H, Ewers M (2010) Automated detection of brain atrophy patterns based on MRI for the prediction of Alzheimer's disease. *Neuroimage* **50**, 162-174.

[13] Misra C, Fan Y, Davatzikos C (2009) Baseline and longitudinal patterns of brain atrophy in MCI patients, and their use in prediction of short-term conversion to AD: results from ADNI. *Neuroimage* **44**, 1415-1422.

[14] Fan Y, Batmanghelich N, Clark CM, Davatzikos C (2008) Spatial patterns of brain atrophy in MCI patients, identified via high-dimensional pattern classification, predict subsequent cognitive decline. *Neuroimage* **39**, 1731-1743.

[15] Haller S, Nguyen D, Rodriguez C, Emch J, Gold G, Bartsch A, Lovblad KO, Giannakopoulos P (2010) Individual prediction of cognitive decline in mild cognitive impairment using support vector machine-based analysis of diffusion tensor imaging data. *J Alzheimers Dis* **22**, 315-327.

[16] Haller S, Bartsch A, Nguyen D, Rodriguez C, Emch J, Gold G, Lovblad KO, Giannakopoulos P (2010) Cerebral microhemorrhage and iron deposition in mild cognitive impairment: susceptibility-weighted MR imaging assessment. *Radiology* **257**, 764-773.

[17] Kononenko I, Šimec E, Robnik-Šikonja M (1997) Overcoming the myopia of inductive learning algorithms with RELIEFF. *Applied Intelligence* **7**, 39-55.

[18] Haug H (1987) Brain sizes, surfaces, and neuronal sizes of the cortex cerebri: a stereological investigation of man and his variability and a comparison with some mammals (primates, whales, marsupials, insectivores, and one elephant). *Am J Anat* **180**, 126-142.

[19] Haller S, Borgwardt SJ, Schindler C, Aston J, Radue EW, Riecher-Rossler A (2009) Can cortical thickness asymmetry analysis contribute to detection of at-risk mental state and first-episode psychosis? a pilot study. *Radiology* **250**, 212-221.

[20] Chen G, Ward BD, Xie C, Li W, Wu Z, Jones JL, Franczak M, Antuono P, Li SJ (2011) Classification of Alzheimer disease, mild cognitive impairment, and normal cognitive status with large-scale network analysis based on resting-state functional MR imaging. *Radiology* **259**, 213-221.

[21] Zhang D, Wang Y, Zhou L, Yuan H, Shen D (2011) Multimodal classification of Alzheimer's disease and mild cognitive impairment. *Neuroimage* **55**, 856-867.

Combinatorial Markers of Mild Cognitive Impairment Conversion to Alzheimer's Disease - Cytokines and MRI Measures Together Predict Disease Progression

Simon J. Furney[a], Deborah Kronenberg[b], Andrew Simmons[a], Andreas Güntert[a], Richard J. Dobson[a], Petroula Proitsi[a], Lars Olof Wahlund[c], Iwona Kloszewska[d], Patrizia Mecocci[e], Hilkka Soininen[f], Magda Tsolaki[g], Bruno Vellas[h], Christian Spenger[i] and Simon Lovestone[a,*]

[a]*King's College London, Institute of Psychiatry and National Institute of Health Research (NIHR) Biomedical Research Centre for Mental Health, London, UK*

[b]*National Institute for Health Research (NIHR), Biomedical Research Centre Guy's and St. Thomas' NHS Foundation Trust and King's College London, London, UK*

[c]*Department of Neurobiology, Care Sciences and Society, Section of Clinical Geriatrics, Karolinska Institutet, Karolinska University Hospital, Huddinge, Stockholm, Sweden*

[d]*Department of Old Age Psychiatry & Psychotic Disorders, Medical University of Lodz, Lodz, Poland*

[e]*Section of Gerontology and Geriatrics, Department of Clinical and Experimental Medicine, University of Perugia, Perugia, Italy*

[f]*Department of Neurology, University of Eastern Finland and Kuopio University Hospital, Kuopio, Finland*

[g]*Third Department of Neurology, Aristotle University of Thessaloniki, Thessaloniki, Greece*

[h]*Department of Internal and Geriatrics Medicine, Hôpitaux de Toulouse, Toulouse, France*

[i]*Department of Clinical Science, Intervention and Technology, Karolinska, Institutet, Stockholm, Sweden*

Abstract. Progression of people presenting with Mild Cognitive Impairment (MCI) to dementia is not certain and it is not possible for clinicians to predict which people are most likely to convert. The inability of clinicians to predict progression limits the use of MCI as a syndrome for treatment in prevention trials and, as more people present with this syndrome in memory clinics, and as earlier diagnosis is a major goal of health services, this presents an important clinical problem. Some data suggest that CSF biomarkers and functional imaging using PET might act as markers to facilitate prediction of conversion. However, both techniques are costly and not universally available. The objective of our study was to investigate the potential added benefit of combining biomarkers that are more easily obtained in routine clinical practice to predict conversion from MCI to Alzheimer's disease. To explore this we combined automated regional analysis of structural MRI with analysis of plasma cytokines and chemokines and compared these to measures of APOE genotype and clinical assessment to assess which best predict progression. In a total of 205 people with MCI, 77 of whom subsequently converted to Alzheimer's disease, we find

---
*Correspondence to: Simon Lovestone, King's College London, Institute of Psychiatry and National Institute of Health Research (NIHR) Biomedical, De, Crespigny Park, London SE5 8AF, UK. Tel.: +44 20 7848 0239/0550, Fax: +44 20 7848 0632; E-mail: simon.lovestone@kcl.ac.Uk.

biochemical markers of inflammation to be better predictors of conversion than APOE genotype or clinical measures (Area under the curve (AUC) 0.65, 0.62, 0.59 respectively). In a subset of subjects who also had MRI scans the combination of serum markers of inflammation and MRI automated imaging analysis provided the best predictor of conversion (AUC 0.78). These results show that the combination of imaging and cytokine biomarkers provides an improvement in prediction of MCI to AD conversion compared to either datatype alone, APOE genotype or clinical data and an accuracy of prediction that would have clinical utility.

INTRODUCTION

The challenge of the neurodegenerative diseases is daunting; it is estimated that the global prevalence of dementia will rise from 24.3 million cases in 2005 to 81.1 million cases in 2040 [1]. Alzheimer's disease (AD) is the commonest form of dementia [2]. Rising to the challenge posed by this health burden, there are many potential disease modification therapies in development with approximately 10 compounds for AD in phase III and more than 50 in phase II [3]. There is a consensus that disease modification therapy is most likely to be efficacious very early in the disease process and because of this there is an increasing drive towards very early identification and diagnosis. Given the inherent difficulty of very early, and even prodromal, diagnosis, biomarkers are likely to play an important role. They are incorporated into the proposed revision of diagnostic criteria [4] for AD and have been increasingly examined for their potential to predict which people with mild cognitive impairment (MCI) are most likely to progress to full dementia [5]. This is important as only a minority with MCI progress to full dementia in the time frame of a typical clinical trial. A recent meta-analysis showed an annual conversion rate of 8.1% and a cumulative proportion of 33.6% for MCI conversion to AD [6] and in a previous systematic review we found study-related variables including recruitment strategy to be the most important factors predicting conversion [7].

The primary focus in the search for biomarkers for AD to date has been on neuroimaging, and on Aβ and tau proteins in cerebrospinal fluid (CSF) [8, 9]. Various studies using structural MRI have identified brain regions within the medial temporal lobe, particularly the hippocampus and entorhinal cortex, as potential biomarkers of conversion from MCI to AD [10–14]. In addition molecular imaging using amyloid PET ligands also report efficacy as markers predictive of conversion [15]. CSF is an excellent fluid for biomarker discovery in neurodegeneration as it is in direct contact with the extracellular space of the brain and is therefore supposed to reflect biochemical changes occurring in the brain [16]. Recently Shaw *et al.* showed in the US Alzheimer's Disease Neuroimaging Initiative (ADNI) study that the t-tau/$A\beta_{1-42}$ ratio discriminated between those who will remain MCI subjects and those who will convert to AD within one year follow-up [17]. In addition it has been reported that MCI subjects with abnormal results on both FDG-PET and episodic memory were more likely to convert to AD [18]. However, structural MRI is not sufficiently predictive of conversion [14, 19], PET imaging is a highly specialised approach available in relatively few centres, and lumbar puncture for CSF, although non-traumatic and without side effects in the majority of patients, necessitates a high level of skill and a hospital setting. A blood-based biomarker would be hugely advantageous especially in large-scale population and community based studies of elderly frail people.

Previously we and others have demonstrated using proteomics that blood-based biomarkers were feasible and reproducible in independent studies [20–22]. However, the most impressive evidence for a specific and sensitive marker of MCI conversion to date comes from a study reporting that 18 signalling proteins in blood plasma could be used to predict conversion from MCI to AD 2–6 years later with an accuracy of 91% [23]. However these results have not yet been independently replicated. Recently, O'Bryant *et al.* developed a serum protein-based classifier for the prediction of AD patients and controls [24].

For the most part, these studies have concentrated on single modality biomarkers although there are theoretical reasons and increasing data from combinatorial studies to think that combining biomarkers might have added benefits [25–28]. Some studies have combined imaging with clinical variables to try to increase predictive power, with mixed results. One such study found no added benefit of combining structural MRI data with clinical measures [12] whereas another developed a predictor including three clinical predictors

(SRT immediate recall, FAQ and UPSIT) as well as two imaging markers (hippocampal and entorhinal cortex volume) [29]. Davatzikos *et al.* recently integrated MRI and CSF biomarkers and noted improved predictive accuracy compared to either individual data type [9] and Ewers *et al.* investigated the accuracy of MRI and CSF biomarkers and neuropsychological tests for predicting the conversion from MCI to Alzheimer's disease [30].

However no study, to our knowledge, has investigated the potential added benefit of combining biomarkers that are readily obtained in routine clinical practice. To explore this we combined automated regional analysis of structural MRI with analysis of serum cytokines and APOE genotype to assess if the combination of data types improved prediction of progression in a small cohort of participants from the AddNeuroMed study, a European ADNI-like biomarker study [31]. In addition, we have examined the predictive accuracy of a cytokine panel in a larger dataset, which includes the AddNeuroMed cohort.

MATERIALS AND METHODS

Subjects

The study population used in this report was derived from the AddNeuroMed study, a European multi-centre study, aiming to identify biomarkers for AD [31] and the Alzheimer Research Trust–funded cohort at King's College London (KCL-ART) [32]. The participating AddNeuroMed clinical centres were in Kuopio, Perugia, Lodz, Thessaloniki, Toulouse and London. Subjects were patients who attended local memory clinics and received a diagnosis of MCI. Diagnosis of dementia was made according to NINCDS-ADRDA criteria and DSM IV, amnestic MCI diagnosis was based on CDR (CDR = 0.5), MMSE (MMSE ≥ 24) and amnestic cognitive impairment according to word list learning recall task of the CERAD (<1.5 SD of population mean adjusted for gender, age and level of education).The follow-up period was one year. At baseline and follow-up information was obtained on demographic characteristics, medical history, current health status, medication use and family history. In addition to the clinical data, blood and urine samples were obtained and participants underwent a neuropsychological assessment.

In the KCL-ART cohort, per MCI converter case we randomly sampled two MCI non-converters matched on gender and age. In the AddNeuroMed cohort, per

MCI converter case we randomly sampled one MCI non-converter matched on gender and year of baseline assessment, sampled in five-year age categories. For the integration of cytokine levels with imaging measures, data from AddNeuroMed subjects who had undergone successful baseline structural MRI imaging, and whose APOE status and cytokine levels were determined were used (cytokine-imaging cohort; $n = 48$).

Assessment of the patient samples was conducted in a randomized fashion. Demographics can be found in Table 1.

Samples

At baseline and follow-up blood samples were drawn by veni-puncture and collected into EDTA glass tubes, after a minimum of 2 h fasting prior to draw. After coagulation for 30 minutes serum was obtained by centrifugation for 8 min at 3,000 g at 4°C. Samples were aliquoted and frozen at −80°C until further use.

Cytokine multiplex analysis

Serum samples were analyzed for 36 cytokines and chemokines (supplementary table 1) using a commercially available Cytokine Human 30-plex panel and a customized 6-plex (Biosource International). Samples were measured at baseline and follow-up in duplicate and according to the manufacturer's recommendations. The samples were measured in a randomized and blinded fashion using the antibody bead mix in duplicate with a biotinylated detection antibody followed by streptavidin-phycoerythrin. The plate was read using the Luminex platform (BioRad), and data were collected for 100 beads per cytokine from each well. Cytokine concentrations were calculated using Bio-Plex Manager 5.0 software with a five parameter curve-fitting algorithm applied for standard curve calculations.

Neuroimaging

Data acquisition

Data acquisition took place using six different 1.5T MR systems (four General Electric, one Siemens and one Picker). At each site a quadrature birdcage coil was used for RF transmission and reception. Data acquisition was designed to be compatible with the Alzheimer Disease Neuroimaging Initiative (ADNI) [33]. The imaging protocol included a high resolution sagittal 3D T1-weighted MPRAGE volume (voxel size

Table 1
Demographics of MCI converter and non-converter cytokine cohort and cytokine and imaging cohort, including mean APOE ε4 dosage and p-values of difference between Non-Converters (MCI-N) and Converters (MCI-C). (MMSE, Mini Mental State Exam, Maximum score = 30)

	Cytokine MCI-N ($n = 128$)	Cytokine MCI-C ($n = 77$)	p-value	Cytokine/imaging MCI-N ($n = 26$)	Cytokine/imaging MCI-C ($n = 22$)	p-value
Age	80.4	77.5	0.003	74.1	73.4	0.68
Female %	55	59	0.77	58	41	0.38
MMSE	27.1	26.2	0.006	27.1	26.6	0.39
APOE ε4 dosage	0.31	0.54	0.009	0.35	0.77	0.02

$1.1 \times 1.1 \times 1.2 \, \text{mm}^3$) and axial proton density / T2-weighted fast spin echo images. Full brain and skull coverage was required for both of the latter datasets and detailed quality control carried out on all MR images [34, 35]. All MR images received a clinical read by an on-site radiologist in order to exclude any subjects with non-AD related pathologies.

Image analysis

A highly automated structural MRI image processing pipeline developed by Fischl et al and producing both regional cortical thickness measures and regional volume measures was utilized for data analysis [36–38]. Cortical reconstruction and volumetric segmentation included removal of non-brain tissue using a hybrid watershed/surface deformation procedure, automated Talairach transformation, segmentation of the subcortical white matter and deep gray matter volumetric structures (including hippocampus, amygdala, caudate, putamen, ventricles) intensity normalization, tessellation of the gray matter white matter boundary, automated topology correction, and surface deformation following intensity gradients to optimally place the gray/white and gray/cerebrospinal fluid borders at the location where the greatest shift in intensity defines the transition to the other tissue class. Surface inflation was followed by registration to a spherical atlas which utilized individual cortical folding patterns to match cortical geometry across subjects and parcellation of the cerebral cortex into units based on gyral and sulcal structure. All volumes were normalized by the subjects' intracranial volume.

The regional cortical thickness was measured from 34 areas and the regional cortical volume was measured bilaterally from 24 areas (supplementary Table 2).

ApoE genotyping

The APOE haplotype was determined using two allelic discrimination assays (rs7412 and rs429358) based on fluorogenic 5' nuclease activity, the Taq

polymerase single nucleotide polymorphism genotyping assay (TaqMan, Applied Biosystems Inc., www.appliedbiosystems.com).

Statistical analysis

As an initial step unsuccessful cytokine readings with less than 50 bead counts were excluded from the analysis.

Observations with more than 50% missing values and/or outliers were consequently excluded from further analysis. Outliers were any data values which lay more than 1.5 times the interquartile range (IQR) below the first Quartile (Q_{25}) or above the third Quartile (Q_{75}).

Machine-learning approach

Datasets

The total sample size with cytokine data (AddNeuroMed + KCL-ART] was 205 (MCI-N = 128, MCI-C = 77). This cohort was divided into an approximate two thirds -one third stratified training set – test set where the training set sample size was 136 (MCI-N = 85, MCI-C = 51) and the test set size was 69 (MCI-N = 43, MCI-C = 26). Using the training set only we created 5 different datasets containing: (1) APOE ε4 dosage, (2) Age, Gender and MMSE score (Clinical data), (3) Cytokine data, (4) A subset of 7 cytokines in common with the panel of 18 identified by Ray et al. [23] (EGF, G-CSF, GDNF, IL-1α, IL-3, MCP-3 AND TNF-α; see supplementary table 1 for details), and (5) Cytokine, APOE ε4 dosage and Clinical data. Missing values were replaced using global class means.

The number of subjects with both imaging and cytokine data was 48 (MCI-N = 26, MCI-C = 22). This cohort was divided into an approximate two-thirds-one third stratified training set – test set where the training set sample size was 31 (MCI-N = 17, MCI-C = 14) and the test set size was 17 (MCI-N = 9, MCI-C = 8). Using the training set only we created 8 different datasets containing: (1) APOE ε4 dosage, (2) Age, Gender and

Table 2
Classification area under the ROC curve for the training and test datasets for entire cohort (best training set classifier in bold)

	Training SVM (all data)	Training SVM (10 attributes)	Training SVM (5 attributes)	Test
Cytokine, clinical + APOEε4	**0.69**	0.67	0.67	0.61
Cytokine	**0.64**	0.63	0.62	0.65
Cytokine subset	**0.66**	N/A	N/A	0.60
Clinical	**0.72**	N/A	N/A	0.59
APOEε4 dosage	**0.59**	N/A	N/A	0.62

MMSE score (Clinical data), (3) Cytokine data, (4) Imaging data, (5) Cytokine and Clinical data, (6) Imaging and Clinical data, (7) Imaging and Cytokine, and (8) Imaging, Cytokine, APOE ε4 dosage, and Clinical data.

Classification

Feature selection and class prediction by machine-learning was conducted using Weka [39]. To address the class imbalance between the two classes with cytokine data (MCI-N = 128, MCI-C = 77), a cost-sensitive approach was employed (weka.classifiers.meta.CostSensitiveClassifier) using a cost matrix of the ratios of the two classes. The class imbalance in the dataset with both cytokine and imaging data was relatively minor (MCI-N = 26, MCI-C = 22) and therefore a cost-sensitive classifier was not used. Three different approaches were assessed using a ten-fold cross validation on the training data with 100 iterations : (1) A Support Vector Machine (SVM - the SMO algorithm in Weka) using default settings (Polykernel kernel) and all the data variables, (2) a within-loop feature selection using the best 10 attributes for classification with an SVM (weka.classifiers.meta. AttributeSelectedClassifier). The feature selection phase was conducted using the SVMAttributeE-val (weka.attributeSelection.SVMAttributeEval) and Ranker (weka.attributeSelection.Ranker) algorithms, and (3) a within-loop feature selection using the best 5 attributes for classification with an SVM. Approaches (2) and (3), which incorporate feature selection, were not conducted for the datasets comprising APOE ε4 dosage only or the Clinical data only.

The effect of the SVM complexity parameter (C) was investigated by setting C = 0.01, 0.1, 1 (the default value) and 10 and the C value resulting in the highest AUC in the training set was used in evaluating the test set.

For each dataset, the machine learning approach resulting in the highest area under the ROC curve

(AUC) after the ten-fold cross validation was applied to the relevant test dataset. To obtain proper probability estimates, the option that fits logistic regression models (-M) to the outputs of the support vector machine was used. An accuracy (ACC), sensitivity (SN), specificity (SP), positive predictive value (PPV), negative predictive value (NPV) and area under the curve were calculated for each test set.

RESULTS

Cytokine dataset

We successfully measured 35 cytokines for analysis in a total of 205 subjects. Only one cytokine - RANTES – showed evidence of technical failure and was excluded from all analyses. In addition IL-17 and IL-1B were excluded from the multivariate analysis because of the high proportion of missing values (>50%). Baseline cytokine levels of three MCI non-converter subjects, were excluded from the analysis, because of overall highly elevated cytokine levels (i.e. more than 60% of all cytokines measured showed apparently arbitrarily high levels) or because more than 50% of all cytokine measures were missing.

Multivariate analysis

A machine-learning approach (Support Vector Machines) to class prediction was used to identify a set of combined analytes that might discriminate between converters and non-converters. Support Vector Machines (SVMs) are used extensively in computational biology as they have been shown to predict binary outcomes with high accuracy and possess the ability to model diverse and high-dimensional data [40].

The total number of subjects with cytokine data was 205 (MCI-N = 128, MCI-C = 77). The feature selection stage did not improve the accuracies of any of the classifiers and therefore the model built with all of the data

for each of the training datasets was applied to the relevant test dataset (Table 2). The AUCs (Figure 1) from the test datasets were 0.62 (APOE ε4 dosage), 0.60 (Cytokine subset), 0.61 (Cytokine data, Clinical data and APOE ε4 dosage), 0.59 (Clinical data) and 0.65 (Cytokine data).

Cytokine and imaging dataset

We then sought to assess whether combining structural MRI data with the cytokine data would improve classification accuracy. MRI brain scans of a subset of the subjects were processed and the regional cortical thickness was measured from 34 areas and the regional cortical volume was measured bilaterally from 24 areas (see Methods for details).
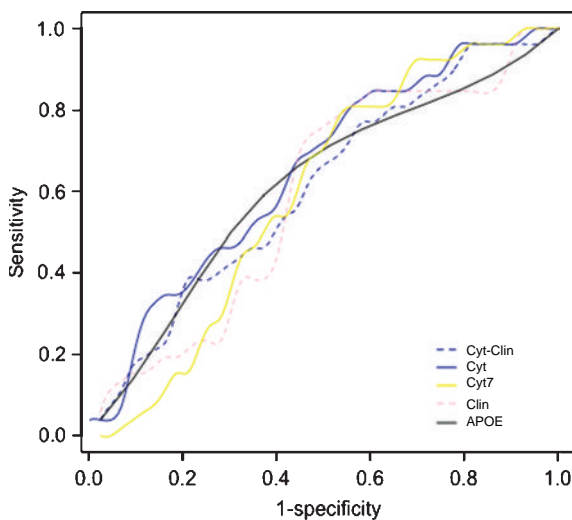
Fig. 1. Entire cytokine cohort receiver operating characteristic (ROC) curves of most accurate training classifiers applied to the test datasets. Cyt-Clin = Cytokine and Clinical data, Cyt = Cytokine data, Clin = Clinical data, Cyt7 = subset of 7 cytokines in common with the panel of 18 identified by Ray et al. , and APOE = APOE ε4 dosage.

The number of subjects with both imaging and cytokine data was 48 (MCI-N = 26, MCI-C = 22). Feature selection improved the training set prediction accuracy for the Cytokine dataset and the combined Cytokine and Clinical dataset. The other datasets showed greatest accuracy when including all data (Table 3). The most accurate model for each training dataset was then applied to the relevant test dataset.

In this smaller dataset, the cytokine data by themselves do not classify the test subjects particularly well (AUC = 0.60). In fact, in this cohort APOE ε4 dosage alone (AUC 0.74) is a better predictor of conversion than the cytokine or imaging data (Table 3). The combination of the cytokine and imaging data is the most accurate classifier (AUC = 0.78) showing a modest improvement over APOE ε4 dosage.

The imaging or cytokine data alone predict the test subjects with AUCs = 0.68 and 0.60, respectively. The sensitivity, specificity, positive and negative predictive values of each classifier is shown in supplementary table 3.

DISCUSSION

This study focused, for the first time, on combinatorial biomarkers using readily available techniques in order to identify a marker set predictive of conversion from MCI to dementia within the time frame of a typical disease modification trial. Alone, cytokine levels showed some predictive value for MCI conversion while imaging data showed a modest predictive accuracy. However, the predictive model using combined cytokine levels and imaging measures outperformed either individual classifier (Table 3 and Figure 2). The cytokine classifier exhibits low sensitivity and a higher specificity (supplementary table 3) whereas the converse is true of the imaging classifier. When the two data-types are combined the classification accuracy is improved (Table 3 and supplementary table 3).

Table 3
Classification area under the ROC curve for the training and test datasets for cohort with cytokine and imaging data (*n* = 48; best training set classifier in bold)

	Training SVM (all data)	Training SVM (10 attributes)	Training SVM (5 attributes)	Test
Cytokine + imaging + clinical + APOEε4 dosage	**0.60**	0.50	0.50	0.74
Cytokine + imaging	**0.56**	0.51	0.54	0.78
Cytokine + clinical	0.49	0.50	**0.50**	0.53
Imaging + clinical	**0.63**	0.54	0.52	0.67
Cytokine	0.48	0.50	**0.50**	0.60
Imaging	**0.62**	0.52	0.54	0.68
Clinical	**0.50**	N/A	N/A	0.50
APOEε4 dosage	**0.59**	N/A	N/A	0.74
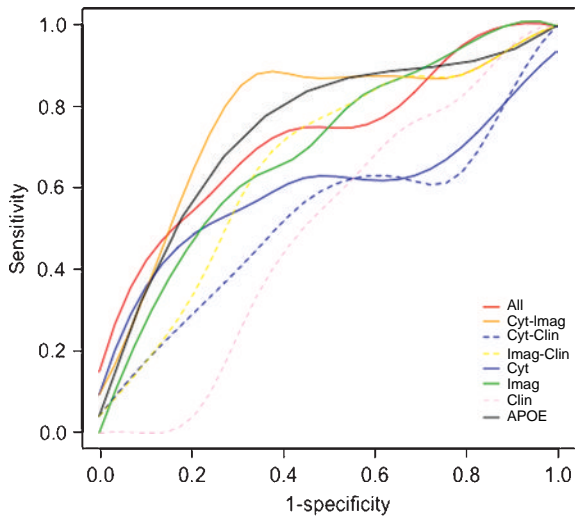
Fig. 2. Cytokine and imaging cohort receiver operating characteristic (ROC) curves of most accurate training classifiers applied to the test datasets. All = Cytokine, Imaging, Clinical data and APOE ε4 dosage, Cyt-Imag = Cytokine and Imaging data, Cyt-Clin = Cytokine and Clinical data, Imag-Clin = Imaging and Clinical data, Cyt = Cytokine data, Imag = Imaging data, Clin = Clinical data, and APOE = APOE ε4 dosage.

Considering that the potential disease modifying therapies are non-hazardous and aim to focus on an early stage of the disease the ideal predictive model would have a high negative predictive value and a high specificity. From a clinical point of view our here introduced model combining imaging and cytokine measures is favorable above combined imaging measures alone, which have been a point of primary interest in the literature so far.

Previous studies have looked at a number of brain regions (e.g. volumes of hippocampus, entorhinal cortex, ventricles, and whole brain) as potential biomarkers of conversion from MCI to AD [10, 29, 41]. Devanand *et al.* integrated the baseline predictors cognitive test performance, informant report of functional impairment, APOE genotype, olfactory identification deficit, and magnetic resonance imaging (MRI) hippocampal and entorhinal cortex volumes [29]. Ultimately, they used five variables in a predictor: Pfeffer Functional Activities Questionnaire (FAQ; informant report of functioning), University of Pennsylvania Smell Identification Test (UPSIT; olfactory identification), Selective Reminding Test (SRT) immediate recall (verbal memory), MRI hippocampal volume, and MRI entorhinal cortex volume. A recent imaging study, also based upon the AddNeuroMed patient cohort, has analyzed regional MRI volumes and

thicknesses as predictors of conversion from mild cognitive impairment to AD [14]. Analysis of the expanded patient cohort of 103 subjects (22 converters at year one follow up) showed that the bilateral hippocampus and amygdala, and right caudate baseline volumes were significantly smaller in MCI to AD converters compared to stable MCI subjects.

We analyzed a subset of 7 of the 18 signaling proteins for MCI conversion identified by an earlier study [23] (see Materials & Methods for details). We trained an SVM using these 7 cytokines and applied the model to a test set resulting in an AUC of 0.60. Our findings suggest that the inflammatory markers identified by Ray *et al.* may show some differential expression in people with established AD, and we are able to show some prognostic value of these markers for the more demanding, but more clinically important task of predicting MCI conversion.

Some of the cytokines we have examined have been previously implicated in AD as potential markers. Reports describing IL-1β levels in serum of AD patients have been conflicting with some groups describing an increase in IL-1β serum levels in AD patients compared to controls [42, 43], but others finding no change [44]. A meta analysis also found a genetic association of a IL-1β polymorphism and AD [45-47]. It has been hypothesized that proinflammatory cytokines, such as IL-1β are activating a cascade of neurotoxic changes in the brain, that are related with the development of neuritic plaques and neurofibrillary tangles characteristics in AD [48]. VEGF is associated with neuroprotection and regeneration in the brain. It co-localizes with plaques in AD brain [49] and some studies report an increase in VEGF levels in serum and CSF [50, 51], whereas others find a decrease in serum [52] and no change in CSF [53]. In the cytokine/imaging cohort the classifier using APOE ε4 dosage alone performs better than most other classifiers. It is not surprising that APOE performs well as it is clear that the ε4 allele is associated with AD and has previously been associated with the time to progression from MCI to AD [54]. In addition, in this smaller dataset the mean APOEε4 dosage per converting patient is much greater than in converters in the entire cohort (0.77 compared to 0.54 – Table 1).

There are limitations to our study. Most obviously, the sample size of the cytokine and imaging cohort is relatively small ($n = 48$), which meant constructing a predictive model with a training set of 31 subjects. When applying our predictors to the set of 17 subjects, although the combination of cytokines outperforms APOEε4 dosage, the increase in performance is mod-

est. It is noteworthy that adding clinical information (including basic cognitive tests, diagnosis and medical history but not very detailed neuropsychometry) adds nothing to the predictive power. This emphasises that the clinical assessment of MCI alone does not predict conversion.

As such, our predictor would need to be applied to a larger dataset to independently assess its accuracy. Nonetheless, we show preliminary evidence that a combined set of imaging and cytokine measures provides a small improvement in prediction of MCI to AD conversion than either cytokine or imaging data alone. It remains to be seen whether the accuracy reported here may be improved still further by the addition of other biomarkers or by alternative MRI analytical routines. As the prediction in this case was over only one year after test these data hold out the promise of a combinatorial biomarker for use in both clinical practice and, perhaps more pressingly, for patient stratifica-

tion and enrichment in trials of disease modification agents.

Supplementary Table 1
Proteins measured with luminex 30- and 6-plex (HGNC, HUGO Gene Nomenclature Committee)

Cytokine	Official full name (HGCN)	Gene symbol (HGNC)
BDNF	Brain-derived neurotrophic factor	BDNF
DR5	Tumor necrosis factor receptor superfamily, member 10b	TNFRSF10B
EGF	Epidermal growth factor	EGF
Eotaxin	Chemokine (C-C motif) ligand 11	CCL11
FGF	Fibroblast growth factor 2 (basic)	FGF2
G-CSF	Colony stimulating factor 3 (granulocyte)	CSF3
GDNF	Glial cell derived neurotrophic factor	GDNF
GM-CSF	Colony stimulating factor 2 (granulocyte-macrophage)	CSF2
HGF	Hepatocyte growth factor	
IFN-α	Interferon, alpha 1	IFNA1
IFN-γ	Interferon, gamma	IFNG
IL-1α	Interleukin 1, alpha	IL1A
IL-1β	Interleukin 1, beta	IL1B
IL-1RA	Interleukin 1 receptor, type I	IL1R1
IL-2	Interleukin 2	IL2
IL-2R	Interleukin 2 receptor, alpha	IL2RA
IL-3	Interleukin 3	IL3
IL-4	Interleukin 4	IL4
IL-5	Interleukin 5	IL5
IL-6	Interleukin 6	IL6
IL-7	Interleukin 7	IL7
IL-8	Interleukin 8	IL8
IL-10	Interleukin 10	IL10
IL-12	Interleukin 12	IL12
IL-13	Interleukin 13	IL13
IL-15	Interleukin 15	IL15
IL-17	Interleukin 17	IL17
IP-10	Chemokine (C-X-C motif) ligand 10	CXCL10
MCP-1	Chemokine (C-C motif) ligand 2	CCL2
MCP-3	Chemokine (C-C motif) ligand 7	CCL7
MIG	Chemokine (C-X-C motif) ligand 9	CXCL9
MIP-1α	Chemokine (C-C motif) ligand 3	CCL3
MIP-1β	Chemokine (C-C motif) ligand 4	CCL4
RANTES	Chemokine (C-C motif) ligand 5	CCL5
TNF-α	Tumor necrosis factor	TNF
VEGF	Vascular growth factor A	VEGFA

Supplementary Table 2
MRI regional cortical thickness from 34 areas and the regional cortical volume measured bilaterally from 24 areas

Volumes	Cortical thicknesses
3rd Ventricle	Banks of STS
4th Ventricle	caudal anterior cingulate
5th Ventricle	caudal middle frontal
Brain Seg Vol	corpus callosum
Brain Stem	cuneus
CC_Anterior	entorhinal
CC_Central	frontal pole
CC_Mid_Anterior	fusiform
CC_Mid_Posterior	inferior parietal
CC_Posterior	inferior temporal
CSF	isthmus cingulate
Left Accumbensarea	lateral occipital
Left Amygdala	lateral orbito frontal
Left Caudate	lingual
Left Cerebellum Cortex	medial orbitofrontal
Left Cerebellum White Matter	middle temporal
Left Cerebral Cortex	para central
Volumes	Cortical thicknesses
Left Cerebral White Matter	para hippocampal
Left choroid plexus	pars opercularis
Left Hippocampus	pars orbitalis
Left Inf Lat Vent	pars triangularis
Left Lateral Ventricle	pericalcarine
Left non WM hypointensities	post central
Left Pallidum	posterior cingulate
Left Putamen	precentral
Left Thalamus Proper	precuneus
Left Ventral DC	rostral anterior cingulate
Left vessel	rostral middle frontal
Left WM hypointensities	superior frontal
Optic Chiasm	superior parietal
Right Accumbensarea	superior temporal
Right Amygdala	supra marginal
Right Caudate	temporal pole
Right Cerebellum Cortex	transverse temporal
Right Cerebellum White Matter	
Volumes	Cortical thicknesses
Right Cerebral Cortex	
Right Cerebral White Matter	
Right Hippocampus	
Right Inf Lat Vent	
Right Lateral Ventricle	
Right non WM hypointensities	
Right non WM hypointensities	
Right Pallidum	
Right Putamen	
Right Thalamus Proper	
Right Ventral DC	
Right vessel	
Right WMhypointensities	

Supplementary Table 3
Sensitivity (SN), specificity (SP), positive predictive value (PPV), negative predictive value (NPV) and Accuracy (ACC) for the cytokine and imaging cohort classifiers

	SN	SP	PPV	NPV	ACC
Cytokine + imaging + clinical + APOEε4 dosage	0.75	0.67	0.67	0.75	0.71
Cytokine + imaging	0.75	0.78	0.75	0.78	0.76
Cytokine + clinical	0.38	0.78	0.60	0.59	0.59
Imaging + clinical	0.63	0.67	0.63	0.67	0.65
Cytokine	0.50	0.78	0.67	0.64	0.65
Imaging	0.88	0.44	0.58	0.80	0.65
Clinical	0.25	0.67	0.40	0.50	0.47
APOEε4 dosage	0.75	0.67	0.67	0.75	0.71

REFERENCES

[1] Ferri CP, Prince M, Brayne C, Brodaty H, Fratiglioni L, Ganguli M, Hall K, Hasegawa K, Hendrie H, Huang Y, Jorm A, Mathers C, Menezes PR, Rimmer E, Scazufca M (2005) Global prevalence of dementia: a Delphi consensus study. *Lancet* **366**, 2112-2117.

[2] Fratiglioni L, Launer LJ, Andersen K, Breteler MM, Copeland JR, Dartigues JF, Lobo A, Martinez-Lage J, Soininen H, Hofman A (2000) Incidence of dementia and major subtypes in Europe: A collaborative study of population-based cohorts. *Neurologic Diseases in the Elderly Research Group. Neurology* **54**, S10-S15.

[3] Pogacic V, Herrling P (2009) List of drugs in development for neurodegenerative diseases. Update June 2008. *Neurodegener Dis* **6**, 37-86.

[4] Dubois B, Feldman HH, Jacova C, Dekosky ST, Barberger-Gateau P, Cummings J, Delacourte A, Galasko D, Gauthier S, Jicha G, Meguro K, O'Brien J, Pasquier F, Robert P, Rossor M, Salloway S, Stern Y, Visser PJ, Scheltens P (2007) Research criteria for the diagnosis of Alzheimer's disease: revising the NINCDS-ADRDA criteria. *Lancet Neurol* **6**, 734-746.

[5] Modrego PJ (2006) Predictors of conversion to dementia of probable Alzheimer type in patients with mild cognitive impairment. *Curr Alzheimer Res* **3**, 161-170.

[6] Mitchell AJ, Shiri-Feshki M (2009) Rate of progression of mild cognitive impairment to dementia–meta-analysis of 41 robust inception cohort studies. *Acta Psychiatr Scand* **119**, 252-265.

[7] Bruscoli M, Lovestone S (2004) Is MCI really just early dementia? A systematic review of conversion studies. *Int Psychogeriatr* **16**, 129-140.

[8] Diniz SO, Pinto JA, Forlenza OV (2008) Do CSF total tau, phosphorylated tau, and β-amyloid 42 help to predict progression of mild cognitive impairment to Alzheimer's disease? A systematic review and meta-analysis of the literature. *World Journal of Biological Psychiatry* **9**, 172-182.

[9] Davatzikos C, Bhatt P, Shaw LM, Batmanghelich KN, Trojanowski JQ (2010) Prediction of MCI to AD conversion via MRI CSF biomarkers and pattern classification. *Neurobiol Aging*.

[10] Desikan RS, Cabral HJ, Fischl B, Guttmann CR, Blacker D, Hyman BT, Albert MS, Killiany RJ (2009) Temporoparietal MR imaging measures of atrophy in subjects with mild cognitive impairment that predict subsequent diagnosis of Alzheimer disease. *AJNR Am J Neuroradiol* **30**, 532-538.

[11] Devanand DP, Pradhaban G, Liu X, Khandji A, De Santi S, Segal S, Rusinek H, Pelton GH, Honig LS, Mayeux R, Stern Y, Tabert MH, de Leon MJ (2007) Hippocampal and entorhinal atrophy in mild cognitive impairment: prediction of Alzheimer disease. *Neurology* **68**, 828-836.

[12] Fleisher AS, Sun S, Taylor C, Ward CP, Gamst AC, Petersen RC, Jack CR, Jr., Aisen PS, Thal LJ (2008) Volumetric MRI vs clinical predictors of Alzheimer disease in mild cognitive impairment. *Neurology* **70**, 191-199.

[13] Jack CR, Jr, Petersen RC, Xu YC, O'Brien PC, Smith GE, Ivnik RJ, Boeve BF, Waring SC, Tangalos EG, Kokmen E (1999) Prediction of AD with MRI-based hippocampal volume in mild cognitive impairment. *Neurology* **52**, 1397-1403.

[14] Liu Y, Paajanen T, Zhang Y, Westman E, Wahlund LO, Simmons A, Tunnard C, Sobow T, Mecocci P, Tsolaki M, Vellas B, Muehlboeck S, Evans A, Spenger C, Lovestone S, Soininen H (2010) Analysis of regional MRI volumes and thicknesses as predictors of conversion from mild cognitive impairment to Alzheimer's disease. *Neurobiol Aging* **31**, 1375-1385.

[15] Okello A, Koivunen J, Edison P, Archer HA, Turkheimer FE, Nagren K, Bullock R, Walker Z, Kennedy A, Fox NC, Rossor MN, Rinne JO, Brooks DJ (2009) Conversion of amyloid positive and negative MCI to AD over 3 years: an 11C-PIB PET study. *Neurology* **73**, 754-760.

[16] Blennow K (2004) Cerebrospinal fluid protein biomarkers for Alzheimer's disease. *NeuroRx* **1**, 213-225.

[17] Shaw LM, Vanderstichele H, Knapik-Czajka M, Clark CM, Aisen PS, Petersen RC, Blennow K, Soares H, Simon A, Lewczuk P, Dean R, Siemers E, Potter W, Lee VM, Trojanowski JQ (2009) Cerebrospinal fluid biomarker signature in Alzheimer's disease neuroimaging initiative subjects. *Ann Neurol* **65**, 403-413.

[18] Landau SM, Harvey D, Madison CM, Reiman EM, Foster NL, Aisen PS, Petersen RC, Shaw LM, Trojanowski JQ, Jack CR, Jr, Weiner MW, Jagust WJ (2010) Comparing predictors of conversion and decline in mild cognitive impairment. *Neurology*.

[19] Cuingnet R, Gerardin E, Tessieras J, Auzias G, Lehericy S, Habert MO, Chupin M, Benali H, Colliot O (2010) Automatic classification of patients with Alzheimer's disease from structural MRI: A comparison of ten methods using the ADNI database. *Neuroimage*.

[20] Akuffo EL, Davis JB, Fox SM, Gloger IS, Hosford D, Kinsey EE, Jones NA, Nock CM, Roses AD, Saunders AM, Skehel JM, Smith MA, Cutler P (2008) The discovery and early validation of novel plasma biomarkers in mild-to-moderate Alzheimer's disease patients responding to treatment with rosiglitazone. *Biomarkers* **13**, 618-636.

[21] Thambisetty M, Simmons A, Velayudhan L, Hye A, Campbell J, Zhang Y, Wahlund LO, Westman E, Kinsey A, Guntert A, Proitsi P, Powell J, Causevic M, Killick R, Lunnon K, Lynham S, Broadstock M, Choudhry F, Howlett DR, Williams RJ, Sharp SI, Mitchelmore C, Tunnard C, Leung R, Foy C, O'Brien D, Breen G, Furney SJ, Ward M, Kloszewska I, Mecocci P, Soininen H, Tsolaki M, Vellas B, Hodges A, Murphy DG, Parkins S, Richardson JC, Resnick SM, Ferrucci L, Wong DF, Zhou Y, Muehlboeck S, Evans A, Francis PT, Spenger C, Lovestone S (2010) Association of plasma clusterin concentration with severity, pathology, and progression in Alzheimer disease. *Arch Gen Psychiatry* **67**, 739-748.

[22] Thambisetty M, Hye A, Foy C, Daly E, Glover A, Cooper A, Simmons A, Murphy D, Lovestone S (2008) Proteome-based identification of plasma proteins associated with hippocampal

metabolism in early Alzheimer's disease. *J Neurol* **255**, 1712-1720.

[23] Ray S, Britschgi M, Herbert C, Takeda-Uchimura Y, Boxer A, Blennow K, Friedman LF, Galasko DR, Jutel M, Karydas A, Kaye JA, Leszek J, Miller BL, Minthon L, Quinn JF, Rabinovici GD, Robinson WH, Sabbagh MN, So YT, Sparks DL, Tabaton M, Tinklenberg J, Yesavage JA, Tibshirani R, Wyss-Coray T (2007) Classification and prediction of clinical Alzheimer's diagnosis based on plasma signaling proteins. *Nat Med* **13**, 1359-1362.

[24] O'Bryant SE, Xiao G, Barber R, Reisch J, Doody R, Fairchild T, Adams P, Waring S, Diaz-Arrastia R (2010) A Serum Protein-Based Algorithm for the Detection of Alzheimer Disease. *Arch Neurol* **67**, 1077-1081.

[25] Mosconi L, Perani D, Sorbi S, Herholz K, Nacmias B, Holthoff V, Salmon E, Baron JC, De Cristofaro MT, Padovani A, Borroni B, Franceschi M, Bracco L, Pupi A (2004) MCI conversion to dementia and the APOE genotype: a prediction study with FDG-PET. *Neurology* **63**, 2332-2340.

[26] Borroni B, Premi E, Di Luca M, Padovani A (2007) Combined biomarkers for early Alzheimer disease diagnosis. *Curr Med Chem* **14**, 1171-1178.

[27] Visser PJ, Scheltens P, Verhey FR, Schmand B, Launer LJ, Jolles J, Jonker C (1999) Medial temporal lobe atrophy and memory dysfunction as predictors for dementia in subjects with mild cognitive impairment. *J Neurol* **246**, 477-485.

[28] Okamura N, Arai H, Maruyama M, Higuchi M, Matsui T, Tanji H, Seki T, Hirai H, Chiba H, Itoh M, Sasaki H (2002) Combined analysis of CSF tau levels and [(123)I]iodoamphetamine SPECT in mild cognitive impairment: implications for a novel predictor of Alzheimer's disease. *Am J Psychiatry* **159**, 474-476.

[29] Devanand DP, Liu X, Tabert MH, Pradhaban G, Cuasay K, Bell K, de Leon MJ, Doty RL, Stern Y, Pelton GH (2008) Combining early markers strongly predicts conversion from mild cognitive impairment to Alzheimer's disease. *Biol Psychiatry* **64**, 871-879.

[30] Ewers M, Walsh C, Trojanowski JQ, Shaw LM, Petersen RC, Jack CR, Jr., Feldman HH, Bokde AL, Alexander GE, Scheltens P, Vellas B, Dubois B, Weiner M, Hampel H Prediction of conversion from mild cognitive impairment to Alzheimer's disease dementia based upon biomarkers and neuropsychological test performance. *Neurobiol Aging*.

[31] Lovestone S, Francis P, Strandgaard K (2007) Biomarkers for disease modification trials–the innovative medicines initiative and AddNeuroMed. *J Nutr Health Aging* **11**, 359-361.

[32] Hye A, Lynham S, Thambisetty M, Causevic M, Campbell J, Byers HL, Hooper C, Rijsdijk F, Tabrizi SJ, Banner S, Shaw CE, Foy C, Poppe M, Archer N, Hamilton G, Powell J, Brown RG, Sham P, Ward M, Lovestone S (2006) Proteome-based plasma biomarkers for Alzheimer's disease. *Brain* **129**, 3042-3050.

[33] Jack CR, Jr, Bernstein MA, Fox NC, Thompson P, Alexander G, Harvey D, Borowski B, Britson PJ, Ward JLW, Dale C, Felmlee AM, Gunter JP, Hill JL, Killiany DL, Schuff R, Fox-Bosetti N, Lin S, Studholme C, DeCarli C, Krueger CS, Ward G, Metzger HA, Scott GJ, Mallozzi KT, Blezek R, Levy D, Debbins J, Fleisher JP, Albert AS, Green M, Bartzokis R, Glover G, Mugler G, Weiner J, MW (2008) The Alzheimer's Disease Neuroimaging Initiative (ADNI): MRI methods. *J Magn Reson Imaging* **27**, 685-691.

[34] Simmons A, Westman E, Muehlboeck S, Mecocci P, Vellas B, Tsolaki M, Kloszewska I, Wahlund LO, Soininen H, Lovestone S, Evans A, Spenger C (2009) MRI measures of

Alzheimer's disease and the AddNeuroMed study. *Ann N Y Acad Sci* **1180**, 47-55.

[35] Simmons A, Other AN, Other AN, Lovestone S(in press) The AddNeuroMed framework for multi-centre MRI assessment of longitudinal changes in Alzheimer's disease : experience from the first 24 months. *Int J Ger Psych*.

[36] Fischl B, Dale AM (2000) Measuring the thickness of the human cerebral cortex from magnetic resonance images. *Proc Natl Acad Sci U S A* **97**, 11050-11055.

[37] Fischl B, Salat DH, Busa E, Albert M, Dieterich M, Haselgrove C, van der Kouwe A, Killiany R, Kennedy D, Klaveness S, Montillo A, Makris N, Rosen B, Dale AM (2002) Whole brain segmentation: automated labeling of neuroanatomical structures in the human brain. *Neuron* **33**, 341-355.

[38] Fischl B, Salat DH, van der Kouwe AJ, Makris N, Segonne F, Quinn BT, Dale AM (2004) Sequence-independent segmentation of magnetic resonance images. *Neuroimage* **23**(1), S69-S84.

[39] Frank E, Hall M, Trigg L, Holmes G, Witten IH (2004) Data mining in bioinformatics using Weka. *Bioinformatics* **20**, 2479-2481.

[40] Ben-Hur A, Ong CS, Sonnenburg S, Scholkopf B, Ratsch G (2008) Support vector machines and kernels for computational biology. *PLoS Comput Biol* **4**, e1000173.

[41] den Heijer T, Geerlings MI, Hoebeek FE, Hofman A, Koudstaal PJ, Breteler MM (2006) Use of hippocampal and amygdalar volumes on magnetic resonance imaging to predict dementia in cognitively intact elderly people. *Arch Gen Psychiatry* **63**, 57-62.

[42] Alvarez XA, Franco A, Fernandez-Novoa L, Cacabelos R (1996) Blood levels of histamine, IL-1 beta, and TNF-alpha in patients with mild to moderate Alzheimer disease. *Mol Chem Neuropathol* **29**, 237-252.

[43] De Luigi A, Fragiacomo C, Lucca U, Quadri P, Tettamanti M, Grazia De Simoni M (2001) Inflammatory markers in Alzheimer's disease and multi-infarct dementia. *Mech Ageing Dev* **122**, 1985-1995.

[44] Lombardi VR, Garcia M, Rey L, Cacabelos R (1999) Characterization of cytokine production, screening of lymphocyte subset patterns and in vitro apoptosis in healthy and Alzheimer's Disease (AD) individuals. *J Neuroimmunol* **97**, 163-171.

[45] Beloosesky Y, Salman H, Bergman M, Bessler H, Djaldetti M (2002) Cytokine levels and phagocytic activity in patients with Alzheimer's disease. *Gerontology* **48**, 128-132.

[46] Di Bona D, Plaia A, Vasto S, Cavallone L, Lescai F, Franceschi C, Licastro F, Colonna-Romano G, Lio D, Candore G, Caruso C (2008) Association between the interleukin-1beta polymorphisms and Alzheimer's disease: a systematic review and meta-analysis. *Brain Res Rev* **59**, 155-163.

[47] Yasutake C, Kuroda K, Yanagawa T, Okamura T, Yoneda H (2006) Serum BDNF, TNF-alpha and IL-1beta levels in dementia patients: comparison between Alzheimer's disease and vascular dementia. *Eur Arch Psychiatry Clin Neurosci* **256**, 402-406.

[48] Mrak RE, Griffin WS (2005) Potential inflammatory biomarkers in Alzheimer's disease. *J Alzheimers Dis* **8**, 369-375.

[49] Yang SP, Bae DG, Kang HJ, Gwag BJ, Gho YS, Chae CB (2004) Co-accumulation of vascular endothelial growth factor with beta-amyloid in the brain of patients with Alzheimer's disease. *Neurobiol Aging* **25**, 283-290.

[50] Chiappelli M, Borroni B, Archetti S, Calabrese E, Corsi MM, Franceschi M, Padovani A, Licastro F (2006) VEGF gene and phenotype relation with Alzheimer's disease and mild cognitive impairment. *Rejuvenation Res* **9**, 485-493.

[51] Tarkowski E, Issa R, Sjogren M, Wallin A, Blennow K, Tarkowski A, Kumar P (2002) Increased intrathecal levels of the angiogenic factors VEGF and TGF-beta in Alzheimer's disease and vascular dementia. *Neurobiol Aging* **23**, 237-243.

[52] Mateo I, Llorca J, Infante J, Rodriguez-Rodriguez E, Fernandez-Viadero C, Pena N, Berciano J, Combarros O (2007) Low serum VEGF levels are associated with Alzheimer's disease. *Acta Neurol Scand* **116**, 56-58.

[53] Blasko I, Lederer W, Oberbauer H, Walch T, Kemmler G, Hinterhuber H, Marksteiner J, Humpel C (2006) Measurement of thirteen biological markers in CSF of patients with Alzheimer's disease and other dementias. *Dement Geriatr Cogn Disord* **21**, 9-15.

[54] Blom ES, Giedraitis V, Zetterberg H, Fukumoto H, Blennow K, Hyman BT, Irizarry MC, Wahlund LO, Lannfelt L, Ingelsson M (2009) Rapid progression from mild cognitive impairment to Alzheimer's disease in subjects with elevated levels of tau in cerebrospinal fluid and the APOE epsilon4/epsilon4 genotype. *Dement Geriatr Cogn Disord* **27**, 458-464.

This page intentionally left blank

Subject Index

This page intentionally left blank

Author Index